सत्यमेव जयते

INDIAN AGRICULTURAL
RESEARCH INSTITUTE, NEW DELHI

49237

I.A.R.I.6.
GIP NLK—H 3 I.A.R.I.—10-5-55—15,000

THE
REVIEW OF SCIENTIFIC
INSTRUMENTS

EDITOR

GAYLORD P. HARNWELL

ASSOCIATE EDITORS

D. W. BRONK
F. K. HARRIS
P. H. MILLER, JR.
W. A. WILDHACK

EDITORIAL BOARD

Term ending December 31, 1940
C. P. BONER
T. W. BONNER
J. P. HERVEY
A. G. HILL
A. W. LAWSON
J. D. STRONG

Term ending December 31, 1950
W. FOWLER
S. A. KORFF
F. N. D. KURIE
C. D. MONTGOMERY
L. S. TAYLOR
R. E. ZIRKLE

Term ending December 31, 1951
W. BLEAKNEY
J. B. H. KUPER
T. LAURITSEN
J. R. PAPPENHEIMER
L. B. SNODDY
C. H. TOWNES

VOLUME 20, NEW SERIES
JANUARY-DECEMBER, 1949

A publication of the
AMERICAN INSTITUTE OF PHYSICS
57 East 55 Street, New York 22, New York

SUGGESTIONS FOR CONTRIBUTORS

Send **manuscripts** to Gaylord P. Harnwell, Randal Morgan Laboratory of Physics, University of Pennsylvania, Philadelphia, Pennsylvania. Textual material (abstract, body of the paper, tabular material, references, and figure captions) must be in English, typewritten (except mathematical expressions) double spaced with wide margins on a durable, white paper, preferably letter size. The original copy, not the carbon, should be submitted. For general style, spellings, abbreviations, and form, consult recent issues of this journal.

An **abstract** must accompany each article. It should be adequate as an index and as a summary.

All but the simplest **mathematical expressions** should be carefully printed in by hand. Be sure to distinguish between capital and small letters. Indicate clearly superscripts and subscripts by inverted carets and carets, respectively. Avoid complicated superscripts and subscripts. Avoid repetition of a complicated expression by representing it by a symbol. Identify in the margin Greek letters and unusual symbols. Use fractional exponents instead of root signs. Use the solidus (/) for fractions wherever its use will save vertical space.

References should appear as footnotes, numbered consecutively, and arranged thus:

[1] A. B. Smith, Phy. Rev. 41, 852 (1932).

[2] H. Lamb, *Hydrodynamics* (Cambridge University Press, Teddington, England), sixth edition, pp. 573, 645.

Tables may be typewritten on sheets separate from the running text. Each table must have a caption which will make the data in the table intelligible without reference to the text. Avoid complicated column headings.

Wherever possible **figures** should be planned for the width of a column (3 in.). A convenient reduction ratio is about 2:1 or 3:1. Lettering should be large enough on the original that when reduced it shall not be less than about $\frac{1}{16}$ in. (~1.5 mm.). Line drawings must be in *India ink* on white paper or tracing cloth. Coordinate paper is not desirable but if used must be blue lined and the coordinate lines which are to show must be inked over. Photographs should have maximum black and white contrast. Identify each original drawing or photograph on the back with the author's name and the figure number. Figures should be numbered consecutively. Captions should be typed on a separate sheet of paper.

A limited number of **alterations** in proof are unavoidable, but the cost of making extensive alterations after the article has been set in type will be charged to the author.

Proof and all correspondence concerning papers in the process of publication should be addressed to the Publication Manager, American Institute of Physics, 57 East 55 Street, New York 22, New York.

INFORMATION FOR SUBSCRIBERS

The Review of Scientific Instruments is a monthly journal published by the American Institute of Physics and devoted to scientific instruments, apparatus, and techniques. Its contents include original and review articles on instruments in physics and allied sciences and sections on laboratory practices, book reviews, new instruments, new materials, news, and current literature of physics. One volume is published annually.

Subscriptions and orders for back numbers should be addressed to the American Institute of Physics, 57 East 55 Street, New York 22, New York.

Subscription Price

	U. S. and Canada	Elsewhere
To members and associate members of the American Institute of Physics	$5.00	$6.00
To all others	7.00	8.00

Back Number Prices

Vol. 1, 1930–Vol. 6, 1935 (some issues out of print)	None
Vol. 7, 1936–Vol. 19, 1948	$104.00
Yearly rate:	
1930–1935	None
1936 and thereafter	$ 10.00
Single copies	$ 1.00

Advertising rates will be supplied on request.

American Institute of Physics
57 East 55 Street **New York 22, New York**

CONTENTS

JANUARY, 1949

Orbital Stability in a Proton Synchrotron . . . . R. Q. Twiss and N. H. Frank 1

Double-Channel, Direct Reading, Low Frequency Counting Rate Meter and Counting Rate Comparator . . . . Robert M. Kloepper and Frank E. Hoecker 17

Recording Mechanical Pressure Gauge of High Range . . . . Paul M. Higgs 23

Self-Contained Recording Pressure Gauge . . . .
David R. Brown, William C. Galloway, Jack B. Robertson, and Gene A. Silvey 27

Multiple-Reflection Optical Lever . . . . H. O. Hoadley 30

Improved Magnetic Focusing of Charged Particles . . . . Larkin Kerwin 36

Geiger-Mueller Counting Unit and External Quenching Equipment for the Estimation of C^{14} in Carbon Dioxide . . . . W. B. Mann and G. B. Parkinson 41

Apparatus for Cloud-Chamber Investigations with Free Balloons . . . .
. . . . E. J. Lofgren, E. P. Ney, and F. Oppenheimer 48

Statistical Theory of the Dead Time Losses of a Counter . . . . C. E. Clark 51

Apparatus for Determining the Effect of Centrifugal Force on the Potentials of Galvanic Cells
. . . . B. Roger Ray and D. A. MacInnes 52

Circuits for Minimizing Transient Effects on Energy Measurements in Calorimetry . . . . .
. . . . Harold J. Hoge 59

Accurate Gas Metering System for Laminar Flow Studies . . . .
. . . . J. W. Andersen and R. Friedman 61

Optical Properties of Surface Films. II . . . . Alexandre Rothen and Marjorie Hanson 66

Sampling Devices for Determining the Bacterial Content of Air . . . .
. . . . Matthew Luckiesh, A. H. Taylor, and Thomas Knowles 73

Wide-Range Saw-Tooth Generator . . . . Peter G. Sulzer 78

Laboratory and Shop Notes:

Distant Counting of Scintillations . . . . E. P. Blizard and S. DeBenedetti 81

Convenient Method for Checking the Linearity of an Electron Multiplier Circuit . . . .
. . . . George P. Kirkpatrick 81

Method of Linearizing the Voltage Rise of a Relaxation Oscillator . . . . R. J. Watts 81

High Temperature X-Ray Diffraction Techniques . . . . J. J. Lander 82

Regular Features:

New Instruments 83

New Materials 91

FEBRUARY, 1949

Trochotron Design Principles . . . . G. W. Monk and G. K. Werner 93

Servo Employing the Magnetic Fluid Clutch . . . . E. S. Bettis and E. R. Mann 97

Note on Analog Computer Design . . . . J. A. Bronzo and H. G. Cohen 101

Exposure Meter for Precision Light Dosage . . . . Herbert F. Launer 103

Capillary Collector for Measuring the Deposition of Water Drops on a Surface Moving through Clouds . . . . Bernard Vonnegut 110

Apparatus for the Production of Large Metallic Crystals by Solidification at High Temperatures
. . . . Louis Gold 115

Large Helium Liquefier . . . . J. G. Daunt and H. L. Johnston 122

Design of the Radiofrequency System for the 184-Inch Cyclotron . . . .
. . . . . . K. R. MacKenzie, F. H. Schmidt, J. R. Woodyard, and L. F. Wouters 126

Method for Measuring Very High Speed Transient Currents . . . .
. . . . A. M. Zarem and F. R. Marshall 133

Laboratory and Shop Notes:

Pulsed Oscillator for F-M Cyclotron . . . J. W. Burkig, E. L. Hubbard, and K. R. MacKenzie 135

Toggle-Operated Vacuum Valve . . . . Ralph O. McIntosh and John W. Coltman 135

Note on Constant Current Regulators . . . . E. E. Minett, D. A. MacRae, and J. Townsend 136

Lock-In *RC* Oscillator . . . . W. C. Elmore and D. Bancroft 136

D.C. Flat Card Resolver . . . . R. G. Murdick 137

Use of Characteristic Curves for Pump-Speed *vs.* Pressure . . . . Saul Dushman 139

Method of Assessing Transient Stresses in Photo-elastic Substances . . . . . . John S. Stanton 139

Kovar Glass Seals at Liquid Helium Temperatures . . . . C. T. Lane 140

Regular Features:

New Instruments 141

New Materials 145

Index to Advertisers xiii

MARCH, 1949

Counter Pulse Shape . . . . C. D. THOMAS 147
Developments in the Useful Circular Nomogram . . . . DOUGLAS P. ADAMS AND HOWARD T. EVANS, JR. 150
New Techniques Applied to the Buerger Precession Camera for X-Ray Diffraction Studies . . . . HOWARD T. EVANS, JR., S. G. TILDEN, AND DOUGLAS P. ADAMS 155
Conditions for Optimum Luminosity and Energy Resolution in an Axial β-Ray Spectrometer with Homogeneous Magnetic Field . . . . JESSE W. M. DUMOND 160
Tissue Stimulators Utilizing Radiofrequency Coupling . . . . OTTO H. SCHMITT AND DONALD R. DUBBERT 170
Absorption Corrections in X-Ray Studies of Preferred Orientation . . . . R. SMOLUCHOWSKI AND R. W. TURNER 173
Rapid Infra-Red Gas Analyzer . . . . RICHARD C. FOWLER 175
Scintillation Counter as a Proportional Device . . . . ROSALIE C. HOYT 178
Pulse Amplitude Analyzer for Nuclear Research Using Pretreated Pulses . . . . C. H. WESTCOTT AND G. C. HANNA 181
Magnetic Ion Source . . . . CARL BAILEY, D. L. DRUKEY, AND F. OPPENHEIMER 189
Theory of the Solenoid Beta-Ray Spectrometer . . . . E. PERSICO 191
Simplified Chronotron-Type Timing Circuit . . . . J. WARREN KEUFFEL 197
Parallel-Plate Counters . . . . J. WARREN KEUFFEL 202

PHYSICAL INSTRUMENTS FOR THE BIOLOGIST

Equipment and Experimental Methods for Interference Diffusion Studies . . . . LOUIS J. GOSTING, EDWIN M. HANSON, GERSON KEGELES, AND MARGARET S. MORRIS 209

Laboratory and Shop Notes:

Note on the Preparation of Beta-Ray Sources . . . . LAWRENCE M. LANGER 216
On the Design of a Radiofrequency Cockroft-Walton Accelerator . . . . PAUL LORRAIN 216
Rejuvenation of Geiger-Mueller Tubes . . . . L. SHEPARD 217
Thyratron Square Wave Generator . . . . LEONARD REIFFEL 218
New Principle in Controlled Vacuum Leaks . . . . C. H. BACHMAN 219
Absorption Cell and Loader for Use in Microanalysis by Infra-Red Spectroscopy . . . . SEYMOUR H. WOLLMAN 220
Octane Vapor Proportional Counter . . . . R. P. PEPPER 222

Regular Features:

New Materials 223
New Instruments 224
Index to Advertisers xlvi

APRIL, 1949

Errors in Second-Order Measuring Instruments . . . . ELLIOT T. BENEDIKT 229
Design and Performance of a Multicellular Geiger Counter for Gamma-Radiation . . . . DAVID A. LIND 233
Maxwell Bridge at Low Frequencies . . . . VINTON A. BROWN AND B. P. RAMSAY 236
Methods for Reducing Insulator Noise and Leakage . . . . F. M. GLASS 239
Conversion of a Motor Generator into a Low Noise Power Amplifier . . . . H. S. SOMMERS, JR., P. R. WEISS, AND W. HALPERN 244
Wide Range Capacitance-Conductance Bridge . . ROBERT H. COLE AND PAUL M. GROSS, JR. 252
Interferometric Study of Supersonic Channel Flow . . . . DANIEL BERSHADER 260
Cloud-Chamber Equipment for Study of Infrequent Cosmic-Ray Processes . . . . W. Y. CHANG AND J. R. WINCKLER 276
Magnetic Deflector for Mesons Produced in the 184-Inch Cyclotron . . . . WOLFGANG K. H. PANOFSKY AND ERNEST A. MARTINELLI 286
Pressure Regulated Thin Window Geiger-Mueller Counter . . . . MICHEL TER-POGOSSIAN, J. EUGENE ROBINSON, AND J. TOWNSEND 289
Electronic Apparatus for the Determination of the Physical Properties of Freely Falling Raindrops . . . . ROSS GUNN 291
Large Mass Spectrometer Employing Crossed Electric and Magnetic Fields . . . . THOMAS MARINER AND WALKER BLEAKNEY 297
Novel Recording Accelerometer . . . . ARTHUR S. IBERALL 304
Book Reviews 308
Author Index to Books Reviewed 317
Other Books Received 317

Laboratory and Shop Notes:

Electron Trajectories in a Gamma-Ray Spectrometer . . . H. Hurwitz, Jr. 318

Timer for Short Intervals . . . R. StuÀrt Mackay 318

New Discharge Tube for the Hydrogen Atom Spectrum . . W. P. van Oort and C. S. van Heel 319

Improving the Response Characteristic of Graphic Recorders . . P. G. Sulzer and A. H. Waynick 320

Vacuum Tube Relay for Thermostat Control . . . I. Sucher and H. S. Anker 321

Accurate, Simple Recording Microphotometer . . . P. Rosenblum and A. deBretteville, Jr. 321

Vacuum-Tube Current Integrator of Improved Design . . . L. H. v. d. Tweel 323

Modification of the Gouy Modulator . . . L. S. Darken 323

Flexible Vacuum Seal . . . Otto Retzloff 324

Device for Producing an Easily Identified Area on the Electron Microscope Specimen Screen . . . Francis W. Bishop 324

Current Integrator . . . H. T. Gittings, Jr. 325

Regular Features:

New Instruments . . . 326

New Materials . . . 331

Index to Advertisers . . . xlviii

May, 1949

Mass Spectrometer for Continuous Gas Analysis . . . Jack A. Hunter, Ralph W. Stacy, and Fred A. Hitchcock 333

Microwave Polarimeter . . . Alfred E. Schwaneke and Zaboj V. Harvalik 337

Photomicrography of Tracks in Nuclear Research Emulsions . . . Adair Morrison and Fred Morton 341

High Temperature X-Ray Diffraction Camera . . . James W. Edwards, Rudolph Speiser, and Herrick L. Johnston 343

Methane Flow Beta-Proportional Counter . . William Bernstein and Robert Ballentine 347

Ionization Flame Detectors . . . Hartwell F. Calcote 349

Experiments in the Possibility of Increasing the Efficiency of Gamma-Counters . . . Hilding Slätis 353

Improved Low Angle X-Ray Diffraction Camera . Barbara A. Wright and Peter A. Cole 355

PHYSICAL INSTRUMENTS FOR THE BIOLOGIST

Simple Calorimeter for the Simultaneous Determination of Heat Loss and Heat Production in Animals . . . Lawrence R. Prouty, Martha J. Barrett, and James D. Hardy 357

Laboratory and Shop Notes:

New Vacuum Gauge . . . Carlton F. Johnson 364

Simple Electronic Relay . . . Robert H. Linnell and Helmut M. Haendler 364

Apparatus for Producing Powder-Like X-Ray Diffraction Patterns from Single Crystals . . . F. W. Matthews and A. O. McIntosh 365

Large Straight Through Vacuum Valve for Van de Graaff Generators . . . B. Jennings 366

Cells Drawn from Tantalum, Molybdenum, and Platinum for High Temperature Research . . . George W. Ziegler, Jr., Rudolph Speiser, and Herrick L. Johnston 367

Non-Uniform Shrinkage of X-Ray Films . . . M. H. Jellinek 368

Use of Gas Traps in Barometers, Laboratory Mercury Lamps, etc. . . . E. L. Harrington 368

Vibration Absorber for Gas Holders . . . R. S. Craig and W. E. Wallace 369

Construction of Beta-Geiger Counters from Prefabricated Thin Wall Tubing . . . F. E. Senftle, W. Havercroft, and P. Hernandez 370

Percent Transmission Computer for Infra-Red Spectra . . . C. E. Zerwekh, Jr. 371

Use of Anodized Aluminum in the Construction of Calorimeter Heaters . . George W. Murphy 372

Method for Preparing Capillary Tube Samples for X-Ray Diffraction Powder Analysis . . . Paul J. Hagelston and Harris W. Dunn 373

Regular Features:

New Instruments . . . 374

New Materials . . . 379

Index to Advertisers . . . xlviii

June, 1949

Further Improvements in Magnetic Focusing . . Larkin Kerwin and Claude Geoffrion 381

Regulation of Temperature in the Application of High Frequency Induction Heating to Thermodynamic Measurements . . . Rudolph Speiser, George W. Ziegler, Jr., and Herrick L. Johnston 385

Instrumentation for Nuclear Studies with Externally Focused Deuteron Beam from Ten-Mev Cyclotron . . . B. R. Curtis, J. L. Fowler, and L. Rosen 388

New Method of Measuring the Stopping Power of Several Materials for Alpha-Particles . . . F. Emmett Hammer and Frank E. Hoecker 394

Cloud Chamber of Light Weight for Balloon Flights . . . R. P. Shutt, A. L. Johnson, and A. M. Thorndike 398
Magnetic Field Strength Meter Using the Proton Magnetic Moment . . . N. J. Hopkins 401
22-Inch Wilson Cloud Chamber in a Magnetic Field of 21,700 Gauss . . . Wilson M. Powell 403
Magnet Coils . L. G. Coonrod, W. E. Cecconi, C. Gedraitis, K. R. Harper, and R. M. Lewis 408
Counter Controllable High Pressure Cloud Chamber . . . G. E. Valley and J. A. Vitale 411
Differential Counting with Reversible Decade Counting Circuits . . Frederick H. Martens 424
Measurement of the Series-Resonant Resistance of a Quartz Crystal . . . L. A. Rosenthal and T. A. Peterson, Jr. 426
New High Sensitivity Remanent Magnetometer . . . Ellis A. Johnson, Thomas Murphy, and P. F. Michelsen 429
Effect of Temperature on the Steady-State Sensitivity of Vacuum Radiation Detectors . . . I. Amdur and N. L. Brown 435

PHYSICAL INSTRUMENTS FOR THE BIOLOGIST

Modified String Flowmeter for Measuring Breath Velocity . . H. Specht and H. F. Brubach 442
Erratum . . . 447

Book Reviews . . . 448
- Author Index to Books Reviewed . . . 456
- Other Books Received . . . 456

Laboratory and Shop Notes:

- Lead-In Seals for Kinetic High Vacuum Systems Using Rubbers . . . Ralph C. Taylor and Carnot W. Ward 457
- Measurement of the Thickness of Thin Nylon Films . . . A. I. McPherson and D. G. Douglas 457
- Ultimate Vacua of Diffusion Pumps . . . G. W. Sears 458
- Device for Producing Rate-Proportional Damping Signal in Servo Systems . . . L. W. Herscher 459

Regular Features:

- New Instruments . . . 459
- New Materials . . . 465
- Index to Advertisers . . . xlii

July, 1949

Direct Reading Pulse Length Meter and Shape Analyzer . . . Robert Rudin 467
Design for a Metal Mass Spectrometer Tube . . . W. M. Hickam 472
Rotor Balancing with an Electronic Capacitor Gauge . . . H. D. Warshaw 474
Counting Volume of a Cylindrical Ionization Chamber . . . Nelson M. Blachman 477
Instrument for Rapid Determination of Crystal Orientation . . . R. H. Gillette and M. H. Jellinek 480
Erratum: A New Discharge Tube for the Hydrogen Atom Spectrum . . . W. P. van Oort and A. C. S. van Heel 479
Characteristics of Halogen Counters . . . Sidney H. Liebson 483
Circuit for the Study of the Operation of the Geiger-Müller Counter . . . Mario Alves Guimarães and Palmyra Amazonas Sampaio 485
Magnetic Susceptibility Balance for Use at Liquid Helium Temperatures . . . T. R. McGuire and C. T. Lane 489
Large Cloud Chamber Using Rear Illumination . . . E. W. Cowan 492
Ten-Channel Electrostatic Pulse Analyzer . . . Dean A. Watkins 495
Precision Automatic Electrometer . . . N. T. Seaton 500
New Technique for the Determination of Heats of Sublimation of Slightly Volatile Substances . . . O. C. Simpson and R. J. Thorn 504
Measurement of the Spin of a Projectile in Flight . . . H. D. Warshaw 507
Stress-Strain-Time Apparatus for Fiber Testing . . . C. H. Reichardt, H. Scharvitz, and J. H. Dillon 509
Amplitude Bridge for Detection of Nuclear Resonance . H. A. Thomas and R. D. Huntoon 516

PHYSICAL INSTRUMENTS FOR THE BIOLOGIST

Cardiotachometer Based on the Plethysmogram . . . E. E. Suckling 518
Syringe Oxygen Cathode for Measurement of Oxygen Tension in Solution and in Respiratory Gases . . . Julian M. Tobias and Nadine Retondo 519

Laboratory and Shop Notes:

Dry Box for Handling Alkali Metals and Other Extremely Hygroscopic Materials . . . . Eugene E. Ketchen, Forrest A. Trumbore, W. E. Wallace, and R. S. Craig 524
Several Improvements on the "Philip's Gauge" . . . C. Hayashi, K. Hashimoto, K. Kaneki, K. Okamoto, and R. Sagane 524
Some Statistical Considerations on Coincidence Counting . . . . Arthur Sard and R. D. Sard 526
Instrument for Measuring Curvature of Cloud-Chamber Tracks . . . E. R. Gaerttner and M. L. Yeater 526
Cadmium Trap for Arresting Mercury Vapor . . . T. Wilner 527
Device to Deposit Automatically the Proper Thickness of Metals Used in Shadow-Casting in Electron Microscopy . . . Francis W. Bishop 527
Technique for the Production of Silica-Filmed Electron Microscope Screens in Quantity . . . Francis W. Bishop 529
Pantograph and Tilting Stage for Use with Nuclear Plates . . . Ian Barbour 530
Simple Punch for Precision Cutting of Photographic Film in a Cylindrical X-Ray Diffraction Camera . . . E. J. Grill and A. H. Weber 532
Magnetic Beam-Splitting Focusing Device for the Electron Microscope . . . Francis W. Bishop 532
Vibration Detection by a Quartz Oscillator . . . Y. L. Yousef and F. Sultan 533
Lead Brick for Shielding . . . Luther E. Preuss 534

Regular Features:

New Instruments . . . 535
New Materials . . . 539
Index to Advertisers . . . xxxviii

AUGUST, 1949

Precision Vacuum Gauge . . . G. C. Fryburg and J. H. Simons 541
Scintillation Counter. I. The Existence of Plateaus . . . Lawrence B. Robinson and James R. Arnold 549
Use of Multigrid Tubes as Electrometers . . . J. R. Prescott 553
High Current Ion Source . . . Richard B. Setlow 558
Scintillation Counter for Laboratory Counting of Alpha-Particles . . . J. D. Graves and J. P. Dyson 560
Improved Synchronous Detector . . . Walter C. Michels and Esther D. Redding 566
Counting with Geiger Counters . . . Homer E. Newell, Jr. and Eleanor C. Pressly 568
Sample Scanning Mechanism for X-Ray Diffraction . J. W. Hickman and A. G. Kleinknecht 573
Design of Equipment for Thermal Studies . . . Robert J. Teitel 575
Preparation and Use of Tritium and Deuterium Targets . . . E. R. Graves, A. A. Rodrigues, M. Goldblatt, and D. I. Meyer 579
Microsampling and Microanalysis of Metals . Donald F. Clifton and Cyril Stanley Smith 583
Transistor Trigger Circuit . . . Herbert J. Reich and Robert L. Ungvary 586
Fast Recycling Cloud Chamber and Pulsed Magnetic Field Equipment for Use with Pulsed Accelerators . . . E. R. Gaerttner and M. L. Yeater 588
Dynamics of a Synchrotron with Straight Sections . . . Nelson M. Blachman and Ernest D. Courant 596
Operational Features of a New Electron Diffraction Unit . . . Robert G. Picard, Perry C. Smith, and John H. Reisner 601
Erratum: Conditions for Optimum Luminosity and Energy Resolution in an Axial β-Ray Spectrometer with Homogeneous Magnetic Field . . . Jesse W. M. DuMond 616

PHYSICAL INSTRUMENTS FOR THE BIOLOGIST

Frequency Analyzer for Bioelectric Potentials in the Sub-Audio Range . . . Charles Markey, Robert L. Schoenfeld, and Paul F. A. Hoefer 612
Apparatus for Electrode Reversal in the Tiselius Electrophoresis Equipment . . . H. Tint 617

Laboratory and Shop Notes:

"Opener-Upper" for Gas Samples . . . Francis J. Norton 620
System for Preparing Semitransparent Mirrors . . . Claude Frémont 620
Method of Asymmetrical Pulse Duration Modulation . . . Richard John Watts 622
Note on the Preparation of Uniform Metallic Foils . . . S. D. Warshaw 623
Note on Removing the Deuteron-Induced Color from Quartz Target Plates . . . A. A. Schulke and R. E. Nuelle 623
Welder for Attaching Fine Wires to Massive Metal Bodies . . . W. J. Trott 624

New Instruments . . . 625
New Materials . . . 631
Index to Advertisers . . . xliv

SEPTEMBER, 1949

Operation of Voltage-Stabilizing Elements with Current-Stabilized Supplies . . . . J. J. GILVARRY AND D. F. RUTLAND 633
Optimum Conditions for a 180° Beta-Ray Spectrometer . . . . CLAUDE GEOFFRION 638
Calibration of Photographic Emulsions for Low Energy Electrons . . . . L. CRANBERG AND J. HALPERN 641
Microwave Secondary Electron Multiplier . . . . M. H. GREENBLATT 646
Theoretical Background of the Multiple Pressure Tube Anemometer . . . . PAUL R. GOUDY AND HENRY F. COLVIN III 651
Detection of Ca^{45}, I^{131}, P^{32}, and Zn^{65} by Photographic Film . . . . DANIEL STEINBERG AND A. K. SOLOMON 655
Inductance Apparatus for Diamagnetic Measurements . . . . S. BROERSMA 660
Tachometer . . . . A. E. BENFIELD 663
Wet Bulb Temperatures without a Wick . . . . KENNETH H. JEHN 668
Electrolytic Thermistors . . . . F. GUTMANN AND L. M. SIMMONS 674

PHYSICAL INSTRUMENTS FOR THE BIOLOGIST

Versatile Microinjection and Micropipetting Syringe . . . . JOHN B. BUCK 676
Direct Experimental Comparison of Several Surface Temperature Measuring Devices . . . . ALICE M. STOLL AND JAMES D. HARDY 678

Book Reviews 687
- **Author Index to Books Reviewed** 695
- **Other Books Received** 695

Laboratory and Shop Notes:

- **Modification of X-Ray Diffraction Micro-Camera to Permit Study of Long Spacings** . . . . M. E. BERGMANN AND I. FANKUCHEN 696
- **High Power Short Duration Spark Discharge** . . . . LESLIE S. G. KOVÁSZNAY 696
- **Simple Stable D.C. Amplifier for Measurement of Bioelectric Potentials** . . . JOHN W. MOORE 698
- **Geiger Tube Quenching Circuit for a Negative High Voltage Supply** . . RICHARD JOHN WATTS 699
- **Extended Range D.C. Bias Control of Thyratron Plate Current** . . . . LEONARD REIFFEL 699

Regular Features:

- **New Instruments** 702
- **New Materials** 707
- **Index to Advertisers** xlii

OCTOBER, 1949

Wide Range Radiation Instrument . . . . LEONARD REIFFEL AND GLENN BURGWALD 711
Variable Temperature Dielectric Cell of Wide Frequency Range for Solids and Liquids . . . . EDWARD B. BAKER 716
Automatic Scanning and Recording Photometer for Night Sky Studies . . . . DOUGLAS MARLOW AND J. C. PEMBERTON 724
Stabilized High Voltage Power Supply for Electrostatic Analyzer . . . . R. L. HENKEL AND B. PETREE 729
Low Temperature Single Crystal X-Ray Diffraction Technique . . . . H. S. KAUFMAN AND I. FANKUCHEN 733
Construction and Calibration of a Cylindrical Electrostatic Analyzer . . . . . S. K. ALLISON, S. P. FRANKEL, T. A. HALL, J. H. MONTAGUE, A. H. MORRISH, AND S. D. WARSHAW 735

Laboratory and Shop Notes:

- **Effect of Space Charge on the Focusing Properties of a 180° Mass Spectrometer** . . . . CHARLES F. ROBINSON 745
- **Vacuum Lock for Continuously Evacuated Systems** . . . . D. SAXON AND J. RICHARDS 745
- **Electronic Instrument for Rapidly Tracing the Plateaux of G-M Counters** . . . . . . G. H. VAZE 746
- **Empirical Balancing Procedure for FP-54** . . . . F. C. ARMISTEAD 747
- **Electrometer Amplifier** . . . . V. J. CALDECOURT 748
- **Improved Magnetic Focusing of Charged Particles** . . . . H. HINTENBERGER 748
- **Mercury Vapor Trap to Protect Laboratory Workers** . . . . JAMES J. BROPHY 750
- **Improved Multivibrator Quenching Circuit** . . . . C. V. ROBINSON 750
- **Note on the Accuracy of the Buerger Precession Camera** . . . . HOWARD T. EVANS, JR. 751
- **Equipment for Measuring Light Scattering** . . . . M. BIER AND F. F. NORD 752
- **Absorption Corrections in X-Ray Studies of Preferred Orientation** . . . . . . J. F. H. CUSTERS 752

Regular Features:

- **New Instruments** 753
- **New Materials** 759
- **Index to Advertisers** xlvi

November, 1949

New Type of Diffusion Pump . . . E. L. Harrington 761
X-Ray Camera for Obtaining Powder Pictures at High Pressures . . . A. W. Lawson and N. A. Riley 763
Fast Neutron Detector . . . W. G. Moulton and C. W. Sherwin 766
Instrumental Distortions in the Shapes of Continuous Beta-Spectra . . . George E. Owen and C. Sharp Cook 768
Simplified Emission Regulator for Mass-Spectrometer Ion Sources . . . E. B. Winn and Alfred O. Nier 773
Electromechanical Lead Networks for A.C. Servo Mechanisms . . . Donald McDonald 775
High Power Attenuator for Microwaves . . . Daniel Alpert 779
Flexible High Voltage Square Wave Generator . . . Langdon C. Hedrick 781
Photo-Tube Input Impedance for a Voltage Stabilizer . . . E. N. Strait and W. W. Buechner 783
Absolute Noise Thermometer for High Temperatures and High Pressures . . . J. B. Garrison and A. W. Lawson 785
Apparatus for Measurements of Extremely High Internal Friction . . . T'ing-Sui Kê and Marc Ross 795
Device for the Measurement of Rotor Temperature in the Air-Driven Ultracentrifuge . . . Paul Gerard Ecker, Josef Blum, and C. W. Hiatt 799
Application of the Electrical Analogy in Fluid Mechanics Research . . . Philip G. Hubbard 802
Shock Tube: A Facility for Investigations in Fluid Dynamics . . . Walker Bleakney, D. K. Weimer, and C. H. Fletcher 807
Theoretical and Practical Sensitivity of the Pneumatic Infra-Red Detector . . . Marcel J. E. Golay 816
Stark-Effect Microwave Spectrograph of High Sensitivity . . . K. B. McAfee, Jr., R. H. Hughes, and E. Bright Wilson, Jr. 821

PHYSICAL INSTRUMENTS FOR THE BIOLOGIST

Double Pulse Constant Current Stimulator . . . Robert L. Schoenfeld 827

Laboratory and Shop Notes:

Iconoscope Electro-Optical Shutter for High Speed Photography . . . H. A. Prime and R. C. Turnock 830
Preparation of Samples of Active Metals . . . Donald F. Clifton 830
Glass Vacuum Valve . . . John Lamb 831
Straumanis' Method of Film-Shrinkage Correction Modified for Use without High Angle Lines . . . A. J. C. Wilson 831
Helium Cryostat Temperature Control . . . I. Šimon 832
New Source of Radiation for Infra-Red Spectrometers . . . L. W. Herscher 833
A Statitron for a Small Nuclear Laboratory . . . D. R. Inglis, R. W. Krone, and S. S. Hanna 834
Pumping Speed of Diffusion Pumps below Limiting Pressure . . . Clifford E. Berry 835
Parallel Operation of Small Thyratrons . . . Paul G. Hansel 836
Improved Embryological Micromanipulator . . . Howard H. Hillemann 836
Transient Response of High Voltage Resistance Dividers . . . Harry J. White 837
Voltage Stabilization for Electrostatic Generators Using an Electron Gun . . . S. J. Bame, Jr. and L. M. Baggett 839
Simple Automatic Water Distiller . . . Narcisco Cordero and Ireneo L. Lawas 840
Measurement of Betatron Guiding Fields during Electron Ejection . . . E. C. Gregg, Jr. 841
Delays in Rectangular Geiger Counters . . . G. E. Bradley and M. L. Wiedenbeck 841
New Instruments . . . 842
New Materials . . . 847
Index to Advertisers . . . xl

December, 1949

Direct Calorimetry by Means of the Gradient Principle . . . T. H. Benzinger and C. Kitzinger 849
Production and Measurement of Ultra-High Speed Impulses . . . R. C. Fletcher 861
Double Magnetic Lens Nuclear Spectrometer . . . Harold M. Agnew and Herbert L. Anderson 869
Small Differential Analyzer with Ball Carriage Integrators and Selsyn Coupling . . . R. E. Meyerott and G. Breit 874
Slide Rule for Radiation Calculations . . . M. W. Makowski 876
Volumetric Respirometer for Aquatic Animals . . . P. F. Scholander 885
Operation of the 184-In. Cyclotron . . . L. R. Henrich, D. C. Sewell, and J. Vale 887
Fractional Microsecond X-Ray Pulse Generator for Studying High Explosive Phenomena . . . H. I. Breidenbach, Jr. 899

Air Ionization Chamber for Soft X-Rays . . . . HERMAN E. SEEMANN 903
Instrument for Measurement of X-Ray Diffraction Patterns . . . . . . JOHN A. BENNETT 908
Circuit for Rapid Determination of Resolving Power and Other Characteristics of Coincidence-Systems . . . . H. DE WAARD 911
Design Curves for 180° Magnetic Spectrometers . . . . GEORGE E. OWEN 916
Apparatus for Isotope Separation by Thermal Diffusion . . . . W. W. WATSON, L. ONSAGER, AND A. ZUCKER 924
Single Pulse Voltmeter . . . . G. T. RADO, M. H. JOHNSON, AND M. MALOOF 927
Sliding Contacts to Transmit Small Signals . . . . BILLY M. HORTON 930
Gamma-Ray Counting Efficiency for a Lead-Cathode G-M Counter . . . . E. T. JURNEY AND FRED MAIENSCHEIN 932
Secondary-Emission Electron Multiplier Tube for the Detection of High Energy Particles . . . . ROBERT P. STONE 935
High Resolution Scale-of-Four . . . . VAL FITCH 942
Erratum: A Wide Range Radiation Instrument . LEONARD REIFFEL AND GLENN BURGWALD 944
Sensitive Magnetometer for Very Small Areas . . . . DARYL M. CHAPIN 945
Growing and Processing of Single Crystals of Magnetic Metals . . . . J. G. WALKER, H. J. WILLIAMS, AND R. M. BOZORTH 947

PHYSICAL INSTRUMENTS FOR THE BIOLOGIST

Electromagnet Blood Flow Meter . . . . JOHN W. CLARK AND JAMES E. RANDALL 951

Laboratory and Shop Notes:

Electromagnetic Focusing Device for Electron Microscope . . . . HAROLD T. MERYMAN 955
Automatic Stabilization of the Overvoltage on a Geiger Counter . . . . H. R. CRANE 955
Long-Lived Self-Quenching Counter Filling . . . . LLOYD G. SHORE 956
On the Vacuum Properties of Silastic . . . . G. D. ADAMS AND W. C. SHERWIN 957
Formation of Insulating Layers by the Thermal Decomposition of Ethyl Silicate . HAROLD B. LAW 958
Vacuum Tight, Flexible Metal—Glass Seal . . . . KENNETH M. SANCIER 958
Procedure for the Solution of Certain Network Problems . . . . JOHN M. KELSO 959
Small Portable Reflectometer . . . . WILLIAM LIBEN AND NOBEL W. SCOTT 960
Differential Pulse Transformer Bridge Circuit . JOHN ALAN GLEDHILL AND ANDREW PATTERSON, JR. 960
Preparation of Single Crystal Copper Ribbons from Single Crystal Copper Rods . . . . A. A. PETRAUSKAS, E. A. COOMES, AND J. E. MACDONALD 961
Sensitivity of Schwarz-Hilger Thermopiles . . . . E. SCHWARZ 962
Technique for Cutting Metal Single Crystals . . . . . T. R. MCGUIRE AND ROBERT T. WEBBER 962
Pulse-Height Limiting Circuit for a Scintillation Detector . . . . W. C. ELMORE 963
Portable Roentgenmeter for Field Use . . . . C. C. LAURITSEN 964
Statistics of Counting Rate Meters . . . . RONALD E. BURGESS 964
Rapid Response Radiation Alarm . . . . R. L. MACKLIN AND E. R. ROHRER 965
Note on Sealing Nylon Films to Geiger Counters . . . . ROBERT A. BECKER 966
Focusing in a Semicircular Magnetic Spectrometer . . . . C. M. FOWLER, R. G. SHREFFLER, AND J. M. CORK 966

New Instruments 968
New Materials 972
Author Index to Volume 20 973
Analytical Subject Index to Volume 20 979
Volume Table of Contents III
Index to Advertisers xliv

THE
REVIEW OF SCIENTIFIC
INSTRUMENTS

VOLUME 20, NUMBER 1 *JANUARY, 1949*

Orbital Stability in a Proton Synchrotron[*]

R. Q. Twiss and N. H. Frank[**]
Research Laboratory of Electronics, Massachusetts Institute of Technology, Cambridge, Massachusetts

(Received May 27, 1948)

The theory of the electron synchrotron has been amply covered elsewhere, but the proton synchrotron exhibits a number of distinct but important differences particularly at low energies. In the present paper the theory for this latter accelerator is developed with particular reference to the problems of injection and stability in the initial acceleration period. This theory is used to set up criteria relating the dimensions of a proton synchrotron to the conditions for stability and to the beam intensities obtainable.

I. INTRODUCTION

The theory of orbital stability in an electron synchrotron has been discussed by a number of writers.[1] Since the energies of the electrons which are accelerated by synchrotron action lie in the extreme relativistic range, attention has been focused largely on the case where the electron speeds are very close to that of light. There then result a number of simplifications of the general theory; in particular, the frequency of the accelerating r-f voltage may be taken as constant. In the proton synchrotron, however, particles are to be accelerated from initial energies, small compared to their rest energy, and hence the frequency of the accelerating voltage must be increased monotonically and synchronously with an increasing magnetic field. It is just this last feature which chiefly distinguishes the proton from the electron synchrotron, and requires that particular attention be given to the effects on the particle motions of departures from the desired time dependence of radio frequency.

No attempt will be made here to describe the basic principles in detail as these have been amply covered in the papers on the synchrotron listed in reference 1. However, an outline of the process by which the equations of motion are derived will be presented. In order to simplify reference to previous publications, the notation employed here will conform, as far as practicable, to that employed by one of us[2] in an article on the electron synchrotron. An analysis of the proton synchrotron has been presented by a group[3] working at Dr. Oliphant's Laboratory at Birmingham, England.

II. THE EQUATIONS OF MOTION

It has been shown[2] that the equations of motion of a charged particle in an axially symmetric magnetic field $\mathbf{B}=(-B_r, 0, -B_z)$ are

---

[*] This report has been supported in part by the Signal Corps, the Air Materiel Command, and O.N.R.

[**] Work performed as a consultant for the Brookhaven National Laboratory under the auspices of the Atomic Energy Commission.

[1] E. M. McMillan, Phys. Rev. **68**, 143 (1945); V. Veksler, J. Phys. U.S.S.R. **9**, 153 (1945); D. M. Dennison and T. H. Berlin, Phys. Rev. **70**, 58 (1946); D. S. Saxon and J. Schwinger, Phys. Rev. **69**, 702(A) (1946); N. H. Frank, Phys. Rev. **70**, 177 (1946); D. Bohm and L. Foldy, Phys. Rev. **70**, 249 (1946).

[2] N. H. Frank, Phys. Rev. **70**, 177 (1946).

[3] J. S. Gooden, H. H. Jensen, and J. L. Symonds, Proc. Phys. Soc. London **59**, 677 (1947); see also H. L. Oliphant, J. S. Gooden, and G. S. Hide, Proc. Phys. Soc. London **59**, 666 (1947).

$$\left.\begin{aligned} d/dt(m\dot r) &= mr\dot\theta^2 - er\dot\theta B_z, \\ d/dt[mr^2\dot\theta - (e\Phi/2\pi)] & \\ &= (eV/2\pi)\sin\left(\theta - \int\omega dt\right), \\ d/dt(m\dot z) &= er\dot\theta B_r, \end{aligned}\right\} \quad (1)$$

where m is the relativistic mass, e the proton charge,

$$\Phi = 2\pi\int_0^r rB_z dr$$

is the total magnetic flux linking a circle of radius r, V and ω are the peak voltage and angular frequency, respectively, of the r-f field across an accelerating gap at $\theta=0$. Radiation effects are omitted since, in the proton case, they are negligible for energies less than 10^5 Mev.

Circular motion in the median plane $z=0$ is possible for the particles if the parameters in these equations vary with time according to certain definite laws. Particles moving in this circle, of radius r_0, will always arrive at the accelerating gap with the same phase ψ_0 relative to that of the accelerating voltage. This quasi-steady motion is given by the equations

$$\left.\begin{aligned} m\dot\theta &= eB_z, \\ d/dt[r_0^2B_0 - (\Phi_0/2\pi)] &= V/2\pi \sin\psi_0, \\ \psi_0 &= \theta - \int\omega dt. \end{aligned}\right\} \quad (2)$$

Here B_0 and Φ_0 are the magnetic field at, and the flux linking, the circular orbit of radius r_0.

From these equations there follow directly expressions for the kinetic energy E and the required angular radiofrequency ω_0 in terms of B_0 and r_0. They are

$$\left.\begin{aligned} E/m_0c^2 &= (1+(eB_0r_0/m_0c)^2)^{\frac{1}{2}} - 1, \\ r_0\omega_0/c &= \frac{(eB_0r_0/m_0c)}{(1+(eB_0r_0/m_0c)^2)^{\frac{1}{2}}}, \\ m\omega_0 &= eB_0, \end{aligned}\right\} \quad (3)$$

where, for protons, $m_0c^2=938$ Mev. These expressions are plotted as functions of eB_0r_0/m_0c in Figs. 1 and 2. To provide an idea of the orders of magnitude involved, there are presented, in Table I, the design data for a proton synchrotron intended to yield particles of 10^4-Mev energy.

If the machine is to be run during any part of its operating cycle as a betatron with no r-f acceleration, the particles will remain in a stable circular orbit of radius r_0 if

$$r_0^2B_0 = \int_0^{r_0} B_z r dr, \quad (4)$$

the well-known betatron condition.

To find the oscillations about the stable orbit and phase in the general case one sets

$$\left.\begin{aligned} r &= r_0 + x, \\ \omega &= \omega_0 + \omega_1, \\ \dot\psi &= \dot\theta - \omega = \dot\varphi - \omega_1, \end{aligned}\right\} \quad (5)$$

where ω_1 is the departure of the angular radiofrequency from its correct value ω_0, and $\dot\varphi$ is the perturbation in the particle angular velocity caused by the correct r-f field. We take x, ω_1, and $\dot\varphi$ as first-order small quantities, the squares and products of which will be neglected.

If the vertical magnetic field B_z in the median plane $z=0$ decreases with radius in the neighborhood of r_0 according to the law

$$B_z = B_0(r/r_0)^{-n}, \quad (6)$$

then n must satisfy the inequality

$$0<n<1,$$

if the orbit r_0 is to be stable for both vertical and radial oscillations. In the following it will be assumed that n is independent of r.

Substituting from (5) and (6) into (1), for the case when the particle is moving in the plane $z=0$, we obtain, after some algebraic manipulation, the following equations describing the phase and radial oscillations:

$$\left.\begin{aligned} \frac{d}{dt}\left(\frac{B_0\dot x}{\omega_0}\right) &= r_0\omega_0B_0\left\{\left(\frac{eB_0}{m_0\omega_0}\right)^2 - (1-n)\right\} \\ &\qquad\times\left\{\frac{x}{r_0} + \eta\frac{\dot\varphi}{\omega_0}\right\}, \\ \frac{d}{dt}\left[\frac{r_0}{\omega_0}\frac{d}{dt}\left(\frac{B_0\dot x}{\omega_0}\right) + (1-n)r_0B_0x\right] & \\ &\qquad + \frac{V\sin\psi_0}{2\pi} = \frac{V\sin\psi}{2\pi}, \end{aligned}\right\} \quad (7)$$

where

$$\eta = \frac{(eB_0/m_0\omega_0)^2}{(eB_0/m_0\omega_0)^2-(1-n)} = \frac{(m/m_0)^2}{(m/m_0)^2-(1-n)}, \tag{8}$$

with m the relativistic and m_0 the rest mass of the particle, respectively.

From Eq. (8), it is clear that η is a very slowly varying function of time, decreasing monotonically from $1/n$ to 1 as the particle kinetic energy increases from zero to infinity. In the nonrelativistic range of energies, it may be taken as constant and equal to $1/n$. In Fig. 3 η is plotted as a function of eB_0r_0/m_0c.

In the important case where the inequality

$$\frac{4V}{2\pi r_0^2 B_0\omega_0\eta(1-n)^2} \ll 1 \tag{9}$$

is satisfied, the equations of motion (7) can be regarded as describing two independent oscillations; the so-called betatron oscillations, which are independent of V, satisfy the pair of equations

$$\left.\begin{aligned} x/r_0+\dot{\varphi}/\omega_0&=0,\\ \frac{d}{dt}\left(\frac{B_0\dot{x}}{\omega_0}\right)+(1-n)\omega_0B_0x&=0,\end{aligned}\right\} \tag{10}$$

for those particles, the angular momenta of which are such that they can perform stable betatron motion in the circle of radius r_0. The much lower frequency forced oscillations known as the synchrotron oscillations satisfy the following pair of equations:

$$\left.\begin{aligned} x/r_0+\eta(\dot{\varphi}/\omega_0)&=0,\\ (1-n)r_0^2\frac{d}{dt}\left(\eta\frac{B_0}{\omega_0}\dot{\varphi}\right)+\frac{V}{2\pi}\sin\psi&=\frac{V}{2\pi}\sin\psi_0,\\ \dot{\varphi}&=\psi+\omega_1.\end{aligned}\right\} \tag{11}$$

TABLE I. Preliminary design data for a 10-Bev proton synchrotron.

Final energy of the protons	10 Bev
Injection energy of the protons	4 Mev
Orbital radius	24.3 meters
Final magnetic field at orbit	15,000 gauss
Magnetic field at orbit at injection	110 gauss
Final radiofrequency	1.96 Mc/sec.
Radiofrequency at injection	183 kc/sec.
Frequency range	10.65 to 1
Acceleration period	1 second
Average energy gain per revolution	5500 ev

When the inequality (9) is not fully satisfied, the two oscillations are coupled, but the effect

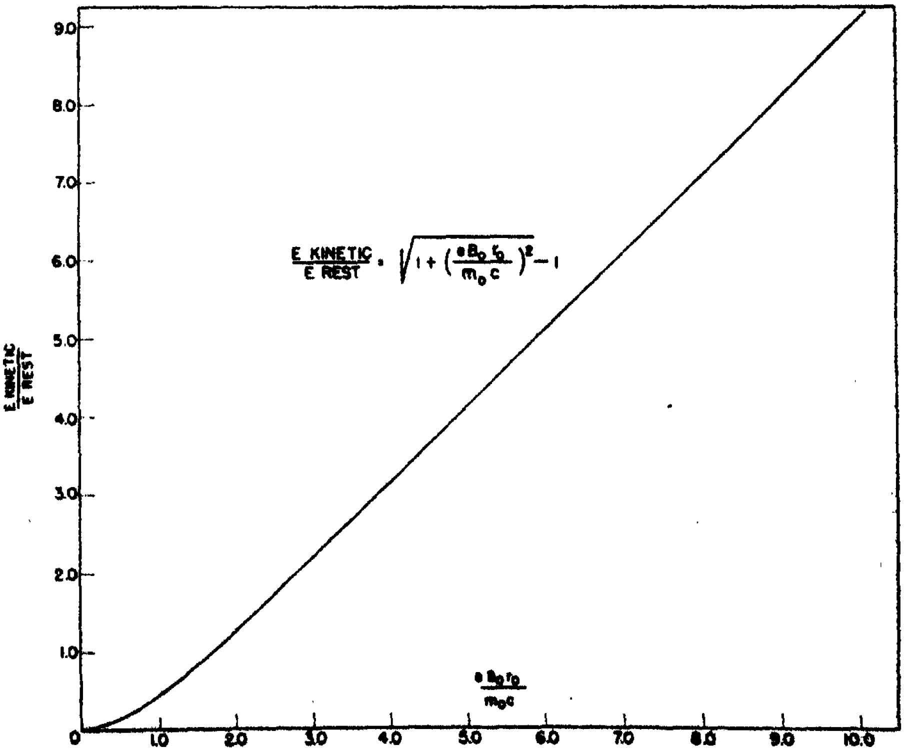

FIG. 1. Kinetic energy of particles as a function of magnetic field.

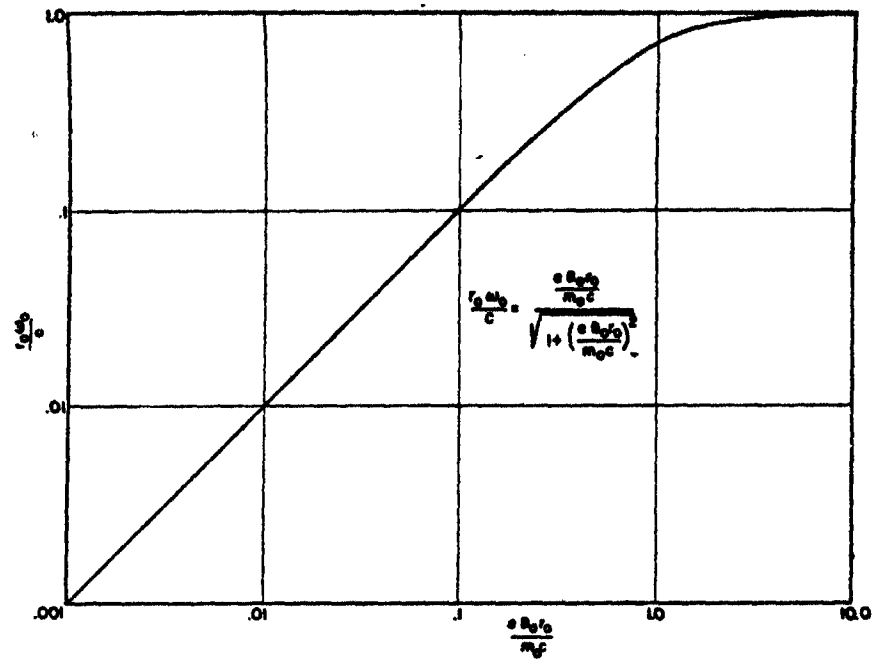

FIG. 2. Angular velocity of particle as a function of magnetic field.

of the small coupling term thus obtained is also small and does not modify appreciably the physical behavior of the protons in the accelerating chamber.

Equations (10) are the well-known equations of oscillation for betatron particles with both B_0 and ω_0 slowly varying functions of the time. The radial oscillations are essentially sinusoidal oscillations of slowly varying frequency $(1-n)^{\frac{1}{2}}\omega_0$ and amplitude which is damped proportional to $B_0^{-\frac{1}{2}}$. Thus, if x_i and $\dot{x}_i$ are the initial values of x and $\dot{x}$, respectively,[***]

$$x(t)=\left(\frac{B_i}{B_0}\right)^{\frac{1}{2}}\left[x_i\cos\left((1-n)^{\frac{1}{2}}\int\omega_0dt\right)\right.$$
$$\left.+\frac{\dot{x}_i}{(1-n)^{\frac{1}{2}}\omega_i}\sin\left((1-n)^{\frac{1}{2}}\int\omega_0dt\right)\right],\quad(12)$$

where ω_i and B_i are initial values. In view of the fact that the betatron oscillations have been fully analyzed elsewhere, (see reference 1) no further discussion of them will be given here and we shall concern ourselves with Eq. (11).

The equation that determines the phase oscillations may be written in the form:

$$(1-n)r_0^2\frac{d}{dt}\left(\frac{B_0}{\omega_0}\eta-\dot{\varphi}\right)+\frac{V}{2\pi}\sin\psi$$
$$=\frac{V}{2\pi}\sin\psi_0-(1-n)r_0^2\frac{d}{dt}\left(\eta\frac{B_0\omega_1}{\omega_0}\right).\quad(13)$$

In general, B_0, ω_0, η, V, and ψ_0 will be slowly varying functions of the time. We exclude for the present the exceptional case of transition from betatron to synchrotron operation, during which V and ψ_0 may vary in a manner which cannot be considered slow. Following McMillan, one may interpret Eq. (13) as the equation of motion of a circular pendulum of slowly varying mass and length, acted on by a unidirectional tangential force together with an irregular forcing term depending on $d\omega_1/dt$. The motion of such a pendulum will be oscillatory if ψ never exceeds the critical angle $\pi-\psi_0$. If it does, the motion will be rotatory in an anticlockwise direction with increasing angular speed under the action of the forcing term $(V/2\pi)\sin\psi_0$. Physically, the particle slips in phase relative to the accelerating voltage and moves continuously from an accelerating to a decelerating phase and back to an accelerating phase, repeating this process. It thus gains no energy from the r-f voltage on the average. The magnetic field, however, is increasing continuously and hence the particle orbit shrinks inward until the particle is lost to the walls, according to the first of Eqs. (11).

[***] x_i is measured from that orbit radius which corresponds exactly to the initial kinetic energy.

III. THE NATURE OF THE SYNCHROTRON OSCILLATIONS

1. Conditions of Acceptance of a Particle into the Acceleration Cycle

Since a necessary condition for continuous acceleration of a particle is that its phase may not exceed $\pi-\psi_0$, restrictions on the initial phase and phase velocity with which a particle is injected into the synchrotron accelerating cycle follow therefrom. An exact calculation would require knowledge of the time variations of η, B_0, ω_1, and V. However, sufficiently accurate information can be obtained by taking $\omega_1=0$ and neglecting the time dependence of η, B_0, ω_0, and V. (This is particularly the case during the initial non-relativistic stages of operation if the magnetic field varies linearly with the time when $\eta B_0/\omega_0$ is constant.)

A first integral of (13) can now be obtained as

$$\dot{\psi}^2=\frac{2\Omega_0^2}{\cos\psi_0}[\cos\psi+\psi\sin\psi_0-\cos\psi_i-\psi_i\sin\psi_0]+\dot{\psi}_i^2, \quad (14)$$

where

$$\Omega_0^2=(V\omega_0\cos\psi_0)/(2\pi r_0^2(1-n)\eta B_0), \quad (15)$$

and ψ_i and $\dot{\psi}_i$ are initial values. Ω_0 is the angular frequency of small synchrotron phase oscillations about the equilibrium phase ψ_0. The equivalent pendulum will oscillate between two limiting values of ψ providing the representative point in phase space lies within the boundary determined by the equation:

$$\cos\psi_i+\psi_i\sin\psi_0-\frac{\dot{\psi}_i^2\cos\psi_0}{2\Omega_0^2}=(\pi-\psi_0)\sin\psi_0-\cos\psi_0. \quad (16)$$

Figure 4 shows the boundary curves for a number of values of ψ_0. The extreme phase angle limits of the oscillatory motion are given by $\psi_1\leq\psi\leq\pi-\psi_0$, where ψ_1 is that solution of

$$\cos\psi_1+\psi_1\sin\psi_0=(\pi-\psi_0)\sin\psi_0-\cos\psi_0,$$

which satisfies the inequality $-\pi\leq\psi_1\leq\psi_0$. In Fig. 5 the total acceptance angle $(\pi-\psi_0-\psi_1)/2\pi$ is shown plotted as a function of ψ_0.

2. Oscillation Periods

Equation (14) cannot be integrated directly except in the special case that $\psi_0=0$. However, it can be integrated numerically for given values of ψ_0, ψ_i, and $\dot{\psi}_i$. In Fig. 6 the normalized oscillation period (the ratio of the period T_0 to $2\pi/\Omega_0$) is plotted as a function of $\psi_i-\psi_0$ for various values of ψ_0 with $\dot{\psi}_i=0$. It will be noted that the period increases monotonically with ψ_i and tends to infinity as ψ_i approaches $\pi-\psi_0$. To get the order of magnitude of the periods involved, we

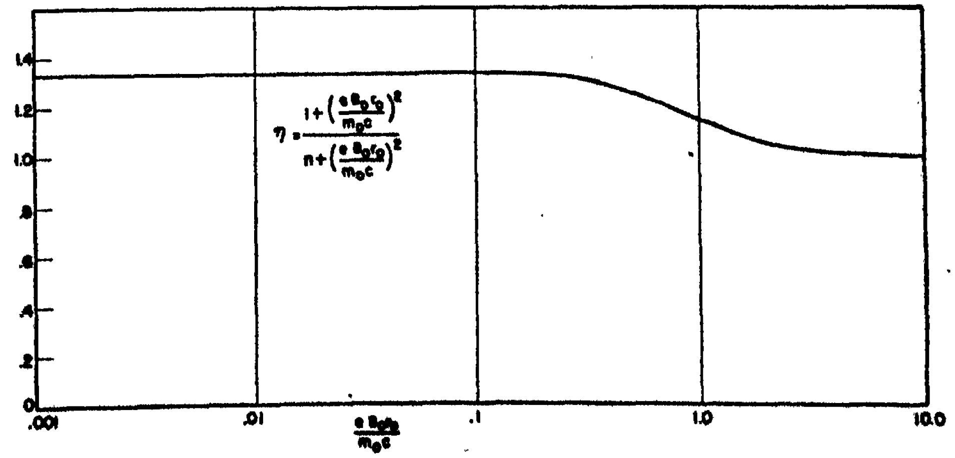

FIG. 3. η as a function of magnetic field.

use the values,

$V = 5500$ volts,
$\omega_0 = 4\pi \times 10^5/\text{sec.}$,
$\psi_0 = \pi/4$,
$n = 3/4$,
$r_0 = 24.3$ m,
$B_0 = 110$ gauss $= 1.1 \times 10^{-2}$ weber/m^2.

This gives $\Omega_0 \cong 2\times 10^{-2}\omega_0 = 8\pi \times 10^3/\text{sec.}$ during the initial stages of operation; i.e., one phase oscillation period occurs in about 50 revolutions of the particle.

3. The Stability of the Phase Oscillations

First consider small oscillations about the equilibrium phase, setting

$$\psi = \psi_0 + \vartheta, \quad \vartheta \ll 1.$$

The equation of undisturbed phase motion becomes

$$\frac{d}{dt}\left(\eta \frac{B_0}{\omega_0}\dot{\vartheta}\right) + \frac{V\cos\psi_0}{2\pi r_0^2(1-n)}\vartheta = 0,$$

and the W.K.B. approximation to the solution of this equation yields

$$\psi = \left(\frac{V\cos\psi_0\eta B_0}{\omega_0}\right)_i^{\frac{1}{4}} \left(\frac{V\cos\psi_0\eta B_0}{\omega_0}\right)^{-\frac{1}{4}} \times \left\{\vartheta_i \cos\int \Omega_0 dt + \frac{\dot{\vartheta}_i}{\Omega_i}\sin\int \Omega_0 dt\right\}, \quad (17)$$

with $\vartheta_i = \psi_i - \psi_0$ and $\dot{\vartheta}_i = -\omega_0 x_i / r_0 \eta$; x_i is the initial radial distance of the mean betatron orbit from the stable synchrotron orbit.

Thus the amplitude A of the phase oscillations varies as

$$A \sim \left(\frac{V\cos\psi_0\eta B_0}{\omega_0}\right)^{-\frac{1}{4}}, \quad (18)$$

where

$$V\sin\psi_0 = d/dt[r_0^2 B_0 - (\Phi_0/2\pi)]. \quad (19)$$

Since $\Phi_0/\dot{B}_0$ will be essentially constant, independent of time, one may write alternatively,

$$A \sim [\eta(\dot{B}_0 B_0/\omega_0)\cot\psi_0]^{-\frac{1}{4}}. \quad (20)$$

The two limiting cases of the non-relativistic motion with $m = m_0$ and the extreme relativistic case with the particle speed practically equal to that of light are of particular interest.

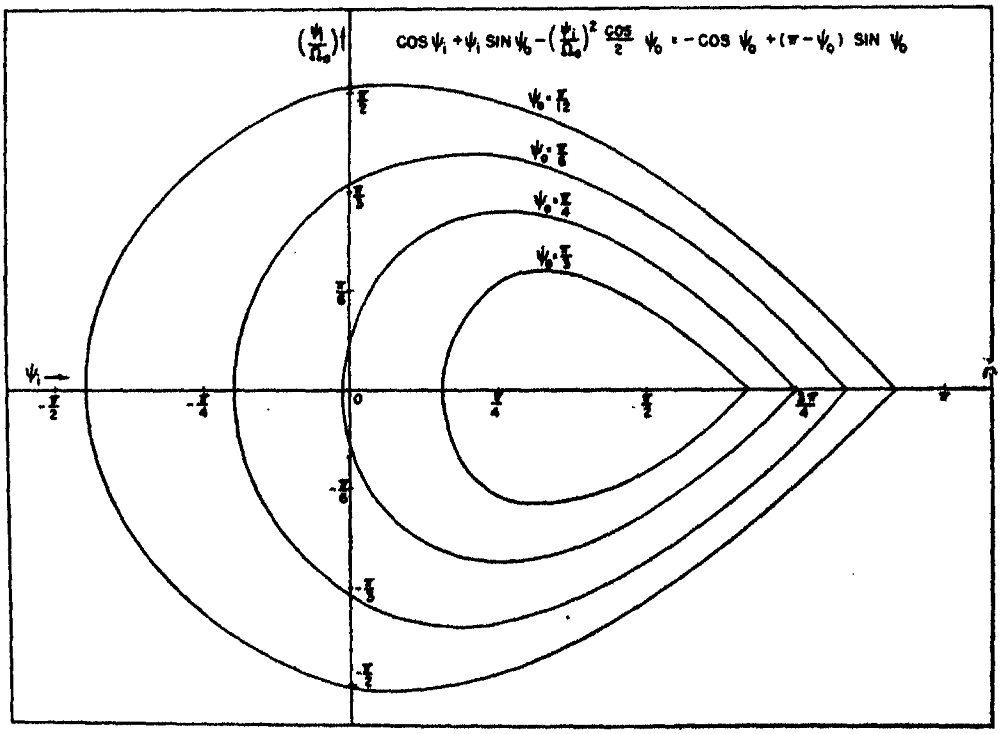

FIG. 4. The acceptance domain in phase space at injection for various values of stable phase ψ_0.

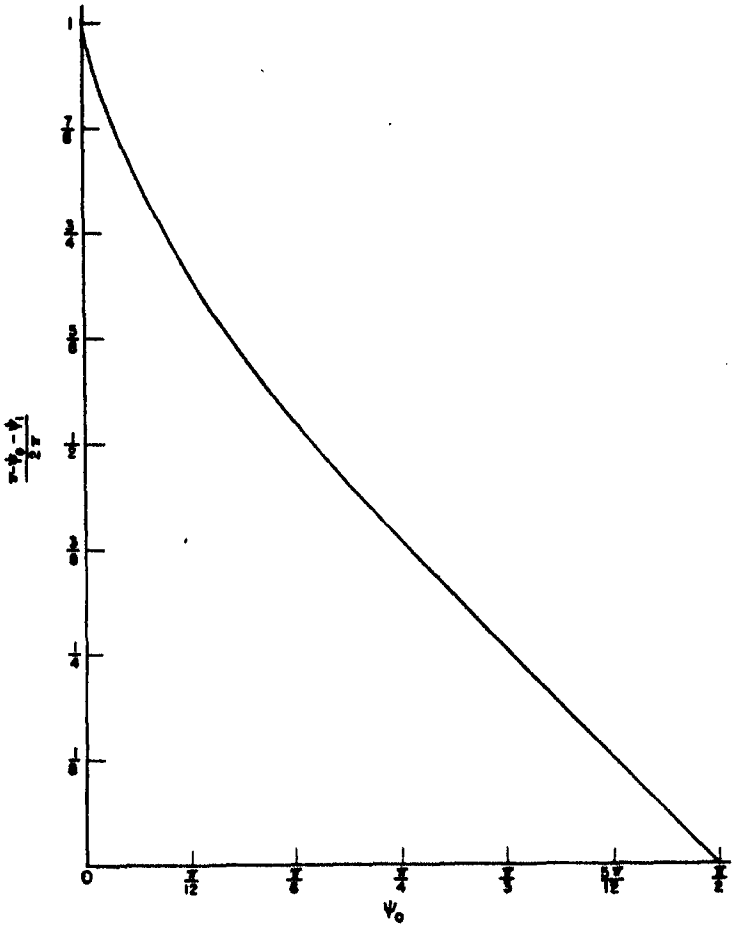

FIG. 5. The normalized injection acceptance angle as a function of the stable phase ψ_0.

The Non-Relativistic Case

In this case $\eta B_0/\psi_0$ is constant and positive amplitude damping will occur only if $V\cos\psi_0$ increases with the time. In practice, $\dot{B}_0$ will increase with time, the initial curvature being due to eddy currents in the magnet core. Injection may occur at the start of this cycle or at any subsequent time. Since $V\sin\psi_0$ is proportional to dB_0/dt, some positive damping can be attained in the early stages of the acceleration cycle even if ψ_0 is kept constant. However, this effect is small and to obtain appreciable damping it is necessary that V be increased more rapidly than $\dot{B}_0$. The effect of the change in ψ_0 is to alter the damping only slightly if $\cos\psi_0$ is near unity.

If V is kept constant, there will be a small increase in oscillation amplitude, proportional to $(\cos\psi_0)^{-\frac{1}{4}}$, so that it is desirable to increase V during the initial non-relativistic stages of acceleration. (A very small additional damping is obtained from the slowly increasing mass during these early stages if $n > \frac{3}{4}$.)

An additional reason for the desirability of positive damping is that of radiofrequency error. Such an error leads to a forcing term $-r_0^2(1-n)(d/dt)(\eta B_0\omega_1/\omega_0)$. The effects of this term will be more or less random, sometimes increasing and sometimes decreasing the oscillation amplitude. As time goes on, there will be an ever-increasing probability that the fluctuating amplitude will exceed the critical limits of Eq. (16) and then the particle will be lost. This probability is of course enormously reduced if steady positive damping is present.

The Extreme Relativistic Case

In this case, ω_0 is constant and the phase oscillation amplitude varies as $(V\cos\psi_0 B_0)^{-\frac{1}{4}}$. The increasing magnetic field provides sufficient damping so that V may be kept constant. As a

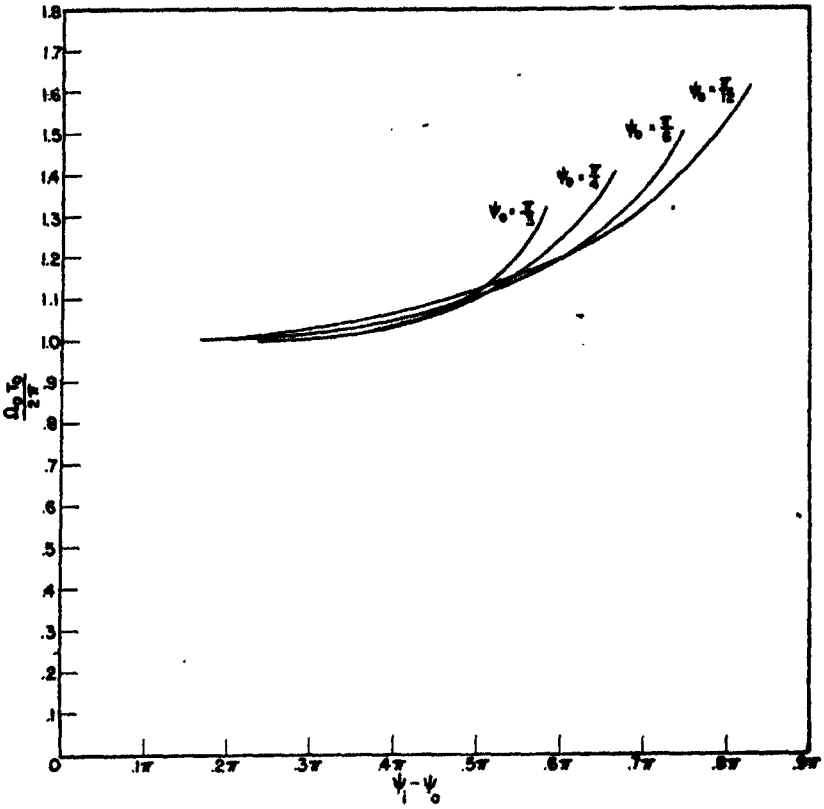

FIG. 6. The period of a synchrotron oscillation as a function of the injection phase.

numerical example of the magnitude of the damping for the whole cycle, we take

$\psi_0=$ constant,
V increasing from 7700 to 10,000 volts,
B_0 increasing from 110 to 15,000 gauss,
$\omega_0/2\pi$ increasing from 180 kc/sec. to 2.00 mc/sec.,
$n=3/4$,
and η decreasing from 4/3 to unity.

Then, according to Eq. (18), the ratio of initial to final amplitude is about 1.9 to 1.

For large amplitudes, the damping may be obtained with the help of the adiabatic theorem. This states that the $\oint p_\psi d\psi$ taken over a complete libration period of ψ is an invariant for slow variations of the parameters in the Hamiltonian of the system, with p_ψ the generalized momentum associated with the coordinate ψ. Now the equation of phase oscillation can be derived from a Lagrangian function

$$L=\frac{1}{2}\left[\frac{r_0^2(1-n)\eta B_0}{\omega_0}\dot{\psi}^2\right]+\frac{V}{2\pi}(\cos\psi+\psi\sin\psi_0),\quad (21)$$

if effects of frequency error are neglected. Hence

$$p_\psi=\frac{\partial L}{\partial\dot{\psi}}=\frac{r_0^2(1-n)\eta B_0\dot{\psi}}{\omega_0},\quad (22)$$

and one has

$$\oint\frac{\eta B_0}{\omega_0}\dot{\psi}d\psi=\text{constant}.$$

If now, at any time, ψ oscillates between ψ_1 and ψ_2, these limiting angles are determined by

$$\int_{\psi_1}^{\psi_2}\left(\frac{\eta B_0 V}{\omega_0\cos\psi_0}\right)^{\frac{1}{2}}[\cos\psi+\psi\sin\psi_0 - \cos\psi_2-\psi_2\sin\psi_0]^{\frac{1}{2}}d\psi=\text{constant},\quad (23)$$

where ψ_1 and ψ_2 are related by

$$\cos\psi_2+\psi_2\sin\psi_0-\cos\psi_1-\psi_1\sin\psi_0=0;$$
$$-\pi<\psi_1<\psi_0<\psi_2<\pi-\psi_0.$$

In the special case $\psi_0=0$, Eq. (23) can be evaluated in terms of complete elliptic functions, and gives

$$k[\sin(\psi_m/2)]=\text{constant }(\omega_0/\eta B_0 V)^{\frac{1}{2}},$$

with $h(k)=E(k)-(1-k^2)K(k)$, K and E being complete elliptic functions of the first and second kind. Figure 7 is a plot of $h(\sin\psi_m/2)$ against ψ_m, the maximum amplitude, and shows that the damping for finite amplitudes is in general less than for small amplitudes in this case.

4. The Stability of the Radial Oscillations

From the solution of the equation for phase oscillations, one obtains the radial oscillations immediately from the first of Eqs. (11). For small oscillations, one has

$$\frac{x}{r_0}=\frac{B_i}{B_0}\frac{(\eta V\cos\psi_0 B_0/\omega_0)^{\frac{1}{4}}}{(\eta V\cos\psi_0 B_0/\omega_0)_i^{\frac{1}{4}}}\times\left\{\frac{x_i}{r_0}\cos\int\Omega_0 dt+\frac{\dot{x}_i}{\Omega_0 r_0}\sin\int\Omega_0 dt\right\},$$

so that the amplitude A is damped according to the law

$$A\sim[\eta(V\cos\psi_0 B_0/\omega_0)]^{\frac{1}{4}}\cdot 1/B_0. \qquad (24)$$

The Non-Relativistic Case

In this case $\eta B_0/\omega_0$ is constant and the radial oscillation amplitude varies as $(V\cos\psi_0)^{\frac{1}{4}}/B_0$. The increase of $V\cos\psi_0$ with time needed to obtain a small phase damping must be less than the increase of $B_0{}^4$ with time to insure positive radial damping. This restriction is purely academic, however, because of the impracticality of attaining such a rapid rate of voltage increase.

The Extreme Relativistic Case

Here ω_0 is constant and the radial oscillation amplitude varies as $(V\cos\psi_0)^{\frac{1}{4}}/B_0{}^{\frac{3}{4}}$. Considering the same numerical example as in the case of phase oscillations, one finds the ratio of initial to final amplitude of radial oscillation to be 48 to 1.

5. The Effects of Frequency Error

From the outset, it should be noted that frequency variations which are rapid compared to the synchrotron oscillations have a negligible effect and will be ignored in the following. Departures in frequency from the correct law affect both the radial and phase motions of the particles. The average position of the particle is displaced according to the formula

$$x/r_0=-\eta(\psi+\omega_1/\omega_0) \quad \text{or} \quad \bar{x}/r_0=-\omega_1\eta/\omega_0. \qquad (25)$$

If this displacement is too great, the particle will be lost to the walls and hence a definite limit exists of the maximum allowed absolute value of the frequency error. With A the *total* oscillation amplitude and $2b$ the width of the accelerating chamber, the fractional frequency error must satisfy the inequality

$$\frac{\omega_1}{\omega_0}<\left(\frac{b-A}{r_0}\right)\frac{1}{\eta}\cong\left(\frac{b-A}{r_0}\right)n \text{ at low energies.} \qquad (26)$$

This requirement is most severe at injection, as then A is a maximum and $1/\eta=n$, a minimum. Thus n should be as large as possible in the proton synchrotron if frequency errors are to be minimized. This is opposite to the betatron case where, to minimize errors in satisfying the betatron flux condition, $(1-n)$ should be large and hence n small.

The general analysis of the effect of frequency error on the phase oscillations is extremely complicated because of the non-linear character of the oscillations. However, the very important practical case of a linear variation with time of the frequency error ω_1 allows a solution. If $\omega_1=\alpha t$, the equation of phase motion becomes

$$r_0{}^2(1-n)\frac{d}{dt}\left(\eta\frac{B_0\dot{\psi}}{\omega_0}\right)+\frac{V}{2\pi}\sin\psi=\frac{V}{2\pi}\sin\psi_0-r_0{}^2(1-n)\frac{d}{dt}\left(\frac{\alpha\eta B_0 t}{\omega_0}\right). \qquad (27)$$

In the low energy range, $\eta B_0/\omega_0$ is constant and (27) takes the form

$$r_0{}^2(1-n)\eta\frac{B_0}{\omega_0}\ddot{\psi}+\frac{V}{2\pi}\sin\psi=\frac{V}{2\pi}\sin\psi_0', \qquad (28)$$

with

$$\frac{V}{2\pi}\sin\psi_0'=\frac{V}{2\pi}\sin\psi_0-\frac{r_0{}^2(1-n)\eta\alpha B_0}{\omega_0}. \qquad (29)$$

Thus the effect of a frequency error is to produce a change in the stable phase angle. This will change the amplitude of oscillation and also alter the limits of stable oscillation from

$$\psi_1<\psi<\pi-\psi_0 \quad \text{to} \quad \psi_1'<\psi<\pi-\psi_0',$$

where

$$\left.\begin{aligned}\cos\psi_1+\psi_1\sin\psi_0&=(\pi-\psi_0)\sin\psi_0-\cos\psi_0,\\ \cos\psi_1'+\psi_1'\sin\psi_0'&=(\pi-\psi_0')\sin\psi_0'-\cos\psi_0'.\end{aligned}\right\} \quad (30)$$

The range of ψ for stable phase oscillations will increase if $|\psi_0'|<\psi_0$, hence if

$$0<\alpha<\frac{\omega_0 V\sin\psi_0}{\pi r_0^2(1-n)\eta B_0}.$$

Thus an increase in radiofrequency from the proper value is less serious than a corresponding decrease. Increasing frequency implies a smaller orbital radius and hence a smaller r-f energy gain per revolution is required to maintain this orbit than an expanded orbit. Particles will be lost if their altered amplitudes exceed the limits of stable phase oscillation corresponding to the new stable phase; i.e., if the representative points in phase space fall outside the appropriate boundary of Fig. 4.

In general the oscillation amplitude will decrease if $|\psi_0'|<\psi_0$, but the amount of this decrease depends on the exact phase when the frequency begins to depart from the correct law. Finally, the speed with which the average radial position follows the frequency change is limited by the period of synchrotron oscillations. Thus essentially no change in radius will occur until an elapsed time equal to an appreciable fraction of the synchrotron period.

As pointed out, a negative frequency error increases the stable phase angle and decreases the stable phase range with a resulting loss of particles.

The principal conclusions may be summarized as follows:

i. The synchrotron oscillation frequency is small compared to the accelerating radiofrequency, from 50–200 times smaller in the case under discussion.

ii. The radial oscillations are heavily damped;

$$A\sim\left(\frac{V\cos\psi_0\eta B_0}{\omega_0}\right)^{\frac{1}{4}}\cdot\frac{1}{B_0}\cong(B_0)^{-\frac{3}{4}}.$$

iii. The phase oscillations are very lightly damped;

$$A\sim\left(\frac{V\cos\psi_0\eta B_0}{\omega_0}\right)^{-\frac{1}{4}}.$$

In the non-relativistic region there is no damping unless V increases with time.

iv. A number of constraints exist on the allowable frequency error. The most important is that the long term error satisfy the inequality

$$\frac{\omega_1}{\omega_0}<\frac{1}{\eta}\left(\frac{b-A}{r_0}\right)\cong n\left(\frac{b-A}{r_0}\right)$$

for the non-relativistic case. This constraint becomes less severe as time increases because A decreases as $1/B_0$.

v. It is desirable to make n as near unity as possible from the standpoint of synchrotron oscillations.

IV. INITIAL BETATRON ACCELERATION

In the majority of existing electron-synchrotrons the machine is operated initially as a betatron in order to obviate the necessity for frequency modulation of the r-f accelerating voltage. It has been suggested that a stage of betatron acceleration be utilized in the proton synchrotron not, of course, to remove the necessity for frequency modulation, but to reduce the range. This will be particularly valuable in a machine that employs a resonant tuned accelerating cavity and yet requires a large accelerating voltage over the whole frequency range. It is correspondingly less useful if an untuned accelerating system is used.

The maximum particle energy attainable in the betatron phase will be determined by economic considerations; the minimum initial energy will depend upon the injection system and will be limited by the necessity of avoiding excessive gas scattering.

There are, however, additional arguments in favor of a betatron acceleration phase, and as some of them are peculiar to the proton synchrotron, they will be discussed in greater detail. It should be emphasized from the outset that we are now only concerned with the case where the betatron phase carries the particles up to energies of a few Mev.

It has been stated above that the amplitude of the horizontal oscillation in a synchrotron is the sum of the high frequency betatron and of the low frequency synchrotron oscillations. If particles are injected into the betatron phase, the low frequency oscillations will not be present, and we can use this fact either to lower the tolerance on the injection energy or to increase the number of particles accepted into the acceleration cycle.

The use of a betatron phase also enables us to get increased phase damping in the early stages. If the r-f voltage be turned on while the betatron condition is satisfied, synchrotron oscillations will take place about a stable phase angle of zero. Under these conditions the stable acceptance angle is equal to 2π. If now the r-f voltage increases linearly with the time to a limiting value V in time T_0, then the particles will be bunched about zero phase.

If

$$\Omega_0^2=\frac{V\omega_0\cos\psi_0}{2\pi r_0^2(1-n)\eta B_0},$$

then the phase of a particle at time T is given by

$$\psi=\frac{\psi_i\Omega_{0i}^{1/3}\Gamma(2/3)}{3^{1/3}T_0^{1/6}}(t)^{1/2}J_{-1/3}\left(\int_0^t\left(\frac{\Omega_0^2\tau}{T_0}\right)^{1/2}d\tau\right),$$

where ψ_i is the injection phase, and we have made the approximate assumption that ψ_i is small. If $T_0\Omega_0$ is $\gg 1$ an asymptotic expansion may be used to yield

$$\frac{\psi_F}{\psi_i}=\frac{1}{(\pi)^{1/2}}\left(\frac{\Omega_{0i}}{\Omega_{0F}}\right)^{1/3}\frac{3^{1/6}\cdot\Gamma(2/3)}{(\Omega_{0F}T_0)^{1/6}}\left(\frac{T_0}{t}\right)^{1/4}$$

$$=\frac{1}{(\pi)^{1/2}}\left(\frac{\Omega_{0i}}{\Omega_{0F}}\right)^{1/3}\frac{3^{1/6}\Gamma(2/3)}{(\Omega_{0F}T_0)^{1/6}}\quad\text{if}\quad t=T_0,\qquad(31)$$

where subscript i refers to initial values and subscript F refers to final values.

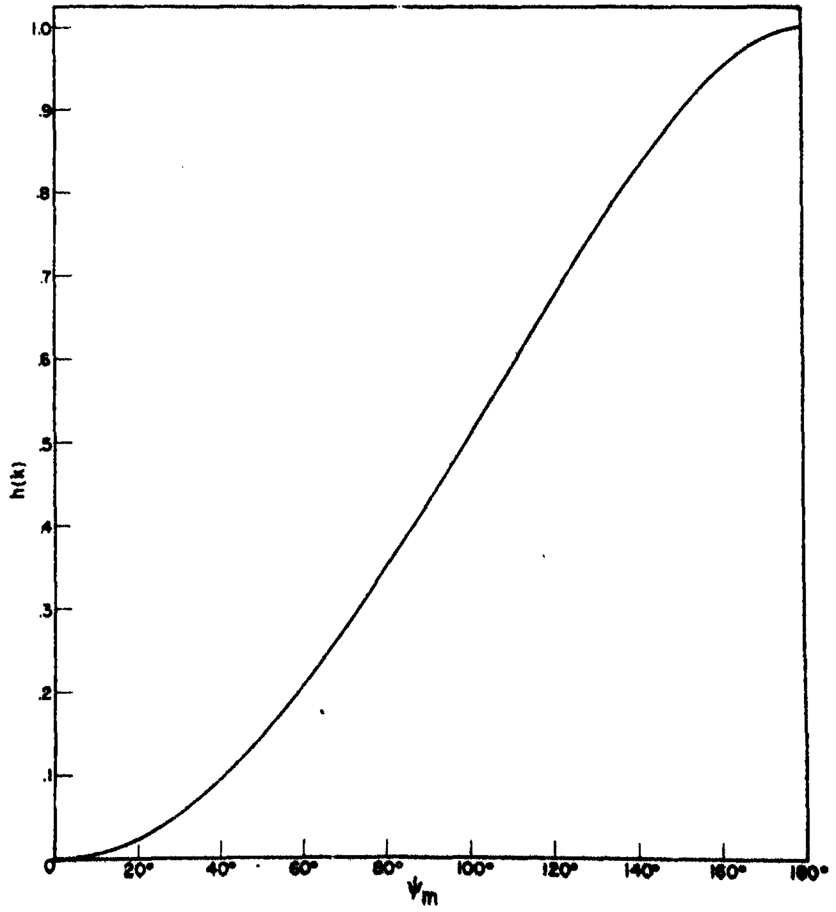

FIG. 7. $H(k)$ as a function of injection angle ψ_m.

In the numerical case quoted above where V is taken to be 10,000 volts and T_0 is the time required to raise the energy of the particle to 8 Mev,

$$\psi_F/\psi_i = 1/2.3,$$

a larger damping than that obtained during the entire synchrotron acceleration period. The damping for large phase angles will be less than this, but even so, by far the great majority of the particles injected will be accepted into the synchrotron acceleration cycle if this prebunching is employed. In addition a much smaller percentage will be lost because of random frequency errors.

It will be noted, from Eq. (31), that the amount of damping obtained depends very little upon the amplitude of the r-f voltage; in fact, $\psi_F \sim V^{-1/12}$. Thus the bunching can be obtained with an r-f voltage only a small fraction of that which would be needed in the synchrotron phase. This may be important if the r-f accelerating system is a resonant one.

To conclude this section we shall give a brief discussion of the effect of an error in the betatron flux condition. In the so-called flux-forcing scheme, prescribed by D. W. Kerst, the betatron coil is placed partly in series, partly in parallel with the field coils, the whole system being powered from the same generator. Under these conditions it can be shown that there is a self-compensation mechanism which automatically preserves the correct field-flux ratio. However a complicated switching problem arises if this scheme is to be incorporated into the proton synchrotron, where the current in the betatron coils has to be turned off at some point in the acceleration cycle. Accordingly, it may be necessary to power the betatron flux coils from a separate generator, and then the possibility arises that the flux is out of phase with the field in the accelerating chamber. One way of avoiding this trouble is to provide an additional field-compensating coil, the current in which is automatically adjusted to give the correct flux-field ratio. Alternatively, the correct orbit can be maintained by a small r-f voltage.

Let it be supposed that the betatron flux departs by a small amount $\Delta\Phi_0$ from the correct value and that the r-f frequency error is ω_1, then the particles in the acceleration chamber will oscillate about a stable phase angle ψ_B given by

$$V \sin\psi_B = \frac{d}{dt}[\Delta\Phi_0 - 2\pi r_0^2 B_0(1-n)\omega_1\eta/\omega_0], \quad (32)$$

and ψ_B can be held small, even with small V, if $\Delta\Phi_0$ and ω_1 are small. If prebunching is used, it may thus be unnecessary to employ any automatic flux compensation even if

$$\Delta\Phi_0/\Phi_0 \gtrless [(1-n)(b-A)]/r_0, \quad (33)$$

where A is the amplitude of the betatron oscillations and $2b$ the width of the acceleration chamber. The inequality (33) gives the condition that the particle be lost to the walls in the absence of an r-f voltage.

V. INJECTION METHODS

A number of injection methods have been proposed for the proton synchrotron. For injection directly into the synchrotron stage of operation, it is convenient to classify these methods into one or more of the four following categories. One attempts to avoid loss of injected particles on subsequent revolutions to the gun by

(1) Adiabatic damping of the oscillations before the particles return to the gun,

(2) Rapid decrease of the free-oscillation amplitude by the use of auxiliary transient fields,

(3) Rapid decrease of synchrotron phase and radial oscillations by rapid alteration of the stable phase angle,

(4) Adiabatic shift of the stable orbit by frequency modulation of the r-f accelerating voltage. With a preliminary betatron stage, methods (1) and (2) are pertinent in addition to the possibility of an adiabatic shift of the betatron orbit.

Most likely injection will take place with energies in excess of 1 Mev, into an initial magnetic field greater than 50 gauss, from an auxiliary accelerator by means of a suitable gun. In practice, intensities will be so low that the effects of space charge, even during injection, can be neglected. We shall not concern ourselves with the nature of this primary accelerator. When injecting directly into the synchrotron phase, it is desirable to minimize the horizontal betatron oscillations by making the injection momentum correspond to the value of B_z at the injection orbit. If particles are injected over a number of r-f cycles while the magnetic field is increasing, one should increase the injection energy in step with the magnetic field. This is not too difficult if the initial accelerator is a low energy transformer but it is much harder if a Van de Graaff accelerator is used and probably impossible if a cyclotron or linear accelerator is employed.

We shall now discuss four alternative injection proposals, chosen to illustrate the four basic methods stated above. The first one is discussed in somewhat more detail than its importance warrants because it serves to clarify the difficulties inherent in injection. The numerical estimates for the number of particles accepted into the acceleration cycle are derived for the machine described by the data in Table I.

1. Adiabatic Damping of Oscillations before Particles Return to the Neighborhood of the Gun

In this system the gun is located vertically above the central orbit and particles are injected over several r-f cycles. It is highly desirable that the particle energy on injection just equal the energy appropriate to the central orbit, so that for maximum intensity the injection gun's energy must be modulated. Let us start by supposing that the injection energy has just the correct value and consider the effects of departure from this energy later. Furthermore let us for the moment neglect the fact that the injected beam has a certain angular spread.

Consider a particle arriving at the acceleration gap with a phase ψ. The initial value of the radial velocity $\dot{x}_1$ is given approximately by

$$\frac{\dot{x}_i}{r_0} = -\frac{\dot{\psi}}{\omega_0 n} = \frac{V(\sin\psi - \sin\psi_0)}{2\pi r_0^2(1-n)B_0},$$

so that during a single revolution the particle moves radially a distance x_1 given by

$$x_1 = \frac{V(\sin\psi - \sin\psi_0)}{(1-n)r_0 B_0 \omega_0} = \frac{eV(\sin\psi - \sin\psi_0)r_0}{(1-n)2E_i},$$

with E_i the injection energy.

If the accelerating gap is located near the gun, x_1 is the radial distance the particle traverses before returning to the neighborhood of the gun. If $x_1 > s$, the half-width of the gun, the particle will certainly not be lost in the second revolution. Another circumstance which allows the particle to miss the gun is that the frequency of the vertical betatron oscillations is $(n)^{1/2}f_0$, where f_0 is the particle rotation frequency. If the particle is injected at a height h above the median plane, it returns to the neighborhood of the gun at a height $h\cos(2\pi(n)^{1/2})$. Thus if $h(1-\cos 2\pi(n)^{1/2}) > t$, the half-thickness of the gun, the particle will not be lost even if $|x_1| < s$. In practice one can choose n so that the particle first returns to the vicinity of the gun after about five revolutions, although ideally it is possible to increase this to $2\pi/\cos^{-1}(1-t/h)$ revolutions if h is increased suitably to allow for the length of the gun and the finite spread of the input beam. This assumes that all but a few particles miss the gun on the first few revolutions.

The particles escaping the gun during the first few revolutions will not return to the gun for a half-period of a synchrotron oscillation. In this time the amplitude of the vertical oscillation will be damped to

$$h\left(\frac{B_i}{B_i + (1/2\Omega_0)(dB/dt)}\right)^{1/2} = h\left[1 - \frac{f_0 V \sin\psi_0}{4\Omega_0 E_i}\right],$$

and if $(hV\sin\psi_0/4E_i)(f_0/\Omega_0) < t$, the particles will not be lost to the gun on subsequent revolutions. In practice, this is impossible to achieve and a certain proportion of the particles will be lost, equal very roughly to $(1/\pi)[\cos^{-1}(1-t/h)]$.

The oscillation period of a particle depends on its injection phase as well as upon B_0, ω_0, and V, all of which change continuously with time. Since the synchrotron period is much larger than a period of vertical betatron oscillations, we can regard their relative phase as a random quantity. With these assumptions, the total number of particles accepted into the machine of Table I is

$$N = 2.5\times 10^7 SI\left(\frac{4}{E_0}\right)\left(2 - \frac{\psi_0}{\pi/4}\right) \times \left[1 - (1/\pi)\cos^{-1}\left(1 - \frac{t}{h}\right)\right]^l,$$

where

$$l\frac{hV\sin\psi_0}{4E_i}\left(\frac{f_0}{\Omega_0}\right) = t,$$

S is the total number of cycles over which injection takes place, E_i the injection energy in Mev, and I the injection current in microamperes.

TABLE II. Number of particles accepted with different injection schemes.

Injection scheme	No. of particles	Gun energy modulated	Injection period
5.2	1.9×10^{10}	No	4 μsec.
5.3	4.6×10^{10}	No	125 μsec.
5.4	7.5×10^{10}	Yes	250 μsec.

If particles are not injected with the correct energy they will have, superimposed on the horizontal synchrotron oscillations, horizontal betatron oscillations of frequency $(1-n)^{\frac{1}{2}}f_0$. This means that the particles will reappear in the vicinity of the gun at intervals during the time required for the radial synchrotron oscillation to move a radial distance equal to the sum of the gun thickness and twice the amplitude of the horizontal betatron oscillations. Thus the possibility of losing particles to the gun is very greatly increased.

2. Single-Shot Injection

In this system an auxiliary electric field is maintained for a time interval less than the rotation period of the particles to remove completely the vertical betatron oscillations. The gun is located exactly as in case (1) and a uniform vertical electric field is established over an arc of the acceleration chamber. The field strength and arc length are to be so chosen that the injected particles emerge into the field-free region with zero vertical velocity, and by tilting the gun the arc length may be shortened. These particles will remain in the median plane until they return to the gun. If by this time the vertical electric field has been removed, the particles will continue to move in the median plane and none will be lost to the gun.

When the finite spread of the injected beam is taken into account, one can show that, as far as subsequent oscillations are concerned, the electric field serves to move the gun into the median plane. In this system particles can be injected only over a single cycle and the resulting loss of intensity may require compensation by the use of an exploded ion source. An important advantage is that initially the particles are essentially all grouped along the central line of the acceleration chamber, while pulsing the source will ensure that no wasted particles are introduced into the chamber. This arrangement is very desirable from the point of view of an automatic frequency control system, which is particularly necessary during the initial stages of operation, and it may well become the determining factor in the choice of an injection system.

If upon injection the particle energy is E_i Mev, one can show that the total number accepted into the acceleration cycle will be equal approximately to

$$2.50\times10^7 I\left(\frac{4}{E_i}\right)^{\frac{1}{2}}\left(1-\frac{2\psi_0}{\pi}\right), \qquad (34)$$

with I the injection current in microamperes and ψ_0 the stable phase angle.

3. Rapid Change of the Stable Phase

If the stable phase angle for synchrotron oscillations be suddenly changed, the particles will execute new oscillations with decreased or increased amplitudes depending on their phase at the instant of change of the stable phase. Thus some of the particles will have their maximum phase velocity and hence their maximum radial displacement from the stable orbit decreased, and one has a mechanism for capturing particles into synchrotron acceleration without hitting the injecting gun.

Since the sine of the stable phase angle is proportional to the time rate of change of magnetic field and inversely proportional to the accelerating voltage, a sudden change in either of these quantities will provide the necessary sudden change in stable phase. Particles are injected from a gun placed on the inside of the accelerating chamber in the median plane (to keep the vertical aperture a minimum).

During injection the r-f voltage is maintained at a constant frequency with a constant magnetic field, so chosen as to keep the stable orbit centered in the accelerating chamber. The machine thus acts as a d.c. cyclotron or as a synchrotron with $\psi_0=0$. The sudden jump in ψ_0 occurs when the a.c. magnetic field is turned on. A particle arriving at the accelerating gap during the injection period with a positive phase will pick up energy and move inwards into the chamber. If the radial displacement in a single revolution exceeds half the gun width, the particle will not hit the gun on the second revolution. In a practical case this radial shift is so large that practically all the particles arriving at the gap with positive phase will miss the gun and all those arriving with negative phase will be lost to the inner walls or to the gun.

During injection the phase motion of the protons is that of the free oscillations of a pendulum with arbitrary initial phase and initial phase velocity given by $\dot{\psi}_i = -n\omega_0 d/r_0$, with d the distance of the gun from the stable orbit of radius r_0. Thus the phase angle ψ is an elliptic function of the time. In particular, if the a.c. magnetic field is turned on at a definite instant of time, the phase ψ_F and phase velocity $\dot{\psi}_F$ at this instant can be written in terms of ψ_i and $\dot{\psi}_i$. If now ψ_0 is the final stable phase angle, it follows readily that the particle will be accepted into the acceleration cycle if the following inequalities are satisfied:

$$\left.\begin{aligned} &\psi_i > 0, \\ &\left(\frac{d}{r_0}\right)^2 \geq \left(\frac{\dot{\psi}_F}{n\omega_0}\right)^2 + 2\left(\frac{\Omega_0}{n\omega_0}\right)^2 \\ &\qquad \times[(\cos\psi_0 - \cos\psi_F) - (\psi_F - \psi_0)\sin\psi_0], \\ &\cos\psi_0 - \cos\psi_F - (\psi_F - \psi_0)\sin\psi_0 \\ &\qquad + \frac{1}{2}\left(\frac{\dot{\psi}_F}{\Omega_0}\right)^2 \lessgtr \cos 2\psi_0 - (\pi - 2\psi_0)\sin\psi_0, \end{aligned}\right\} \quad (35)$$

with $\Omega_0 = n\omega_0 V/[2\pi r_0^2(1-n)B_0]$, the angular frequency of small free oscillations during injection. The first inequality states that the particle does not hit the the gun or inner walls on the first revolution. The second is the condition the amplitude of the new radial oscillations be less than the distance of the gun from the stable orbit, and the third condition ensures that the particle does not move out of the stable phase range for oscillations on subsequent revolutions.

Inserting the expressions for ψ_F and $\dot{\psi}_F$ into the conditions (35) then gives the acceptable injection phase angle as a function of the time of injection of the particle relative to the instant when the magnetic field is turned on. Summing over all injection times for which the acceptable injection phase angle is positive, one then can obtain the total range of acceptable phase angles Θ for all the particles which are injected. This process will not be carried out here in detail but an approximate expression for Θ, obtained by replacing the elliptic functions by trigonometric functions, may be written as

$$\Theta = \frac{f_0}{\Omega_0}\int_0^{\pi}\left[\psi_0 \sin y\left(\frac{2dn\omega_0}{r_0\Omega_0} - \psi_0 \sin y\right)\right]^{\frac{1}{2}} dy, \quad (36)$$

which is valid when $2dn\omega_0/r_0\Omega_0 > \psi_0$. ($f_0$ is the frequency of rotation of the particles.)

If numerical values taken from Table I are inserted, it can be shown that the total number of particles accepted into the stable phase range is given by

$$N \cong 6.3\times 10^7 I\left(\frac{4}{E_i}\right)^{\frac{1}{2}},$$

with I the injection current in microamperes, E_i the injection energy in Mev; ψ_0 has been taken as $\pi/4$, and it may be noted that N varies slowly with ψ_0.

The chief advantages of this scheme are the following:

(a) No auxiliary equipment is required.
(b) It is not necessary to energy-modulate the gun.
(c) There are no critical timing circuits.
(d) The attainable intensity is at least as great as that for any of the proposed alternatives.

4. Adiabatic Shift of the Stable Synchrotron Orbit by F-M Techniques

The scheme described here is essentially that proposed by D. M. Dennison for the electron synchrotron at the University of Michigan. The very different conditions at injection in a proton synchrotron, however, result in considerable difference in detail.

Consider particles injected from a gun at the outside of the accelerating chamber. Initially the radiofrequency is chosen so that the stable orbit passes through the gun and this frequency is so modulated that the stable orbit moves in toward the center at a steady predetermined rate. Particles are injected in bursts over a time interval encompassing a number of revolutions so that energy modulation of the injector is necessary to attain maximum beam intensity.

Particles will miss the gun during the next few revolutions provided they arrive at the accelerating gap with negative phase. Furthermore, if the time required for the stable orbit to reach the center of the chamber is not much longer than the synchrotron oscillation period, particles will not be lost to the gun. If they are lost at all, they will be lost to the inner wall.

The phase acceptance angle ψ_i on the first revolution must lie within the limits $\psi_0' < \psi_i < \pi - \psi_0'$, where ψ_0' is the stable phase angle during injection. As the stable orbit moves inward the phase acceptance angle will decrease, for a given amplitude of synchrotron oscillation, vanishing when the stable orbit reaches the center of the chamber since the maximum amplitude of radial synchrotron oscillation equals the distance d of the gun from the central orbit.

If the frequency error ω_1 has the form

$$\omega_1 = \omega_0[-(nd/r_0) + \alpha t], \tag{37}$$

the first of Eqs. (11) yields

$$x/r_0 = d/r_0 - (\psi + \omega_0 \alpha t / n\omega_0), \tag{38}$$

and the second, in the non-relativistic range which applies at injection, yields for the equation of phase oscillation:

$$\frac{(1-n)r_0^2 B_0}{n\omega_0}\ddot{\psi} + \frac{V}{2\pi}\sin\psi = \frac{V}{2\pi}\sin\psi_0', \tag{39}$$

with

$$\sin\psi_0' = \sin\psi_0 - \frac{2\pi r_0^2(1-n)B_0\alpha\omega_0}{n\omega_0 V}. \tag{39a}$$

From Eq. (38), one sees that the stable orbit, which initially lies at a distance d from the center of the chamber, moves toward the center at a constant rate, so that the frequency law (37) accomplishes the desired result. If the stable orbit is to reach the center in a time less than one synchrotron period, α must satisfy the inequality

$$\alpha > \frac{nd}{r_0}\frac{\Omega_0'}{2\pi} \quad \text{with} \quad \Omega_0'^2 = \frac{\omega_0 n V}{2\pi r_0^2(1-n)B_0}.$$

If furthermore $|\psi_0'|$ is not to exceed $|\psi_0|$, then $\alpha < (\Omega_0'/\omega_0)2\Omega_0' \sin\psi_0$, so that we have, as an additional requirement,

$$\frac{2\Omega_0' \sin\psi_0}{\omega_0} > \frac{nd}{2\pi r_0}.$$

For the 10-Bev machine this inequality is certainly fulfilled and allows a decrease of V during injection with a consequent decrease of Ω_0' and increase of the number of particles accepted into the stable phase range.

We now consider the particles to be injected in bursts with a recurrence frequency f_0 equal to the rotation frequency of the particles. If the phase of a particle injected in the sth burst is ψ_i and the energy is appropriate to the injection orbit, then the particle will not be lost to the gun on subsequent revolutions if

$$\left[\left(\frac{\alpha s}{f_0}\right)^2 + \frac{\{\cos\psi_0' - \cos\psi_i + (\psi_0' - \psi_i)\sin\psi_0'\}nV}{2\pi r_0^2(1-n)B_0\omega_0}\right]^{\frac{1}{2}} < \frac{nd}{r_0}.$$

From this one sees that there is no point in injecting particles after the orbit for which

$$s = (f_0/\alpha)(nd/r_0).$$

The total number of particles accepted is given approximately by

$$N \cong 10^7 I\left(\frac{4}{E_i}\right)^{\frac{1}{2}}\left(1 - \frac{2\psi_0}{\pi}\right)\frac{nd}{r_0}\cdot\frac{f_0}{\alpha},$$

with E_i the average injection energy in Mev, ψ_0 the stable phase, and I the beam current in microamperes.

Since the above expression is inversely proportional to α, the maximum number of particles will be obtained when $\alpha = nd/r_0 \cdot \Omega_0'/2\pi$. In this case

$$N \cong 10^7 I\left(\frac{4}{E_i}\right)^{\frac{1}{2}}\left(1 - \frac{2\psi_0}{\pi}\right)\frac{\omega_0}{\Omega_0'}$$

$$= 4\times 10^8 I\left(\frac{4}{E_i}\right)^{\frac{1}{2}}\left(1 - \frac{2\psi_0}{\pi}\right).$$

It is virtually impossible to attain this value in practice and a much more realistic value is that for which $\alpha = (\Omega_0'^2 \sin\psi_0)/\omega_0$, i.e., with $\psi_0' = 0$. In this case

$$N \cong 10^8 I\left(\frac{4}{E_i}\right)^{\frac{1}{2}}\left(1 - \frac{2\psi_0}{\pi}\right).$$

If the gun is not energy-modulated, injection will start when the energy required in the *central* orbit equals the injection energy, and will cease when the energy appropriate to the *injection* orbit equals the injection energy. The accepted number of particles will then be very much reduced and is probably no greater than that obtained by single-shot injection.

The numerical results obtained in this section are displayed in Table II. In all cases we have taken, $E_i=4$ Mev, $\psi_0=\pi/8$, $I=1$ milliampere. Since the period over which injection takes place varies widely from scheme to scheme it may seem unfair to assume that the peak injection current is the same in all cases. However, the general problem of obtaining high density proton beams at several Mev is still too uncertain to warrant any other assumption.

We have now given one example of each of the four main alternative injection schemes. Of these, if intensity is not the primary consideration, the single-shot scheme is most attractive. In contrast to the other methods, the injected ions are caught into the acceleration cycle and lie initially in the central orbit. This is highly desirable in view of the proposed frequency-control system which, with this injection system, can operate right from the beginning when control requirements are most critical. In the other schemes, a large number of particles not caught into the accelerating phase will drift to the inner wall. Until all these have been removed, the frequency-control system cannot begin to function properly.

If maximum intensity is the primary factor, probably scheme (3) is next best because of its simplicity. No energy modulation of the gun, no auxiliary electric fields or special frequency-modulation techniques are required, and the timing of the various steps in the injection process is not critical.

It must be emphasized once again, however, that a large number of alternative injection schemes of greater or lesser complexity can be evolved, each with advantages peculiar to itself. In a practical case a choice can only be made when all the relevant factors are taken into account.

THE REVIEW OF SCIENTIFIC INSTRUMENTS VOLUME 20, NUMBER 1 JANUARY, 1949

A Double-Channel, Direct Reading, Low Frequency Counting Rate Meter and Counting Rate Comparator*

ROBERT M. KLOEPPER AND FRANK E. HOECKER
Department of Physics and Astronomy, University of Kansas, Lawrence, Kansas

(Received August 30, 1948)

A two-channel, direct reading counting rate meter for measurement of low frequency (average random or uniform) pulse rates in either channel or in both channels simultaneously is described. The outputs of two degenerative vacuum-tube voltmeter integrating circuits are combined into a bridge circuit whereby the equality of pulse rates in the two channels may be determined on a null-reading galvanometer. An impulse register amplifier is provided on each channel for operation of impulse counters for monitoring and/or calibration. The five ranges provided are 0–100, 200, 500, 1000, and 5000 pulses per minute. Although primarily designed for the specific purpose of adjusting two atmospheric pressure wire plate alpha-particle detectors (W. Y. Chang and S. Rosenblum, Phys. Rev. 67, 221 (1945)) to equal average pulse rates, the circuit design may be modified to detect pulse rate ratios other than unity, pulse rate differences, and/or pulse rate ranges other than those enumerated above.

1. INTRODUCTION

THE instrument to be described was developed for the purpose of matching the counting rates of two atmospheric-pressure alpha-particle detectors used in measuring the range of alpha-particles in various substances. Two alpha-particle detectors were used in order to balance out the effects of factors which might affect the counting rate of a single detector such as fluctuations in supply voltage, temperature,

---

* This work was sponsored by the Office of Naval Research under Contract N6onr-260-TO-1.

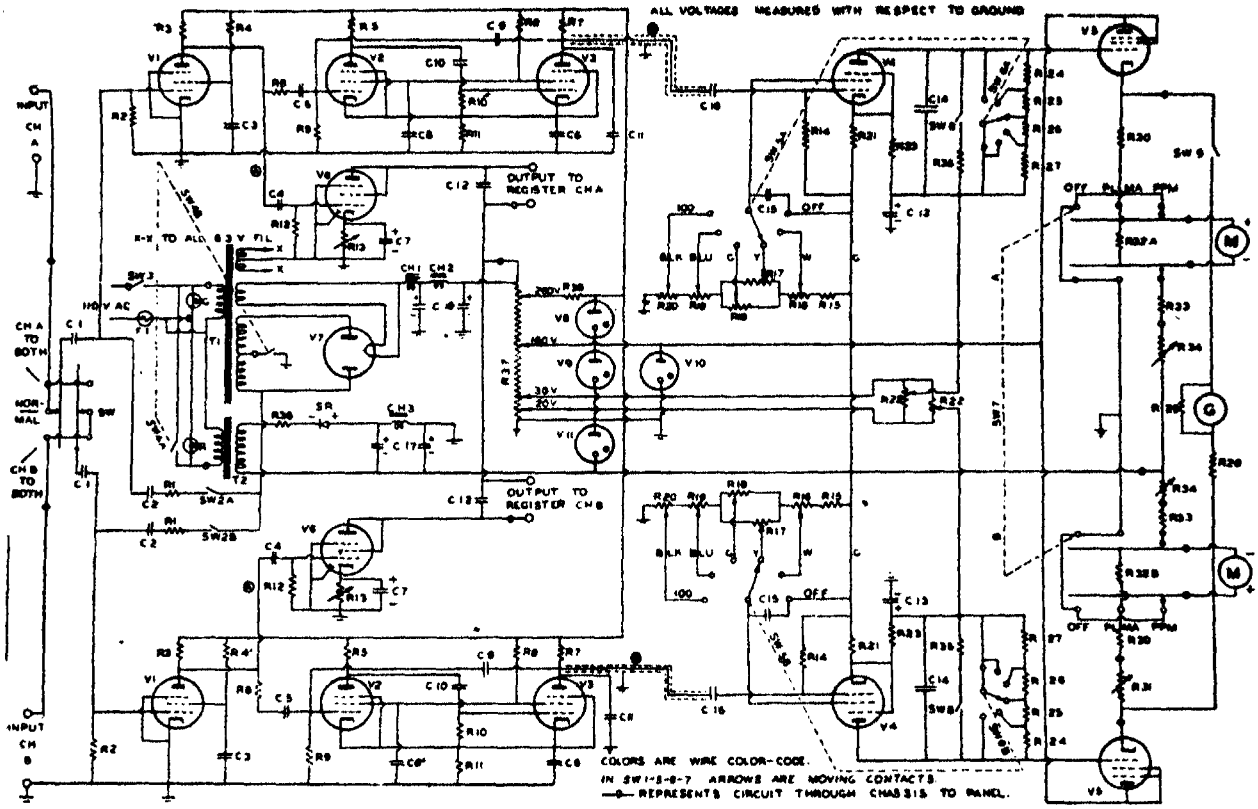
ALL VOLTAGES MEASURED WITH RESPECT TO GROUND
INPUT CH A
INPUT CH B
OUTPUT TO REGISTER CH A
OUTPUT TO REGISTER CH B
110 V AC
X-X TO ALL 6.3 V FIL.
CH A TO BOTH
NORMAL
CH B TO BOTH
250V
150V
30V
20V
BLK
BLU
OFF
ON
MA
PPM
COLORS ARE WIRE COLOR-CODE.
IN SW1-5-6-7 ARROWS ARE MOVING CONTACTS.
—○— REPRESENTS CIRCUIT THROUGH CHASSIS TO PANEL.

FIG. 1. Circuit diagram.

Part number	Value*
C1 A-B**	0.01, mica
C2 A-B	0.003, mica
C3 A-B	0.25, 600 v
C4 A-B	0.0005, mica
C5 A-B	0.0005, mica
C6 A-B	0.5, 400 v
C7 A-B	10, 50 v electrolytic
C8 A-B	0.25, 600 v
C9 A-B	0.0005, silver mica or ceramic
C10 A-B	0.0002, ceramic
C11 A-B	0.005, 400 v
C12 A-B	0.02, 400 v
C13 A-B	10, 50 v, electrolytic
C14 A-B	2, 600 v, Dykanol A
C15 A-B	0.1, 400 v
C16 A-B	0.00012, silver mica or ceramic
C17	50×50, 150 v, electrolytic
C18	8×8, 450 v, electrolytic

Part number		Value*
R1 A-B**	1 Meg	½ w.
R2 A-B	500M	½ w.
R3 A-B	200M	1 w.
R4 A-B	330M	½ w.
R5 A-B	250M	1 w.
R6 A-B	330M	½ w.
R7 A-B	250M	1 w.
R8 A-B	1 Meg	½ w.
R9 A-B	100M	½ w.
R10 A-B	1 Meg	½ w.
R11 A-B	10M	1 w.
R12 A-B	1 Meg	½ w.
R13 A-B	2M	Rheo.
R14 A-B	500M	1 w.
R15 A-B	10M–40M***	1 w.
R16 A-B	25M	Pot.
R17 A-B	25M	Pot.
R18 A-B	25M	Pot.
R19 A-B	15M	Pot.
R20 A-B	20M	Pot.
R21 A-B	3300	2 w.
R22 A-B	1M	Pot.
R23 A-B	30M	1 w.
R24 A-B	10 Meg	½ w.
R25 A-B	20 Meg	½ w.
R26 A-B	10 Meg	½ w.
R27 A-B	20 Meg	½ w.

Part number	Value*	
R28	1000	½ w.
R29	27	½ w.
R30A	3000	5 w.
R30B	2900	5 w.
R31	200	Rheo.
R32 A-B	25#	Meter shunt
R33 A-B	12M	1 w.
R34 A-B	2M	Rheo.
R35 A-B	1 Meg	½ w.
R36	50	1 w.
R37	10M	200 w.
R38	3M	5 w.
Ch1–Ch2	8–16h., 150 ma	
Ch3	10h., 15 ma	
SR	Selenium rectifier, 130 v, 100 ma	
T1	375-0-375 v, 160 ma, 5 v, at 3 amp. 6.3 v at 5 amp.	
T2	110 v to 140 v	

Part number	Value*
Sw1	2-circuit, three position toggle
Sw2 A-B	Push button, s.p.s.t., normally open
Sw3	S.p.s.t. toggle
Sw4 A-B	D.p.s.t. toggle
Sw5–6 A-B	4-circuit, six position, rotary
Sw7 A-B	4-circuit, three position, rotary
Sw8	Push button, s.p.s.t., normally open
Sw9	S.p.s.t. toggle
V1 A-B	6SJ7
V2 A-B	6SJ7
V3 A-B	6SJ7
V4 A-B	6SJ7-GT
V5 A-B	6AC7
V6 A-B	6AG7
V7	5Z3
V8 & V9	VR105-30
V10	VR150-30
V11	VR105-30

Part number	Panel control title
R13 A-B	ADJUST OUTPUTS CH A-B
R16 through R20 A-B	CALIBRATION controls
R22 A-B	ADJUST BIAS CH A-B
R31	BRIDGE ZERO
R34	METER ZERO CH A-B
Sw1	CHANNEL INPUTS
Sw2 A-B	3600 PPM INPUT CH A-B

Part number	Panel control title
Sw3	POWER ON-OFF
Sw4	HIGH VOLTAGE ON-OFF
Sw5-6 A-B	RANGE CH A-B
Sw7	METER SWITCH
Sw8 A-B	CHANNEL RESET CH A-B
Sw9	BRIDGE ON-OFF

---

*Capacity is given in microfarads; resistance in ohms.

** The letter (or letters) following the part number designates the channel (or channels) in which that part may be found.

*** Must be adjusted by trial.

humidity, and atmospheric pressure. This was accomplished by using the counting rate of one of the detectors having a fixed source and source-distance as a reference to which the counting rate of the measuring detector was adjusted, both detectors being operated from the same high voltage source. The adjustment of counting rate of the measuring detector was effected by varying the distance between the alpha-particle source and the detector.

Pulses from the two alpha-particle detectors are fed into the separate channels of the two-channel pulse rate comparator. The circuit of this instrument consists of two essentially identical channels, each composed of an input amplifier, a pulse equalizer, and a pulse amplifier of variable gain for range selection which is directly coupled to an RC integrating circuit and to a vacuum-tube voltmeter. The vacuum-tube voltmeter circuits are coupled to form a pulse rate comparison bridge. The bridge balance indicates equality of average pulse rates.

2. THE CIRCUIT

The two channels of the counting rate meter are essentially identical as may be seen by reference to the circuit diagram, Fig. 1. Switch Sw1 permits the input pulses from either input jack to be placed in both channels simultaneously, principally for calibration or for calibration checking, or to be placed through their channels individually. The tubes V1, V2, and V3 comprise the input amplifiers and pulse equalizer circuits which are essentially those of Kip *et al.*[1]

The theory of the integrating RC "tank" circuit and its associated statistical limitations are adequately discussed elsewhere.[1–3] It may be shown[1] that the voltage on the integrating condenser is proportional to the frequency of the impressed pulses, the value of the RC tank leakage resistor, and the size of the pulses impressed upon the integrating condenser.

TABLE I. Tabulated RC, percent probable error (p) and equilibrium time (t_0) for the chosen compromise in the counting rate meter design.

Counting rate (PPM)	R (megohms)	RC* (minutes)	p (%)	t_0 (minutes)
200	60	2	2.4	7.5
100	60	2	3.5	6.8
50	60	2	4.8	6.1
20	60	2	7.4	5.2
500	40	4/3	1.9	5.3
200	40	4/3	2.9	4.7
100	40	4/3	4.2	4.2
50	40	4/3	6.0	3.8
1000	30	1	1.5	4.4
500	30	1	2.2	4.0
200	30	1	3.4	3.5
100	30	1	5.0	3.1
5000	10	1/3	1.2	2.3
2000	10	1/3	1.8	2.1
1000	10	1/3	2.5	1.9
500	10	1/3	4.9	1.8

* Capacity of C is 2 microfarads.

The method of range switching and of coupling the pulses from the integrator tube (V4) to the vacuum tube voltmeter (VTVM) circuit is adapted from that of Kip *et al.*[1] The rotary switch RANGE CH A[4] (see Fig. 1) consists of Sw5 and Sw6, ganged on a common shaft. The gain of the integrator tube (and, therefore, the amount of charge transferred to the RC tank circuit per pulse) is controlled by variation of the screen voltage of the tube (V4). Sw5 selects the output voltage of the potentiometer appropriate to the screen voltage of the integrator tube for the range chosen. At the same time that the gain control is selected by Sw5, Sw6 changes the value of the leakage resistor R24–27: since the integrating condenser C14 remains constant, this change in leakage resistance modifies the time constant of the memory circuit in accordance with the values of Table I, selecting those values of RC which are a compromise between long equilibrium times and large fractional probable errors resulting from statistical fluctuations. A ganged Sw5–6 is provided for each channel. The OFF position of Sw5–6 puts a direct short across the tank condenser at the same time that the integrator screen voltage is lowered nearly to cathode potential so that the stage gain is zero.

The location of the tank circuit requires that the VTVM grid operate at the plate potential of

---

[1] Kip, Bousquet, Evans, and Tuttle, Rev. Sci. Inst. 17, 323 (1946).

[2] N. S. Gingrich, R. D. Evans, and H. E. Edgerton, Rev. Sci. Inst. 7, 450 (1936).

[3] L. I. Schiff and R. D. Evans, Rev. Sci. Inst. 7, 456 (1936).

[4] CH A and CH B mean Channel A and Channel B, respectively.

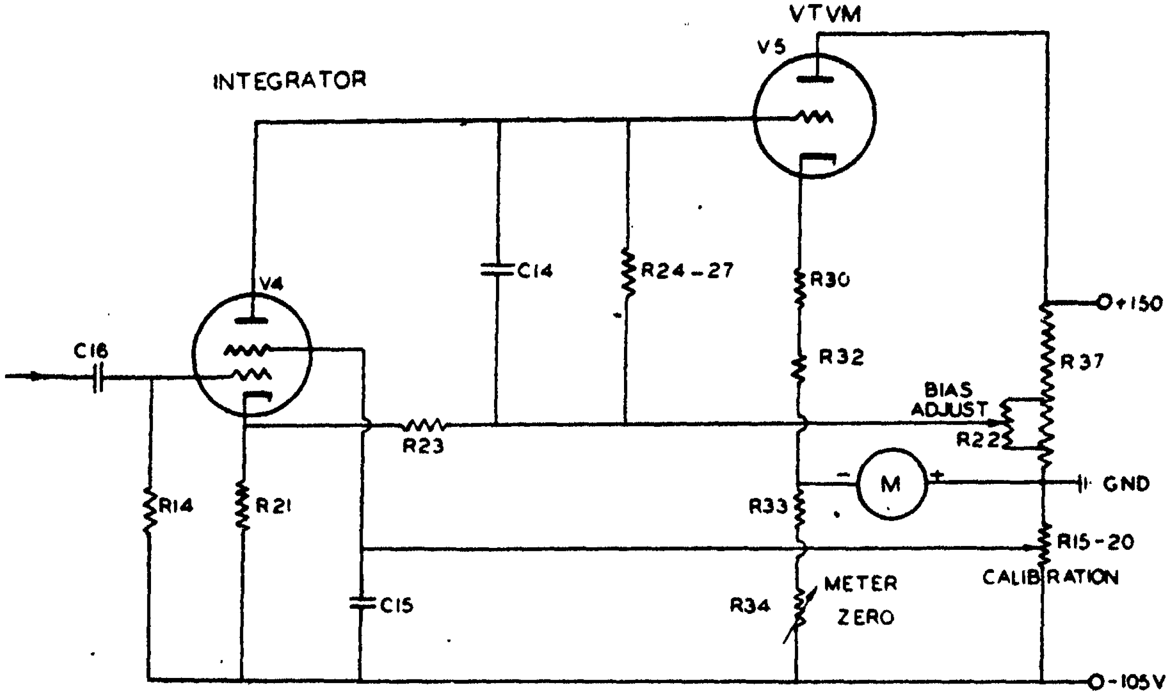

NOTE ALL VOLTAGES MEASURED WITH RESPECT TO GROUND

FIG. 2. Simplified diagram of the integrator and vacuum-tube voltmeter circuits, showing method of bias application to the latter.

the integrator. Rather than allow the VTVM to "float" at a potential of 105 volts above ground, the cathode of the integrator tube was lowered to 105 volts below ground potential. This circuit places the plate of the integrator tube only slightly above ground potential by the amount of positive bias on the VTVM grid. This circuit has the additional necessary advantage over that of Kip *et al.*[1] that the bias and, consequently, the plate current of the VTVM may be adjusted.

The plate voltage of the VTVM is that between ground and the +150-volts supply. R30 is the VTVM degenerative resistor; its value of 3000 ohms gives a voltmeter sensitivity of approximately full-scale deflection of the meter (5 ma) at a tank condenser voltage of 15 volts. It serves the additional function of a bridge arm resistor in the bridge rate comparator circuit.

The design of this circuit allows the "negative" power supply to furnish not only plate voltage to the integrator tube but also bucking voltage to the meter circuit. The negative pulses as applied to C14 by the integrator tube, V4, cause the VTVM plate current to decrease with rising frequency (rising tank voltage). The bias adjustment is used to adjust the VTVM plate current to 8 ma.

The METER SWITCH Sw7 is a rotary three-position, four-circuit gang switch; it controls the meter-switching in both channels simultaneously. With the METER SWITCH in the OFF position, the meters are shorted. In the PL ma position the meter switch inserts the shunts R32 A–B across the meters and inserts these shunted meters in series with the cathode leads with the correct polarity to read the cathode and plate current of the triode-connected VTVM tubes (6AC7). The shunts are wound on one-watt, 100,000-ohm resistors as forms and are carefully adjusted so that the meters require nearly (within about 3 percent) 10 ma for full-scale deflection but more particularly that they require the *same* currents within ½ percent for full-scale deflection when the shunts are used. In the PPM position the following changes take place: (1) the shunts are removed from the meter circuits, (2) the polarity of the meters is reversed, (3) the bucking current circuit is closed and the meter circuit function becomes that shown in Fig. 2. The bucking circuit is not completed in any other meter switch position.

In use, as the plate current falls with rising frequency the constant bucking current source causes the meter to read upscale. This upscale reading will be a linear function of frequency if the VTVM responds linearly to voltage on the integrating condenser and if the bucking current is constant. In this circuit this linearity is realized within ½ percent.

It is entirely possible to use the bucking circuit to set the counting-rate meter at zero against any reasonable background count and, therefore, to record one counting rate in the presence of another.

The bridge circuit is shown in a simplified form without the complicating bucking circuits in Fig. 3 as if Sw7 were in the PL ma position. With identical voltages on C14A and C14B the plate currents may be adjusted by the BIAS ADJUST controls to equal values as read by the two plate meters. By variation of the BRIDGE ZERO control R31 the resistances of the two arms, composed mainly of the cathode degenerative VTVM resistors R30, may be made equal as indicated by a null of the galvanometer G when Sw9 (BRIDGE ON-OFF) is closed.

Counting rates may be read directly from the appropriate channel meter with due regard for the statistical limitations[1,2] as set by the value of the time constant RC of the memory circuit, counting rate and equilibrium time t_0. Table I will be found helpful in judging the operation limitations of the counting-rate meter. The equilibrium time may be reduced by artificial adjustment of the vacuum-tube voltmeters nearly to equilibrium values. The CHANNEL RESET switch Sw8 is placed in series with R35 across the tank condenser C14 to permit this adjustment by rather rapid discharge of C14 to any desired value.

If identical voltages are placed on C14A and on C14B by identical pulse rates in the separate channels, a null-reading of the galvanometer will indicate this identity. Resistor R29 damps the oscillation of the galvanometer on random pulses. A high impedance voltmeter, used to replace the galvanometer in this bridge circuit, could be calibrated directly in terms of pulses per minute difference of pulse-rate in the two channels.

A convenient and rapid method of determining whether the rates are identical is to set the vacuum-tube voltmeters artificially to the same reading (bridge galvanometer at zero) and to observe the direction of drift of the galvanometer.

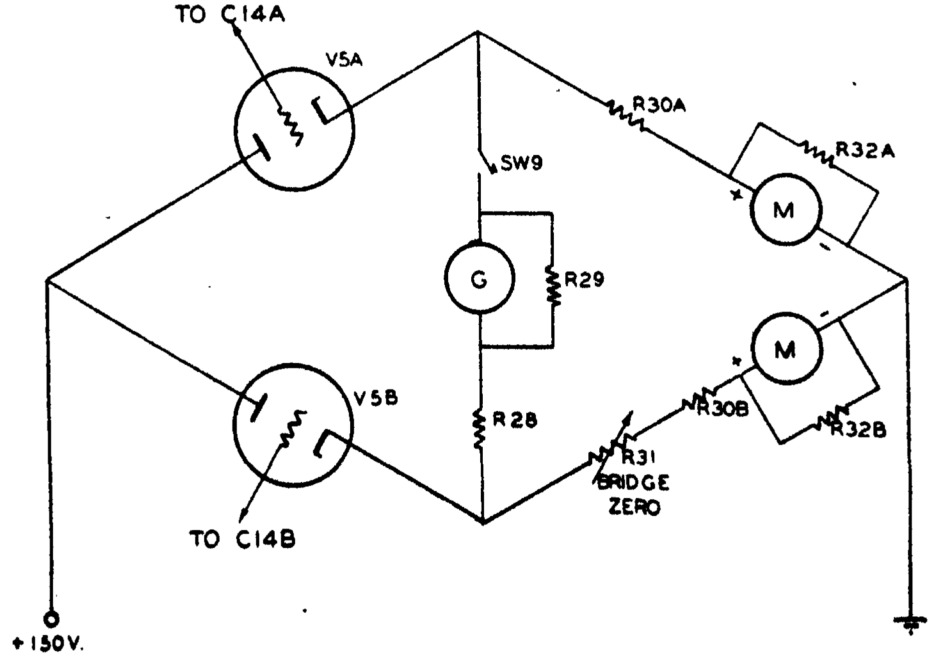

FIG. 3. Simplified pulse rate comparator bridge circuit.

If the impedance of the galvanometer circuit is comparable to the bridge arm resistor values, the counting rate indications of the meters will be erroneous when the BRIDGE ON–OFF switch is on because the galvanometer circuit has a tendency to equalize the meter indications.

The impulse register circuits are driven by the input amplifiers. The positive pulses at point *A* are fed through the coupling capacitor C4 to the grid of a 6AG7, V6. This tube was chosen because it has a very high transconductance, 8000 micromhos, and operates into a low plate load resistance; therefore, it is ideally suited for coupling to an impulse register. The variable resistor R13 (ADJUST OUTPUT) in the V6 cathode return affords a convenient method of varying the current output to the register to permit application of various types of registers as well as relays of varying sensitivities. Another use to which the OUTPUT TO REGISTER terminals may be put is the operation of a speaker for aural monitoring. Normally, no plate current may flow to the 6AG7 unless some resistive connection is made across the OUTPUT terminals. One of these terminals in each channel is maintained at about +300 volts; this provides the high voltage supply to the calibrator.[1]

The calibration may be conveniently checked on the 5000 PPM scale for variations in time by pressing the appropriate 3600 PPM INPUT button. If the channel meter rises to 3600 PPM, there is good assurance that the other channel calibrations have not changed.

Adequate shielding and decoupling must be provided between the two channels to prevent interaction. Care must be taken to prevent voltage fluctuations due to an impulse register load from affecting the output of the pulse-equalizer circuits. If the sensitivity of the input amplifier is increased by lowering the value of R11, shielding becomes of primary importance.

The rate of approach (rise or fall of the VTVM plate current) to equilibrium may be different in the two channels even though identical pulse rates are impressed upon both channels. Such operation is neither unusual nor unreliable. The equilibrium value of the VTVM plate current is dependent upon the value of the leakage resistor of the RC integrating circuit but is independent of the size of the integrating condenser. Hence, the fact that the time constants (and, therefore, the rates of approach to an equilibrium value) of the two channels differ does not indicate that the equilibrium values will differ.

It should be pointed out that a cathode-ray oscilloscope, in general, disturbs the pulse shape enough so that the counting-rate meter cannot be calibrated with a cathode-ray oscilloscope on the circuit.

A 5-ma pen and ink recording milliammeter may be inserted directly in series with the VTVM plate meter. No circuit or calibration modifications are necessary *if* the resistance of the pen recorder is so low that its insertion does not appreciably affect the total value of the cathode degeneration resistance; if it does, recalibration is required because of the changed VTVM sensitivity.

If this plate current is similarly applied across a two or three-ohm standard resistor, the resulting potential drop will actuate a Leeds and Northrup recording potentiometer (20-Mv full scale) without any circuit modifications. This inserted resistance is insignificant and no recalibration is necessary.

THE REVIEW OF SCIENTIFIC INSTRUMENTS VOLUME 20, NUMBER 1 JANUARY, 1949

A Recording Mechanical Pressure Gauge of High Range*

PAUL M. HIGGS
Applied Physics Laboratory, University of Washington, Seattle, Washington

(Received March 23, 1948)

An instrument of rugged construction for recording very large and rapidly fluctuating pressures in liquids and gases is described. The pressure sensitive element is a thick, flat, circular diaphragm, rigidly mounted and fluid damped. The pressure *versus* time record is engraved upon the surface of a rotating polished metal disk by a stylus fastened directly to the diaphragm. The record may be read with a precision of better than one percent of full deflection. The instrument will record pressures up to 1000 pounds per square inch at frequencies from zero to five hundred cycles per second.

INTRODUCTION

THE recording pressure gauge was designed to measure large and rapidly fluctuating pressures of the order of hundreds of pounds per square inch as a function of time and at all frequencies below 200 cycles per second, *including zero*, both in air and under water. Since pressures having these characteristics occur only in the vicinity of abnormally large explosive charges, further design requirements were that the instrument should be self-contained, stable, and sufficiently rugged to withstand the rough treatment it would receive in use. These same requirements almost precluded *a priori* the use of electronic components since reliable operation under the relatively unknown conditions of use was essential. It was also desired that the record be made in as indestructible a form as possible to prevent the loss of data from damaged instruments and possible delay in the recovery of instruments after tests. This is particularly important where sea water with its corrosive effects is involved. An instrument of this or similar design may prove useful in the general study of large scale blast phenomena or where a detailed record of large and rapidly fluctuating fluid pressures is required. A suggested application is the study of transient phenomena in hydraulic systems.

GENERAL DESCRIPTION

Figure 1 is a schematic drawing showing the details of the essential parts of the instrument with the exception of the record disk drive mechanism which is clearly seen in the photograph, Fig. 2. In Fig. 1, (*A*) is the pressure sensitive element of the gauge, a flat circular disk of 24-ST aluminum. This diaphragm is 10 inches in diameter and is clamped over a one-inch face around the periphery, leaving a free or effective diameter of 8 inches. Since the use of gaskets in the diaphragm assembly was not permissible, joints were made liquid tight by painting the bearing faces with red glyptol at the time of assembly. No difficulty due to leakage under high pressures was encountered. Three thicknesses of diaphragms were used in the instruments to give an expanded range of sensitivities. Table I gives the approximate characteristics of these diaphragms.

Figure 3 is a plot of experimentally determined deflections of the gauge diaphragms for applied steady hydrostatic pressures for diaphragms that had been pre-stressed by the application of pressures equal to the maximum allowable. The

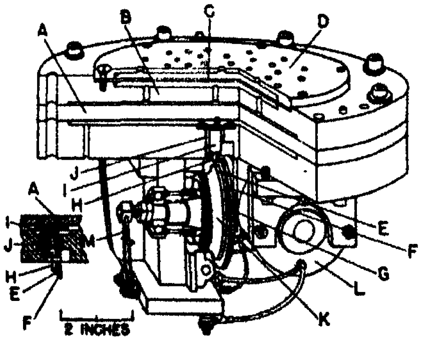

FIG. 1. Gauge in partial section.

---

* This work was undertaken in association with The Applied Physics Laboratory, The Johns Hopkins University, under a Section T Series Contract, NOrd-7818, sponsorship of the Bureau of Ordnance, United States Navy.

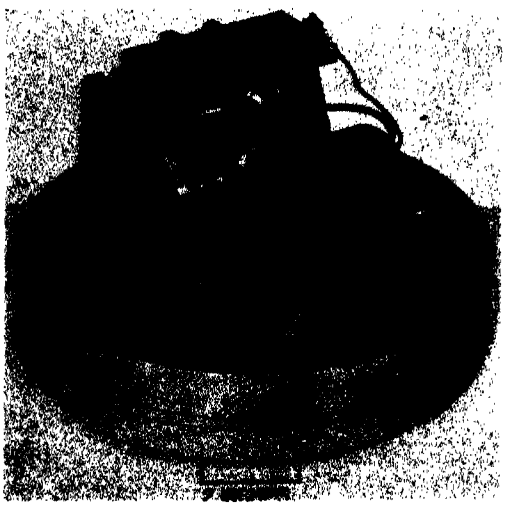

FIG. 2. Recording pressure gauge.

TABLE I. Diaphragm characteristics.

Diaphragm thickness	Pounds per square inch to produce 0.001-inch deflection	Maximum allowable pressure in pounds per square inch
¼"	2.48	300
$\frac{5}{16}$"	4.70	600
⅜"	8.13	1000

relationship

$$d = PR^4/4Et^3$$

(where d = deflection at center of diaphragm, in inches, P = pressure in pounds per square inch, R = radius of diaphragm to supporting edge in inches, E = modulus of elasticity = 1.0×10^7, and t = thickness of diaphragm in inches) is found to hold to a close approximation for the experimental data. It should be pointed out that the diaphragm is not clamped with perfect rigidity; there is some elastic yield of the entire structure under the application of pressure. If the diaphragm thickness is known, the above equation may be relied upon to give an accuracy of about 5 percent.

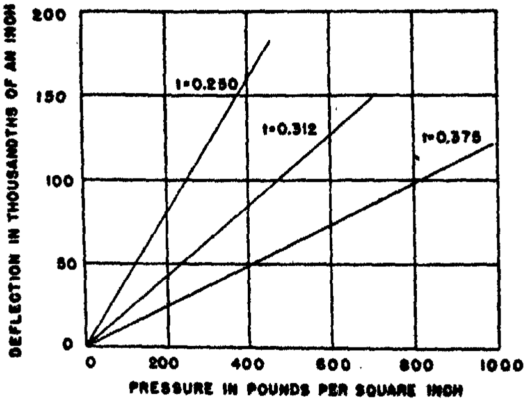

FIG. 3. Deflection of diaphragm as a function of static pressure and thickness of diaphragm.

As a simple clamped diaphragm of the above dimensions would be far under-damped it is necessary to provide a controlled damping mechanism to give the device the proper frequency response characteristics. Damping is provided by a fluid system using Dow Corning Fluid No. 200 as the damping medium. A grade of this silicone fluid having a kinematic viscosity of approximately 1000 centistokes was chosen. One characteristic of this material is a low variation of the coefficient of viscosity with temperature. The damping liquid is in contact with the outer or pressure face of the diaphragm (A), Fig. 1, and receives pressure from the air or water surrounding the instrument through a perforated baffle plate (B), a neoprene barrier diaphragm (C), and a perforated protective cover plate (D). The $\frac{1}{16}$-inch space between the diaphragm and the baffle plate is completely filled by the damping fluid which communicates with the fluid-filled space between the baffle plate and the barrier diaphragm through 30 $\frac{11}{64}$-inch holes drilled through the baffle plate which is $\frac{7}{16}$-inch thick at this section. The design of this damping or baffle plate was based upon computations involving the constants of the diaphragm and the associated damping mechanism. By a proper choice of the damping liquid viscosity and damping orifice dimensions it is possible to adjust the response characteristics of the instrument to an optimum value. The space between the barrier diaphragm and the cover plate is filled with water when the instrument is submerged for use. If the gauge is to be used for *air blast* measurements, the ports in the cover plate should be considerably enlarged over those shown in the drawing or the cover plate should be replaced by a diaphragm retaining ring, leaving the face of the barrier diaphragm exposed. The combination of the small ports in the protective cover with the enclosed air-filled cavity under the cover results in an acoustic filter which greatly attenuates the higher frequencies in the case of an air blast.

When this cavity is filled with water its influence upon the over-all frequency characteristic is small.

Figure 4 shows the response of an instrument having a ⅜-inch diaphragm to a step pulse produced by suddenly dropping a steadily applied hydraulic pressure of 300 pounds per square inch, gauge, to atmospheric pressure. This was accomplished by bursting a heavy lucite window or port in a pressure chamber. The system shows a natural damped frequency of about 360 cycles per second. The diaphragm reaches full deflection in about 2 milliseconds and has practically ceased vibrating in 5 milliseconds. There is very little overshooting. A high frequency vibration corresponding to a coupled motion of the diaphragm plus the baffle plate probably accounts for the slight irregularity of the motion of the recorder stylus during the steep part of the pulse. Figure 5 shows a smoothed plot of this experimental step pulse response plotted on an expanded time axis.

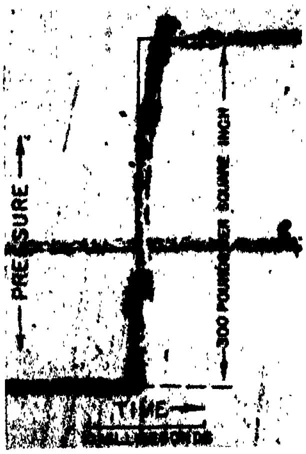

FIG. 4. Record of response of gauge to a step pulse change of pressure.

The over-all characteristic of the moving system is that of a low pass filter having small steady state response to frequencies above 500 cycles per second but permitting approximately full response to a step pulse in about two milliseconds.

The metal parts of the entire diaphragm assembly with the exception of screws and other minor parts are of dural. This gives a light strong structure with no difficulties caused by such effects as differential thermal expansions.

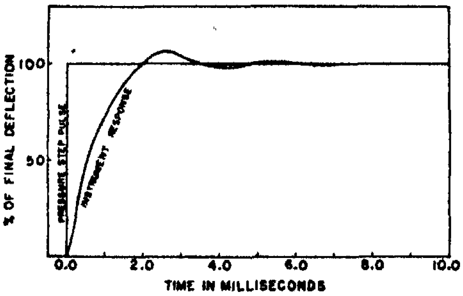

FIG. 5. Smoothed plot of gauge response to pressure step pulse.

The pressure *versus* time record is engraved in the form of a polar coordinate curve upon the polished surface of a chromium plated steel disk. The record disk, which is cut from photographic ferrotype sheet is 3 inches in diameter and has a thickness of about 0.020 inch. Another successful technique involves the use of a glass disk with a thin uniform coating of graphite deposited from Acheson Graphite Dispersion No. 41. The stylus engraves a sharply defined transparent line in this opaque coating and the method is satisfactory where extreme ruggedness and the maximum of resolution is not required. The record disk is shown at (*E*) in Fig. 1. The record disk is mounted upon the turntable (*K*) by means of a ⅛-inch thick backing plate (*F*) and a locking nut (*G*).

The engraving or "writing" tool of the instrument is the tip of a "permanent" type of phono-

FIG. 6. Two gauges installed in case for under water blast pressure measurements.

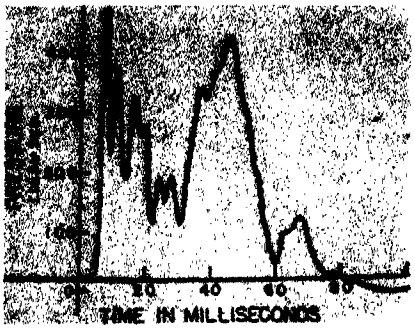

FIG. 7. Record of a water hammer transient in a hydraulic system.

graph needle such as is used in coin-operated automatic phonographs. The needle tip is a smooth, almost spherical surface of hard metal alloy which will press a sharply defined groove in the hard polished surface of the record disk. The stylus tip is soldered through a hole in a flat steel spring (*H*) which is clamped in a slot in the end of the stylus holder (*I*), which is rigidly attached to the diaphragm (*A*). The stylus assembly is steadied against lateral vibration by an accurately fitting bearing sleeve (*J*).

The turntable (*K*) is driven by an electric motor (*L*) through a combination spur and worm gear train. The motor used in the field instrument was an automobile accessory motor modified to increase its ruggedness and speed stability. The motor was powered by "Hot Shot" dry batteries. Under laboratory conditions it would be desirable to use a small a.c. synchronous motor. The mechanical design of this turntable drive was worked out with the guidance of field tests where the submerged recorder was mined with 600-pound charges of T.N.T. at short range. The turntable is carried in a cone bearing and is held firmly seated by a heavy-duty ball thrust bearing.

In the interest of ruggedness and simplicity of construction, no traverse motion is provided to separate the records produced for successive revolutions of the turntable, so in the absence of a pressure variation the stylus will follow a single circular track around the record disk. This is of an advantage in the case of records of less than one revolution duration, as the trace during the quiescent portion of the run will provide a reliable fiducial line for pressure measurement. Overstrain of diaphragms or other damage affecting calibration is also immediately evident.

In the measurement of very large scale, underwater blast pressures the motor circuit is closed and the gauge put into operation by switches actuated by radio control or by the direct action of the explosion, whichever occurs first. The motor is stopped after the turntable has made a predetermined number of revolutions by means of the simple device shown at (*M*) in Fig. 1. A nut floats on the threaded extension of the turntable shaft. It is held from turning by a loop of wire threaded through a hole in the nut and secured by lugs to two binding posts. The nut travels back along the shaft as the turntable rotates until it jams against the turntable bearing lock-nut; it then rotates, breaking the wire loop and opening the motor battery circuit.

Figure 6 is a photograph of one of the cases in which the instruments were installed for the measurement of large scale blast pressures. Two gauges are shown mounted in position on the lid. The case is of heavy construction, weighing approximately 1200 pounds and designed to withstand external hydrostatic pressures in excess of 1000 pounds per square inch. The case furnishes a substantial mounting surface for the gauges and houses the recording mechanism of the instruments. Other applications of the gauge would, in general, not require such ponderous or elaborate installations.

In order to obtain a publishable record as made by the instrument the gauge was installed in a 12-inch water main the flow in which could be stopped by the sudden closure of a valve. Figure 7 is a record of the resultant "water hammer" transient. In addition to the initial transient of the type shown persistent pressure fluctuation due to reflections from remote parts of the hydraulic system was recorded over periods of several seconds duration.

ACKNOWLEDGMENTS

The author wishes to acknowledge the valuable assistance given by various members of the staff of the Applied Physics Laboratory, University of Washington; the cooperation of the Thirteenth Naval District in furnishing necessary manufacturing and testing facilities; and the interest and help given by the Hydraulics Laboratory of the University of Washington in the application of the instrument to the measurement of hydraulic transients.

THE REVIEW OF SCIENTIFIC INSTRUMENTS VOLUME 20, NUMBER 1 JANUARY, 1949

A Self-Contained Recording Pressure Gauge*

DAVID R. BROWN,** WILLIAM C. GALLOWAY,*** JACK B. ROBERTSON, AND GENE A. SILVEY
Applied Physics Laboratory, University of Washington, Seattle, Washington

(Received March 23, 1948)

This instrument is a self-contained time *versus* pressure recording device capable of measuring pressures up to 1200 pounds per square inch at frequencies from 0 to 200 cycles per second over a period of five seconds. The instrument is set in operation by the arrival of a pressure wave above a predetermined threshold, triggering a locking mechanism and permitting compressed springs to drive the record surface past an engraving stylus actuated by a pressure-sensitive diaphragm.

INTRODUCTION

THE self-contained recording pressure gauge was designed as a companion instrument to other pressure-measuring devices such as that described in the preceding paper.[1] In the interest of reliability of operation and ease of installation and recovery, it was decided that this instrument should be relatively small, rugged, and self-contained to the extent of being independently triggered by blast pressures and not dependent upon auxiliary starting devices.

DESCRIPTION

The pressure-sensitive element of the recorder is a rigid, peripherally mounted, circular dural diaphragm (1) (see Fig. 1) with an effective diameter of six inches. Damping is obtained by a sponge rubber pad (2) compressed into a counter-bore between the diaphragm and the steel housing (3). Construction time for the particular use of the instrument did not permit the use of a more elaborate damping system such as used in the recorder described by Higgs.[1] An

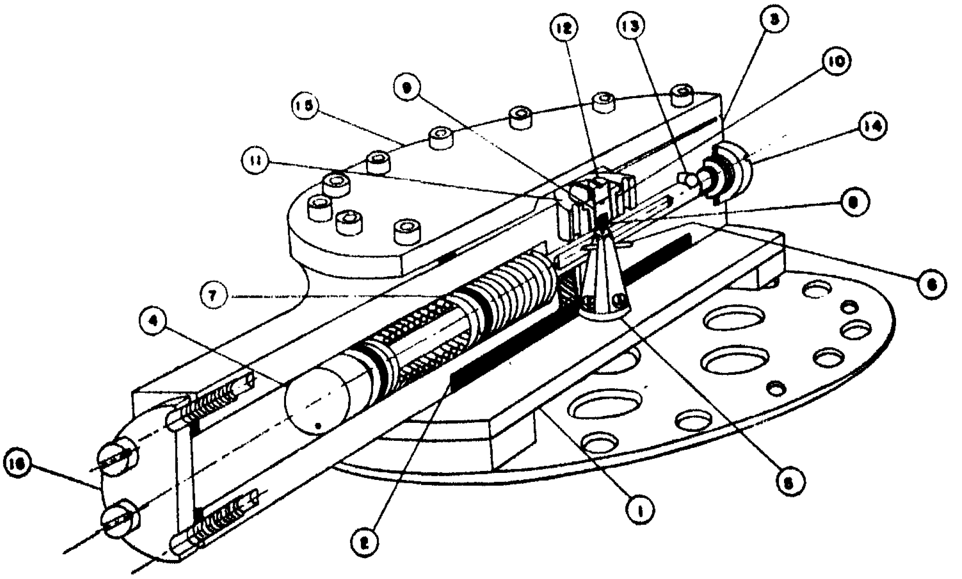

FIG. 1. Sectional drawing of pressure gauge.

---

* This work was undertaken in association with The Applied Physics Laboratory, The Johns Hopkins University, under a Section T Series Contract, NOrd-7817, sponsorship of the Bureau of Ordnance, United States Navy.

** Now at Servomechanisms Laboratory, Massachusetts Institute of Technology, Cambridge, Massachusetts.

*** Now at Research Laboratory of Electronics, Massachusetts Institute of Technology, Cambridge, Massachusetts.

[1] Paul M. Higgs, "A recording mechanical pressure gauge of high range," Rev. Sci. Inst. 20, 23 (1949).

FIG. 2. Pressure gauge showing one method of mounting.

over-all view of the gauge appears in the photograph, Fig. 2, showing the instrument with its steel mounting feet. The instruments were secured either by welding the mounting feet to the supporting structure for air blast measurement or by suspending them by means of wire cables for underwater measurements. The pressure *versus* time curve is recorded on the flattened portion of the dural plunger (4), Fig. 1. The stylus arm (5), fastened to the diaphragm, serves as a mount for the stylus (6) which scribes directly onto the flattened portion of the plunger which was polished to minimize machine marks. The stylus is made from a commercial phonograph recording needle ground thin near the tip to give a spring action to hold the cutting point in contact with the recording surface.

The time axis is obtained from a motion given to the plunger by two compressed helical springs (7) oppositely wound, which drive the plunger through an accurate bore in the steel housing past the engraving stylus. The two springs force the piston face against entrapped silicone stopcock grease[2] which escapes through a carefully dimensioned orifice that is bored through the piston face of the plunger. The rate of motion is controlled by four factors:

1. Spring pressure.
2. Diameter of bore.
3. Viscosity of fluid.
4. Diameter of orifice in plunger.

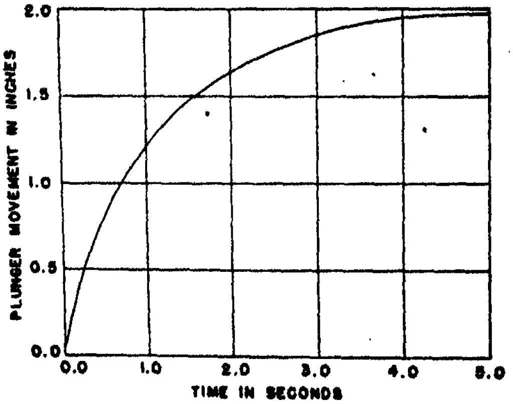

FIG. 3. Displacement of plunger as a function of time.

A plot showing the displacement of the plunger as a function of time is given in Fig. 3. Two oppositely wound springs, a right and a left, are used in pairs to minimize the torque on the dural plunger as the springs elongate. The force exerted by the springs, when fully compressed, is of the order of 230 pounds. It is necessary to select springs whose force constants are matched and lie within a narrow range if uniform performance for several such instruments is desired.

The plunger movement is initiated when the diaphragm is first displaced inwardly, as would occur when the first pressure wave arrives. The inward displacement of the diaphragm closes the firing circuit when the stylus holder contacts the insulated lead contact (8). As the force to be measured is large compared to the force necessary to indent the insulated contact, the damping effect was found to be negligible. The contact plug (9) screws into the flanged plug (10) which is held to the housing by a phenolic insulator (11). The gap setting is determined as follows: first, by advancing the contact plug containing the lead contact until it touches the set screw on top of the stylus holder as indicated by a meter across these points; the points are then separated a predetermined distance by backing off the contact plug, making allowance for the depth of water at which the instrument is to be operated. For these particular instruments, the contacts were set to complete the circuit when the diaphragm was deflected inward one-tenth of its maximum allowable pressure range above the static pressure in which it operates. The gap is fixed after this setting by the locking plug (12).

When the contact points are closed, a current passes through a detonating cartridge held in a steel cartridge plug which ejects the firing pin

---

[2] Dow Corning Stop-Cock Grease, Dow Corning Corporation, Midland, Michigan.

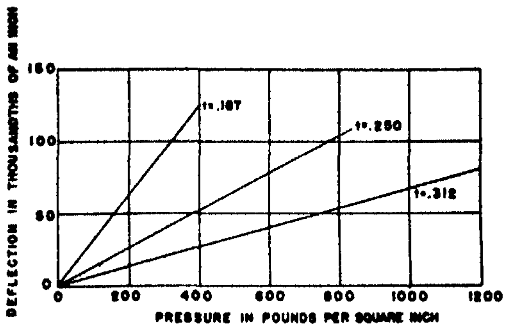

FIG. 4. Deflection of diaphragm as a function of static pressure and thickness of diaphragm material.

(13). This releases the plunger from a locked position. The energy to fire the detonating cartridge is supplied from two small flashlight batteries wired in series and contained in a separate bore in the housing.

The two seal plugs (14), the diaphragm, the bottom plate, and the end cap (16) with their respective gaskets are fastened to the housing, thereby forming the water seals. Because these instruments were used under water for the most part, at depths up to one hundred feet for extended periods of time, it was necessary to give special attention to the seals used. The gaskets found to be satisfactory for the bottom plate and the end cap were rings approximately one-fourth-inch wide placed just inside the bolt circles, and were made of $\frac{1}{32}$-inch thick, hard, service-type sheet asbestos. The seal plug gaskets were made of thin copper pressed over an asbestos core, similar to automobile spark plug type gaskets, and were lubricated with white lead before tightening the seal plugs. At the metal-to-metal contact of the diaphragm to the housing, non-hardening gasket cement[3] was used.

TABLE I.

Diaphragm thickness in inches	Pounds per square inch to produce 0.001-inch deflection	Maximum allowable pressure in pounds per square inch
0.187	3.23	400
0.250	7.76	800
0.317	14.90	1200

Diaphragms were provided in three thicknesses to extend the range of sensitivities. In Table I the approximate characteristics of each thickness of diaphragm is tabulated. Figure 4 is a graph of experimentally derived data plotting the deflection of the three thicknesses of diaphragms as a function of pressure. It was found during the course of this investigation that the diaphragm had to be pre-stressed by the uniform application of pressure equal to the maximum allowable pressure in order to give a linear deflection with pressures up to the elastic limit of the diaphragm material. The following is an experimentally determined relationship:

$$d = (PR^4/4Et^3),$$

where d = deflection at center of plate in inches, P = pressure in pounds per square inch, R = effective radius of diaphragm in inches, E = modulus of elasticity in pounds per square inch, and t = thickness of diaphragm in inches. The above relationship was found to be accurate within five percent for the particular geometry and plate material used.

Figure 5 shows a publishable record made with this recorder during a test of "water hammer" effects caused by the sudden closing of a check valve in water flowing through an eight-inch pipe at approximately six feet per second. The initial peak indicates a maximum pressure of

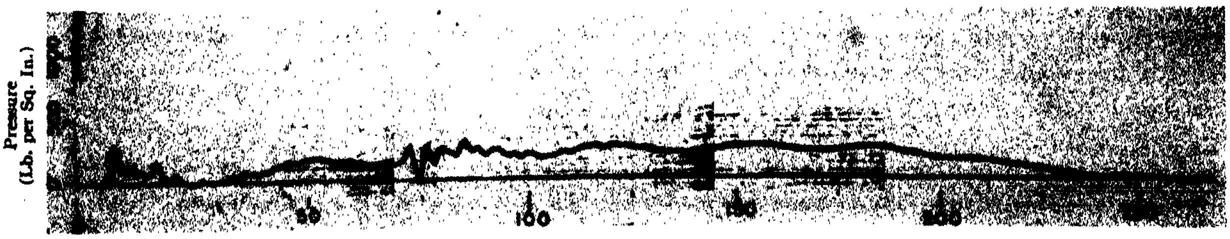

FIG. 5. Record obtained of pressure variation due to sudden closing of a check valve in a hydraulic system.

---

[3] Permatex Number Two, Permatex Company, Inc., Sheephead Bay, New York.

280 pounds per square inch. The base line was made at atmospheric pressure. Measurements for these data were taken from a photograph at a magnification of twenty times.

ACKNOWLEDGMENT

The authors wish to acknowledge specifically the efforts and cooperation put forth by the Engineering and Production Departments of the Puget Sound Navy Yard without whose aid these instruments could not have been completed in the time allotted for preparation. Also the interest and cooperation of the Hydraulics Laboratory of the University of Washington is acknowledged in the application of the instruments to the "water hammer" tests. An appreciation is expressed by the authors for the helpfulness of Dr. J. E. Henderson, Director of the Laboratory, who originally suggested the problem and method of approach.

THE REVIEW OF SCIENTIFIC INSTRUMENTS VOLUME 20, NUMBER 1 JANUARY, 1949

A Multiple-Reflection Optical Lever*

H. O. Hoadley
Kodak Research Laboratories, Rochester, New York

(Received October 2, 1948)

A detailed description is given of the principles of an optical lever which secures increased sensitivity by means of multiple reflections from a single small mirror. It is of particular use where space is limited, or where the mirror must have minimum size and mass, as in a galvanometer. Its limitations are an inherent restriction of the measurable range, and a comparatively rapid loss of light with increasing number of reflections. A model system was constructed, which demonstrates that no special difficulty is met with in making an optical lever according to these principles up to seven reflections. Tests made with the fifth-order reflection proved the model to be quite satisfactory.

INTRODUCTION

THE usual form of optical lever makes use of a single reflection of a beam of light from a rotating mirror, which means that the reflected beam is deflected by twice the angle of rotation of the mirror. Another frequently used form consists of a fixed plane mirror placed opposite the moving mirror, with the beam of light reflected back and forth between the two. The deflection of the emergent beam is that for the single mirror, multiplied by the number of reflections from the moving mirror. The main disadvantage of this latter type of mirror system is that the moving mirror must be large enough so that the successive intersections of the beam fall at different positions; if they overlap, the complete beam cannot escape from the ends of the system. This requirement makes the system unsuitable for use where small mass or size of the moving mirror is important.

The multiple-reflection optical lever described here is designed to remove this objection, while retaining the multiplied sensitivity. The optical system is such that light leaving the rotating mirror in one direction is returned to the same place on the mirror, but from a different direction. The mirror may therefore be made very small.

BASIC PRINCIPLES OF THE OPTICAL LEVER

The construction and performance of the optical system are complex, and therefore a step-by-step explanation of the ideas behind them is given.

On Fig. 1, the arc, SS', represents the surface of a spherical mirror of radius r, the center of which is at C. The two blocks, M and M', are two small plane mirrors, the surfaces of which lie in a plane which passes through C, and the midpoints of which lie the same distance, d, from the point C. The line CV is drawn perpendicular to the plane MM'.

---

* Communication No. 1215 from the Kodak Research Laboratories.

Assuming d to be a small fraction of the radius of the spherical mirror, view the two mirrors, M and M', from any point, P, on the surface of the spherical mirror. The surface normal, of course, passes through C, and M and M' subtend approximately the same angle on either side of the normal. The distance PM' exceeds the radius by the same amount that the distance PM is less than the radius (or vice versa, if the point P is on the other side of CV). Therefore, a bundle of rays proceeding to any section of the spherical mirror from the point M will be focused, to a close approximation, at the point M'.

Speaking mathematically, we say that the center of a spherical reflecting surface has a magnification of -1. A line element at this point is imaged on itself, but reversed.

In Fig. 2 is shown the path of the beam which constitutes the optical lever. The path is laid out in the following way: A ray is drawn perpendicular to the mirror M', intersecting the spherical mirror at P_a. The spherical mirror directs the reflected ray to M, which, in turn, sends it back to the spherical mirror at P_b. This means that a ray directed into the system at P_b would retrace its path from the reflection at M', and leave the system again at P_b, having been reflected once at M' and twice at M. To get five reflections from M and M', instead of three, the spherical mirror is extended to reflect the rays once more at P_b. The dashed line indicates how the two rays, entering and emerging, are directed again to the mirror M', and leave the system at P_c. The path as defined in this way will be referred to as the undeviated beam.

Effect of Rotating the Mirrors

In the case of three reflections, as shown by the solid lines in Fig. 2, it will be seen that rotating the mirror M counter-clockwise by a small angle, α, around the axis perpendicular to the plane of the drawing produces a counter-clockwise deviation of approximately 4α in the emergent ray. However, rotating the mirror M' in the same direction by the angle α produces a *clockwise* deviation of 2α in the emergent ray. **Therefore, in order that the deviations shall be additive, it is necessary that the two mirrors, M and M', shall be rotated in opposite sense.**

This requirement is fulfilled if M' is a virtual image of M, produced by placing a long plane mirror on the line CV. When this is done, the actual path of the rays is as shown in Fig. 3. The solid lines indicating three reflections, and the dashed lines indicating two more reflections, correspond to the rays shown in Fig. 2. To avoid confusion, the system will still be shown "open," as in Fig. 2, but it should not be forgotten that CV represents a plane mirror, and that everything shown to the left of CV is a virtual image.

The Collimating Lens

If we consider a complete beam of light traveling through the system, rather than just a single central ray, it is evident that objectives and field lenses are needed. The spherical mirror acts as a field lens at each reflection, but there must be a collimating lens in front of the mirror M. This lens must render parallel a bundle of rays proceeding from the point P_b, focus the reflected rays again at the point P_a, and similarly for the other reflections. The lens should be as close as practicable to M, its axis in the plane of the drawing, and parallel to CV. The mirror M should be placed so that a perpendicular to CV from the point C passes through the virtual image of the mirror, as seen through the collimating lens. From this it is seen that the focal

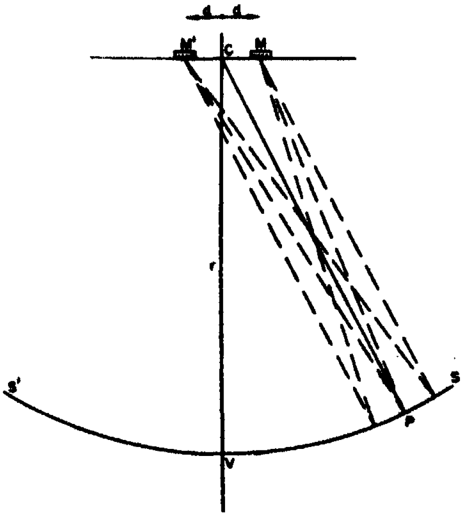

FIG. 1. Diagram of a spherical reflecting surface, showing how a point lying a small distance from the center is imaged to a close approximation on a point diametrically opposite.

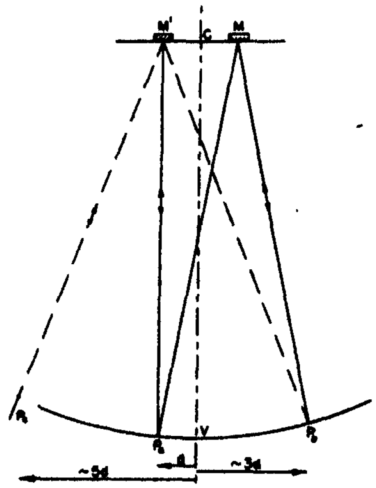

FIG. 2. Schematic view of the path of the light beam in the optical lever.

length of the lens must be slightly less than the radius of the spherical mirror.

Preferably, the collimating lens is corrected for chromatic and spherical aberration, and its field is curved on a radius approximately equal to its focal length. Coma and color magnification are corrected automatically, since the lens and its virtual image form a completely symmetrical objective, with the mirror M as the stop. In the working model described below, an ordinary telescope objective has proved to be quite adequate for the purpose.

The collimating lens, L, is shown in Fig. 3. Because the drawings are of a schematic, rather than pictorial, nature, the lens is not shown in Figs. 4–7, but it should be understood that it is necessary in the actual construction. The proper converging power could be obtained by using a concave mirror at M instead of the lens, but the field of such a concave mirror is curved in the opposite direction from that of the lens, and therefore will not match the curvature of the fixed concave mirror.

Position of the Deviated Images

In Fig. 4(a) is shown the system with three reflections, as explained in Fig. 2. The solid lines represent the path of the rays when the deflection mirror is perpendicular to the plane mirror, CV, while the dashed and dotted lines are the path of the deviated ray, when the mirror is rotated by an angle, α. The first reflected ray is deviated by the angle 2α, and strikes the spherical mirror at P_a', from where it is sent to M'. The distance between P_a and P_a', which will be called δs, is approximately equal to $2r\alpha$. After reflection at M', the returning ray, now indicated by the dotted lines, intersects the spherical mirror again at P_a'', is reflected once more by the mirror M, and emerges at the point P_b''. Since 2α is added to the deviation of the ray at each reflection by M or M', it may be seen that the distance P_aP_a'' is approximately $2\delta s$, and the distance P_bP_b'' is approximately $3\delta s$, or $6r\alpha$.

A similar drawing for a system with five reflections is shown in Fig. 5(a), indicating that the resultant deviation of the ray is approximately $10r\alpha$.

In actual practice, the deviated emerging ray falls on a scale having the same curvature as the spherical mirror. The beginning point for the fixed entering ray is a reference line in the focal plane of an eyepiece, or an index mark or slit illuminated by a condensing lens. In the first case, the exit pupil of the eyepiece is the image of the moving mirror; in the second case, the condensing lens images the light source on the moving mirror.

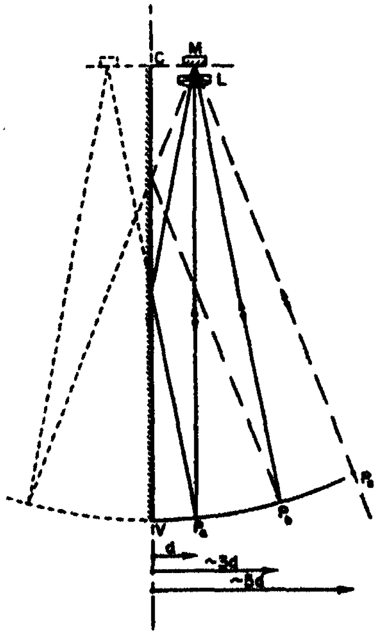

FIG. 3. The actual path of the beam when a plane mirror is placed along the vertical center line, CV.

This means that the emerging ray should not follow exactly the path of the entering ray. The two may be separated by directing the entering ray toward M from a point slightly below the plane of the drawing of Fig. 4(a). In Fig. 4(b) is shown what happens in that case. Figure 4(b) is a view in elevation of the same rays shown in plan in Fig. 4(a). The two squares are the mirrors M and M', viewed normally, and the line MM' is the plane of the drawing of Fig. 4(a). The solid line indicates again the path of the undeviated ray, and the solid dots the intersections of this ray with the spherical mirror. The intersections of the deviated ray are indicated by the small circles.

The ray enters the system at the point P_0, directly under P_b. The successive intersections with the spherical mirror are then P_1, which is above P_a, P_2 below P_a, and the final point P_3 above P_b. Separation between entering and emerging rays in the vertical direction is thus achieved. The points of intersection with the spherical mirror of the deviated ray are then, successively, P_1' above P_a', P_2' below P_a'', and the emergent point P_3' above P_b''.

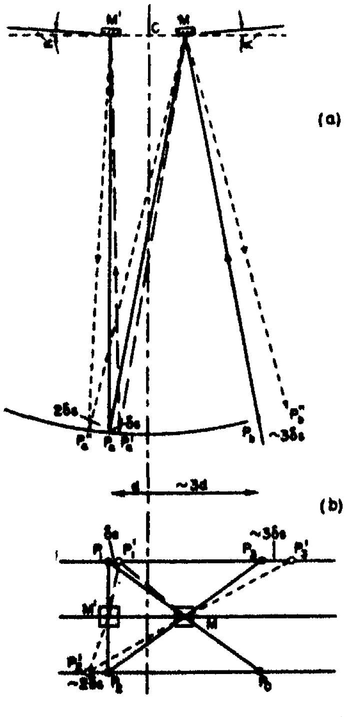

FIG. 4. The deviation in the beam caused by rotation of the mirror, M, for a system of three reflections: (a) a plan view; (b) the elevation.

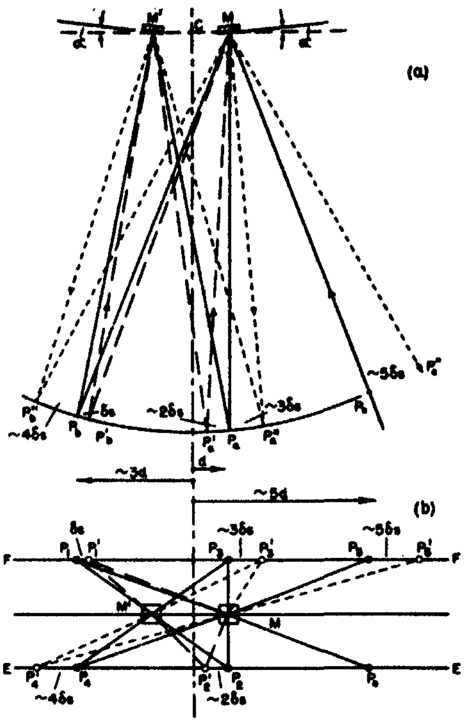

FIG. 5. The deviation in the beam for a system of five reflections.

A similar plan view for the case of five reflections is shown in Fig. 5(b).

In Fig. 6, the drawings of Figs. 4(b) and 5(b) have been reproduced, but with the virtual images to the left of the fixed plane mirror, indicated by dotted lines, and the intersection points shown where they actually occur to the right of that mirror, as in Fig. 3. The path of the deviated ray has not been drawn, but its intersection points are shown.

Limitations on the Measurable Angle

From Fig. 6 may now be seen how the total deviation of the ray is limited by the dimensions of the system. Referring first to the case of three reflections (Fig. 6(a)), we see that the distance between the points P_2 and P_0 is approximately $2d$. Since P_0 is the entering point, and P_2' must fall on the reflecting surface, the maximum possible deviation is reached when P_2' reaches the position of P_0, which means that $2\delta s = 2d$. It was shown earlier that $\delta a = 2r\alpha$, and therefore the largest measurable angular deviation of the mirror M *in this direction* is $\alpha = d/2r$, and the largest scale deflection produced is $3\delta s = 3d$. If

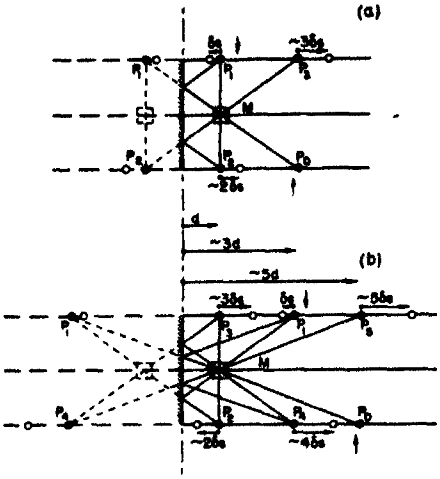

FIG. 6. Plan views for systems of (a) three reflections, and (b) five reflections. These are Figs. 4(b) and 5(b) replotted to show the actual path of the beam with the plane mirror along the center line.

the mirror M is rotated in the opposite direction, the limiting position is reached when the point P_2' meets P_1'. For this position, $4\delta s=2d$; the maximum angle is $\alpha=d/4r$; and the maximum scale reading $1.5d$.

It should be noted that, in order to take full advantage of both directions for the deflection, it is necessary that the spherical mirror have different lengths above and below the center plane, as indicated by the vertical arrows in Fig. 6. Although the beam returning to a position directly above the entrance aperture has been called the "undeviated" beam, there is no reason why the zero of the moving mirror should not be adjusted to lie at some other part of the scale. The concept has been used only for convenience in the explanation.

For the system of five reflections (Fig. 6(b)), the deviation in the direction shown in the drawing is limited by the point P_4' reaching P_0. Then, $4\delta s=2d$, the maximum angle is $\alpha=(1/4)(d/r)$, and the maximum scale reflection is $5\delta s=2.5d$. In the opposite direction, the limiting position is that where P_1' and P_4' meet, which means that $6\delta s=2d$. The corresponding angle and scale deflection are, respectively, $\alpha=(1/6)(d/r)$ and $5\delta s=(5/3)d$.

The total maximum measurable angles and maximum scale deflections will be the sum of those in both directions, as follows:

	Max. angle	Max. scale
$3x$:	$0.75(d/r)$	$4.5d$
$5x$:	$0.41(d/r)$	$4.1d$

It may be seen from this that the maximum measurable angle for a given number of reflections is directly proportional to d. However, the larger the value of (d/r), the less closely the actual dimensions of the system approach the approximate values given above, and the greater the departure from linearity of the scale reading as a function of the mirror deflection, α. No calculations have been made as to the amount of non-linearity that might be expected in such a system.

The non-linear errors will, of course, be greater, and the maximum measurable angle smaller, when the "mechanical advantage" of the system is increased by using more than five reflections from the moving mirror. The approximate dimensions of such a system may be found by using the same arguments as given above for systems of three and five reflections.

Systems with an Even Number of Reflections

The system as illustrated in Fig. 2 always results in an odd number of reflections from the

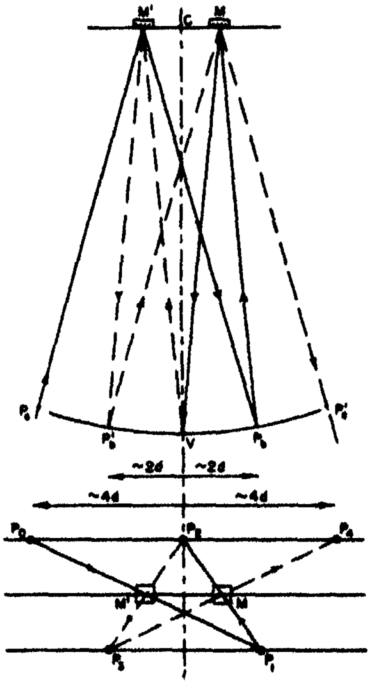

FIG. 7. The path of the beam for an even number (4) of reflections.

moving mirror. Systems with an even number of reflections may be developed by starting the ray from the point *V* toward the moving mirror, as shown in Fig. 7. The elevation view of the system indicates that the emerging ray always follows the path of the entering ray, and cannot be separated from it in the vertical direction. Another disadvantage of such a system is that the undeviated ray falls exactly on the joint between the spherical mirror and the fixed plane mirror.

DESCRIPTION OF THE MODEL

A simple model of the optical lever was constructed, and a photograph of it is shown in Fig. 8. The spherical mirror and the fixed plane mirror should be easily identified in the photograph. The former was cut from a lens element having a surface of the desired curvature, and the latter is a strip from a piece of good-quality plate glass. The moving mirror is attached to the galvanometer movement, and the collimating lens is mounted in a simple focusing mount which replaces the window originally furnished on the galvanometer. The galvanometer mirror is only 3×4 mm. This particular model was intended to detect a yes-or-no deflection, so the slit was extended both above and below the meridian plane, and the small rectangular mirror with a vertical knife-edge placed next to the slit to reflect the emerging beam into a photo-cell.

The vertical entrance slit is 22 mm long, and the height of the mirrors is 25 mm. The collimating lens is a telescope doublet, with an aperture of 18 mm. The radius of the spherical mirror is about 20 cm, *d* is 1 cm, and the distance of the slit from the fixed plane mirror is 5.5 cm, so that the beam undergoes five reflections from the galvanometer mirror when it is perpendicular to the fixed mirror. Accordingly, the model shown has a sensitivity equal to that of a single-reflection optical lever one meter long.

The galvanometer-adjusting knob may be turned counter-clockwise until the first-order reflected image of the slit falls back on the entrance slit. As the knob is turned clockwise from this position, the first-order image moves across the spherical mirror. When it reaches the joint between the mirrors, the second-order image starts across. When these two images coincide, the third-order image may be found at the entrance slit. With further rotation of the knob, the successive orders follow across the mirror. Seven orders are easily visible, even though the system was laid out to use only five. The optical image quality of all visible orders is good. Of course, in this particular application the even orders might be used as well as the odd, since the emerging beam does not have to be imaged on the entrance slit, nor separated vertically from it.

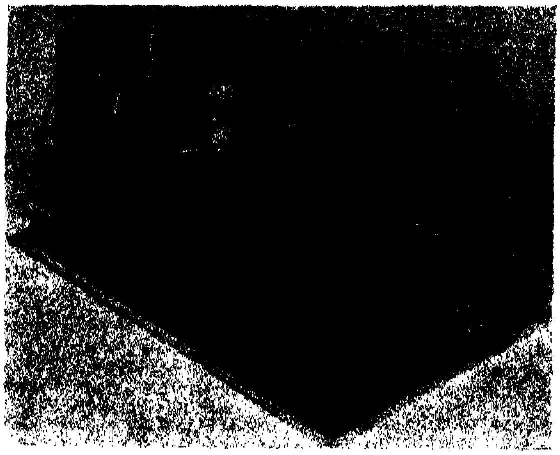

FIG. 8. A working model of the multiple-reflection optical lever.

One other limiting factor of this type of optical lever became apparent in the model: the loss of light in the high order reflections. Each additional reflection from the galvanometer mirror requires two other reflections from the fixed mirrors and two passages through the collimating lens. Although the two fixed mirrors have good evaporated aluminum first-surface coatings, and the lens has an antireflection coating on both surfaces, still each reflected image of the slit looks about half as bright as the image of the next lower order.

Geometrically, the model demonstrates very nicely the principles of the system, and no special mechanical difficulties were encountered in its construction.

THE REVIEW OF SCIENTIFIC INSTRUMENTS VOLUME 20, NUMBER 1 JANUARY, 1949

Improved Magnetic Focusing of Charged Particles

LARKIN KERWIN
Department of Physics, Laval University, Quebec, Canada

(Received September 20, 1948)

A general theory of geometric magnetic focusing of charged particles is developed. Some special cases are discussed. One proves to be the type of focusing in general use; another, equally simple, eliminates second-order aberrations.

I. INTRODUCTION

THE majority of experimental mass spectrometers constructed during the last decade have utilized the second-order focusing properties of wedge-shaped magnetic fields as described by Barber[1] and Stephens.[2] The general appearance of the ion beam trajectory is shown in Fig. 1A. In undertaking the construction of such an instrument in this laboratory, some thought was given as to how the edges of the magnetic field might be reshaped so as to improve the focusing, and possibly reduce the size of the magnet.

II. PERFECT FOCUSING

It is of interest to consider what symmetrically shaped uniform magnetic field would give theoretically perfect focusing of an ion beam of wide divergence. In Fig. 2, where OY is the axis of symmetry, it is desired that all rays leaving a source A should refocus through a point B, such that $AO=OB=a$. We shall here only consider rays in the plane AYB, which is the median plane (midway between and parallel to the pole pieces).

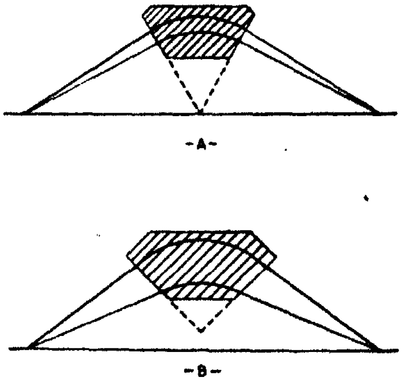

FIG. 1. Typical mechanical appearance of normal and inflection type magnetic fields.

Symmetry imposes the condition that all beams should cross OY at right angles and, therefore, that the center of curvature of the ion beam while in the magnetic field should lie on OY. For a beam leaving A at any angle θ with AB, it is a simple problem in geometry to obtain the point (x, y) where it must enter the magnetic field in order to cross OY at right angles with a given radius of curvature R centered on OY. From Fig. 2 we then have

$$\begin{aligned} y/(a-x) &= \tan\theta \\ &= x/(R^2-x^2)^{\frac{1}{2}}, \end{aligned}$$

whence

$$y = x(a-x)/(R^2-x^2)^{\frac{1}{2}}. \qquad (1)$$

Tracing the points (x, y) for various values of θ gives a symmetrical field as shown by the shading in the figure. This field will give perfect focusing at B of any ions coming from A.[3] Various values of the ratio R/a give the field shapes as shown in Fig. 3.

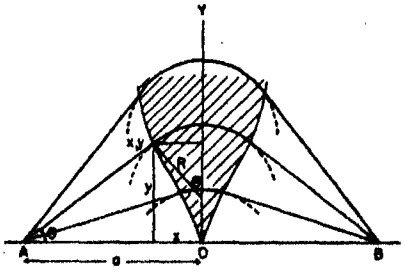

FIG. 2. Geometric composition of perfectly focusing magnetic field.

---

[1] N. F. Barber, Proc. Leeds Phil. Soc. 2, 427 (1933).

[2] William E. Stephens, Phys. Rev. 45, 513 (1934).

[3] It has been brought to our attention that H. Hintenberger has recently published an article [Zeits. f. Naturforschung 3a, 125 (1948)] in which similar considerations are presented, and our Eq. (1) is developed. To date, we have not been able to obtain copies of his paper.

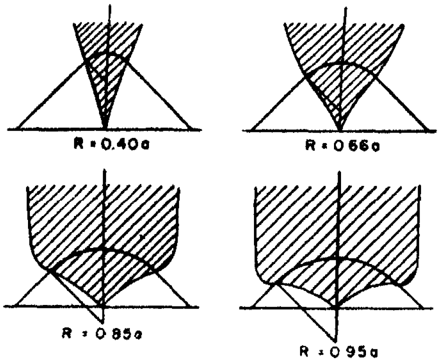

FIG. 3. Variation of ideal field shape with ratio R/a.

III. GENERAL EQUATION

Should the theoretically ideal field as given by Eq. (1) be changed in some way, then an ion leaving A in a given direction would not pass through B, but would have its point of intersection with the line AB displaced. As will be discussed later, aberration, dispersion, image width, etc. may all be considered as being caused by the ideal field's being approximated by some other. Therefore, we shall develop the general equation giving the displacement of the point of intersection with the base line AB produced by any approximation to the ideal magnetic field shape.

In Fig. 4 is shown the path traversed by a charged particle leaving a source O and recrossing the base at L after being deflected by a uniform magnetic field of arbitrary shape. Using the notation as shown and putting $\theta=(\phi+\epsilon)$ where ϵ is small, it may be shown that

$$OL=2x_1-2a+2R\sin\theta-\frac{(x_1-a)(x_2-x_1)}{R\cos^2\theta\sin\theta}+\frac{2(x_1-a)}{\cos^2\theta}. \qquad (2)$$

If we use a uniform magnetic field of the shape as determined by Eq. (1), then the above expression gives the focusing point of the various ion beams. If the ideal magnetic field boundaries are then changed, as indicated in Fig. 5, there will be a displacement dL of the point of intersection as given by Eq. (2). This may be shown to be

$$dL=\frac{2\eta}{[\tan\theta+f'(x)]^2}\left[\tan\theta+f'(x)+\frac{\tan\theta(a-x)f'(x)}{R\cos\theta\sin^2\theta}\right]. \qquad (3)$$

In this expression, $f(x)$ is given by Eq. (1).

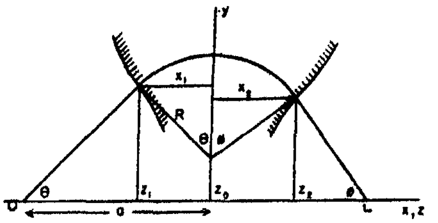

FIG. 4. Path of a charged particle leaving O and being deflected by an arbitrary field.

IV. STRAIGHT LINE APPROXIMATIONS—ABERRATION

Equation (3) gives the displacement dL of the intersection point due to the displacement of the magnetic field boundaries by an amount whose y component is η. In general, η is also a function of x, and it is convenient to express dL in terms of this function. More particularly, it is useful to obtain the expression for straight line approximations, as these are the simplest to use in practice. Thus, in Fig. 6, we see that if the ideal boundary is approximated by a straight line crossing the ideal boundary at a point P, then a ray entering the field at an angle ω with the ray through P has, in effect, the field boundary displaced a certain distance from the ideal. Its point of intersection with the line AB will therefore be displaced an amount dL, which is the aberration due to the approximation. We may now conveniently rewrite Eq. (3) in terms of ω. We see that $\eta=F(\Delta x)$, and since it may be shown that

$$\Delta x=(a-x)\omega/[\tan\theta+f'(x)]\cos^2\theta,$$

we may finally write for a beam divergence of 2ω (ω on either side of the central ray):

$$dL=\frac{2}{[\tan\theta+f'(x)]^2}F\left[\frac{(a-x)\omega}{[\tan\theta+f'(x)]\cos^2\theta}\right]\times\left[\tan\theta+f'(x)+\frac{\tan\theta(a-x)f'(x)}{R\cos\theta\sin^2\theta}\right]. \qquad (4)$$

Equation (4) gives the aberration produced by any straight line approximation to the theoretically perfect curve in terms of the half-divergence ω of the incident beam. It is now necessary to find straight line approximations for which $\eta=F(\Delta x)$ is small if the aberration is to be small.

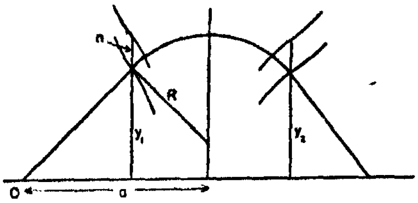

FIG. 5. η is the y component of a displacement of the magnetic field boundary.

V. NORMAL CASE

In Fig. 7, the point P is such that the distance AP is a minimum, i.e., AP is normal to the curve. In finding this point by expressing AP as a function of x and equating the derivative to zero, it is found that for this condition $R=a\sin\theta$. In other words, the tangent to the curve at P passes through O, and $PO=R$. This tangent is a good approximation to the curve at P, and if we expand the ideal boundary equation in a Taylor series at the point P, then the tangent equation will differ from it only in terms of the second degree and higher. That is,

$$\eta=\tfrac{1}{2}f''(x)dx^2+\cdots. \quad (5)$$

By substituting this expression in (4), along with the relations established from Fig. 7, we obtain for the aberration in this case,

$$dL=a\omega^2.$$

If the aberration is measured at the image point normal to the central ion trajectory, it becomes

$$dL=a\omega^2\sin\theta. \quad (6)$$

We note that this case is exactly that developed by Barber, Stephens, and others. In other words, the type of magnetic focusing currently in use is that operating on this tangent to the ideal boundary as shown in Fig. 7. It will hereafter be referred to as *normal focusing*.

VI. INFLECTION CASE

From Eq. (1) it may be shown that the ideal curve has an inflection point given by

$$x_f=3a+(9a^2-8R^2)^{\frac{1}{2}}/2. \quad (7)$$

Therefore, we may closely approximate the ideal curve by a straight line tangent to the curve through the inflection point, as shown in Fig. 8.

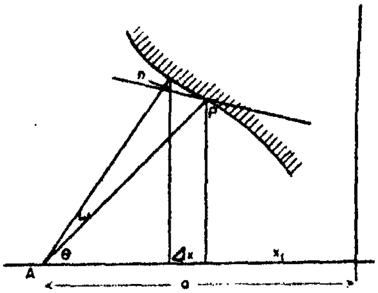

FIG. 6. General case of straight line approximation to ideal curve.

In this case we see that the straight line equation differs from the Taylor expansion of Fig. (1) at the point P only in terms of the third degree and higher. That is,

$$\eta=1/6f'''(x)dx^3+\cdots. \quad (8)$$

Ignoring higher orders and substituting this expression in (4), together with the relations established in Fig. 8, we obtain for the aberration, measured as before,

$$dL=2/3\omega^3[(3a-x)(3a-2x)\sin\theta/6x(a-x)^{\frac{1}{2}}]. \quad (9)$$

This type of focusing will hereafter be referred to as *inflection focusing*. We see that for small values of ω, the aberration produced by this approximation to the ideal field will be smaller than that due to normal focusing.

VII. OTHER CASES

Any other straight lines approximating the ideal curve will be either tangents at some point, or will cut it at an angle. In all cases they will differ from the ideal curve by at least the second degree in the Taylor series, and will produce aberrations of the second order. Theoretically, fields bounded by curved edges will approach the ideal even more closely than the inflection field. For example, third-order aberration will result from the use of magnetic fields whose edges are in the shape of circles. The centers of these circles are located on the extended lines of the central ion beam's initial and final directions, and their radii are given by[4]

$$R_m=R\cot^3\theta.$$

---

[4] This radius is obtained by finding the radius of curvature of the function given by Eq. (1) at the "tangent" point as defined in Section V. In a paper currently in press, K. T. Bainbridge reveals that he is constructing a

Application of Eq. (3) gives the aberration produced by this shape of field as

$$dL = R\omega^3.$$

Obviously, the ideal field may be approximated closely by the arc of a circle at any other point as well. A limiting case is the circle of infinite radius at the inflection point, a case discussed as inflection focusing.

Similarly, field edges in the shape of two arcs of circles centered on the normal to the ideal curve at the inflection point, and tangent to it from opposite directions, would give a better approximation than the tangent line at this point. If the length of field edge to be used extends a distance k on either side of the inflection point, then the radii of the circles to be used are given by

$$1/R = f''(x) + [f'''(x)/4]k,$$

where $f(x)$ is given by Eq. (1). In this case, the *average* of the third-order aberrations of a beam width extending over the distance k is equal to zero.

VIII. DISPERSION

The dispersion produced by an inflection field does not differ greatly from that produced by a normal field. It is possible to express the dispersion as a function of η, and so Eq. (4) provides a convenient means for evaluating it exactly. It may be shown that the dispersion for the general case is given by

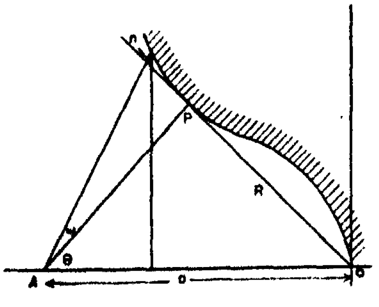

FIG. 7. Normal approximation to ideal curve. Point P is such that AP is normal to tangent.

$$D = 2\Delta R \sin\theta + \frac{\eta}{[\tan\theta + f'(x)]^2}\left[\tan\theta + f'(x) + \frac{\tan\theta(a-x)f'(x)}{R\cos\theta\sin^2\theta}\right]. \quad (10)$$

When the conditions for the normal field are substituted and measurement is made normal to the central ion beam at the image, this becomes

$$D_n = 2a\Delta R/R \sin\theta. \quad (11)$$

This is the familiar case[3] and verifies the correctness of the theory. For the inflection field, substituting the proper expressions gives

$$D_f = 2\Delta R/R(a - x/3) \sin\theta. \quad (12)$$

D_f will therefore have a value between D_n and $2/3D_n$. In the usual case, as discussed later, D_f is approximately $0.9D_n$.

IX. WIDE SOURCES

The theory developed in the previous paragraphs has treated only point sources. If the source section in the median plane is a straight line of width s perpendicular to the central ion trajectory, then it is possible to use Eq. (4) to calculate the image produced by the various approximations. It has thus been verified that the image in both normal and inflection cases is a straight line equal to the source in width, but is inverted.

X. PRACTICAL CONSIDERATIONS

It has been shown that magnetic focusing devices such as mass spectrometers may be designed so as to utilize inflection focusing. This will eliminate second-order aberrations, yet re-

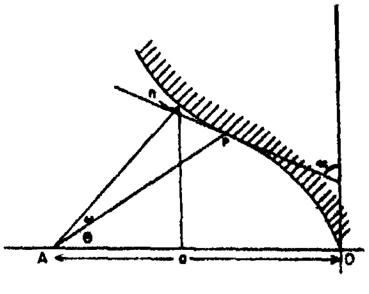

FIG. 8. Inflection approximation to ideal curve. Point P is inflection point of curve.

---

spectrometer in which the aberration is reduced by curving the edges of the magnetic field. He gives as the expression for the radius of curvature $R_m = R\cot^3\theta(\cot\theta - \alpha)$ where α is the half-divergence. This is practically identical with our own. Dr. Bainbridge also gives the expression for correcting the shape of the pole pieces when only one side is available for the purpose.

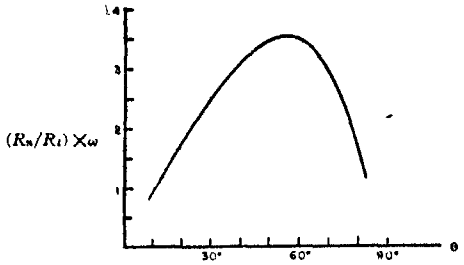

FIG. 9. Ratio of resolving powers of inflection and normal type magnetic fields as a function of θ.

tain simple, straight line field boundaries. The appearance of such a device is suggested by Fig. 1B, where it is seen to bear close mechanical resemblance to the normal focusing device of Fig. 1A. Of some interest is the ratio of the resolving powers of the two fields for various values of θ and a point source. Considering the resolving power as being proportional to the dispersion divided by the aberration, this ratio of resolving powers becomes

$$R_f/R_n = 6x(a-x)^{\frac{1}{2}}/2(3a-2x)\omega. \qquad (12)$$

This has been calculated for various values of θ, and is shown graphically in Fig. 9. We see that there is an optimum ratio near 60°, in which case the usual divergence of 2ω equal to about 4° would give the inflection instrument a resolving power about 10 times higher than that of the normal instrument. It is interesting to note that the optimum case corresponds to a value of α (see Fig. 8) of 90°, in which case the magnetic field profile becomes a single straight line, like those used for 180° deflection in normal spectrometers. In Table I are set down some pertinent data which may be of interest to designers.

The discussion presented here, however, deals with geometric focusing in the median plane, whereas many other factors enter into the design of actual instruments. Rays whose trajectories are not in the median plane are subject to other aberrations. Those whose paths lie at an angle to this plane will experience a dispersion due to the shortening of their velocity component parallel to the median plane. If we include this effect, then the total aberration for a line source becomes in the normal case

$$A = R\omega^2 + R\beta^2,$$

where ω is half the angle of divergence in the xy plane as discussed before and β is the angle of divergence in the z direction permitted by a source of length h. β is given by[6]

$$\beta = h/[2R(\cot\theta + \theta)].$$

In the usual instrument, β^2 is less than $0.1\omega^2$, so that the aberration due to this effect may be neglected. A similar divergence is produced by a variation in the energies of the ions furnished by the source. It is usually made small by using high accelerating voltages. These effects will be somewhat diminished by inflection fields whose dispersion is less than that of normal fields.

For the inflection case, where the rays do not enter the magnetic field normal to its boundaries, rays not in the median plane suffer another defocusing effect due to the fringing magnetic field. Since the field lines at the fringe are curved, the non-median rays will not cross them at 90° and, because of their angle of entry, there will be a small component of the fringing field normal to both the ion trajectory and the main field. This will defocus the beam in the z direction. Therefore, the image of the source will be longer than the source and, unless the exit slit is as long as the image, there will be a loss of current intensity to the collector.

It may be shown from geometric considerations that the resolving power of the direction focusing instrument is given by

$$RP = R/I + F + A,$$

where R is the radius of curvature of the ion path in the magnetic field, I is the image width (equal to the object width), A is the total aberration due to various causes, and F is the exit slit width. Whether or not the total aberration has much effect on the resolving power

TABLE I.

θ	R	x	D_f/D_n	A_f/A_n	R_f/R_n	α(Fig. 8)
20°	$0.485a$	$0.166a$	0.95	5.6ω	$0.17/\omega$	30.2°
30°	$0.666a$	$0.333a$	0.89	3.5ω	$0.25/\omega$	46.0°
40°	$0.799a$	$0.513a$	0.83	2.7ω	$0.31/\omega$	61.6°
45°	$0.848a$	$0.600a$	0.80	2.4ω	$0.33/\omega$	71.5°
50°	$0.888a$	$0.680a$	0.77	2.2ω	$0.35/\omega$	80.7°
54° 59′	$0.920a$	$0.750a$	0.75	2.1ω	$0.35/\omega$	90.0°
60°	$0.945a$	$0.818a$	0.73	2.1ω	$0.35/\omega$	94.0°
70°	$0.978a$	$0.919a$	0.70	2.4ω	$0.29/\omega$	125°

---

[6] Claude Geoffrion, Laval University, unpublished.

depends, therefore, on the particular design. For the inflection field, the aberration due to the geometric shape of the field is very small, and it would probably be advantageous in most cases to increase the divergence of the beam in order to obtain increased intensity at little cost in resolving power. The aberration $R\beta^2$ is also usually negligible. In the case of 180° spectrometers it is possible to obtain increased intensity for the same resolving power by using longer, narrower sources of greater area, but producing the same total aberration as the usual short wide source.[5] In the general case this is also possible insofar as the effect is not too greatly reduced by the field fringe effect.

It is suggested that the principle of inflection focusing may be applied so some of the problems to which attention has recently been invited by Auld.[6]

ACKNOWLEDGMENTS

Sincere thanks is due the members of the Physics Department for enlightening discussions, and in particular are tendered to Professor Enrico Persico who provided a neat mathematical development of Eq. (4) and guided the theory's development, to Professor Paul Koenig who instigated the investigation and followed it critically, and to Professor Claude Geoffrion. Appreciation is expressed to Professor Kenneth T. Bainbridge of Harvard University, who kindly permitted us to read the manuscript of one of his papers currently in press.

---

[6] Mary Jane Auld, Phys. Rev. 74, 108 (1948).

THE REVIEW OF SCIENTIFIC INSTRUMENTS VOLUME 20, NUMBER 1 JANUARY, 1949

A Geiger-Mueller Counting Unit and External Quenching Equipment for the Estimation of C^{14} in Carbon Dioxide

W. B. MANN* AND G. B. PARKINSON**
National Research Council, Atomic Energy Project, Chalk River, Ontario, Canada

(Received August 19, 1948)

A counter unit and external quenching circuit for use with carbon dioxide and carbon disulfide mixtures are described. The counter unit consists of a long and short counter to eliminate end effects. The quenching circuit, which depends on the action of a multivibrator, enables the voltage across the Geiger-Mueller counter to be reduced in a controllable manner by any desired amount and for any desired time.

I. INTRODUCTION

THE internal gas-counting technique developed by Miller,[1,2] using Geiger-Mueller counters filled with carbon dioxide and carbon disulfide mixtures, is especially suitable for the determination of the activity of C^{14} samples that can readily be converted into carbon dioxide. For accurate measurements, however, it is necessary to use an external quenching circuit for the Geiger-Mueller counter that is consistent and stable in operation and can be adjusted to suit the characteristics of the counter. It is also necessary to make corrections for, or eliminate errors caused by, the end effects of the Geiger-Mueller counter. These two requirements have been met by the use of a compensated Geiger-Mueller counter, described in Section II, and a multivibrator quenching circuit described in Section III. By these means it has been possible to obtain highly reproducible measurements.

II. COMPENSATED GEIGER-MUELLER COUNTER

In using gas counters for the assay of C^{14} it is necessary to be assured that the end corrections are either small, or are eliminated, and that there is no appreciable correction for beta-particles originating near the wall and entering the material of the wall without giving rise to an electron avalanche.

---

* Medical and Biological Research Branch.

** Technical Physics Branch. This author designed the external quenching circuit and wrote Section III of this paper.

[1] W. W. Miller, Science 105, 123 (1947).

[2] S. C. Brown and W. W. Miller, Rev. Sci. Inst. 18, 496 (1947).

Calculations based on the probable number of ion pairs produced per millimeter in carbon dioxide show that any wall effect of the type referred to is likely to cause only a small error. Calculations for the end effect, however, show that counts arising from beta-particles entering the cathode volume from the ends may amount to as much as 25 percent for a two-inch-long counter of half-an-inch diameter, with ends one-inch long.

Such a calculation for the end effect takes into account, however, only one element of possible error, namely, that due to beta-particles entering the cathode volume. A further possibility of error arises in the distortion of the electric field at each end and its penetration into the region of space beyond each end of the cathode volume. The magnitude of the error arising from this is difficult to estimate.

The total end effect may, however, be completely eliminated by taking a pair of counters of suitably different length but having the same cross-sectional dimensions and similar end geometries. Such a unit constructed from half-inch-diameter platinum tubes, 0.004-inch tungsten wire, and soft glass is shown in Fig. 1. If the short counter is long enough to provide a small length in the middle having only a radial component of electric intensity, the divergence of electric field at the ends should be identical for both counters. The difference in the counts will, therefore, correspond to an amount of radioactive gas contained in a cylindrical volume equal to the difference in volume of the long and short cathodes. This idealized cylindrical volume will have an electric intensity which is normal to tne wire everywhere along its length (the difference in length of the long and short cathodes), and no correction is required for particles entering the open ends of the cathodes provided the end geometries are approximately similar. The need to use very long counters to reduce the correction caused by the ends is thus obviated.

Fig. 1. Compensated counting unit.

III. MULTIVIBRATOR QUENCH CIRCUIT

It is well known that in a non-self-quenching Geiger-Mueller counter the discharge can be quenched by reducing externally the voltage across the counter, by a sufficient amount and for a sufficient period, following each discharge. Various circuits devised for this purpose have appeared in the literature.[3–9] Miller used a Neher-Pickering circuit to provide external quenching for his counters filled with carbon dioxide and carbon disulfide. The circuit described here, shown in Fig. 2, is believed to be superior to the circuits previously used, and in particular to the Neher-Pickering or Neher-Harper type of circuit, the reason being that in this circuit the voltage is quickly lowered below the threshold of the counter, held there for a predetermined period, and then promptly restored to the operating value. The counter is thus never operating at an intermediate voltage for more than an infinitesimal part of the time. It is also different from most simple multivibrator circuits in that the multivibrator itself is not used to apply the quenching voltage directly to the counter.

In the circuit of Fig. 2, a discharge in the counter causes the grid of V_1 to be driven negative, and this in turn causes the circuit to operate, generating a large negative square pulse which is applied to the anode of the counter through C_2. At the end of this pulse the voltage on the counter anode is restored to its original value, at which it remains until the next discharge occurs. For a short period immediately following the square pulse the circuit is inoperative, and it is a necessary condition for satisfactory operation that, should a count occur during this period, the discharge current of the counter must not be so great as to cause a substantial drop in its anode potential through charging C_2.

---

[3] C. E. Wynn-Williams, British Patent No. 421341.

[4] H. V. Neher and W. W. Harper, Phys. Rev. 49, 940 (1936).

[5] I. A. Getting, Phys. Rev. 53, 103 (1938).

[6] H. V. Neher and W. H. Pickering, Phys. Rev. 53, 316 (1938).

[7] J. A. Simpson, Phys. Rev. 66, 39 (1944).

[8] A. L. Hodson, J. Sci. Inst. 25, 11 (1948).

[9] H. Maier-Leibnitz, Rev. Sci. Inst. 19, 500 (1948).

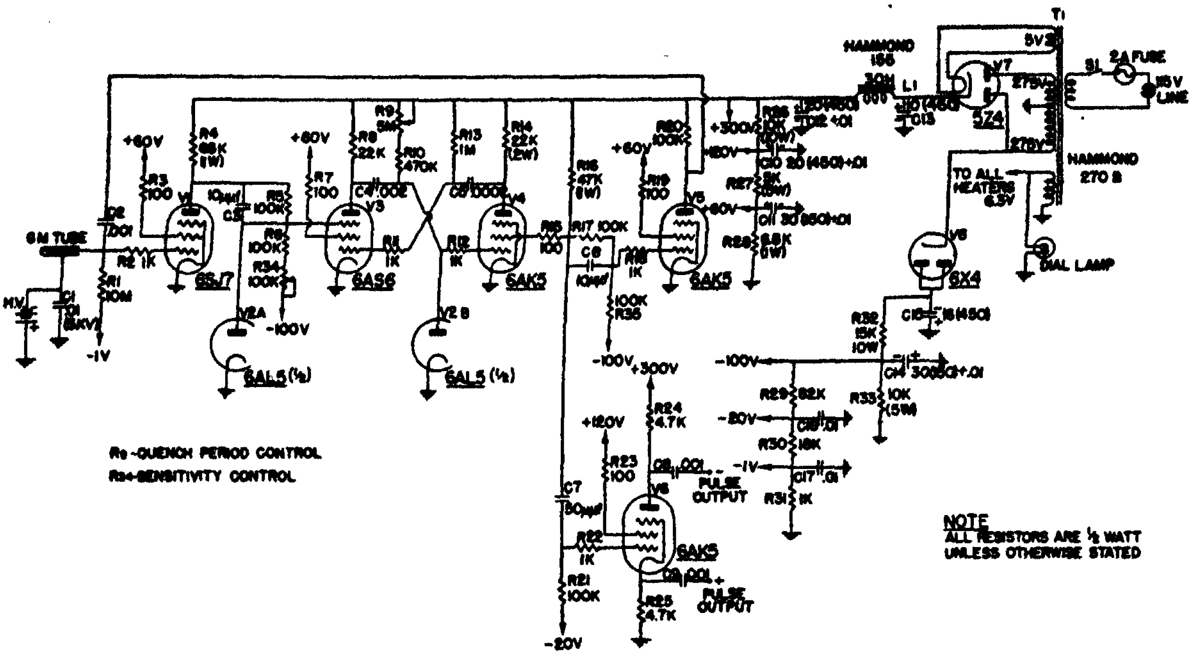

R9-QUENCH PERIOD CONTROL
R34-SENSITIVITY CONTROL

NOTE
ALL RESISTORS ARE ½ WATT UNLESS OTHERWISE STATED

FIG. 2. Multivibrator quench circuit.

A detailed description of the circuit operation follows.

When a discharge occurs in the Geiger-Mueller counter it causes a negative voltage pulse to appear at the grid of V_1; this causes a positive pulse to appear at the plate of V_1, and at the suppressor of V_3 through R_5, C_3. The suppressor of V_3, which is a dual-control tube, is normally biased beyond cut-off, so that no plate current flows. When the voltage on this suppressor is raised sufficiently, by the positive pulse, to allow plate current to flow through R_8, the grid of V_4 is driven negative, causing the plate and screen currents of V_4 to be interrupted. Consequently, the screen potential of V_4 rises sharply, and so does the grid potential of V_5, which is normally biased beyond cut-off. As the grid potential of V_5 rises, plate current begins to flow through R_{20}, causing a negative square wave—the quenching pulse—to be applied to the Geiger-Mueller anode, and the grid of V_1, through C_2. This process is shown diagrammatically in Fig. 3.

The circuit remains in this state, with V_1, V_4 cut off, and V_3, V_5 conducting, until C_4 has discharged sufficiently, through R_{10}, R_9, to allow the grid potential of V_4 to recover far enough for V_4 to conduct again. When this happens the process is reversed; V_5 is cut off, the voltage on the Geiger-Mueller anode is restored, and V_1 becomes conducting; this drives the suppressor of V_3 negative so that the plate current of V_3 is cut off, allowing C_4 to recharge, through R_8 and V_{2B}.

The duration of the negative square wave applied to the Geiger-Mueller anode—the quench period Q—is then determined by the time constant of C_4 and R_{10} in series with R_9. R_9 is made variable, so that the quench period can be adjusted.

At the end of the quench period, V_4 conducts, plate current flows through R_{14}, and the grid of V_3 is driven negative, so that V_3 becomes completely cut off. V_3 remains cut off until C_5 has discharged sufficiently, through R_{13}, to allow its grid potential to recover, at which point V_3 begins to draw screen current again, but not plate current, since its suppressor is now negative. C_5 recharges during the next quench period.

While the grid of V_3 is thus driven negative, this tube cannot draw plate current, so that the circuit is insensitive to further operation until the grid potential of V_3 has recovered. The time required for this recovery—the delay time δ—is determined by the time constant of C_5 and R_{13}. The purpose of this delay time is to allow C_4 to recharge, and to allow the other capacitors—the "speed-up" capacitors C_3, C_6, and the coupling capacitor C_2—to regain their normal potentials before the circuit is retriggered. In this way the operation of the circuit is made independent of the counting rate and of the random time distribution of the pulses from the Geiger-Mueller counter.

Should a count occur in the Geiger-Mueller counter during the delay time, it is not ignored, even though the circuit cannot operate immediately to produce a quenching pulse. In this event the Geiger-Mueller counter continues to discharge, drawing current through R_1 and so biasing off V_1, so that the plate voltage of V_1, and the suppressor voltage of V_3 rise until the suppressor can no longer prevent the flow of plate current in V_3. At the end of the delay time the grid potential of V_3 has recovered to approximately ground level, and V_3 becomes conducting; plate current will now flow through R_8 since the suppressor is no longer biased off. The grid of V_4 is thus driven negative, and the cycle of operation, as described above, is repeated, so that a quench pulse is again produced and applied to the Geiger-Mueller anode. Thus a count occurring during the delay time is quenched at the end of this time.

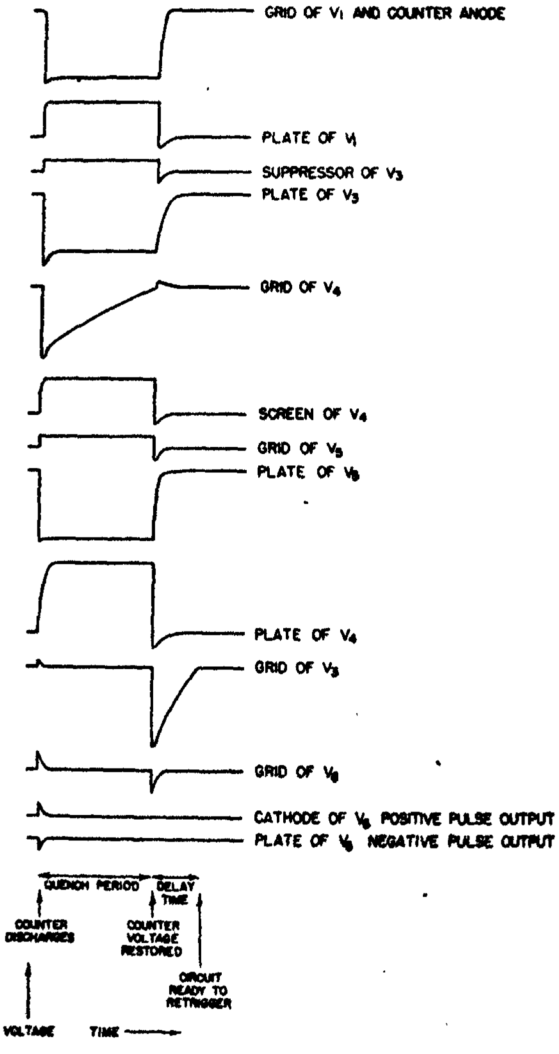

FIG. 3. Wave forms illustrating quench-circuit operation.

The output is obtained by differentiating, through C_7 and R_{21}, the positive square pulse appearing at the screen of V_4 during the quench period. A sharp positive pulse is thus applied to the grid of V_6 at the beginning of the quench period and a sharp negative pulse at the end. Since V_6 is biased beyond cut-off, only the positive pulse causes this tube to conduct, producing a positive output pulse at the cathode and a negative output pulse at the plate. These output pulses are suitable for operating a scaler, oscilloscope, or other auxiliary apparatus. V_6 acts as a buffer, preventing the output loading from having any effect on the operation of the circuit.

The duration of the quench period is variable from approximately 180 to 1800 microseconds. This range has been found sufficient for most applications, but it can be extended, in either direction, by altering the value of C_4. The delay time is approximately 50 microseconds; this also can be changed if required by altering the value of C_5. The magnitude of the quench pulse applied to the Geiger-Mueller anode is determined by the voltage drop across R_{20} when V_5 is conducting; since R_{20} is large, this is substantially equal to the $B+$ voltage supplied to the plate of this tube. For Geiger-Mueller counters operating below 1500 volts, a quench pulse of 250- to 300-volts amplitude is generally quite sufficient; for counters operating above 2000 volts a 500-volt quench pulse is found to be more suitable.

The variable resistor R_{34} controls the bias voltage on the suppressor of V_3, and therefore the triggering level of the circuit. At minimum sensitivity (with R_{34} adjusted to zero resistance), the circuit will be triggered by a pulse of approximately 1- to 2-volts amplitude at the grid of V_1; this is sufficient sensitivity for most counters, but with certain special types it may be desirable to increase the sensitivity somewhat. As the sensitivity is increased a point may be reached beyond which the circuit becomes unstable and goes into self-oscillation, whether a counter is connected to it or not. For this reason it is not advisable to work with the sensitivity control set too close to the point of instability, since this may give rise to spurious and repetitive counts.

The peak amplitude of the output pulses is approximately 30 volts and their width 5 microseconds. This has been found satisfactory for most purposes.

It will be seen (Fig. 2) that it is necessary to apply the high potential to the counter as a negative voltage on the cathode, the anode resting at approximately ground level. The stray capacitance of the wiring connecting the grid of V_1, R_2, R_1, C_2, and the input terminal should be kept as low as possible—so also should that of the lead from the counter anode to the input terminal. If possible, this lead should be short and unshielded. In cases where the counter capacitance is high, or where a shielded lead is necessary, so that the stray capacitance to ground at the input terminal is unavoidably high, a further point arises in connection with the circuit operation, as follows: At the end of the quench period V_5 is cut off and its plate potential rises towards the $B+$ level, with time constant determined by R_{20} and the stray capacitance at the input, simultaneously restoring the counter anode to its operating potential. If this time constant is too long the voltage at the grid of V_1 will not have recovered sufficiently for V_1 to become conducting by the end of the delay time. In this event the suppressor of V_3 will not be biased off, so that V_3 will draw plate current and the circuit will be retriggered, whether a discharge has occurred in the counter or not. The circuit will go into self-oscillation, which will cease as soon as the excessive stray capacitance is removed. To overcome this difficulty, it is merely necessary to increase the delay time to a safe value, by increasing C_5.

In constructing this circuit it is advisable to use accurate resistors (±1 percent) for R_4, R_5, R_6, R_{16}, R_{17}, R_{25}, R_{28}, R_{29}, R_{30}, R_{31}; the rest of the components can be of normal tolerance (±10 percent). R_{26}, R_{27}, R_{32} should be adjusted if necessary, with the circuit in its quiescent state, to correct the +120-, +60-, and −100-volt supplies to within ±2 percent; the $B+$ voltage should be between 260 and 310, but is otherwise not critical; C_4, C_5 can now be adjusted, using an oscilloscope, to give the desired range of quench period and delay time. This procedure will take care of the normal nonuniformity of tube characteristics and will minimize the work involved in setting up.

When operating with a 500-volt quench pulse, it is preferable to replace V_5 by a 6AG5, since it has a higher plate voltage rating than the 6AK5; the auxiliary 500-volt $B+$ supply necessary for this operation (for the plate supply to V_5) is not shown in the diagram. A 6AS6 (made by Western Electric) was chosen for V_3, since it appeared to have a sharper control characteristic on the suppressor than any other available tube. A 6SJ7 was chosen for V_1 because of its low grid current characteristic, although there are doubtless other suitable tubes. It appeared desirable to make R_1 large, so that if the counter should go into continuous discharge the voltage developed across R_1 would be sufficient to operate the circuit and quench the counter. The large negative quench pulses, which are applied to the grid of V_1, certainly exceed the peak voltage rating of this tube by a considerable margin, especially with 500-volt operation. However, there appears to be no satisfactory remedy for this since the only tubes rated for these voltages have otherwise unsuitable characteristics. So far no trouble has been experienced with the 6SJ7 in this respect, but it remains a point to be watched.

IV. RESULTS

Plateaux were obtained using the multivibrator quenching circuit with a four-inch long platinum cathode of half-an-inch diameter, comprising one limb of a compensating counting unit, and varying mixtures of carbon dioxide and carbon disulfide. These mixtures were varied over a wide range—the carbon disulfide from approximately 0.001-cm Hg up to 2-cm Hg pressure, and the carbon dioxide in approximately 5-cm steps from 5 to 20 cm Hg. A typical set of plateaux, using an external gamma-ray source and a quench period Q of 780 microseconds, is shown in Fig. 4. Good working plateaux were obtained even with approximately

0.01-cm Hg pressure of carbon disulfide—an amount which is small enough to neglect in measuring the pressures of carbon dioxide (say 10 to 20 cm Hg) to determine the quantity of carbon dioxide in the effective counting volume.

The effect of changing the quench period Q is shown in Fig. 5 where plateaux are plotted for a number of quench periods between 100 and 780 microseconds.

V. DEAD TIME CORRECTION

In order to obtain absolute counting rates it is necessary to know the correction for counts lost during the dead time of the quenching circuit.

The recorded counts consist of those which occur during delay intervals and those which occur during the quiescent intervals that follow the delay intervals. When a pulse occurs during a quiescent interval, the dead time that follows, during which pulses cannot be recorded, is Q. If a pulse occurs during a delay interval, the dead time consists of the remainder of the delay time δ in addition to the quench period Q, since the circuit cannot record more than one pulse occurring in the delay time. The dead time for such a pulse is $Q+f\delta$, where $f\delta$ is some fraction of δ (e.g., pulse C in Fig. 6).

Let C_A be the recorded counting rate, C_T be the true counting rate, and τ be the effective dead time of the circuit. Further, let us consider the state of affairs existing at the end of a quench period following a count, e.g., as X following count B in Fig. 6. The probability of no further counts occurring in the subsequent delay time δ is then equal to $\exp(-\delta C_T)$.

The probability of one or more counts occurring during this delay time is, on the other hand, equal to $1-\exp(-\delta C_T)$.

In other words, if we consider events occurring immediately after a time corresponding to X in Fig. 6, the probability of the *next* count occurring after the delay time δ, i.e., in a quiescent period, is $\exp(-\delta C_T)$, while that of its occurring during the delay time δ is $1-\exp(-\delta C_T)$.

The number of counts which occur per second during quiescent periods, and are recorded, is $C_A \exp(-\delta C_T)$. Each of these is followed by a dead time Q.

The number of recorded counts which occur per second during delay times is $C_A(1-\exp(-\delta C_T))$. Each of these is followed by a dead time $Q+\eta$ where η is the average value of $f\delta$ for all recorded pulses occurring per second in a delay time.

But for an effective dead time τ the counting system is unable to record counts for a total time of $C_A\tau$ per second. We have, therefore, that

$$C_A\tau = C_A \exp(-\delta C_T)Q + C_A(1-\exp(-\delta C_T))(Q+\eta),$$

i.e.,

$$\tau = Q+\eta(1-\exp(-\delta C_T)). \qquad (1)$$

It is now necessary to determine η.

Consider times t and $t+dt$ after X and *during* the immediately subsequent delay time δ.

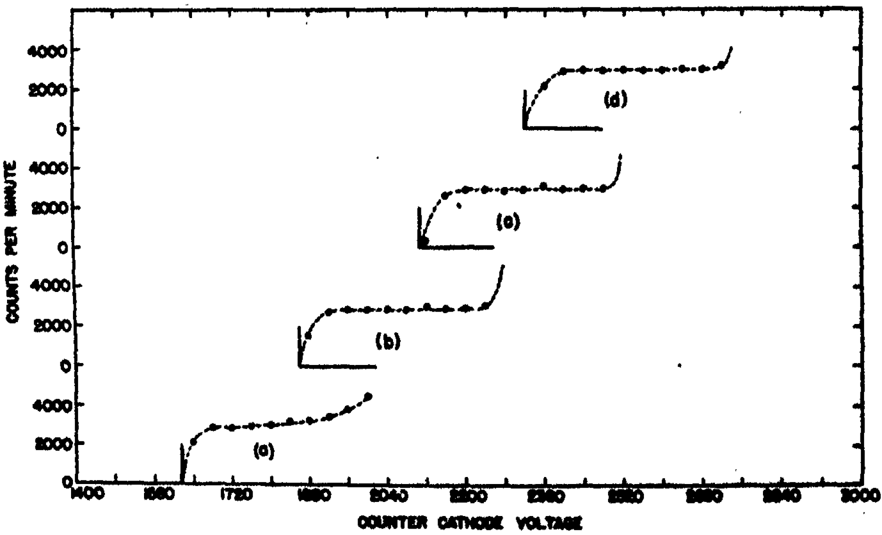

Fig. 4. Plateaux obtained with carbon disulfide at 2.12-cm Hg pressure and carbon dioxide at pressures of (a) 4.84 cm Hg, (b) 9.63 cm Hg, and (d) 19.63 cm Hg.

Then the chance of no counts occurring during t is $\exp(-tC_T)$, while that of a count occurring in dt is $C_T dt$.

The chance, therefore, of the first pulse after X occurring in the interval t to $t+dt$ is $C_T\exp(-tC_T)dt$.

The average value of t for all counts recorded in delay times is thus given by

$$\bar{t}=\frac{\int_0^\delta C_T\exp(-tC_T)tdt}{\int_0^\delta C_T\exp(-tC_T)dt},$$

which is equal to

$$\frac{1-\exp(-\delta C_T)(1+\delta C_T)}{C_T(1-\exp(-\delta C_T))}.$$

The time required is, however, the average time remaining in the delay time δ *after* a pulse.

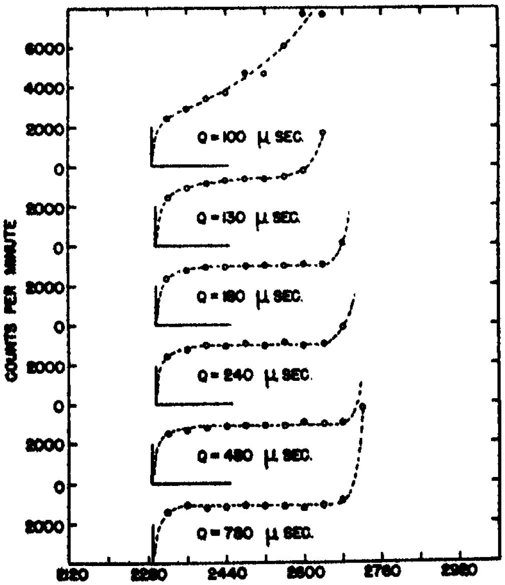

FIG. 5. Effect on plateaux of altering quench period.

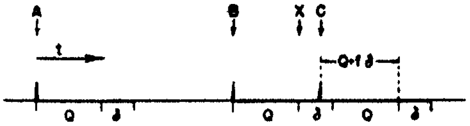

FIG. 6.

This is

$$\eta=\delta-\bar{t}=\delta-\frac{1-\exp(-\delta C_T)(1+\delta C_T)}{C_T(1-\exp(-\delta C_T))}. \quad (2)$$

Substituting this in (1) gives

$$\tau=Q+\delta-\frac{1}{C_T}(1-\exp(-\delta C_T)). \quad (3)$$

If the exponential term in (3) be expanded, we obtain the rapidly converging expression

$$\tau=Q+\tfrac{1}{2}C_T\delta^2-\tfrac{1}{6}C_T^2\delta^3+\cdots. \quad (4)$$

The time $Q+\delta$ can be measured by increasing R_9 until the multivibrator becomes unstable and goes into self-oscillation. When this happens a scaler connected to the output will register pulses, the number of which per second is equal to the reciprocal of $Q+\delta$. The value of Q may be deduced from the setting of the quench-period control which, in turn, is calibrated by connecting a cathode-ray oscilloscope, having a calibrated sweep, to the grid of V_8.

Alternatively, τ can be measured experimentally by, say, the two-source method.

VI. CONCLUSION

Further experiments using the type of counter described, with radioactive C^{14}, have been carried out by one of us in collaboration with Mr. R. C. Hawkings and Mr. R. F. Hunter, to whom our thanks are due for extensive testing of the quenching unit. We also wish gratefully to acknowledge the help of Mr. F. N. MacGillivray, who measured the quench periods for various settings of R_9 using a cathode-ray oscilloscope.

THE REVIEW OF SCIENTIFIC INSTRUMENTS VOLUME 20, NUMBER 1 JANUARY, 1949

Apparatus for Cloud-Chamber Investigations with Free Balloons

E. J. Lofgren, E. P. Ney, and F. Oppenheimer
University of Minnesota, Minneapolis, Minnesota

(Received August 19, 1948)

Apparatus for taking cloud-chamber pictures in free balloon flights is described. The twelve-inch cloud chamber is photographed once per minute by stereo cameras. The complete equipment for a six-hour operation at 90,000 to 100,000 feet weighs 65 pounds and is housed in a 30-inch diameter gondola equipped with temperature control.

INTRODUCTION

Balloons have been developed by the General Mills Company which are capable of carrying 60 or 70 pounds to altitudes of 90,000 to 100,000 feet and remaining there for periods of hours. These balloons are of the open appendix constant volume type and are pear shaped, 70 feet in diameter by 100 feet long. They are made of poly-ethelene one one-thousandth inch thick. The load is carried by strips of tape which also seal the seams. The balloons were used in cloud-chamber and photographic emulsion investigations of cosmic rays. They were flown at Camp Ripley, Minnesota by the Aeronautical Research Group of General Mills.

DESCRIPTION OF APPARATUS

The cloud chamber and associated equipment are housed in a 30-inch diameter spherical gondola spun from 0.020 inch aluminum. The gondola is sealed and has 15 p.s.i. absolute pressure maintained in it at all times. Since gas is supplied for chamber expansion, it is necessary to have a pressure relief valve to hold the pressure constant. Although the expansion ratio of the chamber is temperature compensated in a manner to be described later, the gondola temperature is maintained near room temperature by regulating the amount of solar heating of the section of the sphere containing the cloud chamber. The arrangement is shown in Fig. 1. An insulating wall of Styrafoam[1] separates the sphere into two sections, the lower of which contains the apparatus; this section is internally insulated with fiberglass and is covered on the outside with aluminum foil. A small polar zone on the outside of the upper hemisphere is painted black. With this arrangement, the lower section would reach a temperature below 21°C and the upper section a temperature well above it. When the section containing the apparatus cools below 21°C, a thermostat turns on a blower which circulates warm air from the upper section. Figure 2 is a graph of the temperatures in the two sections of the gondola during a winter flight. Because of the great variation in the angle of the sun in Minnesota throughout the year, it is necessary to make an adjustment in the fraction of the sphere which is painted black. The reason for this is that the insulating barrier between the top and bottom allows some heat to flow when the blower is not on. The black polar zone was 35 inches in diameter on the February flight whose record is shown. The adjustment of

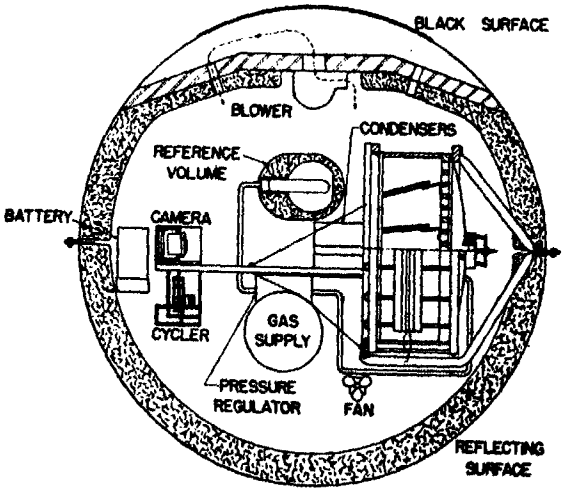

Fig. 1. The sphere and major components are shown. Air is blown through the upper hot compartment by a thermostat-controlled blower to provide temperature regulation.

---

[1] Styrafoam is a form of polystyrene for insulating purposes. It is made by the Dow Chemical Company, Midland, Michigan.

the size of the black zone has not been correctly made on all flights, and temperatures have become as high as 30°C at the end of some flights. During the first hour in which the balloon ascends to 60,000 feet, there is a larger heat loss than at the equilibrium high altitude conditions. This is clearly evident in the initial dip of the temperature curve. Batteries which could be jettisoned at 50,000 feet were used to make up this loss on some flights, but their weight was excessive and they were later replaced by a candle and oxygen supply sufficient for 1½ hours.

Figure 1 also shows the main components of equipment. The twelve-inch diameter cloud chamber is of the rubber diaphragm type whose expansion ratio is determined by compression to a fixed pressure. Most of the experiments have been carried out with either four or five quarter-inch thick lead plates in the chamber. The clearing field is applied between the plates. The chamber is fabricated from aluminum and magnesium and weighs 12 pounds without plates. The aluminum is anodized wherever it is in contact with the sensitive volume of the cloud chamber. The photographs are taken by two cameras between whose optic axes there is an angle of 27°. The lenses are 26-mm focal length and $f/4$ aperture and cover a frame 15/16 inch square on 35-mm film. The film is driven continuously by the motor which drives the cycling cams. The camera bodies are one-piece magnesium castings. The cameras weigh 1 pound each. The chamber is illuminated by a pair of flash lamps with immersion lens systems which have been previously described.[2] The flash lamps[3] are designed to operate at 1000 volts and can be triggered at voltages as low as 400 volts. The lamps are operated by applying a voltage pulse to a model airplane spark coil connected to the aluminized reflector on the lamps. The flash lamp condensers are Mallory Electrolytics with etched plate cathodes, type W.P. There have been no failures of these condensers. They weigh ⅓ as much as oil filled condensers for the same stored energy. Each light has three 350-volt 120-microfarad condensers in series which are charged successively from a 400-volt battery made of sections of Mini-Max Battery No. 493. The cyclic charging is accomplished by a switch on the timing motor. The illumination system complete with a battery to last seven hours weighs 5½ pounds. The clearing field for the chamber is obtained from the voltage across one condenser.

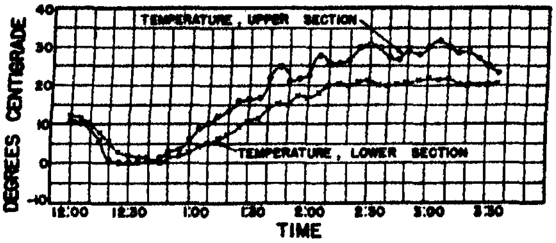

FIG. 2. Observed gondola temperatures in the two sections of the sphere during a February flight.

The cycling is carried out by a constant speed d.c. motor with a cam arrangement.[3] This is shown in Fig. 3. The motor consumes one watt at six volts. Doubling the voltage changes the speed less than ½ percent. Cam set *A* consists of cams for short circuiting the clearing field, expanding the chamber and flashing the lights. In order to achieve accuracy in setting these cams, the shaft which operates them turns approximately 36 r.p.m. The chamber is expanded once per minute so Cam *B*, which actuates a micro switch, functions as a permissive switch, allowing cam set *A* to operate the chamber only when *B* is actuated. Figure 3 also shows the switch, *C*, which cycles the condenser charg-

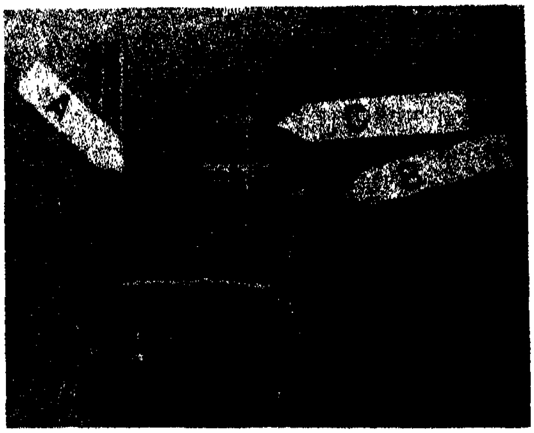

FIG. 3. Constant speed d.c. motor. *A*—Light trigger, chamber expansion, and clearing field contracts. *B*—Permissive switch operating once a minute. *C*—Condenser charging switch.

---

[2] Lofgren, Ney, and Oppenheimer, Rev. Sci. Inst. 19, 271 (1948).

[3] Made by Anglo Corporation, 4234 Lincoln Avenue, Chicago.

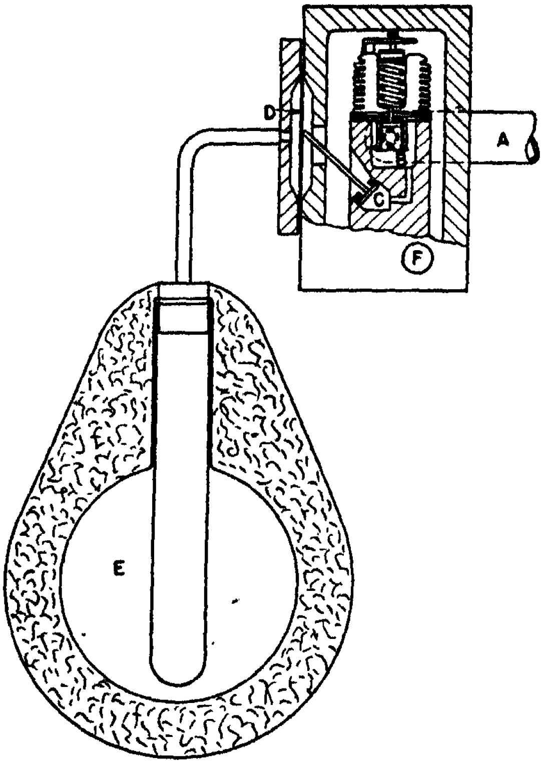

FIG. 4. Pressure regulating system. *A*—High pressure inlet. *B*—spring loaded first stage valve, pressure reduced to 30 p.s.i. *C*—Second stage valve. *D*—Diaphragm whose motion actuates second stage valve. *E*—Insulated reference volume containing air and alcohol. The tubular diaphragm in the reference volume prevents migration of the alcohol. *F*—Outlet to cloud chamber.

ing battery. This motor, the blower, and the fan are powered by Vitamite[4] storage batteries.

The gas for chamber expansion is supplied from a 500-cu in. Air Forces oxygen tank which is filled to 800 p.s.i. The gas supply is sufficient for a six-hour flight. The pressure is reduced and regulated by means of a modified Air Corps two-stage regulator valve. The second stage is constructed in such a way that gas is allowed to flow to compress the chamber until the pressure is equal to the pressure in a reference volume (see Fig. 4). The pressure in the reference volume then determines the compressed pressure and volume of the cloud chamber. If Δp is the difference between expanded and compressed pressures and p is the expanded pressure, then with our chamber to get the best tracks at any temperature, $\Delta p/p$ must increase with temperature about 1 percent per degree C. This can be accomplished if the pressure in the reference volume increases faster with temperature than the expanded cloud-chamber pressure. With argon and a mixture of 70 percent ethyl alcohol and 30 percent water by volume in the cloud chamber, and with a permanent gas and pure alcohol in the reference volume, the desired compensation was obtained over a temperature range of at least 15°C. In order to have the system operate while the temperature was changing, it was also necessary to make the thermal time constant of the reference volume the same as that of the chamber. This was approximated by adjusting the quantity of alcohol and the insulation of the reference chamber. A rubber diaphragm in the reference volume keeps the alcohol from distilling out of the volume. This is a modification of a system used by Leighton.[5]

The entire assembled system weighs about 65 pounds. Figure 5 shows the complete apparatus with the top hemisphere removed.

OPERATION

Eight cloud-chamber flights have been made. Six were recovered and of these five have yielded about 500 useful photographs. Some of the

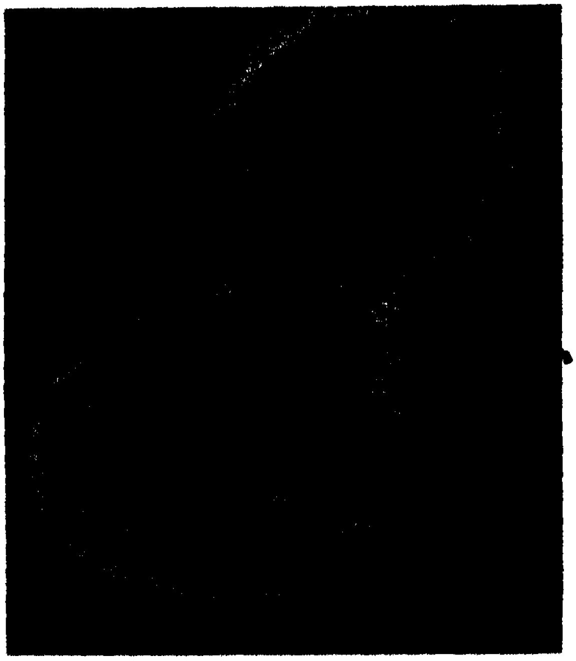

FIG. 5. General view of the completed apparatus. All of the components are attached to the horizontal flange.

---

[4] Made by the Vitamite Company, 227 W. 64th St., New York City.

[5] Robert B. Leighton, Rev. Sci. Inst. 19, 274 (1948).

FIG. 6. Burst of penetrating particles and heavily ionizing particles produced by a penetrating particle. Altitude 83,000 feet.

results have already been published.[6] One photograph, Fig. 6, is included here as an example. It shows a nuclear disintegration produced at 83,000 feet by a fast penetrating particle. The disintegration contains fast penetrating and slow highly ionizing fragments.

We wish to express our appreciation for the ONR support which made this work possible and to Dr. Urner Liddel for his continued interest. These flights would not have been possible without the full cooperation of the General Mills Corporation and especially of T. R. James and Henry Stinger. The recovery was made possible in most cases because of the assistance of Captain Swenson and other pilots at Wold Chamberlain Field. We wish to thank J. T. Tate for his encouragement, and Rudolph Thorness and George DeWitt for help in the design and construction of the apparatus.

---

[6] Freier, Lofgren, Ney, Oppenheimer, Bradt and Peters, Phys. Rev. **74**, 213 (1948).

THE REVIEW OF SCIENTIFIC INSTRUMENTS VOLUME 20, NUMBER 1 JANUARY, 1949

The Statistical Theory of the Dead Time Losses of a Counter

C. E. CLARK
Mathematics Department, Emory University, Emory University, Georgia

(Received April 9, 1948)

In the case of events at random times, the number of events must be estimated from the number of counts recorded by a counter. In this article we study the statistical distribution of the unknown number of events. We show that this distribution is approximately normal, and we approximate the standard deviation.

A COUNTER such as a Geiger counter misses some counts because parts of the instrument have dead time intervals following any one of the impulses that are being counted. Let μ-impulses occur, and let ν be the number of these impulses recorded by the counter. For the case in which the impulses occur at random times, there have appeared in the literature methods of approximating $E(\mu)$, the expected value of μ, assuming ν is known.[1] In this article we extend these results by studying the statistical distribution of μ. We show that μ is approximately normally distributed with standard deviation

$$(E(\mu)[E(\mu)-\nu]/\nu)^{\frac{1}{2}}. \tag{1}$$

This information is needed before we can infer that a small difference between $E(\mu)$ and ν implies a small difference between μ and ν. Moreover we can use a counter when $E(\mu)-\nu$ is large because we have fiducial limits for μ, and we know how many counts we must have for $E(\mu)$ to be an adequate estimate of μ.

To derive the distribution of μ we note that μ could theoretically be any integer not less than ν. The probability $P(\mu)$ that given ν-counts, the unknown number of impulses is μ, is proportional to the probability that ν-counts would be recorded in a run of μ-impulses. Since the probability that an impulse is counted is $p=[\nu/E(\mu)]$, we obtain from the theory of probability that

$$P(\mu)=(k\mu!/\nu!(\mu-\nu)!)p^{\nu}q^{\mu-\nu},$$

where k is the constant of proportionality mentioned above, and $q=1-p$. To determine k we note that, summing from $\mu=\nu$ to $\mu=\infty$,

$$\sum P(\mu)=k\left\{p^{\nu}+\frac{\nu+1}{1!}p^{\nu}q+\frac{(\nu+1)(\nu+2)}{2!}p^{\nu}q^{2}+\cdots\right\}.$$

---

[1] See, for example, L. Alaoglu and N. M. Smith, Jr., Phys. Rev. **53**, 832 (1938).

Since $q<1$, this expression reduces to a convergent binomial series expansion, and we have that

$$\sum P(\mu)=kp^{\nu}(1-q)^{-\nu-1}=(k/p).$$

Since probability theory gives $\sum P(\mu)=1$, we have $k=p$ and

$$P(\mu)=(\mu!/\nu!(\mu-\nu)!)p^{\nu+1}q^{\mu-\nu}.$$

Relations between the binomial and normal distributions imply that approximately

$$P(\mu)=\frac{p}{\sigma(2\pi)^{\frac{1}{2}}}\exp\left\{-\frac{(\nu-p\mu)^2}{2\sigma^2}\right\},$$

where

$$\sigma^2=\mu pq.$$

Setting $\rho^2=q/p$ and rearranging we see that

$$P(\mu)=\frac{1}{\rho(2\pi\mu)^{\frac{1}{2}}}\exp\left[-\frac{\left(\mu-\frac{\nu}{p}\right)^2}{2\mu\rho^2}\right].$$

Setting

$$\mu=\frac{\nu}{p}+(\nu)^{\frac{1}{2}}y \tag{2}$$

and multiplying $P(\mu)$ by $d\mu/dy=(\nu)^{\frac{1}{2}}$ we obtain the probability distribution of y as

$$P(y)=\frac{(\nu)^{\frac{1}{2}}}{\rho\left[2\pi\left(\frac{\nu}{p}+(\nu)^{\frac{1}{2}}y\right)\right]^{\frac{1}{2}}}\times\exp\left\{-\frac{\nu y^2}{2\rho^2\left(\frac{\nu}{p}+(\nu)^{\frac{1}{2}}y\right)}\right\}.$$

We see that for large ν, approximately

$$P(y)=\frac{(p)^{\frac{1}{2}}}{\rho(2\pi)^{\frac{1}{2}}}\exp\left\{-\frac{py^2}{2\rho^2}\right\}.$$

Hence y is approximately normally distributed with mean zero and standard deviation $\rho/(p)^{\frac{1}{2}}=(q)^{\frac{1}{2}}/p$. This with (2) shows that μ is approximately normally distributed with mean $\nu/p=E(\mu)$ and standard deviation $(\nu q)^{\frac{1}{2}}/p$. Since $p=[\nu/E(\mu)]$, the standard deviation of μ can be reduced to (1).

THE REVIEW OF SCIENTIFIC INSTRUMENTS VOLUME 20, NUMBER 1 JANUARY, 1949

An Apparatus for Determining the Effect of Centrifugal Force on the Potentials of Galvanic Cells

B. ROGER RAY* AND D. A. MACINNES
Laboratories of The Rockefeller Institute for Medical Research, New York, New York

(Received October 7, 1948)

An apparatus is described with which electric potentials, developed as a result of phenomena occurring in the rotor of a centrifuge, can be measured within one microvolt, and radial temperature differences in the rotor can be determined and controlled within 0.01°. Rotation in a vacuum minimizes the rise of temperature of the rotor, which can also be measured. The speed of rotation is controlled by a friction drive within 0.01 percent and maintained at definite values, between 400 to 7200 r.p.m., corresponding to stroboscopic patterns. The instrument was designed to measure the effect of centrifugal fields on simple galvanic cells.

THE effect of centrifugal fields on simple galvanic cells has been studied by des Coudres[1] and by Tolman.[2] Some preliminary measurements have also been reported by MacInnes.[3] In the investigations by Tolman, and by MacInnes, the galvanic cells were of the type

$$(\mathrm{Pt}) : \underset{r_2}{\mathrm{I_3}}, \mathrm{KI}, \underset{r_1}{\mathrm{I_2}} : (\mathrm{Pt})$$

in which two, otherwise identical, iodide-iodine electrodes were placed at radii r_1 and r_2 in a centrifugal field. The limiting form of the thermodynamic equation for the resulting potential, E, is

---

* National Research Council Fellow, 1945–47; Merck Fellow in the Natural Sciences under the National Research Council, 1947–48. Present address, Chemistry Department, University of Illinois, Urbana, Illinois.

[1] T. des Coudres, Ann. Physik **49**, 284 (1893); **57**, 232 (1896).

[2] R. C. Tolman, Proc. Am. Acad. **46**, 109 (1910); J. Am. Chem. Soc. **33**, 121 (1911).

[3] D. A. MacInnes, Ann. New York Acad. Sci. **43**, 243 (1942).

$$EF = 2\pi^2 n^2 (r_2^2 - r_1^2)[t_K(M_{KI} - \bar{V}_{KI}\rho) - (M_I - \bar{V}_I\rho)], \quad (1)$$

in which F is the faraday, n is the number of rotations per second, t_K is the transference number of the cation constituent, ρ the density of the solution, M_{KI} and $\bar{V}_{KI}$ are the molecular weight and partial molal volume of potassium iodide, and M_I and V_I are the atomic weight and partial atomic volume of iodine. Since all the other terms are known or can be measured, this furnished a method for determining the transference number, t_K. The method provides a means for investigation of salts in non-aqueous solvents, for which other procedures have proved inadequate.

The apparatus to be described is the result of a long research undertaken with the purpose of making the centrifugal method an accurate means of obtaining transference numbers and ionic mobilities in solutions. The method involves (a) precise measurement of the potential of the cell; (b) adequate speed control and measurement; (c) control of the temperature gradient across the rotor; (d) measurement of the temperature of the rotor; and (e) control of the atmosphere surrounding the galvanic cell. In addition the constants r_1 and r_2 of Eq. (1) must be very accurately known.

The apparatus and the electrical connections are shown diagrammatically in Fig. 1. the rotor $R-R$ is turned by means of the pressure of the disk D on the plate P, which is rotated by the synchronous motor M. The rotor speed can be varied by changing the position of the disk D with relation to the plate P. The potential between the electrodes E_1 and E_2 of the cell C is measured, during the rotation, by electrical contacts through the mercury commutators G_3 and G_4. The difference of temperature at radii corresponding to the positions of E_1 and E_2 is obtained by means of the thermojunctions $J-J$ (actually arranged around the cell C), the thermopotential being measured between the commutators G_3 and G_4. Finally, the temperature of the rotor is found, using a single junction in the rotor, the commutators G_1 and G_2, and the external ice bath K.

THE CELLS

Two forms of galvanic cells are used. For the type shown in Fig. 2A the cylindrical vessel A was machined from the plastic CR 39, kindly furnished by the American Plate Glass Company. This plastic is chemically resistant and is not readily deformed. One of the electrodes, E_2, rests on the bottom of vessel A and the other, E_1, on a shoulder of the vessel. The closing cap consists of two parts, B and K, the first made of CR 39, and the other of Lucite. The two materials are necessary since the CR 39 is too brittle to support the screw threads of the nuts used in sealing the cell, as described below. Three holes pass through the cap B, two of which are used for the leads L_1 and L_2 to the two electrodes, and another for filling the cell. The cap K carries three Lucite nuts, D_1, D_2, and D_3, which exert pressure on Lucite washers, F, and the Neoprene gaskets, N. The filling hole is closed by the use of a Neoprene gasket and a CR 39 plug R with an attached circular disk replacing the washer. The vessel A and the caps are enclosed in a silver plated brass shell H. Four longitudinal slots (not shown) are cut into the cylindrical wall of this shell, so that the filling process can be observed through the transparent walls of vessel A. A threaded brass ring M provides pressure through a Pliofilm gasket P holding the caps against the vessel A.

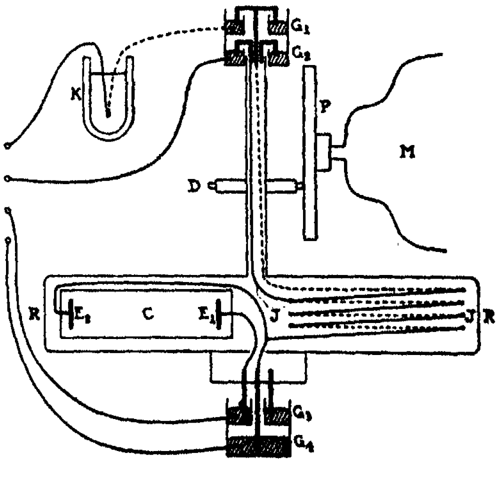

FIG. 1. Diagram of apparatus.

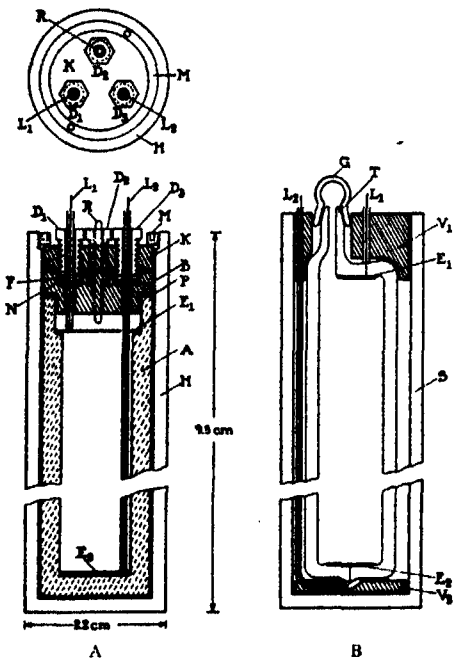

FIG. 2. The galvanic cells.

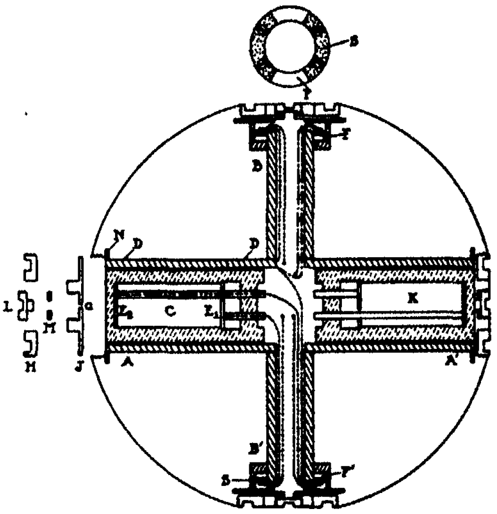

FIG. 3. Horizontal cross section of rotor.

The electrodes E_1 and E_2 are made of disks of platinum, respectively 13 mm and 11 mm in diameter, and 0.2 mm thick, to which No. 24 platinum wire is welded. These wires are enclosed in soft glass tubing, which, at the point of contact with the electrode, is sealed to the wire with lead glass.

These cells have the advantages that they are not fragile and that the dimensions, from which values of r_1 and r_2 of Eq. (1) can be obtained, can be measured accurately with a depth gauge. As a result of their complexity they are somewhat hard to keep clean. Glass parts replacing the plastic vessel A and the cap B have been constructed but have not yet been fully tested.

A simpler cell which has also been used is shown in Fig. 2B. In this design the electrodes E_1 and E_2 are sealed into the Jena 16 III glass wall of the cell. The platinum wire leads, L_1 and L_2 are enclosed in flexible plastic tubing. Filling and removal of solution are carried out through the tube T which is closed with a ground glass cap G. The whole glass cell is enclosed in the brass shell S, the space between the shell and cell being filled with vaseline. This semifluid material helps to equalize the pressure on the two sides of the glass walls and bottom of the cell when in a centrifugal field. Two Bakelite spacers, V_1 and V_2, hold the glass cell in a fixed position in the shell S. Though the dimensions of this cell cannot be obtained with the accuracy of the plastic cell described above, it is more readily cleaned and manipulated. It can also be calibrated with the aid of data obtained with the other cell.

THE ROTOR

The rotor, which is shown in horizontal cross section in Fig. 3, and in vertical cross section in Fig. 4, is constructed from a disk of magnesium 23 cm in diameter, and 5 cm thick. Two cylindrical channels, A–A' and B–B', of 25-mm and 13-mm diameter, respectively, are bored at right angles through the disk. In order to show details of construction clearly, the diameters of these channels and their constants relative to their lengths have been doubled in Fig. 3 but are in the correct proportions in Fig. 4. In the channel A–A' of Fig. 3 is placed the cell C and the counterpoise K. This counterpoise is made to resemble the cell closely, since a precise balance has been found necessary to eliminate vibration, for the speed control, and to be sure that the rotor turns around its geometrical center. The channel B–B' provides readily accessible electrical connections to the cell and the thermojunctions. The channel is lined with an insulating tubing. Bakelite rings, F and F', at each end of the channel carry metal insulated sectors S, which are fitted with screws for fastening the ends of wire leads. One of these rings is shown at the top of the figure. At the ring F' the two leads from the cell C pass to the metal sectors, which are, in turn, connected by wires to the commutators G_3 and G_4, as shown in Figs. 1 and 4.[4]

The cell C is enclosed by a thin cylindrical Bakelite shell D–D in which are embedded the copper-constantan wires which form 22 junctions, 11 of which are at a radius corresponding to electrode E_2 and 11 corresponding to E_1. The terminal leads of these junctions are connected to metal sectors on the insulating rings F and F' from which copper wires pass to the commutators G_2 and G_4, and a constantan wire connects through a sector on ring F to G_1. It is possible to remove this cylindrical shell without disturbing the leads to G_1 and G_2 which pass through the hollow shaft on which the rotor is suspended. As explained above, the purpose of the multiple junctions is to determine the difference of temperature existing between the electrodes E_2 and E_1.

In order to control the atmosphere surrounding the cell C arrangements are made for sweeping out the free spaces in the channels A–A' and B–B' with a gas, such as nitrogen, and to keep the gas from escaping while the measurements are being made. For this purpose the end of each channel is furnished with a closing device, the separate parts of which are shown on the left hand side of channel A–A'. The threaded annular ring H presses against a disk J which in turn compresses the Neoprene gasket N which is recessed into the wall of the channel, thus forming a gas-tight seal. A cylindrical projection from the disk J is fitted with a threaded plug L.

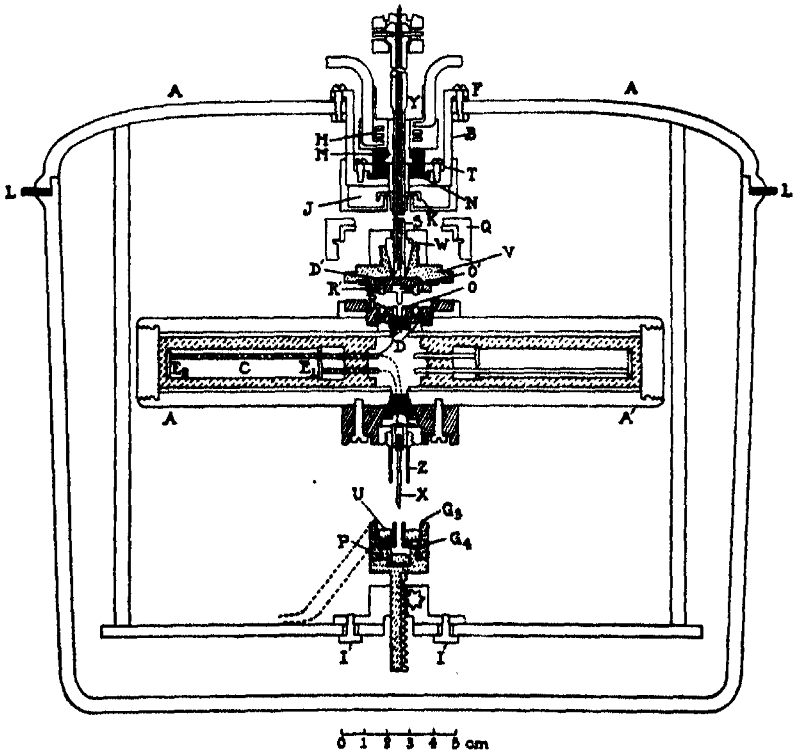

FIG. 4. Vertical cross section of rotor and vacuum chamber.

---

[4] It is necessary to connect the wires from the cell C to the sectors S on the ring F' before inserting the cell into the channel $A-A'$. The lead wires must therefore be long enough to extend out of the open end of this channel. On inserting the cell the extra lengths of the wires (not shown) are looped into the channel $B-B'$ and toward the ring F. To pull the wires in this direction as the cell C is slid into place, there is a cord attached to a small slip ring passing around both wires. This cord is detached after use. For the lead wires a light, many-stranded insulated cable, such as is used with hearing aids, is serviceable. For connecting to the cell C these wires are soldered to tiny screw clamps which grip the platinum leads from the electrodes. An annoying tendency of the leads to break at the soldered joint has been overcome by the use of a low melting alloy, Cerrolow 117, made by the Cerro di Pasco Company.

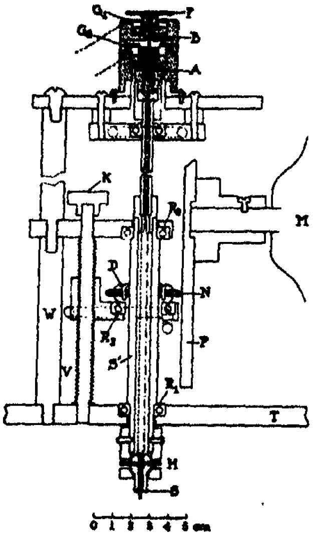

Fig. 5. Speed regulation mechanism.

This, with the washer *M*, is used to close the small hole, *a*, which is used for the entrance and exit of gas. In order to sweep out the channels with nitrogen the plug *L* is replaced with a threaded brass tube connected to the source of the gas. Similar tubes are placed at the ends of the other channels, and bubble tubes are attached to indicate the rate at which the gas is passing. After the channels are fully swept out the threaded plugs *L* are replaced, one at a time, while the gas continues flowing. It is quite essential that the channels should be gas-tight since during a determination the rotor is surrounded by a vacuum and leakage would reduce the vacuum and might also result in disturbance of the solution in the cell.

Further details of construction of the rotor are shown in vertical cross section in Fig. 4. Since it is convenient to be able to remove the rotor without disturbing the copper and constantan leads that pass through the hollow shaft *S*, a special connector for these leads has been provided. The constantan wire from the rotor passes to a small cylinder *O* of that material and the copper wire is connected to a copper ring *R*, the two being fitted into a Bakelite disk *D*. This disk holds a small rubber stopper through which both wires pass and which forms a gas-tight seal. A rubber ring under the disk completes the seal. The wires passing down through the shaft *S* terminate in a constantan pin *O'* and a copper ring *R'*. These are set into a Bakelite disk *D'* which is fastened into the steel member *V* which, with the aid of the chuck *W*, is firmly attached to the flexible shaft *S*. To fasten the rotor to the member *V* and thus to the shaft *S* the collar *Q* is brought into place so that its screw threads engage those on the rotor, with the result that the electrical connections are also made. A rubber washer under the copper ring *R* assures a firm contact with *R'*. During this process the rotor is held by four clamps, one of which can be seen on a supporting post in Fig. 6.

The bottom surface of the rotor carries the leads to the commutators G_3 and G_4 which will be described below.

The vacuum chamber in which the rotor turns has been made by modifying a commercial aluminum pressure vessel, a cross section of which is indicated in Fig. 4. The rim of the vessel has been turned down so that the gasket *L* is on the outside edge. As can be seen in Fig. 6 the cover of this vessel is supported by the framework. From this cover *A–A* of Fig. 4 are suspended the stationary parts of the commutators G_3 and G_4.

In this cover is also mounted a vacuum-tight, water cooled bearing through which passes the flexible shaft *S*. To obtain correct values of the centrifugal potential of the galvanic cells *C*, it is necessary to prevent the development of a radial temperature gradient across the rotor, and it is further desirable that the rotor temperature should not rise during a determination. Rotation in a vacuum of 1μ or less prevents the production of appreciable heat through gas friction. The temperature at the bearing can be controlled by appropriate cooling. In practice the radial temperature differences have been reduced to less than 0.01° by empirically choosing the temperature of the water circulating around the bearing. This cooling water comes from a small thermostat, and is driven through the coils *H* with the aid of a "Marco" diaphragm pump. The coils are joined to the bronze bearing *M*, which is, in turn, fitted into the Neoprene mounting *N*, which gives additional flexibility to the rotating system. An annular projection of this mounting is fastened to the brass cup *B* by means of the ring *T*, the cup itself being joined solidly to the cover with the gas-tight seal *F*. The space *Y* holds vacuum pump oil, which lubricates the bronze bearing *M*. Since there is a pressure difference of one atmosphere across this bearing the oil is slowly forced along the shaft. It is, however, thrown into the chamber *J* by the disk *K* which is attached to the shaft.

THE SPEED CONTROL

Details of the arrangement for speed control are shown in Fig. 5. The hollow shaft S' turns on the ball bearings R_1 and R_2. At the lower end of this shaft is a universal joint which supports and rotates the flexible hollow shaft, *S*, of Fig. 4, to which the rotor is attached. Around the shaft S' and running on the ball bearing R_3 is the disk *D* carrying a ring of Neoprene *N*. This presses lightly on the flat circular aluminum plate *P* which is rotated 1800 r.p.m. by the ⅛ h.p., G.E., synchronous motor, *M*. This motor is mounted on an extension of the supporting plate *T*, and is furnished with an adjusting screw and bolts (not shown) so that the pressure of the Neoprene ring *N* on the rotating plate *P* can be adjusted and held at a definite value. The disk *D* is keyed into a vertical slot on the shaft S' so that disk and shaft turn together. The position of the contact point of the ring and the plate can be shifted by use of the knurled knob *K* which operates the threaded rod *V*. With this arrangement the rotational speed can be adjusted with high accuracy from 400 to 7200 r.p.m. The top end of the shaft S' carries a stroboscopic disk *F* with one white radial band on a black background. With a stroboscopic lamp illuminating this disk with pulses of light at a constant frequency a series of symmetrical patterns are observed as the rotational speed is varied. The use of these patterns to establish speeds with high precision is described in a paper from this laboratory.[8] Since this method requires a rough preliminary knowledge of the speed a pointer moving with the disk *D* passes over a scale attached to the post *W*. This is shown in Fig. 6. With occasional slight manual adjustments it has been found that the speeds can be readily held within 0.01 percent at any desired value within the range of the apparatus.

THE MERCURY COMMUTATORS

The detail that probably contributed most to the success of the apparatus is the design of the mercury commutators, G_1 and G_2 of Fig. 5 and G_3 and G_4 of Fig. 4. It was possible, with these connections from the stationary to the rotating parts of the apparatus, to make measurements of potentials within 1 microvolt. This precision is necessary because the highest potentials determined are of the order of a millivolt. As shown in Fig. 4 the leads from the electrodes E_1 and E_2 of the cell *C* pass through a small rubber stopper, and then to supports for the copper needle *X* and the hollow copper tube *Z*. Below these is shown a Lucite cylinder in which there is a small pool of mercury *P* and an annular ring of mercury *U*. By a rack and pinion motion the Lucite cylinder can be raised so that the copper pin is inserted into the pool of mercury and the hollow tube into the annular ring. Adjusting screws *I–I* make an accurate centering possible. The contactors *X* and *Z* must not rub against the Lucite walls or potentials will be developed. Repeated tests of this pair of commutators have been made in which the leads to the cell have been shorted

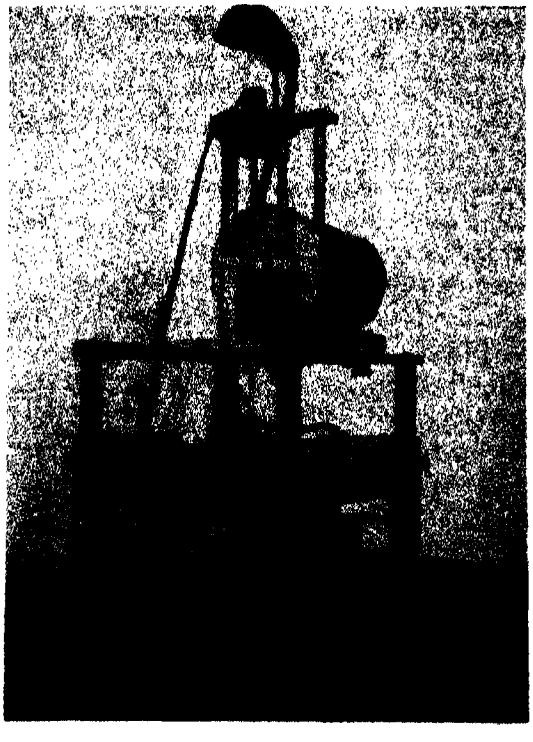

FIG. 6. Apparatus and support.

---

[8] D. A. MacInnes, Rev. Sci. Inst. 14, 14 (1943).

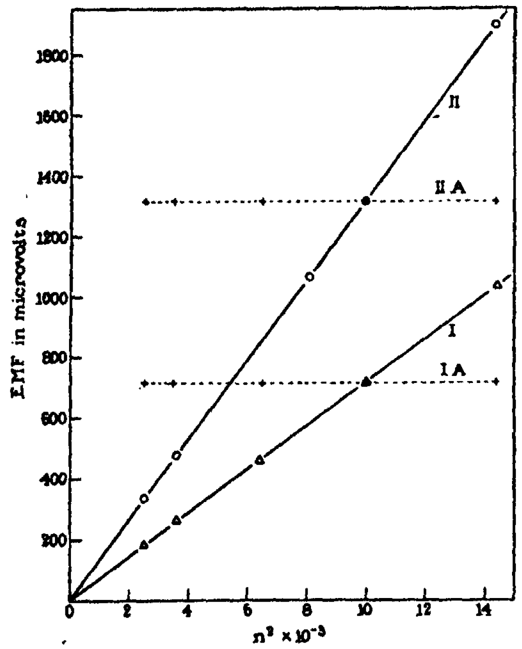

FIG. 7. Typical results. E.M.F. of cell in microvolts *vs.* square of revolutions per second.

and the speed of rotation increased to its highest value. In no case has the observed potential been over 1 microvolt, and it is usually less than this. It has been found desirable to have the tube *Z* of small diameter (8 mm) to reduce peripheral speed and with a smooth, well amalgamated surface. The mercury reservoirs should not be too small otherwise potentials will develop, probably due to heat effects.

Because of their position the design of the commutators G_1 and G_2 of Fig. 5 is slightly different from those just described. The copper and constantan wires which pass up through the shaft *S′* end respectively in a copper tube *A* and a constantan pin *B* which are insulated from each other. Connection from this pin to the annular ring of mercury in the commutator G_1 is made with the overhang sleeve of constantan attached to the lower side of the stroboscopic disk *F*. A similar sleeve joins the copper tube *A* with the mercury in commutator G_2.

SOME TYPICAL RESULTS

The results of two typical experiments are shown in Fig. 7, in which values of the potentials, *E*, in microvolts, are plotted as functions of the square, n^2, of the speed of rotation in seconds. In this plot line *I* refers to data obtained with an aqueous solution of 0.2-normal potassium iodide and 0.01 iodine, using the plastic cell shown in Fig. 2A. Line II is the corresponding plot for a solution of 0.2 N KI and 0.07 N I_2 in pure methanol, in the glass cell of Fig. 2B. According to Eq. (1) these relations should be linear. That they are straight lines to very high accuracy is shown by plotting the slopes, E/n^2, against values of n^2 as shown in I A and II A. These slopes are seen to be constant within a very small limit of error.

To anticipate conclusions which will be published in full elsewhere, the interpretation of the results on a series of measurements on the aqueous solutions of potassium iodide and iodine leads to values of the transference number, t_K, in very close accord with those found by Longsworth[6] by the quite independent moving boundary method for determining these constants. The data, and a modification of Eq. (1), based on a more complete understanding of the cell process, have also yielded a quite new method for demonstrating the presence of the complex ion I_3^- in these solutions.

Up to the present it has not been possible to obtain transference numbers in non-aqueous solutions by the Hittorf and moving boundary procedures. This is due to disturbances arising from Joule heat effects. The results obtained with this centrifugal method for solutions in methanol indicate that transference numbers can now be obtained in many non-aqueous solvents. Together with conductance determinations these constants can be used to obtain ion constituent mobilities, and with e.m.f. measurements on simple galvanic cells they will serve for the computation of activity coefficients in solvents other than water.

ACKNOWLEDGMENT

The authors wish to express their indebtedness to the Institute instrument maker, Mr. Josef Blum. His skill and ingenuity have been invaluable in the development of the apparatus described in this paper.

---

[6] L. G. Longsworth, J. Am. Chem. Soc. 57, 1185 (1935).

THE REVIEW OF SCIENTIFIC INSTRUMENTS VOLUME 20, NUMBER 1 JANUARY, 1949

Circuits for Minimizing Transient Effects on Energy Measurements in Calorimetry

HAROLD J. HOGE
National Bureau of Standards, Washington, D. C.

(Received September 20, 1948)

Transient effects on electrical energy measurements in calorimetry will be minimized if P, the power developed in the heater, satisfies the condition $dP/dR=0$, where R is the resistance in which the power is developed. It is shown that this condition is satisfied if the resistance U between the two points of the supply network to which R is connected is kept equal to R. Circuits for maintaining this condition are described.

THE electrical energy supplied to a calorimeter in a heating period of length t is $Q=\int_0^t EIdt$, where E is the e.m.f. across the heater and I is the current through it. A series of suitably timed readings of both E and I is ordinarily made, from which the power $P=EI$ may be computed as a function of time. This permits the integral to be evaluated accurately even though, as is usually found, both E and I show small, more or less uniform upward or downward trends. There may, however, be rapid changes at the very beginning of a heating period which cannot be conveniently followed in the measurements of E and I. These are caused by a change in the resistance of the heater which results from its rapid rise in temperature. If it is assumed that the power during the period of rapid change is the same as that observed later in the heating period, an error may be introduced. In many calorimeters this error is negligible. Osborne, Stimson, and Ginnings[1] found this to be the case, using a ballistic galvanometer to integrate the effect. The possibilities of error become larger, however, (1) if the heating period is short, (2) if the heater is in poor thermal contact with the calorimeter, or (3) if the heater has a relatively high temperature coefficient of resistance. All three of these conditions occasionally arise in practice.

Calorimetric workers do not seem to be generally aware that errors due to transient effects can be greatly reduced by an approximate matching of the resistance of the supply circuit to the resistance of the calorimeter heater. If the resistance U of the supply circuit is made equal to the resistance R of the calorimeter heater, the power developed in the latter satisfies the condition $dP/dR=0$. Probably the most widely used power-control circuit for calorimetry is the simple series circuit of Fig. 1a. It is commonly used either with $A<(1/10 \text{ to } 1/5R)$ or with $A>(5 \text{ to } 10R)$. The first condition tends to keep E constant as R changes, throwing the variation into I; for the second condition the converse is true. Either of these arrangements is satisfactory where transient errors are unimportant, which is normally the case. However, if there is reason to expect transient effects to be appreciable, it is preferable to operate in the matched condition ($U=R$, $dP/dR=0$). Matching might be more often adopted if it did not mean that the resistor A (Fig. 1a) is no longer available as a means of adjusting the power.

It is not difficult to design control circuits which permit the power to be adjusted by means of resistors, and which may still be kept matched at all times. One of the simplest of such circuits is that of Fig. 1b. It consists of a potential divider D connected across a bank of cells, with an adjustable resistor A in series with the movable tap. The required range of adjustment of A is generally only a small fraction of its maximum resistance. In addition there are a standard resistor in which I is measured and a milliammeter for convenience in adjusting the current. In both the circuits of Fig. 1 the condition of matching is properly met if the resistance from point 1 to point 2 is equal to R by either the right-hand or left-hand path. For circuit *a* this is evident from first principles. Letting the resistance from 1 to 2 via the right-hand path be U and letting the e.m.f. of the battery on open circuit be $E\infty$, it is easily shown that the power developed in R is $P=RI^2=R\{E\infty/(R+U)\}^2$ and that $(R/P)(dP/dR)=(1-R/U)/(1+R/U)$. Hence, $dP/dR=0$ when $R=U$, $P_{\max}=E^2\infty/4U$ and $P/P_{\max}=4/(1+R/U)(1+U/R)$. The expressions for $P/P_{\max}$ and for the logarithmic derivative $(R/P)(dP/dR)$ are particularly useful because they depend only on the ratio of R to U.

---

[1] N. S. Osborne, H. F. Stimson, and D. C. Ginnings, "Measurements of the heat capacity and heat of vaporization of water in the range 0° to 100°C." J. Research Nat. Bur. Stand. 23, 197–260 (1939).

By properly defining $E\infty$ and U, these results may be made to apply to any resistance in any network of resistances and batteries. According to Thévenin's[2,3,4] theorem, any two points on such a network may be considered to be the terminals of an equivalent cell. The current which may be drawn from the two points by connecting them with an additional conductor is the same as that which could be drawn from a cell of e.m.f. $E\infty$ and internal resistance U, when $E\infty$ and U are the e.m.f. and resistance between the two points of the network before the additional conductor is attached. In applying the theorem to circuit b, the two points chosen are 1 and 2, *before* either R or the dummy is connected. Since the entire right-hand side of the circuit is equivalent to a cell of e.m.f. $E\infty$ and internal resistance U, the current which will flow when R is connected is $I=E\infty/(R+U)$. But this expression is the same as that for the simple series circuit a, and hence all the results found above for it apply to this circuit also. They apply in fact to any network of resistances and batteries which may be devised to supply power to the calorimeter.

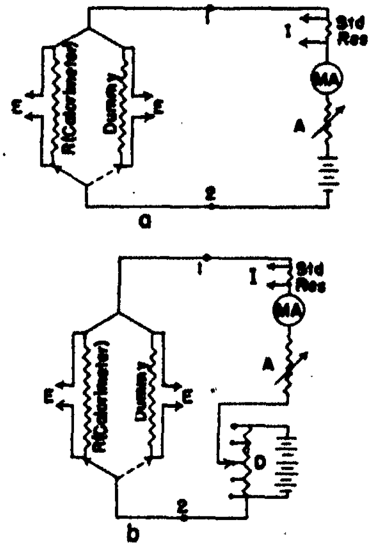

FIG. 1. Two circuits for controlling the power supplied to a calorimeter. Circuit a is the one most commonly used. Circuit b is preferable when the resistances of calorimeter and supply network are to be kept matched.

The author has used circuit b in calorimetric work and found it to be satisfactory. The potential divider D is composed of several fixed resistors in series, as a single resistor with a sliding contact was found to be too unsteady. The condition of matching $(U=R)$ is maintained by adjusting A (between heating periods) to compensate for changes in R caused by changes in temperature. A convenient method of making the adjustment makes use of the fact that when $R=U$, $E=E\infty/2$. First the dummy is made equal to R by means of readings of E. Then resistances A and D are adjusted as desired until, when the resistance of the dummy is made infinite, the e.m.f. across it is doubled. If it is preferred not to interrupt the current long enough for $E\infty$ to be measured, the dummy may be arranged so that its resistance can be changed by several percent. The power is then measured for two values of the dummy resistor, $\Delta P/\Delta R$ computed, and the circuit adjusted to make this quantity zero.

Fortunately $P/P_{\max}$ plotted *versus* R/U has a fairly broad maximum. Hence, the adjustment to make $R=U$ does not need to be made with very great accuracy, and it may in some cases be permissible to use a fixed resistor for A. Assuming the battery to have zero resistance, the combined contribution of D and the battery to U varies from 0 to $D/4$, having its minimum value when the tap is at either end and its maximum value when the tap is in the middle. If A is properly chosen U will never differ from R by more than $D/8$ as a result of adjustment of D. Hence if D is a relatively low resistance and the changes in R are not large the circuit will never be very far from the matched condition.

---

[2] Frank Wenner, "A principle governing the distribution of current in systems of linear conductors," Proc. Phys. Soc. **39**, 124–43 (1927).

[3] L. Thévenin, "On a new theorem of dynamic electricity," Comptes rendus **97**, 159–61 (1883).

[4] William Littell Everitt, *Communication Engineering*, 2d ed., p. 47 (McGraw-Hill Book Company, Inc., New York, 1937). A very satisfactory discussion of the application of the theorem to a.c. circuits.

If for any reason it is desired actually to measure the power during a transient period it is generally best to observe either E or I but not both. This greatly increases the speed with which observations may be made and it does not require the matched condition to be given up. Whether the supply circuit is complicated or simple, $E_\infty = (R+U)I = E+UI$. Hence if E_∞, U, and E are known I can be calculated or if I is known E can be calculated. This calculation is made of course only for the transient period. During the period of steady heating both E and I are measured in the usual way. To determine E_∞ and U, auxiliary measurements are made in which E and I are observed for a widely different value of R (in this case R is the dummy resistor). These, together with any pair of corresponding values of E and I observed during the period of steady heating, permit both E_∞ and U to be calculated. Since E_∞ and U may change slowly with time, the auxiliary measurements should be made just before or just after the heating period in question.

THE REVIEW OF SCIENTIFIC INSTRUMENTS VOLUME 20, NUMBER 1 JANUARY, 1949

An Accurate Gas Metering System for Laminar Flow Studies[*]

J. W. ANDERSEN AND R. FRIEDMAN[**]
University of Wisconsin, Naval Research Laboratory, Madison, Wisconsin

(Received October 18, 1948)

The design and performance of an accurate flow system utilizing critical velocity orifices is described. Results indicate that an absolute accuracy of three parts in a thousand is realized over a flow range of 0.002 to 2 cubic feet per minute. Calibration of the flow system was accomplished by means of a specially modified and carefully standardized wet test gas meter. Descriptions of the components of the flow system and of subsidiary calibrating equipment are presented.

Critical flow orifice discharge coefficients are found to be independent of the type of gas; however, because of gas impurities, prediction of relative rates of flow of various gases through an orifice by use of theoretical relationships is uncertain, and experimental data are given to illustrate this.

INTRODUCTION

As the prerequisite for a variety of scheduled studies with laminar flames and flowing gases, it was required to design, construct, and calibrate a gas flow system of unusual accuracy. This system was designed to meet the following specifications:

a. be able to handle three separate streams of gas;
b. each stream to have a range from 0.002 to 2 cubic feet per minute;
c. each stream adjustable independent of the others;
d. fluctation-free flow.

Essentially the system includes the following features: sensitive pressure regulators, interchangeable critical flow orifices coupled with ten-foot mercury manometers, and accompanying specially modified calibration equipment.

CONTROL AND INDICATION OF GAS FLOW

A diagrammatic sketch of the flow system is presented in Fig. 1. It is seen that there are three independent and identical lines which converge in a mixing chamber. One of these lines will be discussed in detail.

Gas is reduced to a 100-p.s.i. gauge from a high pressure cylinder by a conventional two-stage regulator. Because of the Joule-Thomson effect, it is necessary to bring the gas back up to room temperature. This is accomplished by an electrical gas heater which utilizes porous bronze disks for efficient heat transfer, the disks also serving as gas filters. A sensitive regulator[1] to

---

[*] This work was undertaken with the support of Bureau of Ordnance Contract NORD 9938, University of Wisconsin, Naval Research Laboratory.

[**] Present address: Westinghouse Electric Corporation Research Laboratories, East Pittsburgh, Pennsylvania.

[1] Nullmatic Regulator, Moore Products Company, Philadelphia, Pennsylvania.

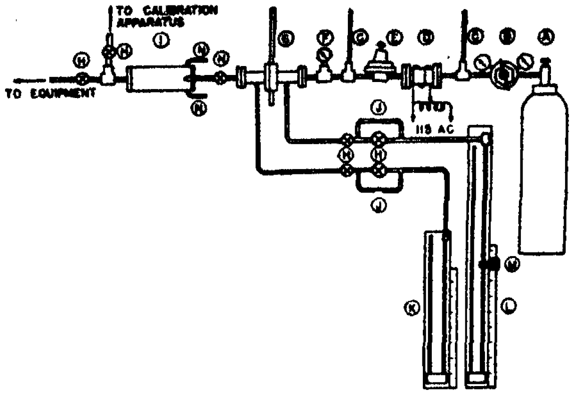

FIG. 1. Diagrammatic sketch of the flow system. A gas cylinder, B reducing valve, C thermometers, D heater, E millmatic regulator, F pressure gauge, G orifice assembly, H stopcocks, I mixing chamber, J constrictions, K four-foot butyl phthalate manometer, L ten-foot mercury manometer, M manometer level indicator, N inputs from flowlines 2 and 3.

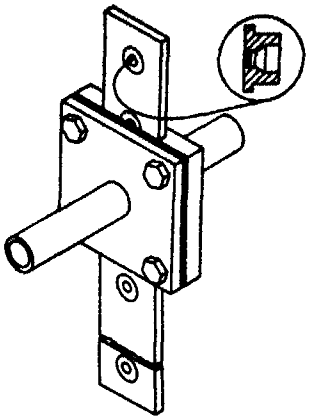

FIG. 2. Orifice assembly and orifice sizes. Jewel sizes (mm): 6/120, 8/120, 12/200, 17/230, 24/230/, 32/230, 44/200, 64/230, 94/260, 110/230. Flow ranges for oxygen (c.f.m.): 0.0023–0.0065, 0.0055–0.016, 0.0080–0.021, 0.016–0.044, 0.032–0.085, 0.057–0.15, 0.10–0.28, 0.22–0.60, 0.27–0.73, 0.50–1.4.

control the upstream pressure to the critical flow orifice[2] is next. The delivery pressure from this regulator is varied from 15 to 56 p.s.i. gauge. Since the flow through a critical flow orifice is directly proportional to the upstream pressure and independent of downstream pressure, as long as the pressure ratio is below the critical (because of sonic velocity at the throat), it follows that the flow rate may be varied 2.8-fold for any one orifice. In order to cover a 1000-fold flow range, a series of ten orifices mounted in a movable steel strip are clamped between rubber-faced flanges, as shown in Fig. 2. The orifice sizes are chosen so as to provide overlapping of ranges. Sapphire cap bearing jewels[3] are used as orifices because they are extremely durable; their contour approximates that of a convergent nozzle, and their use avoids the problem of making extremely small orifices. Diameters of the jewel holes ranged from 6 MM to 110 MM (1 MM = 0.01 millimeter, jewelers' notation).

The pressure on the upstream side of the orifice is measured relative to the atmosphere by means of a ten-foot mercury manometer, the critical portions of which are precision-bore tubing.[4] This permits calculation of pressure from measurement of the lower leg only. The manometer tubes are mounted in a four-inch standard steel channel, the upper and lower ends of the tubes being supported in steel blocks with rubber gaskets, shown in Fig. 3. There is a constriction with a by-pass in the line to the manometer, which guards against blowing out the manometer. A manometer level indicator is shown in Fig. 4. This device may be moved up or down on a 48-inch steel scale and includes a cross-hair with which the mercury level may be measured to 0.01 inch.

Although flow rate is independent of pressure downstream from the orifice, a butyl phthalate manometer is provided to measure this pressure.

To allow for mixing, a heavy-walled cylindrical tube packed with steel wool is provided.

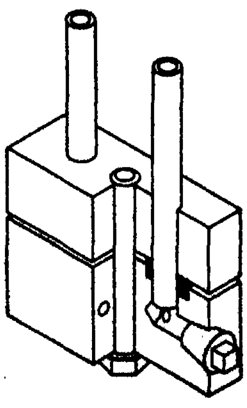

FIG. 3. Manometer foot block.

---

[2] *Fluid Meters, Their Theory and Application*, A.S.M.E. Research Publication (Published by A.S.M.E., 29 West 39th Street, New York).

[3] These were suggested by members of the laboratory of Linde Air Products Company, North Tonawanda, New York, and were procured from Henry Paulson and Company, 37 South Wabash Avenue, Chicago 3, Illinois.

[4] Fischer and Porter Company.

CALIBRATION OF FLOW SYSTEM

1. The Wet Test Meter

An accurate as well as convenient standard was required for the calibration of the thirty orifices in the complete flow system; a wet test meter rated at 50 cubic feet per hour was selected as the most satisfactory device. However, usual operation of the wet test meter does not insure accuracies much better than two percent because of calibration difficulties and maintenance of constant water level. Consequently, the meter was modified in two ways:

a. A method which is capable of measuring the water level to within 0.001″ was installed (Fig. 5). Essentially, an electric circuit was completed when a depth micrometer contacted the water surface in the meter side-arm. The side-arm diameter was increased to 1.5 inches to minimize capillarity. In actual operation the original water level indicator supplied with the meter was lowered approximately $\frac{1}{8}''$ below the surface. Thus, indication of contact with the water by the micrometer was readily accomplished by use of an ohmmeter, the reading dropping sharply from "infinity" to about 10,000 ohms when contact was established.

To insure reproducibility, the meter was rotated at least one complete revolution, always terminating at the zero point on the meter face, and then allowed to drain for five minutes before determining water level. Following this procedure, successive readings were checked to within 0.001 inch. Care must be taken so that the micrometer tip is dry before the determination is made.

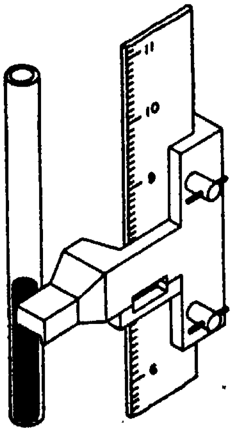

Fig. 4. Manometer level indicator.

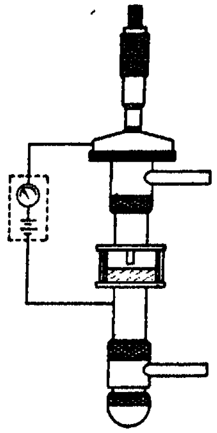

Fig. 5. Wet test meter level indicator.

b. It is obvious that the precautions discussed above must be supplemented by an accurate plumbing of the meter. The spirit level supplied was not sufficiently sensitive, and was replaced by a 12-inch plumb line permanently installed and shielded from drafts by a glass cylinder.

Since the readings of the wet test meter may be affected by the method of calibration, it was decided to calibrate the meter under conditions identical to those used in subsequent orifice calibrations. Thus, while the usual practice of meter calibration is to pass a measured volume of gas slowly through the meter, the initial and final readings being taken with the meter at rest, the system which was constructed is capable of passing through the meter a measured volume of gas at controllable rates of flow up to 0.8 c.f.m., the meter revolving at a constant rate *throughout* the test.

Figure 6 illustrates the system for the calibration of the meter. The sequence of operations is as follows:

a. Saturated air is drawn into the entire system through line *H*.

b. With valves *I* and *J* closed, pressure is applied above distilled water in the fifteen-gallon vessel *B*. Approximately 20 p.s.i. were applied at the higher rates of flow (0.8 c.f.m.).

c. Valve *I* is opened. Water then flows into a four-liter, heavy-walled filter flask. This serves to act as an induction period for the establishment of the rate of flow and elimination of entrained air. During this period the meter reaches a constant rate of rotation.

d. From vessel *C* the water then operates float switch *D*, actuating an electric circuit, thus indicating the instant at which the measured volume begins passing through the meter. This instant is recorded by means of an idler needle which follows the meter pointer until stopped by a solenoid. The circuit is then broken and the idler needle re-engaged.

The needle is stopped again after the water fills the calibrated five-gallon bottle *F* and contacts float switch *E*. After this point the flow may be stopped. By coupling the float switches to a solenoid operated stopwatch, the interval of the run is timed.

It is seen that the primary standard for the entire calibration depends on precise knowledge of the volume of bottle *F*. This volume was determined by weighing the quantity of distilled water required to fill the bottle with the special brass closure clamped in place. Weighings were made on a large analytical balance, and temperature and buoyancy corrections were applied. A drainage correction to account for water left in the bottle from each previous run was made.

Results of the meter calibration showed that there was no detectable change in the calibration factor for rates between 0.1 and 0.8 c.f.m. Therefore it was possible to use the same meter factor "*F*" (ratio of true volume to meter reading) for all flow rates up to 0.8 c.f.m., keeping the water level always constant.

2. Calibration of the Critical Flow Orifices

After the establishment of the wet test meter factor it was possible to calibrate the thirty critical flow orifices with various gases. The theoretical equation governing the behavior of critical flow orifices[2] may be expressed in the following form:

$$w = CA_2p_1[(gMk/RT)(2/k+1)^s]^{\frac{1}{2}}, \tag{1}$$

where w = mass flow rate, C = discharge coefficient, A_2 = orifice cross section, p_1 = upstream pressure, k = specific heat ratio, g = gravitational constant, M = molecular weight, R = gas constant, T = absolute upstream temperature, and $s = (k+1/k-1)$. Upon reduction of Eq. (1) to a convenient set of units, the following result is obtained:

$$V = 3.617CA_2p_1(K/d)^{\frac{1}{2}}, \tag{2}$$

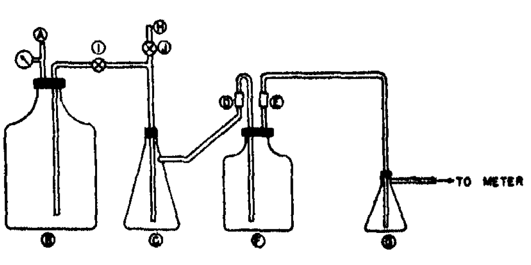

Fig. 6. Calibration system for wet test meter.

where V = volumetric flow rate, cubic feet per minute at 25°C and one atmosphere, A_2 = orifice cross section, square inches; p_1 = upstream pressure, inches of mercury (25°C); d = gas density, pounds per cubic foot at 25°C and one atmosphere; $K = k(2/k+1)^s$.

It may be seen from Eqs. (1) or (2) that the discharge rate is theoretically independent of downstream pressure and varies directly with the absolute upstream pressure. This assumes that the orifice has the proper contour. Independence of downstream pressure was checked experimentally at a pressure ratio of about three to one, and it was found that the rate of discharge did not vary measurably when the downstream pressure was varied ten percent, holding upstream pressure constant. Linear dependence of flow upon upstream pressure was found to hold to within experimental error for all gases over the entire range of orifices.

Since it is difficult to measure with sufficient accuracy the diameter of very small orifices, the product CA_2 should be considered instead of C alone when comparing flows of different gases through the same orifice. Discharge coefficients for the various orifices varied from about 0.8 to 0.95, as calculated from approximate measurements of A_2.

The general plan for the calibration of the thirty orifices with various gases included two phases: the calibration of each orifice with nitrogen, thus obtaining CA_2, and establishment of the ratio of flow of the test gas to that of nitrogen. It will be shown later that C is independent of the gas and that the theoretical formula when properly modified for gas impurities describes relative rates of flow of different gases through a given orifice. Adoption of this procedure materially reduces the labor of the calibration and results in a more flexible flow system.

In actual calibration, discharge rates were corrected to 25°C and one atmosphere by the following formula:

$$V = (rF/\theta)(T_1/T_2)(p_B - p_W/p_B)(p_B/760) \times (298.16/T_1)(T_3/298.16)^{\frac{1}{2}},$$

where V = volumetric flow rate, cubic feet per minute at 25°C and one atmosphere; r = meter reading, cubic feet; θ = time of test, minutes;

TABLE I. Data for the calibration of orifice B-60 (24/230 MM) with nitrogen.

p In. Hg. (abs.)	V (c.f.m.) 25°C, 1 atmos.	Deviation of V from the best straight line through the data: $P_1=0.0005460$ V	Deviation (%)
140.57	0.07679	+0.00004 c.f.m.	+0.05
128.27	0.06999	−0.00005	−0.07
116.23	0.06349	+0.00003	+0.05
104.06	0.05692	+0.00010	+0.18
92.16	0.05030	+0.00004	+0.08
80.02	0.04364	−0.00005	−0.11
68.12	0.03710	−0.00009	−0.24
			Av. = 0.11

F = meter factor = ratio of true volume to meter reading; T_1 = temperature of gas entering meter, degrees Kelvin; T_2 = temperature of meter, degrees Kelvin; T_3 = temperature of gas entering orifice, degrees Kelvin; p_B = barometric pressure, millimeters of mercury (25°C); and p_W = vapor pressure of water at T_1, in millimeters of mercury.

The calibrations were performed by saturating with water vapor just before the gas passes through the meter; hence the formula corrects back to dry gas.

CRITICAL DISCUSSION OF PERFORMANCE

The limiting accuracy of each of the steps in the calibration is as follows:

1. *Calibrated bottle.* The volume was measured four times, the mean deviation from the average value being 2.5 parts in 10,000.

2. *Meter calibration.* (a) Precision of calibration. Sixteen runs were made under nearly identical conditions. The mean deviation from the average value of the meter factor was 2.0 parts per thousand. (b) Water level. The water level could be reproduced to within 0.001 inch. This variation causes a change in the calibration factor of 1.5 part in 10,000.

3. *Orifice calibration with nitrogen.* A given orifice was tested seven times with nitrogen, the mean deviation from the best straight line through the data and the origin being one part in a thousand, when flow rate is plotted against pressure. This includes errors caused by meter reading, meter timing, pressure fluctuation, and pressure measurement. (All runs were made of such length that the number of meter revolutions was an integer.) In order to illustrate the caliber of data which may be obtained, a calibration run is given in Table I.

TABLE II.

Test gas	Av exp. ratio: flow rate of test gas / flow rate of nitrogen	Theoretical ratio: flow rate of test gas / flow rate of nitrogen	Difference rel. to exp. (%)
Nitrogen	1.0000	1.0000	—
Oxygen	0.9349	0.9344	−0.05
Air	0.9908	0.9852	−0.57
Hydrogen	3.666	3.736	+1.91
Helium	2.616	2.806	+7.27
Argon	0.8770	0.8883	+1.29
Carbon dioxide	0.7960	—	—

4. *Orifice calibration with different gases.* Flow rates of seven different gases were measured through each of six orifices varying in diameter from 0.06 to 0.64 millimeter. For nitrogen, oxygen, hydrogen, and argon, each of the results presented in the table below is an average of about thirty independent runs with that gas. For air, helium, and carbon dioxide, each of the values is an average of ten independent runs. The value which best represents the mean deviations of these sets of data is three parts per 1000. No trends in the ratio of flow rate of any given gas to the flow rate of nitrogen (through the same orifice) were observed. It follows that the flow rate ratio is independent of orifice size within the limits studied (see Table II).

The theoretical values were calculated with Eq. (2), assuming that the discharge coefficient C is independent of the type of gas, and using molecular weight M and heat capacity ratio k on the assumption that the gases were perfectly pure. It will be observed from the above table that there are discrepancies between theoretical and experimental values. In the cases of helium and hydrogen, these discrepancies can be explained by a consideration of the reported purity of the gases:

Nitrogen	99.7=0.1%
Oxygen	99.5=0.1%
Hydrogen	99.5=0.1%
Helium	98.2% min.
Argon	99.8% min.
Carbon dioxide	99.5% min.

Assuming that the impurity is always nitrogen, the theoretical ratios may be corrected by computing molal averages of M and k. It is to be noted that the mixture molecular weight of hydrogen or helium would be particularly sensitive to a relatively high molecular weight impurity, such as nitrogen. Unfortunately, since exact analyses of the gases are not available, and vigorous averaging procedures are not thoroughly understood, detailed correction calculations are not presented, but preliminary calculations indicate that application of such corrections would probably make the theoretical and experimental ratios indentical.

It may be concluded that the discharge coefficients are in actuality independent of the type of gas, and that the theoretical equation (2) would correctly describe the dependence of flow rate upon molecular weight and heat capacity ratio for pure gases.

THE REVIEW OF SCIENTIFIC INSTRUMENTS VOLUME 20, NUMBER 1 JANUARY, 1949

Optical Properties of Surface Films. II[*]

ALEXANDRE ROTHEN AND MARJORIE HANSON
Laboratories of The Rockefeller Institute for Medical Research, New York, New York

(Received July 9, 1948)

Measurements of ellipticity of light reflected from a film-coated metal surface have been made for films varying in thickness from 25 to 40,000A. It was found that the approximate formulas of Drude which express as a function of the film thickness the ratio and phase difference of the components vibrating in the plane of incidence and perpendicular to it are valid for thin films. The general formula of Drude expressing the phase shift as a function of the film thickness represents with a fair approximation the experimental results obtained with metallic slides coated with films of Ba stearate whose thickness is up to the order of the wave-length of light. Thus, for the first time, Drude's theoretical formulation has been verified experimentally. For films whose thickness is many times the wave-length of the light used, there is a progressive divergence from Drude's general formula, the cause of which can possibly be due to the birefringence of the films which has been neglected in this work.

Thin Films

THE first attempt to correlate the change in ellipticity of reflected light with the thickness of thin films was made by Drude more than fifty years ago.[1] Since then various formulas have been developed, but the only ones which can be submitted to a practical test are those derived by Drude himself and some of the subsequent modifications of his original formulas.[2,3] In the form in which they are given, Drude's formulas are first approximations, valid only for films whose thickness is small compared to the wave-length of light. When the technique for the deposition of thin films of known thickness was developed, mainly by Langmuir and Blodgett,[4] these formulas could be checked with experimental data. Tronstad[2] was the first to verify them using monomolecular films of fatty acids deposited on a mercury surface. He found close agreement between calculated values and the length of the fatty acid chains.

When a beam of light is linearly polarized at 45° to the plane of incidence it becomes ellipitically polarized on reflection from a metallic surface, and the presence of a film on the metal alters the ratio ψ of the electric vectors vibrating in the plane of incidence and perpendicular to it, as well as their difference of phase Δ. Drude's formulas correlate the parameters ψ and Δ, with the optical thickness of the layer, the angle of incidence ϕ, and the optical constants of the metal. Since these optical constants depend to some extent on the condition of the metallic surface, it was desirable to determine the optical constants of the same stainless steel slides that were used for the deposition of the layers in our experiments.

DETERMINATION OF THE OPTICAL CONSTANTS OF STAINLESS STEEL SLIDES

The optical constants ν and κ correlated to the complex index of refraction $n=\nu(1-i\kappa)$ can be calculated from the equations

$$\nu=\sin\bar{\phi}\tan\bar{\phi}\cos 2\bar{\psi} \quad\text{and}\quad \kappa=\tan 2\bar{\psi}.$$

---

[*] See Part I, Rev. Sci. Inst. 19, 839 (1948).

[1] P. Drude, Ann. d. Physik und Chemie 36, 865 (1889).

[2] L. Tronstad, Trans. Faraday Soc. 31, 1151 (1935).

[3] F. A. Lucy, J. Chem. Phys. 16, 167 (1948).

[4] K. B. Blodgett and I. Langmuir, Phys. Revs. 51, 964 (1937).

TABLE I.

Angle of incidence	49.2°	69.2°	74.2°
ψ'	38.6_5°	32°	29.3°
Δ'	160.5°	127°	109.8°
$\psi-\psi'(l=24.4\text{A})$	0.00°	0.34°	0.61°
$\Delta-\Delta'(l=24.4\text{A})$	1.37°	3.6°	3.55°

In these equations $\bar{\phi}$ is the angle of principal incidence, i.e., the angle at which metallic reflection brings about a phase shift of 90° between the components vibrating in the plane of incidence and perpendicular to it. The principal azimuth $\bar{\psi}$ is the ratio of the two components after reflection at this angle.

To determine $\bar{\phi}$ the $\lambda/4$ plate of the ellipsometer is set in the two positions in which its principal directions are perpendicular and parallel to the plane of incidence, and in each position the angle of incidence is found for which the light is again linearly polarized after compensation. If the plate is exactly $\lambda/4$, this angle is the same for both positions. With most plates, however, two different values are obtained, and the true angle of principal incidence may be taken as halfway between these values if the $\lambda/4$ plate is not too far from 90°.

To determine $\bar{\psi}$, the light is reflected at the true angle of principal incidence and the resulting ellipse analyzed by adjusting the $\lambda/4$ plate and analyzer simultaneously to produce complete compensation. From the experimental value of θ thus obtained and the known value of δ, the ellipticity ϵ can be calculated according to Eqs. (1) and (3) of the previous section.* The ellipticity in this case is identical to the principal azimuth $\bar{\psi}$.

For the stainless steel slides used, the following values were found:

$$\bar{\phi}=77.5°, \quad \bar{\psi}=28°,$$

from which

$$\nu=2.46, \quad \kappa=1.48.$$

Drude's Formulas

Drude's formulas express as a function of the film thickness the ratio and phase difference of the components vibrating in the plane of incidence and perpendicular to it. They are

$$2\psi-2\psi'=\sin 2\psi'\frac{4\pi}{\lambda}\frac{\cos\phi\sin^2\phi\,\alpha'}{(\cos^2\phi-\alpha)^2+\alpha'^2}\times(1-n_1^2\cos^2\phi)\left(1-\frac{1}{n_1^2}\right)l,$$

$$\Delta-\Delta'=\frac{4\pi}{\lambda}\frac{\cos\phi\sin^2\phi(\cos^2\phi-\alpha)}{(\cos^2\phi-\alpha)^2+\alpha'^2}\left(1-\frac{1}{n_1^2}\right)l,$$

where ψ' and Δ' are the values of ψ and Δ where there is no film, ϕ is the angle of incidence, n_1 the index of refraction of the film of thickness l, and α and α' two constants obtained from ν and κ by

$$\alpha=\frac{1-\kappa^2}{\nu^2(1+\kappa^2)^2}, \quad \alpha'=\frac{2\kappa}{\nu^2(1+\kappa^2)^2}.$$

From the above given values of ν and κ for the metal used, $\alpha=-0.0193$, $\alpha'=0.0479$.

The simplest way to test Drude's formulas would be to determine the position (β) and ellipticity (ϵ) of the ellipse characterizing the reflected light for one given film thickness and from these two parameters to calculate the values ψ and Δ to be compared with the theoretical ψ and Δ. This procedure would not make the best use of the ellipsometer which is most sensitive as a differential instrument with a half-shadow arrangement. Therefore, the experimental procedure was as follows. The light before reflection vibrated linearly at 45° in the second and fourth quadrant for an observer looking toward the light. The $\lambda/4$ plate was placed so as to compensate with its fast axis in the first and third quadrant. The positions of the analyzer and the $\lambda/4$ plate for maximum

TABLE II. Ellipticity of light reflected from slides coated with 1, 3, 5, and 7 monolayers of Ba stearate. (Calculated from Drude's formulas.)

Monolayers Ba stearate	Incidence	ϵ	β	$\lambda/4$	ϵ'	β'
1	49.2	10.3	38.3	38.3	0.2	−10.3
1	69.2	24.5	24.7	25.9	0.9	−24.4
1	74.2	28.2	13.0	9.9	3.7	−28.2
3	49.2	11.6	38.2	38.3	0.2	−11.7
3	69.2	27.5	22.4	25.9	−0.1	−27.6
3	74.2	30.6	8.4	9.9	1.36	−30.7
5	49.2	12.9	38.1	38.3	0.15	−13.0
5	69.2	30.4	18.9	25.9	−1.2	−30.8
5	74.2	32.0	2.04	9.9	−1.1	−32.8
7	49.2	14.2	37.7	38.3	0.5	−14.1
7	69.2	32.9	13.8_5	25.9	−2.5	−34
7	74.2	33.5	−6.2	9.9	−3.8	−35.3

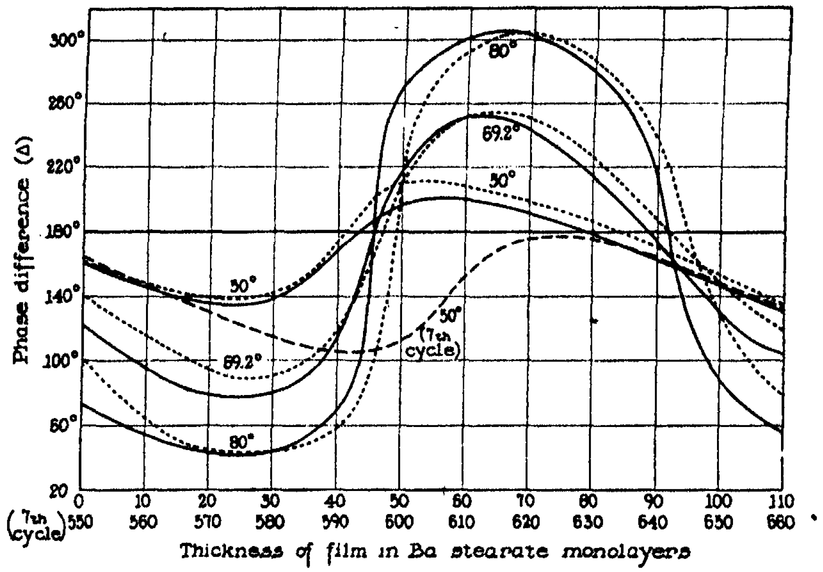

FIG. 1. Phase shift produced by films of Ba stearate at 50°, 69.2° and 80° incidence. The dotted curves are theoretical, and the solid lines and the dashed line are experimental.

extinction were determined for reflection from clean uncoated metal slides at incidence of 49.2°, 69.2°, and 74.2°. The values of ψ' and Δ' determined from these positions are given in Table I. The error involved in a reading of this kind can be neglected here, as ψ' and Δ' are to be used as references to obtain differential values. Then slides were covered with one and three monolayers of Ba stearate as previously described, and the position of the analyzer read for which both half-fields appeared of the same intensity, the position of the $\lambda/4$ plate being so chosen to produce good compensation of both ellipses. Additional layers of Ba stearate were successively deposited on the slide and the corresponding analyzer positions for matching half-fields were read, the $\lambda/4$ plate position remaining unchanged. It remained to check these analyzer positions with those that should be obtained if the reflected light obeys the theoretical formulas. For the above angles of incidence the values of $\Delta-\Delta'$ and $\psi-\psi'$ were calculated from Drude's formulas for one monolayer of Ba stearate ($l=24.4$A, $n=1.495$) and are given in Table I. The values for more than one monolayer are the corresponding multiples of these. From these theoretical values the corresponding ellipses of orientation β and ellipticity ϵ were calculated as well as the theoretical ellipses of small ellipticity resulting when the light goes through the $\lambda/4$ plate of known position and phase retardation. The results have been summarized in Table II. ϵ and ϵ' are the ellipticities of the reflected light before and after going through the $\lambda/4$ plate (85.3° retardation), respectively. The angles from the fast direction of the plate to the perpendicular to the plane of incidence are tabulated under the heading $\lambda/4$. The value of β corresponds to the angle from the major axis of the ellipse of ellipticity ϵ to the perpendicular to the plane of incidence. The values of β' are the angles from the major axis of the ellipses ϵ' to the fast direction of the $\lambda/4$ plate.

These two ellipses of small ellipticity resulting from the compensation of the light reflected from the half-fields which differ in thickness by 49A can be made of equal ellipticities and of opposite sign by proper adjustment of the $\lambda/4$ plate. In this case, the direction transmitted by the analyzer, when both half-fields appear of the same intensity, would be the bisector of the angle made by the minor axis of the ellipses. However, since for successively thicker films the $\lambda/4$ position remains unchanged in actual practice, the direction indicated by the analyzer for equal illumination does not bisect the angle made by the axis but is nearer to the minor axis of the ellipse with the greater ellipticity. The position of optical equilibrium can be calculated from

$$\sin^2\epsilon_1\cos^2\alpha_1+\cos^2\epsilon_1\sin^2\alpha_1=\sin^2\epsilon_2\cos^2\alpha_2+\cos^2\epsilon\sin^2\alpha_2$$

with the condition $\alpha_1+\alpha_2=\alpha$, where α is the angle made by the axes of the two ellipses with ellipticities ϵ_1 and ϵ_2; α_1 and α_2 are the angles from position of equilibrium to the respective axis of the ellipses. This formula reduces to $\sin^2\epsilon_1+\sin^2\alpha_1=\sin^2\epsilon_2+\sin^2\alpha_2$ for small values of α.

Using the calculated values of ϵ' and α' for the theoretical ellipses the positions of the analyzer corresponding to equal illumination for half-fields covered with one and three, three and five, five and seven monolayers were calculated to be 25.9°, 29.3°, and 33.2° for an angle of incidence of 69.2°. Therefore, the calculated angle by which the analyzer should be rotated when one double layer of Ba stearate is deposited on an optical gauge of one and three monolayers is 3.4°. The experimental value is 3.2°. However, it was also found experimentally that the ratio $\Delta\alpha/\Delta N$, N being the number of layers of Ba stearate deposited on an optical gauge, diminishes linearly with the increase in N for the $\lambda/4$ position used and the value $\Delta\alpha/\Delta N$ extrapolated for $N=0$ was 3.4° in perfect agreement with the theoretical value calculated from Drude's formulas. For a film thickness of 50A the experimental value $\Delta\alpha/\Delta N$ is 7 percent smaller than the calculated one, and this difference increases for thicker films.

At an angle of incidence of 49.2°, $\Delta\alpha/\Delta N = 1.3_5°$ (calculated) compared to $\Delta\alpha/\Delta N = 1.4°$ to 1.25° (experimental) depending on whether the double layer was deposited on an optical gauge of one to three layers or seven to nine layers. In other words, at this angle of incidence the experimental values $\Delta\alpha/\Delta N$ vary much less with N than at higher angles of incidence. At 74.2° incidence the following values were obtained for a double layer deposited on a gauge of one to three layers. $\Delta\alpha/\Delta N = 4.9$ (calculated); $\Delta\alpha/\Delta N = 4.5$ (experimental). These results show that Drude's formulas represent the experimental data well. The formulas not only give the right values for the ellipticity at one particular angle of incidence but also describe correctly the variations of the ellipticity as a function of the angle of incidence. At 49° incidence the experimental values remain in good agreement with the theoretical ones up to film thicknesses of about 250A.

Thick Films

Thus, Drude's formulas fit remarkably well the experimental values of the change in ellipticity of reflected light produced by thin films of known thickness. On the other hand, these formulas are first approximations and cannot be expected to hold when the thickness of the film is not small compared to the dimension of the wave-length used. Calibration curves[5] show that the angle $\Delta\alpha/\Delta N$ by which the analyzer has to be turned when a few successive double layers of Ba stearate are deposited, decreases with the number of double layers N, thus showing the beginning of a deviation from Drude's formulas. It was, therefore, of interest to determine the ellipses resulting from reflection when the thickness of the film varied from a few hundred angstroms up to several times the wave-length of the light used.

Experiments were carried out in which successive double layers of Ba stearate were deposited on an optical gauge of one and three monolayers. The ellipses characterizing the light reflected from these films were determined at three different angles of incidence, the readings being made by adjusting both the $\lambda/4$ plate and the analyzer to obtain a position of maximum uniform darkness. Each value obtained with this method is intermediate between those which would be found if accurate readings could be made of each half-field separately.

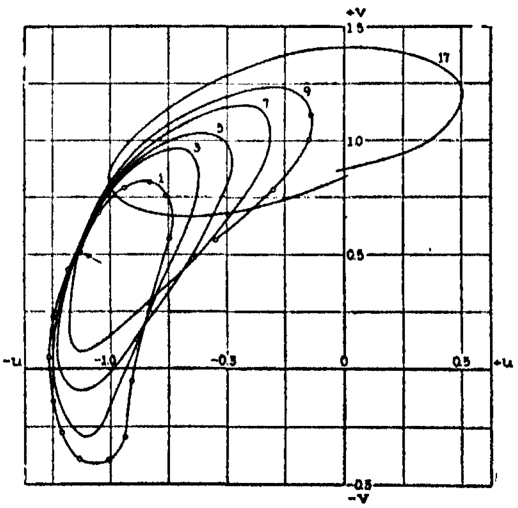

FIG. 2. Ellipticity of reflected light at 50° incidence produced by films of Ba stearate from 0 A up to the equivalent of 17 wave-lengths of light (λ5893). Arrow indicates beginning of the first cycle. All cycles are described clockwise.

---

[5] A. Rothen, Rev. Sci. Inst. **16**, 26 (1945).

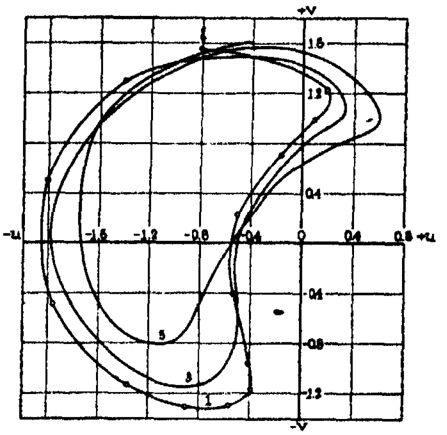

FIG. 3. Ellipticity of reflected light at 69.2° incidence, produced by films of Ba stearate from 0 A up to 5 wave-lengths of light. Arrow indicates beginning of first cycle.

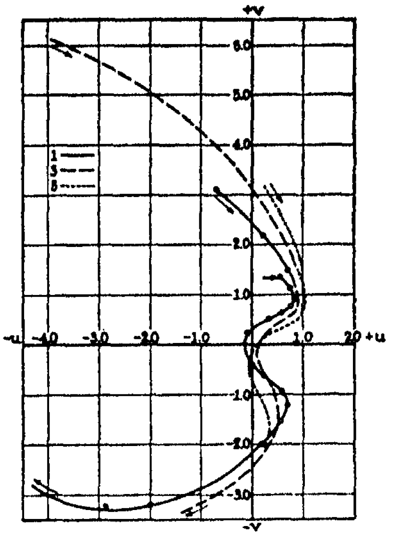

FIG. 4. Ellipticity of light at 80° incidence, produced by Ba stearate films from 0 A up to 5 wave-lengths of light. The described cycles are not closed on account of the rapid change of phase for certain critical thicknesses (45 monolayers for the first cycle) where half of the cycle is described *in a few monolayers of Ba stearate.*

The experimental values of the phase shift Δ between the components parallel and perpendicular to the plane of incidence as a function of the thickness of the film are represented in Fig. 1. The calculated number of monolayers of Ba stearate which produce a path difference of one wave-length of Na D light at the angles of incidence of 50°, 69.2°, and 80° are 93.3, 102.5, and 105, respectively. These figures compare favorably with the experimental values which show that the periods are completed at thicknesses of 92.5, 102.2, and 105 monolayers. Two curves have been plotted to represent the results at 50° incidence. The lower curve was obtained when the slide was coated with 550 to 650 monolayers of Ba stearate, thus representing the seventh complete period. It is to be noticed that this curve is displaced laterally and vertically, a fact which will be discussed later on.

In looking for a theoretical basis for the above experimental curves, it can be noted that Drude's approximate formulas for the light reflected from these films can be obtained from a general equation which should apply to films of any thickness on a reflecting surface. Drude showed that the ratio of the components before (I) and after reflection (R) of the light vibrating either in the plane of incidence (OP) or perpendicular to it (OS) can be quite generally expressed by

$$\frac{R}{I}e^{i\delta}=\frac{r_f+r_m e^{-(4\pi itn\cos\phi/\lambda)}}{1+r_f r_m e^{-(4\pi itn\cos\phi/\lambda)}},$$

where δ is the phase shift, r_f and r_m the Fresnel coefficients representing the amplitudes and phase shift of the components after reflection from the film (r_f) and the metal (r_m), t the thickness of the film, n its index of refraction, and ϕ the angle of refraction in the film. In the case dealt with in our experiments, that of a transparent film deposited on a metal slide, r_m is complex but both r_f and n are real. It also results from the experimental conditions that the incident components perpendicular (OS) and parallel (OP) to the plane of incidence are equal and in phase. Thus, the determined ratio ψ or OP/OS as well as the phase difference Δ produced by reflection from the coated slide is given by

$$tg\psi e^{i\Delta}=\frac{(r^p{}_f+r^p{}_m e^{-ix})(1+r^s{}_f r^s{}_m e^{-ix})}{(1+r^p{}_f r^p{}_m e^{-ix})(r^s{}_f+r^s{}_m e^{-ix})} \qquad (1)$$

when x stands for $(4\pi t/\lambda)n\cos\phi$.

Formula (1) shows that the change of phase is a periodical function of x, a period being completed when the film thickness is such that the optical path difference between the rays reflected from the film and from the metal is equal to one wave-length of light. This formula can be developed as was done by Vasicek[6] in the case of glass reflection. The only difference is that the coefficients r_m are complex and can be represented by $r^{p,s}=X^{p,s}+iY^{p,s}$.

---

[6] A. Vasicek, J. Opt. Soc. Am. 37, 145 (1947).

After separating the imaginary from the real quantities one obtains for the phase difference brought about by film coated metal slides

$$tg\Delta=\frac{AB'+A'B}{AA'-BB'} \tag{2}$$

where

$$A=r_f^p[1+X^{p^2}+Y^{p^2}]+X^p[1+r_f^{p^2}]\cos x + Y^p[1+r_f^{p^2}]\sin x$$

$$A'=r_f^s[1+X^{s^2}+Y^{s^2}]+X^s[1+r_f^{s^2}]\cos x + Y^s[1+r_f^{s^2}]\sin x$$

$$B=-X^p[1-r_f^{p^2}]\sin x+Y^p[1-r_f^{p^2}]\cos x$$

$$B'=X^s[1-r_f^{s^2}]\sin x-Y^s[1-r_f^{s^2}]\cos x.$$

The coefficients $r_f^{p,s}$ are calculated from the Fresnel equations. The quantities $X^{p,s}$, $Y^{p,s}$ are related to the phase shifts δ^p and δ^s (abbreviated $\delta^{p,s}$) and the corresponding amplitudes ρ^p and ρ^s (abbreviated $\rho^{p,s}$) of the components after reflection from an uncoated metal surface by the following formulas

$$tg\delta^{p,s}=(Y^{p,s}/X^{p,s}),\quad \rho^{p,s}=(X^{p,s^2}+Y^{p,s^2})^{\frac{1}{2}}.$$

The quantities $\delta^{p,s}$ and their difference $\delta^p-\delta^s$ as well as $\rho^{p,s}$ can be computed from the optical constants of the clean metal surface by means of equations which can be found, for instance, in the Handbuch der Physik, Volume 20, page 242. It appears from (2) that the phase change Δ is not a sinusoidal function of x since it involves a ratio of polynomials containing not only $\sin x$ and $\cos x$ but also $\sin x \cos x$, $\sin^2 x$ and $\cos^2 x$ terms, in other words, terms corresponding to a periodicity of $2x$. When the calculations were carried out the calculated $\Delta=f(x)$ was in remarkable agreement with the experimental curves (see Fig. 1). Thus the validity of Eq. (1) has been demonstrated for the first time experimentally for transparent films of known thicknesses from a few A up to a wave-length of light.

Further experimental data was obtained for film thicknesses up to 40,000A. The method of Poincaré was adopted for condensed graphical representation of these series of ellipses. Since an ellipse is completely characterized by the ratio of two components and their phase shift, it can be represented on the complex plane by a single point $u+iv$ of modulus $\cot\psi$ and argument Δ. The rectangular coordinates of each point are therefore

$$u=\cot\psi\cos\Delta,\quad v=\cot\psi\sin\Delta,$$

and $u+iv=\cot\psi e^{i\Delta}$.

With this representation all points on the u axis correspond to linear vibrations whereas all points on the v axis correspond to ellipses whose axis are oriented along OS and OP. The points $u=0$, $v=\pm1$ are two circular vibrations of opposite sense. The results obtained at 50°, 69.2°, and 80° have been summarized in Figs. 2 to 4. The points indicated on the initial cycles correspond to thickness intervals of 146A (six monolayers of Ba stearate). From the positions of these points it can be seen that the rate at which the cycle is described is not uniform. This is another way of saying that $\delta\Delta/\delta N$ and $\delta\alpha/\delta N$ are not constant over the period. According to formula (1) the successive cycles (corresponding to one wave-length of light) should be identical. It is especially evident from the results obtained at 50° incidence that the cycles do not superimpose. Each cycle does correspond to an optical thickness of one wave-length of light but the successive cycles precess clockwise around the origin as the approximate center of rotation. The seventh cycle (corresponding to thicknesses from 558 to 650 monolayers of Ba stearate) has rotated by about 60°. Thus, there is a second periodicity on top of the one which corresponds to an optical path difference of one wave-length

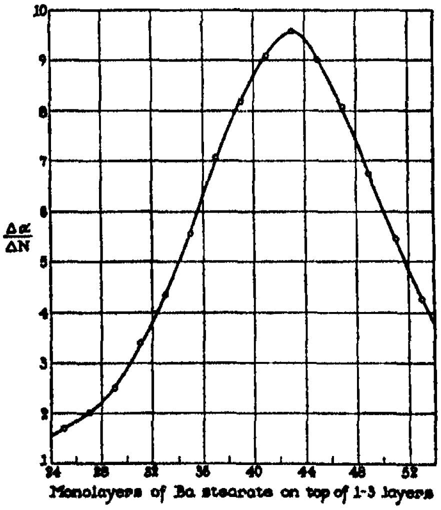

FIG. 5. Calibration curve for 24 to 52 monolayers of Ba stearate, with the fast direction of the λ/4 plate turned 20° counterclockwise from the perpendicular to the plane of incidence.

and this progressive shift affects both ψ and Δ. At 50° incidence the seventh cycle does not cross the u axis (Fig. 2). In other words, the phase shift is never greater than 180°. This can also be observed on the curve of Fig. 1. The precession cannot be predicted from the formula (1). It may be due, however, to the birefringence of the film which has hitherto been neglected. It is known that Ba stearate films are positive uniaxial crystals with indices $n_0=1.491$ and $n_e=1.550$.[3] It was found impossible to build up enough layers to complete the larger period to see whether a cycle would be obtained having the same orientation as that of the first one (0 to 92 layers).

From the practical aspect of the measurement of film thickness, the curves of Fig. 1 exhibit some very interesting facts. A calibration curve[6] is the plot of the position α of the analyzer for equal illumination of both half-fields against the thickness of the film for a fixed position of the $\lambda/4$ plate. In general, the change in phase shift per layer is such as to exert more influence on the orientation of the re-established light than does the change in ψ, so that the analyzer reading shows greatest sensitivity $\delta\alpha/\delta N$ when the change of phase shift $\delta\Delta/\delta N$ is greatest. N is the thickness of the film expressed in double layers of Ba stearate. At 69.2° incidence for a film under 100A thick, $\delta\Delta/\delta N\sim 6°$ and $\delta\alpha/\delta N\sim 3°$. In other words, the analyzer has to be turned 3° for a variation in thickness of 48A. However, $\delta\Delta/\delta N\sim 24°$ and $\delta\alpha/\delta N\sim 9.6°$ when the thickness of the film is about 45 monolayers of Ba stearate. For the same range of thickness at 80° incidence, $\delta\Delta/\delta N\sim 96°$ and $\delta\alpha/\delta N\sim 14°$. It is thus apparent (see Fig. 1) that the range of maximum sensitivity of the apparatus occurs for thicknesses of the order of 45 monolayers of Ba stearate. For thicknesses from 70 to 100 monolayers the sensitivity is still large, although less on account of the skewness of the curve. Finally, there are regions where the sensitivity is very small ($\delta\alpha/\delta N\rightarrow 0$) for thicknesses from 20 to 30 or 55 to 65 monolayers. The plot $\delta\alpha/\delta N$ for N extending from 24 to 55 layers at 69.2 incidence can be seen in Fig. 5. Since with the half-shadow arrangement analyzer positions can be obtained within ±0.02° the maximum sensitivity expressed in terms of thickness of film can then be calculated: $49\times 0.02/9.6=\pm 0.1$A.

Another practical aspect worth considering is the range of thickness which can be determined with a single $\lambda/4$ plate position. Obviously, if the orientation of the ellipses (β) did not change, a single calibration curve could express any range of thicknesses. This condition would be fulfilled if the ratio of the components parallel and perpendicular to the plane of incidence were always one ($tg\psi=1$). All the ellipses would then have their major and minor axis oriented at 45° to the plane of incidence. This condition is approached only as the angle of incidence is decreased. However, on account of the condition $tg2\beta=tg2\psi\cos\Delta$ it can be seen that when $\cos\Delta$ and $tg2\psi$ vary in opposition directions with the increase of the thickness of the film then ($\delta tg2\beta/\delta N$), is small, and the range of the calibration curve is wide.

If the $\lambda/4$ plate does not produce an exact 90° phase shift, some interesting effects are produced. In order to fully compensate an ellipse with such a plate (see part I) its principal directions make an angle β_1 with the axis of the ellipse. In this case even when the orientation remains constant the plate has to be turned if the ellipticity changes, in order to satisfy the equation $\sin 2\beta_1 = (tg2\epsilon/tg\delta_1)(\delta_1=$ phase shift produced by the plate). It may happen that the angle ($\delta\beta_1$) by which the approximate $\lambda/4$ plate should be turned on account of a change in ellipticity may be compensated by the rotation ($\delta\beta$) of the ellipse produced by a change in Δ or ψ or both. In this case the range of thickness covered by a single calibration curve is extended. Because of a combination of this effect and the one described in the preceding paragraph, it was possible to cover a range of thickness from 1500A to 2740A in one calibration curve. The value of the plate used in this case was 76.7°.

SUMMARY

Measurements of ellipticity of light reflected from a film coated metal surface have been made for films varying in thickness from 25 to 40,000A.

It was found that the approximate formulas of Drude are valid for thin films and that the general formula expressing the phase shift as a function of the film thickness represents with a fair approximation the experimental results obtained with films whose thickness is of the order of the wave-length of light.

THE REVIEW OF SCIENTIFIC INSTRUMENTS VOLUME 20, NUMBER 1 JANUARY, 1949

Sampling Devices for Determining the Bacterial Content of Air

MATTHEW LUCKIESH, A. H. TAYLOR, AND THOMAS KNOWLES
Lighting Research Laboratory, General Electric Company, Nela Park, Cleveland, Ohio

(Received September 20, 1948)

Appraisal of air contamination by micro-organisms which are responsible for infectious diseases or result in spoilage of products requires devices for sampling the air to determine bacterial content. The simplest technique involves the use of open petri dishes containing culture media upon which colonies of the organisms can grow. However, quantitative data require the use of devices which will sample the bacterial content of definite volumes of air.

Air samplers which yield quantitative data may be roughly divided into bubbler and impinger types. In the former type a definite quantity of air, with or without atomization, is bubbled through water, thus collecting a large part of the organisms. In the impinger types the organisms are deposited on the culture medium, either by use of high linear velocity of the air or by application of an electrostatic field.

The authors have developed two types of impinger samplers. One of these, weighing approximately 12 pounds, employs an electrostatic field of about 7000 volts. It can be used wherever 110–120-volt, 60-cycle current is available. The other sampler, called a duplex radial-jet air sampler, uses a high velocity air flow to impinge the organisms on the culture medium. Examples of the use of the latter sampler in important laboratory studies are described and typical experimental results are presented.

MODERN air sanitation has for one of its objectives the reduction of air-borne micro-organisms which may be instrumental in the spread of infectious diseases or the contamination of foodstuffs and other products. The oldest and most commonly used method is ventilation, replacing contaminated indoor air with relatively fresh outdoor air. In the past decade two other methods have been introduced; *viz.*, the use of germicidal vapors and air irradiation with ultraviolet of the wave-length λ2537 which is highly destructive to such organisms.

The appraisal of air contamination and its improvement by air sanitation procedures necessitates the use of some method of air sampling which will indicate the concentration of air-borne micro-organisms. This usually involves the collection of the organisms directly onto a culture medium upon which colonies of the organisms will grow, or else their collection in a liquid by bubbling the air through it and incorporating a portion of this liquid in a culture medium. Since no single culture medium will grow all types of the organisms which may be collected, it is never possible to determine accurately the total concentration of such organisms in the air. By proper choice of the culture medium, the concentration of specific types can be determined.

Many air-sampling methods and devices have been developed and used. The simplest of these is the exposure of open petri dishes, containing a culture medium, in the air to be sampled. Since only the heavier particles in the air will settle out, and since air currents disturb the natural settling due to gravity, this method is selective in its results and is erratic and inefficient. Furthermore, the results cannot be related to a definite quantity of air. Some droplet nuclei may be so small that they will never settle out.[1]

Air sampling devices fall generally into two distinct classes, impinging and washing or

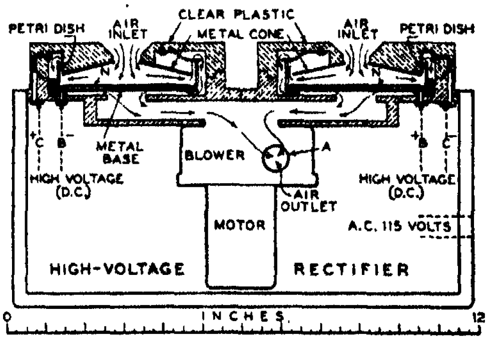

FIG. 1. Diagrammatic sketch of the Luckiesh-Holladay-Taylor electrostatic bacterial air sampler. Air entering the sampler is subjected to an electrostatic field (7000 volts) which increases in intensity towards the edges of the petri dish, as a result of the shorter spacing of the electrodes.

---

[1] E. B. Phelps and L. Buchbinder, "Studies on micro-organisms in simulated room environments. I. A study of the performance of the Wells air centrifuge and of the settling rates of bacteria through the air," J. Bact. **42**, 321 (1944).

bubbling devices. In the impinging types the air-borne organisms are collected on the culture medium by impingement from air moving at fairly high linear velocity, or by use of an electrostatic field to attract charged particles to the culture medium. In the bubbling devices the air is drawn through water in such a way that fine air bubbles are formed, it being assumed that most of the organisms will be collected by and remain in the water. In one sampler[2] the air passes through an atomizing chamber before passing through water.

One of the earliest samplers operating on the impingement principle was the Wells air centrifuge.[3] It employs a rotating glass cylinder, the inside walls being coated with the nutrient material upon which the organisms grow colonies. The organisms in the air drawn through the sampler are impinged, by centrifugal action, upon the walls of the cylinder which is rotating at high speed.

The United States Public Health Service has made an extensive study of the above two sampling devices and six other types.[4] That study showed that the highest bacterial counts are obtained with the bubbler and atomizer-bubbler types of samplers. The most plausible explanation for this finding is the theory that the micro-organisms are carried in the air in

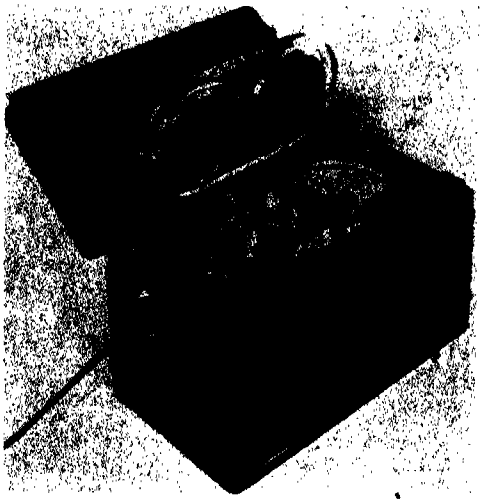

FIG. 2. Photograph of the present model electrostatic bacterial air sampler.

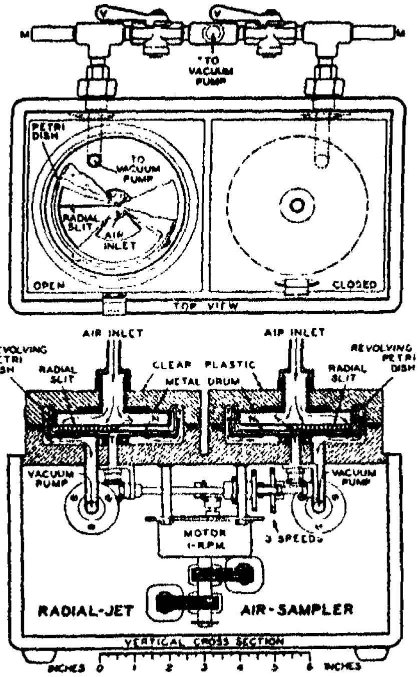

FIG. 3. Diagrammatic sketch of the duplex radial-jet air sampler which has two identical sampling units. The petri dish with culture medium rotates slowly below a stationary radial slit, visible in the open lid, through which air issues at high velocity, impinging the micro-organisms on the culture medium.

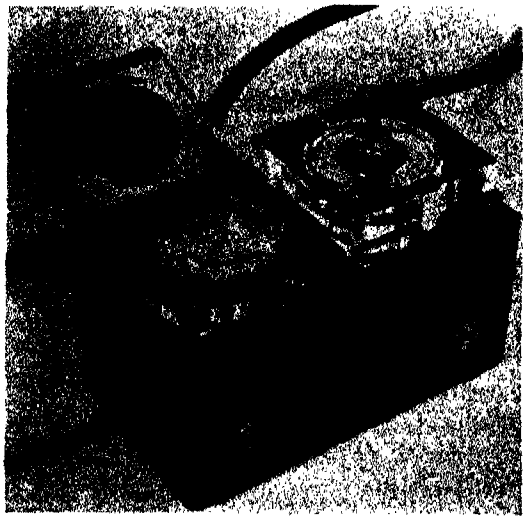

FIG. 4. Photograph of the duplex radial-jet air sampler shown in Fig. 3.

---

[2] S. Moulton, T. T. Puck, and H. M. Lemon, "An apparatus for determination of the bacterial content of air," Science 97, 51 (1943).

[3] W. F. Wells, "Apparatus for the study of the bacterial behavior of air," Am. J. Pub. Health 23, 58 (1933).

[4] H. G. du Buy, Alexander Hollaender, and Mary D. Lackey, "A comparative study of sampling devices for air-borne micro-organisms," Supplement No. 184 to the Public Health Reports, U. S. Government Printing Office, Washington, D. C., 1945.

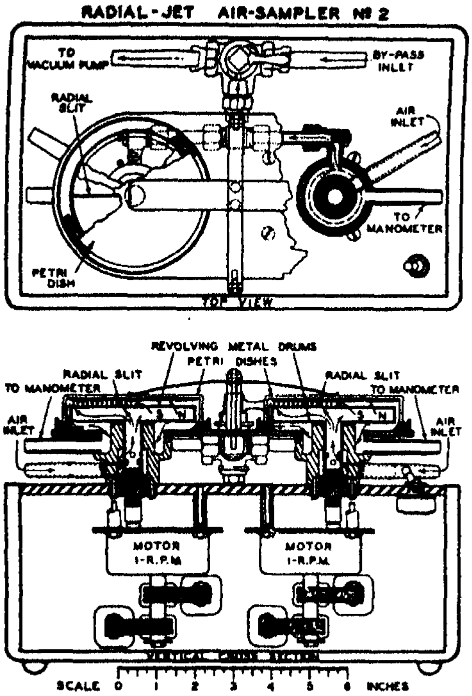

FIG. 5. Diagrammatic views of an improved duplex radial-jet air sampler. The petri dishes are stationary, held in place against rubber gaskets, and the drums containing the radial slits rotate at 1 r.p.m. The outside surfaces of the dishes do not become contaminated by the air being sampled.

"clusters." The bubbler-type samplers apparently break up these clusters so that the maximum numbers of colonies develop, whereas the impingement-type samplers do not break up the clusters and only a single colony develops from a cluster.

ELECTROSTATIC BACTERIAL AIR SAMPLER

About three years ago the authors and their colleague, L. L. Holladay, developed a portable air sampler employing an electrostatic impingement principle.[5] It is illustrated in the diagram and photograph of Figs. 1 and 2. It consists of two sampling units, each holding one petri dish. Each dish rests on one electrode of a high voltage d.c. circuit (approximately 7000 volts), one electrode being negative and the other positive. A metal cone above each dish has a polarity opposite to that of the one on which the dish rests. A small blower mounted in the cabinet below the dishes draws air over each dish, through an electrostatic field which increases in intensity as the air approaches the edge of the dish, as a result of shorter spacing between the electrodes. The air is finally expelled at the back of the sampler cabinet. The apertures are adjusted to give an air rate of ½ cubic foot per minute through each unit. The complete sampler weighs approximately 12 pounds; hence it is readily portable. Its operation is very simple and comparative tests with the sampler to be described next show it to be highly efficient. However, it is improbable that it breaks up "clusters" of organisms. It is probable that this could be accomplished with this sampler by collecting the organisms in water and then violently agitating it before incorporating an aliquot part of it in a culture medium.

AN IMPROVED DUPLEX RADIAL-JET AIR SAMPLER

A single-unit radial-jet air-sampler has already been described by the authors.[5] Although developed independently in this laboratory, it is essentially a modification of the slit sampler first developed by Bourdillon, Lidwell, and Thomas.[6] This type of sampler is highly efficient and is very useful in the laboratory.

In the original designs of Bourdillon *et al.* and of the authors, the sampler consisted of a single sampling unit. By means of a vacuum pump, air is drawn into a hollow drum and issues at high velocity through a radial slit onto the culture medium in a petri dish which is rotating slowly underneath and close to the drum. The sampler we described was the result of extensive investigations of the optimum velocity and character of

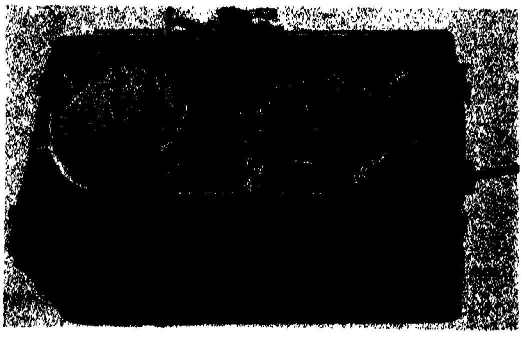

FIG. 6. Photograph of the improved duplex radial-jet air sampler.

---

[5] Matthew Luckiesh, L. L. Holladay, and A. H. Taylor, "Sampling air for bacterial content," General Electric Rev. 49, 8 (1946); J. Bact. 52, 55 (1946).

[6] R. B. Bourdillon, O. M. Lidwell, and J. C. Thomas, "A slit sampler for collecting and counting air-borne bacteria," J. Hygiene 41, 197, 224 (1941).

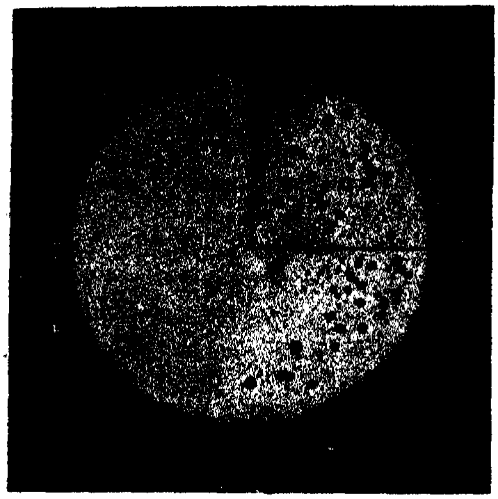

FIG. 7. Typical petri dish illustrating one way in which the sampler can be used to measure the rapid change of bacterial air contamination (see reference 3). It represents periods of 15 seconds before and 45 seconds after exposure of the room air to a 30-watt germicidal lamp. At sampling point the intensity of germicidal energy was 30 microwatts per sq. cm.

the flow of air. The authors later modified this original design to incorporate two identical sampling units, one of which could be used for the control and the other for the test.[7] Used in this way it is a valuable tool in measuring the lethal effect of ultraviolet upon various types of micro-organisms. It can also be used to determine the relative value of different culture media for specific types of organisms or for sampling air in two places in a room simultaneously. The first design of the duplex radial-jet air sampler is illustrated in Figs. 3 and 4. As will be seen, the air flows over the outside of the petri dishes after passing over the culture media, thus allowing possible contamination of the outside of the dishes by bacteria which escape collection. Furthermore, the construction is such that the sampler cannot be autoclaved.

The authors have recently modified the design of the sampler so that the contaminated air does not pass over the outside of the petri dishes. The modified design is illustrated in Figs. 5 and 6. In operation the petri dishes are stationary and are inverted over rotating drums. They are held in place against rubber gaskets by means of a flat spring clamp. Air from the two units after sampling is brought together just ahead of a three-way valve. This valve makes it possible to by-pass air around the sampler while changing petri dishes. Two constant-speed Telechron motors rotate the drums at one revolution per minute. The upper part of the sampler can be removed from the case containing the motors and can be autoclaved without damage. This is an important advantage, especially when sampling pathogenic organisms or molds.

One great advantage of the duplex radial-jet air sampler is that it may be used to measure rapid changes in concentration of air-borne bacteria, such as may occur when a germicidal lamp is turned on in a room. This is illustrated in Fig. 7, a time-indexed photograph of a petri dish after incubation. It shows the concentration of respiratory micro-organisms at a given point in a room 15 seconds before and for 45 seconds after uncovering a 30-watt germicidal unit irradiating the upper air in the room which was 17 feet square and 11 feet high.[7] The test position was in the center of the room, one foot above the mounting height of the lamp. The intensity of the germicidal energy (λ2537) at the sampling position was approximately 30 microwatts per

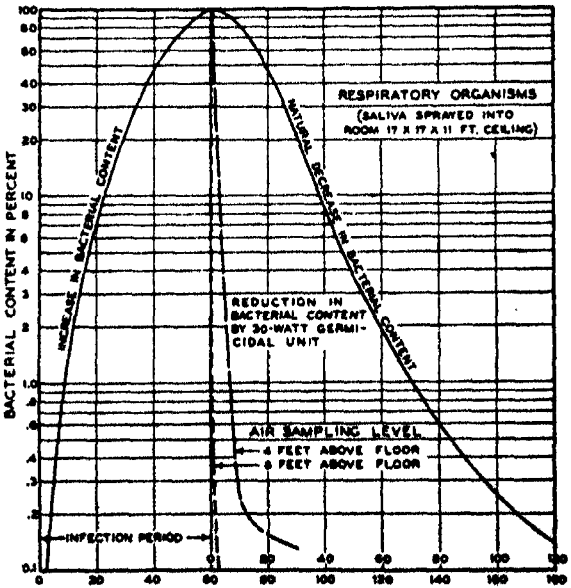

FIG. 8. Some experimental results obtained with the duplex radial-jet air sampler. Saliva was atomized into the air of a closed room for an hour, the air being sampled frequently. At that time the atomizer was stopped and a single 30-watt germicidal lamp unit irradiating the air above the 7-foot level, was turned on. Air samplings at two levels in the center of the room with and without the germicidal unit show its effectiveness in destroying these organisms.

---

[7] Matthew Luckiesh, A. H. Taylor, and T. Knowles, "Killing air-borne respiratory micro-organisms with germicidal energy," J. Franklin Inst. 224, 267 (1947).

sq. cm. Saliva was nebulized into the room air for approximately 20 minutes before starting the test and ***nebulization continued throughout the sampling period.*** Bourdillon, in a letter to one of the authors, indicated that he has used his sampler in this same way to measure the rate of change in air contamination resulting from the use of a mercury lamp.

The rapid decrease of respiratory organisms in the air of the above room when a single 30-watt germicidal lamp unit was turned on after nebulization of saliva for one hour is also shown graphically by Fig. 8. Data from two tests have been combined to show the natural rate of decrease after nebulization ceased when no lamp was used and the highly accelerated decrease produced by the germicidal energy when the lamp was used in the second test.

The authors have found the duplex radial-jet air sampler very valuable in studying the effect of varying the exposure of specific air-borne organisms to germicidal ultraviolet energy. A simplified diagram of apparatus used for this purpose is shown in Fig. 9. Water containing the organisms is nebulized into an infection chamber, volume approximately 25 cubic feet. Air from this chamber is drawn directly into one unit of the sampler which serves as a control, to indicate the concentration of organisms *before* irradiation. The other unit of the sampler receives air which has passed through an irradiation chamber. This chamber has two quartz windows through which the air is irradiated by 8-watt germicidal lamps. The number of lamps used can be varied from one to fourteen and their distances are also variable over wide ranges. These variations are sufficient to determine lethal curves for organisms varying widely in resistance. Room air entering the infection chamber and air passing out of the sampler is disinfected by passing through glass tubes in which are enclosed 30-watt germicidal lamps.

Instead of using one unit for the control and the other for the test, when determining the lethal effect of ultraviolet, a single unit can be used in the following way. Let the drum make a half revolution with the air being irradiated, then cover the lamps and continue the sampling for the other half of the plate. Possible errors due to changes in concentration during the transition period can be avoided by counting the colonies in 160° rather than 180°. Use of a single plate in this way avoids errors caused by lack of symmetry between the two units.

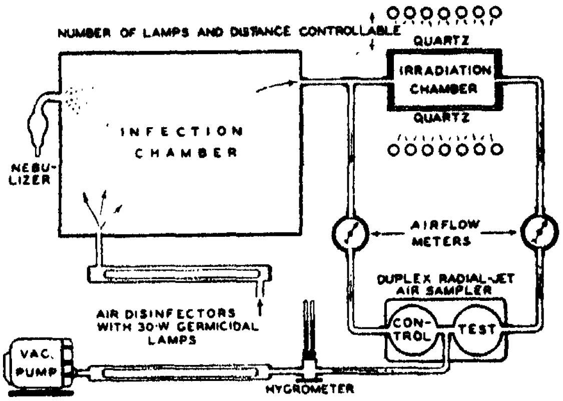
NUMBER OF LAMPS AND DISTANCE CONTROLLABLE
QUARTZ
IRRADIATION CHAMBER
QUARTZ
INFECTION CHAMBER
NEBU-LIZER
AIRFLOW METERS
DUPLEX RADIAL-JET AIR SAMPLER
CON-TROL
TEST
AIR DISINFECTORS WITH 30-W GERMICIDAL LAMPS
VAC. PUMP
HYGROMETER

FIG. 9. Simplified diagram of the arrangement of apparatus used to study the lethal effect of germicidal energy on air-borne organisms of various types.

The electrostatic air sampler is much more easily portable than the radial-jet sampler. The latter requires the use of a vacuum pump which, with motor, weighs nearly 30 pounds. It also requires flow-rate meters in order to maintain the correct air-rates. However, in laboratory studies such as those described above, the jet sampler has distinct advantages.

The sampling efficiency of any air sampler is difficult to appraise, since there is no single method which can be assumed to be 100 percent efficient. Furthermore, as discussed above, some air samplers break up clusters of organisms and produce a larger number of bacterial colonies than those which do not break them up. Also, there is usually no assurance that two samplers operating simultaneously will be sampling homogeneous air. Many tests must be made before valid comparisons are possible. Another factor which may affect sampling efficiency with any particular sampler is the size of the particles carrying the organisms: e.g., dust particles, fine or coarse droplet nuclei, etc. One method of analyzing performance is to put two samplers in series, the second in line to be one known to have a high efficiency. Tested in this way, both of the samplers described above appear to be quite efficient. In many cases reliability and consistency may be more important than the highest possible efficiency. Both of these samplers have proved to be satisfactory in these respects.

THE REVIEW OF SCIENTIFIC INSTRUMENTS VOLUME 20, NUMBER 1 JANUARY, 1949

A Wide-Range Saw-Tooth Generator

PETER G. SULZER
Department of Electrical Engineering, The Pennsylvania State College, State College, Pennsylvania

(Received October 2, 1948)

A new and comparatively simple saw-tooth generator is described. The circuit is capable of operating over the range from 15 cycles to 500 kilocycles with good linearity and rapid flyback.

EVER since the advent of the thyratron saw-tooth generator,[1] various attempts have been made to extend the upper-frequency limit of the linear time base. These have usually taken the form of a modification of Abraham and Bloch's multivibrator.[2] Probably the most successful modification is that due to Puckle,[3] in which one of the multivibrator tubes is used for discharging a condenser, which is subsequently charged through a constant-current device. Although this circuit extended the frequency range by a factor of 10 over the thyratron generator, it has not seen wide application because it requires three tubes. More recently, Keen has described a circuit[4] which performs well with only two tubes.

This paper describes a simple saw-tooth generator that is capable of operating at frequencies as high as 500 kilocycles. Although but a single tube is employed, it appears to function as well as the more complicated circuits mentioned above. The new circuit has been found to be particularly useful as an auxiliary unit for extending the frequency range of already existing oscillographs.

It was thought that a useful time-base generator might be derived from the cathode-coupled multivibrator.[5] Although such a circuit[6] has

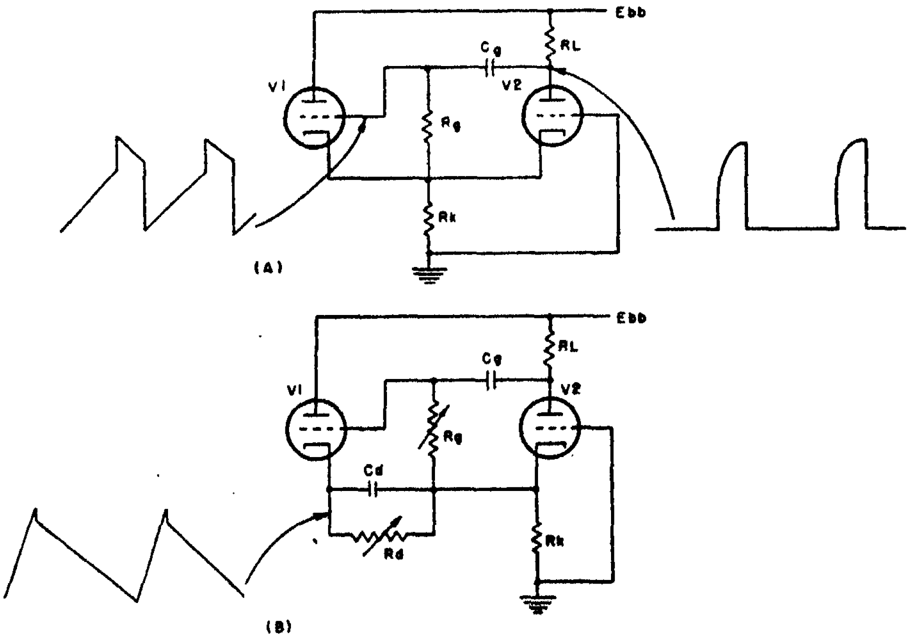

FIG. 1. Cathode-coupled multivibrator.

---

[1] R. St. G. Anson, British Patent 214754.

[2] H. Abraham and E. Block, "Notice sur les Lampes-valves à 3 Electrodes et leurs Applications," Publication No. 27 of the French Ministère de la Guerre, April, 1918.

[3] O. S. Puckle, *Time Bases* (John Wiley & Sons, Inc., New York, 1943), p. 30.

[4] A. W. Keen, W. Eng. **25**, 210 (1948).

[5] Keats A. Pullen, Jr., Proc. I.R.E. **34**, 402 (1946).

[6] J. L. Potter, Proc. I.R.E. **26**, 713 (1938).

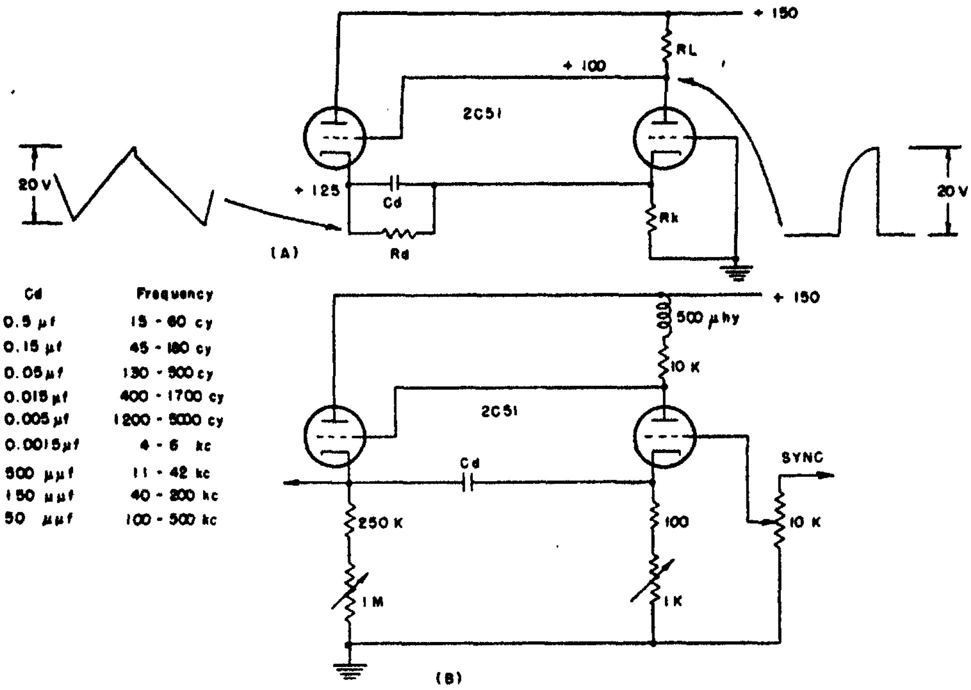

Cd	Frequency
0.5 µf	15 - 60 cy
0.15 µf	45 - 180 cy
0.05 µf	130 - 500 cy
0.015 µf	400 - 1700 cy
0.005 µf	1200 - 5000 cy
0.0015 µf	4 - 6 kc
500 µµf	11 - 42 kc
150 µµf	40 - 200 kc
50 µµf	100 - 500 kc

FIG. 2. Sweep circuit derived from the cathode-coupled multivibrator.

already been obtained, it does not give constant output with variable frequency, which is so desirable in oscillographic work.

CATHODE-COUPLED MULTIVIBRATOR

In considering the cathode-coupled multivibrator, Fig. 1(A), it is convenient to start with V_1 cut off, and V_2 conducting. Thus the grid of V_1 is negative with respect to its cathode because of the charge on C_g. As C_g discharges through a path containing R_g as the most important element, the bias on the grid of V_1 will fall to a point where the tube starts to conduct. When it does, the cathode current of V_1, flowing through R_k, biases the cathode of V_2, decreasing its plate current, increasing its plate voltage, and thus, through C_g, applying a positive voltage to the grid of V_1. The result of this regenerative process is that V_1 conducts heavily, and V_2 is cut off. During this time, C_g is being charged through a path containing R_L, the grid-cathode resistance of V_1, and R_k. As C_g becomes fully charged, the current through it decreases, reducing the positive bias on the grid of V_1, which starts a reverse regenerative process. By a suitable choice of parameters the charging time-constant, which is roughly R_LC_g, can be made much smaller than the discharging time-constant, which is very nearly R_gC_g. Thus the cathode current of V_1 can be made to flow in a series of short pulses.

CIRCUIT MODIFICATIONS

This fact suggests the placing of a parallel $R-C$ combination in the cathode lead of V_1, as is shown in Fig. 1(B). A saw-tooth voltage would be produced across C_d by charging it for a short time by means of the cathode current pulses, and discharging it for a longer time through R_d. The frequency of the resulting sweep oscillator would be determined by both of the time constants, namely, R_gC_g and R_dC_d. Operation of the circuit would be complicated by the fact that it would be necessary to vary R_g and R_d simultaneously to obtain constant output.

It is possible, however, to avoid this difficulty by using the circuit of Fig. 2(A), which dispenses with R_g and C_g. Thus only one time-constant need be considered. Operation of the device is as follows:

Assume that V_1 is cut-off because of a large voltage across C_d, and V_2 is conducting. With the circuit values of Fig. 2(A), the voltages are as shown at this instant of time. C_d will then

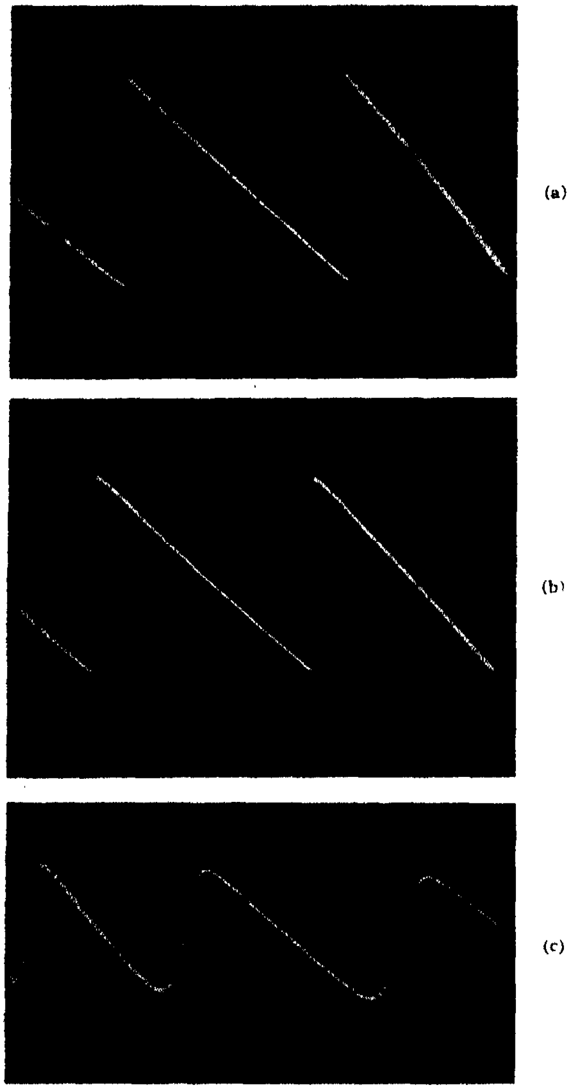

FIG. 3. Oscillograms of the output of the circuit made at (a) 50 cycles, (b) 5 kilocycles, and (c) 500 kilocycles.

discharge through R_d until the cathode voltage of V_1 is lowered sufficiently to allow conduction. The cathode current of V_1 flowing through R_k will place a positive bias on the cathode of V_2, increasing its plate voltage, and making V_1 conduct more heavily. Eventually V_2 will be cut off, as C_d charges through R_k. It is of particular interest to note that V_1 acts as a cathode follower at this time, permitting very rapid charging of C_d through R_k, which is a low resistance. This is desirable for a rapid flyback of the sweep. As C_d becomes fully charged, the current through it decreases, allowing V_2 to conduct, and cutting off V_1. C_d then discharges slowly through R_d, producing the long portion of the saw-tooth, which is used as the active portion of the sweep. Since the saw-tooth is only a small portion of the average voltage between the cathode of V_1 and ground, excellent linearity is obtained without the use of a constant-current device such as a pentode.

It should be noted that the voltage between the cathode of V_1 and ground is not a true saw-tooth because of the small pulse appearing across R_k, which is added to the saw-tooth appearing across C. The amplitude of this pulse is so small, however, that it does not affect the operation of the circuit as a time base.

Figure 2(B) shows a practical circuit using a type 2C51 dual triode. A four-to-one frequency ratio is obtained by varying R_d, while ranges are changed by switching C. The accompanying table shows values of C and the corresponding frequencies covered. With the values shown the circuit produces a 20-volt saw-tooth over the range from 15 cycles to 500 kilocycles. Operation is improved somewhat at the higher frequencies by inserting an inductance in series with R_L.

Synchronization is obtained by applying at least 0.2 volts peak to the grid of V_2, which is normally grounded. Thus synchronizing voltage can be introduced easily without disturbing the other functions of the circuit.

When setting-up the circuit, R_k should be adjusted for a reasonably short flyback with R_g set to a low value and with one of the large condensers switched in for C. Shorter flyback and a higher maximum frequency are obtained with low values of R_k. However, if R_k is set too low, the lower portion of the saw-tooth may be clipped.

Figure 3 contains three oscillograms of the saw-tooth output of the circuit. These were made at frequencies of (a) 50 cycles, (b) 5 kilocycles, and (c) 500 kilocycles. It will be noted that the linearity is good, and that a reasonably short flyback is obtained, even at 500 kilocycles.

CONCLUSION

A new one-tube time-base has been described. It is thought that the circuit could be used to replace the thyratron time base for most oscillograph work.

Laboratory and Shop Notes

Distant Counting of Scintillations*

E. P. Blizard and S. DeBenedetti
Oak Ridge National Laboratory, Oak Ridge, Tennessee
October 7, 1948

TWO limitations to the use of scintillation counters with photo-multipliers are: (a) the photo-multiplier will not operate in strong magnetic fields, and (b) the pulse-height distribution is perturbed by the direct response of the multiplier to radiation. These limitations can be circumvented by separating crystal and photo-multiplier, and focusing or canalizing the scintillation light. To test this point an anthracene sample was mounted at the focus of a hemispherical mirror 1⅝ in. in diameter at one end of an internally reflecting tube of equal diameter and one meter long. A liquid nitrogen cooled 1P21 photo-multiplier was placed at the other end, and the whole assembly made light-tight. With this arrangement we could count with 100 percent efficiency the alpha-particles from a polonium source in contact with the anthracene. With 80 volts per stage the alpha-particle pulses were much larger than those of the photo-multiplier background. Under the same conditions the efficiency for beta-rays of $E_{\max}=0.87$ Mev was also 100 percent within the limits of accuracy of source calibration. Satisfactory results were also obtained with dry ice cooling, and with improved optical techniques it might be possible to dispense with cooling altogether.

---

* This work was performed under Contract No. W-35-058, eng. 71 at Oak Ridge National Laboratory.

A Convenient Method for Checking the Linearity of an Electron Multiplier Circuit

George P. Kirkpatrick
United States Radium Corporation, Almedia, Pennsylvania
October 7, 1948

IN making photometric observations of the brightnesses of phosphors, many workers use electron multipliers and high sensitivity galvanometers. These galvanometers must have a linear response to the output of the multiplier; though this response has been checked initially, very small vibrations do upset the response, and one can do a great deal of work before suspecting the non-linear response. The fact that the suspension of a galvanometer swings freely does not mean that its response to signal strength is linear.

Luminous zinc sulfide deck markers provide a convenient means for checking the linearity of the electron multiplier and galvanometer. The writer uses a set of these markers varying in brightness from 9.0 to 0.30 microlamberts. The set has aged sufficiently so that the breakdown is very slow; weeks are required before a perceptible change in brightness occurs. The markers are also checked (for brightness in microlamberts) against radioactive foil-phosphor light standards. The latter undergo even a slower breakdown than the markers, since the radium exciting source is removed from the phosphor when the standard is not in use.

If the brightest marker is used as a secondary standard, the others may be calibrated in terms of it. First, filters of the proper neutral density are placed between the photocell and the standard marker to give a deflection of approximately 400 mm to 500 mm; the other markers are then observed and their brightnesses computed. The filters are then varied so that the second brightest marker gives the above deflection, and the other markers' brightnesses are computed, assuming the first observed brightness of the second marker. This proceedure may be repeated a number of times using successively fainter markers for the full-scale deflection. The observed brightness of a marker will then be independent of the scale reading, if the response of the circuit is linear.

Method of Linearizing the Voltage Rise of a Relaxation Oscillator*

R. J. Watts
Ohio State University, Columbus, Ohio
August 16, 1948

SOME recently described circuit techniques[1,2] suggest the application of the "bootstrap" generator to the relaxation oscillator in order to obtain a more nearly linear rise voltage. In Fig. 1 is shown a circuit which has been used

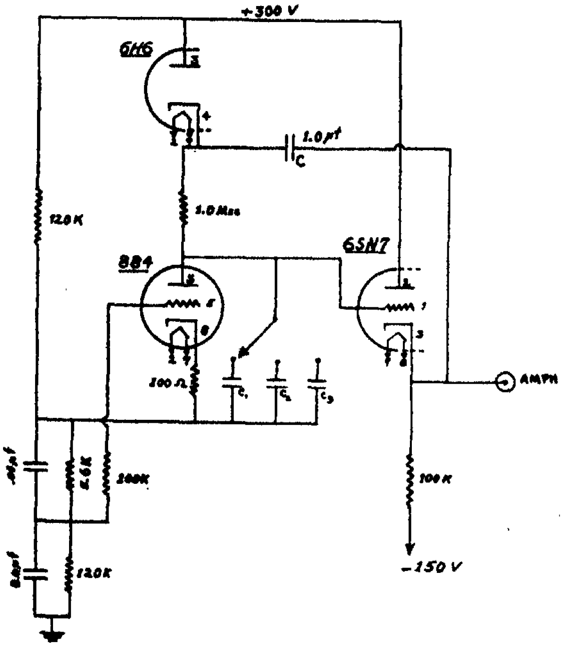

Fig. 1. Circuit for linearizing the voltage rise of a relaxation oscillator.

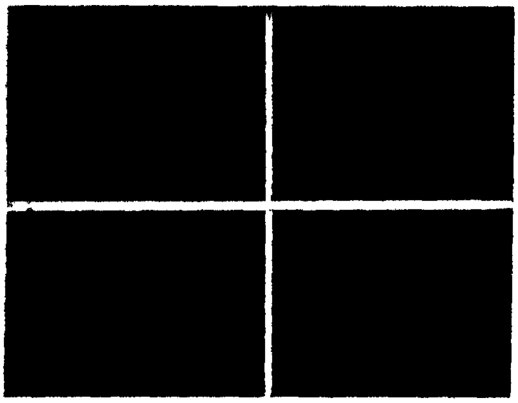

FIG. 2. Oscillograph traces of the voltage wave shapes. *A* is the wave shape of normal relaxation oscillator at 215 cycles/sec.; *A'* is the wave shape observed with circuit described at 215 cycles/sec. *B* is the wave shape of a normal relaxation oscillator at 5.4 kilocycles/sec.; *B'* is the wave shape observed with circuit described at 5.4 kilocycles/sec. (three complete voltage waves are presented in each case).

in this laboratory. In this circuit the "clamp tube" of the usual generator has been replaced by a type 884 thyratron.

The oscillograph pictures shown in Fig. 2 indicate the improvement over the normal relaxation oscillator at two frequencies. Part *A* shows the wave form of the voltage at the output as presented on a Du Mont type 241 oscillograph when the feed-back condenser *C* is disconnected from the cathode of *6H6*. With condenser *C* disconnected, the circuit operation is essentially that of a normal relaxation oscillator. The repetition frequency in this case was 215 cycles/sec.; three complete cycles are shown on the oscillograph trace. No detailed investigation of the linearity of the oscillograph sweep was made, but it was assumed that the central portion of the sweep most nearly approaches linearity. Part *A'* of Fig. 2 shows the wave form observed when feed-back condenser *C* was connected with repetition frequency unchanged. An estimate of the improvement introduced can be obtained by comparison of the central portions of the oscillograph traces. Parts *B* and *B'* show the corresponding results obtained when the repetition frequency was 5.4 kilocycles/sec.

A useful variation of the circuit may be obtained by biasing the thyratron in such a way that the cathode follower 6*SN7* is non-conducting for part of the cycle. In this case, one obtains a saw-tooth voltage with the teeth separated in time from one another by the time during which the cathode follower is non-conducting. The "off period" is useful if one desires to apply keying pulses to some associated circuit, such as those used in television systems.

If, in addition, the thyratron grid is also biased in such a manner that the tube is in a non-repetitive state, a single delayed sweep can be obtained by applying a positive pulse to the grid. The delay time is the time that the cathode follower is non-conducting. This delay time is limited by the useful sweep voltage.

The useful sweep voltage can be increased by the use of a push-pull output. A satisfactory push-pull output can be obtained by using the second triode of the 6*SN7* as a "gain of minus one" amplifier of the type described by Fitch and Titterton.[2]

---

* This work was done in connection with a research contract No. W28-099-ac-179 between the Ohio State University Research Foundation and the Watson Laboratories of the Air Materiel Command, Red Bank, New Jersey.

[1] Britton Chance, Rev. Sci. Inst. 17, 396 (1946).

[2] V. Fitch and E. W.Titterton, Rev. Sci. Inst. 18, 821 (1947).

High Temperature X-Ray Diffraction Techniques

J. J. LANDER
Bell Telephone Laboratories, Murray Hill, New Jersey

November 8, 1948

THREE types of accessories for x-ray studies of materials at high temperatures have been built, and these are sketched in Fig. 1. Accessories (A) and (B) are suitable for the study of materials maintained in high vacuums or controlled atmospheres, and (C) may be adapted for high vacuum but has been used with controlled atmospheres. In either (A) or (B) the incident and diffracted beams pass through strategically placed glass foil sealed to the surrounding glass tube. Since the furnace and containing glass envelope are simply attached to standard equipment (cameras or spectrometer), this technique results in certain simplifications compared with more conventional practice.

The unit (A) can be mounted on an x-ray spectrometer. The glass windows are approximately 1.5 mils thick and are bowed inwards. With CuK_α-radation the ratio of intensities of diffracted feature to background is almost as good as the best obtainable with the glass capillary technique. A range in 2θ of 90° is provided. The powder to be examined is spread on a platinum sheet which is held in the furnace by the thermocouple leads. Temperatures as high

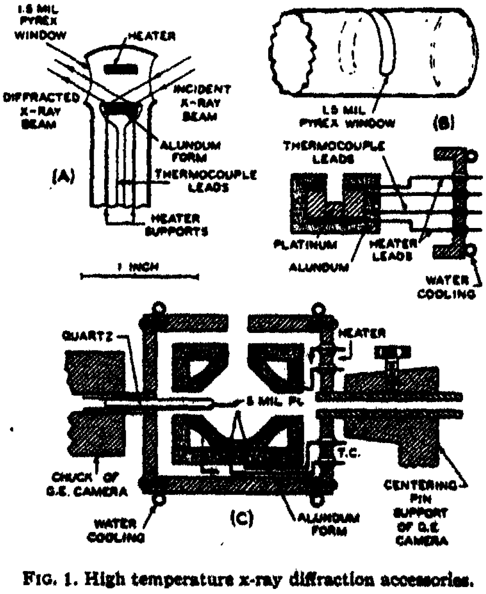

FIG. 1. High temperature x-ray diffraction accessories.

as 1400°C have been maintained and observed with an accuracy of about 5°C, if the coating is thin and adherent. With this accessory and an x-ray spectrometer the time between observations can be reduced to a few seconds. Thus, this technique is ideally suited to the observation of phase transitions and reaction rates, and we have studied the phase transitions of the alkaline earth carbonates in this way.

Materials in test electronic vacuum tubes and cold cathode tubes have been examined by constructing the tubes with opposing glass windows such as are featured in (A). Since the electrical characteristics of the tubes can be measured simultaneously, this technique avoids ambiguity which does result from the use of indirect methods.

Unit (B) is designed to provide a complete powder pattern. It is mounted along the axis of a standard powder camera. The powder to be examined is spread thinly on a wedge filed in a notch in a platinum rod, the ends of which are surrounded by the heater. The temperature of the powder is the more accurately observed, the thinner the powder and the deeper the notch in the rod and the surrounding heater elements. Under favorable conditions the specimen may be held at 1400°C and the temperature observed with an accuracy of about 5°.

Unit (C) is an adaptation of more familiar high temperature equipment.[1] However, the unit is mounted on standard parts of a standard camera. In the design of (C), high vacuums are sacrificed to provide for rotation of the specimen. The furnace design of (C) is also superior since the specimen is almost completely surrounded by heater, and the thermocouple junction is exposed to radiation in a fashion almost identical with that of the sample. Obviously, this feature can be built into (B) and a mechanism provided for rotating the specimen.

---

[1] See, for example, W. Hume-Rothery and P. W. Reynolds, Proc. Roy. Soc. (London) A167, 25 (1938).

New Instruments

W. A. Wildhack: Associate Editor
in Charge of this Section
National Bureau of Standards, Washington, D. C.

These descriptions are based on information supplied by the manufacturer and in some cases from independent sources. The Review *assumes no responsibility for their correctness.*

Regulated Power Supply

A new regulated power supply for an output of 300 volts, 200 milliamperes, has been announced by the Howard Company. Regulation is obtained, within 1 volt, from 0 to full load and line variation from 105 to 125 volts. Ripple is less than 10 millivolts at full load with 115 volts input, and less than 25 millivolts between 0 and full load with line voltage variations from 105 to 125 volts. The supply is stable within 1 volt during long periods of operation at full load.

This power supply is designed to provide a stable source of d.c. for experimental set-ups and is suitable for continuous operation at full load in permanent installations. It is light, compact, and inexpensive, and can be supplied in the cabinet shown or panel mounted for rack installations. The unit measures 17″×10″×9″, weighs 28 pounds, and is priced at $89.00.—Howard Company, *934 Argyle Road, Drexel Hill, Pennsylvania.*

RCA Electron Diffraction Unit

An electron diffraction unit developed by RCA to aid in observing and measuring conditions on surfaces or in thin layers of materials such as metals, ceramics, plastics, organic films, and biological materials, will permit chemical analysis of substances weighing as little as 1/28 millionth of an ounce.

Provisions are included in the instrument for producing electron diffraction patterns by either the reflection or the transmission method. The instrument will also produce shadow micrographs—an essential feature for examining the area of the specimen from which diffraction patterns are obtained.

The new instrument, which resembles RCA's universal model electron microscope in size and shape, consists of an optical system, power supplies, a vacuum system, and a control panel.

The optical system is comprised of an electron gun which produces the electron beam, an anode which accelerates the beam, an electromagnetic lens system to position and focus the beam, an object chamber which allows for introduction and manipulation of the specimen, a viewing screen to make the pattern visible, and a built-in camera to provide for photography of the pattern.

Through the correct choice of apertures and pole pieces, either extremely small illuminating spots may be obtained or wide areas of the specimen may be irradiated. Patterns may be focused by lenses either above or below the specimen.

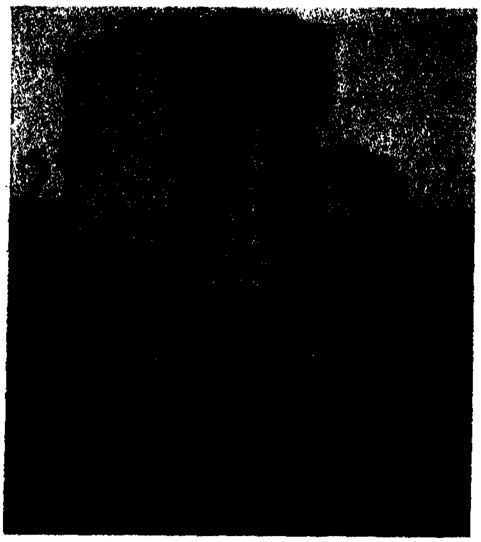

Five external controls provide for positioning specimens up to 1-inçh square at any desired angle. A transmission specimen holder which takes six specimens on ⅛-inch disks of 200-mesh screen is provided, so that it is possible to carry at all times a calibration sample while unknowns are being studied. A beam stop is provided to reduce undesirable halation. A built-in, rock-steady camera is utilized for photographing the diffraction patterns on 4-in.×5-in. plates.

A power supply similar to that used in the electron microscope provides a 50-kilovolt d.c. supply for the diffraction instrument. The vacuum system evacuates the electron column from atmospheric pressure to an operating pressure below that indicated by 1 micron of mercury in only one and a half minutes. All metal vacuum lines and electromechanical valving are features of this system. A special control panel which provides for complete control of the equipment, a built-in charge neutralizer, and ports for accessories are also included.—Radio Corporation of America, *RCA Victor Division, Camden, New Jersey.*

Precision-Regulated D.C. Power Supply

A d.c. power supply with output voltage regulation better than 0.1 percent, and ripple less than 0.01 percent, is announced by the Hastings Instrument Company.

The precision-regulated power supply is adjusted by the manufacturer for optimum regulation at any specified load from 5 to 30 milliamperes, and for any output voltage from 0 to 100 volts. Regulation is thus obtained within ±0.1 percent for input line voltages varying from 75- to 135-volts a.c. at frequencies from 50 to 400 cycles per second.

Developed for use with instruments requiring highly stable d.c. voltages, the power supply is well suited for resistance thermometers, wire strain gauges, position potentiometers, and many other industrial and laboratory instruments. Because of its unusually low output ripple, it may be used with all types of recording oscillographs.

The unit pictured measures 4″×5″×6″ and weighs 6 pounds. It is well designed for laboratory use and is small enough to be readily adapted as a built-in power supply component for large instruments.

Power supplies designed on the same circuit principles for output voltages above 100-volts d.c., units for operation from other current supplies (i.e., 24-volts d.c.), and units having non-standard chassis construction are available on special order. The regular price is $50.00 f.o.b., Hampton, Virginia.—Hastings Instrument Company, Inc., *P. O. Box 1275, Hampton, Virginia.*

Toroidal Coils

Wound toroids ranging from ⅜-inch o.d. up are available from Lenkurt Electric Company, Inc., as an addition to that company's previous line of molded magnetic parts and assemblies. Cores of Permalloy or molded iron powder can be used as required.

Toroidal coils are supplied cased or uncased, impregnated or plain, tapped or not, with an inductance range up to 15 henries and Q as high as 300. Inductance tolerances as close as 0.1 percent can be met. Coils are available with two balanced windings or with a closely coupled secondary superimposed for impedance matching applications.

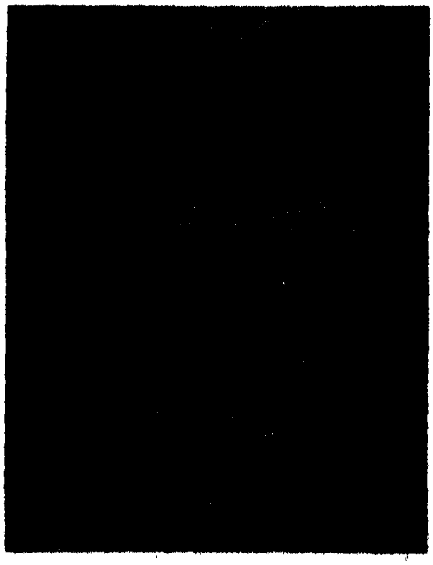

Space savings attained with these toroids range up to 75 percent over helical coils with the same parameters because of improved magnetic efficiency with minimum flux loss.

A few sizes of toroidal cores are molded by Lenkurt as well and are available unwound (up to 3 inches o.d.). Three standard powders are used with applicable frequency ranges: up to 90 kc, up to 5 mc, and up to 200 mc. For special requirements, however, these cores can be molded from any existing ferromagnetic powder.—LENKURT ELECTRIC COMPANY, *1121 County Road, San Carlos, California.*

Multirange Kilovoltmeters

Beta Electronics Company announces the Series 121 multirange kilovoltmeters, with full-scale ranges of 15/30 and 25/50 kv, at 50,000 and 25,000 ohms per volt.

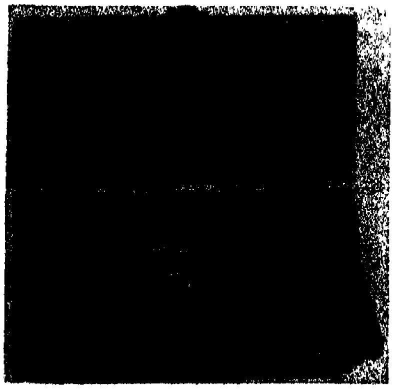

The input resistance on these voltmeters is constant on both ranges, giving a sensitivity of approximately 50,000 ohms per volt on the lower voltage range and 25,000 ohms per volt on the higher voltage range. The meter movement is 20 microamperes full scale and is shunted by proper resistors for the two ranges.

A Lucite safety handle is provided to permit connection of the voltmeter to the source of high voltage.—BETA ELECTRONICS COMPANY, *1762 Third Avenue, New York 29, New York.*

Continuous Hydrogenation Unit

High pressure, high temperature chemical reactions, such as hydrogenations, oxo-syntheses, and general organic syntheses of various sorts require specialized equipment. For general laboratory use, it is necessary that such equipment be compact, simple to operate, and flexible enough for diversified use.

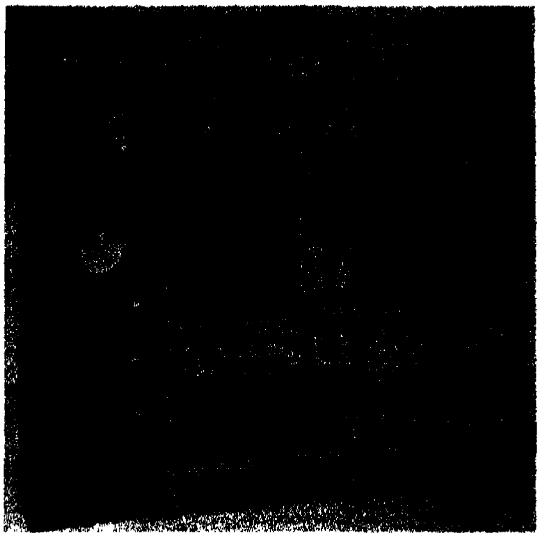

Such a unit has been designed by Autoclave Engineers, Inc., to serve as a research tool or pilot plant for the study of high temperature and high pressure reactions.

The unit as shown consists essentially of two high pressure, high temperature reactors, one high temperature separator, one low temperature separator, two preheaters, feed pumps, valves and fittings, furnace and control equipment for proper operation at pressures to 15,000 p.s.i., and temperatures to 1000°F.

Instruments and control equipment consist of a pressure recorder and controller, multiple-point temperature recorder, two furnaces, temperature indicators and controllers, and six variable transformers for adjusting the flow of current to furnaces and preheaters.—AUTOCLAVE ENGINEERS, INC., *P. O. Box 110, Titusville, Pennsylvania.*

Magnetic Flux Meter

The Model 327 Smith magnetic flux meter provides a new, simple, complete means of measuring a.c., d.c., and transit magnetic flux densities, which eliminates the present search coil errors.

A small probe, thin enough to be readily inserted in the air gap of the average electrical machine, is used for measuring fields approaching a point area.

Probes can be supplied in special thicknesses to suit specific measurement applications.

Simplicity of operation is its outstanding feature.

The interchangeable probe contains a copper constantan thermocouple, and for very accurate results a temperature compensating formula can be applied. Turning the probe in the magnetic field indicates the direction of flux. The maximum reading is obtained when the probe spirals are perpendicular to the field.

Standard range: 0 to 26,000 gauss; special ranges are available. Calibrated accuracy: 1 percent. Connections are provided for oscillographic studies of flux.

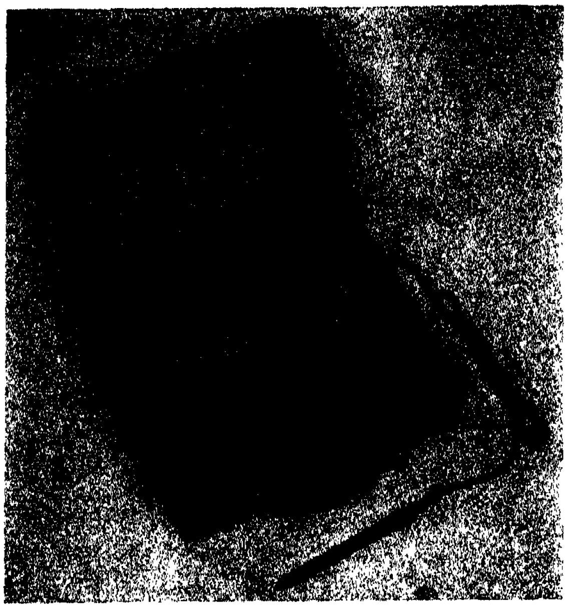

A compact, 13½-in.×11-in.×5½-in. portable, its self-contained probes are interchangeable.—Associated Research, Inc., *231 South Green Street, Chicago 7, Illinois.*

Absolute Pressure Gauge

The absolute pressure gauge manufactured by Airplane and Marine Instruments, Inc., is a custom-calibrated instrument intended for use where precise measurements are required in the ultra-low pressure range. It is adaptable to metering in filling electron tubes, indication of pressures in test tanks and distillation chambers, measurement of condenser pressures, and general laboratory use. A and M welcomes inquiries as to its adaptability to other specific applications.

The instrument consists of aneroid-type capsules whose movement is transferred to a needle by suitable linkage. The principle is unique in that the measured medium is introduced into the inside of one capsule, and the movement of this capsule is opposed by an evacuated capsule. The resultant movement is utilized to position the pointer. The interior of the case is not evacuated, so only a dust-proof case is required. Rugged stops are provided to prevent damage should the instrument go off scale.

Accuracy is said to be 1 part in 500, with a sensitivity of 1 part in 1000. The scale diameter is 6 inches, and the scale length is 15 inches.

The following are available as standard ranges: Model 1001-50, 0 to 50 mm Hg; Model 1001-100, 0 to 100 mm Hg; Model 1001-200, 0 to 200 mm Hg. The scales for these ranges may be graduated as requested by the customer. Inquiries for special ranges are invited.—Airplane and Marine Instruments, Inc., *Clearfield, Pennsylvania.*

Pulsed X-Rays

A technique borrowed from wartime radar sets has provided the peak power flashes needed to make super-speed x-ray motion pictures.

Mr. Donald C. Dickson, of the Westinghouse Research Laboratories, recently stated at the National Electronics Conference that a special high voltage, radar-type pulse transformer and an electronic tube are key units in making exposures of 10 millionths of a second on x-ray film moving at 150 frames a second. The tremendous surges of high voltage power necessary to make these exposures are similar to the split-second pulses required to transmit radar signals.

The electronic tube is flashed at 150,000 volts, and the power during pulses exceeds 5 million watts. The tube used for x-ray movie work is a 14-inch long cylinder. This is immersed, along with the radar-type transformer, in an insulating oil bath and is placed 3 feet from the x-ray film.

In order to generate the type of x-radiations needed, it was necessary to heat the tube filament to a temperature where tube life would be limited to 15 minutes. At 150 frames a second, 135,000 individual radiographs could be taken, requiring more than 6 miles of 9½-inch wide film to record them.

For medical and other industrial uses, longer power surges, greater x-ray penetrations, slower exposures, and larger operating fields may be required.—Westinghouse Electric Corporation, *Bloomfield, New Jersey.*

Magnetic Test Set

A new type of test set for magnetic materials in laminar form is announced by the General Radio Company.

Measurements of permeability and core loss are made at 60 cycles and at low levels such as are encountered in inductors and transformers used in communication systems.

Test sample can be a single lamination or a few duplicate strips in parallel. Minimum length of sample is 2¼", maximum width is ⅜".

Measurements are made on a Maxwell bridge of the inductance and loss of a solenoid surrounding the sample, which is clamped in test yoke so designed that its reluctance is negligible compared to that of the sample.

The sinusoidal magnetizing force applied to the test sample is adjustable from one millioersted to six oersteds. A d.c. magnetizing force up to 2 oersteds can also be applied for incremental measurements. Permeability range is 25,000 full scale for a specimen cross section of 10 sq. mm, for which the dial reads directly in permeability.

Accuracy of absolute measurements depends upon the precision with which the specimen cross section is known. Similar samples of identical cross section can be compared with an accuracy of 2 percent.—GENERAL RADIO COMPANY, *275 Massachusetts Avenue, Cambridge 39, Massachusetts.*

Midget Meter

International Instruments announces the development of a midget meter, 1 inch in diameter, with a scale arc of 270°. This will provide a scale chord even longer than that obtainable on 3½-inch conventional meters.

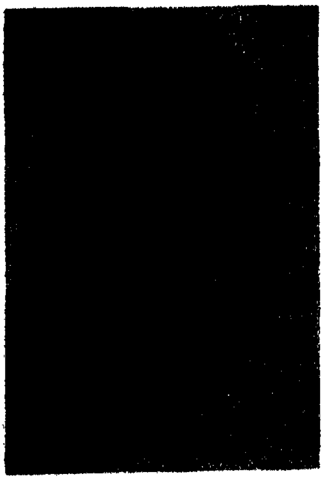

The 1-inch instrument is being developed for special uses in aircraft applications, where size and weight limitations are of prime importance. Other applications are anticipated by the manufacturer, to include radio and television fields, laboratory test equipment installations, and other instances where the use of miniature meters of high accuracy is required. Accuracy is stated by the maker as 2 percent. These midget meters operate on the same general principles as do the conventional D'Arsonval moving-coil types.

The meter is stated to be ruggedly constructed to withstand vibration and shock. The instrument can be made watertight and is designed to mount by means of a threaded ring.—INTERNATIONAL INSTRUMENTS, INC., *331 East Street, New Haven 11, Connecticut.*

Ion Chamber Charger-Reader

A new Model 2050 charger-reader, designed to be used in conjunction with pocket-type ionization chambers, is announced by the Nuclear Instrument and Chemical Corporation. The ionization chambers are used as health monitoring devices in the presence of gamma- or x-ray types of radiation.

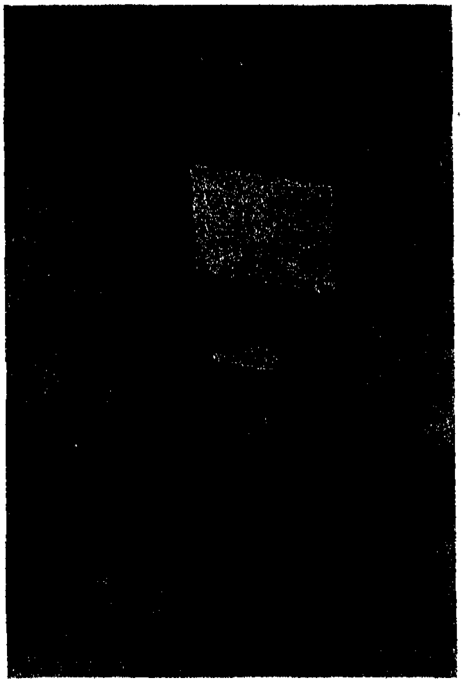

The functions of the Model 2050 are twofold. It will charge the ion chamber to a known voltage, and it will measure the residual chamber charge after exposure to radiation. This 110-volt a.c. operated electronic voltmeter and electrometer will charge and read the nuclear Model 3340 diaphragm-type pocket meter, and, by rotation of a selector switch, the non-diaphragm type-pocket ion chamber can also be checked. All "charge" and "read" observations are made on a 3-inch meter with a linear scaler. Accuracy is ±2½ percent of full scale.

Operation of the 2050 is very simple. The regulating circuits will allow stable operation with an a.c. power variation of from 95 volts to 130 volts. The unit is housed in a smooth grey-finish steel cabinet 6″×5″×10½″, and provision is made for storing up to seven pocket ion chambers within the case cover.—Nuclear Instrument and Chemical Corporation, *223 West Erie Street, Chicago, Illinois*

Beta-Gamma-Scaler

The new Kelley-Koett beta-gamma scaler, Model K-280, is 22″×11″×15″ (deep) and weighs only 47 pounds. It was designed and developed for the precise measurement of radioactivity. It may be used for research work, for assaying of metals, and for many other research or routine counting jobs. Incorporated in the scaler are such features as a scale of 256, scale selector, autocount, and autotime. The scaler has a resolving time of 5 microseconds or better. The high voltage supply is continuously variable from 500 to 2000 volts, with regulation of 0.02 percent for 1 percent change in line voltage. The G-M input terminals are located on the front and rear of the scaler. A Highinbotham scaling circuit is incorporated in the Keleket scaler. A detailed bulletin containing a complete description, specifications, and illustrations will be mailed upon request.—Instrument Division, Kelley-Koett Manufacturing Company, Department B, *Covington, Kentucky.*

Vibration Meter

The new Calidyne vibration meter is designed to read vibration levels directly in r.m.s. inches or r.m.s. inches per second when used with the velocity pick-up made by the MB Manufacturing Company.

The vibration meter is a self-contained, battery-operated unit with internal calibration requiring no external power connection—thus offering the utmost convenience for field testing.

Integration of the velocity pick-up signal to provide displacement measurements directly is effected by throwing a switch. No scale factor or conversion is required.

The instrument is handsomely cased in walnut, is only 7×8¾×11 inches in size, and 14 pounds in weight. Range from 0.001 to 50 inches per second; 0.001 inch up for displacement. Price $350, f.o.b., Winchester, Massachusetts. —The Calidyne Company, *751 Main Street, Winchester, Massachusetts.*

r-f Z-Angle Meter

Another step ahead in speedy, efficient, accurate measurements of complex electronic circuits is announced by the Technology Instrument Corporation engineers with the presentation of the recently developed r-f Z-angle meter. Wherever this new instrument has been shown during the months of testing before its formal announcement to the electronics industry, it has been acclaimed for the way in which it provides direct reading of impedance and phase angle at radio frequencies.

The r-f Z-angle meter has been developed by the engineers who produced the Z-angle meter, which has found wide acceptance for measuring at audiofrequencies, the impedance and phase angle of loudspeakers, transformers, transmission lines, and complex networks without the need of extensive mathematical calculations. The instrument promises to provide the same ease of measurement, at radio frequencies, of broadcast antennas and transmission lines, and for general laboratory measurements which, heretofore, have been avoided because of the cumbersome equipment and calculations involved. The r-f Z-angle meter

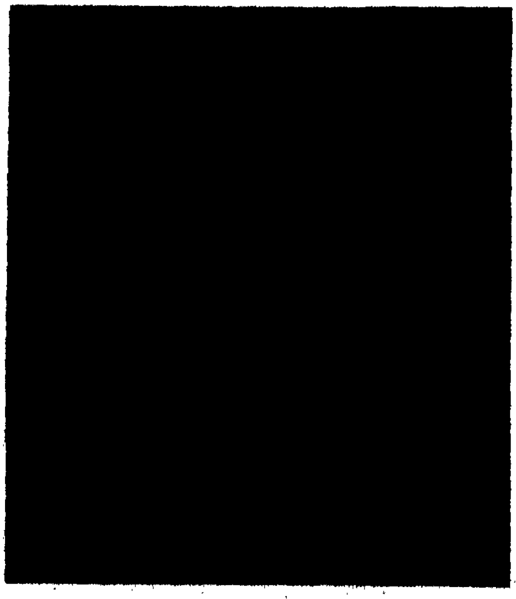

is carefully engineered and produced to the exacting specifications which assure users of electronic measuring devices of a highly efficient and practical instrument.

Technical data, prices, and other information are available on request from the TECHNOLOGY INSTRUMENT CORPORATION, *1058 Main Street, Waltham 54, Massachusetts.*

Fatigue Tester

Accelerated fatigue tests by reverse bending at natural or resonant frequencies are obtained with this pneumatically operated fatigue tester. The pneumatic resonant principle is employed, and a relatively small air supply is required.

The fatigue tester consists of an air-operated fatigue motor, a telescope, a pressure regulator, and an air valve.

The test sample, which may be a material specimen or a finished part, is clamped in a holder. The free end is vibrated by air pressure through a tuned air column until the piece fails.

Samples with resonant frequencies between 50 and 300 cycles per second can be tested. Amplitudes of vibration up to 0.5 inch on the free end may be obtained. The specimen is vibrated under conditions which simulate the actual dynamic loading conditions, and, since the specimen is vibrated at its own resonant frequency, test duration is usually short.

The fatigue motor is made up of a holder in which the specimen is clamped, 2 small pistons which are easily attached to the free end of the specimen, and an adjustable air column. This motor operates from a compressed air supply of 20 lb. per square inch minimum pressure and requires approximately 20 cu. ft. per minute. The adjustable air column can be made tunable over a vibration frequency range of roughly 50 to 300 cycles per second, with the use of seven "trombones" provided with the fatigue tester.

A telescope mounted on the fatigue motor is used to measure the displacement of the vibrating specimen directly in thousandths of an inch.

The pressure regulator maintains a constant air pressure on the fatigue motor up to 20 lb. and can be used for air pressure up to 90 lb. Since the power available from the fatigue motor is a function of air pressure, the pressure regulator is adjusted to the air system, to obtain maximum power. Generally, 20 to 30 lb. per sq. in. is sufficient to drive most specimens.

An air valve is supplied for insertion in the air line between the pressure regulator and the fatigue motor. This is used to control vibration displacement of the specimen.—GENERAL ELECTRIC COMPANY, *Schenectady 5, New York.*

High Accuracy Mercury Manometer

A new type of mercury manometer has been designed and built by the Taylor Instrument Companies to meet requirements of positive actuation, dependable performance, and greater adaptability in flow, liquid level, and differential pressure measurement. The new manometer is designated as Model 1500 to signify its 1500 p.s.i. working pressure and is available in differential pressure ranges of 10 to 400" of water. It is built for use on indicating, recording, or controlling instruments, and two manometers can be mounted on a single case for recording two flows or ratio flow control.

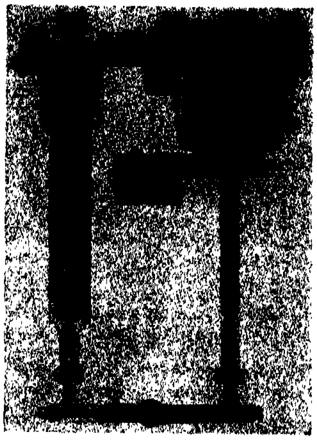

A few of its outstanding features include: (a) *Greater energy output* which is made possible by the use of a large diameter float and long float travel. (b) *Specially designed pressure tight bearing* of stainless steel with Teflon bearing surfaces—the new synthetic plastic whose self-lubricating characteristic assures no freezing, reduces friction to a minimum, and gives leak-proof performance. (c) *Positive overrange protection* is provided with positive-acting, non-sticking check valves submerged in mercury. These valves give protection against loss of mercury from overrange, sudden fluctuations, and flow reversal. (d) *Leakless damping adjustment* under full-rated pressure is assured with an uniquely designed damping device. (e) *Interchangeable range chambers* contribute greatly to the adaptability of the new manometer which now gives continuous ranges from 10 to 533" of water. No piping changes are necessary when changing from one range to another.—TAYLOR INSTRUMENT COMPANIES, *Rochester 1, New York.*

Piezoelectric Gauges

For those who need to measure pressures of "instantaneous" or "explosive" nature, piezoelectric gauges which will give faithful measurements of transient pressures varying from a few pounds to 30,000 p.s.i. are now available commercially.

The remarkable piezoelectric gauge, developed during the war under U. S. Navy contract, is now available for peacetime industrial and laboratory applications. The gauge works on the principle that when certain types of crystals are placed under sudden compressive stress, an electric charge is generated which is proportional to the stress. This charge can be measured and the stress computed, or indicated by suitable instrumentation.

Piezoelectric gauges are applicable only to rapid transient pressures or "explosive" pressure rises. They will not record slow pressure changes regardless of amplitude. Their usefulness lies in their ability to measure shocks of high magnitude when transmitted through liquids, gases, and, in some cases, through solids. Piezoelectric gauges were used to measure air and underwater pressure at the Bikini atom bomb tests. They are used in measuring "artificial earthquakes" set up in geophysical oil field exploration. They may also be used for such applications as measuring the explosive forces in the firing chambers of big guns and in the cylinders of internal combustion engines. The large gauge shown is for blast pressures in gaseous mid-air, and the small one is for underwater use.—Cambridge Thermionic Corporation, *Concord Avenue, Cambridge 38, Massachusetts.*

Earth-Shock Acceleration Detector

A new instrument which measures the intensity of explosion shock waves passing through the earth has been announced by General Electric's Special Products Division.

Called the "earth-shock acceleration detector," the new device is about the size of a small tin can. It is designed so that it can be buried near the scene of test explosions, enabling engineers to determine the underground velocity and acceleration of shock waves caused, for example, by the use of high explosives on large construction projects. The instrument can register shocks up to 1500 times the force of gravity, and as many as 10,000 impulses per second.

The acceleration detector contains crystals which generate a voltage when under stress. Signals from the crystals are carried through cables to amplifiers and delicate recorders above ground.

Four of the new instruments, recently used on the site of Watauga Dam, near Elizabethton, Tennessee, gathered data on what sort of shocks occur 130 ft. below a half-million pounds of high explosives. The explosions were set off by the Tennessee Valley Authority in constructing an earth dam.

These acceleration detectors are not stock items but are "custom built." In each different case, the specific design of the detector is determined by the individual application for which it is to be used. For further information contact the Special Products Division, General Electric Company, *Schenectady 5, New York.*

Manufacturers' Literature

Instrument Notes—8-page brochure, No. 5, Oct.-Nov. 1948, on temperature compensation of bridge-type transducers, describes methods of compensation for two types of errors caused by ambient temperature variations; it includes circuit diagrams.—Statham Laboratories, Inc., *9328 Santa Monica Boulevard, Beverly Hills, California.*

Technique—Vol. 2, No. 4, *Muirhead Journal of Instrument Engineering* features articles on phase displacement, variable air capacitor of zero loss angle, and screens and guard rings in electrical measurements.—Muirhead and Company, Limited, *Beckenham, Kent, England.*

Tracelog—12-page house organ, No. 13, features a description of the improved radiation survey meter, includes a list of more available C-14 tagged compounds, and other items of interest.—Tracerlab, Inc., *55 Oliver Street, Boston, 10, Massachusetts.*

The Experimenter—8-page General Radio bulletin, Vol. XXIII, No. 5, gives a complete description of a new coaxial connector for the laboratory, with cut-away photographs, sketches, and charts.—GENERAL RADIO COMPANY, *275 Massachusetts Avenue, Cambridge 39, Massachusetts.*

Pressure and Vacuum Gauges—A new catalog, 31 pages, gives full descriptions of various indicating and recording gauges and controllers. It is well illustrated with schematic drawings, photographs, and diagrams.—THE BROWN INSTRUMENT COMPANY, *Wayne and Roberts Avenues, Philadelphia 44, Pennsylvania.*

Taylor Instruments—A completely revised illustrated edition of *Taylor Guide to Correct Instrument Selection*, Bulletin 98170, gives a bird's-eye view of the companies' entire industrial instrument line. The field of application of each type of instrument is covered, as well as its principle of operation and range limits.—TAYLOR INSTRUMENT COMPANIES, *Rochester 1, New York*

Speed Measuring Instruments—A new 28-page bulletin 35-30 presents the description, operation, and selection of chronometric, centrifugal, and resonant reed tachometers. A selection of ranges up to 100,000 r.p.m. are available in single and multirange instruments.—JAMES G. BIDDLE COMPANY, *1316 Arch Street, Philadelphia 7, Pennsylvania.*

Micromax Model S—32-page illustrated catalog ND44(1), just issued, lists, for the first time in one publication, the complete line of stripchart micromax recorders and controllers for measuring a wide variety of process variables.—LEEDS AND NORTHRUP COMPANY, *4934 Stenton Avenue, Philadelphia 44, Pennsylvania.*

RCA Technical Bulletins—Two technical data sheets—one on the 4-250A/5D22 power tetrode, forced-air-cooled, for use as an a-f power amplifier and modulator as well as r-f power amplifier and oscillator, and one on the 308S2, and 408S2 eight-inch speakers of the permanent magnet type—have recently been issued.—TUBE DEPARTMENT, RADIO CORPORATION OF AMERICA, *Harrison, New Jersey.*

Deposited Carbon Resistors—2-page catalog data bulletin B-4 gives complete electrical characteristics and mechanical specifications on the IRC precistors which feature high stability and low voltage coefficient.—INTERNATIONAL RESISTANCE COMPANY, *401 North Broad Street, Philadelphia 8, Pennsylvania.*

***p*H and Conductivity**—Catalog No. 15-12 features *p*H and conductivity control and their application to different industrial processes. This 43-page catalog is fully illustrated with photographs and schematic drawings.—BROWN INSTRUMENT COMPANY, *Wayne and Roberts Avenues, Philadelphia 44, Pennsylvania.*

New Materials

Forest K. Harris: Associate Editor
in Charge of this Section
National Bureau of Standards, Washington, D. C.

Titanium

Titanium, one of the least exploited metals, is widely distributed as a minor constituent or impurity in many minerals and is the ninth most abundant of the elements, being 23 times as abundant as carbon. The fact that it is difficult to separate from its ores as a pure metal has kept it in the class of laboratory curiosities until quite recently, and little is known concerning the metallurgy and properties of its alloys. A successful method of refining it was developed by the Bureau of Mines recently, and it is now being produced in a ductile form by du Pont in a pilot plant having 100 pounds daily capacity.

It is a silver-white metal having a density of 4.5 and a melting point of 3140°F. Its yield strength is about 70,000 p.s.i. in the annealed form, and about 100,000 p.s.i. when cold worked. In the ductile form it is easily worked. Also, it has excellent corrosion-resistant properties. Tests have shown that, without protection it withstands atmospheric and salt-water corrosion better than most structural materials. In strength and corrosion resistance it compares with 18-8 chromium-nickel stainless steel, but weighs only about half as much per unit volume.

The use of titanium oxide, as a pigment in paints, and for certain other special applications, has been realized commercially during the past 20 years, but the possible industrial uses of the metal itself have not been explored. Enough is known to indicate that it can be used where a high strength-weight ratio is needed. An early major use may be in high speed planes. It may find applications in corrosion resistant equipment, particularly where heat and pressure are great.

Research on titanium metal and its alloys is being actively pursued by a number of organizations. It is now available in sponge form (99.5 percent pure) at a price of $5 per pound in 100 pound lots, and will shortly be produced in ingots. Mass production will, of course, make it possible to reduce the price sharply. The du Pont Company will supply small samples without charge to industrial and university laboratories for testing.—E. I. DU PONT DE NEMOURS AND COMPANY, *Wilmington 98, Delaware.*

Small Aluminum Tubing

A kit, containing an assortment of small bore aluminum tubing, has been made up for the use of instrument repairmen, to match the mass and inertia of instrument pointers which must be replaced. *3-S* aluminum alloy tubing in outside diameters of 0.0155, 0.019, 0.023, and 0.026 inch and *52-S* aluminum alloy with an outside diameter of 0.019 inch are included. Wall thicknesses are 0.0015 and 0.002 inch. The tubes are of convenient lengths and the kit contains a total of 25 feet of tubing.—PRECISION TUBE COMPANY, *3826 Terrace Street, Philadelphia 28, Pennsylvania.*

Castable Refractory

Firecrete 3x, a new castable refractory for use up to 3000°F, is supplied dry and mixed with water just before use. It may be cast or poured into wood or metal forms to produce special shapes such as burner blocks, door linings, covers, and complete furnace linings. The casting is air-cured for 12 hours and then heated slowly to a temperature above that at which furnace operation will be held. A cubic foot of construction requires 135 pounds of material. Shrinkage is said to be negligible.—JOHNS-MANVILLE SALES CORPORATION, *22 East 40 Street, New York 16, New York.*

Heat-Resistant Polystyrene

Koppers P-8, is a heat-resistant, low shrinkage, polystyrene molding compound made by a new process in which a close control is held over molecular structure. It is stated to mold as easily as the regular grades of polystyrene and to result in a glass-clear product. The manufacturer reports that it has a heat-distortion temperature of 204°F or better when tested in accordance with ASTM D648 and that when a molded piece supports only its own weight, short-time immersion in boiling water does not soften the material enough to warp it materially. Molded articles were unaffected by a 15-minute immersion in boiling water.—KOPPERS COMPANY, INC., *Chemical Division, Pittsburgh 19, Pennsylvania.*

Plastic Pipe

Light-weight plastic pipe, designed for working pressures up to 650 p.s.i. and temperatures up to 100°F, is now being produced on a commercial scale. Standard tees, ells, and joints can be used with this pipe. It is stated to handle a variety of fluids including water, organic solvents, alkalis, etc., as well as natural and manufactured gas. 3½ feet of the 1″ pipe weighs 1 pound. This pipe is now available in standard, heavy-wall pipe sizes from ½″ I.D. to 3″ I.D.—EXTRUDERS, INC., *8509 Higuera Street, Culver City, California.*

Thermosetting Adhesive Film

Scotch-Weld Bonding Film, is applied as a transparent film between surfaces to be joined. Pressures from 25 to 100 p.s.i. and temperatures from 300 to 500°F, for times from 5 to 60 minutes are used in bonding. In a test application, 0.064″ aluminum bonded to itself, was said to develop a shear strength of 3500 p.s.i. in the joint. Only conventional cleaning is required to prepare surfaces. The film is available in rolls of from ¼″ to 36″ width and in film thicknesses from 0.002″ to 0.008″. It is not tacky to the touch when removed from the roll.—MINNESOTA MINING AND MANUFACTURING COMPANY, *902 Fauquier Avenue, St. Paul 6, Minnesota.*

Ultra-Fine Abrasive Powders

Type A-5175 alpha-aluminum oxide has a hexagonal crystal structure and a hardness of 9 on the Moh scale. Its particle size is 0.3 micron, and its apparent density is 4 g/cc. *Type B-5125* gamma-aluminum oxide has a cubic structure and a hardness of 8. Its particle size is under 0.1 micron, and its apparent density is 3.6 g/cc. Both are suitable for metallographic or other fine polishing work and may be applied either dry or in slurry. Both are also suitable for use as ingredients in the manufacture of phosphors and as catalyst carriers.—LINDE AIR PRODUCTS COMPANY, *32 East 42 Street, New York 17, New York.*

Rust Preventive Wrapper

Nox-Rust Wrapper is a special kraft paper impregnated with a chemical which, on slow vaporization, passivates the surface of metal to prevent corrosion. The presence of the impregnant does not particularly alter the appearance or strength of the wrapper, and it is stated to be non-toxic and odorless. Its action does not depend on the package being sealed, and its stability is such that its protection is "for an indefinite period of time." The manufacturer reports tests which show complete protection to the contents of unsealed packages over a period of 45 days in a relative humidity of 100 percent at a temperature of 120°F. Since it does not require sealing and is effective on uncoated metals, it should offer considerable economies in packaging steel parts.

Samples and further information may be secured from the manufacturer.—NOX-RUST CHEMICAL CORPORATION, *2419 South Halstead Street, Chicago 8, Illinois.*

Lens Cleaner

Klr-Vu, a liquid cleaner for optical glass surfaces, is stated to leave an invisible film which gives long-lasting protection against fogging or frosting under severe conditions. The manufacturer also states that glass which has been treated with the liquid has measurably increased light transmission and remains clean considerably longer than normally.—SAX KLEEN COMPANY, *11 Bleeker Street, Albany 2, New York.*

THE REVIEW OF SCIENTIFIC INSTRUMENTS

VOLUME 20, NUMBER 2 *FEBRUARY, 1949*

Trochotron Design Principles

G. W. MONK* AND G. K. WERNER
Carbide and Carbon Chemicals Corporation, Oak Ridge, Tennessee
(Received July 23, 1948)

A simple derivation of the perfect focusing properties of the trochoidal type mass spectrometer, which leads to convenient methods of correlating the many variables for design purposes, is given. Nomographs and general trochoids are given which apply to charged particles in crossed, uniform, electric, and magnetic fields.

I. INTRODUCTION

THE perfect focusing properties of the crossed electric and magnetic fields of a trochotron were first pointed out by Bleakney and Hipple[1] who also described two small experimental units and gave a chart to simplify calculation of the focal distance of such an instrument. A much larger prolate instrument with a focal distance of 40 cm was built at this laboratory and described briefly by Monk, Horton, and Graves,[2] while more recently a 9-cm trochotron for low mass isotopic assay was also constructed here. All of these instruments demonstrated that the unique focusing properties of the trochotron are easily obtained in practice with moderately precise equipment.

Many of the following advantages of the trochotron were first pointed out by Bleakney and Hipple:[1]

(a) The focal distance is independent of the angle with which the ions enter the analyzing fields. This is true for all angles and means that only two precise slits are required, one to define the position of the source and the other placed at the focal point to limit the mass range received by the collector plate. If photographic detection is used, only the source slit is required.

(b) The focal distance is independent of the energy or velocity with which the ions enter the analyzing fields. This, in combination with (a) means that any of a great variety of sources can be used since any ions passing through the source slit will be focused at a distance dependent only upon m/e and the fields.

(c) For fixed analyzing fields the focal distance is proportional to m/e of the particle. If a photographic plate is used for a detector, the masses will be linearly spaced along the plate. This linearity also indicates that the trochotron has twice the resolution of a 180° instrument with the same focal distance.

The disadvantages are predominantly ones of size or mechanical consideration:

(a) The magnetic field must be maintained uniform over a larger region than in any other type of mass spectrometer of the same performance.

(b) A uniform electric field must be maintained over a relatively large region inside the vacuum tank.

(c) The focal point for a given m/e is not unique in that ions of different m/e may pass through that focal point on the way to their own focus, and negative ions of the same numerical m/e will be focused at the same point as the positive ions if they have enough energy to enter the analyzer. This difficulty is easily eliminated in a practical design.

(d) The number of variables which can take a wide range of values makes calculations of performance under various conditions somewhat more involved than with conventional instruments.

The motion of ions in crossed, uniform, electric, and magnetic fields has been studied, both neglecting[1,3,4] and considering[5,6] the relativity effect. The purpose of this paper is to present a simple method of demonstrating the focusing properties of such fields and give practical curves, nomographs, and equations as an aid to computation.

---

* Now at Camp Detrick, Frederick, Maryland.

[1] W. Bleakney and J. A. Hipple, Jr., Phys. Rev. **53**, 521 (1938). Patent No. 2,221,467, *Focusing and Separation of Charged Particles* issued to Walter Bleakney Nov. 12, 1940 and assigned to Research Corporation of New York.

[2] G. W. Monk, J. L. Horton, and J. D. Graves, Rev. Sci. Inst. **18**, 796 (1947).

[3] L. Page and N. I. Adams, Jr., *Principles of Electricity* (D. Van Nostrand Company, Inc., New York, 1931), p. 282.

[4] N. D. Coggeshall, Phys. Rev. **70**, 270 (1946).

[5] L. Page and N. I. Adams, Jr., *Electrodynamics* (D. Van Nostrand Company, Inc., New York, 1940), pp. 241–246, 478–483.

[6] W. R. Smythe, *Static and Dynamic Electricity* (Edwards Brothers, Inc., Ann Arbor, 1936).

Coggeshall[4] describes another arrangement having perfect focusing properties in which the magnetic field is uniform but the electric field strength is proportional to the distance from some axis along the magnetic field. No advantage over the uniform fields is apparent, however, and the difficulty of maintaining such an electrostatic field is great.

The term "trochotron" apparently was first used in a published paper by Monk, Graves, and Horton[2] but recently[7] was also applied to a vacuum tube in which the electron paths were trochoidal.

II. FOCUSING PROPERTIES OF CROSSED, UNIFORM, ELECTRIC AND MAGNETIC FIELDS

Consider a rectangular coordinate system oriented as shown in Fig. 1 with the origin on the ion of mass m, and charge e—at a time when its velocity is v—making an angle, θ, with the positive x axis. Relativity effects will be neglected and, unless otherwise specified, c.g.s.-electrostatic units will be used—except in the case of the magnetic field which will be measured in gauss and assumed large compared to the electric field E.

Instead of calculating the force exerted by the magnetic field on the particle as a result of its total velocity, v, consider two components of v, as shown in Fig. 2, so that one, v_A, is equal to Ec/H along the positive x axis.[8] This component is of such a magnitude and direction that the magnetic force, Hev_A/c, generated by it along the negative y axis, is just equal and opposite to the total electrostatic force, Ee. Thus the problem reduces to combining this uniform translatory motion with the motion that results from a velocity, v_P, in the magnetic field alone. Of course, if this v_P were the velocity of the ion in the magnetic field alone it would execute a circle in a time given by

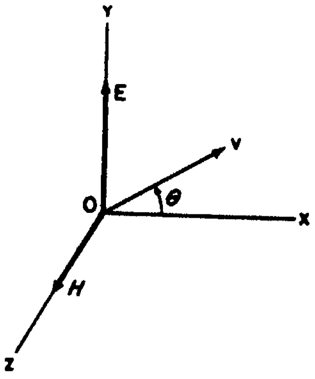

FIG. 1. Orientation of the axes with respect to the fields and the charged particle.

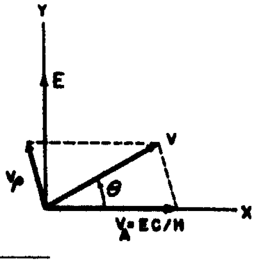

FIG. 2. Components of the initial velocity, v, that are used in the derivation.

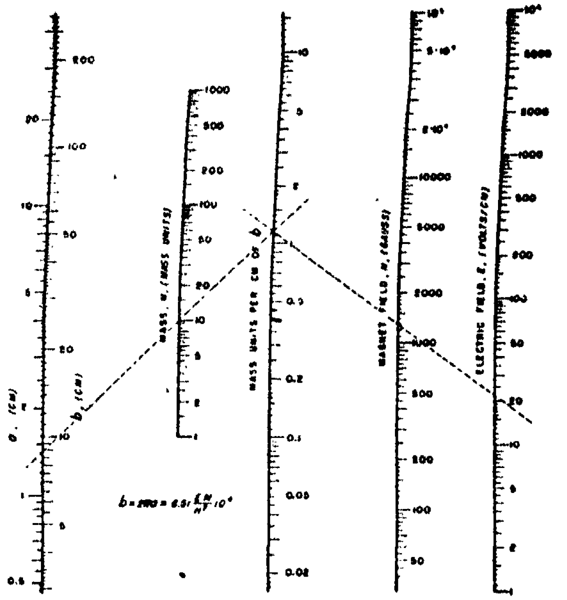

FIG. 3. Nomograph for correlating the variables in Eq. (4). The dotted lines show typical operating values of a trochotron having a focal length of 8.9 cm and receiving mass 10.

$$T = 2\pi mc/He, \tag{1}$$

which is independent of v and θ. At the end of this time the entire circle will be traversed and the translatory velocity, Ec/H, will have moved the particle along the x axis a distance

$$b = v_A T = 2\pi mc^2 E/H^2 e, \tag{2}$$

which is also independent of v and θ. *Thus the particle executes circles while simultaneously being carried along the x axis at a uniform rate, and the length of a cycle does not depend upon the angle or velocity with which the ion enters the fields.*

Such a path is trochoidal in shape and, if the translated circle is thought of as being carried along by a rolling circle, the latter must be assigned a circumference b and hence a radius

$$a = b/2\pi = mc^2 E/H^2 e. \tag{3}$$

However, the concept of a rolling circle can be very confusing because of the difficulty in locating the line along which it rolls for given initial conditions.

The value of v_P can be obtained easily from Fig. 2 by the law of cosines, and hence the radius, ρ, of

---

[7] H. Alfven and H. Romanus, Nature 160, 614 (1947).

[8] A somewhat similar demonstration was used by W. G. Dow, *Fundamentals of Engineering Electronics* (John Wiley & Sons, Inc., New York, 1937), pp. 66–70.

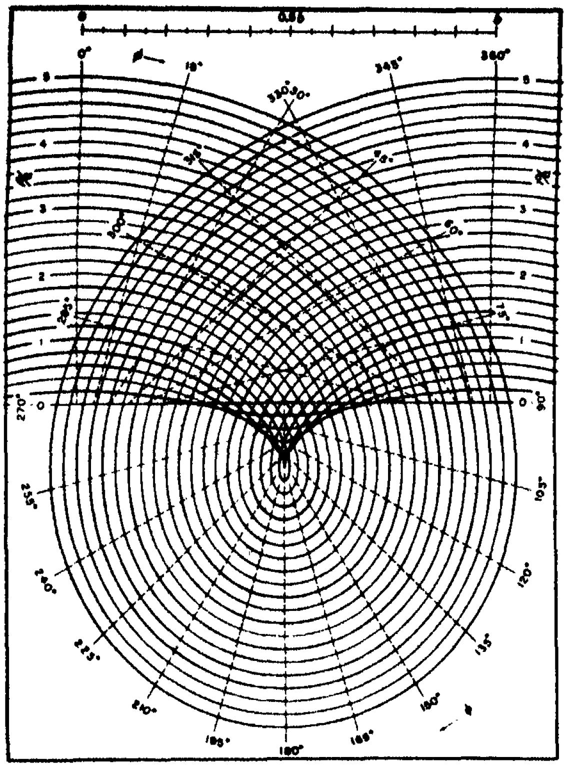

FIG. 4. General trochoids drawn by machine with the same b and difference values of ρ/a.

the circle being translated is calculable. If $\rho > a$, the path will be called a prolate trochoid; if $\rho < a$, it will be called a curtate trochoid; if $\rho = a$, it will be called a cycloid. This definition of prolate and curtate agrees with Bleakney and Hipple[1] but is reversed from that given by Page and Adams.[3,5] Actually the calculation of v_ρ and ρ is not necessary in determining the details of the path by means of the nomographs and charts to be given here.

III. USE OF THE NOMOGRAPHS AND GENERAL TROCHOIDS

The focal length of a trochotron is given by Eq. (2), which can be written in the more practical form

$$b = 6.51(ME/H^2)10^4 \text{ cm}, \tag{4}$$

where M is the mass of a singly charged ion in mass units, E is the electric field in volts per cm, and H is the magnetic field in gauss. Figure 3 is a nomograph for correlating the variables of Eq. (4). Any two straight lines that intersect the center index at the same point connect values of b, M, E, and H that satisfy (4). The center index is calibrated in mass units per centimeter of b to indicate the "mass density" along the focal plane. The dotted lines show typical operating conditions for the 8.9-cm trochotron receiving mass 10.

General trochoids, drawn by machine with different values of ρ/a but the same b are reproduced in Fig. 4. It is intended that the starting point in this chart for given conditions be ascertained by the method to follow, tracing paper laid over the curves, and the proper trochoid sketched in, to give a scale drawing of the ion paths. To find the starting point, first find the ratio, σ, of the initial velocity, v, to the average velocity, v_A, by means of the nomograph given in Fig. 5. The dotted lines are for typical operating conditions in the 8.9-cm trochotron. Now using this value of σ and the given initial angle, θ, construct the triangle shown in Fig. 6 with the vertical leg one unit long. The angle ϕ will be the phase angle given in Fig. 4 and is determined by the fraction of b that the translatory velocity has carried the center of the circle, and is equal to the angle of rotation of the rolling circle. The manner of measuring ϕ in Fig. 6 has been adjusted to correspond to the way the trochoids were

FIG. 5. Nomograph for computing the ratio of the initial velocity to the average velocity.

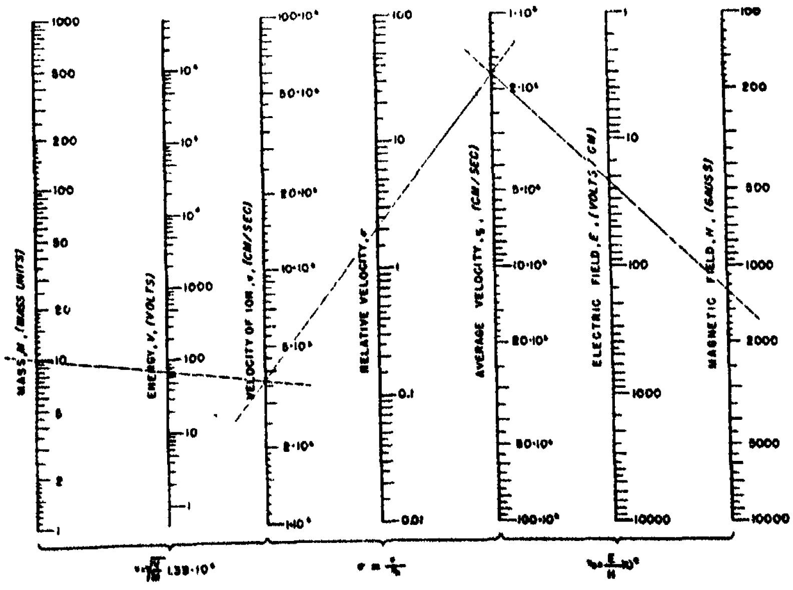

constructed in Fig. 4. The side opposite θ in Fig. 6 will be equal to ρ/a. Now the trochoid corresponding to this ρ/a can be located on Fig. 4, and its intersection with the proper ϕ coordinate will determine the starting point at which the ion had the velocity v at an angle θ. Other points on the path have the same ρ/a, but σ and θ change as the ρ/a vector in Fig. 6 rotates clockwise. Sketch the curve in the direction of increasing ϕ up to $\phi=360°$. Then move the tracing so that this end falls on the same ρ/a curve at $\phi=0°$ and complete the cycle.

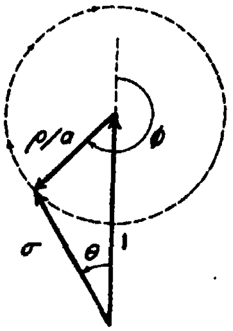

FIG. 6. Construction to allow the graphical evaluation of ρ/a and ϕ.

The y coordinate of the particle is equal to the y coordinate of the end of the ρ/a vector in the construction. The x coordinate of the particle is equal to the x coordinate of the end of the same vector plus ϕ (in radians).

The validity of this construction is easily shown by dividing each side of the velocity triangle in Fig. 2 by $v_A=Ec/H$. Lines of constant σ and lines of constant θ could be superimposed on the general trochoids of Fig. 4 to eliminate the need of any construction; this method was tried, but the result was found to be crowded and confusing.

The curves in Fig. 7 were traced according to the procedure outlined using initial conditions for the 8.9-cm trochotron. Curves 1, 2, and 3 are for the normal operating conditions indicated on the nomograph of Fig. 5 for an accelerating voltage of 75 volts and entrance angles of 75°, 90°, and 105°, respectively. Curves 4, 5, and 6 are for the same angles and mass but with an accelerating voltage of 100 volts. Curve 7 shows part of the path of an ion of twice the mass leaving the source normally at 75 volts when the electric field is one-half its value for the other curves.

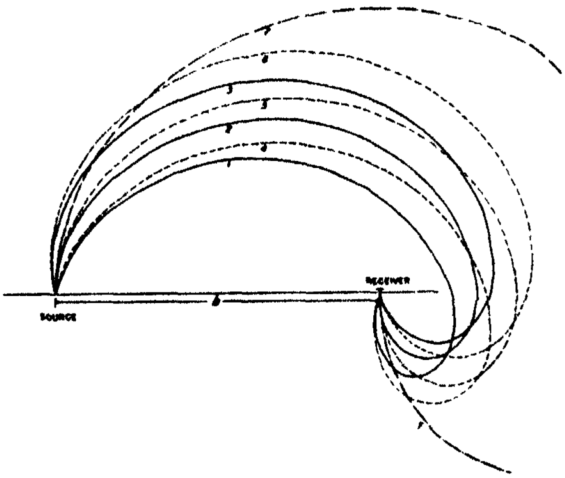

FIG. 7. Typical ion paths in a trochotron sketched from the general trochoids in Fig. 4.

The general theorem of Bleakney[9] is, of course, applicable to the trochotron and indicates that for particles of different e/m to follow the same path from source to collector tuning should be accomplished by varying either the magnetic field or the initial velocity in proportion to the electric field. In the case of the trochotron, this latter possibility implies that with a fixed angle of entrance the accelerating voltage could be varied proportionally with the electric field to avoid changes in the path of the received ion.

This document is based on work performed during 1947 under Contract No. W-7405-eng26 for the Atomic Energy Commision at the Carbide and Carbon Chemicals Corporation, Oak Ridge, Tennessee, and was released for publication on July 19, 1948.

---

[9] W. Bleakney, Am. Phys. Teacher 4, 23 (1936).

THE REVIEW OF SCIENTIFIC INSTRUMENTS VOLUME 20, NUMBER 2 FEBRUARY, 1949

A Servo Employing the Magnetic Fluid Clutch

E. S. BETTIS AND E. R. MANN
NEPA Project, Fairchild Engine and Airplane Corporation, Oak Ridge, Tennessee

(Received August 13, 1948)

A simple servo unit is described. The device utilizes the electromagnetic fluid clutch developed by J. Rabinow of the National Bureau of Standards. Simplicity in design and construction, relatively high torque inertia ratio obtainable, and high power transmission capabilities appear to be the chief merits of such a servo system. Performance data on a prototype servo unit are submitted.

INTRODUCTION

SERVO-MECHANISM design is often a difficult process. The complexity of the process is increased when it becomes necessary to meet rigid specifications of performance and reliability. Hence, a laboratory not equipped to develop a servo system satisfying its unique application requirements must either adapt a commercially available unit, or rely upon servo development by a specially qualified organization. Excessive expense and lack of versatility are too frequently the results of these practices.

Utilizing the principle of the electromagnetic fluid clutch (developed by Rabinow at the National Bureau of Standards),[1] a prototype positioning servo unit has been constructed in the Controls and Instrumentation Section of the Air Force-Fairchild Engine and Airplane Corporation's NEPA Project in Oak Ridge, Tennessee. With this assembly, the applicability of the clutch to use in a servo mechanism has been studied, and preliminary determinations of its torque, response, driving speed, reliability, and other pertinent characteristics have been made.

In the electromagnetic fluid clutch, the air gap of a conventional magnetic coupling is replaced by a fluid having high magnetic susceptibility. Such a fluid is an oil base containing a suspension of fine particles of magnetic material, such as soft iron. The coupling efficiency of the clutch can thus be increased appreciably, and wide variations in transmitted torque can be obtained by means of a simple and continuous control.

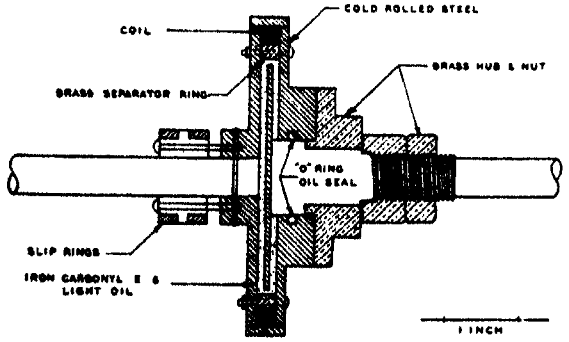

FIG. 1. Magnetic clutch.

Exciting coils for the electromagnet can be arranged in parallel to provide a low inductance electrical circuit. As a result, the exciting current can be varied quickly, producing a rapid response to a command signal.

The possibility of applying this clutch to the solution of a servo problem is apparent. Simplicity of design and construction is one of its more practical advantages. In an operational sense, proportional power transmission control is possible with a relatively weak signal, and the system possesses inherent charactoristics of high torque-inertia ratios, which offer short time responses. Advantage may therefore be taken of the system's momentum, to supply the peak power necessary for the rapid motion of large masses.

The prototype servo assembly noted above incorporates the simplest form of magnetic clutch mechanism. Clutch faces, consisting of cold-rolled steel disks, are arranged in such a manner that the surrounding fluid is energized by a single exciting coil. The fluid in current use is comprised of GAF carbonyl iron powder "*E*" suspended in light oil in proportions of three units of iron to one of oil by weight. Construction details of the clutch are shown in Fig. 1.

Control of the torque transmitted through the clutch is obtained by varying the exciting current in the coil, thereby changing, in a corresponding manner, the intensity of magnetization of the iron particles suspended in the fluid. Since these particles do not have the property of permanent mag-

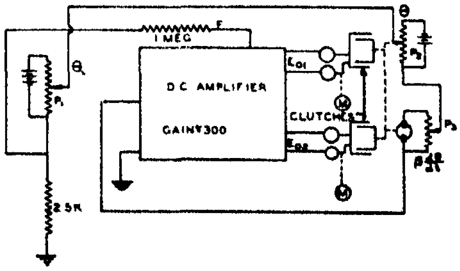

FIG. 2. Servo block diagram.

---

[1] Jacob Rabinow, United States Department of Commerce, National Bureau of Standards Technical Report 1213.

netism, the only torque transmitted between the clutch faces in the de-energized state is that caused by viscous drag in the fluid.

To provide forward and reverse motion, two contra-rotating clutch systems, with an intermediate power take-off, are utilized. Thus the direction and degree of motion may be chosen by energizing the corresponding clutch. The driven clutch faces are mechanically interconnected, with the result that the viscous drag of each balances that of the other. Motive power is provided by two quarter-horsepower electrical motors. An alternate arrangement might incorporate reverse gearing with a single motor.

A small d.c. derivative generator, connected to the output linkage, provides adequate damping of the system; accurate setting of the critical damping is accomplished by varying the generator output.

THEORY AND DESCRIPTION OF EXPERIMENTAL UNIT

A block diagram of the servo system is shown in Fig. 2. The operation of the servo as indicated by the block diagram is quite straightforward. The input to the d.c. amplifier consists of the sum of three voltages: (i) a voltage proportional to θ_i, the angular displacement of potentiometer P_1; (ii) a voltage proportional to θ, the angular displacement of P_2; (iii) a fractional part of the voltage $\beta(d\theta/dt)$ determined by the setting of potentiometer P_3, where β is the e.m.f. of the generator produced by an angular velocity of one radian per second. When the sum of these voltages is of the order of one volt with respect to ground, the amplifier output voltages Eo_1 and Eo_2 are equal to zero, and the servo is at rest position.

As shown on the diagram, potentiometer P_2 is connected to the servo-mechanical output, while P_1 can be rotated in any desired manner to introduce a displacement request signal to the system. The potentiometer P_3 is set to provide proper damping of the system from an equilibrium point.

If P_1 is rotated, the input voltage to the d.c. amplifier produces a signal at either Eo_1 or Eo_2, depending on its direction of rotation. This signal energizes one of the clutches, so that a change in the servo-mechanical output occurs. This change, by reason of the directly coupled potentiometer P_2, causes the voltage proportional to θ to compensate for the initial signal at P_1, and a new equilibrium point for the system is reached. The voltage $\beta(d\theta/dt)$ operates in the usual manner of a derivative signal, providing the equivalent of an anticipatory balance voltage proportional to the rate of change of the servo displacement, thereby preventing servo overshoot.

The connection "*F*" between the amplifier and the input circuit represents degenerative feedback for stabilizing the high gain d.c. amplifier. The schematic of the amplifier is shown in Fig. 3. The amplifier is extremely stable, and has caused no trouble in the numerous applications in which it has been used. The gain, without degeneration, is 1200. For the servo application this is degenerated to approximately 300, which provides ample sensitivity for the purpose.

The output of the d.c. amplifier is fed into 6AS7 tubes connected as cathode followers as shown in the schematic of the circuit. The bias on the followers places their operation on the linear portion of the characteristic curve. In the set-up used, each clutch has an overlap in exciting current, as the balance point of the amplifier energizes each with about 100 milliamperes. The linearity obtained by operating the 6AS7 tubes at this point is better than that experienced when higher bias with resulting lower clutch current is used.

The exciting coils for the clutches are scramble

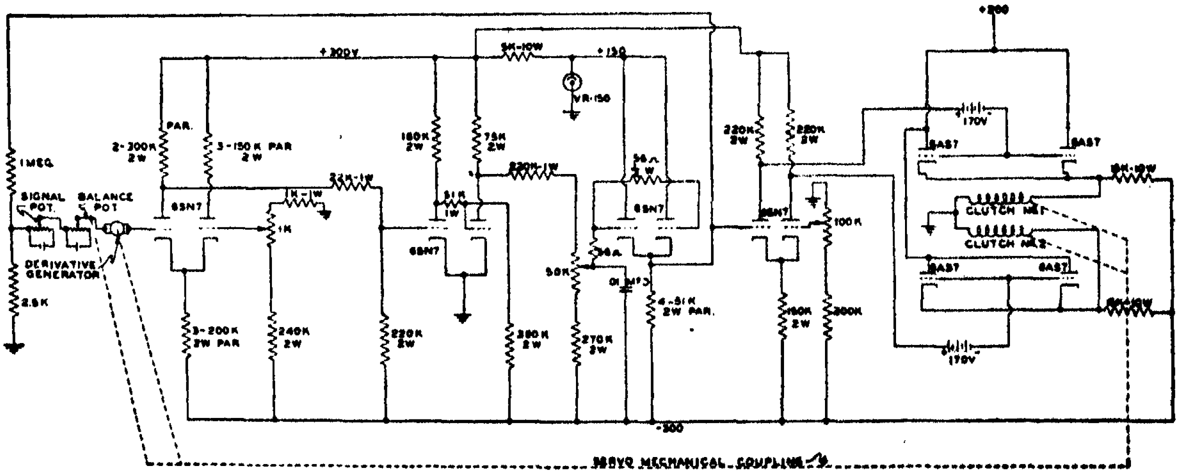

FIG. 3. D.c. amplifier schematic.

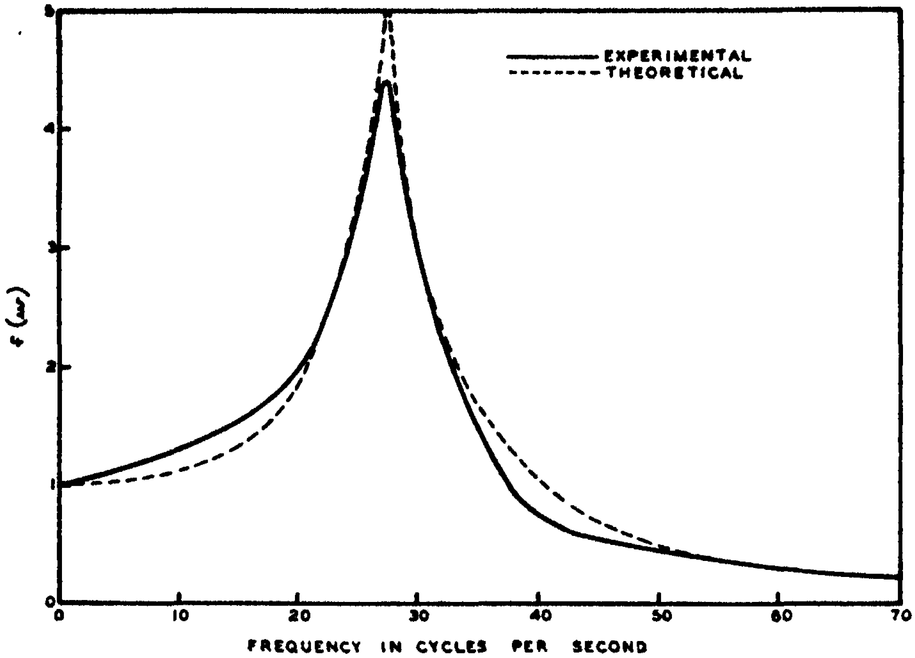

FIG. 4.

wound of No. 34 Formvar wire and have a d.c. resistance of 170 ohms. The inductance of the coils measured on a bridge at 1000 cycles is 0.13 henrys. These values do not necessarily represent optimum points. They are given only to indicate the design characteristics of the prototype servo.

The voltage impressed across the exciting coils ranges between zero and 75 volts as the input signal is changed. With an exciting current of the order of 500 mils, maximum torque is transmitted from the motor through the excited clutch. For values of exciting current between zero and 500 mils, the transmitted torque is proportional to the magnitude of the exciting current.

The differential equation for a damped servo system of the above type is

$$J(d^2\theta/dt^2)+K\beta(d\theta/dt)+K(\theta-\theta_i)=0, \qquad (1)$$

where J = moment of inertia, $\theta-\theta_i$ = angular displacement error, θ_i = requested angular position, K = gain of amplifier and clutch (in torque per unit angular displacement), and β = e.m.f. in volts of derivative generator produced by angular velocity of one radian per second.

If a sinusoidal voltage is used as a request signal, then

$$\theta_i=\theta_m \sin\omega t, \qquad (2)$$

where θ_m = amplitude, ω = angular frequency, and the differential equation (1) becomes

$$J(d^2\theta/dt^2)+K\beta(d\theta/dt)+K\theta=K\theta_m \sin\omega t. \qquad (3)$$

The solution of this equation for θ is

$$\theta=K\theta_m \sin(\omega t-\alpha)/[K^2\beta^2\omega^2+(K-J\omega^2)^2]^{\frac{1}{2}}, \qquad (4)$$

where α is the phase lag between θ and θ_i.

DISCUSSION OF PERFORMANCE

In Eq. (4) the factors K, β, and J represent servo parameters. These parameters were determined by rather indirect means, primarily because the moment of inertia, J, of the system was not known, and

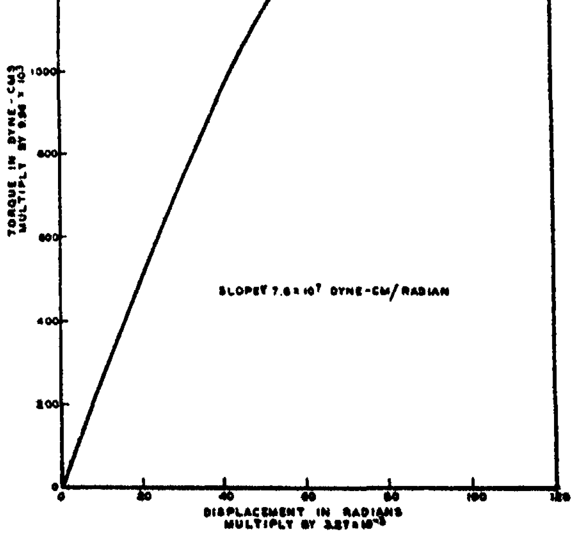

FIG. 5.

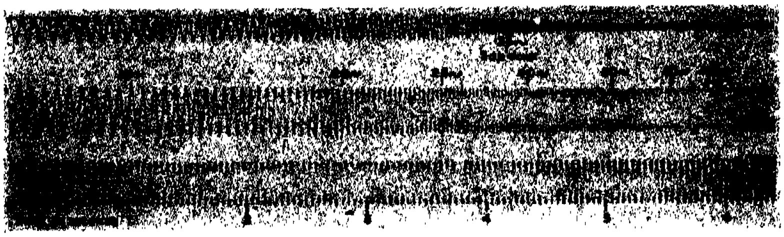

FIG. 6.

because the exact natural resonant frequency could not be determined directly. The frequency response, determined experimentally by driving the servo with an audio oscillator, gave the solid curve shown in Fig. 4. Here the peak amplitude does not occur at the exact undamped resonant frequency, but is shifted slightly below the resonance point. The magnitude of this shift is a function of the damping.

In the above equation, if it is assumed that θ_m is unity, the amplitude of θ can be expressed as a function of ω such that

$$f(\omega)=1/[\beta^2\omega^2+[1-(\omega/\omega_0)^2]^2]^{\frac{1}{2}}, \qquad (5)$$

where $\omega_0=(K/J)^{\frac{1}{2}}$ = resonant angular frequency of the system.

In Fig. 4, the dotted curve is a plot of $f(\omega)$ as a function of frequency for a hypothetical servo of identical type having the values $\beta=10^{-3}$ (i.e., 1 millivolt) and $\omega_0=182.1$, or $f_0=29$ cycles per second.

The close agreement between the two curves in Fig. 4 indicates that the parameters of the actual and hypothetical systems are for all practical purposes the same. Therefore, this value of $f_0=29$ cycles per second was taken as the undamped natural frequency of the actual system.

For the conditions $\beta=0$ and $\omega_0=182.1$, the denominator of Eq. (4) vanishes, and the quotient $K/J=\omega_0^2=33{,}160$. Either K or J must be determined in order to evaluate the desired parameters.

Figure 5 is a plot of torque (in dyne centimeters) *versus* angular displacement of the input signal potentiometer (in radians) for the servo system. Data for this curve were obtained by clamping a lever arm on the servo output shaft, and connecting a spring balance to this lever arm in such a way as to measure the stalled torque of the system. The input signal was introduced by rotating the input potentiometer in incremental steps and taking the resultant torque for each angular step of potentiometer rotation.

This curve is seen to be linear for values of torque output from zero to about 12×10^6 dyne-centimeters. Beyond this value, saturation of the amplifier output followers occurs, and the relationship becomes non-linear. Over the linear range, the slope of this curve gives the over-all gain of the system, K. This slope is determined (from the curve) to be 7.6×10^7 dyne-cm per radian. Substituting in the equation $K/J=33{,}160$ gives a value of $J=2300$ g-cm^2.

The frequency response oscillogram (Fig. 6) is self-explanatory. The bottom trace is a twenty-cycle timing wave, the middle trace is the sinusoidal input signal to the servo, and the top trace is the servo response. The input signal frequency was increased approximately uniformly by manually turning the frequency dial of the input signal generator.

Figure 7 is an oscillogram of the response of the system to a step request. A toggle switch was used to introduce a voltage step which demanded a rotation of 120° of the output shaft. The timing wave in this oscillogram had a frequency of 100 cycles per second.

CONCLUSIONS

Data obtained to date with the magnetic servo described above cannot be accepted as optimum for a family of such assemblies, yet they indicate the high degree of applicability of the magnetic clutch to servo use. In comparison to commercially available units, the magnetic servo offers relatively short response times. Perhaps the most important practical feature of the magnetic servo is its comparative simplicity of design and construction. This places servo development well within the reach of the average laboratory, using readily available tools in the hands of shop technicians.

One undesirable feature of the current magnetic clutch servo assembly has become apparent during experimentation. Because of the abrasive property of the iron-oil mixture, and resultant wear on bearing and sealing surfaces, some difficulty has been experienced in retaining the fluid with conventional

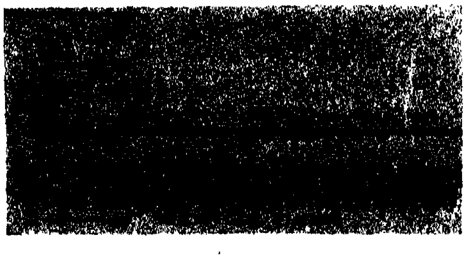

FIG. 7.

oil seals. Although preliminary experimentation has indicated that this effect is slight, its significance can be more rigorously determined during life tests of the assembly. This feature, if significant, may be eliminated through the use of improved seals or varied clutch geometry. Investigation of the problem of oil leakage is being continued, and various seals are being given extensive life tests.

The authors are indebted to Mr. G. R. Nelson, Mr. Lyle Martin, Mr. E. E. St. John, and Mr. J. B. Ruble of NEPA Project for development work on the prototype unit.

THE REVIEW OF SCIENTIFIC INSTRUMENTS VOLUME 20, NUMBER 2 FEBRUARY, 1949

A Note on Analog Computer Design

J. A. BRONZO AND H. G. COHEN
Brown University, Providence, Rhode Island

September 10, 1948

A method is proposed for the simplification of computers designed to solve certain types of partial differential equations. The equations are those in which the spatial derivatives may be replaced by finite difference expressions. The resulting difference—differential equations are reformulated as a system of linear simultaneous equations by making use of Laplace transforms and matrix notation is introduced. By applying a similarity transformation to the matrix a new system is obtained which lends itself more readily to the construction of an analog. As an example, the analog of the equation of the vibrating string with fixed ends is discussed.

THE electrical analog computer method for solving problems involving linear simultaneous algebraic or ordinary differential equations has received some attention in recent scientific and engineering publications.[1] This method is applicable also to linear partial differential equations since they may always be approximated by difference-differential equations.

The authors have been concerned with the development of an electrical analog computer to solve certain linear partial differential equations subject to special boundary conditions. The formulation is reduced to a linear difference-differential equation, after replacing the spatial derivatives by their finite difference equivalents. Operational units are then assembled in a manner dictated by the given equation. The differentiations and integrations with respect to time required are performed continuously by electronic differentiating or integrating amplifiers. Initial conditions are set in each element as proportional electrical quantities before the computing begins. Now it may happen that the analog will be somewhat simplified if a change of variables is made in the difference-differential equation before constructing the analog. If this new equation is then solved by analog methods, the solution of the original problem is known from the equation giving the new variable in terms of the old. Thus the analog yields not the solution directly but something bearing a known relation to it. A group of such transformations which will take a system described by a matrix equation with certain characteristic roots into another system with these same roots is the "similarity" transformation.[2]

Let us consider the solution of

$$F(y,y',y'',\cdots,y^{(n)})=a_1\frac{\partial y}{\partial t}+a_2\frac{\partial^2 y}{\partial t^2}+\cdots+a_n\frac{\partial^n y}{\partial t^n},\qquad(1)$$

where F is a linear function. This can be written in the form

$$F(y,y',y'',\cdots,y^{(n)})=L(p)y+K(p)\qquad(2)$$

by making use of Laplace transforms. Initial conditions are absorbed in $K(p)$. After replacing y', y'', etc. by their finite difference equivalents we have a system of equations which can be written in matrix form as

$$[A_{ij}]Y_j=L(p)Y_j+K_j(p),\qquad(3)$$

where $[A_{ij}]$ is composed solely of numbers. This might also have been written as one difference-differential equation. We call the analog for this system A_1.

Let us now apply to $[A_{ij}]$ a similarity transformation in the following manner. Between $[A_{ij}]$ and Y_j we can insert $[Q_{ij}][Q_{ij}]^{-1}$ without altering the equality. We next premultiply both sides of the equation by $[Q_{ij}]^{-1}$. The only restriction we need make on the matrix $[Q_{ij}]^{-1}$ is that it be non-singular. Then, letting

---

[1] Ragazzini, Randall, and Russell, "Analysis of problems in dynamics by electronic circuits," Proc. I. R. E. 35, 444 (1947); G. A. Korn, "Elements of d.c. analog computers," Electronics, 12, 122 (1948).

[2] C. C. MacDuffee, *Theory of Matrices* (Chelsea Publishing Company, New York, 1946), p. 69.

$$[Q_{ij}]^{-1}\cdot[A_{ij}]\cdot[Q_{ij}]=[B_{ij}], \tag{4}$$

$$[Q_{ij}]^{-1}Y_j=\tilde{Y}_j, \tag{5}$$

we have

$$[B_{ij}]\tilde{Y}_j=L(p)\tilde{Y}_j+\bar{K}_j(p). \tag{6}$$

If (3) gives rise to a stable solution, i.e., if the roots of the characteristic equation in the transform variable p do not lie in the right-half p-plane, then (6) is also stable, by the nature of the transformation. Consider the analog of this new system of equations, calling it A_2. It may happen that A_2 is more economically realized or easier to construct than A_1. To get the answer to the original problem, however, requires premultiplication of $\tilde{Y}_j$ by $[Q_{ij}]$. For a particular $[Q_{ij}]$ it may happen that this additional premultiplication is of a fairly simple nature, while the analog A_2 is preferred over A_1 for reasons of economy.

It might be pointed out that the transformed mathematical formulation may not appear to have any physical significance, but this need not affect the feasibility of building an analog for it.

Example: We shall consider the case where the difference-differential expression is of the form (the classical vibrating string problem)

$$X_{j+1}+X_{j-1}-2X_j-k\frac{\partial^2 X_j}{\partial t^2}=0, \quad j=1,2,\cdots n \tag{7}$$

and the boundary conditions $X_0=0$, $X_n=0$. Taking Laplace transforms,

$$\bar{X}_{j+1}+\bar{X}_{j-1}-(2+kp^2)\bar{X}_j=-p\bar{X}_j(0)-(\partial\bar{X}_j(0)/\partial t). \tag{8}$$

The stability of this analog may now be determined by investigating the eigenvalues of this set of equations.[3] In this case we are assured that the system is stable since it describes the particle-loaded string.[4] Note that on the left hand side of the equation quantities appear with both algebraic signs. An extra component will be required, in general, to change sign. Therefore it may be advantangeous to build an analog, not of Eq. (7), but rather of the following equation

$$\bar{\bar{X}}_{j+1}+\bar{\bar{X}}_{j-1}+2\bar{\bar{X}}_j+(\partial^2\bar{\bar{X}}/\partial t^2) =p\bar{\bar{X}}_j(0)+(\partial\bar{\bar{X}}(0)/\partial t). \tag{9}$$

This equation may be obtained by transforming the original matrix in the following manner:

$$\begin{bmatrix} 2+kp^2, 1, 0, \cdots \\ 1, 2+kp^2, 1, 0, \cdots \\ 0, 1, 2+kp^2, 1, 0, \cdots \\ \cdot \quad \cdot \quad \cdot \quad \cdot \quad \cdot \quad \cdot \\ \end{bmatrix} = \begin{bmatrix} 1, 0, 0, \cdots \\ 0, -1, 0, \cdots \\ 0, 0, +1, 0, \cdots \\ 0, 0, 0, -1, \cdots \\ \cdot \quad \cdot \quad \cdot \quad \cdot \end{bmatrix}$$

$$\cdot\begin{bmatrix} 2+kp^2, -1, 0, \cdots \\ -1, 2+kp^2, -1, 0, \cdots \\ 0, -1, 2+kp^2, -1, 0, \cdots \\ \cdot \quad \cdot \quad \cdot \quad \cdot \quad \cdot \quad \cdot \quad \cdot \\ \end{bmatrix}\cdot\begin{bmatrix} 1, 0, 0, \cdots \\ 0, -1, 0, \cdots \\ 0, 0, +1, 0, \cdots \\ 0, 0, 0, -1, 0, \cdots \\ \cdot \quad \cdot \quad \cdot \quad \cdot \quad \cdot \end{bmatrix}$$

where $[Q_{ij}]$ is now merely

$$\begin{bmatrix} 1, 0, 0, \cdots \\ 0, -1, 0, \cdots \\ 0, 0, 1, 0, \cdots \\ \cdot \quad \cdot \quad \cdot \quad \cdot \end{bmatrix}.$$

This corresponds to a desired change in the analog since a sign change is removed. The actual physical change corresponding to $[Q_{ij}]$ may be as simple as a polarity inversion created by adding or removing a stage of amplification. Since the analog solves for $\bar{\bar{X}}_j$, x_j must be found from the relationship

$$X_j=[Q_{ij}]\bar{\bar{x}}_j.$$

Although a group of acceptable transformations has been found, the particular one used in any given analog will depend on the economy it introduces and upon its mathematical complexity. This may call upon more than a little ingenuity on the part of the designer in finding the optimum relationship between an economical analog and an easily interpreted transformation.

---

[3] It has been demonstrated by Professor J. A. Krumhansl of Brown University that the solution of the difference-differential equation always converges to the solution of the partial differential equation it approximates.

[4] Slater and Frank, *Introduction to Theoretical Physics*, (McGraw-Hill Book Company, Inc., New York, 1933) p. 128.

THE REVIEW OF SCIENTIFIC INSTRUMENTS VOLUME 20, NUMBER 2 FEBRUARY, 1949

Exposure Meter for Precision Light Dosage

HERBERT F. LAUNER[*]
National Bureau of Standards, Washington, D. C.

(Received September 9, 1948)

The exposure meter is an electronic device of the type in which a photo-tube charges a capacitor to the firing voltage of a trigger tube, whose pulse is amplified by a thyratron. The device has been adapted to high intensity sources and is used for the regulation of carbon arc light dosage in the standardization of light-sensitive paper at the National Bureau of Standards. The device, including a modification for automatic extinction of the source when the desired light dosage is obtained, is described, and is shown to be capable of very high reproducibility. Two instruments simultaneously viewing a gradually aging monochromatic source gave count values whose ratios showed a coefficient of variation of 0.32 percent in two weeks of continuous measurement. One instrument, viewing a controlled tungsten lamp, showed a coefficient of variation of 0.18 percent in counts per watt hour over a period of nine days, after which the values changed—the result, presumably, of changes in the lamp.

The instrument was tested for suitability of application by comparing counts with reflectance changes of light-sensitive paper under arc exposure. The results showed that the instrument could control light dosage adequately in spite of large changes in arc voltage, glass filters, and time of exposure.

The instrument was used to test the variability of the uranyl oxalate actinometer, frequently used in photo-chemical work, by simultaneous exposure to a carbon arc. It was found that the actinometer was capable of higher precision than previous investigators had found, in that the coefficient of variation was 1.4 percent, less than ¼ as large as formerly believed.

I. INTRODUCTION

THE technique of precision light dosage appears to be a relatively unexplored field. It involves a device which totals the light, or more strictly, radiant energy, during an exposure, and allows the exposure to be promptly terminated, manually or automatically, when the desired quantity has been received.

The need for such a device arose in connection with the development and production, at the National Bureau of Standards, of light-sensitive papers,[1] used as controls for industrial testing arcs and for technological and scientific research. A carbon arc is employed as a master lamp to produce secondary comparison standards from the papers by exposure to standard light doses. This arc changes, principally because of small variations in controlled voltage, in cored carbon electrodes, and in the glass filter for excluding the far ultraviolet. For precision light dosage, a totaling device, usable over extended periods of time and responding only to the effective portion of the spectrum (near ultraviolet and visible violet blue) of the arc, was required.

Approximate totaling of light is frequently accomplished in photo-chemistry by obtaining the product of time × power, assuming constant behavior of the light source between the isolated radiometric measurements. This simple procedure usually meets photo-chemical needs, and can be considerably improved by continuous radiometric measurement using a recorder but, if applied to a carbon arc, is still incapable of giving immediate, precise values because of the necessity of integrating areas under the erratic power curves.

The ordinary type of thermopile is difficult to correct for the infra-red. The differential thermocouple, developed by Coblentz, Stair, and Hogue,[2] can be corrected to a considerable extent, and a differential thermopile with automatic filter changer was constructed for use with a recorder, but the arrangement was found to lack the required degree of precision.

Certain types of photo-tubes are spectrally suitable but are not constant when operated at a level sufficient to drive the most sensitive recording microammeters available at present, 0 to 10 microamperes, which, furthermore, are not precision instruments.

Another method of totaling light depends upon photo-chemical changes of pure substances or of standardized materials. Among the former, the uranyl oxalate actinometer, in which the photochemically decomposed oxalic acid is determined by titration with permanganate, has received the most intensive study as a laboratory device by Büchi,[3] Leighton and Forbes,[4] Forbes and Heidt,[5] Brackett and Forbes,[6] and for industrial applications by Werkenthin and associates.[7]

Although this actinometer is superior, for relative studies, to intermittent radiometric measurement, experimental evidence** establishing its precision as adequate for the present application is lacking; it is, furthermore, ill adapted for giving an immediate running indication of light totals.

---

[*] Now at Western Regional Research Laboratory, Department of Agriculture, Albany, California.

[1] Herbert F. Launer, J. Research Nat. Bur. of Stand. 41, 169 (1948), RP1916.

[2] W. W. Coblentz, R. Stair, and J. M. Hogue, J. Research Nat. Bur. of Stand. 7, 723 (1931), RP370.

[3] Paul F. Büchi, Zeits. Physik. Chemie 111, 269 (1924).

[4] W. G. Leighton and G. S. Forbes, J. Am. Chem. Soc. 52, 3139 (1930).

[5] G. S. Forbes and L. J. Heidt, J. Am. Chem. Soc. 56, 2363 (1934).

[6] F. P. Brackett, Jr., and G. S. Forbes, J. Am. Chem. Soc. 55, 4459 (1933).

[7] T. A. Werkenthin, David Richardson, R. F. Thornley, and R. E. Morris, India Rubber World 105, No. 2 (Nov. 1, 1941). See also Federal Specification ZZ-R-601a.

In the class of standardized materials, the light-sensitive paper[1] previously discussed has found application as a relative light-totaling control without fixed standards, and is able to give a fairly prompt running indication, but it is not normally intended for high precision use.

For precise, immediate indication, electronic devices appear the most promising. The fundamental basis for one such device is a photo-tube which charges a capacitor to the firing voltage of a "trigger" tube, the pulse of which is amplified to operate an electromagnetic counter. Each count then represents a definite quantity of light, and the total count shows the total light received. Instruments of this type have been developed by Rentschler[8] and Kuper, Brackett, and Eicher,[9] among others. The latter estimated a precision of 1 to 2 percent for their instrument under laboratory conditions. Several commercial models of this type are available for photographic and similar purposes.

Another type of device recently developed by Gilbert[10] totals electric current over time intervals by utilizing the time period of a galvanometer relay actuating an electromagnetic counter. If the source of current is a barrier layer cell or thermocouple, light can be totaled in this way.

Douglas[11] has developed a device for use in atmospheric transmissometry, employing a circuit particularly promising for precision application. Several instruments of this type were constructed with the modifications required by the relatively intense arc to which they apply. In this form no data for precision or reproducibility were available.

The purpose of this paper is to describe the instrument used at the Bureau for predetermined light dosage of light-sensitive papers and to show its suitability for the purpose.

II. DESCRIPTION OF THE INSTRUMENT

The Douglas[11] transmissometer and instruments of like type were specifically designed for measurements at extremely low intensities, and are thus much too sensitive for the relatively enormous intensities involved in the present application. The radiant power, 1080 watts, of the arc to be controlled, is far higher than can be tolerated for reliable performance of photo-tubes, directly exposed, except at impractical distances. For example, using the unmodified transmissometer, the counting rate would be some 20,000 times too high. The optical and electrical changes, along with other features, necessary to adapt the instrument for the present purpose, are described in the following.

A. Optical

The light-sensitive paper, during standardization, is mounted at 25 cm from the arc on a drum rotating horizontally at 1 r.p.m. A position on this drum is a logical place for a receiver, which thus scans the arc from all angles and eliminates effects of arc asymmetry. At this distance the radiant intensity must be decreased some 400-fold to keep the photo-tube current below one microampere, even when allowing for a blue filter. The device for achieving this must be quantitatively unaffected by long exposures to intense light, at temperatures above 60°C in the presence of water vapor, and should preferably be spectrally non-selective from 300 to 490 millimicrons.

The use of metal screens is not practical because of their high transmissions, usually over 30 percent. Recently, Banning[12] has described the use of films of evaporated Chromel A, and has shown them to be almost non-selective in the visible. Although no data on stability are available, such films appear promising for applications of the present nature.

A simple and satisfactory reduction of intensity was obtained by using the first reflection of polished glass. Reflection from the second surface was eliminated by choosing a red glass of low transmission, <0.05 percent, for the wave band of interest. Since the reflectivity of one piece of glass is near 0.05, far too great for the purpose, two pieces were used at 90° from each other. The arrangement is indicated in Fig. 1, showing the receiver *R* mounted on drum *D*, which rotates around the arc. The photo-tube is inside the case near the "*R*," facing away from the arc. It views, through a Corning polished filter 5850, the lower piece of the 90° red glass double reflector, which in turn receives its image of the arc from the upper red glass. A piece of ultraviolet transmissive glass, Corning 791, keeps dust from the reflectors. The fraction of the incident beam coming from the double reflector varies somewhat with the refractive index of the red glass from 0.00258 at 303 millimicrons (calculated from the Fresnel expression, taking the angle of incidence at 45°) to 0.00224 at 486 millimicrons, thus producing a small spectral distortion in favor of the shorter wavelengths.

After passing through a Corex-D glass filter, the portion of the arc spectrum usually effective for

---

** See Section VI of this article.

[8] H. C. Rentschler, J. A. I. E. E. 49, 576 (1930).

[9] J. B. Horner Kuper, F. S. Brackett, and Maynard Eicher, Rev. Sci. Inst. 12, 87 (1941).

[10] R. W. Gilbert, Rev. Sci. Inst. 18, 328 (1947).

[11] C. A. Douglas, Electronics 20, 106 (1947).

[12] Mary Banning, J. Opt. Soc. Am. 37, 686 (1947).

testing materials extends roughly from 290 to 490 millimicrons, with the principal maximum near 388 millimicrons. This region lies within the sensitivity range of the RCA 929 photo-tube, which—corrected with the 5850 filter—extends from 300 to 490 millimicrons with a median maximum near 385 millimicrons.***

B. Electrical

The circuit is shown in Fig. 2. It was developed by Douglas for this type of application and is considerably simpler than his circuit for the transmissometer,[11] notable differences being the use of the cold-cathode trigger tube**** instead of the neon tube and the use of the thyratron-operated electromagnetic counter without previous signal inversion.

The size of C_1, the silver-mica totaling capacitor, determines the counting rate inversely, and was made as large as physically convenient in order to obtain a desirable counting rate. As used, C_1 was 10^2 to 10^3 times larger than usual, and thus introduced uncertainty concerning the ability of the trigger tube to handle the unusually large discharge.

The exposure meter consists of a shielded, grounded receiver connected by a shielded cable to an amplifier counter. It is imperative that the components of the receiver be close together, connected by air-insulated conductors, to reduce the leakage that is usually too high in even the best of insulated cable. It is, therefore, not permissible, although it would often be very convenient, to separate the photo-tube from the trigger tube. Beyond the trigger tube, the effect of leakage becomes negligible.

C. Mechanical

(*1*) *Slip Ring Connection for Receiver*

The rotation of the receiver around the arc necessitated sliding electrical contacts. This was done by means of a polystyrene-mounted copper slip ring, *S*, and a copper graphite brush, *B*, shown in Fig. 1. The other side of the receiver circuit was grounded to the rotating drum, which was, in turn, grounded through a steel spring contact (not shown). Good contacts are necessary since any interruption in the circuit gives rise to spurious pulses. This arrangement has been functioning satisfactorily for two years.

(*2*) *Thermostating of Receiver*

Since the temperature within the receiver hovered near 50°C, the maximum permissible for the photo- and trigger tubes, cooling was necessary. Since, furthermore, the photo-tube output varies 0.3 percent per °C, positive control is necessary. The receiver frame was, therefore, provided with a water jacket and fed from an annular trough (not shown) mounted on top of the rotating drum, which received water maintained at a constant temperature. Thus, constant liquid contact was provided, and the temperature was controlled to within 0.5°C.

III. PREDETERMINED COUNTER

It was desirable to provide for the automatic extinction of the arc when the desired light dosage had been received. Devices for this purpose are commercially available but are very costly, usually require more power than simple counters, and some of them do not indicate the current light dosage.

By a few simple modifications of the electromagnetic counter† used in this work, the counter itself was made to extinguish the arc at any desired count. When all of the digit wheels indicate

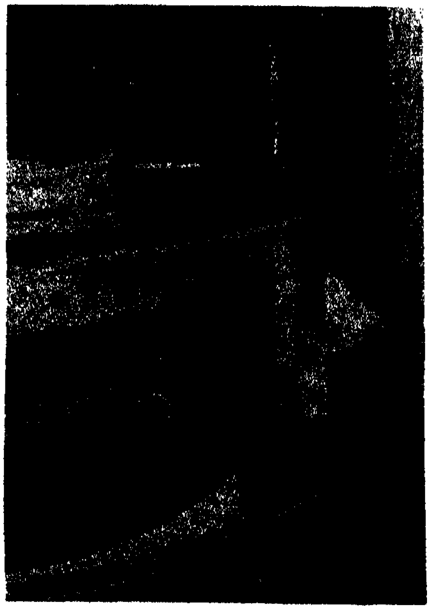

FIG. 1. Exposure meter. Receiver *R* is mounted on rotating sample drum *D*, thus scanning arc at 1 r.p.m. Pulses reach amplifier through slip ring *S* and brush *B*.

*** The photo-tube-filter combination has a very small response to red and infra-red. This was determined by interposing a piece of Corning 2404 glass, which transmits only red and infra-red, between the receiver and the arc. No pulses were recorded in the time interval normally giving 600 pulses. The same experiment was repeated with a tungsten incandescent lamp, arranged to provide some threefold higher infra-red intensity, under which conditions 1 pulse was recorded through the red glass compared to 600 without.

**** The trigger tube, known as the WL-759 Glow Relay Tube, was purchased from the Westinghouse Co., Bloomfield, N. J. as being specially selected for constancy of performance over the anode voltage range 245 to 270 volts. Its characteristics have been studied by W. B. Nottingham, Rev. Sci. Inst. 11, 2 (1940).

† Wizard counter, model EC-7 made by Production Instrument Company, Chicago, Illinois.

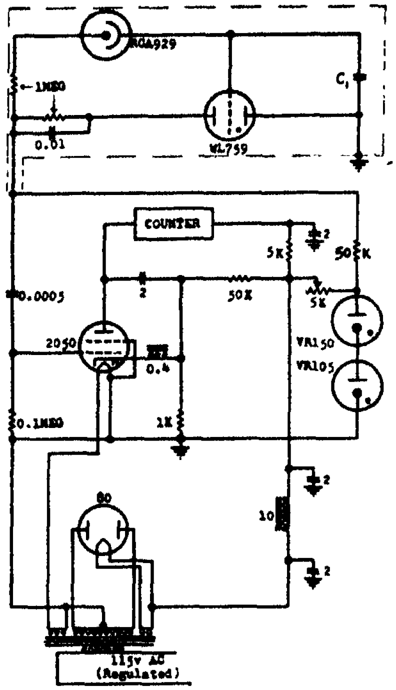

FIG. 2. Circuit diagram of exposure meter. C_1 is the totaling capacitor (must be silver-mica type) whose size determines the counting rate. For the present application it was 0.025μf. The two 5*K* and the 50*K* resistors are rated at 10 watts. The current through the *VR* tubes is adjusted to 20 m.a. The counter is a Wizard model EC-7, rated at 115 v d.c., made by Production Instrument Company, Chicago, Illinois. *Other counters of similar load characteristics will answer* the purpose, but may require some changes in circuit constants. A ¼-watt neon lamp (not shown) is in parallel with the counter and its 5*K* resistor, thus furnishing a visual indication of each pulse. A switch in series with the counter has also been found very convenient. The 2-μf capacitors are of the type Cornell Dubilier TLA6020. Power transformer and 10-henry choke are Halldorson L66 and B4-839 products. Any 0.4-henry choke will suffice, and often a 100-ohm resistor may be substituted.

nines, one more count moves all wheels to zero simultaneously. By placing a lifting cam on the extreme left wheel a small switch was made to operate on the last count. The cam consisted of a thin finishing nail with a rounded polished head, and the switch was made of two 8-mil phosphor bronze spring strips, 4×30 mm, mounted on Bakelite. This switch has been handling its load of 40-ma a.c. satisfactorily.

In the commercial counter the digit-wheel shaft is notched for the width of all the wheels, so that the latter may be simultaneously, but not singly, turned to zero. This shaft was replaced by one 1½" longer, with a notch the width of only one wheel at 1¾" from the left end. By sliding this shaft laterally, each wheel may be turned separately to set up any desired number. To eliminate groping, the left end of the shaft indicates the position of the notch on a marked glass tube placed over the protruding end of the shaft to exclude dust.

Operation of the switch on the desired number is secured by setting up the complement, minus one, of the desired number. For continued use it was desirable to cover the digits with bandage tape, stamping numbers in the reverse order thereon. It is thus a simple matter to turn up the desired number on the wheels. In operation, the counter uncounts, showing, at any time, the counts still needed to reach zero, whereupon one more count extinguishes the arc. In the present application this was done by breaking the holding coil circuit of a manual reset switch. The counter in its present form requires appreciably no more power than normally and is interchangeable with the conventional type.

IV. VARIABILITY OF THE EXPOSURE METER

The variability of the instrument may be expressed as the variation in counts for a given quantity of light received.

No high precision reference method of measuring and totaling light quantities was available, but variability may be determined with a constant tungsten incandescent lamp, measuring time or electrical energy input *versus* counter values. An entirely different method of determining variability consists of two instruments viewing the same monochromatic light source, which need not be constant in output. The results using these two methods are described in the following.

A. Test with Controlled Light Source

A tungsten incandescent lamp, in an arrangement described in footnote (a), Table I, was used as light source in combination with a blue glass filter, Corning 5850.

TABLE I. Test of exposure meter with a constant light source.[a]

Mean[b] power input[c] to lamp watts	Mean[b] counts per watt hr.	Mean[b] counts per minute[d]
507.5	6.052	51.20
508.8	6.042	51.24
508.9	6.044	51.27
508.2	6.043	51.18
508.4	6.031	51.10
508.0	6.044	51.17
507.9	6.062	51.32
508.3	6.062	51.36
508.1	6.062	51.33
508.8	6.010	50.96

[a] The light source was a 500-watt, 115-volt tungsten incandescent airport beacon lamp operated at 110 volts from a 500-watt Raytheon voltage stabilizer. To avoid a conventional socket, the prefocus base of the lamp was securely soldered into a brass tube, itself rigidly mounted with respect to the receiver at a distance of 62 cm. The leads to the lamp terminals were soldered. The equipment was housed in a temperature- and humidity-controlled room, with due precautions to avoid stray light. During dark periods the stabilizer was kept at equilibrium operating conditions with a dummy lamp of equal rating. The source was always burned at least ½ hr. before measurements.

[b] Each of the ten values is the mean of ten individual runs. These 100 experiments lasted ten days.

[c] Power input was calculated from energy input, measured with a certified G.E. standard watt-hour meter, model IB10 to the nearest 0.01 watt hour.

[d] Time was measured with a stopwatch to the nearest 0.2 sec. The experiments lasted 10 to 26 minutes each.

Ten continuous series of ten experiments each were performed with a dark period, either overnight or ten minutes, between each series. The quantities measured were counts, time, and energy input to the lamp in watt hours, noting lamp voltage once each experiment, which lasted from 19 to 26 minutes, to give 1000 to 1400 counts. From these quantities were calculated the watts, the counts/watt hr., and counts/min.

The means of each series of ten experiments are given in Table I. The first nine mean values for counts/watt hr. and counts/min. indicate a high precision and constancy for the exposure meter over a period of 9 days, with coefficients of variation[††] of 0.18 and 0.17 percent, respectively. Within each individual series the coefficients of variation were, for counts/watt hr., 0.48, 0.57, 0.46, 0.42, 0.34, 0.40, 0.43, 0.31, 0.39, and 0.46 percent, in the order of Table I. The voltages within a series varied by 0.3 to 0.4 volt. The 10th mean values show a deviation from the first nine. It was of interest to determine the direction of any further deviations, and the experiments were repeated three weeks later.

TABLE II. Variability of exposure meters from simultaneous performance of two instruments.[a]

Running time[b] hr.	Time[b] periods hr.	Counts 1	Counts 2	Ratios of counts	Counts[b] per hr.
39.8	39.8	17020	8703	1.9556	428
43.8	4.0	1671	856	1.9521	418
46.9	3.1	1316	674	1.9525	425
72.0	25.1	10243	5250	1.9510	408
111.0	39.0	15171	7785	1.9488	389
115.0	4.0	1479	760	1.9460	370
129.1	14.1	5009	2587	1.9362	355
133.1	4.0	1417	730	1.9411	354
139.1	6.0	2139	1100	1.9445	356
153.1	14.0	4943	2529	1.9545	353
158.1	5.0	1703	870	1.9575	341
164.6	6.5	2209	1129	1.9566	340
177.8	13.2	4432	2264	1.9576	336
182.8	5.0	1644	841	1.9548	329
185.8	3.0	975	501	1.9461	325
200.0	14.2	4654	2393	1.9448	328
204.0	4.0	1314	675	1.9467	328
208.1	4.1	1333	681	1.9574	325
223.6	15.5	4972	2550	1.9498	321
228.7	5.1	1646	843	1.9526	323
232.8	4.1	1292	660	1.9576	315
271.4	38.6	11823	6089	1.9417	307

Mean of ratios: 1.9502.
Coefficient of variation: 0.32 percent.

[a] Two receivers were rigidly mounted, as close together as possible, at 175 cm from a 400-watt, type H-1, mercury vapor lamp, also firmly mounted on the same soapstone slab. A light-tight ventilated box over the lamp prevented stray light. All but the middle 76-mm portion of the arc was normally masked, although in another series of experiments the unmasked portion was only 12 mm. The light emerged from the box through Corning filters 5850 and 3389, absorbing all but the 436-mμ line and some red and infra-red lines to which the response was negligible. The lamp was operated at constant voltage to avoid erraticisms in the gradual decrease of intensity through lamp aging.

[b] "Time" and "Counts per hr." are not used for the determination of the ratios but are given as guides. The latter indicate the gradual aging of the lamp and were calculated for meter No. 1.

The next 100 runs gave results as constant as before but the average counts/watt hr. was 5.936, 1.8 percent lower than before, whereas the wattage input increased by only 0.05 percent. After this second series of 100 runs, the next 20 runs resulted in an average of 5.896 counts/watt hr., another decrease of 0.7 percent. The cause of this large change lay either in the lamp or in the receiver[†††] or both. It should be pointed out that the lamp was used much more drastically than corresponds to the usual radiometric practice, and, therefore, these results might be regarded as tentative.

Although it had been hoped to develop, in this manner, a fairly reliable, simple method for checking the performance of such instruments, it is apparent that this procedure must be used with caution and that a comparison against specially designed standard incandescent lamps, operated with all possible precautions (including the measurement of color temperature), is required at intervals of approximately two weeks, for precision over long time periods. For the present application, such refined checks are to be carried out by the Photometry and Colorimetry Section of the Bureau.

B. Test with Two Exposure Meters

If a part of the change noted in the last section arises from variability of the exposure meters, this should manifest itself when two instruments are viewing the same monochromatic source. If an instrument always gives a certain number of counts for a given quantity of light, then two reproducibly functioning instruments should maintain a constant *ratio* of counts, even if the intensity of a monochromatic source is changing. However, if two instruments do *not* maintain a constant ratio, one or both must be varying. It is the fact of such variation which it is desirable to establish, and for which the following experiments (Table II) were planned.

Two receivers viewed a monochromatic source in an arrangement described in footnote a, Table II. The ratios of counts given in column 5, with a coefficient of variation of 0.32 percent, in fair agreement with the results in the foregoing section using a different method, show that the two instruments functioned reproducibly with respect to each other over a continuous period of almost two weeks (terminated by a thyratron failure), in spite of the extensive decrease in intensity of the lamp by aging,

---

[††] Coefficient of variation, percent $= 100s/\text{mean}$, where $s =$ standard deviation $= [\text{sum of (deviations)}\ 2/(n-1)]^{\frac{1}{2}}$.

[†††] The amplifier of the instrument was checked for itr pulse-counting fidelity by parallel operation with anothes amplifier, and found to be perfect for many thousands of counts. Furthermore, minor changes in *VR* tubes were noted, but changes of 5 to 10 percent in voltage on the particular trigger tubes were found to have negligible effect.

TABLE III. Comparison of exposure meter results with reflectance change of light-sensitive paper under various arc conditions.[a]

Exp. No.	Type of filter[b]	Arc volts[c]	Exposure time hr.	Counts[d]	Change in reflectance[e]
	Experiments excluding short ultraviolet				
1	New Corex-D	42.5	13.7	18823	0.202
2	Old Corex-D	42.5	15.4	18823	0.200
3	Old Corex-D	43.5	15.0	18823	0.197
4	Old Corex-D	40.0	18.1	18823	0.198
5	New Pyrex	42.5	14.0	18823	0.196
6	Old Pyrex	42.5	14.3	18823	0.197
	Experiments including short ultraviolet				
7	Corning 791	42.5	14.2	18823	0.276
8	No filter	42.5	13.6	18823	0.396
9	Corning 791	42.5	9.5	12654	0.210
10	No filter	42.5	3.7	5111	0.203

[a] The changes in conditions given in this table are much more extreme than ever obtained in practice. See footnotes b and c.

[b] The new filters were completely unused; the old filters had been used approximately 4000 arc hr. Neither would be used in practice. Ordinarily, a filter is allowed to burn-in 100 hr. and is discarded after 2000 hr. From these data, for the particular samples used, it appears that Pyrex is the more resistant to solarization. Pyrex, Corex-D, and Corning 791 ("high-silica") differ principally in their ascending order of ultraviolet transmission, the last having a cut-off near 220 mμ. The ultraviolet differentially transmitted by the first two glasses, especially when new, occurs in the region below which the photo-tube-filter combination is sensitive and explains the slightly higher reflectance changes in experiment 1. For the same reason it was not expected that experiments including short ultraviolet would give valid results. The values were included to show the extent of departures in reflectance (experiments 7 and 8) when the counts were used as a guide, and in counts (experiments 9 and 10) when reflectance was used as a guide.

[c] The arc voltages are the mean values for each run, taken from a recording voltmeter curve. Since the voltages were measured at the electrode holders, they include the *IR*-drops along the electrodes. This amounts to approximately 3.6 volts, which must be subtracted from the values in Table III to give true arc volts. These voltage differences between experiments 2, 3, and 4, or even between 2 and 3, 2.3 percent, are much larger than may be expected in practice, since the primary voltage is controlled by a mechanical regulator operating over a band width of ±0.5 percent.

[d] Exposure to a given number of counts corresponds to the usual practice.

[e] Changes in reflectance were obtained by measuring the reflectance at 45° from normal incidence, for 578 mμ, near the wave-length of greatest change, before and after exposure. For further details see references 1 and 13.

as indicated in column 6. This is evidence that the instruments were individually constant in operation, inasmuch as systematic variations necessary to give fortuitously constant ratios are improbable in view of the complexity of the electronic processes.

The experiments were repeated a number of times under a variety of conditions: (1) the receiver circuit was operated from very constant B-batteries instead of rectified a.c.; (2) the totaling capacitor was changed from 0.025 to 0.0005μf, thus decreasing the size of the electric pulse fiftyfold; (3) the diaphragm opening limiting the size of the arc was decreased from 76 to 12 mm, thus improving the geometry of the arrangement considerably; (4) the receivers were accurately thermostated; (5) the photo-tubes†††† were replaced by others of the same type; (6) the receivers and lamp were more rigidly mounted on a steel beam instead of a soapstone table top; (7) the counting rates were increased fivefold. None of these changed conditions affected the constancy of ratios appreciably.

The results in Table II were obtained for only one wave-length, but it is not reasonable to expect essentially different behavior at other, nearby wave-lengths. The experiments were intended, furthermore, to afford an insight into the reproducibility of photo-tube response under the ideal conditions of constant photon energy. The performance of the instrument for the spectrally varying and inhomogeneous carbon arc is shown in the next section.

This type of experiment suggests the desirability of having two or more instruments viewing the arc at all times, thus providing a ratio which should serve as an indication of the behavior of the exposure meters. This, combined with frequent checking against a working standard incandescent lamp (taking trends caused by aging and other causes into account) and the whole referred to highest precision incandescent standard lamps, appears to afford a reliable method of measuring light dosage over extended periods of time.

V. SUITABILITY OF THE EXPOSURE METER FOR THE APPLICATION

The arc[1] used for the standardization of light-sensitive papers is usually fairly constant in operation, with occasional extreme differences of three to four percent, and light dosage may thus be approximated on a time basis, but fractional parts of a given light dosage are rendered uncertain by the variation of arc power with electrode length. Furthermore, the glass filter, which surrounds the

TABLE IV. Precision of the uranyl oxalate actinometer[a] using the exposure meter to measure light dosage.

Oxalic acid decomposed[b] milliequivalents	Counts	Milliequivalents per count $\times 10^5$
0.811	35154	2.307
0.832	35605	2.337
0.621	26315	2.360
0.710	30831	2.303
0.797	33582	2.373
0.819	35722	2.293
0.829	35851	2.312
0.482	21303	2.263
0.588	25290	2.325
0.812	35457	2.290
Mean		2.316
Coefficient of variation, percent		1.4

[a] The chemical procedure given in Federal Specification for Rubber, ZZ-R-601a, II-18, "Resistance to light," was followed, except for slight changes in titrimetric technique. The central 80 percent of the face of the thin silica cell was exposed through a diaphragm, and the rest of the cell was covered by a light-proof, internally blackened, snugly fitting case. The case was rigidly mounted on the drum, rotating about the arc at 1 r.p.m., and faced away from the arc, at such an angle that the cell was illuminated by the image of the arc in a piece of polished red glass, also rigid with respect to the case. This reduced the light intensity 20-fold, as described in Section IIA, and allowed exposures up to 12 hr., instead of ½ hr. with direct exposure. The photon receiver was also mounted on the drum. Another method of reducing the intensity, by mounting the cell in a fixed position at 170 cm from the arc, next to a photon receiver mounted there, gave essentially the same results.

[b] The amount of oxalic acid decomposed was calculated from difference in permanganate titer of the uranyl oxalate solution before and after exposure, and usually amounted to 8 to 9 ml of 0.1*N* $KMnO_4$.

---

†††† The original photo-tubes in the two receivers had similar responses, within a few percent, to the 365, 405, and 436-mμ mercury lines; the replacement tubes differed almost two-fold.

arc to eliminate short ultraviolet, deteriorates with use, undergoing a decrease in transmission—and thus causes a gradual decrease in intensity, especially in the shorter wave-lengths. The use of a device for measuring out light doses and fractions thereof is, therefore, required, and it must be responsive to the same factors that affect quantity and quality of radiant energy as the light-sensitive papers.

Experiments designed to test these points were performed. Light-sensitive paper of uniform initial reflectance was exposed for an equal number of counts under conditions varying much more than expected extremes: high and low arc voltage, old and new filters of both Pyrex and Corex-D glass, and normal electrode variations. The reflectance changes undergone during exposure by the light-sensitive paper were measured.[1, 13] These changes in reflectance must correlate with counts for the various conditions under which the exposure meter is to indicate light dosage reliably (see Table III).

The results given in Table III show that, in spite of the abnormally large variations in conditions, the exposure meters reliably indicated light dosage for the light-sensitive paper, provided that the short ultraviolet was eliminated. When the latter was included, as in experiment 7 with Corning 791, a glass transmitting down to 220 millimicrons, or as in experiment 8 without a filter, the fading of the paper was much greater than the exposure meters indicated, or conversely, as in experiments 9 and 10, for equal fading, far less time and fewer counts were required. It is of interest to note the large differences in time for the various conditions.

VI. COMPARISON WITH THE URANYL OXALATE ACTINOMETER

The possibility of precise light dosage using the exposure meter led to a comparison with the uranyl oxalate actinometer, inasmuch as the latter was, at one time, considered for use in measuring light dosage in the standardization of light-sensitive papers. From the very careful work of Leighton and Forbes,[4] for their typical experiments 14–27, a coefficient of variation of 5.8 percent may be calculated. The uncertainties involved in their method of intermittently measured light dosage, however painstaking, may account for much of the variation.

Several series of experiments were performed, using the actinometric technique developed in the rubber industry[7] and using the standardizing arc, measuring light dosage with an exposure meter. The details are given in the footnotes to Table IV.

The results given in Table IV show a coefficient of variation of 1.4 percent. Two other similar series showed 1.9 and 1.1 percent, but in the latter series a result differing, unexplained, by 8 percent from the mean, was omitted. The results, furthermore, were from one batch of C.P. reagents; another batch gave mean values differing consistently from the others by more than 20 percent, pointing to the necessity of great care in purification, as already stressed elsewhere.[4] These results do not indicate the reproducibility of the uranyl oxalate actinometer for a variety of carefully purified batches of reagents, which would constitute the real criterion of its usefulness, but they do indicate that this actinometer is less variable, for a given set of reagents, than had been previously reported.

The writer thanks Paul J. Shouse for assisting in construction and measurement, and William K. Wilson for performing some of the uranyl oxalate experiments.

---

[13] Herbert F. Launer, J. Research Nat. Bur. Stand. 27, 429 (1941) RP 1430.

THE REVIEW OF SCIENTIFIC INSTRUMENTS VOLUME 20, NUMBER 2 FEBRUARY, 1949

A Capillary Collector for Measuring the Deposition of Water Drops on a Surface Moving through Clouds

BERNARD VONNEGUT[*]
Massachusetts Institute of Technology, Cambridge, Massachusetts

(Received September 24, 1948)

An instrument has been devised for the purpose of measuring the amount of water impinging on a small area moving through clouds, rain, or snow. From measurements of this sort, the liquid water content of the atmosphere can be evaluated.

The instrument uses capillary phenomena to collect and retain water drops striking a small porous surface. Its function is the same as small scoops which have been used to measure water collection in flight, but it has the advantage that its response rate is sufficiently rapid to measure collection rate over a very short interval of time. It has been successfully used in wind tunnel and flight tests. With slight modification, the instrument should find application in measurements on other liquid aerosols.

PRINCIPLES OF OPERATION

Components

THE device consists of a collector made of porous material exposed to the air stream so that particles suspended in the air collide with its collecting surface. Figure 1 shows schematically the essential parts of the apparatus. The collecting head of the unit consists of a piece of porous material held in a holder sealed around its edge so that one surface is exposed to the atmosphere while the other is on the inside of the holder. The holder is connected by a tube to the measuring part of the apparatus, in this case a calibrated glass tube. The apparatus is filled with water from the collecting head to the measuring system. If the proper constants are used in the design of the apparatus, the drops from the atmosphere which hit the surface of the porous material will be drawn into the system and their volume can be measured almost immediately on the measuring device.

Capillarity

Figure 1 includes a greatly enlarged idealized drawing of the cross section of a pore in a piece of porous material such as is used in this instrument. It can be seen from the drawing that the interior of the apparatus is filled with water which forms a meniscus in each pore of the porous material on the outside surface. If we assume that the pores are circular, having a radius r, the liquid has a surface tension γ, and contact angle of the liquid with the pore walls is θ, then the pressure difference, P, between the inside and the outside of the meniscus is given by

$$P=(2\gamma\cos\theta)/r. \tag{1}$$

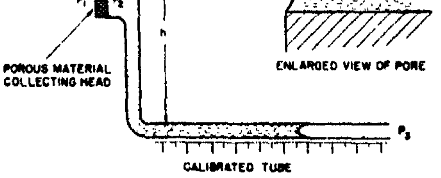

FIG. 1. Schematic diagram of collector.

This pressure difference resulting from surface tension forces causes the pressure in the liquid phase to be less than that in the gas phase when the contact angle is less than 90° (that is when the liquid wets the porous material). If one causes the pressure of the liquid phase to vary with respect to the gas phase, the contact angle of the liquid will change so that the surface tension forces balance the pressure difference. If the pressure difference is increased, the contact angle will decrease. The maximum pressure difference which the surface tension forces will support is limited by the smallest contact angle which the meniscus of the liquid can assume with the wall of the pore. For surfaces wet by the liquid, this angle is substantially zero. Therefore, the maximum pressure difference which can be supported is

$$P=(2\gamma)/r. \tag{2}$$

Because the pressure of the liquid is less than that of the atmosphere, water drops touching the surface of the porous material will be drawn into the body of the liquid while air will remain on the outside. The meniscus can be regarded as sort of a semipermeable membrane, admitting liquid but excluding gases.

We may analyze the situation in the apparatus in Fig. 1 by letting P_1 = pressure on air side of porous material in dynes/cm², P_2 = pressure on liquid side of the porous material in dynes/cm², P_3 = pressure of air at end of measuring tube in dynes/cm², r_1 = pore radius of porous material in cm, r_2 = radius of measuring tube in cm, θ_1 = contact angle of porous material and water, θ_2 = contact angle of measuring tube and water, γ = surface tension of water in dynes/cm, h = height of collector above measuring system in cm, and ρ = density of water in g/cm³. The pressure difference existing across the porous collector (P_1-P_2) is then (neglecting the density of air)

---

[*] Present address: General Electric Company, Research Laboratory, Schenectady 5, New York.

$$(P_1-P_2)=\rho gh+\frac{2\gamma\cos\theta_2}{r_2}+(P_1-P_3). \qquad (3)$$

The maximum pressure difference which the surface tension forces of the liquid in the porous material can support is, from Eq. (2),

$$P_{\max}=(2\gamma)/r_1. \qquad (4)$$

By adjusting P_3, the pressure at the end of the measuring system, so that P_1-P_2 is less than $2\gamma/r_1$ but greater than zero, the system is made stable so that all water touching the collector is immediately drawn into the system while no air is admitted. Because of the incompressibility of the liquid column, the rate of response is very rapid when the viscous forces opposing motion of the liquid are small.

Porous Materials

The porous collector can be made of a great variety of porous materials. Sintered metal, alundum, fritted glass, porous clay, cloth and leather have all been used. Sintered metal seems to be the most desirable material because of its strength, ease of fabrication, and uniformity. The porous metal used was furnished by the Moraine Products Division of the General Motors Corporation in Dayton, Ohio. The metal is made by sintering together a uniform powder of very small bronze spheres. Their product, Porex grade 3, having an effective pore size of approximately 30 microns, was used. After fabrication the collector was thoroughly cleaned of any oil film by washing it out for a few minutes with sulfuric acid-potassium dichromate cleaning solution. The presence of an oil film increases the contact angle of water on the metal and thus lowers the maximum air pressure which the wet porous material will support. Porex grade 3, when clean, should support air pressures of from 40 to 50 centimeters of water. The maximum air pressure which wet porous material will support is limited by the capillary effects in the largest pore, so that uniformity of pore size is very important. Occasionally, samples of porous material are unusable because of a single large pore.

Aerodynamic Pressure Effect and Pore Size

In the discussion concerning the pressures existing in the various parts of the apparatus, it was assumed that a uniform pressure existed in the atmosphere over the collecting area of the porous material. When the collector is moving through the air, the pressure over the collecting surface will not be uniform because of aerodynamic effects. Consequently, provision must be made in the design so that at no point will the pressure drop across the material either force air into the porous material or suck water out of it. The maximum pressure variation which can exist over the surface of any shape of collector is probably several times the pitot static head, but by proper design this pressure variation can be greatly reduced. In the case of collectors having a large aerodynamic pressure variation over the collecting surface, it is necessary to use a porous material having a very small pore size in order to withstand the pressure range. The maximum rate at which water will flow through the porous material is governed principally by the size of the pores. Greater suction can be used with material having a small pore size, but the viscous forces opposing flow increase rapidly as the pore size is decreased. For a given shape and size of collector, the maximum flow rate is approximately proportional to the pore diameter. The maximum flow rate of a collector should, of course, exceed the maximum rate at which water is to be collected. The maximum flow rate can be readily determined by flooding the surface of the collector with water and measuring the rate at which it enters the system.

The early instruments had a wide range of aerodynamic pressure variation over their surfaces and it was, therefore, necessary to use a collector having very small pores. A suction of about six feet of water was used. The maximum flow rate possible through the collector was barely enough to handle the highest liquid water content produced in the wind

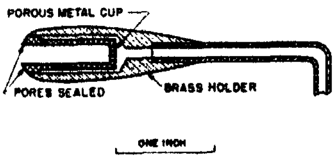

FIG. 2. Section of collector head.

FIG. 3. Collector head.

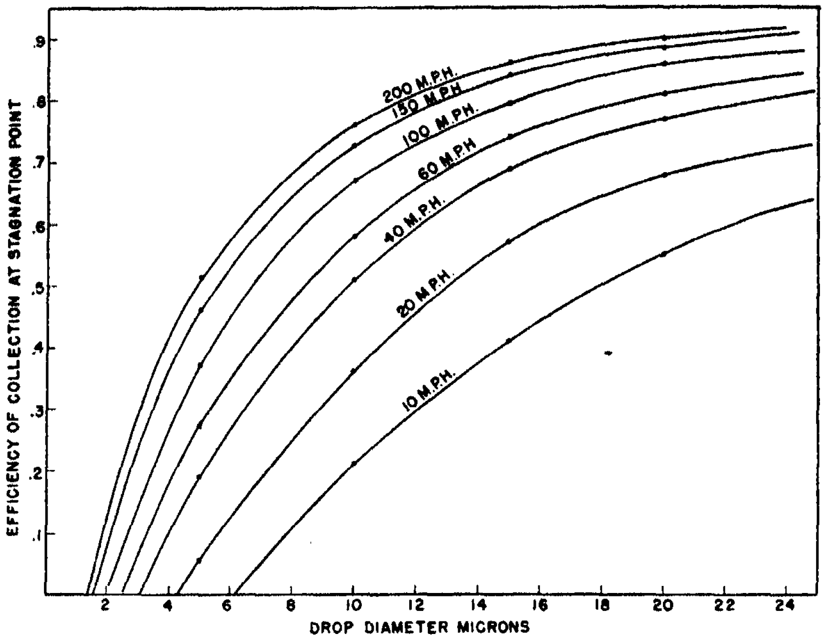

FIG. 4. Approximate efficiency of collection of capillary collector as a function of air speed and drop size from computations of Langmuir and Blodgett. Calculation based on efficiency of collection at the stagnation point of a one-half inch diameter sphere at a pressure of 960mb and a temperature of 10C.

tunnel. It was found that the maximum flow rate gradually decreased with time because of clogging of the pores, and thus caused difficulty. The present design minimizes the aerodynamic pressure variation, permitting the use of larger pores, lower suction, and greater flow rates.

When the porous collector is used at high air speeds, the aerodynamic pressure difference between the collecting head and the measuring system must be taken into account. The most satisfactory method of doing this is to balance out this pressure by connecting the measuring system to a total head tube in the air stream.

Evaporation Losses

Because the water in the pores of the collector is exposed to the atmosphere, evaporation takes place from the system when the atmosphere is not saturated with water vapor. The rate of evaporation from the collector is approximately proportional to the pressure difference between the saturation vapor pressure of water and the partial pressure of water in the atmosphere. The rate of evaporation is also proportional to the airspeed. This can be expressed analytically as follows:

Let V = true air speed in m.p.h., L = evaporation loss in g per minute per sq.cm of projected collecting area, p_s = vapor pressure of water at temperature of collector in centimeters of mercury, p_p = partial pressure of water vapor in the air in centimeters of mercury, and K = constant of evaporation loss for collector. Then

$$L=KV(p_s-p_p). \tag{5}$$

The constant of evaporation loss varies considerably with the design of the collector. It can be reduced to a minimum by constructing the collector so that the airflow over the porous surface is as small as possible. The present design of the collecting head, which is described in the next section, is constructed with this in mind. The constant as measured for this design is 2×10^{-4}. This means, for example, that if measurements are being made in rain at a temperature of 60°F, a relative humidity of 60 percent, and a velocity of 200 m.p.h., the correction for evaporation is 0.021 g/cm²/min. This corresponds to a correction of 0.04 gram per cubic meter, which is not very large compared to rain densities usually measured.

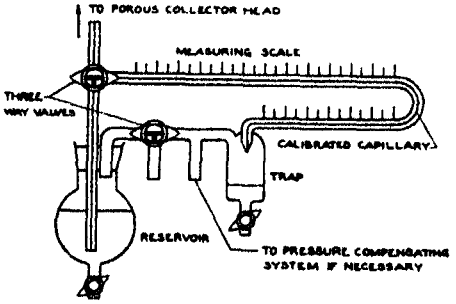

FIG. 5. *Measuring system for capillary collector.*

When the instrument is used for measurements in clouds above freezing, the evaporation rate is negligible because the atmosphere is saturated. Even under conditions when saturation exists, there will be a slight evaporation loss because of the adiabatic temperature rise of the air flowing around the collector. With air speeds of around 200 m.p.h., the temperature differences of a few degrees cause negligible evaporation. At much higher speeds, the temperature rise becomes appreciable, and evaporation losses must be corrected for.

When the capillary collector is used at air temperatures below freezing, the collecting head must be heated. Preferably its temperature should be maintained at a constant value just above the freezing point. The maximum rate of evaporation loss when the atmosphere is below freezing will occur at very low temperatures, when the partial pressure of the water vapor in the atmosphere is negligible compared to the vapor pressure of water at the freezing point. The maximum rate of evaporation for a heated collector of the present design operated at very low air temperatures can be computed from Eq. (5). Substituting the vapor pressure of water, 0.456 cm of mercury, for the term $p_s - p_p$, at 200 m.p.h. gives an evaporation loss of 0.018 g/cm^2/min. Several designs of electrically heated porous collectors have been made and tested, both in the wind tunnel and in flights. Their operation was quite satisfactory in the wind tunnel where the heat losses were quite constant and the temperature regulation was not difficult. However, in flight the temperature control system was found inadequate and large temperature fluctuations occurred in the collector causing excessive and variable evaporation losses of the same order of magnitude as the rates of collection.

DESIGN OF CAPILLARY COLLECTOR SYSTEM

Collecting Head

A wide variety of shapes and sizes of capillary collector heads have been used in wind tunnel tests. The design can be varied to suit the conditions of use. For the purposes of our work, the design shown in Figs. 2 and 3 has proved the most satisfactory.

The hollow shape of the collector gives a large area of porous material in relationship to the collecting area, thus providing a large flow capacity. With a suction of 25 cm of water, the collector can handle a flow rate corresponding, at 200 m.p.h., to a liquid water content in excess of 50 grams per cubic meter. As has been mentioned, the evaporation loss is quite low for this design. The hollow shape is well adapted to measurement of rain and snow. Rain drops or snowflakes have sufficient mass to carry them into the end of the cup, and there is very little loss from splash. The pores of the collecting cup have been sealed for a distance of $\frac{1}{8}$ inch inside of the cup to lower the aerodynamic pressure effect and to cut down the evaporation on the edge of the cup where the air flow is quite rapid.

In general, an object moving through a cloud collides with only a fraction of the particles in the volume it sweeps out. This fraction, known as the collection efficiency, is a function of the size of the collector, its velocity, and the drop size. The smaller the size of the collector, the higher is its efficiency of collection. Using the computations of Dr. Langmuir and Dr. Blodgett** of the General Electric Company Research Laboratory, R. Cunningham has calculated the approximate collection efficiency of this collector under different conditions (Fig. 4). These calculations were made on the assumption that its collection efficiency is the same as that at the stagnation point of a sphere of the same diameter (0.50 inch).

If two or more collectors having different sizes are used simultaneously in making measurements, the average drop size can be computed from their relative collection rates. The liquid water content can then be computed if the average drop size is known.

FIG. 6. Photograph of capillary collector and total head tube on B-17.

FIG. 7. Photograph of measuring system in nose of B-17.

** I. Langmuir and K. B. Blodgett, *A Mathematical Investigation of Water Droplet Trajectories*. Work done under Army Contract W-33-038-ac-9151, December, 1944—July, 1945.

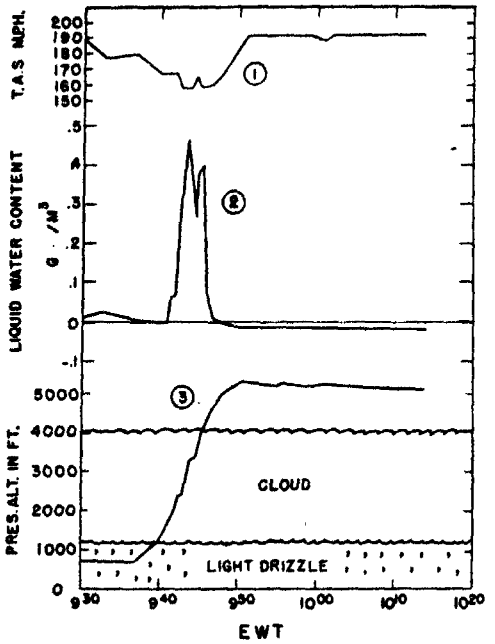

FIG. 8. Flight data taken with collector near Boston, May 19, 1945.

Measuring System

In most of the work a calibrated fine bore glass capillary tube having a volume of 0.01 cc per cm has been used to measure the rate at which water is being collected. The design of this system is shown in Fig. 5. By manipulation of the stopcocks, the system can be filled or drained. Measurements are made by observing the position of the water in the capillary tube as a function of time. One or two successful flights have been made using a microrotameter type of flow meter to measure the rate of water collection. It is planned to describe this in a later paper.

Flight Tests

A number of flights with the capillary collector have been made at temperatures above freezing. These tests were made in a B-17 airplane through the cooperation of the M.I.T. Radiation Laboratory. Photographs of the installation of the collector and measuring system are shown in Figs. 6 and 7. The results of data taken on one of these flights is shown in the diagram in Fig. 8. The instrument is in regular use at the present time on flights being carried out by the M.I.T. Weather Radar Group.

ACKNOWLEDGMENTS

This work was done under U. S. Army Contract W-33-038-ac-5443 (for the period July 1, 1944 to June 30, 1945). The author wishes to thank Mr. W. V. Westerlund of Wright Field and his associates for their help in this work as well as Professors H. G. Houghton, R. M. Cunningham, R. E. Katz, and the members of the M.I.T. De-Icing Research Laboratory for their advice and cooperation. The author is indebted to Dr. V. J. Schaefer of the General Electric Company for his helpful suggestions, to the Moraine Products Company for their cooperation in fabricating the porous metal parts, and to Mr. J. W. Miller and Mr. Arthur Bent of the M.I.T. Radiation Laboratory for arranging flight tests from the Bedford Air Base.

THE REVIEW OF SCIENTIFIC INSTRUMENTS VOLUME 20, NUMBER 2 FEBRUARY, 1949

An Apparatus for the Production of Large Metallic Crystals by Solidification at High Temperatures[*]

Louis Gold
Metals Research Laboratory, Brown University, Providence, Rhode Island

(Received September 28, 1948)

The design and operational aspects of an apparatus suitable for large-scale production of metallic crystals is described and the various high temperature difficulties indicated.

1. INTRODUCTION

THE commercial production of large single crystals is rapidly making available specimens of inorganic compounds for research purposes and special applications. The Harshaw Chemical Company is growing halide crystals in pound denomination;[1] the earlier researches of Stockbarger are being used to good advantage.[2] The Verneuil method for preparing synthetic sapphires[3] has been developed by the Linde Air Products[4] who are producing not only large sapphires, but a number of other refractory oxides. Considerable interest in the problem of growing adequate sized piezoelectric quartz crystals has been manifested, and progress is being made in this direction.[5]

The literature contains ample evidence of extensive investigations pertaining to the preparation and properties of metallic crystals. In general, only the lower melting metals such as zinc, lead, cadmium, etc., have been grown with some consistency with dimensions that might be considered as appreciable;[6] copper and certain alloys (gold-copper, alpha-, and beta-brass, for example) have been prepared in sizes of some note,[7] but beyond the range of approximately 1100°C, the results are quite sporadic.[8]

Although large crystals of metals having high melting points can be prepared by other methods which avoid high temperature complications,[**, 9] solidification from the melt apparently is most amenable to large-scale operation.[10]

Recently there has developed as a result of wartime researches marked awareness of the need for large metallic crystals.[11] In particular the desirability of suitable delay lines and similar storage devices[12] have intensified the importance of such materials.[13] The present paper is an outgrowth of these developments.

The apparatus to be described evolved from the desire to fulfil the considerations of having a relatively simple arrangement for growing large crystals of metals with design features which would allow for reasonable flexibility. The various schemes for growing crystals from the gaseous, liquid, solid, and solution states were critically re-examined and the decision to prepare the specimens from the melt made.

2. THE APPARATUS DESIGN AND CONSTRUCTION

The sundry variations of growing the crystals from a melt are all based on the underlying process of controlled solidification with due observance of the principles of nucleation and growth. The techniques of Bridgman,[14] Stoeber,[15] Czochralski,[16] and Obreimov-Schubnikov[17] were carefully evaluated,

---

[*] This paper is based on work performed at the Metallurgical Project, Massachusetts Institute of Technology, under Contract No. W-7405-eng-175 for the Atomic Energy Project.

[1] H. C. Kremers, Chemical and Engineering News, July 7, 1947.

[2] D. C. Stockbarger, Rev. Sci. Inst. **7**, 133–136 (1936); J. Opt. Soc. Am. **27**, 416–419 (1937).

[3] M. A. Verneuil, Ann. de Chemie et Phys. **8**, 320–48 (1904).

[4] "Synthetic Sapphire, Ruby, and Spinel," (Linde brochure, 1946).

[5] D. R. Hale, Science **107**, 393–394 (1948).

[6] C. A. Cinnamon, Rev. Sci. Inst. **5**, 187–190 (1934); M. F. Hasler, Rev. Sci. Inst. **4**, 656–660 (1933); B. B. Betty, Proc. Am. Soc. Testing Materials **35**, 193–200 (1935) II. R. F. Miller, Trans. A.I.M.E. **111**, 135 (1934).

[7] K. W. Hausser, and P. Scholz, Wiss. Ver. Siemens-Konzern **5**, 144–164 (1927); S. Siegel, Phys. Rev. **57**, 537–545 (1940); J. S. Rinehart, Phys. Rev. **58**, 365 (1940); W. Webb, Phys. Rev. **55**, 297–305 (1939).

[8] J. A. M. Van Liempt, Proc. A.I.M.M.E. Tech. Pub. **15**, 358 (1927); S. Kaya, Sci. Rep. Tohoku Univ. **17**, 1157–1177 (1928); Sci. Rep. Tohoku Univ. **17**, 17, 839–883 (1928).

[**] The other methods referred to are the strain-anneal and electroplating techniques. Metals having allotropic transformations between room temperature and their melting points may be thus most effectively grown as large crystals (see reference 9).

[9] H. C. H. Carpenter, Metal Industries **44**, 557–560, 584–587, 637–638 (1934); T. Erdly-Gruz and R. F. Kardos, Zeits. f. physik. Chemie **178**, 256–265 (1939).

[10] C. Kurylenko, Rev. Opt. (Theor. Instrum.) **23**, 1–19 (1944).

[11] D. L. Arenberg, M.I.T. Rad. Lab. Report 932 (1946). Also see J. Acous. Soc. Am. **20**, 1–26 (1948).

[12] TRE Report T1539, Aug. 1943, *Preliminary Experimental Enquiry into the Possibility of using Solid Materials for Supersonic Transmission Media for Delay Cells and other Devices.*

[13] A. G. Emslie and R. L. McConnell, *Radar System Engineering* (McGraw-Hill Book Company, Inc., New York, 1947), Vol. i, Chap. 16.

[14] P. W. Bridgman, Proc. Am. Acad. Arts and Sci. **60**, 305–383 (1925); *ibid.* **63**, 351–355 (1929).

[15] F. Stoeber, Zeits. f. Krick. **61**, 299–314 (1925).

[16] J. Czochralski, Zeits. f. physik. Chemie **92**, 210–221 (1917); J. Chem. Soc. **112**, 302 (1917).

[17] I. Obreimov and L. Schubnikov, Zeits. f. Physik **25**, 31–36 (1924).

FIG. 1. General view of apparatus.

and the Bridgman method finally selected because of its apparent popularity. Descriptions of apparatus utilizing the Bridgman method, some of which are rather crude and other which are quite elegant in their construction, may be found in the literature.[18] The vacuum furnaces used by Nix[19] and Siegel[20] were considered as best representative of what could most probably serve effectively for most metals since the exclusion of air is generally mandatory. The wire suspension arrangement for raising and lowering the specimens into and out of the furnace was thought to be inadequate for large melts of reactive metals; the method of moving the melt on a mercury column which had been used by both Quimby *et al.*[21] and Gwathemly and Benton[22] in different forms was further modified as will be described.

Figure 1 shows the equipment which has been used to prepare a wide variety of large metallic crystals; copper specimens of the order of 2 inches in diameter and 6 inches in length, for example, have been produced with relatively little difficulty. Metals and alloys in the range from 1100°-1600°C have also been grown in reasonable denominations with the basic limitation of resistance type furnaces restricting operation beyond this range. Although the apparatus has been limited to vacuum operation, it can readily be adapted to usage with inert atmospheres if desired, as would be the case when dealing with highly volatile metals. The apparatus will now be described in terms of its basic components, which are

A. The vacuum system.
B. The furnace chamber.
C. The furnace unit.
D. Power supply and temperature control.
E. The lowering-raising mechanism.

A. The Vacuum System

Gasket seals, waxed joints, and stopcocks were eliminated wherever possible, particularly on the high vacuum side to minimize leak troubles; most of the joints were hard soldered or welded. A vacuum of 5×10^{-6} mm could be maintained with the usual arrangement of Welch Duo-Seal two-stage fore-pump and Distillation Products three-stage vertical diffusion pump. In the course of a run, however, severe out-gassing would reduce the vacuum to approximately 10^{-3} mm. Because of the wide variations in gas composition, it was found that the standard gauges were not serviceable in this range. Instead, a Lepel high frequency oscillator (commonly known as a spark-coil) was used to gain an approximate estimate of the pressure; in any event, it could detect if and when a leak occurred.

B. Furnace Chamber

Figure 2 shows the furnace chamber extending to the bottom of a mercury well (33) on one end and sealed at the top by a steel cover and gasket (7), (8). The steel sidearm pumping lead, hard soldered to the chamber, is bolted to the diffusion pump and the seal made via an indium metal gasket. *** There are several openings on the chamber. Three windows (21) each at a different level provide for sighting. These were not used in any of the runs made, but should prove of value in studying solidification or other processes at much lower temperatures. These windows are made by a special process and are adequately described in the Tube Shop Handbook of the M.I.T. Radiation Laboratory. Their novel feature is the distortionless view one sees through them—of material importance in many instances. Below the bottom window is another opening (22) through which a thermocouple (23) can be inserted. The outside of the chamber is wrapped with approximately 150 feet of ⅜-inch copper tubing (9) which is soft soldered into place; the water cooling provided will dissipate more than 5 kw with the chamber wall running a bit warm. A steel ring (25) was welded into place on the inside to support the furnace unit.

C. Furnace Unit

Because of the high temperatures and prolonged periods of operation, and because of the gradient requirements necessary for single crystal propagation, the furnace design proved to be most formidable; the difficulties appeared to be most marked when attempting to grow the larger sized specimens. Also there were complications resulting from vapors attacking ceramics and the general misbehavior of the insulation at high temperatures.

---

[18] A. G. Hoyem, Proc. Iowa Acad. Sci. **36**, 301 (1929).
[19] F. C. Nix, Rev. Sci. Inst. 9, 426–427 (1938).
[20] S. Siegel, Phys. Rev. **57**, 537–545 (1940).
[21] S. L. Quimby, Phys. Rev. 39, 345–353 (1932).
[22] A. T. Gwathemly and A. F. Benton, J. Phys. Chem. **44**, 34–42 (1940).

*** Indium is better than lead for this purpose because it is softer and less inclined to work-harden.

An Alundum core (16) RA-98 or RA-1139 (supplied by the Norton Refractory Company) is wound with the required number of turns of molybdenum wire (15) of predetermined diameter. A layer of special grade Alundum cement (silica free) (14) is applied over the windings and pre-fired up to 300°C. The current carrying capacity of the return leads is enhanced by using three strands of wire, each of which is encased in an individual alundum tube (12) for protection. The core is slipped over the lip (19) of a steel bucket (11) which is then filled with coarse grain silica free Alundum sand (13). A pair of holes close to the upper rim of the bucket allows for the ready insertion and removal of this unit by a pair of steel hooks. The bare wires protruding above the level of the sand are inserted into a stainless steel sleeve (6) and held firmly in place by a number of set-screws; this arrangement provides the necessary rigidity for facilitating the job of making electrical contact in a vacuum and also serves to protect the embrittled "moly" leads from repeated handling.

The stainless steel sleeves pass through a Lavite plug (10) which centers them and also offers insulation above the furnace. Two lock nuts (7) fasten the power-leads in place. A pair of connectors (5) are fastened to the power-leads by set-screws. Between steel bucket and ledge is a section of Lavite insulator (24) which is braced by a thin steel section not shown.

D. Power Supply and Temperature Control

Evidently temperature control in high power-high temperature furnaces cannot be handled in conventional fashion.[23] For temperatures over 1000°C thermocouples cannot be relied upon for dependable performance. There are two recommended approaches:

(1) Control thermocouple at some convenient point in furnace below 1000°C, but so arranged as to give temperature control in the hot zone which may be well above this temperature.

(2) Maintenance of constant power by using a voltage-stabilized supply.

Because of the uncertainty of the nature of the gradients within the furnace, method (2) seemed preferable; for a furnace relatively free of gradients, method (1) is inherently capable of more accurate control, but method (2) will generally be adequate since, in the range of temperatures of present interest, temperature control better than a few degrees is practically meaningless—primarily because of the limitations of the temperature measuring devices.[24]

A General Radio 7 KVA variac rated at 220 v and 30 amps was operated off a two-phase 60-cycle 220 v-30 amp. line. The power was introduced into the vacuum furnace by means of the power leads (4) indicated in Fig. 2. These leads were made up as a unit which was then soft soldered into the steel cover plates. They are very sturdy in nature and can be made to sizes which will carry currents of the order of hundreds of amperes. A long section of 705-2 glass permits one to see the contact made. For high vacuum operation the contact is best made by dry fits, but for low vacuum or inert atmosphere operation mercury contacts may be used.

The temperatures were read with a Leeds and Northrup optical pyrometer through the 1-inch window (3) by sighting a glass prism (2) in the brass housing (1). In actual practice, no apparent temperature fluctuations were observed during the course of operation of the furnaces. The thermal inertia of the furnace was such as to eliminate rapid fluctuations of temperature even though the voltage were to fluctuate for any reason. Moreover, some approximate data taken on the voltage-temperature characteristics of the furnace indicated that a one-volt change would result in a temperature change of only a few degrees. Still another

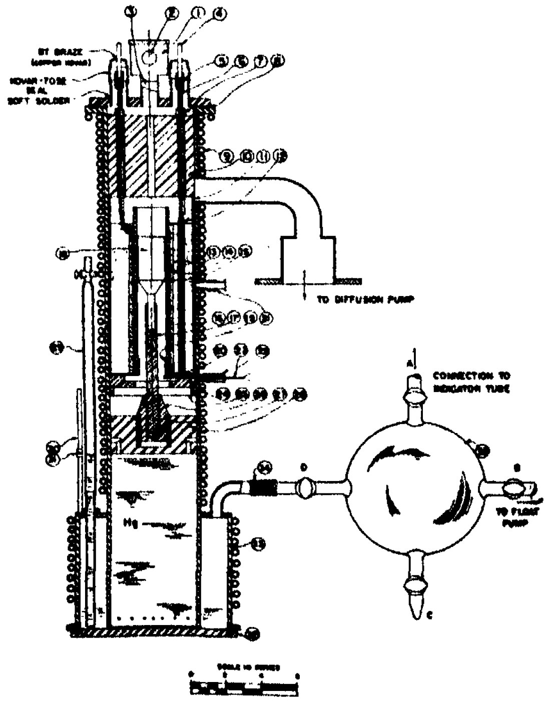

FIG. 2. Sectional view of furnace chamber.

---

[23] N. R. Stansel, *Industrial Electric Heating* (John Wiley & Sons, Inc., New York, 1933).

[24] American Institute of Physics, *Temperature, Its Measurement and Control in Science and Industry* (Reinhold Publishing Corporation, New York, 1941).

indication of the temperature regulation possible was shown by the ability to hold a constant temperature on some particular object in the furnace for hours at a stretch by merely setting the voltage at a given level.

E. The Lowering-Raising Mechanism

Reference to Fig. 2 will indicate the arrangement used to vary the position of specimens in the furnace chamber. The principle of altering the height of a mercury column which was used successfully by Quimby and independently by Gwathemly and Benton was carried out by the former by draining off mercury through a rotating stopcock into an evacuated chamber and by the latter simply by varying the height of a leveling bulb which was slowly lowered by a gear reduction system.

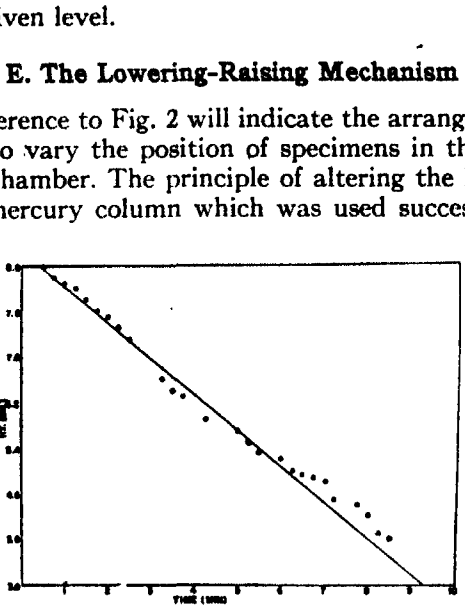

FIG. 3. Typical plot of mercury level *vs.* time showing fluctuations at rapid lowering rates.

The present design is thought to have advantages over the afore-mentioned techniques; the height of the mercury column is varied by regulating the pressure in the steel reservoir (33). This was done by a sequence of manipulations on the stopcocks attached to the volume tank (35); bellows (34) were inserted as indicated to minimize the stresses on the glass connections during the various stages of manipulation. An indicator tube (29) provided with a scale and lens viewer (30) and (31) was used to determine the height of the column (and thus the position of the specimen).

A uniform rate of lowering is possible only under certain conditions, foremost of which is the maintenance of relatively lower pressures in the volume tank than in the reservoir.[25] The uniformity of lowering was checked up to rates of approximately 6 mm per minute, at which point slight fluctuations of the kind shown in Fig. 3 were noted. Since the rates used in the crystal growing runs were never greater than 2.5 mm per minute, the lowering rate was uniform; exceedingly slow rates of the order of mm per hour were not amenable to careful regulation because of stopcock difficulty—it was found important that stopcock *D* be greased properly if good performance were to be had. Grease or dirt in the stopcock hole will give trouble. This possible source of interference could be readily eliminated by inserting a tee branch between the reservoir and the volume tank; one branch could be used for evacuation and raising purposes, while the other could have a metal capillary valve for the lowering process. This suggestion is made for future experimentation.

The steel float (28) is inserted into the chamber prior to the installation of the mercury and the bottom plate (32). The float design was carefully considered in terms of the amount of tilting which would be experienced by melts supported at some distance from the face of the float. If the fit between the float and chamber is too close, there is a tendency for sticking and general erratic behavior; on the other hand, if too loose, the tilting effect is enhanced. Thus, it was necessary to make a simple analysis of the variation of the amount of tilting with the degree of clearance between the float and the furnace chamber. A working formula which applies for the conditions prevalent is

$$\delta = [L(W-w)/h],$$

where delta (δ) is the amount of horizontal displacement, W is the inside diameter of the furnace chamber, w is the diameter of the float, L is the length of the crucible support plus crucible length, and h is the height of the float. For the set-up used calculation based on the above formula indicated that a clearance of several thousandths should not give significant values for delta (δ). It is also a safe precaution to have the inside wall of the chamber free of scratches and bumps.

Figure 2 shows a particular pedestal arrangement (17), (20), and (27). In the course of developing growth techniques for various metals and alloys a variety of pedestal designs were devised. These are shown in Fig. 4. The shapes and materials of construction were altered to modify the temperature gradients in the charge. In general, they were composites of graphite, firebrick, and Lavite.

To achieve the proper levels of the specimen, both during the melting operation and the final solidification state, it was necessary to select the proper relative dimensions for the reservoir and the furnace chamber. Some degree of flexibility was required to accommodate the different sizes and weights of the many specimens; this was accomplished by varying the amount of mercury in the reservoir. The mercury can be siphoned in and out through the indicator tube as the situation might demand. Occasionally the indicator tube, as well as the mercury in it, would become sufficiently dirty to make readings difficult by virtue of the meniscus becoming anomalous and the general obscuring of its position. The tube and mercury were readily cleaned from time to time by admitting dilute nitric acid, water, and acetone in proper sequence via the stopcock shown. It is important to eliminate all traces of water or acetone in the tube prior to starting up again for operation; if this is not done, bubbles will form beneath the mercury in the tube to interfere with proper operation by rising to the surface when a run is in progress.

---

[25] L. S. Marks, *Mechanical Engineers Handbook* (McGraw-Hill Book Company, Inc., New York, 1941), "Flow of compressible fluids," p. 353–361.

3. OPERATIONAL PROCEDURE

Having described the individual design aspects of the components, we will now delineate the manner in which the apparatus may be used for a typical run. By no means are the following details unique: a broad range of variations is possible and, as a matter of fact, additional modes of operation have been utilized. The operational sequences can conveniently be classified as:

A. Loading.
B. Starting-up.
C. Out-gassing and pre-heating the furnace.
D. Raising and melting the specimen.
E. Lowering the specimen.
F. Finishing the run.

A. Loading

The specific nature of the run determines the kind of pedestal, crucible, and furnace to be used. The pedestal is inserted into the hole of the steel float with the crucible or crucible holder in place; the maximum and minimum position of the crucible is then checked by raising and lowering the mercury column. The column is raised by connecting stopcock *A* or *C* to a compressed air line and then keeping the proper cocks closed or open. Lowering is accomplished by simply letting the compressed air in the volumn tank escape. The maximum and minimum position of the crucible in the furnace can be adjusted by varying the quantity of mercury in the reservoir and the height of the pedestal. Different sizes and denominations of specimens require that these adjustments be made.

With these preliminaries dispensed with, the furnace is then lowered onto the Lavite insulator above the steel shelf by means of a pair of steel hooks. The task of getting the crucible into the furnace opening is facilitated by having the float completely lowered before the furnace is inserted. Having set the furnace into position, one can again check the maximum and minimum positions of the crucible.

The Lavite plug is then slipped over the protruding stainless steel connecting rods and lowered into position by a pair of pointed tongs inserted into the sighting hole. The lock nuts are put into place to hold the connector-rods rigidly in place and the connector-cups fastened into place.

The gasket on top of the furnace chamber is well greased and the steel cover carefully lowered into place as the power-leads make contact with the connector-cups. The steel cover is subjected to a slight rotary motion which serves to assure good contact and to spread the grease film under it to effect a good seal.

B. Starting-Up

A rubber hose connection is made between the indicator tube and stopcock *A* on the volume tank. The float pump is then started up and the mercury column slowly raised up the entire length of the indicator tube and just beyond the opening of the stopcock to eliminate all the air. The indicator tube is closed off and the hose connection removed. The volume tank is next evacuated with stopcock *D* on the closed position.

At this point the fore-pump is turned on and the furnace chamber evacuated. To prevent the mercury column rising too far into the chamber, it is important to balance the pressures on both sides of it. This is accomplished by noting when the mercury in the indicator tube begins to fall and as it does, stopcock *D* is slowly opened to decelerate the downward motion of the mercury column. With both sides of the mercury column evacuated, the diffusion pump is then turned on, followed by the water cooling system.

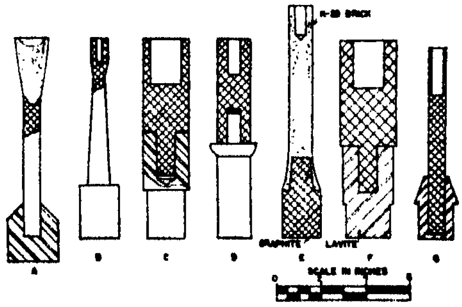

FIG. 4. Pedestal design.

C. Out-Gassing and Pre-Heating the Furnace

The power supply is connected to the furnace leads, and the power gradually increased. Too rapid heating is avoided in order to prevent thermal stresses from causing cracking of the furnace core or crucible. A furnace being used for the first time gives off voluminous amounts of water vapor and carbon dioxide. A new furnace is generally out-gassed overnight at a dull red heat. Subsequent usage of the furnace will not require out-gassing periods of long duration. The furnace is heated above the maximum point of operation to be effective in the melting operation to drive off gas that might otherwise be slowly evolved at the lower operating point.

D. Raising and Melting the Specimen

The specimen is slowly raised into the furnace by careful manipulation of the stopcocks on the volume tank. The raising process is watched through the window on the steel cover via the right angle prism in the brass case. When the specimen has been raised to desired height (as shown by the position of the mercury level in the indicator tube), stopcock *D* is closed and the volume tank evacuated in readiness for the lowering operation.

Temperature readings are taken periodically to follow the progress of the melting operation. If the power required to effect melting has not been predetermined in some preceding run, the voltage is gradually increased until melting is noted. Since some specimens will not show a clear liquid melt,† it is of considerable help to plot the temperature readings *versus* time and get a heating curve from which the melting halt can be detected. After some experience, the halts can be noted without the necessity of plotting the data, but in some instances this cannot be dispensed with.

The temperature readings are subject to a number of sources of error and must therefore be corrected.[26] Where a clear liquid surface can be observed (as in the case of copper, for example) it is not unusual to experience an apparent drop in temperature although actually the temperature has increased. In some instances the drop has been as much as approximately 150°C. This phenomenon can be attributed to the marked change in the spectral reflectivity at the melting point.

To minimize possible reactions of the melt with the crucible or even of the crucible with the holder, and also to minimize evaporation, it is important to avoid overheating the molten change. Yet, one must be certain to have effected complete melting.

E. Lowering the Specimen

Having melted the specimen and allowing sufficient time for the elimination of any solid present in the melt, the solidification process is initiated. The temperature is stabilized at approximately 100°C above the melting temperature. Lowering the specimen out of the furnace is then begun by cautiously turning stopcock *D* to the open position; the volume tank must first be completely evacuated to the point where no glow discharge can be excited with a spark coil. Air escaping into the volume tank as stopcock *D* is opened will give rise to the glow discharge and thus indicate that lowering has commenced. The opening of the stopcock is adjusted until the desired rate of lowering is achieved. This is done by a series of alternating back and forth maneuvering, sufficient time being allowed for equilibrium to set in for each stopcock setting.

F. Finishing the Run

When the specimen has reached the minimum position, or when solidification is known to be complete, the power is gradually reduced. Reducing the power too rapidly may cause cracking of the furnace core or other ceramic materials in the hot zone. With the power completely off it may take hours for the furnace to cool, particularly if it is well insulated. So to accelerate the cooling process the specimen may be raised back into the furnace after the furnace has cooled below the melting point region. This step will simultaneously anneal the specimen and remove thermal stresses that might have been left by the original gradient condition that existed during the solidification.

The cooling operation completed, the usual operation of shutting the diffusion pump and the fore-pump is followed by admitting air through the bleeder-valve on the steel cover. It has been found advisable not to attempt to remove the specimen while the furnace is still in place. By removing the furnace first, one can carefully extract the crucible containing the specimen.

4. DISCUSSION

In the course of the numerous runs made with the apparatus, the complexities arising from prolonged, large scale operation at high temperatures were made evident. A number of these are directly attributable to the presence of a metallic charge and others originate because of the inherent difficulties of high temperature operation.

The crucible problem for metallic melts is much more severe than for inorganic compounds. The technique of thin-walled metal crucibles devised by Stockbarger[3] cannot be utilized because of obvious alloying effects. Refractory crucibles made of Alundum, beryllia, graphite, etc. when in contact with molten metals for prolonged periods will react or show marked penetration. This gives rise to contamination and sticking; silicon, for example, in an Alundum crucible will not come out readily and the crucible needs to be broken away. The need for high gradients also causes difficulty with crucibles by favoring thermal stress cracking.

---

† Reactive metals such as aluminum, beryllium, etc. form oxide skins even in a high vacuum. The oxide skin on the surface of the melt obscures the nature of the charge below.

[26] W. E. Forsythe, *Measurement of Radiant Energy* (McGraw-Hill Book Company, Inc., New York, 1937).

Resistance-wound furnaces are a potential source of trouble because of a number of deleterious effects, foremost of which is electrical breakdown at elevated temperatures. This can be reduced somewhat by designing the furnace for low voltage—high current operation; one cannot carry this process too far because of the wire size limitations. Resistance-wound furnaces are also subject to attack metal vapors. Some degree of minimization of this difficulty is possible by proper shielding of the furnace walls. One cannot, however, completely obscure the surface of the charge because of the necessity of sighting it during the course of a run.

The longevity of such furnaces is seriously handicapped by gradual evaporation of the resistor element and increasing embrittlement of the furnace core. The presence of high gradients is certainly not beneficial.

There appears to be some evidence which indicates that the Bridgman method may not be the best means for introducing the gradient into the molten charge. The large cross-sectional area of melts with relatively high thermal conductivity tends to level-off the gradients existing at the bottom of the furnace. For this reason it was found necessary to support the crucibles on graphite pedestals in order to create sufficiently high thermal gradients in the charge. The graphite pedestals, however, markedly increased the power requirements. It was found necessary to use combinations of graphite and insulators such as Lavite and firebrick to compromise between power-loss and thermal gradients. The Obreimov-Schubnikov technique of instituting the gradient after melting has taken place by introducing a heat sink was surmised to be a more efficient procedure. Some preliminary attempts in this direction were quite encouraging.

The relatively higher degree of impurities in the metal specimens further distinguishes the growth of metallic crystals from inorganic crystals. Insoluble matter in the metal will settle out when the specimen is kept molten for some time. The presence of the insoluble impurities is probably responsible for the observance of an optimum rate of solidification for producing large crystals.

It was generally evidenced that increasing the dimensions of the specimens not only altered the optimum conditions, but also augmented the tendency of parasitic grains appearing. Although a number of specimens were not truly single crystal, i.e., such parasitic grains were evident, their general usefulness was not seriously interferred with. Thus, the term single crystal was avoided in the title of this paper for the sake of completeness and accuracy; moreover, the distinction between the true single crystal and the mosaic crystal is not well enough defined to permit one to use the terminology of single crystal with impunity.

ACKNOWLEDGMENT

The author is indebted to several members of the Metallurgy Department of M.I.T. for making this research possible. In particular, the interest and advice of Professors Chipman, Cohen, and Kaufmann served as a source of constant encouragement during the difficult stages.

Thanks are also due Mr. Holbrook for operational assistance and Mr. Sanroma of the Research Laboratory of Electronics for most of the basic constructional work.

THE REVIEW OF SCIENTIFIC INSTRUMENTS VOLUME 20, NUMBER 2 FEBRUARY, 1949

A Large Helium Liquefier

J. G. DAUNT AND H. L. JOHNSTON
The Cryogenic Laboratory, Department of Chemistry, and The Department of Physics, The Ohio State University, Columbus, Ohio

(Received October 2, 1948)

A large helium liquefier is described which produces 7.5 liters of liquid helium per hour through a Joule-Thomson expansion valve when operated from a compressor giving 21 cu ft./min. flow at a pressure head of 320 lb./sq. in. The liquid helium can readily be transferred into exterior cryostats. The consumption of liquid hydrogen, used to pre-cool the helium gas, during the process of liquefaction is 1.3 liters of hydrogen per liter helium. The liquefier fits into a container 6′ long by 8″ in diameter.

I. INTRODUCTION

A LARGE helium liquefier has been put into satisfactory operation in the Cryogenic Laboratory at the Ohio State University, and in view of the simplicity and stability of its operation, it is thought that a brief description of it might be of interest.

The liquefier is based on some features of the designs for small scale helium liquefiers using the Joule-Thomson expansion method of liquefaction previously developed both at the Ohio State University[1] and at the Clarendon Laboratory, Oxford[2] and utilizes some features of the large helium liquefier in use at the University of California (courtesy of Professor W. F. Giauque).

The liquefier is an all-metal construction immersed in a glass Dewar which contains liquid hydrogen. It is therefore possible to view continuously the level of liquid hydrogen through slits in the silvering of the Dewar, a feature which is found convenient during the operation of the liquefier.

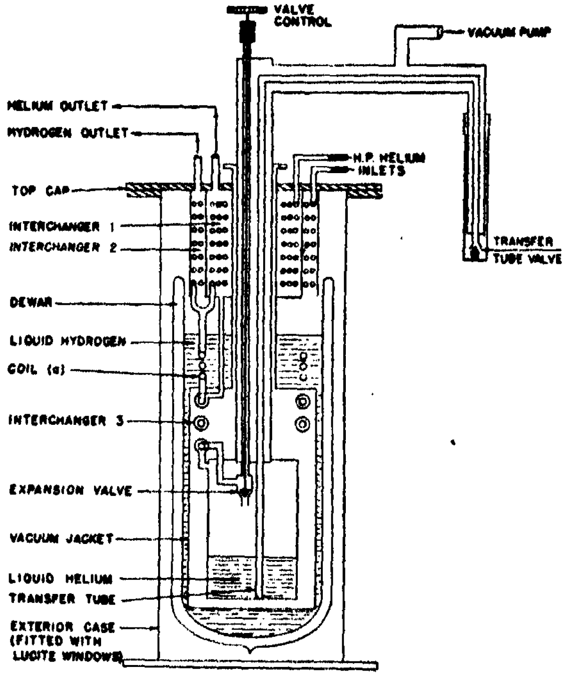

FIG. 1. Helium liquefier.

Observation of the level of liquid helium produced is not critical, since the volume of helium liquefied can be readily obtained from observation of the helium gas-holder level. It was therefore decided to dispense with a direct visual observation of the helium chamber, a process which greatly simplified the construction.

The liquefier does not use liquid air or liquid nitrogen as a pre-coolant, but instead the high pressure input helium gas is allowed to enter at room temperature and to be cooled to liquid hydrogen temperatures by means of heat interchangers. This interchanging system between room temperature and liquid hydrogen temperature is in two parallel sections, one interchanging with the return cold low pressure helium gas and the other with the hydrogen evaporating from the Dewar.

The liquid helium is transferred out of the liquefier into exterior cryostats or storage vessels by means of a vacuum jacketed transfer tube built integrally with the liquefier. It is found that the losses in transfer are small and that the rate of transfer is very fast, a few seconds being sufficient to transfer 1 liter of liquid helium into an exterior cryostat.

II. GENERAL DESCRIPTION OF LIQUEFIER

A schematic diagram of the liquefier is given in Fig. 1 and Fig. 2 shows to scale detail of the more important dimensions.

The helium high pressure input is split into two parallel paths outside the liquefier and the two inputs lead separately to interchangers 1 and 2. Both these interchangers are built concentrically and are of the Hampson type, using a construction developed and patented by Giauque.[3] Interchanger

---

[1] J. G. Daunt and H. L. Johnston, Phys. Rev. 72, 161 (1947) and Rev. Sci. Inst. 20, (1949).

[2] J. G. Daunt and K. Mendelssohn, J. Sci. Inst. (in press).

[3] We are indebted to Professor W. F. Giauque for the information concerning these interchangers and for permission to use his patent design.

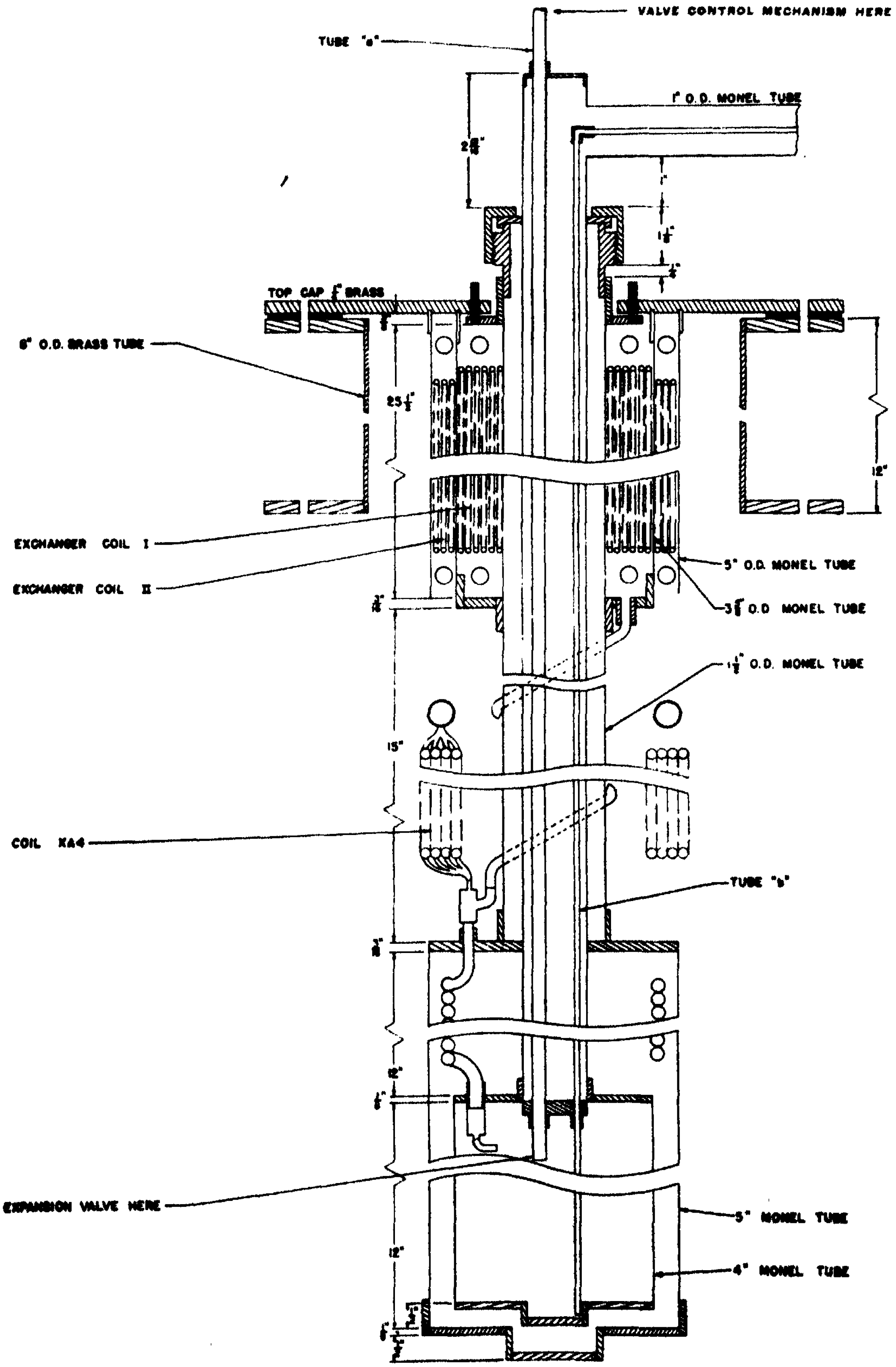
VALVE CONTROL MECHANISM HERE
TUBE "a"
1" O.D. MONEL TUBE
1"
TOP CAP ½" BRASS
8" O.D. BRASS TUBE
25½"
12"
EXCHANGER COIL I
EXCHANGER COIL II
5" O.D. MONEL TUBE
3⅝" O.D. MONEL TUBE
1½" O.D. MONEL TUBE
15"
COIL XA4
TUBE "b"
12"
EXPANSION VALVE HERE
5" MONEL TUBE
4" MONEL TUBE
12"

FIG. 2.

1 has 6 layers of copper tubing ($\frac{1}{8}''$ o.d. and 35 thousandths of an inch wall thickness), and is comprised of 15 high pressure tubes in parallel each of length 23 ft. 8 inches. The return low pressure helium passes through the moderately open network between the high pressure tubes. Interchanger 2 is of the same general construction having 3 layers of the same $\frac{1}{8}''$ copper tubing comprising 9 parallel high pressure paths of length 34 ft. 8 inches each. The evaporating hydrogen vapor passes through the spaces left between these high pressure tubes.

The lower 10 inches of this double interchanger system fits into the top of a glass Dewar vessel which is 54 inches long by $5\frac{5}{8}$ inches i.d. This Dewar is placed in a brass vessel, fitted with Lucite windows, similar to the hydrogen cryostats developed at Ohio State University by one of us,[4] and serves to hold the liquid hydrogen. By this construction the level of the liquid hydrogen within the liquefier can be readily inspected.

Below the room temperature to liquid hydrogen temperature interchanger system, within the Dewar, the liquefier follows essentially the construction described for the small liquefiers previously developed.[1,2] The main components are (a) a high pressure helium coil immersed in liquid hydrogen, serving to cool the incoming helium gas to 15°K, which is the temperature maintained by the liquid hydrogen, (b) a vacuum jacket, which is continuously evacuated by an oil diffusion pump, (c) an interchanger (interchanger 3 of Fig. 1) between 15°K and helium temperature (4.2°K). This interchanger uses the cold of the returning low pressure helium gas which is not liquefied at the expansion valve, (d) an expansion valve, (e) a helium chamber to collect the liquefied helium and (f) a transfer tube which enables the liquid helium to be drawn off into a cryostat outside the liquefier.

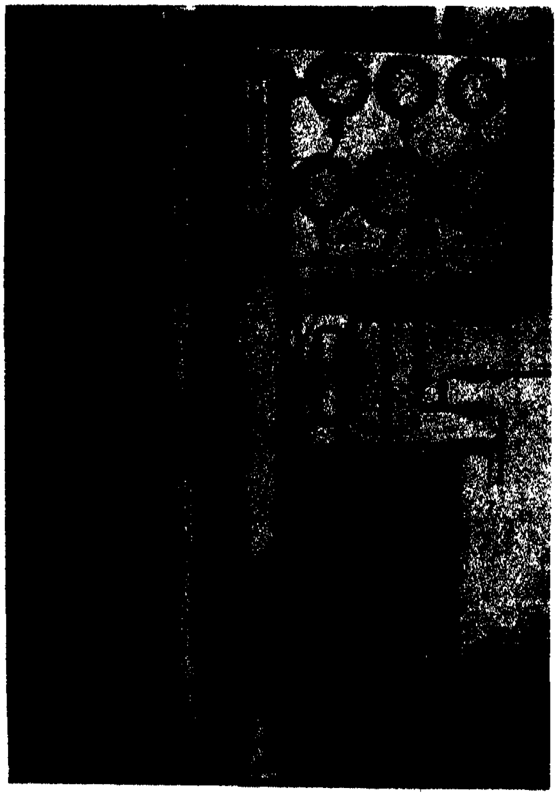

FIG. 3.

In addition, not shown in Fig. 1, there is a gas thermometer attached to the expansion valve and a "valve warmer" which consists of a small bore tube leading directly from a supply of pure helium gas at room temperature outside the liquefier to the expansion valve so that warm gas can be blown onto the valve. This is used if the valve sticks at low temperature.

The high pressure helium coil (a) consists of 4 parallel paths constructed of $\frac{3}{16}$-inch copper tubing, wall thickness 35 thousandths of an inch, each of approximate length 19 ft.

The vacuum jacket (b) is made of monel tubing 5-inch o.d. and 45 thousandths wall thickness. The length of the vacuum jacket is $24\frac{5}{16}$ inches.

The interchanger (c) between hydrogen temperatures and helium temperatures is of the Linde type, chosen in order to minimize conduction losses to the helium chamber. This interchanger is made from $\frac{1}{2}$-inch o.d. copper tubing, length 20 ft., in which is placed four $\frac{1}{8}$-inch o.d. copper tubes, the whole arrangement then being wound in the form of a helix and bound rigidly with asbestos string. The four $\frac{1}{8}$-inch copper tubes take the high pressure gas, the tubes being arranged in parallel. The return helium gas flows back through the space left between the $\frac{1}{8}$-inch tubes inside the main $\frac{1}{2}$-inch tube. In order to increase the length of the return path, the high pressure tubes had wound on their outsides a helical coil of 22 a.w.g. wire of open pitch, the wires subsequently being soldered at intervals to the $\frac{1}{8}$-inch tubes. From the observed high liquefaction coefficient it is evident that this construction is highly efficient.

The expansion valve (d) is a needle valve operated from the top of the liquefier by means of a $\frac{3}{16}$-inch o.d. monel tube, 25 thousandths wall thickness, this control rod being contained in a sheath made from $\frac{1}{4}$-o.d. monel tubing, 15 thousandths wall thickness. The valve was arranged so that the sheath was at high pressure. This arrangement insures a minimum risk of air impurities flowing through the packing at the top of the control mechanism and also serves to allow an easy attachment to be made at the top of the liquefier to measure the high pressure at the valve. It should be mentioned that the valve is mounted *inside* the helium chamber, thereby allowing the operation of a valve warmer.

---

[4] A detailed description of this is being submitted to The Review of Scientific Instruments.

The helium chamber (e) is made from a 4-inch o.d. monel tube 11⅝ inches long. The capacity for helium is approximately 2.2 liters, when allowance has been made for the position of the valve, etc. It is possible therefore to collect helium in amounts of the order of 2 liters between any two transfers to the cryostats outside the liquefier.

The transfer tube (f) consists of a ⅛-inch thin walled monel tube which is carried in a vacuum isolated jacket outside the apparatus into the external cryostats. The exit end (cryostat end) of this transfer tube bears a needle valve to open and close. This transfer tube, the valve and valve controls, the gas thermometer and the valve warmer are all mounted as a unit on a 1¼-inch o.d. monel tube which extends the whole length of the liquefier. This tube can be withdrawn easily without disturbing any of the interchangers, etc., and consequently makes the problem of construction and repairs greatly simplified. At the top of the liquefier this tube makes a vacuum tight joint to the rest of the vacuum jacket by means of a rubber gasket (Fig. 2).

The remaining general arrangements are illustrated in Figs. 1 and 2 and are self-explanatory. A photograph showing the completed liquefier suspended alongside its brass cryostat is given in Fig. 3.

In addition to the liquefier itself a purifier is used to clean the incoming high pressure helium gas. This purifier consists of a high pressure charcoal trap mounted in liquid air. The activated charcoal is contained in a spiral tube 1 inch o.d. and 25 ft. long, which fits inside a glass Dewar vessel 36″ long by 5½″ inside diameter. Between this charcoal trap and room temperature an interchanger is mounted so that the outcoming high pressure helium is approximately at room temperature and so that a minimum loss of liquid air occurs.

TABLE I.

Output	7.5 liters liquid helium/hour
Liquefaction coefficient	14 percent
Temperature of hydrogen bath	15°K
Input pressure	320 lb./sq in.
Gas flow	21 cu ft./min.
H_2 consumption (liquid)	1.3 liters per liter liquid helium

The interchanger consists of four Linde type interchangers mounted in parallel.

III. PERFORMANCE

The performance of the liquefier is given in Table I.

To start the machine it is initially cooled with liquid nitrogen. About one hour is required for this. After liquid N_2 temperature has been reached, the liquid nitrogen is syphoned out of the Dewar and liquid hydrogen introduced. The initial consumption of liquid hydrogen required to cool the machine to 15°K is approximately 20 liters. 10 minutes is allowed to elapse after the introduction of hydrogen and then the helium gas flow is started, and simultaneously the pumping of the liquid hydrogen to low pressure is commenced. Helium liquefaction commences approximately 30 minutes after the flow is started. The high liquefaction coefficient and the liquid hydrogen consumption are comparable with that for other large liquefiers described elsewhere[5] and indicates good interchanger efficiencies.

The liquefier is easy to handle and shows excellent running stability.

IV. ACKNOWLEDGMENTS

This work was carried out with the assistance of a contract between the Office of Naval Research and The Ohio State University Research Foundation.

---

[5] W. H. Keesom, *Helium.* (Elsevier Publishing Company, Inc., New York, 1942.)

THE REVIEW OF SCIENTIFIC INSTRUMENTS VOLUME 20, NUMBER 2 FEBRUARY, 1949

Design of the Radiofrequency System for the 184-Inch Cyclotron

K. R. MacKenzie,* F. H. Schmidt,** J. R. Woodyard, and L. F. Wouters
Radiation Laboratory, Department of Physics, University of California, Berkeley, California

(Received November 2, 1948)

A description is given of the frequency-modulated oscillator and its associated r-f circuits, as used in the 184-inch cyclotron for accelerating deuterons to 190 million volts or alpha-particles to 380 million volts. A 9C21 water cooled tube is used in a grounded-grid circuit, which is tightly coupled to the single-dee resonant circuit so that the oscillator follows the frequency of the dee over the wide range required. During normal operation the oscillator delivers approximately 20 kw of r-f power to the dee system at an efficiency of 60 percent, giving 20 kv at the front of the dee, although the oscillator is capable of considerably more output. The frequency is swept from 12.5 mc to 9.0 mc approximately 100 times per second by a rotating condenser connected to the dee by a half-wave transmission line. Much of the history of the design, and reasons for choices made, are given, as it is felt this may be useful to others designing frequency-modulated oscillators for cyclotrons.

GENERAL FEATURES

THE design of the radiofrequency system for the 184-inch cyclotron was started about April, 1946, shortly after the successful demonstration of the synchrocyclotron principle by the 37-inch cyclotron at Berkeley.[1] Initial thoughts regarding the exact form of the design were varied, but a single dee with some form of mechanical frequency modulation by a rotating condenser were fairly certain features. Consideration was given to the arrangement in which a rotating condenser is mounted directly at the rear of the dee, but eventually it was decided to build a high power version of the system used on the 37-inch cyclotron. This system had been tested and, although cumbersome, it seemed easier to design and build and was known to work; in retrospect, the exceptional ease of operation of the 184-inch cyclotron may be attributed in no small measure to this decision and to the experience gained with the smaller synchrocyclotron.

The r-f resonant system thus consists of a single dee and separate rotary capacitor connected by a transmission line, operating with a node near the middle, i.e., essentially the half-wave mode. The frequency range required for 200-Mev deuterons is 11.5 to 9.8 mc. Additional leeway is provided for tolerance and adjustment. It may be worth while to review the considerations involved in the initial choice of this arrangement for the 37-inch, and subsequently for the 184-inch cyclotrons:

(1) The rotary capacitor could operate outside of the magnetic field. (2) Dee and capacitor design and construction could proceed independently. (This saved considerable time, as the dee design was essentially complete before a number of basic questions regarding the rest of the r-f system had been answered.) (3) Many of the problems involved in the design of the capacitor had been worked out. (4) Vacuum systems for the cyclotron dee and for the capacitor could be independent; little was known at that time concerning the relative vacuum requirements of the two units. (5) It was shown in the 37-inch cyclotron that positive bias on the dee very often increased the beam current, and it was felt desirable to retain the possibility of similarly biasing the 184-inch dee. In addition, a bias on the dee is the surest way of providing a sweeping field to remove electrons trapped in an r-f discharge. (6) The oscillator could be coupled to the r-f system in air near the nodal point of the transmission lines, greatly simplifying oscillator design and adjustment. (7) The system is readily adjustable to give the desired shape of dee voltage *versus* frequency.

DESIGN OF RESONANT SYSTEM

As mentioned, the theoretical frequency shift required is 11.5 to 9.8 mc. At the time it was considered undesirable to have the frequency-time curve convex upward in any part of the useful range. It was thus decided to allow most of whatever extra range was provided at the high frequency end. The ions could then start (as well as finish) where the curve was concave upward. The desirable frequency limits were tentatively set at 12.5 and 9 mc. In order to insure that the higher limit would be sufficiently high, the initial layout was designed for operation between 13 and 9.5 mc. It was planned to increase the line length in order to lower both limits if necessary, by insertion of an extra line section. For this reason, the oscillator and rotary condenser are mounted on a truck, which can move back as much as 3 feet on rails. The rail arrangement also permits more facile assembly and disassembly of the r-f system, as well as withdrawal of the dee face plate (also mounted on a truck) from the vacuum tank.

It was obvious that if the rotary condenser was

---

* Now at the University of California at Los Angeles, California.

** Now at the University of Washington, Seattle, Washington.

[1] Richardson, MacKenzie, Lofgren, and Wright, Phys. Rev. 69, 669 (1946).

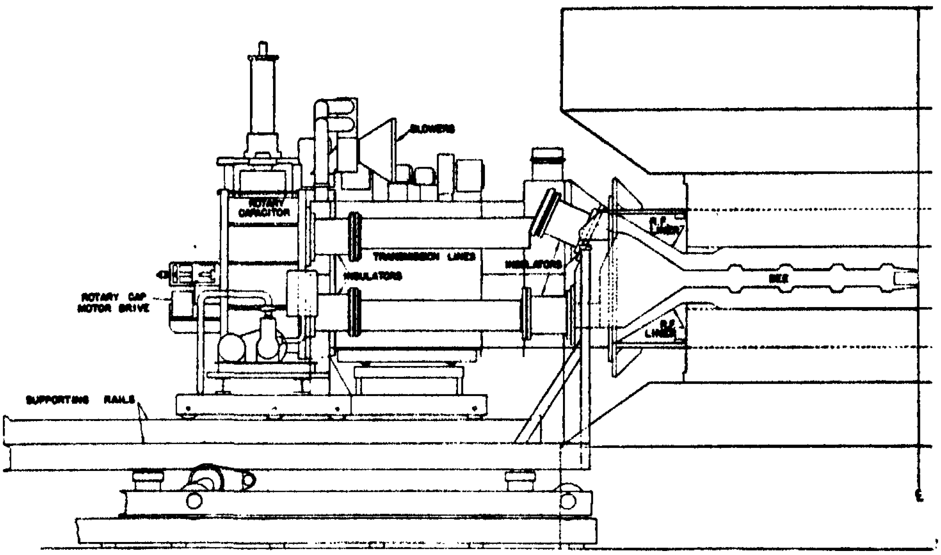

FIG. 1a. Resonant system —elevation.

to be in a negligibly weak field, the line connecting the dee to the condenser had to be quite long and, consequently, of the lowest possible impedance (around 10 ohms). An easy way to reduce impedance was to add lines in parallel, which had the advantage over a single low impedance line that something like an optimum ratio of inner to outer conductor could be maintained.

Since it seemed mechanically desirable to support both the dee and the rotary condenser stator assembly on sets of four large insulators, a four-line system was the natural choice. The arrangement shown in Figs. 1 and 2 has the advantage of permitting almost any desired degree of coupling to the oscillator without the use of auxiliary transmission lines. It conveniently permits an oscillator structure which fits in the distance between the capacitor and the dee tank.

The inner transmission line conductors consist of rolled sheet copper cylinders with appropriate cut-outs for the coupling loops, water lines, and so forth (Fig. 2). They are supported directly by their connections to the corresponding dee and condenser insulators. The outer transmission line conductor

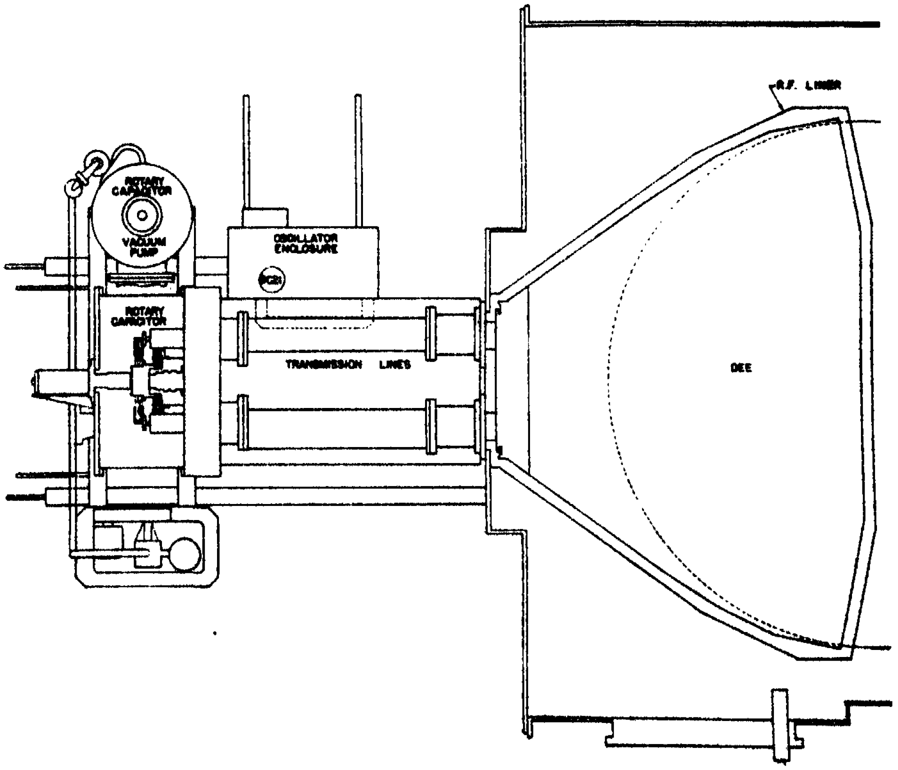

FIG. 1b. Resonant system —plain view.

FIG. 2. Transmission lines and rotary capacitor. Note slots in lines for coupling loops. The vertical pipes are air ducts for insulator cooling.

consists of an aluminum angle frame mounted on a truck, with provisions for increasing its length by replaceable end sections. This frame is the support for copper-lined masonite panels, reinforced on the edges by aluminum angles.

To minimize r-f power losses, all steel surfaces exposed to r-f fields are copper-plated. Wherever pressure contacts exist outside of the vacuum systems, good contact is established by the use of strips of thin soft copper sheet backed by foam rubber pads. Oscillator doors and transmission line covers are lined in this manner all around their edges. Under pressure from suitable clamp, these contact strips deform to match the irregularities of the surfaces which they contact, hence increasing manifold the contact area for r-f current flow.

The dee design progressed quite rapidly. In shape, it tapers from a maximum width of 15′3″ to a width of 4′3″, at the same time thickening from a height of 7″ to a height of 36″ at the back end (Fig. 1a), where the vacuum space bulges out around the pole pieces as illustrated. Its structure consists essentially of a copper covered frame having cross-wise reinforcing members, at the back of which are attached four long, sturdy, threaded shafts. These shafts support the weight of the dee on the four dee insulators, the mechanical system being so arranged that the upper two insulators are under pure compression, the lower two under pure tension. The threads permit slight lateral and vertical adjustment of the dee position. The r-f current is carried through the insulators by means of large sheet copper cylinders.

The r-f liners are simply copper sheets bolted to the magnet pole faces within the vacuum chamber. Their rear edges are crimped over the edge of the vacuum tank opening so that upon fastening the dee face plate, they contact a copper sheet lining on that face plate, thereby completing the r-f current return path within the vacuum system. On the air side of the dee face plate, the return path for the current carried to the condenser by the transmission lines is formed by the transmission line housing, whose ends are firmly connected to the insulator flanges both at the dee face plate and at the condenser vacuum tank cover plate.

The condenser copies the 37-inch rotary capacitor design in its fundamental aspects.[2] It is similar in general appearance, but of course has many more sets of blades as shown in Fig. 3. A total of seven disks, two feet in diameter, with 24 teeth each, are used in the rotor. The 8 stator rings with a matching set of blades are mounted by means of four cylindrical stems onto the four large insulators, which are in turn fastened to the condenser vacuum tank cover plate. The rotor ground coupling capacitor consists of seven solid rotor disks spaced 0.05″ from a similar set of grounded disks. In order to prevent appreciable bypassing of r-f current through the steel rotor shaft, the rotor parts are fastened to the shaft by means of two doughnut-like zircon insulators. The shaft is hollow and carries water cooling through a concentric pipe arrangement to the sealed hollow space within the rotor insulator. Because of the residual capacitance of the rotor to its shaft, 100 $\mu\mu$f or so, it is necessary to protect the bearings at each end of the rotor shaft by sets of brushes which bypass the residual r-f current.

The condenser rotor is mounted on the same steel plate as the stator insulator assembly in order to facilitate alignment of the two sets of teeth. The entire weight of the rotor is supported on a set of bearings fastened to this plate. It is driven by a removable shaft which engages the rotor at the other end and which also serves as a means of introducing the cooling water. This permits easy accessibility since the shell-like capacitor vacuum tank, and the driving shaft, together with the vacuum pumps, are mounted on a truck which may be moved completely out of the way on the rail system. The rail arrangement is shown in Fig. 1. In practice during repairs and overhauls, the capacitor cover plate (which is also mounted on its own truck), remains undisturbed. As was later determined, the effective capacity range of this rotary condenser is 400 $\mu\mu$f to 2400 $\mu\mu$f.

It should be mentioned that extensive air and water cooling is provided for all surfaces carrying r-f current, since operation at a power level as high as 100 kilowatts was originally contemplated. The condenser stator rings and support stems are cooled by copper water lines soldered to them, as are the insulator flanges and dee support stems. Likewise the dee and liners have a labyrinthian network of cooling pipes. All such pipes at r-f potential are brought to sets of hose connections in the vicinity of the nodal region; these connecting sections also serve to cool the transmission lines. The water circuit is completed to ground potential by means of sets of flexible polyethylene tubing, each several feet long. Treated water of low conductivity is used here to minimize current leakage resulting from the dee bias voltage.

---

[2] F. H. Schmidt, Rev. Sci. Inst. 17, 301 (1946).

Air blast cooling from a blower is directed onto the rotary condenser insulators. On its way through the transmission line housing the air serves to cool the outer panels. It finally funnels past the dee support insulators and leaves the system. Total air flow in this system is about 2000 c.f.m.

A major structural and electrical problem in connection with the resonant system design was posed by the feed-through support insulators used for both the dee and the condenser stator stems. These are 15 inches in diameter and 18 inches long. A test apparatus consisting essentially of a high-Q quarter-wave resonant line was constructed.[3] At the open end of the line, the insulators could be operated under simulated vacuum and electrical cyclotron conditions. Over 50-kilovolt r-f could be developed across the insulator at 13 mc by a 5-kilowatt oscillator. Under the most severe test conditions, air blast cooling of the insulators was found necessary.

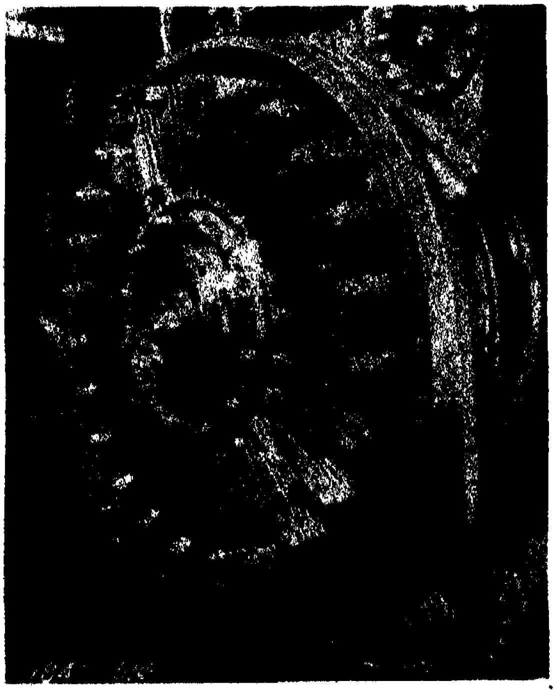

FIG. 3. Rotary condenser.

The same apparatus was employed to measure breakdown between test condenser blades under conditions likely to prevail in the actual rotary capacitor. It was found that a 0.080″ gap between copper or copper-plated surfaces having a reasonable polish would hold a maximum of 50 kilovolts at 13 mc at a pressure of about 5×10^{-6} mm. It was therefore expected that a voltage of about 40 kv could be held in the operating unit. The behavior of the capacitor and of the insulators in actual practice will be discussed.

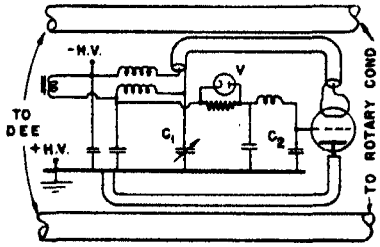

FIG. 4. Oscillator circuit: Two of the 4 lines from dee to rotary condenser are shown. The filament loop couples to the upper and the plate loop to the lower. $C_1=500$ $\mu\mu$f. $C_2=750$ $\mu\mu$f. V = rectifier to prevent positive d.c. on grid due to secondary emission.

SCALE MODEL TESTS

The design had thus progressed a long way, even though a number of dimensions were not well established. The rotary condenser capacitance and the transmission line length were particularly uncertain, but because of the flexible arrangement, they could be easily adjusted within reasonable limits. For the accurate determination of these values, as well as for determining r-f power requirements and testing oscillator layout designs, it was necessary to build a scale model of the r-f system. For reasons of convenience, a quarter scale was chosen. The resonant frequency is then increased fourfold and all inductances and capacitances are reduced by a factor of four. The frequency range is thus around 40 to 50 mc, which is still not too high to be handled by ordinary triodes. For a given dee voltage, the required power is doubled. If an accuracy scaled version of the coupling arrangement is used, the impedance as seen by the oscillator is halved, the Q of the scaled system being one-half the Q of the actual system.

The criterion used for determining the capacitance and line length, besides that imposed by the frequency range, was that the capacitor voltage should not exceed the dee voltage at the highest frequency. This is, of course, realized if the minimum capacity of the condenser just equals the effective capacity of the dee. The basis for this adjustment of the resonant system is that since the insulators are the weakest link in the r-f system, it is preferable to arrange matters so that the condenser insulators are not under any worse condition than the dee insulators.

---

[3] F. H. Schmidt, *High Frequency Insulator and Vacuum Breakdown Tests.* (AEC Report No. MDDC-473, declassified).

The scale model tests immediately showed that under such conditions the line length in air would have to be about 10 feet; at 12.5 mc the required capacitance would then have to be 700 $\mu\mu$f; at 10 mc it would have to be 1850 $\mu\mu$f. The dee and condenser voltage became equal at about 13.5 mc where the minimum capacitance is 500 $\mu\mu$f. This indicated that the effective dee capacitance would be 500 $\mu\mu$f, even though a capacitance measurement indicated it to be 1600 $\mu\mu$f. To the extent of this difference, the dee acts as a line, because of its appreciable size relative to a wave-length.

THE OSCILLATOR

The choice of a grounded grid oscillator was an almost foregone conclusion in view of the unequalled success of this arrangement in all recent Radiation Laboratory r-f installations requiring high power at moderately high frequencies. The oscillator circuit was chosen identical to that of the 37-inch oscillator,[4] since this type of circuit produces the desired[5] r-f voltage rise during acceleration (Fig. 4).

The oscillator unit is mounted on rails so that it can be rolled away from the dee stem enclosure for major servicing or replacement. The oscillator enclosure is made of $\frac{1}{4}''$ steel. Consequently, this house serves as a magnetic shield for the oscillator tube. A crude replica ($\frac{1}{16}$ size) was tested by the magnetic measurements group, using the $\frac{1}{16}''$ scale 184-inch model magnet, and this shielding was found sufficiently effective, the field being cut from 140 gauss to less than 20 gauss. This is further reduced at the 9C21 elements by means of a $\frac{1}{2}''$ steel sleeve over the cooling jacket. The magnetic force on the oscillator housing amounts to 450 lb. The housing and components are shown in Figs. 5 and 6.

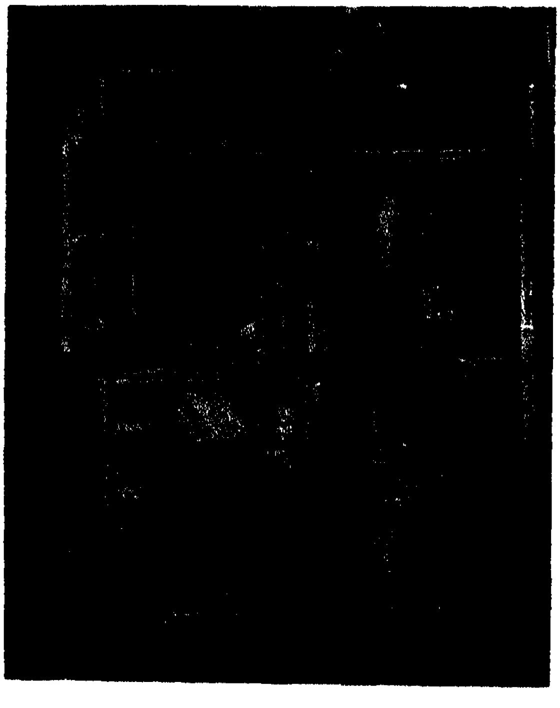

FIG. 5. Front view of oscillator with doors open. Anode water jacket is in lower right-hand corner, grid grounding capacitors in upper right, filament chokes and filament loop phase correcting capacitors in upper left, and filament transformer in lower left.

The choice of a 4-line resonant system makes it very easy to couple plate and cathode loops thereto with the shortest possible uncoupled lengths. These emerge through the rear wall of the oscillator box, each opposite a transmission line, and fit into slots cut in those lines to achieve maximum coupling with adequate high voltage clearance. These slots may be seen in Fig. 2. The end of each loop is thus automatically located opposite the particular tube electrode to which it is connected. The plate loop (lower) is directly grounded to the oscillator box at its other end. The high voltage power supply thus operates with its positive side grounded, eliminating the necessity of supplying low conductivity water to the tube jacket, the water lines being piped through the plate loop. The cathode loop (upper), which is bypassed to ground at its far end by means of a ring of 10 fixed vacuum condensers (about 500 $\mu\mu$f total), serves as one side of the filament heating circuit, the other side consisting of 4 heavy cables passing through the loop. The ring of high vacuum condensers also acts as the cathode circuit phasing capacitor to correct for the phase difference introduced between cathode voltage and plate voltage by the cathode loop self-inductance. Adjustment is obtained by exchanging one or more of the condensers for one or more of different value.

The grid is grounded for r-f voltage by a similar ring of fifteen 50-$\mu\mu$f capacitors. The total capacity is chosen so that in conjunction with the grid leak, its charging time is small enough when compared to the charging time of the resonant circuit to prevent intermittent oscillation.

In this coupling loop arrangement there exists a negligible amount of coupling between plate and cathode circuits; consequently, that parasitic mode in which most of the energy is in the plate loop cannot be excited.

The degree of amplitude modulation depends on the plate-loop resonant frequency, decreasing in percentage as this frequency is raised as far as possible above the cyclotron frequency. On the other hand, if the plate-loop resonant frequency can coincide with a harmonic of the dee system frequency, a serious dip will occur in oscillation amplitude as the f-m cycle passes through that frequency. Since the tube capacity and loop inductance put an upper limit to the plate loop frequency of about 20 mc, it was necessarily lowered by addition of the vacuum capacitors shown between water jacket and ground, until the frequency was under 18 mc (twice the lower limit of the cyclotron frequency). Again, this can be adjusted by exchange of vacuum condensers, hence serving as a convenient means of control of the percentage of amplitude modulation.

---

[4] K. R. MacKenzie and V. Waithman, Rev. Sci. Inst. 18, 900–907 (1947).

[5] D. Bohm and L. I. Foldy, Phys. Rev. 72, 649–661 (1947).

This argument does not apply to the filament loop, so that its frequency was made as high as possible by taking great pains to reduce the self-inductance not serving as mutual inductance in the dee circuit. This has the desirable effect of reducing the phase shift between cathode and plate r-f voltage, and of insuring that the excitation represents a fairly constant fraction of the dee voltage. Actually, because of the dee voltage rise with lowered frequency the excitation also rises, although not quite so rapidly. This is desirable, since the tube must supply considerably more power at the low frequency end, and consequently requires more cathode driving voltage. While this power increase is principally due to the increase in dee voltage, it is also in part due to the fact that the condenser losses are greatest when the teeth are fully meshed.

OSCILLATOR MODEL TESTS

For the purpose of coupling loop measurements, it was necessary to electrically duplicate in the scale model the behavior of the 9C21. The only low power tube then available which seemed to fit the scale requirements, as well as having easily accessible electrodes, was the 304TL. This tube operates with about the same effective plate resistance as the 9C21, but since the load impedance in the model is reduced by a factor of two (because of the non-scaling of Q) it was necessary to use two tubes in parallel. This arrangement had the fortuitous circumstance of having scaled interelectrode capacitances about equal to those of the 9C21. However, the 304-TL requires approximately twice the relative grid driving voltage. With a ¼-scale version of the coupling loops, the 304TL's were thus underdriven by almost a factor of two and operated at around 40 percent efficiency at the low frequency end of the range. This corresponds to about 75 percent efficiency in the actual cyclotron oscillator. Operation of the model under these conditions was thus much more difficult than of the full scale oscillator, but had the advantage that if the model worked, the full scale version was even more certain to work. Because of this non-linear scaling of efficiency it became difficult to predict the amplitude modulation shape from the behavior of the model. The ¼-scale model oscillator is illustrated in Fig. 7.

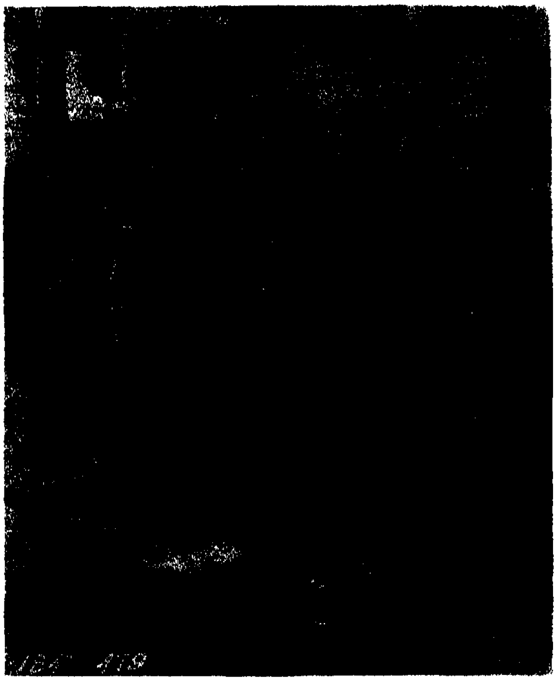

FIG. 6. Rear view of oscillator house showing coupling loops.

OPERATING CONDITIONS AND EXPERIENCES

Initial tests of the full scale r-f system disclosed a re-entrant cavity resonator mode between the two pole pieces of the magnet with the vacuum tank walls as the return circuit, resonant near the lower frequency limit. This was easily suppressed by strapping the pole pieces together at their outer edge. It was also found that the frequency range did not extend low enough by almost one megacycle, even after extensive padding of the resonant system. Since the extra line section had not been made, the easiest solution was the removal of one of the two transmission lines not associated with the oscillator coupling system. This more than sufficiently reduced the frequency limits (about 10 percent). While the effect of this change had previously been measured on the model, it had not been seriously intended that a correction be made in this way. The consequent reduction in efficiency was of no importance, as the high r-f dee voltage of 40 kv was not found necessary. The evident discrepancy in transmission line length was eventually traced to a cumulative error of about two inches in various small errors in model dimensions.

The plate circuit resonant frequency turned out to be too close to the second harmonic of the lower limit of frequency modulation, as evidenced by severe amplitude modulation. Considerable plate capacity was eventually added to improve this

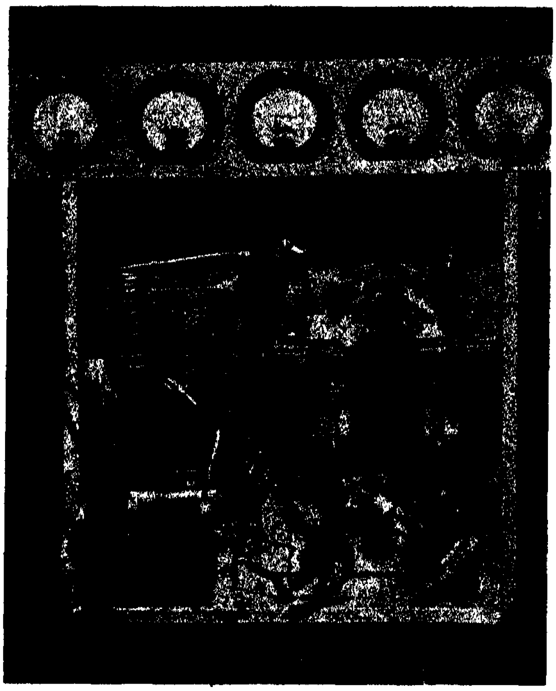

FIG. 7. Model oscillator using 304TL tubes. Front view.

situation. The lack of sensitivity of the beam to even such severe amplitude modulation is of particular interest. Figure 8 plots the amplitude and frequency modulations as a function of time.

Under vacuum, some difficulty was experienced as a result of discharges in the large spaces around the dee. It was easily shown that r-f field conditions can exist which permit electrons to execute resonant oscillations at these frequencies and the appearance of the discharges seem to fit such a theory fairly well. In the particular case of those discharges quite far removed from the immediate vicinity of the dee, where the r-f field is relatively weak, the picture of resonant electrons fits better than does the picture of the non-resonant type of discharge as exists in Philips ion gauges. It is suspected that secondary electron multiplication ("multipactor action") may also be taking place. This does not preclude the Philips gauge type of discharge near the dee, since here an electron has ample time and energy to perform numerous vertical excursions during a positive r-f cycle. All discharges were eliminated by cutting down the available volume by means of perforated shields around the sides of the dee, by adding a grounded "dummy" dee, and by applying a negative bias to the dee.

There is sufficient magnetic field at the rotary condenser to allow a Philips gauge discharge when positive bias is applied; a negative bias is therefore imperative. Fortunately the beam does not seem sensitive to bias, as it often was in the 37-inch cyclotron with positive bias voltage. The increase in beam obtained there may presumably have been due to just such a discharge which increased the ion supply near the ion source.

Several days after the beam was obtained with but 15-kv r-f dee voltage,[6] troubles occurred with the rotary capacitor, characterized by increasing sparking and mechanical sticking. This was found to be due to warpage of the copper-plated stainless steel disks used in the bypass condenser because of poor heat conduction. Spacings were increased, but this afforded only temporary relief. Copper replacement parts then became available and no further difficulties have occurred since their installation.

The blade gap only holds about 30-kv r-f and this may be attributable to the lessened clearance (0.06″ instead of 0.08″) in the final unit, in addition to the severe over-all roughening of the surfaces by discharges taking place during bakeout and sometimes during operation. Occasional water leaks occur around the rotor insulator gaskets, but these have been insufficiently frequent to warrant any major revision.

The r-f insulators have given no trouble whatever since installation one year ago, though at the time of assembly, their fragility was evidenced insofar as shear forces were concerned. The care taken in insuring that only pure tension and compression forces would be applied was thus well justified.

The average power required for a given dee voltage is essentially the same as predicted from the model and is around 40 kilowatts for an amplitude variation from 20 to 30 kilovolts through the f-m cycle. Provision was made in the power supply for arbitrary amplitude modulation by insertion of three parallel 893-power triodes in the d.c. plate power circuit, but they have been used thus far only as current limiters and voltage adjusters.

The authors wish to express their gratitude to Professor E. O. Lawrence and the staff of the Radiation Laboratory for advice and encourage-

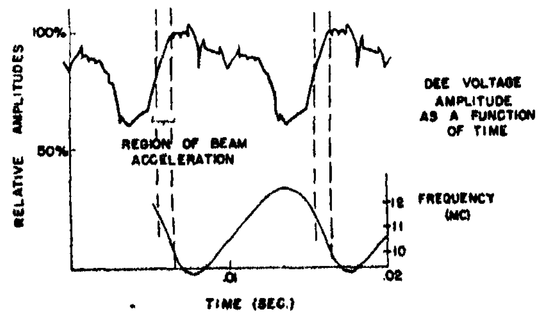

FIG. 8. R-f system frequency as a function of time. Dee voltage amplitude as a function of time.

---

[6] Brobeck, Lawrence, MacKenzie, McMillan, Serber, Sewell, Simpson, and Thornton, Phys. Rev. 71, 449 (1947).

ment throughout the progress of the work. In particular, the assistance and suggestions of W. M. Brobeck, R. L. Thornton, E. M. McMillan, and L. W. Alvarez have been greatly appreciated. The authors also wish to thank certain groups of people in the laboratory who contributed no small part to the successful operation of the r-f system for the 184-inch cyclotron. The model tests and high voltage tests were conducted by J. Riedel, R. Anderson, F. Yeater, and W. R. Baker. The metering and control circuits were devised by C. Park and J. C. Kilpatrick, and the mechanical parts were designed by J. Bell, R. Peters, and O. Callahan under the direction of W. M. Brobeck.

This paper is based on work done under the auspices of the Atomic Energy Commission.

THE REVIEW OF SCIENTIFIC INSTRUMENTS VOLUME 20, NUMBER 2 FEBRUARY, 1949

A Method for Measuring Very High Speed Transient Currents

A. M. Zarem* and F. R. Marshall
U. S. Naval Ordnance Test Station, Pasadena Annex, Pasadena, California

(Received October 2, 1948)

A deflection coil suitable for use in measuring very high speed transient currents is described. When used with a type 912 cathode-ray tube operated at a 15,000-volt accelerating potential, this coil provided a spot deflection of one inch at approximately 50 amperes of current.

A mutual inductance device was constructed to extend the range of measurement of the deflection coil. This device consists of two loops of wire ¾″ in diameter and coaxially positioned with adjustable spacing. The current under study is allowed to flow in one coil, and the other coil is connected to the deflection coil.

Results are given of an analysis of the transient response of such a circuit, taking into account increased losses caused by the transient skin effect. Accurate design of a transformer and deflection coil system to meet specific requirements is facilitated by the analysis.

The deflection coil and transformer described herein has excellent response for transients as long as two microseconds in duration.

IN the course of a recent investigation of spark discharges, there was a need for measuring transient high currents of microsecond duration. The use of a resistive shunt in conjunction with an electrostatic-deflection cathode-ray tube was not possible for the following reasons:

(a) The use of a current shunt of resistance high enough to develop directly the necessary voltage for deflection causes excessive disturbance of the circuit conditions.

(b) The use of a lower resistance shunt in conjunction with an amplifier proved unsatisfactory because of the frequency distortion introduced by the amplifier.

A subsequent study of magnetic deflection demonstrated that it was entirely feasible to obtain satisfactory fidelity by allowing the current under study to flow in a specially designed deflection coil. In Fig. 1 is shown the one-turn deflection coil used with the current path indicated by arrows. It is constructed of copper sheet for low inductance and resistance.

When used with a type 912 cathode-ray tube operated at a 15,000-volt accelerating potential, this coil provided a spot deflection of one inch at approximately 50 amperes of current. This sensitivity was much too great for the application, since currents of from one thousand to ten thousand amperes were under study.

A mutual inductance device was constructed to

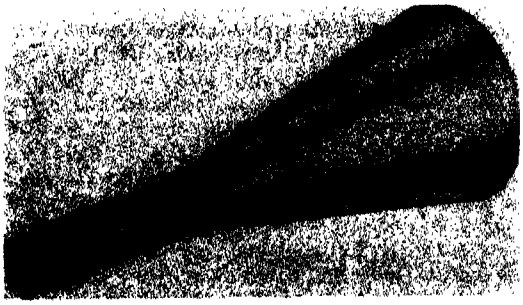

Fig. 1. Deflection coil. Arrows indicate the current paths.

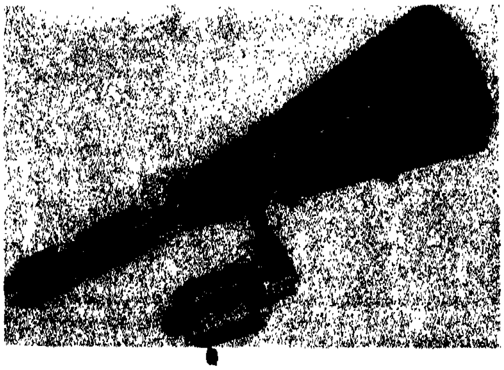

Fig. 2. Transformer and deflection coil in place on cathode-ray tube.

---

* Present address: Stanford Research Institute, Transamerica Building, Los Angeles, California.

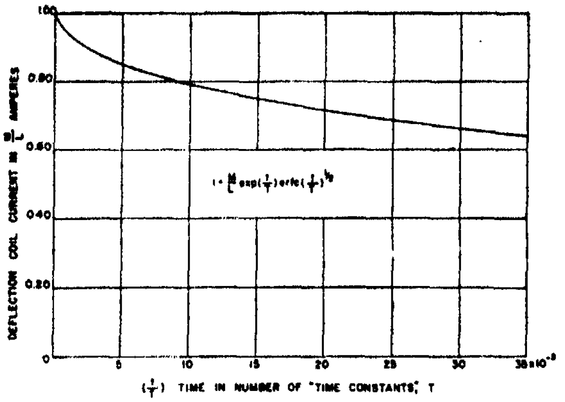

FIG. 3. Response of transformer for unit current suddenly initiated in the primary circuit.

extend the range of measurement of the deflection coil. This device consists of two loops of wire ¾″ in diameter and coaxially positioned with adjustable spacing as shown in Fig. 2. The current under study is allowed to flow in one coil, and the other coil is connected to the deflection coil. If the resistance of the secondary is neglected, the ratio of current flowing in the secondary i_s, to the current flowing in the primary i_p, is

$$i_s/i_p = M/L, \tag{1}$$

where M is the mutual inductance between primary and secondary, and L is the total inductance in the secondary—including the deflection coil.

An analysis of the transient response of such a circuit was undertaken to determine how closely the wave form of current in the deflection coil resembles the primary current. In this analysis it was necessary to consider the increased losses due to the skin effect of current flowing in the conductors. For unit current suddenly initiated in the primary at zero time, the secondary current is given by the expression

$$i_s = (M/L)\exp(t/T)\,erfc(t/T)^{\frac{1}{2}}. \tag{2}$$

Here

M = mutual inductance between coils of the current divider,
L = total inductance in the secondary circuit,
t = time,

$$erfc(x) = [2/(\pi)^{\frac{1}{2}}]\int_x^\infty \epsilon^{-x^2} dx,$$

T = a "time constant" of the secondary circuit giving a measure of the decay time due to skin effects under transient conditions,

$$T = [L/(l/s)(4\pi\mu\rho/10^9)^{\frac{1}{2}}]^2 \quad \text{(practical units)}, \tag{3}$$

where

l/s = ratio of length of conductor to perimeter of conductor (if the conductor perimeter is not constant, use the expression $\oint_l (dl/s)$),
μ = conductor permeability,
ρ = conductor resistivity.

Equation (2) is correct up to the time when current (initially flowing on the surface only) penetrates into the conductors for a distance comparable to the conductor radius. Thus the expression gives quite exactly the first part of the transient response (in which we are interested). A plot of Eq. (2) is given in Fig. 3 for values of time between zero and $0.035T$.

The design of a transformer and deflection coil system is approached as follows:

(a) Estimate the probable duration of the transient to be studied.

(b) Chose the acceptable distortion and determine the value of T from Fig. 3.

(c) Using the formula for T, determine the optimum design of circuit which will give the desired response.

The deflection coil and transformer shown in Fig. 2 (for which $T = 640$ microseconds) has excellent response for transients as long as two microseconds.

Laboratory and Shop Notes

Pulsed Oscillator for F-M Cyclotron*

J. W. Burkig, E. L. Hubbard, and K. R. MacKenzie
Department of Physics, University of California, Los Angeles, California

October 28, 1948

In the 41″ f-m cyclotron at U.C.L.A., the useful frequency range is 16 percent of the total cycle. Since the dee voltage is limited by the plate dissipation of the oscillator tubes, it has been possible to increase the dee voltage by pulsing the oscillator, so that it is in operation only during the useful part of the f-m cycle.

The cyclotron oscillator using four Eimac 304-TL tubes in parallel has been described by MacKenzie and Waithman.[1] The pulsing has been obtained by replacing the grid leak resistor of the oscillator by the plate to cathode resistance of a 304-TH tube. When this tube is conducting, the oscillator operates normally. When it is not conducting, oscillation is stopped, since the grid leak resistance becomes infinite.

A diagram of the circuit for the control tube is shown in Fig. 1. The loop L is inserted into the outer conductor of the transmission line connecting the dee and rotary capacitor, so that the loop and coil are magnetically coupled to the tank circuit of the oscillator. The coil is tuned just below the frequency at which the ions emerge (18 mc). When the frequency coincides momentarily with the resonant frequency of the coil, a high r-f voltage appears on the grid of the control tube which accordingly draws grid current and acquires a negative bias. As soon as the oscillator frequency passes beyond the coil resonance frequency (in the direction of decreasing frequency), the r-f voltage on the control tube vanishes and the negative bias prevents the flow of plate current. The 304-TL oscillator tubes, however, still draw grid current, and the accumulating charge rapidly biases the tubes to cut off. The charge leaks off the condensers c_1 and c_3, and the control tube becomes conducting again after a time dependent upon the time constant $R_2(C_1+C_3)$. R_2 has been adjusted so that the oscillator is off during about ¾ of the frequency cycle. Resistor damage due to r-f is prevented by the small condenser C_3.

The pulsing circuit is mounted in a shielded cage which is connected to the grids of the oscillator tubes. This cage is mounted on insulators adjacent to the oscillator tubes. The cage voltage to ground is equal to the oscillator plate supply voltage plus grid bias.

The repetition rate required is about 1000 c.p.s., which requires that the oscillator be shut off for a period of ¾ millisecond. The time required for sufficient charge to leak off condensers (C_1+C_3) is not easily estimated, since it is a function of the initial charge, which is in turn a function of the coupling between the loop L and the dee stem. R_2 and the coupling are adjusted empirically to give the required off time. The coupling is not critical and is adjusted to give around 1000 volts r-f on the grid. The resistor R_1 is necessary to damp any tendency of the circuit to act as an r-f amplifier for any stray pick-up coming in on the filament leads.

The 304-TH tube proved to be more satisfactory than the 304-TL for control purposes, since it was much easier to cut off. Trouble was experienced when the 304-TL was tried, because the tube was incompletely cut off, which allowed the oscillator to start oscillating before the 304-TL control tube d.c. plate resistance had reached a low enough value. The oscillator would then immediately cut off again, as in the usual "blocking" oscillation caused by too high a grid leak grid condenser time constant.

Installation of the pulse circuit has allowed a 50 percent increase in dee voltage with one-half the previous plate dissipation. The present normal average power consumption, under pulse conditions, is approximately 4½ kw input for 12 kv on the dee, although the tubes, operating with their present efficiency, will allow a 6-kw input. Operation at the higher power level is more unsteady due to frequent tripping of overload relays. Throughout the construction of this circuit the authors have been indebted to Mr. S. H. Plunkett for suggestions and assistance.

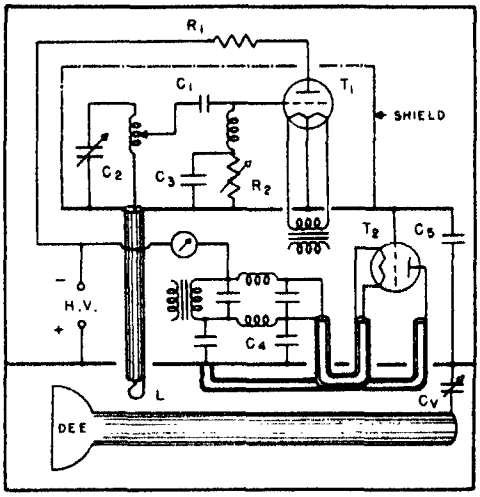

FIG. 1. Oscillator circuit. Pulse operation is obtained by replacing the oscillator grid leak by the components inside the shield. L = loop, C_1 = 0.001μf, C_2 = 0–500μμf, C_3 = 250μμf, C_4 = 200μμf, C_5 = 1500μμf, C_v = 200–700μμf rotary capacitor, R_1 = 100 ohms, R_2 = 150,000 ohms, T_1 = 304-TH, and T_2 = four 304-TL tubes in parallel.

---

* Assisted by the Joint Program of the Office of Naval Research and the Atomic Energy Commission under project number NR022-053.

[1] K. R. MacKenzie and V. B. Waithman, Rev. Sci. Inst. 18, 900 (1947).

Toggle-Operated Vacuum Valve

Ralph O. McIntosh and John W. Coltman
Research Laboratories, Westinghouse Electric Corporation, East Pittsburgh, Pennsylvania

October 21, 1948

A SIMPLE, compact, positive-action valve has been made for use on high speed, high vacuum systems. The valve utilizes a toggle mechanism to obtain positive wide opening and high closing pressure with simple construction. A standard mechanical shaft seal has been found to be suitable for use with high vacuum.

The design of the valve is shown in Fig. 1 in the open position. A circular plate (1) carries an O-ring[1] gasket (2) in a suitably shaped groove. This gasket seals against the smooth top surface of the lower flange (3). The toggle mechanism, which consists of a link (4) and a crank (5) operated by a shaft (6), is connected to the circular plate by means of a screw (7) for adjustment of closing pressure. A lock nut (8) for fixing the adjustment is provided. Maximum travel for the space occupied and a high mechanical advantage during compression of the gasket are features obtained by the use of the toggle action. A set-screw (9) is positioned in the body of the crank to bear against the link when the valve is closed. Adjustment of this screw permits convenient setting of the throw-over of the toggle to take advantage of its inherent locking action.

A cage is formed around the circular plate by three guide pieces (10) to act as a track for the plate in any position of the valve. The crank is set-screwed to the operating shaft (6)

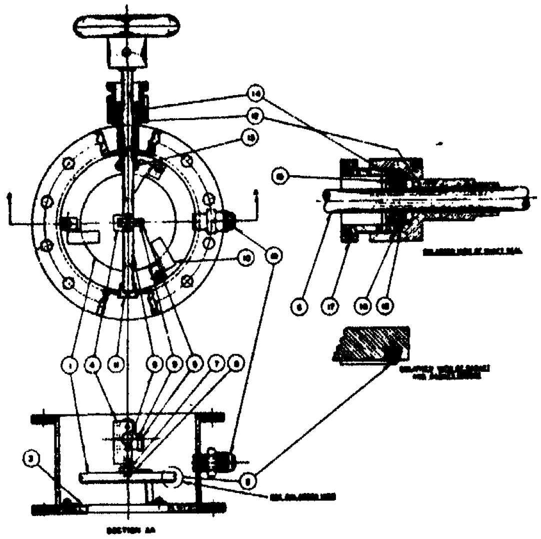

FIG. 1. 4-in. vacuum toggle valve.

which rotates in a blind bearing (11) and passes out of the valve body through a ventilated bearing (12), being positioned by a thrust collar (13). The shaft seal uses an assembly (14) which is commercially available[2] in a variety of sizes. This assembly is held in place by a sprocket-shaped screw (15) and is sealed on the outside rim of its metal frame by a Neoprene gasket (16) which is compressed by screwing in the ring (17) against a washer (18) which is slotted to clear the sprocket-shaped screw. The shaft is $\frac{1}{32}$ inch larger in diameter than the manufacturer recommends. If these sealing assemblies were obtainable with a Neoprene gasket bonded to the metal rim, the arrangement of the shaft seal could be greatly simplified. The assembly has been successfully mounted by soft-soldering it directly to the end of a simpler shaft bearing instead of using a clamping arrangement but great care is required during the soldering.

Several valves of this design have been in use for more than a year with very satisfactory results. The valve was intended to be used such that, when closed, the air pressure on the circular plate would tend to compress the seating gasket, but in practice no such precaution is necessary. A rough-down connection (19) was provided to reduce the pressure preparatory to opening the valve. This is useful to reduce the amount of gas admitted to the diffusion pump in the system, but the valve can easily be open with atmospheric pressure tending to hold it closed.

[1] The O-rings used here were obtained from Linear, Inc., Philadelphia, Pennsylvania.

[2] The shaft seal assembly used here is a "Type L Garlock Klosure," obtained from the Garlock Packing Company, Palmyra, New York.

Note on Constant Current Regulators

E. E. MINETT,* D. A. MACRAE,** AND J. TOWNSEND***
Carbide and Carbon Chemicals Corporation, Oak Ridge, Tennessee

October 21, 1948

NUMEROUS measurement and instrument problems require the establishment of a source of constant direct current. Current regulating circuits have been described in the literature[1] which are variations of the standard electronic voltage regulator. In the case of a constant current regulator, the controlling voltage is the difference between the potential drop across the load, or across a series resistor in the current output line, and a reference voltage derived from a gas regulator "*VR*" tube.

The above circuit works well in principle. However, in practice it is frequently difficult to obtain a potential drop-current relationship in the series resistor or load which will not change with time as the resistor heats up. The essential difficulty arises from the fact that the dropping resistor must carry the full regulated output current. Considerable wattage must be dissipated if large currents are to be handled and when a substantial voltage drop is desired. If ordinary wire-round resistors are used, it is found that ambient temperature control must be provided, even with resistance wire which has a low temperature coefficient. This is inconvenient and frequently expensive.

In the course of improving the current regulation in a mass spectrometer magnet supply, it has been found advantageous to use an incandescent lamp filament as the dropping resistor. The filament is operated at incandescence, so that the heat losses are very largely radiative and independent, within a few parts in ten thousand, of normal variations in room temperature. Because of the low heat capacity of the filament, equilibrium is reached within several seconds. Because of their non-linear voltage-current characteristic, for a given change of current tungsten lamps furnish approximately twice as much signal voltage to the regulating tubes as do linear resistors operating at the same voltage and current.

It has been found possible to regulate a 250-ma current to 2–3 parts in 10,000 over periods of many hours, using a 25-watt, inside-frosted, gas-filled, tungsten Mazda lamp as series resistor, a VR-90 to provide the reference voltage, a 6SJ7 as control tube, and parallel 807's as series regulator tubes.

* Now at Radio Corporation of America, RCA Victor Division, Camden, New Jersey.

** Now at Warner and Swazey Observatory, Case Institute of Technology, Cleveland, Ohio.

*** Now at Washington University, St. Louis, Missouri.

[1] Alfred O. Nier, Rev. Sci. Inst. **18**, 402 (1947), Fig. 5.

A Lock-In *RC* Oscillator

W. C. ELMORE AND D. BANCROFT
Swarthmore College, Swarthmore, Pennsylvania

November 30, 1948

RECENTLY, in connection with the design of a laboratory time standard the problem occurred of converting a continuing sequence of regularly spaced pulses into a sinusoidal wave. At low audiofrequencies—for instance, 50 c.p.s.—inductors with high Q's are impracticable, so one cannot use tuned *LC* circuits for this purpose. It is possible, of course, to employ an electromechanical filter such as an electrically driven tuning fork. If one contemplates securing a series of frequencies in the low audio range, this solution to the problem does not appear attractive. We have found that a satisfactory way of converting pulses to sine waves is by means of an electronic oscillator whose frequency is locked to that of the non-sinusoidal wave form. The use of such a *lock-in* oscillator for this purpose is certainly not new. The circuit devised by us, however, possesses several novel features which make it worth describing here. It will be assumed that the oscillator has impressed on it a periodic signal consisting mostly of fundamental component. Since it turns out with the circuit devised that a signal of only one-tenth of a volt is satisfactory for a reliable frequency lock, one can remove a considerable fraction of the high frequency components by a simple *RC* filter, which also can serve as part of an attenuator.

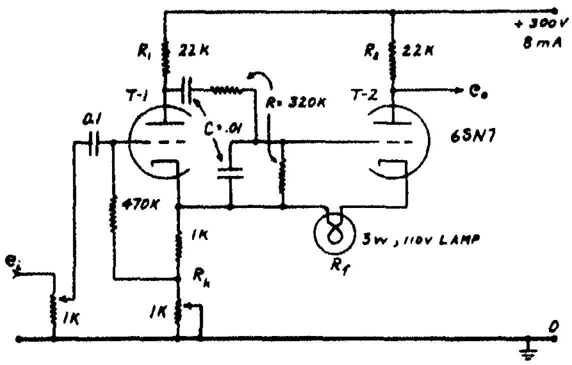

FIG. 1. Lock-in *RC* oscillator for 50-c.p.s. operation.

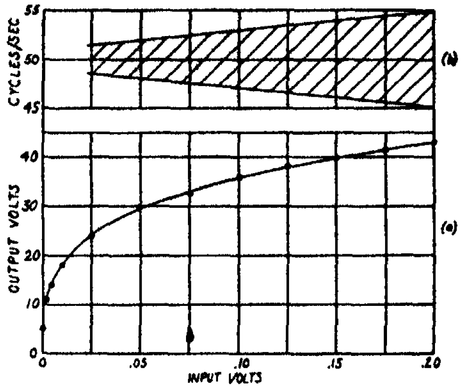

FIG. 2. Locking characteristics of oscillator.

The basic oscillator circuit is a modification of the much-used Wien-bridge circuit.[1] The present circuit, Fig. 1, differs from the conventional one in that the feed-back loop is completed by a regenerative connection between the cathodes of two triodes. The regenerative path consists of a 3-watt, 110-volt lamp that serves to stabilize the amplitude of oscillation within the range of linear (Class A) operation of the tubes. The arrangement adopted leaves the grid of one tube (*T*-1) free for the injection of the locking signal. In addition, the plate circuit of the other (*T*-2) has a considerable degree of isolation from the remainder of the circuit, and can serve as a source of the sinusoidal output signal. (The isolation would be nearly perfect if a pentode were used for *T*-2.) The variable portion of the cathode resistor R_k permits setting the regenerative feedback at a point where resistance changes in the lamp serve to stabilize the amplitude of oscillation. It is found expedient to set the amplitude of oscillation in the absence of an injected signal at a low level. The reason for this choice will become evident in subsequent discussion.

The resistors and capacitors in the Wien-bridge network (*R*, *C*) are so chosen that the frequency of oscillation is close to that of the input signal. Part of one or of both the resistors may be made adjustable to permit fine tuning of the oscillator. The resistance *R* should be high compared with the plate-load resistance R_1 to minimize the effect on frequency of changes in plate resistance. The values given in the figure have been found suitable for 50-c.p.s. operation.

Grid bias for *T*-1 is obtained from a tap on the cathode resistor R_k. Bias for *T*-2 is furnished by the *IR* drop across the lamp.

Let us now consider the operation of the circuit when a periodic signal of nearly the same frequency as the natural frequency of oscillation is applied to the grid of *T*-1. If the signal has sufficient amplitude—a tenth of one volt is sufficient if the injected signal has a more or less square wave form, the frequency of oscillation locks to that of the injected signal and the amplitude of oscillation increases. The increased signal amplitude has an important consequence in that *it causes the resistance of the lamp to increase beyond the value fulfilling the condition for oscillation.* The circuit becomes, in effect, a band-pass amplifier whose gain is greatly magnified by regenerative feedback. As long as the signal amplitude maintains the resistance of the lamp above the value required for spontaneous oscillation, the circuit responds chiefly to the fundamental frequency component of the injected signal. It is not possible for it to oscillate at its own natural frequency which may differ slightly from that of the input signal. In practice it is found that the breadth of the resonance curve (of the regenerative band-pass amplifier) is sufficient that the natural frequency of oscillation can depart several percent from that of a square-wave input signal before the circuit breaks into its own mode of oscillation. The loss of control is very definite when it occurs and results from a decrease in amplitude of the amplified signal which, in turn, reduces the resistance of the lamp to the value fulfilling the condition for oscillation.

When the magnitude of the input signal is held within suitable limits (0.05 to 0.2 volt), the output signal appears to be sinusoidal when viewed on a cathode-ray oscilloscope. No measurements have been made of the small amount of harmonic distortion that may be present.

The stabilizing action of the lamp tends to reduce variations in the amplitude of the output signal for small changes in input level and for small frequency deviations. This feature is illustrated in (*a*) of Fig. 2 which shows a plot of output voltage against input voltage when the input frequency and the natural frequency of oscillation (50 c.p.s.) coincide. For the purpose of this test the input signal was made sinusoidal. In (*b*) of the same figure are shown the frequency limits within which the output signal stayed within 70 percent (3 db) of the maximum occurring at 50 c.p.s. In these tests the r.m.s. amplitude of free oscillation was set at five volts. Definite failure of locking occurred when the frequency departed sufficiently from 50 c.p.s. for the amplitude to drop to about 5 volts.

It should be noted that the resistance of the lamp depends both on the direct current and the alternating current through it. For this reason the plate supply voltage should be stabilized.

---

[1] F. E. Terman, R. R. Buss, W. R. Hewlett, and F. C. Cahill, Proc. I.R.E. 27, 649 (1939).

D.C. Flat Card Resolver

R. G. Murdick
Aeronautics and Ordnance Systems Division, General Electric Company, Schenectady, New York

August 9, 1948

THE purpose of this paper is to introduce an accurate, compact, and inexpensive d.c. resolver. Methods of producing in d.c. computing networks voltages proportional to the sine and cosine of the input angle have frequently involved either the use of more equipment than is desirable or loss of accuracy. Of all known devices, the most compact is the flat card resolver with four brushes to give ±sine θ and

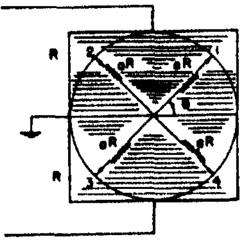

FIG. 1. Flat card resolver.

±cos θ where θ is the angle of rotation. (See Fig. 1.) The brushes are displaced 90° from each other. The amount of the resistance of R measured from ground that is subtended by the brush at 1 is proportional to sine θ and that subtended by 2 is proportional to cos θ. Similar relations hold for brushes 3 and 4.

If the total resistance of the resolver is $2R$, then the ratio of the resistance load on one brush to the resistance of the resolver between a terminal point and ground is a and is called the cascade ratio. If a is large, this device is excellent. However, in many computations a is necessarily restricted to values below ten. A plot of the errors for various cascade ratios is shown in Fig. 2. These errors were computed by usual loop analysis methods. Figure 3 shows the schematic form of the network on which the set of equations required to determine the output voltage was based.

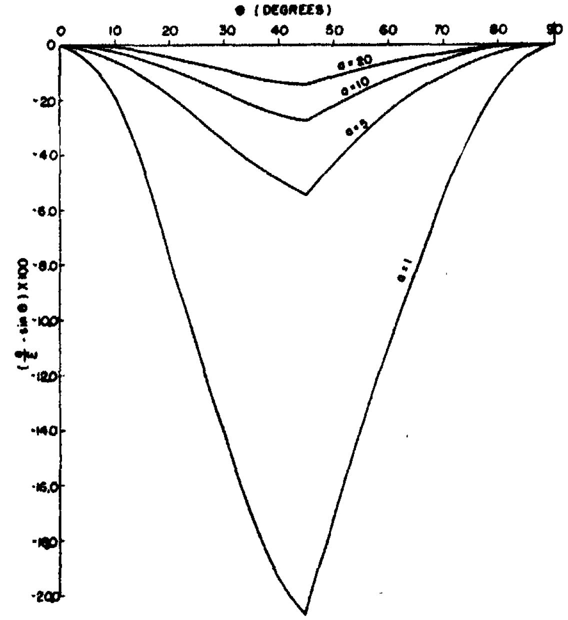

FIG. 2. Error for four-brush resolver. Cascade ratios of 1, 5, 10, and 20.

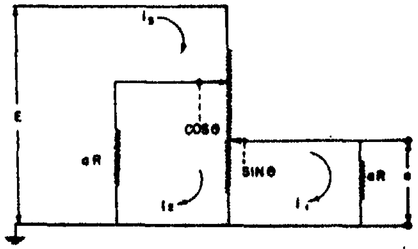

FIG. 3. Schematic diagram of section resolver used for loop analysis.

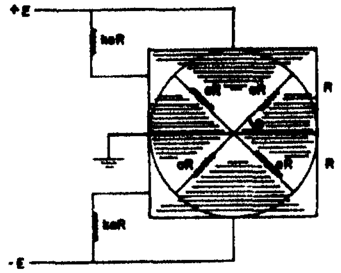

FIG. 4. Modified flat card resolver.

$$(aR+R\sin\theta)i_1-R\sin\theta i_2=0,$$

$$-R\sin\theta i_1+(aRR\cos\theta)i_2-aRi_3=0,$$

$$-aRi_2+[R(1-\cos\theta)+aR]i_3=E.$$

This set of equations is solved for i_1 and e is determined as i_1aR. Since it is desired that $e/E=\sin\theta$, the error plotted in Fig. 2 is obtained by plotting $[(e/E)-\sin\theta]$ *versus* θ. From these results, it is apparent that with a cascade ratio as high as ten, the error is of such magnitude as to preclude this type of resolver in the design of accurate computing nets.

In Fig. 4 a modified flat card resolver is shown that is approximately ten times as accurate as that in Fig. 1 when the cascade ratio is three in each case.

If $a=3$ and the resistances kaR are connected at the points $\theta=\pm 45°$ and k is chosen so the loading error is zero for $\theta=\pm 45°$, then the loading errors are shown in Fig. 5. These errors were computed by a loop analysis similar to that shown above for the resolver shown in Fig. 1. Thus k is determined by the relationship necessary to give the proper voltage division at $\theta=\pm 45°$, i.e.,

$$[a/2]/[(a/2)+ka]=\sqrt{2}/2,$$

$$k=(\sqrt{2}-1)/2.$$

A comparison of the errors shown in Fig. 5 to those shown in Fig. 2 for a cascade ratio of three indicate the great gain in accuracy through use of the modified flat card resolver. If only two of the trigonometric functions are desired, dummy resistor loads may be attached to the remaining brushes.

In Fig. 5 it is apparent that the positive error is numerically greater than the negative error. By varying k, the positive and the negative values of the error may be made equal, thus reducing the variation in output from the desired output still further.

Why was 45° chosen as the point to tie in the resistors? The 45° point was originally chosen since the error was maximum at that point in the simple type resolver (see Fig. 2). Although several other points were tried after this, the range of the error was not decreased. However, since the methods used here were numerical rather than analytical, it is not implied that the 45° point is the best.

The use of four resistors is a considerably more difficult problem to solve since it involves choosing values of the resistors and points of tie-in both. In addition, there is the design difficulty in making the additional taps on the resolver winding.

In the actual manufacture of the resolver, the wire is wound on a flat card of resin-bonded, glass cloth laminate. The wire is wound on the card by servo-controlled winding machines that are capable of winding wire with a diameter varying from 0.0015 inch to 0.0063 inch with resistance varying

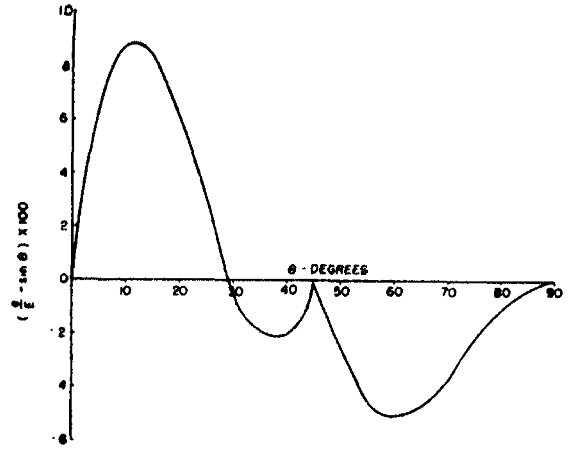

FIG. 5. D.c. resolver error.

from 290 ohms per foot to 7.4 ohms per foot. This wire is wound with turns as close together as practical; usually a space factor of 70 percent to 80 percent is obtained. A stencil exposing a circle for the brush track is laid against the wound card and the exposed insulation is buffed off. The brush at the end of a springlike arm is of a gold and platinum alloy, Paliney No. 7, with a rounded contact point. With present servo winding machines, the sides of the square cards may be varied from 1.5 inches to 2 inches.

Use of Characteristic Curves for Pump-Speed *vs.* Pressure

SAUL DUSHMAN
Research Laboratory, General Electric Company, Inc., Schenectady, New York

December 6, 1948

In many cases it is of interest to be able to derive from the speed characteristic of a pump the total period of time required to exhaust a system from atmospheric pressure to some very low value. The following discussion is intended to describe a method that may be used for this purpose.

Let V = volume of system, P = value of pressure in the system at any instant of time, t, and S = speed of pump. The latter is defined by the relation

$$-V(dP/dt) = S(P-P_f),$$

where P_f = ultimate pressure. Since this is usually much less than P, we can write the last relation in the form

$$-V(dP/dt) = SP. \tag{1}$$

This can be written in the form

$$dt = -(V/S)(dP/Pdt). \tag{2}$$

Hence

$$t_2 - t_1 = V\int_{P_2}^{P_1}(d\ln P/S), \tag{3}$$

where P_1 and P_2 denote the values of P at t_1 and t_2, respectively, and $t_2 > t_1$, $P_1 > P_2$, and *ln* denotes the natural logarithm.

In general, S is plotted on a linear scale *versus* log P and cannot be expressed as a simple function of P. But Eq. (3) indicates that if $1/S$ is plotted *versus* P on semilog cross-section paper, then $t_2 - t_1$ can be derived by merely measuring, or calculating in some approximate manner, the *area* under the curve for $1/S$ *versus* log P between the limits P_1 and P_2.

Obviously, the calculation becomes very simple for the range P_1 to P_2 for which S is constant. In that case

$$t_2 - t_1 = (2.30\,V/S)\log(P_1/P_2),$$

where log denotes logarithms to base 10.

For the other ranges of pressures, in which the value of S varies with the pressure, mechanical integration may be used, or an equivalent method.

The value of $(t_2 - t_1)/V$ gives the *time per unit volume*, and the units are the same as those used for expressing S. Thus, if the latter is given in cubic feet per minute, then $(t_2 - t_1)/V$ gives the period of pumping down in minutes per cubic foot.

A Method of Assessing Transient Stresses in Photoelastic Substances

JOHN S. STANTON
Naval Ordnance Test Station, Pasadena Annex, Pasadena, California

December 6, 1948

A NOVEL method has been found for measuring the transient stresses within photoelastic substances when the latter are subjected to dynamic loading forces of any type. The method consists essentially of combining techniques of the conventional static photoelasticity and of the spark shadowgraph as used in the study of air shock waves.

A photograph (Fig. 1) is obtained of the instantaneous photoelastic pattern by use of a critically damped spark which gives an exposure time of the order of 1/10 microsecond. The model is mounted in a conventional manner as for static photoelastograms. The photograph may be taken either by camera or shadow.

The model may be dynamically loaded in various ways as by transmitted shock, electrodynamic pulsing, collision, and so on. The model shown here was dynamically loaded at the left end of the "neck" (already shown deformed) by a steel ball having a velocity of some 400 feet/second. The stress wave has traveled down the neck as a nearly plane wave, spreading into the widened portion in the complicated fashion shown. This photograph is a shadow picture of the model, and plane polarized light was used to illuminate the model.*

A time delay, variable to alter the time between initiation of loading and exposure, is provided by a conventional multivibrator circuit built into the shadowgraph employed for this photography.**

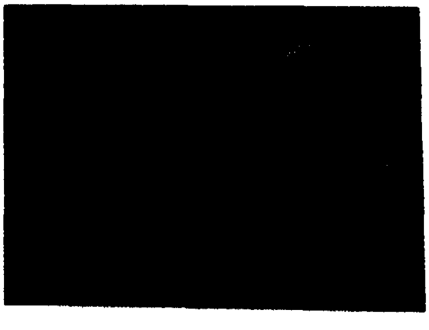

FIG. 1. Transient photoelastogram. Exposure: 10^{-7} second, taken 36 microseconds after collision with a steel ball at the left end of "neck." Model: Plexiglas, 9/16" thick by 3" high.

Any type of photoelastic substance is susceptible to the method here described. The author has employed gelatin models to detect air shock impinging on a photoelastic medium; the model used for the photograph shown here was Plexiglas. Non-photoelastic substances in the elastic region can be studied by the use of photoelastic models if a simple change of time scale is made. By the bonding of photoelastic elements to various points of a non-photoelastic structure, it is possible to extend the study beyond the elastic limit.

---

* Author desires to acknowledge the aid of Dr. D. S. Clark, California Institute of Technology, and of Dr. W. M. Cady of this station in suggesting this and other valuable experiments.

** The shadowgraph employed for this work was designed by Mr. D. G. Marlow and Mr. C. R. Nisewanger of this station and kindly loaned to the author for his use.

Kovar Glass Seals at Liquid Helium Temperatures

C. T. Lane
Sloane Physics Laboratory, Yale University, New Haven, Connecticut

November 22, 1948

In recent months several inquiries have been received by us concerning the problem of metal to glass seals usable at the temperature of liquid helium. A brief summary of current practice in this laboratory may therefore be of some use to other workers in the low temperature field.

We have found the Kovar to Pyrex glass type of seal very satisfactory for use in the liquid helium region, both above and below the λ-point, and we are now using this type of seal exclusively in all our work. Our chief source of supply for these seals has been the Stupakoff Ceramic Company, Latrobe, Pennsylvania, although, on occasion, we have made use of seals fabricated by our own glassblower with equally satisfactory results.

We have not had any experience with this type of seal in sizes much above ½-inch diameter, but there does not appear to be any reason why the larger sizes would not work equally well. In addition to single seals we have on occasion used double ones, i.e., a Kovar tube joined to glass at both ends and this latter form has proved equally successful.

The Kovar seal has shown itself to be exceptionally rugged, much more so than the copper-glass "Housekeeper" seal where, of necessity, the metal has to be very thin at the joint. The resistance of the Kovar seal to repeated thermal shock is also very good. Our current practice is always to have the apparatus in our helium Dewars at liquid nitrogen temperature (77°K) prior to filling with liquid helium at 4.2°K. In so doing the Kovar seal experiences a sudden drop in temperature of over 70°C in a minute or so and in some cases the same seal has been used a number of times without failure. We have used these seals in the helium II region without detecting any porosity to the superfluid, which is a very severe test.

We have also used these seals as "lead-ins" through the metal cap on the Dewar flask, the metal section being either soft soldered or silver soldered to the cap with the glass section then immediately inside the Dewar. This is a much more satisfactory procedure than bringing the glass tube directly through the cap and using a rubber washer, wax, or shellac. We have also found the small Kovar-glass terminals supplied by the Stupakoff Company invaluable for bringing electrical leads into the Dewar through the metal cap. Due to their small size a large number of separate wires may be introduced into even a small Dewar, with excellent insulation. Since these terminals are soldered directly to the cap, excellent vacuum tightness can be attained in the flask.

There is one drawback to the use of Kovar glass seals, namely, the fact that Kovar is ferromagnetic which would preclude the use of such seals in some work. There are, however, many more applications where the magnetic properties are unimportant. Also since Kovar copper produces large thermoelectric effects, it is preferable to use lead-in terminals of the hollow tube type* rather than of the solid rod type in measurements where thermoelectric effects are important. The copper wires can then pass through the Kovar tube into the flask and be sealed to the tube with a drop of solder.

---

* I am indebted to Dr. R. T. Webber for this suggestion.

New Instruments

W. A. Wildhack: Associate Editor
in Charge of this Section
National Bureau of Standards, Washington, D. C.

These descriptions are based on information supplied by the manufacturer and in some cases from independent sources. THE REVIEW *assumes no responsibility for their correctness.*

Ultrasonic Generators

Central Scientific Company announce two new models of ultrasonic generators. They are portable, popularly priced, and generate high power.

These new ultrasonic generators are stable, efficient, and easy to operate for physical, chemical, biological, and industrial research or control.

The Ultrason generates mechanical energy in the crystal holder to vibrate solids, liquids, and gases.

Typical uses in chemical reactions and in other applications are:

to activate ozone to peroxide;
to remove fatty acids from semirefined oils;
to emulsify oils;
to disperse pigments;
to accelerate extractions;
to hasten or retard growth of bacteria, mold, and enzymes.

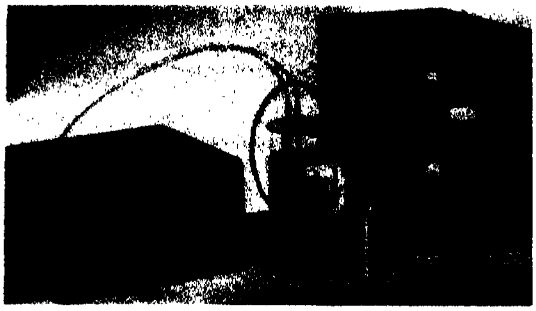

The U-300 Ultrason crystal delivers 300 watts of mechanical energy to the oil bath. A maximum of 10 watts of power per square centimeter of crystal area (a 76-mm crystal) is permissible without fracture of crystal. The crystal oscillating circuit is energized by 900 watts supplied by the low voltage, high frequency generator from a 115-volt, 60-cycle line. Model 100 Ultrason delivers a maximum of 6 watts at the crystal. Both units operate at 450 kc and provide instant and accurate reproduction of power and frequency conditions. The units are provided with built-in safety features and are designed for continuous operation and trouble-free service.—CENTRAL SCIENTIFIC COMPANY, *1700 Irving Park Road, Chicago, Illinois.*

Atomic Clock

In a radical departure from all conventional methods of measuring time, an atomic clock—invariant with age and for the first time independent of astronomical observations—has been developed by the National Bureau of Standards. Based on a constant, natural vibration frequency of atoms in the ammonia molecule, the atomic clock is a scientific achievement which offers an entirely new primary standard of frequency and time. The principle of the atomic clock promises to free man from age-old methods of fixing time by the daily rotation of the earth on its axis as it revolves around the sun. Not only does the new clock promise to surpass in accuracy any time measurement heretofore known, but the primary standard, the earth, is very gradually slowing down. In addition, unaccountable fluctuations in the rate of rotation have sporadically lengthened and shortened the day by a few thousandths of a second. The new method offers an invariant master clock against which the variation in timekeeping of the earth could be measured.

This first atomic clock has run with a constancy of better than one part in 20 million and is already being improved. By use of the proper atomic system a potential accuracy of a part in ten billion is theoretically indicated.

Because it is a standard of frequency as well as of time, the new method may be applied to the precise control of radio-frequencies, eliminating the "drift" allowances in present band-width allocations, and thus providing additional room in the ultra high frequency bands. The maximum utilization of available space in the radio spectrum depends on the accuracy with which the frequency of an individual station can be controlled, especially at the higher frequencies where quartz-crystal control cannot be used. These higher frequencies, which are used by radar, television relays, and microwave equipment, could be controlled by atomic elements. Such control would also make possible the permanent establishment of radio channels on such an exact basis that tuning could be made as automatic as the dialing of a telephone number.

Based on a principle developed by Dr. Harold Lyons, Chief of the Microwave Standards Section of the Bureau's Central Radio Propagation Laboratory, the new clock was constructed under his direction and with the assistance of B. F. Husten and E. D. Heberling. According to Dr. E. U. Condon, Director of the National Bureau of Standards, the method should prove an invaluable tool for basic research and will affect every technical field where precise measurements of time and frequency are crucial.

In recent years, vibrations of atoms in molecules, giving rise to molecular spectrum lines, have been found in the very high frequency (microwave) region of the radio spectrum. Very precise measurements of these lines are now possible by using extremely sensitive radio methods. When it became evident that such spectrum lines could be used as new primary frequency standards, scientists at the National Bureau of Standards began seeking a means of utilizing one of these lines

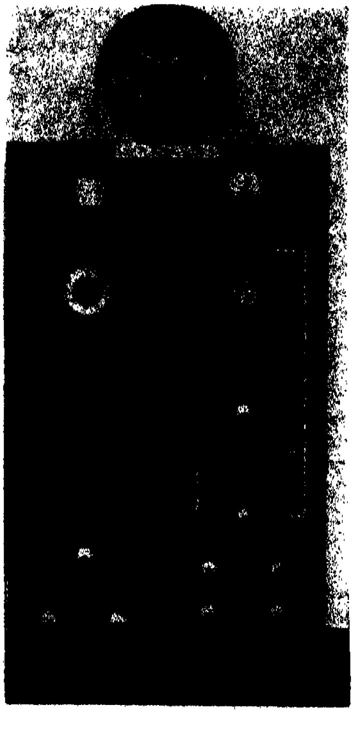

to control an oscillator, which in turn could be used to drive a clock. Because the resulting equipment, the atomic clock, is controlled by the invariable molecular system of ammonia gas, it is independent of astronomical determinations of time and unaffected by temperature, pressure, and aging.

The National Bureau of Standards atomic clock consists essentially of a quartz crystal oscillator, a frequency multiplier, a frequency discriminator, and a frequency divider, all housed in two small cabinets on the top of which are mounted a special 50-cycle clock and a wave-guide absorption cell—a 30-foot copper tube wound in a compact spiral around the clock and filled with ammonia gas. The crystal oscillator generates a fundamental driving signal at a low radiofrequency. A frequency-multiplying chain transforms this into a microwave (very high frequency) signal, which is then compared with a natural vibration frequency of the ammonia molecule. If these two frequencies are different, an "error signal" adjusts the oscillator to bring them into agreement. The oscillator which is inclined to "drift" slightly with age—that is, change in frequency—is thus "locked" to the ammonia molecule. It can then control an electrically driven clock with extreme accuracy.

Present time and frequency standards are based on astronomical determination of the period of rotation of the period of rotation of the earth. Essentially, a telescope is pointed toward a star, and the interval between the exact moment it passes the cross hairs until the exact moment 24 hours later that the star reappears is taken as the standard of time. The "twinkling" of the star, which makes its position difficult to fix, affects the accuracy of such measurements. The atomic clock gives a time standard of high precision continuously available in any interval of time desired instead of every 24 hours, whether it is a millionth of a second or ten hours. Moreover, the atomic clock is invariable so that a given interval of time, whether measured today or a hundred years from now is truly reproducible. The atomic method automatically and continuously controls the rate of the clock without delay or human intervention and is independent of weather.

Another advantage of the atomic method is that if an atomic clock were run continuously over a period of a year, our knowledge of the length of the year could be improved. The time it takes the earth to travel around the sun (a year) is completely independent of the time it takes the earth to rotate once on its axis (a day). This independence causes all the trouble with the calendar, necessitating leap years so that the seasons will always come at the same time during the year. With an atomic clock measurements could determine whether the mean sideral year is more accurate than the mean solar day, as some astronomers believe may be the case.

In terms of the regular 24-hour-day broadcasts of time and frequency by the National Bureau of Standards, which serve the nation and much of the world for standards of radiofrequencies and time, an atomic clock means a precision of both time and radiofrequency standard signals hitherto impossible.

The atomic clock gives the Bureau a time standard analogous to the Bureau's new atomic standard of length furnished by the single isotope of mercury which, if adopted internationally, will provide man with the ultimate standard of length. Both of these recent developments stem from the application of atomic physics to practical problems.—NATIONAL BUREAU OF STANDARDS, *Washington 25, D. C.*

Hydrostatic Impulse Gauge

This mechanical, self-recording gauge may be lowered into a well or connected to a pressure chamber to measure directly the total impulse per unit area generated by pressure waves resulting from underground explosions or other high pressure sources. In operation, the hydrostatic impulse forces mercury through a capillary passage and into a collector; the weight of mercury discharged is proportional to the impulse per unit area in p.s.i.-sec., from 10 to 400 p.s.i. The gauge is entirely self-contained and of simple construction, for convenience in field use. Its applications include geophysics, internal combustion studies, blast damage determination, and water hammer research.—ENGINEERING RESEARCH ASSOCIATES, INC., *St Paul 4, Minnesota.*

Radioactivity Demonstrator

Tracerlab has developed its new radioactivity demonstrator in response to the need for an inexpensive instrument for teaching basic principles of radioactivity in high schools and colleges. Radiation is indicated by three different means: by loudspeaker, by a flashing neon light, and quantitatively with a counting rate meter. The meter reads in counts per minute and will indicate up to 2500 counts per minute. This instrument has sufficient accuracy to permit carrying out simple classroom and laboratory demonstrations of basic principles of radioactivity.

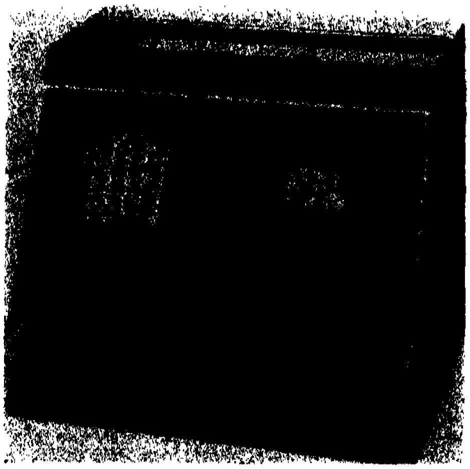

A removable shield is mounted in front of the Geiger tube, to completely eliminate beta-rays when it is desired to measure only gamma-radiation. A switch permits the meter also to indicate the voltage across the Geiger tube which can be varied from about 500 to 1100 volts. The instrument operates on 110 volts a.c.

Sources of beta- and gamma-activity are included at no extra charge, together with an instruction manual, experiments, and a discussion of radioactivity suitable for use in elementary lectures. With the radioactivity demonstrator it is possible to illustrate some of the properties of beta- and gamma-radiations, take background readings, plot the characteristic Geiger tube curve of counting rate *versus* applied voltage, and to make rough qualitative checks of the amount of radioactivity in various natural substances. For additional information and price, write for the Radioactivity Demonstrator Bulletin.—TRACERLAB, INC., *55 Oliver Street, Boston 10, Massachusetts.*

Selenium Rectifiers

The International Rectifier Corporation has developed a complete new line of selenium rectifiers covering the range from 2 volts and 150 milliamperes to 5000 volts and 10,000 amperes. The individual plate sizes range from 1¼"×1¼" to 6¼"×7¼".

The individual selenium plates are capable of withstanding 24 volts r.m.s. maximum in the reverse direction and can be overloaded up to 10 times rated load for periods of 7 seconds or less. The characteristics are also extremely stable since the leakage is less than 1 ma/cm² at maximum reverse voltage. Efficiency varies from 65 percent to 85 percent depending upon the circuit employed, and the change in voltage is less than 5 percent after the first 10,000 hours of operation.—INTERNATIONAL RECTIFIER CORPORATION, *6809 S. Victoria Ave., Los Angeles 43, California.*

Civilian Walkie-Talkies

Portable radio transceivers for public use between homes, automobiles, offices, plants, farms, and many other person-to-person radio telephone applications are now in pilot plant production by the Citizens Radio Corporation which has received the first F.C.C. type approval for equipment to be used on the 465-megacycle band allocated for civilian use.

The equipment is one-fourth the size of the famous wartime walkie-talkie, and is the result of more than two years of research and engineering in which many new techniques, including subminiature tubes and the use of silver-on-ceramic circuits, have been perfected for practical push-button, person-to-person radio communication for public use.

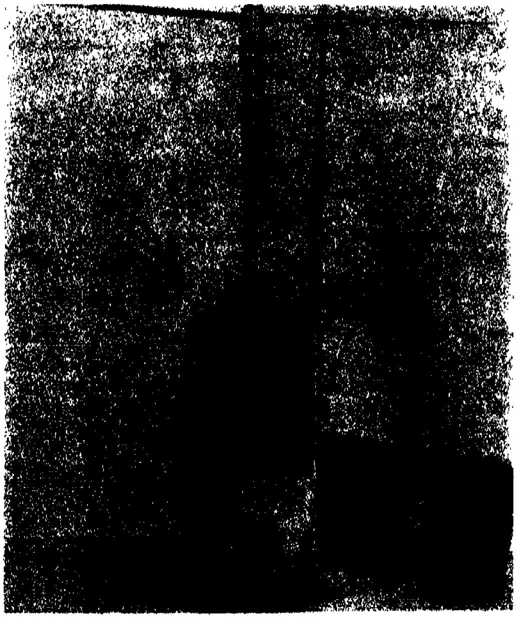

The transceiver, two of which are required for person-to-person air contact, is housed in a tiny case measuring 6"×2¾"×1¼" topped by a small folding antenna. This pocket-sized radio station includes all necessary equipment except a tiny headphone and batteries carried in a separate case about the size of a miniature camera.

The model 100-B citizen's radio is a transceiver for Class B stations only; it operates at 465 mc, tolerance 0.4, input 3 watts, emission A-3 with 30 percent maximum modulation. The transmitting section uses a Sylvania 6K4 subminiature oscillator and the receiver is super-regenerative, using three Sylvania 1V5 subminiature tubes. The transceiver weighs 11 ounces, including antenna; total station equipment, including batteries, is only two and one-half pounds.—CITIZENS RADIO CORPORATION, *Cleveland, Ohio.*

Vibration Measurement Equipment

The new Massa Model GA-1006 vibration measurement equipment was developed to meet several recent demands for extending both the frequency and dynamic ranges of generally available vibration measurement instruments. This new apparatus employs an extremely rugged accelerometer which is designed to give a uniform electrical output for constant acceleration over the entire frequency range 10 cycles to 20 kc. Its output is linearly proportional to mechanical vibrations corresponding to accelerations ranging from less than 0.001 g to more than 100 g.

The accelerometer responds only to vibrations applied along its principal axis, and it can therefore be used to measure the absolute vector components of any vibration existing at any point on the structure under test. Because the phase shift between the mechanical vibration and the generated electrical voltage is independent of frequency over the entire frequency range to 20 kc, very accurate transient vibrations may be electrically reproduced without changes in wave shape of the vibrations. Remote electrical indications of the vibrations can be conveniently made. A self-contained power supply unit makes the equipment conveniently portable for field applications. The new equipment is designed so that it can also be used as a wide-range sound pressure measuring instrument for making both conventional low level measurements as well as for making blast wave analyses of gunfire or other intense sound fields or explosions.—MASSA LABORATORIES, INC., *3868 Carnegie Avenue, Cleveland 15, Ohio.*

Slotted Line and Standing Wave Indicator

A new type of slotted line section, –hp–805A, incorporating a radical departure from conventional design is in production by the Hewlett-Packard Company.

Slotted lines are a fundamental tool for measurements in microwave circuits. By determining the pattern of a standing wave in a transmission line, the character of the load may be calculated. Both magnitude and phase may be determined. In many cases, knowing the standing wave ratio and phase is more important than knowing the impedence itself.

Slotted Line

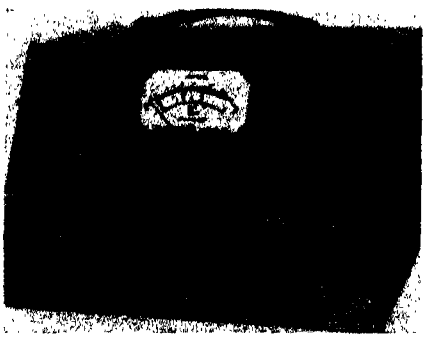

Standing Wave Indicator

The –hp–805A substitutes two parallel planes and a rigid central circular conductor for the conventional coaxial arrangement. This configuration has several important advantages over the standard slotted section.

First, parallel planes may be made mechanically rigid while also providing a rigid probe carriage. Second, the central conductor is proportionately larger and thus can be similarly rigid, eliminating tendency to bow. The depth of probe penetration is much less critical and carriage inaccuracies are all but eliminated.

This design also makes possible a very small effective slot opening. In the –hp–805A the slot opening is less than 0.001 inch referred to a coaxial system, and this serves to keep leakage very low. Residual VSWR can be held to less than 1.04.

Position of the probe is controlled with a cable system driven by a central stationary knob. The probe circuit is tunable over the entire frequency range, and the position may be read to 0.1 mm. Frequency range of the new slotted line is 500 to 4000 mc, and characteristic impedence is 50 ohms.

Hewlett-Packard Company has also in production the new –hp–415A Standing Wave Indicator to measure relative audio-voltages detected by a crystal rectifier or bolometer. It is designed for use with the –hp–805A Parallel-Plane Slotted Line, but may also be used with other slotted line systems. In conjunction with a slotted line it will determine flatness of a coaxial or wave-guide system, measure impedence, locate sources of reflection, and determine percentage of reflected power.

The new indicator consists of a high gain amplifier having a very low noise level and operating at a fixed audiofrequency. The output of the amplifier is measured with a square-law indicating vacuum tube voltmeter. The meter face of this voltmeter is calibrated both in decibels and in voltage standing wave ratio. Input circuits are provided for use with either a crystal or barreter. Equivalent "Q" of the over-all amplifier is 205.

The instrument is powered by any 115-volt a.c. source. The –hp–415A Standing Wave Indicator operates on a single fixed tuned frequency of 1000 cycles per second. However, other frequencies from 300 to 2000 cycles per second can be supplied on special order.—HEWLETT-PACKARD COMPANY, *395 Page Mill Road, Palo Alto, California.*

Manufacturers' Literature

Teledyne and Teleflight Instruments—Single sheet bulletins describe instruments of the electrical bridge type using bonded wire strain gauges, especially valuable in telemetering from aircraft and guided missiles. Teledyne pressure transmitters are available in ranges from 0–100 p.s.i. to 0–500 p.s.i. Teleflight pressure transmitters measure either positive or negative pressures, in ranges up to ±50 p.s.i., and are especially useful where small size is important. Teleflight accelerometers measure accelerations in ranges up to ±200 g.—ENGINEERING PHYSICS DIVISION, FREDRIC FLADER, INC., *North Tonawanda, New York.*

Type RV2 Precision Potentiometers—8-page bulletin includes specifications, photographs, drawings, and prices. Both linear and non-linear functional windings are available.—TECHNOLOGY INSTRUMENT CORPORATION, *1058 Main Street, Waltham 54, Massachusetts.*

Silicone Fluids—31-page booklet, *Dow Corning Silicone Note Book*, Fluid Series No. 3, presents a comprehensive body of information on the properties and behavior of DC200 Silicone Fluids. Charts and graphs of properties are presented. —DOW CORNING CORPORATION, *Midland, Michigan.*

Tubular Rheostats—Bulletin 41, 12 pages, describes various styles of standard, screw-drive, double, graded, switchboard, metal-caged, and non-inductive Jagabi "Lubri-tact" tubular rheostats. Diagrams and applications are shown in a "how to select" section.—JAMES G. BIDDLE COMPANY, *1316 Arch Street, Philadelphia 7, Pennsylvania.*

Decade Counter and Radiation Survey Instrument—Bulletin 485, 4 pages, describes decimal decade-scaling type instrument with built-in impulse register (recording clock), scale of 100 or scale of 1000 Higinbotham scaling circuit. Bulletin 486, 4 pages, describes Model SM3 portable battery-operated instrument for the measurement of radiation intensities.—EL-TRONICS, INC., *2647–67 N. Howard Street, Philadelphia 33, Pennsylvania.*

Phase Microscopy—24-page bulletin, *Phase Microscopes*, presents historical background, theory, and bibliography on phase microscopy and includes a catalog section on phase microscopes.—SCIENTIFIC INSTRUMENT DIVISION, AMERICAN OPTICAL COMPANY, *Buffalo 15, New York.*

New IRC Resistor—Bulletin B-1, 12 pages, gives comprehensive data on characteristics and specifications of new, advanced type BT insulated fixed composition resistors. Performance standards given for ¼-, ½-, 1-, and 2-watt types.—INTERNATIONAL RESISTANCE COMPANY, *401 N. Broad Street, Philadelphia 8, Pennsylvania.*

Accelerometers—Instrument Notes No. 6, December 1948, 8 pages, presents an article on "Calibration and test of accelerometers," illustrated with four figures.—STRATHAM LABORATORIES, *9328 Santa Monica Boulevard, Beverly Hills, California.*

Precision Electrical Instruments—Bulletin describing Muirhead precision instruments of the following types: miniature tuning fork, acoustic strain gauge, portable dark room, the Ipot (toroidal auto transformer), D'Arsonval galvanometer, and phonic motors.—MUIRHEAD AND COMPANY, LTD., *Beckenham, England.*

Radioactive Isotopes—12-page bulletin, *Tracerlog*, No. 14, December 1948, contains information on simulated phosphorus −32 and iodine −131 reference sources, including a procedure for standardizing with these simulated standards. Also presented is a list of uses for radioisotopes.—TRACERLAB, INC. *55 Oliver Street, Boston 10, Massachusetts.*

Instrumentation, Vol. 3, No. 5, fourth quarter, 1948, contains items of interest on applications of scientific instruments and automatic controls in industrial processes and in research laboratories.—MINNEAPOLIS-HONEYWELL REGULATOR COMPANY, *Brown Instruments Division, Wayne and Roberts Avenues, Philadelphia 44, Pennsylvania.*

Wire Wound Resistors—24-page catalog of high quality wire wound resistors, including both *non-inductive* and *inductive* types. Resistors with power ratings of ½ watt to 30 watts are listed.—INSTRUMENT RESISTORS COMPANY, *1036 Commerce Avenue, Union, New Jersey.*

Occupational Safety Posters—72-page 1949 Directory contains 744 illustrations and a convenient index for locating posters on specific accident hazards. Permission granted to reproduce posters. Price, 50 cents.—NATIONAL SAFETY COUNCIL, *20 North Wacker Drive, Chicago 6, Illinois.*

Television Components—4-page folder P-1 gives essential information on a line of television components.—TRANSVISION, INC., *460 North Avenue, New Rochelle, New York.*

Gas Analyzers—Bulletin No. 213, 8 pages, describes instruments for rapid control analysis of gas mixtures containing carbon monoxide, carbon dioxide, methane, oxygen, hydrogen, or nitrogen.—BURRELL TECHNICAL SUPPLY COMPANY, *1942 Fifth Avenue, Pittsburgh 19, Pennsylvania.*

Retaining Rings—8-page bulletin gives comprehensive specification data on Spirolox retaining rings.—SPIROLOX DIVISION, RAMSAY CORPORATION, *3693 Forest Park Boulevard, St. Louis 8, Missouri.*

New Materials

Forest K. Harris: Associate Editor
in Charge of this Section
National Bureau of Standards, Washington, D. C.

Ultra-Sensitive Photographic Emulsion

A new emulsion for nuclear track plates is so sensitive as to present a problem in preventing premature exposure by cosmic rays during shipment to research workers. Packing the emulsion in dry ice affords protection, because of the reduction of sensitivity at low temperatures. It must be continuously refrigerated and allowed to warm up just before exposure. The emulsion is characterized by high concentration of silver halides and by uniform sensitivity. It is approximately four times as sensitive as Eastman's present nuclear track plates and has successfully recorded electron tracks which are ten times as long as those previously recorded.

An additional suggested use is in precision autoradiography. In this application, sections of tissue containing radioactive isotopes are placed in contact with the emulsion so that radiation from the tissue exposes the emulsion. Examination of the developed plate permits identification of the location and amount of radioactive penetration in the tissue.

The new emulsion has been made so far only on an experimental basis and is not yet generally available.—EASTMAN KODAK COMPANY, *Rochester 4, New York.*

Synthetic Calcium Tungstate Crystals

Successful production of water-white single crystals of pure calcium tungstate in research quantities has been accomplished. Single crystals are now being grown in rods having a ⅜-inch square section and lengths up to 2 inches. Representative samples are colorless and their clarity varies from transparent to slightly cloudy. Development work is proceeding on the growing of uniformly clear crystals and on the production of other sizes and forms.

Indicated applications include the use of the material in scintillation counters in the detection and measurement of radioactivity and as screens in x-ray fluoroscopy. Crystals are available in research quantities in the square ⅜" rods, in lengths from ¼" to 2" in ¼" increments. The manufacturer has facilities for the fabrication of special windows or mosaica from the rod now available, and will be glad to consult with prospective users regarding possible applications and techniques of fabricating desired shapes.—NEW PRODUCTS DIVISION, THE LINDE AIR PRODUCTS COMPANY, UNIT OF UNION CARBIDE AND CARBON CORPORATION, *30 East 42 Street, New York 17, New York.*

Copper-Tungsten Contacts

Gibsiloy UW 6 is a powder-metal mixture of copper and tungsten made in various contact shapes and sizes. It is designed for handling heavy currents with minimum erosion. The units are molded to shape and one face is coated with silver solder for brazing in place. The cross strength is 135,000 p.s.i., and the hardness is 90 on the Rockwell B scale.—GIBSON ELECTRIC COMPANY, *8353 Frankstown Avenue, Pittsburgh 21, Pennsylvania.*

Flexible Copper Tubing

Vacuum-tight flexible tubing made of seamless copper may be obtained in lengths up to ten feet or in multiples of this length by welding end to end. The tubing measures $\frac{7}{32}$ inch i.d. and $\frac{11}{32}$ inch o.d. and has a pressure capacity up to 300 p.s.i. without requiring outside reinforcing braid. Fittings may be specified as well as lengths made up of corrugated and plain sections.—JOHNSON METAL HOSE, INC., *221 Mill Street, Waterbury 88, Connecticut.*

Sealed Terminal Bushings

A new line of tinned steatite-sealed terminals have been designed for use on metal enclosures. The terminals are made of glazed steatite that is resistant to rough handling and thermal shock. A tinned surface, permanently bonded to the steatite body, permits rapid and easy soldering to the enclosure after insertion in a hole of the proper size. Leads are brought through an axial hole in the bushing and soldered to the tinned lug provided at the end of the bushing. On special order terminals can be supplied which will operate at temperatures up to 200°C.—GENERAL CERAMICS AND STEATITE CORPORATION, *Keasbey, New Jersey.*

New Resin

Isopol is a hydrocarbon resin of moderately high molecular weight, made up of approximately three parts of styrene to one part isoprene, exactly the opposite proportions to those used in synthetic rubber. It is clear, hard, nearly water-white in appearance, possesses many of the chemical properties of rubber, and is completely soluble in petroleum naphtha. It is best described as a modified polystyrene in which the isoprene acts as an internal plasticizer. Thus the advantages of polystyrene have been retained while the disadvantage of brittleness has been partly eliminated.

In the solid state its use is suggested as a stiffener for both natural and synthetic rubber. Because of its chemical similarity it can be milled and cured in the same way. Because of its solubility in naphthas, aromatic hydrocarbons, chlorinated solvents, esters, and ketones, it offers possibilities in coating applications. In this field it has the advantages that solutions of the resin may be sprayed (in contrast to polystyrene) and that a film may be obtained without using a plasticizer. It shows some tack which may be of advantage in special applications where a finish coat of a different nature is contemplated and where an inert but mildly tacky base coat is desired. The resin may be readily emulsified and shows promise as an impregnant for cloth, paper, or wood. Technical data sheets and samples for laboratory investigation may be obtained from the manufacturer.—UNION BAY STATE CHEMICAL COMPANY, *50 Harvard Street, Cambridge, Massachusetts.*

Heat-Resistant Plastic Tubing

Templex 105 is a plastic tubing approved by the Underwriters Laboratories for continuous use at temperatures up to 105°C. In addition, manufacturer's tests show very favorable results in regard to retained elongation, tensile strength, flexibility, and dielectric strength after exposure to temperatures up to 150°C. 1000-hour exposure to transformer oil shows little effect. The tubing has continuous, abrasion-resistant identification marking. Complete information and samples may be secured from the manufacturer.—IRVINGTON VARNISH AND INSULATOR COMPANY, *Irvington, New Jersey.*

Instrument-Cleaning Solutions

Zenith solutions have been compounded specifically for the cleaning and rinsing of instrument and meter parts without leaving harmful residues. The manufacturer states that they are non-toxic and non-flammable, and they have been thoroughly laboratory and field tested. The cleaning solutions are stated to clean faster and brighter than any others on the market, and the rinses dry quickly without spotting. They are also low in cost, economical in use, and may be used with standard cleaning equipment. Samples will be furnished on request.—ZENITH MANUFACTURING AND CHEMICAL CORPORATION, *52 Beeckman Street, New York 7, New York.*

Anti-Fogging Cleaning Cloth

Specloth is a lens cloth impregnated with a synthetic detergent that coats the lens with a transparent film which prevents moisture from condensing on the surface of the glass. This film is non-greasy and is stated to fog-proof the lenses for as much as 24 hours. These lens cloths are inexpensive and remain effective for many weeks of daily use.—KLEER-VUE CLOTH PRODUCTS, *334 West 37 Street, New York 17, New York.*

Wetting Agent

Santomerse 30-X is a low cost liquid wetting agent and detergent of the alkyl aryl sulfonate type, which is expected to be of interest to the textile industry. It is a clear, light colored liquid containing 30 percent solids (85 percent active sulfonate, 15 percent sodium sulfate), and is resistant to decomposition by either strong acids or alkalis even under extreme conditions. It is suggested for the wet processing of textiles and for other applications where reduction of surface tension and quick wetting are desired. Its high detergent value and viscosity are said to make it also suited for liquid cleaners.—MONSANTO CHEMICAL COMPANY, *St. Louis 4, Missouri.*

Strippers for Organic Finishes.

Strippers S-17 and *S-19* are new room-temperature strippers for synthetic enamels. Stripper S-17 is stated to be a clear, quick-evaporating stripper used at room temperature for removal of all types of synthetic enamels, including heavy coatings of enamels that accumulate on work holders and hooks. For such cases the various layers of enamel exfoliate, leaving the work holders clean. It is particularly recommended for the removal of clear synthetic enamels from highly polished surfaces such as brass, gold plate, and silver. It does not tarnish metals and it has no significant odor. Stripper S-19 is similar to Stripper S-17 in its action and appearance except that it is slightly ammoniacal in composition and is used in certain special cases for removal of synthetic enamels where Stripper S-17 is not satisfactory. Both strippers are used with water seals to minimize evaporating losses, and rinsing is not necessary after their use. The work to be stripped is immersed in the strippers at room temperature. After a few seconds to several minutes, the enamel is completely removed from the surface of the metal and the parts can be removed. The stripper evaporates quickly and the part is ready for refinishing.—ENTHONE, INC., *442 Elm Street, New Haven, Connecticut.*

Self-Adhesive Wire Markers

Flag-It wire markers are designed for coding wires having diameters up to 0.2 inch. They may be wrapped around the wire to form an encircling marker, or the ends may be pinched together to form an upright, numbered flag. It adheres without moistening, is unaffected by moisture or heat, and may be removed without harming the wire surface. The fabric of the marker is coated to make it resistant to grease, dirt, and liquids. Standard cards are preprinted, black-on-white, in numbered or alphabet series, or can be printed to specification. They are attached to a 10-inch card, 40 to the card, from which they may be individually removed as needed.—FLAG-IT WIRE MARKER COMPANY, *320 Rose Street, Los Angeles, California.*

THE
REVIEW OF SCIENTIFIC
INSTRUMENTS

VOLUME 20, NUMBER 3 *MARCH, 1949*

Counter Pulse Shape

C. D. Thomas
West Virginia University, Morgantown, West Virginia

(Received August 30, 1948)

The shape of the decay pulse from a self-quenching counter depends on the circuit constants as well as on the motion of the positive ion sheath. This is considered mathematically and a formula developed to take account of these factors in determining pulse height and form. In order to check this relation experimentally, data obtained from photographed single pulses are presented and compared to the calculated values. These curves cover a wide range of values of circuit resistance and capacity.

THE calculation of the voltage which develops on the wire of a self-quenching counter due to the motion of the positive sheath has been checked by schemes which permit a fairly accurate reproduction of the relation. However, if the series resistance, as well as wiring capacity, is not of negligible importance, the shape of the discharge pulse may be quite different, depending on the values of R and C_p (Fig. 1). It was thought desirable to extend the calculations to the case cited here, since in practice the shunting capacity (C_p) may exceed the capacity of the counter C_g by many times and since the value R used will also materially influence the shape. It is obvious that if R approaches zero the wire voltage will be held constant, while if R becomes very large the discharge will be very nearly that caused by the sheath's motion alone until the cylinder is reached.

If the wire is considered charged and isolated, at some instant after the electron avalanche has been collected, the space within the counter may be treated as a problem in electrostatics, and the relation obtained between the voltage across the counter (ϕ), the charge per unit length of wire (q_0), the radius of the positive sheath (r), and the charge per unit length of the sheath (q). The relation so obtained is

$$\phi=2q_0\ln(b/a)+2q\ln(b/r). \tag{1}$$

When the sheath has moved to the cylinder (b), the voltage on the wire will have returned almost to its original value V. The difference in voltage is due to the fact that q_0 has been reduced slightly because of the negative charge collected on the wire. Equation (1) may be put into time-dependent form by assuming a constant ion mobility, a constant wire charge, and that the sheath is located at position r_0 at time t equal zero:

$$r^2=r_0^2+4kt[q_0+(q/2)]. \tag{2}$$

This situation, however, will not fit the case of Fig. 1 where the supply voltage V tends to return the wire potential to its original value in time comparable to, or less than, the time of motion of the sheath. The equation which determines the wire potential is then given by:

$$R(dQ_t/dt)+\phi=V,$$

where Q_t is the total charge on the wire and the shunting capacity. Equation (1) relates the wire

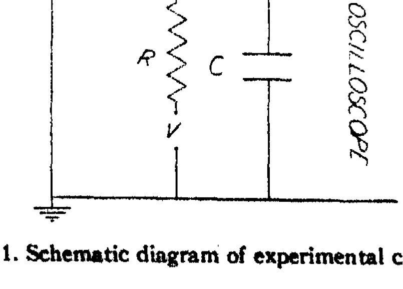

FIG. 1. Schematic diagram of experimental circuit.

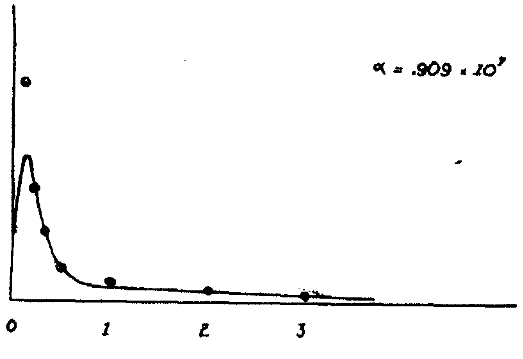

FIG. 2. Full line is the observed pulse height plotted to an arbitrary scale. Circled dots are calculated values. The curves are matched at 0.5 microsecond; $\alpha = 9.09 \times 10^6$ sec.$^{-1}$

charge to ϕ and, since the parallel capacity is constant, its charge also may be expressed in terms of ϕ, yielding

$$R(C_g+C_p)(d\phi/dt) \\ -2RC_gq[d/dt][\ln(b/r)]+\phi=V. \quad (3)$$

In order to solve this, Eq. (2) may be substituted in the second term. The coefficient of t in Eq. (2) is considered as a constant although this is no longer quite accurate, for the charge on the wire is no longer constant during the sheath motion. However, since q is much less than the total charge, the resultant inaccuracy in r (t dependence) may be expected to be slight, and the approximate field for determining the ions' motion may be found by use of q_g^0, the wire charge per unit length before the ionizing event occurs. Upon making this substitution, Eq. (3) becomes

$$[1/\alpha][d\phi/dt]+[qRC_g/(A+t)]+\phi=V, \quad (4)$$

where

$$\alpha=1/(R(C_g+C_p)), \quad A=r_0^2/4kq_g^0.$$

The boundary condition for this equation is obtained from the value of ϕ at time zero. Since the total charge on the wire and parallel capacity is reduced by the amount of the collected charge, its value at $t=0$ is

$$Q(0)=V(C_g+C_p)-qp,$$

where p is the length of the sheath. By use of Eq. (1) $q_g(=q_g^0-q)$, and hence $Q_t(0)$, may be evaluated in terms of the wire potential, $\phi(0)$, and r_0. By equating these two values of Q_t and solving for $\phi(0)$, the initial condition is found to be

$$\phi(0)=V-[2qC_g/(C_g+C_p)]\ln(r_0/a).$$

The solution of Eq. (4) is found to be

$$\phi=V-[qC_g/(C_g+C_p)]\{2\ln(r_0/a)E^{-\alpha t} \\ +E^{-\alpha(A+t)}[\langle Ei\rangle_M\alpha(A+t)-\langle Ei\rangle_M(\alpha A)]\}, \quad (5)$$

where $\langle Ei\rangle_M$ is the exponential integral function.

EXPERIMENTAL PROCEDURE

In order to check results of the above calculation, a circuit such as Fig. 1 was connected to an oscilloscope adapted to photographing single pulses. The capacity of the counter alone, and when in the circuit, was measured in order to get both C_g and C_p. In addition, the circuit was arranged to permit insertion of dummy capacity as well as for interchange of resistance values. Four different counter tubes whose characteristics and dimensions were quite different were used in the tests.

For comparing the photographs with the calculations based on Eq. (5), two schemes were used. For general shape, the photographs were projected onto cross-section paper, but for more accurate check, especially near the end of the pulse where differences were small, the height measurements were taken by use of a low power microscope with micrometer screw. The later device was also used for checking and correcting the time base.

In attempting to evaluate Eq. (5), all factors except q, r_0, and k (or A) may be obtained directly from the physical size of counter and electrical components. The charge q occurs as a multiplier in both terms which vary with time, and since no attempt was made to measure absolute pulse heights, this multiplier will not be needed. The ratio of radius of sheath origin to wire radius is not accurately known, but beaded wire experiments have shown that it is in the neighborhood of 2. The uncertainty in the value of A is still greater since it involves both r_0 and k. With the assumption that r_0 is equal to twice a, and that k is about 2 cm per sec. per volt per cm, the values of A for the counters used were of the order of 0.5 to 1.5×10^{-6} sec. As indicated in the discussion of the initial condition, the time origin is at the instant when the avalanche has been collected and the sheath has not appreciably moved. Experimental evidence on rise time, as well as calculation of the electron velocity in the field near the wire, indicates

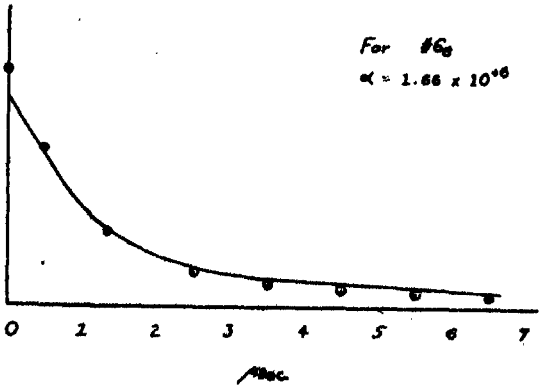

FIG. 3. Full line is the observed pulse height plotted to an arbitrary scale. Circled dots are calculated values. The curves are matched at 1.25 microseconds; $\alpha = 1.66 \times 10^6$ sec.$^{-1}$

that the error thus introduced in the time origin is a small fraction of a microsecond.

Since a great number of different values of α were used with each counter, only typical examples are shown here. Figures 2, 3, 4, and 5 are for a small counter with 5 mm of amyl acetate as the quench-in gas. The cylinder diameter of this counter is approximately 1.9 cm, its wire diameter 0.01 cm, and its length 8 cm. The curves shown are for a wire voltage of 1050, about 90 above threshold voltage. In each case the full line represents the photographed trace beyond peak value and the circles are calculated values which were matched to the experimental height at one point. In order to show most of the length and, at the same time, not to mask the departure from calculated value, as a logarithmic scale would do, the lower end appears very close to zero. The fit at this end is, however, very good. It is noticed that near the pulse peak there is considerable departure. This can be accounted for by the rough approximation made in estimating A, to which the curve is most sensitive for small times. It is also known that in this region of high field the mobility is not a constant as was assumed here.

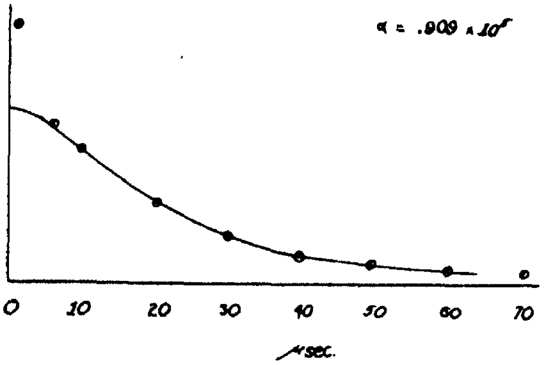

FIG. 4. Full line is the observed pulse height plotted to an arbitrary scale. Circled dots are calculated values. The curves are matched at 10 microseconds; $\alpha = 9.09 \times 10^4$ sec.$^{-1}$

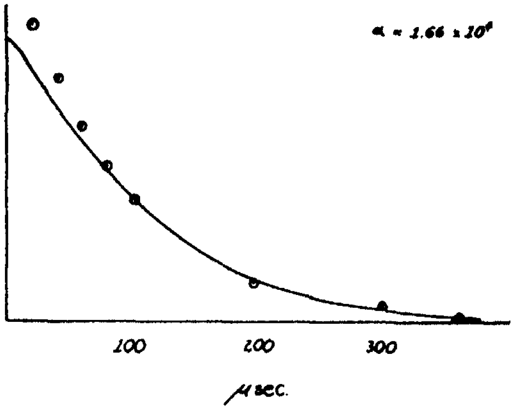

FIG. 5. Full line is the observed pulse height plotted to an arbitrary scale. Circled dots are calculated values. The curves are matched at 100 microseconds; $\alpha = 1.66 \times 10^4$ sec.$^{-1}$

It should be pointed out that while the resistance has a very great effect on the shape of the pulse, the motion of the sheath is not changed very much, and hence the field near the wire and the counter dead time are practically independent of R.

---

[1] H. G. Stever, Phys. Rev. 61, 38 (1942).

[2] Serge A. Korff, *Electron and Nuclear Counters* (D. Van Nostrand Company, Inc., New York, 1946).

THE REVIEW OF SCIENTIFIC INSTRUMENTS VOLUME 20, NUMBER 3 MARCH, 1949

Developments in the Useful Circular Nomogram*

Douglas P. Adams and Howard T. Evans, Jr.
Section of Graphics, Massachusetts Institute of Technology, Cambridge, Massachusetts

(Received August 30, 1948)

The particular type of alignment diagram for the function $U\cdot V=W$ in which the U and V scales lie on the circumference of the same circle and the W scale along a diameter is developed in detail. The forms of the diagram for which certain intervals on these scales are maximized in their spread are derived and described. Such maximized diagrams, it is found, have certain characteristic properties of symmetry. These developments are illustrated with examples.

BACKGROUND

A NOMOGRAM, or "law in graphical form," is a diagram designed to represent graphically a functional relationship between varying quantities. In particular, a nomogram consists of points, lines, or curves—each calibrated in one of the varying quantities of the relationship. When all the quantities but one have known values in a relationship for which a diagram has been prepared, the value of the unknown one can be found by reference to a point, line, or curve, characteristic of the solution, established by the known values. Extended use of the diagram can also often be made to determine compatible values of more unknowns than one.

The ordinary network chart is such a nomogram. Thus, for the equation $U\cdot V=W$, it might take the form of Fig. 1(a) or Fig. 1(b). On reference to the point P_j, characteristic of the solution established by known values U_j and W_j, the unknown value V_j can be read from the chart. The alignment diagram is likewise such a nomogram. It could take, for instance, either of the well-known forms of Fig. 2(a) or Fig. 2(b). On reference to the line K_j characteristic of the solution established by the known values U_j and W_j, the unknown value V_j can be read from the diagram.

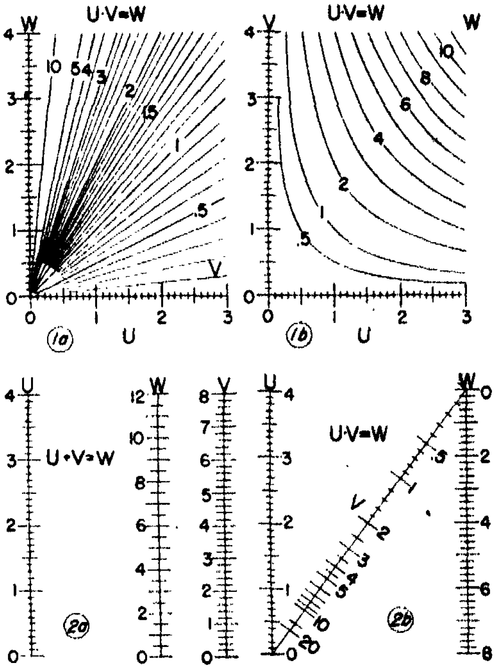

Figs. 1a, 1b, 2a, and 2b. Elementary forms of network chart and alignment diagram.

The generalized alignment diagram for the three-variable equation,

$$F(U,V,W)=0,$$

can be schematically represented in the form of Fig. 3. The U, V, W curves may partake of any definable form. Thus, one of them might be circular (Fig. 4). This type of diagram is not especially rare in the literature. It is clearly distinguished from the type which is of special interest in this article.

THE CIRCULAR NOMOGRAM

The equation $U\cdot V=W$ can also be represented in alignment diagram form by the use of a pair of coincident, circular U and V scales and a third straight-line W scale lying along a diameter of the circle. The values $U, V, W=0$ coincide at one end of the diameter and the values $U, V, W=\infty$, $U, V, W=-\infty$ coincide at the other end (Fig. 5). This diagram, extremely useful for certain purposes, seems to be employed by current English nomographers, but to be practically unknown in this country. In a survey of seventeen hundred nomograms appearing in the technical periodical literature in this country for the years 1925–1947, only one, designed by an Englishman, was found which partook of this form.

Geometrical Relationships

In Fig. 6, let line ABC be a random line of collineation cutting proposed U, V, W scales at points A, C, and B, respectively. Draw lines OA and OC defining peripheral angles θ and ϕ, which vary directly with arcs EA and EC. Construct line

---

* The circular nomogram has been given a thorough introductory treatment in *Elements of Nomography* by R. D. Douglass and D. P. Adams (McGraw-Hill Book Company, Inc., New York, 1947). The present authors believe that treatment to be the first in American texts.

ED parallel to line AC and draw line DC. Since $DC = AE$,

$$\measuredangle DOC = \measuredangle AOE,$$
$$\measuredangle DOC = \theta,$$
$$\measuredangle OAC = \measuredangle ODC.$$

Triangles OAB and ODC are similar and

$$OB/OA = OC/OD,$$
$$OA = 2a\cos\theta,$$
$$OC = 2a\cos\phi,$$
$$OD = 2a\cos(\phi-\theta).$$

Let OB, the distance from O to the cutting point B along the proposed W scale, be called S_W. It is the scale distance measured from point O out along the diameter to the point of location of any particular value W.

$$S_W = 2a\cos\theta\cos\phi/(\cos\theta\cos\phi+\sin\theta\sin\phi),$$
$$S_W = 2a/(1+\tan\theta\tan\phi).$$

Let the U and V scales be defined upon their circular arcs by the relationships:

$$U = \tan\theta, \tag{1}$$

$$V = \tan\phi, \tag{2}$$

$$S_W = 2a/(1+U\cdot V),$$
$$S_W = 2a/(1+W). \tag{3}$$

Thus, the W scale equation is observed to be identical with that for the diagonal scale for the N-type diagram, Fig. 2(b), when the latter is measured from the $V=\infty$ end.[1] This makes it possible to compound the circular diagram with the N diagram. A completed circular diagram appears in Fig. 7.

DISCUSSION

Range and Scope of the Circular Nomogram

The great advantage of the circular nomogram lies in its closure, which permits infinite ranges of all three variables to be present. This property is in contrast to the diagrams for the same basic formula for multiplication presented in Fig. 2(b). More generally, one can have the two arrangements presented schematically in Fig. 8. Any adaptable portion of such a diagram will be a valid alignment diagram.

Changing the Distribution of Graduations

Figure 7 shows the unit values of all three scales on a vertical line through the center of the circle. Fortunately, this distribution of values along the scale can be varied. Assume

$$P\cdot Q = R,$$
$$mP\cdot nQ = mnR.$$

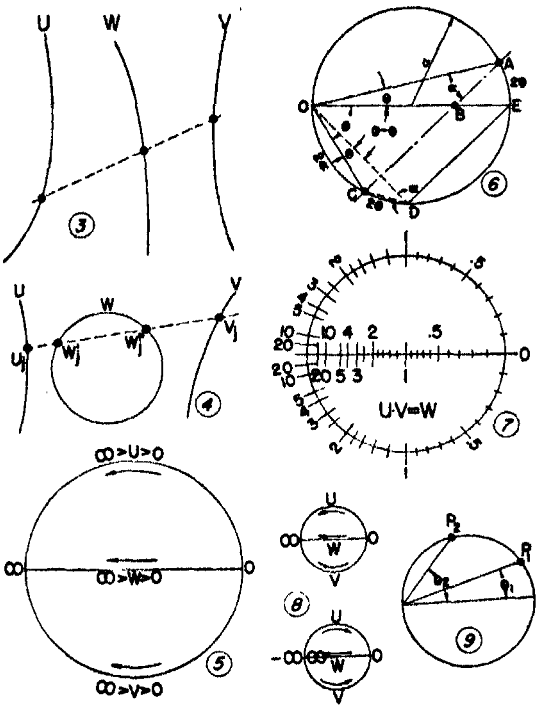

FIGS. 3–9. Basic characteristics of the circular nomogram.

Let

$$U = mP,$$
$$V = nQ,$$
$$W = mnR;$$

then

$$U\cdot V = W.$$

A diagram in U, V, W can be drawn in the standard form of Fig. 7. However, the diagram graduated in the original variables P, Q, and R will be such that these variables along the vertical line through the center of the circle will be $P_0 = 1/m$, $Q_0 = 1/n$, and $R_0 = 1/mn$. Great freedom of distribution of values is thus achieved. The standard equations 1, 2, and 3 will now be

$$P = \tan\theta/m, \tag{4}$$

$$Q = \tan\phi/n, \tag{5}$$

$$S_R = 2a/(1+mnR). \tag{6}$$

Maximizing Intermediate Scale Intervals

If the lowest values of the more useful ranges of the variables P and Q are greater than zero and the highest values of these ranges are finite, the more useful range of the R scale will not contain $R=0$ or $R=\infty$. The *spread* of this useful range will vary with m and n. A preliminary plan of the diagram may show this more useful range to be embarrassingly small. However, it can be maximized as follows. Let R_1 and R_2 be the lowest and highest values in the more useful range of R. Let this R

---

[1] R. D. Douglass and D. P. Adams, *Elements of Nomography* (McGraw-Hill Book Company, Inc., New York, 1947), p. 100, Note 2.

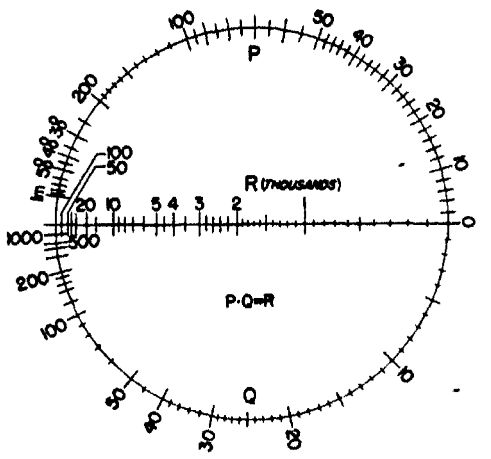

FIG. 10. A simple circular nomogram with maximized ranges.

range be maximized as a problem independent of the other scales. The R scale is characterized by the multiplier $l=mn$:

$$\begin{aligned} S_R&=2a/(1+lR),\\ S_{R_1}&=2a/(1+lR_1),\\ S_{R_2}&=2a/(1+lR_2),\\ T&=S_{R_1}-S_{R_2}. \end{aligned}$$

Then T, the spread of the most used range of R, is to be maximized with respect to the variable l:

$$T=2a\left(\frac{1}{1+lR_1}-\frac{1}{1+lR_2}\right),$$

$$\frac{dT}{dl}=2a\left(\frac{R_2}{(1+lR_2)^2}-\frac{R_1}{(1+lR_1)^2}\right).$$

For a maximum,

$$R_1(1+2lR_2+l^2R_2^2)=R_2(1+2lR_1+l^2R_1^2),$$

$$l=1/(R_1R_2)^{\frac{1}{2}},$$

$$\left.\begin{aligned} S_{R_1}&=2a/[1+(R_1/R_2)^{\frac{1}{2}}]\\ S_{R_2}&=2a/[1+(R_2/R_1)^{\frac{1}{2}}]\\ S_R&=2a/[1+[1/(R_1R_2)^{\frac{1}{2}}]R] \end{aligned}\right\}. \tag{7}$$

It is interesting to observe that the position of this spread upon the diameter is symmetric with respect to the center of the circle. Thus,

$$\frac{S_{R_1}+S_{R_2}}{2}=\frac{2a}{2}\left(\frac{1}{1+(R_1/R_2)^{\frac{1}{2}}}+\frac{1}{1+(R_2/R_1)^{\frac{1}{2}}}\right)$$
$$=a.$$

Maximizing the circular scale intervals, one has (Fig. 9):

$$\begin{aligned} \theta_1&=\tan^{-1}mP_1,\\ \theta_2&=\tan^{-1}mP_2,\\ A&=2(\theta_2-\theta_1). \end{aligned}$$

Then A is the spread of the most used range of P and is to be maximized with respect to m.

$$dA/dm=2[(P_1/(1+m^2P_1^2))-(P_2/(1+m^2P_2^2))].$$

For a maximum,

$$-P_1-m^2P_1P_2^2+m^2P_2P_1^2+P_2=0,$$
$$m=1/(P_1P_2)^{\frac{1}{2}}.$$

Correspondingly,

$$n=1/(Q_1Q_2)^{\frac{1}{2}}.$$

These ranges are also distributed symmetrically with respect to a vertical line on the circle, for

$$\begin{aligned} \tan\theta_1&=(P_1/P_2)^{\frac{1}{2}},\\ \tan\theta_2&=(P_2/P_1)^{\frac{1}{2}},\\ \tan\theta_1&=\cot\theta_2\\ &=\tan(90°-\theta_2),\\ (\theta_1+\theta_2)/2&=45°. \end{aligned}$$

Let the P and Q ranges be maximized independently and the R range be regarded as dependent.

$$\begin{aligned} P_1Q_1&=R_1,\\ P_2Q_2&=R_2,\\ l&=mn,\\ l&=1/(P_1Q_1P_2Q_2)^{\frac{1}{2}},\\ l&=1/(R_1R_2)^{\frac{1}{2}}. \end{aligned}$$

Thus, the R range is also maximized.

In this way, a circular diagram may be drawn with maximum dispersions for the most useful portions of all three scales. In addition, the maximization process, because of its symmetry with respect to the vertical diameter described above, produces a chart in which the index line (e.g., line ABC in Fig. 6) makes the greatest angle with the dependent scale on the diameter, thus allowing the most accurate measurement of R. Hence, the problem of optimum placement of scales for intermediate ranges of the variables in the circular nomogram achieves a pleasing and classical simplicity.

APPLICATIONS

Illustrative Problem 1

Figure 10. Design a circular nomogram six inches in diameter for the equation $P\cdot Q=R$ where infinite ranges of the variables are desirable but the ranges of P from $P_1=50$ to $P_2=100$, of Q from $Q_1=20$ to $Q_2=30$, and of R from $R_1=1000$ to $R_2=3000$ are subject to especially heavy use.

$$\begin{aligned} m&=1/(50\cdot 100)^{\frac{1}{2}}=0.01414,\\ n&=1/(20\cdot 30)^{\frac{1}{2}}=0.04082,\\ l&=1/(1000\cdot 3000)^{\frac{1}{2}}=0.0005773,\\ \theta&=\tan^{-1}0.01414P,\\ \phi&=\tan^{-1}0.04082Q,\\ S_R&=6/(1+0.000577R). \end{aligned}$$

Illustrative Problem 2

Figure 11.[2] Design a circular nomogram six inches in diameter for the equation

$$(\log \sin A)(B^3-4)=7\cos^2 C.$$

Place the B scale on the diameter of the circle. All first-quadrant values of the angles A and C are useful but the range of A from $A_2=10$ to $A_1=50$ and of C from $C_1=10$ to $C_2=50$ are heavily used.

Solution: Since the variable B is to be recorded upon the diameter, write the equation in the form

$$\begin{aligned}(\log \sin A)(1/7\cos^2 C)&=1/(B^3-4),\\ U'&=-\log \sin A,\\ V'&=1/7\cos^2 C,\\ W'&=-1/(B^3-4),\\ U_1'&=0.1158,\\ U_2'&=0.7603,\\ m&=3.37,\\ V_1'&=0.1473,\\ V_2'&=0.3457,\\ n&=4.44,\\ l&=14.95.\end{aligned}$$

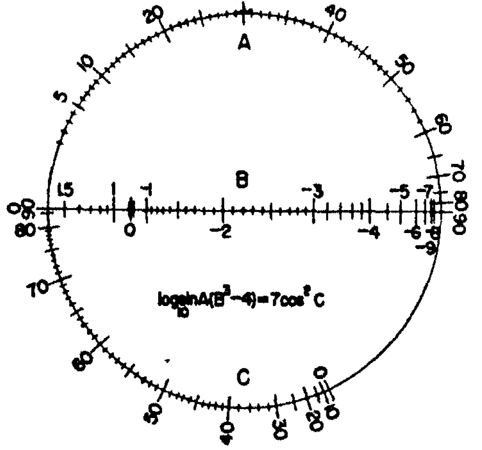

FIG. 11. An advanced circular nomogram with maximized ranges.

Then useful scale equations[3] for plotting this diagram are:

$$S_A=-6(3.37\log \sin A)\quad\text{or}\quad S_A=-6/3.37\log \sin A;$$
$$S_C=6(4.44/7\cos^2 C)\quad\text{or}\quad S_C=6(7\cos^2 C/4.44);$$
$$S_B=6/[1-(14.95/(B^3-4))].$$

Illustrative Problem 3

Figures 12 and 13.[4] Design a nomogram for the

$$s=r_s\cot\cos^{-1}(\cos\bar{\mu}-d^*),$$

equation where $\bar{\mu}$ ranges from 0° to 35°, d^* ranges from 0 to 1.0, s ranges from 10 to 70, r_s ranges from 15 to 40, in steps of 5. s is the dependent variable in practice. Experience indicates that it has a most heavily used interval from $s=25$ to $s=60$.

Analysis

The presence of four variables, three of them independent, precludes the possibility of a single alignment form for the diagram and requires a compounding of diagrams. Let

$$U=\cot\cos^{-1}(\cos\bar{\mu}-d^*).$$

Then,

$$s=r_s U.$$

Since U is given by $\tan\theta$ in the preceding theory, the presence of the cotangent function militates strongly in favor of the circular nomogram.

Let α be the complementary angle to θ, Fig. 12(a). Then $U=\tan\theta$ is properly recorded as $U=\cot\alpha$. Let

$$\begin{aligned}\alpha&=\cos^{-1}(\cos\bar{\mu}-d^*),\\ \cos\alpha&=\cos\bar{\mu}-d^*=x/2a,\\ x&=2a(\cos\bar{\mu}-d^*).\end{aligned}$$

The problem of the last equation is easily solved by a diagram of the form of Fig. 12(b). Let the x scale be tangent to the circle at the vertex A of angle α, have zero value there and be $2a$ units long. Let the $\bar{\mu}$-scale be located pleasingly upon the vertical center line of the circle. Let the values $\bar{\mu}=0$ and $d^*=0$ be on a level with $x=2$. Distances along the x scale can be conveniently transferred to the U scale by concentric arcs about point A, particularly with the aid of corresponding arbitrary graduations on the x and U scales (Fig. 12(c)).

Derivation of the Scale Equations

s scale: To maximize the most favored s interval,

$$l=1/(25\cdot 60)^{\frac{1}{2}}=0.0258;$$
$$S_S=10/(1+0.0258s)$$

for a circle of ten inches diameter ($a=5$).

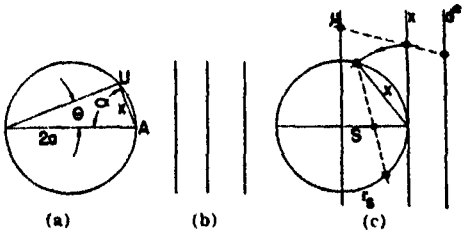

(a) (b) (c)

FIG. 12. Breakdown of parts for nomogram for camera.

---

[2] Compare with Fig. 88 in Douglass and Adams, reference 1, p. 156, where no interval has been maximized.

[3] For derivation and application of scale equations for the circular nomogram, see Douglass and Adams, reference 1, Chapter XVII.

[4] H. T. Evans, Jr., S. G. Tilden, Jr., and D. P. Adams. "New techniques applied to the Buerger precession camera for x-ray diffraction studies," Rev. Sci. Inst. 20, 155 (1949).

In practice, this diagram has been found to be practically indispensable to the efficient use of the equipment whose behavior is represented by this equation.

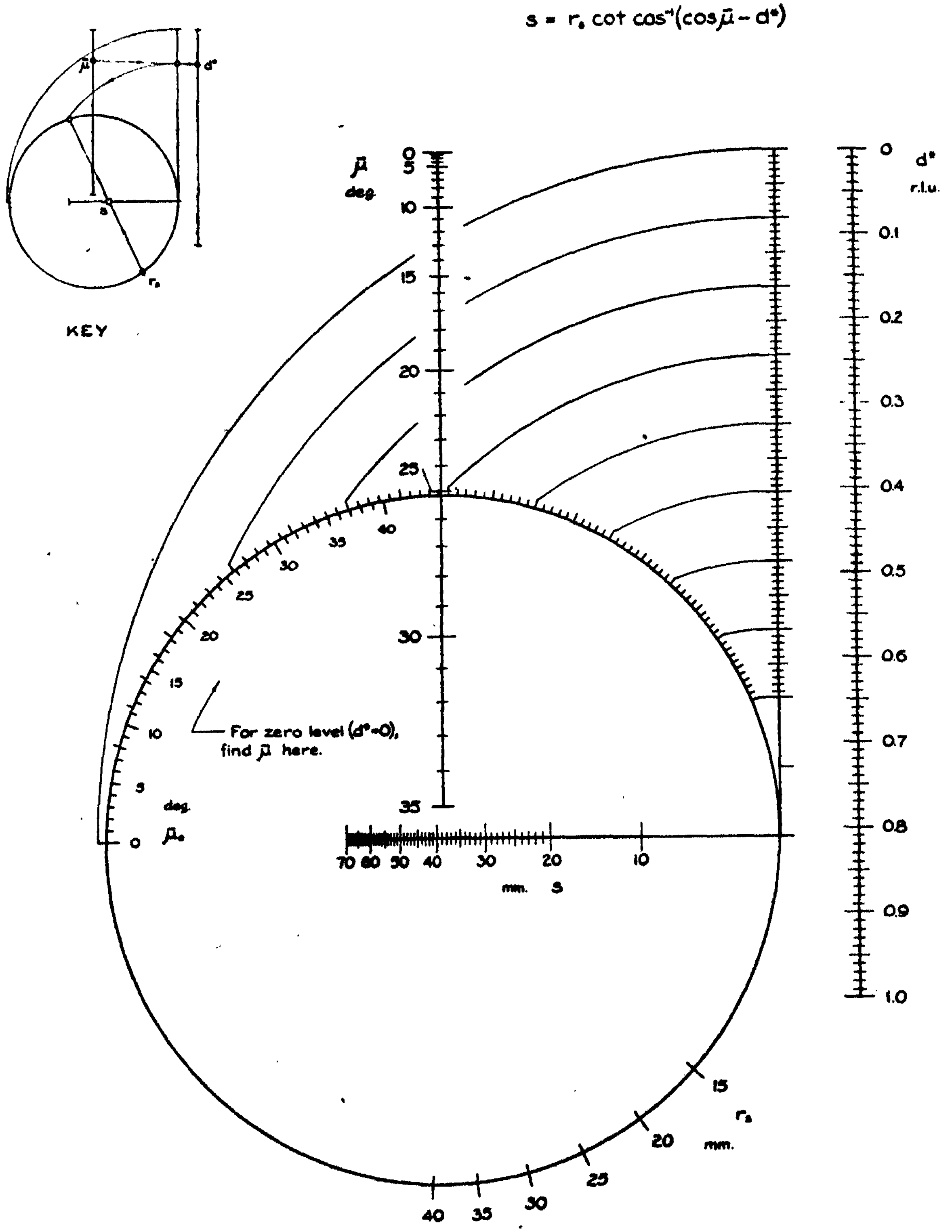

Fig. 13. Final Buerger precession camera nomogram.

r_s scale: The original equation now reads

$$ls=(nr_s)[m\cot\cos^{-1}(\cos\bar{\mu}-d^*)].$$

The device employed requires that

$$\cot\alpha=m\cot\cos^{-1}(\cos\bar{\mu}-d^*).$$

Hence $m=1$, $n=l$ in this scheme and neither of the circular scales can be varied for maximization. The value of r_s on the vertical center line will be

$$r_s=1/l=38.73.$$

The resulting r_s scale does lie in part to the left of the center line and has a satisfactory spread without maximization. A convenient scale equation for drafting the r_s scale will be

$$S_{r_s}=10r_s.$$

x scale: The scale factor of the x scale is unity. The sum of the scale factors of the d^* and $\bar{\mu}$ scales will equal their product and the distances of these scales from the x scale will be proportional to these scale factors.[5] Of these four quantities, only the distance of the $\bar{\mu}$ scale has been fixed (at five inches) by the present design.

$\bar{\mu}$ scale and d^* scale: The equations for these scales, reduced to scale measurement upward from the horizontal center line of the circle, can accordingly be

$$S_{\bar{\mu}}=52.6(\cos\bar{\mu}-0.810),$$
$$S_{d^*}=12.34(0.810-d^*).$$

The d^* scale is 1.17 inches from the x scale.

---

[5] For a description of the derivation of scale factors and scale equations for the parallel-line diagram, see Douglass and Adams, reference 1, Chapter IX.

THE REVIEW OF SCIENTIFIC INSTRUMENTS VOLUME 20, NUMBER 3 MARCH, 1949

New Techniques Applied to the Buerger Precession Camera for X-Ray Diffraction Studies

HOWARD T. EVANS, JR.,* S. G. TILDEN, AND DOUGLAS P. ADAMS
Section of Graphics, Massachusetts Institute of Technology, Cambridge, Massachusetts

(Received August 30, 1948)

The usefulness of the Buerger precession method for single crystal x-ray diffraction studies is increased by the following techniques: (1) The use of a nomogram to facilitate the setting and operation of the instrument; (2) the simplification of orientation and lattice measurement techniques; and (3) the application of the Dawton photographic method to precession photographs for obtaining quantitative intensity data, together with a graphical method for determining Lorentz and polarization corrections.

IN 1944, a new method of obtaining x-ray diffraction data from single crystals was described by Buerger.[1] By use of a camera of novel design, aptly called the "precession" camera, layers of the reciprocal lattice were photographed directly without distortion. This instrument has since been made available commercially and has earned favor in several laboratories.[2] It seems apparent, however, that the full possibilities of this instrument have not been generally realized. Therefore, some of the techniques developed in this laboratory in connection with the precession method will perhaps be of interest.

INSTRUMENT SETTINGS

In preparing the instrument for a run, five separate adjustments must be made for each photograph, defined as follows: (1) F, the film-to-crystal distance; (2) $d^{*\prime}$, an adjustment of the film position for proper registration of the upper levels of the lattice; (3) $\bar{\mu}$, the angle between the direct beam and the normal to the plane being photographed; (4) r_s, the radius of the layer-line screen; (5) s, the screen-to-crystal distance.

F is an independent adjustment determined by the desired magnification of the lattice image, and $d^{*\prime}$ is simply the product of F and d^* the reciprocal lattice spacing normal to the planes being photographed. $\bar{\mu}$, r_s, s, and d^* are, on the other hand, related in a rather complex way, as shown by Buerger, thus: $s=r_s \cot\cos^{-1}(\cos\bar{\mu}-d^*)$.

s is usually the last adjustment made and, hence, may be regarded as the dependent variable of the equation. In his monograph, Buerger gives a chart permitting rapid determination of s over a range of d^* (0 to 1.0 reciprocal lattice units) for two values of r_s (15 and 30 mm) and a fixed value of $\bar{\mu}$ (20°). Although these restrictions on r_s and $\bar{\mu}$ are not inconvenient in a majority of cases, there are many times when a greater flexibility of these variables is desirable.

It is possible to present the behavior of the variables in the equation in an alignment diagram which will give the value of s for all useful values of r_s, $\bar{\mu}$, and d^*. By using this diagram, reproduced in Fig. 1, it is an easy matter quickly and accurately to arrive at an optimum value for each of the settings involved. The key to the diagram shows the general scheme to be the employment of two elementary types of alignment diagrams. The first of these is the familiar three-parallel-line diagram; the second is the less familiar circular nomogram. The further adaptation of the latter to the special needs of the

---

* Present address: Laboratory for Insulation Research, Massachusetts Institute of Technology.

[1] M. J. Buerger, "The Photography of the Reciprocal Lattice," ASXRED Monograph No. 1 (1944).

[2] See for example, G. L. Clark and H. Kao, J. Am. Chem. Soc. 70, 2151 (1948).

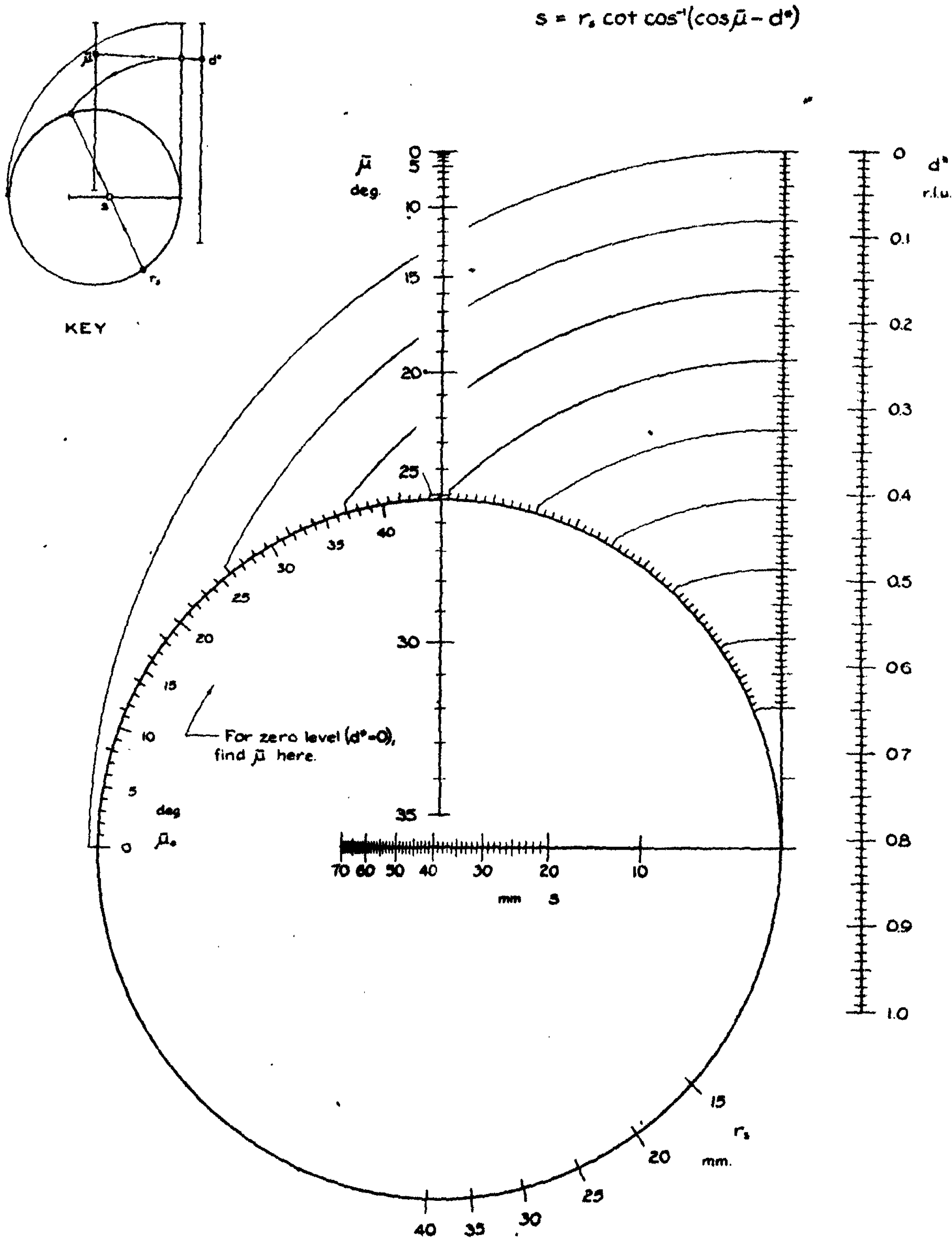

FIG. 1. Nomogram for setting the Buerger precession camera.

equation at hand appears to the writers to be new, and is described in detail elsewhere.[8] Also, its form has accurately maximized along the circle's diameter the spread of the most useful range of the dependent variable, s (25 to 60 mm).

ORIENTATION OF CRYSTALS

The use of the Buerger precession camera in the orientation of crystals has been described in detail by Buerger.[1] If the crystal has a zone of faces parallel to the dial axis, which carries the goniometer head, the optical autocollimator attached to the standard x-ray collimator may usually be used to align the crystal without any trial photographs. Alternatively, the crystal may be brought into orientation by means of a series of trial photographs from which the setting errors are estimated by observing the traces of the zero level reflections on the film.

---

[8] D. P. Adams and H. T. Evans, Jr., "Developments in the Useful Circular Nomogram," Rev. Sci. Inst. 20, 150 (1949).

We have found that another very convenient method is provided by drilling two very small holes (No. 80 drill) in the back of the film holder under the spring clip. These holes admit just enough light to mark the film. A line is thus determined which is accurately located parallel to the dial axis. The angle between this line and a lattice row line thus can be measured accurately to find directly the error of setting of the goniometer head arc parallel to the film. Two such photographs taken 90° apart on the dial supply the data necessary to bring a roughly oriented crystal into perfect alignment. In Fig. 2, which shows such a photograph, two sharp spots are visible near the extreme ends of the horizontal central lattice line. The arc error, measured between the line of these spots and the adjacent lattice line, in this case is 2° 20′. (The orientation of the film is indicated by a cut in the upper right corner, which corresponds with a mark on the film holder.)

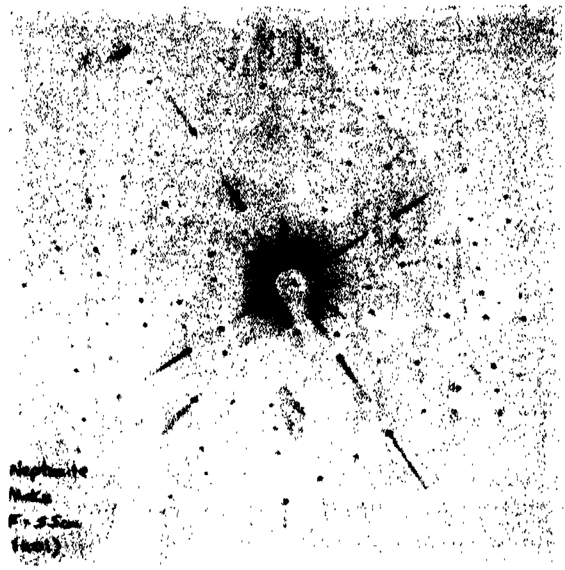

FIG. 2. Zero level precession photograph, showing orientation marks (neptunite, monoclinic).

This method, combined with those described by Buerger, makes the instrument extremely valuable for the purpose of orienting crystals, especially when only anhedral fragments are available. The ease with which the lattice of a crystal may be located, oriented, and explored with the precession instrument makes the latter a very fitting adjunct to the Weissenberg camera with its far-reaching range.

LATTICE MEASUREMENTS

The Buerger precession camera has been found to provide measurements of lattice spacings of considerable accuracy. Our instrument has been calibrated with a quartz crystal, as suggested by Bradley and Jay.[4] The (*h*0*l*) reciprocal net plane of the crystal was photographed with the film-to-crystal distance, F, set as closely as possible with the vernier to 6.000 cm. Two values of F were measured from the spacings on the film, as follows: 5.998 cm; 6.002 cm. The accuracy apparent from these measurements, better than 4 parts in 10,000, has been confirmed by comparative measurements on other crystals. Such precision can be obtained with the Weissenberg only with some trouble involving extrapolations and corrections. One advantage of the precession method is that the spacings of a whole row of spots on a film may be averaged simultaneously bv alignment with a hair-line. Thus, two settings of the hair-line are usually sufficient to provide data of the quality indicated, without any further corrections. The performance of this instrument testifies not only for the nature of the method, but also for the skill of the machinist who built it.[5]

INTENSITY MEASUREMENTS

The precession method has been found to be well suited to the recording of intensity data over a limited range, which, for many cases, is adequate. The Dawton photographic technique[6] is readily adapted to precession photographs. The spots on the film are round and uniform and very con-

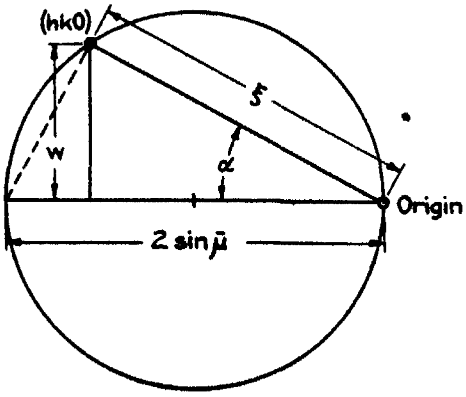

FIG. 3. (See text.)

---

[4] A. J. Bradley and A. H. Jay, Proc. Phys. Soc. London 45, 507–22 (1933).

[5] Mr. Charles Supper of Newton Center, Massachusetts.

[6] R. H. V. M. Dawton, Proc. Phys. Soc. London 50, 419 (1938).

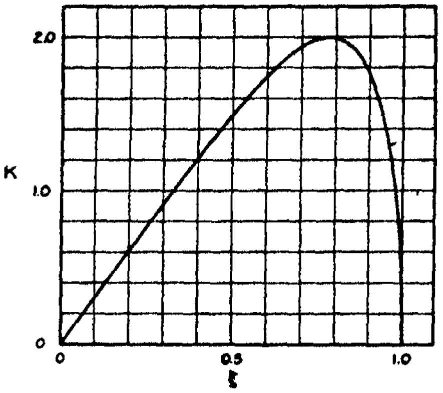

FIG. 4. Lorentz-polarization correction, K, for zero level.

veniently arranged, lending themselves to rapid and straightforward photometric measurement. The maximum range is obtained by using an inclination angle of $\bar{\mu}=30°$, and a film-to-crystal distance of $F=5.5$ cm. With this setting, a circular area of the zero level 11 cm in diameter is recorded on the 5 inch square film. This corresponds to a diameter of 2.0 reciprocal lattice units, and, if molybdenum radiation is used, covers a range just greater than that recorded by the Weissenberg camera using copper radiation. Actually, it has been found that, for most purposes, efficient application of the Buerger precession camera depends on the use of molybdenum radiation.

The form of the Lorentz factor for the precession method has been described by Buerger.[1] Figure 3 is a view normal to the zero level of the reciprocal lattice. One lattice point and the origin are shown. The circle is the intersection of the lattice plane and the unit sphere of reflection. With the quantity w defined as shown in Fig. 3, Buerger derived the following expression for the Lorentz factor:

$$1/L=w\sin\bar{\mu}\cos\bar{\mu}. \tag{1}$$

For the zero level, it appeared that a more convenient expression would combine both the Lorentz and polarization corrections, in terms of $\bar{\mu}$ and the radial coordinate ξ (in r.l.u.; see Fig. 3), the latter being readily measured directly from precession films. Such an expression may be derived as follows:

$$\begin{aligned}\sin^2\alpha&=w^2/\xi^2,\\ \cos^2\alpha&=\xi^2/4\sin^2\bar{\mu},\\ 1&=w^2/\xi^2+\xi^2/4\sin^2\bar{\mu},\\ w&=[\xi(4\sin\bar{\mu}^2-\xi^2)^{\frac{1}{2}}/2\sin\bar{\mu}].\end{aligned} \tag{2}$$

Substituting (2) into (1), there results:

$$1/L\doteq 1/2\xi\cos\bar{\mu}(4\sin^2\bar{\mu}-\xi^2)^{\frac{1}{2}}. \tag{3}$$

The polarization factor is readily derived from the classic formula:

$$1/p=(2/1+\cos^2 2\theta). \tag{4}$$

For the zero level,

$$\begin{aligned}\xi&=\lambda/d=2\sin\theta,\\ 2\sin^2\theta&=1-\cos 2\theta,\\ \cos^2 2\theta&=[1-(\xi^2/2)]^2.\end{aligned}$$

Substituting in (4) gives:

$$1/p=4/(8-4\xi^2+\xi^4). \tag{5}$$

Combining (5) with (3), we obtain:

$$\frac{1}{Lp}=\frac{4\xi\cos\bar{\mu}(4\sin^2\bar{\mu}-\xi^2)^{\frac{1}{2}}}{8-4\xi^2+\xi^4}. \tag{6}$$

If we adopt the settings suggested above ($\bar{\mu}=30°$, $F=5.5$ cm) universally for the taking of zero level quantitative Dawton photographs, this correction is very easily determined for all reflections by means of a simple graphical device. This consists of a template with a set of rings graduated according to $1/Lp$, and whose positions are determined by Eq. (6). By superposing the template directly on the precession film, the correction may be read off directly for each spot by its position with respect to the rings. When $\bar{\mu}=30°$, Eq. (6) may be written:

$$\frac{1}{Lp}\sim K=24.34\frac{\xi(1-\xi^2)^{\frac{1}{2}}}{8-4\xi^2+\xi^4}. \tag{7}$$

This function is scaled arbitrarily to allow $1/Lp$ to range between 0 and 2.00, as shown by the graph illustrated in Fig. 4. In Fig. 5, a chart made from Eq. (7) is shown in place on a precession photo-

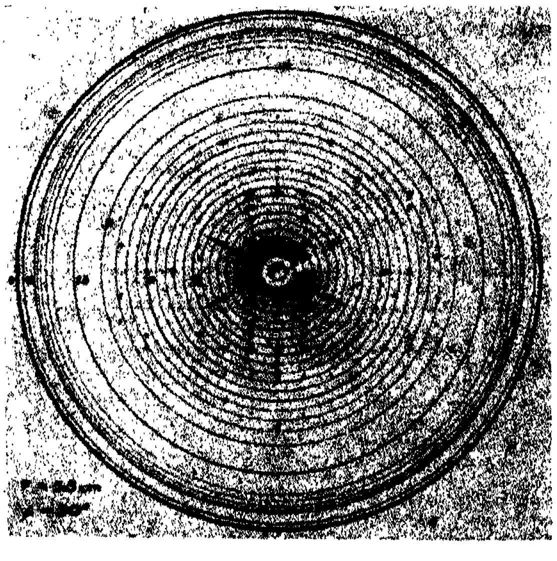

FIG. 5. Template for Lorentz-polarization correction in place on zero level photograph ($K_6TeMo_6O_{24}\cdot 7H_2O$, orthorhombic).

graph. The chart is best prepared photographically from an original drawing, which may be easily made from the data given in Table I.

The precession method is not well adapted to the quantitative photography of upper levels, for several reasons. The range recorded for upper levels is much smaller; the central blind area increases very rapidly with the distance of the lattice plane from the origin (d^*); and the Lorentz-polarization correction is much more awkward to evaluate. Thus, the precession method is practically limited to two-dimensional Fourier studies of crystal structures at present. For three-dimensional studies, the equi-inclination Weissenberg method will maintain its superiority.

SUMMARY

New techniques and aspects of the Buerger precession method for single crystal x-ray studies have been described. The utility of the instrument is greatly increased by the use of a nomogram which quickly solves the rather awkward setting relationships for any case. Other aspects of the method that have been dealt with are the following:

(1) A new method of measuring orientation errors, together with earlier known techniques, speeds the process of locating and aligning the lattice of a crystal, even when crystal faces are totally lacking.

(2) The Buerger precession camera has been found to give reliable measurements of lattice dimensions, accurate to better than 4 parts in 10,000, directly without corrections or extrapolations.

(3) The precession method is convenient for making intensity measurements by the Dawton photographic technique, for zero level reflections. Its range, when molybdenum radiation is used, is comparable with that of the Weissenberg method used with copper radiation. The Lorentz-polarization correction is easily measured by the use of simple graphical methods.

TABLE I. Tabulation of Lorentz-polarization corrections for zero level precession photographs made with the settings $\bar{\mu}=30°$ and $F=5.5$ cm.

Calculated from Eq. (7):		Read from graph of Fig. 5:	
ξ (r.l.u.)	K	K	$5.5\times\xi$ (cm)
1.00	0.000	0.00	5.50
0.99	0.672	0.50	5.47
0.98	0.932	1.00	5.38
0.97	1.117	1.30	5.26
0.96	1.263	1.50	5.15
0.95	1.383	1.60	5.08
0.94	1.490	1.70	5.01
0.93	1.566	1.80	4.90
0.92	1.640	1.90	4.75
0.91	1.707	1.95	4.63
0.90	1.760	2.00	4.30
0.88	1.844	1.95	3.90
0.86	1.907	1.90	3.72
0.84	1.952	1.80	3.43
0.82	1.978	1.70	3.19
0.80	1.994	1.60	2.97
0.78	2.000	1.50	2.76
0.76	1.992	1.40	2.56
0.74	1.980	1.30	2.37
0.72	1.960	1.20	2.18
0.70	1.932	1.10	1.99
0.65	1.851	1.00	1.80
0.60	1.740	0.90	1.62
0.55	1.619	0.80	1.44
0.50	1.491	0.70	1.26
0.40	1.221	0.60	1.08
0.30	0.908	0.50	0.90
0.20	0.607	0.40	0.72
0.10	0.304	0.30	0.54
0.00	0.000	0.20	0.36
		0.10	0.18
		0.00	0.00

ACKNOWLEDGMENT

The observations described in this paper were made in the Laboratory for Insulation Research, at the Massachusetts Institute of Technology. We wish to express our appreciation to Professor Arthur R. von Hippel, director of the laboratory, for his encouragement of the work.

THE REVIEW OF SCIENTIFIC INSTRUMENTS VOLUME 20, NUMBER 3 MARCH, 1949

Conditions for Optimum Luminosity and Energy Resolution in an Axial β-Ray Spectrometer with Homogeneous Magnetic Field

JESSE W. M. DUMOND
California Institute of Technology, Pasadena, California

(Received October 18, 1948)

In a β-ray spectrometer with axial homogeneous magnetic field, it is shown that optimum energy resolution and luminosity are obtained when the trajectories make an angle close to 45° with the field and that an annular resolving slit should be provided at a determined radial and axial location relative to the source. The combined effect of three independent sources of instrumental energy line width is analyzed for the optimum condition. Formulas are given for the optimum dimensions, the energy resolution and the luminosity.

THE improvement recently obtained in the precision of absolute measurement of nuclear energy levels by the direct crystal diffraction of short wave-length nuclear gamma-rays[1] makes it a matter of considerable interest to develop a β-ray spectrometer of high resolving power and high precision comparable to that obtainable in the crystal diffraction method. The low reflecting power of crystals for wave-lengths of order 30 x.u. and less necessitates the use of extremely strong gamma-ray sources and hence practically eliminates this method as an exploratory technique. Its great advantage on the other hand, lies in the high absolute precision which it affords. It thus complements very satisfactorily the qualities of the β-ray spectrometer since the latter instrument has high luminosity but is very difficult to calibrate with absolute precision. The thought here is that if a β-ray spectrometer of sufficiently high resolving power and reproducibility can be designed, its calibration in terms of absolute β-ray energies can be accomplished by utilizing a number of nuclear gamma-ray lines (precisely standardized by the crystal diffraction method) to eject photoelectrons from known and precisely measured electronic energy levels in appropriately selected secondary radiators. The β-ray spectrometer, so calibrated, can then be used for the accurate measurement of both β-ray and gamma-ray energies from a wide variety of sources and the high absolute precision of the crystal diffraction method can thus be propagated over a much wider domain of measurements.

Many types of the β-ray spectrometer exist or have been proposed. Under the auspices of the Office of Naval Research[2] S. Frankel and E. C. Nelson have very recently made a valuable survey of many of these and have discussed their properties. They fall into three general classes.

(*1.*) *Spectrometers in which the central ray of an electron beam or pencil lies in a plane essentially perpendicular to the magnetic field.*—The electrons execute circular orbits which may consist of arcs greater or less than 180° and the field may be uniform or tapered in various ways to obtain various types of focusing. Notable among these is the Siegbahn-Svartholm[3] so-called double-focusing type.

(*2.*) *Spectrometers of the helical focusing type.*—The magnetic field may be approximately uniform (utilizing the field from a long solenoid) or it may be set up by a more-or-less concentrated coil and may merely have axial symmetry. Electrons leave a more or less concentrated source point on the axis at one end and execute paths more or less helical in form passing through various restricting stops and returning to the axis at the other end where they enter the window of a counter. First suggested by Kapitza in 1923 this type, in various modifications, has been used and described by Tricker,[4] Klemperer,[5] Witcher,[6] K. Siegbahn,[7] Deutsch, Elliot and Evans,[8] and T. Lauritsen and R. F. Christy.[9]

(*3.*) *Spectrometers utilizing electrostatic deflection of the β-rays.*—It is pointed out by Frankel and Nelson[2] that for a fast electron whose velocity nearly equals that of light the same curvature may be produced by a magnetic field of 1000 gauss (which is conveniently small) as by an electric field of 300,000 volts per cm (which is uncomfortably large). Such instruments, which possibly have some importance for the formation of images in electron microscopy have therefore not played an important role in β-spectrometry.[10]

---

[1] DuMond, Lind and Watson, "Precision wave-length and energy measurement of gamma-rays from Au^{198} with a focusing quartz crystal spectrometer." Phys. Rev. **73**, 1392 (1948), Jesse W. M. DuMond, "A high resolving power, curved crystal focusing spectrometer for short wave-length x-rays and gamma-rays," Rev. Sci. Inst. **18**, 626 (1947).

[2] Contract N6onr-238 T.O. 5.

[3] K. Siegbahn and N. Svartholm, Nature **157**, 872 (1946); Arkiv. f. Mat. Astr. o. Fysik, **33A**, No. 21 (1946); N. Svartholm, *ibid.*, **33A**, No. 24 (1946).

[4] R. A. R. Tricker, Proc. Camb. Phil. Soc. **22**, 454 (1925).

[5] O: Klemperer, Phil. Mag. **20**, 259 (1940). Klemperer was apparently the first to propose the concentrated coil or "thin magnetic lens."

[6] Clifford M. Witcher, Phys. Rev. **60**, 32 (1941).

[7] Kai Siegbahn, Arkiv. f. Mat. Astr. o. Fysik, **30**, No. 1 (1943); Phil. Mag. **37**, 162 (1946).

[8] M. Deutsch, L. G. Elliot, and R. D. Evans, Rev. Sci. Inst. **15**, 178 (1944). Includes a painstaking analysis of the thin lens type.

[9] T. Lauritsen and R. F. Christy, Phys. Rev. **73**, 536 (1948).

The helical focusing type seems so obviously advantageous as regards the utilizable solid angle of β-rays emanating from the source that this was chosen as the object of the first analysis (the one herein presented) to determine the optimum conditions for simultaneous high resolving power and high luminosity. It is not entirely certain, however, that other and radically different types cannot be devised which will be superior to this one and a program of analysis of other types is now being planned.

The choice of a homogeneous magnetic field (rather than the more complicated field from a concentrated coil) for the β-ray spectrometer here described was based on the following considerations. (1) The analysis is considerably simplified. (2) A homogeneous field is not difficult to realize with a high degree of precision by means of a long solenoid. (3) Small geometrical distortions of such a field by external magnetic influences are more readily detected than they would be in the case of more complicated fields. (4) Since the applied magnetic field is everywhere uniformly strong over the useful region, errors from external magnetic effects are everywhere at a minimum. (5) The adjustment of the spectrometer relative to the field coil is less critical since it depends in first approximation only on the orientation and not on the position. This is a consideration which becomes important because of the high accuracy sought. As Frankel and Nelson[2] point out the thin lens β-spectrometer is more efficient as regards the cost for copper and for power than the solenoid type with uniform magnetic field, but Lauritsen and Christy[9] have shown it to have a poorer resolution for the same range of angles within which the β-rays emanate from the source. The thick lens spectrometer is a compromise between the superior resolving power of the solenoid type and the cheaper thin lens type.

It is a rather surprising fact that the use of a ring shaped annular resolving slit in this type of spectrometer was not suggested until rather recently[11] although the existence of a ring-shaped focus for the bundle of β-rays appears to have been clearly apparent in earlier papers. In a homogeneous magnetic field (solenoid) a bundle of β-rays *of specified energy* leaving a source point on the axis of the spectrometer at colatitude-angles θ in the range $\theta_1<\theta<\theta_1+d\theta$ will focus in a ring whose plane is normal to the axis and whose radius and distance from the source can be readily calculated. It is this type of focusing with which we shall be concerned in this paper.

The trajectory of an electron in a uniform magnetic field is a helix. Let us consider a point source S from which electrons of definite kinetic energy, T, emanate with equal probability in all directions in space. Let us measure the kinetic energy of these electrons in terms of the dimensionless parameter, $\epsilon=T/(m_0c^2)$ (ratio of the kinetic energy to the electron rest-energy, 0.5108 Mev). As x-axis we take a line through the point source S in the direction of the magnetic field whose intensity is H. Let the angle between the helical trajectory and the magnetic field be θ. After one complete turn of the helix the trajectory will once more intersect the x axis in a point S'. Let the diameter of the helical trajectory be R and the distance SS' be L. Then, if e is the electronic charge it is easy to show by elementary considerations that

$$R=2(m_0c/He)[(\epsilon+1)^2-1]^{\frac{1}{2}}\sin\theta, \tag{1}$$

$$L=2\pi(m_0c/He)[(\epsilon+1)^2-1]^{\frac{1}{2}}\cos\theta. \tag{2}$$

For brevity let $K=2(m_0c/He)$ and $Q=K[(\epsilon+1)^2-1]^{\frac{1}{2}}$. The assemblage of helical trajectories emanating from S form a triply infinite family of helices characterized by the three parameters; (1.) the azimuth angle of the trajectory at S, (2.) the colatitude angle θ at S, and (3.) the parameter Q depending on the kinetic energy ϵ and the field strength H.

If we consider the entire sub-class of trajectories having a specified value $\theta=\theta_1$ and $Q=Q_1$ but all values of the azimuth angle at S, these helices will all be found to lie on a cigar shaped surface of revolution having the x axis as axis of revolution and having a sinusoidal profile or trace on a plane through the x axis. Figure 1 illustrates a side view of this surface of revolution with a few of the individual helices traced upon it. Only the part of each helix on the side of the surface of revolution toward the observer is drawn, to avoid confusion. The trace or intersection of this surface of revolution with a plane through the x axis will henceforth be designated simply by the word "trace," and the cartesian coordinates x and y describing the equation of a trace will be taken in a plane through the x axis at any arbitrary azimuth angle. Clearly the angle made by the trace at the origin S with the x axis is equal to θ, since there is one of the helical trajectories which is tangent to the trace at S. We shall henceforth be much more concerned

---

[10] Relatively little attention, however, has been paid to the possibilities of combining electrostatic and magnetic deflections for β-spectrometry.

[11] The suggestion appears to have been first made by Witcher, (see reference 6) who did not, however, make the most of this very ingenious idea. In a letter to the editor of the Physical Review by S. Frankel, Phys. Rev. 73, 804 (1948) the large gain in solid angular luminosity for a specified high resolution obtainable by this ring focus is explained and emphasized. In a still more recent letter to the Physical Review, E. Persico gives his conclusions as to the optimum finite source size and angle of electron departure from the source. E. Persico, Phys. Rev. 73, 1475 (1948).

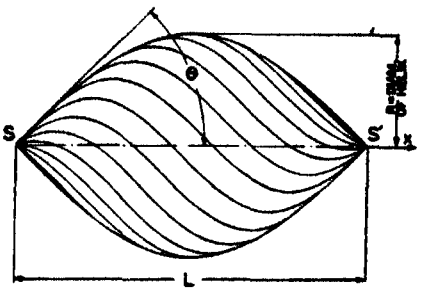

FIG. 1. Illustrating that a family of helical trajectories of specified θ and Q lie on a sinusoidal surface of revolution. L is one full turn of the helix.

with the traces than with the helices. The general equation of a trace is

$$y = Q\sin\theta\sin[x/(Q\cos\theta)]. \tag{3}$$

The traces starting from the origin S form a doubly infinite family of sinusoids characterized by the parameters Q and θ. Now suppose we hold the kinetic energy of the particles and the magnetic field intensity constant (i.e., Q constant) and impose a slight variation on θ. Two closely adjacent traces for a slight variation of θ will be found to have an ultimate intersection point P which will not be situated at S' but somewhere between S' and the summit of the sinusoidal trace. Figure 2 shows the geometry of two such adjacent traces. Let us compute the coordinates x_i and y_i of this ultimate intersection point, by equating

$$Q\sin(\theta+d\theta)\sin\frac{x_i}{Q\cos(\theta+d\theta)} = Q\sin\theta\sin\frac{x_i}{Q\cos\theta}.$$

A straightforward calculation rejecting terms of higher order than the first gives

$$x_i = (Q_1\cos\theta_1)\psi_i, \tag{4}$$

$$y_i = (Q_1\sin\theta_1)\sin\psi_i. \tag{5}$$

Here Q_1 and θ_1 are the particular values of Q and θ which characterize the traces having the ultimate intersection at x_i, y_i, while ψ_i is an angle related to θ_1 by the transcendental equation

$$-\psi_i\tan^2\theta_1 = \tan\psi_i. \tag{6}$$

In Fig. 3 we plot the various branches of the curve $\tan\psi_i$ and also the straight locus $-\psi_i\tan^2\theta_1$. The intersections of these two loci give the solutions for ψ_i, the solution of interest to us being that one which lies in the range $\pi/2 < \psi_i < \pi$. Clearly when

$$\theta = 0, \quad \psi_i = \pi,$$

and when

$$\theta = \pi/2, \quad \psi_i = \pi/2.$$

By substituting a series of values of ψ_i between these limits it is an easy matter to calculate the corresponding values of θ, from the equation

$$\tan^2\theta_1 = -(\tan\psi_i/\psi_i), \tag{7}$$

and the curve of Fig. 4 has been traced in this way. Table I gives the relation between ψ_i and θ_1 numerically.

Geometrically ψ_i is the abscissa coordinate *in angular measure* of P the ultimate intersection point, that is

$$\psi_i = x_i/(Q_1\cos\theta_1). \tag{8}$$

(The half-wave-length L of the sinusoidal trace is $\pi Q_1\cos\theta_1$.)

The ultimate intersection point P on the sinusoidal trace is obviously the focal place where the ring focus defining slit should be located in order to select a specified small band of kinetic energies. Clearly this slit must be an annular opening defined by a pair of diaphragms normal to the x-axis of the instrument.[12] We shall return later to a more careful consideration of the choice of the width of this opening. Its mean radius is given by y_i (Eq. (5)). In Fig. 5 we show a family of different sinusoidal trace-pairs for one and the same initial angle θ_1 but different values of Q_1 (i.e., different kinetic energies or magnetic field intensities). The ultimate intersection points are seen to lie along a straight line which also passes through the origin S.[13]

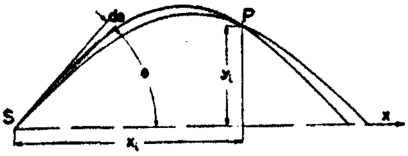

FIG. 2. Showing how two adjacent traces of constant Q but slightly different θ determine an ultimate intersection point P.

We now attack the problem of selecting the best value of θ_1, the colatitude angle at which the β-rays to be used in the instrument are to issue from the source S. If we fix the two points S and P on a certain sinusoidal trace T_1 characterized by the parameters Q_1 and θ_1, P being the ultimate intersection point for T_1 with coordinates x_i, y_i given in Eqs. (4) and (5), and then consider the family of other sinusoidal traces which also pass through S and P in the neighborhood of the trace T_1, these will be characterized by parameters θ and Q in such a way as to establish a functional dependence between these two parameters. For these neighboring traces, as θ departs from θ_1 Q will depart from Q_1, but since the point P *was purposely selected as an ultimate intersection* for the trace T_1 (with its immediate neighbors) we have good reason to expect that the departure of Q from Q_1 corresponding to a specified departure of θ from θ_1 *will be a smaller order of infinitesimal quantity than the latter.* Now what we aim to do is to select θ_1 in such a way that, for small deviations $d\theta$ on either side thereof, the largest possible solid angle at the source S results in the smallest possible inhomogeneity of kinetic energy. To do this we substitute the coordinates x_i, y_i of the ultimate intersection point into the general equation of the sinusoidal trace. This gives us

---

[12] S. Frankel (see reference 11) recommends that the defining edges of the diaphragms lie on a cone with vertex at the source and axis parallel to the magnetic field.

[13] This line is an element of the cone referred to by Frankel (see references 11 and 12).

$$\frac{Q_1 \sin\theta_1}{Q \sin\theta} \sin\psi_i = \sin\left(\frac{Q_1 \cos\theta_1}{Q \cos\theta} \cdot \psi_i\right). \tag{9}$$

Equation (9) is the implicit expression of the above mentioned relationship between Q and θ which obtains for the family of traces passing through the points S and P. We must remember that ψ_i is a function of θ_1 but not of θ. The *solid angle* of β-rays emanating from the source point S is what we wish to maximize or more significantly still *the fraction of the total sphere* into which the β-rays can be projected. Let us define $d\phi$ as this fraction of the total sphere. Then

$$d\phi = \tfrac{1}{2} \sin\theta d\theta. \tag{10}$$

Since we are only interested in small deviations of θ away from θ_1 and of Q away from Q_1 we define two small dimensionless quantities r and δ as follows:

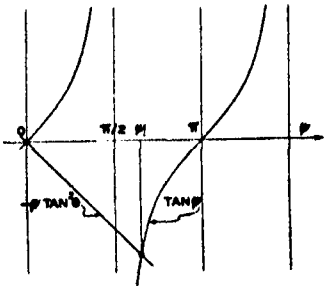

FIG. 3. Graphical solution of the equation relating ψ_i and θ.

$$\frac{Q-Q_1}{Q_1} = r \ll 1; \quad \frac{\cos\theta - \cos\theta_1}{\cos\theta_1} = \delta \ll 1.$$

We may confidently expect r to be an infinitesimal, at least one order of magnitude smaller than δ for the reason explained previously. Rejecting infinitesimals of higher order than the second, one obtains

$$\frac{Q_1}{Q}\frac{\sin\theta_1}{\sin\theta} = 1 + \frac{\delta}{\tan^2\theta_1} + \frac{1}{2}\frac{\delta^2}{\tan^2\theta_1} + \frac{5}{4}\frac{\delta^2}{\tan^4\theta_1} - r,$$

and $(Q_1/Q)(\cos\theta_1/\cos\theta) = 1 - \delta + \delta^2 - r$.

Substituting these values into Eq. (9) and solving for r one obtains

TABLE I.

ψ_i		θ_1
Degrees	Radians	Degrees
90	1.571	90°
91	1.588	80°30′
92	1.606	76°40′
93	1.623	73°40′
94	1.641	71°20′
99	1.73	63°20′
108	1.886	52°00′
117	2.041	44°25′
126	2.20	38°20′
135	2.358	33°10′
144	2.513	28°20′
153	2.671	23°30′
162	2.829	18°40′
171	2.984	13°00′
180	3.141	0°

$$r = \tfrac{1}{4} \cos^2\theta_1 [6 + (5/\tan^2\theta_1) + 2\psi_i^2 \tan^2\theta_1]\delta^2; \tag{11}$$

now since

$$\delta = \frac{\cos\theta - \cos\theta_1}{\cos\theta_1} \cong \left[\frac{d(\cos\theta)}{\cos\theta_1}\right]_{\theta_1},$$

and $d\phi = \frac{1}{2}\sin\theta d\theta$, we obtain $d\phi^2 = \frac{1}{4}(\cos^2\theta_1)\delta^2$. So that Eq. (11) becomes

$$r = \left[6 + \frac{5}{\tan^2\theta_1} + 2\psi_i^2 \tan^2\theta_1\right](d\phi)^2. \tag{12}$$

This shows that our prediction was correct, i.e., that r is indeed a smaller order of infinitesimal than δ or than $d\phi$.

Clearly if we are to minimize the inhomogeneity of kinetic energy we must minimize r. In fact calculation shows that for constant field H

$$d\epsilon/\epsilon = [(\epsilon+2)/(\epsilon+1)]r. \tag{13}$$

Our problem is thus reduced to the evaluation of the bracket of Eq. (12),

$$B(\theta_1) = 6 + 5\cot^2\theta_1 + 2\psi_i^2 \tan^2\theta_1$$

which is a function of θ_1 only (since ψ_i is a function of θ_1 see Eq. (6). Figure 6 shows the value of this bracket $B(\theta_1)$ plotted as a function of θ_1 and

FIG. 4. Graph of ψ_i as function of θ. See also Table I.

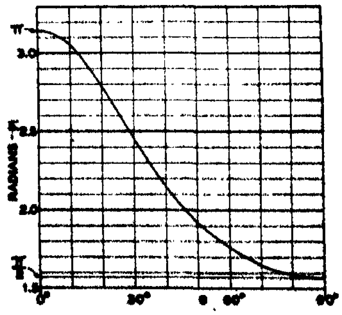

Table II gives the numerical values. It was a matter of considerable surprise to the author to discover that $B(\theta_1)$ is very nearly symmetrical about its minimum point and that this latter appears to occur very nearly at $\theta_1 = 45°$. Neither of the preceding statements is rigorously correct[14] but clearly from the numerical calculations the minimum in B is sufficiently flat to insure that there will be no significant loss of energy resolution if θ_1 is chosen anywhere within the range $40° < \theta_1 < 50°$. For $\theta_1 = 45°$ the value of B is about 19. At 40° and 50° it is about 20.

We now pass to the discussion of the appropriate shape and finite extension to give to the source and the appropriate width and disposition of the annular resolving slit. It appears to the author that when an extended source is necessary symmetry considerations dictate a source in the shape of a small very thin flat disk at S normal to and concentric with the x axis since this is the only shape for which all β-particles emerge at the same angle with the surface (45°). The small but unavoidable retardation of those particles which traverse the active layer from different depths will thus be minimized.

It is clear that the β-ray energy spectrum given by the spectrometer will have three[15] independent instrumental sources of line broadening, (1) the "spherical aberration" coming from the use of a finite angular aperture $\theta_1 < \theta < \theta_2$, (2) the finite spectral width of the selected energy band determined by the width of the resolving slit at the ring focus, (3) the radius of the source disk which we shall denote by ρ. Each of these sources of broadening alone would, if the effect of the other two were reduced to negligible proportions, yield its own characteristic spectral line profile (corresponding to a sharp line in the true energy spectrum). Figure 7 shows the shapes of these three profiles. With all three sources of broadening operating simultaneously the instrumental spectral line profile will be the *fold* of the three characteristic profiles, each with its own peculiar width parameter (determined by the stops and the source radius ρ selected). This resultant (folded) profile will have a resultant width parameter which will determine the resolving power of the instrument. At the same time, each of the three above mentioned sources of broadening contributes its factor to the counting rate of the instrument. The counting rate is in fact jointly proportional to the area of the source disk (ρ^2), to the width of the energy band selected at the ring focus (we assume, sufficiently high resolution so that all the spectral distributions studied can be regarded as continua) and to the solid angle defined by the aperture stops.[16]

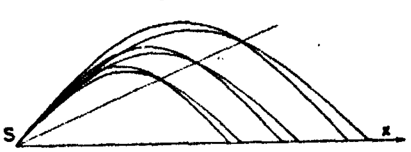

FIG. 5. A family of different trace pairs for the same initial angle θ_1 but different Q, i.e., different energies or magnetic intensities.

TABLE II.

θ_1 Degrees	B
0	∞
10°	167.6
20°	45.8
30°	25.0
40°	19.62
50°	20.0
60°	26.5
70°	48.2
80°	169.2
90°	∞

The problem we must pose is how to apportion the line broadening effects of the above mentioned three causes so as to minimize the resultant line breadth while maximizing the counting rate. The problem is complicated by the curious way in which the width parameter of the resultant folded profile is related to the width parameters of each of the three components.

A brief discussion and justification of the three component profiles of Fig. 7 is first in order. The profile I coming from the finite aperture angle has an infinite ordinate at $\epsilon = \epsilon_0$ but a finite area under the curve since the curve follows an inverse half-power dependence on $\epsilon - \epsilon_0$. This last may be shown as follows: Equation (12) implies that, for angles θ (of β-ray departure) differing slightly from θ_1, the energy ϵ selected by an infinitesimally small ring focus slit (of appropriate position and radius to focus an infinitesimal bundle of rays of angle θ_1)

---

[14] The value of θ_1 which makes $B(\theta_1)$ a minimum can be easily obtained by expressing B as a function of ψ_i,

$$B = 6 - \psi_i(5\cot\psi_i + 2\tan\psi_i).$$

The minimum of this function occurs at $\psi_i = 117.5$ degrees and substituting this value into Eq. (7) one obtains the corresponding value of $\theta_1 = 44°4'$ as the minimum point of $B(\theta_1)$. This differs slightly but not significantly, from the value 42°20′ given by Persico (see reference 11). It is so close to 45° that we shall use the latter value in design calculations since there is a gain in simplicity by this choice.

How nearly the function $B(\theta_1)$ is symmetric can be appreciated from the fact that even where B is enormous near $\theta = 0$ and again near $\theta = \pi/2$, i.e., for vanishingly small angles η, $B(\eta):B(\pi/2-\eta) = 5:\pi^2/2$.

[15] A fourth source of broadening coming from the finite *thickness* of the source is here ignored.

[16] The radius of the source disk has an important influence on the counting rate chiefly *in the case of direct sources of β-rays.* It is to such cases that the remainder of the discussion in this article primarily applies. When the primary source is a gamma-ray source which is to eject secondary β-rays from a converter it may be that the counting rate will not increase with the size of the secondary β-ray source. Then only the causes I and II (of line broadening) enter into the discussion.

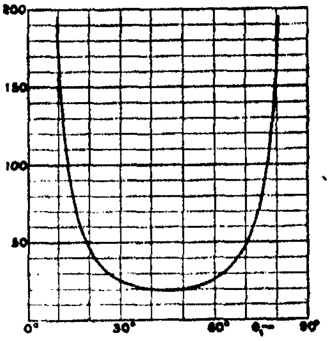

FIG. 6. The bracket $[6+5\cot^2\theta_1+2\psi_i^2\tan^2\theta_1]$ plotted as a function of θ_1. See also Table II.

will differ from ϵ_0 in first approximation by an amount proportional to $(\theta-\theta_1)^2$. This is illustrated by the parabolic characteristic of Fig. 8. If k_1 is a positive constant

$$(\epsilon-\epsilon_0)=k_1(\theta-\theta_1)^2. \qquad (14)$$

Now dj the flux of β-particles for small deviations of θ away from θ_1 will be proportional to the zone width $d\theta$ inside of which they are emitted. Differentiating Eq. (14) gives

$$d\theta=\tfrac{1}{2}k_1(\epsilon-\epsilon_0)^{-\frac{1}{2}}d\epsilon \qquad (15)$$

which proves the asserted inverse half power dependence of β-particle intensity j on $\epsilon-\epsilon_0$. The base width A_1 in Fig. 7 over which this distribution extends is fixed by the finite range of angle $2\Delta\theta$ for which the angular aperture stop is set. From Eq. (12) it is easy to show that to first-order this base width is given by,

$$A_1=(\Delta\epsilon)_1=[\epsilon(\epsilon+2)/(\epsilon+1)]B(\theta_1)\tfrac{1}{2}\sin^2\theta_1(\Delta\theta)^2. \qquad (16)$$

The origin of the profile *II* of Fig. 7 is obvious. If we consider β-rays emanating from a fixed point in the source, say the center, at a fixed sharply defined angle θ_1, then a ring focus slit of narrow but finite width can be considered divided into adjacent infinitesimal elementary rings by each of which slightly different β-ray energies are selected. Energy and position in the slit are linearly related. Because of the narrowness of the entire slit the β-ray flux per unit width of ring and per unit small energy domain will thus be constant across the slit opening yielding the rectangular characteristic shown. The following formula may be readily derived from Eq. (4) and (5) to give the base width A_2 of the rectangular characteristic in terms of the ring focus slit geometry

$$A_2=(\Delta\epsilon)_2=K^{-1}(\sin\psi_i\sin\theta_1)^{-1}\times(\epsilon+1)^{-1}\epsilon^{\frac{1}{2}}(\epsilon+2)^{\frac{1}{2}}\Delta y_i; \qquad (17)$$

$$=K^{-1}(\psi_i\cos\theta_1)^{-1}(\epsilon+1)^{-1}\epsilon^{\frac{1}{2}}(\epsilon+2)^{\frac{1}{2}}\Delta x_i. \qquad (18)$$

$$K=2(m_0c/He)$$

Δy_i and Δx_i are, respectively, the radial and axial widths of the ring focus slit which in formulas 17 and 18 is assumed to have its outer and inner edges lying on the cone whose vertex is at the source in the way first suggested by Frankel,[11] see Fig. 9.

The finite size of the source disk yields the semi-elliptical line profile shown in Fig. 7 at *III*. This conclusion is arrived at as follows: Consider for the moment the trajectories of β-rays which pass through a single point P in the ring focus slit and which take off from the source under a well defined angle θ. Set up cartesian coordinates ξ and η on the source disk with origin at the center such that the η-axis lies in the axial plane through P and the ξ-axis is perpendicular thereto. If now we displace the source point over the source in the η-direction holding θ and P fixed the energy selected will vary for, small displacements, substantially linearly with the displacement because a radial displacement η at the source with P fixed produces the same result as holding the source point fixed and executing a radial displacement $-\eta$ of the point P. On the other hand small displacements of the source point along the ξ-axis will result in no first-order variation whatever of the energy selected because such displacements are equivalent to holding the source point fixed and displacing P tangentially in the ring focus slit. Thus if the source disk is explored holding the point P and the angle θ constant a contour map of lines of constant selected energy can be plotted on the disk and these will simply be a set of equidistant straight lines parallel to the ξ-axis. If ϵ_0 is the energy selected when the source point is at the center of the disk, then each differential energy domain will have associated with it a flux of β-rays proportional to the area between two of the adjacent parallel contours, that is to say proportional to the length of one of the chords of the circle while the distance of the chord from the center is proportional to $\epsilon-\epsilon_0$ as indicated in Fig. 10. Thus, the flux of β-rays per unit spectral energy interval will obey a law

$$y=k_3[A_3^2-(\epsilon-\epsilon_0)^2]^{\frac{1}{2}} \qquad (19)$$

which is in general the elliptical profile shown at *III* in Fig. 7. The half-width of this profile at the base is A_3 and is given in terms of the radius ρ of the source disk by the formula

$$A_3=(\Delta\epsilon)_3=K^{-1}(\epsilon+1)^{-1}\epsilon^{\frac{1}{2}}(\epsilon+2)^{\frac{1}{2}}\times(\sin\psi_i-\psi_i\cos\psi_i)^{-1}(\sin\theta_1)^{-1}\rho. \qquad (20)$$

A few remarks are now in order regarding the validity of *folding* the three profiles of Fig. 7 to obtain the resultant instrumental line profile. For this to be a strictly valid procedure the shape of each profile must be completely independent of changes in the variables upon which the other two profiles depend. Thus, for example, as we vary ξ and η in our exploration over the surface of the source disk

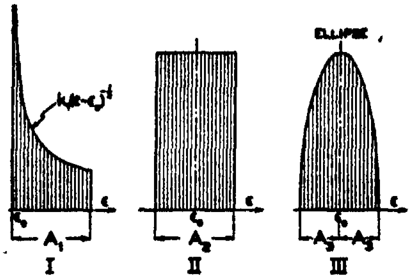

FIG. 7. Illustrating the three spectral profiles introduced by, (I) Finite angular aperture, (II) Finite width of ring focus slit, and (III) Finite size of source disk.

holding the point P in the ring focus slit stationary, is it possible by means of appropriate stops to insure that θ will also remain essentially constant as we have supposed it does in the above derivation of the elliptical profile? The answer is affirmative to a first approximation from the following reasoning. We suppose, to simplify the argument, that the diaphragm opening which selects the range of values, $\theta=\theta_1\pm\Delta\theta$, is placed at such a point along the axis of the instrument that the helical β-ray trajectories shall execute just *one-half of a turn*[17] in going from this diaphragm to the ring focus slit. (For a spectrometer in which $\theta_1=45°$ this situates it at about 0.15 the distance from S to S'.) If this is done then displacements of the source point on the source disk along the η direction (direction of greatest rate of change of energy) *produce tangential displacements* of the trajectory in the θ-selecting slit so that θ remains constant to the first order. Furthermore, displacements of the source point over the source disk along the ξ-direction produce changes in the limiting values of θ which can also be shown to affect the value of the energy only to the second order. This arises from the fact that the maximum displacement ρ over the source disk turns out to be small in comparison to the width of the θ-selecting slit for an instrument of reasonably high resolving power such as $\Delta\epsilon/\epsilon=1/1000$. Thus, we are reassured that the instrument affords a means essentially equivalent to holding ρ and the point P fixed while varying ξ and η over the source disk. The other two cases are much more easily perceived and need hardly be discussed beyond a mere statement of each. They are: Hold θ and the source point ξ, η fixed while varying the point P in the ring focus slit. Hold P and the source point ξ, η, fixed while varying θ.

We must now decide what width parameter (of the folded resultant of profiles *I*, *II*, *III*) to choose as a measure of the instrumental resolving power. If we choose *the base width* W_B of the resultant line for this measure, this will be given very simply by summing the base widths of the components, i.e., $W_B=A_1+A_2+A_3$. Now since the counting rate is proportional to the product $A_1^{\frac{1}{2}}A_2A_3^2$, if we wish to maximize this rate while holding $W_B=A_1+A_2+A_3$ at some specified constant value it is a simple matter to show that we must make $A_1=W_B/7$, $A_2=2W_B/7$ and $A_3=4W_B/7$. To the writer, W_B does not seem to be a satisfactory measure of resolving power however. It is too conservative a choice. A much better measure is the *width at half-maximum height* which we shall designate simply as W. To get this we must actually fold profiles *I*, *II*, and *III* together.

It is a well-known fact that the operation of folding several functions together gives a resultant whose shape is independent of the *order* in which the folding operations were performed. Let us fold profiles *I* and *II* together first. We shall call the half-maximum width of the resultant, W_{12}. Because of the discontinuous nature of the functions it is necessary to distinguish two cases corresponding, respectively, to $A_1<A_2$ and $A_2<A_1$. Perhaps the easiest way to obtain the fold is to decompose profile *II* into two step functions, one positive the other negative, with a displacement A_2 between the discontinuities. The fold of each step function into the inverse half-power curve then gives a parabola with horizontal axis. By such reasoning we obtain the results shown in Fig. 11. The case $A_2<A_1$ breaks into two sub-cases according to whether $A_2<(16/25)A_1$ or $(16/25)A_1<A_2<A_1$. For the latter sub-case the half-maximum width becomes $W_{12}=A_2+A_1-(A_2A_1)^{\frac{1}{2}}$. This then is the sub-case within which the half-maximum width makes the transition from its lower boundary value A_2 to its upper boundary value $21A_2/16$. The important thing to notice about this bizarre behavior of the half-maximum width W_{12} is that it remains within the very narrow range, $A_2<W_{12}<21A_2/16$, *both upper and lower bounds of which are independent of* A_1 *no matter how large* A_1 *may become.* Since the counting rate is proportional to $A_1^{\frac{1}{2}}$ one might at first be tempted, by greatly increasing the half aperture angle $\Delta\theta$, to make A_1 very large indeed since it will not result in any increase in the half maximum width W_{12}. This however would be unwise because such an increase in A_1 merely *adds intensity by lengthening the tail* of the line to the

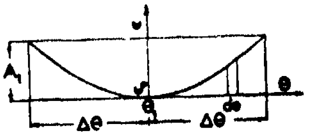

FIG. 8. Dependence of $\epsilon-\epsilon_0$ on $\theta-\theta_1$ from which profile *I* is derived.

---

[17] One-half turn of the helical trajectory corresponds to one-quarter turn round the principal axis of the instrument since the latter is on the circumference, not on the axis of the helix. This choice of position for the θ-selecting slit simplifies the discussion but is not to be regarded as imperative. The point where the two extreme traces of the pencil are radially farthest apart might be an even better place to locate it.

right (Fig. 11). That part of the line which is useful in resolving it from other lines is the core or essentially the part inside the two half-maximum points and as A_1 increases (A_2 constant) there is no gain in the intensity associated with this core beyond the point $A_1=A_2$. Increasing A_1 beyond the value A_2 therefore merely adds to the background distortion in an objectionable way without usefully increasing the intensity of the core of the line. On the other hand as A_1 is decreased below A_2 the intensity associated with the core of the line diminishes. We conclude therefore that the optimum is probably achieved if $A_1=A_2$ in which case the line assumes the simple form shown in the second diagram from the top of Fig. 11. It is this profile then which we shall fold with the elliptical profile *III* of Fig. 7.[18]

Four values of the ratio A_3/W_{12} have been selected for plotting namely, $A_3/W_{12}=0.5$, 0.75, 1.00, 1.25. In each case the folded profile has been plotted and W the width at half-maximum has been determined in terms of $W_{12}=A_1=A_2$. If we think of the half maximum width W as held constant we can thus express the three width parameters A_1, A_2, A_3, of Fig. 7 as multiples of W for the case of each of the four ratios A_3/W_{12} chosen. Now the total counting rate will be proportional to the product $A_1^{\frac{1}{2}}A_2A_3^2$ as we have already stated so that it is possible to compute a number which will be proportional to the total counting rate for constant W as a function of various ratios A_3/W_{12}. Table III shows the data with which this has been done.

In Fig. 12 we show the numbers (proportional to counting rate) in the last column of Table III plotted as a function of A_3/W_{12}. It seems clear that the optimum value occurs somewhere very close to $A_3/W_{12}=1$ or in other words the condition $A_1=A_2=A_3$ in all probability comes very close to giving the greatest counting rate for the least resultant width at half maximum. In Fig. 13 we show the resultant optimum line profile to be expected under this condition. Note that this profile has a width at half maximum which is 1.62 times each of the three equal parameters A_1, A_2, or A_3. Only a slight vestige of the asymmetry which results from the influence of the profile *I* can be detected when we examine Fig. 13. The width parameter $A_1=A_2=A_3$ is shown to scale in the figure.

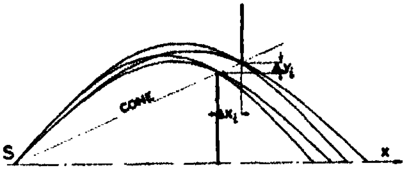

FIG. 9. Showing geometry of ring focus slit with its edges lying on a conical surface with vertex at *S*.

The author makes no claim that the above analysis for the optimum relationship between the parameters A_1, A_2, and A_3 is highly rigorous. He is well aware that the procedure of first choosing the optimum condition $A_1=A_2$ using the width W_{12} as a criterion *before* folding *I* and *II* into *III* is strictly open to criticism. The condition $A_1=A_2=A_3$ is not here laid down as giving *accurately* the greatest intensity for a specified resolving power. It seems likely however that it defines the optimum condition so closely that no significant gain in intensity would be effected by modifying it.

The radius ρ of the source disk should obviously then be chosen so that the loss of energy resolution A_3 from this cause alone shall be equal to A_1 the loss of energy resolution from the solid angle $d\phi$ (or from the range $\Delta\theta$) given in Eq. (16) also the width of the ring focus slit should be chosen to make $A_2=A_1$ using Eqs. (17) and (18) to proportion the radial and axial spread of the slit. The condition $A_3=A_1$ gives the following formula for the radius of the source disk

$$\rho=K\epsilon^{\frac{1}{2}}(\epsilon+2)^{\frac{1}{2}}B(\theta_1)(\sin\theta_1)$$
$$\times(\sin\psi_i-\psi_i\cos\psi_i)(d\phi)^2;\quad K=\frac{2m_0c}{He}. \tag{21}$$

For the optimum design with $\theta_1=45°$ and $\psi_i=2.03$ rad., this gives

$$\rho=36R(d\phi)^2 \tag{22}$$

in which

$$R=\sqrt{2}(m_0c/He)[(\epsilon+1)^2-1]^{\frac{1}{2}}. \tag{23}$$

R is the maximum radial distance of the median traces from the axis of the instrument. We shall take it as a convenient geometrical unit in terms of which all the other linear dimensions are to be expressed.

The condition $A_2=A_1$ leads to the following formulas for the dimensions of the ring focus slit,

$$\Delta y_i=K\epsilon^{\frac{1}{2}}(\epsilon+2)^{\frac{1}{2}}\sin\psi_i\sin\theta_1B(\theta_1)(d\phi)^2, \tag{24}$$

$$\Delta x_i=K\epsilon^{\frac{1}{2}}(\epsilon+2)^{\frac{1}{2}}\psi_i\cos\theta_1B(\theta_1)(d\phi)^2. \tag{25}$$

FIG. 10. Iso-energy bands and coordinates ξ, η on the source disk. To illustrate derivation of profile *III*.

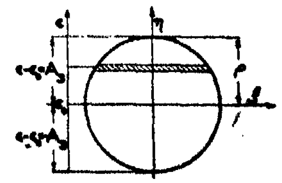

---

[18] If the case in point is one in which the finite radius of the source disk plays no part in giving an increased counting rate (γ-ray sources for example) so that the loss of resolving power from cause III can be kept small in comparison to that from causes I and II without any sacrifice of counting rate, then the discussion from this point on concerning the effect of folding in the elliptical profile *III* should be ignored and the final profile will be essentially the second one from the top in Fig. 11 with the width at half maximum height $W=W_{12}=A_1=A_2$.

For the optimum design with $\theta_1=45°$ and $\psi_i=2.03$ radians these become

$$\Delta y_i=18R(d\phi)^2, \qquad (26)$$

$$\Delta x_i=41R(d\phi)^2. \qquad (27)$$

Clearly, for a given energy ϵ, Eq. (23) shows that we may take R as large as we please provided we can make H small in inverse proportion. There is an advantage in large dimensions because by Eq. (22) ρ is proportional to R and hence the utilizable area and strength of source increases as ρ^2 and R^2. The practical limit to this occurs either when the cost becomes prohibitive or when H must be made so small that uncontrollable outside magnetic influences disturb the field distribution intolerably.

Figure 14 is a schematic axial section through the instrument showing its geometry and the nomenclature of its principal dimensions. We append below a list of the principal useful formulae and relations for the optimum case of $\theta_1=45°$, the nomenclature being that indicated in Fig. 14. Attention is called to the θ-selecting stop that is required to define the two extreme traces on either side of the median trace ($\theta_1=45°$). This is placed one-half turn of the helical β-ray trajectory nearer to the source than the ring focus slit.[17] Other stops which do not define the beam but serve merely to reduce scattering will doubtless be found advantageous. A heavy lead core to protect the counter from gamma rays is also commonly provided. These are omitted however in Fig. 14.

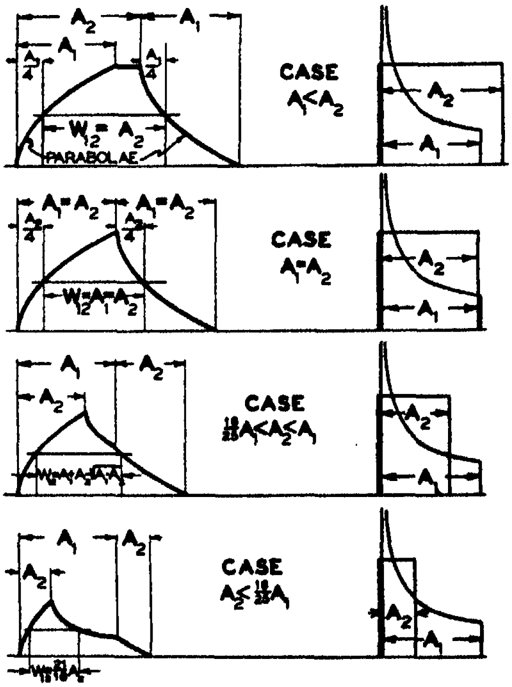

FIG. 11. Illustrating the various cases which arise when profiles I and II of Fig. 7 are folded together. In the above figure A_2 has been progressively diminished holding A_1 constant. The component profiles are shown in each case on the right, the folded resultant on the left. Note that the half-maximum width W_{12} of the folded resultant never becomes less than A_2 or greater than $(21/16)A_2$.

TABLE III. Case of $W_{12}=A_1=A_2$.

A_3/W_{12}	W	$A_1=A_2$	A_3	$A_1^{\frac{1}{2}}A_2A_3^{\frac{1}{2}}$
0	1.00 W_{12}	1.00 W	0	0
0.50	1.19 W_{12}	0.84 W	0.420 W	0.135
0.75	1.40 W_{12}	0.714 W	0.535 W	0.173
1.00	1.62 W_{12}	0.617 W	0.617 W	0.185
1.25	2.00 W_{12}	0.500 W	0.625 W	0.138
∞	A_3	0	1.000 W	0

Resume of Formulas for Optimum β-Spectrometer Design ($\theta_1=45°$)

Fundamental Radius

$$R=\tfrac{1}{2}\sqrt{2}Q_1=\sqrt{2}(m_0c/He)[(\epsilon+1)^2-1]^{\frac{1}{2}}. \qquad (28)$$

Luminosity or Utilizable Fraction of all β-emissions

$$d\phi=\tfrac{1}{2}\sin\theta_1 d\theta_1. \qquad (29)$$

Energy Uncertainty Parameter A_1 Caused by Angular Aperture

$$A_1=(\Delta\epsilon)_1=\epsilon(\epsilon+2)(\epsilon+1)^{-1}20(d\phi)^2. \qquad (30)$$

Radius of Source Disk (to make $A_3=A_1$)

$$\rho=40R(d\phi)^2. \qquad (31)$$

Radial Width of Ring Focus Slit Opening (to make $A_2=A_1$)

$$\Delta y_i=18R(d\phi)^2. \qquad (32)$$

Axial Width of Ring Focus Slit Opening (to make $A_2=A_1$)

$$\Delta x_i=41R(d\phi)^2. \qquad (33)$$

Mean Radius of Ring Focus Slit

$$r_s=0.896R. \qquad (34)$$

Mean Axial Distance of Ring Focus Slit from Source

$$S=2.03R. \qquad (35)$$

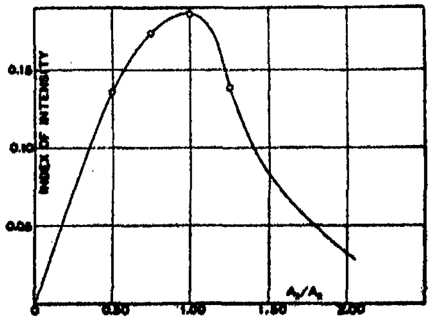

FIG. 12. Curve indicating the optimum ratio of A_3/A_1 to yield maximum intensity for a specified breadth W (at half maximum) of the resultant of the three profiles I, II, and III.

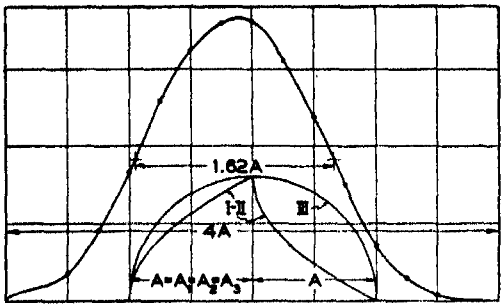

FIG. 13. Resultant instrumental line profile for the optimum case, $A_1=A_2=A_3$. The half-maximum width, W, turns out to be $1.62A$ where $A=A_1=A_2=A_3$. The base width is $4A$. The component profiles *I–II* (fold of *I* into *II*) and *III* are shown. Profile *III* may be thought of as the one which moves across profile *I–II* to give the resultant shown. A vestige of the asymmetry of *I–II* can be seen in the resultant.

Mean Axial Distance of Counter from Source

$$L=\pi R. \tag{36}$$

Linear Extension of β-Ray Beam on the Axis at the Counter

$$C=2\pi\sqrt{2}Rd\phi. \tag{37}$$

Axial Distance of θ-Selecting Slit from Source

$$A_\theta=0.459R. \tag{38}$$

Mean Radius of θ-Selecting Slit

$$r_\theta=0.444R, \tag{39}$$

Half-Radial Width of θ-Selecting Slit

$$\Delta r_\theta=0.854Rd\phi=2.42Rd\phi. \tag{40}$$

In a magnetic β-ray spectrometer of the type here described if the resolving power is very high the geometrical axis defined by the source and stops must be very accurately aligned parallel with the magnetic field, otherwise the ray traces will not register correctly and simultaneously all around the annular defining slit. For this reason it will be wise to provide for a slight amount of angular adjustment so that the orientation of the vacuum chamber with its source holder, stops and counter can be slightly varied relative to the solenoid which furnishes the magnetic field.

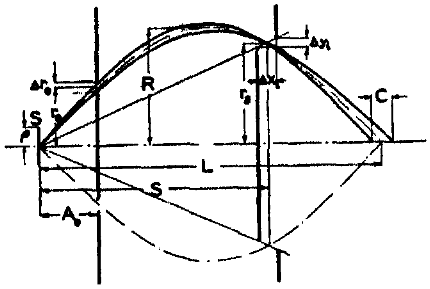

FIG. 14. Schematic axial section through β-ray spectrometer giving nomenclature of optimum dimensions.

It appears from the present analysis that by adhering to the optimum proportions as indicated above it should be possible to design a β-ray spectrometer with a direct β-ray source in which the utilized fraction of the total sphere around the source is $d\phi=0.01$ and in which for the three cases, $\epsilon\ll 1$, $\epsilon=1$, $\epsilon\gg 1$, the resolution is given respectively by $\Delta\epsilon/\epsilon=0.0065$, 0.0049, 0.0032 wherein $\Delta\epsilon$ is the full instrumental line width at half maximum in ϵ-energy units and ϵ is the energy at which the line occurs expressed as a fraction of the electron rest energy. The radius of the source disk should be for such a case $\rho=0.004R$ where R is the fundamental radius of the instrument (or the maximum radial distance from the central axis attained by the median ray of the pencil of electron trajectories). If the source disk can be made indefinitely small without loss of intensity (case of γ-ray source with converter) then $\Delta\epsilon/\epsilon=0.004$, 0.003, 0.002 for the above three cases.

The author wishes to acknowledge with gratitude very helpful criticisms and discussions of this paper by E. R. Cohen and by Professor R. F. Christy.

THE REVIEW OF SCIENTIFIC INSTRUMENTS VOLUME 20, NUMBER 3 MARCH, 1949

Tissue Stimulators Utilizing Radiofrequency Coupling*

OTTO H. SCHMITT AND DONALD R. DUBBERT
Departments of Zoology and Physics, University of Minnesota, Minneapolis, Minnesota

(Received October 18, 1948)

Voltages of arbitrary wave forms, such as those employed for stimulating biological tissues, are normally obtained from "grounded" signal generators. Isolation of such signals from ground can be accomplished by utilizing radiofrequency transmission of energy. The signal generator voltage serves as the source of plate power for a midget radiofrequency oscillator which converts the signal to amplitude-modulated carrier energy. This radiofrequency energy is then transmitted across a small air gap to a receiving circuit where it is demodulated and filtered. The voltage thus recovered is a faithful reproduction of the original signal but is isolated from the input circuit as well as from ground. One model of this radiofrequency link which was developed for nerve stimulation and which has performed well in the laboratory is described in detail.

DURING recent years many excellent designs for electronic tissue stimulators have appeared in the literature of biophysics. As the need for special forms of stimulus has arisen, e.g., step wave, square wave, pulse, double pulse, modulated tetanus, etc., electronic circuits have been evolved in various laboratories which adequately meet each of these special requirements, and it is economical, wherever possible, to utilize these developments instead of devising new but essentially similar apparatus.

A shortcoming of all usual stimulators is the electrical return path to ground, either conductive or capacitive, which they invariably exhibit. This return path greatly reduces the flexibility with which multiple stimuli can be combined and practically requires the use of a differential amplifier except in the simple cases where miniature transformers can be tolerated. Even the best of such transformers have considerable interwinding capacitance, and none can deliver unidirectional wave forms.

By utilizing a radiofrequency link as described in a preliminary note,[1] it is possible to use the pulse, step wave, d.c., or other stimulating wave form or combination wave form as obtained from conventional "grounded" stimulator systems and still retain electrical isolation. The stimulus itself becomes the source of plate power for a midget radiofrequency oscillator, and this radio power is transmitted across a small air gap to be received and demodulated by a tiny coil and varistor type rectifier system. The output voltage now faithfully reflects the wave form of the input but is electrically isolated from it and from ground.

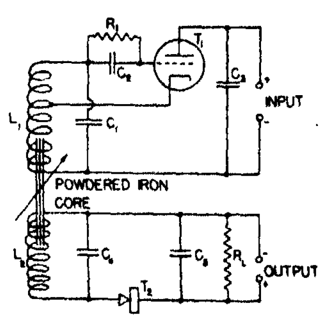

FIG. 1. Basic stimulator circuit. C_1, C_4, 20 μμf; C_2, C_5, 100 μμf; C_3, 25 μμf; R_1, 2200 ohms; R_L, 22,000 ohms; T_1, 6J6; T_2, 1N34; L_1, L_2, 17 turns No. 24 heavy Formvar wire; cathode tap on L_1 4 turns from grid end of coil. Tubular ceramic condensers and ½-watt resistors are used throughout.

Voltage generated in this manner can be treated as though it originated from a completely isolated power source, and several different stimuli similarly generated can be mixed at will or applied to different points on the tissue without reference to grounds. Since the radiofrequency link actually derives its plate power from the stimulus source, it can be used with any standard stimulator.

While there is nothing intrinsically difficult in the design of a unit embodying these principles, it will be found that considerable engineering design effort is required to develop a unit which is physically compact, electrically stable, efficient, and linear in output. One form of this stimulator has been standardized in this laboratory and for some months has given dependable satisfactory service. This stimulator together with its performance characteristics will be described in some detail so that it can be duplicated conveniently. It is hoped that this design will serve as a basis for further development.

The essential circuit of the stimulator is shown in Fig. 1. A small tank circuit together with a 6J6 miniature type tube with both triode sections connected in parallel constitute a Hartley grounded-plate oscillator. An inductively coupled tuned secondary or receiving circuit terminates in a 1N34 germanium crystal diode and filter. The oscillator

---

* This work was supported in part by grants from the Graduate School of the University of Minnesota and from the Rockefeller Foundation.

[1] O. H. Schmitt, "A radiofrequency coupled tissue stimulator," Science 107, 432 (1948).

is plate modulated, the necessary plate power being furnished by the stimulating voltage generator. The only additional source of power required is 6.3 volts at 0.45 ampere for the filament of the 6J6. This power may be d.c. or a.c. and may be grounded or ungrounded. Condensers C_1 and C_4 constitute the primary and secondary tank capacitances, respectively. Approximate tuning of the oscillator and receiver circuits depends upon the choice of these capacitances while the fine tuning is accomplished by adjusting a powdered iron core which can be moved axially inside the coil form by means of a threaded shaft. Since increased inductance in one coil is accompanied by decreased inductance in the other, adjustment for double-tuned resonance is easily found.

The grid leak resistor R_1 is adjusted for proper bias to give maximum efficiency consistent with stability of operation. The grid condenser should not be so large as to encourage intermittent oscillations nor so small as to decrease oscillator efficiency greatly. In addition, the reactance of this condenser at the highest frequency component of the modulating voltage should be at least twice the grid leak resistance in order to preserve linearity of modulation. The by-pass condenser at the input to the oscillator must have low reactance at the oscillator operating frequency but must offer a high impedance to the modulating voltage. If a shielded input cable is used, its distributed capacitance will usually suffice for this capacitance.

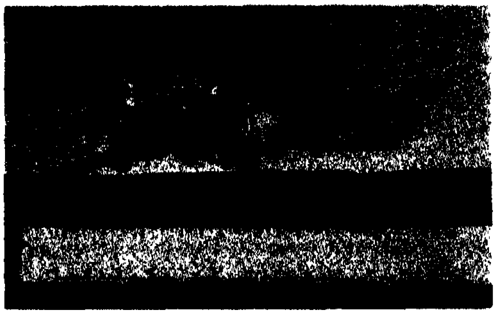

FIG. 2. Side view of complete stimulator.

The resistive load across the oscillator coil for maximum efficiency is easily determined experimentally and the receiver circuit is then designed to reflect this load into the oscillator circuit. It has been shown both experimentally and analytically that the equivalent input impedance to the rectifier filter circuit is approximately one-half the load resistance R_L and is essentially resistive. Thus the turns ratio of the primary to the secondary coil windings can be determined once the load resistance is established or the reverse.

Analysis of the rectifier and filter circuit using actual experimental characteristic curves for the 1N34 germanium diode instead of assuming ideal characteristics shows that a 20 percent loss of power in the crystal is inevitable. The maximum output voltage which the stimulator can produce with reasonable linearity is determined by the peak inverse voltage rating of the crystal diode rectifier. Theoretically, the rectifier should be able to produce an output voltage about one-half the inverse peak rating of the diode. With the 1N34 this rating is 60 volts and, consequently, 30 volts of output should be available. Usually at least 30 volts output can be obtained and with selected 1N34 units as much as 40 volts can be realized linearly. If very high voltages are required, several 1N34 units can be used in series, raising the output to 60, 90, or more volts and special rectifiers such as the 1N38 and 1N39 with higher inverse ratings up to 200 volts are obtainable.

FIG. 3. View of stimulator showing receiver section.

The filter section of the receiver circuit is designed so that its time constant RC is large compared with the time for one carrier oscillation but small compared with the period of the highest important frequency component in the stimulating voltage. Consequently, the ratio of carrier frequency to highest signal frequency should be at least 100. For normal requirements, carrier frequencies between one and twenty megacycles per second prove satisfactory. Design is simplest in the vicinity of five megacycles per second.

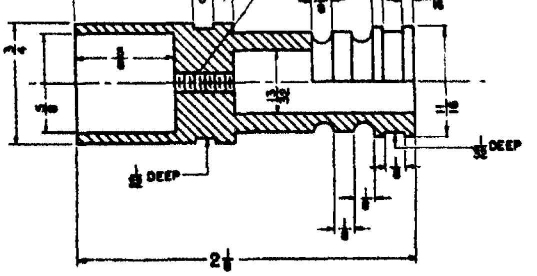

FIG. 4. Dimensional sketch of plastic frame for stimulator.

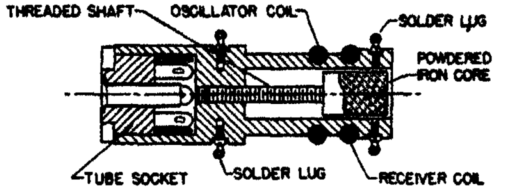

FIG. 5. Section view of plastic frame showing general placement of components.

Figures 2 and 3 show two detailed views of one completed form of the stimulator. The stimulator proper takes the rough form of a cylinder about 1″ in diameter and 4″ over-all including the tube. It is often convenient to mount the unit in a small Lucite stand as shown. It may be detached from this stand in a moment by loosening a single setscrew. As the pictures indicate, the unit is physically small and is thus easily installed in existing equipment close to the tissue to be stimulated. All the components including the miniature tube socket are mounted on a cylindrical frame machined from 1422 Textolite. A dimensional sketch of this frame is given in Fig. 4, and the general placement of components is shown in Fig. 5. The oscillator and secondary coils each consist of 17 turns of No. 24 heavy Formvar wire wound in grooves on the frame. The coils are approximately circular in section. The inductance of each coil is 6 microhenries with a Q of about 65. The presence of the powdered iron core increases this inductance by a factor of about 2 thus giving an adequate tuning range without changing the Q appreciably. The cathode tap of the oscillator coil is 4 turns from the grid end of the coil. The values of the remaining components are included in Fig. 1. Maximum output and best efficiency are achieved when the two coils are tuned for operation at around 7.5 megacycles per second. Tiny solder lugs fastened to the plastic frame by 0–80 machine screws aid in mounting the individual components and a coat of polystyrene based coil dope protects the coils and holds them rigidly in place.

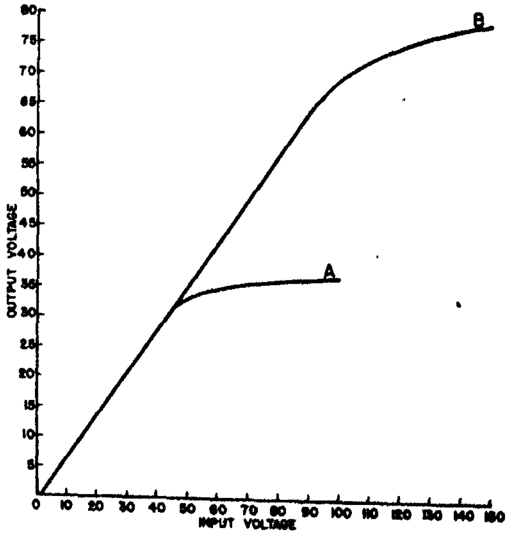

FIG. 6. Stimulator transfer characteristics. Curve *A* shows output *versus* input voltage when the receiving circuit utilizes a single 1N34 germanium crystal diode rectifier. Curve *B* shows the transfer characteristic using two 1N34 units connected in series. In each case the load resistance is 22,000 ohms.

Linearity of the stimulator response is shown in Fig. 6 where output voltage is plotted against input voltage. The rectifiers used in the receiving circuit for these cases consisted either of a single 1N34 crystal diode or of two diodes connected in series. These crystals were not specially chosen to give best results but represent better than average diodes of this type. As one might expect, linearity with a single crystal extends to about 30 volts and with two crystals to over 60 volts. In each case, however, the output in the linear region is roughly ⅔ of the input voltage when working into a load of 22,000 ohms. It will be noted that an initial signal of about 1.3 volts is required to set the oscillator into operation. Where extreme linearity is required even to very small output levels, a d.c. bias of this value may inserted in the input circuit.

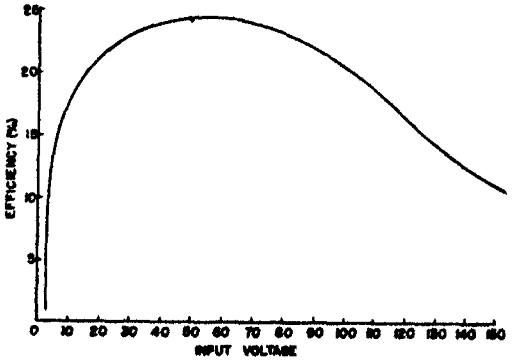

FIG. 7. Over-all stimulator efficiency curve (operating conditions corresponding to curve *B*, Fig. 6).

Figure 7 illustrates a typical stimulator efficiency curve. The oscillator itself has an efficiency of approximately 50 percent. Efficiency of the stimulator without the rectifier and filter circuits is between 30 percent and 40 percent and, as the figure shows, the over-all efficiency of operation has a maximum value of approximately 25 percent remaining fairly constant over the useful operating range.

Measurements with a sensitive capacitometer indicate a capacitance from output to input of approximately 5 micromicrofarads. If shielding is used to prevent direct transfer of residual radiofrequency signal to the tissue circuit, this capacitance may be slightly greater. Ordinary tissue amplifiers have little response at radiofrequencies and it is necessary only to hold down r-f pick-up to a level where the amplifier is not driven beyond its linear characteristic.

Although the r-f coupled stimulator was specifically designed to provide voltages isolated from ground to be used in connection with single nerve fiber studies, there appear to be several other applications where the basic principle is equally useful. Wherever a control or signal voltage appearing at some d.c. voltage level must be applied to circuits at a different voltage level, it is a simple and compact device for providing the transition.

THE REVIEW OF SCIENTIFIC INSTRUMENTS VOLUME 20, NUMBER 3 MARCH, 1949

Absorption Corrections in X-Ray Studies of Preferred Orientation*

R. Smoluchowski and R. W. Turner
Carnegie Institute of Technology, Pittsburgh, Pennsylvania

(Received October 18, 1948)

A general formula is derived for the evaluation of correction factors in the study of preferred orientations in flat specimens. These factors depend on orientation of the sample, angles of diffraction, thickness of specimen, etc. In practical applications a graphical presentation of the absorption correction proves to be particularly useful.

MOST of the qualitative investigations of preferred orientation in flat specimens are limited to comparison of x-ray patterns obtained with the direction of the x-ray beam perpendicular to the specimen. The various factors affecting the intensity of the x-ray diffraction in that case are well known and easy to take into account.

For accurate investigations, however, patterns obtained with the x-ray beam inclined to the surface of the specimen are necessary, and the correction for absorption becomes rather complicated. Recently formulas for this corrective factor applicable to pole figure work with a Geiger counter x-ray spectrometer have been published.[1] They are, however, not general enough for the standard photographic method, and thus it seemed advisable to report on formulas and graphs used for some time in our laboratory in the study of preferred orientation.

Let us consider a flat specimen as shown in Fig. 1, which also illustrates the quantities used: t—thickness of sample; α—angle between beam and normal to surface of sample; $c=(t/\cos\alpha)$—sample thickness in the direction of the beam; x—distance along c traversed by beam before a given individual reflection occurs; β—angle around the reflection ring on the film; the point at which $\beta=0°$ is determined by the intersection of the film and the plane containing both the x-ray beam and the surface normal of the sample.

For a reflection which strikes the film at β, the thickness of sample traversed after reflection is given by

$$[(c-x)\cos\alpha]/A$$

where $A=\cos\alpha\cos 2\theta+\sin\alpha\sin 2\theta\cos\beta$. Hence, the intensity as the beam reflected between x and $x+dx$

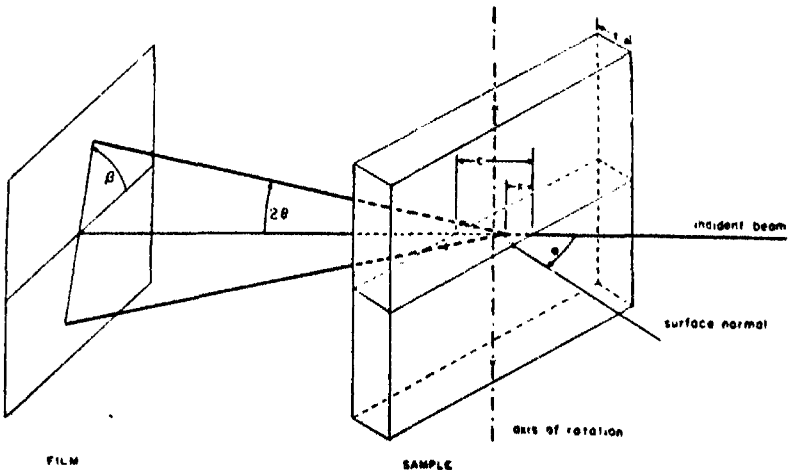

FIG. 1. Diffraction of x-rays in a sample inclined to the beam.

---

* This work was supported by the Atomic Energy Commission.

[1] Decker, Asp, and Harker, J. App. Phys. 19, 388 (1948).

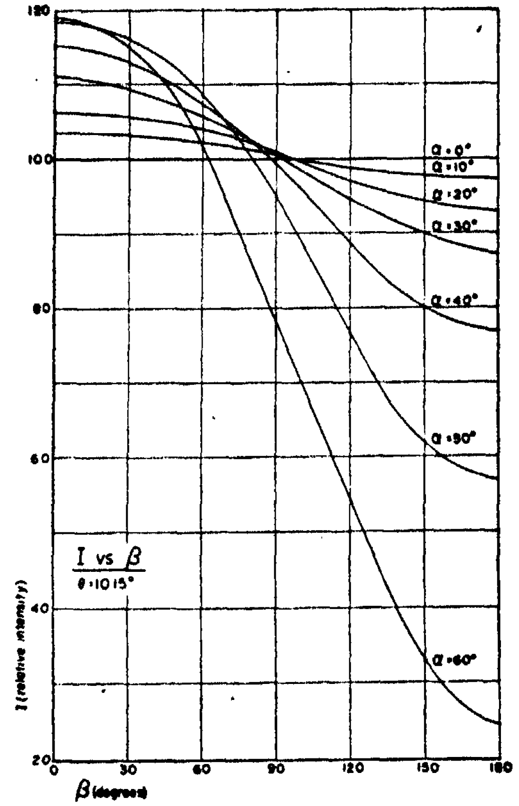

FIG. 2. Relative intensity around reflection ring. For various sample positions. (50% Fe—50% Co alloy. 0.025 mm thick, (110) reflection, Mo$-K\alpha$ radiation.)

leaves the sample is

$$dI = I_0 e^{-\mu x} \exp\{-\mu[(c-x)\cos\alpha/A]\}dx. \quad (1)$$

(All constant factors, such as the structure factor for the reflection, which will be cancelled by taking the ratio of two intensities about one reflection ring, have been dropped.) The total intensity of the given reflection is found by integrating (1) from $x=0$ to $x=c$, and the final result is

$$I = (A/A - \cos\alpha)[e^{-\mu t/\cos\alpha} - e^{-\mu t/A}]. \quad (2)$$

It is most convenient to express this as a graph of I *vs.* β for each of a series of values of α, θ being held constant. For simplicity and accuracy in making such plots, it is best to transform Eq. (2) by converting the exponentials to hyperbolic functions. By this method, the equation can be reduced to the form

$$I = Ke^{-K(1+m)}\left[\frac{\sinh K(1-m)}{K(1-m)}\right] \quad (3)$$

where

$$K = (\mu t/2\cos\alpha), \quad m = 1/(\cos 2\theta + \sin 2\theta \tan\alpha \cos\beta).$$

Figure 2 shows a typical plot of Eq. (3) obtained for the (110) reflections of an alloy of 50 percent Fe and 50 percent Co, in a sample 0.001-inch thick. The values of I have been adjusted to a value of 100 for $\alpha = 0°$. Plots of this type were made in this laboratory and proved to be of great value in quantitative evaluation of photographic measurements. In certain cases formula (3) can be greatly simplified. If $|K(1-m)| \leqslant 0.25$ then the expression $I = Ke^{-K(1+m)}$ represents the correct intensity to within one percent, and if $|K(1-m)| \leqslant 0.5$, to within less than five percent.

It should be emphasized that these plots give only relative intensities; any one point in a reflection ring may be selected as unity, with other points expressed as fractions or multiples of that. One may then correct observed intensities accordingly and determine the true relative intensities reflected in the various directions.

The corrective factor derived by Decker, Asp, and Harker is a particular case of our formula (2) for $\beta = 0$ and with zero value of α taken at the point at which $\alpha = \theta$.

The authors wish to thank Mr. R. Louis Bright for his help in evaluating the formulas, and Mr. Albert Kimmel for his careful work in plotting the graphs and figures.

THE REVIEW OF SCIENTIFIC INSTRUMENTS VOLUME 20, NUMBER 3 MARCH, 1949

A Rapid Infra-Red Gas Analyzer

RICHARD C. FOWLER
Department of Physiology and Vital Economics, School of Medicine and Dentistry,
University of Rochester, Rochester, New York

(Received October 28, 1948)

A brief description of an apparatus, together with a few representative curves, is presented, suitable for measuring the composition of very small amounts of any gas having at least one near infra-red absorption band or, if measured in the presence of other gases, at least one unique absorption band. With the bolometers used, 90 percent full scale response is obtained in 0.15 seconds on a 0.5 cc sample, permitting a 0.4 cm optical path and a very nearly linear response over the range usually found in physiological concentrations and anesthesia.

IN connection with many problems in physiology, cardio-respiratory disease, anesthesia, etc., an instantaneous means for analyzing quantitatively and continuously the respired gas during the respiratory cycle is desirable. Various ingenious methods have been devised to accomplish this, each with a particular limitation. Some of these schemes, together with their outstanding features follow:

(a) The classical fractional sampling of a single expired volume of gas[1,2] lacks time or volume-composition "resolution," involves laborious chemical analysis and is not instantaneous.

(b) The thermal conductivity method again is not instantaneous, with a minimum time lag of 15 to 30 seconds,[3–6] but is commercially available in reliable form.

(c) The acoustic methods[7] are now largely in the developmental stage. They are operable for some gases including oxygen, but have not proven satisfactory for carbon dioxide and some other gases. Since some interfering gases must be removed, and because of the electrical circuit used, they will have an appreciable delay.

(d) The mass spectrometers[8,9] have a small delay, largely in the sampling device, are quite cumbersome and expensive, but have the particular advantage of multiple simultaneous analyses. There is still some question of accuracy, however, as a result of the relative velocity of gases of different characteristics.

(e) The "spectrophotometric" method, developed by Dr. Lilly[10,11] involving the continuous sampling, subsequent ionization and photoelectric measurement is relatively expensive and cumbersome and

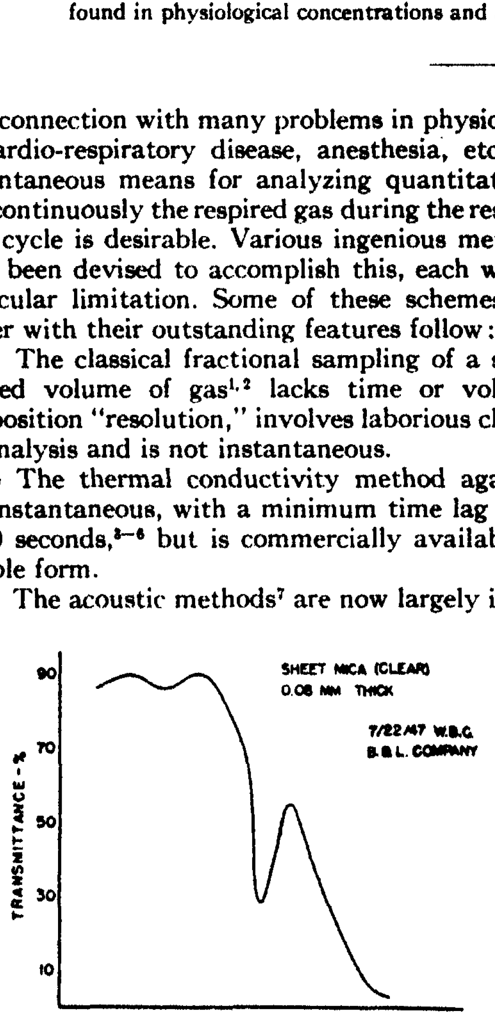

FIG. 1.

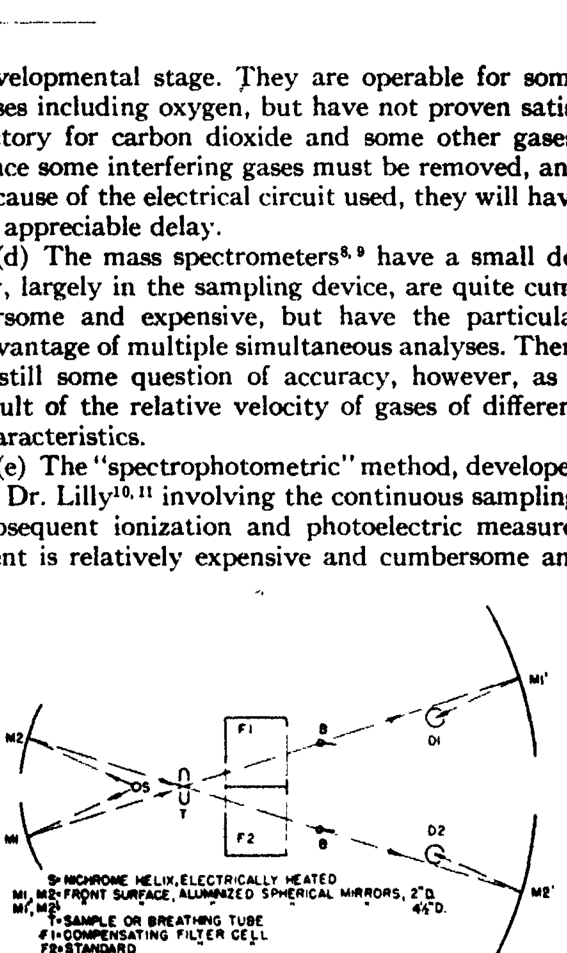
M1'
M2
F1
B
D1
OS
T
M1
F2
B
D2
M2'
S-NICHROME HELIX, ELECTRICALLY HEATED
M1, M2-FRONT SURFACE, ALUMINIZED SPHERICAL MIRRORS, 2" D.
M1', M2' " " " " " 4½" D.
T-SAMPLE OR BREATHING TUBE
F1-COMPENSATING FILTER CELL
F2-STANDARD " "
B-FLAGS FOR OPTICAL BALANCE
D1, D2-WESTERN ELECTRIC "BETT" ELEMENT BOLOMETER BRIDGE CONNECTED.

FIG. 2. Infra-red analyzer.

---

[1] J. S. Haldane, *Respiration* (new edition) (Yale University Press, New Haven, 1935), pp. 19.

[2] A. L. vonMuralt, *Einfuhrung in die Praktische Physiologie*, (Verlag-Julius Springer, Berlin, 1943).

[3] Gow-Mac Instrument Company, brochure.

[4] Cambridge Instrument Company, list No. 144.

[5] H. A. Daynes, *Gas Analysis by Measurement of Thermal Conductivity*, (Cambridge University Press, London, 1933)..

[6] R. H. Munch, "The analysis of gases by thermal conductivity methods," Ind. and Eng. Chem., Ind. Ed. 37, 85 (Aug. 1945).

[7] E. Woods and H. Helmholtz, Mayo Clinic, Demonstration, Rochester, Minnesota, Sept. 1948.

[8] A. Hemingway, A. O. Nier, and R. Varco, University of Minnesota, Demonstration, Minneapolis, Minnesota, Sept. 1948.

[9] R. W. Stacy, J. A. Hunter, and F. A. Hitchcock, "A Mass spectrometer for the rapid continuous analysis of respiratory gases," Am. Physiol. Soc., 57th Ann. Meeting, Atlantic City, New Jersey.

[10] J. C. Lilly, NRC–CAM Report No. 299; also: Army Air Forces, Air Materiel Command, Eng. Div., Memorandum report on nitrogen meter, August 30, 1946, Ser. No. TSEAA-660-107.

[11] J. C. Lilly, "Studies on the mixing of gases within the respiratory system with a new type nitrogen meter," Fed. Proc. 15, No. 1 (March 1946).

FIG. 3.

will have a time lag of the same order as the mass spectrograph and many of the same criticisms apply, but it is quite versatile and should be capable of considerable accuracy.

(f) The interferometric method,[12] while reportedly very accurate, requires constant manual adjustment and has a response lag of the order of 25 seconds.

(g) The paramagnetic oxygen analyzer[13,14] has proven to be a highly satisfactory device and is available commercially in a very reliable form[15] but is limited in usefulness and has a time lag of the order of 15 seconds.

(h) The optical gas analyzers, principally infrared,[16] depend on the unique absorption bands of the various gases, and consequently are limited in their usefulness to those having sufficiently strong absorption in a useful range. In addition, their time response is limited to the rate of response of available infra-red detectors. The instruments on the market at present require a considerable volume of sample[17,18,19] resulting in a poor volume-composition "resolution," and are relatively slow. An infrared "acoustic" device has been described, but has not been developed commercially.[20] A new instrument, developed by Phillips Laboratories, seems to have eliminated most of the objectionable features, but is expected to be quite expensive and is not available commercially as yet. British devices utilize a similar method and are available.[21] A further exposition of the problem is adequately covered by Fastie and Pfund[22] and Williams.[23]

An infra-red gas analyzer has been developed in this laboratory which has been found useful for a number of gases of physiological importance, including carbon dioxide, ether, carbon monoxide, acetylene, and others, and no trouble has been encountered with interference including that from water vapor. The principle features which make this instrument useful are: (a) the use of crossed beams from a common source to keep the sample as small as possible and to reduce the effect of variations of source temperature, (b) the use of inert mica windows (wave-length-transmission curve, Fig. 1) which allow the passage of near infra-red energy without hygroscopic or chemical action, and (c) the use of a rapid, sensitive detector made possible by Western Electric's "SETT" element, a "thermistor" bolometer. The use of selective filters may prove useful but have not been found to be essential.

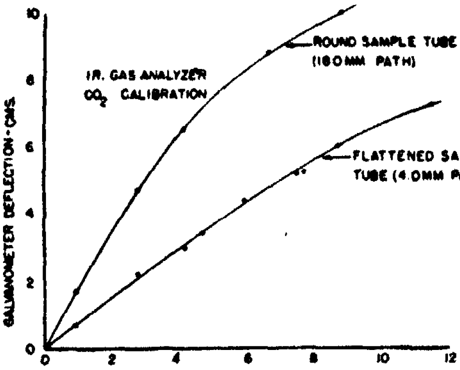

FIG. 4.

The apparatus is shown schematically in Fig. 2, and as built in Fig. 3. The source (S) is a helix of nichrome wire heated electrically (40 watts) and operated at a bright red heat, and the supports and box are water cooled to reduce temperature effects. The two spherical concave front surfaced aluminized or evaporated gold mirrors of 10-cm focal length (M_1, M_2), focus slightly enlarged superimposed images of the source at the center of the sample or breathing tube (T), which, for carbon dioxide, was constricted at this point to give a path length of about 4 mm in order to operate on the straighter first portion of the exponential concentration-absorption curve in the physiological range (0–9 percent). The two beams then continue through the 5.0-cm gas filter cells (F_1, F_2) one of which contains a mixture of all interfering gases in the test sample and the other contains all but the gas to be measured. Since the path through the filter cell is so long, all interfering radiation is filtered out before reaching the detectors. The second pair of mirrors, also of 10-cm focal length, (M_1', M_2'), similar to the first but larger in diameter, refocus a considerably reduced image of the source on the sensitive area (0.2×2.0 mm) of the detectors (D_1, D_2). The size of the source and optical components are so chosen that this reduced image just a little more than covers the active area of the bolometers. The two adjustable opaque flags (B) following the filter cells are essential for balancing the radiant energy in the two beams or spurious deflections will result. The chamber containing the mirrors and bolometers was constructed so that an additional filter gas might be introduced here also.

---

[12] T. Benzinger and C. Kitzinger, "Photographische registrierung interferometrischer gas analysen," AAF Aero Med. Center, Heidelberg, Germany, 1946.

[13] L. Pauling, R. E. Wood, and J. H. Sturdivant, "An instrument for determining the partial pressure of oxygen in a gas," J. Am. Chem. Soc. 68, 795 (1946).

[14] C. A. Dyer, "A paramagnetic oxygen analyzer," Rev. Sci. Inst. 18, 696 (1947).

[15] Arnold O. Beckman Company, Pasadena, California.

[16] E. D. McAlister, "Spectrographic method of measuring carbon dioxide concentration," Phys. Rev. 49, 704 (1936).

[17] Baird Associates, Cambridge, Massachusetts.

[18] Leeds and Northrup Company, Philadelphia, Pennsylvania.

[19] N. Nelson, The N.D.R.C. infra-red gas analyzer for the determination of rapidly changing CO concentrations, A.M.R.L. Proj. No. T-9, May 18, 1945.

[20] M. L. Vengerov, "An optical acoustic method of gas analysis," Nature (London), 158, 28 (1946); "Spectrophone," Comptes Rendus 46, 182–185 (1945).

[21] C. R. Barber, "Thermal and mechanical instruments shown at Physical Society's Exhibition," J. Sci. Inst. 24, 143 (1947).

[22] W. G. Fastie and A. H. Pfund, "Selective infra-red gas analyzers," J. Opt. Soc. Am. 37, 762 (1947).

[23] VanZ. Williams, "Infra-red instrumentation and techniques," Rev. Sci. Inst. 19, 135 (1948).

Considerable attention was given to a suitable source, and while other means such as glass, oligoclase, etc.[24] might peak more energy at a particular absorption band, a considerable decrease in sensitivity would be experienced for another absorption band and furthermore, the high voltage and auxiliary heater made these cumbersome and dangerous. The Nernst glower proved quite fragile and short lived. Nichrome wire, operated at bright red heat, has a very broad peak at about 4 microns which extends relatively little into the visible and so is a good and convenient source.[25] No reason for replacement of the unit was noted after several hundred hours of severe operation.

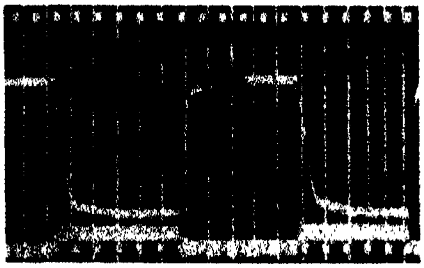

FIG. 5.

The detectors were chosen for their sensitivity and their relatively high speed of response. Other detectors, considerably less expensive may be used at the sacrifice of speed. For a gas having an absorption band in the near infra-red, considerably cheaper and faster detectors may be used (lead sulfide, thalofide cell).

The recorder consists simply of an electrocardiograph string galvanometer, sens. 1 mv per cm, 1500 ohm, with its associated camera, coupled to the high impedance bolometer bridge (each arm 3.0 megohms) through a single coupling vacuum tube with its steady state plate current bucked out. A more rugged pen recorder has been used in conjunction with a breaker type amplifier at the sacrifice of speed, but with greatly increased sensitivity. An indicating meter may thus be used for static measurements of isolated samples.

The calibration curve (Fig. 4) shows the effect obtained by decreasing the optical path through the breathing tube from 18 to 4 mm. The cylindrical tube first used, while quite simple, did not provide sufficiently linear response without extensive electrical compensation, and the short path (0.4 cm) flattened tube, proved quite satisfactory.

Figure 5 is included to indicate the electrical response (bolometer, circuit and galvanometer) obtained by blocking a very small portion of the radiation to one bolometer by means of a small signal magnet, thereby unbalancing the circuit to simulate blocked radiation. Simultaneously another signal magnet interrupted the beam to the camera. The two magnets were interchanged in order to rule out possibility of variations in response and similar results were obtained. The vertical time markers are 0.2 second apart. This shows a 90 percent electrical response in about 0.1 sec. and a slow rise for about 0.4 sec. The over-all response is very nearly the same. The irregularity on the descending portion of one record was due to chattering of the signal magnet.

A record of CO_2 of the respired air during a normal and complete expiration of a normal person is shown in Fig. 6 together with the expired velocity. The over-all speed of response is shown on inspiration where the CO_2 curve drops quickly to the base line. The inspiratory phase is designated by the flat portion of the velocity curve. The lag between the onset of expiration and rise of the CO_2 curve corresponds very closely to the volume of air trapped in the portions of the respiratory tree where gaseous exchange does not take place, the so called "dead space." The continued rise during expiration has

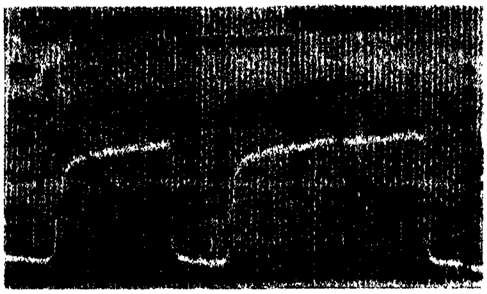

FIG. 6.

---

[24] W. W. Coblentz, Supplementary investigations of infrared spectra, Carnegie Institution of Washington, 1908.

[25] General Electric Company, Lamp Bulletin.

been explained by the continuous diffusion of CO_2 into the lungs from the blood. Variations in this pattern have been found.

This device is believed to have a number of advantages over those existing. These are: (a) relatively low cost, (b) rapidity of response, (90 percent of maximum in 0.15 second over-all), (c) ease of recording, (d) full scale sensitivity obtained with fairly linear response from 0–9 percent CO_2, and (e) insensitiveness to normal pressure and temperature variations. The unit may be used with a number of gases mentioned and with proper alignment and construction, simultaneous measurements may be made of a number of gases.

The need and basic idea for such an analyzer was first brought to our attention by Professor W. O. Fenn, Department of Physiology. In addition to acknowledged sources of information, further material help and suggestions have been made by Dr. B. O'Brian, Colonel A. Gee, Dr. F. Paul, and Mr. W. Klinkert of the University of Rochester, Department of Optics; Dr. A. F. Turner and Staff of the Bausch and Lomb Optical Co.; and Dr. H. Rahn, Dr. A. B. Otis, Dr. H. A. Blair, Dr. W. S. McCann, and Mr. G. Rosenworth and numerous others at the University of Rochester Medical Center. The work was made possible by a fellowship from the John and Mary R. Markle Foundation and was supported in part by the Air Materiel Command at Wright Field.

THE REVIEW OF SCIENTIFIC INSTRUMENTS VOLUME 20, NUMBER 3 MARCH, 1949

The Scintillation Counter as a Proportional Device*

Rosalie C. Hoyt**
The University of Rochester, Rochester, New York

(Received November 2, 1948)

The statistical distribution of fluctuations in the gain of a 1P21 photo-multiplier tube has been investigated and standard deviations of 36 percent to 48 percent have been found. The distribution in photo-multiplier output pulse heights obtained with Po alphas incident on a ZnS screen has also been investigated and standard deviations of 27 percent to 80 percent found. The importance of the contribution from the fluctuations in gain is shown to be small in this case.

I. INTRODUCTION

It has been hoped that the phosphor-photomultiplier counter may be useful as a proportional device, giving output pulses whose sizes are a measure of the energy lost by the incident particle in the phosphor. For particles of short range that are stopped in the phosphor the output pulse heights should be a measure of the energy of the particles, while for particles of large range that pass through the phosphor the pulse heights should be a measure of the energy they lost in the phosphor and thus of their specific ionization. Thus, two particles of differing specific ionization should be distinguishable.

However, for particles losing the same amount of energy in the phosphor there will be a statistical spread of pulse heights, and the width of this spread will determine the degree to which such a counter may be used to distinguish between particles. Therefore, a preliminary investigation has been made of the statistical distribution in pulse heights from a monoenergetic source of particles, and an attempt has been made to determine the relative importance of some of the various factors that contribute to the spread of this distribution.

II. STATISTICAL DISCUSSION

The statistical spread in output pulse heights will be due to several causes, of which the following may be mentioned: (a) statistical fluctuations in the over-all gain (multiplication factor) of the multiplier tube, (b) fluctuations in the efficiency of the photo-cathode of the multiplier tube, (c) fluctuations in the number of light quanta emitted by the phosphor per particle passing through it, and (d) fluctuations in the fraction of these quanta that are collected by the optical system and fall on the photo-surface.

The larger the number of photoelectrons starting out from the first stage of the photo-multiplier tube the smaller will be the relative effect due to cause *a* above on the over-all spread of pulse heights. Likewise, the larger the number of quanta emitted in the phosphor, the smaller will be the effects due to causes *b*, *c*, and *d*, as well as that due to cause *a*.

The purpose of this investigation was to determine the magnitudes of the contribution due to *a* and to the other three taken together and, in addition, to determine the average number of photoelectrons necessary to make the contribution due to *a* negligibly small.

---

* This work was carried out with the support of the Office of Naval Research.

** Now at Bryn Mawr College, Bryn Mawr, Pennsylvania.

Let X = multiplier gain, Y = number of photoelectrons produced by an incident particle, Z = number of output electrons produced by an incident particle. It is then obvious that

$$\bar{Z}=\bar{X}\bar{Y}, \tag{1}$$

where $\bar{Z}$, etc. represent average values. H S. Snyder,[1] of the Brookhaven National Laboratory, has analyzed the statistical problem of the photomultiplier tube, assuming no specific shape for the distributions, and in particular has shown that

$$\langle Z(Z-1)\rangle_{Av}=\langle Y(Y-1)\rangle_{Av}\bar{X}^2+\bar{Y}\langle X(X-1)\rangle_{Av}. \tag{2}$$

Now, $X\sim 10^6$, and therefore $X-1\sim X$. Also, $\bar{Y}\geqslant 1$, therefore $Z-1\sim Z$. Thus Eq. (2) becomes

$$\langle Z^2\rangle=(\langle Y^2\rangle-\bar{Y})\bar{X}^2+\bar{Y}\langle X^2\rangle. \tag{3}$$

From (1) and (3) it is easy to show that

$$(\langle Z^2\rangle-\bar{Z}^2)/\bar{Z}^2=[1/\bar{Y}][(\langle X^2\rangle-\bar{X}^2)/\bar{X}^2] \\ +[(\langle Y^2\rangle-\bar{Y}^2)/\bar{Y}^2] \tag{4}$$

or

$$\sigma_z^2=(1/\bar{Y})\sigma_x^2+\sigma_y^2. \tag{5}$$

Where σ_z^2, etc., are the fractional mean square deviations of the distributions.

From the experimental data to be presented, σ_z^2, $\bar{Y}$, and σ_x^2 were obtained, and from these σ_y^2 was calculated. Thus the relative contributions of σ_x^2 (cause *a*) and σ_y^2 (causes *b*, *c*, and *d*) to the over-all σ_z^2 were determined. (Snyder has also derived relationships from which the higher moments of the distribution for Y can be determined; these, however, have not been experimentally determined in the following).

From Eq. (5) it can be seen that the smaller is $\bar{Y}$, the larger is the contribution of the first term of Eq. (5) (cause *a*) to the over-all distribution. However, it must be remembered that a smaller $\bar{Y}$ means a smaller number of photoelectrons per incident particle and thus a smaller number of quanta emitted per incident particle. The second term of Eq. (5) (causes *b*, *c*, and *d*) will be affected by the smaller number of quanta in the same way that the first term is affected by a smaller number of photoelectrons, although Eq. (5) does not show this explicitly. Thus, as $\bar{Y}$ decreases, not only will the contribution of the first term increase, but that of the second term will increase also.

III. EXPERIMENTAL METHODS AND RESULTS

While the organic phosphors have been found to be very efficient detectors of weakly ionizing radiation, they apparently are not as efficient as some of the inorganic phosphors for detecting heavily ionizing radiation such as alpha-particles. Thus, since the most convenient source of monoenergetic particles to use was a thin polonium alpha-source, activated zinc sulfide was employed as the phosphor throughout this investigation.

The ZnS in the form of commercial x-ray screen (Patterson *D*) was placed directly on the envelope of a 1P21 photo-multiplier tube. (*Note:* The same 1P21 tube, operated at 1230 volts, was used throughout, and thus the results presented below refer only to the *one* tube studied.) A hemispherical mirror was placed over the tube and phosphor, and the polonium source was inserted through a hole at the top of the mirror to within 1 cm of the phosphor screen. The whole assembly was placed in a container which was kept in a bath of liquid nitrogen.

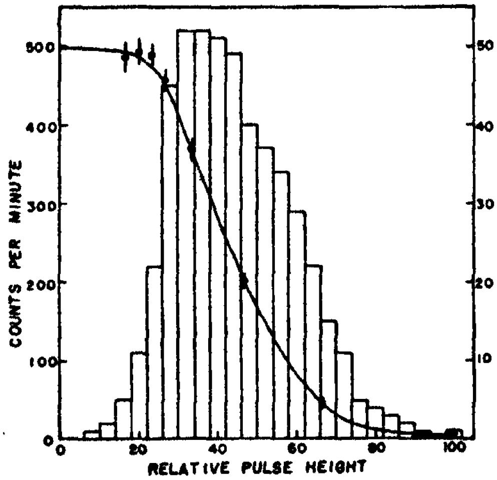

FIG. 1. Integral bias and distribution curves of the photomultiplier output pulse height when a weak light flux is incident on the photo-surface. The ordinates on the left refer to the integral bias curve and are in counts per minute. The ordinates on the right refer to the histogram and are in counts per minute per pulse height interval.

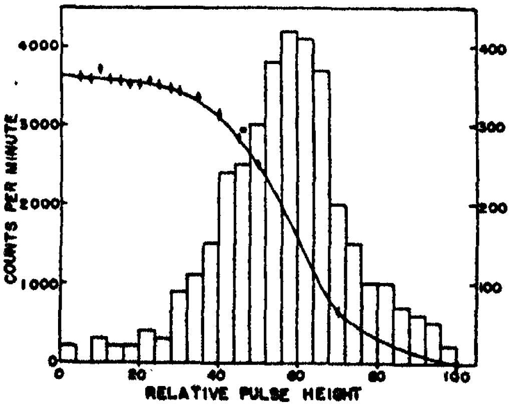

FIG. 2. Integral bias and distribution curves of the photomultiplier output pulses when alpha-particles are incident on ZnS. The ordinates on the left refer to the integral bias curve and are in counts per minute. The ordinates on the right refer to the histogram and are in counts per minute per pulse height interval.

---

[1] Private communication.

The output from the photo-multiplier tube passed through a cathode follower stage into a model A-1 amplifier.[2] The discriminated output from this amplifier was fed into a Tracerlab Autoscaler.

The distribution in multiplier gain (the X distribution in the notation of the previous section) was obtained by taking an integral bias curve (counting rate against discriminator bias setting) with a weak light flux falling on the tube. The light flux was made weak enough so that the probability of observing multiple primary electron pulses rather than pulses from single primary electrons was small. A second integral bias curve of dark noise pulses was obtained and subtracted from the first, yielding a resultant integral bias curve due to single photoelectrons. Such a resultant curve is shown in Fig. 1. From the smooth curve drawn through the experimental points the step distribution curve was obtained. The fractional mean square deviation obtained from the data of this curve was $\sigma_x^2=0.13$. Only one tube was tested; however, it is reasonable to expect that other 1P21 tubes should show standard deviations of the same order of magnitude. A second set of data for the same 1P21 tube gave a distribution curve for which the value of σ_x^2 was 0.23. Most bias curves do not approach as constant a value with decreasing bias as that shown in Fig. 1.

To obtain the pulse height distribution from alpha-particles two integral bias curves were obtained, with and without a 1.5-mil foil of aluminum (sufficient to stop Po alphas) surrounding the polonium source. By subtracting the first bias curve from the second, the effects resulting from the dark noise output and any possible α- and β-ray contamination in the source, mirror, etc., could be subtracted out. In this way the typical integral bias curve and distribution histogram for alpha-particles alone, shown in Fig. 2, was obtained. Analysis of this data gave a mean square deviation of $\sigma_z^2=0.084$. (Other sets of data gave values of σ_z^2 ranging from 0.07 to 0.64).

In order to apply Eq. (5), it is necessary to know the actual numerical value of $\bar{Y}$ rather than the relative pulse heights, H, as measured on the dial of a bias potentiometer. This was done by determining

$$\bar{Y}=\bar{Z}/\bar{X}=[(\bar{H}_z)/(G_z)C]/[(\bar{H}_x)/(G_x)C],$$

where G is the amplifier gain setting and C is a constant conversion factor. In this way $\bar{Y}$ was found to be 35 for the curve of Fig. 2.[3]

Application of Eq. (5) then gives

$$\sigma_y^2=\sigma_z^2-(1/\bar{Y})\sigma_x^2=0.084-0.004=0.080,$$

indicating that the contribution of σ_x^2 to σ_z^2 is practically negligible compared to that of σ_y^2.

It is thus seen that in the above case where $\bar{Y}=35$, the main contribution to the over-all distribution comes from the spread in number of photoelectrons starting out from the photo-cathode, rather than from the spread in distribution caused by the multiplication stages. If however, $\bar{Y}$ had been smaller, this latter effect would have been more serious. However, a smaller value of $\bar{Y}$ would also probably mean a larger value of σ_y^2 (as indicated earlier).

IV. DISCUSSION

From Fig. 2 it can be seen that if $Y>35$, then two particles losing differing amounts of energy in the phosphor can be distinguished to a fair degree of accuracy if both distribution curves have been obtained. If, however, it is desired to distinguish between single particles whose distribution curves cannot be obtained, then from the distribution curve of Fig. 2 an estimate can be made of the probable error of any one pulse height from the mean. Since Fig. 2 agrees in a qualitative way with a Gaussian distribution (as also does Fig. 1), it is reasonable to assume that the probable error of any single measurement from the mean will be of the order of σ_z, and thus, for Fig. 2, of the order of $(0.084)^{\frac{1}{2}}=29$ percent. This figure then gives an idea of the degree to which this counter as operated could distinguish between individual alpha-particles of differing energy.

The zinc sulfide used in this investigation was obtainable only in powders and screens of small grain size, and it is reasonable to expect that the statistical spread in the Y distribution (σ_y) would, if anything, be narrowed if a large transparent phosphor were used.

It is thus seen that this device can be used to give an indication of the energy or specific ionization of the particle, but with a precision that is poor unless the number of quanta emerging from the phosphor is fairly large. This means that for weakly ionizing particles of long range, large transparent phosphor samples must be used, so that a large fraction of the light quanta emitted over the long path may be collected.

---

[2] W. H. Jordan and P. R. Bell, Rev. Sci. Inst. 18, 703 (1947).

[3] A number of other curves were obtained for which the value of $\bar{Y}$ varied up to a maximum of 92. The low value of 35 obtained for the data of Fig. 2 may have been due to improper positioning of the mirror resulting in poor focusing.

THE REVIEW OF SCIENTIFIC INSTRUMENTS VOLUME 20, NUMBER 3 MARCH, 1949

A Pulse Amplitude Analyzer for Nuclear Research Using Pretreated Pulses[*]

C. H. WESTCOTT[**] AND G. C. HANNA
Division of Atomic Energy Research, National Research Council, Chalk River, Ontario, Canada

(Received November 2, 1948)

A pulse analyzer is an instrument used to record the number of pulses occurring in a given time whose amplitudes lie between certain limits. In the present equipment records are obtained from 30 "channels" simultaneously, the upper amplitude limit for any one channel being the lower amplitude limit of the next. Used in conjunction with an ionization chamber and linear amplifier of suitable design, the equipment gives detailed information of the frequency of occurrence of ionization pulses of various amplitudes.

The present equipment is an advance over previous designs in several respects. It is designed to deal with relatively fast counting rates and with pulses having a wide variety of shapes and durations. In order to avoid having to change the circuits of each of the 30 channel units to suit the pulse shape, the pulses are "pretreated" to yield signals of standard form before being passed to the channels for analysis. Further advantages of the present equipment concern the ease of calibration and of monitoring the behavior of the circuits. The whole is built into a console of convenient shape and reasonable mobility. Interchangeable plug-in channel units are employed.

I. INTRODUCTION

THE use of a pulse amplitude analyzer in the investigation of particle energy spectra has been discussed by Freundlich, Hincks, and Ozeroff.[1] In such an analyzer the pulses are divided into groups according to amplitude, and the number of pulses in all the groups are counted simultaneously. The equipment has a number of "channels" corresponding to the number of groups, each group comprising those pulses which are large enough to operate one channel but not large enough to operate the next. The whole of the amplitude spectrum is therefore covered without gaps, and if, as is usually the case, the channel thresholds are uniformly spaced, the spectrum is obtained directly. In this way results can be obtained much more quickly than from bias curve measurements. Consider, for example, the case when there are in time t a number n of counts in a particular group, and a number N of counts of greater amplitude. Then, using the pulse analyzer, the statistical error of the determination of n is $(n)^{\frac{1}{2}}$, whereas from a bias curve, counting for a time t on each setting, counts of $N+n\pm(N+n)^{\frac{1}{2}}$ and $N\pm(N)^{\frac{1}{2}}$ are obtained, so that the determination of n by difference is subject to the error $(2N+n)^{\frac{1}{2}}$. This is always greater, and may indeed be much greater, than $(n)^{\frac{1}{2}}$, and a time $2t$ is required for the determination.

The instrument described by Freundlich *et al.*[1] is, as they pointed out, somewhat limited in scope since the acceptable counting rate is rather low and special attention must be paid to the shape of the input pulses. A desire to improve the flexibility of such a device led to the development of the present instrument. In its design we have departed from the simple system where each "channel" receives a replica of the original signal. The incoming

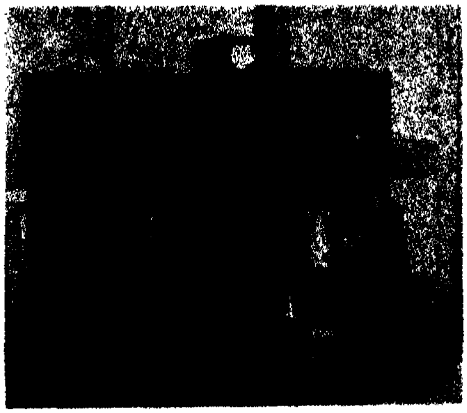

FIG. 1. Photograph—front view.

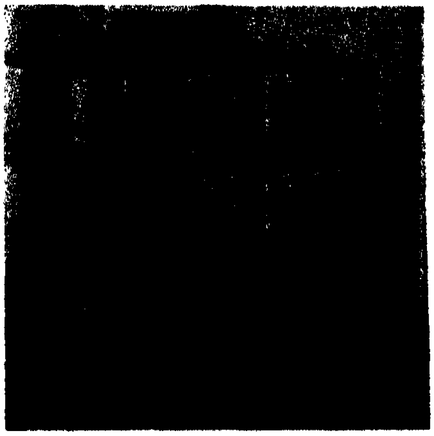

FIG. 2. Photograph—rear view.

---

[*] This document is based on an unpublished report of the National Research Council of Canada. G. C. Hanna and C. H. Westcott, *The 1945 Kicksorter*, CRP-291 (September 24, 1946).

[**] Now at Physics Department, Birmingham University, England.

[1] H. F. Freundlich, E. P. Hincks, and W. J. Ozeroff, Rev. Sci. Inst. 18, 90 (1947).

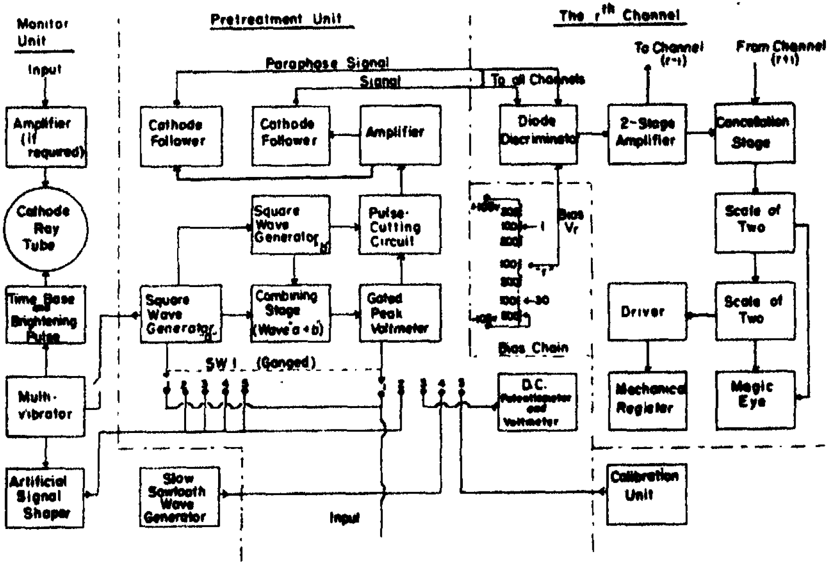

FIG. 3. General schematic diagram.

signal is fed into a "pretreatment unit" where a square wave signal of standard duration is manufactured having the same amplitude as the peak of the incoming signal. This square wave is then passed to the channel units for analysis. It is now possible to accept a wide variety of types of input signal by a simple adjustment to the pretreatment circuit without having to make changes in all the channels.

II. PHYSICAL FORM OF THE EQUIPMENT

The pulse analyzer is built in the form of a console (Fig. 1) for convenience in operation. The channels are interchangeable plug-in units accessible by removing the three rear panels (Fig. 2). Each channel is so arranged that its wiring is accessible for monitoring purposes even when plugged in the rack. The channels are 3½″ wide and are arranged in two rows of 15 alternately above and below a 3″ strip of panel on which are mounted, in a single row, the 30 mechanical registers, each with a "magic eye" underneath, which are used to record the count in each channel. The bias adjusting potentiometers associated with each channel are staggered alternately above and below the registers to indicate whether a particular register is driven from a channel in the upper or lower row. The space at the rear of the lower part of the console, and above the kneehole, is occupied by filament transformers and a large power supply: arrangements are made to deflect the hot air rising from this unit away from the channels above it. The space on either side of the kneehole is used for the pretreatment and monitor units. Each of these has a triangular control panel which fits into a recess in the console table.

III. GENERAL MODE OF OPERATION

Figure 3 shows a schematic arrangement of the equipment. Neglecting for the moment the monitoring circuits shown on the left of the diagram, we may follow the incoming signal from the bottom of the figure, through *SW*1, in its normal position (position 1) into two parallel chains of circuits. In the left-hand chain the arrival of any signal above a preset threshold initiates two successive square waves of duration "*a*" and "*b*," respectively. In the right-hand chain a peak voltmeter circuit records the maximum amplitude reached by the incoming signal and stores this information until the end of the period "$a+b$." A pulse cutting circuit forms a pulse during the period "*b*" only, of amplitude given by the peak voltmeter circuit, and this square pulse, after amplification, is passed to the channels. A smaller paraphase pulse is also fed to the channels for capacity neutralizing purposes.

A biased diode controls the channel operating level, each successive channel being biased more heavily. Two stages of amplification follow the diode discriminator, to provide a large voltage swing for the next ("cancellation") stage. The cancellation stage will only pass a pulse provided that the channel "above" has not operated; in this way each channel records only pulses with an amplitude lying between its own operating threshold level and that of the next channel above. The output from the cancellation stage drives a scale-of-four circuit which in turn feeds an impulsing pair driving a mechanical register.

A feature of the equipment is the section devoted to monitoring operations. This consists essentially of a unit providing artificial pulses of adjustable repetition frequency, and controllable shape and amplitude, synchronized with a time-base on a cathode-ray tube. This basic arrangement can be altered to allow the incoming pulses from the counting system to fire a single sweep time base. Another arrangement allows for accurate calibration of the system.

As shown in Fig. 3 the equipment sorts pulses of sizes between 1.5- and 100-volt amplitude into 30 equi-spaced channels. If it is desired to examine the amplitude spectrum in more detail, a narrower range of pulse amplitudes may be selected. A separate unit is used in this case which cuts a fixed amount from the size of each pulse and amplifies what remains until the desired range extends over 100 volts in amplitude. This unit, developed by Cranshaw and Harvey, is described elsewhere.[2]

IV. THE PRETREATMENT UNIT

The purpose of this circuit is to convert the input pulses, which may have any rise time between 1 μsec. and 3 msec., into square pulses 80 μsec. long of amplitude accurately proportional to the input amplitude.

The input pulse (+100-v max.) triggers a square wave generator *V*1, 2, 3 (see Fig. 4). The duration "*a*" of this square wave is adjustable in steps from 0.2 to 15 msec., and is made just greater than the time the input pulse takes to decay to the triggering threshold level. This threshold, controlled by the bias on the grid of *V*3, is normally set to 1.5 volts.

From the back edge of wave "*a*" *V*4 produces another square wave of duration "*b*" (80 μsec.). *V*6 combines these two into a single wave of duration "*a*+*b*"; there is necessarily a sharp crevasse in this wave but the response of *V*4 is fast enough to ensure that it does not drop below +110 v (see Fig. 5). Thus whenever this chain is triggered the discharging diode *V*7 is cut off for a time "*a*+*b*," during which the input pulse, fed in via a buffer stage *V*8, charges the 0.002 μf reservoir condenser through *V*8*A*. The isolating cathode follower *V*9 imposes a negligible load on the condenser. This then holds the full peak-amplitude charge for the time "*a*+*b*," after which it is rapidly discharged through *V*7 to a level controlled by the bias applied to *V*6 ("d.c. level 1"). The cathode of *V*9 therefore follows the rise of the input signal up to its peak amplitude and remains there until the end of the period "*a*+*b*."

The grid of *V*12 is held by the diode *V*11 at a potential set by "d.c. level 2," except during period "*b*" when the positive square wave from *V*4, applied through the 0.25-megohm resistance, pulls it up to the level of *V*9 cathode, further travel being arrested by conduction of *V*10. Here then we have a square pulse of duration "*b*" and amplitude equal to the input (less the losses in the cathode followers *V*8, 9) plus an adjustable "zero control" voltage set by d.c. level 2. It is necessary for the correct operation of this diode circuit that the quiescent level of *V*9 cathode, set by d.c. level 1, be more positive than the quiescent level of *V*12 grid, set by d.c. level 2.

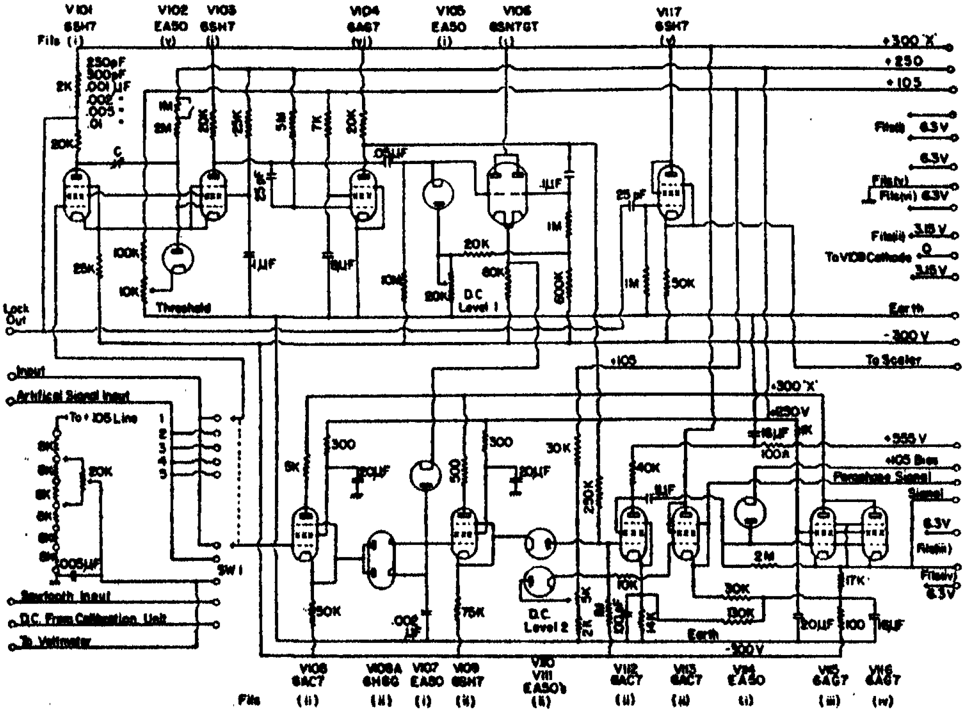

FIG. 4. Pretreatment—circuit. For *V*101, *V*102 ··· *V*117 read *V*1, *V*2 ··· *V*17.

---

[2] T. E. Cranshaw and J. A. Harvey, Can. J. Research A26, 243 (1948).

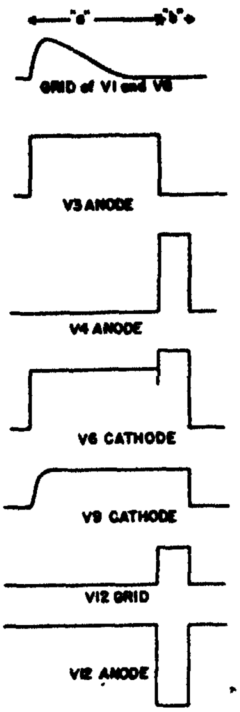

FIG. 5. Pretreatment—wave forms.

The gain of $V12$ is 2.5; consequently there appears on its anode a 220-v (max.) negative going signal of duration "b," which is "d.c. restored" in $V14$ against the +105-v bias line, that is, against the positive end of the resistor chain from which the discriminator diodes in the channels are biased. It is then fed out through the high power cathode-follower stage $V15$, 16 to operate the channels.

From the cathode of $V12$ the positive 80-v (max.) wave is fed out to the channels through the cathode follower $V13$ to act as a capacity-neutralizing paraphase signal. For efficient neutralizing the wave forms at $V15$, 16, and $V13$ cathodes, both of which work into highly capacitative loads, should be identical. This cannot be realized in practice, but the shapes have been made sufficiently similar by shunting the cathode load of $V12$ with a small condenser and smoothing slightly the pulse applied to the grid of $V13$.

Subsidiary features of the circuit include a negative "lock" pulse for driving the monitor unit from the input signals (from $V1$ anode circuit) and short pulses fed out through $V17$ suitable for driving a scaler to check the total number of counts.

The above applies during normal operation, when the monitor unit is driven from the input pulses (arriving at random) and provides a single-sweep time base for studying the operation of the equipment on the oscilloscope. As an alternative, however, the pretreatment unit can be driven from the monitor unit; this arrangement is particularly useful for calibration and fault-finding. Artificial pulses of adjustable amplitude, shape, and repetition frequency from the monitor unit can be fed in directly (position 2 of the input selector switch), and can also be used to trigger the square wave generator ($V1$, 2, 3) while a constant voltage, obtained from a built-in potentiometer system, is applied to $V8$ (position 3). In this case pulses are generated with an amplitude corresponding to the level of $V8$ grid. That is, if $V8$ grid is connected to a source of +50 v (say), which can be measured accurately with a precision voltmeter, the output of the pretreatment unit is the same as though pulses of peak amplitude 50 v were applied to $V8$. This equality is maintained provided the pulse rise time to maximum is less than 10 μsec. Input pulses with a rise time of 2.5 μsec. will record at a level about 5 percent below that of a steady voltage of the same amplitude, but the input/output characteristic of the system is still linear to 1 percent. The equivalence of d.c. and pulse input is not, however, quite exact due to the imperfect cut-off of the diode $V8A$. When a steady voltage is fed in, the reservoir condenser continues to charge up very slowly over the whole of the period "$a+b$." The net effect is a zero shift, the magnitude of which increases with period "a" up to about ¼ volt for "a" equal to 10 msec. This behavior is discussed in greater detail in the report CRP-291.

Fast rising pulses are in general of short duration: consequently period "a" may be shortened and the size of the reservoir condenser reduced, since it need not hold its charge so long. This will increase the accuracy of response to fast pulses and reduce the difference between d.c. and pulse input. In fact the instrument has recently been operated with a 200-$\mu\mu f$ reservoir condenser which permits rise times of less than 1 μsec. to be used. A single switching wave 80 μsec. long derived from a slightly modified square wave generator circuit was employed, gating the peak voltmeter circuit as before and driving $V12$ to produce the channel operating pulse directly. The rise time of this pulse was of course the same as that of the input pulse; provided this is less than about 10 μsec., the channel operation is not affected.

Position 4 of the input selector switch connects $V8$ grid to the slow sawtooth wave provided by the monitor unit (see Section VI), and position 5 to the calibration unit. This unit consists of 30 100-ohm precision resistances connected across a stabilized 100-v line monitored with a standard voltmeter. The junctions of these resistances are, clearly, at potentials corresponding to the transitions between successive channels. A selector switch enables these potentials to be applied in turn to $V8$ for setting up the channels. This unit was found more convenient in use than the potentiometer and voltmeter arrangement available in position 3.

Several power supply voltages are used in the pretreatment unit. The 300-v "*X*" line (semi-stabilized—see Section VII) provides most of the h.t. current. Where high stability is required—for example for screen supplies to ensure constancy of valve characteristics-stabilized +250-v and +105-v lines are available. The large anode swing of *V*12 necessitates the provision of a stabilized +550-v supply. The negative h.t. lines are both stabilized.

The filaments of *V*15, 16 (iii and iv) are heated from a 12.6-v center-tapped, low capacity screened transformer winding, the center wire being driven by the cathode. This supply also feeds all the channel diodes (*V*101 Fig. 6). Filament supply (i) is biased to +90 v (in the main power supply) so that the cathodes of the valves it feeds may rise to +180 v without exceeding the insulation rating. The cathode insulation of the charging diode *V*8*A* is important since it determines the rate of discharge of the reservoir condenser. Consequently this valve is heated from a low capacity transformer winding, the center-tap of which is driven by *V*9. *V*8 and *V*10–13 are also fed from this supply (ii). The other valves are heated by the main 12.6-v system with earthed center-tap (v and vi).

The filament supplies (i), (ii), (iii), and (iv) are derived from a transformer fed from a constant-voltage transformer. This renders the performance of this unit substantially independent of mains voltage. Drifts caused by warming up are reduced by the use of generously rated wire-wound resistances at all strategic points; the circuit is stable within ten minutes of switching on.

V. THE CHANNEL UNITS

Figure 6 shows the circuit of a channel unit. The cathodes of the diodes (*V*101) in all the channels are connected to the output of the pretreatment unit (*V*15, 16 Fig. 4) and the anode load resistances to successive points on a resistance chain. This bias chain consists of 30 200-ohm wire-wound resistances and 30 100-ohm preset potentiometers with suitable padding resistances at each end connected in series between the +105-v and −105-v bias lines. (See Fig. 3.) The preset controls, readily accessible from the front of the instrument, allow small adjustments to be made to the bias voltage of each channel.

Consider the operation of the *r*th channel, i.e., the one biased to a voltage V_r by the *r*th potentiometer of the bias chain counting from the positive end. If the original input pulse is insufficiently large to cause the cathode of *V*101 to drop from its quiescent level of +105 v to below V_r, *V*101 will not conduct. A paraphase signal fed through a small adjustable condenser neutralizes the effect of the diode self-capacity (for wave forms see Fig. 7).

If the cathode of *V*101 falls below V_r, *V*101 conducts and a negative pulse appears on the grid of *V*102. *V*102 runs, during the quiescent period, at the limit of grid current; this assists in the rapid restoration of the original potentials after the pulse is over, since the coupling condenser is recharged by the flow of grid current rather than through the 10-megohm leak.

It should be mentioned here that before a channel conducts it imposes capacitative loads of 2 and 5 $\mu\mu$f on the signal and paraphase inputs respect-

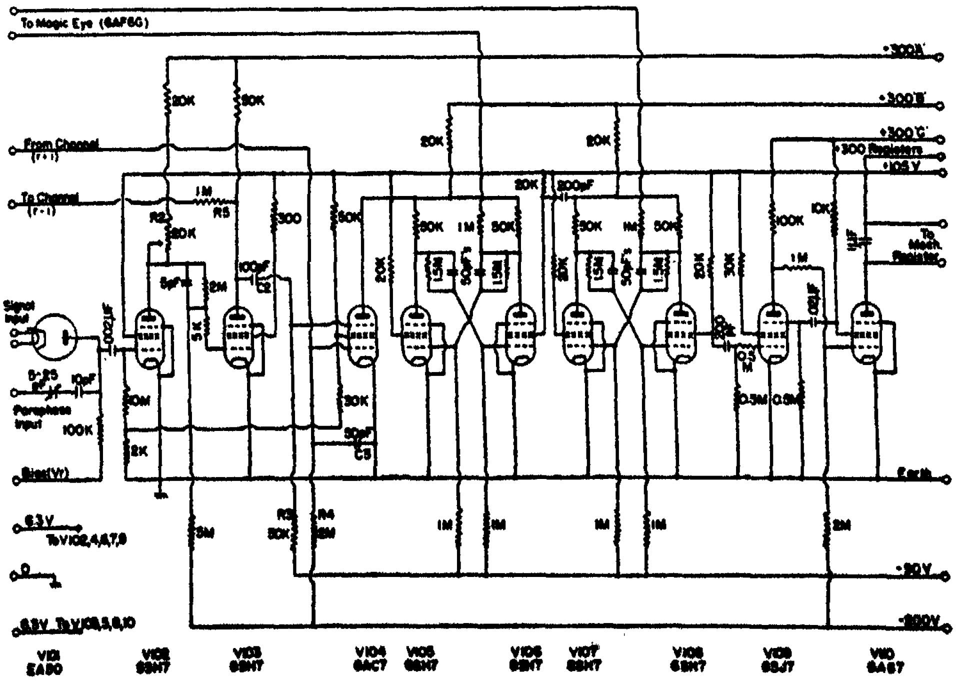

FIG. 6. Channel—circuit.

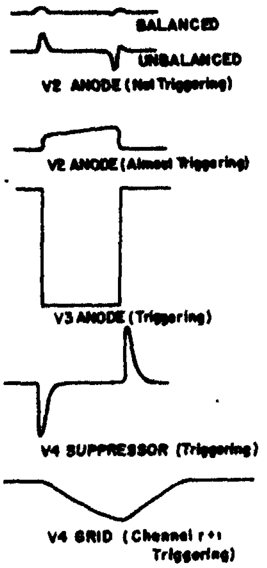

FIG. 7. Channel—wave forms. For $V2$, $V3$, $V4$, read $V102$, $V103$, $V104$.

ively. When the diode conducts the former load becomes 10 μA per volt above threshold, and the latter 17.5 $\mu\mu$f. These conditions determine the design of the output cathode followers $V15$, 16, and $V13$ in the pretreatment unit. The load current of course returns through the bias chain. The center point of this is earthed and each bias point connected to earth through a 1-μf condenser. This arrangement ensures that the threshold voltages are not displaced by more than 20 millivolts (mean) for a total counting rate of 2000/min.

The anode potential of $V102$ is set at +80 v by R_2. Its gain is about 160; consequently a pulse $\frac{1}{4}$ volt in amplitude applied to its grid will cause its anode to rise to +120 v. At this point $V103$ starts to conduct, a further change of 4 v in the anode potential of $V102$ causing $V103$ anode to fall from +300 v to about +30 v. Thus pulses of less than $\frac{1}{4}$ volt on $V102$ grid (resulting for example from imperfect neutralization) will have no effect, while a pulse exceeding this threshold by 25 millivolts will give a full-size negative square wave, of 80-μsec. duration, at the anode of $V103$.

In the canceling stage, $V104$, the suppressor is normally held at −90 v. The control grid is near earth potential drawing 150 μA of grid current. At the end of the negative square wave on $V103$ anode a positive "pip," obtained by differentiating with a 5 μsec. time constant ($C3$ and $R3$), allows a short pulse of anode current to pass which operates the first scale-of-2 circuit ($V105$, 106). If, however, the cathode potential of $V101$ falls below V_{r+1} the next $(r+1)$th channel will operate in a similar fashion. The anode of $V103$ in channel $(r+1)$ will drop to +30 v and the grid of $V104$ in channel r will start to fall, as current flows out of the 50-$\mu\mu$f condenser $C3$ through the resistances $R4$ and $R5$. By the end of the 80-μsec. wave it will have fallen to about −80 v, recovering over the next 30 μsec. Thus all current in $V104$ is cut off for a time comfortably greater than the duration of the positive "pip" on the suppressor and the scaling circuit is not operated.

The scaling circuits are of conventional type using two scale-of-2 pairs in tandem. The state of each pair is shown on a "magic eye" (a double tuning indicator type 6AF6G) fed from the anode of the second valve in each pair through a one-

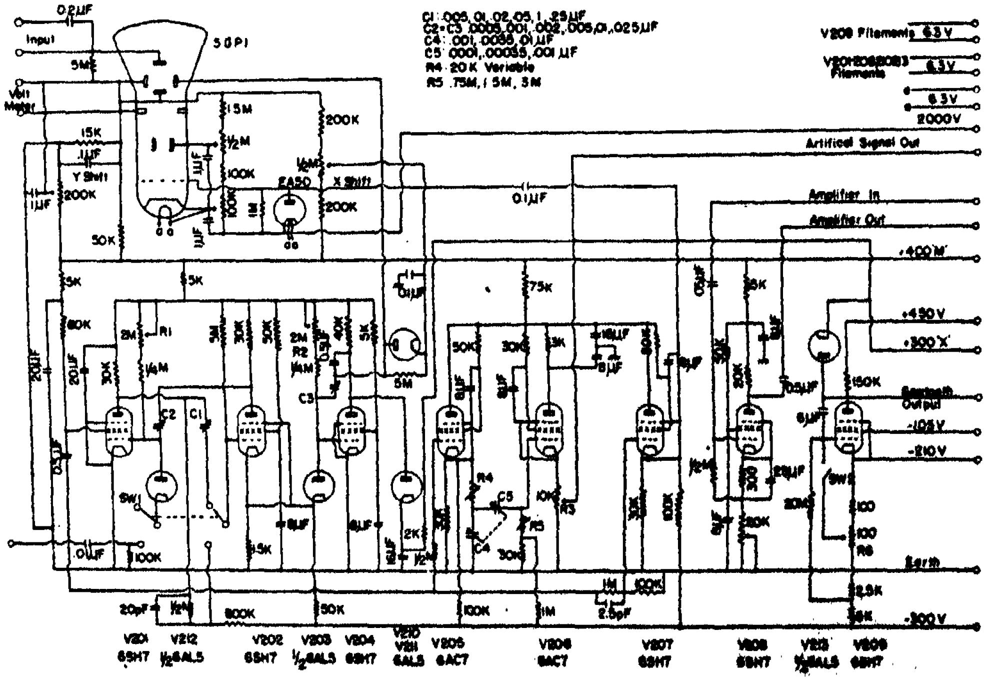

FIG. 8. Monitor—circuit.

megohm resistance which effectively isolates the valve from the self-capacity of the wiring to the magic eye.

The second scaling circuit drives a trigger circuit (*V*109 and *V*110) which provides a 50-ma current pulse lasting about 20 msec. to drive the mechanical register. A telephone call meter (GPO England, Type 100C) was chosen for this on account of its small size and cheapness. Unfortunately these machines are not very reliable at high counting rates and frequent checks of maximum operating speed are made (using the monitor unit). Registers failing at less than 15 operations/second are replaced; tightening the return spring frequently provides a satisfactory cure. The maximum counting rate which a channel can handle is determined entirely by the register. A counting rate of 720/min. (180 register clicks/min.) will be subject to a 1 percent loss; if a 10 percent loss is tolerable the rate may be increased to about 1600 counts/min. The register is highly inductive (about 30 *H*, its d.c. resistance being 2300 ohms). A 1-μf condenser is therefore connected across it to limit the instantaneous voltage surge which would otherwise break down the insulation.

Several h.t. supplies are used. A stabilized +105-v line is used as a screen supply. The +300-v "*A*" line provides a fully stabilized supply for *V*101 and *V*102 whose exact operating conditions are important. 300-v "*B*" and "*C*" are semistabilized supplies for the less critical circuits. Unstabilized lines are used for the register (*V*110 anode supply) and the magic eye. Such subdivision prevents feedback and simplifies circuit design, and is in any case not uneconomical since the total current drain on each supply is large enough to justify its separate existence.

TABLE I.

Line voltage	Current (ma)	Stability	To feed
+550	4	NS	Pretreatment V12
+450	3	NS	Monitor V209
+300 "*A*"	220	S	Channels
+300 "*B*1"	120	SS	Channels 1–15
+300 "*B*2"	120	SS	Channels 16–30
+300 "*C*"	80	SS	Channels
+300 registers	(pulses)	—	Channels
+300 "*X*"	120	SS	Pretreatment
+250	25	NS	Pretreatment
+105	330	S	Channels & pretreatment
+105 bias	25	NS	Bias chain & pretreatment
− 90	8	(NS)	Channels
−105	33	NS	All circuits
−210	−9	NS	Monitor V209
−300	160	S	All circuits
+400 "*M*"	60	—	Monitor*
+230	115	—	Magic eyes*

* These supplies are separately switched.

VI. THE MONITOR UNIT

The main purpose of this unit is to provide artificial signals for fault finding and calibration. They are generated by a self-running multivibrator which also drives a time base circuit for the oscilloscope. This multivibrator can be switched so that it operates only on external triggering pulses, thus providing single-sweep operation of the oscilloscope for monitoring the input to the pulse analyzer during normal operation. The circuit diagram is shown in Fig. 8.

When *SW*1 is raised *V*201 and *V*202 run freely. A set of switched condensers, *C*1, determines the repetition frequency and another set, *C*2, the duration of the positive square pulse on *V*202 cathode. This pulse cuts off the diode *V*203 and the anode potential of *V*204 falls almost linearly with time, from +300 v set by the "catching" diode *V*211, towards earth at a rate determined by *R*2 and *C*3. *C*3 is ganged to *C*2 so that the amplitude of the time base sweep (*V*204 anode) remains constant for different duration times. In addition, the variable parts of *R*1 and *R*2 provide a continuous and separate control of the duration and speed respectively of the time base.

A positive pulse is taken from the screen of *V*201 to brighten the oscilloscope for the duration of the time base and is fed to the cathode ray tube through *V*207.

The artificial signal is obtained from this positive pulse using the shaping network *R*4*C*4*R*5*C*5 driven by a cathode follower *V*205. *R*4*C*4 determines the rising and *R*5*C*5 the falling times of the signal. Its amplitude is adjustable by *R*3.

*V*208 is a simple amplifier with a gain continuously variable up to about 120. Its main use is the checking of h.t. lines for smoothness.

*V*209 provides a slow sawtooth wave rising from a little below earth potential to +100 v in about five minutes. This can be fed into the pretreatment unit input, which is meanwhile triggered by the artificial signal pulses, to check the equality of channel widths. Since the wave rises linearly with time and the pulse repetition frequency is constant, the count recorded in any channel will be proportional to its width. With *SW*2 closed the potential of *V*209 anode is set a few volts below earth using *R*6. As soon as *SW*2 is opened the 6-μf condenser starts to discharge through the 20-megohm resistance and the anode potential rises linearly, operating the first channel as soon as it exceeds earth potential. Thus a change in the setting of *R*6 merely alters the time between *SW*2 being opened and the check run starting. The 6-μf condenser has been chosen for high insulation resistance, any appreciable leak affecting the linearity of the sawtooth wave. *V*213 prevents excessive voltage appearing across the condenser when *SW*2 is left open indefinitely.

When the pulse analyzer is being used normally the monitor unit may be switched off. Alternatively *V*201 and *V*202 can be driven by an external negative lock (obtained from the pre-treatment unit) *SW*1 being depressed so that *V*202 is normally biased off. The duration controls and the time base stage, *V*204, operate as described above, giving a single-sweep time base of adjustable speed and duration locked to the input to the pre-treatment unit.

The oscilloscope itself is mounted on top of the console. Connections to it are made using multicore screened cable except for the vertical deflector plate input, which is a separate "flying" lead in the interests of low capacity. An external voltmeter may be connected to the vertical shift system if measurements of pulse amplitudes are required.

VII. POWER SUPPLIES

The power consumed by the pulse analyzer is approximately 2.5 kw at 115 v 60 c.p.s. The bulk of this power is taken straight from the mains, but two circuits are fed from a small mains-stabilizing transformer rated at 2 amps. These circuits are the rectifier system from which the +550-v supply is derived, and the heater transformer "*B*" which feeds valves in the pretreatment unit (see Section IV).

Closing the main switch energizes a large heater transformer "*A*" which feeds the other valves in the instrument from its 12.6 v 50 amp. center-tapped secondary. It also energizes the mains stabilizing transformer and, consequently, transformer "*B*." A relay prevents the +550-v supply from being energized immediately: this relay remains open until the h.t. switch is closed.

The h.t. power may be switched on after a 40-second thermal delay switch has closed. Circuits of all the rectifying and stabilizing circuits are not given but the requirements are listed below (see Table I). Three types of stabilization are used: "*S*," fully stabilized using a series valve controlled by a d.c. amplifying stage balanced against a neon discharge tube; "*SS*," semistabilized where the current is taken from the cathode of a power pentode with grid and screen held constant; and "*NS*," neon stabilized, i.e., across a glow-discharge tube (in the case of the neon stabilized lines below the +300-v level, the supply resistance is taken to an already stabilized line). The −90-v bias line for the channels is obtained from the −105-v line through a 2000-ohm dropping resistance and is decoupled to earth with a 16-μf condenser.

VIII. SUMMARY OF PERFORMANCE

The instrument will handle pulses of any shape provided that the rise-time is greater than 1 μsec. and the total pulse duration less than about 15 msec. These limits can, however, be extended in both directions by comparatively simple modifications to the pretreatment unit.

The maximum counting rate per channel is 700 counts/minute for 1 percent loss. The total counting rate acceptable is, of course, merely limited by the input pulse length when long pulses are being used, since the probability of two pulses overlapping must always be kept low if reliable analysis is required. For example with $a+b=500$ μsec. a total speed of 1200 counts/minute will give a 1 percent overlap probability. For short pulses the ultimate limit is set by the 80 μsec. channel-operating wave, giving 1 percent loss at 7500 counts/minute. In general these limitations are not serious, since the amplitude analysis yields information so much more rapidly than do successive measurements of points on a bias curve, that a reduction of the counting rate can usually be tolerated.

The channel positions are stable to within 0.04 volt (or 1.2 percent of 1 channel width) against mains voltage changes from 105 v to 120 v. They are subject to long term drift (over a period of weeks) of about 0.05 volt. The general reliability of the instrument is very good.

IX. ACKNOWLEDGMENTS

The work described in this paper was part of the research programme of the Atomic Energy Division of the National Research Council of Canada. The authors had the benefit of discussion with their colleagues throughout the work, and in particular they wish to acknowledge the contribution of Mr. A. G. Ward in the initial stages of planning the design of the instrument.

THE REVIEW OF SCIENTIFIC INSTRUMENTS VOLUME 20, NUMBER 3 MARCH, 1949

A Magnetic Ion Source

CARL BAILEY,* D. L. DRUKEY, AND F. OPPENHEIMER
Department of Physics, University of Minnesota, Minneapolis, Minnesota

(Received November 8, 1948)

An ion source for particle accelerators is described. The ion source utilizes an axial magnetic field for collimation of ion and electron beams and provides an electric field-free region for ion formation. The ion source has afforded yields of 500 microamperes of resolved protons when used in conjunction with a 200-kv high voltage set. A feature of the ion source is the possibility of obtaining favorable atomic to molecular ion ratios.

A MAGNETIC ion source yielding fairly large ion currents has recently been installed on the 200-kv ion accelerator[1] at the University of Minnesota. Sources utilizing a similar principle have been described by at least two authors.[2,3] The Minnesota source was patterned after one built at the University of California by one of us.

The essential features, although not the constructional details, of the present source are indicated in Fig. 1. The hydrogen supply, not shown, is from a supply tank with an electrically heated palladium leak. The field coil, about 400 turns of $\frac{3}{8}$-inch o.d. copper tubing cooled by kerosene flowing internally, supplies an axial magnetic field with its maximum intensity at the center of the arc chamber. The field is adjustable to an upper limit of about 1800 gauss. The filament consists of one and a half turns of 0.060-inch tungsten wire. The space between filament and arc chamber is about $\frac{1}{4}$ inch. The arc chamber is a non magnetic stainless steel cartridge with 0.050-inch molybdenum end plates and is so constructed that it can be removed as a unit from the brass shell of the source. The holes in the molybdenum plates at the filament and probe ends are, respectively, $\frac{3}{16}$ inch and $\frac{1}{16}$ inch in diameter. The $\frac{1}{16}$ inch is bevelled to an angle of 60° on the side facing the probe in order to improve the focussing properties of the gap somewhat. The entrance hole in the non-magnetic stainless steel probe is $\frac{1}{4}$ inch in diameter, and the gap between the probe and the molybdenum plate is $\frac{1}{8}$ inch. The focus electrode is also constructed of non-magnetic stainless steel. Liners of the same material hold the assembly in place. The insulators for the probe and filament leads are special spark plug type seals.

The accelerating tube consists of porcelain insulators very kindly supplied by R. G. Herb of the University of Wisconsin and steel spinnings similar in design to those used in the Wisconsin accelerator. The first few sections of the tube are indicated in Fig. 2. There are eight sections comprising a tube 20 inches long.

Power for the operation of the source is supplied by three generators located in the high voltage shell and driven by insulating belts from motors at ground potential. The first of these, a 3-kw, 32-volt d.c. generator, supplies up to 100 amperes to the field coil and is controlled by a series resistance and/or field rheostat. Normal power consumption is about 750 watts. A 250-volt d.c. generator supplies voltage to accelerate the electrons from the filament and maintains the arc. Control consists of a 70-ohm series resistor to limit the arc current. A 110-volt a.c. generator supplies power to operate the filament, heat the palladium leak, and for the probe high voltage supply. The filament is heated from the secondary of a 10-volt, 1-kw transformer with primary controlled by a Variac and uses about

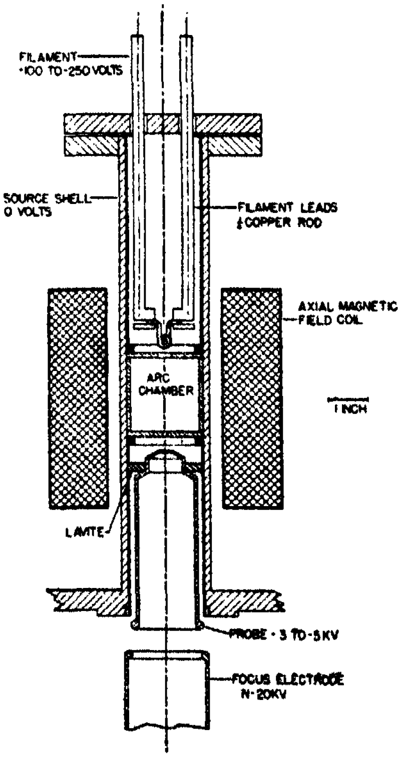

FIG. 1

---

* Now at Concordia College, Moorhead, Minnesota.

[1] J. H. Williams, W. H. Wells, J. T. Tate and E. L. Hill, Phys. Rev. 51, 434 (1937).

[2] A. Theodore Finkelstein, Rev. Sci. Inst. 11, 94 (1940).

[3] M. von Ardenne, Physik. Zeits. 43, 91 (1942).

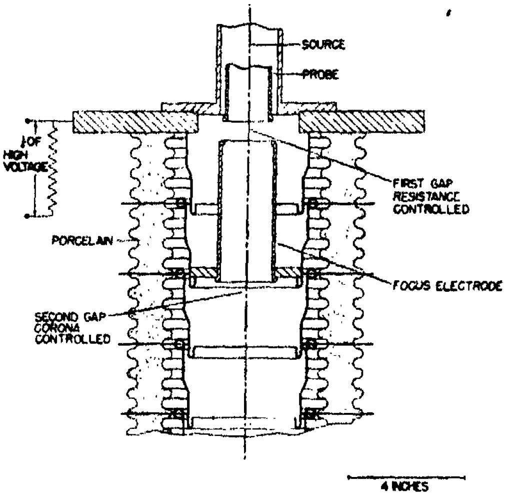

FIG. 2.

60A at 2.5 v. The palladium leak is likewise supplied by a transformer and Variac. The probe high voltage supply is a half-wave rectifier capable of delivering up to 10 kv at 20 ma. The high current rating is necessitated by the large current to the probe under certain defocusing conditions. Control is provided by a Variac in the primary of the high voltage transformer. Voltage to the focus electrode is supplied by a resistance divider across part of the main high voltage supply. For the above reason, this divider has been designed to carry 2 ma of current. Voltage on the spinnings is supplied from a series of corona gaps, the first of which is adjustable. Source body, filament, and magnet coil are cooled by kerosene pumped up from ground potential through insulating tubing. Rough measurements on the hydrogen flow to the source indicate that the gas is used at the rate of 10±5 standard cc per hour at maximum proton yield. At this flow, the pressure at the source is about 0.02 mm Hg, and at the ground end of the accelerating tube it is about 1×10^{-5} mm Hg. Differential pumping is not employed.

By proper manipulation of probe, focus electrode, and second gap voltages, the beam can be focused into a spot ⅛ inch to ¼ inch in diameter on a target seven feet from the source. A magnetic analyzer and a ½-inch diameter diaphragm serve to resolve the beam according to mass. A ⅜-inch diameter diaphragm located between the first diaphragm and the target, and at considerable negative potential, effectively prevents secondary electron emission from the insulated target cup.

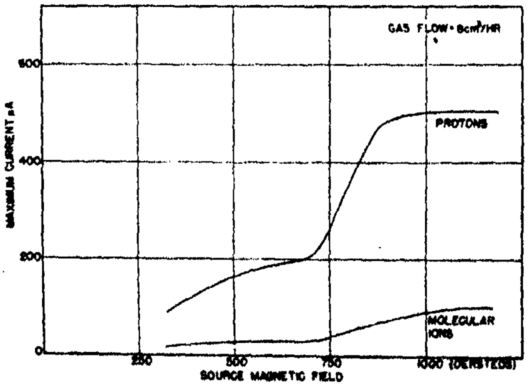

FIG. 3.

Performance curves for 160-kv accelerating voltage are given in Figs. 3 and 4. They show that a source magnetic field of 1000 gauss affords a good yield and that an excess of protons over molecular ions is obtained under usual conditions. This situation is reversed, however, if the gas flow is increased fourfold and the source magnetic field is reduced to about 400 gauss, in which case proton currents of about 100 μA and molecular currents of 200 μA are obtained. It is thus possible to obtain relatively heavy molecular beams also. With the filament, arc chamber, and probe aligned, it is found that optimum yields are obtained when the source magnetic field is coaxial with the source.

Use of a 0.080-inch diameter hole in the second molybdenum plate of the arc chamber resulted in a 20 percent increase in ion yield over that from the $\frac{1}{16}$-inch hole. The gas flow, however, increased by a factor of two with resultant increase in tube pressure. It is felt that the increase in yield might have been better with differential pumping, since tube pressure seems to have a strong influence on yield at these low energies.

Filament life with this design has proved good with operating lives of several hundred hours not uncommon. The arc starts readily, and when the tube is properly outgassed, nearly the maximum proton current is attained after a few minutes of operation.

The functions of the source magnetic field in improving the yield of the source are threefold. The electron beam is collimated by the magnetic field so that most of the arc is in regions from which the ions might be used. For a given gas flow, the yield is higher because the magnetic field keeps the ions from diffusing to the walls of the arc chamber and being lost. The ratio of ion density to arc pressure is thus higher in the presence of the magnetic field. At this field the average ionic radius of curvature is of the order of the diameter of the exit hole. The formation of atomic ions appears to be in large part a two-step process which is thus greatly facilitated by the increased ratio of ions and electrons to un-ionized molecules. The high ratio of protons to molecular ions obtained with this source and the dependance of that ratio on source pressure seem to bear out this point of view. The present limitation on the available ion current seem to be largely due to the inability of the present probe geometry to focus the ions leaving the plasma when the ion density of the plasma is increased by larger arc currents. At larger arc currents, the ion beam bombards the probe or other electrodes and is lost from the beam. Probe and focus electrode currents of several milliamperes have been observed under such defocused conditions so that it seems likely that this amount of current is really available for the beam. A calculation of the space charge limitation resulting from plane geometry with dimensions similar to that of the source indicates a current density such that from a $\frac{1}{16}$-inch aperture only about half as much current as actually reaches the analyzer might be expected. It thus seems necessary to open the exit hole or change the probe design so that larger voltages or smaller gaps can be used without defocusing the beam too badly if large currents are to be obtained.

The source in its present form does not represent a final design. It would be desirable to have the magnet coil removable over the head flanges, and differential pumping would be desirable and even necessary for a longer accelerator. It seems quite likely, on the basis of the present experience, that a permanent magnet might be substituted for the field coil with much saving in the cooling requirements for the source as a result of the much decreased power consumption.

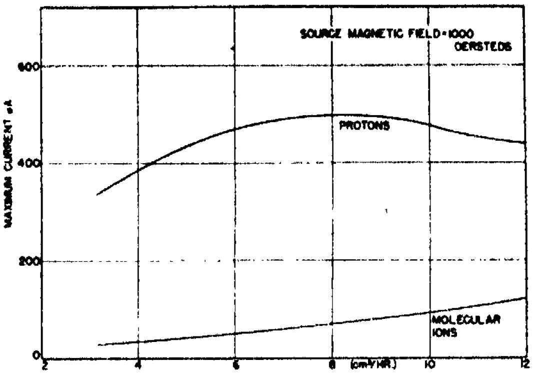

FIG. 4.

This research was done under the partial support of the Office of Naval Research, Contract N5ori-147. It was also materially assisted by the University of Minnesota Technical Research Fund subscribed to by General Mills, Inc., Minneapolis Honeywell Regulator Company, Minneapolis Star Journal and Tribune Company, Minnesota Mining and Manufacturing Company, and Northern States Power Company.

THE REVIEW OF SCIENTIFIC INSTRUMENTS VOLUME 20, NUMBER 3 MARCH, 1949

A Theory of the Solenoid Beta-Ray Spectrometer

E. PERSICO
Université Laval, Québec, P. Q., Canada

(Received November 22, 1948)

A theory of the magnetic lens beta-ray spectrometer utilizing the uniform field of a long solenoid is developed. First the case of a point source is considered, and it is found that the resolving power, for a given solid angle, is maximum when the emission angle α (average angle between the rays leaving the source and the axis) is 45° 37′. Then the theory is extended to the case of a disk source, and it is found that for a given intensity (product of the source area by the solid angle) there is an optimum source diameter and an optimum emission angle, ranging in practical cases between 36° and 40°. The problem of optimum conditions when the quantity of copper in the solenoid and the electric power available are limited by economical considerations is also studied, and it is found that the optimum α-value is in this case about 21°.

INTRODUCTION

AMONG the different types of spectrometers used for analyzing beta-ray spectra, the solenoid spectrometer proposed by Kapitza in 1923[1] has been successfully employed by other physicists,[2] especially in cases where the radioactive material could not be concentrated on a very small area. This instrument is a particular kind of magnetic lens spectrometer, in which the focusing field is the uniform field produced by a long solenoid: this permits a rigourous calculation of the trajectories, and a study of the geometrical properties, which would be very difficult in the other types of magnetic lens spectrometers utilizing non-uniform fields.

A theory of the solenoid spectrometer has been given by Witcher,[2] but it is confined to the case of a point source and does not investigate the conditions giving the maximum resolving power for a given intensity. In this paper we start the theory for a point source in a manner more suitable to its exten-

---

[1] P. Kapitza, Proc. Camb. Phil. Soc. **22**, pt. 3 (1924).

[2] R. A. R. Tricker, Proc. Camb. Phil. Soc. **22**, 454 (1924); C. M. Witcher, Phys. Rev. **60**, 32 (1941); K. Siegbahn, Ark. for Mat., Astr. och Fys. **28A**, 4, N°17 (1942).

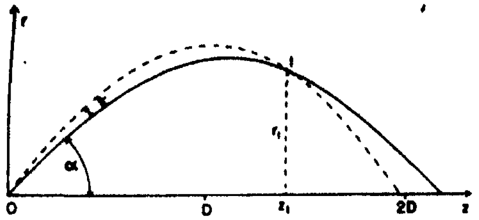

FIG. 1. Formation of the "ring image." The emission angle, α, has been chosen equal to 45° 37′, optimum value for a point source.

sion to the case of a source of finite area. Then we develop simple approximate formulas for the latter case, and apply them to find the optimum source diameter and the optimum emission angle (average inclination, with respect to the field, of rays leaving the source).

RING IMAGE OF A POINT SOURCE

Let us consider a point source, emitting isotropically electrons of momentum p, in a uniform field H. We shall assume cylindrical coordinates z, r, ψ (with the z axis parallel to the field, and the origin in the source) and put for conciseness:

$$D=2p/(eH), \tag{1}$$

(e being the electron charge in e.m.u.). This length determines roughly the linear dimensions of the apparatus.

The trajectory of any electron leaving the source at an *emission angle* α with the z axis will be, as is well known, a cylindrical helix of pitch $\pi D \cos\alpha$ and diameter $D \sin\alpha$, having the z axis as a generatrix. The equation for r will be (also in relativistic mechanics)

$$r=D \sin\alpha \sin\zeta, \tag{2}$$

where

$$\zeta(z)=z/(D \cos\alpha). \tag{3}$$

The sinusoid representing r as a function of z (Fig. 1) will be called, conventionally, a "trajectory," although it represents only the motion in a meridian plane revolving around the z axis so as to contain always the instantaneous position of the electron. We shall consider only the first half-wave-length of the sinusoid, that is, suppose as usual, that the electrons make less than one revolution. Let us now consider another electron leaving the source at an angle $\alpha+d\alpha$: its trajectory will intersect the preceding one at a point I such that

$$(\partial r/\partial\alpha)_I=0. \tag{4}$$

From (2) one gets for such a point

$$[\zeta^{-1} \tan\zeta]_I=-\tan^2\alpha. \tag{4′}$$

It will be useful in the following to introduce the function $\beta(\alpha)$ defined by

$$\tan\beta/(\pi-\beta)=\tan^2\alpha, \quad 0\leqslant\beta\leqslant\pi/2, \tag{5}$$

(whose diagram is given in Fig. 2). Then we have

$$\zeta_I=\pi-\beta, \tag{6}$$

$$z_I=(\pi-\beta)D \cos\alpha, \tag{6′}$$

and from (1)

$$r_I=D \sin\alpha \sin\beta. \tag{7}$$

If the rays where limited by a diaphragm with an infinitely narrow annular slit, so as to admit only rays with α ranging in an infinitesimal interval, they would produce, in the plane $z=z_I$, a circumference of radius r_I, which may be called a "ring image" of the source (giving a generalized meaning to the word "image").

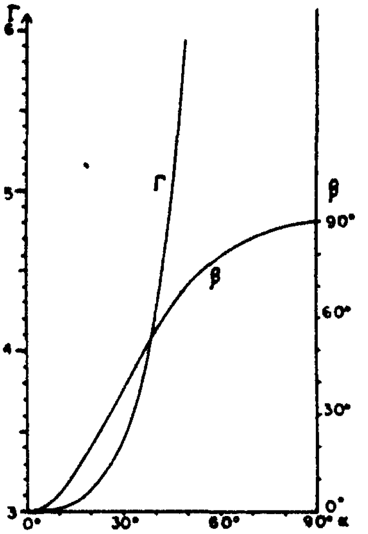

FIG. 2. The auxiliary functions $\beta(\alpha)$ and $\Gamma(\alpha)$.

If the diaphragm slit has a finite width, the ring image will be no longer an infinitely thin line, but will acquire a certain width, as a result of the difference in the spherical aberration of rays with different values of α. To take this effect into account we consider the trajectories leaving the source at angles $\alpha\pm\epsilon$ and develop (2) in Taylor series, neglecting powers of ϵ higher than the second and using (4):

$$r=r_I+(\partial^2 r/\partial\alpha^2)_I\epsilon^2/2. \tag{8}$$

As is seen, to this order of approximation the two trajectories corresponding to $\alpha+\epsilon$ and $\alpha-\epsilon$ fall together on the image plane, and so the width of the ring produced by all rays between $\alpha-\epsilon$ and $\alpha+\epsilon$ is

$$\Delta r=(\partial^2 r/\partial\alpha^2)_I\epsilon^2/2. \tag{9}$$

Differentiating (2), taking into account (4′) and introducing for simplicity the function of α defined by

$$\Gamma(\alpha)=3+\cos^2\alpha \tan^2\beta, \tag{10}$$

(whose diagram is shown in Fig. 2) one gets:

$$\Delta r = (D/2)(\sin\beta/\sin\alpha)\Gamma\epsilon^2. \tag{11}$$

RESOLVING POWER

We define the resolving power P by

$$P = p/\Delta p, \tag{12}$$

where Δp is the increase to be given to the momentum p of the electrons in order that the radius of the ring image be changed by an amount equal to its width (it will be noted that in this virtual change of p, α does not remain constant, its value being determined, for each value of p, by the radius and position of the diaphragm slit). This definition of the resolving power is somewhat more stringent than that usually adopted in optics, because it takes into account the *total* width of the spectral line instead of its half-value width.

Now, from (1) and (4) we get

$$dr_I = (\partial r/\partial D)_I(D/p)dp,$$

so that, identifying dr_I with the ring width Δr and dp with the corresponding Δp, we have

$$P = (\partial r/\partial D)_I D/\Delta r.$$

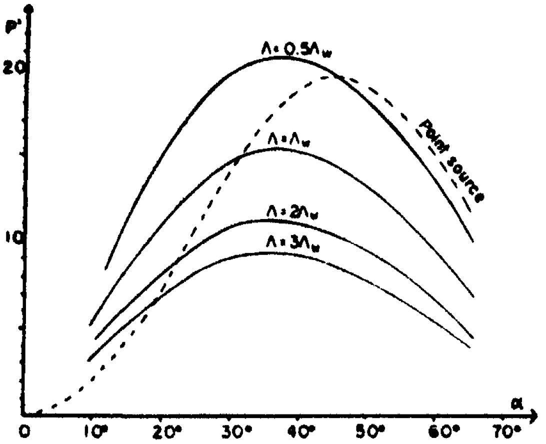

FIG. 3. The broken line represents (in an arbitrary scale), the resolving power *versus* emission angle for a point source (the scale of ordinates depends on the width of the diaphragm slit). The full lines represent the resolving power *versus* emission angle for a disk source of the optimum diameter, for different slit widths, corresponding to different values of Λ; ($\Lambda_W = 3.26\cdot 10^{-6}$).

Differentiating (2) with respect to D (contained also in ζ) and remembering that Eqs. (6) and (6′) apply to point I, we get

$$(\partial r/\partial D)_I = (\sin\beta)/\sin\alpha,$$

and therefore

$$P = (D \sin\beta)/(\Delta r \sin\alpha). \tag{13}$$

Putting in this formula the expression of Δr given by (11), we obtain the resolving power for a point source and a diaphragm admitting rays of emission angles between $\alpha-\epsilon$ and $\alpha+\epsilon$:

$$P = 2/(\epsilon^2\Gamma). \tag{14}$$

OPTIMUM VALUE OF α FOR A POINT SOURCE

In the case of a point source of given activity, the *intensity* of the electron current actually received on the detector will be proportional to the solid angle Ω filled at the source by all rays passing through the diaphragm, which is

$$\Omega = 4\pi\epsilon \sin\alpha. \tag{15}$$

Now suppose we try different values of α and for every one adjust the slit width so as to have always the same intensity: how will the resolving power vary? To find this, we eliminate ϵ between (14) and (15) and obtain for the resolving power

$$P = (32\pi^2 \sin^2\alpha)/(\Omega^2\Gamma). \tag{16}$$

This function is shown in Fig. 3 (broken line) for an arbitrary value of Ω (i.e., in an arbitrary ordinate scale). As is seen, it has a maximum which can be found by differentiation of (16) and elimination of $\tan\alpha$ with (5). After some reductions, one obtains the following equation for $x = \tan\beta$:

$$x/(\pi - \text{arc}\tan x) = (x^4 - 2x^2 - 3)/(x^2 + 3).$$

Numerical solution gives $x = 2.104$, whence $\beta = 64°\,35'$ and $\alpha = 45°\,37'$ (for any value of Ω). With this value of α, (16) gives the following relation between the optimum resolving power and the solid angle for a point source:

$$P_0 = 31.2/\Omega^2. \tag{17}$$

The coordinates of the ring image are obtained from (6′) and (7) and are $z_I = 1.408D$, $r_I = 0.645D$. Figure 1 shows the shape of this trajectory (full line) and the position of the image. The intensity and the resolving power are independent of D, that is of the linear dimensions of the apparatus.

EFFECTS OF THE WIDTH OF THE SOURCE

In most cases it is impossible to concentrate the radioactive substance on an area so small as to be considered a point source. So we shall now suppose

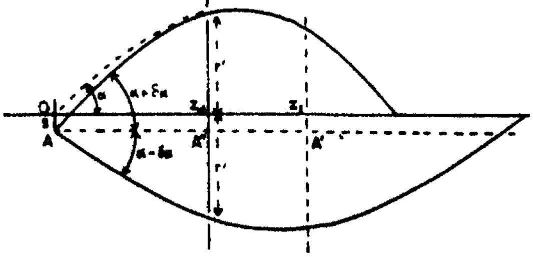

FIG. 4. Origin of "distortion."

that the source is no longer a point but a disk of radius $s=D\sigma$, perpendicular to the field, radiating isotropically, and that a practical limit is imposed not on the total quantity of radioactive substance but on its surface density. Then the intensity of the beam received by the detector will be proportional to the area of the source and to the (average) solid angle utilized, i.e., to the quantity $L=D^2\Lambda$, where

$$\Lambda=\epsilon\sigma^2\sin\alpha. \tag{18}$$

To see how the resolving power is affected by the finite diameter of the source, let us first of all study the ring image of a point A on the edge of the source, supposing the diaphragm slit infinitely narrow, that is $\epsilon=0$. To a first approximation (that is, ignoring the spherical aberration) one could consider A exactly like the point source of the preceeding theory and infer that it will give rise to a ring image centered on A', orthogonal projection of A on the image plane (Fig. 4). The image of the whole source, obtained by superposition of the ring images of all its points, would be a ring of width $2s$. But an additional blurring will be produced by an indirect effect of the spherical aberration, existing even if the slit is infinitely narrow (in which case there would be of course no *direct* effect of the spherical aberration). To see this, consider (Fig. 4) in the diaphragm plane $z=z_d$, an annular narrow slit of radius r', admitting the rays leaving the source center 0 at angle α. For a peripheral point A of the source (projected in A'') the slit is eccentrically placed: the distance of its points from A'' range from $r'-s$ to $r'+s$ and therefore the emission angle of the rays admitted will range from $\alpha-\delta\alpha$ to $\alpha+\delta\alpha$, where $\delta\alpha$ is given (neglecting second order terms) by

$$(\partial r/\partial\alpha)_{z=z_d}\delta\alpha=s. \tag{19}$$

Owing to spherical aberration, the rays emitted in different meridian planes will then meet the image plane at different distances from A', and the ring image of A will no longer be circular but will be flattened into an oval: we shall call this effect "distortion."[*] The superposition of the distorted ring images of all points of the source will give rise to a circular ring of width approximately given by (11), where ϵ is replaced by $\delta\alpha$.

If the slit has a finite width, so as to admit rays, from the source center, of emission angles $\alpha\pm\epsilon$, it will admit, from the source edge, rays of emission angles $\alpha\pm(\epsilon+\delta\alpha)$: therefore the effect of distortion may be approximately taken into account by replacing ϵ by $\epsilon+\delta\alpha$ in (11). One sees that $\delta\alpha$, and therefore the importance of distortion, depends on the position of the diaphragm: the nearer it is to the source, the greater is $\delta\alpha$. As far as distortion is concerned, it would seem advisable to put it as near the image plane as possible, but other practical reasons suggest locating it near the middle instead. We shall suppose it is put in the symmetry plane of the central trajectory (that is the plane where r is maximum). Then, from (19) and (2), one gets

$$\delta\alpha=\sigma/\cos\alpha. \tag{20}$$

Now let us consider the image of the whole source, obtained by the superposition of the distorted ring images of all its points. It will be a ring of width

$$\begin{aligned}\Delta r&=2s+(\partial^2r/\partial\alpha^2)_I(\epsilon+\delta\alpha)^2/2\\&=2s+(D/2)(\sin\beta/\sin\alpha)\Gamma(\alpha)(\epsilon+\delta\alpha)^2.\end{aligned}$$

Putting this expression in (13) we obtain for the inverse resolving power in the case of a disk source

$$1/P=2\sigma(\sin\alpha/\sin\beta)+\Gamma(\alpha)(\epsilon+\delta\alpha)^2/2. \tag{21}$$

If we neglect distortion this formula becomes

$$1/P=2\sigma(\sin\alpha/\sin\beta)+\Gamma(\alpha)\epsilon^2/2. \tag{22}$$

In the ensuing discussion we shall always begin with this formula and then estimate the corrections introduced by distortion.

OPTIMUM SOURCE DIAMETER

Suppose we vary the source diameter and also the slit width so as to get always the same intensity: how will the resolving power vary? To determine this, let us eliminate ϵ from (18) and (22):

$$1/P=2\sigma(\sin\alpha)/\sin\beta+\Lambda^2\Gamma/(2\sigma^4\sin^2\alpha). \tag{23}$$

Considering $1/P$ as a function of σ (for constant α and Λ) one finds easily, by differentiation, that it has a minimum (and therefore the resolving power a maximum) for σ given by

$$\sigma_0=\Lambda^{2/5}\Gamma^{1/5}\sin^{1/5}\beta\sin^{-3/5}\alpha, \tag{24}$$

or, if we prefer to express it in terms of ϵ, by means of (18),

$$\sigma_0=(\Gamma\epsilon^2\sin\beta)/\sin\alpha. \tag{24'}$$

This gives the optimum value of the source radius for a given α and a given intensity. Putting it in (23), we get for the resolving power

$$P=(2/5)\Lambda^{-2/5}(\Gamma\sin^2\alpha\sin^{-4}\beta)^{-1/5}. \tag{25}$$

Note that the factor 5/2 in $1/P$ comes from the addition of 2, from the first term in (23), and $\frac{1}{2}$, from the second (the expressions multiplying these factors becoming equal for $\sigma=\sigma_0$): so we can say that *the optimum source diameter is that contributing to the image width four times the width due to aberration.*

OPTIMUM EMISSION ANGLE FOR A GIVEN FIELD

Suppose we vary the emission angle α, adopting for each value of it the corresponding optimum source diameter and the slit width giving always the same intensity, that is the same Λ. Then (25) shows that the resolving power will vary proportionally to the function

---

[*] Of course this effect must not be confused with the aberration of the same name in the theory of ordinary (point) images.

$$\Gamma^{-1/5}\sin^{-2/5}\alpha\,\sin^{4/5}\beta. \tag{26}$$

This function has a maximum: it can be found by logarithmic differentiation of (26) which gives, after some transformations, the equation

$$(1+2\cos^2\alpha)\tan^4\beta+(2-\tan^2\alpha)\tan^2\beta-9\cos^{-2}\alpha=0, \tag{27}$$

which, together with (5), determines the values of α and β corresponding to the optimum. These are: $\alpha=40°\,25'$, $\beta=57°\,10'$. Inserting these values in (6′) and (7) we find the coordinates of the ring image of the source center: $z_I=1.63D$, $r_I=0.544D$. The corresponding resolving power (optimum for a given Λ and a given D) is

$$P_0=0.308\Lambda^{-2/5}. \tag{28}$$

The source radius is given by (24): $\sigma_0=1.69\Lambda^{2/5}=0.52/P_0$. The latter relation can be also written

$$2s_0/D=1.04\Delta p/p, \tag{29}$$

whence the following practical rule: *when the optimum emission angle is adopted, the source diameter, expressed in terms of D, must be equal to the desired* $\Delta p/p$.

Figure 5 shows the image position and the shape of the trajectory corresponding to the emission angle 40° 25′ (full line). The large diameter of the ring image makes obviously impractical the use of a conventional front-window counter for detection, suggesting instead the use of a counter with lateral windows covering almost the whole circumference, as is shown in the figure,** or some other device.

ECONOMICAL OPTIMUM

The optimum conditions we have discussed till now are those for a given value of D (and therefore of the field intensity H). If, in a disk-source spectrometer, we increase D, that is, increase all the linear dimensions of the apparatus in the same ratio, the resolving power will remain constant while the intensity will increase as the square of this ratio (owing to the increase in the source area). However it must not be forgotten that the background of spurious counts of the G-M counter increases with its surface: so the ratio between the intensity and the background will be almost independent of D, and the advantage of a bigger apparatus will be chiefly that of getting the same number of counts in a shorter time (which is important especially with short-lived isotopes).

A practical limit to the dimensions of the apparatus is given of course by economical considerations. If these, more than the signal-background ratio, are taken into account, the problem of the optimum must be put in a slightly different manner.

Calling l the solenoid length, R its average radius, t the thickness of the winding, the quantity of copper (for a given insulator-copper section ratio) is approximately proportional to the quantity $Q=tRl$, and the electric power needed to produce the field intensity H turns out to be approximately proportional to H^2Rl/t, that is to the quantity $w=Rl/(tD^2)$. The space in which field uniformity is required is that between source and image slit, that is, a cylinder of radius $r_{\max}=D\sin(\alpha+\epsilon)$ and length $z_I=(\pi-\beta)D\cos\alpha$. To insure uniformity in this space the solenoid must be given a supplementary length, proportional to its radius, which can be taken as three times the latter, if small supplementary windings are used to correct the field.[3] Then we can take, approximately (neglecting ϵ)

$$R=D\sin\alpha,\quad l=D(\pi-\beta)\cos\alpha+3\,D\sin\alpha,$$

and therefore

$$Q=tD^2y(\alpha),\quad w=y(\alpha)/t,$$

where

$$y(\alpha)=[(\pi-\beta)\cos\alpha+3\sin\alpha]\sin\alpha.$$

Now the problem is to find such values of t, D, σ, ϵ, α, that the whole set of four functions $-Q$, $-w$, L, P of these five variables is "simultaneously optimum," by which we mean that for any small variation of the variables one at least of the four functions decreases. This problem is equivalent to that of finding the maximum of P subject to the condition that Q, w, L (instead of D, Λ) have constant values, and can be solved in the routine way.

One finds that the optimum source radius is still σ_0 given by (24) or (24′), producing an image width four times that due to the aberration. With this value of σ the resolving power, as a function of α, is

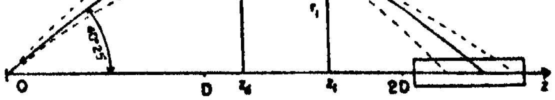

FIG. 5. Shape of trajectory and image position for the optimum emission angle with a disk source of the optimum diameter.

** In this figure we have put the two edges of the image slit in the same plane. As Stanley Frankel, Phys. Rev. 73, 804 (1948) has suggested, it is advantageous to put the inner one a little nearer the source and the outer one a little farther. This improves the "shape" of the resolution curve, but does not affect its total width. Besides, Frankel's reasoning holds only if the first limiting diaphragm is very near the source.

[3] G. Hall, unpublished.

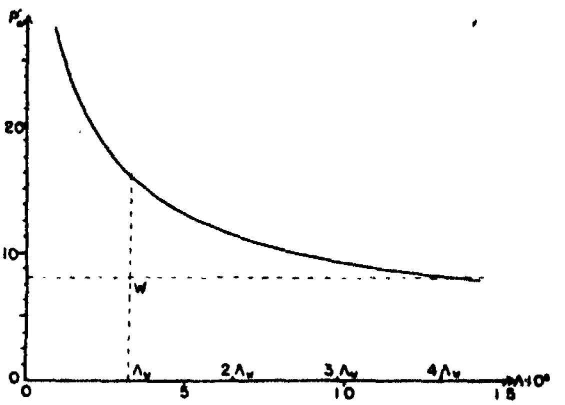

FIG. 6. Resolving power *versus* intensity in the optimum conditions for a given magnetic field.

given (neglecting distortion) by

$$P=(2/5)(Qw/L)^{2/5}(\Gamma\sin^2\alpha\sin^{-4}\beta)^{-1/5}y^{-4/5}.$$

This function has a maximum, which by numerical calculation results about at $\alpha=25°$: this is therefore the most economical angle when distortion is negligible.

With this value of α, formulas (6′) and (7) give, for the coordinates of the ring image: $z_I=2.39D$, $r_I=0.206D$. The optimum source radius and the corresponding resolving power are

$$\sigma_0=1.85\Lambda^{2/5},\quad P_0=0.225\Lambda^{-2/5}, \tag{31}$$

so that, instead of (29), we have

$$2s_0/D=0.83\Delta p/p.$$

EFFECTS OF "DISTORTION"

In the preceding calculations we have disregarded the effect we have called "distortion": so the formulas we have obtained for the disk source are valid only as a limiting case for very small slit width. We shall now take this effect into account and find the corrections for finite slit width. To this end we must start with (21) instead of (22): using (18) and (20), this formula gives (if we call P' the resolving power corrected for distortion)

$$1/P'=2\sigma(\sin\alpha/\sin\beta)+(1+\sigma^3\Lambda^{-1}\tan\alpha)^2\Lambda^2\Gamma/(2\sigma^4\sin^2\alpha). \tag{32}$$

Differentiating with respect to σ and equating to zero we get the optimum value of σ, corrected for "distortion."

$$\sigma_0'=\sigma_0(1+\varphi/2-\varphi^2/2)^{1/5}, \tag{33}$$

where σ_0 is defined by (24), and φ by

$$\varphi=\sigma_0'^3\Lambda^{-1}\tan\alpha. \tag{34}$$

This correction to the source radius is of no practical importance: with ordinary conditions it may amount to a few units percent. Of considerable importance however is the effect of distortion on the resolving power. If, neglecting the difference between σ_0 and σ_0', we replace σ in (32) by σ_0 given by (24), we get

$$P'=P[1+(2/5)\varphi_0+(1/5)\varphi_0^2]^{-1}, \tag{35}$$

where $\varphi_0=\sigma_0^3\Lambda^{-1}\tan\alpha$. The resolving power is therefore reduced by an amount depending on Λ. Figure 3 shows its dependence on α (supposing D fixed) for different values of Λ (expressed as multiples of $\Lambda_W=3.26\cdot10^{-6}$, which is the value of Λ in Whitcher's apparatus). One sees that the optimum is shifted to about 36° for the whole represented range of Λ, and the maximum resolving power ranges from 20.9 for $\Lambda=0.5\Lambda_W$ to 9.43 for $\Lambda=3\Lambda_W$.

These results are better represented by Fig. 6, showing the corrected resolving power *versus* Λ (and therefore *versus* the intensity), assuming a fixed D and for each Λ the optimum α and σ. Point W represents Λ and P for Witcher's spectrometer ($\alpha=18°$): one can see that there is the theoretical possibility of doubling the resolving power while keeping the same intensity, or of quadrupling the intensity for the same resolving power.

If the corrections for "distortion" are applied to the determination of the most economical conditions, one finds similar results. For instance, for $\Lambda=\Lambda_W$ the most economical angle is shifted to about 21°, the corresponding resolving power is $P_0'=12.7$.

The author is glad to express his sincere appreciation for the valuable help given him by Professor G. Hall, who proposed this problem, made part of the calculations and contributed many useful discussions. Thanks are also due to Professor L. Kerwin for revising the manuscript.

THE REVIEW OF SCIENTIFIC INSTRUMENTS VOLUME 20, NUMBER 3 MARCH, 1949

A Simplified Chronotron-Type Timing Circuit

J. Warren Keuffel*
California Institute of Technology, Pasadena, California

(Received November 8, 1948)

A timing circuit is described similar in principle to the Neddermeyer "chronotron," but with the following simplifications and modifications: parallel-wire polythene-tape line to eliminate co-ax "plumbing," germanium crystal detectors, and a delay-line presentation circuit. This circuit uses a single common amplifier for all pulses, which increases stability, makes adjustment easy, and effects a tenfold saving in the number of tubes. It simultaneously records time intervals in two ranges, e.g., 0–0.1 and 0–5 μsec. The precision is 1×10^{-9} sec., but may be increased at the expense of the range. Problems connected with coupling the instrument to parallel-plate counters are discussed.

I. INTRODUCTION

THE timing circuit to be described below was developed in conjunction with the parallel-plate counters discussed in the preceding paper. An instrument having a precision of the order of 10^{-9} sec. is required if the full potentialities of the new counters for the measurement of ultra-short time intervals are to be realized.

Now the pulse from a parallel-plate counter is easily adequate for direct deflection of the plates of a cathode-ray tube, but the problems of providing a precision time base and of recording the measurements photographically are formidable ones. A very elegant timing circuit, the chronotron, has been described by Neddermeyer and co-workers;[1] this instrument uses as a "time base" the precisely known motion of electromagnetic pulses on transmission lines and permits easy photographic recording. In the form developed by these authors, however, it is quite cumbersome, with over 100 tubes, and rather difficult to adjust and maintain. Both these difficulties have been overcome in the present design, and it is believed that the performance has been improved in some respects.

The basic principle of the chronotron is as follows. Two pulses whose time difference we wish to determine are applied, one to each end of a transmission line. They travel towards each other, and their point of intersection is ascertained by a suitable array of detectors distributed along the line. If the pulses are applied simultaneously to the ends of the line, they will evidently meet in the middle, while if one pulse is delayed with respect to the other, the meeting point will be shifted towards the side of the later pulse. The time interval between the two pulses is given by $2x/c$, where x is the distance from the center of the line to the point of intersection and c is the velocity of propagation of the pulses on the line.

In order that the detector array may indicate the point of intersection, a detector must respond differently to two pulses which traverse it simultaneously and two pulses which pass at different times. If the detector responds like a peak voltmeter, for example, then the pulses produce twice the output from the detector located at their meeting point than they produce from detectors some distance away from this point.

A plot of the detector outputs against the detector positions along the line is called a *superposition locus*, and the position of the peak of this curve gives, of course, the meeting point of the pulses.

If the number of detectors is limited, the detector spacing determines both the range of the instrument and its precision; close spacing gives a high precision but a limited range of measurable intervals. The pulse width must, of course, be chosen somewhat greater than the detector spacing for any particular setup.

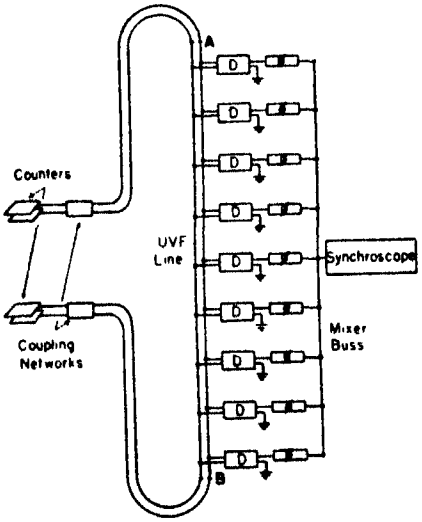

FIG. 1. Chronotron timing circuit. The array of detectors D determines the point of intersection of the pulses from the counters along the UVF line. Video pulses from the detectors are "sorted out" by the delay lines ϕ, so that they appear in order on the synchroscope screen.

---

* Now at Princeton University, Princeton, New Jersey. This paper is based on part of the work done for the doctoral thesis at the California Institute.

[1] S. H. Neddermeyer, E. J. Althaus, W. Allison, and E. R. Schatz, Rev. Sci. Inst. 18, 488 (1947).

A block diagram of the present instrument is shown in Fig. 1. The detectors produce video pulses proportional in amplitude to the detector outputs, *but which are very much broader than the original pulses on the line and are not used as direct carriers of time information to the synchroscope.*** These pulses are sorted out by a series of delay lines, each slightly longer than the next, and present upon the trace of a synchroscope the *superposition locus* corresponding to the event being recorded.

To facilitate the discussion of the instrument, it is convenient to introduce the term "ultra video-frequency" (*UVF*) to describe wide-band circuits for the range of approximately 50 to 1000 mc/sec. and pulses of the order of 5×10^{-9} sec. in duration. Some such terminology is necessary to distinguish between the pulses produced by the detectors, which are in the usual video range, and the actual *UVF* pulses on the timing line.

Before proceeding to a detailed discussion, it might be well to mention a possible generalization of the instrument to the study of arbitrary fast wave forms. If a gate pulse which is short compared to the wave form of interest, but higher than the peak of that wave form, is sent down the timing line in one direction and the wave form of interest sent in the opposite direction, the superposition locus will trace out the wave form of interest. (The detectors may be biased to respond only to voltages greater than the gate pulse.)

Finally, it should be pointed out that the presentation system described in Part V offers possibilities for recording any multiple set of data which may be translated into video pulses.

II. THE *UVF* LINE

The use of an open parallel-wire line is very tempting indeed from the standpoint of ease of construction and manipulation, especially now that there is on the market a flexible parallel-wire line embedded in polythene tape.*** The radiation from the line has not proved serious; the chief difficulty has been found to be with the unbalanced currents.

A characteristic impedance of 300 ohms is a reasonable compromise between the following two desiderata: (a) the capacitors coupling the counter to the line should be small, to minimize the energy which flows in the spark; hence the characteristic impedance of the line should be *large* to preserve a suitable coupling *RC* time constant; (b) the detector impedance being more or less fixed by crystal characteristics and stray capacitances, the characteristic impedance of the line should be *small* for low loading of the line by the detectors.

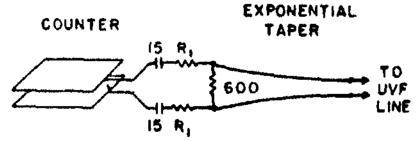

FIG. 2. Coupling network. The step-function wave form from the parallel-plate counter is differentiated to form an ultra-short pulse on the *UVF* line of the chronotron.

A 300-ohm parallel-wire line was therefore adopted. The section along which the detectors are mounted is an air dielectric line, made of No. 14 copper wire spaced 3/8″ center to center. Connections are made with the flexible polythene tape, as are also fixed delay sections which may be introduced to shift the detector section about with respect to the midpoint. In this connection it should be noted that, although the velocity of light on the polythene tape line is slower by about ten percent than in air, the velocity is independent of frequency, and hence the line is non-dispersive, provided only that the dielectric constant of the polythene is independent of frequency over the *UVF* band.

Even if this condition is not strictly true, the velocity is very insensitive to changes in the dielectric constant since so little of the space about the line is filled with dielectric, and because the square root of the dielectric constant enters the equation.

Finally, it may be remarked that no difficulty has been encountered with reflections on the line from supports and from soldered joints between sections of line. Coupling between adjacent sections of line has likewise not been troublesome; a spacing of a few inches has been easily adequate.

III. COUNTER-TO-LINE COUPLING

The present instrument is designed to work with the parallel-plate counters described in the preceding paper. The counters are coupled to the *UVF* line through small capacitors (10 to 15 $\mu\mu f$) for two reasons: (a) the effective capacitance in shunt with a counter must be kept low to minimize the charge, and hence the total energy, which flows through the counter per discharge; (b) the step-function wave form of the counter proper must be converted to a short pulse. Since the line looks like a pure resistance if it is either matched or long compared to the pulse length,**** we have here the usual differentiating circuit which will give us just the wave form desired, if the time constant is properly chosen.

The coupling network is shown in Fig. 2. The exponential taper section† converts the 300-ohm

---

** We shall point out later how they may *also* be so used for the measurement of time intervals in the 0.3- to 5-μsec. range.

*** Amphenol "Twin Lead" designed for television and f-m lead-ins.

**** There may, of course, be reflected pulses in the case of the unterminated line, but the pulse which starts down the line is still the same as in the terminated case.

† See, for example, F. E. Terman, *Radio Engineer's Handbook* (McGraw-Hill Book Company, Inc., New York, 1943), p. 196.

line to a 600-ohm impedance; it was made by splitting the last 30 cm of the polythene tape line and supporting the wires on appropriate Lucite spacers.

The coupling network also matches the counter impedance to the line, so that pulses travelling back along the line towards the counter are absorbed. The elimination of unwanted reflected pulses in the timing circuit is, of course, essential. The coupling network shown here was tested for reflections by connecting the counter and coupling network directly to the end of the timing line. A pulse from another counter was then sent down the line towards the network to be tested, and the superposition locus of the incident pulse plus its reflections, if any, was observed. It was found that the reflected pulse was less than 1/10 the amplitude of the incident pulse and of the opposite polarity. It was also found that the resistors R_1 could be left out without seriously impairing the line-to-counter match. They may be given any value up to a few hundred ohms if a longer *RC* constant is desired.

So far, the performance of ordinary midget resistors in the *UVF* band has been consistent with the assumption that they look like approximately their nominal resistance in parallel with 0.5 $\mu\mu$f.

IV. DETECTORS

Figure 3 shows the circuit diagram of a detector, together with the video pulse-forming network. A small fraction of the voltage pulse appearing on the *UVF* line at the location shown is impressed across the crystal and C_2 by means of the voltage divider R_3R_4. If the pulse is positive, the capacitor C_2 then charges up to the peak voltage across R_4—provided that the time constant involved is less than the duration of the *UVF* pulse. In the case of a negative pulse, the backwards resistance of the crystal is so great (150,000 ohms for the 1N34) that negligible current flows.

The charge on C_2 now flows off, relatively slowly, through *L* and R_5; since these elements, together with C_2, form a resonant circuit which is approximately critically damped, the wave form appearing at the grid of the 6AK5 cathode follower is a sort of half-sinusoid with an exponential tail. The output of the detector is thus a video pulse of width about 0.3 μsec. whose amplitude is proportional to the peak voltage which appeared on C_2. These pulses are then fed into the presentation circuit, which will be discussed in the next section.

To avoid confusion, note that the sole function of these video pulses is to carry to the synchroscope one particular set of data—the peak voltages at the several detectors. They do not directly carry time information to the trace of the cathode-ray tube.

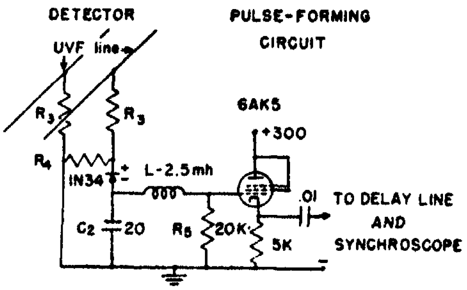

FIG. 3. Detector and pulse-forming circuit. The output is a pulse whose amplitude is proportional to the charge placed on C_2 by the detector.

The detector cannot be coupled directly to the 300-ohm *UVF* line, since the impedance of the crystal is too low and the line loading too great. At the same time, the charging time constant of C_2 must be kept low. A voltage divider of some sort is therefore required. The resistive coupling which was adopted has the advantage that the dispersion of the pulse produced by the presence of the detectors is to the first approximation zero.

The loading effects of detectors on the line have been calculated, and we may summarize the results as follows. With the resistive detector shown in Fig. 3, the attenuation is 0.30 db per detector over the central portion of the *UVF* band and the frequency at which the attenuation caused by stray shunt capacitance in the midget resistors is equal to the attenuation produced by the pure resistance alone is about 1500 mc/sec. Since it is voltage and not power which is our primary concern, it is thus possible to use about 20 detectors for a maximum voltage ratio from one end of the detector line to the other of two-to-one.

It is not essential that a detector operate strictly as a peak voltmeter, but only that it should discriminate between two pulses arriving at different times and two pulses arriving simultaneously. If the crystal is operated along a portion of its characteristic which follows approximately a square law, such discrimination is provided. However, the crystal characteristics are not exactly identical, and may change with use; these disadvantages are minimized if the charging time constant is made so small that the detector behaves as a peak voltmeter. In practice, a value of 300 ohms for R_4 has been found to give a satisfactory compromise between the demands of a short charging time and a large output voltage, even though this resistance, plus the estimated 100-ohm forward resistance of the crystal, gives a time constant of 8×10^{-9} sec. It is to be noted that C_2 may not be reduced, in order to reduce this time-constant, below 10 $\mu\mu$f or so, because the charge stored on it would then leak off through the backward resistance of the crystal rather than through the pulse-forming network.

V. PRESENTATION CIRCUIT

By "presentation circuit" we shall mean the circuit which takes the information contained in the series of charges stored on the detector condensers and transforms them into laboratory data—for example, pulses on a synchroscope screen. There are, no doubt, many ways to do this; the present system is quite simple and, in addition, has the major advantage that all the pulses pass through the same amplifier. The shape of the superposition locus therefore depends only on passive, relatively stable circuit elements and cathode followers.

As already mentioned in the preceding section, the charge stored on a particular detector condenser (C_2 in Fig. 3) flows off through L and R_5, forming a rounded pulse roughly 0.3 μsec. wide at the grid of the 6AK5 cathode follower. The pulses from the pulse-forming circuits are next passed through delay lines (ϕ in Figs. 1 and 4) whose function is to sort them out so that they appear in order upon the trace of the synchroscope. These delay lines are of the continuously loaded coaxial-line type,†† with a characteristic impedance of 1000 ohms and a delay of 0.6 μsec./foot.

Since the attenuation of this delay line is about 2.5 db per μsec., the shortest pulse which may be passed without serious dispersion should be used if many pulses are to be sorted out by this method. The 0.3-μsec. pulses used suffer but very little dispersion in traversing a 5-μsec. delay line. The attenuation introduced by the longer lines is compensated by a potentiometer in the output of each line. This system is now functioning satisfactorily with ten detectors, using 0.3-μsec. pulses spaced 0.5 μsec. center to center.

The unidirectional mixer circuit (Fig. 4) is of considerable importance. It functions as follows: consider a pulse coming from one of the delay lines, and further, suppose that the amplitude of this pulse is larger than any of the voltages at the other potentiometer outputs at this instant. Only the crystal at the output of the line we are considering will conduct, provided that the response of the cathode-follower grid circuit is fast enough. The pulse emerging from this line therefore sees an impedance which is approximately the 1000-ohm resistance of the output trimmer potentiometer; this match is adequate to prevent troubles from reflected pulses. Furthermore, the voltage at the cathode-follower grid is the voltage of the pulse of interest only; the voltages at the other outputs produce no flow of current in the grid resistor since the other crystals are nonconducting. The delay line whose output voltage is, at any given instant, the highest thus dominates the others.

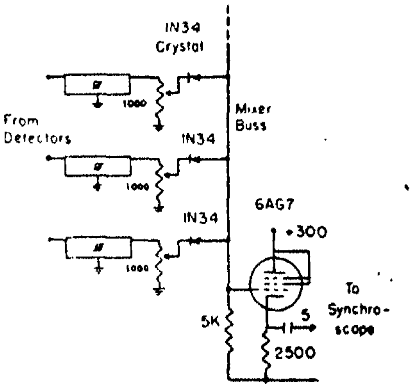

FIG. 4. Presentation circuit. The time delays of the video delay lines ϕ differ by 0.5 μsec. increments, so that signals applied almost simultaneously from the detectors appear in sequence on the synchroscope trace.

TABLE I. Chronotron tests. Polarities of pulses are reckoned with respect to detectors on line. In (a), (b), and (c), two simultaneous pulses are produced by dividing the signal from a single counter at a junction.

Test	Connection to *UVF* line at *A*	Connection to *UVF* line at *B*	Superposition locus
(a)	Pos. pulse	Pos. pulse	Max. at center
(b)	Pos. pulse	Neg. pulse	Null at center
(c)	Neg. pulse	Pos. pulse	Null at center
(d)	Pos. pulse	Terminated in Z_0	No max. or min.
(e)	Neg. pulse	Terminated in Z_0	Locus everywhere zero
(*f*)	Pos. pulse	Open end	Max. at *B*
(g)	Neg. pulse	Open end	Locus zero
(h)	Pos. pulse	Shorted end	Dip at *B*
(i)	Neg. pulse	Shorted end	Dip at *B*
(j)	Pos. pulse	15 additional ft. of line, shorted at the end	Flat (as (d))

This has a twofold effect: first, the "tails" of neighboring pulses do not contribute underneath the dominating pulse, making possible the small pulse separation cited above; second, the video lines can all be connected to the cathode-follower grid without the large voltage losses which a linear matching network would entail.

The output of the final cathode follower is fed directly to the 70-ohm input of a synchroscope††† whose amplifier has a gain of several thousand and a rise time of 0.1 μsec. The 3BP1 cathode-ray tube of this synchroscope was replaced by a 3FP7 tube, with 5000 volts on the post-deflection accelerator electrode. The superposition loci were recorded photographically. With the f:4.5 lens which was available, it was necessary to reduce the 10-pulse picture to about 2×5 mm on the film to obtain sufficient intensity; the present photographic image, viewed through a small magnifier, was large enough to determine with ease which pulse of the superposition locus was highest. It was not dense enough, however, to make reproduction possible here.

---

†† Now manufactured by James Millen Manufacturing Company, Malden, Massachusetts.

††† U. S. Navy type "LZ" oscilloscope.

VI. PERFORMANCE

The instrument was set up for tests as follows. One end (*A* in Fig. 1) of the *UVF* line was connected to a parallel-plate counter, while the other end (*B*) was terminated in a 300-ohm resistor. The synchroscope sweep was triggered by the counter pulses. The detector outputs were then roughly equalized by means of the potentiometers at the delay-line outputs. The final adjustment was made by alternately reversing the direction of travel of the pulse on the line, and leveling the video pulses on the synchroscope screen as well as possible considering the attenuation the *UVF* pulse suffers in traveling past the detectors. For these tests, the pulses were about 5 feet long, and the detector spacings 2 feet.

The qualitative tests described in Table I were then made. These tests confirm in every case the behavior of the superposition locus to be expected for pulses about 5×10^{-9} sec. in duration.

In accord with the predictions of electromagnetic theory, there is for the electric vector a reflection with polarity inversion at a shorted line, a reflection without inversion at an open ended line, and no reflection at a line terminated in its characteristic impedance. Maxima and minima appear in the superposition locus only where two pulses, or a pulse and its reflection, meet.

In addition, a quantitative test was made by using the arrangement in (a), Table I, but inserting several different lengths of Twin-Lead in either side. The displacement of the superposition locus as a function of the length of lead added to one side is shown in Fig. 5. (At the time the test was made there were five detectors spaced two feet apart.) The velocity of propagation of the Twin-Lead as measured by the slope of this graph is 0.90c, while from measurements of the resonant frequency of a length of Twin-Lead it is 0.87c.

These checks, together with the general consistency of the results of the preceding paper on the counter reaction times, provide a very satisfactory verification of the chronotron performance. As regards stability, it has not been found necessary to change the trimmer settings over a period of a couple of weeks. In any case, it is a very simple matter to take an occasional calibration picture as a routine check while taking data.

The over-all precision of the instrument is evidently a function of the detector spacing; precise measurements call for close spacing, with the width of the *UVF* pulses being measured made correspondingly short. For some applications it will be necessary to sacrifice some precision to obtain a wide range of measurable intervals. The possible number of detectors will be limited by the detector loading, and it may be necessary to go to special platinized glass resistors to get away from the shunt capacitance of the midget resistors now used. The precision of the present instrument, with detectors spaced two feet apart, is about 1×10^{-9} sec.; its range (with 10 detectors) is 40×10^{-9} sec. Better photographic and oscilloscopic equipment should make it possible to improve the precision for the same range, or to get a range of, say, 0.1 μsec. with a precision of 1×10^{-9} sec. Work is continuing along these lines in connection with meson decay experiments.

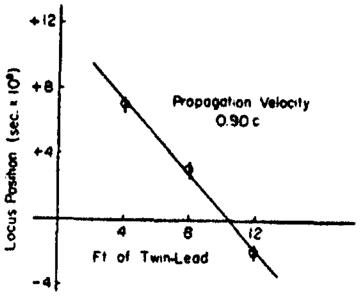

FIG. 5. Test of chronotron. Fixed delay sections of polythene tape line were inserted in one side of the timing line and the shift in the locus position observed. There was a fixed 10-foot delay line in the other side of the loop.

A pulse from a single counter was divided at a 3-way junction to supply a precisely simultaneous pair of pulses.

VII. TIME MEASUREMENTS IN THE MICROSECOND RANGE

It is interesting to inquire as to the appearance of the synchroscope picture if two pulses appear on the line separated by a time interval of the order of several μsec., rather than an interval short compared with the video pulses formed by the detectors. Evidently the pattern to be expected will consist of two flat superposition loci, the one displaced several μsec. with respect to the other, and this shift can thus be used to measure such an interval, without any changes in the instrument or its adjustment. No experimental verification of this effect has yet been carried out, but there appears to be no reason why the chronotron cannot be simultaneously used as a dual-range instrument in this manner. This rather fortuitous circumstance is expected to aid greatly in the study of meson decay, which is now being undertaken and where this instrument and parallel-plate counters are used.

ACKNOWLEDGMENT

The author is indebted to Professor H. V. Neher for several stimulating discussions of the problems arising in this work.

THE REVIEW OF SCIENTIFIC INSTRUMENTS VOLUME 20, NUMBER 3 MARCH, 1949

Parallel-Plate Counters

J. WARREN KEUFFEL*
California Institute of Technology, Pasadena, California

(Received November 8, 1948)

The counter characteristics of a discharge tube using plane-parallel electrodes have been investigated, particularly with regard to the short time lags inherent in the streamer type of spark which occur with such a geometry at near-atmospheric pressure. Construction details for parallel-plate counters with good counter characteristics are given. Spurious counts were minimized by an argon-xylene filling mixture and the use of a univibrator quench circuit. The uncertainty in the reaction time of the counters is $\pm 5\times 10^{-9}$ sec.

I. INTRODUCTION

THERE has been considerable interest lately in the measurement of very short time intervals between ionizing events. This problem arises, for example, in studying the various mesotron decay phenomena and the gamma-decay of metastable states of nuclei. Until now, time measurements have been limited by the variable lags of the conventional Geiger-Müller tube, which introduces an uncertainty of about 0.1 µsec.[1, 2]

It has been known for some time, thanks to the work of White,[3] Wilson,[4] and Newman,[5] that the time lag of breakdown of overvolted plane-parallel spark gaps is exceedingly short, and indeed Wilson found at 100 percent overvoltage lags of the order of a few times 10^{-9} sec., with no apparent lower limit as the overvoltage was increased. The short lags of the streamer-type spark are due primarily to the important role played by photo-ionization,[6] but even apart from the spark lag studies one would expect from elementary considerations a shorter lag with the plane-parallel geometry—where the field strength is everywhere sufficient to propagate a Townsend electron avalanche—than with the cylindrical shape, where the initiating electrons must first drift into the strong field near the wire.

Here, then, was a prospective fast mechanism. Could a parallel-plate spark gap be made to trigger if and only if an external agent produced an electron within the active volume? In the answer to this question, it was realized, lay the key to the problem. A preliminary investigation of the origins of ions within the active volume was undertaken, and it turns out that one has to deal with after-effects of previous discharges similar, if not identical, to the spurious counts observed in conventional cylindrical counters. These after-effects are very poorly understood, but it has been possible, nevertheless, to minimize them to the point where the spurious counting rate is but a small fraction of the true counting rate, for a considerable range of overvoltages, and thus produce a workable parallel-plate counter. Although the feasibility of using the fast streamer spark mechanism as a counter has been demonstrated, many questions have yet to be answered. It seems worth while, however, to report the work which has been accomplished so far.

Parenthetically, it should be noted that the parallel-plate counters are "fast" only in the sense of a very short reaction time. They are not capable of high counting rates because of the large quench time (0.01 to 0.05 sec.) which has so far been necessary, although there is some hope of improvement along these lines.

A timing circuit which permits the measurement of time intervals commensurate with the fast reaction time of the parallel-plate counters is described in a companion paper which follows this one.

II. DESCRIPTION OF PARALLEL-PLATE COUNTERS

A. Counter Characteristics

In this section we discuss the characteristics of parallel-plate counters other than the reaction time, which is reserved for Part V.

An external electronic quench circuit (see Part IV) is necessary with a parallel-plate counter for two reasons. First, unlike the cylindrical G-M tube, the space-charge geometry is not such that the discharge is self-quenching. Second, the intensity of after-effect or spurious activity is such that a "cooling off" period has been found necessary. Evidently this "cooling off" time or quench time, T_Q, is a parameter which must be specified when discussing a counter operated with such a circuit; in what follows, it has the value 0.05 sec. unless otherwise stated.

The first experimental counter consisted of molybdenum disks spaced 3.0 mm and 3.1 cm^2 in area. The counters to be discussed in this paper are rectangular sheets of copper or copper-plated steel spaced 2.5 mm and 35 cm^2 in area; the early counter and the present counters differ significantly only in the higher background rate of the larger counters (approximately a factor of 11 as would be expected from the areas). The filling used in the present counters is 6 mm of xylene plus argon to give a total pressure of ½ atmos.

---

* Now at Princeton University, Princeton, New Jersey. This paper is based on part of the work done for the doctoral thesis at the California Institute.

[1] C. W. Sherwin, Rev. Sci. Inst. 19, 111 (1948).

[2] B. Rossi and N. Nereson, Phys. Rev. 62, 417 (1942).

[3] H. J. White, Phys. Rev. 49, 507 (1936).

[4] R. R. Wilson, Phys. Rev. 50, 1082 (1936).

[5] M. Newman, Phys. Rev. 52, 652 (1937).

[6] L. B. Loeb, *Fundamental Processes of Electrical Discharge in Gases* (John Wiley and Sons, Inc., New York, 1939), p. 426.

A typical plateau for such a counter is shown in Fig. 1. With careful preparation, this plateau was consistently reproducible.

If we assume that only one electron is required to initiate a discharge, the calculated efficiency of the counter filled with the above argon-xylene mixture for a singly charged fast particle passing normal to the plates is about 98 percent. The validity of the above assumption depends on the distance of the single electron from the anode and on the overvoltage, according to the streamer theory of Loeb and Meek, and the efficiency is therefore expected to increase with overvoltage.

A rough experimental check on the efficiency may be made by comparing the coincidence rates obtained in the course of the uncertainty time measurements (see Fig. 7) with the rates calculated from the known cosmic-ray intensity in the basement of the laboratory. The rates agree within the rather large uncertainties of the method (say ±25 percent) but, since the coincidence rate is very sensitive to counter inefficiency, the efficiency must be of the order of 90 percent for overvoltages of 500 or more.

Although the coincidence rate increases with overvoltage, a part of this increase probably results from edge effects. No very definite conclusions may be inferred until further experiments have been made.

In a recent note, Madansky and Pidd[7] report efficiencies of 10 percent for parallel-plate counters. The overvoltages they used, however, were considerably lower than 500, and this explains the discrepancy.

The counters tested to date have exhibited a useful lifetime of one or two months of background-rate counting, at overvoltages of 500 to 1000 and a quench time of 0.05 sec. The usefulness of the counter ends invariably with the occurrence of "spot bursts," localized bursts of spurious counts from one or two points on the cathode. Most counters may then be washed, re-baked and re-filled to produce a counter good for another month or two.

The quench time has been held at 0.05 second largely because the longer quench time is thought to prolong the lifetime. Most counters may be run at quench times of a millisecond or less for short periods with no apparent harm, but at present little is known about the effect of quench time, overvoltage, external circuit capacitance, and counting rate on the useful lifetime.

Finally, two more characteristics of parallel-plate counters should be mentioned. First, the discharge is localized in a fine, plainly visible streamer channel presumably in the neighborhood of the initiating ion. This has obvious possibilities as a means of determining the path of a particle, and it also makes the study of the spurious count phenomena considerably easier. Second, the amplitude of the pulse from a parallel-plate counter is several hundred volts; unlike the cylindrical counter, which is a constant-charge device, the voltage swing is substantially independent of the external circuit capacitance. The latter should be kept small, however, to minimize the energy which flows in the spark and hence the intensity of after-affects. The voltage swing is large even just above the counting threshold, because the streamer persists until the voltage has fallen well below this value.

B. Construction

A counter construction which has been used for experimental work is illustrated in Fig. 2. The ground joint makes it possible to take the tube apart without glass blowing. This joint is sealed with beeswax and rosin. It is located about 4″ below the electrode structure so that the important parts of the tube may be outgassed and the electrodes baked at 500 degrees C, while the ground joint, which projects from the oven, is maintained at room temperature with the aid of a blower.

Two profiles have been used, the one a rounded 45-degree bevel, the other flat with edges rounded by emery paper. These are illustrated in Fig. 2. No significant difference in performance between the two has been noted, but the beveled-edge construction with copper-plated steel as the material is far better mechanically and can be made flat to within perhaps 2 mils if bent around a form in a brake. The precision with which the plates must be held parallel depends on the precision desired for time measurements. We shall discuss this in Part V.

The electrodes have in all cases been polished with successively finer grades of emery cloth, ending up with crocus cloth. Just before final assembly they

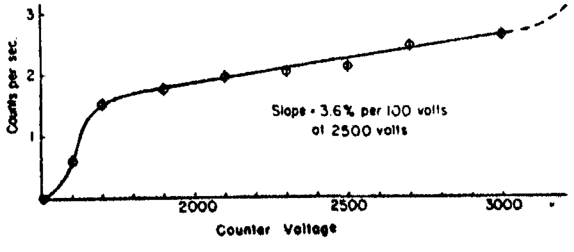

FIG. 1. Typical plateau for a counter filled with argon and xylene. Quench time: 0.05 sec.

---

[7] L. Madansky and R. W. Pidd, Phys. Rev. 73, 1215 (1948); also a discussion with these authors.

are thoroughly swabbed with xylene, and after the tube has been assembled, rinsed with xylene, alcohol, distilled water, and alcohol. The tube is next evacuated to a high vacuum and baked at 500 degrees C for two hours; in the case of the copper electrodes, hydrogen is admitted for 10 min. or so at this temperature to reduce off oxides. The tube is again evacuated to 10^{-5} mm or better, cooled, and filled. Successful results have been obtained only when the xylene has been admitted first, followed by the argon; indeed, the best counters have resulted when the argon rushing into the tube has actually condensed droplets of xylene on the envelope, so that the tube has contained saturated xylene vapor. (The threshold then becomes slightly temperature dependent, but with the parallel-plate counter operated far above threshold, the change is not important in a normal laboratory room.) The importance of admitting xylene first is possibly due to the formation of a layer of xylene on the cathode.

III. THE AFTER-EFFECT

As a first step in studying the parallel-plate counter, an external quench circuit (see Section IV) was constructed which permitted the device to be studied under conditions which would otherwise lead to a continuous discharge. The counter, initially charged only to a small clearing potential, is rapidly charged to the full potential and isolated. A discharge then occurs when an electron appears in the active volume. At a known time T_Q following the discharge, the counter is recharged, and so on. The quench time, T_Q, is adjustable from milliseconds to minutes.

The presence of spurious counts is indicated if the mean interval (as measured, say, with an integrating circuit) between the charging of the plates and the subsequent discharge is much shorter than is to be expected on the basis of the natural background radiation. In an extreme case, the counter counts just as rapidly as the quench circuit will permit.

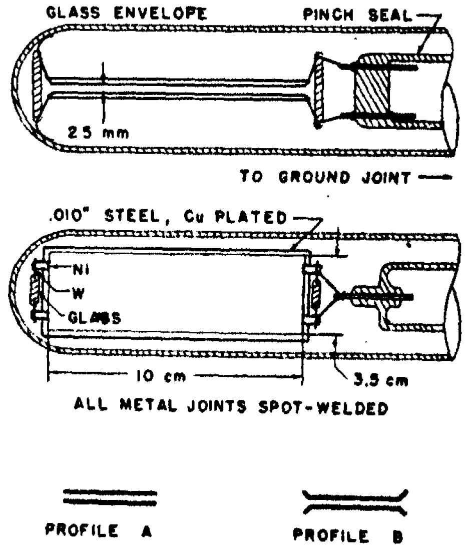

FIG. 2. Schematic drawing of the experimental parallel-plate counters.

Using this circuit, the following conclusions were reached: (a) all counters so far studied need a quench time of at least 0.01 to 0.05 sec. but (b) if a counter is "bad," the spurious activity has a persistence so long (of the order of minutes) that to circumvent it by increasing the quench time is impractical. The use of a quench time of the order of 0.01 second is thus a necessary, but not a sufficient, condition.

The length of the plateau is not very sensitive to the quench time, although the situation was complicated by the fact that the leads to the electrodes began to count at voltages in the vicinity of the upper end of the plateaus of "good" counters. (The end of the plateau is almost by definition the voltage at which the aftereffect begins to mask the true counting rate.)

Another requirement for the suppression of the aftereffect seems to be the use of a small percentage of organic vapor in the tube. Counters filled with pure argon or pure air exhibited no plateau at all even at the longest quench times, although a somewhat critical mixture of 3.4 mm air and ½ atmos. argon did produce a workable counter; the plateau slope was about 10 percent per 100 volts, about three times the slope for a typical argon-xylene counter.

Now it is well known that the addition of one of the so-called "self-quenching" vapors to the conventional G-M counter enables it to be used with a low value of external resistance in a "fast" circuit. The vapor is believed to have two effects. First, it suppresses the production of photoelectrons at the cathode by absorbing ultraviolet photons. Second, it greatly reduces the production of secondary electrons by positive ion bombardment. With a parallel-plate counter operated at a quench time of 0.05 second, however, neither of these effects enter the picture: we wish to point out that in this case, at least, the primary function of the vapor is the suppression of the after-effect.

In addition to the use of a quench circuit and the admixture of organic vapor, a third factor of importance in suppressing the aftereffect is the preparation of the electrodes; successful results have been obtained only when the baking and hydrogen treatment outlined in Section II has been followed.

The plateau slope for an argon-xylene counter, constructed according to the foregoing section, is invariably about 4 percent per 100 volts. To investigate the origin of the plateau slope, plateaus were taken at two widely different quench times. It was found that the slope changed from 4.4 percent at a 0.05-sec. quench time to 2.9 percent at 3.4-sec. quench time. The plateaus were, of course, measured by plotting the reciprocal of the mean interval between the charging of the plates and the subsequent discharge, since the longer quench time was very much longer than the mean interval between natural background counts.

Some, at least, of the plateau slope is therefore to be attributed to the aftereffect. The remainder is due to an increase in the efficiency with overvoltage, a fringing of the field at the edges of the plates, or some other unknown cause.

While a carefully prepared argon-xylene counter is substantially free of aftereffect, it eventually deteriorates. The usefulness of the counter ends invariably with the occurrence of "spot-bursts;" spurious counts are observed to originate from one or more very definite spots on the cathode, the counts occurring in bursts which are easily distinguishable from the normal background counts which are scattered in a random fashion over the surfaces of the plates. At first these bursts choke themselves off, presumably when, by chance, genuine counts occurring elsewhere in the counter give the spot a chance to "cool off." Once such a spot starts, it gets worse and bursts occur more and more frequently. Although lengthening the quench time helps somewhat, as does reducing the overvoltage, in all cases the spot eventually develops until even at the longest quench times the counter counts at the spot almost as fast as the quench circuit recharges the electrodes. The spot may be remedied only by rebaking and refilling, and in the worst cases the counter must be taken apart and the spot swabbed with xylene.

Because of their localization, the spot bursts must be connected with the state of the electrodes. It is not merely a matter of the formation of a sharp point, as the spots do not alter the threshold nor do the sparks favor the spots at low voltages. Indeed, until the spot is very bad the counter operates stably at lower voltages.

In Section II we have mentioned the importance of admitting the xylene first, followed by the argon. The other order of filling, despite ample time for diffusion, exhibited invariably a very bad aftereffect and, in addition, the threshold voltage and visual appearance of the sparks were markedly different, being very similar to the characteristics of pure argon counters.

This effect and the spot bursts are consistent with the suggestion of Professor H. V. Neher that surface films on the cathode and anode play an important role in determining the characteristics of a counter. According to this picture, the aftereffect is suppressed by a film of xylene on the electrodes. A spot burst occurs when the film is locally altered or destroyed in some manner.

An alternative picture would be to suppose that the ultraviolet absorption of the vapor is chiefly responsible for the suppression of the aftereffect, while the spot bursts are caused by an accumulation of material deposited on the electrodes by the action of the sparks. While this picture is inconsistent with the behavior of counters filled with argon and xylene in that order, we feel that more information is needed before a definite conclusion may be reached.

As to the actual mechanism of the spurious counts, one can only say that the evidence points towards the Paetow effect.[8, 9] Submicroscopic bits of insulating materials such as dust or oxides are charged up by photons or positive ion bombardment from the sparks. High fields are formed because of the extremely small size of the particles, and delayed electrons or photons are produced either by breakdown of the insulating matter, field emission, or some other process.

IV. QUENCH CIRCUIT AND AUXILIARY ELECTRONICS

A. Quench Circuit

The quench circuit used with the parallel-plate counters is shown in Fig. 3.

The very fast negative-going pulse from the positive counter plate triggers the univibrator T_1T_2, which in turn causes T_3 to conduct for the duration T_Q of the univibrator swing. When the univibrator flops back, the counter is rapidly recharged and the circuit is ready for another count. The counter is very loosely coupled to the univibrator in order that very little of the charge stored in the stray capacitances of the circuit may flow through the counter during the breakdown, which occurs very much faster than the univibrator swing.

None of the circuit parameters is very critical, nor is the adjustment of the bias on T_1 particularly ticklish since a pulse of several hundred volts is supplied by the counter.

Some factors which influenced the design of the circuit are low current drain on the counter high voltage supply, wide range of quench times, good response to random pulses, and a recharging time short compared with the mean interval between counts (to avoid longer lags due to discharges occurring before the counter reaches the full potential). The use of a receiving-type tube at T_3 has given no trouble, despite the fact that the rated plate voltage is exceeded by a very large factor; the plate dissipation is, of course, kept very low. It is important that T_3 be a sharp cut-off pentode.

B. Auxiliary Electronics

Figure 4 shows how two counters may be connected simultaneously to a common quench circuit

---

[8] H. Paetow, Zeits. f. Physik 111, 770 (1939).

[9] Reference 6, p. 498.

as well as to an auxiliary coincidence circuit without appreciably disturbing the initial *UVF* pulse** which each counter sends down the timing line. The time constants are such that a counter is "left alone," so to speak, until the *UVF* pulse is over; the large series coupling resistors also minimize the charge which flows through a counter and hence the energy in the spark, as a result of external circuit capacitance.

Both counters are connected to the same quench circuit for three reasons: it eliminates the need for another quench circuit, it minimizes relative lags due to different voltages on the counters, and it increases the coincidence rate in the case where the quench time is of the same order of magnitude or larger than the mean interval between background counts.

The voltages V_{C1}, V_{C2} clear the tube of residual ions during the quench periods and compensate for individual variations in counter thresholds; they must not, however, be more negative than -600 volts for complete quenching.

The 1N34 crystal diodes form a simple coincidence circuit of the type discussed by Howland *et al.*[10] The large voltage swing of the parallel-plate counter makes it possible to use a resistance-capacitance divider instead of the conventional amplifier required to drive the circuit with cylindrical counters. The coincidence output is coupled to succeeding circuits through a cathode follower since stray capacitances *must* be kept small at this point. The resolving time of the circuit is around 1 to 2 μsec.

Originally, the resistance-capacitance divider had a 2-μμf capacitor across the 10,000-ohm midget resistor, but the stray shunt capacitance alone is adequate to drive the coincidence circuit.

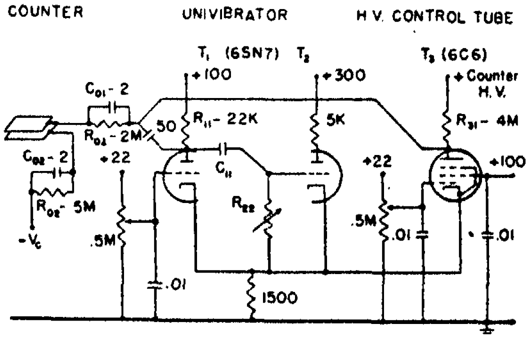

FIG. 3. Quench circuit. Capacitances are in μμf except for the three 0.01-μf bypass condensers; resistances are in ohms, with $K=10^3$, $M=10^6$. For a quench time of 0.05 sec., R_{22} is $20M$, C_{11} is 0.002 μf. V_c is a "clearing field" of about 500 volts.

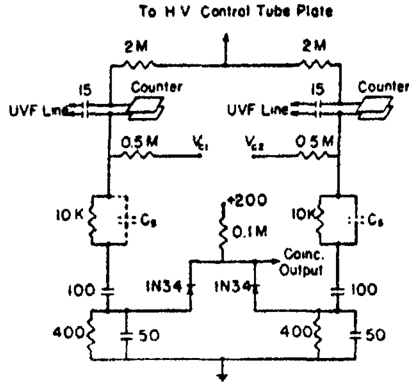

FIG. 4. Two counters coupled to a single quench circuit and to a simple coincidence circuit. Large resistances isolate the counters from these circuits during the initial fast transients, which are sent down the *UVF* timing line. C_s is the stray capacitance of the 10*K* resistors (about 0.5 μμf).

V. THE REACTION TIME

A. Experimental Arrangement

In order to ascertain the precision with which a time interval between two ionizing events may be measured, one needs to know the uncertainty in the reaction time of the parallel-plate counters. The reaction time itself—the time between the appearance of an ionizing event in the counter and the maximum of the short electromagnetic pulse sent down the timing line—is fortunately of less interest, since it would be much more difficult, if not impossible, to measure.

The reaction time uncertainty was measured as follows: two argon-xylene counters of the type described in Part II were placed directly one above the other with their plates horizontal. The auxiliary coincidence circuit described in Part IV selected those events where a particle from the cosmic radiation passed through both counters; because of the proximity of the two counters and the speed of a particle capable of penetrating the counter envelopes and plates, it could be assumed that the counters were tripped simultaneously. As a result, however, of the uncertainty in the time lag between the initiating event in a counter and the electromagnetic pulse which it sends to the timing line, the pulses will enter the timing line not simultaneously but separated by a small time interval ΔT.

A distribution curve of the relative lags ΔT then gives a measure of the uncertainty in the reaction time.

The resolving time of the auxiliary coincidence circuit in the above measurement was about 1 to 2 μsec. This is large enough so that we may safely assume no true coincidences will be missed, yet small enough so that the rate of accidental coincidences is only a few per day.

The timing circuit (similar in principle to the Neddermeyer "chronotron"), used for the very short

---

** In this paper and in the companion paper describing the timing circuit, the term "ultra-video-frequency" (*UVF*) will be used to describe pulses of the order of 5×10^{-9} sec. in duration.

[10] B. Howland, C. A. Schroeder, and J. D. Shipman, Jr., Rev. Sci. Inst. 18, 551 (1947).

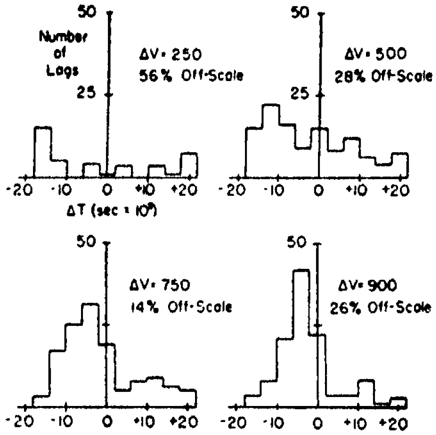

FIG. 5. Distribution of relative lags between two counters tripped simultaneously by a cosmic-ray particle. A relative lag is "off scale" if it lies outside the chronotron range, -20×10^{-9} to $+16\times10^{-9}$ sec. Distributions are given for four different overvoltages, ΔV.

time measurements, is described in a companion paper. The instrumental error is approximately 1×10^{-9} sec., using ten detectors spaced two feet apart; the range is from -16×10^{-9} to $+20\times10^{-9}$ sec. Cases where the coincidence circuit records a coincidence but the chronotron shows no peak in the superposition locus are recorded as "off scale" lags, that is, lags which lie outside of the above range. The superposition loci are recorded by photographing the synchroscope screen.

From the appearance of the superposition locus it is always possible to tell whether two pulses have passed (whether or not they intersect in the measurable range) and thus check the operation of the coincidence circuit. The width of the superposition locus peaks gives a measure of the rise time of the slowest of the two pulses which met, but this rise time tells us very little, of course, about the reaction time itself; it may be some time between the formation of the initiating ion pair and the first observable voltage surge.

B. Results

In Fig. 5 we present distribution curves of the relative lags between two parallel-plate counters. The ordinates of these histograms represent the number of lags occurring in a range 4×10^{-9} sec. wide in approximately 18 minutes of counting; the total number of coincidences is not the same for each graph, however, as will be noted from the variation in coincidence rate shown in Fig. 7.

If we define the uncertainty $\langle\Delta T\rangle$ to be such that one-half the lags (including those off scale) fall within $\pm\langle\Delta T\rangle$ of the center of the distribution curve and plot this uncertainty against overvoltage, the curve in Fig. 6 is obtained. We see that the uncertainty varies from 17×10^{-9} sec. at an overvoltage of 250 to about 5×10^{-9} at 900 volts.

Pulse rise times as measured from the width of the superposition loci at half-maximum range from 8×10^{-9} sec. at the lower overvoltage to 3×10^{-9} sec. at an overvoltage of 900. As mentioned before, these figures represent little more than a lower limit on the absolute reaction time.

C. Discussion of Results

In Fig. 5 we notice that the centers of the lag distributions fall to one side of the zero point. This means that the average lag of one counter is slightly greater than that of the other. Recent results with counters of better mechanical tolerances show that this effect may be greatly reduced; any remaining effect may be corrected by a calibration of the counters.

Also from Fig. 5 we note that the percentage of "off scale" lags decreases as the overvoltage is raised up to approximately 750 volts, after which the percentage increases by a significant amount. This trend is borne out by measurements made using visual observation of the synchroscope at overvoltages up to 1250. However, at the higher overvoltages the superposition loci exhibit sharper peaks with subsidiary maxima and the counters tend to deteriorate rapidly. For these reasons, the behavior of the counters and timing system at overvoltages greater than 1000 require further study before quantitative data may be presented.

Because the percentage of long lags increases at the highest overvoltages, while at the same time the peaks of distribution curves narrow markedly, it seems likely that we are dealing here with at least two effects, which we will, for convenience, refer to as short lags and long lags.

The long lags are probably connected with sparks occurring in the weaker fringing fields at the edge of the plates. To estimate the magnitude of this effect, we note that the effective area of a counter 1.5 in. ×4 in., spaced 0.1 in., increases by about 18 percent if we suppose the field to fringe out a distance equal to the spacing. Bearing in mind that a lag results if *either* counter is triggered in the edge region, this figure must be doubled. The magnitude of the effect is of the right order. In support of this interpretation

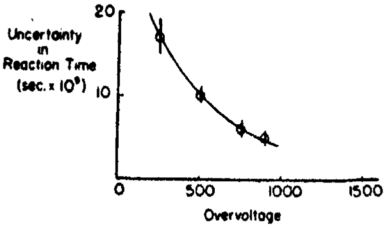

FIG. 6. Uncertainty in the reaction time, $\langle\Delta T\rangle$, as a function of overvoltage. Half the relative lags of two counters tripped simultaneously fall between $\pm\langle\Delta T\rangle$ of the center of the distribution. Data from Fig. 5.

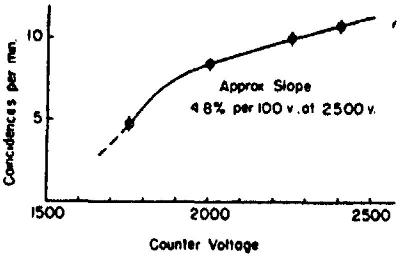

FIG. 7. Coincidence rate *vs*. voltage for two counters, one 6 cm directly above the other, with their plates horizontal.

are the following: (a) the *increase* in percentage of long lags at high overvoltages; (b) the increase as shown in Fig. 7 of the coincidence rate with voltage; (c) an increase in the number of sparks visually observed to go at the edges at the higher overvoltages.

Since the superposition locus has no peak if only one pulse passes down the line, such an occurrence would be recorded as an "off scale" reading. Such cases are fortunately easily recognizable by the fact that, if only one pulse passes down the line, attenuation along the line gives the pattern a tilt one way or the other which is balanced out in the two-pulse case, and it was thus possible to reject this explanation of the long lags with certainty.

Since the reaction time is a function of the field strength at the point where the streamer occurs, non-uniformity of the plate spacing will introduce an uncertainty in the reaction time. The variations from point to point in the spacing of the present counters may be as large as 5 percent. To estimate the importance of uniform spacing, the field strength on one counter was varied by varying the voltage, while the other counter voltage was held constant, and the shift in the position of the maximum in the lag distribution curve was observed. A shift of about 1×10^{-9} sec. was produced by a one percent change in total voltage in the vicinity of 900 volts overvoltage. We conclude from this that the shorter lags are at least in part caused by non-uniformity of the plate separation.

Until further, more detailed investigations have been carried out, it is not possible to state how much of the uncertainty observed in this experiment is due to edge effects and non-parallelism and how much to the ultimate statistical fluctuations in the streamer build-up.

Improvements in the geometry of the counters should virtually eliminate lags due to the former cause, while the lags due to the latter may be minimized in two ways: one may, by further work on the spurious count problem, produce a counter which may be operated at still higher overvoltages, and one may use greater spacings or higher pressure, thus smoothing out the scatter resulting from statistical variations in the number of ion-pairs formed by the initiating event.

ACKNOWLEDGMENTS

The author is deeply grateful to Professor H. V. Neher for advice and guidance. Acknowledgment is also due Professor C. D. Anderson for encouragement during the early stages of the work, Professor L. B. Loeb for a very stimulating discussion, and Betty H. Keuffel for her help in preparing the figures.

THE REVIEW OF SCIENTIFIC INSTRUMENTS VOLUME 20, NUMBER 3 MARCH, 1949

Physical Instruments for the Biologist

Detlev W. Bronk
Associate Editor in Charge of this Section
Eldridge Reeves Johnson Foundation for Research in Medical Physics,
University of Pennsylvania, Philadelphia, Pennsylvania

Equipment and Experimental Methods for Interference Diffusion Studies

LOUIS J. GOSTING, EDWIN M. HANSON, GERSON KEGELES,* AND MARGARET S. MORRIS
Laboratory of Physical Chemistry, University of Wisconsin, Madison, Wisconsin

(Received May 28, 1948)

A single lens convergent light apparatus is described with which diffusion in liquids may be studied by an interference method. Details of the optical elements and their mounting and alignment are given as well as the design of a temperature control regulating near 0°C to within 0.01°C. A modified Polson sharpening technique has been used successfully in forming diffusion boundaries in a Tiselius cell. A modification of the Rayleigh interferometer has been employed as an aid in the measurement of the refractive index increment parameter, j_m, which is required for the evaluation of the diffusion coefficient. During diffusion a reference slit image obtained by the employment of special cell and plate masks permits more accurate measurements of the undeviated slit image position than have been obtained from the interference diffusion fringe picture. Results indicate that the apparatus is capable of 0.1 percent precision.

INTRODUCTION

WHEN monochromatic light from a horizontal slit is brought to a focus by a lens system, and a column of liquid containing a diffusing boundary is placed in the optical path, an interference phenomenon is produced in the focal plane below the undeviated slit image. The description and qualitative explanation of this phenomenon were published by G. L. Gouy in 1880.[1] In recent companion papers, the theoretical basis for converting the interference fringe spacing into an interpretation of the diffusion phenomenon,[2] and the verification and practical utilization of this theory for evaluating diffusion experiments[3] have been reported. In addition, Longsworth[3] has described innovations in equipment and technique which were employed in experimental studies of diffusion with this method.

It is the purpose of this paper to present features of equipment design and methodology developed and employed in this Laboratory during the past year for diffusion studies with the interference method.

APPARATUS DESIGN AND CONSTRUCTION[4]

The study of Longsworth[3] has shown that a high quality single lens convergent light apparatus such as the horizontal slit source and schlieren lens of his electrophoresis schlieren scanning apparatus[5, 6] together with a photographic plate replacing the schlieren diaphragm in the plane of the slit image, constitutes a precise optical system for the photographic observation of the diffusion interference fringes. For the present studies the equipment has been arranged as shown schematically in Fig. 1. The framework supporting the bath and optical parts of the system consists of two parallel 5×8 inch I beams bolted on top of three concrete pillars of about 2000 pounds each. To insulate the system from vibration, mats of Keldur[7] of proper area to bring the dead load up to that specified by the manufacturer are placed between these pillars and the floor. The bath stirrer and refrigeration coil are mounted separately on a stand bolted to the floor. As a result of the use of a condensing lens for the illumination of the slit source, heating of the slit mechanism is reduced, and filters can be mounted

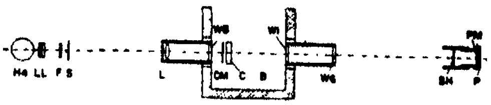

FIG. 1. Apparatus for interference diffusion studies. Schematic side view, not drawn to scale.

H4—G.E. AH4 lamp
LL—Condenser lens
F—Wratten filter No. 77
S—Source slit
L—Convergent lens
*W*1, 8, 6—Windows
CM—Cell mask
C—Cell
B—Water bath
SH—Shutter
PM—Plate mask
P—Photographic plate

---

* Present address: Biochemistry Section, National Cancer Institute, Bethesda 14, Maryland.

[1] G. L. Gouy, Comptes Rendus 90, 307 (1880).

[2] G. Kegeles and L. J. Gosting, J. Am. Chem. Soc. 69, 2516 (1947).

[3] L. G. Longsworth, J. Am. Chem. Soc. 69, 2510 (1947).

[4] Described in Doctoral Thesis of L. J. Gosting, Universtiy of Wisconsin, 1947.

[5] L. G. Longsworth, J. Am. Chem. Soc. 61, 529 (1939).

[6] L. G. Longsworth, Ind. Eng. Chem. Anal. Ed. 18, 219 (1946).

[7] Hobaite Products Company, Inc., 550 Cortlandt Street, Belleville 9, N. J.

on the lamp side of the slit rather than in the optical system proper. The apparatus makes use of a single 170-cm focal length, 6.3-cm clear aperture, air-spaced compound lens[8] corrected for mercury green and yellow lines, and designed to project at full aperture a sharp image of the slit source on the optic axis, at unit magnification. While the use of this long focal length lens results in lower light intensity at the photographic plate than when using the optical equipment of the conventional electrophoresis apparatus,[6] the greater optical lever arm so obtained gives proportionally greater fringe displacements below the undeviated slit image. This allows observation of the diffusion for a longer time than is feasible with a lens of shorter focal length.

The windows[8] for the water bath thermostat are borosilicate crown glass, 10 cm in diameter and 1.5 cm thick, with surfaces flat to one-half wave and parallel to within 30 seconds of arc. Since the water bath is operated near 0°C to minimize refractive index and reduce density fluctuations with changes in temperature, enclosed dry gas spaces[6] adjacent to each bath window are employed to prevent condensation of moisture on the optical elements. Dry nitrogen is passed through those spaces as needed by means of the tubes shown in Figs. 2 and 3. In addition, certain new mounting features render the optical system independent of the water bath position, provide for maximum rigidity of the optical elements, and at the same time afford flexibility of adjustment. Details of the mounting are shown diagrammatically in Fig. 2 and photographically in Fig. 3. The water bath itself is insulated with Foamglas,[9] and all joints and spaces around this insulation are filled with asphalt roofing cement. Along the optical channel, the insulation is further sealed from the atmosphere and the water in the bath by means of hard rubber flanges and pipe[10] fastened to both walls of the bath. Window 6, Fig. 2, or the lens in its cell, is mounted in a bronze collar 5 and fastened to the main bronze tube 3 with alternate pressure and tension screws, so as to make tilting adjustments possible in all directions. Connections between the optical assembly and the water bath are made only through two large synthetic rubber diaphragms of $\frac{1}{16}$-inch Fairprene,[11] which serve to seal the assembly while providing for independence of the bath position. To permit tilting of the entire assembly and adjustment of the inner window, the bronze tube 3 is held firmly in a cast iron bracket, Fig. 3, mounted to channel iron across the supporting I beams with pressure and tension bolts. Further adjustment is possible by rotation of the channel about a vertical axis. Focusing and alignment of this assembly and the slit source were accomplished by alternate use of a leveled surveyor's transit and a Gauss eyepiece telescope. In final adjustment the flat side of the compound lens is parallel with all window faces within about 30 seconds of arc and the normals to these surfaces are horizontal within the same limit of error. No appreciable distortion of the windows resulting from making them water-tight has been detected

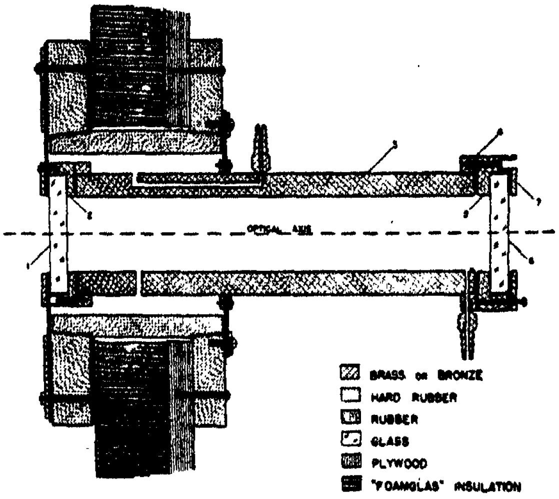

FIG. 2. Diagram of bath double window mounting.

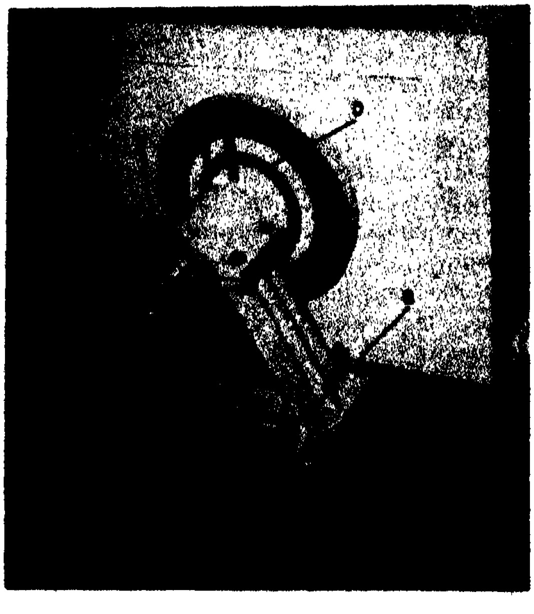

FIG. 3. Photograph of lens mounting.

B = Adjusting bolt
D = Rubber diaphragm
H = Adjustable lens holder
L = Lens

---

[8] Supplied by the Perkin-Elmer Corporation, Glenbrook, Conn.

[9] Pittsburgh-Corning Corporation, Port Allegany, Pennsylvania.

[10] B. F. Goodrich Company, Akron, Ohio.

[11] E. I. du Pont de Nemours and Company, Fabrics Division, Fairfield, Connecticut.

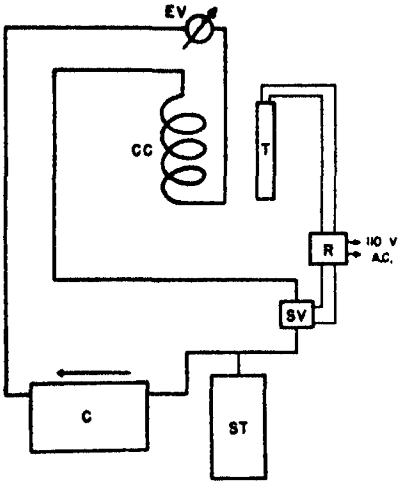

FIG. 4. Refrigeration system.

EV—Expansion valve
CC—Cooling coil
T—Mercury thermoregulator
R—Relay
SV—Solenoid valve
ST—Surge tank
C—Compressor

from Gauss eyepiece reflections, which appear the same whether the bath is empty or filled with water. Without lateral or vertical movement, or rotation, the leveled transit could be focused alternately on the slit source and on the slit image projected when the lens was screwed into place, thus precisely defining the optic axis. In order that the photographic plate could be aligned perpendicular to the optic axis within about 20 minutes of arc, the telescoping camera tube (outside diameter, 4 in.), to which the plateholder adapter and shutter were fixed, was mounted in a cast iron bracket similar to that shown in Fig. 3. The camera tube was focused carefully by eye to bring the emulsion side of the photographic plate to the focal plane of the lens.

Prior to assembly the window thicknesses were measured with micrometer calipers. Their refractive indices were obtained by focusing the microscope of a Gaertner slide comparator on a fine line scratched on a metal plate, and refocusing to obtain the apparent change in position of the line after interposing the windows of known thickness. For measuring the distances between the various optical elements, special inside calipers were constructed of long brass rods with collars at intervals, threaded into rods of larger diameter, with lock nuts for setting. These could be measured after each setting with a 24-inch vernier caliper. The optical distance **b**, from the center of the diffusion cell to the photographic plate, thus mechanically measured, was calculated to be 306.45±0.02 cm in vacuum, assuming the bath and cell to be filled with water at 0.5°C.

In order to obtain diffusion measurements accurate to 0.1 percent, it is necessary to regulate the temperature of the diffusion column to 0.025°C. The method successfully employed to maintain the water bath temperature constant is illustrated diagrammatically in Fig. 4.[12] The mercury thermoregulator (*T*) which is placed close to the cooling coil (*CC*) controls through a relay (*R*) the solenoid (*SV*) in the suction line. On closing, the solenoid instantaneously stops all refrigeration of the bath. The surge tank (*ST*) is then exhausted by the compressor unit (*C*) until the unit pressure control switch shuts off the compressor motor. When the thermoregulator reopens the solenoid, a rapid surge of refrigerant into the tank provides adequate cooling in 10 to 15 seconds, with better than 0.01°C control of the entire bath, and no icing of the coil even below 0.4°C.

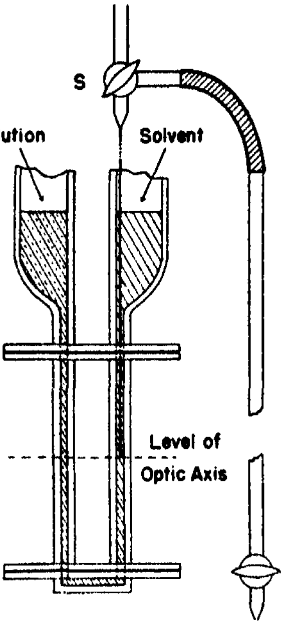

FIG. 5. Capillary siphon for boundary sharpening.

TECHNIQUE OF MEASUREMENTS

The diffusion measurements have been performed with a long center section Tiselius cell[13-15] whose top section is extended with tubes reaching above the bath water. However, the disturbance[8] of the boundary during shifting from behind the opaque horizontal plates where it is formed has been rectified by a slight modification of the boundary sharpening technique due to Polson.[16-18] In

---

[12] The authors are indebted to the Robinson Brothers, Refrigeration Maintenance Corporation, Madison, Wisconsin, for essential parts of the refrigeration control design.

[13] A. Tiselius, Trans. Faraday Soc. **33**, 524 (1937).

[14] L. G. Longsworth, Chem. Rev. **30**, 323 (1942).

[15] L. G. Longsworth, Ann. N. Y. Acad. Sci. **41**, 267 (1941).

[16] A. Polson, Onderstepoort, J. Vet. Sci. Animal Ind. **20**, 159 (1945).

[17] A. Polson, F. J. Joubert, and D. A. Haig, Biochem. J. **40**, 265 (1946).

[18] D. S. Kahn and A. Polson, J. Phys. and Colloid Chem. **51**, 816 (1947).

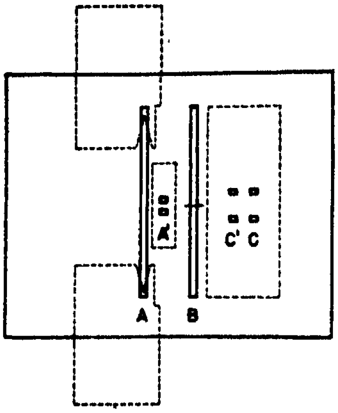

FIG. 6. Diffusion cell mask.

filling the cell, Fig. 5, the bottom section, both channels of the center section, and the left arm of the top section are filled with solution. The right arm of the top section is filled to the same level with solvent, or less concentrated solution. For equilibration to bath temperature, the top section is aligned with the bottom section, and the center channels remain isolated by displacement to one side. Immediately after sliding the center section to the position shown in Fig. 5, a capillary of about 0.5 mm outside diameter, connected to a siphon through a stopcock, is lowered by rack and pinion[18] until the tip is within 0.5 mm of the optic axis, Fig. 5. To locate the optic axis conveniently for positioning the capillary tip, a fine wire is incorporated into the cell mask, as shown in slot *B*, Fig. 6.

Incorporation of the double slits in sections *C* and *C'* into the sliding section of the cell mask, Fig. 6, makes it possible to use the optical system as a Rayleigh interferometer[19] to aid in the evaluation of the refractive index increment of the dissolved solute. If the slits in section *C* are separated by a vertical distance of about 1 cm, the sharpened boundary may be centered between them so that the original solution is in front of the lower slit and and solvent is in front of the upper one, and Rayleigh fringes of a convenient breadth (0.167 mm) may be photographed at the camera plate. The theory for the diffusion interference phenomenon[2] shows that the number $\mathbf{j}_m$[2] of waves retardation by the solution as compared with the solvent is given to the next larger integer by the inequality $\mathbf{j}_m \leqslant \mathbf{N}$, where $\mathbf{N}$ is the number of bright fringes wholly or partly resolved from the undeviated slit image in the diffusion interference pattern. This choice of the integral part of $\mathbf{j}_m$, i.e., $\mathbf{N}-1$, is confirmed below and elsewhere[2,20] by diffusion data for a single homogeneous solute. For this case the same value of the diffusion coefficient is obtained from each fringe of a given photograph as predicted by theory[2] when calculations are based on the correct value of $\mathbf{j}_m$. Use of the wrong integer for $\mathbf{j}_m$ results in values which drift markedly with increasing fringe number. The additional fraction comprising $\mathbf{j}_m$ may be obtained by observing the fractional downward displacement of the Rayleigh interference fringes within the central diffraction zone when solvent replaces the solution in front of the upper slit.[21] In use, section *C*, Fig. 6, is aligned with the cell while light from *C'* passes through the adjacent water bath to provide a reference. With the Tiselius cell in its open position, and the sliding mask moved to align section *C* with the cell, it is possible to cover either *C* or *C'* by rotating a long vane, supported by a heavy vertical wire fastened to the cell holder frame.

To prevent superposition of successive fringe system photographs from sections *C* and *C'*, the mask shown in Fig. 7 is used in front of the photographic plate. Part "a," Fig. 7, was made to fit snugly into the slot in front of the photographic plate. This part was constructed of three sheets of metal firmly fastened together with small screws after the middle sheet was cut as indicated by the dotted line. The thin metal slide, "b," Fig. 7, could be lowered inside "a" through the opening at position 2, and moved so that any one of the levels *A*, *B*, or *C* was located in opening 1. Opening 1 was cut at the level of the undeviated slit image. There is sufficient friction between parts "a" and "b" to hold the slide wherever it is set.

With the cell filled and the capillary adjusted as shown in Fig. 5, section *C* of the cell mask, Fig. 6, is aligned with the right channel of the cell, slot *B* of the slide "b," Fig. 7, is adjusted at the opening 1 in the plate mask "a," and the vane turned to close off light coming through section *C'* and the water bath. The plateholder dark slide is then opened and exposure is made with the manual shutter, Fig. 1. Immediately thereafter, the vane is turned to close off light coming through the cell and section *C*, slot *A* of the slide "b," Fig. 7, is aligned with the opening in the plate mask "a" without disturbing the photographic plate, and a reference photograph is taken. Slot *C* of Fig. 7 is included in the slide to make possible a reference picture both before and after the cell photograph to check periodically the over-all stability of the optical system. Typical photographs are shown in Fig. 8a. The stopcock is then opened, and siphoning commences. As this proceeds, the boundary is swept down to the capillary tip. Schlieren observation with the telescope placed behind the slit image plane, as well as direct observation of the diffusion interference fringes, indicates considerable boundary disturbance during this period. When the boundary reaches the level of the capillary tip, sharpening takes place very rapidly. To insure that gradients of concentration are swept away from the cell walls above the boundary, siphoning is continued at a rate of from 0.3 to 1.5 ml per minute for a time sufficient to replace the liquid in that region at least three times. Throughout this period successive Rayleigh fringe photographs through the cell and the water bath are made as described above. Typical photographs, showing the displacement of the fringe system on replacement of solution by solvent in the cell in front of the upper slit, appear in Fig. 8b. The evaluation of the successive photographs serves to determine whether all refractive index gradients have been swept out from above the thin opaque layer between the slits. The diffusion experiment is started by closing the three-way stopcock *S*, Fig. 5, between the capillary and siphon. The capillary is immediately withdrawn with the rack and pinion. Then the center section of the cell is closed off to prevent any possibility of condensation of atmospheric moisture into the diffusion column. With the cell in this position, the mask, Fig. 6, is moved so that the slot *A* is aligned with the right arm of the cell containing the diffusion column. The vane attached to the frame then serves to screen off either section *A* or section *A′*. During the diffusion experiment, photographs are made through the cell with slot *A*, whose upper and lower ends are made V-shaped to reduce diffraction, and are arranged so they may be opened symmetrically about the boundary as it spreads.[3] The V-shaped ends are produced by thin sheet brass plates, shown with dotted lines, which are actuated to move in vertical ways by a single vertical rod having right- and left-hand threads.

---

[19] Lord Rayleigh, Proc. Roy. Soc. 59, 203 (1896).

[20] L. J. Gosting and M. S. Morris, paper presented at the 113th meeting of the American Chemical Society, Chicago, Illinois, April 22, 1948.

[21] The application of the Rayleigh interferometer has been made in an entirely equivalent fashion by Coulson, Cox, Ogston, and Philpot, Proc. Roy. Soc. A192, 382 (1948) in their independent development of the Gouy interference method, and their paper presents the complete theory for this application.

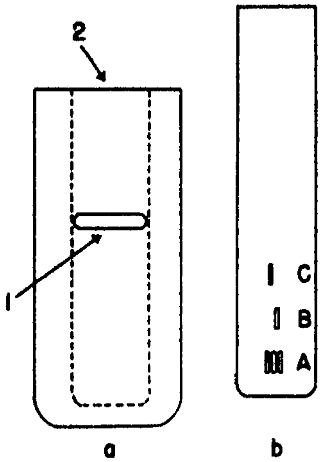

FIG. 7. Photographic plate mask for refractometer photographs. a. Slide holder. b. Slide.

The detachable plate *A′* contains two slits symmetrically located about the level of the optic axis. The purpose of the double slit in section *A′* is to provide reference photographs for each diffusion photograph so that the position of the undeviated slit image may be located. The double slit separation in *A′* is less than in *C′* so that wider openings of the source slit, required for early diffusion photographs, may be used without blurring the fringes in this reference pattern. Photographs of the diffusion interference fringes are followed immediately in each case by the reference double slit interference photograph through section *A′* and the water bath adjacent to the cell. To prevent the alternate diffusion and double slit exposures from superposing on the photographic plate, which must be absolutely stationary between these exposures, interchangeable masks, shown in Fig. 9a for diffusion and 9b for reference photographs are inserted in front of the plateholder. Satisfactory control of exposures is accomplished by the manually operated shutter.

A typical photograph showing both diffusion and double slit reference fringe systems is shown in Fig. 10. The central portion of the pattern shows successive steps taken through increasing thicknesses of gelatin filter according to the technique described by Longsworth.[8] The central maximum of the double slit pattern denoted by "Ref." determines the undeviated slit image position independently. Since this pattern is symmetrical about the center of the slit image, the position of the latter can be located accurately from the two sur-

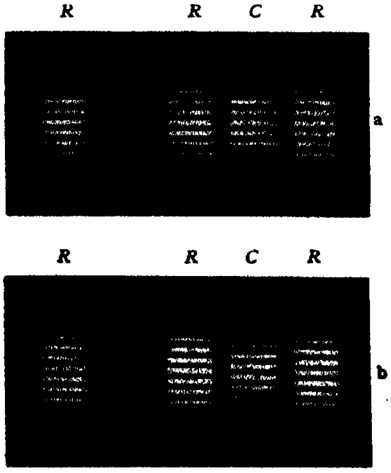

FIG. 8. Sample refractometer photographs, with reference pictures "*R*" and cell pictures "*C*." a. Capillary inserted, but before siphoning, i.e., solution is in front of both slits of *C*, Fig. 6. b. During sharpening, i.e., solvent is in front of upper slit of *C*, Fig. 6, while solution is in front of the lower slit.

rounding minima. Because the double slit pattern is obtained at all times from the same small portions of the lens near its center, this reference is not subject to the same spherical aberration errors as the slit image itself photographed through portions of the lens which approach the periphery as the diffusion proceeds. The precision depends on the stability of the optical track, but the time intervening between the reference and diffusion photographs is so short that the present equipment has in the majority of cases been found to give slit image positions self-consistent to within two or three microns.

On comparison of Rayleigh fringe photographs taken through the cell when filled with homogeneous liquid with those through the adjacent thermostat using reference *A′*, Fig. 6, a constant displacement, δ, was noted that is doubtless due to small prismatic effects in the cell and/or bath windows. This was added to the measured displacement of each fringe below the reference slit image position to give the correct downward displacement, $\mathbf{Y}_j$, of each fringe from the true undeviated slit image.

The optical quality of this combination of bath windows and cell walls was tested by successively placing other double slits with gradually increasing spacings ranging from about 3.3 to 23.3 mm behind the cell and measuring successive "δ" distances as described above. Water filled the cell during these tests, and each pair of slits was always symmetrically spaced about the level of the optic axis. The value of δ decreased slightly as the slit separations were increased, but had not changed by more than 5 microns when slit separations of 20 mm were reached. Thus the central portion of the cell and windows, from which all diffusion data are derived when the slit image position is obtained from a reference double slit beside the diffusion cell, were found to be of good quality.

TEST OF THE APPARATUS

As a demonstration of the precision attainable with the equipment and procedure described above the results of a typical experiment on the diffusion of sucrose in water are summarized in Tables I and II. In the first table the refractometric data, together with the results for a typical diffusion fringe photograph are presented. In the second column of Table I are given the observed displacements, $\mathbf{Y}_j$, from the undeviated slit image position of the fringes whose numbers, j, are indicated in the first column. The third column contains the theoretical[8] values of these displacements in normalized units while the last column gives the ratio, $\mathbf{C}_t$, of the observed and theoretical values. If the theory is valid, and if sucrose diffuses as an ideal solute, the values of $\mathbf{C}_t$ in Table I should be constant for each fringe and this is seen to be accurately true.

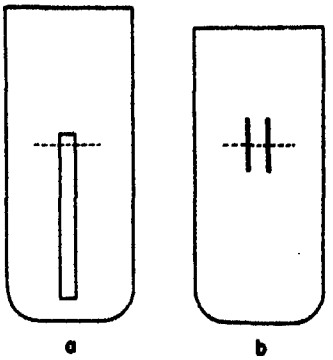

FIG. 9. Photographic plate masks for diffusion. a. Mask for diffusion pictures. b. Mask for reference pictures.

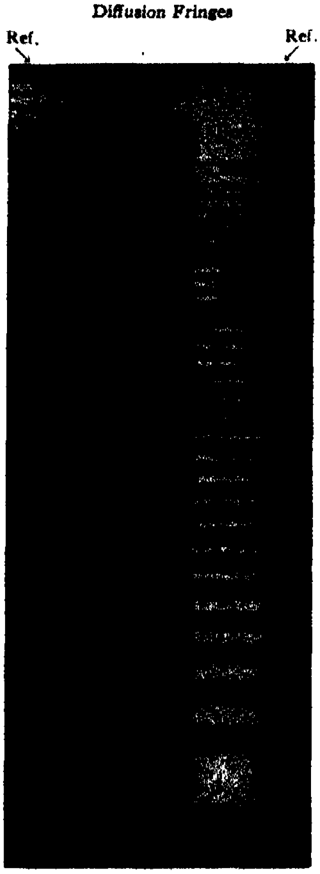

FIG. 10. Sample diffusion interference fringe system, with reference picture "Ref."

The diffusion coefficient, $\mathbf{D}'$, is given by the relation

$$\mathbf{D}' = (\mathbf{j}_m\lambda\mathbf{b})^2/(4\pi\mathbf{C}_t^2\mathbf{t})$$

in which the wave-length, λ, is 5462.2A, the optical distance, **b**, is 306.45 cm, and **t** is the time after cessation of the boundary sharpening procedure. If each of the diffusion fringe photographs is analyzed as is illustrated by Table I the results for the complete experiment may then be summarized

TABLE I. Data for one photograph of a sucrose diffusion at 1.00°C. "Solvent"—2.001_7 g per 100 ml solution. Solution—2.502_5 g per 100 ml solution. Photograph taken 30060 seconds after start of diffusion. Number of diffusion fringes in pattern $= N = 34$. Displacement of Rayleigh fringes on replacing solution by solvent in front of upper slit $= (0.41 \pm 0.01) \times$ (fringe spacing) $\therefore j_m = (N-1) + 0.41 = 33.41$. Displacement of Rayleigh fringes through cell from reference $= \delta = 0.0008$ cm.

1 j (minima)	2 Y_j (cm.)	3 $e^{-z_j^2}$ ($j_m = 33.41$)	4 $Y_j/e^{-z_j^2} = C_t$
0	0.5388	0.90402	0.5960
1	0.4966	0.83347	0.5958
2	0.4624	0.77655	0.5954
4	0.4065	0.68210	0.5960
6	0.3588	0.60240	0.5956
8	0.3168	0.53197	0.5955
10	0.2789	0.46823	0.5956
12	0.2442	0.40978	0.5959
14	0.2120	0.35566	0.5961
16	0.1819	0.30525	0.5959
18	0.1534	0.25814	0.5943
20	0.1273	0.21401	0.5948
24	0.0797	0.13392	0.5951
28	0.0382	0.06438	0.593

as shown in Table II. Here the values of **D′** in the second column show a slight downward drift with time which is due to the fact that the boundary at zero time is not infinitely sharp as required by the theory. Correction for this initial mixing is made[3] by plotting **D′** *versus* 1/**t** to obtain a zero time correction, **Δt**, that amounts to 30 seconds in the present experiment. Column 3 of Table II then gives the final value of the diffusion coefficient, **D**, after application of this zero time correction. The results indicate that the method is capable of a precision of 0.1 percent.

TABLE II. Diffusion coefficients of sucrose in air-saturated water at an average concentration of 2.252_1 g per 100 ml of solution. Temperature—1.00°C. j_m—33.41.

1 t (sec.)	2 $D' \times 10^6$ cm²/sec.	3 $D \times 10^6$ cm²/sec.
1300	2.384	2.331
1830	2.368	2.330
2490	2.356	2.328
3870	2.346	2.328
5790	2.343	2.331
7410	2.342	2.333
9450	2.332	2.325
12210	2.334	2.328
15210	2.334	2.330
17250	2.335	2.331
19230	2.333	2.330
20370	2.334	2.331
24900	2.329	2.326
25260	2.332	2.329
28260	2.331	2.328
30060	2.333	2.331
34230	2.332	2.330
36510	2.336	2.334
38730	2.331	2.329
41730	2.335	2.333
	Mean	2.330
	Av. Dev.	$0.001_7 = 0.07\%$

ACKNOWLEDGMENTS

The authors wish to thank Dr. J. W. Williams for his interest and for placing the facilities of his laboratory at their disposal. They also desire to thank Dr. L. G. Longsworth for his careful reading of the manuscript.

This work was supported in part by grants from the Wisconsin Alumni Research Foundation, The Rockefeller Foundation, and the U. S. Public Health Service.

Laboratory and Shop Notes

Note on the Preparation of Beta-Ray Sources

LAWRENCE M. LANGER
Indiana University, Bloomington, Indiana

January 7, 1949

IN order to measure the true momentum distribution of beta-particles in a nuclear spectrometer, it is important to avoid introducing distortion because of the preparation of the source. Several problems arise in connection with the preparation of a suitable source. Although the solution to these problems is not unique, it is believed that the following suggestions may be of interest.

In order to minimize distortion of the spectrum because of scattering, it is necessary to mount the radioactive sample on an extremely thin backing of low atomic number material which is isolated at some distance from the walls of the spectrometer. Since the materials usually used for making the thin backings (Zapon, Collodion, Formvar, etc.) are usually very good insulators and since the electrical capacity of the source is small, it is found that with strong radioactive deposits the source may charge to several kilovolts, with respect to the vacuum chamber, in a rather short time. Such a charging of the source may introduce an electrostatic acceleration of the emitted particles which will affect the spectrum distribution at very low energies. It will also result in shifting the energies of beta-spectra end points and of internal conversion lines.

The charging of sources may be avoided in many ways. One can, of course, deposit, by evaporation in vacuum, a thin metallic film on the backing material which is mounted on a grounded aluminum ring. This, however, may not always be convenient and the following two techniques are simple effective ways of keeping the source at ground potential. It is found that a solution of Zapon in amyl acetate can be loaded with colloidal graphite ("Aquadag"). Films made from such a solution are much poorer insulators. Such foils, however, do not have the strength of normal Zapon and so must be sandwiched between unloaded films. Another method which may be used satisfactorily with spectrometers employing sources of large area is to stretch a fine hair across the aluminum source supporting frame. The hair is then made conducting by painting with a suspension of colloidal graphite in alcohol. The thin layers of backing are then laid down over the hair in the usual way. For a source which is several millimeters wide, the scattering from the 0.001″ hair is quite negligible.

It is sometimes necessary to prepare the source from solutions which chemically attack the usual backing materials. For this purpose, it is found that backing films can be prepared from clear LC 600[1] which when dry are resistant to acids, alkalis, or alcohol. LC 600 films may be prepared by the usual technique of spreading on a surface of clear water.[2] One drop of one part LC 600 to four parts LC 600 thinner yields a double film of about 0.006 mg/cm^2. Such films do not spread over as large an area as Zapon films, since the solvent dries much more rapidly. They are as a result not as uniform as Zapon films and therefore, when prepared by this technique, are not too suitable for Geiger counter windows.

It is found that deposits of certain chemical compositions tend to break thin backings, presumably by mechanical action, during the last stages of drying. For the preparation of such sources, it may be necessary to use two or more layers of backing in order to obtain sufficient strength. When such a stack of films is prepared wet, there is little tendency to trap air bubbles between layers. The stack should then be thoroughly dried before laying down the sample.

Samples laid down from solutions have, in general, a tendency to clump or "ball-up" while drying. As a result, such deposits may have local thicknesses much greater than that of the average. It is found that such effects are almost completely eliminated by first treating the backing material with a thin layer of insulin.[3] A drop of Lilly insulin diluted with 20 parts of water is led over the backing surface with a dropper so as to wet the area desired for the source. The excess insulin is then drained off with the dropper. When a drop of radioactive solution is now placed on the wetted area, it immediately spreads uniformly to fill the entire area. The source is then dried by evacuation, care being taken to avoid freezing.

This work was supported by a grant from the Frederick Gardner Cottrell fund of the Research Corporation and by the joint program of the ONR and AEC.

---

[1] LC 600 is a synthetic resin coating material manufactured by Lithgow Corporation, Chicago, Illinois.

[2] Lawrence M. Langer and C. Sharp Cook, Rev. Sci. Inst. 19, 256 (1948).

[3] V. J. Schaefer and D. Harker, J. App. Phys. 13, 427 (1942).

On the Design of a Radiofrequency Cockroft-Walton Accelerator

PAUL LORRAIN
Laboratory of Nuclear Studies, Cornell University, Ithaca, New York

December 13, 1948

IT seems that Cockroft-Walton accelerators (Fig. 1),[1,2] which have been used so extensively in the range of energies between a few hundred thousand and a few million electron volts, have always been operated at frequencies of the order of a few hundred cycles per second or less. However, relatively small Cockroft-Walton (henceforth written CW) generators, supplying up to 200 kilovolts and operating at frequencies of the order of 10 kilocycles per second, are now commercially available.[3,4] The numerous advantages gained by using a high frequency have long been recognized. It was thought worth while to investigate the upper frequency limit and the difficulties to be expected at high frequencies, so as to exploit these advantages to their full extent.

Let us call f the operating frequency, C the capacity of one of the condensers, v the peak-to-ground alternating voltage at the source S, and n the number of stages (one-half of the total number of condensers). Then,[2] for ideal rectifiers and for a load

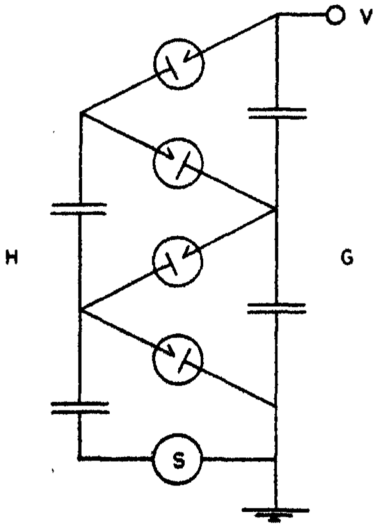

FIG. 1.

current i, the average output voltage V is given by

$$V=2nv-(i/12fC)(8n^3+9n^2+n),$$

and the ripple voltage δV at the output is

$$\delta V=\pm(i/4fC)n(n+1).$$

Practical units are used.

Obviously, the product fC should be large. Now the most economical way to do this is to use as large an f as possible, and then to choose C accordingly. The reason for this is that the cost of a condenser increases much more rapidly with capacity than does the cost of a source of alternating voltage with frequency. Other advantages of lower capacity condensers, aside from their lower cost, are their smaller weight and smaller volume. Also, for a sufficiently high frequency, the number of stages "n" could be made fairly large for a given generator internal impedance or a given ripple voltage. This means that lower voltage ratings for both the condensers and the rectifiers would be permissible. The total number of condensers and rectifiers would be increased proportionately, but their total cost would nevertheless be considerably reduced. Finally, the ripple could have a very low value to facilitate accurate energy measurements.

All this is particularly interesting in view of the fact that high voltage, low capacity "television" condensers are now available at very low prices. For example, a 30-kilovolt 0.0012-microfarad condenser which sells for about three dollars is roughly one inch long and two inches in diameter.[3]

The upper frequency limit is fixed by the electron transit time in the rectifiers. Beyond this frequency, the voltage drop in the rectifiers would increase, with a resultant increase in the internal impedance of the generator. In a two-stage model, this voltage drop was found to be approximately the same at sixty cycles per second and at radiofrequencies ranging up to 21 megacycles per second. The internal impedance was constant for any given current as long as the product fC was sufficiently large to make the second term on the right-hand side of the first equation negligible. The no-load output voltages were in the neighborhood of 1200 volts and currents up to a few milliamperes were drawn. The upper frequency limit thus appears to be above 21 megacycles per second. A rough calculation shows that it cannot be much higher. At the high r-f voltages required for an accelerator, the upper frequency limit would be somewhat lower than at the voltages used, but by less than one order of magnitude.

With small condensers and at high frequencies, stray capacities would be important. The stray capacity between column H (Fig. 1) and ground, and between the two columns, would have two effects. First, the r-f voltages on the condensers of column H would be reduced. This would lower the output voltage even at no load. Second, large r-f currents would flow in the condensers, particularly in the lower ones. These effects could be largely cancelled by using an r-f choke of the proper inductance, with a blocking condenser, in parallel with each rectifier (Fig. 2). However, these effects should preferably not be too large. Then f should not be much higher than a few megacycles and C not much smaller than 0.001 microfarad.

The rectifier filaments are thus provided with a very convenient source of power, for the chokes can be used as transformers to heat the filaments without reducing their Q value significantly (Fig. 2). Usually this power is supplied by storage batteries, or by generators run through a belt from a motor at ground potential, both methods being quite objectionable for various reasons. A two-stage model connected as in Fig. 2, with type 8016 rectifiers and 0.01-microfarad mica condensers operated satisfactorily. Some care has to be used, however, to operate the filament of this tube at the proper brightness, as suggested by the manufacturer. No attempt was made to tune the chokes so as to cancel the effects of the stray capacities, as these are important only for high r-f voltages and small condensers. The filament power can be applied independently of the high tension by opening the plate circuit of the diode nearest to ground.

The ion source could be fed from a transformer in the same manner as the filaments.

The upper limits for the voltage and for the voltage gradient attainable with this generator are comparable to those attained with the electrostatic generator. The output currents could be relatively high and there would be no moving parts.

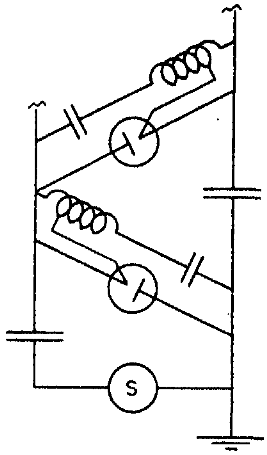

FIG. 2.

The following is a tentative design for a 500-kv generator: $f=5$ megacycles per second; $C=0.0012$ microfarad, 30 kv; $v=15{,}000$ volts; $n=17$; ripple voltage about ±50 volts for a load current of 1 milliampere; rectifier type 1B3 for currents up to 1 milliampere, or type 8013A for higher currents; total cost of condensers and rectifiers, three hundred dollars with the 1B3 and four hundred and seventy dollars with the 8013A (list prices). This is less than for a low frequency design by a factor of about 10. The whole accelerator should be submerged in oil or pressurized (this would require special rectifier tubes designed to withstand the pressure) to reduce the length of the accelerating tube and to facilitate shielding the r-f and other stray radiations.

[1] J. D. Cockroft and E. T. S. Walton, Proc. Roy. Soc. **136A**, 619 (1932).

[2] A. Bouwers and A. Kuntke, Zeits. f. tech. Physik **18**, 209 (1937).

[3] Beta Electronics Company, 1762 Third Avenue, New York 29, New York.

[4] G. J. Siezen and F. Kerkhof, Proc. I.R.E. **36**, 401 (1948).

[5] Jeffers Electronics, Inc., Dubois, Pennsylvania.

Rejuvenation of Geiger-Mueller Tubes*

L. SHEPARD
Department of Physics and Laboratory for Nuclear Science and Engineering, Massachusetts Institute of Technology, Cambridge, Massachusetts

January 3, 1949

IT is well known[1] that Geiger-Mueller tubes filled with a self-quenching mixture of argon and ethanol deteriorate with use, and that refilling the tubes with new gas, though it may improve the operation somewhat, does not restore the original counting characteristics. We wish to report that a simple treatment has been found which, in conjunction with replacing the gas, restores the tube to its original state. This treatment consists of heating the center wire to a dull red by an electric current for about ten minutes while the tube is evacuated, preparatory to filling with new gas.

The tubes for which this treatment has been used are made from a one-inch diameter brass cylinder with a 0.005-inch tungsten central electrode, which is supported at each end by a Kovar glass seal. The assembly is such that an electrical connection can be made at each end of the central wire. In one group of 52 tubes ranging in length from ten inches to thirty inches, the plateaus extended from 900 volts to 1150 volts for each tube. After some months of use during which time about 10^8 counts occurred in each tube, the thresholds had risen to 1000 volts and the plateaus terminated at about 1050 volts. Merely changing the gas brought the thresholds back to 900 volts but the plateaus still extended only to 1050 volts. When the tubes were again evacuated and refilled after the center wire had been heated, the plateaus were the same as when the tubes were first made. Of the 52 tubes so treated, the original characteristics were not restored in only three tubes.

The heating current of about 0.5 ampere is supplied from a Variac, which is adjusted until the wire, as observed through one of the end seals, is visibly red.

---

* Assisted by the joint program of the ONR and the AEC.

[1] See, for instance, S. C. Brown, Nucleonics 2, 10 (1948).

A Thyratron Square Wave Generator

Leonard Reiffel*
Department of Electrical Engineering, Illinois Institute of Technology, Chicago, Illinois

November 10, 1948

The purpose of this note is to describe a simple versatile circuit for generating square wave pulses of large amplitude via a gas filled triode. Under special operating conditions, a thyratron may be used as a trigger tube for the production of approximately square voltage pulses, in discontinuous or continuous wave trains, with widely variable amplitude and symmetry characteristics. If a thyratron with plate supply voltage E_{bb} and a load resistance R_1 is fired at a time t_1, the voltage across the tube will fall rapidly from E_{bb} to E_0, the arc drop; thus a voltage step of amplitude $(E_{bb}-E_0)$ will appear across the tube. If at a time t_2, the thyratron could be made to deionize, the voltage across the tube would rise from E_0 to E_{bb}. This sequence of events would thus produce an approximately square pulse of amplitude $(E_{bb}-E_0)$ and duration (t_2-t_1). It is evident that if the thyratron were ionized (and deionized) N times per second, a square wave of frequency N would appear across the tube.

The mechanism for firing the thyratron offers no difficulty since the mere application of a grid over-voltage will serve to ionize the tube. However, deionization ordinarily can only be commenced by opening the plate circuit or by driving the plate current to zero by applying an inverse voltage across the tube. It is evident that neither of these possibilities is well suited to the production of square waves in the manner outlined.

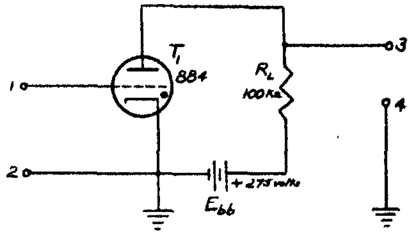

FIG. 1. Thyratron square wave generator.

Under normal operating conditions attempts to interrupt the plate circuit arc by driving the *grid* negative are unsuccessful. This is true because once the plate arc has been formed, the grid structure is immersed in a plasma which effectively shields the plate circuit from voltage variations of the grid. Any variations in grid voltage serve merely to change the thickness of an ion sheath which forms around the grid. The ion sheath thickness can be made as great as desired by raising the grid potential and/or decreasing the plate arc current.[1] If the current in the plate circuit of the thyratron (in which the arc is formed) is limited to a very low value by use of a large plate resistor and the grid is driven sufficiently negative, it is perfectly possible to get a positive ion sheath to extend across the entire discharge region in the tube. This ion sheath effectively cuts the arc in two and causes the plate current to go to zero (i.e., extinguishes the arc).[2]

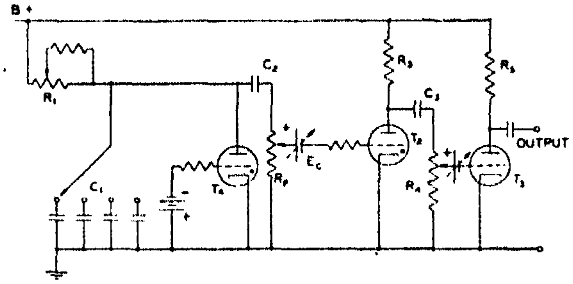

FIG. 2. Thyratron square wave generator.

The circuit of Fig. 1 with thyratron T_1 operating under the special conditions above, becomes, in essence, a square wave generator. Positive and negative pulses must be supplied at terminals 1–2 so as to alternately fire and extinguish T_1 and thus produce *approximately* square pulses across terminals 3–4.

If the squareness of the pulses to be generated at terminals 3–4 is not too critical, the grid (terminals 1–2) may be driven from an ordinary sine wave generator such as is found in most electronics laboratories. The circuit of Fig. 1, with the components listed, produces square waves suitable for many applications across terminals 3–4 at the sine wave oscillator frequency from 10 to about 5000 cycles per second and amplitude 250 volts. It is to be noted that the output impedance of such a circuit will be very high since the high resistance R_1 prevents appreciable current flow through a load impedance coupled to the generator at terminals 3–4. High impedance output is, of course, undesirable if any amount of power is required by the load across terminals 3–4, and a more versatile circuit is shown in Fig. 2.

It has been found that a relaxation oscillator is ideally suited to provide the alternating grid voltage necessary for driving

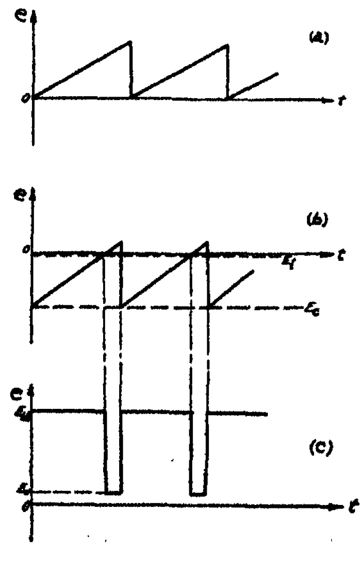

FIG. 3. Thyratron square wave generator.

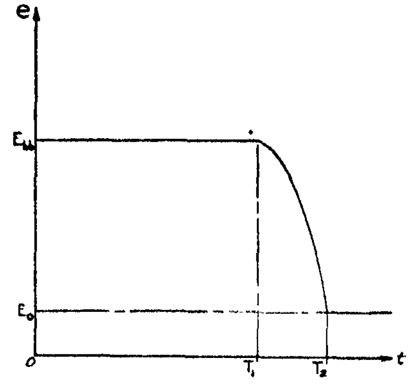

FIG. 4. Thyratron square wave generator.

the grid of the main thyratron T_3. The thyratron T_4 is arranged in such a variable frequency relaxation oscillator. The period of oscillation P of the relaxation oscillator is controlled by varying the magnitude of R_1 and/or C_1. Thus C_1 is used as a frequency range selector and R_1 is used as a frequency vernier. Since this type of relaxation oscillator produces sawtooth wave forms, the mere addition of a variable grid bias on the main thyratron T_3 permits control of the symmetry of the final square wave output, as indicated in Fig. 3.

Figure 3a shows the sawtooth output of the relaxation oscillator; Fig. 3b shows the total grid voltage applied to the main thyratron T_3 (sawtooth plus bias) and Fig. 3c shows the resulting square wave which appears across thyratron T_3. It is evident from the figure that the further the sawtooth is dropped below the level E_i of Fig. 3b, the more asymmetric the resulting square wave will be. Obviously, the upper limit to this procedure is the point at which the peak of the sawtooth falls at the level E_i, since any further increase in bias will prevent the tube T_3 from firing entirely. Also, since E_c must be large enough to extinguish the arc, there is a lower limit on the variation of E_c.

An obvious alternative method of symmetry control consists in varying the amplitude of the sawtooth wave form while maintaining a constant grid bias on T_3. The amplitude of the sawtooth may be conveniently controlled by the potentiometer at the output of the relaxation oscillator.

To accomplish the very desirable reduction of output impedance and increase of power output mentioned earlier, the square wave output of thyratron T_3 is coupled to a low mu, high power output triode.

It should be mentioned that the coupling networks between the relaxation oscillator and thyratron T_3 and between thyratron T_3 and the amplifier consist of 1.0-microfarad condensers (C_2 and C_3 of Fig. 2) and 1.0-megohm resistors (R_3 and R_4 of Fig. 2). This combination yields a time constant of 1.0 second which permits the passage of 20-cycle per second square waves with little or no distortion.

In addition to the distortion in square waves introduced by stray circuit parameters, the thyratron square wave generator produces variations from the ideal output via "ionization time distortion" and "deionization time distortion." The curve of plate voltage *versus* time for a thyratron upon the application of a grid over-voltage represents the best possible "rise curve" of the output square wave, and has been found experimentally by A. E. Harrison[3] and others to be of the form shown in Fig. 4.

The time lag portion of the ionization time, about 1 microsecond long, produces no square wave distortion, but merely a slight asymmetry in the final output. However, the breakdown time portion of the ionization time represents the *minimum rise time* of the output square wave, about 0.2 microsecond for type 884 thyratrons. Although the figure of 0.2 microsecond applies only to the circuit of Fig. 1 with no load, the rise time of the circuit of Fig. 4 with its additional capacitive loading is adequate for most applications.

The deionization time of the thyratron represents the minimum decay time of the output square wave. Ordinarily the deionization time in a type 884 thyratron ranges from 10 to 1000 microseconds. However, there are two factors contributing to a substantial reduction in the recovery or deionization time of the gas. Both the very low arc current being used, and the fact that the grid is driven considerably negative as deionization commences, lead to a much shorter recovery time (about 5 microseconds).

It is possible, by employing hydrogen-filled tubes,[4] that the rise and decay times of square waves produced by thyratron square wave generators can be considerably reduced. The deionization time limits the frequency at which good square waves can be produced to approximately 12,000 cycles per second for argon-filled tubes. Here again, hydrogen-filled thyratrons hold a promise of extending this upper frequency limit to perhaps 40 kilocycles per second.

It is evident from the theory of the basic square wave generator circuit of Fig. 1 that the only limit on the amplitude of the square waves produced is the maximum plate voltage that the thyratron can withstand. Thus, with the proper tube,[5] square waves of 1000-volts in amplitude are easily produced by the basic circuit.

---

[*] Now at Institute for Nuclear Studies, University of Chicago, Chicago, Illinois.

[1] J. Millman and S. Seely, *Electronics* (McGraw-Hill Book Company, Inc., New York, 1941), p. 319.

[2] The negative grid voltage required to extinguish the arc varied from tube to tube, however, a 25-volt pulse was usually found to be sufficient for type 884 and 885 tubes. A similar method has been used to quench tubes in some counting circuits described in the literature and in a transient visualizer described by Reich.

[3] A. E. Harrison, Trans. A.I.E.E. **59**, 747ff. (1940).

[4] H. Heins, Electronics **19**, 92–102 (July 1946).

[5] The tube geometry is of great importance because of the mechanism utilized for extinguishing the arc. No investigation has been made with high voltage commercial tubes.

A New Principle in Controlled Vacuum Leaks

C. H. BACHMAN
Syracuse University, Syracuse, New York

December 20, 1948

MEANS for admitting small quantities of gas to a vacuum system (controlled leaks) have depended upon constrictions for their operation. Typical examples are finely drawn glass capillaries, flattened copper tubing, the porosity of unglazed porcelain, and needle valves of various designs.[1] These all have two basic weaknesses. They are not easily adaptable to be varied over wide values of leak rate, and they are subject to fluctuations in leak rate as particles of dust are drawn into the constrictions.

In an attempt to develop a means of moving strip film into and out of a vacuum chamber between two rubber rollers, it was found that removal was easily accomplished but insertion of the film was always accompanied by some air, apparently carried in on the surfaces of the rollers. This has led to the application of a completely different principle for the operation of controlled leaks which obviates both of the basic weaknesses indicated above in connection with constriction or capillary type leaks.

Instead of introducing gas at a slow steady rate through a constriction, it is introduced in short bursts or pulses through a comparatively large opening. The amount of gas in each pulse as well as the pulse frequency is controlled. With such an arrangement dust particles can have no effect and the leak rate can be adjusted through great ranges.

Two types of pulsed leaks are being investigated currently. These two types are indicated in Figs. 1 and 2. Each has certain advantages and disadvantages which make its use preferable for certain applications.

In Fig. 1 is shown an arrangement consisting of a metal shaft having pits drilled or bored into its surface as indicated. The pick-up tube leading to the vacuum system is inserted into the rubber collar which is shaped to fit the rotating shaft. The collar is held against the shaft with sufficient pressure to give a good vacuum seal between pits. Lubrication with vacuum oil or grease is essential. As the shaft is rotated each pit delivers its volume of gas to the evacuated pick-up tube and moves on to be recharged.

The capacity of this leak is governed primarily by the volume of the pits and the pit or pulse frequency. The bore of the pick-up tube is definitely out of the class of capillaries, being ¼ in. or larger. The pulse frequency is limited by the geometry of the pick-up tube and pit diameters, and by the relative linear speed of the two members. At linear speeds much greater than about 1 foot per second, lubrication and heating problems develop.

Using a variable speed drive the leak rate may easily be adjusted over a 100 to 1 range. The vacuum attained, of course, will depend upon the pump speed and the pit volumes for any given pulse frequency. For extremely slow leak rate a smooth shaft may be used in place of a pitted shaft. Arrangements are easily made to interchange shafts to provide different leak rate ranges.

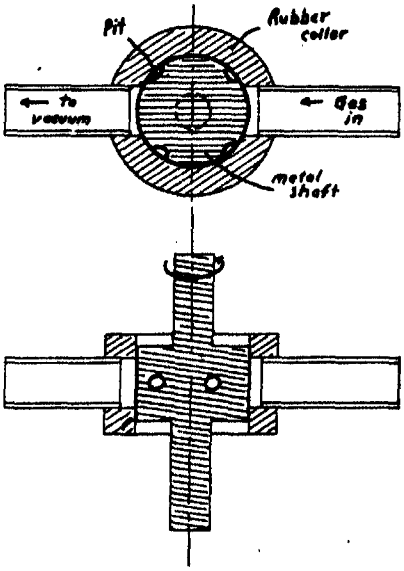

Sectional Views

FIG. 1. Principle of rotary pulsed leak.

This type of leak has the great advantage that its capacity or leak rate can be predicted from a knowledge of the pit dimensions and operating speed (pulse frequency). When used in this type of application care must be used that the pit volume not be reduced during operation by accumulated oil from the lubricated running surface.

Using the displacement of a Hg pellet in a capillary tube as a means of checking the flow rate, repeated measurements on a rotary pulsed leak showed the actual leak rate to check the calculated rate to within a few percent. These measurements were made at pressures below one mm Hg.

One disadvantage possessed by the rotary leak for some applications is the presence of vapor from the lubricating oil. The arrangement of Fig. 2 eliminates this difficulty. The line drawing depicts a rather simplified version of a cam-operated valve. As the cam rotates the rubber cap opens and closes the opening to the pick-up tube.

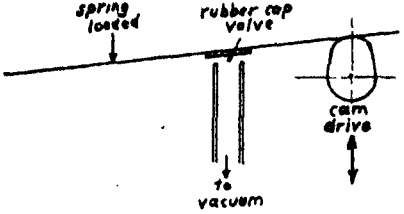

FIG. 2. Principle of valve type pulsed leak.

This leak, although operating on the pulsed leak principle, differs from the rotary leak in that for normal cam speeds the leak rate does not depend directly upon rotational speed. For a given pick-up tube size, the relative open and closed times determine the rate and this is set by the position of the cam. The cam should be adjustable along the line shown by the double-headed arrow. In one extreme the valve will ride open during the complete rotation. In the other extreme it will remain closed. Intermediate positions give "open to closed ratios" between these extremes. The pulsed valve leak, although eliminating the oil vapor, does not lend itself to precalculated design as does the rotary pulsed leak.

Such a pulsed leak, provided with a screw adjustment of cam position, easily controlled the pressure from atmospheric down to 10^{-4} mm Hg. The pumping system consisted of a Welch Duo-Seal No. 1400 mechanical pump, and at the lower pressures a D.P.I. two-stage glass oil diffusion pump was in operation. Pressures were read with Hg manometer, thermocouple gauge, and ionization gauge, each in its range.

Either the rotary or the valve type leak lends itself nicely to applications where a desired vacuum value is held by balancing the leak rate against the pumping speed. The results are even more striking, however, when the pulsing leak is turned on and off by a vacuum switch such as the SMCI[2] monitor, or the type recently described.[3] Although these switches may be used directly with solenoid valves, the use of the proper pulsed leak gives extremely accurate control and eliminates overshooting and relay chattering.

Many variations of the two basic types of pulsed leak described here are possible and a large number have been tried successfully, including the use of solenoid mechanisms instead of motor drives. Both types may be adapted to introduce gas of desired content. Investigations now under way are concerned with the operating characteristics of some of the better designs, and the accuracy with which the leak rate of the rotary pulsed leak can be precalculated.

Although the work to date has been in connection with vacuum systems, the pulsed leak principle should be useful in any application where it is desired to have control over the transfer of gas from a high pressure region to one at lower pressure.

[1] C. H. Bachman, *Techniques in Experimental Electronics* (John Wiley and Sons, Inc., New York, 1948).

[2] *Skaneateles Manufacturing Company*, Inc., 122 Dickerson Street, Syracuse 2, New York.

[3] C. H. Bachman, Instruments 22, 33–36 (January 1949).

An Absorption Cell and Loader for Use in Microanalysis by Infra-Red Spectroscopy*

Seymour H. Wollman**
Sloan Kettering Institute for Cancer Research, New York, New York

December 6, 1948

IT has become recognized that certain substances of great biological activity occur in small quantities in living organisms. Because of the small quantities present it is difficult to

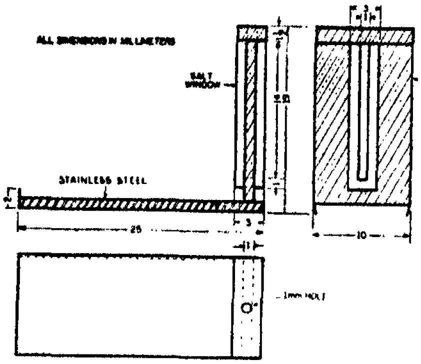

FIG. 1. Absorption cell.

obtain a sufficient amount to give quantitative and qualitative analyses. Any tool which would allow analysis of small quantities of chemicals should be a very useful tool in biological research and medicine. In recent years infra-red spectroscopy has proved useful as an analytical tool. This paper presents a simple modification of a commercially available automatic recording infra-red spectrometer[1] which makes it possible to reduce the quantity of material required for analysis by a factor of ten to thirty or more.

In the spectrometer, radiation from a glow bar is focused on the entrance slit of the spectrograph by a mirror (aperture approximately f:4.5). The sample cell is held in the convergent beam of radiation 2 cm in front of the entrance slit. At this distance the beam has a width of 7 mm.

Since, according to Beer's law, the percent of radiation transmitted through a sample depends only on the number of the particular absorbing molecules per square cm, i.e. on the concentration of molecules times the cell thickness, it is possible to reduce the area of the absorbing cell and thereby its volume, and hence the number of molecules required without changing the absorption spectrum. It is possible to reduce the cell size without reducing the amount of radiation transmitted simply by placing the absorption cell very close to the entrance slit, in as narrow as possible a part of the convergent beam of radiation.

In the following paragraphs a narrow absorption cell and a new cell holder, which holds the absorption cell close to the entrance slit, will be described. A cell loader to take care of difficulties in the handling of small amounts of solution will also be described.

Absorption cell: A diagram showing construction of the absorption cell is given in Fig. 1. The absorption cell consists of a brass spacer mounted on a stainless steel platform which fits on and slides over a track to the window of the cell holder. The cell is mounted with 2 mm of the entrance slit, and since the convergence of the beam is about f:4.5, the minimum allowable width for the absorption cell is about 0.7 mm. A slot in the spacer determines the height and the width of the cell, while the spacer thickness determines the thickness of the absorption path. The absorption cell which is 1 mm thick has a height of 12 mm and a width of one mm (volume about 12 mm^3).*** The slot in the spacer is covered with one-mm thick salt plates cemented in position with an adhesive which is insoluble in CS_2 (National Starch Products, Inc. Adhesive No. 2654) and resistant to acetone (used as a cell cleaner). At first the salt crystals used as windows were cut the width of the spacer. These were found to be unsatisfactory for the small cells since it did not seem to be possible to make the volume available to solution between spacer face and salt plate small enough. This space was present because of the small lack of planarity of the salt windows. It was difficult to fill the space with an inert material without having the material flow into the path of the beam of radiation. A satisfactory solution lay in cutting the salt plates to overlap the space beyond the slot by no more than one mm, and in clamping them in position before painting the edges with adhesive. The top of the spacer is covered with a brass block with a one-mm diameter filling hole. This hole can be stoppered by covering it with lead foil and universal wax during absorption measurements. It is vital that the seal be airtight since CS_2 is volatile, and losses of solvent due to evaporation will be a considerable percent of the total solvent volume if care is not taken. If this happens, the absorption curve will be distorted.

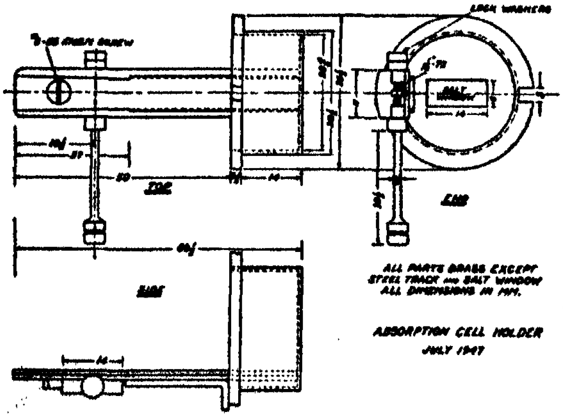
LOCK WASHERS
SALT WINDOW
TOP
END
SIDE
ALL PARTS BRASS EXCEPT STEEL TRACK AND SALT WINDOW ALL DIMENSIONS IN MM.
ABSORPTION CELL HOLDER
JULY 1947

FIG. 2. Absorption cell holder.

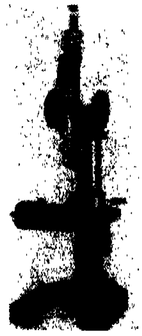

FIG. 3. Absorption cell loader.

Cell holder: Construction of the new cell holder is shown in Fig. 2. It is installed very simply. The spectrometer cover has a window in front of the entrance slit. This window is mounted in a slip ring and can be easily removed and replaced by the cell holder (provided that a baffle is removed from in front of the entrance slit). The cell holder has a small rectangular hole in its end into which a thin rectangular salt crystal window is cemented with Glyptal. The end of the cell holder just misses touching the adjustment screws in the jaws of the slit. An adjustable stainless steel track is installed in the cell holder so that the absorption cell can be accurately lined up in front of the slit. With such a narrow cell this lining up must be done each time the spectrometer cover is removed and replaced. The track is dovetailed in section so that the absorption cell cannot be brushed off accidentally. A notch in the face of the cell holder is provided so that the cell holder can be rotated on its axis until the cell is parallel to the slit; the holder must then be fastened in position by a screw which fits into a hold drilled into the spectrometer cover.

The small volume of a volatile solvent used in the 1-mm cell may be considered an objectional feature; of course it is possible partially to avoid this difficulty by making the cell thicker, increasing the volume of solvent, and reducing the concentration of absorber proportionately. However, with increasing cell thickness two difficulties arise: (a) the solvent itself begins to absorb with consequent difficulties in the detection and analysis of absorber spectrum; (b) the solute molecules are not used as efficiently.

Cell loader: To make it easy to handle small quantities of solutions a cell loader was developed (Fig. 3). It consists of a ¼-cc tuberculin syringe modified by fitting on a capillary pipette to the end. The syringe is fitted with a screw control for fluid delivery, and is mounted on an old microscope base, the stage of which is modified to mount controls to hold and manipulate the absorption cell into position, relative to the pipette. In dealing with small quantities of solution all the solution must be in the pipette and none in the syringe chamber in contact with the plunger. If the plunger is wet, by the solution there may be significant material losses.

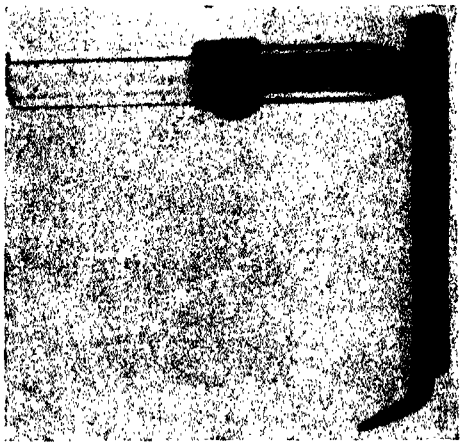

FIG. 4. Sample holder.

If the top of the pipette is centered in the cell, the delivered solution will not flow to the bottom of the cell, but instead will rise up between the absorption cell and the pipette, overflow, and be lost. In order to fill the cell the pipette tip must be placed in contact with the side of the absorption chamber near the top, and the solution must be poured down the side of the chamber. There does not seem to be any corresponding difficulty in recovering the sample. The pipette tip is introduced into the top of the chamber and solution is withdrawn as the pipette is moved to the bottom.

Since the quantities of material, both solute and solvent, are small, unknowns can be stored in small tubes made from small bore glass tubing. A simple tube holder has been made, as shown in Fig. 4, which allows mounting the tubes on the track of the loader stage for convenience in dissolving samples and loading them into the capillary pipette.

I want to thank Dr. K. Dobriner for pointing out the need for these gadgets, and Mr. A. Schreiner for valuable design suggestions.

---

* Presented at the Spectroscopy Symposium at Ohio State University, June, 1947.

** At present at the National Cancer Institute, Bethesda 14, Maryland.

[1] Perkin-Elmer infra-red spectrometer model 12A.

*** For less soluble materials a larger cell with three, mm spacer thickness (volume about 40 mm³) has been designed. It has a slot with trapezoidal cross section because of the converging beam of radiation.

Octane Vapor Proportional Counter

T. P. Pepper
Division of Atomic Energy Research, National Research Council of Canada, Chalk River, Ontario

January 14, 1949

CHEMICALLY pure *n*-octane vapor at room temperature has been used in a proportional counter for the study of the relative yields of the concurrent nuclear reactions: D(*d*, *p*)T, and D(*d*, *n*)He³.

The 3-Mev protons, 1-Mev tritons, and 0.8-Mev He³ particles so produced penetrated a thin Formvar counter window and emerged into the counter in a cone of semi-angle 20°. The thinner the window the easier were the detection and resolution of the ionization pulses from the three groups of charged particles. An octane-filled counter behaved as expected by giving a pulse distribution similar to that of a methane-filled counter at roughly six times the pressure. A representative pulse distribution as recorded on a 30-channel pulse analyzer is given in Fig. 1. The He³ peak could be narrowed to resemble the T peak of Fig. 1 simply by reducing the counter stopping-power and allowing the He³ particles to dissipate most of their energy in the far wall of the counter.

This preliminary success suggests using the saturated vapor of organic compounds of large molecular stopping-power for filling proportional counters. Two useful properties peculiar to such counter fillings are the following:

1. They present molecular stopping power at least equal to the heaviest gases normally used (e.g. Xe), a large fraction of which ($\geqslant \frac{1}{2}$) is due to the hydrogen constituent. This aids experiments requiring low pressure fillings containing one or other of the hydrogen isotopes. Such, for example, is the detection of the reaction D(*T*, *n*)He⁴, an experiment recently performed using the 1-Mev tritons from the reaction D(*d*, *p*)T mentioned above.

2. The pressure, hence stopping-power, of the counter filling is a function of the temperature alone. A liquid reservoir attached to the counter can be thermostatically controlled, thus enabling the counter pressure to be held constant or altered as desired without resort to opening or closing any part of the system to permit the flow of gas. (To avoid condensation

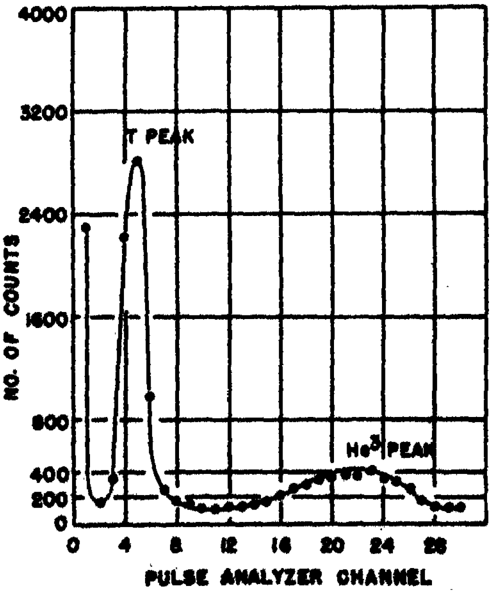

FIG. 1. *T and He³ peaks from the nuclear reactions* D(*d*, *p*)T and D(*d*, *n*)He³ presented on a 30-channel pulse analyser. Proportional counter filling: *n*-octane vapor at room temperature (~20°C). Counter window: Formvar 0.12 mg per cm².

TABLE I.

Organic compound	Molecular weight	Vapor pressure in mm Hg at 20°C
butylethylene	84	138.8
2,2-dimethylpentane	100	84
2,2,4-trimethylpentane	100	38.7
heptane	100	35.5
n-octane	114	10.45
2,5-dimethylhexane	114	38.5

within the counter the reservoir must be kept cooler than the counter.) Pressure determined by temperature alone permits some leakage of the counter filling, thus permitting the use of normally unacceptably thin, porous windows between the counter and evacuated source of charged particles. Flow of vapor through the window keeps purer the filling of the counter, thus lengthening its life.

The work of Farmer and Brown[1] on the life of methane-filled Geiger counters suggests that proportional counters filled with selected vapors would be long-lived. Other important properties, e.g., electron attachment and degree of dissociation of molecular ions, must be investigated for the individual vapor used. Table I presents selected organic compounds of large molecular stopping-power and vapor pressures of a few cm Hg at room temperature whose vapor may, therefore, be suitable for filling proportional counters.

---

[1] E. C. Farmer and S. C. Brown, Phys. Rev. 74, 902 (1948).

New Materials

Forest K. Harris: Associate Editor
in Charge of this Section
National Bureau of Standards, Washington, D. C.

Silicone Rubber

The chemical steps involved in the production of G.E. silicone rubber may be briefly outlined as follows. Elementary silicon, prepared by the reduction of silica sand with carbon, is reacted directly with methyl chloride in the presence of a copper catalyst. Dimethyldichlorosilane is then obtained by fractional distillation of the resulting mixed methylchlorosilanes. This product is treated with water, which replaces the chlorine atoms with hydroxyl groups. These, in turn, react with each other to form the methyl silicone polymer. The addition of the methyl organic group imparts flexibility, plasticity, and even fluidity to what would otherwise be a purely inorganic silicon oxide. The properties of the silicone polymer are determined by the organic group and its size in relation to the silicon-oxygen framework. The polymerized silicone has great chain length and high molecular weight and possesses elastic properties. When it is milled with fillers and curing agents it can be cross-linked (vulcanized) to form a synthetic rubber-like substance.

The compounded and cured elastomer has the same characteristic of exceptional thermal stability as other silicone products. G.E. silicone rubber can be continuously exposed to temperatures of 300 to 325°F, and for short periods up to 520°F without decomposing or becoming brittle or tacky. It contains no plasticizing or other components which tend to evaporate under high temperature or vacuum. Room temperature flexibility is retained down to −70°F. It has been used successfully in contact with many lubricants and industrial chemicals and is highly resistant to oxidation, ozone, corona, ultraviolet radiation, and fungus growths. Over its entire temperature range it is a good insulator, its electrical properties remaining unchanged even after prolonged exposure to high temperature. Its resiliency is comparable to that of natural rubber at room temperature. The tendency to recover its original size and shape after deformation is a necessary characteristic in many gasket applications and is retained even after long exposure to high temperature. Heat does not make it tacky or adhesive. When used in gaskets, sealing rings, and the like, it can be removed easily from metal surfaces without tearing. High speed shaft seals do not tend to grab or tear. However, it has good adhesive properties when cured on glass, ceramics, or steel, and it may be reinforced with glass cloth or asbestos where high strength is essential.

In view of the non-adhesive characteristics of the cured silicone rubber, a high temperature adhesive G.E. No. 12509 has been developed for bonding the cured compound to metals, glass, or to itself. Possessing high thermal stability, the adhesive combines chemically with the silicone rubber to form a continuous phase with no distinguishable glue line. It may be used for laminating layers of sheet stock, for butt-joining flat stock and gaskets, and for incorporating metal inserts in silicone rubber molded parts.

G.E. silicone rubber may be extruded or compression molded (using a pressure of 100–200 p.s.i.). It is also available in flat stock in 14″×14″ sheets with thicknesses ranging from $\frac{1}{32}$″ to 1″, and as a coated glass cloth in widths up to 36″.

The above material was abstracted from a General Electric booklet entitled *Silicone Rubber*.—PLASTICS DEPARTMENT, GENERAL ELECTRIC COMPANY, *Pittsfield, Massachusetts.*

Plastic for Film or Fabric

Velon plastics are modified copolymers of the polyvinyl and vinylidene series. They are combined with plasticizers and stabilizers and other compatible synthetics to secure abrasion resistance, toughness, high tensile strength, tear resistance, and control of elasticity. *Velon* is produced in three major forms: as a film, as a heavier gauge sheeting, and as a filament. The film is non-flammable (does not support flame), is resistant to staining, and may be cleaned with a damp cloth and soapy water. It is produced in thicknesses from 0.004 inch up, and in addition to its extensive applications in yard goods is used for making waterproof covers, liners, bags, etc. The sheeting, embossed with a grain design or polished as a patent leather, may replace leather in many applications. It has advantages in being scuff-resistant, non-absorbent, and easily cleaned. Its abrasion resistance is several times that of leather, and it is capable of withstanding considerable stress, either continuously or intermittently applied. It is also fungus, mold, and mildew proof. In addition to uses in luggage and upholstery, it has special applications as protective fronts for coats and aprons in chemical and allied industries.

Velon filaments, woven in a conventional mesh, make a screening which is superior to metal cloth. It is weatherproof even under severe salt air conditions, can easily be cleaned, and has many times the impact strength and resilience of metal cloth. For textile applications it has been produced both as a monofilament and as a multifilament yarn. The monofilament is made from a resin composed principally of vinylidene chloride with a small portion of vinylchloride. The resin is melted and extruded through orifices in a die. The emerging hot monofilament is plunged into water and then stretched to four times its original length. This treatment orients the structure and increases the tensile strength of the filament by 10 times.—FIRESTONE PLASTICS COMPANY, *Akron, Ohio.*

High Strength Varnish

Harvel 1012 C is an internal-curing insulating varnish developed particularly for the impregnating of wound structures which require very high mechanical bonding strength. It is finding application for the treatment of windings operating at high peripheral speeds and for those subject to high mechanical stress. It is fast curing and the cured film is oil proof, has good chemical and moisture resistance, and excellent resistance to decomposition under high temperature operating conditions. Full information and test samples may be obtained from the manufacturer.—IRVINGTON VARNISH AND INSULATOR COMPANY, *Irvington 11, New Jersey.*

Metal Stripper

Enthone Metal Stripper has been developed for chemically dissolving nickel and other metal coatings from steel without attacking the base metal. It is alkaline in nature, requires no electric current, and can be contained in a steel tank. The parts to be stripped are immersed in a solution of the stripper salts, at a temperature between 160 and 180°F. Stripping speed varies from 0.0002″ to 0.001″ per hour depending on concentration and operating temperature. The base steel is not etched nor attacked in any way, but is left in the same condition as it was prior to plating. In most cases the work can be replated after an acid dip. In addition to nickel, the stripper is effective in removing copper, silver, cadmium, and zinc plate from steel. It is not suitable for removing nickel coatings from zinc-base die castings or copper alloys.—ENTHONE, INC., *442 Elm Street, New Haven, Connecticut.*

Graded-Glass Seals

Technological advances in the art of processing various glasses have made possible a mechanical procedure for making graded seals from fused quartz to soft glass. Substitution of a mechanized process for the previous highly skilled handcraft has made price reductions of the order of 40 percent possible. The present process is applicable to the fabrication of graded seals up to two inches in diameter.—HANOVIA CHEMICAL AND MANUFACTURING COMPANY, *Newark 5, New Jersey.*

New Instruments

W. A. Wildhack: Associate Editor
in Charge of this Section
National Bureau of Standards, Washington, D. C.

These descriptions are based on information supplied by the manufacturer and in some cases from independent sources. THE REVIEW *assumes no responsibility for their correctness.*

Microwave Dielectrometer

The Central Research Laboratories' microwave dielectrometer is now available for measuring the dielectric constant and loss of a wide variety of materials at nominal frequencies of 1000, 3000, and 9000 megacycles. The instrument consists of a slotted wave guide, precision traveling probe, modulated klystron oscillators, probe output amplifier, associated power supplies, and equipment. The sample to be measured is inserted ahead of a short-circuiting plug, and the effect of this arrangement on the standing-wave pattern in the guide provides data for calculating the dielectric constant and loss of the material.

At 1000 and 3000 megacycles, the wave guide is used as a coaxial line operating in the *TEM* mode, and at 9000 megacycles, either as a circular pipe operating in the TE_{11} mode or as a coaxial line operating in the TE_{10} mode. Solids are measured directly in the wave guide in the form of cylindrical samples 1 inch in diameter and about 1 to 2 inches long with a ⅜-inch hole coaxial with the outer surface except when the guide is operated as a circular pipe at 9000 megacycles. Auxiliary sample holders can be used for measuring liquid samples and also for measurements at controlled high and low temperatures. The range of measurement of dielectric constant extends from 1 to 100; of dissipation factor from 0.0001 to 1.0. With ordinary care in sample preparation, an accuracy of 1 to 2 percent can be achieved for most materials.

To insure dimensional stability, ruggedness, and precise alignment, the wave guide is machined out of a solid 2-inch diameter copper bar and mounted on a substantial heat-treated Meehanite support which also carries the necessary mechanical assemblies. The crystal-detector probe is mounted on a precision ball-bearing carriage permitting longitudinal motion along the center line of the wave-guide slot. A spring-loaded, backlash-free, drive mechanism allows setting and reading probe position to 1 micron (0.001 millimeter). The maximum error in measuring displacements of 100 millimeters is approximately 30 microns.

The detector-output indicator is a selective amplifier tuned to the repetition frequency of the square-wave klystron-modulating voltage together with a logarithmic step attenuator and a linear output meter. An auxiliary overload meter with a nearly logarithmic range of 60 db is provided as an aid in tuning.

Routine maintenance is facilitated by built-in test features for measuring all critical circuit voltages and currents. Necessary adjustments are made by convenient screw-driver controls.

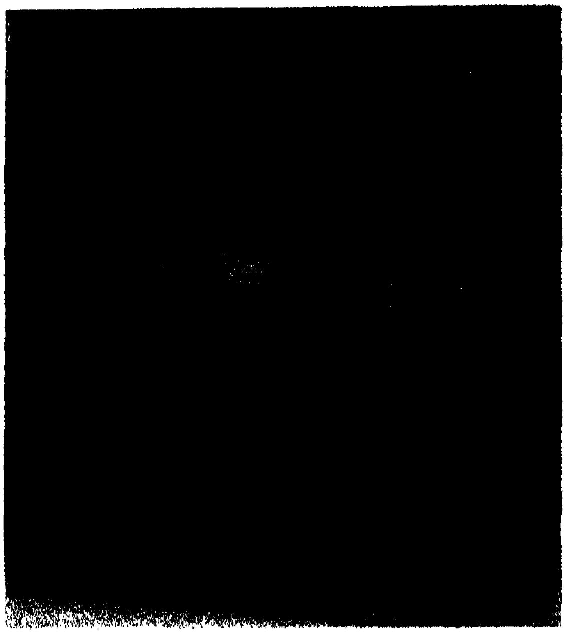

A line-voltage stabilizer and electronically-regulated power supplies provide optimum operating conditions in spite of line voltage fluctuations. Power consumption is 500 watts at 115 volts, 60 cycles.—CENTRAL RESEARCH LABORATORIES, INC., *Red Wing, Minnesota.*

Wide Band Chain Amplifier

The Model 200A chain amplifier is a traveling wave amplifier with a band width of 200 megacycles and a gain of 10 db per stage. With a useful range from 100 kilocycles to 220 megacycles at an impedance level of 200 ohms, the amplifier is especially adapted for use in television testing, nuclear instrumentation, oscillography, and general laboratory measurements. The transmission

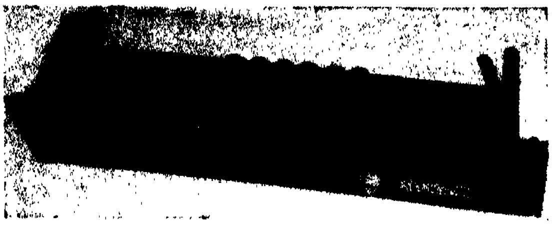

characteristic is ±1.5 db from 100 kilocycles to 200 megacycles, and the standing wave ratio is less than 1 db over this band. Phase shift in the amplifier is substantially linear within the pass-band, owing to mutual-inductance coupling between adjacent sections. Each stage has a tube complement of six 6AK5 tubes. Either one-stage or two-stage amplifiers are available in standard rack or table mounting. For additional information write to: SPENCER-KENNEDY LABORATORIES, INC., *Dept. SI, 186 Massachusetts Avenue, Cambridge 39, Massachusetts.*

Radiation Standards

High accuracy radiation standards, developed for the calibration of Geiger counters and other instruments measuring radioactivity, are now being supplied by the United States Radium Corporation. In addition to the conventional type standard, consisting of hermetically sealed capsules containing a radium salt, the company is offering a new type of calibrated source based on the incorporation of radium or its related elements in foil.

The new type standard is available as a point source or linear source, calibrated for alpha-, beta-, and gamma-radiation. It offers new latitude in design as compared to capsules, making it possible to fit the configuration of the standard to the specific instrument or counter tube, and also making possible the accurate duplication of standards.

While radium is a suitable source of radiation and is used in most of the items discussed, arrangements can frequently be made to supply standards utilizing a source of either virtually pure beta- or gamma-radiation alone. The methods of preparation are applicable to standards of almost any radiation intensity but can be particularly well applied to those of low radiation intensity, standards normally the most difficult to prepare accurately. Stable and accurate alpha-ray sources present no more difficulty than the more readily prepared beta- and gamma-sources.

The wider use of radioactive materials, stimulated by the Atomic Energy Commission's program of releasing new isotopes for research, medical, and industrial use, has created a demand for accurate and reliable measuring equipment. Such equipment, in the form of Geiger counters, ionization chamber survey instruments, and dosage meters, is supplied by a number of manufacturers and is normally furnished with a reasonably accurate initial calibration. Through mechanical shock or vibration, weakening of the power supply, radioactive contamination of the equipment, aging of the counter tube, and many other causes, this initial calibration usually changes in time, and recalibration is necessary. For dependable results in survey work, and especially for the highly accurate measurements required in research, industry, and medicine, dependable, accurately calibrated radiation standards must be available at all times for recalibration or on-the-spot checking of radiation-measuring equipment.

All radiation standards of the United States Radium Corporation are produced to special order, being constructed to meet the specific requirements of the instrument with which they will be used. Correspondence as to their applicability and use to meet new situations is invited by the company.—UNITED STATES RADIUM CORPORATION, *535 Pearl Street, New York 7, New York.*

Micromicroammeter

A new shunt box, type MV-171, converts the MV-17a Millivac vacuum tube millivoltmeter for d.c. into a highly sensitive wide range ammeter. With a total of 23 ranges, it covers all d.c. measurements between 10 micromicroamperes and 10 amperes. Due to a time constant of only 0.3 second, readings are practically instantaneous. Other outstanding features are heavy overloading (100,000 fold on low ranges) without damage to the instrument and exceptionally small voltage drops (1 mv on low ranges, 25 mv from 1 microampere up). With an external voltage source, resistance measurements up to 100 meg-megohms (10^{14} ohms) can be made. The shunt box and meter are operated from 115 v, 60 cycles, no batteries being required.—MILLIVAC INSTRUMENTS, *Post Office Box 3027, New Haven, Connecticut.*

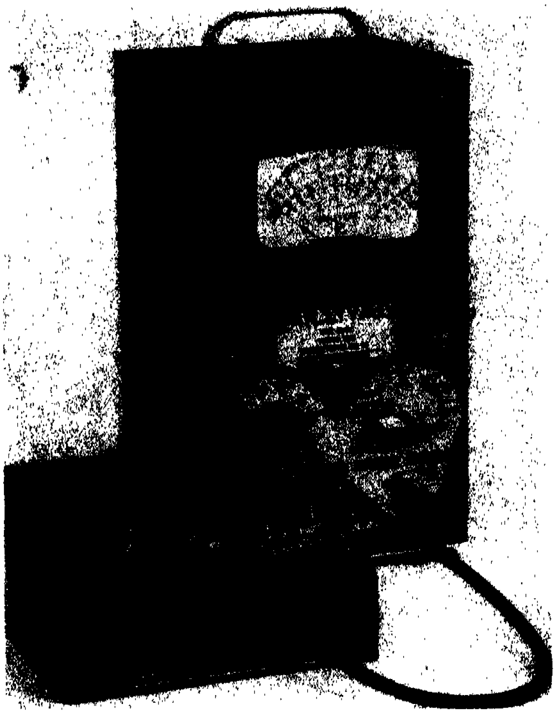

Hand Alpha-Counter

The RCL hand alpha-counter is a completely self-contained assembly which consists of two alpha-sensitive, ten-wire, air proportional counters and a recording electronic circuit which is calibrated to read from 0–20,000 counts per minute. The air proportional counters themselves are designed such that electric field stresses on the insulators are as low as is consistent with good practice, thereby eliminating spurious pulses. Each counter is electrically heated to minimize humidity effects. An Aquadagged Nylon film two ten-thousandths of an inch thick protects the counter volumes from dust, yet permits transmission of alpha-particles. The Nylon film is protected by stainless mesh. The counters are so arranged that close proximity to the hand is assured. Operating in the proportional region, the counters are very stable.

The electronic circuit of the RCL hand alpha-counter consists of a linear amplifier, a multivibrator to equalize the incoming pulses, an *RC* tank circuit, a vacuum tube voltmeter calibrated to read directly in counts per minute, and a regulated high voltage power supply. An internal calibration de-

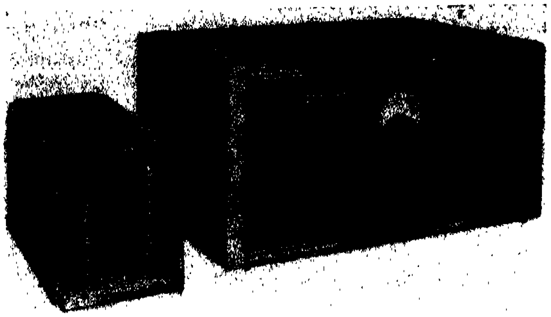

vice enables the user to check the panel meter at will. A convenient output jack permits connection of a recording milliammeter, or an auxiliary alarm circuit, if desired. The counting rate ranges are 0–200, 0–600, 0–2000, 0–20,000 counts per minute and the counter operates at approximately 2150 volts from a 115-volt, 60-cycle power supply.—Radiation Counter Laboratories, Inc., *1844 W. 21st Street, Chicago 8, Illinois.*

"Super-Regulated" Power Supply

The Model 252 regulated d.c. power supply, for applications where super-regulation at moderate power is required, has the following characteristics:

Input:	115 volts, 60 cycles, 400 watts.
Output:	Adjustable from 260 to 300 volts d.c., negative grounded.
Regulation:	With load changes from 400 to 600 milliamperes, the output voltage change at any setting is less than 0.05 percent, varying between individual units from 0.015 percent to 0.04 percent. Equal stability exists with respect to minor line voltage changes.
Noise Level:	Less than 0.001 percent.

This power supply has applications wherever extremely good regulation and stability are required. This includes computer circuits, television amplifier circuits, servomechanism directors, etc. The warm-up time required until the drift is less than 0.005 percent is approximately four hours. After steady state is reached, the instability is less than 0.001 percent per minute.

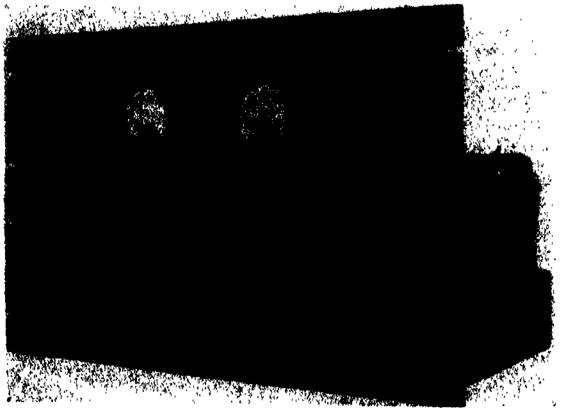

The power supply can be either relay rack panel mounted or supplied in a cabinet.—Beta Electronics Company, *1762 Third Avenue, New York 29, New York.*

Spiral Contractometer

The spiral contractometer, a new direct-reading instrument developed by Abner Brenner and Seymour Senderoff of the National Bureau of Standards, offers a convenient and accurate method for measurement of stress in electrodeposits. Compression or tension in a specimen coating deposited on a standard helix is immediately read from a dial as the helix changes curvature in response to forces acting within the plated layer. The device is rugged and self-contained, requires no auxiliary apparatus, and is well adapted to both industrial process control and laboratory research.

Essentially the new instrument consists of a flat metal strip wound in the form of a helix and mechanically connected to the pointer of a dial on which the rotation of the free end of the spiral with respect to its fixed end is indicated. The helix is connected at its upper, fixed end to a negative lead and suspended vertically in a plating solution along with a suitable anode. As it is plated with a sample coating on the outside, the stress in the deposit causes it to wind more tightly or to unwind, depending on whether the stress is compressive or tensile. A rod running down the axis of the helix is attached to its lower or free end so that rotation of this end due to stress is transmitted to the rod. The rotation of the rod, in turn, is applied to a gear train which produces a tenfold magnification in the rotation of the dial pointer. The angular displacement of the rod is read directly from the dial in degrees and converted to units of stress on the basis of the calibration of the helix used.

In making a stress determination, the helix is first cleaned and, when necessary for good adherence of the deposit to be tested, a "strike" plate is applied. After the helix has been dried and weighed, the inner side is brushed with thinned "stop-off" lacquer to prevent plating on this surface. The helix is then dipped in hot alkali and acid baths, or other preplating dips, and rinsed before it is mounted in the contractometer and immersed in the plating solution.

The helix may be allowed to twist as plating progresses, and a record kept of the displacements with time, or twisting may be prevented until the end of the run by clamping the pointer. Both methods give the same results within the experimental error.

At the end of a run the helix is taken out of the solution, cleaned, and dried, and the lacquer is removed from the inside with acetone. The deposit may then be stripped off as soon as it has been weighed to determine its average thickness. Stress is calculated from the observed deflection of the pointer, the physical constants and dimensions of the helix, and the average thickness of the coating.

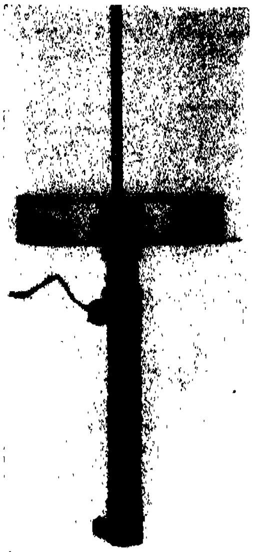

A single helix can be used almost indefinitely without appreciable change in its dimensions, elastic moduli, or deflection constants, provided reasonable precautions are taken in handling and storing.—NATIONAL BUREAU OF STANDARDS, *U. S. Department of Commerce, Washington 25, D. C.*

New Alpha-Particle Counter

A new methane flow proportional counter designed for the efficient detection of alpha-particles is announced by Nuclear Instrument and Chemical Corporation, 223 West Erie Street, Chicago 10, Illinois. The outstanding feature of this new Model D45 Detector is its ability to count alpha-particles in the presence of high beta-activity with 50 percent geometry and low coincidence losses.

When this detector is used with a high gain linear amplifier and a "fast" scaler, it is possible to count alpha-particles in the presence of a beta-activity of 5 $(10)^9$ disintegrations per minute. Measurements of this type are particularly useful in chemical, physical, and biological research.

The counter chamber of Model D45 has a very highly polished cylindrical cathode. The anode is 0.002" diameter tungsten wire mounted between glass insulators. Construction is designed to permit easy decontamination both inside and outside. The sample holder, mounted on a stainless steel sample changer, is designed for standard one-inch diameter samples, with provisions for raising the sample up into the counting volume for improved geometry. Flow of methane gas through the chamber is controlled by means of valves and an attached bubbler. Connection of a coaxial cable is made to the center wire via a well insulated connector on rear of the cover.—NUCLEAR INSTRUMENT & CHEMICAL CORPORATION (formerly Instrument Development Laboratories, Inc.), *223–233 West Erie St., Chicago 10, Illinois.*

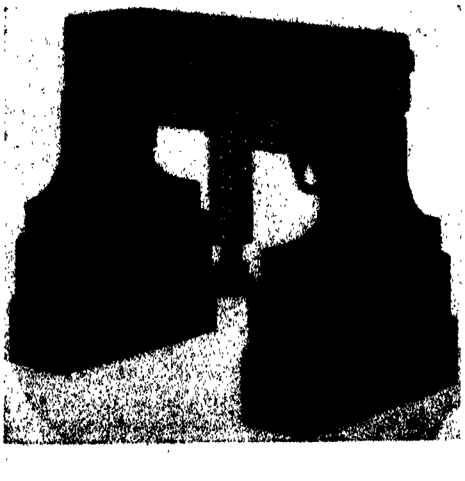

R-F Capacitance Meter

The Type 1612-A r-f capacitance meter is designed for rapidly measuring and testing small capacitors (up to 1200 micromicrofarads) such as are used in radiofrequency equipment. It is equally useful in the laboratory and in production testing and, for the latter use, a simple test jig can be devised to facilitate connections.

Measurement is made by a substitution method in which the capacitance of a calibrated air capacitor is reduced to re-establish resonance after an unknown capacitor is connected. Resonance is indicated by maximum deflection of a meter. Two ranges are provided, 0 to 80 $\mu\mu$f and 0 to 1200 $\mu\mu$f, and range switching is accomplished automatically as the dial is rotated. Measurements are made at a frequency of one megacycle.

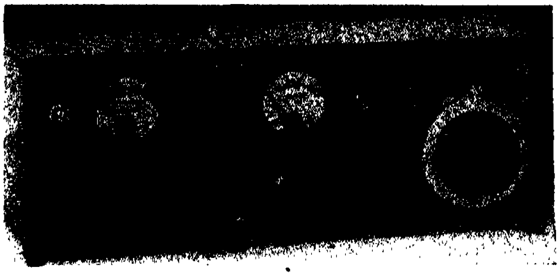

Maximum meter deflection can be also used as an indication of loss, and hence as a basis for rejection of high loss capacitors when compared to a standard sample.

The instrument operates from a 115-volt power line, either a.c. or d.c. Dimensions are $12\times6\frac{5}{8}\times7\frac{3}{4}$ inches over-all.

Weight is 11 pounds.—GENERAL RADIO COMPANY, *275 Massachusetts Avenue, Cambridge 39, Massachusetts.*

Manufacturers' Literature

High Stability Carbon Resistors—8-page catalog describes high stability carbon film resistors, normally supplied to 1 percent tolerance up to 50 megohms, and pyromatic resistors in ranges up to 10^6 megohms. Technical data and price schedules are given.—WELWYN ELECTRONIC COMPONENTS, INC., *234 East 46th Street, New York 17, New York.*

Insulation Tester—Bulletin 21-20-30 describes the "Megger" heavy-duty type insulation tester. All improvements and accessory features are described and illustrated, and specifications are given.—JAMES G. BIDDLE COMPANY, *1316 Arch Street, Philadelphia 7, Pennsylvania.*

Photographic Plates for Scientific and Technical Use—A 44-page booklet describes special plates available for spectroscopy, astronomy, and nuclear research. Information on spectral sensitivity and suggestions on the selection of plates for observation in various regions of the spectrum are given.—INDUSTRIAL PHOTOGRAPHIC DIVISION, EASTMAN KODAK COMPANY, *343 State Street, Rochester 4, New York.*

Cathode Press—A quarterly periodical which reports news of the electronic industry at large, with particular emphasis on the publisher's role in development of new electron tubes, improvement of current models, and applications of new tubes.—MACHLETT LABORATORIES, INC., *Springdale, Connecticut.*

Power Tubes—Technical data sheets on new power tubes:

1. RCA-5762, power triode, 2.5-kw plate dissipation.
2. RCA-5770, power triode, 50-kw plate dissipation.
3. RCA-5771, power triode, 22.5-kw plate dissipation.
4. RCA-5786, power triode, 0.6-kw plate dissipation.
5. RCA-4×150A, power tetrode, 0.15-kw plate dissipation.

—TUBE DEPARTMENT, RADIO CORPORATION OF AMERICA, *Harrison, New Jersey.*

Electric Laboratory Furnaces—Bulletin No. 48A describes a new electric laboratory furnace with a useful temperature range from 300°F to 2000°F. Applications include experimental testing, enameling, fusing, igniting, precipitate drying and ashing in physical and chemical laboratories, and as pilot furnaces in metallurgical laboratories.—COOLEY ELECTRIC MANUFACTURING COMPANY, *38 S. Shelby Street, Indianapolis, Indiana.*

Precision Resistors—NBS Circular 470, *Precision Resistors and Their Measurement*, gives a systematic discussion of the characteristics of precision resistance apparatus, and of the methods used by the Bureau of Standards for measuring resistance. 20 cents per copy.—U. S. GOVERNMENT PRINTING OFFICE, *Washington 25, D. C.*

Ultracentrifuge—8-page folder describes a new Spinco ultracentrifuge, adaptable to the purification and particle-size determination of proteins, viruses, polymers, and other such colloids.—SPECIALIZED INSTRUMENTS CORPORATION, *1106 O'Neill Avenue, Belmont, California.*

Ultracentrifuge—8-page booklet-size pamphlet describing the development qualities and construction of the PHYWE-ultracentrifuge and its accessories. This instrument is planned for exhibition at the German Industrial Show in New York on April 9–24, 1949.—PHYWE AG, *Goettingen, Germany (British Zone).*

Hydraulic Cylinders—A 20-page book, Catalog Section No. 103, illustrates and describes all standard cylinders, with complete diagrams and information to aid in laying out circuits.—GEROTOR MAY CORPORATION, *Baltimore 3, Maryland.*

Thermometer—Bulletin T describes stainless steel thermometers, supplied in variable stem lengths from 4" to 42" for temperature ranges up to 1000°F.—W. C. DILLON AND COMPANY, INC., *5410 W. Harrison Street, Chicago 44, Illinois.*

Portable Hardness Tester—Single-sheet bulletin describes a portable hardness tester for Rockwell Readings. The instrument weighs only 3 lb., 6 oz.; net weight including a carrying case and accessories is 6 lb., 7 oz. Rockwell scale: *A, B,* and *C.*—RIEHL TESTING MACHINES DIVISION, AMERICAN MACHINE AND METALS, INC., *East Moline, Illinois.*

Time Delay Relays—A 6-page bulletin describes new Agastat electro-pneumatic time delay relays which provide an initial time delay of one minute. Thereafter, a power failure will cause the relay to switch off, but restoration of power within 15 seconds immediately re-establishes the circuit. For a power failure longer than 15 seconds, there is a time delay proportional to the length of time of power failure.—AGASTAT DIVISION, AMERICAN GAS ACCUMULATOR COMPANY, *1029 Newark Avenue, Elizabeth 3, New Jersey.*

Measuring Microscopes—Bulletin 161–48, 24 pages, describes and illustrates micrometer microscopes, traveling microscopes, micrometer slide comparitors, and related equipment. Introductory section outlines selection, use, calibration, and construction of measuring microscopes.—THE GAERTNER SCIENTIFIC CORPORATION, *1201 Wrightwood Avenue, Chicago 14, Illinois.*

Slide-Wire Resistance Box—Single-sheet bulletin describes Type 110 slide-wire resistance boxes. Two ranges, 0–11,000 ohms and 0–110,000 ohms, are available, with a useful frequency range of about 110 kc.—TECHNOLOGY INSTRUMENT CORPORATION, *1058 Main Street, Waltham 54, Massachusetts.*

Thermocouples—Bulletin P1238, 56 pages, contains detailed information on thermocouples, protection tubes, and other pyrometer accessories. Engineering information to guide selection of a thermocouple and protection tube is given.—THE BRISTOL COMPANY, *Waterbury 91, Connecticut.*

Recording Vibrometer—A 4-page bulletin describes a recording vibrometer which measures and records frequency, displacement, and wave shape in mechanical vibration. A permanent record is made on waxed paper.—APPARATUS DEPARTMENT, GENERAL ELECTRIC COMPANY, *Schenectady, New York.*

Recording Instruments—Catalog ND46(1), 44 pages, describes Speedomax Type G instruments. High speed, high sensitivity instruments and recording controllers are described, with uses for which they are available.—LEEDS AND NORTHRUP COMPANY, *4934 Stenton Avenue, Philadelphia 44, Pennsylvania.*

Goniometer—A 4-page circular describes a two-circle goniometer designed to measure the angles of crystal faces. Built-in accuracy makes unnecessary numerous provisions for adjustment, so characteristic of earlier instruments.—L. C. EICHNER, *437 Bloomfield Avenue, Bloomfield, New Jersey.*

Thermocouple A.C. and D.C. Meters—A 4-page bulletin describing portable thermal meters and thermal multimeters with vacuum thermocouples for the measurement of a.c. or d.c.—RAWSON ELECTRICAL INSTRUMENT COMPANY, INC., *Cambridge, Massachusetts.*

THE
REVIEW OF SCIENTIFIC
INSTRUMENTS

VOLUME 20, NUMBER 4 *APRIL, 1949*

Errors in Second-Order Measuring Instruments

ELLIOT T. BENEDIKT
North American Aviation, Inc., Inglewood, California[1]

(Received July 19, 1948)

The various types of error which affect the result of a measurement performed by an instrument behaving as a second-order linear instrument are defined.

The theoretical systematic error is shown to be caused by the (dynamical) lag with which the instrument responds to the signal. If the damping is high, this type of error turns out to be proportional to the rate of change of the signal.

The accidental error resulting from input noise and accidental changes of the instrument constants is considered. It is shown that all these effects can be represented by an effective input noise. A formula for the mean square error in the indication of the instrument is given in terms of the correlation function of the above effective noise.

Related theoretical questions on random functions are discussed in the Appendix.

1. INTRODUCTION

CONSIDER a device used for the purpose of the determination of a quantity $F(t)$ variable with the time; we shall assume this device to behave as a second-order system having a (generalized) mass M, resistance R, and elastance S. The (generalized) coordinate θ (usually an angle or a displacement), in terms of the value of which the quantity $F(t)$ is determined, would satisfy the differential equation,

$$M(d^2\Theta/dt^2)+R(d\Theta/dt)+S\Theta=F(t), \tag{1}$$

if there were no accidental effects superimposed upon the quantity to be measured, and no accidental variation in the coefficients M, R, S would occur. If such variations occur, an erroneous value θ' will be determined by the equation:

$$M'(d^2\Theta/dt^2)'+R'(d\Theta/dt)'+S'\Theta=F'(t), \tag{1'}$$

where

$$M'=M+m(t), \tag{2}$$

$$R'=R+r(t), \tag{2'}$$

$$S'=S+s(t), \tag{2''}$$

$$F'=F+f_0(t). \tag{3}$$

The quantities $m(t)$, $r(t)$, $s(t)$, $f_0(t)$ are of the nature of random functions[2] and small in absolute value so that their square can be considered negligible.

Accidental variations of the instrument constant of the considered type can be caused, e.g., in an electrical instrument by deformation of the geometry of its parts which would cause a change in its inductance and elastance, by a temperature fluctuation which would change its resistance, etc. Accidental variations in the input (or effective input) of such instrument could be caused by stray magnetic fields, fluctuations of e.m.f.'s in the circuit, shot-effects in vacuum tubes, etc.

2. ERRORS

Under static conditions and in the absence of any accidental errors, Eq. (1) becomes

$$S\Theta=F. \tag{4}$$

The quantity F is usually determined, assuming this relation to be true, even under dynamic conditions and in the presence of random effects; that is, the incorrect value

$$\mathfrak{F}(t)=S\Theta', \tag{5}$$

---

[1] Now at U. S. Naval Ordnance Test Station, Pasadena, California.

[2] For a definition of the concept of random function, see James, Nichols, and Phillips, *Theory of Servomechanisms* (McGraw-Hill Book Company, Inc., New York, 1947), p. 266.

is assumed for F,[3] so that the error

$$\varphi = \mathcal{F} - F = S\Theta' - F, \tag{6}$$

in its determination is committed.

Subtracting (1) from (1′), taking into account (2), (2′), (2″), and (3), and putting

$$\theta = \Theta' - \Theta, \tag{7}$$

we obtain, neglecting infinitesimals of second order, the differential equation:

$$M(d^2\theta/dt^2) + R(d\theta/dt) + S\theta = f(t), \tag{8}$$

with

$$f(t) = f_0(t) + f_1(t), \tag{9}$$

$$f_1(t) = -m(t)(d^2\Theta/dt^2) - r(t)(d\Theta/dt) - s(t)\Theta. \tag{9'}$$

Using (7), expression (6) can be written in the form

$$\varphi = S(\Theta + \theta) - F = \varphi^0 + \varphi', \tag{10}$$

where

$$\varphi^0(t) = S\Theta - F, \tag{11}$$

represents the systematic error due to the dynamical lag of the instrument, and

$$\varphi'(t) = S\theta(t), \tag{12}$$

represents the accidental error due to the presence of random phenomena in the components of the instrument.

3. SYSTEMATIC ERROR

Assuming

$$\Theta(0) = (d\Theta/dt)_{t=0} = 0, \tag{13}$$

we shall obtain, integrating Eq. (1)

$$\Theta(t) = (1/M\omega_0)\int_0^t F(\tau)e^{\gamma(t-\tau)} \sin\omega_0(t-\tau)d\tau, \tag{14}$$

where

$$\gamma = R/2M,$$
$$\omega_0 = [(S/M) - (R/2M)^2]^{\frac{1}{2}}.$$

If the constant γ is large, the factor $e^{\gamma(t-\tau)}$ will be negligible for non-negligible values of $t-\tau$. Expanding $F(t)$ in series we shall have, then, with sufficient approximation:

$$\int_0^t F(\tau)e^{-\gamma(t-\tau)} \sin\omega_0(t-\tau)d\tau$$

$$\simeq F(t)\int_0^t e^{-\gamma(t-\tau)} \sin\omega_0(t-\tau)d\tau$$

$$-\dot{F}(t)\int_0^t (t-\tau)e^{-\gamma(t-\tau)} \sin\omega_0(t-\tau)d\tau$$

$$= [F(t)/(\omega_0^2+\gamma^2)][\omega_0 - e^{-\gamma t}(\gamma \sin\omega_0 t + \omega_0 \cos\omega_0 t)]$$

$$-[\dot{F}(t)/(\omega_0^2+\gamma^2)^2]\{2\omega_0\gamma + e^{-\gamma t}[(\omega_0^2-\gamma^2)\sin\omega_0 t$$

$$-2\omega_0\gamma \cos\omega_0 t] + (\omega_0^2+\gamma^2)te^{-\gamma t}[\gamma \sin\omega_0 t$$

$$+\omega_0 \cos\omega_0 t]\}.$$

Neglecting in the last result terms in which $e^{-\gamma t}$ appears as a factor, we have:

$$\int_0^t F(\tau)e^{-\gamma(t-\tau)} \sin\omega_0(t-\tau)d\tau$$

$$\simeq [\omega_0/(\omega_0^2+\gamma^2)]F(t) - [2\omega_0\gamma/(\omega_0^2+\gamma^2)]\dot{F}(t).$$

Replacing this result in (14) and (11) we obtain:

$$\varphi^0(t) = -(R/S^2)\dot{F}(t).$$

4. ACCIDENTAL ERRORS

Integrating (8) under the assumptions:

$$\theta(0) = (d\theta/dt)_{t=0} = 0, \tag{15}$$

we obtain

$$\theta(t) = \int_0^t K(\tau,t)f(\tau)d\tau, \tag{16}$$

where

$$K(\tau,t) = (1/M\omega_0)e^{-\gamma(t-\tau)} \sin\omega_0(t-\tau). \tag{17}$$

Squaring both members of (16) we obtain:

$$\theta^2(t) = \int_0^t\int_0^t K(\tau,t)K(\tau,'t)f(\tau)f(\tau')d\tau d\tau'. \tag{18}$$

For the ensemble average of θ^2 we shall have then:[4]

$$\langle\theta^2(t)\rangle = \int_0^t\int_0^t K(\tau,t)K(\tau,'t)\Lambda(\tau,\tau')d\tau d\tau'. \tag{19}$$

---

[3] The rigorous determination of $F(t)$ from the observed response $\theta(t)$ would imply the solution of an integral equation of the first kind [Eq. (14) of the following article].

[4] We shall indicate with

$$\langle A(t)\rangle = \lim_{N\to\infty}\left[\sum_{i=1}^N A_i(t)/N\right],$$

the *ensemble average* of a quantity $A(t)$ (whose repeated measurement under the same controllable conditions at the time t yields results A_i, and with

$$\langle A(t)\rangle = \lim_{T\to\infty}\left[\int_{-T/2}^{T/2} A(t)dt/T\right],$$

its time average. The ensemble and time averages of quantities which depend upon measurements performed at the times t_1, $t_2\cdots t_m$ are respectively defined by

$$\langle A(t_1, t_2\cdots t_m)\rangle = \lim_{N\to\infty}\left[\sum_{i=1}^N A_1(t_1, t_2\cdots t_m)/N\right],$$

$$\langle A(t_1, t_2\cdots t_m)\rangle = \lim_{T\to\infty}\left[\int_{-T/2}^{T/2} A(t_1+t, t_2+t, \cdots t_m+t)dt/T\right]$$

A_i being the result of measurements performed at the times t_1, $t_2\cdots t_m$.

where

$$\Lambda(\tau,\tau') = \langle f(\tau)f(\tau')\rangle, \tag{20}$$

is the (auto-) correlation function of the random process represented by $f(t)$.[5] φ'^2 can be obtained immediately from the value of $\langle\theta^2\rangle$ through Eq. (12).

5. EMPIRICAL DETERMINATION OF THE CORRELATION FUNCTION

Predictions of $\langle\theta^2\rangle$ with the above method can only be obtained if $f(t)$ (that is, all the random processes involved), are independent of the response $\Theta(t)$ of the system. We shall assume this condition to be satisfied in what follows.

The determination of the correlation function (20) for a random function of the type (9) can then be obtained in general, with the method outlined in Appendix I. For the case under consideration, this would involve the determination of the ensemble average of the error in the output of the system for at least 16[6] different, appropriately chosen, responses. Such a procedure, of course, would be extremely lengthy.

A much more rapid determination of Λ can be obtained if the process represented by $f(t)$ is stationary.[7] In this case we shall have:

$$\Lambda(\tau,\tau') = \Lambda(\tau'-\tau) = f(\tau)f(\tau'), \tag{21}$$

which can be approximated numerically from an experimental determination of the function $f(t)$ over a sufficiently long period of time.

It should be noted that, for all practical purposes, the function $f(t)$ will be stationary only if $f_0(t)$ is stationary and $m(t)$, $r(t)$, and $s(t)$ are zero or negligible. Even if these last functions are stationary, their linear combination (9′) will, in general not be stationary. (See Appendix II.)

Once $\Lambda(\tau,\tau')$ is determined, $\langle\theta^2(t)\rangle$ can be determined by numerical integration from formula (19). Usually, however, an approximate evaluation of the integral (19) defining $\langle\theta^2(t)\rangle$ is sufficient, the purpose of which can be reached by approximating the experimentally determined correlation function by an appropriate analytical expression.

6. THEORETICAL METHODS

Further methods can be applied to the problem treated in the present paper if the random function $f(t)$ describes a process of a better specified nature.

If this process is Gaussian,[8] a method due to Rice can be applied; for a Markoffian[9] process, the method of Fokker-Planck-Kolmogoroff can be used with advantage. Details of these methods can be found in the original papers of Rice[10] and of S. Chandrasekhar[11] and Ming Chen Wang and Uhlenbeck.[12] In the latter two papers, a detailed treatment of the statistical properties of the solution of an equation of the type (8) can be found if $F(t)$ is the type of a force acting on a colloidal particle undergoing Brownian motion. An extensive bibliography can be found in these papers.

Due to the fact that the main purpose of the present work was to examine instrument errors from an empirical point of view, and since a comprehensive treatment of the theoretical aspects of the above special cases can be found in the cited publications, no further discussion of these matters will be given here. We shall, however, apply the methods previously established to the case in which the errors are stationary and of a type having considerable theoretical and practical importance.

If the error is simultaneously Markoffian and Gaussian, its correlation function must be of the form[13]

$$\Lambda(\tau,\tau') = \alpha^2 e^{-\beta(\tau'-\tau)} \quad (\tau' \geqslant \tau).$$

Replacing this into (19) and making use of (17) we obtain

$$\begin{aligned}\langle\theta^2\rangle &= (\alpha^2/M\omega_0^2)\int_0^t\int_0^t e^{-\gamma(t-\tau)}\sin\omega_0(t-\tau)e^{-\gamma(t-\tau')} \\ &\qquad\times\sin\omega_0(t-\tau')e^{-\beta(\tau'-\tau)}d\tau d\tau' \\ &= (\alpha^2/M\omega_0^2)\int_0^t\int_0^t e^{-(\gamma-\beta)\sigma}e^{-(\gamma+\beta)\sigma'}\sin\omega_0\sigma \\ &\qquad\times\sin\omega_0\sigma' d\sigma d\sigma' \\ &= \alpha^2 J(\gamma-\beta)J(\gamma+\beta)/M\omega_0^2,\end{aligned}$$

---

[5] I am indebted to S. O. Rice of the Bell Telephone Laboratories for suggesting the above method of determination of $\langle\theta^2\rangle$.

[6] This number can be reduced (to not less than 4) if some of the random processes involved in $f(t)$ can be considered uncorrelated a priori.

[7] A process defined by a random function $x=x(t)$ is said to be stationary if

$$\langle X(x_1x_2\cdots x_m)\rangle = \langle X(x_1x_2\cdots x_m)\rangle,$$

where X is an arbitrary function of the quantities $x_i=x(t_i)$. A relation of this type cannot in general be established on theoretical grounds and is, therefore, assumed whenever this seems justified. Such an assumption made for a given system is referred to as ergodic hypothesis.

[8] The process is said to be Gaussian if the probability of the simultaneous occurrence of the values $x_1,x_2,\cdots x_N(x_i=x(t_i))$ is given by a (pluridimensional) Gaussian function.

[9] A discontinuous random process defined by the series $x_1, x_2\cdots x_N$ is said to be Markoffian if the probability of occurrence of a given term x_i depends only on the value of previously occurred term x_{i-1}. A continuous Markoff process is the limiting case for $t_i-t_{i-1}\to 0$ of a discontinuous one.

[10] S. O. Rice, Bell Sys. Tech. J. **23**, 282 (1944); **25**, 45 (1945).

[11] S. Chandrasekhar, Rev. Mod. Phys. **15**, 1 (1943).

[12] Ming Chen Wang and G. E. Uhlenbeck, Phys. Rev. **17**, 323 (1945).

[13] This result was established by J. L. Doob, Ann. Math.; **43**, 351 (1942).

where

$$J(\xi)=\int_0^t e^{-\xi\sigma}\sin\omega_0\sigma d\sigma$$
$$=[\omega_0-e^{-\xi t}(\omega_0\cos\omega_0t+\xi\sin\omega_0t)]/[\xi^2+\omega_0^2].$$

Making use of the above identity, we obtain

$$\begin{aligned}\langle\theta^2\rangle=[\alpha^2/M\omega_0^2P(\beta)]\{&\omega_0^2+\omega_0^2+\gamma^2-\beta^2/2e^{-2\gamma t}\\&-\omega_0^2[e^{-(\gamma-\beta)t}+e^{-(\gamma+\beta)t}]\cos\omega_0t\\&-\omega_0[(\gamma-\beta)e^{-(\gamma-\beta)t}+(\gamma+\beta)e^{-(\gamma+\beta)t}]\sin\omega_0t\\&+e^{-2\gamma t}[\omega_0^2-\gamma^2+\beta^2/2\cos2\omega_0t\\&+\omega_0\gamma\sin2\omega_0t]\},\end{aligned}\tag{22}$$

where

$$P(x)=x^4-2(\gamma^2-\omega_0^2)x^2+(\gamma^2+\omega_0^2)^2.$$

If the source of the error is a monochromatic disturbance, that is, represented by a sinusoidal function with angular frequency ω_1, amplitude a, and random phase, the correlation function will be of the form![14]

$$\Lambda(\tau_1\tau')=(a^2/2)\cos\omega_1(\tau'-\tau),$$

which replaced into (19) gives:

$$\langle\theta^2\rangle=(a^2/2M\omega_0^2)\int_0^t\int_0^t e^{-\gamma(t-\tau)}\sin\omega_0(t-\tau)e^{-\gamma(t-\tau')}$$
$$\times\sin\omega_0(t-\tau')\cos\omega_1(\tau'-\tau)d\tau d\tau'.$$

The latter expression can be written in the form

$$\langle\theta^2\rangle=(a^2/2M\omega_0^2)\mathcal{R}e\int_0^t\int_0^t e^{-(\gamma-i\omega_1)\sigma}e^{-(\gamma+i\omega_1)\sigma}$$
$$\times\sin\omega_0\sigma\sin\omega_0\sigma'd\sigma d\sigma'$$
$$=a^2\mathcal{R}eJ(\gamma-i\omega_1)J(\gamma+i\omega_1)/2M\omega_0^2,$$

where $\mathcal{R}e$ indicates the operation "taking the real part of." Applying formula (22) we obtain

$$\begin{aligned}\langle\theta^2\rangle=[a^2/2M\omega_0^2P(i\omega_0)]\Big\{&\omega_0^2+\frac{\omega_0^2+\omega_1^2+\gamma^2}{2}e^{-2\gamma t}\\&+\omega_0\exp[-\gamma(t)](\omega_0+\omega_1)\cos(\omega_0-\omega_1)t\\&+(\omega_0-\omega_1)\cos(\omega_0+\omega_1)t+\omega_0\gamma\exp[-\gamma(t)]\\&\times[\sin(\omega_0-\omega_1)t+\sin(\omega_0+\omega_1)t]\\&+e^{-2\gamma t}\left[\frac{\omega_0^2-\omega_1^2-\gamma^2}{2}\cos2\omega_0t+\omega_0\gamma\sin2\omega_0t\right]\Big\}.\end{aligned}$$

Errors due to the superposition of uncorrelated random processes of known nature, as of the ones described above, can be evaluated by making use of the easily proved fact that the correlation function and, consequently, the mean square errors are in this case additive.

7. ACKNOWLEDGMENTS

The author wishes to thank Dr. S. H. Browne of North American Aviation, Inc., and Mr. S. O. Rice of Bell Telephone Company, for helpful discussion on this subject, and Dr. M. Neustadt of North American Aviation, Inc., for assistance in the preparation of the present paper.

APPENDIX I

On the determination of the auto- and inter-correlation functions of a system of random functions.—Consider the linear combination

$$y(t)=\sum_{i=1}a_i(t)x_i(t),\tag{I}$$

of the random functions $x_i(t)$, the coefficients $a_i(t)$ being (deterministically) known functions. We shall assume the x_i's to be independent of the a_k's. The ensemble average of the product

$$y(\tau)y(\tau')=\sum_i\sum_k a_i(\tau)a_k(\tau')x_i(\tau)x_k(\tau'),$$

will be

$$\Lambda(\tau_1\tau)=\sum_i\sum_k a_i(\tau)a_k(\tau)\Lambda_{ik}(\tau_1\tau'),$$

where Λ is the (auto-) correlation function of y and

$$\Lambda_{ik}(\tau_1\tau')=\langle x_i(\tau)x_k(\tau')\rangle,$$

are respectively the auto- and inter-correlation* functions of the x_i's, according as to whether $i=k$ or i k. It should be noted that unless the random functions x_i, x_k are stationary, $\Lambda_{ik}\neq\Lambda_{ki}$.

The functions Λ_{ik} can then be determined from the experimental determination of ensembles of values $y^{(l)}(t)$ of the linear combination (I) for at least n^2, (or not less than n^2 if some of the processes represented by the x_i's are uncorrelated), properly chosen sets of coefficients $a_i^{(l)}(t)$.** If data for a larger number of sets are taken, the consistency of the hypothesis of the independence of the x_i's upon the a_k's can be verified, and the values of the functions Λ_{ik} can be determined by means of the least square method.

APPENDIX II

On the non-validity of the ergodic hypothesis for the process represented by a linear combination of stationary random functions.—Let $x(t)$ be a stationary random function, that is, a function necessarily satisfying the relation

---

[14] See James, Nichols and Phillips, (reference 2), p. 275.

* This terminology seems more appropriate to the author than the term "cross-correlation function" frequently used.

** The choice is, of course, restricted by the relations to which the members of the sets $a_i^{(l)}(t)$ are subjected.

$$\langle x(t)\rangle = x = \lim_{T\to\infty}\left[\int_{-T/2}^{T/2} x(t)dt/T\right].$$

Consider now the random process defined by the function $a(t)x(t)$, $a(t)$ being a known function. We shall have

$$\langle a(t)x(t)\rangle = a(t)x(t) = a(t)\bar{x},$$

which is, in general, different from

$$\langle ax\rangle = \lim_{T\to\infty}\left[\int_{-T/2}^{T/2} a(t)x(t)dt/T\right].$$

The process represented by $a(t)x(t)$ is therefore not stationary.

It follows that a time dependent linear combination of stationary random functions is not generally stationary.

THE REVIEW OF SCIENTIFIC INSTRUMENTS VOLUME 20, NUMBER 4 APRIL, 1949

Design and Performance of a Multicellular Geiger Counter for Gamma-Radiation

David A. Lind
California Institute of Technology, Pasadena, California

(Received October 28, 1948)

The design problems for Geiger counters which have a high gamma-radiation sensitivity are discussed. A description of a Geiger counter consisting of nine individual counters in the shape of pillboxes mounted inside a single envelope is given. The individual pillboxes are 3 inches in diameter. The anode has the shape of a four-pronged spider which is centered in the box. The nine section counter has a flat plateau of about 150 volts, and intrinsic sensitivity of 25 percent. Its lifetime is better than 10^7 counts.

INTRODUCTION

THE problem of a detector with high intrinsic sensitivity for gamma-radiation has not been solved satisfactorily, although, recently the development of the scintillation counter by Deutsch[1] and others has shown considerable promise. Sometime before these developments took place, the same problem presented itself in connection with the curved crystal gamma-ray spectrometer[2] developed in this laboratory. Since the radiation detector was a very important part of the whole apparatus, it was decided to attempt to construct a counter of the Geiger-Muller type but with enhanced sensitivity.

The requirements of the counter were as follows: It must have high sensitivity for gamma-radiations in the energy range 0.025 to 1.0 Mev, and accept an approximately parallel beam about two inches square. Furthermore, a very low background would be desirable, but extremely short counter recovery time would not be necessary on account of low counting rates. It was doubtful if even the scintillation counters could satisfy these requirements, especially the large beam cross section, without considerable development work.

DESIGN

The problem of intrinsic sensitivity of a Geiger counter to radiation is discussed by several authors.[3,4] The intrinsic sensitivity[*] may be represented by the expression:

$$\epsilon(E) = C(\tau R_\tau + \sigma \bar{R}_\sigma + 2\chi \bar{R}_\chi). \tag{1}$$

τ, σ, χ represent, respectively, for photo, Compton, and pair production, the linear absorption coefficients for radiation of energy E in the cathode material. R_τ, $\bar{R}_\sigma$, $\bar{R}_\chi$ represent the mean electron ranges, respectively, for the three corresponding processes. These ranges must be evaluated for the electron energies which result when the initial quantum of energy E interacts with the material. The constant C must be determined experimentally. The expression further assumes that the cathode wall thickness is such that other absorption effects may be neglected. Bradt *et al.*[4] show curves of the dependence of ϵ on E, the quantum energy, and Z, the atomic number of the cathode material, for the optimum design in each case, i.e., when the cathode wall thickness is just equal to the range of the most energetic secondary electrons. Since τ varies as Z^4

---

[1] M. Deutsch, *Scintillation Counters with Naphthalene* (Lab. for Nucl. Sci. and Eng., M.I.T.), Tech. Rep. 3 (Dec. 1, 1947).

[2] J. W. M. DuMond, Rev. Sci. Inst. **18**, 626 (1947).

[3] F. Norling, Arkiv. f. Mat. O Fys. **27A**, No. 27 (1941).

[4] Bradt, Gugelot, Huber, Medicus, Preiswerk, and Sherrer, Helv. Phys. Acta **19**, 77 (1946).

[*] By intrinsic sensitivity is meant the fraction of all photons passing through the counter which register counts.

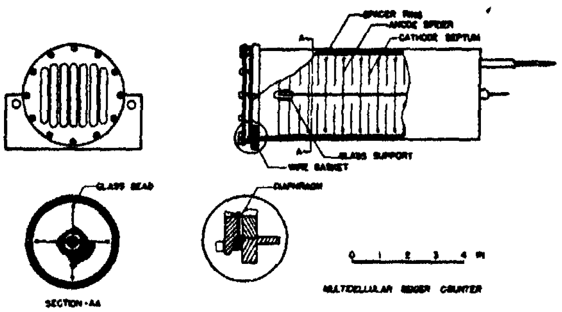

FIG. 1. Schematic drawing of the multicellular Geiger counter showing the main features of construction.

it is advantageous to use plates of high atomic number. On the other hand, if the quantum energy is low, the range of the electrons becomes very small. In this case, it is better to rely on the gas for absorption where every secondary electron produced will register a count.**

It is evident that the efficiency of a counter will vary by a considerable factor especially at low quantum energies. It is impossible to design a single counter of the conventional type, which will have reasonably good efficiency for a wide range of quantum energy, if one must rely only on the cathode for ejection of secondary electrons. Hence, separate counters are used for different energy ranges. In each case the cathode wall thickness is adjusted to some optimum value. The nature of the cathode surface also has an effect on the sensitivity. Evans and Mugele[5] showed that there was considerable advantage in the use of wire gauze for the cathode. This is primarily on account of the increased mass of cathode material effective for production of secondary electrons which penetrate the active volume of the counter. Considering all factors, lead appears to be the best cathode material, providing the natural radioactive contamination can be eliminated. To decrease the effect of this contamination, the plates were silver plated to a thickness of 0.001 inch. The counter designed for optimum sensitivity at 0.5 Mev used a lead cathode of 450 mg/cm^2 surface density. The cathode surface was embossed by rolling it between pieces of 80 mesh wire gauze to increase the surface area.

The counter geometry was such that the sensitive volume had a projected area of at least the cross section of the incident beam of radiation. Consequently, each counter section had the shape of a pillbox approximately three inches in diameter. The anode consisted of a four-pronged spider mounted so the plane of the wires lay midway between the end plates of the box and parallel to them. Electrostatically, the geometry represents a straight wire spaced midway between parallel plates to a fair approximation. A calculation of the field about such a wire leads one to expect a reasonable plateau from this geometry.[6]

The increased sensitivity of the counter is obtained by merely connecting a number of these pill-box counters in parallel in the same envelope. Of course, this arrangement requires that the threshold voltages of the individual sections shall coincide closely enough so that the multicellular counter may exhibit a plateau. This was indeed accomplished by the construction and treatment described below.

CONSTRUCTION

The constructional details of the counter are shown in Fig. 1. The case is made of Shelby tubing, 3 inches inside diameter and 8 inches long, to which an end plate was silver soldered in a hydrogen furnace. The end plate carried the pumping lead and a Stupakoff glass insulator bushing for the central wire. The opposite end was fitted with a flange and a grill to support the 2 mil nickel foil window. The seal was made with an aluminum or lead wire gasket in a vee groove as shown in the detail view. The clamping ring was a grill identical to the inside one. This furnished support to the window which allowed the unit to be pressure tested for leaks. This method of construction permitted rapid opening and resealing of the unit and has given no trouble whatsoever.

The counter sections themselves consisted of circular disks of silver-plated wire gauze or lead sheets 3 inches in diameter. At the center a $\frac{3}{8}$ inch hole was punched to allow the supporting rod for wire spiders to pass down the axis. The spiders

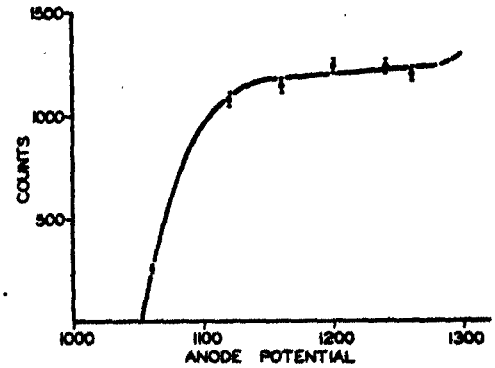

FIG. 2. The counting characteristic for a counter of nine sections.

** Mr. W. West of this laboratory has succeeded in making xenon-argon petroleum ether filled counters operate satisfactorily with high quantum efficiency up to about 0.070 Mev energy.

[5] R. D. Evans and R. A. Mugele, Rev. Sci. Inst. 7, 441 (1936).

[6] S. C. Curran and J. M. Reid, Rev. Sci. Inst. 19, 67 (1948). In this paper several different counter geometries and the plateau to be expected are discussed.

consisted of four radial 0.01 inch tungsten wires, silver soldered to a monel tube 0.050 inch outside diameter. The tips of the wires were beaded with glass to prevent discharge at these points. Each spider was etched by a.c. electrolysis in NaOH solution to clean the wires of all scale and sharp points. A 0.040 inch drill rod was soldered in the Stupakoff bushing and extended down the axis of the counter. As each disk was set in the counter, a spider was slid on this central rod and centered between each pair of disks. In this manner, a maximum of nine complete sections was built up in the cylindrical envelope. The free end of a central rod was supported in a glass bushing to keep the spiders centered on the axis.

No special treatment was given the counter once it was assembled. Of course, during assembly great care was taken to exclude any foreign matter. The counter was merely pumped out and tested to assure that no leaks were present and then filled with a 3 percent mixture of petroleum ether and argon to 20 cm of mercury. It was necessary to wait several hours at least before the counter became stable, but thereafter, the threshold and plateau were quite constant. Furthermore, the characteristics of several counters of this type could be made nearly identical.

PERFORMANCE

The threshold of the counter was about 1100 volts. As Fig. 2 shows, the plateau was flat to about 5 percent per hundred volts and had a length of 150 volts. These characteristics are independent of whether a quench circuit was used or not. The lifetime of the counter was of the order of 10^7 counts, at least.

The efficiency of two of the nine section counters was measured by a coincidence technique using annihilation radiation (0.51 Mev) and found to be approximately 25 percent averaged over the whole face of the counter. Tests made with a collimated pencil of gamma-radiation from a radium source showed that the sensitivity was almost constant over the entire face with the exception of the axis of the counter where the cathode plates were punched out.

The pulses from the nine section counter are not uniform in height, but over the plateau they have a certain minimum height which, of course, increases with the over-voltage. Because of the relatively large capacity of the wire, it is desirable to use a circuit which is a little more sensitive than those ordinarily used. An interesting observation was made on the pulses from a single counter section. The pulse heights are distributed as 1:2:3:4; the interpretation is that the pulse height is just proportional to the number of wires which discharge. The methods by which the discharge spreads are two. The initial ionizing event may produce ions in the vicinity of one or more wires, or the discharge which is propagated by photon emission[7] along one wire may also be propagated from one wire to the others by the same mode. The number of pulses of each height decreases as the height increases.

FIG. 3. Photograph showing the multicellular counter and a bank of six anticoincidence counters in the lead housing.

In the application for which the counter was intended, it was important that the background be as low as possible. If cosmic-ray counts are subtracted by means of a battery of six conventional counters, placed in an arc situated immediately above the gamma-ray counter and connected so as to operate the scaling circuit in anticoincidence with the latter, the background per counter section, when shielded by four inches of lead, is about 11 counts per minute. Figure 3 shows the counter and its anticoincidence counters in the lead housing. There could be some decrease in this rate if the axial dimension of the individual counter sections could be decreased. Spacings of 0.375 inch between the cathode plates have been used but, as would be expected, the operation is somewhat more satisfactory with the larger spacing.

The counter has a sensitivity for gamma-radiation comparable with a good scintillation detector. However, its greatest advantage is that the sensitive volume has a relatively large cross-sectional area. The construction is rather easy and the performance comparable with Geiger counters of more conventional geometry.

The author wishes to acknowledge the assistance of Dr. J. W. M. DuMond under whom the work was carried out. The work was supported by the Office of Naval Research under Contract N6onr-244 Task Order IV.

---

[7] H. G. Stever, Phys. Rev. 59, 765 (1941).

THE REVIEW OF SCIENTIFIC INSTRUMENTS VOLUME 20, NUMBER 4 APRIL, 1949

The Maxwell Bridge at Low Frequencies

Vinton A. Brown and B. P. Ramsay
Naval Ordnance Laboratory, Silver Spring, Maryland

(Received August 2, 1948)

The Maxwell bridge has been found useful for measuring inductance L and a.c. resistance R_{ac} at periods from 0.01 sec. to 200 sec. In some applications, the inductors had solid ferromagnetic cores and inductances of several hundred henries. The effect upon the bridge circuit of induced currents in the ferromagnetic material is expressed as a first approximation in terms of the equivalent mutual inductance M. The resulting equations expressing the frequency dependence of L and R_{ac} are in qualitative agreement with experiment. Because of harmonic frequencies generated by magnetic hysteresis, the bridge cannot be completely balanced when measuring L and R_{ac} of ferromagnetic-cored inductors. Analysis of the precision of measurement indicates that the effect of the residual voltage at best balance is a reduction in bridge sensitivity. Factors determining the choice of bridge resistors and of balance indicator are discussed, and typical graphs of L and R_{ac} as functions of frequency are presented.

INTRODUCTION

THE Maxwell bridge (Fig. 1) is a well-known circuit for the measurement of capacitance or inductance and a.c. resistance. The series combination of inductance and resistance in one arm is balanced by the parallel grouping of resistance and capacitance in the opposite arm. The equation of balance of the general four-arm bridge,[1] of which the Maxwell bridge is an example, is

$$Z_1Z_4=Z_2Z_3, \tag{1}$$

where the Z's are the complex impedances of the respective arms. Substitution of the appropriate expressions for the impedances of the arms of the Maxwell bridge yields the equation

$$(R_1+j\omega L_1)\left(\frac{R_4/j\omega C_4}{R_4+(1/j\omega C_4)}\right)=R_2R_3. \tag{2}$$

The real and imaginary components of this equation are the familiar equations of balance,

$$R_1R_4=R_2R_3, \tag{3}$$

$$L_1=R_2R_3C_4. \tag{4}$$

Thus inductance may be measured in terms of capacitance, or *vice versa* by means of Eq. (4). If the unknown is an inductance, Eq. (3) yields its a.c. resistance R_1, at the frequency and excitation of measurement. If R_1 and L_1 are independent of frequency and excitation, Eqs. (3) and (4) express the balance conditions for all frequencies and excitations. If not, R_1 and L_1 must be considered to be the effective series resistance and inductance at any particular frequency and excitation; Eqs. (3) and (4) then specify the conditions of balance at that frequency and with that excitation only. In either case the balance is complete; that is, an indication of null voltage is always obtainable by proper adjustment of R_2, R_3, R_4, and C_4.

In its usual application the Maxwell bridge is employed at audiofrequencies. Its proven range of usefulness has been extended in measurements at

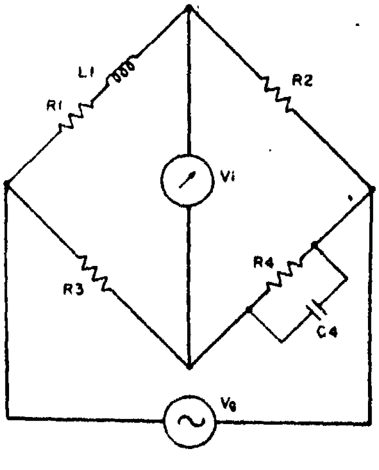

FIG. 1. The Maxwell bridge.

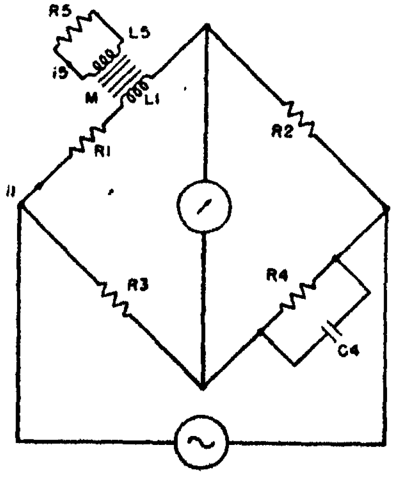

FIG. 2. Effect of mutual inductance upon balance of the Maxwell bridge.

---

[1] B. Hague, *Alternating Current Bridge Methods* (Isaac Pitman, London, 1938), p. 51.

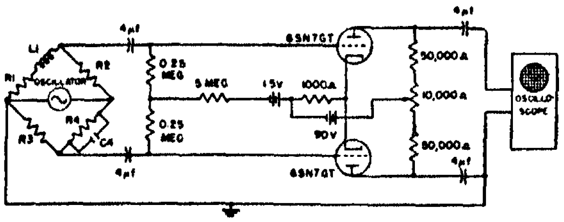

FIG. 3. Balanced amplifier for use with cathode-ray oscilloscope as balance indicator.

the Naval Ordnance Laboratory to frequencies as low as 1/200 cycle per second. In most of these applications, the unknowns were induction coils having solid ferromagnetic cores and inductances of several hundred henries. The effect of eddy currents in the ferromagnetic core upon the balance of the bridge is represented schematically in Fig. 2 by means of a coupled secondary circuit. The current i_5 in the secondary circuit consisting of inductance L_5 and resistance R_5 is a simplified representation of the continuum of eddy currents circulating in the solid core. The equations of balance of this circuit are derived as follows.

EFFECT OF MUTUAL INDUCTANCE

Reference to Fig. 2 shows that the voltage e_1 across the inductive arm is

$$e_1=(R_1+j\omega L_1)i_1+j\omega M i_5. \tag{5}$$

Application of Kirchhoff's law to the secondary circuit gives

$$0=(R_5+j\omega L_5)i_5+j\omega M i_1. \tag{6}$$

Hence the impedance Z_1 of the inductive arm is

$$Z_1=\frac{e_1}{i_1}=R_1+j\omega L_1+\frac{\omega^2M^2}{R_5+j\omega L_5}. \tag{7}$$

Thus Eq. (1) becomes

$$\left(R_1+j\omega L_1+\frac{\omega^2M^2}{R_5+j\omega L_5}\right)\frac{R_4/j\omega C_4}{R_4+(1/j\omega C_4)}=R_2R_3. \tag{8}$$

Separation of reals and imaginaries yields the equations of balance,

$$R_5(R_1R_4-R_2R_3)=\omega^2R_4[L_5(L_1-R_2R_3C_4)-M^2], \tag{9}$$

$$L_5(R_1R_4-R_2R_3)=-R_4R_5(L_1-R_2R_3C_4). \tag{10}$$

It is evident that the conditions of balance for the Maxwell bridge will satisfy Eq. (10). Equation (9), however, becomes

$$0=-M^2\omega^2R_4. \tag{11}$$

Thus, Eq. (9) is not satisfied by Eqs. (3) and (4) except under the trivial condition described by Eq. (11).

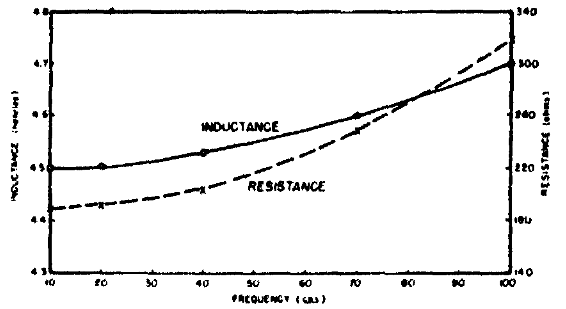

FIG. 4. Inductance and a.c. resistance of a 20-ft. square Helmholtz coil system. 300 turns per coil.

The condition which prevails when the trivial solution is eliminated from consideration can be clarified by separating the adjustable bridge parameters R_2, R_3, R_4, and C_4 from those which are characteristic of the induction coil, namely, R_1, L_1, R_5, L_5, and M. Simultaneous Eqs. (12) and (13) in which this separation is effected follow directly from Eq. (8).

$$R_1+R_5(\omega^2M^2/R_5^2+\omega^2L_5^2)=(R_2R_3/R_4), \tag{12}$$

$$L_1-L_5(\omega^2M^2/R_5^2+\omega^2L_5^2)=R_2R_3C_4. \tag{13}$$

Since L_1 is the inductance and R_1 is the a.c. resistance of the coil in the absence of eddy currents, the effective inductance L and a.c. resistance R of the coil with a conductive core are shown by Eqs. (12) and (13) to be

$$R=R_1+R_5(\omega^2M^2/R_5^2+\omega^2L_5^2), \tag{14}$$

$$L=L_1-L_5(\omega^2M^2/R_5^2+\omega^2L_5^2). \tag{15}$$

This presentation indicates that the a.c. resistance R of a coil with a conductive core will increase with frequency more rapidly than R_1, the a.c. resistance of the coil exclusive of the effects of eddy currents in the core. However, the inductance L of the coil with conductive core is less than L_1, the inductance exclusive of the effects of eddy currents in the core. Equation (15) does not indicate that the inductance of a coil with a conductive core is less than that of an air-cored coil, but it does show that the inductance of a coil with a metallic core is reduced by the effects of eddy currents. Since only eddy-current effects are included in these equations, they are not sufficiently inclusive to describe all effects which are observed with coils having ferromagnetic cores. In particular, they do not take into account the generation of harmonics of the fundamental frequency which result from magnetic hysteresis. Because of hysteresis, a complete balance of the bridge cannot be effected by any adjustment of R_2, R_3, R_4, and C_4 in the case of coils with ferromagnetic cores.[2]

---

[2] A similar conclusion applies to A. T. Starr's bridge (Phil. Mag. 12, 265–280 (1931)), in which the mutual inductance is

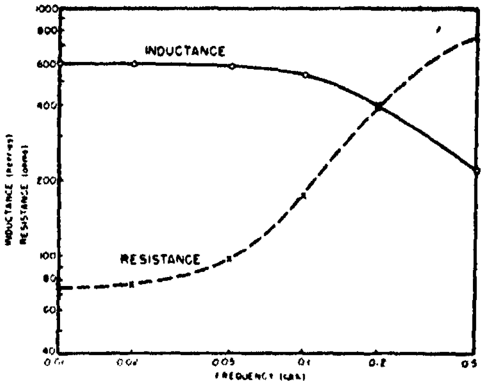

FIG. 5. Inductance and a.c. resistance of search coil with solid ferromagnetic core.

In spite of the impossibility of completely balancing the Maxwell bridge when magnetic hysteresis is present, the conventional Maxwell bridge has been employed for the measurement of L and R_{ac} of ferromagnetic-core inductors on the assumption that the equations of balance [Eqs. (3) and (4)] are applicable when the a.c. voltage drop across the indicator is a minimum. The justification for this assumption is the smallness of the hysteresis effect in comparison with that of inductance. For example, at a period of 10 seconds, the minimum peak-to-peak indicator voltage was 1/1000th of the voltage developed across the inductor. Hence it is concluded that the imperfection of the balance is not sufficient to materially affect the applicability of the usual equations of balance to the problem of determining L and R_{ac}. The precision of measurement is reduced, however, by the residual voltage at best balance, which reduces the sensitivity of the bridge, as shown in the following discussion.

BRIDGE SENSITIVITY

The definition of sensitivity of a Maxwell bridge for which a complete balance cannot be obtained may be developed along lines followed in treating the conventional bridges.[8] With R_4 and C_4 dials set at the positions of best balance, the voltage V_i across the indicator terminals is a minimum. If either dial is displaced from this position while the other remains at its position of best balance, the change ΔV_i in indicator voltage is directly proportional to the deviation in impedance Z_4 from the balance setting, provided this deviation ΔZ_4 is small. Hence,

$$\Delta V_i = SV_g\Delta Z_4, \tag{16}$$

where V_g is the generator voltage. The proportionality factor S, which is a function of frequency, is known as the sensitivity of the bridge. This relation, in the form

$$\Delta Z_4 = (\Delta V_i/SV_g) \tag{17}$$

determines the minimum detectable increments in R_4 and C_4, provided ΔV_i is here considered to be the least change in indicator voltage that can be distinguished from spurious fluctuations. Thus the minimum increments ΔR_4 and ΔC_4 depend upon the following factors:

(1) Sensitivity of the indicator, a factor in determining ΔV_i.
(2) Magnitude of spurious voltage fluctuations relative to V_g, which contributes to $\Delta V_i/V_g$,
(3) Bridge sensitivity S.

In practice, obtaining sufficient indicator sensitivity presents no problem. Experience indicates that it is the magnitude of spurious voltage fluctuations arising in electronic and mechanically driven oscillators at the low frequencies considered here which is the principal limiting factor in the determination of the accuracy of the measurements. If it were possible to obtain a perfect balance independent of frequency, the anomalies in generator voltage would not be detectable at balance. In the actual case, the imperfection of balance reduces the accuracy of measurements to a value determined by the magnitude of the fluctuations in indicator voltage at best balance. The accuracy attained is estimated to be ±2 percent at a period of 1 sec., and ±5 percent at 100 sec.

BRIDGE DESIGN

Choice of resistances for the bridge was based upon several considerations. (a) Since available variable condensers have small capacitance, the value of the product R_2R_3 by which C_4 is multiplied to obtain L_1 must be large to permit measurement of inductances in the range of interest, that is up to 800 henries. (b) It is of course desirable that the factor R_2R_3 have a simple numerical value, in order that inductance may be read off at once from the condenser setting. (c) For maximum bridge sensitivity, R_2 should be of the same order of magnitude as R_1 which, in the applications of greatest interest, was approximately 100 ohms. Such a small value of R_2 would require that R_3 be as large as several megohms. This would introduce leakage problems. To avoid such difficulties R_2 and R_3 were fixed at 20,000 ohms each. The value of the inductance in henries is then 400 times the capacitance in microfarads.

As constructed, the bridge incorporates a decade resistance box as R_4 and a decade condenser as C_4. For measuring inductances above 400 henries, capacitance C_4 is increased to a maximum of 2.11 μf by shunt connection of an auxiliary 1-μf standard condenser. A rheostat controls the current through the bridge, which is ordinarily limited to

---

balanced by modification of the opposite arm so that it becomes the inverse network of the inductive arm. In the presence of a ferromagnetic core, the capacitors in the inverse network do not compensate for the effects of magnetic hysteresis.

[8] See reference 1, pp. 81–85.

40 μa in order to avoid saturation of the ferromagnetic cores of induction coils under test.

The galvanometer need not be one of especially high sensitivity since a minimum deflection of appreciable magnitude, rather than a null, is obtained. The galvanometer's natural period of vibration, however, is fairly important. A portable spotlight galvanometer of 2-sec. period has been found satisfactory at a.c. periods up to 10 sec. For longer periods of the applied voltage, a ballistic galvanometer of natural period 30 sec. has proved more useful, as it smooths out the minor fluctuations in the mechanically driven power supply.

A type of indicator which has proved useful in a somewhat higher frequency range, namely from 1 to 100 c.p.s., is the cathode-ray oscillograph and an appropriate amplifier (Fig. 3). In order to permit the use of a grounded oscillator and a grounded oscilloscope, the input circuit of the amplifier is balanced relative to ground and one side of the amplifier output circuit is grounded. This apparatus has been used in measuring inductance and resistance of large magnetic generators[4] of which the conventional Helmholtz coil and the solenoid are familiar examples.

TYPICAL MEASUREMENTS

Figure 4 presents as typical results, the inductance and a.c. resistance of a 20-ft. square Helmholtz coil system. Both inductance and resistance, which are apparent values, increase with frequency as predicted from consideration of the effect of distributed capacitance.[5]

Figure 5 shows the inductance and resistance of a typical search coil having a solid ferromagnetic core. Resistance increases with frequency because of the effect of eddy currents, as predicted by Eq. (14), and also because of the effect of distributed capacitance. Inductance decreases with increasing frequency, in accordance with Eq. (15). The decrease in inductance is attributed to eddy currents, which delay the penetration of the magnetic field into the interior of the core so that the field strength in the interior is less than the field strength at the surface.[6] The magnetic induction and the inductance are thereby reduced. The agreement of the observed frequency dependence of inductance and resistance with the predictions of Eqs. (14) and (15) justifies the first approximation concept of eddy-current effects in terms of mutual inductance.

---

[4] B. P. Ramsay and F. L. Yost, "Facilities Provided by the Kensington Magnetic Laboratory," Terr. Mag. 52, 357–367 (1947).

[5] L. Page and N. Adams, *Principles of Electricity* (Van Nostrand Company, Inc., 1931), p. 598.

[6] R. M. Bozorth, "Magnetism," Rev. Mod. Phys. 19, 60 (1947).

THE REVIEW OF SCIENTIFIC INSTRUMENTS VOLUME 20, NUMBER 4 APRIL, 1949

Methods for Reducing Insulator Noise and Leakage

F. M. Glass
Instrument Department, Oak Ridge National Laboratory, Oak Ridge, Tennessee

(Received December 14, 1948)

A recent study of the insulator problem involved in radiation detection instruments disclosed the fact that insulators, in high impedance input circuits, are the predominate source of background noise when subjected to high voltages and high humidities. Methods for eliminating this trouble in some of the commonly used circuit components, and new and superior insulating materials, were found.

SERIOUS insulation problems have arisen with the widespread use of radiation detection instruments. In certain types of detection devices such as alpha-chambers, proportional counters, and electrometers having high input impedances, the necessity for good insulators cannot be overemphasized. In many instances where background noise is of sufficient amplitude to make accurate counting difficult or impossible, the spurious counts can be traced to insulator noise. However, as a result of experience with past applications of insulators in the electronic field, engineers are prone to take the quality of insulators for granted. Even if the best insulating materials available are selected, the insulator may be made into a constant source of trouble by improper milling or molding technique. It is the intent of this article to point out some of the insulator troubles encountered and to suggest some preventive measures.

Let us consider some of the common circuit components that are a potential source of trouble as a result of poor insulation. Figure 1 shows a conventional preamplifier for use with an alpha-chamber or proportional counter. In the grid circuit we note that the filter condenser, C-1, the coupling condenser, C-2, and any other supporting insulators

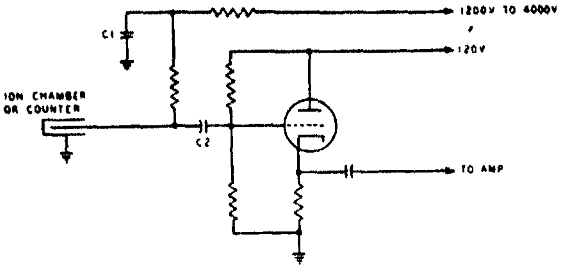

FIG. 1. Conventional preamplifier circuit for radiation counters.

in the chamber or cable and cable connectors are subjected to high voltage. All these components are possible noise makers, especially in the presence of high humidity. Since the humidity is not always a controllable factor in the use of radiation detection instruments, it is necessary to provide insulators which are noise-free at humidities approaching saturation.

DESCRIPTION OF TEST

In order to determine the pulse characteristic, frequency, and cause of insulator noise in such circuits as Fig. 1, a series of tests were made under simulated operating conditions. The equipment used in these tests consisted of an Oak Ridge National Laboratory A-1 amplifier[1] and preamplifier with a combined voltage gain of 300,000, a 5000-v power supply, a 248 DuMont oscilloscope, a Higinbotham scaler,[2] a Tobe line filter, and a humidity controlled test chamber (see Fig. 2). The test chamber was constructed with two compartments. One of these contained the high voltage filter in dry air to prevent surface noise on the $0.01\text{-}\mu F$ 10,000-v Glassmike filter condenser.[3] The other compartment, in which the insulator under test was placed, was humidity controlled. A special noise-free feed-through insulator that could take 5000-v at 96 percent humidity was used to feed the 5000-v through the partition. A hygrometer mounted on the side of the chamber and extending through the wall made it possible to keep a constant check on the humidity. The humidity was controlled by passing dry or saturated air through two valves provided for that purpose. A small fan motor on top of the chamber, with the shaft extending through an air-tight seal, drove a small fan which thoroughly mixed the incoming air. This arrangement provided a means for testing an insulator at any given humidity, and at the same time maintained a zero-count background.

It was observed that all insulator noise could be traced to one of four sources. The first and most annoying source of noise in good insulators is surface noise resulting from high humidity. When the insulator is subjected to high voltage, random pulses are produced with characteristics so nearly like those from ionization chambers, and with amplitudes of such height as to make it impossible to discriminate against them, when counting pulses of low amplitude. These pulses have a rise time of $\frac{1}{8}$ microsecond or less, and amplitudes as high as 3 millivolts.[4] Since shot effect and thermal noise in well designed amplifiers may be as low as 3 microvolts r.m.s. or lower, depending on band width, it is quite obvious that defective or noisy insulators may well be the determining factor in the effective sensitivity of the amplifier.

The second source of noise, although annoying, need not be a serious handicap. It is caused by a change in dielectric strain resulting from a sudden change in voltage across the insulator. This noise appears to be piezoelectric pulses resulting from discontinuity in the mechanical motion of the dielectric when seeking equilibrium. As a rule this phenomenon is more pronounced in materials of crystalline structure. However, ceramics, being comparatively free of this noise, are an exception. Only insulating materials considered suitable for radiation detection instruments were tested for this source of noise. Mica was found to produce the most pulses, while teflon[5] fluorothene[6] and polyethylene produced no pulses. This noise is relatively unimportant in any insulator if the high voltage is turned on one or two minutes before the instrument is put in use, and if no sudden changes of voltage greater than 100-v occur while in operation. (See Fig. 3.)

The third source of noise may offer some difficulty unless a few simple precautions are taken. It is most pronounced in polystyrene or polystyrene substitutes and results from stresses set up in machining. Annealing these materials at 65°C for an hour or more will sufficiently relieve them of stresses set up in the machining processes. These stresses can be visually recognized by use of crossed polaroids. After the insulator has been annealed, care should be exercised in mounting to prevent unnecessary mechanical strain. If these two precautions are taken, the insulator will be free of noise as a result of mechanical stresses.

The fourth source of insulator noise results from leakage through the insulating material. The chief offender among frequently used insulating materials is mica-filled Bakelite. This noise is not present in high grade insulating material such as polystyrene, mica, and teflon and fluorothene. Since it is assumed the designer will use only good insulating materials, this article will carry no further discussion on this type of noise.

---

[1] W. H. Jordan and P. R. Bell, Rev. Sci. Inst. 18, 703 (1947).

[2] W. A. Higinbotham, J. Gallagher, and M. Sands, Rev. Sci. Inst. 18, 706 (1947).

[3] Type ASG, manufactured by Condenser Products Company, 1375 North Branch Street, Chicago 22, Illinois.

[4] Measurements were made using polystyrene sample having a $\frac{3}{4}''$ leakage path, in 90 percent humidity with 5000-v potential across the sample.

[5] Manufactured by E. I. du Pont de Nemours Company, Inc., Plastics Department, Wilmington, Delaware.

[6] A fluoro-ethylene polymer, manufactured by Carbide and Carbon Chemicals Corporation, Oak Ridge, Tennessee.

CABLE CONNECTORS

Cable connectors head the list of trouble makers. Many of the commercially available connectors were tested and none of them were found satisfactory for pulse work when subjected to high voltages and high humidities. The results of these tests are shown in Table I. This table shows the average counting rate for five samples each of the connectors tested. Pulses were recorded over a period of ten minutes for each individual test. Each time the voltage was advanced, a two-minute delay was made before starting the next count. This prevented the recording of counts as a result of change in dielectric strain.

TABLE I. Table shows pulse repetition rate of cable connectors as a function of voltage and humidity.

Sample	Voltage	Pulses/min. at 5% humidity	60%	90%
Amphenol 93-C and 93-M	1500	0	0	7
	3000	0	0.2	420
	5000	0	2.5	>60,000
Amphenol-P. L. 259	1500	0	0.2	420
	3000	0	64	>60,000
	5000	0	498	>60,000
Cannon Q-1-22C and Q-1-SL	1500	0	0	68
	3000	0	0	>60,000
Q-1-22C with polystyrene insulation installed in place of original insulation	5000	0	>60,000	>60,000
Amphenol A.N. No. UG-58U	1500	0	0	4470
	3000	>60,000	>60,000	>60,000
	5000	>60,000	>60,000	>60,000
Amphenol 83-1SPY	1500	0	0	>60,000
	3000	8	8	>60,000
	5000	51	81	>60,000
Amphenol 83-1SPN with phenolic insulation	1500	50	571	704
	3000	25,600	>60,000	>60,000
	5000	>60,000	>60,000	>60,000

As a result of these tests, engineers at Amphenol, working with the Oak Ridge National Laboratory, developed a pulse fitting that is noise-free at 5000-v and 96 percent humidity. This cable connector has teflon insulation which can be successfully cleaned when it gets dirty. The minimum surface leakage path is ½″. The shell has spring fingers for low impedance ground connections, and the center connector is designed to give corona-free service. The Amphenol stock numbers on these connectors are 82-804 and 82-805.[7]

COUPLING CONDENSERS

The data obtained from tests run on coupling condensers were even more discouraging than that obtained from the cable connector tests. However, the noise was eliminated without design changes. Only two of the many condensers tested showed any promise of being satisfactory. Centralab's type #850 high voltage ceramic series[8] were by far the best condensers tested. They were found to be entirely satisfactory at low humidities but very unsatisfactory at high humidities. Table II shows some of the data obtained from this test. Since these condensers are noise-free in dry air, a search was made for a method of surface treating the ceramic shell to make it less hygroscopic.

Silicones were discarded because the temperature necessary for baking exceeds the melting point for the soft solder used in the condenser assembly. Since it had already been demonstrated that a good polystyrene surface produced no pulses, several attempts were made to coat the ceramic shell with polystyrene. A successful method was finally worked out, and is described as follows:

(1) The condenser is washed in petroleum ether, or benzene, then in 180-proof ethyl alcohol, and finally rinsed in distilled water.

(2) It is then baked in a vacuum oven for about one hour at 100°C, after this the oven is cooled to 60°C and dry air admitted.

(3) The condensers are removed from the oven and while still warm, dipped in Amphenol 912 coil dope that has been cut by adding an equal quantity of 916 thinner.

(4) They are then air-dried for 2 hours and baked at 60°C for one hour. The condensers can then be soaked in water for several hours and tested at 90 percent humidity at 5000 v and no pulsing will occur.

FILTER CONDENSERS

Another source of trouble has been filter condensers. The Glassmike, Plasticon ASG, silicon-filled, made by Condenser Products Company, seems to be the most promising condenser for high

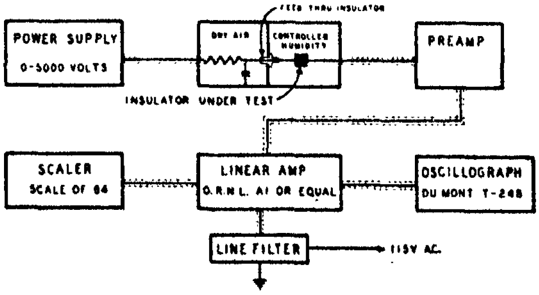

FIG. 2. Block diagram of equipment used in noise tests.

---

[7] Manufactured by American Phenolic Corporation, 1830 South 54th Avenue, Chicago, Illinois.

[8] Centralab Division, Globe Union, Inc., 900 East Keefe Avenue, Milwaukee 1, Wisconsin.

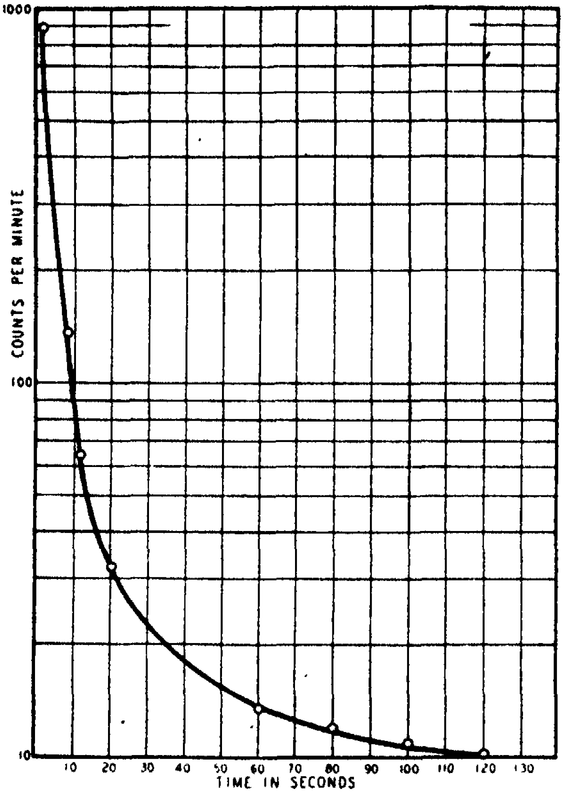

FIG. 3. Curve showing pulse frequency decay with time, resulting from a sudden 1000-v change in voltage across a 0.0001-μf, 2500-v silver-mica condenser.

voltage applications. These condensers produce no pulsing internally, but give considerable trouble on the shell surface at high humidities. However, if the shell is properly cleaned, no trouble will be encountered below 3000 v at any humidity. Alcohol alone will not do the job, as it is not a good solvent for the flux that is used in soft soldering the ends on the glass case. To clean these condensers properly, carbon tetrachloride should be used first to remove the flux. Then they should be washed thoroughly in alcohol. If voltages higher than 3000 v are used, the surface can be further improved temporarily by applying a very thin coat of ceresin wax. This is accomplished by dissolving a piece of ceresin the size of a pea in about four ounces of benzene and dipping the condenser in the solution. The condenser will then stand 5000 v at 90 percent humidity without pulsing. This surface, if not protected from dust, will soon be inferior to the plain glass surface that has been well cleaned. Therefore, if voltages lower than 3000 v are used, it is strongly recommended that no ceresin be applied.

TABLE II. Table shows pulse repetition rate of condensers as a function of voltage and humidity.

Sample	Voltage	Pulses/min. at 5% humidity	60%	90%
50-uuf Centralab ceramic not treated	1000	0	0	128
	3000	0	28	>60,000
	5000	0	578	>60,000
50-uuf Centralab ceramic condenser with shell sealed	1000	0	0	0
	3000	0	0	0
	5000	0	0	0
0.0001 microfarad 2500-v Sangamo silver-mica condenser	500	0	1	16
	1000	0	2	8167
	1500	0	11	>60,000
	2000	6	122	>60,000
0.01 microfarad 5000-v Glassmike condenser	1500	0	0	0
	3000	0	0	0
	5000	0	0	1

STAND-OFF INSULATORS

At the present there are no stand-off or feed-through insulators on the market that are noise-free. They should be machined from teflon or fluorothene, or molded from polystyrene, if possible. If molded from polystyrene, the molds should be so constructed that the use of wax is not required for unloading the mold. The mold should have an optical finish, and be kept immaculately clean. From the standpoint of surface noise, the insulator cannot be any better than any foreign materials that might be deposited on the surface. If teflon or fluorothene is used, it can be easily machined, and no polishing is required. The only precautions necessary are to use a clean cutting tool and to prevent the finished insulator from coming in contact with the hands or anything dirty or greasy. When machining and polishing polystyrene the following techniques will produce good insulators.

(1) When turning on a lathe, as little chuck pressure as possible should be employed, and the stock material within one-half inch of the chuck is not considered usable. With a milling machine one must use as little clamp pressure as possible and take only light cuts to prevent setting up mechanical stresses.

(2) A sharp cutting tool that has been thoroughly cleaned with alcohol must be used. Sapphire cutting tools are recommended.

(3) Polishing is done slowly with emerald or diamond powder and distilled water, using a clean lint-free rag. Chamois is not used as there is always some oil present. Slow polishing speeds are required to prevent surface heating and consequent imbedding of the polishing agent. Powdered carborundum may be used with extreme care to prevent overheating. *Note:* It is almost impossible to get a pulse-free surface using metallic oxide polishing agents.

(4) The insulator is then polished with talc until an optically polished surface is obtained.

(5) The insulator is then removed from the lathe with clean padded tongs and dropped in a container of distilled water until ready for use. The hands should never come in contact with the insulator during the milling or polishing process. Once dirty, no satisfactory method of cleaning polystyrene insulators has been found.

(6) When the insulator is ready for installation it should be removed from the jar of distilled water and rinsed thoroughly in fresh distilled water and dried in a vacuum oven.

Note: Almost all surface leakage is a result of poor polishing technique or mishandling the insulator after it leaves the machine shop.

SELECTOR SWITCHES

High input impedance electrometers place the same exacting demands on insulators as do the input circuits of high gain amplifiers. In addition to the circuit components already mentioned as sources of trouble, we have the problem of procuring a good selector switch for changing input resistors to the electrometer. These switches often must have a d.c. leakage resistance exceeding 10^{15} ohms at humidities as high as 90 percent. They must be comparatively free of contact and stress potentials. It is also often desirable that they be compact for use in portable test equipment. Efforts to obtain these switches commercially have been unsuccessful. Therefore an intensive study of the commercially available switches was made to determine the feasibility of altering or surface treating the most promising of these so that they would fulfill our needs. Centralab's ceramic series, the most promising of the commercially available switches, was studied first. These switches were found to be very good from the standpoint of contact and stress potentials. Tests were then run on leakage resistance, and very discouraging results obtained. Tests in a humidity controlled test chamber showed the resistance to vary from 5×10^{14} ohms at 2 percent humidity to 8×10^{12} ohms at 90 percent humidity. This indicated that if the switch were properly cleaned and sealed against moisture, the insulating properties of the ceramic would be satisfactory for our present needs. Other minor changes in the switch assembly made further improvement by lengthening the shorter leakage paths. After these switches had been treated according to the following process, the leakage resistances exceeded 10^{15} ohms and were independent of humidity.

(1) The switch assembly should be removed from the indexing assembly and cleaned thoroughly with carbon tetrachloride and a stiff brush, then rinsed thoroughly in ethyl alcohol, followed by a distilled water rinse.

(2) The assembly is then baked for 2 hours at 100°C under vacuum, after which dry air should be admitted.

(3) The switch is then removed from the vacuum oven and dipped while still hot in Amphenol 912 coil dope that has been thinned with two parts of Amphenol 916 thinner, agitating it until all the bubbles which form on the ceramic surface are gone. After dipping, it will be necessary to sling off all excess coil dope.

(4) After allowing the switch to dry for 20 minutes in clean, dust-free air, the rotor should be rotated with a clean screw driver to remove the coil dope from the contacts.

(5) After the switch has dried for three additional hours, the switch may be assembled using a polystyrene connecting link or shaft between the indexing assembly and the switch assembly. The metal spacers should also be replaced by spacers made from ¼″ polystyrene dowels ⅜″ in length, drilled and tapped for 5–40 screws. *Caution:* Do not drill all the way through the dowel or spacer as this provides another surface leakage path. Surfaces should be well polished. Also, the hands or anything that is greasy or dirty must not be allowed to come in contact with the ceramic insulation at any time after starting the cleaning process. Switches should be kept in dust-proof containers until such time as they are used. If these suggestions are followed carefully these switches will be found to have a leakage resistance exceeding 10^{15} ohms regardless of humidity. Some of these switches have been in service for ten months and still appear to be satisfactory.

METAL-TO-GLASS SEALS

Other insulators that play an important part in many detection devices are metal-to-glass (Kovar) seals. They are often used in metallic chambers to support the center electrode. Fortunately this type of glass is free of noise if properly cleaned and installed. One successful method of cleaning is to remove all traces of flux from the surface with Zapon #5 thinner, then wash in alcohol and rinse in distilled water. Dry in a vacuum oven, if available. Seals having a flash-over voltage rating of eight times the operating voltage, should be used to insure noise-free operation. If these precautions are taken, no trouble should be encountered with these insulators.

CONCLUSIONS

Insulator noise presents a difficult problem. Especially is this true when the counter voltage exceeds 1500 v and the humidity is above 60 percent. Under such conditions the problem becomes extremely difficult when counting pulses of amplitudes less than 150 microvolts. When accurate counting at low rates is required, it should preferably be done in an air conditioned room, with a humidity not exceeding 50 percent. The insulators should be designed to offer a minimum surface leakage path of ½″. The number of parallel leakage paths should be held to a minimum. From the standpoint of economy and performance, teflon or fluorothene insulation should be used. The labor cost for machining teflon or fluorothene is about 10 percent of that required for machining and polishing polystyrene. These materials produce fewer pulses as a result of mechanical or dielectric strain, and produce far less surface noise at high humidity. If a polystyrene insulator is accidently touched by the hand, it is ruined. Teflon and fluorothene, on the other hand, may be successfully cleaned many times. Neither type of insulator should be dried by rubbing with a cloth as this charges the insulator causing it to attract dust. Only extreme care and patience will solve the insulator problem in radiation detection instruments.

The author takes this opportunity to thank Mr. P. R. Bell of Oak Ridge National Laboratory for bringing to the author's attention the need for this investigation and for the many helpful suggestions which he contributed.

THE REVIEW OF SCIENTIFIC INSTRUMENTS VOLUME 20, NUMBER 4 APRIL, 1949

Conversion of a Motor Generator into a Low Noise Power Amplifier

H. S. Sommers, Jr., P. R. Weiss, and W. Halpern*
Department of Physics, Rutgers University, New Brunswick, New Jersey

(Received November 16, 1948)

The noise output of motor-generator sets is so large as to impair their use in precision control work. This paper describes a method for reducing this noise by incorporating a motor generator in an electronic feed-back circuit. The method is based on the use of a high frequency output channel in parallel with the generator to permit cancellation of the higher harmonics of the noise. Design, construction, and performance of an amplifier based on a ⅓-kw M-G set are described. The noise output of this unit is ⅕ percent of the normal noise of the generator.

A. INTRODUCTION

Problem

FOR certain types of physical measurements—for instance, in magnetic measurements requiring a controllable field and in calorimetry—it is necessary to hold a direct current constant to a high degree of precision. If the load impedance is sufficiently high and the power requirement not exorbitant, precision control can be achieved with feed-back circuits using vacuum tubes throughout.[1,2] No high fidelity feed-back control has yet been described in the literature for these cases where it is not practical to drive the load from vacuum tubes. Conventional controls for cyclotrons or mass spectrographs,[3,4] for example, are limited in both their precision of control and speed of response. This is because available high power sources are not suitable for incorporation in high gain, fast acting feed-back circuits. Generators or thyratrons give trouble because of their inherently large output ripple; this noise may produce unwanted fluctuations in the load current, but more important, it introduces large signals into the feed-back amplifiers which can overload and block them. This latter difficulty limits the possible feed-back gain and hence the quality of control achievable. On the other hand, the size, expense, and upkeep of a storage battery make it undesirable when the power requirements are high.

The present paper describes a practical method of converting a motor generator into a low noise, constant gain power amplifier. Our particular problem has been the development of a current regulator for a 40-kw electromagnet to facilitate its use in the study of the shape of the lines due to resonance absorption by nuclear magnetic moments. The circuits here described apply to a small pilot model generator which excites a magnet; however, they are being adapted to the generator for the large magnet. The method used and the bulk of the circuits have a much wider application than this, for they can be applied to other types of load and other power levels by appropriate scaling of the power stage and the filters.

TABLE I. Power amplifier—noise output.

Frequency	Generator output noise Without feedback	 With feedback	Reduction factor
30–60 c.p.s.	0.40 v r.m.s.	0.15×10^{-3} v r.m.s.	2500
below 1500	0.50	0.50	1000
all frequencies	0.65	1.3	500

Generator Noise

Table I gives the principal harmonic components in the output of the generator used in our pilot model. The largest components are nearly one percent of the generator output. The frequencies of the noise are harmonics of the rotational speed of the machine and are associated with assymetries in the armature and field and with the commutator segments and armature slots. The tolerable output noise is dictated by the gain required to achieve the desired degree of control. Our pilot model control requires the generator output noise be reduced by a factor of 500 at all frequencies below 1 kc/sec. The reasoning which determines the reduction factor will be explained in detail in a forthcoming paper describing the scaling of this power amplifier for use in the current control feed-back circuit for our 40-kw magnet.

Filtering of the generator output with an *LC* circuit is not a feasible means of reducing the noise. Aside from the expense of the filter elements capable of handling the high power, the design of a suitable filter is very difficult because of the high inductance and low resistance of the load. (For the large magnet, the load will have an inductance of 10 henries and a resistance of 2 ohms.) A matched filter requires impracticably large condensers, while an unmatched one either gives circuit instability or excessively long time constants. Shortening the time constants or damping the filter sections results in prohibitive power dissipation.

---

* Now at Airborne Instruments Company, Long Island, New York.

[1] M. E. Packard, Rev. Sci. Inst. **19**, 435 (1948).

[2] D. S. Hughes, W. L. Pondrom, and G. B. Thurston, Phys. Rev. **73**, 647(A) (1948).

[3] W. Y. Chang, Phys. Rev. **69**, 60 (1946).

[4] M. C. Henderson and M. G. White, Rev. Sci. Inst. **9**, 19 (1938).

Our method of reducing the generator output noise was to incorporate it into an inverse feed-back amplifier and remove the ripple by dynamic filtering. This paper will give the design and performance of a feed-back amplifier, incorporating a 100-volt, 1-kw generator working into a 1-ampere magnet, which has been built as a pilot model for the 40-kw system.

Terminology and Symbols

The following conventions will be used in this paper. By transfer function of a component is meant the complex ratio of the output voltage delivered by the component into its load to the input voltage. In case there exists a feed-back channel external to the component, the transfer function is the voltage ratio when the feed-back path is broken. The gain at a certain frequency is then the absolute value of the transfer function at this frequency.

Figure 1 gives a block diagram of a typical feed-back loop. The symbol μ will be used for the forward transfer function, i.e., the voltage ratio without feed-back. β will be used for the feed-back transfer function due to the feed-back net. The loop transfer function will then be $\mu\beta$; it will be considered to be positive if, in the center of the band pass, the vector difference of input voltage and feed-back voltage is less than the input voltage. The quantity $K=\mu/(1+\mu\beta)$, the net transfer function, then describes the behavior of the degenerative amplifier treated as a black box, while $|K|$, the net gain, gives the amplitude of the response as a function of frequency. $|K_0|$ will mean the function evaluated at zero frequency.

B. DESIGN

The purpose of this design is to convert a standard motor generator set into a power source with low noise output and with precisely controllable and variable output voltage. The upper limit on acceptable output noise is 1 mv r.m.s. at frequencies below 1000 c.p.s. The output, working into an electromagnet, must be variable from zero to full voltage.

It is possible to degenerate the output noise (Table I) by incorporating the generator into an inverse feed-back power amplifier provided the section of the closed loop which contains the generator maintains its gain at high frequencies. The cut-off frequency of the loop transfer function can be estimated by the following rough calculation. Suppose the 200-c.p.s. noise is to be reduced by 60 db (i.e., the loop gain is to be 1000 at 200 c.p.s.), and the high frequency cut-off is to be at the rate of 10 db per octave.[5] Then the gain must exceed unity for all frequencies below $200\times 2^6=13{,}000$ c.p.s.

The generator by itself is not a suitable series element for a feed-back amplifier because of its narrow band and non-linear response. These two factors together prevent the generator from satisfactorily degenerating even the 30-c.p.s. component of its own noise output. The bad non-linearity gives serious frequency multiplication of the feed-back frequencies,[6] and the higher harmonics resulting from the multiplication are not attenuated because the generator will not respond to them. One attempt to feed the noise back through the generator illustrates the results to be expected. The generator was driven by a d.c. amplifier and the generator output fed back inversely to the amplifier input. With a rather small amount of degeneration ($\mu\beta$ small), the 30-c.p.s. component of the generator output noise was reduced by a factor of ten, but harmonics with amplitudes comparable to the original 30-c.p.s. noise were added to the output. Increasing the loop gain to remove these higher frequencies made the components well outside the band pass of the generator overload and block the amplifier. To prevent this overloading and blocking of the amplifier, the band limiting must occur in the early stages rather than in the power stage.

It thus becomes evident that a successful method of applying dynamic filtering to the generator output requires a drastic extension of the band width of the power stage. This extended band width has actually been obtained by paralleling the generator output with a hard tube as indicated in the block diagram of the power amplifier, Fig. 2. This tube serves as the high frequency output for the amplifier, while the generator retains its original function

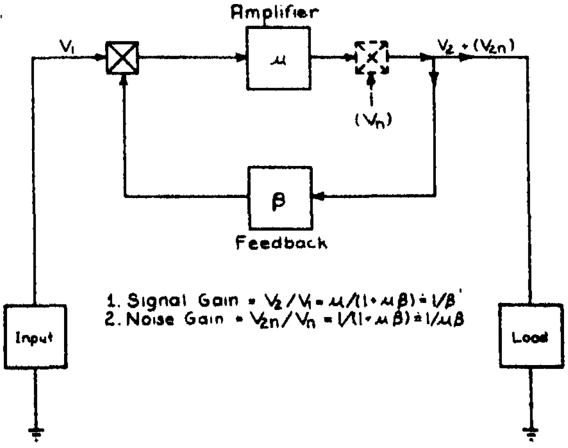
Amplifier
V_1
μ
$V_2+(V_{2n})$
(V_n)
β
Feedback
1. Signal Gain = $V_2/V_1=\mu/(1+\mu\beta)\doteq 1/\beta$
2. Noise Gain = $V_{2n}/V_n=1/(1+\mu\beta)\doteq 1/\mu\beta$
Input
Load

FIG. 1. Feed-back amplifier—block amplifier.

---

[5] H. Bode, *Network Analysis and Feedback Amplifier Design* (D. Van Nostrand Company, Inc., New York, 1948), Chapter 18.

[6] M.I.T. Electrical Engineering Staff, *Applied Electronics* (John Wiley and Sons, Inc., New York, 1943), see p. 528.

of passing the d.c. and low frequencies. As shown in the theoretical analysis, Section C, the gain ($\mu\beta$) of the composite amplifier is the sum of the individual gains of the two outputs by themselves. This addition to the generator output maintains the gain of the power stage (Fig. 2) up to 100 kc/sec., in contrast to the generator itself, whose gain starts to drop at a few cycles/sec. In its essential features, the problem has now become equivalent to the design of a highly stabilized, hard tube power supply.

Components

The components discussed below are shown in detail in the power amplifier block diagram (Fig. 2) and the power amplifier schematic (Fig. 3).

Comparator

The comparator is an adding net which derives the difference between the input voltage and the feed-back voltage. Although pictured as a unit in the block diagram, it is physically integral with the first stage of the voltage amplifier; the difference is obtained by sending the input signal to the grid and the feedback directly to the cathode. This permits the comparison of the two voltages without loading down the input signal, which may come from a high impedance source.

Voltage Amplifier

The voltage amplifier has a gain of about 150,000 and a band pass of 100 kc. This insures the loop transfer gain ($\mu\beta$) will always exceed 1000, with the over-all d.c. transfer gain ($1/\beta_0$) of 55 while the band easily satisfies the requirement that the internal amplifier introduce no appreciable phase shift in the region of frequencies below the loop cut-off. The desired high frequency cut-off of the entire power amplifier can then be obtained by insertion of appropriate passive elements so that the tube characteristics will not influence the loop cut-off. This means the only effect on the amplifier of tube variations will be a change in over-all gain, not in stability. At the same time, the output noise must be kept low, below one part in 10^6 of the maximum signal, which gives an upper limit to the noise (referred to the input) of 20 microvolts in the band between 0.1 and 60 c.p.s.

Figure 3 gives the circuit diagram of the voltage amplifier. The required gain and band width and correct feed-back polarity are obtained by using four direct-coupled stages. The gain per stage is held to about 20 so that each stage can have a band of greater than 100 kc/sec. Even at that, to nullify stray capacities several types of high frequency compensation were incorporated. The largest stray capacity is introduced by the coupling batteries, and this was eliminated by isolating each battery from both the following grid and preceding plate by a pair of series resistors and then shunting the whole with a small condenser. Further compensation is provided by shunting the cathode resistor with a small by-pass condenser; the same scheme is used in the screens. Careful staggering of these various time constants will make the response as flat as one wishes. In this particular case, a slow change in gain has little significance and no special care was taken in choice of condensers. The actual response begins to rise somewhat around 50 kc/sec.

To keep down the noise level, certain standard practices are resorted to. The filaments are operated on d.c., wire-wound resistors are used on the input and first stage, and bias batteries are used to couple from plate to grid. The effect on the output noise of the time constants associated with the plate loads

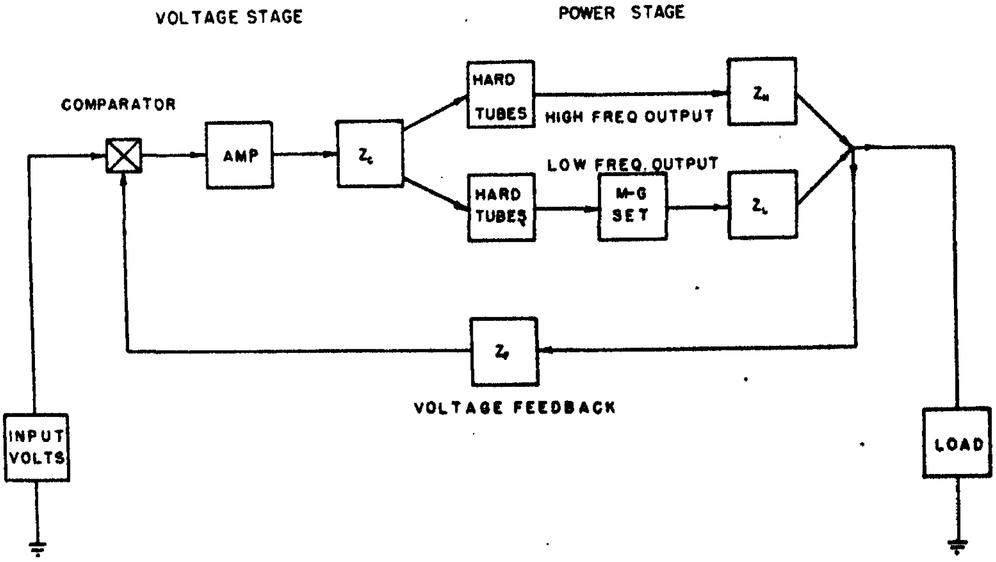

FIG. 2. Power amplifier—block diagram.

of the second, third, and fourth stages, which have been inserted for stability reasons, is discussed at the end of the section on components.

Feedback is derived from a potentiometer (Z_F) across the magnet with center tap feeding into the cathode of the first stage. The impedance of this potentiometer should be high to keep the power dissipation down to a convenient magnitude, while for servicing it is convenient to have an output from the generator when the input grid to the amplifier is grounded. These two conditions, plus the fact that the cathode resistor is specified and the factor $1/\beta_0$ must equal approximately 50, determine the values of the resistances[7] in the feed-back net. The 4-μf condenser makes β increase to about $\frac{1}{3}$ at higher frequencies, thus increasing the a.c. degeneration while maintaining the d.c. net gain.

Generator Branch

The generator field excitation, $\frac{1}{2}$ ampere at 100 volts, is supplied from a bank of hard tubes. Either a small motor generator set or an amplidyne would drive the generator field, but both of these introduce new complications to the problem because of the additional time constants and the high noise output of such units. Even less desirable is a thyratron driver, which is difficult to control over the range from zero to 100 volts output, has a large noise output, and has a considerable variation in characteristics with ambient temperature.

Details of the driver circuit are shown in Fig. 3. The generator field winding, 24 henries and 200 ohms, is the plate load for the five 6L6 driver tubes. These tubes have a common plate connection to the field winding, except for the 10 ohms parasitic suppressors, but each has its own cathode resistor and screen by-pass, which balance the plate currents in the various tubes and suppress parasitic oscillations between them. The separate grid resistors likewise help prevent parasitics besides preventing coupling between these tubes and the parallel output branch to the magnet.

The actual power source for the field is an unregulated half-wave rectifier and a π-section LC filter which delivers a nominal 400 volts. Ripple and lack of regulation have no undesirable effect, for the feedback gives high degeneration for noise introduced at the output of the amplifier, provided no interaction occurs between this supply and other elements of the circuits. Because of dangers of such interaction, the generator driver power supply is separate from the normal plate and screen supplies as well as from the supply for the hard tube output branch of the power amplifier.

The blocking reactor (Z_L), though schematically it enters in the generator output branch, is functionally a unit of the hard tube output branch and will be discussed in the next section.

Hard Tube Branch

The hard tube output branch of the power amplifier is a single 6Y6 cathode follower condenser-

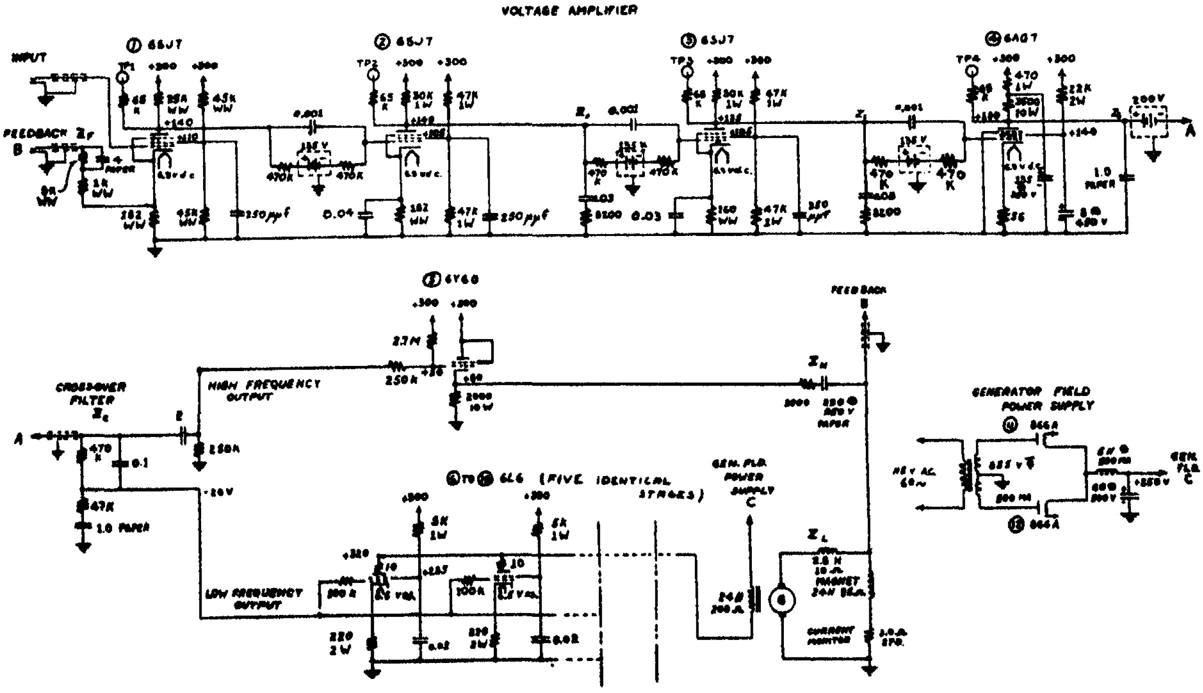

FIG. 3. Power amplifier—schematic.

---

[7] See E. L. Ginzton, Electronics 17, 98 (1944), for the method of calculating the resistances.

coupled directly to the magnet. The design is determined by two principal factors, voltage swing and stability.

1. Voltage swing.—The swing of the output of this branch must be greater than one-half volt r.m.s. at 30 c.p.s. in order to cancel the noise output of the generator. This half-volt must be developed across the load of the cathode follower, this load being the magnet in parallel with the generator output circuit. As the generator armature itself has negligible impedance, the blocking reactor is inserted between the magnet and the generator to increase the impedance presented to the cathode follower. This effectively makes the load into which the coupling net looks just the impedance of the blocking reactor, for its inductance and resistance are much less than those of the magnet.

The maximum voltage swing of the cathode follower is determined by the product of the current capacity of the tube and the inductance of the blocking reactor. Since the blocking reactor must carry the entire magnet current without saturating, it is expensive to make its inductance very large, and so the cathode follower must pass considerable current. However, in this case the magnet available utilized only 15 percent of the generator current rating and a single 6Y6 was sufficient to drive the 2.8-henry inductance of the blocking reactor.

2. Stability of the coupling net and magnet.—Since the coupling net (Z_H) and magnet form a series LC circuit, sufficient damping must be incorporated to prevent internal oscillations in the cathode follower output. Although direct coupling of the 6Y6 to the magnet would remove the possibility of oscillations, condenser coupling makes the design easier because it prevents the d.c. voltage across the magnet from changing the operating point of the cathode follower.

The 1000-Ω resister incorporated in Z_H overdamps the output circuit of the cathode follower. The value of 1000Ω is chosen here because it works well with the coupling condenser and reactor (Z_L) which happened to be available.

In a high power application, a smaller value for Z_L would be used because of the expense of the inductance. To maintain the low frequency response, the 1000-Ω damping resistor would likewise have to be reduced. Critical damping can still be maintained, however, if electrolytic condensers are used for coupling.

Location of Cut-Off Filters

The shapes of the desired loop transfer functions (Section D) determine the high and low frequency cut-offs of both the high frequency and low frequency output channels but do not specify how these cut-offs should be obtained nor where the necessary components should be located. A large part of the frequency response of the loops is inherent in the major components, such as the generator, the magnet, and the blocking reactor. Compensation for the response of these units to give the desired over-all frequency characteristic is accomplished by introducing appropriate RC high pass or low pass filters. Two factors are important in determining the best location of these filters, the actual location being determined by a consideration of the conflicting requirements of the two factors.

1. Because of their effect on noise, these filters should be located as late in the circuit as possible. Insertion of a filter narrows the band width of the amplifier. Since the signal passes through the entire amplifier, the attenuation of the signal is the same no matter where the band limiting occurs physically. The attenuator cuts down the noise band width only for noise originating before the filter; hence the output signal to noise will be best if all the filtering occurs in the output stage.

2. Because of blocking in the amplifier, the band limiting should be introduced at low level. Only those signals can block the amplifier whose frequencies lie outside the loop band width, for the degeneration of the closed loop keeps all extraneous signals inside the band at very low level. Blocking from out-of-band noise must be prevented by limiting the band pass of the feed-back loop at a sufficiently early stage to prevent this noise from overdriving any of the stages inside the amplifier.

A compromise between these two factors is achieved by inserting cut-off filters Z_1, Z_2, Z_3, on the outputs of the second, third, and fourth stages.

C. THEORETICAL ANALYSIS

The use of feedback to reduce the noise is particularly effective in the present instance since the noise source (the generator) immediately precedes the load. This permits the noise voltage across the load to be reduced by a factor equal to the loop gain, which can be made very large. A block diagram of the feed-back circuit is shown in Fig. 1 in which the noise voltage is appropriately shown as added separately immediately before the load. The entire voltage output V_0 is related to the input signal V_I and the noise N by

$$V_0=\mu(V_I-\beta V_0)+N, \tag{1}$$

so that

$$V_0=[\mu/(1+\mu\beta)]V_I+[N/(1+\mu\beta)]. \tag{2}$$

The expression (2) shows that when the loop gain, $\mu\beta$, is large the over-all gain is $1/\beta$, the reciprocal of the feed-back gain, and also the noise content of the output is reduced by the loop gain. If the noise source is situated earlier in the circuit, the noise is reduced by only a fraction of the loop gain.

To utilize this scheme, it is necessary that the over-all circuit have an extremely broad frequency

Table II. Power amplifier—transfer function elements.

SYMBOL	CIRCUIT ELEMENT	CIRCUIT	EQUIVALENT CIRCUIT	FORMULA	VALUES
Y_H	LOAD	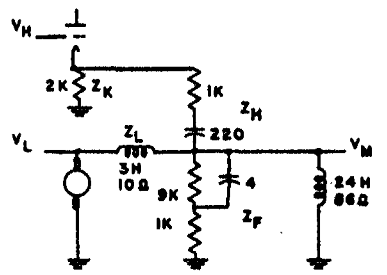 V_H 2K Z_K 1K Z_H Z_L 220 V_L V_M 3H 10Ω 9K 4 24H 86Ω 1K Z_F	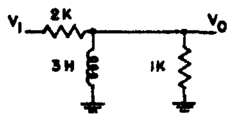	$G_H \frac{T_M p}{T_M p+1}$	$G_H = 0.2$ $T_M = .005$ SEC
Y_L	LOAD		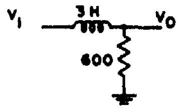	$\frac{1}{T_N p+1}$	$T_N = .005$ SEC
Y_{CH}	Z_C	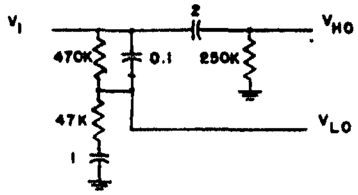 V_I 2 V_{HO} 470K 0.1 250K 47K V_{LO} 1		1	
Y_{CL}	Z_C		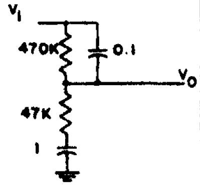	$\frac{(T_{C0} p + 1)^2}{(T_{C1} p+1)(T_{C2} p+1)}$	$T_{C0} = .05$ SEC $T_{C1} = 0.5$ $T_{C2} = .005$
Y_G	MG SET	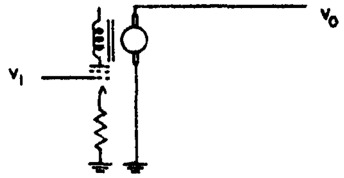	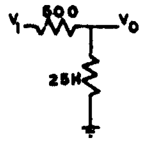	$\frac{G_G}{(T_{G1} p+1)}$	$G_G = 2.5$ $T_{G1} = .05$ SEC
Y_A'	VOLTAGE AMPLIFIER		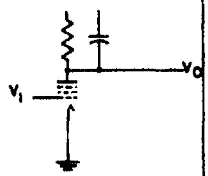	$\frac{G_A}{T_A p + 1}$	$G_A = 1.5 \times 10^5$ $T_A = .003$ SEC
Y_β	Z_F	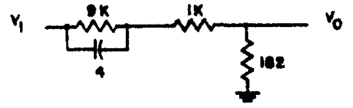	SAME	$\frac{T_{\beta 1} p + 1}{T_{\beta 2} p + 1}$	$T_{\beta 1} = .04$ SEC $T_{\beta 2} = .004$

response for reasons outlined in Section B. The addition of a high frequency channel to produce this response introduces, besides the possibility of instability in the entire circuit, the added possibility of near cancellation of the responses of the two channels in the frequency region where the gains are nearly equal. Were the latter to occur, the loop gain would be small in the stated frequency region and the noise there not filtered effectively. In addition, the circuit might become unstable with small changes in some of the parameters of the circuit.[7] It is possible, in other cases, for the circuit to be unstable even though the responses of the two channels add and maintain a high value of the gain. This occurs, for example, when the low frequency channel falls at −12 db/octave while the high frequency channel rises at +12 db/octave. The sum of the vector responses of the two channels gives a high value of the gain, but the over-all transfer function is such as to make the Nyquist diagram enclose the point (−1, 0), showing that the circuit is unstable. Incidentally, in the extreme situation described the individual channels are separately unstable. If the usual criterion of ±10-db/octave change rates were observed in order to make these channels separately stable, the over-all circuit would be unstable, nevertheless.

A simple criterion with respect to instability can be stated in terms of the relative phases of the transfer functions of the two channels at cróss-over. It can be expressed in terms either of the phases or of the rates of change of the amplitudes of the transfer functions, since phase and rate of change of amplitude are intimately connected.[**] If the amplitude changes as $6n$ db/octave over several octaves, the phase is $n(\pi/2)$ degrees at the center of the region on a log frequency scale. The criterion is: if the relative phase at cross-over is 180° or greater, the system is unstable. Moreover, if the relative phase is close to 180°, near cancellation takes place. A proper design is one in which the relative phase at cross-over is small.

Certain elements were introduced into the circuit to properly shape the high frequency cut-off and to obtain a suitable type of cross-over. These are the cut-off filters Z_1, Z_2, and Z_3 in the amplifier and the cross-over network Z_c, shown in the circuit diagram Fig. 3. The shaping of the high frequency cut-off followed standard criteria.[5] For a discussion of the location of these filters in the circuit, see Section B.

The proper design of the cross-over net, however, requires an analysis of the circuit. This is also true when any scaling is performed to adapt the circuit to loads different from that described here. It is necessary for this purpose, however, to include in the analysis only those time constants of the order of 3×10^{-3} sec. and larger since the cross-over region extends from about 3 to 50 c.p.s.

The voltage across the magnet V_M is a linear combination of the voltage output of the generator, V_L, (whose armature has essentially zero impedance) and the voltage on the grid of the hard tube (the 6Y6), V_H,

$$V_M = Y_H V_H + Y_L V_L. \tag{3}$$

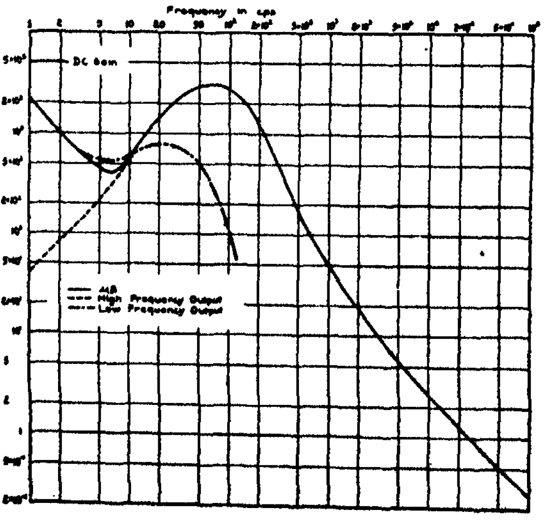

FIG. 4. Power amplifier—transfer function.

The transfer functions Y_H and Y_L refer to the load circuit as it affects the high and low frequency channels, respectively. They, like the transfer functions which follow, are described in Table II. Included in the table are simple equivalent circuits appropriate to the various transfer functions. The symbol "p" in the transfer functions denotes the complex frequency; the numerical values of the time constants and the gains are listed in the last column. Some of the transfer functions listed are only approximate but are sufficiently accurate in the stated frequency region for design purposes. The simplicity of the expressions listed for Y_H and Y_L arises from the fact that in the immediate vicinity of the cross-over point the two capacitances, 220 μf and 4 μf, have negligible impedances.

On tracing the voltages V_L and V_H back toward the comparator it is seen that

$$V_H = Y_{CH} V_A \tag{4}$$

and

$$V_L = Y_G Y_{CL} V_A, \tag{5}$$

where V_A is the voltage output of the amplifier. Y_{CH} in (4) is the transfer function of the cross-over net as it affects the high frequency channel. In the cross-over frequency region, as well as at higher frequencies, this is unity. Y_{CL} in (5) is the transfer function of the cross-over net as it affects the low frequency channel; it is described in Table II. Y_G in (5) is the transfer function of the generator, the ratio of the output voltage of the generator to the grid voltage of the 6L6 tubes.

The voltage amplifier and the feed-back network are common to both channels. The voltage output of the amplifier is

$$V_A = Y_A V_E, \tag{6}$$

where V_E is the output of the comparator and Y_A is the transfer function of the amplifier. When the input is zero,

$$V_E = Y_\beta V_M. \tag{7}$$

Here Y_β is the transfer function of the feed-back network.

On composing the various elements which are in series, the loop transfer functions of the high and low frequency channels are readily seen to be

$$\begin{aligned}(\mu\beta)_H &= Y_H Y_{CH} Y_A Y_\beta,\\ (\mu\beta)_L &= Y_L Y_G Y_{CL} Y_A Y_\beta.\end{aligned} \tag{8}$$

Finally, (3) shows that the over-all loop transfer function is the sum of these:

$$\begin{aligned}\mu\beta &= (\mu\beta)_H + (\mu\beta)_L\\ &= (Y_H Y_{CH} + Y_L Y_G Y_{CL}) Y_A Y_\beta.\end{aligned} \tag{9}$$

A plot of the transfer function $\mu\beta$ is shown in Fig. 4 where log amplitude is plotted against log frequency. Actually, this curve is an experimentally determined one; the graph of (9) agrees with it in all essential details. The cross-over frequency is 10 c.p.s., and the gain there is ~700. The lowest value of the gain in this region is ~500. In the region immediately about the cross-over point the low frequency channel rises at somewhat less than +6 db/octave while the high frequency channel rises at +12 db/octave. Consequently, the circuit stability is not destroyed by the behavior at cross-over. Also the gain remains high. These results are achieved by insertion of the cross-over network, which causes the low frequency channel to decrease its gain beginning at 0.3 c.p.s. and then to increase its gain at 5 c.p.s. The effectiveness of the cross-over net is brought out by considering the circuit without it; the transfer functions are obtained from (8) and (9) by deleting Y_{CH} and Y_{CL}. The cross-over now occurs at 20 c.p.s.; at the intersection $(\mu\beta)_H$ increases at a rate of roughly +6 db/octave and $(\mu\beta)_L$ at a rate of roughly −6 db/octave. The relative phase of the two channels at cross-over is just within the criterion for stability. A large degree of cancellation takes place so that $(\mu\beta)$ is small in spite of the individual gains at the intersection being 350. The near cancellation almost makes the system unstable and detracts seriously from the filtering action on the large 30-c.p.s. component of the generator output.

[**] See reference 5, Chapter XIV.

D. PERFORMANCE

Transfer Function

The performance of the unit as a power amplifier is determined by two factors, the circuit noise and the loop transfer function $\mu\beta$. The methods used to keep the circuit noise at a low level were discussed in Section B. The following paragraphs will discuss determination of the transfer function and its significance.

The amplitude of the transfer function, $|\mu\beta|$ of the composite amplifier is shown as the solid curve in Fig. 4. It is measured by opening the connection between Z_F and the comparator and feeding an input signal to the comparator in place of the interrupted feed-back voltage and measuring the output from Z_F. The ratio of this output to input is $|\mu\beta|$.

Figure 4 shows the measured transfer functions of the high and low frequency outputs as well as the composite one. The high frequency output was obtained in the same manner as the composite transfer function except that during its measurement the generator was shut off. Similarly, the low frequency output was measured with the input to the 6Y6 magnet driver removed.

The stability of the circuit is determined by the slope of the composite transfer function at the high frequency cut-off and the slopes of the two output functions in the region where their gains are equal (cross-over region). The high frequency cut-off will not render the closed loop unstable because the slope in the neighborhood of unity gain is −6 db/octave. Moreover, since this slope is maintained far on either side of the unity gain point (25 kc/sec.) the stability will be maintained in spite of wide variations in the gain of the amplifier. It was to achieve this reliability that the band width of the basic amplifier was extended to 100 kc/sec.

An attempt was made to keep the relative phase less than 120° in the cross-over region in order to maintain a large value for the amplitude of the composite transfer function. This was achieved in the region above 10 c.p.s. but just below this, where the composite curve is beneath the low frequency output, the phase somewhat exceeds 120°.

One of the features of this circuit is that a change in the gain of the voltage amplifier will have no effect on the stability in the cross-over region, for this amplifier is common to both outputs and will not change their relative phase. The gains of the sections of the amplifiers which are not common to both are small, being 2.5 for the low frequency output and 0.6 for the high. Hence, nothing but a major component failure can seriously disrupt the performance in this region.

The relative phase can be adjusted by a passive filter (Z_c) only if the gains at cross-over are high. This is achieved by making T_M large and T_{G1} small (Table II). At the same time, the coupling condenser in Z_H must be large enough to present a negligible impedance in this region.

The noise reduction when the loop is closed is given in Table I. The column labeled "Generator output noise without feedback," gives the measurements of the noise made between the blocking reactor and the magnet with the generator field excited from batteries, and so includes the static filtering provided by the blocking reactor. The next column, "Noise with feedback," shows the effect of the dynamic filtering produced by closing the feedback loop. The d.c. output was around 100 v for these measurements. The table shows the noise reduction factor for the 30-c.p.s. and 60-c.p.s. components taken together is 2500, which corresponds satisfactorily with the measured amplitude of the transfer function in this region (Fig. 4).

Besides this high frequency noise, there are low frequency variations of the generator output arising from other sources. One of them, the d.c. drift, is due to temperature changes affecting the resistances in the feed-back net. No temperature compensation was included in this model. The d.c. drift after warm up was 4×10^{-5} part/min. measured over a 6-minute interval. There was also present a low frequency fluctuation of about 0.1-c.p.s. frequency and 4-mv peak amplitude which was in some way associated with changes in the rotational frequency of the generator.

This work was supported by the Rutgers University Research Fund and by the joint program of the ONR and the AEC.

THE REVIEW OF SCIENTIFIC INSTRUMENTS VOLUME 20, NUMBER 4 APRIL, 1949

A Wide Range Capacitance-Conductance Bridge*

ROBERT H. COLE AND PAUL M. GROSS, JR.**
Metcalf Research Laboratory, Brown University, Providence, Rhode Island

(Received December 14, 1948)

The bridge described has been developed for reasonably accurate measurement by direct balance of capacitance and conductance in the frequency range 50 c/sec. to 5 mc/sec., and over most of this range is essentially direct reading in the two admittance components with negligible unbalance from lead effects or guard circuits of the unknown. These properties are realized by using two circuits developed from the work of others. The first employs inductively coupled ratio arms to minimize residual impedance effects and unbalance by guard circuits, the second, a conductance shifter wye network with good high frequency properties and an essentially linear conductance reading. Design considerations and limitations of these circuits are discussed, as are suitable test cells and auxiliary equipment.

I. INTRODUCTION

THE bridge described here has been developed for use in investigations of complex dielectric constants of polar liquids and solids over a wide frequency range, the primary objectives having been to obtain data of reasonable precision in as convenient and simple a form as possible. To achieve these ends, the circuit design has been arranged to achieve adequate precision on a direct rather than substitution balance, unwanted impedances can be neutralized to the extent that they do little or no harm, and the adjustments for balance are so arranged as to be essentially direct reading in both capacitance and conductance of the unknown.

The basic circuits by which these properties are obtained are by no means new, and all that can be claimed for the present work is their development into a tested instrument usable over a wide range of experimental conditions. The first of the characteristic features is the use of a closely coupled transformer with unity turns ratio as equal ratio arms in a Wheatstone bridge circuit, as shown in Fig. 1(a). This scheme was, so far as we know, first described by Starr[1] (hybrid coil method), and has the advantage over the conventional use of matched impedances that, because of the transformer action, any residual impedance or voltage developed across one coil is reflected across the other by the mutual inductance between the pair. By this arrangement, unbalancing effects in the bridge proper are largely neutralized, and, what is even more useful, unwanted admittances[2] which are necessarily associated with the unknown admittance or its connection to the bridge can likewise be made unimportant.

A typical unknown is indicated schematically in Fig. 1(b) as a three-terminal test condenser comprising test electrodes *D* and *R* and a guard electrode *E*, the latter to be maintained at the potential of *D* in order to prevent surface leakage and, if desired, provide a better defined geometric capacitance between *D* and *E*. The admittance between *E* and *R* ordinarily affects the balance conditions, however connected, and must be accounted for by a second balance with a different connection to the bridge.[3] In the present circuit, the admittance *ER* is connected to the correspondingly lettered terminals of the bridge in Fig. 1(a) and is across one transformer winding. To the extent that the transformer is ideal, no change occurs in balance conditions because the admittance is electrically reflected across the other winding and the ratio arms remain equal.

The third admittance of the three-terminal unknown, between *D* and the guard electrode *E*, appears across the detector, and hence the only effect is on the sensitivity of the detector. The final result is thus that only the direct admittance between *D* and *R* affects the bridge balance. The capacitance and leakage of necessary leads from the unknown to the bridge can also be taken care of in the same way by employing coaxial shielded leads from electrodes *D* and *R*, the shields being connected to point *E* (normally grounded). The cables, to the extent that they can be regarded as simple two-terminal admittances, then are connected across either the ratio arm *ER* or the detector, with the effects already described. The guard compensation effect was apparently first employed by Young[4] in a bridge designed for measurement of small vacuum tube interelectrode admittances with a working frequency of 465 kc/sec.

---

* This paper is based in part on a portion of the thesis submitted by P. M. Gross, Jr., in partial fulfillment of the requirements for the degree of Doctor of Philosophy in the Graduate School of Brown University, October, 1948.

** Present address: University of Virginia, University, Virginia.

[1] A. T. Starr, Wireless Eng. and Exptl. Wireless, 9, 615 (1932). See also B. Hague, *A. C. Bridge Methods* (Pitman Publishing Corporation, London, 1945), 5th Ed..

[2] In this paper, we describe an electrical property as an admittance rather than its reciprocal, impedance, whenever this is more simple and natural.

[3] See, for example, L. Hartshorn, *Radio Frequency Measurements by Bridge and Resonance Methods* (John Wiley & Sons, New York, 1941).

[4] C. H. Young, Bell Lab. Record 24, 433 (1946).

For dielectrics and electrolytic systems, the measures of admittance are most conveniently made capacitance and either conductance or dissipation factor. Suitable variable standards of capacitance are a relatively minor problem, but measurement of the dissipation components with convenience and accuracy has long been a serious measurement problem, particularly at radio frequencies. For the present bridge, a conductance shifter circuit has been developed on the basis of an arrangement in the vacuum tube bridge mentioned above.[4] Young does not describe the conductance circuit used by him in detail, but it was apparently not designed for precision measurement or for use at more than one frequency (465 kc/sec.).

The basic scheme from which our conductance network was evolved is shown in Fig. 1(c). The three terminal wye network is connected across the standard and unknown arms of Fig. 1(a). The conductance G sets the range of conductance unbalance between these arms which can be effected by shifting the tap on a low resistance divider between points L and R. The use of the divider thus splits the conductance G into two variable parts, one across each bridge arm. If the tap is moved to the left, the conductance across LD increases while that across RD decreases, the variation of conductance being nearly linear if the product of the total divider resistance $2r_0$ and conductance G is sufficiently small compared to unity. The range of conductance change which can be produced to compensate an unknown equivalent parallel conductance in the right arm is evidently the value of the conductance G, which can be chosen within quite broad limits to give desired ranges.

The advantages of this conductance shifter are: it is essentially direct reading in conductance; its range can be simply changed; the major residual errors are small and quite simply investigated. The nature and magnitude of residual errors in both this network and in the ratio arms must, of course, be considered, as is done in the next section and in Section III.

II. RATIO ARMS

A. Design Considerations

The compensation by inductive coupling of admittances or induced voltages across one coil of a transformer used for ratio arms is perfect only when the transformer is ideal, i.e., when the two coils are identical with unity coupling and no losses. As discussed below, matching of the two coils to better than 0.1 percent is readily possible, and the discussion here is confined to the effects of imperfect coupling and losses.

As is well known, inductances in general and mutual inductances in particular are in practice far from ideal, owing to distributed capacitances and dissipative losses resulting from skin effect, core losses, dielectric leakage, etc., as well as ohmic resistance. The effects are not accurately described by any simple equivalent circuit containing only fixed, simple impedances, but a sufficient approximation to the properties of coupled ratio arms for this discussion is shown in Fig. 2. The coils are represented by an inductance L and resistance r in series, and a common mutual inductance M. Distributed capacitances are represented by the admittances y_1 and y_2 across L and r, which can also represent any other shunting admittances, such as guard to ground admittance of an unknown. If y_1 and y_2 are not equal, the point E will not be the electrical midpoint between points L and R and the admittances Y_L and Y_R in the standard and unknown arms must be different if the bridge is to balance (potential of D equal to that of E).

The effect of dissipation ($r>0$) and imperfect coupling ($M<L$) is conveniently expressed by the difference between Y_L and Y_R necessary to obtain balance. Letting $Y_L-Y_R=\Delta Y$ and $\frac{1}{2}(Y_L+Y_R)=Y$, we obtain by standard methods the result in complex notation that at balance

$$\frac{\Delta Y}{Y}=(y_1-y_2)\frac{r+j\omega(L-M)}{1+\frac{1}{2}(y_1+y_2)[(r+j\omega(L-M)]}, \quad (1)$$

if the approximation is made that $L+M=2M$, i.e., the coupling is good, but not so good that the difference $L-M$ can be neglected.

At sufficiently low frequencies, distributed capacitance is unimportant and only resistive unbalance of the shunting admittances y need be considered. If $y_1-y_2=1/r'$ and the second term of the denominator in Eq. (1) can be dropped, we obtain

$$\Delta Y/Y=r/r'+j\omega[(L-M)/r']. \quad (2)$$

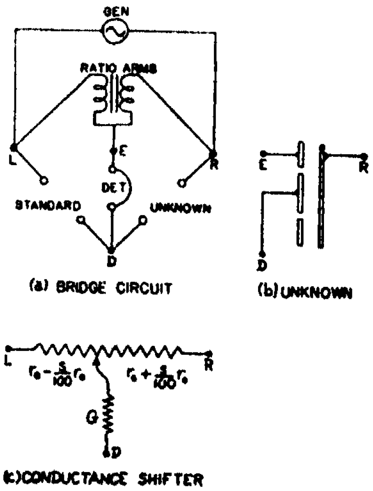

(a) BRIDGE CIRCUIT (b) UNKNOWN

(c) CONDUCTANCE SHIFTER

FIG. 1. Basic bridge circuits.

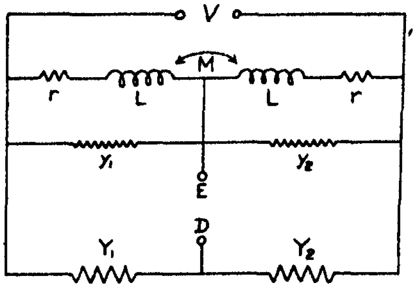

FIG. 2. Equivalent circuit of ratio arms and balancing admittances.

If the unknown admittance Y_R is a pure conductance G and the balance error ΔY is written as $\Delta G+j\omega\Delta C$, we obtain from Eq. (2) the two conditions

$$\begin{aligned}\Delta G/G&=-r/r',\\ \Delta C&=-(L-M)G/r',\end{aligned}\tag{3}$$

the assumption being made that $\omega C\ll G$ and hence $Y\cong G$. These results can be conveniently used to verify experimentally the adequacy of the equivalent circuit of Fig. 2, as shunting one ratio arm by a known resistance r' should require conductance and capacitance changes independent of frequency, the former only to the extent that the equivalent coil resistance is independent of frequency. This has been found true at audiofrequencies for suitable ratio arms, except that the conductance change ΔG increased slowly with frequency, as would be expected because of non-ohmic losses.

At high frequencies, a capacitative shunt admittance has the most serious unbalancing effect on the ratio arms. Consider a difference of shunting admittance given by $y_1-y_2=j\omega C'$ and assume that the unknown is primarily capacitative so that to a sufficient approximation $Y=j\omega C$. Then the balance errors are from Eq. (1) given by

$$\begin{aligned}\Delta G&=-\omega^2rCC',\\ \Delta C&=-\omega^2(L-M)CC',\end{aligned}\tag{4}$$

the second term in the denominator of Eq. (1) again being neglected.[5] The coil resistance r at high frequencies increases with frequency roughly as a fractional power of the frequency. The conductance error ΔG will thus increase somewhat more rapidly than frequency squared, and the capacitance error roughly as the square of frequency. These conclusions have been verified at radiofrequencies by placing a fixed condenser across one ratio arm, with results consistent with Eqs. (4).

B. Construction and Performance

A number of ratio arms have been wound, and the details of three of these, which together cover the range 50 c.p.s. to 5 mc/sec., are given in Table I. The use of several pairs of ratio arms for the entire range of frequencies simplifies design, although it might be possible to wind a single pair of coils sufficiently well balanced and of sufficient inductance.

For the lowest frequencies (50 c/sec. to 20 kc/sec.), the core of a small audio transformer was used. The final winding was balanced to less than 0.05 percent by removing two turns from one coil and adding about 0.07-ohm resistance to this coil. The values of equivalent series resistance r at 1 kc/sec. and the inductance coupling defect $L-M$ were determined from Eqs. (3) as described in Section II-A. The self-inductance of either coil was estimated from its impedance variation with frequency and voltage resonance. At the low frequencies for which this pair of ratio arms is intended, distributed capacitance effects are not important, and

TABLE I. Constants of inductively coupled ratio arms.

Ratio arms, range	Form	Winding	$L(\mu h)$	$C(\mu\mu f)$	r(ohms)	$(L-M)(\mu h)$
A. 50 c.p.s.–20 kc/sec.	Laminated iron core. Winding space, 1.6 cm square by 0.7 cm deep	250 turns each coil, No. 30 dcc wire, wound in opposite directions from center top	4300 (1 kc/sec.)		5.9 (1 kc/sec.)	17
B. 5 kc/sec.–500 kc/sec.	Toroidal dust core. 4.0 cm I.D., 1.4 cm wide, 0.45 cm thick	220 turns each coil, No. 24 enamel wire, wound as a pair in two layers	200	1500	0.8 (10 kc/sec.) 1.0 (200 kc/sec.) 3.4 (500 kc/sec.)	1.8
C. 200 kc/sec.–5 mc/sec.	Toroidal dust core 1.2 cm I.D., 0.7 cm diameter section	30 turns each coil, No. 26 dcc wire wound as a pair in one layer	7.3	45	1.0 (1 mc/sec.)	0.54

---

[5] This approximation is not necessarily a good one if both shunt admittances, y_1 and y_2, are large. If, for example, these y's are capacitative, a resonance denominator of the form $(1-\omega^2(L-M)C)$ results. Equations (4) must therefore be used with some caution.

no attempt was made to estimate the equivalent shunt capacitance.

The ratio arms for the frequency range 5 kc/sec. to 500 kc/sec. were made by winding a pair of wires in two complete layers on a toroidal powdered iron core, the turns and dimensions being as indicated. The equivalent circuit parameters r and $L-M$ were obtained by the effect on bridge balance of unbalanced capacitance across one coil and use of Eqs. (4). The self-inductance L and shunt capacitance C were estimated by voltage resonance with and without an added known capacitance in parallel. The large value of 1500 μμf for C may seem surprising, but it is to be expected from the method of winding which puts turns with a large potential difference in close proximity. The unbalance of the two coils was found to be less than 0.02 percent without adjustment. Two remarkable features of such toroidal windings in practice are the closeness of balance obtained if the coils are wound as a pair, and the fact that considerable maltreatment by displacing and squeezing turns makes only trivial, barely measurable changes.

The ratio arms for the range 200 kc/sec. to 5 mc/sec. are a small scale version of the second coil already described, with a smaller form and fewer turns. The initial balance was off less than 0.2 percent up to 5 mc/sec. The parameters r, $L-M$, and L were determined in the same way as for the preceding ratio arms but at higher frequencies as indicated in Table I. This coil is the least satisfactory of the three, as its coupling is decidedly poorer, and it cannot be used as generally to compensate guard and lead capacitances as can the other two at lower frequencies. This type of use is, however, increasingly academic at frequencies much above 1 mc/sec. because of distributed impedances in connections to an unknown.

Examples of the accuracy to which the ratio arms can be balanced have already been cited, and it remains to illustrate the effectiveness of compensation for unbalanced admittances across these arms. Representative data for each of the ratio arms described in Table I are given in Table II. In this table are listed the changes in conductance ΔG and capacitance ΔC which are necessary to rebalance the bridge after shunting one ratio arm with the impedance stated. These changes, of course, depend upon the admittances in the standard and unknown arms, and these are also stated. The calculated unbalance values were computed from Eq. (1) using these initial values of G and C and the values of the ratio arm resistance r and uncoupled inductance $L-M$ given in Table I.

The effectiveness of the ratio arms in minimizing undesired unbalance from guard or lead admittances across one coil is evident from Table II. At 200 kc, for example, a capacitance of 1000 μμf so placed changes the balance for a direct capacitance one-third as large by less than 1 μμf (<0.3 percent). The compensation is least effective at the highest frequencies, owing to the relatively larger uncoupled inductance of ratio arms C. The conductance unbalance for a shunt of 1000 ohms is even at 2.5 mc/sec. about one-thirtieth what it would be if this resistance were placed in one of the working arms of the bridge.

TABLE II. Effect on bridge balance of shunting one ratio arm.

Ratio arms, frequency	Ratio arm shunt	Initial admittance G(μmho)	Initial admittance C(μμf)	Admittance unbalance ΔG(μmho) Obs.	Admittance unbalance ΔG(μmho) Calc.	Admittance unbalance ΔC(μμf) Obs.	Admittance unbalance ΔC(μμf) Calc.
A, 100 c/sec.	1000 ohms	0.5	300	0.0031	0.0027	1.9	1.6
	1000 μμf	50	300	<0.001	6×10^{-7}	0.3	0.25
A, 5 kc/sec.	100 ohms	0.5	300	0.027	0.035	19.2	18
	1000 μμf	0.5	300	0.0021	0.0018	<0.05	0.006
B, 5 kc/sec.	100 ohms	5.0	300	0.040	0.036	2.9	2.5
	1000 μμf	5.0	300	<0.001	3×10^{-4}	<0.05	0.005
B, 200 kc/sec.	100 ohms	50	300	6.6	7.1	2.5	4.0
	1000 μμf	50	300	0.62	0.7	0.6	0.9
C, 200 kc/sec.	100 ohms	50	300	2.04	2.0	2.4	2.6
	1000 μμf	50	300	0.12	0.43	0.16	0.20
C, 2.5 mc/sec.	1000 ohms	50	10	1.2	1.3	0.05	0.03
	1000 ohms	50	300	34	38	0.50	0.3
	50 μμf	50	300	3.0	4.0	1.8	1.9

An equally interesting result is the generally good agreement between observed and computed unbalances, which gives one confidence in the use of the simple equivalent circuit of Fig. 2 and of the unbalance expression, Eq. (1), to predict the effect of residual impedances on measurements.

III. CONDUCTANCE SHIFTER NETWORK

This circuit is subject to a number of limitations, the more important of which are a non-linear scale for too large values of the range conductance G, failure of this element to be a pure conductance of constant value, and residual effects causing the tapped low resistance not to act as a simple divider at high frequencies.

A. Non-Linearity

If the divider is made up of resistances so as to give a linear change of resistance with tap setting,

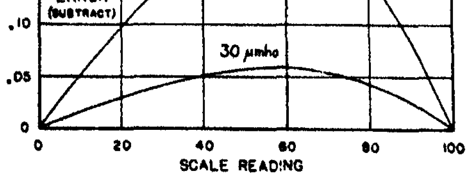

FIG. 3. Corrections for non-linearity of conductance shifter network in 100- and 30-μmho ranges. The scale error is referred to a full scale reading of 100 divisions.

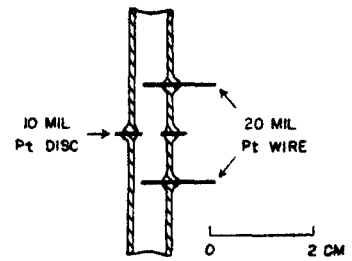

FIG. 4. Vertical section of electrolytic cell for conductance network tests. The body of the cell is 10 mm o.d. tubing. Cell constant approximately 10 cm^{-1}.

the resistances to left and right of the tap in Fig. 1 can be expressed as $r_0 - r_0(s/100)$ and $r_0 + r_0(s/100)$, where the setting s varies from 0 to 100. The equivalent conductances thrown across the standard and unknown arms are readily shown from the wye-delta-transformation[6] to be

$$G_L = \tfrac{1}{2}\frac{1+(s/100)}{1+\tfrac{1}{2}Gr_0(1-(s/100)^2)}G,$$

$$G_R = \tfrac{1}{2}\frac{1-(s/100)}{1+\tfrac{1}{2}Gr_0(1-(s/100)^2)}G.$$

The conductance difference for a given s is then

$$G_L - G_R = \frac{1}{1+\tfrac{1}{2}Gr_0(1-(s/100)^2)}(s/100)G. \quad (5)$$

If the product $\tfrac{1}{2}Gr_0$ is neglected, this reduces to

$$G_L - G_R = (s/100)G, \quad (6)$$

and the conductance difference is linear with setting s of the resistance divider, the range being from zero to G.

The departure from linearity increases with the value of the product Gr_0. In the present circuit $r_0 = 100$ ohms, and the largest value of G used is 100 μmho, whence $Gr_0 = 0.01$. From Eq. (5), the maximum absolute error in G is 0.19 μmho at a setting of 57 μmho and the maximum fractional error 0.5 percent at small settings.

This non-linearity becomes negligible for sufficiently small values of G (10 μmho or less for less than 0.05 percent error) and the small correction for somewhat larger values of G is simple to make. The procedure adopted by us has been to calculate and plot a series of differences to be subtracted from observed readings so that the corrected reading s_1 gives the actual change in G when used in Eq. (6). The formula for the purpose is readily shown from Eqs. (5), and (6) to be

$$s - s_1 = \frac{(1-(s/100)^2)}{1+\tfrac{1}{2}Gr_0(1-(s/100)^2)}(\tfrac{1}{2}Gr_0).$$

Values of the correction $s - s_1$ as a function of s for the values $r_0 = 100$ ohms, $G = 100$, 30 μmho are plotted in Fig. 3.

B. Effects of Residuals

Neither the range conductance G nor the divider circuit can be assumed to be purely dissipative elements because of their distributed inductance and capacitance. The resistances used for G in our applications exceed 10,000 ohms in value and for such resistances the dominant residual is shunt capacitance. If the divider were a pure resistance, small compared to $1/G$, a change of its setting would merely "split" the capacitance of G in proportion to the setting and a simple correction to the apparent measured capacitance would suffice.

Actually, of course, any divider must have residual impedances. In our case, this divider is made up of constant, low inductance one- and ten-ohm decade resistors, a 100-ohm fixed resistor and a one-ohm slide wire, as shown in Fig. 5. The major residual effect is from the series inductances of these elements, the total series inductance L being about 1.7 μh. Because of the constant inductance feature of the decades, the primary effect of inductance is to increase the total impedance of the divider by the factor $1+(\omega L/2r_0)^2$, where $2r_0$ is the total divider resistance. This factor makes the apparent conductance of the unknown larger than the true value, the error being 2.5 percent at 3 mc/sec. for the values $L = 1.7$ μh, $r_0 = 100$ ohms of the circuit used.

The second important residual limiting the accuracy of the conductance network has been found to be the increase in value of the conductance G at high frequencies. The conductances used by us were Western Electric Type 170,176A deposited carbon resistors. The tests described below indicate that, as stated by the makers, the frequency for a given percentage increase varies inversely with the value of G. For a one percent effect the ratio f/G was found to be 0.07, where f is expressed in mc/sec. and G in μmho, and the error at lower frequencies varied roughly inversely as the frequency. Thus a resistance of 10^4 ohms can be used up to 7 mc/sec. with less than one percent effect, while for a resistance of 10^6 ohms the corresponding limit is 70 kc/sec.

A number of other residuals should be considered: the variation in inductance of the slide wire with setting, skin effect in the divider resistances, incipient LC resonance of the divider inductance and the capacitance of G, and various direct or mutual impedances of connecting leads. Rough calculations for the components used indicated these effects to be unimportant compared with the residuals discussed above. This conclusion was verified by three types of tests, as follows:

---

[6] See, for example, reference 3, p. 128.

(a) Conductances of several ½-watt carbon resistors were measured at several frequencies for each of two or more values of range conductance G. Comparison of these data established the effect of frequency on the values of these conductances.

(b) Conductances of several pairs of ½-watt resistors were measured singly and in parallel. The agreements between the measured and calculated conductance series at frequencies up to 5 mc/sec. established that there were no significant errors depending on slide wire and decade settings.

(c) Conductances of KCl solutions of various concentrations were measured as a function of frequency. This was done using the simple cell shown in Fig. 4, the function of the grounded disk between the platinum electrodes being to eliminate dielectric losses of the glass walls from the direct admittance measurement. On the assumption that ionic relaxation effects were negligible at the frequencies and concentrations used, the measured conductance should be frequency independent. The observed variations were found to be accounted for by a divider inductance of 1.7 μh and the previously found dependence of range conductance value on frequency. This inductance value is in fair agreement with a value of 2.0 μh estimated from manufacturers' specifications for the divider decades and other tests of the slide wire (estimated inductance, 0.07 μh).

The errors in conductance measurements are evidently determined mainly by the frequency dependent values of the range conductance G below about 1 mc. For dielectrics, the effect is conveniently described by errors in the dissipation factor $G/\omega C$, which does not exceed 0.0003 for a capacitance of 100 $\mu\mu$f or more over the range 50 c/sec. to 1 mc/sec. About 1 mc/sec., the divider inductance gives rise to larger errors, the effect amounting to several percent for conductances of the order 100 μmho at 5 mc/sec.

The conductance circuit residuals also cause small errors in capacitance measurement. The first of these is due to the shunt capacitance of the range conductance, which is about 0.8 $\mu\mu$f as the circuit is arranged. The measured capacitance error is not necessarily this great as it is partially compensated by the series divider inductance, which has the effect of a negative shunt capacitance of magnitude approximately given by $(LG/2r_0)$. For the circuit constants employed by us, this compensating capacitance is -0.85 $\mu\mu$f for $G=100$ μmho and on this range thus almost exactly balances the real capacitance of G. This was found experimentally by measuring the capacitances of the electrolytic cell of Fig. 4 for different concentrations of KCl. No dependence of apparent capacitance on conductance setting was observed for the range $G=100$ μmho, as would be true for small dielectric constant changes of the solution and no net capacitance effect of the divider. The apparent capacitances of the smaller range conductances were determined by obvious methods of intercomparison and gave values increasing to 1.1 $\mu\mu$f for the smallest value of G used (0.1 μmho).

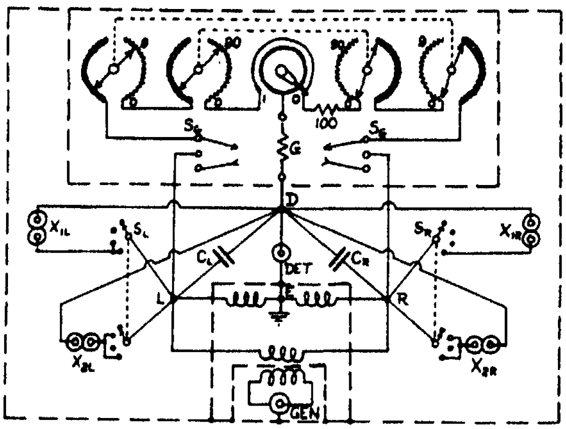

FIG. 5. Schematic wiring diagram of the bridge. Long dashes indicate shielding, short dashes ganged switches.

IV. BRIDGE CONSTRUCTION AND USE

A. Circuit Components and Arrangement

A schematic circuit of a bridge employing the circuits already described is shown in Fig. 5, the components being arranged in roughly the same relative positions as in the instrument. A view of the bridge is shown in Fig. 6. The conductance shifter network is mounted in a shielded box at the top between the precision condensers C_L and C_R, and the coupled ratio arms and input transformer are plugged into a lower box through the door visible in Fig. 6. The switches S_L and S_R connect either of two pairs of external terminals X_L and X_R to twin arms of the bridge. The arrangement of parts has been made as symmetrical as possible.

The divider setting of the conductance network is accomplished by use of ganged pairs of General Radio Type 668 inductance-compensated decade resistance units with ten- and one-ohm steps, and a three-quarter turn slide wire of 26-gauge manganin wire with one-ohm total resistance. The decade resistances are so connected in the two sides of the divider that as one step is removed from one side an equal step is added in the other. A slider on the manganin slide wire makes contact also to an adjacent turn of copper wire connected to the conductance G.

The range conductances G are a set of Western Electric Type D-170176A deposited carbon resistors, chosen for their excellent high frequency characteristics. These conductances, with values of 100, 30, 10, 3, 1, 0.3, 0.1 μmho (10,000 ohms–10 megohms) are mounted on a drum type selector switch, and thus any one of these values can be made the full scale reading of the shifter network. In order to make divider settings from zero to 100 correspond to percent of full scale change, the connections and initial settings of the decades and slide wire are made as shown in Fig. 5. The fixed 100-ohm resistor in the right side is added to make the zero setting of decades and slide wire give the initial balance correctly. The switch S_G interchanges or removes the connections of the divider to the rest of the bridge.

The wiring of the network is made as short and direct as possible to minimize residual impedances, and the inductance of the slide wire has been reduced by running the lead from one end back as a copper strip parallel and close to the manganin wire. The opposing magnetic fields thus partially cancel and the total inductance of the slide wire is reduced to about 0.07 μh, a figure which could probably be improved considerably.

The balancing condensers C_L and C_R are National Type NPW precision condensers with a total capacitance of 650 $\mu\mu$f, which are driven by National micrometer dials. The capacitance change of these condensers is approximately logarithmic with dial setting over 450 $\mu\mu$f of the total range, and a very open scale for balancing small capacitance changes is thus obtained. The necessity for a non-linear calibration chart or graph is the accompanying disadvantage.

In order to avoid the conversion when desired and also provide higher ranges of capacitance and conductance, a supplementary admittance panel has been provided. This contains a 500-$\mu\mu$f variable linear condenser, also driven by a National micrometer dial with 500 divisions, and decades of capacitance and conductance. The former decade (General Radio Type 380-N) provides a total capacitance of 0.01 μf in steps of 0.001 μf and a 500-$\mu\mu$f mica condenser can also be switched. The two conductance decades provide conductance increments up to 0.011 mho in steps of 100 μmho and were assembled from General Radio Type 500 resistors compensated by trimmer condensers for excess inductance.

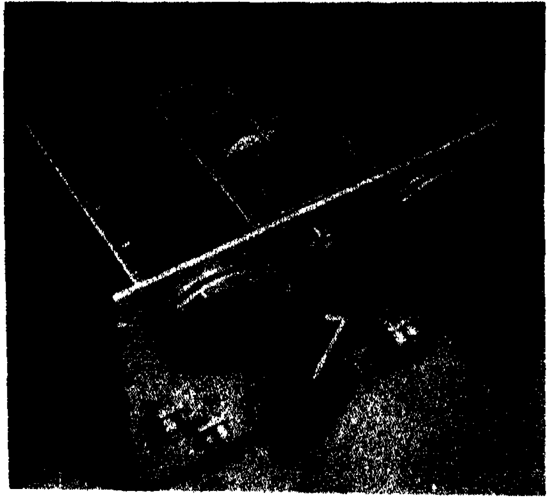

FIG. 6. View of the bridge showing conductance shifter circuit, standard condensers, and panel.

The generators and detectors so far used are conventional. At frequencies below 70 kc/sec. a Hewlett-Packard Type 200 DR oscillator is employed and a General Radio Type 805-C signal generator is used for higher frequencies. A DuMont Type 208B oscillograph preceded by an amplifier with a gain of 65 db and response flat to 100 kc is used at frequencies up to 200 kc. At higher frequencies, the modulated voltage of the signal generator is fed via the bridge to a Type 348-P receiver and the filtered 1000-cycle unbalance output applied to the oscillograph. Either a sweep or signal or modulation frequency can be used for horizontal deflection and the various desired combinations are selected on a switching panel.

Coupling of the generators to the bridge must be done with some care. As the circuit is arranged a balanced voltage about ground is required. This could be induced in the coupled ratio arms by a primary winding on the same core, as has been done by Starr[1] and by Young,[4] but we have preferred to use a separate transformer in order to provide greater flexibility in testing and use of the bridge. In either case, it is important that there be a minimum of electrostatic coupling between windings, as this acts to unbalance the ratio arms by asymmetrical leakage currents flowing from the generator. This effect is not as serious as in conventional bridges because the compensation action of the coupling between the ratio arms is effective for unbalanced voltages as well as admittances, as noted by Young.[4] As a result it has been found possible to use standard bridge transformers (General Radio) up to about one megacycle without appreciable error. At higher frequencies, however, small leakage capacitance and conductance between the windings can cause serious error. To minimize this effect, a special transformer, similar to one described by Field and Easton[7] was made with a carefully overlapped and insulated shield between windings. The leakage capacitance can be estimated from the change in bridge balance on reversing the connections of the primary winding to the generator and ground and was found to be of the order 0.01 $\mu\mu$f. With this small a value, the transformer works satisfactorily to 10 megacycles.

Another effect which must be considered carefully in the bridge design is that of direct coupling between the generator and detector either by induction or a common impedance. This is particularly true in the present circuit, as it is intended for measurement by direct balance, rather than by substitution balances which would minimize such effects. They have been reduced to negligible importance for frequencies up to several megacycles in the present circuit by suitable disposition of leads and grounds and use of coaxial leads.

---

[7] R. F. Field and I. G. Easton, General Radio Experimenter 21, No. 11, (April, 1947).

B. Accuracy

The effects of residuals in the ratio arm and conductance circuits have been considered and it remains to discuss the accuracy at intermediate frequencies for which they are not important. The standard condensers used can be set consistently to one-tenth division out of five hundred total, which because of the roughly logarithmic scale permits an internal consistency of 0.1 percent or better for capacitances larger than 50 $\mu\mu$f, the range being 650 $\mu\mu$f. These figures are characteristic more of the condenser and drive than of the rest of the bridge.

The precision and reproducibility of settings of the conductance is often of the order 0.02 percent, but the accuracy is not as good. The main source of error is the temperature coefficient of about 0.03 percent/°C, which results in an apparent conductance difference of 0.3 percent for 10°C change in ambient temperature. A better performance in this respect might well be secured but some sacrifice has been tolerated in the present design in order to have the good high frequency properties of these resistors. A smaller but comparable source of error is in the lack of consistency of the divider resistance decades. The accuracy of these was found to be better than the tolerances of ±0.1 percent (10-ohm steps) and ±0.25 percent (1-ohm steps) quoted by the makers, and an error of not more than 0.1 percent results. Contact resistances of the decade switches cause variations of the order of 0.02 percent at most with reasonable attention to their cleanliness. (It is worth noting that the slide wire contact, an annoying source of noise in some bridge circuits, causes virtually no trouble here, as its resistance is in series with a resistance of at least 10,000 ohms.)

C. Measuring Cells

The bridge circuit as described has been developed and used primarily for studies of dielectrics and electrolytes. For such systems, the advantage of direct reading scales of both capacity and conductance together with elimination of separate balances and corrections for guard circuit and lead effects have proved very desirable. As the circuit is arranged, the direct admittance between the ungrounded terminals of a three-terminal admittance is measured. This value is not necessarily the same one obtained by a grounded point measurement in the case of a two terminal admittance, but it is the desired one in most designs of cells with guard rings, and the variety of such designs in the literature can be used simply with the present circuit.

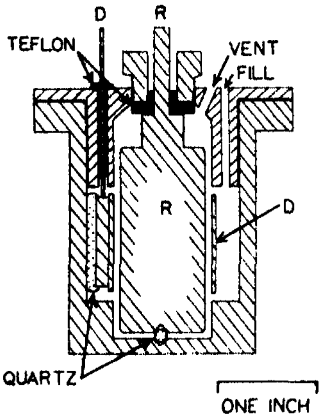

FIG. 7. Dielectric constant cell for liquids, $C_0 = 10$ $\mu\mu$f.

An example of a convenient cell for dielectric constants of liquids is shown in Fig. 7, this particular cell having been made for a study of dielectric constants of hydrogen peroxide-water solutions.[8] The central rod R is connected to terminal R of the bridge and insulated by washers of Teflon from the grounded case. Coaxial with this electrode is the guarded electrode D in the form of a tube with three raised axial slots on its outer surface. The tube is supported and insulated from the body of the cell by quartz rods sprung into the gap and positioned by the slots.[9] Capacitances in air of from 1 to 10 $\mu\mu$f are easily obtained by choice of central electrode diameter, a range readily extended in either direction by change in dimensions. This particular cell was made of stainless steel and electrolytically polished to prevent decomposition of the solutions studied.

It is important that the design of the cell should be such that there is no insulation other than air or the liquid dielectric between the high potential and guarded electrodes. With this arrangement and the guard compensation effect of the bridge, the desired dielectric constant of the sample is merely the ratio of measured capacitances when filled and empty. The specific conductance is also directly obtained from the observed conductance, as the conventional cell constant k defined in electrolytic conductance work is determined from the air capacitance C_0 by the relation

$$k\ (\text{cm}^{-1}) = 0.0885/C_0\ (\mu\mu\text{f}).$$

D. Other Applications

The bridge as described is naturally adapted to studies of dielectrics and electrolytes, but its characteristic features may well be useful for other purposes. Considerable simplification of measurement and reduction of data should be possible in systems for which guard circuits are necessary or desirable. The cancellation of lead effects might well prove valuable when leads must be subjected to unknown displacements which would otherwise cause errors, as in work at pressures other than atmospheric. The simplicity of the basic circuits and their use makes them adaptable to course demonstrations and experiments, and the compensation effect of the ratio arms is an interesting application of electromagnetic induction.

---

[8] To be submitted to the J. Am. Chem. Soc.

[9] We are indebted to Dr. P. M. Gross of Duke University for suggesting this scheme.

THE REVIEW OF SCIENTIFIC INSTRUMENTS VOLUME 20, NUMBER 4 APRIL, 1949

An Interferometric Study of Supersonic Channel Flow*

DANIEL BERSHADER
Palmer Physical Laboratory, Princeton University, Princeton, New Jersey

(Received December 14, 1948)

The Zehnder-Mach interferometer has been applied to the study of supersonic flow of air expanding from a pressure tank into the atmosphere through channels of rectangular cross section. This was made possible by using plane-parallel glass plates for a pair of opposite walls of the channel. Two such channels were used, each about one centimeter in width and two centimeters in depth, one being a divergent channel (half-angle$=4.0°$) and the other a Laval nozzle constructed by the "characteristics" method for $M=1.7$. It was found possible to measure the density distribution with a rather small estimated probable error (two percent or less). Knowledge of the stagnation temperature and pressure made it possible also to compute pressure, temperature, and velocity. Results obtained for the potential flow agree, for the most part, within one percent with the well-known theory of isentropic channel flow. The interferometric technique has been used also as a guide in improving the Laval nozzle, giving quantitative data on the inhomogeneities resulting from small errors in construction. Further quantitative data was obtained on the degree of non-uniformity of the flow in the throat regions of both channels. The boundary layers, which reach a thickness of about ten percent of the channel width near the orifice of the Laval Nozzle, introduce further accuracy problems into the study of channel flow by interferometry. These are taken up in some detail. Some of the considerations here will also apply to the interferometric analysis of flow in larger supersonic wind tunnels whose working sections are essentially channels of rectangular cross section.

I. INTRODUCTION

THE equations of isentropic expansion of a gas from a storage chamber through a convergent-divergent type nozzle into a receiver provide for a flow regime in which the gas moves with subsonic speed in the convergent portion, sonic speed at the throat, and supersonic speed in the divergent part.[1] The compressibility effects associated with the higher subsonic and especially the supersonic flows produce corresponding changes in the refractive index of the gas stream. It is then that optical methods become a powerful tool in flow analysis.

Early in the present century, the German physicists, Prandtl[2] and Meyer,[3] as well as Magin,[4] constructed channels (or nozzles) of the convergent-divergent type and of rectangular cross section in which a pair of opposite walls consisted of plane-parallel glass plates. By means of Toepler's striation ("schlieren") method,[5] they demonstrated the difference in nature of the flow downstream of the throat. This region was found to contain a pattern of stationary waves (Fig. 1) similar to those first observed by E. Mach in his studies on bullet flight and which are now known as Mach lines or Mach waves. The angle α between the Mach line and streamline at any point is simply related to the Mach number of the flow at that point by

$$M=\csc\alpha. \qquad (1)$$

The quantitative feature of these early experiments consisted in calculating the Mach numbers from angle measurements by means of the above equation.

Similar to the channels employed in the above-mentioned investigations, those used in the present study, also have rectangular cross sections and plane-parallel glass plates for one pair of walls. However, a method of optical analysis has been applied which is superior to others for accurate,

---

[*] Extract from dissertation *Interferometric Analysis of Supersonic Flow through Rectangular Channels at Mach Number 1.7*, presented to the Faculty of Princeton University in candidacy for the degree of Doctor of Philosophy, May, 1948.

[1] [a] G. I. Taylor and J. W. Maccoll, *The Mechanics of Compressible Fluids, Aerodynamic Theory* (Ed. by Durand Reprinting Committee, Pasadena, 1943), pp. 222–227.

[b] H. W. Liepmann and A. E. Puckett, *Aerodynamics of a Compressible Fluid* (John Wiley and Sons, Inc., New York, 1947), pp. 23–28.

[2] L. Prandtl, "Neue Untersuchungen über die strömende Bewegung der Gase und Dämpfe," Physik. Zeits. **8**, 23–30 (1907).

[3] T. Meyer, "Ueber zweidimensionale Bewegungsvorgänge in einem Gas, das mit Ueberschallgeschwindigkeit strömt," Mitteilungen über Forschungsarbeiten auf dem Gebiet des Ingenieurwesens **62**, 31–67 (1908).

[4] E. Magin, "Optische Untersuchung über den Ausfluss von Luft durch eine Lavaldüse," Mitteilungen über Forschungsarbeiten auf dem Gebiete des Ingenieurwesens **62**, 1–31 (1908).

[5] H. Schardin, "Das Toeplersche Schlierenverfahren," Forschungsheft 367, 5 (1934).

quantitative work—namely, interferometry. In this method establishment of the gas flow changes the optical path of one of two interfering light beams and produces a measurable shift in the previously adjusted interference fringe pattern. Values of density may be directly obtained from these fringe shifts. The interferometer used for studies in gas dynamics is the Zehnder-Mach type, named after the men who first developed instruments of this type in order to study problems in ballistics. A comprehensive bibliography on the instrument and its application to gas dynamics may be found in the paper of J. Winckler.[6]

The systematic study in this country of high speed gas flow by interferometry began at Princeton in 1943 with the program started by Professor R. Ladenburg. He suggested the present problem and the work was performed under his direction.** This paper is concerned firstly with establishing by experiment the validity of the application of interferometry to "enclosed flows" as represented by flow in a rectangular channel, and secondly with some useful information obtainable by the method.

II. APPARATUS AND EXPERIMENTAL PROCEDURE

A. Apparatus

The two channels used will be characterized by the names "divergent channel" and "Laval nozzle," the latter in honor of the Swedish engineer, de Laval, who made investigations of the flow of steam through nozzles. The channels are open at the downstream end so that the gas discharges into the atmosphere. For the divergent channel the supersonic section contains two plane steel walls, each making an angle of 4.0° with the axial plane of symmetry; in the Laval nozzle the walls, after an initial widening immediately following the throat, become parallel in such a way as to produce a uniform flow with constant Mach number and zero pressure gradient. The contours are shown in Fig. 2 while Table I gives the pertinent dimensions. The dimensions of the divergent channel are practically identical with those of Magin's channel.[4] The design of the Laval nozzle will be discussed in IV.

FIG. 1. Typical schlieren photo of channel showing Mach lines.

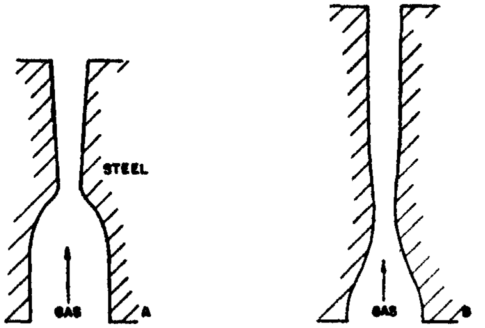

FIG. 2. Channel contours. A—divergent channel; B—Laval nozzle.

The assembled channel, ready for mounting on the pressure tank, is shown in Fig. 3. It is seen that the glass walls extend beyond the orifice of the channel proper. The design*** is such that the contact between the glass and steel walls is made air-tight by squeezing a rubber gasket which surrounds the glass plate, thus avoiding undesirable pressure on the glass by metal parts. If the junction is not air-tight, disturbances in the flow pattern are visible (see Fig. 4).

The position of the channel with respect to other components of the interferometer assembly is shown in Fig. 5. Notice the presence of a compensating chamber in the path of the second beam. This contains glass plates of thickness identical with that of the glass channel walls. All four pieces were cut

TABLE I. Channel dimensions in mm.

	Divergent	Laval
Orifice width	12.75	10.50
Throat width	7.33	7.65
Area ratio (orifice-throat)	1.739	1.372
Depth	19.05	19.05
Throat-orifice length	40.6	66.0

---

[6] J. Winckler, "The Mach interferometer applied to studying an axially symmetric supersonic air jet," Rev. Sci. Inst. 19, 307–322 (1948).

** This research was sponsored by the ONR, Contract N-7ONR-399.

*** Dr. J. Winckler was instrumental in designing this mounting apparatus for the channel.

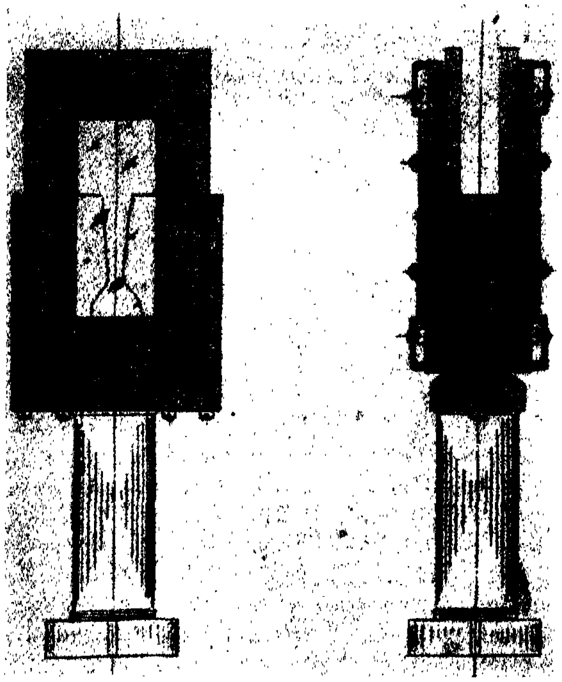

FIG. 3.

out of one ground and polished plate and installed in such an orientation with respect to each other as to minimize any inhomogeneities. Atmospheric conditions prevailed inside the chamber at all times during the present experiments.

The lens L-1 makes the light parallel before it enters the interferometer while the lens L-2 serves as a camera objective to focus the center of the channel on a photographic plate (not shown). The light source is a magnesium spark of about one microsecond in duration. A pressure switch causes the spark to flash at any desired pressure up to 100 lbs. above atmospheric. The photographic plates used were the Eastman 103-0 series, which are sufficiently sensitive in the region of the magnesium blue line, $\lambda = 4481$A, chosen by the monochromator. The interferograms were taken at a magnification of unity. The interferometer plates, on loan from Dr. R. B. Kennard, are the same ones used by Winckler[6] and by Ladenburg *et al.*[7] Further details on the interferometer and associated instrumentation may be found in these papers.

Since the interferometer plates were smaller than the region to be studied, it was necessary to take three pictures of different sections in order to include the whole of the supersonic portion of the divergent channel while for the Laval nozzle four pictures were required. Brass spacers were used to vary the position of the channel assembly with respect to the interferometer plates and thus to determine the section to be photographed. The spacer fits inside the lead-in tube of the channel until it comes up against a shoulder. This shoulder, the spacer, and the outlet-tube all have the same diameter so that the lead-in tube of the channel slides over the outlet tube of the pressure tank up to this shoulder or up to the bottom of one of the spacers. The lower part of the lead-in tube is threaded and accommodates a specially designed nut in such a way that as the latter is tightened, pressure is exerted on a rubber gasket preventing any sliding of one tube around the other. To solve the problem of aligning interferograms of different sections, wires (*w*-1, *w*-2, etc., in Fig. 5) were waxed to the outside of the glass in the overlap regions as reference marks for the fringe shift evaluation. These wires were set at slight angles with the horizontal to avoid the possibility of their being completely covered by one dark interference fringe.

B. Experimental Procedure

For adjustment of the optics, the green line, $\lambda = 5461$A, obtained from a mercury arc and filter was used. Horizontal fringes were established and adjusted to a width of 1.00 mm as a convenient separation. (The magnesium fringes would, of course, be closer together in the ratio 4481:5461.) This careful adjustment of the fringe width is important because only under these circumstances is it possible to align photographs of the different sections. Also important is the stability of the fringe system, for any changes in the pattern be-

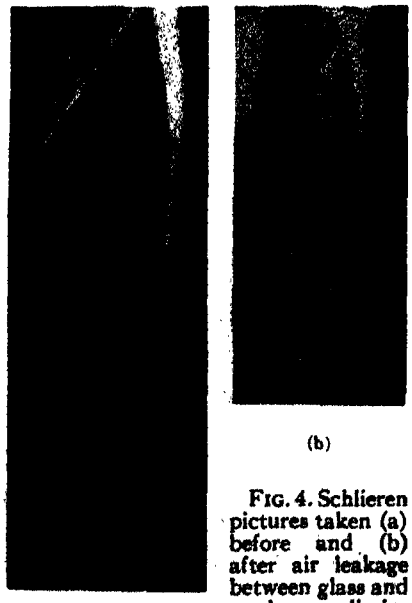

(b)

(a)

FIG. 4. Schlieren pictures taken (a) before and (b) after air leakage between glass and steel was eliminated.

---

[7] R. Ladenburg, J. Winckler, and C. C. Van Voorhis, "Interferometric studies of faster than sound phenomena. Part I. The gas flow around various objects in a free, homogeneous, supersonic air stream," Phys. Rev. 73, 1359–1377 (1948).

tween the time of adjustment and the time the picture is taken are undesirable.

First a photograph is taken of the stationary fringe pattern, quickly followed by a picture taken with air flowing. In some of the later experiments, a final photograph of the stationary fringes was made. Atmospheric pressure and temperature were recorded, as well as the temperature of the air in the tank.

Following the photography of the orifice section, the channel assembly had to be removed and a spacer added. The assembly was put back into place, the fringes again adjusted and the photography procedure repeated for the mid-section, and so on.

C. Evaluation Method

Atmospheric density prevails in the whole channel before the flow, while during the flow a density distribution exists which is, in general, different from atmospheric. If the direction of the light be z and the coordinates in a plane perpendicular to z are denoted by x and y, then in the case that the index of refraction n depends only on x and y, the fringe shift $S(x, y)$ is easily converted to the density $\rho(x, y)$. For if D is the distance between the glass walls, the index of refraction corresponding to a fringe shift S is

$$n = n_a + (S\lambda/D), \qquad (2)$$

where n_a is the index prevailing before the flow. (This assumes, of course, that the optical path through the compensating chamber remain constant in the meantime.) The relation between refractive index and density is given by the Gladstone-Dale formula

$$n - 1 = K\rho, \qquad (3)$$

where K is a constant over a large range of pressures for a given wave-length and a given gas. To get ρ from S, one may combine the two above equations:

$$\rho = \rho_a + (S\lambda/KD), \qquad (4)$$

ρ_a being the density in the channel when the stationary-fringe picture is taken (atmospheric density in the present experiments).

FIG. 5. Optical assembly.

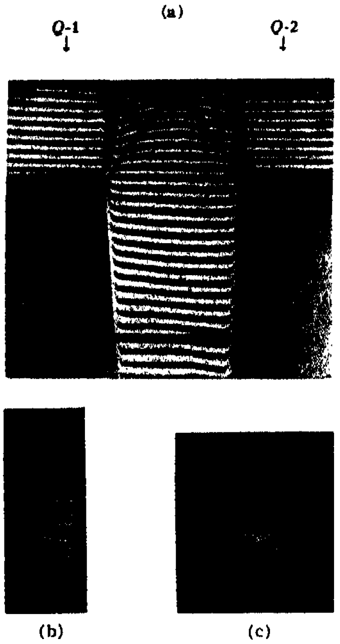

(b) (c)

FIG. 6. Interferograms of (a) orifice section, (b) mid-section, and (c) throat section of divergent channel at $P_0 = 5$ atmospheres.

The interferograms were analyzed by numbering the fringes and measuring their positions with the aid of a comparator. A typical interferogram of the orifice section is shown in Fig. 6a. One of its features is the presence of undisturbed fringes in the regions labeled Q-1 and Q-2, The positions of corresponding fringes in the Q regions of the stationary and flow pictures were carefully compared as were the fringe positions in the overlap regions of the photographs of adjacent sections. When the necessary alignment corrections were made, the whole set of displaced fringes had been numbered and positioned from above the orifice to below the throat as if it were all on one interferogram. It was then possible to assign an undisplaced-fringe number to the position of each displaced fringe and so to obtain the fringe shift S.

D. Auxiliary Experimental Techniques

Additional valuable information was obtained from shadow and schlieren photography as well as from what may be called dynamic interferometry. The former two methods have been well known for some time,[8] and will not be discussed here except to recall that while interferometry measures the density, the photographic effects in schlieren are sensitive to the density gradient in a direction normal to the knife edge whereas the effects in shadow photography are concerned with the second derivative of the density.

---

[8] F. J. Weyl, *Analytical Methods in the Optical Examination of Supersonic Flow* (Navord Report 211–45, December 1945)

The technique of "dynamic interferometry"**** employs a camera with moving film in order to get a continuous record of fringe shifts. A picture of the camera used is shown in Fig. 7. Vertical fringes are focused on the horizontal slit so that each fringe is represented by a point on the film. As the film moves in a vertical direction past the slit, this point will trace a line on the film, the line curving when the fringe begins to shift. Following previous calibration with monochromatic fringes, an intense white light filament source was used and the shift of the central fringe measured. A spark source of light was also focused on the slit and made to flash at a desired tank pressure, marking the place on the film where the fringe shift was to be measured. A moving film trace showing the white light fringes shifting is seen in Fig. 8.

III. ACCURACY OF THE INTERFEROMETRIC METHOD

A. Sources of Error

The errors in the present experiment have been placed rather arbitrarily into four categories which are listed in Table II.

1. *Instrumentation Errors*

The atmospheric pressure and temperature were measured with a mercury barometer and thermometer, respectively, to a high degree of accuracy. The tank pressure P_0 was read to within 0.3 percent (at 60 pounds overpressure) from a gauge which had been cross-checked with other gauges. The tank temperature was taken to be the same as the atmospheric temperature. Later studies with a thermocouple revealed that this might give a value that was too high by one or two degrees, due to efflux of air between the time of the temperature reading and the flash of the spark.

FIG. 7. General radio continuous recording camera.

2. *Miscellaneous Errors*

Considered here was the possible existence of any deviations from steady-state conditions caused by transients, slowly shifting fringes, or oscillations. The only deviation from a truly stationary flow pattern appeared to be a small oscillation of the density about some equilibrium value with a rough periodicity of about 200 microseconds. This is 200 times as long as the duration of the magnesium spark—too long, therefore, to interfere with the sharpness of the photographs. Observation of the moving film record (Fig. 8) shows that the amplitude of these oscillations varies, reaching a maximum of 0.5 fringe. (In all of the present work, a shift of one fringe corresponds to a density change of approximately 0.1 mg/cc.)

The question of whether the Q-regions are truly quiescent during air flow merits consideration because these are used as reference regions for the fringe shift calculations. Results indicate that there is some small disturbance here caused by either a slight change in adjustment of the instrument or else by motion of air. The magnitude of the irregularity leads to the estimate given in Table II.

3. *Geometrical Errors*

The first of these involves the problem of reading the position of the reference wires w-1 and w-2, etc., accurately, for evaluations in lower sections of the channel are dependent on the sectional alignment procedure using these wires. Firstly, the wire was not in perfect focus since it was waxed on the *outside* of the glass; secondly, the fringe pattern sometimes interfered partially. The error in each alignment procedure was estimated at 0.1 fringe. Agreement between results of spark interferograms and moving film traces of a cross section near the throat (see Fig. 9) provided a check on the alignment procedure.

A precision estimate on the measurement of minimum channel width, or throat, is included in Table II because the channel geometry is important for theoretical calculations. The actual position of the throat is difficult to determine because of the small curvature of the walls in this vicinity. Repeated measurements of the throat width yielded the values shown in Table I with an estimated uncertainty of 0.5 percent in throat width and 1.0 percent in throat-orifice distance.

The evaluation of the divergent-channel interferograms was made on the assumption of constant physical conditions from glass to glass. This was investigated by taking an interferogram after having turned the channel through 90° with respect to its usual position. Then the light travels parallel to the glass walls. Of course, it is possible to view the flow field only above the orifice. Pictures of this sort are shown in Fig. 10. They illustrate the smaller density and higher temperature existing in the boundary layer along the glass as evidenced by the curvature of the fringes. Except for this glass layer, conditions are quite uniform from glass to glass up to about 5 mm above the orifice. It is reasonable to extrapolate below the orifice and assume that homogeneity exists there. For the divergent channel, the glass layer is evidently affected by the oblique orifice shock at about 5 mm above the orifice and begins to separate, with the result that the homogeneity in the direction of the light beam is destroyed (Fig. 10a) and fringe shift evaluations become impossible. A more detailed consideration of the glass layer and other boundary layer errors (category IV of Table II) will be given in connection with the discussion of the Laval nozzle where the boundary layers are thicker and therefore play a more prominent role. From these subsequent considerations it was possible to estimate that the error in density due to the boundary layer on the glass was, in the case of the divergent channel, less than 1 percent.

**** See p. 1367 in reference 7.

TABLE II. Survey of experimental accuracy.

	% Uncertainty	Basis for value in previous column
I. *Instrumentation*		
Tank pressure	0.3%	Fineness of graduations on gauge.
Tank temperature**	0.3%	Change in temperature due to efflux before photo is taken.
II. *Miscellaneous**		
Q-1, Q-2 mismatch.		
Effect on density:		
orifice	0.3%	Comparison of stationary and flow pictures.
throat	0.3%	Matching error of 0.1 fringe.
Oscillations.		Analysis of moving film traces.
Effect on density:		
orifice	1.5%	Estimated average displacement of 0.2 fringe from mean value.
throat	0.5%	
III. *Geometrical**		
Overlap alignment.		Study of comparator readings.
Effect on density:		
throat	0.5%	Estimate of a 0.1-fringe error per overlap, resulting in a 0.2-fringe possible error in throat section.
Width of throat	0.5%	Comparator studies on photographic plate.
Position of any wall	0.02 mm	
IV. *Boundary Layer****		
Boundary layer on glass.		
Effect on density at orifice of Laval nozzle, $P_t = 4.80$ atmos.	1.1%	Measurements on interferogram showing this glass-layer.
Corner effect:		
Maximum error—occuring at inner edge of boundary layer.	1.6%	Consistency of postulated corner effects of various magnitudes with other experimental results.
Refraction error—*maximum*	2.9%	Substitution of computed value of density gradient into the derived formula.

---

* Percentage uncertainties in ρ were calculated for divergent channel (ρ orifice $=1.29$ mg/cc, ρ throat $=4.00$ mg/cc). The percentage for the Laval nozzle are smaller since ρ is greater.

** Use of a thermocouple in the Laval nozzle work made this error negligible.

*** In the Laval nozzle work, the calculated ρ was corrected for the glass layer. The refraction error is an extreme case. For the average boundary layer, this was 1 percent or less.

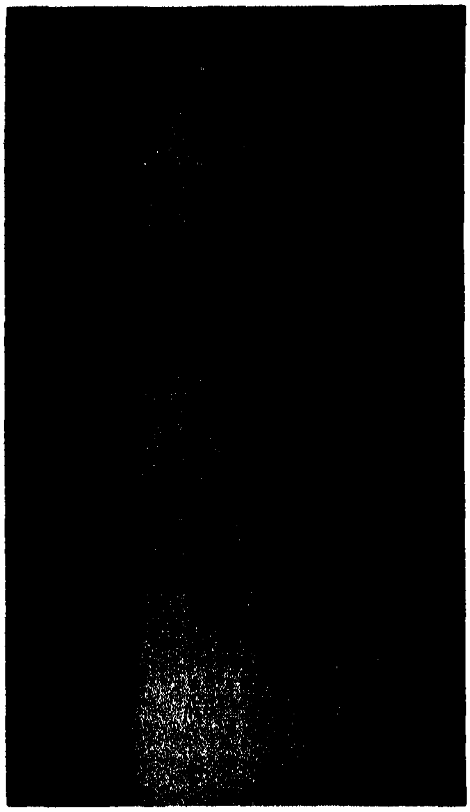

FIG. 8.

B. Potential Flow in the Divergent Channel

A set of interferograms covering the complete supersonic portion of the divergent channel was made and evaluated (Fig. 6). The results for the density were expressed graphically by drawing contours of equal density, known as isopycnals (Fig. 11). Examining this chart, we see first the decreasing density along the axis in the downstream direction, demonstrating the continued expansion. The gradient is largest in the region of the throat. The non-uniformity of the flow is greater in regions where the curvature of the walls is more marked; the homogeneity across the channel grows better as one approaches the orifice.

The isopycnic pattern can be confirmed, within limits, by photography. For if the fringes are made so wide that one fringe covers the entire field and an interferogram is then made, points of equal density will lie on the same fringe (Fig. 12). To do this, however, requires perfect interferometer plates. At least part of the discrepancies between this figure and the isopycnic chart are due to the inhomogeneities in the plates themselves, amounting to some fraction of a fringe.

Since there are no sources of energy dissipation in the channel except in the relatively narrow boundary layer regions, it was possible to obtain

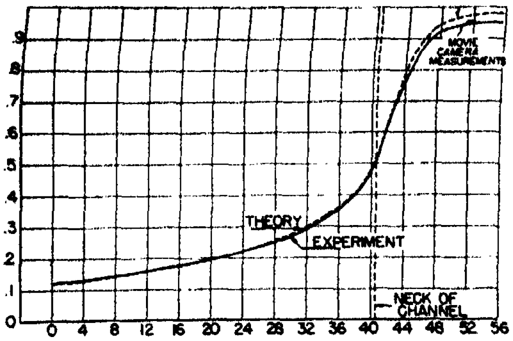

FIG. 9. Plot of P/P_0 *vs.* mm below orifice for divergent channel at $P_0=5$ atmospheres.

pressures and temperatures from the measured density using the well-known isentropic relations. If P_0, ρ_0, and T_0 are the known stagnation values of pressure, density, and temperature, respectively, then the pressure P and temperature T at some point in the channel are related to the density ρ by

$$P/P_0=(\rho/\rho_0)^\gamma=(T/T_0)^{\gamma/(\gamma-1)}, \tag{5}$$

where γ is the ratio of specific heats at constant pressure and volume. The velocity, u, and Mach number, M, may be conveniently calculated from the temperature by the energy equation:

$$u=[2C_p(T_0-T)]^{\frac{1}{2}}, \tag{6a}$$

$$M=[[2/(\gamma-1)][(T_0-T)/T]]^{\frac{1}{2}}. \tag{6b}$$

For comparison with theory, a relation between pressure at some point and the cross-sectional area, A, of the channel at this point was used. The one-dimensional theory of isentropic gas flow gives the relation as

$$(P/P_0)^{2/\gamma}-(P/P_0)^{(\gamma+1)/\gamma}=[(\gamma-1)/(\gamma+1)] \times[2/(\gamma+1)]^{2/(\gamma-1)}[A^*/A]^2, \tag{7}$$

where A^* is the throat area. In view of the small divergence angle of the walls, this one-dimensional theory was considered applicable. In Fig. 9, both experimental and theoretical pressure distribution curves are plotted. Agreement between theory and experiment is around one percent for most of the supersonic portion; deviations up to three percent may be observed in a small region around 32 mm below the orifice.

Schlieren pictures of the divergent channel gave Mach lines which permitted calculation of Mach numbers by Eq. (1). The definition of the lines was not as good as desired with the result that the calculated values of M are estimated as good to ±3 percent. The results for a few well separated places are given in Table III, which contains also the results obtained by interferometry together with results obtained from schlierens by Magin in 1908 with a practically identical channel. Under the heading "Theoretical" are listed Mach numbers *corresponding to the channel areas; the relation, obtained* from the one-dimensional isentropic theory, is

$$A/A^*=[1/M][[1+((\gamma-1)/2)M^2]/[(\gamma+1)/2]]^{\frac{1}{2}[(\gamma+1)/(\gamma-1)]}. \tag{8}$$

The discrepancies between columns 2 and 3 are within the estimated uncertainties of the measurements.

Flow of the gas through the orifice shock involves an increase of entropy and Eq. (5) must be replaced by the Rankine-Hugoniot relation which reads

$$P_2/P_1=[[(\gamma+1)/(\gamma-1)][\rho_2/\rho_1]-1]/[[(\gamma+1)/(\gamma-1)]-[\rho_2/\rho_1]], \tag{9}$$

where the subscripts "1" and "2" refer to opposite sides of the shock. By this equation, pressures downstream of the shock and at the inner edge of the vortex layer along the atmospheric boundary were calculated and found to be equal to 98 percent of the atmospheric value.

(a) (b)

FIG. 10. Interferograms of (a) divergent channel and (b) Laval nozzle showing boundary layer on glass. The lower boundaries represent the orifice. (Magnification of (b) is about 2:1.)

IV. STUDIES WITH THE LAVAL NOZZLE

A. Construction and Revision

An interesting feature of channel flow, for whose study a channel design more suitable than the divergent channel was desired, is the viscous layer or boundary layer existing near the walls. The Laval nozzle was designed to obtain a more fully developed boundary layer with more uniform external conditions such as zero pressure gradient in the flow direction. The purpose of interferometry here was to provide a quantitative check on the proper channel construction.

The equation for two-dimensional steady potential flow may be written as follows:

$$\phi_{xx}[1-(\phi_x^2/a^2)]+\phi_{yy}[1-(\phi_y^2/a^2)] -2\phi_{xy}[\phi_x\phi_y/a^2]=0. \tag{10}$$

Here, ϕ is the velocity potential, a is the local velocity of sound, and the subscripts represent partial differentiation. Starting with certain given boundary conditions, the solution of this equation may be obtained by the "method of characteristics," first applied to supersonic flows by Prandtl and

Busemann[9] in 1929. The method makes it possible to determine the contour of a supersonic nozzle in such a way that the velocity finally becomes unifrom across the entire section. The Laval nozzle used in this work was designed by the "characteristics method" for a Mach number of 1.71. Figure 13 shows the graphical construction for this channel. One assumes $M=1$ at the throat (the validity of this assumption will be discussed later) and produces the expansion by curving the wall and inserting Mach waves in relation to the "wall bending" according to the rules of the method.[10] The quadrilaterals represent, to the approximation used, fields of constant velocity. The smaller the quadrilaterals, the closer the construction approximates the correct solution for the flow field. As the end of the expansion region is approached, the curvature of the walls is so designed as to cancel the reflected Mach lines. When this has been done, the walls of the channel are parallel and the flow field uniform.

A series of preliminary studies which included interferograms and shadow and schlieren pictures all showed the same phenomenon: oblique shocks within the channel (see Figs. 14a and 15a). These shocks are symmetrical and cross the axis at distances of 40.3, 27.4, 14.6, and 2.6 mm below the orifice. Interferometric study revealed that the density ratios varied from 1.01 to 1.03 across the shocks.

A slight revision of the original design and the removal of small machining errors gave an improved channel contour. In this revision the tolerance in the grinding operation was limited to 0.0003" (=0.1 percent of the throat width). The revised dimensions are given in Table IV. The polishing stone was not applied until preliminary shadowgrams were taken for the purpose of obtaining Mach lines. This is shown in Fig. 15b while 15c shows a shadow picture after the final polishing. A quantitative representation of the improvement in uniformity is given in Fig. 16 which shows Mach number distributions before and after improvement as obtained by interferometry. This figure also includes two values of M computed from Mach angle measurements on shadowgrams of the revised but unpolished channel. Agreement with the interferometric results is closer than one percent, itself the estimated degree of uncertainty in the shadowgram measurements. The observed decrease of Mach number with distance downstream, a feature of both curves, is associated with the growing boundary layer which decreases the effective cross section.

The degree to which the pressure gradient near the boundary layer in the direction of the flow was reduced (the main object of the channel revision) is shown in Fig. 17; these calculations were made from the same two interferograms whose axial Mach numbers are plotted in Fig. 16. It was felt that the improved channel gave a very good approximation to uniform flow, although residual non-uniformities are apparent from sensitive schlieren pictures (Fig. 18).

An interesting feature of a well constructed Laval nozzle is the degree to which the flow across the throat is uniform and of Mach number equal to one, inasmuch as the latter is an assumed boundary condition in the "characteristics" construction. In Fig. 19 are shown isopycnic photos of the throats of the two channels, illustrating the relative homogeneity of the flow. The evaluated interferogram of the divergent channel showed that the Mach number increased from 0.97 on the axis to 1.04 at 1.1 mm from the wall, a 7 percent change, whereas for the Laval nozzle the variation was from 1.01 on the axis to 1.05 at 1.0 mm from the wall, a 4 percent change. In the former case the curvature of the walls in the throat region is seen to be rather sharp but in the latter case a very gradual subsonic entrance was drawn with a French curve and a careful attempt was made to provide maximum con-

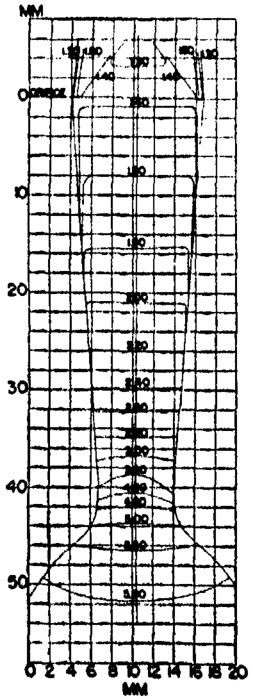

FIG. 11. Isopycnic contours for divergent channel discharging into atmosphere at 5 atmospheres of tank pressure. Contours labeled in mg/cm³. Ordinate readings are mm below orifice.

---

[9] L. Prandtl and A. Busemann, *Näherungsverfahren zur Zeichnerische Ermittlung von ebenen Strömungen mit Überschallgeschwindigkeit* (Stodola Festschrift, Zurich, 1929), p. 499.

[10] A. E. Puckett, "Supersonic nozzle design," J. App. Mech. 13, 265–270 (1946).

FIG. 12. Isopycnic photo (contour fringes) of orifice section of divergent channel.

tinuity with the beginning of the supersonic portion. Figure 20 gives Mach number distributions across the throats of the two channels. From these results it appears quite evident that the assumption of uniform flow of $M=1$ at the throat of a rectangular nozzle is not justified unless the most extreme care is taken to reduce curvatures and discontinuities in this region to the barest minimum.

B. Boundary Layer on the Glass

The evaluation of the Laval nozzle interferograms included a correction for the deviation from truly two-dimensional flow due to the boundary layer along the glass. By taking an interferogram with beam parallel to the glass walls (Fig. 21) one can compute the amount of the necessary correction. In deriving this correction formula, the following notation is used:

S_1 = observed fringe shift in free stream on interferogram made with light beam perpendicular to glass.
Y = coordinate perpendicular to metal walls.
Z = coordinate perpendicular to the glass walls.
$\rho(Z)$ = density at a point in boundary layer Z mm from the glass.
ρ_a = atmospheric density existing in channel prior to gas flow.
ρ_1' = apparent free stream density calculated from S_1.
ρ_1 = true stream density.
$\Delta S(Z)$ = difference in fringe shift between a point in the boundary layer along the glass at Z mm from the glass wall and a point on the same horizontal level in the free stream as observed on an interferogram taken with light beam parallel to the glass walls.

TABLE III. Comparison of Mach numbers for flow in diverging channel.

Distance below the orifice mm	Interferometry	Schlieren	Magin	Area (theoretical)
2.2	1.98	—	1.96	2.01
16.3	1.77	1.79	1.74	1.79
25.6	1.60	1.64	—	1.64
30.7	1.48	1.53	—	1.47

$\Delta\rho(Z)$ = density difference corresponding to $\Delta S(Z)$.
W = width of channel.
D = depth of channel (= glass to glass distance).
δ = width of boundary layer along metal walls (along still air when above the orifice).
ϵ = width of boundary layer along glass wall
$\theta = D - 2\epsilon$.
$\tau = W - 2\delta$.
K = Gladstone-Dale constant.
λ = wave-length of light.

The apparent free stream density is obtained from the optical path change by the relation

$$S_1 \cdot \lambda = K \cdot D(\rho_1' - \rho_a).$$

Allowing for the layer on the glass, the correct expression is

$$S_1 \cdot \lambda = K(\rho_1 - \rho_a)\theta + 2K\int_0^{\epsilon} [\rho(Z) - \rho_a] dZ.$$

The boundary layer density $\rho(Z)$ is less than ρ_1; we put

$$\rho(Z) = \rho_1 - \Delta\rho(Z)$$

and removing ρ_1 and ρ_a from under the integral sign we get

$$S_1 \cdot \lambda = K(\rho_1 - \rho_a)D - 2K\int_0^{\epsilon} \Delta\rho(Z) dZ.$$

By equating the two expressions for $S_1 \cdot \lambda$, there results

$$\rho_1 = \rho_1' + (2/D)\int_0^{\epsilon} \Delta\rho(Z) dZ. \qquad (11)$$

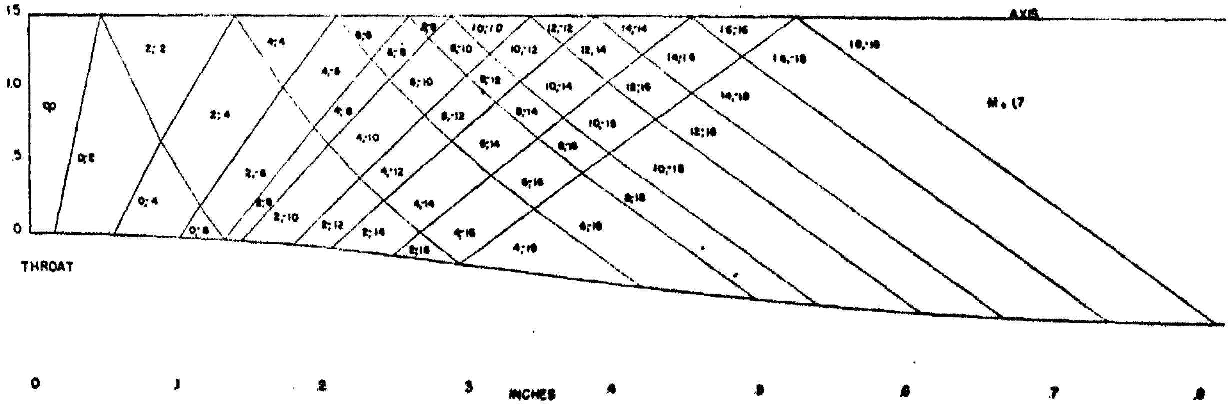

FIG. 13. Design of Laval nozzle contour by method of characteristics. Each pair of numbers gives the magnitude and direction of the velocity in the region indicated.

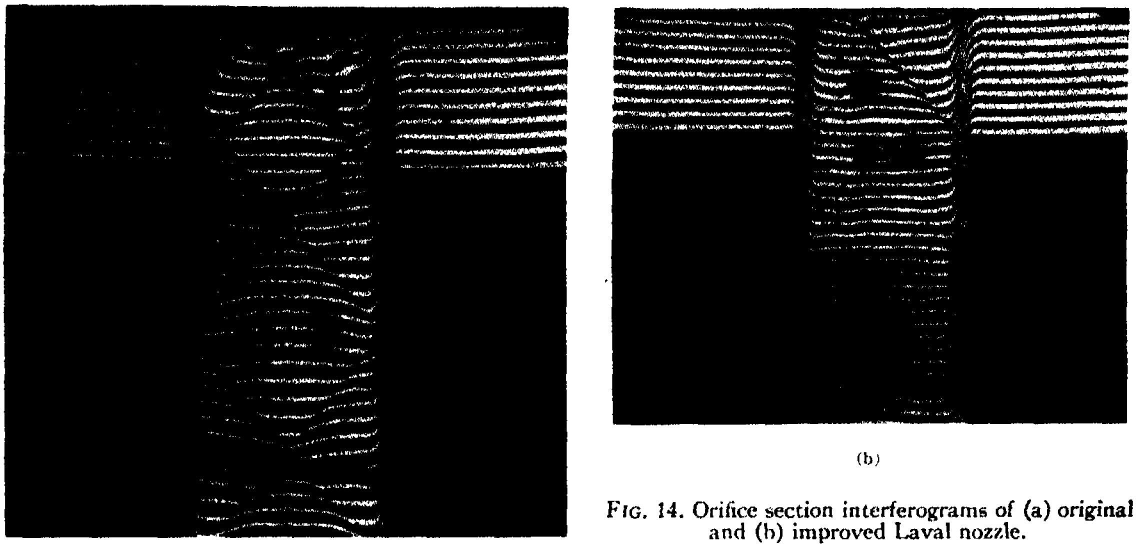
(a)

(b)

FIG. 14. Orifice section interferograms of (a) original and (b) improved Laval nozzle.

Referring to Fig. 21, we consider the two light rays A and B traveling perpendicular to the gas flow but parallel to the glass walls. For the ray A, $Z<\epsilon$ while for B, $Z>\epsilon$ so that the former passes through the boundary layer on the glass while the latter traverses the free stream. The two rays have different histories over a length of path $W\text{-}2\delta$ or τ. The relation between $\Delta\rho(Z)$ and $\Delta S(Z)$ is thus given by

$$\Delta\rho(Z)=(\lambda/K\tau)\Delta S(Z)$$

and the correction formula can be expressed in terms of the measured quantity $\Delta S(Z)$:

$$\rho_1=\rho_1'+(2\lambda/KD\tau)\int_0^{\epsilon}\Delta S(Z)dZ. \qquad (11a)$$

In practice, the correction integral is obtained by measuring the area under the curve of $\Delta S(Z)$ *vs.* Z. Measurements of the correction were made at 0.25, 2.8, 4.3, and 5.8 mm above (downstream of) the

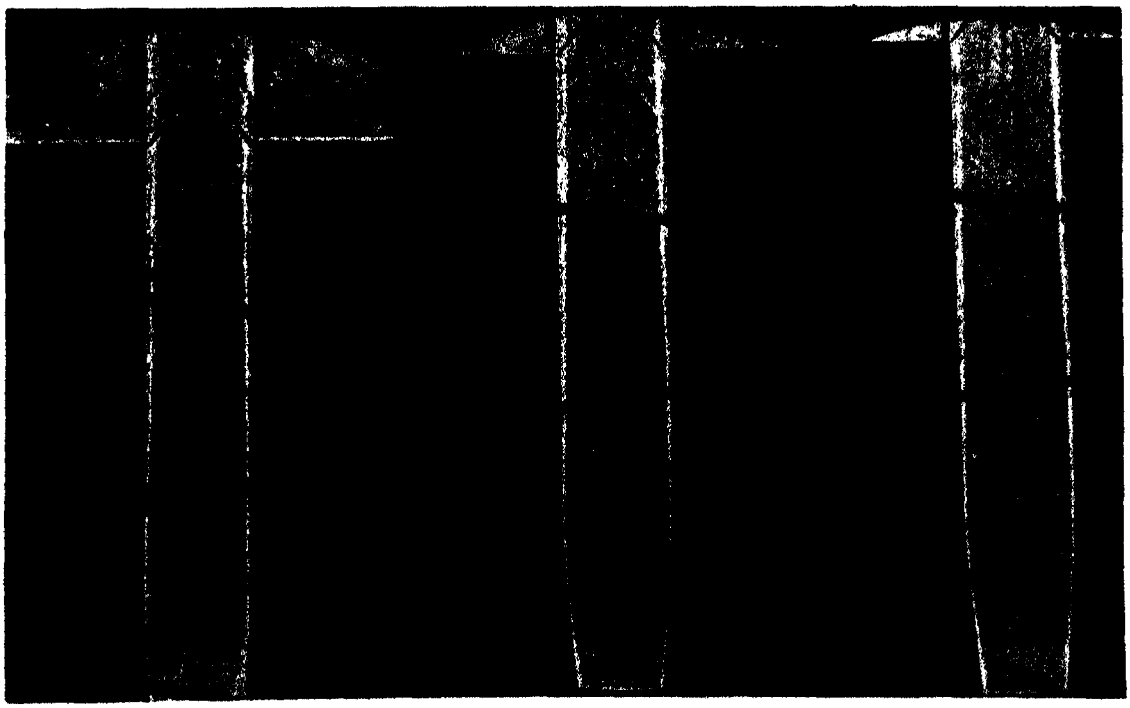
(a) (b) (c)

FIG. 15. Laval nozzle: Shadowgrams showing improvement in design.

TABLE IV. Revised Laval nozzle: Contour dimensions of supersonic portion in inches.

Distance from orifice	Distance from channel axis	Distance from orifice	Distance from channel axis	Distance from orifice	Distance from channel axis
1.500	0.2067	1.900	0.1973	2.300	0.1588
1.510	0.2067		0.1966		0.1580
1.520	0.2067		0.1959		0.1572
1.530	0.2067		0.1951		0.1565
1.540	0.2067		0.1943		0.1559
1.550	0.2067		0.1935		0.1553
1.560	0.2067		0.1927		0.1547
1.570	0.2067		0.1919		0.1541
1.580	0.2066		0.1911		0.1536
1.590	0.2065		0.1903		0.1531
1.600	0.2064	2.000	0.1894	2.400	0.1527
	0.2063		0.1885		0.1523
	0.2062		0.1876		0.1519
	0.2061		0.1867		0.1516
	0.2060		0.1858		0.1514
	0.2059		0.1849		0.1512
	0.2057		0.1840		0.1511
	0.2055		0.1831		0.1510
	0.2053		0.1821		0.1509
	0.2051		0.1811		0.1508
1.700	0.2049	2.100	0.1801	2.500	0.1507
	0.2047		0.1791		
	0.2045		0.1781	(throat)	
	0.2043		0.1771		
	0.2041		0.1761		
	0.2039		0.1750		
	0.2036		0.1740		
	0.2033		0.1729		
	0.2030		0.1718		
	0.2027		0.1706		
1.800	0.2024	2.20	0.1694		
	0.2020		0.1683		
	0.2016		0.1672		
	0.2012		0.1661		
	0.2007		0.1650		
	0.2002		0.1639		
	0.1997		0.1628		
	0.1991		0.1617		
	0.1985		0.1607		
1.89	0.1979	2.29	0.1597		

orifice. The percentage correction for ρ at the orifice in the experiment at 4 atmospheres of tank pressure was

$$100[(\rho_1-\rho_1')/\rho_1]=1.3 \text{ percent.}$$

To obtain data on the correction at various cross sections below the orifice, the variation of the quantity

$$\int_0^{\delta} \Delta S(y)dy$$

along the metal walls was studied and the assumption made that the development along the glass wall was similar. Figure 22 is a test of this assumption. Superimposed on a density profile along metal at 0.50 mm below the orifice are points obtained from the boundary layer on the glass at 0.25 mm above the orifice. The agreement is rather good. All the calculations of the free stream density in the Laval nozzle experiments were corrected for the boundary layer.

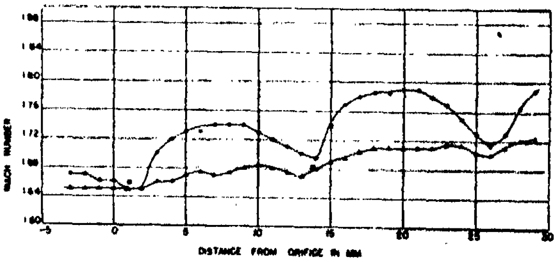

FIG. 16. Laval nozzle: Mach number distribution—
⊙ Before channel revision,
△ After channel revision,
☒ Measurements of Mach angles on the revised but unpolished channel.

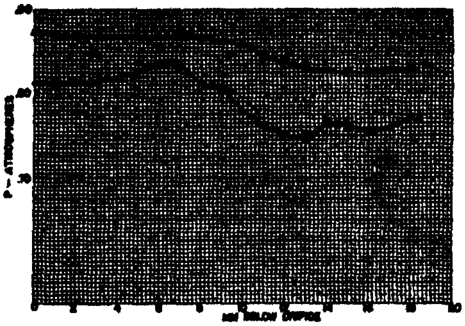

FIG. 17. Laval nozzle: Pressure distributions at 1.5 mm from the wall (a) before improvement and (b) after improvement. $P_0=4$ atmospheres.

The comparison of boundary layers on glass and steel was put on yet a more quantitative basis by replacing *one* of the glass walls with a plane steel plate and comparing directly the boundary layer on this wall with that on the other (glass) wall. Densities were compared at several corresponding points in the two layers. The steel wall showed a somewhat lower density along the whole layer but the average density difference for five cases was only 1.7 percent, too small to conclude that there is any real difference.

C. Refraction Error†

The presence of density gradients in the flow will, in general, cause the light beam to change its direction. This is illustrated schematically in Fig. 23 where a light ray entering the flow field at the point *E* would continue to the point *M* in the absence of a density gradient but actually takes the curved path *EF* in the presence of a downward gradient. This effect will be most marked in regions of high gradient such as boundary layers. Two questions arise:

1. Does the refraction introduce any distortion into the photographic behavior of the system?

---

† A more general and somewhat different treatment of this problem (unpublished) has been given recently by Dr. F. J. Weyl, Naval Bureau of Ordnance, Washington, D. C.

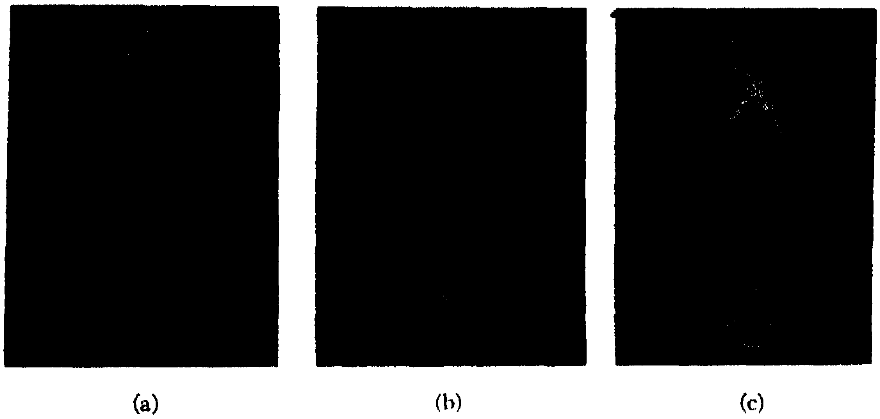
(a) (b) (c)

FIG. 18. Schlieren photographs of the improved Laval nozzle at (a) 4.07, (b) 4.80, and (c) 6.09 atmospheres.

I.e., is the center of the flow field on which the camera lens is focused still being mapped accurately on the screen or photographic plate?

2. By how much is the evaluated density at any point in error due to refraction?

In the following treatment, we make the following assumptions:

(a) The value of the radius of curvature R, of the path EF at E differs negligibly from its value at F so that EF is considered as the arc of a circle.

(b) R is much larger than D, the depth of the working section: $R \gg D$.

(c) The variation of grad$n$ (n = refractive index) between the lines EM and GF in Fig. 23 may be ignored.

(d) The pencil of rays coming from a point in the object plane is narrow enough so that variation of refraction effects between the extreme rays is insufficient to affect the sharpness of the fringes (i.e., optical path difference $\leq \lambda/4$).

(e) The density gradient lies in the plane of the diagram and is perpendicular to the incoming light.

In considering the first of the two questions, notice that under conditions of no flow, the ray shown in Fig. 23 would appear to the camera lens to be coming from point B in the object plane, whereas the presence of flow makes it appear to come from C. We wish to calculate the distance BC or ξ.

Since the tangents to the circle at E and F intersect at H, the line OH bisects the angle ϵ. The following exact relations hold:

$$\sin\epsilon = D/R; \quad \tan\epsilon/2 = EH/R = (D/2+\eta)/R;$$
$$\tan\epsilon = D/(R^2-D^2)^{\frac{1}{2}} = \xi/\eta.$$

From these one obtains

$$\xi = [D\cdot R/(R^2-D^2)^{\frac{1}{2}}][\tan\epsilon/2 - \tfrac{1}{2}\sin\epsilon].$$

Since $D \ll R$, it is possible to neglect D^2 compared to R^2 and to expand the terms in the brackets up to ϵ^3 which gives

$$\xi \cong \epsilon^3\cdot D/8 \cong D^4/8R^3 \cong [D^4/8][|\text{grad}n|^3/n^3].\dagger\dagger \quad (12)$$

The value of ξ was compared with the radius of the "circle of confusion" due to diffraction by the camera lens itself. The half-width Ω of the central maximum of the diffraction pattern formed by the lens of a parallel bundle of light is given by $\Omega = 1.22\lambda f$, where f is the so-called f number, equal to the focal length of the lens divided by its diameter. Measurements of typical boundary layers and an expansion wave in the Laval nozzle gave values of ξ around 10^{-7} cm, whereas Ω was 6×10^{-4} cm. Thus in the fourth column of Table V, ξ is set approximately equal to zero and "photographic distortion" is considered absent. Agreement within the experimental error of 0.003 cm between measurements of channel width on an interferogram at a carefully adjusted magnification of 1:1, and accurate measurements made on the channel itself verified this result.

We now consider the second of the above questions. If ϕ is the angle between the direction of a light ray and the gradient of the refractive index, the radius of curvature of the path is given by

$$1/R = (\text{grad}n/n)\sin\phi.$$

Now, from Fig. 23 we see that

$$MF \equiv \Delta = R-(R^2-D^2)^{\frac{1}{2}} \cong D^2/2R.$$

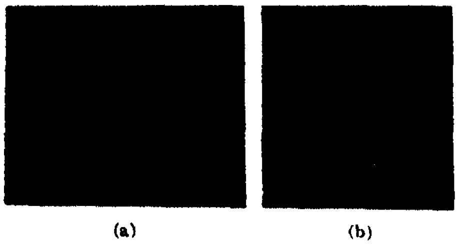
(a) (b)

FIG. 19. Isopycnic photos (contour fringes) of throat sections of (a) divergent channel and (b) Laval nozzle.

---

†† Discussed in next paragraph.

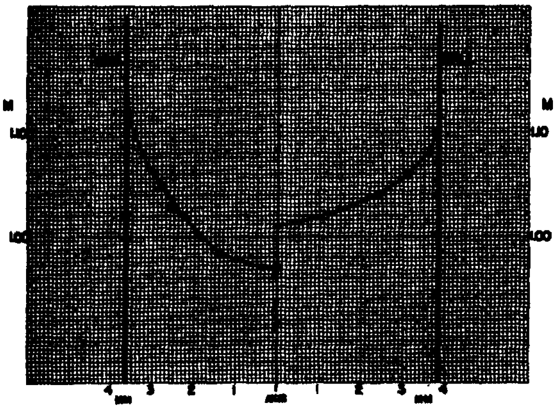

FIG. 20. Mach number distribution across the throat: ×—Divergent channel; ⊙—Laval nozzle.

More generally, if Z be the direction of the incident light with the line EG as the axis $Z=0$, then the deviation, $\delta(Z)$ of any point P lying in EF from the unrefracted path EM will be given by

$$PP'=\delta(Z)\cong Z^2/2R.$$

The average deviation, $\bar{\delta}$, over the path EF will be

$$\bar{\delta}=\frac{\int_0^D (Z^2/2R)dZ}{\int_0^D dZ}=D^2/6R.$$

The actual length of the path EF is

$$EF=R\cdot\epsilon\cong D+(R\epsilon^3/6).$$

Denoting the refractive index along EM by n, we find that the difference, Q, in optical path due to refraction is

$$Q=(n_1+\bar{\delta}\,\mathrm{grad}n)(D+(R\epsilon^3/6))-n_1D,$$

neglecting terms in ϵ^5 compared to ϵ^3. A very good approximate expression for Q may be obtained by allowing

$$\epsilon\cong D/R;\quad 1/R\cong\mathrm{grad}n\quad (\text{i.e., } n=1,\ \phi=\pi/2)$$

and using $\bar{\delta}=D^2/6R$. This gives

$$Q=(D^3/6)|\mathrm{grad}n|^2\cdot[2+(D^2/6)|\mathrm{grad}n|^2].$$

Where the last term in the brackets is much smaller than 1 (it was 10^{-5} or smaller in the present experiments), the expression becomes

$$Q\cong(D^3/3)|\mathrm{grad}n|^2=(K^2D^3/3)|\mathrm{grad}\rho|^2.\dagger\dagger\dagger \quad (13)$$

This extra optical path Q will produce an added fringe shift ΔS, given by $\Delta S=Q/\lambda$; i.e., the *observed* fringe shift will be too great by the amount ΔS. Because of the relationship between ρ and S, the error ΔS will be accompanied by an error $\Delta\rho$ given by

$$\Delta\rho=(\lambda/KD)\cdot\Delta S.$$

Expressing the desired result in fractional form we have

$$\Delta\rho/\rho=(KD^2/3\rho)\cdot|\mathrm{grad}\rho|^2. \quad (13a)$$

$\Delta\rho$ is the amount to be subtracted from the density supposed to exist at the point B according to the observed fringe shift.

Table V gives pertinent data for three cases among the highest gradients measured. The constants associated with these calculations are

$D=1.90$ cm, $\lambda=4.48\times10^{-5}$ cm,
$K=0.229$ cm^3/g, f-number of camera lens $=10$.

To understand the meaning of the bottom row of the table, it should be noted that, in the examples taken here, the higher the gradient, the narrower the fringes. On the present interferograms the narrowest accurately readable fringe width was 0.0080 cm, corresponding to a density gradient of 12.5×10^{-3} g/cc/cm as given in this row of the table. The second row of the table contains a higher gradient value and was included because it represents the highest gradient which was measured, but the data are less reliable. (It is estimated that for this case the uncertainty in gradρ is about 5 percent whereas for the other cases it is about 2 percent.)

The density gradients were computed by taking a region through which the fringe width remained reasonably constant (second column of Table V) and dividing by the total density change. In all cases this region was considerably larger than the maximum deviation, Δ, of the light ray from the unrefracted path so that the assumption of the constancy of gradρ is a valid one.

In boundary layer studies, the exact absolute values of the densities are less important than the shape of the density profile. Distortions of the latter would arise only from variation of gradρ, since for a constant gradient, the refraction error would merely displace the profile parallel to itself. Figure 24 shows a typical boundary layer profile; it is seen

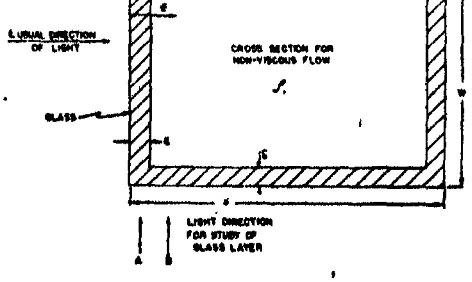
STEEL OR AIR
BOUNDARY LAYER ρ(δ)
δ
USUAL DIRECTION OF LIGHT
CROSS SECTION FOR NON-VISCOUS FLOW
ρ₁
GLASS
δ
δ
W
δ
LIGHT DIRECTION FOR STUDY OF GLASS LAYER
A
B

FIG. 21.

[†††] This is in agreement with the result obtained by Weyl.

that the curvature is small throughout most of the region.

D. Errors Due to Intersecting Boundary Layers

In the corners of a rectangular channel the boundary layers along the two intersecting walls themselves intersect. It is thought that a rounding-together occurs somewhat as shown in the schematic diagram of Fig. 25. The effect on the interferometric evaluation is illustrated by considering the rays labeled *A*, *B* and *C* in this figure. While it is clear that ray *B* does not traverse the boundary layer along the metal as does ray *C*, nevertheless it passes through the thickened "corner layer" and therefore its optical path is different from that of ray *A* (shorter). The difference between *A* and *B* may be mistakenly attributed to the passage of ray *B* through the entire boundary layer along the metal wall. Thus the apparent boundary layer would be thicker than the actual one.

There exists no experimental information on this sort of "corner effect." However, a knowledge of the density profiles in the boundary layers studied has made possible order-of-magnitude calculations which show that the effect of the corner thickening will be, in most cases, an extremely limited one. The first step is to take a typical profile and plot the fringe shift *relative* to the free stream. This was done for the case of a layer at 1 mm below the orifice on an interferogram of the Laval nozzle taken at 5 atmospheres of tank pressure, indicating an apparent boundary layer width of 1.0 mm. One next assumes that the actual boundary layer is thinner, choosing some definite value such as, for example, 0.7 mm and then proceeds to ascertain how much plausibility there is in assigning the remaining 0.3 mm to the "corner layer." It is now necessary to draw an assumed profile for the corner such as is shown in Fig. 25. Then, the procedure is to study a ray parallel to the wall, but somewhat outside the assumed true boundary layer (ray *B* in Fig. 25), say at 0.9 mm from the wall. After measuring the length of path of this ray in the corner layer and using the information given by the fringe shift plot that the difference in optical path was, in this case, equivalent to a relative shift of 0.5 fringe, it becomes possible to calculate an average corner density, ρ_c, which would account for the difference in path. For the example of the assumed 0.7-mm layer, this density was calculated as

$$\rho_c = \rho_1 - 0.5 \text{ mg/cc.}^{\dagger\dagger\dagger\dagger}$$

That such a result is extremely unlikely is apparent if it be noted that the density at 0.1 mm from the wall is only 0.45 mg/cc below the stream density ρ_1, and that the section of corner layer which plays

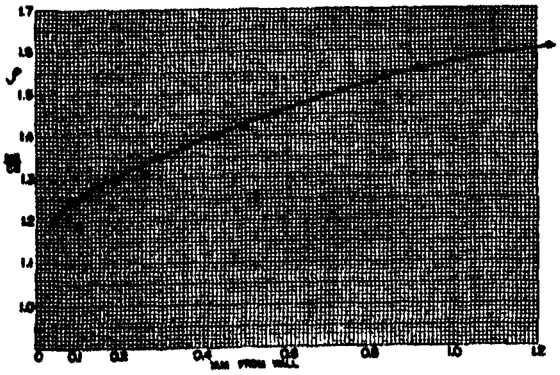

Fig. 22. Laval nozzle: Density profiles in boundary layers on metal and glass. ⊙—Metal wall, 0.5 mm below orifice; ×—Glass wall, 0.25 mm above orifice.

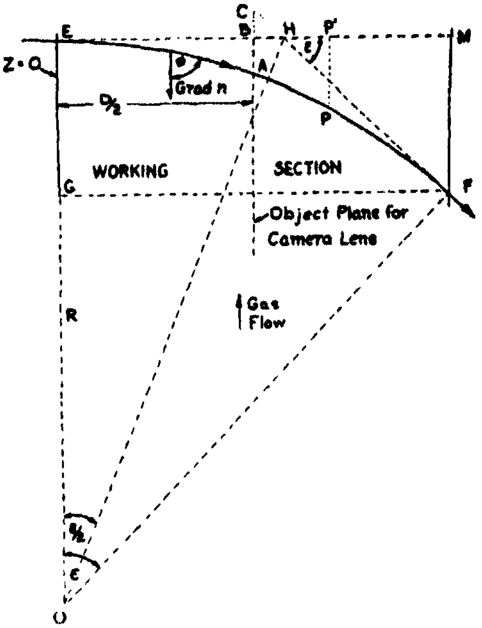

Fig. 23. Schematic diagram of the refraction of a light ray in a gas stream.

Table V. Refraction errors in boundary layers and an expansion wave in a small Laval nozzle ($P_0 = 6.09$ atmos.).

Place	Width of region analyzed (cm)	Grad ρ c.g.s.	ξ	Δ (cm)	$100\frac{\Delta\rho}{\rho}$
Boundary layer 1 mm below orifice	0.082	6.1×10^{-3}	~0	0.0025	0.49%
Boundary layer 1.5 mm above orifice	0.020	15×10^{-3}	~0	0.0061	4.5%
Expansion wave	0.094	8.5×10^{-3}	~0	0.0035	1.0%
Limiting case for accurate fringe readings		12.5×10^{-3}	~0	0.0051	2.9% For $\rho = 1.5\times10^{-3}$ g/cc

---

†††† A shift of 0.5 fringer was equivalent to a density difference of 0.5 mg/cc rather than 0.05 mg/cc because the extra length of corner layer traversed by ray *B* as compared to ray *A* was 0.2 mm, or about one-tenth of the channel depth.

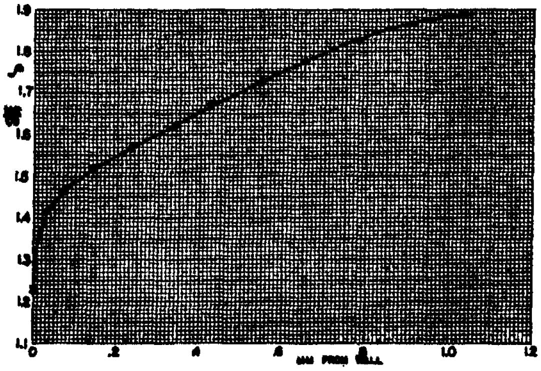

FIG. 24. Boundary layer density profile along channel wall ($P_0=4.80$ atmospheres). See appendix for other pertinent data.

the role in producing the 0.5-fringe shift relative to free stream is 0.9 mm away from the wall. The density must be, in reality, much closer to the free stream value.

One can then assume an 0.8-mm boundary layer and repeat the calculation. In the present case it was concluded that the effect of the corner layer would be limited to causing a relative shift of at most 0.3 fringes relative to free stream in a narrow region at the inner edge of the boundary layer. The result with the Laval nozzle of the dimensions used would be to cause an ambiguity of about 0.1 or at most 0.2 mm in the choice of boundary layer width.

V. SUMMARY AND CONCLUSIONS

This study indicates that the technique of interferometry applied to compressible channel flow is a feasible one which is capable of giving good accuracy in density determinations. Of course, the magnitudes of the various uncertainties depend on the particular apparatus geometry and experimental conditions. In the present experiments an analysis of errors as summarized in Table II leads to the conclusion that values of ρ directly obtained from the interference measurements possess an estimated probable error of about 2 percent. Comparison between interferometric results for potential flow in the divergent channel and the values computed from the one-dimensional theory of isentropic flow show a difference of 1 percent. Independent checks were provided by Mach angle measurements on schlieren pictures and by fringe shift measurements on moving film. In the case of the latter technique, agreement with the results of spark interferograms in the neighborhood of the throat showed that the procedure of studying density fields larger in size than the interferometer plates by aligning interferograms of adjacent sections is reliable.

The deviation from steady flow in channels of the type studied consists in small oscillations about a mean value of the physical variables. There would be corresponding inconsistencies in the absolute values of density calculated from successive interferograms taken at different parts of the oscillation cycle. The estimated uncertainty of this and other errors are given in Table II.

Interferometry can be usefully applied as a guide in nozzle construction since the results of the evaluated interferograms can be quantitatively compared with the desired properties of the nozzle. In particular, the uniformity of flow in the throat can be studied. The present experiments show that the attainment of uniform flow of $M=1$ across the throat is a difficult problem.

There are at least three different boundary layer phenomena which affect the interference pattern in channels having sizable boundary layers:

(a) Boundary layer on the glass.
(b) Refraction error.
(c) Corner intersection of boundary layers.

(a) The density obtained from the observed fringe shift has to be increased by:

$$\Delta\rho=(2\lambda/KD_T)\int_0^s \Delta S(Z)dZ$$

(for notation see Section IV). The percentage correction for the orifice region of the Laval nozzle at $P_0=4$ atmospheres was 1.3 percent. Except for this layer, homogeneity from glass to glass was excellent.

(b) In the presence of a density gradient normal to the light beam, a negative correction to the density will account for the refraction error. This is given by

$$\Delta\rho=(KD^2/3)|\mathrm{grad}\rho|^2.$$

In the present case, an extreme density gradient of 12.5×10^{-8} g/cc per cm was accompanied by a refraction error of 2.9 percent. The shape of a density profile is not altered appreciably by refraction unless gradρ varies strongly.

(c) Semiquantitative calculations give the result that, in the present Laval nozzle experiments, the

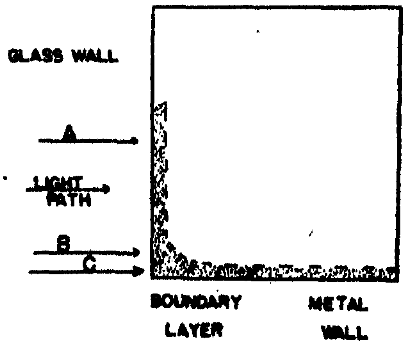

FIG. 25. Schematic diagram illustrating "corner effect."

"corner effect" introduces an ambiguity of about 10 percent in the choice of boundary layer width. Other parts of the interference pattern are unaffected.

ACKNOWLEDGMENT

The writer is indeed grateful to Professor Rudolf Ladenburg who suggested the subject of this research and gave constant guidance in the work. Sincere thanks are also extended to Miss Anne Kenny whose skillful and generous help in many phases of the work, particularly the computations, was of great assistance.

APPENDIX

Notes on boundary layer calculations.—In spite of the relatively small width of the boundary layers (1 mm or less), the sharpness of the interference fringes in these regions made possible an evaluation of density distributions, taking due account of previously mentioned correction factors.

Figure 24, a density profile at 4 mm upstream of the orifice of the Laval nozzle (62 mm downstream of the throat), is typical of many others. Conditions in the free stream near this layer are as follows:

$T_1 = 187°$ K. $\quad M_1 = 1.67$.
$P_1 = 1.02$ atmos. $\quad \rho_1 = 1.91$ mg/cc.
$u_1 = 459$ meters/sec.

The extrapolated value of ρ at the wall is calculated on the assumptions that the wall temperature equals the stagnation temperature of the gas (room temperature) and that the pressure across the throat is constant:

$$\rho_w = P_w/RT_w = P_1/RT_0 = 1.23\text{ mg/cc. } (T_0 = 293°\text{ K.})$$

The ideal gas law may further be used to calculate the distribution of temperature from the known pressure and densities.

As is evident from schlieren pictures (for example, Fig. 18), we are dealing here with turbulent boundary layer flows. Figure 26 shows a laminar-looking layer with an apparent transition to the turbulent form upstream of the uniform section of the channel. The evaluated layers were all considerably downstream of the transition region. The Reynolds number associated with the profile of Fig. 24 is

$$Re = \rho_1 u_1 l/\mu_1 = 4.3\times 10^6,$$

using the distance from the throat as a typical length l. The value of the viscosity coefficient μ_1 corresponding to the temperature T_1 was obtained from the Landolt-Börnstein Tables and found to be equal to 129 micropoises. The Reynolds number for the transition region was calculated to be

$$Re_{\text{trans}} = 1.2\times 10^6.$$

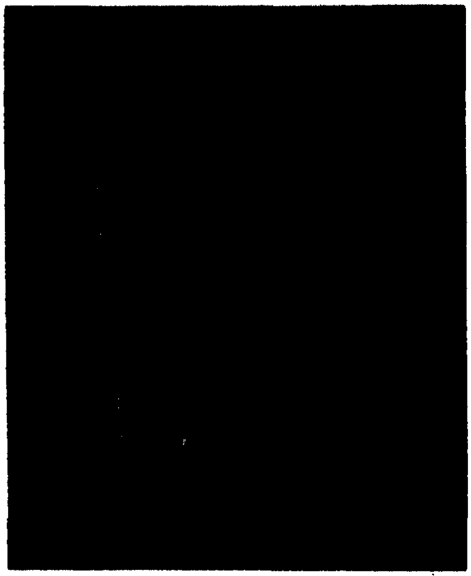

FIG. 26. Schlieren photo of throat region of Laval nozzle showing what appears like a laminar-turbulent transition in the boundary layer.

Of high interest are the velocity distributions in the boundary layers. Values of u were obtained from the energy equation:

$$u = [2Cp(T_0 - T)]^{\frac{1}{2}}.$$

The use of this relation is, in general, not justified for flows of the boundary layer type because of their non-isentropic character. Arguments exist, however, to show that it is applicable in the present case. Preliminary results have been obtained for the velocity distribution but a fuller investigation is planned before these are reported. An extension of the study to other Mach and Reynolds numbers is being undertaken using the larger intermittent supersonic wind tunnel recently constructed at this laboratory under the direction of Professor Ladenburg.

THE REVIEW OF SCIENTIFIC INSTRUMENTS VOLUME 20, NUMBER 4 APRIL, 1949

Cloud-Chamber Equipment for Study of Infrequent Cosmic-Ray Processes*

W. Y. CHANG AND J. R. WINCKLER
Palmer Physical Laboratory, Princeton University, Princeton, New Jersey

(Received January 3, 1949)

The cloud chamber described operates if a particle passes through a vertical telescope and stops before reaching anticoincidence counters under the chamber. The chamber is surrounded by a minimum amount of material, and a large number of the anticoincidence events consist of particles stopping in foils of aluminum, iron, and lead within the chamber. The expansion valve is of the fast electromagnetic type having a thin iron diaphragm which completes a magnetic circuit when closed. Six slow expansions for clearing the chamber occur immediately after each event. The chamber is housed in an insulated room kept within ±0.1°C. The Geiger counter coincidence circuits operate time delays for controlling the expansions, flash lamps, camera, clearing field, and recorders. The electronics is suitable for the study of very infrequent events. Several pictures of meson decay and shower events are presented.

I. INTRODUCTION

INTERACTION phenomena in cosmic rays are generally rare. For example, extensive showers, or showers produced by penetrating particles, or the processes connected with slow mesons occur particularly infrequently—about one in several hours for the usual solid angle of detection. The necessity of using a cloud chamber to observe these events does not need special mentioning. However, for these purposes the cloud chamber, which is of course counter-controlled, and its associated equipment, once adjusted, must be ready at all times to respond to the events. Essentially, the temperature and pressure,[1] in the first place, must be kept constant throughout the whole period so as to maintain the same expansion ratio. Second, the chamber must be cleaned periodically to remove any condensation nuclei so as to provide a clear background. Third, the delay control apparatus, etc., must operate reliably each time.

During the past two years we have built a cloud chamber and automatic control equipment for the study of meson absorption by thin foils.[2] This whole set of apparatus has been working satisfactorily for over a year—the cloud chamber and the counter units, etc., normally are checked only about twice a week (working continuously 24 hours a day). This set of equipment obviously can be used to study other infrequent cosmic-ray phenomena. It may be arranged so that two or more different types of cosmic-ray processes can be studied with the same chamber equipment at the same time, e.g., extensive air showers and meson absorption by thin foils. We feel, therefore, that it may be worth while to report the detailed construction of the cloud chamber and the electronic details of the control units, etc.

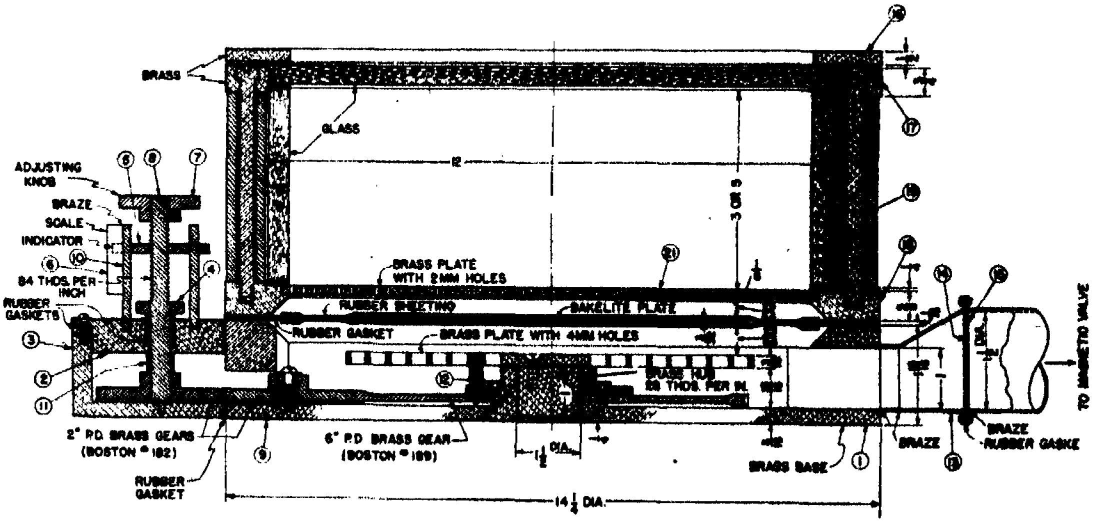

FIG. 1a. Cloud-chamber assembly.

---

* Assisted by the joint program of the AEC and the ONR.

[1] N. N. Das Gupta and S. K. Ghosh, Rev. Mod. Phys. 18, 228–230 (1946).

[2] W. Y. Chang, Phys. Rev. 74, 1236 (1948); Rev. Mod. Phys. 21, 166 (1949).

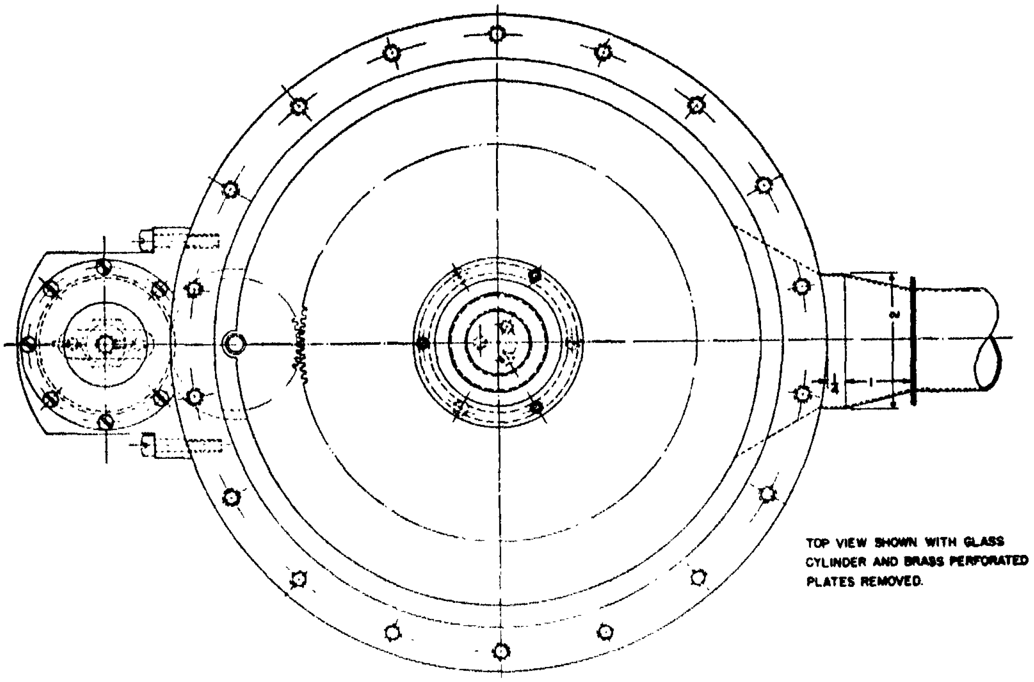
2
$\frac{1}{4}$
1
TOP VIEW SHOWN WITH GLASS CYLINDER AND BRASS PERFORATED PLATES REMOVED.

FIG. 1b. Chamber bottom with gear system.

II. THE CLOUD CHAMBER AND ASSOCIATED APPARATUS

A. The Cloud Chamber

The cloud chamber is in the rubber diaphragm type and has an inside diameter of about 12 inches. Figure 1a shows the assembly. For eventual use with a magnet, the back (dead) space has been made as small as possible. To accomplish this, the position of the perforated brass plate (with 4-mm holes), against which the diaphragm expands, and hence the expansion ratio is varied from outside at the bottom circumference by means of a system of three gears (see Fig. 1b). This brass plate is supported rigidly, by means of three screws, on to the threaded hub. From the plate there are three equidistant brass pins (perpendicular to the plate) which can move along in three brass tubes projected upward from the main gear. Hence, when the gear is turned, a moment is, by means of these pin-tube couplings, applied to the plate, which is thus turned forward or backward. The diaphragm is made of two rubber sheets, with a $\frac{1}{16}$-inch Bakelite plate in between. In this way the diffusion of alcohol from the chamber proper is much slower than without the Bakelite plate. Moreover, the expansion in the neighborhood of the circumference can be as near to that at the center as possible, i.e., more uniform expansion everywhere.

A brass ring (17) is held rigidly to the bottom ring (18) by using only four equally spaced brass cylinders ($\frac{7}{8}$-inch diameter, and with screws (19) inside). The glass window ($\frac{5}{16}$-inch Herculite glass) and the glass cylinder (cut from ordinary battery jar) are held together against the bottom ring (18) by the top ring (16) which can be screwed on to the ring (17). Neoprene gaskets are used for the vacuum seals. In this way we have the least amount of material surrounding the chamber proper. This is an advantage for studying certain cosmic-ray processes taking place inside the chamber, for the number of useless pictures due to the same process at the chamber walls is small. Moreover, the chamber depth can be easily varied (if desired) by simply changing the length of the four spacers and the height of the glass cylinder. The thickness of the over-all dead space at the back is about 2 inches. With argon gas saturated with alcohol-water mixture, the chamber depth can be increased up to 8 inches. Two depths have been used, namely 5 and 8 inches. The deeper chamber has been found to work with smaller turbulence.

Figure 1b shows the arrangement of the three gears, with the outside one in a vacuum-sealed box at the circumference. The expansion ratio can be read from a scale above the box (cf. Fig. 1a, left-hand side). The air passage to the expansion valve is smoothly constricted.

In operating the chamber it is advantageous to employ a back chamber pressure so that the rubber diaphragm is quite clear from the front perforated disk (which is covered with a piece of velvet for the purpose of photography). Thus, the turbulence, which may be created in the neighborhood of the diaphragm during expansion and be transmitted to the chamber proper, can be as small as possible. All

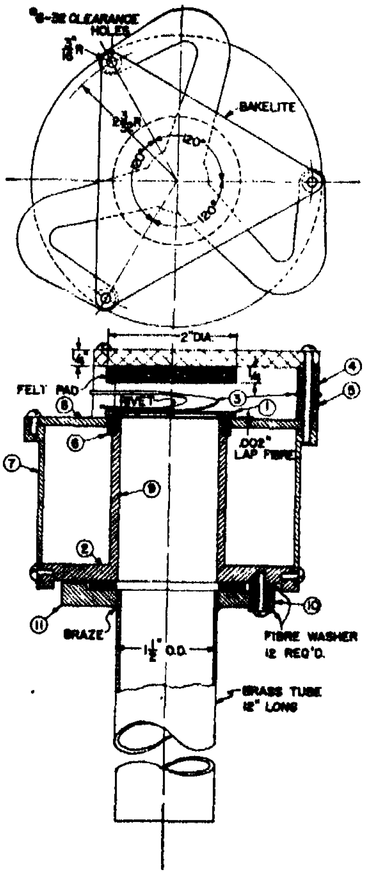

FIG. 2. Expansion valve. The iron diaphragm (1) supported on a Bakelite spider completes the magnetic circuit when closed.

the materials inside the chamber must be very clean, not soluble in the liquid mixture of alcohol-water, and not giving off disturbing volatile substances. Synthetic rubber for the diaphragm and gaskets is found to give a smaller background than gum rubber, for presumably the former does not dissolve in the alcohol-water mixture easily. In using lead foils as absorbing material inside the chamber, the oxide layers found on the surfaces must be carefully cleaned with steel wool and then washed thoroughly with alcohol. No water is used for the cleaning purpose, for lead is oxidized very easily by water. Thus the background at expansion ratios, smaller than the ion limit, will be very small.

B. The Fast Expansion Valve

The fast expansion valve is of a solenoid type. Figure 2 shows its assembly. The inner cylinder ((9) in Fig. 2) is made of steel, with the flange at the lower end, and the solenoid (No. 18 copper wire) is wound upon it. The outer cylinder (7) and the cover ring (8) are also made of steel. The magnetic circuit is thus completed except at the circular gap where the Bakelite ring (6) is. The Bakelite ring (6) provides a fiber seat for the iron disk (1), which may be attracted against the seat by the magnetic field so as to make a vacuum seal. The iron disk (1) is held in position by a thin Bakelite spider (3) (canvas base 0.01 inch thick). As shown in the top sketch, the legs of the spider are fixed so that the iron disk can only move along the axis of the valve. The brass tube (1½-inch diameter), which is to connect the expansion valve to the cloud chamber, is insulated electrically from the valve by means of the fiber washers (10) so that the eddy currents induced in the metal parts of this valve will not flow to the chamber metals when the solenoid current is cut off at the instant of expansion. The operating circuit is described in a later section.

In order to keep a constant expansion ratio for many days, the air pressure behind the diaphragm of the cloud chamber has to be maintained the same for each expansion. This is accomplished satisfactorily by a Mason-Neilan No. 40 reducing valve with the top compartment of the valve sealed against the atmosphere. In this way the air pressure behind the diaphragm is regulated against a constant pressure but not the atmospheric pressure, which varies. Better regulation is obtained with a small leak provided in the back chamber.

C. The Photographic Equipment

A Recordak Micro-File Model E camera and a pair of xenon flash lamps have been used for taking photographs. Each lamp is connected across a bank of condensers of about 50-microfarads capacity, charged at a voltage of about 2500. Two ways of focusing the illuminating beams have been adopted. In one case where the chamber depth was 5 inches, each lamp (General Electric 126, 4 inches long) was focused with a parabolic mirror of 1-inch focal length and 4-inch width, while in the other case (chamber depth 8 inches) a lamp of 8-inches length was focused with a Plexiglas lens. The lamps used in this latter case were manufactured by Amglo Corporation of Chicago and were found to work satisfactorily. Each of these lenses is about 4 inches wide and 8 inches high and has a focal length of about 2 inches. Such lenses have been found to give a better defined beam of light than the parabolic mirrors—sharper edges of the beam and more intense and uniform distribution of light intensity across the depth of the cloud chamber. The cloud chamber is illuminated from both sides—cross illumination. The two beams of light are pointed slightly toward the camera, the angles made with the camera axis being about 70 degrees. The duration of light is only a few hundred microseconds, and therefore a large screen of zinc sulphide is used to test the focusing of the light beams. A front-coated mirror is put perpendicular to the chamber at one edge for the purpose of stereoscopic photography.

In order that the ion clusters can grow up to a large enough size for future condensation, the chamber is delayed to expand at 5 to 10 milliseconds after the particle has entered the chamber. Again to have the liquid drops large enough to be photographed, the lamps are made to flash at 50 to 100 milliseconds after the particle entry. Eastman Linagraph Ortho films have been used in most of the cases.

D. Slow Expansion Device

If each fast expansion is followed by a series of slow expansions, the background of the chamber is found to be much smaller and more uniform, especially when the chamber contains many foils and has a very low rate of expansion. We have used a slow expansion unit by which a sequence of four or eight slow expansions can automatically follow each main expansion. This unit consists of a clock motor, lock-in switches, and delay relays, as shown in Fig. 3. When the incoming pulse locks the lock-in switch #1, the motor drives a circular disk. This rotating disk (not shown), which has 4 studs fixed to its lower face, closes the microswitch #1 four times in a revolution, and hence the chamber undergoes four slow expansions. Near the end of the revolution microswitch #2 is closed by another stud of the disk, and this operation unlocks the lock-in switches #1 and #2 after a certain time interval determined by the delay relay #1. The motor then stops. When the switch *S* is on position 2, the motor repeats another revolution before it stops, and eight slow expansions then follow each main expansion.

E. Constant Temperature Control

It is found that if the room temperature changes by about one degree centigrade, the chamber does not work satisfactorily. In order that the chamber can be continuously ready to record cosmic-ray tracks, the room temperature must be maintained constant. The small insulated room (8′×8′×8′) containing the cloud chamber, is first cooled to a few degrees lower than the outside room temperature. This is done by circulating pipe water through an ordinary car motor radiator. The room is then heated by a heater, which is then controlled by some suitable device.

Two devices have been used. When one goes wrong, the other is used as a substitute. The first one is an ordinary mercury switch. The change in the height of a mercury column is used to switch the heater on or off. The mercury switch is connected in the starter anode of an OA4 tube. The anode current of the OA4 operates a relay which then controls the heater. Since in this way the current through the mercury contact is extremely small, the contact surfaces of the mercury and the pointer can be preserved for a long time.

The second method is an electronic one employing a resistance bridge, as shown in Fig. 4. A small a.c. voltage is applied to the bridge. The temperature-sensitive element made of fine iron wire has a resistance of about 100 ohms and is kept inside the cloud-chamber room. The unbalanced voltage, the phase of which corresponds to, say, a temperature lower than the working temperature, is applied to the grid of the 6J6 tube after being amplified by the two 9001 tubes in cascade. This voltage controls the

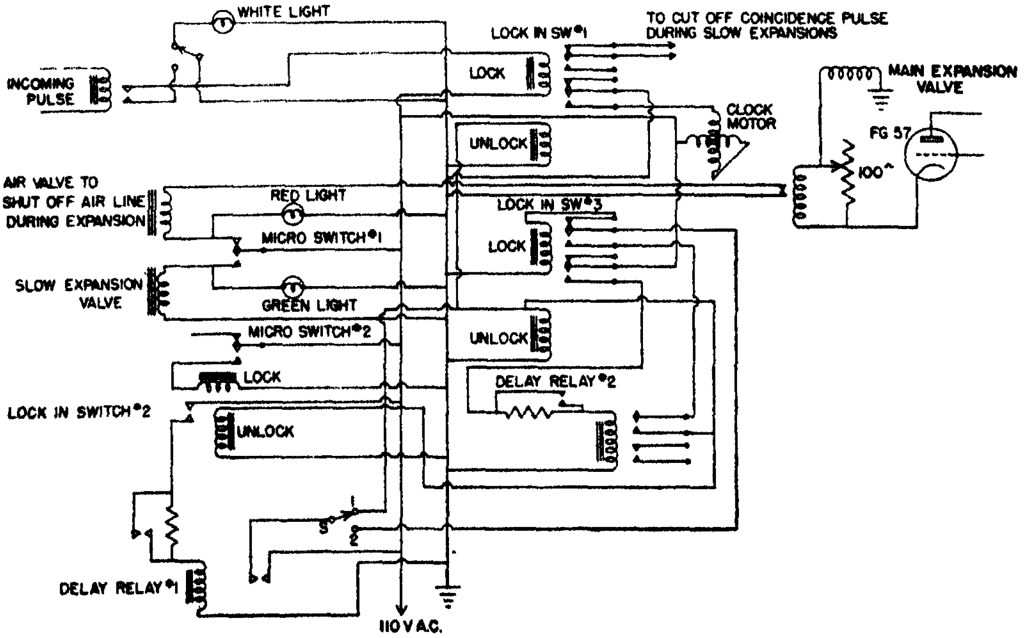

FIG. 3. Slow expansion unit.

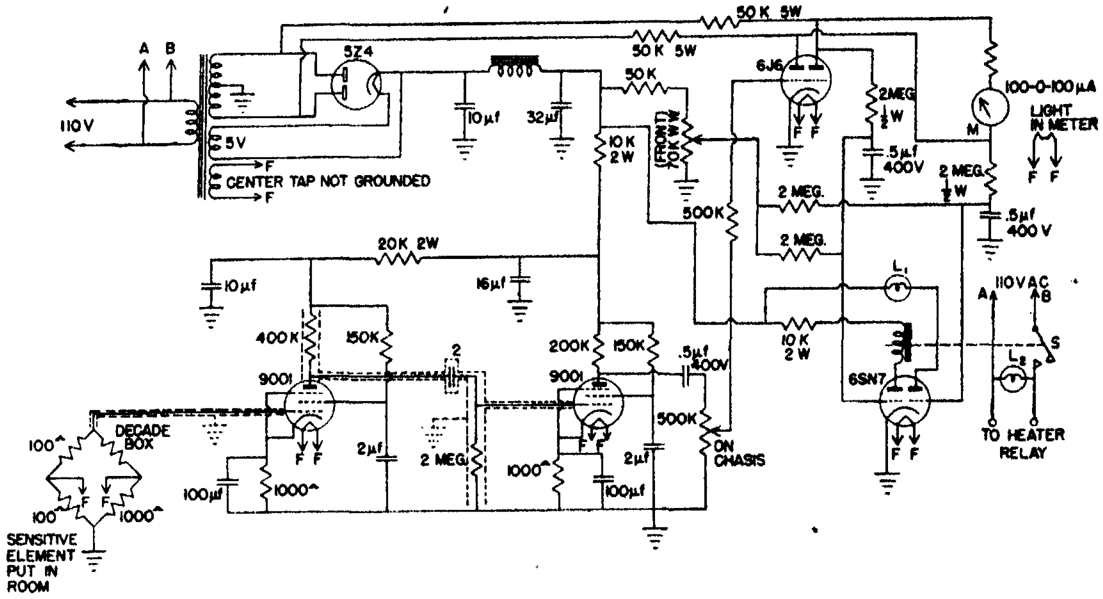

FIG. 4. Electronic temperature control circuit.

6J6 tube against the corresponding anode voltage of the appropriate phase. When the temperature gets lower, the needle of the meter *M* moves to one direction, and the relay in the left anode circuit of the 6SN7 tube closes the heater switch *S*. The indicating lamp L_2 is then lighted. When the temperature becomes higher, the needle of *M* moves to the other direction. The indicating lamp L_1 in the right anode circuit of 6SN7 is lighted. The advantage of this arrangement is that it controls a cooling device (if desired) as well as the heater.

III. ELECTRONIC CIRCUITS

The block diagram of Fig. 5 illustrates the electronic control system. A cosmic-ray particle actuating the three-fold telescope, but not the anticounters below the chamber, begins the cycling process through the coincidence circuits and the electronic gate. The expansion valve, clearing field removal, flash lamps, camera shutter and film advance, mechanical counter, and finally the reset of the gate proceed according to the time schedule, determined by electronic flip-flop circuits with adjustable recovery times. Thyratron-controlled current holds and releases the diaphragm-type expansion valve (cf. Section II-B).

The individual circuits are not shown completely, but some details are presented here, as the task of combining the many units in a reliable manner—especially for use with a very low expansion rate chamber—is time consuming, and many unexpected difficulties with stray pulses, etc., have been overcome in the present work.

A. Counter Circuits

Each tray of the three-fold coincidence counter array is coupled by a conventional cathode follower to a line leading to a pulse sharpener (univibrator), and to a conventional Rossi-type coincidence circuit. The anticoincidence counters are connected in groups to cathode followers which are coupled by crystal diodes to a similar pulse sharpener. This method of rectifier coupling permits paralleling large numbers of counters without undue individual loading. A section of the circuits including the final mixer tube is shown in Fig. 6. The discharge of one of the anticounters, along with the telescope, results in a negative pulse being applied to the control grid of the second section of the mixer tube, thus preventing the transmission of the signal from the telescope.

B. Gate Circuits and Time Delays

A 75-volt negative pulse of a few microseconds' duration from the mixer tube of the coincidence circuits serves to trip the gate (Fig. 7), which is a fast d.c. coupled "flip-flop" circuit, so arranged that it is stable with either tube #1 or tube #2 conducting. The coincidence pulse from the mixer tube causes tube #2 to conduct, and the negative pulse from its plate is led out to the various time delay circuits. Further coincidence pulses have no effect until a reset pulse occurring at the end of cycling again puts tube #1 in the conducting state instead of #2. The gate is insensitive to small pulses because of the method of triggering on the screen grid of tube #1. Triggering on the control grid of tube #1 was found to be unsatisfactory, as in this case the

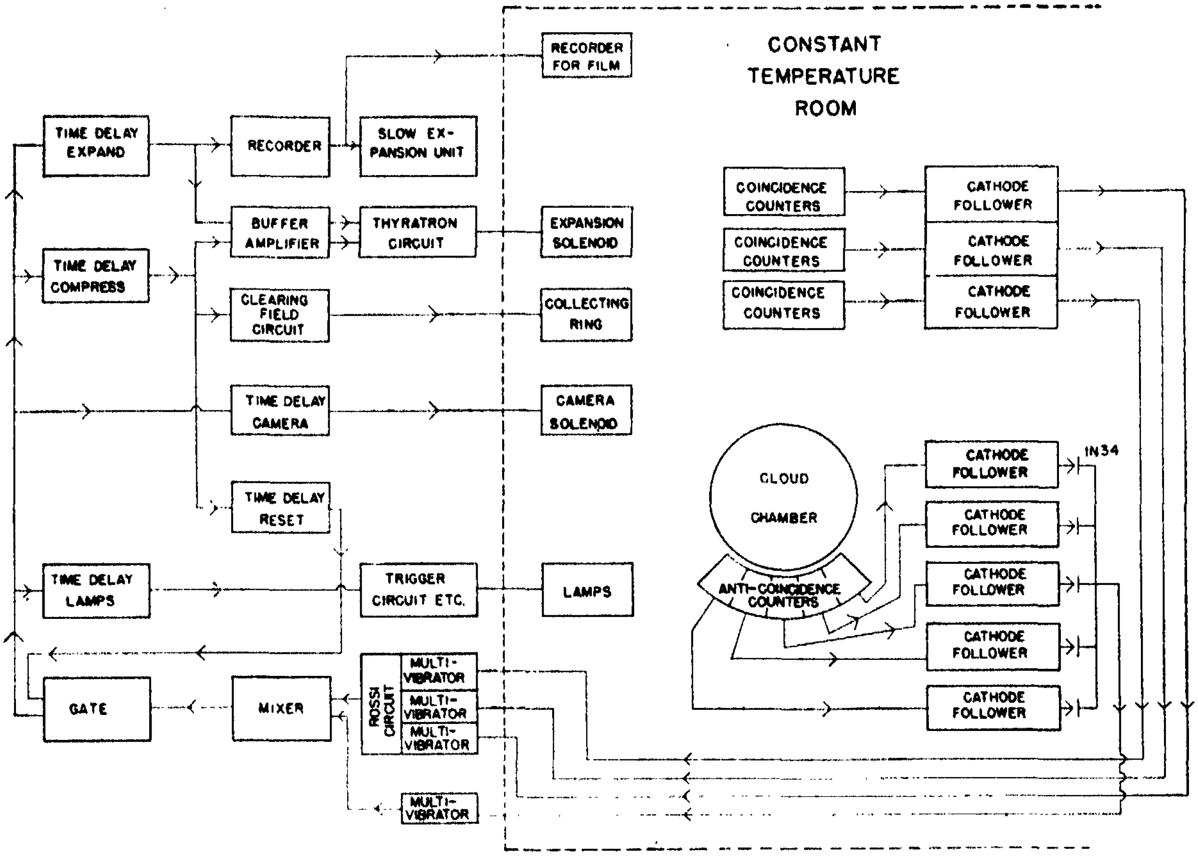

FIG. 5. Block diagram of electronic units.

triggering pulse appears on the output and begins cycling even though the gate is "closed." If the suppressor is used for triggering, the plate-suppressor capacity transmits the pulse to the grid of tube # 2, and the gate may be reopened prematurely before cycling is completed. The input and output connections are electrically isolated, and filtering is provided liberally on power connections. Manual

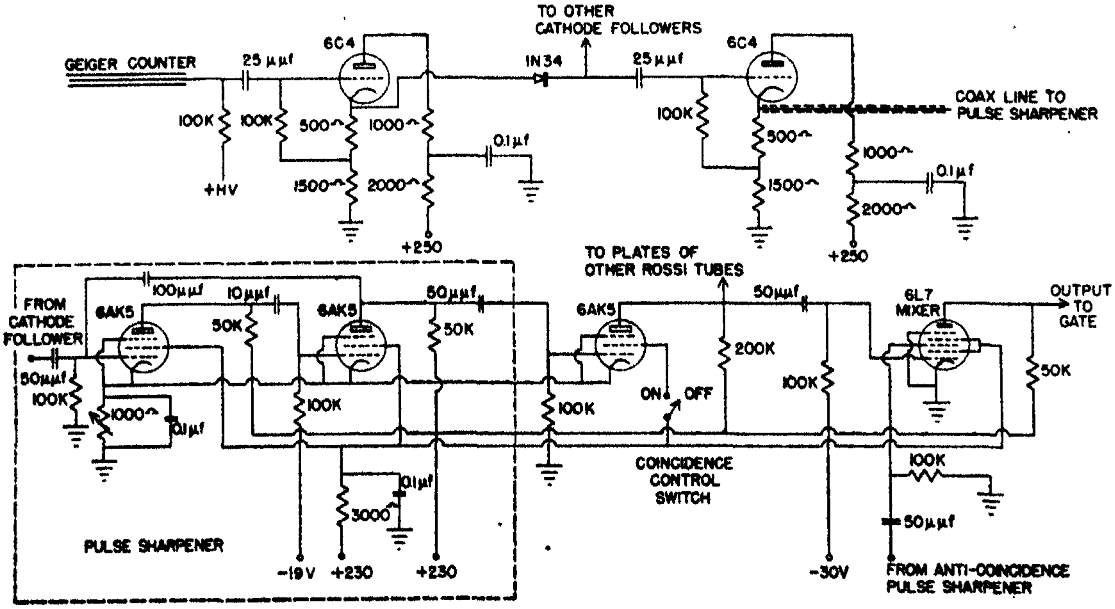

FIG. 6. Cathode follower, coincidence, and anticoincidence circuits.

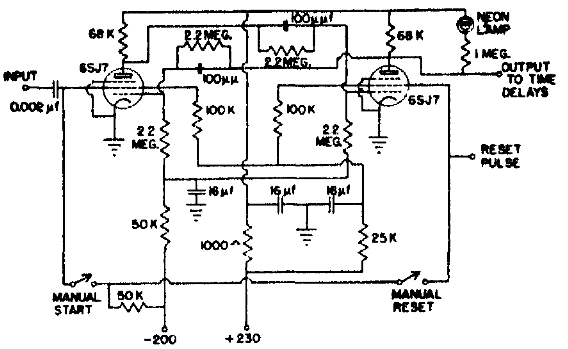

Fig. 7. Gate circuit. This circuit remains closed until cycling is completed.

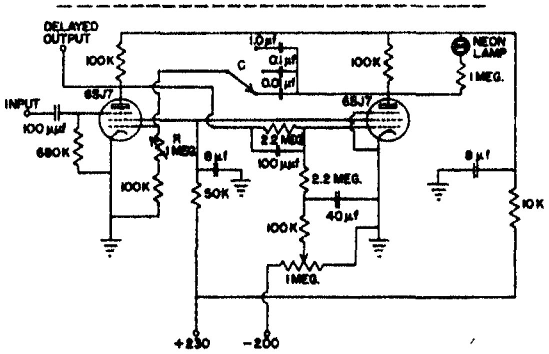

Fig. 8. Typical time delay circuit.

buttons permit operation of the gate by hand when conducting tests of the chamber.

The time delay circuits (see Fig. 8) are conventional univibrators, the period being controlled by the $R-C$ coupling network. The circuit is actuated through the suppressor grid of tube #1, to reduce sensitivity and isolate the input and output circuits.

C. Expansion Valve Circuit

The release of the expansion valve is accomplished by extinguishing the FG57 thyratron which carries the valve current by reducing its plate voltage to zero (see Fig. 9). A second thyratron, type FG17, is used for this purpose, discharging a condenser C through the common load resistance R of the two thyratrons when ignited by a pulse from the time delay expand circuit (see Fig. 5).[8] A pulse from the time delay compress circuit fires the first thyratron and closes the valve. The action is quite rapid, the valve opening with a miniature explosion. With a magnetizing current of about two amperes, the valve is able to sustain one atmosphere over pressure with negligible heating. It was found necessary to isolate the thyratrons from the time delay circuits by a buffer amplifier to prevent the feedback of spurious pulses into other delay circuits.

D. Lamp Circuits

As described in Section II-C, xenon-filled flash lamps (General Electric 126 and Amglo Corporation lamps) are used for illumination, fired from a capacitor bank of 50 or 100 microfarads charged to about 2500 volts. A fine wire wrapped about the capillary of the lamp and excited by the secondary of an automobile ignition coil serves to start the discharge. The coil is energized by a small thyratron which discharges a capacitor through the primary (Fig. 10). The charging and firing circuits must be carefully shielded, and the input from the lamp time delay filtered, as shown, against radiofrequency interference from the discharge circuits. The strong inductive pulse generated when the lamps discharge is an especially bad source of interference, not only to the cloud-chamber circuits, but to other high gain equipment within a radius of 25 feet or more.

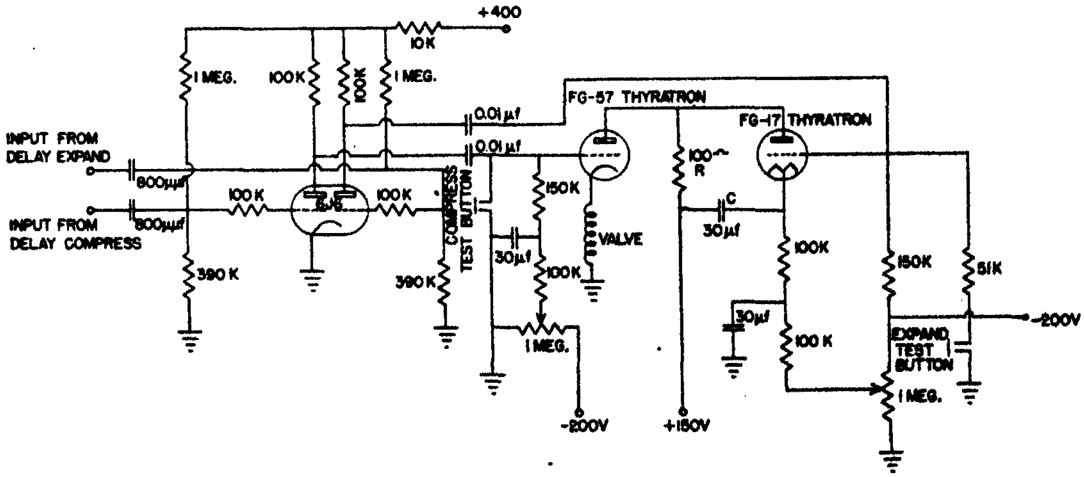

Fig. 9. Valve operating circuit.

---

[8] F. L. Allen, Rev. Sci. Inst. 19, 24 (1948).

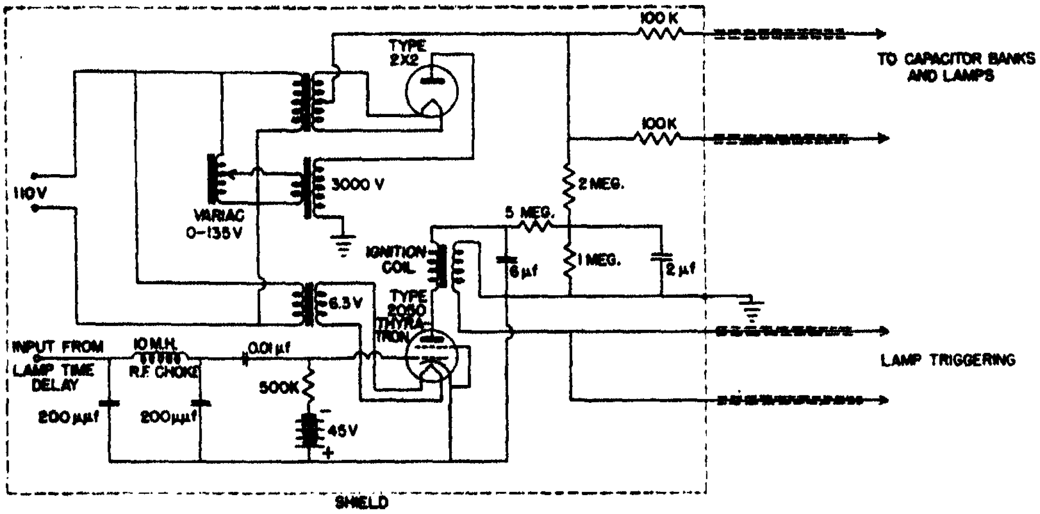

FIG. 10. Lamp firing circuit.

E. Clearing Field and Recording Circuits

The chamber clearing field is applied constantly, and removed at the earliest possible moment after the passage of the particle, by means of a d.c. amplifier connected to the time delay compress circuit. This time delay circuit triggers with the coincidence (see Fig. 5) and returns to normal at the time of compression, when the clearing field is reapplied.

The mechanical counter which is photographed along with the illuminated chamber in each exposure is turned by a simple cold-cathode thyratron circuit (Fig. 11).

IV. SOME CLOUD-CHAMBER PICTURES

In conducting the experiments on meson absorption by thin foils, a three-fold coincidence telescope has been used on the top of the chamber, and many anticoincidence counters in the form of an arc have been employed to surround the bottom circumference of the cloud chamber (see Fig. 5). Eleven (sometimes less) thin foils of thickness approximately equivalent to the range of a 12-Mev (or 2-Mev for Al) proton have been rigidly supported on a Lucite frame inside the chamber. The vertical beam of mesons before entering the telescope has to pass through a lead block of about 30-cm thickness. This lead block has two purposes: to filter off the electronic components of the incident beam, and to increase the intensity of the slow mesons. The whole setup for these experiments is shown schematically in Fig. 12.

In principle, the chamber expands only when a particle after passing through the telescope is absorbed by a foil or by the chamber and counter

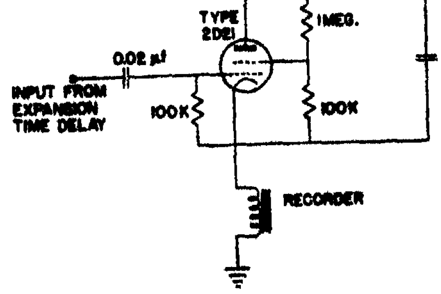

FIG. 11. Mechanical recorder. *Note:* The number under TYPE in the figure should read: *1D21*.

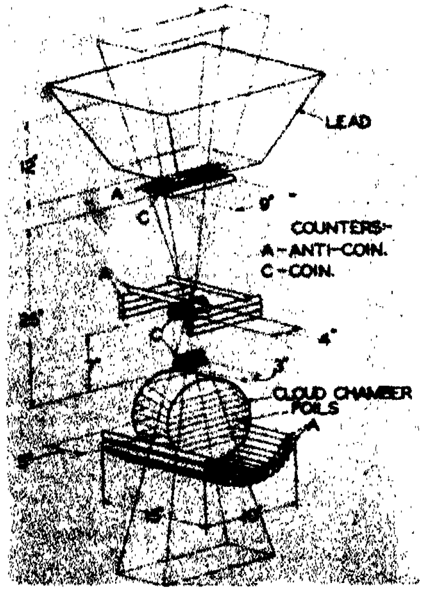

FIG. 12. Apparatus—meson absorption experiment.

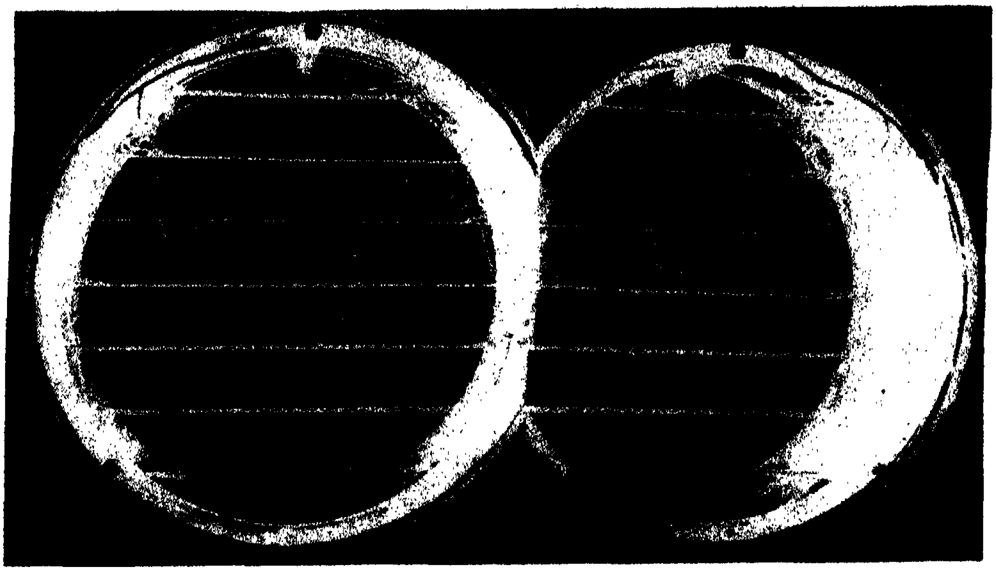

FIG. 13. Side showers covering whole chamber (Fe foils).

walls. To reduce stray coincidences, each tray of the telescope is protected against side showers by anticoincidence counters, and the bottom anticoincidence counters are arranged to cover a solid angle larger than geometrical necessity so as to receive scattered particles. On the average the chamber was triggered about once per 40 minutes, and one useful picture (a particle stopping at a foil) was obtained in about 35 pictures. The variation of ionization from foil to foil has been used to identify a proton, a meson, or an electron. Multiple scattering has been used for reference also.

Here we have presented some pictures of general interest. Figure 13 shows a large shower, which must have been produced in the back of the chamber. Here the chamber is seen to contain many short but straight tracks. The frame on the right-hand side is the stereoscopic picture, and the foils are iron foils (0.028 inch). In Fig. 14, simple cascade showers are produced at the iron foils by some vertical incident particles, presumably electrons. A meson decaying into a light particle, presumably an electron, is shown in Fig. 15. Here the meson stops in the last Al foil (0.002 inch) and the decay electron is emitted upwards to the right (see the direct picture on the left).

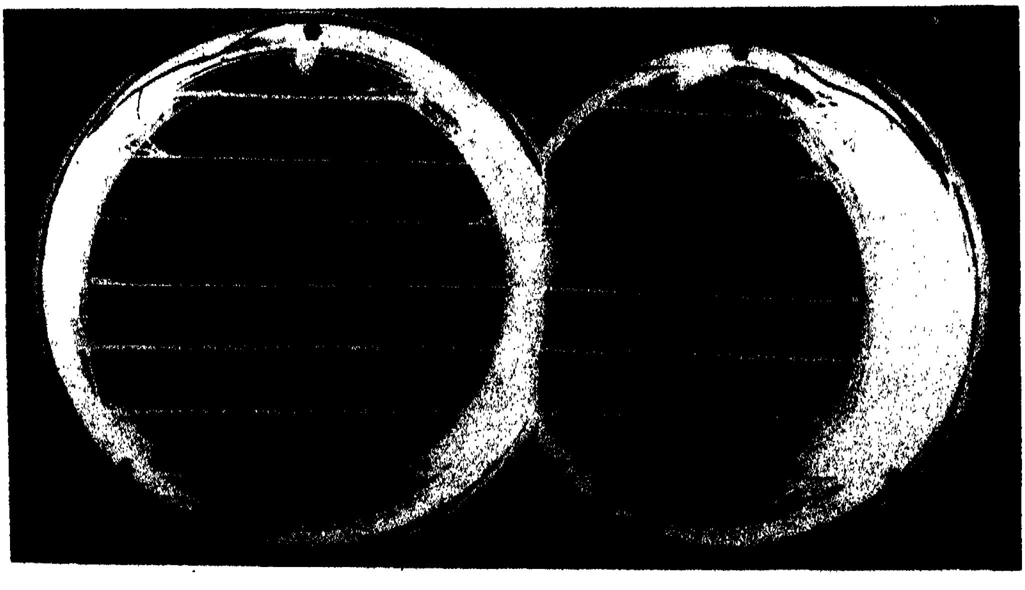

FIG. 14. Simple cascade showers (Fe foils).

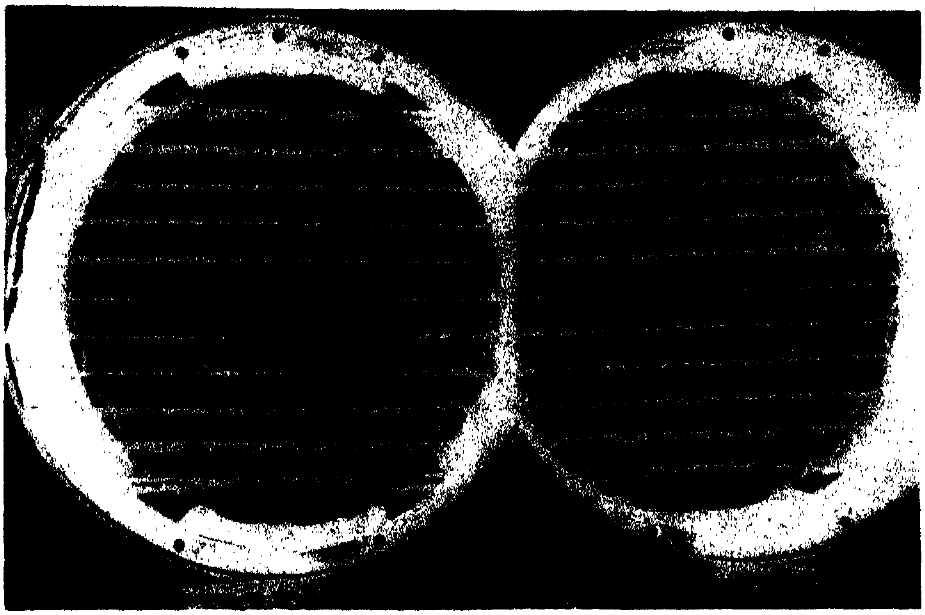

FIG. 15. A meson decaying in a 0.002-inch Al foil.

In conclusion, we should like to express our sincere thanks to Mr. D. B. Davis and his staff for building the cloud chamber and the control equipment, to Dr. T. Coor and Mr. F. J. Darago for their help in designing the electronic temperature control, and to Dr. L. G. Lewis for the valve design.

THE REVIEW OF SCIENTIFIC INSTRUMENTS VOLUME 20, NUMBER 4 APRIL, 1949

Magnetic Deflector for Mesons Produced in the 184-Inch Cyclotron

WOLFGANG K. H. PANOFSKY AND ERNEST A. MARTINELLI
Department of Physics, Radiation Laboratory, University of California, Berkeley, California

(Received January 3, 1949)

A magnetic deflector has been constructed which makes the mesons artificially produced in the 184-inch cyclotron by alpha-particle bombardment available outside the cyclotron tank. The deflector consists of a magnetic shield especially designed to operate in very high external magnetic fields. The effect of the magnetic shield on the internal cyclotron beam has been compensated by pole shims. The deflector yields a total meson flux of approximately 500 mesons per minute.

THE artificial production of mesons by means of high energy α-particles in the 184-inch cyclotron at Berkeley[1] indicated the desirability of making mesons available outside the cyclotron tank in order to make investigations possible by means other than photographic plates inside the tank. A magnetic deflector to draw mesons out into a re-entrant chamber in the cyclotron wall was therefore constructed.

The circulating α-particle beam strikes a target at a radius of 80½ inches from the center of the cyclotron. The magnetic field at the target position is close to 14,000 gauss, so that low energy mesons are unable to leave the cyclotron. The magnetic deflector consists simply of a magnetic shield placed in such a manner that it shields the meson beam and permits it to enter a re-entrant chamber in the cyclotron wall (Fig. 1).

A magnetic shield for this purpose has to meet four requirements: 1. The field in the channel must be sufficiently low to permit exit of the mesons from the field. 2. It must have a sufficiently high geometrical aperture. 3. The shield must not disturb the field at a radius less than target radius. 4. The shield must not interfere with the electrostatically deflected beam[2] in the cyclotron.

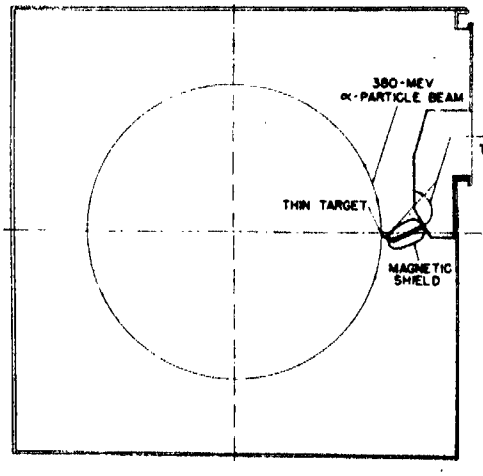

FIG. 1. Geometrical distribution of meson deflector and target in the magnet of the 184-inch cyclotron. Note the trajectory of the alpha-particle beam and the mesons produced in the target.

The problem of shielding magnetically to a sufficient extent in an external field of 14,000 gauss is made difficult by the saturation of iron. Saturation effects are reduced if the shield is not circular but has its large dimension perpendicular to the field; this will only give a small increase in flux density in the iron relative to the external field. These considerations lead to the choice of a shield approximately an ellipsoid whose smallest axis is parallel to the field. The ellipsoidal shape is superior to any rectangular geometry since corners would saturate and thus not contribute to the shielding while still contributing to the disturbing field.

The ellipsoidal shape can be easily analyzed

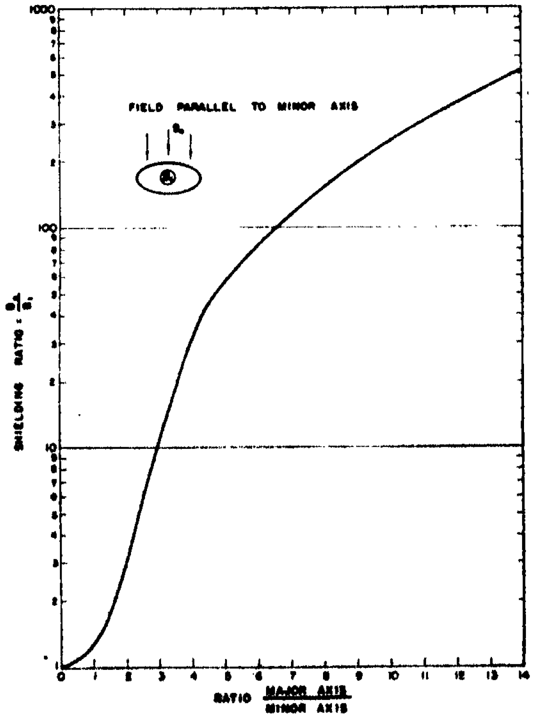

FIG. 2. Theoretical shielding ratio of an oblate-spheroidal shield with cylindrical hole as a function of axial ratio of the spheroid in an external field of 14,000 gauss.

---

[1] E. Gardner and C. M. G. Lattes, Science 107, 270 (1948).

[2] Powell, Henrich, Kerns, Sewell, and Thornton, Rev. Sci. Inst. 19, 506 (1948).

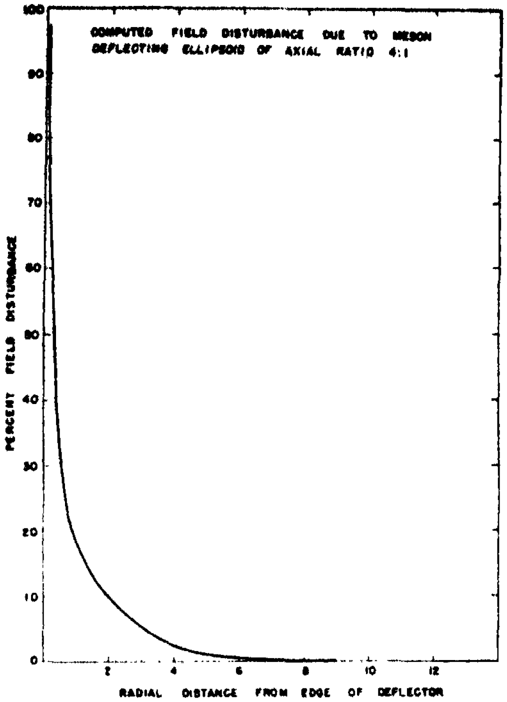

FIG. 3. Percent field disturbance due to spheroidal shield of axial ratio 1 to 4 on the magnetic field in the cyclotron.

mathematically for a given magnetization curve of the iron used. Figure 2 shows a theoretical plot of the shielding ratio attainable with an oblate spheroidal[8] shield with a small cylindrical hole inside the spheroid. The curve is computed for cold rolled steel in an external field of 14,000 gauss. Note the rapid improvement of the attainable shielding ratio with increase in axial ratio of the ellipsoid. An axial ratio of 4:1 was chosen here.

The theoretical disturbance in the field resulting from the ellipsoid is shown in Fig. 3 for an ellipsoid of 12-in.×3-in. axis. The shield was placed 3½ inches from the target radius, thus disturbing the field by approximately 3½ percent. This disturbance is compensated by shims supported on the cylcotron poles, in accordance with the method of Powell *et al.*[2] A radial experimental field plot and the field corrected by the shims is shown in Fig. 4. The position and geometry are also shown in Fig. 4.

Owing to the fact that the shielding action of the iron cannot be computed accurately, it was necessary to estimate the meson trajectory first, construct a deflector, compute the trajectory, and then build a new deflector to conform to the computed trajectory. The final shape of the shield and the position of the meson trajectory is shown in Fig. 5. Figure 6 shows the magnetic field in the channel with and without the shield. Owing to the curvature of the trajectory and the ellipsoidal cross section of the shield, the shield is constructed of 12 layers of hot rolled steel plate, flame-cut to proper shape and bolted together. The hole for the trajectory tapers from an initial hole of 1½-in. vertical ×1-in. horizontal to 2½-in.× ½-in. square at the exit end. Figure 7 shows the assembled deflector.

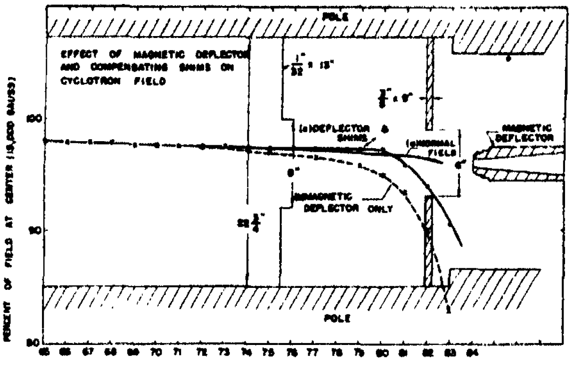

FIG. 4. Radial magnetic field in the cyclotron under the following conditions: (a) Before introduction of meson deflector. (b) After introduction of meson deflector, but uncompensated. (c) Meson deflector in place and compensated with shims as shown.

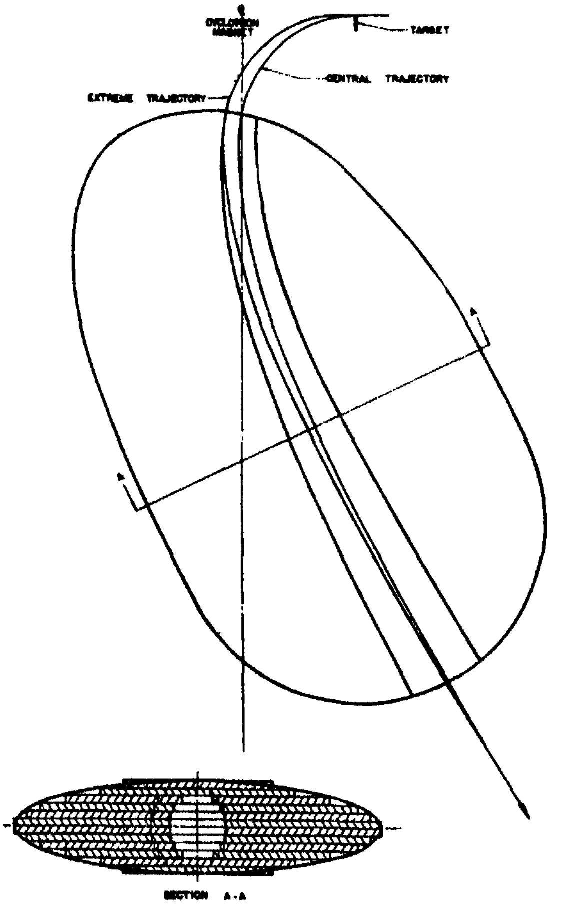

FIG. 5. Meson trajectories from target through meson deflector, as plotted from field measurements.

---

[8] For solution of potential problem, see e.g., H. Smythe, *Static and Dynamic Electricity* (McGraw-Hill Book Company, Inc., New York, 1939), pp. 156ff.

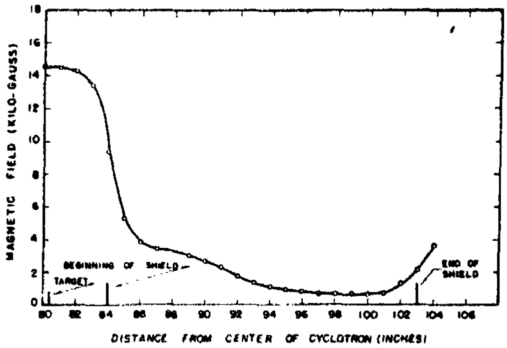

FIG. 6. Experimental magnetic field as a function of position along meson trajectory through meson deflector.

FIG. 7. Photograph of meson deflector in retracted position.

The deflector is designed for a central trajectory corresponding to $B\times\rho=147{,}000$ gauss-cm, corresponding to an 8.5-Mev μ-meson (taking the mass of the μ-meson as $215m_e$) or a 6.0-Mev π-meson (taking the mass of the π-meson as $286m_e$). The deflector will accept beams of vertical divergences of ±6°, horizontal divergences of ±7.2° (at central value of energy); the range of momenta accepted is ±12 percent about the central value.

At this date the deflector has been used only in conjunction with the photographic means of detection. With a cyclotron bombardment of 3×10^{-7} amp. of α-particles for 30 minutes the meson yield is about 30π-mesons in the edge of a 100-micron emulsion; this corresponds to a total flux of about 500 mesons/minute out of the aperture of the deflector.

The problem of deflecting mesons by means of a magnetic shield was suggested by Professor L. W. Alvarez. We are greatly indebted to the magnetic measurements group of the laboratory, notably D. C. Sewell and A. J. Hulse for making magnetic measurements and to Professor Wilson Powell for valuable discussion. This work was performed under the auspices of the AEC.

THE REVIEW OF SCIENTIFIC INSTRUMENTS VOLUME 20, NUMBER 4 APRIL, 1949

Pressure Regulated Thin Window Geiger-Mueller Counter*

MICHEL TER-POGOSSIAN, J. EUGENE ROBINSON, AND J. TOWNSEND**
Department of Physics, Washington University, St. Louis, Missouri

(Received January 13, 1949)

The use of very thin Zapon or Formvar windows for G-M counter tubes in beta-spectroscopy is limited by the fact that the filling mixture of the counter diffuses or leaks through the window, which forbids the use of very thin windows. A pressure regulator is described which will permit the maintenance of a constant pressure of filling mixture even if the window of the counter allows the slow escape of the gas. A thin window G-M counter presenting some improvements is also described.

PRESSURE REGULATOR

THE window separating a G-M counter from the vacuum system of a beta-ray spectrograph should be as thin as possible in order that low energy electrons may be observed. Zapon and Formvar films, prepared according to well-known techniques,[1,2] have been used in this laboratory. Multiple layers were usually used to decrease the probability of holes occurring. Satisfactory films having electron cut-off energies of higher than 5 kev are easy to prepare. However, it has been found that thinner films (~2 kev), even those which do not leak when first used, develop slow leaks after a period of days. This is attributed to the occurrence of very small holes or cracks accompanying the observed stretching of the film caused by the gas pressure in the counter.

A counter in this condition is difficult to use, since the plateau shifts continuously as the pressure decreases. The use of lower pressures of filling mixture in the counter is helpful in preventing window leakage, but a lower limit of 3 to 5 cm Hg is set by the fact that at lower pressures the efficiency of the counter becomes appreciably less than 100 percent, and changes with electron energy.

The connection of a large ballast volume of filling mixture to the counter affords some improvement but is not entirely satisfactory. A system in which there is a continuous flow of gas into the counter, with the excess flowing out through a mercury bubbler, was also tried. It was found that this system was not capable of maintaining the pressure sufficiently constant.

The following scheme was found to be satisfactory. A filling mixture of the proper composition is prepared and stored in a container at approximately atmospheric pressure. This container is connected to the inlet of the device shown in Fig. 1. The outlet is connected to the counter. If the pressure in the counter falls below the preset level, the tungsten contacts sealed into the mercury manometer close and actuate a relay which powers the coil. The iron plunger rises, lowering the mercury level to a point where more filling mixture can flow through the porous glass plug. The device operates smoothly over a wide range of flow rates, and the manometer is observed to vary not more than $\frac{1}{2}$ millimeter.

Care should be taken that sparking does not occur at the manometer contact, as this has a tendency to decompose the quenching vapor in the mixture. The use of a d.c. relay operating on a few milliamperes of current, together with a resistance and capacitance connected in series across the manometer contacts will prevent sparking.

THIN WINDOW GEIGER-MUELLER COUNTER

The conventional G-M counter as used in most laboratories is usually constructed in a semipermanent manner with heat-treated seals of glass, Kovar, or solder. A counter so constructed renders itself quite awkward for experimentation, since a change in design requires either the construction of an entirely new counter or the careful breaking of the heat-treated seals. The counter herein described

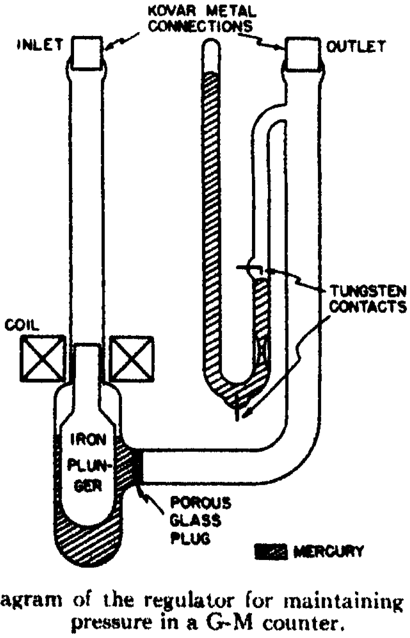

FIG. 1. Diagram of the regulator for maintaining a constant pressure in a G-M counter.

---

* Assisted by the joint program of the ONR and AEC.

** Atomic Energy Commission Predoctoral Fellow in the Physical Sciences of the National Research Council.

[1] John Backus, Phys. Rev. 68, 59 (1945).

[2] K. Siegbahn, Ark. f. Mat. Ast. o. Fysik 30A, No. 20 (1944).

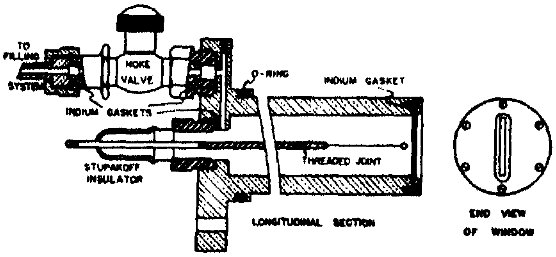

FIG. 2. Thin window G-M tube designed for easy assembly.

eliminates these difficulties by providing gasket seals which may be broken easily and quickly without damage to any portion of the counter mechanism.

The body of the present counter is bored in a piece of brass cylinder, highly polished inside, and chromium plated. The purpose of plating the inside is to obtain a stainless, hard surface, easy to clean when the counter is taken apart.

The filling mixture from the pressure regulator is fed into the counter through a bellows-type Hoke valve (type No. 431). This type of valve has been tried on several counters and has always been found to be gas tight. The Hoke valve is screwed into a stainless steel plug and soft soldered to assure a perfect tightness. This plug is screwed into the flange of the counter. A 0.010″-thick indium gasket assures the tightness of all joints. Three of these gaskets are used in the present counter. A flexible brass tubing connects the counter to the pressure regulator.

In the counter constructed here, which has a cathode diameter of 1″, the anode used is a tungsten wire 0.006″ in diameter and 1¼″ long, the end of which is insulated by a glass bead. It is hard-soldered into a brass threaded plug which is screwed into the central lead. This arrangement permits the easy replacement of the wire. No dimensions except those quoted above will be given, since other dimensions are not critical and can be readily adjusted to the purpose of the counter.

The central lead is a stainless steel rod, hard-soldered to a Stupakoff glass Kovar seal, which is itself soft soldered to a threaded plug similar to the one used with the Hoke valve. An indium gasket makes the joint tight. The window of the counter is a thin film of Zapon cemented with Formvar to the end plate which is attached to the body of the counter by six screws. In this case again an indium gasket assures the tightness of the system. All of the surfaces inside the counter have been carefully polished and all the sharp edges broken. The plateau of this counter is flat between 1400 and 1600 volts when filled to 8 cm Hg of an argon (80 percent)-ethylene (20 percent) mixture.

No rubber has been used in the system described above.[3] All the tubings are sylphons and the joints are similar to the one shown in Fig. 2, the tightness being obtained by the use of indium gaskets. This counter can be taken apart, cleaned with alcohol or ether, and, when mounted, will not show any variation either in the threshold or in the efficiency.

The pressure regulator and G-M counter described have been added to a 180° beta-ray spectrometer[4] in this laboratory and have given satisfactory service during the course of investigations.[5]

ACKNOWLEDGMENTS

The authors wish to thank Mr. O. Retzloff for his excellent machine work in the construction of the Geiger counter.

---

[3] It is the superstition of the authors that it is preferable to avoid the use of rubber or neoprene in G-M counters.

[4] F. N. D. Kurie and M. Ter-Pogossian, Phys. Rev. **74**, 677 (1948).

[5] M. Ter-Pogossian, E. Robinson, and C. S. Cook, Phys. Rev. **75**, 995 (1949).

THE REVIEW OF SCIENTIFIC INSTRUMENTS VOLUME 20, NUMBER 4 APRIL, 1949

Electronic Apparatus for the Determination of the Physical Properties of Freely Falling Raindrops

ROSS GUNN
Physical Research Division, U. S. Weather Bureau, Washington, D. C.

(Received January 13, 1949)

An apparatus is described for measuring the mass, velocity of fall, sign, and free electric charge of individual falling raindrops. Two vertically separated rings are so arranged that naturally charged raindrops fall through them and induce pulses on the grid of a vacuum tube amplifier which in turn operates a tape oscillograph. From the characteristic double pulses produced, the charges and transit times may be determined. The mass of the droplet is simultaneously determined by measuring the size of the spot produced when the drop falls on blueprint paper tape traversing the oscillograph. Short cuts for the reduction of data on drop sizes are given.

SURPRISINGLY little information is available in the literature on the physical and electrical properties of natural precipitation, particularly in relation to the characteristics of single elements. It is the purpose of this paper to outline briefly the principles, design, and calibration of a new electronic instrument that has made possible a detailed study of natural raindrops in relation to their mass, velocity of fall, rate of evaporation, and transported electrical charge. It is believed that the instrument will be generally useful in further studies of the precipitation processes and the physical phenomena associated therewith. Improved methods for the rapid determination of approximate raindrop masses by the use of blueprint paper are outlined, since this method forms a valuable adjunct to the strictly electronic equipment. Perhaps the greatest value of the apparatus resides in the fact that it easily collects information on a large number of individual events, and these appear to be more descriptive of weather processes than statistical results.

BASIC PRINCIPLES

It is an observed fact that a large fraction of all naturally falling raindrops or snowflakes carry appreciable electric charges. Moreover, it has been found practicable to indicate the proximity of such charged precipitation by suitable electronic amplifying equipment appropriately connected to an oscillograph.[1] For example, if a carefully shielded and highly insulated induction ring is so positioned that a charged water droplet falls through it, the charge on the droplet by inducing an opposite charge on the ring, can be arranged to produce a pulse on the grid of a vacuum tube, which in turn can operate an amplifier and associated oscillograph. The magnitude and sign of the electrical charge on the droplet is measured by the direction and magnitude of the pulse recorded on a moving tape oscillograph. It is further easy to see that by positioning two similar inducing rings, separated by a known distance, and making provisions for the rain droplet to pass successively through both inducing rings, a double pulse will be recorded. Now, since the time between the two pulses may be measured by their relative displacements on a moving tape oscillograph, and this is the time it took the droplet to travel the distance between the fixed electrodes, it is clear that the velocity of the droplet may be easily and quickly determined.

Because of the mechanical forces caused by turbulence and the electric fields occurring in the atmosphere, the velocity of fall of natural raindrops of a given size is variable. For this reason, it was necessary to measure the mass of the falling raindrops by an independent means. Earlier work[2] has demonstrated that the mass of natural raindrops can be quickly and conveniently determined by allowing them to fall on blueprint paper. The rain droplets produce spots on the coated paper which can be made semipermanent by developing the paper with light. The method is an adaptation of one widely employed by early German experimenters who used ordinary absorbent paper, and dusted a water soluble dye over the spots to preserve the record.[3] To a first approximation the area of the spot is proportional to the mass of the impinging droplet, and, therefore, the size of the spot is readily calibrated in terms of its mass.

The new apparatus combines the above elements in such a way that the signature traced by a droplet and the spot size are presented as simultaneous events on a moving paper tape. Thus, for each event the mass, velocity of fall, and sign and magnitude of the electric charge on each droplet may be determined. Obviously, such an apparatus is important in any study of the precipitation processes.

THE APPARATUS

The general arrangement and design of the first successful instrument is shown in Fig. 1. The outer

---

[1] Ross Gunn, Phys. Rev. 71, 181 (1947).

[2] Ross Gunn, Naval Research Laboratory Technical Report A676A (October 1944).

[3] J. Wiesner, Wien. Sitz.-Ber. 104, 1397 (1895); P. Lenard, Meteorol. Zeits. 21, 249 (1904).

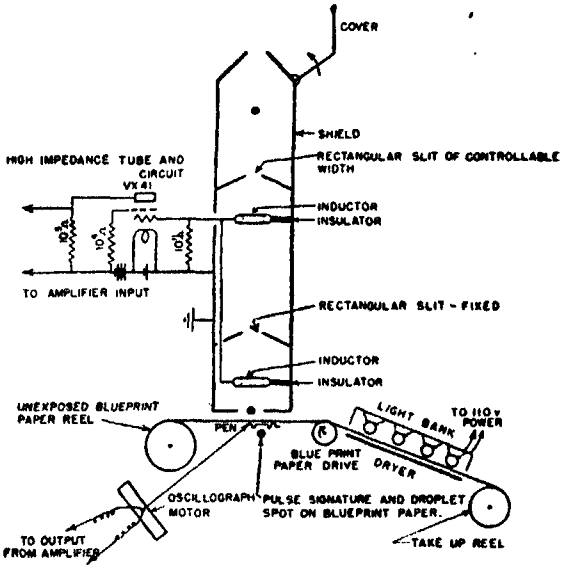

FIG. 1. Arrangement of the apparatus and electrical circuits.

shield of the instrument was an aluminum tube 18 inches in diameter and about 10 feet high. The top of this tube was a cone having an angle of about 45 degrees and arranged with a 6-inch hole at the top. A cover was provided as shown that could be turned back and be entirely clear of the hole. About 4 feet below the top, another cone with a hole about 4 inches in diameter was arranged as shown. A slit was mounted over this hole in such a way that its surfaces were about 45 degrees to the horizontal. It was found convenient to make this slit 4″ long and variable in width from about ¼ inch to ¾ inch. Eight inches below the first slit, a highly insulated brass cylinder 6 inches in diameter and 6 inches long was mounted, concentric with the supporting tube and centered immediately below the first slit. Four feet directly below the first slit a second slit was mounted on another internal cone. This second slit was 4″×¾″ and was so aligned as to be immediately under the first slit. Below the second slit another highly insulated inductor electrode identical with the top one, was mounted and these two were joined electrically by an air insulated wire running down the large tube near its wall.

Mounted in a dry compartment inside the large supporting tube was an electrometer tube having a high input impedance (such as the Victoreen VX-41). Its control grid was connected directly to both inducing electrodes as shown in Fig. 1. The screen and plate voltages on this tube were adjusted by experiment so that the tube would modulate either upward or downward by the same amount for opposite potentials of the same magnitude on the grid. The magnitude of the input resistance placed across the grid and filament of the electrometer tube plays an important part in determining the characteristic response of the apparatus to the electric charge. For example, when the product of the input resistance, *R*, and the input capacity, *C*, or the electrical relaxation time is appreciably greater than the transit time of the charged particle through the electrode, the amplitude of the output pulse measures the total quantity of the electricity on the droplet. On the other hand, if the relaxation time is notably less than the transit time, the magnitude of the pulse is determined by the current flowing and is proportional to the electric charge on the droplet and to the velocity with which it traverses the electrode. Thus, when it is desired to use the apparatus to measure free electrical charge, the resistance-capacity product should be made large, and the charge magnitude may then be immediately scaled from the oscillograph trace. It has been found, on the other hand, that if the device is to be used to measure accurately the velocity of a particle traversing the inducing electrodes, then it is desirable to reduce the input resistance to make the relaxation time smaller than the transit time. The signature given by a traversal of the latter type may be more accurately measured in terms of velocity than the signature normally produced when the relaxation time is large. Characteristic signatures for the two conditions outlined are shown in Figs. 2a and 2b.

Immediately below the tube containing the slit and inductor system, a shelf is provided to carry the oscillograph. The oscillograph was a Brush Laboratory double channel Type BL-202 fed by one of their Type BL-905 amplifiers. The standard recorder paper provided by the manufacturer was replaced by a roll of unexposed blueprint paper about 4″ wide that was pulled through the feed by the small synchronous motor built into the oscillograph. The oscillograph is arranged to be movable on the shelf and is positioned in relation to the projected area of the slits in such a way that a droplet falling with a mean velocity of 400 cm/sec., arrives at the blueprint paper just at the position where the pulses produced by the same droplet are traced by the moving oscillograph pen. Thereafter, the blueprint paper with its spot of water and continuously inked trace is pulled through the oscillograph drive and thence down a trough about five feet long lined with 50-watt electric light bulbs, where the wet spots are dried and the blueprint paper exposed to make a semipermanent record. The paper finally proceeds to a take-up reel driven by a weak friction clutch onto a final process roll. At the paper speeds usually employed, namely 2.5 cm/sec., the blueprint paper was adequately exposed to the light and sufficiently dried to wind up on the final spool. It has been found economical and convenient to buy the blueprint paper in wide rolls and cut them up into rolls of width to fit the oscillograph.

In practice the apparatus operates as follows: the top door of the instrument is opened, and a drop falls through the top cone and succeeds in passing the first slit. If it is not making a large angle with the vertical, it will pass the inducing ring at some distance from its wall, and thence proceed to the second slit about a meter below. If the droplet is not well lined up, it does not get through the second slit and only a single pulse will be recorded. However, if the drop is moving in a substantially vertical direction, it will pass through the second slit and traverse the second inductor, landing finally on the moving blueprint paper immediately below. A pulse will be produced on the grid of the electrometer tube by the droplet as it traverses both the first and second inductors. Thus, characteristic double pulses are traced on the oscillograph paper for droplets so lined up as to traverse both slits. The direction and amplitude of these pulses determine the sign and free electric charge actually resident on the drop. Having traversed the slit and inductor system, the droplet falls on moving blueprint paper adjacent to the trace of its own double pulse, and the size of the spot it produces permits one to determine its mass by an independent measurement. A little experience enables one to associate the double pulses of the oscillograph with the proper spot on the blueprint paper. However, a certain small fraction of the incoming raindrops are electrically neutral or discharge themselves by touching the edge of the slit, and these frequently confuse the interpretation.

A number of typical signatures and rain spots produced by natural raindrops are reproduced in Fig. 2 both for positively charged droplets giving an upward pulse, and for negative ones producing a downward pulse. It may be noticed that the passage of an electrical charge through the highly insulated inductor system modifies the charge on the grid of the electrometer tube when high input resistances are employed, and thus, shifts the zero position of the oscillograph. For this reason, the second pulse is slightly displaced, although its magnitude in relation to the new zero is the same as the original one. It may be noted, further, in Fig. 2a that the width of the second pulse is somewhat less than for the first one. This difference in width results from the different geometry of the lower inductor in relation to its surroundings. At first this difference was considered a misfortune, but actually it has been most useful in defining the signature for an actual passage of a single drop. For example, two droplets occasionally traverse the first inductor only, in about the right sequence to produce a nearly typical signature, but by careful examination it is possible by the above characteristic to separate out these occasionally recurring pulses from the typical signature for a single droplet.

It should be evident from Fig. 2 that the velocity of fall of the droplets may be easily measured by determining the time interval between two succeeding pulses of a given signature. Further, since the average terminal velocity for large numbers of naturally falling raindrops are now available as a result of investigations with this apparatus, it becomes practicable to determine the mass of a falling raindrop which has not been touched or contaminated in any manner simply by knowing this measured time interval. It is clear that such a "weighing process" is most convenient in a number of measurements of the physical properties of raindrops.

The reduction of the data displayed on the blueprint paper tape has been considerably simplified by the adoption of a convenient classification of raindrop sizes together with the use of a transparent mask upon which is reproduced the various spot sizes equivalent to various droplet masses. The added convenience of these short cuts suggests that the method will be generally used in further experiments. The magnitude of the electric charge on naturally falling raindrops is readily scaled from the oscillographic trace when the electrical circuits are calibrated with the standard to be described in a later paragraph.

THE BLUEPRINT PAPER METHOD FOR THE MEASUREMENT OF THE MASS OF RAINDROPS

Early German experimenters[3,4] made extensive use of the absorbent paper method for measuring drop size because of its convenience. Originally the droplets were collected on a suitable absorbent paper and the droplets developed by dusting the paper with a soluble dye. The size of the spot for uniform absorption by the paper may be calculated by equating the area of the spot multiplied by its effective thickness of absorbed water, to the volume of the incident raindrop. It is well known that this is only an approximation under most conditions and the effective thickness, determined by calibrating

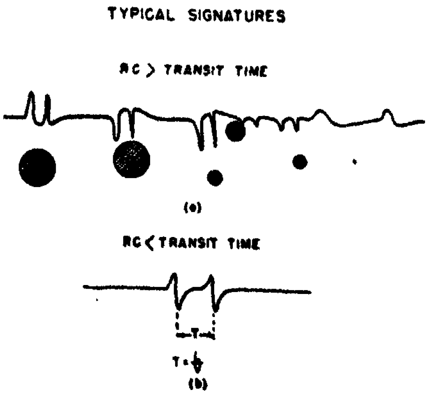

FIG. 2. Characteristic signatures produced by natural rain.

---

[4] E. Niederdorfer, Meteorol. Zeits. 49, 1 (1932).

measurements, varies slightly from the larger drops to the smallest ones. Niederdorfer[4] has estimated the various sources of errors and states that the average error for the above method ranges from 6 percent for the large drops up to 15 percent for droplets as small as 40 micrograms.

The convenience of the original spot method encouraged one to see if the method could not be appreciably improved. It was found that a good quality standard blueprint paper is practical for the determination of the mass of falling raindrops. Such paper, prior to its coating, is carefully freed of all grease and the sensitive coating is uniformly applied. This sensitized coating, being easily wetted, promotes the spread of the impinging droplet in such a way that the produced spots are nearly circular and, therefore, easy to measure with fair accuracy. However, the over-all accuracy that may be achieved by the use of blueprint paper is about that obtained with ordinary absorbent paper sprinkled with dye unless unusual care is taken in the calibration of the paper, the control of its original moisture content, and in the reduction of the data.

It has been found that the determination of the actual masses from the size of the spot produced on the blueprint paper may be greatly facilitated by a classification scheme and by the adoption of a transparent photographic film provided with a large number of circles of graded size that may be slid over the various spots to determine their area. It is pointed out that because of the continuous deformation and vibration of the freely falling raindrops, their diameter has little meaning, whereas the mass of the droplet is specific. Moreover, because the masses of natural raindrops vary from 10 to more than 100,000 micrograms, it seems necessary to adopt some method to collapse the scale. Critical examination of the problem suggests that the best and most convenient scale of raindrop masses will result if one adopts as a classification standard the Briggsian logarithm of the mass expressed in micrograms. On such a scale, raindrops from the finest mist to the largest droplets fall in the range 0.00 to 5.00, while fog and cloud droplets are to be found in the range from 0.00 to -5.00. With such an adopted scale of masses, as many significant figures may be retained as the accuracy of the data suggest.

In developing means for rapidly classifying raindrops from the size of spot produced on blueprint paper, it has been sufficiently accurate to divide the most common range of measurable droplets into 65 intervals of 0.05 unit each. Such an arbitrary subdivision yields a scale in which each interval represents a 12.2 percent increase in mass over the preceding interval, but this represents only a 3.9 percent increase in the effective diameter of the droplet. It should be clear that by the adoption of a uniform fractional increase in the mass for each interval, the area of the droplet spot produced on blueprint paper is similarly increased fractionally by the same amount. Thus, if broken circles are drawn on a large chart in such a way that their areas form a geometric progression of common ratio $R=1.122$ ($\log R=0.05$), and if the assumption is made that the paper absorption or the mass of water per unit area of the spot is a constant, then it follows that the logarithm of the mass for each circle increases by uniform steps and appropriate mass values can be assigned to each circle. The above selection was made because a photographic reduction of such a chart preserves the relative sizes and any selected mass per unit area may be exactly produced by adopting the proper photographic reduction. Thus, a carefully prepared master chart in which the relative diameters are accurately drawn permits one, through easy photographic techniques, to produce a transparent mask that accurately fits any selected blueprint paper. By this means, the masses and radii of the original droplets may be directly read off of the mask when the appropriate circle is fitted to an actual spot on the blueprint paper. A reproduction of such a mask is given in Fig. 3.

In order to determine the effective thickness of the water film absorbed by the paper, it is necessary to make calibration measurements. This was accomplished by letting a number of droplets of known mass fall upon the blueprint paper at their terminal velocity. The size of the spots produced thereby was measured to determine the area corresponding to the known mass. From these data the photographic reduction factor to be applied to the original chart of circles was determined. In general, 4 or 5 masks, all having slightly different reduction factors grouped about the calculated reduction were produced, and by the selection of one of these, the size of circle corresponding to a given droplet mass could be adjusted for a perfect fit. On the assumption that the effective thickness of the water film was constant, all other circles were automatically fitted, and the actual masses could, therefore, be read directly off the transparent mask. Slight departures from the basic assumption occasionally led to corrections for the smaller droplets. In practice, it has been found that the ordinary variations in the behavior of the paper, errors of judgment, and absence of a perfectly sharp edge to the various spots are as great as the departures from the basic assumptions. In general, one attempts only to find the circle on the mask that best fits the spot to be measured. By carrying on the matching processes under a low power binocular microscope, it is found that different observers easily agree to within 0.05 classification unit or to about 12 percent of the mass. Careful and experienced observers can successfully interpolate, but the spot method is not a very pre-

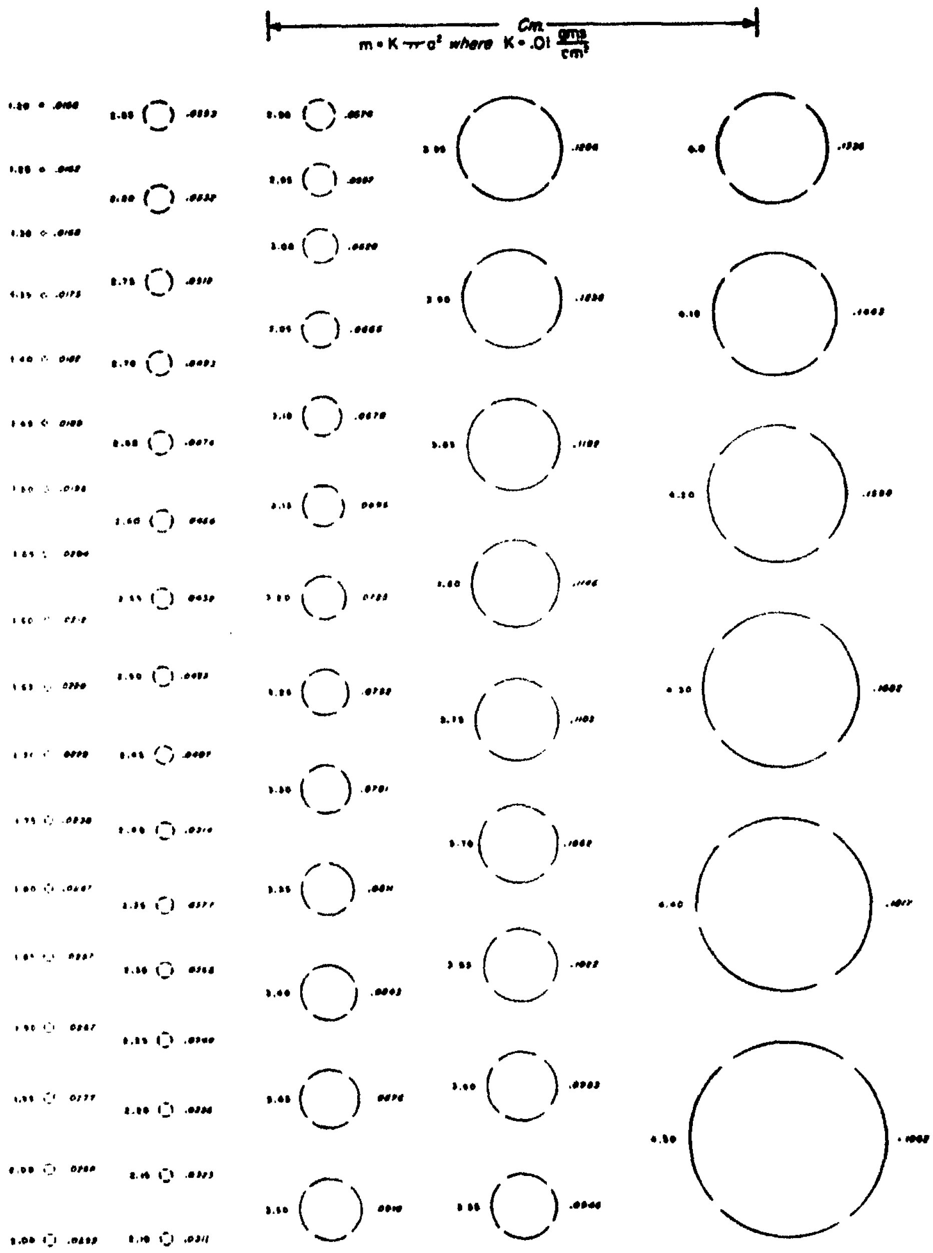

FIG. 3. Cut of transparent film mask for the determination of droplet masses. Logarithm of the mass in micrograms to the left of the circle, equivalent radius in centimeters to the right.

cise one, and it is valuable principally because of its convenience.

In the calibration of the blueprint paper, two methods for measuring the mass of the water droplets were employed. These two methods overlapped for droplets of medium size and gave identical results. For the large droplets the masses were determined by catching one to several drops in a covered aluminum can with a layer of cotton lying on its bottom, covering the can immediately to stop evaporation and carefully weighing on a precision chemical balance. The mass of the smaller drops are most easily determined by catching the droplets in a shallow glass pan filled with vacuum pump oil, covering the droplets as soon as caught by the oil, and measuring their diameter with a calibrated low power microscope. If this method is used for the larger drops, the vertical diameter, measured conveniently by the use of a small, total reflecting prism immersed in the oil, must be determined along with the horizontal diameter. A small camels' hair brush is employed when the droplets are first caught to cover them with oil. If the measurement of the diameter is made within a few minutes of capture, the absorption of the water in the droplet by the dry oil is negligible.

ELECTRICAL CHARGE CALIBRATING UNIT

In order that the above described apparatus may be of the maximum utility and that the absolute

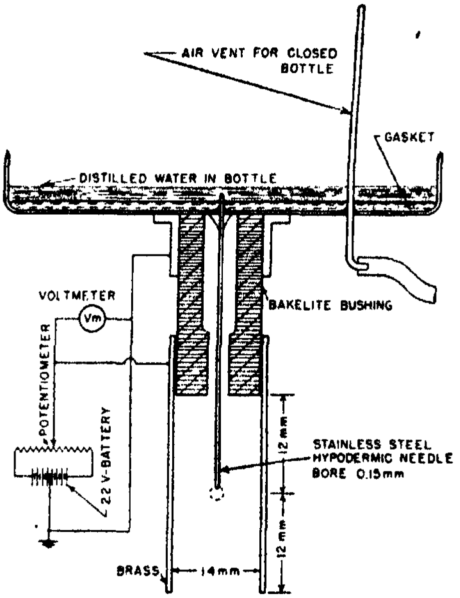
AIR VENT FOR CLOSED BOTTLE
GASKET
DISTILLED WATER IN BOTTLE
VOLTMETER
Vm
POTENTIOMETER
22 V-BATTERY
BAKELITE BUSHING
12 mm
STAINLESS STEEL HYPODERMIC NEEDLE BORE 0.15mm
12 mm
BRASS
14mm

FIG. 4. Construction and circuits for calibrating dropper to produce successive droplets of constant mass and constant electrical free charge.

value of the electrical charge on falling raindrops may be accurately determined, it is important to produce a standard impulse in the apparatus for its calibration. This has led to the development of a standardizing dropper that simultaneously produces consecutive drops of nearly uniform mass and places a free electrical charge of predetermined amount on each. It is theoretically possible to calibrate the apparatus by an absolute method employing ball bearings half submerged in a metallic plate and exposed to a charged parallel plate some distance away in such a way that when the ball is dropped, it carries a known and easily calculable charge. The method was tried with some success, but difficulty was encountered in getting the falling ball to detach itself from the supporting mechanism in a reproducible manner. A more practical solution is to construct a water dropper and arrange an inducing electrode so that each droplet carries an induced electrical charge of selected sign upon it. The design of the calibrating dropper is shown in Fig. 4 and is seen to consist of a bottle to supply the water, a hypodermic needle, and an insulated cylinder concentric therewith. Water slowly dropping from the end of the needle, which has been carefully cleaned and ground to be at right angles to the axis of the needle, is exposed to an electric field produced between the needle and the cylinder by a battery of known and constantly measured potential. With appropriate care and keeping the drop rate close to one drop per second, it is found that the probable variation in the mass of each droplet is less than 2 percent, and the charge induced on each droplet by the surrounding cylinder is constant to better than 1 percent. The mass of each droplet may be determined by the methods outlined elsewhere in this paper, and the average electrical charge on the droplets may be determined by catching a hundred (for example) droplets in an insulated cup directly connected to a calibrated electrometer and condenser system whose voltage sensitivity and capacity are accurately known. This calibration can be carried out with little difficulty and the constant for the calibrating dropper determined once and for all. It is found over a limited range, that the charge induced on each droplet is proportional to the radius of the droplet and to the voltage difference applied between the water droplet and the surrounding cylinder, appropriately corrected for contact electromotive force. Thus, if Q is the charge on each droplet in e.s.u.,

$$Q = KR(\varphi + \Delta), \tag{1}$$

where K is the constant of proportionality and R is the radius of the droplet in centimeters. φ is the battery potential applied to the cylinder, and Δ is the contact potential, each expressed in e.s.u. With the particular dimensions shown in Fig. 4 and employing droplets having a mass of about 10,000 micrograms, the constant of proportionality K as determined by calibration measurements is 1.03. The contact potential between the brass cylinder and water in our experiments amounted to about 0.25 volt and was in such a direction as to put a small negative charge on each droplet. Thus, if an inducing voltage of 30 volts is applied to the inducing electrode, the corrections for contact e.m.f. may be kept to less than 1 percent.

In practice, it has been found convenient to construct an assembly consisting of a supporting metallic plate, the water reservoir, and inductor assembly, together with necessary batteries and a reversing switch, all arranged in such a way that the whole calibrating unit can be conveniently placed in position on top of the electronic analyzer so that the calibrating droplets fall through the apparatus. It has been practical to use this standard unit before every run in order to check the behavior of the apparatus since it is calibrated in terms of absolute electrical values, and the known mass of the droplets from the standard, can be used to calibrate the blueprint paper employed for recording purposes.

THE REVIEW OF SCIENTIFIC INSTRUMENTS VOLUME 20, NUMBER 4 APRIL, 1949

A Large Mass Spectrometer Employing Crossed Electric and Magnetic Fields

THOMAS MARINER* AND WALKER BLEAKNEY
Palmer Physical Laboratory, Princeton University, Princeton, New Jersey

(Received January 17, 1949)

Because of continued general interest in this type of instrument and because of relationship with previously published work it has seemed desirable to report here the progress made, up to cessation of work in 1940, on a large crossed field mass spectrometer, the basic design features of which were directed toward a resolution of about 25,000 in order to permit its use for mass measurement. Although the instrument was necessarily diverted to less exacting applications before development was sufficiently complete to permit attainment of this high resolution, nothing in experience with the instrument indicated that the goal could not substantially have been reached.

INTRODUCTION

EARLY in 1937 the experiments of Bleakney and Hipple[1] had proceeded far enough to give promise of realizing in practice the advantages of perfect focus, linear mass scale, high intensity, and high resolution which they had predicted theoretically for an m/e analyzer consisting of electric and magnetic fields at right angles to each other. Owing to the advantages which this type of analyzer appeared to have over the "double-focus" mass spectrometers,[2-6] we were encouraged to undertake immediately the development of a high resolution instrument employing the new arrangement of fields. With the hope of attaining a precision at least equal to that of existing mass spectrometers[6] we planned for a resolution of about 25,000 using a slit-to-image separation of about 250 mm and an entrance slit width of about 0.01 mm. This would lead to a dispersion of 2.5 mm for 1 percent mass difference, and it was expected that a precision of mass measurement of about 2 to 4 in 10^6 would be achieved.

Our plans were so disrupted by the circumstances concomitant to the recent war that the instrument was not developed to a state suitable for mass measurement. It was, however, put in operable condition and applied to other problems,[7] which fact in itself makes it desirable that the instrument be described in the literature. Further stimulus for presenting a description arises from the hope that some of the findings may be helpful in connection with other instruments of this type which have been or are being constructed. It will be of primary interest that we encountered in our work no phenomena which indicated that the ultimate goal could not have been attained. In particular, we found no evidence for radical departure from theoretical resolution such as has recently been reported for a similar analyzer.[8]

If the description of the progress on the large mass spectrometer could have been presented when development work was stopped in 1940, the details of design might have been of sufficient general interest to justify protracted treatment. Now, however, since the intervening years have brought many of the particulars of design and technique into the realm of general practice (and some into the state of obsolescence), an attempt will be made to present the description as briefly as possible. A considerably more detailed treatment, including extensive drawings and photographs, can be made available to anyone desiring further information.[9]

CONSIDERATION OF THE ORBITS

The first detailed step in design was the selection of suitable orbits for the ions, in the discussion of which we shall use the notation of Bleakney and Hipple, except that in place of β (defined by their Eq. (13)) we shall use a parameter β_1 defined as V_0/E, the ratio of accelerating potential in the ion gun to the analyzing field. This simply postpones consideration of mechanical details of design.

Since it was proposed that the relative advantages of the curtate and prolate orbits be investigated in the new mass spectrometer, a number of trochoids of each type were drawn using the trochoid drawer described by Bleakney and Hipple.[1] More or less intuitively a well-shaped trochoid of each type was then selected for trial as a mean orbit. The first criterion of a good orbit, obviously, was that it remain within the boundaries of a conveniently shaped vacuum chamber. In selecting the prolate trochoid a further consideration was that when adjusted for normal incidence on the focal plane it should have a wide enough cusp to permit the use of a photographic plate or slit carriage of reasonable size. For the curtate trochoid special precautions were taken to avoid a sharp cusp, since failure to do so might lead to undesirable space-charge effects. Preliminary consideration of the mechanics of design indicated that a 3″ magnet gap would be used and that a 20″ pole diameter would accommodate the prolate trochoid enlarged to the size required for a resolution $m/\Delta m$ of 25,000 without placing any part of the orbit outside the probable uniform part of the magnetic field, which was taken to have a radius equal to the pole radius less the gap width. Actually, under this limitation, it was possible to enlarge the chosen prolate trochoid to a total span of 340 mm, with a slit separation $b=262$ mm, so that a resolution of 26,200 would be anticipated with an entrance slit 0.01 mm wide. The curtate trochoid was then enlarged to make use of the total available span in the focal plane, so that for this orbit $b=340$ mm and the theoretical resolution is 34,000 for the slit width considered. One of the selected mean orbits is shown in Fig. 1.

---

* Now at Armstrong Cork Company, Lancaster, Pennsylvania.

[1] W. Bleakney and J. A. Hipple, Jr., Phys. Rev. 53, 521 (1938).

[2] F. W. Aston, Nature 130, 357 (1936).

[3] Josef Mattauch, Phys. Rev. 50, 617 (1936).

[4] A. J. Dempster, Proc. Am. Phil. Soc. 73, 762 (1935).

[5] K. T. Bainbridge and E. B. Jordan, Phys. Rev. 49, 421A (1936).

[6] K. T. Bainbridge and E. B. Jordan, Phys. Rev. 50, 282 (1936).

[7] T. Mariner and W. Bleakney, Phys. Rev. 72, 792 (1947).

[8] G. W. Monk, J. D. Graves, and J. L. Horton, Rev. Sci. Inst. 18, 796 (1947).

[9] T. Mariner, Ph.D. thesis, Princeton, January 1947.

After the chosen orbits had been enlarged to the proper size, the parameters b, $y_{\max}$, and $y_{\min}$ were measured for each. Then a, ρ, and ψ_0 were computed using Eqs. (9), (17), and (18) of reference 1. Since a, θ, and β_1 seemed to be the most convenient orbit parameters to use in connection with later mechanical and electrical considerations, θ and β_1 were also computed. The expression for $\tan\theta$ in terms of known parameters was readily obtained by taking the ratio of Eqs. (13) and (14) of reference 1, and β_1 was computed from the relationship

$$\beta_1=(\rho^2\cdot\sin^2\psi_0/2a\cdot\sin^2\theta),$$

which, in turn, was obtained by using Eq. (13) of reference 1 in the expression for the initial kinetic energy: $V_0e=mv^2/2$. Finally, the ratio of the minimum energy of the ions to their initial energy was computed from the relationship:

$$V_{\min}/V_0=1+y_{\min}/\beta_1.$$

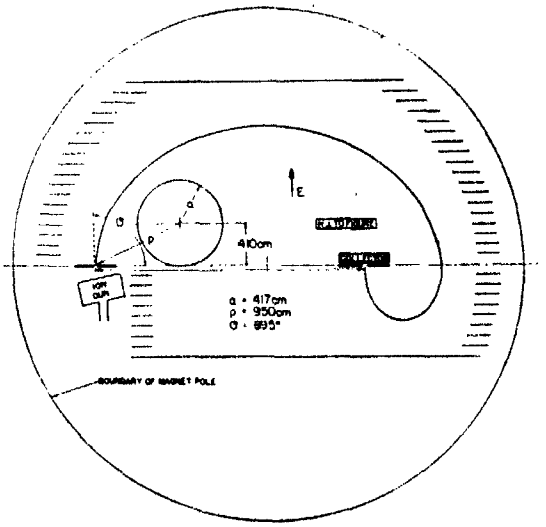

FIG. 1. Schematic drawing of the arrangement of the electrodes in the crossed-field mass spectrograph.

The values of the orbit parameters thus computed for the two selected orbits are listed in Table I.

The parameters thus far considered are associated only with orbit shape and position with respect to the focal plane. They involve relationships between V_0, E, and H without specifying their order of magnitude, so that operating conditions are not fully defined until one of these has been selected for ions of a particular mass-to-charge ratio. A value $E=200$ v/cm was chosen after canvassing the power supplies already at hand. With this value of E, the initial and final energy of the ions would be 1760 volts for the prolate orbit and 820 volts for the curtate orbit. These values are sufficient to give photographic traces in exposures of a few minutes.[10] With $E=200$ v/cm the minimum ion energy would be 685 volts for the prolate orbit and 45 volts for the curtate orbit. Since it would be possible to nearly triple E and $V_{\min}$ for the curtate orbit employing the power supply under consideration, and since it would be possible to build higher voltage equipment if required, the selected orbits seemed satisfactory from the standpoint of convenient shape, adequate final energy of ions, and adequate energy to minimize space charge effects. They were therefore adopted and the instrument designed around them.

THE ANALYZING CHAMBER

The Enclosure

The vacuum chamber is a short cylinder 4¾″ high outside and about 21″ O. D. A 1″-thick Armco iron cover rests on a recessed ridge cut into the top of the ¾″-thick sidewall (which was made of 18-8 stainless steel on account of the low magnetic permeability of this material) and a 1″-thick Armco iron bottom is arc-welded to the sidewall. 18-8 SS tubes of large diameter are welded into the sidewall at appropriate places to accommodate ion guns, slit mechanisms, pumping lines, and cold traps; and thirty smaller side tubes permit attachment of demountable Kovar glass seals through which electrical connections are made from an external voltage divider to the electrodes for the analyzing electric field, E. (Use of an internal voltage divider[8] would be more desirable from the point of view of structural simplicity, but less convenient for carrying out proposed tests on the effect of non-uniform electric fields.)

---

[10] K. T. Bainbridge, J. Franklin Inst. 212, 498 (1931).

The Electrodes for the Analyzing Electric Field

In principle the electrode arrangement for providing the analyzing electric field is a condenser with end plates spaced 27 cm apart and with guard rings or "picture frames**" every centimeter to reduce edge effects. The assembly fills most of the vacuum chamber, shown in Fig. 2 with the cover removed. The end plates are made of fine mesh 18-8 SS screen, and the guard rings are made of 0.006″ Nichrome *V* sheet. Each guard ring has a rigid retaining frame of $\frac{5}{32}''\times\frac{3}{8}''$ Nichrome *V* on each side of it to keep it planar, and these unit assemblies are spaced from one another by mica washers. Six grounded tie rods of Nichrome *V*, insulated from the unit assemblies by Pyrex tubing and from the end plates by Pyrex blocks, are used to compress the whole array into a rigid unit.

The guard rings project into the analyzing region past their retaining frames for a distance about equal to their separation, and the $\frac{3}{4}''$ high ion beam clears all but two of the guard rings by a distance equal to about half their separation.

There is no guard ring in the plane that passes through the axis of the analyzing chamber since the frame in this position holds the slit carriages. The adjacent guard rings therefore project into the analyzing region farther than the others and clear the ion beam by only $\frac{1}{32}''$.

The Slit Assemblies

For mass measurement investigations it was proposed that an entrance slit of fixed width would be used and that a camera, operated through the exit slit port, would handle the plates on which the mass spectra would be recorded. For preliminary survey work greater flexibility seemed desirable, and the slit mechanisms constructed for this purpose were the only ones built.

Three independent adjustments of the entrance slit are possible. These are effected through extensible bellows so that all adjustments may be made while the instrument is in operation. One adjustment permits locating the entrance slit in the optimum position in the incident ion beam, another permits adjustment of slit width, and the third permits alignment of the slit with the magnetic field to secure maximum resolution. Parallelism of exit slit and magnetic field is first secured by tilting the whole vacuum chamber.

Two independent adjustments are possible on the exit slit while the instrument is operating. One external control adjusts the slit width and another turns a lead screw to which the exit slit carriage is attached, so that it is possible to scan mechanically a mass range with extreme values of m/e in the ratio of about 2:1. The ion collector is mounted on the exit slit carriage, and the collector lead and its associated shield are arranged to telescope so that they are effective at all positions of the exit slit.

TABLE I. Characteristics of the selected mean orbits.

Orbit \ Parameter	b cm	$y_{\max}$ cm	$y_{\min}$ cm	a cm	ρ cm	ψ_0	θ	β_1 cm	$V_{\min}/V_0$
Prolate	26.2	13.6	−5.4	4.17	9.5	64.4°	89.5°	8.8	0.39
Curtate	34.0	3.78	−3.88	5.42	3.83	90.75°	35.0°	4.1	0.055

The slit carriages and the central frame in which they are tracked were all made of Nichrome *V* since preliminary tests indicated that this alloy could be run satisfactorily against itself in a vacuum. At infrequent intervals, however, the exit slit was locked by a ball of Nichrome *V* torn either from the central frame or the slit carriage by the other. This effect was eliminated by wiping both parts very lightly with a clean cloth slightly dampened with Lytton molecular lubricant *C*.

In addition to the slit carriages, the central frame also retains a thin sheet of Nichrome *V* to cut off "*N*th order" ion beams. If there are no obstacles in the analyzing region, ions of mass to charge ratio m/Ne, where N is an integer greater than 1, will be detected under the same conditions which permit detection of ions of mass to charge ratio m/e. Where prolate orbits are involved, the general condition for eliminating this possibility is somewhat more critical than that stated by Bleakney and Hipple[1] for curtate orbits, and requires that a length somewhat greater than $b/2$ be blocked off in the focal plane in one piece either beginning at the entrance slit or ending at the exit slit.

THE VACUUM SYSTEM

All of the demountable joints in the vacuum system are sealed with rubber gaskets, neoprene being used where there is exposure to oil vapors.

FIG. 2. Photograph of the vacuum chamber with top cover removed. The size may be estimated from the 30-cm scale at the top of the photograph.

** An apt descriptive phrase borrowed from reference 8.

Permanent joints in the vacuum chamber itself are arc-welded, except that the stainless steel bellows associated with the slit controls are attached with solder. Solder was also used in the pumping lines. Electrical connections are brought into the vacuum through tungsten pinches in the Kovar glass seals, which are themselves mounted on rubber gaskets.

The seam welds of the stainless steel bellows were the only troublesome source of leaks until they were sealed with clear glyptal, which proved sufficiently flexible not to fail in use. Only one or two leaks were found in the other welded and soldered joints, and none in the metal-glass seals. Of all the rubber gasketed joints only the cover seal leaked, and this only when the magnetic field was on. Wedges between the top pole piece and the cover rectified this trouble.

A temporary vacuum system consisted of a four-stage Leybold Hg diffusion pump backed by a Hypervac. In addition to the liquid air trap on the vacuum chamber proper, there was also one on top of the diffusion pump. The small throat of the diffusion pump (1″ diameter) limited the pumping speed at low pressures, and the small forevacuum lead (¼″ diameter), which is an integral part of the Leybold pump, prolonged evacuation time; thus the system was not satisfactory.

The final vacuum system consists of a metal fractionating oil diffusion pump (employing Octoil-*S*), which evacuates the mass spectrometer through a 4½″-diameter line, and a Kinney model CVD556 mechanical pump operating through a 1″-forevacuum line. A large manifold above the oil pump contains a copper liquid air trap. Although the speed of the diffusion pump was not measured, it is commonly accepted to be 80 litres/sec. Valves are provided to isolate the diffusion pump, a backing volume, and the manifold, so that the diffusion pump can be kept operative while the vacuum chamber is at atmospheric pressure. "Roughing" of the vacuum chamber can then be effected through a 1″-diameter bypass tube.

The performance of the vacuum system proved entirely satisfactory. One test was made to get rough data on the speed of evacuation. The mass spectrometer was initially at atmospheric pressure while the manifold was being continuously evacuated by the oil diffusion pump working into the backing volume. After the Kinney pump was started, the bypass valve was opened for 2½ minutes and then closed, immediately after which the gate valve between the diffusion pump and the mass spectrometer was opened. One-half minute later the pressure in the manifold above the diffusion pump was only forty percent greater than normal ultimate pressure. After a total elapsed time of ten minutes the filament of the ion gun was safely lit.

No attempt was made to measure absolutely the ultimate vacuum attained since the performance of the mass spectrometer itself was the final test. However, Pirani gauges and ionization gauges were used in leak hunting and the latter provide a reasonable basis for estimating the ultimate vacuum. The Western Electric D-79510 and D-79512 gauges are operated from a modified Ridenour Lampson[11] circuit which maintains 10-ma grid current at 300-v grid voltage under running conditions and has convenient arrangements for outgassing the gauges. One gauge is inserted at the top of the manifold above the diffusion pump and the other is mounted on the mass spectrometer shell among the leads to the analyzing field electrodes. With liquid air on the manifold and vacuum chamber traps, plate currents of the order of 0.7 microampere were customarily obtained on both gauges. Extrapolation of the data of Jaycox and Weinhart[12] to a grid voltage of 300 volts gives an estimated pressure of 1×10^{-6} mm Hg under the operating conditions.

Before the temporary pumping system was discarded, a test was made to compare the efficacy of the old and new arrangements. With the Hg pump working, the plate current of the vacuum chamber ionization gauge was read and the intensities of the background ion beams in the low mass range were measured. The stopcock to the Hg pump was then closed, the gate valve to the oil diffusion pump opened, and similar measurements taken again. The results given in Table II indicate the superiority of the oil diffusion pump and the larger pumping lines.

It was hoped that tests could be made to determine the degree of necessity for the liquid air trap above the oil pump, but time did not permit. Data bearing on this point have subsequently been obtained by others.[13]

THE MAGNET

General Remarks

The pole radius was selected by consideration of the probable minimum slit widths and the maximum resolving power desired, allowances being made for probable loss in usable radius due to edge effects. The loss was taken to be equal to the effective gap width; and this was justified by subsequent measurements of the field distribution both parallel and perpendicular to the pole pieces. The other dimensions of the magnet were made compatible with the cross section of the pole, with work space requirements, and with space needed for windings. Room was left for more windings than required for the immediately proposed application in order that the magnet should not be too restricted in usefulness. Rough calculations indicated that the shape of the magnet would have little effect on the cost within the limits of practical design; therefore, convenience was given first consideration. Of great assistance*** in designing the magnet were the data on the model magnet for the cyclotron.[14]

---

[11] L. N. Ridenour and C. W. Lampson, Rev. Sci. Inst. 8, 162 (1937).

[12] E. K. Jaycox and H. W. Weinhart, Rev. Sci. Inst. 2, 401 (1931).

[13] T. D. Morgan, Rev. Sci. Inst. 18, 926 (1947).

The Coils

In order to be able to utilize as nearly as conveniently possible the maximum power output of any one of three different generators which might be assigned to the mass spectrometer, it was necessary that the total winding for which room was provided be split into twelve separate coils wound with No. 6 copper wire. Square wire was selected to minimize winding losses and to aid in cooling; and asbestos plus single cotton insulation was selected for durability and heat resistance.

Each coil is a 330-pound "pancake" (44⅜" O. D. ×1⅜" thick) of 373 turns, with a resistance of 1.1 ohms. After being wound, each coil was baked and impregnated with transformer varnish, not only to exclude vapors, but also to make the coils rigid and to aid in cooling. Twelve such coils could utilize a maximum of 17.4 kilowatts from a 20-kilowatt 120-v d.c. generator, or 39.3 kilowatts from a 40-kilowatt 120-v or 240-v d.c. generator. The corresponding current densities are 222 amp./cm^2 and 334 amp./cm^2. With twelve coils these upper limits of current density correspond to 21,300 and 32,100 ampere-turns/cm of gap, and the model magnet data indicate that about 14 kilogauss may be obtained at the lower power using cylindrical poles, whereas about 18 kilogauss may be obtained at the higher power using complex poles.

Although original plans called for twelve coils with water-cooled separators, only eight were installed. These were air-cooled, since the need for very high fields was not in view. Moreover, development work on the mass spectrometer had to be terminated while tests were in progress on electronic control of the synchronous motor generator set assigned to the mass spectrometer. Storage batteries were therefore used in the application of the instrument already reported.[7]

The Core

The core**** of the magnet looks somewhat like a cyclotron magnet core 62" long, 55" high, and 20" wide in outside dimensions. It was made as a one piece 6.5 ton casting of Armco electromagnet iron so proportioned as to present to the flux approximately the same total cross section throughout. After the casting was made, part of the center section was cut out and the pole tips machined. In order to provide for the possibility that contoured poles might be desirable in future applications of the magnet, a six-inch length of each pole tip was made removable. With the pole tips in place, the gap is 5", but this is reduced to an effective 3" by the cover and bottom of the vacuum chamber. The pole tips vary in diameter from 20" to 20¼" and are out of vertical congruence by $\frac{3}{32}$" in the worst place. The 5" gap is uniform to within 0.002" in the worst place, and there is no evidence of voids in the casting.

VOLTAGE SUPPLY, STABILIZER, AND CONTROL FOR THE ANALYZING ELECTRIC FIELD

To be consistent with the initial goal with regard to resolution, the analyzing field should have a stability of about one part in 250,000, at least for periods of a few minutes, and for convenience should generally be coupled to the ion accelerating voltage in such a way as to maintain a constant ratio of the two. Only preliminary progress was made toward the first objective, and consideration of practical schemes for realizing the second was not undertaken.

In the previously reported application of the mass spectrometer[7] the analyzing field was supplied from a 27-segment voltage divider with a total resistance of 2.7 megohms. This was attached to the output of a degenerative stabilizer based on the circuit of

TABLE II. Comparison of backgrounds with Hg and oil diffusion pumps (liquid air on all traps).

Ionization gauge plate current	With Hg pump 1.8–2.0 μa	With oil pump 0.6–0.7 μa
m/e	Approximate peak height in arbitrary units	Approximate peak height in arbitrary units
12	6.0	0.8
14	44.0	9.0
15	7.0	<1.0
16	25.0	4.0
17	23.0	10.0
18	92.0	41.0
20	3.0	1.0
21	7.0	2.5
28	580.0	100.0
29	17.0	6.0
30	2.0	<1.0
32	84.0	22.0
34	1.5	<1.0
36	1.8	0.6
39	2.0	1.2
40	13.0	2.0
41	16.0	7.5
42	4.0	1.3
43	19.0	9.5
44	25.0	4.2

*** We are indebted to Dr. M. G. White for the use of these data prior to publication.

[14] M. C. Henderson and M. G. White, Rev. Sci. Inst. 9, 19 (1938).

**** Made by the American Rolling Mill Company, Middletown, Ohio.

Fig. 9 in the paper of Hunt and Hickman.[15] A full wave voltage doubler rectifier supplied the input to the stabilizer. The output voltage of the stabilizer was adjustable over the range 1100 to 5400 volts by variation of a resistance constituting part of a bleeder in parallel with the voltage divider. Conveniently, the output voltage of a degenerative stabilizer of this type varies nearly in inverse proportion with the control resistance, with the obvious consequence that the control resistance is nearly proportional to the *m/e* of the ions being observed.

A basic feature in the design of the analyzing chamber was that the slit plane be at ground potential, which, in turn, required that the voltage divider supplying the analyzing electric field be grounded at a point not common to either side of the rectifier or stabilizer. Since all leakage currents from the power supply to ground must complete their circuits through the voltage divider in such an arrangement, it is desirable, first, to minimize such currents by using specially selected or specially constructed power supply components, and, second, to minimize the importance of the currents by using a large divider current. The decision to use an existing power supply for the work of reference 7 limited the extent of possible compliance with the second consideration. However, in keeping with the first consideration, it was found possible to substantially improve the stability of the analyzing field by rebuilding several critically located circuit components. Since greater refinement was not required for the purposes at hand, work was terminated when the d.c. fluctuations in the voltage divider had been reduced to about one part in 30,000 and ripple had been reduced to amplitudes of 3.7 and 1.5 parts in 10,000 in the negative and positive branches of the load, respectively. The ripple probably arose mostly from leakage between the primary and secondary of the high voltage transformer, there being only 10^{10}-ohm resistance between them.

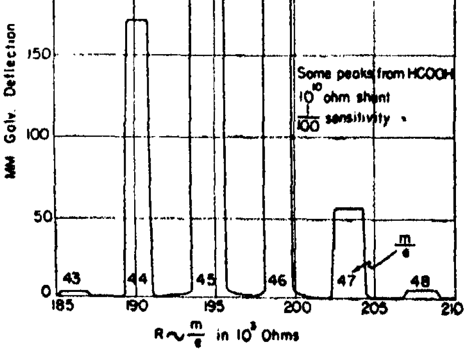

FIG. 3. Spectrum of formic acid in the mass range 43 to 48.

THE ION GUN

No development work was done on ion guns designed to take advantage of the permitted large angular spread in the ion beam. For survey work and for application to the investigation already mentioned[7] a conventional type of ion gun was built. Storage batteries were used to heat the conveniently replaceable tungsten filament whose emitted electrons were accelerated downward in two independently adjustable steps. After passage through the ionization chamber the electrons impinged upon a collector held positive with respect to the ionization chamber in order to suppress secondary emission. A vacuum tube microammeter patterned after that of Shepard Roberts[16] was used to measure the collector current. The sample gas was led through a reentrant tube and introduced directly into the ionization chamber in a stream (directed counter-current to the electron beam) in order to gain a factor of about two in ion intensity.[17]

Before encountering the entrance slit to the analyzing chamber the ion beam passed through three slits in the ion gun. The first of these was generally only a few volts negative with respect to the ionization chamber. Between the second slit and the ionization chamber only 10 percent of the total ion accelerating voltage was applied in order to minimize penetration of the ionization chamber by the accelerating field. The final slit was at ground potential so that no electric field was present between it and the entrance slit to the analyzer. Since the ion gun had to be tilted with respect to the entrance slit plane in order to fulfill conditions for the selected orbit, a non-uniform field would otherwise have prevailed, making it difficult to compute the ion orbit between the ion gun and the slit plane.

The relative positions of the slits in the ion gun were selected after the orbits of the electrons and ions had been calculated under several sets of conditions. (The orbits can be treated by the same equations which apply to the orbits within the analyzing chamber if the electric fields within the ion gun are assumed to be uniform.)

---

[15] F. V. Hunt and R. W Hickman, Rev. Sci. Inst. 10, 6 (1939).

[16] Shepard Roberts, Rev. Sci. Inst. 10, 181 (1939).

[17] Leonard B. Loeb, *Kinetic Theory of Gases*, 2nd Edition (McGraw-Hill Book Company, Inc., New York, 1934), p. 309.

The position of the ion gun was adjusted to be consistent with the requirements for securing the selected prolate orbit in the analyzing region. Energy for accelerating the ions was provided by a stabilized power supply basically the same as that used for the analyzing field, but operating at lower voltage. For convenience, the output meters of the two stabilizers were made to read the same when $\beta = 8.8$ as required for the orbit selected.

THE ELECTROMETER TUBE AMPLIFIER

The ion currents were measured on a Barth type amplifier[18, 19] using a Western Electric D-96475 tube and a Leeds and Northrup galvanometer with a maximum current sensitivity of 9×10^{-11} amp./mm at 1 meter, which can be reduced by an Ayrton shunt. The sensitivity of the amplifier is 108,000 mm/volt on highest galvanometer sensitivity. Random fluctuations were generally of the order of 0.75 mm on 10^{10}-ohm shunt, full sensitivity. Both electrostatic and magnetic shielding were provided for the electrometer tube, and its enclosure was evacuated.

Conclusion

As mentioned at the beginning of the paper, the original purpose in building the mass spectrograph was to obtain an instrument of high resolving power, high intensity, and great utility. Circumstances permitted only a few studies of ionization processes, in which the high resolving power was not required and hence not exploited. The operating parameters used for our research were $b = 262$ mm, $H = 2200$ gauss, exit slit width 3.17 mm, and entrance slit width 0.05 mm. The slit widths represent nominal values inasmuch as no attempt was made to secure accurate alignment with the magnetic field. The theoretical resolution was thus about 81, and the observed resolution differed from this by less than 5 percent.

Although the above result means little with regard to ultimate resolving power, one can see from the slope of the sides of the peaks in Fig. 3† that this must be quite high, probably greater than 1000, even with slits not carefully aligned. Certain preliminary runs made under somewhat different conditions than those quoted above implied considerably higher values of ultimate resolving power, and nothing in our experience with the instrument indicated that the goal of 25,000 could not substantially be reached.

In other respects the device measured up to expectations. The peak shapes were uniformly symmetrical and the tops were really flat. Intensity was excellent, and stability was very good except in a few instances when the effects of improvisations in some of the circuits became apparent. Although vacuum conditions were about as expected, reduction of background would have been undertaken prior to more exacting applications of the instrument.

ACKNOWLEDGMENTS

The greater part of the machine work on the mass spectrometer was executed in the Palmer Laboratory machine shop, to the personnel of which the authors are indebted for their contributions.

The assistance of C. S. Cummings, Robert Matheson, and George Reynolds in constructing and testing some of the electrical circuits is greatly appreciated, as is the aid of Roger Sutton in leak-hunting.

---

[18] G. Barth, Zeits. f. Physik. 87, 399 (1934).

[19] D. B. Penick, Rev. Sci. Inst. 6, 115 (1935).

† The peaks at $m/e = 44$ and 46 are narrower than the other peaks because of a slight lack of precision in the elements of the control resistor, R, of the analyzing field stabilizer. Each of the two peaks in question encompasses a range on the resistance scale within which the combination of resistance elements was changed, a large one replacing the sum of ten smaller ones.

A Novel Recording Accelerometer

ARTHUR S. IBERALL
National Bureau of Standards, Washington, D. C.

(Received January 3, 1949)

The novel features of a small recording accelerometer of slow chart speed are described. Principally, these are its compactness—the recorder, less power supply, fits into a panel type aircraft instrument case—and the use of spark recording to obtain a visible record on a paper chart. Components selected to achieve compactness are a timing type synchronous motor to drive the chart; a 35 mm film cartridge to store the chart, and a model airplane spark coil to provide a high voltage repetitive spark. A simple preliminary chemical treatment for ordinary paper was developed to obtain an intensified trace on the record chart. Small or panel type recorders of other physical quantities can be similarly built, applying the main features of this design.

INTRODUCTION

At the request of, and with the financial support of the Aero Medical Laboratory of the U. S. Air Force, the National Bureau of Standards undertook the development of a recording accelerometer to be used in testing personnel in flight. It was essential that the size be small. Other requirements were a range of 12 g, accuracy within 4 percent of full scale, a natural frequency of 10 c.p.s., a permanent record visible while recording, a paper speed between 4 to 12 inches per minute uniform to within 5 percent, and, if electrically operated, operation from 28 volts d.c.

The method of design, illustrated in an experimental model, may be followed in constructing other small or panel type slow speed recording instruments using certain existing sensitive elements without seriously modifying them.

An exploded isometric drawing of the recorder is shown in Fig. 1, and a schematic diagram of the power supply is shown in Fig. 2. The description of the recorder can best be followed by reference to the figure.

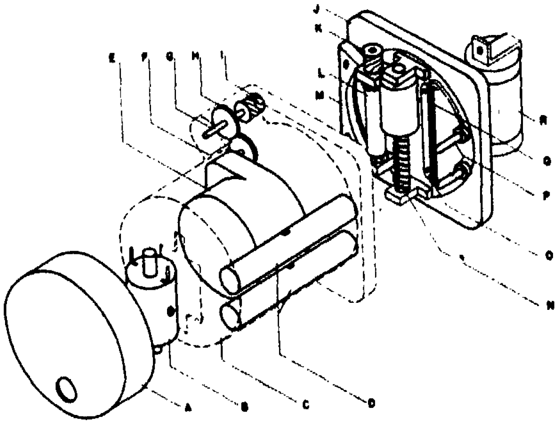

FIG. 1. Schematic layout of component parts of the accelerometer recorder. (A—false bottom, B—spark coil, C—case, D—high voltage receptors, E—motor, F—motor spur, G—shaft, H—shaft spur, I—shaft spiral gear, J—cover, K—driven spiral gear, L—sprocketed roller shaft, M—slotted guide bar, N—accelerometer element, O—plate electrode, P—banana plugs, Q—cartridge slot, R—cartridge.)

CASE

A small recording instrument desirably should be designed to fit into a case of moderate depth, with a small, round or square dial. The preference for a conventional aircraft installation for this instrument led to the choice of a standard aircraft panel type case. The case of a rate-of-climb indicator, C, Fig. 1, is particularly suitable because of a setting shaft, G (part of the zero setting mechanism) built into one square corner. The setting shaft is utilized to transmit power from a motor (placed in the back of the case) to the front of the case without encumbering the inside of the case.

MOTOR

Small synchronous timing motors are suitable for a chart drive because of their small size, their uniform speed, their operation at the common supply frequency of 60 c.p.s., and their availability in a wide range of shaft speeds (integral gear trains provide shaft speeds from 10 r.p.m. to 1 r.p.d.) with a torque output up to 30 in.-oz at 1 r.p.m. Their application depends upon being able to design a chart drive sufficiently free of friction. It is estimated that these motors cannot be used to obtain linear chart speeds in excess of 100 inches per minute. However, they are satisfactory for chart speeds of about 10 inches per minute.

A 2-r.p.m., 3-watt, 24-volt, 60-c.p.s. motor, E, was chosen for the recorder. It is mounted back in the case on tubular shims and fastened from the back of the case with screws. Its location in the case is chosen so that its shaft overlapped the setting shaft to permit gear coupling.

GEARING

A set of spur gears, F and H, of approximately one to one ratio connects the motor to the setting shaft. The only limitations on the gear sizes are that the shaft spur must be large enough to permit its teeth to project from the setting shaft pocket, but small enough to fit in the pocket, and the motor spur gear diameter must be large enough to clear the motor and engage the shaft spur gear. In the experimental model, the shaft and motor spurs had 40 and 60 teeth respectively.

Rotary motion is transformed from perpendicular to parallel to the plane of the cover by means of a set of like-rotation spiral gears, I and K, one of which is mounted on the setting shaft. The spiral gears have the advantage of establishing the axis of rotation as far over to one side of the case as possible, leaving the front end of the case still relatively free.

RECORD DRIVE

The proximity of the spiral gear axis to the side suggested that the record chart could be pushed through the case for the short remaining distance. Considerations of loading and storing the record chart pointed to the desirability of mounting, driving and storing the chart on the cover (see J). The favorable mating characteristics of spiral gears made them the logical breaking point of the driving connection.

The cover glass of the conventional case was therefore removed and replaced by a thick transparent plastic disk. The second spiral gear, K, was pressed on a shaft retained by two bearings mounted on the inside of the cover. Since 35 mm appeared to be approximately the widest record width practicable, and made possible the use of replacement parts from cameras, this size was adopted. A sprocket drive from a 35 mm camera was therefore adapted to drive the record chart by pressing it on the same shaft as the driven spiral gear. The chart thus passes underneath the sprocketed roller shaft, L, in the inside plane at the cover. The cover is undercut in narrow slots underneath the sprocket teeth.

The record chart is stored in a 35 mm film cartridge. The cartridge, R, is mounted from the outside of the cover in a semi-cylindrical hole (not visible in the figure), formed as far over to the side of the cover opposite the sprocketed roller as possible. A slot, Q, cut in the bottom of the hole permits the tangent lip of the film cartridge to project into the case. The record chart is thus drawn from the cartridge with minimum number of contacts by the sprocketed roller.

In order to pass the chart out of the case, a U-shaped slot (not visible in the figure) was cut in the case and a slotted guide bar, M, attached to the cover, was put in this space. With the gearing and motor used, a chart speed of 6½ inches per minute was obtained.

ACCELEROMETER ELEMENT

A range of about 12 g-units and a natural frequency of about 10 c.p.s. were required for the accelerometer element. Coupled with small-size for the recorder and the consequent use of a recording paper 35 mm wide, this led to the use of a simple mass and spring element, without mechanical multiplication of the mass displacement. A scale sensitivity of about one g-unit per 1/16 inch was obtained.

A fixed shaft, on which a bob slides, was mounted in two bearings attached to the inside of the cover plate between the film cartridge and the sprocketed drive roller (see N). The bob size was chosen to be as large as could safely fit in the available space (limited by the motor, the cover plate, the cartridge, and the roller). The shaft size was chosen to have high rigidity. A spring of appropriate diameter (0.02-inch wire) was wound to slide freely on the shaft. In order to restrain the bob from rotating (so that an electrode might be mounted on it), a V-groove was cut in the shaft, and a steel ball was inserted in a snug radial hole which passes through the bob. The ball was retained in the groove by a set screw. The spring was attached at one end of the shaft to an externally threaded sleeve, keyed to the shaft, and at the other end, to a similar sleeve threaded into the bob.

The use of a porous oil-impregnated metal for the sleeve inside of the bob provided some damping.

RECORDING MEANS

The repetitive puncture of a paper chart by a high voltage spark was used to obtain a record trace. This system has the advantages of permitting recording at the back of the paper, securing a record visible immediately at either front or back

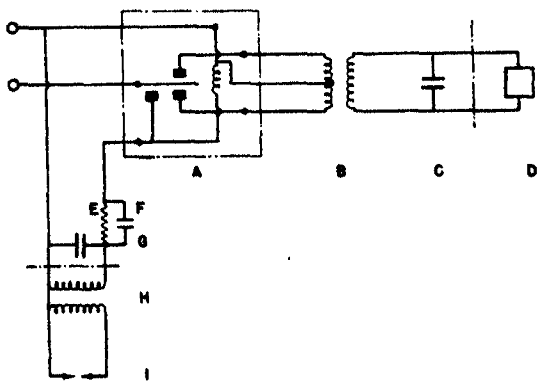

FIG. 2. Schematic layout of the power supply for the accelerometer recorder. (A—vibrator (5 terminal, 28 v, 50 w, 60 c.p.s.), B—coupling transformer, C—filter condenser (16 m.f.d.), D—motor (25 v, 60 c.p.s., 2 r.p.m., 3 w), E—limiting resistor (15 ohm, 25 w), F—bypass condenser (100 μf), G—tuning condenser (4 μf), H—spark coil (model airplane coil), I—spark gap.)

without the need of subsequent development, and of having no writing friction.

The recording electrodes consist of a nickel tip screwed into the bob (a point electrode) and the edge of a plate, O, mounted directly under this tip on the inside of the cover (a line electrode). The electrode spacing is approximately 0.008 inch. The electrode plate is countersunk in the cover and is slightly wedge-shaped so that the edge, underneath the point electrode, projects slightly above the plane of the cover. The paper rides over this edge and is punctured along this line as the bob deflects.

In order to minimize the risk of shock to personnel and to permit free removal of the cover, the plate electrode is made the high voltage electrode, leaving the bob at low potential. The supply voltage to both electrodes is brought in by conducting strips from banana plugs, P, screwed into the cover plate. Mating receptors, D, are fastened to the inside of the case. A small spark coil, B, furnishing the high voltage, is mounted in a slot cut in the back of the case. The slot is covered over by a false bottom, A, added to the case.

POWER SUPPLY

The electrical requirements of the recorder are a 24 volt, 60-c.p.s. sine wave for the synchronous motor, and a high voltage for the sparking electrodes, preferably in the form of a repetitive voltage "pip." The supply voltage available in aircraft is 28 volts d.c. The requirements were successfully met through the use of a 60 c.p.s. vibrator. The vibrator used, A, Fig. 2, has a main driving reed contact and an additional set of single-pole double-throw contacts. The description of the power supply may be followed by reference to Fig. 2.

Two half waves from the double throw contacts are coupled together in the center tapped primary of a small transformer, B. The transformer and a shunt condenser, C, form a filter circuit for the 60 c.p.s. wave. This furnishes the motor supply voltage (see D).

The main reed contact passes a voltage consisting of 28 volts d.c., while the reed contact is closed, and a "pip" of opposite polarity while the reed contact "breaks," due to the inductive delay of the vibrator coil. The only spark coil of minute size available is a model airplane coil, H, operating on 3 volts, so that a matching circuit had to be devised to permit using the vibrator output.

The d.c. component from the reed contact is reduced by a dropping resistor, E, shunted by a large capacitance, F, which passes the "pip." This supply is then fed to the spark coil. The spark is intensified by the use of a shunt capacitance, G, across the primary of the spark coil. The two shunt capacitances have the additional function of quenching the reed contact spark.

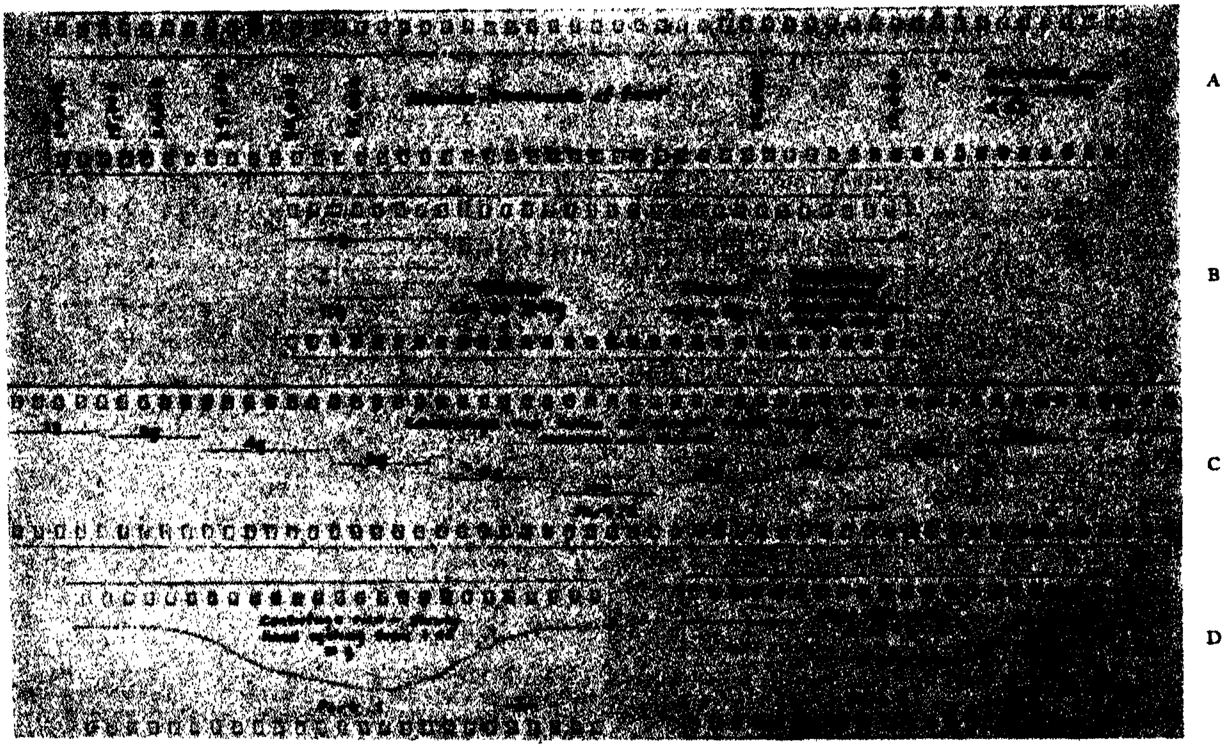

FIG. 3. Typical calibration and performance records obtained with the accelerometer recorder. (A—trace at simulated altitude, B—trace with rapidly oscillating accelerations, C—static calibration trace, D—trace under cyclic accelerations).

In order to avoid external lines for the high voltage, the spark coil is built into the instrument case, for which the only available space is behind the motor.

The remainder of the power supply elements—vibrator, transformer, resistors, capacitances—are housed in a small radio chassis. The operation of a switch simultaneously starts or stops the motor and spark.

PAPER

A 35-mm single weight perforated photographic paper from which the emulsion had been removed was chosen for the record chart. It was found that a higher energy level than available from the small spark coil was necessary to form a trace easily visible at ordinary reading distances. A chemical treatment was developed for the paper that would intensify the trace as it formed. Among the various chemical solutions tried, the following was found to be quite satisfactory. The function of each chemical is given in parenthesis.

In one liter of distilled water dissolve

100 g potassium nitrate (oxidizing agent)
50 g gum acacia (binder)
5 g potassium chloride (catalyst)
5 g ammonium nitrate (oxidizing agent)
0.3 g potassium hydroxide (alkali)
0.5 ml formaldehyde (hardening agent)
6 drops of 5 percent Aerosol OT (wetting agent).

The paper was immersed in this solution for one minute and then passed over a heated dryer. The belt tension of the dryer was adjusted to produce as little distortion as possible in the paper.

PERFORMANCE

The experimental accelerometer was given some laboratory tests to determine its performance before being delivered to the Aero Medical Laboratory. Figure 3 shows some representative data. The first strip, A, Fig. 3, shows the effect of reduced pressure (simulated high altitudes) on the dispersion of the trace; the second strip, B, shows the adequacy of the trace under oscillatory conditions; the third strip, C, shows the static calibration of the accelerometer in a centrifuge, and the fourth and fifth strips show, D, the performance of the accelerometer in a centrifuge under cyclic accelerations chosen to simulate flight turns.

ACKNOWLEDGMENTS

The author wishes to acknowledge the invaluable help and advice given him by the following Bureau of Standards personnel: Jack Sargent, electrical circuit; Leo Schubert, chemical record intensification; Russell Baum, construction.

Book Reviews

The General Properties of Matter

Fourth edition. BY F. H. NEWMAN AND V. H. L. SEARLE. Pp. 431+xi, Figs. 103. Longmans Green and Company, New York, and Edward Arnold & Company, London, 1948. Price $5.25.

This textbook, originally published in 1929 and now in its fourth edition, is clearly intended for students of physics, chemistry, and engineering with special emphasis on the first-named group. It is written with the special aim, however, of including material of interest and application to all three groups which shall be so thoroughly correlated as to emphasize the essential unity of the entire body of information. Readers from each group are thus encouraged to study more closely the related subjects in fields adjacent to their own. The broadening effect on students in these days of extreme specialization should be most beneficial and welcome.

The title is so inclusive that almost any material whatever in physics, chemistry, or engineering *could* be covered by it. The preface gives no clue to the choice of material, but a careful examination shows that the authors have restricted themselves almost exclusively to topics which can be roughly designated as *classical* or *nineteenth century physics*. Only slightly more than two pages are devoted to the statement of a few consequences of the restricted theory of relativity (at the end of Chapter III which bears the title *Gravitation*). The huge body of experimental and theoretical information which has grown up almost entirely in the present century and which, in this country, usually goes by the name of physics of the solid state (cf. Frederick Seitz, *Modern Theory of Solids*, for example) is almost completely ignored. Nothing whatever that could be termed either atomic or nuclear physics is included in the book. Nothing is said of the Uncertainty Principle. The fundamental particles of matter are not discussed. Electricity and magnetism, light (optics, spectroscopy, etc.) per se, even in the classical aspects of these subjects are omitted. Since, however, this reviewer knows of no traditional limits for a book or a course bearing the title *General Properties of Matter*, the above statements are intended as information to the prospective purchaser rather than as strictures. It is quite possible that this text is specifically designed to cover material traditionally offered in certain courses in this country or in England of which this reviewer is ignorant.

The material covered by the text might be roughly outlined as follows: Chapters I to IV inclusive: Elementary mechanics of particles and rigid bodies, gravitation and gravitational potential, gyroscopic problems. Chapter V: Theory and applications of elasticity. Chapter VI: Surface tension. Chapter VII: Viscosity. Chapter VIII: Kinetic theory. Chapter IX: Fourier series. Chapter X: Osmosis, diffusion, and Brownian motion. Chapter XI: Production and measurement of low pressures. Chapter XII: Elementary dynamical problems (such as simple and damped harmonic motion, motion under inverse square law of attraction, motion of projectile in viscous medium). Chapter XIII: Equations of fluid motion. Chapter XIV: Equations of wave motion. Chapter XV: Units and dimensions. Some of the chapters bear rather curious titles. Chapter XII for instance, is called simply "Dynamical Basis—Including Vibrations" and Chapter XIII on fluid dynamics is called simply "Equations of Motion."

The text is written on an elementary or intermediate level so that it can be used by any student who has mastered elementary calculus. It would be suitable for majors in physics in their junior or senior years. Although it contains a great deal on the subject of dynamics, the treatment is entirely on an elementary level—the methods of advanced dynamics, generalized coordinates, LaGrange's and Hamilton's equations etc., are not touched upon.

Within the above roughly outlined framework of its content, *the book is excellently constructed.* It is exceptionally thorough in its treatment. The exposition is lucid and leaves little for the reader to supply from other sources. It is outstandingly well furnished with footnote references to the original papers (extending as far back as the beginning of the nineteenth century and as far forward as the present day), a rare virtue indeed in texts at this level. The problems at the end of each chapter are well selected and interesting. The answer to each problem is given. Each topic is brought up to date with commendable thoroughness. Thus, for example, in the discussion of the numerical value of the universal constant of gravitation, the latest (1942) results of Heyle are given, and in the discussion of the determinations of Avogadro's number, Birge's 1941 results are cited.

The enormous impetus that the "new physics" has received from the tremendous discoveries of twentieth century research has drawn the attention of physicists away from many of the solid and useful achievements of the earlier "classical" period. This book serves a very useful purpose, therefore, in recalling in compact form this earlier store of fundamental information which the beginning student, bewildered with the glamour of betatrons, cosmic rays, and chain reactors might otherwise overlook or ignore. This reviewer prizes it as a valuable addition to his library.

JESSE W. M. DUMOND
California Institute of Technology

Physico Chemical Experiments

BY ROBERT LIVINGSTON. Pp. 267, Figs. 72, Macmillan Company, New York, 1948. Price $3.30.

This is the second edition of the well-known laboratory manual prepared as a companion book to F. H. MacDougall's text, *Physical Chemistry*. There have been very few changes: One experiment has been dropped and two added; the text has been revised in some places.

Forty-two experiments are discussed. These are designed to give the student laboratory experience in the fields which are usually included in the elementary physical chemistry course and should be useful in connection with any textbook or course of lectures on the subject. The specific subjects covered are: Measurements, errors, and computations; the gaseous state; the liquid state; the solid state; the structure of atoms; physical properties and molecular constitution; solutions; thermochemistry; equilibrium; heterogeneous equilibrium; chemical kinetics; electrical conductance; equilibria involving ions; electromotive force; electrolysis and polarization; photochemistry; and the colloidal state.

Discussions of the theory related to the individual experiments are not given in the manual except in a few cases. This seems highly desirable since there is not space for a thorough exposition, and reference to a standard theoretical text is certainly preferable to the inclusion of a sketchy account which the student may accept in preference to looking for a more adequate one elsewhere.

Each experimental discussion includes a preliminary brief outline of the experiment and techniques; a list of apparatus and materials required; a description of procedure that is sufficiently detailed to permit the student to proceed without too much assistance from the laboratory instructor; and a list of computations to be made on the basis of the data obtained in the laboratory. In addition, there are a number of special sections on the use of various pieces of apparatus such as the barometer, the Lind electroscope, the differential thermometer, the polarimeter, the Westphal balance, the Abbe refractometer, etc.

Especially praiseworthy is the introductory section on "Measurements, Errors, and Computations," to which 52 of the 255 pages of the text are devoted. The exposition of the theory in this section is admirable because of its completeness, suitability for its purpose, and the abundance of illustrative examples. In this section the subjects, physical laws and measurements, dimensions, significant figures, exponential notation, distribution of errors, best values, application of error theory to experimental data, evaluation of constants of empirical equations, and graphical methods of computation are discussed.

Notable omissions from the manual are experiments concerning the heat capacities or thermal conductivities of gases; the diffraction of x-rays by solids; the dielectric properties of chemical substances; the magnetic properties of chemical substances; and the distribution of solutes between solvents. It would seem that such experiments would be quite valuable accompaniments of the usual course of lectures in elementary physical chemistry.

The experiments are quite generally designed to require relatively simple equipment which is, in general, desirable at this level. However, there are no experiments included which give the student familiarity with high vacuum techniques, use of electronic equipment, use of modern recording meters of various types, etc.

The printing and binding are excellent.

Clyde A. Hutchison, Jr.
University of Chicago

Velocity-Modulated Thermionic Tubes

By A. H. W. Beck. Pp. 180, Cambridge University Press, The Macmillan Company, New York, 1948. Price $3.75.

This volume of the series on *Modern Radio Technique* edited by J. A. Ratcliffe is intended to acquaint the reader, who is familiar with prewar radio technique, with the principles of operation of velocity-modulation tubes and their limitations. The author's intention was not to write a formal textbook with full documentation but rather a personal account of a division of research which is still progressing rapidly. He has attempted to build up the theory from simple postulates by successive refinements so that physical facts dominate mathematical considerations, and has stuck mainly to the theoretical side, only occasionally remarking that the results are (or are not!) in satisfactory agreement with experiment. Mr. Beck was a Senior Scientific Officer in the Admiralty Signal Establishment at Bristol and was personally responsible for much of the research reported. Naturally most of his applications are drawn from British practice, but the liaison between British and American laboratories during the war was sufficiently good that all our contributions of importance are covered. The book abounds in references to the European literature and especially the work of Warnecke in France.

Following a brief historical introduction, the first chapter deals with the elementary principles of velocity-modulation tubes and describes the principal types. Next is a chapter giving the essential minimum of information on cavity resonators, including some discussion of relaxation methods for approximating the resonant frequencies. The major part of the work is Chapter 3 in which the theory of velocity modulation is developed. Following a chapter on focusing of high current electron beams, which is most important for an understanding of the limitations of velocity-modulation tubes, the various types of v.-m. tubes of practical importance are treated in four chapters.

Chapter 5 covers amplifiers and frequency multipliers including some discussion of multiresonator (cascade) amplifiers. The klystron oscillators are considered next, including a brief treatment of the Heil and Samuel tubes. Reflex klystrons are covered in Chapter 7, and miscellaneous types in Chapter 8. Here we find discussion of the v.-m. mixer, the monotron, v.-m. reactance tubes, and the multireflection tube.

The next chapter deals (all too briefly, I fear) with the limitations and defects of v.-m. tubes, considering maximum frequencies at which klystrons will operate, hysteresis, and problems of modulation. Chapter 10 is devoted to design requirements and manufacturing techniques applicable to v.-m. tubes, and the book is completed with two appendices and a collection of tables useful in calculating v.-m. tube performance. The first appendix gives an example of the application of the results obtained to the design of a moderately high powered C. W. klystron, and the second treats the traveling wave tube.

The author is to be congratulated on a well-rounded and clear presentation of the basic principles of v.-m. tube operation. Most all topics of interest have been covered at least briefly, and this reviewer's principal comment is that in spots the treatment could have been improved by a little expansion. I should like to have seen somewhat more comparison of the theoretical results with experiment and discussion of those cases where agreement is poor, but this may be only a personal preference. As it stands the book is written mainly for tube designers, while incorporation of a little more material of value to the circuit designer would broaden its audience considerably. Specifically the treatment of hysteresis effects, and of noise output could have been expanded, and some mention of phase aberrations due to mechanical defects in the reflector (such as tilt) might have been worth while. Since the book is largely concerned with theory, the material on construction techniques in Chapter 10 seems a bit incongruous, but it should prove valuable to anyone contemplating the construction of experimental tubes. The author's optimism concerning the future importance of v.-m. tubes as microwave mixers may well be unwarranted in view of further studies of space charge suppression of shot noise.

The typography is excellent and the proofreading was done with great care; therefore, it is a piece of really bad luck that Eq. 43 of Chapter 2, said to give correct results for the Q of a cavity in all cases, lacks a factor 2π. But these are minor points and the book can be recommended to engineers and physicists interested in microwaves or to students at the graduate level who wish a general account of the velocity-modulation field.

J. B. H. Kuper
Brookhaven National Laboratory

Radioactive Tracers in Biology

By Martin D. Kamen. Pp. 281, Figs. 38. Academic Press, Inc., New York, 1947. Price $5.80.

This book is an answer to the demand for collected information on the biological applications of radioactive tracers. Although many detailed chemical procedures and experimental techniques are given, this is far from a scientific cook book or a laboratory manual. Three chapters, constituting almost 19 percent of the book are devoted to the fundamentals of nuclear structure, nuclear reactions, and the properties of nuclear radiations. A fourth chapter discusses the principles of instrumentation and the corrections and statistics involved in making assays with radioactive isotopes. In this chapter the emphasis is placed primarily on G-M counters with relatively little space devoted to electrometers. These useful instruments should not be sold short. The Lindemann electrometer, which has proved quite useful in the assay of C^{14} is not even mentioned. The average non-physicist is apt to be more familiar with G-M counters than with electrometers and, consequently, may need more information about them.

About one-half of the book is devoted to the discussion of the uses of specific radioactive elements of biological importance. Typical syntheses and methods of assay are given and illustrative examples and typical protocols help to steer the biologists through the necessary mathematics. The value of the illustrative calculations would have been enhanced if they had been set apart from the text.

For many readers the most-used part of the book will be the chapters devoted to the general aspects of tracer methodology and their applications to specific problems and isotopes. One hesitates to disagree with the choice of material by an author with a well-established reputation in the field. However, several rather important radioactive elements are not mentioned in the text. For example, there is no discussion of the tracing of lead, bismuth, and other elements of some interest. It is also regretted that a complete isotope table was not included. Isotope tables are available in several places but it is a convenience to have the data in the same volume with the text.

The discussion of radiation hazards is very sketchy, taking up less than two pages and giving only scanty references to the literature. The readers of this book are precisely the ones who must understand the hazards of radiation and methods of protection against them. It is unfortunate that an opportunity for a thorough indoctrination was missed.

Given identical material, no two authors would write identical books and the criticisms given should be considered as differences in viewpoint and interest. This book contains a wealth of information badly needed by many workers who are invading a new field of research, and will serve as a valuable reference book to those who are more familiar with the use of radioactive isotopes.

Howard L. Andrews
National Institute of Health

The Measurement of Stress and Strain in Solids

By London Institute of Physics, Pp. 114+xvi, Figs. 33, Plates 8. London Institute of Physics, London, 1948. Price $4.00.

There are twelve papers in this very readable and worth while survey of the subject of stress and strain measurements. The papers can be divided by subject matter into about three groups: First, there are a set of three papers on the wire-resistance strain gauge; second, there are a set of three papers on photoelasticity; and finally, there are two papers on the measurement of strain by x-rays. There are several papers which do not fall into this classification, notably one which deals mainly with mechanical and optical devices for measuring strains.

The papers on wire strain gauges are interesting and informative. In the first of these, E. Jones discusses "Some Physical Characteristics of the Wire-Resistance Strain Gauge." Jones states that without special precautions strains can be measured with an accuracy of ±2 percent. He then goes on to describe the various types of wire-resistance gauge. He discusses the proper selection of the three elements, i.e., the wire, the plastic in which the wire is imbedded, and the adhesive. The article gives details on the effects produced by high humidity, temperature changes, high gauge current, imperfect sticking, and high frequency. Zero drift, fatigue, and the range of the instrument are discussed. The rather complete numerical bits of data given are very useful. Only a few references are quoted. In another article, F. Aughtie treats "The Use of Resistance Strain Gauges in Combination—With Particular Reference to Component Loads." In this article the problem of how n gauges, each having an indication which depends on n factors, shall be connected so that the resulting indication depends only on one of the n factors. A theoretical analysis of the problem is given. Applications to temperature compensation, to the measurement of tensile strain in a bar also undergoing bending, and to more complicated situations are given. E. P. George discusses "High Frequency Strain Gauges." In this article the author points out that the change in the resistance of a strain gauge made, using ferromagnetic wire, is as much as forty times as great at a frequency of 20 megacycles as it is if direct current is used. The change in resistance is not proportional to the strain over any appreciable strain range.

W. A. P. Fisher gives "A Review of Some Recent Developments in Photoelasticity." This article is a review of the progress which has been made in this field in the past eight years. The newer more sensitive resins are described, as are the use of polaroid and the changes which these improvements cause in the optical arrangement. Since as many as 12 fringes may pass a given point on the specimen during loading, monochromatic light must now be used. The accurate observation of boundary stresses is discussed. Three methods of investigating stresses in three-dimensional models are described. The "freezing" method which is most widely used depends upon the fact that glyptal and certain resins, if loaded at high temperature and cooled under load, will lose only a very small proportion of their strain and birefringence upon removal of the load. A plane slice is then cut out of the model and the "frozen" birefringence is examined. Pictures are given. In plane photoelasticity the separation of the principal stresses is discussed. Applications to special problems are mentioned. The references given seem quite complete. H. Mc. G. Ross describes methods used in "The Photography of Photoelastic Stress Patterns."

C. E. Phillips gives "A Review of Some Strain Measuring Devices." This article deals chiefly with optical and mechanical devices. The problem's accuracy and sensitivity are discussed in general, and then a number of instruments in current use are briefly described. In some cases the sensitivities are given. A rather complete set of references are given.

D. E. Thomas describes "The Measurement of Strain in Metals by X-Rays." The author describes how, by making measurements on the Debye rings, a quantitative value for the strains in the surface of a metal specimen can be obtained. In industrial steels, the accuracy obtainable for the lattice constant is one part in 20,000. In some cases five times this accuracy can be obtained. Practical details and examples from the author's experience are given. References to other work are incomplete.

In general the summary given of the progress made during the war years in the application of physical methods to the measurement of stress and strain is a most valuable contribution to our literature.

James S. Koehler
Carnegie Institute of Technology

Technique of Organic Chemistry Vol. II

By V. I. Komarewsky and C. H. Riesz, W. A. Noyes, Jr. and V. Boekelheide, and S. Swann, Jr. Pp. 229, Figs. 66, Tables 10. Interscience Publishers, Inc., New York, 1948. Price $5.00.

Catalytic Reactions (V. I. Komarewsky and C. H. Riesz)—The chief contribution of this portion of the book is the material found in Part III on "Laboratory Techniques in Catalysis." This part includes discussions of batch and continuous flow systems at atmospheric pressure, low and high temperature flow systems, batch and flow systems at reduced pressures, and batch and flow systems at elevated pressures. Emphasis is placed on basic procedures and equipment used in carrying out catalytic reactions under the conditions noted above. The survey of equipment in general use is well presented and is accompanied by a large number of excellent illustrations. General availability of the various types of equipment is considered, and leading references to the literature on catalysis are included. Expansion of the material on basic procedures used in catalytic reactions, as well as the inclusion of a larger number of specific examples of catalytic reactions, would increase the value of Part III for the average reader.

The section on "General Principles" (Part I)is too brief to be of any practical value. Its brevity may actually lead to erroneous conclusions on the part of the chemist who is not already well versed in the principles of catalysis.

"Catalysts and Their Preparation" is also presented in too brief a manner in Part II. The methods for preparing, activating, and storing of catalysts are so essential to the practice of catalysis that this section can scarcely be considered to be adequate. The brief and general nature of this section is further weakened by the lack of a sufficient number of examples.

Photochemical Reactions (W. A. Noyes, Jr., and V. Boekelheide)—The authors of this article have done an excellent job in condensing a large mass of material and have succeeded in giving an accurate and relatively broad picture of the techniques employed and results obtained in this field. The reader quickly becomes aware of the continuity of the presentation and of the orderly and logical manner in which he is led through the general principles to the practical applications. The usefulness as well as the limitations of photochemical reactions are considered.

The study of photochemical reactions is divided into two main parts: (1) the primary process or the immediate effect of light on the absorbing molecules; and (2) secondary reactions or reactions produced by the primary process. This section (Part II), which also includes a discussion of light absorption of monatomic gases, diatomic and polyatomic molecules, is clearly presented. The treatment of light sources, selection according to the nature of the reactants and the intensities needed (Part III), is quite adequate.

The discussion of the "Concept of Quantum Yield," although brief, is sufficient for the obvious purposes of *Photochemical Reactions*. This section also considers radiation standards and methods for the measurement of light intensity. Part V "Factors Influencing Design of Photochemical Apparatus," includes effect of absorption coefficient and of type of absorption, flow and static systems, temperature regulation and effects of intensity, vessel dimensions and effects of impurities. These two sections contain very useful information and the presentation is of the same high quality as noted for the previous sections.

In Part VI a variety of photochemical reactions are discussed. A sufficient number of types are included to give a good, general idea of photochemical applications to organic chemistry.

Electrolytic Reactions (S. Swann, Jr.)—The section on "General Theory" (Part II) includes definitions, mechanism of electrolysis, and calculation of the theoretical amount of current necessary for a given reaction. The discussion of the mechanism of electrolysis covers conductance, reactions at electrodes, polarization and overvoltage, depolarization and catalysis. Part II is quite brief, considering the number of topics covered. Most courses in undergraduate physical chemistry discuss this subject matter in greater detail. Presumably the reader will have had such a course and so the brief resume of general theory may be sufficient. Other than that, the material is well chosen and presented.

The discussion of "Apparatus and General Procedure" includes general equipment, electrodes, electrolytes, diaphragms, and general procedures which are used in carrying out electrolytic reactions. This section (Part III), although brief, is compact and contains much useful information.

Parts V and VI consider "Reactions at the Cathode" and "Reactions at the Anode," respectively. A large number of reduction reactions are included in Part V. A critical examination of the controlling factors in electrolytic reduction reactions, such as composition of the catholyte, cathode material, current density, temperature, etc., is presented in this section. Part VI deals with reactions at the anode in a similar manner. In general, the subject material in Parts V and VI has been carefully selected and the general procedures have not been neglected. *Electrolytic Reactions* serves a useful purpose in pointing out the applications of electrolytic techniques to organic reactions.

It is difficult to predict just how useful this book will prove to be. It will undoubtedly serve to stimulate interest in the three fields which are surveyed. Because of the brevity of the book, however, it can scarcely compete with more comprehensive works. In general, the book is well written and is relatively free of the minor errors which are sometimes found in first editions.

ALLAN R. DAY
University of Pennsylvania

Cathode Ray Tube Displays

EDITED BY THEODORE SOLLER, MERLE A. STARR, AND GEORGE E. VALLEY, JR. Pp. 746+xvii. McGraw-Hill Book Company, Inc., New York, 1948. Price $10.00.

This is Vol. 22 of the now well-known M.I.T. Radiation Laboratory Series devoted to radar and allied techniques. Three editors and twenty-one authors have cooperated to summarize within the confines of a single volume the information accumulated by the Radiation Laboratory, during the war, on cathode ray tubes and the associated circuitry required for the production of visual displays for radar applications. An idea of the extent of utility of cathode ray tubes for display and measurement purposes may be had from the fact that nearly three million tubes were manufactured during the war.

This book is extremely informative not only to persons in the field of radar, but also to those interested in oscilloscopes and their less familiar applications. Since some of the radar display techniques described are similar to those used in television, the television engineer will find in the book considerably helpful information, although there are only a few pages that deal directly with television.

The title *CRT Displays* is somewhat misleading since the reader might expect the discussion to be limited to the displays on the face of *CRT*s. Essentially, the book deals with cathode ray tubes and with the technique of radar display production.

The general lack of references in the book not only detracts from its value, but may leave the reader with the impression that little work was done in the field prior to the war. Certainly it must be admitted that television techniques developed prior to the war form the basis for the techniques used in producing radar displays.

The more basic work on cathode ray tubes was done prior to the war at a relatively leisurely rate in this country and abroad. The task during the war was to adopt and extend this basic work to radar application as quickly as possible. The rapid progress demanded by the war necessarily placed greater emphasis on results than on understanding.

The book consists of 18 chapters and 5 appendices. The introductory chapter gives a general survey of cathode-ray tubes, radar displays and signal discernibility, and resolution. This chapter should be of considerable value to the novice and a good refresher to those who have already forgotten.

Eight chapters (2, 3, 8, 9, 12, 16, 17, 18), for some reason scattered throughout the book, deal with the cathode ray tube and its accessories. The chapter entitled "Cathode Ray Tubes" gives some theory of electron guns and condenses a great deal of functional information on cathode ray tubes used during the war. Many users of electrostatically deflected cathode ray tubes will find very useful the section which deals with the adjustment of the mean potential of the deflection plates in order to obtain optimum spot size. It might have been well to point out more clearly why magnetically deflected tubes are the logical choice for intensity modulation and electrostatically deflected tubes for deflection modulation. A chapter devoted to spot size gives the most extensive discussion on spot size measurement at present available in published form. Four chapters are concerned with focus coils and magnets, deflection coils, pattern distortion in magnetic cathode ray tubes, and special deflection coils and magnets for off-centering. The chapter dealing with mechanical and optical devices describes such practically important accessories as shields, optical filters, optical superposition devices, video mapping, direct projection by means of reflective optical systems, and photographic projection. The longest chapter in the book (97 pages) is concerned with luminescent and dark-trace screens for cathode ray tubes. Unlike the rest of the book, luminescent screens are not treated from the functional point of view. The treatment of dark-trace screens is quite detailed and is the most complete available in published form.

The remaining chapters cover circuit techniques, displays, and technique of display production. One chapter describes in considerable detail a number of deflection-modulated displays including the J-scope generally recommended for the accurate measurements of time intervals, and a high speed oscilloscope. Four chapters deal with general circuit techniques including high voltage power supplies, the fundamental problems and means of transmitting position data, electronic markers and indices, and driving circuits for deflection yokes. Four more chapters describe in considerable detail particular methods for obtaining rectangular-coordinate displays, radial-time-base displays, sector displays, and range-height displays.

Last but not least, five appendices supply data on construction of focusing coils and magnets, construction and characteristics of deflection coils, impregnation of deflection and focus coil, characteristics of 40 types of cathode ray tubes including some of the presently used television tubes, and characteristics and circuit diagrams of eight video amplifiers.

Although, because of the magnitude of the task, the treatment of many topics is necessarily superficial and the arrangement of the material not the best, the editors and authors are to be congratulated for so ably presenting so much useful information within the covers of one volume.

Cathode Ray Tube Displays will undoubtedly serve as a fitting memorial to the hundreds of scientific workers and engineers whose work this book describes.

V. K. Zworykin
RCA Laboratories

Radio at Ultra-High Frequencies, Vol. II, 1940-1947

Edited by RCA Review. Pp. 485, Figs. 260, Summaries 22, Appendices 2. Radio Corporation of America, Princeton, New Jersey, 1948.

Reviewing *Radio at Ultra-High Frequencies, 1940–1947* may be likened to reviewing an issue of the Proceedings of the I.R.E. Subjects of the various papers here reprinted include antennas, transmission lines, propagation, reception and receivers, microwaves (a not-elsewhere-classified category), measurements, radio relay systems, and aids to navigation. The unifying ties are that the papers are all from RCA sources (geographically from Rocky Point, New York, Harrison, Princeton, and Camden laboratories), and the title, which serves to distinguish this collection from other RCA volumes on television, facsimile, etc.

The book tends to show (presumably its purpose) that RCA has had an active research interest in problems in many aspects of the field specified by the title. That the reprinted papers happen to cover an interval in which there was great development in the field occasionally yields a touch of antiquity to the reading—1940 is a long time ago in ultra-high frequency work—but on the whole the group is relatively up-to-date and many of the papers are excellent.

Brown and Woodward in the leading paper, on the measurements of impedance characteristics of cylindrical antennas, fail to confirm a conclusion of Brillouin, and point to the need of more experimental work in an area in which there has been theory. Iams describes a phase-front plotter of considerable interest. The development of some antennas for producing circularly polarized waves (for ground-to-airplane communication) is described, as well as some work on slot antennas. Noise studies and a discussion of receiver sensitivity and signal-to-noise ratio in u-h-f receivers follow.

A 110-page group of articles "Aspects of Reception at Ultra-High Frequency" is an excerpt from lecture notes for a u-h-f course of the 1941–42 variety. Judged by the material, however, the course must have been a good one and possibly superior to the standard course of the time.

Radio relay systems are now in operation and in certain fields—telegraphy, for example—are supplanting previous methods of transmission. An interesting incidental from one of the papers on such systems points out that RCA had one in operation in 1923 (at 182 kc/sec.).

The aids to navigation section gives only summaries of papers, including some on shoran and teleran. Topics of other papers in the book range from the high frequency spectrum of ignition noise to the absorption of microwaves by gases. A bibliography of about 300 RCA papers in or touching on the u-h-f field is given.

All the papers in the book including those given only in summary form and the excerpts from the u-h-f course have appeared in print previously.

J. G. Brainerd
University of Pennsylvania

Principles of Mathematical Physics

Second edition. By William V. Houston. Pp. 363+xii, Figs. 43. McGraw-Hill Book Company, Inc., New York, 1948. Price $5.00.

This is the second edition of an excellent and deservedly popular text intended as an intermediate course for juniors, seniors, and first-year graduate students in those branches of physics requiring mathematical analysis. There is little new material in the second edition, but rather the emphasis has been on increasing the clarity of the explanation by rewriting the difficult passages with more drawings and illustrative examples.

The student is expected to have had a course in elementary physics, analytic geometry, and calculus. Without having to wait until the student has also had differential equations, vector analysis, and the calculus of variations these subjects are supplied in sufficient detail for the analysis of physical phenomena. The treatment does not take the place of a thorough sequence in mathematics, but enables the student to get on with the physics without having to wait until graduate school before being able to tackle some of the more theoretical aspects.

The physics treated is mechanics, thermodynamics and statistical mechanics, and electricity and magnetism: the usual intermediate sequence with the exception of optics. The book hits the high spots of the courses in these subjects not shrinking in doing so from a point of view sufficiently sophisticated to enable the student to cope with the more advanced courses. There is no quantum mechanics, but the classical analysis and methods included will aid the student in quantum mechanics. No use is made of the Laplace transform or of the analogy between mechanical vibrations and electrical circuits, methods which seem to be gaining favor in some quarters today.

The treatment admittedly leaves some scope for the ability of the instructor which tends to give it a categorical flavor. The problems are an integral part of the development of the theory. Equations are derived in some problems and applications illustrated in others. This has the advantage that the student gets a grasp of the subject as he must work it out for himself. Even if he cannot work all the problems he will at least be able to understand the development when it is explained to him. In a few places, on the other hand, as for example in the discussion of moving axes, the principle of leaving it to the instructor to explain could be relaxed just a little with considerable gain in clarity for the student. The physical significance of what is happening is kept continually in mind, and physical arguments are employed as in the case where the smallness of forced oscillation of the frequency is high enough. The author has a happy facility for anticipating just what is going to bother the student and answering his question in the next phrase. He states clearly what he is going to do, what he is not going to do, and what the assumptions are. If something is left out it is stated or put in a problem and the student is not left to wonder whether he should be able to prove it or not.

The m.k.s. units are used throughout, but the Gaussian system is also explained and conversion tables given. This is in line with the growing popularity of these units. It might help to overcome the objections of some of the most violent opponents of m.k.s. units if peculiar properties were not assigned to empty space. A constant of proportionality in a physical equation which depends only on the units used should be treated merely as such and not as a characteristic of space. This outburst is prompted by the author's care in pointing out that the "apparent role of κ_0 as the 'permittivity of a vacuum' is not taken as suggesting the possibility of polarization in a vacuum." Let us lay the ghost of κ_0 as a property of space in the first place.

Electricity and magnetism are treated following Maxwell with just a paragraph on Lorentz in conclusion. These chapters have clearly been written from the experience gained by watching students flounder around in the electromagnetic field. The author has a knack of foreseeing the block on which the student is about to stumble and of pushing it out of his path. This well written intermediate text ends with some properties of the Lorentz transformation and the equivalence of mass and energy.

C. W. Ufford
University of Pennsylvania

Electrical Measurements in Theory and Application

Fourth Edition. By Arthur Whitmore Smith. Pp. 371, +xix, Figs. 250. McGraw-Hill Book Company, Inc., New York, 1948. Price $4.25.

This is the fourth edition of Professor Smith's book on electrical measurements. The previous editions appeared in 1914, 1924, and 1934 (Rev. Sci. Inst. 5, 381 (1934)). This book may be used as both a text and a laboratory guide. The explanations of experiments are not set apart from the other material, but are indicated in the Table of Contents by a star.

The author writes, as he states in the Preface, for "students who have had one year of college physics and desire further knowledge of electrical and magnetic matters." However, little previous knowledge is presumed, and the elementary ideas of electron flow and the fundamental definitions of mechanical and electrical units are given in the Introduction. The first chapter contains simple experiments for the instruction of "students with little laboratory experience." "Those with college laboratory training can pass on to the advanced subjects and more complicated methods." "The simple and more fundamental ideas are treated in the first chapters, and in the first part of each chapter, more difficult measurements and methods requiring more extended knowledge are reserved until the student has attained greater proficiency."

This is a book on electrical measurements and its scope is well outlined in the Table of Contents. The first eight chapters deal with the study and use of the ammeter, voltmeter, ballistic and current galvanometers, Wheatstone bridge, potentiometer, and the fundamental measurements of current and power. Electron tubes are introduced in Chapter Nine and a few important electronic instruments are pictured later. The magnetic circuit, measurements of magnetic flux and magnetomotive force, and magnetic tests of iron and steel are given in three chapters. Simple a.c. circuits are clearly treated in terms of vector diagrams and the fundamental differential equations. Measurements of capacitance and inductance particularly by bridge methods are treated quite extensively. The text concludes with a brief chapter on the calibration of alternating current instruments.

The book is illustrated with clear diagrams and useful pictures of modern apparatus. The meter-kilogram-second system has been employed throughout. A few examples and problems, some with answers, are given, mainly for d.c. and a.c. circuits. Calculus is used, but with each step clearly indicated so that it may be easily followed by a student not too familiar with such mathematics.

This text is restricted to the field of electrical measurements, and, as the title indicates, the principle ideas presented are the theory and application of methods for measuring fundamental quantities such as current and power, charge, resistance, voltage, inductance, capacitance, magnetic flux and intensity, magnetomotive force; and some of their complexities such as temperature variations, electron emission, and hysteresis. The whole field of electricity and magnetism is not covered to the extent that might be needed by an undergraduate student of today in the physical or biological sciences. Perhaps no one text can cover such a broad field.

There are a few short additions that might have been made, however, such as: the mention in the opening paragraph of neutrons in the atom, a brief explanation of diamagnetism, and a diagram of a cathode-ray tube.

In the field for which it is intended, this book, with the material clearly and simply presented, should be a welcome help to the students for whom it was written.

Margaret N. Lewis
Boston University

Vacuum Tube Amplifiers

Edited by George E. Valley, Jr. and Henry Wallman. Pp. 743+xvii, Figs. 391, 22½×15 cm. McGraw-Hill Book Company, Inc., New York, 1948. Price $10.00.

Vacuum Tube Amplifiers is Vol. 18 in the Massachusetts Institute of Technology Radiation Laboratory Series and, like other volumes in the series, represents the combined efforts of a group of specialists to set down the knowledge, experimental and theoretical, which they found useful during the active days of the Radiation Laboratory. Although most of the material in the volume is of importance in radar, much of it will have a continued interest to physicists and engineers who have occasion to design electronic circuits. This is because the various authors have endeavored to emphasize principles of design and have assigned a secondary role to the discussion of specific radar circuits.

It is evident that an effort was made by the editors and by the contributing authors to achieve a unified volume. Nevertheless each chapter, or group of related chapters, bears the stamp of the individual authors, and for the most part forms a self-contained account of a particular aspect of amplifier design that can be read independently of the remainder of the book. This is perhaps an advantage in a volume that will find its greatest usefulness as a reference work. In view of the joint authorship and the variety of topics considered, it appears advisable to mention each chapter in turn.

Chapter 1, "Linear-Circuit Analysis and Transient Response," by Richard Q. Twiss (70 pages) is a concise, formal account of network analysis based on the Laplace transform. The chapter should appeal to the reader who has some prior knowledge of its contents and wishes to improve his understanding of the modern method of computing the transient response of linear networks.

Chapter 2, "High-Fidelity Pulse Amplifiers," by Robert M. Walker and Henry Wallman (42 pages) contains a valuable discussion of the theoretical aspects of the high-fidelity amplification of pulses, together with a number of practical circuits for use with pulses. The number of complete amplifiers is unfortunately limited.

Chapter 3, "Pulse Amplifiers of Large Dynamic Range," by Harry J. Lipkin (53 pages) is concerned with a problem that is peculiar to radar in which a high gain, low pass amplifier is called on to amplify signals from a few microvolts to several volts without blocking for an appreciable time. One gathers that the chapter summarizes a development that required considerable time, effort, and ingenuity on the part of the group working on this problem. It appears unlikely that the design procedures described here will have a very general application in other branches of electronics.

Chapter 4, "Synchronous and Staggered Single-Tuned High-Frequency Bandpass Amplifiers," by Henry Wallman (35 pages) contains a clear mathematical analysis of these types of wide-band amplifiers, illustrated by several practical examples. Emphasis is placed on design considerations. This is the first of four chapters devoted to wide-band bandpass amplifiers.

Chapter 5, "Double-Tuned Circuits," by Richard Q. Twiss (31 pages) constitutes an extension of the usual theory of the double-tuned interstage coupling to the wide-band case. The treatment is mathematical and is illustrated by three examples.

Chapter 6, "High-Frequency Feedback Amplifiers," by Harry J. Lipkin (42 pages) considers the improvement in the gain-band width product and other properties of bandpass amplifiers incorporating inverse feedback.

Chapter 7, "Bandpass Amplifiers: Pulse Response and General Considerations," by Henry Wallman (37 pages) discusses the transient response of bandpass amplifiers to a carrier-frequency pulse, as well as problems arising in the large scale production of bandpass amplifiers. This, and the preceding three chapters constitute an exhaustive account of the design of bandpass amplifiers for radar applications.

Chapter 8, "Amplifier Measurement and Testing," by Yardley Beers and Eric Durand (32 pages) considers methods of measuring the frequency response and the transient response of low pass and bandpass amplifiers used in radar.

Chapter 9, "Low-Frequency Amplifiers with Stabilized Gain," by Duncan MacRae, Jr. (51 pages) deals with the design of very stable amplifiers used in electronic computers. The material in this chapter is capable of rather wide application in the design of electronic circuits. It should appeal to a greater class of readers than the material in the preceding chapters devoted to bandpass amplifiers.

Chapter 10, "Low-Frequency Feedback Amplifiers," by Harold Fleischer (25 pages) is concerned with the theory and design of low-frequency selective amplifiers based on the use of a twin-T or bridged-T network in the feedback loop of the amplifier. The material here should be of considerable general interest.

Chapter 11, "Direct-Coupled Amplifiers," by John W. Gray (87 pages) contains a wealth of practical data pertaining to the design of circuits for amplifying d.c. signals. This chapter should be extremely useful to the circuit designer.

Chapter 12, "Amplifier Sensitivity," by E. J. Schremp (108 pages) is essentially a monograph analyzing the origin and the properties of thermal and shot noise. The treatment is rigorous and requires considerable background in mathematics and physics on the part of the reader. The chapter constitutes a definite contribution to the theory of fluctuation noise.

Chapter 13, "Minimal Noise Circuits," by Richard Q. Twiss and Yardley Beers (80 pages) is concerned with the design of practical circuits for achieving the highest possible signal-to-noise ratio in the case of bandpass amplifiers used in detecting radar signals. The chapter contains considerable information that can be applied in the design of other types of amplifiers, e.g., the pulse amplifiers of nuclear physics.

Chapter 14, "Measurement of Noise Figure," by Yardley Beers (26 pages) describes methods of measuring the performance of amplifiers in detecting weak signals. The methods described are intended to be used with the types of amplifiers described in early chapters and in Chapter 13.

W. C. Elmore
Swarthmore College

Electromechanical Transducers and Wave Filters

By Warren P. Mason. Pp. 419+xii, Figs. 147. 16×23½ cm. D. Van Nostrand Company, Inc., New York, 1948. Price $6.00.

This is a second edition of a scholarly and thorough book on the theory of electrical networks and vibration of coupled acoustical, mechanical, and electrical systems employing electrical, mechanical, and acoustical analogies. The author is an outstanding authority in the field of network and vibration theory and the book follows, for the most part, the field in which he has made outstanding contributions. The new material in the second edition is an outgrowth of the work on filters and transducers made during the war. Eighty-six pages and twenty-seven figures have been added. All the new material is placed at the end of the book. For those who are not familiar with the first edition, a brief review will be given of this portion of the book. This will be followed by a review of the new material.

The treatment throughout the book is almost self-sufficient. However, a considerable knowledge of network theory is required to obtain a working knowledge of the material in the text. The illustrations are adequate and well done.

The electrical network theory in this book shows how the characteristics of the ladder and T sections can be derived from the lattice. A table of filters useful in the design of acoustical and mechanical systems is included. The application of network theory or analogies to the solution of mechanical and acoustical systems, together with both the direct and indirect analogies, is treated in considerable detail. Another subject is the propagation of sound in systems with distributed constants such as pipes and horns. The theory of the vibration of plates and membranes and the use in telephone receivers and as elements in an acoustical filter is also treated in this section of the book.

In the field of electromechanical converting systems, the following transducers are considered: electrostatic, piezoelectric, magnetic, dynamic, and magnetostrictive types. A horn loudspeaker and a crystal-driven ultrasonic radiator are used to illustrate the application of the theory.

Another valuable chapter deals with electromechanical impedance elements in electrical filters. The consideration of mechanical elements for filters includes a very complete treatment of piezoelectric as well as magnetostriction systems. In this field, Mason has been the principle contributor in the literature.

The addition to the book in the new edition includes wave guides and wave guide filters. One very interesting subject and a new concept is the application of a gyroscope as an impedance element. The propagation of sound in air- and liquid-filled ducts as well as the subject of ducts lined with absorbing materials is covered. In the field of underwater sound, consideration is given to the construction and design of directional underwater transducers and the description of a water tank with absorbing walls. Another new subject is torsional vibrating crystals. Altogether, the revision contains an excellent addition to the first edition, which was a valuable and outstanding contribution.

HARRY F. OLSON
RCA *Laboratories*

Practical Spectroscopy

BY HARRISON, LORD, AND LOOFBOUROW. Pp. 605, illustrated. Prentice-Hall, Inc., New York. Price $6.65.

The appearance of *Practical Spectroscopy* by Harrison, Lord, and Loofbourow is very opportune in view of the recent history of that branch of physics. The science of spectroscopy had a long slow growth in which the development of instruments and techniques far outdistanced their use. The consequence was that the sudden outburst of activity on the part of the physicists which took place after the first World War was able to solve in principle in a few years' time most of the fundamental problems of the external structure of atoms and molecules. A great mass of detailed analysis remains to be done by the few remaining physicists interested in such problems. On the other hand, to the astrophysicist, spectroscopy has become his most powerful tool and he already feels the failure to complete the job. The chemists and biologists also are now large "users" of the spectroscope and of spectroscopic data in purely scientific fields; but probably the largest group of "users" is the great number of industrial scientists who find in spectroscopy one of their most powerful analytical tools. These facts, coupled with the scarcity of competent trained spectroscopists in university laboratories, make it increasingly necessary that books such as that under review should be written.

Practical Spectroscopy is addressed to the "users" of spectroscopy whose chief concern is with the results that it will furnish to them. Consequently, it is not a compendium of present day knowledge of the art as was "Kayser" in 1901 or "Baly," the English counterpart of Kayser. It is, rather, a well considered selective condensation of our present knowledge of techniques in all the branches of the subject. Very wisely, the authors have not hesitated to give their judgments on the choice of instruments instead of facing the inexperienced user with unweighted alternatives.

As with all books, there are bound to be details with which any particular reviewer will disagree. Some points of this sort are the following. In Chapter 4, where various mountings of the concave grating are discussed, there is no general formula for the dispersion given. In fact, on page 85 a serious error of statement occurs because such a formula was not used. The statement is that the dispersion of the fourth order of the red end of the spectrum by a 15,000-line per inch grating in a 3-meter Eagle mounting is 1.3A per mm, whereas it should be about 0.4A per mm. I missed also any reference to the very useful fact that Rowland ghosts are displaced from the parent line by a definite fraction of its wave-length, usually 1/1000 or 1/750. The discussion of the concave grating in the Wadsworth mounting is, I think, insufficient, considering the usefulness of that mounting for analytical work. It should be mentioned that the focal curve, over its usable length, can scarcely be distinguished from a circle of radius $r = R/2 + 3\cos i$), which is the actual radius of curvature at the normal. For some uses, it may also be important to know that due to the off-axis position of the mirror and grating, there is a slight astigmatism.

I particularly appreciated the discussion in Chapter 6 on the illumination of the slit. It is a subject usually treated in a very cursory manner in spite of its essential importance. It is natural that Chapters 12 and 13 on the measurement of intensities should be excellent since this is a field in which Professor Harrison is an expert. The recent work on the use of photoelectric cells for the measurement of intensities may have a considerable effect, but it seems fairly certain that photographic techniques will hold their own for some time. The chapter on quantitative analysis, although it draws largely on previous chapters, seems to me too short. On the other hand, the chapters on the vacuum ultraviolet and on interferometry are correctly kept within small compass, since they are unlikely to be of interest to most present users of spectroscopy. It should, however, be noted that in Chapter 20 the authors have transformed Professor R. W. Wood into a superman who can observe the green line of mercury in the seventh order of a 15,000-line grating!

At the present low ebb of spectroscopic training in the universities, those who need spectroscopic techniques for the solution of their problems will have to rely more and more on such books as this. Especially in the industrial laboratories will it be indispensable.

A. G. SHENSTONE
Princeton University

Principles of Servomechanisms

BY GORDON S. BROWN AND DONALD P. CAMPBELL. Pages 400, Illustrations 207, Tables 21. John Wiley and Sons, Inc., New York, 1948. Price $5.00.

The development of the theory of servomechanisms has been rapid over the past ten years, in fact, so rapid that not until the publication of *Principles of Servomechanisms* has there appeared a correlated work suitable for use as a textbook in engineering schools.

The book is confined to linear closed-loop servomechanisms, and attention is centered on their frequency response, the use of which has proved itself a powerful tool not only in the analysis but in the synthesis of servomechanisms.

After an introduction to the elements of automatic control and the problems of synthesis, the differential equations of several simple systems are examined to provide the student with a "feel" of the subject. The transient response of an elementary positional servomechanism is worked out in detail along classical lines and criteria of good performance based on experience are stated.

The theory of the Laplace transform is summarized in Chapter 3 to furnish a systematic means of solving differential equations and to lay the groundwork for the definition of the transfer function which is an important concept in synthesis when systems become at all complex.

Chapter 4 introduces the student to the frequency response of servomechanisms and its correlation with transient response. Chapter 5 is a well prepared discussion of equivalent circuits, transfer functions, and block diagrams. By means of several examples, it is shown how the transfer functions of devices like motors, electron tube amplifiers, and hydraulic transmissions can be formulated.

The bulk of frequency response theory is covered in Chapters 6 through 8. Several techniques of plotting frequency response data are given: Nyquist diagrams, inverse plane diagrams, log magnitude and angle *versus* frequency diagrams, and log magnitude *versus* angle diagrams. Each of these techniques is important for the light it sheds on the performance of servomechanisms and for the familiarity it gives the student with presentations current in the literature.

Chapters 9 and 10 are concerned, respectively, with systems subject to output as well as input disturbances and with experimental procedures. The experimental procedure chosen is limited to servomechanisms with synchro data systems, and it seems that the value of the chapter could be measurably increased by presenting the matter of testing in a more general way. For instance, in closed-loop servomechanisms with electrical data systems, the servomechanism can be left intact and a signal inserted in series with the controller input across a low impedance. This makes it possible to test servomechanisms such as those using bridges or potentiometers where the input cannot be rotated continuously at reduced amplitude to obtain the desired signal. The signal required for testing a so-called d.c. servomechanism is sinusoidal and that for a carrier frequency servo is a double-sideband suppressed carrier signal produced by sinusoidal modulation. Several ways of generating such signals suggest themselves.

Especially valuable is the last chapter on approximating the transient response from the frequency response. The reviewer feels that the method of trapezoidal approximation given is the simplest yet devised. Computations are facilitated by a four place table of sin x/x which appears in the chapter. However, the use of the contour integral to obtain the inverse Laplace transform in the proof of the method is somewhat confusing after having been introduced to partial fractions in Chapter 3. It might have been better, though somewhat harder on the student, if the inverse transform had been performed by evaluating the contour integral to begin with.

In general, the book is well organized and understandably written. Illustrations are freely used to amplify the text and the tabulations of equations and pertinent data are extremely helpful. The back of the book contains a complete bibliography to which references are made throughout the text and an adequate set of problems arranged by chapters. The book should be very helpful to engineers interested in servomechanisms and should find widespread acceptance among instructors as a textbook.

W. J. Brackmann
Norden Laboratories Corporation

Distillation and Rectification

By Emil Kirschbaum. Translated by M. Wulfinghoff. Pp. 426, Figs. 236. Chemical Publishing Company. Inc., Brooklyn, 1948. Price $10.00.

This is not the complete up-to-date book on distillation for which so many of us have been waiting. However, it does present a fairly good coverage of material in this field except for developments which have occurred during the past twelve or thirteen years. It is the translation of a book first published in German in 1940 and covers in a comprehensive manner only information up to about five years before that time.

The treatment of the fundamental principles involved in distillation is thorough and good discussions of the various types of partial pressure-composition, temperature-composition, and equilibrium diagrams are included. These descriptions show the applications to miscible, immiscible, binary, multicomponent, and azeotropic systems. The effect of pressure is discussed at some length. Information regarding the design, construction and the various methods of operating distillation equipment is presented. A long section is devoted to the details of construction and behavior of bubble caps in operation. There are many useful illustrations interspersed with the text, the total number of figures being 236 within the 426 pages.

Methods for determining the size of column required for a given separation for both batch and continuous distillation are illustrated with a few numerical examples. Where possible, graphical methods have been employed in preference to those which require involved calculations. Ample consideration is given to the use of the enthalpy-concentration diagram as applied to binary mixtures. Other subjects considered include the use of sieve plates and packed columns, details of heat exchangers and control equipment, and the fundamentals of molecular distillation.

Interesting features not included in previous books on the subject are: the presentation of empirical graphs for estimating the permissible vapor velocity in plate columns; photographs showing fluid motion and distribution on bubble cap trays; tables of vapor-liquid equilibrium data and 8″×8″ graphs on loose sheets depicting these for 63 systems. The translator has included a rather inadequate review of progress made since the original publication. This takes the form of a series of short abstracts of some articles which have appeared in technical journals in this country from 1940 to 1946.

The book is written more in the fashion of a dissertation or thesis rather than an American technical book as it contains no chapters but merely headings and sub-headings throughout. It will be difficult for those in this country to read chiefly because of the use of symbols entirely different from those to which we are accustomed. In addition, the diagrams, graphs and illustrations are lettered in German but do have captions in English and translations beneath the figures. The index and bibliography are decidedly incomplete.

This translation will prove interesting to those well versed in the art of distillation due to its different approach to many of the topics but it will not fill the need for those who wish to learn of recent developments. Libraries will find it useful as a reference for the subjects, such as bubble cap operation, which have been treated thoroughly.

A. Ralph Thompson
University of Pennsylvania

Author Index to Books Reviewed

Beck, A. H. W. *Velocity-Modulated Thermionic Tubes* 309

Boekelheide, V.—see Komarewsky, V. I. 310

Brown, Gordon S. and Donald P. Campbell. *Principles of Servomechanisms* 315

Campbell, Donald P.—see Brown, Gordon S. 315

Harrison, G. R., Lord, and Loofbourow. *Practical Spectroscopy* 315

Houston, William V. *Principles of Mathematical Physics* 312

Institute of Physics, London. *Measurement of Stress and Strain in Solids* 310

Kamen, Martin D. *Radioactive Tracers in Biology* 309

Kirschbaum, Emil. *Distillation and Rectification* 316

Komarewsky, V. I., C. H. Riesz, W. A. Noyes, Jr., V. Boekelheide, and S. Swann, Jr. *Technique of Organic Chemistry, Volume II* 310

Livingston, Robert. *Physico Chemical Experiments* 308

Loofbourow—see Harrison, G. R. 315

Lord—see Harrison, G. R. 315

Mason, Warren P. *Electromechanical Transducers and Wave Filters* 314

Newman, F. H. and V. H. L. Searle. *General Properties of Matter* 308

Noyes, W. A., Jr.—see Komarewsky, V. I. 310

RCA Review. *Radio at Ultra-High Frequencies, Volume II,* 1940–1947 312

Riesz, C. H.—see Komarewsky, V. I. 310

Searle, V. H. L.—see Newman, F. H. 308

Smith, Arthur Whitmore. *Electrical Measurements in Theory and Application* 313

Soller, Theodore, Merle A. Starr, and George E. Valley, Jr. *Cathode Ray Tube Displays* 311

Starr, Merle A.—see Soller, Theodore 311

Swann, S., Jr.—see Komarewsky, V. I. 310

Valley, George E., Jr.—see Soller, Theodore 311

——— and Henry Wallman. *Vacuum Tube Amplifiers* 313

Wallman, Henry—see Valley George E., Jr. 313

Other Books Received

Advances in Biological and Medical Physics. Volume I. Edited by J. H. LAWRENCE AND J. G. HAMILTON. Pp. 484+xi, Figs. 49. Academic Press, Inc., New York, 1948. Price $8.60.

Methods in Medical Research. Volume I. Edited by V. R. POTTER. Pp. 372+xii, illustrated. Year Book Publishers, Inc., Chicago, 1948. Price $8.00.

Microwave Antenna Theory and Design. MIT Radiation Laboratory Series. Pp. 721+xviii, Figs. 300, McGraw-Hill Book Company, Inc., New York. Price $8.00.

Principles and Methods of Telemetering. PERRY A. BORDEN AND GUSTAVE M. THYNELL. Pp. 230, illustrated. Reinhold Publishing Corporation, New York, 1948. Price $4.50.

Principles of Radar. DENIS TAYLOR AND C. H. WESTCOTT. Pp. 141. The Macmillan Company, New York, 1948. Price $3.50.

Scientific Foundations of Vacuum Technique. SAUL DUSHMAN. Pp. 882+xi, Figs. 324, Tables 222. John Wiley and Sons, Inc., New York, 1949. Price $15.00.

Sources of Engineering Information. BLANCHE H. DALTON. Pp. 109. University of California Press, Berkeley, 1948. Price $4.00.

Techniques Générales du Laboratoire de Physique. Volume 1. J. SURUGUE. Pp. 433, Figs. 438. National Center of Scientific Research, 1947.

Vacuum-Tube Circuits. LAWRENCE BAKER ARGUIMBAU. Pp. 668, Figs. 676. John Wiley and Sons, Inc., New York, 1948. Price $6.00.

Velocity-Modulated Thermionic Tubes. A. H. W. BECK. Pp. 180, Figs. 56. The Macmillan Company, New York, 1948. Price $3.75.

Waveforms. MIT Radiation Laboratory Series. Edited by CHANCE, WILLIAMS, HUGHES, MACNICHOL, AND SAYRE. Pp. 535+xxii, Figs. 704. McGraw-Hill Book Company, Inc., New York, 1949. Price $6.00.

Laboratory and Shop Notes

Electron Trajectories in a Gamma-Ray Spectrometer

H. Hurwitz, Jr.
Knolls Atomic Power Laboratory, General Electric Company, Schenectady, New York*

February 9, 1949

IN designing a gamma-ray spectrometer of the type recently described by Lawson,[1] it is necessary to compute the trajectories of electrons emitted radially inward from a target near the edge of a cylindrically symmetrical magnetic field. The deflection, φ, of the electrons when they have returned to the radius, r_0, of the target is given by the formula

$$\varphi=2\epsilon\int_{r_m}^{r_0}\frac{Hdr}{(1-\epsilon^2u^2)^{\frac{1}{2}}}=\pi-2\epsilon\int_{r_m}^{r_0}\frac{udr/r}{(1-\epsilon^2u^2)^{\frac{1}{2}}}, \tag{1}$$

where

$$ru(r)=\int_r^{r_0}rHdr,\quad \epsilon=e/cp.$$

Here p is the momentum of the electron, and r_m is the radius at which ϵu is unity. For large p or a uniform field φ is given by

$$\varphi=2\arctan\left[\epsilon\int_0^{r_0}Hdr\right]. \tag{2}$$

This formula is surprisingly accurate even when p is comparatively small and the field is not uniform. For electrons of small energy, the numerical computation of φ can be done most conveniently by use of the following alternate form of Eq. (1):

$$\pi-\varphi=\frac{2}{\epsilon}\int_0^1\frac{dy}{u+rH},\quad u=\frac{(1-y^2)^{\frac{1}{2}}}{\epsilon}. \tag{3}$$

To integrate Eq. (3), u is first computed numerically as a function of r. Then $u+rH$ can be obtained as a function of u, and hence of y.

After the deflection, φ, of an electron at r_0 has been computed by Eq. (2) or (3), the additional deflection $\Delta\varphi$ corresponding to the path from r_0 to a larger radius r_e is given by

$$\Delta\varphi=\epsilon\int_{r_0}^{r_e}\frac{udr/r}{(1-\epsilon^2u^2)^{\frac{1}{2}}}. \tag{4}$$

---

* The Knolls Atomic Power Laboratory is operated by the General Electric Research Laboratory for the AEC. The work reported here was carried out under Contract No. W-31-109 Eng-52.

[1] James L. Lawson, Phys. Rev. 75, 433 (1949).

A Timer for Short Intervals*

R. Stuart Mackay
Department of Physics, University of California, Berkeley, California

January 25, 1949

IN a forthcoming study of the stoppage of centricular fibrillation by electrical impulses, it was desired to pass pulses of current of variable duration through a heart. Because the currents involved would be one or more amperes, it was necessary either to use rather large thyratrons in some form of inverse parallel connection, or to construct a device activating a fairly rugged relay. The latter was thought preferable from a standpoint of simplicity if a satisfactory unit could be designed. Interval times involving the gradual charging of a condenser through a resistor to some predetermined voltage are well known, but few have been specifically designed to act for times less than the period of the a.c. supply line frequency. In fact, most such timers have made use of the passage of the voltage into negative values to deionize a thyratron. The present circuit was built to cover the range of times from 0.01 second to 10 seconds, but with small changes in the circuit time constants it gave satisfactory results from about 0.002 second to several minutes. These short time intervals were accurately calibrated by counting with a scaling circuit the number of cycles passed by the relay from a 10-kilocycle oscillator. The oscillator used was the horizontal sweep circuit of a standard oscilloscope. A single RC differentiating circuit sharpened the pulses sufficiently to work a standard scaling circuit. The scaling circuit was also used to calibrate the oscillator frequency by counting the number of cycles produced in a five-minute interval.

The relatively large plate currents drawn by relays of substantial enough design can most efficiently be handled by a small thyratron. Because of the short time intervals involved one cannot depend on an alternating plate voltage to deionize the tube and thus release the relay. Also, a relay to be used on the plate current pulses of an a.c. fed thyratron must be made extra slow in acting so that it will not chatter. For these reasons the thyratron in the present circuit is fed with filtered direct current. The thyratron is normally on and the current it passes holds the relay open. The relay is allowed to fall closed by breaking the plate current for a time less than the timing interval, but greater than the deionization time of the tube. This momentary current interruption is produced by a single pole double throw snap-switch arranged to complete the circuit in both of its positions. However, during the transit time of the moving member neither pole is connected for a suitable instant, thus allowing the grid to regain control. The relay, after it has fallen closed, completes the external circuit through one set of contacts, and starts the charging of condenser C (Fig. 1) through resistance R by means of the other set. After a time roughly equal to RC, the condenser will charge to a voltage high enough to ionize the gas in the neon bulb, whereupon the condenser starts to discharge through the bulb and the 15,000-ohm resistor. The positive pulse so produced is applied to the thyratron grid to reionize it and pull in the relay, thus again opening the external circuit. At the same time the other set of contacts shorts the condenser through the 10,000-ohm resistor, thereby discharging the condenser ready for another cycle.

The relay used, because of ready availability, had a 300-ohm coil resistance. An extra 1000-ohm current-limiting resistor then had to be placed somewhere in the circuit, and it was used so as to act as part of a voltage divider to supply cut-off bias once the tube is extinguished. It is to be noticed that it is shown shunted by a one-microfarad condenser. Without this, though the timing interval was always correct, the tube wouldn't deionize with every flip of the switch. This condenser then maintains the falling cathode potential quite positive for the time required for deionization. The positions of relay coil and resistor could be interchanged if a higher resistance relay was to be used.

In the present version of this circuit, C was a one-microfarad paper condenser in all cases, while R was made the variable

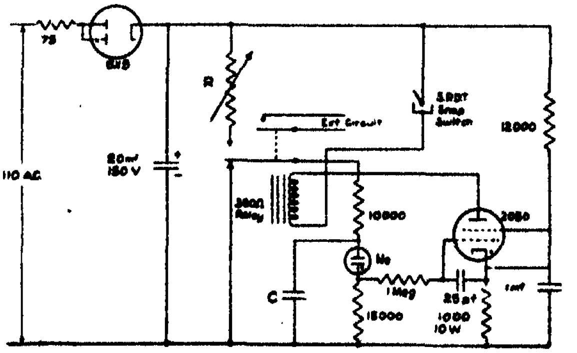

Fig. 1. A timing circuit in which the relay is deenergized for a time of approximately RC. Especially at the short intervals, a power supply with better regulation will give greater reproducibility.

element. It is preferable in the low ranges to use a linear wire wound potentiometer of say 100,000 ohms for R and a series of fixed resistors and a step switch in the higher ranges. For an increased range one should also allow C to vary. The shortest time interval was produced with an R of zeró ohms because then the charging current was limited only by the 10,000-ohm resistor. This resistor was so placed that it not only determined the shortest time, but also, at the end of an interval, it discharged the condenser gradually rather than abruptly, as would be the case if the condenser were shorted directly by the contacts. There seems to be some evidence that this is advantageous to the condenser as well as to the relay contacts.

The neon bulb, before installation, was placed in series with a suitable resistor across the a.c. line for a week of aging in order to reduce any tendency towards a change in characteristics. Since the life of such a bulb depends on the time integral of the current passed, and since this bulb is only required to pass one small pulse for each timing cycle, it should provide long and stable operation. Variations in the characteristics of the thyratron, of course, do not matter since it is merely pulsed at the proper time by the neon bulb. If left unregulated, variations in the line voltage will still somewhat affect the interval by changing the condenser charging rate, but at least the firing point will not also be variable. Since the neon bulb breaks down at a time when the condenser is only about half-charged, the derivative of the charging curve is still high at the operating point, thus making for positive reproducible action. The size of the resistor delivering the pulse isn't critical since, though it does control the neon bulb current, in any case the size of the pulse will be the difference in the neon bulb firing and operating potentials (the latter, though approximately constant, taken at the stated current). The 25-$\mu\mu$f condenser was introduced to minimize the possibility of a positive plate transient ending the timing interval too soon (by raising the grid potential).

We might now consider the main feature contributing to the high speed of response of this circuit. It is only after the relay has completely fallen closed that the external circuit is completed and the condenser starts to charge. Thus it does not matter how sluggish the relay is in dropping out, as only its pull-in time limits the speed of operation. This latter time can be rather small even for relays usually considered big and slow in action. Furthermore, it is reduced from its normal value by the large initial current surge from the one-microfarad condenser upon ionization of the thyratron. This discharge current is limited only by the relay impedance since the condenser is effectively placed across the relay coil and thyratron by the low impedance of the power supply. If the relay impedance is small then these initial currents will be high and will cause a fast snap in action. The thyratron is quite capable of carrying momentary high current surges, and since it turns the relay on, there is no danger of welding the contacts of even a small switch.

In conclusion, the application of this system to the activation of various other mechanical elements might be mentioned. For example, at present it is being used in conjunction with a high speed magnetic shutter activated by a light integrating photo-cell on an automatic enlarger. It was found impossible to turn the light off quickly enough when the proper exposure was reached so a shutter had to be used. Its magnet is placed in a circuit similar to the magnet of the relay except that R is replaced by a multiplier photo-tube aimed at the light reflected from the emulsion. When the proper quantity of light has impinged on the paper the exposure is terminated by pulling the shutter closed. Here also the opening time does not matter as any light passed during this phase is monitored by the photo-cell and counted toward the total desired.

---

* This circuit was developed at the request of the Harold Brunn Cardiovascular Institute of Mount Zion Hospital in San Francisco, California.

A New Discharge Tube for the Hydrogen Atom Spectrum

W. P. van Oort and A. C. S. van Heel
N. V. de Bataafsche Petroleum Maatschappij, Laboratorium, Amsterdam, Holland

January 6, 1949

A DISCHARGE tube emitting strong Balmer lines is of great importance for refractometry. The Balmer lines are very sharp and extend over the whole visible range of wave-lengths. The source of light which has been generally used until now is a Geissler tube, which gives good Balmer lines, though of a very low intensity A Geissler tube consumes about 1 watt. This is inconveniently small especially when handling colored solutions.

A new tube will be described which emits Balmer lines of high intensity and has a long lifetime. The power consumption is 400 watts and the lifetime reaches at least 500 hours. The tube is shown in Fig. 1.

The material of the tube is Thuringer glass. The electrodes are of aluminum sheets of 2 mm thickness and are mounted in such a way that the discharge has to turn once through 180° and once through 90° before reaching the capillary tube, in which we do not want metal particles. The avoidance of metal in the capillary tube is necessary to obtain a pure hydrogen atom spectrum. Aluminum has been chosen for the electrodes because of its very low sputtering caused by ion bombardment.

As the ends containing the electrodes are placed sideways the radiation of the capillary tube in the longitudinal direction can be utilized ("end-on"). In this way a small but very strong source of light is obtained. The diameter of the capillary tube is 3 mm, its length 80 mm.

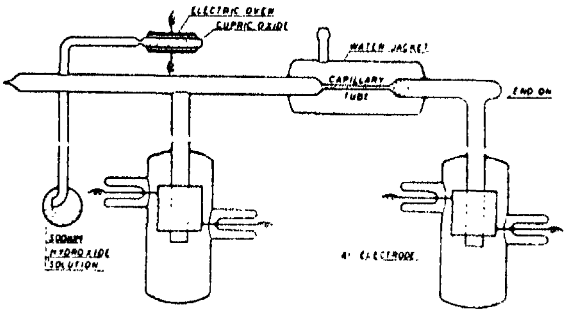

FIG. 1.

The tube is filled with water vapor. During the discharge water is dissociated and hydrogen ions and atoms are obtained. As long as an adequate amount of oxygen is present no H_2 molecules can exist and the H atom spectrum is emitted. However, the oxygen will be taken up by the Al of the electrodes and H_2 molecules will appear in the tube. As a result the blue H_2 molecule spectrum will be emitted. This spectrum is undesirable because of its many lines in the visual range of wave-lengths.

In the new tube all H_2 molecules which may be formed are removed by the following device. A tube filled with CuO rods is sealed to the discharge tube and is heated by a small electric oven to 270°C. At this temperature the H_2 molecules reduce the CuO to Cu and H_2O is formed. If no H_2 molecules are present, nothing happens and the tube is in the right condition. The CuO rods are cylinders with a diameter of 0.5 mm and a length of 5 mm.

A very strong solution of NaOH in H_2O ensures the right vapor tension of H_2O in the tube. At room temperature the vapor pressure will be about 1 mm.

The diffusion of H_2 to the CuO and the combustion to H_2O take place at a rapid rate, thus enabling operations to go on continuously for hours on end.

The total life of the tube is restricted by the amount of oxygen present in the CuO. With an amount of CuO of 10 grams more than 500 working hours may be counted on. An increase of this amount of CuO immediately results in a longer lifetime.

The tube is fed by means of a transformer on the mains. The power taken up is 400 watts at a terminal voltage of 1360. The current amounts to 300 mamp. For a short period a current of 500 mamp. is allowable, in which case the energy taken up is 700 watts.

The power consumption of the small electric oven is 35 watts.

A new type of gas discharge tube emitting Balmer lines of high intensity is described. The tube is useful in refractometric work. The power consumption of the tube amounts to 400 watts. The tube can be used continuously for at least 500 hours.

Improving the Response Characteristic of Graphic Recorders

P. G. Sulzer and A. H. Waynick
Electrical Engineering Department, The Pennsylvania State College, State College, Pennsylvania

January 25, 1949

It is frequently desirable to record fluctuating, variable voltages with a sensitive graphic recorder such as the Esterline-Angus Model AW. When continuous and long-term recordings are to be made, such as the recording of radio wave field strengths, it is further desirable to utilize a sensitive movement so that the power requirements for the meter amplifier will be small.

Experience with a recording system utilizing an Esterline-Angus 0.001-ampere, full-scale recorder driven by a 6SN7 amplifier has indicated that fluctuations of less than about five percent of the total deflection are not recorded. The frictional forces between the pen and the paper prevent response to the small torque involved when the pen pressure is adequate for trouble-free, long-term recording. Consequently, the recording could only be accurate to within ten percent of full scale which is quite inadequate for the above and many other purposes.

A solution of this problem which permits recording to within the accuracy of the meter movement alone was obtained by means of the circuit shown in Fig. 1. The circuit is a conventional bridge comprised of the plate loads and plate resistances of V_1 and V_2 and the two 10-K resistors in series with the relevant portions of R_1. It is unbalanced by an amount which is a function of the magnitude of the input signal, when the latter is applied, with consequent proportional meter deflection.

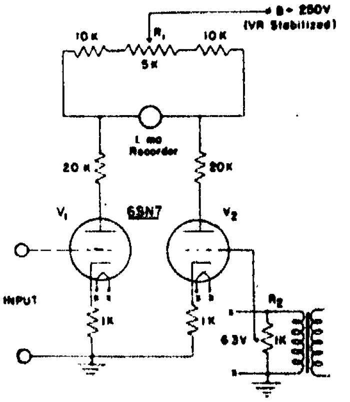

Fig. 1. Schematic diagram.

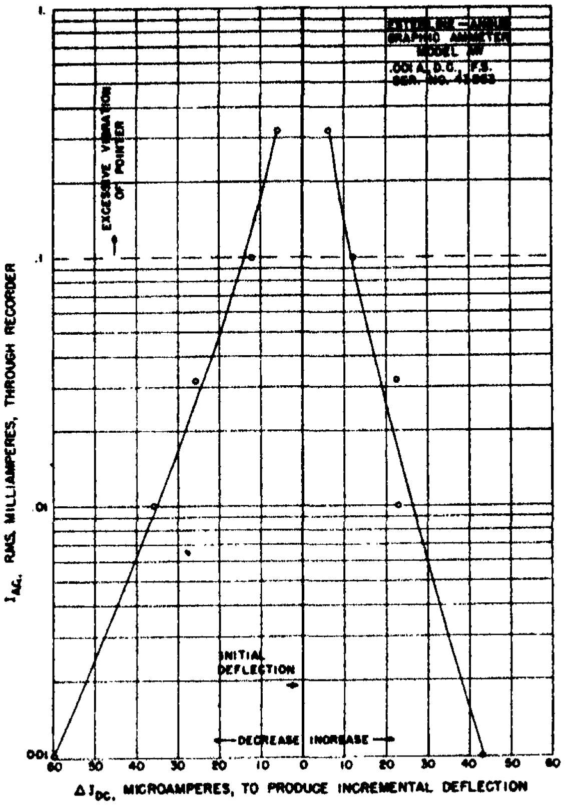

Fig. 2.*

The unusual feature of the circuit is the injection of a 60-cycle voltage into the grid circuit of the "sleeper" tube, V_2 The magnitude of this "jitter" voltage is controlled by the adjustment of R_2. Since the recorder frequency response drops off very rapidly above a few cycles per second, the recorder cannot follow the "jitter" current fluctuations. However, the vibratory forces set up in the meter movement are found to greatly reduce the friction of the meter pen with the recording paper, with consequent improvement in the accuracy of the recording.

A simple experiment, whose results appear in Fig. 2, illustrates the improvement that may be obtained by this method of operation. Referring to the figure it will be noted that the abscissa indicates the increment in d.c. signal current required to produce an increment in recording pen deflection. The ordinate is in r.m.s. a.c. "jitter" current through the recorder. It was found that "jitter" currents of less than one microampere had negligible effect on the recorder operation. As indicated on the figure, $I_{a.c.}$ greater than 0.1 milliampere resulted in excessive vibration of the recorder pointer with consequent broadening of the recorder trace. By utilizing an $I_{a.c.}$ of slightly less than 0.1 milliampere a.c., the increment in $I_{d.c.}$, required to produce an increment in the deflection was reduced by a factor of four in comparison with the value required for zero $I_{a.c.}$. It was determined that the magnitude of the initial deflection and the recording paper speed, for values less than about 6 inches per hour, had no significant effect on the above results.

Three Esterline-Angus 0.001-ampere recorders have been in continuous operation for one year using the above technique with excellent results.

A Vacuum Tube Relay for Thermostat Control

I. Sucher and H. S. Anker*
Department of Biochemistry, Columbia University, New York 32, New York
January 25, 1949

The determination of the density of water by the "falling drop" method is simple and accurate and has proven valuable for the measurement of the abundances of the hydrogen and oxygen isotopes in experiments using the tracer technique.[1] The apparatus required for the application of the falling drop method has been described in detail.[1,2] It includes a thermostat controlled to better than ±0.001°C by a thyratron relay.[2]

However, the high cost and limited life of the thyratrons as well as the bias battery necessary prompted the development of a self-contained high vacuum tube relay. Such a relay has operated for several years without trouble in this laboratory. Its circuit is given in Fig. 1. The relay operates in the following manner: If the temperature increases, the contacts of the toluene regulator close so that zero bias is applied to V_2. This tube consequently passes current through R_3, thereby biasing the V_1's negatively. The V_1's do not conduct in this condition. The impedance of the primary of T_1 is therefore high so that very little current is drawn through the heating element (H). At the same time a blower (F) connected in parallel with the primary of T_1 is energized blowing on the surface of the thermostat and cooling it by increasing the rate of evaporation of the water. On opening of the toluene regulator contacts, the actions of V_2 and V_1 are reversed, lowering the impedance of the primary of T_1 which permits a large current to flow through the heater and cutting the fan off. In using this device it should be remembered that in contrast to a mechanical relay the heater is not completely shut off and that the wave form of the heater current is seriously distorted. A differential output of about 200 w is obtained for the heating element. In operation the toluene regulator is shaken mechanically due to vibration of the stirrer resulting in very rapid switching. Thus very smooth control of the thermostat is obtained.

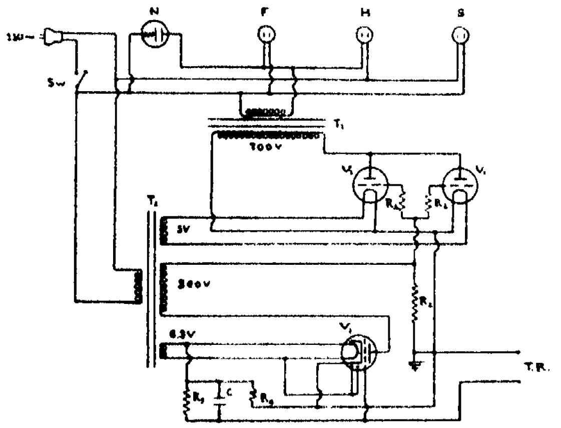

Fig. 1.

N: Neon lamp; NE 30
F: Fan outlet; (25-w motor)
H: Knife heater outlet; (500 w)
S: Stirrer (Cenco No. 18850)
T_1: Stancor P-6314
T_2: Stancor P-6119
R_1: 10,000 ohms; carbon; ½ w

R_2: 100,000 ohms; carbon; 2 w
R_3: 5 megohms; carbon; ½ w
R_4: 20,000 ohms; carbon; 1 w
C: 0.1 μf; paper; 400 v
V_1: 2 $A3$
V_2: 6 $SQ7$
T.R.: Toluene regulator

Note: Since all tubes are operated by unrectified alternating current, the secondary voltages of T_1 and T_2 must be connected in phase. This is achieved as follows: The filament windings of T_2 are connected permanently and V_2 is inserted into its socket. The high voltage winding of T_2 is now connected in such a manner, that on shorting the terminals T.R. a large bias voltage appears across R_3. Then after insertion of the V_1's and of a 200-w lamp into the outlet H, T_1 is connected in such a way that on shorting the terminals T.R. the lamp extinguishes nearly completely. For safety the relay is ground to a water pipe.

---

* Present address: Department of Biochemistry, University of Chicago, Chicago, Illinois.

[1] Keston, Rittenberg, and Schoenheimer, J. Biol. Chem. **122**, 227 (1937).

[2] D. Rittenberg and I. Sucher, Rev. Sci. Inst. **14**, 51 (1943).

Accurate, Simple Recording Microphotometer

P. Rosenblum and A. deBretteville, Jr.
Signal Corps Engineering Laboratories, Fort Monmouth, New Jersey
January 25, 1949

A MICROPHOTOMETER, suitable for the study of x-ray diffraction film, was designed in the Squier Signal Laboratory. This instrument may be of general interest since it is applicable for recording a wide range of film and glass plate photographs. The results of tests made with this microphotometer proved to be satisfactory. The instrument was designed with only essential components in order to facilitate manufacture in the laboratory shop. It was also possible to use a simple optical system of low resolving power because of the large grain size of the film used in x-ray diffraction work in contrast to fine grain spectroscopic plate. Perrine has described a microphotometer using an optical system which is somewhat similar.[1] Brentano also describes a microphotometer for x-ray diffraction work.[2] Most laboratory microphotometers use photographic type recorders. However, to facilitate the rapid analysis of results, electrical type recording was chosen. A standard electronic recorder was found applicable for this purpose.

Figure 1 shows a general picture of the microphotometer. A light beam emerges from the right and left of the large horizontal tube which contains the light source in the middle. The left beam passes into a compensating photo-cell, while the right beam after passing through the x-ray film enters an appropriate slit in front of the scanning photo-cell. The compensating and scanning photo-cell are in a Wheatstone Bridge circuit with the recorder across the bridge, registering the unbalance.

A 6–8-volt light bulb wired as a light source for the photometer is mounted on a rod which can slide in and out of an opening in the tube. A set screw locks the rod in the correct position on the optical axis. The optimum focusing adjustment for the scanning lens is by a rack and pinion. The lens for the compensating system can be adjusted and the amount of light altered by an iris diaphram.

The film holder consists of two highly polished chromium bars which are held on the film carriage by four thumb screws. Several spring clips fit into holes on these bars which

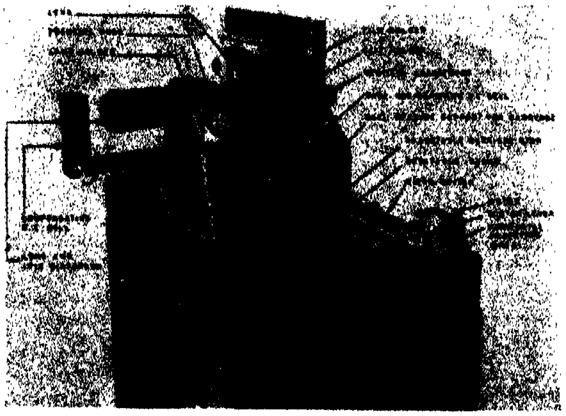

Fig. 1. Microphotometer showing component parts as indicated.

hold the film securely in place. By spacing the bars apart, a large range of film and glass plate photographs is easily accommodated An adjusting knob (Fig. 1) on the side of the film holder positions the film vertically. The small hand wheel on the right is used for quick horizontal alignment.

The movable film carriage track uses rollers which are of the ball bearing type fixed on the inner race to the film carriage while the outer race is free to rotate on the heavy round chromium plated bar Extreme accuracy is possible using this method of construction since there are so few moving parts.

The drive for transporting the film carriage across the light beam uses a lead screw mounted on the base which rotates in a split nut enabling the film to move back and forth. A 1-r.p.m. reversible motor with a simple lever-operated clutch drives the lead screw through two spur gears. It is possible to easily change film speeds by interchanging the spur gears between the clutch and the lead screw.

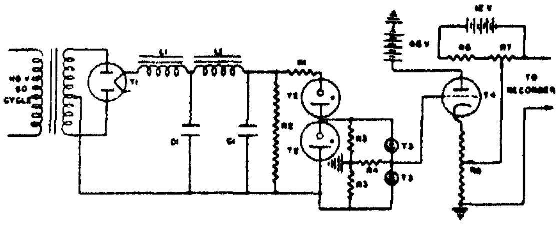

FIG. 2. Wiring diagram of power supply for photo-cells and impedance matching cathode follower for voltage recorder.

$T1$ = 5U4-G
$T2$ = 150-VR
$T3$ = 918 P.E. cell
$T4$ = 5692
$C1$ = 4 μf
$L1$ = 20H

$R1$ = 2K
$R2$ = 1M
$R3$ = 25K
$R4$ = 20M
$R5$ = 1K
$R6$ = 3K
$R7$ = 1K

The main base is constructed of heavy steel plate bent and welded at the corners. It is reinforced by steel channels for rigidity.

The electrical system as mentioned above should be so designed as to minimize the fluctuation of the light source and the power source. A Superior Electric Company "Stabiline" No. 1 E 5101 which is an electronic voltage regulator circuit, was used to obtain constant input voltage for the entire electrical system. To minimize the fluctuation of the light source, the two photo-cells are mounted in a bridge circuit as shown in Fig. 2.

The lamp is operated through the voltage regulator circuit using a "Variac" to change the lamp intensity.

Since the recorder has a low impedance transformer input and the photo-cells have a high output resistance, a cathode follower was used to match impedances. A 5692 tube was used successfully for this purpose. To overcome drift in the output, the plate of the 5692 was reduced to 45 volts and the filament voltage was supplied by a 6-volt storage cell instead of an a.c. transformer.

The optimum fixed slit is selected for the type of film one desires to measure. The film is then adjusted on the carriage for scanning. A trial setting is made using the sensitivity adjustment (or cathode follower potentiometer, R-5). The starting point of the pen is then set by means of the biasing potentiometer (R-7). It takes a few minutes to find the optimum sensitivity setting that will cover the chart.

In order to obtain maximum integrated area from the chart curve, the greatest possible expansion ratio is used. A planimeter then can be used to measure the line areas and thus determine the integrated intensity with the minimum error. This expansion is accomplished by reducing the film carriage speed to the minimum of 1¼ inches per hour and increasing the chart speed to a maximum of 120 inches per hour, giving a 96:1 expansion.

In order to insure stability, the background should always be checked to obtain a straight line output without scanning, i.e., for a fixed position of the film.

This adjustment can be obtained by lowering the sensitivity of which there is more than an adequate amount, and increasing the lamp voltage if need be. In order to check the stability, a Debye x-ray pattern was recorded by scanning the same portion of the film in opposite directions. The record obtained is shown in Fig. 3. The area of the peaks for the left and right traverses should be equal. However, the human element enters in selecting the background so the authors each measured the areas for their own chosen background. Both ob-

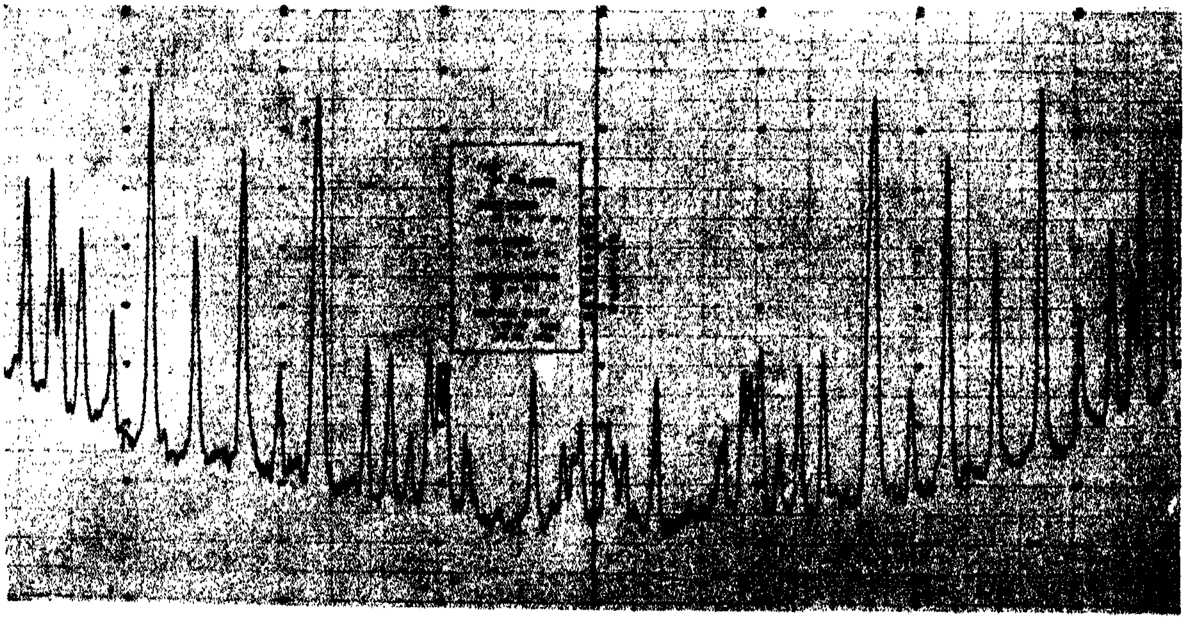

FIG. 3. Record obtained on a 10-inch chart by electronic recorder (Brown Model No. 153X12V-X-30Y10 range 0–50 M.V.) of a Debye x-ray diffraction picture of $AlPO_4$ powder.

servers found the area on each side of the reversing point to differ by less than one percent, and the mean area for each observer differed by 1 percent which was due to the different backgrounds chosen.

The authors wish to thank Dr. R. Brill for his suggestions in the building and testing of the instrument; also Mr. F. Priebe for assistance in the electrical circuit design. The authors wish especially to thank Mr. E. Limpier and Mr. F. F. Cruell of the Squier Signal Laboratory for their excellent craftsmanship in the construction, and without whose ability the photometer would not have been possible.

---

[1] J. O. Perrine, J. Opt. Soc. Am. (1924).
[2] J. C. M. Brentano, Rev. Sci. Inst. 16, 309–315 (1945).

A Vacuum-Tube Current Integrator of Improved Design

L. H. v. d. Twerl
Wetenschappelijke Adviezen, bouw Wetenschapp. Apparaten, Lijnbaansgracht 284b., Amsterdam, Nederlands

February 1, 1949

VARIOUS types of current integrators have been used employing a gas-discharge tube and a condenser charged to the breakdown voltage of the glow tube. It is obvious that some disadvantage is inherent in these methods. The currents to be measured by these methods were limited at the low side to 10^{-10} ampere. Recently,[1] a method has been described lowering this limit, but many precautions have to be taken and special construction of the discharge tube is essential. Another drawback is the variation of the breakdown voltage of gas tubes.

Using neither relay nor gas tube, the circuit diagram is given in Fig. 1 and is essentially a normal one-shot multivibrator. At the beginning of the cycle the control-grid voltage of tube *V1* is well below cut-off and increases steadily when the grid capacitance is charged through *R1* (which may be a photo-tube, an ionization chamber, or a high resistance) until tube *V1* reaches its cut-off. At this moment the triggering mechanism starts and pulls down the current-drawing cathode of *V2*; and as the current in *V1* is limited by the anode resistor *R2*, the cathode falls to a potential of a few volts above ground, depending upon the type of *V1* being used. The grid current of *V1* discharges the condenser *C1*. The coupling circuit *R3 C3* is chosen to have an *RC*-time long enough to provide for this discharge. After this, the flip-flop returns to its zero condition and the cycle begins again. Since *V1* is used below cut-off during the greatest part of the cycle, the major part of the leakage is due to insulation faults in this tube. Grid current is drawn only at the end of the cycle; but as the anode current remains very small, the grid current will be small also.

A tube particularly well suited to this application is the Philips type CF 50. This tube is to be recommended particularly because of its high insulation (10^{13} ohms or better) and its high transconductance at low anode currents. This high transconductance is important to minimize the fluctuations in the voltage at which triggering action starts. Variations in this triggering voltage result from variations of the contact potential of *V1* and of the bias at which *V2* draws a current given in the first approximation by V_g^2/R_k.

If desired, the cathode potential can be given continuously by a meter connected to the common cathodes. When used as a dosimeter the cathodes may be adjusted at approximately 15 volts using a variable resistor to give one roentgen per cycle. The apparatus behaves extremely well in a current range from 10^{-9} to 10^{-11} ampere.

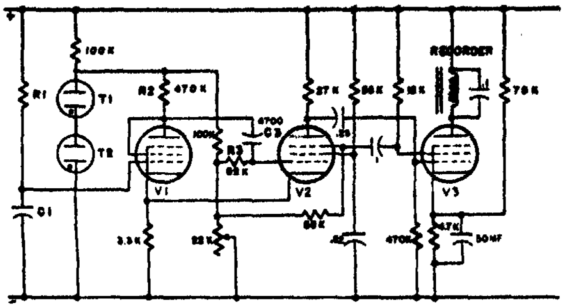

FIG. 1. Circuit diagram of current integrator.

Other types of trigger units may also be used but the author has only tried this one believing it to have certain advantages. The rest of the circuit is designed to lengthen the pulse with a minimum of parts. It consists of a multivibrator coupled to the suppressor of the EF 50 tube; but any conventional pulse-lengthener may be used.

I wish to express my sincere thanks to Professor Dr. J. Clay of the Amsterdam Laboratory for Cosmic Radiation, for his hospitality, and to Dr. H. den Hartog and Mr. F. A. Muller who added so much to the development of this instrument.

---

[1] A. B. Pal, Rev. Sci. Inst. 19, 529 (1948).

A Modification of the Gouy Modulator

L. S. Darken
Research Laboratory, United States Steel Corporation of Delaware, Kearny, New Jersey

February 1, 1949

GOUY,[1] in attempting to improve the automatic temperature control of an ordinary laboratory water thermostat, found he could decrease the cyclic temperature variation by a factor of twenty by substituting a mechanically driven oscillating contact for the normally stationary contact in his mercury in glass thermoregulator. Reid[2] describes a modification for furnace control involving the addition of an oscillating voltage to the thermocouple voltage. He obtained this oscillating voltage by passing a small current through a resistance consisting of a resistance wire immersed to a periodically varying depth in mercury. Reid reports a fifteenfold increase in the sensitivity of the controller by means of this device. Several other modifications of the Gouy modulator have been reported, at least one of which is commercially available.

This communication describes a small simple generator which may be used to produce the oscillating voltage in series with the thermocouple. It may also be used in conjunction with other types of elements which respond electrically to temperature variation. This generator is shown in Fig. 1. It consists of an Alnico magnet which is rotated by an electric motor about a fixed coil. The Alnico magnet is about 2½ inches in diameter; pole pieces ½″×½″×1½″ of soft iron were added. The synchronous motor is geared down to rotate the magnet at one revolution per minute. The coil (20 ohms) is an old galvanometer coil of about one hundred turns on a rectangular form about ½″×1″. The electromotive force produced was nearly sinusoidal with a maximum of 0.7 mv. To reduce this voltage to the optimum, a variable shunt (50 ohms) was initially used. This may be replaced by a fixed shunt when the proper resistance is determined. A schematic diagram is shown in Fig. 2. This modulator is now used in conjunction with a platinum-platinrhodium thermocouple and a commercial controller to control a tubular "Globar" furnace

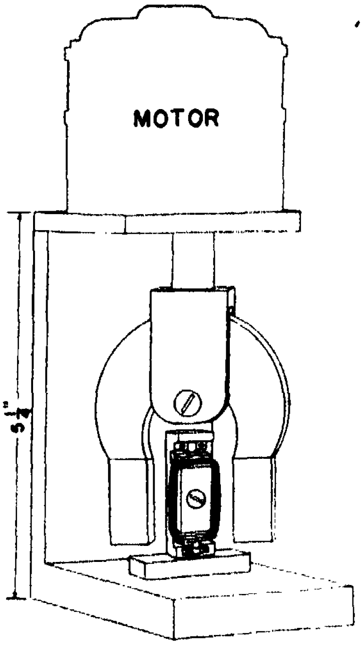

FIG. 1. Gouy modulator (modified).

at temperatures up to 1650°C. The cyclic temperature variation (near 900°C) was reduced from 8°C to 0.3°C by the use of this modulator. An 8-ohm shunt which leads to the addition of ±0.1 mv (corresponding to ±9°C) to the thermocouple voltage was found satisfactory. The cyclic voltage may be varied over rather wide limits (perhaps a factor of two) without markedly affecting the sensitivity but should not be less than the initial sensitivity of the controller else the gain in sensitivity is markedly decreased. On the other hand too large a cyclic voltage leads to drift—i.e., response to line voltage changes.

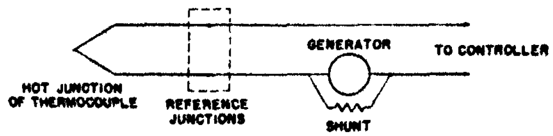

FIG. 2. Modulator circuit.

The advantages of the above described modulator over others include: (1) Absence of any moving contacts in the thermocouple circuit; (2) absence of any wired connection between thermocouple circuit and any other circuit (no leaks are likely); (3) true zero mean cyclic voltage; (4) failure of the modulator leads merely to absence of modulation and does not otherwise disrupt control; (5) no metal other than copper is used in the circuit.

---

[1] M. Gouy, J. de Phys. 6, 479 (1897).

[2] W. T. Reid, *Temperature—Its Measurement and Control in Science and Industry* (Reinhold Publishing Company, New York, 1941), p. 611.

A Flexible Vacuum Seal

OTTO RETZLOFF
Department of Physics, Washington University, St. Louis, Missouri
February 9, 1949

IT is often necessary to move an object inside a vacuum from outside. The Wilson seal is perhaps the best known of the devices which have been invented for this purpose. This note describes a device which enables one to rotate an object in a vacuum and also to displace it in any direction within wide limits. It consists essentially of a sphere fitting in a spherical socket and made vacuum tight by an O-ring (Fig. 1). The center rod A slides along a diameter of the sphere and the junction is made vacuum tight by an O-ring. The sphere B, 1 inch in diameter, fits in a spherical socket which consists of two parts, C and C_1 as shown. The sphere and spherical sockets are machined to within 0.001″ accuracy by means of two homemade tools of simple design. The vacuum is maintained by a suitable O-ring between the sphere and the spherical socket. The half of the spherical socket, C_1, next to the vacuum chamber can be attached to it in many ways, two of which are shown in the diagram. In the left half of Fig. 1 is shown a way of attaching C_1 by means of a set of bolts (one of which is shown) and a suitable O-ring. In the right half of Fig. 1 is shown how it may be attached by soldering.

The O-rings used in this seal can be purchased from the Linear, Inc., State Road and Levick, Philadelphia, Pennsylvania. If the proper O-rings are used and the grooves cut according to the instructions of the Linear company there is no difficulty at all in securing vacuum tight joints. With a vacuum of 10^{-4} mm or more inside the vacuum chamber, it is possible to rotate the sphere in any direction within 30° of the central position as well as to push the center rod in and out and also to rotate it, without impairing the vacuum.

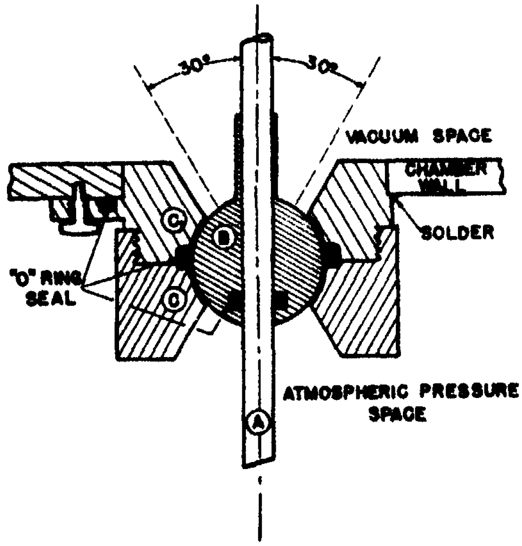

FIG. 1.

This work was supported partly by the joint program of the Office of Naval Research and Atomic Energy Commission.

A Device for Producing an Easily Identified Area on the Electron Microscope Specimen Screen*

FRANCIS W. BISHOP
Department of Radiation Biology, University of Rochester, School of Medicine and Dentistry, Rochester, New York
November 22, 1948

THERE occasionally arises the need of examining a specimen both in the electron microscope and the optical microscope. It also may be desirable to reinsert given specimen into the electron microscope and relocate exact field.

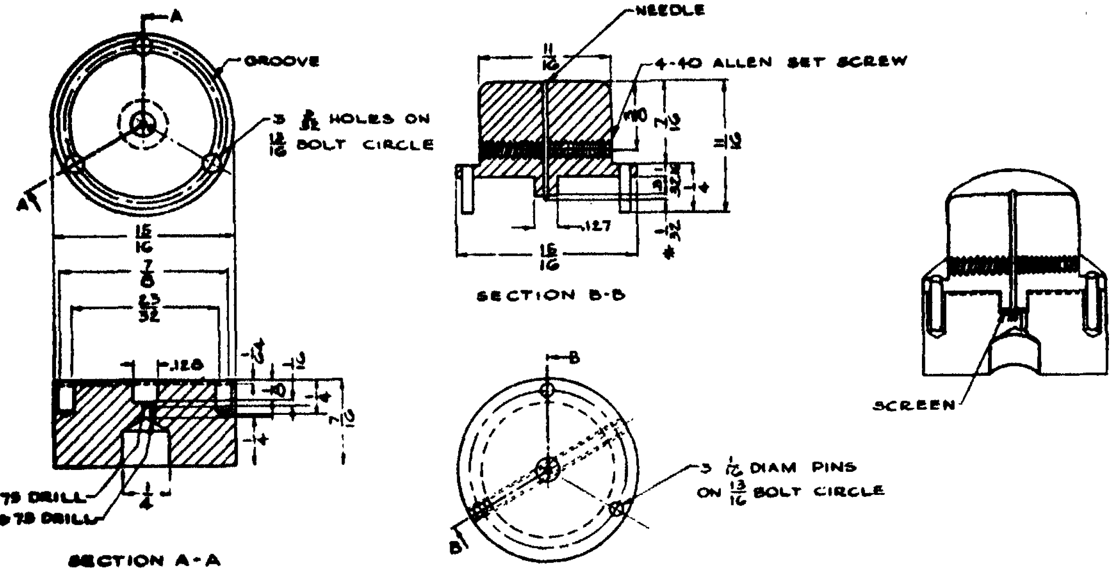

FIG. 1. Note: * dimensions adjustable according to size of hole desired in screen.

A device which would mark the specimen screen in some way would be of great assistance in providing a reference point in the relocation process. Many times the marked area of the screen itself will contain a suitable portion of the object to be examined in the microscope.

To achieve this end, a simple marking device was constructed in the laboratory. It consists of a female brass block, counter-bored to hold a specimen screen and a male element which holds a sewing needle of appropriate dimensions. The point of the needle may be adjusted for any degree of penetration into the specimen screen and is locked in place and centered by two opposing set screws (Fig. 1). When a wire mesh screen is used, the wires are forced slightly apart where the needle enters, resulting in a circular opening which is easily found and identified in either the optical or electron microscope (*A* in Fig. 2).

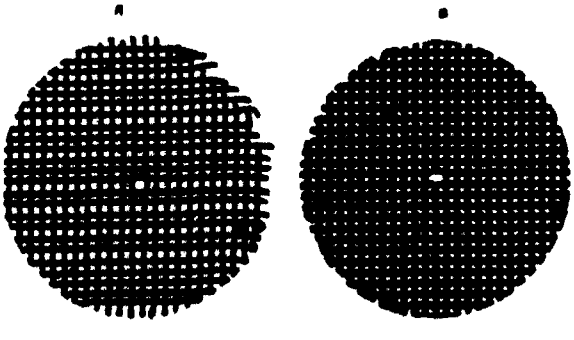

FIG. 2.

Lektromesh screens have no loose wire to be displaced by the needle, but usually a portion of the mesh is broken and may take the appearance of the screen *B* in Fig. 2. In either case, the hole is sufficiently distinctive to be used as a landmark.

As a result of the punching by the needle, the screen may bulge, and should therefore be flattened against a plane surface by means of a roller.

In order to facilitate the examination of the specimen in the optical microscope, a small brass specimen holder was constructed. It accommodates the usual specimen cap and specimen and permits examination with up to a high dry objective. When it is desired to save a specimen for a considerable time before it is examined, or if it is to be re-examined at a later date, we employ a small, knurled brass plug which is inserted into the specimen cap and holds the specimen firmly. This ensemble is kept in a suitable bottle until needed. It also provides a practical way of shipping a given specimen to another laboratory.

* This paper is based on work performed under contract with the United States Atomic Energy Commission at the University of Rochester Atomic Energy Project, Rochester, New York.

A Current Integrator

H. T. GITTINGS, JR.
University of California, Los Alamos Scientific Laboratory, Los Alamos, New Mexico

January 25, 1949

A CURRENT integrator has been developed to measure the number of positive ions in the ion beam of an electrostatic accelerator. The ions are collected in a Faraday cage with a secondary-electron barrier.

A capacitor between the cage and ground will accumulate a positive charge which is the integral of the beam current and is proportional to the number of ions collected. An amplifier with its input across the capacitor is designed to operate a relay when the capacitor has accumulated a predetermined amount of charge. The relay contacts short the capacitor which drops out the relay and restarts the cycle. The relay contacts also operate a mechanical counter which is calibrated in microcoulombs per count.

There are, however, several factors to be taken into consideration before such a system will be adequate. The relay must operate at precisely the same value of coil current each time and it must operate fast. A very satisfactory relay is the Western Electric 275B, which is a sealed, mercury type. The capacitor must have low dielectric absorption. Polystyrene or Glassmike capacitors are suitable. The Faraday cage should not swing in potential with respect to ground, if it does leakage current will be more troublesome, the cage and cable

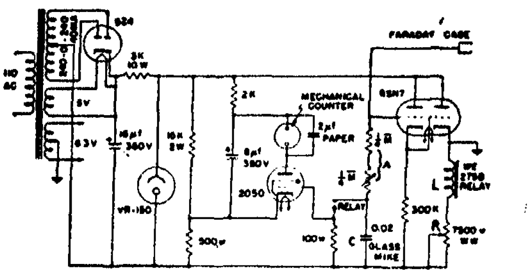

FIG. 1.

w = ohms
K = ohms × 10³
M = ohms × 10⁶
WW = wire wound
W = watts

capacity to ground will appear as an undesired shunt capacity (appreciable when high accuracy is desired), and the electron barrier potential will vary. The amplifier across the capacitor must have very high input impedance and low output impedance. The relay inductance introduces into the relay circuit a voltage proportional to the rate of change of the relay coil current and hence to the rate of change of charge on the capacitor, which is proportional to the beam current. It can be shown that precise compensation for this voltage, irrespective of time-variations of beam current, can be achieved for any capacitor, C, and relay (inductance, L, resistance, R)-if a particular value of resistance, $r=L/(RC)$, is placed in series with the capacitor (Fig. 1).

When the relay contacts short the capacitor, the discharge current is limited by a 100-ohm resistor. If the relay has double-pole contacts the other contacts may be used to operate a mechanical counter, if not, the voltage pulse across the 100-ohm resistor can be used to trigger a thyratron which will operate the counter.

It can be seen from Fig. 1 that the Faraday cage (the input grid) varies in potential only a very small amount since the power supply swings with respect to ground.

The calibration procedure is to adjust the rheostat in series with the relay coil to give the desired sensitivity using a very low value of charging current so the inductive effect is small. The charge, q, is determined by measuring the current with a potentiometer and the time with a stop clock. Then at the highest charging current the compensating resistor is adjusted to give the same sensitivity. Careful tests have shown the sensitivity of 1.00 microcoulomb per count to be constant to within 0.2 percent from 0.005 microampere to 10 microamperes. Changing relays will probably require recalibration but the sensitivity is practically independent of the 6SN7.

New Instruments

W. A. Wildhack: Associate Editor
in Charge of this Section
National Bureau of Standards, Washington, D. C.

These descriptions are based on information supplied by the manufacturer and in some cases from independent sources. THE REVIEW *assumes no responsibility for their correctness.*

Infra-Red Analyzer

The Perkin-Elmer Corporation announces the development of the Model 12-D infra-red analyzer for continuous automatic analysis of as many as six different components in a flowing stream of sample. The stream may be either in the liquid or gas phase.

The instrument consists of the following units:

Infra-red Monochromator—Similar to that used in the Perkin-Elmer Infra-red Spectrometer.

Turret—Automatically driven, twelve point (one reference standardization point and one absorption point for each of six components).

Recorder—Leeds and Northrup, 12-point, strip chart, specially designed for this instrument. Automatically synchronized with turret.

Amplifying Circuit—Highly stable, a.c. operation. Compensates for changes in ambient temperature, source intensity, window dirt, etc.

The cycling time for a six-component analysis is about 6 minutes.

The analyzer is particularly time-saving in the pilot plant in determining optimum process conditions. Operating variables such as temperature, contact time, flow rate, etc., may be varied continuously and evaluated immediately from the automatic analytical record. In a continuous, multi-stage process, sampling may be performed at intermediate stages for independent evaluation.

In the process plant, the instrument provides a permanent, accurate record of product concentration and purity, as well as an immediate indication warning of process troubles.—THE PERKIN-ELMER CORPORATION, *Glenbrook, Connecticut.*

Color Computing Device

The General Aniline-Librascope tristimulus integrator integrates continuously over all portions of the visible spectrum, will tell immediately whether a given color will match another color, and, if not, will describe the difference between them. Without the integrator, an answer to this question may take hours to get, and even then be less accurate.

The instrument was designed for use with the General Electric spectrophotometer invented by Professor Arthur C. Hardy, of M.I.T. Only minor modifications of the spectrophotometer are required, and the computer may be placed inside the existing case.

Although the eye can tell whether or not two colors are the same, no one can describe color differences in words which mean the same thing to everybody. Color scientists, however, have developed an internationally accepted mathematical procedure for obtaining numbers which unambiguously specify any color.

In order to understand this method and the operation of the new computer, it is necessary to know that color as we see it is composed of three parts: first the light, which is energy radiating from the sun or a lamp; second the dyed, painted, or naturally colored material under observation which reflects or transmits varying percentages of light of different wavelengths, and finally the eye itself. Internationally accepted data on the light and the eye are available, and reflectance or transmittance may be measured on a spectrophotometer. These three factors must be combined mathematically to give three numbers, known as the tristimulus values, which are a unique specification of any color observed. Even a color-blind person can make the necessary calculations and evaluate the color of any material.

Until the invention of the tristimulus integrator, this procedure required multiplication of the three values at scores of wave-lengths and addition of the products. The integrator, an electronically controlled ball and disk mechanism which is connected directly to the spectrophotometer, instantly gives the correct result with a precision of five-hundredths of one percent. Together, the two instruments—the recording spectrophotometer and the tristimulus integrator—not only measure and analyze color in 2½ minutes, but yield a numerical specification of what we see with hitherto unobtainable accuracy.—General Aniline and Film Corporation, *230 Park Avenue, New York 17, New York.*

Multichannel Switch

The Applied Science Corporation of Princeton announces the development of a new multichannel switch driven by a 60-cycle synchronous motor. The use of a synchronous motor assures constant sampling rates and allows the convenient use of an a.c. line voltage source whose frequency is automatically synchronized with the sampling operation. The 4-pole model shown here is 2″×3″×4″ in physical size and has 30 contacts per pole. The wiper is of the shorting type for flexibility of use. Standard models have sampling rates of 720, 360, 240, 180, or 90 r.p.m.

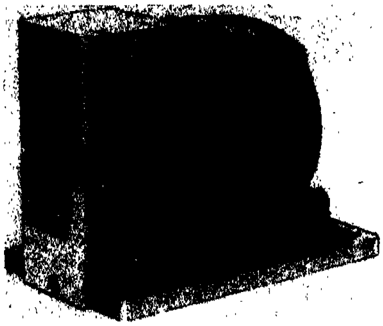

These switches facilitate investigation of a large number of separate quantities or of a single quantity under a number of various conditions. In addition to telemetering applications, they may be used for the display of characteristic curves and multichannel voltage comparison. Electrical operations may be synchronized with mechanical motion by appropriate attachment of switch rotor.—The Applied Science Corporation of Princeton, *P. O. Box No. 44, Princeton, New Jersey.*

Hivolt Power Supplies

Condenser Products Company announces the addition to their line of Hivolt power supplies of Numbers PS-5, PS-10, and PS-30, which have respective outputs of 5000, 10,000, and 30,000 volts. Input voltage is 118 volts, 60 cycles. Containers are gray, lacquer-coated terne or tin-plated and are hermetically sealed and oil-filled.

Hivolt power supplies are used for oscilloscopes, radiation counters, insulation testers, electrostatic precipitators, photoflash devices, projection television, spectrographic analyzers, Van de Graaff generators, etc.

The new Hivolt power supplies weigh:

PS-5	8.5 lb.
PS-10	10 lb.
PS-30	21.5 lb.

The PS-1 (2400 volts) weighs 2.2 lb.; PS-2 (2000 volts) weighs 2.5 lb. These two models are already widely used.

For further information on the complete Hivolt power supplies, write for specification sheet showing regulation and ripple curves and other pertinent information. Special output 60-cycle and higher frequency input supplies on request.—Condenser Products Company, *1375 North Branch Street, Chicago 22, Illinois.*

Low Range Air Cells

Two new Tate-Emery air cells having load ranges of 0–1.2 to 0–6 lb. and 0–2 to 0–10 lb. in tension and compression are announced by The Baldwin Locomotive Works, Philadelphia 42, Pennsylvania. The lowest capacity previously available was 0–30 lb. Other air cells are built with capacities up to 1200 lb. These load-weighing devices were designed for use on testing machines of any type or capacity to give high precision measurement of small loads such as in testing plastics, textiles, cord, paper, and other material. They can also be used independently for such purposes as weighing chemicals, or controlling chemical processes.

When a standard Tate-Emery indicator with 66-in. scale is connected with the cell, the 0–2-lb. range shows a pointer movement of approximately 2 in. for one ounce or 1/16 in. for one gram. Ranges are changed in the indicator.

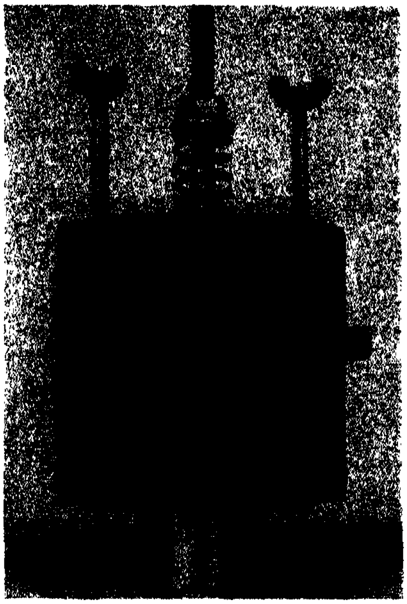

Portable Bourdon gauge type indicators with 22-in. scale are available with these cells when existing indicators do not readily accommodate additional ranges. The minimum range with this type indicator is 0–10 lb.

An air jet and baffle within the cell controls the action of a pneumatic force balance system, so that air pressure automatically balances the load. Total movement of the load-sensitive member is less than 0.0005 in. This air pressure is transmitted to the load indicator.

Accuracy of load measurement is within ½ percent of reading or 0.15 percent of capacity, whichever is greater, when Bourdon gauge type indicators are used. This becomes ½ percent of reading or 0.1 percent of capacity, whichever is greater, for the Tate-Emery load indicator.—The Baldwin Locomotive Works, *Philadelphia 42, Pennsylvania.*

Gyros

Production of telemetering rate gyros calibrated for rotational measurements from 10° to 1000° per second and position gyros with one- and two-axis electrical sensory elements is announced by the G. M. Giannini Company

Gyro accuracies of better than ± 2 percent are offered and production gyros have been standardized with 2000-ohm, 2500-ohm, and 5000-ohm resistance pick-offs. Other resistance ranges furnished on request.

Telemetering rate gyros offer natural frequencies to 40 cycles per second and are available damped or undamped.

Additional detailed information available.—G. M. Giannini and Company, Inc., *254 West Colorado, Pasadena 1, California.*

Tensile Tester

The Instron tensile tester is a new, versatile, precision instrument based on electronic principles that make possible the accurate load-elongation measurements of plastic and textile materials, wire, paper, rubber, adhesives, and similar specimens.

Full-scale load range of the unit extends from 2 grams up to 5000 pounds in some models, representing a spread of approximately a million to one, and a choice of jaw speeds is incorporated ranging from 0.02 to 20 inches per minute. By virtue of the flexibility of the controls, both for changing the sensitivity of the load recording system and for operating the motion of the pulling jaw, a variety of unique testing techniques is available for the determination of special properties, as well as for routine measurements.

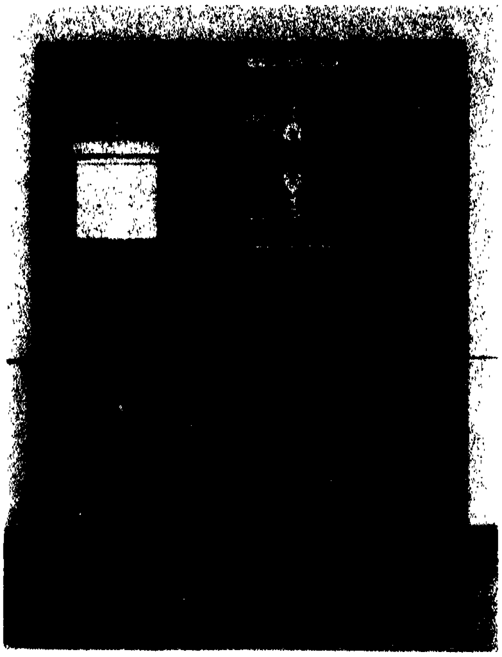

The instrument utilizes an electronic weighing system based on the electric strain gage principle for detecting and recording the load applied to the sample under test. The pulling jaw is operated by an unusual drive that provides a controlled rate of elongation of the sample over a wide range of speeds, in either direction of travel and with instant reversibility. The chart of the high speed recorder is driven at various speed ratios with respect to this jaw, so that tensile load-elongation curves of the material are made accurately at constant rate of elongation.

The main power to actuate the moving crosshead is derived from a servo-controlled drive acting as a "positional follow-up" system. By this means, a low power reference unit, which is driven synchronously at various speeds through a set of light change gears, is able at all times to determine the position of the moving jaw. Instantaneous starting, stopping, and reversal of direction of travel of this jaw is affected through fast-acting computer-type magnetic clutches operating on the reference unit.

As almost no lag or error is introduced at reversal, this system enables measurements to be made of hysteresis under cyclic conditions with accurate correspondence between head position and chart travel being maintained at all times. Operation of the pulling head is controlled by pushbuttons located on the right side of the unit. The operation can be made automatic by adjustable, close-tolerance switches which control the gage length, cycling points, and other functions.

Chart speeds range from 0.2 to 50 inches per minute, which, in combination with the available head speeds, provide magnification ratios up to 1000 to 1.—Instron Engineering Corporation, *2 Hancock Street, Quincy, Massachusetts.*

Rouy Photrometer

Reflecting the latest electronic developments, the new Photrometer is faster, more accurate, and simple to operate, having only two movable parts. It is pre-calibrated for 38 of the most common clinical tests, making it unnecessary to keep a supply of standard solutions on hand. Supplied with every Photrometer is a handbook containing calibration tables for each clinical method, thus eliminating calculation.

The optical system consists of a lamp, precision ground mirror, filters and absorption cell. Light traversing this system falls upon a barrier layer photoelectric cell, generating a current which actuates a direct-reading microammeter.

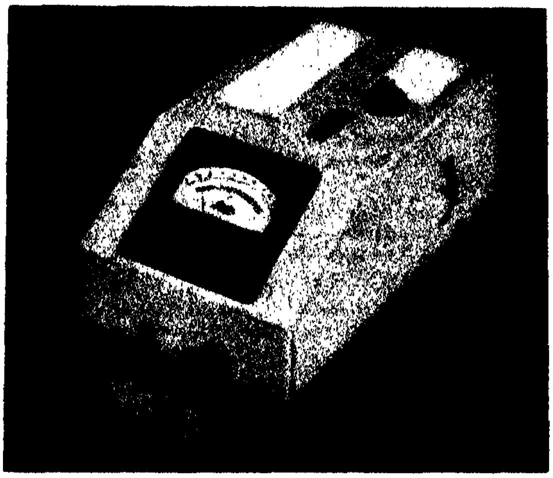

Of twelve filter spaces provided, ten contain narrow spectral band filters which cover the entire visible spectrum. Two other spaces are supplied to allow for special work by the user.

Housed in a compact, white enameled cabinet, the Photrometer is mounted on a base cast from high strength aluminum alloy, making the unit lightweight and easy to handle.—E. Leitz, Inc., *304 Hudson Street, New York 13, New York.*

Precision Warburg Apparatus

Precision Scientific Company has developed an advanced Warburg apparatus for the following uses:

1. For measuring respiratory exchange in yeast, bacteria spores, plant and animal tissues, and for the measurement of lactic acid production by normal and tumor tissues.
2. For reactions in which acid or alkali is produced or consumed in bicarbonate solutions in equilibrium with CO_2 gas mixtures.
3. For the measurement of blood gases and for investigating the reactions of hemoglobin and other blood pigments.

A time-saving convenience is found in that the entire manometer bank can be rotated through 360° in either direction for as many revolutions as desired. The apparatus holds 20 Warburg manometers (or 10 Summerson differential manometers) which can be read in motion or stopped in pairs by an operator from a fixed position.

Operation is further simplified by the simultaneous adjustment of shaking amplitude of the entire range from 1 to 4 centimeters. The shaking rate is also adjustable at any interval from 50 to 150 oscillations per minute.

The function of holding the guaranteed temperature sensitivity of 0.02°C is performed by three units. An improved adjustable Micro-Set Thermoregulator in conjunction with a Merc-to-Merc relay has shown in tests that it responds to temperature changes of less than 0.01°C. The noiseless powerful "Precision" Octo-Mix stirrer circulates approximately 60 gallons of water per minute to assure uniform bath temperature. The auxiliary heater will bring bath temperatures from cold to operating in approximately an hour. Temperature range of heated model is from room temperature to 60°C.

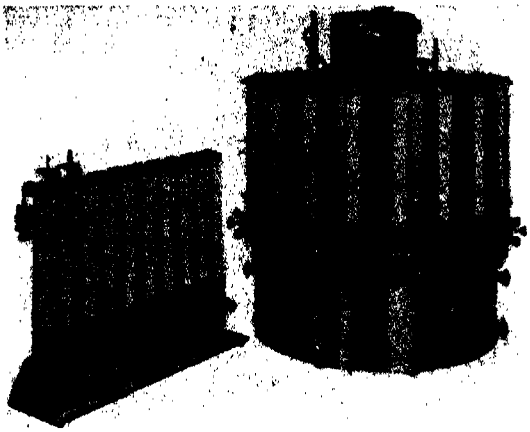

Stainless steel manometer supports with built-in manometer guards have bridge-type construction which eliminates quiviering or wobbling. No twisting motion is employed in their operation. Glassware can be removed from manometer supports by loosening only three thumbscrews.

Careful designing has enabled "Precision" to incorporate these advances in a circular stainless steel apparatus with over-all dimensions only 27″ in diameter by 41″ in height. The Precision Warburg apparatus is available also in a combination heated and refrigerated model with a temperature range of 10°C to 60°C. Apparatus for temperatures lower thân 10°C can be supplied in custom built models.—Precision Scientific Company, *Chicago 47, Illinois.*

Thermoregulator

A new immersion-type Micro-Set Thermoregulator for laboratory use in controlling liquid temperatures in water and oil baths, or air temperature in ovens, etc., has a sensitivity of ±0.02°F over a range of 50 to 220°F. Only 15″ long, its patented design eliminates an outer shell so that there is a minimum of lag in response to slight temperature changes.

The Thermoregulator features a quick-adjustment sleeve which magnetically moves one of two electrodes so that the regulator will turn heating devices on and off to maintain any temperature within its range. The thermometer-shaped device has two capillaries, one with mercury which rises and falls with temperature to make or break contact with the upper metallic electrode. Contact points are sealed in hydrogen under pressure, eliminating corrosion, and load terminals are enclosed to eliminate danger from sparks. The device is for operation with relays such as the Fisher-Serfass Electronic Relay.—Fisher Scientific Company, *717 Forbes Street, Pittsburgh 19, Pennsylvania.*

Hand Torch

The new Torchmaster is a general utility, self-contained hand torch only 2¼" by 13" burning liquid petroleum gas (butane, propane, etc.). It holds enough fuel for an average day's burning. The torch will do light brazing, soldering, and innumerable heating operations. It burns upside down or at any angle and has a filtered "Wind-Pruf" burner that will not clog or blow out. It is of steel construction, satin-chrome finished, and of precision manufacture throughout. A single control valve turns the torch on and off and adjusts the flame from a pencil point to a roaring blowtorch. It is easy to handle, invaluable in cramped quarters, and can be carried or stored anywhere. Amazingly economical, it can be filled from standard containers for three or five cents.—Industrial Engineered Products Company, *7416 Melrose Avenue, Los Angeles 46, California.*

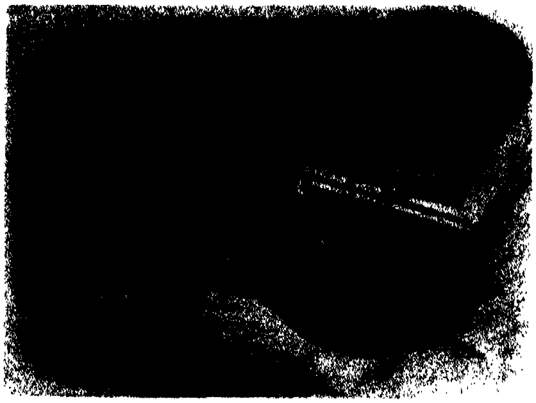

High Stability Carbon Resistors

A new resistor of outstanding characteristics is now available from Welwyn Electronic Components, Inc. Of the "cracked carbon" process of manufacture, the resistor element is a homogeneous film of pure carbon deposited on a porcelain tube. After aging, carefully fitted turned brass end caps are applied, into which the terminal leads are staked and soldered; the completed resistor is then brought to the required resistance value by spiraling in automatic machinery. The completed resistor is then given several coats of silicone, containing lacquer, to protect it from moisture and mechanical damage. This manufacturing technique assures high stability and careful adherence to tolerances. Normally made to 1 percent tolerance, it is expected that all resistors delivered in the American market will adhere to that figure for the life of the component. They can also be had in 2 percent and 5 percent tolerances, and in the sizes of ¼, ½, 1, and 2 watts capacity. American stocks in decade and RMA preferred values will be maintained at New York for immediate deliveries.

The lacquer coating is capable of operating at 150°C, and this factor can permit the resistor to dissipate full power rating in ambient temperatures of 100°C. The temperature coefficient of resistance of cracked carbon is of the order of 0.02 percent/°C, and this value can be taken to hold over the major range of resistance values. Voltage coefficient of resistance can be taken as of the order of 0.002 percent of the resistance value per volt applied.

The noise level to which Welwyn resistors approach is within a very few decibels of the minimum value as determined by the Johnson formula. As the resistance element is a homogeneous layer of carbon of almost monomolecular thinness in the higher resistance values, it can be appreciated that they are free from the customary sizzling and frying noises, so commonly associated with the composition carbon resistors.

The development technique has been so far perfected that these ***high stability*** resistors are offered in a range from 100 ohms to 50 M ohms in 1 percent tolerance, and wider ranges in a 5 percent tolerance of resistance values.—Welwyn Electronic Components, Inc., *234 East 46th Street, New York 17, New York.*

Laboratory Balance

New instrument-making methods and materials have made possible a radically new torsion-principle balance for general laboratory use. With a sensitivity rating of 2 milligrams (1/32 grain), and a capacity of 120 grams (4 oz.) a fast weighing balance of this type has manifold uses below the delicate work for which the accuracy of the enclosed-case, ultra-refined precision balance alone suffices.

The new balance is a torsion balance, with no departure from the principle of a beam balancing by means of ribbon metal bands acting in torsion, rather than pivoting on knife edges. Other than adherence to basic principle, the new product has undergone a complete re-engineering and modernization of design.

The beam graduations are in two parallel scales, one in grains, the other in grams—and one in black and the other in red to guard against confusion.—The Torsion Balance Company, *Clifton, New Jersey.*

Manufacturers' Literature

Technical Review—No. 1, an 8-page illustrated periodical, features a new electrodynamic high speed level recorder with writing speeds up to 1000 db/sec. and a new beat-frequency oscillator with regulating compressor, making possible recordings of frequency responses of microphones, amplifiers, loudspeakers, etc., building-acoustic recordings of sound insulation of walls, and automatic recordings of reverberation curves in halls.—Brüel & Kjaer, *Naerum, Denmark.*

Tracerlog—No. 15, 12-page house organ, includes a description of techniques for the use of beta-radiation and photon absorbers, a description and specifications of the SU-3A Laboratory Monitor for determining small amounts of radiation, and a list of uses for radioisotopes, Part II. Also contains index of all Tracerlog technical articles and data (January 1947 to December 1948).—Tracerlab, Inc., *55 Oliver Street, Boston 10, Massachusetts.*

Recording Paper—A 12-page illustrated reprint from Western Union *Technical Review* describes "Teledeltos," a dry electrosensitive recording paper for facsimile telegraph apparatus and graphic chart instruments. This non-electrolytic recording material is insensitive to light, not readily marked by heat, unaffected by cold, and impervious to fungus growth and parasitic organisms.—Development and Research Department, The Western Union Telegraph Company, *60 Hudson Street, New York 13, New York.*

Oscillographer—Vol. 11, No. 1, 16 pages, features an illustrated article on the Type 250 cathode-ray oscillograph. Other items are notes on improving the performance of Types 248 and 248-A cathode-ray oscillographs, an oscillographic crystal mode analyzer, and a bibliography of papers in contemporary publications of interest to those engaged in the application of the oscillograph.—Instrument Division, Allen B. DuMont Laboratories, Inc., *1000 Main Avenue, Clifton, New Jersey.*

Apparatus Notes—No. 502, a 12-page bulletin, contains detailed information on a variety of laboratory apparatus, including box furnaces, salt fog cabinets, mercury filters, pocket microscopes, program timers, tally counters, microscope lamps, weights, and support frames.—Andrew Technical Service, *4747 North Damen Avenue, Chicago 25, Illinois.*

Dynamometer—Bulletin D, a 4-page bulletin describes the Dillon Dynamometer, a portable, individually calibrated, fatigue-tested dynamometer for measuring traction, tension, or weight from 0–500 lb. to 0–20,000 lb. Unlike ordinary "spring" measuring devices, it operates through deflection of a special alloy steel beam, requiring only 0.040-inch movement to indicate a full-scale reading.—W. C. Dillon & Company, Inc., *5410 West Harrison Street, Chicago 44, Illinois.*

Current Data on High Vacuum Apparatus—8-page bulletin contains article on measurement of low pressures and notes on developments in the field of high vacuum.—Distillation Products, Inc., *755 Ridge Road West, Rochester 13, New York.*

Oscillo-Record Camera Accessories—Details on request of a new universal mount which is adjustable in height to suit any standard oscilloscope, a new adapter for mounting standard 35-mm 1000-ft or 400-ft magazines, and a Binocular Split Beam Viewer. These accessories are for the manufacturers' Oscillo-Record Camera.—W. J. Schubert, Special Camera Division, Fairchild Camera and Instrument Corporation, *88–06 Van Wyck Boulevard, Jamaica 1, New York.*

D.C.-A.C. Chopper—Single page Form 233C lists and describes a new Type 240 Chopper, designed specifically for operation at 0.050 ampere or less, and Type 222 Chopper, listed at 0.5 ampere or less.—Stevens-Arnold, Inc., *22 Elkins Street, South Boston 27, Massachusetts.*

New Materials

Forest K. Harris: Associate Editor
in Charge of this Section
National Bureau of Standards, Washington, D. C.

Hermetic Seals

Cerroseal-35 is an indium solder that adheres directly to glass, mica, and some ceramics, and also bonds to the same metals as ordinary solder. It can therefore be used for hermetically sealing glass to glass or glass to metal. Its working temperature is approximately 260°F on glass, and it can be used for the sealing of glass dial covers on instruments, vacuum seals in glass laboratory apparatus, etc. It has the following advantages over the litharge-glycerine seal: it does not pull loose under vibration; is not dissolved by various vapors to which it is exposed in use; provides leak-tight joints which may be tested immediately after setting; less skill is required for assembling. Samples of this solder together with instructions for its use are available from the manufacturer.—Cerro De Pasco Copper Corporation, *40 Wall Street, New York 5, New York.*

Ductile Cast Iron

Magnesium has been considered to be completely unalloyable with iron but, if properly controlled, it can be incorporated in molten iron to bring about desirable changes. An effective way of doing this is by incorporating a nickel-magnesium alloy in molten iron. The cast alloy is characterized by a graphite structure in the form of spheroids, flake graphite being entirely absent.

The process is operative with practically all types of cast iron including hypo- and hypereutectic, ferritic, pearlitic, acicular, and austenitic varieties. For pearlitic grades of cupola-melted material containing 3.2–3.6 percent of carbon and 1.8–2.8 percent of silicon, the ductile iron (as cast) provides a combination of 85–105,000 p.s.i. tensile strength with some ductility. In contrast to gray cast iron, its strength is only moderately affected by section thickness. Under stress it behaves elastically like cast steel rather than cast iron up to high loads, with a modulus of elasticity of 25×10^6 p.s.i.

The high strength and rigidity of ductile cast iron make it applicable to heavy industrial machinery, while its ductility may provide thermal shock resistance far greater than has previously been available in high carbon castings. Resistance to growth and oxidation give promise of its usefulness in high temperature applications. A number of foundries have arranged manufacturing licenses under the pending patent application.—International Nickel Company, *67 Wall Street, New York 5, New York.*

Flexible Conduit

Flexpansion is a flexible metallic electrical conduit with a Neoprene coating bonded to the metal. The conduit and its fittings are liquid proof, airtight, and chemical resistant, and are stated to completely eliminate the danger that the wire within the conduit will be damaged by oil, grease, or other liquid. It has been developed for use on machine tools, chemical plant wiring, underground wiring, or other places in which ordinary conduit is likely to be short-lived. Nominal sizes range from ¼ to 2 inches. Lengths and end fittings may be specified.—TECHNIFLEX CORPORATION, *55 Jersey Avenue, Port Jervis, New York.*

High Temperature Flexible Tubing

Flextite Hytem is a plastic tubing developed for electrical insulation applications. This tubing is stated to have unusual resistance to high temperatures, good dielectric strength, high resistance to stretching, tearing, or abrasion, and to withstand exposure to oils, acids, and alkalies. Manufacturer's tests show that the tubing is not brittle and will not crack when flexed after 100-hour exposure to heat at 300°C. It is recommended for use under continuous operating temperatures up to 150°C.—MITCHELL-RAND INSULATION COMPANY, *51 Murray Street, New York 7, New York.*

Heat Exchange Tubing

A new fin design on heat exchange tubing makes use of crimped or corrugated helical fins. Tubing with this construction is available in lengths up to 25 feet. Tube diameters range from ⅜ to 1 inch and fin widths from ¼ to ⅜ inch. A typical application is in the construction of blast air-heating and -cooling equipment.—ROME-TURNEY RADIATOR COMPANY, *107 Canal Street, Rome, New York.*

Strapping Tape

No. 320 is a new Scotch paper tape, 13–15 mils thick, reinforced with thread-like fibers running lengthwise through it. It has a tensile strength of 180 pounds per inch of width. Faced with a pressure-sensitive adhesive, it adheres to the work and to itself as it is wound in place. It may be used in packaging structural shapes, pipe, rod, coils, etc., and in preparing such products as plate glass, plastic sheets, etc., for shipment. It is available in 60-yard rolls, in widths from ¼" to 23".—MINNESOTA MINING AND MANUFACTURING COMPANY, *902 Fauquier Avenue, St. Paul 6, Minnesota.*

Fire-Retardant Paint

Flame-Seal is a new fire-retardant and non-toxic paint which does not require mixing and which can be applied directly with brush or spray gun. This paint, when attacked by flame, undergoes a physical transformation, forming a hard protective crust at least 8 times the thickness of the original paint. Sustained exposure for 30 minutes at a single spot to flame from a blow torch at 2000°F is stated to cause some charring, but the coating will not at any time support combustion.

This paint is said to be moisture-proof and termite-proof, and will not craze, chip, peel, or crack. It can be washed with any standard cleaning powder or soap without decreasing its effectiveness as a flame-retardant. It is recommended by the manufacturer for use on all interior raw-wood surfaces.—STALLTON CHEMICAL CORPORATION, *8–14 37th Avenue, Long Island City 1, New York.*

Temperature Indicators

Tempilstiks, *Tempil Pellets*, and *Tempilaq* are the three forms in which this temperature indicator is available. The first is a crayon to mark a surface where temperature is to be read, the second is a pellet to be placed on the surface, and the third is a liquid that is spread or spotted on the surface and allowed to dry. Each will melt at the temperature for which it has been specified. These products are now available with melting points at intervals of 12½°F throughout the temperature range from 113 to 400°F, and with larger intervals up to 1600°F.—TEMPIL CORPORATION, *132 West 22nd Street, New York 11, New York.*

Dry Cell

The *Eveready Ignitor* No. 6 dry cell has been improved to provide 25 percent and 20 percent increase, respectively, in the ASA light intermittent and heavy intermittent test. This should be of advantage to those who use this cell for testing instruments, alarm systems, and similar applications.—NATIONAL CARBON COMPANY, *30 East 42nd Street, New York 17, New York.*

Neoprene Floor Mat

Neo-Sponge Comfort Mat is designed for use by workers who have to stand at their job. It is constructed of Neoprene rubber filled with minute nitrogen bubbles, and has a triangular raised pattern on both sides of the reversible unit. It is not subject to attack by oils, greases, or acids and is stated to be an excellent insulator both against electricity and heat. It is available in 18- and 36-inch widths, in lengths up to 9½ feet, and in ¼- or ⅜-inch thicknesses.—AMERICAN FLOOR PRODUCTS COMPANY, *1524 M Street, N. W., Washington 5, D. C.*

THE
REVIEW OF SCIENTIFIC
INSTRUMENTS

VOLUME 20, NUMBER 5 *MAY, 1949*

A Mass Spectrometer for Continuous Gas Analysis*

JACK A. HUNTER, RALPH W. STACY, AND FRED A. HITCHCOCK
Laboratory of Aviation Physiology and Medicine, The Ohio State University, Columbus, Ohio
(Received October 18, 1948)

An instrument for recording continuously the relative abundance of gases in a three component mixture is described. High accuracy of analysis has been sacrificed in favor of high speed response since the instrument was designed primarily for use in the investigation of respiratory problems. An instantaneous change in gas composition will appear on the record with a lag of less than 0.2 second and will require approximately 0.1 second to settle on this new value.

INTRODUCTION

PROBLEMS existing in several fields have shown the desirability of recording the composition of gas mixtures at various stages of a continuous process. The particular problem that prompted the development of this instrument concerned the changing composition of respired air. In the investigation of such respiratory problems it is necessary that the instrument have a "rise time"** less than 0.2 second with minimum lag.

It was deemed advisable to take the design of an instrument which had already proven itself and incorporate only the necessary modifications to achieve the desired performance. Accordingly, the instrument described in A. O. Nier's papers[1,2] was used as a basis for the design of this spectrometer.

GENERAL DESCRIPTION

Figure 1 is a schematic diagram of the general layout of the mass spectrometer. Air is drawn into the sampling system through a hypodermic needle (B) by a vacuum pump (A). It flows past a needle valve orifice (C) and a portion is drawn into the ion source (D). The ions pass into the magnetic field (E) and the components are deflected to fall on the collector plates (F, F′, F″). Static potentials on plates (G, G′) serve to bring the two outside components to bear on their respective collector plates. The electrometer tubes and the input resistors are mounted inside the receiver end of the spectrometer tube, and connection is made to the preamplifier through shielded cables. The output of the amplifiers is fed into mirror galvanometers which reflect beams of light onto a moving strip of photographic paper.

THE SAMPLING SYSTEM

The sample to be analyzed is pulled through a number 24 hypodermic needle and past the leak by a small vacuum pump,[3] as shown in Fig. 1. The line between the hypodermic needle and the leak has great effect on both time lag of response and the response time, and, therefore, should be kept as short as possible. A six-foot length of ¼″ O.D. copper tubing has been used satisfactorily.

The leak itself, shown in Fig. 2, consists of a needle valve. The needle used was an ordinary sewing needle usually designated as a No. 3 "between" needle, mounted in a brass bolt with a ¼-28-N.F. thread. The seat consists of a cylindrical brass rod 3 mm in diameter and 5 mm in length through which a 0.7-mm hole has been drilled. The variable constriction produced by the needle valve is introduced into the stream of gas in such a way as to obtain a very short flushing time. Readjustment of the needle valve is rarely necessary. The use of a pumping system somewhat larger than usual permits a leak of such dimensions as to reduce the effect of fractionation[4] to below the sensitivity of the instrument for a wide range of operating conditions. To demonstrate this, measurements of apparent relative abundance were made on CO_2 and O_2 in O_2-CO_2-N_2 mixtures. If fractionation exists, then varying the ratio of leak dimensions to mean free path would cause a change in the measured ratio of CO_2 to O_2. The fore pressure on the leak was held constant while the leak dimensions were varied sufficiently to change the vacuum from 10^{-5} to 2×10^{-6} mm Hg, and the ratio of CO_2 to O_2 remained constant to within experimental accuracy (±0.5 mm; 11 cm full scale galvanometer deflection).

---

* The work described in this paper was carried out under contract between the ONR and the Ohio State University Research Foundation.

** "Rise time" is defined as the elapsed time from the beginning of the response to the attainment of a new value, stable to within experimental accuracy, for an instantaneous input change.

[1] A. O. Nier, Rev. Sci. Inst. 18, 398 (1947).

[2] A. O. Nier, Rev. Sci. Inst. 11, 212 (1940).

[3] Such as Welch Duoseal No. 1400-B.

THE SPECTROMETER TUBE

The spectrometer tube is constructed of metal throughout. That portion of the tube which passes through the magnetic field was flattened to slip between the pole faces of the magnet and curved to accommodate the ion beam curvature. This portion was formed from copper tubing $2\frac{1}{4}''$ in diameter with $\frac{1}{16}''$ walls. To this is attached a copper tee, one leg of which goes to the vacuum system. At the other end of the tee, a sylphon bellows is attached to facilitate focusing of the ion beam.[5] The ion source is mounted on a brass plate, which is bolted onto the sylphon end of the spectrometer tube. All temporary connections of the tube are made with grooved flanges fitted with Neoprene gaskets. Permanent connections are made with silver solder. Electrical connections are made through Stupakoff seals soldered into the tube. The receiver end of the tube is constructed from $4\frac{1}{2}''$ diameter brass tubing and is about 18'' long. The receiver assembly is mounted on a brass plate which is bolted onto the spectrometer tube in a manner similar to the ion source.

THE VACUUM SYSTEM

The vacuum system consists of the forepump,[6] a diffusion pump with a capacity of 250 liters per second at 10^{-6} mm Hg,[7] a cold trap in which liquid air is used routinely, a thermocouple gauge, and a Philips ion gauge. All metal parts of the vacuum system except the pumps were boiled in a bright plating bath to clean the surfaces. In practice, we have had no difficulty getting a vacuum of 5×10^{-6}

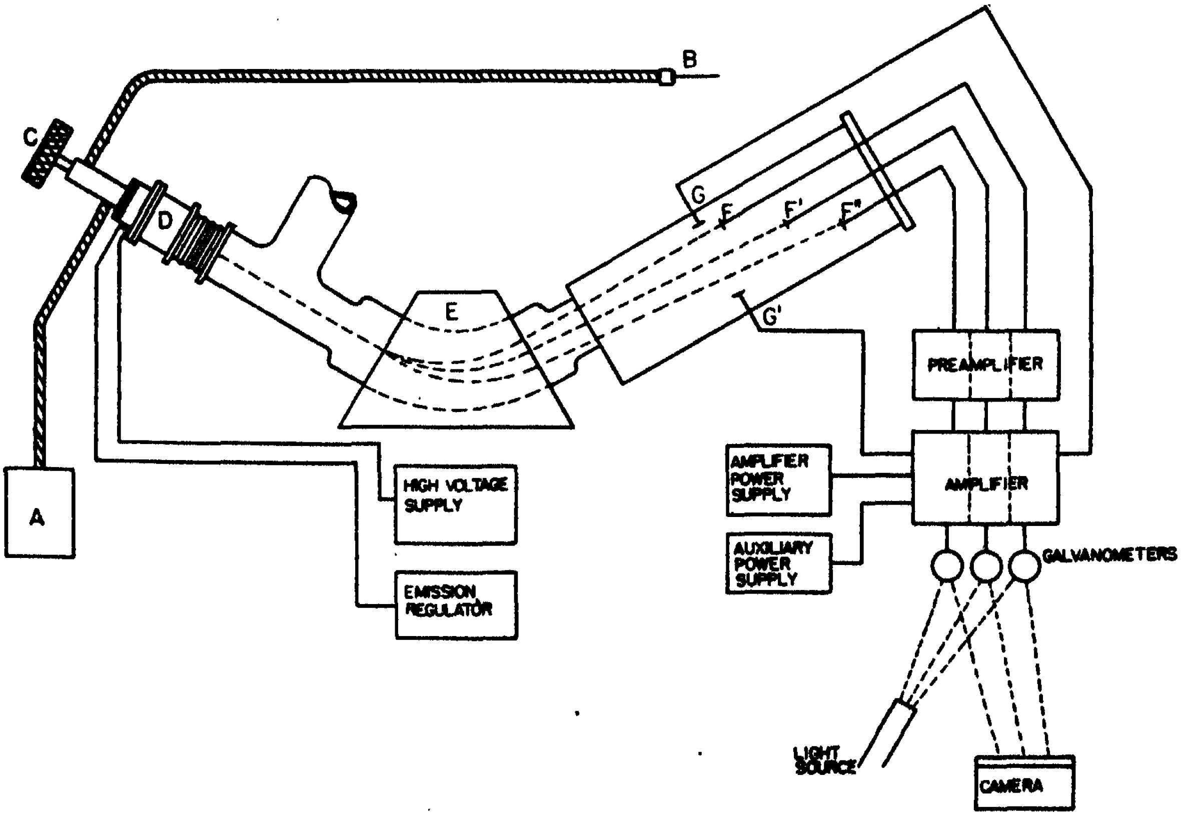

FIG. 1. Schematic diagram of general assembly.

---

[4] R. E. Honig, J. App. Phys. 16, 646 (1945).
[5] W. E. Stephens, Phys. Rev. 45, 513 (1934).
[6] Such as Welch Duoseal No. 1405-B.
[7] Such as Distillation Products, Inc., No. VMF 260.

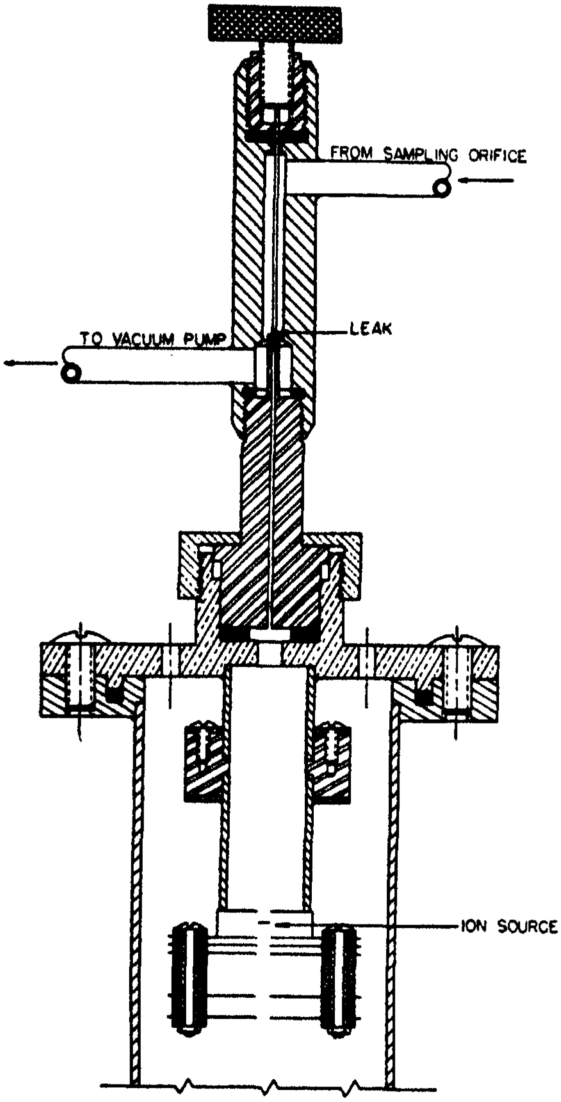

FIG. 2. Leak and ion source.

mm Hg without degassing. After the pressure has been reduced to about 5×10^{-6} mm, the needle valve is opened until the gas flow into the spectrometer tube is sufficient to raise the pressure to 10^{-5} mm Hg.

THE ION SOURCE

The ion source used is basically the same as that of Nier's instrument, except that tantalum was used instead of Nichrome V, and the ionization chamber was so designed as to offer appreciable resistance to flow of gas into the main vacuum chamber. This causes the pressure in the ionization chamber to be about 80 times that in the main vacuum chamber and thus permits the use of an oil diffusion pump even though we are working in the same mass range as the oil vapors. With this ion source total positive ion currents of 10^{-9} ampere are easily obtained with 200 microamperes total emission current.

The design for the electromagnet we have used is taken from Nier.[2]

THE RECEIVER ASSEMBLY

The problem of collecting a multiple beam becomes relatively simple when the masses are as widely separated as in the case of carbon dioxide, oxygen, and nitrogen. The receiver assembly (Fig. 3) consists of three sections, each composed of a

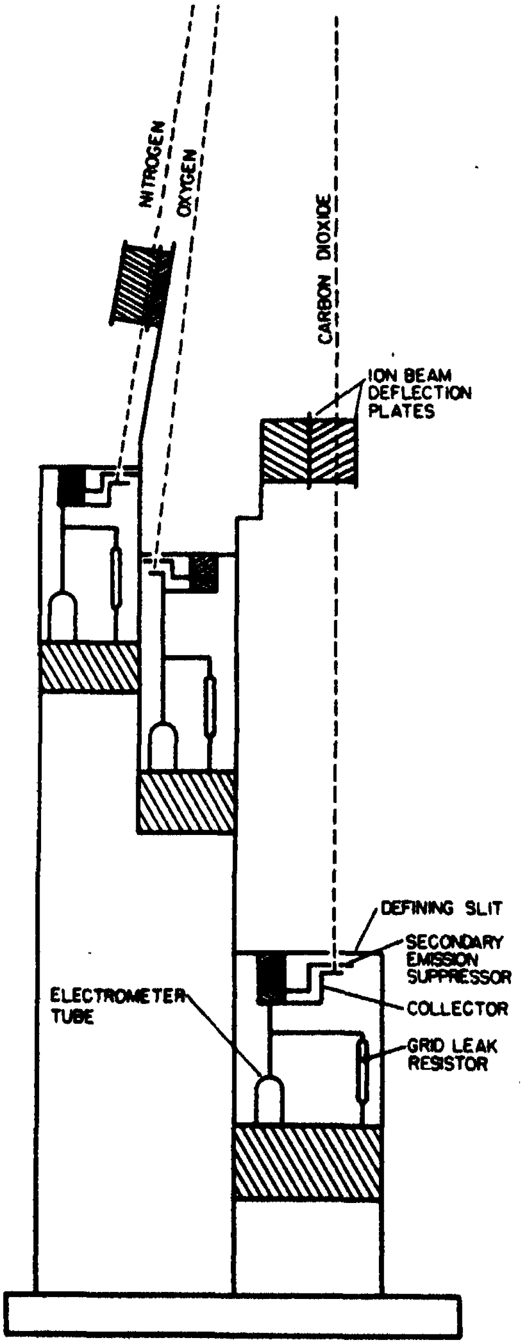

FIG. 3. Receiver assembly.

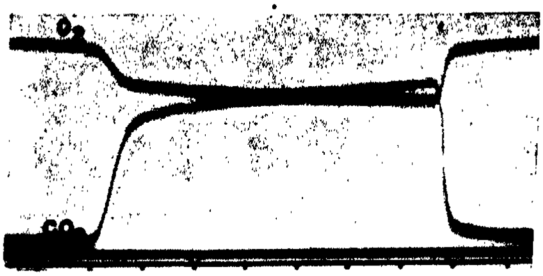

FIG. 4. A typical record of expiration.

defining slit, a secondary emission suppressor slit, and a receiving plate. Since it is difficult to determine exactly the separation between the three components, two sets of deflecting plates were added, through which the CO_2 and N_2 beams pass and are shifted slightly to bring them to bear exactly on their collecting plates when the middle beam is centered on its collector. A stabilized potential of 225 volts is taken from the amplifier power supply and brought to the plates through potentiometers and reversing switches. To reduce the capacitance of the collecting plates and their leads, the preamplifier stages are mounted in the receiver assembly. It is necessary to maintain great rigidity of the receiving plates relative to their surroundings inasmuch as there is appreciable response to low sonic frequencies.

ELECTRONIC COMPONENTS

With the exceptions to be noted for the amplifier and its power supply, the electronic equipment is the same as that of the Nier instrument. The first modification consists of omitting the condensers across the preamplifier grid leak resistors. These condensers were used by Nier to match the time constants of the channels, which is not necessary in our work.

The second modification consists of changing circuit elements of the power supply to increase its current capacity to one-half ampere in order to permit the addition of a third channel in the amplifier, and an extra stage of amplification to each channel in order to drive the relatively insensitive galvanometers we have used.

Finally, the addition of a third channel made necessary some change in the filament supply of the amplifier. In order to keep the filaments of the various stages near the cathode potentials the 12-volt filament tubes were changed to 6-volt tubes and ballast resistors introduced at appropriate points. Similar changes were made in the preamplifiers.

The recording has been accomplished with three type G-6 G. E. galvanometers reflecting light beams onto the lens of a 12-cm Cambridge strip camera. In operation, a film speed of one inch per second has been used. The galvanometers are of the ribbon type and are serviceable up to 500 c.p.s., which, along with their rather low current sensitivity, has been found to be a handicap, since any "hash" picked up from other apparatus is recorded. These galvanometers are to be replaced with recorders[8] which have a full scale response of 250 microamperes in less than 0.25 second.

PERFORMANCE

Figure 4 is a record which is typical of that obtained when a normal expiration is recorded with the sampling orifice placed just in front of the lips. The instrument is calibrated at the end of each recording with a gas mixture of known oxygen and carbon dioxide content. By setting up the relations between calibration excursions and experimental excursions in a simple algebraic ratio, results have been obtained which are consistently accurate to one millimeter partial pressure of oxygen or carbon dioxide. That the oxygen in air sampled had no effect on the carbon dioxide reading was demonstrated by transferring the sampling needle from a stream of 100 percent nitrogen to 100 percent oxygen. When this was done the carbon dioxide reading remained consistently on zero. In a similar manner it was demonstrated that the carbon dioxide in the sample had no effect on the oxygen reading.

The rise time of the instrument was determined by placing the needle orifice in a stream of gas mixture which differed in oxygen and carbon dioxide content from room air, then suddenly removing the needle into room air. The change thus observed begins about 0.2 second after the movement of the needle, and is complete within 0.1 second of the time it begins. The rise time is essentially the same for oxygen and carbon dioxide, indicating that the memory effect due to adsorption of gases onto the metal parts of the ion source (which is seen to the greatest extent in carbon dioxide) is negligible.

ACKNOWLEDGMENTS

The cooperation of the Betatron Laboratory at Ohio State University and of its director, Dr. T. J. Wang has been of great value in the design and construction of the instrument.

---

[8] Such as G. E. photoelectric recorders.

THE REVIEW OF SCIENTIFIC INSTRUMENTS VOLUME 20, NUMBER 5 MAY, 1949

A Microwave Polarimeter

ALFRED E. SCHWANEKE[*] AND ZABOJ V. HARVALIK[**]
University of Missouri, School of Mines and Metallurgy, Rolla, Missouri

(Received December 6, 1948)

A microwave polarimeter is described which enables the determination of rotation of the plane of polarization of microwaves in the 3.2-cm band. The transmitter-analyzer utilizes klystron tube 723 A/B. The microwaves are fed into a horn which acts as a polarizing agent. The analyzer-receiver consists of a horn antenna, rotatable wave guide, a crystal detector, and an indicator. The microwaves are rectified by a crystal rectifier, and are either detected by a microammeter, a galvanometer, or by an amplifier of appropriate design. Changes of angles of rotation can be detected if they are not less than 2° to 3°.

INVESTIGATIONS regarding the behavior of microwaves have disclosed that their physical properties are more or less identical with those of visible light. A certain kind of phenomenon of interaction of microwaves with matter will show a pronounced difference, however, due to differences in wave-length. This difference is even more pronounced with respect to absorption and reflection when microwaves are directed against matter. This paper describes a microwave polarimeter which might prove useful in the investigation of polarized microwaves and their interaction with reflecting and absorbing substances.

The microwave polarimeter, like the optical polarimeter, uses a polarizer and an analyzer, but it differs in that the microwave-polarizer also includes a microwave-generator. A klystron tube (723 A/B) generates microwaves of 3.2-cm wave-length and about 25 milliwatts. The microwaves are fed by a wave guide into a horn which acts as the polarizing agent. In the analyzer a system of horn and wave guide also is used. The microwaves reaching the horn of the analyzer are transmitted by a wave guide to a loop. The microwave energy induced in the loop is transmitted to a coaxial line, which permits the rotation of the horn over a range of 360°. Using a coupling antenna, the energy from the coaxial line is transferred into a wave guide, into which a 1N21 crystal detector is inserted. The output current is fed from the detector into an amplifier or microammeter or galvanometer.

The essential features of the polarimeter are shown in Fig. 1. The polarizer portion consists of a type 723 A/B klystron generator coupled to a short section of a wave guide which radiates energy into space through a pyramidal horn antenna. This antenna radiates a plane-polarized wave that is intercepted by another horn which serves as the antenna of the receiver-analyzer. A special coaxial-line-rotating joint allows the analyzer horn to be rotated in order to measure the polarization characteristics of the received energy. This special joint couples the energy to a semi-resonant section of wave guide terminated in a silicon crystal rectifier (1N23). The output of the polarizer can be fed either into a galvanometer or into an amplifier with the following modification: If the output of the polarizer is amplitude modulated by a 1000-cycle/second wave, this modulation is appearing as a 1000-cycle varying voltage across the crystal rectifier with a steady, true current component of the rectified carrier. This complex current is passed through an impedance transformer (T3 of Fig. 8). The resulting 1000/cycle-second square wave is then sent through the amplifier to a vacuum tube voltmeter which indicates the received signal in-

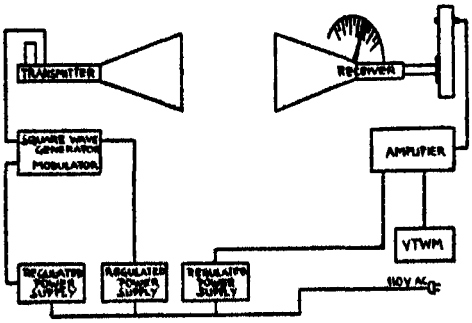

FIG. 1.

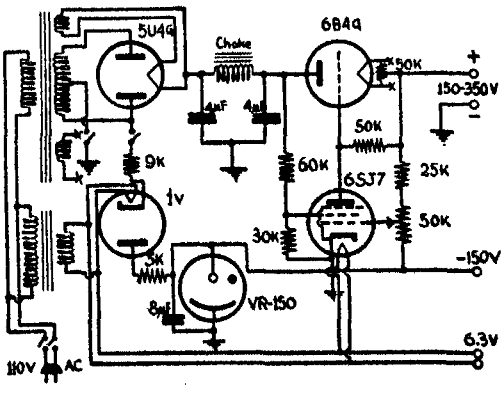

FIG. 2.

---

[*] Now at Central Missouri State Teachers College, Warrensburg, Missouri.

[**] Now at Institute of Science and Technology, University of Arkansas, Fayetteville, Arkansas.

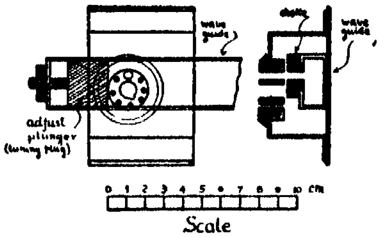

FIG. 3.

tensity. Any change of amplitude in the receiver is recorded by the voltmeter.

Variations in the line voltage would cause variations in frequency and amplitude of currents and voltages appearing in all components of the above described system. Therefore, the power supply must be regulated. The connection of power supply with the transmitter-polarizer is shown in Fig. 2. If an amplifier is used with the analyzer-receiver, an identical power supply is recommended for the amplifier, as well as for the modulator which causes the 1000-cycle/second signal in the transmitter polarizer. These power supplies show a regulation better than 1 percent over the range of 150 to 350 volts output.

TRANSMITTER POLARIZER

The transmitter-polarizer section of the polarimeter is relatively simple in its construction. One end of a wave guide, 15 cm long, is terminated in a flange; the other end is terminated with a close-fitting, rectangular, machined brass plug, which includes an adjusting screw to vary the plug position over a range of about 1 cm. At a distance of 1.0 cm from the central region of travel of the brass plug, a hole is drilled to mount a quarter-wave choke coupling to take the coaxial output line from the klystron. This choke coupling is used to insulate the wave guide from the flange of the line, since the flange is at a beam potential of +250 to +300 volts. A small chassis is placed above this hole. On it is mounted a modified octal socket to receive the klystron, and an octal plug to furnish the various voltages to the klystron. Detail of the klystron mount and the wave guide connection is shown in Fig. 3. The horn antenna is attached to the choke flange at the other end of the wave guide section. This type of construction enables the guide to be excited in its simplest mode, namely, the TE 1.0 mode which radiates a wave from the horn that is plane-polarized parallel to the short dimension of the guide, which, in this case, is vertically polarized.

If the reflector or repeller voltage of a klystron is varied sinusoidally or by a saw-toothed wave shape, the resulting radiofrequency output will undergo ordinary frequency modulation at the rate of the varying voltages applied.

If a square wave variation is applied to the repeller potential, the result will be amplitude modulation of the klystron output power.

To simplify the receiving system, the klystron is amplitude-modulated with a square wave of approximately 1000 cycles/second. The modulator consists of a multi-vibrator which produces essentially a square wave voltage, a positive peak-type tube circuit to insure a flat-topped positive peak, and an amplifier to produce the power output required for best modulation. The output of the square wave amplifier is coupled to the klystron repeller through a 0.5-microfarad capacitor. A diagram of the modulator and its controls is shown in Fig. 4.

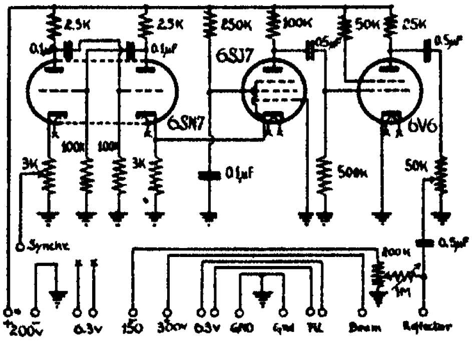

FIG. 4.

RECEIVER ANALYZER

Rotating joints for wave guides have been used extensively in radar work. These joints allowed lateral or azimuth rotation without rotation of the plane of polarization, and a search revealed that no type was suitable for sensitivity to only one plane. Therefore, the receiver analyzer for this instrument, in order to fulfill the requirement of being sensitive to only one plane of polarization, had to be of a special construction. Furthermore, it must contain a device which permits the continuous rotation of the plane of polarization to an axis in line with the transmitted energy from the polarizer. The receiver developed for this instrument is shown in Fig. 5.

A wave guide similar to that used in the transmitter polarizer, with its associated flange, is mounted in lubricated bearings cast of lead with brass sleeves. These bearings allow a free axial rotation of the wave guide. The receiving horn is attached to the flange. The opposite end of the section of the wave guide supports a special rotatable coupling.

A machined brass plug fits tightly into the end of the wave guide. A brass tube, 3.2-cm inside diameter, extends through this plug and serves as the outside conductor of a coaxial line centered in this tube. A wire terminating at the inside of the brass plug in a small loop 0.4 cm in diameter serves as the center conductor of the line. The orientation of this loop determines the response of the receiver to the plane of polarization or the energy in the wave guide. In this case the response must be limited to transverse electro-magnetic fields only (TE 1.0). As all waves have associated magnetic fields at right angles to the electric field, the solution to obtaining a plane-polarization response at the end (plug) of the guide is to mount the loop to respond only to the magnetic lines of force which are parallel to the long dimension of the guide.

The use of the loop with its axis parallel to the long dimension of the guide, in order to link only the magnetic lines of force appearing across the long dimension of the guide, allows a coaxial line to pass out of the geometric center of the plug in the guide. As far as could be determined, this type of coupling has not been used before, for all commercial line-to-wave guide couplings make use of a quarter-wave probe placed parallel to the electric lines of force in the guide. This requires a wire across the short dimension of the guide which necessitates a connection through the sides of the guide. In this case the connection would interfere with the rotation of the receiving horn. A detail of the special coupling is shown in Fig. 6. The loop supports the center wire of the coaxial tube and is soldered to the plug. This makes a rigid support without the use of insulating materials.

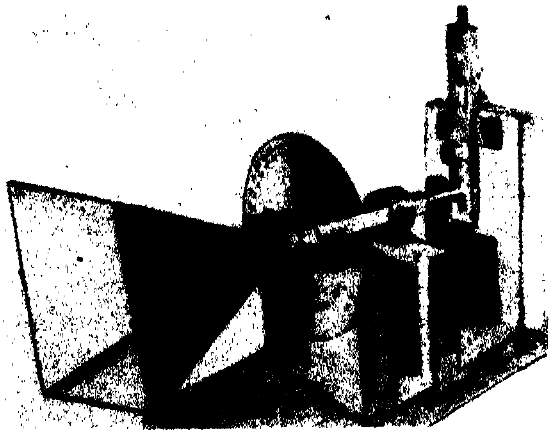

FIG. 5.

The other end of the coaxial tube rotates in a slip ring arranged to allow free mechanical movement and yet maintain good electrical contact. A quarter-wave choke here would reflect high resistance to the two contacting surfaces and would be a desirable refinement. The coupling to the wave guide semi-resonant cavity is usually the familiar quarter-wave probe inserted through the side of the guide. This probe at this end of the coaxial tube is supported by a thin filament of acetate glue placed at a point of high electrical impedance. This movable tubing plug shown in Fig. 6 assures the passage of energy from the probe toward the crystal detector. The crystal is placed slightly off center across the short dimension of the wave guide cavity to afford a better impedance match of the crystal characteristics to the guide or cavity impedance. The systems can be tuned with great ease and stability.

A microammeter or galvanometer attached to the crystal was first used to receive the signal. To increase sensitivity, however, the amplitude modulation voltage appearing across the crystal was amplified and then measured with a vacuum tube voltmeter. A Silver Vomax, Model 900, vacuum tube voltmeter was used. A circuit of the receiver amplifier is shown in Fig. 7.

HORN ANTENNAS

The antennas used in this instrument are identical for receiver and transmitter, and are of standard pyramidal form. Other types can be attached to the choke flanges whenever a special wave, such as a circular polarized one, is desired.

The pyramidal horns are constructed of copper sheeting and are soldered to the flanges. This enables the horns to be attached to the standard flange of the wave guide.

The angle of flare in the horizontal plane is 40°. This angle was chosen to obtain the greatest attenuation of other unwanted modes or planes of polarization while gaining the maximum intensity of the transverse electrostatic plane of polarization. The length of the horns, five wave-lengths or 16 cm, was chosen for constructional ease. The flare in the vertical plane is also 40°. The flare in this plane is not absolutely necessary, but was in-

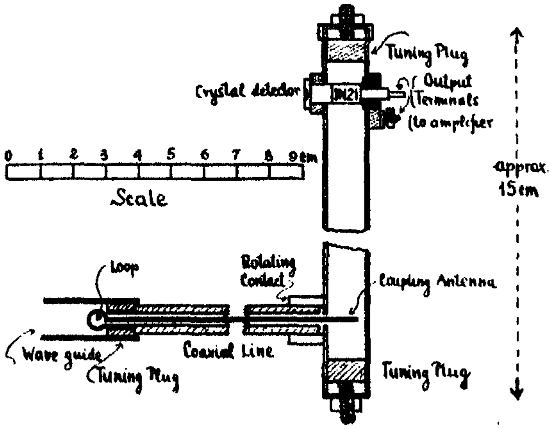

FIG. 6.

corporated to obtain a sharper beam of energy in the vertical plane. The angle used was selected for the same reasons as the other 40° angle, merely for attenuation of unwanted modes and gain for the preferred planes of operation. The calculated beam width, considering the dimensions used, is approximately 20°.

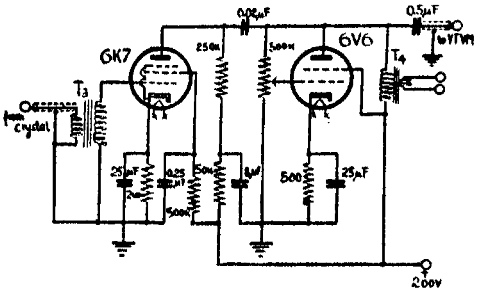

FIG. 7.

According to theory, the area of the opening of the horn becomes a phantom array of phased dipoles: the greater the area, the larger the number of phased units. This accounts for the sharp response of the horn antenna.

OPERATION OF THE POLARIMETER

In operation, the polarizer is clamped to one end of a table, while the receiver-analyzer is clamped a short distance away, facing the transmitter. Celluloid protractors are fixed to the base of the receiver, with the rotating section of wave guide passing through its center. A pointer on the rotating part indicates the angle of movement of the horn. These protractors are marked to 30 minutes of a degree.

With the correct voltages applied to both transmitter and receiver, the receiver-analyzer horn is rotated in small angular steps, and the readings on the vacuum tube voltmeter are recorded for graphing on polar coordinate paper for calibration. Then the samples are placed between the polarizer and analyzer, with the resulting data recorded as above.

The graphs of the voltage readings are not true pictures of the polarization planes or polarization characteristics of the received waves, but the following characteristics may be deduced from them: If the resulting curves do not reach true nodes at two separate 180° settings of the horn, the analyzer waves are probably elliptically polarized. The shape of this ellipse may be shown by drawing the normals to the angular lines representing the voltage for that angle. These normals will be tangent to the ellipse of the received waves. If the normals do not produce an ellipse and the voltages show true nulls, the received waves are plane-polarized. The plane of polarization is then parallel to a line drawn through the nulls. Calibration graph is shown in Fig. 8 and will clarify this point.

It was contemplated to increase the sensitivity as well as a continuous recording of the polarization properties of the sample by rotating the analyzer horn continuously about half a revolution per second with a Selsyn motor. This motor can be synchronized by applying a circular sweep to an oscilloscope with a long persistance screen somewhat on the order of a PP1 radar system. The plane of polarization would then appear instantaneously, and any change in the polarization characteristics of the received wave could be easily recorded.

CALIBRATION OF THE INSTRUMENT

The calibration showed that this instrument is accurate enough to read planes of polarization to within 3°. This calibration graph is shown in Fig. 8 and was taken without any obstructing sample between the polarizer and analyzer. The reference zero is determined by allowing the receiver-amplifier to operate with the transmitter and modulator turned off. The voltage indicated under these conditions will be the noise output generated in the circuit of the amplifier. In all of the measurements made, this reference zero was 0.8 volt or less.

This microwave polarizer is intended to be used to investigate polarization phenomena of materials placed between the transmitter-polarizer and analyzer-receiver.

Of interest are investigations of the Faraday effect in the region of microwaves, rotation of polarization planes by different dielectric materials, refractions in connection with polarization and rotation, phase relationships, and similar phenomena.

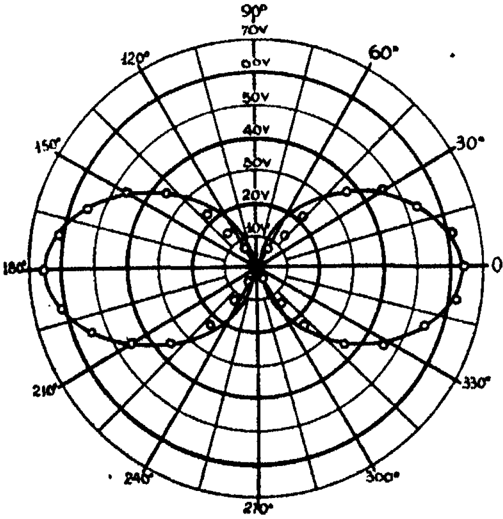

FIG. 8.

This paper is essentially the content of the thesis for partial fulfillment of the requirements for the degree of Master of Science in Physics at the University of Missouri, School of Mines and Metallurgy, Rolla, Missouri. The complete thesis of Mr. A. E. Schwaneke is deposited with the library of said institution.

The microwave polarimeter has been exhibited at the student exhibit of the Colloquium of the College Physicists, S.U.I., Department of Physics, Iowa City, Iowa, June, 1948.

BIBLIOGRAPHY

(1) H. E. Hollman, *Physik und Technik der Ultrakurzen Wellen* (Edwards Brothers, Inc., Ann Arbor (A.P.C.), 1943), Vol. 2.

(2) E. V. Appelton and J. A. Ratcliff, Proc. Roy. Soc. London, **117A**, 576 (1928).

(3) A. L. Green, Proc. I.R.E. *22*, 324 (1934).

(4) W. G. Baker and A. L. Green, Proc. I.R.E. **21**, 1103 (1933).

(5) John D. Kraus, Electronics **20**, *109* (1947).

(6) Harvard University, *Radio Research Laboratory* (*Very High Frequency Techniques*) (McGraw-Hill Book Company, Inc., New York, 1947), Vol. 1, p. 138.

(7) A. B. Brownell and R. E. Beam, *Theory and Application of Microwaves* (McGraw-Hill Book Company, Inc., New York, 1947).

(8) King, Mimno, and Wing, *Transmission Lines, Antennas and Wave-Guides* (McGraw-Hill Book Company, Inc., New York, 1945).

(9) Nathan Marchand, *Ultra High Frequency Transmission and Radiation* (John Wiley & Sons, Inc., New York, 1947).

(10) C. G. Montgomery, *Technique of Microwave Measurements* (McGraw-Hill Book Company, Inc., New York, 1947).

(11) S. Ramo and J. R. Whinnery, *Field and Waves in Modern Radio* (John Wiley & Sons, Inc., New York, 1944).

(12) L. N. Ridenour, *Radar System Engineering* (McGraw-Hill Book Company, Inc., New York, 1947).

(13) Sperry Gyroscope Company, *Microwave Transmission Design Data* (1944).

THE REVIEW OF SCIENTIFIC INSTRUMENTS VOLUME 20, NUMBER 5 MAY, 1949

Photomicrography of Tracks in Nuclear Research Emulsions

Adair Morrison and Fred Morton
Physics Division, National Research Laboratories, Ottawa, Ontario, Canada

(Received November 8, 1948)

A simple projection system and film holder for taking photomicrographs of particle tracks in photographic emulsions of the type used for nuclear research is described. With this film holder a series of exposures covering a considerable length of the track image is obtained on a single film as adjacent segments of track are brought successively into sharp focus and recorded.

In reporting experiments in which nuclear disintegrations, produced by cosmic rays and by fast neutrons, were observed in photographic emulsions, it was found very difficult to produce good photomicrographs of the events. The tracks to be photographed were often several hundred microns long and they usually slanted through the emulsion. With the conventional photomicrographic equipment, a very large number of photographs was required and on each of these only a short length of the track was in focus. The amount of time and material required was excessive and the accurate alignment and assembly of the short lengths into a mosaic was difficult so another method was sought. A fairly successful solution of the problem was found by using a rather simple projection system and a special film holder.

The projection system consisted of a microscope lamp, a shutter, the microscope, a right-angle prism with the 45° surface silvered, and a front-surface mirror. (See Fig. 1.) The beam of light through the microscope, after two reflections, formed an image on the table top beside the microscope. An oil immersion objective and a low power eyepiece (3× or 5×) were used. Either a filament or vacuum-arc type of lamp was used.

The film holder, designed to expose—a few millimeters at a time—a strip of film aligned with

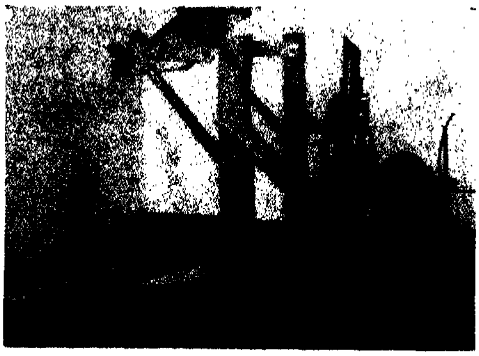

Fig. 1. Projection apparatus consisting of microscope lamp, shutter, microscope, right-angle reflection prism, and front-surface mirror. Microscope and mirror are mounted on a heavy metal base. Film holder in place on white circle representing illuminated field of view.

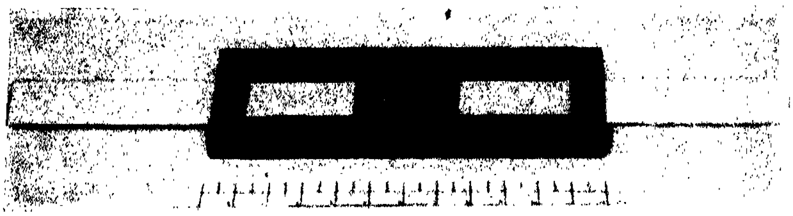

FIG. 2. Film holder for photomicrography of tracks in nuclear research emulsions.

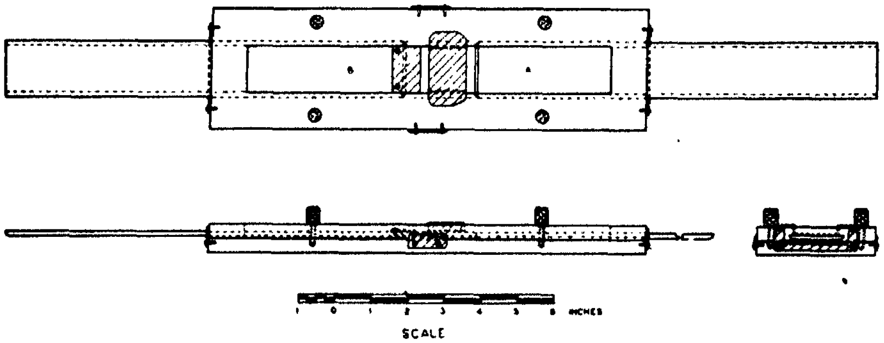

FIG. 3. Drawing showing construction of film holder.

the track, consisted of two pieces of black Bakelite, with the film between them, clamped together with thumb screws. The upper piece had a rectangular opening cut through it directly above the film; this opening could be partly or completely closed by two white slides traveling just above the surface of the film. These traveled in a channel cut into the lower face of the upper Bakelite piece from one end to the other. The dimensions and details of construction are shown in Figs. 2 and 3.

In the first design the ends of the slides were accurately fitted so that they were light-tight when butted together and each was beveled so that it would not cast a shadow on the film when used near the end of its travel. By moving either slide *A* or *B* (Fig. 3) a length of film was exposed and the amount exposed was determined by the separation of the ends. An improvement was made by adding to the end of slide *B* a piece of brass which projected about half an inch over slide *A*, and by placing a brass runner an inch wide in the opening above slide *A*. These then had the function of limiting the length of the exposed area, while slide *A* now acted only as a shutter. The runner was held firmly in place by the spring pressure of its two vertical portions against the walls of the opening. The horizontal portion of this brass piece was just above slide *A*, but not touching it, and was at the same level as the brass piece attached to slide *B*.

Ease of loading in the dark was assured by the guides attached to the lower piece, by the symmetrical placement of the thumbscrews, and by the clamping of the film between the surfaces of the two pieces so that its exact size and position did not matter. Since the device was used in a darkroom, no protection was necessary for the edge of the film.

The loaded film holder, with slide *B* in its extreme withdrawn position, was placed on the table top aligned with the track to be photographed. The runner and the microscope fine control were adjusted so that the sharply focused part of the image lay between the runner and the brass piece on slide *B*. With the shutter in the light beam closed the film was uncovered by moving slide *A* till its end was under the runner. After making the exposure, slide *B* was moved over till the brass extension reached the runner, and slide *A* was moved back till it again touched slide *B*. This process was repeated along the whole length of the film.

With successive strips of this kind, long tracks were conveniently photographed and, from contact prints, a mosaic of the track was assembled on a large sheet of white cardboard. The completed mosaic was photographed to secure final prints of the desired size. The film used was "Kodalith Ortho Thin Base Film," chosen because of fine grain, high contrast, and availability.

It was necessary to adjust the lamp and the microscope very carefully so that the whole field of the projected image was uniformly illuminated.

The particular advantages of this method may be summarized as:

(1) No special photomicrographic camera is needed, since prism and mirror can be obtained cheaply, if not already on hand, and the film holder can be built locally.

(2) Long tracks, either single or radiating from stars, can be quickly photographed on a few films; thus the amount of processing and printing is reduced and the construction of a mosaic is greatly simplified.

THE REVIEW OF SCIENTIFIC INSTRUMENTS VOLUME 20, NUMBER 5 MAY, 1949

A High Temperature X-Ray Diffraction Camera* †

JAMES W. EDWARDS, RUDOLPH SPEISER, AND HERRICK L. JOHNSTON
The Ohio State University, Columbus, Ohio

(Received January 3, 1949)

A high temperature x-ray powder diffraction camera has been designed to yield patterns at temperatures in excess of 2500°K. The sample, in form of a wire, compacted rod, or contained (wherever suitable) in a thin walled quartz or ceramic tube, is heated indirectly by conduction and radiation in a thin walled molybdenum, tantalum, or platinum furnace. The furnace is heated by high frequency (0.5 megacycles) eddy currents induced by a small induction coil. The cylindrically shaped furnace and the sample are held coaxially in the induction coil and slowly revolved. The specimen temperature is maintained constant to ±0.2 percent by an especially designed temperature regulator. A water-cooled copper jacket with slots covered with metal foil to filter the diffracted x-radiation surrounds the furnace and is used to protect the x-ray film from heat and light. The temperature of the specimen is measured with a disappearing filament optical pyrometer at temperatures in excess of 1100°K and a platinum, platinum-rhodium thermocouple at lower temperatures. The camera is either operated with a high vacuum or with an inert gas atmosphere.

INTRODUCTION

THE camera described in this paper has been developed as a part of a research program devoted to the study of the thermodynamic and physical properties of inorganic solids at elevated temperatures. With the aid of induction heating, a high temperature powder diffraction camera has been designed which will yield x-ray photographs at temperatures in excess of 2500°K.

Induction heating[1] was chosen for several reasons:

1. The very high temperatures readily attainable—virtually limited only by the melting points of the furnace elements.
2. The simplicity of camera design possible.
3. The elimination of ceramic material for the support of heating elements—thus problems of extensive outgassing and thermal shock and the use of substances with unfavorably high total emissivity are avoided.
4. The robust construction of the heating elements possible lead to long life furnaces.
5. The very rapid attainment of temperature equilibrium within the furnace—one minute or less—leads to an efficient use of the camera.

In induction heating, the object to be heated (which must be a conductor) is placed in the center of a work coil where it is heated by the eddy currents induced by the r-f current flowing in the work coil. Non-conductors can only be heated by radiation and conduction. For this reason and the fact that conductors of very small diameter cannot be effectively heated by low frequency oscillators, the furnace of the x-ray camera is designed to heat the specimen indirectly. This is accomplished by supporting the specimen to be studied inside a chamber made of a refractory conductor (e.g., tungsten, tantalum, molybdenum, graphite, or platinum). The chamber (furnace) is then placed in a suitable work coil and heated by the induced eddy currents. The minimum size of the furnace is dictated by the frequency of the power source and the maximum size is set by the total allowable radiation losses from the surface of the furnace. Cylindrical chambers of $\frac{3}{8}''$ to $\frac{3}{4}''$ diameter and 1″ high were found to work well with the equipment used in this laboratory.

The x-ray film is effectively protected from the intense heat and light emitted by the furnace by the use of a water-cooled copper radiation shield which completely surrounds the work coil and furnace. The shield is slotted and the slots are covered by metal foil transparent to x-rays of the desired wave-length.

Depending upon the nature of the specimen and furnace elements, the x-ray camera can either be operated at high vacuum or with suitable inert gaseous atmospheres. If platinum furnace elements are used, the camera can be operated in air up to temperatures where the vaporization of platinum becomes excessive—about 1500°C. Tantalum furnace elements have been successfully used in high vacuum up to 2250°C. Undoubtedly, furnace elements made of sintered tungsten would increase the practical temperature limit of operation several hundred degrees.

At low temperatures (room temperature—1500°C), the temperature is measured with a platinum-platinum 10 percent rhodium thermocouple. The thermocouple is shielded to a considerable degree from the r-f-field by the furnace elements, their supporting members and the copper

---

* This work was carried out under contract between the ONR and The Ohio State University Research Foundation.

† Parts of this paper were given at the Fifth Annual Conference on X-Ray and Electron Diffraction, November 1947, and the meeting of the American Physical Society, January 1948, New York, N. Y.

[1] Three high frequency oscillators are used for heating in this laboratory: Two General Electric 15 kilowatt electronic heaters operating at a frequency of 500 kilocycles and one Westinghouse 20 kilowatt oscillator operating at a frequency of 450 kilocycles.

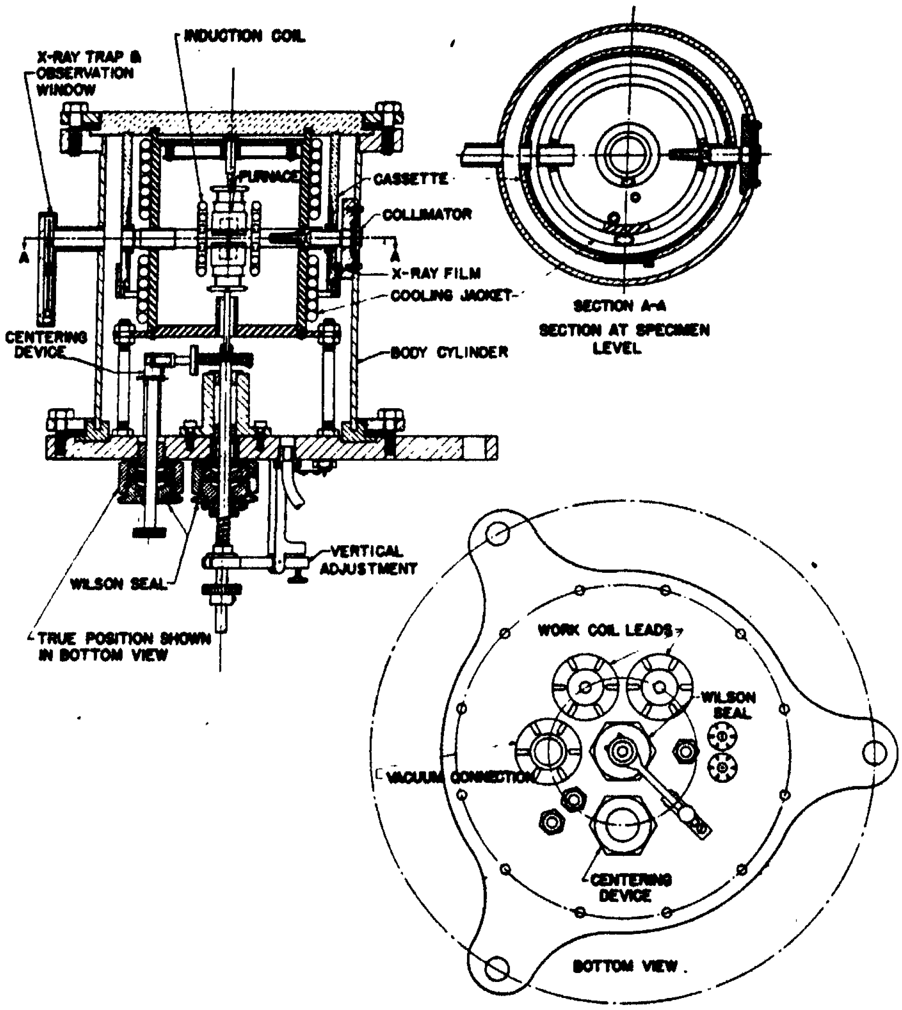

Fig. 1. High temperature x-ray diffraction camera.

cooling jacket and is further shielded by shielding tape outside the heating zone. A filter network is used to eliminate the very small r-f-pick-up that does occur. No difficulty has been experienced in measuring temperatures accurately in this manner.

High temperatures—850°C and up—are measured with an optical pyrometer.

DESCRIPTION OF CAMERA

A general view of the camera is shown in Fig. 1. The specimen in the form of a wire or compacted rod is mounted vertically in tube E (Fig. 2) in the center of the lower furnace element, and extends upward into the upper furnace element. These elements are constructed from 0.010″-tantalum sheet, the inside and outside open-ended cylinders being drawn in suitable dies. The furnace elements are $\frac{9}{16}$″ high by $\frac{3}{4}$″ O.D. and $\frac{1}{2}$″ I.D. The sample holder, E, in the lower cylinder is a tantalum tube 0.03″ I.D. The various parts of the furnace are either riveted or welded together. The holes, D, in the outer cylinder (4 holes in the upper and 4 in the lower furnace elements, 90° apart) are sighted upon with the optical pyrometer in making temperature measurements. The vanes, F, set in at 45° to the axis of the holes help to create a "hohlraum." The furnace elements are supported by tantalum strips which in turn are fastened to small tantalum radiation shields. If these shields absorb too much of the r-f energy, they are cut by several radial slots which minimizes this effect. The open ends of the furnace elements are about 2 mm apart in the assembled camera; the space between being for passage of incident and diffracted x-radiation. The furnace is surrounded by a 1″-I.D. coil (4 or 6 turns) of $\frac{3}{16}$″-copper tubing.[2] This coil is wound so that the turns are essentially horizontal with spacing $\frac{1}{16}$″ except for the middle spacing which is $\frac{1}{8}$″. The latter spacing is for passage of x-rays. The furnace is heated by induced eddy currents when an r-f-current is passed through the work coil.

---

[2] The detailed design of the work coil, that is, the coupling to the work and the number of turns to be used, depends upon the energy input into the work required. An excellent book discussing the theory of induction heating is G. H. Brown, C. N. Hoyler, and R. A. Bierwirth, *Theory and Application of Radio-Frequency Heating* (D. Van Nostrand Company, Inc., New York City, 1947).

A cylindrical copper cooling jacket (see Fig. 1) surrounds the furnace and work coil. This jacket is wound with $\frac{1}{4}''$-copper tubing through which water is passed for cooling. The upper end of the cooling jacket is closed with a closely fitting copper plate $\frac{1}{8}''$-thick. This plate supports the upper furnace element. A monel tube for support of the lower part of the furnace passes through the center of cooling jacket base plate. A $\frac{3}{8}''$-wide horizontal slot around the cooling jacket allows diffracted x-rays to pass. This slot is covered with metal foil (Ni where CuK α-radiation is being used) to prevent heat and light from striking the film as well as for filtering the x-radiation.

The film is held inside a cassette of 11.459 cm diameter and the Straumanis arrangement is used. The ends of the film fall in the shadow cast by the section of the work coil which crosses the specimen level. The film is further protected from light by a slotted mask which slides into the cassette and is held in place by two threaded collars. The slot in the mask is covered with metal foil.

The top of the cassette fits into a shoulder in the body cylinder. This joint is made vacuum-tight by a $\frac{1}{16}''$-thick Neoprene gasket which is held down with a brass ring. The body cylinder is fastened to the base plate in the same way.

The collimator fits into a hole in the body cylinder and passes through holes in the cassette and cooling jacket. A copper jacket fastened to the cooling jacket surrounds the collimator to prevent it from being heated. The hole through the collimator is covered with aluminum foil to maintain a vacuum.

Opposite the collimator are holes through the cooling jacket, cassette, and body cylinder through which the emergent beam passes and through which the furnace can be observed with an optical pyrometer through a lead glass window. Inside the window is a shutter which is actuated from the outside by a small magnet. This shutter is normally closed to prevent material evaporated from specimen and furnace from condensing on the window causing pyrometric readings to be low. The shutter can be opened for observations or moved so as to interpose a fluorescent screen in the x-ray beam.

The specimen is rotated by means of a shaft passing through a double Wilson[8] seal in the center of the base. The upper end of the shaft terminates at a friction joint. A monel tube in the upper part of this joint supports the lower furnace element. By means of the adjusting arm the upper member of the friction joint can be moved laterally to adjust for eccentricity of the specimen. The lower furnace element and specimen can also be adjusted vertically by the vertical adjustment lever. All adjustments of the specimen can be made externally while the camera is in operation.

The vacuum system is connected through the bottom of the camera. (See Fig. 2.) A Distillation Products oil diffusion pump VM2 and a Duoseal fore pump are used to maintain the high vacuum.

TEMPERATURE MEASUREMENT AND CONTROL

The temperatures in the range 850°C and higher are measured with a Leeds and Northrup Model 8622-C disappearing filament optical pyrometer. The pyrometer is sighted through the observation window into the "hohlraum," D (Fig. 2), in the furnace elements. The temperatures in the upper and lower furnace elements are measured. The rotation of the lower furnace element is interrupted momentarily to read the temperature in each quadrant. These temperatures are then averaged to determine the temperature of the specimen. The pyrometer used is calibrated every 100 degrees between 800°C and 2300°C using a General Electric ribbon filament tungsten lamp standardized at 100 degree intervals by the National Bureau of Standards.

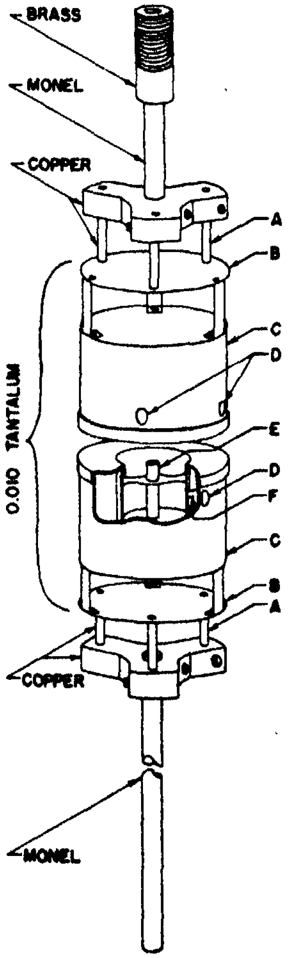

FIG. 2. Tantalum furnace.

---

[8] R. T. Wilson, Rev. Sci. Inst. 12, 91 (1941).

b

a

FIG. 3a. Tantalum-room temperature. FIG. 3b. Tantalum 2000°K.

Since a small temperature difference exists between the furnace elements and specimen, the temperature scale in the camera is established by observing the melting points of small samples of metals such as copper, iron, and platinum placed at the specimen level. The calibrating substances are set in the specimen holder and observed with the optical pyrometer at the same time the temperature of the furnace elements is measured. The accuracy of the temperature measured in this manner is limited by the precision of the pyrometer. The precision of the pyrometer is about 0.2 percent of the absolute temperature at 2000°K depending upon the observer.

For making diffraction patterns of certain oxides in air (in the temperature range room temperature—1400°C), platinum heating elements may be used.

These elements are similar to the design shown in Fig. 2, except that double furnace walls are not used and no holes are drilled in the cylinder walls. Also the copper and brass parts are replaced by monel. The stem that supports the upper furnace element is a hollow monel tube through which a platinum, platinum—10 percent rhodium thermocouple (wire size B and S No. 36) passes into the furnace through the upper element. The junction of the thermocouple is to one side and at the same level at which the x-ray beam passes through the specimen. The thermocouple is placed so that it is in the shadow cast by the work coil and in line with the position where the x-ray film is clasped in the cassette. Thus, no shadow of the thermocouple appears on the exposed part of the film. The thermocouple leads are brought through the bottom of the camera through insulated Stupakoff seals and then over the copper radiation shield to the top where they then pass downward through the hollow tube that supports the upper furnace element. The thermocouple and thermocouple leads as well as the cold junction of the thermocouple are well shielded inside and outside the camera against r-f pick-up. The very small amount of r-f that is absorbed by the thermocouple is eliminated with an r-f filter. A potentiometer of high sensitivity is used to measure the e.m.f. generated by the thermocouple. The rotation of the lower furnace element is interrupted while making the potential measurement. The thermocouple is calibrated against melting point standards supplied by the National Bureau of Standards, and then calibrated again by melting the standards in the camera, the melting point standards being placed in the specimen holder. The accuracy of the temperature measurement is only limited by the precision of temperature control.

The temperature is controlled either manually or automatically to 0.2 percent of the absolute temperature at temperatures above 800°C. This is accomplished in the case of the General Electric oscillator by holding the current in the work coil constant with the aid of a variable inductance placed in series with the work coil.[4] At temperatures less than 800°C the variometer is connected as a variable output transformer. In the case of the Westinghouse oscillator the temperature can be regulated by adjusting the plate voltage.

FILM SHRINKAGE AND CALIBRATION

Since the x-ray film shrinks when placed in a vacuum it is desirable to preshrink the cut film in a vacuum chamber prior to loading into the camera. No additional shrinkage has been observed in film which has been kept in a vacuum for about 24 hours; such film remains tight against the cassette wall.

Each film may be calibrated for shrinkage (or elongation) after being developed by locating centers of symmetrically spaced arcs around incident and emergent beam positions in cases where back reflections are obtained. When suitable back reflections are not obtained calibration is accomplished by measuring distances between shadows cast by the mask.

OUTGASSING

In a high vacuum, the furnace occasionally outgasses as the temperature increases, causing the pressure suddenly to rise high enough to sustain a gaseous discharge. It is then necessary to turn off the r-f current in order to prevent arcing. The system must be allowed to pump down before the power can be applied again. However, arcing within the camera usually does no damage since the overload relays in the oscillator automatically cut off the high voltage to the oscillator tube. Outgassing is minimized by frequent removal of evaporated metal from the work coil and cooling jacket.

---

[4] R. Speiser, G. W. Ziegler, Jr., and H. L. Johnston, Rev. Sci. Inst. (in press).

RESULTS

Using a four turn work coil and exposures of 1¼ to 2 hours, satisfactory diffraction patterns of tantalum and molybdenum have been obtained using a tantalum furnace at high vacuum in the range of temperature 1500° to 2500°K. Satisfactory diffraction patterns of $BaTiO_3$ have also been obtained with a platinum furnace operating in air in the range of temperature 400° to 1600°K.

A diffraction pattern of tantalum at 2000°K is shown in Fig. 3b.

Lattice parameters calculated from back reflections can be obtained with an accuracy of 0.02 percent or better.

THE REVIEW OF SCIENTIFIC INSTRUMENTS VOLUME 20, NUMBER 5 MAY, 1949

A Methane Flow Beta-Proportional Counter*

WILLIAM BERNSTEIN AND ROBERT BALLENTINE
Brookhaven National Laboratory, Upton, New York

(Received January 25, 1949)

A methane flow beta-proportional counter has been designed to detect the high and low energy solid beta-emitters used in tracer experiments. At present, both C^{14} and P^{32} are being counted. The use of a sintered-glass Gooch crucible, both as a filter and sample holder, greatly simplifies the analytical technique involved in such experiments. The instrument is stable and the results are reproducible over long time periods.

CHEMISTS have long accepted the sintered-glass Gooch crucible as an adequate tool in gravimetric analysis. The desirability of combining both the standard analysis for an element with the simultaneous determination of a tracer radioactive isotope has led to the design of a counter adapted to count the sample directly in such a crucible. Figures 1a and 1b show the design finally adopted, which employs the well-known methane-flow proportional counter principle in an end-on version.

This technique has a number of desirable properties. Absence of a window makes it particularly useful for tracers with low beta-energy such as C^{14} and S^{35} (0.15 and 0.16 Mev). It determines high energy betas (P^{32} at 1.7 Mev) equally well. The low background (8–10 c.p.m.) facilitates measure-

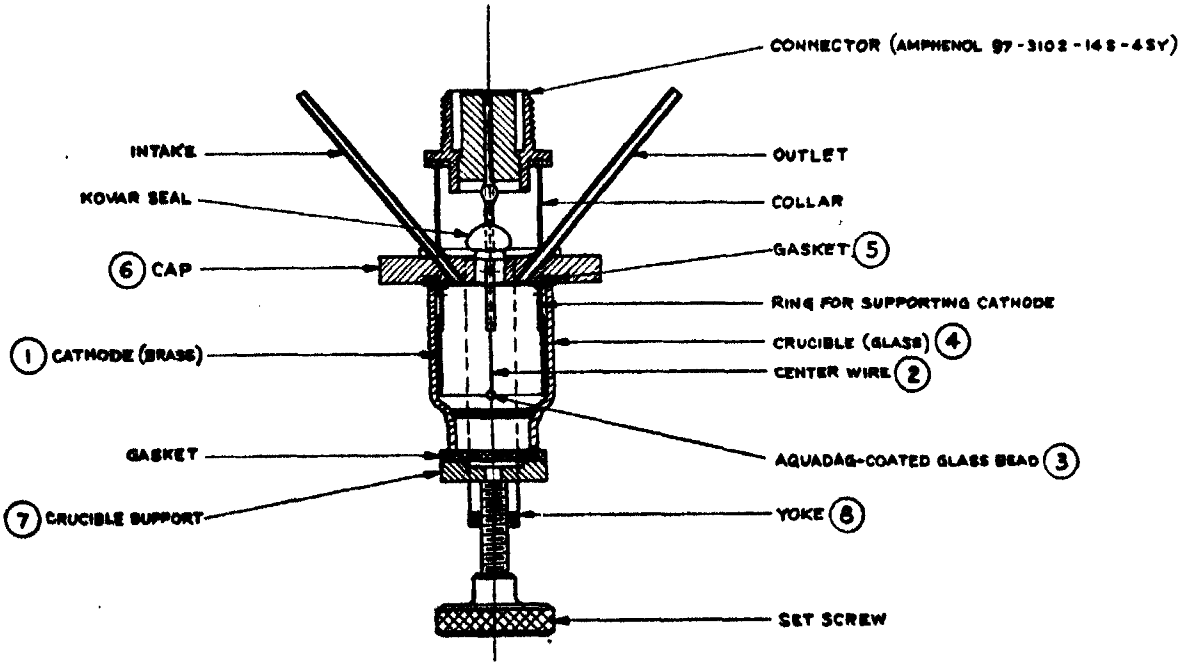

FIG. 1a.

---

* Research work done at Brookhaven National Laboratory under the auspices of AEC.

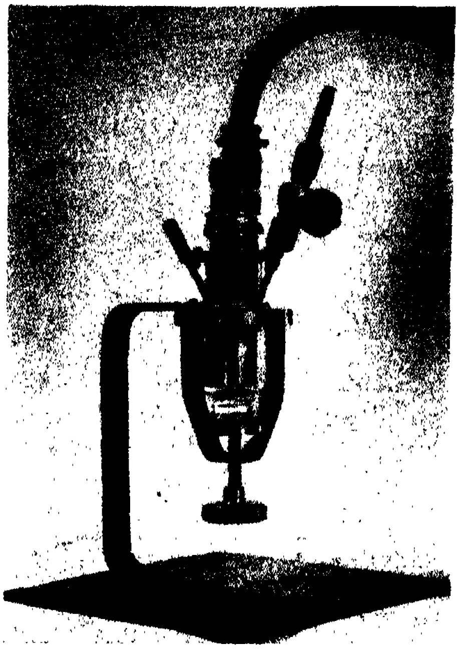

FIG. 1b.

ments on samples of low specific activity, while the coincidence correction factor is negligible even at high counting rates (5×10^4 c.p.m.). Thus, the wide range of both particle energy and sample activity accommodated, coupled with the great stability of this counter, provides a precision instrument for solid sample counting in gravimetric tracer investigations.

The design adopted (see Figs. 1a and 1b) is a cylindrical methane-flow counter. The cathode (1) is constructed of brass tubing and is split to facilitate the dismantling of the counter if decontamination is necessary. The center wire (2) is 2-mil tungsten with an Aquadag-coated glass bead (3) at the end to eliminate sparking and charge accumulation. The weld is shielded by the Kovar lead-through to cover possible points. The Gooch crucible (4), forming the sample holder, and the seal (5) to the brass Cover (6), is held in position by the crucible support (7) and yoke (8). The crucible may be changed by lowering the thumb screw, and swinging the yoke to one side. Crucibles are selected for constant height to maintain the same geometry. A filtration procedure has been discussed by J. Sacks.[1]

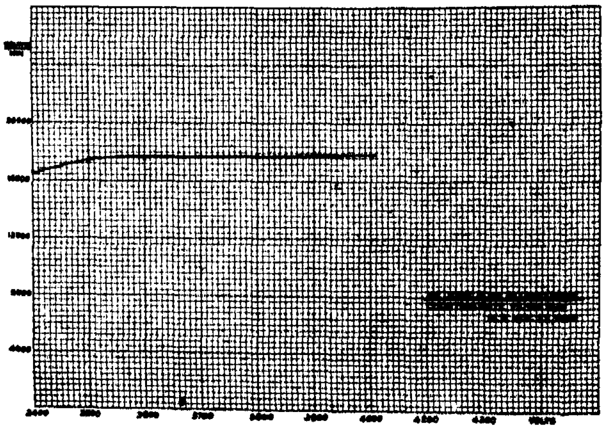

FIG. 2.

The electronic components of this instrument are slight modifications of the IDL proportional counter scaler, Model 162, and the IDL 5000-volt power supply. Since there is still a wide distribution of pulse heights, the input time constant is reduced by a factor of ten to prevent overloading of the amplifier by large broad pulses. This overloading usually results in multiple counting of single pulses. This change does not result in any shift in the operating characteristic of the counter, since the time constant is longer than the rise time of the pulse. Later models will be constructed with a cathode follower mounted directly on the counter to eliminate the effects of cable capacitance, and thereby enable operation at reduced voltages.

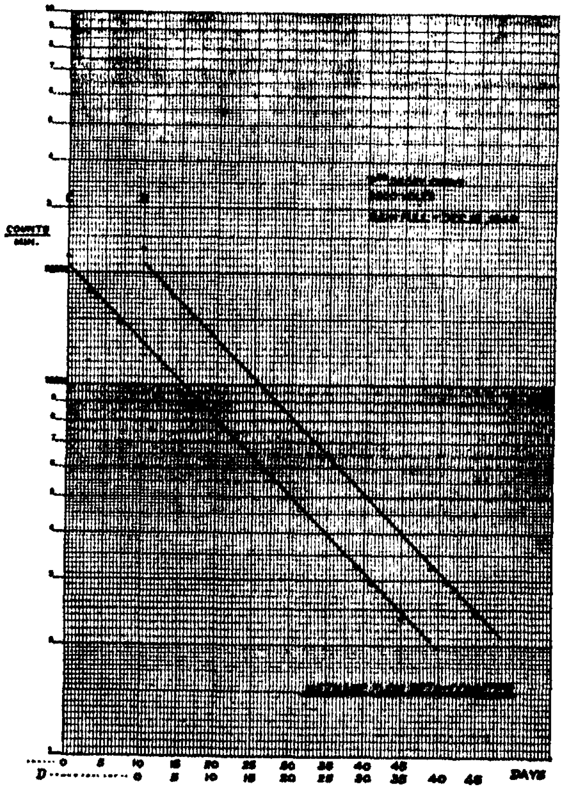

FIG. 3.

The counter has been in use for several months and considerable data has been gathered to date.

---

[1] J. Sacks, *Analytical Chemistry* (in press).

Most data at hand is based on the use of P^{32} betas as the source, although solid barium carbonate sources have been used. The geometry of the instrument is 35 percent according to measurements with a calibrated RaE source by Dr. Benjamin Burtt of the Chemistry Department. Figure 2 is a plot of counting rate against voltage, showing a slope of only about 1.1 percent per hundred volts in the operating region.

The low slope indicates that the counter is operating in the limited proportional region, counting virtually all the beta-particles entering the sensitive volume. Secondly, pulse-height limitation occurs because the more energetic particles expend only a small fraction of their energy in the relatively small sensitive volume. All these factors plus the renewal of the counting gas account for the excellent reproducibility of counts over short and long time periods (decay curve of P^{32}) Fig. 3.[3]

The instrument is sensitive to r-f interference, and some line filtering must be used. Precautions are necessary with the high voltage insulation to eliminate leakage counts. These disadvantages of the described counter are common in all proportional counter work, and in general, they have produced little difficulty in successful operation of the instrument.

The authors wish to acknowledge the interest and advice of many of the members of the laboratory, and the suggestion of Dr. Vaughan T. Bowen and Dr. Jacob Sacks of placing the counter cathode within the crucible.

---

[3] The authors are grateful to Dr. J. Sacks for the data which is not corrected to any standard reference source.

THE REVIEW OF SCIENTIFIC INSTRUMENTS VOLUME 20, NUMBER 5 MAY, 1949

Ionization Flame Detectors[1]

HARTWELL F. CALCOTE[2]
Frick Chemical Laboratory, Princeton University, Princeton, New Jersey

(Received April 23, 1948)

Two new ionization methods of detecting flames are described for use in the measurement of flame speeds. In one the loading characteristics of a high frequency oscillator are utilized by causing the flame to pass through an oscillator tank coil. The second method employs the flame conductivity by placing two ring electrodes around the exterior of a combustion tube, and applying a d.c. voltage across them through a large series resistance. The voltage pulse created by either method when the flame passes the detector is used to trigger an electronic chronoscope.

Both methods have the distinct advantage over previous methods of flame detection in that the direct measurement of flame speeds can be made without the introduction of electrodes or wires into the combustion tube. The oscillator detector has the additional advantage that the point at which the measurement is made can be varied at will.

INTRODUCTION

SINCE the publication in 1883 by Mallard and Le Chatelier[3] of the photographic method of determining flame velocities in tubes, various methods of flame detection for the purpose of measuring flame velocities have been developed. In some cases these were necessitated by the low luminosity of the flame while others were developed as a matter of convenience to avoid the development of film. Thus far all such methods require the presence of electrodes or similar pick-up elements inside the combustion tube, which is undesirable because of the possibility of distorting the flow of flame gases and thus altering the flame velocity.[4]

In both the "spark method"[5] (in which a pair of electrodes, charged just below the sparking potential, are discharged by the high degree of ionization in the flame gases), and in the "flame conductivity method"[6] (in which the ionization in the flame causes an increase in current between two electrodes) it is necessary to have metal probes in the tube. In the "method of melting screen wires"[7] (in

---

[1] The work described in this paper was done in connection with Contract NOrd 7920 with the United States Naval Bureau of Ordnance, as coordinated by the Applied Physics Laboratory, The Johns Hopkins University, and with Contract N6-ori-105 with the ONR, U. S. Navy.

Acknowledgment is also due to Dean Hugh S. Taylor who has general supervision of this project and to Professor Robert N. Pease.

[2] Present address: Experiment Inc., P. O. Box 1-T, Richmond, Virginia.

[3] E. Mallard and M. H. Le Chatelier, Annales des Mines 8, 274 (1883).

[4] L. Khitrin, Tech. Phys. U.S.S.R. 4, 110 (1937); H. F. Coward and F. J. Hartwell, J. Chem. Soc. 132, 2676 (1932).

[5] W. A. Bone, R. F. Fraser, and D. A. Winter, Proc. Roy. Soc. 114, 402 (1927).

[6] W. Unger, Forsch. Gebiete Ingenieurw. 15, 1 (1944).

[7] H. F. Coward and H. P. Greenwald, Bureau of Mines Tech. Paper 427 (1928); R. V. Wheeler, J. Chem. Soc. 105, 2606 (1914).

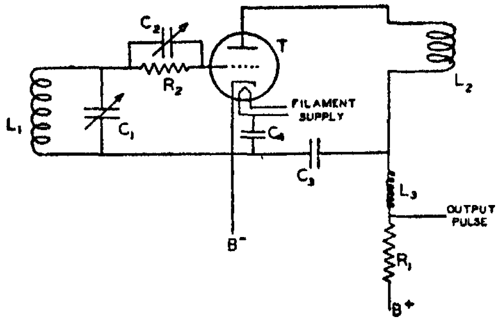

FIG. 1. Oscillator circuit; *T*, 955 Acorn tube; C_1, C_2, 25 mmf tuning condensers; C_3, C_4, 500 mmf midget mica condensers; L_1, Three turns No. 12 copper wire, ½-inch in diameter and ¾-inch long; L_2, Three turns No. 12 copper wire wound close spaced around the reaction tube (28 mm Pyrex); L_3, 2.5 mh R. F. choke; R_1, 1 megohm resistance; R_2, 0.5 megohm resistance. The filament and plate voltages were obtained from an electronically regulated power supply.

which an electric circuit is broken when the hot flame melts a thin wire) it is not only necessary to have a thin wire stretched across the inside of the tube, but it is also necessary that after each measurement the screen wires be replaced.

Two novel methods of flame detection have been developed by the author which avoid these difficulties. In both methods the passage of the flame through the detector generates an electrical pulse which can be used to trigger an electronic chronoscope, or can be used as a time-marker on an oscilloscope screen. One detector utilizes the loading characteristics of a high frequency oscillator; the other relies upon the small change in impedance between two metal rings around the exterior of the combustion tube.

I. THE HIGH FREQUENCY OSCILLATOR AS A FLAME DETECTOR

An increase in ionization of the gas within a coil through which a high frequency current is passing will cause an increase in the absorption of energy from the oscillator, effectively lowering the *Q* of the coil. The coil can be wound around the tube through which the flame is propagated, and, in addition to avoiding the introduction of probes, the coil can be simply moved from one point on the tube to another so that measurements are not confined to one region of the tube. In the measurement of flame speeds two such oscillators are used to trigger a chronoscope "on" and then "off."

Similar applications of loading tank coils to detect ionization have recently been made in electrolytic solutions. Bradhurst[8] used a Hartley oscillator with the tank coil wound around a sector of glass tube in a "decant line." Oscillations were obtained when oil passed through the coil but stopped when a conducting acid entered. Jensen and Parrack[9] used a tuned plate—tuned grid oscillator with the tank coil of the oscillator wound around a titrating flask. The change in plate current due to loading was used as a measure of the change in solution conductivity.

TABLE I. Comparison of oscillator and two-ring detectors.

3.13% *n*-butane in air		
	Peak pulse voltage	
Pressure mm Hg	Oscillator detector[a]	Two-ring detector
150	9.0	—
200	8.0	4.5
300	8.5	—
500	10.	4.3

[a] Not "motorboating."

Circuit Considerations

Since this application of an oscillator depends on the loading of the circuit, i.e., on an increase in the dissipation of energy in the tank coil, it is important that: (1) the normal circuit losses be negligible and (2) the circuit be sensitive to any change in loading of the tank coil. Both requirements demand a high *Q* circuit.[10] In addition, the second requirement suggests that the inductance in the tank circuit should be large compared to the capacity.

Assuming the same type of argument for losses in a conducting flame as for eddy current losses in an iron core transformer,[11] the power loss will be proportional to the square of the frequency so that high frequencies will be required. Yet as the frequency is increased, the effective *Q* of the coil is decreased because of the skin effect so that in practice a compromise must be obtained between the two effects.

The above considerations can be fulfilled by many types of oscillators. However, in addition to changing the efficiency of oscillation, changing the equivalent resistance in an LCR circuit will also change the frequency of oscillation. Therefore additional advantage may be taken of the change in frequency due to a change in the effective resistance of the coil. This can be done by using an oscillator with more than one tuned circuit, such as a tuned plate-tuned grid oscillator. Greater sensitivity could be obtained by placing a crystal in the circuit but this was found unnecessary.

---

[8] J. W. Bradhurst, J. Sci. Inst. 21, 108 (1944).

[9] F. W. Jensen and A. L. Parrack, Ind. Eng. Chem. Anal. Ed. 18, 595 (1946).

[10] A high *Q* means a reduction in time resolving power due to the flywheel effect in a tuned circuit. Therefore if *Q* is made very high a flame which is in the detector for only a short time might give a weak pulse.

[11] See for example: A. S. Langsdork, *Theory of Alternating Current Machinery* (McGraw-Hill Book Company, Inc., New York, 1937) p. 246.

Description and Operation of Oscillator

A tuned plate-tuned grid oscillator, Fig. 1, was used with the plate tank coil wound close-spaced around the reaction tube. In order to obtain the maximum L/C ratio no additional capacity was placed in parallel with this coil, the stray capacity and plate-to-cathode capacity of the tube being utilized. The resulting frequency was approximately 65 megacycles when a 6J5 tube was used and 100 megacycles with a 955 acorn tube.

The coil and circuit components were mounted together to avoid any unnecessary losses in the lead from the coil to the oscillator. The Lucite mounting was supported by a steel rod parallel to the Pyrex combustion tube, thus permitting the measurement of flame speeds over any section of the combustion tube by merely moving the coil and oscillator along the tube.

Tuning of the oscillator was achieved by tuning C_1 for a maximum voltage drop across R_1 or a minimum current in the plate circuit. C_2, which controls the feedback, was then adjusted until the circuit went "in" and "out" of oscillation easily.

The circuit values are not critical, although maximum sensitivity will be obtained when R_1 is as large as feasible. In order to obtain a high Q for the over-all circuit, C_1 should be large compared to L_1, and R_2 should be large. The value of R_2 is usually limited by the fact that when it becomes excessively large the time constant of R_2C_2 will cause the grid bias to build up until the phenomena known as "motorboating" takes place. Although in most oscillators this cannot be tolerated, in this application "motorboating" at a frequency sufficiently high to be filtered out by the choke coil, L_3, is not objectionable. It has, in fact, been found to increase the sensitivity considerably.

With a power supply voltage of 400 volts the d.c. voltage at the point "output pulse" was 35 volts and a pulse of approximately 4 volts peak was obtained. When "motorboating" was allowed the d.c. voltage was 80 volts, and the pulse voltage was approximately 15 volts peak. A few other typical results are recorded in Table I. The pulse shapes were dependent upon the flame, usually having a sharp leading edge with a rather ragged decay.

II. TWO-RING FLAME DETECTOR

A much simpler system for detecting ionization in flames consists of two aluminum foil electrodes wrapped around the outside of the Pyrex combustion tube, a large resistance, and a source of d.c. voltage. The experimental arrangement is shown in Fig. 2.

Theory of Operation

The detector does not act due to a change in the capacity between the electrodes as one might at first assume. An analysis of the circuit shows that, if this were so, a decrease in capacity due to ion formation would produce a positive pulse. The pulse actually obtained is negative as seen on a cathode-ray oscilloscope screen and as deduced from its ability to trigger the electronic chronoscope used.

The two-ring detector may be assumed to depend for its operation upon the momentary migration of charged particles (ions and electrons) in the electric field between the electrodes. The equivalent electrical circuit would then be as shown in Fig. 3. The two condensers are formed by the two metal electrodes, M, and the glass surface, S, inside the tube opposite each electrode.[12] The resistance R' represents the resistance between the two inner glass surface "condenser plates." With no flame in the detector, R' will be determined by the surface resistance of the glass and will be very large. The

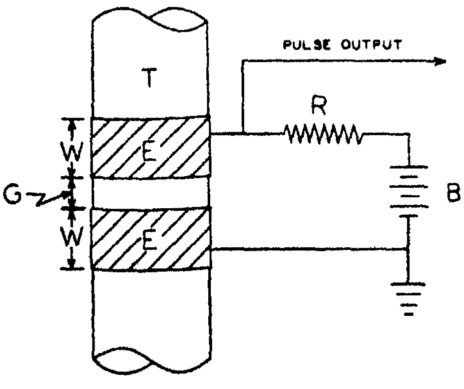

FIG. 2. Two-ring detector; *T*, combustion tube; *E* electrode; *W*, width of electrode; *G*, gap space; *R*, 7 or 10 megohm resistance; *B*, regulated power supply, 350–700 volts.

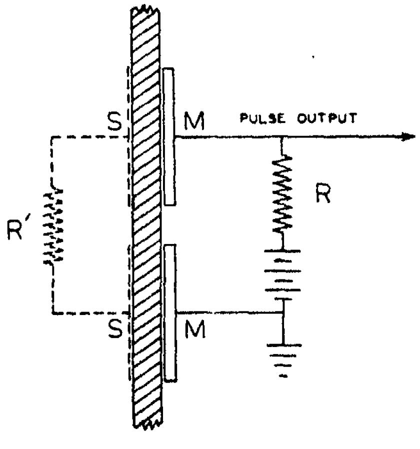

FIG. 3. Equivalent circuit for two-ring detector.

---

[12] Compare the theory of ozonizer action. G. Glockler and S. C. Lind, *The Electrochemistry of Gases and Other Dielectrics* (John Wiley & Sons, Inc., New York, 1939), p. 35.

TABLE II.

3.13% *n*-butane in air at 200 mm pressure
$E = 700$ volts $R = 10$ megohms

Electrode width W, cm	Gap space G, cm	Peak pulse voltage
0.7	0.1	2.0
1.9	0.1	3.8
5.6	0.1	4.5
5.6	0.2	4.8
5.6	0.5	3.3

TABLE III.

3.13% *n*-butane in air at 200 mm pressure
$R = 7$ megohms, $W = 1.0$ cm, $G = 0.1$ cm

Voltage across detector, E	350	600	700
Peak pulse voltage	0.42	1.4	1.5

presence of ions in the flame will reduce this resistance when the flame passes through the detector, so that a very small current, approximately 10^{-6} ampere, will flow in the circuit, producing a voltage drop of the proper sign across R.

Characterization of Detector

A few preliminary observations of the effect of varying certain parameters on the size and type of pulse obtained from the detector were made. Since the pulse was taken from across a 10 megohm resistance, and the input of the C. R. O. used to observe the pulse was only 1 megohm, a cathode follower was used as an impedance matching device.

The effect of varying the electrode width and the gap space is shown in Table II. The output voltage increases with increasing electrode width and decreases with increasing gap width, possibly going through a maximum.

The effect of the power supply voltage is demonstrated in Table III. An increase in power supply voltage causes an increase in the output pulse voltage.

In a *n*-butane-oxygen mixture at a considerably lower pressure the output pulse is much larger than in the air mixtures above. A mixture of 15.5 percent *n*-butane in oxygen at 42 mm of Hg pressure, with the detector described in Table III ($E = 600$ volts), gave a voltage pulse of 18 volts.

The flame speeds in the air mixtures were of the order of 60 cm/sec. and the pulse width at the base approximately 40×10^{-3} sec.; the pulses came to a point and were symmetrical. Several times, particularly at higher pressures, two pulses were observed. In the oxygen mixture the flame speed was approximately 9000 cm/sec. and the electrical disturbance was actually a group of very sharp pulses over a period of approximately 40×10^{-3} sec.

Comparison of Detectors

A comparison of the two-ring flame detector with the high frequency oscillator detector is presented in Table I. Although the two-ring detector has the advantage of simplicity, it is less sensitive than the oscillator detector and has the disadvantage of requiring high voltages which in some instances appeared to give a slight vibration to the flame. Nevertheless, flame speeds measured by the two methods agreed within an experimental error of less than 2 percent.

Other applications readily suggest themselves for these devices. For example, they might be used as "combustion protection control"[13] or the oscillator detector might be used as a quantitative measure of gaseous ionization in the range of 10^8 ions/cc[14] and higher.

---

[13] D. A. Campbell, Instruments 18, 868 (1945).

[14] This is the value most generally given for the ion concentration in flames. See for example: H. A. Wilson, Rev. Mod. Phys. 3, 156 (1931); T. Heumann, Spectrochim. Acta 1, 293 (1940); H. F. Calcote, Third Combustion Symposium, Madison, Wisconsin, Sept. 7, 1948.

THE REVIEW OF SCIENTIFIC INSTRUMENTS VOLUME 20, NUMBER 5 MAY, 1949

Experiments in the Possibility of Increasing the Efficiency of Gamma-Counters*

HILDING SLÄTIS
Nobel Institute for Physics, Stockholm, Sweden

(Received January 3, 1949)

The efficiency of G-M tubes for recording γ-quanta is increased by insertion of concentric ring systems of metal between the wire and the cylinder. When the ring systems get suitable voltages, good plateaus and resolving times are obtained. The efficiency of a counter, which had 3 ring systems with 24 rings in each system, was 2.5 times that of a conventional counter of the same size. This means an increase of 6 times in $\gamma-\gamma$-coincidence measurements. The efficiency of an improved tube (see note added in proof) is 3.2 times that of a conventional counter.

I. PRINCIPLE AND CONSTRUCTION OF THE NEW GAMMA-COUNTERS

AMONG earlier attempts to increase the efficiency of γ-counters may here be mentioned only the multi-cellular γ-counter by Dumond.[1]

With the aim to raise the efficiency, some experiments have been carried out with G-M tubes, where a system of concentric rings was introduced (Fig. 1). The rings were made in three different sizes B_1, B_2, B_3 (see Table I), and all rings of the same size were held together by three axial rods (drill rod), one of which was brought out through the envelope at the end of the tube (only one of these rods is drawn in Fig. 1, namely that from the rings B_3 to the electrode W_3). The ring systems were supported by mica plates M at the ends of the cylinder C. The cylinder C and the rings were made of brass. The anode wire was of tungsten and was stretched by a spring S.

Besides a tube A of common type for comparison purposes, which did not contain any ring system, there were made three γ-tubes B, C, and D of the new type, with 12, 22, and 43 rings of each of the three sizes. The cylinders C and the glasswalls G were exactly equal for all four counters. The tubes were filled with 90-mm argon and 10-mm alcohol vapor.

II. VOLTAGES OF THE RING SYSTEMS

In order to avoid an undesirable deformation of the electric field between anode (wire) and cathode (cylinder) by introducing the ring systems, these should be kept at voltages which correspond to their place in the undisturbed electric field between wire and cylinder. The voltages, which may be given to B_1, B_2, and B_3, assuming that the voltage of the wire is V_a and that of the cylinder 0, are

$$V = V_a[\log(r_c/r)/\log(r_c/a)],$$

if r is the distance of the points considered (the ring) from the axis of the cylinders, r_a the radius of the wire, and r_c that of the cylinder. Assuming that $V_a = 1000$ volt, we obtain for the mean distances from the wire given in Table I, the voltages 179, 92, and 30 volt for the ring systems B_1, B_2, and B_3 respectively.

It was desirable to make the voltages of the ring systems change in the same proportion as the voltage of the wire. Therefore the desired voltage for the ring systems were taken from a potentiometer arrangement connected to the high tension stabilizer.

Figure 2 shows the characteristic curves of the counter C for different voltages on the ring systems. The figures in brackets indicate the voltages for the systems B_1, B_2, and B_3 respectively, for the case in which the anode voltage is 1000 volt. It is seen that the best plateau occurs for values which are in close agreement with the theoretical ones. The curve *a* shows that the plateau is very bad when the rings are at the same voltage as the cylinder. For the rest it is obvious, that a good plateau is attained also for voltages, which are only in the vicinity of the ideal values.

TABLE I. Diameter of the wire: 0.15 mm; dimensions of the cylinder: length 88 mm, thickness 1 mm, inside diameter 25 mm.

Ring system	Inside diam. mm	Outside diam. mm	Mean distance from the wire, mm
B_1	8.00	12.06	5.0
B_2	13.66	17.72	7.8
B_3	19.32	23.38	10.7

III. COMPARISON BETWEEN THE EFFICIENCIES AND RESOLVING TIMES OF THE COUNTERS

The counters were investigated for three different radiations, namely the γ-radiation from Ra, filtered

TABLE II.

Tube	Number of rings in each system	Thickness of the rings, mm	Axial distance between the surfaces of adjacent rings, mm
B	12	1	6
C	22	1	3
D	43	0.5	1.5

---

* Presented at a conference on "Problems of Nuclear Physics," September 14–18, 1948, in Birmingham, England.

[1] J. W. M. Dumond, Rev. Sci. Inst. 18, 627 (1947).

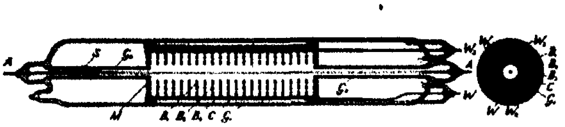

FIG. 1. The new γ-counter.

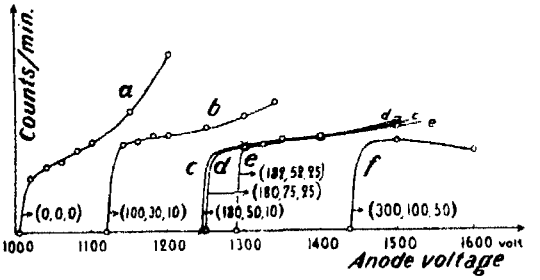

FIG. 2. Characteristic curves for the counter C. The figures in brackets are the voltages of the ring systems B_1, B_2, and B_3, respectively, when $V_a = 1000$ volts.

by 1-cm Pb (≈ 2 Mev), that from Co^{60} (≈ 1.2 Mev) as well as that from Hg^{203} (0.27 Mev). The result was that the relative efficiencies for the different counters were proportional to 100, 182, 244, and 206 for the counters A, B, C, and D, respectively.

Thus, the best result was obtained with the counter C, which contained 22×3 rings. The fourth tube D had almost the double number of rings but with half the thickness. Therefore, the absorbing matter was equal for C and D. It will be seen that the efficiency for the latter tube is a little lower, obviously because a part of the ejected electrons is absorbed in an adjacent ring before the ionization in the gas has occurred (the order of magnitude for the number of ionizations per cm is the same as the number of rings per cm).**

The resolving time for the counters A, B, and C was $(6 \pm 1) \cdot 10^{-4}$, $(1 \pm 0.5) \cdot 10^{-4}$, and $(2 \pm 1) \cdot 10^{-4}$ sec., respectively. The measurements confirm the observations of other authors[2] that the insertion of a grid increases the resolving power of a counter.

IV. THE EFFICIENCY AS A FUNCTION OF THE DIRECTION OF THE INCIDENT GAMMA-RADIATION

The efficiency of the counters was investigated for different angles φ of incidence between the γ-radiation and the "equatorial plane" of the counter. The source was a Ra sample at a distance of 120 cm from the counter. Figure 3 shows diagrammatically the result. The number of counts measured with the tubes A, B, and C are here plotted as a function (radius vector) of the angle φ. Two results of interest are to be noted: (a) the efficiency for the tubes B and C is highest at an angle of incidence 10°–20°; (b) the efficiency is diminished only slightly when φ goes to 90°. In this position, however, the tube will be seen under the smallest space angle from the sample. Hence, the efficiency per space angle is highest for $\varphi = 90°$. This is important by absorption measurements, where a canalized beam is used to reach a right angle traversing of the γ-quanta through the absorbers.

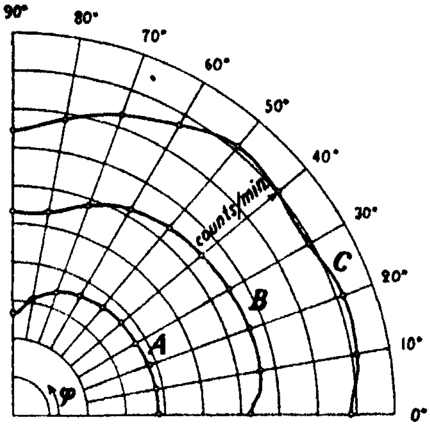

FIG. 3. The measured intensity (radius vector) of the γ-radiation as a function of the angle (φ) of incidence for the tubes A, B, and C.

A more complete description of these experiments appears in Arkiv f. Mat. Astr. o. Fys.[3]

** *Note added in proof:* This interpretation was confirmed by the following experiment. The tube D was filled with 190-mm argon and 10-mm alcohol (e.g. the pressure doubled). Furthermore, in order to prevent the necessary anode voltage from increasing due to higher pressure the central wire was replaced by one of 0.05-mm diameter. The relative efficiency of the counter was by that increased from 206 to 320, or 3.2 times that of a conventional counter of the same size (this means an increase of 10 times in γ–γ-coincidence measurements). Experiments with improved counters will be continued.

[2] W. F. Libby and D. D. Lee, Phys. Rev. **55**, 245 (1939); S. A. Korff and W. E. Ramsey, Rev. Sci. Inst. **11**, 267 (1940). Compare also S. A. Korff, *Electron and Nuclear Counters* (D. Van Nostrand Company, Inc., New York, 1946), p. 88.

[3] H. Slätis, Arkiv f. Mat Astr. o. Fys. **36A**, No. 17 (1948).

An Improved Low Angle X-Ray Diffraction Camera

BARBARA A. WRIGHT AND PETER A. COLE*
United Shoe Machinery Corporation, Research Division, Beverly, Massachusetts

(Received January 25, 1949)

A description is given of a low angle x-ray diffraction camera which incorporates both high resolution and facility in adjustment and alignment of components. A diffraction pattern of the low angle pattern of collagen photographed with this instrument is compared with a similar pattern photographed with commercially available equipment.

INTRODUCTION

THE x-ray diffraction studies of collagen which are being conducted in this laboratory have imposed rigorous instrumental requirements which are not satisfied by the available commercial equipment. The lack of adequate commmercial low angle diffraction equipment has prompted workers in this field to design x-ray diffraction cameras which would be suitable for the examination of collagen. Low angle cameras for this application have been developed by Corey and Wyckoff[1] and by Bear.[2]

The double crystal spectrometer was first used in the study of low angle scattering by Fankuchen and Jellinek[3] and has recently been applied by Kaesberg, Ritland, and Beeman[4] to a direct intensity determination of the low angle diffraction pattern of collagen, thus eliminating the difficulties encountered in photographic intensity measurements.

It would appear that the photographic method will continue to have application in exploratory work and in the study of materials which require the recording of diffraction orders of very low intensity.

It was found that a satisfactory low angle diffraction camera should incorporate the following features:

(1) Sufficient refinements to permit the recording of reflections from molecular spacings as great as 1200A.
(2) Resolution of 3 lines per millimeter at 300 millimeters.
(3) Adjustable slit-widths.
(4) A minimum of scattered radiation.
(5) Sample holder in which the material may be maintained at controlled temperature and humidity.
(6) Facility in alignment of components.

DESCRIPTION

It was desirable to use slits of adjustable width and separation to permit operation of the camera at the optimum conditions for the particular material under investigation. For this purpose, Gaertner bilateral slit mechanisms were employed. Two of the slits were used to collimate the beam. These were mounted separately on stands of adjustable height. In order to minimize the scattered radiation, special lead jaws were required which were flat and parallel to a tolerance of 0.01 mm and tapered to an edge thickness of 0.1 mm. A third slit of similar construction was also used to reduce scatter. This was attached rigidly to a chamber in which the sample was to be located. This last unit was mounted on a separate adjustable stand.

Around the cylindrical sample chamber there was wound a heating coil which operated through a variac. A layer of asbestos paper three-sixteenths of an inch thick was used as insulation for the camera. Within a quarter of an inch of the sample there was located a copper-constantan thermocouple which was connected to a Leeds and Northrup Portable Precision Potentiometer. It was possible to control the temperature of the sample to within 2°F in the range from 75°F to 200°F. Any desired humidity could be maintained within the chamber by introducing air of controlled water vapor content. The air leaving the chamber was passed through a Foxboro Humidity Recorder. With this equipment it has been possible to run a sixty-hour exposure with less than ten percent variation in the relative humidity of the air in the sample chamber.

The sample holder consisted of a pair of parallel jaws of variable separation. These jaws could be translated vertically and rotated as much as 60°

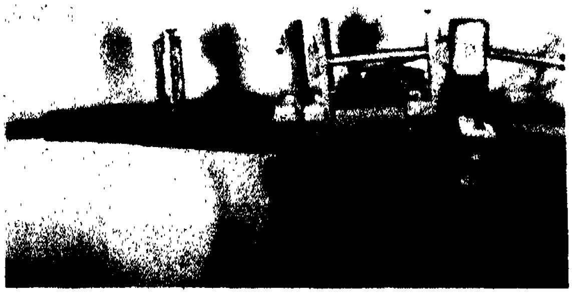

FIG. 1. Improved low angle x-ray diffraction camera.

---

[*] Present address: Dr. Peter A. Cole, National Military Establishment, Research and Development Board, Washington 25, D. C.

[1] R. B. Corey and Ralph W. G. Wyckoff, J. Biol. Chem. 114, 407 (1936).

[2] R. S. Bear, J. Am. Chem. Soc. 66, 1297 (1944).

[3] I. Fankuchen and M. H. Jellinek, Phys. Rev. 67, 201 (1945).

[4] Kaesberg, Ritland, and Beeman, Phys. Rev. 74, 71 (1948).

FIG. 2. Collagen diffraction pattern photographed with commercially available low angle camera.

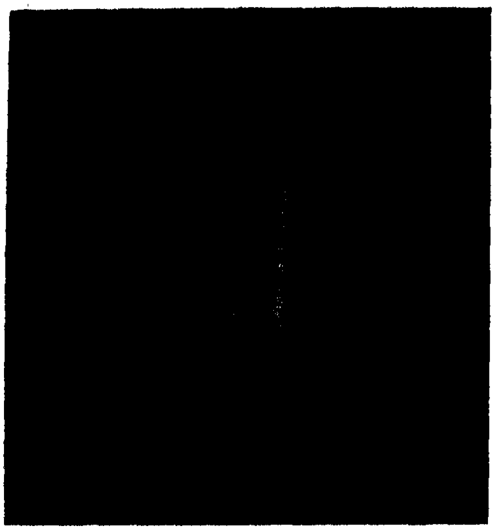

FIG. 3. Collagen diffraction pattern photographed with improved low angle camera.

in the plane perpendicular to the beam. This mechanism provided ease and accuracy in sample alignment. The x-ray beam passed through double mica windows 0.001″ thick separated by a dead air space. These windows made the chamber air tight and minimized x-ray absorption and scatter which would be caused by the condensation of water at high humidity. This construction would also permit the evacuation of the sample chamber or its operation at elevated pressures.

A fourth stand supported a film holder with a beam stop, adjustable both in height and rotation. All stands were mounted on a rigid rail one meter long. The entire assembly was attached to the diffraction unit as shown in Fig. 1. The tube which separated the collimating slits contained limiting diaphragms to reduce scatter occurring between these slits.

DISCUSSION

Figures 2 and 3 are comparable low angle x-ray diffraction patterns of collagen from kangaroo tail tendon. Both patterns were photographed with copper $K\alpha$-radiation, with a distance of 30 cm between the specimen and the photographic film, and with a separation of 30 cm between the collimating slits. For both photographs, the specimens were maintained at 100°F and 40 percent relative humidity. As calculated from the films, the fundamental spacings of both patterns was 627A.

The pattern of Fig. 2 was photographed with a commercially available low angle camera employing silver slits of 0.3-mm opening; that of Fig. 2 was photographed with the improved diffraction camera described above with the slits adjusted to a width of 0.15 mm. In Fig. 3 it is apparent that the first order has been resolved from the main beam, and that all orders are more sharply resolved than in Fig. 2. The effort required for aligning the instrument has been reduced from three hours' work and three six-hour exposures, to ten minutes' work and one six-hour exposure.

In the results of Kaesberg and his associates, the ratio of peak separation to peak width is greater than 10:1. This ratio indicates that the collagen periodicity is much more regular than has been previously supposed from published photographs of collagen diffraction patterns. Figure 3, taken with the new camera described above, provides photographic evidence which begins to approach, in resolving power, the measurements made with the double crystal spectrometer.

THE REVIEW OF SCIENTIFIC INSTRUMENTS VOLUME 20, NUMBER 5 MAY, 1949

Physical Instruments for the Biologist

Detlev W. Bronk
Associate Editor in Charge of this Section
Eldridge Reeves Johnson Foundation for Research in Medical Physics,
University of Pennsylvania, Philadelphia, Pennsylvania

A Simple Calorimeter for the Simultaneous Determination of Heat Loss and Heat Production in Animals*

LAWRENCE R. PROUTY, MARTHA J. BARRETT, JAMES D. HARDY
Department of Physiology, Cornell University Medical College, New York, New York

(Received October 18, 1948)

This paper describes a new type of gradient calorimeter which permits the rapid simultaneous measurement of respiratory metabolism and heat loss. It uses the temperature difference between the inner and outer aspect of a fixed transitional layer of air rather than adiabatic principles. (W. O. Atwater and F. G. Benedict, "A respiration calorimeter with appliances for the direct determination of oxygen," Publication 42, Carnegie Institute of Washington (1905); G. Lusk, Arch. Int. Med. **15**, 793 (1915); E. F. DuBois, *Basal Metabolism in Health and Disease* (Lea and Febiger, Philadelphia, 1936), third edition; Forester, Ferris, and Day, Am. J. Physiol. **146**, 600 (1946); L. Love and H. C. Bazett, Fed. Proc. **7**, 74 (1948); C. P. Yaglou, "Thermal insulation of clothing," unpublished data; T. Benzinger, personal communication.) Application of gradient principles to calorimetry so simplifies heat loss determinations that they become the easiest and most accurate part of the procedure.

DESCRIPTION OF CALORIMETER

Measurement of Heat Production

THE apparatus used for metabolic studies is shown in Fig. 1. Outdoor air is drawn into the system through bottles (*A* and *B*) containing soda lime and sulfuric acid for the removal of carbon dioxide and water vapor, respectively, and then, into the respiration chamber through the air inlet (*C*). The calorimeter proper is composed of two concentric sheet copper (0.02-inch thick) cylinders (*D* and *E*). The animal is placed in a covered wire cage which is thermally insulated from the inner cylinder. The cage rests upon a pan containing a small quantity of mineral oil for the collection of excreta. The calorimeter sets upon rubber insulators on an activity platform for recording animal movements. As the air passes from the calorimeter through the outlet (*H*), aliquot samples are taken for the determination of respiratory metabolism, by means of a Barker gas sampling device.[1] Samples thus received into a master cylinder are transferred to a second sampler which can be attached directly to the Carpenter gas analysis apparatus,[2,3] for the quantitative estimation of carbon dioxide and oxygen. Heat production can be calculated by the usual methods of indirect calorimetry.

Measurement of Heat Loss

An animal placed inside the inner copper cylinder of the calorimeter will lose its heat by radiation and convection to this cylinder. The heat loss by evaporation was measured by collecting and weighing the moisture given off by the animal. The heat loss due to radiation, conduction, and convection is for the most part absorbed by the copper wall of the inner cylinder. There is, however, a small amount of heat which is carried out by the air stream and for which correction must be made. As the inner cylinder is always warmer than the outer cylinder, there will be a transfer of heat between them, and the rate of exchange will be directly proportional to the temperature difference between the two cylinders. That is,

$$Q=K(T_1-T_2), \qquad (1)$$

where $Q=R+C+D$, K = the heat flow constant, T_1 = temperature of the inner cylinder, T_2 = temperature of the outer cylinder. Providing the conditions between the two cylinder walls remain fixed, K is a constant and can be determined experimentally by measuring the other factors in Eq. (1). K, the heat flow constant, thus depends upon the construction of the calorimeter, and it is essential, having once calibrated the instrument, to allow no alteration of conditions between the calorimeter walls. Changes in position of the animal inside the calorimeter have no effect on K, as it is affected only by changes between the calorimeter walls. The use of the outer calorimeter cylinder makes it unnecessary to have a constant temperature room such as was required for the calorimeter described by Day and Hardy.[4]

---

* This research was supported in part by funds from ONR.

[1] S. B. Barker and E. Smyth, "A mechanical pump for the drawing of gas samples," Proc. Soc. Exper. Biol. and Med. **38**, 745 (1938).

[2] Carpenter, Fox, and Sereque, "The Carpenter form of the Haldane gas analysis," J. Biol. Chem. **83**, 211 (1929).

[3] T. M. Carpenter, "An apparatus for the exact analysis of air in metabolism investigations with respiratory exchange chambers," J. Metab. Res. **4**, 1 (1923).

The calorimeter is shown in more detail in Fig. 2. The two concentric copper shells (*A* and *B*) are separated by an air layer one centimeter in width, this separation being rigidly maintained by small rubber insulators. The inner chamber contains a wire cage, fourteen centimeters in height and twenty-two centimeters in diameter, which will accommodate a full-sized cat. Thermocouples, (*D* and *E*) placed in the air inlet and outlet, give the temperature of the air as it enters and leaves the chamber. The top of the inner shell (*H*) is machined to fit tightly and is made air-tight by a seal of stopcock grease. The top of the outer shell (*I*) need not be air-tight as long as there is no appreciable circulation of air between the walls from outside sources.

An electric fan in fixed position is turned directly on the calorimeter. This assists in maintaining the outer shell at room temperature and eliminates the thermal effects of experimenters moving in the neighborhood of the calorimeter. The outer cylinder together with the electric fan thus acts as a heat absorber of large capacity insofar as the movement of heat from the inner wall is concerned. Thermocouples connected in parallel are attached to the surfaces of the inner and outer copper cylinder. These sets of thermocouples can be balanced one against the other to determine temperature difference between the calorimeter walls as shown in Fig. 3. The thermocouples for the inner shell are also arranged to be balanced against a reference standard in order to determine the actual temperature of this inner shell. This is important in making corrections for the heat capacity of the calorimeter. Thermocouples for determining body and skin temperature of the animal are admitted through a latex seal situated just below the air outlet (*I*, Fig. 1).

Electrical Circuit

Figure 3 shows a diagram of the potentiometric circuit used. All temperatures are taken with

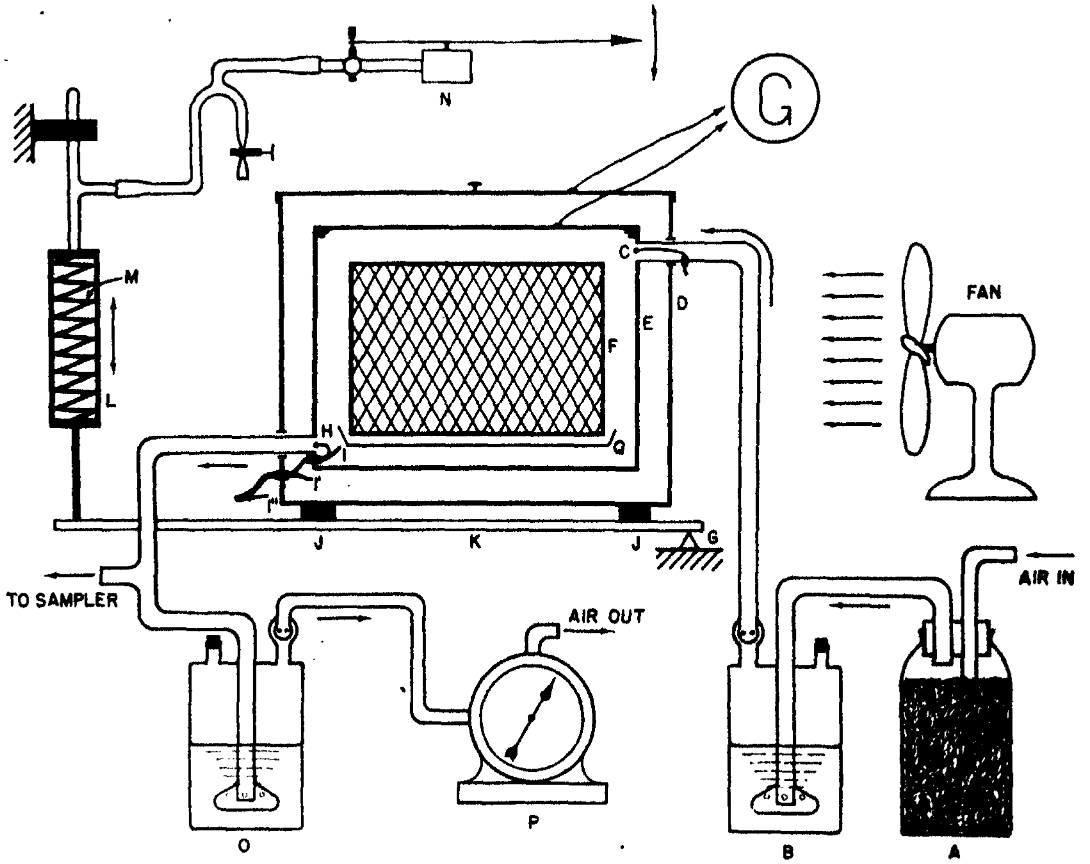

FIG. 1. Small animal calorimeter circuit. *A*—soda lime bottle; *B*—H_2SO_4 bottle; *C*—thermocouple in air inlet; *D*—outer shell; *E*—inner shell; *F*—wire cage; *G*—fulcrum; *H*—thermocouple in air exit; *I*, *I'*, *I''*—animal inner and outer shell thermocouple leads, respectively; *J*—rubber insulators; *K*—activity platform; *L*—rubber tubing; *M*—coil spring; *N*—tambour for pneumographic activity recorder; *O*—H_2SO_4 bottle; *P*—air flow meter.

---

[4] R. Day and J. D. Hardy, "A calorimeter for measuring the heat loss of premature infants," Am. J. Dis. Child. **63**, 1086 (1942).

copper-constantan (size No. 28 wire) thermocouples connected as shown, the solid lines representing copper and the broken lines constantan leads. The minimum requirements for the circuit are a sensitive galvanometer, a dependable slide wire, and a standard cell or meter to insure a constant, known current input. A milliammeter** is used in this case and is more useful than a standard cell because the current input could be altered as desired.

CALIBRATION PROCEDURES

Electric Checks

The heat flow constant, K, is determined by introducing a known amount of heat into the calorimeter and, following establishment of thermal equilibrium, measuring the temperature gradient between the walls, over the range of heat loss value expected during animal experimentation. A ten-watt electric bulb is used as a source of heat, with suitable provisions for shielding, as described by Day and Hardy.[4] The shielding provides more equal distribution of heat in the calorimeter and thereby simulates more closely the situation applicable to an experimental animal. A carefully standardized ammeter and voltmeter are used to measure the heat input. No air was circulated through the calorimeter during the electric checks.

At equilibrium for an electric check we have

$$H=K\times(T_1-T_2), \qquad (2)$$

where $H=0.432\times\text{volts}\times\text{amperes}$ (kg cal./$\frac{1}{2}$ hr.), K = heat flow constant, T_1 and T_2 = temperature of inner and outer walls, respectively. The experimental periods are one-half hour in length as the thermal response time of the lamp and calorimeter system is such that sixty-six percent of thermal equilibrium is obtained in approximately that time. The heat input for this series of electric checks varied from 1.2 to 2.3 kg cal. per half-hour. The temperatures of the inner and outer shells are taken at ten-minute intervals and the average gradient during a half-hour period computed. In order to eliminate the factor of heat storage in the calorimeter, only those periods during which the system is near equilibrium are used to calculate the heat flow constant. Heat input is plotted as a function of the temperature gradient between the inner and outer shells, and is expressed in drum divisions (Fig. 4). The relationship is linear, and the heat flow constant, measured by the slope of the line, is equal to 0.0181±0.004 kg cal. per drum division for a half-hour period.

The value of K is independent of the environmental temperature and the rate of heat loss. It is dependent, however, on the physical situation of the calorimeter relative to its surroundings. Should the position of the calorimeter be changed, particularly with respect to the electric fan, it is necessary to redetermine the constant. The value of K will also shift if the arrangement of thermocouples on the walls of the cylinders is altered. Physical changes made within the inner shell will not affect the heat flow constant, but will alter its heat capacity.

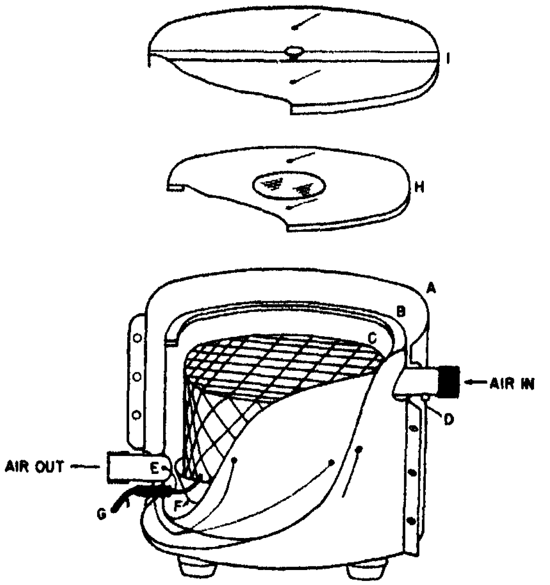

FIG. 2. Cutaway view of small animal calorimeter. *A*—outer shell; *B*—inner shell; *C*—wire cage; *D*—ingoing air thermocouple lead; *E*—outgoing air thermocouples; *F*—oil pan; *G*—thermocouple leads emerging from latex seal; *H*—inner top; *I*—outer top.

The time required for the inner and outer shells to adjust to thermal equilibrium is fifty minutes. Figure 5 shows the temperature changes in the inner and outer shells as well as the changes in thermal gradient and room temperature. It will be noticed that the thermal gradient becomes level fifty minutes after the heat is turned on, although the temperatures of the inner and outer shells continue to rise due to increase in room temperature. Forty minutes after the heat was turned on, the room temperature dropped from 23.3 to 22.8°C, and this produced a change in the temperature of the inner and outer shells as indicated. The effect upon the gradient (lower curve, Fig. 5) is less marked, although it will be seen that errors will be introduced into the measurements of heat loss if rapid changes in room temperature occur during an experimental period. Thus, although, as stated above, a constant temperature room is not required for this calorimeter, it is important that rapid changes in room temperature be avoided. To the right in Fig. 5 are shown the results of an experiment in which the effects of room temperature

---

** Weston, Model No. 62.

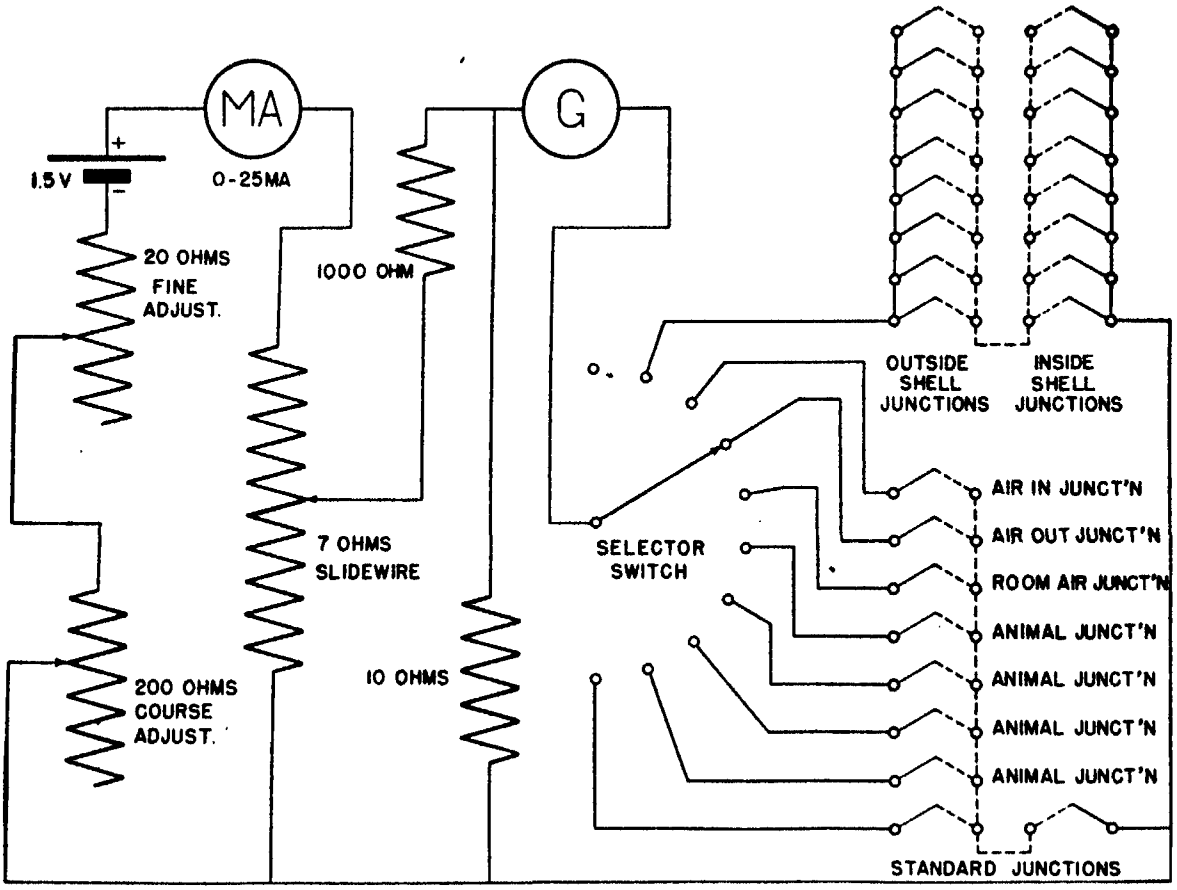

FIG. 3. Electrical circuit diagram. Thermo-junctions on right, potentiometric circuit on left.

changes are pronounced. The heat input during this experiment was maintained at a constant level, and just before the end of the experiment, the room temperature rose 1.6°C in twenty minutes. As this produced a more rapid change in the temperature of the outer shell than of the inner shell, there was an apparent fall in the thermal gradient, indicating a decrease in heat input which did not occur.

Determination of Heat Capacity of Calorimeter

When equilibrium conditions are not present, a correction must be made for the heat which is stored in the walls of the calorimeter. The heat given off by a source within the calorimeter then becomes:

$$H=K(T_1-T_2)\pm S, \qquad (3)$$

where S represents kilogram calories stored, and may be positive if the calorimeter is retaining heat, or negative if losing heat. Both the inner and outer walls may theoretically contribute to this storage factor. In practice, however, it has been found that since the outer shell follows the room temperature so closely, it stores very little heat which is attributable to the source within the calorimeter. The heat storage in the outer wall has been calculated in a large series of experiments, and in every case has been found to represent less than one percent of the total heat loss. Thus, the total storage may be considered as being derived from heat gained or lost by the inner wall.

The thermal capacity of the calorimeter and its contents was estimated from the sum of the weights and specific heat of the copper, rubber, and glass of which the calorimeter and calibrating equipment were constructed. It can also be measured from experiments in which the temperature of the calorimeter is allowed to change. The equation for heat loss by the calibrating lamp for such test periods is

$$H=K(T_1-T_2)+C(T_e-T_b). \qquad (4)$$

In this equation the last term represents the heat stored, S, the thermal capacity of the calorimeter being C. T_e and T_b are the temperatures of the inner and outer shell at the end and beginning of an experimental period, respectively. As pointed out above, K is determined for experimental periods during which there is thermal equilibrium and thus, the storage term is zero. Therefore, K can be used in Eq. (4) to determine the value of C.

The average value for C as determined for twelve experimental periods is 0.39, ±0.02 kg cal. per degree, a value which agrees with the one estimated on the basis of the weights and specific heats of the component parts.

Alcohol Checks

The equation for the heat loss from the alcohol lamp is

$$H = K(T_1 - T_2) + C(T_e - T_b) + 3.1 \times 10^{-4} V \times (T_0 - T_i) + 0.584w, \quad (5)$$

in which the symbols have the same meaning as in Eq. (4) except for V, which is the volume of air passing through the calorimeter during an experimental period, and w, which is the water collected in the sulfuric acid bottles. The last two terms of Eq. (5) represent the heat carried out of the calorimeter by the stream of ventilating air and the heat due to water vapor, respectively. Analyses of gas samples are the most tedious part of the experimental routine and are usually deferred until the day following the experiment or other convenient time, as the cylinders containing gas samples may be stored for several days without change or danger of contamination.

Table I contains the values obtained from six experiments, each experiment consisting of three half-hour periods. The average deviation from the theoretical heat production is +1.7 percent for the measurement of heat loss and −0.1 percent for heat produced. Close agreement between indirect and direct calorimetry indicates that all constants were accurately determined.

Operation of the Calorimeter

In the experimental routine a fasted animal which has been shaved several days prior, is brought to the laboratory about an hour before being put into the calorimeter. Thermocouples are placed on several parts of the body and in the rectum. The animal is weighed and placed in the cage inside the respiration chamber. The top is placed on the calorimeter, the air flow is started, and the first observation period is begun, not sooner than thirty minutes later. At this time the calorimeter begins to approach equilibrium and the experiment is begun. The calculations in a sample observation follow:

February 19, 1948—Cat *A*, fasted eighteen hours, weight—1750 g.

A. Average temperature during half-hour period

1. Calorimeter	30.18°C
2. Rectal	38.57°C
3. Skin (average)	37.42°C

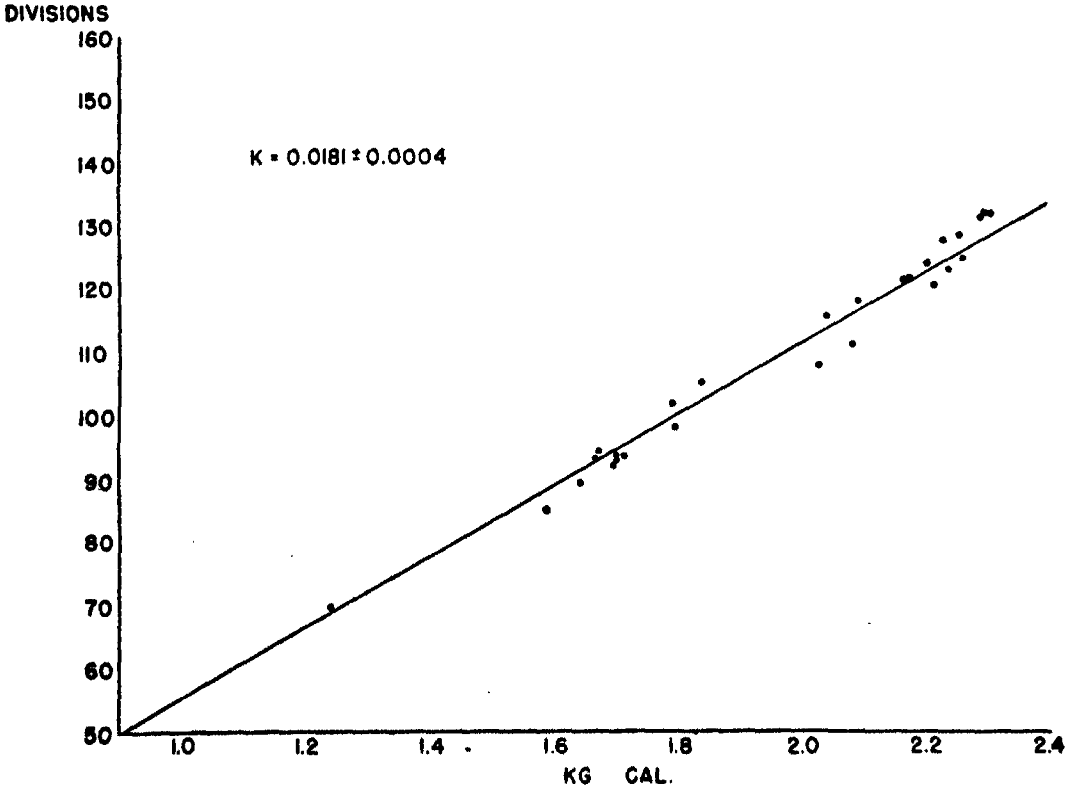

FIG. 4. Plot of heat input to calorimeter in electric check in kilogram calories per half-hour against slide wire drum divisions (to convert °C, multiply by 0.026) to obtain the heat flow constant, *K*.

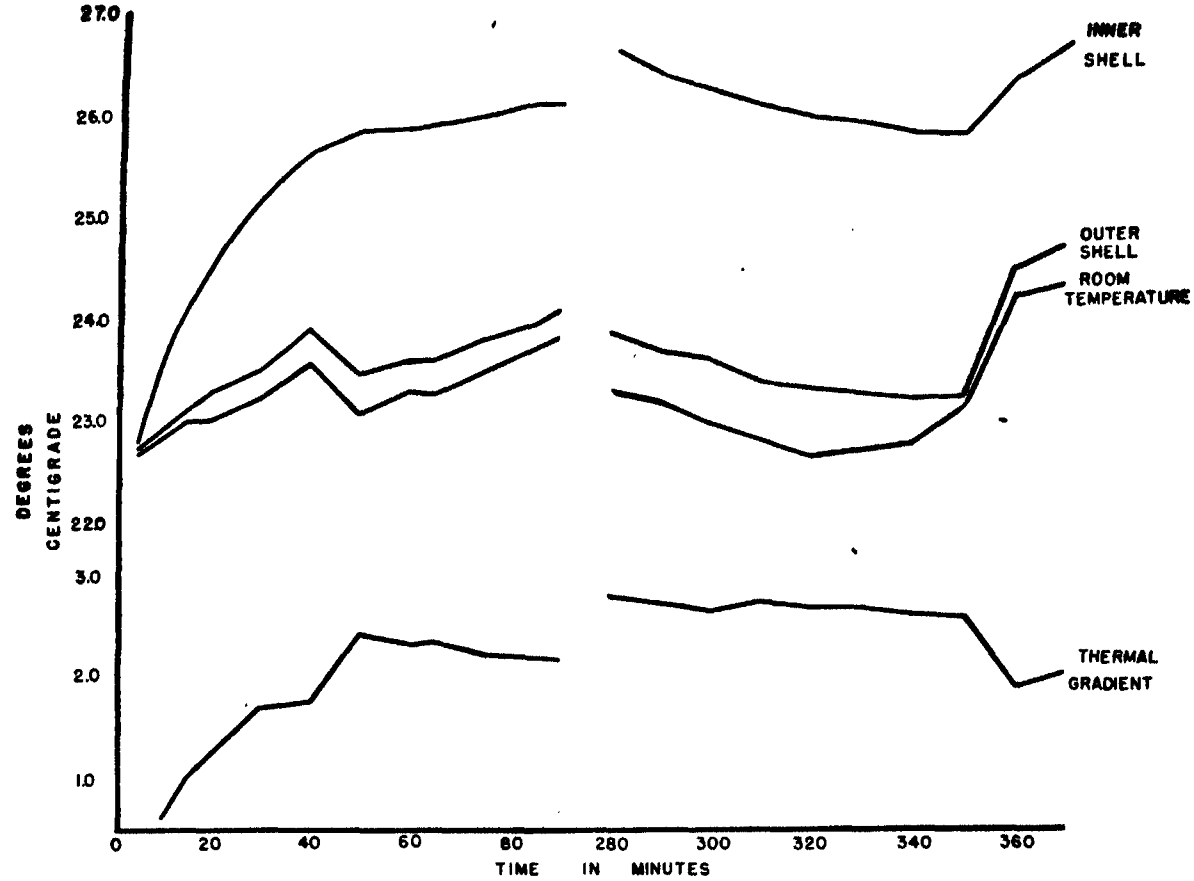

FIG. 5. Inner shell and outer shell temperatures and thermal gradient for two experiments. A. Thermal response of the calorimeter, heat source turned on at time zero. B. Thermal gradient changes for an experiment during which an abrupt change in room temperature of 1.60°C occurred in 20 minutes.

B. Room temperature

1. Beginning of period	27.68°C
2. End of period	27.90°C
3. Change during period	+0.22°C

C. Heat loss

1. To thermal gradient

$H=K(T_1-T_2)$

$=0.6958^{***}(30.20°\text{C}-28.04°\text{C})$

$=1.503$ *Calories*

2. To calorimeter storage

Storage = thermal capacity of calorimeter (T_a-T_b).

$S=0.4(30.36-30.00)=0.144$

3. To circulating air

$A=\Delta T_{\text{air}}\times$ specific heat air $\times 0.026\times$ liters

$=119.8\times 3.1\times 10^{-4}\times 0.026\times 64.1=0.062$ *Calories*

4. To vaporization

$H_v=L\times w$

L = latent heat of vaporization at skin temperature of cat plus heat of expansion and cooling to calorimeter humidity and temperature.

w = weight of water evaporated

$H_v=0.612\times 0.677=0.414$ *Calories*

5. To animal heat storage

$S_{\text{animal}}=$ specific heat $\times$ weight $\times\Delta T_{\text{animal}}$

$=0.83\times 1.75\times 0.07=0.10$ *Calories*

Total metabolism as determined by direct heat method

$H=1.503+0.144+0.062+0.414+0.10=2.22$ *Calories* ½ hr.

D. Heat production

Total metabolism as determined by indirect heat method +*2.20 Calories* ½ hr.

TABLE I. Summary of alcohol checks. Direct and indirect calorimetry values are compared with the theoretical value obtained from amount of alcohol burned.

Date	R.Q.	Direct calorimetry Cal./hour	Direct calorimetry percent	Indirect calorimetry Cal./hour	Indirect calorimetry percent	Theor. Cal./hour
11/14/47	0.657	4.26	+1.4	4.36	+3.8	4.20
12/3/47	0.671	9.46	+1.2	9.20	−1.7	9.36
12/8/47	0.666	8.94	+0.7	8.78	−1.2	8.88
12/11/47	0.665	9.40	+5.6	8.76	−1.5	8.90
12/16/47	0.658	10.04	−0.1	10.06	0.0	10.06
12/29/47	0.659	11.68	+1.3	11.52	0.0	11.52
Average	0.663		+1.7		−0.1	

SUMMARY

A simple heat flow or "gradient type" calorimeter is described, based upon the principle that heat loss by a body contained within two concentric thermally conductive cylinders insulated from one another, will be proportional to the temperature

---

*** *K* here has a value for use with shell temperatures in °C.

gradient between the cylinders. An instrument large enough to contain a full-sized cat, used in connection with the gas sampling apparatus described by Barker, was constructed and tested. The calorimeter may be used with any other satisfactory method of measuring the respiratory quotient.

Electric and alcohol checks were carried out for half-hour periods. The precision of the calorimeter is ±2 percent for an individual period under favorable conditions.

Complete procedure for obtaining heat loss and heat production is described, together with sample calculation for an animal experiment.

The advantages of the calorimeter are: (1) Adequate precision is obtained with inexpensive construction and simple measuring equipment. (2) Rapidity of response permits short experimental periods. (3) Simplicity of operation permits one observer to carry through the complete procedure. (4) It is flexible in application, particularly with regard to study of heat loss and heat production at different environmental temperatures for animals of any size.

Laboratory and Shop Notes

A New Vacuum Gauge

CARLTON F. JOHNSON
Ordnance Research Laboratory, Pennsylvania State College, State College, Pennsylvania
March 8, 1949

OBSERVATIONS have been made in this laboratory on the variation of the motional impedance of a magnetostrictive transducer with air pressure on the face of the transducer.

As is generally known[1] both the resistive and reactive components of a transducer's impedance vary rapidly near the resonant frequency, and often represent a considerable departure from the off resonance, or clamped impedance. If a transducer is series tuned, its impedance at resonance is essentially resistive. The value of its radiation resistance at resonance is a function of the mass density and the velocity of sound of the medium into which the transducer is radiating. Thus, the electrical impedance of a transducer radiating into air should vary with the air pressure. Measurements made in this laboratory on a scroll type magnetostrictive transducer operated at approximately 63.1 kilocycles indicate that this is so, and the change in voltage across the transducer windings (a measure of its electrical impedance) appears to be linear with changes in pressure from atmospheric pressure to a pressure of a few millimeters of mercury.

The transducer and its series tuning capacitance are made one arm of a resistance bridge as shown in Fig. 1 so that when the bridge is balanced, only the *change* in voltage across the tuned circuit is measured. In the present case, when the bridge is fed at a level of about 2.5 volts r.m.s., the bridge can be balanced, at atmospheric pressure, to about 10 millivolts, and at a pressure of less than 10 millimeters of mercury the maximum bridge unbalance amounts to about 80 millivolts. When a pressure of about 1 millimeter of mercury is reached, the bridge unbalance decreases by about 10 millivolts as shown in Fig. 2 to the limit of the roughing pump used. The cause of this reversal is not explained, since accurate estimation of the ultimate degree of vacuum attained has not yet been attempted.

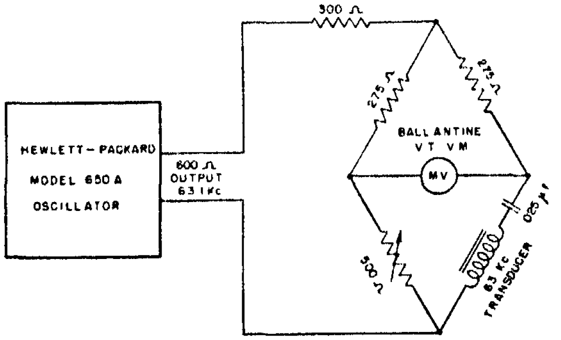

FIG. 1.

The transducer used was originally designed to work in water, hence a considerably greater effect might be measured with one designed to work in air, i.e., one which would be more loaded by air than is the present one. Lower frequency transducers could also probably be used more advantageously, provided that the frequencies chosen were high enough to avoid standing wave effects from reflections of the sound in the vacuum system. However, the standing wave effect would probably be negligible at low pressures. One advantage of the present transducer is that no standing wave effects are apparent in air owing to the relatively small amount of power radiated into the air at the frequency used.

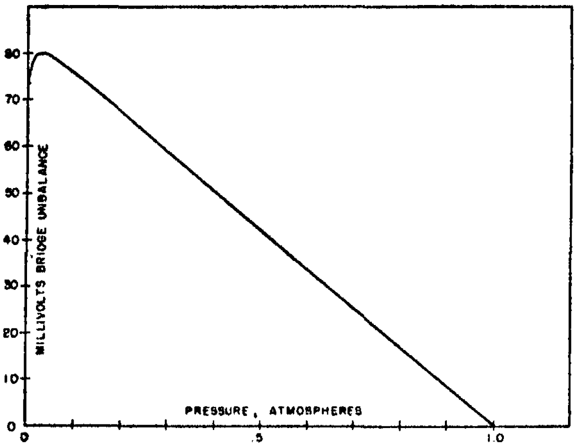

FIG. 2.

It is proposed that with suitable design features a transducer could be used as a vacuum gauge of fundamental nature.

---

[1] A. B. Wood, *A Textbook of Sound* (G. Bell & Sons, Ltd., London, 1944), pp. 72 *et seq.*

A Simple Electronic Relay

ROBERT H. LINNELL* AND HELMUT M. HAENDLER
Department of Chemistry, University of New Hampshire, Durham, New Hampshire
August 30, 1948

AN electronic relay has been constructed using a thyraton tube, the load being placed in the anode circuit. Control of the tube was achieved by applying the filament voltage to the grid 180° out of phase with the anode voltage.

Figure 1 shows the schematic diagram. It is important to note that there is an internal connection in the tube between the heater and cathode (pins 2–4). There will be an a.c. potential difference between heater pin 1 and cathode pin 2, but not between heater pin 4 and cathode pin 2; if this potential is sufficiently large and of proper phase it can be used to control the tube's firing. When the anode of the tube swings

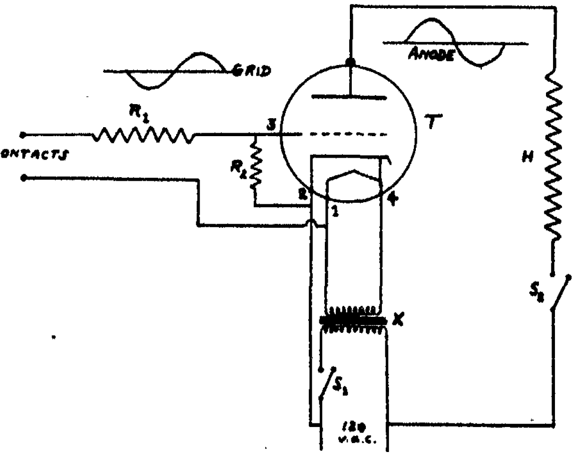

FIG. 1. R_1 2.7 megohm, ½ watt, R_2 330 kohm, ½ watt, S_1 filament switch S_2 anode switch, X transformer, 5 v.a.c. 5a. T General Electric GL-5559/FG57 H heaters.

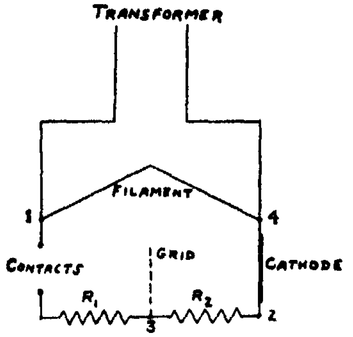

FIG. 2.

positive, the grid must swing sufficiently negative to prevent the tube from firing. Thus an 180° phase difference between grid and anode is necessary. The proper phase is determined by trial. If the tube fires continuously when first connected up, it is only necessary to disconnect the two leads from the filament transformer to the tube heater and switch them in reconnection. The magnitude of the voltage available between pins 1–2 is more than sufficient for grid control and the resistors R_1 and R_2 form a voltage divider circuit which determines the fraction of total filament voltage applied to the grid (see Fig. 2). The values indicated for R_1 and R_2 were chosen to give ample voltage at the grid to ensure control of the tube and yet have a very small grid current. Since the fraction of filament voltage available on the grid is $R_2/(R_1+R_2)$, increasing R_1 will decrease the control voltage put on the grid, and if R_1 becomes sufficiently large the voltage available will be insufficient for operation of the circuit as a relay. For best results the above fraction should be made near unity. It can be seen that decreasing R_1 will cause grid current to increase and since this is undesirable R_2 is made very large so that R_1 can have a large value without making the fraction $R_2/(R_1+R_2)$ significantly smaller than unity. However if R_2 is made excessively large the operation fails due to capacity effects.

In operation, the warming of mercury in the thermoregulator closes the contacts which put the fraction $R_2/(R_1+R_2)$ of the filament voltage on the grid and this prevents the tube from firing, thus heaters in the anode circuit cool. The mercury then contracts breaking the contacts and allowing the tube to fire which warms the heaters in the anode circuit.

The thyraton used (General Electric GL-5559/FG-57) has a rating of 2.5 amperes average anode current and 15 amperes peak anode current. Since the tube carries current only during positive voltage swings of the anode, these tube requirements may be met by using ordinary 120-volt a.c. knife heaters with a rating of 740 watts or less (if more than one heater is used, they should be wired in parallel for maximum power output). This is equivalent to a resistance of approximately 19.5 ohms in the anode circuit. Actually a maximum of about 300 watts will be delivered continuously by the anode load with the above heaters.

This relay has been used to control the temperature of a water bath. A mercury filled regulator with make-break contacts in air showed no appreciable oxidation of mercury after several months of operation. Temperature control to 25.000°C ±0.005° was achieved with an uninsulated Pyrex jar of water.

This same method could conceivably be used on other thyraton tubes, provided grid control voltage was less than filament voltage.

The authors wish to thank Dr. S. N. Van Voorhis of the University of Rochester Physics Department for helpful suggestions.

---

* Present address: Department of Chemistry, University of Rochester, Rochester, New York.

An Apparatus for Producing Powder-Like X-Ray Diffraction Patterns from Single Crystals

F. W. Matthews and A. O. McIntosh
Central Research Laboratory, Canadian Industries, Ltd.
McMasterville, Quebec, Canada

February 25, 1949

OCCASIONALLY it is desirable to identify single crystals without powdering the material. Single crystal rotation patterns can be used to obtain the "*d*" spacings and the unit cell dimensions but these data are not readily used for identification. There are, at present, no determinative tables based on unit cell measurements and the "*d*" spacings obtained from rotation photographs give no indication of the relative intensity of the powder lines. A comprehensive determinative table, based on diffraction powder data, is published by the American Society for Testing Materials.[1] This requires the interplanar spacings, "*d*" and the relative intensities of the powder lines. For identification purposes it is advantageous to obtain the powder data directly from the single crystal. This can be done by imparting to the crystal, placed in the x-ray beam, a very large number of orientations. A method has been described for use in the identification of gemstones.[2,3] This method, designed for use with large mounted specimens, recorded only in the back-reflection area and due to the limited rotations gave arcs in the pattern. For identification purposes the preparation of standard patterns was required. Since the method here described gives results similar to an ordinary powder pattern the standard x-ray powder index can be used.

The instrument (Figs. 1, 2) was constructed around a standard collimator of the General Electric XRD[4] equipment (1). The collimator holder (2) was machined to fit the bearing (3) of the large spur gear. A stationary driving disk (4) is attached to the collimator. Fastened to the large spur gear (5) is the bearing housing (6) which carries the shaft on which the sample is mounted. This shaft is fitted with a rubber disk (7) that is in contact with the driving disk (4). Recessed into the shaft is a small rod (8) at the extremity of which is a smooth surfaced platform (9). To the platform a small flat disk is attached by means of grease. The rod (8) can be adjusted as to height giving longitudinal adjustment of the specimen. The disk, to which the crystal is attached by a glass fiber, can be moved transversely giving the other motions necessary for adjustment. The sample holder is counterbalanced by the weight (11). When motion is transmitted to the large spur gear by the motor (12) through the gear (13) the sample holder rotates about the axis of the collimator. At the same time the disk (4) causes the specimen to rotate about an axis perpendicular to the collimator axis. Thus the crystal is made

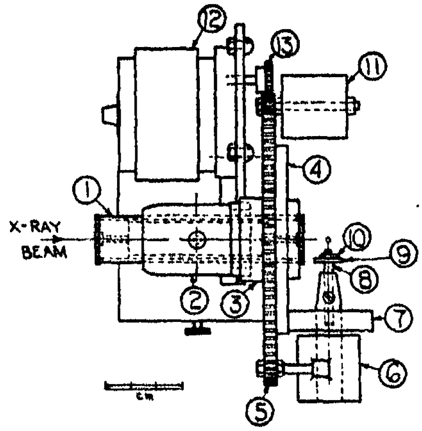

FIG. 1. Scaled drawing in plan of crystal rotating device.

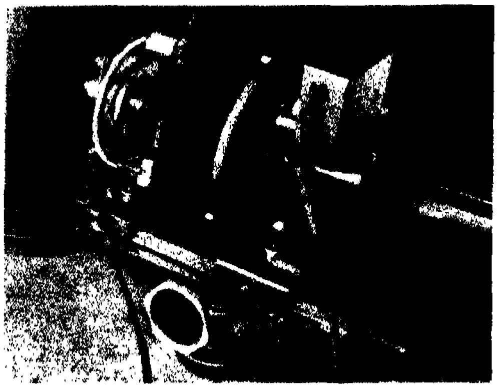

FIG. 2. Crystal rotating device mount on camera track of x-ray unit showing rotating flat film cassette.

to rotate about two mutually perpendicular axes. The pattern is recorded on a flat film rotated about the axis of the beam in the direction counter to the rotation of the crystal.

Patterns made with this apparatus will not be exact duplicates of normal powder patterns which require very many random orientations. Since the equipment described does not give random orientation, difference in intensities will exist. These might be sufficient to remove some lines of the pattern completely. In practice, however, there seems to be qualitative agreement between patterns made from single crystals by this instrument and those made from powdered material. Figure 3 shows the two types of patterns recorded on the same film. The relative line intensity is closely matched in this photograph of sodium chloride which is of high symmetry and in similar photographs of sucrose which has lower symmetry. A contributory factor is that in neither case was a main crystallographic axis used as an axis of rotation thus avoiding planes parallel to the beam, which do not come into the reflecting position.

The instrument can be used for identification of small crystals mounted in the manner usual for single crystal investigations. Larger crystals require an edge to be used so that absorption does not interfere with the relative line intensity. A possible use of this equipment is the quick checking of the identity of crystals before a single crystal pattern is obtained. In this connection it would be useful to design the equipment to take the goniometer head used in the single crystal equipment. A further improvement would be effected if the flat cassette were replaced by a semicylindrical cassette the radius of which was made the same as powder cameras used for routine identification.

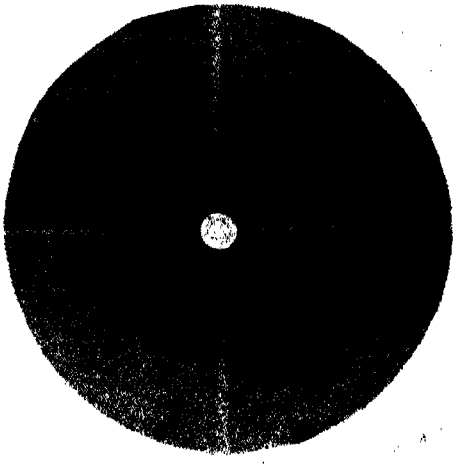

FIG. 3. Sodium chloride diffraction photograph (1) from single crystal (2) powdered sample.

We wish to acknowledge the help of Mr. R. V. Row in the construction of this instrument.

---

[1] American Society for Testing Materials, card file of x-ray diffraction data, Philadelphia Pennsylvania (1942).

[2] S. S. Gordon, Am. Mineral 32, 690 (1947).

[3] G. Switzer and R. J. Holmes, Am. Mineral 32, 351–353, (1947).

[4] *General Electric X-Ray Corporation, XRD Laboratory Handbook*, Milwaukee, Wisconsin.

A Large Straight Through Vacuum Valve for Van de Graaff Generators

B. JENNINGS*
Westinghouse Research Laboratories, East Pittsburgh, Pennsylvania

March 17, 1949

IN order to change targets on an electrostatic generator or external beam cyclotron, it is necessary to have a vacuum valve on the beam tube of special characteristics. This valve must be very tight in the closed position to keep a good vacuum in the main system. It must have a large straight through opening so that the beam cannot splash on the valve parts and produce unwanted disintegrations, and must be easily and quickly closed in case of accident. The valve described here fulfills these requirements.

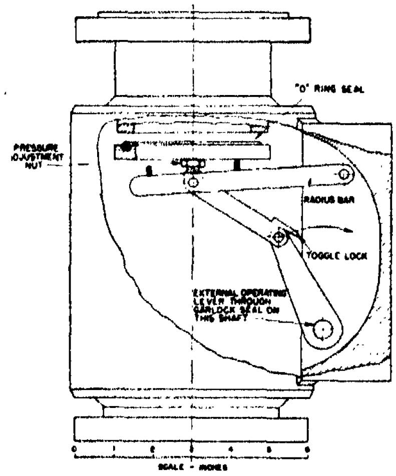

FIG. 1.

The valve[1] consists of a plate carrying a rubber seal of the type known as an "0" ring[2] which is held mechanically against a polished valve seat. This mechanical force is supplied by a lever structure consisting of three bars, one of which is a radius bar to hold the valve plate centrally over the valve seat. The other two form a toggle joint which acts as the compression member of the lever system in the closed position of the valve, as they are locked together in the closed position of the toggle and act as one bar. The mechanical compression on the valve plate can be adjusted by the spacing nut and thread in the valve plate.

To open the valve the lower member of this compression unit is turned clockwise by the outside handle so that the toggle joint unlocks, and the two parts of the cantilever compression member fold together allowing the valve plate to drop down out of the passage way. The radius bar, however, holds the valve plate so that it returns to the correct position when the valve is closed.

The mechanical advantage of the operating lever in starting to swing the valve plate up into position is poor but very little force is required. At the point where the valve is being closed against the valve seat the mechanical advantage has become much better and the force required to snap the toggle is not excessive. About a quarter of a turn of shaft rotation is necessary to close the valve and the action is easy enough so that it could be done by a motor or weight drive for automatic closing in case of vacuum trouble.

The operating shaft is brought outside through a commercial Wilson[3] seal which is applied in the conventional way for rotating a shaft through a vacuum seal.[1]

The valve has been checked for tightness in the closed position with a helium mass spectrograph leak detector, both with the vacuum above and below the seat. No indication of leaks has been found in either direction. This valve is being used as the target valve on the Westinghouse Electrostatic generator at East Pittsburgh, Pennsylvania.

---

* Assisted by the Joint Program of the ONR and the AEC.

[1] R. O. McIntosh and J. W. Coltman, Rev. Sci. Inst. 20, 135 (1949).

[2] Linear, Inc., State Road and Levick Street, Philadelphia 35, Pennsylvania.

[3] Garlock Packing Company, Palmyra, New York.

Cells Drawn from Tantalum, Molybdenum, and Platinum for High Temperature Research*

George W. Ziegler, Jr., Rudolph Speiser, and Herrick L. Johnston
The Cryogenic Laboratory and The Department of Chemistry, The Ohio State University, Columbus, Ohio

March 17, 1949

CYLINDRICAL cells, containers, and furnace elements can be fabricated of tantalum, molybdenum, and platinum sheet for use in high temperature research. These refractory materials have been used to fabricate seamless Knudsen cells employed in vapor pressure measurements,[1] furnace elements in a high temperature x-ray camera,[2] and sample containers for high temperature calorimetry.[3] (In these examples it is important to use seamless cell containers since induction heating is used, and it is essential that the object be uniformly heated.)

Starting with a 0.010-inch tantalum blank, 2 inches in diameter, it takes four draws to make a cylinder ¾ inch in diameter and one inch high (see Fig. 1). The dies are made to nest one within the other. The schedule and die sizes are as follows:

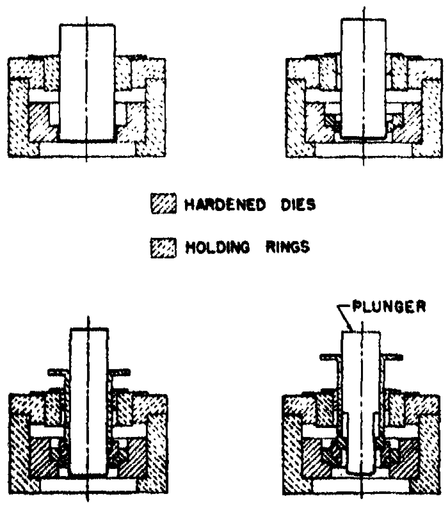

FIG. 1.

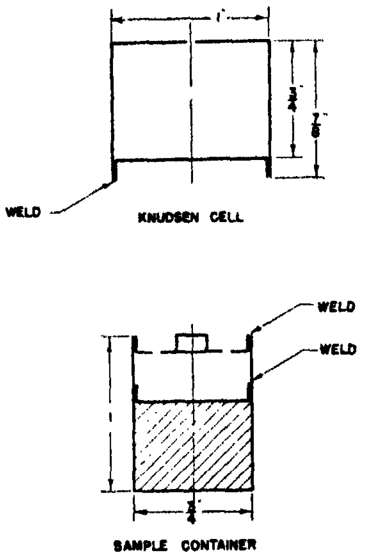

FIG. 2.

Draw	Die size	Radius of curvature of edges of stakes and punches
1st	2" to 1½"	5/32"
2nd	1½" to 1¼"	9/64"
3rd	1¼" to 1"	1/32"
4th	1" to ¾"	1/64"

An arbor press is employed to make the draw and the die assembly is *loosely* clamped with c-clamps.

Before each draw, the sheet, punch and die are thoroughly greased with Vaseline. After the draw, the Vaseline is removed with successive washes of benzene, acetone, and ether. Then the piece is annealed in vacuum (10^{-5} mm Hg with gradually increasing temperature and finally held at 1200°C for a few minutes. After the last draw the cell can be trimmed by placing the punch in a suitable collet and machining off the ragged edge at low speed. The lid is made from the same sheet with a similar die (not illustrated) so as to give a very snug fit inside the cell body as shown in Fig. 2. The lid is welded to the cell body with an electric arc (using a carbon electrode) in a hydrogen atmosphere.

The sample container (for use in a high temperature drop calorimeter) is suspended by a tantalum wire in the furnace. The bail to which the wire must be attached is formed with pliers and inserted into suitable slots cut into the lid and the ends are then melted down to the lid. The 1/32-inch holes drilled into the top of the lid are used for sighting into with an optical pyrometer when measuring temperatures. If the sample is volatile, the sample is sealed into the container with an inner lid as shown in Fig. 2. The space between the inner and outer lids creates a good "hohlraum" to sight into for accurate temperature measurements.

The Knudsen cell body is made from the same set of dies by utilizing only the first three draws. The orifice in the top of the Knudsen cell is made by reaming a hole of the desired size to a knife edge periphery.

The x-ray induction furnace elements are cut from the cylinders obtained from the fourth draw.

Platinum and molybdenum parts are also fabricated in the same manner. Platinum can be arc welded in air and is annealed at a temperature corresponding to a dull red color. Molybdenum is welded under a hydrogen atmosphere and annealed in vacuum (10^{-5} mm Hg) at 1100°C for a short time.

---

* This work was carried out under contract between the ONR and The Ohio State University Research Foundation.

[1] Holden, Speiser, and Johnston, J. Am. Chem. Soc. 70, 3897 (1948).

[2] Edwards, Speiser, and Johnston, Phys. Rev. 73, 1251 (1948).

[3] Ziegler, Speiser, and Johnston, *manuscript in preparation.*

Non-Uniform Shrinkage of X-Ray Films

M. H. Jellinek
Laboratory, Linde Air Products Company, Tonawanda, New York
February 9, 1949

THE application of x-ray back reflection diagrams to measure solid solution compositions has been carried out in this laboratory on samples showing a maximum change of about 1 percent in lattice parameter. Sufficient accuracy was obtained by using Straumanis' type cameras of 57.3-mm diameter. Originally sodium chloride was tried as an internal standard to allow a determination of film shrinkage of no-screen x-ray film but it soon became apparent that non-uniform shrinkage was occurring about the hole punched in the film to accommodate the collimator.

To be able to measure this shrinkage as a function of position on the film a standard index was made by soldering ordinary needles at non-uniform distances to a steel strip. These needles were then used to prick the film in the region of interest before it was loaded to the camera. After the film was developed, fixed, and dried the spacings between pin pricks were measured with a traveling microscope reading to 0.001 mm. The standard was calibrated similarly without processing the film and a direct measure of film distortion was obtained.

The pricking device was made with a larger spacing between the central pins and this section was always placed across the center of the collimator hole in the film. In this way the standard was impressed in nearly the same location on each film. The average results of 37 sets of measurements are given in Table I.

Table I.

Standard pin spacing	Film distortion	Change in mm per mm of film in each region
8.023 mm	−0.016 mm	−0.0020
7.592	+0.003	+0.0004
13.077	−0.052	−0.0040
9.363	+0.015	+0.0016
8.235	−0.039	−0.0047

These results show that a large shrinkage occurred where the hole was punched through the film, that on either side of the hole there was a region where the film stretched slightly, followed in turn by a region of shrinkage.

The results for the region of expansion are probably too low because no attempt had been made to locate the region exactly and it is very possible that a small band showing a high degree of stretch exists.

The Use of Gas Traps in Barometers, Laboratory Mercury Lamps, etc.

E. L. Harrington
University of Saskatchewan, Saskatchewan, Canada
March 12, 1949

THE basic principle underlying the use of traps to capture and to retain residual gases in barometers, mercury lamps, or in other vacuum, mercury-containing chambers may not be new, but the author has noticed only one reference[1] to it in the literature and has not observed any practical application of it in any laboratory other than his own. Two important applications will be described, and two different forms of construction involving the same principle will be shown. Each depends for its action on the reluctance of mercury to enter a fine glass capillary, which makes it possible to trap any traces of gases left by imperfect exhaustion, accumulated from the gradual release of adsorbed gases, or due to other causes.

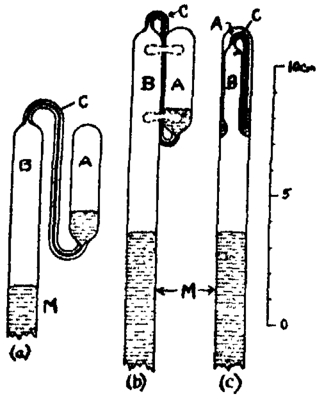

Fig. 1. (a) Diagrammatic representation of a gas trap; (b) the upper end of a barometer tube incorporating the gas trap shown in (a); (c) same except with a different type of trap.

Figure 1 is designed to illustrate the principle itself and also its application to the barometer or to mercury manometers. Referring to Fig. 1(a) it is evident that any trace of gas in the tube, B, above the surface of the mercury M, can be crowded through the capillary C into the chamber trap, A, simply by elevating the mercury in B until a small amount of mercury enters A. As M is lowered to its normal position the mercury thread will break at the upper end of B, leaving the space B free of gas. The amount of gas which normally would be collected in A would be quite insufficient to push the mercury into the A-end of the capillary and then to the height required to escape back into B. This simple operation might well precede any set of readings, but it is found that after the first few months the vacuum is so nearly perfect that little or no further gas is collected.

Figure 1(b) represents the upper end of a barometer tube incorporating the same arrangement as shown in Fig. 1(a) but in a more compact, practical form. It is seen that A is brought more closely adjacent to B and the two chambers are tied together by fused-on braces made of 3-mm solid glass rod in order to obtain greater mechanical strength. To free B from any trace of residual gas one has merely to swing the lower end of the barometer to one side until the surface of the mercury rises to the upper end of B and crowds any trace of gas through C, and then to return the lower end to its normal position. The tendency of the trapping mercury in A to return to B will depend on the pressure in A, but in the case of the first such barometer to be constructed in the laboratory of the Physics Department of the University of Saskatchewan not enough gas was accumulated in twelve years to untrap the gas collected. The form shown in Fig. 1(c) is identical in principle but somewhat neater in form, more compact, and sturdier. The choice between the two forms may depend on the skill of the glass blower and on the diameter of the tubing employed. The first form is easier to make and must be the choice where the tubing is too small in diameter to give room for an inner tube since the latter must be sufficiently large to prevent mercury forming a continuous column and emptying A through siphon action. The pressed-in lump shown in the throat of B in Fig. 1(c) is designed to prevent such action.

The advantages of the modification must be obvious. Our laboratory barometers incorporating this principle give higher readings than are given by the commercial barometers or by one supplied by the meterorological service. In the case of the standard form one is never certain as to whether any appreciable gas pressure exists in the relatively small space above the mercury in the tube, and the sharpness of the "click" made by the impact of M against the top of the tube is too insensitive to be of much use, besides being a risky test to make. One can hardly allow for the depression of the mercury due to

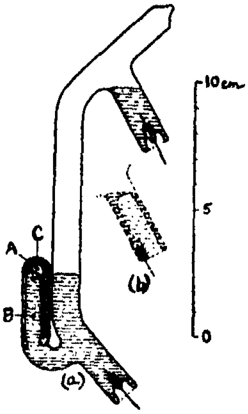

FIG. 2. (a) A laboratory mercury vapor lamp provided with a gas trap; (b) alternative form of electrode well.

this accumulated gas since its effect in any case must depend on the volume of the space above M, hence on the barometer height. Central meteorological stations may call in barometers for servicing, but this merely gives the barometer a fresh start in gas collecting and is both expensive and time consuming. With the improvement suggested even the remote observer can be sure that his reading is correct at all times. Even though with continued use the quantity of gas collectable becomes vanishingly small, it is a source of satisfaction to have at all times the means of quickly making certain of a reliable reading. In the case of mercury manometers forming a part of a McLeod gauge system, for example, where the operation of the trap cannot depend on inclining the apparatus the same result can be accomplished by applying to the system a positive pressure sufficient to cause M to go over the top.

Figure 2 shows the application of the trap to a laboratory mercury lamp of the type which is started by establishing a continuous mercury pool or stream between the two electrodes. To start such a lamp one rotates the lamp clockwise about an axis normal to the plane of Fig. 2 until the two pools are connected, and then very slowly brings it back to its normal vertical position. The arrangement of the trap addition is such that in the horizontal position chamber B is free of mercury and full of its share of any residual gas which may be present in the lamp. As the lamp is righted the gas in B including any extra swept in by the striking arc becomes trapped and crowded over into A through the action of the pressure normally developed during the operation of the lamp. Thus it is seen that with each starting of the lamp the vacuum is automatically improved, in sharp contrast with the usual lamp in which the vacuum gradually deteriorates with increasing life and use. The modified form for each electrode member, shown in Fig. 2(b) has a reentrant tube at the end. This modification reduces the weight of mercury required, almost eliminates hammering, and should greatly reduce the chance of breakage in shipment and in use. The two forms work equally well.

Aside from accidents, the failure of a laboratory mercury lamp is generally due to the gradual increase in the pressure of the residual gas. This gas may contaminate the mercury, but in any case the lamp becomes harder to start and the effective voltage required increases with time. This often leads to more violent mechanical treatment by the student attempting to start the lamp, too frequently ending in fracture. Partially to overcome this difficulty most such lamps have been provided with chambers large enough to take care of the residual gases without building up appreciable pressures, but this makes them more bulky and more fragile, and also reduces their efficiency since a larger radiating surface requires a larger wattage if the same operating temperature is to be maintained. Experience to date has shown that the lamps herein described operate more steadily than lamps of the usual type, that they are more easily started, and that the mercury remains clean. Incidentally, the "click" becomes sharper and this suggests greater caution against rapid turning or shaking just to hear it. All lamps which must be tipped in starting, should be provided with mechanical means of preventing the lamps from being turned in the wrong direction since the exposure of the tungsten leads is likely to cause the failure of the lamp. It will be observed that the upper end of the lamp slopes to the right, in contrast with its commercial prototype. While this aids in keeping full the upper electrode well and makes it possible to use either polarity, it is best to have the upper electrode serve as cathode. If the lower electrode were the cathode a large mercury drop might interrupt its flickering "hot spot," and stop the discharge.

---

[1] C. J. Smith, *Intermediate Physics* (Edward Arnold and Company, London, 1932).

A Vibration Absorber for Gas Holders*

R. S. Craig and W. E. Wallace
Department of Chemistry, University of Pittsburgh, Pittsburgh, Pennsylvania

March 12, 1949

THE vibration of gas holders has often been a source of annoyance to workers in cryogenic laboratories. This is particularly true in those cases in which the system is equipped with selsyn-level indicators or automatic switching devices which are controlled by the level of the holder.

The vibrations are usually caused by a coupling between the gas holder and the compressor. The movable portion of the gas holder and the cushion of enclosed gas effectively form a mass and spring system possessing a characteristic natural frequency. The natural frequency depends upon the quantity of gas enclosed, and hence upon the height of the holder. At some particular level the natural frequency of the gas holder may become equal to the frequency of the pulses from the compressor, under which conditions violent vibration of the gas holder may result. Systems which are particularly prone to vibrate in this manner are those in which the gas holder is

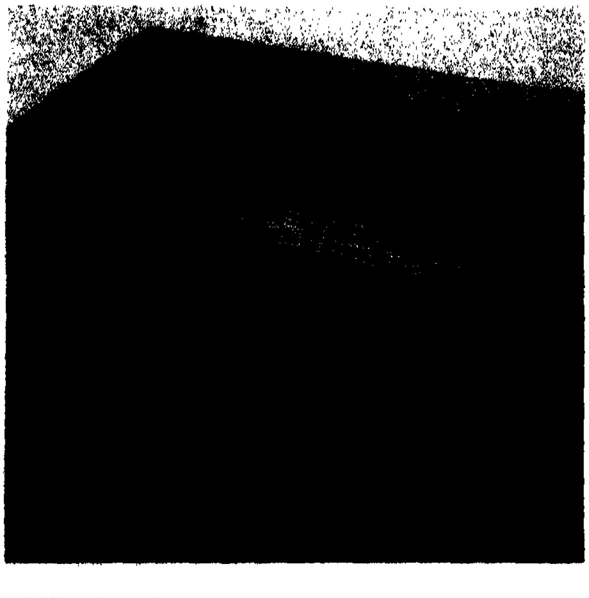

FIG. 1. View of top of gas holder, showing the vibration absorber in position.

designed so that it may be evacuated. In such cases the volume of enclosed gas becomes small as the float approaches its lower position, and the natural frequency may then become sufficiently high to equal the frequency of the pump.

The difficulty was eliminated in an installation in the University of Pittsburgh by a device known as a Dynamic Vibration Absorber.[1] This device consists of a relatively small m-k system in the form of a mass suspended from a spring. The spring is attached rigidly to the offending vibrating system and the magnitude of the mass is adjusted until the frequency of the absorber is equal to that of the forcing vibration (i.e., the frequency of the compressor). Under these circumstances the amplitude of vibration of the gas holder is reduced to a negligible value, and the energy is absorbed almost entirely by the small m-k system.

The gas holder to which this device was applied is a part of the standard equipment for use with the Collin's Helium Cryostat. The movable portion of this holder consists of a steel cylinder open at the top and closed at the bottom. The helium gas is enclosed in the space between the bottom of the floating portion and the outer container, where it is sealed by a large neoprene gasket. The spring was fastened to a support bolted across the top of the gas holder as shown in Fig. 1. The spring had a stiffness coefficient of approximately 500 lb./in., and the magnitude of the suspended mass was 50.4 pounds. This device has proved entirely satisfactory in operation.

* This work was supported by a grant from the Office of Naval Research Contract N6-ORI-43, No. 2, with the University of Pittsburgh.

[1] Den Hartog, *Mechanical Vibrations* (McGraw-Hill Book Company, Inc., New York, 1943).

Construction of Beta-Geiger Counters from Prefabricated Thin Wall Tubing*

F. E. Senftle, W. Havercroft, and P. Hernandez
Radioactivity Section, Bureau of Mines, Canada

March 8, 1949

The construction of thin beta-Geiger counters has been described in the literature and textbooks. The usual method to obtain thin walls has been to draw the glass very thin. Although this can be done manually with some difficulty by a skilled glass-blower, it has become common practice to use a glass lathe where any quantity of tubes are to be made.

Recently the Corning Glass Works has made commercially available, thin wall etched borosilicate glass tubing (Code No. 7740) which has been found to have certain distinct advantages in the construction of Geiger tubes. This prefabricated thin walled tubing is particularly useful where Geiger tubes of uniform diameter are needed or where it is necessary to build a number of tubes with limited glass-blowing facilities. It is the purpose of this paper to describe the new tubing and Geiger tubes made from it. The use of this special tubing has facilitated the construction of certain types of cathodes for Geiger counters, and the increased mechanical strength of such tubes also admits their use in environments of higher than atmospheric pressure.

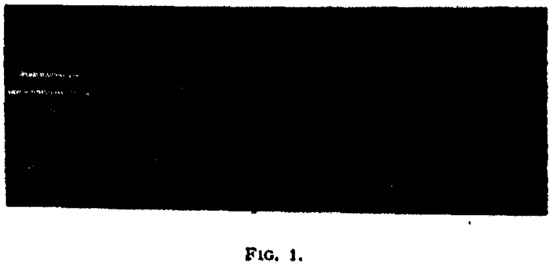

Fig. 1.

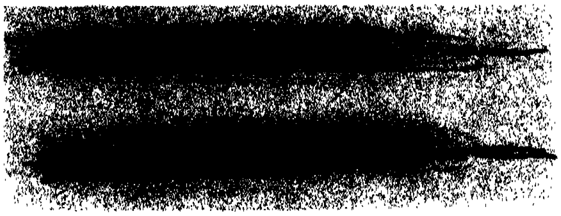

Fig. 2.

Fig. 3.

The thin glass etched blank as received from the manufacturer and the first steps in the construction of the Geiger tubes are shown in Fig. 1. The central section of the blank is the thin wall, and on either end is a short section of ordinary unetched borosilicate glass tubing. The over-all length of the blank is 6″ to 8″. At present two diameters are obtainable, 19-mm and 25-mm O.D. The thin central section is slightly smaller on the O.D. and slightly larger on the I.D. than the heavy section at the end. The wall thickness of the thin section is remarkably uniform, and, depending on the particular blank, the thickness is between 0.006″ to 0.016″, which is about 41 to 110 mg per cm^2. The maximum variation of thickness of the individual blanks tested was found to be about ±0.002″. For low energy beta-counters it is necessary to select blanks with the thinnest wall. However, the majority of blanks which have been tested to date have been found to be sufficiently thin for most work.

The blanks of thin tubing have a substantially uniform bore, and are less fragile than hand-drawn tubing, since they have no extremely thin mid-section which thickens toward the ends. In the hand-drawn and to a lesser extent in the lathe-drawn tubes, the central diameter is slightly smaller than that of the extremities. Hence, any uniform cylindrical cathode could not be conveniently put inside such an envelope. On the other hand, the uniform bore tubing allows the use of a wide copper spiral or open screen as a cathode. These open cathodes allow a free passage of the beta-particles into the active volume while still maintaining a uniform field. Although a close wound wire helix or fairly fine copper screen has an inside area greater than that of a solid cylinder, a condition tending to increase the gamma-efficiency, it has been found that a good beta-counter can be made, if the wires are not too close together. The sectional area to gamma-rays perpendicular to the tube axis is small for an open helix.

Figure 2 shows a typical copper spiral beta-counter and also one with a conventional deposited silver cathode. Both were made with Code No. 7740 glass. If a silver surface is used for a cathode, it is more convenient to deposit it on the thin glass blank prior to any glass-blowing steps as shown in Fig. 1.

Tests on a small number of tubes indicate that they will stand a maximum of 60 p.s.i. external pressure. It is obvious that Geiger tubes made from such tubing would be particularly suitable for beta-measurements under a considerable head of liquid. A tube with a liquid jacket is shown in Fig. 3.

Where radioactive elements or tracers can be used, a constant check on concentration may be maintained. In certain industrial processes, the active solutions are circulated under pressure through the jacket, and the concentration of the beta-active tracer may be continuously monitored. The relatively strong thin wall of these Geiger tubes makes such an arrangement feasible.

Our thanks are due the Corning Glass Works for providing helpful information.

* Permission to publish this paper has been granted by the Director, Mines Forests and Scientific Services Branch, Department of Mines and Resources, Ottawa, Canada.

Percent Transmission Computer for Infra-Red Spectra*

C. E. Zerwekh, Jr.
Humble Oil and Refining Company, Baytown, Texas

January 3, 1949

A DEVICE for converting the usual infra-red intensity wave-length curves to percent transmission curves which was described earlier[1] has been modified to increase its versatility. The incident energy (I_0) and transmitted energy (I) curves are run in a conventional manner on an infra-red spectrometer except that they are superimposed on the same chart. This chart is then placed in another instrument and the curves traced simultaneously by hand with two pointers placed on a single track. One of the pointers selects a voltage E proportional to I and applies it to the other pointer which impresses it across a resistance R proportional to I_0. The current i flowing in the resistor is equal to the quotient of E/R and is thus directly proportional to I/I_0 or the percent transmission.

The infra-red equipment consists of a Perkin-Elmer Model 12-C Infra-Red Spectrometer equipped with a chopped beam detecting system and a Perkin-Elmer Breaker Type D.C. Amplifier.[2] The output of the amplifier is impressed on a suitable filter circuit and then fed to a Brown Elektronik strip chart recorder. The electrical circuit of the computer is illustrated in Fig. 1. All of the electrical components were mounted on a Brown Elektronik recorder chassis that had been stripped of everything except the chart drive motor and associated mechanism. The two resistance cards, specially wound by General Radio so that the total length occupied by the windings was equal to the 0–100 distance on the chart paper, were mounted in the place originally occupied by the Brown slidewires. An additional Brown carriage for carrying the sliding contacts was placed on the carriage track, and contacts were mounted on both carriages. Since each contact had two elements, one of these was cut off so that each carriage and its contact touched only one resistance card. A pointer was mounted on each carriage and aligned with the point of contact between the resistance card and the sliding contact. In addition, two more sliding contacts, one for each card, were mechanically coupled together and mounted on a special carriage at the zero end of the resistance cards. These contacts allow compensation for difference in zero levels. A shorting switch S_2 was also mounted across the input to the recorder to allow the fiducial marks appearing on the original curve to be transferred to the percent transmission curve. This switch was mounted under an accelerator pedal to allow it to be operated by foot. A variable shunting resistor R_3 across the recorder input allows the sensitivity of the recording system to be adjusted to compensate for the changes in battery voltage and, in effect, is a standardizing knob. The chart drive motor on the computer and the recorder were connected to a common switch to allow the computer and recorder charts to be started and stopped simultaneously.

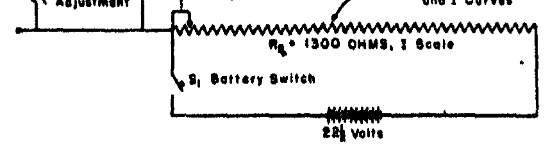
R₁ = 300,000 OHMS, I₀ Scale
Output to Recorder
R₃ = 250 OHMS Shunting Resistance for Range Adjustment
Mechanically Linked Contacts for Zero Adjustment
Sliding Contacts To Follow I₀ and I Curves
R₂ = 1300 OHMS, I Scale
S₁ Battery Switch
22½ Volts

FIG. 1. Circuit diagram of Percent Transmission Computer.

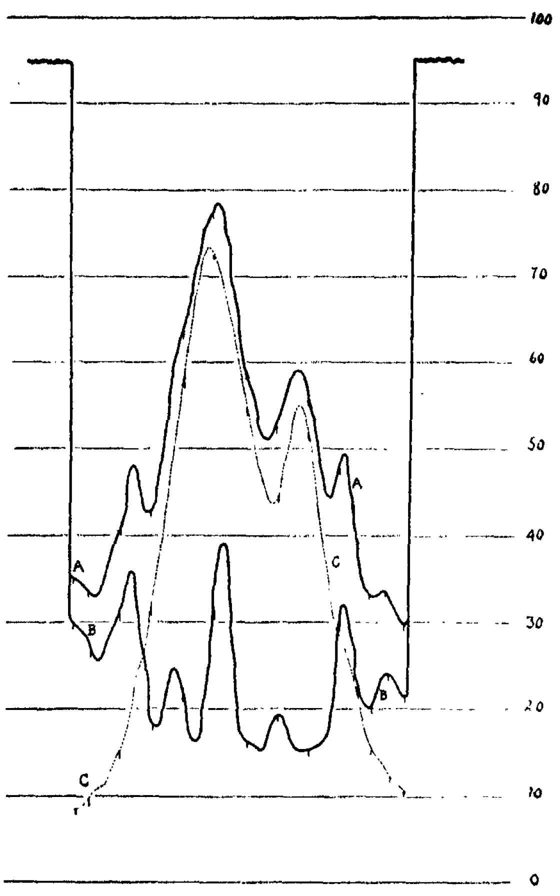

FIG. 2. Curve A: cell filled with sample; curve B: cell filled with reference standard; curve C: percent transmission (curve A×100/curve B) traced by the computer.

To use the instrument, a record of the wave-length intensity curve for the filled sample cell is made in the usual manner. Then the chart is turned back to the starting point and a record is made of the reference. This is very readily done with the Perkin-Elmer Model 12-C Infra-Red Spectrometer since the chopped beam detecting system eliminates practically all zero drift. The chart is then removed from the original recording system, placed in the computer, and aligned for the proper starting position. The zero contacts are then adjusted to the proper zero level. When the start switch is thrown, both charts begin moving simultaneously and at the same speed. The superimposed charts are traced by hand, and whenever a fiducial marker passes under the tracing pen, the marking switch is pressed to place a mark on the percent transmission curve. Figure 2 illustrates the type of results obtained from this instrument. Curve A is the intensity wave-length curve for the 6.70 to 7.00 micron region for a sample cell filled with

0.182 volume percent *trans*-1,3-dimethylcyclohexane in carbon tetrachloride, and curve B is the corresponding curve for the same sample cell filled with carbon tetrachloride. Curve C is the ratio of A to B as determined by the Percent Transmission Computer.

Tests obtained on this computer show that it has an inherent accuracy and reproducibility of ±0.1 percent transmission on the average with a maximum deviation of approximately 0.3 percent. Tests under actual operating conditions give results that are on the average within ±0.7 percent of the actual value, with the maximum deviation occurring when both the incident and transmitted energy curves have steep slopes, such as those occurring in the regions where water vapor absorbs strongly.

---

[*] The work done in connection with this paper was performed at the Humble Oil and Refining Company at Baytown, Texas.

[1] R. M. Fuoss and D. J. Mead, Rev. Sci. Inst. 16, 223 (1945).

[2] Liston, Quinn, Sargeant, and Scott, Rev. Sci. Inst. 17, 194 (1946).

The Use of Anodized Aluminum in the Construction of Calorimeter Heaters

George W. Murphy
Department of Chemistry, University of Wisconsin, Madison, Wisconsin

February 9, 1949

AMONG the desirable features of electrical heaters for introducing measured amounts of energy into calorimeters are those of low heat lag and low heat capacity. For routine work, durability is also an important asset. Where a liquid of negligible electrical conductivity is to be heated, bare resistance wire satisfies the first two requirements admirably; however, in aqueous solutions of electrolytes, which are appreciably conducting, bare resistance wire in contact with the solution cannot ordinarily be used. Furthermore, any attempts to insulate the wire inevitably increase the heat lag and the heat capacity. It is the purpose of this paper to describe a technique for preparing insulated heaters with very low heat lag and heat capacity and high durability.

Anodically prepared layers of aluminum oxide on aluminum have been employed for many years for corrosion protection and for other purposes.[1] These layers are extremely tenacious and durable, and for our purposes, have the important property of being electrically insulating. The thickness of the coating can be controlled within wide limits. Thus if a suitable aluminum heater core is anodized, resistance wire wound on this core will be insulated from it; heat conductivity between the wire and the core should not be seriously impaired because of the thinness of the coating. A casing can be soldered to the core to protect the resistance wire from the solution.

A heater which has been so prepared and used for routine work in the undergraduate physical chemistry laboratory will be described in a forthcoming book.[2] Several variations in design of this heater have been prepared by the author and his associates, and the wide application suggested has prompted this publication of constructional details.

The sequence of operations for preparing a heater is shown in Fig. 1. The heater illustrated is tubular in form so that a stirring propellor can be inserted to improve circulation of the liquid. Pure aluminum is best for anodizing, but the customary alloys will give satisfactory service for this application. Threads are machined on the core for a calculated length of resistance wire. Rounded grooves should be milled between the thread terminals and the outlet holes for the wire, and all sharp corners over which the wire might pass are carefully removed. If this is not done, subsequent breakdown of the coating is likely. The usual anodizing process increases the dimensions very slightly; therefore, the casing should be a free fit around the core before anodizing.

The part to be anodized is degreased in an organic solvent, pickled in 1-molar sodium hydroxide solution until hydrogen is copiously evolved, rinsed thoroughly, and placed in the anodizing bath. The electrolyte in the anodizing bath is 5 percent by volume H_2SO_4.[3] The temperature should not rise much above that of the room for best results. For this purpose tap water may be circulated through a copper cooling tube, which also serves as cathode. A motor stirrer should be provided. A current density of about 0.2 amp./sq. in. yields a satisfactory coating in about 30 minutes. Thicker coatings can be obtained with higher current densities and longer times. After anodizing, the part is rinsed and "sealed" by immersion in boiling water for about 20 minutes. This operation seals the pores by formation of a hydrated oxide.

When both parts have been anodized, the surfaces are tested for short circuits, and if the tests are satisfactory, resistance wire (preferably of Advance or manganin) is wound on. The small outlet hole at one end is reamed to expose the bare metal, since one end of the wire is to be grounded to the case. The casing is now slipped on and soldered to the core with aluminum solder.[4] The oxide coating must, of course, be filed or ground away at the points to be soldered. The grounded end of the resistance wire is soldered to the case.[5] A heavy copper wire lead may be soft soldered to the other end of the resistance wire. No flux should be allowed to flow into the outlet hole of the heater. The lead wire may then be insulated by a tube of Lucite which is sealed to the heater by Lucite cement, or by such other means as may be dictated by the particular problem. The other end can be a strip of aluminum grounded to the case. Additional leads for potentiometer connections can be provided if desired.

The heaters described above were designed for a low voltage (6 volts) and low power dissipation (6 watts). There is nothing in the construction, however, to indicate that these units cannot be used for much higher voltages and power dissipation. Professor Paul Bender and his associates of this De-

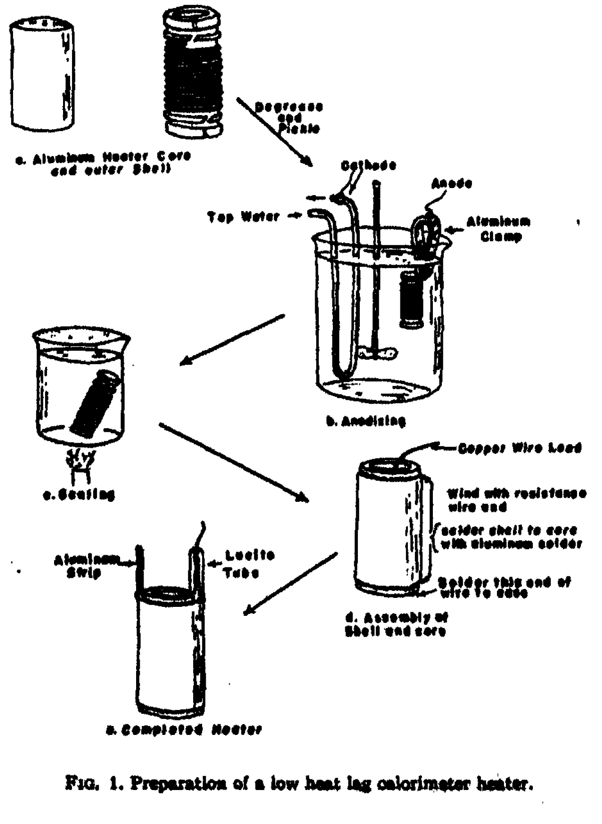
a. Aluminum Heater Core and outer Shell
Degrease and Pickle
Cathode
Anode
Tap Water
Aluminum Clamp
b. Anodizing
c. Sealing
Copper Wire Lead
Wind with resistance wire and
solder shell to core with aluminum solder
Solder this end of wire to case
d. Assembly of Shell and core
Aluminum Strip
Lucite Tube
e. Completed Heater

FIG. 1. Preparation of a low heat lag calorimeter heater.

partment have constructed heaters which operate satisfactorily from a 110-volt power supply and will handle at least 250 watts.[6] These units were totally enclosed in a brass shell and the lead wires were carefully insulated and enclosed in brass tubes.

Rough tests of these units for heat lag have yielded no quantitative data, since the results seem to be influenced as much by the stirring arrangement and thermometer inertia as by the lag of the heater itself.

The heater described above is suitable for use in aqueous solutions which are neither strongly acid nor strongly basic. For acid or basic solutions the heater could be sheathed with gold or other non-corrodable material. It might also be mentioned that tantalum is known to form anodic layers similar in characteristics to those on aluminum. A heater made with a tantalum core would be able to withstand strong acids; furthermore, tantalum might make possible high temperature applications beyond the melting point of aluminum.

The author in collaboration with Mr. W. R. Rowe has also prepared a low heat lag resistance element for temperature control by winding Hytemco wire on an anodized aluminum form. This has given satisfactory service for a year at control temperatures in the neighborhood of 250°C.

The author wishes to thank Mr. Lloyd Lincoln of the departmental shop for his skillful assistance in the machine and soldering work on a number of these heaters. He is indebted to Mr. Harry A. Schopler for preparing sketches on which Fig. 1 was based.

[1] Alex Jenney and W. Lewis, *The Anodic Oxidation of Aluminum and its Alloys* (Chemical Publishing Company, New York, 1940).

[2] Daniels, Mathews, Williams, and staff, *Experimental Physical Chemistry* (McGraw-Hill Book Company, Inc., New York, 1949), fourth edition.

[3] Many variations in electrolyte have been employed (see reference 1). The concentration is not critical.

[4] Aladdin Rod, a solder made by the Aladdin Rod and Flux Manufacturing Company, is satisfactory. The manufacturer's instructions for using this solder should be carefully followed.

[5] If the aluminum core is tinned with aluminum solder at this point, soft solder may be used between the resistance wire and the core. Aluminum solder will not in general wet the resistance wire.

[6] These heaters will be described in more detail in forthcoming publications by Bender and associates.

Method for Preparing Capillary Tube Samples for X-Ray Diffraction Powder Analysis*

Paul J. Hagelston and Harris W. Dunn
Carbide and Carbon Chemicals Corporation, Y-12 Plant, Oak Ridge, Tennessee

February 1, 1949

FILLING of capillary tubes with powder samples for x-ray diffraction work is usually accomplished by thrusting the capillary into a quantity of powdered sample material, each thrust forcing some of the powder into the tube until the required amount is enclosed therein. The tube is then end-sealed.

Under the following increasingly common conditions, the usual method is not at all satisfactory.

1. Handling of hygroscopic materials in a dry box is difficult since it necessitates wearing cumbersome gloves extending through the ports while manipulating small tubes. Too, the likelihood of moisture pick-up is a danger during the period of removal of the sample for sealing.
2. Contamination by dirt and dust from air, vessels, and hands is an ever-present possibility even with stable samples.
3. Samples extremely limited in quantity, such as enriched isotopes, make capillary filling virtually impossible.

Gibons and Bicek[1] have recently outlined a method for filling capillaries which requires the use of a vacuum set-up. The points of great caution they cite as necessary in their method are believed to be non-existent through use of the following technique. In addition, the limiting conditions numbered above are virtually eliminated.

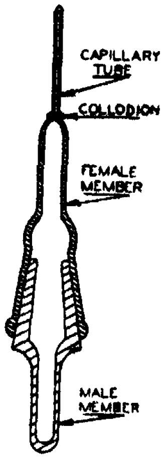

FIG. 1. Capillary filling jig final assembly.

Figure 1 shows a capillary filling jig, consisting of an amended 10/30 pyrex ground joint whose male member is closed at the tubular end. The female member has a small hole in its tubular end into which is placed the open end of a capillary tube whose other end is sealed. The capillary is held in position by application of collodion or other suitable thick fluid to its junction at the tip of the female member.

To assemble this filling jig, a difficult and unsatisfactory job when done by hand, an assembly jig is used, one head of which is shown in Fig. 2. The sealed end of the capillary is stuck in a plastic-clay-filled hole on the bottom of the lower knurled knob on the screw column of the assembly head, and the amended 10/30 ground joint assembly placed in position by inserting the tubular end of the male member in the base hole provided. The capillary is positioned directly above the female member tip hole through use of the rotational, horizontal, and vertical adjustments provided. The lower knob, which is attached to but free to rotate upon the vertical screw shaft, is held while the screw shaft is rotated downward, bringing the capillary the desired distance into the tip of the female member. Collodion or other material is applied, allowed to dry, and the lower knob again held while the shaft is retracted.

To fill the then assembled jig, the ground joint is separated and the sample material placed in the female member. The male member is refitted and a fine-cut file drawn across the assembly, the resultant vibration forcing the material into the capillary. When the latter is filled to within about one-quarter inch of the collodion joint, it is sealed-off by a hot pin-point flame.

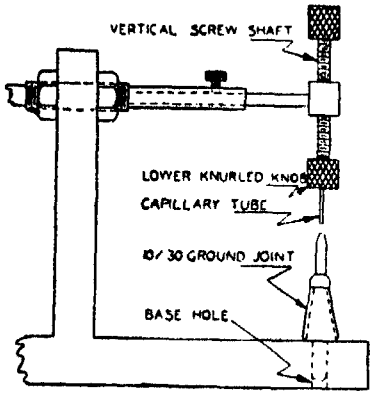

FIG. 2. Assembly jig head.

With hygroscopic materials, the component parts of the jig are allowed to dry in the dry box, the material placed in the female member, and the male and female parts refitted. The assembly may then be removed from the dry box and the capillary filled and sealed-off as above. Throughout the procedure, parts can be kept clean and very little possibility of contamination presents itself.

When dealing with materials of extremely limited quantities, it is necessary to assemble the filling jig so the junction of the capillary to the tip of the female member is essentially a butt joint.

---

* This document is based on work performed for the AEC by Carbide and Carbon Chemicals Corporation, at Oak Ridge, Tennessee.

[1] G. Gibons and E. J. Bicek, *Anal. Chem.* 20, 884 (1948).

THE REVIEW OF SCIENTIFIC INSTRUMENTS VOLUME 20, NUMBER 5 MAY, 1949

New Instruments

W. A. Wildhack: Associate Editor
in Charge of this Section
National Bureau of Standards, Washington, D. C.

These descriptions are based on information supplied by the manufacturer and in some cases from independent sources. THE REVIEW *assumes no responsibility for their correctness.*

Nucleometer

The Mark 9, Model 3, RCL Nucleometer-Scaler Type is a complete instrument for counting alpha-, beta-, or gamma-radiations with extreme precision and reliability. It consists of the counter tube, high voltage supply for the counter tube, amplifier, pulse equalizer, scaling circuit, a supply of gas and a regulator. With reasonable precautions the reproductibility of the RCL Nucleometer-Scaler Type will be within statistics.

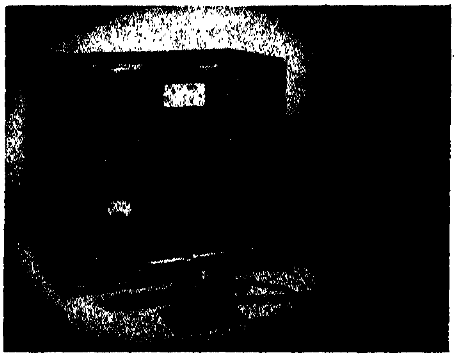

The counter tube through which the hydrocarbon gas flows, operates in the proportional region as differentiated from the Geiger region. This results in the following advantages:

a. Low resolution loss at all counting rates—less than 2 percent at 100,000 counts per minute.
b. Exceedingly flat and long plateau.
c. With an airlock to introduce samples directly into the counter, the tolerance to air is several orders of magnitude greater for a given accuracy than a Geiger counter tube, permitting shorter flushing time.
d. The chemical breakdown of the gas, forming undesirable deposits on the inside surface of the counter, is approximately in the ratio of the voltage pulses from Geiger and proportional counter tubes, being on the order of 1000 times less obnoxious for the proportional counter tube than for the Geiger counter tube.

The counter tube is available in either an internal sample or external sample type. With the internal sample type, the radioactive sample is placed in a "well" and slid directly into the counter volume giving 50 percent geometry and no window absorption. This counter tube is used for counting samples with soft radiation and when sensitivity is of utmost importance. The external sample type has a thin window and is furnished with standard Lucite mount. It is used where variations in geometry are desired, as well as when absorption measurements are required. Since both counter tubes operate slightly above atmospheric pressure all consequent leakage problems are eliminated.

The counter tube is operated at 4200 volts from a regulated supply with a stabilizing factor greater than 200. The voltage may be varied from 2200v to 5000v permitting determination of the counter tube characteristic curve.

Since the counter tube operates in the proportional region an amplifier is used between the counter and scaler. In order to advantageously use the fast characteristics of the counter a fast linear amplifier is employed. Use of the proportional counting region requires that the pulsed amplitudes be equalized before scaling.

The scaler is of the time tested Higinbotham type and contains a scale of 512 in order that one may count at the high rates permitted by the low resolution loss of the counter, with alternate selection of scales of 64, 128, and 256. It is complete with panel mounted Standard Electric Timer and Wizard Recorder.

The gas is specially purified methane and is furnished through a two-stage regulator, which informs the operator of delivered pressure as well as an indication of gas remaining in the tank.—RADIATION COUNTER LABORATORIES, INC., *1844 West 21st Street, Chicago 8, Illinois.*

Radiation Meter

Radiation Meter, model number RM-1 is a portable survey meter which has the following features:

1. Continuously variable high voltage supply from 400 to 1500 volts, permitting the use of end-window as well as cylindrical type G-M tubes. High voltage is obtained from inexpensive 67.5-volt batteries.

2. A meter range covering three ranges of activity: 5000, 50,000, and 500,000 counts/minute. At the upper range, more than four times tolerance dosage of x- or gamma-radiation can be measured. Intensities considerably above tolerance levels for the various alpha- or beta-emitting radioactive isotopes can also be readily determined.

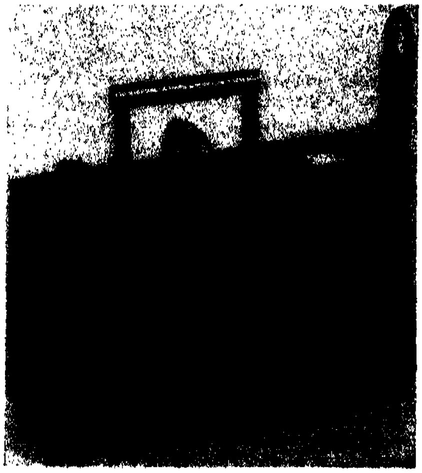

3. Meter accuracy of better than 2 percent, full scale. This permits use of the instrument as an inexpensive count rate meter for quantitative assay, besides its regular application for health monitoring and contamination detection.

4. The instrument is of rugged construction. It can be used in all kinds of weather. It is supplied with earphones. It is particularly suitable for prospectors for radioactive ores.—THE NUCLEONIC CORPORATION OF AMERICA, *497 Union Street, Brooklyn 31, New York.*

Alpha-Particle Counter

The outstanding feature of the Model D45 detector is its ability to count alpha-particles in the presence of high beta-activity with 50 percent geometry and low coincidence losses.

When this detector is used with a high gain linear amplifier and a "fast" scaler, it is possible to count alpha-particles in the presence of a beta-activity of 5×10^9 disintegrations per minute. Measurements of this type are particularly useful in chemical, physical, and biological research.

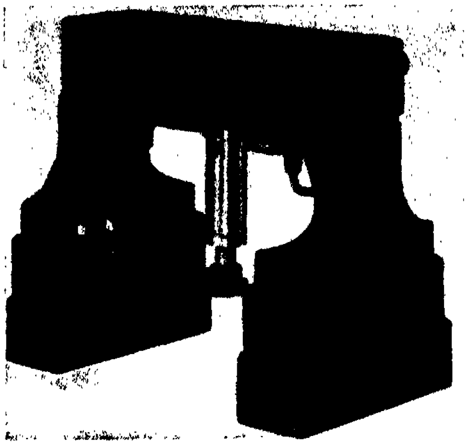

The counter chamber of Model D45 has a very highly polished cylindrical cathode. The anode is 0.002" diameter tungsten wire mounted between glass insulators. Construction is designed to permit easy decontamination both inside and outside. The sample holder, mounted on a stainless steel sample changer, is designed for standard one-inch diameter samples, with provisions for raising the sample up into the counting volume for improved geometry. Flow of methane gas through the chamber is controlled by means of valves and an attached bubbler. Connection of a coaxial cable is made to the center wire via a well insulated connector on rear of the cover.—NUCLEAR INSTRUMENT AND CHEMICAL CORPORATION, *223 West Erie Street, Chicago 10, Illinois.*

Wide-Range Power Supply

A new wide-range power supply apparatus featuring a continuously-variable voltage output from 500 to 50,000 volts with a maximum current output of 1 milliampere has been announced by the General Electric Company.

Designed for laboratory applications where a variable voltage at low current is required, the new wide-range power supply can be used in electron diffraction studies, mass spectroscopy studies, research on high intensity screens for cathode-ray studies, electron microscopy, and projection television experiments.

The high voltage is attained through the use of a radio-frequency oscillator, power amplifier, r-f transformer, and a ladder-type voltage tripler circuit. Use of the r-f source, about 40 kc, makes possible reduction of the output ripple to a low value by simple filtering means. This minimizes the equipment's weight (350 lb.) and size (23×84×20 in.).

The wide-range power supply has been designed with exceptional stability as to output voltage, ripple, and load regulation. Output power, supplied through a 15-ft. x-ray cable, is not affected by variations in line voltage or frequency. Full compensation is made for ambient temperature changes, and precision regulation is attained through the use of two regulating loops in cascade.

A switch on the control panel provides for the selection of two ranges: 500 to 5000 volts and 5000 to 50,000 volts. Output voltage may be turned on or off by easily accessible, momentary push buttons. A gravity-operated grounding device shorts the output terminals when the high voltage is turned off. The output voltage and output current may be read on two panel-type meters at the top of the equipment. Controls are provided to turn the supply on or off, to adjust the voltage, and to adjust the plate current in the oscillator tubes.

Power requirements are 100–130 volt r.m.s., 60 cycles, with commercial stability. Full load power consumption is approximately 1000 watts. Ripple is between 0.006 percent and 0.04 percent, depending upon output voltage and load. Drift is less than 20 parts per million per minute on the low voltage range and less than 100 parts per million per minute on the high voltage range.—SPECIAL PRODUCTS DIVISION, *General Electric Company, Schenectady 5, New York.*

Ultrasonic Generator

A new type "CL" (clinical-laboratory) ultrasonic generator has recently been developed by Ultrasonic Engineering Company. The principal feature of the new equipment is the special convertible "transducer" for transmitting the high frequency vibrations to the skin of the patient, or to the specimen of tissue or other material under treatment. The transducer is connected to the generating unit by a coaxial cable carrying low voltage (less than 100 volts) high frequency current.

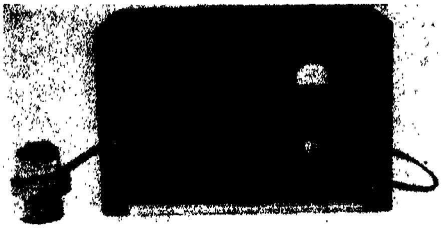

The base of the transducer comprises a transparent Lucite tube, surrounded by a ring containing the primary winding of the step-up Tesla coil, from which a handle projects, with the connecting cable leading through it.

Inside the tube is the secondary winding of the step-up coil. The crystal is mounted above the secondary coil upon Nylon rods, between Bakelite and glass disks. The tube is closed by a cap containing a Bakelite diaphragm 1/100 inch thick, mechanically connected with the vibrating crystal by oil which fills the entire assembly.

This diaphragm, placed against the skin of the patient under treatment, effectively transmits the ultrasonic vibrations generated by the crystal, which is one and one-half inches in diameter and from approximately one-eighth to one-quarter inch thick, depending upon the frequency desired.

A second Lucite tube is provided, which may be screwed to the top of the base assembly and filled with oil, into which a test tube or other vessel containing either solid or liquid material to be treated may be immersed. Through this feature of convertibility, the equipment is readily adapted to most requirements of clincial or laboratory work.

The generating unit, operated by standard 115-volt, 60-cycle current, uses full-wave rectification with adequate filtering. The self-excited oscillator is coupled to the crystal circuit, and is frequency-controlled by it. Thus the frequency of the oscillator is prevented from drifting out of phase with the natural period of the crystal, assuring constant and maximum energy delivery. Power control is adjustable, and is metered in the crystal circuit.

Standard frequency of the generator is 450 kc, with alternate crystal and coil available for quick conversion to 900 kc. Other frequencies are available upon special order.

A series of larger models have been developed for industrial laboratory and production work and will soon be available. Particularly interesting is a model designed for continuous-flow processing of liquids in manufacturing applications.

The new "CL" Ultrasonic Generator is designed to provide the clinic, laboratory, or physician with compact, flexible, inexpensive equipment for experimental research or treatment work.—Ultrasonic Engineering Company, *Dept. 33, Main Street and Eighth Avenue, Maywood, Illinois.*

Sound Measurement

Model GA-1002A sound pressure measurement equipment is a newly designed instrument incorporating important structural refinements resulting from the experience acquired during manufacture and use of its predecessor. Major improvements include a specially isolated socket tip which effectively separates the microphone clamping structure from the preamplifier extension tube. This isolation eliminates mechanical resonances that might otherwise result in the extreme high frequency range due to standing waves which could be set up in the preamplifier extension tube under certain conditions of use. The M-101 standard microphone, which is part of the equipment, has been re-designed to provide more accurate polar symmetry of the mechanical structure, resulting in exact acoustic symmetry about the normal axis of the microphone even at frequencies above 20 kc.

Sound pressures from less than 1 dyne/cm^2 to 20,000 dynes/cm^2 (160-db level) may be directly measured, and a times-ten multiplier is available for extending the upper range to 200,000 dynes/cm^2 (180-db level). A built-in calibrating circuit permits setting the system gain so that exactly 1 millivolt/dyne/cm^2 is delivered across the 10,000-ohm output circuit.

The acoustic impedance of the standard microphone is virtually infinite so that accurate sound pressure measurements may be made even in very high impedance environments such as inside small enclosures at the higher frequencies. Complete lack of phase distortion permits exact reproduction of sound pressure transients over the complete audio frequency spectrum.—Massa Laboratories, Inc., *Cleveland, Ohio.*

Graphic Recorder

Model FRA, a direct ink-recording instrument, automatically plots a curve of any slowly or rapidly changing measurable quantity that can be converted into a d.c. or a.c. voltage. The measuring ranges can be selected and recorded either on a logarithmic or linear scale.

This recorder may be applied to the fields of acoustics, electroacoustics, noise and vibration, loudness, strain and pressure, and field strength.

This instrument is available in 56 double chart speed combinations from 45 inches per minute to ½ inch per hour and for recording frequency ranges from 2 to 200,000 c.p.s.

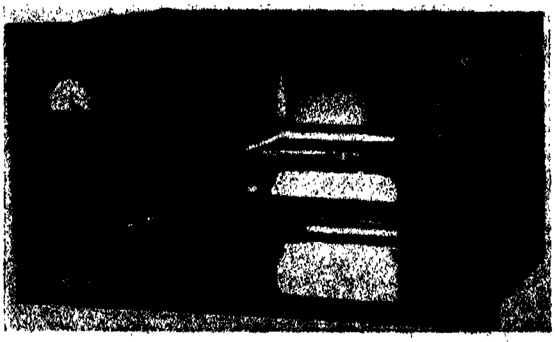

It is completely cased for portable field use or laboratory rack mounting in 10½″ rack space, incorporates built-in cali*bration control, and is unaffected by line voltage changes.*—Sound Apparatus Company, *Stirling, New Jersey.*

Electron Multiplier Photometer

The Farrand Electron Multiplier Photometer has been designed for general purpose measurement of very low light intensities. Photo-multiplier tubes affording high sensitivities are used as detectors and obviate the need for additional amplifiers.

The main features of this photometer are: Selective wide range of sensitivity, linear response, measurements in the ultraviolet and visible region, dark current balance control, constant voltage, stable battery power supply, interchangeable photo-multiplier tubes, flexible utility, compactness, and simplicity of operation.

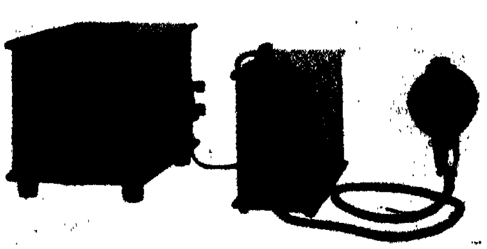

By choice of a photo-multiplier having optimum characteristics in the ultraviolet or visible region of the spectrum, the use of the photometer is readily extended to numerous and broad applications concerned with photometry.

The photometer is comprised of three units: (1) detector, (2) power supply and controls, (3) galvanometer. This arrangement makes it convenient to use directly or to attach the photometer to various instruments.

A detailed description of the Farrand Electron Multiplier Photometer is contained in Bulletin 804.—Farrand Optical Company, Inc., *4401 Bronx Boulevard, New York 66, New York.*

Microwave Power Meter

The Hewlett Packard Company announces a new microwave power meter. The new instrument is known as the −hp−430A Microwave Power Meter, and is designed automatically to indicate power developed in a standard barreter. Power level is read directly on a 4″ square meter face. No calculation or knob-twisting is necessary once range selection and zero set are made. The −hp−430A is automatically self-balancing, and may be used over any frequency, depending on the associated barreter and mount.

This instrument consists of an a.c. bridge, one arm of which is a barreter. The bridge is in balance with zero r-f power in the barreter. As r-f power is applied to the barreter, an equivalent a.c. (audio) power is automatically removed; thus the bridge remains in balance. A vacuum tube voltmeter reads the change in audio power level. This meter, calibrated in milliwatts, gives a direct indication of the r-f power in the barreter.

The indicating meter is calibrated in dbm in addition to the linear milliwatt calibration. The 5 power ranges are selected on a convenient front panel switch.

From a technical standpoint, the new −hp−430A covers a power range of from 0.02 milliwatt to 10 milliwatts. Ranges are related in 5 db steps, and continuous readings are available from −20 dbm to +10 dbm (0 dbm equals 0.001 watt). This power range may be extended by the use of attenuators or directional couplers. Accuracy of the meter is within 5 percent of full scale readings.

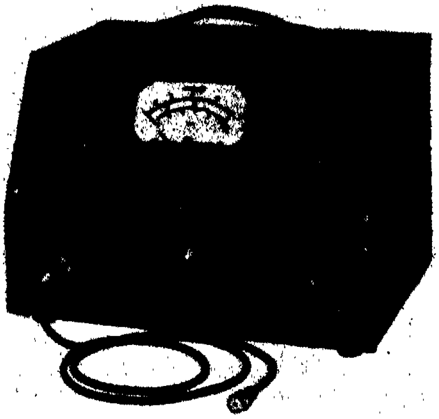

This power meter measures 12″ wide by 9″ high, and is 9″ deep and is powered by any 115 volt, 60 c.p.s., a.c. source.—Hewlett Packard Company, *395 Page Mill Road, Palo Alto, California.*

Coatingage

The "Coatingage" is an instrument for measuring the thickness of non-magnetic coatings on iron or steel. Measurements are made rapidly, without damage to the coating, and the thickness is indicated directly on the meter of the instrument. Two concentric scales cover a range of 0.0001″–0.50″. The instrument's lightweight and self-contained battery power supply permit its use in the field as well as in the laboratory or on the production line.

The "Coatingage" head contains a coil, connected in a bridge circuit. Coating thickness is measured by the effect of changes in the reluctance of the magnetic circuit. When the coil is in direct contact with the base metal the reluctance is low and the self-inductance of the coil is high. The bridge is then balanced for zero thickness. An increase in the gap between the coil and the base metal unbalances the bridge, and causes current to flow through the indicating microammeter.

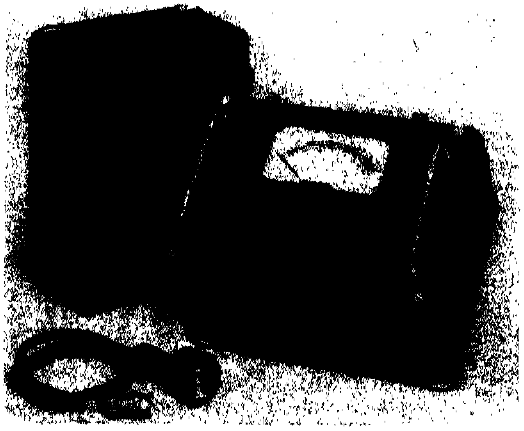

The instrument is housed in a luggage-type carrying case, 8″ high, 9″ wide, and 6″ deep, weighing 10 lb. Power is furnished by two 67½-volt batteries and one 1½-volt battery, contained in the instrument. Thickness readings are within 10 percent of the actual thickness.—Branson Instruments, Inc., *436 Fairfield Avenue, Stamford, Connecticut.*

Manufacturers' Literature

Sonic Energy—4-page brochure discusses potentialities of sonic energy for laboratory and production applications.—ULTRASONIC CORPORATION, *61 Rogers Street, Cambridge 42, Massachusetts.*

Electronic Counters—4-page catalog is a brief guide to the company's line of high speed electronic counters, scalers, counter chronographs, and special electronic frequency measuring and computing equipment. A discussion of the electronic counting principle, methods of count detection, and typical applications are included.—POTTER INSTRUMENT COMPANY, INC., *136-56 Roosevelt Avenue, Flushing, New York.*

Alarms—Bulletin 300 describes various types and applications of Panalarms, sound and visual alarms which indicate failure or abnormal conditions when actuated by a remote switch, thermostat, float switch, or other switch.—PANALARM PRODUCTS, INC., *7216 North Clark Street, Chicago 26, Illinois.*

Universal Tester—Bulletin M, 4 pages, describes a multilow range universal tester. An 8-inch dial indicator is calibrated in 4 scales, up to 100 pounds.—W. C. DILLON AND COMPANY, INC., *5410 West Harrison Street, Chicago 44, Illinois.*

Manometer—Publication No. TP-30-A describes recent improvements in new models of the W and T Precision Dial Manometer.—WALLACE AND TIERNAN PRODUCTS, INC., *Belleville 9, New Jersey.*

Self-Lubricating Bushings—A 7-page pamphlet describes the uses and properties of Graphalloy self-lubricating bushings. These contain no oil, and are particularly useful in inaccessible equipment; at temperatures where oil solidifies or volatilizes; for current-carrying bearings; for submerged bearings, etc.—GRAPHITE METALLIZING CORPORATION, *1050 Nepperhan Avenue, Yonkers 3, New York.*

Standardization—Pamphlet contains a series of papers on the subject "What Good Are Standards?" which were presented at the 1948 annual meeting of the American Standards Association. These papers include discussions of various problems, such as the legality of standardization, the standardization work of the Munitions Board, and the functions of standardization in such company operations as purchasing, manufacturing, and marketing. Available for $1.00 from AMERICAN STANDARDS ASSOCIATION, INC., *70 East 45 Street, New York 17, New York.*

Hydraulic Cylinders—Catalog Section No. 103, a 20-page illustrated booklet, describes all standard hydraulic cylinders, with complete diagrams and information. Engineering data in the new catalog includes displacements and theoretical forces for cylinders.—GEROTOR MAY CORPORATION, *Baltimore 3, Maryland.*

Metals—24-page booklet, PM 13, is a brief survey of the manufacturer's metals, alloys, and chemicals and their uses. Booklet available in English, French, and Spanish editions.—MUREX LIMITED, *Rainham, Essex, England.*

High Speed Motion and Still Photography—129-page illustrated booklet (reprints of papers presented at 1948 Convention) describes various high speed cameras as well as techniques used by governmental and industrial agencies. Specific topics include electrical flash photography and a new high speed stroboscope, lamps for high speed photography, motion picture equipment for very high speed photography, methods of analyzing high speed photographs and the uses of high speed photography in the armed forces, automotive and other industries and research. $1.50.—SOCIETY OF MOTION PICTURE ENGINEERS, *342 Madison Avenue, New York 17, New York.*

Socket-Turret—A single-page illustrated bulletin describes various types of new and unique terminal structures on which the circuit components associated with a vacuum tube may be neatly connected directly at the socket.—VECTOR ELECTRONIC COMPANY, *738 East Third Street, Los Angeles 13, California.*

Explosilite—Bulletin No. DT-4 describes the M.S.A. Explosilite, a simple and dependable automatic means of warning when dangerous atmospheres contaminated by natural gas or petroleum vapors occur. This device continuously samples the air of a working place, flashing an alternate bright and dim red signal light when flammable gas concentrations reach a predetermined danger point.—MINE SAFETY APPLIANCES COMPANY, *Braddock, Thomas and Meade Streets, Pittsburgh 8, Pennsylvania.*

pH Equipment—Circular 1176A describes pH meters, pH electrodes, flow, and immersion type assemblies, and miscellaneous accessories.—CENTRAL SCIENTIFIC COMPANY, *1700 Irving Park Road, Chicago 13, Illinois.*

Edgewise Panel Instruments—A 4-page brochure "Electrical Measurements" is devoted to edgewise panel instruments, explaining their desirability for accuracy and a description of various instruments which are available in the edgewise panel case.—SENSITIVE RESEARCH INSTRUMENT CORPORATION, *9-11 Elm Avenue, Mount Vernon, New York.*

Vacuum Tube Voltmeter—Bulletin GEC-461 describes Type AA-1, vacuum tube voltmeter, with a calibrated range of 0.001 volt to 300 volts at all frequencies from 10 cycles to 1.5 megacycles. This voltmeter is graduated in decibels, covering a range of −52 to +52 db from a reference level of 1 milliwatt at 600 ohms, and contains a 10-position pushbutton switch for selection of any working range instantly.—GENERAL ELECTRIC COMPANY, *Schenectady 5, New York.*

High Vacuum Apparatus—The winter 1949 publication of DPI features an article on the "Measurement of low pressures" and includes other high vacuum techniques of interest.—DISTILLATION PRODUCTS, INC., *Vacuum Equipment Division, Rochester 13, New York.*

CEC Recordings—A 6-page house organ, Vol. 3, No. 1, features a description of a new sampling probe (Type 18863) for the Consolidated Leak Detector, a description of an automatic high vacuum bakeout oven to speed up and greatly improve the cleaning process of vacuum system parts, and other items of interest.—CONSOLIDATED ENGINEERING CORPORATION, *620 North Lake Avenue, Pasadena 4, California.*

UHF Noise Diode—Publication 86-30B describes the Type TT-1 temperature-limited diode used as a noise source in measuring receiver sensitivity for frequencies up to approximately 3000 mc. Having coaxial-line construction, it is readily adaptable to wide-range (untuned) coaxial circuits. A maximum temperature-limited emission of 100 ma enables the measurement of receiver noise factors up to about 20 db. This brochure is fully illustrated with a photograph of the tube, schematics, and characteristic curves.—ECLIPSE-PIONEER DIVISION, BENDIX AVIATION CORPORATION, *Teterboro, New Jersey.*

New Materials

Forest K. Harris: Associate Editor
in Charge of this Section
National Bureau of Standards, Washington, D. C.

Glass

"Glass is an inorganic product of fusion which has been cooled to a rigid condition without crystallizing" (A.S.T.M.). Usually 60 percent or more of sand is fused together with various percentages of two or more oxides of Na, Ca, K, Pb, B, Mg, and Al. About 600 different glasses are made commercially which can be classified into five chemical types of silicate glass.

Soda-Lime glasses have been made for more than 5000 years, and are still used for 90 percent of all glassware. Their raw materials are the least expensive and they are among the easiest to melt and shape. Only within the past 40 years have they been studied scientifically to improve their properties. Silica is used as the glass-forming oxide, Na_2O and K_2O as alkaline fluxing ingredients to lower the fusion temperature, and CaO and MgO as alkaline earth fluxing agents to increase chemical durability. At the present time 70–75 percent of silica is used with seldom more than 17 percent of alkali and 5–15 percent of alkaline earths. Controlled amounts of minor ingredients are used to fit the glasses to different purposes.

Lead glasses were first produced in 1675 and have been extensively used in cut and engraved glassware. Their indices of refraction are high and they are used in compound lenses. They also have higher electrical resistivities than soda-lime glasses. Today they are used for insulators, in some radio tubes, for lenses, prisms, and fine art glass. Lead oxide is a good fluxing agent and in percentages from 20–40 it replaces most or all of the lime and some of the soda or alkali content. Excluding x-ray absorbing and optical glasses, compositions are in the range 53–67 percent SiO_2, 5–10 percent Na_2O, 1–10 percent K_2O, 0–6 percent CaO, and 20–40 percent PbO.

Silica glass (fused quartz or fused silica), 99.8 percent silica, can be made by fusing quartz crystals or sand. The fusing temperature is high (about 3150°F) so that special melting techniques must be used. Also the molten glass is so viscous that it is difficult to make it homogeneous and free from bubbles. It is difficult to shape and its use has been restricted to small and simple forms. It has been used for the envelopes of ultraviolet light sources, for chemical laboratory ware, combustion tubing, thermocouple sheaths, furnace windows, etc. First commercial production was about 1910.

Borosilicate glasses (1910) are of a type in which the melting point of the silica is lowered by the addition of boric oxide (B_2O_3) and aluminia (Al_2O_3) with only the smallest possible amounts of alkali. They have high intrinsic resistance to corrosion and to thermal shock but are difficult to manufacture and work. Thermal expansion coefficients may be as low as 25×10^{-7}/°C, whereas soda-lime and lead glasses have coefficients around 90×10^{-7}/°C. Pyrex laboratory and oven glassware are of this type. Present day compositions of commercial borosilicate glasses are in the range 73–82 percent SiO_2, 3–10 percent Na_2O, 0.4–1 percent K_2O, 0–1 percent CaO, 0–10 percent PbO, 5–20 percent B_2O_3, and 2–3 percent Al_2O_3.

Ninety-six percent silica glasses, developed in 1939, employ a revolutionary process in manufacture. An article is formed from conventional borosilicate glass and a heat treatment causes the glass to separate into two intermingled phases. One phase contains nearly all the alkalies and can be leached out by hot acids to leave a sponge-like glass containing 96 percent silica and 3+ percent of B_2O_3. The pore diameters average 20A in size. The leached glass is so refractory that subsequent heating can close the pores completely without any change in the shape of the article even though there is a linear shrinkage of about 14 percent. Thus the difficulties of working a glass of high silica content are circumvented and the resulting 96 percent silica glass is practically as ideal as fused quartz. Also large and intricately shaped objects can be made. "Vicor" brand glassware is of this type and has such uses as range burner plates, crucibles, laboratory ware, germicidal lamps, thermocouple protection tubes, induction furnace linings, and electrical insulation. Such glass can be used at a red heat and plunged into ice water repeatedly without cracking.

The above material was abstracted from an article in the "Burrell Announcer" written by H. G. Vogt of the Corning Glass Works.—BURRELL TECHNICAL SUPPLY COMPANY, *1942 Fifth Avenue, Pittsburgh 19, Pennsylvania.*

Cellulose Gum

Considerable new information on the physical and chemical properties of *Hercules CMC* cellulose gum is contained in a revised technical booklet on this chemical, just released by the manufacturer.

Hercules CMC is a refined, odorless, and tasteless grade of cellulose gum (sodium carboxymethylcellulose). Solutions of this gum can be evaporated to leave flexible films which are unaffected by oils, greases and most organic solvents. Certain salts and acids react with the gum to give films which are relatively insoluble in water. Tensile strength of CMC films ranges from 9600 to 11,600 p.s.i., and their percentage elongation from 1.7 to 4. The film-forming properties are used in the formation of barrier coatings on paper board, where it adds resistance to penetration of oils, waxes, and ink. This property is also utilized in textile sizing and finishing. In addition, it also has marked suspending, thickening, and stabilizing properties. It is used to stabilize oil-in-water emulsions; to control viscosity in resin emulsion paints; as an additive to detergents where its suspending properties help to eliminate the redeposition of dirt; as a thickening agent in latex solutions; and as a binder in the ceramic industry in various glaze applications. The purified food-grade type of this gum is finding use in the food and pharmaceutical industries to control viscosities, stabilize emulsions, as a suspension agent, or as a water-soluble film-former.—HERCULES POWDER COMPANY, *Wilmington, Delaware.*

Plastic Bell Jar

Lucite bell jars, developed by the manufacturer for use in vacuum equipment for precision casting, are now generally available in-seven-in. and ten-in. diameters. They can also be made on quantity order in other specified sizes for evacuation work.—DURABLE FORMED PRODUCTS, INC., *6–8 Greene Street, New York 13, New York.*

Silicone Fiberglas Sleeves

A sleeve employing silicone rubber reinforced with Fiberglas has been developed for flexibly connecting lengths of rigid duct carrying air heated to 550°F. An internal pressure of ten p.s.i. is withstood at this temperature without leakage. The sleeve will also remain flexible at temperatures as low as −75°F. The manufacturer is prepared to supply sleeves in diameters between a fraction of an inch and several feet, with the length and wall thickness appropriate to the application.—CONNECTICUT HARD RUBBER COMPANY, *405–9 East Street, New Haven 9, Connecticut.*

Glass Phenolic Laminate

Grade 170 Laminate is characterized by very low water absorption (0.06 percent) and low power factor. Its tensil and flexural strengths are both very high, 52,000 and 69,000 p.s.i., respectively. Its density is 1.78, and its dielectric strength is 580 v.p.m. It is available in natural color and semi-glass finish with standard NEMA tolerance for grade *G-3*, in thicknesses from 1/32 in. to 2 in., and sizes 36×36 in. and 36×48 in. The manufacturer suggests that the use of this material may eliminate the necessity for fungicides and other special handling required for tropical and high humidity applications.—St. Regis Paper Company, Panelyte Division, *230 Park Avenue, New York 17, New York.*

Insulating Bushings

Compression type lead-through bushings of steatite and Neoprene, designed for use in hermetically sealed transformers and capacitors (including oil-filled types) are now generally available. They are stated to have high resistance to mechanical and thermal shock even at extreme temperatures, and to be free from tracking tendencies. Voltage and current capacities are high for the space occupied.—Lundey Associates, *694 Main Street, Waltham 54, Massachusetts.*

Carbide Milling Cutters

Carbo-Mills form a new series of carbide cutters having 1/8-in. shanks. They are made of solid carbide in a single piece, cutting heads and shanks being integral. There are 12 different shapes in the series, chosen to meet the widest possible range of applications. These mills are suited to the deburring and machining of parts made from materials that are abrasive, tough, or of hardness ranging up to 60-C Rockwell.

The single piece construction simplifies the problem of balance at high speeds, making possible precise work in intricate or exacting operations. The prices are less than for similar mills of two-piece construction; and they can be repeatedly reground to give results comparable to new tools at each regrinding.—Severance Tool Industries, Inc., *710 Iowa Street, Saginaw, Michigan.*

Carbide Blanks

Cylindrical carbide blanks are available in lots of 50 or more in any one of 7 grades of carbide. Lengths range in 1/16-in. steps from 3/16 in. to 1½ in., and diameters in 3/32-in. steps from 3/32 to ½ in. Ground or unground finish may be specified.—Carboloy Company, *11167 East 8 Mile Road, Detroit 32, Michigan.*

Tungsten Powder

Tungsten powder of closely controlled particle size and distribution is now available as a result of newly installed facilities for producing tungsten in powder form for the manufacture of tungsten carbide tools. This material will contain at least 75 percent of individual particles measuring below 5 microns.—Sylvania Electric Products, Inc., *500 Fifth Avenue, New York 18, New York.*

Stainless Steel Clad Sheets

Permaclad is a composite sheet material in which a layer of stainless steel is permanently bonded to a carbon-steel backing plate. The stainless layer forms 20 percent of the total thickness in sheets up to 13 gauge, and 10 percent in heavier gauges. The cost of the material is about half the cost of solid stainless in the same gauge. The bond strength is stated to be equal to that of the component steels. The clad material is metallurgically correct on one side for corrosion-resistant service, and possesses the ductility and other desirable properties of the carbon-steel backing plate. The standard material (type 304 stainless with AISI-1008 backing) can be cold-formed, arc- or spot-welded, soldered, drawn, or stamped without separating the layers and without loss in the corrosion-resistant properties of the stainless steel. Compositions other than the standard may be specified.—Alan Wood Steel Company, *49 Darby Street, Conshohocken, Pennsylvania.*

Phosphor Bronze Wire

By special processing the manufacturer has increased the tensile strength of "Grade-A" phosphor bronze wire by at least 10,000 p.s.i. over established standards, and increased the tensile strength of "Grade-E" to the values covered by standard specifications for "Grade-A." Both types can be had in diameters from 0.0159 in. to 0.182 in., making available to spring makers a better product at no increase in price, according to the manufacturer.—Riverside Metal Company, *Riverside, New Jersey.*

Centrifugal Castings

Cylindrical steel castings, free from defects and of uniform quality, are available in specified alloys. The centrifugal casting process used is licensed on an exclusive basis from Firth-Vickers Stainless Steels, Ltd. Castings up to 42 inches diameter and in lengths up to three feet (depending on diameter) can be supplied. The work is handled in permanent metal molds and the desired heat treatment is applied during the process. The finished casting is machined to remove surface skin and the scale resulting from heat treatment, and examined by x-rays to insure freedom from structural defects. The user employs this blank to machine whatever finished parts are required.—Lebanon Steel Foundry, *First Avenue and Leaman Street, Lebanon, Pennsylvania.*

THE REVIEW OF SCIENTIFIC INSTRUMENTS

VOLUME 20, NUMBER 6 *JUNE, 1949*

Further Improvements in Magnetic Focusing

LARKIN KERWIN AND CLAUDE GEOFFRION
Department of Physics, Laval University, Quebec, Canada
(Received December 20, 1948)

The general theory of magnetic focusing in a plane developed in a previous paper is extended to asymmetric cases. The general asymmetric case being developed, several particular examples are considered, including one which eliminates second-order aberrations, and requires a smaller magnet than the normal design. Methods of minimizing aberrations are discussed.

I. INTRODUCTION

IN a recent paper[1] a theory of magnetic focusing of charged particles in a plane was developed. It is based on an ideal magnetic field of such a boundary shape as to produce perfect focusing, as shown in Fig. 1. Here the field boundary M is symmetrically shaped so that monoenergetic ion beams leaving a source S are deflected so as to focus perfectly at T. The equation of M is a function of the parameters a and R, and is given by:

$$y=x(a-x)/(R^2-x^2)^{\frac{1}{2}}.$$

In the theory was developed a method for calculating the aberration, dispersion, image widths, etc., produced by any approximation to the ideal curve. Among the several practical approximations considered were the normal case—being the line through O tangent to the ideal boundary as shown by N, which is the type of focusing currently in common use—and the inflection case—being the line F tangent to the ideal boundary at its inflection point. The inflection field eliminates second-order aberrations, yet requires a smaller magnet for the same resolving power.

In all of these cases, the discussion was confined to approximations which were symmetrical about the y axis. It is the purpose of this paper to show how further practical improvements may be obtained by using non-symmetrical fields. In designing these, we may use the technique, familiar in optics, of balancing a positive aberration produced by one boundary with a negative aberration produced by the other.

In Fig. 2, M is the ideal field boundary and C is any curve coincident with M at P. Then any ray from S entering the field defined by C at a point other than P will pass through an interval of magnetic field w which will cause it to be aberrated from the focusing point T. We introduce an axis tangent to the ideal curve M and call k the abscissa along the axis. Then if we designate the ordinate of M with respect to k as $f(k)$, and that of C as $F(k)$, we have:

$$w=F(k)-f(k).$$

If, using the magnetic field boundary C on the left, we wish to focus all beams at T, then the point where an extra-P beam leaves the field boundary on the right must not be on M, but a distance w' from it, such that the aberration produced by w' is equal to that produced by w, but of opposite sign. Although not immediately obvious, it may be shown that, to the degree of approximation to be considered, w' must equal $-w$. By finding w' for

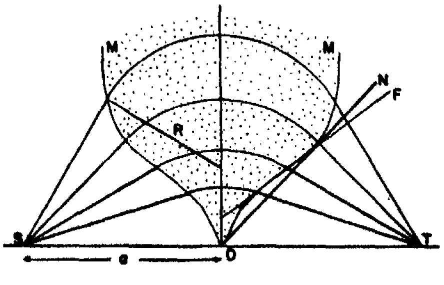

FIG. 1. Ideal magnetic focusing field.

---

[1] Larkin Kerwin, Rev. Sci. Inst. 20, 36 (1949).

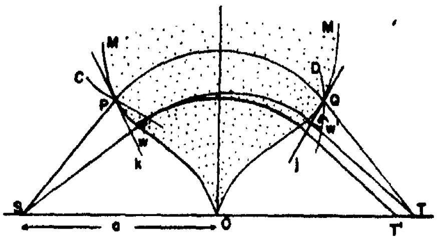

FIG. 2. C is any approximation to the ideal curve M; D is the corresponding approximation which corrects defocusing produced by C.

each ray we establish a curve D, which differs from M by w' and corrects the defocusing effect of C. Placing the equation D equal to $E(j)$ where the j axis is tangent to the ideal boundary at the point Q where the ray through P leaves it, we have:

$$w'=E(j)-f(j).$$

Remembering that $f(k)=f(j)$, we therefore have, as the condition for corrected focusing,

$$F(k)+E(j)=2f(k).$$

Expanding these functions in Taylor series at the points P and Q, neglecting 4th-order terms, and remembering that $f'(k)=0$ and that $\Delta j=\Delta k$ to this degree of approximation, we have

$$\begin{aligned}2[(\Delta k^2/2)f''(k)+(\Delta k^3/6)f'''(k)]\\ =\Delta k[F'(k)+E'(k)]+\Delta k^2/2[(F''(k)+E''(j)]\\ +\Delta k^3/6[F'''(k)+E'''(j)].\end{aligned} \quad (4)$$

Equation (4) enables us to determine the exit boundary shape D which will correct aberrations produced by an entrance boundary shape C. Several practical examples of this asymmetric arrangement will now be considered.

II. NORMAL CASE CORRECTIONS

In the case of the normal approximation, the curve C becomes a straight line tangent to the ideal boundary at P, as shown in Fig. 1. Accordingly, $F(k)=0$, and Eq. (4) simplifies to

$$\begin{aligned}2[(\Delta k^2/2)f''(k)+(\Delta k^3/6)f'''(k)]\\ =\Delta kE'(j)+(\Delta k^2/2)E''(j)+(\Delta k^3/6)E'''(j).\end{aligned}$$

Therefore, since $E'(j)=0$, we see that the curve D must have the same slope as the ideal curve at the point Q, where it coincides. If D is to be approximated by a circle, then we neglect third-order terms, and have

$$(\Delta k^2/2)E''(j)=\Delta k^2f''(k).$$

If we insert the geometric conditions developed in the reference cited[1] we find for the radius of curvature of the circular approximation to D:

$$R_d=R_0(\cot^3\theta)/2,$$

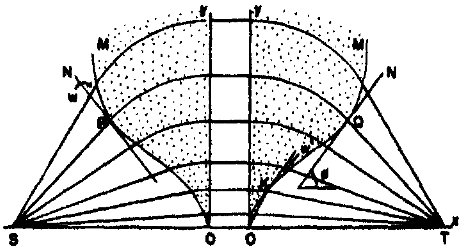

FIG. 3. Aberration produced near P is negative, that produced near K is positive.

where R_0 is the radius of curvature of the ion beam in the magnetic field.[2] A magnetic field bounded by a straight line on one side and an arc of a circle of radius R_d on the other, these boundaries being located according to the theory just discussed, will produce third-order focusing. That is, second-order aberrations will be corrected. Using the same procedure we may verify the case previously suggested,[1] that an entrance field boundary in the shape of a circle of radius $R_0\cot^3\theta$ may be corrected by an exit field boundary in the shape of an arc of a circle of the same radius.

III. INFLECTION CASE CORRECTIONS

In the inflection approximation, the curve C becomes a straight line tangent to the ideal boundary M at its inflection point. Here again $F(k)=0$, and in addition $f''(k)=0$.

Equation (4) therefore simplifies to

$$\begin{aligned}(\Delta k^3/3)f'''(k)=\Delta kE'(j)+(\Delta k^2/2)E''(j)\\ +(\Delta k^3/6)E'''(j).\end{aligned} \quad (5)$$

From this we see that the curve D must have the same slope as the ideal curve M at the inflection point, and further that D must be an inflection curve with the same inflection point as M. If we wish to eliminate second-order aberrations, then we drop third-order terms and D becomes simply a straight line, i.e., the inflection case already discussed.

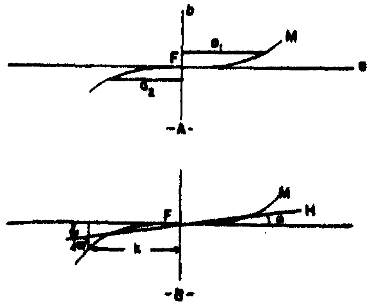

FIG. 4.

---

[2] In a recent paper (Proc. 7th Solvay Congress, Brussels, 1947), Dr. Kenneth T. Bainbridge proposes such a focusing field. We thank Professor Bainbridge for an advance copy of the manuscript.

In the reference cited, it was shown that third-order aberrations may be made to average zero by using entrance and exit boundaries in the shape of arcs of circles tangent at the inflection point and of radius given by

$$R=4\Delta k/f'''(x),$$

where $f(x)$ is given by Eq. (1). Equation (5) points to the fact that we may make the third-order aberrations average zero by curving only one boundary. To effect this it is necessary that

$$E'''(j)=2f'''(k)$$

to the approximation considered. If therefore the exit boundary shape is that of a circle of radius

$$R_{a'}=2\Delta k/f'''(x),$$

then the average of the third-order aberrations over a region $\pm\Delta k$ will be zero.

We note that the radius used depends on the portion of the boundary utilized—i.e., the width of the beam. Also, that as Δk is plus or minus (on one or the other side of the central ion trajectory), the radius reverses sign, i.e., the boundary shape is that of two circles tangent at the inflection point.

IV. ASYMMETRIC IDEAL FIELD

In Fig. 3 we consider the ideal field as consisting of two halves joined along the y axis. The left half deflects the divergent beam from S into a beam parallel to the x axis, while the right side deflects a beam parallel to the x axis into a beam focusing at T. Obviously any section of the left side might be combined with any section of the right side to produce perfect focusing.

Another method of reducing aberrations is therefore based on the observation that the normal or inflection case approximations produce a residual aberration of one sign or the other depending on whether the concave or convex part of the ideal curve is approximated. We may therefore obtain a better correction if we combine the convex part of the boundary P, at the entrance, with the concave section K, at the exit.

In order to correct, say, second-order aberrations in this way, it is necessary that the 2nd-order term component of w at P should equal the second order term component of w' at K. This means that the radius of curvature at P should equal that at K. This enables us to locate the point K, but since the equations involved are very cumbersome, we may use a simpler method of finding K which is illustrated for the normal case.

TABLE I.

θ	R	x_K	y_K	θ'	h
30°	$0.500a$	$0.0890a$	$0.165a$	10.2°	$0.329a$
45°	$0.707a$	$0.193a$	$0.223a$	15.7°	$0.459a$
90°	$1.000a$	$0.628a$	$0.300a$	38.0°	$0.490a$

In Fig. 4A the ideal curve is shown at M, drawn with respect to new axes a and b, through the inflection point F. Then the equation of the ideal curve with respect to these axes may be represented by:

$$b=Aa^3+Ba^4+\cdots,$$

whence:

$$b'=3Aa^2+4Ba^3+\cdots,$$

and

$$b''=6Aa+12Ba^2+\cdots.$$

Therefore the radius of the curve at a_1 is given by:

$$R_1=\frac{(1+9A^2a_1^4)^{\frac{3}{2}}}{6Aa_1+12Ba_1^2}.$$

If we place $a_1=-a_2$, we have:

$$\frac{R_1}{R_2}=\frac{-Aa+2Ba^2}{Aa+2Ba^2}.$$

We see, therefore, that if a is small, or B is small, then $R_1=-R_2$. In the case considered here, 4th-order terms are neglected, i.e., B is small, so that we see that R_1 will equal $-R_2$ when $a_1=-a_2$. In this case, we see that $b_1'=b_2'$. Referring back to Fig. 3, we see then that the ideal curve will have the same radius of curvature at K as at Q when the slope at K equals that at Q. This slope is given by

$$\tan\phi=\frac{a^3\sin^2\theta-2xR^2+x^3}{(a^2\sin^2\theta-x^2)^{\frac{1}{2}}}$$

from which we may easily calculate x_K by numerical methods, and draw through it the line A with slope $\tan\phi$. It is then only necessary to match the central ray through P with the central ray through K, and we have an aplanatic combination, as shown in Fig. 5 for the general case.

From this figure we see that the distance h is still necessary to completely determine the exact

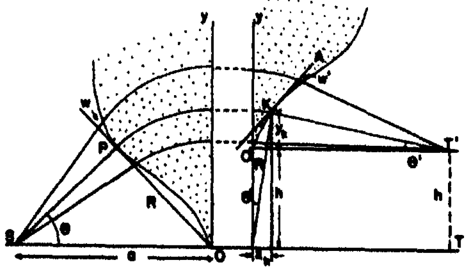

FIG. 5. A combination of negative aberration produced near P and positive aberration produced near K gives an unaberrated image at T'.

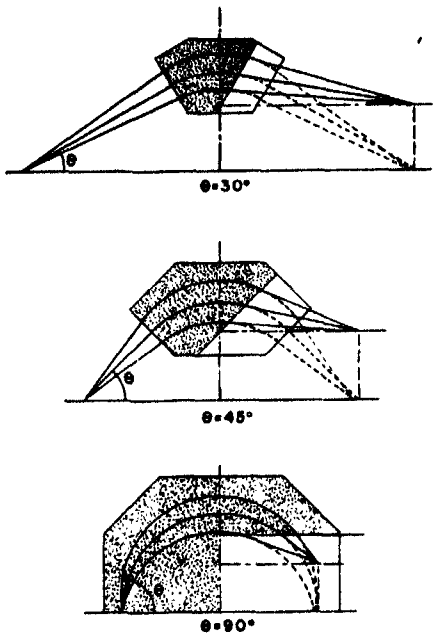

FIG. 6. Comparison of normal focusing and compensated aberration fields.

location of K. This is obtained by putting

$$h=R\cos\theta'-y_K,$$

where y_K is obtained by using Eq. (1), and θ' is determined by

$$x_K=R\sin\theta',$$

where, of course, $R=a\sin\theta$.

These various calculations have been made for a number of instruments, and are given in Table I.

These cases are shown in Fig. 6, with the normal case dotted in for comparison. In addition to the reduced aberration, we see that this field possesses the further practical advantage in being considerably smaller than the normal field, permitting the use of much smaller magnets.

V. MINIMIZING ABERRATIONS

The various approximations to the ideal magnetic field boundary discussed in this theory have this in common: the central ion beam passes through the points of coincidence between the ideal boundary and the approximation and hence is not aberrated, while rays to either side of the central ray are aberrated by an amount which is a function of their distance from the central ray. For all practical purposes, the aberration of an instrument is its maximum aberration, which is provided by the outer rays of the beam. It is possible to reduce the instrument's effective aberration by reducing this maximum aberration, at the expense of aberrating the central rays. In other words, it is possible to minimize the maximum aberration by simple methods, which will be illustrated for the inflection case.

It has been shown[1] that the aberration is proportional to the y component of the displacement of the approximation from the ideal curve. This in turn may be shown to be a function to the w component parallel to the central ion trajectory as it enters the field. In Fig. 4B which shows the inflection approximation F to the ideal curve M we see that the maximum aberration is due to the component w. If instead of F, however, the line H, at an angle β with F, were used as the effective field boundary, then the maximum aberration would be due to w'. The condition for which w' will be a minimum is best found by averaging the squares of the deviations and finding the condition for which the average is a minimum. We thus have:

$$w'^2=1/\Delta k\int_0^{\Delta k}w'^2dk,$$

where

$$w'=1/6f'''(x)\Delta k^3-\Delta k\tan\beta,$$

whence

$$w'^2=\frac{f'''^2(x)\Delta k^6}{252}-\frac{2f'''(x)\Delta k^4}{30}+\frac{\Delta k^2\tan^2}{3}.$$

From this we easily find, as the condition for minimum aberration,

$$\tan\beta=[f'''(x)k^2/10].$$

If the inflection field boundaries are tilted so as to coincide with H, the aberration will therefore be reduced by a factor of about 2.

ACKNOWLEDGMENTS

The authors take pleasure in acknowledging the assistance of Professor E. Persico in mathematical discussions, and thank him for reviewing the manuscript.

THE REVIEW OF SCIENTIFIC INSTRUMENTS VOLUME 20, NUMBER 6 JUNE, 1949

The Regulation of Temperature in the Application of High Frequency Induction Heating to Thermodynamic Measurements*

RUDOLPH SPEISER, GEORGE W. ZIEGLER, JR., AND HERRICK L. JOHNSTON
The Cryogenic Laboratory and The Department of Chemistry, The Ohio State University, Columbus, Ohio

(Received May 20, 1948)

An apparatus to regulate the elevated temperatures produced by high frequency induction heating is described. The regulation is achieved by varying the inductance in series with the work coil in such a way as to hold the current through the work coil constant. Except for a *negligible* error due to a small percentage change in frequency, the energy transferred to the work (in applications described in this paper) can be held constant.

INTRODUCTION

A PROGRAM of research on the structure and thermodynamic properties of inorganic solids, liquids, and gases at very high temperatures is underway in this Laboratory. This program includes: vapor pressure measurements,[1] calorimetry,[2] and structure studies by x-ray diffraction.[3]

The use of high frequency induction heating has been developed as the principal source of energy to carry out the aims of this research because this method of heating is particularly well suited in the temperature range 1000°–3000°K. Employed as generators are two 3-phase, 15-kilowatt, General Electric electronic heaters which operate at a frequency of 500 kilocycles. The power output of these units is varied by changing the plate voltage. For this purpose, the manufacturer has supplied only six voltage taps on the primary of the high voltage transformer in the power supply for the oscillator, thus making available only six different outputs for a given experimental set-up. However, two requirements are necessary for satisfactory application of these generators to high temperature research: (1) The power output must be continuously adjustable to any value desired within the rated capacity of the generator; (2) the energy supplied by the generator must be regulated in such a manner that the temperature of the object being heated is maintained constant with the necessary precision.

The problem of designing a suitable device to satisfy these requirements is greatly simplified by the fact that the methods[1–4] employed in determining the vapor pressure, heat capacity, and high temperature crystal structure of a substance, lead only to a negligible change in its mass and emissivity. Also, the efficiency of heating is not critical because the mass of the object being heated is seldom greater than 50 grams and the power cost in research of this type is insignificant.

It was found that by placing a variable inductance (hereafter called a variometer) in series with the work coil (see Fig. 1a), the current flowing through the work coil, hence the energy, could be varied over limits wide enough to satisfy experimental requirements. In addition, fluctuations in the r-f current in the work coil due to fluctuations in the line voltage (which lead to temperature fluctuations) could be reduced to negligible proportions by *small* changes in the inductance of the variometer.

APPARATUS

A variometer was designed to have a maximum inductance of 35 percent of the total inductance in the tank circuit of the oscillator. The variometer is made of two helices of 13 turns each and of different diameters. The helices are connected in series with opposing windings and are arranged, one within the other, so that the smaller helix can be moved along the common axis with reference to the larger, stationary helix. A diagram of the variometer is

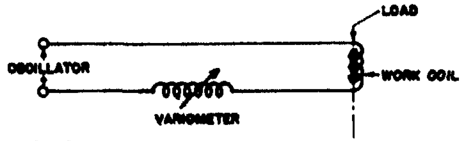

A.- CIRCUIT DIAGRAM - LOADED WORK COIL

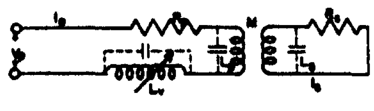

B.- EQUIVALENT CIRCUIT FOR DIAGRAM "A"

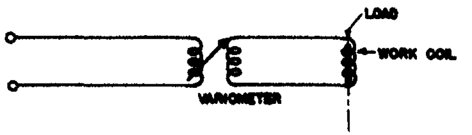

C.- CIRCUIT DIAGRAM – VARIOMOTER HOOKED-UP AS VARIABLE TRANSFORMER

FIG. 1.

---

* This work was carried out under contract between the ONR and The Ohio State University Research Foundation.

[1] Holden, Speiser, and Johnston, J. Am. Chem. Soc. 70, 3897 (1948).

[2] Speiser, Ziegler, and Johnston, "Induction Heating Applied to High Temperature Thermodynamics," Fall Meeting of the American Chemical Society, New York City, 1947.

[3] Edwards, Speiser, and Johnston, Phys. Rev. 73, 1251 (1948).

[4] R. Speiser, Ohio State Univ. Eng. Exper. Station News 19, 12 (1948).

TABLE I.

Variometer inductance	Plate voltage tap setting	Pyrometer temperature °C
Minimum	1	1153
Maximum	1	1239
Minimum	2	1229
Maximum	2	1363
Minimum	3	1300
Maximum	3	Washer melted

shown in Fig. 2. The coils are made of ¼-in. o.d. copper tubing through which cooling water is circulated and are wound on low loss plastic frames. The upper, movable coil is rigidly supported by a plastic arm attached to a counter-weighted brass carriage. The carriage is driven up or down through a gear train and rack and pinion (reduction ratio 6030:1) by a small d.c. motor whose sense of rotation depends upon the polarity of the d.c. signal applied to the armature. The speed of the motor can be varied from 100 revolutions per minute to 3000 revolutions per minute by varying the voltage across the armature of the motor.[5] Limit switches prevent the moving coil from traveling too far up or down. The entire assembly is mounted upon a micarta base 1½-in. thick. To prevent heating by r-f radiation, all parts of the variometer to the right of the dotted line are made of low loss plastics. The variometer parts to the left of the dotted line are made of brass.

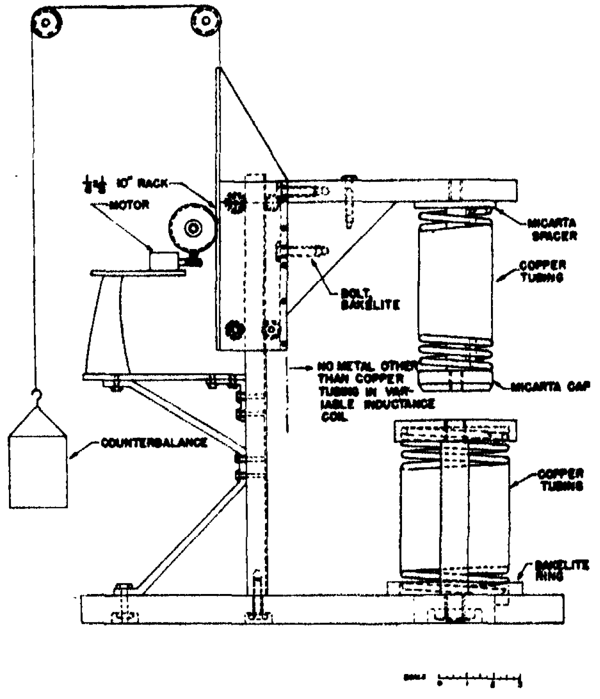

FIG. 2.

The range of the variometer was checked by heating an ⅜-in. iron washer, 1¼-in. diameter, in a work coil of 5 turns, made of ¼-in. copper tubing, 2½-in. diameter and 2½-in. long; the data obtained are given in Table I. These data show that there is a satisfactory overlapping of the available power at each plate voltage setting in the oscillator. Thus a continuous range of output energies are available instead of the six fixed values built into the set.

If the variometer is connected as a transformer, as illustrated in Fig. 1c, temperatures from as low as a few degrees above room temperature up to the highest temperature obtainable with the variometer connected as shown in Fig. 1a, are available without changing the coupling of the work coil to the load. Hence, a continuous range of temperatures from about room temperature to about 3000°K is available through the use of the variometer. The ability to reach lower temperatures through the use of the variometer is especially important in case of the high temperature x-ray work since the need for another type of camera (perhaps resistance heated) to bridge the gap from room temperature to 900°C is thus eliminated.

REGULATION OF TEMPERATURES

Fluctuations in the line voltage lead to small fluctuations of the r-f current flowing through the work coil. These lead in turn to temperature

TABLE II. Automatic regulation of temperature[a]

Time(min.)	T°C	v(volts)
With regulation		
0	1331	206.5
3	1336	207.0
4	1332	206.5
5	1330	207.0
8	1330	206.0
12	1333	207.0
16	1330	205.5
21	1331	205.0
29	1333	208.0
Without regulation		
30	1332	207.5
32	1334	208.0
35	1340	208.0
36	1338	208.0
38	1342	208.5
42	1351	208.5
46	1340	208.0
51	1345	208.0
53	1351	208.5
60	1336	207.0
With regulation		
62	1332	208.0
64	1332	208.0
66	1333	209.0
68	1333	209.0
70	1335	209.5
72	1332	209.5
74	1331	209.0
75	1332	210.0

[a] Tantalum Knudsen cell 2-cm diam. by 2-cm long in a water-cooled, six-turn work coil 3-cm diam. made of ¼-in. copper tubing. The assembly was mounted in a metal vacuum cell whose pressure was less than 2×10^{-4} mm Hg. The temperature was measured with an optical pyrometer.

---

[5] At present, a Delco motor, 27.5 v. d.c., taken from a Sperry Automatic Pilot is being used. The field of this little motor is a permanent magnet.

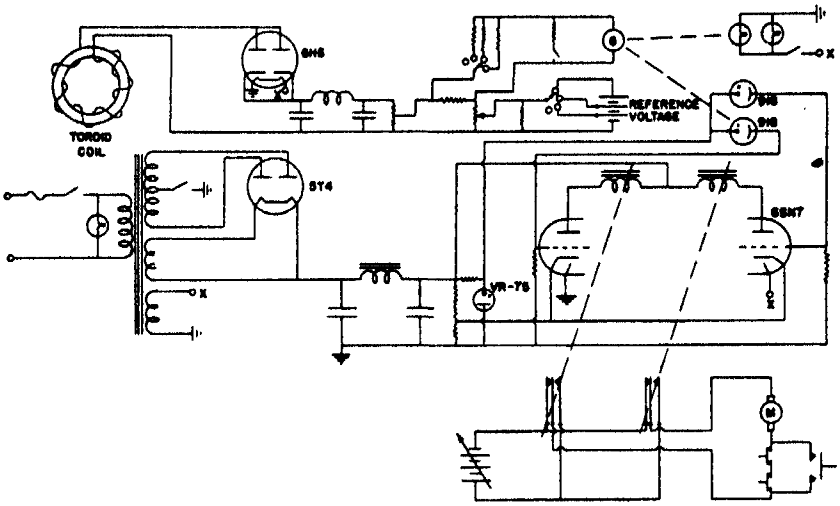

FIG. 3.

fluctuations of the sample being heated. However, small changes in the variometer inductance can be made to counter these deviations so that the temperature is held constant. This can be accomplished manually or automatically. In manual operation the temperature is frequently observed with a pyrometer and the inductance of the motor-driven variometer is adjusted so as to maintain the temperature constant. Temperature control with a precision of 0.2 percent is accomplished in this manner.

A servo-mechanism to maintain constant current in the work coil is shown diagrammatically in Fig. 3. In the Appendix it is shown that, except for a small term that is of negligible magnitude, the power is held constant** when small changes are made in the variometer inductance to compensate for supply line voltage fluctuations. The slight error is due to the small changes in frequency that occur when the variometer inductance is changed.

A toroid is mounted on a straight portion of one lead from the oscillator so that the plane of the toroid is perpendicular to the lead, which is coaxial with the toroid axis. The toroid signal is rectified, filtered, and balanced against a standard reference potential corresponding to the desired temperature. The difference or error signal is impressed upon a galvanometer, *G*, and a light beam reflected from the galvanometer mirror activates one of two photo-cells, the photo-cell being activated depending upon the direction of unbalance. This d.c. signal is amplified so as to actuate a relay which in turn applies a d.c. voltage to the motor *M*. The motor, in rotating, changes the inductance of the variometer in such a way as to oppose the current change in the work coil.

The effectiveness of this method in holding the temperature constant can be judged from the data listed in Table II. The voltage given in the third column is the primary voltage of the transformer used in the high voltage power supply for the oscillator. The temperature regulation is as good as the precision of the optical pyrometer, i.e., 0.1 percent.

APPENDIX

The induction heating circuit shown in Fig. 1a can be represented by the equivalent circuit[6] shown in Fig. 1b. Except for inclusion of the variometer inductance, L_v, the relationship between the generator voltage, V_p, the primary current, I_p, the resistance of the work being heated, R_s, its inductance, L_s, and the mutual inductance between the work and work coil, M, is given by Eq. (9.03) of reference 6:

$$V_p=\left[R_p+j\omega(L_v+L_s)+\frac{(\omega M)^2}{R_s+j\omega L_s}\right]I_p. \tag{1}$$

The power consumed by the work is

$$P=I_p^2\Delta R, \tag{2}$$

where $\Delta R=[(\omega M)^2R_s]/[R_s^2+(\omega L_s)^2]$.

Fluctuation of the line voltage leads to a change in the generator voltage, V_p, and consequently in I_p as shown by Eq. (3).

$$dV_p=\left[R_p+j\omega(L_v+L_s)+\frac{(\omega M)^2}{R_s+j\omega L_s}\right]dI_p. \tag{3}$$

If the variometer inductance, L_v, is varied, then due to the consequent change in frequency, $\omega(\omega=2\pi f)$, R_p and R_s are changed ($R\propto f^{\frac{1}{2}}$), and from Eq. (1),

$$\left[R_p+j\omega(L_v+L_p)+\frac{(\omega M)^2}{R_s+j\omega L_s}\right]\frac{dI_p}{dL_v}+I_p\frac{d[R_p+j\omega(L_v+L_p)+(\omega M)^2/(R_s+j\omega L_s)]}{dL_v}=0. \tag{4}$$

** It can be readily shown that at high temperatures if the power flowing into the work is held constant, the temperature will be held constant too, with rather high precision if the characteristics of the work being heated do not change. This is true as long as the difference is great enough between the temperature of the work and the environment. Under these conditions, the steady state temperature of the work is insensitive to fluctuations of the environment temperature.

[6] Brown, Hoyler, and Bierwith. *Theory and Application o Radio-Frequency Heating* (D. Van Nostrand Company, New York, 1947), Chapter 9.

However, during regulation, L_v is automatically adjusted so that dI_p in Eq. (4) is made equal and opposite to dI_p in Eq. (1). This variation in L_v, in order to keep I_p constant, causes a variation of the frequency so that P in Eq. (2) is not held quite constant and there is a change,

$$dP = I_p^2 d(\Delta R), \qquad (5)$$

which will be shown to be negligible.

Substituting the value of dI_p in Eq. (4) into Eq. (3), $d(\Delta R)$ can be obtained,

$$d(\Delta R) = \pm\frac{2\omega M^2 R_s^3}{(R_s^2+\omega^2 L_s^2)^2}d\omega \pm \frac{\omega^2 M^2(\omega^2 L^2 - R_s^2)}{(R_s^2+\omega^2 L_s^2)^2}dR_s. \qquad (6)$$

If $\omega L_s/R_s$ is set equal to Q, then Eq. (6) can be written as

$$d(\Delta R) = \pm\frac{2M^2}{L_s}\frac{Q}{(1+Q^2)^2}d\omega \pm \frac{M^2}{L_s^2}\frac{Q^2(Q^2-1)}{(1+Q^2)^2}dR_s. \qquad (7)$$

But the fractional error in power control will be

$$dP/P = d(\Delta R)/\Delta R \qquad (8)$$

and

$$\frac{d(\Delta R)}{\Delta R} = \pm\frac{Q^2-1}{Q^2+1}\frac{dR_s}{R_s} \pm \frac{2}{Q^2+1}\frac{d\omega}{\omega}. \qquad (9)$$

It can be readily shown that $d(\Delta R)/\Delta R$*** is a negligibly small quantity. The Q of the secondary circuit is much larger than unity for the frequency range (~0.5 Mc) employed.[6] Thus the magnitude of the factors involving Q in Eq. (9) are less than unity. The maximum change in the frequency, as a result of changes in L_v to compensate for line voltage fluctuations in order to keep the current I_p constant, is approximately 1000 cycles per second. Now the resistance, R_s, varies as the square root of the frequency (reference 6, p. 93), hence, $dR_s/R_s \sim 0.001$; the value of the second term in Eq. (9) is $2/Q^2+1\times 0.002$, and assuming $Q=5$, $dP/P \sim \pm 0.0012$. The fluctuation in temperature as a result of this fluctuation in power is $dT/T = dP/4P \approx \pm 0.0003$. Thus, as is evident from Table II, the servo-mechanism described in this paper can be expected to regulate the temperature to 0.1 percent or better as long as the characteristics of the sample being heated do not change.

*** The result given in Eq. (9) could also have been directly derived from Eq. (2), but at a loss, perhaps, in the clarity of presentation of the working theory of the regulator.

THE REVIEW OF SCIENTIFIC INSTRUMENTS VOLUME 20, NUMBER 6 JUNE, 1949

Instrumentation for Nuclear Studies with Externally Focused Deuteron Beam from Ten-Mev Cyclotron*

B. R. CURTIS,** J. L. FOWLER, AND L. ROSEN
Los Alamos Scientific Laboratory, P. O. Box 1663, Los Alamos, N. M.

(Received February 9, 1949)

A beam of ten-Mev deuterons of about ½ μa has been focused on an area ½ in. in diameter at the center of a 2-ft. diameter reaction chamber 15-ft. away from the cyclotron. In the center of the reaction chamber a gas target is supported with side ports so constructed that nuclear reaction products from the gas can be counted by a proportional counter mounted at the periphery of the chamber. The counter can be rotated through a Wilson seal to make any angle with the beam in the horizontal plane. At the exit of the reaction chamber a Faraday cup is supported. This can be removed to allow the beam to pass between the poles of an analyzing magnet for energy measurements. Tests with charged particle detectors such as a proportional counter or photographic plates show the background to be sufficiently low to allow good resolution of the products from the *d-d* reactions. Using the *d-d* reaction as a neutron source, background neutrons above 12 Mev are only about ten percent. However, the background neutrons above one Mev amount to about 25 times the neutrons from the *d-d* reactions.

I. INTRODUCTION

THE high neutron and gamma-ray background in the immediate vicinity of cyclotrons makes many experiments impossible. In order to avoid this difficulty the beam from the Los Alamos cyclotron has been brought out and focused at the center of a reaction chamber 15 feet from the cyclotron and so located that the three foot water and paraffin shield lies between the reaction chamber and the cyclotron. Figure 1 shows a diagramatic layout of the apparatus. The deflected beam enters a wedge shaped focus magnet about six feet from the beam exit port of the cyclotron.[1] From there the beam, diaphragmed to about ±½ deg., passes into the center of a two-foot diameter reaction chamber. The target is mounted in the center of this chamber. In most of the experiments done to date, gas targets have been used. These are constructed with a beam entrance and exit port and a side port for particle counting. A proportional counter is mounted in the reaction chamber on a movable arm through a Wilson seal in the base of the chamber. The counter can be rotated to make any desired angle with the beam so that it can count the reaction products produced by the beam.

---

* This document is based on work performed at Los Alamos Scientific Laboratory of the University of California under Government Contract W-7405-eng-36.

** Now at Collins Radio Company, Cedar Rapids, Iowa.

[1] L. S. Lavatelli, Los Alamos Report LADC-128.

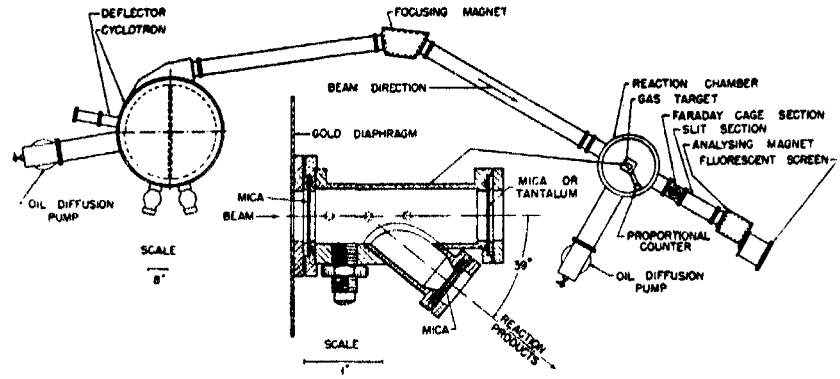

FIG. 1. Diagram of apparatus with enlargement of gas target.

On emerging from the reaction chamber the beam enters a Faraday cage section. From time to time the energy of the beam is determined by lifting the Faraday cup out of its path and allowing it to pass through slits and then between the poles of an analyzing magnet. A simultaneous measurement of the deflection of the beam and the magnetic field gives the deuteron energy.

II. FOCUS MAGNET AND FOCUSING BEAM

The focus magnet used in these experiments was designed and constructed by Feynman, Lavatelli, and Sutton.[1] It consists of a focusing wedge which deflects the deuteron beam through 32 deg. on a radius of curvature of 46 cm. The magnet was designed to provide horizontal and vertical focusing at a first order focal distance 300 cm from the wedge. The field of the focus magnet is held constant during an experiment by electronic controls.[2]

In order to determine the best focal distance and arrangement of the focusing magnet with respect to the reaction chamber, a television camera was used for continuous observation of the focused spot of deuterons as observed on a willemite (zinc orthosilicate) screen placed at the end of a telescoping exit tube.

The beam is defined by the opening of the focus magnet chamber to an area five in. wide by ½ in. high. After focusing, and under optimum operating conditions, a beam of six μa of ten-Mev deuterons can be obtained over an area ¼ in. wide by ⅜ in. high.

Since the target is located at the focus point of the magnet, the beam converges as it enters the scattering chamber and diverges as it leaves. In order to confine the beam to a known direction, a slit 1⅛ in. wide by 11/16 in. high is placed between the focus magnet and the scattering chamber, and a gold diaphragm with a ¼ in. hole is placed at the entry port of the gas target. The beam is thus defined to ±0.63 deg. in the horizontal and ±0.53 deg. in the vertical direction. Under these conditions about ⅓ μa of beam can be obtained through the ¼-in. hole.

To determine the exact direction of the beam as it passes through the gas target chamber, a small aperture (⅛ in. diameter) Faraday cup is mounted on the proportional counter. This is moved through the beam and the current picked up by the cup monitored by a d.c. amplifier and a meter. Thus, the angular spread of the beam can be measured and its angular direction in passing through the scattering chamber determined. A sample curve of the angular spread is shown in Fig. 2. This is the spread expected from the geometry of the experiment. Rutherford scattering due to the front window of the gas target did not appreciably increase the angular spread, since only about 2.5 percent of the beam is scattered more than one degree.

III. THE REACTION CHAMBER ASSEMBLY

Figure 3 is a side view assembly drawing of the reaction chamber and proportional counter. The reaction chamber proper, pump out leads and side ports are of welded steel construction. The lid of the chamber is a 1½ in. thick safety glass plate which rests on two ¼-in. by ¼-in. rubber gaskets which are countersunk in ⅛-in. deep grooves in a ring around the edge of the chamber. At one time a one-in. thick plate glass lid was used and it held under atmospheric pressure. However, the heat

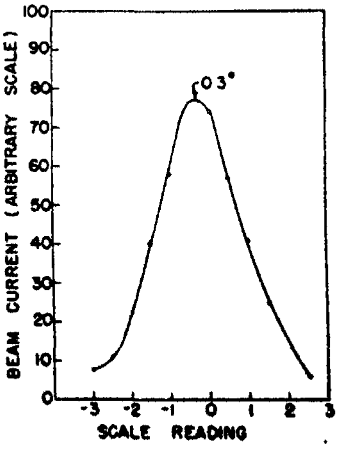

FIG. 2. Spread of beam after passing through gas target. One scale division corresponds to 1/32-in. Beam is limited by a ⅛-in. hole at entrance of gas target 7⅛ in. in front of the position where spread is measured.

---

[2] H. T. Gittings, Los Alamos Report LADC-503.

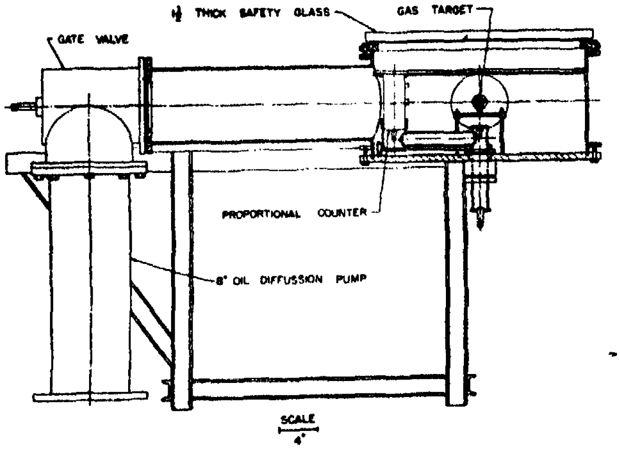

FIG. 3. Assembly drawing of reaction chamber.

from a photo-floodlight left over it produced enough strain to cause it to shatter under atmospheric pressure.

The bottom of the chamber is a ¾-in. brass plate which has a ¼-in. gasket groove to make a vacuum seal to the chamber. In the center of the bottom plate is a Wilson seal through which the proportional counter can be rotated at the desired angle to the beam in the horizontal plane. The lead to the counter passes through the center of its supporting arm. The counter is so mounted that it can be adjusted in height relative to the base plate. The high voltage connections and preamplifiers which can be seen in Fig. 4 are supported at the end of a two-in. tube which passes through the Wilson seal. Mounted within the reaction chamber at about the top of the proportional counter is a ring accurately graduated in degrees from 0–360 deg.

Included in Fig. 1 is a drawing of a typical gas target which is supported on a mount above the base plate so that it can be lined up with the geometrical center of the reaction chamber. The windows over the ports are mica of thickness from one to three mg/cm². The target is so constructed that the proportional counter can only see the beam where it is bombarding the target gas, and hence the charged particle background due to bombardment of windows, etc., is eliminated. Similar targets have been constructed in which the side ports make angle of 20 deg. and 30 deg. with the beam axis. These targets are water cooled.

Figure 4 is a photograph of the reaction chamber, showing the beam entrance tube, Faraday cage section and analyzing magnet.

IV. FARADAY CAGE

In order to determine absolute deuteron cross sections, one has to accurately measure the number of deuterons in the bombarding beam. For this purpose a nine-in. long Faraday cage 1¾ in. in diameter is supported in the six-in. tube at the exit of the scattering chamber (Fig. 1). The Faraday cage is supported by a rod through a Wilson seal so that it can be removed from the path of the beam when a measurement of beam energy is made. The Wilson seal, and therefore the Faraday cage, was insulated by Lucite from ground. Permanent bar magnets arranged on the outside of the vacuum system produce a small magnetic field perpendicular to the direction of the beam in the vicinity of the back of the Faraday cage in order to prevent secondary electrons from escaping from the cage.

The deuteron current collected by the Faraday cage is measured by an electronic current integrator,[3] the Faraday cage being held at a negative potential to prevent secondary electrons produced by the beam in its path from reaching the Faraday cage section. Tests were made on the current as a function of the negative potential where the beam was monitored by the He³ particles produced in a gas target and counted by the proportional counter. Within the accuracy of this measurement the He³ counts per current integrator count were independent of this bias between −40 to −120 volts.

During an experiment in which the deuteron current must be known accurately, the current integrator is calibrated (at approximately four-hour intervals) under as nearly as possible the same conditions as it is used. The Faraday cup is connected to ground through a very high resistance. The negative potential at which the cup is held causes a current to flow through the current integrator and this current is measured either with a calibrated galvanometer or with a standard resistance and type "*K*" potentiometer. With the current constant a timed run is taken with the current integrator. This procedure is repeated with different values of resistance and hence different values of current until one has a calibration curve over the current range expected in the experiment. For most

FIG. 4. Photograph of the reaction chamber, Faraday cage section, and analyzing magnet.

---

[3] H. T. Gittings, Los Alamos Report LADC-520.

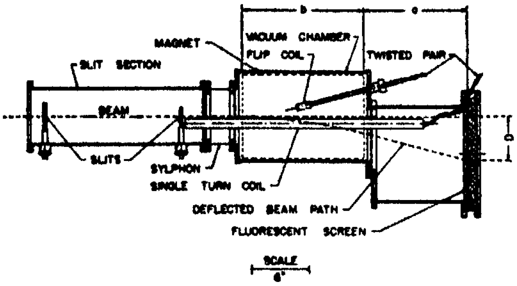

FIG. 5. Slit system and analyzing magnet for energy measurements.

experiments the deuteron current is from 0.1–1.0 μa. With the cyclotron turned on and the beam prevented from reaching the cup, radiation produces a leakage current of about 3×10^{-4} μa.

V. ENERGY MEASUREMENT

The energy of the beam of deuterons is measured by a magnetic deflection method following the general procedure described by Creutz and Wilson.[4] This involves measurement of the deflection of the deuteron beam and the simultaneous measurement of the magnetic field causing this deflection.

The experimental arrangement is shown in Fig. 5. It consists of a magnet with rectangular pole pieces (28.5×25.0 cm), a fluorescent screen for observation of the deuterons, and a single turn rectangular flux coil for measurement of the field. An adjustable slit section is provided between the gas target and the analyzing magnet to define the beam to a line about one mm wide.

The energy of the deuteron beam is given approximately by the following formula, as derived from the equations of motion by Creutz and Wilson.[4]

$$W=\frac{e^2A^2}{2M_0c^2}\left(1-\frac{W}{2M_0c^2}\right)\times\left[1+\left\{\frac{a+b/2(1-e^2A^2/8M_0c^2W)}{D}\right\}^2\right], \quad (1)$$

where, W is the energy of the deuteron beam in ergs, D is the deflection as measured on the fluorescent screen, c is the velocity of light, e is the charge on the deuteron, M_0 the rest mass of the deuteron, and a and b are dimensions of the apparatus as shown in Fig. 5.

The quantity A in the above equation is equal to $\int Hdx$ where H is the change in magnetic field produced by breaking the magnetizing current and dx is measured along the initial direction of the deuteron beam. The value of A is determined by use of the single turn coil, of width W, which extends through the magnetic field from a zero field region on one side of the magnet to a zero field region on the other. The coil was constructed by placing a copper ribbon $\frac{1}{16}$ in. high by 0.001 in. thick around a form of Lucite 25 in. long by 1 in. wide, carefully machined so that the width was uniform to ±0.002 in. The ends of this coil are brought out with a twisted pair to reduce the effect of stray fields and connected to the secondary of a mutual inductance M. The total flux as measured with the coil is equal to $W\int Hdx$ which is equal to $M\Delta I$ where ΔI is the current through the primary of M necessary to balance out the emf developed by the change in flux through the coil. The current ΔI is measured with a potentiometer bridge and standard resistance.

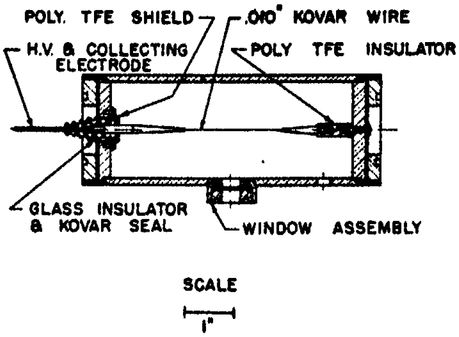

FIG. 6. Sectional view of proportional counter.

Since in this method only single deflection was measured rather than reversing the magnetic field, as in the method of Creutz and Wilson, a small correction was necessary for the residual field of the magnet. This was obtained by using a small flip

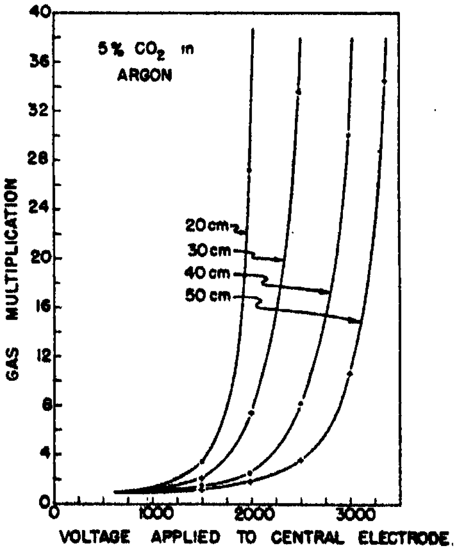

FIG. 7. Gas amplification for proportional counter as function of voltage on central electrode and pressure of gas in cm of Hg in counter.

---

[4] E. C. Creutz and R. R. Wilson, Rev. Sci. Inst. 17, 385 (1946).

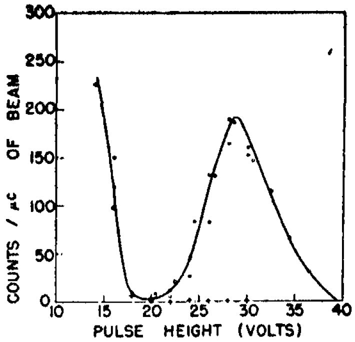

FIG. 8. Distribution of pulses from proportional counter due to He^3 particles which come off from the $D(d,n)He^3$ reaction at 22.7 deg. to deuteron beam.

coil, which was calibrated against the single turn coil so that the residual field could be measured and the correction applied. Since the residual field causes compensating correction in both D and H, the final correction to the energy is small. The use of single deflection requires this correction, but no galvanometer correction is necessary since the galvanometer drift over the time for the field to come to zero is negligible.

The mutual inductance used in these experiments was calibrated by Leeds and Northrup to 0.5 percent accuracy. It was compared with two other inductances, also calibrated by Leeds and Northrup, and found to agree within 0.2 percent.

The width of the undeflected deuteron beam is approximately one mm wide. When deflected, the width increased about 0.5 mm, indicating an inhomogeneity of energy of approximately one percent. The position of the beam could be read to 0.5 mm in 160 mm.

The geometrical constants a, b, and w could be measured to better than 0.5 percent.

Since the energy is proportional to A^2/D^2 the expected accuracy is of the order of two percent.

Several tests were made using aluminum absorbers to take out most of the energy of the deuteron beam and then varying the gas pressure in the target chamber to give a range-absorption curve for the beam. The results of this method showed essential agreement with the magnetic deflection method and indicated that no larger error existed, i.e., a shorted pick up coil, etc.

VI. PROPORTIONAL COUNTER

Figure 6 shows the proportional counter used to determine the absolute intensities of the charged particles resulting from deuteron reactions. The central electrode was made of 10-mil Kovar wire and served both as the high voltage and collection electrode, the signal being taken off through a 5000 volt 0.0001-μf mica condenser. The body of the counter was turned from brass to a wall thickness of $\frac{1}{16}$ in. In order to eliminate background which might result from an (n, alpha) or an (n, p) reaction in the glass insulator a shield of Poly TFE was placed around this insulator. All parts of the counter were furthermore decontaminated in 1–1 HNO_3 before assembly. The counter was found to operate well when filled with argon at pressures ranging from 20 cm to 70 cm Hg and at voltages ranging from 500–2000 volts. (This is the only pressure and voltage region tried to date.) The rise time of the pulses is approximately 1.1 μs when a gas amplification of about ten is utilized.

Figure 7 is a family of gas amplification curves for this counter. Plutonium alpha-particles from a $\frac{1}{10}$ mg/cm^2 foil were used to obtain these curves, both the foil and the counter being mounted in a vacuum system. The argon in the proportional counter was contained by a 1.4 mg/cm^2 mica window. In a similar manner the resolution of the proportional counter was determined by obtaining the energy distribution of the alphas from the above mentioned plutonium foil. The width at half-maximum of the energy distribution curves was found to be 3.5 percent.

A number of background difficulties were experienced when the counter was first tried. The background experienced can be discussed under three categories: gamma-ray background, background due to voltage breakdowns, and particle background. The gamma-ray background was sufficiently reduced by encasing the counter in two in. of lead, except for a $\frac{3}{8}$-in. opening in front of the window. Spurious counts caused by voltage breakdowns inside the counter were essentially eliminated by applying an over-voltage to the counter and permitting it to break down for about five minutes.

Charged particle background was successfully eliminated by the simple device of making certain that the counter could not see the deuteron beam at points where it came into contact with mica windows or diaphragming slits.

Even after eliminating the above sources of background a disturbing amount still remained due to high energy neutron bombardment of the walls of the counter and of the gas in the counter. This could only be eliminated by reducing the neutron background. By use of detectors sensitive to neutrons of energy one Mev and over, it was found possible to eliminate effectively all neutron background of over one Mev coming from the cyclotron tank proper by shielding with water and paraffin as heretofore mentioned.

A considerable number of neutrons of energy greater than one Mev were, however, produced by deuteron bombardment of the diaphragming slits and target windows. This background could not be shielded from the counter by hydrogen containing materials due to geometrical considerations. However, this background was also considerably reduced by utilizing gold diaphragms to define the beam. It was found, for example, that gold gives only about 0.3 the neutron background of brass.

It was also found that a 0.0003-in. tantalum target window produced 0.4 the neutron background of a two mg/cm^2 mica window.

Even after the above mentioned modifications were incorporated into the set-up, the neutron background of energy greater than one Mev was approximately 25 times the neutron flux obtained from the d-d reaction at a point 45 cm from the target. This was the case when a target six cm long containing D^2 at a pressure of 58 cm Hg was used, the beam being diaphragmed by a $\frac{1}{4}$-in. diaphragm in front of the target as illustrated in Fig. 1.

However, when all the above devices were employed for reducing background, the proportional counter gave consistant and apparently precise results. Figure 8, for example, gives the energy distribution of the He^3 particles obtained from the $D+D\rightarrow He^3+n$ reaction using the above counter at 22.7 deg. with respect to the incident deuteron beam. The points shown by crosses were obtained when $H_2{}^1$ was substituted for the $D_2{}^2$ in the target.

VII. CONCLUSIONS

The apparatus described in this paper allows one to do a considerable number of experiments with cyclotrons which otherwise would be impossible due to background. The equipment, of course, is particularly adaptable to the study of scattering and of charged particle reactions. Preliminary results on the differential cross section of the $D(d,n)He^3$ reaction have already been reported.[5] This experiment has been repeated with better resolution and the revised results will be given in a forthcoming paper. By substituting photographic detectors for the proportional counter a number of experiments involving the charged particles from the *d-d* reaction have also been performed.

Experiments which require monoenergetic neutrons are also made possible using this apparatus. With one atmosphere of deuterium gas in a target as shown in Fig. 1, the background neutrons (above 12 Mev) are only about ten percent of neutrons from the $D(d,n)He^3$ reaction. Thus, in this neutron energy region one can perform standard neutron experiments. For instance, the activation of the ten-minute Cu^{62} by the $Cu^{63}(n,2n)Cu^{62}$ reaction has been done as a function of neutron energy for energies from 11–13 Mev. This work will soon be published.

Although the neutron background between one and 12 Mev is rather formidable (Section VI) one can, by use of coincidence techniques, perform experiments with monoenergetic neutrons in this energy region. An example is the possibility of doing *n, p* scattering at 8.0 Mev. A triple coincidence proton recoil counter would be supported on the outside of the *d-d* chamber with its hydrogen containing radiator so mounted as to intercept the neutrons which would lie in the horizontal plane passing through the center of the target and which would come off at an angle of 61 deg. to the deuteron beam. When the bombarding deuterons had an energy of ten Mev these neutrons would have an energy of 8.0 Mev. Then one would rotate the proportional counter in the reaction chamber to 38.6 deg. so as to count the He^3 particles associated with the 8.0-Mev neutrons. The neutron cone is, of course, defined by the diaphragm between the He^3 counter and the target. In doing the experiment one would record the coincidences between the He^3 counter and the proton recoil counter. Thus, the real coincidences would give the number of recoils due to the eight-Mev neutrons and the total He^3 counts would give the total number of neutrons passing through the radiator.

We wish to acknowledge the assistance of Mr. John Slye, Mr. Harry Snowden, Mr. Raymond E. Squires, and Mrs. Louise Spence, who helped construct the apparatus and who operated the cyclotron during many of the tests described above. We also wish to thank Mrs. Mary A. Dodds who assembled many of the figures and material used in this report.

---

[5] Curtis, Rosen, and Fowler, Phys. Rev. 73, 648 (1948).

THE REVIEW OF SCIENTIFIC INSTRUMENTS VOLUME 20, NUMBER 6 JUNE, 1949

A New Method of Measuring the Stopping Power of Several Materials for Alpha-Particles

F. Emmett Hammer* and Frank E. Hoecker
Department of Physics, University of Kansas, Lawrence, Kansas

The application of an atmospheric pressure alpha-particle detector to the measurement of the relative stopping power of thin films of absorbing material for alpha-particles was investigated. The air-equivalent of absorbing films was measured directly by balancing the counting rates of two detectors in air, and again when an absorbing film is inserted between one of the detectors and its source. Measurements of the air-equivalent and relative stopping powers of films of mica, polystyrene, and aluminum are given. The relative stopping powers determined agree well with previous values. The errors of the method are discussed and an attempt is made to specify the magnitude of the probable error in the result.

INTRODUCTION

DATA published by different observers on the relative stopping powers of heavy substances for alpha-particles differ by as much as 10 percent.[1] More complete and precise data on this subject are desirable as a basis for revision of present theoretical treatments.

The application of a variation of the wire-plate alpha-particle detector, described by Chang and Rosenblum,[2] to the measurement of the relative stopping powers of certain substances has been studied. Data which are in close agreement with the best available values on mica and aluminum, and data on polystyrene (not previously available), are presented. These measurements are in the nature of preliminary tests to determine the applicability of the method of measurement to heavy substances.

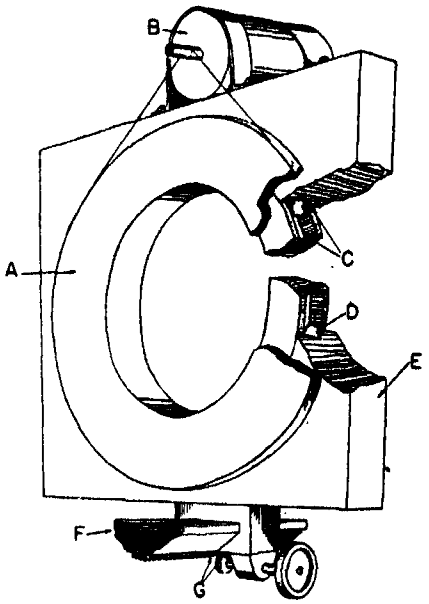

FIG. 1. Film rotating mechanism. *A*—Rotating ring. *B*—Drive motor. *C*—Ball-bearing raceway. *E*—Frame.

APPARATUS AND MEASUREMENT PROCEDURE

The apparatus consists basically of an alpha-particle detector and an associated electronic circuit[3] which counts individual alpha-particles after their passage through chosen thicknesses of absorbing material.

The detector consisted of a circular brass plate 2.5 cm in diameter with a stem threaded through a back plate mounted on a frame of insulating material. An alloy wire approximately 0.07 mm in diameter was stretched across the insulating frame in front of the circular brass plate. The threaded stem permitted adjustment of wire-plate spacing which was maintained at approximately 1 mm. The high voltage negative (2500 to 3000 volts) was connected through a 20-megohm resistor to the brass plate, and the wire connected to ground through a 100,000 ohm resistor. This provided negative pulses to the amplifier on breakdown. A capacity of 250 $\mu\mu f$ was connected between plate and wire to provide a sufficiently large pulse to operate the amplifier.

The alpha-particle sources used were polonium plated on silver.[4]

The films used were aluminum, prepared from various numbers of thin foils, mica,[5] and polystyrene. The polystyrene films were prepared by pouring a solution of polystyrene in amyl acetate of suitable concentration onto a glass plate. Evaporation of the amyl acetate left a thin film of polystyrene which could be removed from the plate. The films were mounted in lucite rings which fitted into the rotating mechanism. (Fig. 1.) Rotation of the films provided a means of averaging out non-uniformities and gave results depending on the average film thickness.

---

* Now at Oklahoma City University, Oklahoma City, Oklahoma.

[1] M. S. Livingston and H. A. Bethe, Rev. Mod. Phys. 9, 271–272 (1937).

[2] W. Y. Chang and S. Rosenblum, Phys. Rev. 67, 222 (1945).

[3] Robt. M. Kloepper and Frank E. Hoecker, Rev. Sci. Inst. 20, 17 (1949).

[4] Rutherford, Chadwick, and Ellis, *Radiations From Radioactive Substances*. (The Macmillan Company, New York, 1930 edition), p. 555.

[5] John Strong, *Procedures in Experimental Physics* (Prentice-Hall, Inc., New York, 1938 edition), p. 388.

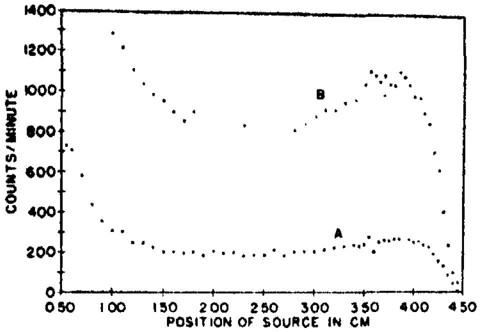

FIG. 2. Characteristic counts-per-minute *vs.* distance curves. Curve *A* is for a narrow source, curve *B* for a wide source.

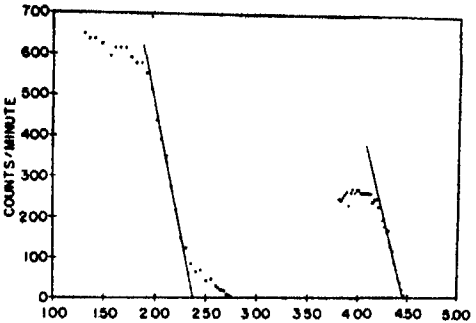

FIG. 3. End-of-range curves for air and mica using narrow source. Left-hand curve is for mica. Slope approximately 1750 counts/min. Right-hand curve is for air. Slope approximately 875 counts/min.

Errors due to variations in voltage, temperature, humidity, and atmospheric pressure on the counting rate of a detector were minimized by using two detectors, one having a fixed and the other a movable source. A dual channel counter amplifier and pulse rate comparator, designed by Kloepper and Hoecker,[5] was used to determine when the counting rate of the two detectors was equalized. A mechanical counter (Cyclotron Specialties Company type 401-A) was also connected to the output of each channel.

The two detectors were adjusted for equal counting rates in air. A film of absorbing material was then inserted between the movable source and its detector and the source position again adjusted for equalized counting rate. The difference between the two positions is the air-equivalent[6] of the absorbing film. Since any determination of a balance position may be in error due to random emission from the sources, the mechanical counters were connected for approximately 4000 counts and the difference in counting rates converted into a position correction by use of the average slope of the end-of-range curves.

The operating point used for equalizing the counting rate was approximately the inflection point of the end-of-range part of the counts-per-minute *versus* distance curve. As seen from Fig. 2, this curve is similar to a number-distance curve. There is a peak, however, toward the end of the range, which indicates that the detector is somewhat sensitive to the ionizing power of the alpha-particles. It will be noticed that the slope of these curves varies greatly with the width of source used, and also that any balance position error will vary inversely as the slope of the curve.

The effect of the geometry of the apparatus upon the counting rate, associated with different film thicknesses, was compensated for by the shape and size of source used. The air-equivalent was corrected to air at 15 degrees C and 760 mm of mercury. The absorbing films were weighed and the relative stopping power determined.[7]

CORRECTIONS FOR GEOMETRY OF THE APPARATUS

The effect of the geometry of the apparatus upon the determination of air-equivalent is divided into two parts. These are the effect of the solid angle subtended by the detector wire and the effect of obliquity of the path of particles through flat sheets of absorbing material.

An extended theoretical and experimental study of the characteristics of this type of detector with respect to geometrical and other types of errors is in preparation. This study indicates that the solid angle effect can be represented approximately by a $1/d$ function where d is the distance between the source and the detector. The result of the solid angle effect is to increase both the slope and the maximum counting rate when an absorbing film is in place. This is shown by Fig. 3.

The effect of flat sheets of absorbing material is to produce a greater reduction in the residual air range for particles traveling obliquely through the material than for particles traveling normally. The normal component of this loss in residual range due to obliquity of path is given by $\Delta R = R_0(\cos\theta_0 - \cos\theta_1)$, where θ_0 is the angle between the path

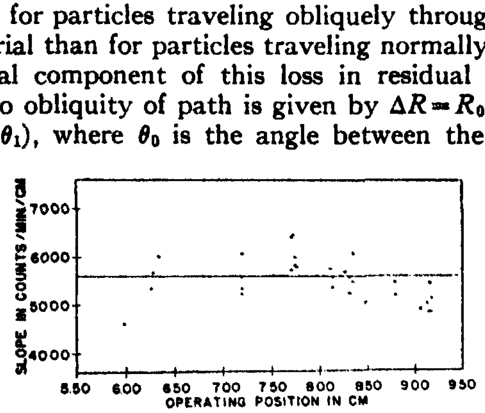

FIG. 4. Values of slopes of end-of-range curves for air and polystyrene films *vs.* operating position. Group of six points at extreme right of figure is for air curves.

---

[6] The air-equivalent of a film is the thickness of air in centimeters to which the film is equivalent for the stopping of alpha-particles.

[7] The relative stopping power of a substance is defined as the weight in mg/cm^2 which is equivalent to 1 cm of air (1.22 mg/cm^2) at 15 degrees C and 760 mm of mercury for the stopping of alpha-particles.

Table I. Air-equivalent of various films. (Air-equivalent in cm of air to which the film is equivalent in stopping power.)

			A. Polystyrene films				
Date	#12.5	#11	#17	#18	#20	#25	#50
June 28	1.860	2.614	1.350	1.229	0.864	0.774	0.349
June 29	1.856	2.598	1.347	1.232		0.772	0.355
July 9	1.838	2.604	1.386	1.233	0.956	0.768	0.354
July 10	1.844	2.596	1.342	1.233	0.963	0.772	0.352
Fig. 5	1.862					0.791	
Fig. 6	1.844		1.391			0.796	

			B. Mica films				
Date	#1	#2	#3	#6	#7	#8	#9
June 30	2.103	2.013	1.491				
July 9	2.136	2.062	1.890	0.880	2.347	1.141	2.842
July 10	2.242	2.057	1.502	0.884	1.174	1.148	2.838
Fig. 5		2.055		0.921			
Fig. 6		2.049	1.493	0.870			

	C. Miscellaneous films	
Date	Nylon	Metal
July 1	0.813	
July 9	0.825	2.176
July 10	0.352	2.171
July 27		2.171
Fig. 5	0.836	2.185
Fig. 6	0.827	2.195

of the particle in air, and the axis of the apparatus, θ_1, is the angle between the particle path through an absorbing film and the axis, and R_0 is the range of the alpha-particles in air. This residual range loss for particles having an oblique path results in a reduction in the slope of the end-of-range curve.

From the above considerations, it was concluded that the solid angle effect and the effect due to obliquity of path through flat sheets of absorbing material could be balanced against each other by a proper choice of size and shape of source. Since the quantitative determination of the above effects is rather difficult theoretically, the conditions for balance were determined experimentally.

A wide source in the form of a portion of a cylinder of 1-cm arc, having a radius of curvature of 0.56 cm and a length of 2.5 cm, was plated with polonium. This was placed with its axis parallel to, and the concave side toward, the detector wire.

Figure 4 shows the values of the slopes (calculated from plots of end-of-range curves) obtained for several polystyrene films plotted against the approximate operating position for each film. It will be observed that these slopes are essentially constant regardless of the distance between the source and the detector. An arbitrary average of 5600 count/min./cm was used in making the corrections to the balance positions.

The curvature of the source might be expected to introduce an error in the determination of the air-equivalent. This point was examined experimentally. The air-equivalents of several films determined from carefully made plots of end-of-range curves using the flat source, Fig. 5, were compared with the air-equivalents of the same films determined from plots of end-of-range curves using a curved source, Fig. 6.

While taking data for these curves, the voltage across the detector was controlled so that the maximum point for each curve was approximately 2000 counts/min. It will be seen that the slope is approximately constant in both cases. Using points on the curves at which the counting rate was 900 counts/min. as reference points, the air-equivalent was determined by measuring the horizontal distance between the reference point on the air curve and that on the film curve. The measurements labeled Fig. 5 and Fig. 6 in Table I show the resultant air-equivalents. It will be seen that there is good agreement between the pairs of values. Four of six pairs agree within 0.01 cm.

From these considerations, it was concluded that any variable effect the curvature of this source had on the shape of the end-of-range curve, was negligible over the part of the curve used for measurement; and that the source curvature introduced no observable variation in the position of the balance point with variation in film thickness.

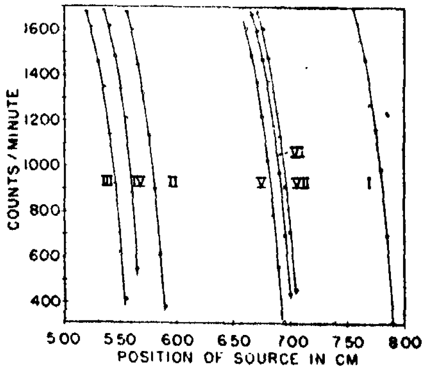

Fig. 5. End-of-range curves for several films using flat source. Curve I is for air, II and VII polystyrene, III aluminum, IV and V mica, and VI Nylon.

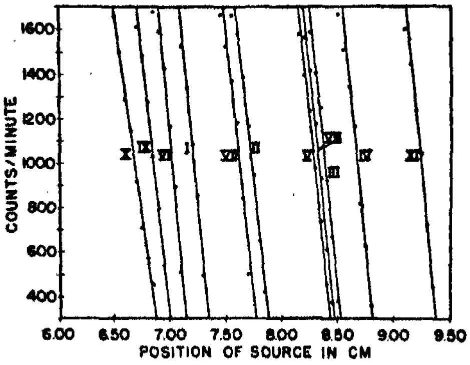

Fig. 6. End-of-range curves for several films using curved source. Curves I to IV inclusive are for polystyrene, V to VII are for mica, VIII for Nylon, IX and X for aluminum, and XI is for air. Curve X is for the non-uniform Al film No. M-2.

DETERMINATION OF PROBABLE ERRORS

Random Errors

Table I shows the air-equivalents of various films measured under the heading of the date on which the measurements were made.

Application of a test described by Simon[8] to the measured air-equivalents of a group of five polystyrene films indicated that the errors were random in nature.

The probable error in the air-equivalent of each of these films varied from ±0.001 cm to ±0.003 cm. Since the number of measurements was rather limited, the probable error specified for the group is that for the films with the largest error.

It should be pointed out that while the probable error in the slope of any one end-of-range curve is quite large, the error in the air-equivalent is small because the variations in slope are caused largely by slow variations in the sensitivity of the detector. When the balance positions for air and for the film being measured are taken in immediate succession, there is usually not much change in the sensitivity of the detector between the readings. Rapid changes may account for the rather unreliable readings for film number seventeen.

The probable error in the weight of any film was estimated from observed variations in the set of weights used. This set was self-calibrated with an estimated probable error in any one weight of ±0.03 mg. The probable error in the weight of any film was estimated as ±0.05 mg.

The probable error in the area of the films was estimated as ±0.025 cm^2 from measurements made on the cutter used to cut film sections for weighing.

The probable error in the relative stopping power was calculated from the propagated errors in the air-equivalent, the weight, and the area.

Assignable Errors

There are certain constant errors which can be assigned. Figure 4 shows that the slopes of the end-of-range curves in air are somewhat less than the average for the polystyrene films. (The group of six points at the right of Fig. 4 is for air curves.) This difference in slope corresponds to an error of 0.012 cm in the air balance position for all measurements.

The average slope of the end-of-range curves for the mica films measured was 7600 counts/min./cm instead of 5600 counts/min./cm for all other films. This slope difference corresponds to a position error for the mica films of 0.043 cm.

TABLE II. Relative stopping powers of various absorbing films (in mg/cm^2 equivalent to 1 cm of air at 15 degrees C and 760 mm Hg for the stopping of alpha-particles).

Material	Film no.	Air-equivalent in cm	Rel. stopping power
Mica	#6	0.994	1.41
	#8	1.199	1.47
	#3	1.550	1.46
	#2	2.102	1.51
	#1	2.175	1.48
	#9	2.895	1.43
		Average	1.46
Polystyrene	#50	0.365	1.02*
	#25	0.791	1.06
	#20	0.971	1.06
	#18	1.224	1.05
	#17	1.375	1.05
	#12.5	1.864	1.06
	#11	2.615	1.10**
		Average	1.06
Aluminum	#1	0.113	1.35*
	#2	0.211	1.50
	#4	0.368	1.53
	#6	0.560	1.56
	#8	0.811	1.59
	#M-1	2.192	1.63
	#M-2	2.367	1.74**

* Errors large due to thinness of films.
** Measurements excluded from calculation of probable error.

Probable Error of the Relative Stopping Power

Table II shows the calculated relative stopping powers for the films measured. The starred measurements were not included in the calculations of probable error. Two of them are for very thin films where the error is consequently quite large. The polystyrene film number eleven is a very thick film and seems definitely out of line with the rest. The film numbered M-2 was a very non-uniform aluminum film. Since no effort was made to allow for the change in slope due to non-uniformity, this measurement was also excluded.

The probable error in the relative stopping power for the mica films was calculated on the basis of the deviations from the average value shown in Table II. It is somewhat larger than the value calculated from the propagated errors in the air-equivalent, weight, and area. Since the sampling of measurements is small, the larger error, ±0.014 is specified.

The probable error in the average value for polystyrene is ±0.003. The probable error in a single determination for a film of average thickness, as calculated from the propagated errors in air-equivalent, weight, and area, is ±0.007. It is believed the polystyrene measurements are sufficiently reliable to justify specifying the smaller error.

If the starred aluminum films are excluded from consideration, there is still a noticeable increase in relative stopping power for the thicker films. This is in accord with the findings of Taylor[9] and others that the relative stopping power increases with decreasing velocity of the alpha-particle. This means that any heavy film is less effective as an absorber near the end of the range than it is near the source.

---

[8] Leslie E. Simon, *Engineers' Manual of Statistical Methods* (John Wiley & Sons, Inc., New York, 1941 edition), pp. 41–51.

Since the alpha-particles from polonium have an initial energy of approximately 5.3 Mev, and all the films measured were placed quite close to the source, the value of relative stopping power specified for aluminum will be that found for film number two and for alpha-particles of approximately 5 Mev. This value is 1.50±0.039. The probable error is that calculated from the propagated errors in air-equivalent, weight, and area.

CONCLUSIONS

The value determined for the relative stopping power of mica (1.46±0.014) compares quite well with previous values.[10] The value for aluminum (1.50±0.039) is in good agreement with a recent value by Rosenblum.[11] No published values for polystyrene are available.

It is believed that this method holds promise of high precision if further investigation of the proper size and shape of source leads to a reduction in the slope deviation of the end-of-range curves for various types of films to be measured.

This work was supported in part by ONR Contract No. N6-onr-260-TO-1.

---

[9] T. S. Taylor, Phil. Mag. 18, 604 (1909).

[10] See reference 1, p. 272.

[11] S. Rosenblum, Ann. d. Physik 10, 408 (1928).

THE REVIEW OF SCIENTIFIC INSTRUMENTS VOLUME 20, NUMBER 6 JUNE, 1949

A Cloud Chamber of Light Weight for Balloon Flights

R. P. Shutt, A. L. Johnson, and A. M. Thorndike
*Brookhaven National Laboratory, Upton, New York**

(Received February 1, 1949)

Some constructional details of cloud chambers used for balloon flights are described. Details are given on the fabrication of transparent plastic front walls and cylinders for the cloud chambers. A relatively large number of bicycle spokes is used for holding the chamber together, thus distributing material stresses, enabling one to make the aluminum parts of the cloud chamber quite light.

The back and front walls of the cloud chambers are somewhat spherically curved, resulting in considerable reduction of material thicknesses. By the same means a piece of slightly curved metal gauze is sufficient to limit the motion of the rubber diaphragm in the compressed position.

A mechanism used for adjusting expansion ratios can be removed before a balloon flight. Gas and liquid can be inserted through bicycle valves.

The cloud chambers are 12 inches in diameter, 3¼ inches deep, and weigh approximately 6 pounds.

IN the Spring of 1948 several lightweight cloud chambers for balloon flights were constructed, some of which have been in operation during the summer and fall. A few of the constructional details of these cloud chambers will be described in this article.

The weight of the cloud chambers is reduced by the following means. A plastic material is used for the transparent walls of the cloud chamber. Most of the other parts consist of tin-plated aluminum. The plastic front wall of the cloud chamber and the walls limiting the motion of the rubber diaphragm bringing about the expansions are somewhat curved and therefore could be made thin. The remaining parts are also kept thin by distributing material stresses, making use of a relatively large number of bicycle spokes for holding the chamber together, rather than the usual smaller number of heavy bolts. In order to adjust the expansion ratio, a mechanism which is removed before a flight is attached to the cloud chamber. It will be seen that besides saving weight, the latter feature also reduces the amount of compressed air to be carried along for operating the cloud chamber. The resulting cloud chamber is 12 inches in diameter, 3¼ inches deep, and weighs 6.3 pounds. It is felt that by making use of magnesium where possible, and admitting higher material stresses, one might save another one or two pounds in a similar design. Photographs of the cloud chamber are shown in Fig. 1.

Some of the parts of the cloud chamber and, where of interest, their fabrication, will now be described. Reference will be made to the assembly drawing shown in Fig. 2.

The plastic front wall, Part 109 in Fig. 2, ⅛ inch thick and 12¼ inches in diameter, is spherically curved with a radius of 24 inches. A plane flange is retained for clamping it to the remainder of the chamber. Plexiglas** is used as the material. After heating the Plexiglas sheet evenly in an oven to a temperature of 160°C, it is clamped over the top of an open vessel which then is immediately connected to an evacuated tank. Thus, the Plexiglas sheet is drawn into the vessel. When the Plexiglas has reached the desired shape its depth is held constant by regulating the degree of evacuation until it has cooled off. Since in this way the surfaces of the plastic do not come in contact with any other surfaces, the plastic remains quite clear and transparent, and since the wall is only slightly curved and its thickness turns out to be practically constant, no optical distortions are observable, compared to the usual distortions of tracks encountered in any cloud chamber.

---

* Research carried out at Brookhaven National Laboratory under the auspices of the AEC.

The Plexiglas cylinder, Part 110 in Fig. 2, is seamless, 3½ inches deep, with an outside diameter of 12 inches and a wall thickness of approximately ⅛ inch. It is manufactured in the following way. A sheet of Plexiglas, $\frac{3}{16}$ inch thick, again heated to a temperature of 160°C and then clamped over the top of the vessel, in this case is drawn in by evacuating until a cylindrical Neoprene-covered form, 6 inches deep and 11¾ inches in diameter, can be set inside and clamped securely to the top of the vessel. Air is now admitted into the vessel, whereupon the still hot plastic shrinks back tightly over the form. After the plastic has cooled off, the form is removed, and a cylinder of a depth of 3.5 inches is cut out. The remaining sections of the cylinder are useless because they are either too thin or too uneven. The resulting seamless cylinders have a wall thickness tapering from $\frac{3}{16}$ inch at one end to $\frac{3}{32}$ inch at the other and have withstood a force of 5 tons applied along their axes. Optically, the cylinders are comparable to the Pyrex glass cylinders usually used for cloud chambers.

By combining the techniques indicated, the transparent walls of the cloud chamber have also been made in one piece complete with front wall, cylinder, and flange for clamping to the remainder of the assembly. This unit will be used in future designs.

Two short-stemmed bicycle valves, Part 222, passed through holes in the plastic cylinder, serve to admit gas and liquid into the chamber, and to measure the internal pressure, respectively.

A piece of tin-plated brass gauze pressed into spherical shape and soldered to a tin-plated aluminum ring,*** Part 112, determines the position of the rubber diaphragm, Part 218, when the cloud chamber is compressed. The gauze is made of wire 0.013 inch in diameter, and has a mesh of 30×30. Its radius of curvature is again 24 inches. In order to obtain a dark optical background, velvet is sewed to the gauze.

The remainder of the assembly is contained in a flanged aluminum cylinder, Part 108. Through thirty holes in the flange, bicycle spokes, Part 212, are passed to the clamping ring, Part 101, in order to hold the cloud chamber together. Thus the material stresses are distributed so that none of the parts are warped.

The back wall, Part 105, again of spherical curvature of 24 inches radius, and tin plated for soldering, slides in the aluminum cylinder. A seal is provided by an "O-ring" gasket, Part 211. Several ribs, approximately $\frac{1}{16}$ inch high, provide a space between this wall and a layer of aluminum gauze acting as a limit for the movement of the rubber diaphragm when an expansion is made, in order to let the air escape quickly from the back slide of the diaphragm. Three helical surfaces have been milled into the ring supporting the back wall. These surfaces ride on three matching surfaces milled into a ring, Part 106, which in turn rides on a flange extending inward from the back side of the containing aluminum cylinder, Part 108. Upon turning the latter ring the position of the back wall, Part 105, is shifted, in this way changing the expansion ratio of the cloud chamber. Since there is always gas pressure on the back wall, the frictional forces along the helical surfaces are quite large. Adjusting the expansion ratio is therefore facilitated in the following manner. An assembly consisting of an auxiliary cylinder and piston, Parts 116 and 120, sealed with a rubber diaphragm, is attached to the back cylinder, Part 108, by inserting it into a bayonet lock. By means of a bicycle pump, air is now pumped into the auxiliary cylinder, thus pushing the piston against the back wall of the cloud chamber until the internal pressure on the back wall is balanced. The ring, Part 106, can

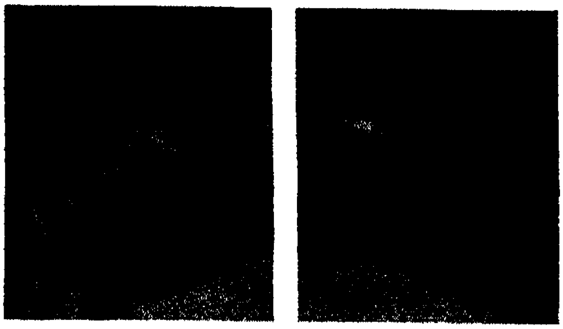

FIG. 1. Photographs of frontside and backside of a cloud chamber designed for balloon flights. The cloud chamber is 12 inches in diameter and 3.5 inches deep. Two lead plates are mounted inside.

** Although Plexiglas and Lucite are assumed to have identical chemical compositions, in the fabricating process described, clear surfaces were obtained more easily with Plexiglas.

*** Aluminum and brass parts were tin-plated by the Sperry Corporation, Lake Success, New York.

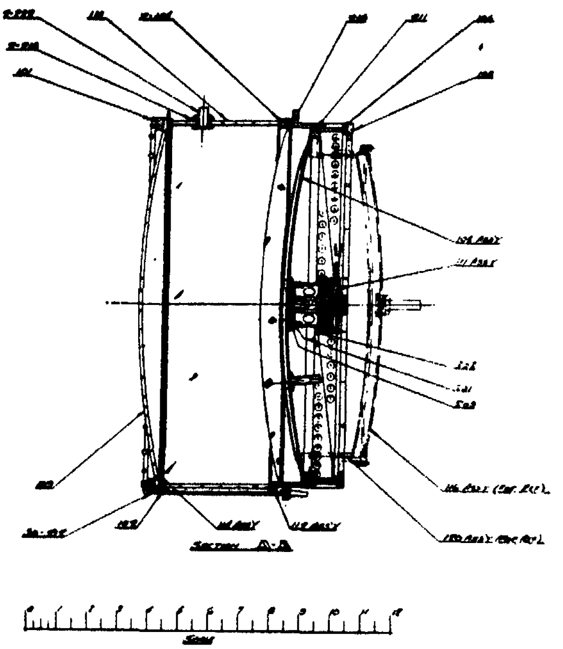

FIG. 2. Assembly drawing of balloon cloud chamber.

now be turned easily in order to change the expansion ratio. Of course, this pressure-equalizing assembly is removed before a balloon flight.

The electromagnetic expansion valve assembly shown, Parts 111, 201, 202, and 209, operates on dry cells with a power consumption of 0.2 watts. With an inductance of 1 henry and a resistance of 200 ohms, it is felt that in connection with suitable control circuits this valve will open fast enough for counter-controlled operation. In order to improve the reliability of operation for many hours without supervision, the design is such that the spring closing the valve after expansion is extended when the valve is opened. It was found that the usually employed compressional springs jam too easily.

Admittedly the construction of a cloud chamber of light weight is accomplished rather simply when, in the compressed position, the movement of the rubber diaphragm is not limited by mechanical means such as the brass wire cloth, Part 112. Since, in this case, only the air pressure behind the diaphragm determines the degree of compression of the cloud chamber, no mechanism is necessary to change the expansion ratio except for some pressure control device. However, in this case the expansion ratio is quite sensitive to small changes in temperature, necessitating compensating apparatus. Therefore, the present design was preferred, employing mechanical stops in both the expanded and compressed position. Pressure-controlled cloud chambers for balloon flights have been described and operated successfully by several authors.[1,2]

A few words may be in order on the use of Plexiglas in cloud chambers. The advantages of Plexiglas are not only its light weight and simplicity of shaping, but also the fact that Plexiglas consists of elements of low atomic number, may be important for many applications. The disadvantage of Plexiglas is its slight swelling and softening when exposed to water or alcohol, both liquids commonly used in cloud chambers. However, several cloud chambers have been in operation for a number of months without any mechanical defects developing due to softening of the cloud chamber walls. At some points where local pressure was applied to the plastic by members supporting lead plates inside the cloud chambers, some crazing was observed. If after some additional time the plastic should soften too much, new plastic parts will be used, since they are easily made in reasonable quantities by the methods described above.

The tracks photographed in these cloud chambers appear to be as good as those obtained in conventional cloud chambers, as far as both their contrast and straightness are concerned. At times there may have been indications that a cloud chamber with plastic walls tends to give general background fog somewhat more readily than one with glass walls, but there are many other factors which may have caused fog in the observed cases. A program to study these questions more carefully is under way. If as a result, glass should turn out to be superior in spite of its relatively high density, glass parts can be substituted for the plastic cylinder and front disk in the present design. For this purpose curved front glass plates and cylinders, approximately $\frac{1}{8}$ inch thick, have been procured.****

ACKNOWLEDGMENT

The authors wish to express their appreciation and gratitude to Mr. K. J. Kristoffersen and to Mrs. S. H. Cornish for developing the described methods for manufacturing the Plexiglass parts of the cloud chambers, and to Mr. S. G. Hasselriis who has been responsible for the manufacture of all of the other parts.

---

[1] R. B. Leighton, Rev. Sci. Inst. 19, 274 (1948).

[2] E. J. Lofgren, E. P. Ney, and F. Oppenheimer, Rev. Sci. Inst. 20, 48 (1949).

**** The curved front glass plates have been obtained from the Lancaster Lens Company, Lancaster, Ohio. The thin-walled glass cylinders were made by Warren L. Kessler, Inc., Bethpage, Long Island, New York.

THE REVIEW OF SCIENTIFIC INSTRUMENTS VOLUME 20, NUMBER 6 JUNE, 1949

A Magnetic Field Strength Meter Using the Proton Magnetic Moment

N. J. Hopkins
Radiation Laboratory, McGill University, Montreal, Canada

(Received January 25, 1949)

A simple, portable instrument is described which employs the nuclear absorption method and the known value of the proton magnetic moment to determine magnetic field strength. No known fields and no geometrical calculations are required for calibration. The range covered by the present instrument is approximately 3000 to 19,000 gauss. No upper limit is inherent in the method. Homogeneity is required over a small cylindrical volume. Absolute accuracy of better than ±0.2 percent is obtainable, depending only on precise measurement of frequency. Higher accuracy is possible in comparing fields and in measuring field changes.

INTRODUCTION

It has been suggested in a number of places that either the nuclear absorption method[1] or the nuclear induction method[2] might be used both as a means of stabilizing a magnetic field and as an accurate measure of field strength. Packard[3] has used the induction method for automatic control of the current supplied to a magnet. The instrument described herein used the absorption method for measuring fields.

The basis of operation may be reviewed briefly as follows. A proton sample (distilled water contained in a glass cell) is mounted within a small coil which is inserted in the magnetic field to be measured, with the axis of the coil at right angles to the direction of the field. R-f oscillations are set up in this coil at a frequency determined by the setting of a tuning capacitor. When this frequency coincides with the Larmor precessional frequency of the protons, transitions occur which result in an absorption of energy from the r-f field. With a suitable detector circuit this energy drop appears as a V-shaped dip in a horizontal C.R.O. trace. Also necessary to bring about this display are auxiliary "wobbling" coils which carry the unknown magnetic field back and forth at 60 c.p.s. through its resonant value.

In making a measurement the tuning capacitor is varied until the resonant dip appears on the C.R.O. screen. The field strength is then determined from the well-known equation for the precessional frequency which in this case reduces to

$$H=(234.8_7\pm0.2_9)\times10^{-6}f,$$

where H is the magnetic field strength in gauss; and f is the Larmor frequency in c.p.s. (The proton magnetic moment used is the corrected value quoted by Bloch, Nicodemus and Staub.[4])

No difficulty is experienced in locating the resonance signal and no manipulative skill is required in the operation of the instrument. The apparatus is very simple and a similar instrument could be built quickly in any laboratory.

Four interchangeable sample coils are used to provide coverage of a range from 3000 to 18,900 gauss.

DESCRIPTION OF THE APPARATUS

The sample coil and tuning capacitor are incorporated in a probe together with a 6AK5 regenerative detector and the wobbling coils. The probe is a rectangular box with dimensions dictated by the size of the frequency-linear tuning capacitor, its dial and the space required for mounting the 6AK5, the r-f chokes and the regenerative control potentiometer. It is important that no magnetic materials be used in the probe.

The dial used is calibrated from 0 to 100 over 270°, diameter $2\frac{3}{4}$ inches. It is driven by a friction vernier. To avoid realignment difficulty in the event of tube failure, the capacitor is mounted rigidly on the end plate of the probe with one plug-in type connection to the 54-$\mu\mu$f condenser and with its other connection to a chassis ground.

From this part of the probe a brass tube, diameter $\frac{3}{4}$ inches, length 6 inches extends with an axial lead. This forms a low loss line to the sample coil which plugs into terminals at the tip. Soldered to the tip is a copper shield can which also supports the wobbling coils. These are wound in bakelite forms and each consists of 140 turns of No. 24 cotton covered wire, inside diameter $\frac{3}{4}$ inch, outside diameter $1\frac{1}{2}$ inches, length of winding $\frac{1}{4}$ inch. They are separated by a distance of 1 inch center-to-center and the outside thickness of the whole is $1\frac{9}{16}$ inches. (See Fig. 1.)

Wobbling amplitude amounts to 55 gauss peak-to-peak given by variac range of 0 to 43 volts. The amplitude may be varied down to zero, although it is normally used at maximum. As constructed the instrument can measure magnets with gap widths larger than $1\frac{9}{16}$ inches for pole diameters up to 13 inches and with gap widths greater than

---

[1] Purcell, Torrey, and Pound, Phys. Rev. **69**, 37 (1946); Bloemenbergen, Purcell, and Pound, Phys. Rev. **73**, 679 (1948).

[2] Bloch, Hansen, and Packard, Phys. Rev. **69**, 127 (1946).

[3] Martin Packard, Rev. Sci. Inst. **19**, 435 (1948).

[4] Bloch, Nicodemus, and Staub, Phys. Rev. **74**, 1025 (1948).

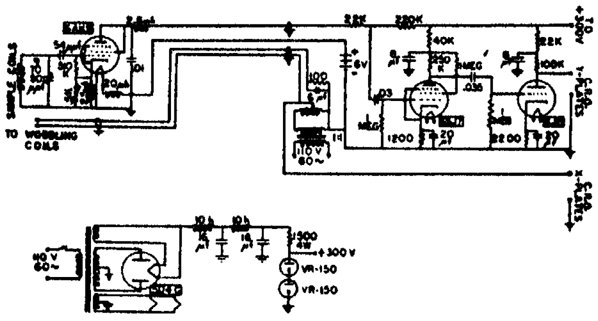

FIG. 1. Circuit diagram; magnetic field strength meter.

3½ inches for larger diameters. The minimum gap width could be reduced without difficulty to ¾ inch if the wobbling coils were removed and others wound on the pole pieces of a particular magnet being measured.

Four sample coils are used having 3, 9, 14, and 25 turns, respectively. The water sample in each is enclosed in a thin-walled glass cylinder inside length 1.2 cm, inside diameter 0.5 cm. These are quickly and satisfactorily made by using glyptal cement to seal each end of suitable lengths of glass tubing.

The remainder of the apparatus is mounted on a single chassis and consists of a standard two-stage audio amplifier, plate and filament power supply and the 60 c.p.s. wobbling voltage supply.

OPERATION

For ordinary measurements calibration curves are useful. They allow rapid translation of the dial reading into the field strength and can give accuracies of ±0.3 percent with the dial described above. They may be plotted easily, using the following procedure.

The regeneration control is advanced until oscillations are just maintained. (This point is easily determined by the behavior of the C.R.O. trace when it is reached.) A standard variable-frequency source is loosely coupled with the sample coil and varied to obtain a zero-beat note on the oscilloscope screen, indicating that the two frequencies are the same. In this way the frequency and hence the field strength corresponding to any dial setting may be determined.

Slight errors may be introduced in taking the dial reading and through change in oscillation frequency with regeneration control setting. These may be eliminated for the most accurate work by making use of the above procedure for each field measurement, the dial setting and regeneration control setting being left unchanged when the resonance dip has been located. In this way the accuracy can be made practically the $\pm 0.1_2$ percent upper limit dictated by the possible error in the numerical constant of the equation given above.

Best sensitivity in measurement will be attained when the regeneration is just sufficient to maintain oscillations. However, this adjustment is not critical.

The horizontal width of the C.R.O. trace is just the wobbling amplitude in gauss. Thus to use the instrument for exploring a field the resonance dip can be located and adjusted to mid-screen with the sample at the center of the field. As the sample is moved away from the center, the field change will be indicated by the change in position of the resonance dip. This type of measurement will be most effective if the wobbling amplitude is variable and its value is known for different settings of the varying control. The method of determining the amplitude is to read the frequency change which moves the resonance dip from one side of the screen to the other.

It is to be noted that the accuracy limitation imposed on absolute measurements does not apply in the case of field changes as discussed in the preceding paragraph. Nor does it apply when the instrument is used for comparing fields since this involves only ratios of frequencies.

The width of the resonance dip is an indicator of homogeneity, allowing use of the instrument for locating the most homogeneous point in a field or for establishing the boundaries of the region in which a field is uniform.

CONCLUSIONS

The operation of the instrument was tested in fields from 1883 to 16,214 gauss, the upper range being in the McGill University cyclotron and the lower range in a laboratory magnet.

The 6AK5 operated normally in the fields available for test and it seems probable that the range of the instrument could be extended considerably higher with no constructional changes beyond winding coils to oscillate at higher frequencies.

The lower limit was set at 3000 gauss since below this the signal became difficult to locate. It was still recognizable down to 1900 gauss.

Radial fall-off in the cyclotron field is approximately 15 gauss per inch, so that inhomogeneity of at least this amount is tolerated with clearly defined signals.

In view of the simplicity of the apparatus, the accuracy obtainable and the ease of operation, the method appears to have advantages over others used for the same purpose.

The author wishes to thank D. A. Anderson for suggesting this work and for much valuable advice, particularly in the design of the probe circuit.

THE REVIEW OF SCIENTIFIC INSTRUMENTS VOLUME 20, NUMBER 6 JUNE, 1949

A 22-Inch Wilson Cloud Chamber in a Magnetic Field of 21,700 Gauss

WILSON M. POWELL
Radiation Laboratory, Department of Physics, University of California, Berkeley, California

(Received March 22, 1949)

A Wilson cloud chamber 22 inches in diameter in a magnet producing a magnetic field of 21,700 gauss at the center of the chamber is described. The magnet is pulsed in synchronism with the 184-inch Berkeley cyclotron and can be operated with a steady field of 10,000 gauss. The use of the instrument for identifying light atoms is discussed briefly.

INTRODUCTION

THE 184-inch cyclotron has recently undergone a conversion so that it accelerates protons up to an energy of 350 Mev. A large cloud chamber with magnet for use with the cyclotron has been designed so that particles with $h\rho$ up to 3×10^6 gauss cm will produce cloud chamber tracks of measurable curvatures. In order to accomplish this, the cloud chamber must be in a high magnetic field and a long section of the particle's path must be observable. This magnet produces a field of 22,000 gauss and the cloud chamber has a useful diameter of 19.5 inches. The track of a 350 Mev proton crossing the diameter of the chamber would have a sagitta of 2.3 cm and thus a very accurate curvature measurement can be made.

THE MAGNET

The magnet, Fig. 1, consists of a pair of coils, two poles, and an iron yoke. The coils were made of bare copper strap, 1 inch by $\frac{1}{4}$ inch in cross section, wound in eight pancakes of 75 turns each and insulated between turns with two layers of glass tape 7 mils thick. The pancakes were separated by wooden spacers $\frac{5}{16}$ inch thick and $\frac{3}{4}$ inch wide, so arranged as to direct the cooling oil back and forth across the pancakes as shown in Fig. 2. These wooden spacers were attached to wooden rings which insulated the pancakes from the $\frac{1}{4}$ inch thick iron tank that contained them. The inner wooden rings were $\frac{1}{2}$ inch thick so that the inside diameter of the pancakes was only $1\frac{5}{8}$ inches greater than the $19\frac{1}{2}$-inch inside diameter of the coil tank. The pancakes were dropped into the iron tank, the re-entrant lid dropped on top of them, and great pressure applied to the lid as it was welded down. This was done to prevent the motion of the pancakes inside the coil tank.

The bottom pole fills the cylindrical space bounded by the inside of the coil tank. The upper pole has a conical hole which allows the camera to see a circular region having a diameter of 50 cm.

The current for the magnet is supplied by a navy pulse generator with a five-ton flywheel. It is energized by a 150 hp motor and pulsed once a minute. In order to build the current up rapidly, the circuit to the magnet is interrupted by opening a contactor while the current in the generator field windings is rising to its maximum value. Then the contactor is closed after the terminals of the generator have reached full voltage. During a pulse the speed of the generator and flywheel is reduced by 10 percent. Figure 3 shows how the field at the center of the gap rises with time reaching a peak value in about 2.1 seconds and remaining constant for 0.2 second. At a time 2.3 seconds after closing the contactor, the generator field winding circuit is opened and the current to the magnet drops from 1000 amperes to about 30 amperes in the conductor in 7 seconds. Shortly after this, the contactor is opened, the field windings energized and the generator is ready for another pulse.

The two coils are connected in series, the current passing through each coil in four parallel paths. When the magnet is pulsed as described above, the maximum current is 4000 amperes and the power 800 kilowatts; this produces a field of 21,700 gauss at the center of the gap. The field is constant over the 0.2-second period of steady current; during this time, the cyclotron is pulsed and the cloud chamber expanded. The magnet can also be operated with a steady field of 10,000 gauss; this requires 1300 amperes and 85 kilowatts. Figure 4 shows the magnetization curve measured at the center of the magnet and Fig. 5, the shape of the field at 10,000 and 21,700 gauss.

The coils of the magnet are cooled by oil which circulates through an oil-water heat exchanger (see Fig. 6) mounted on the frame supporting the magnet. During the pulsed operation the temperature of the cooling oil rises to 45°C after several hours. In order to protect the cloud chamber from the heat radiated by the coils, water-cooled, stainless steel pads line all the surfaces of the magnet that are exposed to the cloud chamber. See heat shields, Fig. 1. The temperature of the water circulated through these pads is maintained at 19.3°C. Heavy foam rubber pads protect the chamber from the outside and a small fan circulates the air around the chamber to keep it at a uniform temperature.

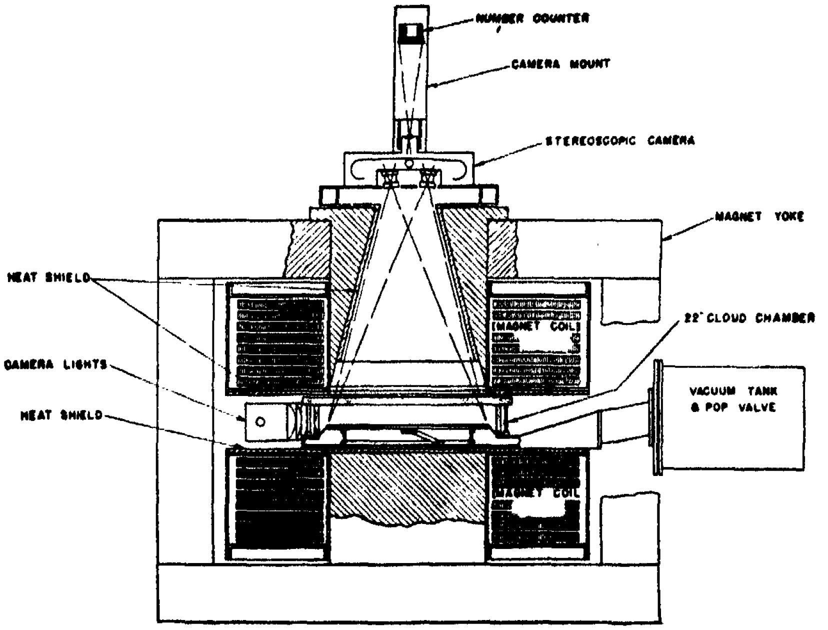

FIG. 1. The cloud-chamber magnet showing the location of the cloud chamber, the camera, and the lights.

THE CLOUD CHAMBER

The cloud chamber, Fig. 7, is built on a duraluminum manifold, circular except for a neck that extends out beyond the magnet coils and to which the expansion valves may be connected. The upper part of the cloud chamber consists of a 22-inch Lucite cylinder, 3½ inches high, and with a ¾-inch wall topped by a one-inch thick Tufflex disk which is attached to the manifold through a dural clamping ring. In order to keep the height of the cloud chamber at a minimum, both the top glass and the clamping ring are bevelled at an angle of 30° to the perpendicular so that the top surface of the clamping ring is level with that of the top glass.

The diaphragm consists of a ⅜-inch Lucite disk, 20½ inches in diameter, with $\frac{1}{16}$-inch gum rubber glued to its top surface. The rubber has a diameter of about 23½ inches so that it extends beyond the edge of the Lucite and makes the seal between the manifold and the bottom of the Lucite cylinder. There is a pantagraph connecting the Lucite disk to the bottom of the manifold; its purpose is to guide the disk during the expansion so that it moves parallel to the cylinder walls. The motion of the

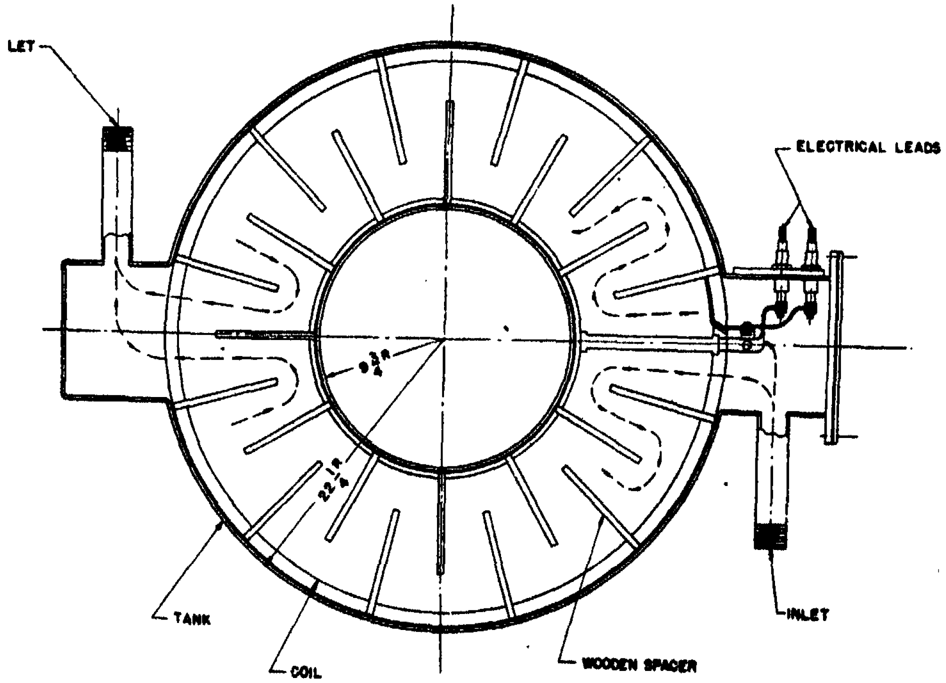

FIG. 2. Plan view of a magnet coil, showing the flow of the cooling oil.

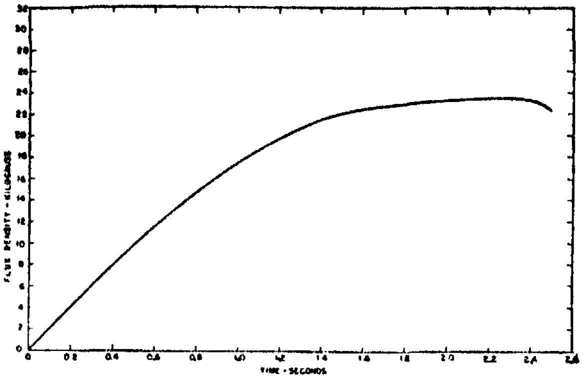

FIG. 3. The rise of the magnetic field at the center of the cloud chamber as a function of time.

disk is stopped by ⅜-inch neoprene pads which cover the bottom of the manifold except for three air channels, each three inches wide.

Several problems arose owing to the eddy currents that are induced in metal parts of the chamber when the field is rising and falling. The forces that were produced were large enough to move the whole chamber. For this reason a hole 19½ inches in diameter was cut in the bottom of the manifold and the duraluminum replaced by a ½-inch thick iron disk. When the chamber is in place, this disk becomes part of the lower pole and serves to increase the field at the center of the chamber as well as to prevent any violent motions of the chamber since it is attracted to the lower pole when the field comes on. The clamping ring that holds the top glass to the chamber has been broken and clamped together with a layer of paper insulation at the break. In addition, the studs that go between the clamping ring and the manifold have been insulated from the clamping ring by paper washers.

The clearing field voltage is applied across two grids of wires. The high voltage is connected to a set of parallel wires spaced ¼ inch apart and supported by a Lucite hoop just below the top glass, while the ground connection is made to a corresponding set under a layer of black velvet that is glued to the top surface of the diaphragm. It is not sufficient simply to ground the manifold since the rubber diaphragm is an insulator. Two aquadag rings were painted near the top and bottom edges of the Lucite cylinder and connected to ground to prevent the surfaces from charging up.

THE OPTICAL SYSTEM

The cloud chamber is illuminated through the Lucite walls of the cylinder by a pair of General Electric FT. 422 flash tubes. Each tube is wrapped in aluminum foil except for a strip $\frac{3}{16}$ inch wide going the length of the tube. The foil was held on by winding 5-mil tungsten wire in a spiral with half inch spacing around the tube; this wire and the aluminum foil acted as the tickler electrode. Although the width of the light source is reduced, the intrinsic brilliance increases so that the intensity of the illumination reaching the lens is reduced by only 20 percent. This lens is cylindrical, 18 inches long and 2¼ inches wide; it provides a beam of light approximately two inches wide at the center of the chamber. Because of the aberration appearing when rays pass obliquely through the cylindrical lenses, it was necessary to place baffles covered with black velvet between the lens and the source in vertical planes perpendicular to both. These louvres were spaced every two inches starting three inches from the center of the lens. The Lucite surfaces of the cloud chamber cylinder scattered light onto the black velvet in an intensity amounting to about 2 percent of the intensity at the center of the chamber. The resulting background made it necessary to use the Eastman Orthochromatic Linagraph film instead of Super XX. This film is at least twice as sensitive

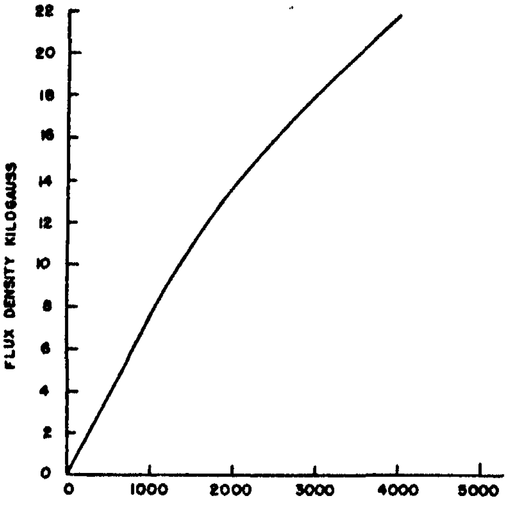

FIG. 4. The magnetization curve of the magnet.

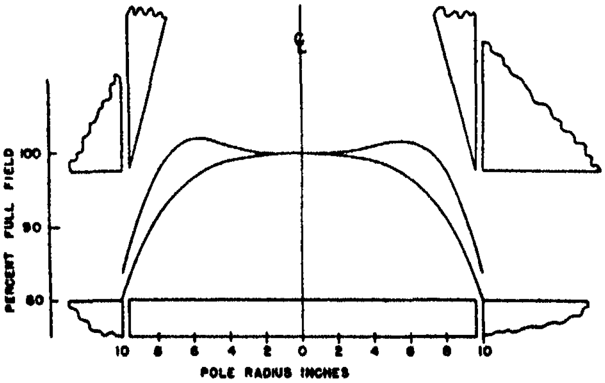

FIG. 5. The upper curve is the percentage of the field at the center of the chamber as a function of radius when the chamber is operated with 10,000 gauss at the center. The lower curve refers to a field at the center of 21,700 gauss.

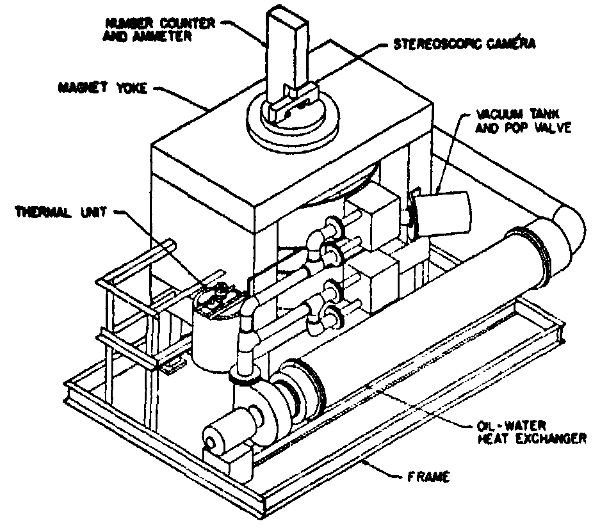

FIG. 6. General assembly of the cloud chamber and magnet.

to the light from the flash tubes and has much greater contrast.

460 μf at 1600 volts were discharged through each flash tube. The combination of the resulting surge of current and the magnetic field produces forces large enough to break the tube. This difficulty has been overcome by bringing the ground lead back along the tube and binding it tightly so that it produces a force on the tube in the opposite direction. Wherever possible, the two leads coming to the tube are twisted.

The stereoscopic camera uses a pair of Leitz Summar, F2, 50-mm lenses separated by 4.5 inches. The camera is located about 25 inches above the center of the cloud chamber with each lens toed in toward the other so that the optic axis of each makes an angle of 5° with the perpendicular to the cloud chamber. The film gate is tipped at an angle of 0.34 degree from the perpendicular to the optic axis in the proper direction to keep all parts of the chamber in the best possible focus when the camera is placed directly above the center of the chamber. A third lens in the back of the camera permits a counter and an ammeter showing the magnet current to be photographed at the instant when the cyclotron is pulsed. This is accomplished by discharging a condenser through a flash light bulb illuminating counter and meter at the proper time.

TIMING

Two sets of cam driven switches control the timing of the cloud chamber. The slow timer with seven cams driven continuously by a variable speed motor performs the following operations: (1) rings a warning bell ten seconds before an expansion, (2) turns on the magnet, (3) resets the clearing field, (4) resets the generator circuit, (5) operates a valve to make the cloud chamber expand slowly as many times as desired. The cams are made adjustable by clamping onto them the desired number of dogs which operate microswitches. The maximum time for one revolution is four minutes, the shortest 1.5 minutes. By doubling the number of dogs the cycle can be repeated twice in one revolution.

The second set of cams controls the more rapid sequence and is called the fast timer, Fig. 8. A small synchronous motor running continuously is coupled to the cam shaft by means of a solenoid operated clutch. The cam shaft makes one revolution in half a second. Only five of the seven cams are used. Dogs are attached to the cam wheels at suitable intervals as in the slow timer, and each microswitch is mounted on a wheel which can be rotated by means of a worm gear from the front panel. The microswitch wheels are coaxial with the cam shaft but do not rotate with it. Scales marked in hundredths of a second intervals are pasted to the

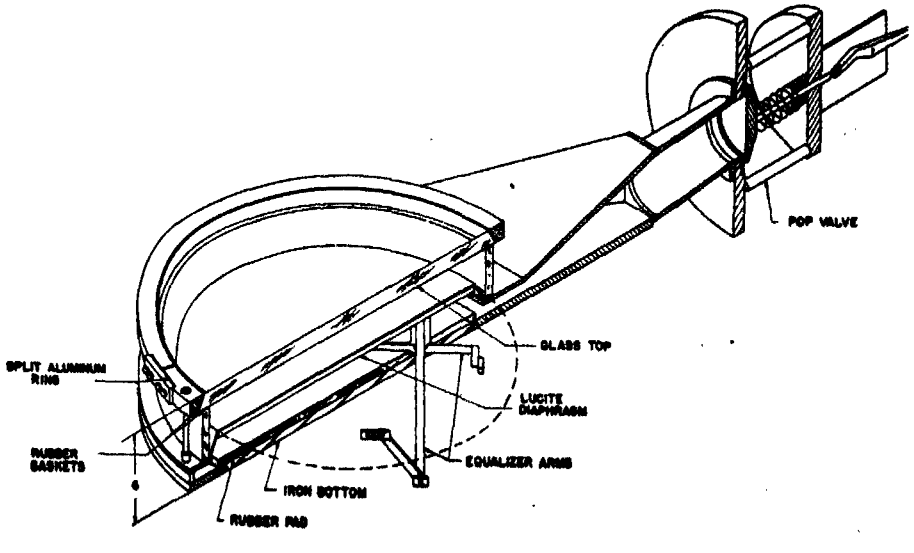

FIG. 7. Cross section of the Wilson cloud chamber.

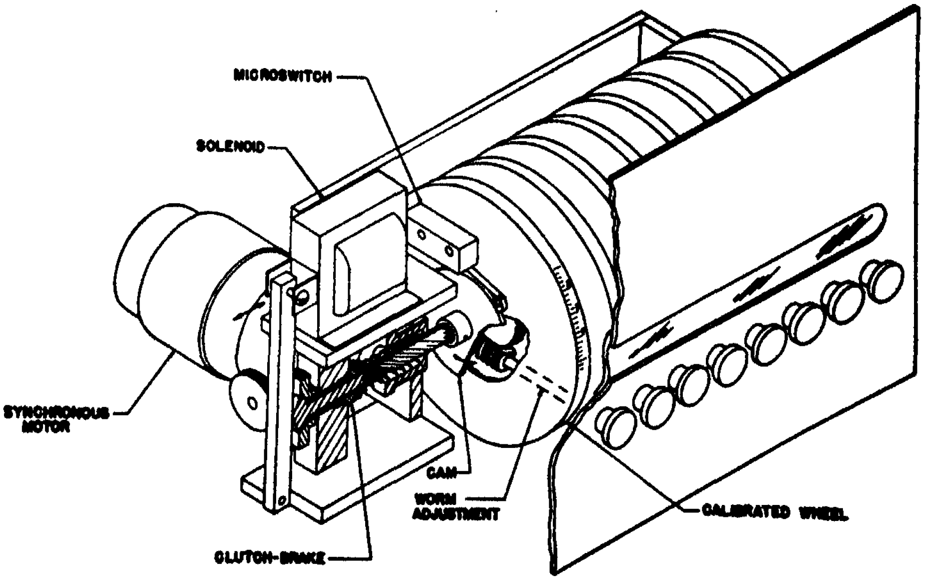

FIG. 8. The fast timer.

edges of the wheels so that their phasing may be read on the front panel and adjusted by means of the worm gear. Cam 1 turns off the clearing field, cam 2 expands the chamber, cam 3 turns on the rf oscillator on the cyclotron, cam 4 pulses the ion source in the cyclotron, and cam 5 flashes the lights. Cam 6 interrupts the current going to the magnetic clutch so that the cam shaft stops rotating. The timing sequence is as follows when operating with 100 cm pressure of helium when the chamber is expanded and using water vapor. The time of starting of the cam shaft will be called zero. The clearing field is turned off 0.12 second later, the chamber expanded at 0.16 second, the rf turned on at 0.18 second, the arc pulsed at 0.21 second, the lights flashed at 0.23 to 0.24 seconds. For gases of higher molecular cross section, greater time must be allowed between the arc pulse and the lights. Higher gas pressures increase this time also. If the arc is pulsed 0.02 second earlier, then about half the time the tracks appear slightly broadened because the ions have diffused before the chamber has reached the appropriate supersaturation to start forming drops. There is a jitter of 0.01 second in the time interval between the expansion of the chamber and the pulsing of the arc. This arises from the fact that the beam from the cyclotron comes out in pulses 0.01 second apart arbitrarily phased with the timing of the cloud chamber. Good pictures can be obtained with both arc and light excitation 0.02 second later, but the longer time makes the tracks less straight in the pictures taken without magnetic field.

TRACK ENDINGS

This cloud chamber and magnet may be used not only to make accurate curvature measurements on the tracks of fast particles but also to identify the slow particles that result from the disintegrations of nuclei. Figure 9 has been prepared to demonstrate how the lightest nuclear fragments may be identified near the end of their range. The lighter particles have a longer range for the same curvature and, hence, curl up more in the magnetic field. It is necessary to use hydrogen or helium gas at 100 cm of mercury or less with water vapor if a distinction between tritons and alpha particles is to be made. Even under these conditions about 20 percent of the tritons will show curvatures identical with those for an alpha particle over the last 20 cm of the track. Protons, alpha particles, and deuterons can be distinguished with little ambiguity in this range.

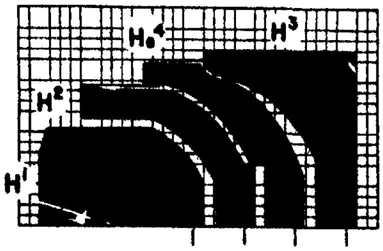

FIG. 9. Track endings in a field of 21,700 gauss with 100 cm. Hg pressure of helium and water vapor at 19.3°C. Last 22 cm all tracks perpendicular to base line.

ACKNOWLEDGMENTS

The major portion of the engineering of the magnet and cloud chamber was done by Paul Hernandez. Walter Hartsough, Dr. Evans Hayward, and Keith Brueckner were responsible for much of the work necessary for successful operation of the chamber, and Marguerite Hayward for the photography. This work was performed under the auspices of the Atomic Energy Commission.

THE REVIEW OF SCIENTIFIC INSTRUMENTS VOLUME 20, NUMBER 6 JUNE, 1949

Magnet Coils

L. G. Coonrod, W. E. Cecconi, C. Gedraitis, K. R. Harper, and R. M. Lewis
Laboratory for Nuclear Science and Engineering, Massachusetts Institute of Technology, Cambridge, Massachusetts

(Received March 3, 1949)

Methods of winding magnet coils using copper tape as the current-carrying element are described. Difficulties with unsatisfactory arrangements are pointed out. One satisfactory system is described in detail, providing an efficient design for magnet winding to yield relatively high copper cross section while permitting the removal of heat at a high rate.

During the past three years a number of magnet coils and Helmholtz coils for the production of magnetic fields from 1700 to 17,000 gauss have been constructed by us for the Laboratory for Nuclear Science and Engineering. These coils have been built to designs of and for use by Professor George E. Valley, Professor Robert Williams, Dr. Robert Thompson, and Dr. William Preston, all now or formerly of this Laboratory. In the construction of these coils several features have been found to contribute to the over-all performance.

Magnet coils should be designed to provide a large value of gauss-cm^3 in the air gap per watt of exciting power. This is especially true for electromagnets to be used with portable power supplies. This can best be achieved by realizing a high ratio of copper cross section to total winding space. Another necessary objective is to provide a design with low thermal gradients from copper to cooling medium so that maximum temperature utilization of the materials is achieved. In the effort to satisfy these requirements a decision was made to use copper strip. This has been followed in all the magnets described herein. Copper strip is usually obtained in 350-foot lengths. It is often desirable to use 2500-foot lengths in coil winding. We have found that lapped joints (tape overlapped approximately 8 to 10 inches), soft-soldered with gas torch, to be the most satisfactory joint. Silver soldering was not satisfactory. The strip must be wound under back tension of several hundred pounds. This is provided by a friction detent, spring-loaded (see Fig. 3). When wound under tension, we have realized actual build-up equal to 112 percent of calculated [no. of turns × (thickness of copper + thickness of insulation) × 1.12 = actual build-up].

In using copper strip on a bobbin such as is shown in Fig. 1(A), the heat developed within the conductor as I^2R loss is readily transferred to the edges of the copper strip by conduction. If the insulating gap to the spool-head is kept small and is thoroughly filled with solid dielectric and varnish, the temperature drop across the gap can be held to low limits. By suitable selection of spool-head thickness with appropriate spacing of cooling tubes, it is possible to limit the temperature drop here to low values. Cooling tubes, for magnets with low power consumption, may be used only on the periphery (Fig. 1(A)), or for larger power consumption, a set of tubes may be added in the position shown dotted in Fig. 1(A). In mounting copper tubing in such position, we flatten the tubing slightly before applying it to the spool-head. It is attached to the spool-head with soft solder, gas-heated, to obtain a low resistance thermal bond. If several bobbins, or pies, are to be stacked or wound as multiple units, the spool-heads may have a recess routed out as shown in the right-hand and center section of Fig. 1(B). The copper tube is then soldered into this groove, leaving no interfering protuberances.

In a typical example[1] six pies, wound on two triple bobbins (similar to Fig. 1(B) and having spool-heads ½ inch thick and approximately 39-inch outside diameter, dissipate 50 kw into 30 gallons per minute of water with a 30°C average temperature rise of copper above water inlet temperature. With the mica and fiberglass construction it would undoubtedly be safe to operate these coils at 100 kw input.

The inner end of the conductor, in all the coils discussed here in, is brought out radially as shown in Fig. 2. The conductor tape is given a 90° lateral bend by folding at 45°. An additional 90° fold brings the end out vertically. The bobbin core is flattened as shown in Fig. 2(A) to accommodate the extra thickness here. A recess is provided in the spool-head to permit this radial lead to clear the normal winding. The radial lead is half-lapped with fiberglass tape and is sandwiched with mica as shown in Fig. 2(B). To prevent slipping during early stages of winding, the inner end is secured by two textolite pins inserted in the bobbin core; these are long enough to penetrate the double thickness of conductor near the 45° fold. (See Fig. 2(B).) This method of attaching and bringing out the inner end of the winding has been entirely trouble-free. The inner end and outer end of the winding are normally terminated on a rectangular textolite block located at some convenient point on the circumference to permit attaching heavy current leads. Naturally the radial groove for the inner lead is designed to point toward this block. The details of attachment have varied from job to job.

---

[1] G. E. Valley and J. A. Vitale, "A counter controlled high pressure cloud chamber," Rev. Sci. Inst. 20, 411 (1949).

Originally 0.004 inch electrical Kraft paper wound in alternate layers was tried for interlayer insulation. It was planned to impregnate the entire assembly under vacuum, as is common in transformer practice. This proved impossible as the varnish penetration was inadequate. The coils so treated were quite unsatisfactory since temperature cycling caused breathing of moisture bearing air, followed by small leakage currents causing electrolysis and rapid deterioration.

The next step, suggested by Dr. Thompson, was spiral wrapping of the copper which was then wound without additional interlayer insulation. See Fig. 3(A). During winding the successive bobbin layers were painted with Ajax Varnish No. 02025. The tight wrapping caused the varnish to squeeze out to the ends of the layers, giving a very tight fill. It should be noted that the spiral tape is butted, not half-lapped, to preserve space-factor. This is not a comfortable expedient as gaps could occur opposite one another to permit leakage. However, the varnish appears to supply adequate fill. A set of coils as described was operated for six weeks in Colorado, in a trailer, at 13,500 feet, and has subsequently been in intermittent use at sea level for four months and still shows insulation resistance better than 10 megohms per pie.[1] Incidentally, any coil showing less than 1 megohm may be expected to give trouble ultimately. Some of our more recent coils show insulation resistance of 3 to 4×10^8 ohms. The spiral wrapping was applied by a Segur Taping Machine, Model 1-109A, modified to take tape width and winding pitch to meet our requirements. This required very close speed adjustment to produce an accurately butted spiral wrap.

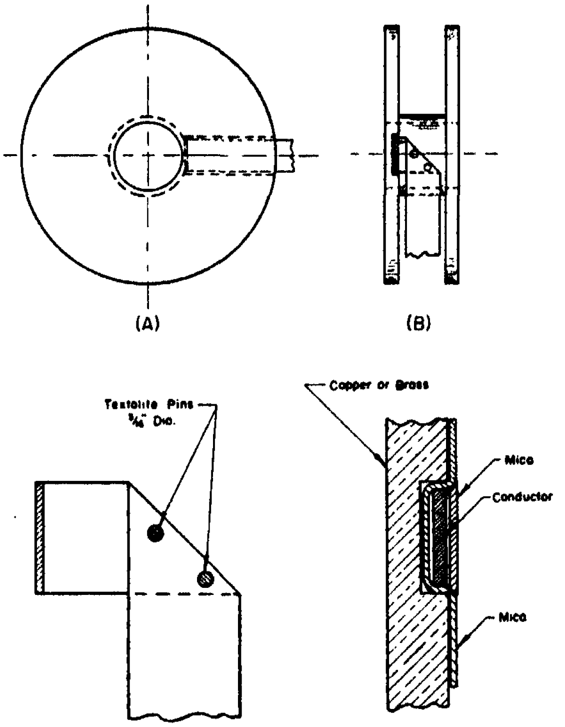

FIG. 2.

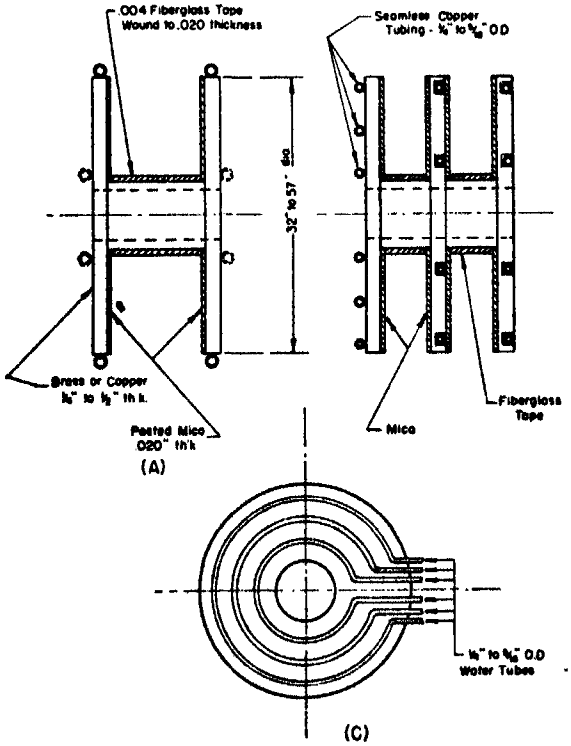

FIG. 1.

An improved method of insulation has just been tried. Availability of wider fiberglass tape made this possible. This consists of a strip of tape folded laterally about the copper tape (see Fig. 3(B)) so that a continuous seam ("*S*" in Fig. 3(B)) comes on top. As this always meets a continuous strip of tape on the next layer, leakage paths are long. Winding presented some problems which were successfully met in the following manner (see Fig. 4):

1. The flat tape was induced to fold by rotating brushes. (See "*RB*," Fig. 4.) These did not crease or crack the tape but firmly brought it over.
2. Rubber friction wheels ("*W*"—Fig. 4) brought the tape snugly over the copper. The amount of tension is controllable by the angle of the wheel.
3. Electrical Scotch Tape is applied by a roller ("*T*"—Fig. 4). This holds the "packaged" copper.
4. A grooved roller ("*G*"—Fig. 4) presses the package tight without causing folded creases. The grooves appear to be necessary.
5. After the "packaged" copper is safely bedded on the bobbin, the Scotch Tape is pulled off since it is not needed in a permanent coil; indeed, it is detrimental, wasting in this case

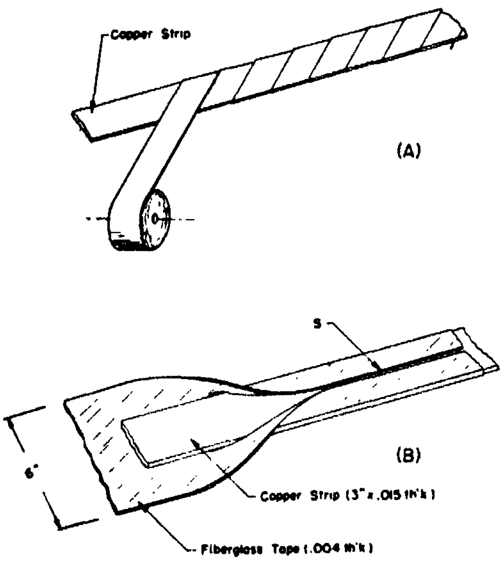

FIG. 3.

1 inch winding space in 300 turns or 12 percent. The tape returns via an idler (Fig. 4) where it is returned to roller "*T*" for reuse.

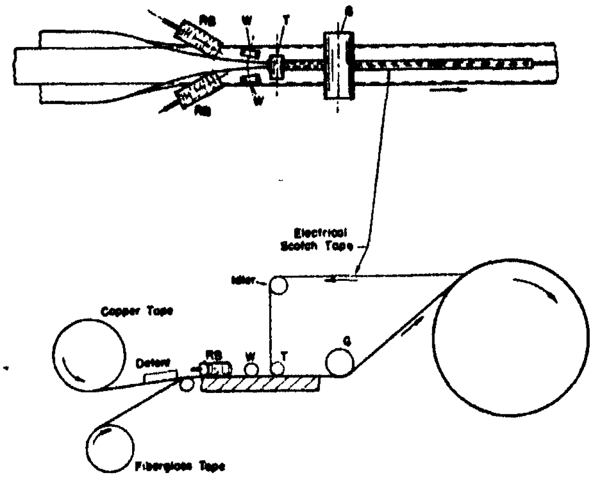

FIG. 4.

Oddly enough the Scotch Tape can be reused for many times. It stretches and from time to time lengths must be cut out. The speed of the rotating brushes is not critical. They can be started in advance of the winding rotation. In our set-up, vacuum cleaner brushes were used, driven by electric hand drills rotating at approximately 1200 r.p.m. One drill was reconnected to provide counter clockwise rotation. The equipment can operate at winding speeds up to approximately 6 r.p.m., being limited by the speed of the operator applying varnish. We expect to mechanize this in the future.

One advantage of the winding last described is that non-circular bobbins can be wound. A shape, roughly pentagonal, gives erratic linear speeds for constant angular velocity of the winding arbor. This would completely prohibit the butted spiral wrap. No difficulty was experienced with the last method in winding such a form.

The construction of the coils described above was in pursuance of research in nuclear physics and cosmic rays supported by the joint AEC–ONR program.

THE REVIEW OF SCIENTIFIC INSTRUMENTS VOLUME 20, NUMBER 6 JUNE, 1949

A Counter Controllable High Pressure Cloud Chamber*

G. E. VALLEY AND J. A. VITALE
Physics Department and Laboratory for Nuclear Science and Engineering, Massachusetts Institute of Technology, Cambridge, Massachusetts

(Received March 3, 1949)

A high pressure cloud chamber is described which is so designed as to be as easily counter controlled as an ordinary cloud chamber. The instrument is fitted with a magnet capable of producing a field of approximately 10,000 gauss continuously. It is mounted in a trailer and can be readily transported to mountain sites.

PROPERTIES OF HIGH PRESSURE CLOUD CHAMBERS

A HIGH pressure cloud chamber combines the properties of an ordinary cloud chamber with those of a thick emulsion photographic plate. It can, as a result, yield information which cannot be obtained otherwise.

Compared with an ordinary cloud chamber which operates near atmospheric pressure, a high pressure instrument possesses the following advantages and disadvantages:

(1) The stopping power of the gas is much higher and so is the probability of making a nuclear collision with a gas atom.

(2) The sensitive time is much longer. When random expansions are made for cosmic-ray studies, this is an obvious advantage; when the instrument is counter controlled by cosmic rays, or used with a high voltage accelerator, this ceases to be an advantage and may even be a hindrance because of the background of uninteresting phenomena.

(3) The time required to reach thermal and vapor diffusion equilibria between expansions is much greater. For random expansions this effect is more than outweighed by the increased time of sensitivity. Thus, with 100 atmos. of argon we get forty times as many cosmic-ray tracks per picture, but only twice as many per unit time as compared to an ordinary cloud chamber. If, however, we are interested in observing reactions in the gas, each of these figures must be multiplied by 100 (at 100 atmos.). Thus, we can get 4000 times as much information per picture and so can gather statistics on phenomena so rare that they cannot be observed at all in a one-atmosphere instrument, because of the practical impossibility of scanning the huge number of pictures which would be involved.

(4) Coulomb scattering increases as the square root of the pressure and, under many circumstances, makes any achievable magnetic field give only qualitative information. This is an important effect when argon is used at 100 atmos. or higher. When hydrogen or helium are used, scattering can be reduced to negligible importance by easily obtainable magnetic field strengths. Even when argon is used, it is very useful to have a magnetic field because it enables electrons to be easily distinguished from more interesting particles. This effect is discussed in detail in Appendix I.

(5) Although the time of sensitivity is much increased and a background of tracks is present in every counter-controlled picture, this is considerably ameliorated by another effect. It is well known[1] that, relative to the ion diffusion constant, the ion mobility increases in proportion to the pressure. Moreover, the coefficient of electron attachment is very high, so that both positive and negative ions are heavy. Now, because of the high pressure, it is possible (indeed, necessary) to apply much higher clearing potentials than are commonly used in cloud chambers. One achieves drift velocities, in 100 atmos. of argon, for instance, on the order of several cm/sec. The result is that many tracks, and in particular many counter controlled tracks, are observed to be split into two perfectly sharp and distinct parallel components. By measuring the separation of the positive and negative ion components of different tracks in the same picture, one can determine their relative time of occurrence to at worst ±0.04 sec., which is quite comparable to the resolving time of an ordinary one-atmosphere instrument. In some cases this is not possible because ions of one sign may have drifted outside the illuminated region.

In comparison with photographic plates the high pressure cloud chamber has the following properties:

(1) By choice of pressure and atomic number of the gas, it is possible to determine at least the sign of charge, and often the momentum of particles, by the use of practically obtainable magnetic field strengths (10,000 gauss).

(2) The material in which reactions take place is pure (it requires less than 2 g of alcohol to make tracks in a volume containing 60 moles of argon at 150 atmos., for instance), and can be changed—hydrogen, helium, nitrogen, and argon are practical gases which can be used at present. Oxygen is most dangerous, and krypton and xenon are very expensive. Of the heavy organic gases, only CF_4 remains gaseous at 3000 p.s.i., to our knowledge.

(3) The instrument can be triggered like any other cloud chamber, and there is little question as to whether the tracks seen are germane to the experiment at hand. Moreover, the results do not depend on the time elapsed before the emulsion is developed.

(4) Since the illuminated volume is relatively thick compared to its diameter, it is practicable and useful to take stereoscopic photographs.

(5) A major disadvantage is that ionization density of a track can only be crudely estimated. Neither grain nor droplet counting is possible because the ion density even from a minimal ionizing particle is so high as to produce a completely homogeneous track. Track width however, gives some indication of ion density, so that star fragments are easily distinguished from high velocity particles. The theory of this is given in Appendix II.

CHARACTERISTICS OF THE PARTICULAR INSTRUMENT CONSTRUCTED

The design objective which we set was to achieve the properties listed above within the following limits:

(1) The instrument was to be transportable to a mountain site. This limited its dimensions to fit in a trailer of standard road and railway clearances.

---

* Assisted by the joint program of the ONR and AEC.

[1] L. B. Loeb, *Kinetic Theory of Gases* (McGraw-Hill Book Company, Inc., New York, 1934), Chapter XI.

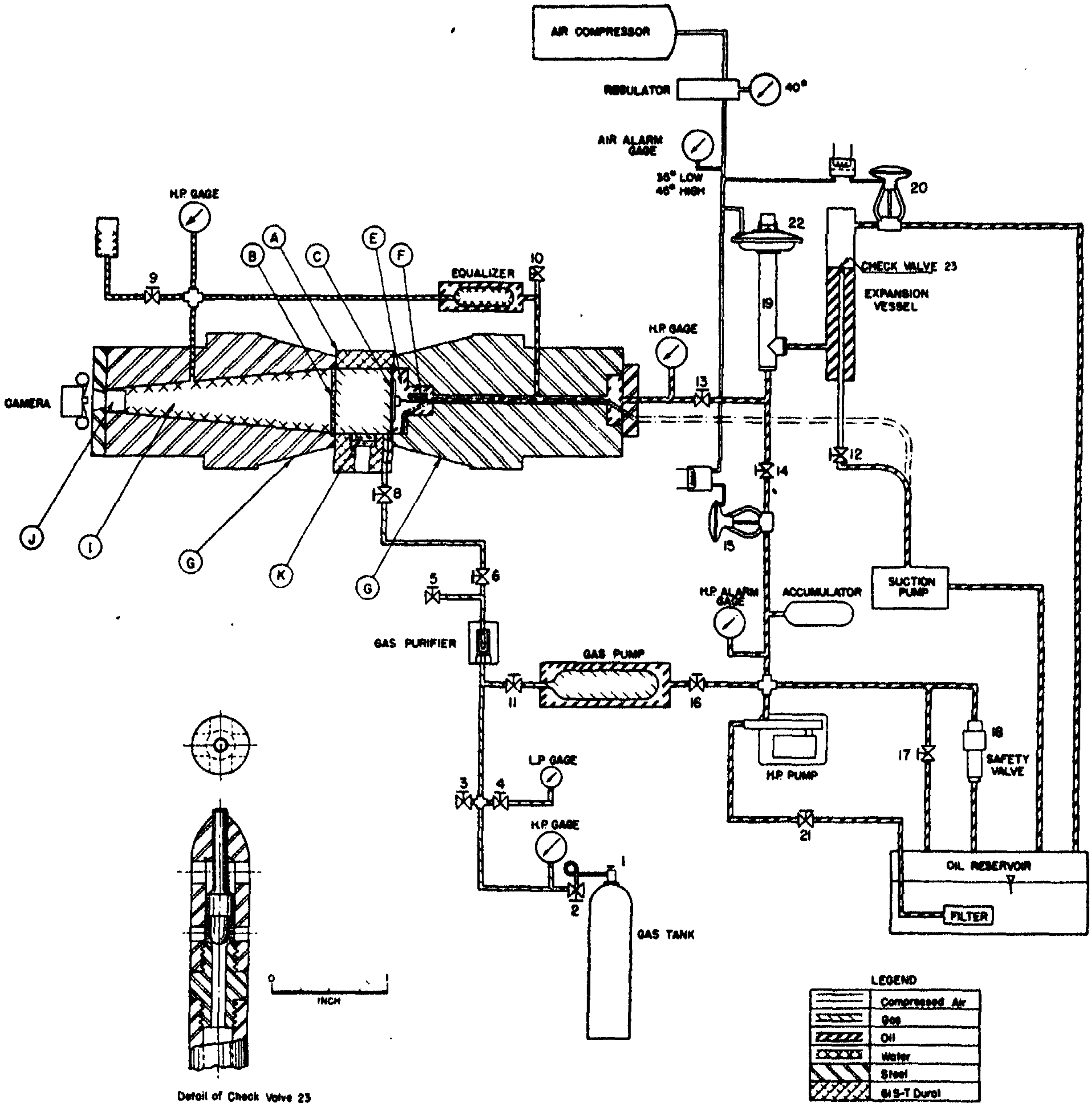

FIG. 1. Schematic of hydraulic system and section in elevation of cloud chamber and magnet without coils.

(2) The fuel required could not exceed what was practical to truck up the mountain.

(3) The instrument was to be capable of rapid assembly and disassembly for repair, with a minimum of physical effort because of the serious loss in effectiveness of personnel at high altitude.

(4) The wall of the cloud chamber was to have the smallest surface density consistant with a contained pressure of 200 atmos.

(5) The configuration of the instrument was to place a minimum of restrictions on the experiments that might be performed with it.

We arrived at a design which yields an illuminated volume 9 in. in diameter and 2½ in. deep, in a magnet which produces 8800 gauss for 43 kw. and which can dissipate 100 kw. given 10°C intake water. The instrument less trailer and generators weighs 8 tons and occupies about 40 percent of the available floor area of a trailer of 25-ton capacity. The surface density of the cloud-chamber wall is 15 g/cm^2 and since the material is of low atomic number, there is little probability of shower production by electrons or photons in the wall. The exterior of the chamber is accessible and almost any arrangement of lights, triggering devices, absorbers, etc. can be used. It requires 90 min. to remove the cloud chamber from the magnet; of this time, 60 min. is required to release the gas and other fluids.

The design evolved is shown in Figs. 1–3. The cloud chamber proper is defined by the machined aluminum alloy cylinder *A*, the circular glass plate *B*, and the rubber diaphragm sealed piston *C*. The piston is caused to move by pumping oil into the chamber *E* until rheostat *F* balances the bridge circuit of which it forms one arm. The piston is caused to move back, thereby expanding the chamber, by releasing a measured quantity of oil from chamber *E* into another vessel. A system of pneumatically operated valves with electrical control allows this cycle to be repeated automatically.

This assembly is made pressure tight by rigidly clamping it between the poles *G* of an electromagnet by means of four studs *H*. The thin glass plate *B* is supported hydrostatically by water in chamber *I* which is automatically kept at the same pressure as the oil in chamber *E*.

Stereoscopic photographs are taken through the thick glass windows *J* and light is admitted to the chamber through window *K*.

THE MAGNET

A general view of the instrument, with magnet coils removed to show the shape of the magnet, appears in Fig. 2. The magnet was cast and machined for us by the Boston Navy Yard.** The material satisfies Navy specification 49-S-1 Class F (carbon 0.3 percent, manganese 0.6 percent, phosphorous 0.05 percent, sulfur 0.05 percent, silicon 0.2–0.3 percent, nickel 0.85–1.00 percent, chromium 0.4 percent).

The pole shape and yoke dimensions were based on previous experience with a smaller magnet.[2] These dimensions were then altered to provide a structure of sufficient strength to withstand a pressure of 3000 p.s.i. on and in each pole.

Each pole is a frustrum of a right circular cone of diameters 13 in. and 18 in. and 10⅞ in. in length. Both poles are hollow.

The cavity *E* is circular in cross section, and is made just large enough to house the piston-bearing, control-rheostat, and the high voltage lead.

The cavity *I* (cf. Fig. 1 and Fig. 3) is defined by the volume of two skewed circular cones of common base. This shape of cavity produces the most rigid structure consistant with the requirement that an unobstructed view of the illuminated volume be obtained from each of the two windows *J*. This cavity was cored and its surfaces were not machined. They were coated with Malacca #810 Neoprene*** compound applied in several successive coats and then cured by an air blast (150°F) for 24 hours. This coating has thus far protected the cavity surface from rusting.

At a pressure of 3000 p.s.i., the force tending to push the poles apart is 260,000 lb. This force is transferred through the magnet yoke to four 2½-in. studs *H* (Fig. 3). The portion of the yoke which is perpendicular to the axis of symmetry is designed to be a beam of uniform strength loaded at the center. It is seen from Fig. 2 that every section of the beam taken parallel to the axis of symmetry is a "T" section. The web of the "T" section is shaped as two parabolas whose vertices are at the end supports. Since the structure was cast, this shape introduced no difficulties of fabrication and yielded a net saving of 1000 lb. as compared with a magnet yoke of uniform cross section, calculated to give the same deflection under pressure.

Type 49-S-1 Class F steel has a tensile strength of 85,000 p.s.i., and a yield point of 53,000 p.s.i. The most highly stressed part of the yoke occurs at the tip of the pole which contains the water column *I*. Here the metal is approximately 1.5 in. thick. Strain gauge measurements over this region at 3000 p.s.i. indicate that the outside surface is stressed to 6750 p.s.i., from which the inner surface is calculated to be stressed to 8700 p.s.i.

The four 2½-in. studs *H* which hold the yoke together are machined from Elastuf Type A-2 alloy machinery-steel. This steel has a tensile strength of 140–160,000 p.s.i. and a yield point of 125–145,000 p.s.i. with 16–20 percent elongation. Each stud is

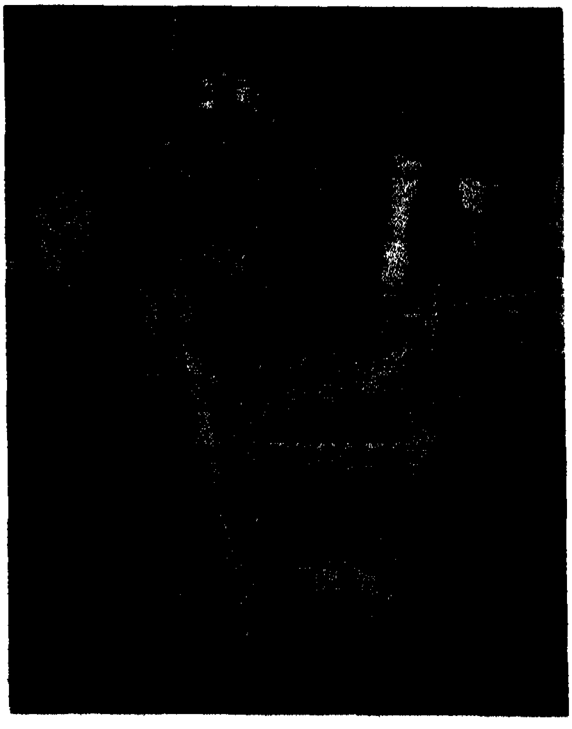

FIG. 2. Photograph of front end of magnet with coils removed.

** We wish to record our indebtedness to Commander F. B. Merkle and his staff at the Boston Navy Yard for their efficient effort in making this magnet.

[2] G. E. Valley, Phys. Rev. 72, 772–83 (1947).

*** Glover Coating Company, Malden, Massachusetts.

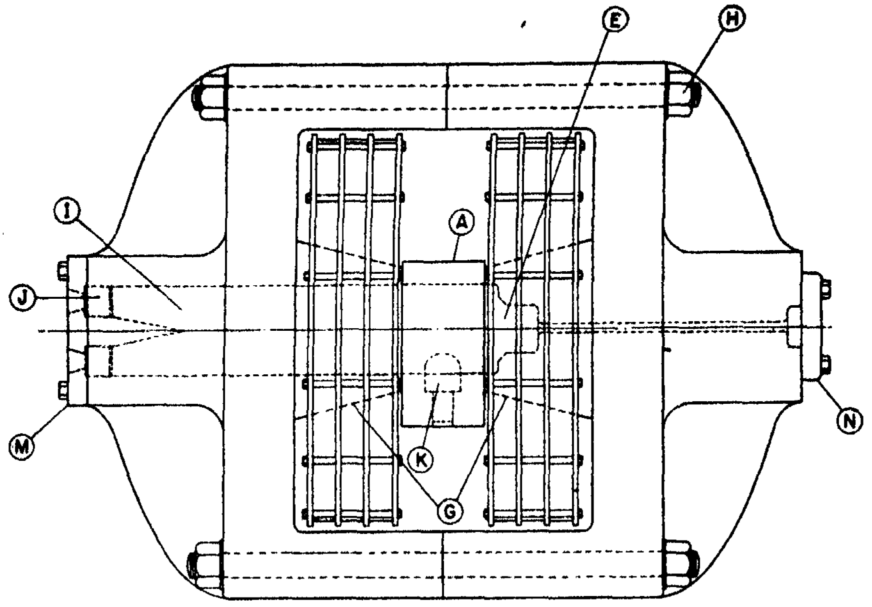

FIG. 3. Plan view of magnet with coils.

loaded to 15,000 p.s.i., and withstands a total of 65,000 lb. when the chamber is pumped up to 3000 p.s.i. Under this condition each stud elongates by 0.020 in. Thus, if the studs are initially unstressed, the magnet poles will separate by 0.020 in. due to this cause alone, upon application of pressure. Prestressing of the studs could of course nullify this effect, however, since the poles separate by an additional 0.005 in. anyway, due to bending of the yoke under pressure, we have not chosen to prestress the studs. Instead, we use a system of gaskets which remain tight for a relative displacement of the poles by more than 0.030 in.

We tried to mount the magnet as far above the trailer floor as was safe in view of the position of the center of gravity of the loaded vehicle. The center line is actually supported 38 in. above the floor, which gives ample room for placing other detecting devices beneath the cloud chamber. The frame supporting the front half of the yoke slides on triangular ways, propelled by means of a screw and wheel (Fig. 2). All parts of the frame in contact with the magnet yoke are made of Type 304 nonmagnetic stainless steel. The yoke is bolted to the frames with push-pull screws so that it can be leveled and aligned to the precision required by the gasket system.

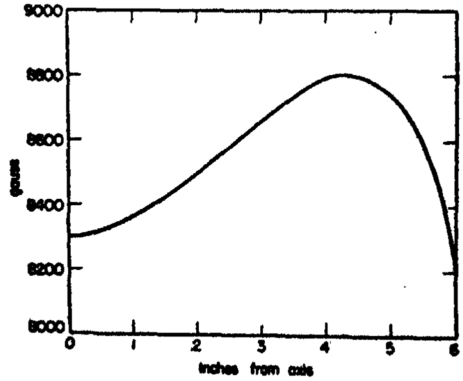

FIG. 4. Axial component of magnetic field along horizontal radius in median plane at 38 kw.

Because of the hollow poles and the comparatively poor magnetic properties of the steel of which the magnet is made, we regard the field distribution (Fig. 4) as being quite satisfactory. Figure 4 shows the axial field component along a horizontal radius; in this direction the cavity *I* is effectively a cylinder. The distribution along a vertical radius differs from that of Fig. 4 by less than 1 percent. This observation indicates that if one is going to put a hole in a magnet pole, there is little gained by using a conical hole rather than a cylindrical one of equal base radius. It will be noted that the maximum difference in axial field component shown in Fig. 4 is 500 gauss in 8500. The field may therefore be said to be uniform to ±3 percent. The method of construction of the coils is described in an accompanying paper.[3]

THE CLOUD CHAMBER PROPER

The cloud chamber is shown in detail in Fig. 5. The chamber wall is essentially a cylinder of 9 in. i.d. and 13.5 in. o.d. and is 8 in. long. As shown in insert *A* of Fig. 5, the wall of this cylinder had to be considerably thickened where the illumination window *K* was to be inserted in order not to weaken the structure. This eccentric configuration itself introduced new problems of stress distribution which we solved by approximate methods.

---

[3] Coonrod, Cecconi, Gedraitus, Harper, and Lewis, Rev. Sci. Inst. 20, 408 (1949).

This configuration gives us a surface density of 15.5 g/cm^2 over half the surface of the cylinder and approximately that value over the surface of the illumination window *K*. Since the cylinder is only clamped between the magnet poles, it can be rotated about the axis of symmetry to place the thin sections in best orientation for a particular experiment. Thus, for anticoincidence triggering, we orient the thin section to the bottom and allow the counter-telescope collimated incident radiation to enter through window *K* after passing through the lamp *L*; whereas, for an experiment to observe the decay of ordinary mesons, we might reverse this orientation.

The choice of the material from which the chamber wall was made depended upon its availability, machineability, corrosion resistance, and upon its density in proportion to its strength. Table I shows wall surface densities for various materials when a safety factor of five is assumed for a 9-in. i.d. cylinder to contain 3000 p.s.i.

TABLE I. Attainable wall surface densities for various materials.

Material	Yield point (p.s.i.)	Wall thickness (cm)	Density (g/cm)	Surface density (g/cm^2)
Stainless steel	60,000	3.4	7.9	27.0
Beryllium copper	95,000	2.0	8.3	16.5
Red brass (hard)	55,000	3.7	8.8	32.4
Aluminum alloy 61S-T	40,000	5.7	2.7	15.5
Magnesium alloy ASTM No. L	26,000	10.7	1.7	18.6

It is seen from Table I that either aluminum alloy 61S-T or beryllium copper might have been chosen. Because of its lower atomic number and greater availability, we chose to make the cloud chamber of aluminum alloy 61S-T. This alloy was chosen instead of other higher strength aluminum forging alloys because of its greater resistance to intergranular stress corrosion when subjected to contin-

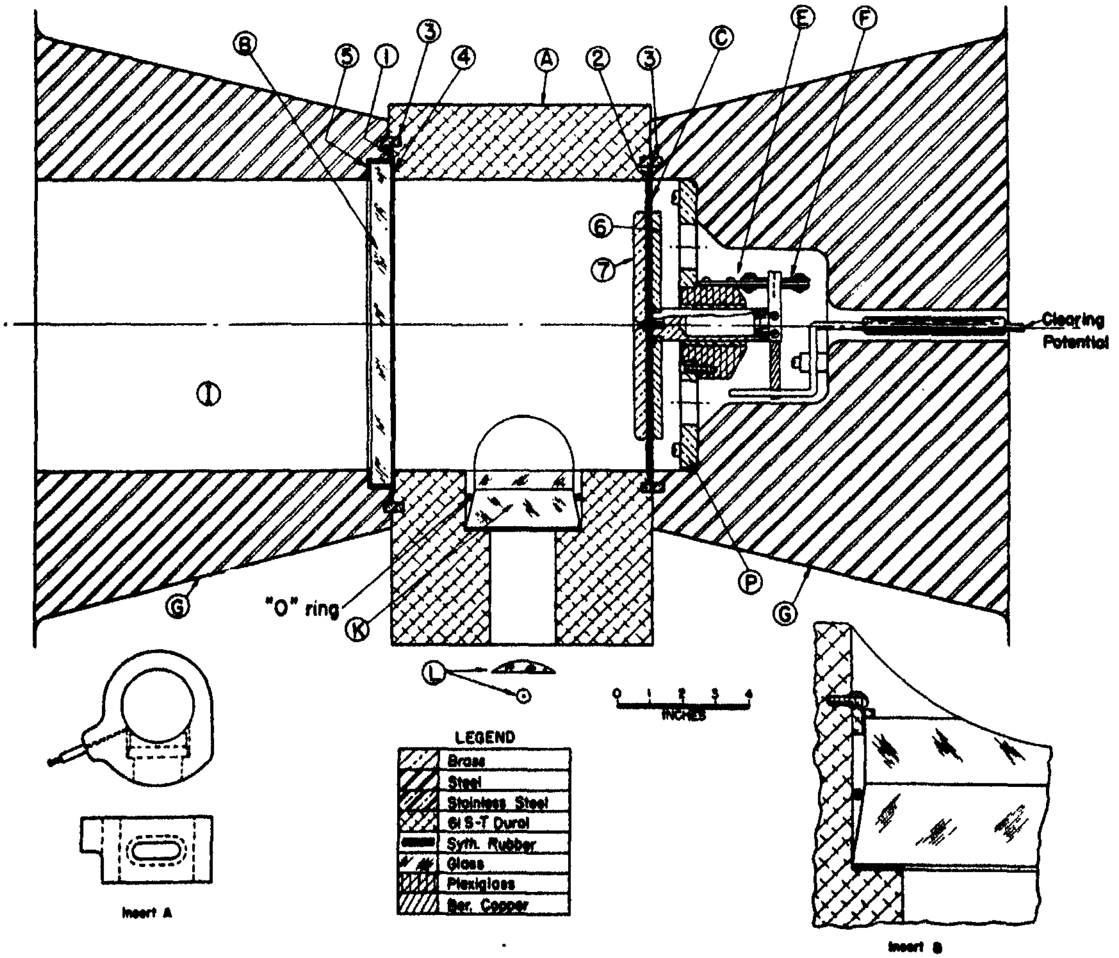

FIG. 5. Detail side elevation section of cloud chamber showing electrical connections; insert *A* shows plan and front elevation of cloud chamber; insert *B* shows pressure seal of window *K*. Inserts *A* and *B* are not to scale.

uous stress in the presence of liquids.[****] The chamber was machined from a forged biscuit 20 in. in diameter and 9 in. thick. In order to protect the aluminum and to prevent undesirable light reflection, the finished chamber was anodized black all over.

A strain rosette cemented to the chamber wall at its thinnest section showed a principal stress of 4000 p.s.i. corresponding to a stress of 6400 p.s.i. on the inner surface, when the contained gas pressure was 3000 p.s.i. It will be noticed from Table I that we calculated safety factors from the yield points rather than from the ultimate strengths of the various materials. This was because any yielding of the material would prevent proper functioning of the pressure seals and would constitute a practical failure. Thus, as far as explosion hazard is concerned, the safety factors are larger than given here and may in some cases change the order of apparent desireability of the various materials.

The glass window *K* is supported by a ¾-in. shoulder as shown in Fig. 5. A rubber-asbestos gasket $\frac{1}{32}$ in. thick is inserted between the glass and the metal in order that the surface of the metal shoulder need not be polished to avoid locally stressing the glass. This gasket is only for mechanical support of the glass, and is not a pressure seal.

The pressure seal is obtained by tapering and polishing the edge of the glass (taper $\frac{3}{16}$ in. in 1¼ in.) and inserting an "O"-ring[4] gasket of ⅛-in. diameter between the glass edge and the polished wall of the cavity into which it fits. This is an application of P. W. Bridgeman's "unsupported area" principle. It is readily seen that the greater the pressure the further into the tapered groove is the O-ring forced, and the tighter is the seal.

The glass is 1¼-in. selected plate prestressed† by the usual heat treatment after being ground and polished to the desired shape.††

Such a 2-in. by 6-in. light of Herculite is expected to fail at an applied pressure of 22,000 p.s.i. which gives us a factor of safety of 7.3 at our maximum working pressure of 3000 p.s.i. Although a safety factor of 10 is usually recommended, we consider this adequate since we can pretest individual pieces of glass to 4500 p.s.i. by filling the entire chamber with water, and also because there is no clamping frame needed to hold the window in position.

Heat-toughened glass has initial compressive stresses on the surface and a tensile stress at its mid-plane. A fully "tempered" plate (4000-μ/in. center tension) has stress of about 9200 p.s.i. at the center. The surface compression has a higher value. A test at 3000 p.s.i. using strain rosettes cemented to the outer surface of the Herculite window showed that the maximum principal stress was 5250 p.s.i. tensile. Thus the window has in use, a residual surface compression in excess of 2000 p.s.i.

It will be observed that whereas the chamber diameter is 9 in., the maximum unobstructed width of the window is only 6 in. It was therefore necessary to insert a plano-concave diverging lens in order to illuminate the entire chamber. This was ground from a piece of plate glass of the same original size of that from which the window *K* was made. It would have been easier to use a plastic for this but we find that Lucite, when exposed to air after a previous exposure to alcohol, develops surface cracks and becomes cloudy for that reason; polystyrene is not subject to this difficulty but is less desireable mechanically. The cylindrical surface has a radius of 4½ in. and so serves also to make the inside of the chamber smooth. This lens simply rests on the Herculite window, being held from falling out by a pair of ¼-in. square brackets screwed to the cavity walls. The resultant illumination is satisfactorily uniform over the entire chamber diameter.

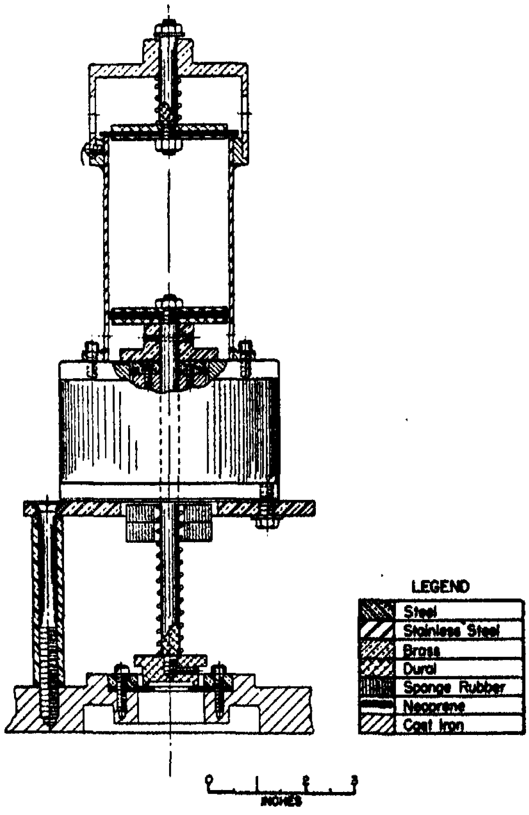

FIG. 6. Assembly drawing of valve 22, air pilot valve for main expansion valve 19.

[****] We are much indebted to Mr. W. G. Dow of the Aluminum Company of America, and to the members of their research laboratory who checked the stress-corrosion behavior of these alloys under stress in an alcohol-saturated atmosphere.

[4] F. N. D. Kurie has discussed the use of "O"-rings for vacuum seals, Rev. Sci. Inst. 19, 485 (1948).

† The Pittsburgh Plate Glass Company's Herculite process.

†† All our glass parts were ground and polished by the A. D. Jones Optical Company, Cambridge, Massachusetts.

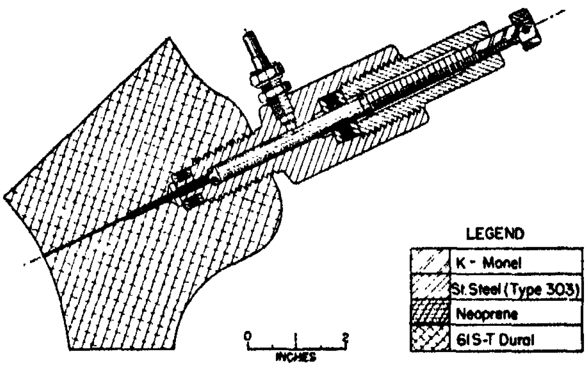

FIG. 7. Section of needle valve 8, shown as mounted in cloud chamber wall.

The crevices required for the sealing gasket are filled with a soft wax. This is made by mixing equal parts of petrolatum and paraffin, blackened with carbon-paper pigment. This material is soft enough to transfer the gas pressure to the O-ring seal at all normal temperatures.

The positions and shapes of the gaskets required to seal the chamber to the magnet poles are shown as Parts 1 and 2 in Fig. 5. Because of the shape of the pole faces between which the cloud chamber was to be mounted and the inevitable deflection of the yoke, ordinary gaskets were unsatisfactory to seal the chamber to the pole faces of the magnet. A satisfactory gasket scheme for this application must (1) be leakproof at 3000 p.s.i. even when the initial or tightening pressure is relaxed due to the yoke deflection; (2) be easily assembled and disassembled; (3) not require too close machining tolerances; and (4) not be very position sensitive.

The gaskets used are cut from $\frac{1}{8}$-in. Neoprene sheet (45 durometer) and are flat. The gasket seat on the chamber is tapered so that when the cylinder is tightly clamped between the poles, the gasket is $\frac{1}{16}$ in. thick at the stainless steel ring (Part 3 in Fig. 5), and $\frac{1}{8}$ in. thick at the inside diameter of the chamber. Gasket (2) being a solid sheet also serves as the moving diaphragm *C* of the cloud chamber and separates the oil in cavity *E* from the gas in the chamber. These gaskets also make use of the unsupported area principle.

A half-size model of this gasket arrangement was built and tested prior to incorporation in the final design. In the model, two flat plates were used for pole faces and the model tested to 6000 p.s.i. with the end plates (poles) moved progressively further apart.[8] This test indicated that the gasket system would remain tight if the magnet poles separated by as much as 0.050 in. under pressure. The measured total separation of the poles of the final instrument was 0.025 in. at 3000 p.s.i., which includes the 0.020-in. bolt elongation and 0.005-in. yoke deflection.

The rings (3) serve to locate the cloud chamber between the poles and also prevent gaskets (1) and (2) from blowing out as the poles separate. These rings slide freely in both the dural cylinder and in the pole faces and enter $\frac{1}{4}$ in. into each. The poles need be moved apart only 1 in. from the closed position shown in order to insert or remove the chamber.

Gasket (4) is a conventional flat gasket made of 80-durometer rubber. Item (5) is not a complete ring gasket but is sectioned to serve as a cushion for preloading gasket (4). The diaphragm gasket (2) was first made of Chemigum and vulcanized to the piston plate (6). The present design makes the clearing field electrode (7) a $\frac{3}{8}$-in. thick brass plate. A tongue and groove clamping ring of $\frac{1}{4}$-in. diameter is cut on the electrode and piston plate. Thus, any diaphragm material can be used and changed at will by simply removing one screw.

A combination of parts like (1) and (3) (Fig. 5) was also used to seal the end plates *M* and *N* (Fig. 3).

The two windows *J* (Figs. 1 and 3), have conventional flat gaskets (80-durometer Neoprene) between the glass and the end plate (*M*). A flanged cup fits over each glass plug and is screwed to the end plate to preload its gasket. When under pressure, the ratio of light area to gasket area is sufficient to ensure a tight seal.

HYDRAULIC SYSTEM

The mode of operation of the hydraulic system for actuating the cloud-chamber piston is essentially

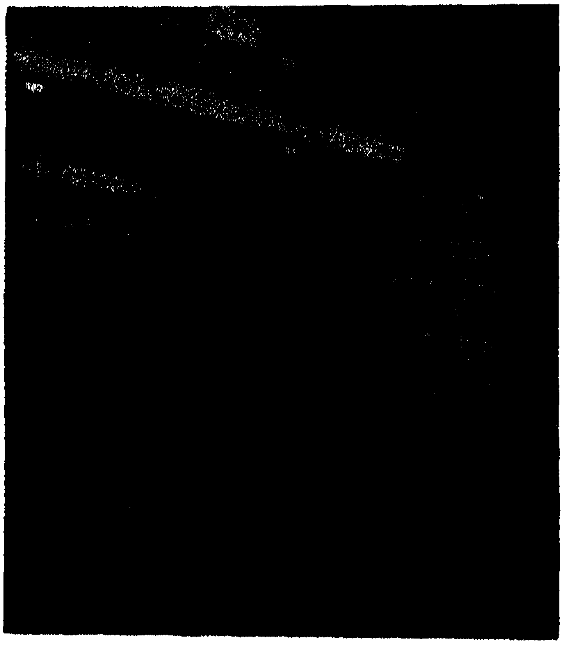

FIG. 8. Photograph of rear of magnet showing hydraulic system and water cooling pipes for magnet.

---

[8] J. A. Vitale, L.N.S.E., Technical Report No. 1, 1947.

that described by Johnson, DeBenedetti, and Shutt.[6] We have made use of commercially available parts wherever possible. These are listed in Table II. The piping diagram is shown in Fig. 1. Figure 8 is a photograph of the rear of the magnet and shows the hydraulic system. The water-oil pressure equalizing system consists of a water-filled Buna-S bag immersed in oil which is contained in a strong steel cylinder. The interior of the bag is connected to water cavity *I*, and the interior of the steel cylinder is connected to oil cavity *E* as shown in Fig. 1. Obviously a change in oil pressure is immediately transmitted to the water and both remain always at the same pressure. Since the piston is free, the oil pressure in turn always equals that of the gas in the cloud chamber. Consequently, the water and gas are also at the same pressure and there is no net force on the glass plate *B*.

The brass piston rod slides in a stainless steel bearing insulated from but supported by a perforated brass disk *P* (Fig. 5).

Prior to an expansion, all valves, except the throttle valve #13 and valve #12, are closed and the expansion vessel is partly filled with oil and partly evacuated. To make an expansion the compressed air, which holds valve 19 closed, is released. This release of air is achieved by means of the permanent magnet Fussell type valve 22,[7,8] shown in detail in Fig. 6. Valve 22 is designed to open valve 19 suddenly. It is held shut by a permanent magnet in order that it shall not open in case of power failure. The dash pot arrangement shown in Fig. 6 is required to prevent valve 22 and therefore valve 19 from reshutting before the piston has finished moving (i.e., before the expansion vessel is completely full of oil). Valve 22 is made to open by means of the system of LePrince-Ringuet as described by Chu and Valley.

After the expansion, the expansion vessel is filled with oil but none escapes through valve 12 because of the check valve 23 on the end of the vertical pipe which is inserted in the expansion vessel. Two seconds after the expansion, the dash pot on valve 22 allows it to close and immediately thereafter valve 19 closes, thus isolating the expansion vessel from the remainder of the system; therefore, the next two operations, of recompressing the cloud chamber and of re-evacuating the expansion vessel, can proceed independently of one another and in any time sequence. We therefore do not provide a timed sequence of operations; instead, we allow the system to recock itself under the control of its interlocking relays alone.

For instance, the high pressure oil pump is actuated, and valve 15 is opened, by any unbalance of the bridge circuit of which rheostat *F* is a component which indicates that the piston has moved in the expanding direction by more than 0.005 in. This is subject only to the condition that the main valve 19 is closed. Thus, while the chamber is standing cocked, any leaked oil is automatically repumped. It should be remarked that we have kept the instrument at 1500 p.s.i. for several weeks at a time and have, during such

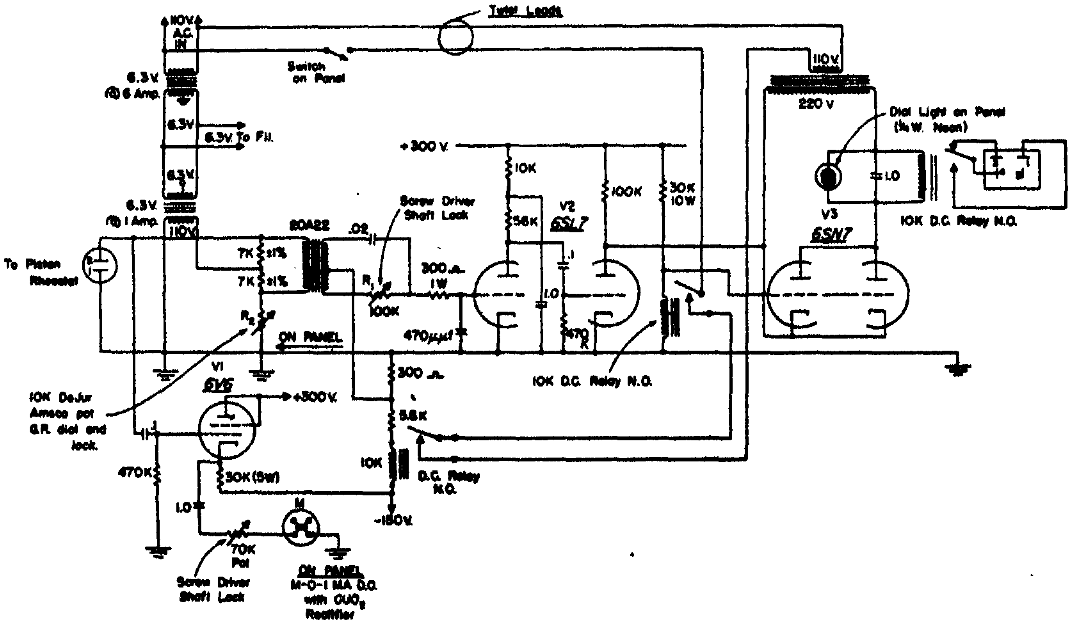

FIG. 9. Schematic wiring diagram of piston control bridge.

---

[6] Johnson, DeBenedetti, and Shutt, Rev. Sci. Inst. 14, 265 (1943).
[7] L. Fussell, Jr., Rev. Sci. Inst. 10, 321 (1939).
[8] F. H. Chu and G. E. Valley, Rev. Sci. Inst. 19, 496–99 (1948).

TABLE II. Components for high pressure cloud-chamber hydraulic system. (See Fig. 1.)

Part	Type	Manufacturer
Valves 15 and 20	#108, ½-in. port, air-to-open	Mason Neilan Reg. Company
Valve 19	#37, ½-in. port, air-to-close	Mason Neilan Reg. Company
Valve 13	#222-H-¼-in. bar stock globe valve	Crane Company
Valve 18	#1130-½-in. hydraulic relief valve	Crane Company
Valve 22	Special air valve	See Fig. 6
Valve 8	Special needle valve	See Fig. 7
Valve 23	Special check valve	See insert, Fig. 1
Valves 2, 3, 4, 5, 6, 9, 10, 11, 12, 14, 16, 17, 21	Nos. 222-H, 222½-H ¼-in. bar stock globe valves	Crane Company
Air valves to operate valves 15 and 20	P32-X solenoid valve	Automatic Switch Company
High pressure gauges	#0-5000 p.s.i.	Ashton Valve Company
Air alarm gauge	#0-100 p.s.i.	Ashton Valve Company
Accumulator	DD3-100	Greer Hydraulics, Inc.
Equalizer	DD3-100 (modified accumulator)	Greer Hydraulics, Inc.
Gas pump	GD7-100 (modified accumulator)	Greer Hydraulics, Inc.
Gas purifier filter	F1WE carbon tube	R. P. Adams Company, Inc.
Suction pump	"Pressovac"	Central Scientific Company
High pressure oil pump	GMD 1-92-100-T	Milton Roy Company
Fittings, pipe	Spec. for 3000-p.s.i. working pressure	Crane Company
Fittings, tubing	Ermeto	Weatherhead Company

periods, never actually observed any gas, water, or oil leakage.

Oil is removed from the expansion vessel by the vacuum pump as soon as the check valve 23 is opened. This occurs as soon as valve 20 opens and allows the pressure in the expansion vessel to fall to zero. The vacuum pump then pumps out the oil in the expansion vessel until its level falls to the port of valve 23; thereafter it removes any residual gas. The evacuated volume of the expansion vessel is obviously the same as the change in volume of the cloud chamber. It can be changed by raising or lowering the tube which holds valves 23 and 12. At present we allow the vacuum pump to operate continuously. The evacuated volume produced in the expansion vessel is satisfactorily reproduceable for expansions made at equally spaced intervals. When expansions are made at irregular intervals controlled by counters, the system of allowing the pump to operate continuously is not completely satisfactory, and we propose in the future to pump the expansion vessel for a fixed interval of time only, after each expansion.

We have found it desirable to interlock the system fairly completely. Valve (#22) cannot be triggered unless valve 20 is closed, nor while the piston controlling bridge is unbalanced nor, after an expansion, until the high pressure oil pump has started to recompress the chamber. Valve 20 in turn cannot be opened unless valve 19 is closed and the air pressure is 40±5 p.s.i. This is required because the main valve 19 will leak if the air pressure is below 30 p.s.i., and valve 22 will spontaneously open if the air pressure is above 55 to 60 p.s.i. In addition, the high pressure oil pump is turned off and an alarm is sounded by a time clock, if it pumps for 10 sec. longer than the average time observed to be required at the expansion ratio in use; and if this fails to stop the pump, its power is cut off by the high pressure alarm gauge at a pressure 500 p.s.i. in excess of operating pressure. All electrical controls failing to stop the pump, safety valve #18 will open at 3500 p.s.i. and bypass the system to the oil reservoir which is at atmospheric pressure. The last two safety devices prevent the entire apparatus from exploding; the previously mentioned devices prevent the more delicate structure of the piston from being broken.

ELECTRONICS

Piston Control Bridge

This circuit (Fig. 9) consists of an ordinary resistance bridge powered by 110 v 60 c from the mains. The unbalance signal is amplified and limited by V_2, and applied to the cathode of the phase sensitive detector V_3. Tube V_3 is rendered phase sensitive by using 60 c 220 v (also derived from the mains) as its plate supply voltage. The grid of V_3 is kept at a fixed bias voltage. Obviously the grid potential of V_3 can be adjusted so that it will conduct only when V_2 drives its cathode negative during the half-cycle when its plate is positive. Since there is a reversal of the phase of the signal from V_2 when the bridge passes through balance, the initial phases can be set so that V_3 conducts only when the bridge is unbalanced in one direction.

Because of the high gain and limiting action of V_2, its output signal is essentially a square wave. Consequently, when V_3 conducts, it functions as a normal half-wave rectifier to drive the relay shown in its plate lead. When a relay is used whose coil resistance is 10,000 ohms, a 1-μfd condenser is a sufficient filter to prevent chattering of the relay contacts.

The bridge is isolated from the mains and from the grid of V_2a in order that one side of the piston rheostat can be grounded. The piston rheostat consists of two pieces of resistance card (as used on General Radio Company Model 301A, 20K potentiometer) mounted side by side. The sliding contact is mounted on the piston shaft by a Bakelite arm, and so is insulated from the high clearing potential which is applied directly to the piston. The sliding contact is made of Paliney #7 contact metal††† (high palladium—low gold alloy).

The bridge is so connected that V_3 conducts (and so activates the high pressure oil pump) when the resistance of the piston rheostat is too low for balance. Thus, if the rheostat breaks, the pump will not run. Tube V_3 is driven by its cathode so that the pump will not run if V_2 burns out. Sufficient gain and output signal voltage is provided by V_2 to drive a Type 6AS7 tube as V_3 (grid biased at −50 v with respect to ground) should it be desirable to drive a heavier load than the small relay shown. When a 6SN7 is used for V_3, its bias can be adjusted over a range of 50 v without noticeable effect on performance; likewise the adjustment of phase control rheostat R_1 is very uncritical.

Tube V_1 is a cathode follower which reads the voltage across the piston rheostat. This tube drives a recording milliameter which records the piston position. It is important to know the piston position at all times since the unbalanced force exerted on it is over 100 tons during expansion, and mechanical stops can obviously not be provided; it is, therefore, necessary to be certain that the piston is pumped sufficiently far forward during the compression cycle, so that it will not exceed its allowable traverse during expansion. The compressed position of the piston depends on the resistance required to balance the bridge; this can be set by adjusting R_2. Although the piston position can be set to ±0.005 in. by this device, such precision is unnecessary because the piston position affects the volume of the cloud chamber before expansion, but does not set the expansion ratio directly, since this is determined by the evacuated volume of the "expansion" chamber. Consequently, an error in the bridge balance affects the expansion ratio only to a second order.

MAIN SEQUENCE CONTROLLER

The only time interval which needs to be precisely controlled is that between the opening signal for the main expansion valve (valve 22 controlling valve 19) and that which fires the lamp.

The circuit (Fig. 10) consists of a slow relaxation

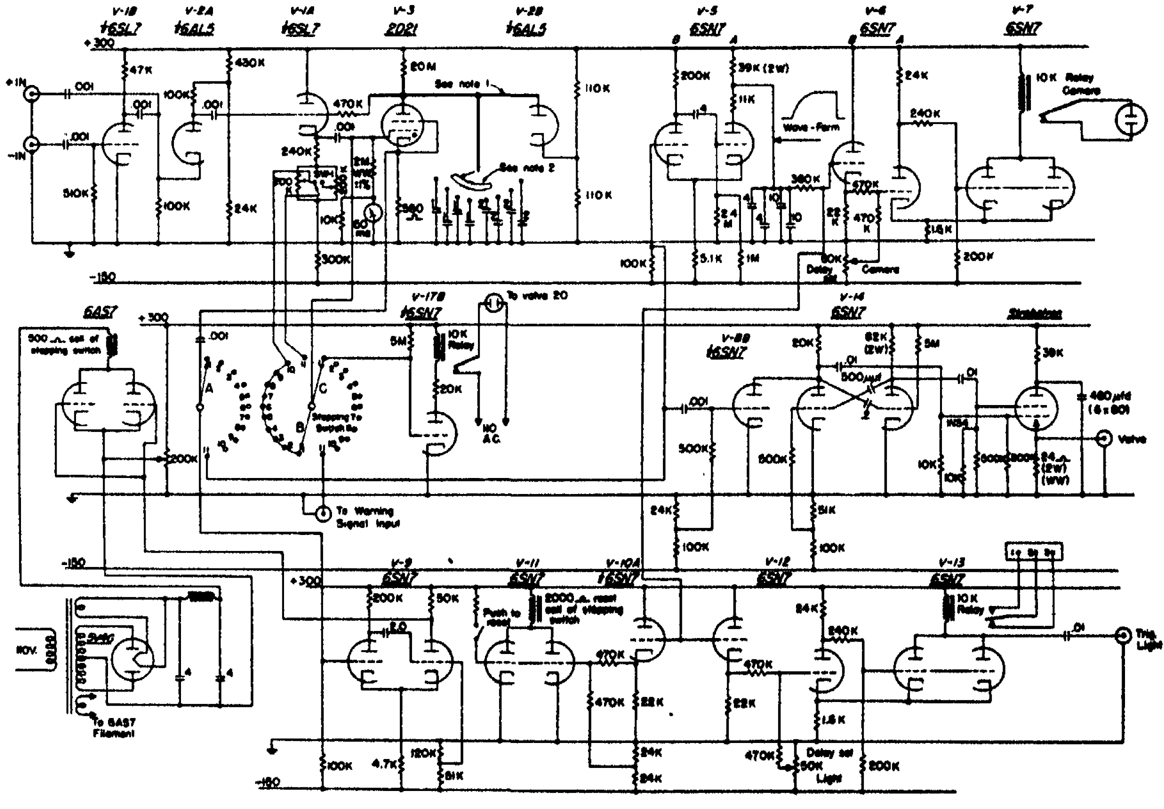

FIG. 10. Schematic wiring diagram of main sequence control circuit. *Notes*: (1) Double lines indicate wires to be insulated for 2000 v. (2) Ceramic switch shorts 1 to 8 contacts when turned.

---

††† From the J. M. Ney Company.

oscillator (V-1A, V-3, and V-2B) which fixes the interval between expansions, and a delay circuit V-5 which controls the interval between inception of an expansion and illumination of the cloud chamber. The remainder of the circuit consists of elements controlled by these two.

The slow relaxation oscillator consists of the thyratron V-3 which is grid controlled by cathode follower V-1A. After the thyratron fires, the condensers connected to its plate recharge through its 20-megohm plate resistor; consequently, the control grid potential of V-3 slowly increases toward the potential at which it will fire again. It is seen that the cathode circuit of V-1A has a split load resistor with two taps, either of which can be selected by a switch SW-1. The voltage obtainable from the left tap can rise to the firing potential of V-3; that from the right tap can rise only to within a few volts of firing potential. With the switch in the right position the thyratron can only be fired if a positive pulse is applied via limiting diode V-2A, and if its plate condenser has had time to charge. Limiting diode V-2B prevents the grid of V-1A from approaching so close to the potential of its plate that a trigger pulse could produce no effect. The relaxation period of V-3 can be selected between 0.3 and 4 min. by choice among several values of plate condenser.

The period of V-3 is multiplied by ten by means of the stepping switch shown.†††† Several features of the circuit are determined by the peculiarities of this switch, which was the only one with a reasonably high coil impedance available to us.

This switch makes one step whenever V-3 fires. A pulse is taken from the cathode of V-3 when it fires and is applied to the grid of V-9A of flip-flop V-9. The signal from V-9 turns on the grid-controlled rectifier 6AS7 which furnishes the 14 watts necessary to actuate the stepping switch. This arrangement requires a separate floating power supply which has not proven unsatisfactory. The alternative would be to put a pilot relay in the plate circuit of V-9B and use this to control the step switch—one still needs 14 watts of d.c., and no reduction of complexity results. Flip-flop V-9 is required because the pulse from V-3 is far too short to actuate the stepping switch. Another method of actuating this switch would be to discharge a large electrolytic condenser through its coil by means of a gas tube. Since the condenser could be recharged slowly, power could be taken from the regulated supply; furthermore, no flip-flop would be required to lengthen the pulse. A condenser of about 100 μfd at 300 v would be required.

The control grid of thyratron V-3 is connected to moving contact B of the stepping switch; this contact can bear successively on any one of eleven fixed contacts; of these the first ten are permanently connected to the higher potential side of SW-1. In consequence, the thyratron fires automatically until arm B, after 9 periods of V-3, finally rests on contact eleven. The position of the moving contact of SW-1 can then determine whether the thyratron fires automatically or not at the end of the tenth period.

When arm A of the stepping switch is at position eleven, the cathode signal of V-3 can, besides triggering V-9, also trigger valve 22, thus expanding the cloud chamber, and can also trigger the delay flip-flop V-5 which controls the flash lamp. Thus, when SW-1 is in the left position the cloud chamber operates automatically (making "random" expansions), and when SW-1 is in the right position the chamber waits until expanded by a Geiger counter pulse arriving via V1-B and V-2A.

Initially, in flip-flop V-5, element V-5A is nonconducting and element V-5B is conducting; this situation is reversed when V-5A receives a positive grid pulse from V-3 via contact A-11 of the stepping switch. The length of time during which V-5B conducts on the time constant of the resistor-condenser combination of the plate circuit of V-5A and the grid circuit of V-5B. This is adjusted to be about 5 sec. The plate of V-5B is made to increase in potential slowly by means of the 28-μfd condenser shown and the output wave form of V-5B is as shown on the diagram. This wave is applied to "pulse-height discriminators" V6, 7 and V12, 13 which control the camera and light, respectively.[9] These devices can be set to function at a particular amplitude of the wave form V-5 and therefore at a particular time after V-3 has fired. The extra width provided for the output wave form V-5 is for the purpose of keeping the camera relay shut long enough to change the film. Although this arrangement allows the time at which the film starts to move to be precisely set, this is a feature of no great value.

The stepping switch is of the type which requires resetting after each cycle; a spring and ratchet combination is built in for this purpose. The pawl is automatically lifted for resetting by a magnet energized by tube V-11 which is turned on by the output signal from V-5 as shown.

After the switch is reset, arm C of the stepping switch applies the grid voltage of V-3 also to the grid of V-17B thereby turning it off. This de-energizes the relay in the plate circuit of V-17B and this causes valve 20 to open. Valve 20 therefore stays open for a full period of V-3.

When arm C is at position eleven, the V-3 grid voltage is applied to frequency modulate an audio oscillator which sounds a warning note whose frequency increases as the instant of expansion is approached. We have found this to be an invaluable device.

---

†††† Stepping switch type Guardian R.E.R.

[9] Cf. Rad. Lab. Tech. Ser., *Cathode Ray Tube Displays* (McGraw-Hill Book Company, Inc., 1948), Vol. 22, p. 234 ff.

The strobatron which energizes the trigger coil of valve 22 is triggered by the biased-off multivibrator *V*-14, whose driver tube *V*-8*B* is triggered directly by the cathode signal from *V*-3 via contact *A*-11 of the stepping switch. A circuit similar to that of *V*-5 could alternatively have been used to trigger the strobatron. It is always desirable to drive both grids of a strobatron with as large voltage pulses as are conveniently obtainable; it is also desirable to mount a small panel light next to the strobatron to keep its cathode illuminated. With these precautions the device is entirely reliable.

OPERATION

The clearing potential which is applied to the piston, is required to be about 4000 v. The surface resistance of the rubber diaphragm is ohmic and depends greatly upon the vapor present in the cloud chamber, but is independent of the gas pressure. When absolute propyl alcohol is used, the resistance is about 20 megohms; any amount of water vapor is harmful and can decrease the surface resistance by as much as an order of magnitude. The current which flows across the rubber membrane produces fog from electrolytic ions; fortunately this fog does not reach the illuminated volume until after the tracks have been photographed. However, it is necessary to allow it to settle out after each expansion if the chamber is to operate for any length of time.

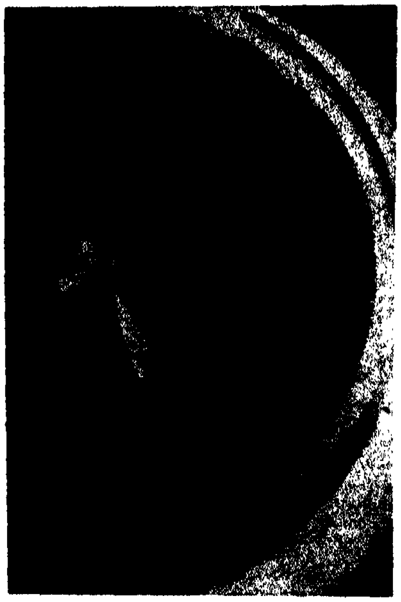

FIG. 11. Cloud-chamber photograph showing sharp negative and positive ion tracks due to a single particle. Range *vs.* scattering measurements indicate that the particle is a proton. The heavy plumes of ionization are caused by corona from the sharp corners of the slot in the head of the screw which holds the clearing field electrode to the piston.

Absolute propyl alcohol is very good as far as this effect is concerned but requires rather a long interval between expansions; absolute ethyl alcohol is faster but has also a higher conductivity. We have obtained best results with a 3:1 mixture of propyl and ethyl alcohols. With either variety of absolute alcohol, the volume expansion ratio at 100 atmos. of argon and with an excess of liquid present, is 1.063. If water is added, the expansion ratio decreases to 1.04,[10] but the performance is considerably worse. At a pressure of 167 atmos. of hydrogen, the expansion ratio for a minimal expansion ratio mixture of alcohol and water is 1.08.

By using the cloud chamber itself as a gas thermometer, we have determined that the time after expansion required to establish thermal equilibrium is 5 to 7 min. The smallest interval between expansions which can be used is 20 min. if the device is to be counter controlled and is to operate reliably for a long time. The extra time is required to establish vapor equilibrium and we are now studying means to reduce this.

We normally operate the chamber unsaturated—i.e., with no excess liquid present. We have operated continuously for as long as 3 weeks on one charge (1.5 cc) of alcohol; the required expansion ratio gradually increases with time as alcohol is absorbed by the rubber membrane. The effect of temperature on required expansion ratio is no greater than for any ordinary one-atmosphere instrument with liquid excess. This procedure does not appreciably decrease conduction across the rubber membrane but has a number of minor advantages.

A photograph taken with this instrument under counter control has already been published.[11] Another is shown in Fig. 11 in which the splitting of the positive and negative ion component can be more clearly seen.

We find that the shortest time after inception of the expansion at which tracks can be photographed is 0.6 sec. This has relatively little to do with the speed of expansion. Actually, we find that the chamber tends to develop a fine general fog if the expansion is too fast. We usually operate with throttle valve 13 nearly closed, a procedure which yields the desired reliability.

The sensitive time is very long; it can be compared to that of an ordinary cloud chamber by observing the average numbers of cosmic-ray tracks which are photographed per expansion. We estimate the sensitive time to be about 5 sec. at 100 atmos. of argon and a clearing field of about 250 v/cm. It is very noticeably longer at 150 atmos. The sensitive condition exists before the expansion and not after it, and is due to the small diffusion and drift velocity. Consequently, it cannot be measured by use of a fast motion picture camera as is often suggested. We have demonstrated that it can be changed by variation of the clearing field in the expected way.

---

[10] Cf. J. S. Laughlin, Rev. Sci. Inst. 19, 918 (1948).

[11] Valley, Leavitt, and Vitale, Phys. Rev. 75, 201–203 (1949).

We do not find that an unduly long period of time is required to clear dust from the filtered gas after filling the chamber. From twelve to twenty expansions starting at a ratio of 1.01, repeated at four-minute intervals, and graded into the steady regime, suffices. This requires about three hours.

ACKNOWLEDGMENTS

We have been fortunate in having the assistance of Mr. Thomas Mersereau during the assembly and testing of the instrument. Its development was first proposed to us several years ago by Professor Bruno Rossi and we have since enjoyed the support and encouragement of him and of Professor J. R. Zacharias. We avoided many pitfalls because of the mature advice of Mr. M. M. Hubbard.

Thanks are due Mr. Lewis Coonrod and his competant machinists for their excellent machine work on such a complex assembly.

APPENDIX I

The mean square Coulomb scattering angle for a particle of known constant momentum traversing a given thickness of matter is given in Rossi and Greisen's review article.[12] If we call this angle θ, and then calculate the magnetic deflection angle φ for the same path length, the ratio θ/φ can be taken as the fractional error in magnetic deflection caused by scattering. It is obvious that this is also the fractional error in measured momentum due to scattering. If the formulas for scattering and magnetic deflection are combined, we have

$$\theta/\varphi=(K/\beta H)(P/x)^{\frac{1}{2}}, \tag{1}$$

where H is the magnetic field strength in gauss, P is the pressure in atmospheres, and x is the path length in centimeters of the particle whose velocity is $\beta=v/c$.

K is a constant dependent on the material and has the values shown in Table III.

TABLE III. Values of scattering error constant for different gases.

Material	K
Argon	465
Tetra-fluoromethane (CF_4)	500
Air ($Z_{eff}=7.2$)	275
Helium	56
Hydrogen (H_2)	41

APPENDIX II

The ions are originally produced along a line, and then diffuse radially to produce a track of apparent width w at a time t. The problem is to calculate how w depends on t and the initial number of ions, formed per unit length of track, I.

Let the track be vertical, and the x axis be horizontal and perpendicular to the line of sight. Then the observed surface density of ions is just the number which have diffused to the element dx at x during the time t.

This is

$$\rho_x=\frac{I}{2(\pi t/D)^{\frac{1}{2}}}\exp-(x^2/4t/D),$$

where D is the diffusion constant of the ions in the gas.

We now assume that the optical density of the photograph is given by $d=\log\rho_x$. This implies that the light from one droplet is not obscured by another; this needs only be true near the edge of the track where ρ_x is smallest.

Since the tracks appear sharp, and since the film is developed to yield maximum contrast, we identify an optical density d_0 as defining the observable track edge. Then,

$$d_0=\log I_1-\log 2(\pi t/D)^{\frac{1}{2}}-(w_1^2/16t/D)+\text{const.},$$

where w_1 is the apparent width after a time t of a track produced by a particle whose specific ionization was I_1. And for a second particle:

$$d_0=\log I_2-\log 2(\pi t/D)^{\frac{1}{2}}-(w_2^2/16t/D)+\text{const.}$$

Then, if the two specific ionizations are to be compared, we have, if t/D is the same in both cases,

$$I_1/I_2=\exp((w_1^2-w_2^2)/16t/D).$$

Thus, a comparison can be made when t/D is known to be the same for both tracks; this could be done for counter controlled pictures, but the results are very sensitive to the observed width. This in turn depends on the level of illumination in the chamber, a fact which probably means the method is only good for distinguishing between tracks of particles of very different specific ionizations. We regard the comparison of tracks of differing ages to be very rough indeed, although obviously possible in principle.

---

[12] B. B. Rossi and K. Greisen, Rev. Mod. Phys. **13**, 240–309 (1941).

Differential Counting with Reversible Decade Counting Circuits*

FREDERICK H. MARTENS
University of New Mexico, Albuquerque, New Mexico

(Received March 1, 1949)

Three circuits were designed and built to apply a reversible decade counting circuit to the direct measurement of the difference in the counting rate from two counter tube telescopes used in cosmic-ray research. The circuits are equally applicable to the direct measurement of the difference in the strength of two radioactive samples. An input circuit prevents two pulses from the Geiger tubes from arriving simultaneously at the first ring-of-ten. A driving circuit switches and shapes the pulses for correct bi-directional operation of the ring-of-ten. A coupling circuit permits two decade rings to be operated in cascade, giving a differential electronic scale of 100.

INTRODUCTION

THE difference in the counting rate from two sources of electrical pulses may be measured with a reversible ring-of-ten.[1] The pulses from one source must be applied alternately to each lead of one pair of input terminals in order to advance the pattern of the ring in a clockwise direction. The pulses from the other source must be applied alternately to each lead of the other pair of input terminals to advance the ring counter-clockwise.

An *input circuit* is required to prevent the simultaneous arrival of pulses from both sources. A *driving circuit* must distribute pulses of correct shape alternately to each lead of one pair of input terminals of the ring-of-ten. A *coupling circuit* is needed when two reversible rings-of-ten are placed in cascade. The coupling circuit provides for the transmission of a correct coupling pulse to the second ring-of-ten whenever a full decade is added or subtracted from the first ring-of-ten.

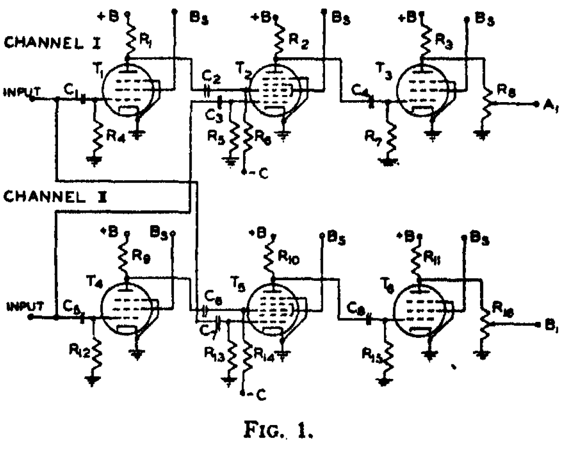

FIG. 1.

Input Circuit	
$C_1, C_2, C_3, C_4, C_5, C_6, C_7, C_8$	25 μμf
$R_1, R_2, R_3, R_9, R_{10}, R_{11}$	47,000 ohms, 2w
$R_4, R_5, R_6, R_{12}, R_{13}, R_{14}$	100,000 ohms, ½w
R_7, R_{15}	2.2 megohms, ½w
R_8, R_{16}	500,000 ohm pot.
T_1, T_3, T_4, T_6	6SJ7
T_2, T_5	6SA7

$+B$, +250v; B_s, +180v; $-C$, −20v

THE INPUT CIRCUIT

The input circuit (Fig. 1) is composed of two identical channels, each fed from its respective source of pulses and each designed to drive the first reversible ring in an opposite direction. Each channel is composed essentially of an anti-coincidence circuit required for preventing simultaneous pulses in the two channels. Consider only channel *I* as marked in Fig. 1. The input pulses, negative in sign, are fed to tube T_1 and also to the first control grid of T_5. The positive pulse from T_1 is used to drive T_2, the anti-coincidence tube. This positive pulse on the second control grid of T_2 will be transmitted only if the first control grid is not receiving at the same time a negative pulse from the input to channel *II*. Thus, if two source pulses should occur simultaneously in the two channels, no pulse would be transmitted. This is necessary because two pulses fed simultaneously into the ring circuit would cause an erroneous reading. The pulse from the anti-coincidence tube is inverted by T_3. This gives a positive pulse to trigger the driving circuit described in the next section.

An identical pulse is delivered by tube T_6 in channel *II* for each input pulse from the other source when not simultaneously accompanied by a pulse in channel *I*.

THE DRIVING CIRCUIT

Each pair of input terminals, *PQ* and *ST* (Fig. 2), for the reversible ring-of-ten is fed by a trigger circuit of the type described by Regener.[2] If fed from channel *I* at A_1 (compare Fig. 1) the trigger circuit T_1, T_2, supplies the necessary positive pulses to the "clockwise" pair *PQ* of input terminals of the first ring-of-ten. The cathode follower circuit, T_3, is used to reduce the load on the trigger circuit. An identical trigger circuit is placed between channel *II* at B_1 and the "counter-clockwise" input terminals *ST* of the first ring-of-ten.

---

* This work was done in a partial fulfillment of the requirements for the degree of Master of Science in Physics at the University of New Mexico, Albuquerque, New México.

[1] V. H. Regener, Rev. Sci. Inst. 17, 375 (1946).

[2] V. H. Regener, Rev. Sci. Inst. 17, 180 (1946).

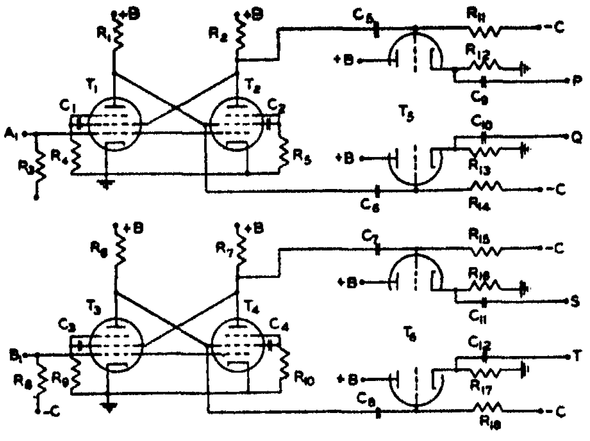

FIG. 2.

Driving Circuit

C_1, C_2, C_3, C_4, C_5, C_6, C_7, C_8	25 μμf
C_9, C_{10}, C_{11}, C_{12}	0.005 μf
R_1, R_2, R_6, R_7	47,000 ohms, 2w
R_4, R_5, R_9, R_{10}	470,000 ohms, ½w
R_3, R_8	22,000 ohms, ½w
R_{11}, R_{14}, R_{15}, R_{18}	470,000 ohms, ½w
R_{12}, R_{13}, R_{16}, R_{17}	2,000 ohms, 2w
T_1, T_2, T_3, T_4	6AK6
T_5, T_6	6SN7
$+B$, +250v; $-C$, −20v	

THE COUPLING CIRCUIT

The coupling circuit providing directional feed from the first ring to the second ring is shown in Fig. 3. It consists of two pentodes, T_1 and T_2, which permit only one pulse to pass for each complete revolution of the first ring-of-ten. As explained below, T_1 will pass such a pulse only when the ring is proceeding in the counter-clockwise direction (from position "0" to position "9"), and T_2 will pass such a pulse only when the ring is proceeding in the clockwise direction (from position "9" to position "0"). A driving circuit of the type shown in Fig. 2 must be connected between points A_2, B_2, and the "clockwise" and "counter-clockwise" pairs of input terminals to the second ring-of-ten, respectively.

The control grids of T_1 and T_2 are biased beyond cut-off. They are coupled by condensers to the plates of two opposite tubes, T_A and T_F, in the first ring. The screens are connected directly to the two plates of two adjacent tubes, T_C and T_D, of the first ring. T_1 can pass a pulse only when its screen is at a high potential, i.e., when tube T_C of the first ring is cut off. Similarly, T_2 can pass a pulse only when tube T_D is cut off.

Let us now assume that tubes T_A, T_B, T_C, T_D, and T_E in the first ring are conducting. Their plates are at a low potential. As the electrical pattern of the ring advances clockwise, tube T_A cuts off and tube T_F turns on. A positive pulse is fed to T_1. However, since the screen grid of T_1 is at a low potential, no pulse is transmitted. A negative pulse is fed to the grid of T_2, but negative pulses have no effect on either T_1 or T_2 because these tubes are biased beyond cut-off anyhow, no matter what their screen potential is. There is no occurrence when tube T_B shuts off next. When tube T_C cuts off, the screen grid of T_1 is raised to a high potential, so that a future positive pulse on the control grid will turn T_1 on and thus feed the second ring by one step in the counter-clockwise direction. Tube T_D turns off next. This puts T_2 in a condition to transmit a future positive pulse which arrives on its control grid. The following pulse causes T_A to conduct and T_F to cut-off. This puts a positive pulse on the control grid of T_2, which feeds the second ring by one step in the clockwise direction. As the electrical pattern continues to advance around the first ring there is no further action, except for the lowering of the screen grid potentials when tubes T_C and T_D turn on. So, for one clockwise revolution of the first ring, we have one pulse transmitted to the clockwise input of the second ring. A similar analysis shows that one pulse is fed through T_1 to the counter-clockwise input B_2 of the second ring when the first ring advances counter-clockwise by one complete revolution.

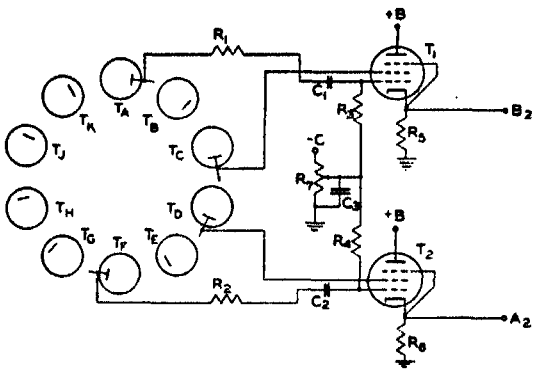

FIG. 3.

Coupling Circuit

C_1, C_2	25 μμf
C_3	4 μf, 50v
R_1, R_2	22,000 ohms, ½w
R_3, R_4	47,000 ohms, ½w
R_5, R_6	22,000 ohms, 2w
R_7	500,000 ohm pot.
T_1, T_2	6AK6
$+B$, +250v; $-C$, −20v	

A small pulse occurs at the plates of T_A and T_F when any of the other tubes in the ring change condition. The control grids of the triodes in the decade rings must be at zero bias so these pulses will not be large enough to disturb the coupling circuit.

This work was facilitated by a Frederick Gardner Cottrell Special Grant-in-Aid from Research Corporation, New York, for cosmic-ray research at the University of New Mexico.

The Measurement of the Series-Resonant Resistance of a Quartz Crystal

L. A. Rosenthal and T. A. Peterson, Jr.
Rutgers University, Dept. of Electrical Engineering, New Brunswick, New Jersey

(Received September 10, 1948)

Three instruments are described which will measure the equivalent resistance of commercial quartz crystals in the range of 80 kilocycles to 100 megacycles. Information on the theory and operation of these instruments is given. Some data are shown indicating the results to be expected.

I. INTRODUCTION

IT has long been the desire of the engineer working with crystal oscillators to have available an equivalent circuit for the crystal upon which a design could be based. Unfortunately, certain non-linearities enter the picture and make any equivalent circuit exist for but one current level and temperature. As next best substitutes, the less complex ideas of activity, figure of merit, and performance index[1] were introduced. These ideas serve their purpose in comparing crystal units, but they are all based on the equivalent circuit, in which the resistance is a particularly important parameter.

The instruments described in the following sections were used in the investigation on commercial quartz crystals of the plated and pressure mounted varieties in the frequency range of 80 kilocycles to 60 megacycles.

II. THEORY OF THE CRYSTAL AND ITS RESISTANCE MEASUREMENT

The electro-mechanical equivalent circuit for a crystal operating at any mode has been shown to consist of a series resonant motional arm in parallel with a static holder capacity as in Fig. 1a.[2] The admittance of this parallel combination can be represented as a circle diagram* (Fig. 1b). A vector joining the origin to any point on the circle represents the total admittance. Four critical points are observed on the circle diagram. These are:

a. Minimum impedance } Along the line passing through
b. Maximum impedance } the origin and center of the circle (O').
c. Series resonance-unity power factor } along the real axis.
d. Anti-resonance-unity power factor }

From simple geometry, the points we are concerned with can be expressed in terms of R_x and ωC_0.

$$\text{a.}\quad Z_{\min}=\frac{2R_x}{(1+a^2)^{\frac{1}{2}}+1}\qquad a=2R_x\omega C_0,$$

$$\text{c.}\quad R_s=\frac{2R_x}{1+(1-a^2)^{\frac{1}{2}}}.$$

The two unity power factor conditions cease to exist if "a" is greater than 1. In addition, with no crossing of the real axis, there can be no inductive component associated with the crystal and it is useless for many oscillator applications (e.g. Pierce, Miller).

For the low impedance region that we are concerned with, it is important to realize that minimum impedance and unity power factor occur at different frequencies and that the series resonant resistance for the crystal network is different from the motional arm resistance. These differences depend on the quantity "a" which is generally very small.

In order to measure the resistance, the crystal is made the controlling element of an oscillator which operates the crystal in the vicinity of the low impedance resonance. In this way the frequency stability which is associated with crystal control is maintained by the oscillator for the wide range of crystals accommodated. The test oscillator must have provisions for the measurement of the crystal impedance and a check for operation at unity power factor. Resistance can be measured by a substitution method or a calculation method, each of which is described below.

In the substitution method, a resistor is made to replace the crystal unit keeping the amplitude of oscillation, as measured by the rectified grid current, unchanged. If the frequency does not change upon the substitution of the resistor it can be further assumed that the crystal was operating in a purely resistive fashion. At this single frequency the substituted resistance is equal to the total impedance of the crystal.

In the calculation method, the voltage drop across the crystal, as well as the current through the unit, is measured. As an example, the crystal can be made the series arm of a "half T" section and a resistor the shunt arm. By measuring the input and output voltages of this network, the crystal resistance can be calculated as:

$$R_x=(V_{\text{in}}/V_{\text{out}}-1)R_1$$

where R_1 is the terminating resistance. Of course, the above equation can be applied only for a purely resistive crystal and therefore some series resonance check must be incorporated. The simplest method for the latter check is through the use of a Lissajous phase shift pattern between the input and output voltages. When these voltages are in phase, corresponding to a straight line pattern, the crystal must be purely resistive.

---

[1] Biggs and Wells, J. Inst. Elec. Eng. **93**, Pt. 3, 29 (1945); C. W. Harrison, Bell Sys. Tech. J. **24**, 217 (1945); and R. A. Heising, *Quartz Crystals for Electrical Circuits* (D. Van Nostrand and Company, New York, 1946).

[2] K. S. Van Dyke, Phys. Rev. **25**, 895 (1925).

* Providing "ωC_0" is assumed to be constant.

Combinations of the above methods were used in the test oscillators described in following sections. Problems arise that may disqualify one method or the other in certain cases. The circuits finally chosen gave the most reliable results.

III. THE TEST OSCILLATORS

The low frequency crystal test set (Fig. 2) consists of a two stage tuned amplifier transformer coupled to a "pi" attenuator feedback network, of which the series arm is the crystal. It is basically a modified Heegner[3] oscillator, capable of dissipating large amounts of power in the crystal. The input and output voltages to the attenuator are measured and their relative phase angles observed by a Lissajous figure method.

To operate, a resistor is put across the crystal and the gain adjusted so that the circuit oscillates continuously over the tuning range. When passing through the crystal frequency, the crystal's low impedance shunts the resistor and opens up the phase shift pattern from that of a straight line. The resistor can then be removed, leaving the crystal alone to control the frequency of oscillation. By tuning, the crystal phase shift can be controlled so that series resonance is readily located. Various crystal currents can be obtained under this same condition by adjusting the oscillator's over-all gain. This low frequency apparatus proved to be very reliable in performance between the frequencies of 50 to 150 kilocycles. The transformer provided the chief limitation of the frequency range.

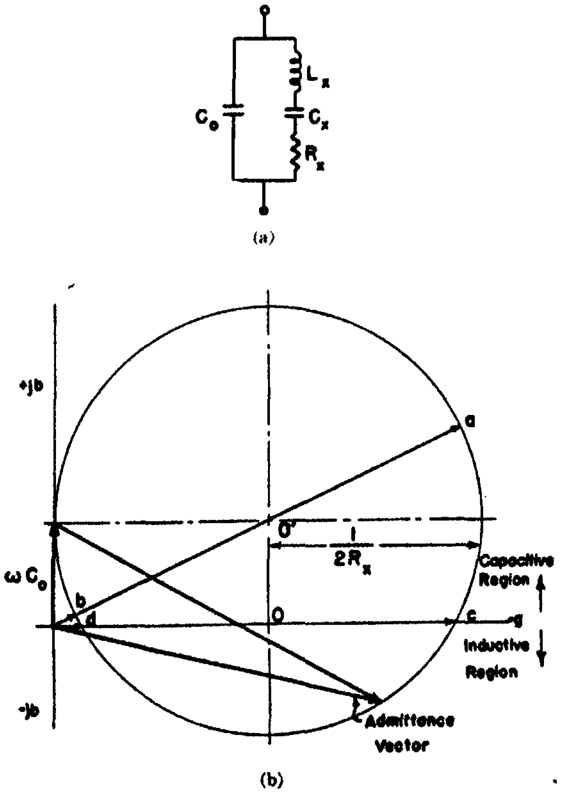

(a)

(b)

FIG. 1. Crystal equivalent circuit and polar admittance diagram.

TABLE I.

Nominal crystal frequency-mc	Resistance at harmonic mode Ohms	Harmonic mode
50	14	3
50	26	3
50	42	3
50	19	3
50	68	5
50	52	5
60	23	3
60	17	3
60	31	3
60	42	3
60	15	3

The medium frequency test oscillator used (Fig. 3) was a circuit developed by the Signal Corps Engineering Laboratories and known as the Crystal Impedance Meter.[4] With the proper choice of tuning inductors, crystals between 200 and 15000 kilocycles could be tested. This meter consists of a crystal in a low impedance feedback network with tuned half sections on either side for impedance matching to a pentode power amplifier. Rectified grid current and crystal current are measured. Since the substitution method is used, a calibrated variable resistance network can be made to replace the crystal unit. Series resonance exists at the point where the substitution of a resistor causes no frequency change as determined on a stable receiver.

In operation, a crystal is inserted in the feedback network and the oscillator tuned for a peak in the amplitude of oscillation as indicated by the rectified grid current. This peak is generally accompanied by a maximum of feedback current through the crystal. The crystal is now in the region of minimum impedance and quite close to series resonance for these medium frequency units. Then by a process of repeated substitution of resistance for the crystal, and retuning, a point is obtained where neither the amplitude nor frequency of oscillation change in the substitution. This value of the substituted resistance is then considered to be the series resonant resistance of the crystal. Various crystal currents can be obtained by adjusting the screen grid voltage of the amplifier tube.

---

[3] K. Heegner, E.N.T. 15, 364 (1938).

[4] C. J. Miller, Jr. *Long Range Planning for Quartz Crystal Units* (Sig. Corps Labs. Pbl., October 15, 1945).

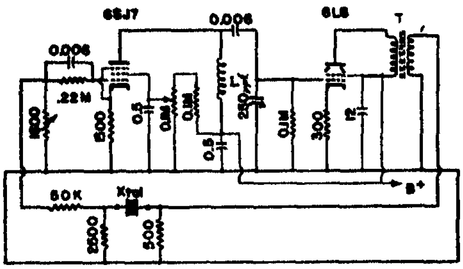

FIG. 2. Low frequency test oscillator.

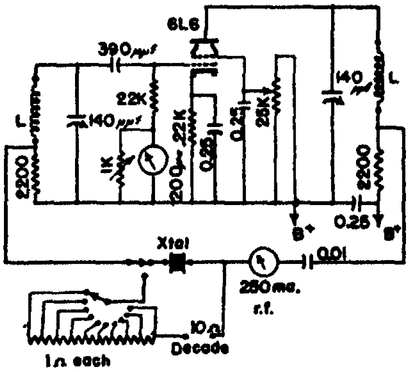

FIG. 3. Medium frequency test set.

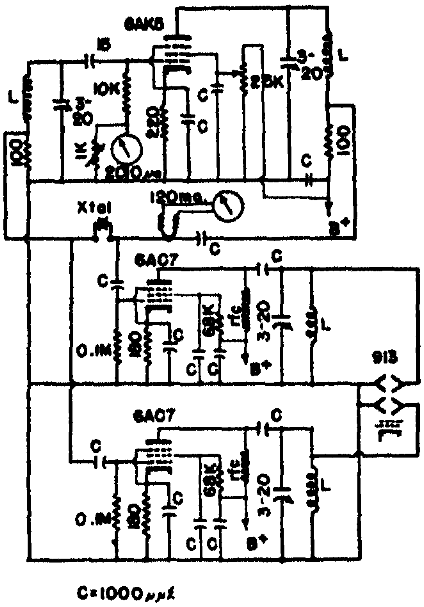

FIG. 4. High frequency test set.

The circuit used for the high frequency meter (Fig. 4) was the same as the medium frequency meter. Components have been changed to allow for differences at the high frequencies, so that the circuit will oscillate up to about 100 megacycles. However, this oscillator will tend to operate the crystal at minimum impedance if the tuning depends upon a maximum of either d.c. grid or feedback crystal current. It has been shown that minimum impedance may have more than a negligible separation from series resonance. To assist in locating series resonance, an oscilloscope with tuned amplifiers was added to indicate the phase shift across the crystal.

The operation of this combination is still simple. A crystal is made to oscillate in the meter and a receiver tuned to that frequency. A short circuit is substituted for the crystal and the meter is retuned to the crystal frequency on the receiver. The two amplifiers on the oscilloscope are then tuned for a maximum deflection which is a straight line at an angle of 45°. The crystal is now put in place of the short circuit and the oscillator is tuned for zero phase shift. By substitution of resistors the resistance of the crystal may be found, as was done with the medium frequency meter.

IV. RESULTS OBTAINED AND DISCUSSION

Some typical curves of the resistance as a function of the current level for low and medium frequency crystals are included (Figs. 5 and 6). The observed data give, firstly, an idea of the impedance level to be expected, and secondly, the variation of resistance with current level or amplitude of oscillation.

On Fig. 5 the four apparently identical low frequency units have impedance levels between 1000 and 3000 ohms. The resistance generally increases with crystal current, but may have erratic variations. The non-linearities that are present in many units can probably be ascribed to the coupling of extraneous modes into the fundamental response. The effect of these parasitic modes will vary with the temperature of the quartz and may increase the resistance by as much as 500 percent.[5] The disturbing fact is that these modes are unpredictable

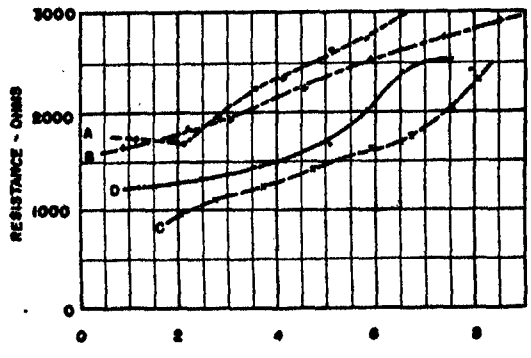

FIG. 5. Crystal resistance *vs.* current for low frequency units. Four crystals "*DT*" cut at 81.94 kc.

---

[5] Armour Res. Found., *Parasitic Vibrations in Quartz Oscillator Plates*, Report No. 11, July, 1947.

among the usual commercial units as shown by these four units of the same cut, frequency, and manufacturer.

The medium frequency units were all "*AT*" or "*BT*" cuts (Fig. 6). The resistance is more uniform at low current levels, but at higher levels may rise very rapidly.

The high frequency units which were tested were of the harmonic mode shear type. A table of some observed resistances at a level of 50 milliamperes is included.

ACKNOWLEDGMENTS

The results presented in this paper were obtained under the Signal Corps Engineering Laboratories Contract No. W36-039 sc 32081. Our thanks are extended to the Frequency Control Branch which furnished much of the equipment and all of the crystals tested.

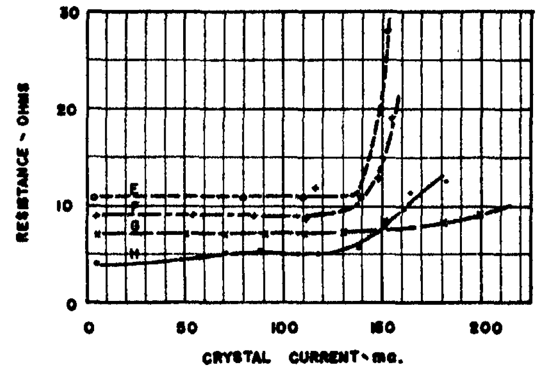

FIG. 6. Crystal resistance *vs.* current for medium frequency units. *E*—8400 kc pressure mounted, *F*—7000 kc plated, *G*—7375 kc pressure mounted, *H*—8000 kc plated.

THE REVIEW OF SCIENTIFIC INSTRUMENTS VOLUME 20, NUMBER 6 JUNE, 1949

A New High Sensitivity Remanent Magnetometer

ELLIS A. JOHNSON, THOMAS MURPHY, AND P. F. MICHELSEN
Carnegie Institution of Washington, Washington, D. C.

(Received March 8, 1949)

The remanent magnetometer, sturdily constructed for use in a mobile field laboratory, is capable of measuring magnetic moments of rocks as small as 2×10^{-8} c.g.s. unit per cc. A sample of rock of 25- to 50-cc volume is rotated over a pick-up coil at 10 cycles per second, and the induced alternating voltage, after amplification, is measured in both intensity and phase, and the direction and intensity of magnetization determined. The apparatus is calibrated with a needle-magnet of known magnetic moment. It has been used successfully in measurements of polarization of the glacial clays of New England and sedimentary rocks of the western states.

INTRODUCTION

IN September, 1938, one of us[1] published a description of an apparatus designed to measure small magnetic moments such as those encountered in samples of a few cubic centimeters of magnetically polarized clay or rock. This apparatus was found generally satisfactory in the course of a long series of measurements, but some disadvantages were encountered in its use which it was hoped could be avoided when constructing another unit. The synchronous commutator detector was in constant need of attention and adjustment and did not operate satisfactorily over long periods. It was planned to eliminate this unit in any new design.

Furthermore, the apparatus was not sturdy enough to withstand the effects of transportation to a working site in the field, and samples were brought from the field to the laboratory. This procedure was not above criticism for, in the course of handling and transportation, clay or rock specimens would be subjected to shocks and heavy vibrations, and might be exposed to magnetizing fields. Finally, the small sample utilized, a 1.5-cm cube, was difficult and laborious to make, so that a finished sample might easily differ considerably in both size and shape from what was specified.

With these points in mind, it was concluded that further work required a more sturdy apparatus which would need minimum maintenance, and be able to operate for long periods out of range of a laboratory. Greater sensitivity in the new apparatus was desirable. The apparatus described here, while modeled on the old one, fully satisfies the requirements just outlined, and incorporates as well recent improvements in electronic components and techniques.

The old apparatus was used in the laboratory from 1937 to 1939 for measurements of the magnetic polarizations of glacial clays deposited in Connecticut about 20,000 years ago, and of ocean bottom sediments from the North Atlantic, probably dating back 400,000 years. Both clays and ocean sediments

---

[1] E. A. Johnson, Rev. Sci. Inst. 9, 263–266 (1938).

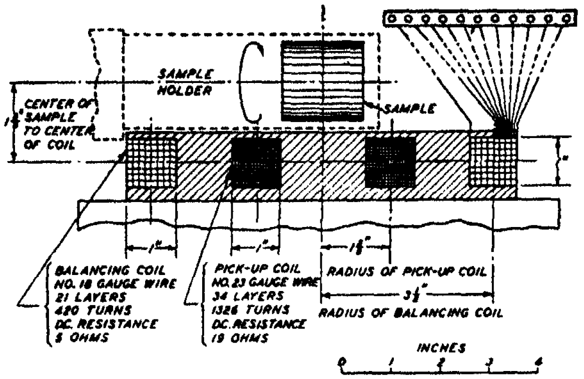

FIG. 1. Pick-up coil.

showed slow and restricted variations with time in the direction of the horizontal component of magnetization (the component corresponding to declination of the earth's magnetic field).[2]

The apparatus described in the present paper was used in New England in 1947 for the measurement of the polarization of 5000 years of deposition of glacial clay[3] and in the western United States in 1948 for measurements on sedimentary rocks ranging in age from 10 million to 150 million years.[4]

The new apparatus has also been used to measure the magnetic moments of very thin films of iron, down to 10^{-7} mm, in an attempt to verify Kittel's[5] theory that very thin films should act as single domains. Preliminary measurements indicate that this is indeed the case, since the moments of films ranging from 10^{-7} to 10^{-4} mm appear to have a natural and constant value per cm of thickness and cannot be demagnetized.

MECHANICAL PARTS

As in the old apparatus, the sample of clay or rock is rotated at the end of a shaft, over a system of coils in which it induces a small alternating voltage. The voltage after amplification is measured both in intensity and phase, and from the results the magnetization of the sample can be deduced.

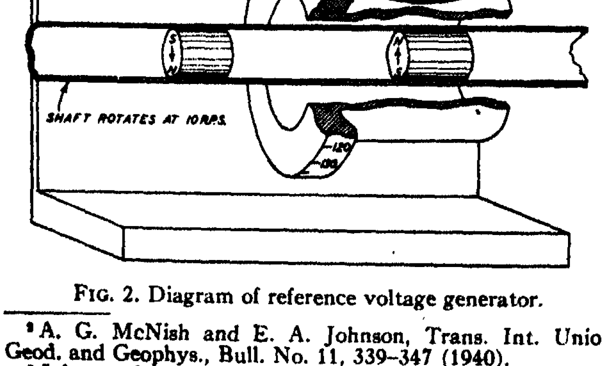

FIG. 2. Diagram of reference voltage generator.

The original theory and design appears to be satisfactory with respect to design parameters. Attempts were made to improve sensitivity using balanced coils on an iron core. These failed because of the critical requirements for shaped pole pieces, and the considerable phase distortion and increased 60-cycle pick-up in the iron-cored detectors.

A shaft consisting of a tube of dural one inch in diameter and four feet long is supported horizontally in bronze sleeve bearings, on massive mounts fixed to the heavy base of the apparatus. The shaft is driven at one end, through a reduction gear, by a standard synchronous motor, and rotates at ten revolutions per second. The motor is shock-mounted on the base and connected to the shaft by a flexible coupling. The base of the apparatus consists of two 4-inch I-beams of dural six feet long, bolted to dural sheet ½ inch thick and one foot wide. On the end of the shaft remote from the motor, any one of a variety of holders, all constructed entirely of a plastic material, can be attached in which to mount the sample under investigation. The pick-up coil system is attached to the base immediately below the sample holder. A large aluminum box, with walls ½ inch thick, which helps to shield the coil and sample holder electrically and also to prevent their being damaged, completely encases the coil and the end of the shaft. Other subsidiary devices necessary for the measurements are attached to the base, but these will be dealt with later. All parts of the apparatus except the motor and the magnets (described later) are constructed of non-magnetic materials.

PICK-UP COIL SYSTEM

Johnson,[1] in the paper cited earlier, described the design of coil systems suitable for his early apparatus; now, however, the development of 10-cycle transformers with a step-up ratio of 275 has reduced the number of turns required on the pick-up coils. The new system, like the old, consists of two coils as shown in Fig. 1. The main coil has 1326 turns, with a mean diameter of 2¾ inches, and the total number of turns on the outer, or "balancing" coil, is 420, the mean diameter being seven inches. The balancing coil has taps taken off at close intervals to permit fine adjustment, and the leads from the two coils are joined in opposition. The number of turns on the outer coil was determined by trial and error, the number being varied until a signal voltage of less than 0.001 volt resulted when the complete system was placed in a uniform 60-cycle a.c. field of 2 oersted, a field very much bigger than one would expect to encounter. The coils are wound on

---

[2] A. G. McNish and E. A. Johnson, Trans. Int. Union Geod. and Geophys., Bull. No. 11, 339–347 (1940).

[3] Johnson, Murphy, and Torreson, Terr. Mag. **53**, 349–372 (1948).

[4] Torreson, Murphy, and Graham, Phys. Rev. **75**, 208–209 (1949).

[5] Charles Kittel, Phys. Rev. **70**, 965–971 (1946).

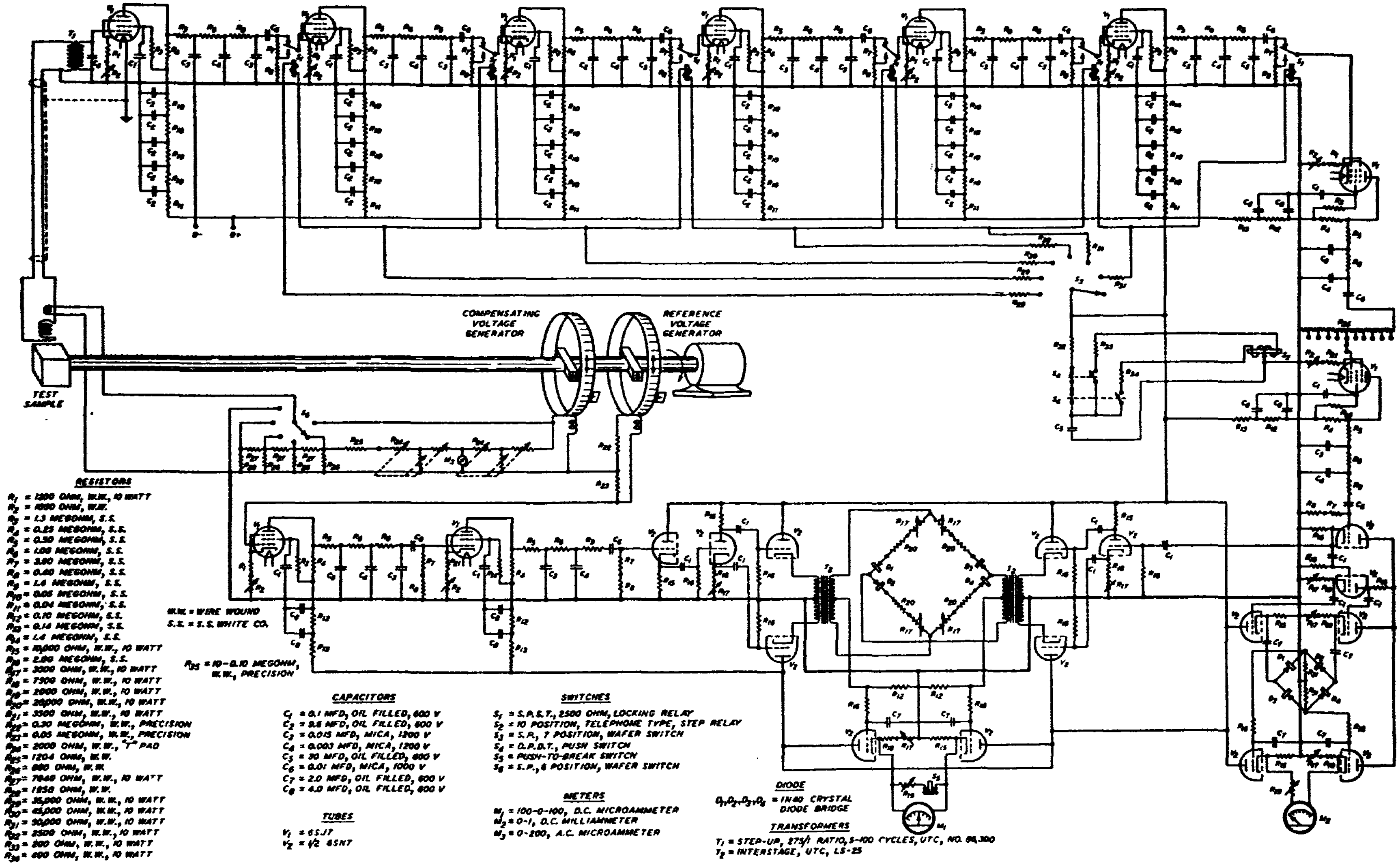
COMPENSATING VOLTAGE GENERATOR
REFERENCE VOLTAGE GENERATOR
TEST SAMPLE
RESISTORS
R1 = 1200 OHM, W.W., 10 WATT
R2 = 1000 OHM, W.W.
R3 = 1.3 MEGOHM, S.S.
R4 = 0.25 MEGOHM, S.S.
R5 = 0.30 MEGOHM, S.S.
R6 = 1.00 MEGOHM, S.S.
R7 = 3.00 MEGOHM, S.S.
R8 = 0.40 MEGOHM, S.S.
R9 = 1.4 MEGOHM, S.S.
R10 = 0.05 MEGOHM, S.S.
R11 = 0.04 MEGOHM, S.S.
R12 = 0.10 MEGOHM, S.S.
R13 = 0.14 MEGOHM, S.S.
R14 = 1.4 MEGOHM, S.S.
R15 = 10,000 OHM, W.W., 10 WATT
R16 = 2.00 MEGOHM, S.S.
R17 = 3000 OHM, W.W., 10 WATT
R18 = 7500 OHM, W.W., 10 WATT
R19 = 2000 OHM, W.W., 10 WATT
R20 = 20,000 OHM, W.W., 10 WATT
R21 = 3500 OHM, W.W., 10 WATT
R22 = 0.30 MEGOHM, W.W., PRECISION
R23 = 0.05 MEGOHM, W.W., PRECISION
R24 = 2000 OHM, W.W., "T" PAD
R25 = 1204 OHM, W.W.
R26 = 800 OHM, W.W.
R27 = 7840 OHM, W.W., 10 WATT
R28 = 1950 OHM, W.W.
R29 = 35,000 OHM, W.W., 10 WATT
R30 = 45,000 OHM, W.W., 10 WATT
R31 = 50,000 OHM, W.W., 10 WATT
R32 = 2500 OHM, W.W., 10 WATT
R33 = 200 OHM, W.W., 10 WATT
R34 = 400 OHM, W.W., 10 WATT
W.W. = WIRE WOUND
S.S. = S.S. WHITE CO.
R35 = 10-0.10 MEGOHM, W.W., PRECISION
CAPACITORS
C1 = 0.1 MFD, OIL FILLED, 600 V
C2 = 9.8 MFD, OIL FILLED, 600 V
C3 = 0.015 MFD, MICA, 1200 V
C4 = 0.003 MFD, MICA, 1200 V
C5 = 30 MFD, OIL FILLED, 600 V
C6 = 0.01 MFD, MICA, 1000 V
C7 = 2.0 MFD, OIL FILLED, 600 V
C8 = 4.0 MFD, OIL FILLED, 600 V
TUBES
V1 = 6SJ7
V2 = 1/2 6SN7
SWITCHES
S1 = S.P.S.T., 2500 OHM, LOCKING RELAY
S2 = 10 POSITION, TELEPHONE TYPE, STEP RELAY
S3 = S.P., 7 POSITION, WAFER SWITCH
S4 = D.P.D.T., PUSH SWITCH
S5 = PUSH-TO-BREAK SWITCH
S6 = S.P., 6 POSITION, WAFER SWITCH
METERS
M1 = 100-0-100, D.C. MICROAMMETER
M2 = 0-1, D.C. MILLIAMMETER
M3 = 0-200, A.C. MICROAMMETER
DIODE
D1, D2, D3, D4 = 1N40 CRYSTAL DIODE BRIDGE
TRANSFORMERS
T1 = STEP-UP, 275/1 RATIO, 5-100 CYCLES, UTC, NO. 86,300
T2 = INTERSTAGE, UTC, LS-25

FIG. 3. Circuit diagram of remanent magnetometer.

a massive form of clear plastic which is bolted rigidly to the longitudinal I-beams of the base.

REFERENCE VOLTAGE GENERATOR

The phase of the signal voltage is measured by an electronic wattmeter. This requires a synchronous generator of variable phase and low noise, and a permanent magnet generator is used for this purpose, as shown in Fig. 2. The magnet of the generator is a cylindrical alnico magnet 0.75 inch long and 0.9 inch diameter, magnetized to saturation along a diametric plane, which is inserted in the shaft near the motor end. The generator coil has 1700 turns and is mounted on a clear plastic drum. The drum, which can be rotated by hand, is coaxial with the shaft and carries a graduated circle, the zero of which can be adjusted. In operation, the magnet rotating with the shaft acts as a line of dipoles of infinitesimal size and induces in the coil a signal of very pure wave form. When the drum carrying the coil is rotated, the phase of the signal is changed, the amount of change being read off on the circle. This signal is referred to in later discussion as the "reference voltage."

The rotating magnet also induces a parasitic voltage in the main pick-up coil and this is balanced out by magnetic and electrical means. First, another similar magnet is inserted in the shaft close to the original one but antiparallel to it. A third and much smaller magnet is mounted nearer the motor at the end of the shaft and, by adjusting its distance and orientation, it is possible to compensate for the signal produced by the magnets, the motor, and the traces of magnetic material in the shaft and components, and reduce the effect to a quite small value, equivalent to a moment of 2×10^{-5} c.g.s. unit at the center of the sample holder. This "residual signal" does not stay constant but varies within small limits, due possibly to temperature differences between the compensating magnets. To eliminate the "residual," resort is had to electrical means. A second generator, very similar to the first, is made by installing a small coil near the second balancing cylindrical magnet. The current from this coil is fed through an attenuator to a small coil located beneath the main pick-up coil, as shown in the circuit diagram of the whole apparatus in Fig. 3. By varying the phase and intensity of the signal from this compensating generator, it is possible, with surprising ease, to reduce the "residual" below the limits of measurement of the detecting apparatus.

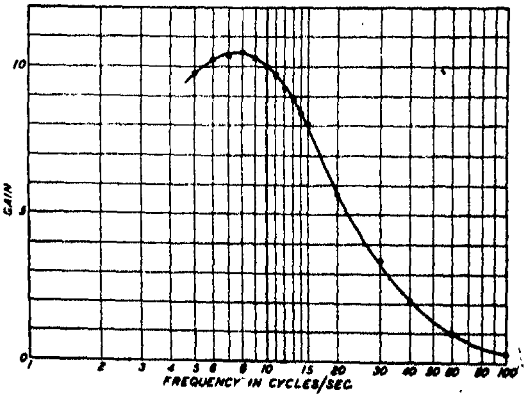

FIG. 4. Frequency response of unit amplifier.

AMPLIFIERS

The main pick-up coil is coupled to the amplifiers by a transformer. This is of a special type made by the United Transformer Company for use at frequencies between 5 and 100 cycles per second. It is made to match impedances of 10 and 750,000 ohms. The turns' ratio is 275/1. A small capacitor is joined across the output terminals, acting as a filter for frequencies higher than 10.

The amplifier is constructed in eight units, the units being almost identical. Each unit amplifier has a high gain pentode (6SJ7) operating with about two percent feedback, and an *R–C* filter network. The values of the impedances and the feedback are so chosen that the over-all gain per stage is ten at ten cycles per second, the final adjustment being obtained by changing the value of the cathode resistor within narrow limits.

Each of the first six of the unit stages has at its terminal a pair of resistors with values in the ratio of 9 to 1. A relay-operated switch connects the grid of the tube of the next unit stage across one or both of these resistors to provide either one of two gains, ten or one. The seventh stage has ten equal resistors at its terminal, to provide any unit gain from one to ten. The eighth stage always operates at a gain of ten.

By means of two controls, one operating the switches between stages, the other the ten-position potentiometer of the seventh stage, it is possible to choose the over-all gain of the amplifier in a range of values from 10 to 10^7. All the stages are always in operation.

The filter network serves several purposes. It discriminates strongly against 60-cycle signals arising from large 60-cycle gradients, and it decreases the band width, which prevents overloading of the final stages by noise when the amplifier is used at high gain. It also filters out undesired harmonics. Figure 4 shows the frequency discrimination for each stage.

The negative feedback stabilizes each stage so that it is independent of large changes in plate and filament supply. The gain of each stage is found to stay constant within one percent over long periods.

The grid bias on the tubes in each stage except the last one is approximately one volt. In the last stage it is 1.8 volts. The impedances in the plate circuit are so chosen that no damage can result if any stage is accidentally overloaded.

The over-all frequency response of the apparatus, including the coils, transformer, amplifiers, output stage, and voltmeter, is given in Fig. 5. The band width measures 6.5 cycles. The peak occurs at 7 cycles and is the result of trying to achieve a narrow band width and a large discrimination against 60 cycles at the same time, without too elaborate a filter and too much loss in gain. The first tube was chosen for low flicker noise. The measured noise at ten cycles is about twice the thermal noise in the first grid circuit.

POWER SUPPLY

Power for the amplifiers and the remainder of the electronic equipment is obtained from the 60-cycle commercial power circuits or from a 60-cycle portable generator. One regulated 300-volt d.c. power pack provides a "*B*" supply for the first six amplifier stages, each stage incorporating its own decoupling circuit. The other two stages and equipment are fed from a similar power pack. In the remaining parts of the circuit, a constant-voltage "*A*" supply is necessary, so the complete filament supply comes from a regulated d.c. power pack of variable voltage. The voltage is about 6.2 volts. The amplifiers will operate quite well with no noticeable increase in noise if a 6.3-a.c. voltage is used in the filament circuits instead of a d.c. supply.

INTENSITY MEASUREMENT

The signal picked up by the coil is amplified at a chosen gain value until the output voltage of the amplifier lies between two and eight volts, as read from a meter on the instrument panel. A cathode follower is used in an output stage and the signal, split into two parts, is fed into the remainder of the circuit. For the intensity measurement, one part is measured in a vacuum-tube voltmeter circuit, which uses germanium diodes for rectification and has a period of four seconds.

The intensity meter reading in volts is readily converted to intensity of magnetization when the apparatus is calibrated. Calibrating is done with a small alnico magnet embedded in a piece of plastic of the same size and shape as the specimen. The magnetic moment of this magnet, of the order of 1 c.g.s. unit, is known from magnetometer readings. Since the gain of the amplifier is known, moments within the range from 10^{-6} c.g.s. to 20 c.g.s. units can be measured easily in absolute magnitude to an accuracy of a few percent.

DIRECTION OF MAGNETIZATION

The direction of magnetization is determined by measuring the phase of the amplified signal with respect to an arbitrary zero. The arbitrary zero is chosen along one side of the cubical specimen. To measure phase the signal voltage is compared to the reference voltage, the latter amplified to eight volts to approximately equal the signal voltage, in an electronic wattmeter using a ring modulator circuit. The d.c. output of the ring circuit, amplified in a d.c. amplifier having a time constant of four seconds, operates a meter with a central zero on the instrument panel. The phase of the reference voltage is varied until the meter reading is zero. In this position, the two voltages differ in phase by $\pi/2$ and hence, by geometry, the direction of magnetization in the sample can be obtained.

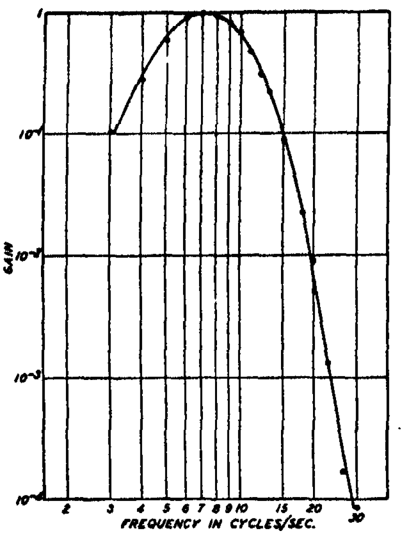

FIG. 5. Frequency response of remanent magnetometer.

The particular advantage of the wattmeter is that it acts as a very narrow band detector. Even when the signal is of the same order as the noise of the first tube, the wattmeter responds, on the average, only to the steady 10-cycle component and is relatively unaffected by the noise, which, although it has the same frequency, has random and rapid changes of phase. It is possible therefore to measure the phase of signals whose intensity is about one-tenth that of the thermal noise in the grid of the first tube. Furthermore, for such weak signals, by changing the phase of the reference voltage until it agrees with that of the weak signal, the bridge circuit measures intensity. Voltages as low as 8×10^{-11} volt can be detected in the pick-up coil circuit by this means. This corresponds to a rotating moment in the specimen holder of 5×10^{-7} c.g.s. unit.

FIELD EQUIPMENT

The complete equipment is solidly constructed and installed in a large "six by six" Army truck. The electronic equipment is mounted in a relay rack which is shock-mounted from the truck body.

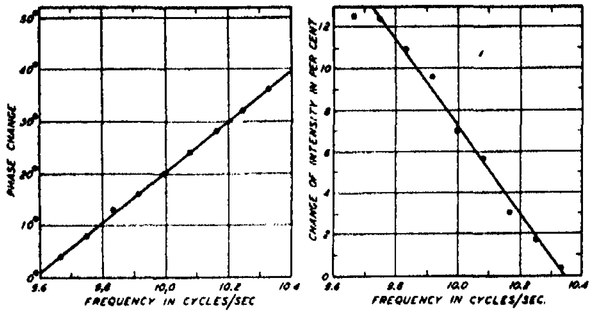

Fig. 6. Change of phase and of intensity with frequency of remanent magnetometer.

The rotary apparatus is mounted on a heavy wooden table-top with a thin layer of rubber between to allow some relative movement. The table-top is rigidly fastened to the truck body. All the metallic parts of the equipment are joined electrically together through the screening in the connecting cables. A separate ground system for the electronic equipment is used, and this is joined to the outside screen at only one place, namely, at the cathode of the first tube. No outside ground is used and has never been found necessary either in the laboratory or in the field.

METHOD OF MEASUREMENT

The samples used in the apparatus are of two kinds, cylinders and cubes. When working with clay, the sample is taken by inserting a cylindrical cup of bakelite bonded paper directly into the clay bank. Suitable means of recording the orientation are used. The cup holding the sample fits directly into the specimen holder. The sample so taken measures 1½ inches long and 1½ inches in diameter. Rock samples 1⅝ inches in diameter are taken with a diamond coring tool and cut with diamond-impregnated saws to 1⅝ inches in length. These cylindrical samples fit into the holder of the apparatus exactly like the cups of clay. Using cylinders, the direction and intensity of magnetization can be measured in only one plane which is sufficient in some cases. For a complete evaluation of the magnetization, the cylinders are cut into cubes 3 cm on a side. These specimens are measured in the apparatus by rotating on the three different axes. Computation gives the intensity, but the direction is usually plotted on a stereographic net. The volumes of the clay and rock cylinders are approximately 40 and 50 cc, respectively, as compared with 27 cc for the cubes.

The chief source of error in the apparatus is in the use of a synchronous motor to drive the shaft. As the frequency of the power supply varies, so does the frequency of the signal induced in the coil. The amplifiers are tuned quite sharply and a small change in frequency produces a moderate change in intensity of the amplified signal and a large change in phase. Figure 6 shows this effect.

A frequency meter with a range of 58 to 62 cycles per second is used to measure the frequency of the power supply and to indicate any sudden changes. In practice, whenever the power frequency fluctuates more than 0.1 cycle per second over a few minutes while measurements are being made, the small standardizing magnet is used at frequent intervals to check the phase and intensity readings. The portable power supply is used in the field and is fitted with a frequency control. Although its frequency fluctuates rather rapidly over a range of 0.3 cycle per second, the average stays fairly constant and the resultant effect is to increase the over-all noise in the apparatus slightly. However, in work so far undertaken, any error attributable to this cause has been much smaller than the other experimental errors encountered and no remedial changes have been considered necessary.

It has been found that the apparatus is capable of measuring magnetic moments in the range from 20 to 10^{-4} c.g.s. unit to an accuracy of two percent in intensity and to within 0.2° in direction. In the range 10^{-4} to 10^{-5} the intensity can be measured within three percent and the direction within 2°. For values less than 10^{-5} c.g.s. the intensity is probably accurate to 10 percent and the direction to 5°. The value of 2×10^{-6} c.g.s. unit is looked on as the practical limit of measurement; below this value traces of impurities and inhomogeneities in the sample are thought to play a big role, and external electrostatic effects on the specimen and the specimen holder become prominent. The smallest moment which is detectable is 5×10^{-7} c.g.s. unit which corresponds to about 2×10^{-8} c.g.s. unit per cc of sample. When the humidity is very low the plastic sample holder collects large electrostatic charges and the pick-up coil must be electrostatically shielded from the holder if the limit of measurement is to be reached.

Effect of Temperature on the Steady-State Sensitivity of Vacuum Radiation Detectors

I. AMDUR AND N. L. BROWN
Department of Chemistry, Massachusetts Institute of Technology, Cambridge, Massachusetts

(Received March 28, 1949)

The steady-state sensitivities of two vacuum radiation thermocouples of very different design and a vacuum compensated bolometer have been measured at 298°, 205°, and 96°K, and the effect of temperature has been found to vary widely for the three detectors. The observed results have been accounted for quantitatively in terms of theoretical sensitivity relations which are based on exact heat flow theory and take into account the specific structural characteristics of the detectors. The treatment is sufficiently general to permit the prediction of steady-state sensitivities as a function of temperature for any vacuum radiation thermocouple or bolometer whose structural characteristics are known.

THE temperature dependence of the steady-state sensitivity of a vacuum radiation detector, such as a radiation thermocouple or a bolometer, does not seem to have been systematically investigated although occasional experiments have been performed near liquid air temperature.[1] These particular experiments showed a greatly enhanced sensitivity at the low temperature for the specific detectors which were used, and, as a result, it is frequently assumed that the steady-state sensitivity of all types of detectors may be expected to increase rapidly with decreasing temperature.[2] Since this is not universally true, it seems desirable to study carefully the temperature dependence of radiation detectors of widely different design, and to attempt to correlate the results with theoretical predictions based on heat flow equations appropriate to the various detectors.

THEORETICAL

Since experimental results were obtained for two radiation thermocouples (of very different design) as well as for a compensated bolometer, it is necessary to derive sensitivity relations for both types of detectors, whose important features may be summarized as follows:

I. Radiation thermocouples

A. Detector with very large receiver area (detector A)

This thermocouple contains a circular platinum receiver, 0.279 cm in diameter, blackened with Aquadag on its upper surface and tinned with solder on its under surface. The receiver is fastened to two constantan wires (one of which serves only as a support), 0.0013 cm in diameter, and to a Chromel *P* wire, 0.0015 cm in diameter, which are symmetrically spaced, 120° apart, and mounted so that the electrical length of each wire, 0.257 cm, is greater than its thermal length, 0.178 cm. A previous description[3] of this detector gives complete structural details and shows the reason for assigning different lengths to the wires for purposes of estimating electrical resistance as compared with thermal resistance.

B. Detector with very small receiver area (detector B)

This thermocouple was made by using a condenser discharge to butt weld a 0.0013 cm diameter constantan wire, 0.318 cm long, to a 0.0015 cm diameter Chromel *P* wire, 0.318 cm long. No receiver is attached to the welded wires which are merely covered with a coating of Aquadag (thereby increasing the diameters to 0.00164 cm and 0.00184 cm, respectively) and mounted so that the thermal and electrical lengths are the same, namely, 0.318 cm. Additional structural details for this detector appear elsewhere.[4]

II. Compensated bolometer (detector *C*)

The bolometer has a detector element consisting of an Aquadag covered platinum wire, 5.6×10^{-4} cm in diameter (diameter of wire core $=2.74\times10^{-4}$ cm) and 0.476 cm long, which, like the welded thermocouple, acts as its own receiver. A bolometer of this type has also been described previously.[5]

The temperature rise experienced by a radiation thermocouple is usually so small (less than 0.05 degree) that it is not necessary, in considering the effect of ambient temperature, to distinguish between the temperature of the cold junction (assumed to be equal to that of the surroundings) and the average temperature of the entire thermocouple. This is not the case for a bolometer whose heating current may cause temperature differences as high as 100° between the midpoint and ends, so that a true average temperature must be used in deriving the sensitivity relation. In order, therefore, to use

---

[1] F. S. Brackett and E. D. McAlister, Rev. Sci. Inst. 1, 181 (1930); C. H. Cartwright, Rev. Sci. Inst. 4, 382 (1933).

[2] J. Strong, *Procedures in Experimental Physics* (Prentice-Hall, Inc., New York, 1939), p. 340.

[3] I. Amdur and H. Pearlman, Rev. Sci. Inst. 10, 174 (1939).

[4] I. Amdur, C. F. Glick and H. Pearlman, Proc. Am. Acad. Arts Sci. 76, 101 (1948).

[5] I. Amdur and C. F. Glick, Rev. Sci. Inst. 16, 117 (1945).

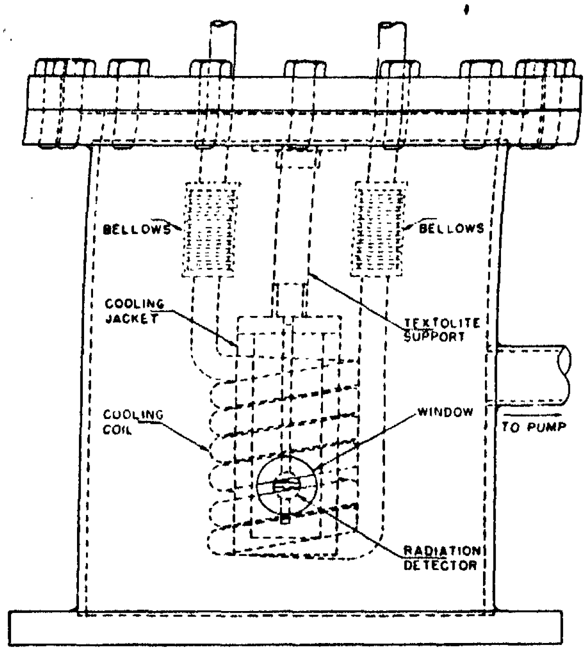

FIG. 1. Vacuum chamber.

a minimum number of symbols, temperatures and temperature differences, averaged over the active receiver area of the detector, will be used for the radiation thermocouples as well as for the bolometer.

The derivation of the sensitivity equation for a radiation thermocouple of the type of detector *A* is very similar to that given by Cartwright[6] and, in view of its brevity, is repeated as an effective method of indicating the basic assumptions involved in arriving at the final relation. The symbols which will be used are as follows:

E = power absorption by thermocouple
E_r = power loss by radiation
E_c = power loss by wire conduction
E_p = power loss by Peltier-heat effect
σ = Stefan-Boltzmann radiation constant
S = radiating surface of thermocouple
$\langle T\rangle_{\text{Av}}$ = average absolute temperature of receiver
ϵ = emissivity of radiating surface
$\langle \Delta t\rangle_{\text{Av}}$ = average temperature difference between receiver and cold junction
K_1 = thermal conductivity of constantan at $\langle T\rangle_{\text{Av}}$
K_2 = thermal conductivity of Chromel *P* at $\langle T\rangle_{\text{Av}}$
r_1 = radius of constantan wire
r_2 = radius of Chromel *P* wire
l = thermal length of constantan or Chromel *P* wire
P = thermoelectric power of thermocouple at $\langle T\rangle_{\text{Av}}$
i_g = current through galvanometer
V = emf developed by thermocouple
G = resistance of galvanometer
R = resistance of thermocouple at $\langle T\rangle_{\text{Av}} = \rho_1 L/(\pi r_1^2) + \rho_2 L/(\pi r_2^2)$
ρ_1 = resistivity of constantan at $\langle T\rangle_{\text{Av}}$
ρ_2 = resistivity of Chromel *P* at $\langle T\rangle_{\text{Av}}$
L = electrical length of constantan or Chromel *P* wire

When steady-state conditions are reached, the power lost by the thermocouple through radiation, wire conduction, and Peltier-heat effect, becomes equal to the power which it absorbs, so that

$$E = E_r + E_c + E_p \tag{1}$$

where

$$E_r = 4\sigma S\langle T\rangle_{\text{Av}}^3 \epsilon \langle \Delta t\rangle_{\text{Av}} \tag{2}$$

$$E_c = (2K_1\pi r_1^2/l + K_2\pi r_2^2/l)\langle \Delta t\rangle_{\text{Av}} \tag{3}$$

and

$$E_p = P i_g \langle T\rangle_{\text{Av}}. \tag{4}$$

Since the e.m.f. developed by the thermocouple, connected directly across the galvanometer terminals, is

$$V = i_g(G+R) = P\langle \Delta t\rangle_{\text{Av}}, \tag{5}$$

the galvanometer current may be written

$$i_g = P\langle \Delta t\rangle_{\text{Av}}/(G+R) \tag{6}$$

and the sensitivity as defined by Cartwright, namely,

$$Q = i_g(G+R)^{\frac{1}{2}}/E, \tag{7}$$

becomes

$$Q = \frac{P}{(G+R)^{\frac{1}{2}}}\left[4\sigma S\langle T\rangle_{\text{Av}}^3\epsilon + 2K_1\pi r_1^2/l + K_2\pi r_2^2/l + \frac{P^2\langle T\rangle_{\text{Av}}}{G+R}\right]^{-1}. \tag{8}$$

For detector *B*, the relation for *Q* is somewhat different, because the absorbed power, instead of

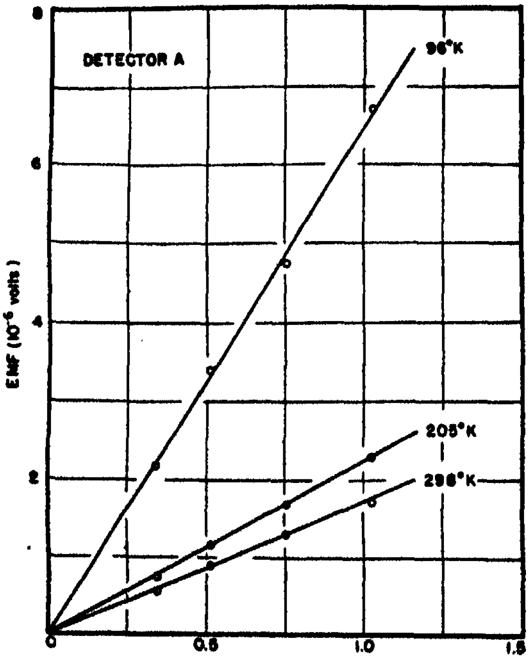

FIG. 2. Response of radiation thermocouple with large receiver area.

---

[6] C. H. Cartwright, Zeits. f. Physik 92, 153 (1934).

being concentrated on a central receiver of essentially uniform temperature, is distributed over the entire length of the detector wires. The heat flow equations for the latter case are the same as those for an electrically heated wire, heat stationed at the ends, and have been considered in connection with the theory of the steady-state sensitivity of a vacuum bolometer.[5] Application of the bolometer results to detector B results in replacing Eq. (3) by

$$E_c=(1+1.1\times10^{-9}\langle T\rangle_{Av}^3)(3K_1\pi r_1^2/l+3K_2\pi r_2^2/l)\langle\Delta t\rangle_{Av}\quad(9)$$

where $(1+1.1\times10^{-9}\langle T\rangle_{Av}^3)$ is a small correction term resulting from the loss of a small fraction of absorbed power by radiation. Since, in the present

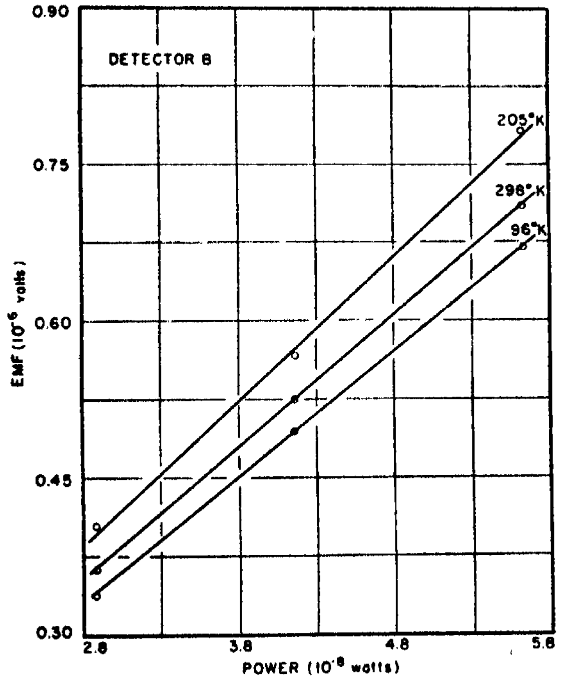

FIG. 3. Response of radiation thermocouple with small receiver area.

application, this correction has a maximum value of only 3 percent at room temperature, it is given in the above form, specific for detector B, rather than in its general form. Substitution of numerical values into Eq. (9) reveals that the power lost by wire conduction is nearly equally divided between the two wires. The junction of these wires, therefore, will have a maximum temperature difference, $\langle\Delta t\rangle_{\max}$, which, for the present case where radiation losses are small, has the following relation to the average temperature difference, $\langle\Delta t\rangle_{Av}$,

$$\langle\Delta t\rangle_{\max}=1.5\langle\Delta t\rangle_{Av}.\quad(10)$$

Equation (5) must therefore be replaced by

$$V=i_s(G+R)=P\langle\Delta t\rangle_{\max}=1.5P\langle\Delta t\rangle_{Av}\quad(11)$$

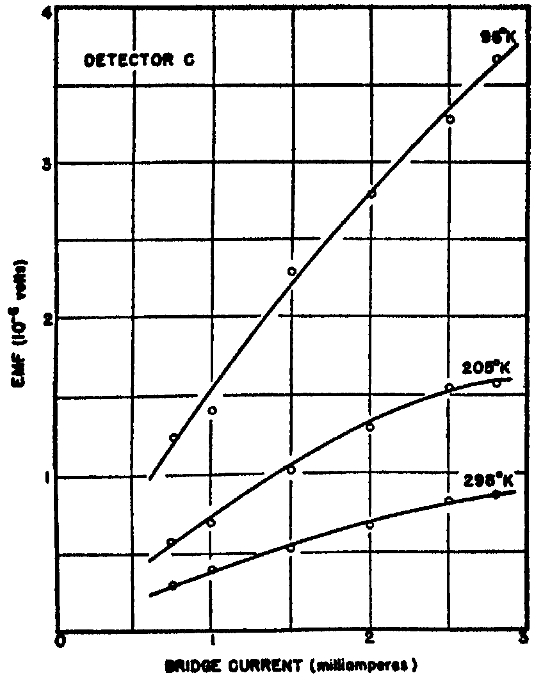

FIG. 4. Response of bolometer.

and the sensitivity equation appropriate to detector B becomes

$$Q=\frac{1.5P}{(G+R)^{\frac{1}{2}}}\bigg[4\sigma S\langle T\rangle_{Av}^3\epsilon+(1+1.1\times10^{-9}\langle T\rangle_{Av}^3)\times(3K_1\pi r_1^2/l+3K_2\pi r_2^2/l)+\frac{1.5P^2\langle T\rangle_{Av}}{G+R}\bigg]^{-1}.\quad(12)$$

The sensitivity equation for a compensated bolometer contains many of the symbols already listed, except that the subscripts 1 and 2 are not used with K, r, or ρ, since the sensitive element of the bolometer is a single platinum wire whose thermal and electrical lengths are equal. Additional symbols which appear are:

α = temperature coefficient of resistance of bolometer and of compensator
T_0 = absolute temperature of surroundings and of ends of bolometer
R_0 = resistance of bolometer and of compensator at T_0 $=\rho_0 l/(\pi r^2)$
ρ_0 = resistivity of bolometer at T_0
K_0 = thermal conductivity of bolometer and of compensator at T_0
N = resistance of each of manganin resistors in Wheatstone network
r' = radius of bolometer including blackening

The expression for Q for a compensated vacuum bolometer, in the type of Wheatstone network used in the present experiments, has been previously derived[5] and has the form

$$Q=\frac{\alpha R_0(G+R)^{\frac{1}{2}}}{R^{\frac{1}{2}}(R+N+2G)}\frac{\left[4\sigma S\epsilon\langle T\rangle_{\mathrm{Av}}{}^3\langle\Delta t\rangle_{\mathrm{Av}}+\frac{12}{l}K_0\pi r^2\langle\Delta t\rangle_{\mathrm{Av}}(m+n\langle\Delta t\rangle_{\mathrm{Av}})\right]^{\frac{1}{2}}}{\left\{4\sigma S\epsilon(\langle T\rangle_{\mathrm{Av}}{}^3+3\langle T\rangle_{\mathrm{Av}}{}^2\langle\Delta t\rangle_{\mathrm{Av}})+\frac{12}{l}K_0\pi r^2(m+2n\langle\Delta t\rangle_{\mathrm{Av}})+\frac{\alpha R_0}{R+N+2G}\left[4\sigma S\epsilon\langle T\rangle_{\mathrm{Av}}{}^3\langle\Delta t\rangle_{\mathrm{Av}}+\frac{12}{l}K_0\pi r^2\langle\Delta t\rangle_{\mathrm{Av}}(m+n\langle\Delta t\rangle_{\mathrm{Av}})\right]\right\}} \tag{13}$$

where

$$m=1+\frac{2\epsilon\sigma r'T_0{}^3l^2}{15r^2K}\quad\text{and}\quad n=\frac{2\epsilon\sigma r'T_0{}^2l^2}{5r^2K}-\frac{\alpha}{5}.$$

To the first order of small quantities, Eq. (13) is valid for both positive and negative differences between radiation loss and self-heating due to the increase of wire resistance with temperature, although the original derivation assumed that the difference was positive (which is usually the case at room temperature or higher). The general applicability of the end result is due to relationships between hyperbolic trigonometric and circular trigonometric functions which appear in solutions of the second order differential heat flow equations for the two cases. The original derivation should be consulted for the basic assumptions and for a description of the procedure for calculating theoretical values of Q.

EXPERIMENTAL

Each detector was suspended inside a cylindrical copper cooling jacket, 1 inch I.D., 1¼ inch O.D., and 3$\frac{9}{16}$ inch long, which was slotted to permit radiation to strike the receiver surface. Refrigerant (acetone at dry ice temperature or liquid nitrogen) was circulated through ⅜-inch copper tubing coiled around and soldered to the cylinder which was supported and thermally insulated from the cover of a metal vacuum chamber (6 inch O.D. and 8 inch high) by a Textolite rod and Adnic (high thermal resistance alloy) bellows. Two copper-constantan thermocouples, one soldered to the bottom of the cooling jacket, and the other, to the detector case, emerged, together with the detector leads, through metal-glass seals in the vacuum chamber cover. National Bureau of Standards carbon filament lamps were used as sources of radiation which entered the vacuum chamber through a plane Pyrex window (calibrated for transmission and reflection) sealed to a copper-glass Housekeeper seal in the chamber wall.

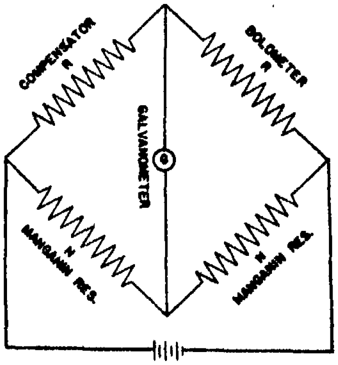

FIG. 5. Wheatstone bridge network.

The essential features of the cooling jacket and vacuum chamber are shown in Fig. 1. All surfaces inside the vacuum chamber were blackened to reduce scattered radiation.

At the lower temperatures, refrigerant was circulated through the coil of the cooling jacket in the presence of about 1 cm of helium to improve heat conduction between the radiation detector and the surrounding cylinder. After temperature equilibrium had been reached, the pressure was reduced to 10^{-5} mm or lower for the duration of the runs, during which circulation of refrigerant was continued to prevent temperature rise resulting from radiation and heat leak through supports and lead wires. Responses of the detectors were measured with a special potentiometer using a galvanometer amplification device[7] as in previous experiments.[5, 6]

Detector A was irradiated with a standard lamp which had been calibrated at four currents, and detector B, with a lamp which had been calibrated at three currents. The bolometer, detector C, was irradiated with a single power density at six different Wheatstone bridge currents. The experimental results are shown in Figs. 2–4, where the temperatures are those corresponding to the readings of the copper-constantan thermocouple fastened to the detector case inside the cooling jacket. The ordinates in Figs. 2 and 3 are the open circuit potentials developed by the radiation thermocouples, and the abscissas, the powers absorbed by the detector receivers. For detector A this power is given by

$$E=\gamma E_a\pi(r')^2 \tag{14}$$

---

[7] I. Amdur and H. Pearlman, Rev. Sci. Inst. 9, 194 (1938).

where: γ, the absorptivity of the Aquadag surface, is taken as 0.67, independent of temperature, for all lamp currents; E_a, the power density reaching the receiver, is known from the National Bureau of Standards lamp calibration and the window transmission (0.839 to 0.763 for lamp currents between 0.400 and 0.250 amperes); and r', the radius of the hole in a mask above the receiver is 0.0813 cm. For detector B the absorbed power is

$$E=\gamma E_a 2(r_1'+r_2')l \qquad (15)$$

where l, the length of the constantan or Chromel P wire, is 0.318 cm; and r_1' and r_2', the radii of the constantan and Chromel P wires (including the Aquadag coating) are 8.2×10^{-4} and 9.2×10^{-4} cm, respectively. The ordinate in Fig. 4 is the open circuit potential produced upon irradiation as measured by connecting the galvanometer leads in Fig. 5 to the special potentiometer. (Figure 5 shows the circuit corresponding to the definition of Q in Eq. (7).) The abscissa is the total network current, of which a known fraction passes through the bolometer. The constant power, E, absorbed by the bolometer was 1.15×10^{-8} watt corresponding to values of 0.67, 64.4×10^{-6} watt/cm², 2.8×10^{-4} cm, and 0.476 cm, respectively, for, γ, E_a, r', and l in the relation

$$E=\gamma E_a 2r'l. \qquad (16)$$

DISCUSSION

Figures 2 and 3 show extremely different characteristics for detectors A and B whose important difference is the absence of a relatively large receiver in detector B. The slopes of the straight lines define one type of sensitivity, S^*, namely the open circuit potential produced upon absorption of unit radiant power. For detector A, decreasing temperature increases this sensitivity markedly, the values being 1.70, 2.23, and 6.48 volts/watt at 298°, 205°, and 96°K, respectively, whereas detector B exhibits very little effect as shown by sensitivity values of 12.6, 13.8, and 11.8 volts/watt at the same respective temperatures. In the case of the bolometer, detector C, the experimental potentials are directly proportional to the sensitivity, S^*, at any bridge current since the absorbed power was constant at 1.15×10^{-8} watt. At low values of the bridge current, there is relatively little effect of temperature on sensitivity (in fact, as the current approaches zero, the sensitivity approaches zero at any temperature). As the temperature of the bolometer wire is raised by increasing the bridge current, the temperature effect on the sensitivity becomes very marked as shown by values of 74.7, 135, and 319 volts/watt for a bridge current of 2.80 ma at 298°, 205°, and 96°K, respectively. Except for the very large difference in absolute values, the change of sensitivity with temperature for detector C parallels that of detector A. It is the primary purpose of this paper to show that the widely different results which have been observed are sufficiently in accord with theory to permit a reasonably accurate prediction of the effect of temperature upon the sensitivity of a radiation detector of known structural characteristics.

TABLE I. Parameters and constants for calculating Q for detectors A and B.

A. Temperature independent values.

	Detector A	Detector B
σ, watts/deg.⁴-cm²	5.74×10^{-12}	5.74×10^{-12}
S, cm²	0.127	3.48×10^{-3}
ϵ	$0.55=\frac{1}{2}(0.47+0.63)$	0.47
r_1, cm	6.50×10^{-4}	6.50×10^{-4}
r_2, cm	7.50×10^{-4}	7.50×10^{-4}
l, cm	0.178	0.318
L, cm	0.257	0.318
G, ohms	55	55

B. Temperature dependent values.
1. Values common to both detectors.

	298°K	205°K	96°K
K_1, watts/deg.-cm	0.242	0.206	0.163
K_2, watts/deg.-cm	0.171	0.151	0.124
$\|P\|$, volts/deg.	6.44×10^{-5}	4.89×10^{-5}	3.08×10^{-5}
ρ_1, ohm-cm	5.01×10^{-5}	5.00×10^{-5}	4.98×10^{-5}
ρ_2, ohm-cm	7.07×10^{-5}	6.84×10^{-5}	6.57×10^{-5}

2. Detector resistance, R.

	298°K	205°K	96°K
Detector A	20.0 ohms	19.6 ohms	19.2 ohms
Detector B	24.7	24.2	23.7

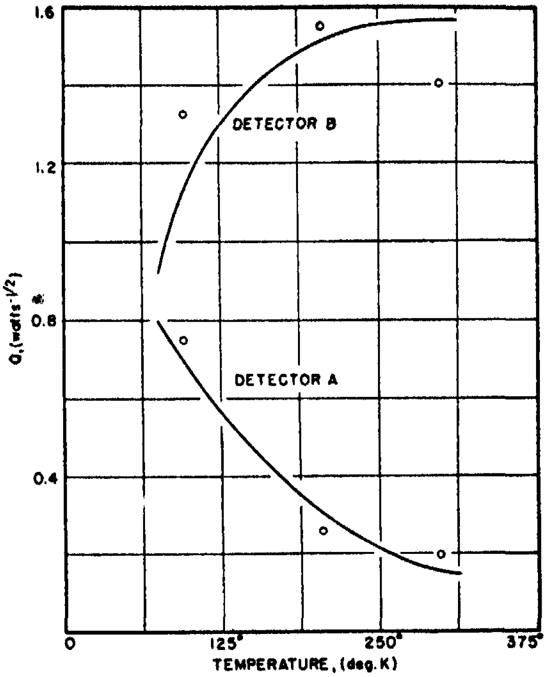

FIG. 6. Theoretical and experimental sensitivities of radiation thermocouples.

Before comparing theoretical and experimental

TABLE II. Parameters and constants for calculating Q for detector C.

A. Temperature independent values.

E, watts $= 1.15\times10^{-8}$
S, cm^2 $= 8.4\times10^{-4}$
r, cm $= 1.37\times10^{-4}$
r', cm $= 2.8\times10^{-4}$
$l(=L)$, cm $= 0.476$
N, ohms $= 51.00$

B. Temperature dependent values.

	298°K	205°K	96°K
α, deg.$^{-1}$, $\times10^3$	3.55	5.30	15.6
R_0, ohms	87.99	58.93	23.01
ρ_0, ohm-cm, $\times10^6$	10.9	7.30	2.85
K_0, watts/deg.-cm	0.700	0.682	0.767

results, the observed sensitivities must be put into the form of Eq. (7). The case of detectors A and B, which must be considered separately from that of detector C, will be treated first.

Since the responses of the radiation thermocouples were measured as open circuit potentials, no current flowed through the galvanometer and the Peltier-heat effect given in Eq. (4) was absent. Under these conditions, a somewhat larger value of $\langle\Delta t\rangle_{Av}$ results from a given power absorption by the detector and the open circuit potential, V_{exp}, is somewhat larger than V as defined in Eqs. (5) or (11). In practice, however, the magnitude of $(P^2\langle T\rangle_{Av})/(G+R)$ or $(1.5P^2\langle T\rangle_{Av})/(G+R)$ is negligible in comparison with the other terms in Eqs. (8) or (12), so that the value of V_{exp} differs negligibly from V and the experimental value of Q for comparison with theory may be written

$$Q_{\mathrm{exp}}=\frac{V_{\mathrm{exp}}}{E(G+R)^{\frac{1}{2}}}=\frac{S^*}{(G+R)^{\frac{1}{2}}} \qquad (17)$$

where S^* has been previously defined as the open circuit potential produced by unit power absorption and is therefore equal to V_{exp}/E.

Before theoretical Q values can be calculated from Eqs. (8) or (12), it is necessary to have values of P, K_1, K_2, and R as functions of temperature. A constantan-Chromel P thermocouple was calibrated from 76.9°K to 300°K and the results represented by the equation

$$V=(10.26-0.0149T-8.30\times10^{-5}T^2)\times10^{-3}\text{ volt} \qquad (18)$$

so that the desired relation for P becomes

$$dV/dT=P=-(0.0149+16.60\times10^{-5}T)\times10^{-3}\text{ volt/deg.} \qquad (19)$$

In calculating numerical values of P from Eq. (19), the results are expressed as absolute values in order to obtain positive sensitivities from Eqs. (8) or (12).

Eucken and Dittrich[8] give values of the thermal conductivity, K_1, and resistivity, ρ_1, for samples of constantan which were subjected to a variety of annealing and working treatments. Since the sample which they describe as "strongly deformed" was judged to correspond most closely to the bare drawn, unannealed wires which were used in detectors A and B, it was decided to use the values which they give for this sample, namely: at 80°K, $K_1=0.157$ watt/deg.-cm, $\rho_1=4.98\times10^{-5}$ ohm-cm; at 273°K, $K_1=0.232$ watt/deg.-cm, $\rho_1=5.01\times10^{-5}$ ohm-cm. Values at the desired temperatures, 298°, 205°, and 96°K, were obtained by linear extrapolation and interpolation. In the case of Chromel P, the literature provides insufficient information on K_2 and ρ_2. However, the values $K_2=0.189$ watt/deg.-cm at 373°K and $\rho_2=7.06\times10^{-5}$ ohm-cm at 293°K were given by the manufacturer as appropriate values for the wire which was used in the construction of the detectors. The temperature coefficient of resistivity was determined experimentally from measurements of the resistance of a sample of Chromel P and values of ρ_2 were computed from the relation

$$\rho_2(T)=7.07\times10^{-5}[1+3.98\times10^{-4}(T-298)]\text{ ohm-cm.} \qquad (20)$$

Values of K_2 were then obtained by assuming that, at any given temperature, the Wiedemann-Franz

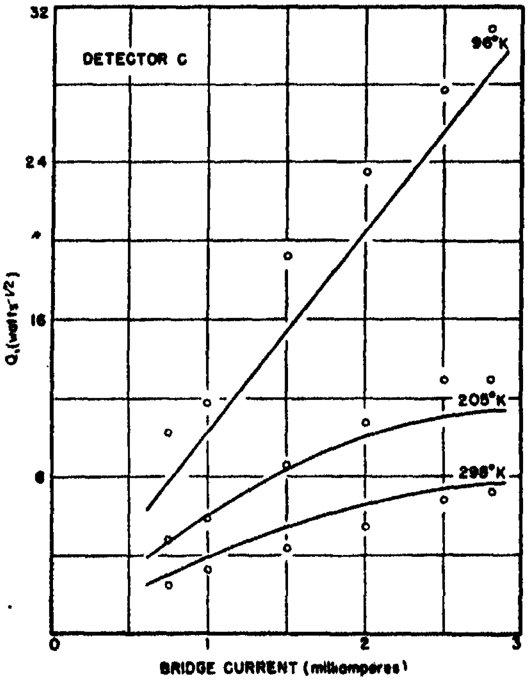

FIG. 7. Theoretical and experimental sensitivities of bolometer.

---

[8] A. Eucken and K. Dittrich, Zeits. f. physik. Chemie 125, 211 (1927).

relation could be expressed by

$$K_1\rho_1 = K_2\rho_2. \tag{21}$$

The reliability of this method of estimating K_2 appears to be confirmed by the fact that it predicts a value at 373°K which is within 1 percent of that given by the manufacturer. The desired values of the detector resistance, R, were computed from the ρ_1 and ρ_2 values since the electrical lengths and radii of the constantan and Chromel P wires were known.

Numerical values of all the parameters and constants which are required for the calculation of Q as a function of $\langle T\rangle_{Av}$ are collected in Table I.

A comparison of calculated and experimental values of Q for detectors A and B is shown in Fig. 6 where the curves correspond to values calculated from Eqs. (8) and (12) and the points to values from Eq. (17). For detector A, the average absolute deviation between calculated and experimental sensitivities is 15.6 percent, and for detector B, 9.7 percent. This agreement is considered satisfactory in view of the extremely large difference in the values of Q_{exp} for the two detectors, both with respect to absolute values and temperature dependence.

The procedure for calculating the average absolute temperature, $\langle T\rangle_{Av}$, of the bolometer wire at any network current, and the theoretical value of Q as a function of $\langle T\rangle_{Av}$ from Eq. (13) has been presented in detail.[5] Results for the present bolometer will be given without repetition of derivations or explanations which appear in the original reference.

Table II lists all the parameters and constants which are required for calculating experimental and theoretical values of Q. The entries for α, ρ, and K have been obtained by graphical interpolation of results for platinum given by Rolf.[9] Table II does not include σ, $\epsilon(=0.47)$, and G since these appear in Table I.

A comparison of calculated and experimental values of Q for detector C is shown in Fig. 7 where, for simplification in plotting, the bridge current, rather than the average bolometer wire temperature, $\langle T\rangle_{Av}$, has been used as the abscissa. The relation between $\langle T\rangle_{Av}$ and bridge current for the three ambient temperatures of the bolometer (entered as $\langle T\rangle_{Av}$ for zero bridge current) is shown in Table III.

TABLE III. Values of $\langle T\rangle_{Av}$ as function of bridge current.

Bridge current (milliamperes)		$\langle T\rangle_{Av}$ (deg. K)	
0	298	205	96
0.75	303.0	211.3	101.5
1.00	306.5	216.4	106.4
1.50	317.2	229.6	121.2
2.00	330.5	248.0	145.0
2.50	345.6	268.5	176.5
2.80	356.0	282.1	196.0

The curves in Fig. 7 correspond to values calculated from Eq. (13), and the points to values calculated from the relation

$$Q_{exp} = \frac{2V_{exp}(G+R)^{\frac{1}{2}}}{E(R+N+2G)} = \frac{2S^*(G+R)^{\frac{1}{2}}}{R+N+2G} \tag{22}$$

which has been derived previously. The agreement between calculated and experimental sensitivities for detector C is about as satisfactory as that for detectors A and B, since the average absolute deviation for all the points is 12.8 percent.

The present results can be summarized in qualitative terms as follows:

The steady-state sensitivity of a vacuum radiation thermocouple may be expected to increase with decreasing temperature if it has a very large receiver area (detector A), and therefore, at room temperature, loses most of its incident energy by radiation. The increase in sensitivity will be due to the diminution of this radiation loss at the lower temperatures. It must be remembered, however, that the decrease of thermoelectric power of the thermocouple with decreasing temperature will tend to offset the advantage gained from the decreased radiation loss. As a result, a vacuum radiation thermocouple with a very small receiver area (detector B) which, at room temperature, loses little of its incident energy by radiation, may be expected to gain relatively little sensitivity, or actually to lose sensitivity, with decreasing temperature.

The steady-state sensitivity of a vacuum wire bolometer (detector C) may be expected to increase with decreasing temperature due primarily to the decrease of bolometer resistance at the lower temperatures. If the radiating area of the detector is large (as in a ribbon bolometer) the decrease in radiation loss with decreasing temperature will augment the effect of decreased resistance and result in a still larger increase in sensitivity.

---

[9] P. Rolf, Phys. Rev. 65, 187 (1944).

THE REVIEW OF SCIENTIFIC INSTRUMENTS VOLUME 20, NUMBER 6 JUNE, 1949

Physical Instruments for the Biologist

Detlev W. Bronk
Associate Editor in Charge of this Section
Eldridge Reeves Johnson Foundation for Research in Medical Physics,
University of Pennsylvania, Philadelphia, Pennsylvania

Modified String Flowmeter for Measuring Breath Velocity

H. SPECHT[*] AND H. F. BRUBACH[**]
Laboratory of Physical Biology, Experimental Biology and Medicine Institute, National Institutes of Health,
U. S. Public Health Service, Bethesda, Maryland

(Received October 18, 1948)

An instrument is described which measures instantaneous breath velocities without incurring high flow resistances. It records reciprocating flows, such as those of the full breath cycle, within the limits of normal breath velocities with high frequency resolution and yields accurate and reproducible measurements when suitably calibrated. The system described incorporates an automatic control over a valve system insuring directed flow of the respired gases through a closed breathing circuit, permitting measurement of breath velocities at simulated high altitudes. The advantages, disadvantages, and idiosyncracies of this type of instrument as used in physiological measurement are discussed.

IN the course of work requiring measurement of breath velocities a flowmeter has been developed in this laboratory patterned after that constructed by Lee and Silverman[1] but with modifications which permit its use at low atmospheric pressures, as in a decompression chamber where pure oxygen must be supplied to the subject, for the recording of expiratory and inspiratory flows in a continuous fashion. This instrument, although largely a composite of equipment components already at hand in the laboratory, has certain characteristics which may be of critical interest to others contemplating work in this field. It is recommended that reference 1 be read for details of structures common to both instruments, and their aerodynamic characteristics.

CONSTRUCTION

The apparatus, as used to collect data on breath velocities at different densities of inhaled gases,[2] consists grossly of a mask, flowmeter unit, valve, and connecting tubing as shown in Fig. 1. The spirometer and carbon dioxide removing filter are not shown.

A McKesson Metabolor type mask (*A*) is fixed in a stand in such a manner that pressing the face into the inflated rim (*B*)[***] will not deflect the flowmeter unit from the optical path directed to the recording system. The mask provides for nasal breathing but does not preclude mouth breathing if the subject cannot properly breath through his nose. The opening (*C*) in the mask for the passage of the breath is made directly before the subject's nose and mouth, but some deflection of the breath is unavoidable due to the fact that the lead-off is horizontal. The subject sits before the mask on an adjustable seat integral with the mask stand and flowmeter bench so that head position in the mask is comfortable with the spine erect. A second opening (*D*) in the mask, approximately in a direct line with the air stream from the nose is provided for a control unit to be described subsequently.

The mask and valve unit are hermetically integrated with the flowmeter unit by means of thin-walled rubber tubes (*E*) made of dental dam which serve to isolate the flowmeter unit from shock or vibration. The gap between these units covered by the tubing is about one millimeter.

The flowmeter consists of a 1.25-inch i.d. brass tube (*F*) which is placed in the breathing circuit as an integral part through which all air entering or leaving the mask must pass. It is made 10 diameters long to minimize turbulent flow during quiet breathing. This is aided by a set of collimating surfaces (*G*) placed in the ends of the tube to correct cross currents due to irregular inflow from the mask and valve. These collimators are made from a one inch ribbon of brass shim stock folded into a screen with approximately hexagonal openings about 5 mm in diameter. At right angles and passing through the axis of the tube midway in its length is a fine nickel wire (*H*) (0.001-inch diameter) which is deflected by the air passing through the tube. At right angles to the tube and to the axis of the wire a pair of opposing windows (*I*) permits the passage of a beam of light focused in the plane of the wire. The shadow thrown by the wire is optically magnified and photographically recorded. The wire is constructed long enough (*ca.* 20 cm) to allow angular displacement at the points of suspension to be negligible with the maximum deflection expected in use. The wire is suspended vertically from an adjusting head and is maintained under tension by a small tungsten spring (*Y*) (filament from a flashlight bulb) similar to the method used in reference 1. Free oscillation of the wire is effectively prevented without recordable effect on the timing of the response by passing it through 3 drops of spermacetti oil each suspended in a small wire loop surrounding the wire. These damping droplets (*Z*) are spaced in such a manner as to affect the larger harmonic oscillations that might be expected to interfere grossly with the legibility of the respiratory velocity pattern.

---

[*] Senior scientist.

[**] Technologist.

[1] R. C. Lee and L. Silverman, Rev. Sci. Inst. **14**, 174 (1943).

[2] Specht, Marshall, and Hoffmaster, Am. J. Phys. **157**, 265 (1949).

[***] In order to prevent excessive inflation at altitude due to the change in barometric pressure the rim of the mask was evacuated and then snugly filled with water, providing a good fit to the face under all our experimental conditions.

The source of illumination (*J*) was first a Hanovia Labarc unit which gave enough visible light for inspection of the projected image and made good photographic records. It also served to give very fine time lines, inasmuch as the light is interrupted twice during each cycle of the voltage change in the current supply. Later, a motion picture projection lamp replaced the Labarc and has been found quite satisfactory for recording. A Pyrex #3966-M-829 heat filter (*K*) is interposed between the source and the focusing lens (*L*) to reduce the heat transmitted by the projection lamp. The focusing lens is mounted on the frame of the flowmeter on an adjustable bracket, and the focal point of the source adjusted to maximum brilliance on the wire within the expected limits of deflection.

The shadow of the wire is projected by means of a telescope system (*M*) giving about 350× magnification and a field large enough to cover the maximum expected deflection of the wire. In this instance this is achieved by using the inner element (*N*) of an old Leitz #5 microscope objective and the focusing element (*O*) of a motion picture projector lens system mounted integrally on an optical bench with the flowmeter and the light source. It was found desirable to install a ring-shaped warming element (*P*) at the telescope window of the flowmeter in order to prevent condensation of the breath moisture on the window. Heat from the source is apparently sufficient to prevent fogging of the opposite window.

Photographic registration is made by means of a long paper camera (*Q*) fitted with a cylindrical lens (*R*) of about 2-inch aperture in order to gather sufficient light for proper contrast on the photographic paper.

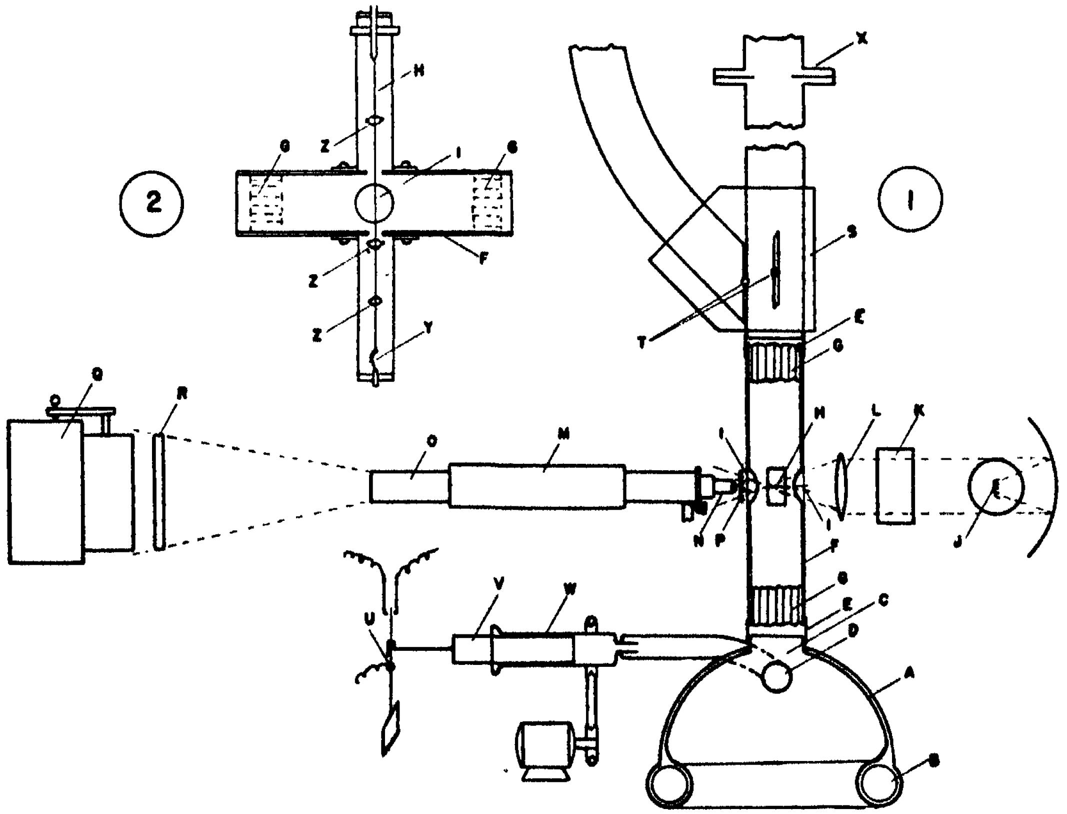

Fig. 1. Schematic layout of flowmeter and accessory devices (1) and a vertical detail of the flowmeter unit (2). See text for description of labeled parts.

Since a record of both expiratory and inspiratory flows was desired it was decided to use the same instrument for both measurements, thus eliminating discrepancies in timing between separate instruments. This choice necessitated a valve (*S*) distal to the flowmeter and thus introduced dead space whose effect must be recognized.†[3]

In the interest of reducing the resistance of the circuit, a valve was developed which does not require the force of the breath for closure except in that it initiates this action. This valve offers a very low resistance to all flows in the range we encountered. It is completely open to inspiration or expiration as alternately set by the breath pressure. The valve is a gang-connected butterfly doublet (*T*) mounted in a block bored for the breathing circuit. It is moved by a spring opposed solenoid. The latter is energized by a breath pressure switch (*U*) of special design, requiring only minute pressure differences to be operated. Inspiration is arranged straight through the valve and expiration at an angle of 45°.

The timing of the automatic valve is adjustable. In most instances it was loaded in the direction of automatic operation after expiration, thus anticipating the following inspiration. Many patterns show a vibration mark at the instant of valve action, and thus we were able to calculate the efficiency, a measurement which is not possible with other types of valves during use. The inherent lag of this system is about 1/10 second, and at rest, the breath patterns indicate a 50 cc backflow. This

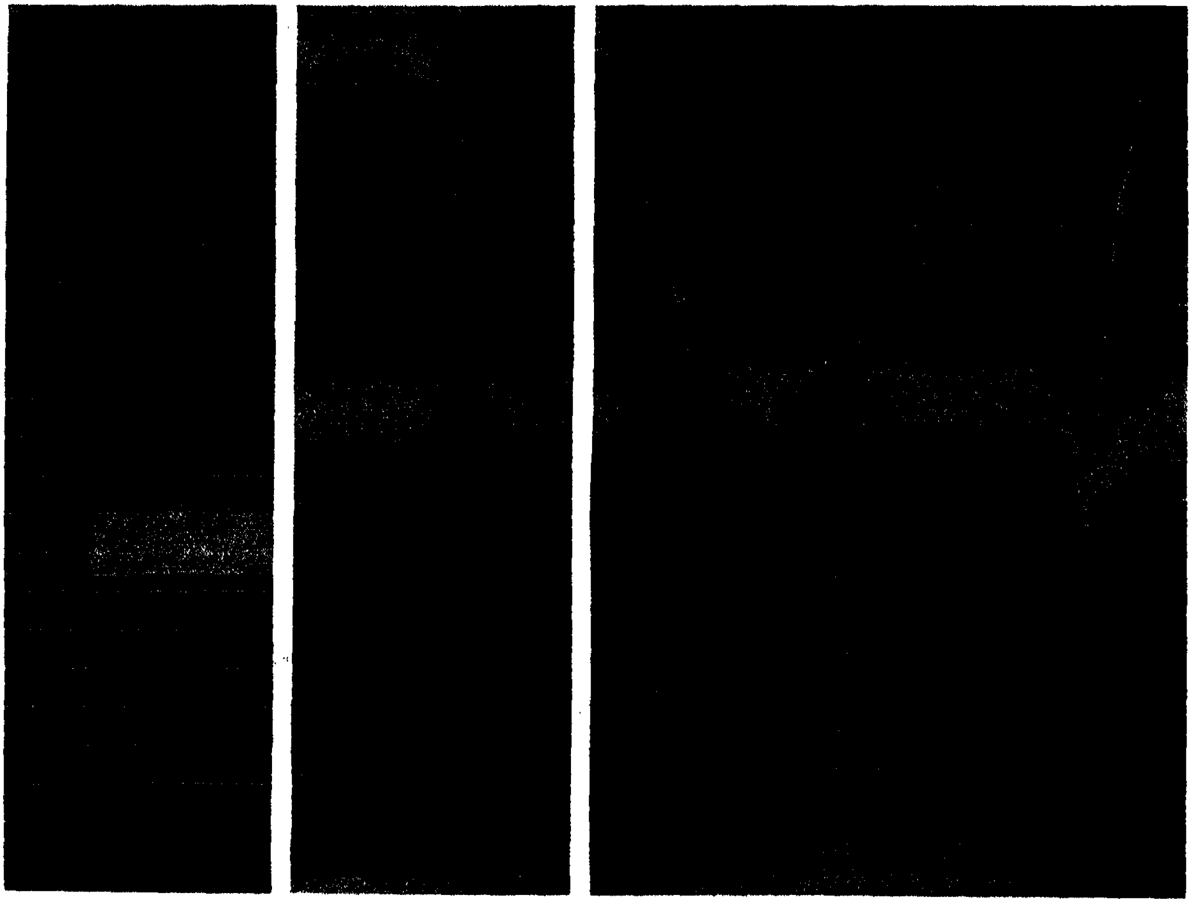

FIG. 2. (a) Trace of the response of the flowmeter to mechanical deflection, i.e., restoration from half-scale deflection. The displaced position is above the upper margin of the figure and the first trace is only faintly seen. Four reversals are distinguishable before the resting position is assumed. The period is about 1/80 second. Time lines of 1/240 sec., alternately black and white, form the background of the figure. (b) Trace beginning at upper left shows the displacement of a plunger in a cylinder connected to the flowmeter. Trace beginning at the center of the figure shows the response of the flowmeter to the air movement induced by the plunger. The upward sweep of the first trace has no counterpart in the flowmeter trace since it was caused by accidental parting of the connecting line. (c) Same as (b) but at somewhat slower rate of displacement. Ink lines show the beginning and end of plunger displacement and, in the first displacement, the attainment of maximum velocity is marked by an ink line across both traces.

---

† Data presented by Stannard and Russ (see reference 3) on the effects of added dead space of about 150 cc, slightly more than the volume of this flowmeter, resulted in a gain of about 16 percent in the tidal volume, but they found no consistent effect on the breathing rate.

[3] J. N. Stannard and E. Russ, J. App. Phys. 1, 326 (1948).

is comparable to that given for sensitive rubber valves developed for similar purposes.[1] In common with the latter, efficiency rises with ventilation.

The valve is actuated by a relay system tripped through a switch operated by the breath pressure through the floating plunger (*V*) of a rotated dry syringe barrel (*W*)[4] connected to the mask aperture (*D*) mentioned earlier. This control system can be balanced or unbalanced to anticipate either inspiration or expiration. In its final form it is arranged to reset itself for tripping the valve at the earliest possible moment after reversal of the breath velocity.

The valve openings are connected distally to a closed oxygen circuit of 1.25-inch rubber tubing disposed in such a manner as to avoid sharp turns and connect with a recording spirometer which has a CO$_2$ absorption filter in the exhalation line. An adjustable iris diaphragm (*X*) for selected resistance in the inspiratory line was provided for demonstrating effects of high resistance on the breath velocity pattern.

OPERATING CHARACTERISTICS

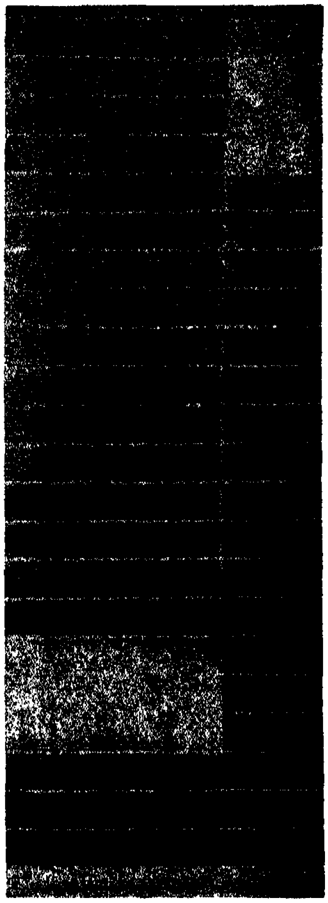

FIG. 3. Response of the flowmeter to a stepwise change in airflow, from about 30 to 100 liters per minute. Time for the change is 0.04 sec.

The natural period of the wire and spring is very short (*ca.* 1/80 sec.) and with damping shows a 95 percent restoration from half-scale deflection within 1/20 second, as shown in Fig. 2(a). It will be seen here also that the first crossing of the baseline occurs within 1/240 second of release. Figures 2(b) and 2(c) show the record of the manual displacement of a piston and the concomitant response of the wire. In Fig. 2(b) the piston marker was accidentally released at the end of the stroke showing an upstroke which is spurious. Figure 2(c) shows a similar run at a slightly slower rate of movement and then a return movement at a still slower rate. Vertical lines have been drawn to indicate the correspondence of the beginnings and endings of the piston movements and in the first stroke the time of attainment of peak velocity is marked by a vertical line. Figure 3 shows the response of the wire to a step change in flow, *ca.* 30 to 100 *L*/min., which was effected by clapping a flat plate over a bypass duct as air was drawn through the flowmeter. The time from low to high flow is about 0.04 second. Our calibrations of this wire as illustrated in Fig. 4 show it to be linear only on log-log plot. This would be in contrast to the findings of Lee and Silverman,[1] who assume linearity on arithmetic coordinates, if it were not a matter of degree, since they actually show certain deviations from linearity and dismiss them as minor. It is likely that the magnitude of this deviation is dependent on the wire diameter and spring characteristics which are obviously not the same in the two instruments. Our calibrations were made with a rotameter whose range is indicated by the data in Fig. 4. Readings at the low flows cannot be made accurately and thus account at least in part for gross internal inconsistencies. It is seen, however, that the curves form well-defined families which indicate good internal consistency over the rest of the range. These considerations led us to calculate regression lines for each calibration run and to base our flow measurements on such derived curves. It was found necessary to make calibrations for each day that experiments were run because there were real but unpredictable changes in the level of response of the wire as shown in Fig. 4 by the families of unbroken and broken lines, respectively, taken on 5 different days. There are several probable causes of these changes, the most frequently applicable being temperature changes which alter the spring tension, and relaxation of the spring suspension through constant stress. It was also found accidentally that otherwise unaccountable changes in shadow width of the wire were related to deposition of material on the wire either during use or in calibration. This was most easily recognized after the calibrating gas source had been drawn through the CO$_2$ filter bed

---

[4] H. F. Brubach, Rev. Sci. Inst. 18, 363 (1947).

TABLE I.

	Expiration	Inspiration
20 *L*/min.	1.4 mm H_2O	1.1 mm H_2O
40	2.2	—
50	3.9	2.0
70	5.8	3.0
80	7.5	—
100	9.0	4.0

inadvertently. In this instance, a noticeable deposit could be removed from the wire with a fine brush. While this was a gross effect, it is possible that the moisture carried over the wire by the exhaled breath may cause the accretion of particles, or solids in solution, on the wire which alters its resistance to air flow.

It was found necessary to make separate calibrations for opposed flows as shown in Fig. 4; unbroken lines being "inspiratory" and broken lines being "expiratory" calibrations. The observance of respective zero positions as shown in Fig. 2(c) was also necessary. This change in resting position is a common difficulty with lightly stretched suspensions which are required to pass through the zero position, as in the registration of deflections of opposite sign. This behavior of the wire was not due to the damping system used here since such displacements were also observed and recorded when the oil droplets were absent. Although the magnitude of this effect may not be great, it should be recognized in all cases where the wire is allowed to come to rest before registering an opposed flow, as is the case in breath velocity patterns in which a post-expiratory pause is interposed, as shown in Fig. 5(b) and 5(d).

Measurement of the overall flow pressure from mask to spirometer with a series of constant flows through a rotameter in place of the subject was made with a slant manometer. "Expiration" pressures were measured across the circuit including the CO_2 filtering bed, while "inspiration" pressures were measured only across the duct and flowmeter. The pressures at the several rates of flow are given in Table I.

Measurements with oxygen instead of air gave essentially equivalent values indicating that orifices in this system were large enough to have only a negligible influence with this difference in density at the flows tested. It should be emphasized that the velocities in exercise may reach beyond the range indicated. The calculated critical velocity for turbulent flow for the flowmeter tube is 48 *L*/min., which happens to coincide with the break in slope of the expiratory pressure-flow table values. We feel that this is fortuitous, since the inspiratory pressure drop values follow a linear course. It is likely that the change in slope of the expiration values is due to characteristics of the CO_2 filter

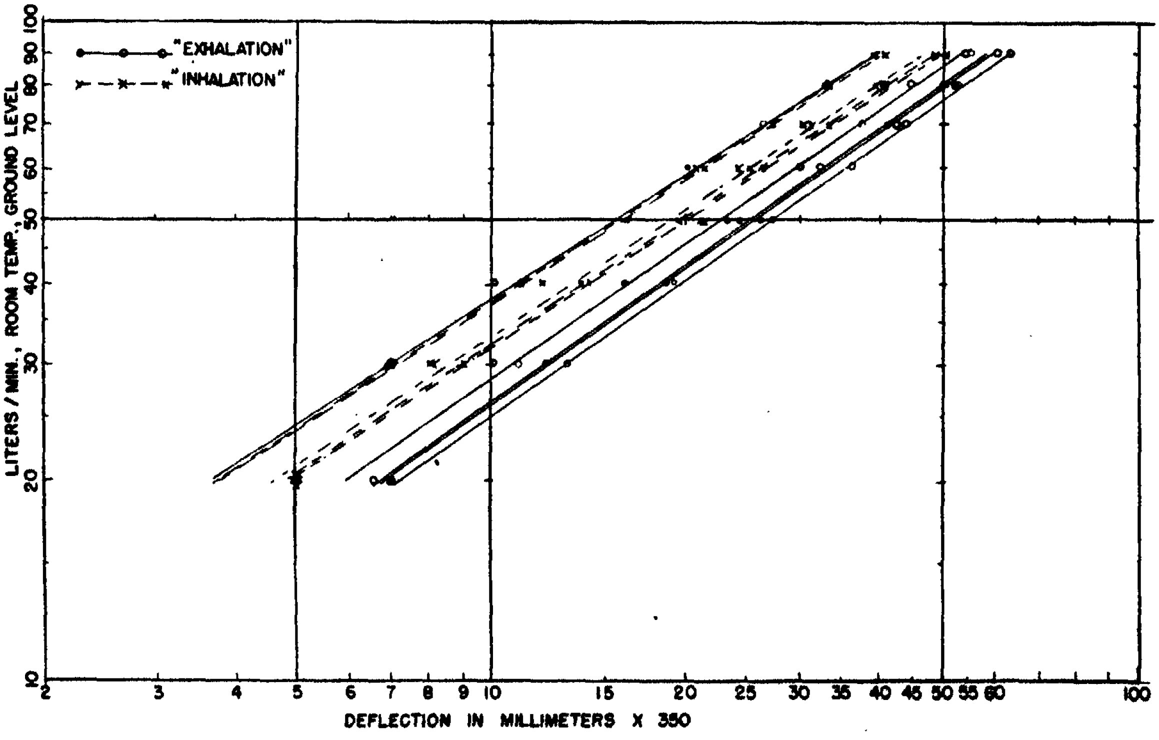

FIG. 4. Sample calibrations of the flowmeter for five different days. Calibrations were made with a rotameter covering the whole range shown on the ordinate. Pairing of exhalation and inhalation data is not indicated in the figure but the relatively independent variation of these values is indicated by the position of one set of exhalation values at the extreme left of the whole group.

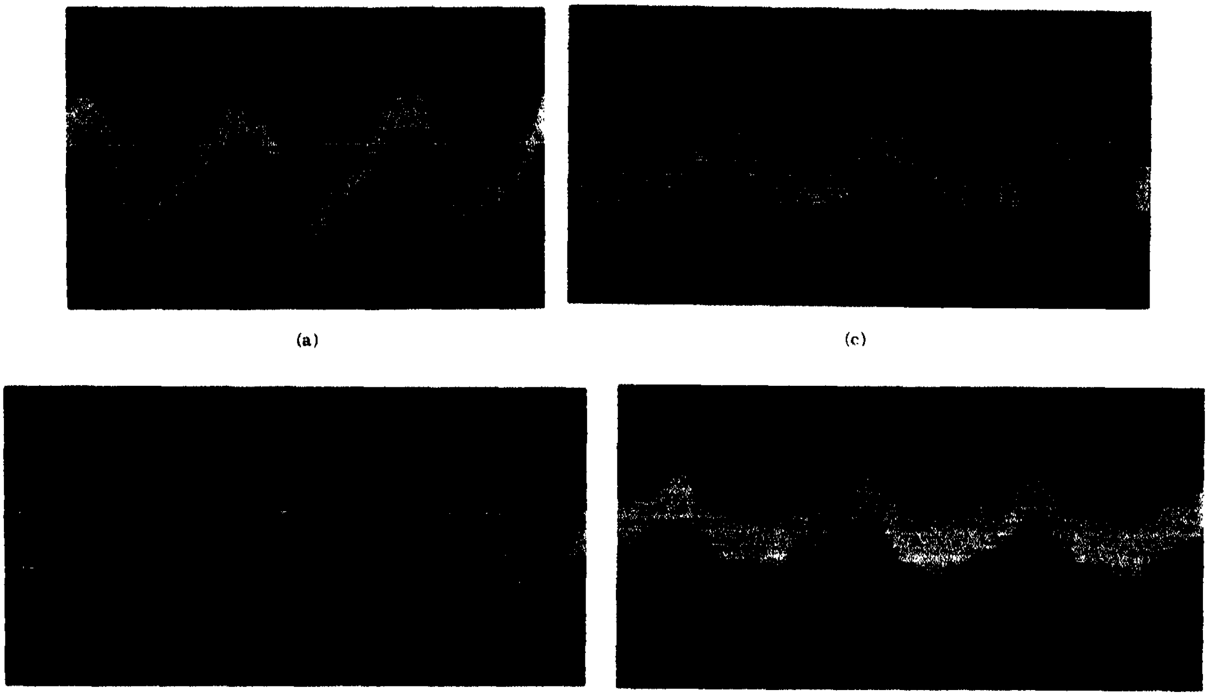

(a) (c)

(b) (d)

FIG. 5. Breath velocity patterns made on each of two subjects in full oxygen at ground level (a and c) and at 30,000 feet simulated altitude (b and d). In each record the upper margin of the shadow trace is to be compared to the control level marked by a grid line superimposed on the 5 mm uniform grid. Time, in seconds, proceeds from left to right. Inhalation rises and exhalation falls below the control level. The sensitivities of the ground level and altitude deflections differ, the latter being the less sensitive; maximum velocities for inhalation and exhalation respectively are (a) 52 and 58 *L*/min., (b) 80 and 96 *L*/min., (c) 40 and 35 *L*/min., (d) 38 and 42 *L*/min. It is to be noted that in the altitude records (b and d) there appears a protracted arrest of the breath flow after exhalation.

bed. There is little reason to believe that the flow pressures throughout the range usually encountered in exercise (up to *ca.* 120 *L*/min.) would be greater than a linear extrapolation of the values given here. It is not clear, however, that pressures exerted by constant flows are comparable to those encountered in intermittent flows such as the breath cycle presents. Apparatus for measuring such transient pressures accurately has not been available to us, but our attempts to compare the velocity patterns from pressure-drop methods as devised by Silverman, Plotkin, and Lee,[5]†† to those from the wire deflection method used here show that transients are seriously damped out, even though the recommended precautions regarding resistance of the pressure conducting lines were fully considered.

We feel, furthermore, that the range of the present instrument is limited in its application not so much through the resistance of its own structure but mainly that of the ducts which are used for various purposes such as in our own experiments.[2] While it is obvious that the diameter of the trachea must itself induce turbulence under these conditions, the mounting pressure drop through the whole test system places additional high and unnatural loads on the physiological mechanisms which are to be studied. Thus it might be possible to work at a higher range of flow values by using larger bores in the flowmeter and ducting but sacrificing sentitivity at low flows since the instrument depends on linear velocity for the deflecting force.

---

[5] Silverman, Plotkin, and Lee, Rev. Sci. Inst. 19, 513 (1948).

†† A portable model built by Warren E. Collins and loaned to us through the courtesy of the Naval Medical Research Institute, U. S. Naval Medical Center, Bethesda, Maryland.

Erratum

The Central Research Laboratories, Inc., Red Wing, Minnesota, has called our attention to an error in publishing the stated range of the pre-focused interchangeable optics for their monochromator. In an advertisement on page xxxvii of the May, 1949, *Review of Scientific Instruments*, the range was given as from 0.15 to 52 microns. The range should have been given as from 0.15 to 25 microns. The publisher was responsible for this error and regrets the inconvenience to readers and to the Central Research Laboratories, Inc., which might have arisen from inquiries based on this error.

Book Reviews

Microwaves and Radar Electronics

By E. C. Pollard and Julian M. Sturtevant. Pp. 426 +vii, Figs. 192, Tables 12. John Wiley & Sons, Inc., New York, 1948. Price $5.00.

The authors of this book have drawn upon their wide experience in the development of microwave radar to put together a survey of the by-products of that tremendous concentration of scientific and technological effort by which the Allies turned a wave-length into a weapon. Their subject is not radar as a function, but the new devices and techniques that comprise, in patent language, the radar art, with special emphasis on the role of these techniques in postwar research. One chapter near the end of the book contains an explanation of the elements of the radar problem, illustrated by a few typical radar systems, but the rest of the book is devoted to magnetrons, klystrons, wave guides, pulse circuits, cathode-ray tubes, amplifiers, servo-mechanisms, and so on.

This vast assortment could not have been covered without drastic condensation and many compromises—compromises that will make the specialist wince when he turns to the chapter on his specialty. But the microwave specialist is not the reader the authors had in mind. The success of the book can properly be judged only by the student who turns to it to find out what this elaborate microwave business is all about, and what one can do with microwaves and the circuit tricks of radar that he could not do before. If the student is willing to move rapidly from exhibit to exhibit, accepting ingeniously condensed explanations, he will cover a lot of ground and accumulate a staggering load of facts.

A small amount of misinformation, and several careless statements, will be found along the way: We are told that "waveguide does not have the property of a guaranteed mode of excitation which is so useful in a coaxial line" (p. 112); the field configuration in the celebrated TE_{01} mode is misrepresented in Fig. 4.13; an antenna matching device is said to do two *different* things, (a) cancel the reflection, (b) build up the intensity so that all the power can be radiated—hence two variables are needed (p. 100); "Like charges should repel, but the observed fact is that moving charges attract one another" (p. 7). Another small fraction of the information is now obsolete, which is not surprising, but it is surprising that in a book described as a "postwar book on postwar problems" such flat statements as the following should be left unqualified: "Powers up to 3 megawatts in pulse form at 9 centimeters or longer, or 30 kilowatts at 1 centimeter, can be obtained with magnetrons."

Much of the book, in short, reads like a 1945 status report; the authors are describing the trees, not the woods or the vistas beyond. They have not entirely abandoned the point of view of the radar systems engineer who is concerned mainly with what a piece of "plumbing" will do, not why it does it. In its relation to the electronic art, the cathode is one of the most remarkable and important parts of the magnetron; in the 14-page section on magnetrons the cathode is allotted two or three sentences, one of which describes it as the source of r-f energy! The section on crystal detectors begins, "Crystals are usually mounted in a special cartridge, one of which is illustrated in Figure 4.1", and continues in the same vein. No hint here of the intense research in the physics of semiconductors which has led to the widely used germanium diode and, more recently, the transistor.

Despite their shortcomings, these chapters do give as compact and fast-moving an account of a rich field as could well be devised. The figures are abundant and excellent; carefully selected and condensed explanations of the basic electromagnetic theory are inserted where they will be most helpful. The very comprehensive index—so complete as to include the entry "main bang"—is a substantial asset.

In the last two chapters, "Microwave Communications," and "Microwaves in Physical Research," the authors make good on their promise to give us a glimpse in the direction of future developments. Certainly much remains to be done to exploit the microwave art for communication purposes as fully as it was exploited for radar. It is good to see an adequate description of the experiments of the pioneers in microwave spectroscopy, Cleeton and Williams. Pollard and Sturtevant also explain the peculiar feature of the ammonia molecule that accounts for its unique role in the story of microwave spectroscopy. The Lamb-Retherford experiment gets only two sentences, however—surely a perfunctory treatment of the most important physics experiment the microwave development has yet fostered. The inclusion of a good discussion of thermal radiation at radiofrequencies, and of Dicke's microwave radiometer, was an excellent idea, for the implications of this work are not yet widely appreciated. All of this material, together with brief discussions of microwave particle accelerators and microwave measurements of superconductivity, will certainly leave the reader sharing some of the authors' enthusiasm for the shiny contents of our new toolbox.

E. M. Purcell
Harvard University

Rocket Propulsion Elements

By George P. Sutton. Pp. 294, Figs. 130. John Wiley & Sons, Inc., New York, 1949. Price $4.50.

The major new developments of World War II—atomic bombs, radar, proximity fuzes, and rockets—were produced without benefit of standard text books and reference books on these subjects. In the first three cases this is understandable since the basic principles underlying these developments had been discovered in the years just preceding the beginning of the war. In the case of rocket aircraft and ordnance it may appear surprising as the fundamental principles of rocket propulsion have been known for many years. The answer is of course to be found in the fact that prior to World War II the number of professional scientists and engineers interested in rocket propulsion was very small. Rocket development was largely pursued by amateurs primarily interested in space navigation. Few schools presented courses in the subject and thus there was no great demand for textbooks, and in fact, there were no teachers with teaching experience in the subject to write them.

The situation is considerably different at the present time but only a few textbooks for undergraduates and first-year graduate students have appeared since the war, presumably because of security restrictions. One of these few texts is *Rocket Propulsion Elements, An Introduction to the Engineering of Rockets*, by George P. Sutton, Supervisor, Propulsion Development, North American Aviation, Inc. and Instructor, University Extension, University of California. Even in this book as noted in the preface, "The text and the figures have been submitted and checked by military authorities. This requirement limited in part the amount of experimental and calculated data which could be presented, since a large part of the technical information on this subject cannot be published for security reasons." Nonetheless, the book brings together many of the fundamental mechanical, thermodynamic, thermochemical, and ballistic principles which were known at the start of World War II as well as some applications developed during the war which are no longer classified. As such it will be very useful in the instruction of present-day students on whom to a large extent our future security depends.

The treatment of nozzle theory and thermodynamic relations and of rocket propellant performance is conventional, but the material on these subjects is presented in an excellent manner for the student familiar with the basic physical, chemical, and engineering laws who is approaching rocket problems for the first time. No attempt is made to derive or to elaborate upon the fundamental laws but the application of these laws to rocket propulsion is made directly and discussed in some detail. Copious references to existing texts on the basic principles are given.

The major portion of the text is devoted to rocket devices employing liquid propellants, three chapters being devoted to the propellants, motors, and feed systems of such devices. The treatment of solid propellant rockets in the final chapter is admittedly sketchy. The chapters on flight performance and rocket testing are satisfactory for an introductory text.

Unfortunately the treatment of the basic mechanism of rocket flight given in the first chapter is not too well done. Momentum is correctly defined as mass times velocity, but the quantity called momentum in Eq. (1-1) is actually the impulse transmitted to the rocket per second. To make the confusion complete, momentum is given the units of ft.-lb. at the end of the chapter when it should be in lb.-sec. or slugs-ft./sec. The difficulty arises from the fact that mass flow rate rather than mass appears in the equation for the force on the rocket. In addition, the discussion of efficiencies which are rarely used in designing rocket units will only lead the student into the apparent paradoxes which always arise in this connection without being explicit or detailed enough to be of real help. The efficiencies defined are all instantaneous efficiencies dependent on instantaneous power considerations and yet they are all defined initially in terms of relative energy values.

The book contains a considerable number of good illustrations and there are many tables of data. There are good problems and a summary of symbols at the end of each chapter. English engineering units are used consistently throughout. The sketch of rocket history in Chapter II is readable and interesting. With the exception of the points noted above, the book is an excellent one and should be of wide use in introductory courses on rocket aircraft and ordnance.

William A. Fowler
California Institute of Technology

The Optical Principles of the Diffraction of X-rays

By R. W. James. Pp. 623+xv, Figs. 217+vii, 22×14 cm, Vol. II of *The Crystalline State* edited by Sir Lawrence Bragg. The Macmillan Company, New York, 1948. Price $17.50.

Under the title *The Optical Principles of the Diffraction of X-rays*, Professor R. W. James of the University of Cape Town has written the second volume of the series entitled *The Crystalline State*, originally planned and edited by W. H. and W. L. Bragg and now continued under the editorship of W. L. Bragg. The first volume *A General Survey* covered, as its title implied, the whole field of the x-ray analysis of crystals, and provided a continuation of the series of editions of *X-rays and Crystal Structure* in which the Braggs summarized so elegantly their original researches and those of others into the field of the x-ray analysis of the fine structure of matter.

In this volume, Professor James treats of the basic problem of x-ray analysis. He discusses the way in which the intensities of the x-ray diffraction pattern depend on the arrangement of the atoms within the scattering material and on the quantum mechanics of the electrons within the atoms of that material. His program is comprehensive and he carries it through in a way which is astounding to one who has worked for many years in the study of a few small parts of this large field.

It is impossible within the space and the time allotted to this review to examine critically all the chapters of the present work, even if the reviewer felt himself qualified to do so. The book provides basic material for those who are interested in the use of x-ray diffraction and other diffraction techniques for the determination of the electronic configurations of atoms, and also for those who are completely disinterested in the detailed structure of atoms and are only interested in the gross stereochemistry of large organic and inorganic molecules. It is concerned with the way in which the texture of natural crystals, in their departure from the ideal crystalline state, affects the diffraction phenomena. It is, of course, this last phase of the problem which is the crux of the situation as far as the x-ray analysis of material structures is concerned. We have a fairly complete theory, and Professor James presents it well, of the diffraction of x-rays from a "perfect" crystal. The reader of the book will find himself with a very good summary of the theory and the experimental results of the literature and will be well prepared to find and read the original papers on the subject. We also have a very complete theory of the "perfectly imperfect" crystal and this is also admirably presented here. Of real importance to the subject of x-ray analysis of structures of crystal molecules and of texture problems of the crystals themselves, is the region between the "perfect" crystal and the "perfectly imperfect" crystal, for it is in this region that almost all crystals which can be grown or which occur naturally are to be found. In this section of the book Professor James excels, for he has himself been involved in many of the most fundamental experimental and theoretical investigations in the field. His treatment of the effect of thermal motion seems admirable to the reviewer who has read it largely for his own education, and without any real qualification for criticism.

At the present moment the attitude of the x-ray analyst is that the values of $|F(hkl)|^2$ can be determined from the x-ray diffraction intensities. The only problem which remains is the determination of the phases of the Fourier coefficients $F(hkl)$ of the electron density distribution. Professor James discusses this problem also and gives an excellent summary of the various processes which had been developed up to the time of completion of his manuscript. In the reviewer's opinion, however, the timeliness of this book lies in its application to researches which have been published in the last year and which are now in progress. It now seems that given *accurate* values of $|F(hkl)|^2$, it will be possible in the not too distant future to select by routine procedures, a relatively small number of structures which will be consistent with the x-ray data. The power of the procedures which have been proposed by Harker and Kasper and the generalizations of these methods which are under development by Karle and others will depend on the availability of highly accurate values of $|F(hkl)|^2$. Professor James does not provide the complete secret for such accurate determinations, but he does summarize very completely the work which has been carried out so far in this direction, and the future developments which are needed can well be based on his summary.

Individual research workers in a particular small subdivision of the field covered by this book will undoubtedly be able to criticize it. The reviewer has found one or two places in which his own taste differs from that of Professor James. Objective thought indicates however that these differences are only in methods of treatment and the reviewer gladly forgoes his priviledge of minor criticism in return for the inspiration of the first reading and the tremendous value of the continued use of the book as a reference. Sections of the book will provide potent material for graduate seminars in x-ray diffraction, if the students and the professor are willing to face concentrated material of great importance. The book can be recommended without reservation to any one who has any interest in research in any one of the many fields included in the title.

Technically the book is excellently produced. The reviewer has found only a few typographical errors. The price seems high to one who wishes that the book could reach the hands of many students, but the number of text and plate figures and the number of formulas indicate that the book would be difficult to produce at a lower figure.

A. L. Patterson
Bryn Mawr College

Recent Advances in Biological and Medical Physics

EDITED BY JOHN H. LAWRENCE AND JOSEPH G. HAMILTON. Pp. 450+xi, Figs. 49, Tables 60. Academic Press, Inc., New York, 1948. Price $8.60.

The title of this book is somewhat misleading for the subject matter is concerned not with biophysics but with the application of stable and radioactive isotopes to problems in biochemistry and medicine. The misnomer reflects a growing tendency on the part of biologists and physicists alike to regard biophysics as any biological study which utilizes a mass spectrograph or a Geiger counter as its method of analysis. One might equally well define biophysics as the study of renal function because elaborate physical methods are sometimes employed for analysis of the urinary constituents. Biophysics is more properly concerned with the physical properties of cells and tissues but this is not the subject matter of the volume under review.

Although the title is misleading, this book fulfills an important need for a comprehensive reference source in a field which is expanding with great rapidity. The volume consists of ten chapters, each chapter being written in review form by an outstanding contributor to the field. Five chapters are devoted to those recent advances in the biochemistry of intermediate metabolism, which have been made possible through the use of isotopic tracers. These chapters include the metabolism of carbon and nitrogen in vivo, phospholipid metabolism, the nucleic acids, and the metabolism of iodine and iron. In the opinion of the reviewer, these sections supply the most valuable material of the book. Two chapters are offered on the fundamentals of radioactivity, its nature, production, and detection. Both chapters are masterpieces of condensation, but the scope of the subject is too broad to be clearly presented in 98 pages. The remaining chapters are concerned with clinical applications of radioactive materials to the control of malignancies, with the effects of radiation on the human organism as a whole, and with protection from radiation.

The scientist who is unfamiliar with applications of nuclear physics to biochemistry will find this book valuable as a general survey of the field. From this point of view the book may be particularly helpful to workers in countries which have not, as yet, had full access to the detailed literature. To the biochemist, the book will be constantly useful as a reference source.

JOHN R. PAPPENHEIMER
Harvard University

The Structure of Matter

BY F. O. RICE AND E. TELLER. Pp. 361, Illustrations 77, John Wiley & Sons, Inc., New York, 1949, Price $5.00.

The Structure of Matter is a clear, absorbing, non-mathematical account of the entire broad field indicated by its title. Omitting only a discussion of fundamental particles (which from the point of view of the book are presumably matter without structure), the reader is taken from that simplest form of matter, the hydrogen atom, uniformly into more and complex aggregates to find himself finally dealing familiarly with problems of composition and stability of the stars. The course of this progression to the stars includes the structure of atoms, atomic spectra, the chemical bond and structure of molecules, molecular dipoles, Van der Waals' forces, molecular spectra, the solid state, electric and magnetic properties of matter, radioactivity, and nuclear chemistry.

Naturally this book of 350 pages cannot serve as a reference for the broad field covered, or as a rigorous development, but only as an incisive introduction. It's style and scope reminds the reviewer of Wells' *Pocket History of the World*, where each century of history rushes past—but not before the reader is made to feel he is satisfyingly aware of its true meaning and relation to the entirety of human experience. The book is not a superficial summary of physical and chemical information, but a logical and penetrating presentation of ideas, principles, and results. The authors' thorough familiarity with wide areas of the material covered have enabled them to choose the important ideas, to express them simply and yet accurately, and to correlate and give perspective to the many phases of their account.

Perhaps the most delighted readers will be the trained physicists and physical chemists—even though the book is non-mathematical and very simply written. They will find in *The Structure of Matter* a fascinating and easily read story, new points of view, a general cultural education in physics and chemistry, and some sparks of humor.

The success of this book as a classroom text is debatable. An advanced undergraduate of first-year graduate course based on it would certainly be an interesting and worth while experiment. The words will be easily read by a student of this level. However, quantum mechanics is used as a basis for discussion almost throughout, and many advanced ideas are introduced. The hazards are that in spite of the clarity of style the student may be left breathless by the wealth of new ideas or because of difficulties in assimulation may come to regard the whole discourse as somewhat unreal. He may be better served by a slower and more rigorous approach.

Mathematics is avoided almost to a fault. Although many advanced quantum-mechanical ideas are used and discussed, no mathematics as complicated as a differential equation (including Schrödinger's equation) is involved. This is, of course, contrary to usual practice since students advanced enough in our present educational system to deal with probability distribution, quantum-mechanical resonances, and tunneling effects are usually capable of handling somewhat more mathematics than the authors allow themselves.

As supplementary material for advanced students, *The Structure of Matter* should be readable and valuable. In fact, for most physicists and physical chemists the only unreadable part will be the closing expression of "that's all" in Greek.

CHAS. H. TOWNES
Columbia University

Principles of Radar

BY DENIS TAYLOR AND C. H. WESTCOTT. Pp. 141, 8 in. × 6 in. Figs. 51. The Macmillan Company, New York, 1948. Price $3.50.

This compact little book forms one of a series on modern radio technique which is intended to describe advances in radio technique made during the war. The whole subject of radar is included in this volume which covers essentially the entire British technique ranging from long wave flood lighting radar to microwave radar. The elements of radar beacons are also included, again over a wide range of wave-lengths. Ground and airborne radars are both included.

This is, of course, a very considerable subject to cover and the authors have attempted to present the fundamental features which underlie radar rather than spend much time on the description of specific sets. This is a very desirable approach and indeed a little volume such as this published during the war would have been invaluable to those who were struggling with the whole problem of the wise choice in radar for various purposes. The authors succeed in their aim and the result is a very attractive presentation of the way in which the problems of radar have been solved for equipment over a wide range of wave-lengths.

As an example of topics which are covered simply and adequately, we can include the calculation of maximum range, propagation problems, methods of height finding, and a rather interesting appendix on scattering areas.

By way of a certain amount of criticism, one wonders why the book is so entirely confined to techniques which are primarily British. There is no doubt that the British contribution to radar was the most significant and of the first magnitude, still there did result methods which are present in American sets which could have been included to make the book more complete. For example, there is no mention of rapid scanning radar such as the GCA or the APQ7, both of which represent important contributions to radar methods. This slant in the direction of British methods is also expressed in the language and one feels a sense of profound regret that a subject which was so entirely interlinked in research effort during the war should nevertheless be developing a national form of language. Thus, one sees "centimetric" radar in place of "microwave" and "time base" in place of sweep and so on. This is not at all significant, but it does underline the fact that there is a tendency for language to diverge even in the technical field.

The book does not look forward very much and one feels that it represents a description of the whole art as it applied in early 1945, with very little included beyond this time. It is also interesting to note that the one serious divergence of thinking between English and American practice, namely, that of feeding an antenna, is markedly shown in the illustrations in this book.

The book should be read by anyone with a certain amount of knowledge of radar who wishes to widen his understanding of the subject. For English readers it could well serve as an introductory book, but it would be found by American readers that the illustrations were not apt, although the method of presentation is excellent, the language clear and well conserved and the actual material very well chosen. One small defect lies in the fact that no more advanced reading is suggested and this is rather an omission in an elementary book.

Ernest C. Pollard
Yale University

General Techniques of the Physics Laboratory, Vol. 1

Edited by J. Surugue. Pp. 433, Figs. 438. Centre de Documentation due Centre National de la Recherche Scientifique, Paris, 1947. In French.

This book constitutes the first volume of a series which promises to be a detailed collection of useful experimental procedures for the physicist. It is not written for the specialist in a given field, but for the experimenter who has to make use of or choose between certain techniques with which he is not too familiar.

In the foreword to this volume, Professor Joliot-Curie points out that scientific research is furthered in part by manufactured equipment (which is especially true in this country), but to a larger extent by special apparatus which every research worker must design and construct for himself and put into operation. It is during the latter process that one often encounters technical problems which may have been solved already in a satisfactory manner by other people, perhaps working in an unfamiliar field. A good compilation of modern research techniques is therefore a welcome aid and convenience for the experimenter.

The present volume, written by various experts, treats the following subject matter: Principles of Construction of Scientific Apparatus (H. Gondet), Principal Operations of Glass Blowing (Ch. Amate), Vacuum Technique (J. Surugue), Production of High Temperatures (G. Ribaud), General Techniques of Optics (A. Arnulf), Light Sources and Filters (G. Dupuy), Photoelectric Cells (A. Lallemand and M. Munsch), Procedures of Recording (H. Gondet), and Regulation and Rectification of Voltages and Currents (M. Demontvignier).

The book is perhaps best compared to *Procedures in Experimental Physics* by J. Strong (Prentice-Hall, Inc., New York, 1945), which is widely used in this country. Many of the techniques described are similar to those given by Strong. Some parts are treated in greater detail, as, for example, the subject of ovens and furnaces and the use, adjustment, and testing of various optical instruments. The material in the last two chapters of the volume is for the most part not mentioned by Strong: the chapter on recording techniques presents chemical, mechanical, electrical, and optical methods for recording. The chapter on electrical regulation and rectification discusses resistance, inductance, and discharge tube regulators, various solid and vacuum tube rectifiers, and has a section on the operation and construction of filters.

From the point of view of the contents, *General Techniques of the Physics Laboratory* is excellently written. The material is organized in a clear and logical manner, which is a speciality of French scientists. The index, which is important in this kind of a book, is good. The clarity of some of the figures might perhaps be improved.

As far as the usefulness of the presented information to an American physicist is concerned, it is more difficult to give a completely enthusiastic opinion. For there exists in different countries a vague pattern of certain preferred techniques, which is generally determined by practical circumstances. For example, due to the very high industrial development in this country, the American physicist makes use of many techniques which lean heavily upon industrial equipment (which does not mean that these techniques are necessarily better than those used elsewhere). Therefore, in some cases a book like Strong's will give more useful information to an experimenter in this country. This is especially true with respect to comparative performance characteristics of apparatus manufactured by competitive firms, which the French book lacks completely.

Yet, many American physicists will find this book a source of most welcome and useful information.

W. E. Meyerhof
University of Illinois

Waveforms

Edited by Britton Chance, Frederick C. Williams, Vernon Hughes, Edward F. MacNichol, and David Syre. Pp. 535+vii–xxii, Figs. 704. McGraw-Hill Book Company, Inc., New York, 1949. Price $10.00.

The Radiation Laboratory series has once again presented us with a volume packed from cover to cover with useful, practical information. In spite of the fact that some twenty-odd thick volumes have already appeared in this series, which, after all, covers only a relatively small segment of applied physics, the books continue to present new material and to present it divorced from the original application so that the reader interested in the general fields of electronics and applied physics cannot fail to find the series of major importance.

Waveforms is an excellent example. Starting with the radar problem of generating suitable waveforms for timing and indicating purposes, the authors have assembled material covering the circuits and techniques for generating and handling wave forms of almost any conceivable type. Having developed this circuitry, they then illustrate some of the applications, to modulation, to frequency division and counting, and to numerous mathematical operations. Although much of the fundamental material dates back to prewar days, the demands of radar required the development of precision circuits, and it is primarily because this precision is available that many of the applications discussed in the book are possible.

The merits of the book, then, lie in its encyclopedic discussion of the techniques of generating precision waveforms and its indication of the present and future applications of these circuits.

Early in the book two particularly interesting chapters deal with operations on waveforms with linear and with non-linear circuit elements. In discussing the non-linear elements, a large number of unusual tube characteristics are presented. It is refreshing to see such material emphasizing the non-linear behavior of tubes in contrast to the conventional linear approximations. The treatment of linear circuit elements is interesting but not altogether satisfying. In view of the widespread use of operational methods, it would seem that they deserve more than a cursory reference.

The book is liberally illustrated with actual circuit diagrams and cathode-ray oscilloscope photographs. The diagrams generally contain the circuit constants and therefore should be of inestimable value to the engineer and physicist interested in applying the material to practical problems. It is interesting to note the inclusion of some circuits and techniques developed in England. These have not always been translated into American tube types. It would have been helpful to include a table of approximate equivalents, or better yet, a brief technical description of the few British tubes mentioned.

The scope of this work is such as to appeal to a wide variety of interests. For example, the chapters on generating waveforms and on modulation, particularly time modulation, will prove of interest to communication and television engineers. The chapters on mathematical operations on waveforms, storage tubes, delay lines are of immediate application to the field of high speed electronic computation. Form the point of view of the experimental physicist, the techniques of measuring and controlling waveforms occurring in intervals of a microsecond or less, present him with a new tool which should prove of increasing importance in the future.

The book ends with a glossary of terms which includes a number of words and phrases new to those of us who are not specialists in this field. The authors state that they are attempting to replace the colloquialisms currently used by more precisely defined terms. For example, a flip-flop is changed to a monostable circuit. They are to be congratulated on their efforts, but when a picturesque colloquialism is once entrenched in the language it cannot be removed, it can only be paralleled by the scientific term. In this particular case, the classification of multivibrator type circuits into astable, bistable, and monostable would seem particularly apt and it is to be hoped that these terms will receive general currency.

This reviewer must confess that once again he is delighted to find a volume of the Radiation Laboratory series which, although the work of many contributing authors, has the continuity and readability of a first class reference book. The editorial staff and the authors have done an excellent job. Let us hope that the title does not imply to prospective readers that the book is limited to some specific radar problems, for it is indeed a book of wide scope and general interest with applications to numerous fields. No experimentalist can afford to overlook it.

W. H. Pickering
California Institute of Technology

Microwave Antenna Theory and Design

Edited by Samuel Silver. Pp. 721+vii–xviii, Figs. 300. McGraw-Hill Book Company, Inc., New York, 1948. Price $8.00.

The extension of radiofrequency techniques to the microwave range marks a new era in antenna theory and design. In this range, the conventional low frequency techniques are combined with the optical techniques on the one hand to achieve directivity, gain, and efficiency; on the other hand, new design principles are made available to obtain special effects. This book, edited by Samuel Silver, represents a documentary report covering the important antenna development during the war at the Radiation Laboratory, M.I.T., and to a limited extent other allied laboratories.

According to the subject material, the book can be divided into two parts. The first half of the book from Chapter 2 to Chapter 7, written by Silver, deals with the general principles of microwave antennas. The author collects material which is scattered among textbooks and articles of diversified topics. It covers circuit theorems, microwave transmission lines, radiation from current distributions, geometrical optics, and scattering and diffraction. The author has placed enough emphasis on mathematical rigor, and the material is well arranged, so that the first part is appropriate for classroom use.

The second part of the book deals with the design principles of various types of antennas. It starts with a chapter on dipole antennas and feeds used in connection with reflectors and other optical systems. In spite of their simple geometry and dimensions, they are not readily susceptible to accurate analysis. Experimental results and descriptions of different dipole arrangements are presented. The wave guide and horn feeds are covered in another chapter by J. R. Risser who has made a thorough and highly creditable experimental study of the impedance and radiation properties of electromagnetic horns. The results are presented here together with some theoretical analysis. The practical matter of pressurization is also touched upon.

In the chapter on "Linear Array Antennas and Feeds" by J. E. Eaton, L. J. Eyges, and G. G. Macfarlane, the latter from Telecommunication Research Establishment, England, the first third is devoted to the pattern theory, general formulas, uniform array, and beam synthesis. This is followed by a discussion of array elements. The outstanding work on slot radiators by British and Canadian scientists during the war is included. The impedance aspect of arrays, a few typical broadside arrays for beacons and feeds, and endfire arrays are described in detail.

Lenses and reflectors are treated in two chapters by Risser and Silver, respectively. The well-known metal-plate lenses developed by W. E. Kock, and the briefly mentioned parallel-plate systems, represent two of the radical departures from the optical systems at optical frequencies.

Although beam shaping is a standard practice at the standard broadcasting frequencies, the stringent requirements to provide proper coverages for radar mapping from the air, or air search from the ground, necessitated the development of new techniques. L. C. Van Atta and T. J. Keary give a well-balanced treatment of the theory, experimental results, and applications. Some early development, however, is omitted.

The practical aspects of microwave antennas are treated in the last three chapters. In "Antenna Installation Problems" by Van Atta and R. M. Redheffer a description of importnat considerations of installing antenna systems on ground, ship, and aircraft is given. A condensed treatment of the electrical aspect of the dielectric housing, or radome, is included.

Microwave antennas usually involve four-dimensional problems. Theoretical analysis can, at best, serve as a guide to the design of a practical system. One relies heavily upon the measurements of the performance of the components for most of the detailed design information. "Antenna Measurements—Techniques" by H. Krutter, who is personally responsible for many of the techniques, summarizes the practical techniques and their fine points instrumental to microwave antenna designs. The book is concluded with a brief chapter on "Antenna Measurements Equipment" by O. A. Tyson, who made the research work possible in the antenna group of the Radiation Laboratory by supplying them with new instruments for reliable and accurate measurement.

As a whole, the second half of the book contains a tremendous amount of reference material which is invaluable to designers and others seeking practical understanding of microwave antennas. The general organization of the book is to the credit of the authors and the editor.

The antenna systems discussed in this book are necessarily restricted to those used in microwave radar systems, although most of them can be used for other applications. There are, unfortunately, a few omissions, among which are the off-focus properties of optical systems and special systems for rapid scanning.

L. J. Chu
Massachusetts Institute of Technology

Scientific Foundations of Vacuum Technique

By Saul Dushman. Pp. 882, Fig. 324. John Wiley & Sons, Inc., New York, 1949. Price $15.00.

Of many books of undoubted value, it can be said that any one of a number of authors could have accomplished as much. It is doubtful whether anyone else could have done this piece of work. Dr. Dushman, recently retired as assistant director of the General Electric Company Research Laboratory, has spent nearly forty years working and studying in this field and its associated phases and has been a leader all the way.

His 1922 volume, *The Production and Measurement of High Vacua* brought together at that early date the known vacuum information. In a conversation during the preparation of his present volume, Dr. Dushman told this reviewer that he was not too happy about some of the things in the earlier book and this time he was giving every effort to produce a comprehensive, scholarly treatise of permanence and of which he could be proud. The result is a beautiful piece of work.

For those who do not already know the author by his works, it may be said that the writing style is clear and concise and the presentation orderly. The book is extremely readable.

The contents, by their nature, require many references. These are taken in stride with facility and without adverse effect on the subject matter. Liberal use has been made of direct quotations of sections of references as well as of illustrations. When expertly done this is a good thing. Valuable information, often lost thru interpretation of anothers work, can be saved by skillful quotation of pertinent material.

Apparently every effort has been made to give credit to all sources of information. The name index runs to well over a thousand. The footnotes are studded with acknowledgments of "private communication" and "copy of manuscript before publication," testifying to a wide and active acquaintanceship among workers in the field and assuring that no source of information has been neglected.

The above paragraphs bear witness to the capabilities of the author and the quality of his work. In his choice of contents he has drawn upon the fields of physics, chemistry, and metallurgy—the applications and fundamentals of vacuum technology extend into all of them with increasing importance.

The first two chapters contain a treatment of the kinetic theory of gases and of gas flow through orifices. The pertinent information is included without padding and together with some of the material of the later chapters would serve as an excellent basis for a practical course in kinetic theory.

Three chapters cover the various types of mechanical and vapor pumps. Descriptions and characteristics of many pumps, both historical and presently available are given. Information on pump speeds and design of pumping systems are included. In the case of vapor pumps such items as design information, nozzle characteristics, and available types of pump fluids are adequately discussed.

Chapter 6, entitled "Manometers for Low Pressures," contains about 125 pages and illustrates well the ingenuity of man as well as the effectiveness of the author's literature dragnet. Over one hundred different gauge constructions are referred to. Admittedly many are variations of a common principle. Certainly there exist only half a dozen or so basic physical phenomena upon which gauges may be built. Examples of ingenuity, although perhaps not of convenience, are the application of a Michelson interferometer to the measurement of small mercury displacements in a manometer, and the construction of a hot wire gauge in the capillary of a McLeod gauge! Those gauges more commonly in use, such as the McLeod, the ionization gauge, and various hot wire gauges, have been given thorough treatment. This chapter also includes a section on leak detection in which the mass spectrograph and the halogen ion detector are discussed.

Up to this point, about the halfway mark, the material, although masterfully and thoroughly presented, would be available without too much reference work. It is the second half of the book which, in the reviewers opinion, will prove to be of greatest ultimate value. The mere gathering of this material would have been a forbidding undertaking. Its intelligent interpretation in the interests of vacuum technology is a real contribution.

Two chapters are used in the presentation of sorption phenomena, one for metal, the other for charcoal, silicates (glasses), and cellulose. Particularly detailed are the sorption data for charcoal and glass. One chapter discusses the solubility of gases in metal and techniques of degassing.

Clean-up of gases at low pressures is discussed under two headings. In chemical clean-up are discussed the use of getters and the reaction of gases with incandescent filaments. Under electrical clean-up are found some of the explanations which have been offered for that rather nebulous but real phenomena, the disappearance of gas under certain conditions of low pressure discharge.

A chapter on vapor pressures contains extensive tables of vapor pressures of metal and other materials, and describes practical methods of evaporation. The final chapter gives numerous data on dissociation pressures and oxidation rates and discusses the logarithmic and parabolic laws of rates of oxidation.

The completeness of this work must be emphasized. Where gaps appeared the author, when possible, performed the necessary experiments or calculations to close them. Such an instance is found in the case of the vapor pressure tables 1 and 2 of Chapter 11.

By virtue of its scope, this is a reference book. It is also a book in which to browse. It will be serving both purposes adequately for many years to come.

C. H. Bachman
Syracuse University

Principles and Methods of Telemetering

By Perry A. Borden and Gustave M. Thynell. Pp. 230, Illustrated. Reinhold Publishing Corporation, New York, 1948. Price $4.50.

Instrumentation which provides remote indication or recording of variable physical quantities has added a distinct phase to the field of electrical communications. This phase of communications, called telemetering, has fostered the development and application of many unique systems and measurement devices. Although telemetering systems have been employed for many years, there has been a relatively small amount of literature which deals exclusively with the field. This book provides a description of many types of telemetering equipment which are presently in use or have been employed in the past. Consideration of the principles of telemetering is chiefly related to the specific equipment being discussed.

With consideration of the electrical variable, the telemetering systems are classified as: (1) current, (2) voltage, (3) frequency, (4) position, (5) impulse. Seven chapters are devoted to the description of representative equipments in each of the classifications together with a brief discussion of the system principles and methods. Consideration of basic characteristics and limitations of the systems is almost nonexistent. In many instances the reader must deduce the principal characteristics of the system from the method of operation of the described apparatus. In this respect, however.

the authors define their position as compilers of information relating to the essentials of the various apparatus.

The measurement field is considered with a reasonable breadth of types of apparatus. Emphasis is given the measurement of liquid level and flow, mechanism displacement and position, and electrical quantities related to power applications. The descriptions of the apparatus and the methods of operation are presented fully and the reader should have no difficulty in understanding the devices.

One chapter deals specifically with interconnecting circuits and channels. Illustrations are given of the use of simplex, phantom, and other similar methods for the transmission of telemetering signals over circuits which carry other intelligence. The chapter on carrier current goes into some detail on the equipment employed and discusses the application methods and problems.

The practical application of telemetering apparatus establishes additional requirements for equipment to properly associate information from various sources. It is necessary to perform operations upon this information so that the desired result is presented in the most easily used form. Consideration of these problems together with a description of typical apparatus is contained in the chapter on coordinating, totalizing, computing, and integrating. The final chapter discusses the general relationship of typical application problems and the type of telemetry which should be employed.

An interesting classified list of patents in telemetering and allied fields is included.

The authors' viewpoint is "prior to the advent of the electron tube" which does not bring forth discussion of some of the more promising possibilities of telemetry. In addition, practically no consideration is given to telemetering via a radio link. This is felt to be a serious omission since radio telemetering provides the means for a vast new field of instrumentation.

The book will undoubtedly be of considerable interest for those desiring descriptive information about commercial apparatus employed in stationary installations. It will be of little value to those seeking knowledge of the fundamentals of telemetering.

T. W. Sheppard
The Johns Hopkins University

Methods in Medical Research, Vol. I

Edited by V. R. Potter. Pp. 372+xiii, Illustrated, 16×24 cm. The Yearbook Publishers, Inc., Chicago, 1948. Price $8.00.

The annual volumes, of which this is the first, should be valuable additions to the biological literature, since there has been no similar systematic presentation of current methodology in this field. Although intended primarily to cover techniques of particular concern to medical research, many of the articles are of broader biological interest. It is also possible that some of the methods, such as those for measuring fluid flow and those for certain chemical studies, contain ideas of use to experimenters in non-bilolgical fields.

Each volume is to "be divided into four or five principal, self-contained sections, each of which shall, for that volume, represent one of the broad fields of medical research: biochemistry, physiology and pharmacology, microbiology and immunology, and biophysics, including radiobiology." Within each of these broad fields it is planned "year by year, to select various topics wherein a restatement of techniques seems timely." The stated purpose is to provide a place for appraisal of the various methods proposed for solution of a particular experimental problem and to offset the present difficulty of obtaining publication of adequate descriptions of technique, especially in the field of physiology. For each topic selected, an expert is chosen to serve as associate editor who picks contributors to describe particular methods.

The subjects treated in this volume include the following: Section I: Assay of antibiotics (65 pages). This covers the assay of potency of penicillin, streptomycin, tyrothricin, and bacitracin, by biological, chemical, and physical methods.

Section II: Circulation and blood flow measurements (188 pages). This includes an extraordinary number of devices for measuring flow of blood, mostly contrived to cause a minimum disturbance in pressure relations of the system in which flow is measured. There are volume-displacement methods, drop recorders, a "bubble" flow meter, a critical and condemning discussion of thermostromuhrs, differential pressure flow meters, and a section on methods for following pulsatile flow. In an electromagnetic flow meter, measurement is made of the voltage generated between two electrodes on opposite sides of an intact blood vessel as the blood crosses a strong magnetic field. Systems for perfusing various organs are considered. Methods are discussed for measuring blood flow indirectly in certain regions by microscopic observation, by skin temperature recording, by plethysmographs, by nitrous oxide exchange (human brain), etc. There is also a discussion of several methods for determining cardiac output and for studying vascular tone.

Section III: Selected methods in gastroenterological research (18 pages). These concern the study of gastric acidity in man and the use of animals for certain tests of liver function and for evaluation of treatments for peptic ulcer.

Section IV: Cellular respiration (74 pages). This section briefly covers the measurement of respiration of intact animals of various sizes by a closed volume method and then more extensively considers applications of the Warburg manometer technique to slices and homogenates of excised tissues. The biochemical details are given for determining the concentrations of particular enzymes in homogenized tissues. Finally, a system is described for rapid freezing of tissue samples and subsequent analysis for various substances, including enzymes, of interest in carbohydrate metabolism.

The authoritativeness of each contribution has been increased in a way which may recommend itself to future editors of similar surveys. Each article has been submitted to at least one other experienced investigator for review. The reviewer is given real responsibility for critical comment by noting his name at the end of the article, frequently the comments themselves are printed. This appears to be of considerable value in assessing many of the methods now employed in biological research, where procedures are often not standardized and where additional precautions and controls seem needed for almost every new application.

Martin G. Larrabee
University of Pennsylvania

Sources of Engineering Information

By Blanche H. Dalton. Pp. 109. University of California Press, Berkeley, 1948. Price $4.00.

To meet the need for "a compilation listing source material (in engineering) for American engineers and librarians," the engineering librarian of the University of California has prepared a revised edition of a syllabus originally written for use with lectures on library materials for those engaged in research in engineering.

The organization of the compilation makes it an excellent tool for students and librarians. Mrs. Dalton correctly places the emphasis on periodical literature, where the chief attention belongs in tracing scientific information. The first three sections of the book form a unit—"Indexes to Periodical and Serial Literature," "Abstracts," and "Location of Articles and Identification of Periodicals." The third section contains suggestions for the searcher not familiar with the services a library can offer in finding the periodicals needed.

The fourth section, "Bibliography," should be useful to the researcher who needs not only a list of bibliographies, but also directions for preparing a bibliography for himself; and the fifth section is a list of reference books, classified by general type—for example, technical dictionaries and handbooks—and by subject within the type. The brief section on the trade catalog collection describes the organization of such a collection, and the four pages devoted to standards and specifications gather into a good working-list the names of national standardizing bodies and of important publications in this diffuse and frequently confusing field.

The various lists cover the ground thoroughly; the organization under headings and subheadings follows familiar library patterns, and the book will not only guide librarians in organization and method, but also provide a check list for library holdings. Whether the practicing engineer or research worker will take the time and trouble to look through the classifications till he finds what he needs is another matter; he would doubtless prefer a subject index for quick reference rather than the subject classification only, which he must first learn before he can use the book with speed or can be sure he has not overlooked the source of the information he needs.

ROSE E. LONBERGER
SARAH D. JONES
University of Pennsylvania

Vacuum-Tube Circuits

BY LAWRENCE BAKER ARGUIMBAU. Pp. 668 Figs. 676. John Wiley & Sons, New York, 1948. Price $6.00.

The text *Vacuum-Tube Circuits* presents no new material but does bring together, under one cover and in a coherent manner, many of the necessary relationships between vacuum tubes and present-day communication circuits. The title does not indicate that the book covers only applications of vacuum tubes to the communications fields.

The text assumes a firm foundation in alternating current circuit theory and the associated mathematics. Some previous knowledge of the fundamental concepts of vacuum tubes themselves is assumed even though the second and third chapters (Diodes and Rectifiers and Triodes, Pentodes, and Linear Amplifiers [Including Random Noise]) review these facts to some degree. The first and foremost consideration is the association of the tube to its circuit which is brought about with expedience.

Chapter Four is entitled "Transient Response of Video Amplifiers." The chapter begins with a discussion of the fundamentals of television in an attempt to place restrictions on the operation of the video amplifiers. This discussion is necessarily brief and somewhat out of place here, particularly in view of the wide application of the term "video amplifier" to broad-band amplifiers in general. The presentation of the subject is, however, thorough and of great practical worth. Design criteria are given for broad-band amplifiers under all conditions of operation, with special reference to transient response.

Chapter Five discusses "Amplitude Modulation and Tuned Amplifiers" which includes the relationship between modulation band width, circuit Q and the operation of the radio-frequency coupling circuits in current use.

"Power Amplifiers," Chapter Six, discusses the theory of class A, B, and C amplifiers. Of particular interest is the fact that the author devoted time and space to the step-by-step determination of the correct operating conditions for class B and C amplifiers. Although this information can most certainly be found elsewhere, it is a valuable addition in providing background for a book of wide coverage such as this.

The chapter on oscillators (Chapter Seven) provides all the usual ramifications, including well presented design criteria. The best portion of the chapter is the section on stabilized oscillators of many forms. Amplitude and frequency stability under varying operating conditions are discussed in detail.

The cathode-follower as an example of inverse feedback (Chapter Eight) receives complete treatment including the choosing of proper quiescent operating conditions. Negative feedback as a whole is presented with lucidity by the use of equivalent circuits and examples. The effect of negative feedback on noise, distortion, band width, and amplifier stability is illustrated.

Chapter Nine (Amplitude Modulation) continues the study of class C amplifiers as applied to the modulated output stage of an amplitude-modulated transmitter. Improvement of linearity of modulation by the use of negative feedback is shown. Other topics discussed are: single-side-band transmission, frequency changers, detectors, and automatic volume control as applied to amplitude modulation. Particular attention is paid to the correct operation of the diode detector in minimizing the different types of distortion which might arise in such a circuit.

In Chapter Ten, frequency modulation theory and history, transmitters and receivers are discussed. The advantages of FM over AM are brought out. The effect of pre-emphasis on signal-to-noise ratio is discussed. The relationship between modulation index, deviation ratio, pre-emphasis, and signal-to-noise ratio is not clearly defined. The ratio detector (or discriminator) is omitted.

The problems connected with television pulse generators, sweep circuits, and synchronism of television signals are the concern of Chapter Eleven. For the allotted space the coverage is good, but many items of importance such as d.c. restorers and sound "traps" are eliminated.

The last chapter discusses the generation of microwave frequencies by triodes, magnetrons, and klystrons. Multiple-cavity and reflex klystrons are both considered.

The text as a whole should be of much practical value due to its wide, up-to-date coverage, clear presentation, and frequent practical references and examples. The value of the author's bibliography is increased by brief summaries of the content of articles in many cases.

JOE CYRIL MAY
Yale University

Author Index to Books Reviewed

Arguimbau, Lawrence Baker. *Vacuum-Tube Circuits*—— 455

Borden, Perry A. and Gustave M. Thynell. *Principles and Methods of Telemetering* 453

Chance, Britton, Frederick C. Williams, Vernon Hughes, Edward F. MacNichol, and David Syre. *Waveforms* 451

Dalton, Blanche H. *Sources of Engineering Information*— 454

Dushman, Saul. *Scientific Foundations of Vacuum Technique* 453

Hamilton, Joseph G.—see Lawrence, John H. 450

Hughes, Vernon—see Chance, Britton 451

James, R. W. *The Optical Principles of the Diffraction of X-rays* 449

Lawrence, John H. and Joseph G. Hamilton. *Recent Advances in Biological and Medical Physics* 450

MacNichol, Edward F.—see Chance, Britton 451

Pollard, E. C. and Julian M. Sturtevant. *Microwaves and Radar Electronics* 448

Potter, V. R. *Methods in Medical Research, Vol. I* 454

Rice, F. O. and E. Teller. *The Structure of Matter* 450

Silver, Samuel. *Microwave Antenna Theory and Design* 452

Sturtevant, Julian M.—see Pollard, E. C. 458

Surugue, J. *General Techniques of the Physics Laboratory, Vol. I* 451

Sutton, George P. *Rocket Propulsion Elements* 448

Syre, David—see Chance, Britton 451

Taylor, Denis and C. H. Westcott. *Principles of Radar* 450

Teller, E.—see Rice, F. O. 450

Thynell, Gustave M.—see Borden, Perry A. 453

Westcott, C. H.—see Taylor, Denis 450

Williams, Frederick C.—see Chance, Britton 451

Other Books Received

Advances in Electronics, Vol. 1. EDITED BY L. MARTON. Pp. 475+xi, Figs. 155, Academic Press, Inc., New York, 1948. Price $9.00.

Components Handbook. EDITED BY J. F. BLACKBURN. Pp. 626, Figs. 369, Tables 91. McGraw-Hill Book Company, Inc., New York, 1949. Price $8.00.

Cosmic Ray Physics. D. J. X. MONTGOMERY. Pp. 370+viii, Profusely illustrated. Princeton University Press, Princeton, 1949. Price $5.00.

Electronic Time Measurements. EDITED BY CHANCE, HULSIZER, MACNICHOL AND WILLIAMS. Pp. 538+xviii, Figs. 383, McGraw-Hill Book Company, Inc., New York, 1949. Price $7.00.

Modern Operational Calculus. N. W. MCLACHLAN. Pp. 218+xiv, Figs. 29. The Macmillan Company, New York, 1948. Price $5.00.

Photoelectricity and Its Application. V. K. ZWORYKIN AND E. G. RAMBERG. Pp. 494+xii, Figs. 780. John Wiley & Sons, Inc., New York, 1949. Price $7.50.

Practical Analysis. FR. A. WILLERS. Pp. 422, Figs. 132. Dover Publications, Inc., New York, 1949. Price $6.00.

Principles of Electricity and Electromagnetism. G. P. HARNWELL. Pp. 670+xvi, Figs. 351. McGraw-Hill Book Company, Inc., New York, 1949. Price $6.00.

Principles of Mechanics. J. L. SYNGE AND B. A. GRIFFITH. Pp. 530+xvi, Figs. 164. McGraw-Hill Book Company, Inc., New York, 1949. Price $5.00.

Quantum Mechanics. LEONARD I. SCHIFF. Pp. 404+xii, Figs. 30. McGraw-Hill Book Company, Inc., New York, 1949. Price $5.50.

Radioactive Measurements with Nuclear Emulsions. H. YAGODA. Pp. 356+ix, Figs. 75. John Wiley & Sons, Inc., New York, 1949. Price $5.00.

Scientific and Industrial Glass Blowing and Laboratory Techniques. W. E. BARR AND V. J. ANHORN. Pp. 388, Illustrations 212. Instruments Publishing Company, Pittsburgh, 1949. Price $6.00.

Stochastic Processes and Their Application to the Theory of Cosmic Radiation. N. ARLEY. Pp. 240, Figs. 53. John Wiley & Sons, Inc., New York, 1949. Price, $5.00.

The Atmospheres of the Earth and Planets. EDITED BY G. P. KUIPER. Pp. 366, Illustrated. University of Chicago Press, Chicago, 1949. Price $7.50.

Laboratory and Shop Notes

Lead-In Seals for Kinetic High Vacuum Systems Using Rubbers

Ralph C. Taylor and Carnot W. Ward
Naval Research Laboratory, Washington, D. C.

IN using kinetic high vacuum systems in tube development, metal sputtering, and other applications, the effective sealing of leads is often a perplexing problem. The common methods employed using low vapor pressure waxes and resins, have the disadvantage of being clumsy and time consuming.

While working with high vacuum systems requiring electrical leads it was found that metallic conductors imbedded in a rubber matrix could be used successfully for seals in the range 10^{-6} to 10^{-7} mm. Designs similar to that shown in Fig. 1 have proved most satisfactory.

Various types of synthetic rubbers have been used, but it was noted that many of the compounding ingredients, such as carbon black, oils, and plasticizers in the rubbers contribute in making the elastomers gassy.

Silicone and neoprene elastomers, when properly compounded with low vapor pressure materials, give good results but a butyl rubber GR-I was used because of its low permeability and good electrical properties. The following recipe, Table I, has been tried and found to function well and permit rapid evacuation of the system.

Table I.

Butyl Rubber GR-I	100.00
Zinc Oxide	5.00
Stearic Acid	2.00
Sulfur	2.00
Tuads	1.00
M.B.T.	0.50
Titanium Dioxide	40.00
	150.50
Gaskets Vulcanized 35 in. at 300°F.	

Various designs have been used, hollow tubes, solid rods or flat metal strips have been employed as conductors, but the gasket most often used has been of the type shown in Fig. 1.

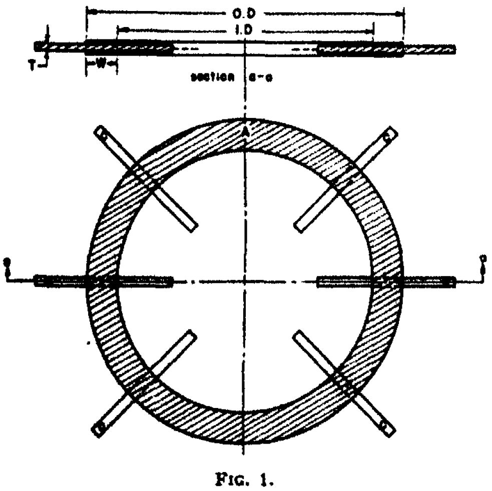

Fig. 1.

The gasket is a flat rubber ring (*A*), with the dimensions governed by the application, i.e., the I.D. of the bell jar or flange of the tube. Any metal may be used as the conductor (*C*) but silver, copper or nickel ribbons or tubing plated with brass have been found to give best adhesion to the rubber. The total thickness (*T*) is sufficient to give approximately $\frac{1}{16}$–$\frac{1}{8}$ in. on the top and bottom of the metal. The width (*W*) is usually $\frac{1}{2}$ to 1 in.

The gasket is vulcanized in a mold with the metal inserts in place. Adhesion is obtained to the metal by the usual methods common in the rubber industry utilizing commercial adhesive cements such as Ty-Ply Reanite or Cycle-Weld.

Gaskets of this design with as many as eight conductors imbedded in the vulcanized rubber have been successfully used for a period of nine months.

Measurement of the Thickness of Thin Nylon Films

A. I. McPherson and D. G. Douglas
McGill University, Montreal

April 4, 1949

AN optical method of measuring the thickness, and from it the mass per unit area, of thin mica windows has recently been described in this journal.[1] This method however is not applicable to the very thin windows currently being used in most beta-ray spectrometers. For these an optical method is especially desirable since a small window is too light to be weighed with acceptable precision on an ordinary chemical balance. Furthermore, if the film is removed from its supporting frame for weighing or testing, cementing it in place becomes much more difficult.

We have recently made some thin nylon films for use as windows for a Geiger counter, following rather closely the method of Brown, Felber, Richards, and Saxon.[2] It has proved convenient to pick up the films on a frame cut from mica, as many as 8 layers being picked up on one frame to build up any desired thickness.

We have found it possible to measure the thickness of these thin films quickly with a Michelson interferometer set for white-light fringes, and showing fringes from yellow sodium light at the same time. The film on its frame was introduced into one arm of the interferometer, and the amount of displacement of the central black fringe was measured.

For example, for two circular films 1.5 cm across, made up of 6 and 8 layers respectively, the displacement of the dark fringe was 0.8 fringe-width and 1.2 fringe-width. This corresponds to an increase of optical path $n\lambda = 2t\ (\mu - 1)$ and thus is equal to 0.8λ and 1.2λ where λ is the effective wavelength of the light used, t the thickness and μ the refractive index of the nylon film. The refractive index μ was found to be between 1.50 and 1.62, as determined from Brewster's angle for the film for sodium yellow light measured with a spectrometer and Nicol prism. The thickness of these films is thus determined within about 10 percent, being between 0.38 and 0.47 micron for one, and between 0.57 and 0.71 microns for the other. (Since our mean value $\mu = 1.56$ agrees well with the mean value $\mu = 1.55$ for nylon fibres kindly furnished by Dr. R. D. Bennett of the Nylon Division, Canadian Industries Limited, the accuracy obtained by using the mean is probably very much better than 10 percent.

The density of the nylon chips from which the thin films were made was found to be 1.10 gm per cm^3 by weighing in air and in water; assuming the same density for the films and the chips this gives for the two films discussed, masses between 0.042 and 0.052 mg per cm^2, and 0.063 and 0.078 mg per cm^2, or using the mean value of $\mu = 1.56$, masses of 0.046 and 0.069 mg per cm^2.

This method of measurement of thickness is quick, and its accuracy is satisfactory for the purpose, especially for comparing one film with another, and also for examining a film for uniformity of thickness and constitution in terms of the distortion it produces in the fringe pattern. Our films are uniform over their entire area to better than one-twentieth of a fringe-width. Since the films are measured and examined on the mica frames on which they are formed, it is possible to select a film suitable for the particular purpose considered.

---

[1] F. W. Brown, III and A. B. Willoughby, Rev. Sci. Inst. 19, 820 (1948).
[2] Brown, Felber, Richards, and Saxon, Rev. Sci. Inst. 19, 818 (1948).

Ultimate Vacua of Diffusion Pumps

G. W. Sears*
General Electric Company, Schenectady, New York

February 25, 1949

Any evacuated system represents a balancing of rates of evolution and rates of removal of gases to give a steady state pressure characteristic of this balance. Any arbitrary distinction between static and dynamic vacuum systems tends to obscure the utility of this principle for static systems.

In at least one important instance the elementary procedure of material balancing appears to have been over-looked. A typical curve of pumping speed *vs.* log pressure for a diffusion pump is shown in Fig. 1, curve *A*, in accordance with Dayton.[1] It will be noted that the pumping speed slowly rises to a plateau value with decreasing pressure. It then remains constant over a long range of pressure and falls rather rapidly to zero at the ultimate or limiting pressure of the pump.

For clarity a brief description of a pumping speed determination is given, Gas is admitted to the high vacuum side of a diffusion pump at a measured rate (volume/time), a measured pressure, and a known temperature. The steady state pressure at the throat of the pump is measured and the temperature of the flowing gas is assumed to be equal to the temperature of the admittance chamber. If S^* is the effective pumping speed at the throat of the pump (volume/time), S_M is the measured rate of introduction (volume/time), p is the admittance pressure, and P is the throat pressure, we write

$$S^* = pS_M/P. \tag{1}$$

The various factors which complicate the absolute measurement of pumping speed do not concern the present paper and will not be considered.

This paper is concerned with the behavior of the pumping speed curve in the low pressure cut-off region. The operation, of a diffusion pump depends on gas molecules from the region being evacuated effusing into the directed vapor stream of the pump. Some of the directed momentum of the vapor molecules is imparted to the gas molecules. The vapor stream effectively exerts a pressure gradient on the gas causing it to flow through the pump. This process would seem to be independent of pressure once the pressure had been lowered by a backing pump to a value at which molecular flow or effusion could occur. It is indicated that the pumping speed should rise to a plateau value and remain there for all lower pressures.

It is postulated that such is actually the case and that effective pumping speeds in the cut-off region are not true pumping speeds. This is explained on the basis that the rate of gas evolution by the pump becomes appreciable and even exceeds the measured rate of introduction of gases into the vacuum during pumping speed measurements.

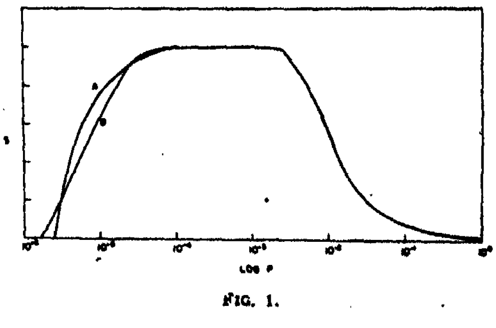

FIG. 1.

If the ultimate pressure of a diffusion pump is P_0, the true pumping speed is S, and the mass rate of evolution of gases by the pump is π, we may write

$$P_0SM/RT = \pi \tag{2}$$

where M is the average molecular weight of the evolved gas, T is the absolute temperature of the evolved gas, and R is the gas constant. For pressures P, greater than P_0, but still on the plateau, we write as a consequence of Eqs. (1) and (2)

$$S^* = S(1 - P_0/P). \tag{3}$$

Qualitatively this equation describes the pumping speed cut-off curve at low pressures. It predicts a low pressure limit for a diffusion pump as well as the plateau region. Figure 1, shows the comparison between calculated effective pumping speed, curve *A*, and measured effective pumping speed, curve *B*. The discrepancies between the precise contours of the two curves is explained in that the mass rate of gas evolution by the pump is dependent on previous history. Obviously, a pump that has operated for a short time will evolve more gases than one which has operated for a longer period. We would expect the ultimate pressure of a pump to decrease with operating time and to assymptotically approach a final value characteristic of the particular pump and pumping fluid.

Experimentally the true pumping speed is the plateau value, and the rate of evolution of gas by the pump, π, may be estimated from Eq. (1) using the experimentally determined cut-off pressure. It should be noted that π includes not only gas evolution from the pump, but also non-measured residual evolution from the system as well. By using a well outgassed glass system the contribution from the system can be made negligible.

This immediately allows some valuable conclusions to be made concerning the design of vacuum systems for low ultimate operating pressures.

The gases evolved by a diffusion pump arise from two sources, decomposition of pumping fluid and outgassing of the pump and its contents during operation. The outgassing gases are undoubtedly most significant at the start of pumping operations and become progressively less important as the pumping time increases. Decomposition gases are obviously not present in the case of mercury as a pump fluid. Of the organic and silicone pump fluids it would be expected that decomposition would occur to a markedly lesser degree for the latter. In the later stages of an evacuation operation the decomposition gases represent substantially all of the pump gas evolution and limit the ultimate pressure which may be reached.**

Mercury offers the best properties for lowest ultimate pressures. It cannot decompose and only evolves adsorbed and dissolved gases. After prolonged operation the rate of gas evolution becomes very small.

Equation (1) determining the ultimate vacuum of a diffusion pump contains a pumping speed factor. For a given amount of pumping fluid, the pump design having the greatest speed factor would give the lowest ultimate pressure. For a given pump the lowest boiler temperature compatible with the maximum attainable pumping speed would give the lowest ultimate pressure.

Copley, Simpson, Tenney, and Phipps[3] have described a long divergent nozzle pump having a speed factor of 0.5 theoretical. Such a pump with a pumping speed of 50 liters/sec. is comparable in dimensions and volume of mercury to a two-stage diffusion pump with a pumping speed of 10 liters/sec. Since both pumps evolve gases at substantially the same rates Eq. (2) predicts that the limiting pressure of the expanding nozzle pump should be lower by a factor of five than the limiting pressure of the two-stage pump.

---

* Research Associate, General Electric Research Laboratory.

[1] B. Dayton, Ind. Eng. Chem. 40, 795 (1948).

** It is important to note that the rate of decomposition of a hot organic or silicone pump fluid is very sensitive to material it contacts. Metal surfaces would tend to catalyze the decomposition process. In the construction of metal pumps it would be expected that the low pressure characteristics might be markedly improved by plating the inner pump surfaces with a metal catalytically inactive for the oil in question.

[2] Copley, Simpson, Tenney, and Phipps, Rev. Sci. Inst. 6, 265 (1935).

Device for Producing Rate-Proportional Damping Signal in Servo Systems

L. W. Herscher
The Dow Chemical Company, Midland, Michigan

February 9, 1949

CONSIDERABLE trouble with the usual slide wire and commutator type d.c. generator methods of providing a damping signal was encountered in the operation of a double-beam infra-red spectrometer.[1,2] The sliding contacts of both systems required very frequent servicing.

Installation of the system shown schematically in Fig. 1 has proven to be a practical method of avoiding the uncertain prospect of finding a cure for the contact troubles. A variable air condenser is rotated through a maximum of approximately 130 degrees by a gear pair coupling to the beam balancing servo motor and generates a current proportional to the rate of change of angular position of the condenser.

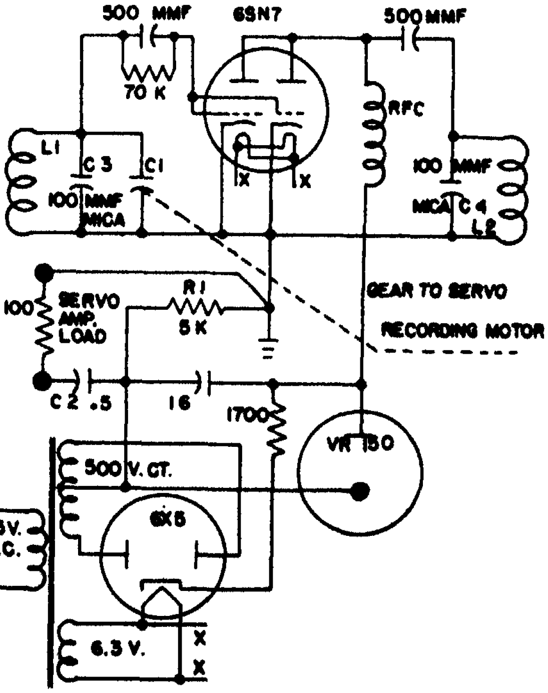

Fig. 1.

The circuit employed is a self biased tuned plate-tuned grid oscillator. The strength of oscillation and therefore the plate current of the tube is varied by changing the grid tank tuning with C_1 which is the control element coupled to the balancing motor and has a range of 10- to 50-$\mu\mu$f linear with angular position. By operating in the proper portion of one side of the grid tank resonance curve a constant output current throughout the entire scale range is obtained for a fixed speed of pen travel. The voltage across R_1 changes from 18 to 54 volts when the recorder is moved from one end of the scale to the other and a current of approximately five microamps flows in the servo amplifier input circuit at maximum pen speed of two seconds across the chart. The correct polarity for the required counter e.m.f. for damping can be obtained by the choice of direction of rotation of C_1 or by adjusting C_3 and C_4 to choose the side of resonance at which the grid is tank tuned. The amount of current can be adjusted by varying C_3 or R_1. L_1 and L_2 are broadcast receiver r.f. coils. C_1 should have low friction bearings and preferably a pig-tail connection to the rotor. The connections to this condenser are made through a two-foot length of coaxial cable.

The system has been in use several months and has required no further attention or adjustments since installation.

---

[1] N. Wright and L. W. Herscher, J. Opt. Soc. Am. 37, 211 (1947).

[2] Baird, O'Bryan, Ogden, and Lee, J. Opt. Soc. Am. 37, 754 (1947).

New Instruments

W. A. Wildhack: Associate Editor
in Charge of this Section
National Bureau of Standards, Washington, D. C.

These descriptions are based on information supplied by the manufacturer, and in some cases from independent sources. THE REVIEW *assumes no responsibility for their correctness.*

Interpolator for UHF Measurements

The interpolating frequency standard is a precision interpolator for use with heterodyne frequency meters in making accurate frequency measurements at ultra high frequencies up to about 3000 megacycles. When used with such a frequency meter, whose accuracy is, at best, 0.1 percent, the over-all accuracy of measurement is improved to about 0.001 percent (ten parts per million).

The instrument provides a series of harmonics of a nominal 1-megacycle signal, whose fundamental is adjustable over a range of 1 percent. At the 100th harmonic and above, therefore, complete coverage from one harmonic to the next is obtained. Consequently, when a frequency lying between 100 and 200 megacycles is measured aproximately on a frequency meter, it can be matched and determined accurately with the interpolating frequency standard.

This instrument is designed particularly for use with the General Radio Company's Type 720-A heterodyne frequency meter, which covers a fundamental range of 100 to 200 megacycles. Higher frequencies, up to 3000 megacycles, are measured by using harmonics of the heterodyne frequency meter.

An additional series of harmonics, based on a 0.1-megacycle fundamental, is also generated by the device, for use with the General Radio Type 620-A heterodyne frequency

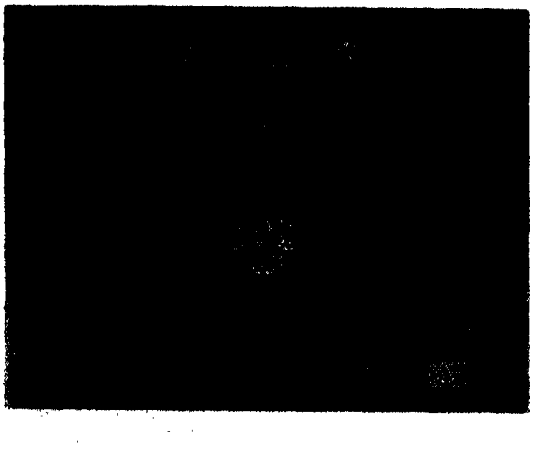

meter, for measurements in the range between 10 and 300 megacycles.

The adjustable frequency generated by the interpolating frequency standard is determined primarily by a quartz-crystal oscillator. If increased accuracy is desired, the system can be standardized periodically in terms of standard-frequency radio transmissions from the National Bureau of Standards Station WWV.—General Radio Company, *275 Massachusetts Avenue, Cambridge 39, Massachusetts.*

Sky Compass

The National Bureau of Standards has developed a sky compass which indicates the direction of flight from which, with other data, the position of aircraft can be determined. The sky compass is based on the investigations made by the late Dr. A. H. Pfund, of The Johns Hopkins University, and is an outgrowth of his twilight sextant.

The Pfund sky compass, not to be confused with the sun compass, operates on the principle that the light of the sky during the day is partially plane polarized, the polarization being a maximum at right angles to the incident beam from the sun. The plane of polarization at any point in the sky thus contains both the observer and the sun. Establishment of this plane also gives direction since it points to (or away from) the sun.

The principal advantage of the sky compass over the sun compass (which measures the direction of the sun directly) is its use during twilight, and when the sun is several degrees below the horizon, as well as when the region of the sky containing the sun is overcast, so long as there is a clear patch of sky overhead. The sky compass is thus of particular value when the sun compass and the sextant are not usable. Since the extent of polarization of the sky's light is greatest at right angles to the incident beam of sunlight, the compass is most accurate in the polar regions, where it is also most useful, because of the long duration of twilight and the weakness and inaccuracy of the magnetic compass at high latitudes.

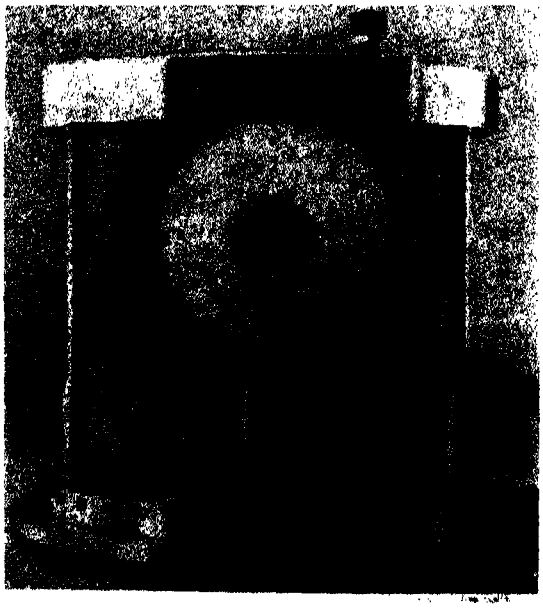

Essentially, the sky compass consists of an analyzer for determining the plane of polarization of the light, an azimuth circle on which the sun's computed azimuth can be set, and a clock which drives a chosen reference line in synchronization with the sun's apparent motion, that is, one revolution in 24 hours. For convenience in observing a portion of the sky around the zenith through the analyzer, the analyzed beam is turned from vertical to horizontal by means of a mirror.

The analyzer consists of a circular sheet of polaroid and a star-shaped half-wave plate of cellophane placed over the center portion of the polaroid. As the compass is turned, the intensity of the light seen through the polaroid will change. If the light source is completely plane polarized, the intensity variation will include two maxima and two minima (zero intensity) in one complete revolution, the maxima occurring in the plane of polarization, the minima, at right angles to it. In general, the sky light will be only partially polarized, so that the minimum intensity will not be zero. Even when the maximum is pronounced with respect to the minimum, it is difficult for the human eye to judge with much exactness when this maximum occurs. To facilitate accurate judgment, the half-wave plate is used to rotate the plane of polarization of the light by an angle which depends on the orientation of the plate's "optical axis" to the plane of polarization. When the optical axis of the half-wave plate is parallel to the plane of polarization, it does not rotate; when it is at right angles to it, the plane of polarization is rotated 180°, or effectively not at all. Thus, at four points in every revolution, when the optical axis is 0°, 90°, 180°, and 270°, the half-wave plate will not rotate the plane of polarization.

Using this effect, together with that of the polaroid, a setting may be made by matching the intensities rather than by estimating maximum intensity. The light which has passed through the half-wave plate appears in the form of a star at the center of the field of view of the instrument, on the background of the light which has passed only through the polaroid. At four points in a complete revolution, as indicated above, the intensity in the two light paths will be the same, and the field will blend into a homogeneous whole. Two of these matches will be "dark," the other two will be "light," so that a light match determines the plane including the sun, and it is necessary to be able to distinguish only the general directions "toward" and "away from" the sun.

On the ground, an accuracy of 1° may be obtained in measuring the sun's direction. On an airplane, the accuracy is expected to be somewhat less with the experimental model, because of such factors as difficulties in leveling. Both the accuracy and simplicity of use increase as either the north or south pole is approached, because of the lower altitude of the sun and because the deviation of the sun's azimuth from that corresponding to local apparent time is negligible. The compass may be read when the sun is as much as 7° below the horizon, but accuracy drops quickly when clouds obscure the zenith.—National Bureau of Standards, *Washington 25, D. C.*

Projection Oscilloscope

Beta Model 701 portable projection oscilloscope, compact in size, produces a large-size picture which can be viewed by a group of people. Important and obvious uses of this oscilloscope are in educational institutions, where it is desired to show oscillograms of various wave forms to groups of students. The trace on the screen is bright enough to be viewed in a normally lit classroom. The oscilloscope can be used at seminars and lectures, for industrial monitoring, in experimental work, and wherever it is desired to display electrical wave forms to a group of people.

The oscillogram presented on the screen is approximately 16 in. wide and 12 in. high. When folded, the cabinet is 13 in. wide, 16 in. high, and 19 in. deep. The screen upon which the oscillogram is projected is contained inside the cabinet, when folded for carrying. The complete unit weights approximately 60 lb.; a carrying handle is provided.

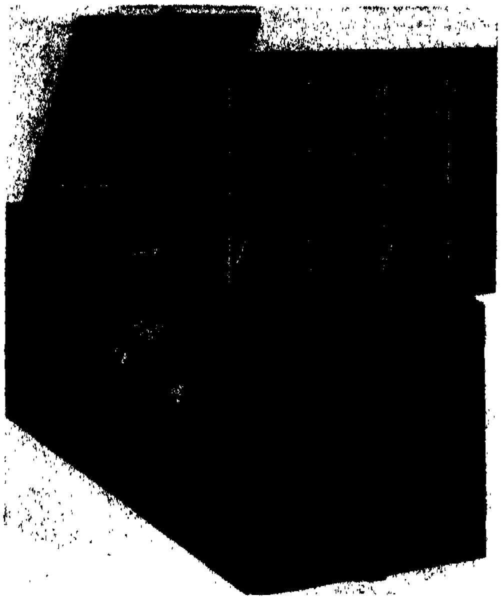

The vertical amplifier response of the Model 701 PPO is good to 50 kc and usable to 100 kc. Horizontal sawtooth sweeps are good to 2 kc and usable to 5 kc. Vertical deflection sensitivity is approximately 60 mv (r.m.s.) per inch, or 0.6 v for full scale deflection; horizontal deflection sensitivity is 0.65 v (r.m.s.) per in., or 1.0 v. full scale.

The controls of the Model 701 PPO include on-off, intensity, focus, coarse and fine amplitude, sync amplitude, vertical and horizontal centering, vertical and horizontal gain, sweep selection (internal or external), and retrace blanking. Provisions are made for external, 60-cycle, or internal sweep synchronization. The "Norelco" projection system is employed.—Beta Electric Corporation, *1762 Third Avenue, New York 29, New York.*

Signal Generator

The Model 614A UHF signal generator is a new signal generator for fast, direct readings between 800 and 2100 mc. The new instrument does away with charts and interpolations, since readings are made direct in either microvolts or decibels. For ease of operation, carrier frequency is also set and read directly on a large central tuning dial.

This signal generator has an internal impedance of 50 ohms, and accuracy is ±1 decibel throughout the frequency range. R-f output ranges from 0.1 volt to 0.1 microvolt and may be continuous, pulsed, or frequency modulated at power supply frequency. The instrument can be modulated either externally or internally and may be synchronized with positive or negative pulses or sine waves.

The -hp- Model 614A is designed for convenience in making the following measurements: receiver sensitivity and alignment, signal-to-noise ratio, conversion gain, standing wave ratios, antenna gain, and transmission line characteristics.—Hewlett-Packard Company, *395 Page Mill Road, Palo Alto, California.*

Recording System

The AIL Type 373 rectangular coordinate recording system provides, in Cartesian coordinates, an inked plot of voltage, or of the logarithm of voltage, as a function of the displacement angle of a measured element. Usable chart width is ten in., corresponding to a voltage range of 10,000 to 1, or 80 db. Both pen and paper feed are servo controlled with chronograph paper feed optional. Maximum pen speed is 40 in. per sec., equivalent to 320 db per sec. At full scale expansion, the maximum paper feed rate is 10 in. per sec.

The system finds application whenever it is desired to record voltage as a function of time or an angle. It can be used for recording light intensities, sound pressures, and heat levels at writing rates higher than formerly available. As originally designed to plot logarithmically the field strength pattern of narrow beam radar antennas, the system consists of a selective amplifier, pen and paper servo amplifiers, a power supply, and the recorder. The system operates from 115 volts, 60-cycle power, and can be supplied in portable carrying cases or in standard rack and panel construction.—Airborne Instruments Laboratory, *160 Old Country Road, Mineola, New York.*

Slotted Line and Video Oscilloscope

The FTL-30A slotted line is a precision device designed for making impedance and wavelength measurements in the range of 60 to 1000 mc per sec. Measurements can also be made with somewhat slightly reduced accuracy in the range between 1000 and 2000 mc. It is a coaxial line 250 cm long having a surge impedance of 51.0

ohms+0.5 ohm. Fine design features and highly precise machining and components used in the fabrication of the line, together with great structural rigidity, assure enduring accuracy.

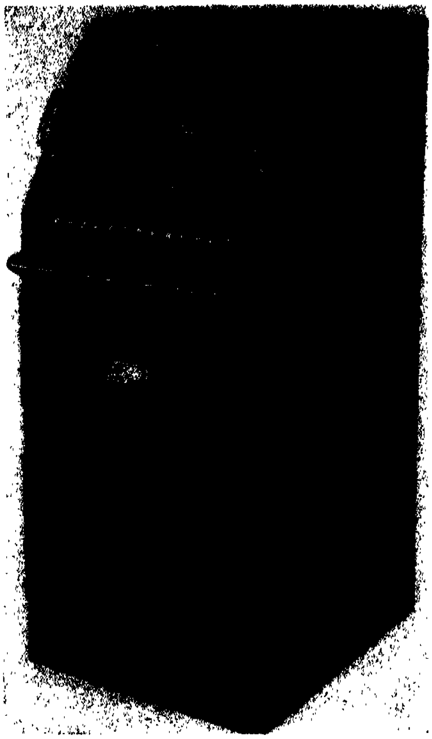

The FTL-32A oscilloscope enables the observation of wave forms having frequency components as high as 50 mc per sec. and as low as 10 c.p.s. This wide band frequency response is obtained with sufficient amplification to provide deflection sensitivity of 0.1 peak to peak volts per inch. The horizontal amplifier has a band width of 10 c.p.s. to 10 mc. Both repetitive and triggered sweeps are incorporated with time durations consistent with the 50-mc band width. Synchronization from either an internal or external source is independent of the synchronizing signal amplitude, provided a minimum of 0.1 v is exceeded.

The oscilloscope is housed in a castered console cabinet. The cabinet outline is such as to provide convenient space to rest other instruments on the top surface, and a drawer which will accommodate all probes, accessories, and other small-laboratory instruments.—Federal Telecommunication Laboratories, Inc., *500 Washington Avenue, Nutley 10, New Jersey.*

Electronic Motor Control

A new simplified circuit for stepless speed control of fractional horsepower motors makes possible an economical electronic control system without sacrificing desirable operating features. Operating from either a 110-v or 220-v (50–60 c) a.c. power source, the power unit utilizes full-wave gaseous rectification to supply both the armature and field of a specially designed, ball bearing, d.c. motor. The magnitude of the voltage furnished to the armature is controlled by an electrical "brain" which reacts to change in motor load or upon instructions from the operator.

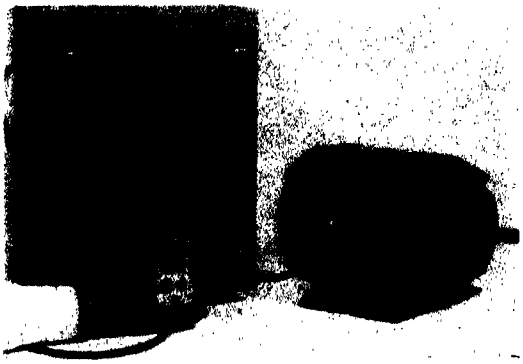

The control unit, which can be at a considerable distance from either the motor or power unit, permits the selection of any desired speed over a range greater than 20 to 1 (80 r.p.m. to 1800 r.p.m. standard, other speed ranges available). The selected speed is maintained substantially constant from no load to full load. An "idle" switch on the control unit is used to start or stop the motor without changing the speed setting.

Reversing control units are available at small additional cost. The specially designed motor in connection with dynamic braking permits applications incorporating the reversing feature to achieve full speed reversals within one second.

Two models are available which include various type motors up to and including ¼ hp. Most types are available for immediate delivery from stock.—Servo-Tek Products Company, *4 Godwin Avenue, Paterson 1, New Jersey.*

Vibration Measurements

Type 410-X5 vibration integrator, and Type 410-X6 calibrated vibration pick-up, enable convenient measurement of vibration displacement, velocity,

and acceleration in the audio frequency range. These instruments were designed for use with the Type 410-A sound level meter.

With Types 410-X5 and 410-X6, displacement can be measured from 0.14μ in. to 0.028 in.; velocity from 51.3μ in. per sec. to 10.3 in. per sec.; and acceleration from 0.15 in. per sec. per sec. to 3900 in. per sec. per sec. over a frequency range of 25 to 3000 c. Response is flat from 60 to 1000 c.

Easy operation requires only that the Type 410-X5 vibration integrator be inserted in place of the microphone on the sound level meter. Small size enables the vibration pick-up to be held in one hand while readings are taken from the sound level meter held in the other hand. A tripod is available for fixed positioning of the sound level meter, and a table is provided for converting decibels to units of displacement, velocity, and acceleration.—HERMON HOSMER SCOTT, INC., *385 Putnam Avenue, Cambridge 39, Massachusetts.*

Viscosimeter

The Texaco viscosimeter is an instrument available for the study of plastic fluids and thixotropic suspensions. Applications are suggested in laboratories dealing with the study of non-Newtonian fluids, such as drilling muds, cement, concrete, adhesives, asphalt, paint, plastics, ceramics, and certain food products.

The viscosimeter is designed to accommodate either the specially designed laminar cup and rotor, or a standard Stormer cup and rotor, for making comparative Stormer readings. A synchronous motor drives the rotor through a geared shaft system and a five-speed transmission, with no clutches to slip. Rotor speeds of 100, 225, 400, 600, and 900 r.p.m. are provided. A stroboscopic arrangement on the shaft provides a convenient check on the synchronization of the motor.

The sample cup and water bath rest on the torsion table. Thus, the torque of the rotor is transmitted through the sample directly to the torsion table, in proportion to the viscosity of the sample. The table is free to rotate through about 150°, and the deflection is indicated on a dial mounted on the table.

The torsion table hangs suspended by a heat-treated beryllium-copper torsion wire. This torsion wire is secured in a vernier-calibrated torsion head at the top of the instrument. Another wire from the under side of the table provides for proper tension on the torsion wire and centering of the table.

By rotating the torsion head, the table may be returned to zero deflection. This eliminates any torque effect from the lower wire and increases the deflection range to the elastic limit of the torsion wire. The correct deflection may then be read very accurately from the vernier scale of the torsion head.

By proper selection of motor sizes, gear ratios, and torsion wires, great flexibility of operation is available.—SOUTHWESTERN INDUSTRIAL ELECTRONIC COMPANY, *2831 Post Oak Road, Houston 19, Texas.*

Miniature Adjustable-Speed Drive

New design possibilities are created by the introduction of the new Metron miniature variable-ratio speed changer, which weighs less than 6 oz. It can deliver up to 70-oz.-in. torque and 0.025 hp. Possible applications include business machines, recorders, controllers, computers, indicating mechanisms, and similar devices.

The ratio of input to output speeds is infinitely adjustable between 1:6 increase and 6:1 decrease, with a total speed range of 36 to 1. A dial and pointer indicate ratio setting, and the adjusting knob is equipped with friction drag to prevent ratio wander. Efficiency, speed regulation, and no-load loss characteristics are good. Maximum output torque is obtainable at zero speed, and operating speeds as high as 20,000 r.p.m. are practical.

Internal construction employs rollers contacting disks on input and output shafts. Speed is adjusted by changing the radius at which the rollers make contact. Novel "lock-up" devices are provided to increase contact pressure automatically when the load torque is increased, insuring high maximum output torque, minimum reduction in speed with increased load, and at the same time providing low loss when lightly loaded. Other design features are ballbearings on all rotating parts, permanent lubrication, overload protection, and sealed construction.

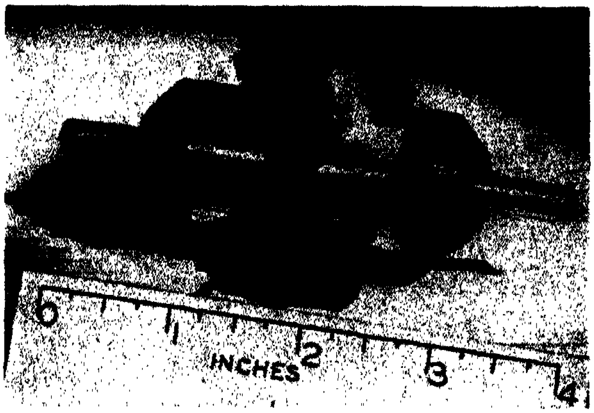

This variable unit complements the Metron fixed-ratio speed changer, having the same body diameter, mounting foot, and shaft height above the mounting surface. As a result, fixed-ratio gear sections can be supplied integral with the variable-ratio unit to obtain any nominal output speed range, and the unit can be driven by any speed motor without loss in horsepower rating.—METRON INSTRUMENT COMPANY, *432 Lincoln Street, Denver 9, Colorado.*

Sensitive Integrator A new industrial integrator, Model 808, provides means for simple and effective integration of d.c. potentials or currents with respect to time. Fundamental elements of the integrator are the Weston Model 806 integrating relay, an electronic relay circuit with associated sealed reed type relays, and a counting mechanism. The Model 806 is the primary element, operating the relay circuit to initiate an oscillatory action, the frequency of which is proportional to the input. The counter totalizes the number of cycles to provide a running time-integral of the input.

The unusual sensitivity of the Model 808 integrator makes it ideal for applications in light integration (using a photronic photo-electric cell) totalizing the amount of light, d.c. ampere-hour integration from low potential shunts, watt-hour integration using thermal converters, total radiation integration using thermopiles, integration of nuclear radiation (in combination with Geiger counters or ionization chambers), and integration of quantities measured by changes in transmitted light.

The unit is chassis mounted and enclosed in a cast aluminum weatherproof case. Unlimited service life may be expected, according to the manufacturer, with routine vacuum tube replacements only at about 2000 service hour intervals.—Weston Electrical Instrument Corporation, *617 Frelinghuysen Avenue, Newark 5, New Jersey.*

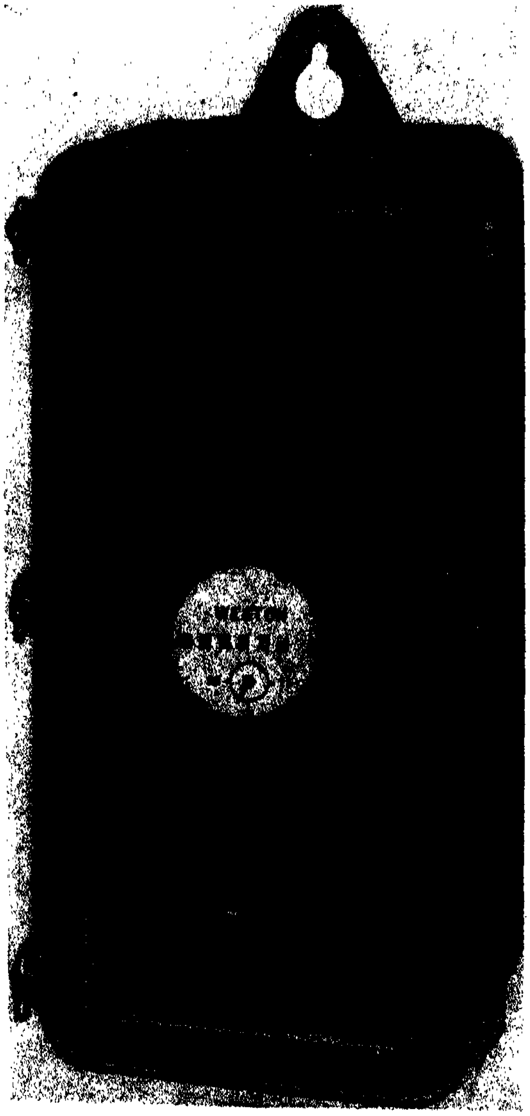

Phase Meter Type 320-A phase meter makes possible the measurement of phase difference between two voltages at audio- and supersonic frequencies, essentially independent of voltage amplitude, frequency, and wave shape. Direct readings of phase angle are indicated on a panel-mounted meter having four full-scale ranges of 360°, 180°, 90°, and 36°. 180° phase-reversing switches are provided for each channel, so that the expanded 90° scale may be moved to any of the four quadrants.

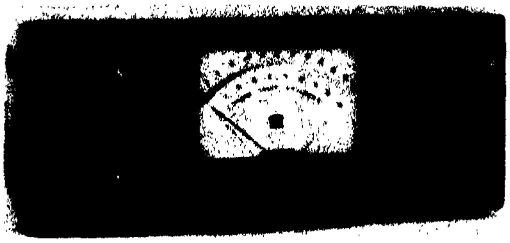

In the phase meter, the two signals being compared are converted into two trains of short pulses, which occur at the zero-axis crossings of the respective signals. The time displacement between corresponding pulses of the two pulse trains is indicative of the phase angle between the two signals. The pulse trains are fed into a "flip-flop" circuit, which measures the ratio of time displacement to the pulse repetition period. For a given phase angle, this ratio is independent of frequency.

The frequency range of the phase meter is 20 c.p.s. to 100 kc. Sufficient meter damping is provided to permit satisfactory use of the instrument at frequencies as low as 2 to 5 c.p.s. With the 180° phase-reversing switches in the same corresponding positions, and over the frequency range 20 c.p.s. to 100 kc, accuracy is within 2 percent of full scale, or 3.5°, whichever is larger.

Terminals for connecting a recorder are provided at the back of the instrument. The power consumption is approximately 100 watts, 105–125 volts, 50–60 c.p.s.—Technology Instrument Corporation, *1058 Main Street, Waltham 54, Massachusetts.*

Manufacturers' Literature

Laboratory Equipment— No.49 3 34, 16-page *Announcer*, contains an article "The evolution of modern glasses" and information on new laboratory equipment.—Geo. T. Walker and Company, *324 Fifth Avenue South, Minneapolis, Minnesota;* Burrell Technical Supply Company, *1942 Fifth Avenue, Pittsburgh 19, Pennsylvania;* Eberbach and Son Company, *200 East Liberty Street, Ann Arbor, Michigan.*

Instrumentation—Quarterly publication, Vol. 3, No. 6, 32 pages, contains articles on measurement and control in industrial processes and an article on electrolytic conductivity.—Minneapolis-Honeywell Regulator Company, Brown Instruments Division, *Wayne and Roberts Avenues, Philadelphia 44, Pennsylvania.*

Reticles—Reticle Production is a technical bulletin describing the new photographic, mechanical, and high vacuum techniques employed in producing precise reference lines in the focal planes of optical systems.—W. AND L. E. GURLEY, *Troy, New York.*

Liquid Level Transmitter—Bulletin 98069, 4 pages, explains operating principle, design features, and gives application drawings of Taylor force-balance liquid level transmitter.—TAYLOR INSTRUMENT COMPANIES, *Rochester 1, New York.*

Altimeter—Publication No. T.P. 24A, 4 pages, describes sensitive altimeters designed for quick, accurate results in such applications as aerial surveys, topographic mapping, gravity meter surveys, and profiles for highway locations.—WALLACE AND TIERNAN PRODUCTS, INC., *Belleville 9, New Jersey.*

Tracerlog—No. 17, 12 pages, features a 7-page article on radioautography.—TRACERLAB, INC., *55 Oliver Street, Boston 10, Massachusetts.*

Radioactivity—New 36-page catalog of instrumentation for radioactivity.—NUCLEAR INSTRUMENT AND CHEMICAL CORPORATION, *223 West Erie Street, Chicago 10, Illinois.*

Nuclear Research—Brochures describe two new scalers, Model 2000 automatic scaler and Model 1000B scaler.—BERKELEY SCIENTIFIC COMPANY, *Sixth and Nevin Avenue, Richmond, California.*

Vacuum Tubes and Applications—Application notes AN-139, 8 pages, "Characteristics of pentodes and triodes in mixer service." Application notes AN-138, 4 pages, "Mixer-oscillator circuit for f-m and a-m RCA-6J6 or RCA-19J6." Booklet CTV-1004, 32 pages, "RCA television components for kinescope RCA-16AP4." Technical bulletins on the following: RCA-715-C pulse amplifier tetrode, RCA-5825 half-wave rectifier tube, RCA4-65A VHF power tetrode, RCA-16AP4 16-inch "metal" picture tube, RCA-5763 VHF beam power amplifier, RCA-3RP1 3-inch oscillograph tube, RCA-12S8-GT triple diode—high mu-triode, RCA-5794 fixed-tuned oscillator triode for radiosonde service at 1680 mc, RCA-408S3 8-inch PM Speaker.—TUBE DEPARTMENT, RADIO CORPORATION OF AMERICA, *Harrison, New Jersey.*

The Capacitor—Vol. 14, No. 4, 16 pages, contains an article on simple methods of measuring inductance of air-core and powdered-iron-core coils.—CORNELL-DUBILIER ELECTRIC CORPORATION, *Hamilton Boulevard, South Plainfield, New Jersey.*

Thin Resistors—Bulletin 138 describes new, wire-wound, vitreous-enameled thin-type resistors. Dimensional drawings of resistors and a table of values of resistance are given.—OHMITE MANUFACTURING COMPANY, *4835 Flournoy Street, Chicago 44, Illinois.*

Motors—Bulletin No. 49-A describes twenty models of hysteresis type fractional hp motors available in one-, two-, and three-speed units.—ELECTRIC INDICATOR COMPANY, *Stamford, Connecticut.*

Temperature-Compensated Relay—Application notes No. 3 give complete description and listing of a new temperature-compensated relay, for operation at constant voltage regardless of temperature or at decreasing voltage with increasing temperature.—SIGMA INSTRUMENTS, INC., *45 Ceylon Street, Boston, Massachusetts.*

Reflectogage—Bulletin 3700 describes theory and general application of the Sperry Reflectogage to non-destructive measurements of plate and sheet stock, tanks, pipe, etc.—SPERRY PRODUCTS, INC., *Danbury, Connecticut.*

Rectifiers—**Rectifier News**, A new 4-page periodical will feature technical articles and circuits concerning new developments in dry-plate rectifiers. Subscriptions available without charge if requested on company stationery.—INTERNATIONAL RECTIFIER CORPORATION, *6809 South Victoria Avenue, Los Angeles 43, California.*

Nickel Alloys—Technical bulletin T-3, 44 pages, discusses the resistance of high nickel alloys to corrosion by sulfuric acid. The bulletin contains tables, charts, and photographs, in addition to text material covering over 30 various nickel-bearing materials.—THE INTERNATIONAL NICKEL COMPANY, INC., *67 Wall Street, New York 5, New York.*

New Materials

Forest K. Harris: Associate Editor
in Charge of this Section
National Bureau of Standards, Washington, D. C.

Industrial Preservative

Milmer 1, copper-8-quinolinolate, is capable of protecting a wide variety of industrial products from degradation by microorganisms. It is claimed by the manufacturer to be one of the most powerful rot and mildew preventatives known; virtually non-toxic to man, it does not irritate or sensitize the skin and is not decomposed or deactivated by ultraviolet light. It is also heat stable, resists leaching, and is not lost to the atmosphere. A 15-page bulletin has been prepared by the manufacturer on the basis of extensive laboratory and field experience, giving a description of the material, and methods of formulation and application to protect textiles, plastic-coated fabrics, protective coatings, and other products.

Although it is extremely difficult to remove *Milmer 1* from textiles, present knowledge does not indicate that it forms a chemical bond with cellulose or other fibers on which it is used. Since long term protection depends on its retention in the fabric, the carrier or resin finish which bonds the preservative to the cloth fibers must be of a permanent nature. In paints and plastic coatings the material to be preserved acts as its own bonding agent. In soft textiles, however, it must be bound by a carrier or a textile finish. The permanence of the protection depends largely on the permanence of the vehicle that holds it in the fabric. Beyond this the only critical point is adequate concentration of the preservative in the finished fabric. In most cases, a concentration of approximately 1 percent by weight is recommended and gives a reasonable safety factor to assure adequate protection over long periods of severe exposure. In plastic-coated fabrics it has a dual protective role. It must not only protect the base fabric, but also prevent the growth of fungi on the plastic coatings which may contain plasticizers or other nutrient materials of animal or vegetable origin. Commercial paints, lacquers, or varnishes may themselves be nutrients for microorganisms or they may be applied to materials which are susceptible to attack. Where film clarity or color is not of primary importance, *Milmer 1* may be added as a pigment; special formulations must be used, however, for clear films. Asphalt used for impregnating cotton in the manufacture of wire and cable insulation has been found to be very susceptible to attack by microorganisms but is completely protected by the addition of 1 percent of the preservative. In this connection it is interesting to note that recent tests indicate that measurable increases in conductivity in plastic insulation can be traced to fungus growth on the surface. This increased conductivity is assumed to be due to the hygroscopic nature of the fungal growth which causes the insulating material to absorb excessive moisture. The use of a fungicide in the formulation of extruded plastic insulation shows promise of cutting down these losses.—MONSANTO CHEMICAL COMPANY, *St. Louis 4, Missouri.*

Felt Gaskets

Chrome-Lock is a specially compounded felt, containing zinc chromate as a corrosion inhibitor, designed for protective gasketing or sealing-in flanged, lapped, or butted joints. Under bolted, screwed, or nailed pressure the resins traverse within the felt and are extruded onto the faying surfaces sufficiently to form a positive dam. The resultant seal will exclude or retain air, water, dust, and other materials. It has a pressure-sensitive backing, making it simple to apply even on vertical or inverted surfaces. It is stated to remain pliable indefinitely, and to resist permanent distortion (75–100 percent recovery after pressure release) insuring stability in storage and unlimited service life. Under bolted pressure it fills in surface irregularities in the joint as well as in and around bolt and rivet holes, reducing or eliminating the need for expensive machining. It's compressibility and laminating quality permit low bolt pressures and, consequently, light flanges. The resins extruded on the joint facings hold the metal in a passive state, preventing rust in new installations, arresting it in old installations and inhibiting electrolytic action between dissimilar metals. Its continued pliability and cushioning qualities provide protection against vibration and mechanical shock, and its use is suggested by the manufacturer for new or replacement gasketing in electrical instruments. It is available in thicknesses from $\frac{1}{32}$ to $\frac{1}{4}$ inch and in widths from $\frac{3}{16}$ to 72 inches. Where non-flammable installations are required, *Chrome-Lock Type N* may be specified. Samples and Engineering Folder PRC-1021 may be obtained from the manufacturer.—PRODUCTS RESEARCH COMPANY, *5426 San Fernando Road, Glendale, California.*

Protective Coating for Metals

Metalast, based on vinyl and other resins, is a protective coating applicable to any metal and is designed to prevent corrosion, fouling, and abrasion. It can be applied at any temperature between 5°F and 90°F, dries in less than 20 minutes, and is unaffected by temperatures up to 200°F. It is stated to be characterized by extreme chemical inertness, excellent toughness and flexibility, good clarity, non-flammability, and high resistance to aging and weathering.—C. A. WOOLSEY PAINT AND COLOR COMPANY, *229 East 42 Street, New York, New York.*

Nylon Anode Bags

Nylon bags have been developed for covering nickel, copper, silver, zinc, and other metal anodes used in electroplating solutions. They are stated to be over 50 percent stronger than comparable cotton bags and to retain their strength in acid or alkaline solutions at temperatures up to 150°F. For example, in a bright nickel-plating solution operating at a *p*H of 3.5, no measurable change in tear or bursting strength could be determined after 2 months immersion. The bags are usually supplied 4 inches longer than the anode to allow for sludge accumulation and are provided with a nylon draw cord. Their cost is stated to be less than, or equal to, comparable cotton bags.—ENTHONE, INC., *442 Elm Street, New Haven, Connecticut.*

New Nickel Alloys

Recent alloys, developed primarily for electronic applications, include 4 which are essentially pure nickel. These are designated as *220, 224, 225,* and *230* nickel. Principal applications are for cathodes, anodes, and other structural parts of vacuum tubes, furnace lead-in wires, support wires in incandescent lamps, etc. *Monel 326* represents a slight variation from conventional monel to make it non-magnetic. Its principal uses are for cable shielding, mass-spectrometer parts, structural parts of cathode-ray tube guns and vacuum tubes, and compressed knit mesh for shielding gaskets.—INTERNATIONAL NICKEL COMPANY, *67 Wall Street, New York 5, New York.*

Strong Laminate

Formica RN-30 is a new laminate reported to have greater and more uniform strength, to machine better, and to have a smoother finish and better electrical properties than fabric-based laminated plastics now in common use for cams, pinions, gears, bearings, and similar applications. Woven, fabric-base laminates which are widely used in mechanical and electrical applications have a definite weakness; although they have good strength parallel to the weave in both directions, they have poor strength diagonally. The new laminate has uniform strength in all directions, due to the matted, unwoven cotton fibers distributed evenly throughout. Parts made from it wear more evenly because of its uniformity. The smooth finish sometimes required in special applications, and previously obtainable only in premium linen grades, is now available in this laminate at lower cost. It is stated to be smoother in texture than even the fine-weave linen laminates.—THE FORMICA COMPANY, *Cincinnati 32, Ohio.*

Plastic Field Lens

The *Kodak Ektalite Field Lens* is a thin flat plastic lens whose surface is molded into a series of concentric grooves which refract light in the same manner as the unbroken curve of a glass lens. Its weight is about 10 percent of that of a comparable glass lens of conventional shape and it can be produced far more cheaply. While it is not a precision lens, it is expected to find applications as a television magnifier, inspection lens, etc. It is already used in the viewing system of the "Kodak Reflex II" camera and in the "Kodaslide" viewer. Its advantages are not limited to the fact that it can duplicate the performance of a conventional lens; its lightness makes possible lenses of large area which could not be made economically by conventional means. Furthermore, spherical aberration, common to simple lenses, is almost eliminated by the thinness of the plastic lens. It is produced by molding flat sheet stock in a brass mold. The manner of forming the ridges in cutting the mold determines the characteristics of the lens. There are over 200 ridges to the inch, reproducing the curvature of segments of a conventional lens. Near the edge the groove faces are inclined at a rather steep angle and they become flatter as the center of the lens is approached. Light entering through the back of the lens passes out through the arc-sided grooves and is refracted just as it would be in a conventional lens.—EASTMAN KODAK COMPANY, *Rochester 4, New York.*

THE
REVIEW OF SCIENTIFIC
INSTRUMENTS

VOLUME 20, NUMBER 7 *JULY, 1949*

A Direct Reading Pulse Length Meter and Shape Analyzer

ROBERT RUDIN*
Bell Telephone Laboratories, Murray Hill, New Jersey

(Received December 20, 1948)

An electronic circuit is described which allows determination of the length and shape of a voltage or current pulse in the microsecond range, by measuring the pulse duration at different levels of the pulse and reading these figures directly on a meter. Comparison with other measuring methods shows good agreement of the results.

THE instrument described in this article was designed to measure the duration of repeated current or voltage pulses and to determine the form of the pulse by measuring the width at different heights. These measurements are especially important in studying the operation of pulsed devices of which the magnetron is an example, and in the accurate investigation of modulators for producing the pulses.

The cathode-ray oscilloscope is generally used for the analysis of the pulses in electronic circuits. Although the shape of the pulse can obviously be observed in great detail, precise quantitative measurements are difficult and of limited accuracy, largely because of difficulties related to the sweep circuit. This is especially true when delay networks must be introduced. A calculation of the pulse length, for instance, at the average pulse height can be made by measuring the recurrence frequency, the average current and the peak current; but this latter measurement is difficult and may be unreliable unless special arrangements are used and all sources of error have been carefully eliminated. The circuit described below has therefore been developed in an effort to determine pulse shapes and dimensions independently of the oscilloscope.

In order to explain how the circuit works, let us first consider a simplified circuit which would measure the duration of a strictly rectangular pulse, as indicated in the schematic diagram Fig. 1.

THE BASIC CIRCUIT

The current pulse is carried through a resistor R_0 and the voltage developed by the drop is applied to the control grid of V_1 which is normally conducting, but is biased beyond cut-off by the pulse. If the voltage of the pulse is appreciably higher than the voltage required for cut-off, the time during which V_1 is nonconducting will depend only on the duration of the pulse and not on its height. The plate current of V_1, in flowing through R_1, biases V_2 beyond cut-off so that V_2 will conduct only during pulses. In flowing through R_L, the plate current of V_2 thus produces at the plate of V_2 a negative voltage pulse whose amplitude is determined by the constants of V_2 and the circuit elements, and whose duration is equal to that of the pulse through R_0.

These constant voltage pulses pass through C_1, R_3 and the diode V_3 and charge the combination

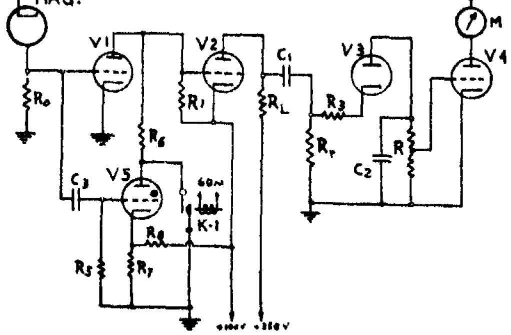

FIG. 1.

---

* Present address: Physics Department of Columbia University, New York 27, New York.

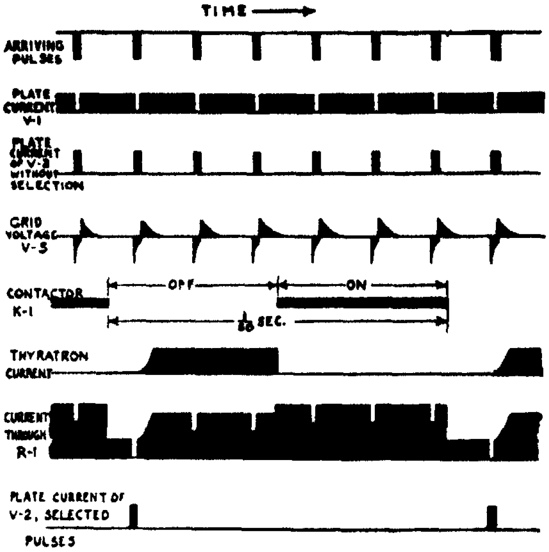

FIG. 2.

C_2-R which has a time constant of approximately 0.5 second, to an average voltage which depends only on the time for which V_2 conducts. A fraction of this voltage is applied to the grid of the meter tube V_4, reducing the plate current with increasing voltage across C_2, so that the reading of the meter M will depend on the number of coulombs delivered to C_2 through the diode and the rate of discharge through R. This circuit therefore gives a meter reading depending on the product of pulse length and recurrence frequency. A direct calibration of the meter in pulse length is possible only when the recurrence frequency is known. As it was desirable that the instrument read pulse duration directly and that the reading be independent of recurrence frequency, a constant "local" recurrence frequency of pulses reaching V_2 is introduced. This is accomplished by a selection of pulses, passing only a predetermined number of pulses per second through the measuring channel.

THE PULSE SELECTOR

The plate of a thyratron V_5 is connected, through a resistor R_6, to the plate of V_1. The cathode is biased to a positive potential of about 20 V through R_7 and R_8 so that no plate current flows. The grid is connected to the pulse input through a differentiating circuit C_3R_5 having a time constant short in relation to the pulse to be measured. When a negative pulse is applied to the input, a negative charge appears at the left plate of C_3 and reaches the grid of V_5 without any effect on V_5 other than to drive the grid further negative with respect to the cathode. But at the decay of the pulse, the negative charge of the left plate disappears, freeing the charge of the right plate, so that a positve voltage impulse appears at the grid, firing the thyratron. V_5 remains conducting even after the positive impulse to the grid disappears. Since its anode voltage is supplied through R_6 and R_1, a current sufficient to cut off V_2 will flow through R_1, even when V_1 is biased beyond cut-off. Thus C_2 will be given no additional charge, because subsequent pulses will not cause V_2 to conduct until the thyratron is extinguished by external means. For this purpose, a relay K_1 is connected across V_5, closing its contact in regular intervals, e.g., at the frequency of the power supply, i.e., 60 times per second. At the closing of the contact, the current through R_1 is actually slightly increased but V_5 is extinguished so that when the contact of K_1 opens, no plate current will flow through V_5 until the next pulse arrives and, at its decay, fires V_5 again through C_3R_5. The action is repeated after every contact of K_1 and as that contact opens the next pulse passes through V_1, V_2, V_3, applies a certain charge to C_2 and at its decay fires V_5 so that subsequent pulses will not pass through V_2.

As the relay closes its contact for about half the time, it remains open for about 1/120 second and when the recurrence rate of the pulses to be analyzed is higher than 120 per second, one pulse will pass at every opening of the relay. The recurrence frequency of pulses arriving at V_3 is therefore 60 per second, independent of the actual recurrence frequency. (Where the electrostatic field of a pulse can be strong enough to ionize the gas of the thyratron, shielding must be used in order to insure correct and stable operation.)

Figure 2 shows diagrammatically the interaction of the different elements. The original pulses, shown in the first line, cause corresponding cutoffs of V_1 (second line) and, without any selection, would result in plate current pulses of V_2 as shown in the third line. The fourth line shows the voltages appearing at the grid of the thyratron as a result of the differentiating elements C_3R_5. The fifth line symbolizes the opening and closing of K_1.

At the beginning of the diagram, K_1 is closed and the thyratron remains extinguished, even during the first pulse. But at the time of the second pulse, K_1 has already opened and, as shown in the seventh line, the current through R_1 has assumed the normal value, as in the second line. This second pulse cuts off V_1 and opens V_2 so that a pulse passes through C_1, V_3, etc. At the decay of each incoming pulse, a positive voltage appears at the grid of the thyratron and fires it. The plate current starts flowing and reaches its full value after a short delay in the microsecond range (ionization time of the thyratron), as indicated in the diagram. The seventh line shows that the plate currents of V_1 and V_5 add through R_1, so that subsequent pulses will not allow V_2 to conduct. With the next closing of K_1

the situation remains nearly unchanged, the current through K_1 substituting for the plate current of V_5. The opening of K_1 causes the circuit to be ready for the next pulse to pass through V_2 and to carry a certain charge into C_2 as indicated in the last line.

THE BIASING CIRCUIT

While the circuit as described above is suitable for measuring the width of rectangular pulses, the pulses encountered in practice usually are not rectangular. In order to measure the pulse width of nonrectangular pulses at any desired height, a bias is applied to the input circuit, rendering it insensitive for the part of the pulse below this level.

As shown in the complete circuit diagram Fig. 3, a diode V_6 is inserted in the path of the incoming pulse. The cathode of V_6 is biased positively with respect to the plate by the adjustable voltage divider $R_{10}R_{11}$. Obviously no current will flow through V_6 unless the voltage of the incoming negative pulse is greater than this positive bias. A small positive bias is also applied to the cathode of V_1 by the cathode resistor R_9. This bias is such that an incoming negative pulse of approximately 0.3 volt, added to the thermionic voltage of V_6, will reduce the plate current of V_1 sufficiently to initiate plate current in V_2 and a pulse voltage of approximately 2 volts will cut off V_1 completely and allow full plate current for V_2.

Now suppose the positive bias to the cathode of V_6 is adjusted to the value of h (see Fig. 4). None of the pulse below h will pass through V_6. As a negative voltage of $dh=2$ volts is sufficient to bias V_1 to cut-off and allow full current to flow in V_2, the measuring circuit will measure the pulse width at a height of approximately $h+dh/2$. In the model developed, the pulse amplitude is adjusted to approximately 30 volts by a method described later and dh is very nearly 2 volts. Since the level h can be varied by the control R_{10}, the width at different

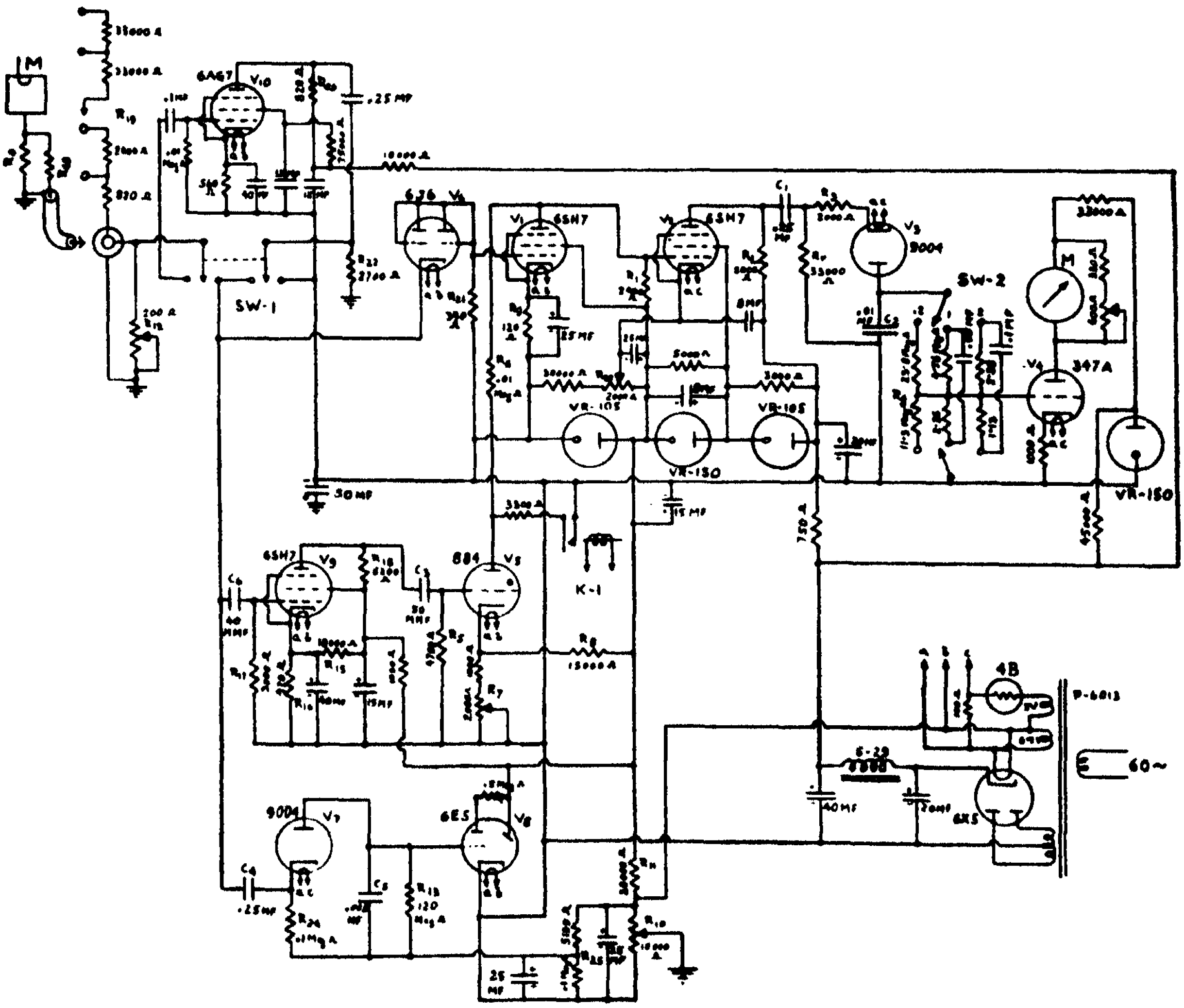

FIG. 3.

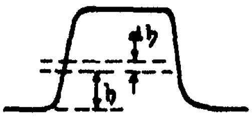

FIG. 4.

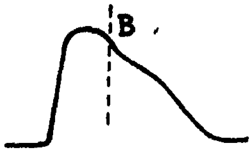

FIG. 5.

heights can be measured and the shape of the pulse thus determined.

PEAK MEASURING CIRCUIT

In order to measure the shape as described in the preceding paragraph, the amplitude of the pulse reaching V_6 must be held to a fixed value irrespective of the amplitude of the original pulse to be analyzed. This is accomplished by adjustment of the variable resistor R_{12} as determined from the measuring circuit consisting of V_7 and V_8. The pulse to be analyzed passes through C_4 and V_7 to charge the peaking circuit C_5R_{13}. The negative voltage developed across C_5 is applied to the grid of the magic eye tube V_8. The grid return is biased, through the bleeder R_{25}, by the positive voltage across the 10,000-ohm control R_{10} which has been fixed to approximately 30 volts.

With no pulse applied and the lower plate of C_5 at cathode potential (by shorting R_{10}), V_8 will be biased by the thermionic voltage of V_7 which is approximately 1 volt and the shadow will be closed about halfway. This position can be marked on V_8 as a reference level. Now since R_{13} is very high compared to the internal resistance of V_7, an incoming pulse charges C_5 to nearly the full peak value. (See later). When the input control R_{12} is adjusted to open the shadow of V_8 to the index mark, the peak voltage of the pulse is very close to the voltage developed across R_{10}; the error is probably less than 2 percent of the pulse height. In the model constructed, R_{10} is a wire-wound potentiometer with a linear characteristic and the position of its slider can therefore be calibrated in percent of pulse height. Its setting will thus define the level, *h*, at which the pulse duration is measured. Accordingly when a pulse is being analyzed, the input resistor R_{12} is adjusted so that the magic eye is opened to the index mark. The width at any setting of R_{10} is then read directly on the dial of the milliammeter in the plate circuit of V_4 as described later.

THE DELAYING CIRCUIT

The meter as thus far described has proved quite reliable for pulses which have a more or less flat top. But if the pulse decays slowly, two difficulties appear: (1) if the decay of the pulse is too slow, the recharge of C_3 will deliver only a very small voltage to the grid of V_5 so that the thyratron will not be fired and V_5 will not remain cut off; (2) if the pulse be shaped as shown in Fig. 5, the rate of decay at *B* can be sharp enough to deliver a positive pulse to the grid of V_5 thus causing it to fire too early and prevent the remainder of the pulse from being analyzed. These two difficulties have been eliminated by the introduction of the delaying tube V_9.

This sharp cut-off pentode (Fig. 3) is biased slightly beyond cut-off by the bleeder R_{15}–R_{16}. The front of the incoming pulse passes through the condenser C_6, drives the grid of V_9 still further negative and has no other effect. However, because of the differentiating action of the circuit C_6–R_{17}, a positive voltage impulse will be applied to the grid of V_9 during the decay of the pulse. This renders V_9 conducting, causing plate current to flow through R_{18}. This causes the left plate of C_3 to become less positive and sends a negative impulse through C_3 which in turn has no effect other than to drive the grid of V_5 still further negative with respect to the cathode. At last, after the completion of the primary pulse which is to be studied, the positive impulse at the grid of V_9 will disappear and current will cease flowing in R_{18}; C_3 will discharge through R_5, as described above, giving a positive pulse which fires the thyratron V_5. By this combination, the thyratron can be fired only after the decay of the primary pulse is complete and premature action is eliminated.

INPUT CONNECTIONS

For the measurement of current pulses, the magnetron current is passed through a non-inductive resistor R_0 of 3 to 6 ohms and the voltage developed is fed to the input through a concentric line, matched at the input by a 68 ohm series resistor R_{68} and loaded by the input control resistor R_{12}. The adjustment of R_{12} will obviously control the input voltage to the circuit.

For the measurement of voltage pulses a tapped low inductive bleeder R_{19} is connected in series with the input control resistor R_{12}; adjusting this resistor changes the voltage drop across R_{12}.

THE PHASE INVERTER TUBE

The arrangement as thus far described operates only on negative pulses since the pulse must drive the grid of V_1 beyond cut-off. In order to measure and analyze positive pulses, a phase inverter tube V_{10} is employed. The pulse to be measured is applied to the grid of V_{10} and the output is then connected ahead of the input to V_6, V_7 and V_9 by a switching arrangement shown in the complete circuit diagram Fig. 3. When the switch is thrown to the left, the control resistor R_{12} is connected to the input to V_{10} and used to bring the pulse applied to V_6, V_7 and V_9 to the proper value as checked by V_8.

STABILITY OF OPERATION

In order to insure a constant calibration certain precautions must be taken. Changes in plate supply voltage of V_4 would affect the reading of the meter, therefore the plate supply voltage is stabilized by a *VR*-150 gas tube. Similarly the screen and plate supply voltage of V_2 is stabilized by a *VR*-105 and *VR*-150 tube in order to keep the voltage drop across R_L constant. The *VR*-105 tube across the plate supply voltage of V_1 is necessary to insure stable operation of the d.c. coupled amplifier stage.

Stabilizing the plate voltage alone is not sufficient to keep the zero readings and the calibration constant, because changes of heater voltage, due to line voltage fluctuations or heating of the power transformer, result in variations of cathode temperature which in turn influence the thermionic voltage (contact potential). Although this change is unimportant in some tubes, there are 4 tubes where any change of thermionic voltage would cause troubles: during the pulse, the grid of V_2 is connected to a positive bias by the control R_{20}. The thermionic voltage will add to this bias and therefore influence the plate current. Similarly a change of the thermionic voltage will affect the zero reading of V_4. The stability of the thermionic voltage of the diode V_3 is of even greater importance, because the thermionic voltage of V_3 adds directly to the voltage across C_2 and any change would show on the meter. The thermionic voltage of V_7 affects the reading of V_8 and although this reading is not critical, the heater of V_7 has also been stabilized, as this could be done without any additional elements. The heater currents are stabilized by a ballast lamp (type *WE4B*) to a heater voltage of 6.3 volts.

The meter cannot be calibrated by comparison methods because no time standards are available. Therefore the calibration must be calculated from the circuit elements. As a matter of fact, the voltage which appears across C_2 can be calculated easily and exactly and the meter can be calibrated by connecting a d.c. voltmeter across C_2 and applying a d.c. voltage corresponding to the calculated value.

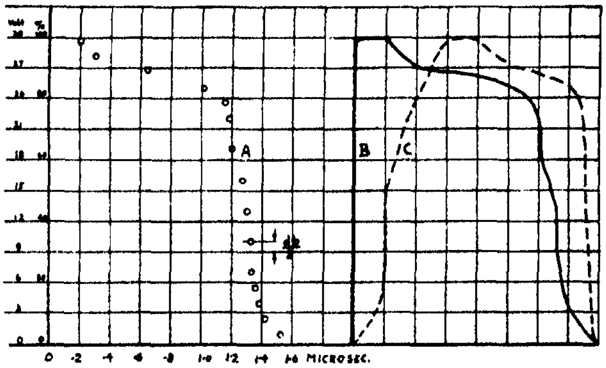

FIG. 6.

When a pulse has been measured at different heights, e.g., at 10 percent, 20 percent · · · 90 percent, the results are then translated into pulse shape. Obviously, pulses shaped like *B* or *C* in Fig. 6 will give the same meter readings, but the experimenter will usually know how to interpret the readings, especially when the pulse is also viewed on a *CR* scope. As an example, the pulse width curve *A* has been drawn from the readings:

Setting	100 percent	95	90	85	80	75	70	60
$h+dh/2$		99	94	89	84	79	74	64
Reading	0	0.20	0.30	0.64	1.02	1.13	1.18	1.20
Setting	50 percent	40	30	20	15	10	5	0
$h+dh/2$	54	44	34	24	19	14	9	4
Reading	1.27	1.30	1.32	1.33	1.35	1.38	1.42	1.52

Comparison of the pulse length as measured by this instrument and as computed from average and peak values shows agreement better than 5 percent in the settings, which is within the limits of accuracy usually expected.

THE REVIEW OF SCIENTIFIC INSTRUMENTS VOLUME 20, NUMBER 7 JULY, 1949

Design for a Metal Mass Spectrometer Tube

W. M. Hickam
Research Laboratories, Westinghouse Electric Corporation, East Pittsburgh, Pennsylvania

(Received March 3, 1949)

A 90° sector type mass spectrometer tube made of Monel is described. The design is such that the electrode assemblies and analyzer section are easily removable without destroying the slit alignment. A double gasket arrangement is used for making the necessary high vacuum seals. The tube can be operated at an elevated temperature with no cold spots which is particularly desirable for degassing and for studying samples which have low vapor pressures. Operation of the analyzer section at any desired potential with respect to ground is permitted.

WITHIN the past few years a number of mass spectrometer tubes have been built for use in routine analysis[1] and research applications.[2–4] The tube to be described in the present paper (it is not in production commercially), permits easy access to and removal of the entire electrode structure and analyzer section. It incorporates features such as simple sealing procedure, operation at elevated temperature with no cold spots, easy slit alignment, and an insulated analyzer section. The ease with which the inner parts of the tube may be changed makes it particularly useful as a research instrument and also satisfactory for routine analysis.

DESCRIPTION

The mass spectrometer tube was constructed of Monel and has a 90° sector with a five-inch radius of curvature. The main envelope parts were machined and then assembled by copper brazing in a hydrogen atmosphere, arc welding, and atomic hydrogen welding. Monel was chosen since it could be welded or brazed satisfactorily, and the atmospheric purity required in a hydrogen furnace for maintaining a clean surface was not as severe as in the alloys containing chromium.

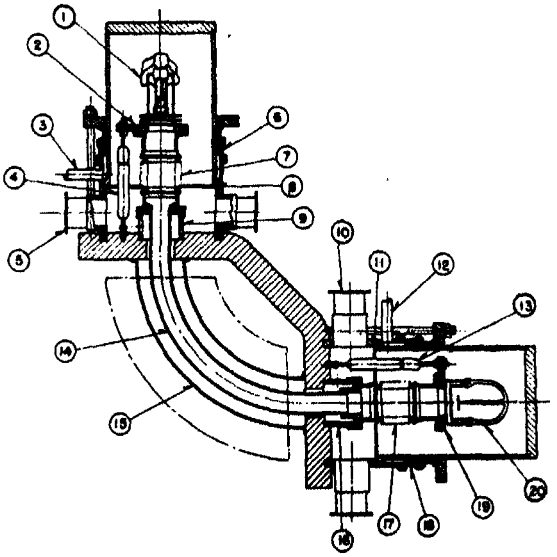

FIG. 1. Schematic of mass spectrometer tube.

Shown in Fig. 1 is a schematic of the mass spectrometer tube. Caps at either end can be easily removed for access to the ion source #1 or exit assembly #20. The sealing of these caps consists of a double gasket arrangement. The inner gaskets #8 and #11 are of 0.020-inch diameter gold wire. The outer gaskets #6 and #18 are of $\frac{1}{16}$-inch rubber sheet. The separation of the gasket surfaces is such that the rubber gasket seals before the gold gasket. Further compression of the rubber gasket permits making the high vacuum gold gasket seal. Pumping leads #3 and #12 serve to maintain a guard vacuum between the rubber and gold gaskets. Six $\frac{1}{4}$-inch studs threaded into the main base plate provide the necessary compression for making the seal. Cooling coils are shown on either side of the rubber gasket. The outer sections to which the cooling coils are attached are of thin wall material to permit greater heat transfer across the inner wall of the guard vacuum region. This permits the gold gasket to be heated along with the rest of the tube. The life of the gold gasket is of the order of 50–100 sealing operations and some three times greater than that of the rubber gasket.

The initial slit alignment procedure is simple and may be carried out in a short time. Removal of the ion source or exit assembly does not destroy this alignment. Mounting rings #2 and #19 have conventional pin stops for orienting the slits. Each of the rings is fastened to three supports such as #4 and #13 through dowels. The dowels, as well as the opposite ends of the mounting ring supports which are threaded into the main base plate, are of Monel. In constructing the supports the Monel parts are drilled such that a $\frac{1}{8}$-inch diameter tungsten rod can fit into the appropriate end. Heating of the Monel and tungsten with an oxygen-acetylene reducing flame results in the Monel wetting the tungsten and giving a very strong joint. The two tungsten ends can then be joined by the central glass section which provides the insulation. In aligning the mounting ring, the six supports are screwed into the main base plate and the tube properly located in a jig to which the mounting rings are attached. Heaters wound on quartz tubing are placed over the glass section of the supports. These serve to raise the temperature of the glass to its softening point and permit locating the dowels such that the slits will be correctly aligned. Annealing of the glass is easily carried out and one merely releases the nuts of the dowels in the cooling process to prevent cracking the glass due to contraction. Although the shrinkage of the glass was neglected in making the jig, it could be taken into account if necessary.

---

[1] J. A. Hipple, J. App. Phys. **13**, 551 (1942).
[2] J. E. Taylor, Rev. Sci. Inst. **15**, 1 (1944).
[3] N. D. Coggeshell and E. B. Gordon, Rev. Sci. Inst. **14**, 125 (1943).
[4] A. O. Nier, Rev. Sci. Inst. **18**, 398 (1947).

Outer #15 and inner #14 analyzer sections are rectangular in cross section. The outer section is machined as a semi-circular channel. This channel is cut in half and welded together to give a 90° arc of rectangular cross section. The inside section is of sheet material cut to the proper dimensions and atomic hydrogen welded along the four corners, followed by cleaning in a hydrogen atmosphere furnace. At either end the inner section fits into metal supports which are insulated from the main base plate by glass cylinders #9 and #16. Holes in the glass cylinders permit pumping through the analyzer section. In practice the entire tube is pumped from the ion source end, although provisions are made for pumping at both ends should the need arise. Stainless steel Sylphons #7 and #17 connect the analyzer to the mounting rings. The Sylphons serve to shield the ion beam and to give flexibility which prevents severe strains on the glass cylinders and supports. The inner analyzer section is designed such that it can be removed at the ion source end without disturbing the exit assembly. The rectangular analyzer section permits a larger cross section area for the ion beam to pass through than can be obtained on circular construction using the same magnetic gap. It would be possible in such construction to decrease the magnet gap by having the sides of the outer analyzer section made of soft iron that conformed to the shape of the pole faces. This would enable having a gap width of nearly the same dimension as the ion beam. The double analyzer with its insulated inner section permits operating the analyzer at any desired voltage with respect to ground. This feature makes it possible to operate the tube in a manner such that metastable ions[6] may be studied.

In general, in the sector type tube a magnet is used for focusing the electron beam. In this instrument a small permanent magnet supported by the ion source mounting ring serves this purpose. The magnet consists of two Alnico pole pieces each $\frac{1}{4}$ inch × $\frac{1}{2}$ inch × $\frac{3}{4}$ inch and a soft iron yoke. The field obtained with a $1\frac{1}{2}$-inch gap is 150 gauss. No difficulty has been experienced in maintaining a well defined electron beam even when the magnet is heated to 300°C. Placing the magnet inside the tube enables the gap to be decreased to approximately the length of the electron beam.

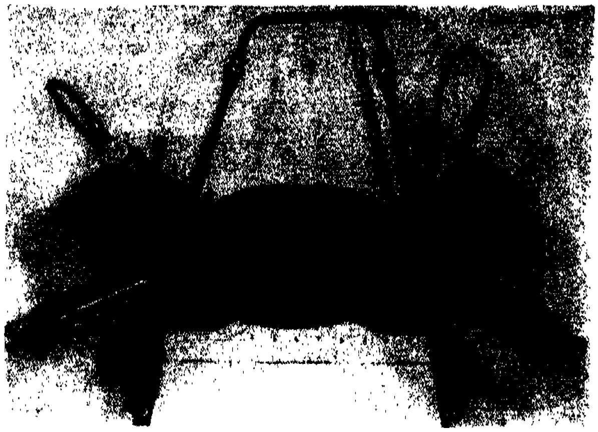

FIG. 2. Completed mass spectrometer tube.

The external electrical connections into the tube are made through standard octal glass presses except where special presses are required. The presses are sealed in all cases to Kovar eyelets and these atomic hydrogen welded to Monel eyelets such as #5 and #10. A particular advantage of welding the Kovar and Monel lips in this manner is that it permits easy replacement. The weld can be ground away and only a small amount of the lip destroyed. It is found possible to make as many as five welds before destroying the lips. Connections for measuring the electron and ion current are made through special presses of #707 Corning glass. The resistance of this glass is higher than Pyrex and is particularly superior at an elevated temperature. Pin-jacks are used for making connections to the various electrodes inside the tube.

The ion source and exit assembly used are of similar construction to those described by Hipple.[1] A detailed description of the assemblies will be omitted since the design employed is often of a specialized nature. In the present construction it is only required that the electrodes containing the ion defining slits include stops of known orientation with respect to the pins in the mounting rings.

OPERATION

In operation the tube is found to perform satisfactorily. A well-focused electron beam is obtained as determined by the ratio of the total emission current from the filament to the electron current which passes through the ion source. The resolution is as expected—about one in one hundred and fifty mass units. To obtain this resolution it is necessary that the tube be operated at a temperature of at least 100°C since this is in the neighborhood of the Curie point for Monel. Where this resolution is not required, the tube can be operated at room temperature. The guard vacuum can be raised to about 100 microns before detecting oxygen in the tube. Degassing of the tube starting from atmospheric pressure may take a little longer than in the conventional glass tube, but the ultimate vacuum is of the same magnitude. If electric heaters are used, the power required to heat the tube to 300°C is approximately three kilowatts. Figure 2 shows the completed mass spectrometer tube.

---

[6] J. A. Hipple and E. U. Condon, Phys. Rev. 68, 54 (1945).

ACKNOWLEDGMENT

The author wishes to acknowledge the suggestions of Dr. J. A. Hipple,* who supervised the construction, and Mr. A. G. Sharkey,† who followed much of the early engineering work.

---

* At present with National Bureau of Standards, Washington, D. C.

† At present with Bureau of Mines, Bruceton, Pennsylvania.

THE REVIEW OF SCIENTIFIC INSTRUMENTS VOLUME 20, NUMBER 7 JULY, 1949

Rotor Balancing with an Electronic Capacitor Gauge*

H. D. Warshaw
The Franklin Institute, Laboratories for Research and Development, Philadelphia, Pennsylvania

(Received February 9, 1949)

A variable air-gap capacitor is formed between an unbalanced rotating member and a stationary plate. The output of an oscillator is modulated in accordance with the variations in air gap, the modulated wave being displayed on the screen of a cathode-ray oscilloscope for continuous observation. Cyclic displacements at the periphery of the rotor of 0.0005 in. are easily detected. A contactor on the rotor shaft provides the means for locating the point of unbalance.

INTRODUCTION

DYNAMIC balancing machines have been developed which are capable of indicating the magnitude and phase of unbalance of rotating parts, and these machines are indicated whenever production balancing is required. The field man is often called upon to balance rotating machines in place. In other cases, commercially available machines cannot be employed because the rotors are vertically mounted on step bearings or because of other special construction. This paper describes a technique whereby electronic equipment which is portable and is easily employed in the field can be adapted to specialized balancing problems.

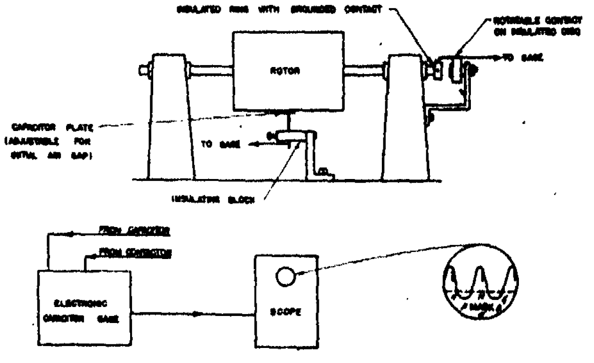
INSULATED RING WITH GROUNDED CONTACT
ROTATABLE CONTACT ON INSULATED DISC
TO GAGE
ROTOR
CAPACITOR PLATE (ADJUSTABLE FOR INITIAL AIR GAP)
TO GAGE
INSULATING BLOCK
FROM CAPACITOR
FROM CONTACTOR
ELECTRONIC CAPACITOR GAGE
SCOPE
MARK

FIG. 1. Block diagram of complete system.

CAPACITOR

The measuring element of the gauge is a stationary capacitor plate mounted near the periphery of the rotor to be balanced, so that the plate and rotor form an electrical condenser. Changes in air gap produce changes in capacity (C) of the condenser in accordance with the formula $C=KA/d$ where $K=$ a constant, $A=$ area of plate, and $d=$ thickness of air-gap. During rotation, unbalance of the rotor produces cyclic changes in capacity that modulate the gauge circuit output displayed on the screen of a cathode-ray oscilloscope as shown in Fig. 1. In this diagram, the rotating machine is represented by a rotor and its bearing mounts, and the capacitor plate is shown supported by a threaded post insulated from the frame of the machine. The capacitor plate is electrically connected to the gauge circuit which is also connected to the shaft contactor.

CIRCUIT

Figure 2 shows the complete circuit diagram of the electronic capacitor gauge. A crystal-controlled oscillator supplies a 100-kc carrier of constant frequency and amplitude to the tank circuit. The carrier amplitude in the tank circuit is modulated in accordance with the variations in capacity of the measuring element. The tank circuit is operated near resonance, the exact point being determined by the shape of the calibration curve to be obtained. This will be discussed further in the section on calibration. The output of the tank circuit is passed through a cathode follower to a clipper circuit, which is adjusted to remove approximately 70 percent of the carrier. The remainder is fed to the vertical deflection amplifier of a Dumont Type 164E oscilloscope. This procedure allows the oscilloscope amplifier to be operated at high gain without overloading. A clamping circuit holds the clipped side of the carrier in a fixed position on the screen of the cathode-ray tube so that the screen can be calibrated directly in terms of rotor displacement.

---

* This paper is based on work done for the Office, Chief of Ordnance, Department of the Army.

SHAFT CONTACTOR

The equipment thus far described provides an indication of the amplitude of vibration of the rotor high point. However, the location of the high point requires a reference to a fixed point on the rotor. This is obtained by means of a shaft contactor (see Fig. 1) which consists of a grounded projection on the rotor shaft that strikes a flat spring contact once every revolution. The flat spring is connected to the line marked TO SHAFT CONTACTOR in Fig. 2. During the instant of contact, approximately 50 percent of the modulated signal at the cathode follower is by-passed to ground. Hence, as observed on the oscilloscope screen, every cycle of the modulated wave is notched at the same point with respect to the peak of the wave. The phase angle between the notch and the peak corresponds to the angle between the point of shaft contact and the high point of the rotor. For higher accuracy, the flat spring is mounted on a rotatable assembly that may be turned until the notch is at the peak of the modulated wave. The point of shaft contact and the rotor high point are then coincident.

APPLICATION

Figure 3 shows an installation of a capacitor gauge for balancing a wheel that is to rotate at high speed about a vertical axis. Due to an irregular profile at the rim, it was more convenient in this application to mount the gauge above the wheel near its rim, as shown.

The capacitor plate consists of a brass block (approximately 2 in. × 1 in.) supported on a threaded post that passes through a block of insulating material. This assembly is designed to permit adjustment of the plate for parallelism with the upper surface of the wheel, and to allow accurate setting of the initial air gap. The shaft contactor (not shown) is similar to that of Fig. 1 except that the rotatable contact is positioned by an electric motor drive controlled from a remote station.

The display on the screen of the cathode-ray tube of a pure sinusoidal modulation at the rotational frequency of the wheel indicated the absence of wheel vibration (as a thin plate). Hence, the vertical displacement of its rim was essentially proportional to the horizontal, for the small displacements involved. The ease and accuracy with which the rotor high point was located during numerous balancing operations was further evidence of the suitability of the gauge mounting used in this particular application.

CALIBRATION

The curve of capacity *versus* air gap, shown in Fig. 4, is based on calculated values for the capacitor installation of Fig. 3. With a linear electronic measuring circuit, the over-all sensitivity for air gaps greater than 0.004 in. would be relatively low. However, it has been pointed out that the measuring circuit is not linear, the tank circuit is adjusted to operate over a non-linear portion

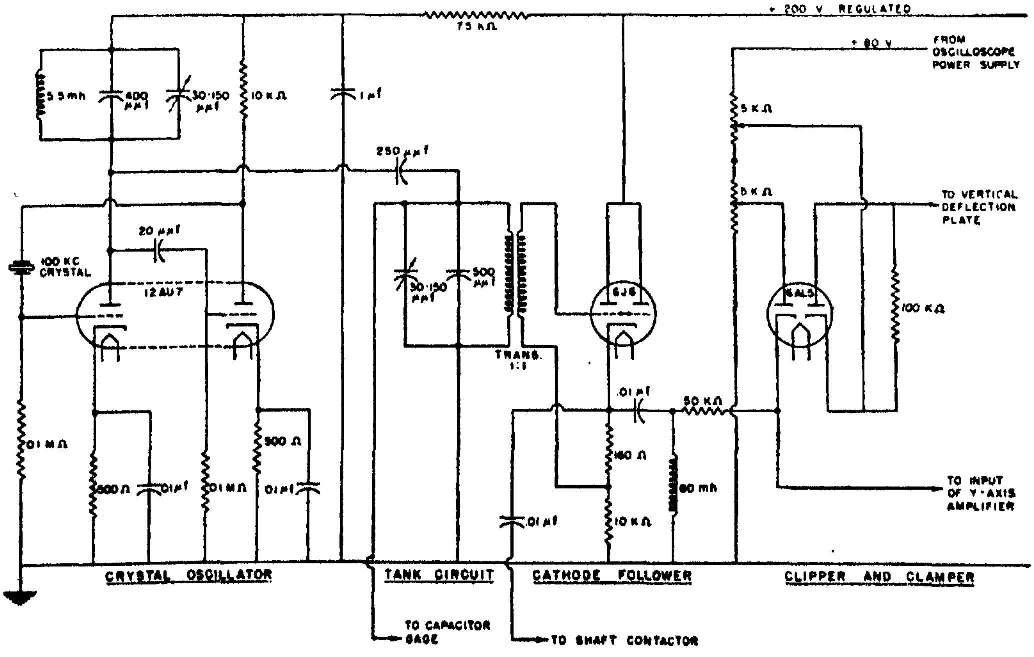

FIG. 2. Electronic capacitor gauge circuit.

FIG. 3. Capacitor gauge installation.

of its resonance curve. When properly adjusted, the over-all calibration curve of signal amplitude *versus* air gap, as shown in Fig. 4, is obtained. The sensitivity at the wider air gaps is sufficient to allow this electronic capacitor gauge to clearly indicate rotor displacements covering a maximum range from zero to 0.008 in.

BALANCING

To balance the rotor shown in Fig. 3, the capacitor plate is adjusted so that a uniform air gap of approximately 0.010 in. is obtained. The image on the screen of the cathode-ray tube will consist of a solid band (the 100-kc carrier) approximately 0.4 in. high. A calibrated mask is placed over the screen of the tube and the band is positioned so that its upper edge coincides with an arbitrarily selected horizontal line representing zero rotor displacement. The lower edge of the band will remain straight and fixed in position at all times since the carrier has been clipped and clamped at this level. When the rotor is driven, displacements of its upper surface that reduce the air gap will appear on the screen as deflections above the zero line, and displacements that increase the air gap will appear below. The latter deflections are small since the sensitivity decreases rapidly for air gaps greater than 0.010 in. However, since these deflections are not useful or necessary, they are ignored.

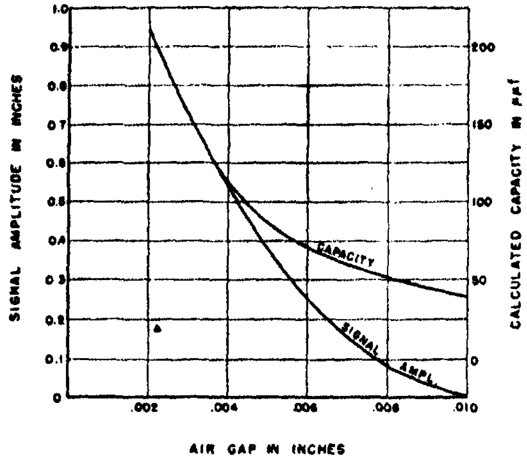

FIG. 4. Calibration curves.

Near the first critical speed of the unbalanced rotor, the upward deflections on the screen become prominent and the position of the notches relative to the peaks of the waves are observed. As the rotor speed varies, the oscilloscope sweep frequency is adjusted to one-half or one-third the frequency of rotation so that 2 or 3 cycles of the modulated wave will appear stationary on the screen. The speed of rotation is carefully controlled so that the amplitude of vibration does not exceed 0.008 in. The shaft contactor is then driven to a position such that the notches in the scope pattern are directly at the peaks of the waves. The rotor is then brought to rest and its heavy point located by observing the point of contact of the shaft contactor. Material is removed from the rotor at the heavy point and the process is repeated until the rotor displacement at the critical speed is of the order of 0.003 in. From the calibration curve it may be seen that the signal amplitude will be small (0.15 in.) and difficult to observe. Therefore, the capacitor plate is readjusted so that the initial air gap is reduced to 0.005 in. The signal amplitude for a rotor displacement of 0.003 in. will now be 0.6 in. The above procedure is repeated until the desired degree of balance is obtained. When surface irregularities produce signals of the order of magnitude of the signals due to unbalance, further refinements in balancing are useless.

ACKNOWLEDGMENT

The author wishes to thank Drs. N. H. Smith, C. T. Chase, and Mr. R. E. Benn for their encouragement and assistance.

THE REVIEW OF SCIENTIFIC INSTRUMENTS VOLUME 20, NUMBER 7 JULY, 1949

The Counting Volume of a Cylindrical Ionization Chamber*

NELSON M. BLACHMAN
Brookhaven National Laboratory, Upton, New York

(Received March 1, 1949)

The effect on the electric field inside a circular-cylindrical ionization chamber of the end plates is determined. The field lines terminating on the collecting wire at the ends of the guard sleeves determine the volume in which the freed electrons are collected by the wire. Formulas and a graph for determining this counting volume are exhibited. In appendices effects of the sleeves are considered, and the inverse-square integral evaluated for both cylindrical and spherical ionization chambers.

A ROTATIONALLY symmetric ionization chamber is shown in Fig. 1. The guard sleeves are assumed to have the same radius and to be maintained at essentially the same potential as the collecting wire. Away from the ends of such a long cylindrical ionization chamber the electric field is purely radial, and the volume in which the freed electrons are collected by the wire is defined by the right circular cylinder with bases at the ends of the sleeves (*A*, Fig. 1). With this cylinder as a first approximation, one must correct for the effect of the end plates.

The chamber will be assumed sufficiently long that neither end plate influences the opposite end. Thus, we shall treat the effect of each end plate as if the chamber were semi-infinite. The electric field configuration in the vicinity of an end plate is shown qualitatively in Fig. 2. It is seen that the end plate *increases* the counting volume, since, with the end of the guard sleeve at *A*, the counting volume is that to the right of *CAC* rather than *BAB*.

With the wall and end plate at potential zero and the wire and sleeve at potential V, we may write the potential ϕ at any point, because it is independent of azimuth, as a sum of solutions of Laplace's equation of the two forms $\log(b/r)$ and $Z_0(kr/b)e^{-kz/b}$, where r denotes the distance from the axis and z distance from the end plate. $Z_0(kr/b)$ is a linear combination of the Bessel functions $J_0(kr/b)$ and $N_0(kr/b)$,[1] say $Z_0(kr/b)=J_0(kr/b)+n_kN_0(kr/b)$; k and n_k are chosen so that $Z_0(kr/b)$ vanishes both on the wire and sleeve, at $r=a$, and on the wall, at $r=b$. The coefficients of the terms in the sum are obtained on imposing the boundary condition: $\phi=0$ for $z=0$ and $a<r\leqslant b$. Thus,

$$\phi=[V/\log(b/a)][\log(b/r)-\textstyle\sum_k A_kZ_0(kr/b)e^{-kz/b}], \quad (1)$$

where

$$A_k=(2/k)(a/b)Z_1(ka/b)\log(a/b)/[Z_1^2(k)-(a/b)^2Z_1^2(ka/b)], \quad (2)$$

and the summation is to be taken over all positive k's satisfying the foregoing condition. $Z_1(kr/b)=J_1(kr/b)+n_kN_1(kr/b)$.

On account of the factor $e^{-kz/b}$ in Eq. (1), the summation becomes small compared to the $\log(b/r)$ term for z of the order of $(b-a)$ or larger. We may thus treat it as a perturbing field superposed on the $\log(b/r)$ field that would obtain in the absence of any end plate.

The effective part of this perturbation is that arising from $\partial\phi/\partial z$, to which is due the departure of AC in Fig. 2 from AB. The slope of AC away from radial (AB) at any point is the ratio of axial to radial electric field, $(\partial\phi/\partial z)/(\partial\phi/\partial r)$. From the logarithmic term we have approximately

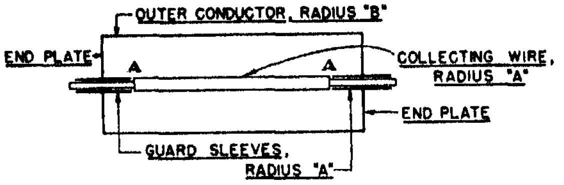
OUTER CONDUCTOR, RADIUS "B"
END PLATE
A
A
COLLECTING WIRE, RADIUS "A"
END PLATE
GUARD SLEEVES, RADIUS "A"

FIG. 1. Circular-cylindrical ionization chamber. (The "B" at the top of the figure and the "A" at the extreme right should both be lower case.)

$$\partial\phi/\partial r=-[V/\log(b/a)]/r. \quad (3)$$

Thus, the slope of AC away from radial is approximately

$$d\zeta/dr=[\log(b/a)/V]r\partial\phi/\partial z, \quad (4)$$

where $\zeta(r)$ is the distance between AC and AB at radius r.

Substituting $\partial\phi/\partial z$ from (1) and (2) into (4) and integrating, we have

$$\zeta(r)=\textstyle\sum_k A_ke^{-kz/b}[rZ_1(kr/b)-aZ_1(ka/b)], \quad (5)$$

for which z has been assumed to be essentially constant, being, say, the z at A. The volume included between CAC and BAB is

$$\int_a^b 2\pi r\zeta(r)dr=\pi b^3\textstyle\sum_k A_ke^{-kz/b}[4k^{-2}Z_1(k)-(1+4k^{-2}-a^2b^{-2})(a/b)Z_1(ka/b)]. \quad (6)$$

---

* Work done under the auspices of the AEC.

[1] The "Neumann function" is denoted by N_0 by Jahnke and Emde (see reference 2) but by Y_0 by Watson.

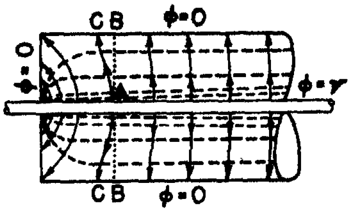

FIG. 2. Distortion of the field due to an end plate.

Each end plate increases the counting volume by this amount, which may be expressed in the form

$$b(b-a)^2[K_1e^{-p_1z/(b-a)}+K_2e^{-p_2z/(b-a)}+\cdots], \quad (7)$$

in which it is convenient to use $p=(b-a)k/b$ rather than k. Here z is the distance from the end plate to the end of the sleeve. For z of the order of $(b-a)$ or larger, terms in (7) beyond the first may be neglected; the error involved will be of the order of the second term. K_1 and p_1 are functions of the ratio (a/b) and are exhibited in Fig. 3, which is plotted with $(a/b)^{\frac{1}{2}}$ as the abscissa to improve the accuracy. K_2 lies between ±0.1 in the practical case, and p_2 is about 6.0.

The writer wishes to acknowledge discussions of this problem with Drs. Isaac Halpern, John Hornbostel, Everett Hafner, and Ernest Courant.

APPENDIX A

In the limit as the wire and sleeve radius a approaches zero, n_k goes to zero, and Z becomes J. Then the values of k become the positive roots of the equation $J_0(k)=0$, which are listed by Jahnke and Emde,[2] the first two being $k_1=p_1=2.4048$ and $k_2=p_2=5.5201$. Correspondingly, K_1 becomes 1.4477 and K_2 -0.0796. In this limit Eq. (2) becomes

$$A_k=2/[k^2J_1^2(k)]$$

and

$$K=-8\pi/[k^4J_1(k)].$$

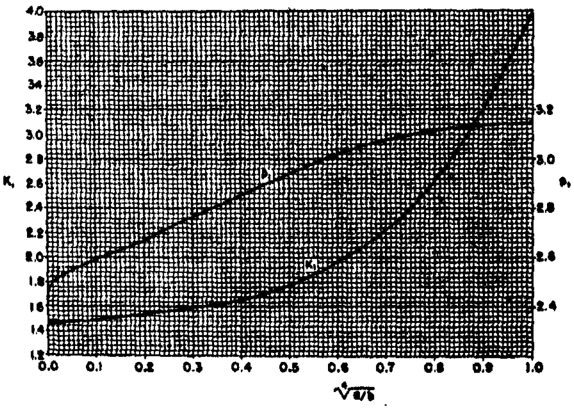

FIG. 3. K_1 and p_1 *vs.* $(a/b)^{\frac{1}{2}}$. Increase in counting volume due to one end plate is approximately $K_1b(b-a)^2\exp-[p_1z/(b-a)]$.

APPENDIX B

In the opposite limit, as the wire and sleeve radius a approaches the wall radius b, the field becomes two-dimensional and is readily obtained in closed form by use of the mapping by the complex function

$$w=(2V/\pi i)\log\cos\omega,$$

where $\omega=\xi+i\eta$, $\xi=\frac{1}{2}\pi(b-r)/(b-a)$, and $\eta=\frac{1}{2}\pi z/(b-a)$; $w=\phi+i\psi$, with ψ a stream function. Thus,

$$\phi=(2V/\pi)\tan^{-1}\{\tan[\tfrac{1}{2}\pi(b-r)/(b-a)]\tanh[\tfrac{1}{2}\pi z/(b-a)]\},$$

and

$$\begin{aligned}\partial\phi/\partial z&=[V/(b-a)]\sin[\pi(b-r)/(b-a)]/\\&\qquad\{\cos[\pi(b-r)/(b-a)]+\cosh[\pi z/(b-a)]\}\\&=[2V/(b-a)]\{e^{-\pi z/(b-a)}\sin[\pi(b-r)/\\&\qquad(b-a)]-e^{-2\pi z/(b-a)}\sin[2\pi(b-r)/(b-a)]+\cdots\}.\end{aligned}$$

The radial electric field is, in the limit, constant and given by

$$\partial\phi/\partial r=-V/(b-a).$$

Proceeding as before, we have

$$\begin{aligned}\zeta(r)=(2/\pi)(b-a)[&e^{-\pi z/(b-a)}\{1+\cos[\pi(b-r)/(b-a)]\}\\&+\tfrac{1}{2}e^{-2\pi z/(b-a)}\{1-\cos[2\pi(b-r)/(b-a)]\}+\cdots].\end{aligned}$$

Thus, the increase in the counting volume due to one end plate is

$$2\pi b\int_a^b\zeta(r)dr=4b(b-a)^2[e^{-\pi z/(b-a)}+\tfrac{1}{2}e^{-2\pi z/(b-a)}+\cdots]$$

if wire and wall diameters are nearly equal.

APPENDIX C

In case the radius of the collecting wire is less than that of the sleeve, there is an additional distortion of the field which *decreases* the counting volume of the chamber. This effect is difficult to calculate precisely, because of the complicated shape of the center conductor, essentially a thin wire coming out of the flat end of a thicker wire. The effect is due to the inside right angle at the base of the thin wire, on account of which the electric field line emerges from the corner at a 45° angle, as well as to the change in radius.

If we consider the field that obtains when a uniform wire of radius a at the center of a grounded cylindrical surface of radius b has potential V for $z>0$ and potential V' for $z<0$, with $V'>V>0$ (Fig. 4), we see that there is an equipotential $\phi=V$, PQ, that includes the surface of the right half of the wire, making a right angle with itself at Q. This equipotential has radius a for z sufficiently positive and, with $V'=\{1+[\log(c/a)/\log(b/c)]\}V$, radius c for z sufficiently negative; c represents the radius of the sleeve. Thus, the field in this case should be very much like that we wish to study.

The potential ϕ is easily found by decomposing it into its even and odd components as functions of z, of which the former is the usual logarithmic potential, and the latter exactly like (1);

$$\begin{aligned}\phi=[V/\log(b/a)]\{&\log(b/r)\\&+\tfrac{1}{2}[\log(c/a)/\log(b/c)]\textstyle\sum_k A_kZ_0(kr/b)e^{-kz/b}\},\end{aligned}$$

with k and Z_0 as before and A_k given by (2).

The point Q (Fig. 4) may be determined as that point $r=a$, $z=z$ where $\partial\phi/\partial r$ vanishes. The field line QR, which bisects the right angle at Q, bounds the counting volume. It may be determined from the relation $d\zeta/dr=(\partial\phi/\partial z)/(\partial\phi/\partial r)$, but now $\partial\phi/\partial r$ cannot be accurately approximated by the first term of the series; z/b is small along QR, and the series converges slowly. This makes even the determination of the point Q difficult. However, it is thus possible at least in principle to determine the approximate diminution in the counting volume, $2\pi\int_a^b r\zeta(r)dr$, resulting from this difference in sizes of sleeve and collecting wire.

---

[2] E. Jahnke and F. Emde, *Tables of Functions* (Dover Publications, New York, 1943), p. 166.

This size difference will also have an effect on the field due to the end plates. However, one may compute the end-plate correction for each central-conductor size and use an intermediate value, as the two will not differ greatly.

In the special case where $c-a\ll b-a\ll b$, the field configuration can be obtained directly by the Schwarz transformation mapping the upper half of the τ-plane onto the t-plane with $dt/d\tau=[1+(2/\pi)(c-a)/\tau]^{\frac{1}{2}}$ and $t=z+i(r-a)$. If this condition obtains, one finds approximately that $\zeta=(1/\pi)\times(c-a)\log[2\pi e(r-a)/(c-a)]$, whence the diminution in the counting volume due to the change in central-conductor size from c to a is approximately

$$2b(c-a)(b-a)\log[2\pi(b-a)/(c-a)].$$

The change at the other end of the chamber from a to c subtracts another equal amount from the counting volume.

APPENDIX D

When a cylindrical ionization chamber of length $2L$ and radius R is used with an external point source of radiation at distance A from its axis and equidistant from its ends, it is necessary in calculating the cross section of the ionizing gas to know $\int d\tau/\rho^2$ over the volume of the chamber, where ρ is the distance from the source to the point of integration. This integral may be written

$$\int d\tau/\rho^2=\int_{-L}^{L}\int_0^R\int_0^{2\pi} rd\theta drdz/(A^2+z^2+r^2-2Ar\cos\theta).$$

The integration over θ is carried out by means of Peirce[3] No. 300. The substitution $s=r^2$ then allows the next integration to be done by No. 160. With the substitution of $\sec^2\phi$ for the argument of the logarithm thus obtained, the last integral is converted to the standard form of the incomplete elliptic integral of the second type $E(k,\phi)$ except that $k=A/R>1$. Thus,

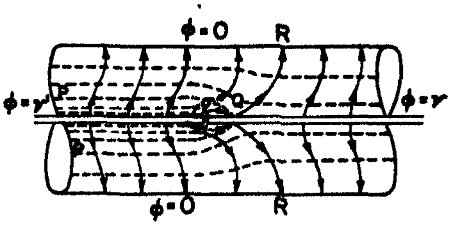

FIG. 4. Approximation to field at end of sleeve.

$$\int d\tau/\rho^2=4\pi L\log\sec\phi_1+4\pi R\int_{\phi_1}^{\phi_2}(1-k^2\sin^2\phi)^{\frac{1}{2}}d\phi,$$

where

$$\sin\phi_2=R/A$$

and

$$\sec^2\phi_1=\{R^2+L^2-A^2+[(R^2+L^2-A^2)^2+4A^2L^2]^{\frac{1}{2}}\}/2L^2.$$

Unfortunately there seems to be no table of this incomplete elliptic integral for k greater than unity. The contributions to the integral due to the end plates, etc., may be added separately. Since they are small, it is sufficient to use an average value of ρ^2 for them.

In taking into account the effect of absorption in the chamber wall it is necessary to have an expression for the cosine of the angle between the line joining the source and point of integration and the normal to the wall at the point of intersection. This cosine turns out to be $[\rho^2-z^2-(Ar/R)^2\sin^2\theta]^{\frac{1}{2}}/\rho$.

The integral $\int d\tau/\rho^2$ has been evaluated for a source at distance A from the center of a sphere of radius R with $A>R$; here $\int d\tau/\rho^2=2\pi R-(\pi/A)(A^2-R^2)\log[(A+R)/(A-R)]$.

---

[3] B. O. Peirce, *A Short Table of Integrals* (Ginn and Company, Boston, 1929).

Erratum: A New Discharge Tube for the Hydrogen Atom Spectrum

[Rev. Sci. Inst. **20**, 319 (1949)]

W. P. van Oort and A. C. S. van Heel
N. V. de Bataafsche Petroleum Maatschappij, Laboratorium, Amsterdam, Holland

THE authors have requested that the above address be completed as follows:

N.V. de Bataafsche Petroleum Maatschappij, Laboratorium,
Amsterdam, Holland,
Laboratorium voor Technische Physica der Technische,
Hogeschool, Delft, Holland.

THE REVIEW OF SCIENTIFIC INSTRUMENTS VOLUME 20, NUMBER 7 JULY, 1949

An Instrument for Rapid Determination of Crystal Orientation

R. H. GILLETTE AND M. H. JELLINEK
Laboratory of The Linde Air Products Company, Tonawanda, New York

(Received February 25, 1949)

The rapid orientation of crystals is accomplished by the use of an apparatus employing a Geiger counter and x-ray focusing. The instrument can be used for precise orientation or to sort samples into various tolerance ranges. Applications to sapphire are discussed in detail. The instrument has also been used in connection with rutile and barium titanate orientations.

THE mechanical, optical, and other properties of synthetic single crystals of scientific and commercial interest are often profoundly influenced by crystallographic orientation. To mention but a few examples: rutile has widely different refractive indices and dielectric constants parallel and perpendicular to the optic axis and these are important, for example, in cutting this substance as a gemstone. Piezoelectric crystals such as barium titanate must be sliced in carefully controlled directions for maximum effect. Sapphire with its relatively high refractive index and low dispersion might have applications to lens design if cut perpendicular to the optic axis where birefringence effects would be minimized. To insure uniform wear of sapphire phonograph needles the C axis must lie in the plane of the record and tangent to the groove. In some of these applications precise knowledge of crystallographic orientation is essential and the techniques for obtaining this information have been studied extensively in connection with quartz.[1] In many cases, however, a range of orientations is permissible and the number of individual units to be determined is so great that the more exact methods cannot be justified. It is the purpose of this paper to describe a simple device for sorting crystals into predetermined orientation ranges in a rapid, but reliable, manner.

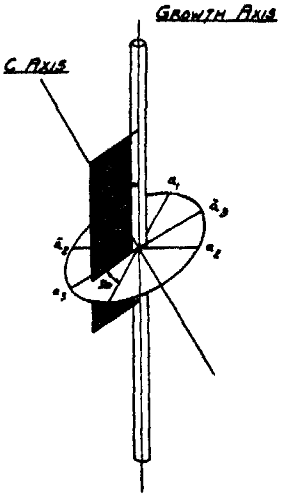

FIG. 1. Definition of ρ and φ.

For the sake of definiteness, sapphire, which crystallizes in the hexagonal system, will be used as an illustration although the extension to other crystals will be immediately obvious. When grown by the Verneuil technique, this material is in the form of rods or boules, the growth axis of which forms a convenient line of reference for specifying orientation in terms of two angular parameters ρ and φ defined as follows and illustrated in Fig. 1:

ρ is the angle between the crystallographic C axis and the growth axis of the rod or boule.

φ is the angle between a negative A axis of the crystal and the plane defined by the C axis and the growth axis, subject to the restriction that it lies between 30° and 90°.

It is clear that ρ specifies how much the crystal has been tilted with respect to the growth axis, while φ defines the extent of the rotation of the crystal about its own C axis. The evaluation of these parameters for the different crystallographic planes is described in *Dana's System of Mineralogy*[2] although the definition of φ used here differs slightly from that of reference 2.

For an important application it has been empirically determined that ρ and φ should equal approximately 60°. The crystallographic n planes, having hexagonal Miller Indices $22\bar{4}3$, can be shown to have $\rho = 61.20°$ and $\varphi = 60°$. This means that in a 60–60 rod (or boule) the n plane is nearly perpendicular to the growth axis, being tilted only 1.20°. Furthermore, this plane gives a strong Bragg reflection. In the powder data of the ASTM card index the spacing of the n plane is given as 2.08A and the relative reflection intensity as 0.84. (Of course, the later value is related to the multiplicity of the reflecting plane, but the single crystal has more than enough intensity for present purposes.)

Orientation of massive crystals of this type, having no definite crystal faces visible, can be accomplished by back reflection Laue diagrams and gnomonic projections, or by other more elaborate methods using two crystal reflections.[3] However, for purposes of economy, it was felt that no longer than 15–20 seconds could be spent on each sample to determine whether it fell in the range $\rho = 60 \pm 5°$, $\varphi = 60 \pm 5°$ on a go, no-go basis.

---

[1] See, for example, R. A. Heising, *Quartz Crystals for Electric Circuits* (D. Van Nostrand Company, Inc., New York, 1946).

[2] Palache, Berman, and Frondel, *Dana's System of Mineralogy* (John Wiley & Sons, Inc., New York, 1946), Vol. 1.

Since the spacing of the *n* plane is 2.08A, its Bragg angle using copper *Kα*-radiation is 21.8°. This means that a correctly oriented crystal placed in an x-ray beam so that the end face normal to the growth axis makes an angle of 21.8° with the incident beam will show a strong reflection at 43.6° to the incident beam. This reflection could be detected by some suitable device as a film, fluorescent screen, or a Geiger counter. In this case, the presence of the reflected ray will be independent of rotation of the crystal rod around its own axis. Furthermore, it would be impossible to observe a reflection from any other plane because no other plane of corundum can reflect at the above angle when copper radiation is used.

If a rod has an orientation somewhat different from the optimum, the *n* plane will be tilted by an amount which for small angles is very nearly equal to the angle of disorientation. When such a rod is introduced into the beam, two possible adjustments may have to be made:

(1) Rotation of the specimen about its own axis until the $22\bar{4}3$ plane is vertical and

(2) Rotation of the rod about the end that is in the beam until this plane makes the Bragg angle with the beam. When this has been done, the amount of disorientation of the rod is given directly by the amount by which the specimen had to be adjusted from the position in which a correctly oriented crystal would reflect.

In this work a range of orientations was desired and the apparatus was designed for this purpose. As basic equipment, a standard x-ray generator and a quartz crystal orientation unit were used. A special crystal holder was constructed for the orientation unit that accomplished this purpose. Figure 2 diagrammatically shows the incident x-ray beam impinging on the crystal and the reflected ray with the reflecting face lying along the center of rotation of the two arms of the orientation unit. Also shown in this figure are the extreme rays so that the geometry of the instrument for maixmum permissible departure from ideal orientation is clear. It is evident that a hollow cone of 10° solid angle centered on the theoretical position for the $22\bar{4}3$ plane will limit the movement of the crystal rod so that ρ and φ cannot vary from 60° by more than ±5° in any direction. Further the total area covered by the reflected ray for all possible positions is shown at the Geiger tube slit position. Consequently, if a suitably dimensioned slit is properly located before the Geiger tube and if the crystal movement is limited by the chosen cone, then the presence of the desired reflection when the crystal is at any position in the cone is all that is required for selecting desired crystals. The crystal can be made to occupy all positions in the cone by rotating the cone relatively rapidly upon its own axis and displacing the crystal slowly from a central location to the edge.

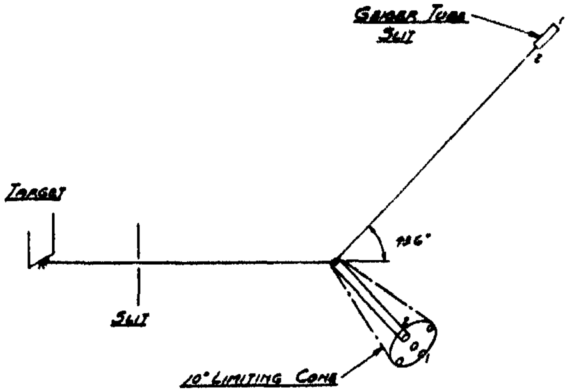

FIG. 2. Crystal orientating instrument.

The final instrument was produced by redesigning the specimen post on a quartz crystal unit and by adding a preamplifier and one stage of amplification to the electronic equipment of the Geiger counter to yield sufficient output to give full scale deflection for a correctly oriented crystal on a microammeter of 150 μamp. full scale. Figure 3 shows the specimen holder from the front and the cone into which the crystal is placed is evident as is the entrance slit to the counting tube. The gear

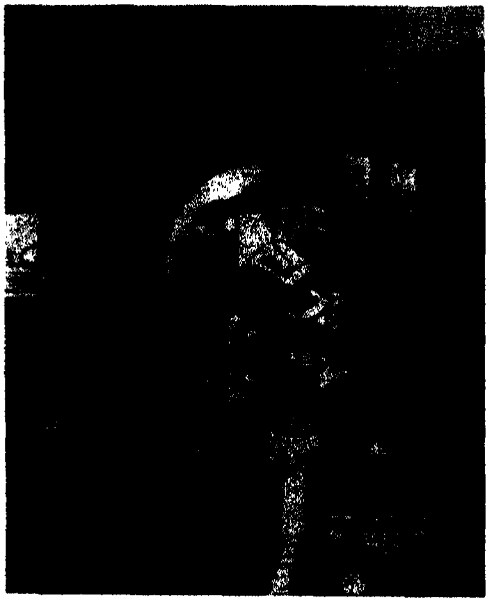

FIG. 3. Specimen holder; front view showing cone and Geiger tube slit.

---

[3] I. Fankuchen, U. S. Patent 2,392,528.

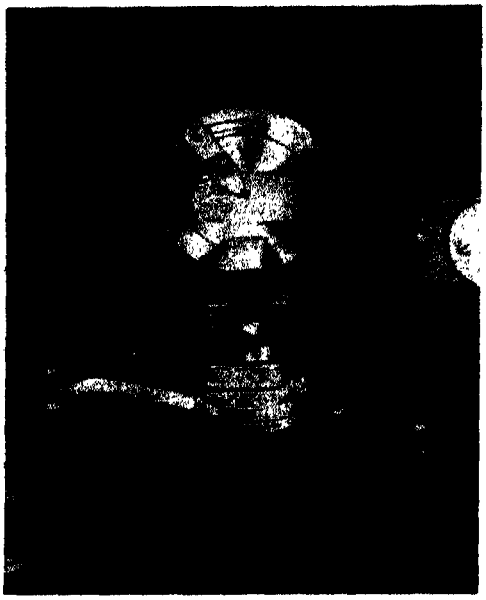

FIG. 4. Specimen holder; rear view showing ring cam to operate alignment plate.

and flexible cable allow the operator to manipulate the crystal holder to either release the crystal or ready the apparatus for a new one. When the lever is thrown in one direction, a cam removes the pressure on three small steel points that hold the crystal firmly so that it is not pushed through or pulled from the x-ray beam while still allowing it to be moved about in the cone. Simultaneously the cam drops a flat surface across the small end of the cone located in such a way that the crystal face is correctly placed when it is against this surface. This cam arrangement and locating plate is shown in Fig. 4. When the lever is reversed, the pins firmly grasp the rod before the plate is withdrawn. The complete unit is shown in Fig. 5. The operator works the cam with the left hand and inserts crystals with the right.[4]

In actual operation it turned out that rotation of the cone was unnecessary because the operator could easily move the crystal about in it and pass through all positions in several seconds. If the crystal were in the desired range, it was promptly noted by movement of the meter needle completely across the scale. Total time required per sample is between 15 and 20 seconds. Further, the apparatus can never pass an unacceptable crystal, although it may occasionally reject a "good" one.

To illustrate briefly the results obtainable, eight white sapphire and ruby rods were selected at random and surveyed, allowing 15 seconds in the cone per sample. Back reflection Laue diagrams were made of these samples and gnomonic projections were prepared. The projections of samples No. 2, 4, 5, 6, and 7 were not measured because it was obvious that they were far removed from ρ and φ equals 60±5° while the results of the remaining three are given in Table I. Only sample 8 was selected by the orientation instrument as being in the desired range.

TABLE I. Orientation of sapphire by Laue methods.

Sample	Orientation rho (ρ)	phi (φ)
1	38½°	70°
3	38½°±1°	70°±1°
8	61°	57½°

The instrument described has been in constant use for well over a year and has been operated entirely by technicians with no previous training in x-ray techniques. During the period of use several thousand crystals have been oriented to a ±5° tolerance at an average time per crystal of less than 15 seconds. It is of course impossible for the device to pass an incorrectly oriented piece, and, although several efforts have been made to check this point, the instrument is not known to have rejected a correctly oriented piece.

Obviously any desired orientation could be checked in this same way by suitably tilting the axis of the cone to the incident x-ray beam. Frequently, however, it is useful to use another plane. For example, when crystals having $\rho=45°$ and

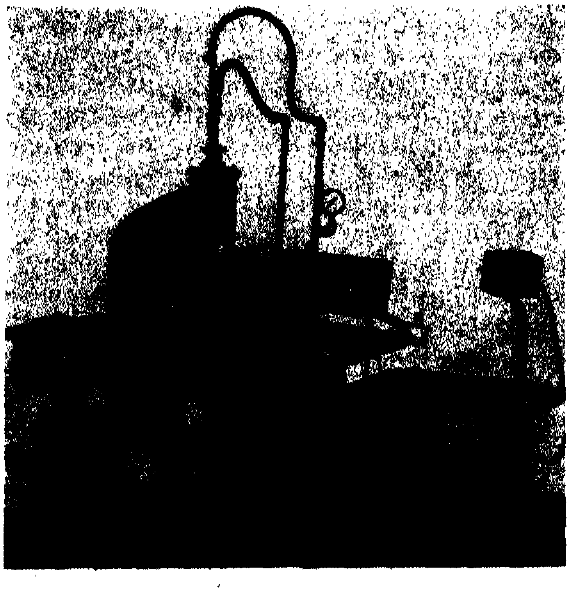

FIG. 5. Complete orientation unit showing x-ray unit, goniometer, operating controls, sample holder, and electronic equipment.

---

[4] Anyone desiring working blueprints of the crystal holder may obtain them by writing either of the authors.

$\varphi=60°$ are desired the $11\bar{2}3$ plane which has the values 42.3° and 60° for these parameters is evidently well suited, and has indeed been used.

Similar laboratory equipment has been used to determine the orientation of rutile rods and boules and barium titanate crystals by the selection of suitable reflecting planes in each instance.

The advice and assistance of Professor Horace Winchell in the preliminary consideration of this equipment is gratefully acknowledged.

THE REVIEW OF SCIENTIFIC INSTRUMENTS VOLUME 20, NUMBER 7 JULY, 1949

Characteristics of Halogen Counters

Sidney H. Liebson
Naval Research Laboratory, Washington, D. C.

(Received March 3, 1949)

Some characteristics of halogen counters have been obtained which enable their preparation for given operating voltages. Other factors influencing their behavior are discussed with a view toward obtaining optimum results.

SELF-QUENCHING halogen counters have previously been described.[1,2] The figures presented in the earlier work[2] were based on parameters more conventionally used by workers in nuclear physics and included data which are not generally useful in the preparation of halogen counters. Accordingly, an experimental investigation was made of operating characteristics of halogen counters employing various concentrations of what was found to be the optimum admixture ratio, four parts of argon to one of chlorine in a predominantly neon filling.

THRESHOLD CHARACTERISTICS

The threshold for counting action in halogen counters is sharply defined, no appreciable proportional counting region being evident. This would appear to indicate a copious production of photons for propagating the discharge once amplification has set in.

Within limits of experimental error, ±1 percent on voltage measurements and ±5 percent on pressure measurements, it was found that the threshold characteristics for these counters could be fitted by an empirical curve of the form

$$\log E/p=-A\log(pr_a+1.15)+4.85, \qquad (1)$$

where E is field strength at the wire in volts per cm, p is the total pressure of $A+Ne+Cl_2$, r_a is the wire radius, and A is a constant, depending on percentage admixture, given in Fig. 1. These measurements were taken on numerous counters with anode radii varying from 0.0063 cm to 0.063 cm, cathode radii from 0.32 cm to 5 cm and total pressure from 5-cm Hg to 60-cm Hg. The measured threshold voltages were in agreement with the empirical fit to about ±3 percent. The form of Eq. (1) was approximated by simple theoretical analysis. No variation in threshold characteristics was observable for counters prepared with chrome-iron or tantalum cathodes, although there is good evidence to believe that photoelectric processes at the cathode play an important part during the initiation of the discharge.[2] Deviations from Eq. (1) generally occurred only when operating in the low-voltage region where pre-threshold oscillations were evident.

PLATEAUS

The plateaus of halogen counters are determined by many factors. There were some general rules which were followed for preparation of counters with slopes as low as 1 or 2 percent for a hundred volts. The more important of these was the use of as high a value of pr_c (total pressure X-cathode radius) as was consistent with other operating characteristics. Both deadtime and threshold voltage increase with an increase of pr_c, and decrease with a decrease in percentage admixture, so that

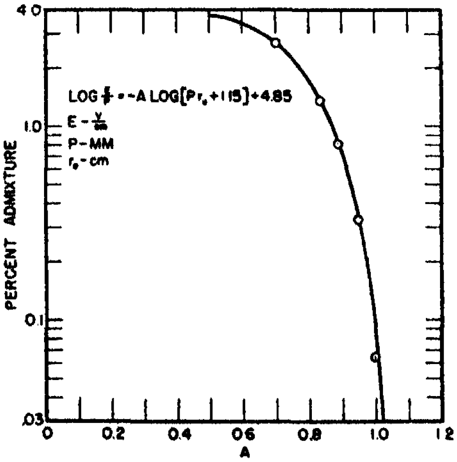

Fig. 1. Values of the empirically determined constant A.

---

[1] S. H. Liebson, Phys. Rev. 72, 181 (1947).

[2] S. H. Liebson, H. Friedman, Rev. Sci. Inst. 19, 303 (1948).

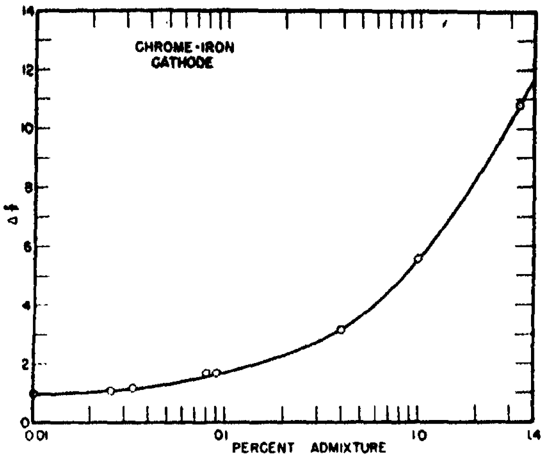

FIG. 2. Plateau characteristics of typical halogen counter.

an increase of pr_c can be compensated by a decrease in percentage admixture, except when operating the counters in the region characterized by prethreshold oscillations. Since pr_c is related to the number of collisions which an atom or ion may make before encountering the cathode, it is seen that the criterion for optimum plateau lengths as stated above is equivalent to providing increased quenching of the metastable atoms.

For low values of pr_c, the discharge mechanism appeared to be different, resulting in counting action with pulse sizes many times that of conventional alcohol-argon fillings.

Preparation of the cathode surface for cathodes such as chrome-iron or tantalum influences markedly the slope and length of plateau. A recently published abstract has erroneously claimed slopes of 6 percent per hundred volts to be inherent to halogen counters.[3] L. B. Clark, Sr. of this laboratory has prepared counters with nitrogen bombarded chrome-iron cathodes in which the slope had changed from about 15 percent per hundred volts before bombardment to less than 2 percent per hundred volts after bombardment. Of interest was the fact that $\Delta(E/p)$, the length of the plateau expressed in terms of the variation of (E/p) from threshold to the end of the plateau, was almost constant, depending only on the percentage of admixture present, for counters whose cathodes had been prepared in the same manner. Figure 2 shows a typical curve for $\Delta(E/p)$ measured with a counter having a 30-mil diameter center wire and a 2-cm diameter chrome-iron cathode. It should be emphasized that the absolute values of $\Delta(E/p)$ varied depending on cathode treatment. The relative constancy of $\Delta(E/p)$ would seem to indicate a critical excitation or a critical production of excited states within the gas at the end of the plateau.

To check the amount of impurity which may be present and still obtain counting action, various other gases such as N_2, O_2 and air, were added in amounts approaching 25 percent of the partial pressure of admixture within the counter. The results showed the prime effect to be an increase in the slopes of the counter, but the counting action itself was unimpaired.

Since the halogen counters are internally quenched, and since large currents may be passed by the counter without danger of excessive breakdown of the gaseous constituents such as is common to organic vapor type counters, these counters operated satisfactorily with anode resistors as low as 1000 ohms. In one instance, dissipation of 30 watts within the counter for two minutes, had no appreciable effect on the counter characteristics other than to increase the slope of the plateau from about 4 percent per 100 volts to about 10 percent per 100 volts which was presumed to have been due to gas liberation by the cathode or anode.

COSMIC-RAY OPERATION

In use as cosmic-ray coincidence counters, particular attention should be placed on maintaining the entire active volume of the counter at sufficiently large values of (E/p) to minimize negative ion formation. For tubes with wire sizes of 30 mils diameter and 2-cm cathode diameter containing a mixture of neon, argon, and chlorine at about 30-cm total pressure, operating at about 400 volts, the cosmic-ray efficiency was close to 100 percent.

The slower rise time of counters operating in the low voltage region may make such counters unsuitable for coincidence measurements. However, operation with argon-chlorine counters would afford the life and temperature characteristics typical of these counters and provide rise-times of the same order of magnitude as organic-vapor quenched counters operating at the same voltages.

DEAD TIME[4]

The dead time for halogen counters, as for other types of self-quenching counters, will vary with operating conditions, and is about 350 microseconds (measured from the start of the pulse) at $(E/p)=7.5$ to about 65 microseconds at $(E/p)=65$, for counters with 30-mil center wire diameter and 2-cm cathode diameter.

The greatest difficulty connected with the preparation of halogen counters is a suitable choice of anode and cathode materials for use within the tube. The prime requirements of these materials are sufficient conductivity to prevent accumulation of static charges, and chemical inertness not only with respect to neutral chlorine, but also the chlorine ions in the discharge.

---

[3] A. B. Willoughby, Phys. Rev. **75**, 1460 (1949).

[4] H. G. Stever, Phys. Rev. **61**, 38 (1942).

THE REVIEW OF SCIENTIFIC INSTRUMENTS VOLUME 20, NUMBER 7 JULY, 1949

A Circuit for the Study of the Operation of the Geiger-Müller Counter

MARIO ALVES GUIMARÃES AND PALMYRA AMAZONAS SAMPAIO
Departamento de Fisica, Universidade de S. Paulo, S. Paulo, Brasil

(Received March 8, 1949)

The vacuum tube circuit described in this paper was designed in order to measure the effective dead-time (σ') of a Geiger-Müller counter and, the probability (α') of occurrence of spurious discharges within a given interval of time ($\zeta-\sigma'$) after an initial discharge. The experimental results obtained permit, by means of an adequate formula [M. A. Guimarães, Thesis for Doctor's degree, to be published], the determination of (α') and, in some cases, (σ').

INTRODUCTION

An ideal Geiger-Müller counter must present a well defined plateau and should be sensitive only to particles from a given source. Frequently it happens however that, after a discharge takes place, the counter discharges spontaneously even in the absence of an ionizing particle (spurious discharges). In the present work, a vacuum tube circuit is described whereby one can measure the percentage of eventual spurious discharges occurring in a given interval of time ($\zeta-\sigma'$) (which may be varied conveniently within certain limits), following the initial discharge. In order to do this, ζ is kept constant and, by varying the intensity of the source, the probability (α') of spurious discharges is determined.

THEORY

The pulse from the Geiger-Müller counter goes to a trigger circuit amplifier which feeds, simultaneously, a multivibrator circuit and one of the grids of an anticoincidence twin tube; the other grid is fed by the output pulse from the multivibrator (Fig. 1). The arrangement is such that, one of the plates of the anticoincidence tube is not sensitive if the two grids receive *simultaneous* pulses. Let us suppose now that two pulses from the amplifier follow each other within an interval of time ζ corresponding to the operating time of the multivibrator and the first one triggers the multivibrator. The second pulse cannot trigger the multivibrator and then, the anticoincidence tube will be fed only through one of its grids (the one fed by the amplifier). Therefore, its plates will be sensitive to the second pulse. Hence, one of the plates is sensitive to all the pulses coming from the amplifier, while the other is sensitive only to the pulses which are not registered by the multivibrator.

Let (σ) be the real dead-time of the counter[1] and (σ') the minimum time interval that must elapse in order that the amplifier amplifies the next pulse after a discharge of the Geiger-Müller counter. Call A the average number of particles entering the counter per unit of time, and A_1 the average number of pulses registered by the amplifier per unit of time.

Assuming 100 percent intrinsic efficiency of the counter, we have:[2]

$$A_1=\frac{A}{1+A\sigma}e^{-A(\sigma'-\sigma)}.$$

For a low counting rate, that is, when $A(\sigma'-\sigma)\ll 1$, the previous result may be modified expanding the exponential term in power series and neglecting the terms in $A(\sigma'-\sigma)$ which appear with exponents >1; we have:

$$A_1=\frac{A}{1+A\sigma}[1-A(\sigma'-\sigma)]=A\left[1-\frac{A\sigma'}{1+A\sigma}\right]$$

$$=A[1-A_1\sigma' e^{A(\sigma'-\sigma)}]$$

$$=A\left\{1-A_1\sigma'\left[1-A(\sigma'-\sigma)+\frac{A(\sigma'-\sigma)^2}{2!}\right]\right\}$$

$$=A[1-A_1\sigma'+A_1\sigma' A(\sigma'-\sigma)\cdots].$$

Since $A(\sigma'-\sigma)\ll 1$, we may neglect the terms $A_1\sigma'[A(\sigma'-\sigma)^i/i!]$ for $i\geqslant 1$, which are very small compared with $A_1\sigma'$. Follows then

$$A_1=A(1-A_1\sigma').$$

Hence, for low counting rates, everything happens as if the counter and the amplifier work together with the resolving power (σ').

Let A_2 be the number of pulses from the multivibrator per unit of time. Suppose, moreover, that $(n+1)\sigma'>\zeta>n\sigma'$ (with n an integer and greater than zero).

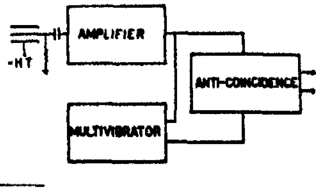

FIG. 1.

---

[1] H. G. Stever, Phys. Rev. 61, 40 (1942).

[2] A. E. Ruark and F. E. Brammer, Phys. Rev. 52, 322 (1937).

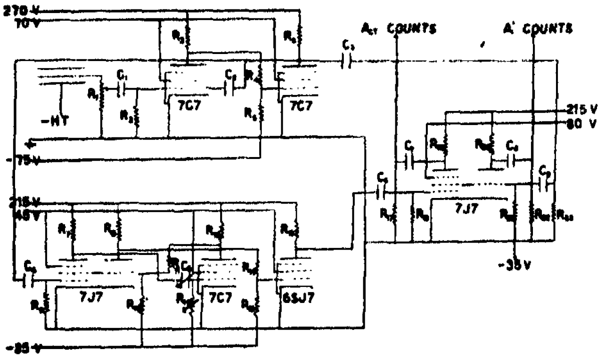

FIG. 2.

$R_1 = 1 M\Omega$
$R_2 = R_8 = R_9 = R_{10} = R_{13} = R_{16} = R_{17} = R_{18} = R_{19} = R_{21} = R_{22} = R_{23} = 100{,}000\Omega$
$R_3 = 75{,}000\Omega$
$R_4 = 50{,}000\Omega$
$R_5 = 150{,}000\Omega$
$R_6 = 250{,}000\Omega$
$R_{11} = 125{,}000\Omega$
$R_7 = R_{12} = R_{15} = R_{20} = 500{,}000\Omega$
$R_{14} = 220{,}000\Omega$

$C_1 = C_9 = 0.00005\ \mu f$
$C_2 = C_3 = 0.00001\ \mu f$
$C_4 = C_6 = C_7 = C_8 = 0.0001\ \mu f$
$C_5 = 0.002;\ 0.00025\ \mu f$

In these conditions, the following relation holds (1):

$$A_1 = A_2 + A_2\left\{n - \sum_{m=0}^{n-1}\sum_{k=0}^{m}\frac{\{A[\zeta-(m+1)\sigma']\}^k}{k!}\times\exp[-A[\zeta-(m+1)\sigma']]\right\}.$$

In the first approximation, that is, when $A_1(\zeta-\sigma')/1-A_1\sigma'\ll 1$, $A_1\sigma'\ll 1$, and $\zeta-\sigma'\cong\sigma'$, we have

$$(A_1 - A_2/A_2) = A_1(\zeta-\sigma'). \qquad (1)$$

But $A_1 - A_2$ gives us the multivibrator losses, A_{cc}, which are measured directly at one of the plates of the anticoincidence tube, while A_1 is measured directly at the other plate. Hence (1) will become:

$$(A_{cc}/A_1 - A_{cc}) = A_1(\zeta-\sigma').$$

This formula holds for the case in which the counter does not give spurious discharges within an interval of time $>\sigma'$ following an initial discharge.

Consider now the case in which the counter gives a certain percentage of spurious pulses. When the number of particles counted by the counter is relatively small, we have already seen that:

$$A_{cc}/(A_1 - A_{cc}) = A_{cc}/A_2 = A_1(\zeta-\sigma').$$

This means that, in such cases, the probability of a discharge during the interval $(\zeta-\sigma')$, due to particles counted by the counter is $A_1(\zeta-\sigma')$. Now, if α is the probability of occurrence of spurious pulses in a time interval $>\sigma'$, the actual number of pulses from the counter per unit of time is

$$A_1(1+\alpha+\alpha^2+\cdots) = (A_1/1-\alpha) = A_1'. \qquad (2)$$

Since to each discharge (spurious or not) that triggers the multivibrator the probability of missing the next pulse (due to the law of random distribution of the particles) is given by $A_1(\zeta-\sigma')$, it follows that the number of such losses by the multivibrator per unit of time, is

$$A_{cc} = A_2A_1(\zeta-\sigma').$$

If, now, $\alpha'\leqslant\alpha$ is the probability that a spurious discharge will occur within the interval of time $(\zeta-\sigma')$ that follows a discharge (spurious or not), the number, per unit of time, of losses of the multivibrator due only to spurious pulses is

$$A_{cs} = A_2\alpha'.$$

But, it may happen that a casual discharge during the interval $(\zeta-\sigma')$ overlaps a spurious discharge; these cases are included both in the calculation for A_{cc} and A_{cs}. The probability of such an occurrence is $\alpha' A_1(\zeta-\sigma')$; hence, the number of such occurrences per unit time will be $A_2A_1\alpha'(\zeta-\sigma')$.

Calling A_{ct} the total number of pulses lost by the multivibrator, per unit time, we have:

$$A_{ct} = A_2A_1(\zeta-\sigma') + A_2\alpha' - A_2A_1\alpha'(\zeta-\sigma'),$$

hence

$$A_{ct}/A_2 = A_1(1-\alpha')(\zeta-\sigma') + \alpha'.$$

From (2), it follows that

$$A_1 = A_1'(1-\alpha),$$

and hence

$$A_{ct}/A_2 = A_1'(1-\alpha')(1-\alpha)(\zeta-\sigma') + \alpha'.$$

It is evident from this that, plotting $A_{ct}/(A_1' - A_{ct})$ in function of A_1', we obtain, for low counting rates, a straight line cutting the ordinate axis at a point corresponding to the value α'. If the counter has not registered spurious pulses during an interval $>\sigma'$, $\alpha' = \alpha = 0$, and the straight line will pass by the origin, and from its slope we can calculate $(\zeta-\sigma')$. If we know the value of ζ, we may then calculate σ'.

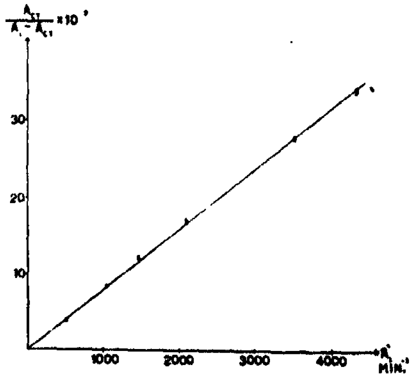

FIG. 3. Curve corresponding to a counter that does not show spurious counts in the interval $\tau-\sigma'$ with $\tau = 10.5\times 10^{-4}$ sec.

DESCRIPTION AND OPERATION OF THE CIRCUIT

(a) *The trigger amplifier* is constituted by two 7C7 tubes connected as a multivibrator; the first tube is direct-coupled to the second whose plate is connected to the grid of the first through a condenser. The first tube conducts normally, and the voltages and resistances are adjusted in such a way that the second is normally non-conducting. The effect of a negative pulse coming from the counter is to make the first tube non-conducting, thus allowing the second to conduct. Adjusting conveniently the size of the pulse coming from the counter, we obtain as a result a pulse at the plate of the second tube, which is, in shape, approximately square of a duration of about 1.5×10^{-5} sec., after which the equilibrium condition of the multivibrator is restored.

(b) *The multivibrator* uses two tubes, a 7J7 and a 7C7, to which we shall refer as (I) and (II), respectively. (I) is a twin tube and one of its sections, I_a, has two control grids, one of which, G_{ab}, controls also the other section I_b. Tube (II) is a pentagrid tube whose plate is coupled by means of resistances to the grid G_{ab} common to both sections of I.

The positive pulse coming from the plate of I_b is rendered negative by means of a phase inverting tube, in this case a 6SJ7. Under normal conditions sections I_a and I_b are conducting, while (II) is non-conducting. A negative pulse at G_a will trigger the multivibrator, and a negative square pulse is obtained at the plate of tube 6SJ7. The multivibrator resolving time depends on the negative voltage at the control grid of II, on the resistance R_{12} connected to this grid, and on the condenser C_6 which couples the plate of I_a to the control grid of II.

(c) *Anticoincidence tube.* The 7J7 tube was employed. The control grid G_a is connected to ground by means of a resistance and the grid G_{ab} common to both sections is maintained at a negative potential. Normally, I_a and I_b are non-conducting. There are three possible cases:

(1) a pulse enters at G_a;
(2) a pulse enters at G_{ab};
(3) a pulse enters at G_a and *simultaneously* another pulse enters at G_{ab}.

Every time that grid G_a receives a pulse from the multivibrator, the grid G_{ab} receives simultaneously a pulse from the amplifier. It may happen, however, that the multivibrator misses a pulse from the amplifier, and in this case, only the grid G_{ab} receives a pulse from the amplifier. We can conclude, consequently, that case (1) never occurs; case (2) can only occur when the multivibrator misses a pulse from the amplifier; case (3) occurs every time that the multivibrator is triggered by a pulse coming from the amplifier. In both cases, (2) and (3), a pulse comes out of the plate of I_b while only in the second case a pulse comes out of the plate of I_a. Therefore, we have registered through I_b all the pulses from the amplifier and through I_a only counts missed by the multivibrator.

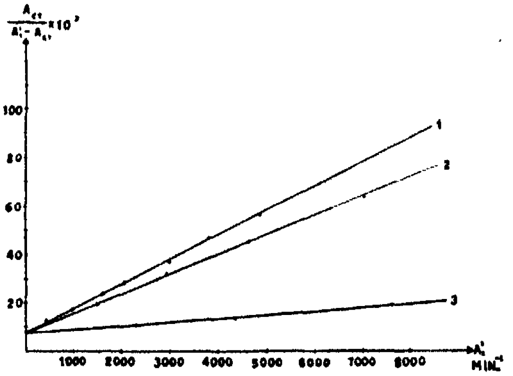

FIG. 4. Curves (1), (2), and (3) correspond to $\tau_1=10.5\times10^{-4}$ sec., $\tau_2=9.3\times10^{-4}$ sec., and $\tau_3=5.3\times10^{-4}$ sec., respectively, with voltage applied to the counter equal to 1080 volts.

An explanation is due here as to the meaning of the term "*simultaneously*" which was stressed above. Actually, the part of the square pulse coming from the amplifier which feeds the grid G_{ab} is the positive part, while the first (negative) part of this pulse feeds the multivibrator which, in turn, feeds at the same time grid G_a. Hence, when we say that the two grids are fed simultaneously, it means only that the two pulses which feed these grids originate from a unique pulse of the amplifier. In reality, the pulse at the grid G_{ab} is delayed in time relatively to the pulse at the grid G_a by a certain interval of time which depends on the duration of the square pulse at the amplifier. In this way, it is easy to understand the reason why the plate of section I_a is not sensitive to the third case. In fact, suppose that the grid G_a receives, at a given instant, a negative pulse from the multivibrator. If this pulse lasts during an interval of the time greater than the delay of the positive pulse which enters at the

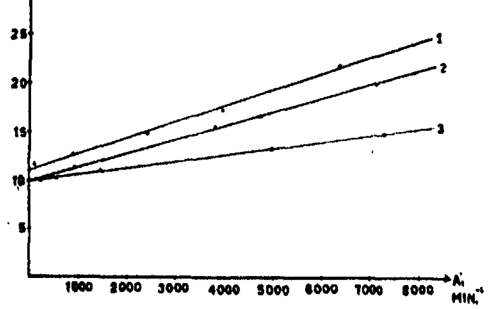

FIG. 5. Curves (1), (2), and (3) correspond to $\tau_1=10.5\times10^{-4}$ sec., $\tau_2=9.3\times10^{-4}$ sec., and $\tau_3=5.3\times10^{-4}$ sec., respectively, with voltage applied to the counter equal to 1160 volts.

grid G_{ab}, the plate of I_a will not conduct because, at the moment when the positive pulse enters, the grid G_a is still negative. Nevertheless, section I_b is sensitive to this pulse because it is controlled only by the grid G_{ab}.

EXPERIMENTAL RESULTS

By means of the method described above, we tested two Geiger-Müller counters having a brass cylinder cathode; one 30 cm long and 5 cm in diameter, and the other 10 cm long and 2.5 cm in diameter; both were filled with alcohol and argon at pressures of 9 cm and 1 cm Hg, respectively. The first counter was tested after intermittent use for around three years. Two different voltages applied to the counter, 1300 and 1360 volts. It can be seen from the result obtained (Fig. 3) that the counter did not register spurious discharges during the interval $\zeta-\sigma'$ where $\zeta=10.5\times10^{-4}$ sec. On the other hand, the experimental curve allows us to determine σ'. We found $\sigma'=(5.82\pm0.12)\times10^{-4}$ sec., a value which was the same for both voltages used. Figures 4 and 5 correspond to the second counter, which also had been in use for about three years. Measurements were also made with two different voltages applied to the counter (1080 and 1160 volts). Three different values of ζ were used, namely: $\zeta_1=10.5\times10^{-4}$ sec., $\zeta_2=9.3\times10^{-4}$ sec., and $\zeta_3=5.3\times10^{-4}$ sec. The experimental results obtained are given by the curves (Figs. 4 and 5). With the potential of 1080 volts (Fig. 4) we see that the percentage α' of spurious discharges for the three different values of ζ given above was the same, the value of α' being $(8.9\pm1.2)\times10^{-3}$. With the potential of 1160 volts we found a value for $\alpha'=11\times10^{-2}$ corresponding to ζ_1, and $\alpha'=10\times10^{-2}$ corresponding to ζ_2 and ζ_3.

DISCUSSION

The characteristic curve of a G-M counter (counting rate in function of voltage) presents a region called plateau in which the counting rate remains approximately constant. What in general is observed is that in the plateau region there exists a small increase in the counting-rate as the voltage increases. Curran and Rae[3] attribute this increase mainly to the multiple discharges produced by bombardment of the cathode by positive ions produced in the discharge. Nevertheless, it seems that the method employed by those authors does not appear to be sensitive enough to measure the percentage of spurious discharges accurately even when the percentage of spurious counts is high. Moreover, it seems also that their method of measurement does not provide enough sensitiveness to measure percentage of spurious counts smaller than 1 percent. The method presented above has the advantage of measuring with reasonable precision percentages of 0.1 percent. By the experimental results obtained we could explain the slope of the plateau as due to the existence of spurious, the origin of which was not yet investigated by us. In this way, for the counter employed to obtain the curve of Fig. 3 the background counting rate obtained with the two voltages, 1300 and 1360 volts were the same and it was not possible to observe the existence of spurious counts during the interval $(\zeta-\sigma')$ following an initial discharge. For this reason, we believed that, in this case, $\alpha'=\alpha=0$ and then we could compute σ' by means of the relation $tg\theta=\zeta-\sigma'$. As to the second counter (Figs. 4 and 5), the background counting rate obtained with the two applied voltages 1080 and 1160 volts were different; on the other hand, with the higher voltage, we obtained a percentage of spurious counts which explained satisfactorily the increase of background counting rate.

ACKNOWLEDGMENTS

We acknowledge our indebtedness to Dr. P. A. Pompeia for the construction and adjustment of some of our experimental equipment, and to Professor M. D. Souza Santos, Professor O. Sala and Dr. P. T. Bittencourt for some helpful discussions.

---

[3] S. C. Curran and E. R. Rae, Rev. Sci. Inst. **18**, 871 (1947).

THE REVIEW OF SCIENTIFIC INSTRUMENTS VOLUME 20, NUMBER 7 JULY, 1949

Magnetic Susceptibility Balance for Use at Liquid Helium Temperatures

T. R. McGuire and C. T. Lane
Sloane Physics Laboratory, Yale University, New Haven, Connecticut*

(Received March 11, 1949)

Data are presented on the design and performance of an apparatus for the measurement of magnetic susceptibilities at the temperatures attainable with liquid helium. After extensive trials, the instrument has proved itself easy and reliable in operation and especially suited to measurements on small specimens.

INTRODUCTION

In the past few years a number of different pieces of apparatus have been built and used in this laboratory for the purpose of making magnetic measurements at low temperatures.[1-3] We have never been entirely satisfied with any of these designs for work in the liquid helium region.

In a recent article[4] Hutchison and Reekie have described a new type of magnetic balance which appears to work very satisfactorily for measurements at liquid nitrogen temperatures. We have constructed one of these balances with a number of improvements and modifications and this has been in use for work in the liquid helium region for nearly a year. The instrument has proved itself very satisfactory, and in many respects much better than previous ones employed here, and we feel that some description of its construction and performance may be useful to others working in this field.

If a body of volume v and susceptibility k (per unit volume) is placed in an inhomogeneous field H, it experiences a body force given by

$$\mathbf{F}=[(k-k_0)/2]v\nabla H^2,$$

where k_0 is the susceptibility of the surrounding medium. A magnetic balance is required to measure forces of the order of a few dynes with accuracy. For work in the liquid helium range, the whole balance must be capable of evacuation so that the specimen can be surrounded with helium gas at a few mm Hg pressure for heat exchange purposes.

Although this method does not, in general, permit of absolute measurements of k owing to the difficulty of determining the field gradient accurately, this defect is not a drawback since a calibrating substance of known susceptibility can be used. The fact that very small specimens can be used is an advantage in many cases where these are of rare material or have to be homogeneous single crystals.

CONSTRUCTION

Figure 1 shows schematically the balance, as evolved by us, for use at liquid helium temperatures.

The balance arm B, made of Lucite, is supported between two uprights by means of a stretched flat metallic ribbon S. The use of Lucite is recommended because of its light weight and the absence of any ferromagnetic impurity. The specimen X is at one end of the arm B supported by a quartz wire. The other end of the arm has a counterpoise W whose distance from the point of suspension may be varied, both W and B being threaded. Arm B also carries a small galvanometer mirror M as shown. Inside the gap of a small permanent magnet P is the compensating coil C. This magnet is from a 5-in. loudspeaker, and for C we used the voice coil of the speaker. It was believed that the field of this magnet (approximately 2000 gauss) was sufficiently high so that errors due to stray fields would be negligible.

The electrical leads to C were of very fine flexible wire (No. 40 copper); one was connected directly to the brass base plate D; the other came through a small insulated Stupakoff terminal (not shown) in D. The restraining force on B due to these leads is negligible. The weight of balance arm plus coil was approximately 7 g.

Attached to the coil form of C were several strips of aluminum foil which, in the magnetic field of P, served as an electromagnetic damper.

The balance housing H is of Pyrex glass and for the vacuum seal between H and D we used Apiezon "Q" compound. A tube (not shown) passing through D was used for evacuating the balance, and filling with helium gas.

A rather critical element in the design is the thin-walled glass tube T which houses the specimen X. The heat capacity of this tube had to be as small as possible consistent with sufficient mechanical strength, for reasons which will presently be discussed. The helium (D_H) and nitrogen (D_N) Dewars were of conventional design, silvered and with viewing slits, and both made of Pyrex glass. The

---

* Assisted by the ONR.

[1] S. H. Browne and C. T. Lane, Phys. Rev. 60, 899 (1941).

[2] J. A. Marcus, Phys. Rev. 71, 559 (1947); Thesis Yale (1947).

[3] S. G. Sydoriak and J. E. Robinson, Phys. Rev. 75, 118 (1949).

[4] T. S. Hutchison and J. Reekie, J. Sci. Inst. 23, 209 (1946).

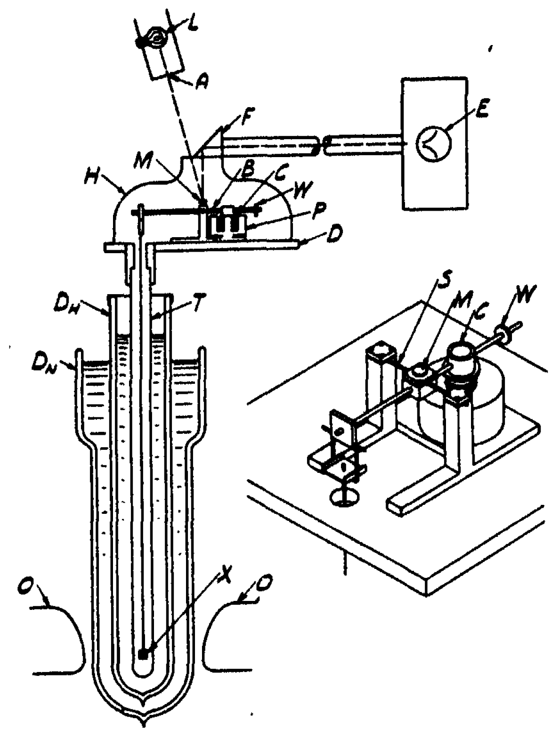

FIG. 1. Schematic drawing of the balance.

pole pieces of the Weiss electromagnet 00 were of the type used by Föex and Forrer.[5] These have the advantage of making $H(\partial H/\partial x)$ relatively constant over a distance of several millimeters and hence, a certain leeway is permissible in replacing the measured specimen by the calibration specimen. With our magnet and these pole pieces, a maximum field of about 7000 gauss was obtainable at the gap (4.2 cm) necessary to accommodate the Dewar flasks.

Reference has been made to the special requirements for tube T. The helium Dewar is filled at the liquefier and transported to another room where the balance is set up. This latter contains a few mm Hg pressure of pure helium gas. With the magnet out of the way (it slides on rails), T is precooled with liquid nitrogen. This precooling flask is removed and replaced by the liquid helium Dewar as rapidly as possible. With T about ½-in. diameter by 0.01-in. wall, the loss of liquid helium is nominal.

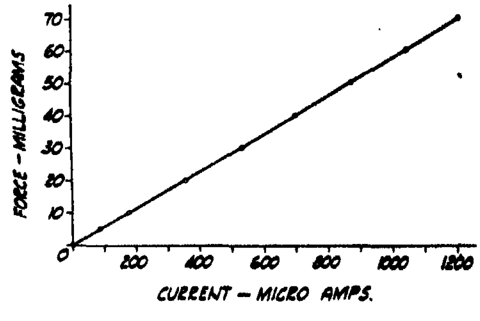

FIG. 2. Relation between force on the balance and compensating current.

Of the several materials tried for suspension S, phosphor bronze and nichrome were found to be best. This was usually a ribbon, approximately 0.005-in. thick, cold rolled in three stages from 0.012-in. diameter wire with gas flame anneal between each rolling. Nevertheless, in measurements at liquid helium temperatures, difficulties were at first experienced due to hysteresis in the suspension. At these temperatures the resistivities of many metals (especially single crystals) are extremely small. Hence, in changing the magnetic field, large and persistent eddy currents are induced in the sample and these give rise to very large diamagnetic forces on the specimen. Thus, very large deflections of the balance occur and these were found to result in a semi-permanent set in the suspension S such that the zero would change with time. We overcame this by placing stops (not shown) near the balance arm such that the latter's motion was limited to a very small amount.

Although we have not, as yet, tried it, it seems possible that the following modification of the balance suspension would be usable. In place of S a rigid rod could be used, each end of which terminated in a micro ball bearing** attached to the uprights. Such a "fiber" would, of course, have virtually zero restoring torque and be free from the above difficulty.

The optical system of the balance consists of a light source L (32 cp auto bulb), a prism F and a Type 920 split cathode photo-tube E. The two cathodes of E form two arms of a Wheatstone bridge, the remaining two arms containing two fixed 10-megohm resistors. The bridge is supplied by a 135-v "B" battery, and a galvanometer is used as the indicating instrument. A spot of light, which is the image of the circular aperture A, is reflected as shown. The photo-tube is adjusted mechanically until a position is obtained where the galvanometer reads zero. A small deflection of B throws the bridge off balance and the current is adjusted in C until the galvanometer again reads zero. This compensating current is thus a measure of the force on the specimen. With a constant light source and the photo-tube and balance shielded from stray illumination, the stability of the galvanometer spot was found to be excellent and a magnification of 200 times was obtained using this circuit. In addition to better sensitivity, much less

---

[5] G. Föex and R. Forrer, J. de phys. et rad. 7, 180 (1926).

** Such micro bearings in non-magnetic material are obtainable from New Hampshire Ball Bearings, Inc., Peterborough, New Hampshire.

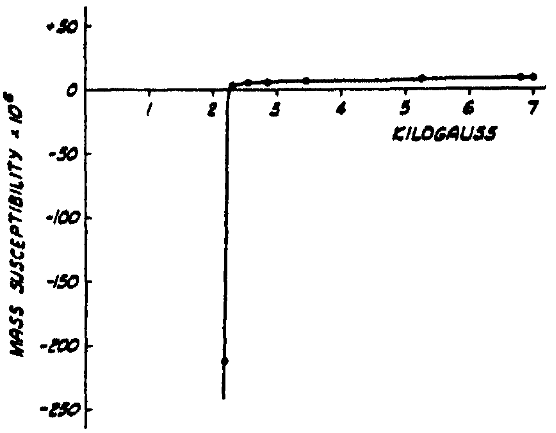

FIG. 3. Magnetic susceptibility of vanadium at 3.5°K.

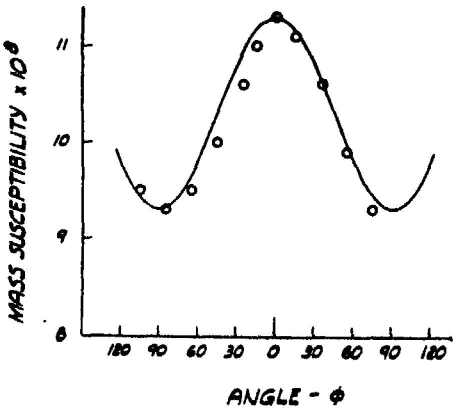

FIG. 4. Magnetic susceptibility of a single crystal of mercury at 4.2°K.

eye fatigue is experienced with this arrangement as compared to the usual microscope and slit system.

We used spectroscopically pure (Johnson, Matthey and Company) polycrystalline bismuth as our calibrating substance, taking the room temperature mass susceptibility as 1.34×10^{-6}. In all measurements the susceptibility of the medium (k_0) is negligible. A difficult field gradient measurement and the necessity of determining the forces in absolute units is thus evaded.

PERFORMANCE

Figure 2 shows that the balance is satisfactorily linear over a wide range of forces. A force of 1/20 of a dyne is detectable. From a large number of measurements carried out in the past year we have selected two examples to illustrate the performance of the instrument. Figure 3 shows the susceptibility of a polycrystalline vanadium specimen as a function of magnetic field at 3.5°K. The sample was roughly spherical in shape with a diameter of about 3 mm and weighed approximately 0.17 g. The material was about 99.8 percent pure. At about 2.2 kilogauss the vanadium suddenly becomes highly diamagnetic, indicating a transition into the superconducting state.

Figure 4 shows the diamagnetic susceptibility of a single crystal of mercury as a function of the angle (ϕ) between the magnetic field and the principal axis of the crystal. The mercury crystal was of extreme purity (impurity 6×10^{-4} percent) and the measurement was made at 4.2°K in a field of 5250 gauss. The solid line in Fig. 4 is the expected $(\text{cosine})^2$ law, provided that no field dependence of susceptibility exists (DeHaas-van Alphen effect) and the circles are the experimental points.

By replacing the electromagnet with suitable air-core solenoids or Helmholtz coils, the device should be well suited for magnetic measurements in the superconducting phase.

THE REVIEW OF SCIENTIFIC INSTRUMENTS VOLUME 20, NUMBER 7 JULY, 1949

A Large Cloud Chamber Using Rear Illumination

E. W. Cowan
California Institute of Technology, Pasadena, California

(Received November 30, 1948)

A large cloud chamber is described that makes use of rear illumination by means of a transparent piston and back plate. This system of illumination is particularly advantageous for a large cloud chamber since the increase in the amount of scattered light for small angles of scattering from droplets reduces the total light required.

A LARGE cylindrical cloud chamber 87 cm in diameter and 15 cm in depth was constructed by Anderson and Neddermeyer in 1937. This same chamber with a few modifications has recently been placed in the pressurized cabin of a B-29 airplane and 3500 pictures have been taken without magnetic field at altitudes up to 13,500 meters. Since the chamber has operated very satisfactorily for these experiments and is of somewhat unconventional construction, the following description is given.

A photograph of the chamber mounted in the cabin of the airplane is shown in Fig. 1. A cross-sectional view of the chamber in Fig. 2 indicates the method used to obtain an axial expansion. A circular glass diaphragm, connected to the chamber by a ring-like rubber membrane, is supported by rollers resting on the lower part of the chamber walls. Compressed air admitted to the cavity behind the diaphragm (on the side opposite to that of the cloud chamber) moves the diaphragm forward and compresses the gas in the chamber, which is 10 or 20 cm Hg pressure above the outside pressure with the chamber in the expanded position. Expansion is accomplished by suddenly releasing this compressed air into the cabin through a large valve.

Eight equally-spaced push-rods are connected to a brass ring that surrounds the glass plate forming the diaphragm. The push-rods pass through sleeves in the rim of the cavity behind the chamber to aid in guiding the diaphragm. Alternate push-rods are supplied with adjustable nuts that limit the forward motion of the diaphragm and thus control the expansion ratio. Springs on the other push-rods are adjustable so that the diaphragm will remain perpendicular to the axis of the chamber during the expansion.

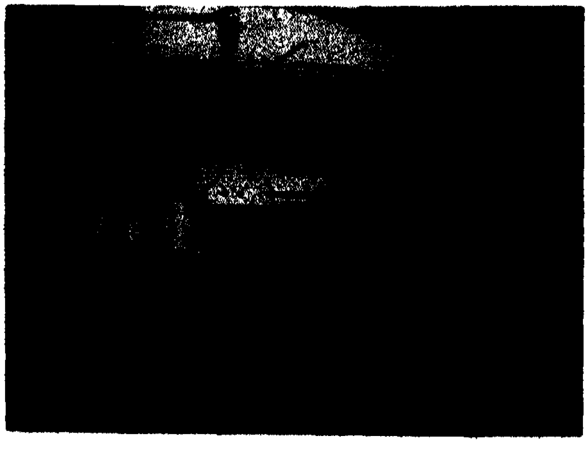

Fig. 1. Front view of cloud chamber mounted in cabin of B-29 airplane. Cameras appear on stand in front of chamber.

Figure 3 shows the manner in which three horizontal plates, one of carbon and two of lead, have been arranged inside the chamber for the high altitude experiments. Four wires, supported above and below the set of plates, and the center one of the three plates, are lowered to a potential of from 500 to 1000 volts below the potential of the outer two plates and the chamber walls to provide a sweep field for the chamber. An electric field of the order of 50 to 100 volts per centimeter is thus maintained in the chamber until the moment of the expansion.

As the diaphragm moves to expand the chamber, a mechanism connected to the push-rod at the top of the diaphragm short circuits the sweep-field circuit and reduces the sweep field to a small value. Simultaneously the same mechanism uncovers a hole and drops a small shot. The short flash of light illuminating the chamber to photograph the tracks also photographs the shot during its fall. In Fig. 5 the shot is indicated by an arrow just below the center of the bottom plate in the chamber. From a measurement of the distance the shot has fallen, the time interval between the short-circuiting of the sweep field and the instant of taking the picture may be calculated.

Tracks produced by particles passing through the chamber before the removal of the sweep field are spread out or separated by the action of the sweep field on the ions. The tracks appearing unseparated in the photographs are therefore caused by particles passing through the chamber after the removal of the sweep field. For a particle to produce a track appearing on the photograph, its passage also must have preceded the light flash by at least the time required for droplets to grow large enough about the ions to be photographed. Therefore the period of time between the removal of the sweep field and the light flash, as measured by the fall of the shot, minus the time required for droplets to grow large enough to be photographed (of the order of 0.050 to 0.100 seconds) is the sensitive time for tracks which show no separation by the sweep field. This is true provided that the flash of light is delayed only a sufficiently short time (of the order of a few tenths of a second) after the expansion so that the gas of the chamber is still capable of forming droplets about ions and is thus sensitive to particles at the time when the flash of light occurs.

Two Type K-25 aerial cameras have been modified for use with the chamber by adding an 0.75-diopter lens immediately in front of the camera lens, which is normally focused for large distances. The cameras are placed as shown in Fig. 4. Simultaneous pictures are taken from two different angles to provide a stereoscopic view of the chamber. Each camera takes 50 pictures, 13.9 cm by 11.4 cm, on a 6-meter roll of triple-X (exposure index 200) panchromatic film. Most of the pictures have been taken with a lens aperture of f:16.

Illumination is provided by four krypton-filled flash bulbs, each connected to a 23 μf condenser charged to a potential of 2000 volts. These flash bulbs and their power supplies are part of a Model S-1169 Army Signal Corps light identification unit. Since this unit is designed to operate on the standard 24-volt d.c. aircraft supply, it can be used with only minor modifications. Four of the Model X-400 flash-bulb units arranged in a straight line approximate the desired line source and are rugged and simple to mount.

The front plate of the chamber, the diaphragm, and the back plate of the air-filled cavity behind the chamber are all of "Tuflex" glass so that the chamber is essentially three transparent circular disks arranged to form a cylinder, with the center disk the movable diaphragm. This allows the chamber to be illuminated from the rear (side opposite from that of the cameras) as shown in Fig. 4. Because the spherical droplets in the chamber scatter many times more light per unit solid angle through a small angle of deviation than through a large angle, such rear illumination requires only a small fraction of the energy for lighting demanded by right-angle illumination with the light sources at the sides of the chamber. An arrangement of chromium-plated iron mirrors, shown edge-on in the side view in Fig. 4, helps distribute the light in the chamber so that tracks in different parts of the chamber will scatter more nearly equal amounts of light into the cameras.

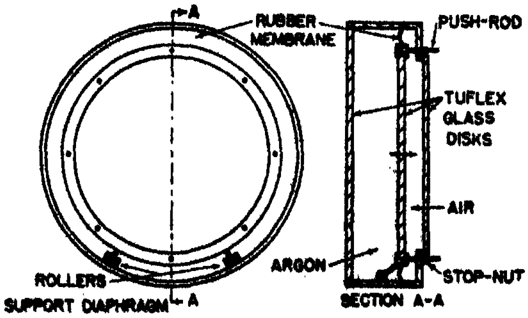

FIG. 2. Method of obtaining expansion of chamber.

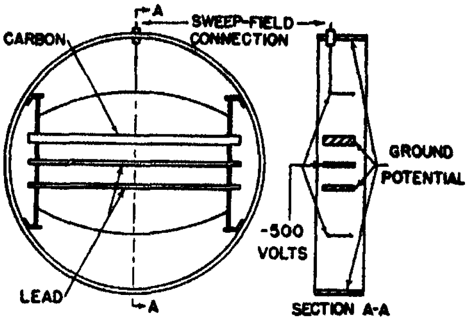

FIG. 3. Arrangement of plates in chamber.

The arrangement of the mirror system is symmetrical with respect to a horizontal plane through the center of the chamber. A more even distribution of illumination can be obtained by using brighter lights at a greater distance from the chamber. However, this was not permitted by the space available in the cabin of the airplane. Direct rays of light and rays scattered through only a very small angle are prevented from entering the cameras by arranging the source and mirrors so that they are hidden behind the carbon and lead plates mounted in the chamber, in the manner indicated in Fig. 4.

Argon gas saturated with ethyl-alcohol vapor is used to fill the chamber. Although the chamber has been tested to withstand a pressure of one atmosphere above the surrounding atmospheric pressure, a pressure somewhat less than half of this value (with the chamber in the compressed position) has been used for most of the high-altitude experiments because of the possible danger of losing pressure in the pressurized cabin in which the chamber was placed.

In order to insure that the gas near the top of the chamber is saturated with alcohol vapor, alcohol is pumped from a small pool in the bottom of the chamber through a filter and check valve up to two small pipes entering the top of the chamber. From these pipes the alcohol squirts onto the rubber part of the diaphragm and runs down again to the pool at the bottom of the chamber, providing a surface of alcohol of considerable

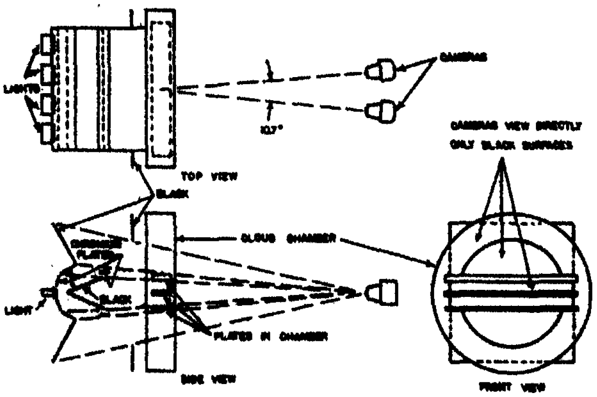

FIG. 4. Cameras and illumination.

area from which evaporation can take place. The alcohol pump is run only for a few seconds during the waiting part of the cycle of operation, when the diaphragm is in the position which compresses the chamber gas.

Regulation of the air pressure which controls the position of the diaphragm is accomplished by means of pressure-reducing valves and electrically-operated shut-off valves. Since the rubber part of the diaphragm is not perfectly stiff, changing the differential pressure across the diaphragm changes the chamber volume slightly even when the diaphragm is against the stops, thus providing a fine adjustment of the expansion ratio in addition to the rather coarse mechanical adjustment of the stops. Adjustment of the springs that control the angle of the diaphragm during its movement is best accomplished by watching as the chamber expands the relative motion of the images of a small light reflected in the three glass plates.

The air used to compress the chamber is dried to prevent the appearance of a cloud of water droplets behind the diaphragm on expansion and is warmed slightly to prevent cooling of the diaphragm and the resultant condensation of alcohol on the chamber side of the glass.

Operation of the chamber is controlled electrically by means of conventional circuits. Pictures have been taken both with the chamber expanded at predetermined intervals and with counter control. A cycle of operation with the former type of control requires approximately one minute. Although a slow expansion during each cycle is desirable for a few cycles when first placing the chamber in operation after filling it, further slow expansions are not necessary.

A typical photograph obtained with a random expansion at an altitude of 12,100 meters is shown in Fig. 5. A light delay long enough to take advantage of most of the sensitive time of the chamber was used. In some of the flights the length of time the light was delayed after the expansion was considerably reduced to decrease the number of tracks and the resultant confusion in each photograph. When the pictures are viewed stereoscopically, the effect of separating the tracks in a third dimension makes their interpretation clearer. Views from both cameras are shown in the final enlargement in Fig. 5. In Fig. 5 the photograph at the upper right shows an enlarged view of the region of the chamber enclosed by the rectangle shown in the left-hand photograph. A further enlargement is shown in the lower right-hand view which includes that part of the chamber enclosed by the rectangle which appears in the upper right-hand view. The successive enlargements show the large amount of detail which appears on these photographs, and show also the number and variety of tracks recorded by a single expan-

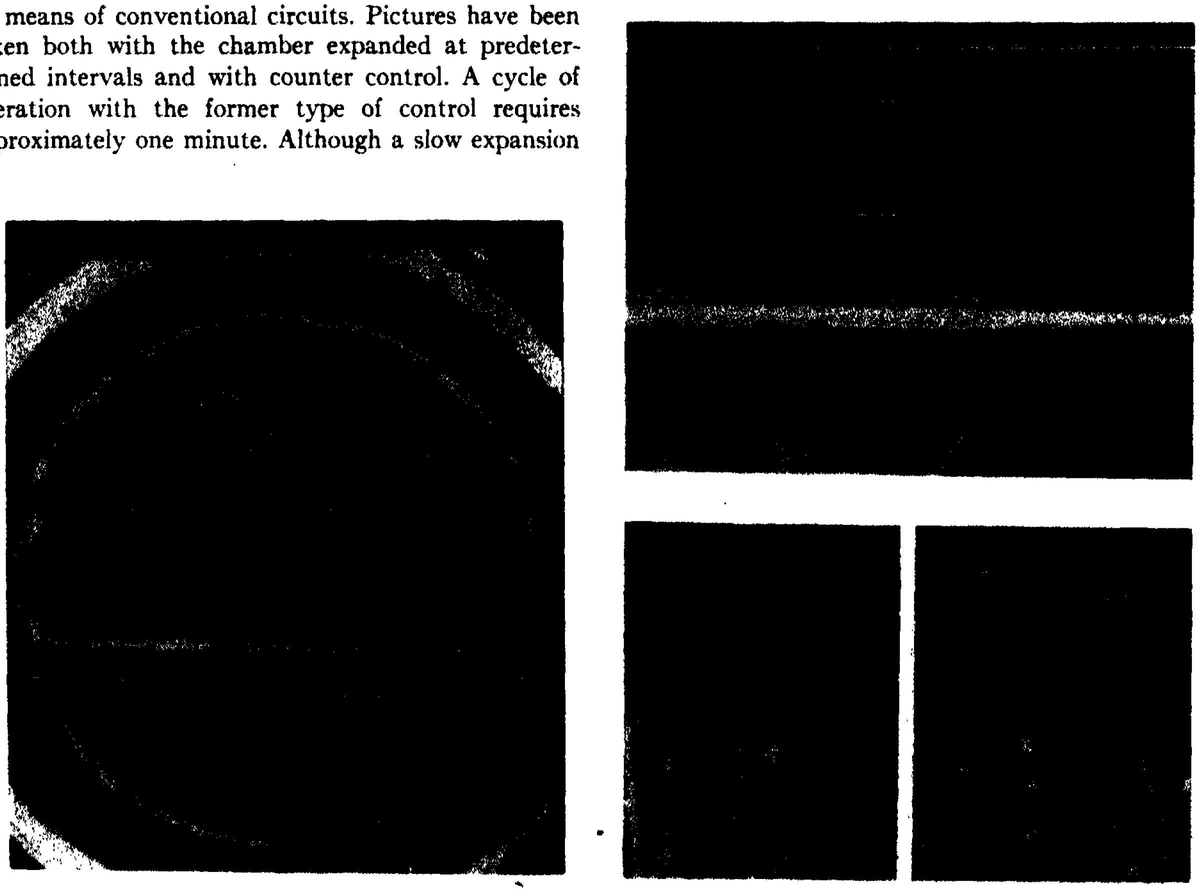

Fig. 5. Typical chamber photograph (long light delay) at 12,100 meters altitude. Enlargements show detail in right center of picture.

sion of the chamber at high altitude. Some results obtained with this equipment have previously been reported.[1,2]

I wish to express my indebtedness to Professor C. D. Anderson, who provided much helpful advice in the course of these experiments.

---

[1] E. W. Cowan, Science **108**, 534 (1948).

[2] Adams, Anderson, and Cowan, Rev. Mod. Phys. **21**, 72 (1949).

THE REVIEW OF SCIENTIFIC INSTRUMENTS VOLUME 20, NUMBER 7 JULY, 1949

The Ten-Channel Electrostatic Pulse Analyzer

DEAN A. WATKINS
Los Alamos Scientific Laboratory, Los Alamos, New Mexico

(Received March 17, 1949)

A ten-channel pulse height discriminator using a beam deflection tube is described. The instrument provides one-volt channels and has a high degree of stability. Essential circuits are given so that the analyzer may be readily duplicated. Performance and limitations are discussed.

TO determine the energy spectra of particles in nuclear experiments, one method is to measure the height of pulses produced by the particles in an ionization chamber. Ordinarily these pulses are amplified and then sorted and counted by means of a counting circuit which incorporates a pulse-amplitude discriminator. In its usual form, this discriminator will produce a standard output pulse for input pulses exceeding a certain amplitude and will produce no output if the pulses are less than this amplitude. The discriminator level, or bias, is adjustable, and by taking consecutive sets of data, the well-known integral-bias curve is obtained. Another method employs a discriminator that responds to voltage pulses in a certain interval and does not respond to pulses outside this interval. Taking successive sets of data gives a differential-bias curve.

A device employing "*n*" single-channel discriminators responding to adjacent voltage intervals has been described by Freundlich, Hincks, and Ozeroff.[1] These analyzers employ 12, 20, and 30 channels. Similar instruments using ten channels have been built and are now being used at the Los Alamos Laboratory. These analyzers, although having several disadvantages, have proved very useful. In spite of regulated power supplies, it has been necessary to recalibrate them frequently, each of the ten channels having to be set individually. The smallest channel width obtainable has been about two to four volts. Physically, the analyzers are large and employ 168 vacuum tubes.

To overcome these limitations, a ten-channel analyzer using an electron beam tube has been devised. The analyzer is shown in Fig. 1. It occupies six 8¾-inch chassis in a standard relay rack. The units are, from top to bottom, (1) a pulse generator for calibration, (2) a pulse amplifier, (3) the analyzer chassis, (4) five "scale-of-sixteen" scalers, (5) five "scale-of-sixteen" scalers, and (6) the analyzer power supply. The ionization chamber and its preamplifier are the only additional items of equipment required.

Deflection Tube

The heart of the analyzer is the X150 beam deflection tube shown in Fig. 2. Its internal structure is shown in Fig. 3. The tube was developed by the Federal Telecommunication Laboratories at Nutley, New Jersey, as an outgrowth of their work on beam tubes for electronic switching and multiplexing.[2]

The operation of the tube as a pulse amplitude discriminator is shown in Fig. 4. The pulses from the amplifier are made push-pull and applied to the deflection plates. Initially the beam is deflected above the region of the dynodes by applying a d.c. voltage to the deflection plates. As the pulse is applied, the beam travels downward a distance proportional to the amplitude of the pulse, causing it to fall on one of the dynodes. In practice the beam is cut off during the first part of this interval by a negative bias on the focusing and gating electrode. One microsecond after the beginning of the input pulse the beam is gated on for 1.5 microsecond. Since the beam is off during the rise and fall of the input pulse, an output signal actually occurs only during the flat top portion of the pulse, thus avoiding an output signal on other dynodes during its rise and fall. The result is a 1.5-microsecond voltage pulse appearing across the corresponding dynode load resistor. This pulse is amplified and counted.

---

[1] Freundlich, Hincks, and Ozeroff, Rev. Sci. Inst. **18**, 90–100 (1947).

[2] Grieg, Glauber, and Moskowitz, Proc. I.R.E., **35**, 1251–1257 (1947).

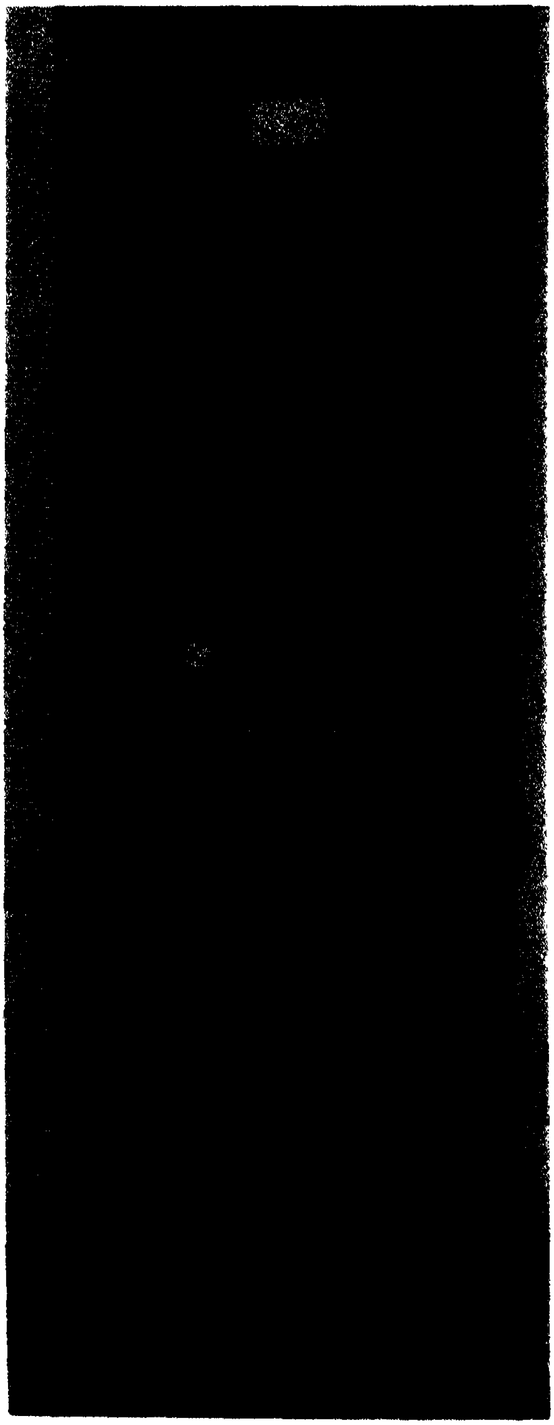

Fig. 1. The ten-channel analyzer. Units are from top to bottom, (1) a pulse generator for calibration, (2) a pulse amplifier, (3) the analyzer chassis, (4) five "scale-of-sixteen" scalers, (5) five "scale-of-sixteen" scalers, (6) the analyzer power supply.

Fig. 2. The ×150 beam deflection tube.

The dynodes are operated at a voltage somewhat less than that of the anode to encourage secondary emission. In the ×150 tube the dynode current with the beam centered on a dynode is of the order of 100 microamperes. The deflection sensitivity of the tube is about 1.5 volts per dynode width. The ratio of beam width to dynode width is such that the dynode output current goes to zero when the beam strikes between two dynodes. A plot of dynode output *versus* deflection voltage is given in Fig. 5. The beam is line focused.

Analyzer System

A block diagram of the system employing the ×150 deflection tube is shown in Fig. 6. The Model 101 pulse amplifier is of the feed-back type with a gain of 74 db. It has a rise time of 0.5 microsecond and will produce 125-volt positive pulses without overloading. At its input, the pulses from the chamber preamplifier are differentiated (clipped) with a time constant of 3 to 5 microseconds. The remainder of the system with the exception of the scalers and registers occupies a single chassis (Fig. 7), the complete schematic for which is shown in Fig. 8. The pulses from the amplifier are fed into a pulse-lengthening circuit which generates flat-topped pulses having a duration of 3 microseconds. Each pulse has an amplitude proportional to that of the corresponding input pulse. The input pulse is also applied to a 1-microsecond delaying amplifier. The delayed pulse triggers a univibrator which generates a rectangular gating pulse of about 65-

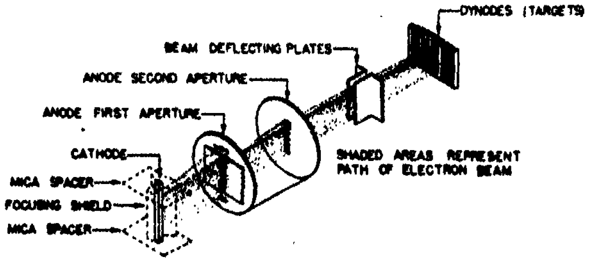

Fig. 3. The internal structure of the ×150 tube showing path of electron beam.

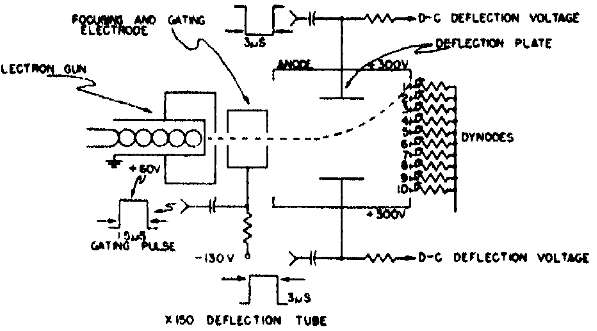

FIG. 4. The deflection tube schematic showing operating voltages and input signal.

volt amplitude having a rise time of less than 0.05 microsecond and a length of 1.5 microsecond. This pulse goes through a cathode follower and is then applied to the gating and focusing electrode.

The ten dynodes of the deflection tube are coupled to ten two-stage pulse amplifiers which drive cathode followers. The cathode followers are coupled with short lengths of cable to the ten scaler-registers.

Controls and Adjustments

The front panel controls and their uses are as follows:

1. "*Run-Stop*" *Switch.* This switch inactivates the gating pulse generator, thus preventing the analyzer's responding to input pulses.

2. "*Discriminator Bias.*" This control consists of a two-gang, ten-turn helical potentiometer with a linearity of 0.1 percent. It changes the d.c. deflection voltage on the tube, thus permitting the operator to slide the ten channels up or down the voltage spectrum over a range of from zero to 100 volts.

3. "*Attenuator.*" The attenuator is just what the name implies. Set on "1," the ten channels cover a range of 10 volts and are thus 1-volt channels. With the attenuator set at "10," the input pulses are attenuated by a factor of 10. Hence, the ten channels cover an effective range of 100 volts giving 10-volt channels. In this position the operation covers in one setting the entire voltage range up to the limit of the amplifier.

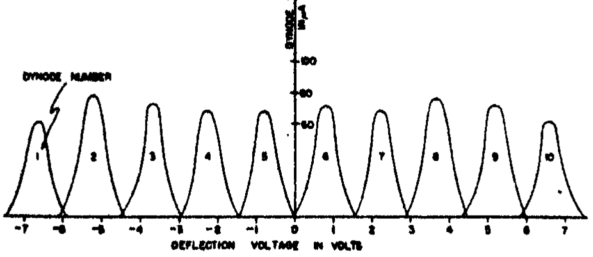

FIG. 5. A plot of dynode output current *versus* deflection voltage for the X150 beam tube.

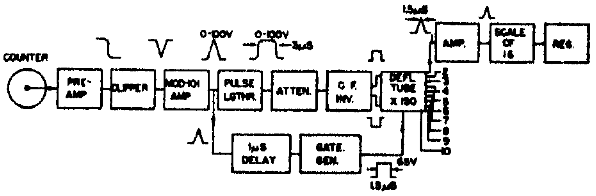

FIG. 6. A block diagram of the analyzer system.

The remainder of the controls are screwdriver adjusted. The potentiometer marked "Calibration" is set so that the ten channels occupy an effective interval of ten volts. The "Focus" control is adjusted for optimum beam focus as observed with an oscilloscope tied to two adjacent dynodes. The "Gating Bias" control is also adjusted for optimum focus with pulses applied to the analyzer. The "Dynode Voltage" potentiometer is set for maximum secondary emission.

Channel Width

The channel widths are set individually by means of bias controls on discriminators at the inputs of the ten scalers. A plot of channel width *versus* pulse height is given in Fig. 9, which shows that the individual channels occupy half the interval from channel to channel. Actually, by resetting the discriminators, the channels can be made to occupy the whole interval.

Scalers and Power Supply

The scalers used in this instrument are conventional "scale-of-16" scalers driving Production In-

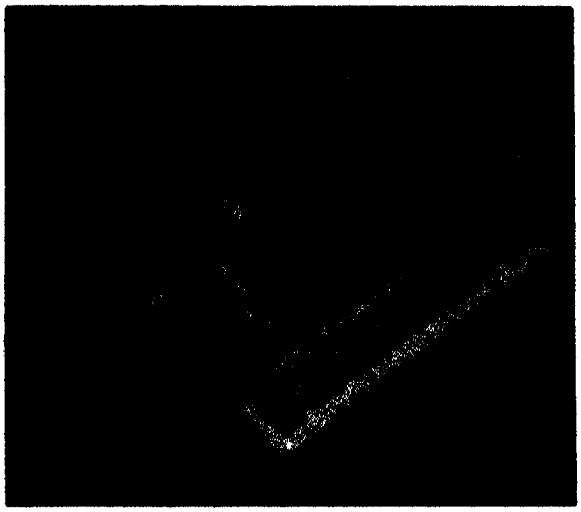

FIG. 7. Rear view of the analyzer chassis showing arrangement of components.

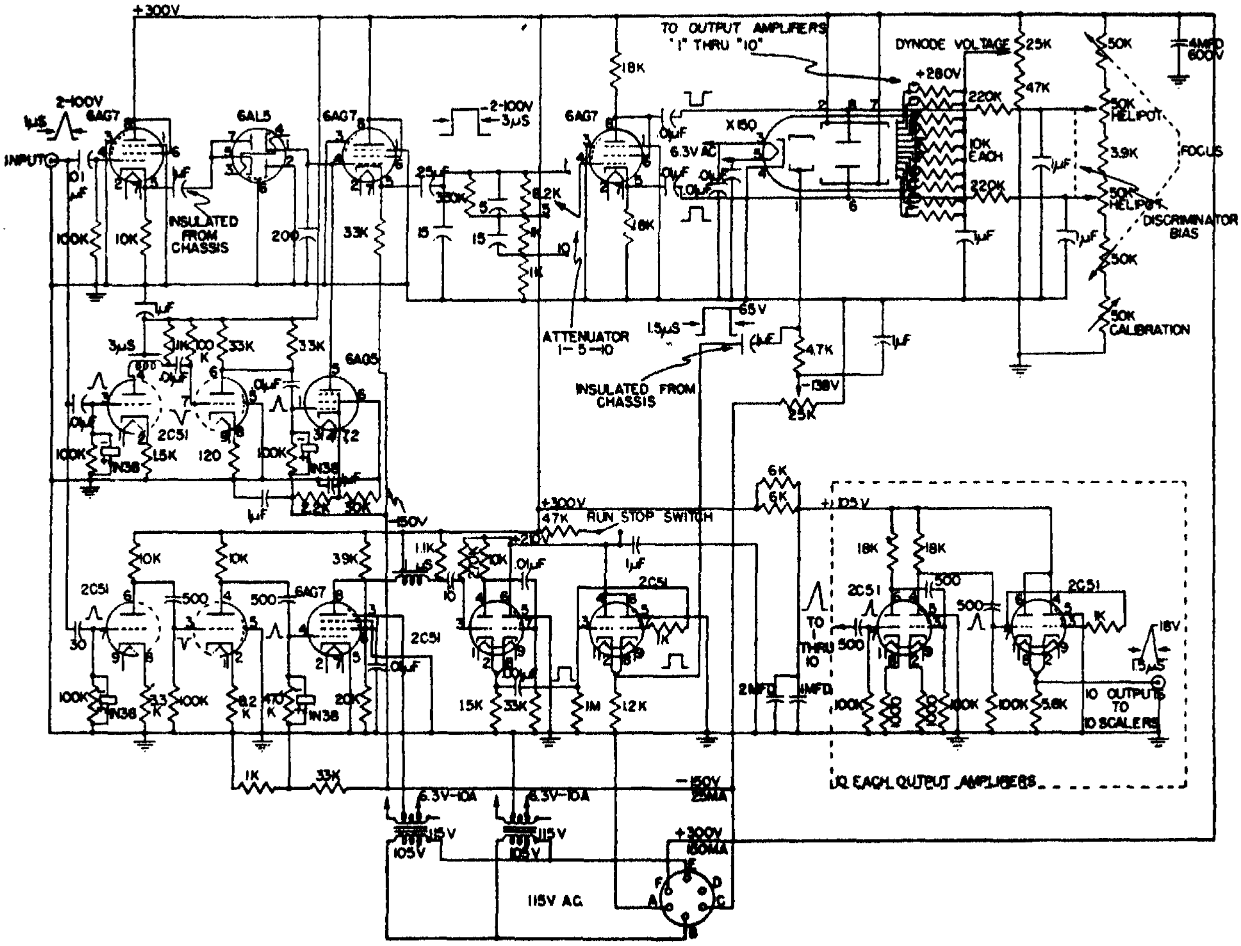

FIG. 8. Complete schematic for the analyzer chassis.

struments Company registers capable of about 20 counts per second. This makes possible a counting rate of 320 per second per scaler for regularly spaced pulses, or an over-all rate of about 2500 counts per second for the analyzer.

The power supply for the analyzer chassis is an electronically regulated type delivering 300 volts at 150 ma and −150 volts at 25 ma. The circuit is given in Fig. 10.

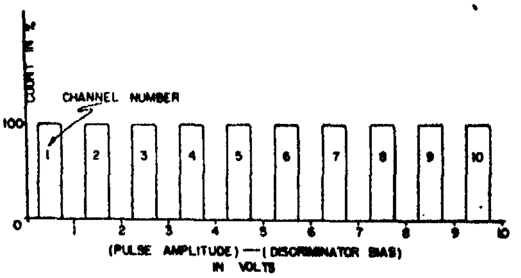

FIG. 9. Calibration chart for the analyzer showing channel width *versus* pulse height. Each channel occupies half the interval from channel to channel.

Performance

The performance of the analyzer depends largely upon the conditions existing in a given experiment. The important factors to consider are (1) average counting rate, (2) rise time of the input pulses, and (3) over-all stability.

(1) The highest permissible counting rate for the analyzer is determined by the capacity of the mechanical registers and the statistical error which can be tolerated. For less than 1 percent loss, the average density should be 250 counts per second assuming that the pulses are uniformly distributed over the ten channels.

(2) For the unit here described, the input pulses must rise to full amplitude in 1 microsecond or less. However, by changing the two delay lines the analyzer may be used with pulses having a rise time as long as 10 or 15 microseconds. Since the pulses are differentiated at the input of the amplifier, the decay time of the chamber pulses is not important.

(3) The over-all stability of the analyzer de-

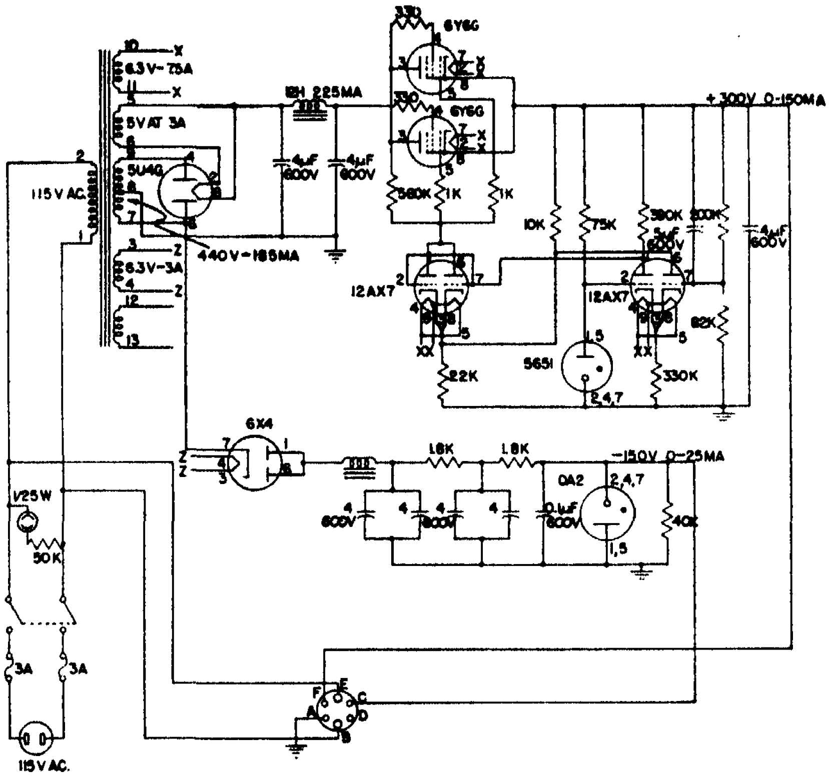

FIG. 10. Analyzer power supply schematic.

pends on (a) the stability of the pulse amplifier, (b) the stability of the voltages on the deflection tube, and (c) the stability of the discriminators preceding the scalers.

(a) The stability of the amplifier has proved to be excellent. The stability factor (βK) is 100 and it is operated from its own electronically regulated supply.

(b) The voltages on the deflection tube are also obtained from a regulated supply whose output voltage is within 0.03 percent for ten percent line and load fluctuations.

(c) The voltages on the scaler discriminators are also well regulated and are insensitive to line fluctuations.

No measurable change in calibration of the overall system has been detected since it was first adjusted. However, to satisfy the operator, a pulse generator is provided in order that the various calibrations may be checked from time to time.

ACKNOWLEDGMENTS

The development program for the analyzer was begun by Mr. H. G. Weiss at Los Alamos. Mr. Weiss is now employed by the Raytheon Manufacturing Company of Waltham, Massachusetts. Other members of the Laboratory Electronics Group, including Mr. R. W. Freyman, made valuable contributions to the program. The co-operation of Mr. A. K. Wing and Mr. M. W. Wallace of the Tube Department, Federal Telecommunication Laboratories, is gratefully acknowledged.

THE REVIEW OF SCIENTIFIC INSTRUMENTS VOLUME 20, NUMBER 7 JULY, 1949

A Precision Automatic Electrometer*

N. T. Seaton
Department of Physics, University of California, Berkeley, California

(Received July 19, 1948)

A triple-range portable electrometer suitable for the precision measurement of currents of the order 10^{-11} to 10^{-14} amp. is described. Current is measured in terms of the automatically registered time interval required to charge a condenser up to a certain voltage. The use of negative feedback and special operating conditions for the input FP-54 Pliotron allow current to be simply determined to within 0.1 percent. Radiotype dry batteries, which operate the instrument completely except for a timer, are contained within the amplifier and will last at least 250 hours.

INTRODUCTION

MANY of the important characteristics of radioactive substances can best be determined from measurements with an ionization chamber and electrometer. In cases where a large number of such measurements involving currents of the order of 10^{-11} to 10^{-14} amp. are to be made with great accuracy, the construction of a suitable electrometer may pose a problem. The present electrometer, although more expensive to construct than most of those described previously in the literature, gains considerable advantage in accuracy and convenience of operation. The simultaneous measurement of two currents can be accomplished with an extension of the method employed, with the result that, even though they may both arise from a widely fluctuating source, an accurate value of their relative intensity can be obtained.

THEORY

The fundamental theory of the instrument, involving the application of negative feedback, has been discussed previously by Roberts,[1] and more completely by Lea;[2] the elements of the theory are as follows:

Referring to Fig. 1, suppose we add a charge dQ to the input electrode, thereby changing its voltage by an amount dE. The output voltage will then change by $dV=-AdE$ and we will have

$$\begin{aligned} dQ &= C_0dE+C(dE-dV) \\ &= -CdV[1+(C+C_0)/AC] \\ \bar{i} &= -\frac{CV}{t}\left(1+\frac{1+C_0/C}{A}\right). \end{aligned}$$

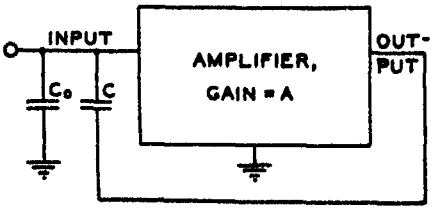

Fig. 1.

where t is the time interval in which the output voltage changes an amount V. The use of a fairly large amplification (say 10^4) not only reduces the determination of $\bar{i}$ to readily measurable quantities but, because of the subsequent limitation of the range in the input voltage to a small value $(\Delta E \mp -V/A)$, it also limits the conduction current in the input-system insulators and permits a special method of stabilizing the input electrometer tube. The permissible ground-feed-back capacity ratio, C_0/C, depends upon the accuracy desired and the stability of the amplifier. Again referring to Fig. 1, we have for R, the dynamic output resistance of the amplifier

$$1/R=g_mC/(C+C_0)+g_m/A, \qquad (2)$$

where g_m is the over-all transconductance. The percent error caused by a drift, ΔI, in the output-current conditions over the time t is therefore

$$r=\frac{-100\Delta I\cdot A(C+C_0)}{Vg_m(C+C_0+AC)}\cong\frac{-100\Delta I}{Vg_m}(1+C_0/C). \qquad (3)$$

The relative uncertainty in a measurement introduced by random fluctuation in the current source is proportional to $(CV)^{-\frac{1}{2}}$. This uncertainty in a measurement by an integrating instrument is less than that of a measurement occupying the same time interval and obtained with any other type of instrument.

APPLICATION OF THE THEORY

As shown in the photograph, Fig. 2, the instrument consists of an electrometer head connected through a five-foot cable to the main amplifier which operates the timer. The electrometer head is an evacuated brass box containing an FP-54 Pliotron, a special relay, three feed-back condensers, and a range switch (operated by the knob on the side). These components are indicated within the dotted area at the upper left of the circuit diagram given in Fig. 3. The main amplifier contains the additional amplifying tubes, a special relay, and all the batteries necessary to operate the instrument; these components are shown in the remainder of the circuit diagram. When standardized readings are desired, the fixed voltage $V\cong 4.5$ v can be measured to within 0.1 percent with a suitable external voltmeter or potentiometer (not shown in the photograph). The time interval t is read to 0.1 sec. with the sixty-cycle timer shown. Error due to drift, which automatically shows up at the end of a reading, will generally be less than 0.1 percent for time intervals up to 1000 sec. and a capacity ratio, C_0/C of ten or less.

---

* This instrument was partially completed at the National Research Council, Ottawa, Canada.

[1] S. Roberts, Rev. Sci. Inst. 10, 181 (1939).

[2] D. E. Lea, J. Sci. Inst. 3, 89 (1937).

CIRCUIT AND OPERATION

The initial stage of the amplifier consists of an FP-54 operated as a stable voltage amplifier with a grid current less than 10^{-17} amp. The conditions under which this may be done have been discussed in some detail in a previous article.[3] The intermediate stage employs the triode section of a 3A8GT and has a gain of approximately 30. The internal construction of this latter tube secures considerable stability when the filament is connected as shown. The final stage, giving a gain of 1000, consists of the pentode section of the above tube with another 3A8GT pentode section as a load resistance. The use of a pentode as a load resistance has been described by Meissner,[4] Schmidt,[5] and Horton.[6] The remaining 3A8GT triode section is used as an amplifier to control the 1C21 thyratron which in turn operates the relay system. The correct conditions for a stable degenerative amplifier have been given by Nyquist[7] and are met here by the introduction of the phase-shift network $R_9C_9R_{10}C_{10}$ in the input of the final stage and the capacity C_7 across the output. The constants in this system are chosen, however, on the assumptions that any capacity between the output system and the FP-54 plate lead is eliminated, and that the capacity to ground of the latter is kept less than $100\mu\mu f$.

The over-all operation of the circuit is as follows: If switches S_2 and S_3 are in positions 3 and 2, respectively, the relay M_1 will ground the input and the output will be "grounded" to $10\frac{1}{2}$ v. When the timer is stopped (by adjustment of P_6 if necessary), the microammeter will indicate the d.c. balance of the amplifier: the filament control P_2 and the coarse and fine zero-setting controls P_3, P_4 may then be adjusted. The precise adjustment of the timer control P_6 can be accomplished by first backing it off, whence a flick of S_3 will deionize the thyratron and thus start the timer, and then advancing it slowly until the timer "just stops." The instrument can now be put in the current-measuring state by first setting S_2 in position 2 and then giving S_3 a momentary depression. The release of the relay M_2, brought about by the depression of S_3, changes the output voltage from $10\frac{1}{2}$ to 6 v, starts the timer and finally opens the circuit for the relay M_1. The relay M_1 first frees the input circuit and then the output. After the presence of input current has caused the output to drift through $4\frac{1}{2}$ v, the thyratron will fire and the relay M_2 will close. The closing of M_2 stops the timer and activates the relay M_1. Upon completion of the cycle of operations thus, any accumulated amplifier drift will show up on the galvanometer. The instrument may, of course, be removed from the current-measuring state at any time by setting S_2 in position 3. If the instrument has been warmed up for fifteen minutes or so, the initial adjustment of P_2 and P_3 should last at least ten hours while P_6 may require adjustment every two or three hours. *Successive measurements are thus just a matter of reading the timer, and depressing S_3 for each measurement, coupled with an occasional adjustment of P_4.* When standardized readings are desired, the measurement of the voltage V may be accomplished as follows. After setting S_3 in position 3 and S_2 in 1, one may connect the external voltmeter or potentiometer to the jacks V, adjust P_1 for zero galvanometer reading, and then adjust it again with S_3 in position 1. When the measurement has thus been obtained the voltmeter or potentiometer should be disconnected. Since the load on the "C" battery supplying the voltage V is only $\frac{1}{4}\mu c$ per current-measuring cycle, such a determination of V is good for a considerable time, barring of course large temperature fluctuations.**

FIG. 2. A photograph of the electrometer. Attached to the input is a small ionization chamber.

Construction Details

Some of the more significant details employed in the construction of the electrometer head are as follows. The three feed-back condensers all employ guard-ring construction and polished*** polystyrene insulation. The insulator for the smallest feed-back condenser should be preferably of rod rather than disk shape. The two smaller feed-back capacities are adjustable from beneath the base to give convenient scaling. Metal bellows keep the vacuum here as well as for the range-switch mechanism. The range-switch employs a polished polystyrene rod for the rotor insulation while the stator contacts are supported from the condensers. The input lead insulator should be made from a length of good-

---

[3] N. T. Seaton, Can. J. Research F, 26, 302–309 (1948).
[4] E. R. Meissner, Electronics 6, 195 (1933).
[5] O. H. Schmidt, Rev. Sci. Inst. 4, 661 (1933).
[6] J. W. Horton, J. Frank. Inst. 216, 749 (1933).
[7] H. Nyquist, Bell Sys. Tech. J. 11, 126 (1932).

** Mean temp. coeff. per cell is 1.0×10^{-3} v/°F between 63 and 70°F (International Critical Tables VI, 316).

*** Polystyrene can be readily polished with jeweler's rouge in oil; afterwards it should be thoroughly washed in ethyl alcohol.

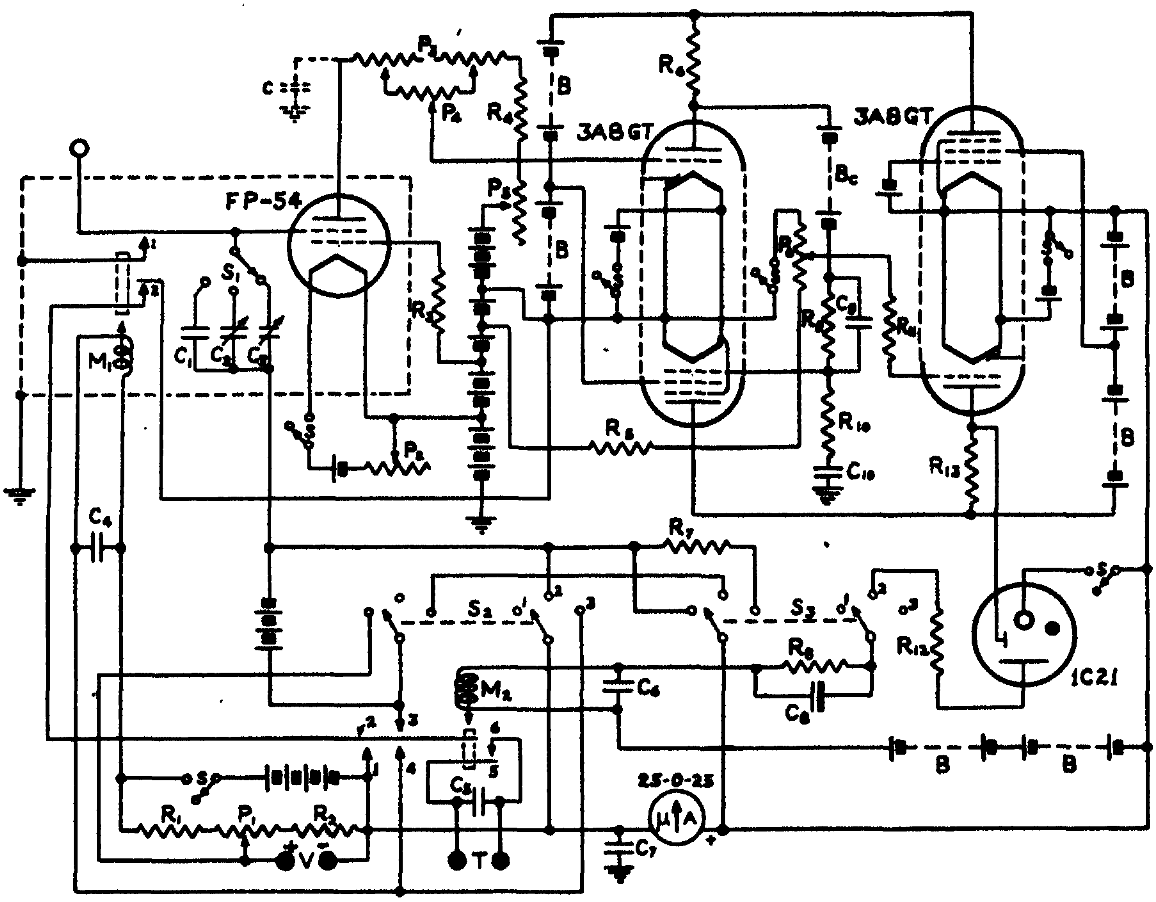

Fig. 3. Circuit diagram of the electrometer.

Parts list:

R_1	50	~
R_2	1.5	*K*
R_3	1*	*M*
R_4	30*	*M*
R_5	5	*M*
R_6	4	*M*
R_7	25	*K*
R_8	30	*K*
R_9	20	*M*
R_{10}	2	*M*
R_{11}	20	*M*
R_{12}	2	*K*
R_{13}	2	*M*

C_1	220 μμf
C_2	22 μμf
C_3	2.20μμf
C_4	0.10μf
C_5	0.10μf
C_6	0.25μf
C_7	0.05μf
C_8	10 μf
C_9	50 μμf
C_{10}	2000 μμf
c	lead capacity (see text)
B	67½-v Minimax
B_c	75-v hear. aid bat. (min. cap. to grnd.)
	Other batteries of voltage indicated, at 1.5 v per cell

P_1	1 *K*
P_2	6 ~
P_3	10 *M* (dual)
P_4	0.5 *M*
P_5	10 *M*
P_6	5 *M*
S_1	range switch (see text)
S_2	DP3Pos. lever
S_3	DP3Pos. lever (spring ret. 1 to 2)
s	6PST on-off sw.
M_1	170 ~ spec. rel.
M_2	10 *K* (see text)

* Varies with diff. FP-54*s*.

quality fused-quartz tubing (8 mm O.D.). After a thorough washing with alcohol, then water, it should be heated to 300°C or so, and from then on the insulating surface should never be touched with anything. The input lead and the insulator itself are readily sealed in place with De Khotinsky medium cement. The remainder of the leads are brought out at the rear through Kovar seals. The FP-54 is mounted horizontally and should have a grounded coating of Aquadag almost to the shoulder of the bulb. As the FP-54 is quite sensitive to magnetic fields, the relay M_1 should be of the completely enclosed type. Polished platinum is satisfactory for use in the two sets of self-wiping contacts of this relay. It is essential that the contact set 1 should open before set 2 at the beginning of each current-measuring cycle. De Khotinsky medium cement is satisfactory for sealing the top cover plate in place, however, the remainder of the box should not be overheated as otherwise the polystyrene insulators will soften. The electrometer head is evacuated (through a small needle valve in the rear) primarily to reduce ionization currents in the feed-back condensers arising when the instrument is operated in the presence of radiation. Since for this purpose a vacuum of several millimeters is sufficient, continual outgassing of walls should not necessitate re-evacuation more than two or three times a year.

The construction of the main amplifier is quite straightforward. It is, however, necessary to *completely* shield the FP-54 plate lead (and attached network) not only from the output but also from any external fields. The connecting cable therefore consists of a separate beaded coaxial cable (low capacity) for the FP-54 plate lead and an eight conductor shielded cable for the remainder of the leads. If, as shown in Fig. 2, ordinary cable connectors are used, it is necessary to ground the caps and cover any slots in them as well as put sleeves over the junctions. The shielding requirements of any system attached to the input are just as stringent. The relay M_2 was carefully constructed from an old audio-transformer and some telephone relay contacts. The contact system is depicted in Fig. 4. When the relay is closed, 2 and 4 contact 1. As the relay opens armature 2 breaks from 1, then contacts 3, and *while* these *remain* in contact, 1 and 4 are broken. Contact should be made by 5 and 6 before 1 and 4 break. Any tendency for the contacts 2 and 3 or 5 and 6 to bounce on closing must be eliminated by suitable damping. In order not to shunt the high output resistance, $A/g_m \cong 3$ meg, some care may be necessary in insulating from ground the coil of the relay M_1 and the various batteries associated with the output system. The only other sources of trouble may result from excessive grid current in the triode sections of the 3A8GT's and from anomalous oscillation or a shifting cathode spot in the 1C21 thyratron which can cause the relay M_2 to open spontaneously.

MODIFICATIONS

When relative current measurements are being made, the sensitivity of the instrument may be decreased by increasing the battery supply for V up to 45 v; in the case of ionization current measurements, a similar effect may also be obtained by using the ionization chamber as an additional feed-back capacity. With both methods the precision of the instrument is increased (see Eq. (3)). If the instrument is used for measuring high resistances, the source of e.m.f. supplying the current should be at least 1 v if the instability variations of the input are to be negligible in comparison with it.

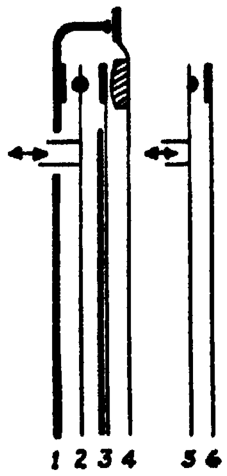

FIG. 4. Contact system of relay M_2. Numbers correspond to those on the circuit diagram, Fig. 3.

The over-all consistency of operation of the electrometer may be conveniently checked by placing in series a high sensitivity voltmeter and 6 v battery from the output (V^- terminal) to ground. If the instrument is then put in the current-measuring state, the meter reading should drop from 4.5 v to 0 v and remain steady there without any noticeable drift in 15 minutes or so. This range of 4.5 v in the output voltage represents the range through which the condenser is charged, and it is therefore essential that it be reproducible within a few millivolts each time the instrument is put in and out of the current-measuring state (use switches S_3, S_2). Such an additional external battery and voltmeter are useful for detecting small output voltage changes, and hence background currents down to 10^{-17} amp. can be estimated in a reasonable length of time. The internal vacuum of the electrometer head may also be measured with this method in combination with an external radioactive source to set up ionization in the gas between the feed-back condenser plates.

Current may also be determined with a somewhat similar instrument that utilizes a fixed time interval and requires a measurement of the change in output voltage, a measurement not difficult because the dynamic output resistance is of the order of several hundred ohms. In this case the equivalent relays of M_1 and M_2 become slightly more complicated and must be contained within the electrometer head, however the main amplifier is considerably simplified. If the "fixed" time interval for such a monitor electrometer is obtained from the main electrometer (Fig. 2), we obtain the simultaneous measurement of two currents.

THE REVIEW OF SCIENTIFIC INSTRUMENTS VOLUME 20, NUMBER 7 JULY, 1949

A New Technique for the Determination of Heats of Sublimation of Slightly Volatile Substances

O. C. Simpson and R. J. Thorn
Argonne National Laboratory, Chicago, Illinois

(Received January 3, 1949)

A technique is described which enables one to measure relative vapor pressures by measuring the rate of change of transmissivity of thin deposits as they are formed by condensation from the vapor. From the temperature dependence of this rate the heat of sublimation of slightly volatile substances can be determined. In the case of graphite, deposits of the order of 0.1 μg per cm^2 can be detected.

I. INTRODUCTION

THERE are two general methods of determining the heat of vaporization or sublimation. One method is based upon the measurement of the slope of the plot of log$p$ against the reciprocal absolute temperature and requires only relative vapor pressure measurements as a function of temperature; the other, based upon the calculation of the absolute entropy difference of the vapor and the condensed phase, requires the measurement of the absolute vapor pressure at a known temperature plus a knowledge of the pertinent specific heat data. Of these methods the second is usually the more accurate, but the first one possesses the advantages that factors such as the vaporization coefficient must be rather strongly temperature dependent to cause large error, only relative vapor pressure measurements are required, and no specific heat data are needed.

One of the chief difficulties in the application of either method to substances having low vapor pressures, such as graphite for example, is that ordinary techniques for determining the small rates of evaporation require long times. The technique described in this report enables one to measure extremely small rates of evaporation (actually condensation) and hence enables one to employ the first method conveniently. The same technique can also be used in the second method provided a proper calibration is made.

The authors are employing this technique for the determination of small rates of evaporation to determine the heat of sublimation of graphite. It will be some time before the authors' investigation is concluded, but the experimental technique is described here since others may have use for it.

II. THEORY

The technique presented herein is essentially as follows: a fraction of the material evaporating from the top surface of a cylinder heated in an evacuated space is collected on a circular target placed above and parallel to the surface. The time rate of deposition of the material is determined by measuring the time rate of change of the transmissivity of the target. The light from the incandescent material serves as a light source for this measurement. At feasible temperatures for substances such as graphite the rate of deposition is so small that ordinary methods such as weighing do not permit its determination within reasonable times. However, the use of an optical pyrometer constitutes a very sensitive method for the determination of this rate. From the dependency of the deposition rate on temperature it is possible to calculate relative vapor pressures and therefrom the heat of sublimation. The experimental arrangement is represented schematically in Fig. 1.

If light of spectral radiant intensity $(J_\lambda)_0$ and wavelength λ emitted from the top surface of the cylinder at some high temperature T°K is intercepted by the layer of the material deposited on the quartz target, then the decreased intensity J_λ of light entering the optical pyrometer is given in terms of the thickness x of the deposit by the relation

$$J_\lambda = (J_\lambda)_0(1-r_1)(1-r_2)(1-r_3)e^{-kx-k_qx_q}. \tag{1}$$

In this equation r_1, r_2, and r_3 are the reflectances of the deposit-vacuum, the deposit-quartz, and the quartz-vacuum interfaces respectively; k and k_q are the absorption coefficients of the material and quartz; and x_q is the thickness of the quartz. More correctly there may be additional terms due to the window on the apparatus and a prism. These terms, however, can be omitted from this discussion, although they must be considered when it is necessary to measure the true temperature of the cylinder.

If we assume that the spectral intensity $(J_\lambda)_0$ emitted from a non-black body with a spectral emittance e_λ is given by Wien's law,* we can write

$$(J_\lambda)_0 = e_\lambda c_1 \lambda^{-5} e^{-c_2/\lambda T}. \tag{2a}$$

Corresponding to the decreased intensity J_λ there is some apparent absolute temperature T_a°K such that

$$J_\lambda = e_\lambda c_1 \lambda^{-5} e^{-c_2/\lambda T_a}. \tag{2b}$$

If Eq. (2b) is divided by Eq. (2a) and the expression for $J_\lambda/(J_\lambda)_0$ so obtained is substituted into Eq. (1), then an equation relating the apparent temperature T_a to the thickness and reflectances is obtained. That is,

---

* For $\lambda = 0.665\mu$ and $T = 2500$°K, $e^{c_2/\lambda T} = 5.5\times 10^3$. Hence one is justified in using Wien's law rather than Planck's. Whether Wien's law is strictly applicable to non-black bodies, however, is another question which will not be discussed.

$$\frac{1}{T_a}=\frac{1}{T}+\frac{\lambda}{c_2}(kx+k_qx_q)-\frac{\lambda}{c_2}\ln[(1-r_1)(1-r_2)(1-r_3)]. \quad (3)$$

If the thickness x of the material deposited on the quartz is increasing with time due to molecules condensing on the target (in this discussion we are assuming that the vapor is composed of a single molecular species), the dependency of T_a on time can be found from the elementary kinetic theory relations. The result is

$$\frac{1}{T_a}=\frac{1}{T}+\frac{\lambda k_qx_q}{c_2}-\frac{\lambda}{c_2}\ln[(1-r_1)(1-r_2)(1-r_3)]$$
$$+\frac{\lambda kFA_s}{c_2DA_d}\left(\frac{M}{2\pi R}\right)^{\frac{1}{2}}\frac{p}{(T)^{\frac{1}{2}}}t. \quad (4a)$$

In this expression F is the fraction of the molecules evaporating which condense on an area which intercepts the light entering the pyrometer; A_s is the area of the top surface of the cylinder; A_d is the area of the deposit through which light passes to the pyrometer; D is the density of the deposit; M is its molecular weight; R is the molal gas constant; p is the vapor pressure of the material; and t is the time. In the derivation of this equation there is the inherent fact that when $t=0$, r_1 is zero and $r_2=r_3$, since no deposit is present on the target. For very small values of t, r_2 becomes different from r_3, and r_1 becomes greater than zero, but neither is necessarily independent of t (hence x) due to the fact that reflection of light takes place not only from the outer atomic layer but from a finite number of atomic layers. However, for sufficiently large values of t these reflectances become constant since the deposit is then sufficiently thick to permit the maximum reflection characteristic of the interfaces. Hence for values of t greater than this minimum and for constant values of the temperature of the cylinder, Eq. (4a) assumes the form

$$\frac{1}{T_a}=A_0+\frac{A_1pt}{(T)^{\frac{1}{2}}}. \quad (4b)$$

This relation shows that the reciprocal of the apparent absolute temperature is, under the conditions already specified, a linear function of time with a slope

$$a=\frac{\lambda kFA_s}{c_2DA_d}\left(\frac{M}{2\pi R}\right)^{\frac{1}{2}}\frac{p}{(T)^{\frac{1}{2}}}. \quad (5)$$

Since the Clausius-Clapeyron equation,

$$dp/dT=\Delta H/T\Delta V, \quad (6)$$

can be expressed in a form involving the derivative of the logarithm of the vapor pressure, determination of the temperature rate of change of a quantity which is proportional to the vapor pressure (such as the slope a in the present case) is sufficient for the determination of the heat of sublimation. Equation (6) can be expressed in the desired form by neglecting the volume of the solid phase compared with the gaseous phase and assuming the latter to be a perfect gas. If the value of p given by Eq. (5) is then substituted in this relation, we find

$$\frac{d\ln(a(T)^{\frac{1}{2}})}{d\left(\frac{1}{T}\right)}=-\frac{\Delta H}{R}. \quad (7)$$

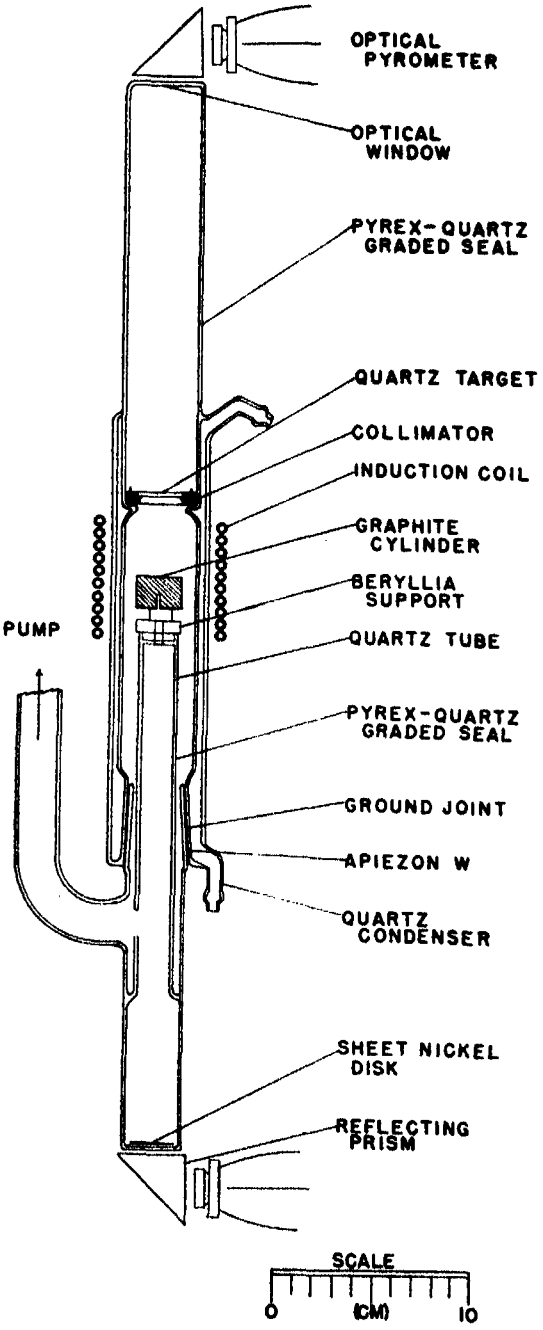

FIG. 1. Experimental arrangement used to determine rate of evaporation of solids.

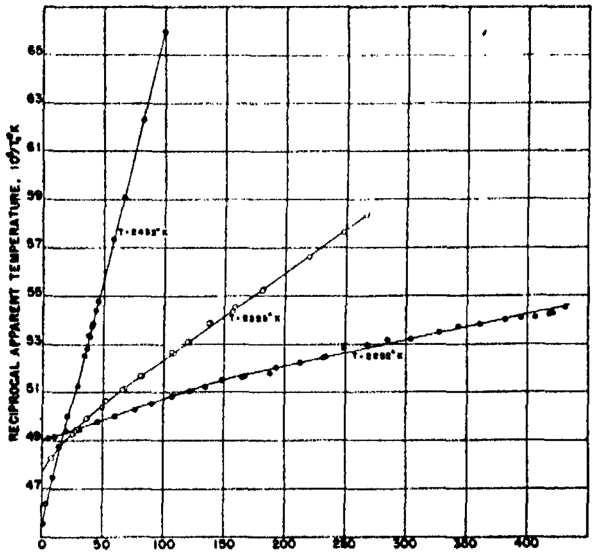

FIG. 2. Relative rates of deposition of graphite.

Hence the heat of sublimation is equal to 4.575 times the slope of the plot of $\log(a(T)^{\frac{1}{2}})$ *vs.* $1/T$.

Provided the absorption coefficient can be evaluated, then the technique described herein can be used to determine the absolute vapor pressure of the material at a given temperature (see Eq. (5)). From this the heat of sublimation can be calculated according to statistical mechanical relations.*

III. EXPERIMENTAL EXAMINATION OF TECHNIQUE

Typical examples of the plot of the reciprocal apparent absolute temperature T_a measured through graphite deposits as a function of the time are given in Fig. 2. These curves are characterized by a slight negative curvature in the initial region which becomes less with increasing time until the curve finally becomes linear. The length of the non-linear region depends upon the temperature of the cylinder, increasing with decreasing temperature. This initial curvature is to be expected according to Eq. (4a), since during this period the reflectances r_1 and r_2 are time dependent and are changing in such a manner as to make $d\ln[(1-r_1)(1-r_2)]/dt$ a negative quantity which decreases numerically to zero when r_1 and r_2 become constant. Hence $1/T_a$ *vs.* time has a negative curvature until r_1 and r_2 become constant.

The possibility that this non-linear region might have an effect on the calculated slope a can be excluded in two ways. In one procedure the slope of only the linear region is calculated, this region being defined as follows: If t_1 is the minimum time which for all practical purposes is necessary for the attainment of the linear region at some temperature T_1, then the equivalent time t_2 necessary at some other temperature T_2 is

$$t_2=t_1\frac{T_2}{T_1}\exp\left[\frac{\Delta H}{R}\left(\frac{1}{T_2}-\frac{1}{T_1}\right)\right]. \tag{8}$$

Since the linear region is readily discernible at the high temperature end of the permissible range, one of these runs can be selected arbitrarily for estimating t_1. The corresponding t's for other temperatures can then be calculated with the aid of this equation provided a rough estimate of ΔH has been made. Since accurate values of the t's are not required, ΔH can be estimated by considering $1/T_a$ *vs.* t to be linear for all values of t. In essence this procedure is equivalent to selecting regions of equivalent thickness. Another procedure of eliminating the initial region is to make an initial deposit at a relatively high temperature before measurements of T_a *vs.* time are made. When this procedure is used $1/T_a$ is linear in time.

The deposits whose transmissivities are represented in Fig. 2 range in total weight from 23.7 μg at 2252°K to 143 μg at 2433°K for an area of about 3 cm^2. Since one can readily read a temperature difference of 3° with an optical pyrometer, the limit of detection of the presence of the deposit is 0.11 μg per cm^2. This corresponds to a thickness of about 5×10^{-8} cm or about three or four atomic layers. This conclusion agrees with that of Estermann and Stern,[1] who found that deposits of two or three molecules in thickness are visible because of aggregation. The thickness of the graphite deposit at which the curvature becomes zero or at which the reflectances become constant is about 3.6×10^{-6} cm or about 250 atomic layers.

IV. POSSIBLE ERRORS

The possible sources of error which may be considered as being inherent in the transmissivity technique are (1) the dependency of the absorption coefficient on thickness, (2) the dependency of the absorption coefficient on temperature, (3) the deviation of non-black body radiation from Wien's law, (4) the thermal expansion of the deposit, and (5) the radiation from the deposit.

In general the effect of factors (1) and (3) if operative would be to make $1/T_a$ other than a linear function of time. Since we have observed a linear dependence with graphite aside from the initial effect of reflectances, we conclude that these factors cause no error in this case unless a fortuitous combination of them causes effective cancellation. It is doubtful that the absorption coefficient of graphite changes sufficiently with temperature to cause any error since the transmissivity curve of thin graphite deposits as a function of wave-length shows no absorption peaks in the neighborhood of 0.665μ. The thermal expansion of graphite would cause $\log a(T)^{\frac{1}{2}}$ to change by less than 0.02 percent for the temperature range given in Fig. 2. If the deposit on the quartz target emits radiant energy and if this energy is of the same order as that from the cylinder transmitted through the deposit, then values of a will be in error. However, the ratio of these intensities is $e^{-c_2/\lambda T_d}/\tau e^{-c_2/\lambda T}$ in which T_d is the temperature of the deposit and τ its transmissivity. Crude measurements showed that $\tau \cong 0.01$ (for the thickest deposit) and $T_d \cong 1000$°K. Hence for the ratio we obtain 8×10^{-4} at $T=2200$°K showing that the amount of radiant energy emitted by the deposit is negligible in our experiments compared with that transmitted from the cylinder.

---

* See, for example, K. K. Kelley, U. S. Bur. Mines, Bull. 383 (1935).

[1] I. Estermann and O. Stern, Zeits. f. physik. Chemie **106**, 399 (1923).

The sources of error which are not necessarily inherent in the transmissivity technique but which may be present under the conditions of the experimental procedure are (1) temperature gradients in the material, (2) variation of the vaporization coefficient with temperature, and (3) variation of the condensation coefficient with temperature. For metals temperature gradients will usually cause no trouble since their thermal conductivities are high and temperatures above 2000°C are not usually required. However, at temperatures above 2000°C these gradients become appreciable, especially in the case of graphite, and they must be taken into consideration by calculation of an "average" temperature. One of the best ways of eliminating the variation of the vaporization and condensation coefficients with temperature is to employ conditions such that they are unity. In the case of the vaporization coefficient a unit value can be assured if the material is vaporized in a small furnace cavity and permitted to effuse through an orifice in the furnace. In all probability the vaporization coefficient will also be unity if the surface of the material is chemically clean. A value of unity for the condensation coefficient can be approached by employing a water-cooled target.

The authors wish to acknowledge the help of Dr. George H. Winslow in subjecting the technique to a detailed analysis.

THE REVIEW OF SCIENTIFIC INSTRUMENTS VOLUME 20, NUMBER 7 JULY, 1949

Measurement of the Spin of a Projectile in Flight*

H. D. WARSHAW
The Franklin Institute, Laboratories for Research and Development, Philadelphia, Pennsylvania

(Received February 9, 1949)

Projectile spin is measured by recording the voltage generated in a pick-up coil as the rotating field of a transversely magnetized projectile passes the coil.

A permanent magnet within a brass sleeve (for magnetic insulation) is inserted in a projectile of mild steel. Rotation of the projectile as it passes the pick-up coil generates a sinusoidal e.m.f. which is displayed on the screen of a cathode-ray tube and photographed for subsequent analysis.

INTRODUCTION

In ballistic studies, information regarding the movement of the projectile in flight is highly useful. Projectile spin measurement falls into this category and is the subject of this paper.

PICK-UP COIL

Figure 1 shows the laboratory set-up and a block diagram of the associated equipment used for measuring and recording projectile spin. The pick-up coil consists of 1200 turns of number 30 Formex insulated copper wire wound on a rectangular coil form 30×6 inches. The coil is positioned so that its long sides are parallel to the line of flight. As the rotating projectile passes the coil, a voltage is

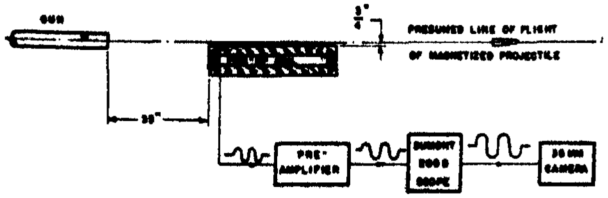

FIG. 1. Gun, pick-up coil, and recording equipment (pick-up coil viewed from above).

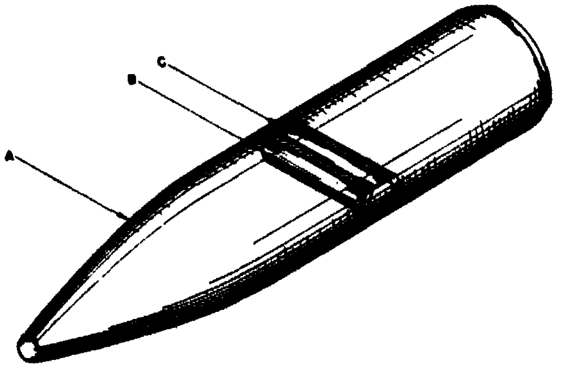

FIG. 2. Cut-away sketch of projectile. (A) Cold rolled steel projectile. (B) Magnetic insulator (brass sleeve). (C) Magnetized insert (hardened drill rod).

---

* The paper is based on work done for the Office, Chief of Ordnance, Department of the Army.

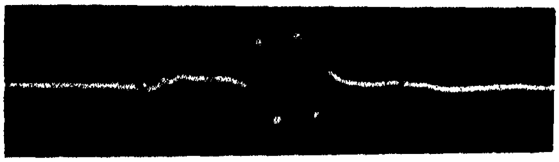

FIG. 3. Oscilloscope record of projectile spin.

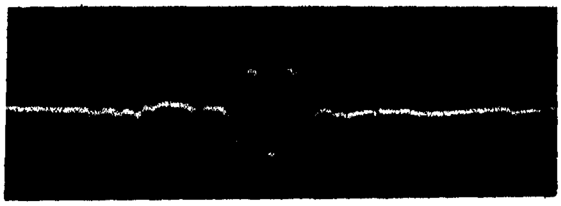

FIG. 4. Oscilloscope record of projectile spin.

generated in that side of the coil nearest the line of flight. Any voltage generated in the opposite side of the coil will reduce the signal output, which is the difference in voltage generated in the two sides. However, the signal reduction is negligible since the intensity of the magnetic field due to the projectile is negligible at the far side of the coil.

The coil is mounted on a sturdy *wooden* frame. The presence of sizable quantities of iron or steel within a few inches of the coil will concentrate the earth's magnetic field sufficiently to cause spurious signals to be generated with the slightest relative movement between coil and metal. These movements are produced by the gun blast. Since the coil cannot be protected by armor plate, a reasonably accurate gun must be used.

RECORDING EQUIPMENT

The signal output of the coil is passed through a pre-amplifier and then to the vertical deflection amplifier of a Dumont Type 208*B* cathode-ray oscilloscope. The over-all voltage amplification of the system is approximately 10,000. The oscilloscope, modified for single sweep, is triggered by a switch in the breech mechanism of the gun. Permanent records are obtained by photographing the trace that appears on the screen when the projectile passes the coil.

PROJECTILES

The caliber .50 projectiles used in these tests were made of cold-rolled steel. This material has high magnetic permeability but low retentivity. This is unfortunate since it implies the following:

1. The projectiles cannot be permanently magnetized.
2. If a permanent magnet insert is used, a large part of its field will be shunted by the body of the projectile.
3. If a steel slug having high magnetic retentivity is inserted and then magnetized, most of the field from the magnetizer will be shunted. The small portion that is stored by the slug will be shunted by the body of the projectile.

From the standpoint of manufacturing problems and availability of materials, it was decided to develop the method suggested under No. 3. A satisfactory design was evolved in which a hardened steel insert was magnetically insulated from the projectile. A cut-away drawing of this design applied to a caliber .50 projectile is shown in Fig. 2.

The drill rod insert ($\frac{1}{8}$-in. diameter) is hardened but not tempered. It is pressed into the brass sleeve ($\frac{3}{16}$-in. O.D.) which is in turn pressed into the projectile. The projecting ends are then ground even with the body of the projectile. The axis of the insert passes through, and is normal to the axis of the projectile.

The brass sleeve is a magnetic insulator and is essentially equivalent to an air gap between the insert and projectile. It permits effective magnetization of the insert after assembly and greatly reduces the shunting effect of the body of the projectile on the field of the magnetized insert.

MAGNETIZER

Prior to firing, the assembled projectile is clamped between the pole pieces of a magnetizer. The ends of the insert are clamped by the pole tips which are also $\frac{1}{8}$ in. in diameter. The magnetizer provides sufficient flux to saturate the insert. After magnetization, the field strength of the insert is measured with a General Electric Company Gauss-Meter. If the field strength is 50 to 60 Gauss at the exposed tip of the insert and approximately 0.75 Gauss at one inch from the tip, the projectile is ready to be fired.

RESULTS

Figures 3 and 4 are photographic records obtained with the equipment described. Calculations based on the linear velocity of the projectile and the rifling twist in the gun indicate that the projectile should execute two full revolutions while passing the pick-up coil. In Fig. 3, it may be seen that two complete sine waves of voltage were generated in the pick-up coil. However, due to the spurious signal that preceded the desired signal, the base line of the sine waves is not parallel to the zero signal base line (at the extreme left end of the trace). The true base line is midway between, and parallel to the lines joining the peaks of the sine waves. Thus, the number of revolutions of the projectile as it passes the coil may be determined.

DISCUSSION

In Fig. 3, it should be noted that the signal started and ended at zero voltage. Apparently, the magnetized insert in the projectile was normal to the plane of the coil when passing the leading and trailing edges of the coil. Occasionally, this condition may be duplicated, provided the projectile is accurately positioned in the gun prior to firing. However, this is not a necessary prerequisite, since in Fig. 4 the number of revolutions is accurately determined, even though the insert was in a position to generate a voltage as it passed the leading edge of the coil. As shown on the photograph, it is necessary to extrapolate the signal to the point on the trace at which the insert passed the leading edge of the coil.

The term "projectile spin" refers to rotation with respect to a known distance in the direction of flight (the length of the pick-up coil in this case). "Angular velocity" refers to rotation with respect to time. Although angular velocity was not measured, it may be obtained simply by the addition of time-markers to the oscillograph trace. This could be accomplished by modulating the intensity of the trace with pulses of a known frequency.

THE REVIEW OF SCIENTIFIC INSTRUMENTS VOLUME 20, NUMBER 7 JULY, 1949

Stress-Strain-Time Apparatus for Fiber Testing

C. H. Reichardt,* H. Schaevitz,** and J. H. Dillon***
The Textile Foundation and Frick Chemical Laboratory, Princeton University, Princeton, New Jersey

(Received March 11, 1949)

A stress-strain apparatus for testing individual fibers is described. The apparatus employs a ring dynamometer in conjunction with a linear variable differential transformer. A constant rate of elongation apparatus is fully described and a schematic diagram of a constant rate of loading apparatus is discussed. The use of linear variable differential transformers allows simple a.c. amplifiers to be employed and thus removes many of the difficulties involved in d.c. bridge circuits. Load ranges from 50 grams to 1 gram per ten chart inches can be obtained with a sensitivity of several milligrams. By changing the size of the ring dynamometer employed, an apparatus giving the greater load ranges necessary to test yarns can be constructed.

THE original Sookne-Rutherford Autographic Load Elongation Apparatus[1] for fibers in use at the Textile Research Institute Laboratories, Princeton, New Jersey, is one of the first sensitive, automatic stress-strain testers to have been developed. It has been of great value in studies of the mechanical properties of fibers; however, it does possess several limitations which are more or less inherent in the chainomatic balance type of stress-strain apparatus. The two major limitations, which might possibly be removed by redesign of the instrument, are:

(1) "hunting," which increases with the sensitivity, particularly at or near zero load, and
(2) the fact that the maximum usable load range, which obtains the same precision as obtained at low load ranges, is limited by the type and size of chain that is used.

The first limitation presents a difficulty in the proper analysis of stress-strain curves since, in order to maintain sensitivity and at the same time prevent "hunting" at the zero load position, the test fiber must always be maintained under a small positive stress; thus, zero stress cannot be attained at any time during the experiment. The second problem appears to be almost insurmountable and limits the use of the apparatus to the testing of textile fibers with low breaking strengths, prohibiting its use with even the finest yarns. The Sookne-Rutherford apparatus and the more recent Sookne-Harris modification[2] do have two salient features that other types of apparatus do not: namely, (1) the point of stress measurement remains at a fixed position in space and thus mathematical corrections do not have to be made for displacement of the stress-measuring device with increasing stress, as is the case with various other applications employing strain gauges; and (2) the balance type of machine does not possess the large inertia effects inherent in the pendulum and inclined plane type of tester.

A more versatile type of instrument with all the advantages, including better sensitivity, but without the major limitations of the Sookne-Rutherford apparatus has been greatly needed. There exist, as commercially available products, numerous devices which are capable of incorporation in a stress-strain apparatus. Some of these are: (a) the magnetic strain gauge,[3] employed in conjunction with a stress beam or weigh bar, (b) the resistance strain gauge bonded to a stress

---

* Fellow of Textile Research Institute.

** Schaevitz Engineering, Camden, New Jersey.

*** Director of Research, The Textile Foundation and Textile Research Institute, Inc.

[1] A. M. Sookne and H. A. Rutherford, J. Research Nat. Bur. Stand. 31, 25–31 (1943).

[2] Harris Research Labs., 1246 Taylor Street, N.W. Washington, D. C.

[3] J. W. Ballou, ASTM Bulletin, No. 150, pp. 38–112 (1948).

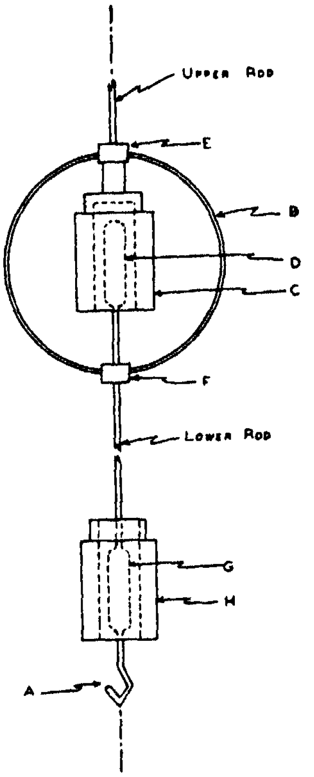

FIG. 1. Schematic diagram of the stress-measuring mechanism.

beam or weigh bar,[4] (c) the unbonded type of resistance gauge,[5] and (d) the Linear Variable Differential Transformer used in conjunction with a stress beam or ring dynamometer.[6] The last is adapted easily to a satisfactory stress-strain apparatus since simple alternating current amplifier circuits may be used. Furthermore, a simple modification of this type of equipment allows the construction of a stress-strain apparatus in which the stress-measuring point can be maintained at a fixed point in space, regardless of stress imposed.

As Ballou has recounted in a recent paper,[3] there are two major types of stress-strain apparatus available, those employing constant rate of stress, and those using constant rate of strain. The Linear Variable Differential Transformer (hereafter referred to as the LVDT), in conjunction with a ring dynamometer, affords application in the construction of either type of instrument. In both cases, the electrical circuit is the same, the only differences occurring in the mechanical design. This paper is concerned mainly with a constant rate of strain type of stress-strain apparatus. A brief description of the arrangement for the constant rate of stress application is included to show the versatility of this device.

The constant rate of strain, stress-strain apparatus consists of three main sections: (1) the constant rate of strain mechanism which has a range of rates of movement from 1.0 inch per minute to 0.001 inch per minute, with practically instantaneous commencement, reversal or cessation of motion at any given rate, (2) the stress-measuring mechanism which includes the LVDT attached to a ring dynamometer, the amplifier, and the recorder, and (3) the stress-point, zero-positioning mechanism, which maintains the upper jaw or stress-measuring jaw at a fixed point in space.

A. The Stress-Measuring Mechanism

The force applied to the upper sample jaw, *A* (see Fig. 1), is translated into a linear displacement of the ring dynamometer, *B*, for which displacement is directly proportional to imposed force, either compressional or tensile. This linear displacement is identical with that of the iron core, *D*, of the LVDT, *C*. Hence, the output of the LVDT[6] which is linear with core displacement, changes linearly with the applied force. The output voltage of the LVDT is thus available to drive the recorder, which will be described later.

The theory of ring dynamometers is to be found in several standard engineering texts. The National Bureau of Standards employs them in the measurement of large stresses to a high degree of accuracy. Most of the applications, however, have employed ring dynamometers for the measurement of large stresses. To obtain a ring dynamometer for use with single fibers, i.e., with extremely small loads and which will have a linear relationship between imposed stress and the displacement of the ring, several dimensional limits, not normally encountered, must be considered. In order that the displacement be directly proportional to the imposed force, the radial thickness of the ring must be small in comparison to the radius of the ring. At the same time, however, the radial thickness of the ring must not be so small that local buckling occurs at the points at which stress is applied to the ring. Consequently, for the construction of ring dynamometers for different load ranges, the ratios of radial thickness to ring width and radial thickness to radius must be altered for each case. Any proportional change of the two ratios might bring one or the other difficulty to bear. In addition to these dimensional limits, the ring supports, or to be more exact, the points at which stress is applied to the ring, must be diametrically opposite or non-linearity occurs. Again, linearity is lost if the ring is not properly supported or clamped. The National Bureau of Standards, in their applications with heavier rings, have "bossed" diametrical shoulders on the rings, the rings being clamped through these shoulders. The clamps in use at present for the light rings are somewhat different and are described in detail in the following paragraphs. H. Schaevitz[7] has indicated some success recently with a method in which two rods are silver-soldered to the ring, the two rods having the same axis and passing through diametrically opposite holes in the ring. More extensive tests must be carried out, however, before this latter method can be proved satisfactory, although the results to date are very promising.

---

[4] Recently developed by the Instron Engineering Corporation.

[5] R. D. Meyer, Instruments 19, No. 3 (March 1946).

[6] H. Schaevitz, Proc. Soc. Exper. Stress Analysis IV (No. 2), 79–88 (1947).

[7] H. Schaevitz, unpublished communications.

As is seen in Fig. 1, an upper rod supports the coil body of the LVDT, *C*, and by means of the upper clamp, *E*, the ring dynamometer also. The lower clamp, *F*, supports the core of the LVDT and a lower rod leading to the upper stress measuring jaw, *A*. There is no mechanical connection between the upper and lower clamps except through the ring. The axes of the upper and lower rods, the LVDT coil body and core, and a diameter of the ring dynamometer must be identical with the force axis. The LVDT core is rigidly attached to the lower clamp, but the attachment of the LVDT coil body allows it to be displaced linearly along the axis of force to allow adjustment of the position of the core in the coil body.

The clamps have a rounded edge (radius *ca.* 0.01 in.) in contact with the inner surface of the ring. The ring is held in place against these edges by a flat metal surface pressing against the outer surface of the ring. This flat face is so constructed that, when the two sections of the clamps are rigidly fastened, the surface exerts just enough pressure on the ring to prevent its slippage from position under normal handling. As was stated previously, the lines of contact made between the rounded edges of the two clamps and the inner surface of the ring must be (1) perpendicular to the plane of the ring and (2) diametrically opposite.

As a guide to any future construction, one of the difficulties encountered in the development of the instrument is mentioned here. Originally a paper shim was used in the ring clamps between the outer ring surface and the flat surface of the clamp. The principle of the paper shim was to exert enough pressure to prevent slippage of the ring but not enough to hinder the bending of the ring. However, the force exerted by the expansion and contraction of the paper through adsorption and desorption of water vapor caused a deflection of the ring and a corresponding large humidity sensitivity of the instrument. Unfortunately, this reason for the humidity sensitivity of the apparatus was not detected immediately.

The output of the LVDT in the ring dynamometer is placed in "series bucking" with the output of a similar LVDT in the recorder (see Fig. 2) by means of the circuit given in Fig. 3. Examination of this circuit shows essentially, that the output voltages of the two LVDT's are bucked against each other, the error voltage being fed into a three-stage resistance-coupled voltage amplifier, feeding a power stage consisting of a 6L6 with the plate circuit transformer-coupled to one phase of a two-phase induction motor. The other phase of the recorder motor is connected directly to the line voltage. Any displacement of the ring activates the motor of the recorder in such manner that the micrometer moves the core of the LVDT of the recorder to its proper position. At the same time, this displacement of the core, caused by the micrometer, is transformed into a linear pen movement which is directly proportional to the original displacement of the ring dynamometer. Other components of the circuit shown in Fig. 3 will be discussed in later paragraphs.

B. Stress-Point, Zero-Positioning Mechanism

An LVDT core, *G* (Fig. 1), is made an integral part of the lower rod leading from the lower ring clamp. This core passes through an LVDT coil body, *H*, which is rigidly fastened to the framework. The output of the LVDT, *H*, is fed into an amplifier identical to the one used in the stress-measuring mechanism. In this case, however, the amplifier operates a motor which is linked through a worm and worm gear to the upper rod of the stress-measuring mechanism. When the core, *G*, is moved out of the null-balance position of the coil by reason of a change in the force exerted on the upper jaw (displacing the ring), the amplifier drives the motor so that the core is instantaneously brought back into the null-balance position. The upper jaw is then maintained at a constant position in space. The necessity and accuracy of this zero-positioning mechanism can be demonstrated by consideration of the operation of the light ring dynamometer. A force of 50 grams elongates the ring about 0.05 inch. In testing a normal fiber with a breaking strength of approximately 10 grams, the upper jaw would move a maximum of 0.01 inch without the stabilizing mechanism. This 0.01 inch displacement represents an error of 10 percent in the elongation of a fiber 1 inch in length strained 10 percent. The stabilizing mechanism, however, maintains the upper jaw at a position well within 50 micro inches of the original setting, reducing the error from this cause to less than 0.05 percent.

Several factors which are not readily apparent must

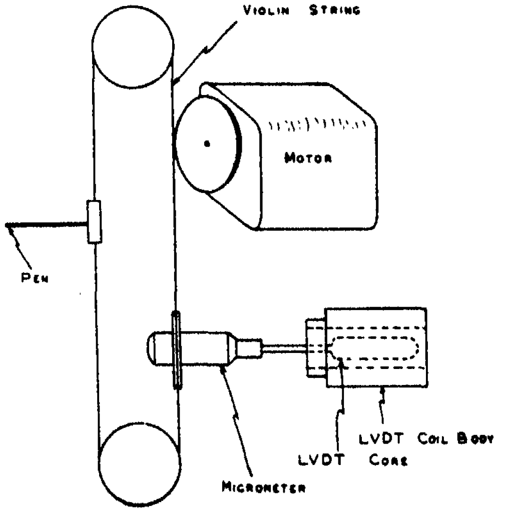

Fig. 2. Schematic diagram of the recorder.

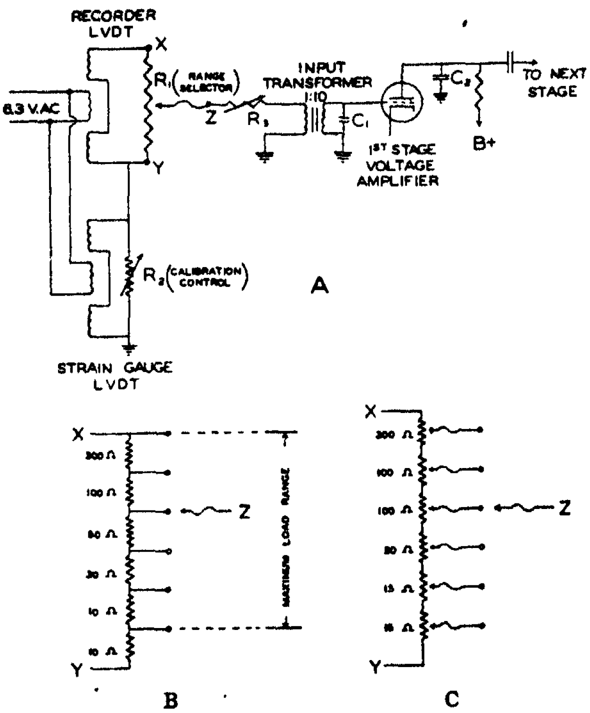

Fig. 3. Diagram showing circuit employed.

be considered in the actual construction of such an apparatus. If the core and coil body of an LVDT are not coaxial, a sideward force is exerted on the core by the field. The factors which might permit this force to come into play are removed or reduced in several ways. The upper rod is passed through a bushing in the framework such that all motion except that along the axis of the rod (and therefore the force axis) is prohibited. The LVDT coil body of the zero-positioning element has an inside diameter approximately twice that of the other LVDT coil bodies. This precaution decreases the sideward force exerted without serious reduction to the sensitivity of the compensating LVDT as a whole. All necessary joints, including ring dynamometer clamps, in the complete mechanism must be rigid and free from play. Another factor to be considered in the overall design is the influence of the two transformers on one another. Any such interference can be removed by keeping each one outside the effective magnetic fields of the other (about eight inches is sufficient) and by electrically insulating the two cores (i.e., the lower rod between the positioning core and the ring clamps should not be metallic).

While construction precautions involving the use of LVDT's are being considered another point is worthy of mention. Although it is obvious that any magnetic metal brought near the LVDT would greatly influence its output, it is not obvious that any large mass of a non-magnetic metal (brass, aluminum, etc.) immediately surrounding or within a few inches of the LVDT coil body also produces an effect on the output of the transformer. The main difficulties produced by a non-magnetic mass appear to be in changing the waveform of the output. For this reason, all of the LVDT's used in this apparatus have been mounted in a Plexiglas housing slightly larger than the LVDT coil body and in such a manner that the coil body may be adjusted to various positions in the Plexiglas mount. This plexiglass housing is then held in position by other Plexiglas or thin brass rods.

C. The Constant Rate of Strain Mechanism

The normal type of elongation apparatus in which commencement or reversal of motion is obtained by reversing the motor which drives an elongating mechanism through a gear train is considered inadequate, mainly because of the lag in reversal, commencement, or cessation of motion introduced by the necessarily loose-fitting gears in most gear trains. In addition, a change in rate of elongation in such mechanisms usually involves replacing gear boxes, which is considered harmfully time consuming in some instances.

One way of solving the lag problem is to reverse, start, and stop the mechanism through the use of adequate instantaneous reversing clutches at the point where the angular motion is transformed into linear motion. This practice has the advantage of keeping the number of points at which lag can be introduced to a minimum. At the same time, such a system allows the construction of a variable speed reducer, with a wide variety of output speeds (see Table I), and a transmission in which elimination of lag is not a difficult problem since the motor operates continuously in one direction.

There are numerous ways in which this can be accomplished as well as, or better than, the one chosen; it would only be fair to mention that the gear array designed for the apparatus described herein was designed to employ equipment already on hand. A more efficient and more compact speed reducer and transmission can be constructed if the utilization of available commercial equipment is not involved.

In the apparatus constructed at the Textile Research Institute Laboratories, a 1/15 h.p. continuous-rated constant-speed induction motor drives five different Boston Gear Works, Series LA, Speed Reducers in parallel. The output of any one of these can be taken off by means of sliding gears. These, in turn, drive a gear box which affords an additional 5:1, 1:1, or 1:5 ratio leading into two magnetic clutches attached to two miter gears which drive a third miter gear attached to a vertical-threaded shaft. The magnetic clutches and pinion gears constitute the reversing and starting mechanism. The vertical-threaded shaft drives a complex nut, designed to eliminate "play" between two angle beams. The lower sample jaw is attached to the complex nut and moves vertically with the complex nut as the latter is driven up and down by the threaded shaft.

D. The Recorder

The general operation of the recorder is described in Section A; however, the range selector (see Fig. 3), has not been described previously. A variable resistance, R_1, has been placed across the output of the recorder LVDT. Increasing the resistance increases the load range, i.e., the number of grams represented by one chart inch. Thus, by switching in any one of several preset resistances, the calibration can be changed to any desired fraction of the maximum load range of the ring dynamometer.

The range selector (R_1, Fig. 3A) can be constructed in several ways, two of which are indicated here. In Fig. 3B, a number of precision resistors are placed in series across the Recorder LVDT and connected with a switch to Z. The values shown give load ranges of 50, 20, 10, 5, 2, 1 grams full scale for a 50 gram ring dynamometer using LVDT's with resistances of approximately 100 ohms. In Fig. 3C, a number of potentiometers are connected in series across the Recorder LVDT with the center taps connected with a switch to Z. The potentiometers are then permanently set at the required resistances.

A variable resistance, R_2, is connected across the Strain Gauge LVDT as a calibration control. When the arrangement shown in Fig. 3C is used, R_2 may be a fixed precision resistor and all calibrations carried out with the load selector potentiometers.

For optimum operation of the recorder it is advisable that R_1 and R_2 have approximately the same resistance; if the resistances of R_1 and R_2 vary appreciably the phase relationships of the two LVDT's are incorrect and non-linearity will result. In other terms, if Z is connected directly at X, the two LVDT cores should have the same displacements at each balance position for optimum operation of the recorder. Circuit C is the more easily adaptable of the two, as Circuit B can be used only when the mechanical design of the recorder is such that the displacement of the ring dynamometer for the maximum usable load causes very close to the desired scale deflection of the recorder pen. Under some conditions, for example when excessive building vibrations are present, it is advantageous to introduce a variable resistance R_3 as a sensitivity control with the amplifier operating at maximum gain rather than controlling the over-all gain of the amplifier.

In order for the recorder motor to operate, the field voltage and control voltage must be 90 degrees out of phase. The phase relationship of the error voltage from the two LVDT's may be controlled by placing a capacitor across either the primary or secondary of the input transformer of the amplifier. This capacitor also tends to reduce the high frequency "noise" in the circuit. In this case it was found that a capacitor of the order of several microfarads in the primary circuit of the input transformer was necessary to control properly the phase relationship of the error voltage. At the same time a capacitor, C_1, of the order of 0.0X m.f.d. only, across the secondary of the input transformer gives much more satisfactory phase control. Further, following normal servo amplifier practice, a small capacitor, C_2, from plate to ground in the first stage of the voltage amplifier generally improves the action of the mechanism.

TABLE I. Rate of movement of the lower sample jaw (inches/minute).

Primary gear ratio \ Gear box ratio	25:1	100:1	300:1	600:1	900:1
5:1	1.00	0.25	0.083	0.0417	0.0278
1:1	0.20	0.05	0.0167	0.0083	0.0055
1:5	0.04	0.01	0.0033	0.0016	0.0011

In the operation of the apparatus it is often convenient to be able to adjust the position of the pen with regard to the chart paper. Examination of the apparatus shows that this can be accomplished in either one of two ways: (1) by moving the LVDT coil body of the ring along its axis, and (2) by moving the LVDT coil body of the recorder along its axis. Once the core of the ring LVDT has been located at null-balance when the apparatus is at the zero load position there is no advantage to be gained by moving the ring LVDT coil body. Maintenance of the ring LVDT at null-balance at zero load allows any sensitivity range of the recorder to be employed without changing the zero load position of the pen. Movement of the recorder

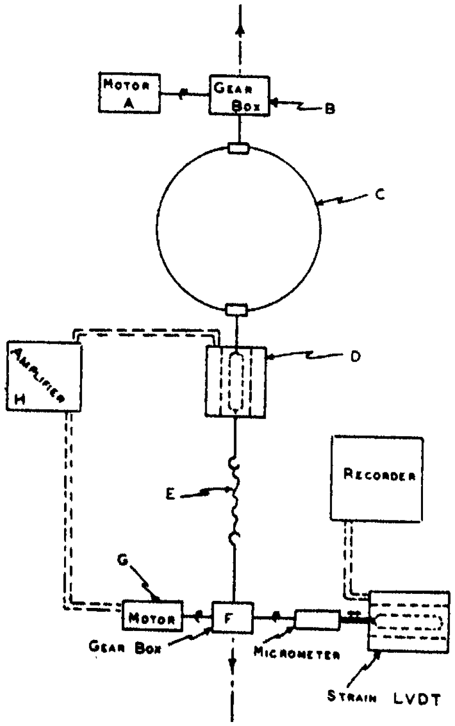

FIG. 4. Schematic diagram of the constant rate of stressing, stress-strain apparatus.

LVDT coil body along its axis allows the position of the pen to be moved along the chart without' disturbing the null-balance at the zero load position. Thus, it is advantageous to mount the recorder LVDT coil body so that it may be moved along its axis. At the same time, if the axis of movement of the recorder LVDT core, the axis of the core itself, and the axis of the recorder LVDT coil body are not identical, non-linearity of the recorder results. Obviously, then, extreme care must be taken in the construction of the entire apparatus.

A Gorrell and Gorrell Monodrum is used to drive the chart, affording twenty different chart speeds, each successive speed being 10/16 that of the previous. As the chart moves at a constant rate and the lower sample jaw moves at a constant rate, the abscissa can be transposed from time to strain values. By installing a reversing, double magnetic clutch, the chart can be made either to rotate continuously in one direction or to reverse direction with the strain mechanism, allowing the recorder to plot a curve continuously in one direction or hysteresis loops.

E. A Constant Rate of Stressing, Stress-Strain Apparatus

Essentially, the modification of a constant rate of strain apparatus to a constant rate of stressing apparatus involves an interchange of the two motor drives with their controls (shown schematically in Fig. 4).

The reversible constant speed motor, *A*, drives the gear box, *B*, which moves the upper clamp of the ring dynamometer, *C*, in a vertical direction. Thus, the upper clamp of the ring is moved at a constant rate of speed and if the lower clamp is held motionless, force is applied to both clamps at a constant rate.

The test sample, *E*, is held between two hooks. The upper hook is supported by the lower clamp of the ring dynamometer, *C*. (The core of the fixed LVDT, *D*, is an integral part of this linkage.) The lower sample hook, attached to the vertical elongation drive mechanism, is moved in a vertical direction by the motor, *G*, operating through the gear box, *F*.

The amplifier, *H*, activated by the output of the

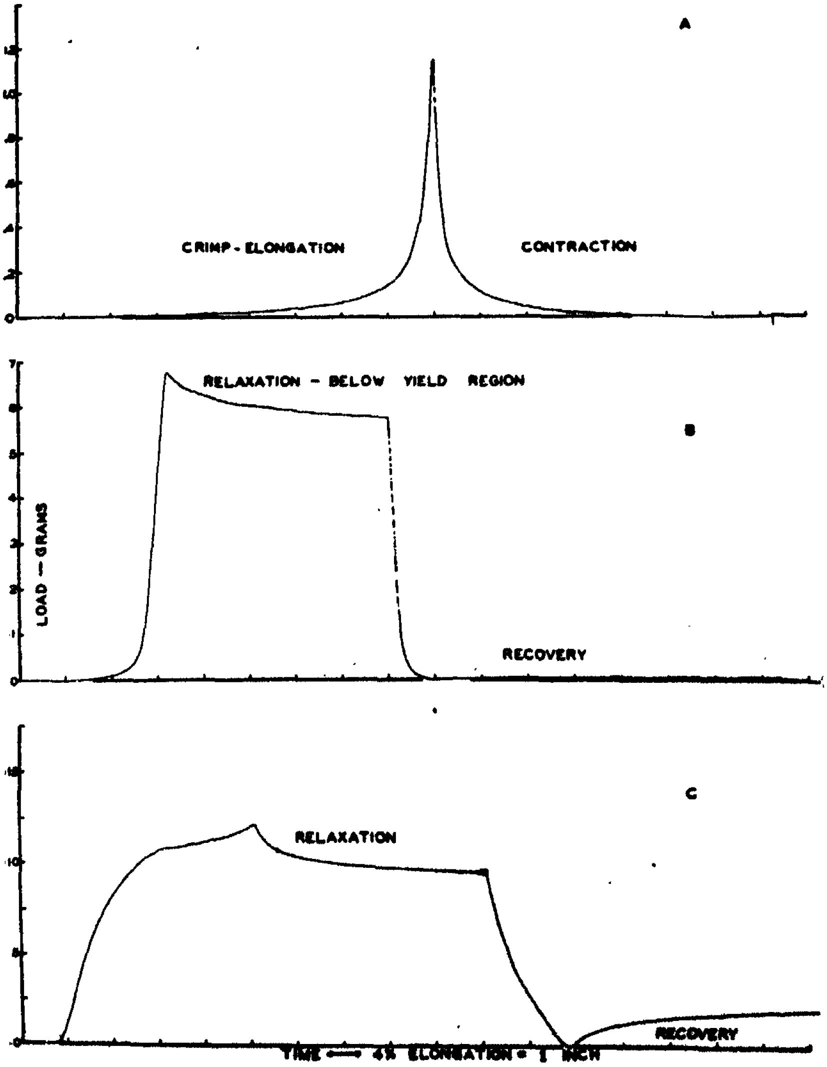

FIG. 5. Typical stress-strain curves of Rambouillet 56's wool.

LVDT, *D*, operates the motor, *G*, in the following manner. When the upper clamp of the ring dynamometer, *C*, is moved upward at a constant rate, the lower clamp of the ring dynamometer would follow it at the same rate, if the fiber did not tend to hold it in place. At the same time, if the lower clamp of the ring dynamometer moves, it also moves the core of the LVDT out of null-balance. Any movement of the core, however, activates the motor, *G*, which in turn strains the fiber so that the stress on the fiber equalizes the stress of the ring dynamometer and maintains the upper sample hook (and thus the lower clamp of the ring dynamometer) at a constant point in space.

The construction of a recorder for this apparatus is similar to that of the constant rate of strain apparatus, with possible simplification in the case of a yarn tester. The stress axis is, naturally, also a time axis in a constant rate of stress apparatus. In the case of a yarn tester, the maximum elongation is normally about ten inches and, thus, the pen can be attached directly to the lower sample hook, i.e., to the elongation drive, with the strain being registered directly on the chart. For fiber studies, where the maximum elongation seldom attains one inch, a more complicated strain recorder is necessary. (This recorder can also be used in the yarn tester if it is desired that the recorder be remote from the tester.) Essentially, the same recorder as used in the constant rate of strain apparatus is employed.

The movement of the strain mechanism is reduced to the linear limit of the LVDT through the use of a micrometer. The arrangement is such that an LVDT core attached to the micrometer moves in an LVDT coil body in direct proportion to the movement of the strain mechanism. The output of this LVDT is placed in series bucking against that in the conventional recorder. The recorder pen then gives a linear reproduction of the movement of the strain mechanism.

F. Operation

The apparatus described herein uses a ring dynamometer which has a displacement of 0.050 inch under a load of 50 grams. In the recorder circuit, a set of potentiometers varying from 300 ohms to 15 ohms gives a set of load ranges varying from 50 grams in 10 chart inches to 1 gram in 10 chart inches. A sensitivity of several milligrams is obtained in all load ranges. In all load ranges, the recorder traverses full scale (10 inches) in less than two seconds. The record drawn is a smooth line except when the load is increasing or decreasing slowly, i.e., approximately 0.02 gram per second or less. In this latter case, the record drawn consists of small steps the magnitudes of which are approximately the width of the pen line. The response of the recorder is rapid and, if no lag of reversal or starting is present in the elongation mechanism, there is no perceptible lag in the reversal or commencement of the recorder. Figure 5 shows several stress-strain curves of a single fiber of Rambouillet 56's wool at 60 percent relative humidity. The three curves were taken successively at the same rate of elongation and identical chart speeds, but at varying load ranges. Curve 5*A*, with a load range of 200 milligrams per original chart inch, shows the stress-strain characteristics of the crimp in the wool fiber. Curve 5*B*, with a load range of 1 gram per original chart inch, shows the relaxation and recovery of the wool fiber below the yield point. Curve 5*C* shows one complete cycle including relaxation, contraction and recovery of the wool fiber with a load range of 2.5 grams per original chart inch. It will be noticed that there is a small step-wise action of the recorder, particularly when the load is changing slowly. These steps can be eliminated by increasing the gain of the amplifier; however, increasing the gain, increases the sensitivity and any rapid or jarring action is liable to instigate hunting in the recorder. A balance between the two extremes is thus necessary and a slight step-wise action must be accepted if extreme stability is desired.

The apparatus is operated in an ordinary, non-conditioned laboratory. The stress-measuring mechanism (the ring dynamometer and LVDT) is enclosed in a case, the only opening in which is a small hole in the bottom of the case for the lower rod supporting the upper sample hook. No drift of the recorder was noticed for periods of observation that lasted from twelve to forty hours for any of the load ranges. For normal operation, the amplifiers are "on" continuously; separate switches which interrupt the line voltage across the field coils only of the induction motors are turned "off" when the apparatus is not in use.

G. Conclusions

A constant rate of strain, stress-strain apparatus, employing a linear variable differential transformer with a ring dynamometer which has eliminated the load range limitations but has maintained the stationary stress-measuring point of the Sookne-Rutherford autographic balance, has been constructed. The LVDT and ring dynamometer also readily lend themselves to application in a constant rate of stress apparatus.

Sensitivity to within several milligrams is obtained in any of several load ranges varying from one gram to fifty grams. The recorder may be switched from one load range to another during an experimental run, since all of the load ranges have the same non-drifting, zero position. By moving the recorder LVDT coil body, the one-gram load range may be obtained at any point in the entire 50-gram load capacity. By using a heavier ring dynamometer, it should be possible to obtain load ranges up to 1000 pounds with the same "degree" of sensitivity, if, naturally, the rest of the apparatus is more heavily constructed. Similarly, ring dynamometers can be used to give increased sensitivity for very low loads.

The authors wish to thank Mr. Harold Lambert, Mechanician of the Textile Research Laboratory, for his valuable suggestions and excellent craftsmanship in the construction of many parts of the apparatus. It is also a pleasure to acknowledge the cooperation of the Quartermaster Corps which supported this work, in part, under Contract No. W44-109-qm-1890.

THE REVIEW OF SCIENTIFIC INSTRUMENTS VOLUME 20, NUMBER 7 JULY, 1949

Amplitude Bridge for Detection of Nuclear Resonance

H. A. Thomas and R. D. Huntoon
National Bureau of Standards, Washington, D. C.

(Received March 17, 1949)

A circuit for detecting nuclear resonance absorption is described that, unlike the rf bridge, is simple to construct and adjust and very insensitive to microphonics. The voltages in two branches of an rf network, one of which contains the coil and sample, are rectified by diode detectors and the audio outputs combined in such a way that noise modulation from the rf generator is balanced out but the desired signal is not. Experimental performance is discussed and typical signal-to-noise ratios are given.

FOR the measurement and stabilization of magnetic fields or other similar applications of nuclear resonance where a relatively strong absorption can be used, it is desirable to simplify the circuits and greatly reduce the disturbances due to microphonics at the expense of maximum signal-to-noise ratio.

The radiofrequency bridge method developed by Bloembergen, Purcell, and Pound[1] approaches the theoretical minimum noise figure but is extremely microphonic, because small phase changes as well as small amplitude changes give rise to an unbalance signal into the detector. Small vibrations alter the reactances in the bridge as a first-order effect and the resistances only as a second-order effect. Thus a considerable reduction in microphonic response can be expected if the rf voltage in each half of the bridge is rectified by a diode and the outputs are combined in an audiofrequency bridge adjusted to balance out audiomodulation noise originating in the rf supply. Changes in reactance at audio frequencies due to microphonics are extremely small so that this arrangement is quite insensitive to them.

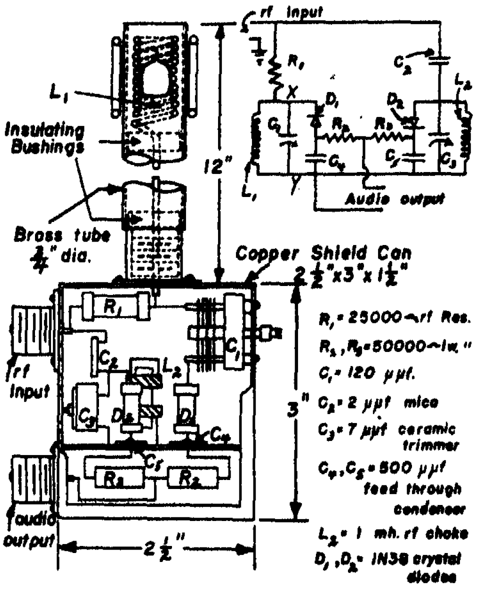

FIG. 1. Amplitude bridge.

The resulting bridge will detect only amplitude changes in the rf and is appropriately called an amplitude bridge.[*] It requires only an audio amplifier as an unbalance indicator instead of a complete radio receiver.

These advantages of circuit simplification and reduced response to vibration are obtained at the expense of signal-to-noise ratio because of the noise contributions from the diode detectors which are located at the point where the signal is still small.

Figure 1 shows the details of a typical amplitude bridge for detecting resonances near twenty megacycles. The rf coil, L_1, which contains the sample, is grounded directly to the upper end of the brass tube which forms the probe. The tuned circuit, L_1-C_1, is fed through resistance R_1, which has a value much higher than the resonant impedance, R_0, of L_1-C_1 so that the low impedance of the signal generator will not lower the Q of the tuned circuit appreciably.

If the noise and hum modulation in the output of the rf generator supplying the bridge circuit is not excessive, sufficient reduction of this noise at the audio output can usually be obtained by merely adjusting C_3. How-

---

[1] Bloembergen, Purcell, and Pound, Phys. Rev. **73**, 679 (1948).

[*] The amplitude bridge was first called to the authors' attention by the wartime research of Dr. C. H. Page of the National Bureau of Standards.

FIG. 2. Proton resonance line using a water sample adjusted with ferric nitrate.

ever, in some cases it may be desirable to obtain a more complete audio balance by making R_2 and C_4 adjustable.

Magnetic sweeping is accomplished by applying a low-frequency voltage to the small Helmholtz coils located on either side of the upper end of the resonance absorption probe. In this way the resonance line can be displayed on an oscilloscope. Figure 2 shows a proton resonance line using a water sample adjusted with ferric nitrate. The value of the polarizing field was 4700 gauss, the line width 0.25 gauss, and the amplifier band width extended from 5 to 2000 cycles.

As predicted by the theory [1] there is an optimum operating level for the rf field in the sample. Figure 3 shows the absorption pip voltage out of the bridge *vs.* the rf voltage across L_1. The total noise of bridge and amplifier and the signal-to-noise ratio for two types of diodes are also shown plotted against rf level. It will be noticed for both the crystal diodes and the oxide-coated cathode high vacuum diodes that the noise voltage increases linearly with the rf level and hence the optimum signal-to-noise ratio does not coincide with maximum absorption signal. The noise shown is mainly due to the diodes, and in the case of the high vacuum diodes, results from the flicker effect. The amplifier and thermal circuit noise were relatively quite low.

It can be shown theoretically that the noise figure of a properly designed system with high vacuum diodes should be less than 10 if shot noise from the diodes were the sole source of noise aside from the Johnson noise of the circuit elements. The noise figure for optimum operating conditions is found to be of the order of 500 to 1000 for the diodes used. The crystal diodes shown were expected to be noisy but were used in the interests of simplicity. High vacuum diodes were expected to be better but were found to offer only a small improvement because of the flicker effect from the oxide cathodes. Figure 3 shows a comparison of the results obtained for the two different types of diodes. Tungsten filament diodes, which should not suffer from flicker effect, were tried but the expected improvement was not observed because of other difficulties such as loss of rectification efficiency and noise from the filament supply.

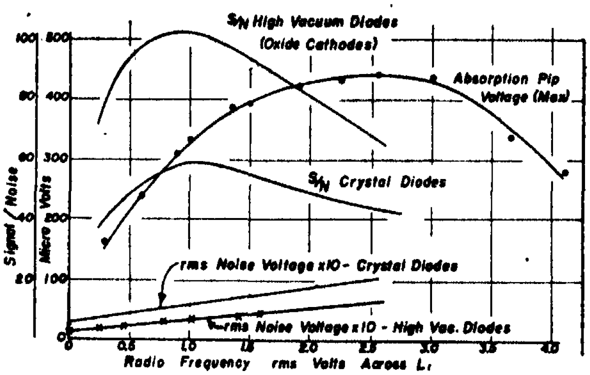

FIG. 3. Signal and noise characteristics of amplitude bridge.

As will be seen from Figs. 2 and 3, quite usable signal-to-noise ratios were achieved in spite of the relatively high noise figure. With the addition of an audio phase detector, or lock-in amplifier, the signal-to-noise ratio was greatly improved, as would be expected. Such an arrangement has been used successfully in a feed-back loop to control a magnetic field by injecting correction current into auxiliary coils on the main magnet. A stability of 2 parts per million for a 1 percent change in main exciter current was observed.[2]

Those who have had experience with balancing an rf bridge at these frequencies will appreciate the simplicity of adjustment of the amplitude bridge. Tuning the absorption coil to resonance and rough equalization of the two detector outputs by adjustment of C_3 is usually all that is required. Experience has shown that once this adjustment has been made, the equipment needs no further attention throughout the useful life of the diodes. Furthermore, the resonance probe may be moved at will in the magnetic field with little or no difficulty due to microphonics.

It should be noted that the amplitude bridge does not respond to what Bloembergen, Purcell, and Pound call the dispersion part of the nuclear resonance signal. Neglecting a very small second order correction only the absorption component is detected.

---

[2] Thomas, Driscoll, and Hipple, Phys. Rev. March 1, 1949 (in press).

Physical Instruments for the Biologist

Detlev W. Bronk
Associate Editor in Charge of this Section
Eldridge Reeves Johnson Foundation for Research in Medical Physics,
University of Pennsylvania, Philadelphia, Pennsylvania

A Cardiotachometer Based on the Plethysmogram

E. E. SUCKLING
Long Island College of Medicine, Brooklyn, New York

(Received March 17, 1949)

An instrument is described which enables the pulse rate in humans to be continuously observed. The pulsations generated in a partially inflated blood pressure measuring cuff are converted into electrical pulses and applied to a counting rate circuit.

THE metering of heart rate in humans is often done from the electrocardiogram. The steep *R* wave which is a millivolt or more in amplitude can be made to operate circuits which will measure either the time duration between pulses[1] or the number of pulses a minute.

In some circumstances it is inconvenient to attach electrodes to the skin of the patient's chest or arms and in other cases electrical interference may cause too great a disturbance to the electrocardiogram to enable reliable signals to be obtained. In these circumstances the unit to be described is useful since it is unaffected by electrical disturbances and connection to the patient involves only a standard blood pressure cuff fastened about the lower part of the calf muscle and inflated to a low pressure. The input signal to the present instrument is derived from the alterations in cuff pressure which accompany the volume pulse in the arterial system. Such changes in cuff pressure are commonly employed to drive recording tambours in the clinical estimation of blood pressure by the oscillatory method.

The cuff comprises a rubber bag enclosed in a bandage with a length of rubber tubing leading from the bag to the tambour and inflater. The tambour is a brass cylinder of two inches diameter covered at one end with 2-mil copper foil. Movements of this copper foil diaphragm are caused by the pressure changes within and are detected by a piezo electric gramaphone pick-up as shown in the photograph (Fig. 1). From this system pulse waves of a few millivolts are obtained when the cuff is inflated to a pressure of 30 millimeters of mercury. Figure 2 shows an oscillogram of the resulting wave. Too great a pressure between pick-up and drum seems to cause fatigue of the crystal and the set screw is adjusted so that a light contact is made when the cuff is inflated. Adjustment is seldom needed.

The amplifier and counting circuits (Fig. 3) are operated from batteries in order to minimize 60 cycle noise which might otherwise cause incorrect triggering of the counting circuit. Three stages of amplification build up a sufficient voltage to pass current through the 1Q5 tube which is normally biased to near cutoff. The relay in the 1Q5 plate pulls in at each pulse and in doing so lights a lamp which gives a visual indication of heart action and shows by its regularity that the unit is operating satisfactorily. In addition this relay has a set of three contacts of which the moving one is connected to condenser *C*5. *C*5 collects a charge from potentiometer *P* during the time between beats and when a beat occurs carries the charge across to share it with *C*6 and *C*7. *C*6 and *C*7 have a slow fixed leakage rate and thus take up a mean voltage which depends on the original potential to which *C*5 is charged and the frequency with which it donates charge to *C*6 and *C*7.

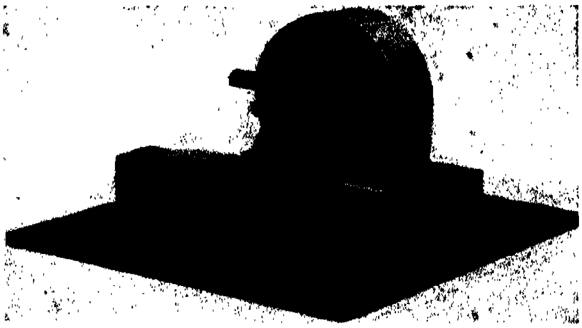

FIG. 1. Tambour with piezoelectric transducer.

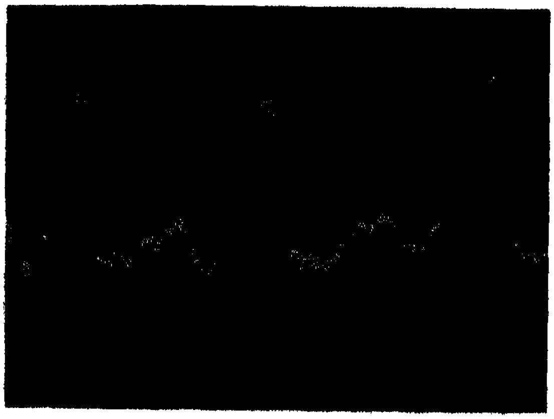

FIG. 2.

---

[1] R. E. Sturm and E. H. Wood, Rev. Sci. Inst. 18, 771 (1947).

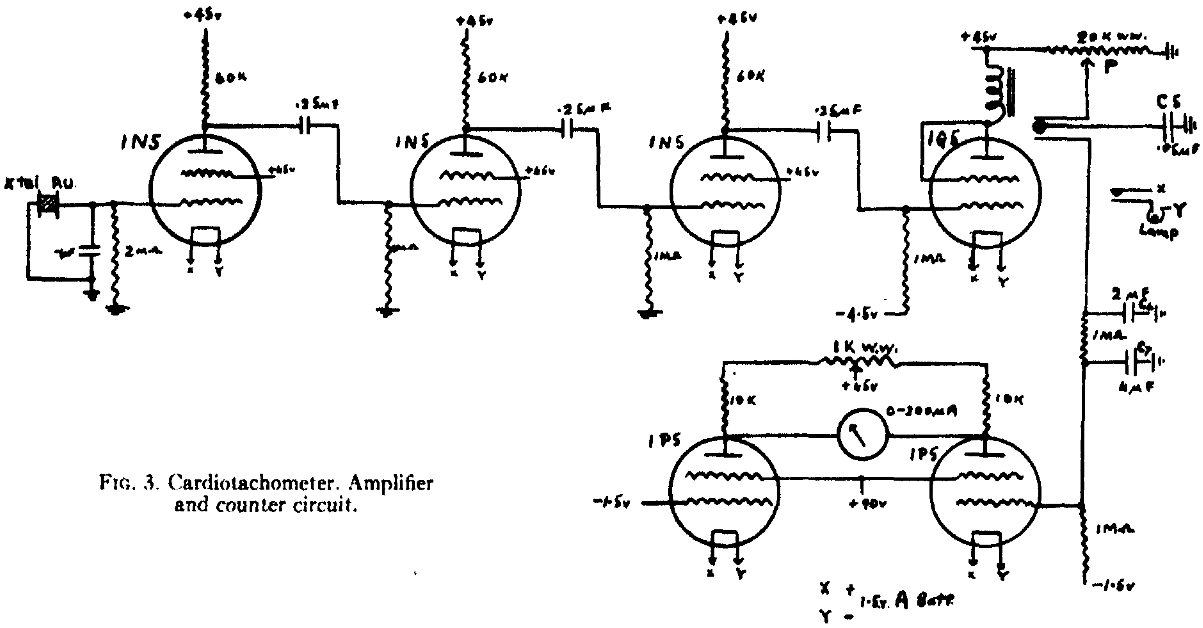

FIG. 3. Cardiotachometer. Amplifier and counter circuit.

The two 1P5 tubes operate as a vacuum tube voltmeter to measure the potential of C7. With the circuit parameters given a 0–200 microammeter can be calibrated fairly linearly for counting rates between about 30 and 200 pulses a minute and the pointer will move only very slightly between pulses.

In use the cuff is attached to the leg (or arm) and inflated to a pressure of about 30 millimeters of mercury. The instrument (Fig. 4) is then turned on and as condensers *C6* and *C7* charge the pointer settles in a few seconds at the position on the dial corresponding to the pulse rate. The lamp flickers steadily in synchronism with the pulse. Any movement of the muscle around which the cuff is bound of course causes extraneous pulses to be generated in the machine but following such a disturbance equilibrium is restored in a few seconds. In anesthetized patients steady indication of pulse rate during an operation has been demonstrated without difficulty.

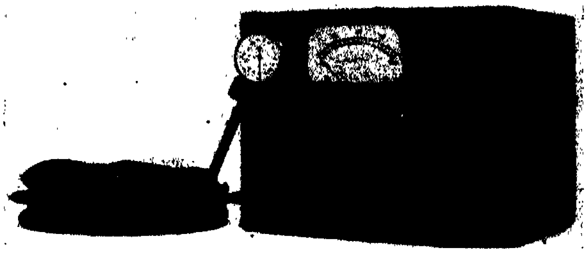

FIG. 4. Complete unit.

THE REVIEW OF SCIENTIFIC INSTRUMENTS VOLUME 20, NUMBER 7 JULY, 1949

Syringe Oxygen Cathode for Measurement of Oxygen Tension in Solution and in Respiratory Gases

JULIAN M. TOBIAS*
with the technical assistance of NADINE RETONDO
Department of Physiology and Toxicity Laboratory, University of Chicago, Chicago, Illinois

(Received February 17, 1949)

A method is described for measuring oxygen tension in Ringer solution which utilizes the principle of the polarograph, but substitutes a platinum wire cathode for the usual dropping mercury electrode. The wire cathode and a calomel anode are mounted in the piston of a hypodermic syringe into which the solution is aspirated for analysis. Sensitivity and reproducibility are evaluated. Extension of the method to the analysis of gaseous oxygen is also described.

SINCE 1924, when Heyrovsky showed that oxygen, dissolved in electrolyte solutions, is reduced at the dropping mercury cathode,[1] this reaction has occasionally been used to follow res-

---

* The present investigation was aided in part by a grant from the Dr. Wallace C. and Clara A. Abbott Memorial Fund of the University of Chicago, and in part under contract between the Medical Division, Chemical Corps, U. S. Army and the University of Chicago Toxicity Laboratory. Under the terms of the contract the Chemical Corps neither restricts nor is responsible for the opinions or conclusions of the authors.

[1] J. Heyrovsky, Trans. Faraday Soc. 19, 785 (1924).

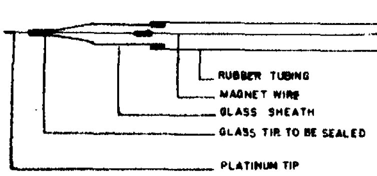

FIG. 1.

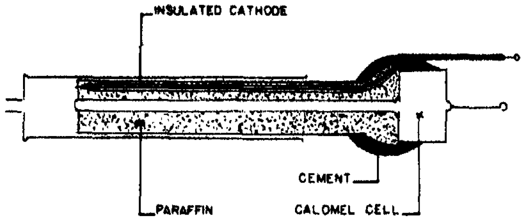

FIG. 2.

piration *in vitro*.[3–9] Cumbersome and costly in commercially available forms, the dropping mercury electrode assembly or polarograph has not been widely used as a respirometer though a simplified modification has been described.[2] A major forward step was taken in 1931[10, 11] when, though the fact had been known before,[12] it was more extensively shown that the dropping mercury electrode could be replaced in a large number of analyses by a platinum wire electrode. Beside the advantage of using platinum rather than mercury in contact with biological systems, such a change makes the entire instrument far simpler and more versatile. In 1938, Blinks and Skow[13] used such an electrode to study oxygen exchange by respiring and photosynthesizing leaves, no further botanical experiments being made with a metal cathode until 1942.[14] To Davies and others working in Dr. D. W. Bronk's laboratory, however, should go the credit for initial extensive experiments with a platinum wire microcathode applied to the measurement of oxygen tension in animal tissues *in vivo* and to the measurement of oxygen consumption by small bits of surviving tissue *in vitro*.[15–22] Others too have used the instrument for measuring oxygen tension in brain, *in vivo*.[23, 24] A platinum microelectrode has also been used for analyses in a flowing stream of electrolyte.[25–27] Similar experiments have been begun by the author.[28] The desirability, in certain instances, of taking the measuring instrument to the tissue left in its near normal environment rather than bringing the excised tissue to the measuring instrument is obvious. Up to now, however, the method has not been made available in simple, inexpensive form even for *in vitro* applications. It is the purpose of this communication to describe and evaluate the oxygen tension measuring performance of a Pt cathode mounted, together with a calomel anode, in the piston of a hypodermic syringe.

For a discussion of theory one should consult the monograph of Kolthoff and Lingane[29] and other cited references. Suffice it here to say that if a Pt cathode immersed in an electrolyte solution be maintained at about 0.8 v with respect to a nonpolarizable anode, then the current which flows is a straight line function of the oxygen tension of the solution (Fig. 4).

CONSTRUCTION

Figure 1 shows the method of insulating the Pt lead; Fig. 2 shows the electrodes as placed in the syringe; Fig. 3 shows the circuit diagram.

A bit of Pt wire (0.1–0.2 mm diam.), soldered to a similar copper lead, is thrust through rubber tubing (2 mm o.d. app.) into a soft glass tip (1–2 cm of 1–2 mm i.d.) until the wire protrudes. After taping the copper lead to the rubber tube, the glass tip is flame sealed to the wire and the wire cut off. How much Pt is left exposed should depend upon galvanometer sensitivity. The smaller the electrode the smaller the current, the more micro the instrument, the more rapidly does the electrode become polarized and the more rapidly can measurements be made.

---

[2] O. Muller, *The Polarographic Method of Analysis* (J. Chem. Ed. Publ., Easton, Pa., 1941).

[3] P. Baumberger, Cold Spring Harb. Symp. Quant. Biol. **7**, 195 (1939).

[4] H. G. Petering and F. J. Daniels, J. Am. Chem. Soc. **60**, 2796 (1938).

[5] K. S. Karsten, Am. J. Bot. **25**, 14s (1938).

[6] R. J. Winzler, J. Cell. Comp. Physiol. **17**, 263 (1941).

[7] H. G. deBuys and R. A. Olson, Am. J. Bot. **27**, 401 (1940).

[8] W. M. Manning, Ecology **21**, 509 (1940).

[9] Beecher, Follanskee, Murphy, and Craig, J. Biol. Chem. **146**, 197 (1942).

[10] S. Glasstone and G. D. Reynolds, Trans. Faraday Soc. **29**, 399 (1933).

[11] S. Glasstone, Trans. Am. Electrochem. Soc. **59**, 277 (1931).

[12] E. Salomon, Zeits. f. physik. Chemie **25**, 365 (1898).

[13] L. R. Blinks and R. K. Skow, Proc. Nat. Acad. Sci. **24**, 420 (1938).

[14] R. Kolkwitz, Ber. der deutsch. bot. Ges. **60**, 306 (1942).

[15] P. W. Davies and F. Brink, Rev. Sci. Inst. **13**, 524 (1942).

[16] P. W. Davies and F. Brink, Fed. Proc. **1**, 19 (1942).

[17] Bronk, Larrabee, and Davies, Fed. Proc. **5**, 11 (1946).

[18] P. W. Davies, Fed. Proc. **5**, 21 (1946).

[19] Posternak, Larrabee, and Bronk, Fed. Proc. **6**, 182 (1947).

[20] Bronk, Brink, and Larrabee, Fed. Proc. **7**, 14 (1948).

[21] Davies, Grenell, and Bronk, Fed. Proc. **7**, 25 (1948).

[22] P. W. Davies and A. Rémond, Proc. Ass. Res. Nerv. Ment. Dis. **26**, 205 (1946).

[23] Roseman, Goodwin, and McCulloch, J. Neurophysiol. **9**, 33 (1946).

[24] Davis, McCulloch, and Roseman, Am. J. Psychiat. **100**, 825 (1944).

[25] Bronk, Brink, Connelly, Carlson, and Davies, Fed. Proc. **6**, 83 (1947).

[26] O. Muller, J. Am. Chem. Soc. **69**, 2992 (1947).

[27] Carlson, Brink, and Bronk, Fed. Proc. **7**, 18 (1948).

[28] J. M. Tobias and R. Holmes, Fed. Proc. **6**, 215 (1947).

[29] I. M. Kolthoff and J. J. Lingane, *Polarography* (Interscience Publishers, Inc., New York, 1946).

FIG. 3.

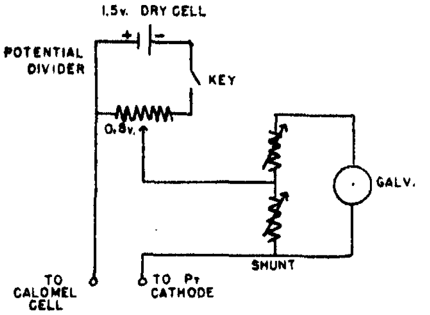

The syringe plunger top is now cut off and the distal end opened by grinding with carborundum.[30] One thus has a hollow tube which fits tightly into the syringe barrel. The Pt electrode and a small calomel half cell (Coleman titration reference electrode 5745) are placed in the piston, their tips flush with the opened distal end. This unit is made rigid by closing the proximal end with de Khotinsky cement. With care to leave the electrode tips exposed, the piston is filled with paraffin, de Khotinsky or some other suitable substance. Such a plunger can now be used to aspirate fluids into or eject them from the syringe. Oxygen tension of the fluid so aspirated can then be measured by the protruding electrodes.

This construction is, of course, variable. For small amounts of fluid smaller syringes and modified anodes can be used. The solid pistons of very small syringes must be replaced by tubing ground to fit the cylinder, or one can use the small Yale syringes for gravity injection which have a sidearm through which the anode or cathode can enter.

Beyond the above one requires only a 1.5 v dry cell, three variable resistors, a switch and a galvanometer. A Rubicon No. 4625 galvanometer (sens. 0.007 μa/mm) is suitable for use with all but very small electrodes. To allow for using electrodes of widely varying resistance, thus obviating the need for their precise reduplication, two resistors are set up as a universal shunt.

OPERATION AND PERFORMANCE IN ANALYSIS OF SOLUTIONS

Statistical evaluations are in terms of standard error given by $(\sum d^2/N)^{\frac{1}{2}} \div (N)^{\frac{1}{2}}$.[31] It should be vigorously emphasized at the outset that the measuring syringe must lie quietly on some surface during and for about one minute before current measurement. Otherwise varying amounts of oxygen are stirred toward the cathode and current readings become uninterpretable. The case of maximum or constant stirring[30] will not be considered here.

The simplest calibration method is to measure current when the syringe contains solutions of differing but known oxygen tensions. A current-oxygen tension curve so obtained gives both sensitivity and a conversion factor. Study of such curves obtained in different ways has revealed pitfalls and ways of avoiding them. All data have been obtained with the cathode 0.8 v to a calomel half cell.

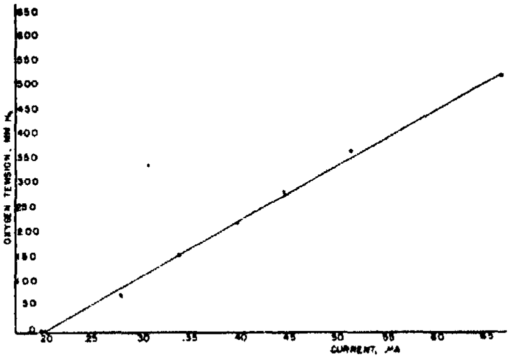

FIG. 4. Typical calibration curve.

A typical calibration curve is shown in Fig. 4. It becomes apparent, on repetition, that the relation is constantly linear, and the curve should consequently be obtainable, with measurable error, from two points. Therefore, performance has been studied using mainly air saturated or essentially oxygen free (bubbled with tank N_2-oxygen partial pressure 0.25–0.5 percent barometric) frog Ringer solution.

First of all, variation of sensitivity was examined from day to day. For one electrode, 19 measurements in 18 days gave an average of 0.3150±0.0173 microampere (μa) per 150 mm mercury partial pressure change in oxygen tension. Extrapolating from this full-scale sensitivity and from the known solubility of oxygen (0.037 cm per cc per mm partial pressure at 25°C) a change of 1 mm on the galvanometer scale is found equivalent to a change of about 0.12 cm oxygen per cc. However, the accuracy indicated is only achieved without more frequent calibration if many (about 20) measurements are made, and, from any two measurements, the determination of a difference may be in large error. It was also found that beside a 5.5 percent S.E. in sensitivity (slope) the absolute value of any one current point could vary considerably. Thus, in 150 measurements chosen at random from several weeks experiments, the current in air saturated solution was found to average 0.3238 ±0.0098 μa (a range of 0.2600–0.5800). Some electrodes have been more stable, the variability perhaps being in surface properties of the cathode and degree of polarizability of the calomel cells. Such data soon accumulate, however, for all electrodes being used and clarify how any one must be controlled for a particular need.

---

[30] J. Strong, *Procedures in Experimental Physics* (Prentice-Hall, Inc., New York, 1943).

[31] R. A. Fisher, *Statistical Methods for Research Workers* (Oliver and Boyd, London, 1946).

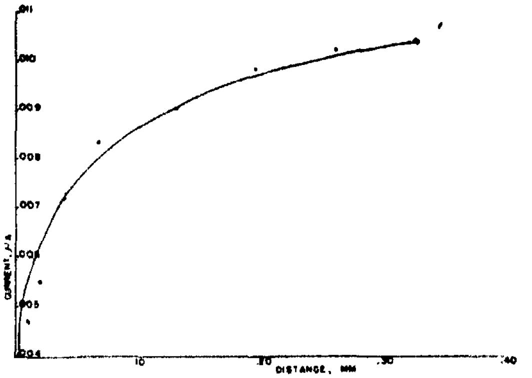

FIG. 5. Shadowing of electrode on approaching a surface.

Even an electrode as variable as the above is much more stable over a shorter time, hours instead of days. Thus, 0.5 cc samples of air saturated or oxygen free solution were aspirated alternately, at 6 minute intervals, over a total time of two hours. In all cases, current was measured at precisely 1 minute after closing the circuit, and the current was not allowed to flow longer than 1 minute. In the interval between measurements polarization effects decay. Under these conditions both sensitivity and absolute current value in air saturated solution are much more constant. Thus, 1 minute current values at air saturation were reproducible with an S.E. of only 0.6 percent of the mean, and the sensitivity values with an S.E. of 0.7 percent of the mean. It is useful to see what this means in terms of changes in oxygen volume. In Ringer solution, at 25°C, the solubility of oxygen is about 0.028 cc per cc at 760 mm. Therefore, the amount of oxygen dissolved changes by about 0.037 cm per cc per mm partial pressure or by about 5.6 cm per cc for full scale sensitivity (full scale = 150 mm p.p.). With the galvanometer used, a 1 mm deflection corresponded to about 3 mm partial pressure or a change in dissolved oxygen of about 0.2 cm per cc. Since it is partial pressure which is actually measured, the sensitivity must increase as the volume decreases. In other experiments, using modified electrodes in a 1 cc tuberculin syringe, comparable stability and reproducibility were achieved with volumes of only 0.02–0.05 cc wherefrom one can calculate that in such volumes a 1 mm deflection on the galvanometer scale should correspond to a change of about 0.004–0.01 cm of dissolved oxygen. For comparison with other microrespirometers see Tobias[32] or Glick.[33] The standard error and reproducibility of this measurement are not yet known. It will, in all likelihood, not be as good as that for full scale sensitivity. However, the use of more sensitive current measuring devices should increase reproducibility as smaller differences are measured.

Experiments have also been done to show the desirability of leaving the current on for only a short period of time. It was found that readings at three minutes after closing the circuit, without impressed intermittent depolarization, yielded air saturation points tending to fall with time (in two cases falling 8 and 21 percent in 1.5–2 hours) and varying with a standard error of 1.4–3.4 percent of the mean. Under these conditions, sensitivity

TABLE I. Reproducibility of current with gas and ringer in syringe.

	Gas			Gas			Gas	Gas	Gas
N_2	Air Current, μa	O_2	N_2	Air Current, μa	O_2	N_2	Air Current, μa	Air Current, μa	Air Current, μ
0.0757	0.8250	3.695	0.0734	0.3820	1.499	0.0730	0.8780	1.858	0.3771
0.0757	0.8630	3.715	0.0734	0.3800	1.698	0.0730	0.8630	1.845	0.3500
0.0757	0.8690	3.695	0.0671	0.3940	1.569		0.8360	1.858	0.3795
0.0775	0.8650	3.715	0.0671	0.3630	1.569	0.0695	0.8320	1.858	0.3695
0.0775	0.8650	3.755	0.0671	0.3750	1.500	0.0730	0.8260	1.780	0.3719
0.0817	0.8900	3.770	0.0650	0.3585			0.8360	1.804	0.3882
0.0796	0.8950	3.770	0.0629	0.3650		0.0695	0.8580	1.699	0.4030
0.0754	0.9310	3.770	0.0629	0.3710		0.0730	0.7470	1.923	0.4300
0.0692	0.8900	3.770	0.0608	0.3775			0.7800	1.671	0.4102
0.0712	0.8840	3.770	0.0608	0.3686				1.725	0.3965
			0.0629	0.3709				1.699	0.4050
				0.3709				1.750	0.3900
				0.3755				1.750	0.4160
				0.3730				1.685	0.4150
				0.3755				1.763	0.4190
				0.3709				1.750	0.4190
				0.3628				1.830	0.4210
				0.3628				1.763	0.4360
				0.3690				1.830	
Means*									
0.0759	0.8937	3.743	0.0658	0.3694	1.566	0.0718	0.8284	1.792	0.3976
±0.0012	±0.0067	±0.0106	±0.0013	±0.0018		±0.0007	±0.0141	±0.0163	±0.0057

* Reliability given as ± S. E.

---

[32] J. M. Tobias, Physiol. Revs. 23, 51 (1943).

[33] D. Glick, *Techniques of Histo- and Cytochemistry* (Interscience Publishers Inc., New York, 1949).

TABLE II. Comparison of analyses for gaseous oxyegn by syringe cathode and Haldane apparatus.*

Syringe cathode		Haldane		Difference	
Partial pressure, mm Hg	Vols. %	Partial pressure, mm Hg	Vols. %	Partial pressure, mm Hg	Vols. %
181	24.4	185	24.9	4	0.5
150	20.1	150	20.1	0	0.0
156	20.9	148	19.9	8	1.0
115	15.4	117	15.7	2	0.3
73	9.8	75	10.3	2	0.5
			Mean	3.2	0.46

* Each datum the average of duplicates.

too was found to decline with time and to vary with a standard error of 2.3–3.3 percent of the mean. Impressed intermittent depolarization (reversing the direction of current flow for a time equal to that of the preceding run) prevented the declines with time but did not materially lessen the standard errors. Therefore, using a short time of current flow, 1 minute as in previous trials, favors both stability of a given point on the curve and reproducibility of sensitivity.

Since the method depends on the rate of diffusion of dissolved oxygen toward the cathode, any thing which interferes with such diffusion must either interfere in a constant or negligible fashion or current readings will not accurately reflect oxygen tension in the body of solution. Thus, if a cathode in a solution of uniform and constant oxygen tension is brought closer and closer to some surface the surface eventually interferes with diffusion toward the electrode, casts a kind of shadow, and the current may fall as shown in Fig. 5. Distance and the effect on current will vary depending on the size of the cathode. As the cathode is made smaller it can approach more closely to a surface without such an effect manifesting itself. The fact is noted here because a solid object in the syringe barrel could cause serious difficulty unless its position were rigidly controlled. Therefore, also, for high precision, unless large volumes are used, calibration probably should be done in the same volume of solution as is to be used for the unknown.

What magnitudes of variation in salt concentration are important is not yet clear. It was found that in pure KCl solutions varying from 0.1 to 0.0025 M, air saturation current was no less stable for all concentrations taken together than for any given concentration. Since, however, there are many instances where the supporting electrolyte makes a great deal of difference,[29] it would probably be wise to measure the effect of concentration on stability in each case considered.

ANALYSIS OF RESPIRATORY GASES

The procedure can also be adapted to analysis for gaseous oxygen. The modification required is that one introduces only a small but constant volume of Ringer solution into the syringe. Then a sample of the gas in question is drawn in, equilibrated with the solution, and the oxygen tension of the solution is measured.

Current reproducibility with nitrogen, air or oxygen in the syringe over frog Ringer is shown in Table I. Different electrodes were used, and it is seen that the current was stable, on the average, within a standard error of about 1.1 percent of the mean.

Calibration curves are similar to that shown in Fig. 4. In all cases a 2 cc syringe was used. After measuring 0.1 cc of Ringer into the syringe, a 1.5 cc sample of the gas mixture to be analyzed was drawn in, shaken with the Ringer and expelled. This was repeated three times. A fourth sample was left in and the syringe tip closed. Gas and Ringer were now vigorously shaken for 30 sec. Following this the syringe was held upside down for 1 minute in a clamp, to drain solution down on to the electrodes. Then the circuit was closed and the current read 1 minute later.

Analyses of several gas mixtures by the electrode method and by the Haldane technique are shown in Table II. The average difference by the two techniques was 3.2 mm partial pressure of oxygen (range 0–8) or about 0.5 vol. percent. Since this application of the technique does not serve the author's main interests, no extensive study of precision has been made. It seems worthwhile, however, to report the method as a potentially useful one.

So much for general description. Details on particular application should be considered in context. Calibration experiments were all done with maximum care. Measurements were made at constant intervals, the syringe was always washed out a constant number of times at a more or less constant rate, and stereotypy in running experiments was carefully cultivated. It is to be anticipated that when used with tissues, with almost surely some protein in solution and with occasional irregularities in technique required, the precision demonstrated here may not obtain. Nor can one freely extrapolate from reproducibility of full scale sensitivity to reproducibility for very small changes. Such evaluation will emerge with use of the instrument.

ACKNOWLEDGMENT

The author is indebted to Dr. J. O. Hutchens for calling his attention to the small Coleman half cell. Dr. M. Morse of the Department of Pediatrics, Billings Hospital, generously made the control analyses of gas mixtures by the Haldane technique.

Laboratory and Shop Notes

A Dry Box for Handling Alkali Metals and Other Extremely Hygroscopic Materials*

EUGENE E. KETCHEN, FORREST A. TRUMBORE,
W. E. WALLACE, AND R. S. CRAIG
Department of Chemistry, University of Pittsburgh, Pittsburgh, Pennsylvania

April 28, 1949

THERE are many laboratory procedures which require the use of materials and reagents which readily absorb moisture from the atmosphere. It is well known that where extremely hygroscopic substances are involved, even the simplest laboratory manipulations become complicated and cumbersome if complete protection from moisture is demanded. At the present time an investigation is under way in this laboratory to determine certain thermochemical characteristics of elemental sodium and potassium and the binary alloys composed of these two metals. Because of the extreme reactivity of these materials toward atmospheric moisture, it has been necessary to devise a special technique for use in handling samples. It has occurred to us that this technique may be of interest to others dealing with substances exhibiting comparable affinities for water vapor.

In the early stages of the work all manipulations were carried out in a rather conventional high vacuum system. Residual gas pressures were reduced to the limit of a good mercury diffusion pump before beginning a given sequence of operations involving the alkali metal samples. The necessary motions in the vacuum system were accomplished using suitable arrangements of ground joints, metal bellows, magnetic devices, etc. Those familiar with high vacuum techniques and remote control operations will recognize that a trouble-free system designed along these lines will be difficult, if not impossible, to construct and maintain. More recently the various operations have been carried out in a specially constructed chamber patterned in principle after the dry boxes which have frequently been employed in handling hygroscopic materials.

The dry box currently in use was constructed of a piece of Pyrex glass pipe 12 inches in diameter and 18 inches long. The glass wall is about ⅜ inch in thickness. The two ends of the pipe are fitted with cadmium plated steel caps which are clamped onto the pipe and provided with Neoprene gaskets to form gas-tight seals. In each of the metal caps there is a hole about six inches in diameter accommodating a Neoprene glove which enables the operator to work in the closed chamber. The Neoprene gloves are held to the metal cap by a gas-tight ring and gasket arrangement that can be removed to permit access to the working chamber. A view of the assembled chamber is shown in the accompanying photograph.

To illustrate the operation of the dry box suppose we consider an actual case. In our work it is frequently necessary to transfer a small sample (about 0.2 ml) of liquid alloy from a stock bottle to a small glass bulb sample container which is subsequently crushed to allow the alloy to react with water in a calorimeter. The stock bottle, sample container, hypodermic syringe, and other needed accessories are placed in the working chamber which is then sealed and evacuated down to 2–3-microns pressure.[1] At this stage it is necessary to provide a means of evacuating the interior of the gloves (where the hands will be inserted later) since they would either inflate and burst or develop porosity while sustaining a full atmosphere pressure differential. The interior of the gloves is evacuate with any auxiliary pump capable of attaining a pressure of a few millimeters or by using the pump which backs the diffusion pump. A metal disk bolted to the metal caps mentioned earlier with appropriate gaskets and provisions for connecting to the pump serves as the vacuum seal for exhausting the interior of the gloves.

FIG. 1. View of the dry box. Parts of the lines for evacuating and flooding the chamber with helium are visible at the right. The metal disks used while evacuating the interior of the gloves have been removed from the metal caps and are to be seen lying on the table.

After the chamber has been evacuated, it is refilled with helium gas which has been purified by passing over activated charcoal at a pressure of 1000 lb./in.^{2} or more and liquid nitrogen temperatures. As a further clean-up procedure, a "getter" of metallic potassium or sodium-potassium alloy is exposed to the helium atmosphere. The chamber is then ready for transferring the alloy sample. The hypodermic syringe is used to pipet a sample of the desired size into a sample bulb blown on the end of a glass tube which terminates on the other end in a standard taper joint. The sample container is then capped with a suitable glass interjoint provided with a vacuum stopcock to isolate the transferred sample from the surrounding atmosphere. The dry box can then be opened, the enclosed sample attached to a vacuum system, the protective atmosphere of helium pumped away and the sample sealed off under vacuum until needed. The weight of the alloy sample can of course be determined from the known weights of the empty and filled bulb after applying certain buoyancy corrections. The samples transferred by the technique described appear to be entirely free of contamination due to moisture, judging from their bright mirror-like surfaces. Sodium-potassium alloys develop a tarnished surface with extreme rapidity when exposed to a moist atmosphere.

The experimental chamber has been used to handle pure potassium (which appears to require an unusually clean atmosphere), a number of sodium-potassium alloys of varying compositions, and certain hygroscopic salts which had to be maintained as nearly anhydrous as possible. It has proved to be quite satisfactory in dealing with these substances and should be readily adaptable to the manipulation of other hygroscopic materials.

---

* Contribution No. 720 from the Department of Chemistry, University of Pittsburgh. This work was supported by a basic research grant from the ONR, Contract N6ori43, No. 2.

[1] In this technique a better vacuum is not necessary since the partial pressure of impurities in the helium protective atmosphere probably exceeds 3 microns by a factor of ten or more.

Several Improvements on the "Philip's Gauge"*

C. HAYASHI, K. HASHIMOTO, K. KANEKO,
K. OKAMOTO, AND R. SAGANE
Department of Physics, Tokyo University, Tokyo, Japan

March 28, 1949

IN an article in this Journal, R. G. Picard** has described the so-called "Philip's gauge," or cold cathode ion gauge. The use of an axial magnetic field with only a few thousand volts of either a.c. or d.c. makes it possible to measure pressures in the range of 1×10^{-3} to 1×10^{-6} mm of Hg. Since this type of gauge greatly

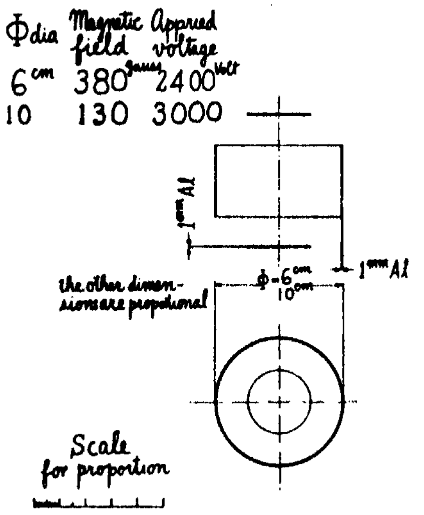

FIG. 1.

simplifies the measurement of low pressures, it is desirable to extend its range to the region of 10^{-6} mm of Hg, as well as to the region 10^{-1} mm of Hg.

During about eight years experience in the use of this type of gauge, our laboratory has developed several desirable improvements, based chiefly, as indicated below, on a variation of its geometrical configuration and dimensions.

1. Use of this type of gauge in the region of 10^{-6} mm of Hg.—The gauge, 10 cm in diameter, which is shown in Fig. 1, is used for this purpose. A current-pressure curve taken under certain fixed conditions is given in Fig. 2. If the dimensions of the gauge are increased, it is possible to measure much lower pressures. The necessary magnetic field strength usually decreases in this case, although several different modes or types of discharge exists. Since pressures lower than 10^{-6} mm of Hg can be measured, this large type of Philip's gauge may easily be used at the high voltage end of a Van de Graaff generator, and in similar applications.

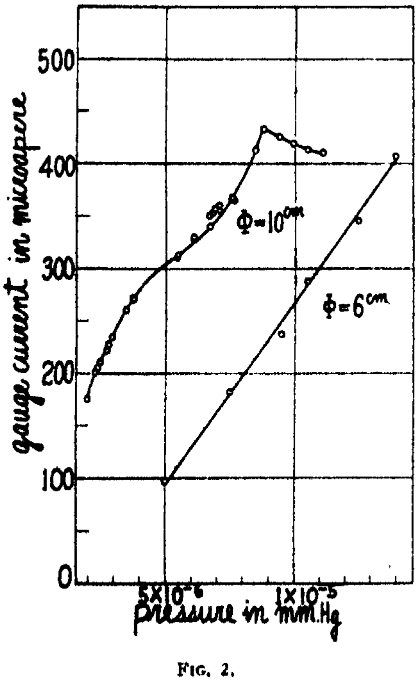

FIG. 2.

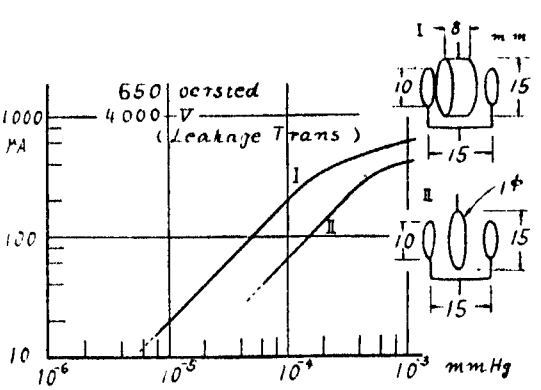

FIG. 3.

2. Use of the cylindrical electrode to increase the current for a given vacuum.—The ring electrode, which is usually used, was replaced by the cylindrical electrode, as shown in Fig. 3. This increased the current by a factor of 2 to 3, and also improved its stability.

Of course, the current for any given vacuum is increased by enlarging the anode. Also the orientation of the cathode and anode affects the stability of the discharge near its high vacuum limit.

3. Use of this gauge to measure pressures of 0.1 mm of Hg and higher.—This can be done by reducing the dimensions and also the applied voltage, although the necessary magnetic field strength is greatly increased (over 1000 oersteds).

4. Use of this gauge as a type of safety relay.—Figures 4 and 5 show several characteristic curves for the gauge using a box cathode and a ring anode. The dimensions of the box were 6 ×15×15 mm. The ring anode was 2 turns of 1-mm copper wire. In Fig. 4 the ring had an inner diameter of 4.5 mm, and in Fig. 5, 2.0 mm. The magnetic field strength in each case was 1070 oersteds.

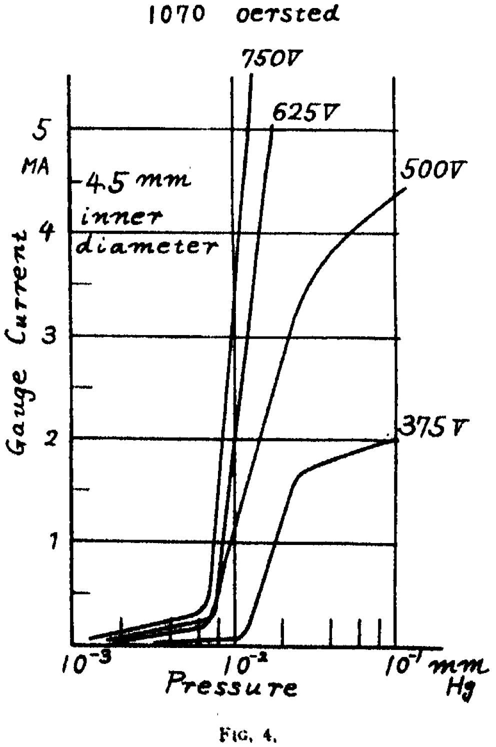

FIG. 4.

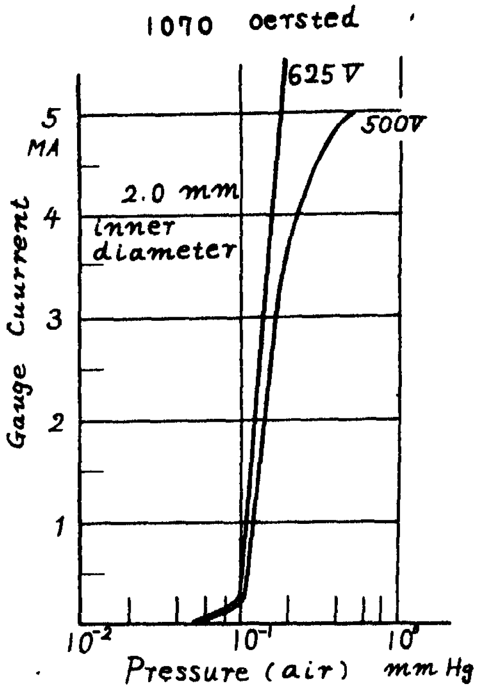

FIG. 5.

The position of sharp increase of current has a very good reproducibility and depends largely on the dimensions of the gauge. Fine adjustments can be made by changing the applied voltage.

The work has been financed by the Applied Research Fund as well as the Scientific Research Fund of the Ministry of Education.

---

* F. M. Penning: Physica 3, 873 (1936); 4, 71 (1937); Philip Tech. Rev. 2, 207 (1937).

** Robert G. Picard, Rev. Sci. Inst. 17, 125 (1946).

Some Statistical Considerations on Coincidence Counting

ARTHUR SARD
Department of Mathematics, Queens College, Flushing, New York
AND
R. D. SARD*
Department of Physics, Washington University, St. Louis, Missouri

April 28, 1949

IN cosmic-ray and nuclear-physics research the coincidences recorded with a particular experimental arrangement are sometimes necessarily the result of two effects. For example, in a recent measurement[1] of delayed coincidences between incident mesons and the electrons resulting from their disintegration, 103 counts were recorded in the double-coincidence channel covering delays from 4.6 to 5.25 microseconds. Some of these 103 counts are due to actual meson disintegrations, the rest to chance coincidences; and there is no way for the apparatus to disentangle the two types of event. But one can calculate, from measurements of individual counting rates and of the channel width, the expected number of chance-coincidences (casuals), which in this example comes out to be 41. One knows, furthermore, that the distribution of the casuals is Poissonian, as is that of the reals; and that the two distributions are sensibly independent. The problem is to estimate the expected number of reals and the standard error of this estimate. Known procedures in the theory of stochastic variables lead to the following estimates. Estimate the mean number of reals as $103-41=62$. Estimate the standard error of the preceding estimate as $(103)^{\frac{1}{2}}$.

We proceed now to justify these estimates. Let x be the number of reals, y the number of casuals, and $z=x+y$ the number of observed coincidences in an experiment. Let the operator E denote taking the expected value (mean), and let α and β be respectively the means of x and y. Then $\alpha=Ex$, $\beta=Ey$, $\alpha+\beta=Ex+Ey=E(x+y)=Ez$. We know further that since x and y are independent Poissonian stochastic variables, z is also Poissonian.[2] Then the probability of a z is

$$\exp(-\alpha-\beta)\,(\alpha+\beta)^z/z!. \tag{1}$$

We know β and we have one observation of the quantity z. We wish to estimate α on the basis of this knowledge. Let α^*, a function of z, be our estimate of α; let σ be the standard error of α^*, and let s, a function of z, be our estimate of σ.

The recommended definitions of α^* and s are the following:

$$\alpha^*=z-\beta, \quad s^2=z.$$

The reasons for adopting these definitions are twofold. First, the estimates are *unbiased*:

$$E\alpha^*=\alpha, \quad Es^2=\sigma^2.$$

(Accordingly, the arithmetic means of the estimates, in repeated independent estimations, converge with probability one to the true values.[3])

Proof:

$$E\alpha^*=E(z-\beta)=Ez-E\beta=\alpha+\beta-\beta=\alpha.$$
$$\sigma^2=E(\alpha^*-\alpha)^2=E(z-\beta-\alpha)^2=\text{ Variance of } z=Ez.$$
$$Es^2=Ez=\sigma^2.$$

Second, the definitions of α^*, s^2 above are the *only* definitions which give unbiased estimates whatever the value of α may be. In effect, the requirement that $Ef(z)=0$ for a range of α's implies that $f(z)=0$. For, by (1), $\exp(\alpha+\beta)\,Ef(z)$ is a power series in $(\alpha+\beta)$ with coefficients $f(n)/n!$, $n=0, 1, 2, \ldots$. Since a power series in a variable t which vanishes for all values of t in an interval must have all its terms identically zero, $f(z)=0$ for all integers z.

It may be of interest to note (as is known) that the above estimates are maximum-likelihood estimates. That is, the *a priori* probability of z occurrences, (1), considered as a function of α, is a maximum when $\alpha=\alpha^*$; and the *a priori* probability of z occurrences, considered as a function of $\sigma^2=\alpha+\beta$, is a maximum when $\sigma^2=s^2$.

---

* Partially supported by the joint program of the ONR and the AEC.

[1] A. H. Benade and R. D. Sard, to be published.

[2] L. Janossy, *Cosmic Rays* (Oxford University Press, London, 1948), p. 368.

[3] J. L. Doob, Trans. Am. Math. Soc. 36, 764 (1934).

An Instrument for Measuring Curvature of Cloud-Chamber Tracks

E. R. GAERTTNER AND M. L. YEATER
Research Laboratory, General Electric Company, Schenectady, New York

May 5, 1949

WHEN large numbers of cloud-chamber tracks are analyzed, it is desirable to use mechanical aids for improving the speed and accuracy of the measurements. The instrument described here for measurement of curvature is an adaptation of the familiar three-point method. It is made in such a way that the three points are adjusted independently to the curve. After each point is adjusted it is locked, so that the fitting is direct and positive. The sagitta is measured with the instrument, and the radius of curvature is read from a calibration curve for the chord length used. The sagitta is read from a precision micrometer scale. Our experience indicates that the tracks of small curvature can be

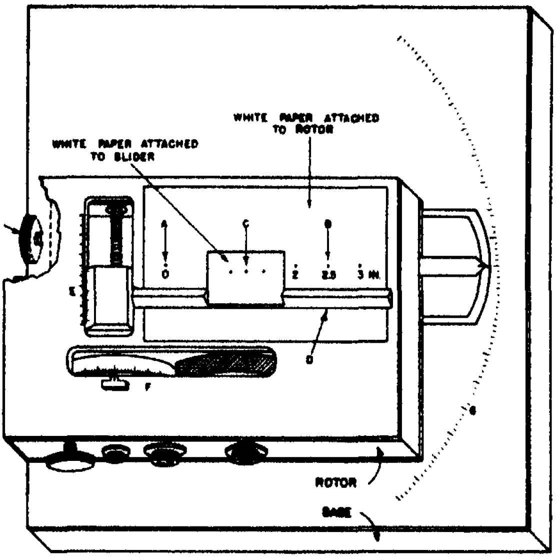

FIG. 1. Instrument for measuring curvature of cloud-chamber tracks.

measured in this way more rapidly and with greater precision than by the procedure of comparing the track image with arcs drawn on a card.

A sketch of the instrument is shown in Fig. 1. The operation is as follows. The image of the track is projected on the top surface from a fixed projector. The whole instrument is moved, sliding on a plate glass surface, until the terminal point *A* intersects the track near one end. The base of the instrument is then locked to the plate glass by partial evacuation of the hollow underside. This fixes point *A*. The upper part of the instrument is rotated about point *A* until one of the points *B* (at chord lengths 2, 2.5, or 3 inches) intersects the track. The thumb screw *T* is used to lock the rotor in this position, fixing point *B*. The appropriate center point *C* is then adjusted to the apex of the track. This point is carried on an arm *D* which is moved by a precision screw. The screw can be rotated at two speeds, for coarse and fine adjustment. The first decimal of the sagitta is read from the vernier scale *E*, and the others are read from the micrometer scale *F*.

The surface on which the tracks are projected is made of white paper. The points *A* and *B* are tiny holes made by pricking the paper with a sharp needle. The resulting dots are smaller than the average droplet in the tracks. The center points *C* are made in a similar way on white paper which is fastened to the arm *D*.

When experimental conditions are adjusted so that multiple scattering[1] is negligible, the width and density of the cloud-chamber tracks are the chief limitations on the accuracy of measurements made with this instrument. The scale can be read to 0.0005 inch, and the dots can be adjusted to the curve to an accuracy of 0.001 inch. The latter number has been estimated from repeated measurements of a straight line. The average error in sagitta for 166 typical electron tracks of various energies, measured by two observers, has been found to be 0.0023 inch; this is for sagittas ranging from 0.025 inch to 0.300 inch, with an average value of 0.079 inch, and for an average chord length of 2.5 inches. Measurements of electron tracks by two observers indicate an accuracy of about 5 percent for tracks of 50-Mev electrons curved in a field of 4000 gauss.

The rotational degree of freedom about the point *A* makes the instrument useful for angle measurement; e.g., the horizontal projection of the angle which a curved track makes with a lamina in the cloud chamber. This measurement is made after the sagitta has been obtained. With the point *C* adjusted to the sagitta of the track, the base is moved so that the points *B* and *C* are again on the curve and *A* is on the lamina. This puts *A* at the intersection of track and lamina even if the track is not visible at the lamina. The angle between the lamina and the chord is then measured directly on the angular scale *G*. The angle between the lamina and the tangent to the track is obtained from this angle and the angle between the chord and the tangent. The latter is derived from the measurement of the sagitta.

---

[1] Compare H. A. Bethe, Phys. Rev. 70, 821 (1946).

Cadmium Trap for Arresting Mercury Vapor

T. WILNER
Thaliavägen 38, Bromma, Sweden

May 9, 1949

FOR vapor traps in connection with producing high vacua the use of liquid air cooling, or alkali metal traps, is sometimes a bit inconvenient. It is here suggested to substitute *cadmium* for the alkali metal, thus doing away with the disturbances owing to oxidation. In Fig. 1 a simple cadmium trap is shown which has been successfully tried. The "pump tube" is a thin-walled steel tube having an O.D. of 1 inch. It acts as a small electric furnace having water-cooled end portions. It is charged with a small steel receptacle containing a few grams of granulated cadmium. In the experiments the temperature has been kept at 300–400°C; it is conceivable, however, that lower temperature may be used. At the cooled portions there will form condensation zones where small cadmium crystals will be deposited. In condensing, the cadmium will alloy itself with the mercury vapor present, forming cadmium amalgam, the vapor pressure of which is very small. It is possible that the trap will, to an extent, act as a getter for other matter than mercury. It should be a relatively simple matter to produce a simple pump provided with diffusion jet of a type suitable for operating with cadmium vapor; such development has, however, not yet been attempted.

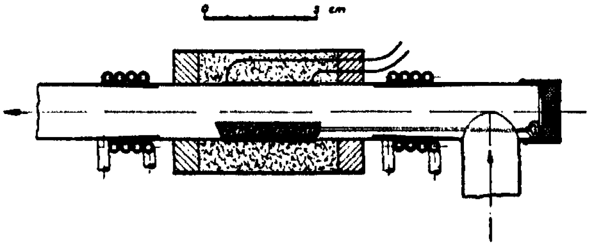

FIG. 1.

A Device to Deposit Automatically the Proper Thickness of Metals Used in Shadow-Casting in Electron Microscopy*

FRANCIS W. BISHOP
Department of Radiation Biology, The University of Rochester, School of Medicine and Dentistry, Rochester, New York

May 2, 1949

WHILE image contrast in the optical microscope may be brought about by differential absorption of the light passing through the object, in the electron microscope it is due to an unequal amount of electron scattering in the various parts of the specimen.

If the object to be examined in the electron microscope is very thin or is made up of such light atoms that its scattering power is not greatly different from that of the supporting membrane or film, the contrast may be so slight that details are not visible.

In such cases shadow-casting of the specimen may well be applied. This technique has been in use for a number of years and has attained a high degree of usefulness.[1, 2] It consists essentially in depositing a thin coating of a heavy metal upon the specimen at an angle so that the metal piles up on exposed surfaces and is not laid down in areas sheltered by elevated portions of the specimen. The shielded areas in the shadow of the specimen retain their transparency to the electron beam while portions covered by the metal are rendered more opaque. The end result is an increase in contrast over the unshadowed specimen. It has been stated that objects too small to be directly resolved by the electron microscope can be made to cast a shadow by the proper technique and thus be detected. In any event, the shadow-casting procedure is a very important adjunct to electron microscope technique.

It is difficult to achieve uniform results with the shadowing unless great care is taken to maintain such factors as distance from the source, amount of metal, evaporating temperature, etc. Visual inspection may be helpful in judging the deposit in the case of certain metals such as gold, but with others, for example uranium, the coating may be invisible.

It was decided to try to construct an apparatus which, by means of resistance-measuring detecting-device mounted in the vacuum jar, would cause a suitable meter to deflect in proportion to the thickness and kind of metal used and also to shut off the current in the evaporating filament when the proper coating was attained (Fig. 1).

Accordingly, an electronic circuit was arranged (Fig. 2) whereby a lowering of the resistance at the detector increased the negative bias of a 6SJ7 and thus decreased the deflection of a meter in the cathode circuit. A selector switch makes it possible to transfer to the grid of a 6J5, voltages from a series of resistors in the cathode circuit of the 6SJ7. A 14,000 ohm relay is placed in the plate circuit of the 6J5 and is normally energized. When the plate current of this tube drops to a value of 2 Ma, the plate relay falls out and energizes a secondary heavy-current relay which in turn interrupts the circuit to the evaporator. The unit is fed from a small power pack which delivers approximately 160 volts d.c.

In use the meter is adjusted to full scale deflection by control R4 before evaporation is started. The point at which the 6J5 relay drops out for any scale selected is set by the individual controls R1, R2, or R3. Point 4 on the switch is for the manual operation of evaporation and while the meter deflects the proportion to the resistance of the metal coating, the 6J5 relay does not operate to automatically cut off the evaporating current.

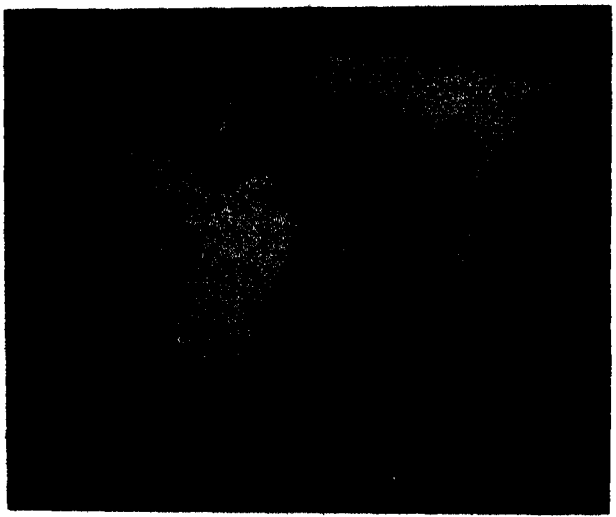

FIG. 1.

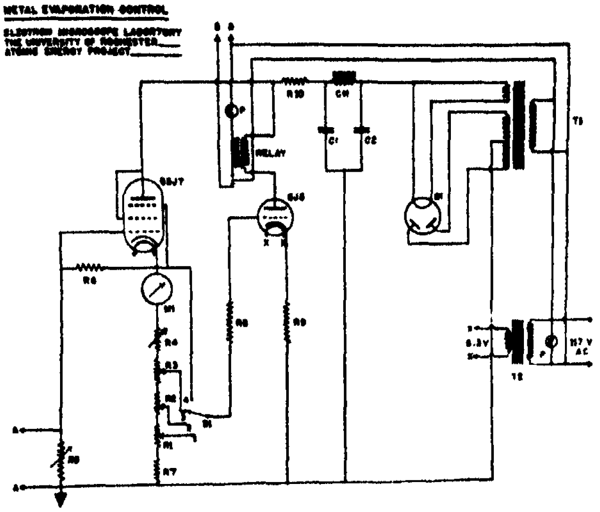

FIG. 2.

R1	10,000-ohm potentiometer
R2	15,000-ohm potentiometer
R3	100,000-ohm potentiometer
R4	150,000-ohm potentiometer
R5	2-megohm potentiometer
R6	75-ohm ½ W.
R7	5000-ohm ½ W.
R8	1.5 megohm
R9	5000-ohm ½ W.
R10	5000-ohm 1 W.
C1	8 μfd
C2	8 μfd
S1	4-point Yaxley switch
P	Pilot light 110 V.
M1	Meter 0–500 microamperes
AA	To detector
BB	To secondary relay coil
T1	Transformer, Stancor P-6149, primary 115 V. Secondaries (1) 100 V. 150 MA. DC. (2) 5 V. 3 A.
T2	Transformer, Stancor P-6134 primary 115 V. Secondary 6.3 V. 2 A.
CH	Choke, Thordarson T-20C52, 8 H 40 MA.

It should be noted that with metals which evaporate very easily, if the temperature of the filament is excessive, considerable evaporation may take place after the filament is turned off and is in the process of cooling. Overshooting of this kind may be minimized by watching the deflection of the meter and controlling the evaporation current accordingly.

The detecting element consists of a burned out filament mount from the RCA electron microscope. These mounts usually have little value around the laboratory; in this case, however, they are able to serve a useful purpose. The short, heavy leads to the filament are cut off leaving the two insulated metal strips which are exposed to the metal vapor during evaporation. It was found that the evaporated film did not make adequate contact with these raised metal strips so that a small amount of Aquadag was used to coat them and also a portion of the mica disk on which they are mounted. This provides an adequate contact area upon which the evaporated metal may fall and bridge the gap between the electrodes so formed.

The detector plugs into an appropriate socket and, incidentally, shields it from the metal vapor. The socket should, of course, be covered at all times when evaporation of conductive materials is done.

Usually a supply of burned out filaments becomes available in time, and while these make a convenient and quickly interchangeable unit, many other arrangements are possible.

A new element must be employed each time evaporation is done, but in case of necessity they can be cleaned and reused.

The resistors associated with taps 1, 2, and 3 on the selector switch are adjusted by trial so that with a given metal, a light, medium, or heavy deposit respectively is obtained. They may also be set to provide the optimum coat of different materials if

FIG. 3.

desired. Usually, however, in the various laboratories one particular metal is preferred so that with this device there is a choice of three degrees of thickness of metal deposit as well as the manual control. Most metal films remain stable, but it was observed that with uranium any exposure to air resulted in an instant conversion to uranium oxide. This may occur slowly in the vacuum system if there should be a small leak. Uranium-shadowed specimens are therefore not coated with the metal but with an oxide. This may account for their great stability in the electron microscope. The resistance of a fresh deposit of the metal on our electrodes is of the order of 15,000 ohms but rises to hundreds of megohms when exposed to air.

A two-megohm potentiometer has been placed across the detector leads in order to simulate the effect of a metal deposit on the detector and through its use, the relay may be set to operate at any desired deflection of the meter. It also provides a rapid method of checking the operation of the device. When not in use, it is set at maximum resistance.

It is now no longer necessary to wonder if or how much evaporation is occurring when the filament is heated for degassing, etc. The moment any deposit of metal of any consequence takes place, a deflection is seen on the meter.

The position of the detector is fixed in relation to the filament and the specimen is also placed at a convenient constant distance (Fig. 3). The detector may be located at any point in the bell jar which is not obstructed by equipment.

A device which automatically deposits with a proper thickness of metal used in the shadow-casting technique in electron microscopy has been described. It has eliminated the guess work from this technique and has produced reliable and consistent results.

A Technique for the Production of Silica-Filmed Electron Microscope Screens in Quantity*

FRANCIS W. BISHOP
Department of Radiation Biology, The University of Rochester, School of Medicine and Dentistry, Rochester, New York

May 2, 1949

MANY laboratories have experienced difficulties in maintaining the integrity of collodion or other plastic films which are used as a specimen support in the electron microscope. Films of oxides of metal and films of silicon dioxide and silicon monoxide have been found to be much more resistant to the heating and other effects of the electron bombardment, but their preparation and mounting on the screen have been difficult.

A number of different methods have been used in the preparation of the collodion films. In most of these a drop of collodion in a suitable solvent, usually amyl acetate, is allowed to fall upon the surface of clean distilled water; the drop spreads, the solvent evaporates leaving a thin film of collodion.

Several possible techniques may be used to transfer this film to the supporting screen. In some laboratories a number of screens are placed on the top of the floating film and, by means of a loop, a section of the film containing the screen is lifted from the water, inverted, and allowed to dry on a suitable peg. Other laboratories may hold the specimen screen in a forceps and, by dipping under the film, are able to pick up a suitable section.

In this laboratory and others it has been the custom to submerge a glass slide carrying a number of screens in a dish, form the film in the usual way, and then to pipette off the water allowing the film to settle on the screen and slide as the tide goes out.

It seemed desirable to develop an apparatus which would simplify the production of the collodion-filmed screens and at the same time be adaptable to the technique of making silica films which has been in use in this laboratory for some time.

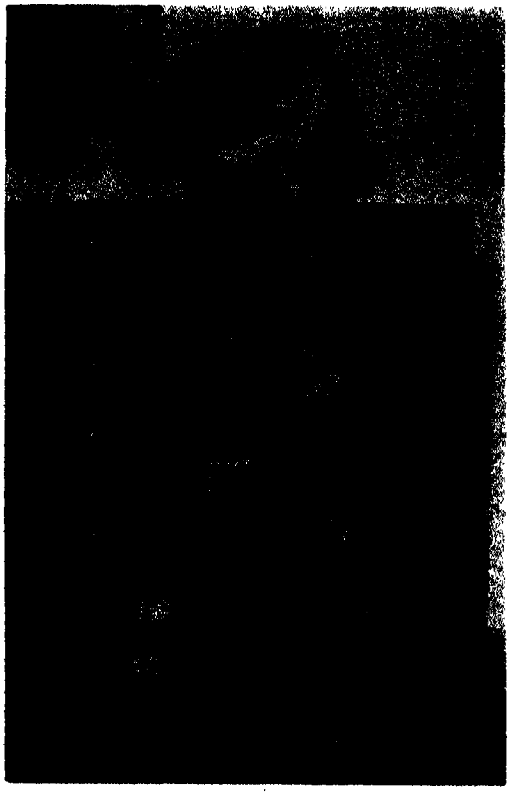

FIG. 1.

---

* This paper is based on work performed under contract with the U. S. AEC at The University of Rochester Atomic Energy Project, Rochester, New York.

[1] R. C. Williams and R. W. G. Wyckoff, J. App. Phys. 15, 712 (1944).

[2] Robley C. Williams and Ralpha W. G. Wyckoff, J. App. Phys. 17, 23 (1946).

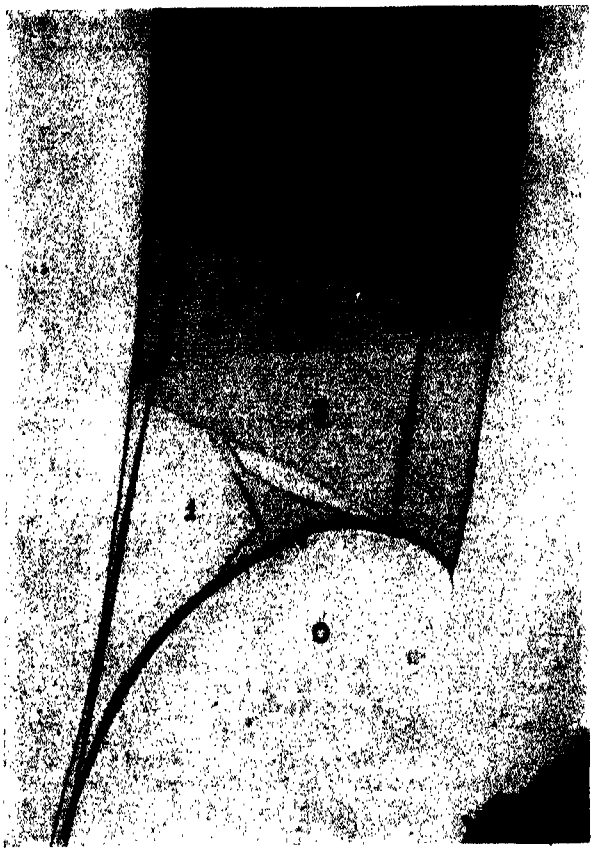

FIG. 2. Transmission of the electron beam through various thicknesses of the folded collodion-silica film. Factors: Magnification 9600×, 50 K V. Objective aperture used, contrast lantern slide plate. Printed on Haloid F-1 paper.

Since we had a distilled water line in the specimen preparation room and a convenient drain line beneath the bench, it was decided to make a fixed installation. Accordingly, a four-inch Pyrex funnel was fitted with a *T* connection and a stopcock as shown in Fig. 1. This funnel will accommodate glass slides of various sizes. The funnel is filled as necessary through the *T* which is connected to the distilled water supply by means of a short length of Tygon tubing and a valve.

In use, a clean glass slide is placed horizontally in the funnel and distilled water admitted until the slide is covered by about ¼-inch of the water. A number of specimen screens are then placed on the slide and a film of collodion is made in the usual way. The funnel is then emptied directly into the drain through the stopcock. The film is allowed to dry *in situ*. The screens are then ready to receive a specimen and upon drying may be placed in the microscope or they may be shadow cast on the slide without being disturbed. The collodion film as it is wrapped around the slide is usually sufficient to hold the specimen screens in place. When not in use, a glass cover protects the device and cleaning is simple. If a source of distilled water is not available in the room, a large bottle may be used to feed the funnel by gravity with another below for drainage.

We have largely discarded the collodion film as a specimen support in this laboratory and have adopted silica, and the device described is extremely useful in a major step in the preparation of silica films. As a preliminary step, the usual two percent collodion solution is further diluted to a point which will just produce consistent films (cir. 0.2 percent). A number of screens are coated in the manner previously described. The resultant film, while too weak to use as a specimen support, is sufficient to act as a temporary base upon which silica can be evaporated.

The silica is placed in a suitable cone-shaped filament of 20-mil tungsten wire and evaporated normal to the surface upon the slide holding the desired number of collodion-filmed screens. Experience is the best guide in determining the amount of silica to be evaporated to produce a strong but transparent film. Specimens are mounted in the collodion-silica-filmed screens in the usual manner and may be shadow-cast if desired.

The films thus formed are rugged and structureless. They may be so transparent that unless a specimen is on the screen, it may be difficult to be sure that a film is actually present. Figure 2 shows a film deliberately broken by scratching with a needle which shows the transmission of the beam through up to 4 thicknesses of the film. No trace of the thin sub-film of collodion can be seen. The silica films may be used in cases where the specimens are contained in solvents which would destroy collodion or Formvar films and where cells in tissue culture are grown directly on the specimen screen, the silica screens may be sterilized by heat or chemical means. The technique makes it possible to prepare the specimen screens easily and in quantity with all of the advantages of silica and without the shortcomings of collodion or Formvar.

A simple device and a technique have been described which make the preparation of collodion-filmed specimen screens and silica-filmed screens for the electron microscope both very convenient and rapid.

** This paper is based on work performed under contract with the U. S. AEC at The University of Rochester Atomic Energy Project, Rochester, New York.

A Pantograph and Tilting Stage for Use with Nuclear Plates*

IAN BARBOUR
University of Chicago, Chicago, Illinois

May 9, 1949

TECHNIQUES using nuclear emulsions have been assuming increasing prominence recently in the study of cosmic-ray and accelerator phenomena. The two attachments described here have been found useful in the microscopic analysis of such plates. In Fig. 1, the "short arm" of a pantograph which we have constructed is seen attached to the moving stage of a leitz microscope at (A). The "fixed point" (B) is rigidly connected to the table, so the "long arm" with its magnetically operated pen (C) traces the motion of the microscope stage with a magnification of 20. When each event is brought into focus at the microscope eyepiece cross-hair, the switch (D) in the pen magnet circuit is closed, leaving

FIG. 1. Pantograph attached to microscope stage.

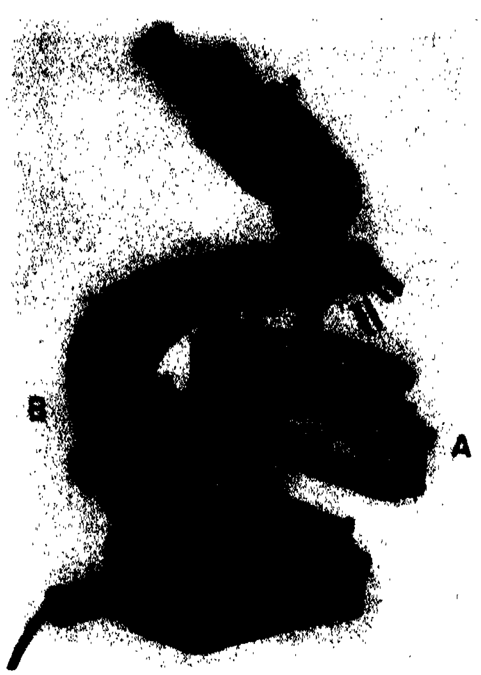

FIG. 2. Microscope with tilting stage.

a dot on the graph paper which can be numbered for identification. Thus a permanent plot of the location of events on the plate is obtained. By using precision ball-bearings at all points of motion of the pantograph members, a ball-point support on the paper, and a counter-weight to relieve the frictional load (the wire can be seen above the pen, passing up to pulleys on the ceiling of the room), the precision in locating points in one region of the plate is about 20 microns, and about 75 microns in comparing points of wide separation. We have found this pantograph useful in tracing meson tracks from one plate to another, particularly in connection with magnetic deflection experiments. In this case the events are located relative to a grid of x-ray dots obtained by exposing a stack or sandwich of plates to an x-ray beam through a Pb plate containing pin-point holes. The "azimuth" angle of the tracks is read off to within ¼° with the eye-piece protractor, seen at (E).

Figure 2 shows the tilting stage for viewing tracks which dip into the emulsion. The original controls for moving the plate in the plane of the stage, as well as the bearing for rotation about a vertical axis, which are standard parts of this Zeiss microscope, have been retained. An additional rotation about a horizontal axis is obtained by the brass arms and bearing (A) on either side, which are accurately machined with no free motion. The microscope has an adjustment screw for moving the objective lens system toward or away from the observer, so the optical axis can be made to pass through the axis of tilt. The tilt angle is controlled and measured to within 5 min. by a divided-head screw and graduated scale (B). The objective and condenser used in these experiments have lens-mount dimensions and working distances which allow a maximum tilt angle at optimum illumination of about 11° with Ilford and Kodak plates. Allowing for shrinkage of emulsion on development, this means that tracks which passed through the plate at angles of up to 26° with the emulsion surface can be brought into the focal plane of the lens. Using above and below the plate an oil of refractive index essentially equal to that of the plate itself, there is no change of illumination upon tilting the plate. Accurate measurements of the "dip" angle facilitates matching track segments due to the same particle in different plates. The tilting stage is also of great value in photographing tracks. Figure 3a shows a conventional photomicrograph of a track whose original dip angle was about 23°. With only a small portion of the track in focus, a mosaic of at least 5 exposures would be required to reproduce this one field of view. In b, after the stage is tilted by 9½°, the same track is in good focus throughout the field of view (100 microns).

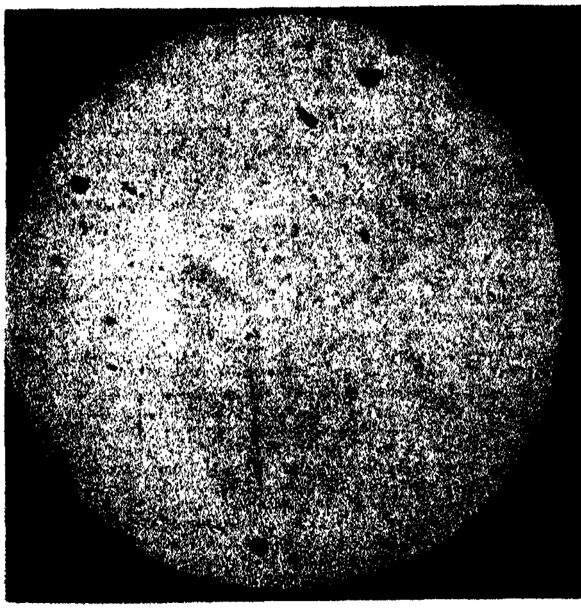

FIG. 3a. Photomicrograph of track which passed through emulsion at angle of 23° with its surface.

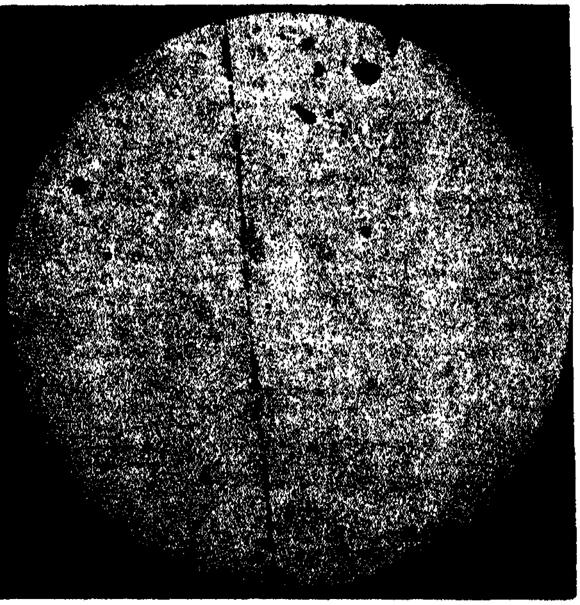

FIG. 3b. Same after stage is tilted.

---

* Assisted by the joint program of the ONR and the AEC.

A Simple Punch for Precision Cutting of Photographic Film in a Cylindrical X-Ray Diffraction Camera

E. J. Grill and A. H. Weber
Saint Louis University, St. Louis, Missouri

April 25, 1949

FIGURE 1 shows a cutter for punching the holes for entrance and exit port assemblies in the photographic film of a standard 114.6 mm diameter cylindrical x-ray powder camera.

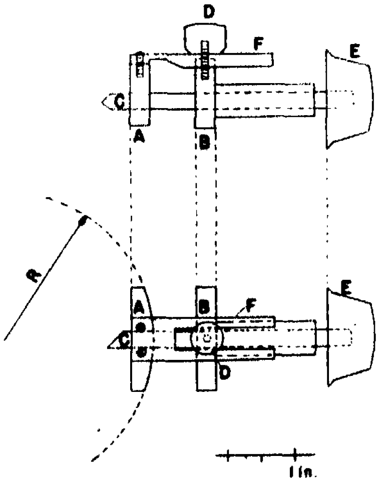

Fig. 1. X-ray diffraction camera film punch. Upper, side view; lower, plan view. *A*, inner guide plate; *B*, outer guide plate; *C*, cutter-plunger; *D*, locking nut; *E*, Bakelite knob; *F*, spacing bar.

The feature of the device is accurate hole cutting with the photographic film in place in the diffraction camera. Once the circular port holes are cut the film is not removed from the camera until it is ready for photographic processing.

In use the x-ray film, cut to proper length and width on a trimming board, is inserted in the film holder of the powder camera from which the exit and entrance tubes have been removed. With the cutter-plunger *C* (Fig. 1) withdrawn so that its cutting end is within the sleeve section of *B*, the inner guide plate *A* is placed against the photographic film (camera cover off) in the vicinity of a camera port. Nut *D* is loosened and the outer guide plate *B* is moved toward *A* to make contact with the projecting camera port; knob *E* is moved with a slow twisting motion so that the cutting end *C* hunts and finds the port hole; nut *D* is tightened lightly; cutting end *C* is advanced against the film and is made to cut through the film by carefully twisting *E* (if care is observed the cutting of the film is an easy smooth operation involving no jolting punch-through of the cutting edge; usually the circular cut-out drops into the hole in *A* and is removed along with the cutting tool).

The cutter is easy to use and results in excellent fitting of the photographic film in the camera. The curvature of *A* can be adjusted obviously to any camera radius.

A Magnetic Beam-Splitting Focusing Device for the Electron Microscope

Francis W. Bishop
Department of Radiation Biology, University of Rochester, School of Medicine and Dentistry, Rochester, New York

May 3, 1949

ELECTROSTATIC beam-splitting devices for use on the electron microscope have been built by RCA and others. They consist principally of two pairs of deflecting plates arranged one above the other and connected to a square wave voltage generator. This square voltage wave applied to the plates causes the electron beam to shift so that it enters the specimen at a slightly different angle than normally. During the zero interval, the beam passes through the specimen in the usual manner. Effectively the beam is split into two components which, if the instrument is not correctly focused, results in two separated images of the specimen. When exact focus is achieved, two images move into coincidence. The effect is similar to that of a range finder of a camera.

Fig. 1.

This method seems to be quite satisfactory in most respects. It has the disadvantage that a new specimen door has to be constructed, since the supply to the plates is commonly brought into the apparatus through the door and it makes impossible the use of the stereoscopic device at the time the beam splitter is in operation.

At the Toronto meeting of the Electorn Microscope Society of America a casual mention was made of the fact that on one of the European microscopes the same effect was achieved magnetically. No details were given.

In view of the apparent simplicity of the idea, it was decided to try this method on our microscope. A pair of relay coils having an ohmic resistance of 2200 ohms each was found in the laboratory. These were connected in series and mounted externally on diametrically opposite sides of the specimen chamber and one was displaced vertically about ¼ inch. As viewed from the inside of the microscope, the polarities should be the same (Fig. 1).

A square wave generator was constructed which was capable of furnishing a current of about 10 milliamperes through the coils at 114 volts (Fig. 2). This unit furnishes a very satisfactory square wave when connected to a non-inductive load of 4400 ohms, but of course the wave shape is modified when fed to an inductive load such as the coils. A small selenium half-wave rectifier was connected in reverse across the coils in order to short circuit a

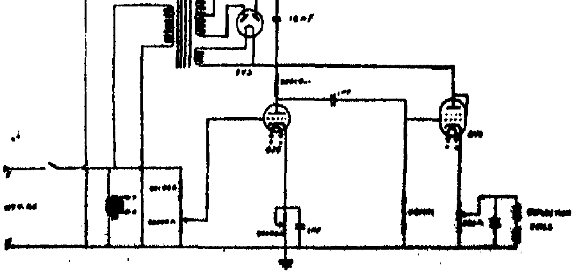

Fig. 2. Square wave generator for magnetic beam-splitting device. Radiation Mechanics Laboratory, The University of Rochester (AEC).

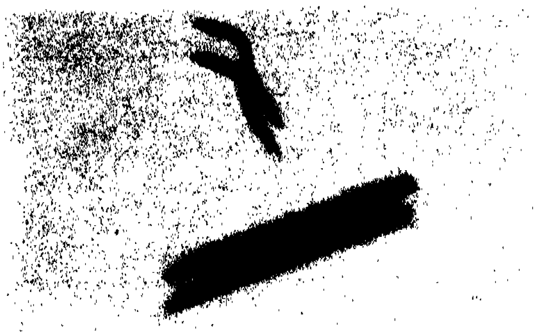

FIG. 3.

a small inverse voltage which appeared without it. The current appeared to be sufficiently constant over the period of time necessary to give a sharp image with the deflected electron beam so that it was decided to try the device even though the wave form deviated slightly from the ideal condition.

During the half-cycle that the output voltage of the generator is zero, the electron beam is undisturbed. During the remaining half-cycle, the beam is deflected by the upper coil and returned to the axis by the second coil. It is important that the deflected and undeflected beams strike the specimen at the same point. This condition is met by adjustments of the position of the deflecting coils. In practice, the double image is more easily seen if the condenser lens current is set at a value different from that required for maximum illumination of the viewing screen. If the condenser is set at cross-over, very exact alignment of the microscope and focusing device is necessary. Since we prefer voltage alignment of our instrument to magnetic alignment, and as these may not coincide, we always find it necessary to use the focusing device at a condition other than cross-over.

After focus is obtained, the voltage supply to the deflecting coils is turned off before actual photographic exposure is made, as any fluctuations in output of the square wave generator might affect the stability of the image during exposure. In practice it is definitely easier to note a change in the image sharpness when the objective current is varied with the beam-splitter than without it. More experience with it will determine its ultimate value.

Figure 3 shows an out-of-focus image with the beam-splitter on. The objective control is set so far off from exact focus that the images are completely separated. Without changing the focus, the beam-splitter is turned off in Fig. 4. Now the image appears to be comparatively sharp although the focus is as inexact as before. In other words, a given degree of unsharpness due to improper setting of objective current is more easily noticed through use of the beam-splitter.

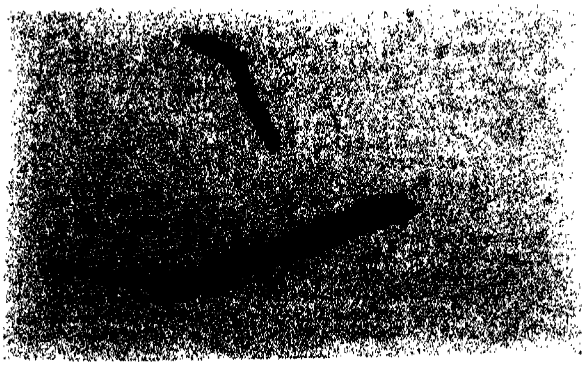

FIG. 4.

An experimental magnetic beam-splitting device has been described which, it is hoped, may prove of interest to operators of the electron microscope.

* This paper is based on work performed under contract with the U. S. AEC at the University of Rochester Atomic Energy Project, Rochester, New York.

Vibration Detection by a Quartz Oscillator

Y. L. Yousef and F. Sultan
Faculty of Science, Fouad I University, Cairo, Egypt

February 25, 1949

IN 1938, Bancroft and Jacobs,[1] in connection with elasticity measurement of thick metal rods, described a method for vibration detection employing the principle of the condenser microphone. The end of the rod is placed about 1/1000 of an inch from a capacity electrode connected to the grid of an impedance-matching valve coupled to a filter and an amplifier. No explicit mention of the sensitivity is made. Recently, Bordoni[2] used an electroacoustic method for elasticity investigations. It is reported that amplitudes as small as 0.1 A could be detected. However, a common objection to these methods is the very close proximity of the capacity electrode from the vibrating material, as this implies a considerable increase in the damping due to air and a consequent decrease in the natural frequency of vibration, especially when the vibrating material has a small inertia.

The present note outlines a method which derives its sensitivity from the comparatively large power output produced by the vibration rather than from the proximity of the capacity electrode or from the high gain of the amplifier, and is, moreover, applicable equally efficiently at infra-sonic as well as ultrasonic frequencies. It utilizes a well established phenomenon in a slightly detuned quartz crystal oscillator, namely, the rapid change of anode current with capacity. The vibrating material forms with a fixed electrode a small air condenser, which itself constitutes a part of the capacity of the tuned circuit. Under appropriate conditions, when the oscillator is working near the mid-point of the steep portion of the crevasse, the circuit is highly responsive to very minute capacity alterations, and is, at the same time, sufficiently stable, even if the slope, which may be partly controlled by the leak resistance between the crystal plates, is as high as 100 ma per micro-microfarad or even more. The small changes of capacity arising from the vibrations set up appreciable proportionate changes of anode current, which can be interpreted directly by a load as voltage variations, and may be amplified and measured on an oscillograph. The change in the load voltage corresponding to a change of 10^{-8} microfarad in the capacity is normally of the order of several volts.

With a 10-watt oscillator operating at a frequency of 8 Mc/sec., it is found that when the slope at the working region is 80 ma/micro-microfarad, the capacity between a test reed (frequency 45 c.p.s.) and the fixed electrode is 0.5 micro-microfarad for a separation of 0.5 cm, the load is 2000 ohms, the voltage amplification of the amplifier is 700 and the sensitivity of the oscillograph is 5 cm/volt, then an amplitude of about 10^{-5} cm will produce a fluorescent track of length 1 cm and can be measured to an accuracy of a few parts percent. It appears that an increase in the amplifier gain to 10^{-6} would probably enable an amplitude of the order of 10^{-9} cm to be detected.

[1] D. Bancroft, and R. Jacobs, Rev. Sc. Inst. 9, 279 (1938).
[2] P. G. Bordoni, Nuovo. Cimento 4, 177 (1947).

Lead Brick for Shielding

Luther E. Preuss
Edsel B. Ford Institute for Medical Research, Detroit, Michigan

April 28, 1949

SOLID lead bricks, 2"×4"×8" in size, are in common use for shielding purposes in many laboratories where radiation from radioactive sources must be reduced below the recommended limit of 0.1 *R* per day. The ordinary bricks, however, suffer from certain deficiencies. They are liable to tip when stacked to an appreciable height and fissures develop between them after brief usage, even with carefully machined bricks. Interlocking lead bricks of tongue and groove design which are made with a minimum of expensive processing have been developed at this laboratory to overcome these difficulties.

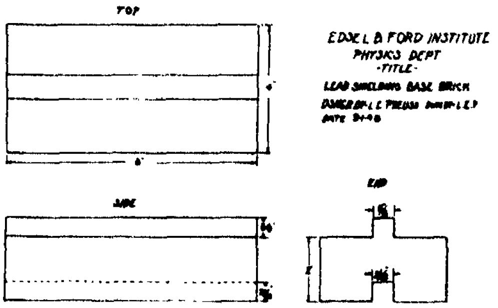

FIG. 1.

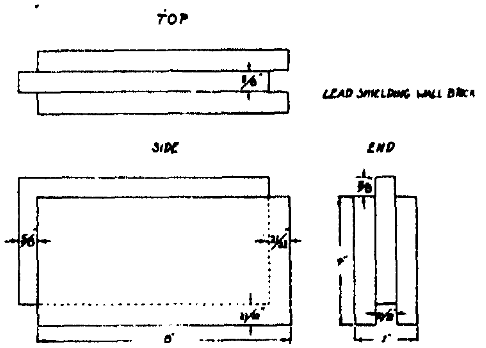

FIG. 2.

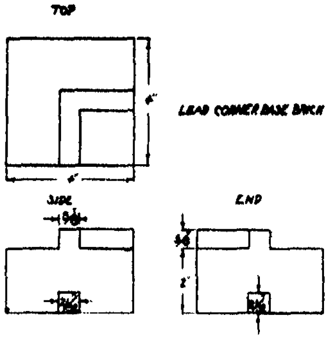

FIG. 3.

Preliminary work indicates that these bricks are useful and superior to the non-interlocking design. They are easy to stack, have no tendency to tip over, are positioned safely on the apron of a hood for radioactive work, and because of the design it is not possible for fissures to develop between them, through which dangerous dosages can escape.

Figures 1–4 show dimensioned, working drawings of the four types which are used. In Fig. 1 the base brick is shown, in Fig. 2 the wall brick and in Figs. 3 and 4 the corner-base and corner-wall bricks, respectively.

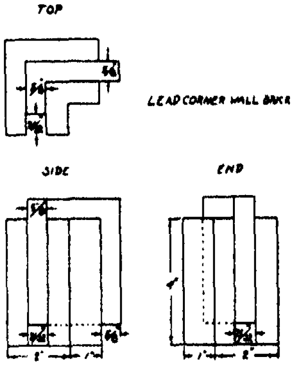

FIG. 4.

The same design could obviously be applied to bricks of iron or other material if such were necessary or practical from either an experimental or economical viewpoint.

New Instruments

W. A. Wildhack: Associate Editor
in Charge of this Section
National Bureau of Standards, Washington, D. C.

These descriptions are based on information supplied by the manufacturer and in some cases from independent sources. THE REVIEW *assumes no responsibility for their correctness.*

Phase-Contrast Microscope

A phase-contrast microscope of a totally new design, developed by Officine Galileo, Italy, a 68-year old scientific optical firm, is now available on the American market.

The revolutionary features of the instrument are: an auxiliary lens built in the microscope tube, replacing the ordinary telescope attachment used for centering the phase ring; a pancratic substage which provides for an annular source of variable diameter to match any phase ring and any condition illumination; and a built-in source of light for visual observation. These improvements open new possibilities to the phase technique of observation and simplify operations considerably. The usual tedious procedure of interchanging from eyepiece to telescope and then back from telescope to eyepiece or to the photographic camera, an ordeal often repeated when observing living preparations, is completely eliminated. By switching the auxiliary lens in and out, the alternate checking of field and illumination can be repeated at will and at any time without touching the set-up for visual, photographic or moving-picture record.

The pancratic condenser makes it possible to switch over instantly from normal bright field technique to phase contrast and from phase contrast to classical dark field ultramicroscopy. The association of these techniques during a single observation is achieved completely for the first time and is of invaluable help.

The pancratic condenser gives a light ring which matches all phase rings, so that any phase objective of any power—and of different makes or design—can be used on the microscope without special adjustment. This character of interchangeability will be heartily welcomed by workers in the field. Also, the flexibility in the working of the substage makes it possible to use low-power condensers for phase-contrast observation of living tissues or cultures prepared on thick cavity slides.

Finally, the new substage provides for a very efficient exploitation of the light flux from the source, so that the specimen is always invested by the minimum amount of radiant energy necessary for comfortable observation at any magnification and aperture, which is no mean advantage when making observation on living matter.

The Galileo Corporation of America has appointed as its sole agent: PFALTZ & BAUER, INC., *Empire State Building, New York 1, New York.*

Raychronometer

The Raychronometer is an automatic beta- and gamma-ray scaling instrument which includes the following major components: Geiger tube voltage supply, counting circuits, computer, Geiger tube fuse, counting rate meter, and control circuits. Several of these components include newly developed features which lead to an instrument of very reliable and simple operation.

The voltage supply may be operated as a conventional, regulated, variable power supply (500 to 2500 volts) or as a pulse-amplitude, regulated power supply. When operated as the latter, the voltage supplied to the Geiger tube is forced, within reasonable limits, to assume the value necessary for the production of pulses of a constant and selected amplitude. The Raychronometer contains a pulse-amplitude regulator circuit to accomplish this purpose. The pulse-amplitude control is variable over the ranges encountered in conventional Geiger tubes.

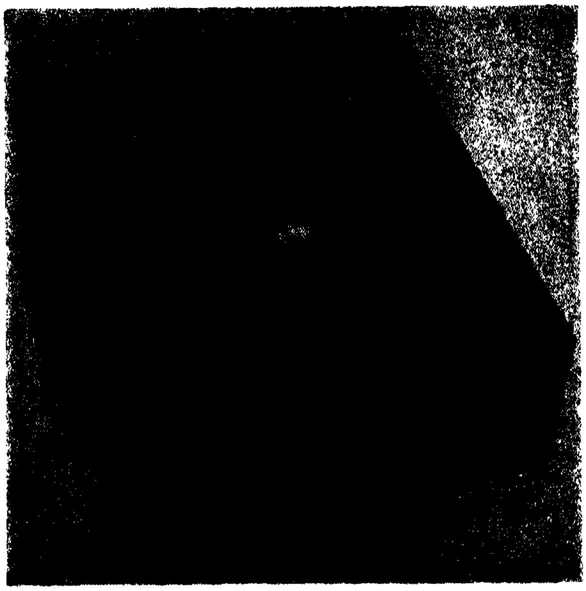

The manner of operation of this circuit is such as to eliminate the necessity for day-to-day adjustments of the Geiger tube voltage. When the instrument is turned on, the Geiger tube voltage will gradually rise to the value necessary for operation at the initially chosen point.

The counting system consists of an electronic scale of 100 followed by two decades of electromechanical scales. Neon interpolation bulbs indicate the progression of counting of these scales.

Incorporated in the Raychronometer is a computer which, in essence, multiplies a constant (the number of counts) by the reciprocal of time (from a synchronous motor) to furnish directly the counting rate with a selected precision. The standard deviation of the measurement may be selected to be 10, 6, 3, 2, or 1 percent. This determines that the number of counts which will be collected is 100; 300; 1000; 3000; or 10,000, respectively.

At the moment the counting process is initiated, a synchronous motor begins the generation of the time function. The error of the computed rate is smaller than 1 percent for any measurement requiring one minute or longer.

Additional features of the Raychronometer include connections from the counting rate meter suitable for driving an Esterline-Angus 1 ma. recording meter, an oscilloscope connector for pulse monitoring, and a separate on-off switch for the Geiger tube voltage supply.

A total of 24 tubes, exclusive of the Geiger tube, are employed. The Geiger tube is not supplied with the instrument.—RADIOACTIVE PRODUCTS, INC., *3201 East Woodbridge Street, Detroit 7, Michigan.*

Portable Scaling-Type Radioactivity Detector

The Nuclear Development Laboratory is presenting for the first time a low-cost, midget, portable Radioactivity Detector which has an accuracy and sensitivity normally obtained only in elaborate and high-priced laboratory type instruments. The development of this new radiation detector (Model PRD1) has been made possible by the invention of a remarkably compact electronic scaling circuit, which is used to automatically add up pulses from a large beta and gamma-ray sensitive Geiger-Mueller counter tube.

The maximum sensitivity of this instrument is limited mainly by the time for which measurements are made, as the accuracy of any one reading is dependent upon the number of counts totalized. For example, under average background conditions, one milligram of radium (or equivalent) at a distance of 100 feet will raise the counting rate of this instrument by 10 percent, and sufficient accuracy to verify this increase may be obtained in a five-minute reading.

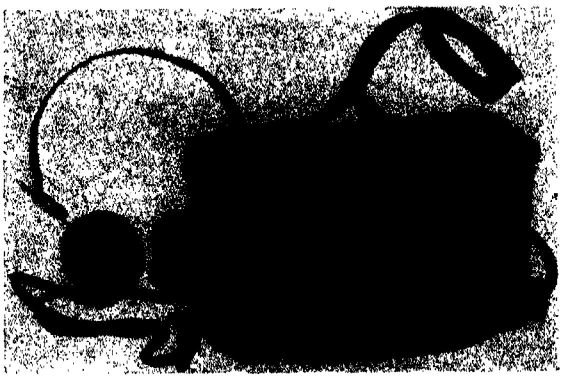

The maximum radiation intensity accurately covered by this instrument is limited by the scaling ratio (25:1) to about 5000 counts per minute. However, where required, this may be easily raised by a factor of 10 or more for applications involving highly radioactive monitoring.

The Nuclear Development Laboratory believes that the outstanding versatility and low price ($79.50) of the Model PRD1 Radioactivity Detector represents a great stride forward in the direction of satisfying the "Atomic Age" requirements for a popular-priced personal radioactivity detector.—NUCLEAR DEVELOPMENT LABORATORY, *Post Office Box 7601, Kansas City, Missouri.*

Geiger Counter for Prospecting

This new Geiger counter employs a 900-volt plug-in type Geiger tube with a 30 mg/cm^2 thin window section, which makes possible the detection of beta-particles as low as 160 kev, as well as gamma-rays. This greatly increases the sensitivity of the instrument, making it equal in sensitivity to the most elaborate and costly type of laboratory equipment.

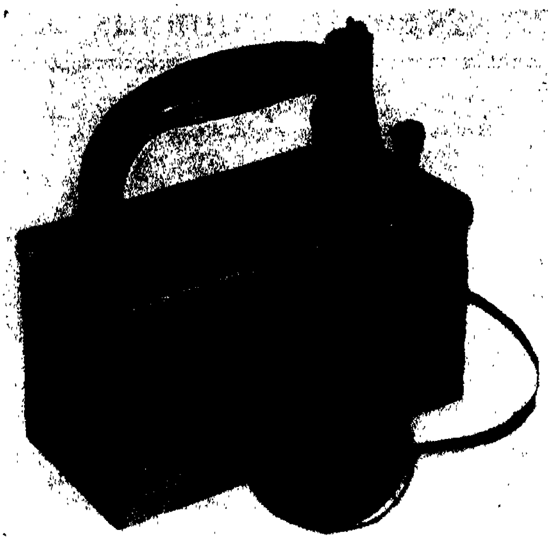

It is suitable for laboratory work where auditory monitoring is used but is designed primarily for field use in locating radioactive ores, where extreme light weight and small size are important. It can be carried on the belt or by its handle.

The weight is approximately 2 lbs. complete, including battery, and the size is only 2¾ in.×3¼ in.×6 in. The large sensitive Geiger tube is enclosed within the case, thus eliminating the need for a probe and cable.

Only one battery is used, which is easily replaceable. The life is its shelf-life of one year with normal use. The life of the Geiger tube is more than one hundred million counts. A crystal earphone and battery are included in the low price of $75.00. It is complete and ready to use.—PRECISION RADIATION INSTRUMENTS, INC., *1101 North Paulina Street, Chicago 22, Illinois.*

Wave-Guide Windows

Glass wave-guide windows, scientifically designed to permit silver soldering, without damage, to micro-waveguide systems operating at frequencies ranging from 3000 to 40,000 megacycles, have been announced by the Electronics Division of Sylvania Electric Products, Inc.

Development of these resonant windows, in which glass stress is eliminated at relatively high temperature differentials required for silver soldering, now makes available a wide range of window shapes and outside contours, for narrow- and wide-band transmissions. Power losses range from 0.02 to 0.1 db. The new windows for frequencies above 3500 mc will stand pressures up to 65 psia.

Applications include pressurized or gas-filled waveguide systems for all types of radar, including navigation, fire control, long- and short-range search, and those for gas analyses and meteorological uses. They are also used in the construction of TR and ATR switching tubes and to isolate portions of vacuum stystems.

Elimination of bending stress in the window glasses is the result of applied research work done by Messrs. Martin, Pease, and Roberts, of the Electronics Division of Sylvania at Boston, Massachusetts, in which glass and Kovar have been combined through the use of special sealing techniques.

Dimensional tolerances, which depend on the frequency of the window as well as the size of the window iris, range from ±0.005 in. at 3000 mc to ±0.0005 in. at 30,000 mc. Glass tolerances vary from 0.001 in. to 0.0001 in. Increased glass-metal seal strength is

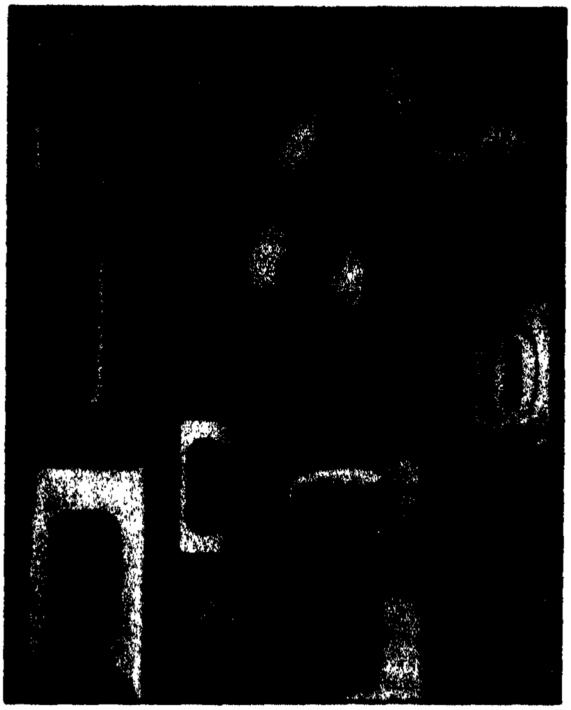

obtained by beveling one or both sides of the Kovar section.—Electronics Division, Sylvania Electric Products, Inc., *500 Fifth Avenue, New York 18, New York.*

Bridger

The Model 100 Bridger provides means for bridging a vacuum tube voltmeter, distortion meter or oscilloscope across any part of an audio frequency circuit through a well-shielded cable, yet without imposing any of the load of the meters or cable on the circuit.

Input Impedance—100 megohms in parallel with 6 uuf when using 3-foot shielded input cable.
Output Impedance—200 ohms, with one side grounded.
Size—5½ in×6 in.×11 in.
Voltage Ratio—Output/Input—0.98 (or −0.2 db) up to 30 volts with low capacity output circuit; and up to 25 volts with usual shielded output cable. This may be extended to 250 volts by adding Model 104 Voltage Divider (10:1 ratio) to tip of input probe.

The Bridger uses an advanced design of cathode follower (with output/input ratio practically unity) and a new development in double-shielded cable. The cable capacity is almost completely balanced out by the circuit configuration. The plastic-jacketed cable was designed especially for this unit; it has unusually low capacity but very high flexibility.—Audio Instrument Company, *1947 Broadway, New York 23, New York.*

Preparative Centrifuge

Application of forces up to 125,000 times g on 150 cc of material, and 60,000 g on quantities ranging upward to 1100 cc, are the purposes of the new Model L Spinco Preparative Centrifuge. The unit, which is completely housed in an enclosure 25 in.×30 in.×36 in., is of the vacuum chamber type to prevent frictional rotor heating (a two-stage mechanical pump creates a usable vacuum within 5 minutes of starting).

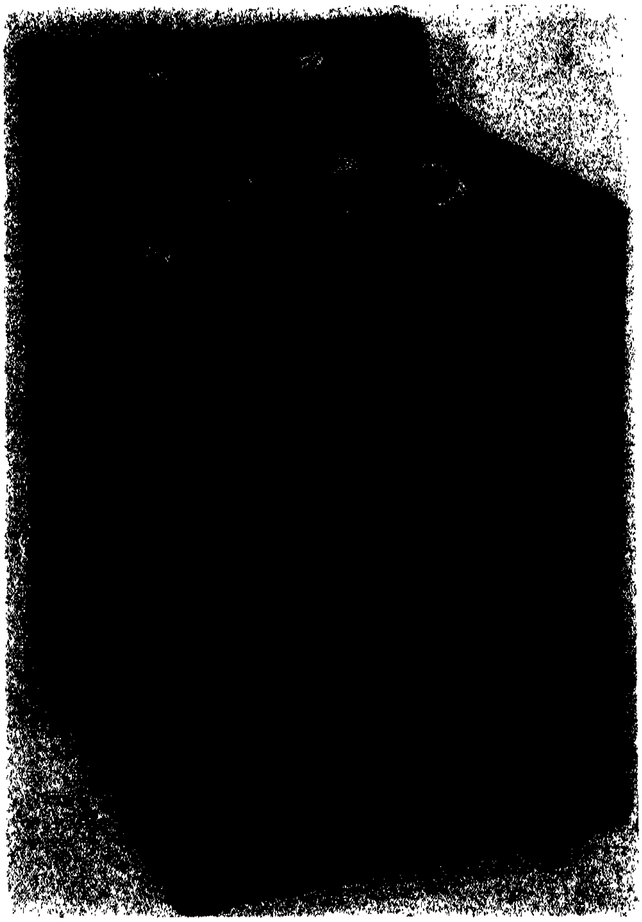

Automatic operation of the machine has been promoted with the provision of an automatic electronic control which accurately limits motor current during starts; by an automatic speed control which holds running speed to its preset value; by automatic braking at rates which can be preset; and by a device which automatically shuts down the centrifuge at the conclusion of a run in addition to a time switch for setting the actual run length.

Several rotors are available. The smallest, 6¾ in. in diameter, holds 150 cc of material and reaches its terminal speed of 40,000 r.p.m. in less than 4 minutes, decelerating again to a standstill in approximately the same time. The largest, 11 in. in diameter, holds over a liter of material, accelerating to its maximum speed of 20,000 r.p.m. in less than 20 minutes.

Prices are approximately $3300 with refrigeration, $3000 without refrigeration, f.o.b. Belmont, California.—Specialized Instruments Corporation, *613 O'Neill Avenue, Belmont, California.*

Regulated Power Supply

The Kepco Model 245 Power Supply, features a high degree of voltage regulation with a small compact unit.

Its specifications for d.c. output are 200 to 450 volts at currents from 0 to 200 milliamperes, regulated; a.c. output is 6.3 volts at 6 amperes, unregulated. Regulation between 200 and 450 volts for both load variation from 0 to 200 milliamperes and input variation from 105 to 125 volts is better than 0.5 percent. The d.c. output voltage is within 0.5 volt between 200 and 450 volts for load variations from 0 to 200 milliamperes. Ripple voltage is less than 5 millivolts; input voltage is 105 to 125 volts a.c., 50 to 60 cycles; power required is 300 watts; and output impedance is less than 2 ohms.

Its front panel is equipped with voltage control; d.c. output terminals (isolated from chassis); a.c. center-tapped output terminals (isolated from chassis); on-off switch and pilot light; d.c. output switch; line fuse; d.c. output fuse; meters 0 to 200 milliamperes d.c. and 0 to 500 volts d.c. A ground terminal connected to the chassis is mounted at the back of the supply.

The unit measures 8-in. high, 8-in. deep, and 16-in. wide and weighs 29 pounds. It is priced at $149.59.—KEPCO LABORATORIES, INC., *149–14 Forty-First Avenue, Flushing, New York.*

Electronic Microammeter

The MacDonald Electronic Microammeter Type 100 is a new instrument designed for measuring very small direct currents. It will fill the need for a high-sensitivity direct-current measuring device much as the vacuum tube voltmeter meets the need of a sensitive voltage-measuring device.

The instrument has an input resistance of 50 ohms and a sensitivity of one microampere full scale. The input can be overloaded by currents as high as ¼ ampere without damage to the instrument. Unlike conventional high sensitivity galvanometers, the MacDonald Electronic Microammeter is not sensitive to position or vibration.

In operation, the instrument combines the characteristics of a magnetic amplifier with those of a vacuum tube output circuit to provide low input resistance, high sensitivity, and input overload safety. An output jack is provided so that the instrument can be used as a high sensitivity d.c. amplifier; as such it will actuate a 1-milliampere 1400-ohm recorder directly. The instrument is available with multiple ranges.—W. S. MACDONALD COMPANY, INC., *33 University Road, Cambridge 38, Massachusetts.*

Manufacturers' Literature

Radio and Electrical Measuring Equipment—General Radio Catalog L 1948 is a complete catalog of General Radio equipment—stroboscopes; variacs, sound-level meters, vibration meters, impedance bridges, signal generators, oscillators, wave analyzers, distortion meters, impedance standards, vacuum-tube voltmeters, frequency standards, broadcast monitors, and parts and acessories. Includes prices.—GENERAL RADIO COMPANY, *Cambridge 39, Massachusetts.*

Industrial Uses of Radioactive Materials—A selected bibliography, 13 pp., probably the most extensive available bibliography on the industrial uses of radioactive tracers, includes references dealing with the fields of petroleum, mining and metallurgy, textiles, instruments, radiography, analysis, pharmaceutical, glass, radioisotope preparation, and miscellaneous industrial applications. This bibliography is available without charge from ARTHUR D. LITTLE, INC., *Cambridge 42, Massachusetts.*

Micro-Line Counter—A 4-page illustrated brochure describes operation and applications of the Micro-Line Counter, an instrument which indicates instantly and accurately counts of individual lines, as in fabrics, in screens of engraving, etc.—MICRO-LITE COMPANY, INC., *44 West 18 Street, New York 11, New York.*

Haydon Timing Motors and Devices—Catalog No. 321, 20-page book, presents the Haydon line of synchronous timing motors, chart drives, timing devices and clock movements, complete with details on the products, photographs and profile drawings of all units, shaft drawings and listings of speeds, voltages, frequencies, shaft sizes and special variations available in each of 10 motor series.—HAYDON MANUFACTURING COMPANY, INC., *Torrington, Connecticut.*

Lucite Acrylic Resin Cast Sheeting—A new 32-page booklet entitled *DuPont Lucite Acrylic Resin* contains general information concerning this material, including a chart listing the properties, a section on handling and fabricating, and a summary of types, forms, and sizes of the sheeting.—PLASTICS DEPARTMENT, E. I. DUPONT DE NEMOURS AND COMPANY, *Wilmington 98, Delaware.*

Testing Machine Accessories—Bulletin 261-A, 12 pages with over 30 illustrations, describes supplementary devices used to adapt testing machines to the widest scope of testing conditions. These include grips, specimen holders and compression plates; auxiliary testing equipment; testing machine accessories; and various testing conveniences.—THE BALDWIN LOCOMOTIVE WORKS, *Philadelphia 42, Pennsylvania.*

Thermocouple and Pyrometer Accessories—Bulletin No. P1238, 56 pages, contains detailed information on thermocouples, protection tubes, and other pyrometer accessories. This bulletin includes a technical section, "Users' Manual" which contains engineering handbook data on such subjects as factors affecting thermocouple life, corrosion and poisoning, thermocouple reproducibility, thermocouple insulation, and information required in selecting the right thermocouple and protection tube for every application.—THE BRISTOL COMPANY, *Waterbury 91, Connecticut.*

Radio and Electronic Equipment—Leaflet, 4 pages, describes Browning radio and electronic equipment, including frequency meters, oscillator grid dip meter, WWV standards frequency calibrator, power supply and square wave modulator, capacitance relay, signal system, oscillosynchroscope, oscillorecord camera, sweep calibrator, audio amplifier, frequency meter calibrator, and FM-AM tuners. Includes prices.—BROWNING LABORATORIES, INC., *742–750 Main Street, Winchester, Massachusetts.*

GAP-R Electronic Analog Computers—Bulletin and preprint describe analog computor components, such as adding, coefficient, integrating, differentiating, augmenting, etc., with which complete analog computors can be constructed incorporating all elements of the class of systems to be studied. Ten fields of technology in which analog analysis is useful are listed.—G. A. PHILBRUCK RESEARCHES, INC., *230 Congress Street, Boston 10, Massachusetts.*

High-Speed Chronoscope—Bulletin 100 describes the Model 100 American High-Speed Chronoscope, an electronic stop-watch for the measurement of time from 10 microseconds to 1 second.—AMERICAN CHRONOSCOPE CORPORATION, *150 South Middle Neck Road, Great Neck, New York.*

Tracerlog—April 1949 issue of Tracerlog, house organ, features an article on the performance characteristics of Geiger tubes and includes an insert on operating instructions for such tubes.—TRACERLAB, INC., *55 Oliver Street, Boston 10, Massachusetts.*

Rotameter with Safety Shielding—4-page illustrated catalog describes various models of the Full-View Rotameter with Safety Shielding.—BROOKS ROTAMETER COMPANY, *Lansdale, Pennsylvania.*

Electrical Measurements—4-page leaflet is devoted to a discussion of the operating principles and available models of high-resistance instruments in which a potentiometer circuit compensates for voltage drop across the current-measuring elements.—SENSITIVE RESEARCH INSTRUMENT CORPORATION, *9–11 Elm Avenue, Mount Vernon, New York.*

The Graphic—Bulletin No. 549 describes Model AW Recording Milliammeters and their applications.—THE ESTERLINE-ANGUS COMPANY, INC., *P. O. Box 596, Indianapolis 6, Indiana.*

Attenuators—Leaflets describe high-frequency step attenuator and attenuator pad for use up to 1000 mc.—WEINSCHEL ENGINEERING COMPANY, *123 William Street, New York 7, New York.*

New Materials

Forest K. Harris: Associate Editor
in Charge of this Section
National Bureau of Standards, Washington, D. C.

Colloidal Graphite

Neolube is an alcohol suspension of Acheson colloidal graphite, designed for application with a brush on a wearing surface. The alcohol evaporates quickly leaving on the surface an adherent film that will not blow or rub off. The film can be rubbed to a high polish that will not stain a fabric following the initial rubbing. It is designed for use on bearing surfaces where any oil drip might be objectionable or where oil may become gummy and lose its lubricating value and may be used on electrical apparatus including contacts, since the film is electrically conducting.—HURON INDUSTRIES, *Port Huron, Michigan.*

Lay-Out Plate

A series of ceramic surface plates is available in sizes ranging from 5 to 24 inches in diameter. The top is finished flat to within 0.001 inch and has a semiglossy surface which is neither slippery nor sticky. It is well adapted for blueing in checking work flatness and can be cleaned with soap powder and water.—NORTON COMPANY, *36 New Bond Street, Worcester 6, Massachusetts.*

Core Binder

Cycor 151 is a thermosetting resin, developed in a research on foundry problems, to make water-resistant sand cores. The amount of binder used and the use of additives may be adjusted to give desired green or baked tensile strengths, permeability, hardness and collapsibility, resulting in cleaner, more uniform castings. The curing temperature is 350°F, and cores containing the binder may be cured in externally heated or dielectric ovens. The finished core will withstand high humidity and long lay-over in molds waiting to be poured.—AMERICAN CYANAMID COMPANY, *30 Rockefeller Plaza, New York 20, New York.*

Casting Sealant

G E Permafil is a liquid resin for sealing porous, light metal castings. It was developed to make possible the salvage of castings which would otherwise be rejected because of porosity, and to permit their use in applications involving oil or vapor pressure. A polyester-type resin, Permafil converts to a tough, clear solid, free from voids, through heat and catalytic action. Castings are sealed by vacuum impregnation with a subsequent short oven-bake. The material is stated to have good storage life under recommended conditions. Further information may be obtained from the manufacturer.—GENERAL ELECTRIC COMPANY, Chemical Department, *Pittsfield, Massachusetts.*

Bonding Process

A process has been developed for bonding dissimilar materials in parts which must withstand high lateral or internal hydrostatic and aerostatic pressure. Primarily designed for bonding plastic or Neoprene to metals, or ferrous to non-ferrous metals, the process uses special equipment and a new bonding agent. In addition to bonding, the process eliminates microporosity by impregnation with the bonding agent, with a wide range of temperature and chemical resistance. Such dissimilar materials as glass to metal, Neoprene to metal, steel inserts to aluminum, brass to aluminum, and aluminum to aluminum have been bonded. Finished parts show no visible signs of treatment, and anodized, plated, or machined areas are not affected. Descriptive literature may be obtained from the manufacturer.—WESTERN SEALANT, INC., *9091–3 West Washington Boulevard, Culver City, California.*

Gasket Coating

Felseal, a modified polysulfide elastomer of the thiokol type, can be applied to any fiber-type base material for use in sealing gaskets with high resistance to pressure, chemical action, and heat. It is not materially affected by mineral or vegetable oils, aliphatic or aromatic hydrocarbons, lower alcohols, carbon tetrachloride, or dilute acids and bases. It contains no free or extractable sulfur compounds and does not corrode or stain copper or aluminum. It is stated to operate efficiently from −30 to +225°F without appreciable change in its characteristics. It is available in coating thicknesses from 0.001 in. to 0.005 in. on base materials such as chipboard, treated paper, and fiber.—FELT PRODUCTS MANUFACTURING COMPANY, *1508 Carroll Avenue, Chicago 7, Illinois.*

Heat Resistant Phenolic

Resinox 10231 is a phenolic molding powder which was developed for use in products which must withstand extremes of thermal shock and still retain a high gloss. It is stated to have withstood 100-hour exposure to temperatures ranging from 400 to 500°F, and to be capable of immediate transfer from room temperature to a hot oven without any evidence of blistering. It is also stated to have improved molding properties and excellent dimensional stability.—MONSANTO CHEMICAL COMPANY, *St. Louis 4, Missouri.*

Use for Dri-Film

G. E. Dri-Film water repellent has been used in a rubber laboratory to reduce the chore of cleaning latex from glass dishes, to a simple rinsing operation. It is stated to be the best material yet found for preventing the adherence of latex to glass. G. E. No. 9987 Dri-Film is diluted to a 10 percent solution, and poured into the dish to be protected. After the excess is drained off, the article is dried 15 minutes at 200°F. Dishes so treated can be used and cleaned 5 times before another application is needed. This formulation of Dri-Film was originally developed for treatment of glass ware and needles used in handling blood, to reduce the clotting rate.—GENERAL ELECTRIC COMPANY, *Pittsfield, Massachusetts.*

Laboratory Quartzware

Quartz has long been known to possess many desirable properties for laboratory apparatus but has been difficult to obtain. A complete line of standard laboratory ware is now available in transparent quartz for use where glass is unsuitable. It may be used continuously at high temperatures, is chemically inert to most reagents except hydrofluoric acid, and is extremely resistant to thermal shock. Its use is especially recommended in micro-work where ordinary glassware tends to introduce impurities into the material. In addition to standard apparatus, a custom fabrication service is available to meet specialized needs.—THE PANRAY CORPORATION, QUARTZWARE DIVISION, *393 Broadway, New York, New York.*

High Temperature Plastic

Kel-F is a polymer of trifluorochloroethylene in which ⅘ of the weight is made up of the 2 halogens, fluorine and chlorine. It is colorless and transparent but can be blended with solid fillers and coloring agents. It is related to the fluorocarbons (in which all the hydrogen of the hydrocarbon has been replaced by fluorine) but differs from them in that some of the fluorine has been replaced with chlorine. The new plastic has the properties of stability and chemical inertness which characterize the saturated fluorocarbons and in addition possesses certain useful physical properties: It is extremely resistant to chemical action but is easily worked in conventional equipment; it is strong and hard but not brittle; it can be used at relatively high temperatures and has satisfactory performance at extremely low temperatures; it is amenable to heat treatment which imparts desirable permanent properties at the use temperature. Because of its chemical inertness (it is not affected by prolonged exposure to concentrated hydrofluoric acid, strong caustics, aqua regia, and other vigorous oxidizing agents) it may be used in pump and valve packing and seats where corrosive gases or liquids are processed. Its transparency makes it an excellent substitute for glass in gauges and flowmeters where glass would be attacked. It can be laminated with wire or glass cloth in applications where inertness must be combined with higher mechanical strength. Its low cold-flow makes it useful as the seating material in safety release valves which are normally closed for long periods of time by constant spring-loaded pressure. Since its properties are satisfactory from −320°F (liquid nitrogen temperature) to +390°F, it could be used in liquid air and oxygen work, in refrigerating systems and in low temperature reaction systems. It is a good electrical and heat insulator and is believed to offer possibilities as a wire insulation in motors and other equipment that must operate at high temperatures under corrosive conditions. Another valuable property is that it is not wetted by water and is unaffected by high humidity, making it a good water sealing agent. It has good fabricating properties in the temperature range of 550–600°F and may be compression, transfer or injection molded, or extruded. It has been made as sheets, films, tubing, rod, or as insulation on wire, and can be punched, drilled, or machined to close tolerances. It is stated to be remarkably amenable to heat treatment, stable properties at one temperature being obtained by suitable heat treatment at a higher temperature. In this way it may be made relatively soft and resilient or harder and less yielding without the use of plasticizers and without the sacrifice of any of its stability characteristics.—W. M. KELLOGG COMPANY, *Jersey City, New Jersey.*

THE
REVIEW OF SCIENTIFIC
INSTRUMENTS

VOLUME 20, NUMBER 8 *AUGUST, 1949*

A Precision Vacuum Gauge

G. C. Fryburg and J. H. Simons
Department of Chemistry, The Pennsylvania State College

(Received February 25, 1949)

A pressure measuring device of the general type first described by Knudsen has been constructed for obtaining precision measurements of gaseous pressures in the range from 1×10^{-5} to 10^{-3} mm of Hg. The instrument has been calibrated, with the aid of a McLeod gauge, in nitrogen, hydrogen, oxygen, methane, ethylene, normal-butane, and iso-butane. The mechanical precision of the instrument seems to be better than plus or minus 0.5 percent and the accuracy of the above calibrations is probably of the order of plus or minus 1 percent. Calibration curves for the above gases have been treated analytically and equations for the different gases have been discussed. An empirical method of calibration has been described for calibrating the instrument in condensible gases whose pressures cannot be measured in a McLeod gauge.

INTRODUCTION

In the ion-beam scattering work conducted in this laboratory,[1] there has been a need for some time for an instrument capable of accurately determining the pressures of hydrocarbon gases and vapors in the range from 1×10^{-5} to 10^{-3} mm of Hg. Mechanical devices like the Pirani gauge and the ionization gauge, while useful in indicating vacua in this region, are not capable of giving precision measurements of the pressure. In addition, they are not reliable when used with gases which are affected by the hot filaments in these gauges. The McLeod gauge, which is the gauge most often used for precision pressure measurements in this range, usually requires a cooling trap to prevent mercury vapor from contaminating the vacuum system. Since all but the most permanent gases will adsorb in this trap, the McLeod gauge is useful for only the most permanent gases under these conditions. Furthermore, even with permanent gases, measurements of the lower pressures in this range with a McLeod gauge are unreliable due to the uncertainty involved in the value of the capillary correction and to the tendency of the mercury to stick in the capillary tubes. An instrument of the Knudsen variety which circumvents both of these difficulties is described below. It is capable of giving precise and dependable pressure readings throughout the entire range from 1×10^{-5} to 10^{-3} mm of Hg. It involves no objectionable medium like mercury and thus may be used without a cooling trap. It may be used for condensible as well as for non-condensible gases, and it gives a continuous reading of the pressure.

DESCRIPTION

The instrument is of the deflecting leaf type of Knudsen gauge. A diagram of it is illustrated in Fig. 1. This type of gauge suffers from the disadvantage that it cannot, in general, be calibrated directly from its dimensions and operating conditions as can the torsion-fibre type of gauge:[2] because the temperature of the deflecting leaf cannot be known and hence will remain uncertain. It is, however, very much simpler to construct and possesses greater sensitivity over a broader range of pressures for a given set of operating conditions.

The deflecting system consists of a strip of aluminum foil (1) 14.3 cm by 2.0 cm by 0.0006 cm, hung from a piece of No. 26 spring brass wire (2) to each end of which is soft-soldered a small pivot (3). The foil is attached to the wire by means of a small amount of Apiezon W wax. A 2-mm edge is bent back along both sides of the foil at right angles to its face to keep the foil rigid and straight at all times. The center portion of the brass wire is bent downward in the shape of a U to allow adjustment of the distance between the pivot points (before attachment of the foil) and to lower its center of gravity. The

---

[1] Russell, Fontana, and Simons, J. Chem. Phys. 9, 381 (1941). Simons, Fontana, Francis, and Unger, J. Chem. Phys. 11, 312 (1943). Simons, Muschlitz, Jr., and Unger, J. Chem. Phys. 11, 322 (1943). J. H. Simons and G. C. Fryburg, J. Chem. Phys. 13, 216 (1945). J. H. Simons and L. G. Unger, J. Chem. Phys. 13, 221 (1945).

[2] M. Knudsen, Ann. d. Physik, 32, 809 (1910).

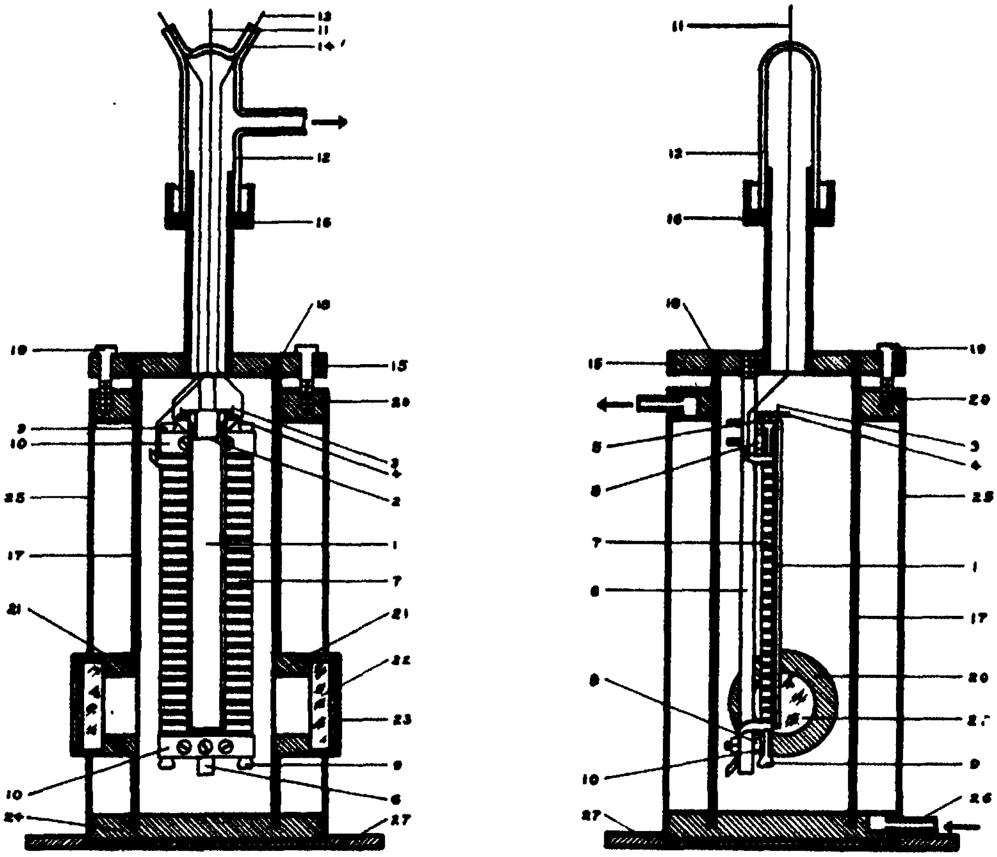

FIG. 1.

pivots themselves were obtained from Permo Incorporated of Chicago and are of K Monel, 0.020 inches in diameter and 3-mm long tipped with an extremely hard alloy of osmium. The tips were accurately ground with a radius of curvature between 0.0075 to 0.001 inches and with a 40 degree included angle. The whole deflecting system weighs 0.0761 g and has its center of gravity about 0.10 cm below the axis of rotation. It is suspended from a case-hardened steel yoke (4), the pivot points resting in the center of two small indentations each ground with a 90 degree included angle and terminating in a slightly concave bottom whose diameter is about 0.02 inches. The surface of these indentations is highly polished. The steel yoke, itself, is bolted in a supporting $\frac{1}{4}$-inch square brass bar (6). Thus electrical contact is obtained between the aluminum leaf and the body of the gauge, a condition necessary to eliminate spurious electrostatic effects. This type of suspension of the deflecting leaf allows deflection without any bending of the leaf in contrast to the usual type of suspension in which the top of the leaf is clamped in place and deflection obtained by bending of the leaf. Bending of the leaf is undesirable as it sets up stresses in the leaf and results in poor ability to re-zero accurately. In our instrument, with proper polishing of the indentations, the leaf re-zeroed to within, at worst, a few thousandths of a millimeter.

The heater element consists of a long piece of flat Nichrome resistance wire wound about two glass rods (9) which are held apart by brass clamps (10). The wire is held in place on the rods by glass thread made from very fine glass wool. This is also mounted on the brass bar (6), directly in front of the deflecting leaf and about 1-mm distant from it. The lower end of the Nichrome ribbon is bolted to the bar thus grounding it to the body of the gauge. The upper end is insulated with glass capillary and brought out through a tungsten seal in the glass tube (12). The element has a resistance of about 15 ohms. Current (about 0.2 amps) is supplied by a six-volt storage battery which is charged while in use to ensure constant supply voltage. The current may be varied by means of a sensitive, variable resistance in series with the heater element. The magnitude of the current is determined by measuring the voltage drop across a standard 5-ohm resistance also in series with the heater, a Leeds and Northrup type K potentiometer being used for this purpose. So that the temperature of the heater can be determined, a small copper-constantan thermocouple is soft-soldered to the back of it. The leads (13) of this are also insulated in fine glass tubing and are brought out through short pieces of glass capillary (14) blown into the top of the glass tube (12). The wires are sealed in place by warming the glass capillary slightly and placing a piece of Apiezon

W wax over the hole in the end. Capillary action draws the melted wax down the bore of the tube and upon cooling makes a very satisfactory vacuum seal.

The body of the gauge consists of a 2-inch copper pipe (17) silver-soldered into a grooved disk (24) of ⅜-inch brass. Two hollow brass cylinders (21) are silver-soldered into sides of the pipe near the bottom of the aluminum leaf so that movements of the leaf can be observed. Plate glass disks (22) are sealed into these with Apiezon W wax and held in place by brass lock washers (23). The top of the gauge consists of another ⅜-inch brass disk (15) into which the supporting bar (6) is screwed and silver-soldered in place. Also silver-soldered into this top is a crows nest (16) by means of which a vacuum tight seal is made to the glass tube (12), with the aid of some Apiezon W wax. In the bottom side of this top (15), a groove, ¼-inch deep, is machined to fit over the copper pipe (17). A close-fitting, annular rubber gasket (18) fits into this groove and the remainder of the space is filled with Apiezon W wax, the rubber gasket having previously been boiled in dilute KOH solution to remove sulfur, etc. To assemble the gauge it is only necessary to fit the groove over the pipe, warm the joint, and then draw the disk down onto the pipe by tightening up on eight steel machine screws (19) which screw into holes in the ½-inch brass flange (20) silver-soldered around the copper pipe. This seal is quite easy to make or break and was never found to leak.

Around the body of the gauge is soft-soldered a piece of sheet copper (25) enclosing an annular space through which water flows, the purpose of which is to maintain the body of the gauge at constant temperature. This in turn is surrounded by large pieces of rock cork cut to fit snugly against the gauge, insulating it from the room. The temperature of the water is determined by means of a thermocouple. The entire gauge is soft-soldered into a circular depression in a square piece of ¼-inch brass which is bolted securely to a large piece of Transite. Also bolted to this Transite is the microscope used to observe the deflection of the aluminum leaf. This is mounted in a machined carriage and is of the filar micrometer type capable of reading accurately to 0.001 mm over a 4-mm range on the object. The Transite piece is mounted on sponge rubber and bolted loosely to a flat board which in turn is mounted on three 3-foot pieces of ½-inch pipe screwed onto the floor. This arrangement gives sufficient stability and yet eliminates all vibrations from the floor.

OPERATION

The construction of this gauge obviously prohibits the use of heat treatment in degassing it. It was, therefore, necessary to exhaust it for some time, before all the gases adsorbed on the large metal surfaces were removed. After pumping for one week, it was found that the pressure in the entire gauge system rose at the rate of only 1×10^{-8} mm of Hg per hour when disconnected from the pumps. This was about as good as could be obtained even with longer pumping. The lowest pressure obtainable was about 5×10^{-6} mm of Hg as indicated by an ionization gauge connected to the instrument. This pressure no doubt arose in part from the vapors given off by the rubber gasket, the Apiezon W wax, and the stopcock grease, though Apiezon N grease was used on all stopcocks.

In operation of a Knudsen gauge there are two common methods employed: one is to keep the temperature of the heater constant, and the other is to keep the current passing through the heater constant. The latter method is the simpler but suffers from the disadvantage that the calibrations will be different for gases having different thermal conductivities. This amounts to a deviation of but a few percent for most gases and is, therefore, of little consequence since it is usually less than the precision of measurement of the gauge. However, with our precision instrument, it was necessary to eliminate this variable, and so this gauge was operated with a constant heater temperature. This temperature was determined by means of the thermocouple soldered to the back of the heater. Differences of 0.001 mv or 0.025°C could be detected. Data were taken to ascertain how sensitive the gauge readings were to changes in the heater temperature. It was determined that the sensitivity of the gauge was altered 2 percent per degree change in the heater temperature. Nearly identical results were obtained with respect to changes in the temperature of the water (flowing around the body of the gauge). By means of the variable resistor which was in series with the gauge heater, it was possible to maintain the heater temperature constant to about plus or minus 0.002 mv or plus or minus 0.05°C. This should contribute an error of only plus or minus 0.1 percent. The water flowing around the gauge issued from a constant temperature bath regulated by a thermostatic regulator similar to that described by Fenske[3]. No variation in the temperature of the water greater than plus or minus 0.001 mv or plus or minus 0.025°C could be detected. Hence negligible error should arise from this cause.

From these preliminary investigations, operating conditions were chosen which would give a 2-mm foil deflection at a pressure of about 1×10^{-3} mm of Hg. This was about the upper limit of pressure for the region in which we were interested, and hence 2 mm would be about the maximum foil deflection. This was kept as small as was feasible in order to keep the distance between the aluminum leaf and the heater, which was about 1 mm to start, as small as possible. The operating conditions chosen were: the temperature of the heater was maintained at a temperature which gave a thermocouple e.m.f. of 2.822 mv (approx. 68.0°C); the temperature of the water was maintained at a temperature of 25.0°C which gave a thermocouple emf of 0.984 mv.

---

[3] Hersh, Fry, and Fenske, Ind. Eng. Chem. 30, 363 (1938).

The precision of the instrument, when operated as above, can be obtained from a comparison of the gauge readings taken during different "runs" for the calibration in a given gas. Some of these "runs" were made as much as two weeks apart. The gauge readings were reproducible to a few tenths of a percent, except at the small deflections. This slight uncertainty in the small deflections, however, arises as a result of the uncertainty in the time readings, which was about plus or minus 0.05 minutes, and is not a characteristic of the gauge.

CALIBRATION OF THE GAUGE

As was stated above, it is not possible to calibrate Knudsen gauges of this type directly from their dimensions and operating conditions. Hence it is necessary to calibrate them against a McLeod gauge. However, for the pressures in the region in which we wished to calibrate the gauge, the readings of the McLeod gauge are unreliable due to the uncertainty involved in the value of the "capillary corrections." In addition, the mercury tends to stick in the capillary tubes at the lower pressures involved. To circumvent these difficulties a dynamic method of calibration was used which did not require measurements at the lower pressures or even an actual evaluation of the higher pressures, thus eliminating all error caused by uncertainty in the "capillary correction."

Gas was allowed to leak into the gauge system through a long slender capillary made by pulling out a piece of ½-mm capillary tubing to a length of about 10 feet. This was inserted into a large U tube of 10-mm Pyrex tubing and the butt end ring-sealed into the tubing. One end of the U tube was joined through a vacuum stopcock to the gauge system and the other end was connected to a glass bulb and a closed-tube mercury manometer. This "backing system" could be evacuated and filled with any desired gas. The gauge system consisted of the instrument itself, a large McLeod gauge equipped with a cooling trap to prevent mercury vapor from entering the rest of the system, an ionization gauge, and a mercury diffusion pump equipped with cooling trap and suitable backing pump. All of these parts were connected to a common manifold through large vacuum stopcocks so that any one of them could be cut out of the system at will. The ionization gauge was always cut out before allowing any gas to leak into the system and was used only to determine the limiting pressure. With the instrument operating and the capillary leak cut into the system, it was only necessary to cut out the pumps and the pressure in the system rose as a linear function of the time. The movable leaf deflected as the pressure increased, and the deflections were read at convenient intervals as denoted on an accurate electrical timer. Hence if the "leak" through the capillary were calibrated, the pressure in the system would be known at any time, from which a plot of gauge deflection versus pressure could be obtained. The "leak" was calibrated with the aid of the McLeod gauge. After the pressure had increased to a sufficient magnitude so that sticking of the mercury in the capillary tubes was not too troublesome, the mercury in the McLeod was raised to the 10^{-5} mark in the closed capillary. This was adjusted accurately with the aid of a cathetometer capable of reading 0.01 mm. This McLeod gauge was constructed with an open 8-mm tube in addition to the usual open capillary tube, and the difference in height between the mercury columns in the 8-mm tube and in the closed capillary was measured with the cathetometer. This was, of course, not the pressure in the system but was greater than it by the difference in the capillary depressions in the two tubes. Nevertheless, this "difference" or "capillary correction" in contrast to the "capillary correction" between the two capillary tubes, is fairly constant, since the mercury was always brought to the same place in the closed capillary and since any variations in the diameter of the 8-mm tube would have negligible affect on the small depression in it. It was not necessary to know the magnitude of this "capillary correction" for it is only the *rate* of increase of pressure which is required. This was obtained by plotting the above-mentioned differences in height, taken at definite intervals of time, against the time. This plot is a straight line the slope of which is the rate of increase of pressure and the intercept of which on the y axis is the sum of the "capillary correction" and the small initial pressure, p°. With this value of the slope it was possible to make a plot of gauge deflection $(D-D^\circ)$ against the increase in pressure $(p-p^\circ)$ thus obtaining the desired calibration curve. Here, p° is the small limiting pressure existing in the gauge at zero time, and so $(p-p^\circ)$ is the increase in pressure caused by the leak. D° is the position of the leaf of the gauge at zero time and so $(D-D^\circ)$ is the deflection caused by the increase in pressure. The deflection could be plotted against the total pressure, p since p° can be measured with the ionization gauge. However, in our scattering experiments we desire the increase in pressure, and hence the use of $(p-p^\circ)$.

In calibrating the gauge it was found necessary to take the McLeod gauge readings and the deflection readings during different "runs." This was due to the fact that the raising and lowering of the mercury in the McLeod caused a light change in the pressure of the system. This was detected in the effect it had on the deflections of the gauge, causing an increase in deflection with some gases and a decrease with others. Consequently, the data of foil deflections versus time were usually taken without taking any McLeod gauge readings. The McLeod gauge readings were taken during separate "runs," and no more than two or three were taken without pumping out the system and starting over again. Corrections were made on the values of the second and third readings from observations of the deviations produced in the foil deflection and from a knowledge of an approximate value of the rate of increase of pressure. This amounted to 0.1 or 0.2×10^{-4}

mm of Hg in most cases. In order to take these readings at different times, it was essential that the rate of increase of pressure remain constant. The number of moles of gas leaking through the capillary was very small and a simple calculation showed that the value of the rate would not drop 0.5 percent in less than six months. Hence, it was only necessary to establish the same room temperature each day to insure a constant rate. However, to obtain results reproducible to a few tenths of a percent it was also necessary to keep the level of the mercury in the McLeod gauge at the same place (in order to maintain a constant volume in the system), and to keep the cooling mixture on the McLeod gauge trap at the same level for each "run" and during a "run."

In the actual McLeod gauge measurements, sticking of mercury was still troublesome. Therefore, three or four readings were taken at each timer interval and the average of these used. The method of least squares was then applied to these averages and the rate of increase of pressure was obtained as the slope of the line. The mean deviation between the experimental averages and points calculated by using this rate of increase of pressure was about 0.13 mm. This amounted to but a few tenths of a percent of the experimental values, so it is evident that they all lay close to a straight line. The rates of increase of pressure used were of the order of 30×10^{-6} mm of Hg per hour.

The above method of calibration was used for nitrogen, hydrogen, oxygen, methane, and ethylene, though for the last two gases, dry-ice-acetone mixture had to be substituted in place of liquid air on the McLeod gauge trap due to a small amount of adsorption. However, this method could not be used for more easily condensed gases, such as butane, for these would be readily adsorbed in the cooling trap. Hence an expansion method was used for the calibrations of the two butane isomers. The system was modified by inserting two stopcocks in the manifold in series between the McLeod gauge and the instrument; the volume between the stopcocks being very small (about 1 cc). This effectively separated the system into two distinct parts connected only through the two stopcocks. The one part consisted of the McLeod and accompanying trap. Bulbs containing nitrogen and the butanes were connected to this so that samples of these gases could be admitted to it at pressures ranging from 0.3 mm to 1.25 mm. The other part consisted of the gauge and the pumps, the ionization gauge and the capillary leak having been removed.

The method of calibration consisted merely of expanding some butane gas from one of the bulbs into the McLeod gauge system up to some pressure within the range mentioned above. These pressures were high enough that the vapor pressure of mercury at room temperature amounted to a negligible percentage of the total pressure. As a result, no cooling of the McLeod gauge trap was necessary and hence, no harmful adsorption occurred. The pressure of the gas in this system was read with the McLeod gauge; accurate measurements being easily obtained at such high pressures. The gas in the small volumes between the two stopcocks was then trapped off and quickly expanded into the gauge, the pumps having been cut out from this region just previous to the expansion. This resulted in a deflection of the leaf of the gauge and in a drop in the temperature of the gauge heater. However, it was found possible to maintain the temperature of the heater constant by quickly increasing the current passing through it. With a little practice it was possible to do this and read the deflection of the foil within a minute after the expansion. Equilibrium seemed to be reached very quickly as no change in the deflection was noticeable after this except for the small gradual increase caused by the natural leakage of the system. This amounted to only 0.001 mm per minute and was not significant when the readings were obtained within one minute after cutting out the pumps.

If the ratio of the volume of the space between the stopcocks to the volume of the gauge system is known, one can easily calculate the final pressure in the gauge system from the previous measured pressure by means of Boyle's law, and thus calibrate the gauge. Accurate measurements of these two volumes by the usual methods would be quite cumbersome. However, as the gauge had previously been calibrated in nitrogen, this gas could be used to calculate the ratio of these volumes by actual measurements of pressures before and after expansion. Numerous values of this ratio were taken with nitrogen over the entire range of pressures and at widely different times during the actual butane calibrations. The ratio remained constant to plus or minus 0.5 percent or plus or minus 0.000005 out of 0.00115, this latter number being the value obtained for the ratio. It was, of course, necessary to keep the temperature of the room constant during measurements of this type, just as in the other method of calibration.

As a check on the method, two points were taken with methane and two with ethylene, the gauge having already been calibrated in these gases by the other method. For methane, values for $(D-D^\circ)$ of 1.507 mm and 0.788 were obtained at pressures of 68.94×10^{-6} and 34.56×10^{-6} mm of Hg, respectively. The values for these same pressures taken from the calibration curve were 1.507 mm and 0.785 mm. For ethylene, values for $(D-D^\circ)$ of 1.774 mm and 1.114 mm were obtained at pressures of 85.4×10^{-6} and 50.9×10^{-6} mm of Hg. The values taken from the calibration curve were 1.782 mm and 1.119 mm. The agreement in the case of the methane is very good. That for the ethylene is in error by 0.4 percent which is within the precision of the measurements.

The results obtained by this method were as precise as those obtained by the dynamic method and had the advantage of being easier to take.

TABLE I. Calibration results.

$D-D^\circ$	$P-P^\circ$ in mm of Hg $\times 10^6$					
(mm)	N_2	H_2	O_2	CH_4	C_2H_4	C_4H_{10}
0.100	4.15	4.5	4.1	4.1	4.05	4.1
0.200	8.45	9.2	8.4	8.4	8.35	8.4
0.300	12.7	13.9	12.6	12.8	12.7	12.8
0.400	17.1	18.7	16.9	17.2	17.2	17.2
0.500	21.5	23.4	21.25	21.6	21.6	21.6
0.600	26.0	28.2	26.25	26.1	26.1	26.3
0.700	30.6	33.1	30.1	30.7	30.75	31.25
0.800	35.1	37.9	34.55	35.3	35.4	36.25
0.900	39.7	42.85	39.0	39.9	40.2	41.6
1.000	44.3	47.7	43.6	44.7	45.0	47.0
1.100	48.9	52.8	48.1	49.4	49.9	52.75
1.200	53.6	57.8	52.9	54.1	54.9	58.7
1.300	58.5	63.0	57.6	59.0	59.95	64.6
1.400	63.2	68.15	62.3	63.9	65.1	70.75
1.500	68.0	73.4	67.0	68.8	70.3	77.1
1.600	72.9	78.5	71.9	73.8	75.4	83.75
1.700	77.8	83.8	76.7	78.9	80.8	90.4
1.800	82.8	89.1	81.5	83.9	86.2	97.25
1.900	87.7	94.5	86.5	89.0	91.9	104.1
2.000	92.8	99.9	91.5	94.1	97.4	111.25

RESULTS

The results of the calibrations of the above-mentioned gases were plotted on a large piece of graph paper with $(D-D^\circ)$ as the ordinate and with $(p-p^\circ)$ as the abscissa. One millimeter along the ordinate corresponded to 0.005-mm deflection of the foil and one millimeter along the abscissa, to a pressure of 0.25×10^{-6} mm of Hg. These results are presented here in Table I. The values for all the gases except the butanes represent actual experimental values. Those for the butanes were taken at even values of $(D-D^\circ)$ from a curve drawn through the experimental points. It should be noted that the points obtained for both of the butane isomers fell along the same curve, and that none of them deviated from the curve by more than 0.005 mm. Also, no points could be obtained for the butane calibrations for pressures below 20×10^{-6} mm of Hg, as below this the vapor pressure of mercury amounted to more than 1 percent of the total pressure in the McLeod gauge system. However, the lowest four experimental points fell on the nitrogen, methane, and ethylene curves, which are all identical here, and so it was assumed for pressures below this that the butane calibration was also identical with that of the above three.

The calibration curves for all the gases were of similar shape starting out from the origin as straight lines and gradually dropping off from linearity at higher pressures. Curves of this shape may be represented analytically by an equation of the type

$$y=Ax/(1+Bx) \tag{1}$$

in which y represents the deflection of the foil, $(D-D^\circ)$; x represents the pressure, $(p-p^\circ)$; and A and B are constants characterizing the shape of the curve. Transposing and dividing by x one obtains

$$\frac{y}{x}=A-By \tag{2}$$

which is an equation of a straight line. By adapting the results given in Table I to this equation, it was possible to evaluate A and B for the calibration curve of each gas by applying the method of least squares. The values obtained are given in columns two and three of Table II.

According to Knudsen's theory of the radiometer gauge, the calibration curves for all gases should start out from the origin as straight lines, all having the same slope. This is predicted by his theoretical equation

$$K=\frac{p}{2}\left[\left(\frac{T_1}{T_2}\right)^{\frac{1}{2}}-1\right] \tag{3}$$

where T_1 and T_2 are the absolute temperatures of the heater and the aluminum leaf, respectively; p is the pressure of the gas in the instrument; and K is the repelling force being measured. This equation was derived[2] from simple kinetic theory considerations and the assumption that the distance between the heater and the movable leaf is vanishingly small compared to the mean free path of the gas molecules. Because of this latter assumption, Knudsen's simple linear relationship is applicable only at low pressures, the magnitude of which depend on the geometry of the particular gauge. At higher pressures, as the mean free path of the gas molecules decreases, there results a gradual dropping off from linearity. Since the mean free path varies from one gas to another, it is to be expected that the calibration curves of different gases will begin to drop off from linearity at different pressures, and that they will drop off different amounts as the pressure increases. An examination of our sensitive calibration curve reveals the fact that the curves are all straight lines up to a pressure of about 20×10^{-6} mm of Hg, corresponding to a deflection of about 0.5 mm. In addition, all of these lines, except that for hydrogen, have the same slope within the precision of measurement. This is illustrated in column four of Table II in which the slopes of the curves are given at a deflection of 0.200 mm. These were calculated using the equation obtained upon differentiating Eq. (1); namely,

$$y'=\frac{A}{(1+Bx)^2}. \tag{4}$$

The slope for the hydrogen calibration is quite definitely lower than the others, about 9 percent in fact. This is probably due to the low accommodation coefficient which hydrogen undoubtedly exhibits with respect to the heater element. As a result, the hydrogen molecules rebounding from the heater have an energy corresponding to some temperature below T_1. Also, these molecules upon rebounding from the aluminum leaf have an energy corresponding to some temperature higher than T_2. Both of these effects cause a decrease in sensitivity of the gauge. Amdur, Jones, and

Pearlman[4] have measured the accommodation coefficients of various gases on gas covered platinum at room temperature. They report a value of 0.316 for hydrogen. Beeck[5] has measured the accommodation coefficients of hydrogen and various hydrocarbons on clean nickel at 140°C. He reports 0.310 for hydrogen. With the exception of helium and deuterium, all the other gases investigated by the above authors lie roughly in the same vicinity: between 0.70 and 0.90. For all the other gases investigated by us, the calibration curves have the same slope in the low pressure region. This would seem to indicate that the gauge calibrations are not too sensitive to varying accommodation coefficients but are affected only by large variations or very low coefficients.

Though the calibration curves for the other gases investigated by us start out with the same slope in the low pressure region, there is a definite spreading of the curves as the pressure increases above 20×10^{-5} mm of Hg. From what has been said above one would expect those gases possessing the smallest mean free path to fall off the most from the initial linear relation and those possessing the largest mean free path, to fall off the least. An inspection of Eq. (1) shows that the greater the constant B is, the more the curve falls off from a straight line. An examination of Table II, in which the mean free paths are given for the different gases, illustrates that B increases as the mean free path decreases. These values of the mean free paths, with the exception of that given for butane, were taken from Kennard's "Kinetic Theory of Gases," page 149. The values given are for a pressure of one atmosphere and a temperature of 15°C. They are much smaller at one atmosphere than at the pressures existing in our gauge, but they exhibit the same relative magnitudes in either case. The value given for butane was calculated by the same method as that used by Kennard, the value for the viscosity being obtained from the data of Titani.[6] The viscosities of the two butanes are nearly identical and as a result the mean free paths are the same.

To determine the relationship between the mean free path and the rate at which the calibration curves fall off from a straight line, Eq. (4) was differentiated so that the rate at which the slope decreases may be evaluated. Equation (5) results:

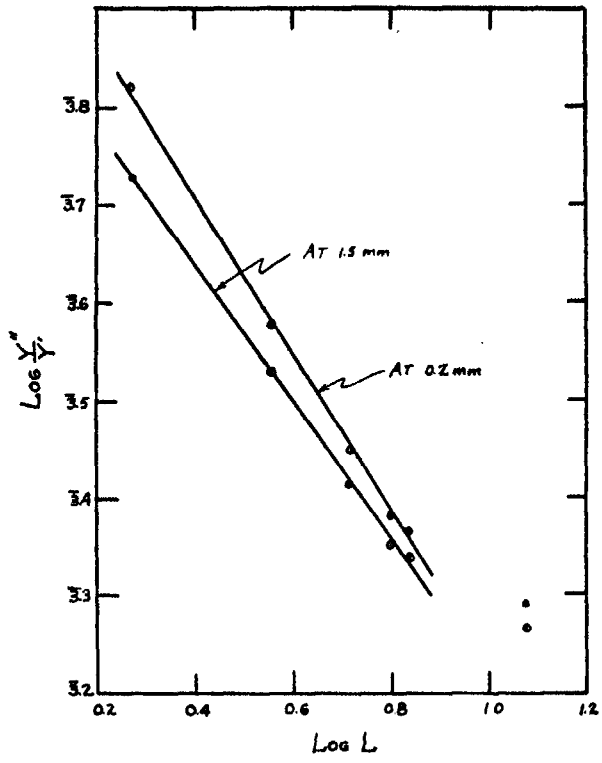

FIG. 2.

$$y''=-\frac{2AB}{(1+Bx)^3}. \qquad (5)$$

The values obtained for this at deflections of 0.200 mm and 1.500 mm are given in columns six and seven of Table II. The ratio of the rate at which the slope is decreasing to the slope itself is given in columns eight and nine for the same two deflections. A plot of this ratio, y''/y', *versus* the mean free path, L, indicated that the calibration curves for different gases dropped off exponentially with decreasing mean free path. A plot of $\log y''/y'$ versus $\log L$ for deflections of 0.200 mm and 1.500 mm, given in Fig. 2, confirms this exponential relationship. With the exception of hydrogen, all the gases lie on a straight line.

TABLE II. Characteristics of the calibration curves.

Gas	A	B	y' at 0.200 mm	y' at 1.500 mm	y'' at 0.200 mm	y'' at 1.500 mm	y''/y' at 0.200 mm	y''/y' at 1.500 mm	$L\times 10^6$ (cm)
H_2	0.02193	$0.0_3 9833$	0.0215	0.0191	$-0.0_4 420$	$-0.0_4 350$	$0.0_2 195$	$0.0_2 183$	11.8
O_2	0.02415	$0.0_2 1179$	0.0237	0.0207	$-0.0_4 553$	$-0.0_4 453$	$0.0_2 233$	$0.0_2 219$	6.79
N_2	0.02387	$0.0_2 1213$	0.0234	0.0204	$-0.0_4 561$	$-0.0_4 457$	$0.0_2 241$	$0.0_2 224$	6.28
CH_4	0.02393	$0.0_2 1422$	0.0234	0.0199	$-0.0_4 657$	$-0.0_4 514$	$0.0_2 281$	$0.0_2 259$	5.16
C_2H_4	0.02425	$0.0_2 1927$	0.0235	0.0188	$-0.0_4 891$	$-0.0_4 638$	$0.0_2 379$	$0.0_2 339$	3.61
C_4H_{10}	0.02467	$0.0_2 3418$	0.0233	0.0154	$-0.0_3 155$	$-0.0_4 836$	$0.0_2 665$	$0.0_2 541$	1.84

L (the mean free path) is given for a pressure of 1 atm. and a temperature of 15 degrees Centigrade.

---

[4] Amdur, Jones, and Pearlman, J. Chem. Phys. 12, 159 (1944).

[5] Otto Beeck, J. Chem. Phys. 4, 680 (1936).

[6] T. Titani, Bull. Chem. Soc. Japan, 5, 98 (1930).

The close adherence to such a relationship of all the gases except hydrogen suggests an empirical method by which calibration curves could be obtained for other gases knowing only the mean free path of the gas molecules and an approximate value of their accommodation coefficient. If the accommodation coefficient is in the range from 0.70 to 0.90, as it seems to be for most gases, it may be assumed that the initial slope of the curve at a deflection of 0.200 mm is approximately 0.0235. Hence, y' is known at a y of 0.200 mm. If L is known, a value of y''/y' for a y of 0.200 mm or any other chosen value of y may be obtained from a plot similar to that in Fig. 2. With this information, A and B in Eq. (1) may be evaluated as follows: Division of Eq. (5) by Eq. (4) yields

$$\frac{y''}{y'}=-\frac{2B}{1+Bx}. \tag{6}$$

Substitution of x in terms of y from Eq. (1) into this and into Eq. (4) yields

$$y'=\frac{(A-By)^2}{A} \tag{7}$$

and

$$\frac{y''}{y'}=-\frac{2B}{A}(A-By). \tag{8}$$

All the quantities in these two equations are known except A and B which may be obtained by solving simultaneously. These may then be placed in an equation of the same form as Eq. (1), giving the desired calibration. This method would not give results as accurate as actual experimental measurements, but they would probably be in error no more than a few percent. Its advantage lies in the fact that it may be used for gases whose pressures cannot be measured with a McLeod gauge and for which, therefore, the instrument could not be calibrated experimentally.

CONCLUSION

The results of this investigation indicate that this gauge may be operated with a mechanical precision of about plus or minus 0.5 percent and may be calibrated, with the aid of an accurate McLeod gauge, with an accuracy of around plus or minus 1 percent. In addition, the instrument is simple to construct and if properly mounted, is fairly rugged and quite dependable. Being of the deflecting leaf type of Knudsen gauge, it suffers from the disadvantage that it cannot be calibrated theoretically from its dimensions and operating conditions. However, for the relatively high pressure region in which we are interested, our results indicate that it is very unlikely that any type of Knudsen gauge would obey its theoretical calibration here with any accuracy approaching that desired by us. This arises from the difficulty in realizing a distance between the heater and leaf that is vanishingly small compared to the mean free path of the gas molecules. In our gauge where this distance is 1 mm at the lowest pressures obtainable, departures from the theoretical linear relationship appear at pressures in the vicinity of 20×10^{-5} mm of Hg in the case of nitrogen. The mean free path of nitrogen at this pressure is about 30 cm, or 200 times the distance between the heater and the leaf which is 1.5 mm at this pressure. Thus the distance between the heater and the leaf must be at least as small as 1/200 of the mean free path of the gas molecules at the given pressure in order for Knudsen's theoretical equation to be obeyed. This is a factor, the magnitude of which has not been fully appreciated by many investigators, and indicates the great difficulty which would be encountered in designing a Knudsen gauge of either type which would obey Eq. (2) up to a pressure of 10^{-3} mm of Hg.

THE REVIEW OF SCIENTIFIC INSTRUMENTS VOLUME 20, NUMBER 8 AUGUST, 1949

The Scintillation Counter. I. The Existence of Plateaus

LAWRENCE B. ROBINSON* AND JAMES R. ARNOLD
Institute for Nuclear Studies, University of Chicago, Chicago, Illinois

(Received February 1, 1949)

A method has been developed whereby inorganic phosphors can be mounted on a photo-multiplier tube in thin films. The ZnS:Ag phosphor is quite satisfactory for use in conjunction with the 931A photo-tube. Plateaus have been established similar to those associated with Geiger-Müller counter tubes and the associated circuits.

INTRODUCTION

RECENTLY the technique of detecting nuclear particles and quanta by using a photo-multiplier tube in conjunction with some fluorescent material (phosphor) has been highly developed. It is desirable to establish the existence of quantitative concepts (common to Geiger-Müller counters) in regard to the scintillation counter if this latter instrument is to be regarded as a "counter" rather than an instrument which gives some response to ionizing particles. A systematic study concerning the existence of these concepts is in progress and, in this report, some of the considerations necessary in establishing plateaus are discussed. In the investigation of the problem of the plateau, the writers found it necessary to compare the counting characteristics of several phosphors, to develop a technique of mounting the phosphors, and to test the performance of the instrument in a typical counting situation.

Three inorganic and two organic phosphors were examined. The inorganic phosphors were obtained in powder form through the courtesy of Dr. R. S. Holmes of the RCA Laboratories, Princeton, New Jersey. Two of the phosphors, ZnS:Ag, Cu, and ZnS:Ag are available commercially from the RCA (Victor Division, Lancaster, Pennsylvania) and the third, $BaSO_4$, is a product of Ilford, Ltd. The composition and spectral characteristics of the RCA phosphors have been described elsewhere.[1] The ZnS:Ag phosphor is presumably the same one as that used by Sherr.[2] The Ilford Phosphor emits a narrow band peaked at 3500A; its time constant is reported to be about one microsecond. The organic phosphors used were naphthalene and anthracene. The naphthalene was a c.p. (chemically pure) commercial product not further purified; the anthracene was purified in collaboration with Dr. Anthony Turkevich.

Alpha-particles from polonium were used as a source of radiation since the resulting pulses were expected to be large and relatively uniform in size. The results obtained are given in graphical form.

APPARATUS

The counting apparatus consists of a 931A photo-tube coupled with a Model 162 scaler (formerly Instrument Development Laboratories, now Nuclear Instrument and Chemical Corporation, Chicago, Illinois). The high voltage of the scaler was connected across both the 931A tube and a one-megohm resistor in series with the tube; resistances of 100,000 ohms were used to couple the stages of the photo-multiplier. The one-megohm resistor is placed in series with the tube, with a condenser to ground between it and the bleeder to reduce the ripple from the high voltage supply and the attendant pulses. Thus only half of the output from the power supply is across the tube. Pulses were taken off through a 50 condenser into the amplifier of the scaler, where they were amplified and counted in conventional fashion. The tube was mounted in a light-tight brass cylinder, with provision for the introduction of phosphors and samples. A slot sample holder insured reproducible sample geometry.

The scaler was furnished with a pulse discriminator, which allowed the minimum size of pulse sufficient to record to vary by a factor of about thirty. The pulse

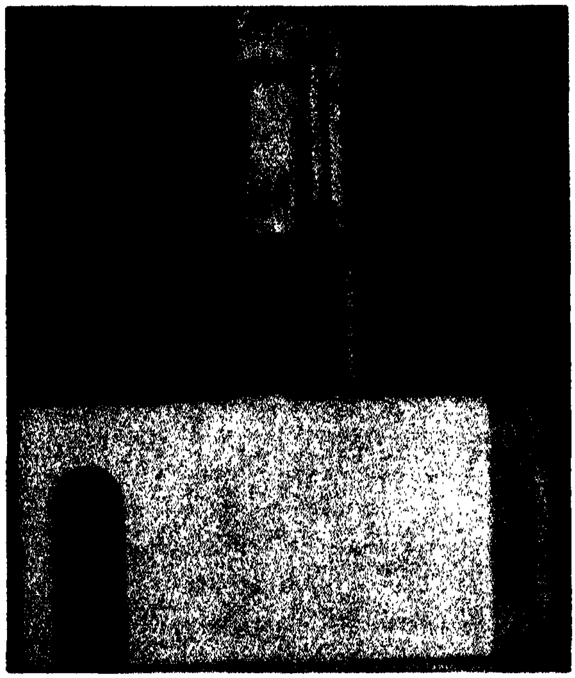

FIG. 1. A thin phosphor screen mounted on a photo-multiplier tube. All films used were about 10 mg/cm² thick.

---

* Present Address: Department of Physics, Howard University, Washington, D. C.

[1] RCA Review 7, 199–230 (1946).

[2] R. Sherr, Rev. Sci. Inst. 18, 767 (1947).

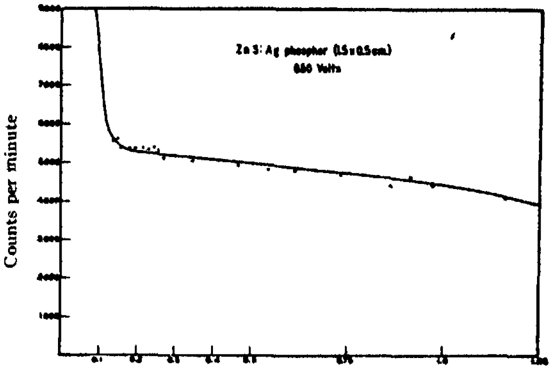

FIG. 2. Bias plateau curve.

discriminator was calibrated with a standard pulse generator.

A supply of 931A and 1P28 photo-tubes was obtained of which the 931A's seemed generally more satisfactory. Two of the six 931A's tried proved satisfactory.

MOUNTING OF INORGANIC PHOSPHORS

Since inorganic phosphors are, in general, opaque to their own radiation, it is desirable to have them mounted as a very thin film, if they are to be used for scintillation counting. One method for mounting these phosphors has been given by R. Sherr.[2] This method involves sprinkling the powder on the tube opposite the cathode and gently tapping the tube so that the powder moves about and leaves a thin layer behind. A volatile liquid is sprayed over the powder which leaves a reasonably stable film upon evaporation. This procedure cannot be used in experiments where a knowledge of the thickness of the film (mg/cm²) is desirable.

We have found the following procedure more satisfactory than Sherr's method of mounting thin films. A dilute solution of rubber cement in benzene (about 0.5 percent cement) is used to form a paste with the phosphor powder, about 0.1 ml of solution for every 200 mg of powder. A previously weighed cellophane strip is then moistened with the rubber cement solution. When the benzene on the cellophane evaporates, the paste can be rolled on the cellophane in any desired thickness with a glass rod. The film can be cut into any desired shape with a razor blade or any sharp cutting instrument. The cellophane strip can be reweighed and the thickness can be determined since the area of the film is easily obtained. The cellophane is then attached to the tube with Scotch Tape. A mounted film is shown in Fig. 1. The optimum size and shape of the film were established by considerations to be mentioned later.

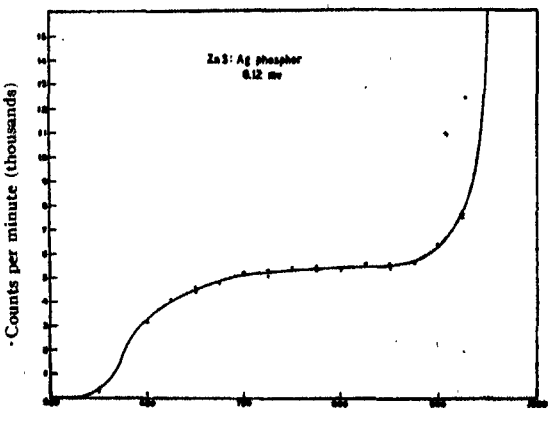

FIG. 3. Operating voltage plateau curve.

EXPERIMENTAL RESULTS

The Po alpha-source had been estimated to yield about 2×10^4 disintegrations per minute. The polonium film was covered with aluminum foil of 0.2 mg/cm² thickness.

Since Po provides an essentially monochromatic source of alpha-particles, one would expect that practically all of the light pulses produced in the phosphor would be of approximately the same intensity. Thus the ideal graph representing counting rate *vs.* pulse height would be similar to the range curve for collimated alphas, i.e., a long flat portion with quite a sharp cut-off, where the slope of the cut-off results from alpha particles straggling. Figure 2 shows a typical curve for the ZnS: Ag phosphor. The abscissa indicates the minimum height of the recording pulses. There is a flat region from 0.1 to 0.8 mv, in which the counting rate changes by 6 percent. In the large pulse region there is a slow drop in a count rate, indicating that there is a broad distribution of pulse heights. In the region of low bias the curve rises steeply, although the background with the sample removed is still small. This unusually high counting rate in the region of small pulses was ascribed to long-lived phosphorescence induced by alpha-particle bombardment. Despite the absence of ideal behavior at either extreme, it will be seen that the ZnS: Ag phosphor is excellently suited to counting alpha-particles.

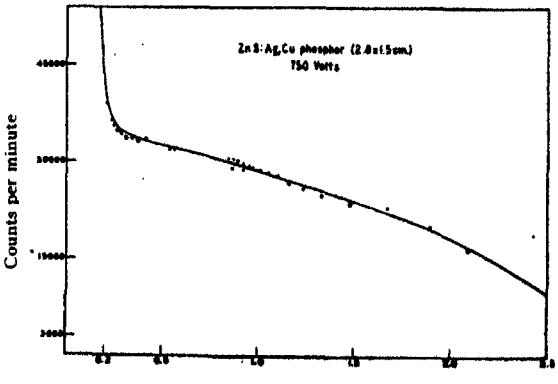

FIG. 4. Bias plateau curve.

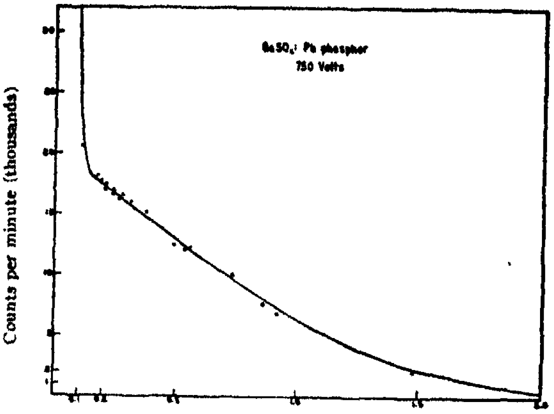

FIG. 5. Bias plateau curve.

A monochromator was used in an attempt to determine the cause of the inhomogeneity of pulse heights. The monochromator consisted of a metal plate about 2 mm thick with a number of 1-mm holes drilled through it. No sharpening of the upper end of the bias curve was observed, indicating that the inhomogeneity of the alpha-particles from the source was not a major source of the spread. Since the tube container was not evacuated, some inhomogeneity could have resulted from collision of alpha-particles with air molecules. The alpha-particles had approximately 2.5-Mev energy upon arriving at the screen.

Changing the operating voltage changes the height of the pulses from the multiplier tube. Thus a curve showing counting rate *vs.* operating voltage is essentially the same as the bias curve discussed above. With a proper choice of pulse height, a plot of counting rate *vs.* operating voltage shows a plateau of the type characteristic of Geiger-Müller tubes. Such a curve is shown in Fig. 3. The plateau is about 400 volts long, and shows a slope of 2 percent per hundred volts.

Figure 4 shows the results obtained using the ZnS:Ag, Cu phosphor. When exposed to daylight, and even artificial lighting, this phosphor shows an intense afterglow which decays with a ten-minute half-life. Thus one must wait three or four hours after assembling the apparatus before measurements can be made. The counting characteristics of this phosphor are apparently not as good as those of ZnS:Ag. The flat region is considerably shorter, while the behavior at the two ends of the bias curve is substantially the same.

The results obtained with $BaSO_4$:Pb are given in Fig. 5. It is apparent that this is the least satisfactory of the three. There is no well established plateau region, while the "turn-up" at low bias begins before the true counting rate has been achieved.

Eastman c.p. anthracene was purified by a process of alternate sublimation from fused KOH and recrystallization from benzene and acetone. The phosphor was mounted in the form of a large flake, about 20 mg/cm² in thickness, directly on the counter tube. Figure 6 shows the behavior of this material. The response is seen to be fairly good, although the pulses are much smaller in size; i.e., they have the same height at 875 volts as the ZnS:Ag pulses at 750 volts. From the gain curve of the tube (Fig. 7), we conclude that the anthracene pulses are about threefold smaller. At 875 volts the tube background at room temperature rises rapidly at low bias. The gain curve as given in Fig. 7 is a plot of bias voltage *vs.* operating voltage with constant counting rate.

Naphthalene in the form of a clear lump 2×1.5×0.3 cm was mounted on the tube with Duco cement. This material gave a poor response to alpha-particles, and was not studied further in this connection. Results are shown in the same graph with anthracene.

To test the counter as a working instrument, a determination was made of the half-life of ThB, on the suggestion of Dr. Truman P. Kohman. The phosphor used was ZnS:Ag, the tube was operated at 650 volts, at a pulse selector setting of 0.24 mv. Lead was plated out without carrier from a solution of $Th(NO_3)_4$ (the salt having stood for several years without purification). The ThB activity obtained could then be followed through its decay products ThC and ThC′. The initial count obtained was about 800 counts/minute; the decay was followed for over six half-lives (Fig. 8). The half-life of 11.2 hours taken from the curve is in good agreement with the literature value of 10.6 hours.[3] An attempt to determine the background of the instrument at this setting resulted in 3 counts in 140 minutes. An intense source of gamma-radiation in the vicinity of the tube produced no increase in background.

REMARKS

The establishment of plateaus with the scintillation counter is in some respects similar to temperature saturation in a two element vacuum tube. Pulses of varying sizes exist in the fluorescence radiation from the phosphors. As the sensitivity of the tube is increased by increasing the operating voltage, the count-

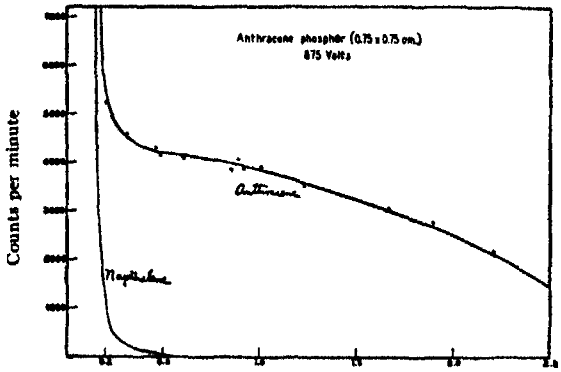

FIG. 6. Bias plateau curve.

---

[3] K. Siegbahn, Arkiv. f. Mat. Astr. o. Fys. 30A, No. 20 (1944).

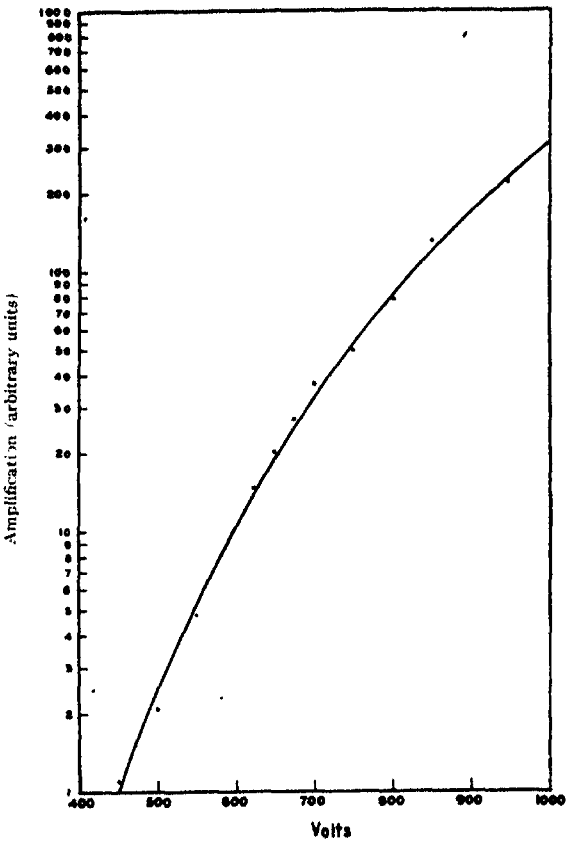

FIG. 7. Amplification as a function of operating voltage.

ing rate will increase because more and more smaller pulses will be registered by the scaler. (This same action can be obtained by keeping the operating voltage fixed and varying the bias control.) Finally when the stage has reached such that all of the pulses produced by ionizing particles are counted by the scaler, further increase in the operating voltage (with the bias voltage fixed) cannot increase the counting rate. When the voltage becomes higher than the desirable operating point (or the tube becomes very sensitive), then other effects occur not characteristic of the actual counting rate alone.

It is then apparent that if the total number of pulses in the fluorescence radiation produced by the alpha-bombardment is small, the plateau will begin at a relatively low voltage and persist for quite some time before effects not characteristic of the true counting rate obtain. On the other hand it is sometimes desirable to operate a higher counting rate. That these two considerations had to be compromised guided these writers in the selection of the size of the phosphor screens. The size used in obtaining the data from which Fig. 2 is prepared was small enough to give a reasonable low counting rate and at the same time large enough to insure sufficient accuracy of counting. That the shape of the phosphor screen should be approximately the same as that as the sensitive element of the tube has also been recognized by others.[4]

An intercomparison of results shows that the response of the phosphor to nuclear radiation bombardment as well as similarity of the spectral characteristics of the phosphor and tube are also important considerations in establishing plateaus with the scintillation counter. The ZnS:Ag phosphor proved to be the best in these respects.

This counter is well suited for counting alpha-particles when films are used which are prepared in the manner described above. Thickness of about 10 mg/cm^2 correspond approximately to the range of the alpha-particles. Consequently practically all of their energy is transferred to the phosphor and the pulses produced are large. Beta- and gamma-radiation transfer a relatively small part of their energy (as a rule) in traversing matter of 10 mg/cm^2 thickness. When films of inorganic phosphors are made thicker, the desired results are not obtained since such films are opaque to their own fluorescence radiation; consequently the counting rate will decrease with increasing thickness. One of us (L.B.R.), with his colleagues and students at Howard University, is studying the problem of modifying the inorganic phosphor film preparations so that beta- and

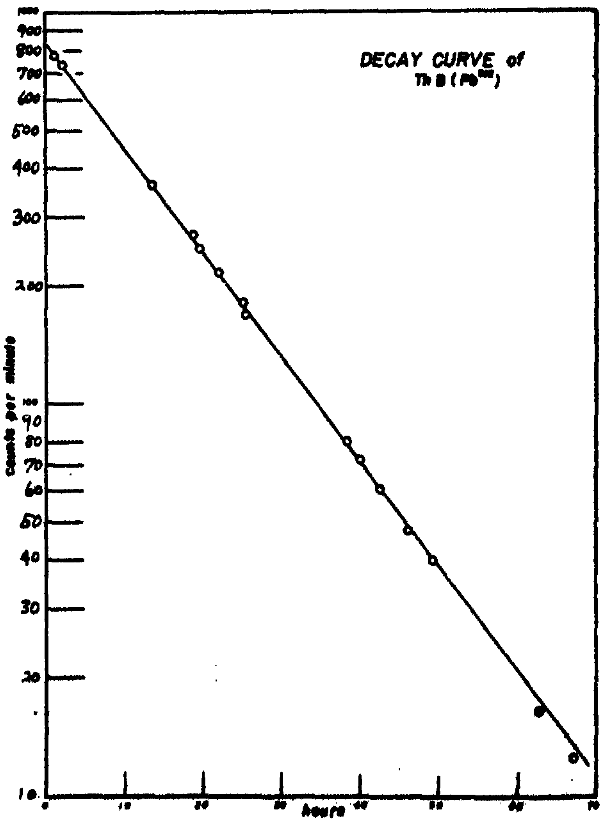

FIG. 8. Decay curve of thorium B.

---

[4] Marshall, Coltman, and Bennet, Rev. Sci. Inst. 19, 744 (1948).

gamma-radiation might be counted. The phosphor powder has been dispersed in a polystyrene base plastic; upon solidification, the translucent plastic can be cut into any size or shape desired. Varying degrees of transparency can be produced by controlling the concentration of the phosphor powder. Details of the results will be submitted in other articles in this series.

We conclude that the scintillation counter, under the conditions described above, is an excellent instrument for counting alpha-particles down to very low specific activity.

The authors are indebted to a number of colleagues for advice and assistance, particularly Dr. John A. Simpson, Jr., Dr. James S. Allen, and Mr. Ernest C. Anderson. They are equally indebted to Dr. W. F. Libby for making available space and equipment for the research, and to the Viking Fund for supporting it in part.

THE REVIEW OF SCIENTIFIC INSTRUMENTS VOLUME 20, NUMBER 8 AUGUST, 1949

The Use of Multigrid Tubes as Electrometers

J. R. PRESCOTT
Melbourne University, Melbourne, Australia

(Received January 25, 1949)

The use of several types of multigrid tubes as electrometers has been investigated. They are shown to possess a number of advantages. Details are given for the 6BE6 and 7A8. Grid currents of between 10^{-13} and 10^{-14} amp. are obtainable with mutual conductances of the order of 5 microamp./volt and an amplification factor of 300.

THE use of conventional tube types as reduced grid current tubes (electrometers) has been described by a number of authors.[1–5]

Multigrid tubes (having five or more grids), ordinarily used as mixers and converters, appear to possess a number of advantages over other types used as electrometers, particularly if grid currents of the order of 10^{-13} amp. can be tolerated.

The present communication describes the results of tests on a selection of multigrid tubes in which the following types were studied: 6BE6, 7A8, 6D8, 1R5, 6SB7-Y. Of these only the 6BE6 and 7A8 proved suitable. The 1R5 and 6SB7-Y were cut off when operated at the low plate voltages necessary to achieve electrometer operation. The 6D8 was rejected because of the impossibility of achieving sufficiently low leakage current between the control grid and other electrodes. This is presumably due to the internal structure, as the control grid is brought out to a cap on the top of the glass envelope and special treatment of the glass did not improve the inter-electrode insulation.

ADVANTAGES OF THE MULTIGRID TUBE

The following sources of grid current in electrometer tubes are discussed by Metcalf and Thompson:[6]

(a) Leakage over glass or insulation,
(b) Ions formed by gas present in the tube,
(c) Thermionic grid emission due to heating of grid by filament power,
(d) Ions emitted by the filament,
(e) Photoelectrons emitted from the grid under the action of light from the filament, and
(f) Photoelectrons emitted by the control grid under the action of soft x-rays produced by the normal anode current.

These represent a positive ion current or its equivalent when the control grid is sufficiently negative to repel all electrons.

The contribution from (b) (gas ionization) may be cut down by operating the tube with much reduced potentials on the plate and screen. Metcalf and Thompson[6] recommend 8 volts as an upper limit. Further reduction in potential is necessary to reduce (f).

In multigrid tubes the screen, which is at a positive potential, completely encloses the control grid and will effectively reduce the number of positive ions formed in the gas which reaches that grid. This permits slightly higher operating potentials. It performs the same function for the positive ions emitted by the cathode. This is the chief source of positive ions at low plate and screen potentials.[6]

The positive grid current can be further reduced by operating the first or second grid or both at a negative potential of up to 2 volts. The effect is twofold: (1) the total current to the plate and screen is reduced and with it the ionization of the residual gas, and (2) the grid constitutes a negative

---

[1] E. A. Johnston, and C. Neitzert, Rev. Sci. Inst. 5, 196 (1934).
[2] P. A. Macdonald, Physics 7, 265 (1936).
[3] G. H. Gabus and M. L. Poole, Rev. Sci. Inst. 8, 196 (1937).
[4] C. E. Nielsen, Rev. Sci. Inst. 18, 18 (1947).
[5] H. S. Aaker, Electronics 20, 138 (June 1947).
[6] G. F. Metcalf, and B. J. Thompson, Phys. Rev. 36, 1489 (1930).

potential "trap" which removes many of the positive ions emitted from the cathode.

Due to the disposition of the electrodes, conventional electrometer tubes and other tube types used as electrometers have an amplification factor of about 1. This is a disadvantage, particularly when the tube is used as the first stage of a direct coupled amplifier where maximum gain is sought with a minimum number of stages of amplification. Since multigrid tubes have a pentode structure between the control grid and the plate, they exhibit the high amplification factor associated with such a structure. In the tubes tested, this factor was of the order of 300.

In amplifiers where electrometer tubes are commonly employed, it is customary to use substantial degenerative feedback. Such feedback can be applied with convenience directly to one of the first two grids. This avoids the necessity for feeding back to the control grid through its very high impedance, a process which results in an appreciable time lag in the application of the degenerative signal. Application of feedback to the control grid is in any case impossible if the input stage is to be operated with the control grid floating. The 7A8 also possesses the peculiarity that under certain conditions plate current is almost independent of heater potential from 2.6 to 3.0 volts. These features will be discussed in greater detail below.

MEASUREMENT OF GRID CURRENT

Two methods are commonly used for the measurement of grid current. For currents greater than about 10^{-12} amp. the method consists in noting the change in the plate current/control grid characteristic when a high resistance is inserted in the grid circuit. This method was used for some measurements in the present investigation. Contact potentials proved troublesome.

The second method, suitable for smaller currents, is to observe the time taken for the potential of the control grid, left floating, to drift over a specified range, using plate current as an indication of the grid potential. The grid current can then be calculated from the known capacity of the grid circuit.

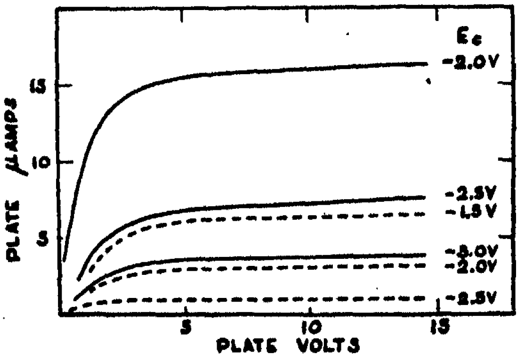

FIG. 1. Pentode plate characteristics for 6BE6 No. N18. Broken and continuous lines correspond to filament potentials of 3 and 4 volts, respectively.

The tube under test was enclosed in a sealed metal box to shield it from light and minor electrical disturbances. It was unnecessary to shield any of the other circuit components, see also Nielsen.[4] The box was not evacuated but contained phosphorus pentoxide as a drying agent. Initially, measurements of actual grid current were carried out after the box had been left sealed overnight, but a test set of measurements taken without drying agent in the box showed no significant difference between "dried" and "non-dried" tubes.

The 6BE6 is a miniature type with the pins sealed directly into the glass envelope. The 7A8 has a loktal base. The pins are sealed directly into the glass and project through holes in the metal base which is readily removed without damage to the tube. After soldering short flexible leads directly to the pins, the surface of the glass was treated in the following way to improve its insulation, with very satisfactory results. After washing with soap, water, and alcohol the glass is sprayed with diethyl-dichlor-silane. This polymerizes on the surface of the glass to form a monolayer of water repellant silicone polymer which is very closely adherent. After further washing with hot water and alcohol to remove excess silane the valve is baked at 70°C and coated with ceresin wax. With this treatment the leakage to the grid pin was usually too small to be detected by "rate of leak" methods using an electroscope. In one or two cases where this was not so, it was found that the leakage resistance could be satisfactorily increased by scraping off again as much of the wax as possible and washing in alcohol. After this discovery (which was accidental) all tubes were given the same treatment. That this apparently elaborate technique was justified is shown by the freedom from trouble due to leakage currents both in the tests and in apparatus using the tubes over a considerable period.

CHARACTERISTICS OF THE 6BE6 AND 7A8

The necessity for reducing the potentials on screen, plate, and filament to a low value has been discussed. In specially designed electrometer tubes such as the FP54 or D-96475, plate potentials may be as low as 4 volts. In using as electrometers, tubes that are normally designed to operate at potentials of some hundreds of volts, it is not always possible to reduce the plate potential as low as this without reducing the plate current and mutual conductance to values too small for practical use. Of these the second is the more important. In choosing operating potentials it is necessary to strike a balance between smallness of grid current and adequate plate current and mutual conductance. Once the collecting potentials are appreciably less than the ionization potential of the residual gas the main source of positive grid current is the emission of ions from the cathode. Under these conditions lowering the heater voltage is more effective in reducing the grid current than lowering the plate voltage. In the present investigation plate and screen potentials were of the order of 9 volts and the heaters, normally rated at 6.3 volts were run at values between 2.5 and 4 volts.

The 6BE6

(a) *Plate Characteristics*

Figure 1 shows plate characteristics of 6BE6 No. N18 for a screen potential of 9.3 volts, heater potentials of 4 and 3 volts and grid 1 connected to cathode (experimental points are omitted). These are typical pentode characteristics.

(b) *Effect of Potential of the First Grid* (g_1)

In Fig. 2 are shown characteristics of plate current against grid voltage for different potentials on g_1 together with the corresponding grid current curves. The ordinate of the latter is plotted on a logarithmic scale, zero grid current is arbitrarily taken at 10^{-14} amp. Heater potential is 4 volts. Screen and plate are operated at 9.3 volts. As expected, increasing the negative bias on the first grid results in a decrease in the grid current. Crosses on both plots indicate corresponding experimental points for 3 volts on the filament and $E_{g1}=0$. Thus grid current can be reduced either by a lowering of heater potential or by increasing the bias on g_1. Both of these also alter the cathode current. It is possible to predict the grid current for a specified combination of E_{fil} and E_{g1} with given E_p from a graph of grid current on the flat portion of the grid characteristic against cathode current.

Grid current was a linear function of cathode current up to 600 microamp., a change in cathode current of 100 microamp. giving an increase in grid current of 6×10^{-14} amp.

An increase in plate potential produces an increase in slope of the line. This characteristic is useful in selecting an operating point where the first grid is to be used for the application of negative feedback in direct coupled amplifiers. Knowing the d.c. level of the feedback, one can choose the filament voltage within limits to give the required grid current.

TABLE I.

	Grid and plate characteristics			6BE6 No. N18
Screen	9.3	9.3	9.3	Volts
Plate	9.3	9.3	9.3	Volts
Heater	4	4	3	Volts
Control grid	−2.7	−2.2	−2.4	Volts
Grid g_1	−0.2	−0.4	0	Volts
i_p	4.2	3.4	2.7	μa
g_{op}	6	4.3	2.6	μa/Volt
μ	330	300	220	
i_g	16	6	5	$\times10^{-14}$ amp.

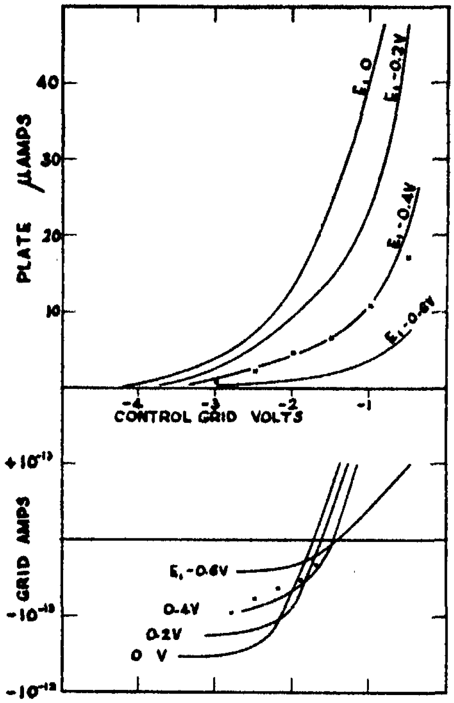

FIG. 2. Plate and grid current characteristics for 6BE6 No. N18—effect of grid g_1.

(c) *Uniformity of Tubes*

Of the six type 6BE6 tested, none differed from the others by more than 10 percent in its plate characteristics. Of the six, two proved unsuitable for electrometer applications because of excessive grid current. Three of the tubes, including the two latter, also showed, under certain conditions, an increase in plate current when the potential on g_1 was increased from 0 to about 0.15 volts negative. Beyond 0.15 volts the plate current again decreased. Care must be exercised in using tubes with this characteristic to avoid positive feedback when negative feedback is intended. Table I summarizes the data for the 6BE6.

The 7A8

The 7A8 tubes tested exhibited characteristics very different from those of the 6BE6. Figure 3 shows the plate current characteristics as a function of E_f with 10.8 volts on plate and screen and g_1 0 volts. These curves exhibit a marked plateau in the neighborhood of 2.8 volts where the plate current not only fails to increase with increasing E_f

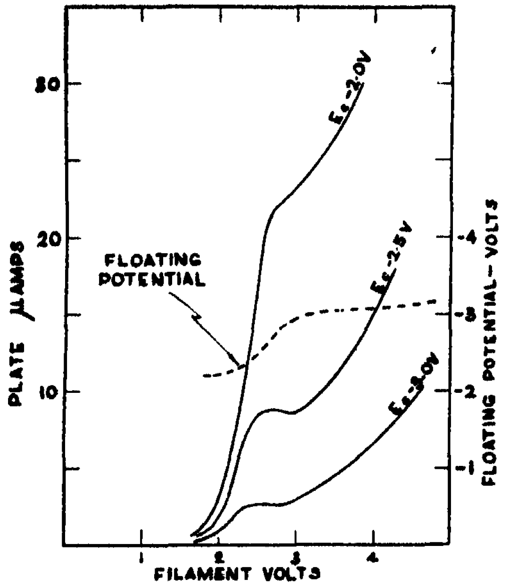

FIG. 3. Plate current and floating grid potential for 7A8 No. I—effect of filament potential.

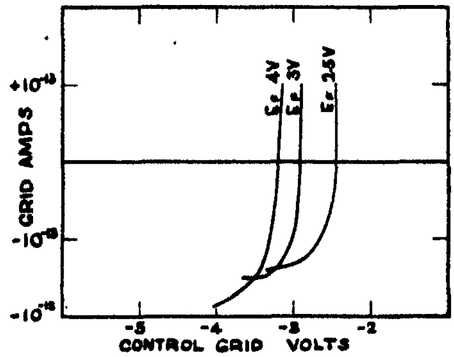

FIG. 4. Grid characteristics for 7A8 No. I—effect of filament potential with grid g_1 O. Volt.

but may actually fall by a small amount. The explanation of this can be found in the onset of space-charge conditions at about 2.5 volts. This effect, which may for convenience be called the "plateau effect," lends itself to a useful application. One of the disadvantages of direct coupled amplifiers designed for long period operation is drift of the zero, caused mainly by falling filament potential in the first stage. Using the 7A8 as the first stage and operating it with E_f 2.8 volts this drift can be virtually eliminated. In an amplifier built to record cosmic ray burst in an ionization chamber, the plate current in the final stage fell from 80 to 60 microamp. when the filament supply to the first stage was changed by 0.5 volts. Using a 6BE6 in the same circuit, a change of about 0.1 volts in E_f was sufficient to reduce the plate current in the final stage to zero.

The usefulness of the plateau effect would be nullified if it were not possible to operate the tube on an appropriate portion of the grid current characteristic curve, namely at a control grid potential more negative than that at which the grid floats. In Fig. 3 the broken curve indicates the floating potential of the grid. It will be noted that the control grid must be operated at negative potentials greater than 3 volts to satisfy this condition, with consequent small values of plate current.

Figure 4 shows the grid current characteristics for different values of E_f with 10.8 volts on plate and screen and g_1 0 volts. It will be seen from this figure that in order to profit from the plateau effect it must be possible to tolerate a grid current of the order of 5×10^{-13} amp.

EFFECT OF GRIDS 1 AND 2 (g_1 AND g_2)

Much smaller values of grid current can be achieved by running g_1 at a negative potential. Increasing E_{g1} at first causes an increase in plate current (up to about 0.5 volts) after which plate current again decreases. For $E_{g1}=-1.0$ volts, the plate current has fallen to the value it had at $E_{g1}=0$. At the same time the plateau effect becomes progressively less pronounced and disappears entirely when E_{g1} is -0.5 volts. This corresponds with the plate current maximum.

Plate and grid current characteristics are shown in Fig. 5 with $E_{g1}=-1$ volt and E_f as a parameter. Plate and screen are at 10.8 volts. The linearity of the plate characteristics is interesting. Similar

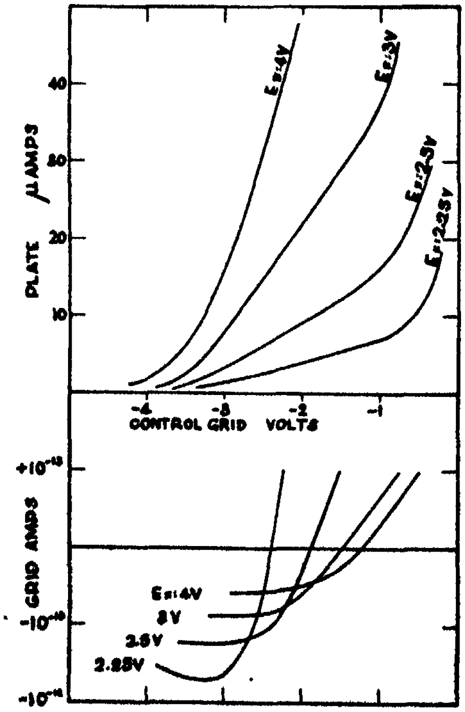

FIG. 5. Plate and grid characteristics for 7A8 No. I—effect of filament potential with grid g_1 at -1 volt. In the lower half of the figure, values of E_f should read from above: 2.25 V, 2.5 V, 3 V, and 4 V.

curves were obtained for a plate and screen potential of 9.3 volts.

g_2 has a much smaller control over plate current than either g_1 or the control grid (a factor of 10 in the latter case) and does not give the increase in plate current produced by g_1 for small negative voltages. Negative feedback may therefore be conveniently applied to g_2 at a d.c. level of up to 3 or 4 volts negative.

Table II summarizes the data for the 7A8. None of the tubes of this type tested differed by more than 15 percent in either plate or grid characteristics. The smallest value of grid current obtained (not shown in the table) was 3×10^{-14} amp.

TABLE II.

	Grid and plate characteristics 7A8 No. I					
Screen	10.8	10.8	10.8	9.3	9.3	Volt
Plate	10.8	10.8	10.8	9.3	9.3	Volt
Heater	2.8	4	2.5	4	4	Volt
Control grid	−3.2	−3.3	−2.8	−3.6	−3.0	Volt
grid g_1	0	−1.0	−1.0	0	−1.0	Volt
grid g_2	0	0	0	0	0	Volt
i_p	2	5	2.1	1	2.3	μa
g_{gp}	4.4	9.2	2.9	2	7	μa/volt
μ	260	350	200	200	300	
i_g	30	63	7	50	13	amp. $\times10^{-14}$

The corresponding values of the various electrode potentials were: $E_p=E_s$, 9.3 volts; E_{g1}, -1.0 volts, E_{g2}, 0 volts; E_f, 3 volts; E_c, -1.8 volts; i_p, $1\mu a$; g_{gp}, $3\mu a$/volt; μ, 180.

EFFECT OF PLATE POTENTIAL ON GRID CURRENT

For a given screen potential a change in plate potential had no significant effect on grid current except for potentials 5 or 6 volts greater, when the grid current begins to increase. At the same time the floating potential moves to less negative values. This effect has been described by Nielsen.[4]

DISCUSSION

It is clear from the characteristics that the low plate current and mutual conductance make multigrid "electrometers" unsuitable for use directly with a current measuring instrument as the indicator unless it is of high sensitivity. If this type of recording is required, the tube may be used in a simple circuit such as that described by Roberts.[7] An instrument similar to Roberts's and using the 6BE6 was designed and has operated successfully over a period of several months as a sensitive millivoltmeter.

Both the 6BE6 and 7A8 have operated successfully as the input stage of a portable direct coupled amplifier used in this laboratory for recording cosmic-ray ionization chamber bursts. The advantages of the 7A8 in minimizing drift have already been mentioned in this connection.

ACKNOWLEDGMENT

The work described was performed as part of the program of the Nuclear Physics Section of the Council for Scientific and Industrial Research.

---

[7] S. Roberts, Rev. Sci. Inst. 10, 181 (1939).

THE REVIEW OF SCIENTIFIC INSTRUMENTS VOLUME 20, NUMBER 8 AUGUST, 1949

A High Current Ion Source

RICHARD B. SETLOW
Sloane Physics Laboratory, Yale University, New Haven, Connecticut*

(Received April 11, 1949)

An ion source is described which utilizes a hot cathode as an electron source and an axial magnetic field for focusing. The electron beam is pulsed for 250 μsec. 60 times a second. Peak ion currents of 100 ma are readily obtainable. At a hydrogen pressure of 25 microns of Hg the proton content of the beam is between 30 and 40 percent. Constructional details and operating conditions are given.

I. INTRODUCTION

THE ion source to be described was designed for use in a high-current resonant cavity proton accelerator.[1] The accelerator, in the last stages of construction, is expected to yield a peak voltage of the order of 10^6 volts at a peak power of 10^6 watts for 250 μsec. repeated 60 times a second. The accelerating distance is about 4 cm. Hence the focusing problem is not of great importance and high-density ion beams may be used. Many different types of ion sources have been described.[2] It was felt that an ion source using a hot cathode and an axial magnetic field would supply the necessary ion current. Thus a source similar to one described by Finkelstein[3] was constructed and tested under pulsed operation. Peak positive ion currents from hydrogen gas of the order of 100 ma were readily obtained.

II. GENERAL OPERATION

A schematic diagram of the ion source is shown in Fig. 1. The electrodes are made of $\frac{1}{32}$-inch copper sheet. The filament supports are $\frac{1}{4}$-inch copper rods hollowed for internal water cooling. These pass through glass sleeves in the end plate, and are waxed over to supply the vacuum joint. The ion source is mounted horizontally inside a three-inch copper tee, the lower opening of which leads to pressure gauges and a diffusion pump with a throat four inches in diameter.

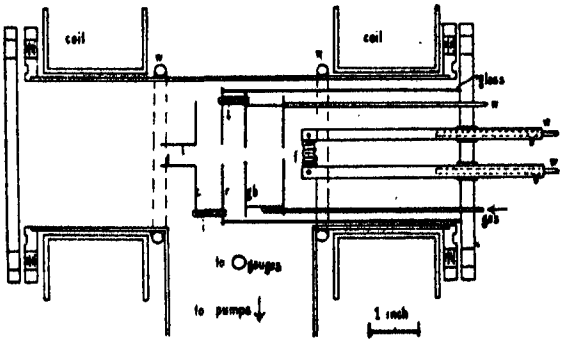

FIG. 1. Schematic diagram of ion source. *f*: filament; *gb*: gas box; *r*: retarding electrode; *c*: collector; *w*: water cooling; *i*: insulators.

The filament and retarding electrode are at ground potential and the gas box is at a positive potential. Electrons emitted by the filament are accelerated toward and pass through the gas box, are then stopped by the retarding potential and return to the filament if they have made no inelastic collisions. The electron beam is focused by an axial magnetic field produced by two air-core coils mounted on the outside of the copper tee. The coils are similar to those described by Finkelstein. In the region of the gas box the electrons bombard hydrogen gas and produce ions which may diffuse out of the field-free region and be accelerated toward either the filament or the collector. The positive-ion space charge is neutralized by the focused electron beam and the beam is well collimated.

Since about half the positive ions formed bombard the filament, it was felt that a pure metal emitter would have a longer life than an oxide-coated one. Accordingly, the filaments were made of 1-mil tantalum foil of $\frac{1}{4}\times\frac{1}{2}$ inch area. The foil was crimped by means of a rack and pinion and then made circular so as to be out of the direct path of the positive-ion beam. More efficient filament structures could undoubtedly be designed. Tantalum was used because it is easier to work cold than tungsten, and has a higher electron emission at ordinary filament temperatures.

It seemed advisable for several reasons to pulse the ion beam. First, under pulsed operation the filament

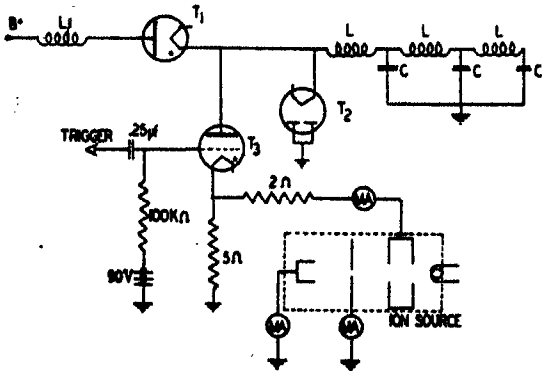

FIG. 2. Ion source power supply. *L*: 160 μh; *C*: 10 μf; L_1: 0.8 h; T_1: 872; T_2: 5R4GY; T_3: GL-5545(GE); *B*+ : 0–300 volts.

---

* Assisted by the joint program of ONR and AEC.

[1] Kolstad, Schultz, and Montgomery, Phys. Rev. 73, 1258 (1948).

[2] For example, S. K. Allison, Rev. Sci. Inst. 19, 291 (1948); R. N. Hall, Rev. Sci. Inst. 19, 905 (1948).

[3] A. T. Finkelstein, Rev. Sci. Inst. 11, 94 (1940).

life is longer, due to the smaller average positive-ion bombarding current. At high average currents the filament heats up from positive ion bombardment. At low currents the operation of the source is satisfactory.[4] Second, the volume of gas associated with a neutralized positive-ion beam of 100 ma is very large. In the present source, a mass-spectrographic analysis (see below) indicates that the ions H^+, H_2^+ and H_3^+ are about equally abundant. This implies that a 100-ma beam is equivalent to about 3500 liters/sec. of H_2 at a pressure of 10^{-5} mm Hg. This figure takes no account of ordinary diffusion from the ion source into the accelerator. Such pumping speeds are prohibitive in a relatively small instrument. Pulsing the ion beam, however, can reduce the average gas flow to amounts which can be handled without too much difficulty.

The ion source is pulsed by discharging an artificial transmission line through a resistance connected between the gas box and ground. The pulse length is 250 μsec. and the repetition rate is 60 sec.^{-1}. A circuit diagram is shown in Fig. 2. The impedance of the ion source varies from several hundred ohms at low currents to a few ohms at ion currents of the order of one ampere. To ensure a satisfactory match with the transmission line over this wide range of currents, the line had an impedance of 4 ohms and the resistance in parallel with the source was 5 ohms.

TABLE I. Typical operating values.*

Peak voltage (volts)	Peak electron emission (amp.)	Peak collector current (ma)
65	0.90	20
74	0.95	21
95	1.1	24
105	2.1	52
120	3.5	180
165	7.7	380
200	38	850

* Pressure: 25 microns; magnetic field: 600 gauss; filament power: 200 watts; gas: H_2.

TABLE II. Percentage ion content of positive-ion beam.*

Pressure (microns)	Peak voltage (volts)	H^+	H_2^+	H_3^+
27	110	36	38	26
27	180	43	30	27
19	180	31	47	23

* *Filament current adjusted to give peak ion current of 30 ma.*

III. OPERATING CHARACTERISTICS

About one-half of the positive-ion beam passes through the retarding electrode and is picked up by the collector. By making the collector positive with respect to the retarding electrode, it is possible to estimate the number of secondary electrons measured as positive-ion current. The secondary electron current is less than 10 percent of the collector current.

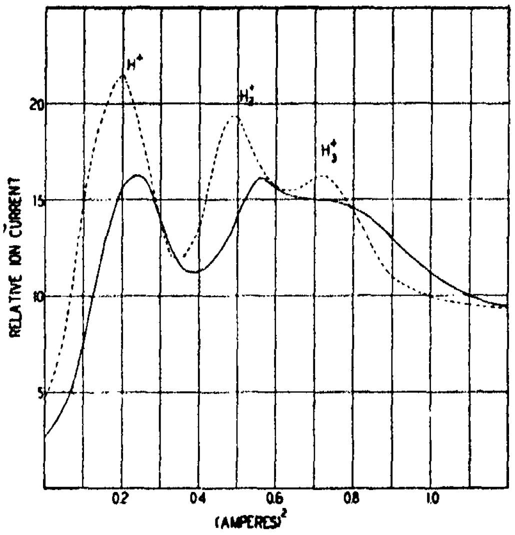

FIG. 3. Relative positive-ion current *versus* the square of the current through the deflecting magnet at a pressure of 27 microns. The solid curve corresponds to a peak voltage of 110 volts; the broken one to 180 volts.

The magnitude of the axial magnetic field does not seem important, although its alignment is rather critical. Variation of the field between 350 and 1000 gauss changes the positive-ion yield by about 50 percent.

The best operating pressure seems to be about 25 microns of Hg. The source will function steadily down to pressures of 15 microns, but below this the operation becomes erratic. These pressures were estimated from the pressure outside the source (see Fig. 1), the known rate of diffusion out of the source (about 20 *l*/sec.) and the measured speed of the oil diffusion pump (about 50 *l*/sec.). The pressures outside the source were two to four times lower than the pressures inside. This low pressure differential was due to the low speed of the oil diffusion pump at high fore-pressures.

In Table I are given typical operating values.

A mass spectrographic analysis of the ion beam was carried out. Since the diffusion pump used in this work was unable to maintain an adequate pressure differential between the gas box and external regions, the hole in the retarding electrode was decreased to $\frac{1}{16}$-inch diameter. This allowed a pressure of about 0.1 micron to be maintained in the mass spectrograph. Under these conditions the gas flow was 100 cm^3/hr. The collector was removed and a circular electrode with a $\frac{1}{4}$-inch hole put in its place. This electrode was kept about 5000 volts negative. The ions were deflected by a magnetic field, travelled about 25 cm and were received by a small collector connected to the vertical plates of an oscilloscope. The deflection of the beam was about 4 cm. With the above geometry, the ion mass-number is proportional to the square of the magnetic field strength.

Figure 3 shows the relative positive-ion current as a function of the square of the deflecting magnetic field. Obviously no attempt was made to focus the positive-ion beam. The areas under these curves represent the relative abundance of the ions. Table II shows the relative abundance under various conditions.

---

[4] F. Oppenheimer and A. Hudgins, MDDC-782 (Declassified March 17, 1947).

IV. CONCLUSION

The ion source described above is very stable under pulsed operation and can yield positive-ion currents as high as one ampere. At these high currents the filament lifetime is of the order of 10 minutes, whereas at ion currents of 100 ma it is at least several hours. Many improvements in design are possible. First among these is a more homogeneous magnetic field and electrodes shaped so as to produce focusing. The use of oxygen-free hydrogen gas might increase the filament life. The gas consumption, as would be expected, is very high, amounting to about 3 liters/hr. with a ½-inch exit hole. This of course raises the problem of maintaining a pressure differential between the ion source and an accelerator. Solution of this difficulty requires the use of a high-speed differential pumping system. It may be necessary also to pulse the gas flow. The operational characteristics of the ion source using helium or argon are approximately the same as for hydrogen.

The author wishes to express his thanks to Dr. Robert Spence for his assistance in the later phases of this work.

THE REVIEW OF SCIENTIFIC INSTRUMENTS VOLUME 20, NUMBER 8 AUGUST, 1949

A Scintillation Counter for Laboratory Counting of Alpha-Particles

J. D. Graves and J. P. Dyson
Naval Radiological Defense Laboratory, San Francisco 24, California

(Received March 1, 1949)

A simple, reliable, wide range alpha-counter has been developed which is suitable for the routine counting accompanying radiochemical laboratory analysis. This instrument utilizes the alpha-scintillation process in conjunction with a photomultiplier tube and a commercial Geiger tube power supply, amplifier, and scaler. Desirable features include low cost, ease of construction, ruggedness, and long life. Tests performed on the completed counter assembly indicated the following operating characteristics: a counting efficiency of 100 percent for 4–5 Mev alpha-particles; a resolving time limited by the electronic circuits (photomultiplier pulses have a rise time of about 0.5 microsecond); a counting rate unaffected by variations in temperature, humidity, or pressure; a background below 10 counts per hour. The chief undesirable feature is the small field of view for high sensitivity. Samples to be counted must be small, about ½ in.×½ in. maximum, and must be confined to a known region on the sample holder.

INTRODUCTION

An instrument for the routine measurement of alpha-particle activities is required for radiochemical analysis in the laboratory. Performance difficulties have been encountered with existing devices for this purpose: parallel-plate ionization chambers, gas-flow proportional counters, and thin-window Geiger tubes. The appearance of the early reports on scintillation counters[1,2] seemed to offer a new approach to the problem and led us to attempt the development of a simple, practical scintillation counting device for the systematic determination of alpha-activities.

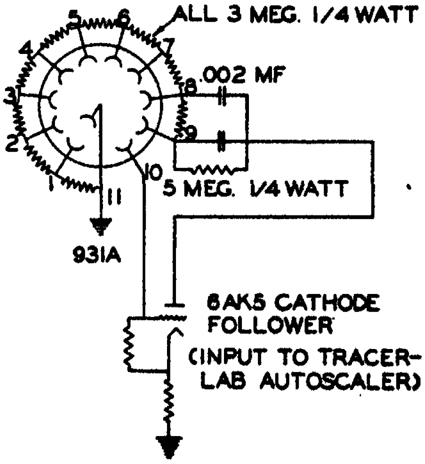

Fig. 1. Photomultiplier tube circuit used with a positive power supply.

To develop this method of detection into a reliable, practical instrument for routine laboratory counting, the following features were examined: electronic circuits, photo-tube, sensitive screen.

THE DEVELOPMENT

The Electronic Circuits

The requirements placed on the electronic circuits were primarily that they be adequate to insure proper operation of the device and secondarily that they be simple and preferably utilize arrangements already in-

---

[1] R. Sherr, Rev. Sci. Inst. 16, 757 (1947).

[2] Fitz-Hugh Marshall and J. W. Coltman, "The photo-multiplier radiation detector," Phys. Rev 72, 528A (1947).

corporated in existing equipment. Tracerlab[3] "Autoscalers" proved adequate for the high voltage supply, discriminator and scaling unit.

Circuits for the photomultiplier tube are shown in Figs. 1 and 2. In each case terminal number 11 is the photosensitive cathode; terminals 1 through 9 are the dynodes; and terminal number 10 is the anode. The voltage dropping resistors between the electrodes are equal and have a value from 1 to 10 megohms, depending on the current available. The anode is isolated from the other electrodes to eliminate pick-up and to prevent pulses from being transmitted to the anode through the circuit.

With a positive power supply available, the output of the photomultiplier tube is connected directly to the grid of the cathode follower in order to isolate the anode.

In the event that a scaling unit which does not include a built-in power supply is used, a negative power supply (Fig. 2) is satisfactory and utilizes a simpler circuit.

Work done with auxiliary amplifiers, discriminators, and filters has established the fact that they do not add to the efficiency of the counter as here employed for counting the alpha-activity of radioactive samples. It is true, however, that the limit of fast counting, or the resolving time of the assembly, is set by the amplifier-scaler, not by the photomultiplier tube or phosphor.

Photomultiplier Tube

The characteristics required of photomultiplier tubes for scintillation counting were known from previous work to be found in selected models of the RCA Type 931A. Since it is one of the least expensive photomultiplier tubes and is readily available, the 931A was chosen as a basis for design of a laboratory alpha-counter.

When voltage is applied to a photomultiplier, there exists in the anode output a dark current caused by the thermal emission of electrons from the surfaces within the tube. This dark current consists of pulses of about 0.1-microsecond duration and maximum amplitude of the order of 1 volt at room temperature with a tube voltage of 1 kilovolt. These dark current pulses must be discriminated against or they will be indistinguishable from the signal pulses to the scaling unit or counter at the anode output. The discriminator of the Autoscaler was found to be in the correct range for eliminating dark current at room temperature. The amplitude of the dark current pulses can be reduced to less than 0.01 of their amplitude at room temperature by cooling the tube to −196°C.

If the cathode of the tube is exposed to identical pulses of light of sufficient intensity to release electrons from the photosensitive surface but not to cause saturation, the pulses observed at the anode will not be identical. This is caused by the statistical dispersion of

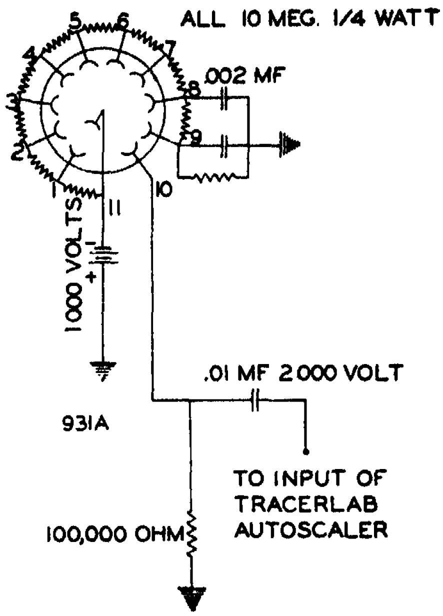

FIG. 2. Photomultiplier tube circuit used with a negative power supply.

the directions and numbers of secondary electrons emitted by the impact of each primary electron on the electron surfaces.[4,5] The anode pulse amplitude distribution extends from some minimum amplitude to a maximum amplitude which is a function of the intensity of the light pulses and the voltage on the tube. As mentioned previously, discrimination must take place to eliminate the dark current pulses. This necessarily results in the loss of those signal pulses lying below the level of discrimination. Fortunately, with the high efficiency phosphor used for alpha-particle detection, the resulting loss of detection efficiency was only of the order of a few percent.

Because a signal pulse height distribution exists and discrimination takes place at a fixed level, a variation in counting rate with applied voltage will occur. It is, therefore, necessary to determine the most efficient operating voltage and the voltage regulation needed to insure counting accuracy. Figure 3 is a graph of the counting rate *versus* applied voltage for two thicknesses of phosphor screen. A 5-Mev monoenergetic alpha-source was used 2 mm from the phosphor screen. In the case of the lighter screen the counting rate increases with applied voltage until all the pulses are above the fixed discriminator level. Thereafter the counting rate remains constant. There is a combination of fixed discriminator level and light signal input (screen thickness) which yields a flat counting rate. For such a combination, the requirements on voltage setting and regulation within the flat portion are very slight. In the case of the heavier screen, however, the counting rate will rise until the limit of the curve—the counting of the dark

---

[3] Tracerlab, Inc., 55 Oliver Street, Boston 10, Mass.

[4] Zworykin, Morton, and Malter, Proc. I. R. E. 24, 351 (1936).

[5] W. Shockley and J. R. Pierce, Proc. I. R. E. 26 321 (1938).

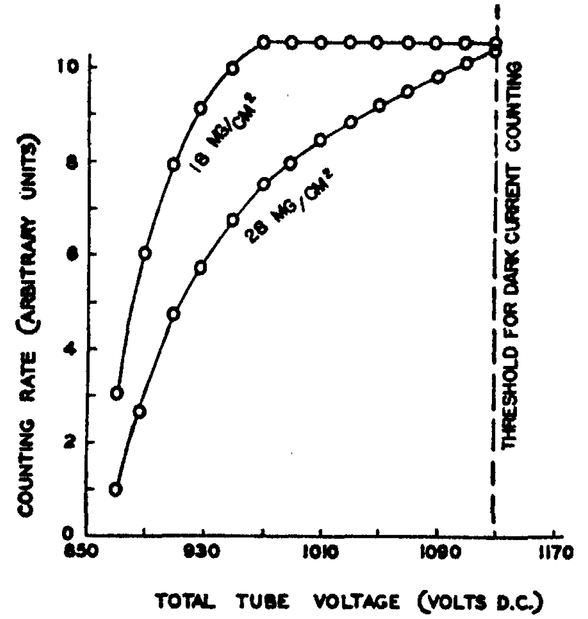

FIG. 3. Counting rate of the alpha-scintillation counter as a function of the photomultiplier tube voltage for two fluorescent screen thicknesses.

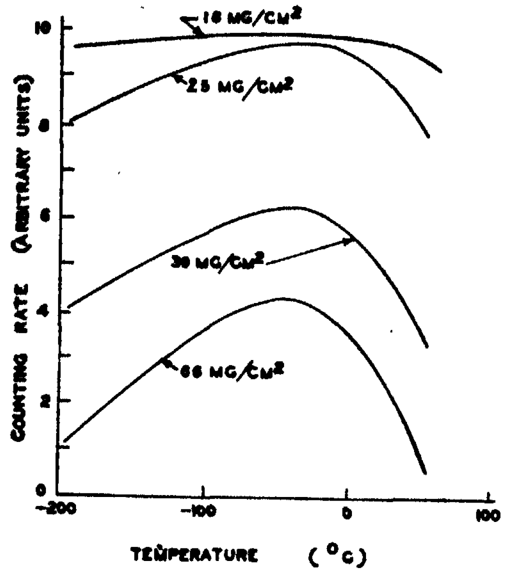

FIG. 4. Counting rate of the alpha-scintillation counter as a function of the fluorescent screen temperature for four fluorescent screen thicknesses.

current pulses—is reached. For such conditions, a 0.10–0.15 percent increase in counting rate per volt is observed. The curves of Fig. 3 were essentially the same for fifteen tubes tested with the exception that each entire curve shifts its position along the voltage axis for different tubes.

The area of light-emitting surface which may be detected efficiently by a 931A has been determined by measuring its field of view.[6] To perform this measurement, a small light source consisting of a fluorescent screen bombarded by a small alpha-source was moved across the outside of the tube envelope as close as possible to the photosensitive cathode. An area of approximately ½ in.×½ in. was observed to have a flat response of maximum sensitivity. An attempt to increase the area of this flat response by removing the source of light one inch from the tube envelope proved somewhat successful but reduced by a factor of 10 the light available to the cathode per scintillation. This small field of view places stringent restrictions on the size of the alpha-source which may be efficiently counted and also on the positions possible for both the fluorescent screen and the alpha-source.

Although the maximum rated output of the tube is 1.0 milliampere, for efficient counting the maximum allowable output current was found to be of the order of 1 microampere. Above this current value the tube begins to fatigue appreciably,[7] resulting in a decreased sensitivity for the tube. With a continuous output current above 1 microampere, the fatigue effect is characterized by an initial rapid decrease in sensitivity, followed by a gradual lessening in the rate of decrease, until after a few hours a very slight constant rate of decrease in sensitivity is reached. For a 3 microampere output the sensitivity is reduced about 12 percent after a period of 2 hours, whereas for an output of 23 microamperes the sensitivity decreases about 75 percent after 5 hours. The sensitivity of the tube will recover to its original value if it is not used for a period of several days after fatigue has taken place. After recovery, upon refatigue, there is no assurance that the sensitivity will decrease in the same pattern as before. Because of this uncertain efficiency of detection, the high counting rates corresponding to currents above 1 microampere are difficult to interpret into absolute terms (such as disintegrations per second from the source). Great care must therefore be taken in using the tube above 1-microampere output.

To determine the types of housing necessary for the 931A for use in the alpha-scintillation counter, the effects of electrical pick-up, mechanical shock, and exposure to external light while in the process of counting were examined. The tube was found to be very sensitive to electrical pick-up, which appeared as spurious counts recorded by the scaler. Complete metal shielding of the tube, tube circuits, and high voltage leads was necessary to eliminate the effects of pick-up. Any exterior light entering the tube while in operation appeared as an increase in the dark current level resulting in a decrease in the detection efficiency of the tube. It was necessary to completely shield the tube against any exterior light to eliminate this effect. The 931A is fairly non-microphonic and, enclosed in a housing as required for electrical and light shielding, was not affected by tapping with a hammer or dropping from a height of a few inches.

---

[6] K. G. Kessler and R. A. Wolfe, J. Opt. Soc. Am. 37, 1933–144 (1947).

[7] Marshall, Coltman, and Hunter, Rev. Sci. Inst. 18, 504 (1947).

Luminescent Screen

The first requirement of a luminescent material to be used in an alpha-scintillation counter is that upon bombardment by alpha-particles it produce scintillations which will appear at the anode of the photomultiplier tube (931A) as current pulses individually distinguishable by the counting circuit. On recommendation of manufacturers, several zinc sulfide phosphors were obtained and tested. Of these, Patterson D, a silver-activated zinc sulfide phosphor, fulfilled this first requirement most satisfactorily. In order to determine its characteristics and limitations, this phosphor was investigated in detail.

To obtain comparable results in the investigation of phosphors, a counter was built using interchangeable phosphor screens. The phosphor was mounted on microscope cover slips 22 mm×22 mm. The cover slips were cleaned by immersion in ethyl alcohol for 10 minutes, dried, and weighed to 0.1 mg. They were then placed in a small beaker with a few milliliters of amyl acetate and the desired amount of phosphor evenly distributed over the surface of the cover slip by gently bubbling air through the solution. The amyl acetate was removed and the phosphor dried. The phosphor was fixed to the surface of the glass by dropping controlled amounts of Duco All Purpose Fixative (1:30 in acetone) upon it, 0.1 mg/cm^2 of this binder being effective in securing the phosphor to the glass. The screen was dried, weighed, and the amount of phosphor per unit area calculated. Such screens were found to be generally uniform and resistant to abrasion and shock.

With the various standard phosphor screens available, it was possible to perform preliminary experiments which revealed a marked dependence on temperature in the counting rate of the scintillation counter. From a practical standpoint it is desirable to know the temperature of maximum efficiency and the temperature regulation which must be maintained for a given counting accuracy at any desired temperature. This information was obtained by measuring the counting rate with fixed discriminator of a scintillation counter using various screen thicknesses as the temperature of the phosphor was varied between −196°C and 50°C (Fig. 4). The percentage change in counting rate with a given change in temperature is observed to be less for decreasing weight per unit area of phosphors. In the case of the 18 mg/cm^2 screen, the long flat portion of the curve (Fig. 4) extending through room temperature is further evidence that all of the scintillations are of sufficient intensity to cause current pulses above the discrimination level throughout this region of temperatures. For these temperature measurements a special container (Fig. 5) was employed within which the 5-Mev-alpha-source, phosphor screen, and photomultiplier tube were contained. The temperature variations were achieved by an initial cooling followed by warming to room temperature and finally by heating in an oven. The special container was first immersed in a vacuum flask of liquid nitrogen. After temperature equilibrium was reached, the bath was discarded and the container placed within a non-operating oven where it was allowed to warm up slowly. Near room temperature the oven was employed to obtain further increases in temperature. The method was dynamic and, accordingly, the results are only approximate.

Effectively all of the temperature dependent variations in the counting rate of the alpha-scintillation counter are attributable to the phosphor. Tests without the phosphor showed that the photomultiplier amplification itself is relatively temperature insensitive. A blackened neon bulb was used in place of the scintillating phosphor and the photomultiplier showed no appreciable output variations with changing temperature. The neon bulb was of an intensity such as to cause a distribution of pulse heights in the output. For 120 pulses per second, about 90 were of a level to be passed by the discriminator and counted.

Randall[8] has found that with ultraviolet excitation many phosphors, including the activated zinc sulfides, exhibit intensities which are dependent upon temperature. The method employed here gives the number of pulses per second occurring above a fixed discriminator level which effectively is a measure of the variation in pulse height distribution and is independent of the total energy per pulse. In the method employed by Randall,

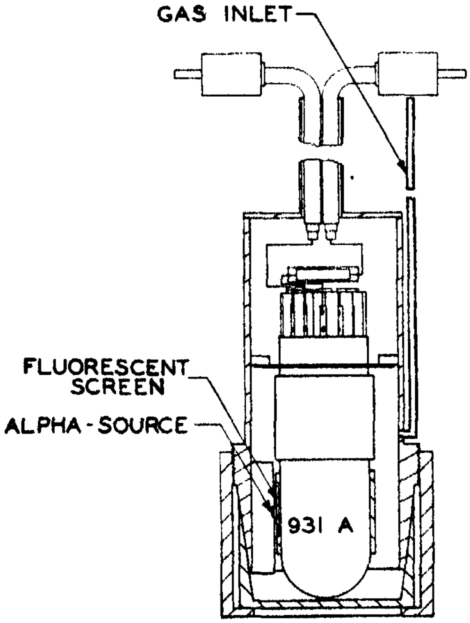

FIG. 5. Cross-sectional view of the apparatus used in the determination of the effect of reduced and elevated temperatures on the photomultiplier tube and fluorescent screen.

---

[8] J. T. Randall, Proc. Phys. Soc. London 49, 46–56 (1937).

the total energy output is measured. It is interesting to note that the variation in total energy output with temperature follows a curve similar to the variation in the pulse height distribution with temperature. This indicates that a change in efficiency occurs, and the change is characterized primarily by a change in amplitude or intensity of the light emitted rather than by any appreciable change in duration.

At any constant temperature, the intensity of the light incident upon the cathode of the photomultiplier tube may be expected to vary with the phosphor thickness due to the absorption and scattering of light produced within the phosphor and due to the relative fraction of the alpha-particle range absorbed therein. To determine maximum efficiency, it is therefore necessary to know the optimum thickness or weight per unit area at which this incident light is maximum. Figure 6 shows the effect of phosphor thickness on the counting rate using a constant 5-Mev alpha-source. It may be seen that the counting rate increases with decreasing weight until a weight of 25 mg/cm^2 is reached, whereupon the counting rate remains constant with a further decrease in phosphor weight. At about 8 mg/cm^2 the counting rate begins to decrease with further decrease in phosphor weight. This constant counting rate for a 200 percent increase in phosphor weight is desirable from the standpoint of screen construction in that it allows variations of phosphor thickness and distribution. Measurement of maximum pulse height throughout this flat portion showed a maximum at a phosphor weight of about 9 mg/cm^2, which is very nearly the range of the alpha-particle. It is evident that the reduction of light at the cathode is affected much less by absorption and scattering within the phosphor than by reduction of light produced within the phosphor. The constant counting rate between 8 mg/cm^2 and 25 mg/cm^2 indicates that essentially all of the signal pulses at the anode of the photomultiplier occur above the discrimination level.

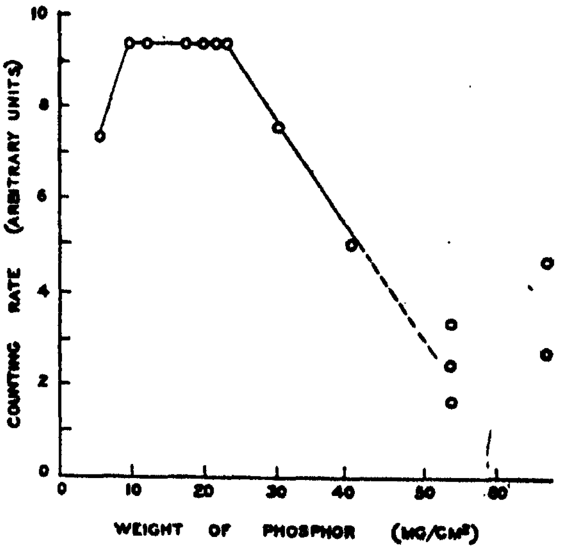

FIG. 6. Counting rate of the alpha-scintillation counter as a function of the fluorescent screen thickness. 5-Mev alpha-particles were used.

The maximum signal pulse height to dark current ratio for this 9 mg/cm^2 weight of phosphor was 18 to 1 with both tube and phosphor at room temperature. The ratio could be increased by better choice of tubes and by operation at a lower tube voltage. However, this ratio was more than sufficient to produce 100 percent counting efficiency.

The resolution possible due to the phosphor will be determined by the change in intensity of the light pulse with respect to time. The electrical pulse dimensions are determined primarily by the emission from the phosphor and the time constant of the associated circuit. These pulses are observed to be about 10 microseconds in duration with a rise time of about ½ microsecond. Using 5-Mev alpha-particles, the resolving time of the scintillation counter, exclusive of the counting circuit, approached ½ microsecond. This, however, is much less than the resolving time of our scaling unit and counters.

Complete shielding of the phosphor from light is necessary both before and during the period it is to be used as an alpha-scintillator. Exposure of the phosphor to daylight results not only in partial transmission of the light but also excitation of the phosphor, causing luminescence. Upon removal from the light the phosphorescence from the phosphor is detected by the photomultiplier and counting circuit for a period of several minutes. This is observed in the output of the photomultiplier as a general increase in the dark current level.

THE COUNTER ASSEMBLY

An exploded view of the complete alpha-scintillation counter based on the above developments is shown in Fig. 7. To facilitate complete interchangeability between the photomultiplier tube and phosphor screen, the phosphor was deposited on flat square microscope cover slips. This method also provided optimum counting geometry for the flat alpha-sources used. As was shown previously, these phosphor screens could vary in weight from 8 mg/cm^2 to about 25 mg/cm^2 with a constant counting efficiency for 5-Mev alpha-particles. A value of 16 mg/cm^2 was used in order to cover a large range of alpha-energies on either side of 5 Mev.

Due to the restricted field of view of the photomultiplier tube, it was important to maintain the phosphor screen in a fixed position with respect to the tube. This was accomplished by use of the screen holder shown in Fig. 7. A slot is provided to hold the screen. This holder clamps to the envelope of the tube and may be rotated until the screen is at an optimum position.

The tube, tube circuit, and phosphor screen are contained in a light-tight metal box. In order to maintain complete darkness within the box while alpha-samples are being changed, a recessed tray which slides under the phosphor screen on light-tight tracks is provided to hold the alpha-sample. Stops are provided to assure correct positioning of the alpha-sample with respect to the phosphor.

The high voltage input and signal output leads are brought out of the counter housing through low-loss connectors. From there these leads continue to the cathode follower of the Autoscaler as shielded low loss coaxial cable.

THE COUNTER PERFORMANCE

For a 5-Mev alpha-source of about 100 disintegrations per second the counter exhibited a "geometry" of about 40 percent. The alpha-source was $\frac{3}{16}$ in. in diameter and was deposited on a platinum disk. Negligible self-absorption was present in the source. This "geometry" includes not only the solid angle subtended but all other factors such as the efficiency of the counter and back scattering. Considering the solid angle subtended by that portion of the phosphor screen which is usable due to the field of view of the photomultiplier, the efficiency of the counter is essentially 100 percent.

To check reproducibility, a continuous series of counts was made at room temperature for a period of four days with the alpha-source mentioned above. The results of this run were analyzed statistically, and the data were found to be consistent. No tube fatigue was noticed and the temperature effect was negligible. The tube was operated at 1000 volts total applied voltage and the temperature variation was about 15 degrees, from 65°F to 80°F.

The natural alpha-background of the scintillation counter proved to be so slight that it was unmeasurable to any degree of accuracy. Operation of the counter with the phosphor screen removed resulted in the counting circuit recording 150 counts over a 16-hour period. These counts were primarily due to the cosmic-ray and laboratory gamma-ray background and to the few very high dark current pulses which occur. Operation of the counter with the phosphor screen in place resulted in 156 counts in a 16-hour period. The total background could be reduced to less than one count per 16 hours by reducing the alpha-efficiency of the counter to 30 percent. In contrast to gas-type alpha-counters, the scintillation counter has a very small sensitive volume—the volume of the phosphor—which may be removed from all surfaces, except its own backing, a distance greater than the alpha-particle range. As a result, the alpha-background may be expected to be very low. Unfortunately, however, the photomultiplier tube is slightly sensitive to other more penetrating radiations and for this reason the small but definite background indicated above is observed. At maximum, the detection efficiency for these normal background radiations is only about 10^{-3} percent.

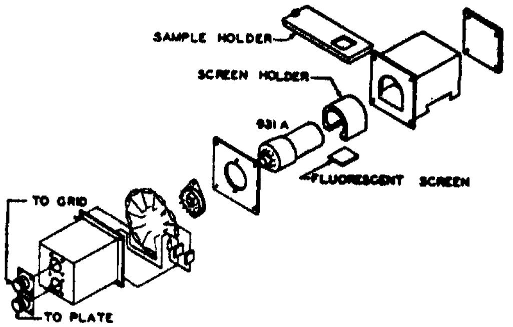

FIG. 7. Alpha-scintillation counter assembly.

The counter was found to be insensitive to applied tube voltage over the range from 950 volts to 1100 volts as indicated in Fig. 4. Striking the counter sharply with a metal bar produced no spurious counts, misalignment of counter elements, or injury of any kind to the counter.

CONCLUSIONS

The development of a scintillation counter for routine laboratory counting of alpha-particles has been described. The counter has many desirable features including:

(1) low cost,
(2) ease of construction,
(3) operation by standard Geiger tube electronic equipment,
(4) reproducibility,
(5) very long life,
(6) insensitivity to room temperature, humidity, or pressure variations,
(7) freedom from microphonic effects,
(8) ruggedness—no thin windows,
(9) very low background—normally below 10 counts per hour,
(10) approximately 100 percent counting efficiency for 4–5-Mev alpha-particles, and
(11) very short resolving time, of the order of 0.5 microsecond.

The chief undesirable feature is the small field of view for high sensitivity. Samples to be counted must be small, about $\frac{1}{4}$ in.×$\frac{1}{4}$ in. maximum (preferably smaller) and must be confined to a known region on the sample plate.

The properties of the alpha-scintillation counter are such as to make it a valuable instrument for the radiochemical laboratory.

An Improved Synchronous Detector*

WALTER C. MICHELS AND ESTHER D. REDDING
Bryn Mawr College, Bryn Mawr, Pennsylvania

(Received March 9, 1949)

The synchronous amplifier design of Michels and Curtis has been modified to minimize feedback and so to allow preamplification and high sensitivity. The resulting instrument has a voltage sensitivity of 2×10^6 mm/volt with an inductive input impedance of 2×10^6 ohms. The frequency selectivity is sufficiently sharp so that the band width is of the order of 0.25 c.p.s. at 800 c.p.s. Advantages and disadvantages of the synchronous detector are discussed.

INTRODUCTION

VARIOUS forms of synchronous detectors[1] have been described in the literature. Instruments of this type possess the common characteristic that they measure an alternating current signal by producing a beat note between this signal and a controlling alternating voltage of the same frequency and by applying this beat note to a deflection instrument which shows a maximum response at zero frequency. The interaction of the measured and controlling signals may be magnetic, in which case the two voltages are applied separately to the coils of an electrodynamometer galvanometer[2,3] or it may be electrostatic, in which case the voltages are applied respectively to corresponding elements of the two tubes of a balanced vacuum tube circuit.[4,5]

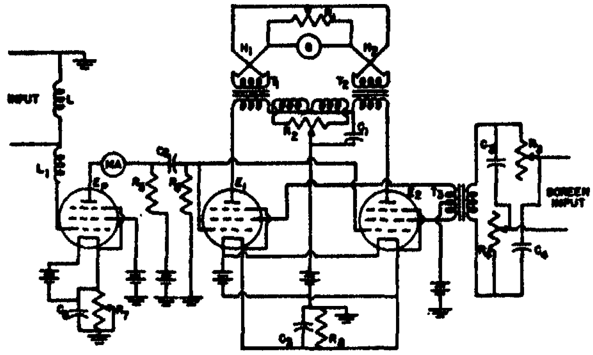

FIG. 1. Wiring diagram. $R_1=40$ ohms; $R_2=2000$ ohms; $R_5=10^5$ ohms; $R_6=10^6$ ohms; $R_7=10^4$ ohms; $R_8=500$ ohms; $C_2=0.25$ μf; $C_5=C_6=12$ μf; T_1 and T_2 are 500,000-ohm : 500-ohm transformers; H_1 and H_2 are vacuum thermocouples with 750-ohm heaters and 6-ohm couples; the screen supplies for all tubes and the plate supply for E_1 and E_2 are 90 volts; the plate supply for E_p is 300 volts; all other circuit constants are discussed in the text.

Synchronous detectors have certain distinct advantages over competing devices:

(1) The frequency selectivity is high and controllable, since it depends almost entirely on the period of the final deflection instrument.
(2) The detector is intrinsically phase selective.
(3) If the signal and the controlling voltage are supplied from the same source (or synchronized sources), the sensitivity is nearly independent of frequency variations in the source.
(4) The response to harmonic frequencies can be reduced to a very low level if the controlling voltage has good wave form.

In spite of these advantages, the synchronous detector has found only limited application. The most serious detriment to its wide use results from the fact that feedback is difficult to eliminate in any instrument to which there is supplied power of large magnitude compared with the signal, at the same frequency as that of the signal. Even small amounts of feedback may produce serious nonlinearities in the response of a synchronous detector of high sensitivity. Difficulties due to this cause limited the voltage sensitivity of the instrument reported in M-C to about 10^5 mm/volt and the input impedance to 10^4 ohms.

DESIGN OF THE DETECTOR

Some photoelectric work now in progress in this laboratory demands an instrument of high frequency selectivity and with a sensitivity of the order of 10^{12} mm/amp at frequencies of about 1000 c.p.s. The instrument to be described meets this requirement. A schematic diagram of the device is shown in Fig. 1. The synchronous detector proper, which utilizes the identical pentodes E_1 and E_2 ($1L4$), differs from the design described in M-C in only two important respects. The phase shifting network (R_3, R_4, C_3, C_4) has been inserted in the controlling voltage supply to the screens of the tubes, rather than between the signal source and the grids. The older arrangement resulted in a variable input impedance, while the present circuit takes advantage of the fact that the screen supply may be from a low impedance source. With R_3 and R_4 adjustable from 0–5000 ohms and C_3 and C_4 having capacitances of 0.05 μf, the impedance of the phase shifter at 800 c.p.s. varies between the limits 2000 ohms and 3000 ohms, so that a negligible load is placed on a transformer or alternator of less than 100 ohms impedance. The transformer T_3 has primary and secondary impedances of 180,000 and 20,000 ohms respectively, so that it, in turn, imposes only light loading on the phase shifter.

---

* A preliminary report on this instrument was presented to the Pasadena meeting of the Pacific Coast Section of the American Physical Society in June 1948.

[1] The term "lock-in amplifier," used previously by one of us, has been abandoned in favor of the present, more descriptive name for this type of instrument.

[2] Frank A. Laws, *Electrical Measurements* (McGraw-Hill Book Company, Inc., New York, 1938), second edition, p. 463.

[3] Walter C. Michels, *Advanced Electrical Measurements* (D. Van Nostrand Company, Inc., New York, 1941), second edition, pp. 155–156.

[4] C. R. Cosens, Proc. Phys. Soc. London 46, 818 (1934).

[5] Walter C. Michels and Norma L. Curtis, Rev. Sci, Inst. 12, 444 (1941). This reference will hereafter be referred to as M-C.

The second change is in the arrangement of the transformers T_1 and T_2 which couple the tubes to the vacuum thermocouples H_1 and H_2. These transformers have a 50,000-ohm: 500-ohm ratio. The large direct components of the plate currents (about 2 ma) are sufficient to saturate the cores of commercially available transformers of high impedance and to cause resultant distortion. To avoid saturation, the arrangement shown in the figure was adopted. The separate plate currents from the two tubes pass through one-half of the turns of each transformer primary, while half of the combined plate currents pass through the second half of the turns in the opposite sense to the currents in the first half. As is shown by Eq. (1) of M-C, the alternating components of the two plate currents are opposite in phase, so that the second half of each transformer winding carries only direct current. This current, assuming perfect balance of the two tubes, is identical with the direct current component in the first half. The condenser C_1, of one μf capacitance, bypasses any small alternating currents which may result from unbalance.

In the work for which this detector is designed, the small alternating signal to be measured is superimposed on a direct current signal of considerably greater magnitude. This fact and the high impedance of the signal source dictate an inductive input impedance. The best available choke for the purpose was one with an inductance of 700 *H* and a resistance of 6000 ohms (Thordardsen *T-37C36*). Because the impedance of this choke is only of the order of two megohms at the operating frequency, a voltage sensitivity of about 10^5 mm/v is required. This, in turn, demands preamplification. The preamplifier tube E_p is a 1*L*4, operated at a plate potential of 90 v and a grid bias of −3 v feedback to the input circuit is minimized in several ways:

(1) The batteries supplying the plate and screen voltages of the preamplifier are distinct from those supplying potentials to the detector stage.
(2) The transformer T_3 is shielded from the preamplifier by soft iron.
(3) The input choke *L* is mounted in a 6-mm thick iron case and is connected to the grid of the preamplifier by coaxial cable.

In spite of these precautions, a small amount of feedback was originally encountered. This feedback was quite reproducable, and was traced to magnetic coupling. It was satisfactorily eliminated by inserting the small coil L_1, consisting of four turns of about 1.5 cm diameter, in the input circuit. This coil is mounted near the transformers T_1 and T_2 in such a way that it can rotate about an axis perpendicular to itself. With the grid of the preamplifier grounded, it is easy to find a position of the coil which results in zero output of the detector. After the coil has been locked into this position, the sensitivity of the instrument is constant and the linearity good to better than one percent.

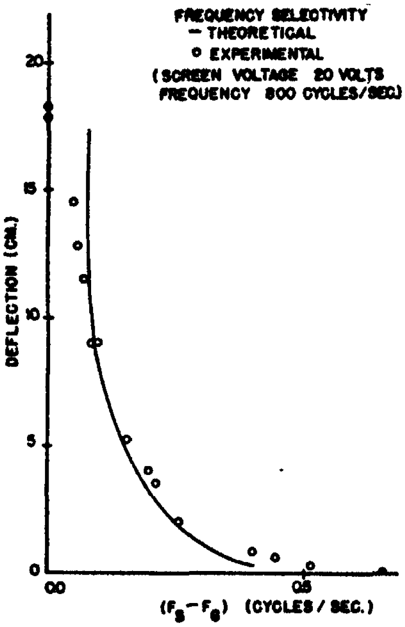

FIG. 2. Frequency selectivity curve. F_S is the frequency of the controlling voltage applied to the screens of E_1 and E_2, F_G is the frequency of the signal voltage applied to the grid of E_p. The amplitudes of both voltages were held constant for all readings.

The variable biasing resistor R_7 and the milliameter MA are used to maintain steady operating conditions regardless of the direct current component of the input. The direct component of the plate current of the preamplifier is maintained at two milliamperes by adjustment of R_7.

SENSITIVITY AND SELECTIVITY

The complete instrument, including batteries but excluding the input choke, has been mounted in a portable steel carrying case, weighing 35 lb. To achieve the desired sensitivity, however, it is necessary to use a high sensitivity galvanometer, which is not readily portable. The one used here is a Leeds and Northrup Type HS, with a sensitivity of 10^7 mm/volt and a resistance of about 20 ohms. With this galvanometer used as a deflection instrument and with a screen input voltage of 30 volts at 800 c.p.s., a sensitivity of 2×10^8 mm/volt or 4×10^{11} mm/amp can be obtained with excellent stability. Higher screen voltages cannot be used without introducing harmonic response, as the 1*L*4 tubes do not maintain linearity for screen grid swings appreciably in excess of ten volts r.m.s.

It is shown in M-C that the response of a synchronous detector falls off very rapidly with departure of the signal frequency f_G from the controlling frequency f_s. The difference of the output of the two tubes E_1 and E_2 is a complex wave, but it includes only one component, the beat frequency (f_G-f_s), which is sufficiently slowly varying for the thermocouples H_1 and H_2 to follow. If the thermal time constant of these couples is τ the galvanometer will be able to follow the beat frequency only if

$$|f_G-f_s|\leq 2\pi/\tau.$$

Letting $\omega=2\pi|f_G-f_s|$, this condition reduces to $\omega\tau\leq 1$. It is shown in Eq. (6) of M-C that the ratio of the sensitivity for any ω satisfying this condition to the sensitivity for $\omega=0$, is

$$\theta_\omega/\theta_0=\omega_0^2/(\omega^2-\omega_0^2)\omega\tau,$$

where ω_0 is 2π divided by the natural period of the galvanometer.

The solid line of Fig. 2 shows a plot of the theoretical deflection against the difference in frequency between the signal and controlling voltages. The circles show the observed deflections, which were obtained by applying to the input inductance a signal produced by two synchro-variable transformers. These transformers were excited by the same source that supplied the controlling voltage and were driven mechanically at measured speeds between one-tenth and ten revolutions per second.[6] It will be noticed that the agreement between measured and predicted deflections is excellent over the range of 0.1 to 0.3 c.p.s. The theory is not good below the lower limit, and the departure from the theoretical curve at the higher frequency differences is probably due both to noise and to small amounts of feedback. Even with these disturbances present, the $1/e$ width of the response curve is 0.24 c.p.s., and the response has dropped to 1.7 percent of maximum for a frequency difference of only 0.5 c.p.s.

This instrument was designed and built in connection with a program of work on the surface properties of solids which is being assisted by a Frederick Gardner Cottrell Grant of the Research Corporation. The authors wish to express their gratitude for this help.

---

[6] Deflections were not measurable at frequency differences between one and ten c.p.s.

THE REVIEW OF SCIENTIFIC INSTRUMENTS VOLUME 20, NUMBER 8 AUGUST, 1949

Counting with Geiger Counters

Homer E. Newell, Jr. and Eleanor C. Pressly
Naval Research Laboratory, Washington, D. C.

(Received April 1, 1949)

The coincidence rate of a perfectly efficient two-counter telescope is obtained in terms of the radiation intensity and the effective dimensions and separation of the counters comprising the telescope. Formulas are presented for the counting rate in a field of isotropic radiation and in a field where radiation varies with the zenith angle in accordance with a cosine squared law. By means of the formulas the counting rate may be located between an upper and a lower bound which in most practical cases differ by only a few percent. The information embodied in the formulas is also presented graphically in a form convenient for ready calculation of the ratio of coincidence rate to radiation intensity once the effective dimensions and separation of the counters are known.

PART A. ANALYSIS AND FORMULAS

I. INTRODUCTION

THE coincidence rate N_2 of a two-counter telescope is given by an expression of the form

$$N_2=GI,$$

where G is a factor which depends, among other things, upon the geometry of the telescope and the character of the radiation in which the telescope is embedded. If the radiation is isotropic, I is the unidirectional intensity factor; but if the radiation varies with zenith angle ζ in accordance with a cosine squared law, then I $\cos^2\zeta$ is the radiation intensity.

The isotropic case was discussed in a recent paper.[1] Subject to certain simplifying conditions, formulas were obtained expressing G as a function of the effective length, diameter, and separation of the counters. The underlying assumptions were:

- (*a*) that the effective volumes of the two counters comprising the telescope were exactly equal right circular cylinders;[2]
- (*b*) that the counters were placed with their axes parallel to each other and normal to the line joining the centers of the axes;
- (*c*) that the radiation surrounding the telescope traveled in rectilinear paths which were unaltered in traversing the telescope; and, finally,
- (*d*) that all and only those rays, the paths of which traversed both counters, were counted.

---

[1] H. E. Newell, Jr., Rev. Sci. Inst. 19, 384 (1948).

[2] Henceforth the term "counter" shall mean the effective volume of the counter.

Retaining the assumptions (*a*)–(*d*), the present paper continues the discussion of the isotropic case, and in addition treats the cosine squared law case. Part A contains an analytic discussion of the subject. In it formulas are presented which may be used to calculate the factor *G*. Curves for the graphical determination of N_2 in both the isotropic and cosine squared law cases are presented in Part B.

II. PRELIMINARY DISCUSSION

Select a set of mutually orthogonal axes *O-XYZ* in space, oriented with *OY* parallel to the counter axes and *OZ* parallel to the telescope axis, that is, to the line joining the centers of the counters. Consider an arbitrary ray *OR* making an acute angle η with *OZ*, as shown in Fig. 1. The ray may be thought of as the intersection of the two half-planes *YOR* and *XOR*. But these two half-planes are uniquely determined by the angles α and β which they respectively make with planes *YOZ* and *XOZ*. There is accordingly a bi-unique correspondence between the directions **OR** and the pairs $[\alpha, \beta]$. Both α and β are shown in Fig. 1 as great circle arcs on the unit sphere about *O* as center.

Let $\sigma(\alpha, \beta)$ be the plane area normal to *OR* which a ray travelling parallel to *OR* must cross in order to pass through both counters of the telescope. Then the coincidence rate of the telescope is given by

$$N_2 = \iint_{\Sigma} I(\alpha, \beta)\sigma(\alpha, \beta)d\Sigma, \qquad (2.1)$$

where $I(\alpha, \beta)$ is the unidirectional intensity factor in particles per unit area-unit solid angle-unit time, and Σ is the solid angle over which $\sigma(\alpha, \beta)$ does not vanish. In the earlier paper it was shown that σ is given over most of the range of integration by

$$\sigma = \frac{a^2}{(1-\sin^2\alpha \sin^2\beta)^{\frac{1}{2}}} \times \Bigg\{ (\delta - \sin\alpha)(\Delta \cos\beta - \cos^2\alpha \sin\beta) + \left[\frac{\delta^2}{4} \arccos \frac{2\sin\alpha - \delta}{\delta} + \tfrac{1}{2}(\delta - 2\sin\alpha)(\delta \sin\alpha - \sin^2\alpha)^{\frac{1}{2}} \right] \cos\alpha \sin\beta \Bigg\}, \qquad (2.2)$$

where $\delta = d/a$ and $\Delta = l/a$. The quantities *a*, *d*, and *l* are respectively the separation of the centers, the diameter, and the length of the counters.

III. FORMULAS FOR THE COINCIDENCE RATE: THE ISOTROPIC CASE

Using the expression (2.2) for $\sigma(\alpha, \beta)$, it was shown in the previous paper that N_2 in the isotropic case satisfies the inequality

$$N_{2m} \leq N_2 \leq N_{2M},$$

where[3]

$$N_{2m} = 8I \int_0^{\alpha_0} \int_0^{\beta_1(\alpha)} \sigma(\alpha, \beta) d\Sigma \qquad (3.1)$$

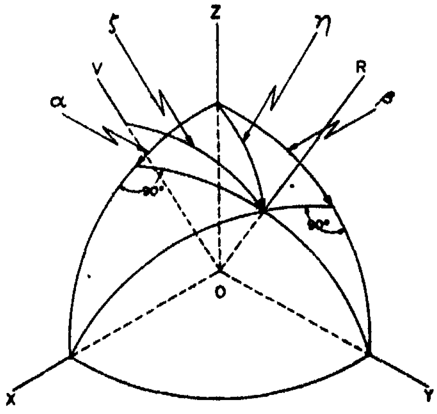

FIG. 1.

Fig. 2*a*. Counting rate of a two-counter telescope: isotropic case.

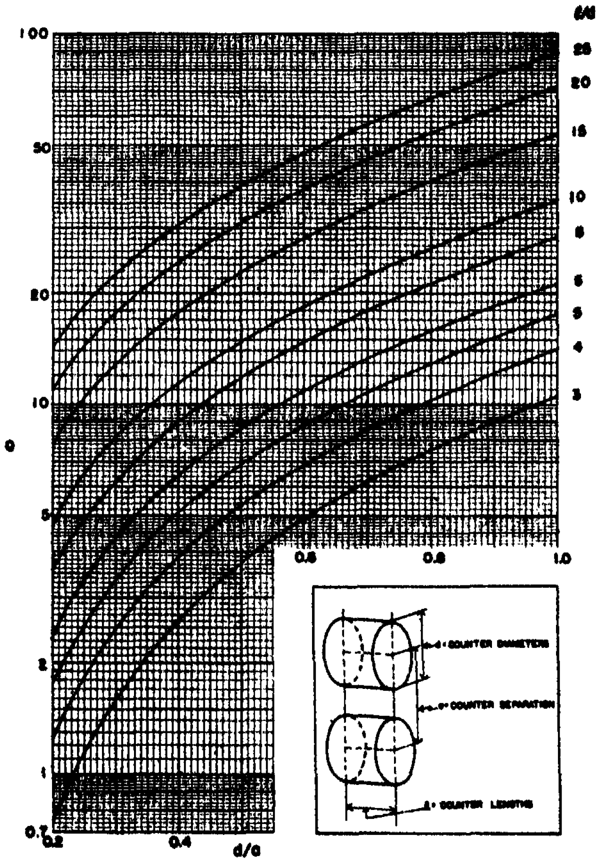

FIG. 2*a*. N_2 = Coincidences per unit time (from entire sphere). I = Unidirectional radiation intensity in particles per unit area—unit solid angle—unit time. (The number of particles crossing area $d\sigma$ in unit time from solid angle $d\Sigma$ in direction normal to $d\sigma$ is $I\,d\sigma d\Sigma$.) $N_2 = Qa^2I$. Formula used to calculate Q gives value too large by no more than E percent, Fig. 3.

Fig. 2*b*. Counting rate of a two-counter telescope: isotropic case.

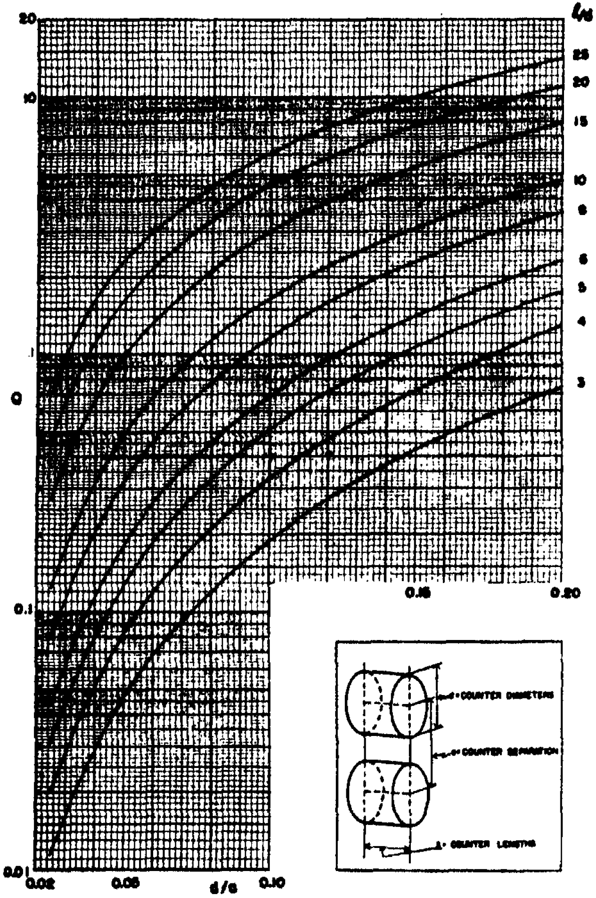

FIG. 2*b*. N_2 = Coincidences per unit time (from entire sphere). I = Unidirectional radiation intensity in particles per unit area—unit solid angle—unit time. (The number of particles crossing area $d\sigma$ in unit time from solid angle $d\Sigma$ in direction normal to $d\sigma$ is I $d\sigma d\Sigma$.) $N_2 = Qd^2$I. Formula used to calculate Q gives value too large by no more than E percent, Fig. 3.

$$N_{2M} = N_{2m} + 8I \int_0^{\alpha_0} \int_{\beta_1(\alpha)}^{\beta_0(\alpha)} \sigma(\alpha, \beta_1(\alpha)) d\Sigma. \tag{3.2}$$

$$d\Sigma = \frac{\cos\alpha \cos\beta}{[1-\sin^2\alpha \sin^2\beta]^{\frac{1}{2}}} d\beta d\alpha,$$

$$\beta_1(\alpha) = \text{arcctn}\left\{\frac{\cos\alpha}{\Delta}[\cos\alpha - (\delta \sin\alpha - \sin^2\alpha)^{\frac{1}{2}}]\right\}, \tag{3.3}$$

$$\beta_0(\alpha) = \text{arcctn}\left\{\frac{\cos\alpha}{\Delta}[\cos\alpha - (\delta^2 - \sin^2\alpha)^{\frac{1}{2}}]\right\}, \tag{3.4}$$

and

$$\alpha_0 = \arcsin\delta. \tag{3.5}$$

Here again $\delta = d/a$ and $\Delta = l/a$.

Integrating first with respect to β, the formulas for N_{2m} and N_{2M} become[3]

$$N_{2m} = 4a^2 I \int_0^{\alpha_0} \left\{ \Delta(\delta - \sin\alpha)\left[\arctan\frac{\Delta}{A} + \frac{\Delta A}{\Delta^2 + A^2}\right] - \frac{\Delta^2(\delta - \sin\alpha)\cos\alpha}{\Delta^2 + A^2} + \frac{\Delta^2 B}{\Delta^2 + A^2} \right\} d\alpha. \tag{3.6}$$

and

$$N_{2M} = N_{2m} + 8a^2 I \int_0^{\alpha_0} \frac{\Delta^2}{\Delta^2 + A^2} \{(\delta - \sin\alpha)(A - \cos\alpha) + B\} \times \left\{\left[\frac{\Delta^2 + A^2}{\Delta^2 + C^2}\right]^{\frac{1}{2}} - 1\right\} d\alpha; \tag{3.7}$$

Fig. 3. Closeness with which text formulas approximate counting rate of a two-counter telescope: isotropic case.

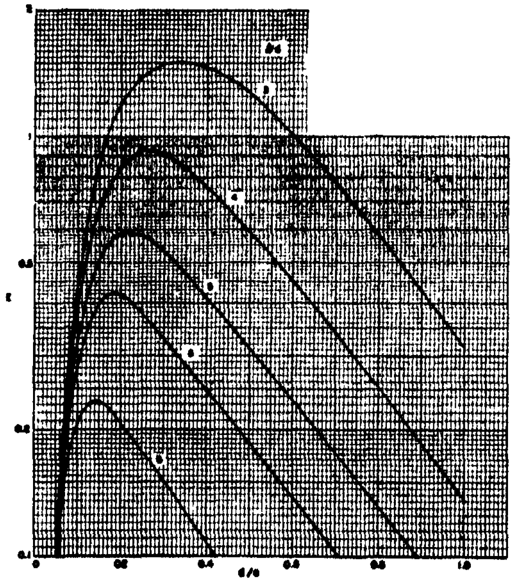

FIG. 3. N_2 = Coincidences per unit time (from entire sphere). N_{2m} given by 3.6. N_{2M} given by 3.7. Then $N_{2m} \leq N_2 \leq N_{2M}$. $E = 100(N_{2M} - N_{2m})/N_{2m}$.

where

$$A = \cos\alpha - (\delta \sin\alpha - \sin^2\alpha)^{\frac{1}{2}}, \tag{3.8}$$

$$B = \tfrac{1}{2}\left[\delta^2 \arccos\left(\frac{2\sin\alpha - \delta}{\delta}\right) + 2(\delta - 2\sin\alpha)(\delta \sin\alpha - \sin^2\alpha)^{\frac{1}{2}}\right], \tag{3.9}$$

and

$$C = \cos\alpha - (\delta^2 - \sin^2\alpha)^{\frac{1}{2}}. \tag{3.10}$$

For a single set of values of l, d, and a, the integrals in (3.6) and (3.7) can be evaluated graphically to within a fraction of a percent in a few hours. The percentage error in using these formulas to approximate N_2 does not exceed

---

[3] Note that (3.1), (3.2), (3.6) and (3.7) count all rays from the entire sphere which can cause coincidences.

$$E=100\frac{N_{2M}-N_{2m}}{N_{2m}}.$$

Graphs of E were presented in Fig. 6 of the previous paper, and are given in different form in Fig. 3 below.

IV. FORMULAS FOR THE COINCIDENCE RATE: THE COSINE SQUARED LAW CASE

When the radiation intensity varies with zenith angle ζ in accordance with a cosine squared law, $I(\alpha, \beta)$ is given by

$$I(\alpha, \beta)=I\cos^2\zeta(\alpha, \beta),$$

where I is constant. Formula (2.1) then becomes

$$N_2=I\int_\Sigma\int\cos^2\zeta(\alpha, \beta)\sigma(\alpha, \beta)d\Sigma.$$

Fig. 4*a*. Counting rate of a two-counter telescope: cosine squared law case.

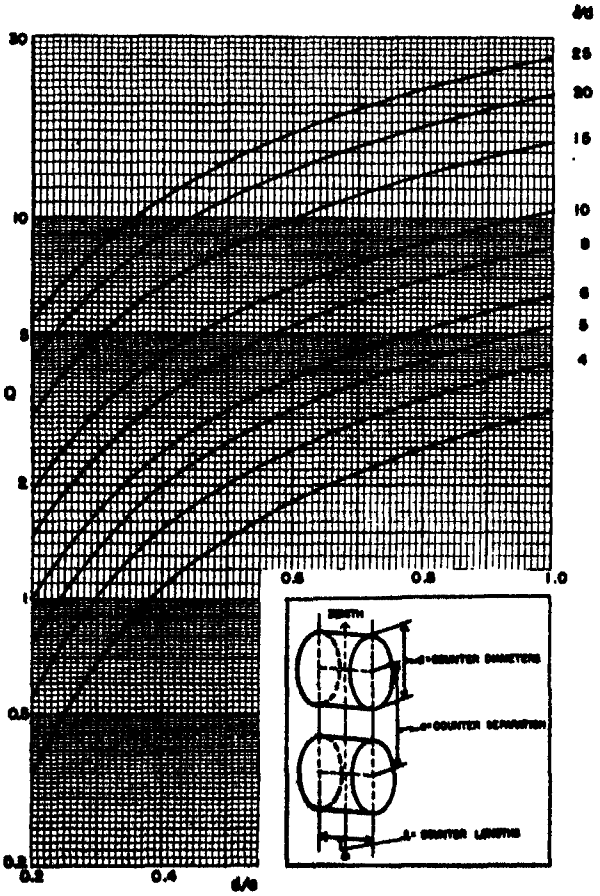

FIG. 4*a*. N_2 = Coincidences per unit time (from upper hemisphere only). $I\cos^2\zeta$ = unidirectional radiation intensity in particles per unit area-unit solid angle—unit time. (The number of particles crossing area $d\sigma$ in unit time from solid angle $d\Sigma$ in direction normal to $d\sigma$ is $I\cos^2\zeta d\sigma d\Sigma$.) ζ = zenith angle. $N_2=Qd^2I$. Formula used to calculate Q gives value too large by no more than E percent, Fig. 5.

If the axis OZ of the telescope is inclined at an angle to the vertical OV, as shown in Fig. 1, the integrand is not symmetric in α and β. Thus, *counting rays from a single hemisphere only*,

$$N_2=I\int_{-\alpha_0}^{\alpha_0}\int_{-\beta_0}^{\beta_0}\cos^2\zeta(\alpha, \beta)\sigma(\alpha, \beta)d\Sigma, \tag{4.1}$$

where β_0 and α_0 are as given in (3.4) and (3.5).

This formula may be used when the cosine squared law is valid over the entire solid angle viewed by the telescope. But if the solid angle includes directions below the horizon, the formula must be modified to account for shadowing by the earth and departures from the cosine squared law.

When the telescope axis is vertical, OZ coincides with OV in Fig. 1, and ζ coincides with η. In this case

$$\cos^2\zeta=\frac{\cos^2\alpha\cos^2\beta}{1-\sin^2\alpha\sin^2\beta}.$$

Fig. 4*b*. Counting rate of a two-counter telescope: cosine squared law case.

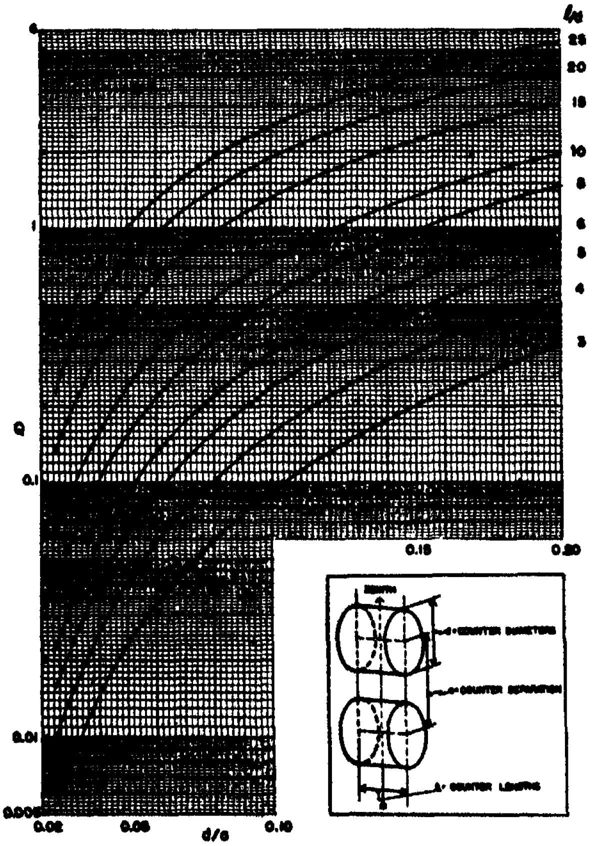

FIG. 4*b*. N_2 = Coincidences per unit time (from upper hemisphere only). $I\cos^2\zeta$ = unidirectional radiation intensity in particles per unit area-unit solid angle—unit time. (The number of particles crossing area $d\sigma$ in unit time from solid angle $d\Sigma$ in direction normal to $d\sigma$ is $I\cos^2\zeta d\sigma d\Sigma$.) ζ = zenith angle. $N_2=Qd^2I$. Formula used to calculate Q gives value too large by no more than E percent, Fig. 5.

Fig. 5. Closeness with which text formulas approximate counting rate of a two-counter telescope: cosine squared law case.

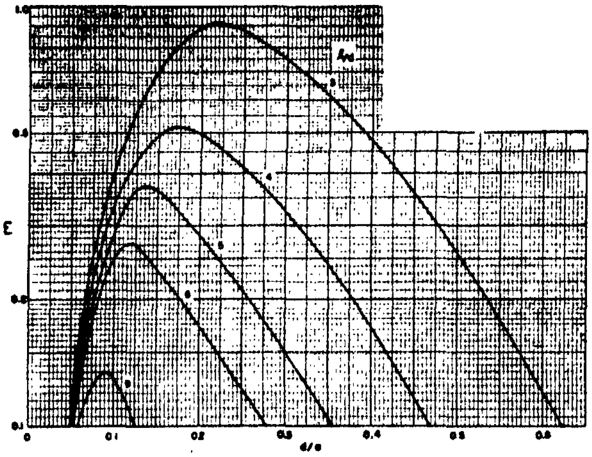

FIG. 5. N_2 = Coincidences per unit time (from upper hemisphere only). N_{2m} given by 4.4. N_{2M} given by 4.5. Then $N_{2m} \leq N_2 \leq N_{2M}$. $E = 100(N_{2M} - N_{2m})/N_{2m}$.

As a consequence (4.1) becomes

$$N_2 = 4I \int_0^{\alpha_0} \int_0^{\beta_0} \frac{\sigma(\alpha, \beta)\cos^3\alpha \cos^3\beta}{[1-\sin^2\alpha \sin^2\beta]^{5/2}} d\beta d\alpha.$$

Set

$$N_{2m} = 4I \int_0^{\alpha_0} \int_0^{\beta_1(\alpha)} \frac{\sigma(\alpha, \beta)\cos^3\alpha \cos^3\beta}{[1-\sin^2\alpha \sin^2\beta]^{5/2}} d\beta d\alpha, \quad (4.2)$$

and

$$N_{2M} = N_{2m} + 4I \int_0^{\alpha_0} \int_{\beta_1(\alpha)}^{\beta_0(\alpha)} \times \frac{\sigma(\alpha, \beta_1(\alpha))\cos^3\alpha \cos^3\beta}{[1-\sin^2\alpha \sin^2\beta]^{5/2}} d\beta d\alpha, \quad (4.3)$$

where $\beta_1(\alpha)$ is given in (3.3). Then

$$N_{2m} \leq N_2 \leq N_{2M}.$$

The quantities N_{2m} and N_{2M} differ from N_2 by no more than

$$E = 100 \frac{N_{2M} - N_{2m}}{N_{2m}}$$

percent.

Integrating with respect to β, (4.2) and (4.3) become

$$N_{2m} = \frac{a^2 \Delta I}{2} \int_0^{\alpha_0} \left\{ (\delta - \sin\alpha) \left[\Delta A \frac{3\Delta^2 + 5A^2}{(\Delta^2 + A^2)^2} + 3 \arctan \frac{\Delta}{A} \right] + 2\Delta[B - (\delta - \sin\alpha)\cos\alpha] \frac{\Delta^2 + 2A^2}{(\Delta^2 + A^2)^2} \right\} \cos^2\alpha d\alpha, \quad (4.4)$$

and

$$N_{2M} = N_{2m} + \frac{4a^2\Delta^2}{3} I \int_0^{\alpha_0} \frac{\cos^2\alpha}{(\Delta^2 + A^2)^{\frac{3}{2}}} \times \{(\delta - \sin\alpha)(A - \cos\alpha) + B\} \times \left\{ \frac{2\Delta^2 + 3C^2}{(\Delta^2 + C^2)^{\frac{3}{2}}} - \frac{2\Delta^2 + 3A^2}{(\Delta^2 + A^2)^{\frac{3}{2}}} \right\} d\alpha. \quad (4.5)$$

where A, B, and C are given in (3.8)–(3.10).

V. DISCUSSION OF ACCURACIES

Subject to the conditions (*a*)–(*d*) set forth in the introduction, formulas (3.6) and (3.7) can be used as an approximation to N_2 in the isotropic case. The closeness of this approximation can be estimated from the graphs of Fig. 6 in the previous paper and Fig. 3 below. Similarly the graphs of Fig. 5 below furnish an estimate of how closely (4.4) and (4.5) approximate to N_2 in the cosine squared law case. It is estimated that an *additional* error of ±3 percent exists in the N_2 graphs of both the present and earlier papers due to integration and plotting errors.

PART B. GRAPHS[4]

VI. GRAPHS OF THE COINCIDENCE RATE: THE ISOTROPIC CASE

For the convenience of the experimenter, the information contained in the graphs of the previous paper is replotted below in different form, (Figs. 2 and 3), to show the variation with l/d instead of l/a.

VII. GRAPHS OF THE COINCIDENCE RATE: THE COSINE SQUARED LAW CASE

Using the approximation given by (4.5), the coincidence rate in the cosine squared law case is plotted in Fig. 4. The error made by using (4.5) is in the positive direction and is in percentage less than the quantity E graphed in Fig. 5.

VIII. ACCURACY OF THE GRAPHS

The graphs in Sections VI and VII of coincidence rates all contain integration and plotting errors not exceeding ±3 percent. Those of E contain similar errors of not more than ±10 percent.

---

[4] For as long as they last, full scale copies of these graphs may be obtained from the authors upon request.

THE REVIEW OF SCIENTIFIC INSTRUMENTS VOLUME 20, NUMBER 8 AUGUST, 1949

Sample Scanning Mechanism for X-Ray Diffraction

J. W. Hickman and A. G. Kleinknecht
Westinghouse Research Laboratories, East Pittsburgh, Pennsylvania

(Received March 28, 1949)

An automatic scanning mechanism is described for the study of preferred orientations in worked materials for pole figure representation. The device maintains a fixed specimen to film distance and permits tilting to 75 degrees from the normal to the beam about horizontal and vertical axes. The yoke support is constructed to clear conventional film holders so that close specimen to film distances can be obtained. The sample holder can be easily removed and adapted to suit any specimen as required. An area of 2.38 square centimeters per hour is scanned when the beam is perpendicular to the plane of the specimen.

INTRODUCTION

It is well known that many of the properties of worked metals are dependent upon crystal grain orientations. For the investigations of worked metals it is thus desirable to know whether preferred orientation exists, as well as the extent and the type of preferred orientation. In drawn wires working results in identical treatment in all directions orthogonal to the wire since preferred orientations appear only along the axis of the wire. In this case the orientation is unidirectional. In the case of rolled sheet metal, the sheet is subjected to treatment which is not identical for all directions orthogonal to the rolling direction. This results in preferred orientation in two directions; namely, the rolling and cross-rolling directions.

The only feasible method for studying two-dimensional preferred orientation is to make a pole figure for the specimen. In those cases where the sample is so fine grained that spotty diffraction patterns do not result, the specimen may remain stationary. In many cases, however, the grain size of the sample is so large that spotty patterns are given when the sample remains stationary. In these cases it is necessary that the x-ray beam scan the sample during the exposure. The scanning technique results in a great saving both in labor and time since many x-ray diffraction patterns are superimposed on one film. The scanning may be obtained by oscillating the specimen through a slight angular range by using an oscillating crystal camera or by shifting the specimen in its own plane by some mechanism during the exposure.

An integrating camera which sweeps the beam over large areas of sheet specimens has been described by Smith.[1] Blueprints of this camera have been made available by the Research Laboratories of the Aluminum Company of America. Recently Hay[2] has described a simple scanning mechanism which fits directly onto the track of the General Electric XRD Unit. The Hay design has the advantage that both front and back reflection photographs may be taken simultaneously. This instrument, however, does not permit the photographic plates to be brought close to the sample when scanning is occurring at relatively small angles of sample to beam direction. Furthermore although the sample may be set at any angle about a vertical axis, no provisions are made for setting at angles other than 90° to a horizontal axis. To overcome these limitations an instrument has been designed which permits front and back reflection photographs to be taken simultaneously where the specimen to plate distances may be set at values as small as 3 cm. In addition both horizontal and vertical angular settings were considered desirable, these limits being set at ±60° about each axis. It is also possible to scan horizontally along a wire, for example, without vertical travel. Furthermore, all positions of the sample are obtained while keeping the specimen to film distance constant.

In order to obtain small sample to plate distances a narrow base is provided consistent with the necessary mechanical bearing surface. This base forms part of a supporting frame, shown in Fig. 1, which fits onto the camera slide. The frame has two vertical supporting

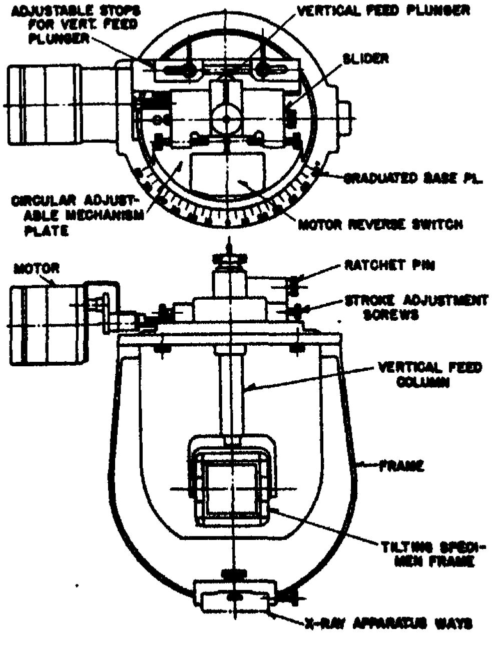

Fig. 1.

---

[1] D. W. Smith, "Symposium of Radiography and X-Ray Diffraction," A.S.T.M., Philadelphia (1939); Proc. A.S.T.M. 200 (1936).

[2] R. H. Hay, Rev. Sci. Inst. 18, 801 (1947).

horns raised to such height that the mechanism carried on it clears the tops of the standard General Electric Circular Back Reflection film holders. The two film holders and scanning mechanism fit on to the common camera slide.

The specimen to be scanned is held in the specimen frame which can be tilted to any desired horizontal angle by means of an indicating dial graduated in degrees. This dial is fastened to the yoke which holds the tilting frame. The tilting frame is held and turned in the yoke which is attached to the vertical feed column which moves up automatically in small increments (0.040 inch) at each end of the horizontal stroke.

The mechanism for accomplishing these motions consists of a pawl which engages in teeth cut in the vertical feed column in such a manner that the vertical feed plunger, to which the pawl is pinned, upon being forced inward by the adjustable stops, raises the feed plunger through the pawl by the required amount at each end of the stroke. This entire mechanism is contained in a slider by means of which the horizontal motion is obtained. This slider also contains a ratchet pin whose function is to click in at each rise to keep the vertical feed column from falling back. A sliding key is provided to keep the vertical feed column from rotating in the slider.

The horizontal motion of this slider is derived from a screw working in a nut tapped in the slider body. This screw, in turn, is driven through two small spur gears, by the reversible motor. The motor reversing switch, with stroke adjustment screws which actuate the switch, reverses the slider travel while the adjustment screws determine the length of the stroke.

The complete operating mechanism of the scanner is carried on a circular adjustable mechanism plate which in turn has a bearing in a base plate with graduations in degrees. The circular adjustable plate can thus be rotated about a vertical axis in order to give the specimen the desired angular displacement.

In order to reset the mechanism after the vertical feed column has completed its upward travel the ratchet pin is withdrawn and given a slight turn for permanent disengagement. The pawl is then pressed outward disengaging the teeth and the vertical feed column is lowered to the starting position, the ratchet pin is reengaged, and the mechanism is ready for another cycle of operation.

Another novel feature of the device is the adaptability afforded for holding any body in any manner by simply detaching the yoke and tilting specimen frame by means of the knob at the top of the vertical feed column. Any other holding device to accomplish the desired purpose may be substituted for the yoke and tilting specimen frame. The original specimen frame permits angular displacements to ±60° and carries a scale for tilting to ±45°. An alternative sample holder has been designed by Mr. H. H. Plotkin with two sides of the square frame cut out for visibility at large angles. The circular adjustable plate can thus be rotated to ±75° and a tilting frame graduated to ±90° is also provided.

The beam traverses the sample horizontally to the end of the stroke where the vertical feed column elevates the sample 0.040 inch when the horizontal reverse mechanism moves the sample in the opposite direction. A total time of 6.1 hours is required to completely traverse a sample of 1.5 in.×1.5 in. (3.81 cm) when the beam is perpendicular to the plane of the specimen. In this position an area of 2.38 square centimeters per hour is scanned.

The choice of materials in constructing the instrument was made with special regard to lightness consistent with strength. The yoke is made of aluminum as well as the motor switch box. The base plate and upper structure are made of rust proofed steel and the slider is of bronze in order that best wearing conditions obtain. The vertical feed column and all the contact surfaces are hardened to resist wear. The yoke was given a crackle finish and the specimen frames are made of brass.

THE REVIEW OF SCIENTIFIC INSTRUMENTS VOLUME 20, NUMBER 8 AUGUST, 1949

Design of Equipment for Thermal Studies

ROBERT J. TEITEL
Brookhaven National Laboratory, Upton, New York

(Received April 11, 1949)

A versatile metallurgical furnace for high temperature investigations of metals and alloys is described. Its uses to conduct thermal analysis and thermal treatments on beryllium-iron alloys are described in detail. In order to apply thermal analysis to these alloys, a special thermal crucible was designed and found successful.

INTRODUCTION

IN the course of a recent investigation into the beryllium-iron system,[1] a metallurgical furnace was designed and built to carry out thermal analyses and solution treatments on high melting point alloys. Due to its versatile design, this furnace can be adapted to many other types of metallurgical experiments. Therefore, a more detailed description of the furnace and its uses, in particular, for thermal analysis and solution quenching from high temperatures, will be presented here.

FURNACE

A cross section of this furnace is shown in Fig. 1. Two concentric seamless steel tubes, when welded to metal rings above and below, form a water jacket. The top and bottom are closed by brass plates using rubber gasket seals. Two smaller pipes are introduced through the water jacket to provide vacuum and electrical connections, thus leaving the top and bottom free for the removal and replacement of furnace shields and cores. This water jacket accommodates cores having diameters up to four inches.

A high speed, high vacuum oil diffusion pump (DPI model 275CM) is connected to the vacuum port and a Welch Duo-Seal mechanical pump is used to maintain the fore pressure.

The advantages of this design are listed below:

1. Various core sizes can be substituted quickly and easily.
2. The type, amount, and kind of insulation needed for the best control of the furnace at any temperature can be placed into the apparatus with ease.
3. Since the gaskets are all clamped down, inert atmospheres at high pressures can be used as well as vacuum. In order to do this properly, a valve should be placed between the fore pump and the diffusion pump.
4. The special port for the electrical and gauge connections eliminates the necessity of providing these connections in every furnace cover.
5. The water jacket cools the outside shell and the gaskets. Therefore, effective use of the furnace with little chance for leaks to develop is insured.

In the following sections, the application of this apparatus to the thermal analysis and solution treatment of beryllium-iron alloys will be described. Treatment of these alloys presents more difficulties than are ordinarily encountered in investigations of phase systems.

Due to the chemical activity, high melting point and high vapor pressure of beryllium, protection of thermocouples becomes a problem. Beryllium, iron and their alloys melt at high temperatures (above 1150°C). Therefore, crucible and furnace problems are added.

THERMAL ANALYSIS

Furnace Arrangement

An Alundum furnace core, 1½ inches in diameter and 12 inches long, is used in this investigation (Fig. 1). It is wound with molybdenum wire. Alundum cores placed concentrically about the core form radiation shields and insulating brick is used for the top and bottom.

The internal arrangement used for thermal analysis is shown in Fig. 2. A special beryllia thermal crucible, the fabrication of which will be described in greater detail later, rests upon an Alundum tube base in the center of the core. Temperature measurements are made by a platinum-rhodium thermocouple which is introduced into the furnace at the bottom and passes up through an insulating brick base, a Lavite base, an

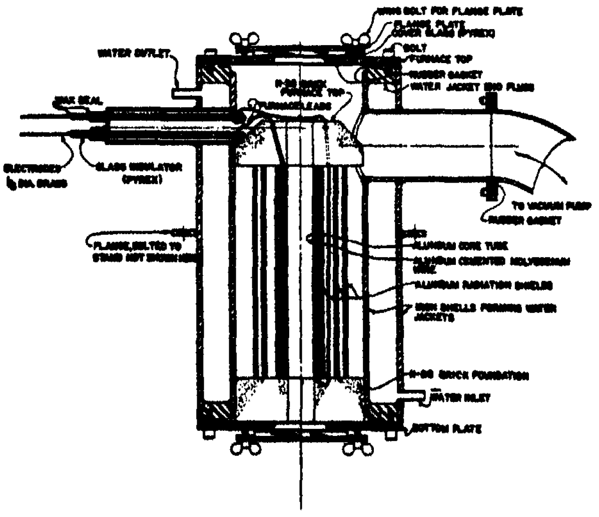

FIG. 1. Vacuum furnace.

---

[1] R. J. Teitel and M. Cohen, "The beryllium-iron system, TP 2550 E," J. Metals, 285 (April, 1949).

Alundum base and then into a thermocouple well integral with the bottom of the crucible. Since the thermocouple insulator is thin ($\frac{3}{32}$-inch diameter) and fragile, a silica tube is placed around it for support in the cool zones of the furnace while an Alundum tube is used for this purpose in the hot zones. The thermocouple is adjusted by moving the silica tube through the rubber seal at the bottom of the copper tube. This adjustment is made with the unit, which includes the parts mentioned above, outside of the furnace and afterwards this assembly is raised into the furnace.

Thermal analysis also requires a method for raising and lowering the temperature slowly and uniformly. This is accomplished by using a synchronous motor to drive a dry induction regulator. The regulator is not entirely effective unless the input voltage is stabilized. Consequently, a saturated core stabilizer is used for this purpose. The voltage regulator acts as a variable transformer; i.e., it raises the output from 0 to 200 percent of the input voltage. Therefore, the rate of voltage rise or descent is adjusted by varying the speed of the motor drive through a train of gears. Further control is possible with the aid of a variac on the input side of the regulator. Using such a control, the rate of rise or descent is adjusted within 1 to 2.5°C/minute.

Thermal Analysis Procedure

Pieces of alloy, previously prepared in a vacuum induction furnace, are loaded into the thermal crucible shown in Fig. 2. After lifting the crucible into the furnace, the vacuum pumps are turned on and the temperature of the furnace raised as quickly as possible. The thermocouple wires protruding from the bottom of the furnace are joined to the copper leads of a recording potentiometer. These junctions are immersed in an ice bath and maintained at 0°C. When a halt in the heating curve is noticed on the potentiometer, the induction regulator is turned down in order to level the temperature of the furnace at about 100°C to 200°C above the melting point. Then the synchronous motor is fixed into place and the cooling curve automatically is plotted on the potentiometer. Heating curves are made by simply reversing the synchronous motor. One complete analysis takes 10 to 15 hours and includes an investigation from the melting point down to approximately 500°C. When more precise data are necessary, precision Leeds & Northrup K2 potentiometer and a timer are used to obtain the thermal curves.

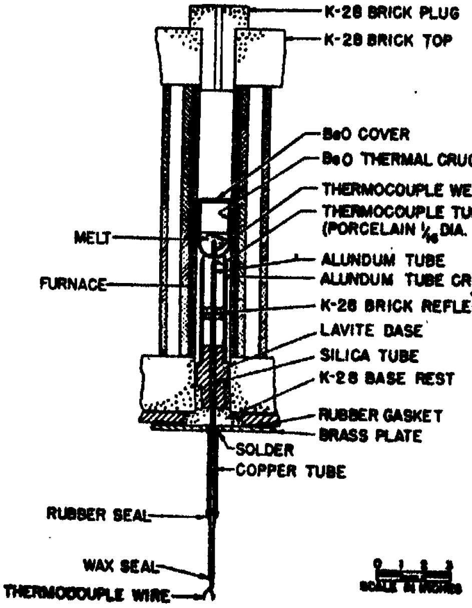

FIG. 2. Thermal analysis arrangement.

Examples of the recorder plots derived from a thermal analysis for both heating and cooling are shown in Fig. 3. An inverse rate plot using the K2 potentiometer is shown in a previous article.[1]

Fabrication of Thermal Crucibles

A slip casting procedure used to produce these unusual shaped crucibles is reported by V. Mahady.[2] The steps of the procedure are given below:

1. Preparation of plaster mold—A large glass test tube with a brass rod protruding through a hole on the bottom (Fig. 4a) is inverted and luted to a cardboard form with plasticene clay (Fig. 4b). The plaster is carefully cleared of lumps and bubbles and then poured into the form. After the plaster has set, the glass tube is removed leaving the test tube shape with a hole at the bottom of the plaster mold (Fig. 4c). The mold is then thoroughly dried.

2. Preparation of slip—Beryllia (−20 mesh refactory grade) is supplied by Clifton Products, Inc. A mixture (800 grams of beryllia and 600 grams of water) is ground in a tungsten carbide ball mill for 65 hours. Afterward the mill is rinsed with 500 cc of water. The mixture is leached by adding 100 cc of dilute hydrochloric acid and after 24 hours, the acid is decanted from the beryllia. Then it is washed with distilled water a few times and 0.1 percent by volume of gum arabic (in water solution) is added.

3. Graphite rods—The thermocouple well in the bottom of the crucible is formed by slip casting a graphite rod. These graphite rods, $\frac{1}{8}$-inch diameter and 2 inches to 3 inches long, are machined and dried in a furnace. They are dipped 2 or 3 times into beryllia slip (specific gravity of 1.16) to a depth of $\frac{1}{2}$ to $\frac{3}{4}$ inch (the desired length of the thermocouple well). After each dip they are partially dried for 20 to 30 minutes in air.

4. Slip casting—The coated graphite rods are placed into the plaster mold with the bare section of the rod in the hole in the bottom of the mold. Slip (specific gravity 1.45–1.49 and *p*H 4.5) is poured into the mold and allowed to settle for 26 seconds. This gives a wall thickness of $\frac{3}{32}$ inches. After trimming the excess slip

---

[2] V. M. Mahady, "The preparation of slip cast beryllia crucibles with projecting thermocouple protection tubes," M.I.T. Metallurgical Project Memorandum (July 24, 1946).

from the mold, the mold and crucible are placed in a drying oven for two hours at 50°C. Then the crucible is removed from the mold and dried for 24 hours.

5. Firing—An oxy-propane furnace is used for this step. The crucibles are placed into the furnace in an upright position and heated slowly to 1800°C over a period of six hours. They are held at temperature for 15 minutes and then slowly cooled. The graphite rods burn out between 750° and 950°C leaving a reentrant thermocouple well in the bottom of the crucible. The density of the slip cast beryllia is 90 percent that of the solid.

After some experimentation, a reaction between beryllia and the porcelain thermocouple insulator was detected. This reaction causes frequent thermocouple failures. Therefore, it was found advisable to dip the graphite rods into Alundum slip first. This procedure gives an Alundum coating inside the thermocouple well and prevents the reaction.

The advantages of this design of crucible are the following:

1. The thermocouple is accurately located with respect to the melt.
2. The thermocouple is protected from contamination by fumes or vapors.
3. The melt can be completely covered, thus preventing large metal losses during the long periods required for thermal analysis.
4. The alloy sample need not be machined especially to fit into the crucible.

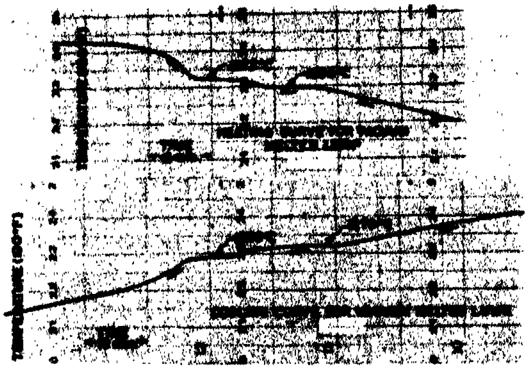

FIG. 3. Record of thermal analysis of beryllium automatically plotted.

SOLUTION TREATMENTS

Furnace Arrangement

The same furnace core is used for thermal solution quenching experiments with a different internal arrangement (Fig. 5). The specimens are loaded into iron capsules for guidance and identification through the apparatus. These capsules can accommodate either powder or solid specimens. In the former case, the powder is placed into a beryllia lining which fits into the iron capsule. In the latter case, the beryllia lining is used only when the temperature of the treatment is above the solidus of the alloy.

These capsules are placed into the Pyrex glass tube shown in the upper right corner of Fig. 5. By moving the magnet, a pusher in the tube forces the capsules through a hole in the tube one by one, thus introducing the specimens into the furnace. The center sketch in Fig. 5 shows the path of the capsule through the furnace. Each capsule is guided into the furnace by a molybdenum funnel and an Alundum tube. It is halted by a molybdenum vane in an iron block located in the center of the furnace. After the prescribed time, the vane is moved aside and the capsule drops through the Lavite funnel at the bottom of the furnace into the oil quenching bath.

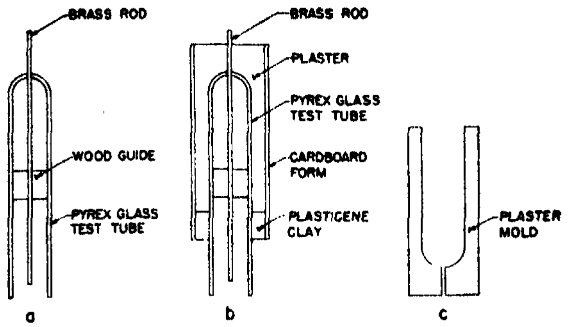

FIG. 4. Sketch of mold fabrication for thermal analysis crucible.

The iron block is supported in the center of the furnace by three molybdenum rods as shown in the left sketch in Fig. 5 and the temperature of this iron block is controlled by a thermocouple and potentiometer controller.

All operations are controlled and watched from the top by a vane port and sight tube respectively.

The silicone oil in the quenching tank is cooled by a copper cooling coil surrounding the tank. A beaker of water placed around the tank improves the contact between the cooling coil and the tank.

If repairs to any part of the heat treatment apparatus are needed, the top and iron block are removed as one unit. Here again, all adjustments are made outside the furnace.

Quenching Procedure

Capsules containing the specimens are loaded into the Pyrex glass tube which is forced through the rubber seal at the top of the furnace. The capsules are treated in turn and allowed to collect in the tank below. After the furnace has been turned off and the vacuum broken, the tank is removed and the capsules recovered. Then they are cleaned in carbon tetrachloride and acetone.

The identification of each specimen is preserved by keeping records of the numbers marked on the iron capsules.

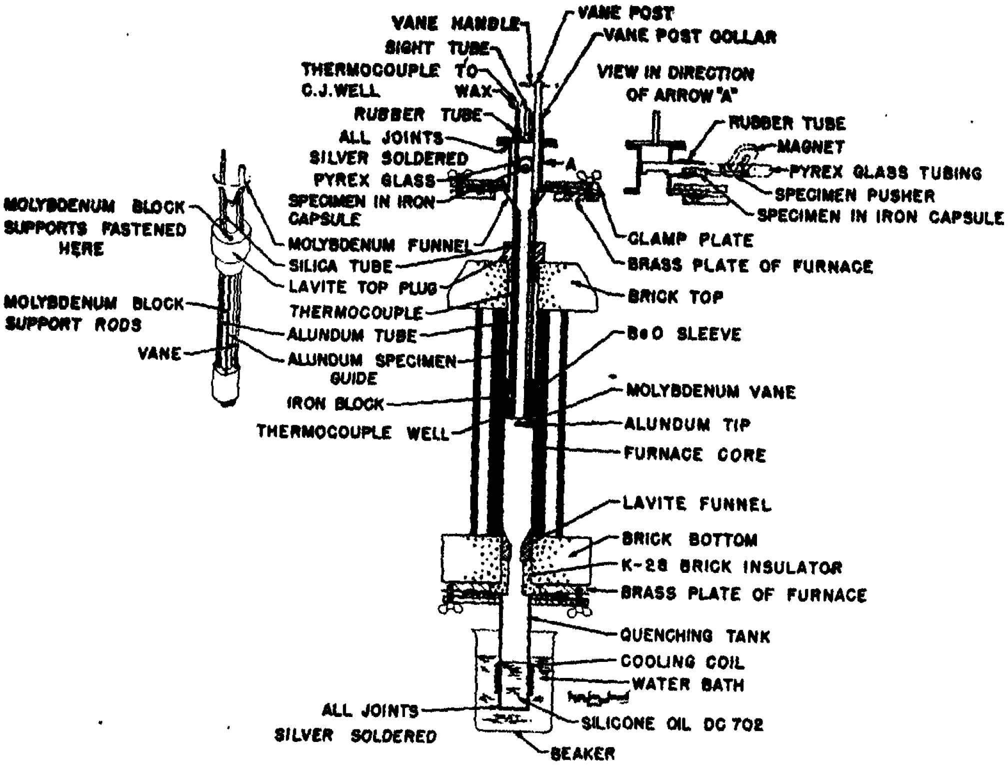

FIG. 5. Internal arrangement thermal solution treatments.

CONCLUSIONS

A metallurgical furnace and its application to high temperature thermal analysis and thermal treatments have been described. Thus furnace can accommodate various cores and amounts of insulation. It also can be used for investigations up to 1600°C in either vacuum or an inert gas atmosphere for the protection of metals under observation.

ACKNOWLEDGMENTS

The author wishes to thank Dr. M. Cohen and Dr. A. R. Kaufmann, Professors at M.I.T., for their advice, and Mrs. V. M. Mahady for making the special thermal crucibles and other ceramic objects.

This research was carried out in the Department of Metallurgy at M.I.T. under the auspices of the Manhattan Project, Contract No. W 7405-eng-175.

THE REVIEW OF SCIENTIFIC INSTRUMENTS VOLUME 20, NUMBER 8 AUGUST, 1949

Preparation and Use of Tritium and Deuterium Targets*

E. R. GRAVES, A. A. RODRIGUES,** M. GOLDBLATT, AND D. I. MEYER
Los Alamos Scientific Laboratory, Los Alamos, New Mexico

(Received May 23, 1949)

Methods are described for preparing Ta-H and Zr-H targets for economic use of tritium. Ratios of hydrogen isotope to metals of about 1.0 were obtained. The use of these targets under deuteron bombardment is discussed.

I. INTRODUCTION

THE use of the deuterium-tritium reaction as a fast neutron source involves the problem of conservation of tritium. While a recirculating system is possible, using tritium either as a bombarding ion or as a target, this system is tedious and subject to accident. While a tritium gas target with a thin window for beam penetration may be used at higher voltages its use is impossible with bombarding energies of less than a few hundred kilovolts. A stable solid form of tritium constitutes the best target. Tritium ice would seem useful. Extensive tests were made on the use and conservation of minimum quantities of ice (using deuterium ice). Water vapor was stored in a reservoir which included a liquid air trap and the pressure measured to determine the quantity of D_2O. Repeated transfers of the vapor from the reservoir to the target and back always resulted in a gain of water vapor from elsewhere in the system in spite of careful auxiliary trapping. In addition thin layers of ice were found to be evaporated rapidly by deuteron bombardment. The consequent dilution of the original target material by these effects, together with the problems of the chemical disintegration of the tritium water molecule due to its own radioactivity were considered sufficient reasons to render tritium ice an impractical target material.

After consideration of various compounds and their properties it was decided to concentrate on the use of metals which absorb quantities of hydrogen and retain it. This property is known for a number of elements.[1–5] Among those which absorb the most are palladium, tantalum, zirconium, titanium. It was required that the hydrogen isotope, once absorbed, should remain trapped in the target under bombardment by a beam in a vacuum. Pd absorbs and emits gas at too low a temperature and hence was ruled out as a possibility. Since Ta exhibits the phenomenon of absorption at very high temperatures, it was investigated for its applicability first. At a later time Zr was used. Ti, desirable for its lower atomic number, has not been used to date. Targets have been successfully prepared using both Ta and Zr. The Zr targets have been by far the more successful type both from the standpoint of preparation and of use. However, the procedures developed for making both and for using them in a 200 kv Cockcroft-Walton accelerator will be discussed.

II. PREPARATION OF TARGETS

The vacuum systems and apparatus employed in the production of target foils are diagrammed in Figs. 1–3. It will be noted that the systems used were functionally identical for both tantalum and zirconium. Logically, the systems were composed of three sections each: the first section was used for purification and storage of the hydrogen isotope; the second section was employed for absorptions; and the third portion of each system enabled the recovery of unreacted tritium gas. However, as indicated by the diagrams, the Ta was heated as a ribbon conducting current between electrodes, whereas the Zr was placed on a W backing and heated by induction.

In order to insure the removal of impurities which might have been with the hydrogen isotope, the tritium or deuterium was reacted with uranium to form UX_3 and the impurities were exhausted.

Tantalum Procedures

From tantalum sheet, either 0.001 inch or 0.004 inch thick, a piece was cut having an exposed area of ⅞ inch by ½ inch. This was clamped to the flattened surface of molybdenum rods, approximately ¼ inch in diameter which served as current carrying leads. Careful adjustment was necessary in mounting, in order that the tantalum neither sag too much nor sever due to decreased tensile strength when heated. Heating current was supplied by four 220 v power-stats in parallel supplied in turn by a variac. This circuit was capable of supplying 190 amperes at approximately 10 volts. The high current carried by the leads necessitated air cooling on the leads and ground joint which was waxed.

After the ribbon assembly was installed and the system pumped down to $\ll 10^{-5}$ mm Hg, the outgassing procedure, which was the essential feature of the preparation, was begun. The heating current was slowly raised until the tantalum reached approximately

---

* This document is based on work performed at Los Alamos Scientific Laboratory of the University of California under Government Contract W-7405-eng-36.

** Deceased.

[1] D. A. Wright, Nature 142, 794 (1938).

[2] Mary R. Andrews, J. Am. Chem. Soc. 54, 1845 (1932).

[3] G. Hagg, Z. Phys. Chem., B, 11, 433 (1931).

[4] F. M. Penning and J. H. A. Moubis, Physica IV, 1190 (1937).

[5] Donald P. Smith, *Hydrogen in Metals* (University of Chicago Press, Chicago, 1948). Published since the work of this paper was completed, this book also contains an excellent bibliography.

1900°C, measured with a Leeds and Northrup Optical pyrometer. When the tantalum is first heated there is an initial surge in pressure due to the liberation of absorbed and adsorbed gases. The temperature of the tantalum was maintained at 1900° until the pressure dropped to a constant value. Owing to excessive heating of the leads and ground joint it was sometimes necessary to carry on this process intermittently, alternating heating with brief cooling periods. The temperature was raised progressively to 2000°, 2100°, and 2200°C. At 2200°C it was found best to degas by heating for a few seconds followed by cooling periods of 10–30 seconds. Degassing time is reduced by "flushing" the metal with H_2. This is accomplished by heating in H_2 at a pressure of several millimeters of mercury, cooling and pumping as before. When the pressure in the closed system after a 2200°C flash rose to less than 0.2 microns, read on the Pirani gauge, the foil was ready for filling.

A measured amount of gas was transferred from the storage section to the "reaction" section by means of a Toepler pump. Pressures from 2 to 5 mm of Hg were used, measured by the McCleod gauge. In the closed reaction system the tantalum was slowly heated, taking about one minute to reach approximately 1900°C. At this time the heat was cut off by means of a switch and the system allowed to drop to an equilibrium temperature and pressure. Absorption began immediately with cooling and 15 minutes were allowed for reaching equilibrium. The final pressure measured on the McCleod gauge, together with the initial pressure and the known volume of the system, provided a measure of the gas absorbed. Any residual tritium was pumped into the recovery section.

Results of Tantalum Absorption

Tests with deuterium produced foils with a maximum ratio D:Ta of 0.8→1.0. This value was calculated from the estimated gas absorption in the central area used for a target and was checked by comparison of the yield from the d-d reaction in this target with that from a heavy ice target. It was also shown that 0.004 inch tantalum foil absorbed approximately four times as much gas as 0.001 inch foil.

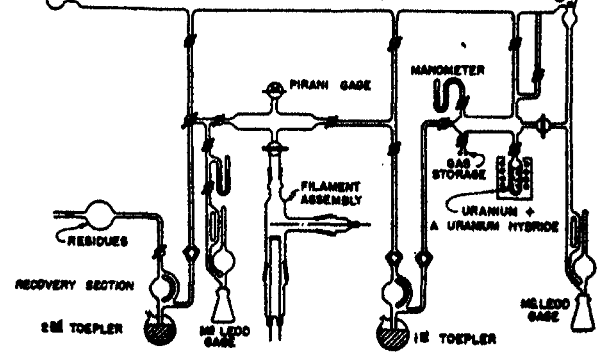

FIG. 1. Apparatus for preparing tantalum foils.

The gas impregnated foils were warped, presumably due to uneven heating, and extremely brittle. This caused formidable problems concerning mounting as a target. As described in Section III, a good thermal contact is necessary between the target foil proper and a cooled backing. Since the tantalum reaches 2200°C during processing it is almost impossible to plate it with anything or bind it to any backing before impregnating. One attack was to evaporate gold onto one side of the foil after preparation. The equipment used is shown in Fig. 2. Although a layer was deposited without any apparent loss of deuterium from the already filled tantalum foil, the gold peeled after removal from the system. A copper backing was applied by touching the hot tantalum with a copper wire as the tantalum cooled during the absorption of deuterium. The copper wet the tantalum very well but there was no observable absorption of deuterium. Attempts at heating the tantalum to the necessary temperature by induction heating in the hope of reducing warping were unsuccessful with the equipment available.

In view of the extreme brittleness of the processed foils, the first tritium impregnated ones were purposely made with only one-fourth the gas content of the best deuterium ones. Use of these is described in Section III.

Zirconium Foils

These structural difficulties with tantalum led to a search for a foil material which would be less fragile, less laborious to degas and which would absorb hydrogen at a lower temperature. A reasonable metal to replace Ta appeared to be zirconium. J. Fitzwilliam and C. Squire[6] in their magnetic studies on Zr-H reported that zirconium specimens would begin to take on H_2 at 900 degrees K. They estimated that the Zr was filled to 66 atomic percent with hydrogen. Although by pumping on the Zr-H at 1000 degrees K, the hydrogen was completely removed, there was no evidence that the zirconium would lose hydrogen at room temperature.

Early in our investigations it was discovered that if the Zr were allowed to melt onto a tungsten plate, the Zr would readily absorb deuterium. The zirconium adhered very well to the tungsten backing, probably because of the formation of the compound W_2Zr at the interface of the foil and the backing. The adopted procedure for making deuterium and tritium containing foils was as follows.

The tungsten backing was a 0.030 inch sheet which was cut into the shape of the target. Before the zirconium foil was fastened to the backing, the tungsten piece was cleaned and degassed. The backing was placed on a quartz pedestal in the reaction section

---

[6] J. Fitzwilliam and C. Squire, J. Chem. Phys. 9, 678 (1941).

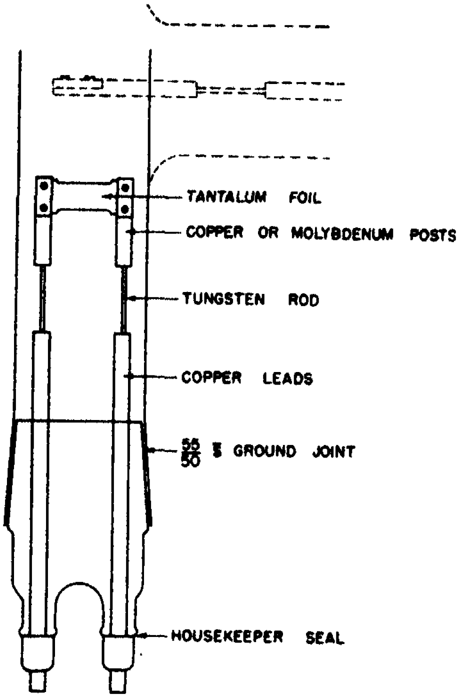

FIG. 2. Detail of assembly for heating tantalum ribbon. For sputtering and tinning, two electrode pairs were used as indicated by dotted lines.

(Fig. 3) and inductively heated in a vacuum to nearly 2000°C for about one minute. Power for heating was supplied by a 20-kw Thermonic generator. A five-minute cooling period was allowed. The cycle was repeated until less than a micron change in pressure was noted in the closed reaction section during a cycle of heating. After cooling, the clean backing was removed from the reaction vessel and a 0.001 inch zirconium foil, in the shape of the backing, was then spot welded to the tungsten at several places. The foil and backing were again placed on the quartz pedestal, and the system was evacuated to 10^{-6} mm Hg. In all the induction heating procedures care was taken to eliminate mercury vapor from the reaction section with cold traps.

A nearly complete fusion was made between the Zr and the W when the target pair was heated to about 1600°C and kept at this temperature for about two minutes. A cooling period of several minutes was allowed. To insure complete fusion and degassing of the zirconium the foil temperature was raised to 1800°C, the melting point of the Zr, for nearly one-half minute. The 1800°C heating was performed only twice because at this temperature there was a slow distillation of the zirconium. However, it was found that no successful foil could be made of Zr without degassing the metal at its melting point. After the last 1800° treatment the foil temperature was dropped to 1500°C for five or ten minutes to allow more degassing.

Upon the cooling of the foil to room temperature, hydrogen isotope gas was pumped into the reaction section by means of the first Toepler until a pressure of three to five millimeters of Hg was reached. Then the foil, in the atmosphere of deuterium or tritium, was heated to a temperature of 1100°C and maintained at this point for about two minutes. Again the foil was allowed to cool to room temperature, and the final pressure of the system was noted. From the change in pressure and the volume of the system, it was possible to estimate the amount of gas absorbed. The unreacted gas was pumped off before the foil was removed from the reaction vessel.

Results on Zr Foils

An inspection of the several absorptions of tritium in 0.001 inch zirconium foil showed that the average occlusion produced a foil which had a ratio of hydrogen isotope atoms to zirconium atoms of 0.65. The highest atomic ratio obtained was nearly unity. Similar results were obtained with deuterium and zirconium.

III. TARGET USAGE

In practice it is desired to use a given tritium target for an indefinite length of time with negligible loss of yield from the d-t reaction in the target. There are two main factors which cause loss of yield. First, if the target becomes too hot tritium gas will be released and lost. Second, if a layer of "gunk" deposits on the target the yield will drop. The first difficulty is avoided by operating the target below some critical temperature and the second is minimized by operating at elevated temperatures. It is essential to be able to control the temperature of the target.

First there must be adequate thermal contact to the target foil itself. This problem was taken care of for Zr foils by the tungsten backing onto which the Zr was melted. Contact to the Ta foils was very difficult. The physical properties of the tantalum changed upon gas absorption such that it became extremely brittle, the degree increasing with gas content. Owing to the nonuniform heating during preparation the foils were very warped. The foil itself could not be used as a gas tight

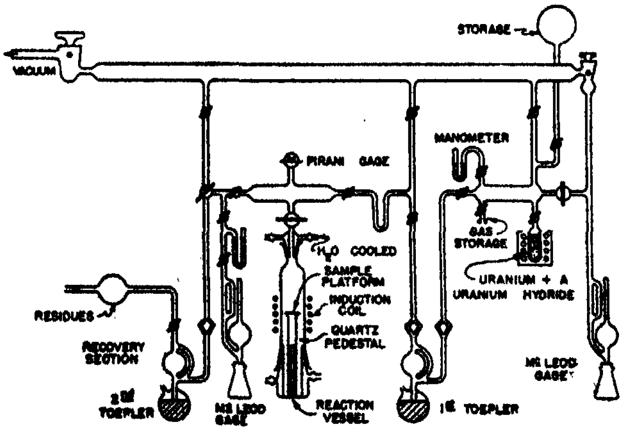

FIG. 3. Apparatus for preparing zirconium foils by induction heating.

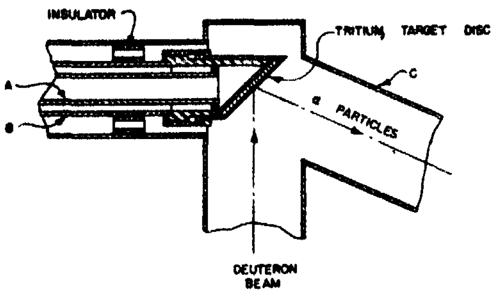

FIG. 4. Target assembly showing mounting arrangement used in accelerator.

membrane. After impregnation the foil released tritium at considerably less than red heat. Attempts to provide a bond to Ta at an earlier stage which could be soldered at low temperature after gas was absorbed have been described in the previous section. In addition to these, various other schemes were tried to provide thermal contact in mounting. Successful use was made of Ta filled targets where the ratio hydrogen isotope to Ta was less than about 1:2, by cementing the foil to a perforated 0.003 inch silver backing with Conductalute cement. Other glues and cements which were tried failed in test bombardments.

Figure 4 shows the target mounting assembly used for both type targets. Cooling or heating was provided to the end plate by circulating air (or freon refrigerant in some cases) down tube *A* and out through tube *B*. A thermocouple (not shown) mounted on the side of the end plate measured the temperature at this point. The tantalum-silver disk assembly or the zirconium-tungsten disk was clamped down against the end plate by the collet arrangement shown. The deuteron beam impinged on the target as shown and the reaction yield was monitored by counting the alpha particles emerging into a proportional counter through a window at the end of tube *C*.

It is possible to distinguish between loss of tritium and "gunk" deposit as a cause of yield loss by counting the x-ray strength of the targets in a standard geometry. The x-rays originate in the stopping of tritium beta-rays by the heavy metal atoms and are almost entirely bremsstrahlung. This counting rate monitors the tritium content since the absorption of the bremsstrahlung in the "gunk" layer is negligible. Test showed that the highest safe temperature for operation with a beam was about 100°C. However the deposit rate is sufficiently reduced at 50°C–80°C and this was chosen as an operating temperature range, accomplished by warming the "cooling" air. In addition to this limit on the gross temperature it was found that a limit was necessary on the beam strength because of local heating. This limit for a $\frac{3}{16}$ inch diameter beam is approximately 10 microamperes at 200 kv. Although the Zr targets probably outgas at a lower temperature than Ta, the better heat conductivity of their mounting serves to make operating conditions very closely the same as those for Ta.

It is clear that the focussing of the beam greatly affects the local heating of the target making impossible any precise statements about the outgassing limits of the foils. If the hydrogen is in solution in the metal and possesses the property of flow within the metal, local heating would act like a leak in a gas reservoir. This does not seem to be the case, since targets have developed weak spots during bombardment. One of the earliest Ta targets lost an average of approximately 50 percent of its yield. The x-ray count was also down in rough agreement with this figure. A "geographic count," i.e., taken with a lead mask provided with a small hole, revealed a region toward one side weaker than the rest. Of interest also is the fact that a count of the back side of the foil, i.e., the side away from the deuteron beam, showed the same "geography." Since new targets proved quite uniform in "geography," it is concluded that the tritium is bound in its locations within the metal after the original absorption.

The neutron yield of the best targets for 10 microamperes of 200-kv deuterons is 10^9 neutrons per second. The deposit rate, although small, is such that the yield drops to around half after a few tens of hours of bombardment. It has been possible in many cases to clean the surface with carborundum and recover the target strength, without actually removing an appreciable amount of tritium. This operation is impossible on full strength Ta foils and difficult on weak ones due to their brittleness. This is one of the great advantages of the Zr targets. The process may be repeated as necessary. On the other hand, the long life activity induced in the Zr during operation makes monitoring the tritium content after long bombardment difficult. A month or more is needed for decay until a reliable count may be made on the tritium content. Hence long term experiments on operational procedures are made even longer.

Targets of the type described have been in use for standard operation in the Cockcroft-Walton accelerator at Los Alamos since November 1947. It is not possible to state on the basis of present experience that such targets have indefinite lifetimes. However, although the yields from some targets have dropped to 50 or 60 percent of the original, the x-ray count indicates no gross loss of tritium to an accuracy of a few percent. Presumably the original yield may be regained by proper surface cleaning.

The authors wish to express appreciation to J. H. Coon and E. S. Robinson for helpful discussions and assistance.

THE REVIEW OF SCIENTIFIC INSTRUMENTS VOLUME 20, NUMBER 8 AUGUST, 1949

Microsampling and Microanalysis of Metals

DONALD F. CLIFTON AND CYRIL STANLEY SMITH
Institute for the Study of Metals, University of Chicago, Chicago, Illinois

(Received May 9, 1949)

In studies of composition gradients in diffusion samples, or for identifying inclusions, it is often desired to obtain analytical samples from minute and exactly located positions in experimental material. This paper deals with the design and use of a microshaper using a diamond tool to take linear cuts separated by as little as 0.02 mm. A hand-driven drill can be used for sampling circular areas of diameter greater than 0.1 mm. The chips, which may weigh as little as 0.1 microgram, are picked up on an electrified quartz fiber and centrifuged into a capillary which is evacuated and sealed for annealing. A precision x-ray diffraction photograph is then obtained from the annealed chip, and the calculated lattice parameter used as an index of composition. Two examples of the use of the technique are given.

IN studies of diffusion and other problems involving a composition gradient, or in the identification of particles differing from their matrix, it is sometimes desired to analyze samples of minute size obtained from exactly-known locations in experimental pieces. Petrographers[1–3] have made some use of tiny drills and burrs driven at moderately high speeds to cut samples from both equiaxed and elongated areas down to about 0.1 mm minimum dimension. These devices give a powder specimen.

In many metallurgical cases, composition gradients exist perpendicular to a nearly plane interface, and a narrow linear sample such as that cut by a dividing engine gives a larger mass for analysis without loss of spatial resolution in the significant direction. The present paper deals with the design and use of a "microshaper" which makes linear cuts separated reproducibly by as little as 0.02 mm, and describes methods of handling the tiny chips removed thereby and the x-ray diffraction technique used for analyzing them.

Figure 1 is a photograph of the microshaper and Fig. 2 is a schematic cross section. The diamond tool (60° nose angle, 25° negative rake, 45° clearance) is held in a manner that allows complete adjustment of orientation in a clamp at the end of a cylindrical bar restrained to slide kinematically in two Vee guides with a point and plane to prevent rotation. The guides are attached to a plate, which is attached by means of an elastic hinge plate (ribbon hinge) to the main frame of the machine. The tool bar is held in place by a 1 kg tension spring at 45°, attached to a projection below the plate. This allows the tool to rise if overloaded and prevents damage. The spring also pulls the bar backwards against a cam which provides forward feed when it is rotated by a hand wheel on the end of its shaft, which passes through bearings in the main frame at the rear. A 500 g compression spring at the rear supplements the hinge plate and presses the guide plate vertically upwards against an adjustable stop. A second cam, on the same shaft as the first, can depress the rear of the plate, pushing it away from the stop and, by causing rotation around the center of the hinge, raise the cutting tool about 0.25 mm. The cams were designed to cause the tool to lower onto the specimen, move forward, lift out while still moving forward, and return while raised. While cutting, the tool bar guide plate is held against the stop and is thus in an exactly reproducible and fixed position, adjustable, however, to exact parallelism with the surface to be sampled. The position at which the cut begins is determined by an adjustable stop, which sets the length of cut up to the maximum (3 mm) possible. The whole bar can be moved forward or backward over about 8 mm to cause the tool tip to start cutting at the desired point on the sample.

The specimen—preferably a standard metallographic specimen mounted in 1 inch diameter Bakelite to

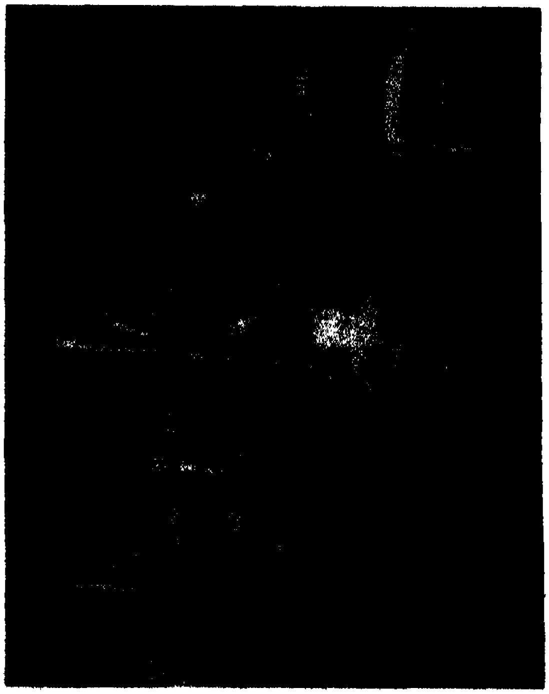

FIG. 1. Microshaper.

---

[1] B. Granigg, *Metal und Erz*, XII (NF III), 193 (1915).

[2] H. Moritz, Centralblatt für Minerologie, Geologie, und Paleontologie A(7), 251 (1929).

[3] M. Haycock, Econ. Geology 26, 415 (1931).

facilitate level polishing, and lightly etched to delineate the structure—is mounted with its surface horizontal by pressing into cement or plasticene on a holder, which is then secured to the stage proper by thumbscrews through slots to allow for adjustment. The stage has two precise motions, at right angles to each other and to the direction of motion of the tool. It slides laterally on cylindrical guides and is moved by a micrometer screw of 0.5 mm pitch. The whole stage and lateral movement is mounted on a keyed cylinder sliding vertically in the main frame and can be raised by another micrometer screw of 1.0 mm pitch working directly against the base plate. Both micrometer screws have large heads, graduated in 100 divisions. No front and back motion is provided on the specimen as this is provided for in the tool motion and does not need extreme precision.

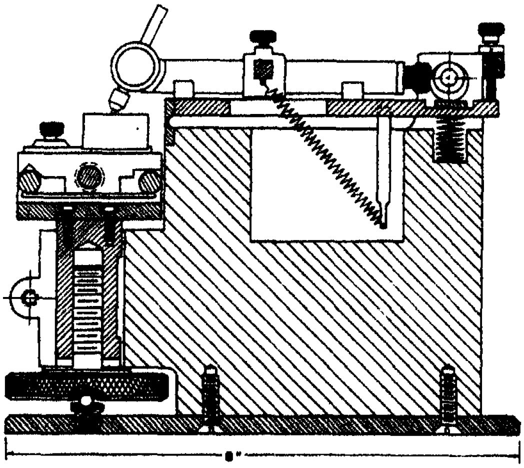

FIG. 2. Schematic cross section of microshaper.

A binocular microscope at about 45° permits the operation of the tool and removal of the clip to be watched. In taking a series of cuts the specimen is raised slowly by the vertical micrometer until it just touches the tool as the handwheel is turned to cut. Leveling is adjusted if necessary, then the specimen further raised to give the desired depth of cut and the first cut taken. The specimen can then be moved laterally any desired amount and a new cut taken. When a cut is desired in a particular location, the exact positioning of the specimen is best done by the use of a toolroom microscope focused vertically on the specimen, the cross-hairs in the eyepiece being adjusted against a trial cut and used to locate the specimen for subsequent ones.

The sample removed by this shaper is in the form of a single chip if the metal is reasonably ductile. In general, cuts about 0.02 mm wide and 1 mm long (giving chips weighing about 3 micrograms) are preferred, although satisfactory analyses have been obtained on as little as 0.1 microgram. Nothing is gained by chips heavier than 50 micrograms. It is difficult to take extremely short cuts, for the tool does not immediately cut a full-width furrow. In a ductile metal the chips are heavily deformed and are much shorter and thicker than the furrow. There is some building up of ridges on the edges of the furrow and cuts closer together than about 0.02 mm cannot be obtained with accuracy.

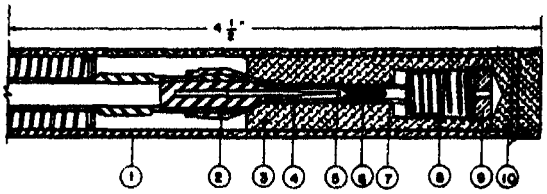

FIG. 3. Specimen holder for centrifuge.

(1) Centrifuge arm
(2) Pin vise
(3) Aluminum housing
(4) Quartz fiber
(5) Sample
(6) Capillary
(7) Capillary supporting sleeve
(8) Capillary expulsion spring
(9) Spring retaining plug
(10) Cap

A great deal of trouble was encountered in handling the chips until the following technique was developed, and even then the loss of critical samples was not unknown. The specimen must be electrically grounded to the frame of the machine, or the chip will become charged and stick to the diamond in awkward spots. The cams must be adjusted to lift the tool out of the sample while it is still moving forward and cutting, otherwise the chip will remain attached to the sample. With skill and practice chips can be made to lie at the end of the furrow or to remain loosely held on the tool tip. All trace of grease must be avoided. The chips are then picked up on a 0.005-inch tip drawn on a quartz rod about 0.02 inch in diameter. This is held in a pin vise and given a charge of static electricity by rubbing with silk, or by picking the charge off a larger and more easily charged rod. The chip is thrown off the rod into a thin-walled capillary by means of a centrifuge, using

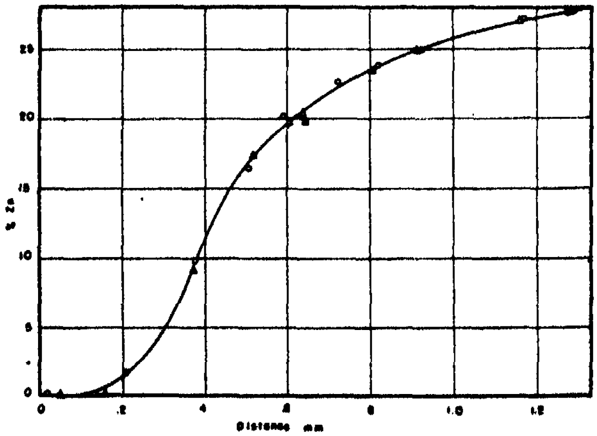

FIG. 4. Composition of annealed diffusion couple formed between copper and α-brass. Points represent results on two series of cuts, 0.02 mm wide and 0.25 or 2.0 mm long (0 and Δ, respectively). Chips analyzed weighed about 0.2 and 2.0 micrograms, respectively.

the holder shown in Fig. 3. About 500 G is ample to transfer the specimen, which is easily seen at the bottom of the capillary.

METHOD OF ANALYSIS

The best of sampling is useless without sufficiently sensitive and accurate analytical methods. The use of precision lattice parameter measurements will generally prove the simplest for quantitative measurements on the micro-chips though it is limited to binary solid solutions in which the lattice parameter is a sensitive function of composition. For multiphase or multicomponent alloys x-ray methods are less satisfactory and often useless, and the more cumbersome microcolorimetric or spectrographic methods may be necessary.

Annealing of the heavily cold-worked chips is generally necessary before x-ray analysis. The capillary containing the chip is evacuated with a mechanical pump and a small length containing the specimen is sealed off with a pin-point flame. The tiny capsule and its contents are then annealed at a temperature that will give sharp diffraction lines but not allow much grain growth. The final stage consists of breaking open the capillary in a steel "diamond" mortar and picking the annealed chip out of the debris on a slightly greased 0.001–0.002-inch diameter tip on a quartz rod which is transferred directly to the camera. The need for a sufficient number of grains to give smooth measurable diffraction lines is one of the factors limiting minimum specimen size. It is for this reason that the large negative rake is used on the cutting tool, for this gives severe deformation of the metal in the chip so that it will recrystallize at a low temperature and to a very fine grain size. Brittle materials which give fairly strain-free powder on cutting usually give satisfactory patterns without annealing. The powder is picked up directly from the surface of the specimen by a greased fiber and transferred to the x-ray camera.

The x-ray diffraction patterns are obtained using a 9 cm Bradley type camera[4] as modified by Zachariasen. This camera has a rotating specimen holder with three mutually perpendicular adjustments, enabling the specimen to be placed on the axis of rotation and in the center of the x-ray beam and camera. The adjustment is made while observing with a 15× toolroom microscope. The camera is housed in a thermostatted box (±0.5°C) and is evacuated to about 1 mm pressure to minimize fogging due to scattering of x-rays by air. Exposures run about 4 to 16 hours—i.e., from two to eight times those needed for normal-sized samples. The films are indistinguishable from those made with large samples.

Figure 4 is an example of the results that can be obtained with these techniques. It shows the compositions of two independent series of cuts, 0.02 mm wide and 0.25 and 2 mm long, respectively, which were taken on a small diffusion sample composed of copper and alpha brass pressure-welded together and annealed for 3½ days at 800°C. Using the Bradley and Jay $\cos^2\theta$ extrapolation, correcting for film shrinkage by the Straumanis method,[5] the error was estimated to be less than 0.0005A, or one-quarter weight percent of zinc.

In another experiment it was shown that there was no detectable difference in composition between samples 0.02 mm wide by 0.7 mm long cut from the grain boundary of 3 mm grain-size bronze containing 1.4 percent tin, and others cut from positions progressively removed from the boundary. The lattice parameters in this case were determined using a modification devised by J. B. Hess of Cohen's extrapolation. The probable error of the tin determination was 0.1 atomic percent.

It is believed that the device will prove especially useful in studying intermediate phases formed by diffusion. It is possible, for example, to make a diffusion pair, anneal to produce intermediate layers of all the phases capable of existence at the annealing temperature, and then to sample them all and determine their structure and parameter variation—all this on a single specimen.

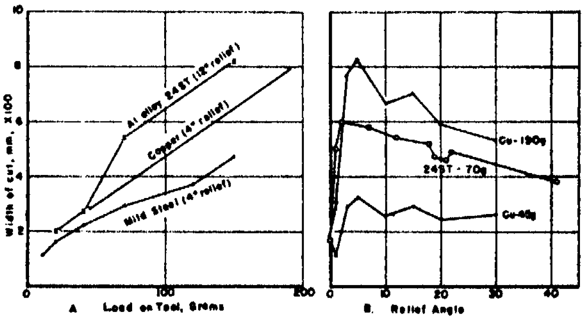

FIG. 5. Width of cut with gravity-loaded tool *vs.* (A) load on tool; (B) relief angle.

Prior to the construction of the micro-planer with a positive feed, use was made of a gravity-loaded diamond tool on a dividing engine. The width of cut varied greatly with hardness of the metal, grain orientation, and other factors. Unless the tool was lowered into position extremely slowly, the initial dent was more important in determining the cut width—even in long cuts—than the stationary load. Some data on cut width as a function of load and tool orientation may, however, be of interest, and are summarized in Fig. 5.

In cases where a sample is to be taken from a small, nearly equiaxed area, drilling is preferable to the use of the shaper. We have had good results with a simple preliminary device using a jeweller's pivot drill, resharpened to a symmetrical pointed chisel edge. This is held in a pin vise mounted in a cylindrical shank sliding in a well-fitted bearing in a frame which also holds a two-way adjustable slide for the specimen. The pin vise shank has a knurled head and is held up by a light spring. It is depressed by hand until it strikes the specimen surface and given one or two twists under manual pressure, taking care to withdraw the drill while still turning. A fixed microscope with cross-hairs locates the specimen under the drill point. The manner of handling the chips is identical with that described above. Areas down to 0.15 mm in diameter have been sampled with the present device. Drilling at a low speed with a fairly deep cut is to be preferred to high speed drilling, as it gives chips rather than powder.

---

[4] Bradley, Lipson, Petch, J. Sci. Inst. **18**, 216 (1941).

[5] M. J. Buerger, *X-Ray Crystallography* (John Wiley and Sons, Inc., New York, 1942), p. 411.

ACKNOWLEDGMENTS

This work would have been impossible were it not for the contribution of Mr. J. Getzholtz of the Physical Science Division machine shop of the University of Chicago. Mr. Getzholtz contributed to the design of the microshaper and provided the exquisite workmanship needed for its construction. Mr. J. B. Hess materially assisted in technique development and made the analyses on the copper-tin alloy.

THE REVIEW OF SCIENTIFIC INSTRUMENTS VOLUME 20, NUMBER 8 AUGUST, 1949

A Transistor Trigger Circuit

HERBERT J. REICH AND ROBERT L. UNGVARY
Department of Electrical Engineering, Yale University, New Haven, Connecticut

(Received March 8, 1949)

Analysis of the characteristic curves of transistors shows that the negative resistance necessary to the functioning of a trigger circuit exists in the base circuit of a transistor. A trigger circuit may therefore be formed by inserting a resistance of proper magnitude in series with the base. Such a circuit has the advantages over vacuum-tube circuits of much shorter triggering time, simplicity, small size, absence of filament power supply, and low operating voltage. The rise and fall times of the output voltage are less than 0.1 microsecond and the circuit is stable from zero triggering frequency up to the maximum frequency used. Although the circuit has been tested only up to 1 Mc, an upper limit of at least 10 Mc is probable. An output voltage of 5 or 6 volts may be readily obtained. Like other types of trigger circuit, the transistor circuit may be converted into a relaxation oscillator or a pulse generator.

THE triggering speed and maximum frequency at which vacuum-tube trigger circuits can be operated is limited by circuit and interelectrode capacitances. The very low interelectrode capacitances and small size of transistors[1] therefore suggest that these devices may provide considerable improvement in maximum frequency limit and in output wave form of trigger circuits.

Because the operation of all trigger circuits depends upon the presence of a circuit element having negative variational resistance, the simplest way in which to determine the manner in which a transistor should be used in such a circuit is to determine from the characteristic curves how the electrode voltages must be varied in order to produce a negative variational resistance.[2] The curves show that in the proper ranges of operation a small increment of voltage applied in the base lead, as in Fig. 1, produces a current increment in opposition to the voltage increment and that a negative variational resistance therefore exists at the point of application.

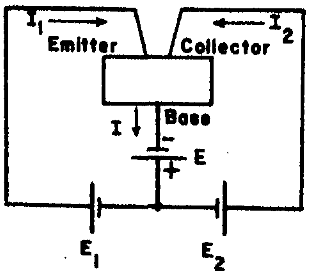

FIG. 1. Transistor negative-resistance circuit.

Figure 2 shows a curve of base current I *vs.* voltage E obtained in the circuit of Fig. 1 at zero emitter supply voltage E_1 and a collector supply voltage E_2 of -2.5 volts. This curve was derived graphically from measured curves of collector current *vs.* emitter current at constant values of emitter voltage and at constant values of collector voltage. The effect of variation of collector voltage upon the currents is so small in comparison with the effect of variation of emitter voltage that little error results from assuming the collector voltage to be constant and obtaining the curve of Fig. 2 from the constant-collector-voltage curve of Fig. 3. (Variation of collector voltage raises the minimum slightly in the curve of Fig. 2 and displaces the minimum toward the right.) The minimum of the curve of Fig. 2 is lowered by an increase in the magnitude of

---

[1] J. A. Becker and J. N. Shive, Electrical Engineering **68**, 215 (1949).

[2] H. J. Reich, *Theory and Applications of Electron Tubes* (McGraw-Hill Book Company, Inc., New York, 1944), second edition, Sec. 10-1.

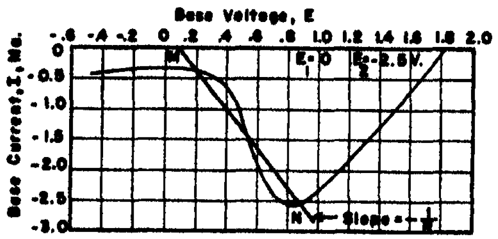

FIG. 2. Curve of base current I *vs.* base voltage E at zero emitter supply voltage E_1 and a collector supply voltage E_2 of -2.5 volts.

the negative collector supply voltage E_2. Although the resulting increase of slope in the negative-resistance region is desirable, the high emitter and collector currents are likely to damage the transistor.* Since points in the curve of Fig. 2 at which the slope is negative correspond to points at which the magnitude of the slope of the curve of Fig. 3 is greater than unity, the region of operation in which negative variational resistance is possible may be determined by inspection of a family of constant-collector-voltage curves.

Triggering of the circuit of Fig. 1 should be made possible by the addition, in series with the voltage E, of a resistance R, if the value of $1/R$ is less than the maximum magnitude of negative slope of the curve of Fig. 2, i.e., if R exceeds the minimum value of negative variational resistance. This fact is shown by the multiple intersections of the curve with the load line MN, which passes through the point on the voltage axis corresponding to the voltage E and has a negative slope equal to the reciprocal of the circuit resistance R.[2] If the value of R is properly chosen, multiple intersections, and hence triggering, are obtained even when E is zero. The minimum magnitude of negative resistance for the curve of Fig. 2 is approximately 625 ohms. Triggering should therefore be possible for values of R greater than this value. These predictions are verified experimentally.

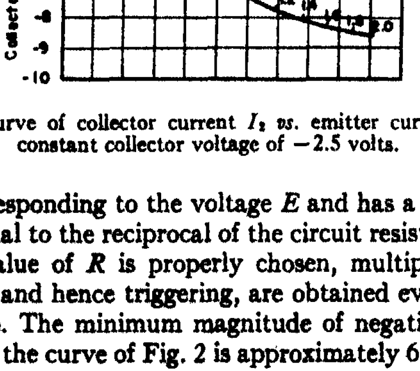

FIG. 3. Curve of collector current I_2 *vs.* emitter current I_1 at constant collector voltage of -2.5 volts.

Analysis of trigger circuits from a somewhat different point of view indicates that triggering is possible only in circuits having positive feedback. Becker and Shive have shown that positive feedback is produced by a resistor in the base lead.[1]

Introduction of resistance in series with the emitter causes the variation of emitter voltage with base voltage E to be decreased, and introduction of resistance in series with the collector causes the variation of collector voltage to be increased. With series resistance in either circuit the path of operation no longer approximates a curve of constant collector voltage, but instead a curve that has smaller slope and cuts through the curves of constant collector voltage. As a result, the minimum of the curve of Fig. 2 is raised and may even disappear. An emitter resistance of a hundred ohms or less may eliminate the negative resistance and thus prevent triggering. The introduction of a resistance of as much as a thousand ohms or more into the collector circuit, on the other hand, has a much smaller effect upon the curve and does not prevent triggering.

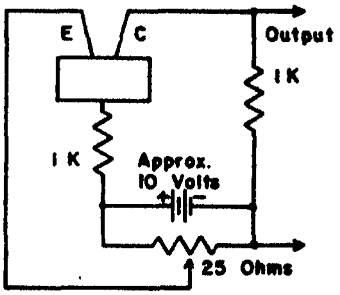

FIG. 4. Transistor trigger circuit.

Because the base current is equal to the difference in the magnitudes of the emitter and collector currents, relatively small output voltage is obtained across the base resistor. A change of 5 volts or more may, however, readily be produced across a resistor in the collector circuit, as shown in Fig. 4. In order to keep circuit time-constants small, it has been found desirable not to exceed collector circuit resistance of approximately 1000 ohms unless high output voltage is essential.

The triggering impulses may be introduced either in series or in parallel with the base resistor. If series input is used, the input source works into a relatively low resistance equal to the difference between the magnitudes of the base circuit resistance and the instantaneous negative resistance. If parallel input is used, the input source works into a conductance equal to the difference between the magnitudes of the conductance of the base resistor and the instantaneous negative conductance. Although the smaller loading of the driving source with parallel input is advantageous, the shunt capacitance of the source increases the triggering time and thus limits the maximum triggering frequency and distorts the output waveform.

Although an attempt has not yet been made to determine the upper frequency limit of triggering, a

---

* The use of continuous currents of magnitudes corresponding to points appreciably to the right of the minimum of the curve of Fig. 2 is not recommended.

"breadboard" model of the circuit of Fig. 4 in which no effort was made to minimize circuit capacitances and inductances was not at all critical in adjustment and required no readjustment from zero frequency up to the maximum value used, 1 Mc. The triggering time, determined by an oscilloscope across the collector resistor, is about 0.1 microsecond. Reduction of circuit capacitances, which included the input capacitance of the oscilloscope, should reduce the triggering time appreciably. There appears to be considerable likelihood that the circuit can be made to trigger reliably at frequencies up to the 10-Mc limit observed in the use of transistors in amplifiers. The output voltage change for the circuit parameters shown in Fig. 4 is approximately 6 volts, but this value can be increased by the use of greater output resistance and higher supply voltage. The input-pulse voltage required to trigger the circuit is approximately 1 volt. Examination of Fig. 2 shows that the required input-pulse voltage can be reduced by adjusting the circuit parameters or voltages in such a manner as to make the maximum magnitude of slope of the current-voltage curve more nearly equal to the reciprocal of the base resistance R.

Negative transistor resistance can also be obtained between the collector and the base if the collector is coupled to the emitter. Unfortunately, however, the coupling circuit must have low resistance because of the high emitter current. Since the high positive conductance of the coupling circuit shunts the effective negative conductance of the transistor, the net conductance is small in magnitude and usually positive.

In addition to improved output wave form and a probable higher frequency limit, advantages of transistor trigger circuits over vacuum-tube circuits include their extreme simplicity, small size, absence of filament power supply, and low operating voltage. Like other trigger circuits, the transistor trigger circuit can be readily converted into a relaxation oscillator or a pulse generator by adding circuit capacitance in such a manner that triggering is followed by exponential rise or fall of potential of one or more electrodes.[3] In the circuit of Fig. 4 this may be accomplished by connecting a capacitor between the collector and ground. Since sustained sinusoidal oscillation may occur if a parallel resonant circuit is shunted by a negative conductance of magnitude greater than that of the circuit conductance, the circuit of Fig. 4 may be converted into a negative-resistance sine-wave oscillator by replacing the cathode resistor by a parallel resonant circuit.[3] An advantage of the transistor circuit relative to a tube circuit in this application is the relatively high magnitude of negative conductance attainable at supply voltages of only a few volts.

---

[3] H. J. Reich, *Theory and Applications of Electron Tubes* (McGraw-Hill Book Company, Inc., New York, 1944), second edition, Secs. 10-8, 10-10, and 10-17.

THE REVIEW OF SCIENTIFIC INSTRUMENTS VOLUME 20, NUMBER 8 AUGUST, 1949

A Fast Recycling Cloud Chamber and Pulsed Magnetic Field Equipment for Use with Pulsed Accelerators

E. R. Gaerttner and M. L. Yeater
Research Laboratory, General Electric Company, Schenectady, New York

(Received May 9, 1949)

The objective of the work described here has been the development of cloud-chamber apparatus for use with new high energy pulsed accelerators, such as the present 100-Mev betatron and the 300-Mev synchrotron now being constructed by the General Electric Company. The present cloud chamber is operated at a repetition period of about 5 seconds. An "overcompression" step in the cloud-chamber cycle causes old tracks to be evaporated by momentary heating of the gas through compression. A pulsed magnetic field of 12-milliseconds duration is used with this cloud chamber. The field is produced by discharging capacitors through Helmholtz coils. With these short current pulses, strong fields (20,000 gauss or more) are obtainable at fast cloud-chamber recycling rates with relatively small heating of the coils.

I. INTRODUCTION

The new high energy accelerators impose some new requirements on the cloud-chamber equipment associated with them and also permit the use of some new techniques. These accelerators are characterized by short radiation pulses and by repetition rates which are fast compared with those of cloud chambers. The 100-Mev betratron of The General Electric Company, for example, can be used to generate x-ray pulses of about 5-microseconds duration[1] at a rate of 60 pulses per second. Owing to the short radiation pulse length, it is possible to use, with the cloud chamber, a pulsed magnetic field of short duration. Short field pulses of large amplitude can be obtained with non-ferromagnetic coil structures at relatively fast repetition rates. The low duty cycle of the exciting current leads to a small heat dissipation in the coils. Since these coils are much smaller and lighter in weight than ferromagnetic structures, the cloud-chamber equipment can be assembled as a compact and portable unit.

It is desirable, in general, to have a cloud chamber with a fast recycling rate in order to accumulate data rapidly. The fast recycling rate which has been obtained with the overcompression technique makes it possible, in our case, to take advantage of the fast repetition rate of the pulsed magnetic field.

---

[1] G. C. Baldwin, private communication.

In order to gain full advantage of the use of this type of cloud chamber, it is necessary to minimize the labor of measuring the curvature of the tracks. We have developed an instrument which has provided measurements with better accuracy and at a faster rate than we have been able to obtain by comparing the tracks with curves of known radii. This instrument is described in a separate note.[2]

II. THE CLOUD CHAMBER

In order to increase the cloud-chamber repetition rate, it is necessary to dissipate old tracks rapidly. This must be done by a method which gives tracks of good quality. By introducing an additional step in the conventional cycle of cloud-chamber operation, causing a momentary "overcompression" of the filling gas, we have increased the repetition rate without altering the other characteristics of the chamber. The nature of the filling gas, the strength of the clearing field, and the timing of the various steps in the cycle are subordinate factors in its behavior at fast recycling rates.

Design Considerations

From the physics of drop formation in a cloud chamber,[3] it can be inferred that, with moderate heating, the old drops in a cloud chamber can be evaporated rapidly to such a size that a strong clearing field can remove them. This heating can be obtained by decreasing the volume of the cloud chamber from its expanded value to a volume less than that which exists just prior to expansion. The cycle involves a conventional adiabatic expansion, followed by an adiabatic overcompression and a relatively slow return to the initial volume. The expansion ratio required is nearly the same as for a chamber operating in the conventional way. An overcompression ratio[4] about equal to the expansion ratio is satisfactory in most cases. The movement of the cloud-chamber piston required for this cycle is accomplished with a mechanism using compressed air to drive auxiliary pistons which are coupled to the cloud-chamber piston.

The nature of the filling gas influences the limiting conditions of operation at increased repetition rates. It is desirable to use a gas with high ion mobility and good thermal conductivity, for most rapid clearing and for maintenance of thermal equilibrium. A monatomic gas is preferred because of the smaller expansion ratio required.

The clearing field should be as large as possible without producing spurious ionization. This is desirable because the droplets can never be completely evaporated by overcompression; hence some fairly heavy ions must be removed from the chamber.

The timing of the chamber is empirically adjusted to provide optimum growth time for the tracks and to maintain good thermal equilibrium.

The size of the cloud chamber is fixed by practical limitations on the size of the field coils in the present case. Small field coils are desirable in order to have a small amount of stored energy in the field. We have arbitrarily chosen an inside coil diameter of nine inches, as a compromise, which requires a stored energy readily obtainable with a capacitor bank of reasonable size and will accommodate a fairly large cloud chamber.

Owing to the rapid change of magnetic flux in the present chamber, the large structural parts near the coils must be non-conducting. Suitable materials for these parts are textolite and polystyrene.

Physical Characteristics of the Cloud Chamber

A functional diagram of the present five-inch cloud chamber is shown in Fig. 1. A photograph of the chamber is shown in Fig. 2. In Fig. 3 the field coils are shown in place. The cylinder surrounding the coils, and the box above the coils, shown in Fig. 2, form a light-tight and thermally insulating structure around

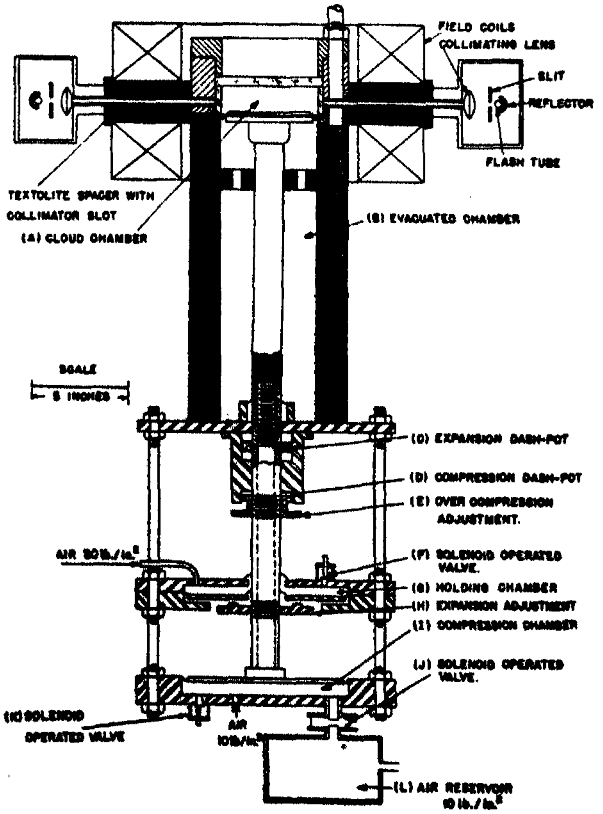

FIG. 1. Functional diagram of cloud chamber, with field coils.

---

[2] E. R. Gaerttner and M. L. Yeater, in press.

[3] *Cf.*, N. N. Das Gupta and S. K. Ghosh, Rev. Mod. Phys. 18, 225 (1946).

[4] By overcompression ratio is meant the difference between the normal and overcompressed volumes, expressed as a fraction of the normal volume.

FIG. 2. Photograph of complete cloud chamber assembly, including camera, optical system and insulating enclosure.

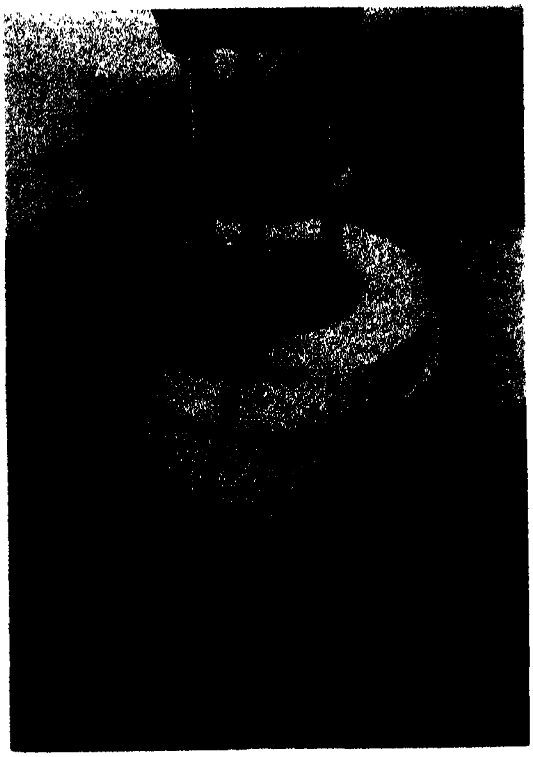

FIG. 3. Photograph of field coils mounted on cloud chamber, with insulating enclosure removed.

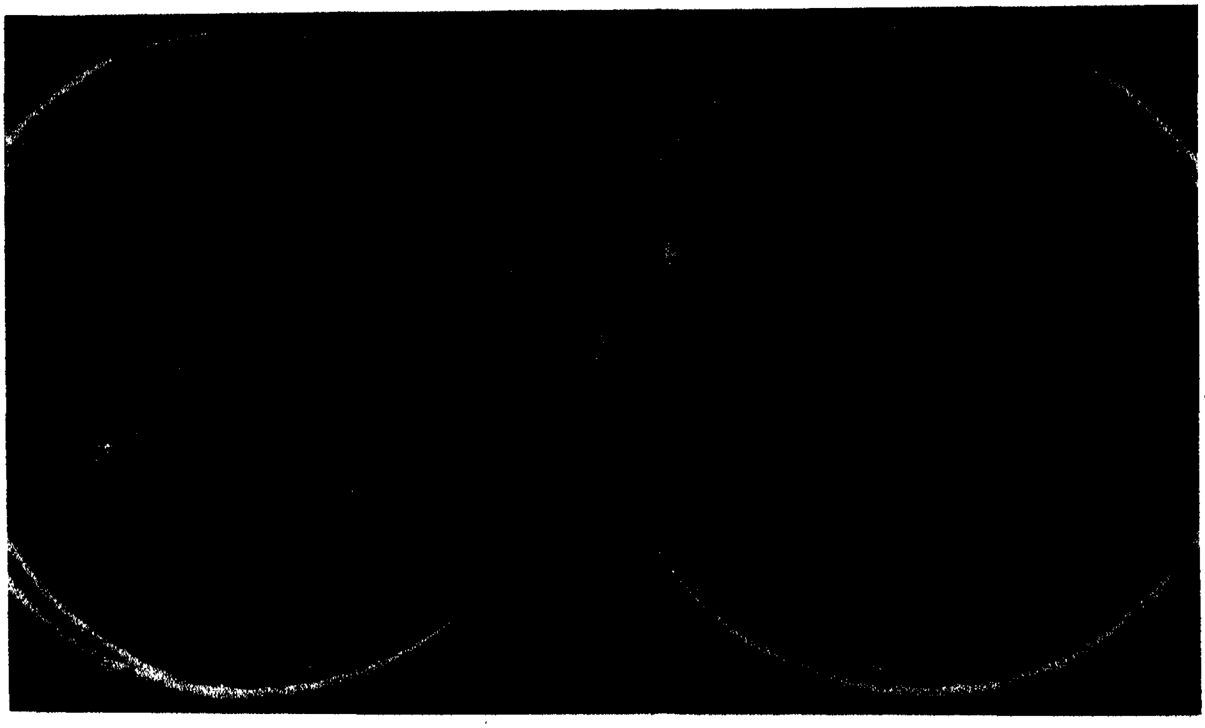

FIG. 4. Typical electron tracks obtained with the cloud chamber. The filling gas consists of equal parts of helium and argon, with equal parts of water and ethyl alcohol added. The repetition rate is one expansion every six seconds. The chamber is irradiated with x-rays from the 100-Mev betatron. This picture shows a pair formed in the gas by a beam of x-rays ¼-inch in cross section; the beam is admitted to the chamber through a thin aluminum window.

Fig. 5. Electron tracks observed with the chamber expanding every two and one-half seconds. There is no magnetic field. The primary x-rays are from the betatron. The filling gas contains helium and argon in the ratio of three to one.

the chamber and stereoscopic viewing system. The boxes at the sides of the chamber contain the flashlamps and part of the lamp trigger circuits and complete the light-tight structure which houses the optical system. The pneumatic driving mechanism is visible at the bottom of the structure. The whole cloud-chamber assembly, with field coils, is mounted on a mobile carriage.

The mechanical operation can be summarized as follows: A conventional glass cylinder and glass top plate, held together by the plastic structural rings as shown in Fig. 1, are used with a piston and diaphragm in the usual cloud chamber arrangement. The piston is held in the starting position by the force of the air in the compression chamber (*I*). This force is made sufficiently large to overcome the force on the cloud-chamber piston produced by the difference in pressure between the cloud-chamber gas and the partially evacuated chamber (*B*); but it is not great enough to overcome the force on the expansion adjustment nut (*H*) produced by the air pressure in the holding chamber (*G*). The cloud-chamber piston, therefore, assumes a rest position determined by the expansion adjustment nut bearing against the holding-chamber piston.

To expand the chamber the solenoid-operated valve (*K*) is released and the cloud-chamber piston drops to a position determined by the expansion dashpot (*C*).

To overcompress the chamber after the expansion, (*K*) is closed and immediately afterward the solenoid-operated valves (*J*) and (*F*), which are normally closed, are opened simultaneously. The air from the reservoir (*L*) rapidly forces the cloud-chamber piston to the upper position determined by the overcompression dashpot adjustment (*E*). This position is above the starting position fixed by the holding chamber. To return the cloud-chamber piston to the starting position, the valves (*J*) and (*F*) are closed and the air pressure in the holding chamber forces the piston down to the starting point, completing the cycle.

Cloud-Chamber Performance

The cloud chamber described above, operating at a period of five to seven seconds, has been used with the 100-Mev betatron and 70-Mev synchrotron to take about 80,000 photographs of electron tracks. A typical picture of electron tracks from this group is shown in Fig. 4.

Tests have been made at faster repetition rates. With an interval of one second between expansions, the chamber is not uniformly sensitive; the new tracks are recognizable, however, at each expansion. With an interval of two and one-half seconds the tracks appear to be satisfactory. A picture taken at this rate is shown in Fig. 5.

The improvement offered by the overcompression technique can be shown by a comparison of cloud-chamber photographs taken with and without overcompression. An example of this is illustrated in Fig. 6,

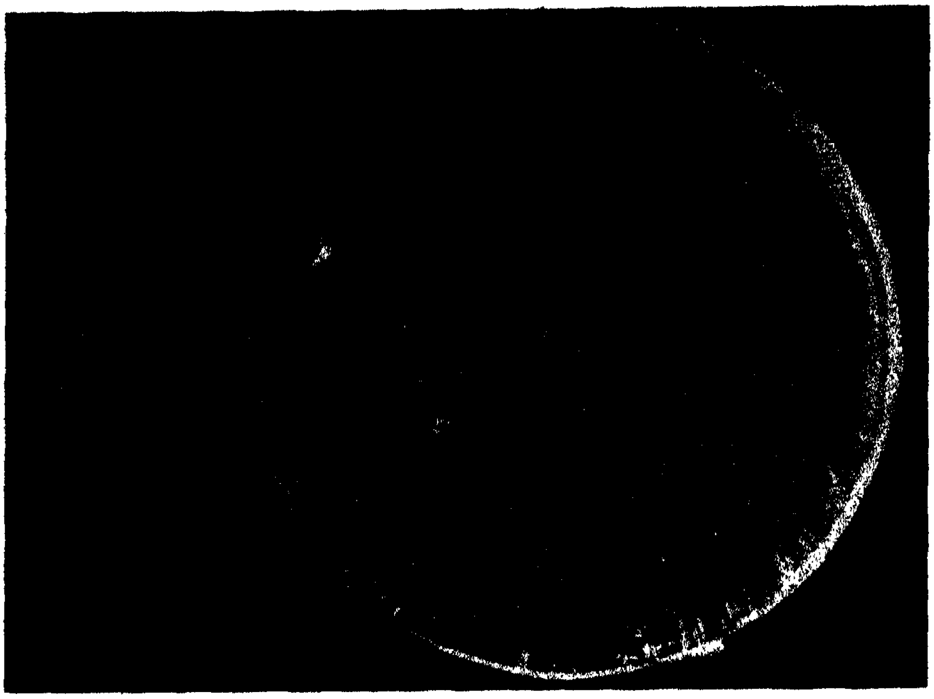

FIG. 6a

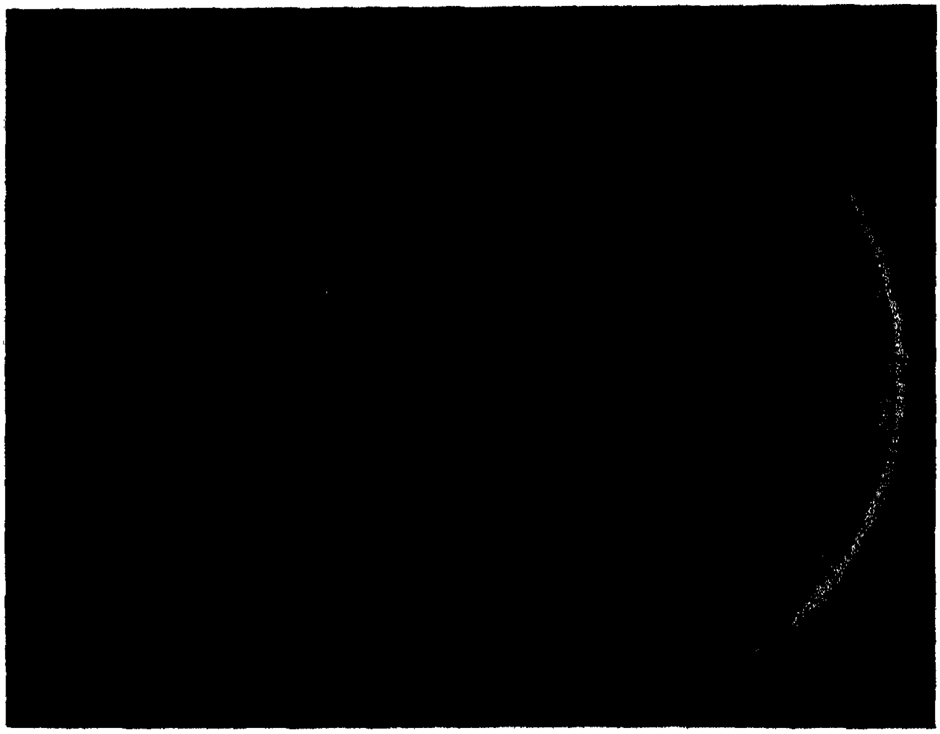

FIG. 6b

which shows the behavior of the chamber when a large number of tracks is present. The time between expansions is seven seconds. The filling gas is the mixture used by us most extensively, consisting of equal parts of helium and argon at atmospheric pressure plus equal parts (by liquid volume) of ethyl alcohol and water. For one picture in each group the chamber is strongly irradiated with a pulse of x-rays from the 100-Mev betatron. For the remaining pictures in each group the chamber is not irradiated. Without overcompression, the tracks formed in the first expansion are still discernible in the third picture, and not until the twelfth picture is the chamber as clear as before irradiation. With overcompression, the first picture taken after

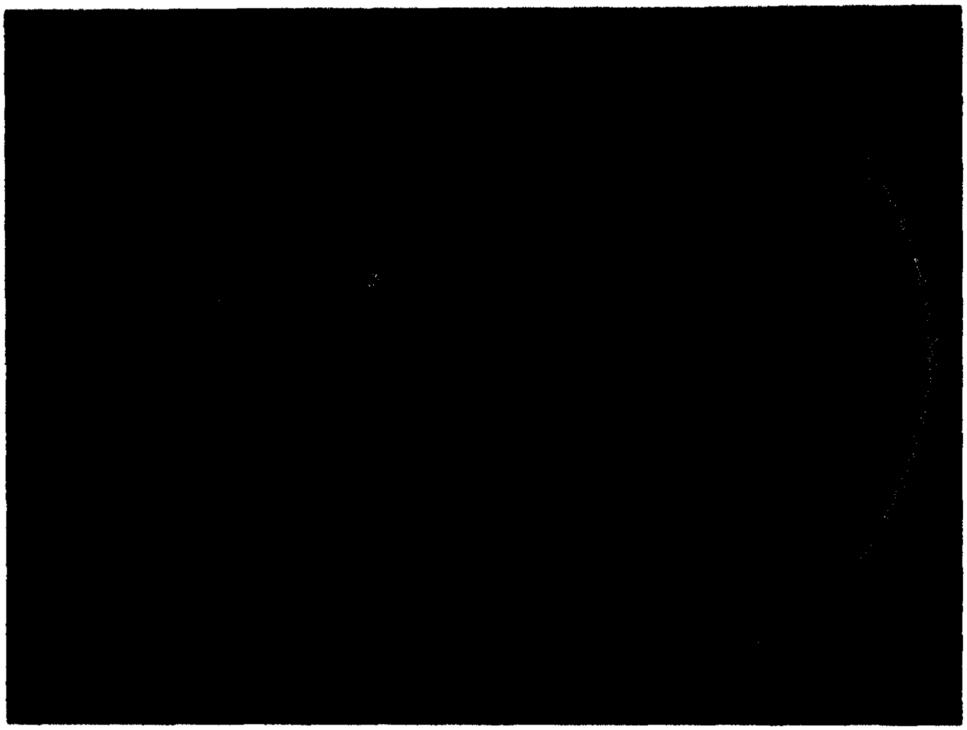

FIG. 6. Representative pictures from sequences of cloud-chamber photographs which were taken to show the effect of overcompression on the rate of clearing. The filling gas is helium and argon in equal parts; the interval between expansions is seven seconds; the magnetic field is 4000 gauss. One sequence was taken without overcompression and one with overcompression. For the first expansion only in each sequence, the chamber was strongly irradiated with x-rays from the 100-Mev betatron, using the same intensity in each case, as shown in *a*. Picture *b* shows the residue of old tracks on the second expansion without overcompression, traces of which remain until the twelfth expansion. Picture *c* shows the relatively slight residue of old tracks on the second expansion with overcompression; the chamber is completely clear on the third expansion in this sequence. (Parts (a) and (b) are on page 592.)

FIG. 6c

the one showing irradiation is fairly clear, and the clearing is complete in the next picture.

For operation at intervals shorter than about five seconds it seems advisable to use a filling gas consisting mostly of helium. Tests made with various mixtures of helium and argon indicate that for the most rapid operation, the best clearing of old tracks is obtained with pure helium. Sequences of pictures similar to those of Fig. 6, taken with a filling of pure helium and a repetition interval of six seconds, show that even without overcompression the chamber is completely clear by the fourth expansion after irradiation. This is to be compared with the twelve expansions required when the filling was half argon.

The cloud chamber appears to be free of turbulence. Maintenance of suitable thermal conditions is favored by the following characteristics of the equipment: (1) the heat dissipation in the magnetic field coils is relatively small, (2) the housing about the chamber and coils is well insulated and can be thermostatically regulated, (2) the net heat flow owing to expansion and overcompression can be controlled by adjustment of the timing. The data indicating the essentially turbulence-free character of the chamber are (1) observation of straight tracks such as those of Fig. 5, (2) observation of electron tracks which describe complete circles in a magnetic field, (3) measurement of the difference in radius of curvature along different sections of the same track curved in a magnetic field. The latter affords good statistical evidence because the conditions can be chosen so that the effect of scattering[5] in the gas is negligible. Using the instrument[2] previously mentioned for measurement of curvature, we have looked for a change in curvature along tracks of electrons with energies near 25 Mev. These tracks are formed in a filling gas containing helium and argon in equal parts, with a field of 4000 gauss. The repetition interval is seven seconds. The average difference in the measured value of the sagitta for two over-lapping sections of a track (the track length is 8.4 cm and the chord used is 5.1 cm) is 0.0075 cm. This is about equal to the discrepancy between repeated measurements of the same section of track. The effect of turbulence is therefore less than other factors contributing to the error in curvature measurement,[6] such as track width and droplet spacing along the track.

A timing sequence[7] which has given good electron tracks at intervals of five to seven seconds is the following: droplet growth time, 200 milliseconds; interval from beginning of expansion to start of overcompression, 300 milliseconds; time during which chamber is overcompressed, 500 milliseconds; time of return from over-expanded position, about two seconds.

---

[5] The criterion for evaluating the scattering has been given by H. A. Bethe, Phys. Rev. **70**, 821 (1946).

[6] The instrumental error is discussed in reference 2.

[7] In the present arrangement, timing is accomplished through the use of multivibrator delay stages. Timing adjustments are facilitated by displaying the multivibrator signals on an oscilloscope having a special sweep circuit which provides several parallel traces, one above the other, to give an expanded time scale.

III. PULSED MAGNETIC FIELD EQUIPMENT

This apparatus provides a magnetic field in the form of a half-sine wave of 12-milliseconds duration. The field is synchronized with the accelerator so that it reaches its peak value when the radiation pulse occurs. We have operated the field equipment automatically at peak fields of 4000, 11,000, and 16,000 gauss,[8] at rates of five seconds, 12 seconds and 30 seconds per cycle respectively. Fields up to 20,000 gauss have been produced during brief tests. For sustained operation at levels above 16,000 gauss, the present capacitor bank of 100 units should be increased. Peak fields of 33,000 gauss can be provided at ten second intervals, for example, with 400 capacitor units,[9] with minor additions to the present charging equipment.

Fields of larger amplitude can be produced in this way, but it seems desirable first to explore the possibility of replacing the capacitor bank with a rotating machine[10] for energy storage, with suitable changes in the auxiliary equipment. The ultimate limit on field strength is probably fixed by the mechanical strength of the coils rather than by the energy reservoir.

The coils now used can accommodate a cloud chamber with an inside diameter of eight inches. With fields up to 33,000 gauss this size of chamber appears adequate for use with the 300-Mev synchrotron now under construction in Schenectady.

Coil Design

The energy E which must be stored in the capacitors to provide a peak induction B at the center of a Helmholtz arrangement consisting of coils of mean radius a can be evaluated approximately from the following equation:

$$E \cong 2.5(L/n^2)B^2a^2 + \text{losses during rise of pulse.} \quad (1)$$

In this equation L is the inductance in henrys and n is the total number of turns; E is expressed in joules, B in gauss and a in cm. For the geometry used, L/n^2 is roughly proportional to a. Therefore, the stored energy E is determined essentially by B^2a^3 and the Q of the circuit.

The most efficient use of the stored energy can be obtained with coils of small radius, since the maximum particle energy which can be measured is proportional to Ba. One further consideration, however, is that the Q of the coils decreases with decreasing radius. A final design must, therefore, be a compromise which takes into account energy storage, heat dissipation in the coils, and a practical lower limit to the cloud-chamber diameter.

The field coils which we have been using are shown in the photograph of Fig. 3. Each coil has an inside diameter of 9 inches, a mean radius of 6.25 inches and a 3.5-inch square cross section. The separation between the coils is 2 inches. Each coil is wound with 129 turns of one-fourth inch square double-cotton-covered copper, wrapped with glass tape, and impregnated with Permafil insulating compound. The voltage insulation per coil is 10,000 volts; additional insulation for 10,000 volt surges is provided on the first layer of each coil. The inductance of the coils is 14 millihenrys and the Q of the coils is 31 at the present resonant frequency of 42 cps.

The uniformity of the magnetic field over the volume of the cloud chamber depends on the size of chamber and the separation of the coils.[11] With a two-inch clearance between the coils, the magnetic field is uniform to better than one percent over the volume of the five-inch cloud chamber discussed in Part II.

The heat dissipated in the coils for a magnetic induction of 10,000 gauss and a repetition interval of five seconds is 230 watts. Water cooling can be provided by coils of one-fourth inch copper tubing (not shown in Fig. 3) which can be added to enclose each field coil.

Excitation Equipment

The basic field circuit consists of the field coils, capacitor bank, and switch tube in series. Figure 7 shows our present mode of operation. The sequence is to charge the capacitors, discharge them by triggering the ignitron, and then reverse the capacitor voltage with a special mechanically operated switch. The additional charge required for each cycle is only that lost through heat dissipation in the coils, capacitors and leads. This apparatus is electronically synchronized with the cloud chamber and betatron.

A switch tube which has the required power rating and also affords the necessary precision timing is the GL506 ignitron. This tube can operate up to about 20 kilovolts and 4000-peak amperes in the plate circuit (150 amperes average current). The current capacity of one of these ignitrons is sufficient for production of a field of 33,000 gauss in the coils described above.

Regulation of the peak voltage of the capacitors is necessary to insure a constant amplitude of the magnetic field pulses. In our present arrangement, using a grid controlled rectifier to charge the capacitors, the field is reproducible to better than one percent.

---

[8] These measurements are based on a primary calibration of the field pulses made with a search coil and ballistic galvanometer. (*Cf.*, P. Kapitza, Proc. Roy. Soc. **A115**, 658 (1927). Peak field measurements made in this way are accurate to better than one percent.

[9] This assumes that the capacitor voltage is allowed to change polarity during the discharge. If the polarity is not allowed to change, the capacitors can be operated at twice the rated a.c. voltage, and only one-fourth as many units are needed for the same field. The capacitors now used are the Pyranol-treated capacitors often used for power factor correction. Each unit weighs about 45 pounds, has a volume of about one-half cubic foot, with a capacitance of 10.5 microfarads. They can be operated at a.c. peak voltages up to 7 kilovolts and can sustain higher a.c. voltages for short periods. These capacitor units can be mounted in compact assemblies for the present application, since the heat dissipated in them is negligible at the repetition frequencies used with the cloud chamber.

[10] *Cf.*, P. Kapitza, Proc. Roy. Soc. **A115**, 658 (1927).

[11] A discussion of field uniformity for coils of this type is given by A. E. Shaw, Rev. Sci. Inst. **11**, 57 (1940).

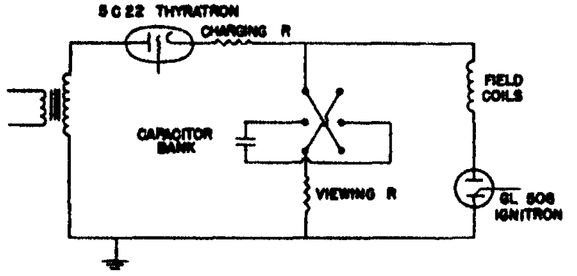

FIG. 7. Basic circuit for the pulsed magnetic field, showing the charge and discharge paths.

The rate at which the field equipment can be recycled depends on the charging circuit. Except for replenishing the charge of the capacitors, the time required for a complete cycle is about a second (primarily determined by the time of reversal of the mechanically operated switch). The re-charging rate can be made as rapid as desired with a large input transformer and a charging rectifier of sufficient capacity. At present we are using a ten kilovolt, ten-kilowatt input transformer, and one 5C22-hydrogen thyratron for the charging rectifier. The total capacitance is 1050 microfarads and the charging resistance is 8000 ohms.

IV. SYNCHRONIZING EQUIPMENT

The synchronizer is an electronic device which limits the betatron output to a single pulse of x-rays which coincides with the sensitive time of the cloud chamber, and also times the magnetic field pulse so that the field will reach its maximum value at the time the x-rays are generated.[12] The operation can be summarized as follows. The synchronizer receives a signal from the cloud-chamber control circuit a few milliseconds after the chamber has expanded. A continuous train of signals from the accelerator injection circuit is also supplied to the synchronizer; these are the signals which ordinarily drive the output stage of the injection circuit. As shown in the block diagram of Fig. 8, the multivibrator A, when triggered by the cloud-chamber signal, provides a gate which is slightly longer than the interval between two injection pulses. This gate and the injection pulses are applied to a coincidence stage B. In the output of B no signals of appreciable amplitude appear except for a pip, a', which results from the simultaneous excitation of B by the gate and the pip a (since it is possible for both a and b to fall within the gate if a occurs just at the beginning of the gate, the primary oscillator is locked in with the line voltage used to energize the accelerator). The signal a' triggers a multivibrator C, which provides a negative gate slightly shorter than the interval between successive injection signals. When this gate is mixed with the original train of injection signals in the coincidence circuit D, only the signal b is passed. This signal is used to drive the output stage of the accelerator injection circuit.

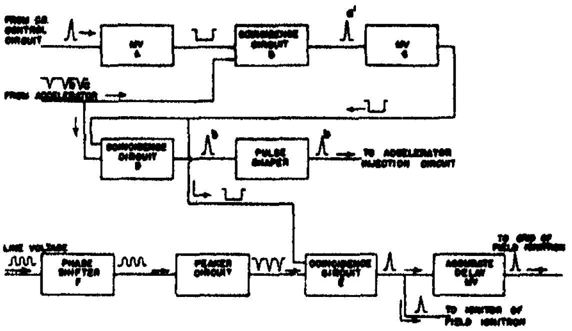

FIG. 8. Block diagram of synchronizer for cloud chamber, pulsed field, and accelerator.

The gate from C is also mixed in E with a series of signals derived from the line voltage. The output of E is therefore a single pulse which is synchronized with the injection signal. This signal from E fires the ignitor of the field circuit ignitron. A precision multivibrator is also triggered by this signal and provides a delayed pulse to trigger the grid of the ignitron. The phase shifter F is used to phase these field signals with respect to the betatron injection signals.

ACKNOWLEDGMENTS

We are indebted to Messrs. Leon Grodzins, Henry Rej, and James Allison for their assistance in the construction of the cloud chamber and field equipment. We wish to thank Dr. E. E. Charlton and the Betatron group for their cooperation in making the 100-Mev betatron available to us. The cooperation and skill of the betatron operators, E. L. Martin and J. McNamara, have been essential to the successful testing of our apparatus. This work has been supported by Contract N7 onr 332 with the Office of Naval Research.

---

[12] The timing can readily be adjusted so that the magnitude of the field at the time of the x-ray pulse is within $\frac{1}{2}$ of one percent of its peak value; the field is constant to this accuracy for 750 microseconds, for the 12-millisecond pulse length.

THE REVIEW OF SCIENTIFIC INSTRUMENTS VOLUME 20, NUMBER 8 AUGUST, 1949

The Dynamics of a Synchrotron with Straight Sections*

NELSON M. BLACHMAN AND ERNEST D. COURANT
Brookhaven National Laboratory, Upton, Long Island, New York

(Received April 11, 1949)

The equations describing the "betatron" and "synchrotron" oscillations of a particle being accelerated in a synchrotron having straight sections are obtained. In particular, the relative increase in the ratio of either betatron-oscillation frequency to the frequency of revolution is found to be approximately half the ratio of the total length of straight sections to the orbit circumference. The effect of magnetic fringing fields is considered. With regard to the synchrotron phase oscillation, it is found that the criterion of non-relativistic adiabatic damping is no longer that n exceed $\frac{3}{4}$ but that it exceed $\frac{3}{4}$ by at least $\frac{1}{4}$ of the ratio of the total length of the straight sections to the orbit circumference.

INTRODUCTION

THE "racetrack" modification of the synchrotron by the insertion of straight sections was proposed by Crane[1] in 1946, and several synchrotrons incorporating this feature are now being constructed or designed. Dennison and Berlin,[2] and Serber[3] have treated the effect of the straight sections on the betatron oscillations. However, it seems desirable to reconsider these oscillations in greater detail and to treat, too, the effect of the straight sections on the synchrotron oscillations. Several authors[4] have obtained the dynamical equations of the various oscillations of the accelerating particle in a circular synchrotron, and we shall see how they are modified by the straight sections.

BETATRON OSCILLATIONS

We shall consider a synchrotron having N straight sections of length L each, and N circular sections of length $360°/N$. The betatron oscillation which a particle executes subsequent to entering a circular section is determined by two initial conditions, most conveniently the displacement and the derivative of displacement with respect to path length on entering the section. The former will be denoted by X_k, with k the ordinal number of the section (modulo N), and the latter by Y_k/λ, where λ is $1/2\pi$ of the wave-length of betatron oscillation; $\lambda = R/(1-n)^{\frac{1}{2}}$ for the horizontal oscillation and $R/n^{\frac{1}{2}}$ for the vertical, with R the radius of the curved sections of the orbit and $n = -(R/H)(\partial H/\partial r)$ thereon. Thus, if s is the path length measured from the beginning of the circular section the particle is in, its betatron displacement is

$$X_k \cos(s/\lambda) + Y_k \sin(s/\lambda).$$

The amplitude of this oscillation is $(X_k^2 + Y_k^2)^{\frac{1}{2}}$, although the maximum may not occur within the circular section. On emerging from the k-th circular section the particle passes through a straight section of length L. Hence, with $a = L/\lambda$,

$$\left.\begin{aligned} X_{k+1} &= X_k \cos\Theta + Y_k \sin\Theta + aY_{k+1}, \\ Y_{k+1} &= -X_k \sin\Theta + Y_k \cos\Theta, \end{aligned}\right\} \tag{1}$$

where Θ is the length of one circular section in radians of betatron oscillation ($\Theta = (1-n)^{\frac{1}{2}}2\pi/N$ for horizontal oscillation and $n^{\frac{1}{2}}2\pi/N$ for vertical). These recursion relations are linear and have constant coefficients. Hence, like similar differential equations, their solution is a sinusoidal function of the independent variable k. The coefficient of k in the argument of the sine is μ, where[2, 3]

$$\cos\mu = \cos\Theta - \tfrac{1}{2}a \sin\Theta. \tag{2}$$

Thus, the general solution of (1) is of the form

$$X_k = A \cos(\mu k + \phi), \quad Y_k = B \sin(\mu k + \psi). \tag{3}$$

However, in order that (3) be compatible with (1), it is necessary that

$$\begin{aligned} A/B &= -(1 + a \operatorname{ctn}\Theta)^{\frac{1}{2}} \\ \text{and} \quad & \\ \sin(\phi - \psi) &= \tfrac{1}{2}a/(1 + a \operatorname{ctn}\Theta)^{\frac{1}{2}}. \end{aligned} \tag{4}$$

As Serber[3] has pointed out, the motion of the particle can be bounded only if μ is real. An upper limit on the length of the straight sections, exhibited in Table I for $n = 0.6$, is therefore imposed by (2).

TABLE I. Limiting lengths of straight sections for $n = 0.6$ and non-relativistic injection.

N	2	3	4	6
L/R for vertical stability	0.950	2.44	3.70	6.00
L/R for radial stability	2.06	4.08	5.86	9.22
L/R for phase stability	4.72	3.14	2.36	1.57

Change in Frequency

With a small, (2) becomes

$$\begin{aligned} \mu &= \Theta + \tfrac{1}{2}a \\ &= (1 + NL/4\pi R)\Theta. \end{aligned} \tag{5}$$

---

* Work done under the auspices of the AEC.

[1] H. R. Crane, Phys. Rev. 69, 542 (1946).

[2] D. M. Dennison and T. H. Berlin, Phys. Rev. 69, 542 (1946); 70, 764 (1946).

[3] R. Serber, Phys. Rev. 70, 434 (1946).

[4] David M. Dennison and T. H. Berlin, Phys. Rev. 70, 58 (1946); N. H. Frank, Phys. Rev. 70, 177 (1946), and Chap. VI, Report T-1, Brookhaven National Lab. (Jan. 15, 1948); D. Bohm and L. Foldy, Phys. Rev. 70, 249 (1946); R. Q. Twiss and N. H. Frank, Rev. Sci. Inst. 20, 1 (1949).

In this approximation the result is independent of the distribution of the straight sections around the orbit. If they are distributed uniformly (N infinite), the particle motion becomes sinusoidal. The ratio $\mu N/2\pi$ of betatron-oscillation frequency to frequency of revolution is increased in the ratio μ/Θ, i.e., by half the ratio of the total length of straight sections to the total length of curved sections.

Thus, the values of n are shifted which produce resonances[5] among the two betatron-oscillation frequencies and the frequency of revolution, i.e., those for which integers p, q, r exist satisfying a relation

$$(2\pi/N)p+q\mu_h+r\mu_v=0.$$

The values of n at which the most serious of these resonances occur are given in Table II for a circular synchrotron, a four-section synchrotron with $L/R=\frac{1}{2}$, such as the Brookhaven proton synchrotron,[6] and a four-section synchrotron with $L/R=0.76$, such as the one at Michigan. The necessity of avoiding these resonances has led to the choice of $n=0.6$ at Brookhaven and Berkeley and $n=0.45$ at Michigan.

A synchrotron with straight sections distributed uniformly around the orbit is equivalent to a circular synchrotron having the same orbit circumference, i.e., of radius $R+NL/2\pi$. To be equivalent for horizontal oscillations, the magnetic field in the circular synchrotron must equal the mean field in the one with straight sections on corresponding orbits, displaced from the equilibrium orbits by equal distances. It follows directly that $(1-n)$ for the circular synchrotron is $(1+NL/2\pi R)$ times $(1-n)$ for the one with straight sections. The effect of the straight sections is, thus, to increase the value of $(1-n)$ for horizontal oscillations. The foregoing result is, therefore, again obtained, since the ratio of horizontal-betatron-oscillation frequency to revolution frequency in a circular synchrotron is $(1-n)^{\frac{1}{2}}$.

To be equivalent for vertical oscillations, the radial component of the magnetic field in the circular synchrotron must equal the mean value of the radial field on a path the same distance above the median plane in the synchrotron with straight sections. Thus, n in the circular synchrotron must be as much larger than n in the other as the magnetic field is smaller, *viz.*, $(1+NL/2\pi R)$. Our foregoing result is, therefore, again obtained, since the ratio of vertical-betatron-oscillation frequency to revolution frequency in a circular synchrotron is $n^{\frac{1}{2}}$.

Amplitude Variation

If a is not small, the square of the amplitude of betatron oscillation, $(X_k^2+Y_k^2)$, varies with time ((3)), the extreme values being, say,

$$\alpha_\pm^2=\tfrac{1}{2}\{A^2+B^2\pm[A^4-2A^2B^2\cos 2(\phi-\psi)+B^4]^{\frac{1}{2}}\}. \quad (6)$$

TABLE II. Values of n at which resonances occur.

$\lvert p\rvert$	$\lvert q\rvert$	$\lvert r\rvert$	n (circ.)	n $(L/R=\frac{1}{2})$	n $(L/R=0.76)$
0	2	1	0.80	0.80	0.80
0	1	2	0.20	0.20	0.20
1	0	1	1.00	0.82	0.65
1	1	0	0.00	0.18	0.35
1	2	0	0.75	0.80	0.83
1	0	2	0.25	0.20	0.17

Given a and Θ and, therefore, μ, we know the ratio A/B and the value of $(\phi-\psi)$ ((4)), and so a pair of values (X_k, Y_k) suffices to determine A and B and, particularly,[2]

$$\alpha_\pm^2=\frac{1\pm\cos\Theta}{1\pm\cos\mu}[X^2-aXY+(1+a\operatorname{ctn}\Theta)Y^2]. \quad (7)$$

The maximum, α_+^2, occurs when $X_k/Y_k=\operatorname{ctn}\frac{1}{2}\Theta$ (and the minimum, α_-^2, which manifests itself through a minimum slope on passing through zero displacement, when $X_k/Y_k=-\tan\frac{1}{2}\Theta$). Hence, a particle which executes such betatron oscillations that it barely strikes the wall of the vacuum chamber will do so when k reaches a value where $X_k/Y_k=\operatorname{ctn}\frac{1}{2}\Theta$. It will be lost to the wall, plainly, halfway around the k-th circular section. Thus, as scattering by residual gas gradually increases α_+, particles will be lost near the centers of the circular sections. For the Brookhaven machine, the maximum amplitude, α_+, exceeds the initial amplitude, X_1, for the case of parallel injection ($Y_1=0$) by a factor of 1.05 for the vertical oscillations and 1.03 for the horizontal.

Gas Scattering

In connection with gas scattering it is important to know the mean-square maximum amplitude of the betatron oscillation executed by a particle because of scattering through angle θ in the plane of oscillation (horizontal or vertical component), since the allowable residual gas pressure for a given percentage loss varies inversely with this quantity. In determining the mean value it is necessary to average over the possible locations at which the scattering can occur, which are distributed uniformly in path length over straight and curved sections, as well as over θ, to take advantage of the fact that $\langle\theta\rangle_{\mathrm{Av}}=0$. It is necessary only to average over one pair of straight and curved sections, but in doing so one must extrapolate the oscillation to determine the values of X and Y at the beginning of the next (or last) curved section.

If α_+^2 does not start out from zero before the scattering but, through scattering, increases from α_+^2 to $(\alpha_++d\alpha_+)^2$, the effect is to add $2\alpha_+d\alpha_++(d\alpha_+)^2$ to α_+^2. Combining (3) and (7) and averaging with respect to k, one finds that the two terms of this increment have equal mean values. Thus, finally, we obtain

---

[5] E. D. Courant, J. App. Phys. **20**, 611 (1949). See also reference 2.

[6] Livingston, Blewett, Green, and Haworth, Rev. Sci. Inst. (in press).

$$\langle (d\alpha_+)^2\rangle_{Av} = 2\alpha_+\langle d\alpha_+\rangle_{Av} = \tfrac{1}{2}\lambda^2\langle\theta^2\rangle_{Av}\frac{\cos^2\frac{1}{2}\Theta}{\cos^2\frac{1}{2}\mu}$$

$$\times\frac{\Theta+a(\frac{3}{2}+\frac{1}{2}\Theta\,\mathrm{ctn}\Theta)+a^2(\mathrm{ctn}\Theta-\frac{1}{2})+\frac{1}{3}a^3}{\Theta+a}. \quad (8)$$

In our paper on "*Scattering of Particles by the Gas* in a Synchrotron"[7] account was not taken of this effect of straight sections. The quantity B^2 defined there, which is the square of the amplitude of betatron oscillation, must be replaced by α_+^2. Comparing (8) with equation (15) of reference 7, we see that the effect of straight sections is to multiply the quantity η, which determines the percentage loss and which is proportional to the residual gas pressure, by the factor

$$\frac{\cos^2\frac{1}{2}\Theta}{\cos^2\frac{1}{2}\mu}\times\frac{\Theta+a(\frac{3}{2}+\frac{1}{2}\Theta\,\mathrm{ctn}\Theta)+a^2(\mathrm{ctn}\Theta-\frac{1}{2})+\frac{1}{3}a^3}{\Theta+a}. \quad (9)$$

In the limit as the number of straight sections N grows infinite, a and Θ go to zero, and this factor becomes

$$1+a/\Theta=1+NL/2\pi R,$$

which is just the increase in the effective value of λ^2 and agrees with our previous result for the relative increase due to the straight sections in the betatron-oscillation frequency, provided one takes account of the concomitant decrease in the actual revolution frequency.

Fringing Fields[8]

The magnetic fields at the ends of the curved sections do not fall to zero abruptly, but decrease continuously. Therefore, the effective length of the curved sections is not, in general equal to their physical length; let the difference be such that a particle of momentum eH_0R/c traveling along the circle $r=R$ in one of the curved sections is deflected through an angle $(2\pi/N+2\delta)$. ($H=H_0$ at $r=R$.) Then the curved section is equivalent to a curved section extending over this angle with no fringing field, and the straight sections are effectively shortened by $2R\delta$. Up to now we have tacitly assumed that this effect has been taken into account in the design of the magnet by making the physical extent of the curved sections $(2\pi/N-2\delta)$. The Brookhaven machine has been designed with 88.2° quadrants. However, if this correction is not made properly, or if the value of δ varies during the magnetic cycle (which it may do because of eddy current and saturation effects), the effects of the fringing fields on the motion of the particles must be considered. These effects will be twofold: distortion of the equilibrium orbit, and changes in the frequencies of oscillation about this orbit.

The equilibrium orbit must have the property that the particle is deflected through an angle of 2π in one revolution, and therefore through $2\pi/N$ in going through one curved section and its fringing fields. This means that we must have

$$(e/pc)\int H ds=2\pi/N, \quad (10)$$

where the integral is taken along the portion of the orbit passing through one curved section and its fringing fields. If we also require that the mean deviation of the orbit from the circle $r=R$ be zero, the length of the path is $(2\pi/N+2\delta)R$, and (10) becomes

$$(2\pi/N+2\delta)eH_0R/pc=2\pi/N,$$

so that

$$p=(1+\epsilon)eH_0R/c, \quad (11)$$

with $\epsilon=N\delta/\pi$, is the momentum the particle must have in order to be deflected by $2\pi/N$ in passing through the curved section near the circle $r=R$. The radius of curvature of the path of a particle of this momentum in the magnetic field H_0 is

$$\rho=R(1+\epsilon). \quad (12)$$

The orbit is therefore approximately $1/N$ of a circle of radius ρ. The orbit will, of course, not coincide exactly with the circle $r=R$; it is easily shown by geometrical arguments that the total radial excursion of the orbit is

$$(2NR\delta/\pi)\sin^2(\pi/2N),$$

which, if $\pi/2N$ is small, is approximately

$$\pi R\delta/2N. \quad (13)$$

To obtain the frequencies of betatron oscillation we consider the general case of a synchrotron in which the magnetic field varies in an arbitrary manner along and near an equilibrium orbit. At any point of this orbit the radius of curvature is

$$\rho=pc/eH, \quad (14)$$

and in the vicinity of this point the motion of the particle is indistinguishable from the motion in a circular synchrotron of radius ρ. The equations of betatron oscillation are, therefore,

$$\left.\begin{aligned} d^2x/ds^2&=-(1-n)x/\rho^2,\\ d^2z/ds^2&=-nz/\rho^2,\end{aligned}\right\} \quad (15)$$

where s is the distance traveled along the orbit, ρ is the radius of curvature at s, x and z are, respectively, the deviations from the orbit in the osculating plane of the orbit and perpendicular to that plane, and n is defined by

$$n(s)=-\frac{\rho(s)}{H(s)}\frac{\partial H(s,x)}{\partial x}\bigg|_{x=0}. \quad (16)$$

---

[7] N. M. Blachman and E. D. Courant, Phys. Rev. 74, 140 (1948); 75, 315 (1949).

[8] We are indebted to Dr. Lloyd Smith for calling the problem of fringing fields to our attention. Some of the results of this section have also been obtained by Dr. Smith and others at Berkeley.

In the case we have considered here, ρ is given by (12) in the curved sections and is infinite in the straight sections. Therefore, the effective value of n in the curved sections, as defined by (16), is

$$n=(1+\epsilon)n_0, \tag{17}$$

where $n_0=-(R/H)(\partial H/\partial x)$ is the value of n referred to the radius R. This is, strictly speaking, true only if n_0 in the fringing field is the same as in the curved sections. If this is not the case[9] but $n=n_1$ in the fringing field, n_0 must be replaced by $(n_0+\epsilon n_1)/(1+\epsilon)$, so that we have, instead of (17),

$$n=n_0+\epsilon n_1. \tag{18}$$

Thus, the synchrotron with a fringing field is equivalent to one without a fringing field, but with radius ρ instead of R, n given by (18), and straight sections of length $(L-2R\delta)$.

The numbers of radians of horizontal and vertical betatron oscillations, respectively, per curved section with fringing fields are, for small ϵ,

$$\left.\begin{aligned}\Theta_h&=(2\pi/N)(1-n_0)^{\frac{1}{2}}[1-\epsilon n_1/2(1-n_0)],\\ \Theta_v&=(2\pi/N)n_0^{\frac{1}{2}}(1+\epsilon n_1/2n_0).\end{aligned}\right\} \tag{19}$$

If $a\ll 1$, so that (5) is valid, we obtain for the ratios of betatron-oscillation frequencies to the frequency of revolution

$$\begin{aligned}\omega_h/\omega&=(1-n_0)^{\frac{1}{2}}[1+NL/4\pi R\\ &\qquad -\epsilon(1-n_0+n_1)/2(1-n_0)], \qquad (20)\\ \omega_v/\omega&=n_0^{\frac{1}{2}}[1+NL/4\pi R+\epsilon(n_1-n_0)/2n_0].\end{aligned}$$

Adiabatic Damping

To a first approximation, at least, straight sections do not affect the adiabatic damping of betatron oscillations; both horizontal and vertical amplitudes decrease inversely as the square root of the magnetic field.

SYNCHROTRON OSCILLATIONS

Synchrotron oscillation involves the departure of three quantities from their equilibrium values; the energy of the accelerating particle, its radial displacement, and its phase angle, i.e., the extrapolated phase angle of the net accelerating field at the time of passage through it. The three departures, which will be designated, respectively, by ΔE, x, and $\phi-\phi_0$, are connected by three equations, two of which are unaffected by straight sections:

$$x=(R/1-n)(E/(E^2-E_0^2))\Delta E \tag{21}$$

and

$$(d/dt)(\Delta E/\omega)=(eV/2\pi)(\sin\phi-\sin\phi_0). \tag{22}$$

in which E and E_0 are the total and rest energies of the particle, respectively, ω is the frequency of the accelerating voltage, e is the charge of the particle, V is the amplitude of the net accelerating voltage per revolution, and ϕ_0 is the equilibrium phase angle.

The third equation has the form

$$d\phi/dt=K\Delta E, \tag{23}$$

where K is a slowly varying constant, $K=-\partial\omega/\partial E$, ω now representing the frequency of revolution of the particle. From the relations $\omega=v/(R+NL/2\pi)$, $v=c(1-E_0^2/E^2)^{\frac{1}{2}}$, and $E^2-E_0^2=(Her)^2=(H_0eR^nr^{1-n})^2$, we have

$$\begin{aligned}K&=-(\omega/v)(\partial v/\partial E)+[\omega/(R+NL/2\pi)](\partial r/\partial E)\\ &=\frac{\omega}{E}\,\frac{E^2/[(1-n)(1+NL/2\pi R)]-E_0^2}{E^2-E_0^2}.\end{aligned} \tag{24}$$

Non-relativistically,

$$K=(\omega/2T)[(1-n)^{-1}(1+NL/2\pi R)^{-1}-1],$$

with $T=E-E_0$ the kinetic energy of the particle; ultra-relativistically, $K=\omega/E(1-n)(1+NL/2\pi R)$.

Limiting Oscillations

Combining (22) and (23), we obtain the differential equation of phase oscillation,

$$(d/dt)[(d\phi/dt)/K\omega]=(eV/2\pi)(\sin\phi-\sin\phi_0), \tag{25}$$

which allows stable oscillations only up to a certain limiting amplitude. During the time required for any instability to manifest itself the change in $K\omega$ will be negligible. Hence, we can obtain a first integral of (25):

$$\tfrac{1}{2}(d\phi/dt)^2+U(\phi)=W, \tag{26}$$

where

$$U(\phi)=(K\omega eV/2\pi)(\cos\phi+\phi\sin\phi_0) \tag{27}$$

may be described as the potential energy of the particle for synchrotron oscillation, $\frac{1}{2}(d\phi/dt)^2$ as the corresponding kinetic energy, and W, the constant of integration, as the total energy for synchrotron oscillation.

If the straight sections are too long—specifically, if

$$L/R>(2\pi/N)[(1-n)^{-1}(E_i^2/E_0^2)-1],$$

where $E_i=E_0+T_i$,— K is negative at injection, because an increase in particle energy then increases its angular velocity more than the concomitant increase in radial displacement decreases it. Later in the acceleration cycle, as E increases, K will become positive. At the moment when K is passing through zero, $U(\phi)$ vanishes identically, and phase stability disappears. The above condition therefore puts a limit on the length of the straight sections in addition to the limits imposed by the requirement that the betatron oscillations be stable. This limit is shown in Table I for $n=0.6$ with non-relativistic injection ($E_i=E_0$).

The straight sections are seen not to affect the shape of $U(\phi)$ or, therefore, the limiting phase angles of stable synchrotron oscillation, which remain $\pi-\phi_0$ and ϕ_1, with $U(\phi_1)=U(\pi-\phi_0)$. For a particle executing the limiting oscillation, $W=U(\pi-\phi_0)$, and using (23), we have

---

[9] H. R. Crane reports (private communication) that n is negative in parts of the fringing field of the Michigan synchrotron.

$$\Delta E=(2^{\frac{1}{2}}/K)[U(\pi-\phi_0)-U(\phi)]^{\frac{1}{2}}. \qquad (28)$$

For a particle injected with phase ϕ, $|\Delta E|$ must not exceed this value if it is to oscillate stably. In view of (27), ΔE is proportional to $(\omega V/K)^{\frac{1}{2}}$. If, in introducing straight sections into the synchrotron, ωV is not changed, ΔE is increased, non-relativistically, in the ratio $[1+(1+n)NL/4\pi Rn]$ if $NL\ll 2\pi R$. From (21) we see that the amplitude of radial oscillation associated with a given amplitude of phase oscillation is increased by the straight sections in the same proportion as ΔE. The amplitude of the limiting radial oscillation at injection (where we may put $E=E_0$), one of the factors determining the required radial aperture, is, from (21), (27), and (28),

$$x_i=R\left[\frac{eV/T_i}{2\pi(1-n)}\,\frac{(\pi-2\phi_0)\sin\phi_0-2\cos\phi_0}{(1+NL/2\pi R)^{-1}-(1-n)}\right]^{\frac{1}{2}}.$$

For the Brookhaven machine, where $\phi_0=150°$, the phase acceptance range at injection is $\phi_1+\phi_0-\pi=189°$. ΔE is maximum for $\phi-\phi_0$ and at injection is 53 kev, while x_i is 8.1 inches out of a useful horizontal semi-aperture of about 15 inches.

Adiabatic Damping

For small oscillations about the equilibrium phase, (25) becomes

$$(d/dt)[(d\phi/dt)/K\omega]=(eV\cos\phi_0/2\pi)(\phi-\phi_0). \qquad (29)$$

The W-K-B approximate solution to (29) is

$$\phi=\phi_0+\Phi(-K\omega/V\cos\phi_0)^{\frac{1}{4}} \times(-K\omega/V\cos\phi_0)_i^{-\frac{1}{4}}\sin\int\Omega dt, \qquad (30)$$

where

$$\Omega=(-K\omega eV\cos\phi_0/2\pi)^{\frac{1}{2}} =\frac{c}{R+NL/2\pi}\left[-\frac{eV\cos\phi_0}{2\pi E} \times\left(\frac{1}{(1-n)(1+NL/2\pi R)}-\frac{E_0^2}{E^2}\right)\right]^{\frac{1}{2}} \qquad (31)$$

is the frequency of synchrotron oscillation, Φ is the initial amplitude of phase oscillation, and the subscript i indicates initial value. In the Brookhaven machine Ω varies from 2600 cycles per second at injection to about 1300 c.p.s. at 2.8 Bev. The phase oscillation damps as

$$(-K\omega/V\cos\phi_0)^{\frac{1}{4}}\propto\left[-\frac{\tan\phi_0}{EdH_0/dt} \times\left(\frac{1}{(1-n)(1+NL/2\pi R)}-\frac{E_0^2}{E^2}\right)\right]^{\frac{1}{4}} \qquad (32)$$

for constant R. Non-relativistically, (32) is

$$\left\{-\frac{\tan\phi_0}{E_0dH_0/dt}\left[\frac{1}{(1-n)(1+NL/2\pi R)}-1 +\left(3-\frac{1}{(1-n)(1+NL/2\pi R)}\right)\frac{T}{E_0}\right]\right\}^{\frac{1}{4}}.$$

Thus, for non-relativistic damping of the phase oscillations, it is necessary, if ϕ_0 and dH_0/dt are constant, that

$$n>1-1/3(1+NL/2\pi R), \qquad (33)$$

which becomes the well known $n>\frac{2}{3}$ for a circular synchrotron, with $L=0$. However, if (33) is not satisfied, the resultant anti-damping is not serious. At Brookhaven ($n=0.6$) the maximum amplitude of phase oscillations will be only 1.018 times the initial amplitude.

Ultra-relativistically, the E_0^2/E^2 term in (32) vanishes. Hence, with ϕ_0 and dH_0/dt constant, the ratio of final (ultra-relativistic) phase amplitude to initial (non-relativistic) phase amplitude is

$$\{(E_0/E)/[n-(1-n)NL/2\pi R]\}^{\frac{1}{4}},$$

in which E is the final energy, and this ratio is increased by the fraction $(1-n)NL/8\pi Rn$ by the straight sections. There is seen to be very little damping of the phase oscillations for a final energy of a few times the rest energy.

The energy spread of the beam is, from (23), Ω/K times the amplitude of phase oscillation. Ultra-relativistically, $\Omega/K=[-EeV\cos\phi_0(1-n)(1+NL/2\pi R)/2\pi]^{\frac{1}{2}}$. The straight sections increase the spread in the output energy of the synchrotron by the fraction $NL/4\pi R$ in addition to the increase in final phase-oscillation amplitude which they effect. As above, the ratio of final to initial energy spread is

$$\{(E_0E/4T_i^2)[n-(1-n)NL/2\pi R]\}^{\frac{1}{4}}.$$

This ratio is 15.0 at Brookhaven, where $T_i=3$ Mev and $E-E_0=2.8$ Bev, resulting in a total spread in the beam of 1.6 Mev.

Again, the relation between energy spread and radial spread of the beam, (21), is unaffected by the straight sections. The latter is increased in the same ratio as the former on account of the straight sections. The radial synchrotron oscillations may be obtained from the phase oscillations by combining (21), (23), and (24):

$$x=(R/\xi\omega)(d\phi/dt) \qquad (34)$$

with

$$\xi=(1+NL/2\pi R)^{-1}-(1-n)(E_0^2/E^2).$$

Their damping may then be obtained directly from the damping of phase oscillations as given by (32). Thus, the amplitude of radial oscillations is $(R\Omega/\omega\xi)$ times the amplitude of phase oscillations, if the latter are small, and, therefore, damps as

$$(\xi\Omega/\omega)(-K\omega/V\cos\phi_0)^{\frac{1}{2}}$$

$$\propto\left\{\frac{E^3 dH_0/dt}{(E^2-E_0^2)^2[E^2-(1-n)(1+NL/2\pi R)E_0^2]\tan\phi_0}\right\}^{\frac{1}{4}}.$$

Hence, non-relativistically the radial synchrotron oscillation amplitude decreases as $T^{-\frac{1}{2}}$ if dH_0/dt and ϕ_0 are constant, while ultra-relativistically it decreases as $E^{-\frac{3}{4}}$. The ratio of final (ultra-relativistic) to initial (non-relativistic) amplitude is

$$\{(4T_i^2E_0/E^3)[n-(1-n)NL/2\pi R]\}^{\frac{1}{4}},$$

where E is the final energy and T_i the kinetic energy at injection. At Brookhaven this ratio is 0.024, resulting in a final total beam width of 0.4 inch (plus betatron oscillations).

THE REVIEW OF SCIENTIFIC INSTRUMENTS VOLUME 20, NUMBER 8 AUGUST, 1949

Operational Features of a New Electron Diffraction Unit

Robert G. Picard, Perry C. Smith, and John H. Reisner
RCA Victor Division, Radio Corporation of America, Camden, New Jersey

(Received March 17, 1949)

A new electron diffraction unit having a three-lens optical system and a maximum effective specimen-to-plate distance of 200 cm is described. The applications of such a system to the study of long interatomic spacings is discussed. Wide variations in the area of specimen irradiated are obtainable. An explanation is given of the design considerations in such an optical system, with special reference to the functioning of the post-specimen lens as both focusing and magnifying lens. The use of the unit as a shadow microscope is explained, and the advantages are given of this instrument over other shadow microscopes with respect to increased size of image, increased size of specimen field available for observation, and greater specimen protection from damage by the concentrated electron beam.

The resolution attainable with the instrument is calculated and a "resolution index" is defined which makes possible intercomparisons of resolution under various operating conditions. Factors which limit accuracy, as opposed to resolution, are discussed critically and the accuracy of data obtainable with the instrument is estimated.

A number of diffraction patterns are shown to illustrate the results obtained under various operating conditions as diffraction camera and shadow microscope, and also to illustrate the techniques of charge neutralization, spot diameter measurement, and internal calibration of plates using a known specimen.

INTRODUCTION

In a previous paper,[1] the authors have described some preliminary investigations on high resolution electron diffraction, and mentioned that a new diffraction unit was under construction. This instrument has been completed and has been in operation for more than two years. It has some unique optical arrangements which have been thoroughly tested, and its new features and their operation form the subject of this paper.

Electron diffraction patterns have long been obtained with instruments having no lenses.[2-4] Unfortunately, such systems use a very small portion of the available electron beam to produce the electron diffraction pattern. Greater intensity in the pattern and sharper lines can be obtained if a lens is used to focus the source on the final screen or plate.

Two factors should be considered in choosing the position for this lens in the optical system: (1) position between source and viewing means, and (2) position with respect to specimen. It is desirable to have the smallest possible spot formed on the photographic plate since spot size limits resolution. Thus, ideally, the power and position of the lens should be so chosen that a reduced image of the source (or limiting aperture) is formed on the plate. This requires that the lens be positioned so that the object distance, u, is greater than the image distance, v, giving a resultant magnification of the source

$$M=v/u<1.$$

This inequality implies that $f<v<2f$ and $u>2f$. From these relations and a knowledge of the total camera length, it is simple to determine the approximate lens strength required.

The second factor of importance is the position of the specimen with respect to the lens. If the specimen is above the lens (on the source side), it is irradiated with an effectively divergent beam, while, if it is below, the beam is convergent. In the former case, changing focus of the lens changes the diameter of the diffraction pattern,[5] while in the latter, changing focus changes the sharpness of the pattern without affecting its size.

---

[1] Picard and Reisner, Rev. Sci. Inst. 17, 484–489 (1946).

[2] Thomson and Fraser, Proc. Roy. Soc. A128, 641 (1930).

[3] Wierl, Ann. d. Phys. 8, 521 (1931).

[4] Kikuchi, Japanese J. Physik 5, 83 (1928).

[5] Picard, J. App. Phys. 15, 678–681 (1944).

A further improvement in resolution and an increase in optical versatility can be accomplished by using two lenses, both above the specimen. If the first lens is very strong, it can form a much reduced image of the source. This image may then be focused on the photographic plate by the second lens.[6] The power and position of the second lens should be chosen so that any magnification of the source image that this lens may produce will be much less than the demagnification obtained with the first lens.

If the second lens is capable of having its focal length varied continuously over a wide range of values, it can form a sharp image of the reduced source image at any position from above the specimen to the final screen or plate. If this image is positioned above and very close to the specimen, a shadow image of the specimen will be formed on the final screen. The magnification of this image is determined by the ratio of the distance from source image to plate and source image to specimen. For all practical purposes, no accuracy will be lost if the magnification is taken as the ratio of specimen to plate distance and specimen to source image distance. The resolution in the magnified image depends on the size of the reduced source image and improves as the spot size is reduced.[7]

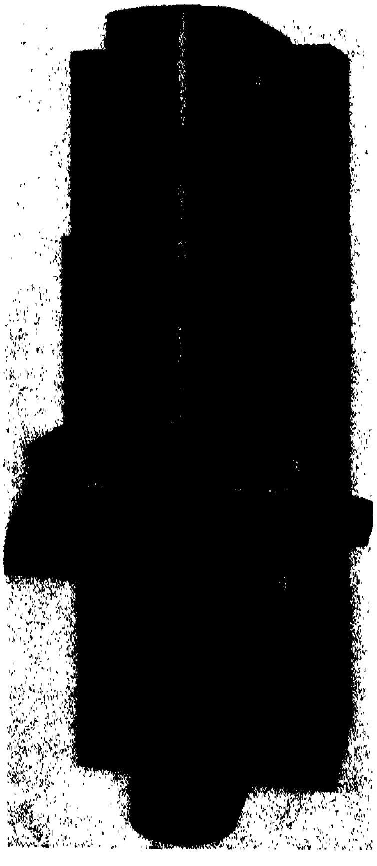

FIG. 1. Over-all view of the diffraction unit.

If the second lens is weakened to form an image of the spot on the photographic plate, a sharp diffraction pattern will result. Gradual defocusing toward the shadow microscope condition will produce on the plate an out-of-focus pattern which becomes more complex as the lens is strengthened. If a single crystal is in the beam, its image may be repeated in a definite pattern by diffracted beams to form what is called a "point" diffraction pattern. A comprehensive treatment of the two lens pre-specimen system is given in the literature,[8] so further discussion at this point is unnecessary.

The inclusion of a lens below the specimen adds an extremely valuable feature for making useful electron diffraction patterns of materials having d_{hkl} spacings greater than 5Å. This lens, in combination with either one or two lenses above the specimen, permits the central portion of the pattern to be enlarged electron optically.[9] The lens or lenses before the specimen form a focused diffraction pattern above the post specimen lens which magnifies this pattern on the final screen or plate.[10] The strength of the lower lens can be so adjusted that the size of the final pattern corresponds to a specimen-to-plate distance much greater than the physical specimen-to-plate distance.

THE OPTICS OF THE DIFFRACTION UNIT

A three lens optical system, including all the properties described in the preceding section, has been built into a practical electron diffraction camera (Figs. 1 and 2). The positions of the various components have been chosen to permit maximum versatility of operation. All of the lenses are electromagnetic with continuously variable focal length. A specially designed pole piece is used in the top lens to make it a very strong lens for spot size reduction. The second lens uses no pole piece, and the bottom lens uses a weak pole piece to obtain equivalent specimen-to-plate distances as great as 200 cm. Without a pole piece in the lowest lens, the magnification obtainable is sufficient to provide an effective specimen-to-plate distance of approximately 100 cm.

The salient features of the optical system as depicted in Fig. 2 are the electron gun, the limiting aperture, two lenses above the specimen, one lens below the specimen, and a viewing and photographic chamber. When lens 1 is used as a very short focal length lens, the source is imaged just below the gap in the pole piece and gives rise to a very wide angle beam which illuminates the inside of the lower half of the pole piece. A 1.5 mm aperture is placed at the top of lens 2 to eliminate reflections from the inside of the pole piece of lens 1. Another aperture is placed at the top of lens 3 to prevent the diffracted beam from striking the inside of this lens or its pole piece and causing spurious reflections or excessive scattering. This last aperture is very large (23 mm) to avoid cutting off any portion of the diffraction pattern and serves only to shield the inner lens surface from the beam.

---

[6] Hillier and Baker, J. App. Phys. 17, 12–22 (1946).

[7] von Ardenne, Electronen-Ubermikroskopie (Julius Springer, Berlin, 1940), p. 71.

[8] Hillier and Baker, J. App. Phys. 17, 12–22 (1946).

[9] A. F. Prebus, "The Electron Microscope," in *Colloid Chemistry* (Reinhold Publishing Company, New York, 1944), Vol. V, p. 181.

[10] Simard, Burton, and Barnes, J. App. Phys. 16, 832 (1945).

The two lenses above the specimen serve a very important purpose in addition to providing control of spot size and position. The ability of the combination to vary the angle of illumination on the specimen permits different sized areas of the specimen to be irradiated and thus contribute to the diffraction pattern. When lens 2 is used without lens 1, the area of specimen irradiated is approximately 0.001 inch in diameter. Such a narrow beam is useful in studying individual components of an inhomogeneous misture distributed over the specimen support in transmission studies. Patterns can be obtained from minute single crystals. Correspondingly small areas of reflection specimens can also be examined. When lenses 1 and 2 are used together, the area of specimen irradiated can be increased up to approximately $\frac{1}{8}$ inch diameter, and the diffraction pattern then gives information arising from the distribution of material over a large area of the specimen.

It is possible to accomplish two important optical effects by means of a lens placed below the specimen in a diffraction camera. Such a lens can be used to form a focused image of *an electron source* and, hence, a diffraction pattern produced by a specimen placed between the source and the lens. Such a lens can also be used to form a magnified image of *a diffraction pattern* produced by specimen and lens combinations preceding the lens. In designing a diffraction camera such as described here the position of a lens between specimen and final viewing screen or plate must be carefully considered as the lens must be used for both purposes described above under somewhat contradictory operating conditions. With a physically fixed specimen to plate distance, the maximum effective camera length possible when a post-specimen *focusing* lens is used is limited to the distance between lens center and final plate. However, maximum *magnification* with the lens occurs when the lens is placed midway between final screen and specimen. These facts are demonstrated in the following crude analysis.

Figure 3 shows the two optical arrangements, (a) the case where the lens is used to *focus* a diffraction pattern on the viewing screen, and (b) the case where the lens is used for *magnification*. Because of the limits in accuracy imposed by the assumption that a magnetic lens of the type actually employed is a perfect thin lens, simple calculations may be used only to indicate optimum position of the lens in the camera. To a sufficiently good approximation, the angular change in direction, ϕ, of a ray passing through a lens is proportional to the distance, r, from the center of the lens at which the ray strikes. If the ray initially makes a small angle with the optic axis,

$$\phi = r/f.$$

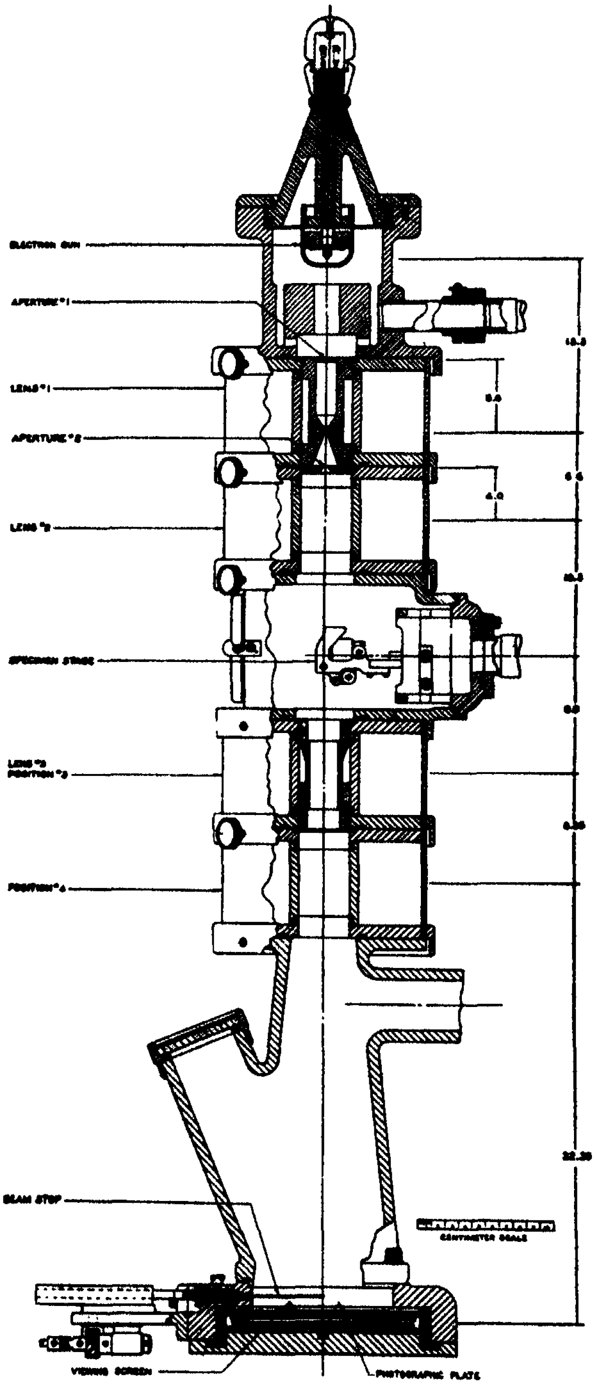

FIG. 2. Cross-sectional view of the optical system of the diffraction unit.

If a specimen is placed a distance A ahead of the photographic plate, a diffraction ring arising from planes in the specimen inclined to the beam at an angle θ will have a radius at the plate of $R = 2A\theta$ if no lens is present (assuming $\theta = \sin\theta = \tan\theta$). If a lens is placed a distance B ahead of the photographic plate but following the specimen, rays contributing to this diffraction ring will strike the lens in a circle of radius

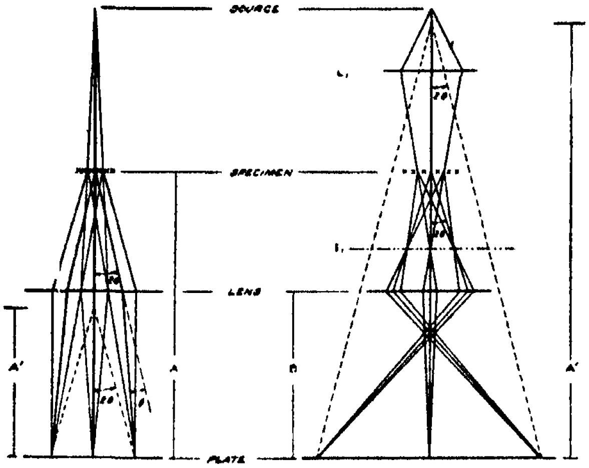

FIG. 3. Ray diagrams illustrating the use of the post-specimen lens as (a) a focusing lens, and (b) a magnifying lens.

$r=2(A-B)\theta$. The lens will reduce the angle of divergence of the rays by an angle ϕ, thus producing a resultant angle $(2\theta-\phi)$ for the remainder of the path to the plate. These rays will then produce a ring at the plate of radius

$$R'=2(A-B)\theta+(2\theta-\phi)B.$$

Since

$$\phi=r/f \quad \text{and} \quad r=2(A-B)\theta,$$
$$R'=2\theta[A-(A-B/f)B]=2\theta A'.$$

The effective specimen to plate distance is

$$A'=A-(A-B/f)B, \tag{1}$$

and is always less than A when a lens of focal length f, placed between the specimen and photographic plate, is used to focus the pattern. A' approaches A as a limit as the lens becomes weaker. Furthermore, when f is varied (as occurs when focusing an electromagnetic lens), R', the ring diameter at the plate, also varies.

If the source is effectively at infinity (parallel illumination of the specimen), a focused pattern will be formed on the plate when $f=B$. Under this condition, $A'=B$. If the source is closer, thus producing divergent illumination on the specimen, as shown in Fig. 3a, the lens must be strengthened to produce a focused image on the plate, f becomes less than B, and $A'<B$. Thus, the maximum effective specimen to plate distance obtainable, using a lens between specimen and plate to produce a focused pattern, is the distance from the lens to the plate.

Equation (1) above fails to take into account the properties of thick lenses and, as a result, the values calculated deviate from practice as shown in Fig. 4. The solid curve represents the effective camera length as a function of lens focal length for a lens in the #3 position (see Fig. 2). It can be seen that the reduction in spot size, and consequent increased sharpness of pattern obtained by using a focusing lens between specimen and plate, is accompanied by a reduction in effective camera length and, hence, does not necessarily result in increased resolution in the pattern. The ratio of spot size at the plate to effective camera length is a good criterion of the instrumental resolution and will be called the "resolution index." The significance of this ratio is discussed in the section on resolution.

The above discussion describes the action of a lens between specimen and plate when the illumination on the specimen is parallel or divergent. These conditions can be produced by using a simple beam collimating system above the specimen or by placing a lens above the specimen in such a position that the source is at the focus of the lens, thus producing parallel illumination of the specimen. If this pre-specimen lens is operated to produce an image of the source *above* the specimen, divergent illumination of the specimen will result. Therefore, the preceding analysis also covers this optical condition.

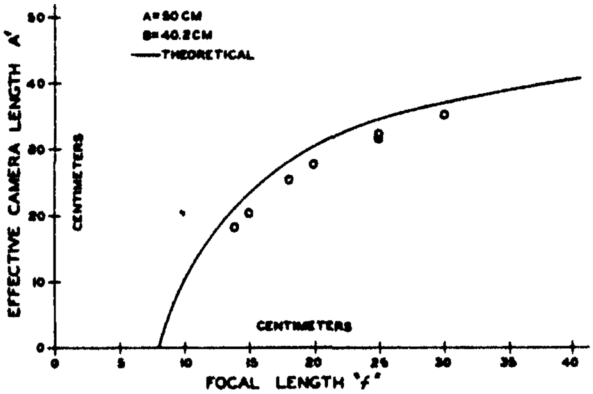

FIG. 4. Effective specimen to plate distance as a function of the focal length of the post-specimen lens.

To produce convergent illumination on the specimen, one or more lenses must be placed between source and specimen and these lenses must be operated so as to produce a focused image of the source *below* the specimen. It is then possible to form a focused diffraction pattern below the specimen, and a subsequent lens can form a magnified image of this pattern (Fig. 3b). Under these conditions, the effective specimen to plate distance, A', may be expressed in terms of the instrumental constants A and B as

$$A'=(AB-B^2-Af/f), \tag{2}$$

where f is again the focal length of the post-specimen lens. To obtain the maximum magnification with this lens for any focal length, the lens must be correctly positioned. This position may be found by determining the maximum value of A' as B is changed. The result is

$$B=A/2. \tag{3}$$

Thus, maximum utilization of such a lens for magnifying diffraction patterns will be obtained when the lens is placed midway between specimen and plate. However, since lens aberrations increase rapidly with the aperture of the lens used, it is desirable to move the magnifying lens as close to the specimen as the strength of the lens permits. This is also the best condition when the post-specimen lens is used for focusing when the specimen is irradiated with divergent illumination. In the actual diffraction unit, a compromise dictates the placement of the lens in position 3 for general use, with position 4 available for special magnification problems.

Figure 5 shows equivalent camera length as a function of lens position for several values of focal length with convergent illumination of the specimen. The lens used in position 4 is sixty percent more effective for magnification than when used in position 3. Figure 6 shows the relation between effective camera length and current through the lens when the lens is in position 3.

The third function of the post-specimen lens, as used in the diffraction unit, is the magnification of shadow micrograph images. As the magnification of a shadow microscope is

$$M \cong \frac{\text{Specimen to plate distance}}{\text{Specimen to point source distance}},$$

any means which will increase the effective specimen to plate distance will increase the magnification. It follows from the equation for M that, theoretically, M can be increased indefinitely by making the denominator of the fraction approach zero. This condition can be fulfilled by the two lens systems preceding the specimen. However, an upper limit in useful magnification is imposed by the dimensions of the spot formed above the specimen as previously mentioned. If the very intense reduced image of the source formed by lens #1 is positioned too closely to the specimen, the specimen supporting film is often broken or the specimen is fused. The use of a post-specimen lens permits high magnification to be obtained without bringing the source image dangerously close to the specimen. In point microscopy, the diameter of the image on the final screen is small since the angle of illumination of the specimen must be small in order to get good resolution in the image. For a given magnification, a wider field may be obtained by forming the reduced image of the source farther from the specimen, thus illuminating a wider area of the specimen, and restoring the original magnification by means of the post-specimen lens.

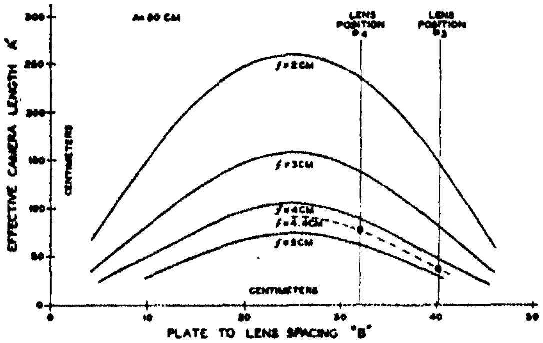

FIG. 5. Effective specimen to plate distance as a function of the position of the post-specimen lens.

While a multitude of lens combinations are available, in practice it has been found most generally useful to employ lens 1 for spot size control or specimen area irradiation control, lens 2 for spot position control, and lens 3 in the number 3 position for magnification.

RESOLUTION

The resolution obtainable with the instrument depends on the fineness of the beam at the plate and upon the image defects produced by the lenses. The first of these factors was carefully investigated by making measurements of the diameter of the undiffracted beam at the plate when the beam was focused on the plate by various combinations of lenses. Since it is practically impossible to measure directly the diameter of such a spot on a photographic plate because of the intense halation produced, the beam was used to trace a line on the plate and the width of the line was measured with a microphotometer. The method was to focus the beam on the plate (a very slow Eastman type 548-0 spectroscopic plate) with no specimen and rapidly but smoothly move the plate in its carriage across the beam path. By this method, a well defined line was traced which showed no halation and could readily be measured. Figure 7 shows a number of microphotometer traces of such lines made under various lens conditions described in Table I. The finest spot is obtained for the conditions described under trace 10, for which lens 1 is operating at high power to produce a maximum reduction in size of the source image and lens 2 is focusing this image on the plate without magnification by lens 3. The spot diameter here is less than 0.04 mm.

It is desirable to be able to express the instrumental resolving power as a number so that intercomparisons may be made among different instruments or different operating conditions with the same instrument. The resolving power of the photographic plate is independent of the position of the image on the plate, but the difference in d_{hkl} spacing corresponding to a given distance on the plate is a reciprocal function of radius

FIG. 6. Effective specimen to plate distance as a function of current in the post-specimen lens used with a weak pole piece.

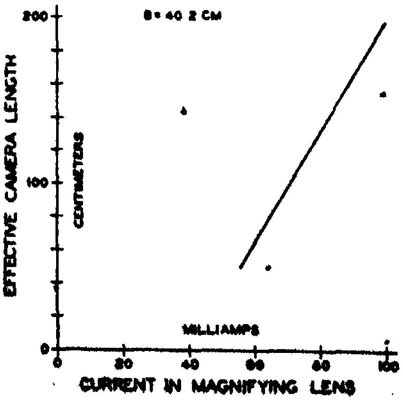

described implicitly by the equation

$$Dd_{hkl}=2L\lambda=K. \qquad (4)$$

Equation (4) gives the relation between diffraction ring diameter, D, and interplanar spacing, d_{hkl}, and is a simplification of Bragg's law for the small angles used in electron diffraction. K is a constant for fixed electron wave-length (accelerating voltage) and L is the specimen to plate distance.

If it is assumed that 2 rings may be detected as separate if they are separated on the plate by a distance ΔD, then

$$\Delta D=-(K/d_{hkl}^2)\Delta d_{hkl}.$$

ΔD is a constant fixed by the resolving power of the photographic plate if, for the moment, no consideration is given to the natural width of the lines of the diffraction pattern. The instrument resolving power is

$$\Delta d_{hkl}/d_{hkl}=(\Delta D/K)d_{hkl}=K'd_{hkl}. \qquad (5)$$

Equation (5) states that the resolving power is proportional to the interplanar spacing, and the constant, K', may be taken as a measure of the resolving power.

If the natural line width of each of two closely spaced lines is no greater than the diameter of the image of the source produced on the final plate, and the resolving power of the plate is finer than this spot size, ΔD can be taken equal to this diameter. In the described diffraction unit, ΔD can be made as small as 0.025 mm. Other typical operating conditions are

$L=500$ mm.

$\lambda=0.055$A (corresponding to 50 kv accelerating voltage).

Under these conditions

$$K'=4.55\times 10^{-4} \text{ per Angstrom unit.}$$

Other factors involved in the photographic process, instrumental instabilities, and factors characteristic of the Bragg reflection itself, such as intensity, line width, etc., contribute to a reduction in resolving power. However, it is safe to assume that two lines may be resolved if they are separated by twice the diameter of the spot on the final plate. Under this assumption

$$K'\cong 10^{-3} \text{ per angstrom unit.}$$

This method of expressing resolving power provides a number for comparison but does not obviously relate this important number to any instrumental constants. This deficiency is particularly prominent in such an instrument as that described because the effective camera length can be varied over a wide range. Magnification of the pattern produces an increase in the size of the image of the source, W, as well as an increase in camera length. It has been found convenient to use the ratio of these two values as a measure of resolution. That this is possible is shown below.

$$\Delta d_{hkl}/d_{hkl}=(\Delta D/K)d_{hkl}=(CW/2L\lambda)d_{hkl}$$
$$=C/2\lambda(W/L)d_{hkl}. \qquad (6)$$

C is a constant and λ, the wave-length, is constant. This leaves the ratio W/L as a measure of the resolution. This ratio, which will be called the "resolution index" may be expressed regardless of the magnification employed in the instrument.

As described above, various combinations of lenses are possible and useful. While other factors than resolution may determine the choice of a combination, it is useful to keep in mind the effect of a combination upon resolution. For this, "resolution index" defined above is applied. Using a 0.025 mm aperture above lens #1, the indices shown in Table I were calculated from photometer traces generated by moving the plate normal to the beam. Several facts are apparent: (a) highest resolution occurs using only pre-specimen lenses, (b) where a post-specimen lens is employed for pattern magnification, resolution increases with magnification, (c) maximum resolution does not correspond to maximum current in lens #1. There is a considerable discrepancy between measured values of "resolution index" and calculated values, the former always being higher. This is due to scattering from apertures, pole pieces, and the specimen. Under some circumstances, the effect is large enough to completely mask changes in spot size attributable to changes in aperture size.

From a theoretical standpoint, using an effective source 5 cm above lens #2 should give about four times more favorable a resolution index when used in conjunction with a lens in the #3 position (trace 13) than when used with lens #2 (trace 10). Again, with the source 20 cm above lens #2 (lens #1 off), the index should be more favorable for lens #3 (trace 18) over lens #2 (trace 14) by a factor of 1.5. Table I shows this factor to be unity. Theoretically, resolution may be increased under conditions of short source to specimen length by using a lens close below the specimen.

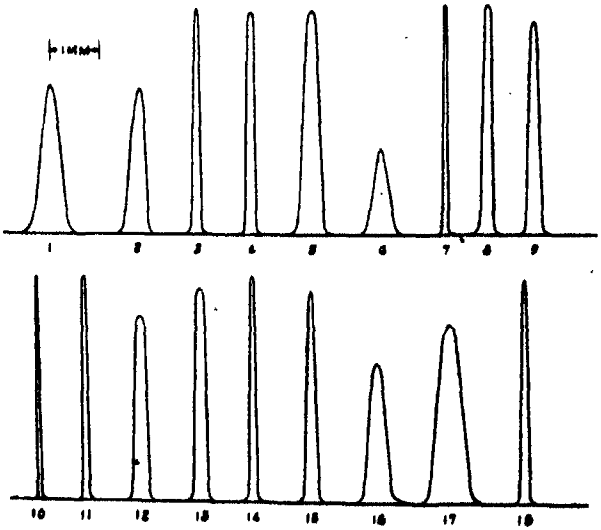

FIG. 7. Microphotometer tracings of lines traced by the focused electron beam under various lens combinations. See Table I.

Disadvantages that result from such a procedure are that (a) there is a reduction in equivalent camera length, and (b) equivalent camera length becomes a function of lens focal length making the determination of crystal constants subject to an additional source of uncertainty.

For exceptional resolution, two pole pieces, each with small apertures, may be used.[8] However, for most work, the simple aperture-lens system described is far more satisfactory since it avoids the very difficult problem of aperture centering and positioning which use of two pole pieces demands.

ACCURACY

Where post specimen lenses are employed, the accuracy must be considered separately from resolution since the magnitude of the diffraction pattern is altered by the lenses by a factor generally different from the alteration in spot size.

Where pre-specimen lenses alone are employed, pattern dimensions are determined by (1) accelerating voltage, (2) specimen-to-plate distance, and (3) crystalline properties of the specimen. Uncertainties in the measurements of voltage and specimen-to-plate distance limit the accuracy of the measurements of diffraction patterns. To these limits must be added the uncertainty in measurement of the plate due to line breadth which may arise from (1) instrumental limitations of spot size or from (2) broadening of lines due to specimen properties and physical condition. In general, it is difficult to measure high voltage to anything like the accuracy possible in the diametral measurement of a diffraction pattern. Likewise, the measurement of specimen-to-plate distance inside the vacuum chamber is extremely difficult to such a degree of accuracy. Measurements show that the short time fluctuation in voltage in the described camera is ±0.002 percent, while the long time stability, e.g., from turn-on to turn-on, is ±0.02 percent, representing an uncertainty of ±0.001 percent and ±0.01 percent in diffraction pattern dimension. Because of high voltage stability but low accuracy of voltage measurement, calibration of the instrument may usually be done with specimens of known spacings from the value of the instrumental constant $K = d_{hkl}D$, which is determined for the fixed specimen-to-plate distance. When this distance is changed, a new constant must be determined.

With the described instrument used with pre-specimen lenses, the instrumental constant is limited by the ability to measure D, the ring diameter. Although a very small residual field must exist in the #3 lens when it is turned off, any influence which such a field has on the electron beam passing through it is less than measurable with the inherent resolution of the diffraction camera.

When a post-specimen lens is utilized, as pointed out above, changes in effective camera length take place. The case where an increase in effective length is obtained gives rise to an increase in instrumental constant which increases slightly with the diameter of the rings. This radial distortion of the pattern is simply pincushion distortion of a lens used at large aperture. Its effect on a diffraction pattern magnified by a lens in the #3 position is small for effective distances up to 200 cm, being less than one percent at 82 mm ring diameter for 200 cm effective camera length.

TABLE I. Lens data for measurements of spot diameter and resolution index.

Trace number	Lens #1 current in ma.	Lens #2 current in ma.	Lens #3 current in ma.	Effective camera length A' in cm	Spot width W in cm	Resolution index (W/A') $\times 10^4$
1	0	0	0	50	0.05	10
2	To focus	0	0	50	0.034	7
3	20	To focus	0	50	0.01	2
4	20	To focus	50	17	0.020	12
5	20	To focus	75	122	0.035	3
6	20	To focus	89	170	0.030	1.8
7	50	To focus	0	50	0.006	1.2
8	50	To focus	50	17	0.015	9
9	50	To focus	75	122	0.022	1.8
10	90	To focus	0	50	0.004	0.8
11	90	To focus	50	17	0.008	4.7
12	90	To focus	75	122	0.030	2.5
13	90	To focus	90	170	0.028	1.6
14	0	To focus	0	50	0.012	2.4
15	0	To focus	50	17	0.014	8
16	0	To focus	75	122	0.040	3.3
17	0	To focus	89	170	0.052	3.1
18	0	0	To focus	35	0.008	2.3

Examination of Fig. 6 reveals that the slope of the camera length vs. current in magnifying lens curve is approximately 3. Thus, if the effective camera length is chosen by setting the current in this lens, an error of 1 ma in adjusting the current will produce an error of 3 cm in the effective camera length. Since the magnifying lens will be used only to obtain effective camera lengths greater than 50 cm (the physical camera length), the error introduced by a current setting error of 1 ma will vary from 5 percent at 60 cm camera length to 1.5 percent at 200 cm.

THE DIFFRACTION CAMERA

While this paper primarily deals with the optical properties of a new diffraction camera, a brief description of the instrument may serve to clarify questions concerning mechanical arrangement. The cross-section of the column is shown in Fig. 2. The electron source is a self-biased electron gun whose high intensity recommends it for the diffraction application. Accelerating potential is provided by a fifty kilovolt stabilized electron microscope supply. The instrument was originally used with a variable voltage supply from 12 to 50 kilovolts. However, diffraction at the lower voltages is so difficult with many substances, due to charging of the specimen in the electron beam and broadening of the lines because of decreased beam penetration into the specimen, that the variable feature was abandoned and the voltage was fixed at fifty kilovolts. The electron

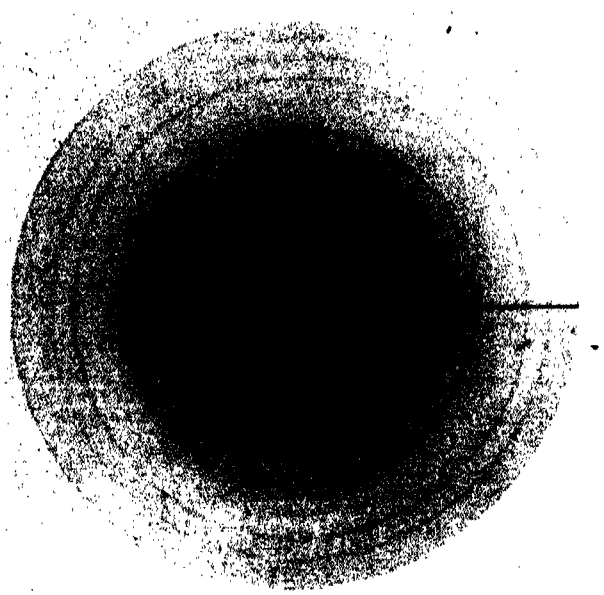

FIG. 8. Pattern of magnesium oxide with a trace made by the undiffracted beam.

gun mounting and all lenses are provided with transverse adjustment screws. All lens spools are identical. Demountable pole pieces provide short focal length lenses where necessary, as in the number 1 and number 3 positions. The specimen chamber is specially designed for diffraction work. It provides a large window for observation of the specimen during adjustment. This is frequently valuable in reflection work since the incident beam often causes the surface of the specimen to fluoresce and it is therefore possible to observe the area being struck. The auxiliary charge neutralizing gun is built into the chamber and can be employed as general illumination for observing the interior of the specimen chamber. An auxiliary port in the chamber is provided to permit the use of mechanical agitators, heaters, and evaporators.

Of extreme importance to successful electron diffraction is a versatile specimen stage providing three translational and one rotational degree of freedom. An additional rotation, dependent upon the first rotation, is also provided to permit adjustment of the grazing angle. Ease of manipulation to provide practically any orientation of specimen in the electron beam has made it possible to obtain diffraction from many specimens which have previously given no results.

Below the specimen chamber are shown one lens spool and one spacer. These components are interchangeable so that the number 3 lens can occupy either the number 3 or number 4 positions in the column if desirable.

The viewing chamber is designed to give a four-inch diameter view on the fluorescent screen. Since the angular aperture of beams used in electron diffraction are frequently quite large, the viewing screen is placed as close to the photographic plate as possible so that a focused beam spot on the screen will be in focus on the plate. A retractable beam stop is included to improve visibility of faint patterns by eliminating the bright central spot which otherwise tends to blind the operator. Its situation close to the viewing screen makes it possible for it to cast a minimal shadow on the plate. For ease of observation, the viewing port is wide enough to permit binocular vision.

Patterns or shadow micrographs are photographed on standard 4×5 glass photographic plates. A single cassette holds three such plates and slides parallel to the viewing screen.

Versatility is the keynote of the diffraction camera described above. For example, it has been found that withdrawal of the beam stop at the last moment of plate exposure marks a dark pattern center on the developed plate which is useful in making plate measurements. The ability to slide the plate with the shutter open and beam on makes it possible to trace the central spot as a fine line across the plate. The fine line is a measure of beam diameter and may be compared to ring widths to study broadening of lines in diffraction. Such a plate is shown in Fig. 8.

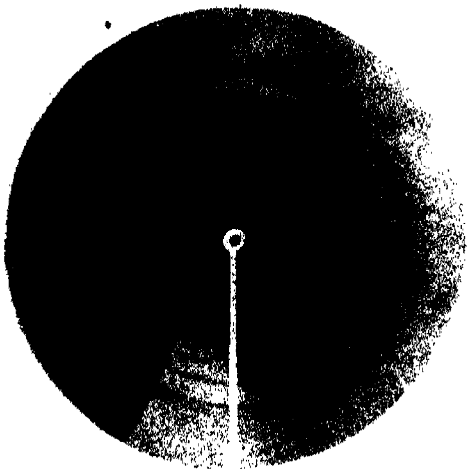

FIG. 9. Pattern of Fuller's Earth with magnesium oxide superimposed upon it to provide internal calibration of the plate.

The use of a specimen holder which accommodates several specimens makes it possible to superimpose unknown and standard diffraction patterns on the same plate. If the shutter is used to expose only half of the plate with the standard, the two sets of rings may readily be distinguished. An example of this technique is shown in Fig. 9.

ELECTRON GUN FOR CHARGE NEUTRALIZATION

When materials are bombarded with a high velocity electron beam, as occurs when a specimen is examined in an electron microscope or electron diffraction camera, electrons are knocked out of the material and, consequently, it acquires a charge. This charge is purely surface phenomenon, as the penetrating power of the electron beam commonly used—50 to 100 kv—is extremely small, generally less that 10^{-3} mm.

The magnitude and duration of this charge depends on both the causative electron beam and the nature of the bombarded material. Beam current and accelerating voltage influence the total magnitude of the charge. The surface and volume conductivities of the specimen and the potential relative to ground of the specimen mount and support determine the duration and equilibrium value of the charge.

The charge, in turn, influences the path of the beam through subsequent portions of the apparatus by imposing an electrostatic field which the beam must traverse. The optical constants of the instrument are not calculated to compensate for this unknown electric field, and, furthermore, the field is seldom sufficiently stable to permit optical elements to counteract it.

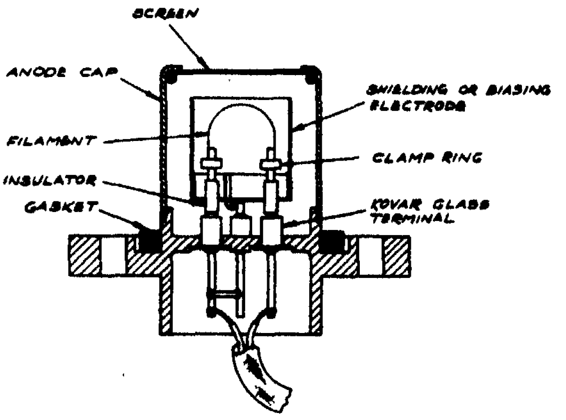

FIG. 10. Constructional details of the gun used for charge neutralization.

In electron diffraction, a charge on the specimen may shift the pattern, cause unsharpness in the lines or spots, and, in many cases, completely destroy the pattern or prevent its formation. The most pronounced charging effects are observed with reflection specimens. In the study of these specimens, the electron beam strikes one surface only, and, if the specimen is a poor conductor, the charge accumulated on the bombarded surface cannot leak off. Not only the specimen, but its method of mounting is important if charging effects are to be avoided. The mounting method should permit specimens to be well grounded, but even this precaution will not overcome electrostatic effects on insulating specimens.

A well known and frequently used method of neutralizing the charge on insulating specimens is to bathe the specimen in a stream of low velocity electrons from an auxiliary electron gun.[11] Several considerations govern the design and use of a generally satisfactory neutralizing system:

(1) General irradiation with electrons of the specimen, specimen holder, and entire specimen chamber provides the best condition for neutralization.

(2) Neutralizing current at the specimen varies widely with the specimen employed, but is generally of the order of 0.5 to 5 milliamperes per square centimeter.

(3) Electron accelerating voltages should be available from 200 to 1000 volts.

(4) The source of electrons should not contaminate the specimen with evaporation products.

A neutralizing electron gun fulfilling the above requirements has been built into the specimen chamber of the described camera and so directed that its axis intersects the optical axis of the camera at the mean point of the range of specimen motion (Fig. 10). The anode cap has a front made of a large disk of fine mesh, stainless steel wire screen. The filament is shielded from the rest of the anode by a cylinder maintained at filament potential or lower. Thus, all the emitted electrons are accelerated toward the anode which has a large open area. This effective aperture may be adjusted by using screens with different numbers of openings per inch.

This gun has very high efficiency for charge neutralization as nearly all of the electron emission is used. Hence, low filament temperature may be used, and the concomitant tungsten evaporation is negligible. The rate of evaporation of tungsten increases by a factor of 10^{16} as the temperature of the filament is raised from 1500°K to 3000°K, the usual operating range of the filament in an electron gun of this type. Over the same range of temperatures, electron emission increases by a factor of 10^{8}.

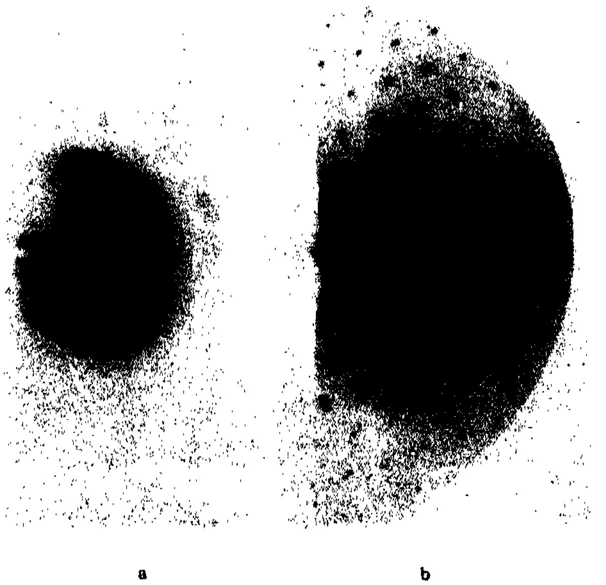
a b

FIG. 11. Reflection pattern from a piece of mica—(a) without charge neutralization, and (b) with charge neutralization.

---

[11] E. I. Alessandrini, J. App. Phys. 16, 94–96 (1945).

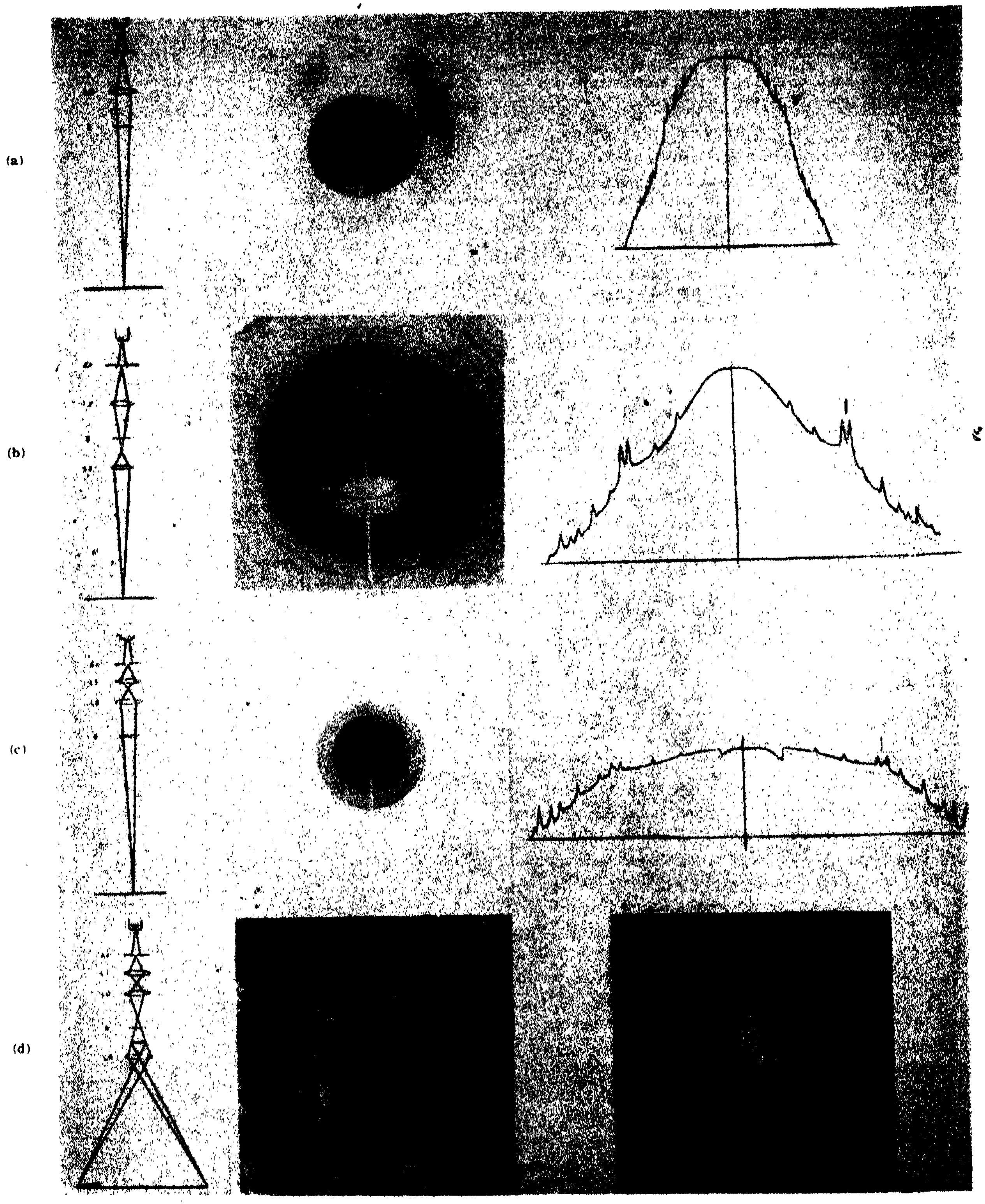

FIG. 12. (a) Pattern of tetraphenyl tin using the optical arrangement shown at the left. The microphotometer curve of this pattern is shown at the right. Specimen-to-plate distance—50 cm. (b) The same but magnified to an effective specimen-to-plate distance of 212 cm. (c) The same with the optical arrangement shown at the left. (d) Shadow micrographs of powdered mica made using the lens combination shown at the left.

Insulating materials, such as mica, have been used to produce electron diffraction patterns, have had surface charges neutralized completely with the gun of Fig. 10, and the pattern has been unchanged after a one hour exposure to the auxiliary electron beam (Fig. 11). With a small aperture gun operating at 500°K higher than the described gun but providing adequate current to neutralize charges on mica, the rate of tungsten deposition on the mica was such as to produce a noticeable dimming of the pattern in two or three minutes, and complete obliteration of the pattern in less than ten minutes.

DISCUSSION OF RESULTS

The extreme versatility of the electron diffraction unit described in the preceding sections is well illustrated in Fig. 12. The pattern obtained with the simplest optics—a single lens above the specimen focusing the source on the plate—is shown at (a) with its microphotometer trace. At (b) is shown the same pattern magnified electron optically by a post-specimen lens in the number 3 position. The striking feature of this pattern is not the increase in ring diameter but the withdrawal of the inner rings from the area of intense halation at the pattern center. This fact is even more vividly illustrated by the corresponding microphotometer trace which was made under identical conditions to the one above it. The explanation of this effect is not completely worked out and is still the subject of some controversy. However, the authors are convinced of the reality of the effect since it has been observed on many plates and always occurs when the pattern is magnified electronically regardless of the relative exposure of the unmagnified and magnified patterns.

Several factors may contribute to the improvement in contrast possible with the use of a post-specimen magnifying lens. This lens acts to deflect the stray and widely scattered electrons from striking the central area of the photographic plate, and thus acts as a stop in the image forming system. The area of plate halation due to the extremely intense undeflected beam is a constant regardless of magnification. This area is small and will affect only the rings of very small diameter. Furthermore, there is a subjective advantage in working with large patterns which generally results in more accurate appraisal of plate exposure times because of the removal of the rings from the vicinity of the bright central spot. In addition, there is an improvement in the effective contrast when using a recording microphotometer on magnified rings because the length of the reading slit becomes a much smaller percentage of the ring diameter.

Figure 12(c) illustrates the improvement in resolution obtainable by using lens 1 to reduce the size of the image of the source. The pattern looks the same as that of Fig. 12(a), but the microphotometer trace has been enlarged 5 times. If this latter fact is born in mind, it becomes obvious that the lines are sharper than in Fig. 12(a). The pair of lines indicated by the arrow show an intermediate line in Fig. 12(c) which is not resolved in Figs. 12(a) and (b), although the pattern of Fig. 12(b) has been sufficiently magnified to make this pair of lines stand out strongly against the background.

Figure 12(d) demonstrates the use of the instrument as a shadow microscope. The post-specimen lens is used to magnify the shadow microscope image. The higher magnification picture is produced by using lens 2 to bring the reduced image of the source closer to the specimen with no change in the power of lens 3.

ACKNOWLEDGMENT

The authors wish to express their indebtedness to Mr. S. M. Zollers and Mr. E. Dornfeld of the Scientific Instruments Section, and Mr. A. M. Rennie, all of whom played essential roles in the design and development of the diffraction unit

THE REVIEW OF SCIENTIFIC INSTRUMENTS VOLUME 20, NUMBER 8 AUGUST, 1949

Physical Instruments for the Biologist

Detlev W. Bronk
Associate Editor in Charge of this Section
Eldridge Reeves Johnson Foundation for Research in Medical Physics,
University of Pennsylvania, Philadelphia, Pennsylvania

Frequency Analyzer for Bioelectric Potentials in the Sub-Audio Range*

CHARLES MARKEY, ROBERT L. SCHOENFELD, AND PAUL F. A. HOEFER
Department of Neurology, College of Physicians and Surgeons, Columbia University, and the Neurological Institute of New York, New York City, New York

(Received January 6, 1949)

An analyzer for sub-audio bioelectric potentials, particularly the human electroencephalogram, is described. The instrument is coupled to the output of a standard EEG amplifier and records twenty frequencies by means of individual filters each coupled to a two-inch cathode-ray oscilloscope. A 35-mm slow moving camera provides a time base while simultaneously photographing, the filter deflections, a cathode-ray trace of the unanalyzed slow wave and one-second time markers produced by a clock driven flashing light. The system employs amplitude modulation of a 1200 cycle carrier; the filters being selective to the lower sideband frequencies which are recorded as horizontal deflections of the oscilloscopes.

The present analyzer, in contrast to others, has a one-half-second time constant and is thus a low "Q" system responsive to activity of short duration. The frequency spectrum obtained is necessarily broad but detailed in the time domain, an aspect of physiological importance, hitherto neglected.

INTRODUCTION

THE electroencephalogram is a continuous time varying potential in the range from 0.5–60 cycles per second. Certain features of the record have been useful in the diagnosis of central nervous dysfunction. Since time varying potentials may often be uniquely described by their frequency and phase spectra, several attempts at electromechanical frequency analyses of the EEG have been made based upon the arbitrary selection of an interval for analysis.

Grass and Gibbs[1] chose a thirty-second strip of record artificially made periodic in the form of an endless belt, rotated at high speed and reproduced photoelectrically so that the record could be analyzed in the audio range with a standard harmonic filter. Walter[2] devised a technique for integrating the response of a number of tuned filters over a ten-second interval, and for recording the resultant analysis superimposed on the primary record. Barbour[3] used a single filter to sweep through the band recording successively the amplitude of each frequency component in the EEG.

No one of these methods indicates the phase spectra but only the amplitude of frequencies present for the time interval considered. In these methods the interval of analysis is long compared to the probability of changes in the potential patterns. Also the time sequence of appearance and disappearance of different frequencies is not indicated.

The present analyzer records twenty components simultaneously with the primary record and provides a method for studying the changes in wave form and frequency that occur.

CIRCUIT OPERATION

A block diagram of the circuit in which the important stages are detailed is shown in Fig. 1. The EEG wave is coupled from the output of any one channel of a standard EEG amplifier. The coupling network attenuates the very low frequencies which would unbalance the modulator stage that follows. This high pass characteristic is compensated for in the filter stages. The signal is amplitude modulated with a 1200-cycle carrier frequency in a balanced modulator stage consisting of two 6L7 heptodes. The 6L7 pentagrid converter provides a simple electronic means of grid modulating the carrier, using resistance-capacity coupled inputs, and assuring isolation of the input circuits by virtue of the two independent control grids which are shielded from one another within the tube. The input signal level is of the order of 0.2 volt while the carrier level is 0.4 volt. The output current can be represented as a power series expansion of the product of these two voltages. Hence it consists of upper and lower sidebands plus very small higher order terms. When the stage is properly balanced by means of the screen voltage potentiometer R_7 and output balancing control R_9, the carrier is suppressed. It is necessary to make a slight adjustment of R_9 before using the equipment, but the balance will remain stable over several hours of operation.

The modulator thus transposes the EEG frequencies to a narrow range on each side of the carrier. The output of the modulator is coupled by means of a

---

* Mr. Charles Sheer contributed valuable assistance in the research that led to the development of the present instrument.

[1] Albert M. Grass and Frederic A. Gibbs, "A Fourier transform of the electroencephalogram," J. Neurophysiol. 1, 521 (1938).

[2] Grey W. Walter, "A new electronic analyzer," Electronic Eng. XVIII (November, 1946).

[3] Ian Barbour, "An automatic low frequency analyzer," Rev. Sci. Inst. 18, 7 (1947).

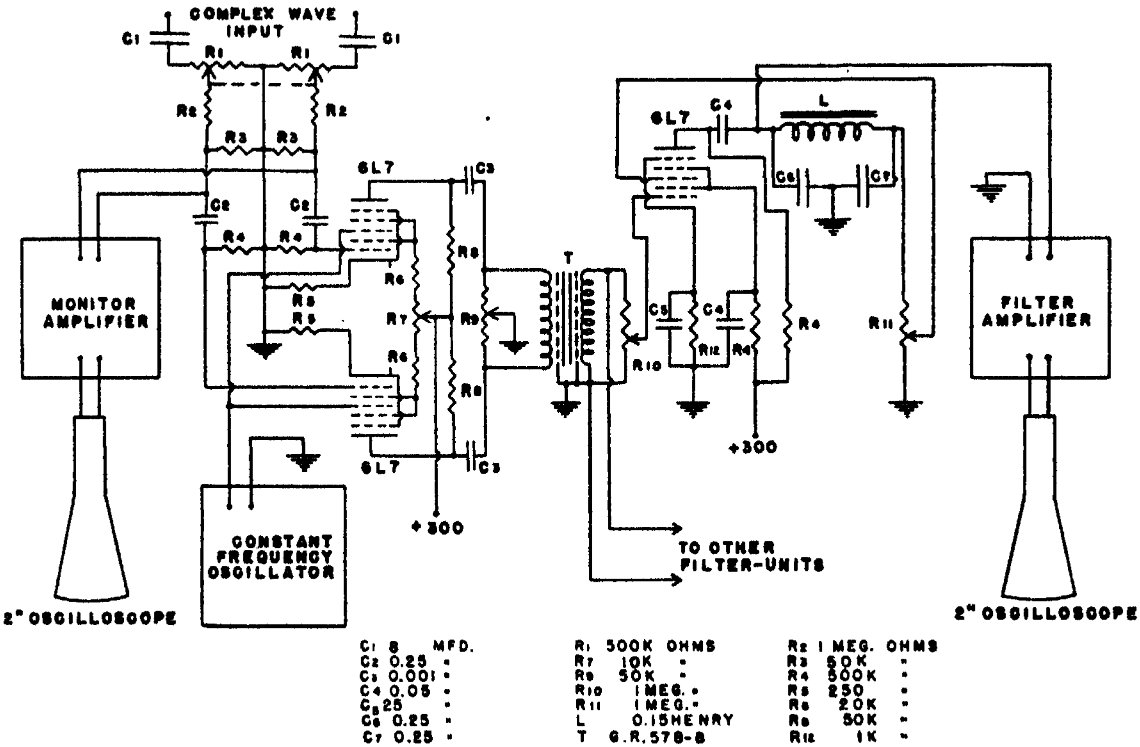

FIG. 1. Block diagram of the analyzer showing the circuits of the modulator and a filter stage.

shielded low capacity transformer to twenty filter stages in parallel. The filter stages, one of which is shown, have high input impedance and do not intercouple in normal operation. Each consists of a frequency selective regenerative amplifier with the feedback accomplished in the second control grid of another 6L7. The amount of feedback is adjusted so that the circuit is highly regenerative but not oscillatory. The intrinsic "Q" of the coil is approximately 50 at the carrier frequency and this is effectively the selectivity of the resonant circuit without the feed-back tube. Since the required "Q" with regeneration is of the order of 2400, it was necessary to use an inductive type resonant element to obtain a high intrinsic selectivity.

The selectivity of the system must be set by means of the feed-back potentiometer R_{11} before taking data. The selectivity will vary about ten percent during a half-hour EEG run so that it is advisable to calibrate the instrument before and after each run for quantitative results. The selectivity adjustment may be accomplished in about ten minutes.

In order to obtain stable operation of the carrier frequency oscillator as well as the filters, the a.c. supply is powered from a Solar constant voltage transformer. The plate supply of all stages with the exception of the oscilloscope high voltage is obtained from a Miller electronic voltage regulator having a stabilization ratio of one part in twenty-five thousand.

Each filter may be made selective to a band width of one cycle or less within the range of the lower side bands of the modulation products. The response of each filter is proportional to the energy distributed in the EEG frequency band to which it is tuned. The filter output voltage is of the order of ten millivolts for best selectivity; this signal being amplified through two pentode stages and recorded as a full-scale deflection on a two-inch oscilloscope. There are twenty-one such oscilloscopes arranged in a horizontal bank, the central one acting as a monitor of the unanalyzed EEG. A slow moving camera with a wide angle lens provides the time base while continuously recording the twenty-one traces. The camera does not resolve the high frequency into identifiable cycles but records the modulating envelope as a shadowgram. In the filter oscilloscopes the beam is positioned to one side for better quantitative recording. The time rate of one second is recorded on the film by a flashing light driven by a clock.

The operation of the system is most easily described for the case when the twenty filters are tuned in integral steps from 1–20 cycles per second, although other tuning may be used. The selectivity is adjusted so that the response of adjacent filters is down to 25 percent of the resonant one. With this selectivity the effective "Q" and time constant "T" are approximately given by:

$$Q=(4f_0/f_2-f_1),\quad Q\gg 1, \tag{1}$$

$$T=(Q/\pi f_0), \tag{2}$$

in which f_0 = frequency to which filter is resonant, f_1 = lower frequency at which filter response is 25 percent of resonant response, and f_2 = upper frequency

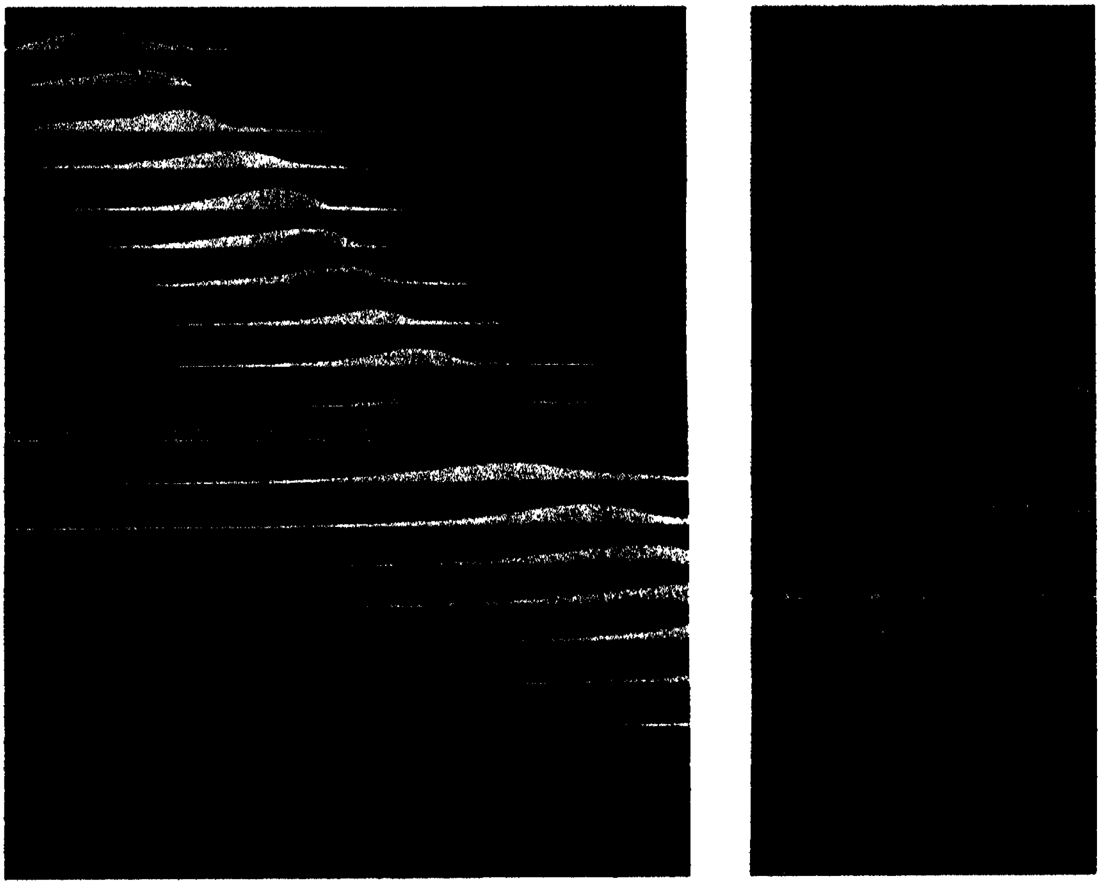

(a) (b)

FIG. 2. (a) Calibration run with 1–20 c.p.s. tuning. Center trace is calibration oscillator signal. Time of one second indicated by bottom dashed line. Frequency traces in steps of one cycle from bottom to top. The oscillator is manually tuned from the higher to the lower frequencies. (b) EEG calibration pulses indicating transient response of the analyzer. Tuning 1–20 c.p.s. as in (a).

at 25 percent of resonant response. Although the actual "Q" of the filters is of the order of 2400, the "Q" referred to the low frequency varies from 2–40.

The filters are calibrated to equal amplitudes with an oscillator (Fig. 2(a)). Its frequency is slowly changed to allow each filter in turn to build up to a steady-state response. As resonance occurs in each filter, the equation of response referred to a simple series resonant circuit will be:

$$i(t)=(V_0/R)\sin\omega_0 t-(V_0/R)\epsilon^{-(\omega_0 t/2Q)}\sin\omega_0 t,\quad Q\gg 1, \tag{3}$$

where $i(t)$—time response of the filter, V_0—amplitude of applied harmonic voltage, R—damping constant of filter, and ω_0—undamped natural angular frequency of filter. It can be seen from this equation that the time constant ($T=2Q/\omega_0$) equals the time necessary for the filter to build up to steady state and to die away from it when the applied sine wave is removed.

If the applied voltage is a complex periodic wave, the "Q" of the filters must be sufficiently large so that each filter responds to only one component. Under these conditions, the filters responding to the different frequency components will all build up to a steady state response. Since the "Q" determines the time constant, this requirement indicates that the fundamental period of the complex wave must be shorter than the time constant of all filters. The analyzer has a time constant of about 0.64 second for all filters in the tuning described so that waves with fundamental periods as low as two cycles per second are resolved.

The short time constant and low "Q" make this system highly responsive to transients (Fig. 2(b)). The requirements for an analysis of transients can be developed in terms of a single step function. The response of a series resonant circuit to a step function of amplitude V_0 is:

$$i(t)=(V_0/QR)\epsilon^{-(\omega_0 t/2Q)}\sin\omega_0 t,\quad Q\gg 1. \tag{4}$$

The spectrum of a step function as given by the Laplace transform is:

$$|V(\omega)|=V_0/\omega, \tag{5}$$

$$V(\theta)=-90°, \tag{6}$$

where ω=angular frequency, θ=phase angle, and V=amplitude of spectrum. In order to make the amplitude of the filter responses directly proportional to the frequencies represented, by comparison of (4) with (5), it follows that:

$$Q \propto \omega,\ R \text{ maintained constant.} \tag{7}$$

In the present analyzer (substituting in Eqs. (1) and (2)), at the tuning mentioned, these values become:

$$Q = \omega/\pi, \tag{8}$$

$$T = 2/\pi. \tag{9}$$

Several sample records are shown (Fig. 3). The time sequence of sinusoidal wave forms may be observed readily. The spike-and-wave pattern is not resolved harmonically because of its slow fundamental. The complexity of typical wave forms is evident. The information obtained lends itself to qualitative study only.

LIMITATIONS OF FREQUENCY ANALYSIS

Frequency analysis of an arbitrary class of time varying potentials is ultimately dependent on the limit of resolving power of resonant elements. A single filter has a time of response that is inversely related to its frequency band width. If the frequency discrimination is increased, the filter takes longer to respond and becomes less sensitive to brief events. If the time of response is shortened, the frequency response becomes less selective. In a fundamental way, therefore, the resolution of the filters is limited and the best design is predicated on the selection of the type of phenomena to which the filters must respond.

By an event we mean any pattern bounded in time that may recur. Any particular class of time varying potentials is characterized by the complexity and duration of events that can be isolated. With periodic waves, for example, the time duration of events is determined by the fundamental period. In most instances of harmonic analysis one deals with periodic phenomena within a limited frequency band so that the duration and complexity of events varies within a restricted range. In the EEG events with a wide

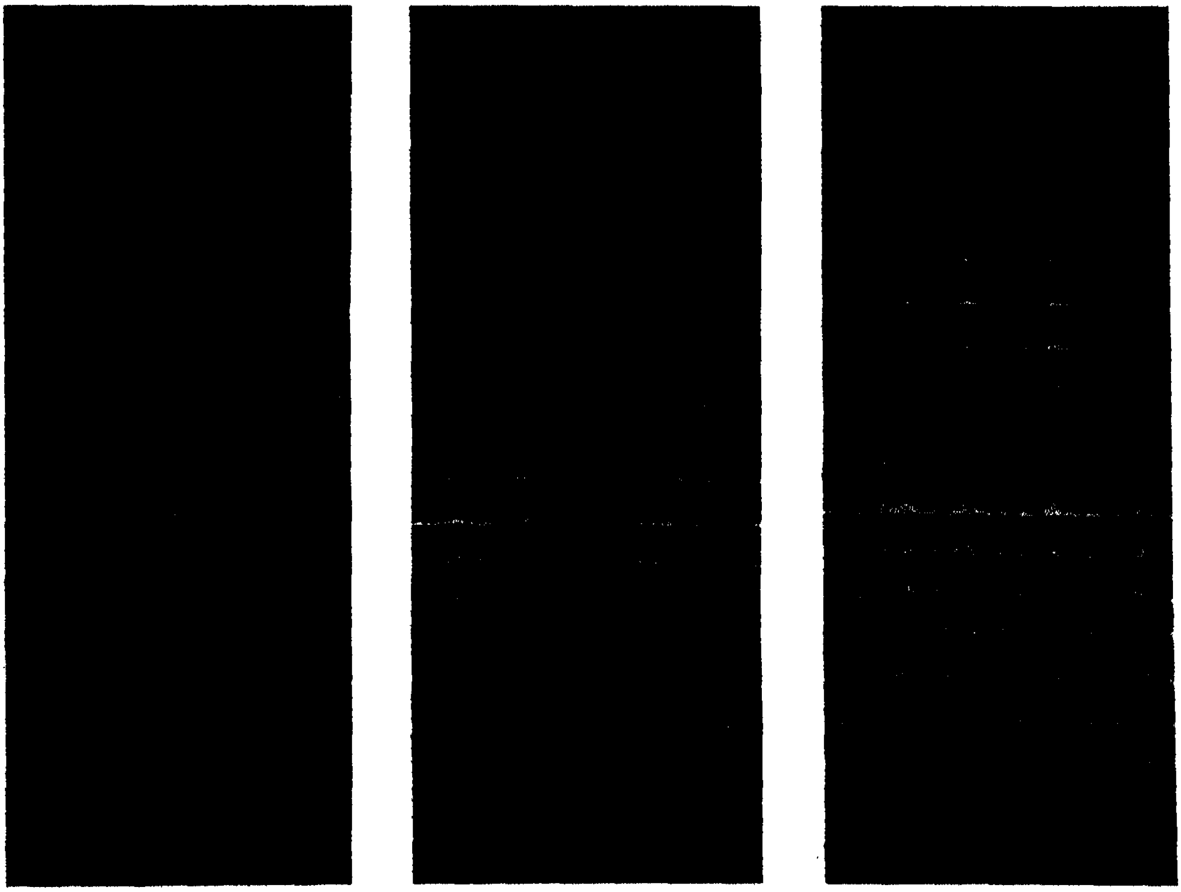

(a) (b) (c)

FIG. 3. (a) Analysis of alpha-groups which are often found in EEG records. Wave forms are almost sinusoidal and frequencies typically vary from 8 to 12 c.p.s. Tuning 1–20 c.p.s. (b) Analysis of slower frequencies. Note the shift from 7 c.p.s. to 2 c.p.s. in predominant frequency, the 7 c.p.s. wave persisting at lower amplitude. Tuning 1–20 c.p.s. (c) Analysis of spike-and-wave pattern found in EEG records from patients with petit mal epilepsy. Note shift in predominant frequency from 4 to 2 c.p.s. Note transient character of spike as shown by wide frequency distribution. Tuning, in this case, from 1–60 c.p.s. Traces 1–6 record 1–6 c.p.s.; traces 7–13, 8–20 c.p.s.; traces 14–20, 25–60 c.p.s.

distribution of duration and relative complexity may be observed. In analyzing this phenomenon some selection of the time interval is presumed and the choice of the most probable time duration implies either foreknowledge of what is significant or an arbitrary choice.

A completely adequate analyzing system should give enough frequency components of events of selected duration to distinguish between them and to relate their frequency characteristics. However, the selectivity of the filter system is determined by the time interval over which the filters must respond. Two extremes of filter design are possible; one with a short-time constant and low "Q," the other one with a long-time constant and high "Q." Short events become lost in a long-time constant system, long events are not resolved in a short-time constant system. The long-time constant system permits a high degree of frequency discrimination, the short-time constant system has a necessarily broad response. The selection of the interval for analysis thus determines the degree of frequency discrimination that is possible.

The present instrument was designed for events of relatively short duration and hence is a short-time constant, low "Q" system. The use of longer intervals for analysis (Grass and Gibbs, Walter) has yielded little information. On the other hand, brief events such as a single spike or spike-and-wave group are of physiological importance. The present analyzer obtains a relatively broad frequency spectrum of such events. It is hoped that comparison of these spectra with others of activity less well understood may extend knowledge of the human electroencephalogram.

Erratum: Conditions for Optimum Luminosity and Energy Resolution in an Axial β-Ray Spectrometer with Homogeneous Magnetic Field

[Rev. Sci. Inst. 20, 160 (1949)]

Jesse W. M. DuMond
California Institute of Technology, Pasadena, California

IN this paper, the quantity (Eq. (10)), $d\phi=\frac{1}{2}\sin\theta d\theta$, is defined in *words* on page 163 as "the fraction of the total sphere into which β-rays can be projected", the implication being that it is the said fraction *corresponding to a specified range $d\theta$ of colatitude angles of emanation from the source.* The value of $d\phi$ however, *corresponding to a specified resulting range of energy inhomogeneity* (from aberration), is twice as great as the formulae throughout the paper indicate. The author's error arose from overlooking the fact that the range from θ_1 to $\theta_1=\Delta\theta$ contributes identically the same energy inhomogeneity as the range from θ_1 to $\theta_1+\Delta\theta$, see Fig. 8. Therefore, in formula 12 and in formulae 21 to 40 inclusive the symbol $d\phi$ should be interpreted as *only half the fraction of the total sphere* into which β-rays can be projected. The happy result of this correction is to make the luminosity of the instrument for a given energy resolution twice as great as represented in the paper, or to make the resolving power four times as great for a given luminosity as that stated in the paper. If the reader will therefore substitute $d\Phi=2d\phi$ throughout the paper and interpret $d\Phi$ as the utilized fraction of the total sphere about the source, all will be correct. The numerical values of the resolution given in the next to the last paragraph should also be revised for this reason. $\Delta\epsilon/\epsilon=0.0065$, 0.0049, 0.0032 should be changed to $\Delta\epsilon/\epsilon=0.0016$, 0.0012, 0.0008. The statement $\rho=0.004R$ should read $\rho=0.001/R$. In the final sentence of the paragraph, the values given as $\Delta\epsilon/\epsilon=0.004$, 0.003, 0.002 should read $\Delta\epsilon/\epsilon=0.001$, 0.0008, 0.0005.

The writer is indebted to Professor F. H. Schmidt of the University of Washington for kindly pointing out this error to him after the paper was published.

An Apparatus,for Electrode Reversal in the Tiselius Electrophoresis Equipment

H. TINT
Wyeth Institute of Applied Biochemistry, Philadelphia, Pennsylvania

(Received May 9, 1949)

An accessory to the standard Tiselius electrophoresis apparatus is described which permits electrode reversal during operation without changing the terminal polarity of the arms of the electrophoresis cell. It thus permits maintenance of the usual silver-silver chloride electrodes in optimum condition in runs of extended duration for critical analytical and preparative electrophoresis without increasing the physical dimensions or complexity of the electrode system. It incorporates a four-position, multiple-way valve, of Plexiglas construction, which is designed to be inserted at the position of the upper section of the standard cell, replacing it as a tubular transfer point of current between the electrode vessels and the limbs of the cell proper.

INTRODUCTION

FOLLOWING the description by Tiselius in 1937[1] of an improved apparatus for the electrophoretic study of electrolytes by the moving boundary method, the application of this technique has undergone fairly widespread laboratory adaptation. The basic form of the equipment and the manipulations and methods involved in its use have been adequately reviewed in the literature.[2,3,4] These principles have been embodied in various commercial designs which are currently available. However, Longsworth *et al.*,[5] have described a form of this equipment which is used in this laboratory and which occurs most frequently elsewhere at the present time.[6]

In this design, the cell-complement includes silver-silver chloride electrodes, immersed in concentrated KCl solution, which serve as terminals for current to and from the cell. The size of the electrode vessels is governed by the volume of buffer which it is desirable to interpose between the electrodes and the cell.[1] This volume is in turn determined by the necessity to have the electrode heating effect, a source of thermal convection, considerably removed from the cell proper. At the same time the volume must be sufficiently large to prevent the products of the electrode reaction from migrating into the cell. For practical purposes, the usual 11-ml analytical cell requires approximately 500 ml of buffer in each electrode compartment; however, smaller volumes are possible if a more concentrated buffer is placed between the electrodes and the dilute buffer in the cell.[7]

The ability to reduce the size of the electrode vessels to a minimum which is practical for ordinary analytical runs under average conditions, is a desirable feature in the design of the equipment considering the physical limitations of the bath. However, this same feature militates against the extension of the use of the same equipment for preparative purposes, using the same analytical cell or, even to a lesser extent, using cells of greater capacity. To compensate for the need for the greater amounts of electricity which are required for preparative runs of long duration, the electrode capacity must be increased by one of several alternative procedures.[4] The size of the electrode cells may be increased proportionately, but the volume increases usually required for adequate preparative runs are usually beyond the practical limits of this particular equipment, and the vessels must be housed outside the bath. With the decreased heat exchange under these conditions, lower potential gradients than are possible with the analytical cell must be used. Other alternatives rest in more or less complicated mechanical systems for buffer circulation[4] which are also beyond the scope of the present equipment. None of these methods, however, provides for replacement of the silver chloride

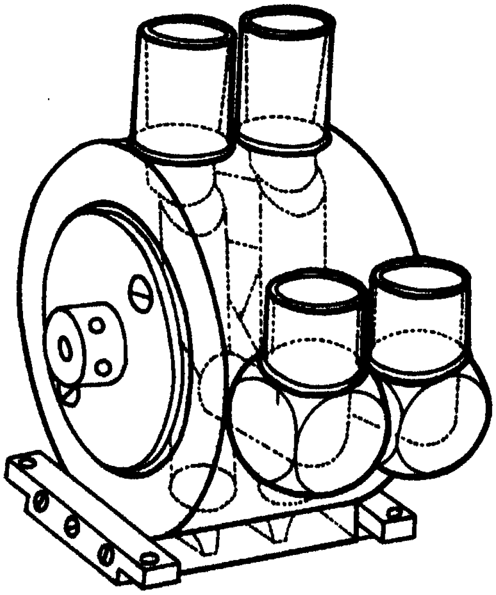

FIG. 1. Channel-reversing valve with mounting brackets.

---

[1] A. Tiselius, Trans. Farad. Soc. 33, 524 (1937).

[2] D. A. MacInnes and L. G. Longsworth, in Jerome Alexander's *Colloid Chemistry* (Rhinehold Publishing Corporation, New York, 1946), Vol. 5, p [illegible]

[3] L. G. Longsworth, Ind. Eng. Chem. 18, 219 (1946).

[4] H. Svensson, Adv. Prot. Chem. 4, 251 (1948).

[5] Longsworth, Cannan, and MacInnes, J. Am. Chem. Soc. 62, 2580 (1940).

[6] Supplied by the Klett Manufacturing Co., New York.

[7] A. Tiselius, Svensk. Kem. Tid. 50, 58 (1938).

layer on the cathode, which becomes depleted in the course of the run.[8]

The most logical alternative for providing large electrode capacity with small buffer volumes is to utilize a method of reversing current direction in the electrode vessels without change in direction through the electrophoresis cell. By periodic reversal during a run, the electrodes serve alternately as anodes and cathodes and are thus alternately self-plating. At the same time the products of electrolysis at the electrodes are confined to the electrode vessels. Thus the smaller buffer volumes which are satisfactory for analytical runs may also be used for longer preparative runs, and by being able to confine the electrode vessels in the bath, the maximum heat-exchange potential of the instrument may be utilized.

Svensson[9] has described a system for electrode reversal in connection with a preparative cell of unique design; however, it extends considerably beyond adaptation to the present available standard equipment. The present writer has designed an accessory unit which in turn is readily adaptable to this standard equipment and is capable of providing reversal of electrodes without changing the direction of migration of the electrolytes under inspection in the cell. At the same time, provision is made to permit the entrance of withdrawing mechanisms into either leg of the cell for the removal of components during the progress of the run. All operations in analytical or preparative runs may be carried out entirely in the bath without any need for disassembling the equipment within the progress of the experiment however long it may be necessary to continue the run.

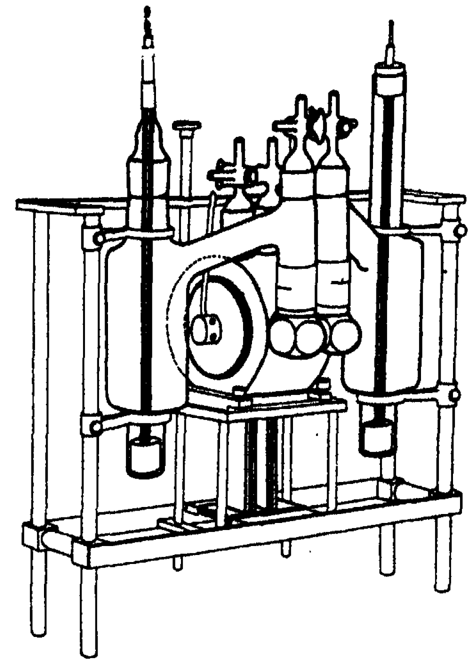

Fig. 2. Assembly of valve with cell and electrode vessels in standard frame. The rack and pinion device for sliding the cell section has been omitted to simplify the diagram.

DESCRIPTION

The principle of this method may be seen in Figs. 1 and 2. In place of the usual upper section of the cell, which provides the bridge between the cell and the arms of the electrode vessels, is substituted a Plexiglas[10] valve constructed after the fashion of a large double stopcock. The plug of the valve is precision-bored in a particular manner as to allow in each of four quarter-turns, either a direct connection between the electrodes and the limbs of the cell, or a reverse one. At the same time, in two of these positions, paths are allowed for direct entrance of sampling tubes into either leg of the cell. The channels in the plug, in each of the four positions, are continuous with the following paired openings in the shell: top, compensating and sampling ports; one-side, connecting to the side arms of the electrode vessels; and bottom, feeding directly to the arms of the electrophoresis cell.

Operating Positions

The arrangement of the channels in the several operating positions is demonstrated in the diagrams of Fig. 3. In position *A*, 0°, the connection between the legs of the cell and the electrodes is direct. At the same time a straight path is provided downward through the plug to either leg for the entrance of sampling or filling tubes. The reversing channels of the plug are sealed-off against the blank side of the shell. With a 90° turn of the plug in a clockwise direction, to position *B*, the connection between the cell and electrodes is still direct; however, the sampling ports are in reverse communication with the cell legs. In this case direct sampling is not possible although the upper ports may be used as terminals for compensating mechanisms. In position *C*, 180°, the electrodes are reversely connected with the cell and again direct sampling is possible. Finally, in position *D*, 270°, the electrode-cell connection is reversed and there are no direct sampling channels.

Construction

The size of the valve and its plug is governed by several considerations. It cannot be made larger than is permitted by the space available for its insertion in the standard frame. Also, increasing size involves concomitant increased sliding-surface area with serious lubrication problems at the reduced operating temperatures of the bath. At the same time, the plug must be sufficiently large to permit boring of relatively large, non-contiguous channels and at the same time retain sufficient plug-to-shell interface which can be adequately sealed with lubricant to prevent leakage. The cross-sectional area of the channels must be sufficiently large to insure minimal resistance to current in the system and well in excess of the cross section of the electrophoresis cell, whether analytical or preparative.

---

[8] R. A. Alberty, J. Chem. Ed. 25, 426 (1948).

[9] H. Svensson, Arkiv. Kemi, Mineral. o, Geol. 22A, No. 10 (1946).

[10] Manufactured by Rohm and Haas Company, Philadelphia, Pennsylvania.

The operating model has a plug which is 7.5 cm long and an average cross section of 8.25 cm, with shell dimensions to conform. The channels are 2 cm in diameter and the distance between the central planes of the channel openings at either end of the plug is approximately 4 cm. The plug is tapered along its length 0.5 cm to fix its position in the shell and, in operation is prevented from coming loose by a spring tension on the smaller end against the shell. The larger open end of the plug bears a metal extension to permit insertion of a lever for rotation while immersed in the bath.

Cemented on the lower side of the shell is a Plexiglas plate which is ground flat to serve as a sliding junction for the central section of the standard glass analytical or preparative cell. In the thickness of this plate, the circular channels which are continuous with those of the plug are tapered to rectangular slits with dimensions and position to conform with those of the cells. The top and side ports in the shell terminate in tubes of external diameter corresponding to those of the arms of the regular electrode vessels. The nipples uppermost on the valve shell are internally ground to accommodate standard-tapered sealing plugs.

Assembly and Operation

To assemble the equipment, the ground surface of the plug is lubricated with a proper consistency of petroleum jelly diluted with mineral oil, inserted in the shell and the spring-lock attached. The shell is then mounted upon the frame and, with the assembly inverted, the cell sections are slid into junction with the Plexiglas plate. A light spring is then pressed against the bottom section of the cell to keep the cell-assembly in firm union with the valve during all subsequent filling and operating conditions. The assembly of the glass parts with that of the Plexiglas valve is made flexible to allow for variable contraction rates of the several parts of differing composition, and thus prevent "freezing" of sliding parts or high pressures leading to breakage of glass parts. The electrode-vessel arms are then attached by rubber tubing to the electrode ports of the shell and the assembly is placed into the bath for equilibration. The apparatus is then filled in the usual manner, insuring that all the channels in the plug are free of air pockets during operation.

The plugs in the sampling ports of the shell are fitted with three-way stopcocks, which may be adjusted for compensation or sampling as desired. When all the parts of the assembly and contents are in hydrostatic and temperature equilibrium, changing the position of the plug introduces no shift in the position of boundaries observable in the continuous cell channel; however, in practice one is insured against the possibility of shifting by the expedient of displacing the bottom cell-section whenever a shift in the operating position of the plug is made. All hydrostatic pressures in the assembly may then be equalized by appropriate adjustment of the stopcocks before the bottom section is replaced.

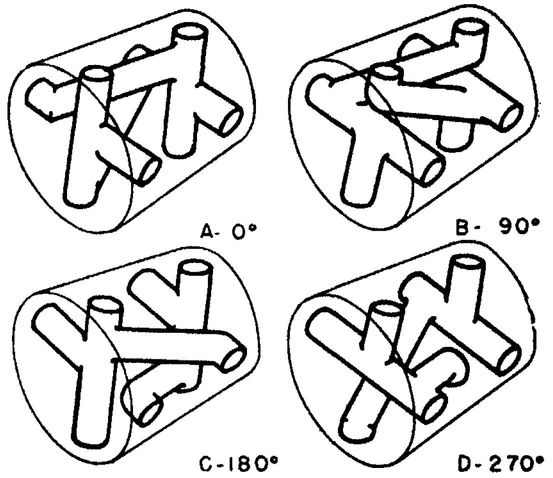

FIG. 3. Operating positions of valve. Electrode to cell connections: *A*, *B*—direct; *C*, *D*—reverse.

When a reversal of the current is desired, the power-supply line terminals are switched, reversing electrode charge, and the plug is then rotated to either of the two positions providing a continuance of the original polarities at the terminal ends of the electrophoresis cell. Thus migration of components in the cell may continue in an unchanged direction.

A typical run with this accessory equipment in the standard Tiselius electrophoresis apparatus was performed upon a standard protein solution (normal bovine serum), with plug positions changed half-hourly with electrode reversal. The amount of voltage required to yield a given current in the run was the same for each of the four plug positions. The run yielded scanned patterns which were typical for this material, and from which mobility and composition data were calculated which were identical with those obtained from a run using the regular three-cell-section equipment, without electrode reversal.

ACKNOWLEDGMENT

The writer expresses his indebtedness to the Institute instrument maker, Mr. John Dura, who contributed materially to the development of the apparatus described in this paper.

Laboratory and Shop Notes

An "Opener-Upper" for Gas Samples

FRANCIS J. NORTON
General Electric Research Laboratory, Schenectady, New York
June 1, 1949

VARIOUS break-off devices have been in use to open gas samples sealed in glass so they can be led uncontaminated into a vacuum analytical system.[1]

By using spherical ground glass joints, available commercially, a device can be made for admitting a gas sample sealed in glass into a vacuum system. An absolute minimum of glass blowing skill is needed. The gas holder is simply a length of glass tubing, sealed at each end. It is scratched with a file or Carboloy scratcher at a suitable point, and placed in the ball-joint container. The ball-joint is of course lubricated with a good vacuum grease. The whole is then put on a vacuum system by the tapered joint, or sealed on, and the outer container evacuated around the gas sample tube. Then when suitable vacuum is attained, the gas tube is broken by moving the lower ball-joint section. This admits the sample, uncontaminated, into the vacuum system. Figure 1 shows the device. A sturdy clamp should fasten the tube above the top of the ball-joint to a substantial support.

A suitable size for the ball-joint is 18/9, of 18-mm ball diameter, 9-mm i.d. tube. This outer tube should be sturdy. The inner gas holder can be $\frac{3}{16}$ inch, or 5 mm diameter, with not too thick walls. It should be scratched at the point of maximum bend.

Various modifications suggest themselves. For a much larger gas holder it would be better to have an extended smaller thinner end which is scratched and broken. For very heavy walled capillary tubing such as might be used for pressure experiments, the outer container could be a metal ball-joint. This metal joint could have an outer sylphon bellows covering it, and stopcock grease avoided entirely. The simplest version first described has proved entirely satisfactory.

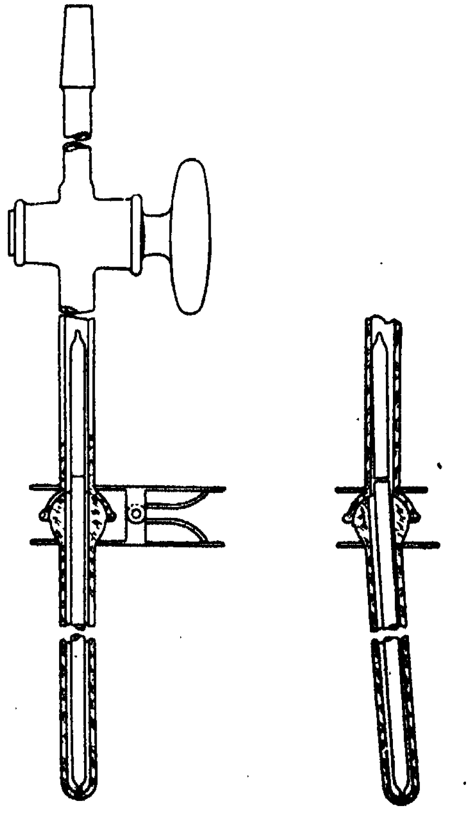

FIG. 1.

---

[1] Barr and Anhorn, *Scientific Glass Blowing* (Instruments Publishing Company, New York, 1949) p. 245; R. T. Sanderson, *Vacuum Manipulation* (John Wiley & Sons, Inc., New York, 1948) p. 67; Farkas and Melville, *Experimental Methods in Gas Reactions* (The Macmillan Company, New York, 1939) p. 148.

A System for Preparing Semi-Transparent Mirrors

CLAUDE FRÉMONT
Department of Physics, Laval University, Québec, Canada
May 14, 1949

IN preparing semi-transparent mirrors for interferometers or other physical instruments by the usual evaporation technique, it is difficult to obtain mirrors with exactly the desired transmission and reflection coefficients. This is due to the light coming from the evaporation filament interfering with the measurements, and to metallic films being deposited on the measuring apparatus.

A system which overcomes these difficulties has been developed in this laboratory. Cross sections of the apparatus with a schematic diagram of the optical system is shown in Fig. 1. The optical flat to be surfaced is placed at *A* in the aluminizing chamber which is evacuated by a diffusion pump. A tungsten filament *D* and *I* heated by d.c. current thorugh a control rheostat vaporizes aluminum metal placed on it. The resultant molecular rays condense on the nearby optical flat. As the process continues, an intermittent beam of light, caused by a motor-driven toothed wheel rotating in front of a light-source *S* and filter *M*, is directed onto the flat *A* through a small semi-transparent mirror *N* placed just below the filament, on the axis of the system, and inclined at 45° to it. The portion of the light transmitted by *A* is focused on the photoelectric cell P_1 by the lens L_1. The portion reflected by *A* returns to *N*, where part of it is transmitted and focused by

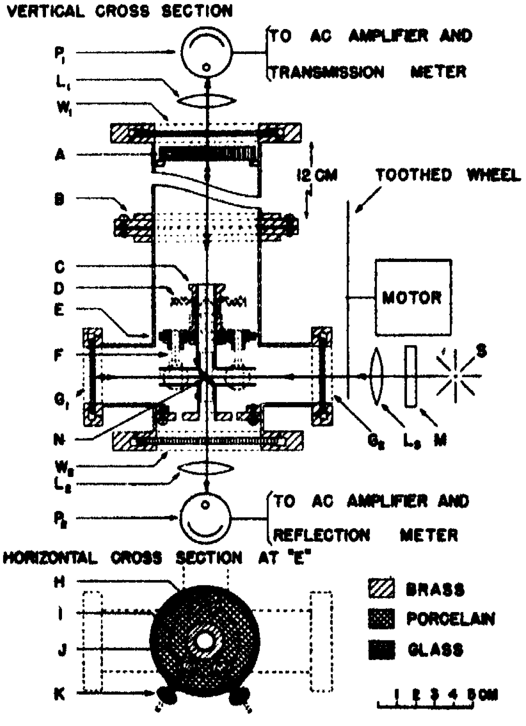

FIG. 1. Vertical and horizontal cross sections of the aluminizing chamber with schematic diagram of the optical system.

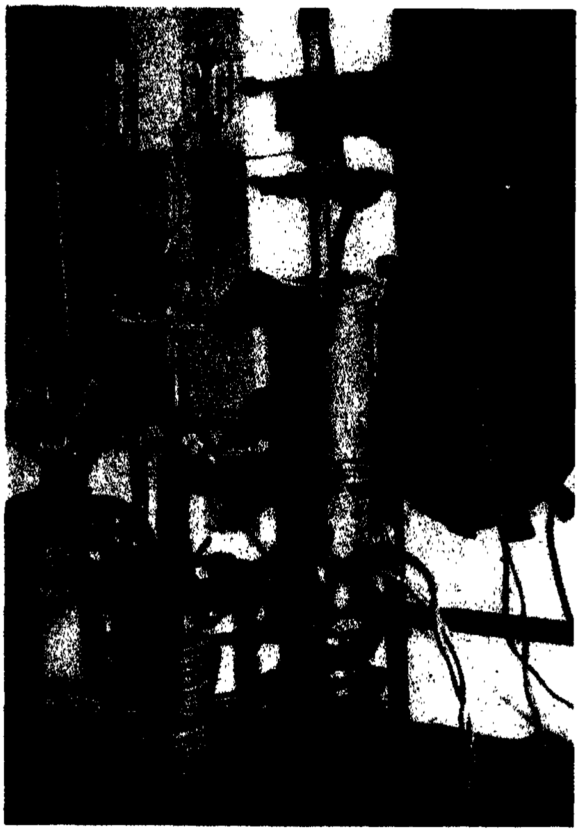

FIG. 2. Photograph of the system.

the lens L_2 on the photoelectric cell P_2. The outputs of these cells are amplified by a.c. amplifiers and measured by specially calibrated meters reading respectively percentage transmission and percentage reflection. Since the photoelectric cells are connected to a.c. amplifiers, the continuous light coming from the evaporation filament either directly or after multiple internal reflections in the aluminizing chamber can in no way affect the measurements.

The various light ports W_1, W_2, G_1 and G_2 are made vacuum tight by compressing glass plates between low pressure rubber gaskets. A rubber-gasketed vacuum joint at B permits easy access to the filament D. This consists of tungsten wire, bent into a series of V's which form a circle, as at I. The whole filament assembly C, D and E, may be removed by simply sliding it up along C. The banana plugs F serve as electrical connections for the filament, being fixed to metal-glass "Kovar" seals at K.

The adjustment of the transmission meter is very simple if the initial transmission of the optical flat is chosen as 100 percent. It is then only necessary to adjust the gain of the amplifier before the evaporation starts so that the meter reads 100 percent. One can also get an absolute value of the transmission by adjusting the meter to 100 percent when the optical flat A is not in the apparatus. With this glass disk in position, measurement of the transmission before, during and after the surfacing is thus possible. It is to be noted that the distance of the luminous source, the light absorbed by the light ports W_1, W_2, G_1 or G_2, the amount of transmission and reflection of the mirror N and the distance to the cells P_1 and P_2 are factors which do not influence the results, as they are constant and their effect eliminated from measurements by adjusting the meter.

The zero of the reflection meter is adjusted when the optical flat A and the reflecting surfaces W_1, L_1 and P_1 are taken off the apparatus. The intermittent light falling on the photoelectric cell P_2 in these conditions comes only from that portion which crosses the semi-transparent mirror N, is reflected by the light port G_1 and again by the mirror N. The intensity of this beam is constant and its effect can be eliminated by the zero adjustment. A plane aluminized mirror, taken as standard, is then placed at A and the gain of the amplifier adjusted so as to read 100 percent of reflection. The intensity of the light reflected by the surfaces W_1, L_1 and P_1 is measured by simply taking off the standard mirror. It was found to be 8 percent of the total reflection and corrected on the scale of the reflection meter. In correcting this meter scale one must keep in mind the fact that the light reflected by these surfaces must cross the aluminized mirror twice and so its intensity will vary as the square of the incident light. In this case it is also possible to adjust the meter so as to read the absolute percentage of reflection instead of the percentage of the maximum reflection. For this adjustment the meter is set to the absolute value of the reflection coefficient of aluminum for the wave-length used[1,2] with the "standard" mirror in position.

The uniformity of the metallic deposit can be calculated[3] and the dimensions of the aluminizing chamber chosen accordingly. In the present case the relative error in depth between the center and side of a 2-cm diameter semi-transparent mirror is less than 0.7 percent.

The surfacing time is a function of the distance from the filament to the mirror and of the filament tempertaure. For a given distance and temperature, the intensity of the transmitted light through the mirror is an exponential function of the time of evaporation as shown by the experimental curve given in Fig. 3. When the filament is turned off, the evaporation stops very rapidly, even with a strong current. This gives a precise control on the value of the transmission coefficients. As a certain amount of absorption takes place in the glass and the metallic film, we cannot expect that the sum of percentage of transmission and reflection will be 100 percent. In fact this difference gives us the percentage of light absorbed in the film.

With this aluminizing system it is thus possible: (a) To measure precisely before, during and after the deposition the transmission and reflection coefficients of semi-transparent surfaces. These coefficients are measured normally to the surface and for a given

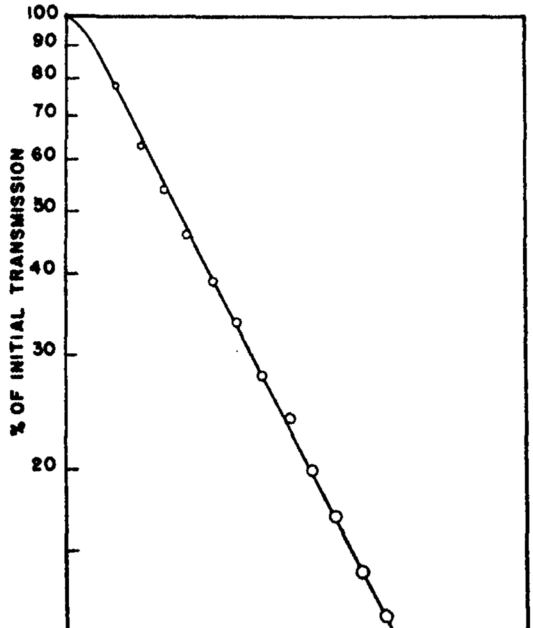

FIG. 3. Percentage of the initial transmission as a function of the time of surfacing for a semi-transparent aluminized mirror.

wave-length. (b) With a slightly modified filament it is possible to evaporate other metals than aluminum. The filament is wound on a suitable form so as to make a series of small helical cones in which are placed some bits of the metal to be evaporated. The molten drops will stay in these small "crucibles" by capillarity without wetting the filament and will be evaporated. (c) By replacing the windows and the small semi-transparent mirror with quartz or plastic plates it is possible to use the same apparatus for wave-length down to the limit of transmission of air. (d) The system might be very useful for studying the optical properties of thin metal films. For example it would be very well suited for examining the variation of transmission and reflection of these films with time, even in vacuum, which phenomenon has been noticed by Edwards and Peterson.[4] It should be easy to modify the system so as to measure simultaneously during the evaporation, the electrical resistance, the transmission, the reflection and and by difference the absorption of the metallic film.

The author wishes to thank Professor E. Persico and Dr. H. P. Koenig for many helpful suggestions in the design and construction of this apparatus. Thanks are also due to Professor L. Kerwin who kindly revised this manuscript.

---

[1] Uljanin, Physik. Zeits. 11, 784 (1910).
[2] E. Hulburt, Astrophys. J. 42, 205 (1915).
[3] John Strong, *Procedure in Experimental Physics* (Prentice-Hall, Inc., New York, 1945), p. 177.
[4] H. W. Edwards, and R. P. Peterson, J. Opt. Soc. Am. 27, 87 (1937).

A Method of Asymmetrical Pulse Duration Modulation

Richard John Watts
Los Alamos Scientific Laboratory, Los Alamos, New Mexico*

April 20, 1949

A WELL-KNOWN electronic circuit in nuclear physics is the pulse height discriminator. This circuit is in general based upon the Schmitt[1] trigger circuit. It is the purpose of this note to point out how this circuit may be made the basis of a method of pulse duration modulation.

The pulse height discriminator is characterized by the property that when the signal voltage on the grid of one of its member tubes exceeds some given value of voltage on the same grid (which may be adjusted) the circuit assumes a quasi-stable state and does not return to its stable state until the signal voltage decreases below the given value. The output of such a circuit is, therefore, essentially a square wave whose duration depends upon the time the signal was above the reference value of voltage.

Figure 1 illustrates by means of a block diagram the method of making use of this characteristic. Block 1 is an audio amplifier whose output varies the voltage on the grid of the discriminator tube in accordance with the incoming audio signal. The important point about this signal is that it is adjusted in peak amplitude so that it never flips the discriminator to its quasi-stable state.

It has been shown by Shannon[2] that if a function $f(t)$ contains no frequencies higher than W c.p.s., it is completely determined by giving its ordinates at a series of points spaced $1/2W$ seconds apart.

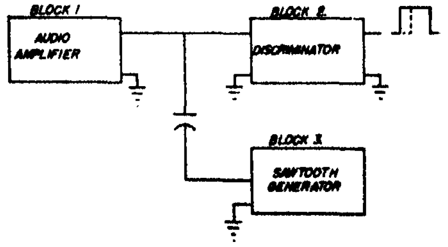

FIG. 1. Block diagram of a method of pulse duration modulation.

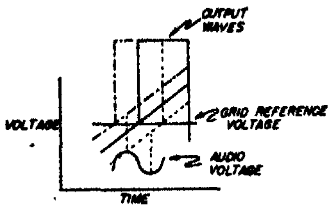

FIG. 2. Voltage and time relationships on the grid of the pulse height discriminator with the duration of the subsequent output waves.

For the system illustrated the $1/2W$ seconds apart sampling rate is obtained by means of a repetitive sawtooth generator.[3] A sawtooth of voltage from this generator is also impressed upon the grid of the discriminator. This sawtooth is large enough to make the discriminator flip. The instantaneous value of the audio voltage on the grid will determine how much more voltage the sawtooth must supply before the discriminator flips and in turn the time the sawtooth voltage is above the reference voltage will determine the duration of the output square wave. This process is illustrated by Fig. 2. Let the horizontal line represent the grid reference voltage at which the discriminator flips. It can be seen that the addition of the audio voltage to the sawtooth voltage will determine the time at which the sawtooth voltage will reach the grid reference voltage. The vertical dotted lines then indicate the duration of the output pulse. Inasmuch as the sawtooth voltage drops rapidly, only one side of the output wave is modulated. The output consists of a series of pulses spaced $1/2W$ seconds apart with the width of each pulse determined by the instantaneous audio voltage.

Figure 3 is a schematic of a circuit used to test the method. The solid lines indicate a d.c. method of connection which has

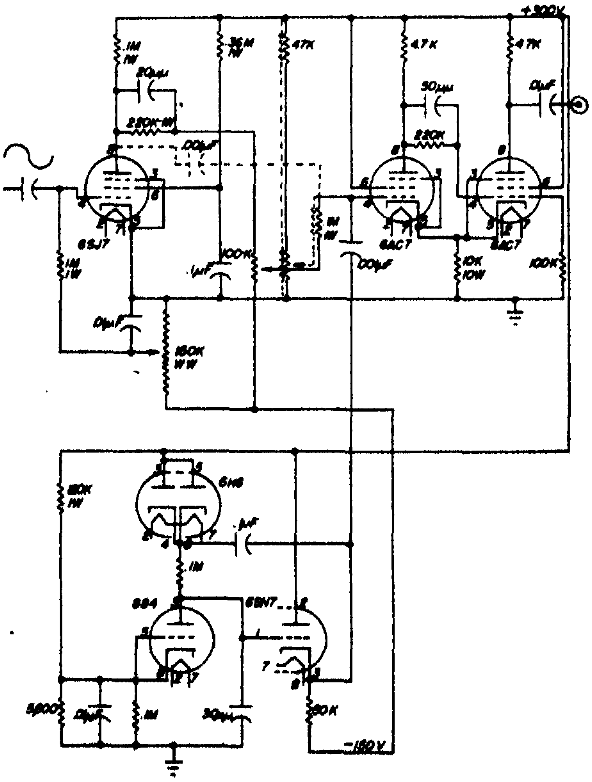

FIG. 3. Schematic of a circuit used to test the method.

been found useful for modulating a slowly varying d.c. voltage. The dotted lines indicate an a.c. method of connection useful in ordinary audio work.

---

* This document is based on work performed at Los Alamos Scientific Laboratory of the University of California under Government Contract W-7405-eng-36.

[1] O. H. Schmitt, J. Sci. Inst. 15, 24 (1938).

[2] C. E. Shannon, Proc. I.R.E. 37, 11 (1949).

[3] R. J. Watts, Rev. Sci. Inst. 20, 81 (1949).

A Note on the Preparation of Uniform Metallic Foils*

S. D. Warshaw
Institute for Nuclear Studies, The University of Chicago, Chicago, Illinois

June 3, 1949

FREQUENTLY, work with low energy charged particles demands the use of metal foils with thicknesses of the order of 0.4 mg/cm^2 or less. While gold and aluminum foils can be obtained commercially, these generally have local non-uniformities of the order of ±20 percent of the average thickness. Such local gradients make these foils unsuitable for, say, a measurement of the energy loss of a collimated beam of charged particles.

With the method described in this note, uniform foils of reasonably known thickness, free of wrinkles and pin-holes, may be prepared from a variety of metals. While the technique is not radically different from that used in electron microscope work,[1] it is felt that it is sufficiently convenient to serve as a useful tool for several applications in nuclear physics, and therefore warrants this note.

Procedure. Carefully cleaned glass slides were first coated with a weakly adherent plastic film by immersion in a 5 percent solution of pyroxylin in a 50 percent mixture of ether and alcohol; the slide was withdrawn in such a way that the excess liquid could drain off. The concentration of the pyroxylin was not found to be critical, but best results were obtained when the liquid flowed easily, and was still just concentrated enough to form a barely visible coat on the glass when dry. (Pyroxylin is sold as "Parlodion" by the Mallinckrodt Chemical Company.) The coated slide was then placed in a vacuum evaporator, on a wire rack at a convenient distance from the source, and, using standard evaporation techniques,[2] covered with metal. After evaporation, the edges of the film on the glass were roughed with a sharp knife, and the film cut across at about 2 cm intervals. The slide was then immersed at about a 45° angle to the surface of a dish of distilled water. The surface tension of the water was usually enough to peel the plastic film off the glass, carrying the foil with it, and leaving the foil and backing floating on the water surface. If the parlodion solution was too dilute, the water generally failed to disengage even the edges of the foil; it was then necessary to soak the slide in an ether-alcohol mixture for a few minutes, and free the foil completely by working at the edges with a wire loop and forceps. However, if the foil were freed under the surface of the liquid, it generally curled up, indicating that it was deposited in a highly strained state. This, of course, made mounting difficult. Small local strains also developed, very often, around dust particles and water bubbles in the plastic solution; therefore absolute alcohol was used and the solution prepared as dust free as possible and stored in a clean, glass-stoppered bottle.

For mounting the foils, it was convenient to use a small brass frame, about 1.5×2 cm, with a 2mm wall. This was placed under the floating foil and raised carefully so that the surface tension would not cause any rupture. The last few wrinkles were removed with the aid of a soft brush dipped in alcohol and the foil then washed free of the plastic by dipping it, mounted on the frame, into the ether alchohol, at right angles to the liquid surface.

Measurement of Thickness. A mirror from a Michelson interferometer was placed in the evaporator bell jar at the same time as the coated slide, and in as nearly the same geometry as possible, but with half of the mirror covered by a shield. The deposit of metal on half of the mirror then corresponded to the amount deposited on the glass slide. Fringes were obtained with yellow (Na-D lines) and the relative displacement of the two sets of fringes—one set from each half of the mirror—then gave the linear thickness of the foil in half-wave-length units, after the displacement was first estimated using white light to determine the integral number of fringe displacements. It was found most convenient to make an enlarged photograph of the fringes, and determine the displacement from this with a traveling microscope. The probable error, obtained by measuring a large number of displacements separately, was about ±2 percent. The linear thickness was then converted to mg/cm^2 by using the usual bulk density of the metal.

A serious objection to this procedure is that the evaporated foils are possibly porous[4] and therefore the bulk density is not appropriate. In order to check on this possibility, several accurately defined areas of the foils were, while still on the glass slide, dissolved in acid and quantitatively analyzed by titrating the 8-hydroxyquiniline precipitate against standard bromate.[3] The internal probable error of the chemical determination was about ±1.5 percent and the chemical result (in mg/cm^2) was about 2 percent lower than the physical. This good agreement may, of course, be fortuitous:[4] a cautious estimate of the error in thickness would then be obtained by adding all of the relative errors without regard to sign. Thus the foils could have been $2+1.5+2=5.5$ percent "thinner" (in mg/cm^2) than the interferometer method implied. Even this figure, however, compares favorably with the errors inherent in the use of hammered or rolled foils; furthermore, for many applications in nuclear physics, the thickness need not be known very precisely.

So far, the method has been used for the preparation of Al, Cu, Au, Ag foils, with thicknesses ranging from 0.04 to 0.3 mg/cm^2 in the case of aluminum, and from 0.1 to 0.4 mg/cm^2 for the heavier metals.

---

* Assisted by the joint program of the ONR and AEC.

[1] V. K. Zworykin *et al.*, *Electron Optics and the Electron Microscope* (John Wiley & Sons, Inc., New York, 1945) p. 328 ff.

[2] John Strong, *Procedures in Experimental Physics* (Prentice-Hall, Inc., New York, 1945), Chap. 4.

[3] I. M. Kolthoff and E. B. Sandell, *Quantitative Inorganic Analysis* (The Macmillan Company, New York, 1936), p. 306.

[4] L. Schulz of the Institute for the Study of Metals has kindly pointed out that porosity may account for 10 percent of the volume in evaporated foils. The only precaution taken against this was to perform the evaporation very slowly, i.e., for periods of from 5 to 10 minutes.

Note on Removing the Deuteron-Induced Color from Quartz Target Plates*

A. A. Schulke and R. E. Nuelle
Department of Physics, Washington University, St. Louis, Missouri

June 6, 1949

QUARTZ plates are frequently employed in this laboratory as a visual aid in the alignment of the various cyclotron target assemblies. These plates are bolted to the end of each target and the bright blue glow observed as they fluoresce under deuteron bombardment. The advantages of this method are that the glow can be observed from a remote position by means of a telescope-mirror arrangement and, since a relatively short bombardment produces a deep purple color in the plates, rough measurements of the beam pattern can be made *in situ*. Disadvantages are that the plates are relatively expensive—$15 to $20 each—and, since the color change is apparently stable under normal conditions, the plates can be used only once. In an effort to restore the plates to their original transparent state, heat treating experiments were conducted. At a threshold temperature of 280°F, the areas which had been colored by the deuterons were observed to give off a strong blue fluorescence which gradually diminished in intensity over a period of ten minutes or so. It was noted that this decrease in intensity was accompanied by an increase in transparency of the plates as the deuteron-induced color disappeared. The end point was difficult to determine. At higher temperatures, 300°F to 400°F, the effect was more intense but the duration shorter. At still higher temperatures, 600°F to 700°F, the plates glowed brightly for a minute or two after which it ceased suddenly leaving the plates perfectly clear.

---

* Assisted by the joint program of ONR and AEC.

Welder for Attaching Fine Wires to Massive Metal Bodies

W. J. Trott*
General Motors Corporation, Research Laboratories Division

April 23, 1949

THE equipment described in this paper was originally developed for welding thermocouple wires of 22 gauge onto the surface of 37-mm armor-piercing shot bodies in order to measure their temperature throughout the heat-treating cycle in an induction furnace. Later the equipment was used to spot thermocouples at various points and depths in 75-mm shell bodies for a heat-treat check and to spot thermocouples for bearing temperature measurements. In these applications, where the temperature is rapidly changing, the usual method of wedging or peening thermocouple wires into small holes provides insufficient heat conduction for consistent and accurate temperature measurements. Some method of welding the wires to the shot bodies was needed.

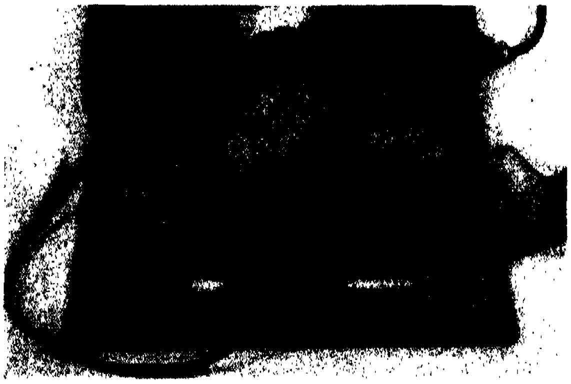

Fig. 1. Complete welding equipment and samples of work.

In the method described in this paper, the heat required for the weld is developed instantaneously to produce equal heating in the weld area of the two parts despite the much larger heat dissipation of the heavier piece.

The operation of the welder is as follows: Condensers are connected to the wire and the mass of metal to which the wire is to be welded. The wire is held away from the mass of metal until the condensers are fully charged. By tripping a spring, the wire is quickly brought against the mass of metal; the sudden discharge of the condensers producing the weld before the mass of metal can carry away the heat. However, if the wire bounces upon contact with the mass of metal, no welding may take place. Consequently a chuck was designed to hold the wire so that it is permitted to slip and thus absorb the bounce by friction between the chuck jaws and the wire, maintaining contact without motion or strain between the parts until the weld is completed. This is accomplished by using a compressive spring to close the jaws of the chuck over the wire.

Figure 1 shows the apparatus consisting of a power supply (upper right), a condenser bank (upper left), a ground plate on which the mass of metal is placed, and a holder for the wire. This figure also shows the method by which welds are made on round stock and various samples of welds which may be made with the equipment.

The instantaneous heat energy required to make a good weld ranges between melting and exploding, or rapid vaporizing, of the wire. This means that the electrical energy, $1/2CV^2$ must be proportional to the cross-sectional area of the wire, or if the capacity remains fixed the voltage must be increased in direct proportion to the diameter of the wire. Penetration of the weld is approximately equal to the diameter of the wire; thus, if the part welded to the wire is thinner than the wire diameter then the voltage is reduced to avoid melting a hole through the piece.

The power supply produces d.c. adjustable from 50 to 225 volts. The diameter of the wire to be welded or the thickness of the piece, whichever is the smaller dimension, determines the voltage required for the weld; this voltage is independent of the material. A tuning eye with a sensitivity control is provided to indicate full charge on the condensers. A switch allows the condensers to charge in the "On" position and shorts the condensers through a resistor for safe handling in the "Off" position.

The wire holder pictured in Fig. 1 is shown in exploded detail in Figs. 2 and 3. The wire to be welded is threaded down through the knob (Fig. 2) "*b*" and out through the chuck "*i*" with normally ⅛ inch of wire extending beyond the chuck jaws. The chuck is held closed by compression of the spring "*a*" drawing it into the tube "*h*" of the driver assembly. This chuck is released by gripping the barrel of the wire holder as shown in Fig. 1 and pushing in the knob "*b*". The driver assembly is cocked in position ready for welding by pulling up on knob "*b*", thus compressing the driving spring "*f*" and fixing latch "*c*" to engage shoulder "*g*" of the driver. When the tuning eye indicates that the condensers are fully charged and the wire holder is in place over the mass of metal the latch is released, the wire is driven against the metal by the impelling spring, the chuck slips along the wire to maintain contact without bounce, and the weld is made.

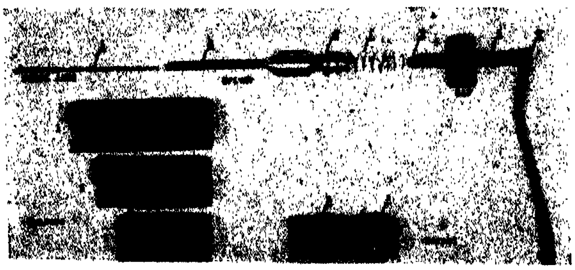

Fig. 2. Exploded view of wire holder.

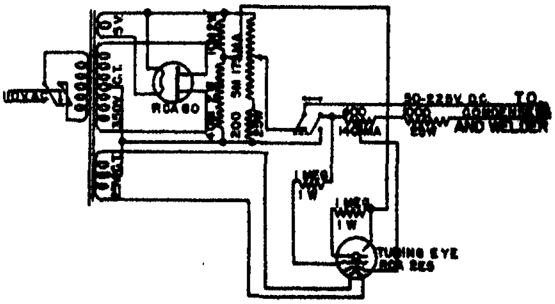

Fig. 3. Drawing of wire holder.

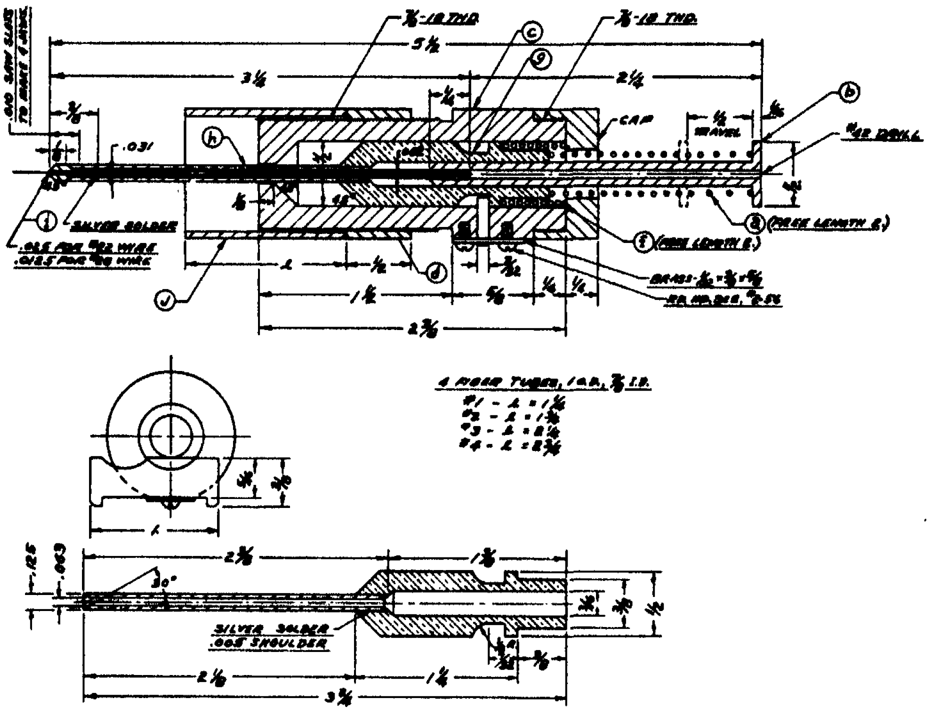

FIG. 4. Power Supply. Percussive welder (universal type).

a.	Spring-chuck clamping	.035 wire
b.	Knob	C.R.S.—case harden
c.	Latch	Fiber
d.	Sleeve-threaded	Fiber
–	Cap	Fiber
f.	Spring-driving	.018 wire
g.	Driver	Brass
h.	Tube-driver	Monel
i.	Jaw-chuck	C.R.S.
j.	Spacer	Fiber

For each weld the driver assembly should reach the end of its stroke with the chuck jaws $\frac{1}{32}$ inch from the surface of the mass of metal. This adjustment is made by choice of length of spacers, and by screwing the threaded sleeve "*d*" along the barrel. Tube "*h*" was made $\frac{1}{8}$ inch in diameter and $2\frac{1}{8}$ inches long to permit welds to be made in the bottom of $\frac{5}{32}$-inch holes to a depth of two inches.

Figure 4 is the wiring diagram of the power supply. The block to the left in Fig. 1 contains several types of welds. One wire was welded in a $\frac{5}{32}$-inch diameter hole to a depth of one inch with the aid of spacer No. 3 in Fig. 2. A piece of paper rolled in a cylinder and placed in the hole in the block insulated the driver tube ("*h*" in Fig. 2) from the steel block. When the weld was completed, a porcelain tube was inserted into the hole to support the wire. If it is desired to weld two wires into one hole the procedure is slightly modified. A two-hole porcelain tube is cut to a length $\frac{1}{8}$ inch longer than the depth of the hole. One of the two holes in the porcelain tube is broken away to a distance less then $\frac{1}{8}$ inch from one end. The first wire is then mounted in the wire holder with the wire extending beyond the chuck by a distance of $\frac{1}{8}$ inch greater than the length of the porcelain tube. The driver assembly is then cocked, the wire is inserted into the one of the two holes in the porcelain tube which was broken away, and the weld is made in the usual manner. When this first wire has been welded, it is bent down below the surface of the upper end of the porcelain tube into the region that was broken away. Thus the first wire is safely insulated during the welding of the second wire, and the second wire is welded in the same way as the first. The other samples consist of a $\frac{1}{32}$-inch thick sheet of aluminum to which 22 gauge Chromel and Alumel wires were welded and a 0.005-inch thick sheet of brass to which a 22 gauge iron wire was welded. These two welds are necessarily weaker, but will stand some abuse.

* Now at Navy Underwater Sound Reference Laboratory.

New Instruments

W. A. Wildback: Associate Editor
In Charge of this Section
National Bureau of Standards, Washington, D. C.

These descriptions are based on information supplied by the manufacturer and in some cases from independent sources. THE REVIEW *assumes no responsibility for their correctness.*

Low-Frequency Oscilloscope

A new low-frequency cathode-ray oscilloscope with optional recording camera has been developed primarily for measurements in the sub-audible frequency range, with adequate high frequency response to handle all significant harmonics of this frequency band. It should prove particularly useful in vibration studies, strain gauge measurements, servo mechanism development, electro-physiological research, and other work of the same general nature.

Signals are displayed on a 5-inch long-persistence cathode-ray tube. Fixed sweep speeds of 1, 2, and 4 inches per second are provided on the time base, which may be either continuously recurring or externally triggered on a single-sweep basis.

On the recording model, a continuous 35-mm photographic record may be made with the internal camera which photographs the cathode-ray tube pattern through the back of the cathode-ray tube bulb. A single control on the front panel is required to operate the camera, and the vertical motion of the spot can be fully observed on the screen while the record is being made. Accurate timing and amplitude markers may be printed on the film by the camera at the same time as the trace is recorded. The camera is daylight-loading, holding 100 feet of the film per loading, the receiving cassette will accept up to 20 feet of record. Recording paper or film may be used, depending on the speed of the traces to be recorded.

The vertical (Y) amplifier is a 4-tube differential amplifier of high sensitivity (300 microvolts/inch). The differential feature allows it to be used in high-hum fields, or under other conditions

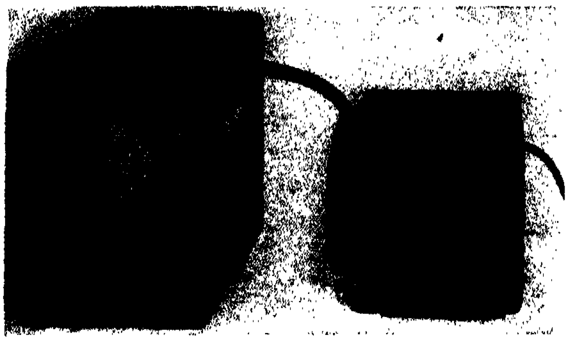

where an undesired signal-to-ground exists on the two push-pull input terminals. By the use of low-frequency compensating circuits, extremely good low frequency response is obtained from the RC-coupled amplifier, and it is flat (3 db) from 1/20 c.p.s. to 1200 c.p.s. A single-ended connection is also provided into the last two stages of the amplifier, giving d.c. response at a maximum sensitivity of 50 millivolts/inch.

The entire instrument is contained in two black crackle-finish units, each weighing roughly 25 pounds and provided with carrying handles. The visual unit (including camera) may be set up in the most convenient operating position, and the power supply unit may be located within range of its 6-foot interconnecting cable.—Special Products Division, Smith and Stone, Ltd., *Georgetown, Ontario, Canada.*

High-Frequency Voltmeter

The new Millivac MV-18A vacuum-tube voltmeter measures r-f voltages down to a single millivolt at frequencies between 1 megacycle and 200 megacycles. Within this frequency range, it is flat within 10 percent. When used for higher frequencies, larger response-corrections have to be made. The instrument can be used for frequencies as high as 2500 mc, 10 mv then being the lowest voltage which can be read.

The MV-18A, for low voltage measurements, uses germanium "pseudo-thermocouples" as a detector and a highly sensitive, high impedance, carrier-type d.c. amplifier which converts the minute d.c. voltages, developed by the thermoelectric effect within the germanium crystal, into meter readings. For high voltage measurements, up to 1000 volts, regular crystal diode rectification is used. Three different germanium probes are available for this purpose which have various capacitive input dividers to "trade surplus sensitivity for minimum circuit loading."

Direct TV and FM field-strength measurements, complete r-f signal tracing through TV and FM receivers at actual operating signal levels, and VHF and UHF laboratory research are among the most important applications suggested for this new instrument.—Millivac Instruments, *P. O. Box 3027, New Haven, Connecticut.*

Accelerometer

Exceptional sensitivities and natural frequency ranges are characteristic of the new Model 18 Accelerometer, which allows direct operation of voltage and current indicators and recorders to higher frequency ranges than previously possible without complicated amplifying equipment.

The Model 18 Accelerometer is a vacuum-tube device, requiring 6.3 volts filament supply and approximately 1 ma plate current, through a suitable load resistor, from a plate voltage supply of 100 to 300 volts. Pick-ups are constructed with stops to limit motion of the sensitive element.

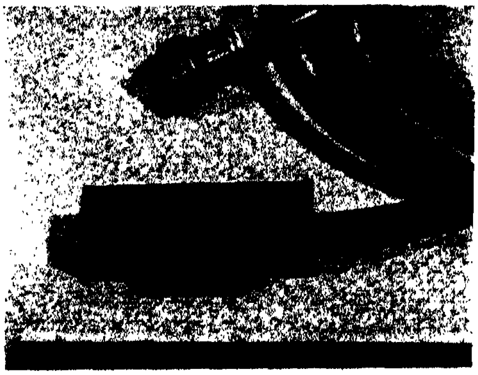

Standard pick-ups, ruggedly cased and protected against overload shocks, weigh two ounces; special designs, uncased, weigh only 5 grams. Pick-ups having natural frequencies from 80 to 450 c.p.s. have a corresponding range of sensitivities from 15 to 0.21 volts per gravity acceleration, and acceleration ranges from 1 to 70 g. Natural frequencies as high as 1700 c.p.s. are obtainable. Suitable damping is provided, and each instrument is individually calibrated.

The accelerometers are d.c. operated and can deliver as much as 400 microamperes into 1000 ohms impedance, or 20 volts into 1 megohm at full range output without amplification.—The Calidyne Company, *751 Main Street, Winchester, Massachusetts.*

Automatic Scaler

The Berkeley Scientific Company has included in their line of instruments a fully-automatic Geiger-Müller scaler, Model 2000.

The number of counts is read directly in numbers on the front panel, eliminating the need for interpolation. A decimal scale of 1000 is used in combination with a new direct-reading mechanical register with zero reset. High voltage is electronically regulated to 0.005 percent and is of the new r-f type which has proved very satisfactory in other equipment.

A direct-reading electric time clock is built-in. Automatic operation for a predetermined number of counts (up to 20,000) may be conveniently reset by selector knobs on the front panel.

An accessory timer is available for automatic operation for predetermined time intervals.

The entire circuit is divided into seven removable plug-in units, which affords complete accessibility and permits rapid exchange, testing and servicing. Three decimal counting units are used to form the scale-of-1000. Other plug-in units contain the high voltage power supply, voltage-regulator circuits, input amplifier and output amplifiers. Forced-air cooling is provided by a quiet built-in fan.

Berkeley has also announced a new Geiger-Müller scaler, Model 1000B, designed for laboratory work and research in all fields. It weighs only 14 pounds and is smaller in size than a portable typewriter.—Berkeley Scientific Company, *Sixth and Nevin Avenue, Richmond, California.*

Temperature Transmitter

The Taylor Transaire with Speed-Act is a new force-balance type pneumatic temperature transmitter. It is designed particularly for applications where it is desirable to have the indication, record or control remotely located from the point of measurement and where it is necessary to have accuracy, high speed of response, small thermal elements, and short range spans within the limits of −375° and +1000°F.

The Transaire Temperature Transmitter operates on the force-balance principle. As temperature increases, pressure within the thermal system increases in direct proportion and causes a diaphragm to move upward. This upward motion results in motion of a lever which causes a baffle to move away from a nozzle and give decreased nozzle pressure. The output air pressure increases and causes an increased downward force to be exerted by bellows, which counter-balances the force on the lever due to the temperature change, and brings the system into equilibrium. The new output pressure is a measure of the new temperature and is transmitted to the remote receiver or receiver-controller. By means of a ¼-inch O.D. copper tubing, this pressure can be transmitted to receivers as far as 1000 feet away, and even farther, depending on conditions.

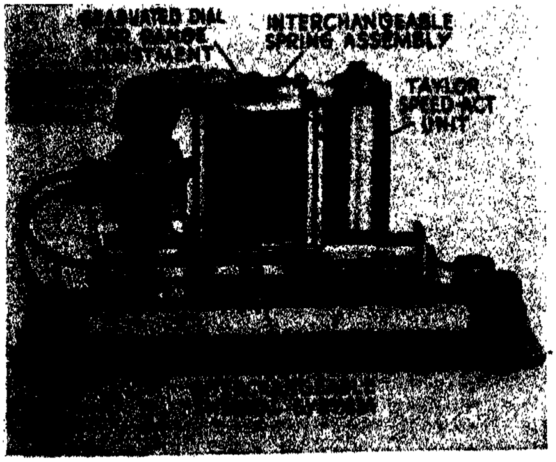

The principle of derivative action is applied to decrease the lag inherently present in the response of any form of thermal measuring element. This feature of the instrument is called "Speed-Act."

Other unique features of the new Taylor Transaire Temperature Transmitter are: (1) Unusually small thermal elements (cigarette size) which contribute to the high speed of response as well as convenience of installation; (2) short range spans to permit closer readings; (3) adjustable operating ranges to permit a wider range of application by individual instruments; (4) fixed air output range of 3 to 15 p.s.i. for full temperature span, linear to 0.1 percent; (5) compensation for barometric and ambient temperature changes; (6) interchangeable unit assemblies; and (7) thermal systems built to withstand over-range temperatures up to 1000°F.

The Taylor Transaire Transmitter is compact, fully encased to give adequate protection from dust and moisture. Convenient mounting brackets are provided for pipe or wall mounting, or an adjustable bracket is supplied when the instrument is used with a separable bushing.—Taylor Instrument Companies, *Rochester 1, New York.*

Deadtime and Recovery of Geiger Counters

An electronic gating instrument has been designed and constructed at the National Bureau of Standards for accurate determination of the deadtime and recovery characteristics of Geiger-Müller counters. The deadtime and recovery characteristics are important not only because the errors in counting depend on them, but also because they are intimately associated with the electrical discharge process.

Incoming radiation in a Geiger counter causes negative electrons to be attracted to the positive wire. The highly mobile electrons reach the positive wire of a Geiger counter within a fraction of a microsecond after ionization has occurred. At the same time, the heavy positive ions begin moving toward the negative outer cylinder. These positive ions still remain in the vicinity of the wire long after the electrons have reached it. They form a sheath around the wire and reduce the field intensity below the value required for another avalanche to take place. If a particle enters the counter while the ions are still close to the collecting wire, Geiger action cannot occur. As the sheath of positive ions moves slowly outward, the electric field around the wire increases, reaching its normal value when the ions arrive at the outer cylinder.

The deadtime is defined as the time interval after a pulse has occurred during which the counter is insensitive to further ionizing events. Physically it is the time required for the positive ions to travel far enough from the wire to let Geiger action resume. Similarly, the recovery time is defined as the time interval that must elapse after a pulse has occurred before a full-size pulse can again occur; physically it is the time required for the positive ions to reach the counter wall. Both the deadtime and the recovery characteristic of a Geiger counter, as well as the input sensitivity of the associated circuits, are involved in the "resolving time," defined as the minimum time interval by which two pulses must be separated to be detected as separate pulses by the counter and its accessories.

Since nuclear disintegrations occur in a random manner, there is a finite probability of two disintegrations occurring within any given time interval. Because the counter is dead for a short period after each pulse, some disintegrations are not detected, resulting in a discrepancy between the number of particles entering the counter and the number of counts recorded.

With the NBS electronic gating instrument, it is possible to study the pulses that occur in the time interval between the end

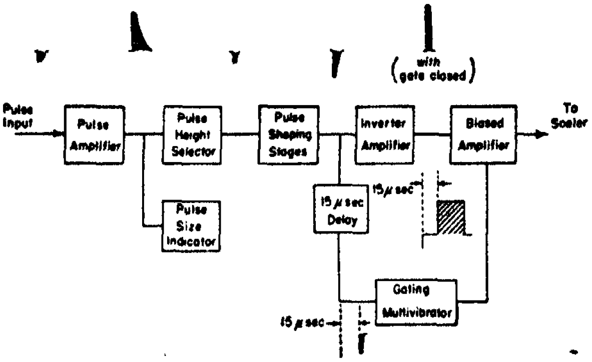

of the deadtime of a Geiger counter and the end of a predetermined gating period. In practice, the counter under test is exposed to a steady source of radiation, and the number of accepted counts is recorded for various gating times. As the gating time is reduced, the number of counts decreases. The deadtime is obtained by plotting a curve of accepted counts *versus* gating time and extrapolating to find the intersection of the curve and the time axis. By adjusting the gating instrument to accept only pulses above a certain size, it is possible to obtain similar curves for which the time-axis intercepts represent the recovery time of the counter for various pulse amplitudes.

When the gating instrument is in operation, random pulses from a Geiger counter are fed through the pulse amplifier to the pulse height selector and pulse shaping circuits to give sharp negative pulses of uniform height. These negative pulses follow two paths: one through an amplifier to a heavily biased stage, and the other through a delay circuit to a gating multivibrator. An initiating pulse entering the system finds Channel 1 blocked by the heavy bias. But by way of Channel 2, it trips the multivibrator and opens Channel 1 for pulses to pass. Because of the delay in Channel 2, Channel 1 is not opened until the initiating pulse has died away. The delay used is 15 microseconds. Subsequent pulses find Channel 1 open, go through it, and are counted. After a time determined by the circuit constants of the multivibrator, Channel 1 is blocked off again and the whole process is repeated. For the usual counting rates, the probability of having more than one pulse during the interval while Channel 1 is open is very small. In effect, the system selects pairs of pulses with a time separation less than a selected value determined by the setting of the controls on the multivibrator, and one count is recorded for each such pair received. In the determination of recovery curves, the bias voltage of the pulse height selector is adjusted to discriminate against pulses of less than a selected size.—NATIONAL BUREAU OF STANDARDS, *Washington 25, D. C.*

Gamma-Ray Detection Tube

An improved type of gamma-ray detection tube which is five to six times more sensitive than standard tubes now used for tracing medicinal isotopes, analytical chemistry, search for radioactive ores, thickness gauges, geophysical studies, industrial control, and radiation survey meters, has been announced by Sylvania Electric Products, Inc.

The increased sensitivity and compactness of the new tube tend to reduce the psychological reactions of patients who have hitherto been faced with apparatus resembling a "cannon" and placed very close to the body. With the new gamma-detector tube, which is only six inches long and two inches in diameter, radiations from isotopes may be measured with the tube several inches from the body. Since the intensity of nuclear radiations follows the inverse square law, relatively remote measurements permitted by the more sensitive tube also tend to give the physician more accurate observations. Also, increased sensitivity permits effective dosage with lower concentration of tracer isotopes.

For tracer chemistry applications in medicine, it is more directional than gamma-tubes hitherto available. Directional characteristics may be increased through the use of external lead shielding, so that maximum effectiveness may be obtained within ten degrees of either side of its "window." With suitable external shielding, the tube provides precise measurements, since it may be aimed at the organ of the body being studied.

The new GG306 gamma-ray detector tube is self-quenching; operates at 960 volts; has an average Geiger threshold of 900 volts; provides 810 counts per minute from 5 micrograms of radium filtered through $\frac{1}{2}$ inch of lead 12 inches from end; has a maximum recovery time of 800 microseconds; has a maximum deadtime of 100 microseconds; is suitable for an input circuit impedance of 5 megohms; and has an ambient temperature rating of −40° to −70°C.—SYLVANIA ELECTRIC PRODUCTS, INC., *500 Fifth Avenue, New York 18, New York.*

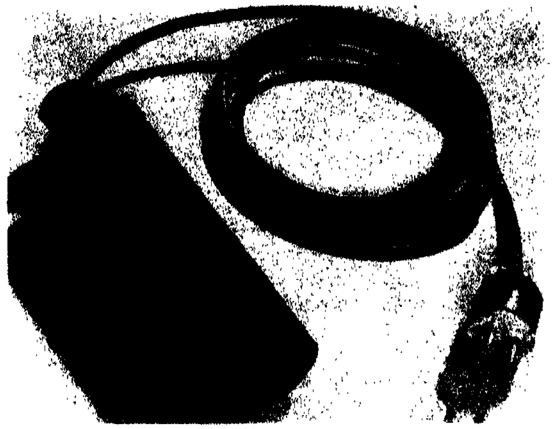

Beta-Gauges

Tracerlab announces the Beta-Gauge, an industrial measuring and control instrument using radioactive isotopes. The essential components of the gauge are a source of beta-radiation from strontium-90 and a radiation detector. Sheet material to be measured is interposed between the source and the detector, and a part of the radiation is absorbed by the sheet material in proportion to its weight per unit area. Weight per unit area or thickness is read on a properly calibrated recorder connected to the detector. The recorder scale can be calibrated in terms of a plus or minus deviation from specifications or as an absolute thickness or weight reading.

For practical purposes, the chemical composition of the sheet being measured does not affect the calibration of the instrument. The Tracerlab Beta-Gauge is comparable to a chemical balance in that it will provide the same information as is obtained by weighing on a balance a known area of the sheet material in question. Moisture, clay, chemicals, etc., affect results only in proportion to their weight in the sheet.

An outstanding advantage of these gauges is the fact that no physical contact is made with the material being measured, causing no marking of delicate or easily marred surfaces, as is the case with mechanical and other contacting gauges.

A few typical uses of the Tracerlab Beta-Gauge are measuring Cellophane and other thin plastic films, plastic and rubber sheets up to $\frac{3}{16}$ inch thick, paper ranging from heavy board to extremely thin condenser paper less than 0.0002 inch thick, sheet metal including steel and brass up to 0.040 inch thick, thin aluminum foil, textile yarn and roving, and coated textiles such as artificial leather.

Model SM-2 Beta-Gauge uses a Brown Electronik Recorder, and the gauge standardizes itself completely automatically every thirty minutes. The inherent accuracy of the Beta-Gauge is ±0.05 percent of sample thickness or ±0.03 mg/cm^2, whichever

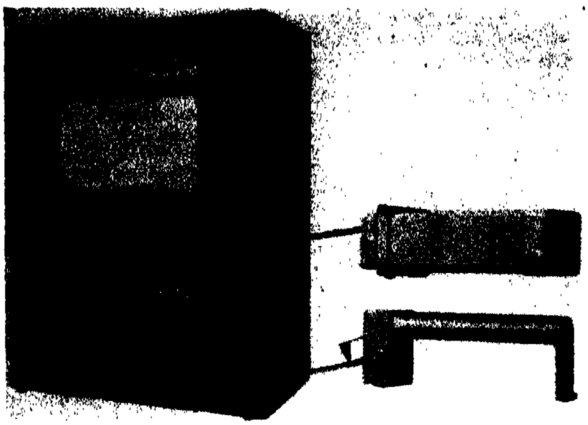

is larger. The amount of drift occurring between standardization periods is within the limits of inherent accuracy of the Beta-Gauge. Long life batteries which require renewal no more often than three a year are used as power supply to eliminate the need for a closely regulated a.c. power supply. Maximum sensitive length of the gauge is 15 inches, while its minimum sensitive length is ¼ inch. A non-recording industrial Beta-Gauge and a laboratory model Beta-Gauge are also available.—TRACERLAB, INC., *55 Oliver Street, Boston 10, Massachusetts.*

Tachometer

A new electronic "pulse counter" for accurate measurement of very high speeds has been announced by the General Electric Company. The equipment consists of a high frequency pulse generator or pick-up, an electronic counting circuit, and two speed indicating units, one for "on the spot" readings and the other for remote readings.

A magnetic pulse generator fits on the periphery of a drum which is attached to the shaft of the machine to be tested. The drum is magnetized, one side containing 150 magnetic poles and the other side 1500. When rotated, the drum generates electrical impulses in the magnetic pick-up; electronic circuits count the pulses at speeds up to 50,000 per second. The indicators do the necessary calculation and interpolation, and flash on an opal glass screen, in figures approximately 1-inch high, the number of revolutions per minute. Continuous readings are made and the figures on the screen change every second to indicate any variations in the revolutions per minute.

Up to 4000 r.p.m. the 1500-pole side of the generator is used, with an accuracy of 0.1 r.p.m., while over 4000 r.p.m., the magnetic pick-up automatically shifts to the 150-pole side and the readings are accurate to 1 r.p.m. Any system which generates electrical impulses can be used in place of the magnetic pick-up. For example, a disk on the shaft of the machine to be tested could be marked with black and white stripes and a photoelectric pick-up used to gather and relay the pulses to the electronic circuit.

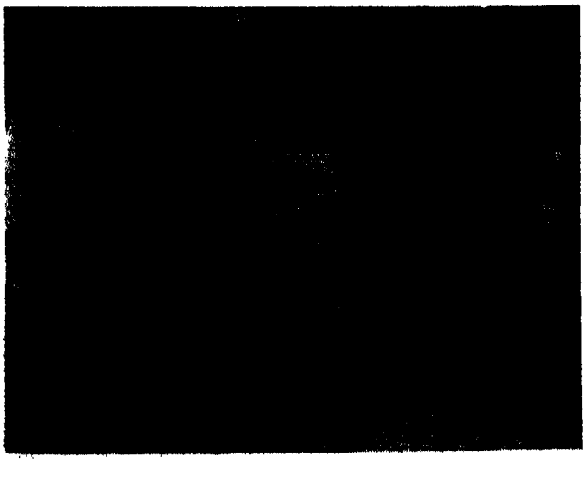

A reading is taken every second. The counting operation requires 8/10 second, while the calculation, interpolation, and indication of the figures utilize the remaining 2/10 second of the cycle. The timing for this fractional split is governed by a 1000-beat tuning fork oscillator which is accurate to about 0.001 percent.

The electronic counting circuit is housed in a 200-pound cabinet which measures about 5'×2'×1½'. The speed indicator is housed in a separate cabinet, approximately 2'×2'×1½'. The electromagnetic tachometer generator weighs about 5 pounds and is approximately 6 in.×8 in.×4 in. Two hundred feet of cable may be used between the tachometer generator and the control cabinet, and another two hundred feet of cable may be used between the control cabinet and the indicating units.—GENERAL ELECTRIC COMPANY, *Schenectady 5, New York.*

Noise Generator

The Type 810-A Noise Generator is a compact and inexpensive source of random noise for use in research engineering and production testing. It provides a random noise with equal power in equal bands throughout the audiofrequency spectrum and a substantial radiofrequency output if desired. A switch enables a noise output conforming to "noise of a general character" as specified by the American Standards Association. This range is particularly useful for calibrating sound level meters.

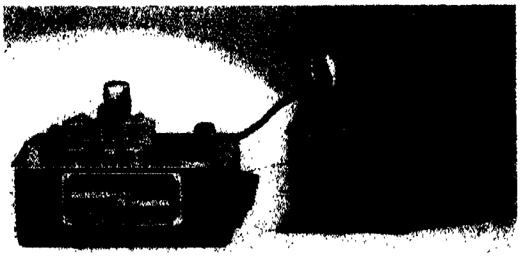

Conveniently operated with the Type 20-A power supply, the Type 810-A uses one 6C4 and one 6D4 tube and has an audiofrequency output voltage from 0 to 0.2 volt. Frequency range is 30 to 500,000 cycles in the r-f range, and 30 to 20,000 cycles in the a-f range.

The necessary power requirements are 6.3 volts a.c. at 0.6 ampere and 250 to 350 volts d.c. at 12 ma, which are provided by the Type 20-A power supply.—HERMON HOSMER SCOTT, INC., *385 Putnam Avenue, Cambridge 39, Massachusetts.*

Counter Tube

The RCL Flow Geiger-Müller Counter was developed to meet the requirements for a reliable, low cost and permanent self-quenching detector for alpha-, beta-, and gamma-radiation. It may be used directly with the usual commercially available scaling circuits, since it operates at approximately 1350 volts.

The counter is cylindrically shaped and has a 1½ inch diameter side window of 2.2 mg/cm^2 aluminum foil. The gas filling, supplied from a cylinder, is flowed slowly through the counter during operation. The gas mixture used has been developed to minimize formation of undesirable deposits on the center wire or cathode during operation, resulting in more reliable performance for an indefinitely long life. Virtual elimination of non-conducting surfaces minimizes troublesome hysteresis effects.

The integral counter and mount design is particularly convenient and readily adaptable to low cost shielding. The standard

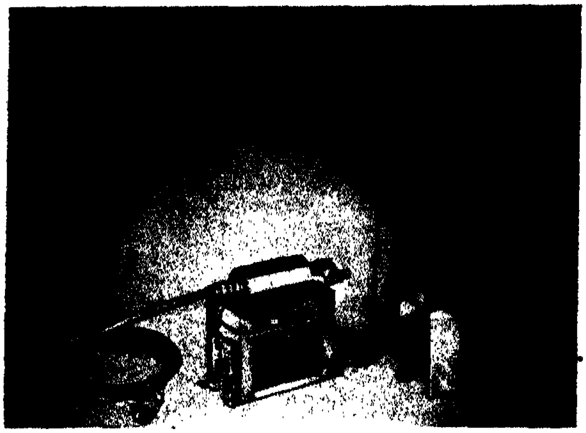

RCL Lucite mount has geometry ranges of 38, 8, 3⅓, 1½, and 0.9 percent and facilitates convenient absorption measurements. External mounting of samples eliminates necessity for long flushing periods. The counter is chrome finished.—Radiation Counter Laboratories, Inc., *1844 West Twenty-First Street, Chicago 8, Illinois.*

Induction Tracer

Induction Tracer Type 154 is a versatile, highly sensitive portable instrument for the tracing of unknown paths of cables and pipes, the tracing of cable faults and breaks in pipe lines, identification of cables, and depth determinations by the induction method.

In use, an a.c. is injected at one terminal of the wire, cable, or pipe line under test, which gives rise to an alternating magnetic field surrounding the conductor concentrically. If the induction tracer is now placed in this field, e.m.f. will be induced in the special coils with which the instrument has been provided, and after suitable amplification, this e.m.f. is made audible in a pair of headphones. The magnitude of the e.m.f. falls off as the radial distance between the conductor and coils increases. By this principle, the induction tracer is capable of tracing accurately current-carrying conductors, and faults in these, as well as determining the orientation and approximate distance of a conductor. Depth determination is based on a potentiometric null method, using headphones as a detector.

The instrument is a self-contained portable unit comprising a wooden carrying case, two special detector coils, a battery, a pair of piezoelectric headphones, and a three-stage amplifier. The last-named component possesses the following operating controls: function selector switch, gain control, depth measuring control, frequency response selector and on-off switch, pilot light. A linear or sharply-peaked frequency response characteristic may be employed. The detectors, as well as the headphones, are provided with plugs so that the amplifier may be employed with other accessories.—Addison Electric Company, Ltd., *163 Holland Park Avenue, London, W.11, England.*

Phase Meter and Field Strength Meter

Model 108-C Phase Meter provides a simple, easily operated, and accurate means for measuring the phase relations existing in directional antenna systems. Provision is also made for remote monitoring of the amplitudes of the currents in the several elements of the array. The phase indication is clearly displayed on a meter marked in two-degree intervals. One-half degree increments can be readily resolved. Although normally supplied for operation in the standard broadcast band, it is adaptable to other frequency ranges on special order.

A new Field Strength Meter, operating in the range of 200 kc to 560 kc, has been designed particularly for the communications and industrial heating fields. Field strengths between 10 micro-

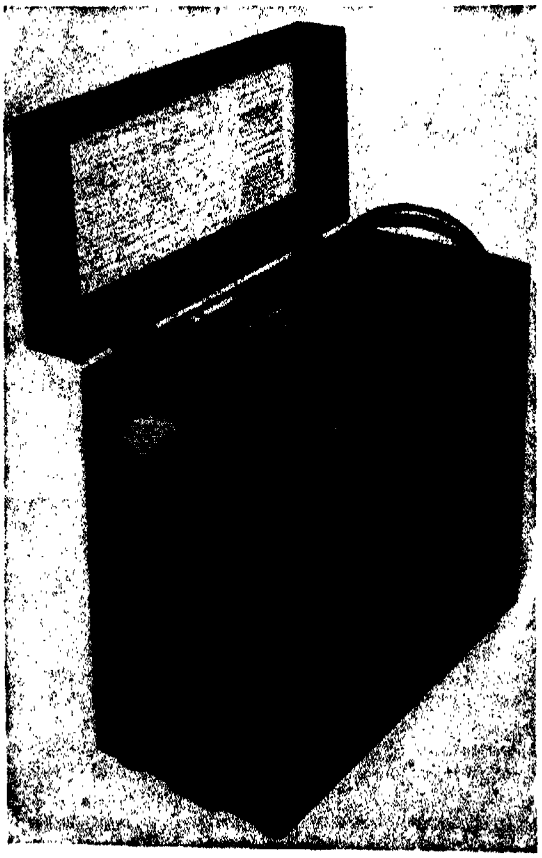

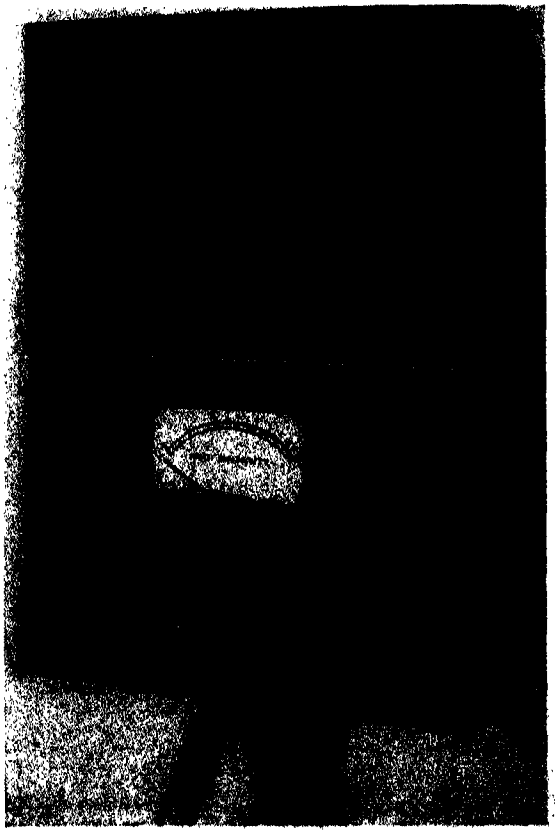

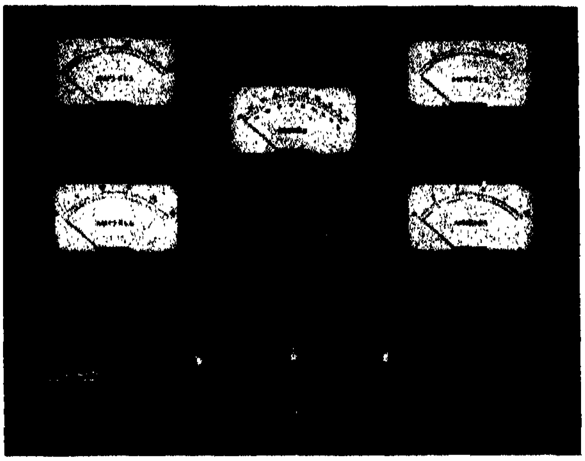

volts per meter and 10 volts per meter are read directly, without recourse to charts, curves, factors, or computations. The instrument is easy to operate and weighs only 12½ pounds; measurements are quickly and accurately made.—CLARKE INSTRUMENT CORPORATION, *910 King Street, Silver Spring, Maryland.*

Manufacturers' Literature

Tracerlog—12-page house organ, No. 19, describes three new types of Geiger tubes and has an article on x-ray counters for K-capture isotopes.—TRACERLAB, INC., *55 Oliver Street, Boston 10, Massachusetts.*

High Vacuum—Revised 48-page Bulletin 10A contains technical information and descriptive data on high vacuum pumps and accessory apparatus.—DEPARTMENT Y, CENTRAL SCIENTIFIC COMPANY, *1700 Irving Park Road, Chicago 13, Illinois.*

Cathode Press—Summer issue, 1949, features articles on high voltage rectifier tubes, new vacuum tubes for very high frequencies, ruggedization of power tubes, and other items of interest.—MACHLETT LABORATORIES, INC., *Springdale, Connecticut*

Announcer—16 pages, Number 49 6 35, features a historical story on the development and manufacture of paper for filtering. Included also are descriptions of various items of laboratory equipment.—BURRELL TECHNICAL SUPPLY COMPANY, *1942 Fifth Avenue, Pittsburgh 19, Pennsylvania.*

Cenco News Chats—Number 64, 25 pages, presents an article on the organization of the American Association of Cereal Chemists, a biographical sketch on Thomas Burr Osbourne, and various items on chemistry laboratory equipment.—CENTRAL SCIENTIFIC COMPANY, *1700 Irving Park Road, Chicago 13, Illinois.*

The Experimenter—8-page General Radio bulletin, Vol. XXIV, No. 1, gives a description of equipment for distortion measurement in the radio broadcasting station. Block diagram of a typical installation and circuit diagrams are shown.—GENERAL RADIO COMPANY, *275 Massachusetts Avenue, Cambridge 39, Massachusetts.*

Electrical Measurements—Separate bulletins describing the following instruments: (1) Williamson DC Voltmeter-Ammeter, accuracy ¼ of 1 percent, 26 ranges of d.c. current and voltage for reading voltage from 1 millivolt to 1000 volts, and current from 10 microamperes to 15 amperes, full scale ranges; (2) Model S DC Polyranger, accuracy ½ of 1 percent, 13 ranges of d.c. current and voltage for reading voltage from 5 millivolts to 1000 volts, and current from 100 microamperes to 1 ampere, full scale ranges.—SENSITIVE RESEARCH INSTRUMENT CORPORATION, *9–11 Elm Avenue, Mount Vernon, New York.*

The Laboratory—Vol. 18, No. 5, 32 pages, features an article on latest progress in the development of cold rubber, in addition to other articles of general scientific interest and descriptions of laboratory equipment and chemicals.—FISHER SCIENTIFIC COMPANY, *717 Forbes Street, Pittsburgh 19, Pennsylvania.*

Phase Contrast—Catalog D-104, 16 pages, contains an explanation of Phase Contrast Microscopy, an article on proven uses of this new technique, and catalog data on phase contrast accessories.—BAUSCH AND LOMB OPTICAL COMPANY, *Rochester 2, New York.*

Photomicrography—4-page descriptive Circular No. 810 and 22-page Technical Information Bulletin No. 812 describe and illustrate exposure photometers for photomicrography and metallography.—PHOTOVOLT CORPORATION, *95 Madison Avenue, New York 16, New York.*

Relays—New "Quick Guide" catalog lists most widely used relays, classified according to function. Data arranged to select relays of suitable electrical and mechanical characteristics.—STRUTHERS-DUNN, INC., *150 North Thirteenth Street, Philadelphia, Pennsylvania.*

Precision Potentiometers—Bulletin 105 describes Models F and G single-turn continuous-rotation potentiometer for which the manufacturer claims accuracy of ±0.5 percent (or 0.05 percent by selection), long life, and low noise. Bulletin 106 illustrates and describes the laboratory model Helipot, with a linearity accuracy of ±0.1 percent, in resistance ranges from 10 ohms to 100,000 ohms.—HELIPOT CORPORATION, *South Pasadena, California.*

Tank Gauges—8-page bulletin describes the "Varec" Electronic Gauger for remote reading liquid level. The system utilizes precision potentiometers whose variations are converted into direct readings in feet, inches, and eighths of an inch at the remote position.—THE VAPOR RECOVERY SYSTEMS COMPANY, *P.O. Box 231, Compton, California.*

Chronographs—Bulletin 171–49, 16 pages, describes and illustrates tape chronographs, drum chronographs, electrically-driven tuning forks, regulator clocks, and accessories.—GAERTNER SCIENTIFIC CORPORATION, *1201 Wrightwood Avenue, Chicago 14, Illinois.*

Timing Motors—Bulletin, 8 pages, gives technical data, selection guide chart, and specifications for Telechron Synchronous Motors and Instrument Movements.—TELECHRON, INC., *Ashland, Massachusetts.*

Instrumentation—Vol. 4, Number 1, 32 pages, contains articles of interest in measurement and control of industrial processes. Articles on precision heat treating, automatic control in coal hydrogenation, temperature as a factor in developing photosensitive glass, and basic concepts of thermoelectric pyrometry are included.—MINNEAPOLIS-HONEYWELL REGULATOR COMPANY, *Brown Instruments Division, Philadelphia 44, Pennsylvania.*

New Materials

Forest K. Harris: Associate Editor
in Charge of this Section
National Bureau of Standards, Washington, D. C.

Conductive Coatings DuPont Conductive Coatings, containing a specially prepared silver powder, produce a surface of low electrical resistance when applied to a variety of non-conducting materials such as glass, porcelain, steatite, wood, plastics, cloth, paper, etc. Aging or exposure to sulfides has only a slight effect on the conductivity of the coating. When applied to metals, the coatings inhibit rust and maintain the inherent surface conductance. It is possible with these coatings to add firmly bonded metallic ,layers to glass, porcelain, mica or steatite products which are used in the insulating parts of resistors, capacitors, transformers and other devices. The coating can also serve as a base for electroplating, a thin layer of copper being first plated on the coating, after which other metals can be plated on the copper by standard methods. Two general types of materials are available. *Type F* is specifically designed for bonding metals to ceramic bases. It contains, in addition to the silver powder, a finely divided, low melting glass in a liquid vehicle and is fired in an oxidizing atmosphere. The square resistance of this type of coating may be less than 0.01 ohm. *Type A* coatings are used chiefly for electrical shields. The coating may be air-dried or baked at a moderate temperature. The square resistance is approximately 2 ohms.

A number of formulations are available with different characteristics designed to meet certain requirements, such as the base material to be coated, the electrical resistance desired, adherence, and film toughness. The various materials, together with their characteristics, recommended thinners and methods of application are given in detail in DuPont's Ceramic Products Bulletin CP2-1248. This bulletin also describes a recommended copper-plating bath and procedure. E. I. DuPont de Nemours and Company, *Wilmington 98, Delaware.*

Silicone-Coated Carbon Resistors

Welwyn "High Stability" carbon resistors are a British product which are now available in this country. They are made by depositing a homogeneous carbon film on a porcelain tube. After aging, turned brass caps with staked and soldered terminal leads are applied and the resistor is brought to the required value by spiral-cutting the film in automatic machinery. Finally they are coated with silicone lacquer to provide mechanical and moisture protection. The lacquer coating is capable of operation at temperatures up to 150°C, permitting the resistor to dissipate rated power at ambient temperatures up to 100°C. These resistors are available in 1, 2, and 5 percent tolerances in capacities of ¼, ½, 1, and 2 watts. In the 1 percent class they are available in resistances from 100 ohms to 50 megohms. A wider range of resistance is available in the 5 percent class. Welwyn Electronic Components, Inc., *234 East 46 Street, New York 17, New York.*

Corrosion-Resistant Immersion Heaters

Carpenter stainless steel Number 20, an alloy having corrosion-resistant properties not found in many types of stainless steel, is used as the sheathing material on a new type of immersion heater designed specifically for use in the presence of highly corrosive acids, for example—sulfuric acid in all concentrations at temperatures up to 176°F; or up to 25 percent concentration at the boiling temperature. The heaters are made for operation on 115 to 550 volts, and in ratings from 200 watts to 5 kilowatts. They can be supplied in straight lengths up to 176 inches and can be bent to a minimum radius of 1¼ inches, allowing the units to be shaped to fit user's specifications. Lug-type terminals are standard but other types can be furnished on order. Electro-therm Inc., *8024 Georgia Avenue, Silver Spring, Maryland.*

Cellulose Ester Thermoplastics

Kodapak Sheet is a thermoplastic cellulose ester with important electrical applications. It is made in two types: *Kodapak* I, cellulose acetate; and *Kodapak* II, cellulose acetate butyrate. Kodapak I has greater rigidity and higher heat resistance, while Kodapak II has better moisture resistance, higher stretch, and greater toughness. These sheetings are manufactured by casting from solvents under rigidly maintained conditions of purity. They can be readily formed by means of heat and pressure, are easily creased, beaded, cemented and dielectrically heat-sealed. They are markedly superior to cellulose for electrical insulation because of (1) greater resistance to moisture, (2) greater resistance to oxidation, and (3) higher dielectric strength. Manufacturer's booklets are available giving their mechanical and electrical properties together with other information to aid in the selection of the most suitable material for particular applications. Cellulose Products Sales Division, Eastman Kodak Company, *Rochester 4, New York.*

Graphite-Filled Nylon

Nylatron G is a new form of Nylon containing graphite as a filler. The manufacturer states that it is less costly than the unfilled Nylon and that it has improved wearing and friction-free qualities. Applications include dry bearings, cams and followers, gears, washers, oil-seal rings and packings. It is available in cylinders ranging from 2- to 7-inches O.D. with wall thickness subject to specification, strip material in widths up to 2 inches and thicknesses from 0.01 to 0.09 inch, and in rods from 0.1- to 2¾-inches diameter. Polymer Corporation, *405 Walnut Street, Reading, Pennsylvania.*

Glycol Synthesis

The synthesis of two new glycols —2-methoxymethyl and 2-ethoxymethyl 2,4-dimethyl-pentanediol-1,5 has been announced. These substituted pentanediols combine the chemical characteristics of glycols and glycol-ethers. The hydroxyl groups in the 1,5 positions make them of special interest for the manufacture of maleic and other alkyd resins, plasticizers and elastomers. The ether groups confer solubility characteristics which make them useful as coupling agents and as solvents for protective coatings, hydraulic fluids, duplicating fluids, metal cleaners, dyes and adhesives. Their water solubility and low volatility suggest their use as softeners and plasticizers in water-soluble resins. The 2-methoxymethyl compound may be used at 15–25 percent concentration as a plasticizer in the milling, moulding, and casting of Nylon resins. The finished articles are stated to possess better flexibility, increased toughness and higher impact resistance, especially at low temperatures. Carbide and Carbon Chemicals Corporation, *30 East 42 Street, New York 17, New York.*

Crystalline Antibiotic

Dihydro-streptomycin sulfate is now commercially available in crystalline form, permitting the establishment of new standards of potency and purity. These include a minimum assay value of 725 mcg/mg (against the present 600) and less than 1 percent unreduced streptomycin sulfate (against the present maximum of 3 percent). This product, previously available only in a non-crystalline form, is available in adequate supply at no increase in cost. Heyden Chemical Corporation, *393 Seventh Avenue, New York 1, New York.*

Lined Steel Pipe

Production of large-size steel pipe lined with *Saran Rubber 187* is announced by the Michigan Pipe Company of Bay City, Michigan. This development complements the line of small-size, saran-lined pipes made by the Dow Chemical Company. The lining material is especially resistant to abrasion and is inert in contact with petroleum products, chlorinated hydrocarbons, bleaching agents, acids and most chemicals. The standard lining is ⅛-inch thick and its general operating range is from −5°F to 167°F, depending somewhat on service conditions. Standard lined pipe and fittings are available in all standard sizes from 8 inches to 36 inches, and the company will fabricate pipes with thinner steel walls or with thicker lining than standard on special order. The Dow Chemical Company, *Midland, Michigan.*

THE
REVIEW OF SCIENTIFIC
INSTRUMENTS

VOLUME 20, NUMBER 9 *SEPTEMBER, 1949*

Operation of Voltage-Stabilizing Elements with Current-Stabilized Supplies

J. J. GILVARRY* AND D. F. RUTLAND**
North American Aviation, Inc., Los Angeles, California

(Received May 9, 1949)

The performance parameters of a voltage stabilizer consisting of a voltage-stabilizing element (such as a *VR* tube) connected across the output of a current-stabilized power supply are determined and a particular parameter (the range-regulation factor Q) suggested as a figure of merit. The advantages of a current-stabilized over an ordinary supply from the standpoints of voltage stabilization and suitability for variable load are emphasized. Stability criteria for the case when the stabilizing element has a negative-resistance characteristic and a graphical analysis for the case of non-linear elements are given. Application to the special case of *VR* tubes is made with experimental results.

A VOLTAGE-STABILIZING element is a two-terminal circuit element whose voltage-current characteristic can be approximated by a constant direct-voltage generator in series with a small resistance. Common examples are the *VR* tubes or the voltage-reference tubes[1] widely used as standard reference voltages in degenerative stabilizers. Other examples are so-called regulating condensers,[2] ceramic materials of the thyrite type,[3] and gas diodes and thyratrons operated in the conducting state. An ordinary electric cell can be considered an element of this type (in fact, storage batteries are frequently connected across the output of motor-generator sets as stabilizing elements).

This paper discusses voltage-stabilizers consisting of such an element connected across the output of a current-stabilized power supply. The current-stabilized supply, for example, may be of the electronic type taking advantage of the form of a pentode characteristic or employing inverse current-feedback.[4]

I. PERFORMANCE PARAMETERS

The characteristic of the stabilizing element is a non-linear relation between the current I and potential E, such that over a range $I_{\min}$ to $I_{\max}$ (the limits of the operating range of current) the corresponding change in potential,

$$\delta = E_{\max} - E_{\min}, \qquad (1)$$

is relatively small. The quantity δ will be referred to as the regulation of the element. For any operating point (I_0, E_0) in the limits of the operating range, the true characteristic will be replaced by the linear equation

$$E = e + rI, \qquad (2)$$

where r is the dynamic resistance $(dE/dI)_0$ at the operating point and e is the (hypothetical) zero-current potential obtained by extrapolation to the voltage axis of the tangent to the characteristic at the operating point.

The equivalent circuit of a voltage-stabilizer consisting of such an element associated with a current-stabilized supply and providing an output current i at a potential E to a load R_L is shown in Fig. 1 (the generator E_L in the load circuit is introduced for mathematical convenience). The equivalent circuit of the current-stabilized supply has been taken as a constant current generator I_S in parallel with an ordinary supply (to which Thévenin's theorem applies) of open-circuit voltage E_S and dynamic internal resistance r_S whose equivalent circuit is in current-generator form. The special case of an ordinary supply therefore corresponds to $I_S = 0$. The parameter E_S will be referred to as the equivalent supply voltage.

The performance parameters of the stabilizer will be taken as the over-all stabilization ratio S and over-all

---

* Now at The Rand Corporation, Inc., Santa Monica, California.

** Now at Institute for Numerical Analysis of the National Bureau of Standards, University of California at Los Angeles, Los Angeles, California.

[1] T. Jurriaanse, Philips Tech. Rev. 8, 272 (1946).

[2] P. McK. Deeley, *Electrolytic Capacitors* (Cornell-Dubilier Electric Corporation, Plainfield, New Jersey, 1938), p. 168.

[3] G. P. Harnwell, *Principles of Electricity and Electromagnetism* (McGraw-Hill Book Company, Inc., New York, 1938), p. 141.

[4] J. N. Van Scoyoc and F. H. Schulz, Proc. I.R.E. 32, 415 (1944).

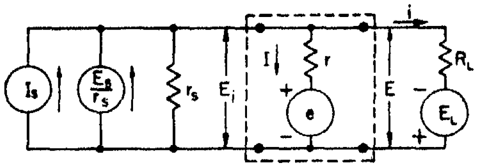

FIG. 1. Equivalent circuit of voltage-stabilizer.

internal resistance R defined by

$$\frac{1}{S}=\left(\frac{\partial E}{\partial E_S}\right)_{E_L},\quad \frac{1}{R+R_L}=\left(\frac{\partial i}{\partial E_L}\right)_{E_S},\tag{3}$$

and the parameter Q defined by

$$1/Q=(\partial I/\partial E_S)_{E_L}\tag{4}$$

and referred to as the range-regulation factor. From the results of Hunt and Hickman,[5] the over-all stabilization ratio S and over-all internal resistance R for any stabilizer associated with a power supply are given by

$$S=S_0(1+kr_S)+r_S/R_L,\tag{5a}$$

$$R\doteq R_0+\frac{r_S}{S_0}\,\frac{1+R_0/R_L}{1+kr_S},\tag{5b}$$

where S_0 and R_0 are the stabilization ratio and internal resistance of the stabilizer itself (exclusive of power supply) defined analogously to S and R in (3) by replacing E_S with the input terminal voltage E_i of the stabilizer, and the parameter k is the equivalent bleeder conductance of the stabilizer defined by $I=kE_i$. Evaluation of the parameters S_0, R_0, and k for the stabilizing element considered as a four-terminal network yields

$$S_0=1,\quad R_0=0,\quad k=1/r,\tag{6}$$

from which one has

$$S=\frac{r_S}{r}\left[1+r\left(\frac{1}{r_S}+\frac{1}{R_L}\right)\right],\tag{7a}$$

$$R=r/(1+r/r_S).\tag{7b}$$

Under the approximation that the absolute value of r is small compared to the parallel combination of r_S and R_L, or

$$1/|r|\gg 1/r_S+1/R_L,\tag{8}$$

which is usually valid in practice, one has

$$S\sim r_S/r,\quad R\sim r.\tag{9}$$

Equation (7b) implies that for r small, a low over-all internal resistance R can be obtained under the condition that r_S/r be large, which is necessary for high stabilization. This behavior differs from that of the usual stabilizer where k is small but S_0 is large, in which case it follows from Eq. (5b) that the contribution $r_S(1+R_0/R_L)/S_0$ of the power supply to the over-all internal resistance can be kept small only by keeping the ratio r_S/S_0 small.[5] In contrast to the usual stabilizer which functions because S_0 is large, it is clear from Eq. (5a) that a voltage stabilizer based on a stabilizing element functions because its equivalent bleeder conductance $k=1/r$ is large compared to $1/r_S$ (since S_0 is unity, a stabilizing element associated with a power supply of zero internal resistance is not a voltage stabilizer).

The range-regulation factor Q is a measure of the change in current through the stabilizing element under variations of the equivalent supply voltage, and is important because the element can stabilize only over the range $I_{\min}$ to $I_{\max}$ of element current as a limit. This parameter is

$$Q=r_S\left[1+r\left(\frac{1}{r_S}+\frac{1}{R_L}\right)\right],\tag{10}$$

or under approximation (8),

$$Q\sim r_S.\tag{11}$$

The parameter Q is independent of the dynamic resistance r of the element under approximation (8), and hence its use as a figure of merit of the voltage stabilizer has an obvious advantage over the use of S, particularly when variations of r from its nominal value occur (as in the case of VR tubes; see Section 5).

Since an electronic current-stabilized supply can generally be designed for much larger internal resistance r_S under the same current drain than an ordinary supply with the same equivalent supply voltage, its use in conjunction with a stabilizing element yields much larger values of range-regulation factor Q and stabilization ratio S for the same dynamic resistance r of the element than the standard practice (ordinary power supply with a series resistor). The disadvantage which must be tolerated is the additional complication of the current-stabilizing circuit.

2. VARIABLE LOAD

The basic design problem in a voltage stabilizer of the type under discussion is to keep the current I through the element within a range I_1 to I_2 (with $I_{\min}\leqslant I_1<I_2\leqslant I_{\max}$) over which the corresponding change E_2-E_1 in potential across the element is sufficiently small to yield the desired stabilization. The limits I_1 to I_2 corresponding to fixed allowable limits on E can be determined directly from the characteristic of the element or from the incremental equation $\Delta I=(\Delta E)/r$ if the dynamic resistance r of the element is sufficiently constant in the neighborhood of the operating point. The range I_1 to I_2 will be taken as fixed, and will be referred to as the operating range. Under constant load, the permissible total variation of equivalent supply voltage E_S is $Q(I_2-I_1)$ for r approximately constant, or $r_S(I_2-I_1)$ under inequality (8). In many practical applications, the

---

[5] F. V. Hunt and R. W. Hickman, Rev. Sci. Inst. 10, 6 (1939).

output voltage need be stabilized only over limits separated by δ, in which case the permissible variation of E_S is $r_S(I_{\max}-I_{\min})$.

In the case of variable load, the element current I is

$$I=I_S-i+(E_S-e)/r_S, \tag{12}$$

under inequality (8) for $|r|$ small. Hence, the double inequality

$$I_1\leqslant I_S-i+(E_S-e)/r_S\leqslant I_2 \tag{13}$$

determines two lines, $I=I_1$ and $I=I_2$, in the plane of the variables i and E_S such that the point of operation (i, E_S) lies in the area between these two lines. Such a line $I=I_1$ (Fig. 2), of slope r_S and intercept I_S-I_1-e/r_S on the i-axis of the i, E_S plane, will be referred to as a range-regulation characteristic. In the range-regulation diagram of Fig. 2 for the operating range I_1 to I_2, the output voltage E is stabilized within the limits E_1 to E_2 for any point of operation between the range-regulation characteristics (solid lines) for $I=I_1$ and $I=I_2$, and hence the limits of variation of load current i and equivalent supply voltage E_S which maintain the required stabilization can be determined directly from the diagram.

If $I_S=0$, corresponding to the case of an ordinary power supply of internal resistance r_S', the positive intercept $e+r_S'I_1$ of the range-regulation characteristic $I=I_1$ on the E_S-axis is more convenient in application. Range-regulation characteristics in this case are shown (dashed lines) in Fig. 2 for the operating range I_1 to I_2. Subject to the restriction $I_1\leqslant I\leqslant I_2$, a maximum load current $i_{\max}'$ exists for such a stabilizer, which is defined by

$$i_{\max}'=(E_S-e)/r_S'-I_1, \tag{14}$$

as a linear function of the equivalent supply voltage E_S. Hence, a maximum load current cannot be associated with the voltage-stabilizer unless the corresponding supply voltage is also specified. In the case of a current-stabilized supply, however, the maximum load current $i_{\max}$ is

$$i_{\max}=I_S-I_1+(E_S-e)/r_S\sim I_S-I_1, \tag{15}$$

which is approximately independent of E_S for r_S sufficiently large. Thus, a maximum load current, as such, can be associated with the voltage stabilizer, and this feature is a salient advantage of the use of a current-stabilized supply in applications involving variable load.

One can show (by noting that I constant implies E constant) that the slope of a range-regulation characteristic $I=I_1$ in the i, E_S plane is strictly r_S, independent of approximation (8). Under approximation (8), however, this slope is approximately Q and can be determined experimentally as the reciprocal slope of the curve of element current I against the equivalent supply voltage E_S, for any fixed load satisfying (8), and a line of constant load resistance R_L is approximately an ordinate in the i, E_S plane.

3. STABILITY REQUIREMENTS

In practice, the dynamic resistance r of the element may be negative over a restricted range of operating current. The elements which are of practical use in voltage stabilization ordinarily have a negative-resistance characteristic (if at all) of the current-controlled type,[6] in which the region of negative resistance is bounded by points of zero resistance, as in the characteristic CC of Fig. 4. At the points of zero resistance, the stabilization ratio S becomes infinite and changes sign.

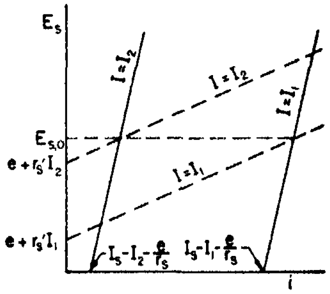

FIG. 2. Range-regulation diagram ($E_{S,0}$ is the operating value of E_S).

The condition[6] for stability on a current-controlled element is that the over-all resistance be positive when the element is considered in series with the associated circuit, or, for the equivalent circuit of Fig. 1, that

$$r_SR_L/(r_S+R_L)+r>0. \tag{16}$$

Hence, if inequality (8) on $|r|$ holds, the stability criterion of (16) is always fulfilled (for r_S and R_L positive). Difficulty due to instability can arise, therefore, only when $|r|$ rises sufficiently on the negative-resistance branch of the characteristic to be of the same order of magnitude as r_S or R_L.

The stability criterion of (16) can be written equivalently as $Q>0$ or $S<0$ (for r_S and R_L positive). Hence, for r negative, the range-regulation factor Q is positive or negative and the stabilization ratio S negative or positive according as the point of operation is stable or unstable. The over-all internal resistance R defined by Eq. (7b) is always negative for stable operation of the element with r negative.

4. GRAPHICAL ANALYSIS

A graphical analysis can be given which is useful in bringing out some points of physical interpretation. If the parallel resistances r_S and R_L are combined into a single resistance r_e, where

$$1/r_e=1/r_S+1/R_L, \tag{17}$$

then the equivalent circuit of the stabilizer becomes that of Fig. 3 when the stabilizing element N is non-linear. In Fig. 4, let $E_{S,0}$ be the point on the E-axis of the element's characteristic CC which corresponds to the operating value of E_S. Then a line of slope $-r_S$ through this point yields an intercept A on the I-axis corre-

---

[6] E. W. Herold, Proc. I.R.E. 23, 1201 (1935).

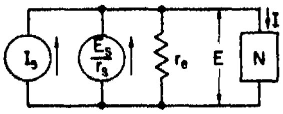

FIG. 3. Voltage-stabilizer with non-linear element N.

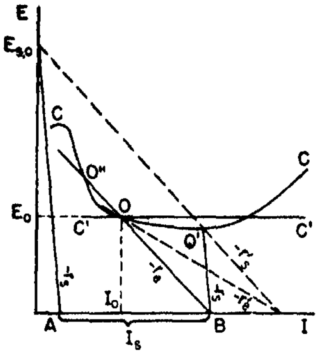

FIG. 4. Graphical construction for non-linear element.

sponding to the current $E_{S,0}/r_S$, and the current $I_S+E_{S,0}/r_S$ corresponds to an abscissa B which is I_S units greater. Lines through B of slope $-r_S$ and $-r_e$ are then the supply lines at no load and under load respectively. The intersections of these lines with the characteristic of the element yield the operating points O' and O corresponding, respectively, to no load and a load R_L, and hence yield E as a function of E_S when $E_{S,0}$ is varied. The corresponding construction for the case of an ordinary supply ($I_S=0$) is shown (heavy dashed lines) in Fig. 4 for supply lines of slope $-r_S'$ and $-r_e'$ at no load and under load, respectively.

If the characteristic has a region of negative resistance, two intersections (such as O and O'' in Fig. 4) of a supply line with the characteristic may exist. The stability criterion of (16) can be rewritten $r_e>|r|$, which requires that the absolute value of the slope of the supply line exceed the absolute value of the slope of the characteristic. Hence, of the points O and O'' in Fig. 4, the point O which meets this condition is stable while O'' is unstable.

The inequality (8) can be interpreted as stating that the slope r of the characteristic is insignificant compared to the slope of the supply line under load, or $|r|\ll r_e$. In this case, the characteristic can be replaced by a horizontal straight line ($C'C'$ in Fig. 4) through O, as far as determining the element current I corresponding to the supply voltage E_S is concerned. With this assumption, one has directly from the diagram that

$$E_S-E_{S,0}=r_S(I-I_0) \tag{18}$$

at constant load. Hence, when inequality (8) holds and r_S is constant, the stabilization characteristic (output voltage E *vs.* equivalent supply voltage E_S for fixed load) consists of a segment of the characteristic of the element multiplied by the scale factor $r_S(\sim Q)$ on the axis of abscissae.

5. *VR* AND VOLTAGE-REFERENCE TUBES

The application of the preceding theory to *VR* tubes and the voltage-reference tubes (RCA 5651 and North American Philips 85A1) requires some comment. The experimental evidence[7] indicates that for most *VR* tubes the characteristic is U-shaped over the limits of the operating range, with a region of negative resistance usually in the low current region. The characteristic over a particular *VR* tube type does not have the degree of definiteness of, say, a triode characteristic over a tube type. The point of zero slope and the regulation δ, for example, vary over somewhat wide limits from tube to tube. Hence, if the design is for operation under unselected tube replacement, one is more or less forced to forego designing for a desired stabilization, and to design merely for a desired range of *VR* tube current. In addition, the *VR* tube characteristic shows variation for a particular tube in the form of hysteresis effects and abrupt voltage changes of various types (both of which are less, to some extent, at high current levels) and sizable drifts due to various causes. Variation of the characteristic over the tube type and in the individual tube is reduced[1] in the voltage-reference tubes.

When extreme stabilization (at constant load) is required, it is usually not possible to maintain a consistently high stabilization ratio with an ordinary supply by selecting an operating point close to the point of zero slope, because of the variation of the characteristic. The use of a current-stabilized supply, however, with its considerably larger internal resistance, makes it possible to achieve a consistently high stabilization ratio for any position of the point of zero slope in the limits of the operating range. For design purposes in this connection, only a rough approximation to the maximum slope of the characteristic over the limits of the operating range is needed, and is provided by the nominal resistance $r_n=\delta_n/(I_{\max}-I_{\min})$, where δ_n is the nominal regulation associated with the tube type by the manufacturer.

The preceding theory has assumed that no reactive element exists in the equivalent circuit of the stabilizing element and that the dynamic resistance is a constant equal to its zero-frequency value r. Experimental tests[7] of *VR* tubes show that, due to ion-inertia effects, a reactive element exists whose magnitude becomes comparable to r in the neighborhood of 100 cycles, at which frequency the dynamic resistance has risen significantly

TABLE I.

	Range-regulation factor Q (ohms)	Stabilization ratio S	Ratio Q/S (ohms)	Measured dynamic resistance r (ohms)
Ordinary power supply	5000	45	110	110
Current-stabilized supply	86,000	890	97	110

---

[7] G. M. Kirkpatrick, Proc. I.R.E. 35, 485 (1947).

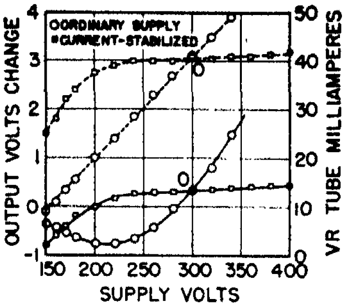

FIG. 5. Stabilization characteristics (solid) and tube-current curves (dashed) for *VR* 105.

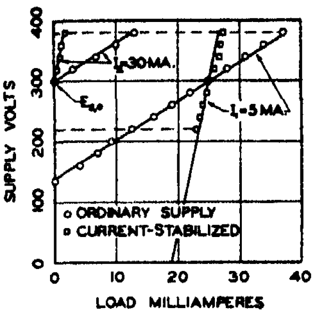

FIG. 6. Range-regulation diagrams for *VR* 105.

compared to its zero-frequency value. Hence, Eq. (7b) for the internal resistance (approximately *r*) of the voltage stabilizer is valid when the stabilizing element is a *VR* tube only for frequencies considerably below 100 cycles, and if a *VR*-tube stabilizer must provide a return path of low impedance for frequencies in the neighborhood of this value or higher, suitable by-pass capacitors must be used. Detailed information on the reactance and frequency variation of internal resistance for the voltage-reference tubes is not available. The considerations above do not affect the validity of the expressions for the range-regulation factor and stabilization ratio as applied to *VR*-tube stabilizers, because the rate of change of input voltage is sufficiently small in general so that the dynamic resistance *r* for zero frequency represents the impedance of the *VR* tube.

It should be pointed out that trouble with oscillation is sometimes experienced in indiscriminate by-passing of *VR* tubes. In this connection, the stability criterion of (16) is only a static criterion.

6. EXPERIMENTAL RESULTS

As a check on the general validity of the theory presented, tests were made on *VR* 105 tubes associated with an ordinary supply and a current-stabilized supply employing a pentode regulator.[8] Curves of tube current in the *VR* 105 (dashed curves) at no stabilizer load and corresponding stabilization of the output voltage (solid curves) with respect to an arbitrary reference voltage are shown in Fig. 5 for the cases of both supplies. The reciprocal slopes, *Q*, of the curves of *VR* tube current and reciprocal slopes *S* of the stabilization curves are tabulated[9] in Table I for the common operating point *O* in the case of both supplies. As a check, the ratio *Q*/*S* is tabulated for comparison with the measured dynamic resistance *r* at *O*, since these are identical from Eqs. (7a) and (10). The ordinary supply was closely linear, and it is clear from Fig. 5 that its stabilization curve corresponds to the *VR* tube characteristic multiplied by the corresponding *Q* of Table I as a scale factor on the abscissae. In Fig. 6, theoretical range-regulation characteristics determined from average measured values of parameters are compared with the corresponding experimental points for supplies of the two types in association with a *VR* 105 tube.

The high stabilization ratio (890 from Table I) obtainable with current-stabilized operation of *VR* tubes even at relatively large values of dynamic resistance *r* indicates the advantage in many cases of such operation of the associated *VR* or voltage-reference tube in the design of highly stable degenerative stabilizers. In conclusion, the authors wish to express their thanks to Doctors W. E. Frye and R. S. Wehner of The Rand Corporation for helpful discussions.

---

[8] Essentially, the current-stabilized supply was that of Fig. 3 in reference 4, using a 6AG7 pentode with its screen-grid voltage stabilized by an auxiliary degenerative stabilizer for the data of Fig. 5 and by a *VR* 150 for the data of Fig. 6.

[9] The tube used for the data of Fig. 5 and Table I was a selected tube whose characteristic was monitored and showed only slight variation (negligible in the neighborhood of *O*) during the measurements.

THE REVIEW OF SCIENTIFIC INSTRUMENTS VOLUME 20, NUMBER 9 SEPTEMBER, 1949

Optimum Conditions for a 180° Beta-Ray Spectrometer

CLAUDE GEOFFRION
Department of Physics, Laval University, Quebec, Canada

(Received April 18, 1949)

The relations existing between source dimensions, beam divergence, luminosity, and resolving power of a 180° homogeneous field spectrometer are established. From these the conditions for maximum luminosity for a given resolving power are derived. By increasing the source height and slightly decreasing the width, the luminosity may be increased without affecting the resolving power.

I. INTRODUCTION

IN the design of β-ray spectrometers, it is always desirable to achieve the greatest possible luminosity for a given resolving power. Studies thus far published have mainly considered the homogeneous field 180° spectrometer in which the source height made only a negligible contribution to the aberration, i.e., the trajectories are all considered as lying in the same plane. If we also consider a beam diverging out of this plane, we find that these divergent trajectories add to the aberration and also increase the luminosity. Consideration of these trajectories shows that there exists an optimum choice of parameters such as source dimensions and slit widths which will provide for maximum luminosity for a given resolving power. It is the purpose of this paper to establish these optimum conditions.

II. IMAGE OF A FINITE SOURCE

Consider a source of finite dimensions located in a homogeneous magnetic field H, as shown in Fig. 1. The origin O is at the center of the source, which lies in the plane XOZ, where the OZ axis is parallel to H. An electron leaving the source from a point $P(x_0, O, z_0)$ will cross the plane XOZ at a point $P'(x, y, z)$ whose coordinates are given by the well-known equations:

$$x = x_0 + 2r\cos\alpha\cos\beta,$$
$$y = O,$$
$$z = z_0 + r(\pi + 2\alpha)\sin\beta,$$

where r is the radius of curvature of the electron trajectory in the magnetic field, equal to p/H where p is the momentum of the electron, α is the angle between the initial direction of p and the plane YOZ, measured positively counter-clockwise from the plane, and β is the angle between the initial direction of p and the plane YOX, measured positively counter-clockwise from the plane.

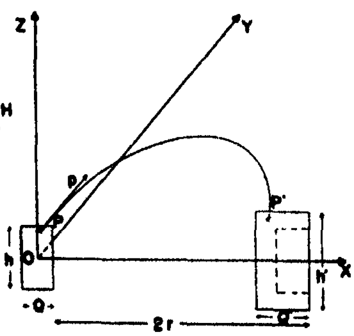

FIG. 1. Electron trajectory in an homogenous magnetic field, with coordinate origin at the center of the source.

If the source has height h and width Q, and the angles α and β are limited to $\pm\alpha_0$ and $\pm\beta_0$ by baffles, then all electrons of the same momentum will cross the ZOX plane in an area whose dimensions are:

$$\text{width:}\quad Q' = Q + 2r(1 - \cos\alpha_0\cos\beta_0),$$
$$\text{height:}\quad h' = h + 2r(\pi + 2\alpha_0)\sin\beta_0.$$

This area may be considered as an image of the source, which would be equal to it in area but for aberrations which are functions of α_0 and β_0. The right edge of this image is located a distance $2r$ (i.e., $2p/H$) from the right edge of the source. Electrons of a different momentum will form a similar image, displaced from the first one. If the images are kept narrow, by limiting α_0, β_0 and Q, the images due to various momenta will be separated, and the resolved beams may be passed one at a time through an exit slit to a measuring apparatus.

The angle β can be limited to any desired value β_0 by making the height h and that of the exit slit each equal to $\pi r\beta_0$. The angle α_0 may be determined (to a first approximation) by placing a diaphragm of height h and width $D = 2r\alpha_0$ perpendicular to the central trajectory near its middle point. Any electrons leaving the source with angles α and β greater than $\pm\alpha_0$ and $\pm\beta_0$ will thus be prevented from reaching the detector and the total solid angle (ω) of those which do reach the detector is given by $2\alpha_0\beta_0$.

We therefore see that the width Q' of the image on the plane XOZ is completely determined once we have chosen Q, h, and the width (D) of the diaphragm. However this width Q' is not the effective width, because the presence of an exit slit may apparently enlarge the image. If the slit of width F and the detector behind it are displaced behind the image of a beam of monoenergetic rays, the image will seem to have a width given by $Q'' = Q' + F$. It is this effective width Q'' that must be used in calculating the resolving power of the spectrometer.

III. LIMIT OF RESOLUTION AND RESOLVING POWER

The limit of resolution of a spectrometer is defined here by the ratio $\Delta p/p$ where Δp is the difference

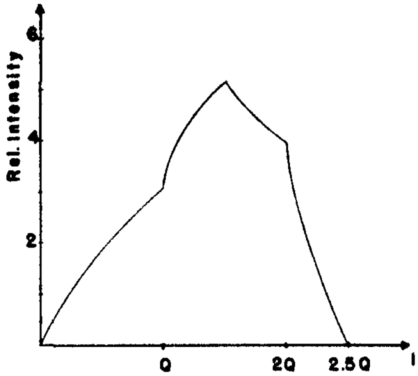

FIG. 2. Monoenergetic electron intensity distribution along the image width, under optimum conditions, for a movable slit of height h and width dF. Coordinate l represents the position of the slit, measured in Q (source width) units positively from the right edge of the image toward the source.

between momenta of two groups of monoenergetic electrons of which the spectrometer gives two images just completely separated and where p is the value of the mean momentum of these electrons. On the other hand, $p=H\cdot r$ and the dispersion of a spectrometer is the ratio $\Delta x/\Delta p$ where Δx is the distance along OX between the right edge of two images of electrons differing in momentum by Δp. At the limit of resolution, the distance Δx equals the width of the image and the ratio $\Delta p/p$ may be expressed by

$$\Delta p/p=(\text{width of the image})/(H\cdot r\cdot\text{dispersion}).$$

Remembering that the image width is $Q''=F+Q+2r(1-\cos\alpha_0\cos\beta_0)$ and that, at 180° from the source, the dispersion of a homogeneous field spectrometer is $2/H$, we find that

$$\Delta p/p=[F+Q+2r(1-\cos\alpha_0\cos\beta_0)]/2r$$

which may be closely approximated by:

$$\Delta p/p=(F+Q)/2r+(\alpha_0^2+\beta_0^2)/2. \qquad (1)$$

The resolving power, which is the criterion of usefulness of the apparatus, is defined by the inverse of the limit of resolution, i.e.:

$$\text{R.P.}=p/\Delta p.$$

IV. LUMINOSITY

The luminosity of the apparatus is defined as the number of monoenergetic electrons coming from the source (of area $Q\cdot h$) which being restricted to a solid angle ω (which we have seen is equal to $2\alpha_0\beta_0$) will pass through a very wide exit slit of height h, per unit time. It will be given by

$$L=KQh\omega/4\pi \qquad (2)$$

where Q and h are defined as before, and K is the number of monoenergetic electrons emitted by the source in all directions per unit area per unit time.

Substituting for ω and for h ($h=\pi r\beta_0$), the expression for luminosity becomes:

$$L=K\cdot Qr\alpha_0\beta_0^2/2. \qquad (3)$$

V. OPTIMUM CONDITIONS

The limit of resolution and the luminosity are thus seen to be functions of the same parameters, Q, r, α_0, and β_0. Therefore, for a given r and limit of resolution $(\Delta p/p)$, there must exist an optimum relation between α_0, β_0, and Q which will give L a maximum value. The relation may be found by using Lagrange's method of undetermined coefficients. If we define a new function ψ equal to $\Delta p/p+\lambda L$, where λ is undetermined, and then make all derivatives of ψ with respect to Q, α_0, and β_0 equal to zero, we obtain the desired relations making L maximum. They are:

$$Q=2\alpha_0^2r, \quad \beta_0=\alpha_0(2)^{\frac{1}{2}}.$$

Substituting these conditions in Eqs. (1)–(3), we find for the limit of resolution:

$$\Delta p/p=F/2r+5\alpha_0^2/2,$$

and for the luminosity:

$$L=2Kr^2\alpha_0^5.$$

Investigation of the energy distribution along the image width shows that there is also an optimum value for the exit slit width F. In Fig. 2 this distribution is shown for an exit slit of height h and very narrow width dF, under the optimum conditions given above; under these circumstances, the image width is $2.5Q$, and $\Delta p/p$ is $5\alpha_0^2/2$. This distribution is calculated by integrating the number of electrons from a unit area of the source, which reach a unit area of the exit slit, over the height and width of the source and over the height of the exit slit; the area under the curve represents what is called the luminosity of the apparatus.

If the slit width is now widened to F, the effective image width and the limit of resolution will be enlarged and the corresponding intensity distribution curve will

FIG. 3. Monoenergetic electrons intensity distribution along the image width, under optimum conditions, for a movable slit of height h and width $F=Q$. Coordinate l represents the position of the left edge of the slit, measured in Q units positively from the right edge of the image toward the source.

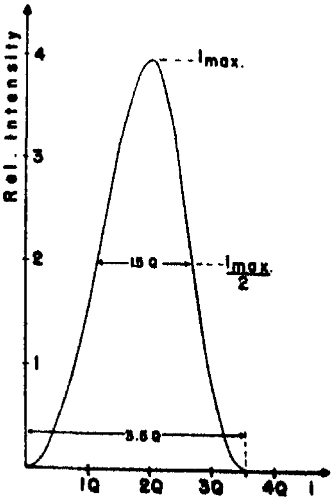

TABLE I.

Type of spectrometer	High source	Usual type	Usual type
Radius "r"	30 cm	30 cm	12 cm
Width of source "Q" and of exit slit "F"	1.2 mm	1.4 mm	0.56 mm
Width of diaphragm "D"	2.7 cm	4.1 cm	1.6 cm
Height of source, diaphragm, and exit slit "h"	6.0 cm	2.0 cm	0.81 cm
Limit of resolution	0.3%	0.3%	0.3%
Luminosity$\times 10^6/K$	32.1	6.16	0.986

have a peak value $I_{\max}$, which is a function of F. Using integration, and Lagrange's method, it may be shown that when F equals Q, $I_{\max}$ has a maximum value $0.63L$ for a given $\Delta p/p$ (Fig. 3).

Substituting this new condition, the limit of resolution becomes:

$$\Delta p/p = 7\alpha_0^2/2.$$

This expression for the limit of resolution is defined for the complete separation of two lines; if it is sufficient to distinguish two lines at only half-intensity, the limit of resolution may be shown to be:

$$\Delta p/p = 3\alpha_0^2/2,$$

and the resolving power is

$$\text{R.P.} = 2/(3\alpha_0^2).$$

The luminosity may now be expressed as a function of K, r, and the limit of resolution or the resolving power:

$$L = 0.725Kr^2(\Delta p/p)^{5/2} = 0.725Kr^2(1/\text{R.P.})^{5/2}.$$

Therefore, for a 180° homogeneous field spectrometer of given r and desired resolving power (R.P.), the parameters giving maximum luminosity should be chosen in this order:

(1) The width of the source (Q) and of the exit slit (F) should equal: $(4/3)r/\text{R.P.}$

(2) The diaphragm width (D) should equal: $2r(2/3\text{R.P.})^{1/2}$.

(3) The heights of the source, diaphragm, and exit slit should equal: $2\pi r/(3\ \text{R.P.})^{1/2}$.

In the following discussion we shall call a high source type spectrometer one operated under these optimum conditions.

It must be remembered that for a large radius, the limit of resolution must be kept small, for the practical reason that a large value will require too wide a gap between the magnet pole faces.

VI. COMPARISON WITH THE USUAL TYPE

It is of considerable interest to compare the luminosity of this "high source" spectrometer with the usual 180° spectrometer of the same radius and resolving power. In the usual type, the source and exit slit height are chosen so small as to make β_0 negligible with respect to α_0. Thus β_0^2 is usually made less than $0.1\alpha_0^2$ by most designers. To have optimum conditions in this case,[1] the source and exit slit widths are made equal to the aberration width $\alpha_0^2 r$. The diaphragm width is made equal to $2\alpha_0 r$ and source, slit, and diaphragm height equals $\pi r\alpha_0/(10)^{1/2}$. We may therefore express the limit of resolution and the luminosity of this type in terms of α_0; thus:

$$\Delta p/p = (93/140)\alpha_0^2 \text{ (at half-intensity)},$$
$$L = Kr^2\alpha_0^5/20,$$

or

$$L = 0.139Kr^2(\Delta p/p)^{5/2}.$$

This shows that the luminosity of the high source type spectrometer is at least 5.2 times greater than that of the usual type for the same limit of resolution and radius r. This is due to a large increase in β_0 and h and a small decrease in α_0 and Q.

In any spectrometer, luminosity could be increased by using larger values of r, but this would require the use of larger magnets, often the restricting factor in design. This difficulty has been overcome in this laboratory by abandoning the usual magnet form in favor of the double mushroom type. Our 1600-pound magnet permits a 30-cm radius, whereas the usual type magnet of this weight provides only about a 12-cm radius. The mushroom type magnet however restricts us to the use of a G-M counter as a detector, since large plates cannot be accommodated.

The following table gives, for comparison purposes, at the same limit of resolution of 0.3 percent:

(1) the luminosity, source, diaphragm, and exit slit dimensions of a 30-cms radius high source spectrometer (optimum conditions),

(2) the same parameters for a 30-cm radius usual type spectrometer,

(3) the same parameters for a 12-cm radius usual type spectrometer (usual type magnet of approximately the same weight as that of a 30-cms radius double-mushroom magnet).

It is to be noted that these comparisons are theoretical. In practice, designers of the usual type make β_0 even smaller than $\alpha_0/(10)^{1/2}$. Examination of some published designs of usual type spectrometers shows that the use of high source type would increase their luminosity by as much as 6.5 times.

VII. CONCLUSION

The preceding calculations show that there exist optimum conditions for the operation of a 180° beta-ray spectrometer; through the use of these conditions, an appreciable gain in luminosity may be achieved. This increased luminosity of the high source homogeneous field spectrometer also compares favorably with that of shaped field or lens type spectrometers.

ACKNOWLEDGMENTS

Sincere thanks are due to Professor E. Persico for his assistance in the mathematical treatment of the problem and to Professor L. Kerwin for many helpful suggestions in the writing of this paper.

---

[1] J. L. Lawson and A. W. Tyler, Rev. Sci. Inst. 11, 6 (1940); K. Siegbahn, Ark. f. mat., ast. o. Fys. 30A 20 (1944).

THE REVIEW OF SCIENTIFIC INSTRUMENTS VOLUME 20, NUMBER 9 SEPTEMBER, 1949

Calibration of Photographic Emulsions for Low Energy Electrons

L. Cranberg and J. Halpern
Physics Department, University of Pennsylvania, Philadelphia, Pennsylvania

(Received April 19, 1949)

Measurements are reported for the dependence on energy of photographic darkening due to electrons of energies between 4.4 and 45 kev. For Ilford *B*-2 plates, in the linear density exposure region, the results can be expressed by the empirical formula $D/Q/A=KE^x$. D is the photometric density, Q/A the exposure in electrons/mm², E the energy in electron-volts; K and x are constants with the values $(0.30\pm0.03)\times10^{-12}$ and 1.45 ± 0.05, respectively. The relationship for two other emulsions tested is complicated by the presence of surface coatings on the emulsions. Reproducibility of results is discussed.

Results are given on density fluctuations due to granularity of Ilford and x-ray emulsions. The limit of sensitivity, using the L. and N. recording microphotometer with scanning beam 1.0 by 1.3 mm, is estimated at 450 electrons/mm² of 40 kev energy for the x-ray emulsion and 680 electrons/mm² for the Ilford plates. The latter is limited by photometric sensitivity.

INTRODUCTION

THE present work aims to provide data on photographic emulsions from which one may estimate the limitations imposed on quantitative beta-ray spectroscopy using photographic detection. The energy region covered is from 4.4 to 45 kev. Items to be considered are the darkening of the emulsion as a function of exposure and energy, reproducibility of results, and the threshold of detection. Photographic density as measured on a Leeds and Northrup recording microphotometer is taken as the measure of darkening. It is assumed always that the quantity of interest is the difference between the densities of adjacent exposed and unexposed areas.

Data are available in the literature[1] illustrating the dependence of density on energy and exposure for various emulsions; but for no one photographic material are all the points of interest covered. Further, the emulsions for which partial data are available are not ones which seem most suitable for beta-ray spectroscopy.

It is well known[2] that at sufficiently low densities the plot of a density-exposure curve for electrons is a straight line passing through the origin. Previous work[2] indicates that this linear relationship extends to densities well within the range to be encountered in most beta-ray spectroscopy work. We have re-examined the extent of the linear region for the electron energies involved in our work, and have thereafter limited exposures to this region. The major portion of our work is concerned with obtaining data on the energy dependence of the sensitivity of several emulsions. Sensitivity is defined here as the slope of a density-exposure curve in the linear region under standard developing conditions. Data were obtained with an electron gun furnishing monoenergetic electrons.

An important handicap of photographic detection for beta-rays is the high threshold of detection. The precision of measurement depends on the ratio of the density produced by a given exposure (the signal) to the fluctuations in density (noise) from all causes in the exposed and unexposed regions under comparison. Few data are available on the latter subject. Albersheim[3] obtained a theoretical result for the root-mean-square fluctuation in density (ΔD), which for small densities reduces to

$$\Delta D=K\left(\frac{A}{A'}D\right)^{\frac{1}{2}}$$

where D is the average specular density, A the projected grain area, and A' the area of the scanning beam of the microphotometer. The factor K is 0.7 for surface deposits and 1.0 for volume distributions of grains. The analysis assumed uniform grain size and neglected effects of diffraction of light around the grains. We have experimentally examined the question of threshold of detection and give data for the same emulsions whose sensitivities have been measured.

The most important criteria for choice of type of emulsion for a given problem[4] are the average size and concentration of silver-halide grains in the emulsion. Large size favors high sensitivity but gives large fluc-

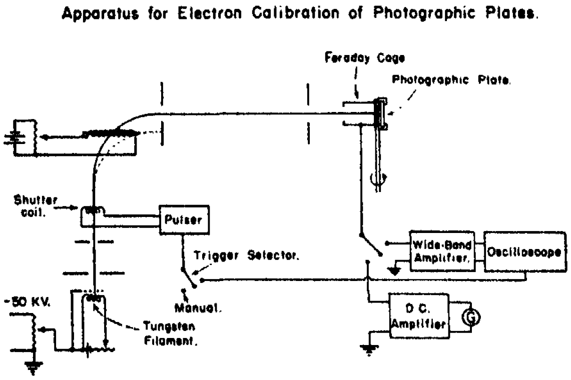

FIG. 1. Calibration apparatus.

---

[1] W. Langendijk and L. S. Ornstein, Physica 7, 475 (1940).

[2] A. Becker and E. Kipphan, Ann. d. Physik. 10, 15 (1931).

[3] W. J. Albersheim, J. Soc. Mot. Pict. Eng. **29**, 236 (1937).

[4] Mees, *The Theory of the Photographic Process* (MacMillan Company, Ltd. London, 1942). Klemperer, ***Einfurung in der Elektronik*** (M. S. Rosenberg, New York, 1944).

tuations. High silver-halide concentration is also favorable to sensitivity. Small grain size correlates with small fluctuations and wide range of linearity of density-exposure curve. Of the four possible combinations of large and small grain size and high and low silver-halide concentration, small-size small-concentration can be ruled out as unpromising. An emulsion with large grain size and high concentration is not available. We have concentrated on the other two cases as represented by the Ilford B-2 nuclear plate* of 50 micron thickness and the Eastman no-screen x-ray film, which is coated on both sides with emulsion 20 microns thick and is covered with a protective gelatine coating one micron thick. Data published on the Ilford plates give 0.4 microns as the average diameter of the grains and a concentration of silver-halide of 80 percent. Microscopic examination of a developed sample of x-ray film reveals a wide range of grain sizes of irregular shape running from a few microns to 25 microns, with an average value of about 10 microns. The concentration of silver-halide is not more than 20 percent. It is assumed in the following that the photographic reciprocity law[4] is obeyed for electrons in the region studied. Since in our work the interval between exposure and development was never more than a few hours, effects due to fading[5] are assumed to be negligible.

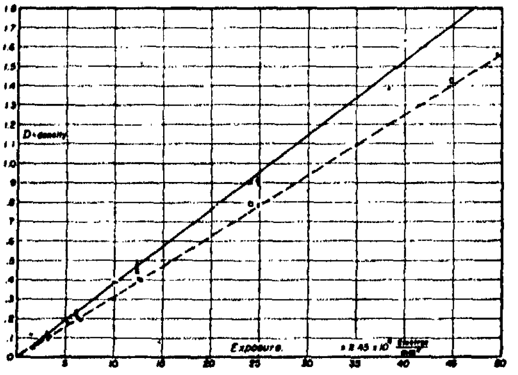

FIG. 2. Density-exposure curves for Ilford B-2 plate at 40 kev.

APPARATUS

The essential elements of the apparatus are illustrated in Fig. 1. High voltage is supplied by a 50 kv stabilized r-f supply provided with a 200 megohm bleeder which can be tapped at ten equidistant points along its length. The design of the electron gun is patterned on that of the RCA 50 kv electron microscope. Electrons are obtained from a battery-powered tungsten filament enclosed in a hemispherical grid structure. The electron beam is deflected 90° (by a battery-powered iron core magnet) to prevent filament light from reaching the emulsions. A series of apertures define a beam of circular cross section $\frac{3}{8}$ inch in diameter at the plane of exposure. A Faraday cage and the holder for the emulsion to be tested are located on opposite sides of a structure mounted on an arm which can be rotated through a Wilson seal.

To keep currents to be measured in a convenient range (10^{-10} to 10^{-11} amperes), exposure times as small as a few milliseconds are required. The pulsing of the beam is accomplished by a beam shutter consisting of an additional air-core coil external to the vacuum system. This coil is normally energized, thus causing the beam to be deflected away from the emulsion as shown by the dotted line in Fig. 13. Exposure is accomplished by triggering an Eccles-Jordan pulser which short-circuits the coil for a time determined by the time-constant for the pulser-coil combination (approx. 3 milliseconds) and thus gives an undeflected beam on the emulsion for a few milliseconds. Exposure is varied by triggering the pulser a desired number of times. Coarse adjustment of beam intensity is provided by a rheostat controlling the filament temperature.

Sample films and plates tested are 1×3 inches. The rod supporting the film holder and Faraday cage can be moved parallel to the long film dimension through the Wilson seal so that seven circular areas can be exposed on each sample with but slight overlap.

Care in locating the apertures defining the electron beam is found to be essential in eliminating objectionable electron scattering. As evidence that difficulties from this source were satisfactorily overcome, it is noted that the density of nominally unexposed areas adjacent to the exposed film areas is the same as that of masked parts of a film sample.

MEASUREMENTS

The voltage furnished by the high voltage supply was measured by observing the current through the bleeder, which consisted of ten 20 megohm resistors connected in a manner designed to minimize corona. These resistors were measured at their working voltage by comparison with precision standards. As a check of the loading action of the electron gun on the bleeder, it was noted that the current through the 90° deflecting magnet (which is sensitive to the energy of the beam) was never dependent on the beam current.

To measure exposure, the beam was first allowed to fall on the Faraday cage, the current to which was amplified by a d.c. amplifier and observed with a sensitive galvanometer. The shutter coil was then energized and periodically short-circuited by triggering the pulser with the sweep of a Dumont CRO type 256-D. This caused the beam to arrive at the Faraday cage in pulses synchronized with the scope sweep. The duration of the pulses could be measured by viewing them on the scope with the aid of the 50 microsecond timing markers available. The pulses obtained were closely trapezoidal, the flat portion comprising at least 85 percent of the total duration. Errors in relative exposure are thought to be not more than one percent and absolute errors not more than 5 percent.

---

* Eastman NTB could not be studied because of excessive peeling of the emulsion in vacuum.

[5] G. Albony and H. Faraggi, Comptes Rendus 228, 68 (1949).

The accuracy of measurement of beam current was limited by its constancy. Variations were not erratic but consisted of slow drift of the galvanometer in one direction. Measurements were always made immediately before and after exposure, and data were discarded when the difference so recorded exceeded 10 percent. As a check on possible errors in current measurement with the Faraday cage due to secondaries or back-scattering, the Faraday cage used in all the measurements was compared with another of 5 times greater ratio of length to aperture. Only for the lowest energy electrons was a difference detectable, and this amounted to about 5 percent of the current.

All development was done within a few hours of exposure using full strength *D*-19 for 5 minutes at 18°C. Fresh developer was always used. Development was carried out in glass cylinders 1½ inches in diameter and 5 inches long filled three-quarters with solution and closed with rubber stoppers. Agitation was provided by systematic rotation and oscillation of the cylinders as recommended in the literature.[6] Stopping and fixing were combined by using Kodak acid-fixer *F*-5 freshly prepared. For the Ilford plates, the hypo-concentration was that recommended by the manufacturers.

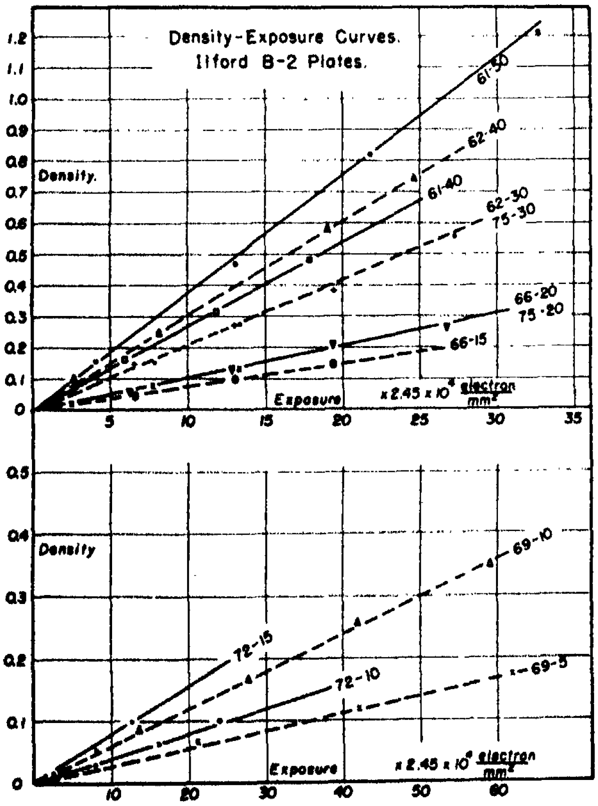

FIG. 3. Density-exposure curves for Ilford *B*-2 plates at various energies.

All density measurements were made with a Leeds and Northrup recording microphotometer with a scanning beam 0.01 by 1.3 mm. Background density measurements were always made in areas adjacent to each of the exposures. Density values shown plotted in the subsequent data are the values obtained by subtraction of this background density averaged over an area equal to the area of exposure scanned by the photometer.

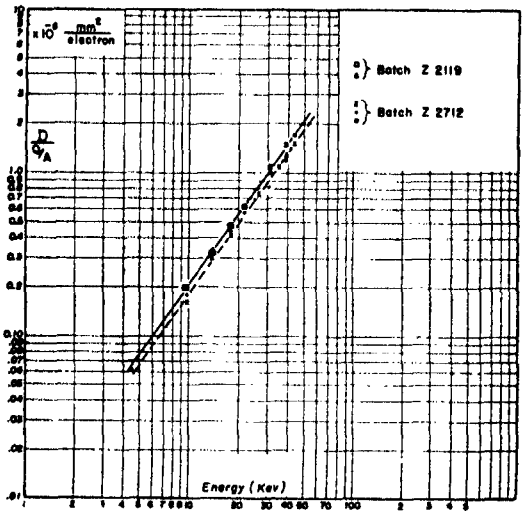

FIG. 4. Sensitivity curves for Ilford *B*-2 plates.

Usually it was found that the density of an exposed area varied smoothly from one edge of the ⅜-inch spot to the other, with the same pattern of variation showing up in all exposures at a given energy. This is thought to be due to the fact that the beam takes about 10 percent of the total exposure time to come in and out of position when being pulsed. A weighted average was taken from the photometric record. Estimated from reproducibility, errors from this source were less than 5 percent. For the fine grained emulsion, this is the limiting error in the measurement of density. At very small densities there must be added to this an uncertainty of 0.002 in density since the smallest density that one can estimate on the instrument is 0.001. For the coarse-grained emulsion the photometer record revealed fluctuations due to granularity, and the reproducibility corresponds to an uncertainty of 0.003 in density reading.

RESULTS AND CONCLUSIONS

As a preliminary check on reproducibility of results with a given emulsion, runs were made at 40 kv to obtain density-exposure curves. The results are shown in Fig. 2 for Ilford plates. These were all of the same emulsion number and processed simultaneously in separate containers. The points scatter between two straight lines whose slopes differ by 20 percent. It is clear, however, that the points corresponding to any given plate do not scatter this much from the best straight line for that plate. In fact, the variations are consistent with the uncertainties in measurement of exposure and density as given in the preceding section. Some of the variation from plate to plate must be due processing. Since the relative sensitivity to different energies is the primary consideration for beta-ray spectroscopy, we have minimized variations in the subsequent work by always comparing densities on the same sample.

---

[6] "A method of development suitable for standardized sensitometry," Phot. J. 80, 341 (1940).

The results of a series of runs on Ilford plates at different energies are given in Fig. 3. The numbers on each curve are the plate-designating number followed by the nominal voltage at which the run was made. It is clear that all exposures were within the range in which the density-exposure relation is linear. These curves illustrate again the variation in slope at a given energy for different plates. The slopes of these curves are shown on a double logarithmic plot in Fig. 4, the absolute values for the 20 kv run being taken as reference. The points corresponding to the data of Fig. 3 are shown as x's. The circles are derived from data taken at three points on two additional plates. The dots are obtained from a run on a single plate exposed once at each point of the energy spectrum at a density well within the range of linearity of the density-exposure curve. All other runs were taken in the latter manner.

The data fall on a well-defined straight line so that one may write the following expression for the dependence of density on energy:

$$D/(Q/A)=KE^{x}$$

where x is 1.45 ± 0.05 and K is $(0.30\pm0.03)\times10^{-12}$, if E is expressed in volts, Q in electrons and A in mm^2.

The curves of Fig. 5 were taken on two batches of commercial x-ray film. These curves fall into two parts. At the upper end of the spectrum they follow a straight line parallel to that for the Ilford plates but displaced upward corresponding to a sensitivity 4.5 times greater. There is a fairly sharp cut-off at the lower energies due presumably to the protective gelatine layer. At 4.5 kv the sensitivity has dropped to values of the order of 10^{-10} mm^2/electron and there is a consistent variation in sensitivity from sample to sample. This suggests variation in thickness of the protective coating. An electron of 7 kv energy will have a range of 1 micron in the gelatine coating.

Data on a third emulsion, an experimental Eastman type *K*, were also taken and are given in Fig. 6. These curves are parallel to the other two at the higher energy region and show effects of a gelatine coating.

Since in the foregoing it was important to be within the limits of linearity of the density-exposure curve and since this criterion is most critical at the lower energies, we have explored the maximum densities permissible. Figure 7 shows data taken at 10 and 15 kv for *B*-2 and x-ray film respectively. At 45 kv, the *B*-2 plate is linear to densities of at least 1.5 and the x-ray emulsion to densities of at least 1.0.

The smallest density which is detectable with a given precision depends on fluctuations or noise superimposed on the record of the signal and background. The background noise has high frequency components due to the granularity of the emulsion, small dust particles and scratches; and low frequency components due to such causes as large-scale fluctuations in grain distribution, irregular development, and variations in focus adjustment of the microphotometer. The amplitudes of those components that are recorded depend strongly on the resolution of the photometer.

The Leeds and Northrup microphotometer has a scanning beam width of about 0.01 mm and a height which was set at 1.3 mm. The effective resolution can

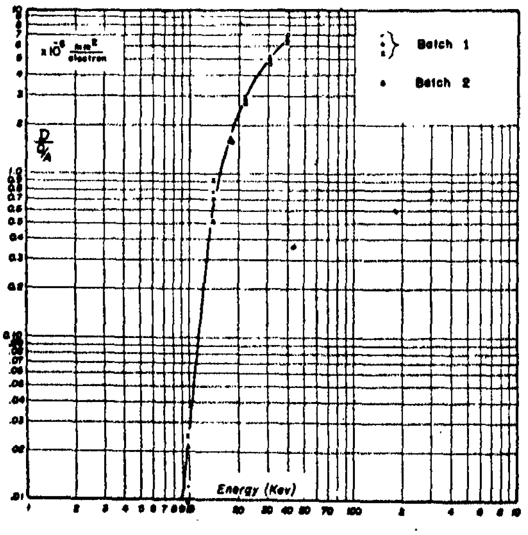

FIG. 5. Sensitivity curves for x-ray film.

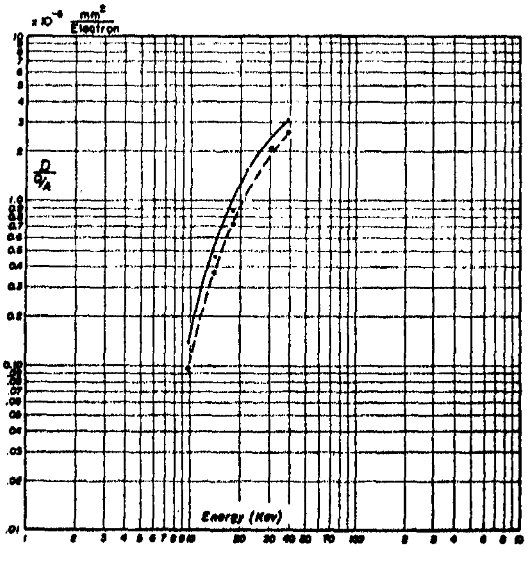

FIG. 6. Sensitivity curves for Type *K* plates.

be varied by changing speed of scan up to a maximum of 50 mm/minute. That is to say, if the scanning is done sufficiently slowly to allow the recording systems to follow the high frequency fluctuations, the record shows the noise corresponding to a resolution of 0.01 mm. As scanning speed is increased, the frequencies generated in the photo-cell circuit exceed the speed of response of the recorder, which then begins to act as a low pass filter. The value of the resolution in this case can be estimated from the minimum wave-length of the fluctuations on the record.

Our observations on fluctuations of background for the x-ray emulsion were made on a sample with average density of 0.135. This value was obtained by treating part of a sample with Farmer's Reducer to dissolve out the silver and by comparing densities of treated and untreated portions to give the density of the silver deposit itself. A speed of 0.2 mm per minute or less (resolution of 0.02 mm) was necessary to resolve clearly noise due to granularity. This amounted to a density fluctuation of 0.03. At the maximum speed of scan (resolution of about 1 mm) the amplitude of the noise dropped by a factor of 10.

In contrast to the situation with x-ray film, noise due to granularity of the Ilford plates could not be detected even at the lowest scanning speed, and an upper limit of 0.001 density units may be taken as its value. The average density of the silver was 0.014 in these measurements. A microphotometer with greater gain could be used with profit. To estimate the improvement that might be gained if precision were limited by statistical fluctuation of the grains, grain counts were made corresponding to the density of 0.014. The grain count was found to be 2500 grains in the 0.01 by 1.3 mm scanning beam. This implies a mean square fluctuation of 50 grains or a density fluctuation of 0.0003. The value calculated from the Albersheim formula is 0.00035.

When a length of developed but unexposed film or plate is run through the photometer, low frequency variations in density are observed amounting usually to a few thousandths in density for the Ilford plates and a few hundredths for x-ray film. The wave-length of these variations corresponds to centimeters on the emulsion. These fluctuations, which are due partially to variations in position of the sample in the focal plane of the photometer, can be minimized by careful background subtraction. It is believed that with sufficient care the precision of a single measurement of background density may be kept down to the value of 0.003 for the x-ray film and 0.001 for the Ilford plate using the photometer as manufactured.

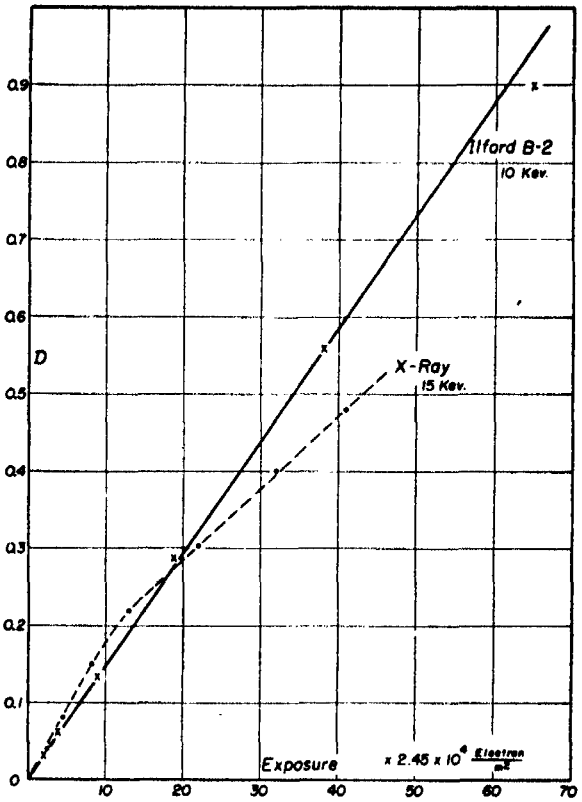

FIG. 7. Density-exposure curves at low energy.

Combining the results of the data on sensitivity and minimum detectable density, one may compare the two emulsions from the point of view of threshold of detectability. Expressing the latter in terms of the exposure equivalent of the limiting density the figures are 450 electrons/mm^2 for x-ray film and 680 electrons/mm^2 for Ilford plates. The above figures are taken for electrons having an energy of 40 kev and for a photometer resolution corresponding to an aperture 1.0 mm by 1.3 mm. The Ilford plate threshold is limited by photometric sensitivity.

The cooperation of Dr. J. Sherman of the Industrial Test Laboratory, Philadelphia Navy Yard, in arranging for use of microphotometer facilities is gratefully acknowledged. Mr. R. Trees assisted in the construction of parts of the vacuum system and electron gun. This work was supported in part by the joint program of the ONR and AEC and by a Faculty Research Grant of the University of Pennsylvania. The work was done while one of the authors (L.C.) held an AEC predoctoral fellowship.

THE REVIEW OF SCIENTIFIC INSTRUMENTS VOLUME 20, NUMBER 9 SEPTEMBER, 1949

A Microwave Secondary Electron Multiplier*

M. H. GREENBLATT**
Randal Morgan Laboratory, University of Pennsylvania, Philadelphia, Pennsylvania

(Received April 18, 1949)

The construction and operation of a dynamic electron multiplier, of the type sometimes called a multipactor, is described. Briefly, the multipactor consists of two parallel secondary emissive plates having an alternating voltage across them. The magnitude of the voltage is adjusted so that the transit time across the gap for electrons starting with zero velocity from one of the plates when the field is passing through zero shall be just one-half the period of the a.c. voltage. In this way, electrons and their secondary descendents can be made to bounce back and forth between the plates and multiplication takes place. The necessary phase relationships between the electrons and the field are discussed.

The multipactor described here uses 10 cm microwave power to get the a.c. voltage. It has been used as a gamma-ray detector in which case the cavity is "broken down" by the multiplication of a Compton electron ejected from the cavity wall by a gamma-ray. This breakdown gives rise to a microwave pulse several millivolts high at a crystal rectifier. The efficiency of this process is about 1.5×10^{-5} count/gamma-ray. The rise time of the pulse is calculated to be about 5×10^{-10} sec. and is measured to be less than 10^{-7} sec. The deadtime is presumed to be about 5 microseconds.

I. INTRODUCTION

THE use of microwave power to operate a secondary electron multiplier should enable one to construct a nuclear particle counter whose pulses have a very short rise time and to gain information about time delays in secondary electron emission. The multiplier described here was developed with these aims in view.

In simplest terms, the multiplier has two flat plates made of a material having a secondary emission ratio, σ, greater than unity. These plates are in the form of a condenser and an alternating voltage $V_0 \sin\omega t$ is applied across them. The voltage is adjusted so that the transit time between plates for an electron starting from rest from one of the surfaces at $t=0$ shall be just one-half the period of the alternating voltage. If any secondary electrons are produced by the first electron at the second surface, the field can now force them back to the first surface and continued multiplication can take place.

A multiplier operating on this principle, but which used 50 mc power instead of 3000 mc, which is used here, has been described by P. T. Farnsworth.[1] He reports stable gains of up to 10^6 for special cases and gains of at least several thousand in any case. The basic theory of operation was subsequently given by Henneburg, Orthuber, and Steudel[2] and others.

II. THEORY OF OPERATION

Consider two flat plates separated by distance d so as to form a condenser and having a voltage $V_0 \sin\omega t$ across them. We shall assume throughout this paper, except where stated otherwise, that the initial velocity of electrons ejected from one of the surfaces is zero and that the time delay in secondary emission is also zero. Let an electron appear at the lower plate at a time τ. The equation of motion is then

$$\ddot{x}=(eV_0/d)\sin\omega t.$$

The solutions of this equation subject to the conditions that $\dot{x}$ and x are both zero at $t=\tau$ are $\dot{x}=(eV_0/md\omega)\times(\cos\omega t-\cos\omega\tau)$ and

$$x=(eV_0/md\omega^2)[\sin\omega t-\sin\omega\tau-\omega(t-\tau)\cos\omega\tau]. \quad (1)$$

We now impose the conditions that if $\tau=0$, x shall equal d when $t=\pi/\omega$, i.e. an electron starting from the lower surface at $t=0$ will arrive at the upper surface exactly one-half period later. This condition, inserted into Eq. (1), leads to the equation

$$\pi=-md^2\omega^2/eV_0. \quad (2)$$

It is of interest to investigate the transit times of electrons starting at times other than $\tau=0$ under the

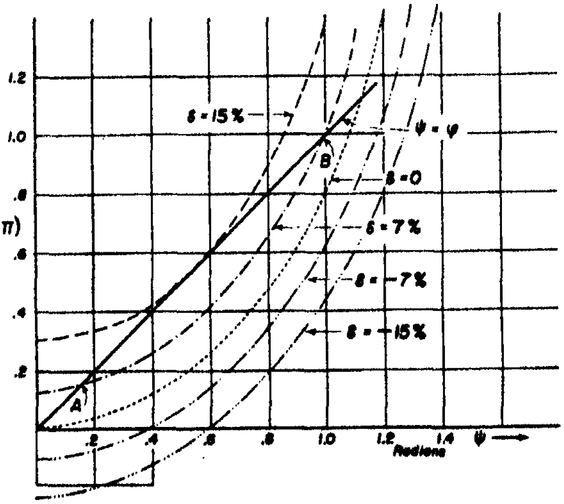

FIG. 1. Arrival time *vs.* departure time for different V_0.

---

* This report contains the essential portion of a thesis in partial fulfilment of the requirements for the degree of Doctor of Philosophy in Physics.

** Now at the RCA Laboratories, Princeton, New Jersey.

[1] P. T. Farnsworth, J. Frank. Inst. **218**, 411 (1934).

[2] Henneburg, Orthuber, and Steudel, Zeits. f. tech. Physik **17**, 115 (1936); Brüche, *E—Elektronengeräte* (Reprinted by Edwards Brothers, Ann Arbor, Michigan, 1944), p. 352ff. L. M. Myers, *Electron Optics* (Chapman-Hall, Ltd., London, 1939), p. 306ff.

conditions stated in Eq. (2) and also to see the effect of small variations in V_0. We shall call the voltage given by Eq. (2) $V_{00} = -md^2\omega^2/e\pi$ and shall refer to any other V_0 by $\delta \equiv 1-(V_0/V_{00})$. A little reflection shows that continued multiplication is possible only for positive δ, assuming zero time delay in secondary emission. (For if V_0 is greater than V_{00}, the transit time for electrons will be less than one-half period and secondaries from the second surface will see a field which has not yet reversed itself and, therefore, pushes them back into the surface with energies too small to produce more secondary electrons.) Equations (1) and (2) can be combined, setting $x=d$, to read

$$-\pi(1-\delta) = \sin\phi - \sin\psi + (\psi-\phi)\cos\psi, \qquad (3)$$

where $\psi \equiv \omega\tau$, the starting phase, and $\phi \equiv \omega t$, the arrival phase.

The solution of Eq. (3) can be obtained in several ways. The straightforward "brute force" method is to prepare a curve of $\pi+\sin\phi$ *versus* ϕ and the series of straight lines $(\phi-\psi)\cos\psi+\sin\psi$ *versus* ϕ on two pieces of graph paper. By superposing the two curves and noting the intersections for different values of ψ, the curve of Fig. 1 for $\delta=0$ is obtained. When the ordinates of the two curves are made to differ by $\pi\delta$, the other curves for various δ are obtained. It is immediately seen from Fig. 1 that ψ must surely be less than 65° for the electron to be able to catch up with the field.

A solution which graphically indicates possible electron trajectories has been given by R. Kompfner.[3] From his representation, many things that are not at all apparent from the "brute force" solution can be seen. For example, it is perfectly possible for an electron to require 3/2 or 5/2 of a cycle to get across the gap and such an electron can still have appreciable energy. It is also possible for electrons to leave the lower surface and return to it within the range $0° < \psi < 65°$ and have appreciable energy. All possible paths except the simple 1/2 cycle crossing will be neglected here.

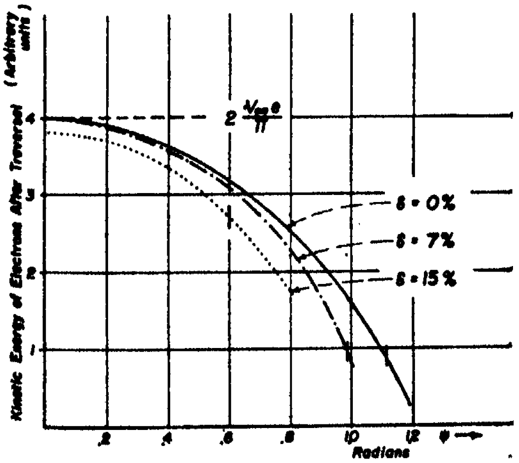

FIG. 2. Kinetic energy *vs.* departure time for different V_0.

The solutions for some different values of δ are shown in Fig. 1. $\phi-\pi$ is plotted against ψ because this gives the phase of arrival of the electrons with respect to the field which will carry them back, and if secondaries are instantly emitted, $(\phi-\pi)$ is also the starting phase for these secondary electrons.

In Fig. 1 it is seen that the 45° line intersects the curve for any δ (less than 15 percent) in two places. An electron must be emitted between 0° and the higher intersection in order to be focused to the phase at the lower intersection. We shall call the phase at the higher intersection $\psi_{\max}$. If δ is greater than 15 percent, all electrons take longer than one-half period to cross the gap and no phase focusing exists.

The expression for the kinetic energy of the electrons as they arrive at the second surface is

$$\text{K.E.} = \tfrac{1}{2}(e^2V_0^2/md^2\omega^2)(\cos\phi-\cos\psi)^2$$
$$= (eV_0/2\pi)(\cos\phi-\cos\psi)^2. \qquad (4)$$

Some curves of kinetic energy as a function of ψ are shown in Fig. 2.

III. APPLICATION TO PARTICLE COUNTING

Three thousand mc microwave power is used to operate this multiplier. The power is fed into a re-entrant cylindrical cavity resonator shown in Fig. 3. The gap between the center post and the top of the cavity is the region where multiplication takes place. Power is fed in through a coupling loop, and a much smaller monitor loop is used to sample the magnetic field in the cavity.

If a gamma-ray goes through the gap and causes an electron to be ejected from one of the surfaces, it may be possible for this electron to start the multiplication process. In computing the probability that an electron with just those properties necessary to start multiplication will be ejected by the passage of a single gamma-ray, the following factors must be considered.

In order to start the multiplication, an electron having nearly zero velocity must appear at one of the gap surfaces at a time between 0° and $\psi_{\max}$. Since $\psi_{\max}$ is, to the first approximation, never larger than 65°, only 65/360 or ~1/6 of the electrons ejected at random times from either the top or bottom surface can be effective in starting the multiplication. Also, since most of the electrons ejected by gamma-rays have high energies (>10 kev), one must consider the probability that these electrons will knock out slow secondaries from the gap surface. These factors have been mentioned only to make the small measured efficiency seem reasonable.

After a gamma-ray has started the multiplication process, the electron current in the gap quickly builds up. These electrons absorb energy from the microwave field during each traversal while energy is being replenished from the source with a time constant $2Q/\omega$. Since this time constant is long compared to the transit time, the power picked up by the monitor loop, which is

---

[3] R. Kompfner, "Transit-time phenomena in electronic tubes," Wireless Engineer 19 (220), 2 (1942).

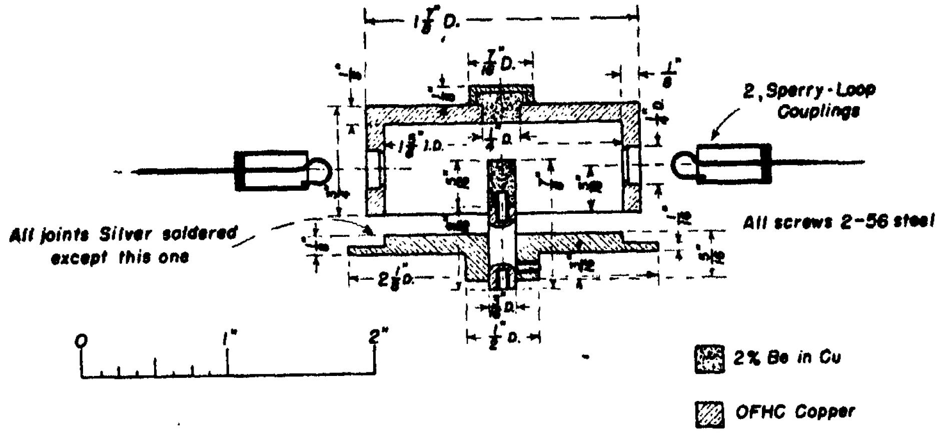

FIG. 3. Diagram of cavity.

a measure of the energy stored in the cavity, decreases, thus producing a pulse with a short rise time.

It is very difficult to give an exact description of the events during and after a pulse. Roughly speaking, it is plausible that the following happens. Multiplication proceeds until the electrons have drained enough energy from the electric field to cause the microwave voltage to fall below the value necessary to sustain multiplication ($\delta > 15$ percent). The microwave voltage will fall somewhat below this value because, although the phase of the electrons will diverge if $\delta > 15$ percent, the electrons can still withdraw energy for a few cycles. At this point the peak of the pulse has been reached. The phase divergent electrons will finally strike one of the surfaces with too small an energy to eject any more electrons, and the gap voltage will gradually build up to its former value.

The above discussion gives rise to the question of whether such a cavity will be self-quenching. The microwave field will certainly overshoot $0.85V_{00}$, and if all sources of renewed multiplication, such as residual ions, electrons, etc., are removed before the microwave field can build up to $0.85V_{00}$ again, then the cavity will be self-quenching.[4] It is experimentally observed, however, that the cavity is not self-quenching. While a few pulses seem to be self-quenched, this might be caused either by statistical fluctuations in the number of ions produced by the electron stream or the secondaries they release or perhaps by noise in the magnetron output.

The rise time of the pulse can be estimated in the following way. The top of the pulse will be reached when the electrons have absorbed enough energy to reduce the microwave voltage below the value required to sustain multiplication. This will occur when the voltage has been reduced by about 2 percent, since, for reasons shown later, the voltage in operation is usually about 2 percent above the minimum required for multiplication. This, in turn, will occur when the energy absorbed by the electrons is about 4 percent of the energy stored in the cavity. The energy absorbed per electron per traversal is nearly $2V_0e/\pi$. We assume that the cavity is a parallel *LRC* circuit where C is the capacity across the gap, L is the inductance of a concentric line having radii equal to the radii of the cavity, and R is the resistance corresponding to losses in the walls of the cavity. The energy stored in the cavity is $\frac{1}{2}CV_0^2$. We now set $n2V_0e/\pi = 0.04CV_0^2$ where n is the number of electrons in the gap at the final multiplication. Substitution of the experimental values $V_0 \simeq 550$ volts and $C \simeq 2\times10^{-13}$ farad leads to $n \simeq 4\cdot10^7$.

The above is a very crude calculation, but indicates that even with a conservative value of 2 for σ, only 24 half cycles of the microwave voltage are necessary for the voltage pulse to build up. If we take the rise time to be the time required for the pulse to rise from 0.1 to 0.9 of its final value we obtain a value of 5×10^{-10} sec. The effect of space charge is neglected because, whereas 10^7 electrons per traversal correspond to about 10 ma, the maximum space charge limited current is about 500 ma for this cavity.

IV. CONSTRUCTION OF MULTIPLIER AND RELATED APPARATUS

The multipliers described here were constructed of oxygen-free high conductivity copper (OFHC) because such copper can be silver soldered in a hydrogen atmosphere without becoming oxidized. All hard soldering operations described here were done in a hydrogen atmosphere. Be-Cu is used as the secondary emissive surface because of the simplicity of activation.[5]

A construction diagram of the cavity used for the detection of gamma-rays was given in Fig. 3. A nomograph, which shows the dependence of center post diameter, kinetic energy of electrons and the power required to operate the cavity, all as a function of gap separation is given in Fig. 4. These curves are calculated on the assumption that the cavity is a simple *LRC* circuit and are based on the measurements of the cavity shown in Fig. 3.

---

[4] It can easily be shown that if 1 ev ions were produced by the electrons, for example, that they would not disappear in time, but it is hard to see where the ions could get so much energy.

[5] J. S. Allen, "An improved electron multiplier," Rev. Sci. Inst. 18, 739 (1947).

The cavity is assembled with silver solder. The joint between the top and bottom halves is made with wax or a gold gasket for ease in disassembly.

After the cavity is evacuated, it is found that no multiplication takes place until the surfaces are activated by the admission of enough power to cause breakdown in the cavity. This latter power level is easily recognized by the fact that the power in the monitor loop suddenly stops increasing as the available input power is increased. After the cavity has remained broken down for a few minutes, the available power can be decreased to the point where the power in the monitor loop just begins to change, and in this region, the cavity is sensitive to gamma-rays.[6] If the power is raised above this point, it will again break down. The cavity is therefore usually operated at a power level only a few percent above the minimum.

The source of microwave power is required to supply a watt or so at a wave-length of about 10 cm, but it is desirable to have considerably more than this available. A QK-59 magnetron (Sylvania) was used in this laboratory.

A block diagram of the equipment used is shown in Fig. 5. Most of the components are used in a standard way. The parts peculiar to this experiment are as follows. The 30 ohm resistor in series with the magnetron power supply enables one to modulate the voltage on the magnetron. In particular, it is used to get pulses to quench the cavity counter by reducing the available power and to pulse the microwave power to test the rest of the equipment. A thyratron which shorts an artificial line is used to get microsecond pulses from a low impedance. The lossy cable is used to reduce the percentage of noise in the microwave power since the absolute magnitude of the noise generated by the magnetron is nearly the same at low levels as at high levels. The 2 microsecond pulser produces a 40 volt pulse every time the cavity breaks down and quenches the cavity. For simple visual observation of the pulses a Kaylab amplifier (voltage gain 10^4) is used and its output is seen on a simple 3-inch oscilloscope. Two Navy #TS-34A/AP 'scopes, which have a frequency response flat out to 4 mc, are used, one merely as an amplifier for the other, to get rough estimates of the size and shape of the pulses.

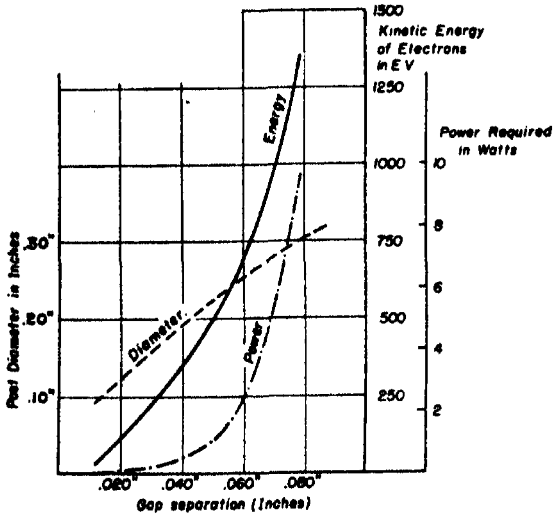

FIG. 4. Nomograph for cavity construction. (Pertinent data for cavities having height = 0.58" and outer radius = $\frac{13}{16}$". Q assumed = 10^3 and $\lambda = 10.9$ cm.)

V. CHARACTERISTICS OF GAMMA-RAY DETECTION

Since this counter is not self-quenching, an external quencher in the form of a pulse to momentarily decrease the magnetron output was employed. An unfortunate consequence of such external quenching is that the pulse shape and size is distorted and takes the form shown in Fig. 6. Because the quenching pulse is necessarily greater than the initial pulse, quantitative information about the pulse height distribution such as might be obtained from a discriminator and scaler is made unobtainable. But visual observation of the pulses shows that they are all of nearly the same height just as is to be expected.

As mentioned previously, the rise time of these pulses is expected to be of the order of 5×10^{-10} sec. Only visual observation of the pulses was employed to measure the rise time and the only conclusion to be drawn is that the rise time is at least as fast as the oscilloscope amplifier and so is probably less than 10^{-7} sec.

The amplitude of the pulses due to gamma-rays is about 3 or 4 times larger than the background noise. This background noise comes primarily from the magnetron.

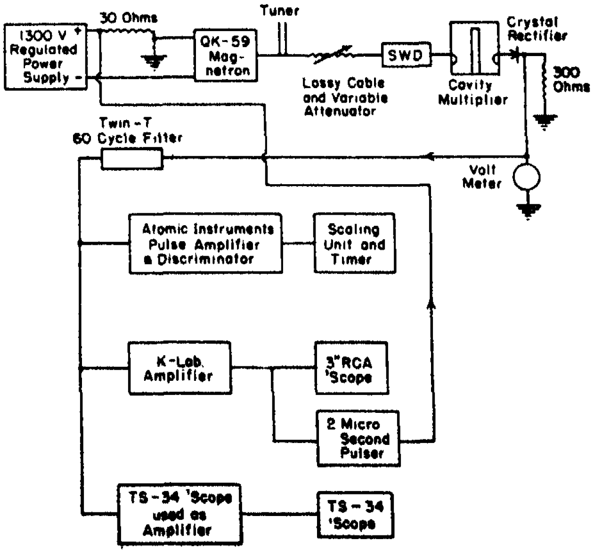

FIG. 5. Block diagram of apparatus.

---

[6] Successful cavities have been examined after the activation by breakdown, and it is found that the gap surfaces are darkly colored. Chemical tests indicate that the darkness is primarily a copper oxide. The presence of BeO is, however, not ruled out.

The magnitude of the background noise at the crystal rectifier is about 1 millivolt r.m.s. The height of the initial pulses due to the gamma-rays is about 4 mv. The quenching pulse is about 3 times as large as this, but the magnitude of the quenching pulse should not be critical. The d.c. voltage across the crystal rectifier is about 0.3 volt. Thus the gamma-ray pulses are between 1 percent and 2 percent of the d.c. voltage—a reasonable figure since the input power level is only a few percent above the minimum necessary for sustained multiplication.

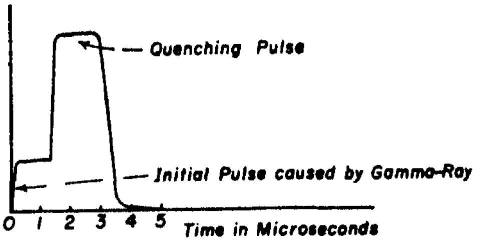

FIG. 6. Typical voltage pulse at crystal rectifier.

The efficiency of this counter is of the order of 1.5×10^{-5} count per gamma-ray.[7] If it is remembered that this counter is sensitive to about one-sixth of the electrons, the efficiency of the surface itself is about 10^{-4} where efficiency now means the number of electrons emitted which are capable of starting multiplication per gamma-ray. This latter figure should be the same order of magnitude as the efficiency of a static electron multiplier having plates of Be-Cu. J. S. Allen[6] reports that the efficiency of his multiplier was of the order of 10^{-4} for gamma-rays.

The number of background counts observed with the cavity counter is of the order of one count every 200 sec.[8] This number, however, is difficult to measure because the magnetron output must be held constant to 1 percent for such a long time.

Two sources of Ra were used to check the proportionality of this counter, and it proved proportional up to 10 counts/sec. This was measured using 10 millicuries of radium and unfortunately a stronger source was not available to check the deadtime. The deadtime, however, must be at least as long as the quenching pulse, and there seems to be no reason for it to be longer than this.

It would be highly desirable to get a curve of the counting rate or efficiency of the counter as a function of the microwave power input because the magnitude of the range of power permitting multiplication would yield information on the maximum time delay in secondary emission.[9] Unfortunately, the counter is sensitive over a very small range of input power corresponding to 70 to 73 arbitrary units and breaks down when this limit is exceeded. Fluctuations of 1 or 2 such units are caused by fluctuations in the high voltage supply and make it exceptionally difficult to obtain such a curve but visual observation of the counting rate on a 'scope indicates that the efficiency remains roughly the same in this range.

It is worth mentioning that sinusoidal modulation of the microwave power can be used to quench the cavity, if the modulation frequency is high enough compared to the average number of counts per second.

ACKNOWLEDGMENTS

In conclusion, the author wishes to thank the faculty and graduate students at the Randal Morgan Laboratory for their helpful suggestions. In particular, a great debt is owed to Dr. P. H. Miller, Jr. for his constant interest and support. A debt of gratitude is due to various firms for expeditious handling of small items, in particular, RCA Laboratories and the Sperry Gyroscope Company. The author also thanks the Navy Bureau of Ships for financial support of this project.

---

[7] In computing this efficiency, 6×10^{10} gamma-rays per second per gram of Ra was assumed. Corrections were made for the fact that 60 cycle hum in the power supply makes the gap voltage fall below $0.85V_{00}$ for about $\frac{1}{3}$ of a cycle. The source used was measured by Radium Service, Philadelphia, Pennsylvania.

[8] This is a higher background than one would expect from cosmic radiation and is probably due in part to thermal electrons.

[9] An attempt was made earlier to make a microwave photomultiplier to get such information but this failed, probably because of ionization difficulties.

THE REVIEW OF SCIENTIFIC INSTRUMENTS VOLUME 20, NUMBER 9 SEPTEMBER, 1949

The Theoretical Background of the Multiple Pressure Tube Anemometer

PAUL R. GOUDY[*] AND HENRY F. COLVIN III[**]
Kollsman Instrument Division of Square D Company, Elmhurst, New York

(Received May 3, 1949)

A recent investigation has resulted in the development of a multiple pressure tube anemometer, which measures both wind speed and direction without moving parts exposed to the wind.

From the expression for the air flow past a quadric surface, it is shown that, by the use of one system of suitably spaced impact holes, it is possible to measure the rectangular components of wind velocity in one quadrant. Another arrangement of holes is presented that takes advantage of the breakdown in flow pattern past 90° to measure wind components in all quadrants without ambiguity.

The components of wind velocity so measured are combined in an electromechanical system which provides indications of speed and direction.

Finally, the experimental instrument embodying these principles is evaluated and performance data taken from it are presented.

SYMBOLS

p = Free stream static pressure.
p_1 = Static pressure in disturbed flow.
$\Delta p_1 = p_1 - p$ = Superstream pressure in disturbed flow.
p_2 = Static pressure at quadric surface.
$\Delta p_2 = p_2 - p$ = Superstream pressure at quadric surface.
Δp_4 = Superstream pressure at top hole in experimental heads.
P = Total pressure.
q = Impact pressure.
V = True wind speed.
V_1 = Wind speed in disturbed flow.
V_2 = Wind speed at quadric surface.
ρ = Air density.
θ = Impact angle of wind.
α = Angle of resultant magnetic field.
K_a = Inertia factor.
E_1, E_2 = Output voltages of potentiometers.

I. INTRODUCTION

EXISTING methods of measuring wind velocity involve the combination of two sensing instruments, one for speed and one for direction. These are of various types, the oldest being the wind-vane. Speed is generally measured by a rotation anemometer, although other instruments such as pressure plates, bridled cups, and pressure tubes are also in use. All, however, are characterized by the fact that they must have some moving part in the sensing element.

A multiple pressure tube anemometer which does not possess this characteristic has been developed.[†] It is the purpose of this paper to discuss the theoretical and practical considerations which make this instrument possible.

II. GENERAL THEORY

Pitot static tubes in use today have been specifically designed to minimize the effect of pitch and yaw. However, a definite relationship exists between the pressure measured by an impact tube and the angle it makes with the wind stream (yaw angle).

Let us assume that air is a weightless fluid of constant density and zero viscosity. It is flowing without turbulence at a free stream velocity V with a free stream static pressure p. The flow is disturbed by the presence of some object, so that the fluid at some point in the vicinity of the object is flowing at the velocity V_1, with a static pressure of p_1, and a superstream pressure of Δp_1.

Any point at which the fluid is brought to rest is called a stagnation point. The corresponding pressure is P and the superstream pressure, called in this case the impact pressure, is q. Then,

$$q = \tfrac{1}{2}\rho V^2, \tag{1}$$

and by Bernoulli's statement of the Law of Conservation of Energy,

$$p + \tfrac{1}{2}\rho V^2 = p_1 + \tfrac{1}{2}\rho V_1^2. \tag{2}$$

Combining (1) and (2) and clearing:

$$\Delta p_1 / q = 1 - (V_1^2/V_2^2). \tag{3}$$

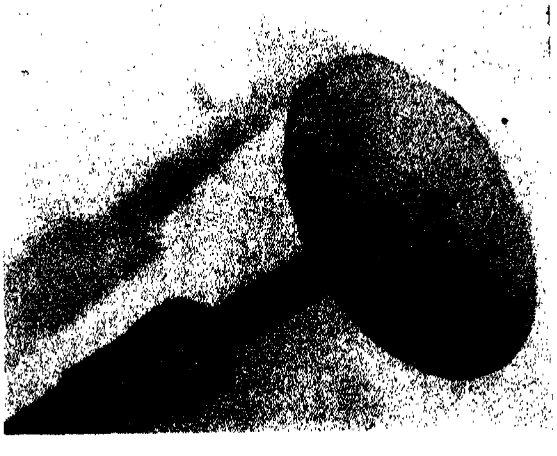

FIG. 1. Test head, showing top reference hole.

---

[*] In charge of Research and Development of Meteorological Instruments.

[**] Engineer.

[†] Developed under Signal Corps Contract No. W36-039-SC-32292.

Lamb[1] has pointed out that a solid moving in translation in a fluid has its apparent inertia increased by a factor K_a, called the inertia factor, which is proportional to the mass of the fluid displaced and is a function of the shape of the solid. For simple quadrics, such as the sphere, ellipsoid, cylinder, etc., the inertia factors have been computed and the results checked experimentally.[2] The inertia factor affects, among other things, the velocity V_2 of the fluid stream along the surface of the body in the following fashion:[2]

$$V_2 = (1+K_a)V \sin\theta, \tag{4}$$

where θ is the polar angle on the quadric.

For a sphere,

$$K_a = 0.5,$$

so that,

$$V_2 = 1.5V \sin\theta, \tag{5}$$

and, combining (3) and (5) and canceling the V^2:

$$\Delta p_2/q = 1 - 2.25 \sin^2\theta, \tag{6}$$

where Δp_2 is the superstream pressure at the quadric.

That is, the ratio of the superstream pressure at any point on the sphere to the impact pressure is a function of the impact angle of that point with relation to the direction of flow.

If a circular plate of zero thickness is placed in the fluid stream parallel to the direction of flow, it will have an inertia factor

$$K_a = 0.$$

Therefore, from (4)

$$V_2 = V \sin\theta, \tag{7}$$

and, combining (3) and (7)

$$\Delta p_2 = \tfrac{1}{2}\rho V^2 \cos^2\theta. \tag{8}$$

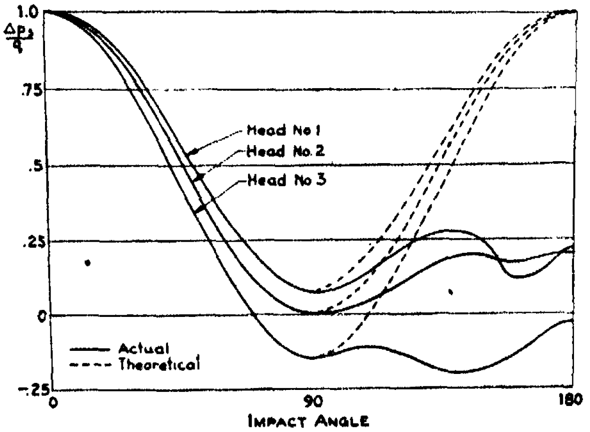

FIG. 2. Variation in measured impact pressure with yaw angle for three experimental heads.

This indicates that the superstream pressure is identical to the impact pressure which would be measured if a wind with a free stream speed of $V \cos\theta$ were blowing directly into the tube.

It is apparent then that the tube is actually measuring the component of the free stream wind velocity which is normal to the tube opening. If a hole at right angles to this tube is considered, the superstream pressure at this hole will be

$$\Delta p_2 = \tfrac{1}{2}\rho V^2 \sin^2\theta, \tag{9}$$

which is equivalent to measuring the wind speed $V \sin\theta$ head on.

Thus, it is apparent that when a wind blows on two perpendicular impact tubes located in a circular plate of zero thickness, the pressures measured in the tubes correspond to the components of wind velocity normal to each tube.

In the more general case of a circular plate with finite thickness

$$K_a \neq 0$$

and

$$\Delta p_2/q = 1 - (V_2^2/V^2), \tag{10}$$

which is a special case of (3).

The superstream pressure for any point on the circumference becomes

$$\Delta p_2 = \tfrac{1}{2}\rho(1+K_a)^2 V^2 \cos^2\theta - \tfrac{1}{2}\rho[(1+K_a)^2 - 1]V^2. \tag{11}$$

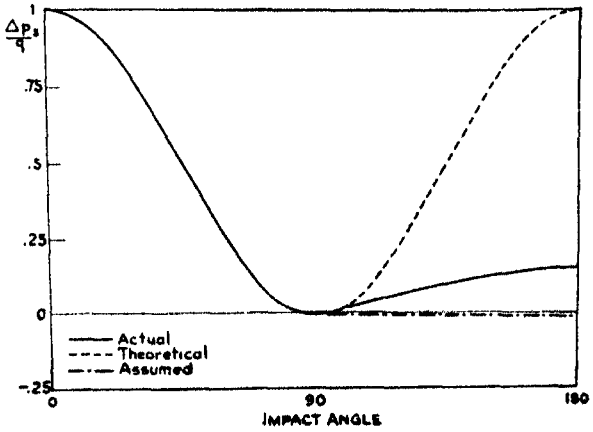

FIG. 3. Yaw angle characteristic for experimental head #4, showing the experimental data, the curve predicted by theory, and the curve assumed in this development.

This means that the superstream pressure at the circumference of the plate is composed of two parts, one dependent on both wind speed and impact angle and the other dependent only on wind speed.

If a pressure equal in magnitude to the part dependent only on wind speed were added algebraically to this superstream pressure, the resulting pressure would be

$$\Delta p_3 = \tfrac{1}{2}\rho(1+K_a)^2 V^2 \cos^2\theta, \tag{12}$$

and it would be possible to measure wind components in the same manner as with the theoretical plate of zero thickness.

---

[1] Horace Lamb, F.R.S., *The Inertia-Coefficients of an Ellipsoid Moving in Fluid*, R & M #623, Advisory Committee for Aeronautics (October, 1918).

[2] A. F. Zahm, *Flow and Drag Formulas for Simple Quadrics*, N.A.C.A. Report #253 (1928).

III. EXPERIMENTAL RESULTS

In this analysis the superstream pressure (Δp_2) at the quadric surface has been considered with reference to the free stream static pressure. Since true static pressure is difficult to obtain in practice, however, the reference pressure in the test heads has been obtained from a flush hole located symmetrically at the top of the head (Fig. 1). A consideration of the streamlines of flow over the head indicates that the pressure at this hole is less than the free stream static pressure by some value Δp_4 which is in effect a negative superstream pressure.

Thus, the differential pressure measured between the impact and top holes may be described as

$$\Delta p_5 = \Delta p_2 - \Delta p_4. \tag{13}$$

Since Δp_4 is proportional to V^2, is independent of impact angle, and is affected in absolute magnitude by the thickness of the head, a head contour exists in which

$$\Delta p_4 = -\tfrac{1}{2}\rho[(1+K_a)^2-1]V^2. \tag{14}$$

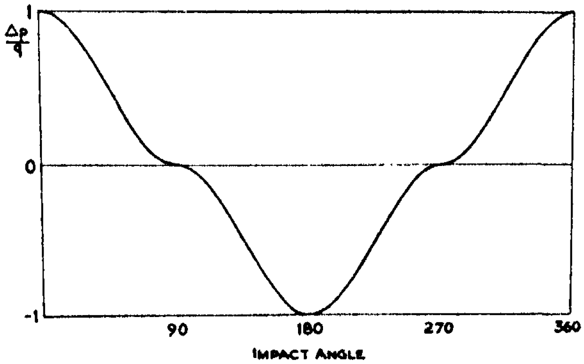

FIG. 4. Assumed variation with yaw angle of differential pressure between diametrically opposed holes in final head.

This relationship makes practicable the operation proposed in arriving at Eq. (12).

The test results obtained from three experimental heads are shown in Fig. 2. Head number 2 conforms to the relationship of Eq. (14), since Δp_5 is equal to zero when $\theta = 90°$.

The discrepancy in these curves between the actual results and theory is caused by the fact that the flow streamlines break away from the surface at impact angles greater than 60° to 90°, depending on the head design. This discrepancy can be avoided in an actual instrument by limiting the use of an impact opening to the region of 0°±90°.

Data from head number 4, shown in Fig. 3, offer another solution to the problem. The variation in pressure in the region 180°±90° is very small with respect to the total change in pressure in the region of 0°±90°. The characteristic in the latter region may be approximated by Eq. (11) and the characteristic between 90° and 270° by

$$\Delta p_2\Big|_{90°}^{270°} = -\tfrac{1}{2}\rho[(1+K_a)^2-1]V^2, \tag{15}$$

(shown in Fig. 3 by the "assumed" curve).

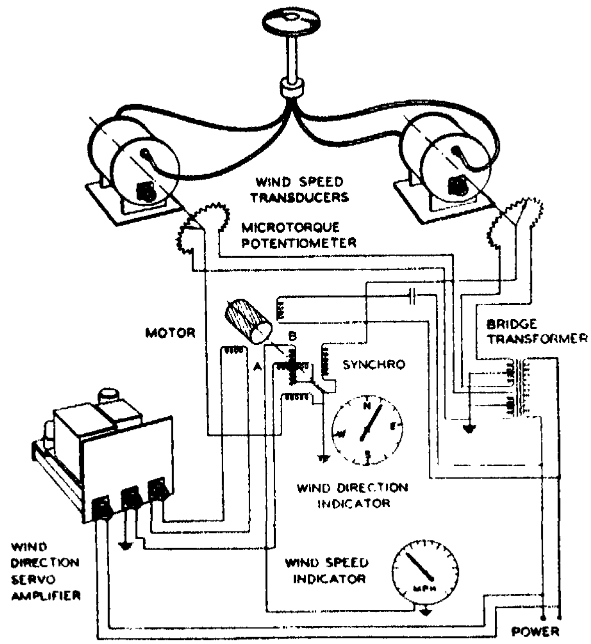

FIG. 5. Schematic diagram of the multiple pressure tube anemometer.

Thus, the differential pressure between two holes 180° apart (Δp) can be represented by the two following equations

$$\Delta p\Big|_{270°}^{90°} = \tfrac{1}{2}\rho(1+K_a)^2V^2\cos^2\theta, \tag{16a}$$

$$\Delta p\Big|_{90°}^{270°} = -\tfrac{1}{2}\rho(1+K_a)^2V^2\cos^2\theta \tag{16b}$$

(equations shown in Fig. 4), representing one component of the wind. Two holes placed on an axis at right angles to that of the first pair will measure the perpendicular component.

IV. COMBINATION OF WIND COMPONENTS

These components may be combined to give wind speed and direction indications in a number of ways. One simple means is provided by connecting each pair of impact holes to a differential pressure diaphragm which, through a suitable mechanism, positions a linear potentiometer in proportion to the square root of the differential pressures.

If these potentiometers are connected as shown in Fig. 5, the a.c. voltages E_1 and E_2 appearing between the potentiometer sliders and ground will be a function of the position of the sliders and hence of the square root of Δp:

$$E_1=K/\sqrt{2}(1+K_a)\rho^{\frac{1}{2}}V\cos\theta, \tag{17}$$

and

$$E_2=K/\sqrt{2}(1+K_a)\rho^{\frac{1}{2}}V\sin\theta, \tag{18}$$

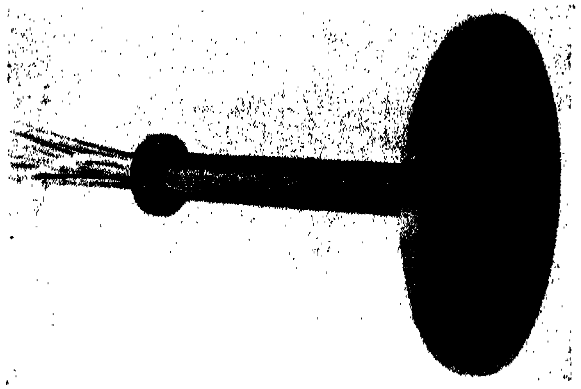

FIG. 6. Final head, with four impact holes.

where K is equal to the electromechanical calibration constant of the system. All of the constant factors may be combined to give

$$E_1=K'V\cos\theta, \tag{19}$$

and

$$E_2=K'V\sin\theta. \tag{20}$$

E_1 and E_2, when applied to two mutually perpendicular coils, create two electromagnetic fields F_1 and F_2 whose magnitudes may be represented by

$$F_1=K''V\cos\theta, \tag{21}$$

and

$$F_2=K''V\sin\theta. \tag{22}$$

The magnitude of the resultant electromagnetic field F, which is the vector sum of F_1 and F_2, is proportional to wind speed,

$$\begin{aligned}F&=(F_1{}^2+F_2{}^2)^{\frac{1}{2}},\\&=((K'')^2V^2\cos^2\theta+(K'')^2V^2\sin^2\theta)^{\frac{1}{2}},\\F&=K''V,\end{aligned} \tag{23}$$

and its direction (α) is representative of wind direction

$$\begin{aligned}\alpha&=\tan^{-1}(F_2/F_1),\\\alpha&=\tan^{-1}(K''V\sin\theta/K''V\cos\theta),\\\alpha&=\theta.\end{aligned} \tag{24}$$

If a rotor carrying two perpendicular windings be placed in this magnetic field, and connected as shown in Fig. 5, the voltage induced in rotor winding A will cause a servo motor to position the rotor to a null. In this position, the axis of rotor winding B is parallel to the direction of the electromagnetic field and has a voltage induced in it. Thus, the position of the rotor indicates the direction of the field, and hence the direction of the wind, and the voltage induced in winding B is proportional to the strength of the magnetic field, and hence to the speed of the wind.

V. ACCURACY OF RESULTS

Certain of the equations introduced in this paper have only approximated the actual test results obtained. In order to justify these approximations, it remains to examine the errors introduced into the theoretical solution by the use of actual results in place of the mathematical relationships.

Table I shows the results of a series of calculations of the wind speed and direction which would be indicated by an instrument operating on the basis of Eqs. (16a) and (16b), and by one based on Eq. (12). Equations (12) and (16) are mathematically identical but are based on different physical circumstances. It will be noted that the errors resulting from the use of two diametrically opposed holes are small and are less than those resulting from the use of a top reference hole.

TABLE I. Experimental results.

A. Calculated by Eq. (12) with data taken using top reference hole.

Wind speed—100 m.p.h.

Wind direction relative to impact hole (degrees)	Error in wind direction (degrees)	Error in wind speed (m.p.h.)
0	6.7	8.2
20	−0.7	7.7
40	−0.8	6.3
60	1.1	7.0
80	0.3	8.6

B. Calculated by Eqs. (16a) and (16b) with data taken using two holes 180 degrees apart.

Wind speed—100 m.p.h.

Wind direction relative to impact hole (degrees)	Error in wind direction (degrees)	Error in wind speed (m.p.h.)
0	0	3.0
20	1.2	2.5
40	−0.6	−1.7
60	−0.1	0.5
80	−2.4	4.6

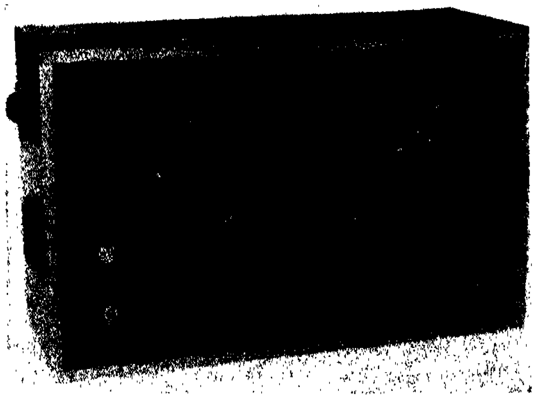

FIG. 7. Wind speed and direction indicator for multiple pressure tube anemometer.

VI. THE EXPERIMENTAL INSTRUMENT

An experimental instrument was constructed which functions in accordance with the relationships of Eq. (16). It consists essentially of a detecting head similar to Fig. 6 with the four pitot openings connected to two electro-mechanical transducers. The two electrical outputs are a function of the differential pressures between the North and South openings and between the East and West openings, respectively. The transducers are connected electrically to an electro-magnetic resolver which presents the values of wind speed and direction on two indicating dials as shown in Fig. 7.

Although the operation of this instrument is adversely affected at low wind speeds, it will, even in the experimental form, measure wind speed and direction at speeds above 10 m.p.h., with an accuracy sufficient for most practical purposes.

A discussion of the construction and operation of the completed experimental instrument will be the subject of a future paper.

THE REVIEW OF SCIENTIFIC INSTRUMENTS VOLUME 20, NUMBER 9 SEPTEMBER, 1949

The Detection of Ca^{45}, I^{131}, P^{32}, and Zn^{65} by Photographic Film

DANIEL STEINBERG* AND A. K. SOLOMON
Biophysical Laboratory, Harvard Medical School, Boston, Massachusetts

(Received June 3, 1949)

The density response of photographic emulsions to the radiations of Ca^{45}, I^{131}, P^{32} and Zn^{65} has been determined. Characteristic curves for all four isotopes against Eastman no-screen x-ray film and Eastman type *M* stripping film are presented, together with certain additional studies on Eastman *NTB* stripping film and Eastman type *K* x-ray film. The relative photographic effectiveness of the isotopes examined increases in the order: Zn^{65}, P^{32}, I^{131}, Ca^{45}, C^{14}. Applications of the data for quantitative radioautography are discussed.

THE present studies are an extension of the research previously reported on the detection of C^{14} by photographic film.[1] In order to determine the response of photographic film to the continuous spectrum of a beta-emitting isotope, nineteen different films were exposed to C^{14}, and their characteristic curves obtained. It has seemed desirable, particularly in view of the importance of radioautographs, to extend this work to include other beta- and gamma-emitters. For this purpose we have selected four isotopes of biological interest whose disintegrations cover a wide range of energies.

EXPERIMENTAL METHOD

The conventional method of determining the contrast and sensitivity of a photographic film involves exposing the film to a uniform source of radiation through an absorbing wedge. A radiator comprising eight small sources of radioactive carbon of graded intensity was previously used[1] to replace the conventional uniform source and wedge. This method has been continued and extended for use with other isotopes. Figure 1 shows the radiator, its collimator which limits the beta-radiation received by the film to a small uniform circle, and an example of an exposed film. Characteristic curves showing the relationship of the logarithm of exposure to density have been obtained by exposing the film to the radiator, developing under standard conditions, and measuring the density with an Ansco-Sweet photoelectric densitometer.

PREPARATION AND CALIBRATION OF SOURCES

A. Simple Beta-Emitters

Ca^{45} was obtained from the Atomic Energy Commission as Ca^*Cl_2. Eight successive dilutions, varying in concentration by a factor of three between steps were prepared. Measured volumes were then evaporated to dryness in the radiator cavities, with the addition of one drop of 1 percent Aerosol OT as a wetting agent.

P^{32} obtained from the Atomic Energy Commission as carrier-free $H_3P^*O_4$ was prepared in the same way.

Sources prepared by evaporation, even with the addition of a wetting agent, do not spread uniformly over flat surfaces. In these preparations the actual distribu-

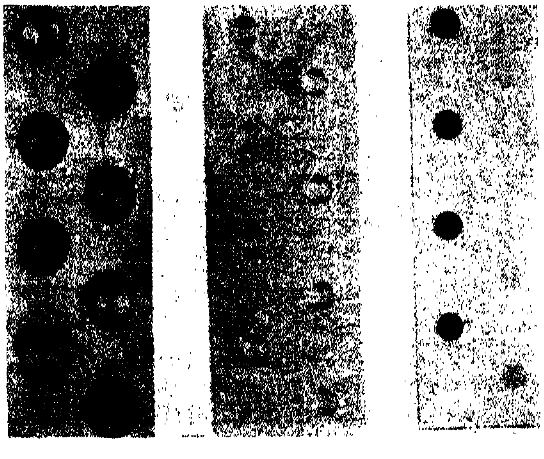

FIG. 1. Radiator with collimating piece and specimen film.

---

[*] Postdoctorate Research Fellow, National Institutes of Health.

[1] J. Cobb, and A. K. Solomon, Rev. Sci. Inst. 19, 441 (1948).

tion consisted of a uniform central area, with a slight accumulation of material at the perimeter. The use of collimators limited the effective source to the uniform central area, as confirmed by displacing the collimator relative to the radiator by a distance up to 2 millimeters and finding no change in the radiation as measured directly by a Geiger counter. A further check was provided by microscopic examination of the image.

B. Complex Beta- and Gamma-Emitters

Because of the high penetrating power of their gamma-rays, it was not practicable to use collimators with isotopes such as I^{131} and Zn^{65}. Uniform sources were therefore prepared from suspensions of precipitated material. I^{131} was obtained from the Atomic Energy Commission as a KI^* solution. Graded dilutions were prepared, and added to a fixed amount of carrier KI. BiI^*_3 was precipitated and transferred to the radiator as a water-acetone slurry with a micropipette. In the course of drying under the infra-red lamp, the precipitate became rather pasty and could then be spread uniformly by a fine beaded glass capillary.

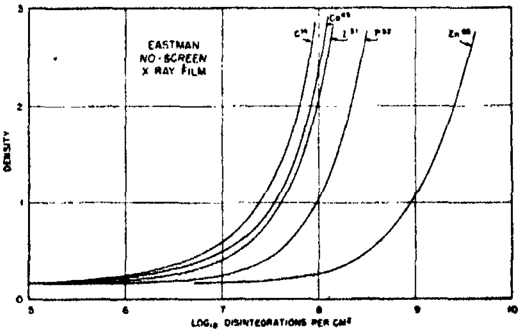

FIG. 2. Characteristic curves for Eastman no-screen x-ray film. Exposure times 1–3 hours. Development 5 minutes at 68°F in *D*-19.

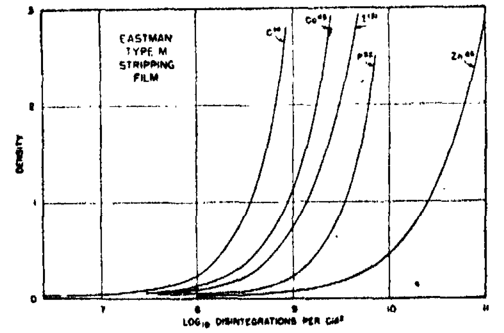

FIG. 3. Characteristic curves for Eastman type *M* stripping film. Exposure times 16–48 hours. Development 5 minutes at 68° in *D*-19.

Zn^{65} as zinc ammonium citrate was obtained from the Massachusetts Institute of Technology cyclotron (deflector plate *D* 4) through the courtesy of Dr. John Gibson and Dr. Robley D. Evans. Graded dilutions were prepared, added to a fixed amount of carrier $ZnSO_4$, precipitated as Zn^*S and transferred as described for iodine.

TABLE I. Eastman no-screen double x-ray, emulsions YC5133-678-X2 and YN5133-676-1.

Isotope	Sensitivity 0.1 above background	 0.6 above background	Contrast At $D=0.1$	 At $D=0.6$
C^{14}	6.42	7.24	0.31	1.15
Ca^{45}	6.42	7.34	0.27	1.13
I^{131}	6.70	7.42	0.31	1.32
P^{32}	7.11	7.85	0.23	1.41
Zn^{65}	7.96	8.77	0.28	1.18
Eastman type *M* stripping film, emulsion N4X-21896-1				
C^{14}	7.69	8.39	0.28	1.47
Ca^{45}	7.84	8.76	0.20	1.40
I^{131}	8.35	8.96	0.35	1.41
P^{32}	8.75	9.39	0.30	1.66
Zn^{65}	9.47	10.20	0.32	1.34
Eastman *NTB* stripping film, emulsion N4X-22271				
C^{14}	7.65	8.41	0.24	1.25
Ca^{45}	7.86	8.78	0.22	1.20
Zn^{65}	9.50	10.28	0.25	1.25
Eastman type *K* industrial x-ray film, emulsion J-S135-420-89				
C^{14}	6.55	7.31	0.25	0.89
Ca^{45}	6.57	7.56	0.23	0.93
Zn^{65}	8.12	9.04	0.25	0.97

CALIBRATION

Accurate calibration of the sources in terms of absolute disintegrations per minute is essential if one is to compare the photographic effect of different isotopes. Fortunately, the presence of the collimator simplified the calibrations of the beta-emitters, Ca^{45} and P^{32}, because the solid angle of the escaping beam could be embraced by the sensitive volume of the thin-window Geiger counter used for the measurements. Thus, we had effective 100 percent geometry for the collimated beam, and it was necessary only to correct for air and window absorption. Correction for air absorption was made only to the surface of the collimating piece, rather than to the source itself. This gave us a direct count of the actual number of particles striking the film. It was possible to verify that the geometry was 100 percent by comparing counting rates with the collimator absolutely on the axis of the tube, and displaced by as much as 2.5 mm from the axis.

The figures obtained in this fashion have been multiplied by 2 to make the data as presented applicable directly to a real source emitting radiation both up and down. Such a source (uniform, flat, infinitely thin) would theoretically produce some blackening of the film, or at least dissipate some of its energy, outside the periphery of the major exposed area. Therefore, an independent check on the equivalence of the exposure-density relation obtained with a real source seemed necessary.

First, a large piece of filter paper was soaked in Ca^*Cl_2

and a radioautograph was prepared with the film separated from the filter paper by 1.5 mg/cm^2 of aluminum foil to prevent chemical fogging. Using the density pattern of this autograph as a guide, a smaller circle of filter paper of uniform radioactivity was cut out to serve as source for a second radioautograph. This uniform source was calibrated against U_3O_8 corrected for backscatter. The exposure-density values obtained with this real source fell within 10 percent of the values obtained with the radiator calibrated against the counter directly.

Another possible source of calibration error considered was that which might arise from scattering of the beta-radiation from the walls of the collimator at an angle outside the calculated solid angle of radiation. The extent of such scattering was considered unimportant for two reasons. First, the measured counting rate, after air and window absorption correction, was unchanged when the radiator-window distance was increased from 2.5 to 3.5 mm. Second, the border of the image was very sharp and microscopic examination showed a steep gradient from image to background.

Zn^{65} was calibrated with a Lauritsen electroscope against a Bureau of Standards radium gamma-ray standard. Extrapolation from the Bureau of Standards[2] figures for the relative gamma-ray efficiency of the Lauritsen electroscope, and the transmission of radium gamma-rays through the aluminum chamber walls was used to determine the gamma-ray activity in a solution of Zn^*Cl_2. The disintegration scheme of Good and Peacock[3] was the basis of the conversion of measured activity to disintegrations per minute.

To avoid effects of adjacent sources when counting, the radiators for the gamma-emitters were cut into eight individual pieces. A small aliquot of the standardized Zn^{65} was prepared in a cup identical with those used in the radiator. The cup of the radiator was then standardized against this both by direct counting with a Geiger counter, and by comparison using photographic film.

TABLE II. Film characteristics.

	Average background	Average grain size (μ)
No-screen x-ray	0.18	6 –8
Type *M* stripping	0.05	1 –2
Type *K* x-ray	0.28	4 –6
NTB stripping	0.04	0.6–0.8

TABLE III. Initial activity required for radioautographs (15-day exposure, 5-minute development in *D*-19).

Density above background	C^{14}	Ca^{45}	I^{131}	P^{32}	Zn^{65}
		Eastman no-screen x-ray film			
0.1	124	124	414	843	4250
0.6	806	1030	2180	4610	27,400
		Eastman type *M* stripping film			
0.1	2280	3260	18,500	36,700	138,000
0.6	11,400	27,000	75,200	160,000	741,000

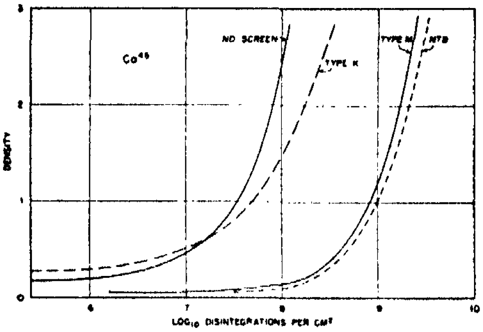

FIG. 4. Comparison of the response of the four films used to beta-radiation from Ca^{45}. Exposure times 1–3 hours for no-screen and type *K* x-ray films; 16–48 hours for type *M* and *NTB* stripping films. Development 5 minutes at 68° in *D*-19.

The I^{131} was standardized both by gamma-radiation against the radium standards and by beta-radiation against a sample of U_3O_8 under a Geiger counter. The decay scheme used was that proposed by Metzger and Deutsch[4] and the corrections for backscatter were taken from Zumwalt.[5] Originally, difficulties were encountered in obtaining agreement between the gamma- and beta-ray standardizations due to losses during preparation of the evaporated sample. Such losses could be prevented by the addition of carrier KI to solutions of NaI* and evaporation at room temperature over night. Under these conditions, we obtained a beta-ray standardization value which agreed within 3.6 percent with the gamma-ray standardization.

FILMS, EXPOSURE, AND DEVELOPMENT

The films chosen for primary investigation were Eastman no-screen x-ray film and type *M* stripping film, as recommended by Cobb and Solomon.[1] These films are of particular interest because of their use in the preparation of radioautographs using the stripping film technique developed by MacDonald, Cobb, and Solomon.[6] Certain additional studies were carried out on Eastman *NTB* stripping film and Eastman type *K* x-ray film.

Films tested were clamped emulsion side down between the radiator and a glass slide, exposed for a measured time interval (1 to 3 hours for no-screen x-ray film; 16 to 48 hours for type *M* stripping film) and developed immediately. Precautions in handling films and procedures for development were those described in the previous paper.[1] Films were developed for exactly five minutes at 20°C in Kodak *D*-19, rinsed 30 seconds in a 1 percent acetic acid stop-bath and fixed in Kodak *F*-5 for twice clearing time.

---

[2] Bureau of Standards, "Suggestions for use of gamma-ray standards."

[3] W. H. Good, and W. C. Peacock, Phys. Rev. 69, 680 (1946).

[4] F. Metzger, and M. Deutsch, Phys. Rev. 74, 1640 (1948).

[5] L. R. Zumwalt, MDDC-1346, U. S. AEC.

[6] MacDonald, Cobb, and Solomon, Science 107, 2786 (1948).

RESULTS

Characteristic curves for the isotopes examined are given in Figs. 2 and 3. For purposes of comparison, measurements have been repeated with C^{14} using the original radiator. In Fig. 2, the density as measured by the densitometer is plotted against the logarithm of the total exposure for type *M* stripping film. Exposure, in terms of total number of disintegrations per cm^2 of exposed film, calibrated as discussed above, has been multiplied by 2 in every case to yield values corresponding to a real source emitting radiation both up and down. Figure 3 is a similar curve for the case of Eastman no-screen x-ray film. In spite of the precautions taken in development, scatter of experimental points on the same radiator is about ±10 percent.

Eastman no-screen x-ray film is a coarse-grained, fast film useful for work with weak sources. It is coated with emulsion on both sides of the support, which contributes to the blackening of the film in those cases (all except C^{14} and Ca^{45}) in which significant amounts of radiation penetrate through the support to the second emulsion. Each coating is 23 microns thick, and the support is 0.203 mm thick. These thicknesses correspond to 6 mg/cm^2 and 25.6 mg/cm^2 respectively (neglecting the 1.2 micron thick gelatin coating on the emulsion). Type *M* stripping film is a fine-grained, slower film which offers better resolution, with an emulsion which is about 10 microns thick, corresponding to about 2.6 mg/cm^2.

The astronomical convention that a density 0.6 above background serve as an index of the speed of the film was followed in reporting the results for C^{14}. Further experience with radioautographs has shown that a criterion of 0.1 density unit above background is of more use in evaluating film for biological investigations. Table I shows the sensitivity and contrast at both values for no-screen x-ray film, type *M* stripping film, *NTB* stripping film and type *K* industrial x-ray film. The contrast in each case is given for the point at which the sensitivity has been measured. As one moves further toward the linear portion of the characteristic curves, the contrast increases to values between 3 and 4. The average grain size as estimated microscopically and average background densities are given in Table II.

Figure 4 shows a series of characteristic curves for Ca^{45} for all four of the emulsions examined. It will be noted that the type *K* film is apparently more sensitive than the no-screen at lower densities. However, this apparent discrepancy between the curve and the values given in Table I disappears when the higher background density of the type *K* film is considered.

For use in radioautographs, it is desirable to know the minimum surface concentration of activity that will produce the desired image density. Table III gives these values in disintegrations/cm^2/minute for densities of 0.1 and 0.6 above background, and fifteen day exposures. If the concentration is markedly non-uniform, the values in Table III will obviously not apply, though in many cases they will provide a first approximation. Scatter, geometry and absorption corrections must be evaluated in relation to the particular technique employed. Latent image fading, for which no accurate data are available for these emulsions, may become important for long exposures.

DISCUSSION

Table I shows that the photographic effectiveness of the isotopes decreases as the maximum energy of the beta radiation increases. Webb[7] has pointed out that the developability of silver bromide grains depends on the number of ionizing events produced within the grain by the passage of a single electron. Since the number of ionizations per micron path reaches its maximum at the end of the path, there is a threshold energy above which the ion pairs are spaced too far apart to permit the formation of a developable grain by a single electron impact. From the examination of electron tracks, Webb assigned a figure of 50 kv for the threshold energy above which electron tracks did not register on Eastman *NTB* film at the time of his paper. This figure is in agreement with that of 50–70 kv obtained by Berriman[8] and of 80 kev obtained by Herz[9] for *NT2a* plates. Since the track lengths that can be observed on the no-screen and Type *M* emulsions are no longer than a very few grains at most, even for C^{14}, it can be inferred that only electrons of less than 50 kv maximum energy will produce developable grains in these films. Every electron must, of course, pass through a range of energies lower than 50 kv, but not all of them will come to this range within the emulsion. Among the elements examined, C^{14} with a maximum range[10] of 27.9 mg/cm^2 (compared to emulsion thicknesses of 6 mg/cm^2 for the first emulsion on no-screen x-ray, and 2.3 mg/cm^2 for type *M* stripping film) should be the most effective, and this is borne out by the data in Table I. The effectiveness decreases with increasing energy of beta-radiation from C^{14} through P^{32} as expected. The new electron plates described by Berriman[11] which are sensitive to electrons of maximum energy would, of course, show a different energy dependence.

From the results obtained with Zn^{65} it can be seen that the contribution of the gamma-ray to the exposure of the film is small, which is to be expected since so little of the energy is absorbed by the film. Qualitatively it would also appear that the contribution of the x-ray is small since the total effectiveness of this isotope is so low. I^{131} falls nicely between Ca^{45} and P^{32} as would be expected from the beta-ray contribution alone, again indicating that the gamma-rays add relatively little to the photographic effect of the isotope.

---

[7] J. H. Webb, Phys. Rev. 74, 511 (1948).
[8] R. W. Berriman, Nature 161, 432 (1948).
[9] R H. Herz, Phys. Rev. 75, 478 (1949).
[10] Solomon, Gould, and Anfinsen, Phys. Rev. 72, 1097 (1947).
[11] R. W. Berriman, Nature 162, 992 (1948).

As a check on the method of calibration used in these experiments, the C^{14} radiator used in the previous work was recalibrated. The results were 17 percent lower than the original values. This may be considered good agreement in view of the uncertainties in the initial calibration and the possibility that the radiator may have lost some activity either by exchange of C^*O_2 from BaC^*O_3 with atmospheric CO_2, or by direct loss through mechanical abrasion. The no-screen and type *M* films were also remeasured to check the characteristic curves. For no-screen, the sensitivity values agree within 5 percent. However, there is an absolute discrepancy in the two values obtained for the type *M* emulsion. The previous emulsion appears to be 1.8 times more sensitive at 0.6 above background than that used in the present series.

It has already been shown[12] that the reciprocity law holds for monochromatic electron beams and x-rays, and so it was to be expected that it would hold for the continuous beta-spectrum. In these experiments, the reciprocity law has been checked with the Zn^{65} radiator and found to hold over the total time range investigated from 1 to 200 hours.

SCINTILLATION INTENSIFIERS

In view of the low sensitivity of films to gamma-radiation, it seemed desirable as suggested in the earlier paper to determine whether fluorescent materials might enhance the response of the film. The following substances were investigated: zinc sulfide, calcium tungstate, fluorescein, anthracene, and naphthalene. In the early phases of our work we did not have available clear crystals of these substances, and so were limited to use of amorphous preparations. Solutions of these were made in dilute celloidin and spread uniformly on a glass slide as support. The resulting smooth sheet was used as a backing for the film during exposure. Calcium tungstate was used in the form of a standard commercial x-ray intensifying screen. Back-scattering from metallic lead strip was also investigated. None of these preparations gave detectable intensification. More recently we have used large clear naphthalene crystals and find that these give quite striking intensification.

USE OF DATA IN RADIOAUTOGRAPHY

The data presented find application both in assay of unknown sources and, reciprocally, in calculation of exposure time for preparations of known activity. In such quantitative applications, rigorous controls must be exercised in handling of films and in processing. For purposes of calibration at the beginning of a study, it is necessary to expose a radiator or other standard source to the film to be used. To eliminate variables in processing and emulsion characteristics, a set of calibrated sources must be exposed along with the unknown and the films developed under uniform conditions.

The autographic method permits assay of the activity of each small area over the entire preparation simultaneously. If it is desired to evaluate the radiation delivered to the film by particular microscopic structures, a microdensitometer may be used. If the definition is fine enough, actual grain counts may be made under the microscope and compared with the series of standard reference exposures.

If it is desired to use the counter data directly to predict optimum exposure times, the characteristic curves given in Figs. 2–4, or the sensitivity values in Tables I and III may be used provided the source of radiation is approximately uniform.

The relation between the sensitivity of no-screen x-ray film and type *M* stripping film provides a most useful index in estimating the exposure time required, particularly for non-uniform sources. It is our practice to put up each series of biological sections against both type *M* and no-screen x-ray film. The first test exposure to no-screen is developed at a time calculated to be less than that required for optimum image. Two or more additional test preparations are then taken off and developed until the optimum value for no-screen exposure is determined. From this value the time required for optimum exposure to the type *M* film may be computed. This procedure is particularly advantageous since the stripping film technique used to obtain high resolution autographs with the type *M* film involves a number of laborious operations, whereas the no-screen exposures can be made quite simply.

ACKNOWLEDGMENTS

The authors wish to express their thanks to Miss Mary Powell Smythe for her valuable assistance in the course of these experiments. This work has been supported in part by the ONR and the AEC.

---

[12] A. Charlesby, Proc. Phys. Soc. London 52, 657 (1940). R. H. Morgan, Radiology 42, 471 (1944).

THE REVIEW OF SCIENTIFIC INSTRUMENTS VOLUME 20, NUMBER 9 SEPTEMBER, 1949

Inductance Apparatus for Diamagnetic Measurements

S. Broersma*
Laboratory for Technical Physics, Delft, Holland

(Received June 1, 1948)

Two types of inductance apparatus have been applied to the measurement of the susceptibility of diamagnetic compounds. With an alternating current apparatus, an accuracy of 0.1 percent of the diamagnetic effect, $\Delta\kappa = 0.7\cdot10^{-8}$, has been obtained. The time of measurement was about 8 minutes. Liquids could be easily measured; solids would give no difficulties. In an apparatus with varying coefficient of inductance, the effect of a moving substance in a magnetostatic field was investigated. To date, its precision is a factor of 10 smaller than that obtained with the first apparatus.

1. INTRODUCTION

In this paper we shall describe two types of inductance apparatus: one operating on a.c. and one in which the sample moves with respect to the magnet. Both have been used for diamagnetic measurements. Detailed information can be found in the thesis of the author.[1]

As voltages generated in secondary coils are measured, we have to investigate the flux Φ threading these coils. Two factors are of interest, *viz.*, the flux Φ_0 as produced by a primary coil carrying a current or by a permanent magnet, and the effect of the sample on this flux. In general one can write:

$$\Phi = (1 + f\kappa)\Phi_0,$$

where f is a "filling-factor" and $\kappa = \mu_r - 1$, the susceptibility referring to unit volume.

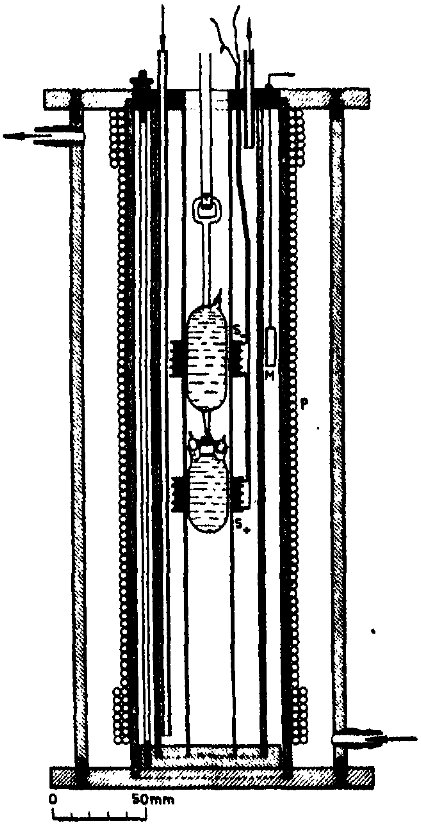

Fig. 1. Coils and cells.

It is obvious that two methods are possible. One can either change the flux $\Phi_0 = M_0 I$ by changing the primary current I, or the filling-factor simply by removing the sample. Assuming in both cases periodic variations of frequency ω, the induced e.m.f. becomes:

$$V = -i\omega M_0 I(1 + f_0\kappa) - i\omega\Phi_0 f_0\kappa/2\sqrt{2}. \qquad (1)$$

Here f_0 represents the case of maximum filling, V and I give the effective values.

The smallest effect to be measured is 0.1 percent of the diamagnetic susceptibility, i.e., $0.7\cdot10^{-8}$. As f_0 does not exceed 0.5, $f_0\Delta\kappa = 3\cdot10^{-9}$. This number emphasizes the difference between the two methods. In the first we have to remove the main term in $1 + f_0\kappa$ which causes most of the disturbances. In the second the diamagnetic effect itself is the main effect. But here the change in the position of the sample, obtained by mechanical motion, introduces disturbances.

2. A.C. INDUCTANCE APPARATUS

With this apparatus the small relative change of $3\cdot10^{-9}$ of an induced e.m.f. has to be measured. In section 3 we shall see that voltage fluctuations of $3\cdot10^{-8}$ v occur so that 10 v have to be generated. Some disturbances, such as capacitive effects, necessitate the use of a low frequency, therefore, 175 c.p.s. was chosen. This fixes the value of $M_0 I$. Further considerations lead to the choice of a mutual inductance apparatus. The use of separate primary and secondary coils offers freedom in the construction. Moreover, the main part of the induced e.m.f. is compensated for by applying two oppositely connected secondary coils.

The calculation of the coefficient of mutual inductance yields

$$M_0 = \mu_0 n N_s S_s. \qquad (2)$$

---

* Now at University of Indonesia, Bandung, Indonesia.

[1] S. Broersma, *Magnetic Measurements on Organic Compounds* (Nyhoff, The Hague, 1947). See also J. Chem. Phys. (to be published).

Here n is the number of primary turns per meter, N_s is the total number of secondary turns, S_s is the cross section of the secondary coil, and μ_0, the permeability in vacuum. Capacitive effects lead to the use of small coils ($M = 0.25$ mh), and primary currents as high as 50 amp.

It is important to watch the filling-factor. An estimate leads to $f_0 = (1-\alpha)r$, where α is the demagnetizing-factor and r the relative amount of volume inside the secondary coil taken in by the sample. We were able to obtain $f_0 = 0.45$.

Figure 1 shows the set of coils used. The solenoid P of length 0.36 m, consists of 90 turns of capillary wire. The two secondary coils S_+ and S_- are composed of four sections of 350 turns each. By adjusting the number of turns, the voltage difference between the two coils can be reduced to 10^{-3} of the main voltage. A small piece of metal M, placed in between the coils, reduces the voltage in phase with the primary current. A horizontal copper plate, outside the primary, cuts the induced voltage down to 10^{-5} of its original size.

The circuit diagram (Fig. 2) shows that the primary current flows through two small resistances, a and b, of 10^{-3} ohm each. The voltages across these resistances are branched off by means of potentiometers. The upper part, containing a variable resistance r and a small resistance c, produces a voltage in phase with the primary current. The lower part consists of an air condenser C of about 2000 $\mu\mu$f and a decade resistance R. The voltage across R:

$$V_{\text{comp}} = i\omega \cdot bRC \cdot I, \tag{3}$$

compensates for the e.m.f. in the secondary coil. Its value is correct within 10^{-5}, at least as concerns voltages of the same phase and for the circuit elements employed.

Both the voltage given by Eq. (3) and the first term in Eq. (1) are proportional to the current and the frequency. Therefore they cancel in the equilibrium condition:

$$M_+ - M_-(1+f_-\kappa) = bC \cdot R. \tag{4}$$

When a substance has to be measured, the lower cell is filled and placed in one of the coils. After R has been adjusted, the sample is brought into the second coil and another reading of R is taken. The difference of both settings then represents twice the effect of the sample. Hence the volume susceptibility can be measured as a change of R, as long as b and C remain constant and M and f reproduce (see section 3b). The upper container serves to compensate for a large part of the diamagnetic effect, of which the values do not vary strongly.

As the factors b, R, C, M, and f for a spherical sample were known, an absolute measurement within 2 percent could be performed. More precisely, the proportionality constant can be found from a calibration with a known substance. A great many results were obtained this way. Comparison with those found with a torsion balance showed agreement within 0.1 percent. By employing relays, most of the measurement is made automatic, with the exception that every 5 seconds a galvanometer reading must be taken. After that, the sample moves and a part of R is short-circuited. R consists of two resistances in series, one to adjust the zero point and one to measure the effect. A measurement takes 8 minutes, filling included. Nine cc of substance are required.

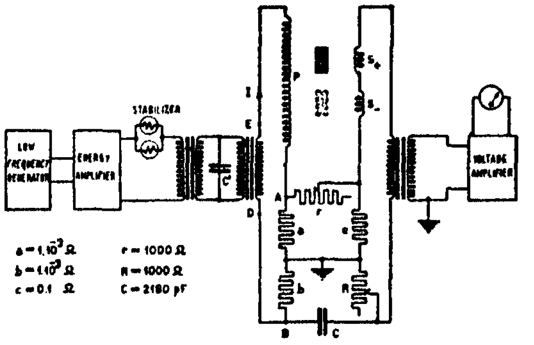

FIG. 2. Circuit diagram.

Some of the auxiliary apparatus is indicated in Fig. 2. An RC generator supplies a signal of constant frequency and small distortion to the energy amplifier which has an output of 200 w. The common point of the primary and secondary circuit has to be grounded. This necessitates the use of an input transformer which also reduces the effect of the amplifier noise. A twin-T network limits the band width to 1 c.p.s.

A galvanometer, whose field coils are supplied with a.c., is used as null-instrument. The galvanometer gets a deflection when a phase relation between field and measuring current exists. The band width is 3 c.p.s.; the scale is linear. Two galvanometers are used: one in phase with the e.m.f. and one 90 degrees out of phase. The phase is adjusted by utilizing the phase change, occurring in the filters employed, near their resonance point.

3. DISTURBING EFFECTS

(a.) Because the apparatus is based upon the measurement of an e.m.f., the voltage fluctuations occurring in resistors and amplifier tubes limit the precision. These voltages are of the order of $3 \cdot 10^{-8}$ v. This value was also imposed as a limit for other disturbances.

(b.) According to Eqs. (1) and (2), V depends upon geometrical conditions like S and f. In connection with the expansion of the surface of the copper coil, a temperature constancy of 10^{-4}°C in the time between two readings is necessary. With a swift oil stream and a regularly moving sample, this can be achieved.

By adding some turns at the end of the primary coil, the inhomogeneity of the field has been reduced to a relative change of 10^{-5} per mm. A displacement of the secondary coil of 0.3 μ is allowed. The value of f remains constant within 0.1 percent if the sample does not move more than 1 mm from a central position.

(c.) The proportionality between the e.m.f. and the primary current is important in connection with the required constancy of the latter. Observation showed that a doubling of the current changed the adjustment by an amount equal to twice the diamagnetic effect. By shunting the coil it was easily found that the supply circuit accounted for no more than two percent of this effect.

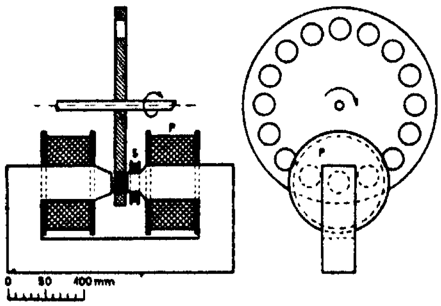

FIG. 3. Apparatus with varying inductance.

An important part of the non-linearities is due to eddy currents in the coil. The magnetic field generates currents in the copper wires which may produce an extra field as large as 0.1 percent of the original. This places a limit upon the size of the wires. Furthermore, for the reproduction of this extra field it is necessary to control the specific resistance of the metal, and hence, the local temperature of the wire within 10^{-3}°C. As the heating of the coil is proportional to I^2t, we can expect a non-linearity depending upon t. Oil cooling of the secondary suppresses this effect.

An instantaneous non-linear effect is caused by ferro-magnetic impurities. An amount of iron of $4\cdot10^{-9}$ g gives a change of 0.1 percent of the diamagnetic effect. The non-linearity is about one-tenth of this. Any impurities present in the copper coils can be compensated by the addition of a piece of iron. The samples are freed from iron by pouring them through a funnel in a magnetic field.

(d.) Both the applied voltage across the primary and the induced e.m.f. in the secondary coil lead to the appearance of capacitive effects. In order to keep these small, one has to use coils of small impedance. As all effects increase with the square of the frequency, this has to be kept low. The effect of the self-capacitance can be studied by assuming a condenser C_s to be placed across each of the secondary coils. If the generated e.m.f. is V_0, then the change of the voltage due to the self-capacitance is:

$$V_{\mathrm{self}} = -V_0\cdot i\omega C_s Z_s \approx 2V_0(\nu/\nu_0)^2. \tag{5}$$

Here Z_s is the impedance of one secondary coil, ν_0 its natural frequency. The factor 2 takes care of the fact that, in our apparatus, the resistance part of the impedance is of the same order of magnitude as the inductive part. As ν_0 is 160 kc.p.s., the voltage represented by Eq. (5) corresponds to 0.3 of the diamagnetic effect. Although the coils compensate each other to some extent, still the frequency has to be kept constant within some tenths of one percent. C_s is kept low by layer-spacing and by dividing the coil into sections; it proves to be 18 $\mu\mu$f.

The phenomenon of mutual inductance can be represented by two condensers connecting the center point of the primary with the center points of the secondary coils. If Z_p is the impedance of the primary coil, one finds a voltage variation of:

$$V_{\mathrm{mut}} = i\omega I\cdot C_m Z_p Z_s \approx V_0\cdot \nu^2 N_s N_p S_p\cdot f(r_p/r_s). \tag{6}$$

This has the same order of magnitude as the diamagnetic effect. A small number of turns is preferable. The geometrical factor is a minimum when r_p/r_s is somewhat larger than two. C_m is 12 $\mu\mu$f.

Moisture on the quartz container causes large dielectric losses. A single touch of the fingers can alter the effect by one tenth. However, a thin tin foil, placed between coil and container, eliminates this entirely. Furthermore, the dielectric properties of the substance then cannot affect the measurement.

4. INDUCTANCE APPARATUS WITH MOVING SAMPLE

This type of instrument, based upon the second term in Eq. (1), seems not yet to have been used for the purpose of susceptibility measurement. A static magnetic field is applied so that an iron core, which increases the flux considerably can be used. In the a.c. apparatus, the flux variations in the neighborhood of a substance were observed by means of a tightly fitting coil. Because of the motion of the sample this is not possible here, but, due to the iron core, the substance is able to produce an overall change in the flux which can be observed somewhat farther away in the circuit. There is a maximum flux variation when the "magnetic resistance" of the sample equals that of the rest of the magnetic circuit, hence, $f_0 = 0.5$.

By using several samples or several magnetic poles, the flux pulses can be made to follow each other in a more or less periodic way. They have to be spaced carefully so that the fundamental obtains a maximum amplitude. If there are several poles, it is advantageous to connect neighboring secondary coils oppositely. This improves the shape of the voltage curve and reduces the effect of current variations in case an electromagnet is used.

The frequency ω, occurring in Eq. (1), depends upon the number of revolutions per second r of the rotating part (either sample or magnet), the number of samples p, and the number of poles. Substituting this in the formula and combining the last factor with Φ_0, we get:

$$V = -i(\pi/\sqrt{2})f_{0\kappa}\cdot rp\cdot\Phi_{\text{tot}} \approx 0.15p\Phi_{\text{tot}} \text{ millivolts.} \quad (7)$$

Assuming that a three-phase motor is used so that $r=25$, and by substituting $f_{0\kappa}=-3\cdot 10^{-6}$, the last member of the equation is found.

In our first apparatus we used a small electromagnet (Fig. 3). The circumference of a circular disk, containing 16 samples, moves through the air gap. As there is no likelihood here of capacitive or temperature effects, large coils can be used. Eddy currents in moving metal, and vibrations of the coil give the main contribution to the voltage disturbance. This disturbance was about 10^{-5} v which is far larger than the usual noise effects. The flux proved to be 1 vsec., while an e.m.f. of 2 mv was observed. This is in agreement with Eq. (7). The accuracy was of the order of 1 percent.

An alternative apparatus, using the principle of a rotating field and stationary sample, also was built. The flux was smaller here than in the previous case as was the accuracy. The advantages of this type of apparatus lie in its adaptability to the measurement of temperature effects and the ready exchange of samples.

This work has been performed in the laboratory for Technical Physics under the supervision of the late Professor E. C. Wiersma. The discussions with Professor P. van der Leeden were of great assistance.

THE REVIEW OF SCIENTIFIC INSTRUMENTS VOLUME 20, NUMBER 9 SEPTEMBER, 1949

A Tachometer

A. E. Benfield
Department of Engineering Sciences and Applied Physics, Cruft Laboratory, Harvard University, Cambridge, Massachusetts

(Received May 23, 1949)

The theory and operation of a simple tachometer are described, in which a direct electrical e.m.f. is generated by attaching a magnet to the rotating member. It is shown how the position and orientation of the magnet affect the magnitude of the generated e.m.f., and suggestions are made for further increasing the e.m.f. generated per rate of revolution.

INTRODUCTION

This paper describes a tachometer which translates revolutions per second immediately into a direct electrical voltage. As the relationship between these two quantities is linear, and as the instrument is very simple and easy to make, it seems worthwhile to describe its theory and operation in some detail, in the hope that it will be useful.

THEORY

In order to understand the principle of operation, consider first a single turn of wire, in which is connected a galvanometer, and imagine passing a bar magnet repeatedly through this circuit at a regular rate, so that the path of the magnet links the circuit n times per second. In such a circuit an alternating e.m.f. will be generated but, as is well known, no direct voltage will appear. Hence the galvanometer, in so far as it is only sensitive to direct current, will not deflect.

However, suppose now that a part (AA' in Fig. 1) of this simple electrical circuit in the neighborhood of the magnet (NS) is a rotating shaft, to which the magnet is rigidly attached by means of a non-conductor, so that the section AA' and the magnet rotate together as a single piece about the axis of AA', while brushes CC' preserve the continuity of the electrical circuit. One

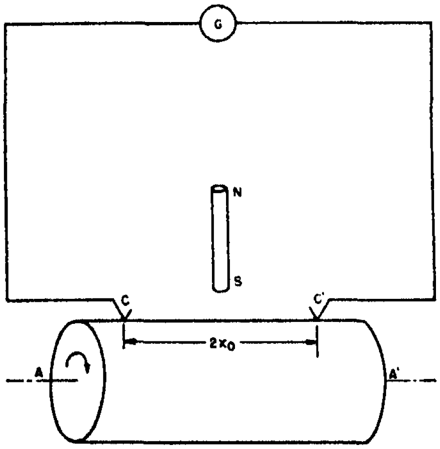

FIG. 1. A schematic diagram of the circuit. The magnet NS is rigidly attached to the shaft AA' by an insulator (not shown), so that NS and AA' rotate together, while the rest of the circuit remains stationary.

would now expect the generated e.m.f. to differ from the e.m.f. appearing in the entirely stationary circuit considered in the preceding paragraph. This is because there is now no movement of the magnetic field with respect to the shaft AA', since both rotate together. Therefore, no e.m.f. should be generated in that part of the circuit lying between the points CC'. Looked at another way, the section CC' is, for the action of the magnetic field, a gap in the circuit, though it is not a gap for the electric current.

It turns out that, for the arrangement shown in Fig. 1, a direct e.m.f. *is* generated. We shall show below how the magnitude of this direct e.m.f. may be calculated.

As no direct voltage appears if the whole electrical circuit including the section CC' is stationary, let us, therefore, calculate for such a stationary circuit the *DC* contribution to the total e.m.f. made by just the section CC' alone. This e.m.f., E_{DC}, will have the magnitude of the direct e.m.f. appearing in the circuit of Fig. 1. This is because this calculation will give the amount of direct e.m.f. lacking from the circuit of Fig. 1, where the magnet NS and the section AA' rotate together.

In making this calculation imagine the magnetic field to be stationary, and a thin wire joining the points CC' to rotate about the axis of AA', generating thereby a cylindrical surface. Such an arrangement is shown in Fig. 2. The length of the magnet, which lies close to the cylinder, is comparable with the diameter $2R$ of the cylinder. Therefore, it is unwise to use the usual approximation for the field of a dipole, which is valid only at distances large compared with the dipole's length. Rather, we shall imagine the magnet to contain equal centers of north and south polarity, of strengths $+m$ and $-m$, situated distances b_N and b_S, respectively, above the top of the cylinder, and we shall calculate the magnetic intensity B at point P for each pole separately, using the inverse square law. From this we shall be able to calculate the e.m.f., $E(t)$, generated in CC' due to its movement across the radial component of B, which is normal to the motion of CC', and from $E(t)$ we shall find E_{DC}.

In Fig. 2 a geometrical construction for the north pole N is shown. An exactly similar construction applies to the south pole S. Using for convenience the electromagnetic system of units the field strength at point P due solely to $+m$ is

$$B_N = m/r^2, \tag{1}$$

where

$$\left.\begin{aligned} r^2 &= x^2+y^2 \\ y^2 &= p^2+(b_N+u)^2 \\ p^2 &= u(2R-u) \end{aligned}\right\}. \tag{2}$$

and

The meaning of the various symbols may be seen in Fig. 2. Combining Eqs. (1) and (2),

$$B_N = \frac{m}{b_N^2+x^2+2u(b_N+R)}. \tag{3}$$

The radial component of B_N at point P may be shown to be

$$\frac{m}{R}\left\{\frac{b_N(R-u)-Ru}{[b_N^2+x^2+2u(b_N+R)]^{3/2}}\right\},$$

where a magnetic field pointing toward the axis is taken as positive. Consequently, the radial component of B at point P due to the combined effect of both the north and south poles of the magnet is

$$\frac{m}{R}\left\{\frac{b_N(R-u)-Ru}{[b_N^2+x^2+2u(b_N+R)]^{3/2}}-\frac{b_S(R-u)-Ru}{[b_S^2+x^2+2u(b_S+R)]^{3/2}}\right\}. \tag{4}$$

If, now, we apply Faraday's Law to an element dx of the line CC', and make use of the fact that $R-u=R\cos\omega t$, (where $\omega=2\pi n$ is the angular frequency of rotation of CC') we see that the e.m.f. generated in x is

$$E(t)=mR\omega\int_{-x_1}^{+x_2}\left\{\frac{(b_N+R)\cos\omega t-R}{[b_N^2+x^2+2R(b_N+R)(1-\cos\omega t)]^{3/2}}-\frac{(b_S+R)\cos\omega t-R}{[b_S^2+x^2+2R(b_S+R)(1-\cos\omega t)]^{3/2}}\right\}dx. \tag{5}$$

Equation (5) may be readily integrated.[1] For the special case of $|x_1|=|x_2|=x_0$, which is of most interest to us, we find that

$$E(t)=4\pi mnRx_0\left[\frac{R-(b_N+R)\cos\omega t}{\{b_N^2+2R(b_N+R)(1-\cos\omega t)\}\sqrt{x_0^2+b_N^2+2R(b_N+R)(1-\cos\omega t)}}\right.$$
$$\left.-\frac{R-(b_S+R)\cos\omega t}{\{b_S^2+2R(b_S+R)(1-\cos\omega t)\}\sqrt{x_0^2+b_S^2+2R(b_S+R)(1-\cos\omega t)}}\right]=4\pi mnRx_0 f(t) \tag{6}$$

---

[1] See, for instance, *A Short Table of Integrals*, B. O. Peirce (Ginn and Company, New York, Third Revised Edition), p. 21, integral No. 138.

As we are interested only in the *DC* term, E_{DC}, we must now find the average value of $f(t)$ between $\omega t=0$ and 2π. What we seek, in fact, is the constant term of the Fourier expansion of Eq. (6), which is

$$E_{DC}=(\omega/2\pi)\int_0^{2\pi/\omega}E(t)dt. \tag{7}$$

However, the expression for $f(t)$ in Eq. (6) seems to be hard to integrate, and so a numerical method of integration has been used for evaluating Eq. (7). As $f(t)$ is an even function, it is only necessary to integrate from $\omega t=0$ to π; eleven values of ωt were used in this interval in carrying out most of the integrations. Values of E_{DC}, calculated by the method described above, will be compared under *Results* below with some experimentally determined values. We shall now describe the experimental arrangements and explain how the observations were made.

EXPERIMENTAL ARRANGEMENTS

A small Alnico bar magnet 4.4-cm long having a roughly circular cross section of about 0.5-cm diameter was used. This magnet had a magnetic moment of 443 e.m.u. as measured on a Hibbert Balance. The centers of magnetism, *N* and *S*, were located by sprinkling iron filings and were found to be each 0.3 cm from the ends of the magnet. Hence the pole strength $m=\pm 117$ e.m.u. This magnet was inserted into a Bakelite holder, which was in turn attached by a set screw to a copper rod, which could be rotated.

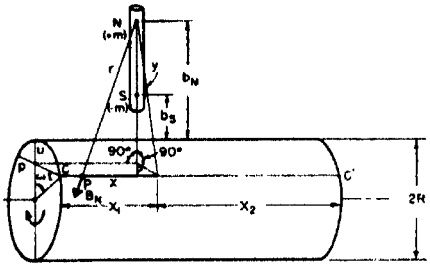

FIG. 2. The section *CC'* of Fig. 1 is shown with the geometrical construction used in the calculations.

For most of the measurements the apparatus was rotated by a 1/75 hp, 1800 r.p.m., 60-cycle synchronous motor, but when a variable speed of rotation was needed a 0.009 hp, 100 volt, *DC* motor was substituted for it, and the rotations per minute were counted with a small Veeder counter. The apparatus may be seen in Fig. 3, which shows a brass counterweight, used for approximately balancing the inertial effect of the magnet, and the brushes corresponding to the contacts *CC'* mentioned earlier. The brushes, which were kept lubricated with light machine oil, surrounded the copper rod and could be moved parallel with its axis. They consisted of crimped phosphor-bronze strip 1-mm wide. It was found advisable to use for the brushes a metal having a low thermo-electric voltage against copper. For some of the measurements copper point contacts, closely resembling those shown schematically in Fig. 1, were used; no difference in the observed values of E_{DC} was found for these two different methods of making contact with the rotating rod. Possibly carbon brushes would also serve. At times the brushes made erratic contact, resulting in an unsteady deflection of the galvanometer.

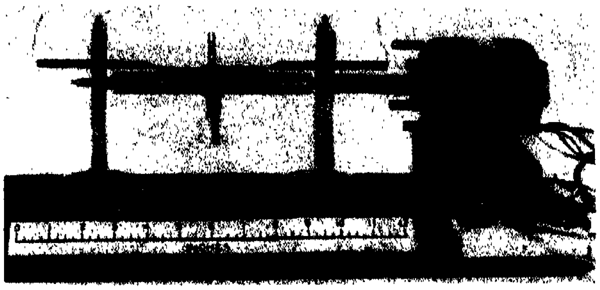

FIG. 3. A photograph of the apparatus. The magnet (below) is attached to the copper shaft, $R=0.92$ cm, by means of a Bakelite holder, to which is attached a brass counterweight (above) for giving approximate dynamical balance during rotation. Two crimped phosphor-bronze brushes surround the copper rod, symmetrically spaced on either side of the magnet, about ⅜-inch apart.

In order to measure the voltage, the contacts or

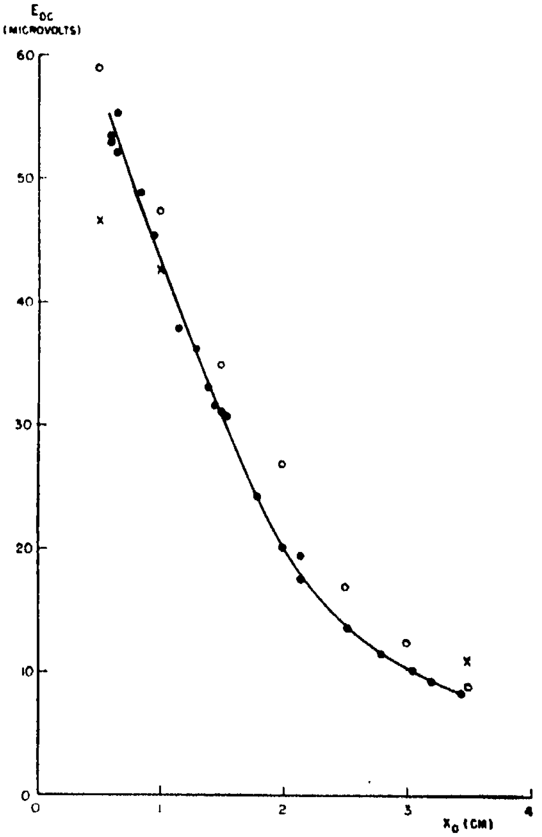

FIG. 4. A plot of E_{DC} against x_0 for $m=117$ e.m.u., $n=30$ rev./sec., $R=0.92$ cm. The solid circles and curve (●—●) are the experimental values. The hollow circles (○○) are the values calculated using $b_S=0.30$ cm and $b_N=3.80$ cm. The crosses (××) show three points recalculated using $b_S=0.40$ cm, with no other changes.

brushes were directly connected to a d'Arsonval galvanometer having a sensitivity of 6.34 μv/cm, which later changed to 3.80 μv/cm, at a scale ditsance of 93 cm, and the deflections of the galvanometer were recorded. In every case a deflection on each side of zero was taken, by reversing the direction of rotation of the shaft, and the mean of the two deflections was used.

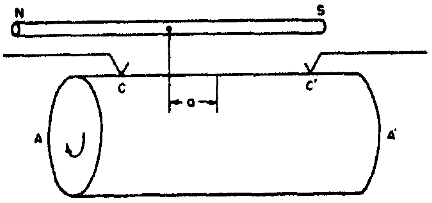

FIG. 5a. The axis of the magnet is now parallel with the axis of AA'. The distance a is the horizontal separation of the center of the magnet NS from the center of the gap CC'. E_{DC} is taken as positive when the direction of rotation and the distance a are as shown.

RESULTS

Figure 4 shows the observed e.m.f. as the distance x_0 is varied, where $2x_0$ equals the separation CC' of the brushes, symmetrically placed with respect to the magnet. Points calculated from the theory are also shown, some using the value of $b_S=0.3$ cm and others assuming a value of $b_S=0.4$ cm. The latter points are included in order to show how sensitively the calculated value of E_{DC} depends on the position of the magnet. The calculated values, depending on the numerical integration of $f(t)$, involve the subtraction of two areas whose difference is sometimes relatively small. Hence the calculated points do not lie on as smooth a curve as might be expected. However, the agreement between the observed and calculated values is reasonably close. Although E_{DC} increases as x_0 decreases, as shown in Fig. 4, reference to Eq. (6) shows that as x_0 approaches zero, $E(t)$ also approaches zero, and so E_{DC} should approach zero for very small values of x_0. Therefore, E_{DC} should pass through a maximum as x_0 goes from zero to 0.5 cm. The experimental arrangements did not permit this to be detected.

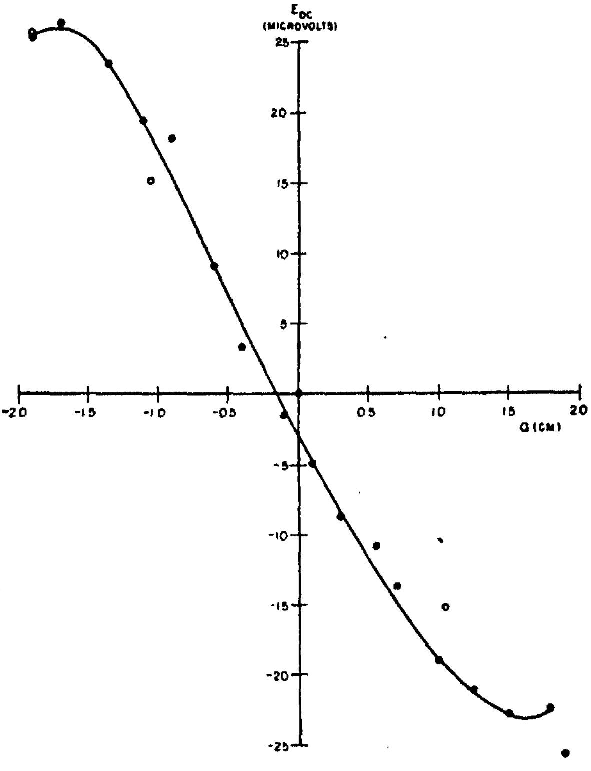

FIG. 5b. The solid circles show the experimental values for the arrangement of Fig. 5a and the hollow circles show calculated values when $m=117$ e.m.u., $n=30$ rev./sec., $R=0.92$ cm, $b_S=b_N=0.90$ cm, $CC'=1.70$ cm. The asymmetry is most likely due to an unsymmetrical intensity of magnetization of the magnet.

Figure 5a shows a different orientation of the magnet, which is now parallel to, rather than normal to, the axis of rotation, and Fig. 5b shows the observed and calculated e.m.f.s, E_{DC}, for different positions of the magnet along the line of its axis. In order to make these calculations, Eq. (5) is integrated with the limits shown, rather than from $-x_0$ to x_0, and this leads to an equation differing slightly from Eq. (6).

Figure 6 shows the result of moving the magnet (now again in the orientation of Fig. 3) to different radial positions. Observations are shown for shafts of three different radii, $R=0.63$, 1.25 and 1.90 cm. In order to have values of b_S less than $+0.3$ cm, a hole was drilled in each copper shaft, into which the magnet could be pushed when required. The presence of these holes was found experimentally to make no noticeable difference in E_{DC} when the magnet was entirely outside the shaft. Notice in Fig. 6 that near $b_S=0$ there is no change in the sign of E_{DC}. A change in sign would be expected from the simple dipole picture used in formulating the theory because, for the simple dipole, the magnetic field in the interior of the magnet would be directed from north to south. In fact, of course, B is continuous, and so the vector of magnetic induction inside the magnet points from south to north. Hence, when one of the poles is inside the shaft, and ωt is in the neighborhood of 0, $E(t)$ will have a different sign from that given by Eq. (6) and a larger magnitude, since roughly the total flux of the magnet, directed from south to north, cuts CC' when ωt is close to 0, 2π, 4π, etc. *Equation (6) is valid, therefore, only when both poles of the magnet are outside the rotating shaft.* When one pole is inside the shaft, the actual E_{DC} may be roughly calculated by taking the value computed from Eqs. (6) and (7) and subtracting it from the e.m.f. generated by the total flux of induction issuing from the magnet and cutting CC'.

It will be noticed in Fig. 6 that E_{DC} is greatest when, roughly, $b_S=-R$, and that E_{DC} increases as R increases. Referring to Eq. (6) one can see that $E(t)$, and consequently E_{DC}, approaches zero as R approaches zero.

A plot of E_{DC} against n for a particular geometry, illustrating the linearity of the device, is omitted for reasons of space.

REMARKS

There are several points to mention.

The e.m.f. E_{DC} reverses, of course, when either the direction of rotation is changed or the magnet is attached to the shaft the other way around. However, changes in the geometry of the circuit on the galvanometer side of CC' produce no noticeable effect on E_{DC}, even when the circuit is deformed quite close to C or C'. For instance, when insulating spacers were introduced between the crimped brushes and the shaft, so that the brushes made contact with AA' over only a small part of a circle, no change in E_{DC} was observed.

E_{DC} is small. This is a disadvantage, since a relatively delicate current-measuring device like a galvanometer is needed in order to measure speeds of rotation with this instrument. However, the magnitude of the generated voltage might be increased in a number of ways. For instance, one might insulate the shaft for those values of ωt where $f(t)$ is positive. Or, better, there seems to be no reason why a factor of 10 or so might not be gained by increasing both the strength and the number of the magnets, and these could be arranged to give dynamical balance to the rotating parts. Or one might use a radially magnetized disk in place of individual magnets. One could also increase the number of magnetic gaps in the circuit, though no obvious way of doing this without the disadvantage of also increasing the number of brushes suggests itself. Another way of increasing E_{DC} would be to pass the generated current through a coil wound around the magnet, in order to increase the total magnetic flux, though possibly not very much would be gained in this way, and E_{DC} would no longer be linear with n.

In this connection, if a large current were to pass between CC' one would expect an appreciable reaction between it and the field of the magnet, of such a nature that the lines of flow of the electric charge would be curved. No net torque on the shaft, however, would be observed, for the magnet is rigidly attached to it.

If one thinks of the device of this paper as a generator, the corresponding motor effect has been observed by the writer. For instance, if a magnet is attached to the upper part of a stainless steel cup floating in mercury freshly cleaned,* and if electrical contact is made through mercury both where the current enters and leaves the float, in order to reduce friction, the cup will rotate. Using the magnet described above, a cup of 5-cm diameter rotated at the rate of about 4 seconds per revolution when 30 amperes DC passed through it. If the entrance and departure of the current is restricted to the axis of rotation of the cup, no complete rotation is observed, which corresponds with the fact noted at the end of Results above that, as R approaches zero, E_{DC} approaches zero.

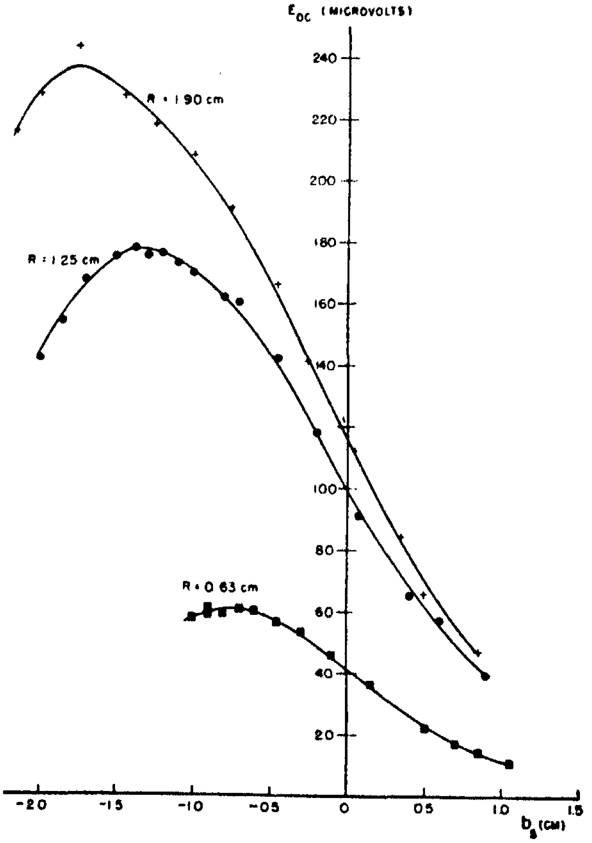

FIG. 6. Experimental values for shafts of three diameters. The magnet, oriented as in Fig. 3 with the north pole pointing out, was moved to different radial distances from axis of AA'. A hole was drilled through a diameter of AA', to permit the south pole of the magnet to be moved into the shaft. In each curve a maximum occurs when b_S roughly equals $-R$. Here $m=117$ e.m.u., $n=30$ rev./sec., $x_0=1.05$ cm.

CONCLUSIONS

A simple tachometer has been investigated which has the advantage of generating in a very simple manner a direct voltage which is linearly related to the rate of rotation. The chief disadvantage is that the magnitude of the voltage is small. Possibly this may be increased by means suggested above or in some other way.

ACKNOWLEDGMENTS

It is a pleasure to thank Mr. Harold Benner for making the apparatus, and numerous colleagues who have shown interest and been of help in discussing the problem, in particular A. G. Emslie, J. R. Hooper, Jr., F. V. Hunt, and M. H. Johnson, Jr.

---

* By passing it through a filter paper containing a pin hole.

THE REVIEW OF SCIENTIFIC INSTRUMENTS VOLUME 20, NUMBER 9 SEPTEMBER, 1949

Wet Bulb Temperatures without a Wick*

KENNETH H. JEHN
Electrical Engineering Research Laboratory, The University of Texas, Austin, Texas

(Received May 23, 1949)

It is desired to determine the feasibility of measuring wet bulb temperatures without a wick. The sensing element is a thermistor bead of small mass and rapid response, which, when dipped into distilled water, retains water in sufficient quantity to register a wet bulb temperature when exposed to the air. The experimental apparatus and procedures are described in detail, and the data presented. It is concluded that wickless wet bulb measurements are feasible, with an accuracy of the order of ±0.1°C.

I. INTRODUCTION

DURING the course of taking low level meteorological measurements along radio paths in connection with microwave propagation studies at this laboratory, it was discovered that the measurement of wet bulb temperatures was complicated by the fact that the rod-shaped thermistors[1] used in this work were not ideally suited to the use of wicking because of their small size and the presence of the lead wires. Moreover, the accumulation of dirt on the wick made frequent changes of the wicking necessary, a delicate task which sometimes resulted in damage to the plastic insulating sheath on the thermistor. These wicking difficulties prompted the search for a scheme which would eliminate them.

Professor Athelstan F. Spilhaus, Dean of the Institute of Technology, University of Minnesota, suggested some time ago that the wick difficulties could probably be eliminated by eliminating the wick itself, using insulated thermistors of small mass and consequently rapid response. Mr. William E. Gordon,[2] Associate Director of the Electrical Engineering Research Laboratory at The University of Texas, recognized the possibilities in such a scheme, and organized some preliminary studies with a non-wicked bead thermistor. These studies seemed to indicate that the wet bulb process was being approximated.

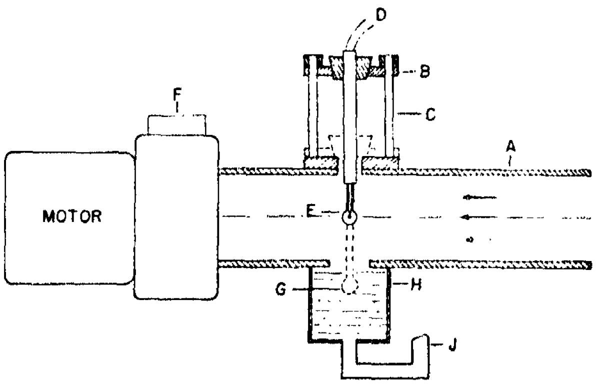

FIG. 1. Schematic drawing of the test instrument. A. Aeration tube. B. Thermistor carriage, actuated by 6-volt relay through system of levers. C. Brass rods on which thermistor carriage rides. D. Flexible leads to amplifier. E. Wire loop and plastic around thermistor bead, the whole unit composing the wickless wet bulb. F. Blower. G. Wickless wet bulb in dipping position. H. Distilled water reservoir. J. Water level gauge. Arrows show direction of air flow.

The principle of the method is to use a thermistor of small mass, which is coated with an electrically insulating material, dipped into distilled water, and then exposed to an airstream whose wet bulb temperature is to be measured. Evaporational cooling lowers the temperature of the element and increases its resistance. This change in resistance can be measured by means of a bridge circuit, and a calibration of temperature *versus* resistance for the thermistor will translate recorder readings into temperatures.

II. EXPERIMENTAL WORK

1. Method of Attack

In order to test the feasibility of wickless wet bulb measurements, the following method of attack was devised. For a given wet bulb temperature, obtain indications of the instrument for different values of the rate of air flow past the thermistor (aeration speed). From these, determine the optimum aeration speed range. Next, for a given wet bulb temperature and optimum aeration speed, obtain indications of the instrument with time. From these data, determine the optimum time of exposure to the airstream (dipping rate), and the lag coefficient of the instrument. Finally, for the optimum aeration speed and dipping rate, plot indications of the instrument against wet bulb temperatures determined with an aspirated psychrometer, to determine whether or not wet bulb temperatures are being obtained, and the degree of accuracy of the measurements.

2. Description of the Test Instrument

A sample of air is drawn through the aeration tube (Figs. 1 and 2) by means of an exhaust fan and variable speed motor. This air moves past the bead thermistor which has previously been dipped into the distilled water reservoir by means of a relay which moves the thermistor carriage through a system of levers (Fig. 3a). This relay can be activated manually, or automatically by means of a cam on the shaft of a synchronous motor.

---

* This research was sponsored by the ONR under Contract N6onr-266, T. O. II.

[1] Solid semi-conductors which have a large negative temperature coefficient of resistance. The thermistor is composed of a combination of metallic oxides which are milled, mixed, formed, and fired, producing a hard ceramic-like structure. The diameter of the rod-shaped thermistors currently in use is about 0.05 inch, and their effective length (between leads) about 0.5 inch. Thermistor literature is not extensive. One of the most comprehensive articles is the following: Becker, Green, and Pearson, Properties and uses of thermistors—thermally sensitive resistors, Electrical Engineering 65, 711–725 (1946).

[2] Now Director of the Microwave Astronomy Project at Cornell University, Ithaca, New York.

The thermistor provides the voltage input to an amplifier, and variations in its resistance due to changes in temperature are recorded on an Esterline-Angus graphic meter model AW (0–1 milliampere). The amplifier is composed of a conventional bridge type electronic voltmeter, using a 6SN7. The power supply utilizes a full wave rectifier tube (5Y3G), with regulation supplied by a pair of VR-105's in series.

Simultaneously, an indicating aspirated psychrometer is functioning and is read at short intervals. This instrument consists of a laboratory thermometer, and aeration tube, exhaust fan, and water reservoir similar to the test instrument. A constant speed motor provides the optimum ventilation for the psychrometer which is continuously wick-fed from the reservoir. The aspirated psychrometer and test instrument are mounted so as to obtain, as nearly as possible, identical samples of air.

The thermistor is an experimental bead type ceramic resistor (V-682)[3] made in the Bell Telephone Laboratories. The bead itself is about 0.035 inch in diameter and has platinum leads about ½-inch long and 0.004-inch in diameter running parallel and continuously through the bead and projecting at either end. The unwanted leads were cut off. The cold resistance of this type of thermistor at 25°C is approximately 100,000 ohms, and the negative temperature coefficient of resistance at 25°C is 4.6 percent per Centigrade degree. The leads from the thermistor pass through a glass tube and rubber stopper mount and are joined to the amplifier circuit by means of two flexible leads (Fig. 3). A double coating of polyisobutyl methacrylate (PBM), applied by dipping, covers the bead and wire loop,[4] as well as the lower ends of the leads.

III. PRESENTATION OF DATA

1. Determination of Aeration Speed

For the determination of the rate of air flow through the aeration tube, it was considered practicable to use a calibrated hot wire anemometer, and to plot aeration speed against aeration motor voltage to obtain a calibration for the aeration tube. By varying the voltage across the aeration motor, then, with the hot wire anemometer mounted at the spot later occupied by the bead thermistor, a calibration of aeration speed *versus* aeration motor voltage was obtained.

2. Indicated Wet Bulb Temperature as a Function of Aeration Speed

For a given wet bulb temperature (T_w) which was nearly constant, indicated wet bulb temperatures (T_{wi}) for the test instrument were read for the range of aeration speeds from zero to 850 feet per minute. Due to the disk-shaped structure of the wet bulb, it was considered advisable to determine such indications for different aspects of the thermistor in the airstream. These were parallel, perpendicular, and at a 45 degree angle to the center line of the aeration tube. The results of these tests are plotted on the same grid of difference between indicated and "true" wet bulb temperature *versus* aeration speed in Fig. 4. Since accuracy was not being investigated at this stage, zero ordinate represents only a uniform ambient wet bulb temperature.

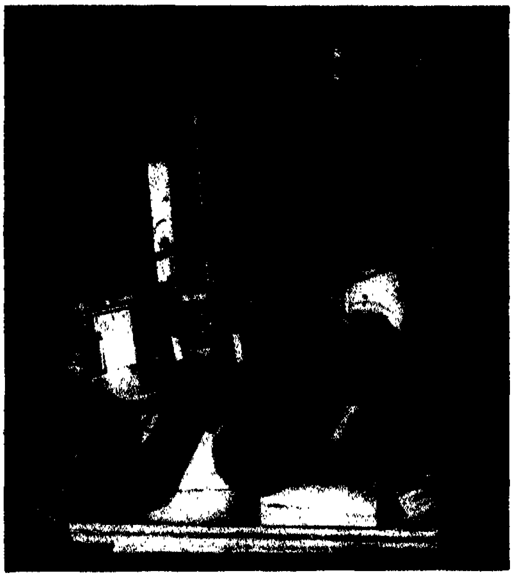

FIG. 2. Test instrument (left) and comparison psychrometer.

Some cooling occurs even with no aeration (water temperature was about 7°C higher than wet bulb), but even a very small air movement of 50 feet per minute past the sensing element produces an appreciable cooling due to convection at the wet bulb surface. As aeration speed increases, the indicated wet bulb temperature approaches the ambient wet bulb temperature until further increases in aeration speed remove water from the wet bulb and reduce the effective cooling. The optimum range is sufficiently large to justify the use of aeration motor voltage as a calibration parameter. It appears that a perpendicular aspect is least desirable, since the separation between indicated and true wet bulbs is largest, even at optimum aeration. From considerations of fluid flow, the parallel aspect should provide optimum ventilation of the bead, with evaporation from both faces proceeding equally rapidly. This is borne out by the lower curve in Fig. 4 which shows the nearest

---

[3] The experimental bead, with some modifications, is now designated D-177232 or D-177703, depending on the arrangement of the leads. Both models are glass coated. Western Electric is the distributor.

[4] In earlier tests, the plastic did not cover the ends of the trimmed leads, and the wire loop became necessary to insure electrical insulation.

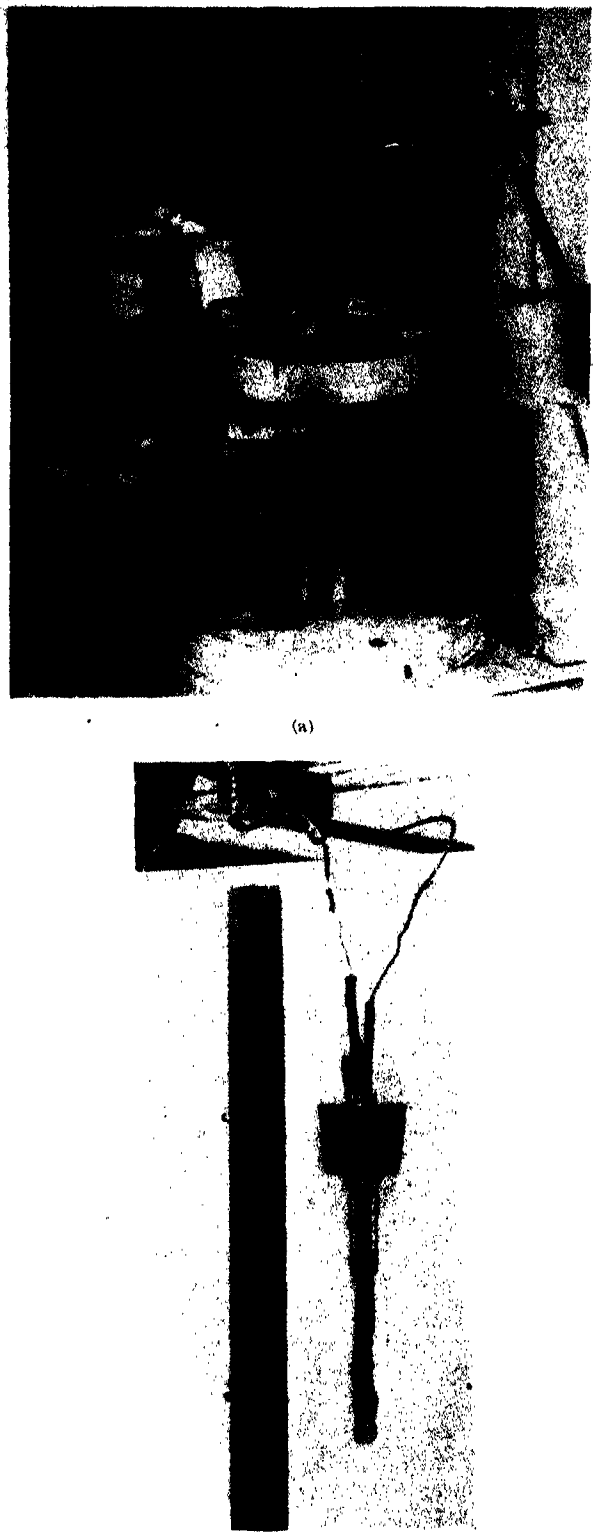

(a)

(b)

FIG. 3. a. Close-up of dipping mechanism. b. Bead thermistor and support.

approach to ambient wet bulb temperature at a slightly higher optimum aeration speed than the other two aspects. It was concluded as a result of these tests that the thermistor should be mounted parallel to the airstream for subsequent measurements, and that an aeration speed of approximately 670 feet per minute would give the best results.[5]

3. Dipping Rate

An examination of some of the records showed that an equilibrium temperature in water was reached in a period of the order of 5 seconds and that a wet bulb temperature was indicated in a period of the order of 15 seconds. Since a cam and 1 r.p.m. synchronous motor combination were to operate the dipping relay, a dipping rate of 10 seconds in water and 20 seconds in air was chosen, giving two wet bulb temperatures per minute (Fig. 5). Individual readings of indicated wet bulb temperature are quite reliable, where in spite of large variations in water temperature, a nearly constant T_{wi} is indicated on the record.

It is worthy of note that in spite of the rapidity of evaporation of water from the sensing element, wet bulb temperature is reached and indicated for periods of the order of 2 or 3 minutes with only one dipping of the thermistor. In Fig. 6a, the test instrument indicated a temperature within 0.2°C of the first indicated wet bulb temperature for approximately 2 minutes; in Fig. 6b, this time was increased to $2\frac{3}{4}$ minutes.[6] Longer exposure of the sensing element in the airstream produces a greater variation in the readings, probably because evaporation becomes unequal from the two faces of the sensing element. In general, the duration of indicated wet bulb temperature was found to be long when the spread between dry bulb and wet bulb temperature was small, and short when the spread was large. A functional relation between these variables was not determined.

4. Lag Coefficient

One result expected of this method of measuring wet bulb temperatures was that the speed of response would be rapid. Since the lag coefficient is a measure of this response, the lag of the bead thermistor used to measure wet bulb temperature was investigated. Lag coefficient theory is discussed elsewhere.[7, 8]

In this study, the initial temperature T_0 is that of the water in the reservoir and the ambient temperature is that of the wet bulb. Temperatures T_t are read at one-second intervals beginning with $t=0$. The method used in determining the lag coefficient was to average $T_t - T_w$ for several minutes, and plot $\log(T_t - T_w)/(T_0 - T_w)$ *versus* time in seconds. The slope of the resulting

---

[5] Aeration speed for a conventional wicked mercurial psychrometer is of the order of 1000 feet per minute.

[6] A more recent record showed wet bulb temperature within 0.2°C for $3\frac{1}{2}$ minutes.

[7] W. E. K. Middleton, *Meteorological Instruments* (University of Toronto Press, Toronto, 1942).

[8] A. F. Spilhaus, "A study of the aspiration psychrometer," Trans. Roy. Soc. South Africa 24, 185–202 (1936).

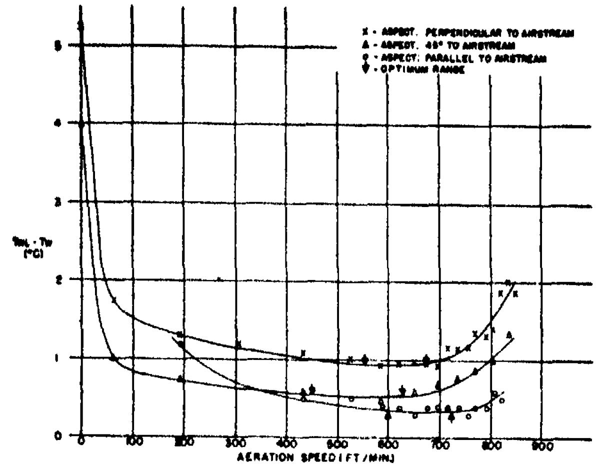

FIG. 4. Indicated wet bulb temperature as a function of aeration speed.

straight line multiplied by 2.3 is the negative reciprocal of the lag coefficient, and the y-intercept is unity. A set of such data is plotted in Fig. 7, with a resulting lag coefficient of 2.7 seconds. Since the lag coefficient of a mercurial psychrometer is of the order of 30 to 50 seconds, it is seen that the bead thermistor used in this investigation has a response of the order of 10 to 15 times as rapid as that of a mercurial psychrometer.

It is interesting to observe in Fig. 7 that the plotted points are not all colinear. In particular, the slope of the curve (and therefore the lag coefficient) is changing rapidly in the first second, where a mean λ of 6.8 seconds is obtained. Since the errors in the time scale, and in particular, the error in the determination of the zero point, are of the order of 0.2 second or less, and since the time delay involved in returning the thermistor from the reservoir to the airstream is of the order of 0.1 second or less, it is concluded that the change in the lag coefficient with time is real. Spilhaus[8] has shown that the lag coefficient depends on the heat capacity of the wet bulb (including the water), atmospheric pressure, ventilation, and range through which indicated wet bulb temperature passes. It is evident, then, that any variation in the lag coefficient for a given set of measurements will be due primarily to a change in the heat capacity of the wet bulb. It is concluded that the larger lag coefficient in the first second is due to the increased heat capacity of the wet bulb, occasioned by the excess of water which clings to the wet bulb when it is first drawn from the water.

5. Accuracy

Four different sequences of T_{wi}, T_w data, representing wet bulb temperatures between 14°C and 24°C were available for accuracy determinations. Ten sets of T_{wi}, T_w were chosen at random from each of the four sequences and plotted on linear coordinates of T_{wi} *versus* T_w, as shown in Fig. 8. The data are presented on two sets of axes so that an expanded scale could be used. The computed correlation coefficient for these 40 independent pairs of measurements was found to be 1.00 and the slope of the line of regression to be 1.006. The root mean square of the residual errors[9] was found to be ±0.05°C. It is evident that the 45° line drawn in Fig. 8 represents quite well the experimental points, and that the accuracy of the test instrument compared to the aspirated mercurial psychrometer is of the order of ±0.05°C.

The comparison psychrometer had been calibrated previously against a laboratory standard mercurial

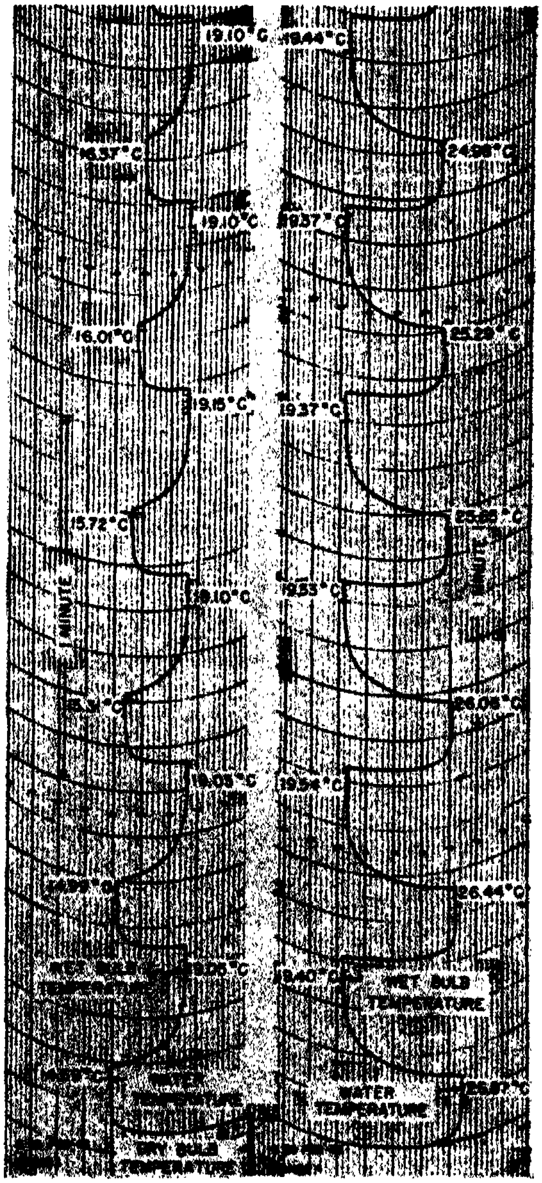

(a) (b)

FIG. 5. Sample records showing indicated wet bulb temperature with a dipping rate of 10 seconds in water and 20 seconds in air. Water temperature (a) below and (b) above wet bulb temperature. Time increasing upward, temperature increasing toward the right.

---

[9] Visually estimated from a plot of T_{wi} *versus* T_w on an enlarged scale.

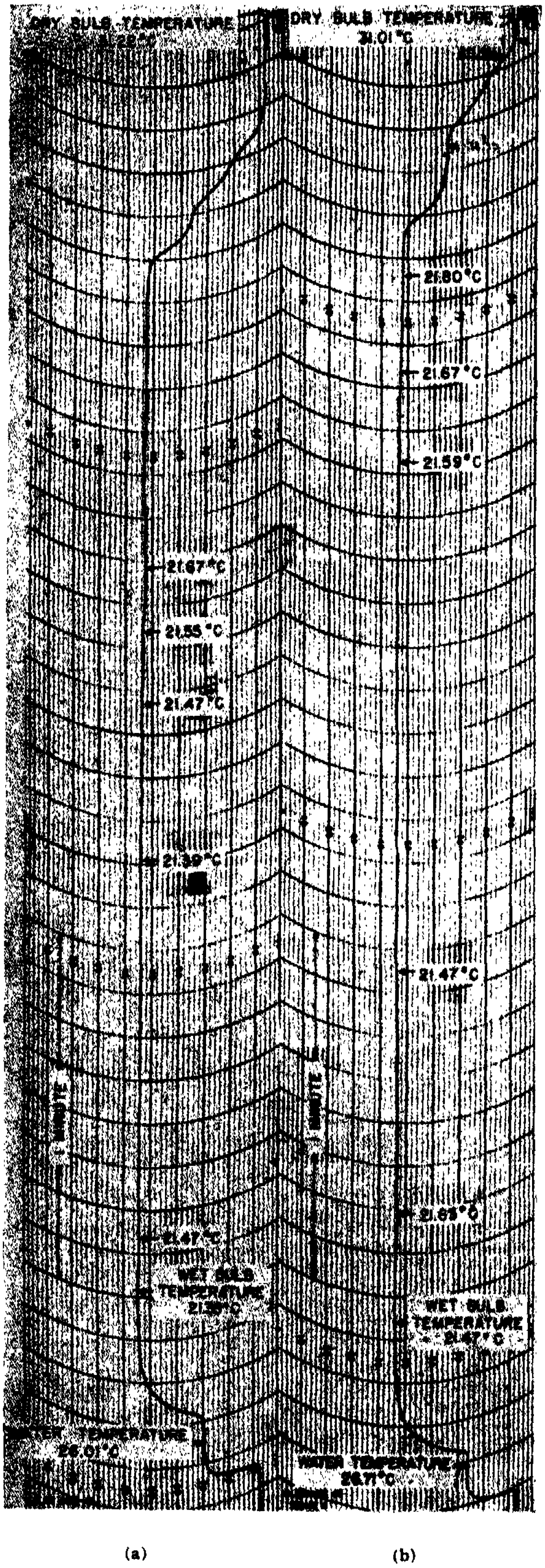

FIG. 6. Sample records showing duration of indicated wet bulb temperature with one dipping of the thermistor. Time increasing upward and temperature increasing toward the right.

thermometer, which in turn had been calibrated by the National Bureau of Standards. Applying the NBS corrections to the standard thermometer made it an effective temperature scale, and it is this scale (T) against which the comparison psychrometer readings (T_w) are plotted in Fig. 8. The computed correlation coefficient for 8 independent pairs of T_w, T over the range 12°C to 24°C was found to be 1.00, the slope to be 1.007, and the standard error of estimate to be $\pm 0.03°C$. The same 45° line therefore represents the T *versus* T_w plot as well as the T_{wi} *versus* T_w plot. It is concluded that the accuracy of the test instrument is in the order of $\pm 0.1°C$, compared to a standard scale of temperature.

The sensitivity of the test instrument varies from 9 recorder divisions per degree at 0°C to 3 divisions per degree at 40°C. Since the recorder paper can be read to the nearest quarter division, the sensitivity becomes approximately $\pm 0.05°C$ in the mean, ranging from about $\pm 0.03°C$ to $\pm 0.08°C$.

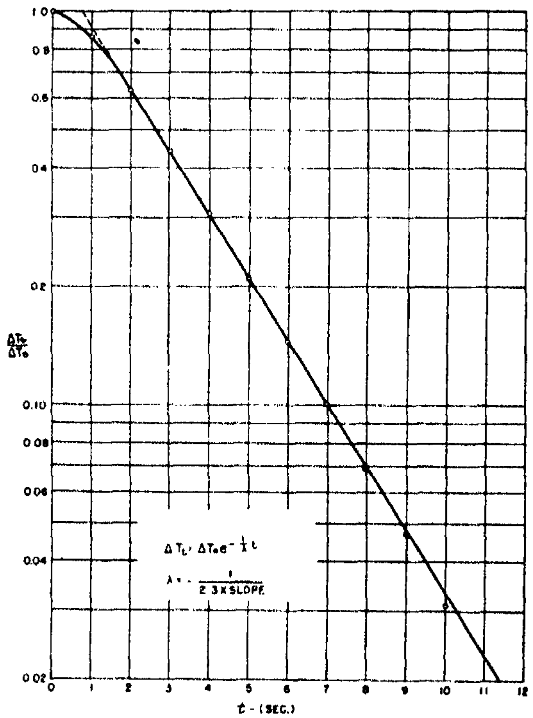

FIG. 7. Determination of lag coefficient: ratio of temperature difference at time t to initial temperature difference *versus* time.

IV. APPLICATIONS OF THE WICKLESS WET BULB DEVICE

Applications of the principle of wickless wet bulb measurements or of the test instrument herein described are best referred to in terms of the advantages of this method over that of wicked thermistors. Certain wick difficulties have been described in the introduction to this paper, and it is concluded that they have been eliminated. Servicing of the non-wicked psychrometer requires only that the reservoir be kept filled; there are means of maintaining a constant level of water in the reservoir. A certain amount of lubrication of the dipping mechanism is required, but in this connection it is well to point out that there may be ways other than dipping to apply water to the thermistor. It is conceivable that water at or near the wet bulb temperature[10] could be fed continually by some means to the thermistor, with a consequent nearly continuous record of wet bulb temperature. With the rapid speed of response of this type of instrument, the measurement of fluctuations in wet bulb temperature would be feasible.

Even with the instrument in its present form, a response to wet bulb fluctuations has been observed, and if it were possible to extend the range of optimum aeration within certain limits of accuracy, the thermistor could be naturally aerated; i.e., exposed to the free air, without the aeration motor and fan.[11] Using thermistors having similar characteristics for the simultaneous measurement of dry bulb temperature would provide a means of measuring fluctuations in vapor pressure[12] in the free atmosphere at a point (or over a small volume). Simultaneous measurements at several levels would make possible a delineation of what might be termed micro-moisture fluctuation patterns, along the lines developed by Gerhardt and Gordon.[13]

ACKNOWLEDGMENT

The assistance in this work provided by members of the staff of the Electrical Engineering Research Laboratory is acknowledged with thanks. Especial thanks go to W. E. Gordon, J. R. Gerhardt, W. R. Guild, and A. F. Spilhaus for stimulating advice and technical assistance. The courtesy of C. B. Green of Bell Telephone Laboratories in providing the bead thermistor used in the investigation is greatly appreciated.

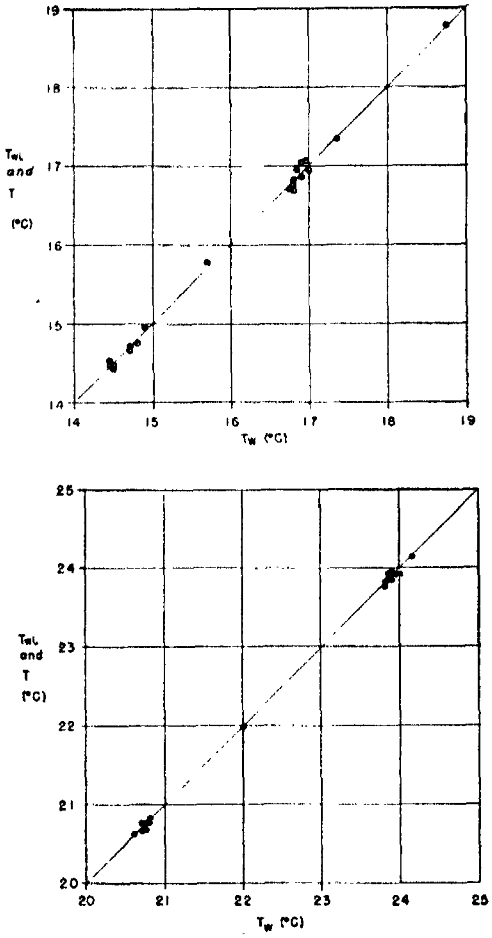

FIG. 8. Correlation plots of indicated wet bulb temperature, T_{wi}, *versus* wet bulb temperature, T_w, (small circles); and wet bulb temperature *versus* temperature scale, T, (black circles).

---

[10] D. B. Brooks and H. H. Allen, Some improvements in psychrometry, J. Wash. Acad. Sci. 23, No. 3 (1933).

[11] It is interesting to speculate on the possibility of using Lorenzen's thermocouple without a wick. His instrument is a very small butt-welded thermocouple, carefully wicked with a few strands of cotton thread. No aeration is required. See C. Lorenzen, Jr., "The Construction and Use of a Thermoelectric Psychrometer," in *Temperature: Its Measurement and Control in Science and Industry* (Reinhold Publishing Corporation, New York, 1941), pp. 660–665.

[12] A "compensated" psychrometer, in which the lag coefficients of the wet and dry sensing elements are made equal, would be required for these measurements (see reference 8).

[13] J. R. Gerhardt and W. E. Gordon, Microtemperature fluctuations, Journal of Meteorology 5, 197–203 (1948).

THE REVIEW OF SCIENTIFIC INSTRUMENTS VOLUME 20, NUMBER 9 SEPTEMBER, 1949

Electrolytic Thermistors

F. Gutmann*
Faculty of Agriculture, University of Sydney, Australia

AND

L. M. Simmons
The Scots College, Sydney, Australia

(Received April 18, 1949)

A thermistor for use with alternating current and having a half-temperature at 300°K of 7.2°C is easily constructed by immersing platinum electrodes in a viscous solution of waterglass. It is three times as sensitive as commercial thermistors, withstands a.c. potentials of more than 240 volts, and its cold resistance and sensitivity are easily controlled. Other electrolytic solutions have been tested, but these, although withstanding high a.c. potentials, are less sensitive.

METHODS for constructing conventional thermistors from heavy metal oxides are described by Becker and collaborators and by Grisdale and others,[1,2] but, as pointed out by Becker *et al.*,[1,3] very close control is necessary for their manufacture. H. Diamond *et al.*, employed sulphuric acid as a temperature-sensitive resistor for low temperature measurements in meteorological investigations.[4] This work, on what may be termed electrolytic thermistors, was extended to mixtures of cuprous chloride, hydrochloric acid, and ethyl alcohol by D. N. Craig.[5]

Wolfson states that typical thermistors have a half-temperature of 20°C at 300°K, that is, a temperature change of 20°C at 300°K will double or halve the electrical resistance of the element.[2] Thus the smaller the half-temperature at 300°K, the more sensitive is the resistance of the thermistor to change in temperature. It would appear from Craig's paper that the half-temperatures of his electrolytic thermistors at 303°K were about 28°C.[5]

The present investigations were undertaken to see whether more sensitive electrolytic thermistors could be readily constructed. Systems consisting of decinormal silver nitrate with silver electrodes, and decinormal cupric sulphate with copper electrodes, were found to be far less sensitive than conventional thermistors. They have, however, the advantage that very high alternating potentials can be maintained across them without irreversible reactions occurring; in the case of the silver-silver nitrate system, this value exceeded 800 volts. This means that the sensitivity of the electrical resistance measurements can be made appreciably greater with them than is possible with the voltages recommended for conventional thermistors.[6]

An attempt was next made to decrease the half-temperature of electrolytic solutions by increasing their viscosity. To this end 15 percent by weight of gelatine was dissolved in the decinormal cupric sulphate, and the half-temperature was then found, by extrapolation, to have fallen from about 62°C to about 43°C at 300°K.

To avoid the instability of gelatine towards heat and electrolytes, a viscous solution of waterglass, sp. gr. 1.38, was tried, the electrodes consisting of platinum wires. The half-temperature at 300°K was found by direct measurement with a.c. to be only 7.2°C. Thus this thermistor had three times the temperature sensitivity of the conventional elements. Furthermore, although this thermistor does not constitute a reversible system as was required by Craig for his purposes,[5] alternating potentials of up to at least 240 volts could be applied without altering its electrical characteristics or producing visible gas evolution. Attempts to use this thermistor with a d.c. bridge were unsuccessful because of polarization effects, even when the bridge voltage was kept at 1.5 volts, i.e., well below the observed decomposition potential of 1.8 volts.

This waterglass thermistor has a smaller temperature range than most conventional solid thermistors, because the boiling point of the waterglass solution is only a few degrees above 100°C. Also, in the present designs, it seems to be rather slower in its response to temperature changes than most commercial thermistors. Over the latter it has the following advantages:

(a) It has greater sensitivity due to its smaller half-temperature.
(b) Much higher potential differences may be applied to it than are recommended for commercial thermistors.
(c) It is readily prepared at negligible cost.
(d) Its cold resistance is easily adjusted to any desired value.

Thermistors were also constructed using diluted waterglass solutions. In one case, one part by weight of the viscous waterglass was mixed with three parts

---

[*] Now with The New South Wales University of Technology, Sydney, N.S.W., Australia.

[1] Becker, Green, and Pearson, Trans. A.I.E.E. 65, 711 (1946); Bell Sys. Tech. J. 26, 170 (1947).

[2] R. O. Grisdale, U. S. Patent 2,258,646 (1941); E. F. Dearborne, U. S. Patent 2,274,592 (1942); E. F. Dearborne and G. L. Pearson, U. S. Patent 2,282,944 (1942).

[3] H. Wolfson, reported by W. Grattidge and F. A. Vick, Nature 162, 625 (1948).

[4] Diamond, Hinman, and Dunmore, Bull. Am. Meteorolog. Soc. 18, 73 (1937); J. Inst. Aero. Sci. 4, 241 (1937); J. Research Nat. Bur. Stand. 20, 369 (1938).

[5] D. N. Craig, J. Research Nat. Bur. Stand. 21, 225 (1938).

[6] Standard Telephones and Cables Ltd., London, "Thermistors," p. 10.

by weight of water, and it was found that the half-temperature at 300°K rose to 43°C. Thus not only may the cold resistance of a waterglass thermistor be controlled, but also its temperature sensitivity.

Attention is drawn to the fact that the high sensitivity of the waterglass thermistor permits the use of very simple electrical measuring devices in place of the more elaborate bridge circuits usually employed. An example of such a simple arrangement is described below as the *constant current circuit*.

Fig. 1 shows the results obtained. The resistances at 27°C have been reduced to the same arbitrary value of 10 units. The curve for the dilute waterglass is practically coincident with that for decinormal cupric sulphate containing 15 percent of gelatine, but the latter has not been explored above 60°C.

E. F. G. Herington and R. Handley have reported that consistent results were not obtained when the tip of a conventional thermistor was dipped into mercury at the bottom of a thermistor well;[7] we have noticed a similar inconsistency when the waterglass thermistor is so treated.

EXPERIMENTAL

The thermistors were constructed by filling thin-walled narrow bore glass U-tubes with the various solutions and inserting down each limb an electrode consisting of a wire of the selected metal. The cold resistance was adjusted by moving the wires up and down the limbs. In most cases the total length of the electrolyte column was about 2 cm.

Each thermistor was attached to the bulb of a thermometer and immersed in a mechanically stirred lagged water-bath whose temperature was controlled by a heating coil and rheostat. The leads from the thermistor were insulated by glass or rubber tubing. Temperatures and resistances were allowed to become steady before reading.

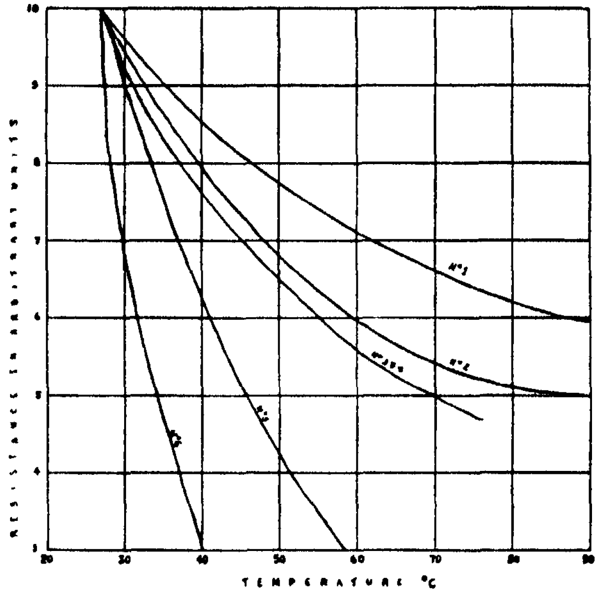

FIG. 1. Temperature/resistance curves: 1. 0.1N-AgNO$_3$. 2. 0.1N-CuSO$_4$. 3. 0.1N-CuSO$_4$+15 percent gelatine. 4. Diluted waterglass. 5. Conventional thermistor. 6. Waterglass sp. gr. 1.38.

Resistances were measured by an a.c. bridge which was first balanced for the cold resistance of the thermistor for capacitance as well as for resistance. A Wagner earth was employed. A resistance decade box was connected in series with the thermistor and at all temperatures this was adjusted so as to re-establish the original balance. The resistance decrement of the thermistor was therefore read directly from the resistance introduced by the decade box. About 20 volt 50 c.p.s. alternating current was supplied to the bridge. The power dissipated in the thermistor was of the order of 10 milliwatts; had the thermistor been thermally isolated, this would have produced a temperature rise of about 0.003°C per second.

The *constant current circuit* previously mentioned as a simple electrical measuring device consisted in passing a constant alternating current through the thermistor and measuring the potential difference across it by means of a vacuum tube voltmeter. The current being constant, the V.T.V.M. readings are directly proportional to the resistance of the thermistor. In order to keep the current constant, the thermistor was connected in series with a *swamping resistor* having a resistance of the order of 100 times the cold resistance of the thermistor, and a constant voltage was applied to the arrangement by means of a constant voltage transformer.

---

[7] E. F. G. Herington and R. Handley, J. Sci. Inst. **25**, 435 (1948).

THE REVIEW OF SCIENTIFIC INSTRUMENTS VOLUME 20, NUMBER 9 SEPTEMBER, 1949

Physical Instruments for the Biologist

Detlev W. Bronk
Associate Editor in Charge of this Section
Eldridge Reeves Johnson Foundation for Research in Medical Physics,
University of Pennsylvania, Philadelphia, Pennsylvania

A Versatile Microinjection and Micropipetting Syringe

JOHN B. BUCK
Laboratory of Physical Biology, National Institutes of Health, Bethesda, Maryland

(Received April 11, 1949)

A screw-driven microinjection syringe capable of delivering volumes as small as 0.1 mm³ with statistically good reproducibility is described. It features interchangeable impellers mounted on a sliding way for simultaneous availability of coarse and fine adjustment, and a mechanical positioner permitting known and reproducible fractional revolutions of the control knob.

I. CONSTRUCTION

THE present instrument (Fig. 1) follows the Chambers[1] plan of a screw-driven hypodermic syringe connected by flexible tubing to a metal holder accommodating replaceable glass capillary needles. Ease of operation and reliability have been improved by substituting ureteral catheter[2] for the usual metal tubing. The syringe is clamped in a cradle (*C*, Figs. 1 and 2) or held by a retaining nut (*RN*, Fig. 3). The plunger (*PL*), with the knobbed end cut-off, is connected to the threaded shaft of the drive mechanism by rubber pressure tubing (*PT*, Figs. 1, 3, 4) which compensates for the slight irregularities in alignment in most commercial syringes. The control mounting, which is of brass except where otherwise noted, has the following major advantages over previous instruments of the type:

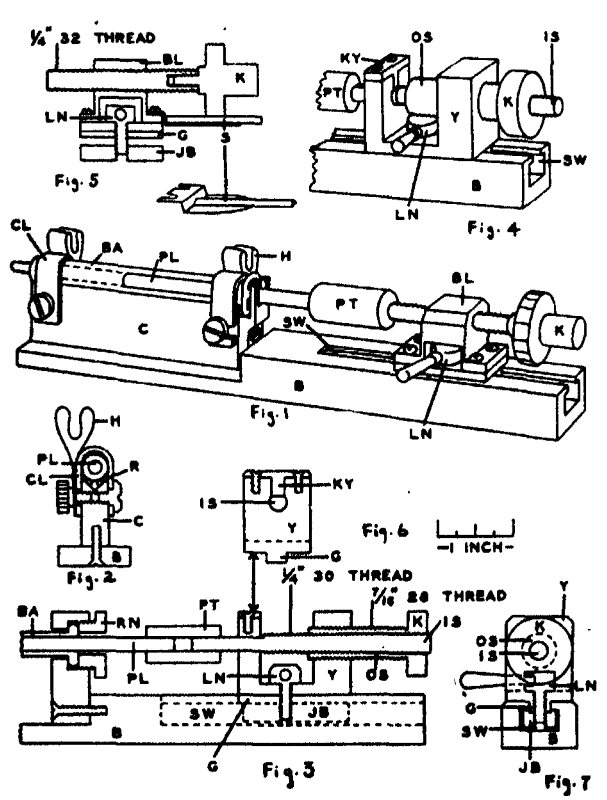

FIGS. 1–7.

Fig. 1. Complete assembly, with 1 cc tuberculin syringe and direct-motion drive. Fig. 5. Side elevation of direct motion drive. Figs. 3, 4, 6, 7, various views of differential motion drive. *B*, base; *BA*, barrel; *BL*, block; *C*, cradle; *CL*, clamp; *G*, gib; *H*, spring clip for needle holder; *IS*, inner shaft; *JB*, jam block; *K*, knob; *KY*, key; *LN*, lock nut; *OS*, outer shaft; *PL*, plunger; *PT*, rubber pressure tubing; *R*, rubber; *RN*, retaining nut; *S*, positioning spring; *SW*, slotted way; *Y*, yoke.

1. Interchangeable direct-motion (Figs. 1, 5) and differential-motion (Figs. 3, 4, 6, 7) impellers, differing 15-fold in sensitivity, are provided. The former impeller has been used extensively for injecting insect larvae and chick embryos, transplanting insect organs, making measured phage platings and quantitative topical application of insecticides. The latter, which is made of steel, is useful where unusually exquisite control is necessary. It requires especially precise alignment to prevent binding, since it does not rotate the plunger as it pushes.
2. The entire drive mechanism for the plunger slides in a slotted way (*SW*, Figs. 1, 4) and can be locked in position at any point by a lock nut (*LN*) which activates a jam block (*JB*, Figs. 3, 5, 7). Fine control is thus provided by the threaded drive, while gross movement, as is needed in filling the instrument or in handling large volumes, is simultaneously available by direct movement of the sliding block (*BL*) or yoke (*Y*).
3. For the direct-motion drive a series of readily interchangeable control wheels (*K*, Fig. 5) are provided, the rims of which are divided by precisely-spaced transverse milled grooves into various equal fractions of one circumference (e.g., 8, 10, 12, 64, 100, 150). As the wheel is turned the grooves pass over a (removable) spring positioner (*S*, Fig. 5) which permits the expulsion

---

[1] R. Chambers and M. J. Kopac, *McClung's Handbook of Microscopical Technique* (1937).

[2] J. B. Buck and H. Specht, Science **106**, 551 (1947).

of known and automatically reproducible volumes of liquid. A similar arrangement could readily be applied to the differential-motion drive.

4. The fact that the grooves in the control wheel make audible clicks as they pass over the spring is extremely useful during continuous microscopic observation, since it permits known volumes to be delivered without ocular supervision.

The instrument is filled by siphoning through the needle-holder, air-bubbles being scrupulously excluded. Boiled water is the most satisfactory liquid for filling the system, the experimental liquid being taken up only in the needle. The seal between barrel and plunger is improved with petroleum jelly.

II. CALIBRATION AND PERFORMANCE

Calibrations of the direct-motion drive made gravimetrically and by a new "areal" method have been presented.[3] They indicate that delivery is linear and highly reproducible over the range 1/100 to 1 revolution of the control wheel. Coefficients of variation[4] range from 1.3 to 2.5 percent for 14 mm^3 (one revolution of the impeller) and from 8 to 14 percent for 0.14 mm^3. These values compare favorably with those obtained with various microburettes, even though such reports, and those claiming even higher "accuracy,"[5] are based on extrapolations from calibrations made on far larger volumes than the instruments' claimed lower limits.[3]

Additional calibrations brought out the important fact that at the standard delivery rate of 14 mm^3/min. (one revolution per minute) the volume actually delivered or withdrawn is slightly but significantly reduced when the diameter of delivery orifice is reduced to 50μ. With a 30μ orifice delivery is very markedly reduced even at a rate of 7 mm^3/min. These anomalies, due to water being forced into the crevice between barrel and plunger, point to the need for careful checking of actual deliveries, particularly when using the minute apertures necessary in microinjection work.

The delivery of the differential-motion drive mechanism is about 1 mm^3/revolution (net piston movement of 1/420 inch). For lack of a sufficiently sensitive method the delivery performance was not calibrated down to its theoretical lower limit (0.01 mm^3).

Thanks are due Mr. Laurence Crisp for designing the differential-motion impeller.

---

[3] Buck, Keister, and Zelle, Anal. Chim. Acta, in press.

[4] These averaged four to five times the standard errors of the means.

[5] Scholander, Edwards, and Irving, J. Biol. Chem. **148**, 495 (1943).

THE REVIEW OF SCIENTIFIC INSTRUMENTS VOLUME 20, NUMBER 9 SEPTEMBER, 1949

Direct Experimental Comparison of Several Surface Temperature Measuring Devices*

ALICE M. STOLL AND JAMES D. HARDY
From The Russell Sage Institute of Pathology in affiliation with The New York Hospital, and the Department of Physiology, Cornell University Medical College, New York, New York

(Received May 9, 1949)

A copper cylinder was constructed and to it four layers of oak-tanned leather were applied. The thermal gradient through the leather was measured by means of thermocouples on the cylinder and between the layers of leather. By suitable extrapolation of this gradient the temperature of the outside leather surface was determined accurately and constituted the standard surface temperature to which the readings of the surface temperature measuring devices were compared.

Several types of surface temperature measuring devices were compared and evaluated on the basis of:

(1) accuracy as determined by agreement with the standard surface temperature,
(2) adaptability to use in a variety of experimentally produced environmental conditions similar to naturally occurring environmental conditions.

It was concluded that:

(1) The radiometric type of skin thermometer was the most dependably accurate instrument of those tested, although requiring corrections when used in "sunlight."

(2) Under normal conditions, the #40 gauge bare wire thermocouple was of the same order of accuracy as the radiometer and was only slightly affected by environmental changes. The accuracy of the coarser bare wire thermocouple was considerably more impaired by such changes.

The thermocouple glued to the surface, or embedded in solder and taped to the surface, or mounted on copper mesh and tied to the surface was less accurate than the bare wire thermocouple. In general, increasing the effective mass of the thermocouple decreased the accuracy of the instrument under normal conditions as well as under the changed environmental conditions.

(3) The Dermalor resistance thermometer was next in order. Errors were not greater than two percent under certain conditions but increased to four or five percent during radiation.

(4) The errors in the disk thermistor readings ranged from −1.2°C to −1.9°C under the conditions studied. The accuracy of this instrument could be increased by calibration *in situ* against a radiometer. However, this would not obviate the error produced by infra-red radiation, for instance. This error amounted to −0.7°C.

Other types of thermistors having much smaller contact surfaces are available and it is reasonable to expect that these instruments would yield readings as accurate as those of a thermocouple. However, they too would be subject to the errors exhibited by thermocouples or any other small instruments in actual contact with the surface. The feasibility of employing a thermistor as a micro-radiometer is under consideration. It presents special advantages to use in this manner in that thermistors can be constructed with a rapid response time, and as they have a high resistance they are particularly well adapted for electronic recording.

(5) The Roll and Mold pyrometers were entirely unsuited to this measurement in the temperature range studied, showing errors of from 3°C to 7°C depending upon the experimental conditions.

(6) Mercury-in-glass thermometers were unsuited to this type of temperature measurement because of the long contact time required which affects the temperature itself, and because of the marked impairment of their accuracy by environmental changes.

INTRODUCTION

The importance of skin temperature in the determination of heat loss from the body has long been recognized. An excellent discussion of the relation of skin temperature to heat loss, the factors affecting skin temperature, and the results of investigations prior to 1938 appears in Murlin's extensive review of the subject.[1] For any significant results in the study of heat loss the average skin temperature over the entire body surface must be known. Therefore, accuracy and rapidity of measurement are essential. Furthermore, recent advances in the evaluation of the environment with respect to its effect upon the individual have indicated the desirability of a more complete delineation of the "comfort zone." In studies of this type, skin temperature has been given weight equal to that of such fundamental physiological measurements as blood pressure, blood flow, and heart rate.[2] Of these interrelated factors, it has been suggested that skin temperature may be the best single objective index of the comfort zone.[3] It is therefore of increasing importance that an accurate method of measurement be made available and that errors prevalent in commonly used methods be ascertained where possible. In this way correction factors could be found and applied appropriately so that the various results of similar studies obtained by different methods of investigation could be brought into agreement.

Many devices and methods have been developed for the measurement of skin temperature and have yielded equivocal results because of the technical difficulties involved. Foremost among these difficulties is the proper calibration of the instrument. Since the temperature to be measured is that of a boundary between two different media, the difficulty of calibration of surface temperature measuring devices other than a radiometric instrument, under actual conditions of use, is readily appreciated. That serious errors may be attributed to discrepancies in the conditions of calibration and the conditions of use has been shown.[4] When contact instruments are used, the problem is further

---

* This work was supported in part by funds from the ONR of the United States Navy.

[1] J. Murlin, Ergeb. d. Physiol. 42, 153 (1939).

[2] Glickman, Inouye, Telser, Keeton, Hick, and Fahnestock, "Physiological adjustments of human beings to sudden change of environment," ASHVE Journal Section, 101 (July, 1947).

[3] "Heating, ventilating, air conditioning guide," ASHVE, New York 27, 222 (1949).

[4] J. D. Hardy, J. Clin. Invest. 13b, 605 (1934).

complicated by the effect of the applicator itself in changing the skin temperature as it measures it. A difference in the temperature of the applicator and of the skin exerts this effect. It is also known that pressure of the applicator on the skin changes the temperature.[5] This may be due to vascular changes on deformation of the skin or, possibly, local sweating. Environmental conditions also influence the surface temperature and at the same time may affect the instrument itself.

At present, because of the differences in calibration and conditions of use there is no basis for wide intercomparison of data from different laboratories. This study was undertaken to develop a method by which several types of instruments may be tested under comparable conditions and thus provide a basis of intercomparison. The same instruments were employed under a variety of experimental conditions designed to simulate actual environmental situations under which they might be used and thereby obtain an indication of the extent and direction of errors due to the influence of the environment on the instrument reading.

MATERIALS AND METHOD

Several types of instruments were selected for comparison:

1. The Hardy Dermal Radiometer.[6]
2. The Dermalor—a resistance wire skin thermometer.[7]
3. Surface Pyrometers (Cambridge Instrument Company).
    (a) The Roll Model—a flat strip thermocouple designed primarily for industrial uses.
    (b) The Mold Model—a small flat bead thermocouple also designed for industrial uses.
4. Thermocouple #5–#40 gauge copper and constantan wire thermocouple glued to the test surface with Duco cement.

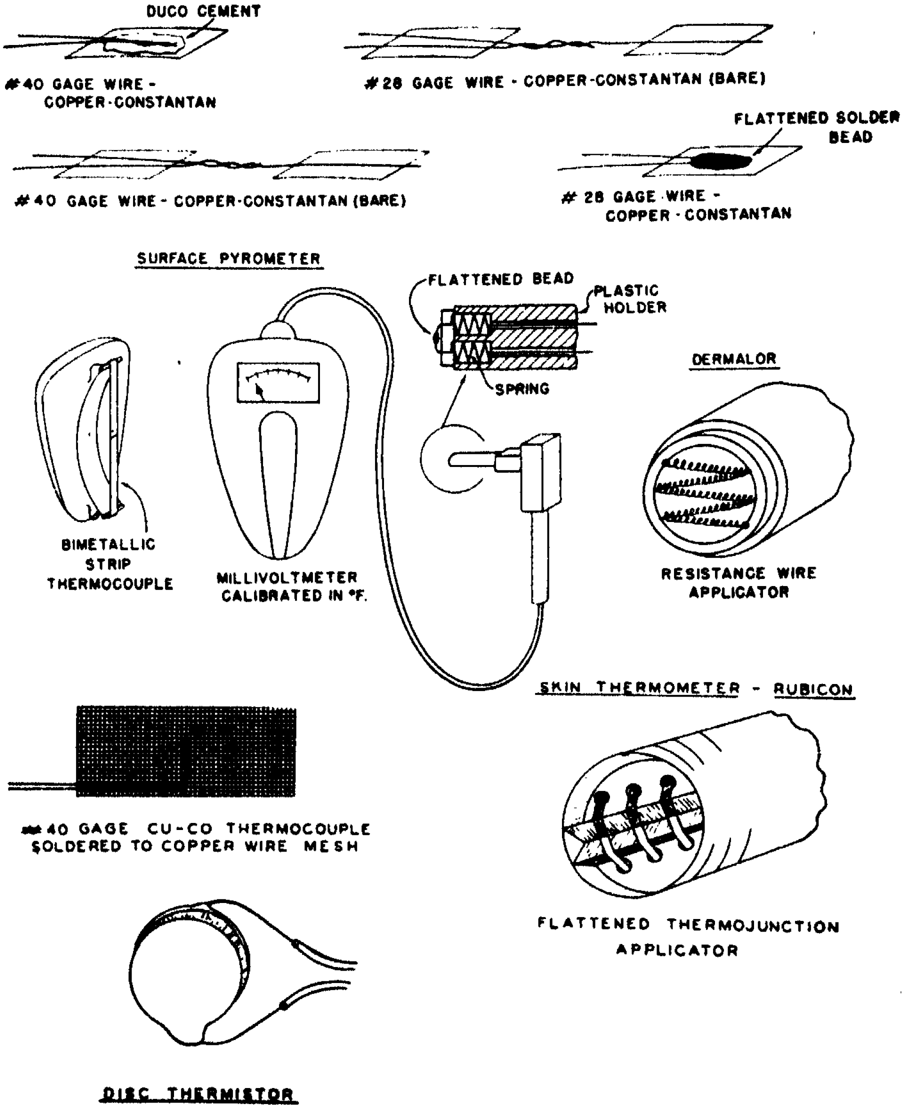
DUCO CEMENT
#40 GAGE WIRE - COPPER-CONSTANTAN
#28 GAGE WIRE - COPPER-CONSTANTAN (BARE)
FLATTENED SOLDER BEAD
#40 GAGE WIRE - COPPER-CONSTANTAN (BARE)
# 28 GAGE WIRE - COPPER - CONSTANTAN
SURFACE PYROMETER
FLATTENED BEAD
PLASTIC HOLDER
SPRING
DERMALOR
BIMETALLIC STRIP THERMOCOUPLE
MILLIVOLTMETER CALIBRATED IN °F.
RESISTANCE WIRE APPLICATOR
SKIN THERMOMETER - RUBICON
#40 GAGE CU-CO THERMOCOUPLE SOLDERED TO COPPER WIRE MESH
FLATTENED THERMOJUNCTION APPLICATOR
DISC THERMISTOR

FIG. 1. Applicators for surface thermometers.

---

[5] N. A. Remizov, Arch. Sci. Biol., St. Petersburg 38, 815 (1935).
[6] J. D. Hardy, J. Clin. Invest. 13a, 593 (1934).
[7] S. S. Samuels, N. Y. State J. Med. 40, 884 (1940).

5. Thermocouple #6–#40 gauge copper and constantan wire thermocouple stretched across the surface and supported at either end with adhesive tape, leaving the thermojunction bare.

6. Thermocouple #7–#28 gauge copper and constantan wire thermocouple imbedded in a flattened bead of solder taped to the surface with adhesive tape.

7. Thermocouple #8–#28 gauge copper and constantan wire thermocouple stretched across the surface and supported at either end with adhesive tape leaving the thermojunction bare.

8. Mercury-in-glass thermometers
   (a) clinical
   (b) general laboratory.

9. The Western Electric disk thermistor (5 mm in diameter by 1 mm thick)—applied to the surface by means of a thread drawn taut over the thermistor and fastened by adhesive tape. The leads were supported by means of a dab of wax inserted between them and the surface.

10. The Rubicon Skin Thermometer—three copper-constantan thermocouples with flattened junctions mounted in a plastic holder.

11. #40 gauge copper-constantan thermocouple—mounted on copper mesh and applied to the surface by means of ties run through the edges of the mesh and tied tightly about the cylinder.[8]

With the exception of the mercury thermometers and the Hardy Dermal Radiometer, these instruments are represented in Fig. 1.

In order to compare the instruments it was necessary to provide a standard surface the temperature of which could be determined accurately within ±0.05°C. This was accomplished in the following manner (Fig. 2): a copper cylinder, 12 inches high and 8 inches in diameter was set up and provided with a stirring device, a thermostatically controlled heater, a Bureau of Standards certified thermometer, and inlets for testing and reference thermocouples. The cylinder was filled with water and its temperature maintained constant within ±0.03°C. On this cylinder four layers of oak tanned leather, each 12 inches high, 12 inches wide and about 3 mm thick, were tightly laced. A thermocouple of #40 gauge copper and constantan wire was inserted between the cylinder and the first layer and between each of the succeeding layers. All thermocouples used in this study were made of specially annealed Leeds and Northrup thermocouple wire. All thermojunctions were about 6 inches from the top and 6 inches from the side edges of the leather strips so that they lay in a straight line from cylinder to surface in the center of the leather covered area. The copper leads from the thermocouples were connected to a rotary switch which in turn was connected to a Type K, Leeds and Northrup potentiometer. The cold junction was inserted into the cylinder within 1 cm of the thermometer and a second thermocouple provided a check on the uniformity of the temperature within the cylinder. For convenience in recording data the thermocouples were numbered as follows:

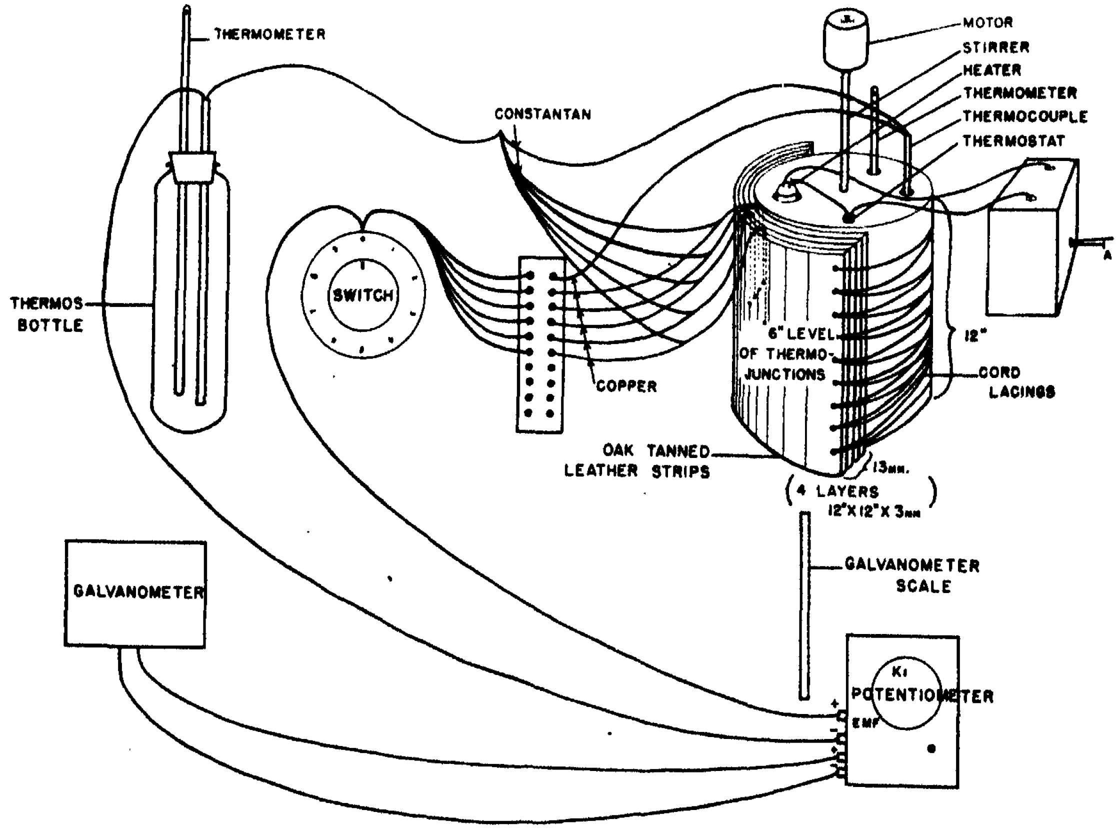

FIG. 2. Schematic representation of apparatus for obtaining a standard surface temperature.

---

[8] E. D. Palmes and C. R. Park, Fed. Proc. 6, 175 (1947).

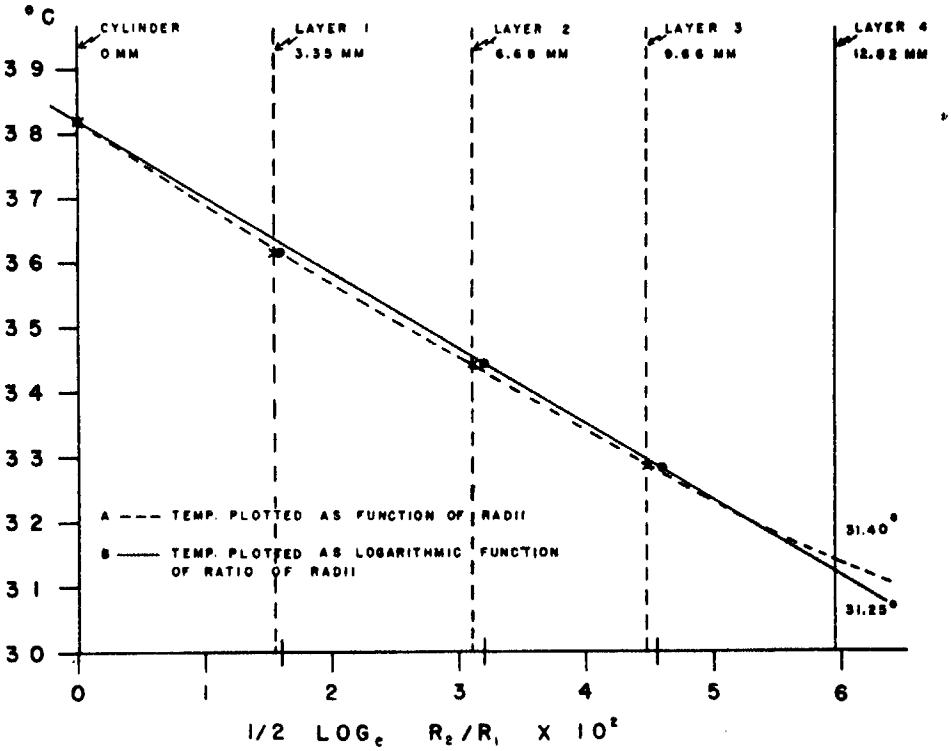

FIG. 3. Method for extrapolation of surface temperature. Curve *A* (dashed line) indicates the temperature gradient curve obtained by plotting the temperature of the surface of each leather layer against the distance of that surface from the surface of the cylinder (see top of chart). Curve *B* (solid line), a straight line, is obtained from the same data by plotting the temperature of the surface of the leather layer against the logarithm of the ratio of radius of each layer to the radius of the cylinder (see points marked off on the abscissa).

#0—within the cylinder at about 6 inches from the reference thermocouple,
#1—between the cylinder and the first layer,
#2—between the first and second layers,
#3—between the second and third layers,
#4—between the third and fourth layers,
#5–#8—test thermocouples on the leather surface.

The temperature of the standard surface was then obtained by extrapolation of the thermal gradient from the cylinder to the outermost leather surface. Because of the curvature of the surfaces it was necessary to employ the equation for heat transmission through the walls of a tube in order to obtain a straight line extrapolation. This equation simplified is:[9]

$$t_2-t_1=K\cdot\tfrac{1}{2}\log_e(r_2)/(r_1)$$

where t_1 = temperature of cylinder, t_2 = temperature of leather layer, K = a constant, r_1 = radius of cylinder, and r_2 = radius of leather layer. The thickness of each layer was measured with a micrometer and the radius calculated. The temperature difference (t_2-t_1) of each of the first three layers was measured in microvolts, converted to degrees centigrade and plotted against the value of $\frac{1}{2}\log_e(r_2)/(r_1)$ for each layer, respectively. The temperature of the outside surface of the fourth layer was then found by extrapolation and was the desired standard surface temperature to which all surface thermometer readings could be referred. Figure 3 illustrates the method by which the surface temperature was determined by extrapolation of the curve obtained on plotting the observed temperatures against $\frac{1}{2}\log_e$ of the ratio of the radial distances (Curve *B*—solid line). Curve *A* (dashed line) is shown for comparison. It was obtained on plotting the same temperatures directly against the radial distances of the layers from the cylinder. It is readily seen that since Curve *A* is not linear, an error of as much as 0.15°C can be made on extrapolation of this line unless the mathematical equation for the curve is set up and solved. Curve *B*, on the other hand, is a straight line and more readily yields the correct surface temperature on simple extrapolation, therefore this method was used throughout.

In making the comparisons the desired environmental conditions were established and the apparatus was permitted to come to thermal equilibrium. The room temperature and the temperature of the cylinder as well as pertinent data such as radiation intensity or wind velocity were recorded. All thermocouples were read successively from the cylinder outward. The surface thermometers were read in an order such that the instrument having the least effect upon the surface temperature during application would be first and that having the greatest effect would be last. Thus the thermocouples affixed to the surface were read first, then the radiometer and others, with the mercury thermometers last. In the instances where the surface temperature was affected by the applicator, sufficient time for the equilibrium to be re-established was permitted to elapse before the next instrument was applied.

EXPERIMENTAL DATA

In each situation studied, preliminary trials were necessary to achieve the best technique as determined by consistency and accuracy of results. The data herein presented represent readily duplicable results of the best performance of each instrument.

---

[9] W. L. Badger, *Heat Transfer and Evaporation* (The Chemical Catalog Company, Inc., New York, 1926), p. 14.

The following conditions were selected for test environments:

1. Normal—ordinary laboratory conditions, which include natural convection and radiation exchange between the leather surface and the walls of the room.
2. Forced convection—simulated wind, derived from an electric fan blowing air directly on the surface at the rate of four feet per second as measured by an anemometer.

TABLE I. Deviation in degrees centigrade from standard surface temperature under normal conditions.

Radiometer	Dermalor	Mold pyrometer	Roll pyrometer	Thermocouple #5	Thermocouple #6	Thermocouple #7	Thermocouple #8
−0.22				0	+0.34	−0.14	−0.17
−0.28				−0.02	−0.22	−0.14	−0.17
−0.15	−1.00			+0.43	+0.07	+0.27	+0.66
−0.12	−0.77	−6.4	−1.4	+0.39	+0.19	+0.32	+0.84
−0.11	−0.44	−5.1	−1.8	+0.19	+0.17	+0.22	+0.32
+0.04				+0.29	+0.12	+0.12	+0.02
+0.04				+0.22	0	+0.02	−0.05
+0.12				+0.22	+0.05	+0.07	+0.07
+0.19	−1.16	−5.0	−3.9	+0.39	+0.24	+0.29	+0.24
+0.13				+0.02	−0.14	−0.10	−0.12
−0.10	−0.20			+0.22	+0.05	+0.22	+0.14
−0.11	−0.36	−5.2	−3.5	+0.39	+0.24	+0.36	+0.29
+0.03	−0.22	−5.4	−4.3	+0.24	0	+0.12	+0.02
+0.06	+0.01	−5.0	−3.3	+0.17	−0.14	+0.17	0
−0.01	−0.56	−5.6	−3.4	+0.32	−0.05	+0.41	+0.05
+0.05	+0.10	−5.3	−3.6	+0.19	+0.02	+0.10	+0.19
−0.19	+0.16	−4.5	−3.4	+0.10	−0.07	+0.02	−0.05
Av. −0.04	−0.44	−5.3	−3.2	+0.22	+0.05	+0.14	+0.13

3. Infra-red radiation—simulating hot walls, derived from an electric hot plate directly facing the leather surface, other conditions "normal."
4. Simulated sunlight—produced by the radiation from a 1500 watt lamp, other conditions "normal."
5. Simulated sunlight and forced convection—"sunlight" as above and "wind" from an electric fan blowing air on the irradiated surface at the rate of two feet per second.

The standard surface temperature under normal conditions ranged from 27°C to about 32°C. Table I presents the deviations in degrees centigrade of the surface thermometer readings from the extrapolated (standard) surface temperature obtained in a series of experiments under normal conditions.

The radiometer and thermocouple #6 yielded the best results, all readings being well within the limits of experimental accuracy. Thermocouples #7 and #8 performed satisfactorily while #5 (glued on surface) showed an average deviation of +0.22°C.

The copper mesh mounted thermocouple readings (not shown in table) fell about 0.34°C below the extrapolated temperature.

The Dermalor, with an average deviation of −0.44°C, fell within the range of accuracy guaranteed by its manufacturers (2 percent, about 0.5°C to 0.6°C at the temperatures measured).

The disk thermistor was carefully calibrated in contact with the bulb of a mercury-in-glass thermometer in an air chamber rather than by immersion in a liquid in order to more closely approximate the conditions of use. A smooth, reproducible calibration curve was obtained. In spite of this precaution, however, an average deviation of −1.21°C (not shown in table) was observed.

The Rubicon Skin Thermometer readings (not shown in table) were in error by −2.85°C under normal conditions. The applicator of this instrument could not be satisfactorily adapted to use on the leather surface. Because of the construction of the holder, good contact could be obtained only by pressing the applicator into the surface. This could not be done sufficiently well on the relatively unyielding leather surface. It is to be expected that on actual skin surfaces into which the applicator could be pressed, a better approximation could be attained.

Both the Roll and the Mold model pyrometers showed wide deviations from the standard which was relatively near the lower limit of their scale range (50°F to 250°F or 10°C to 120+°C).

Mercury thermometer results do not appear in this table. Because of the long reading time required, about three minutes, it was deemed advisable to test them separately. Three techniques were used:

1. The thermometer was rolled on the surface.
2. Spot contact was maintained with the thermometer bulb covered by a notched cork.
3. A combination of the above, the thermometer, under a notched cork, was rolled on the surface.

A short series of observations was made with a clinical thermometer, a large bulb laboratory thermometer and a small bulb laboratory thermometer. It was found that under normal conditions agreement with the standard within between 0 and −0.5°C could be attained but required about three minutes contact time. Rolling under a notched cork reduced this time but introduced the possibility of errors due to friction. Forced convection or radiation falling on the surface increased the reading time by five minutes and the error by two or three degrees centigrade. Because of the long lag in response and their inadaptability to changing environmental conditions, mercury thermometers were not suited to comparison with the other instruments employed. They were therefore eliminated from the study although they could be used to advantage with a very limited set of conditions and a rigid technique developed through trial and error.

Table II presents results obtained under a variety of environmental conditions. These results are best evaluated by comparison with Table I and consideration of the factors influencing the reading of each instrument under given conditions:

1. Forced convection—To study the effects of convection currents, it was necessary to supply an air stream of constant velocity so that equilibrium was established and maintained throughout the experiment.

For accurate results with the radiometer, it was held at an angle such that it did not interrupt the stream of air, and that the air was not deflected into the reflecting cone of the radiometer. With this precaution, convection had no effect upon the accuracy of the instrument.

The Dermalor applicator must necessarily be placed upon the surface since it is a resistance coil dependent upon contact for its effect. Interruption of the air stream during application then resulted in a reading higher than the true temperature. The accuracy of this instrument remained about the same as under normal conditions although the direction of the error was reversed.

Thermocouples #5, #6, and #8 and the copper mesh mounted thermocouple (not shown in table) showed an increased error of about 0.2°C, while #7 (covered with adhesive tape) agreed more closely with the standard temperature than under normal conditions.

The Roll Pyrometer and the thermistor (not shown in table) error remained unchanged while the Mold Pyrometer showed less error than under normal conditions.

The error in the Rubicon Skin Thermometer readings (not shown in table) apparently decreased to −0.84°C during forced convection. However, this effect was only apparent since the actual temperature of the surface approached room temperature during forced convection, while it was about four degrees above room temperature under normal conditions.

2. Infra-red radiation—Accuracy within experimental limits was obtained with the radiometer when it was held in a position such that the area tested was not shaded from the radiation.

The Dermalor readings were in error by −1.75°C (average deviation) due to the shading of the test area and actual cooling of the surface by the applicator. Preheating the applicator to approximately the surface temperature (about 37°C) probably would reduce the error.

The accuracy of thermocouples #5, #6, and #7 was not significantly impaired by this radiation. Thermocouple #9 (copper mesh) readings (not shown in table) were in error by −0.4°C while thermocouple #8 (#28 gauge wire) differed from the standard by as much as −0.5°C.

The error in the pyrometers was greatly increased.

Because of the difficulty in the application of the thermoelement of the Rubicon Skin Thermometer, these readings (not shown in table) were apparently in error by −4.93°C. Under infra-red irradiation, however, the surface temperature was about 9°C above room temperature and the large error reflects poor contact of the thermoelement with the surface.

Since the data obtained with instruments #9, #10, and #11, studied after the completion of tests on the other eight, indicated that the readings were not appreciably different from those of similar instruments in the same situations, these instruments were not subjected to simulated sunshine or this radiation plus convection. It is to be expected that they would exhibit the same type of errors as other contact instruments under the same conditions.

3. "Sunlight."

In testing the performance of the instruments during radiation of energy in the visible range, sunlight itself could not be used because of its variability. It was simulated by the diffuse radiation produced by a 1500 watt lamp about 1.5 meters from the surface, and directed toward the surface through a large lens.

Under the conditions of this experiment, reflection of the radiation into the cone of the radiometer could not be avoided without interrupting the light beam. On placing the radiometer directly on the surface to avoid reflection, this instrument with its diameter of 4 cm, shielded the surface from the radiation and thus cooling of the surface ensued during the 8 seconds required to obtain the radiometer reading. However, since cooling is more readily measured than reflection, this procedure was followed. The cooling amounted to about 0.15°C in the required reading time; the exact amount of cooling under each set of conditions was determined by experiment.

The procedure for making a surface temperature measurement with the radiometer during this irradiation was then as follows: the radiometer was placed directly over the test area and the reading noted at a definite minimal time (8 sec.). The radiometer was then removed and the radiation continued until equilibrium was reëstablished. The cooling effect was then determined after the manner described by Hardy and Oppel:[10] at zero time the radiometer was applied to the surface as above and at the same instant the radiation was cut off by a shutter. The radiometer was read at 8 seconds and at frequent intervals thereafter for about 2½ minutes as the surface cooled. These readings were plotted against the time and the resulting cooling curve was extrapolated back to zero time. The difference between the extrapolated value at zero time and the observed temperature at 8 seconds constituted the cooling correction which was added to the reading of the radiometer obtained in making the surface temperature measurement during irradiation. Figure 4 shows two of the curves for cooling correction obtained in this manner. In order that this procedure be valid, the conditions under which the cooling correction was obtained were necessarily identical with those under which the test determinations were made.

After the addition of the cooling correction, there was no error in the radiometer measurements in "sunlight."

The Dermalor readings were in error by −1.2°C, again due to shading and the difference in temperature between the surface measured and the applicator itself.

Thermocouple #6 (#40 gauge wire uncovered) was not appreciably affected by this radiation, while #5, #7, and #8 showed between −0.4 and −0.9°C errors.

The errors in the pyrometer readings were greatly

---

[10] J. D. Hardy and T. W. Oppel, Physics 7, 466 (1936).

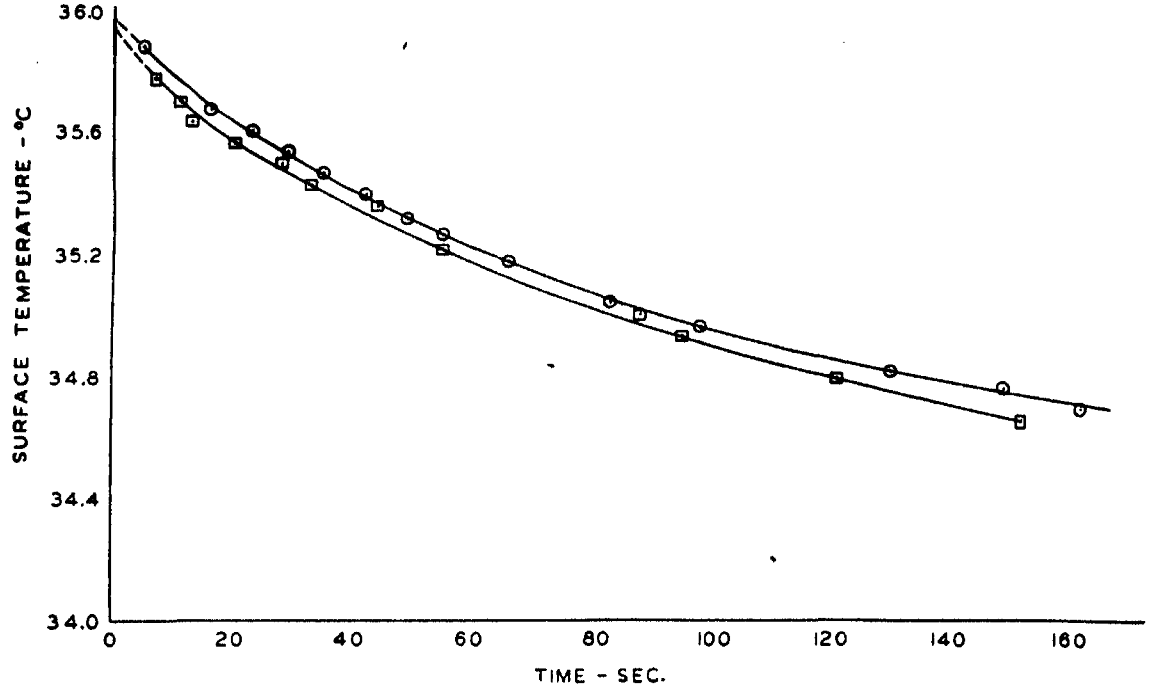

FIG. 4. Cooling curves. Two curves showing the cooling of the standard surface on interruption of the radiation falling on it from the 1500-watt lamp during application of the radiometer. By extrapolation back to zero time the correction factor for cooling under these conditions is obtained.

increased in "sunlight" as they were during infra-red radiation.

4. "Sunlight" and "wind."

When convection currents were superimposed on the "sunlight" falling on the surface a new correction for cooling was determined and applied to the radiometer reading. Thereupon the radiometer readings were brought into complete agreement with the standard surface temperature.

The Dermalor appeared to be more accurate under these conditions (average deviation = −0.1°C). In this instance there was little difference between the temperature of the applicator (25° to 27°C) and the temperature of the standard surface (about 29°C), therefore, there was no appreciable cooling effect from the applicator. The error due to shading was canceled by the interruption of the air stream during measurements.

Thermocouple #6 was the most reliable, while #5, #7, and #8 showed errors of from −0.4°C to −0.6°C.

The pyrometers under these conditions agreed more closely with the standard than under normal conditions but were still grossly in error.

A generalized summary of the foregoing data is presented in Tables III and IV.

DISCUSSION

In any study of surface temperature it is well recognized that there are factors which dictate the type of instrument most suited to the individual problem. This is particularly true when dealing with skin temperature. The measurement of surface temperature depends upon a transfer of energy from the surface to the measuring instrument. Theoretically, surface temperature could be measured in terms of any one of its components, i.e., radiation, conduction, convection or vapor pressure. Convection and vapor pressure measurements are technically extremely difficult to make and have not been employed for this purpose. Because of the relative ease of measurement, radiation and conduction have been

TABLE II. Deviation in degrees centigrade from standard surface temperature under conditions indicated.

				Thermocouple			
Radiometer	Dermalor	Mold pyrometer	Roll pyrometer	#5	#6	#7	#8
Air flow—4 ft./sec.							
+0.05	+0.30	−3.7	−2.6	−0.22	−0.17	−0.07	−0.19
+0.05	+0.60	−4.5	−3.3	−0.33	−0.29	−0.14	−0.33
−0.05	+0.60	−3.0	−3.0	−0.24	−0.39	−0.02	−0.29
Av. +0.02	+0.50	−3.7	−3.0	−0.26	−0.28	−0.08	−0.27
Infra-red radiation							
+0.12	−1.54	−6.3	−5.1	−0.07	+0.05	−0.10	−0.60
+0.02	−1.02	−8.1	−5.3	+0.02	−0.16	−0.16	−0.54
+0.02	−1.68	−4.5	−8.9	+0.02	0	−0.19	−0.34
−0.09	−2.07	−8.4	−4.5	+0.10	−0.24	−0.29	−0.51
−0.12	−2.46	−8.8	−5.9	+0.09	−0.15	−0.17	−0.46
Av. −0.01	−1.75	−7.2	−5.9	+0.03	−0.10	−0.18	−0.49
1500 watt lamp radiation							
+0.13	−1.02	−7.7	−3.8	−0.17	+0.22	−0.73	−0.27
−0.05	−1.30	−5.9	−4.8	−0.37	0	−0.92	−0.44
−0.16	−1.59	−7.5	−7.9	−0.37	+0.07	−0.95	−0.39
−0.15				−0.37	0	−1.04	−0.56
+0.02	−1.03	−6.5	−4.3	−0.50	−0.40		−0.72
−0.03	−0.98	−6.6	−3.9	−0.41	−0.10	−0.93	−0.58
Av. −0.04	−1.18	−6.8	−5.4	−0.37	−0.04	−0.91	−0.49
1500 watt lamp radiation + air flow—2 ft./sec.							
−0.11	+0.49	−3.7	−2.6	−0.29	+0.02	−0.44	−0.27
−0.05	−0.05	−3.5	−2.4	−0.51	−0.05	−0.68	−0.51
−0.04	+0.01	−3.5	−2.9	−0.49	−0.05	−0.58	−0.39
0	0	−3.9	−2.8	−0.41	−0.41	−0.61	−0.41
Av. −0.05	+0.11	−3.7	−2.7	−0.42	−0.12	−0.58	−0.40

used extensively. Since radiation may be measured at a distance from the surface, it would appear to be the more desirable measurement.

The formula for radiation exchange between two bodies at different temperatures may be expressed as

$$R=e_1e_2S_0(T_1^4-T_2^4),$$

where, in the particular instance of skin temperature, R = quantity of energy exchange, e_1 = emissivity of a perfect black body reference block = 1, e_2 = far infra-red emissivity of the skin = 0.989,[11] S_0 = the Stefan-Boltzmann constant, T_1 = absolute temperature of the black body, and T_2 = absolute temperature of the skin. Since all the terms of the equation except R and T_2 are known, T_2 may be determined from the measured quantity R; also as R usually may be determined accurately without affecting T_2, this is theoretically a dependable measurement of skin temperature.

Conduction, on the other hand, may be expressed more simply as

$$C=K(T_s-T_i),$$

where C = quantity of energy exchange, T_s = temperature of the skin, T_i = temperature of the instrument, and K = a constant. However, K depends upon many factors: the contact pressure, the roughness and wetness of the skin, and the size and the conductivity of the applicator. Even when the size of the applicator is minimal and the conductivity optimal, the other factors influencing K are variable and affect the accuracy of the determination.

For practical purposes when rough, quasi-quantitative measurements suffice, conduction methods are usually quite satisfactory. Because of the low cost, sturdiness and ease of operation of various instruments based on this principle, conduction instruments have come into wide usage and consequently have been employed in studies for which they are not suited. Quantitative studies relating skin temperature to heat loss rate and to blood flow measurements, for instance, require a method of greater precision. Theoretically, the radiometric method is most suitable and this is borne out by practical experimental evidence. Of the many devices employed in measuring skin temperature, as yet no single instrument adaptable to every situation has been demonstrated. The radiometer most nearly approaches this ideal because of its accuracy and its applicability to the particular problems of this measurement. With appropriate corrections the Dermal Radiometer maintains an absolute accuracy of ±0.1°C, the limit of accuracy with which the scale of this model may be read, under all conditions of these experiments. This confirms and extends the work of a previous investigation by Hardy.[4] Unlike any other instrument similarly employed, the radiometer does not come in contact with the skin; therefore changes in temperature and possible vascular changes due to pressure or contact with the skin on application of the instrument are obviated. The reading time is short, eight seconds, and relatively rapid changes in skin temperature may be followed readily. The necessity for corrections under certain circumstances and the bulk and fragility of the instrument are decided disadvantages. Also, the radiometer principle has not been adapted for measuring skin temperature beneath clothing or for continuous recording. However, such corrections as are necessary can be made with the radiometer itself and attempts to

TABLE III. Average deviation from extrapolated temperature—°C.

	Experimental conditions				
Instrument	Room (normal)	Wind velocity 4 ft./sec.	Infra-red radiation (hot stove)	1500 watt lamp radiation	1500 watt lamp wind velocity 2 ft./sec.
"Dermal" radiometer	−0.04	+0.02	−0.01	−0.04	−0.05
Thermocouple #40 gauge wire (bare)	+0.05	−0.28	−0.10	−0.04	−0.12
Thermocouple #28 gauge wire (bare)	+0.13	−0.27	−0.49	−0.49	−0.40
Thermocouple solder bead (adhesive tape)	+0.14	−0.08	−0.18	−0.91	−0.58
Thermocouple #40 gauge wire (glued)	+0.22	−0.26	+0.03	−0.37	−0.42
"Dermalor" resistance thermometer	−0.44	+0.50	−1.75	−1.18	+0.11
"Pyrometer" strip thermocouple	−3.2	−3.0	−5.9	−4.9	−2.7
"Pyrometer" solder bead	−5.3	−3.7	−7.2	−6.8	−3.7
Copper mesh thermocouple	−0.36	−0.57	−0.42		
Disk thermistor	−1.21	−1.22	−1.91		
Rubicon skin thermometer	−2.85	−0.84	−4.93		

TABLE IV.

	Performance under experimental conditions				
Instrument	Room (normal)	Wind velocity 4 ft./sec.	Infra-red radiation	1500 watt lamp radiation	1500 watt lamp wind velocity 2 ft./sec.
"Dermal" radiometer	Excellent ±0.05°C	Excellent	Excellent	Requires correction	Requires correction
Thermocouple #40 gauge wire (bare)	Excellent	Fair	Good	Excellent	Good
Thermocouple #28 gauge wire (bare)	Good ±0.15°C	Fair	Poor ±0.90°C	Poor	Poor
Thermocouple solder bead (adhesive tape)	Good	Excellent	Fair	Poor	Fair
Thermocouple #40 gauge wire (glued)	Fair ±0.30°C	Fair	Excellent	Fair	Fair
"Dermalor" resistance thermometer	Fair	Fair	Poor	Poor	Good
"Pyrometer" strip thermocouple	Very poor ±3.0°C	Very poor	Very poor	Very poor	Very poor
"Pyrometer" solder bead	Very poor	Very poor	Very poor	Very poor	Very poor
Copper mesh thermocouple	Fair	Fair	Fair		
Disk thermistor	Poor	Poor	Poor		
Rubicon skin thermometer	Very poor	Very poor	Very poor		

---

[11] J. D. Hardy, Am. J. Physiol. 127, 3 (1939).

reduce the bulk without sacrificing accuracy are now in progress in other laboratories.[12]

It would be of considerable practical value if these experiments could be put to use in deriving correction factors which would bring into agreement skin temperature data obtained by the various methods of measurement. The skin temperature measuring devices fall into two general classes, namely those instruments which cover several square centimeters of skin and thereby alter the normal heat flow pattern, and those which come into contact with the skin at only one point or at most in a single fine line. The bare wire thermocouples belong to this latter group, and an attempt has been made to discover whether these thermocouples are indicating subsurface temperature, surface temperature or the temperature of the air in close proximity to the surface.

Büttner[13] has measured the thermal gradient through the air immediately adjacent to a wall of known temperature higher than that of the circulating air. He found a linear relationship between temperature and distance from the wall such that the temperature fell at the rate of 2°C per millimeter in still air. From this data it is possible to determine whether or not the thermocouples were reading the temperature of the air in the boundary layer. For a #28 gauge thermocouple, 0.6 mm in diameter, one side just touching the surface, it was found experimentally that in still air this instrument was reading 0.13°C higher than the actual surface temperature. It was thus evident that the thermocouple was not reading the temperature of the air in the boundary layer or the surface temperature but an equivalent subsurface temperature. It can be easily shown that the thermocouple was reading the temperature of the leather 0.2 mm beneath the surface, a result which is to be explained on the local banking of heat between the thermocouple and the surface. It is a fact that although thermocouples can be made with very fine wire they will indicate only the temperature of the very small junction at a spot on the skin where the wire is having the most disturbing effects. For example, the #40 gauge thermocouple, 0.2 mm in diameter, gave a reading of the surface temperature which was 0.05°C higher than the true temperature of the surface, again showing evidence of heat banking.

Büttner has also measured the "effective Grenzschicht" or thickness of the boundary layer of air at a surface upon which wind was blowing at various known velocities. Applying his data to these experiments it was found that although the thermocouples were now reading lower than the true surface temperature there was definite evidence of banking of heat between the thermocouple and the surface. From these considerations it became obvious that an exhaustive treatment of the heat flow problem would be necessary to arrive at corrections which could be applied to thermocouple measurements under various environmental conditions, to say nothing of the various methods of applying thermocouples to the skin surface. Such an approach does not appear justifiable in view of the present data. It is believed, however, that if skin thermometers were calibrated against a surface of known temperature under the various circumstances which are to be employed in the biological study, empirical corrections could be arrived at and applied so that a more accurate evaluation of skin temperature could be made. A perhaps even more accurate method would be to calibrate skin thermometers in place on the skin by comparison with radiometer measurements. Studies of this nature are now being made in this laboratory in an attempt to evaluate further the various methods now employed for measuring skin temperature.

---

[12] M. Van Dilla and J. Bochinski, Report R252 Radiometer, A. S. F., QM Climatic Research Laboratory, Lawrence, Massachusetts (October, 1945).

[13] K. Büttner, *Verdunstung und Strahlung in Bioklimatologie und Meteorologie* (Preuss. Meteorol. Institut., Berlin, 1934), Vol. X, p. 5.

Book Reviews

Metal Rectifiers

By H. K. Henisch. Pp. 155+xi, Figs. 55. Clarendon Press, Oxford, 1949. Price $3.75.

This book is the second volume of a new series entitled *Monographs on the Physics and Chemistry of Materials* edited by a distinguished group of British scientists. It is the second English language text to deal exclusively with a phase of the subject of metal-semiconductor rectifiers. The first was the Radiation Laboratory volume on *Crystal Rectifiers* by Torrey and Whitmer.

One distinguishes two general phases of the subject of metal-semiconductor rectifiers, namely, (1) the large area disk type of rectifier used almost exclusively in low frequency power applications, and (2) the metal point contact type of unit applied mainly in high frequency electronic circuits. Henisch's book deals with the former.

The subject of dry rectifiers presents an author with a very complex problem. Semiconductors have electrical properties which are extremely sensitive to structure changes and to impurity inclusions. When one studies the contact between a metal and a semiconductor the sensitivity is often magnified another order of magnitude. Thus, it is easy to see how the thirty or more years of extensive literature can be cluttered with misinformation and conflicting data. Henisch deals with this problem by not attempting to review papers in detail. Instead he describes with the aid of the literature and his own experience what he calls the "characteristic rectifier properties." These are properties, such as, the contact resistance *versus* voltage relation, which are qualitatively the same for most rectifiers and show promise of being subsumed by theory. In addition to this, there are chapters on methods of manufacture and methods for making electrical measurements upon rectifiers. Modern and earlier theories of rectification are discussed, and finally the author's desiderata for future rectifier developments are given.

The description of methods of manufacture will be of interest to those who have not had the opportunity to witness the industrial processes. Two words of caution are in order. Firstly, the author has had to rely upon published material for his descriptions. Because industrial firms are usually unwilling to disclose their latest processes, the descriptions are tinged with obsolescence. For example, his discussion of a vacuum preannealing process (p. 123) imputes novelty to a process which has been superceded for at least ten years. Secondly, it must be realized that rectifier manufacture is still an art, and it must not be supposed that written instructions will suffice to insure that anyone can make good rectifiers at first try. I am, however, sympathetic with the author, and feel that he is working in the right direction to free the subject of cook book magic. I would criticize one item, namely, his description of the preparation of germanium rectifiers. This is inadequate and it would be better if this were left out.

The section on characteristic rectifier properties is quite adequate for the expressed purpose of the book; that is, "to collect and summarize the most important aspects of the subject . . . for practical workers in this field."

The chapter on modern theories provides a good summary for those who are not interested in pursuing the work in more detail. Serious students of the theory will find more satisfaction in consulting papers in the adequate bibliography given at the end of the book. The choice of older theories discussed makes entertaining reading. One criticism I might make is that some of the discussions of the modern theory are disappointingly brief. One launches with interest into a topic and is barely settled when the end of the section abruptly appears.

The book is not intended to give engineering information, but emphasizes the physics aspect of the problem. It would be better if the brief mention of practical matters that is made would be deleted in favor of more space for the theory.

We may summarize by saying that the book is a good summary for research workers who would gain an acquaintance with the field of large area rectifiers, but will not be satisfying to those already expert and desirous of reading new work in the field, or to those mainly interested in point contact rectifiers and transistors.

S. J. Angello
Westinghouse Research Laboratories

Introduction to Statistical Mechanics

By Ronald W. Gurney. Pp. 268, Figs. 60, McGraw-Hill Book Company, Inc., New York, 1949. Price $5.00.

This book was written with the object of presenting statistical mechanics in a form attractive to the experimental physicist and chemist. As a result, the over-all treatment is quite elementary, with an adequate number of illustrative and practical examples.

Gurney's book can be divided into two parts, with Chapter 7 falling between them. The first six chapters derive the most probable distribution of energy among a number of weakly interacting atoms or molecules that have quantized energy states, and apply the resulting partition functions to a discussion of thermodynamic functions, properties of gases, activation energies, crystal order, and fluctuations. The last five chapters present a more conventional, but still elementary, exposition of statistical mechanics in terms of ensemble and phase space, with applications to imperfect gases, condensation, solids, homonuclear diatomic molecules, and quantum statistics. Chapter 7 is a relatively lengthy exposition of solid and liquid solutions, that is informative and makes good use of the preceding material.

The consistent emphasis on simplicity throughout the book, both as to physical ideas and analytical development, leads to a number of excellent and clear qualitative explanations of such matters as the most probable energy distribution, the progress toward this equilibrium distribution, the relation between the partition functions of a gas and a solid, and the concept of temperature. At the same time, it is perhaps an inevitable result that some of the discussions will not satisfy the more inquiring students even in a basic course on this subject. Thus an integral is substituted for a summation on page 95 without any mention of the need for taking the limit of large a, and the similar less justifiable substitution on page 225 leads to the discrepancy between the middle and right sides of Eq. (406). Similar oversimplifications appear in the implication (page 186) that a classical ideal gas shows much greater density fluctuations than a quantum ideal gas, and in the omission of nuclear spin from the consideration of hetero- and homonuclear diatomic molecules (page 226).

With its clear development of basic statistical concepts, and its numerous applications to physically interesting situations, Gurney's book will prove to be of considerable value to undergraduate students of physics and chemistry, and to professional workers in experimental physics, chemistry and metallurgy. By the same token, the older books of Tolman, Fowler and Guggenheim, and Mayer and Mayer, will continue to be indispensable to those who wish to become acquainted with the full power of statistical mechanics, or to follow the analytical details of many applications.

L. I. Schiff
Stanford University

The Instrument Manual

Edited by the Proprietors of Instrument Practice. Pp. 548+cxiii, illustrated. United Trade Press, Ltd., London, 1949. Price L3 10s.

Here is a book that should prove to be a very useful reference for those interested in problems in measurement and control. The purpose of *The Instrument Manual* is perhaps best understood by quoting excerpts from the editor's introduction. "The object of this book is to provide in a convenient form general information of value to all concerned with industrial instruments, that is, manufacturers and users of devices to facilitate observation, make measurements, record data, and manually or automatically control processes. . . . This work can be said to give both overseas and home users and purchasers of instruments detailed information of the British instrument industry, and what it has to offer the world."

The field covered by the manual is very extensive, ranging from simple manufacturing gauges to mass spectrometers. It is a treatise on measurement and control, being primarily devoted to physical principles and methods of measurement and control, rather than to a description of specific equipment.

As is usual in any volume written by a number of authors, the treatment of the various sections is not uniform. An attempt was made to vary the treatment of various subjects in accordance with the general level of interest and the extent of the use of the particular class of instrument.

The manual is divided into twenty one sections as follows:

I. Engineering Precision Instruments (measurement and gauging of screw threads, gears, flatness, and general physical dimensions).
II. Engineering and Mechanical Instruments (stress, strain, impact, hardness, fatigue and wear).
III. Optical Instruments.
IV. Instruments for the Determination of Texture (surface quality, magnetic and supersonic testing).
V. Instruments for the Determination of Compositional Quality (spectroscopy, polarography, gas analysis, calorimetry, mass spectrometry, radiography, and gas analysis).
VI. Measurement and Control of Time and Speed.
VII. Measurement and Proportioning of Weight.
VIII. Measurement and Control of Pressure.
IX. Measurement and Control of Level.
X. Measurement and Control of Specific Gravity.
XI. Measurement and Control of Temperature and Pyrometers for Furnace Temperature.
XII. Measurement and Control of Flow.
XIII. Measurement and Control of Hydrogen Ion.
XIV. Measurement and Control of Humidity.
XV. Automatic Control.
XVI. Electrical Measuring Instruments.
XVII. Review of Electronic Instruments.
XVIII. General Trends in Instrument Design.
XIX. Organisations Interested in Instruments.
XX. Publications Directly Associated with Instruments.
XXI. Directory of Manufacturers.

Each section of the manual includes a fairly complete bibliography (up to 1947 in most cases) as well as a buyers' guide and references to British Standards Specifications. In addition there is a list of recent British patents pertaining to instrumentation. The buyers' guide is a list of British manufacturers only.

The American reader will be disappointed not to see mention made of many new instruments with which he is familiar. This reviewer was pleased, however, to find the thoroughness with which some of the fundamentals of measurement and control are treated. The section on automatic control, for example, covers 100 pages and is well done. There are few volumes which cover so many subjects in this field as well.

The manual can hardly seem to justify the date, 1949, for there are a number of significant advances in recent years that receive little or no mention. In the very interesting section on measurement of time, for example, no mention is made of the possibility of the atomic clock, which is considered by many to be revolutionary as a time standard. Another subject that should be discussed in a book of this character is that of oxygen analysis. No mention is made of the possibility of combustion control from oxygen analysis, nor is any mention made of paramagnetic oxygen analyzers which are being put to numerous uses in this country. These and other omissions may be excused on the basis that certain techniques and equipment have not received general acceptance in England, and therefore are not included.

Judging the manual on the basis of its contents, it is considered to be very well done in general, and should prove of interest to many people. Unfortunately, the life of the manual is likely to be limited by the very poor binding. The reviewer's copy has already begun to collapse.

J. C. Mouzon
Research and Development Board

Atmospheric Electricity

By J. Alan Chalmers. Pp. 175, Figs. 36, 22½×14½ cm. Clarendon Press, Oxford, 1949. Price $3.75.

This book by J. Alan Chalmers is a valuable addition to the literature on atmospheric electricity. The volume serves both as an introduction to the subject and a reference work of limited value. The principal problems and the majority of the important contributions to the field are covered. The material for the book is well organized, the topics have been thoughtfully selected and an attempt made to report the principal results. The text is generally well written and concise.

The opening chapters are devoted to a brief historical review of early observations and their interpretation, together with a summary of the fundamental principles necessary to understand the special problems of atmospheric electricity. The important sections of the book are opened by a review of the numerical magnitudes and characteristic properties of various types of ions in the atmosphere. The factors governing the rate of production of ions, their destruction and their final equilibrium are considered in relation to their influence on the natural conductivity of the atmosphere. A chapter on the vertical electric field well summarizes the experimental data under fair weather conditions.

The various components of the air-earth current and their possible interrelation under storm conditions are considered. The electrical balance of the atmosphere as determined by ohmic conduction, point discharge and mechanical transport is worked out as fully as the experimental data permit. From the results of this investigation, the author concludes that storm conditions over a small fraction of the globe are responsible for the world wide electrification observed in the atmosphere.

The electrical effects that accompany the production of a thundercloud are discussed at some length with the major emphasis placed on experimental methods and results of measurements. The author considers various proposed theories to account for the electrification of raindrops and discusses how these proposed mechanisms can account for the separation of free electrical charge in the thunderstorm. He appears to be well satisfied that available mechanisms will adequately account for the principal features of thunderstorm electrification. The chapter on the measurement and physical characteristics of the lightning flash is a concise and valuable summary of the electrical characteristics of the transient state.

The frequent references to special apparatus and problems associated with the measurement of atmospheric electric quantities add notably to the usefulness and interest of the volume. Explanatory diagrams would, in a number of cases, add further value to these references.

One serious discrepancy has been noted. The author, in order to be consistent with some of the older writers, defines a positive electric field as the space gradient of the potential, instead of the negative space gradient, as used by all modern writers. While this assumption is illustrated in Figs. 1 and 29, the discussion in Sections 16 and 17 and the equations in other sections of the book are hopelessly inconsistent therewith. Understanding of atmospheric electricity would have been advanced if the errors of the past had been corrected and the standard definitions employed by mathematicians and physicists had been adopted.

A careful reader will encounter a number of gaps and examples of misplaced emphasis. The use of data collected at Kew, instead of the more descriptive information collected over the oceans by the research ship, "Carnegie," gives a misleading impression of world-wide atmospheric conditions and discharge rates. Although I have not carefully checked many of the assignments of credit for original contributions by the author, the confusion in the discussion of the electric field meter, inappropriately called a "field mill," indicates that revisions might be necessary in the interest of objectivity and history. This reviewer has personally used the electric field meter to measure atmospheric electric fields on aircraft since 1929 and was surprised to find the author giving 1937 as the date of first application.

Ross Gunn
U. S. Department of Commerce

Ultrasonics

By Benson Carlin. Pp. 270+xi, Figs. 160, Tables 8, 15×23 cm. McGraw-Hill Book Company, Inc., New York and London, 1949. Price $5.00.

This book is primarily concerned with ultrasonic wave propagation as a means for the detection and location of flaws in the fabricated products of industry. A few biological and chemical effects of ultrasonic waves are briefly noted, but no reference is made to the manifold uses of piezoelectric crystal oscillators in the measurement of the physical properties of matter. The book constitutes a useful first reader for one previously unfamiliar with the subject who wishes to utilize ultrasonic phenomena in industrial, chemical or biological research. The text, which is entirely non-mathematical, is praiseworthy throughout for clarity of exposition, but for practical purposes must be supplemented by a considerable knowledge of electronics.

The first two chapters are devoted to descriptions of the propagation of plane longitudinal and transverse elastic waves in a homogeneous, isotropic medium, and the reflection and refraction of these waves at a plane interface between two such media. Propagation in anisotropic media is not mentioned. Chapters III and IV deal with the preparation and mounting of plane, curved and focusing piezoelectric crystal plates suitable for the production and detection of various types of ultrasonic beam in specimens with plane or curved surfaces, and with means for coupling the crystal to the work.

Explanations of the ways in which the phenomena of resonance and of pulse reflection may be employed for the measurement of the thickness of specimen plates are given in Chapter V. The text of this and succeeding chapters is admirably illustrated with clear schematic electronic circuit diagrams and well-conceived functional block diagrams. Chapters VI and VII are concerned with the testing of materials for flaws by means of continuous and pulsed ultrasonic wave trains. Brief reference is made to submarine and seismic echo ranging.

Chapter VIII will be of particular value to those interested in the use of ultrasonic phenomena in chemical or biological research, for it deals in adequate detail with the production of high power ultrasonic beams in liquids. The phenomenon of magnetostriction and the construction of magnetostriction oscillators and receivers are discussed in Chapter IX.

The book closes with a brief review, derived from the author's personal experience, of certain practical considerations in the application of ultrasonics to flaw testing. It is the opinion of the reviewer that the value of the book to workers in this, its primary, field of interest would have been much enhanced if the final chapter had been greatly enlarged and more profusely illustrated with typical oscillographic records.

S. L. Quimby
Columbia University

Radioactive Measurements with Nuclear Emulsions

By Herman Yagoda. Pp. 356, Figs. 75. J. Wiley and Sons, Inc., New York, 1949, $5.00.

Photographic emulsions were instrumental in the discovery, by Becquerel, of natural radioactivity. In the subsequent study of the natural radioactivities, and in their application in many fields, photographic emulsion techniques have played a major role, proceeding in two directions—detection of the radiations by the blackening which they produce, and the development and use of special emulsions, known as nuclear emulsions, capable of recording tracks of individual particles. Because of the short range, in the emulsions, of charged particles of moderate (non-relativistic) energies, the study of individual tracks involves special microscopic observation and recording techniques.

While the potentialities, inherent in the use of nuclear emulsions for the study of nuclear reactions, were recognized quite early (for instance, by M. Goldhaber and co-workers in 1936) the available emulsions have been, until just a few years ago, unable to compete with other charged particle recording devices, such as the cloud chamber. Nevertheless, emulsions were used for the study of radioactivity in many other fields. In the intervening years, important advances in nuclear emulsion techniques were made as a result of the pioneer investigations of Wilkins in this country, of Blau and Wambacher in Europe, and of Zhdanov and Perfilov in the USSR.

In recent years, the nuclear emulsion technique has seen a remarkable revival as a result of the improvements in emulsions, largely through the efforts of Occhialini, Powell, and co-workers. The new nuclear emulsions are more sensitive, enable discrimination between different particles, and can be used to provide a quantitive measure of the charge, mass and energy of the charged particle responsible for the track. Developed primarily as a result of pressure from workers in nuclear physics and cosmic rays, having already to their credit the discovery of the pi-meson and the heavy nuclear component in the primary cosmic radiation, nuclear emulsions are today being fruitfully applied in many fields.

Within the past year, the sensitivity of nuclear emulsions has been further improved to the extent of being capable of recording charged particles of all energies. "Minimum ionization" emulsions are comparable to cloud chambers operated at high pressures (~1000 atmospheres). Their use has already led to the observation of showers of relativistic particles associated with cosmic-ray induced nuclear disintegrations. These new emulsions should be of major importance in tracer studies involving artificial beta-radioactivity.

Reports on the use of nuclear emulsions in radioactivity studies are widely dispersed through the periodical literature. A wealth of useful information, concerning the properties of emulsions, is collected in C. E. K. Mees's encyclopoedic "Theory of the Photographic Process;" the application of nuclear emulsions to nuclear and cosmic-ray studies is admirably described in "Nuclear Physics in Photographs" by C. F. Powell and G. P. S. Occhialini. The volume reviewed herein discusses the application of nuclear emulsions to a variety of fields—nuclear physics, radiochemistry, geology, geochemistry, metallurgy, minerology, crystallography, biology, and cosmic rays. The author appears to be particularly well qualified for an undertaking of such broad scope, having himself contributed in most of these fields.

Chapter 1 contains a painstakingly thorough and interesting review of the history of the development of photographic emulsions as applied to the study of radioactivity and a brief, but complete, summary of the effects which produce a photographic image.

Chapter 2 discusses the scintillation method for detecting charged particles, and its similarity to the emulsion technique. To this reviewer, the similarity seems rather far fetched; the cloud-chamber method, for instance, is much more similar.

Chapter 3 describes in detail many useful methods of source preparation, of sample exposure, and of processing emulsions. The summary of processing techniques is quite complete, but a more detailed discussion of hot-cold techniques for processing thick emulsions and a discussion of the possibilities of physical development would have added to the usefulness.

Chapters 4–9 contain a thorough discussion of the detection of alpha-particles, and of the application of emulsions to the study of alpha-radioactivity.

Chapters 10 and 11 cover beta-ray autoradiography, with applications to biology and metallurgy. Also included, is a brief summary of the methods of slow neutron radiography.

Chapter 12 summarizes recent work in nuclear physics and cosmic rays. In contrast to the subjects treated in other chapters, the work in nuclear physics and, especially, cosmic rays is in the earliest stages. Already, some of the quoted results have been superceded. For instance, the evidence for the existence of the neutretto, based on the first measurement of the pi- to mu-meson mass ratio, is no longer believed. It is necessary to object to the author's discussion on one point: The double star (binery evaporation), observed by Leprince-Ringuet and co-workers, is by no means the same event as the relatively frequently occuring star-sigma-meson-star phenomenon. In the former, both stars appear to result from the capture of a slow meson which, if true, is strong evidence for the existence of a meson still heavier than the pi.

This book is a useful addition to the literature on nuclear emulsions. The complete list of references, liberally refered to throughout the text, is especially useful. While the author's wide range of interests makes for constantly interesting reading, it is also the source of the book's greatest weakness—its diffuseness. Some of the material, like the chapter on scintillation techniques, could have been omitted. On the other hand, the beautiful work on pleochroic halos, recent developments in automatic scanning, recording, and grain counting, and the effects of low temperatures on track fading are given only cursory treatment or completely omitted. Although practically all the available information on processing and measuring techniques can be found in this book, it would have been helpful if the organization had been such that all of this material appeared in a single chapter.

Bernard T. Feld
Massachusetts Institute of Technology

Scientific and Industrial Glass Blowing and Laboratory Techniques

By W. E. Barr and V. J. Anhorn. Pp. 388, 212 illustrations. Instruments Publishing Company, Pittsburgh, 1949. Price $6.00.

In the Preface the authors state, that "In presenting this book we are attempting to fulfill three objectives. First, it is necessary to point out and describe characteristics of various laboratory glasses as well as fundamental techniques involved in handling glass. . . . Our second object is to present advanced techniques as the application of high vacuum, silvering and the evacuation of glass jackets to the construction of glass equipment. . . . Several condensation pumps which are used with mechanical vacuum pumps are described along with auxiliary equipment needed in vacuum work.

"Our third objective is to describe glass equipment for specific applications in the laboratory."

These objectives have been amply fulfilled in the small book of 380 pages, which is a veritable compendium of information for the experimenter and it should be of substantial help in the design and construction of all manner of glass and quartz devices and equipment.

The first eight chapters contain a detailed description of the technique of making glass seals, tube bends, spirals and glass to metal seals. The next three chapters deal with glass vapor pumps, vacuum gages, and the technique for obtaining high vacuums.

The only criticism (which is of a minor nature) that the reviewer would wish to make is that the Knudsen equation on page 225, for the resistance to flow of a tube, is only approximate and involves large errors when applied to relatively short lengths.

Complete descriptions are given of the construction of mercury vapor lamps (for the production of ultraviolet) and fluorescent lamps. The transmission coefficients for various wave-lengths are given for a number of glasses and also information on the compositions of fluorescent materials.

Chapter 12, Gas Adsorption Apparatus for Measuring Surface Areas, 13, The Modified Menzies-Wright Molecular Weight Apparatus, and 14, Swietoslawski Ebulliometers, have been written in collaboration with members of the Mellon Institute of Industrial Research and describe particular applications of glass equipment.

The last chapter deals with the design and construction of distillation equipment for fractionation of different organic liquids.

The book can be highly recommended as an invaluable aid to experimental work in chemistry, physics and even biology.

Saul Dushman
General Electric Company

Photoelectricity and Its Application

V. K. Zworykin and E. G. Ramberg. Pp. 494, Figs. 780. John Wiley & Sons, Inc., New York, 1949. Price $7.50.

Photoelectricity and Its Application is a survey of the field of photoelectric effects, their history, theory, and application. The primary emphasis is placed upon the theory, construction, and uses of photoelectric devices. This fact, and the broad scope of the undertaking, have resulted in a descriptive rather than an analytical presentation of material. In a series of well-written and beautifully illustrated chapters the authors have described the construction and operation of multipliers, image tubes, and camera tubes. Television, picture transmission, and sound reproduction systems are treated in lucid and complete fashion. The miscellaneous uses of photocells as tools in science and industry are described with careful attention to the problems of amplification and noise in photocell circuits.

Two brief chapters are devoted to photovoltaic and photoconductive cells. The discussion of modern photoconductive cells is particularly timely; some characteristics of the lead sulfide cell which is of particular importance for infra-red work are given. It is unfortunate that so much data on this cell are still classified. One also regrets that the recent published material on lead selenide and telluride cells missed inclusion in this book.

The materials, apparatus, and methods for construction of photocells are described in two short chapters. These chapters contain a review of high vacuum technique, which is too brief to be of much practical value to the working physicist. Although the common types of gauges and pumps are described, critical comment and performance data are lacking. The problems of the research worker who wishes to obtain the best possible vacuum are given scant attention.

The treatment accorded the fundamental theory of photoemission from metal surfaces is most disappointing. In a book devoted chiefly to engineering applications one is prepared to accept a somewhat perfunctory discussion of fundamentals but not a completely inadequate and distorted picture of modern achievements. The authors quickly survey the well-known history of pioneer work which culminated in Millikan's verification of the Einstein equation. Only passing reference is made to the classic work of Fowler and no mention is made of the theoretical and experimental work of DuBridge and his coworkers which is surely the most important contribution to an understanding of photoemission since Millikan's research. The authors make the curious statement (p. 28) "In the study of photoemission, the existance of the tail of the distribution curve plays a minor role, . . . " Considering the large amount of fruitful labor which has gone into the study of energy distribution curves and the temperature dependence of the photocurrent as excited by near threshhold radiation, this assertion cannot be accepted.

The inadequacy of the present volume in its treatment of the fundamentals of photoemission is the more keenly felt because the standard American text on the subject, Hughes and DuBridge's *Photoelectric Phenomena*, is now out of date. One can only hope that there will soon appear as adequate a treatment of fundamentals as the present volume offers of engineering applications.

Robert J. Maurer
Carnegie Institute of Technology

Principles of Mechanics

Second Edition. By John L. Synge and Byron A. Griffith. Pp. 530+xvi, Figs. 164. McGraw-Hill Book Company, Inc., New York, 1949. Price $5.00.

The second edition of this excellent elementary text is substantially the same as the original. The principal revision is a major change in the treatment of the motion of a charged particle in an electromagnetic field. A detailed description of the method for finding the principal axes of inertia of a rigid body has been added. Small changes, usually short additions, have been made at some other points, mainly in the treatment of the motion of rigid bodies and in discussions of dimensions and units. A few new exercises have been added and minor corrections made. All in all, old friends of the book will probably find that the changes made are summarized adequately by the statement that about 16 new pages have been added to the 514 very satisfactory old ones.

For the benefit of those not familiar with the first edition, a brief statement of the ground covered will now be attempted. The first half of the book is entitled "Plane Mechanics" and treats the easier topics, in particular those not involving vector cross products. About 35 pages are devoted to the foundations of mechanics, 80 to statics, 10 to kinematics, 100 to dynamics of particles, rigid bodies, and systems, and 15 to impulsive motion. In general, only motions in a plane or parallel to a fixed plane are considered although the generalization to unrestricted three-dimensional motion is usually given in cases where it is easy. The second half of the book is entitled "Mechanics in Space" and contains the three-dimensional treatment of topics requiring vector cross products as well as topics regarded as less elementary than those treated in the first half. About 15 pages are devoted to the algebra of vectors, 60 to statics, 120 to dynamics of particles, rigid bodies, and systems, 15 to Lagrange's equations, and 25 to the special theory of relativity. Finally, there is an appendix on the theory of dimensions.

The topics usual to an undergraduate course in mechanics are treated in a manner that may be inferred from some random observations. Normal modes of vibration are introduced in connection with conservative systems having two degrees of freedom but no mention is made of normal coordinates. The static bending of beams is considered briefly but the vibration of strings is not. The motion of a pendulum is treated by means of elliptic functions but the discussion of resonance in the case of the damped harmonic oscillator is passed over superficially in six lines. The study of motion under central forces covers planetary orbits, the stability of circular orbits with general laws of force, and the study of apsides. The form of Lagrange's equations used contains the generalized forces but generalized momenta, ignorable coordinates, Hamilton's principle, and the Hamiltonian function are not mentioned. Unusual, and welcome, topics are the brief treatment of the relativistic motion of a particle in one space dimension and the discussion of the motion of a charged particle in a static electromagnetic field with particular emphasis on electron optics.

The mathematical preparation demanded of the student includes a fair knowledge of calculus and analytic geometry and some elementary differential equations. Vector algebra and differentiation of a vector with respect to time are used extensively but no previous knowledge is required.

The outstanding feature of this book is the painstaking care with which the student is helped over difficulties. The various difficulties are isolated and treated one at a time. Analogy and example are ably used to guide the students' thinking and break the monotony of a too formal treatment; but they are never substituted for proofs. The division of the book into two parts enables the authors to treat first the simpler aspects of mechanics. With a framework thus provided, it is possible to motivate the explanation of the more difficult details of three-dimensional mechanics before they cause trouble.

An almost necessary consequence of these desirable features is the fact that this book covers less material per page than many. Also one could lose sight of the forest in the explanation of the trees if it were not for the excellent summaries at the ends of the chapters and the summarizing sections scattered through the chapters. The reviewer has the feeling that while the explanations are certainly clear and should be very helpful to the average student, they do not always appear to penetrate as deeply as he would desire. The division into two parts means that there is much backward reference of the second to the first.

Since Lagrange's equations come at the end, the student gets no real chance to apply them. One wonders why the authors do not follow their own advice and introduce them earlier. Then perhaps some of the other material could have been jetisoned to make room for a discussion of general constants of motion and other more advanced and powerful techniques.

The reviewer feels that there are but few minor criticisms to be made. It would seem that one could find more convenient symbols than **q** for velocity, **P** for force, **h** for angular momentum, and **G** for torque. While the many problems at the ends of the chapters are very good and will undoubtedly be useful even to teachers who do not use the book as a text, a few problems in which the solutions were numbers rather than letters should emphasize that mechanics can be physics rather than mathematics. The physical form of the book is the usual excellent product that one expects from its publisher.

This book should have a very great appeal for teachers of undergraduate mechanics courses that come to a climax at Lagrange's equations provided they prefer full explanations to conciseness. The care with which difficulties are explained and the various possible points of view made clear mean that it is particularly to be recommended for those studying alone. Even teachers who wish to cover much material not in this book may find it a desirable text or reference since its use should cut to a minimum the class time devoted to topics it covers.

Leverett Davis, Jr.
California Institute of Technology

On the Theory of Stochastic Processes and Their Application to the Theory of Cosmic Radiation

By Niels Arley. Pp. 240, Figs. 53. John Wiley and Sons, Inc., New York, 1949. Price $5.00.

Crudely speaking, a stochastic process is any sequence of events, which can be described by the methods of the theory of probability. The theory of stochastic processes can be regarded as one of the sturdiest achievements of modern mathematics. However, the theory is not yet very widely known among physicists. There seem to be two reasons for this situation: the lack of books on the theory, written in such a way as to be accessible to physicists, and the lack of experiments which require the use of the theory. The lack of experiments is really only apparent as is evident, for example, from the increasing use of the 'Monte Carlo' method in describing the degradation of high energy radiation in passing through matter. On the other hand, the lack of books suitable for physicists on the theory of stochastic processes is real, and the appearance in this country of Professor Arley's book is quite opportune.

The book was published originally in 1943 as a doctoral thesis at the University of Copenhagen. Its second printing seems to have been done by a lithographic process, but only one of the reproductions has suffered very much as a result.

The book is divided into two parts. The first, a mathematical part, is devoted to an exposition of the theory of stochastic processes. The first chapter gives a survey of the theory in which the fundamental equations of propagation of probability are written down in both differential and integral (Chapman–Kolmogoroff) form. One might have hoped, here, for a slightly gentler introduction to the jargon of set and measure theory, but perhaps the missionary zeal required to write such an introduction for physicists would have been out of phase in a doctoral thesis, particularly in a doctoral thesis published in Scandinavia. Chapters 2 and 3 are devoted to existence and uniqueness theorems for one-dimensional and multi-dimensional stochastic processes. Together with an appendix, Chapter 7, these chapters are an exposition of an important extension of the original work of Feller and Lundberg on so-called discrete stochastic processes.

The second part of the book, a physical part, applies the general theory of stochastic processes to one of the most interesting questions in the theory of cosmic rays: the problem of fluctuations in the number of particles occurring in the cascade showers. Chapter 4 is devoted to the discussion of various statistical models of a cascade shower. The models of Bhabha and Heitler, of Furry, as well as a general model of the author are considered. The last model, the Arley model, has several advantages over the earlier ones. However, it is so complicated that its predictions are difficult to obtain in numerical form. The concluding portion of Chapter 4 gives a useful method of approximating the solutions of the Arley model. Chapter 5 is a brief survey of the theory of cosmic radiation, confined mainly to the theory of the soft component. Finally, in Chapter 6, the various models of a soft shower are applied to predict the probability of a given number of electrons appearing under a given thickness of matter if the shower is initiated by the entrance of a single photon or electron. The predictions are compared with the experimental data, fragmentary in 1943, and still inadequate now. The results are in fair agreement with the Arley model.

The book is an interesting and useful contribution to the literature of mathematical physics, which can be recommended to all physicists who can afford it.

A. S. Wightman
Princeton University

Modern Operational Calculus with Applications in Technical Mathematics

By N. W. McLachlan. Pp. 218, Figs. 29. Macmillan and Company, New York, 1948. Price $5.00.

In the preface the author states that this book is intended to serve as an introduction to modern operational calculus for post-graduate engineers and technologists. For this reason the book is divided into two main parts. The first seven chapters, constituting the main body of the text, introduce the operational calculus and show how the theory is applied to physical problems. The second part contains six appendices of a mathematical nature designed to help the type of reader who lacks the mathematical theory for understanding the main body of the text. In addition the second part contains a set of problems designed to give facility at using the theory and also a short list of Laplace transforms.

The author states that the standard of rigor used in this book is higher than is usual in books directed towards the class of reader mentioned above. In his preface he makes a rather elegant plea for maintaining the standard used in this text. Such topics as the convergence of infinite series and integrals are handled with care and dealt with at some length throughout the text.

In the first chapter the Laplace transform $\varphi(p)$ of a function $f(t)$ is defined by the integral

$$\varphi(p)=p\int_0^\infty e^{-pt}f(t)dt,$$

and this definition agrees with the so-called Heaviside operational form. This definition differs from that commonly used by the majority of mathematicians as they usually employ the same definition without the use of the external "p." In view of the widespread use of the methods of the Laplace transform theory it would be useful if a standard definition and notation were adopted and adhered to in all future writing on the subject.

After dealing with some of the analytical properties of the transform the author goes on, in the second chapter, to derive many of the rules of operation of transform. In addition to the usual rules of operation two new theorems on transforms of functions of the type $\int_t^\infty f(t)dt$ and $f(a(t^2-b^2)^{\frac{1}{2}})$ are obtained.

The first application of the theory is made in the third chapter where the theory is applied to obtain operational solutions of linear differential equations with constant coefficients. Physical applications are illustrated by means of electrical network problems. The next chapter applies the theory to partial differential equations and the diffusion equation is used to show how the theory is applied in a concrete case. Physical applications of the chapter include the problems of plane sound waves in a viscous medium and compressional shock waves. The last application of the theory occurs in the fifth chapter in which evaluation of integrals and derivation of mathematical relations are discussed.

The sixth chapter is again of a mathematical nature and is designed to illustrate, by examples, several methods of finding Laplace transforms of functions. In this chapter the Mellin inversion integral is introduced for the first time.

When the text is read as a whole, one can hardly fail to see the predominant part played in the illustrative examples by Bessel functions. The reviewer feels that in an introductory book of this type more applications involving elementary functions could have been used to better advantage.

Max Wyman
University of Alberta

The Atmospheres of the Earth and Planets

Edited by Gerard P. Kuiper. Pp. 366, Figs. 91, 16 plates. University of Chicago Press, Chicago, 1949. Price $7.50.

This book contains the contributions presented at a Symposium on the Atmospheres of Earth and Planets, sponsored by the University of Chicago on the occasion of the fiftieth anniversary of the Yerkes Observatory. The book is unusually up to date, because the majority of the eighteen contributors have revised their manuscripts after the symposium meetings. The authors range all the way from specialists in meteorology, geology, chemistry, and high altitude research to theoretical astrophysicists, stellar and solar spectroscopists, meteoriticists, and binary star specialists. Because of the variety of viewpoints and also because of the wealth of material presented, this book is difficult to review, albeit an exciting one to read. It covers only those aspects of the earth's atmosphere that can be compared with planetary atmospheres in general. The large subject of the ionosphere and related solar phenomena are, in part, summarized in the Introduction. Interested readers will want to consult another recently published symposium book sponsored by astronomers: Centennial Symposia, Harvard Observatory Monograph No. 7, Cambridge, Massachusetts, 1948. The question of life on other planets can be settled—short of planetary exploration expeditions—only through the study of planetary atmospheres, and this problem has been the motive for much of the work on planetary atmospheres described in this volume.

Kuiper's introductory chapter is followed by Rossby's account of our present knowledge of the general circulation of the lower atmosphere in the light of the technological advances of the past fifteen years and of recent military demands for global weather information. Rossby and his fellow workers have found a great meandering river of air near the tropopause at the northern edge of the trade wind region, moving from west to east with speeds recorded up to 250 miles per hour. Since the study of planetary atmospheres can be made only by means of the radiation received, the study of the *optical* properties of planetary atmospheres is of first importance and is the subject of Chapter III, written by Van de Hulst. This chapter, dealing with a wealth of phenomena, relates theory to observation and suggests future observational needs.

Chapter IV by Greenstein, Clearman and Durand is concerned with the V-2 rocket program and will probably be the chapter of greatest interest to the majority of readers. Astronomers will be particularly interested in the extension of the ultraviolet spectrum of the sun down to 2200A and the exciting possibilities of observations which could be realized with improved, and more complicated, instrumentation. Whipple, Jacchia and Kopal report on seasonal variations in the density of the upper atmosphere as determined from meteor observations. Swings gives a well-documented account of the spectra of the night sky and the aurora and a long list of future observational needs. Spitzer considers the spray region of our atmosphere, or "exosphere," and shows that the temperature of the critical level at the base of the exosphere is all-important in determining the rate of escape of a planetary atmosphere. Chamberlin's paper on the geological evidence in the history of the earth's atmosphere demonstrates that changes in its composition must have been relatively small throughout geological history. Brown's paper however, indicates that the earth's atmosphere is almost entirely of secondary origin, and that it was formed as the result of chemical processes that took place subsequent to the formation of the planet. Papers by Adel and Migeotte show that infra-red spectroscopic observations of the sun are a powerful means of analyzing the earth's atmosphere. Adel identifies nitrous oxide and tentatively identifies HDO and Migeotte has discovered methane in our atmosphere. The classical investigations of the atmospheres of Mars and Venus made with the Coude spectrograph of the 100-inch telescope at Mt. Wilson by Adams and Dunham is described by Dunham in Chapter XI. This work culminated in the discovery of carbon dioxide on Venus and further indicated that the amount of water vapor and oxygen in the Martian atmosphere is less than 0.15 percent of the amount in the earth's atmosphere.

Chapter XII, a survey of planetary atmospheres by Kuiper, is undoubtedly one of the most interesting chapters in the book, giving as it does some of the conclusions reached by him as a result of observations with an infra-red spectrometer using a lead sulfide photoconductive cell. Two conclusions of interest are (1) that the bright desert regions of Mars are composed of igneous rock similar to felsite, and (2) that the Martian polar caps are not composed of carbon dioxide but are almost certainly composed of H_2O frost at a temperature much below freezing. Kuiper provisionally concludes that Saturn's rings are covered by frost, if not composed of ice. The suggestion is made that perhaps the five inner satellites of Saturn, with very high albedos, and densities near unity, are composed of ice. This chapter indicates the need for the development of a much more sensitive infra-red detector.

The interpretation of planetary spectra is peculiarly dependent on producing similar spectra in the laboratory, necessitating the design of low pressure, multiple reflection, spectrographs. Such an instrument, allowing optical paths of over three miles, is described by Herzberg in Chapter XIII and some of the results are given. In the last chapter, Franck discusses Kuiper's infra-red observations of the green areas of Mars. Although the reflection spectrum is somewhat similar to that of lichens and mosses, another possibility is suggested, namely that the variation of color with the seasons may be due to a change in the degree of hydration of minerals or salts concentrated near the equator of Mars.

A surprising number of the papers show a militaristic stimulus, either through the use and application of war-developed tools and instruments (e.g., the V-2 rocket, radar devices, the Cashman cell, the multiplier phototube) or through the sponsorship by the military of programs of scientific investigation. With bombers normally operating at the 40,000 foot level, and rockets and guided missiles reaching 50, 100 and 200 miles altitude, there will be every incentive to learn as much of the nature of the earth's atmosphere as possible, with money available for even fantastically expensive projects.

John B. Irwin
Indiana University

Quantum Mechanics

By Leonard I. Schiff. Pp. 404+xii, Figs. 30. McGraw-Hill Book Company, Inc., New York, 1949. Price $5.50.

The classes in quantum mechanics are large these days, and there is real need for a text in a large class, more, perhaps, than in older times, when a scant dozen students took the course at even the biggest graduate departments of physics. The text is hard to find; those available on the American market tend to be careful discussions of principle over a rather narrow range of application, or very general treatises without much attention to the approximate methods and to the many particular formulations which represent the stock in trade of the quantum mechanical calculator. The present book is the first in America to fill the gap; it covers exactly the most used fields of application for physicists, with real attention to the methods for the handling of detailed problems. The spirit of the book is heuristic nearly throughout; those who seek mathematical rigor and completeness will not find it. But the reader will find something which most physicists value much more, a thorough physical discussion of what lies behind the formalism of the theory.

The text begins with a brief but clear account of the underlying ideas of quantum mechanics, a very Copenhagen-like account of complementarity and its implications. The Schrödinger equation is then built up by a series of plausible generalizations, checked step by step through the examination of their consequences. Finally the general interpretation of operators as dynamical variables is achieved and the usual treatment of the properties of complete normal orthogonal sets given. Especially well done is the discussion of normalization in terms of conditions at great distances, both for discrete and for continuous ranges of eigenvalues. The normalization in a box is adopted at an early stage.

Two typical eigenvalue problems, the harmonic oscillator and the angular part of the central force problem, are given in detail. The spherical harmonics are introduced here, and later are shown to be the basis for representation of the angular momentum matrices. The hydrogen atom solutions are given, but the hydrogen wave functions are not discussed at adequate length for most students.

The treatment of collision theory, so very important for physicists, is unusually complete. The method of partial waves is done out for potentials of finite range and for the Coulomb potential. The familiar time-independent and time-dependent perturbation methods are all done in some detail, with the treatment of the Born approximation and its connection with the Green's function, and the *WKB* method, done a la Langer, being especially good. The calculation of the location of ions along the track of an electron whose wave function is a plane wave is not usual, and well worthwhile.

A brief matrix formulation of the general transformation theory, and a rather well-motivated discussion of the problem of identical particles and of spin wave functions, complete the more general portion of the text. There is a short account of the problems of many-electron atoms, of molecules, and of nuclei. This is too sketchy to be of much help, except for the Thomas-Fermi and Hartree methods in the atomic case, and the Zeeman effect in alkali atoms.

The semiclassical treatment of radiation by atoms is given, but that is not all. After working up through the one-particle Dirac theory (and its solution in the central field problem), the general Lagrangian theory of the second quantization of the Dirac and Klein-Gordon equations is given. The occupation number operators are obtained, and the positron theory briefly discussed. Then quantum electrodynamics and its supplementary condition are tackled, very much according to Fermi, and the semiclassical theory at last justified, as well as the wave-photon quality for light. This whole discussion is made in a thoroughly non-covariant form, so that it is perhaps not enough in itself for students of theory who will want to become acquainted with relativistic language. But the three chapters concerned are indeed meaty, if they have not so much of the physical clarity of the rest of the book.

It would be a mistake to forget the nearly two hundred problems which come at the chapter ends. Most of these are much more than numerical exercises; some contain very useful results. There is a good index, and the book is rather free of errors; the reviewer noticed only a couple of obvious misprints. A little more space for graphs, diagrams, and writing out matrices would have been welcome; where these were given, they were excellent.

P. Morrison
Cornell University

Electric and Magnetic Fields

Third edition. By Stephen S. Attwood. Pp. 475+xi, profusely illustrated. John Wiley and Sons, Inc., New York, 1949. Price $5.50.

The third edition of Professor Attwood's popular intermediate textbook contains about 10 percent more material than the second edition; and over 50 percent more than the original text, which was published in 1932. The new material includes concise discussions of energy density in the magnetic field, of forces on moving changes, of properties of diamagnetic, paramagnetic, and ferromagnetic materials; and of Maxwell's Equations and plane-wave solutions of them. A decimal designation of sections and equations has been adopted, the format has been greatly improved, the the values of the physical constants appear to be up-to-date, and there are some changes in notation designed to agree with modern standards and/or conventions. A few changes and additions have been made in the problems. The order of presentation remains the same: *The Electric Field* (Chapters 1–8), *The Magnetic Field* (Chapters 9–15), and *Combined Electric and Magnetic Fields* (Chapter 16); and three appendices on units and dimensions, atomic theory, and history.

The major change in the new edition is the emphasis throughout on the m.k.s. rationalized system of units. These units are used not only throughout the analytical material but also for tabular and graphical data on ferromagnetic materials. To one who has been engaged for the past 12 years in proselytising students and associates alike in the use of rationalized m.k.s. units, this wholehearted acceptance of the system by an author whose book is directed to students who will later study both communications and machinery, is a particularly good omen. Is it too much to hope that sometime in the future the catalogs of manufacturers of ferromagnetic materials will be devoid of such phrases as ampere-turns per inch, kilolines per square inch, ohms per mil foot, and watts per pound?

Ideas often obscure to students are handled with extreme care; for examples the discussions of the concept of potential gradient, and of the properties of singular points. Similarly when Professor Attwood proceeds from the step-by-step production of the hysteresis loop of a ferromagnetic material to the production of a $B-H$ loop on an oscilloscope by applying alternating current to the coil of the sample, he carefully identifies the result as a *hystero-eddy-current loop*. The same care and clarity permeate the entire book in the form of extraordinarily clear reproductions of drawings of field lines and equipotential. The book has been justly praised for these fine drawings in all editions.

There are minor points open to adverse criticism. Boldface type, or other distinctive marking, is not used for vectors; equations simply have (*vector*) printed after them and there is no way to tell which symbols of such equations represent vectors, and which scalars. There is an over-emphasis of the Bohr atomic model and a corresponding under-emphasis of the idea of electronic energy levels that can be accepted without setting up a mechanical model. Use is made, without detailed explanation, of the unconventional integration of $(-H)$ counterclockwise around a current, instead of the conventional integration of H clockwise around the current. Conduction currents in metals are alleged to correspond to electronic drift velocities of 40 cm per sec. (first edition), 10 cm per sec. (second edition), 1 cm per sec. (third edition); these velocities are usually 3 orders of magnitude less than the average of these values. The dielectric properties of the recently investigated titanates and the properties of electrets are not discussed.

But these latter items simply represent the caviling indulged in by the reviewer who insists on proving that he has examined the book carefully. Professor Attwood's new edition is excellent. It will stimulate students and teachers. It seems likely to extend its usefulness and to continue to grow effectively as it has since it was first published 17 years ago.

S. Reid Warren, Jr.
University of Pennsylvania

Author Index to Books Reviewed

Anhorn, V. J.—see Barr, W. E. 690
Arley, Niels. *On the Theory of Stochastic Processes and Their Application to the Theory of Cosmic Radiation* .. 691
Attwood, Stephen S. *Electric and Magnetic Fields* 694
Barr, W. E. and V. J. Anhorn. *Scientific and Industrial Glass Blowing and Laboratory Techniques* 690
Carlin, Benson. *Ultrasonics* 689
Chalmers, J. A. *Atmospheric Electricity* 688
Griffith, B. A.—see Synge, J. L. 691
Gurney, R. W. *Introduction to Statistical Mechanics* 687
Henisch, H. K. *Metal Rectifiers* 687
Kuiper, G. P. *The Atmospheres of the Earth and Planets* .. 692
McLachlan, N. W. *Modern Operational Calculus with Applications in Technical Mathematics* 692
Proprietors of Instrument Practice. *The Instrument Manual* 687
Ramberg, E. G.—see Zworykin, V. K. 690
Schiff, L. I. *Quantum Mechanics* 693
Synge, J. L. and B. A. Griffith. *Principles of Mechanics* .. 691
Yagoda, H. *Radioactive Measurements with Nuclear Emulsions* 689
Zworykin, V. K. and E. G. Ramberg. *Photoelectricity and Its Application* 690

Other Books Received

The Pulsation Theory of Variable Stars. S. ROSSELAND. Pp. 152+viii, Figs. 25, Tables 10. Oxford University Press, New York, 1949. Price $5.00.

Radioactive Tracer Techniques. G. K. SCHWEITZER AND I. B. WHITNEY. Pp. 241+vi, Figs. 13. D. Van Nostrand Company, Inc. New York, 1949. Price $3.25.

Theory of Dielectrics. H. FROHLICH. Pp. 180+vi, Figs. 47. Oxford University Press, New York, 1949. Price $4.50.

Electric Resistance Strain Gauges. W. B. DOBIE AND P. C. G. ISSAC. Pp. 114+xiv, Figs. 89. The Macmillan Company, New York, 1949. Price $3.50.

Industrial Rheology and Rheological Structures. Pp. 311, Figs. 76. J. Wiley and Sons, Inc., New York, 1949. Price $5.50.

Literature Search on Dry Cell Technology. M. BOLEN AND B. H. WEIL. Pp. 700. State Engineering Experiment Station, Georgia Institute of Technology, Atlanta, Georgia, 1948. Price $5.00.

Histopathology of Irradiation from External and Internal Sources. Edited by WILLIAM BLOOM. Pp. 808, Figs. 516. McGraw-Hill Book Company, Inc., New York, 1948. Price $8.00.

Constructive Uses of Atomic Energy. Edited by S. C. ROTHMANN. Pp. 258+ix, Figs. 52. Harper and Brothers, New York, 1949. Price $3.00.

Introduction to Statistical Mechanics. G. S. RUSHBROOKE. Pp. 334+xiii, Figs. 47. Oxford University Press, New York, 1949. Price $5.50.

Engineering Optics. K. J. HABELL AND A. COX. Pp. 411 +xiv, Figs. 182. Pitman Publishing Corporation, New York, 1948. Price $7.50.

Experimental Physics for Colleges. W. A. SCHNEIDER AND L. B. HAM. Pp. 411+xiv, Figs. 182. The Macmillan Company, New York, 1949. Price $7.50.

Our Sun. D. H. MENZEL. Pp. 326+viii, Figs. 178. The Blakiston Company, New York, 1949. Price $4.50.

Laboratory and Shop Notes

Modification of X-Ray Diffraction Micro-Camera to Permit Study of Long Spacings

M. E. Bergmann and I. Fankuchen
Polytechnic Institute of Brooklyn, Brooklyn, New York

June 16, 1949

IN this note we describe some modifications of the camera originally designed by F. G. Chesley,[1] which we have found useful in our work. This camera is now available commercially from North American Philips Company.

For work with fibers and with biological specimens it is often desirable to be able to obtain details of the diffraction pattern corresponding to longer spacings than are available with the original camera design. An increase in the specimen-to-film distance can be achieved (a) by moving the film holder back toward the rear of the camera and (b) by rebuilding the front part to move both the slit system and the specimen holder forward.

In (a) we eliminated the extension tube by building a new small cassette which fits directly into the tube which normally holds the extension tube.[2] In (b) we replace the front part of the camera by a new part having the same dimensions as the old part, except for the depth which was increased. The slit system and the specimen holder can be inserted into the new part without mechanical modification. The maximum depth of the new front part is limited by the necessity of aligning specimen and slit under the microscope and by intensity considerations. By making both of these modifications and by using x-rays of different wave-lengths we have been able to obtain spacings in excess of 100A.

It is not always advisable to evacuate the camera to eliminate air scattering. Most of the scattering which blackens the central portion of the film occurs directly in front of the film. We were able to eliminate most of this central blackening by pushing a trap from the back of the cassette through the film so that it protrudes approximately 1.5 mm beyond the film. This trap, which was made of brass, has the incidental advantage of holding the film more rigidly in place.

In use it was necessary to clean the slit rather frequently with the help of the tungsten wire supplied with the camera. The Cellophane vacuum seal, which was originally placed directly over one end of the glass capillary, will be punctured during the cleaning. The seal should, therefore, be placed on the outside of the camera.

Calibration of the specimen-to-film distance should be made by coating the specimen with the standard substance, chosen so that its spacings have the right order of magnitude. Because of the small camera constant, errors caused by different thicknesses of the specimen are more important than in ordinary x-ray cameras.

[1] F. G. Chesley, Rev. Sci. Inst. 18, 422 (1947).
[2] Parts of original camera are fully described by Chesley, see reference 1.

High Power Short Duration Spark Discharge

Leslie S. G. Kovásznay
Department of Aeronautics, The Johns Hopkins University, Baltimore, Maryland

June 6, 1949

SPARK photography in large supersonic wind tunnels and especially in ballistic firing ranges requires a large amount of total light output since the areas to be illuminated are rather large The duration of the light is required to be short and the light source has to be small. The three requirements inherently call for an extremely high brilliance of the light source, since the light flux integrated in time must be concentrated to a small area and short time interval.

The standard method for obtaining a spark discharge for shadow photography is to discharge a condenser (0.005–1 μf) through a spark gap.[1] The discharge is usually of an oscillatory nature and the light output has an exponential type of over-all decay depending on the damping characteristics of the discharge circuit.

The duration of the light output from a discharge gap is controlled by two factors. One is the decay of the excitation processes in the luminous gas; the other is the electrical properties of the discharge circuit. Even if the electrical circuit were able to deliver instantly a finite amount of energy into the spark gap, the light output would decay in finite time. It is conceivable that this time would mainly depend on the communicated energy per unit mass of gas (erg/gram) and that higher "energy loading" would involve longer decay. This decay of light output is estimated for low "energy loading" to be of the order of 10^{-8} sec.

Unfortunately, the properties of the electric circuit increase this time of duration by more than an order of magnitude.

The spark gaps in general have rather small impedances (0.2–2 ohms) and the problem is to produce high current (1000–5000 amperes) pulses of short duration (10^{-6} sec. or less). The high current level rules out entirely the use of electron-tube control. Large high voltage commercial condensers usually have so large a self-inductance that their resonance frequency is below 1 Mc. On the other hand, the impedance of the spark gap is well below the resistance value for critical damping of the oscillations. Any damping resistor decreases the amount of energy delivered into the gap and if the condenser's capacity is increased in order to increase the stored energy, the oscillating frequency goes down and the duration gets longer.

Another approach to the problem is the coaxial cable type discharge circuit.[2] The current pulse is formed by the discharge and extinguished by the reflected wave from the other end of the coaxial cable. A serious problem is encountered in matching the low impedance of the spark gap to the high impedance of the coaxial cable and it is customary to obtain the surge impedance required by adding a resistor in series with the spark gap. In most cases 90–98 percent of the energy is lost in the matching resistor. This fact restricts the use of this type of circuit to cases where the light output is a less stringent requirement than the short duration. The duration of the coaxial type spark source is claimed to be of the order of 10^{-7} sec. (although the definition for duration is not specified).

In the present approach the following reasoning has been followed. A certain amount of energy is stored in the condenser. Using dimensional reasoning, the capacity of the condenser is proportional to its linear dimension and the stored energy is proportional to its volume. When the energy is discharged, large currents flow from the place of storage to the discharge gap. All these current paths produce a magnetic field. The energy stored in the magnetic field is proportional to the self-inductance of the system.

Increased damping and shorter duration can be achieved by reducing the self-inductance. To minimize the self-inductance requires a geometrical arrangement confining the magnetic field to a small volume.

An experimental spark gap unit was built in the Department of Aeronautics, The Johns Hopkins University, and the arrangement is shown in Fig. 1. The spark gap itself is on the axis and consists of

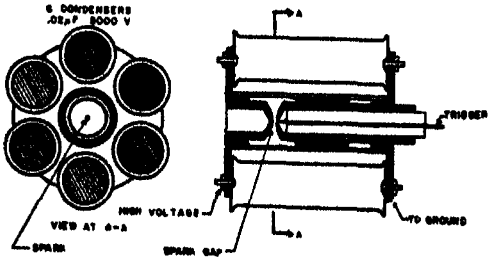

FIG. 1. Concentric condenser spark gap.

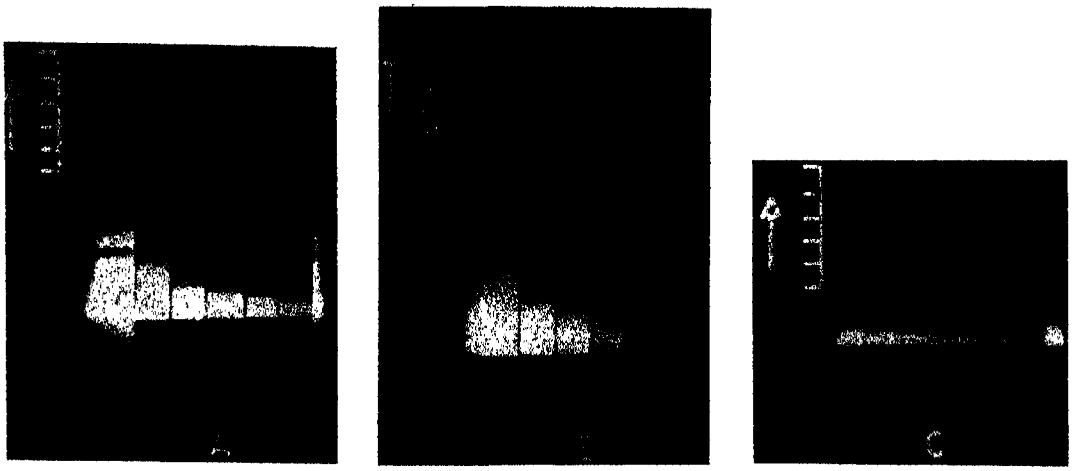

FIG. 2. Rotating mirror records of various sparks.

three electrodes. The spark discharge takes place between the two hollow spherically faced electrodes, and the spark is "triggered" by a needle electrode. The light emerges axially through the hole (approx. 0.5 millimeter). The spark gap is almost identical with that described in reference 1. The energy is stored in the six 0.02-μf condensers (Condenser Products Glassmike) totaling 0.12 μf. The rated voltage of the condensers for continuous use is 5000v d.c. The condensers are the non-inductive type with the tinfoils extending beyond the two ends. The currents are collected by the two annular plates, and the magnetic flux is confined to a toroidal space inside the condenser assembly. The estimated self-induction of the assembly is 0.01–0.02 μHy.

The spark duration measurements were conducted in the Ballistic Research Laboratories, Aberdeen Proving Ground. The total light output of the assembly was slightly greater than the average spark station in the aerodynamics firing range.

The total light output is sufficient for shadow pictures on Eastman Kodak medium lantern slides at a distance of 5 feet, resulting in an average photographic density of 1.0–1.5.

The spark duration was determined by a rotating mirror camera. The time record of the spark intensity was obtained by a novel technique, as follows:

The real image of the spark was produced on the recording film, by a 14-in. focal length lens. With the use of a weak cylindrical lens and a square aperture the small light spot was pulled out into a thin line with uniform light intensity stretching perpendicular to the direction of deflection produced by the rotation of the mirror.

The writing speed of rotating mirror was 3.1 millimeters per microsecond on the film. For calibration purposes a five-step gray filter was placed along the film attenuating the light by known ratios. This way a rough evaluation of the decay of light intensity was possible. Comparison of three spark units was made. They follow:

(A) Standard spark unit of the Ballistic Research Laboratories. The condenser is a commercial 0.5-μf condenser charged 6000 v. The spark gap is at atmospheric pressure and has hollow aluminum electrodes.

(B) High pressure air gap with conventional condenser. Libessart type confined air gap with G.E. 0.1-μf condenser charged 6000 v.

(C) Author's spark. Total capacitance 0.12-μf charged 6000 v. Gap similar to (A).

Figure 2 shows the rotating mirror records of the three gaps. The total light outputs were of the same order although (B) gave somewhat more light than the others (attributed to the better light efficiency of the confined air gap). The units on the time scale are microseconds. The records show clearly that (A) and (B) oscillate although (B) oscillates with a higher frequency; unfortunately for the record presented herein, the oscillation of (B) cannot be seen in the print although it is clearly visible in the original negative. Photo-densitometer readings give the approximate decay curves in Fig. 3. The ratio of the light intensity to its maximum intensity is plotted against the time.

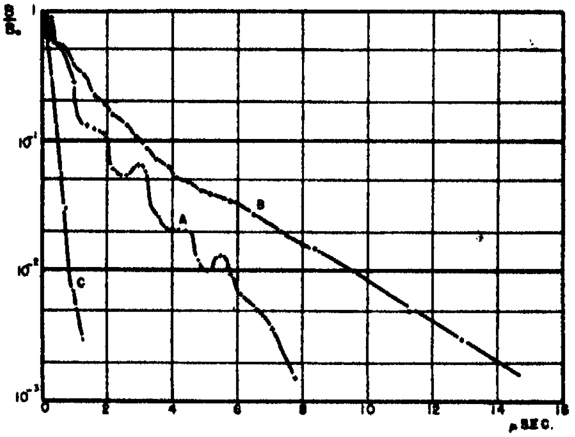

FIG. 3. Decay of light intensity at various sparks.

A definition for duration is quite difficult, particularly when one recalls that an adequate record of detail in a photograph requires a wide range of light intensities. The range of the visual perception of contrast has a threshold of the order of 0.02. This suggests that we can define a realistic duration as the time during which the light intensity drops to 1/50 of its maximum value. The "time constant" of the exponential decay is definitely too short for use as a measure of duration since the visual perception of contrast extends well beyond the point at which the light has attenuated to 1/*e* of its peak value.

Accepting the above definition of duration, the duration of the three light sources are: (A) 4 microseconds; (B) 7.5 microseconds; (C) 0.8 microsecond.

Author is greatly indebted to Dr. A. C. Charters and to his associates for helping with the experiments as well as for their great interest in this work.

---

[1] A. C. Charters, "The spark photography range," presented at the 6th Inter. Congress for Applied Mechanics, Paris, France (September 1946).

[2] Beams, Kuhlthau, Lapsley, McQueen, Snoddy, and Whitehead, J. Opt. Soc. Am. 37, 868 (1947).

A Simple Stable D.C. Amplifier for Measurement of Bioelectric Potentials

JOHN W. MOORE
Medical College of Virginia, Richmond, Virginia

June 3, 1949

TO answer the need for a simple stable amplifier for measurement of injury potentials in research and student laboratories, the amplifier to be described was made. It is a simplified two-stage design adapted from an earlier three-stage circuit. With a single tube power supply circuit, the whole amplifier can be compactly made in a standard cabinet as in Fig. 1. A schematic diagram of the circuit is shown in Fig. 2.

The chief asset of this type of circuit is its very stable and linear operation obtained by multiple feed-back paths. This makes the basic design applicable to many problems other than the one at hand. Its features are: (1) the cathodes of the balanced input tube are run at a high level above the negative supply voltage. The average d.c. output level contributes some feedback against drift along with that of the common cathode resistor. (2) Cathode degeneration and output feedback insure linearity, constancy of amplification (from tube to tube), and low output impedance. (3) The output and input are grounded, necessitating a floating power supply, but no difficulties have been experienced with this. (4) The meter is protected from overload by saturation of the output stage.

Stable operation in the presence of line voltage variation is obtained by the cathode feed-back scheme. Any variation in the average d.c. current to the output stage applies a voltage to the balanced input stage in a manner that removes the variation. There is also considerable resistance common to the two input cathodes so that any variation in that stage alone can be degenerated. With a variation of ±10 percent in the line voltage, a slow (~10 sec.) drift of less than 2 percent of the low sensitivity scale output is observed. The usual voltage fluctuations of a power line are not nearly as severe as the ±10 percent and are of short duration, so that in usual operation, the output is quite steady. Where greater stability is required, in some applications of this type circuit, regulation of the d.c. supply voltage naturally gives improved performance.

The present design for measurement of injury potentials used a Weston 301 galvanometer ($500\,\mu a-0-500\,\mu a$) in the output. Two sensitivity ranges were chosen: one to give full scale deflection with 75-mv input, one with 150 mv. This amplifier has been in constant service for almost two years and has been completely trouble free. The small resistor between the cathodes of the input tube gives the balance adjustment; the value given is sufficient to counteract the balance of the large majority of the type 6SL7

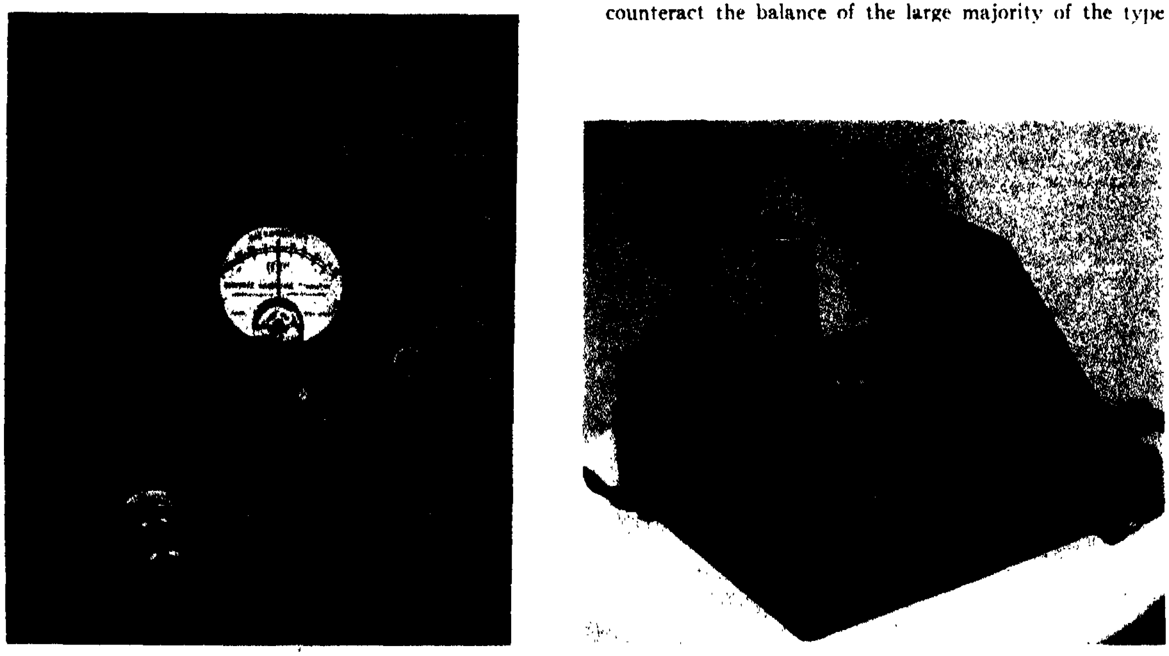

(a) (b)

FIG. 1.

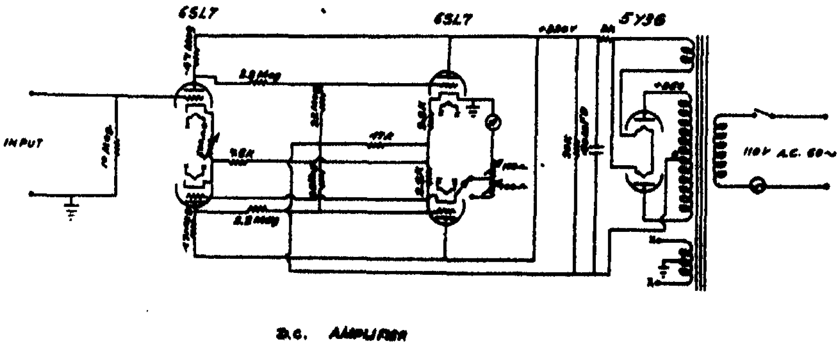

FIG.

tubes tested.[1] This amplifier was made with a 4.7-meg. input resistor. This has been recently increased to 10 meg. with no noticeable difference in performance. When the input leads are open circuited, some of the poorer tubes tested gave more than the quoted drift for line voltage variation. However, when the input is connected to a source of a few thousand ohms (such as the bioelectric source used here), the fluctuations are greatly diminished.

In the two-stage amplifier shown here, most of the gain is used in cathode degeneration for stability; linearity is provided at the same time. In order to have sufficient output gain for feedback to give a good integrating or differentiating amplifier, another stage should be employed. The extra stage (simply inserted between the two shown) can have its cathodes tied together and resistors in the plates and the common cathode about equal. With a polystyrene (or a good paper condenser) of a few microfarads, integration over a period of several minutes can be performed.

The two-stage circuit has also been used with a photo-tube input to make a light intensity meter. This is suitable for determination of exposure time for photo-micrographs, and so on.

The original idea for this type of circuit was developed by Mr. A. W. Vance of the RCA Laboratories. The amplifier described here has been extensively used and tested by Dr. R. W. Ramsey of the Physiology Department of the Medical College of Virginia.

---

[1] Some makes, such as Tungsol, had a much smaller unbalance than others and gave more stability against line voltage variations.

Geiger Tube Quenching Circuit for a Negative High Voltage Supply

Richard John Watts
Los Alamos Scientific Laboratory, Los Alamos, New Mexico*

April 20, 1949

THE following circuit (Fig. 1) illustrates a method of assisting the quenching action of a Geiger-Müller tube. It may be considered a Neher-Harper circuit with two modifications (1) a negative high voltage supply is used. (2) No high voltage need be placed across receiving type tubes not designed for this purpose. Inasmuch as the circuit was designed for portable work a CK569AX tube was selected. However, the method is applicable to heater type tubes.

It should be pointed out that if a very high impedance voltmeter is placed across the electronic tube of a Neher-Harper quenching circuit, it can be ascertained that the tube behaves as a shunt regulator for the high voltage supply. This can lead to some confusion in the length of a G-M tube plateau since the voltage across the G-M tube does not change linearly with supply voltage. If supply voltage changes are used for plotting plateaus with this circuit, it then appears that the length of the plateau has been increased considerably over the plateau obtained from a non-quenching circuit.

In the present circuit one cannot expect this increment in plateau since the high voltage is not across a non-linear medium.

The operation of the circuit is as follows: The circuit constants are chosen such that the plate voltage in the quiescent condition of the CK569AX is 70 volts. When the G-M tube fires there is observed across the one-megohm resistor in series with the high voltage supply a sharp positive pulse of voltage. This pulse is of the order of 100 microsec. in duration with the circuit constants given. The rise time of this pulse as observed with a Tektronix 511 AD oscilloscope is less than 0.2 microsec. This sharp positive pulse of voltage is applied to the grid of the CK569AX. The tube thereby conducts and the plate voltage goes negative sharply. Inasmuch as the central wire of the G-M tube is connected directly to the plate of the CK569AX the G-M tube voltage will be thrust below threshold rapidly.

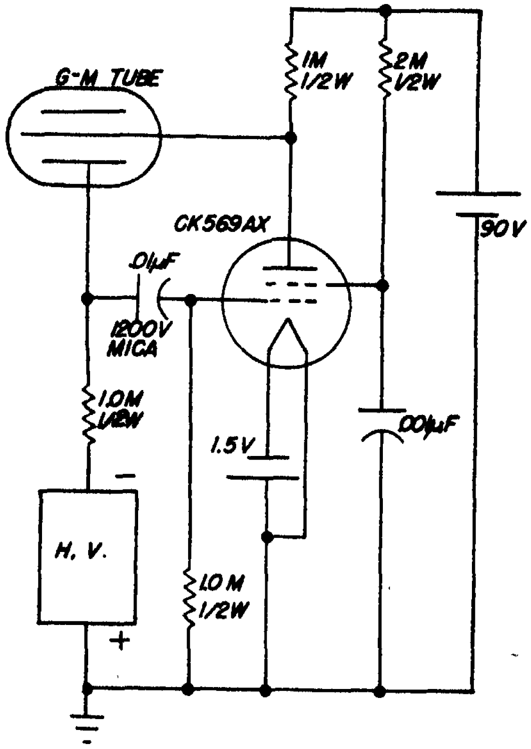

Fig. 1.

It should be noted that the negative pulse obtained by electron collection on the central wire of the G-M tube is the same polarity as the plate voltage drop. Thus the circuit is in a sense regenerative. With the circuit given, the negative voltage pulse on the anode of the CK569AX has been observed to be 250 microsec. in duration with a fall time of about 0.5 microsec. The circuit constants given are not optimum. They were chosen with regard to reasonable battery drain for portable operation. The Geiger tube used was a standard size in common use with a neon-amylacetate filling. The tube was operated in the plateau region at 900 volts.

---

* This document is based on work performed at Los Alamos Scientific Laboratory of the University of California under Government contract W-7405-Eng-36.

Extended Range D.C. Bias Control of Thyratron Plate Current

Leonard Reiffel
Armour Research Foundation, Technology Center Chicago, Illinois

May 26, 1949

THERE are three important basic circuits useful in controlling the average current in a thyratron with alternating plate voltage.

These are:

1. The d.c. grid bias control
2. Variable phase grid voltage control
3. Constant phase plus bipolar d.c. grid bias control.

It is the purpose of this paper to describe the basis of a new technique for thyratron plate current control applicable to shield grid tubes.

Before proceeding, it will be helpful to review briefly the advantages and disadvantages of the already extant methods.

1. The d.c. grid bias control: This system consists merely in applying variable d.c. voltage to the thyratron control grid. The point of firing is delayed as the bias voltage is made more negative.

The maximum delay attainable by this method is 90 degrees of the plate voltage cycle. This delay angle corresponds to approximately 50 percent of maximum d.c. plate current (i.e., the variable bias provides continuous control from full d.c. plate current to one-half of full current). Any attempts to advance the firing point beyond 90 degrees by further reduction in bias cause the plate current to drop abruptly to zero.[1]

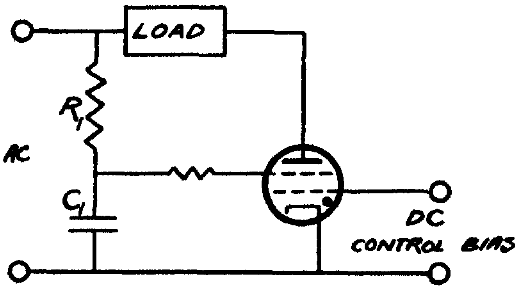

FIG. 1.

This technique has the advantage of extreme simplicity. However, the control range is limited and the bias required for a given current varies somewhat during the tube life because of changes in the critical grid voltage curve. These changes become very important near the 90 degree delay point since the critical grid voltage curve intersects the bias curve nearly tangentially.[2]

2. Variable phase grid voltage control:[3] This method consists in applying to the grid an alternating voltage of (usually) the same frequency as the plate voltage. As the phase angle of the grid voltage with respect to plate voltage is varied from approximately zero degrees lagging to 180 degrees lagging, the d.c. plate current varies smoothly from the maximum (full one-half cycle of conduction) to very nearly zero.

This method, probably the most widely used, has the advantages of full 180 degrees delay range and a high degree of immunity to fluctuations in d.c. current due to changes in the critical grid voltage curve (because of the large angle of intersection between this curve and the grid voltage curve for large amplitudes of grid voltage). This system, however, requires a variable phase shift circuit with its attendant saturable reactor[4] (or manually variable reactor) center tapped transformer and phasing condenser. Usually, when the controlling signal is d.c. a triode etc., is used to control the inductance of the saturable reactor and thus control the phase shift and d.c. plate current. The primary controlling parameter thus becomes the triode grid bias voltage.

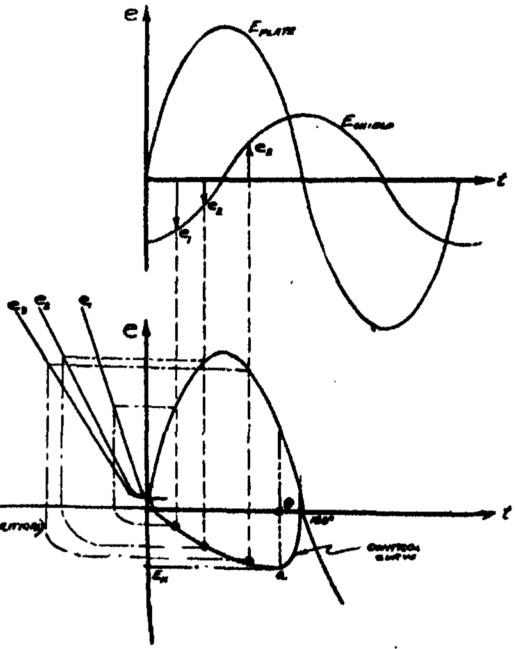

FIG. 2.

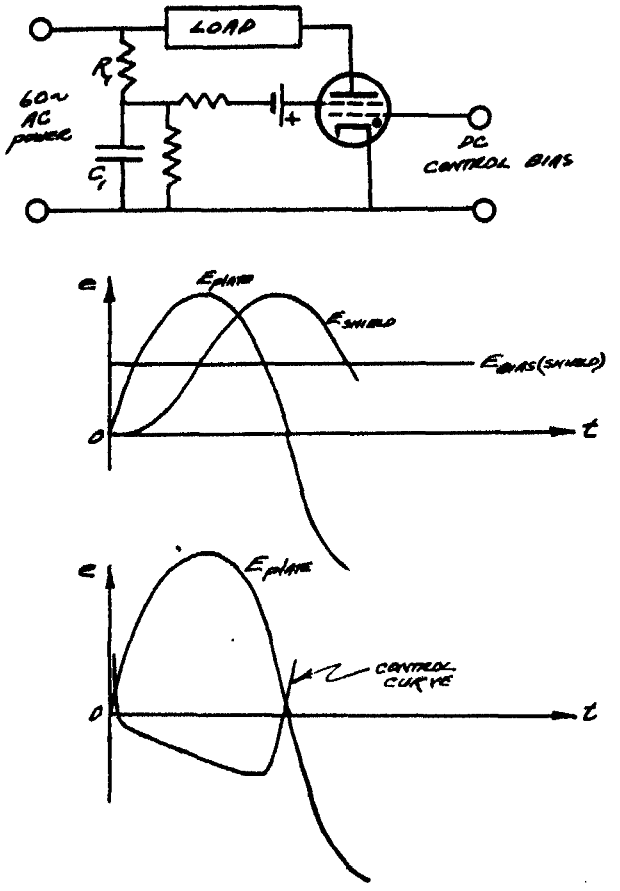

FIG. 3.

3. Phase-bias control:[5] This method is an extension of method 1 in which a phase-shifted (90–150 degrees behind the plate voltage) a.c. voltage is added to the variable d.c. applied to the grid. If the amplitude of the a.c. applied to the grid is E_M, then in order to get full 180 degree control, the d.c. bias must vary from E_M to $-E_M$.

This method will thus yield smooth current control over the entire half-cycle[6] but *bipolar* d.c. bias must be provided and the circuit is not as independent of critical grid voltage curve changes as the preceding method unless E_M is large. This leads to difficulty in supplying the bipolar d.c. bias. Regardless of the amplitude required, if electronic control is to be used, the bipolar bias requires additional circuits.[7]

New circuit.—The principle of the new technique for control of thyratron plate current is illustrated in Fig. 1.

An alternating voltage of amplitude E is applied to the plate of thyratron T_1 and an a.c. voltage of amplitude E_s is applied to the shield grid. This voltage E_s is shifted approximately 90 degrees behind the plate voltage by the *fixed* phase shifting network consisting here of R_1 and C_1. This phase-shifted shield grid voltage introduces an asymmetry in the critical grid bias control curve of the thyratron, since at the beginning of the positive half-cycle of

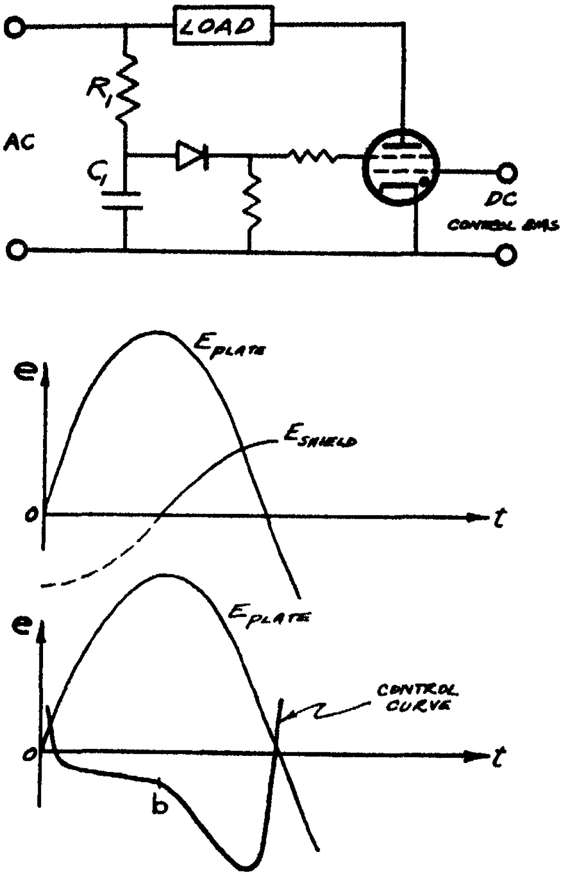

FIG. 4.

plate voltage the shield grid is negative by E_g, while at the end of the positive half-cycle the shield is positive by E_g. Thus the critical control grid voltage is more positive at the beginning of the positive plate half-cycle (0 degrees) and more negative at the end (180 degrees) than it would be ordinarily. This gives rise to a new critical grid voltage curve with its minimum shifted considerably toward the 180 degree point of the plate voltage as shown by the construction in Fig. 2.

By inspection of Fig. 2 it is evident that the point of firing of the thyratron may be delayed more and more by increases in the negative bias on the control grid until the point *a* is reached, at a bias E_K and firing point θ. With the simple circuit of Fig. 1, it has been found that θ can be made as large as 145 degrees.

It is to be noted, however, that there are a number of inherent limitations in the simple system just described. First, the change in the critical grid voltage for a unit change in shield grid voltage at constant plate voltage becomes increasingly less as the shield grid goes more and more positive. This tends to flatten the critical grid voltage curve near point *a* and leads to the limit of 145 degrees maximum delay mentioned above. A possible means of extending this limit will be discussed. Second, during the first 90 degrees of the plate voltage cycle, the shield grid may be sufficiently negative to require a positive grid voltage for firing. This throws the circuit open to the same criticism leveled against the phase-bias system of control. This objection may be overcome in a number of ways, among which are:

1. The shield grid may be biased positively if this is not obviated by other considerations.[8]
2. A rectifier (IN34) may be used to eliminate the negative half-cycle of shield grid voltage; however, the firing point stability will suffer during the first quarter-cycle of plate voltage.

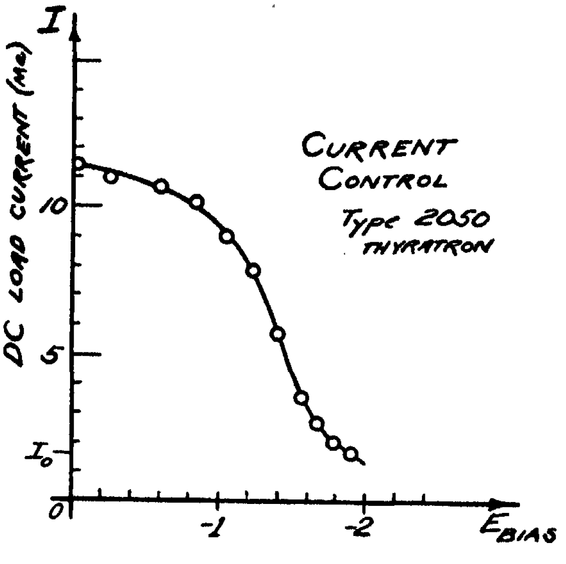

FIG. 5.

3. Tubes may be employed which will fire at negative control grid voltages even with the shield grid near $-E_g$. This is, of course, the most desirable condition and uses the simplest circuit.

The first two suggestions lead to the circuits and control characteristics shown in Figs. 3 and 4. Figures 1 and 2 refer to method three.

As an example the circuit of Fig. 4 was employed with a type 2050 thyratron, a tube not fulfilling conditions in 3 above, and yielded the results shown in Fig. 5 for $I_{\text{d.c.}}$ *versus* E_{bias}.

From the figure it is seen that continuous control of the d.c. plate current may be had with the circuit of Fig. 4 over a range extending from 100 percent to about 15 percent of full current. There is a small region of jitter when the bias is near point *b* of Fig. 4, just before the rectifier applies the shield grid voltage. This may be eliminated by shifting the phase of the shield grid voltage

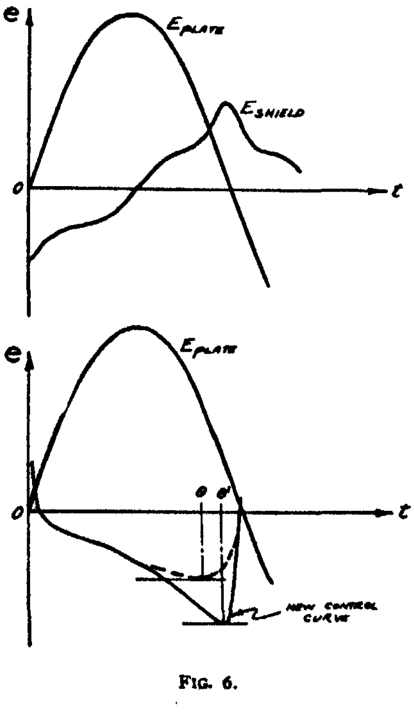

FIG. 6.

by only about 80 degrees with a slight reduction in the control range.

Method one above yields similar results and is preferable from the stability point of view.

Thus it is possible to obtain continuous control of d.c. plate current over a range corresponding to a delay angle of near 0 degrees to about 145 degrees using the proper circuit of those shown previously. This control may be achieved with variable *monopolar* control grid bias. By using moderately large shield grid voltages,[9] the slope of the critical grid voltage curve may be made large which minimizes the effect of aging and small changes in plate voltage as mentioned earlier.

If it is desirable to extend the range of control even further, a peaked wave form, such as generated by a *fixed* saturable reactor, may be applied to the shield grid. This will give greater rates of change of shield grid voltage in those regions where the critical grid voltage varies slowly with shield grid voltage. This scheme is illustrated in Fig. 6 and should permit extension of the control range to about 165 degrees.

[1] Millman and Seely, *Electronics* (McGraw-Hill Book Company, Inc., New York, 1941), first edition, pp. 432–3.

[2] This same characteristic of large variation in d.c. current at fixed bias for small changes in the critical grid voltage curve has prevented wide use of an a.c. bias amplitude control system. See H. J. Reich, *Theory and Applications of Electron Tubes* (McGraw-Hill Book Company, Inc., New York, 1944), second edition, p. 509.

[3] See reference 1, pp. 428–432.

[4] J. C. May *et al.*, "Thyratron phase control circuits," Electronics, 107–9 (July 1948).

[5] See reference 1, pp. 434–5.

[6] Neglecting tube drop, of course as in all the preceding discussion.

[7] See reference 4, p. 108.

[8] A circuit which interchanges the role of the control and shield grids is now under investigation.

[9] The voltage which may be applied is, of course, limited by the possibility of shield grid to cathode breakdown.

New Instruments

W. A. Wildhack: Associate Editor
in Charge of this Section
National Bureau of Standards, Washington, D. C.

These descriptions are based on information supplied by the manufacturer and in some cases from independent sources. THE REVIEW *assumes no responsibility for their correctness.*

Oscillator

Model M oscillator has been designed as a source of power covering the frequency range of 0.25 to 120,000 cycles per second. The frequency is continuously variable from 1 to 120,000 cycles per second in five overlapping ranges, and provision is made for fixed frequencies determined by plug-in units for frequencies as low as 0.1 cycle per second.

The circuit is a new arrangement of the bridge-stabilized type of oscillator, using two separate amplifiers connected together by a four-terminal bridge network. This arrangement affords a means of reducing to a minimum the influence of amplifier parameters on the frequency of oscillation. The circuit is self-balancing. The amplifiers operate in phase opposition, and their output is essentially free of even harmonic distortion. Third harmonic distortion is generated in the AVC element, but it has been kept to a low value by the use of an element with a long thermal time constant.

The power supply is electronically regulated. Deposited carbon resistors are used in the frequency determining networks.

Calibration is accurate within 1½ percent plus 0.1 cycle. Some specifications on "undesired voltages" are as follows: power supply noise, less than 0.01 percent of the output signal; harmonic distortion, less than 0.2 percent at all frequencies from 20 cycles per second to 15,000 cycles per second; microphonic noise, less than 0.01 percent of the output signal.

Power consumption is 140 watts at 115 volts, 60 cycles per second. Dimensions are 9¾ in. high, 18½ in. long, and 12 in. deep. Weight of the unit is 43.5 pounds.—SOUTHWESTERN INDUSTRIAL ELECTRONIC COMPANY, *2831 Post Oak Road, Houston, Texas.*

Polinear Recorder

Model PFR polinear recorder offers the engineer means for recording complete characteristics of electroacoustic and electronic devices with one instrument. The combined features of polar and rectilinear movement permit the recording of angular patterns, frequency response characteristics, and other measurements.

The instrument can record either d.c. or a.c. voltages, selectable by the operator. The turntable, 8½ in.×11 in., is driven linearly by a synchronous motor and is rotated by a selsyn repeater. The latter allows the test turntable to be placed at any distance and any location from the recorder. The turntable of the recorder is equipped with a friction slip clutch which allows the operator to set it at any angular position independent of the selsyn position, or any linear position independent of the drive motor. Both linear and polar motions are reversible.

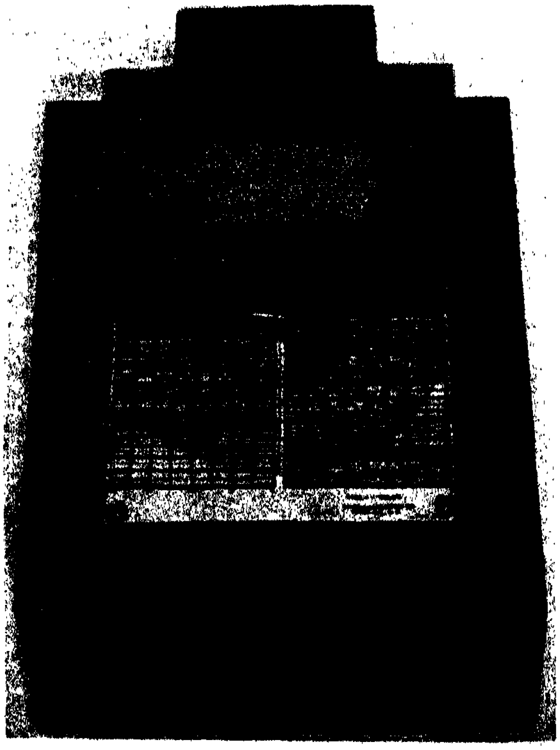

Special combination charts, polar and semilog, are available; however, standard commercial charts of the polar, or semilog type, can also be used on this recorder.

The instrument is housed in a carrying case of 11 in. × 13 in. × 17 in. dimensions.—Sound Apparatus Company, *Stirling, New Jersey.*

Ultrasonic Generator

A new ultrasonic generator, providing a simple and practical method for studying the effect of ultrasonic energy on various materials and processes, has been announced by General Electric's Special Products Division.

The generator converts high frequency electrical power into high frequency mechanical vibrations in the form of sound waves, pitched considerably higher than the range of human hearing. It permits a wide operating range by providing four vibration frequencies: 300, 500, 750, and 1000 kc.

Entirely self-contained in a steel console, the equipment consists of a power unit and a transducer assembly. Simple controls mounted on the sloping front panel of the generator cabinet include on-off switches for the high voltage circuit and the filament circuit, a voltage control to vary the power, and an instrument which indicates the power supplied to the quartz crystal.

The transducer assembly is mounted on top of the cabinet. It consists of a transparent cylinder to hold insulating oil around the high voltage leads coming from the electronic circuit to the crystal. The transducer, or crystal, forms the bottom of a test well which is immersed in the insulating oil. Material to be tested is placed in a suitable container (a beaker or test tube) within this well and is directly exposed to vibrations from the crystal.

Standing 45 in. high, the ultrasonic generator is 21 in. wide and 19 in. deep. The test well measures 1¾ in. in diameter and has a depth of 2⅝ in. Power input is 500 watts at 115 volts, 50 cycles, while power output is 200 to 250 acoustical watts.—General Electric Company, *Schenectady 5, New York.*

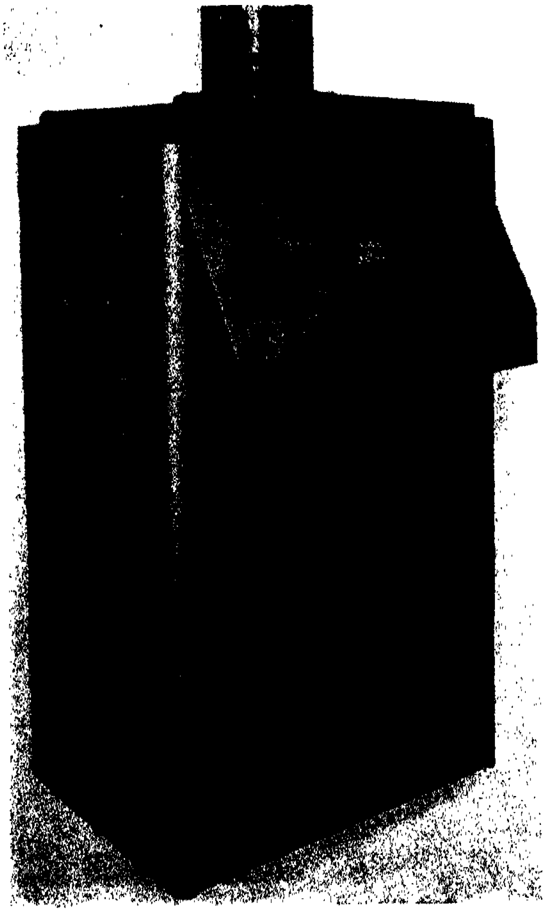

Relaxation Machine

Relaxation tests at temperatures up to 1800°F can be carried out automatically, including a record of the rate of decline of load, by means of a new machine of 4000-lb. capacity announced by the Baldwin Locomotive Works.

Relaxation occurs when a material is stretched to, and held at, a given elongation, as in bolts, particularly at elevated tempera-

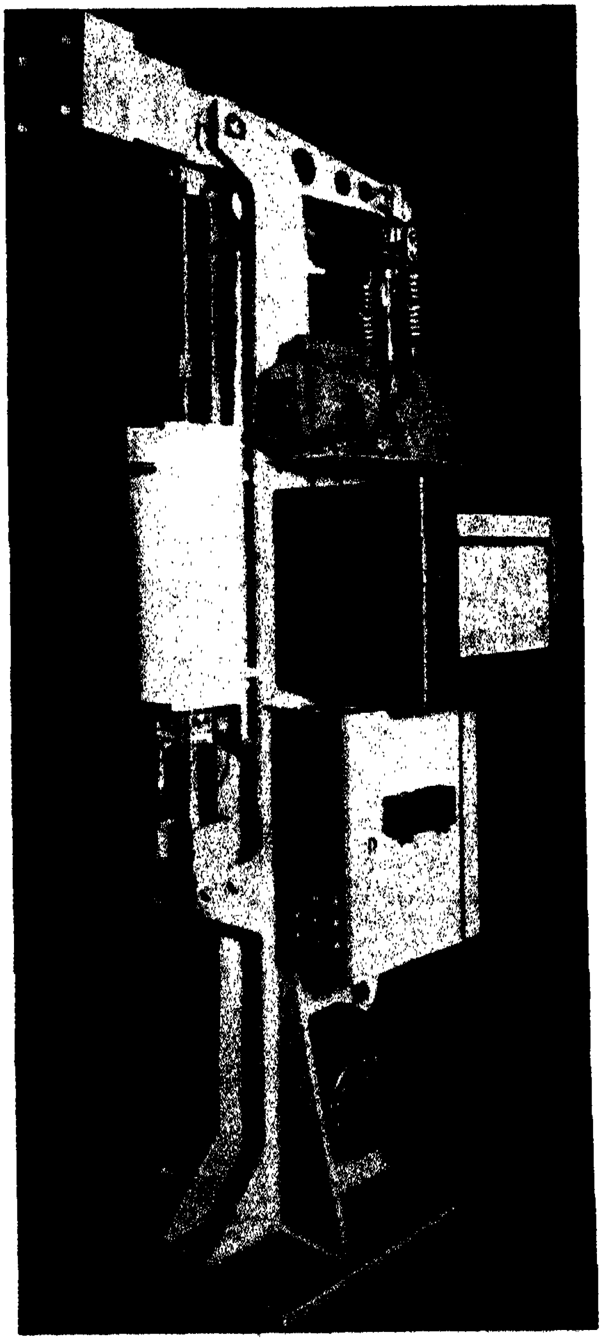

tures. Creep then tends to elongate the bar and release the load. Elastic shortening balances this effect and total strain remains constant. Plastic elongation can be measured by the decrease in stress. Relaxation tests are useful beyond the direct application of data on the behavior of metals at constant total strains. They establish the relative ability of a material to withstand stress at high temperature. They are valuable in estimating creep values in certain ranges of stress and temperature for high strength alloys and in predicting mechanical properties of metals at high temperatures.

The machine automatically relaxes tensional loads from as high as 40,000 lb. per sq. in., permitting strain increments of only 2×10^{-6} in. per in. of the 6-in. gauge length of a standard 0.356-in. diameter specimen. These increases in length are detected by a highly sensitive extensometer with electric contacts that close a 6-volt relay circuit to operate a ¼-hp servo motor which reduces the load enough to open the contacts again and maintain a substantially constant strain.

The load is reduced through a worm and gear box, iso-elastic springs by which the load is measured, and a lever arm with a mechanical advantage of 8:1. Accuracy is approximately 1 percent of load, or 0.25 percent of capacity.

The recorder produces a curve of stress *versus* time on a flat chart slightly less than 10 in. wide. The stress axis is driven indirectly from the spring loading device.

The furnace is 18¾ in. long, 8¼ in O.D. and 2¾ in. I.D. It may be controlled within 5°F or less, or within 2°F or less, depending upon the controller used with it. The machine has a welded steel frame, is 7 ft. high, and occupies a floor area of 25 in.×30 in.—Baldwin Locomotive Works, *Philadelphia 42, Pennsylvania.*

Impedance Bridge

Brown Electro-Measurement Corporation, formerly Brown Engineering Company, announces the versatile new BECO Model 250-A Universal impedance bridge.

Featuring small size and light weight for easy portability, the bridge provides unusually high accuracy by utilizing 0.1 percent precision wire-wound resistors in the bridge arms, and a unique directly calibrated slide-wire consisting of a 0.1 percent precision decade with a coaxially mounted single-turn rheostat for interpolation within the decade steps.

Permanently etched, direct-reading dials increase the ease and rapidity with which measurements can be made.

The bridge can measure resistance, capacitance, and inductance over the following ranges:

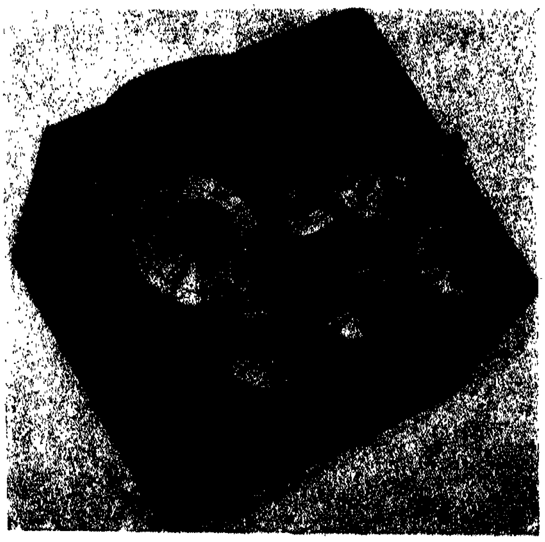

Resistance: 1 milliohm to 1 megohm.
Capacitance: 1 micromicrofarad to 100 microfarads.
Inductance: 1 microhenry to 100 henries.
Storage factor ($Q=X/R$): 0.02 to 1000.
Dissipation factor ($D=R/X$) 0.002 to 1.

Included in the 9¾-in.×10¾-in.×10¾-in. cast aluminum cabinet are four flashlight cells which power the bridge, precision reference standards, 1000-c.p.s. tone generator, zero-center 1 microampere per millimeter suspension galvanometer for d.c. null detection, and headphones for a.c. null detection. Space is provided for the storage of headphones, test leads, and for the companion Model 850-A-amplifier which increases null detection sensitivity on a.c measurements.

All controls and terminals are protected by an attractive cast aluminum cover when the bridge is not in use. Net weight approximately 20 lb.—Brown Electro-Measurement Corporation, *4635–37 S.E. Hawthorne Boulevard, Portland 15, Oregon.*

Counters

A new stainless steel mica end window counter (a) has been announced. Features of this counter are long flat plateaus (several hundred volts long), long life (10^9 counts), low backgrounds, and

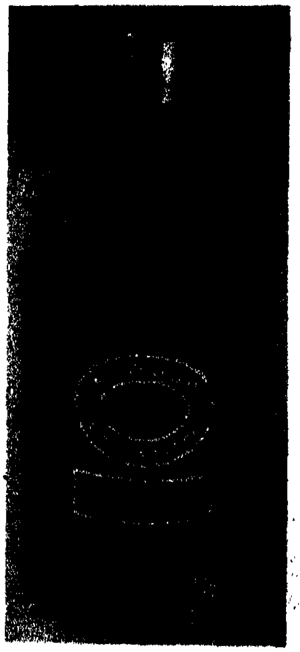

(a)

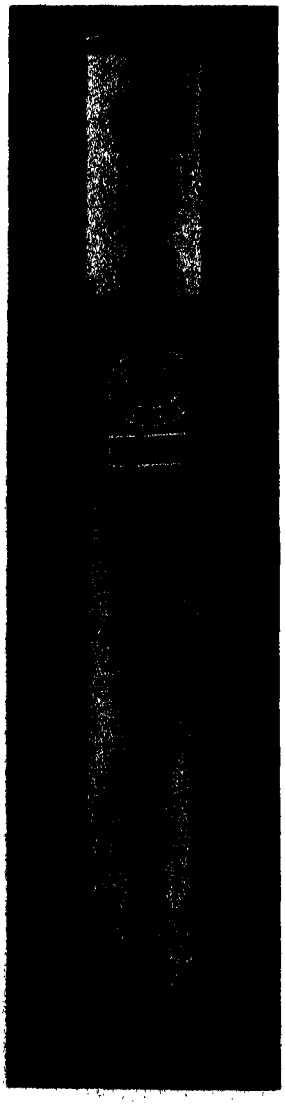

(b)

the seal remains tight. The rise in counting rate is stated to be 2 or 3 percent per hundred volts. This counter can be obtained with a socket-type base.

Also available is an "enriched" BF_3 counter for neutrons (b), which is more than 4 times as efficient as normal BF_3 counters because the boron content is 96 percent boron 10. Sizes available are 1 inch, 1½ inch, or 2 inches in diameter, and 6 to 24 inches in length. Pressures are 30 cm to 45 cm BF_3.—N. WOOD COUNTER LABORATORY, *5646–48 Harper Avenue, Chicago 37, Illinois.*

Vacuum Pump

The HV-1 vacuum pump, combining high performance specifications with simplicity of design and ease of installation, is now available.

The pump is an oil-diffusion type designed to meet exacting production line requirements. It was originally designed by Eitel-McCullough engineers for their use in the manufacture of vacuum tubes; since then, the HV-1 has been tested and proved through millions of hours of operation in all types of applications. Expanding techniques in the field of nuclear science, research, and material processing in vacuum have created a market warranting mass production of the pump, the manufacturer states.

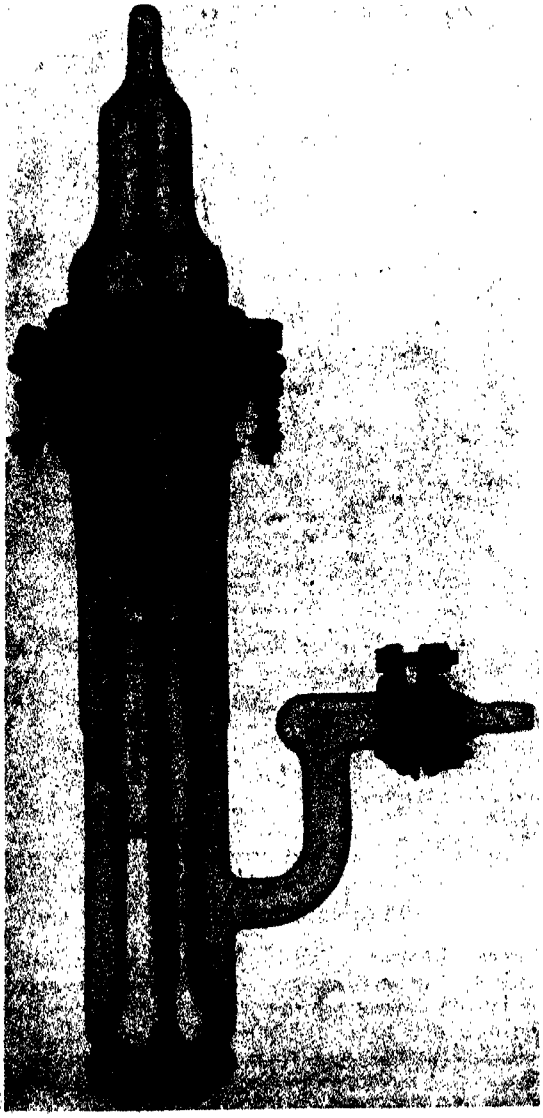

According to the manufacturer, the HV-1 has many outstanding features, including: speeds up to 67 liters per second, attainable vacuum of 4×10^{-7} mm Hg, clear glass pump barrel, no liquid cooling, no charcoal trap, no mechanical wear, and simplicity of mounting and maintenance.—EITEL-MCCULLOUGH, *San Bruno, California.*

R-F Power Supply

Spellman Television Company is now manufacturing a compact, completely enclosed 30-kv r-f power supply suitable for application in dust precipitation, electrostatic painting, and insulation breakdown tests as well as projection television. Power up to 500 microamperes may be drawn with good regulation.

The unit features unusual stability and includes a low voltage d.c. supply. The output voltage is variable from 15 kv to 30 kv through a control on the front panel. The high voltage unit includes a focus control and a voltage tap variable from 4 kv to 6 kv for use with the 5TP4 projection kinescope tube. The high voltage 30-kv–6-kv cables are 3 feet, 11 inches in length, and are of the safety type.

The tube complement includes one 5U4 rectifier, two 6L6 oscillators, and three 1B3 high voltage rectifiers. Dimensions of the power supply are: length 14⅛ in., width 11⅛ in., and height 12⅛ in.

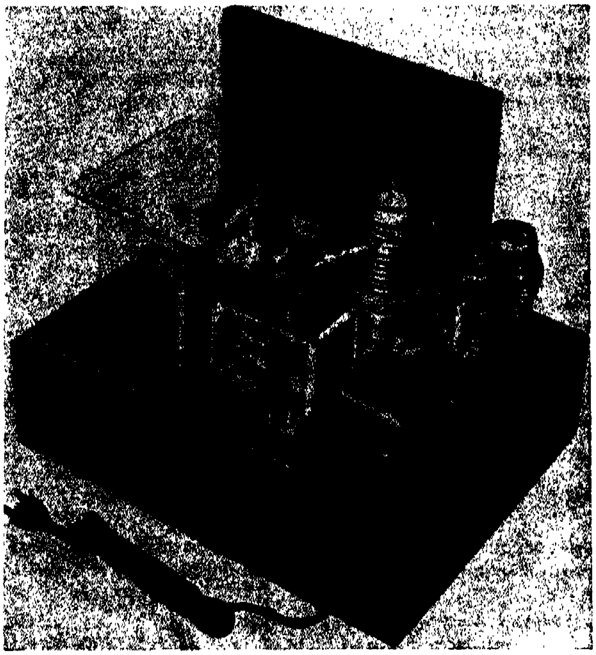

Also available are a 60-kv r-f power supply and a 30-kv r-f regulated power supply with regulation better than 1 percent at 1-milliampere load.—SPELLMAN TELEVISION COMPANY, INC., *130 West 24th Street, New York 11, New York.*

Proportional Counter

Model PC-1 alpha-beta-gamma-proportional counter has an alpha-background, easily maintained at less than five counts per hour. Meson and distributed gamma-background is about 35 counts per minute. The alpha-plateau extends from about 1100 volts to 1400 volts, and the beta-plateau from about 1700 volts to 2000 volts.

The tilt of either is less than 2 percent per 100 volts average, and the best 100 volts has a tilt of less than ½ percent.

The reset control simultaneously resets the register, and the scaling stages and purges the chamber. The operating cycle comprises only the following three operations: (a) exchanging the samples, (b) depressing the combination reset and gas purge lever, and (c) setting and starting the timer. The automatic timer is adjustable up to 56 minutes. The maximum error, including dial setting inaccuracy, is better than 0.2 second at any dial setting.

The unique counter is designed to be an integral part of the instrument. Its compactness makes for laboratory efficiency and eliminates many of the troubles encountered with the use of external chambers, such troubles being leaky high voltage leads, chamber temperature coefficient problems, gas connections, etc.

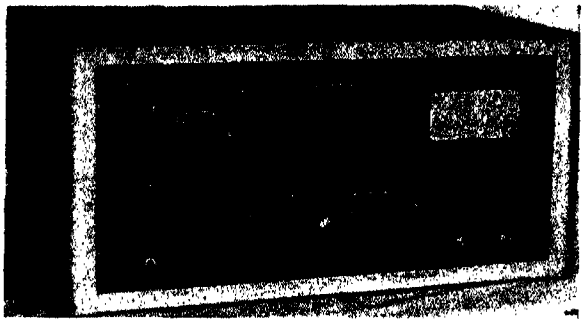

The gas bubbler, which is flush panel mounted and illuminated, is leakproof through either intake or exhaust connections when the instrument is in any position. The accessory built-in gas supply comprises a regulator and brackets with hold-down straps for mounting a 4-in.×12-in. tank of gas on the back of the cabinet. This supply is sufficient for roughly 2000 sampling cycles. The gas mixture is 10 percent C.P. methane in 90 percent argon.

The sample table will accommodate 1½-in. diameter samples up to $\frac{3}{16}$ in. thick. Special sample tables for larger samples are available on special order. Counter construction is such that the entire unit may be decontaminated in less than 10 minutes by the operating personnel.

Both the high voltage and the sensitivity regulation are better than 0.1 percent per percent line voltage change, so that external regulation is unnecessary.—Nuclear Measurements Corporation, *3339 Central Avenue, Indianapolis 5, Indiana.*

Wide-Band Amplifier

Model 100 wide-band amplifier is the first unit of a completely new series of equipments designed for application in the field of nuclear research or for general problems involving the study of transients.

The amplifier has a band width extending from 4000 cycles to 22 megacycles. Response is uniform within 3 db.

Input and output connections of 75-ohm impedance level are provided for use with standard coaxial cables. In addition, a high impedance output connection is available. The amplifier has a voltage gain of 230 at an average output level of 0.4 volt from the 75-ohm output termination, and 250 on the high impedance output connection at a 3.5-volt level.

Miniature tubes and techniques are employed throughout and novel mechanical design results in an extremely compact self-contained unit on a standard rack panel 5¼ in. high by 19 in. wide. The over-all depth, back of front panel, is 4¾ in. Weight complete with tubes is 5 lb. 14 oz. Total power consumption is 26 watts.

A power supply designed for use with the amplifiers, having both regulated plate and heater voltages, will be available.—U. S. Electronic Company, *262 Conner Street, New Haven 11, Connecticut.*

The Speedigram

A new analytical balance, the speedigram, permits untrained personnel to weigh objects quickly with accuracy and without the use of computations or interpolation.

With this new instrument, inexperienced operators have achieved weighing times of less than two minutes. The speedigram is important in production laboratories for volume procedures.

The speedigram analytical balance reads directly up to 100 grams without weights. An extra 100 grams weight is supplied, however, so that the full capacity, 200 grams, is available. The sensitivity of this analytical balance is 0.05 mg at full load.

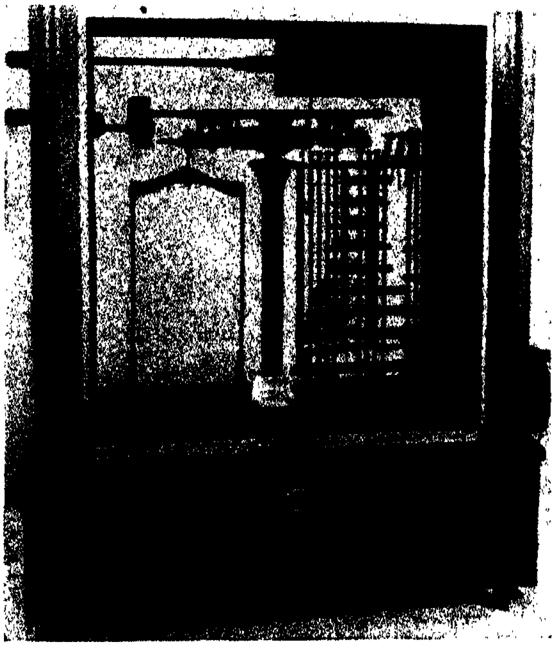

Numerals appearing through the plate over the dials indicate the weights which will be deposited on the pan. Deposition is automatic when the beam is released. Readings are made across the dial so that no arithmetical sums need be computed, thus eliminating a major source of error in analytical weighing.

The speedigram has no complicated parts to get out of order and its working parts are in full view.—Voland and Sons, Inc., *New Rochelle, New York.*

Manufacturers' Literature

Pressure Recorder—Bulletin No. G620 on the new Series 500 absolute pressure gauges describes the instrument and gives data on the new principle of operation employed, which makes it possible to accurately record and automatically control absolute pressure within a scale range as low as zero to 20 millimeters of mercury absolute.—The Bristol Company, *Waterbury 91, Connecticut.*

Electronic Tubes—New issue of the RCA preferred tube types list, Form PTL-501A, has been prepared to assist equipment manufacturers in formulating their plans for future production of electronic equipment.—COMMERCIAL ENGINEERING, RCA TUBE DEPARTMENT, *Harrison, New Jersey.*

Recordings—Vol. 3, No. 2, July 1949, 6 pages, contains articles pertaining to Consolidated's mass-spectrometer-type instruments and dynamic recording instruments.—CONSOLIDATED ENGINEERING CORPORATION, *620 North Lake Avenue, Pasadena 4, California.*

Tin Research Institute—34-page illustrated booklet reviews the activities of the Tin Research Institute during the post-war period.—TIN RESEARCH INSTITUTE, INC., *492 West Sixth Avenue, Columbus 1, Ohio.*

Electrostatic Sampler and Oxygen Therapy Unit—4-page bulletin, CT-9, illustrates and describes the MSA electrostatic sampler, designed for high efficiency atmospheric sampling for all types of particulates in the ceramic, electrical, steel, and chemical processing industries.

Bulletin CW-3 describes the MSA oxygen therapy unit, designed for use in hospitals, dispensaries, offices, or homes. Oxygen flow is automatically adjusted to fit individual breathing needs by this instrument.—MINE SAFETY APPLIANCES COMPANY, *Pittsburgh 8, Pennsylvania.*

Plasticizers—12-page Technical Bulletin O-D-113 contains twenty-two plasticized polyvinyl chloride formulations, noting the outstanding properties of each. Included also is a list of polyvinyl chloride resin, plasticizers, and stabilizers suppliers.—MONSANTO CHEMICALS COMPANY, ORGANIC CHEMICALS DIVISION, *St. Louis, Missouri.*

Electrical Contacts—Technical Data Bulletin 7.101, 12 pages, describes Fastell materials for electrical contacts in various services, from high frequency interruption at low current and voltage to breaker overload protection in currents of several thousand amperes and voltages of several hundred kilovolts.—FANSTEEL METALLURGICAL CORPORATION, *North Chicago, Illinois.*

Selenium Rectifiers—6-page brochure C-349-848 contains operating characteristics, applications, circuit diagrams, design data, and price information on the company's standard line of full-wave, single-phase, bridge rectifiers. The brochure describes cells varying from 1¼ in.×1¼ in. to 6¼ in.×7¼ in. and their operating ranges from 2 volts and 150 ma to 5000 volts and 10,000 amperes.—INTERNATIONAL RECTIFIER CORPORATION, *6809 South Victoria Avenue, Los Angeles 43, California.*

X-Ray Screens—12-page brochure announces a new line of x-ray screens under the name of Rādelin.—UNITED STATES RADIUM CORPORATION, *535 Pearl Street, New York 7, New York.*

Capacitors—Bulletin 214 gives complete details of Type 84P "Telecaps," small molded tubular capacitors in ratings as high as 10,000 volts d.c. and suitable for high temperature conditions met in television, industrial electronics, and various radio applications.—SPRAGUE ELECTRIC COMPANY, *North Adams, Massachusetts.*

•

Colorimetric Comparator—Technical Publication 16-C describes the W+T colorimetric comparator for measuring hydrogen ion concentration (*p*H value) in a simple manner, using permanent, non-fading color standards.—WALLACE AND TIERNAN, *Instrument Department, 1 Main Street, Belleville, New Jersey.*

FCC Measurement Manual—37-page manual gives complete information for making measurements required by amendment (e) to Section 3.46 of "Standards of good engineering practice." The manual states each requirement for both a-m and f-m broadcasters, lists equipment needed to make appropriate measurements, and gives in step-by-step detail proper procedures for measuring, recording, tabulating, and presenting the required data. Offered free on request to radio station chief engineers.—HEWLETT-PACKARD COMPANY, *395 Page Mill Road, Palo Alto, California.*

Index to Gaertner Literature—4-page alphabetical index of all instruments manufactured by the company and reference to the bulletin in which each is described. Also includes a list of more than 30 bulletins in print and in preparation.—THE GAERTNER SCIENTIFIC CORPORATION, *1201 Wrightwood Avenue, Chicago 14, Illinois.*

Tables of Sines and Cosines to Fifteen Decimal Places at Hundredths of a Degree—NBS Publication AMS 5, *Tables of Sines and Cosines to Fifteen Decimal Places at Hundredths of a Degree*, 95 pages, 10¼ in.×7¾ in., 40 cents a copy.—SUPERINTENDENT OF DOCUMENTS, U. S. GOVERNMENT PRINTING OFFICE, *Washington 25, D. C.*

Steel Castings—36-page illustrated booklet, "The steel castings industry," presents word-and-picture discussion of the use of steel castings in many basic manufacturing operations.—STEEL FOUNDERS' SOCIETY OF AMERICA, *920 Midland Building, Cleveland 15, Ohio.*

Flowrator Instruments—Catalog 50, 24 pages, presents principles of operation, construction details, and features of ratomatic instruments for flow rates.

Catalog Section 96 describes the magna-sight, a flow-rate measuring instrument for jobs where accuracy within several percent is satisfactory.—FISCHER AND PORTER COMPANY, *Hatboro, Pennsylvania.*

New Materials

Forest K. Harris: Associate Editor
in Charge of this Section
National Bureau of Standards, Washington, D. C.

Soldering and Brazing

The term "soldering" generally means the joining of 2 metal surfaces by means of another metal or alloy applied in a molten condition. Most satisfactory adhesion is attained when the solder or one of its constituents alloys with the metals it joins. When alloying does not occur an extremely clean surface must be maintained in the operation. For alloys used in soldering, the temperature at which melting begins (the solidus) is lower than the temperature at which it becomes completely molten (the liquidus), except the eutectic composition for which these two temperatures coincide.

Soft solders are used for joining metals at comparatively low temperatures. They will withstand considerable bending without fracture but usually have a low strength compared to that of the metals joined. The soft solders in general use are lead-tin alloys. The eutectic alloy containing 63 percent tin and 37 percent lead melts at about 360°F. All other lead-tin alloys between 20 percent and 97 percent tin have a solidus temperature of 360°F, the liquidus temperature varying with composition. The alloy containing 2 parts lead to 1 part tin has been used for "wiped" joints as it remains partly molten over a wide temperature range and can be molded during solidification. Before the war, 50-50 alloy was used as a general purpose solder, its liquidus temperature being

423°F. Tin is still in scarce supply and its use is at present somewhat restricted. The higher melting points and broader freezing ranges of the lower tin solders make soldering more difficult but with proper techniques and fluxes joints can be made which are practically as satisfactory as those made with 50–50 solder. Most commercial soft solders contain small percentages of other added elements. Antimony apparently increases the strength, whereas bismuth, copper, and silver promote "tinning" or spreading of the solder. Generally the added constituents lower both the solidus and liquidus temperatures. Solders used for joining zinc or galvanized metals should be free from antimony, as this element combines with the zinc to form a brittle, high melting constituent which lowers the strength of the joint. Nominal compositions of a series of lead-tin solders with tin content ranging from 25 to 50 percent are listed in Table I. Lead-silver solders are useful substitutes for lead-tin solders for many purposes. The silver content is usually low, 2.25–2.50 percent. The eutectic alloy, with 2.50 percent silver, is very fluid when molten, but solidifies at a definite temperature. When a freezing range is required, the silver is reduced to 2.25 percent and 3 percent tin is added. The melting temperature of lead solder with 2.5 percent silver (572°F) as well as other lead-silver solders is considerably higher than those of the ordinary lead-tin solders, so that somewhat different fluxes and techniques are required. This type of solder has proven satisfactory for copper, copper-base alloys, iron, steel, and tin-plate.

TABLE I. Lead-base solders.

ASTM class	Nominal composition, percent Sn	Sb (max.)	Cu (max.)	Bi (max.)	Freezing range, °F Solidus	Liquidus
50–50	50	0.4	0.08	0.25	360	423
40–60	40	0.4	0.08	0.25	358	482
—	35	1.50	0.08	0.25	358	493
30–70	30	0.75	0.15	0.25	358	502
25–75	25	0.4	0.08	0.25	361	511

Lead-tin-bismuth solders are characterized by a lower solidus temperature (205°F) than that of the ordinary lead-tin solders, and are useful for soldering alloys classed as pewter. Table II below gives the characteristics of some of these low melting solders.

TABLE II.

Nominal composition, percent Pb	Sn	Bi	Liquidus °F
25	25	50	266
50	37.5	12.5	374
25	50	25	338

An alloy of 95 percent tin with 5 percent antimony, melting at 450°F with a small melting range, has been recommended as a soft solder. It is claimed that joints made with this alloy are somewhat higher in strength than those made with lead-tin solders. Current restrictions on tin limit the application of this solder.

For joints required to withstand higher temperatures than can be met by lead-tin solders, an alloy of 95 percent cadmium with 5 percent silver has been recommended. This alloy has a solidus temperature of 640°F and is completely molten at 740°F.

To secure good adherence in soldering it is necessary that the surfaces of the metal and the solder be free from oxide and dirt. Grease and dirt can be removed by benzene or some other suitable organic solvent. Where permissible, oxide or stained surfaces can best be cleaned by mechanical abrasion, i.e., filing, grinding, or polishing. To enable the solder to "wet" the metal it is necessary to employ a covering material which will remove oxide film and protect the surfaces from air while they are being heated. Such an agent is known as a flux. Fluxes commonly used for soft soldering metals other than aluminum are solutions or pastes containing zinc chloride or a mixture of zinc and ammonium chloride. It is claimed that flux containing zinc and ammonium chlorides in their eutectic proportions (71 and 29 percent by weight, respectively) is best for lead-tin solders. Zinc chloride alone or with small additions of ammonium or stannous chloride have been found satisfactory for lead-silver solders. When the flux melts it partially decomposes with the liberation of hydrochloric acid which enables the flux to dissolve surface oxides. The fused flux forms a protective film that prevents further oxidation. If the flux reaction continues too long, salt deposits occur which make further fluxing or soldering difficult. Consequently, it is best to apply the flux immediately before soldering, with a small stiff brush to assist "wetting." Excessive chloride flux should be removed immediately after soldering, using a large swab and hot water. Since chloride fluxes are corrosive it is sometimes necessary to use a different flux for certain types of work where the last traces of flux cannot be removed after soldering. (Note: Your editor has found it practically impossible, by any cleaning process known to him, to remove flux completely enough to insure that no corrosion occurs in and around the joint over an extended period of time.) Rosin is the only flux known to be noncorrosive in all soldering applications and is commonly used where corrosion is a hazard. It can be dissolved in alcohol in varying proportions to obtain flux of any desired consistency. Wire solder with a rosin core is obtainable commercially. Wetting agents are sometimes added to rosin flux as it "wets" metals more slowly than chloride flux. Also rosin in a modified form, termed a "rosin dimer," has greatly improved wetting properties over ordinary rosin.

A prime requisite in soldering is a constant source of heat which will maintain the surface at the desired temperature with the least amount of oxidation. In soft soldering this is usually accomplished with a preheated "iron" (usually of copper) of good thermal conductivity and large heat capacity, with an electrically heated source, or with a controlled flame. Excessive amounts of either flux or solder should be avoided. The "iron" should be clean and should be covered ("tinned") with a thin layer of molten solder to improve heat transfer. Frequently, prefluxing and pretinning of the bonding surfaces is desirable. When solidification occurs over a wide range of temperature relative motion of the metals at the joint should be avoided during solidification, as this would damage the bond. Clamping the pieces in place during such an operation is desirable. Overheating should be avoided as this increases oxidation and may affect the flux adversely. In soldering galvanized iron or zinc a mixture of ammonium and zinc chloride is widely used. It should be applied sparingly, and the excess removed immediately after joining as it attacks zinc very rapidly. It is important that the soldering "iron" be moved slowly in one direction only as repeated motion over a spot will cause the zinc to dissolve in the solder, making it gritty and brittle. In soldering stainless steel, 50–50 lead-tin solder is used. Hydrochloric acid, diluted with an equal volume of water, is applied first and then, after 5 minutes and without washing off the acid, zinc chloride flux is applied. The soldering operation is then carried out in the usual manner. This class of steel does not solder as readily as other metals.

Soldering and brazing of aluminum.—In general, it is preferable to join aluminum and its alloys by welding, because soldered joints of these metals will corrode rapidly in a moist atmosphere if not adequately protected. Aluminum of at least commercial purity, and wrought aluminum alloys containing not more than 1 percent of manganese or 1 percent of magnesium are the only metals of this group for which soldering is considered advisable. The heat-treatable aluminum or aluminum clad alloys should not be soldered. Most of the soft solders for aluminum contain 50–75 percent tin, and 40 percent zinc is frequently used. Proprietary alloys possessing a wide range of melting points are available for soldering aluminum. Care must be taken that the solidus temperature of the solder is at least 100°F higher than the service temperature of the joint if it is to be subjected to a sustained load. Until recently, the only satisfactory method of removing oxide film was by rubbing or abrading the surface beneath the molten solder with a wire brush or steel wool. Proprietary fluxes are now available from suppliers of aluminum solders, which eliminate the need for the mechanical removal of oxide film. Since the fluxes are corrosive they should be removed after soldering, by use of a large swab and warm water. Rapid corrosion will occur in soldered aluminum joints if not adequately protected in moist atmospheres. Where joints are exposed to humid or marine atmospheres, it is desirable to make long lap or scarf joints. In salt water or salt spray, joints can be cathodically protected by attaching strips of zinc or cadmium very close to the joint. In an ordinary humid atmosphere, or in water where no electrolyte is present, a moisture proof lacquer or paint coating should be used over the joint.

Filler metals and fluxes used in brazing aluminum and its alloys are proprietary and can be obtained from manufacturers of aluminum alloys. Brazing is employed when higher strength is required than can be obtained with soft soldering, and where economy or neatness dictate its use in preference to welding. Thin sections are sometimes brazed because of the poor results obtained in welding. Complex assemblies or castings with heavy sections are not amenable to brazing. Of the wrought non-heat-treatable alloys, only commercially pure aluminum and the aluminum-manganese alloys can be brazed. The heat-treatable magnesium-silicon alloys of aluminum can also be brazed.

TABLE III.

	Nominal composition, percent				Freezing range, °F	
No.	Ag	Cu	Zn	Other	Solidus	Liquidus
1	10	52	38	—	1510	1600
2	20	45	35	—	1430	1500
—	20	45	30	5 Cd	1430	1500
3	30	38	32	—	1370	1410
4	40	36	24	—	1330	1445
5	45	30	25	—	1250	1370
6	50	34	16	—	1280	1425
7	60	25	15	—	1260	1325
8	70	20	10	—	1335	1390
9	72	28	—	—	1435	1435
10	80	16	4	—	1360	1460
11	15	80	—	5 P	1200	1300
12	50	15.5	16.5	18 Cd	1160	1175
—	50	15.5	15.5	16 Cd, 3 Ni	1195	1270
—	50	15	25	10 Cd	1166	1190

Hard solders are distinguished from soft solders in possessing much higher melting points and in making joints which generally have higher strength. The typical hard solders are either precious metal alloy solders or brazing solders.

Silver solders, generally alloys of silver, copper, and zinc, are widely used. They are malleable and ductile and, in many cases, the joints are as strong as the metals themselves. Some of these alloys are listed in Table III. Alloy 11 (proprietary) is widely used and is claimed to be self-fluxing. It is recommended for copper and its alloys but not for iron or steel. Alloy 12 (proprietary) is a recently developed, general purpose solder, suitable for a variety of metals including stainless steel. Tungsten can be soldered to copper with Alloy 7. Silver solder for general use may be made in the shop by melting together 1 part of silver and 2 parts of yellow brass (60 Cu–40 Zn). An alloy containing 85 percent Ag and 15 percent Mn has good characteristics and a high melting range. It was developed for bonding parts having a high service temperature, and can be used with stainless steel.

Gold solders are generally alloys of gold with copper, silver, and zinc. They are generally designated with the karet number of the gold alloy with which they should be used. Fine gold or the higher karet gold alloys may be used for soldering platinum and platinum metal alloys.

Brazing solders (or "spelters") are brasses containing more zinc and having a lower melting point than the commercial brasses or bronzes. Commonly used brazing alloys contain from 40 to 55 percent copper with the remainder zinc. These are brittle alloys and joints made with them, although superior to soft-soldered joints, will not withstand bending and impact as well as those made with silver alloys. The compositions and melting temperatures of some brazing alloys are given in Table IV.

TABLE IV.

		Composition, percent				Melting
Cu	Sn	Pb (max.)	Fe (max.)	Al (max.)	Zn	temperature °F
49–52	—	0.5	0.1	0.1	Remainder	1600
49–52	3–4	0.5	0.1	—	Remainder	1520–1550
68–72	—	0.3	0.1	—	Remainder	1650–1760
78–82	—	0.2	0.1	—	Remainder	1725–1825

For most purposes, borax or a mixture of borax with boric acid (25–75 percent borax) are suitable for use as fluxes with the precious metal and brazing alloys. For soldering silicon bronze or beryllium copper, potassium bifluoride or zinc chloride are added to the flux mixture. When soldering tungsten to copper with Alloy 7, sodium cyanide is a satisfactory flux. Great care must be taken when using cyanide salts that they do not enter the body orally or through skin abrasions. They must be kept dry and should not come in contact with acids, nitrates, nitrides, or other oxidizing agents. Breathing the fumes of a flux containing a bifluoride salt should also be avoided.

Since silver solder and other brazing alloys melt at high temperatures, soldering irons cannot be used. Common methods of application are by dipping the work in molten alloy; by heating with torches or in furnaces; by electrical resistance heating; or by induction heating.

The above material has been abstracted from Letter Circulars 937, 938, and 939 recently written by the Metallurgy Division of the National Bureau of Standards. These letter circulars also contain bibliography material on soldering.—NATIONAL BUREAU OF STANDARDS., *Washington, D. C.*

Asbestos Tubing

Asbestos tubing, originally designed as a heat-resisting base for electrical coils, has other potential uses. Since it is unaffected by high temperatures, it can be used for both electrical and heat insulation in electrical heaters and other heating devices. The tubing is made by spirally winding specially prepared asbestos tape to predetermined sizes around a mandrel. It is then die-formed to shape with square, rectangular or oval cross section. Such tubes can be made in any length with wall thicknesses from 0.01 inch up. The tubing is stated to be unaffected by sudden temperature changes. Further information may be obtained from the manufacturer. PRECISION PAPER TUBE COMPANY, *2045 West Charleston Street, Chicago 47, Illinois.*

Rubber-Insulated Heating Element

Heating elements, in which resistance wires are imbedded in insulating fabric plies between sheets of rubber are available for service up to 300°F. These units may be used to control moisture condensation, to prevent freezing of pipe lines, to free frozen chutes or storage bins, or as a warming pad or heat booster. The sheet material is available under specification as to use, temperature, size and capacity. Almost any size, weight or shape may be obtained. B. F. GOODRICH COMPANY, *448–52 South Main Street, Akron 11, Ohio.*

Protective Coating for Steel

Vinsynite is a liquid material for application to finished steel surfaces prior to finish coating. It adheres to the steel, phosphatizes it, and deposits a thin protective film on the surface. Application of this film is followed by a primer coat of vinyl-resin base that adheres tightly to the initial film and protects against corrosion. This can be followed by any conventional paint. The pre-treatment and primer coating produce a protective film that approaches the durability and service characteristics of plastic sheeting of equivalent thickness. It is stated to withstand salt spray in a 1000-hour test.—THOMPSON AND COMPANY, *1018 Edward Street, Oakmont, Pittsburgh, Pennsylvania.*

Plastic-Coated Steel Tubing

Permatube is thin-walled Electricweld steel tubing combined with *Vinsynite* metal treatment. The vinyl-resin coating has a thickness of 0.0015 inch. The tubing can be fabricated by bending, expanding, flanging, upsetting, and flattening without damage to the protective film, which has lasted for 3000 hours exposure in an accelerated spray test before corrosion appeared. This tubing can be supplied in all standard Electricweld sizes and shapes in lengths to 10 feet.

Electricweld tube is now available in square, rectangular, oval, or special section. Square tubing ranges from $\frac{3}{4}$ in. to 3 in.; rectangular sections can be of any dimensions that do not exceed $3\frac{3}{4}$ in. on the long side; minimum ovals are $\frac{3}{4}$ in. by $\frac{3}{8}$ in.; maximum ovals include any section that will lie in a 4-in. circle. Thickness can be specified in gauges from 14 to 20.—JONES AND LAUGHLIN STEEL CORPORATION, *311 Ross Street, Pittsburgh 30, Pennsylvania.*

Ashless Filter Material

Whatman's Ashless Tablets are a convenient source of ashless pulp for use in the filtration and washing of gelatinous or gummy precipitates as recommended in current techniques. The addition of small amounts of pulp also assists in the retention of fine precipitates, making possible the use of more rapid filter paper with a consequent saving of time. A stock suspension can be prepared using several tablets, or a portion of a tablet may be added to each determination before filtering. The tablets are composed of highly purified pulp washed in hydrochloric and hydrofluoric acids until practically ashless. Each tablet weighs about 2.5 grams and has an ash of 0.0005 gram. BURRELL TECHNICAL SUPPLY COMPANY, *1942 Fifth Avenue, Pittsburgh 19, Pennsylvania.*

Precision Castings

Polystyrene is employed in the place of wax in a new precision casting process. In general, castings in intricate shapes can be made to tolerances of ±0.005 inch, and up to 5 pounds in weight. Plastic patterns are made and assembled in multiple on a gate. They are dipped in a fine slurry of silica sand, air dried, and placed in a stainless steel flask into which silica mold material is poured. When this has solidified it is placed in a curing oven, followed by a furnace where the plastic is burned out at 1800°F, prior to pouring the castings. The process can be employed to cast mild and stainless steel, vanadium steel, tool steel, and high alloy steels. It can also be used for aluminum, brass, copper, and manganese bronze.—ELECTRONICAST, INC., *1729 West Fulton Street, Chicago 12, Illinois.*

Resistance Alloy

Alloy 1000 is an electrical resistance material having a resistivity of 1000 ohms per circular mil foot. Its temperature coefficient of resistance does not exceed ±0.000025/°C and remains substantially constant between 20°C and 100°C. It has high tensile strength and ductility, resistance to surface corrosion equal to that of nickel-chromium alloys, a low coefficient of linear expansion, and a low thermal e.m.f. against copper. The material is stated to solder readily. It is available in wire in diameters from 0.9 mil to 10 mils, and in small ribbon sizes.—C. O. JELLIFF MANUFACTURING CORPORATION, *Pequot Road, Southport, Connecticut.*

Carbide Tubing

Tungsten carbide, combining hardness and strength, and *titanium carbide*, combining hardness with ability to withstand thermal shock, abrasion, and corrosion at high temperatures, are the materials from which tubes are supplied. Sizes range from 0.004 in. to 0.4375 in. i.d., and from $\frac{1}{32}$ in. to $\frac{9}{16}$ in. o.d. The outside is rough extruded 0.010 in. to 0.015 in. oversize; the inside is held to within ±1 percent of specification and is accurately concentric. Orifices and nozzles, thread and wire guides, punch and die parts, gauge parts, guide bushings, burner cores, furnace rollers, and thermocouple protective tubes are representative applications.—KENNAMETAL, INC., *100 Lloyd Avenue, Latrobe, Pennsylvania.*

THE
REVIEW OF SCIENTIFIC
INSTRUMENTS

VOLUME 20, NUMBER 10 *OCTOBER, 1949*

A Wide Range Radiation Instrument

Leonard Reiffel* and Glenn Burgwald**
Institute for Nuclear Studies, The University of Chicago, Chicago, Illinois

(Received May 6, 1949)

A radiation monitoring instrument based on the scintillation counter is described which measures γ- (or β-) radioactivity levels from 1 milliroentgen/hour to 100 roentgens/hour without changing scale. The instrument may thus be entirely unattended even in the vicinity of widely varying sources. Its performance and limitations are discussed, together with means for increasing its ultimate sensitivity.

I. INTRODUCTION

THE purpose of this paper is to describe a radiation instrument capable of monitoring a range in γ- (or β-) radioactivity from 1 milliroentgen/hour to 100 roentgens/hour. This corresponds to tolerance periods ranging from no limit (1 milliroentgen/hour) to 4 seconds/day (100 roentgens/hour). It was deemed very desirable to cover this range without manual scale switching so the instrument could be left completely unattended. Accuracy of approximately 15 percent was considered adequate.

Thus, the requirements placed on the detector unit are that it shall respond to a signal intensity ranging over 5 decades without saturating or requiring attention of any sort. Pulse counting techniques (scaling, etc.) were eliminated because it was felt saturation effects would be exceedingly troublesome at the higher levels; hence, some sort of integrating system was indicated.

It is possible to use an ionization chamber over these ranges providing a sufficiently large collecting voltage is applied. However, the chamber is essentially a very high impedance device and automatic range switching would be difficult but necessary if an electrometer tube or similar method were to be used to lower the impedance level. Because of these real and suspected difficulties, it was decided that a scintillation counter and integrating circuit (low pass filter) be used as the primary radiation detector.

Such a method has the following advantages:

1. The scintillation counter crystal is not troubled by saturation even at the highest levels.
2. The photo-multiplier tube used to detect the scintillations is a reasonably low impedance device.
3. By judicious choice of the photo-multiplier's operating point, a range of 10^5 in output may be had with no adverse effects.
4. The detector is small, sturdy, and readily portable.

II. BASIC CIRCUIT

The detector consists of an Anthracene crystal and Type 931A photo-multiplier tube. The pulse output of the tube is integrated to provide a d.c. level proportional to the pulse rate, and is compared to a balancing voltage by means of a Brown converter.[1] Any difference between the comparison voltage and *PM* tube output is amplified and used to position a servo motor on a

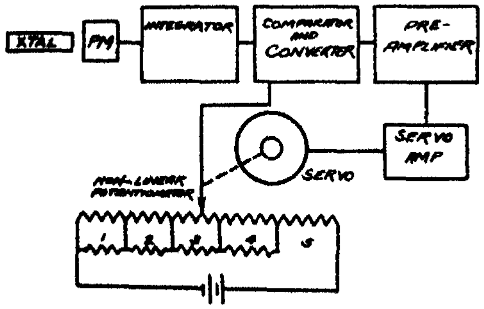

FIG. 1.

---

[*] Now at Armour Research Foundation, 35 West 33rd Street, Chicago 16, Illinois.

[**] Now at Nuclear Instrument and Chemical Corp., 223 West Erie Street, Chicago, Illinois.

[1] Manufactured by Brown Instrument Division, Minneapolis-Honeywell Corporation.

highly non-linear potentiometer geared to an indicator pointer (see Fig. 1). However, the range of *PM* output voltage which may be balanced is 100,000 to 1 because of the special potentiometer used. Figure 2 illustrates the potentiometer, servo motor drive, and indicator unit.

III. COMPLETE CIRCUIT

The scintillation detector consists of a piece of clear, crystalline anthracene approximately $1\times1\times0.5$ cm obtained from Harshaw Chemical Company. The crystal is mounted in paraffin and ground flat on its two larger surfaces. The photo-multipliers used to detect the scintillations are selected 931A tubes. The criterion for selection is low absolute dark current, which, however, is not a difficult requirement to meet since the dark current of all the tubes checked was in the vicinity of 1.0×10^{-9} ampere. This low value may have been fortuitous. However, G. H. Dieke[2] made similar measurements on a series of such tubes and obtained values less than 9.5×10^{-9} ampere for 6 of 9 tubes operating under considerably more severe voltage conditions.

The photo-multipliers used in the instrument are operated in the vicinity of 900 volts which must be well stabilized. Since multiple probes are sometimes used with the same indicator, the sensitivities of the *PM* tubes are matched by adjusting the voltages on the first two stages.

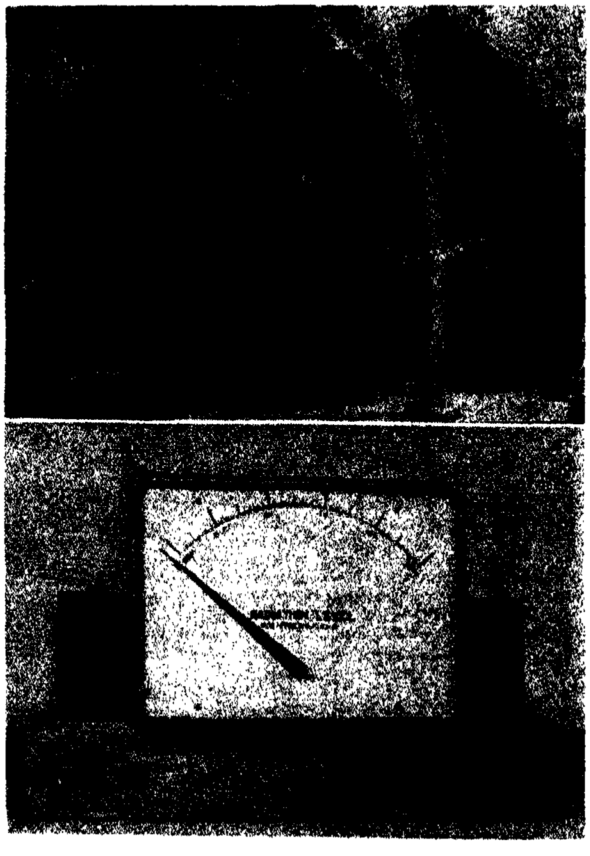
FIG. 2. Top: Servo motor and tapped potentiometer. Bottom: Indicator unit and scale.

The crystal was mounted on the photo-tube and the entire assembly was placed in a cylindrical brass housing, which in turn was mounted on a probe chassis (see Fig. 3), and gasketed for light tightness. Light leakage up through the socket and around the pins was eliminated by blackening the interior of the housing and filling the gap between the tube base and chassis socket.

A more serious problem was the electrical leakage across the socket of the tube. The entire base assembly was, therefore, thoroughly cleaned and coated with paraffin. This procedure reduced the no signal output of the tube by at least a factor of 10.

As outlined in Section II, the problem reduces to that of measuring the d.c. component of the *PM* output which may vary over a range of 10^6. The load impedance usually associated with photo-multipliers in scintillation work is of the order of 50,000 ohms so as to obtain fast pulse decay. In this case, however, the impedance is made large (2.7 megohms) since it is only the d.c. output which is of interest.

The load resistor drives an *RC* low pass filter which serves to eliminate the rapidly varying components of the *PM* tube output so the servo system will not act erratically. This *RC* integrator circuit serves the second important function of slowing down any step function increase in radiation level (and *PM* output) which could block the servo amplifier.

The d.c. output signal of the integrator circuit is fed to a Brown converter along with a d.c. comparison voltage supplied from the servo driven slidewire. Since the impedance level at the Brown converter is of the order of one megohm and the applied signal is of the order of 0.1 millivolt at the low end of the range, considerable hum is introduced by the vibrator driving coil. This pick-up is greatly reduced by opening the converter and rearranging the driving coil leads so that they come out the top of the housing.[3]

The Brown converter, essentially a driven single-pole double-throw switch, is designed so that the contactor arm closes each of the two circuits some 45 percent of a complete cycle, and shorts both circuits together for about 10 percent of a cycle. This action permits the integrating capacitor C_3 to receive charge via the low impedance comparison voltage circuit. The capacitor holds this charge easily until the contactor closes the *PM* tube circuit, and thus the net voltage change as seen by the first amplifier grid is very nearly zero. To prevent this action, a resistor R_{30} is placed in series with the comparison voltage such that the integrating capacitor takes on very little charge from the comparison voltage.

The 60 cycle unbalance voltage derived from the Brown converter is fed to the grid of the first servo preamplifier tube. It was found convenient to heat the filament of this tube by r-f power supplied by a simple tickler oscillator to reduce the 60 cycle pick-up.

---

[2] G. H. Dieke, "A study of standard methods for spectrographic analysis," Report No. W-193, WPB, May 1, 1945.

[3] Components Handbook, MIT Radiation Lab. Series, p. 498.

As seen in Fig. 4, the servo preamplifier consists of two 6AK5's and one 6SL7. This tube line-up yields a gain of the order of 10^6 if the amplifier is linear. The preamplifier is *RC* coupled to two 6N7's which serve as the servo power amplifier. This power amplifier design is taken from the Brown Company "Electronik" recorder, and matches the Brown 160 r.p.m. servo motor used as the indicator and potentiometer drive. The 6N7's deliver a considerable d.c. current to the control phase of the servo motor which causes dynamic braking with its attendant stability.

The servo motor is used to drive the comparison voltage potentiometer and the indicator needle (see Fig. 2). The system is geared so the motor, running at 160 r.p.m., drives the potentiometer through 330° and the needle through 110° in approximately 10 seconds. Since the signal voltage available from the *PM* tube varies over five decades, it is also necessary that the comparison voltage do so. To accomplish this, the potentiometer, which is wire-wound, is tapped at four regularly spaced intervals. A one-ohm resistor is placed across the first interval, 10 ohms across the second, 100 ohms across the third, 1000 ohms across the fourth, and no resistance across the last which is one-fifth of a 50,000 ohm potentiometer or 10,000 ohms. When a voltage is applied across the potentiometer, one ten-thousandth appears across the first interval, one-thousandth across the second—and so on. Thus, the ratio of voltages available from the potentiometer is 100,000 to 1 (i.e., ratio of voltage on one-tenth of the first decade to full potentiometer voltage).

When the indicator is positioned in the last two decades, the servo tends to hunt with an amplitude amounting to approximately 2 percent of a decade. This has not interfered with reading the indicator; however, if the life of the potentiometer is much reduced by this action, steps will be taken to eliminate it.

IV. PERFORMANCE OF CIRCUIT

The instrument was tested and roughly calibrated at radiation levels up to approximately 100 mr/hr. with a 0.3 millicurie Co^{60} γ-ray source. The total potentiometer voltage was adjusted so the 100 mr/hr. level would fall at the end of the second decade. This adjustment is very stable and required 21 volts across the entire potentiometer or approximately 21 millivolts across the second decade.

In order to check performance at high radiation levels, a 0.5 gram radium source was used to yield levels up to 45 r/hr. and higher. The readings predicted on the assumption of linearity were well checked even to the highest radiation levels and no drift has been observed. A more accurate calibration is planned for the near future when time permits.

FIG. 3. Complete radiation instrument; foreground: servo preamplifier, probe pick-up and power supply, indicator unit. Background: Dark current cancellation chassis and typical multiple probe.

V. LIMITATIONS

There are two basic limitations to the performance of the instrument. These are:

1. At very low levels (5 mr/hr. or less)—dark current variations.
2. At very high levels (10 r/hr. or more)—photomultiplier fatigue.

The dark current of the photo-multiplier, due ideally to thermionic emission from the photo-cathode, is strongly temperature dependent and thus may cause a shift in the zero position of the instrument as the temperature varies. However, with tubes selected for low dark current, this effect is small enough to be neglected providing no levels less than 5.0 mr/hr. need be measured to 15 percent accuracy. It was found that a 4°C change in temperature caused a shift of the order of 0.7 μr/hr. This *approximate* relationship was tested over the range +40°C to −4°C. The temperature dependence for our application is, therefore, unimportant.

For those applications requiring higher sensitivity and accuracy, at least two possibilities are open. First, a thermostatically controlled oven operating at about 40°C (to absorb maximum room temperature) has been used successfully. A "Fenwal thermoswitch" (or similar device) and resistor heating element will maintain the temperature to within 0.4°C and thus effect a considerable increase in the minimum measurable signal (at a given accuracy).

Second, a more direct method of *canceling* the dark current *pulses* has been employed. It is found that the pulses making up the dark current of a *PM* tube are considerably smaller than the average current pulse due to a scintillation.[4]

This immediately suggests the use of a pulse height discriminator circuit set to reject dark current pulses. However, any direct pulse height discriminating circuit would become completely blocked at higher radiation levels, and its output would rapidly go to zero.[5] It is thus necessary to employ a discriminator circuit in which blocking does not cause the entire instrument to become inoperative. (At levels which block the discriminator, dark current is unimportant.) This may be done by placing the discriminator circuit in a feed-back loop as shown in Fig. 5(a).

---

[4] G. A. Morton and K. W. Robinson, "A coincidence scintillation counter," Nucleonics, 25–29 (February 1949).

The circuit is designed so as to feed back an *identical* canceling pulse for every photo-multiplier pulse less than the discrimination level. For pulses greater than this level, the phase inverting pulse amplifier feeds back a pulse clipped at the discrimination level. These cancellation pulses are delivered at low impedance to a resistance to ground in series with the photo-multiplier load. Since the multiplier output current is saturated, these feed-back pulses do not affect its output. The circuit operates as a completely fed-back high gain amplifier as long as the clipper is inactive; hence, voltage developed between grid and cathode is very small. When the pulse height exceeds the clipping level, the loop gain is greatly reduced and a considerable output pulse is developed to feed the integrating condenser. For pulses whose amplitude exceeds the clipping level, only that portion below the clipping level is canceled. The voltage on the integrating condenser is thus due only to those portions of the input pulses which are above the clipping level. This eliminates the dark current pulses entirely, at the expense of a factor of three in sensitivity which may be made up elsewhere in the instrument. When the discriminator blocks, its output goes to zero and the full *PM* output charges the integrating condenser.

The adjustment of the loop gain of the circuit is rather critical[6] and for this application, where the pulses are to be integrated, it is possible to simplify the method of cancellation as shown in Fig. 5(b).

Here the cancellation pulses are "pre-integrated" so that they appear as a d.c. level feeding the integrating capacitor and do not influence the pulse amplifier except for shifting the bias on the first tube slightly. There is no danger of regeneration if the "pre-integration" is practically complete.

If the radiation monitor were required to operate over very wide temperature ranges at high sensitivity, it would probably be necessary to combine pulse cancellation and thermostatic control,[7] since there is evidence that the light output of the crystal itself varies somewhat with temperature.[8]

Photo-multiplier tubes, when operated at high light levels, exhibit a fatigue effect wherein the output current decreases steadily with time although the illumination is constant.[9] If the illumination is removed, the tube

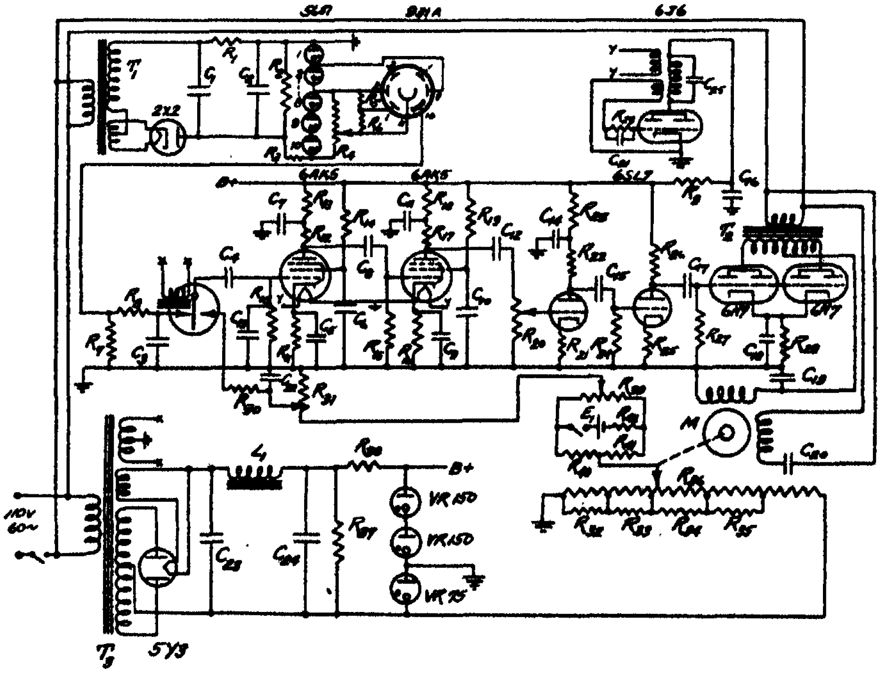

FIG. 4.

---

[5] Some circuits when blocked would still develop an output, but it would not bear any direct relationship to the radiation level.

[6] The loop gain is adjusted to approximately unity, at the pulse input grid, since the cancellation pulses should differ from the *PM* pulses only in sign (neglecting loading by the servo preamplifier). This requires feeding back across a high gain phase inverting amplifier which may regenerate unless great care is taken.

[7] It is of interest to note that by reversing the output of the pulse amplifier in Fig. 5(b), great sensitivity may be obtained at the integrating condenser. This is particularly true if the clipping circuit is revised as a pulse stretching circuit. In this manner, a non-blocking, very high sensitivity instrument is obtained. (For a monotonically increasing reading with increasing radiation level, the pulse amplifier must not block *too* rapidly.) Under these conditions, dark current compensation is necessary so the circuit of Fig. 5(b) is essentially employed twice. Using this method, radiation levels of the order of 50 microroentgens/hr. are easily detected.

[8] Notes on Conference of Scintillation Counters and Crystal Counters, Rochester, New York, p. 8, July, 1948.

[9] See reference 2, p. 43.

will not recover the original sensitivity for some 50 hours.

At lower levels of illumination, the recovery per unit time approaches the fatigue rate and the net loss in sensitivity is small. It is thus important to keep the photo-multiplier output as small as possible at the high radiation levels. In a reasonably good tube, the fatigue is considerably less than 5 percent at a current of 30 microamperes. It is good design to minimize the *PM* tube output and maximize the servo system sensitivity. For this reason, the anthracene crystals need not be large, or backed by a reflecting surface. Since the instrument is designed for approximately 30 microamperes of *PM* tube current at 100 r/hr., the minimum current is of the order of 3×10^{-10} ampere (or about one-third of the dark current of the tube). It is, therefore, desirable that tubes be selected for low absolute current.

In certain installations, there is the possibility of cooling the *PM* tube to reduce dark current, and at the same time maintain a constant temperature. This technique is not without possible drawbacks, however, since there is some evidence to indicate that fatigue effects are greatly increased at lower temperature.[10, 11] No data were obtained in this connection.

ACKNOWLEDGMENT

The authors wish to express their thanks to Dr. H. L. Anderson for suggesting the problem and for facilitating its completion. This work was supported by the Office of Naval Research under Contract N6ori-20, Task Order No. 22.

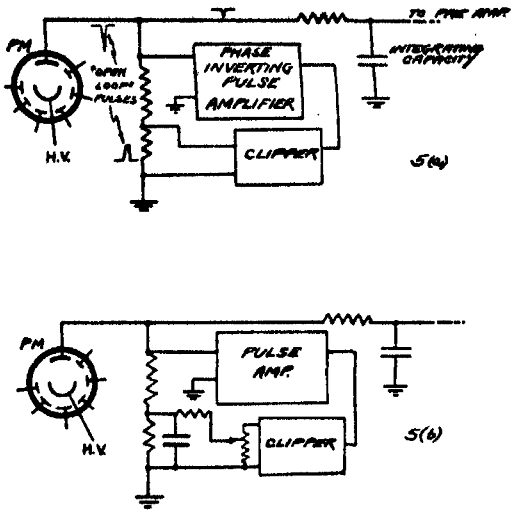

FIG. 5.

PARTS LIST

Resistors

R_1—110 K, 4 watt
R_2—10 M, 1 watt
R_3—47 K, 1 watt
R_4—1 M Pot.
R_5—1 M, ½ watt
R_6—1 M, ½ watt
R_7—2.7 M, ½ watt
R_8—2.7 M, ½ watt
R_9—10 K, 1 watt
R_{10}—1.5 M, ½ watt
R_{11}—3.3 K, ½ watt
R_{12}—1 M, 1 watt
R_{13}—100 K, 1 watt
R_{14}—0.47 M, 1 watt
R_{15}—.47 M, ½ watt
R_{16}—3.3 K, ½ watt
R_{17}—1 M, 1 watt
R_{18}—100 K, 1 watt
R_{19}—0.47 M, 1 watt
R_{20}—0.5 M Pot.
R_{21}—3.3 K, ½ watt
R_{22}—0.5 M, 1 watt
R_{23}—100 K, 1 watt
R_{24}—0.47 M, ½ watt
R_{25}—3.3 K, ½ watt
R_{26}—1 M, 1 watt
R_{27}—0.47 M, ½ watt
R_{28}—500 Ω, 2 watt
R_{29}—39 K, 1 watt
R_{30}—.33 M, ½ watt
R_{31}—50 K Pot.
R_{32}—1 Ω, 1 watt
R_{33}—10 Ω, 1 watt
R_{34}—100 Ω, 1 watt
R_{35}—1 K, 1 watt
R_{36}—10 K, 1 watt
R_{37}—1 M, 1 watt
R_{38}—2.2 K, 2 watt
R_{39}—1 K Pot.
R_{40}—1 K, ½ watt
R_{41}—1 K, ½ watt
R_{42}—33 K, ½ watt

Capacitors

C_1, C_2—0.5 mf, 2000 v
C_3—1 mf, 600 v
C_4—1 mf, 600 v
C_5—100 mf, 15 v, elect.
C_6—0.05 mf, 600 v
C_7—10 mf, 450 v, elect.
C_8—0.01 mf, 600 v
C_9—100 mf, 15 volt, elect.
C_{10}—0.05 mf, 600 v
C_{11}—10 mf, 450 v, elect.
C_{12}—0.01 mf, 600 v
C_{13}—0.0005 mf, 600 v mica
C_{14}—10 mf, 450 v elect.
C_{15}—0.01 mf, 600 v
C_{16}—0.005 mf, 600 v
C_{17}—0.01 mf, 600 v
C_{18}—50 mf, 25 v elect.
C_{19}—1.5 mf, 600 v
C_{20}—1 mf, 600 v
C_{21}—500 mmf, 600 v mica
C_{22}—2 mf, 600 v
C_{23}—20 mf, 450 v, elect.
C_{24}—20 mf, 450 v, elect.
C_{25}—250 mmf, 600 v mica

T_1—(Halldorson P-1930A) 1600 volts at 2 ma, 2 volts at 1.75 amps
T_2, T_3—700 v C. T. at 70 ma; 5 v at 3 amps, 6.3 v at 3 amps (Stancor P-4078)
L_1—15 h., 75 ma (Stancor C-1002)
E_1—1.5 volt flashlite battery
M—Servo motor (Brown 76750-1) 110 volt, 60 cycle, 6 in. oz torque, 160 r.p.m.

---

[10] See reference 2, p. 46.

[11] J. H. de Boer and M. C. Teves, "Sekundarer scheinungen, die auf den primaren photoelektrischen Effekt bei an Salzschichten adsorbierten Casiumatomen folgen," Zeits. f. Physik 74, 604 (1932).

THE REVIEW OF SCIENTIFIC INSTRUMENTS VOLUME 20, NUMBER 10 OCTOBER, 1949

Variable Temperature Dielectric Cell of Wide Frequency Range for Solids and Liquids*

EDWARD B. BAKER
The Dow Chemical Company, Midland, Michigan

(Received April 25, 1949)

A cell was developed with which power factor and dielectric constants of solids and liquids can be accurately and conveniently measured from −25°C to +150°C and 0 to 200 Mc. It uses 7 cc of liquid or a solid disk up to 1.5 in. in diameter and up to 150 mils thick. A rapid means of controlling temperature with a circulating oil stream is provided, with a view toward automatic recording *vs.* temperature at constant frequency. Thermal expansion of solids may be simultaneously recorded. Fringing errors for solids may be eliminated by using a sample of smaller diameter than the electrodes.

INTRODUCTION

THE dielectric cell to be described was designed with the primary purpose of measurement of dielectric constant and loss on a *single specimen* of a solid material, such as a plastic, over the range of frequency and temperature in which dispersion exists. Facility in changing temperature and frequency, ease of introduction of the sample, and high precision of measurement were given consideration. A simple attachment also permits precise measurement of liquids.

The cell was designed with the ultimate purpose of the automatic recording of dielectric properties as a function of temperature at constant frequency, since it is impractical to measure over a wide frequency range at constant temperature in a continuous manner. The design permits the sample to expand and contract thermally and the expansion coefficient may be measured or recorded automatically.

Audio- and radiofrequencies up to 200 Mc can be used in the temperature range −25°C to +150°C. In the audio range the cell is externally connected to a Schering bridge, whereas above ½ Mc one of a set of coils is placed in parallel with the electrodes to form a lumped constant resonant circuit which may be used to measure the dielectric properties by any of the usual methods. For the highest frequencies the cell converts to a re-entrant resonant cavity, capacitatively loaded by the sample, in the manner of Works *et al.*[1] Continuous frequency coverage is not provided although it could be done simply by connection of a parallel capacitance, or variation of sample thickness. Steps of two to three points per logarithmic decade are possible with the coils chosen, for a given sample thickness.

APPARATUS

A. The Cell Proper

As can be seen in Figs. 1 and 2 the cell consists principally of two 1½-in. diameter electrodes, one of which is fastened solidly to the framework and the other to a movable carriage. The electrodes (A) are Invar cups precisely flat and parallel, supported by bolting to quartz tubes, which in turn are clamped to the supports. Electrical connection is made to the cups by means of silver-plated stainless steel flexible bellows. The bellows (B) on the movable electrode, which is at ground potential and connected solidly to the outer cylindrical shield, allows a motion of about ¼ in. when the shield is clamped in place. The bellows (C) on the upper electrode permits switching from resonant cavity to the several coils in the upper chamber (D), or to external leads for audio measurements.

When the cavity is closed off at the top the supporting quartz tubes would not need to be insulators, but for the other switch positions, very good insulation is necessary. The quartz tubes also supply rigid support with low thermal loss, and this loss is further decreased in their design (E) (Fig. 1) by an evacuated jacket. Thermostated oil is circulated through the two electrodes in parallel flow and the oil also must be a fairly good insulator, since it necessarily passes through a region in which an electrical field exists. The connecting bellows are made as thin as possible to obtain high flexibility and low axial thermal conductivity. They are silver plated for minimum electrical losses at high frequencies.

The quartz tubes are accurately ground cylinders on their outer surfaces and the end surfaces to which the electrodes are bolted are square with the cylindrical surfaces. They are vacuum jacketed but not silvered, to reduce thermal loss. The quartz pieces are clamped to Invar "V-blocks" (F), which have the form of two parallel rods bolted at their ends to a plate. The clamps are thin Bakelite tubes having set screws which contact the V-block rods and distort the Bakelite tubes to press the quartz pieces against the V-block rods, establishing line-contact against the rods and quartz pieces. This method of clamping safely distributes stresses and results in low thermal contact, at the same time being precisely rigid.

Due to the low expansion coefficients of Invar and quartz a seal can be made between the electrode pieces and the quartz pieces by bolting, but a very thin (0.002 in.) gasket of Teflon and a spring take-up on the bolts as shown in Fig. 3 are still necessary to prevent leakage over the large temperature range used.

---

* Some of the material in this article was presented at the 17th Annual Meeting of the Conference on Electrical Insulation, National Research Council, October 27–29, 1948, and an abstract was printed in the Annual Report.

[1] Works Dakin, and Boggs., Proc. I.R.E. 33, No. 4, 245–254 (1945).

The frame, or bed, of the instrument consists of a large Invar tube (G) of 3-in. diameter and $\frac{1}{4}$-in. wall, made by drilling out a rod through all but the bottom end, and two $\frac{5}{8}$-in. solid Invar rods, all bolted to steel (chromium-plated) end plates. The large tube serves as the backbone of the frame and the smaller rods as the carriage ways. The carriage rides on five ball bearing wheels arranged "kinematically" to center on the right-hand rod and to guide in the plane of the other rod. A floating plate carrying a similar set of wheels, is attached by spring-backed bolts and holds the carriage against the ways.

The carriage is over-counterbalanced by about seven pounds by means of a single steel tape (H) passing over two ball-bearing pulleys and carrying a cylindrical lead weight (I) which moves inside the larger Invar tube. The counterweight is held from scraping the inside of the tube by six miniature ball-bearing wheels arranged symmetrically in its surface. The lead counterweight moves in air for most of its travel but in oil through the last inch. The end of the counterweight is tapered to prevent shock upon entry into the oil. It is totally immersed in the last $\frac{1}{4}$ in. of travel. The viscous resistance of the oil gives a dash pot action and prevents damage to the electrodes. They may be released at full separation without damage, although this is not good practice, of course.

The upper "head" plate (J) of the bed has a hole in the center through which the upper quartz electrode support passes and the upper V-block rods are bolted near the edge of this hole, overhanging it. On the bottom side of this plate the 6-in. diameter outer shielding cylinder (K), jointly the principal part of the cavity and the coil housing, is bolted by four screws (L) with sliding handles for easy removal. Both geometrical alignment and good electrical contact are assured by a ring knife edge at this point.

The lower two-thirds of this cylinder serves as the cavity wall, being separated by a partition from the upper one-third in the form of a silver-plated brass disk (M), $\frac{3}{8}$ in. thick, with a hole in the center to allow passage of the quartz supporting tube of the upper electrode. The cavity is closed off by a ring knife edge attached to the upper end of the electrode bellows and pressed against the edges of the hole in the partition plate with considerable force by means of a lever and spring mechanism (N). Upon releasing this spring it is possible, using a train of gears extending outside, to turn a contact arm and select one of seven coils mounted on the partition plate, or a banana plug receptacle for direct connection to a cable. Additional external coils can be plugged into the banana receptacle. Connection of the arm to polystyrene-insulated coil contacts which are small cup-shaped silver buttons is then firmly made by the same spring mechanism which closes the cavity. The cavity connection is made between any of the coil connections in which position the contact arm moves down between two of the coil contact stand-off insulators, stretching the bellows to a greater extent.

Coupling of the generator and receiver to the resonant circuit is made through two diametrically opposite

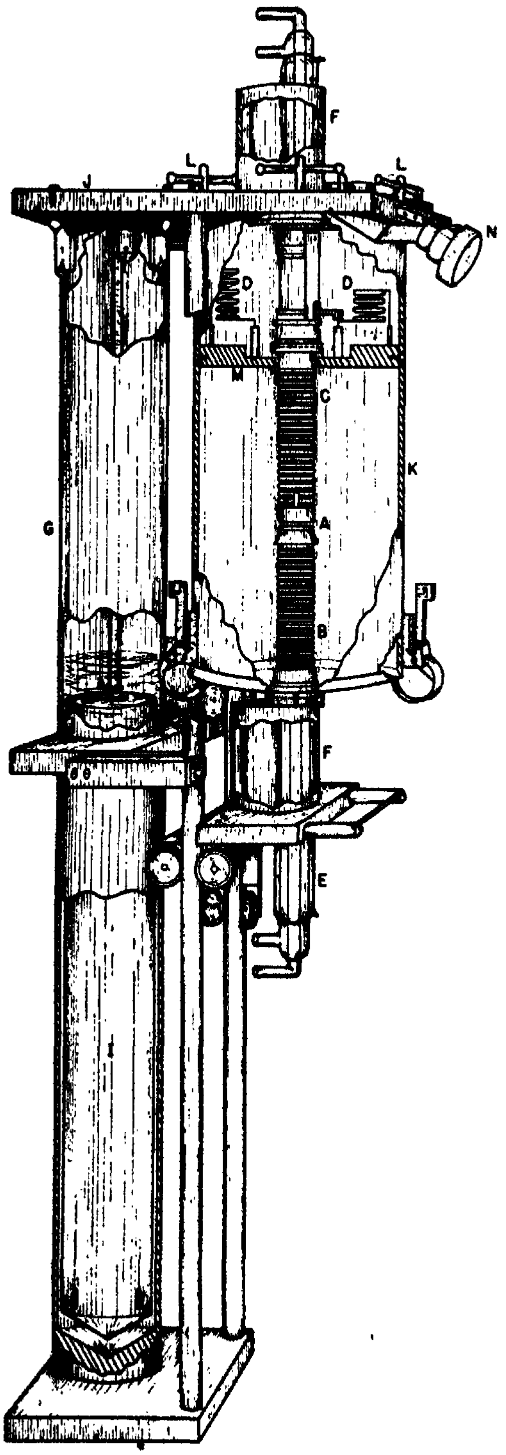

FIG. 1. Cut-away drawing showing electrode mounting, coils, and counterweight.

holes about halfway along the upper electrode. At this point either inductive loops or capacitative probes can couple to the simple cavity. The best arrangement proved to be a capacitative probe to the generator and a loop to the receiver, since by this means the next higher cavity mode is not strongly excited. This means of coupling is satisfactory with the first two coils also down to about 40 Mc. Below 40 Mc the output of the regenerative amplifier described by Towsley[3] is fed through the generator hole with a rod directly connected to the top electrode by a contacting spring mounted on the electrode. In this range a capacitative probe, with a small disk on the end is used for the detector coupling. There is no reason why a regenerative amplifier could not be made and connected thus in the case of the pure cavity, but the present model does not provide enough positive feed-back above 40 Mc to increase the Q appreciably. However, above 40 Mc the Q is already sufficiently high for accurate measurements without the amplifier. The regenerative amplifier has been used down to ½ Mc, with the detector probe coupled, even though the coupling decreases to a low value with the maximum probe capacity (about 3 $\mu\mu$f) available, due to the amplifier gain. Below ½ Mc bridge methods are used.

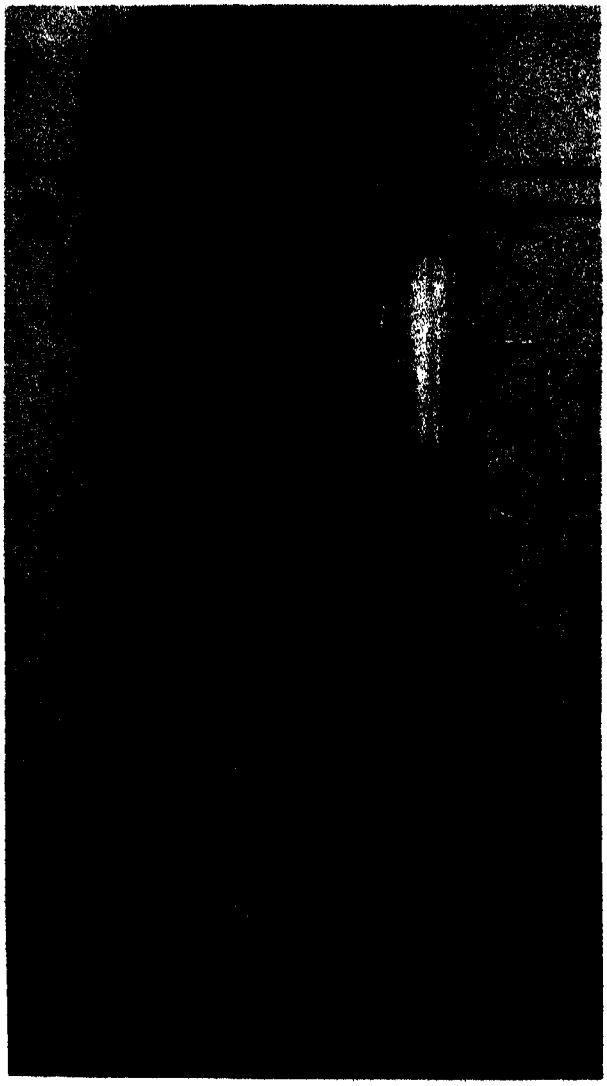

FIG. 2. Front view of complete unit.

When used at audiofrequencies the cell is connected through a cable to the audio bridge, and used as a simple condenser. The inductance correction, if this cable is short, is negligible up to ½ Mc, above which coils are used.

The bottom edge of the cavity cylinder is formed into a circular knife edge and the bottom end plate is held against this by four strong spring clips with snap lever action, so it may be unbuckled and lowered with the carriage to allow access to the interior. The bottom electrode is thus moved entirely clear of the cavity and solid sample disks can be placed upon it, or a quartz retaining ring for liquids, held by a ground joint on the electrode cap (Fig. 3).

The carriage may be clamped at any position by the lever clamp (Fig. 4) which is not fastened directly to the carriage but to the other end of a stainless steel bellows filled with mercury. By turning a micrometer screw plunger into the mercury well through a Teflon gasket the bellows is extended smoothly and accurately in 100:1 hydraulic ratio. Each 1/1000-in. micrometer division corresponds roughly to 10 microinches and may be read to 1 microinch. A Pratt and Whitney electric gauge of the variable reluctance type is also mounted on the carriage and reads the bellows deflection with about the same sensitivity as the micrometer. The electric gauge has a range of only 6/10 mil whereas the micrometer has a range of 10 mils. The electric gauge is used to read deflections produced by the sample; the micrometer is used to produce independent deflection, usually with only air or a liquid in the gap. The electric gauge, used with a recording meter thus will record thermal expansion of a solid sample in the gap.

One has the choice of allowing the gap to close on the solid sample and applying a compression equal to the counterweight overbalance, or clamping at a predetermined fixed distance.

The top plate of the mercury bellows, which carries the clamp, rests on three posts extending from the bottom plate when the bellows is not in use. A needle valve opens the bellows chamber to a small reservoir open to the atmosphere. If the valve is opened before clamping and the micrometer is backed off to the fullest extent and then the valve is closed, the full range of the micrometer is available, starting from the fixed position on the posts. One may adjust the electrical gauge to come on scale at this point.

The absolute separation of the electrodes is read on a Federal jewel-bearing dial gauge, smallest division

---

[3] F. E. Towsley, Annual Report, Conference on Elect. Insulation NRC (1948).

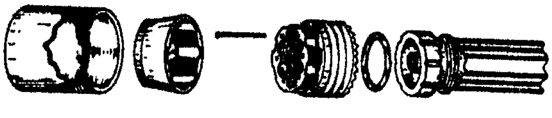

FIG. 3. Exploded view of lower electrode cap mounting, with quartz ring for liquids.

1/10,000 in. and ¼-in. stroke, which is supported from the large tube "backbone" and indicates against the end of an adjustable screw mounted on the carriage. This dial gauge is accurate to approximately one division and leaves something to be desired, but is the best direct indicating instrument available of sufficient range.

A dry atmosphere is provided inside the cavity by connecting a silica gel drying unit to it. A stream of dry air enters the cavity and flows out through a few small holes in the bellows on the upper electrode, passing between the quartz and the surrounding metal and thus prevents the accumulation of moisture and frost on the quartz at low temperatures, with consequent loss of insulating quality.

B. The Oil Circulating System

Several problems arose in the design of the oil circulation system due to the wide temperature range covered, particularly in selection of materials. The most severe of these is the choice of the heat transfer fluid itself which must remain sufficiently fluid over the range −25°C to +150°C, be below flash point at the upper limit, and also be a sufficiently good electrical insulator. The only substance meeting these requirements is one of the silicone fluids (DC 500 fluid, 10 centistokes viscosity) which have abnormally low viscosity temperature coefficients.

The circulation system, partially visible in Fig. 5, consists of an overflow reservoir, pump, cooling unit, electrical heaters, and the electrodes in parallel, in that order, the electrode discharge passing again to the reservoir. The control thermocouple is inserted inside the lower electrode with the leads carried inside the circulation tubes and out the reservoir. A differential thermocouple, for stabilization of temperature control, is inserted as close as possible to the main heater (No. 1) and the leads to it are brought out as tungsten seals, producing a pair of compensating junctions at the tungsten. The functions of the thermocouples will be described in connection with the temperature control circuit.

In order to maintain even approximately constant pumping speed for satisfactory temperature regulation, it is imperative to use a constant displacement pump. Satisfactory performance was attained with a Viking model BFH (Viking Pump Company, Cedar Falls, Iowa) geared down 7:1 from a 1/10 hp 1800 r.p.m. motor, resulting in a flow of ½ g.p.m. Due to the large radiating surface on this pump it is necessary to insulate it with asbestos paste, and even then it is a heavy load on the cooling system.

Heat is supplied to the oil by coil-coil filaments directly immersed in it. One such heater is on the control amplifier output for fast control and the other on a Variac for slow base heating at high temperature.

The base cooling necessary at low temperature operation is furnished by a heat exchanger made from spiralfin tubing by enclosure in a copper foil jacket. A Dewar containing a mixture of dry ice and DC 500 silicone oil of 2 c.k.s. viscosity is raised and lowered on a motor driven elevator. The background heating and cooling are automatically adjusted as will be described at a later point.

The overflow reservoir permits expansion of the oil and effects separation from entrained air. It is vacuum insulated, as are some of the connecting lines, to minimize thermal loss.

The flexible hose connections to the cell were made with DC X6167 silastic tubing slipped inside of large-size thin-walled rubber tubing for mechanical reinforcement. Even though swelled 50 percent by the oil, this silastic retains sufficient mechanical strength to be used if reinforced by the rubber cover. All other kinds of rubber furnish oil soluble contaminants. Teflon is not sufficiently flexible. Red rubber tubing, for example, did not swell much but gave up sulfur to the oil. This did not cause excessive power factor but catalyzed polymerization of the silicone fluid, and eventually even the cross-linked sulfur was removed resulting in destruction of the rubber; the dissolved sulfur attacks most metals in the system.

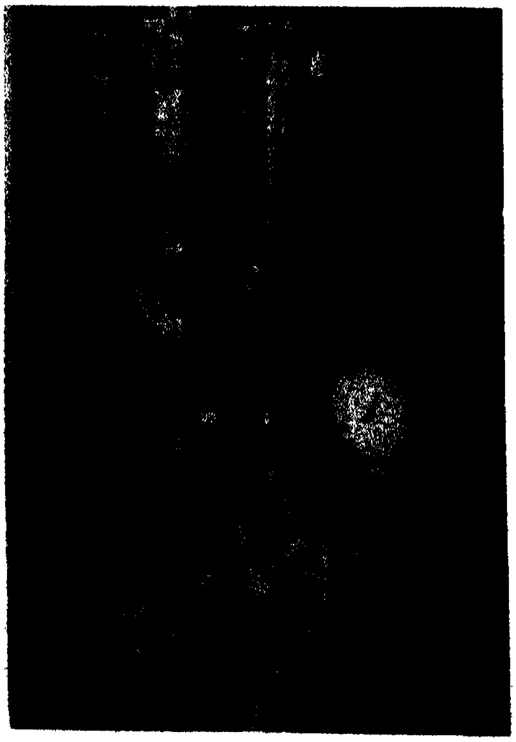

FIG. 4. Photograph of cell with cavity removed, showing carriage mechanism, electrodes, coil switch, and quartz ring for liquids.

C. Temperature Control System

1. General Design

The temperature control system is shown schematically in the block diagram Fig. 6. The control thermocouple, located inside the ground potential electrode, is opposed by the cold junction, a differential thermocouple for stabilization, and the set point potentiometer to give the error signal which is converted to 60 cycles, amplified, synchronously rectified and used to control the power stage thyratrons supplying the main control heater (No. 1). For additional stabilization a low pass filter is inserted.

Background cooling and heating are provided by an auxiliary control system tending to maintain constant current in heater No. 1 by driving either the cooling elevator or the Variac supplying heater No. 2. The error signal is derived by rectifying and bucking out a sample of the thyratron current.

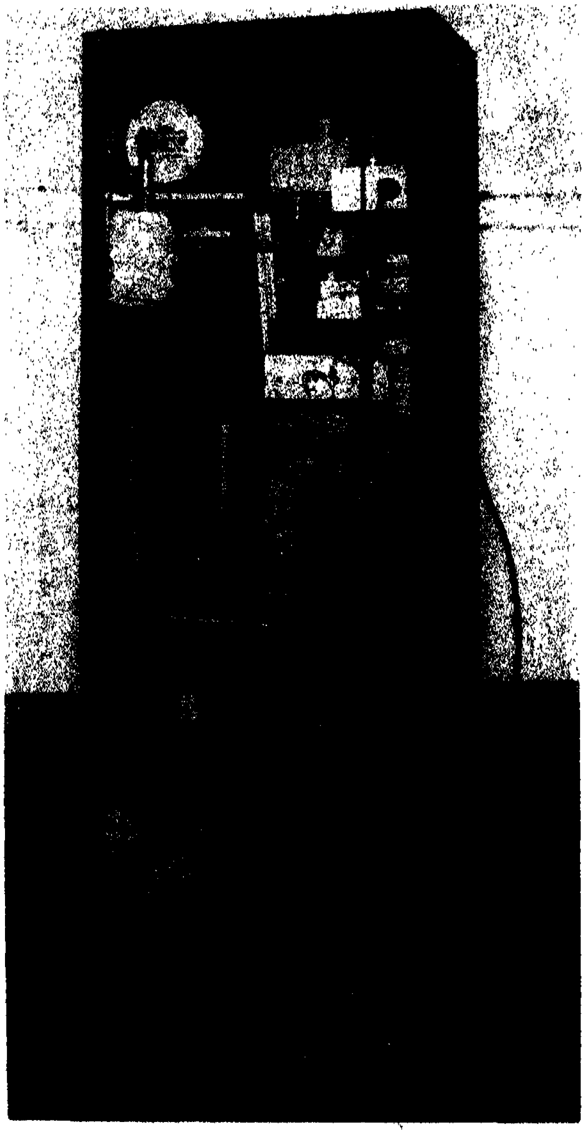

FIG. 5. Back view of unit showing amplifiers and circulation system.

The main control system thus gives fine regulation and corrects fast perturbations whereas the auxiliary system narrows the operating range necessary for the main control and makes it possible to go to low temperatures.

2. Thermocouples and Set Point Potentiometer

Copper-constantan thermocouples are used, the cold junction being kept in a bath of dry ice and DC 500 2 centistokes silicone oil, which attains a constant temperature of −78.1°C. The great advantage of this cold junction bath, which is quite dependable, over an ice bath is that its temperature is outside of the operating range (−25°C to +150°C) and therefore the cell and cold junction thermocouples together produce a voltage of only one sign. This simplifies the design of the potentiometer considerably.

The differential thermocouple, with one junction thermally lagged, provides one of the two means used to slow the amplifier response and eliminate hunting.

The potentiometer circuit (Fig. 7) is quite conventional, being provided with standard cell, switch, and rheostat for calibration, except that with the stepping relay circuit shown in Fig. 8 it is possible either to change the temperature setting continuously or stepwise and to do this either by hand or by motor drive.

For most dielectric measurements discrete steps of roughly five degrees are sufficiently close and a rapid selection of fixed steps is advantageous. When automatically sweeping the temperature, discrete steps allow complete thermal equilibrium at each step. On the other hand, continuous control allows selection of temperatures intermediate to the fixed points, and continuous sweep gives more legible charts in automatic recording.

The automatic operation of the stepping relays (Fig. 8) is accomplished by motor driving the slide wire. As each revolution is completed a limit switch actuates one of the stepping relays, advancing the potentiometer arm to the next fixed step. One stepping switch is for ascending temperatures, the other for descending, selection being made according to the rotational sense of the motor.

Upper and lower limit switches on the potentiometer reverse the sense of the motor, and their positions on the temperature scale are adjustable by two extra arms on the dial. It is thus possible, in automatic operation, to cycle the temperature between two of the fixed points, over the range of interest for the material being measured.

Due to the thermocouple response characteristic the temperature scale is non-linear, being linear in voltage. Each step corresponds exactly to 0.2 mv and roughly to 5°C. It would complicate design considerably to make the temperature scale linear.

As may be seen from Fig. 7 the control amplifier is

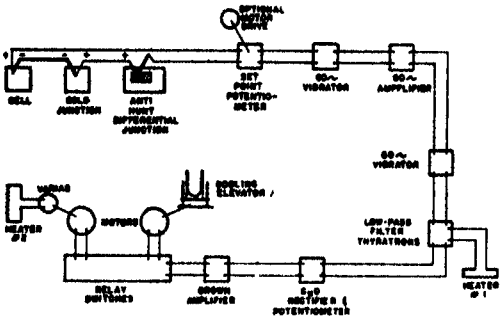

FIG. 6. Block diagram of temperature control system.

also used as a galvanometer in calibration against the standard cell.

3. *Amplifier and Thyratrons*

Voltage amplification of the thermocouple error signal is similar in principle to a Brown[3] amplifier, but to obtain higher gain and freedom from hum the system indicated in Fig. 6 was employed. Brown vibrators are used for input conversion to 60 cycles and for output synchronous rectification. Initial impedance matching is made with a Brown input transformer and the 60 c.p.s. voltage is amplified with a narrow band amplifier of three separate stages, each stage being shielded from the others and having an individual Wien bridge feed-back circuit, thus avoiding regeneration due to phase shift.

A 6K6 power stage and isolation transformer follow to supply the synchronous rectifier. Isolation is necessary because the thyratrons are supplied from 220 volts with grounded neutral and the transformer secondary center-tap must be 110 v a.c. from ground.

Operation of the control thyratron continuously over most of the cycle by the filtered d.c. output of the vibrator is accomplished by superposition on the d.c. signal of a wave form of the kind shown in Fig. 9 produced by distorting the output of the 6H6 half-wave rectifier with an inductance. As this wave form is raised and lowered by the d.c., firing of the thyratron takes place in different portions of the cycle. This thyratron has relatively low power capacity but extreme grid stability and is used to drive the two power thyratrons in parallel by pulsing its output through a transformer and applying the pulse to their grids. The output of the power thyratrons thus varies continuously with the error signal when the latter calls for heat but remains at zero for an error signal of the opposite sense, when heat losses in the system supply the cooling.

It is desirable to have the rate of heating available roughly equal to the rate of cooling as governed by the heat losses, and this symmetry of operation is aided by the auxiliary heating and cooling system.

4. *Auxiliary Control*

Since the thyratron plate current is pulsating d.c., a sample of 60 c.p.s. voltage may be obtained from it and at the same time be isolated by passing it through a small low impedance transformer. This a.c. signal is proportional to the thyratron current and if rectified by a small copper oxide rectifier and bucked out with a potentiometer serves as an error signal for the secondary control system. Amplification through a conventional Brown amplifier provides current to drive either the auxiliary cooler or heater motor. A system of limit switches and relays, shown in Fig. 10, are necessary to pass from heating to cooling automatically according to demand by switching to one motor or the other. Limit switches are also necessary at the maximum position of the heater Variac and at the point of maximum cooling.

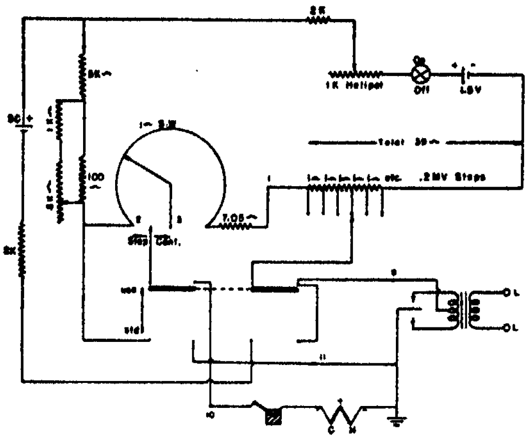

FIG. 7. Potentiometer circuit.

The auxiliary system tends to maintain constant current in the output thyratrons by supplying or removing heat at the correct rate to keep the error signal zero. This system is geared down to operate slowly (approximately 3 minutes from full heating to full cooling) to

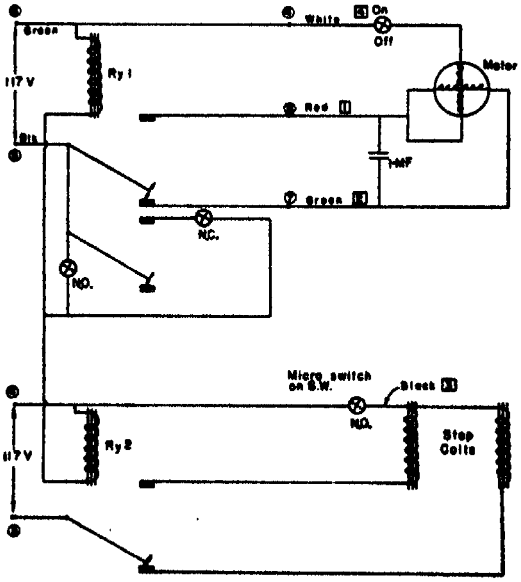

FIG. 8. Stepping relay circuit. N.O. and N.C. = limit switches on stepping relay shaft. ☐ = numbers on slidewire chassis terminal board. ○ = numbers on potentiometer chassis terminal board.

---

[3] The Brown Instrument Company, Philadelphia, Pennsylvania.

avoid hunting in conjunction with the main heater, and thus presents no hunting problem by itself because the gain is low and time lags are small. The electrical gain control on the Brown amplifier may be varied to obtain optimum performance.

Stabilization is obtained with the differential thermocouple, one junction lagged, as shown in Fig. 6, plus the low pass filter shown in Fig. 6 and Fig. 9. With this stabilization it is possible to use the full gain of 1.2×10^6 from thermocouple to heater, and the resulting recovery time for a relatively small disturbance is of the order of 4 or 5 seconds. A change in set point of 5 degrees requires about 45 to 60 seconds for equilibrium, which is determined primarily by the total power output available on rising temperature and the system losses with falling temperature. For larger changes the time to equilibrium is roughly proportional to the change, at the rate of 5 degrees per minute. The maximum sweep rate either continuous or step-wise is thus about ½ hr. for the full range −25°C to +150° and this is about the same whether one large change in set point or a number of small ones are made. For large changes there is considerable overshoot of the auxiliary system, which is desirable for rapid response.

D. Remarks on Methods of Measurement of Dielectric Constant

The dielectric constant is effectively the ratio of the capacity of a given condenser filled with the dielectric to its capacity empty. One method for its measurement is a direct determination of these capacities by comparison with a calibrated variable condenser. There is always a "lead" correction to be made since it is impossible to fill all of the space in the condenser with dielectric; even though one electrode almost surrounds the other it is necessary to bring out a lead from the inner electrode. Then the capacity C of the condenser with dielectric in it is no longer proportional to the empty capacity C_0, but

$$C=\epsilon C_0+C_L,$$

where ϵ is the dielectric constant and C_L is the lead capacity, the part of the condenser which cannot be filled with dielectric.

If the electrodes can be moved relative to each other, $\Delta C=\epsilon\Delta C_0$, and by measurement at two positions, ϵ may be determined independently of C_L. This is possible with liquids, but not with solids. It is also possible to determine C_L by measurement with a standard liquid of known dielectric constant.

If the electrodes are flat and parallel, of equal area A and separation d, the capacity is

$$C=K\frac{A}{d};\quad K=0.225\ \mu\mu\text{f/in.}$$

This formula is approximate, since it assumes the electrical field exists only between the plates and is uniform therein. The form of the correction to be applied depends upon the geometry external to this region. Kirchoff[4] has given a theoretical formula which applies

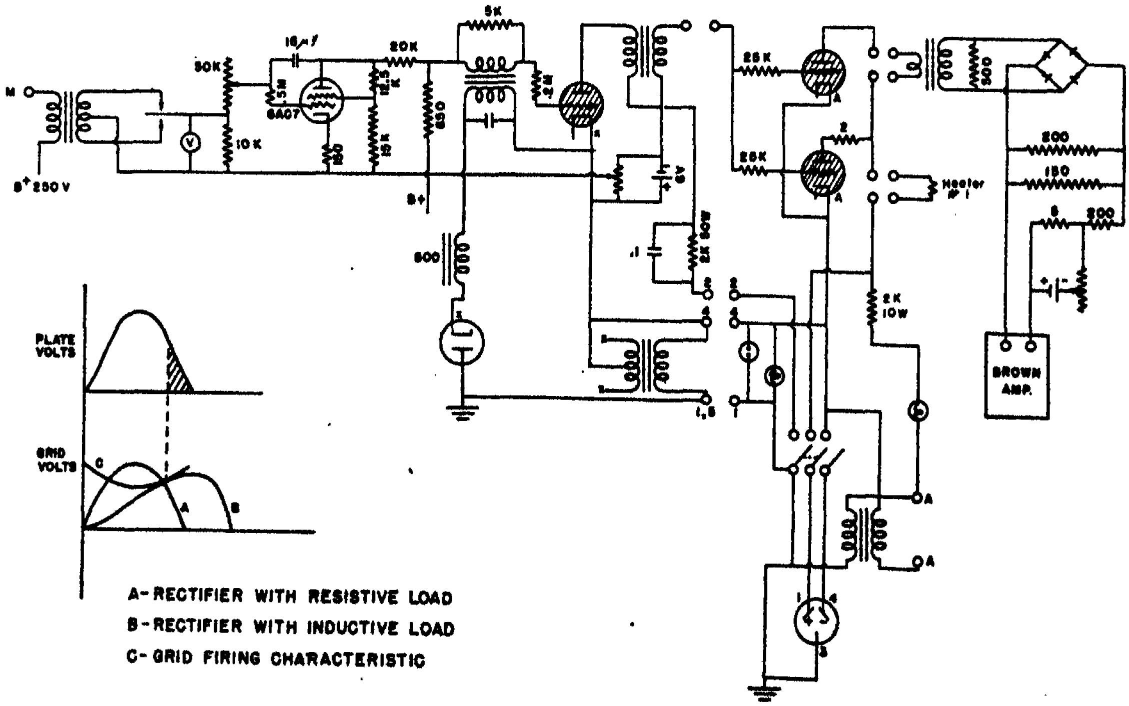

FIG. 9. Power amplifier, with filter and secondary control circuit take-off.

---

[4] See, L. Hartsborn, *Radio-frequency Measurements by Bridge and Resonance Methods* (John Wiley and Sons, Inc., New York, 1941), p. 104, for a discussion of edge effect.

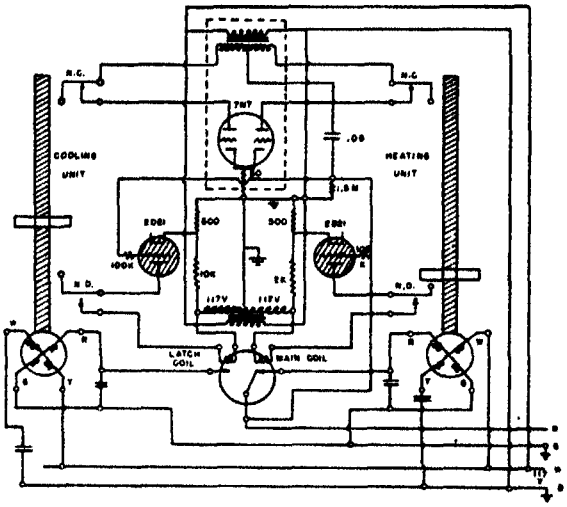

FIG. 10. Auxiliary heater and cooler switching circuit.

to completely isolated electrodes in a vacuum. For the electrode arrangement used here the air capacity was found to have the form

$$C_a = K\frac{A+\alpha}{d} - \beta e^{-\gamma d} + \delta,$$

where α, β, γ, and δ are adjustable constants. At large distances ($\frac{1}{16}$ in.) the exponential term is negligible and α can be determined by varying d. Then β and γ are determined by plotting $C_a - K(A+\alpha/d)$ against d on log paper. The additive constant can be found by measuring benzene at variable distance and adjusting for self-consistency. Since there is some field penetration through the quartz ring a small correction involving a linear term in d is necessary, as well as a small term to take account of the column of liquid outside the gap, also linear in d. Absolute measurement of the dielectric constant of benzene measured in this way is consistent to ±0.0005 from 20 to 120 mils and agrees well with the value listed in I.C.T. The purpose of the formula is simply for interpolation at values of d between those used in the air calibration. In order to obtain the accuracy given above, gauge blocks were used to obtain known displacements of the electrodes, inserted between a stop on the guiding rod and one on the carriage. By moving the gauge blocks in an oscillatory manner between the stops it was found possible to repeat absolute gap distances to $\pm 5\ \mu$ in. as determined by repetition of bridge balance.

In the case of solid samples, the use of a disk of somewhat smaller diameter than the electrodes serves one of the purposes of a guard ring, namely, elimination of errors due to fringing of the field, but of course does not perform the other function of by-passing surface currents. The use of this "phantom guard ring" does not seem to have been reported before, and should increase accuracy of measurement, particularly at high frequencies, where the ordinary real guard ring becomes impractical.[4] An accurate knowledge of the disk diameter is essential and account must be taken of its change with temperature. For an isotropic and not-too-elastic material the necessary information for this correction is obtained simultaneously by the thickness variation under constant load.

One disadvantage of this cell is the large correction which must be determined and applied due to the expansion of the quartz supporting rods. It was hoped that the vacuum jacket construction would reduce this, since the outer wall is larger, heavier, and more nearly at room temperature, but it did not. Provision of a quartz bellows section on the inner tube would seem desirable. Due to the length of the tubes (a total of 15 inches) this correction amounts to about 1.5 mils at 150°C which is a large fraction of sample thickness (70 to 100 mils). However, it is quite reproducible and easily determined.

The accuracy of measurement of solid samples is dependent directly upon distance measurement, which in turn depends upon accuracy of dimensioning of the sample. For this purpose the Schiefer abrasion testing machine,[5] developed by H. F. Schiefer of the National Bureau of Standards, was adapted to grind the disks flat. With this machine it is easily possible to grind the sides flat and parallel to less than one-tenth mil and with a sufficiently sensitive limit switch, such as an electric gauge, they can be ground conveniently to within one-tenth mil of final dimension. If such accuracy of dimensioning is achieved it is not necessary to use tinfoil or silver paint on the sample but simply a thin film of silicone oil (DC 200, 200 c.k.s.) which is not too heavy to flow easily under the electrode pressure used.

The author would like to express appreciation of the aid of Mr. L. W. Burd, who helped with the design and built much of the equipment, and of the personnel of the laboratory shops, who built the remainder.

---

[5] H. F. Schiefer, Textile Research J. 17, No. 7, 360–368 (1947). The machine is made by S. W. Frazier, 953 15th Street, S. E., Washington, D.C.

THE REVIEW OF SCIENTIFIC INSTRUMENTS VOLUME 20, NUMBER 10 OCTOBER, 1949

An Automatic Scanning and Recording Photometer for Night Sky Studies*

Douglas Marlow and J. C. Pemberton
Pasadena Annex, U. S. Naval Ordnance Test Station, Pasadena, California

(Received May 3, 1949)

This paper describes a photoelectric photometer which scans the entire sky in 32 minutes, recording the light energy in a 100A band as a function of altitude and azimuth. The light is chopped by a rotating shutter and detected by a photo-multiplier tube, the output from which is amplified and synchronously rectified to produce a d.c. signal for the graphic recorder. Three different types of automatic scanning are provided, as well as a manual control of the various functions. The minimum energy which may be reliably recorded, using a 4-inch, $f{:}1$ lens, is of the order of 10^{-13} watt.

INTRODUCTION

Studies of the light of the night sky have occupied the attention of astronomers and physicists for many years, not only because the subject is of intrinsic interest, but also because of the potential knowledge to be gained about the upper levels of the earth's atmosphere, where a large fraction of the light is known to originate.

Extensive spectrographic research has shown that the spectrum of the atmospheric component of the night sky within the sensitivity range of the 1P21 photo-multiplier tube includes: 1. A few relatively strong atomic lines (5577A [OI], 6300A [OI], and 5893A NaI) 2. Numerous bands of O_2 and N_2, and 3. A general background of continuous radiation which may be unresolved bands.

Although spectroscopy suffices to establish the general character of the radiation, it is not capable of following rapid changes because of the necessarily long exposure time. This limitation led to the early development of photoelectric photometers which provided a tremendous gain in speed with, unfortunately, a loss of spectral resolution. (Those versed in circuit theory will recognize the analogy with the transmission rate—band-width relation.) Improved photo-cells and circuit techniques have made it possible, in the instrument described in this paper, to record the energy in a 100A band in a time of the order of 1 sec.

The program of night sky investigation at NOTS was initiated utilizing two photometers donated by C. T. Elvey, used by him for studies in the 7500A region.[1] These were soon followed by improved versions but, even so, it was apparent that the extensive program could not be completed in the desired time unless a faster, more stable instrument were made available. Without listing the specific defects of these early instruments, it is sufficient to say that a scan from horizon to zenith required 30 to 40 min., whereas it was desired to scan the *entire sky* in this time.

DESIGN CONSIDERATIONS

A study of the requirements of the research program led to a number of design features which are novel in sky photometry.

The most important of these is the completely automatic recording of luminous energy as a function of altitude and azimuth. Since the design of the amplifier depended to a great extent on the recorder, first consideration was given to a choice of this unit. Because of its ruggedness, simplicity, and freedom from additional power-source requirements, the Esterline-Angus recording milliammeter was chosen.

Because zero shift was the most exasperating fault of earlier photometers, the present instrument is designed to use a.c. amplification and to have the further important property of discrimination between dark current and signal. The latter requirement could obviously not be met by any system which converted the d.c. output of the photo-cell into a.c., since, in such a system, the signal and dark currents are indistinguishable. This leaves only the possibility of chopping the light, an expedient which was, therefore, adopted.

The speed of the system has been improved so that it is possible to scan a hemisphere in 32 min., approximately the shortest time permitted by the recorder time constant (0.5 sec.) which also establishes the minimum chopping rate at perhaps five per second, if use is to be made of the time resolution possessed by the recorder. Faithful response to such frequencies indicates the choice of a photo-multiplier rather than a gas tube, such as had been used originally. Although gas tubes are now available which have a better signal-noise ratio than the 1P21 photo-multiplier,[2] their output is so low that a large anode load resistor (about 10^{12} ohms) must be used in order to obtain a usable signal at the amplifier terminals. The high value of load resistor combined with that of the stray capacities leads to a time constant of the order of 10 sec., which would reduce the response to the chopping frequency essentially to zero. In principle, the time constant can be reduced to any desired amount by negative feedback, but the necessary reduction was so large in this case (frequencies as high as 300 cycles must be passed, for reasons which will appear) that this was not a practical solution.

---

* This paper is based on work performed under ONR Project NR-082-045.

[1] C. T. Elvey, "Observations of the light of the night sky with a photoelectric photometer," Astrophys. J. 97, 65 (1943).

[2] The CE 70 and CE 71 developed by Continental Electric Company following suggestions of G. Kron of Lick Observatory.

Automatic calibration is provided by a solenoid-actuated focal-plane shutter coated with non-phosphorescent radium paint. The shutter is pulled in front of the photo-cell once every four minutes, each time the optical axis returns to the horizon.

Since the batteries used in the older photometers were always a source of annoyance, they have been eliminated by a suitably designed power supply. In order to insure absolute freedom from power frequency interference, synchronous rectification is used in the amplifier output, a feature which will be more fully discussed in a later paragraph.

The scanning motions can be carried out in the following four different ways:

1. *Full scanning:* In this type of operation the photometer starts at the North horizon, sweeps up to the zenith, down to the South horizon, and stops. The base is then turned automatically through 22½ deg. so that the lens is pointing SSW; the photo-cell is calibrated and a new sweep started, from SSW to NNE. The scanning proceeds in this manner until the end of the sweep from NNW to SSE, when the base automatically reverses to North and a new cycle begins. The reversing period is marked on the Esterline-Angus recorder by the left-hand chronograph pen so that the observer, sitting at some distance from the photometer, knows when each cycle starts. The base is reversed instead of being allowed to turn continually in one direction, in order to avoid the use of slip rings to feed the numerous circuits on the rotating member.
2. *Vertical-circle scanning:* This motion is carried out with the azimuth fixed, so that the photometer scans along a vertical circle from horizon to horizon, calibrating at the end of each sweep, as in 1.
3. *Monitoring:* The lens is pointed at a fixed altitude and azimuth and records luminous energy *vs.* time; calibration occurs every 4 min.
4. *Manual control:* All operations of the instrument are under control of the observer by means of switches.

CONSTRUCTION

The construction of the photometer is shown in Figs. 1 and 2. It will be seen to consist of three basic assemblies: a deep base box or compartment, an azimuth plate and fork assembly, and the scanning head.

The base compartment contains the various control relays, switches for manual control, a selector switch, a copper-oxide rectifier for supplying d.c. to the shutter actuators, and the azimuth motor (a Barber-Colman shaded-pole reversible). Three ball-bearing rollers support the azimuth plate, which is restricted to rotation about a vertical axis by a shaft located on its center line. Concentric with this shaft is the azimuth drive gear meshing with the azimuth motor pinion. Vertical supports fastened to the azimuth plate form a fork and carry the ball bearings in which the trunnions of the scanning head turn. Power for rotation in altitude is delivered through a gear train by a Bodine synchronous motor mounted on the side of one of the vertical supports.

The foundation of the scanning head is an aluminum-alloy casting with integrally cast trunnions and lens barrel. All components of the photometer proper are mounted on the casting with the exception of the chopper motor, which is fastened to the cover. By designing the amplifier for miniature tubes it has been possible to mount it on the scanning head in close proximity to the photo-cell, eliminating low-level, high-impedance leads. The cables consist, therefore, of power, control and recorder-output circuits only, insuring freedom from hum and other external interference.

The lens is a specially designed, spherically corrected doublet of 4-in. aperture and 4-in. focal length, mounted in a sleeve which can be screwed in or out along the lens barrel for focusing. Filter holders, not shown, may be slipped over the lens sleeve, in front of the lens, or may be placed inside the barrel just in front of the shutter-actuating solenoids. Inside the lens barrel, on the front surface of the casting, are mounted two Leland rotary solenoids which carry the master and calibrating shutters. Behind the back surface of the casting are located, in order, the chopper shutter, a two by ten degree focal-plane aperture to define the field of view, and the photo-multiplier tube. A commutator is rigidly fastened to the back end of the chopper shaft to provide synchronous rectification of the amplifier output signal. Power for the shaft is delivered through a flexible separable coupling from a Bodine synchronous motor mounted on the cover (a standard *J* box).

In order to prevent transmission of heat into the interior of the cover from the chopper motor, the latter is mounted on phenolic studs. Active cooling is provided by a blower impeller which sucks cold air through a

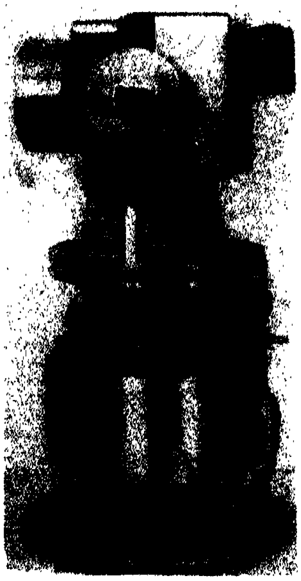

FIG. 1.

light-tight duct open to the atmosphere and through a port concentric with the shaft, expelling it in the space between cover and motor. Temperature considerations likewise dictated the placement of the vacuum tubes on the outside of the case, as shown in Fig. 1. The sockets are mounted on phenolic rings ½-in. high, so designed that no metallic connection other than the wiring exists between the socket and the aluminum casting.

All resistances and condensers for the amplifier are mounted on terminal boards or clamps fastened to the back side of the aluminum casting (Fig. 2), so that when the cover is removed the unit lacks only the chopper-commutator drive to make it complete. The leads for the chopper motor run in a shield along the inner surface of the cover to one half of a separable plug, the mating part of which is fastened to the casting (directly to the right of the altitude motor, Fig. 2), making it very easy to remove the cover for inspection or repairs. The sensitivity switch is remote-operated from the observer's position by a synchro drive, hidden in Figs. 1 and 2. A simple sighting tube is mounted on one trunnion to assist in aiming the lens at a definite point in the sky (e.g., Polaris) when it is desired to monitor.

AMPLIFIER

The amplifier, Fig. 3, is a two-stage, negative-feedback circuit of high stability and linearity.

Direct coupling is employed between the photo-cell anode and the first grid, and in the feed-back path from the second cathode to the input circuit, thus reducing the number of time constants in the loop to one (second grid circuit) and making oscillation impossible. The first-stage heater is operated at reduced voltage in order to eliminate grid current which would upset the bias for high values of the load resistor R_1, and also in order to increase the gain available from the tube. By this artifice, a gain of 600–700 has been achieved from the first grid to the second grid. Because of the direct coupling, it is necessary that the second cathode be at essentially zero d.c. potential, if the first-stage bias is to be maintained; for this reason it is returned to a negative voltage. Small errors in establishing this voltage are of no consequence since the first stage uses cathode self-bias. This is also true of the photo-cell dark current, provided it is small. Loading of the first stage by the input impedance of the second has been overcome by returning the second grid resistor to the cathode circuit, making its apparent resistance approximately 150 megohms.

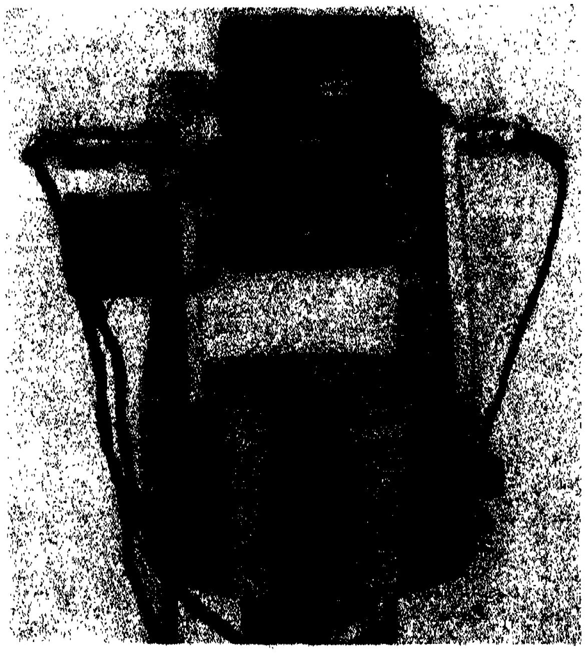

FIG. 2.

The over-all current gain of the amplifier, defined as feed-back current in 20-ohm resistor R_2 divided by photo-current in R_1, is given by

$$G_i = R_1/R_2.$$

Since the recorder resistance is only 1500 ohms as compared to 15,000 ohms for the plate load resistor of stage two, essentially all of the feed-back current passes through the recorder, and G_i, therefore, is also the gain from the photo-cell anode to the recorder movement. The sensitivity is controlled by switching R_1 by a nominal factor of 2 for each step, so that, there being nine positions, the highest sensitivity is 2^8 or 256 times greater than the lowest. The highest value of G_i is about 1.3×10^5, which, combined with the gain of 5×10^6 achieved in some 1P21's, gives an over-all amplification of the photo-cathode current of 6.5×10^{11}. Experience in the field has shown that, because of noise, this is about as high as one can go with the required time resolution and without resorting to refrigeration of the photo-tube. Most of the records to date have been made with a G_i of approximately 10^4, and only on rare occasions has there been need for the maximum value.

The chopper was originally designed to produce a sinusoidal modulation of the light, as this seemed to be the easiest type of signal to amplify and required the least band width, but excessive pen vibration caused by the ripple component of the rectifier output demanded a modification of the wave form. The chopper was changed, therefore, to give a nearly square wave form for which the average rectified d.c. is almost equal to the peak value and the ripple correspondingly low. This change necessitated a greater band width in the amplifier, at least 300 c.p.s. according to the well known rule-of-thumb that the highest frequency required is ten times the fundamental (30 c.p.s. in this case) for good reproduction of square waves. Since the amplifier had appreciable response even at 10 kc this presented no difficulty and there remained only the question of the effect of stray capacity in the input circuit. Because of the feed-back, the stray capacity is effectively reduced to a negligible amount.

The commutator shown in Fig. 3 is schematic only.

If constructed as shown, it would have a frequency twice that of the chopper, which admits light for one half revolution of the shaft and blocks it for the second half. Actually, all four brushes are disposed along the commutator in the same axial plane and the segments are cut as shown in the development of Fig. 4.

The $\frac{1}{2}$-μf condenser across the recorder terminals is largely of psychological value in checking operations, since the high frequency brush noise does not affect the recorder but does make the interpretation of oscilloscope patterns difficult.

The chopping frequency of 30 c.p.s. was chosen in order to eliminate any possibility of interference from 60-cycle power lines. If one assumes an input wave of any form whatever, of fundamental frequency f_0, and operates upon it with a square-wave switching function of the same frequency suitably phased, analysis will show that the output will contain d.c. and all *odd* harmonics of f_0. Therefore, if an expected interfering frequency is any *even* harmonic of f_0, it will not be registered by the recorder. By choosing $f_0=30$ c.p.s., one makes the power frequency and all its harmonics even harmonics of the chopping frequency and hence of no importance unless the interference is so strong as to cause overloading ahead of the rectifier. It is still true, however, that excessive 60-cycle interference will cause needle vibration, and for this reason every effort has been made to keep the residual hum level as low as possible.

The power supply circuit is not shown as it is quite conventional. All amplifier voltages are stabilized by gas regulator tubes and the -1000 v for the photo-cell by a degenerative vacuum tube regulator. The heater winding of the power transformer is not directly grounded, but is connected across a 100-ohm potentiometer, the arm of which is connected to the chassis. By proper adjustment of the latter, the hum level at the recorder terminals with the commutator stopped can be reduced to 2 or 3 millivolts.

CONTROL CIRCUIT

The various mechanical motions required of the instrument are controlled by cam-operated switches driven by the recorder motor, in conjunction with limit switches on the azimuth and altitude axes and several control relays mounted in the photometer base.

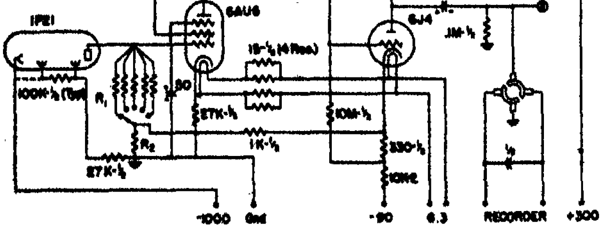

Fig. 3.

Fig. 4.

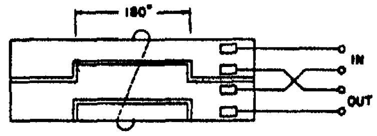

The various scanning motions described under Design Considerations are chosen by a selector switch mounted on the side of the base compartment (knob, Fig. 2). The 3-position toggle switch (Fig. 2) allows the operator to change the altitude independently of the control circuit when the selector switch is in the "monitor" or "manual" position. The push buttons allow manual operation of the master and calibrating shutters in the fourth, or "manual" position of the selector switch.

Since the recorder and altitude motors are both synchronous, there is a one-to-one correspondence between the elevation of the photometer and the angular position of the recorder camshaft, making it possible to synchronize the operation of the calibrating shutter with that of the main shutter even though the latter is controlled by the altitude motor and the former by the recorder motor. Although the altitude motor stops itself by opening its limit switches, it cannot start again until ordered to do so by the recorder motor, so that synchronism between the shutters and the altitude motion of the photometer is always assured.

A temporary loss of synchronism between the altitude and azimuth motions can occur if the instrument is started in an arbitrary configuration, but in the worst case this will mean only that the first two altitude sweeps will be on the same azimuth, after which all the motions will interlock properly. By observing the position of the camshaft and the direction of the azimuth plate, an operator soon learns to start up with no lost motion.

Because of the synchronous drives, a given arc in altitude is always represented by the same length of chart (13.5 in. per 180 deg.), which makes the reading of the records quite easy. When operated from a commercial power line, the length of a record is also an accurate measure of elapsed time (3.2 min. per 13.5 in.) but usually in field work a portable generator is used and time is marked on the record by means of a second chronograph pen controlled through electrical contacts by a spring-driven clock.

Although the control circuitry is complex, it is sufficiently straightofrward that a detailed circuit diagram and explanation are not deemed essential in a paper of this length.

PERFORMANCE

Since August 1948 the automatic photometer has been in operation every clear night during the dark-moon period, that is, about 4 days out of every 28, and has proved to be so productive that new methods of

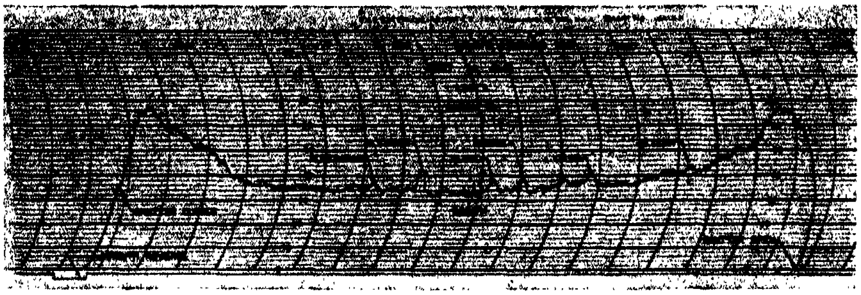

FIG. 5.

analysis have had to be devised to keep up with the flood of data.

Most of the work has been done in three 100A bands, isolated by interference filters chosen to center as nearly as possible on wave-lengths 6300 [OI], 5890–6 NaI, and 5577 [OI].

An example of the data furnished by the instrument is shown in Fig. 5, which is a record of a 5577A sweep, from NNW to SSE, made with an amplifier gain of 3.4×10^4. Combining this figure with the published sensitivity of a 1P21 (14,800 amp. per watt at 5577A) and the maximum recorder current of 0.7 ma read from the record, one obtains for the maximum total power received during this sweep

$$\frac{7\times10^{-4}}{3.4\times10^4\times1.48\times10^4}\approx1.4\times10^{-12}\text{ watt.}$$

The small irregularities in the line are caused by random noise from the photo-multiplier, while the larger bumps represent the various stars identified in the figure. The steady increase in intensity of the 5577A radiation from the zenith to points near the horizons is caused by the increase in optical thickness of the emitting layer as it is viewed more and more obliquely, offset to some extent by the increasing thickness of the absorbing lower atmosphere. Finally, at elevations of about 10 deg., the absorption begins to increase so rapidly that the intensity falls essentially to zero in a few degrees. A detailed presentation of the data and their interpretation will appear in a later paper.[3]

Just below the chart grid is the line drawn by the azimuth-indicating pen. The displacement of this line immediately following the closing of the shutter indicates that the instrument has just finished the final altitude sweep and that the azimuth plate is returning to North to begin a new cycle. No timing marks or calibrating steps are shown on the record because the clock and luminous shutter were not yet finished when the run was made. This record shows also that the instrument is completely free from zero shift. On one occasion only, while using an experimental photo-multiplier at high gain, a shift of several chart divisions was observed and was found to be due to synchronous vibration of the elements of the tube. Substitution of a less microphonic tube corrected the fault, which has not occurred since.

FURTHER DEVELOPMENT

Alterations suggested by four months of field use and by the need for an airborne instrument are now under way. When finished, the instrument will be completely remote-controlled by synchro drives and additional cabling.

In addition to the remote control of the sensitivity switch which already exists, there will be, on a central remote panel, controls for rapid traverse in altitude and azimuth in either direction, the selector switch of Fig. 2, and indication, via synchro drives, of the altitude and azimuth angles. The rapid traverse in altitude will be accomplished by switching the altitude motor from 60- to 400-cycle power. The switches shown on the base in Fig. 2 will be removed so that all control will be vested in a single remote center, that is to say, in a comfortable, heated Quonset Hut, while the photometer alone braves the inclement winter weather which seems to be a cherished tradition of observational astronomy.

ACKNOWLEDGMENTS

The authors express their thanks to Dr. F. E. Roach, Head of the Aerophysics Section, for his support of and belief in their projected designs, to the Optics Section of NOTS under Dr. Roger Estey which designed and fabricated the special lens for the photometer, and to Dr. W. M. Cady, Head of the Physics Division, for shop time.

---

[3] Preliminary notes have been published by F. E. Roach and Daniel Barbier, Pub. Astronom. Soc. Pac. 61, 88–92 (1949).

THE REVIEW OF SCIENTIFIC INSTRUMENTS VOLUME 20, NUMBER 10 OCTOBER, 1949

Stabilized High Voltage Power Supply for Electrostatic Analyzer

R. L. Henkel and B. Petree
University of Wisconsin, Madison, Wisconsin

(Received June 23, 1949)

An a.c. operated power supply has been developed which furnishes voltage for the electrostatic analyzers for the University of Wisconsin electrostatic generator. Voltage is continuously variable from about 5000 to 50,000 with stability and accuracy of measurement within ±0.01 percent. The stabilizer is of the usual degenerative type, but the error signal is amplified by a phototube galvanometer d.c. amplifier and applied to a series impedance in the high voltage transformer primary circuit. The generator beam energy automatically follows adjustments of a low voltage potentiometer used for voltage measurements in this supply.

INTRODUCTION

THE Wisconsin electrostatic generator furnishes positive ions of continuously variable energy which can be determined to about 0.1 percent accuracy. The generator has an automatic energy control system which has been described by Hanson[1] and Ashby.[2] This system is operated by a signal derived from an electrostatic analyzer which measures the energy of the diatomic beam. A second analyzer described by Warren *et al.*[3] may be used to select a portion of the output beam of the generator to give high energy resolution. In practice, the plate spacings of the two analyzers are so adjusted that a single voltage source can be used for both.

Previously a 30 kilovolt stack of dry batteries had been used for precise work using the electrostatic generator. The difficulties encountered in using batteries for a voltage source have been described by Herb *et al.*[4] Varying internal impedance, voltage drifts, and the tedious procedure necessary to obtain a given voltage made the battery source very inconvenient.

It was decided to replace the dry batteries with an a.c. operated power supply having a continuously variable output voltage, which in the range of about 5–50 kilovolts would be known to better than one part in ten thousand. It was also desired to use a standard low voltage potentiometer (0–1.6 volts) for voltage measurement. The vacuum tube amplifier conventionally used in regulators of this type has been replaced by a phototube-galvanometer combination which is simple, free from drift, and insensitive to stray induced voltages.[5,6]

PRINCIPLES OF OPERATION

A block diagram of the system is given in Fig. 1. The power supply proper consists of a conventional rectifier and filter circuit. Primary power is supplied by a 400-cycle, 110-volt alternator, the output of which is stabilized with an auxiliary field regulator. Gross adjustments in voltage are made with a variac by adjusting the 400-cycle voltage applied to the primary of the high voltage transformer. Stabilization is accomplished by means of a variable impedance transformer[7] in the primary circuit of the high voltage transformer. The stabilizing action is as follows.

Reference voltage is furnished by a type *B* Rubicon potentiometer. For regulation, a comparison voltage is picked off the high voltage divider at the 750-ohm taps as shown. Any difference between the comparison voltage and the reference voltage on the potentiometer represents an error voltage and is applied to the phototube galvanometer amplifier,[6,7] the operation of which is described below. The amplified error voltage is applied to two single-stage, direct-coupled, vacuum tube amplifiers. The output of one of these amplifiers furnishes grid bias voltage to a pair of 6*B*4 triodes which form a variable load on the secondary winding of the variable impedance transformer. Specifically, if the output voltage is too high, the amplified error furnishes more negative bias to the grids of the triodes, thereby increasing the series impedance of the transformer and lowering the primary voltage until the error is minimized. Similarly, if the output voltage is too low, less negative bias is applied until the primary voltage is raised to minimize the error. A typical curve showing the regulation action at 20 kilovolts is shown in Fig. 2. The rapid increase in error shown by the error curve is due to the light pattern leaving the phototube, thereby resulting in loss of stabilizing action. One should notice that as long as the regulator is in operation and utilizing maximum gain, the error is less than 0.02 percent. For

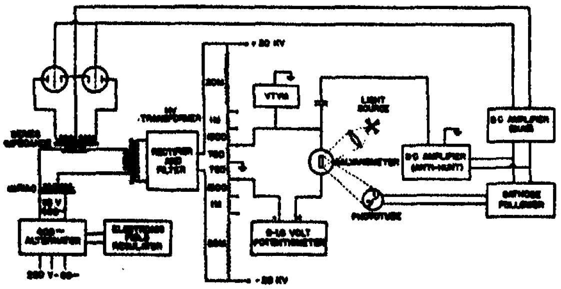

FIG. 1. Block diagram of power supply and regulator.

---

[1] A. O. Hanson, Rev. Sci. Inst. 15, 57 (1944).

[2] R. M. Ashby and A. O. Hanson, Rev. Sci. Inst. 13, 128 (1942).

[3] Warren, Powell, and Herb, Rev. Sci. Inst. 18, 559 (1947).

[4] Herb, Snowdon, and Sala, Phys. Rev. 75, 246 (1949).

[5] Sten von Friesen, *Dissertation Uppsala*, 1935.

[6] R. W. Gilbert, Rev. Sci. Inst. 7, 41 (1936).

[7] L. N. Ridenour and C. W. Lampson, Rev. Sci. Inst. 8, 162 (1937).

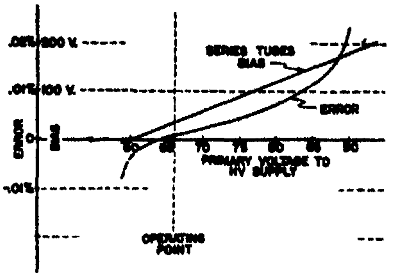

FIG. 2. Regulation curve at 20 kilovolts.

a ±5 percent line voltage change near the operating point, the total error is less than 0.0025 percent (less than ½ volt in 20,000 volts). This curve was taken in the high current output taps (*E*) without auxiliary filtering.

To prevent oscillations caused by overcorrection, the second vacuum tube amplifier supplies a differentiated error voltage to the galvanometer and thereby furnishes viscous damping by electrical means.

While this regulator is in operation, fine adjustments of output voltage are readily made by merely adjusting the potentiometer voltage. The range of control at a single variac setting is about ±30 percent. Larger changes require adjustment of the variac to a new operating range. In the existing model this is done automatically by a thyratron-controlled motor drive on the variac (not shown). If put into operation, this motor control minimizes the error to within some present value and turns itself off automatically.

DESCRIPTION

400-Cycle Alternator and Regulator

A 1.5-kva, 115-v, 400-cycle Leland generator driven by a 3-phase induction motor is used for the source of power. Two field windings are available on this alternator so that a degenerative regulator is easily applied to it. The electronic regulator circuit shown in Fig. 3 was designed by J. L. McKibben.[8] It varies an opposing magnetic field in the alternator to stabilize the peak generated voltage to about one part in 3000. The output is entirely independent of normal line voltage fluctuations. This auxiliary stabilization is required because the inertia and electrical damping of the galvanometer prevent it from correcting for very rapid line voltage fluctuations.

High Voltage Rectifier and Filter

The high voltage rectifier and filter circuit is shown in Fig. 4. The center tap of the output is at ground potential as is necessary for use with the Wisconsin electrostatic analyzers. The 20-second time constant of the voltage doubling capacitors and bleeder resistor, together with the 800 cycles per second charging rate, give a peak ripple voltage of about one part in 30,000. However, an additional resistance capacitance filter section is normally used as it has been found that this reduces the magnitude of small irregular fluctuations which may appear when irregular bursts of current are drawn by the analyzer. Taps *E* are used when the supply is used to furnish high currents. Presumably, the supply will operate for any steady current load within the rating of the high voltage transformer. The condensers used have a resistance greater than 10,000 megohms, so that no correction is necessary for the leakage current.

High Voltage Divider

The characteristics of the high voltage divider determine the stability and accuracy of voltage measurement for the 50-kv supply. Corona currents, leakage currents, or resistance changes will result in a departure from the expected dividing ratio. The divider has been built to give a constant dividing ratio to better than 0.01 percent under all operating conditions. A somewhat similar design has been successfully used at Wisconsin since 1941. The divider consists of forty one-megohm manganin resistors specially manufactured and selected by the Shallcross Company. The resistors are mounted in groups of three each between corona free shields supported by 3-in. Mycalex insulating columns as shown in Fig. 5. Two sections of 20 resistors each are enclosed in 7½-in Lucite tubes which are arranged in an airtight system through which dry air is circulated by a blower in the base. Drying compound is inserted in both ends of the base for initially drying the air. The use of manganin

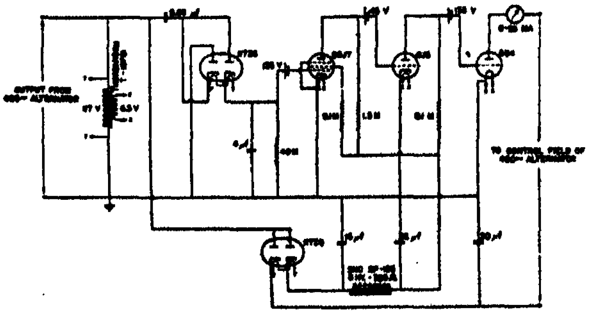
OUTPUT FROM 400~ ALTERNATOR
TO CONTROL FIELD OF 400~ ALTERNATOR

FIG. 3. Electronic stabiliser for 400 cycle alternator.

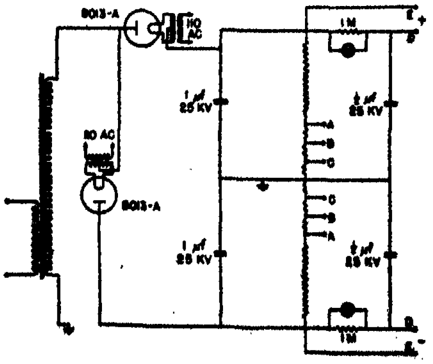

FIG. 4. High voltage rectifier and filter.

---

[8] J. L. McKibben, Phys. Rev. 70, 117A (1946).

wire and circulated air reduces all temperature effects to a negligible amount. Low voltage taps on each section at 750 ohms, 2250 ohms, and one megohm from ground are available for measuring, regulating, and monitoring purposes.

The resistor stack is standardized and checked for long time stability by an occasional measurement of the $Li^7(p, n)$ threshold energy, using the Wisconsin electrostatic generator. No change in ratio has been detected in six months of operation.

Galvanometer-Photo-tube Amplifier

Figure 6 shows the electrical and optical details of the galvanometer-phototube amplifier.[6,7] A Type 920 twin phototube is illuminated as shown, by light reflected from the mirror of a galvanometer. The phototube is positioned so that its output voltage is zero when the galvanometer is undeflected. Under this condition the two cathodes of the 920 are about equally illuminated. If an error voltage is applied to the galvanometer, it will deflect, moving the light pattern parallel to the long dimension of the cathodes. The illumination is thus unbalanced and a voltage will appear at the output terminals, the polarity of which depends upon the direction of galvanometer rotation, or upon the polarity of the error voltage. The gain can be conveniently adjusted to a desired value, by varying galvanometer sensitivity, light intensity, or length of light path. A gain of about 10^6 is used at present.

The deflections of the galvanometer are an indication of the error. As an example of the regulation under unfavorable conditions, i.e., at 5000 volts, 0.01 percent error will cause the light pattern to move about 6 centimeters. In operation, however, deflections are observed to be less than one millimeter. Thus average stability is considerably better than 0.01 percent.

In this connection it should be noted that the normal mechanical drift of the zero position of the galvanometer is less than one millimeter. One millimeter deflection corresponds to 4×10^{-7} applied volt. This low equivalent input voltage drift is the principal reason that the phototube-galvanometer amplifier was used in preference to a vacuum tube amplifier in this regulator.

Vacuum Tube Amplifiers

The high internal impedance of the phototube made it necessary to isolate the following amplifier grids with a cathode follower. These two identical amplifiers are of the series balanced type,[8] capable of amplifying voltages of either polarity, and have gains of about 30.

The output of one amplifier (VT-3) shown in Fig. 7 furnishes voltage which is added to or subtracted from a fixed bias of 35 volts on the grids of the 6B4 variable impedance triodes (VT-5, -6).

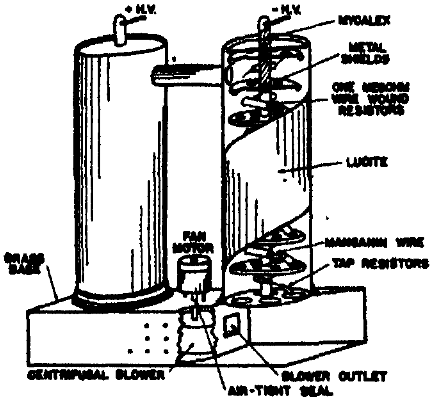

Fig. 5. High voltage resistor stack.

The output of the second amplifier (VT-2) is coupled through a Sprague Vitamin Q condenser (C-1) to one galvanometer terminal. This capacitance and its associated resistances are of sufficiently small time constant that the voltage thus supplied to the galvanometer is effectively the derivative of the error signal. Thus the electrical equivalent of viscous damping is supplied, and the oscillations which will otherwise develop are prevented, without loss of sensitivity. The selection of the differentiating capacitance (C-1) was made by experiment and it is not clear whether the optimum value is being used or not. A front panel gain control for the differentiating amplifier has proved to be convenient.

Indicators and Controls

For convenience in starting, adjusting, and observing the operation of the power supply, panel meters are provided to indicate the output voltage of the bias amplifier (VT-3), and the voltage across one 750-ohm section of the voltage divider. In order to avoid shunting the 750-ohm resistor, a vacuum-tube voltmeter (VT-1) of high input resistance is employed.

The only panel controls needed for operation are a switch for connecting and disconnecting the potentiometer and the galvanometer (S-1), a variable galvanometer shunt resistance (R-15) and switch (S-2), a gain control (R-8) for the differentiating amplifier, and the variac. The remaining variable resistances require only initial adjustment. The bias meter has a switching system (not shown) which allows its use as an indicator for the initial balancing of the circuits.

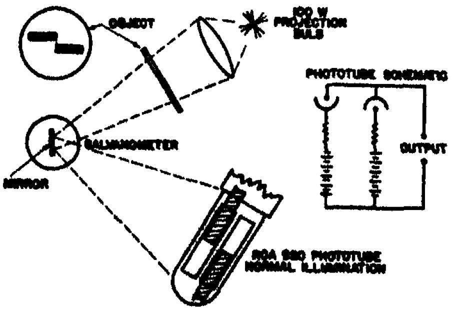

Fig. 6. Photo-tube-galvanometer amplifier.

---

[8] M. Artst, Electronics, August 1945.

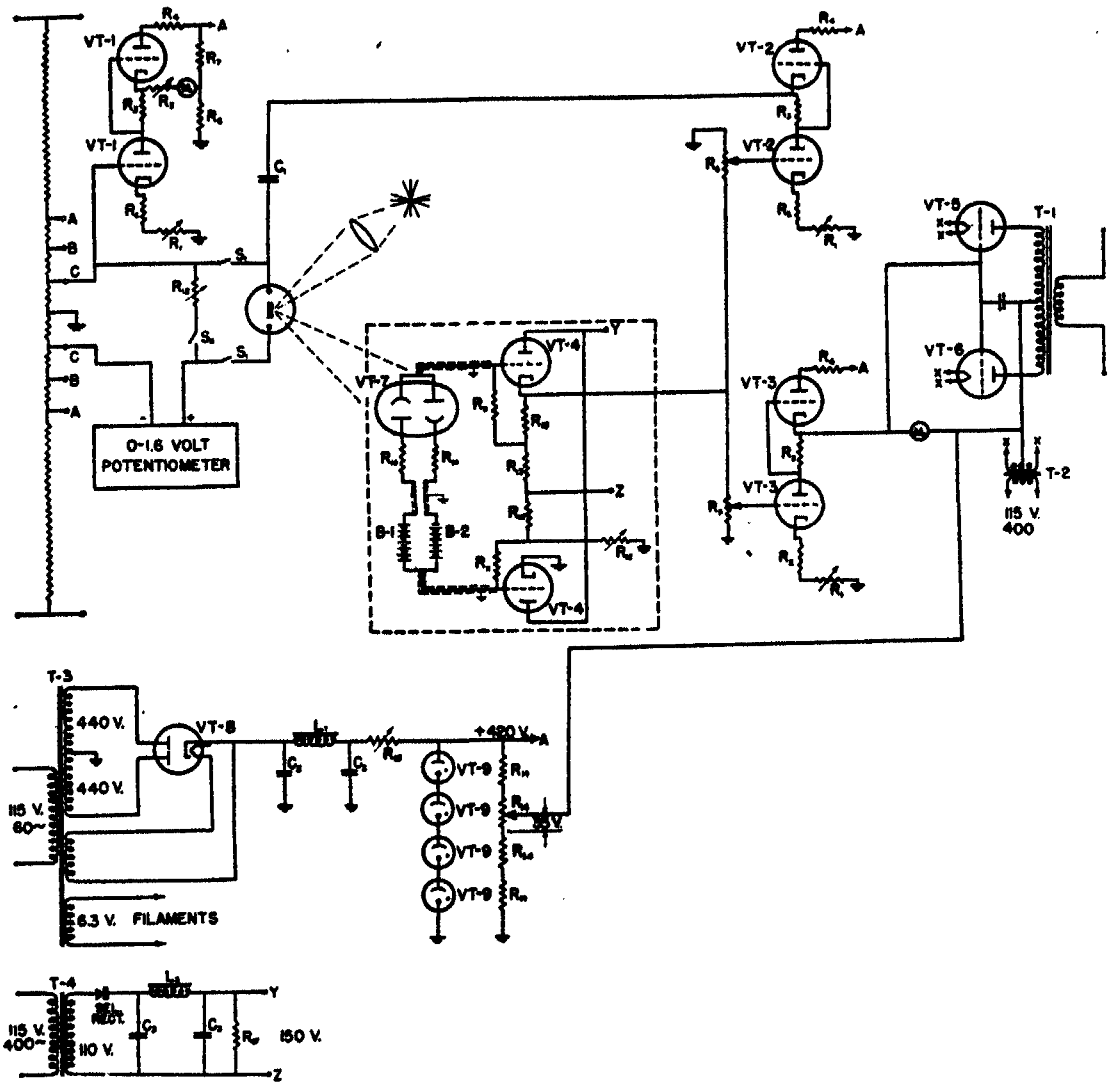

FIG. 7. Circuit diagram of regulator.

VT-1, 2, 3:	6*SL*7	*R*-1:	1*K* 1*W* Pot	*R*-12:	2.5*K* 1*W* Pot	*T*-1:	Power transformer Secondary: 800v *CT* Primary: 30v (several filament windings in series aiding)
VT-4:	12*AU*7	*R*-2:	5*K* 1/2*W*	*R*-13:	47*K* 1/2*W*	*T*-2:	Filament transformer 6.3 volts
VT-5, 6:	6*B*4-*G*	*R*-3:	5.6*K* 1/2*W*	*R*-14:	10*K* 10*W* Wire wound adjustable	*T*-3:	Stancor P6143
VT-7:	920	*R*-4:	11.2*K* 1/2*W*	*R*-15:	1.5*K* 1/2*W*	*T*-4:	Thordarson*T*-21*F*08
VT-8:	5*V*4*G*	*R*-5:	100*K* 1*W* Pot	*R*-16:	6*K* 20*W* Wire wound adjustable	*B*-1, 2:	45 volts
VT-9:	0*B*2/*VR*105	*R*-6, 7:	47*K* 2*W*	*R*-17:	50*K* 2*W*	*M*-1, 2:	200 μa full scale
C-1:	0.25 μf Sprague Vitamin Q	*R*-8, 9:	5*M* 1*W* Pot	*L*-1:	20*HY* 50*MA*		
		R-10:	2.2*M* 1/2*W*	*L*-2:	800*H*4 5*MA*		
C-2, 3:	4 μf 600v oil	*R*-11:	22*M* 1/2*W*				

OPERATION

The following procedure is used in putting the regulator into operation.

With galvanometer disconnected (*S*-1), the shunt (*R*-15) at minimum resistance, and the variac turned to zero, the potentiometer is set to the proper fraction of the high voltage desired. The reading of the vacuum tube voltmeter is noted. The potentiometer is then disconnected, and the variac is turned up until about the same reading is noted. The potentiometer is again connected and the galvanometer switch (*S*-1) turned on. Next, the galvanometer shunt resistor is gradually increased. If an oscillation occurs, it will be indicated by fluctuation of the bias meter and oscillation of the galvanometer light pattern. The oscillation should then be stopped by advancing the gain control of the differentiating amplifier. Finally, the galvanometer shunt is removed (*S*-2) entirely.

When small voltage changes are desired, it is only necessary to change the potentiometer setting. The high voltage follows automatically to the new value. For large changes in voltage, it may be necessary to shunt the galvanometer during the process.

This work was supported in part by the Wisconsin Alumni Research Foundation and in part by the Atomic Energy Commission.

A Low Temperature Single Crystal X-Ray Diffraction Technique

H. S. KAUFMAN* AND I. FANKUCHEN
Polytechnic Institute of Brooklyn, Brooklyn, New York

(Received June 23, 1949)

A low temperature x-ray diffraction technique, especially suitable to single crystal work, is described. Crystals are grown in glass capillaries on the x-ray camera. Position and orientation are determined with the aid of a polarizing microscope on the apparatus. A special specimen holder is used which prevents moisture condensation and permits rotation and oscillation of the specimen while it is being cooled.

A RELATIVELY simple method has been developed for low temperature x-ray diffraction studies of materials which are not normally solid at room temperature. The method is particularly applicable to single crystal work and may also be used for Debye-Scherrer powder diagrams.

Other low temperature methods have been described by, among others, Lonsdale and Smith,[1] Hume-Rothery and Strawbridge,[2] and Vonnegut and Warren.[3] The present procedure has been found to be flexible and has the advantage that crystals are grown in glass capillaries on the x-ray camera under controlled conditions, in the field of a polarizing microscope. This enables the observer to determine the position and orientation of a single crystal (when anisotropic) with relative ease.

In order to achieve the desired flexibility it was necessary to design a special specimen holder which fits on a standard goniometer head. The holder is a double walled cylinder with Bakelite end pieces (see Fig. 1). Its dimensions are: height 4 cm, diameter 3 cm. The walls are made of very thin (0.6 ml) unstressed polystyrene film and are separated by a $\frac{3}{4}$-cm dead air space. This double-walled arrangement provides insulation and prevents the condensation and freezing of atmospheric moisture on the specimen. Thin, unstressed polystyrene was used because of its low absorption of x-rays and its non-interference with the polarized light observations of the growing crystals.

The cooling system consists of a jet of cold compressed gas (usually nitrogen) which impinges on the specimen. The gas is cooled in a copper heat exchange coil which is immersed in dry ice solvent mixture or liquid nitrogen. The gas is directed by a nozzle tipped tube (supported by the top of the camera) into the central hole of the specimen holder. This arrangement permits complete rotation and enables one to obtain a twenty degree angular adjustment of the specimen while maintaining the cooling gas flow.

The upper end piece of the specimen holder has a central tapered hole with a sealed-in, glass nozzle which acts as the gas inlet and directs the cooling gas over the specimen. Two smaller holes on the side of the main central hole provide a gas outlet.

The specimen consists of a sealed-off, thin-walled (0.03 mm) glass capillary tube about $\frac{3}{4}$ mm in diameter which contains the liquid to be studied. This is supported by the lower end piece of the holder so that it is on the axis of rotation of the system and in the path of the nozzle. The length of the specimen is about 3 cm and is adjusted so that 2 or 3 mm of the specimen project into the nozzle tip.

The above described assembly, including goniometer head, is set on a Unicam type single crystal apparatus. A 10 cm diameter cylindrical camera is set around the specimen holder. The camera is of the open side type so that the necessary manual adjustments of the goniometer arcs may be readily made. Film contained in a black paper sheath is secured to the outer circumference of the camera when an exposure is to be made.

The optical system consists of a removable light source behind the x-ray pinhole system, a pair of polaroid plates and a horizontal microscope. One polarizing plate is mounted between the pinhole system and the

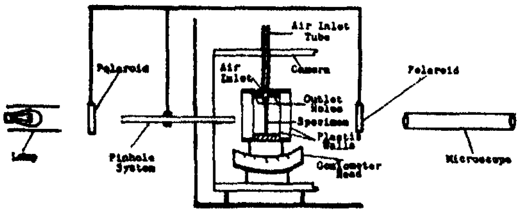

FIG. 1. Sketch of low temperature single crystal apparatus.

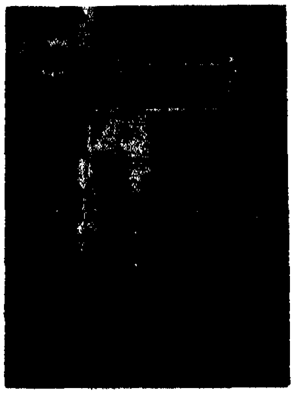

FIG. 2. Photograph of low temperature single crystal apparatus.

---

* American Chemical Society Postdoctoral Fellow 1947–1949.

[1] K. Lonsdale and H. Smith, J. Sci. Inst. 18, 133 (1941).

[2] W. Hume-Rothery and D. J. Strawbridge, J. Sci. Inst. 24, 89 (1947).

[3] B. Vonnegut and B. E. Warren, J. Am. Chem. Soc. 58, 2459 (1936).

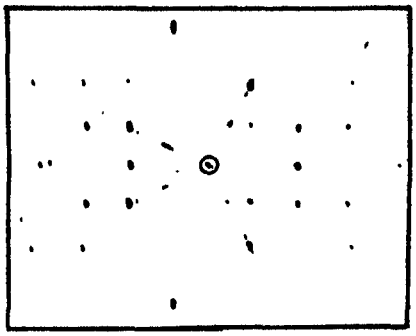

FIG. 3. Low temperature single crystal oscillation diagram of cyclooctatetraene.

lamp and the second (crossed relative to the first) is just in front of the microscope objective. The polaroids are mounted in such a manner that they may be rotated simultaneously about the axis of the x-ray pinhole system. (See *Figs. 1 and 2*).

In practice the capillary containing the specimen is centered in the path of a light beam defined by the x-ray pinhole system. A cold jet of gas is then directed at the specimen. It has been found that fast cooling (rapid gas flow) causes supercooling of the liquid and subsequent instantaneous freezing of the entire liquid column. This results in a multicrystalline powder specimen. For single crystal diagrams the specimen is first frozen as for powder specimens. The gas flow is then shut off, allowing the specimen to partially melt. The melting process begins at the bottom of the capillary tube and gradually creeps up the tube. When all but 2 or 3 mm of the specimen is fluid, the gas flow is resumed at a slow rate. There remain seed crystals in the upper, frozen portion which provide a nucleus for further slow growth. With reasonable care by freezing, melting and refreezing the specimen, one can obtain a satisfactory single crystal.

The freezing process is observed through the polarizing microscope and it is a simple matter (for anisotropic crystals) to determine the orientation and single crystal character of the specimen. Should a desired crystal direction, as indicated by the polarizing microscope, be tilted at an angle the entire specimen holder may be reoriented with the aid of the goniometer arcs. If the crystal is not perfect or at such an angle that it cannot be adjusted with the goniometer, the specimen is again partially melted and slowly frozen. Repetition of this procedure usually results in a satisfactory single crystal. Single crystal specimens appear transparent as compared to the opacity of polycrystalline specimens.

Once a well-oriented specimen has been obtained, one removes the light source and polaroids and the entire unit is placed before the x-ray tube. The x-ray beam being defined by the same pinhole system as was the light beam, it passes through the crystal as observed in the optical system. An oscillation diagram is taken and minor adjustments may be made in the orientation of the crystal. The crystal is then ready for a complete series of diffraction diagrams.

The above described method has been used successfully for single crystal studies of benzene and cyclooctatetraene. These materials melt at 5° and −7° respectively. Using the readily available dry ice-solvent mixtures as refrigerant one can attain specimen temperatures as low as −60° depending upon the rate of gas flow. A representative single crystal diagram of cyclooctatetraene is given in Fig. 3.

THE REVIEW OF SCIENTIFIC INSTRUMENTS VOLUME 20, NUMBER 10 OCTOBER, 1949

Construction and Calibration of a Cylindrical Electrostatic Analyzer

S. K. Allison, S. P. Frankel,* T. A. Hall, J. H. Montague, A. H. Morrish, and S. D. Warshaw**
Institute for Nuclear Studies, University of Chicago, Chicago, Illinois

(Received June 23, 1949)

A cylindrical electrostatic deflector has been constructed with average radius 15 cm, spacing 0.5 cm and deflection 90°, in which the deflecting potential can be in the neighborhood of 50 kv. Thus protons up to 0.75 Mev can be focused. Movable slits have been incorporated in the design, and the geometry of the entrance and exit apertures of the deflecting channel is such that the stray field may be calculated analytically. This has been done for the case in which the deflecting plates are symmetrically charged above and below zero potential. The predictions have been compared with experiments on the focusing of electron beams by the instrument under controlled conditions. Agreement with the calculations is demonstrated within the accuracy of the experiments, which is about 0.3 percent.

Experiments with asymmetric charging of the electrodes are reported and shown to agree with a plausible extension of the theory. Further experiments investigated the effect of small displacements of the slits from the computed focal positions. A set of factors, or calibration constants, has been measured so that, given the coordinates of the centers of the entrance and exit slits, and the potentials applied to the deflecting plates, the kinetic energy of the focused ion beam, as it left its source at zero potential, can be calculated to within 0.3 percent.

I. INTRODUCTION

IN the cylindrical electrostatic analyzer a deviation in direction of a beam of charged particles is caused by passing them into an electric field between conductors which are sections of coaxial cylinders by planes perpendicular to the cylinder axis. Such analyzers have been used in experimental nuclear physics with three rather different objectives in mind.

(1) *An energy selector in the first stage of mass spectrometers.* The analyzer focuses particles of a certain charge and kinetic energy, even if these enter it in slightly divergent directions. Explorations of the theory of the instrument, mainly with this application in mind, are in the literature.[1-3]

(2) *An absolute energy spectrometer.* From the observation that a group of particles traverses the analyzer and is focused at the exit focus, a determination of the kinetic energy of the particles (their charge being known) can be made in terms of the radii of the plates, and the deflecting voltages.[4-10]

(3) *A high resolving power energy selector for high energy ion beams.* By using large radii of curvature, and narrow entrance and exit slits, beams homogeneous in energy to within 200 electron volts can be selected from an approximately parallel 1 Mev beam containing an energy spread of 5000 volts.[11, 12]

The theoretical calculations and the experiments of this report are concerned mainly with the second of the applications listed above.

II. DESIGN

A. General Considerations

The elementary formulas of the electrostatic analyzer, including location of the focal points, have been given by some of the authors previously quoted, and their deduction will not be repeated here. Table I gives the notation used in this article, and some of the elementary formulas.

The relativistic expression for W in Table I applies if the kinetic energy of the ion is small but not negligible compared to its rest mass energy. Remembering that V_1 and V_2 are in volts, and using the second law of motion in the sense that rate of change of momentum, rather than mass times rate of change of velocity, is involved, we obtain

$$z\mathbf{E}_0/q = \dot{\mathbf{p}},$$

or

$$2z\kappa(V_2 - V_1)/q = pv, \tag{9}$$

since the magnitude of $\dot{\mathbf{p}}$ is pv/r.

The following relativistic expressions, with the kinetic energy W in electron volts, are well known.

$$W/q = m_0c^2\left(\frac{1}{(1-\beta^2)^{\frac{1}{2}}} - 1\right), \tag{10}$$

$$p = \frac{m_0v}{(1-\beta^2)^{\frac{1}{2}}} = (1/c)\{(W/q)^2 + 2m_0c^2W/q\}^{\frac{1}{2}}. \tag{11}$$

When substituted in (9), they lead to Eq. (2) when higher powers of $W/(2qm_0c^2)$ are neglected.

In designing an electrostatic analyzer for the collection of particles diverging from a point source, the question of its window or collecting power is of great importance. The collecting power may be defined as the fraction of particles, homogeneous in kinetic energy,

---

* Now at California Institute of Technology, Pasadena, California.

** Assistant in the Institute, supported by the joint program of the ONR and the AEC.

[1] A. L. Hughes and V. Rojansky, Phys. Rev. 34, 284 (1929).

[2] R. Herzog, (a) Zeits. f. Physik 89, 447 (1934); (b) Archiv. f. Elektrotechnik 29, 790 (1935); (c) Zeits. f. Physik 97, 596 (1935).

[3] A. J. Dempster, Phys. Rev. 51, 67 (1936).

[4] Allison, Graves, Skaggs, and Smith, Phys. Rev. 55, 107 (1939).

[5] L. S. Skaggs, Phys. Rev. 56, 24 (1939).

[6] J. Mattauch, Phys. Rev. 57, 550 (1940).

[7] Allison, Skaggs, and Smith, Phys. Rev. 57, 550 (1940).

[7a] A. O. Hanson and D. L. Benedict, Phys. Rev. 65, 33 (1944).

[7b] Herb, Snowdon, and Sala, Phys. Rev. 75, 246 (1949).

[8] L. del Rosario, Phys. Rev. 74, 304 (1948).

[9] F. T. Rogers, Jr., (a) Rev. Sci. Inst. 8, 22 (1937); (b) Rev. Sci. Inst. 11, 19 (1940).

[10] H. V. Argo, Phys. Rev. 74, 1293 (1948).

[11] Warren, Powell, and Herb, Rev. Sci. Inst. 18, 559 (1947).

[12] Fowler, Lauritsen, and Lauritsen, Rev. Sci. Inst., 18, 818 (1947).

TABLE I.

Symbols	Interpretation	Numerical values
	A. Notation and certain numerical values	
r_1, (r_2)	Radius of inner, (outer) wall of deflecting channel	14.750±0.0003 cm 15.250±0.0003 cm
$\bar{r}$	Geometric mean radius; $(r_1r_2)^{\frac{1}{2}}$	14.998 cm
r_0	Radius of a concentric circular orbit traversed by the central ray of a bundle of divergent ionic rays	—
δr_0	$r_0-\bar{r}$	—
δr_f	Radial displacement of the focal line due to stray field outside condenser mouth	−0.156 cm (calculated)
δr_s	Radial displacement of the center of the slit aperture from the uncorrected focus	—
w	$(r_2-r_1)/2$	0.250 cm
(r, θ)	Polar coordinates of an ion in a general position. $\theta=0$ lies at the entrance aperture	Analyzer plates extend from $\theta=0$ to $\theta_{\max}=90°$.
V_1, (V_2)	Deflecting potential, in volts, applied to the inner (outer) electrode	—
φ	V_2-V_1	$0<\lvert\varphi\rvert<60$ kv
z	Charge of an ion in electron units. $z=-1$ for electrons	—
m_0	Rest mass of an ion in grams	—
W	The kinetic energy, in electron volts, of an ion traversing a circular orbit through the analyzer, the orbit being centered on the cylinder axis	$W=14.999z(V_2-V_1)$ (non-relativistic; calculated)
q	Electron volts per erg	$(1.602\times10^{-12})^{-1}$
c	Light velocity; cm/sec.	2.998×10^{10}
κ	$\{2\ln(r_2/r_1)\}^{-1}$	14.999
l_1, l_2	Entrance and exit conjugate focal lengths of the analyzer, measured from foci to the planes $\theta=0$, $\theta=(1/2)\pi$ respectively	—
l	The common value of l_1 and l_2 for equal conjugate foci	5.29 cm (calculated)
W_0, $(\bar{W}_0)$	An ion passing through the analyzer on a concentric circular orbit of radius r, $(\bar{r})$ had the kinetic energy W_0, $(\bar{W}_0)$, in electron volts, when it left the source, at potential zero	$0<W_0/z<750$ kv
$E_0(r)$	The electrostatic field, in volts per cm, well inside the deflecting channel where perturbations due to the entrance and exit apertures have become negligible	—
$E(r, \theta)$ or $E(x, y)$	The electrostatic field at any point	—

B. Basic equations and formulas

$$V_r=V_1+2\kappa(V_2-V_1)\ln(r/r_1) \tag{1}$$

$$W=\kappa z(V_2-V_1)/\{1-\kappa z(V_2-V_1)/2qm_0c^2\} \tag{2}$$

$$\{(l_1-g)(l_2-g)\}^{\frac{1}{2}}=\bar{r}/\{\sqrt{2}\sin(\theta_{\max}\sqrt{2})\} \tag{3*}$$

$$g=\{\bar{r}\cot(\theta_{\max}\sqrt{2})\}/\sqrt{2} \tag{4}$$

$$l=\frac{\bar{r}}{\sqrt{2}}\,\frac{1+\cos(\theta_{\max}\sqrt{2})}{\sin(\theta_{\max}\sqrt{2})} \tag{5}$$

$$W_0=W+z\{V_1+2\kappa(V_2-V_1)\ln(r_0/r_1)\} \tag{6}$$

$$\bar{W}_0=W+\tfrac{1}{2}z(V_2+V_1) \tag{7}$$

$$E_0(r)=(V_2-V_1)/\{r\ln(r_2/r_1)\} \tag{8}$$

* The difference between $\bar{r}$ and $\frac{1}{2}(r_1+r_2)$ is negligible.

and emitted isotropically from a point source, which can be brought to the exit focus. In studying the products of a nuclear reaction produced by an incident beam of i microamperes and having a cross section σ, the collecting power sets a lower limit to the product $i\sigma$, below which insufficient counts will be observed from a given target to obtain acceptable statistical accuracy. In the case of the third application mentioned above, where the incident beam of particles is essentially parallel, the consideration of collecting power is not so important, and for this purpose analyzers of approximately 1 meter radius have been used.

The maximum collecting power of a cylindrical analyzer is approximately $1/4\pi$ times the solid angle subtended at the entrance focus by a rectangle of width (r_2-r_1) and height equal to the height of the beam halfway through the analyzer.

If l_1 is the distance from the point source to the entrance aperture of the analyzer, the collecting power is approximately

$$\frac{h(r_2-r_1)}{4\pi(\frac{1}{2}\theta_{\max}\bar{r}+l_1)^2}, \tag{12}$$

h is the extension of the beam parallel to the cylinder axis as it passes through the midpoint of the analyzer.

The maximum value of the collecting power for any given analyzer will result from $l_1=0$, that is, the source placed directly in the analyzer entrance. This is not convenient experimentally, however, and the present analyzer is used with the two focal distances equal. The collecting power under this condition is

$$\frac{h(r_2-r_1)}{4\pi\bar{r}^2\left(\dfrac{1+\cos(\theta_{\max}\sqrt{2})}{\sqrt{2}\sin(\theta_{\max}\sqrt{2})}+\frac{1}{2}\theta_{\max}\right)^2}. \tag{13}$$

Using the dimensions of our analyzer, and taking $h=1.25$ cm (half of the height of the exit aperture), we obtain 2×10^{-4} for the collecting power.

Thus, small radius of curvature and large (r_2-r_1) contribute to high collecting power. However, changing $\bar{r}$ and (r_2-r_1) in the direction of higher collecting power, rapidly decreases the energy W_0 of the incident particles which can be deflected by a given potential difference between the plates, and thus puts an increasingly lower upper limit on the range of energies to which the instrument can be applied. The design must be a compromise between the two objectives. Both limits become less stringent the higher the deflecting potentials, and thus there is an incentive toward designs which permit high voltages to be placed on the deflecting plates. Previous experience had shown that under standard laboratory vacuum conditions (unbaked metal surfaces large in area exposed in the vacuum; occasional admission of air and re-evacuation; pressure $\leq 10^{-5}$ mm), fields of 100 kilovolts per centimeter could be maintained in an analyzer without unduly increasing the background counting rate of the particle detector. With the dimensions given in Table I, the analyzer, relatively small and light compared to a magnetic deflector of equal power, will focus 750 kev singly charged ions, or 1.5 Mev doubly charged alpha-particles.

B. The Deflector Plates

Figures 1 and 2 are photographs of the interior of the analyzer, and part of its vacuum wall, respectively. The deflecting electrodes are mounted on a quartz post, 3.81 cm in diameter and 14.77 cm long, located at the cylinder axis. The spacing between the aluminum deflector plates clamped on this post remains constant, independent of any warping of the sides of the analyzer under evacuation or due to temperature effects. Furthermore the leakage path for the rather high potentials on the electrodes is entirely along this support. The design is such that contact lines between quartz and metal occur only in regions screened from the electric field, and the maximum electric field lies in the vacuum between the analyzer plates themselves. The quartz post was ground and polished by Mr. Fred Pearson, Jr., of our optical shop, and the diameter was held within a tolerance of ±0.00025 cm. A longitudinal line in the surface of the quartz was straight to within 5×10^{-5} cm, in the region in which the two electrodes were clamped on.

FIG. 1. Interior of the analyzer. The deflector plates are assembled on the quartz post and the slit mechanisms are in place.

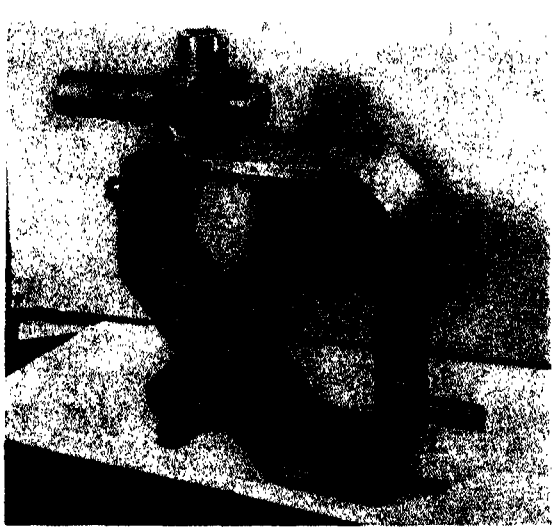

FIG. 2. Part of the vacuum wall, and the target chamber of the analyzer. In the calibration experiments, the target chamber was removed and an electron gun (not shown) attached.

In order to facilitate an accurate calculation of the fringing electric fields at the entrance and exit of the

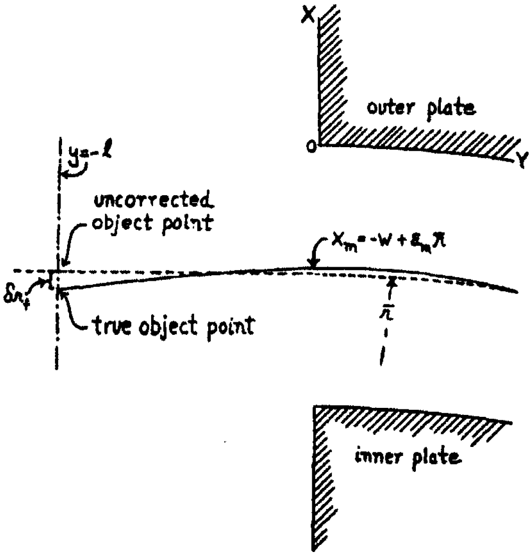

FIG. 3. The solid line indicates a trajectory which, originating at the true object point, will pass through the interior of the analyzer channel along the concentric circle of geometric mean radius.

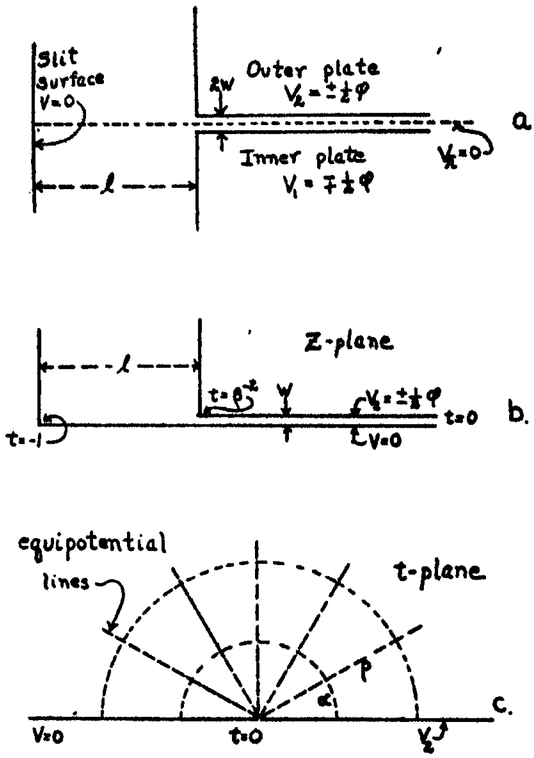

FIG. 4. Stages in the analytical solution of the problem of the fringing electrostatic field at the channel entrance.

deflector channel the design was made to approximate closely the ideal conditions of Fig. 4a. The deflector plates are shaped so that the radial surfaces at the channel apertures extend to each side for a distance of over six times the 0.5-cm channel width. The slit edges were elongated in a direction perpendicular to the slit height so that a grounded radial surface, parallel to the extension surfaces of the deflector plates, was formed at the focal distance. These slit planes were always at ground potential, and constituted a boundary condition for the field.

The charging voltage for the inner deflecting electrode is brought down a brass rod inserted in an axial canal ground into the quartz; the rod is threaded into a transverse arm, and a spring contact touches the inner surface of the clamping collar of the electrode.

The outer electrode is charged through a quartz post, similar in design to the support post, but not precisely machined. This post is inserted through the opposite vacuum wall and carries a metal cap with a spring contact which touches the deflector.

C. High Voltage Insulation

The problem of bringing in the high voltage through the vacuum walls was somewhat complicated by the fact that single quartz posts long enough to provide the required leakage path in air were not available. The quartz posts were held in accurate metal guides inserted in the walls of the analyzer, with about 1 cm of the quartz protruding into the air through the wall. This was capped by a special hollow Lucite bushing extending 16 cm outward from the vacuum wall, and making a rubber gasket vacuum seal by pressure on a flange of the quartz. Care was taken to make the mechanically weak Lucite very thick at points where the compressive stresses necessary to seal the gasket were applied. After the Lucite cap was in place and a satisfactory vacuum had been attained in the analyzer, showing that the electrode seal did not leak, the cavity in the Lucite was filled with a heavy, transparent paraffin oil. No electrical breakdowns have ever been observed in these electrodes. Small sylphons were attached at the tops of the Lucite caps, to serve as flexible couplings and insure that no mechanically rigid attachment could be made to the Lucite, which would eventually warp under shear. The wisdom of this precaution is shown in that after eighteen months of use of the analyzer in various positions these replaçeable sylphons are distorted, but no strains have been placed on the Lucite.

D. The Slits

Figure 3 is a schematic drawing of the entrance aperture. The electric field in the deflecting channel of course extends into the region to the left of the plane $\theta=0$. If the central ray[12a] of a divergent, monoenergetic bundle of ions is to traverse the deflector channel on a circle of radius $\bar{r}$, it must pass through a small region (which we will inaccurately call the true focal "point") displaced toward the center of curvature of the instrument a distance δr_f, as shown. There is, as discussed later, a much smaller displacement, δl_f, of the focal point toward the plane $\theta=0$. The above statements apply to a situation in which the exit aperture and slits are in positions which are mirror images of the entrance arrangements.

In order to explore the situation, the slits were designed so that three different adjustments can be made from outside the vacuum wall.

(1) The slit width is variable from 0 to 0.5 cm.
(2) The radial position (or y-coordinate, Fig. 3) of the center of the slit apertures can be shifted.
(3) The focal position, or the perpendicular distance from the plane of the slit apertures to the plane of $\theta=0$, can be varied.

Quantitative settings for the above motions can be made by readings on scales which are visible through observation windows. At present, no verniers are incorporated in the design and the accuracy of settings is probably not better than 0.02 cm. This seems to be a limiting factor in the accuracy at present, for, as reported later, 0.1 cm variation in δr_f changes the calibration factor by 1.33 percent. Slit settings were made by gears and slides actuated by rods which could be rotated and slid through Wilson[13] seals in the vacuum walls. The slit mechanism was detailed by Mr. D. N. Di Costanzo of our instrument shop.

[12a] The central ray of a bundle is that ray which, well inside the analyzer, follows a circle concentric with the channel.

E. Precision of Dimensions

The design is one in which high precision of dimensions is relatively easy to obtain, since all requirements can be met by careful work on a good lathe.

The most sensitive dimension is the width of the channel, $2w$. If a length λ is set as a tolerance in either of the r's, the maximum fractional error in the calibration constant is λ/w.[13a] The inner walls of the channel were cut on a high precision lathe with the electrodes clamped to an accurate 3.81 cm (1.5 inch) axle, and the surfaces were lapped and polished so that they were of the design dimensions to ± 0.0003 cm, giving $\lambda/w = 0.12$ percent. A line in the surface of the quartz post, parallel to its axis, and of length sufficient to pass through both clamping collars, should not depart from straightness by as much as λ, and the diameter of the post should be constant to within 2λ. These conditions were met in the grinding and polishing of the post.

III. CALCULATION OF THE EDGE EFFECT

A. The Fringing Electric Field

The radial shift δr_f, of Fig. 3, is calculable for certain simple geometrical arrangements of the conductors at or near the entrance and exit ports of the deflector channel. We have made the calculation for an arrangement equivalent to infinitely thick deflector plates, such that conducting planes constitute the surfaces $\theta = 0$ and $\theta = \theta_{\max}$ on both sides of the channel, with a grounded slit plane at $y = -l$ (cf. Fig. 4a). Other conductors, such as the vacuum walls, are assumed to be too far away to affect the stray field, and it is assumed that the instrument is being used with $V_2 = -V_1$. This will be referred to as symmetric charging, and the magnitude of each potential, in volts, will be $\frac{1}{2}|\varphi|$.[14]

The case of the infinitely thick deflecting plates, with the grounded slit plane at finite distance, which is directly applicable to our analyzer, is illustrated in Fig. 4. We shall at first neglect the curvature of the deflecting channel. With symmetric charging, a zero of potential occurs at $\bar{r}$, and the problem can be split into two halves, as in Fig. 4b, since a conducting sheet could be placed along the zero equipotential surface. This reduces the problem to the "bend of a Leyden jar" problem solved in standard texts on electrostatics.[15]

The field distribution is obtained by mapping Fig. 4b, using a Schwartz-Christoffel transformation, into the positive t half-plane and the real t axis, with a singularity at the origin, as in Fig. 4c. Consider the function

$$V_t = -\ln(-t) = -\ln\rho - i(\alpha - \pi), \tag{14}$$

and let $\mathfrak{Im}\,V_t$ represent the potential in the t-plane. When $\alpha = \pi$, $\mathfrak{Im}\,V_t = 0$, and if $\alpha = 0$, $\mathfrak{Im}\,V_t = \pi$. Thus the potential is measured in units of π with 2π volts across the plates.

Let $\beta = -(l/\omega)$ and set

$t = 0$ at a point far inside the channel,
$t = \beta^{-2}$ at the inside corner (Fig. 4b), and
$t = -1$ at the outside corner.

Then the Schwartz differential equation is

$$Z' = dZ/dt = \{A/t\}\{(t-\beta^2)/(t+1)\}^{\frac{1}{2}}. \tag{15}$$

At $t = 0 + \eta$, with η small and real, $Z'/|Z'| = i$ sign A.

At $t = 0 - \eta$, $Z'|Z'| = -i$ sign A. If we choose a left-handed coordinate system in the Z plane, with the y axis increasing to the right, then in order to have t increasing along this line we must have sign A negative.

At $t = \beta^{-2} + \eta$, $Z'/|Z'| =$ sign A, and at $t = \beta^{-2} - \eta$, $Z'/|Z'| = -i$ sign A. This produces at 270° clockwise rotation at the inside corner, and similarly at the outside corner. It can also be shown that all points between the plates are mapped into the positive t half-plane.

Integration of (15) gives

$$\begin{aligned}\pi Z/w = i\ln\{(1+\beta M)/(1-\beta M)\}& \\ +\beta\ln\{(1-iM)/(1+iM)\},&\end{aligned} \tag{16}$$

where

$$M = (1/\beta)\{(1-\beta^2 t)/(1+t)\}^{\frac{1}{2}}, \tag{17}$$

and we may remark that, as defined, β is negative.

Here we have used $A = -l/\pi$, and set the origin in the Z plane at the corner $t = \beta^{-2}$, so that no constant of integration appears. The value of A was chosen by setting

$$Z(t = -1) = -w - il.$$

The field is then given by

$$\begin{aligned}E = E_y + iE_x &= -(dV_t/dZ)(dZ/dt) \\ &= (\pi\beta/l)\{(t+1)/(\beta^2 t - 1)\}^{\frac{1}{2}}.\end{aligned} \tag{18}$$

As $t \rightarrow 0$, i.e., far inside the channel, $E \rightarrow -(i\pi)/w$ or $E_x = E_0 = -\pi/w$, as it should. Thus, we obtain

$$E_x/E_0 = \{(t+1)/(1-\beta^2 t)\}^{\frac{1}{2}} = 1/M\beta. \tag{19}$$

As an example, the calculation of the field at $\theta = 0$, $r = \bar{r}$, or, in the Cartesian coordinates of Fig. 6b, at $x = -w$, $y = 0$, will proceed as follows. Using $Z = x + iy$ in Eq. (16) gives the transcendental equation

$$\begin{aligned}-\pi = i\ln\{(1+M\beta)/(1-M\beta)\}& \\ +\beta\ln\{(1-iM)/(1+iM)\}.&\end{aligned} \tag{20}$$

If we designate the value of M at the point ($x = -w$, $y = 0$) by M_m, then a numerical solution of Eq. (20)

---

[13] R. R. Wilson, Rev. Sci. Inst. 12, 91 (1940).

[13a] In the notes at the end of the paper by Herb, Snowdon, and Sala, J. L. Powell has given a method by which corrections to the analyzer constant can be computed from a survey of the variations in spacing along the channel. We have not carried out such a survey of our instrument.

[14] Herzog, references 2(b) and 2(c), has given an analytical solution to the problem along an extension to the median radius. Rogers, reference 9(b), has obtained a graphical solution for the stray field.

[15] For instance, Jeans, *Electricity and Magnetism* (Cambridge University Press, London, 1927), fifth edition, p. 277.

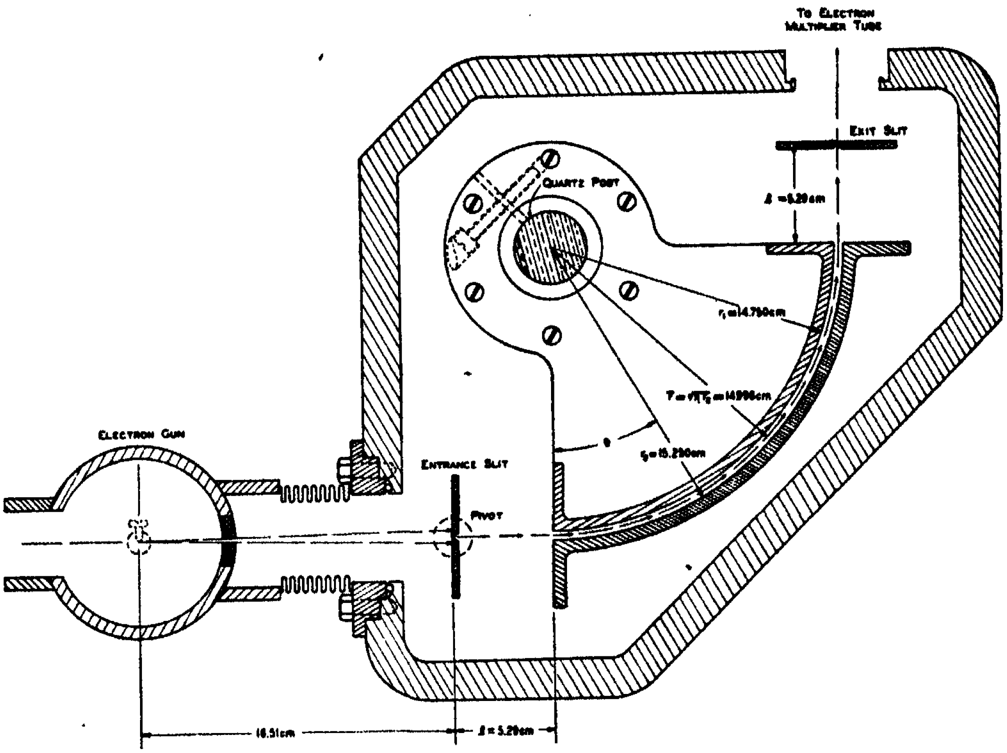

FIG. 5. Relative positions of the electron gun and electrostatic analyzer in the calibrating experiments.

gives $M_m=-0.0567$, using $w=0.25$ cm, $l=5.29$ cm, $\beta=-21.2$. Thus we obtain $E_z/E_0=0.83$. On entering the channel the discrepancy between E_z and E_0 decreases roughly exponentially.[16, 17]

TABLE II. k's for various charging arrangements.

Arrangement	k from Eq. (36)
A. Symmetric charge	$k_A=\kappa\left\{1+\frac{\kappa z(V_2-V_1)}{2qm_0c^2}+\frac{2\delta r_0}{\bar{r}}\right\}$
B. Inner charge ($V_2=0$)	$k_B=\kappa\left(1-\frac{\kappa zV_1}{2qm_0c^2}+\frac{2\delta r_0}{\bar{r}}\right)-\frac{1}{2}$
C. Outer charge ($V_1=0$)	$k_C=\kappa\left(1+\frac{\kappa zV_2}{2qm_0c^2}+\frac{2\delta r^0}{\bar{r}}\right)+\frac{1}{2}$

B. The Focal Spot Shift δr_f

The calculation of the position of the focus can now proceed with consideration of a trajectory which passes through the analyzer along $\bar{r}$. For values of θ well inside the deflector channel, we may put $E=E_0$; near the mouth we must use Eq. (19).

The differential equation of the trajectories may be readily obtained in a form suited to our purpose from the principle of least action. We will proceed using nonrelativistic expressions. The principle may be written

$$\delta(2m(H-V))^{\frac{1}{2}}ds=0, \tag{25}$$

where the integrand is the momentum and ds is an element of path along the trajectory.

Let T be the kinetic energy of an ion at (r, θ) in the analyzer channel. Then, in polar coordinates, Eq. (25) becomes (disregarding the factor $(2m)^{\frac{1}{2}}$)

$$\delta\int T^{\frac{1}{2}}\{r^2+(dr/d\theta)^2\}^{\frac{1}{2}}d\theta=0. \tag{26}$$

Using well-known steps, we obtain

$$(d/d\theta)(\partial/\partial r')\{T^{\frac{1}{2}}(r^2+r'^2)^{\frac{1}{2}}\}=(\partial/\partial r)\{T^{\frac{1}{2}}(r^2+r'^2)^{\frac{1}{2}}\}, \tag{27}$$

---

[16] The effect of curvature of the deflecting channel on the stray field is negligible in our analyzer. It may be calculated as follows. The two parallel equipotential lines of Fig. 4c are mapped into circles through the transformation

$$\xi=\bar{r}\exp\{\gamma(Z+w)\}, \tag{21}$$

where $\bar{r}=(r_1r_2)^{\frac{1}{2}}$ and

$$\gamma=(1/2w)\ln(r_2/r_1)=(1/15)\text{ cm}^{-1}. \tag{22}$$

After some calculation, it is found that

$$\epsilon_r=\frac{1}{\gamma\bar{r}e^{(x+w)}}\mathfrak{Im}\frac{\pi\beta}{l}\left(\frac{t+1}{\beta^2t-1}\right)^{\frac{1}{2}}, \tag{23}$$

$$\epsilon_\theta=\frac{1}{\gamma\bar{r}e^{(x+w)}}\mathfrak{Re}\frac{\pi\beta}{l}\left(\frac{t+1}{\beta^2t-1}\right)^{\frac{1}{2}}. \tag{24}$$

The field on the median line $x=-w$ therefore differs from the field with no curvature by the factor $(\gamma\bar{r})^{-1}$ which exceeds unity by less than 1 part in 15,000 in our instrument. Thus E_x and E_r are indistinguishable.

[17] A plot of the equipotential surfaces and lines of force at the channel entrance is given by Rogers (9a) for the case $V=0$ at infinite distance from the entrance. Our calculations are made for $V=0$ at $y=-l$, where, without the grounded slit plane, E_x/E_0 would have been 0.2. Herzog (2c) has discussed the problem, including the grounded slit plane, and given expressions leading to the location of an "equivalent" entrance plane, the effect of the fringing field being considered as equivalent to the extension of the actual channel.

One of us (S. F.) has solved the analogous problem of the infinitely thin deflector plates with $V=0$ at infinity.

in which $r' = dr/d\theta$. If we treat $\partial T/\partial\theta$ as small, this becomes

$$\frac{d}{d\theta}\frac{r'}{(r^2+r'^2)^{\frac{1}{2}}} = \frac{(r^2+r'^2)^{\frac{1}{2}}}{2T}\frac{\partial T}{\partial r} + \frac{r}{(r^2+r'^2)^{\frac{1}{2}}}. \tag{28}$$

Now let r_0 be the radius of the concentric circle described (well inside the channel) by the central ray of a bundle of ionic rays. Consider a divergent ion of this bundle, at radius $r = r_0(1+\epsilon)$, where ϵ is small. If we use this condition, plus the fact that

$$\partial T/\partial r = -Ez, \tag{29}$$

we may write, from Eq. (28)

$$d^2\epsilon/d\theta^2 = 1-(Er_0z)/2T. \tag{30}$$

Since $zE_0 = qmv^2/r_0 = 2T/r_0$, it follows that

$$d^2\epsilon/d\theta^2 = 1-E/E_0 = 1-1/\beta M. \tag{31}$$

Here, $\theta = \gamma\mathfrak{I}\mathrm{m}Z = \gamma y$. Hence

$$d\epsilon/d\theta = \int_{t=0}^{M} \{(\beta M-1)/\beta M\}(d\theta/dM)dM, \tag{32}$$

where we have put $d\epsilon/d\theta = 0$ at $t=0$ where $M = \beta^{-1}$, equivalent to $\theta = \pi/4$. The integral (32) can be calculated exactly. The approximation ϵ small is not valid outside the entrance aperture, however, and it is best to transform to a rectangular set of coordinates, obtaining $x(y)$ in this region, using ϵ and $d\epsilon/d\theta$ for initial values at the entrance. The value of ϵ is obtained from

$$\epsilon = \int_{\beta^{-1}}^{M} (d\epsilon/d\theta)(d\theta/dM)dM. \tag{33}$$

The goal of the present calculations is to find the displacement of the object focus due to the stray electric field. If the stray field is neglected the object focus is located at $x = -w$, $y = -l$. To find the true position, outside the entrance aperture we write a well-known solution of the integral of least time, namely

$$d^2x/dy^2 = -(1/T^{-\frac{1}{2}})\partial(T^{-\frac{1}{2}})/\partial n. \tag{34}$$

The left-hand member of (34) is a close approximation to the curvature of the trajectory, and the derivative in the right-hand member is with respect to the normal. This leads to

$$d^2x/dy^2 = (1/T)(\partial T/\partial n) = -1/r_0M\beta. \tag{35}$$

Furthermore, by differentiation of Eq. (16) we obtain with $Z = x+iy$,

$$dy/dM = (2\omega\beta/\pi)\{(1/1-\beta^2M^2)-(1/1+M^2)\}. \tag{36}$$

To calculate the deviation of the object "point" (actually, a line parallel to the cylinder axis) consider a bundle of ionic rays having $r_0 = \bar{r}$, and consider the central ray of this group of trajectories. For this ray, at points well inside the channel, $\epsilon = 0$, but ϵ becomes finite near and outside the ports. At the plane of the entrance aperture we have, for the central ray, $x_m = -w+\bar{r}\epsilon_m$, and

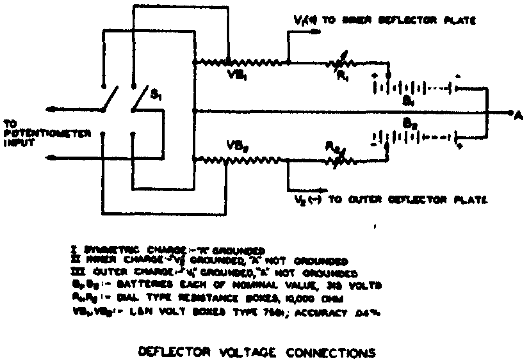
V1(+) TO INNER DEFLECTOR PLATE
VB1
R1
S1
B1
A
B2
TO POTENTIOMETER INPUT
VB2
R2
V2(−) TO OUTER DEFLECTOR PLATE
I SYMMETRIC CHARGE:- "A" GROUNDED
II INNER CHARGE:-"V2" GROUNDED, "A" NOT GROUNDED
III OUTER CHARGE:-"V1" GROUNDED, "A" NOT GROUNDED
B1,B2:- BATTERIES EACH OF NOMINAL VALUE, 315 VOLTS
R1,R2:- DIAL TYPE RESISTANCE BOXES, 10,000 OHM
VB1,VB2:- L&N VOLT BOXES TYPE 7591; ACCURACY .04%
DEFLECTOR VOLTAGE CONNECTIONS

FIG. 6. Electrical connections to the deflector plates in the calibrating experiments. Since there was a current drain on the batteries, the potentials were checked frequently during a run, using a potentiometer and standard cell.

$$x_m' = (d\epsilon/d\theta)_m.$$

Direct integration of Eq. (32) gives $x_m' = -0.000936$, and numerical integration of (33) gives $\epsilon_m = 0.99\times10^{-5}$. Then, outside the channel,[17a]

$$x'(M) = x_m' + \int_{M_m}^{M} (-1/\bar{r}\beta M)(dy/dM)dM, \tag{37}$$

and

$$\delta r_f = x_m - \int_{-\infty}^{M_m} x'(M)(dy/dM)dM. \tag{38}$$

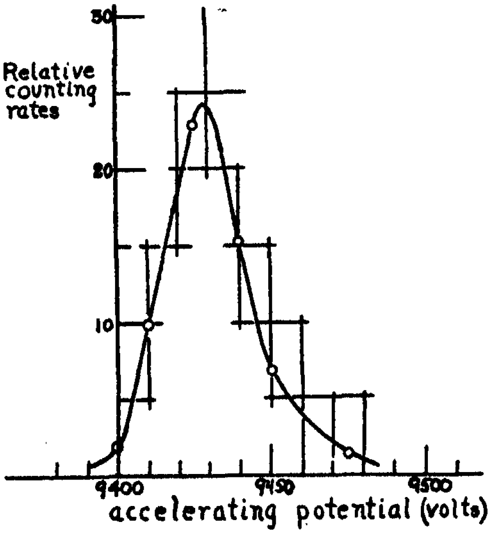

FIG. 7. A profile of the counting rate for electrons vs. accelerating potential in the electron gun. The conditions were as in Table VI.

[17a] These values of x_m' and ϵ_m are so small that replacing either or both of them by zero would not affect our result within the limits of accuracy of our calibration measurements. The fact that they are negligible gives pragmatic justification for not carrying out a more careful calculation of these quantities, in which the tangential, as well as the radial, component of the electrostatic field is included.

TABLE III. k as $f(W_0)$ and charging symmetry.

Arrangement	k calculated for 9.4 kev electrons	k observed
1. Experiments with $\lvert\varphi\rvert=\lvert V_2-V_1\rvert=610.0$ volts; $9.092<W_0<9.704$ kev		
A. Symmetric charge $V_1=305.0$; $V_2=-305.0$ volts	15.448	15.46_2
B. Inner charge $V_1=610.0$; $V_2=0$ volts	14.948	14.95_0
C. Outer charge $V_1=0$; $V_2=-610.0$ volts	15.948	15.95_6
2. Experiment with $\lvert\varphi\rvert=500.0$ volts; $W_0=7.680$ kev		
A. Symmetric charge $V_1=250.0$; $V_2=-250.0$ volts	15.423	15.40_6
3. Experiments with $\lvert\varphi\rvert=410.0$ volts; $6.080<W_0<6.479$ kev		
A. Symmetric charge $V_1=205.0$; $V_2=-205.0$ volts	15.401	15.36_2
B. Inner charge $V_1=410.0$; $V_2=0$ volts	14.901	14.87_4
C. Outer charge $V_1=0$; $V_2=-410.0$ volts	15.901	15.85_0

After integration and numerical substitution it results that $\delta r_f=-0.156$ cm.[18]

C. The Constant of the Analyzer

We define the constant k of the analyzer through the relation

$$k=W_0/z(V_2-V_1), \tag{39}$$

which may be directly determined by experiment. By differentiation of Eq. (6) we obtain

$$dW_0/dr_0=2z\kappa(V_2-V_1)/r_0. \tag{40}$$

Now consider $r_0=\bar{r}+\delta r_0$, and $W_0=\bar{W}_0+\delta W_0$, so that (cf. Table I)

$$W_0=z\left\{\frac{\kappa(V_2-V_1)}{1-\dfrac{\kappa z(V_2-V_1)}{2qm_0c^2}}+\tfrac{1}{2}(V_2+V_1)+2\kappa(V_2-V_1)\frac{\delta r_0}{\bar{r}}\right\}, \tag{41}$$

from which

$$k=\left\{\kappa\left(1+\frac{\kappa z(V_2-V_1)}{2qm_0c^2}\right)+\frac{1}{2}\frac{V_2+V_1}{V_2-V_1}+\frac{2\kappa}{\bar{r}}\delta r_0\right\}. \tag{42}$$

The calculations leading to δr_f enable us to predict the value of δr_0 for symmetric charging, if the position of the entrance slit is known. Let δr_s be the radial displacement of the entrance slit from the point $x=-w$, $y=-l$, the slit being located at $x=-w+\delta r_s$, $y=-l$. Then $\delta r_0=\delta r_s-\delta r_f$ or

$$\delta r_0=\delta r_s+0.156. \tag{43}$$

Experimentally, it is easy to obtain values of k for arrangements other than symmetric charging, but theoretical calculations have not been carried out. Dr. John L. Powell indicated to us how fringing fields from asymmetrical charge distributions can be calculated. In addition to the problem whose solution we have indicated here, where $V_1=\pm\frac{1}{2}\varphi$, $V_2=\mp\frac{1}{2}\varphi$, one must solve the problem for $V_1=V_2=a$. This latter case does not represent a workable analyzer, of course, but when additively combined with the problem we have solved will give the solution for $V_1=\pm\frac{1}{2}\varphi+a$, $V_2=\mp\frac{1}{2}\varphi+a$. In particular, if $a=\frac{1}{2}\varphi$, one obtains the solutions for charge distributions we have experimentally tried. Without completing these calculations, we have made the plausible assumption that δr_0 *is a function of geometry only*, and will be invariant under different charging arrangements. Within the accuracy of our measurements, this assumption is borne out by experiment. Table II shows the various charging arrangements we have tried, with the predicted expression for k.

D. Experimental Calibration

Experimental Arrangements and Procedure

Electrons were passed through the analyzer channel at various kinetic energies in the range 6–10 kilo-

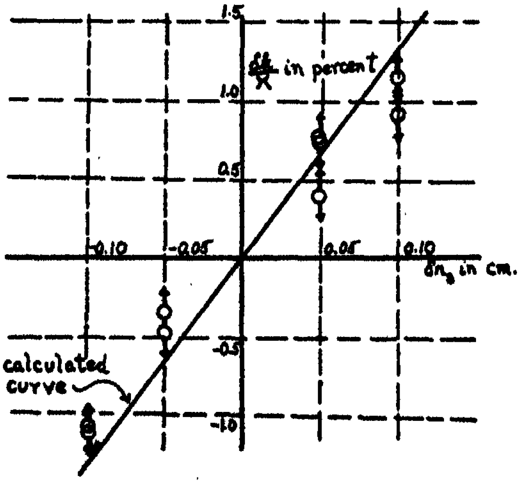

FIG. 8. Calculated and observed values of the variation of the analyzer constant with radial position of the slits. The nonrelativistic value of k_A at the origin of the figure is 15.31_4.

---

[18] The existence of the fringing field has a small effect on the azimuth of the focal point, also. The displacement is toward the entrance aperture of the instrument, and amounts in our case to 0.00313 cm. Such a displacement could produce no measureable effects within the accuracy of our calibration.

TABLE IV. Calculated non-relativistic k values at $\delta r_s=0$ compared with relativistically corrected observations on electrons.

Arrangement	Calculated N.R. k	Observed k, corrected
A. Symmetric charge	15.310	15.29_7
B. Inner charge	14.810	14.79_7
C. Outer charge	15.810	15.78_8

volts, requiring deflector plate voltages in the region from 200–600 volts. The orientation of the analyzer was such that the cylinder axis was horizontal, and the plane of the electronic orbits vertical. Since the electrons moved in orbits of 15 cm radius, a magnetic field with a horizontal component of 20 gauss could produce a comparable curvature. Some iron in the vicinity of the analyzer could not be avoided. With a sensitive compass, the direction of the cylinder axis of the analyzer was rotated in the horizontal plane, until, with the adjacent iron braces, etc., in place, the horizontal component of the magnetic field lay in the plane of the orbits. An earth inductor showed the following:

Horizontal component	0.063 gauss
Vertical component	0.11 gauss
Angle of dip (from the horizontal)	63°

The earth's field clearly was partially screened by iron in the laboratory.

Since the initial direction of the electrons was horizontal and the final vertical, the magnetic field could only produce small deviations parallel to the cylinder axis, which introduce negligible changes in the calibration constant.

The electron gun is shown somewhat schematically in Fig. 5. A brass housing, cylindrical in shape, with an inside diameter of 9.842 cm, had a tungsten wire under spring tension along its axis. The wire was 0.0178 cm in diameter. The wire was parallel to the cylindrical axis of the analyzer. The entire gun was mounted so that it could be rotated about an axis 16.51 cm from the wire and parallel to it, and by means of set screws in the attachment of the gun to the analyzer housing, this axis could be made collinear with the focal line $x=-w$, $y=-l$. A cathetometer was used in this and the following adjustments. The gun was rotated about the focal line until the tungsten wire was in the plane determined by the lines $\{x=-w,\ y=-l\}$ and $\{x=-w,\ y=0\}$. Finally the entrance slit was set by looking through the window in the analyzer wall at the scale, and then, by sighting through the cathetometer, it was verified that the center of the slit aperture lay at the "uncorrected object point" of Fig. 3. These adjustments were correct to within 0.02 cm, which was about the precision to which the slits could be reset.

Figure 6 shows the circuits for determining the deflector voltages, which could be read to about 1 part in 1000. The accelerating voltage for the electrons was supplied by a 540 cycle high voltage half-wave rectifier. The source of the 540 cycle current was a 5 hp synchronous motor a.c. generator combination, with the d.c. field current of the 540 cycle generator supplied from a storage battery used for no other purpose. The only drain on this set was the 200 microamperes, used for voltage measurement, through a 50 megohm wire-wound resistor of 0.1 percent precision. At this low drain a 0.050 microfarad filtering condenser sufficiently suppressed the 540 cycle ripple, and accelerating voltages could be held to 0.1 percent.[19]

TABLE V. Tangential slit displacements.

Symmetric charging: $V_1=305.0$; $V_2=-305.0$ volts
Slits 1 mm wide
Object and image slits at mirror image positions

Object slit position y	x	Observed k for electrons
$-l$; i.e., -5.29 cm	$-w$; i.e., -0.25 cm	15.45_2
-5.50 cm	-0.25	15.44_4
-4.75 cm	-0.25	15.46_7

The electron detector was an Allen[20] electron multiplier tube, and thus extremely low emission currents from the tungsten wire could be used. In making a determination the deflector potentials V_1 and V_2, supplied by B batteries, were set to some desired value, see Fig. 6. The accelerating voltage on the electrons was then changed in steps through the region in which it was expected that the condition of Eq. (41) would be met. Figure 7 shows some of the profiles used in the determination of k, which, experimentally, is simply the ratio

$$W_0/\{-(V_2-V_1)\}.$$

Experiments on k as a Function of Initial Kinetic Energy and Charging Arrangement

Table III shows a series of experiments conducted with the entrance and exit slits each 0.1 cm wide, and at the uncorrected object and image points, where δr_0 of Eq. (43) is $+0.156$ cm.

The value of k for 9.4 kev electrons is relativistically higher than that for heavy positive ions by 0.138, and is 0.113 and 0.091 higher at 7.7 and 6.2 kev respectively. Subtracting these relativistic corrections from their appropriate observed values, and averaging the results gives the *non-relativistic values* in Table IV.

Experiments on the Variation of k_A with Radial Slit Displacements δr_s

It is seen from the equations of the instrument that if a divergent source is located at $x=-(w+\delta r_f)$, $y=-l+\delta l_f$, the non-relativistic value of k_A is κ. Disregarding the negligible shift δl_f,[18] the variation in k

---

[19] The drop of potential along our tungsten filament due to the heating current was in such a direction that this correction was in the opposite sense to the correction for the tungsten work function. The difference, about 1.5 volts, was negligible. Cf. J. W. DuMond, Phys. Rev. 51, 400 (1937).

[20] J. S. Allen, Rev. Sci. Inst. 18, 739 (1947).

TABLE VI. Final measurements on the calibration constant. Symmetric charging: $V_1=305.0$; $V_2=-305.0$ volts. Slits 1 mm wide, located at uncorrected object and image focal points.

Run	50 megohm resistor used	k_A for electrons
1	X	15.43_4
2	Y	15.47_0
3	X	15.46_4
4	Y	15.45_9
5	X	15.46_4
Average k_A for 9.4 kev electrons		15.45_8
Relativistic correction		-0.13_8
Non-relativistic k_A for protons and heavy ions		$15.32_0\pm0.02$
Calculated N.R. k_A from Eq. (42)		15.31_0

as the entrance slit is moved in the x, or radial direction, is obtained from Eq. (42),

$$\delta k/\kappa=2\delta r_0/\bar{r}=\delta r_0/7.50. \tag{44}$$

Entrance and exit slits were always moved together, either in or out, in steps of 0.05 cm. The experiments were carried out with symmetric charging. The graph of Fig. 8 shows the calculated variation and the observed points. The vertical line at each point indicates an error of ±0.15 percent, which corresponds to an error of about 0.02 cm in the setting of the slit centers to any desired δr_s. The slit width was 0.1 cm; $|\varphi|$ was 610.0 volts. The agreement is good, the observed slope being indistinguishable from the predicted in the region $-0.05<\delta r_s<0.05$ cm.

Variation of k with Tangential Slit Displacements δl_s

The theory of the instrument predicts that, relative to the effect of radial displacement, the value of k should be insensitive to displacement of the object slit toward and away from the entrance aperture to the deflecting channel. Table V shows the result of some experiments made to test this point.

Final Determinations of the Analyzer Constant

As the calibration measurements proceeded, the technique of making them improved, and more factors were brought under control. Before disassembly of the calibrating equipment, a final set of runs was carried out. Two precision 50 megohm wire-wound resistances, X and Y, were available and used alternately to detect any temperature effects which might arise. The meter[31] used for reading the current through the 50 megohm resistors was calibrated with a potentiometer immediately before and after the run, etc. The results are given in Table VI.

E. Conclusions

With the present instrument it should be possible to measure energies of moving charged ions in the range $W_0/|z|\gtreqless 1$ Mev with an accuracy of 0.3 percent. The limit is set by the accuracy with which the slits can be set to a given radial position. If, in the future, such instruments are designed with movable slits, the accuracy of setting should be improved.

The observed profiles of Fig. 7 have a half-width at half-maximum less than that predicted by an elementary calculation. Roughly we would expect that the ratio $\delta W_0/W_0$ at half-maximum would be the slit width, 0.1 cm, divided by the $\bar{r}$ of 15 cm, or 1/150. Actually this is observed to be nearer 1/300, and the profile departs considerably from a triangular profile. We have not attempted a precise calculation of this effect.

Operation of the instrument with the object slit located at $y=-5.29$ cm, $x=-0.25$ cm, instead of $y=-5.29$ cm, $x=-0.41$ cm decreases the aperture of the instrument somewhat, and some ions from a divergent source may be lost by hitting the outer plate. This effect can be detected as a variation of the intensity of the image with δr_s, and can be corrected for by moving the slits towards the center of curvature.

Herzog[3] has mathematically investigated certain arrangements of grounded conductors which, if placed just outside the entrance and exit apertures, nullify the shift of the object and image foci due to the stray field. The present work indicates that such auxiliary electrodes are not necessary for the use of the instrument in precise energy measurements. Nevertheless, the possibility of introducing such auxiliary electrodes should not be disregarded, as the design is somewhat simplified if the actual focal points are at the "uncorrected" positions of Fig. 3. On the other hand, when the analyzer is being constructed for the deflection of high energy ions from nuclear reactions, it may occur that the maximum field strength exists between these Herzog shields and the analyzer plates and thus that the presence of the shields determines the maximum deflecting voltage which can be used.

---

[31] Weston Model 622 d.c. milliammeter.

Laboratory and Shop Notes

The Effect of Space Charge on the Focusing Properties of a 180° Mass Spectrometer

CHARLES F. ROBINSON
Consolidated Engineering Corporation, Pasadena, California

June 21, 1949

ASSUME an ion beam in the shape of a narrow ribbon so that the dimension parallel to the magnetic field (here called h) is large compared to the maximum thickness of the beam. Assume a beam having half-angle of divergence α and whose intensity in charge per unit volume is uniform in the neighborhood of any transverse section. Consider a particle having charge q, mass m, velocity v, located in a laminum whose angular position measured from the center of the beam is β, and let the magnetic field strength be B. Using electromagnetic units we find the force on the particle to be given by

$$mv^2/r = vqB \pm 2(\pi Iqc^2/vh)(\beta/\alpha), \tag{1}$$

v being the velocity in cm/sec. and the ± sign referring to particles which are respectively closer to and farther away from the mean center of curvature than the central plane of the beam. I is the total current in the beam.

Solving (1) for r, expressing v in terms of charge and accelerating voltage V, we have

$$r = \frac{1}{B}\left(\frac{2mV}{q}\right)^{\frac{1}{2}}\left[1 \pm \frac{\pi I}{B}\,\frac{mc^2}{qVh}\left(\frac{\beta}{\alpha}\right)\right]^{-1}. \tag{2}$$

The second term in the bracket represents, in situations of interest here, a small perturbation on the radius and the bracket may be expanded in a binomial expansion retaining only the first two terms:

$$r = \frac{1}{B}\left(\frac{2mV}{q}\right)^{\frac{1}{2}}\left[1 \mp \frac{\pi Imc^2}{BqVh}\left(\frac{\beta}{\alpha}\right)\right]. \tag{3}$$

The approximate construction of the perturbed trajectories is a simple matter, the unperturbed trajectories having various values of β being centered on the arc aa' of Fig. 1, while the perturbed trajectories have their centers in the arc bb' which has the same radius

$$r_0 = 1/B(2mV/q)^{\frac{1}{2}}, \tag{4}$$

as the unperturbed trajectory and its center on the line shown, where γ is given by

$$\gamma = (\pi Imc^2/BqVh\alpha). \tag{5}$$

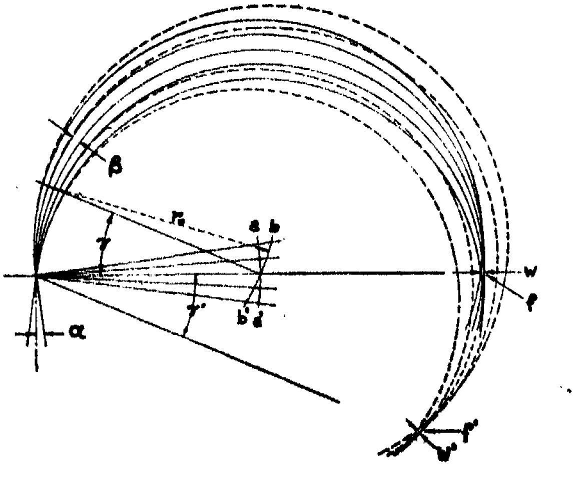

FIG. 1.

It is at once clear from examination of Fig. 1 that in situations in which the ions resolve themselves into a single beam, the first-order effect of space charge is not a widening of the beam at the focus, but a shift of the position at which this focus occurs; f is the (180°) point at which the beam forms a focal spot of width w in the absence of space charge, while f', w' are the corresponding parameters for a beam having appreciable space charge.

It is also evident from a study of the figure, that to the extent to which the arc bb' may be approximated by a straight line, $\gamma' = \gamma$ and the focal line would have the same width in the presence of space charge as if space charge were absent. This is the same approximation which has to be justified to keep spherical aberration within reasonable limits in a conventional instrument and is certainly justified here, so that we may assume $w' = w$, $\gamma' = \gamma$ in the present case. This is to be compared with the conclusion of Smith, Parkens, and Forrester[1] who have apparently overlooked the shift in focal position.

To get an idea of the numerical magnitudes involved, we may assume the following:

γ (shown) = 11° 30′ = 0.2 radian
α = 2° 47′ = 0.05 radian
B = 3500 gauss
V = 1920 volts = 1.92×10^{11} e.m.u.
m = 50 a.w.u. = 8.3×10^{-23} g
q = 1 proton charge = 1.6×10^{-20} e.m.u.

(These parameters correspond to an instrument of five-inch radius.) Under these conditions we find, from (5):

$I = 4.58$ microamperes per cm of beam length.
Using $B = 15{,}000$ gauss, $V = 50{,}000$ volts, $m = 40$

(assumed by Smith *et al.* and corresponding to an instrument of about five-inch radius), and setting $\alpha = 6.8°$, we find $I = 1.6$ ma/cm, which is the same as the result of Smith *et al.*; however, by displacing the resolving slit to the perturbed focal position, we get a beam which is broadened only by spherical aberration and which will pass through a slit less than 1 mass unit in width; in other words, we get a clean separation of adjacent masses in the mass 40 region.

There can be little doubt that this rough analysis will break down to some extent in a practical situation, partly because the assumption that h is large compared to the maximum thickness of the beam will not hold true in a heterogeneous beam and partly because the divergence of the various masses near the focal position complicates the analysis considerably beyond what has been given here. However, there would seem to be equally little doubt that proper allowance for the shift in focal position which results from high space charge will result, in many cases, in a very real improvement in resolution.

---

[1] Smith, Parkens, and Forrester, Phys. Rev. 72, 989 (1947).

A Vacuum Lock for Continuously Evacuated Systems

D. SAXON AND J. RICHARDS
Argonne National Laboratory, Chicago, Illinois

June 30, 1949

IT is desirable on some types of vacuum equipment to provide a mechanical means of inserting items such as counters, sources, probes and the like into the instrument without breaking the vacuum. Two such devices are now in use on a 180° β-spectrometer. One unit facilitates easy replacement of the very thin Nylon windows[1] used on the end window G-M counter while the other is a source quick change. Since space was limited by the pole faces of the spectrometer magnet, the authors were unable to make use of the modified No. 440 Crane split gate valve[2] often used on such devices, and had to use in their place specially built brass stop cocks through which the source and counter pass.

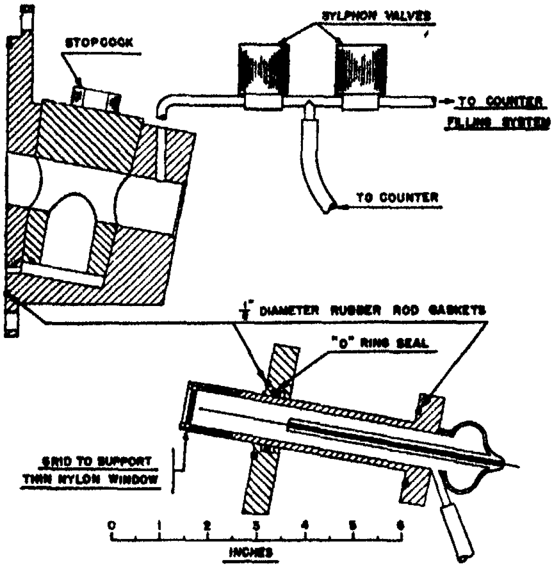
STOPCOCK
SYLPHON VALVES
TO COUNTER FILLING SYSTEM
TO COUNTER
⅛" DIAMETER RUBBER ROD GASKETS
"O" RING SEAL
GRID TO SUPPORT THIN NYLON WINDOW
0
1
2
3
4
5
6
INCHES

FIG. 1. Counter quick change unit.

Figure 1 shows in cross section the counter quick change unit. The two sylphon valves make possible the simultaneous evacuation of both sides of the counter window by the filling system pump before opening the stop cock. After closing the left-hand valve the counter is filled. When in operating position both the counter and the source holder are held in place by hinged studs and wing nuts not shown in the diagrams. The source quick change unit, in Fig. 2, is similar in principle and operation with the exception of the provision made for evacuating the inside of the stopcock when in the closed position. The air which leaks into the counter stop cock when closed is sufficient to break the thin Nylon window when the stop cock is opened. Hence some means for evacuating this volume must be provided. This problem was solved by drilling a small hole from the stop cock well to the spectrometer chamber.

On the source quick change, the leakage problem was solved by using the counter filling system pump to evacuate the vacuum lock and the stop cock. The stop cock surfaces were machined to ±0.0005″ tolerances and then lapped to fit. In addition to the "O" Ring seals, ⅛″ diameter rubber rod was used for some of the gaskets and gave completely trouble free performance.

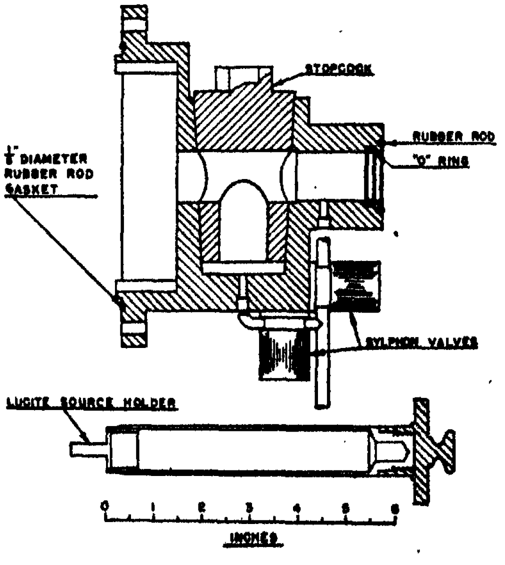

FIG. 2. Source quick change unit.

---

[1] Brown, Felber, Richards, and Saxon, Rev. Sci. Inst. 19, 818 (1948).
[2] F. N. D. Kurie, Rev. Sci. Inst. 19, 485–493 (1948).

An Electronic Instrument for Rapidly Tracing the Plateaux of G-M Counters

G. H. VAZE
Tata Institute of Fundamental Research, Bombay, India

August 3, 1949

THE present day need of large numbers of good counters in cosmic-ray and nuclear research demands a quick method of counter checking. The usual method of tracing the Voltage *versus* Counting Rate curve of a counter takes several minutes. The following electronic circuit is capable of tracing this curve on an oscilloscope in a few seconds.

The circuit essentially consists of a sweep circuit which varies the voltage on a G-M counter linearly and appears as a horizontal sweep for the scope. The integrated counting rate appears as the vertical sweep, thus enabling the spot to trace the required curve. The block diagram of the circuit is given in Fig. 1. The circuit details are briefly given below:

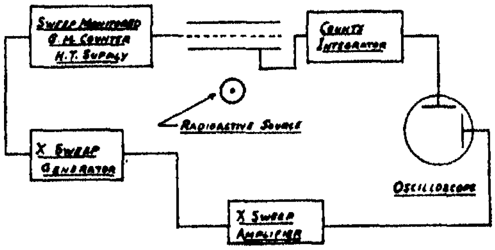

FIG. 1.

The linearly varying voltage required for the G-M counter is taken through a high voltage amplifier. A transmitter tube type 813 is used for this purpose. The plate of this tube is supplied with a high voltage obtained by rectifying 2500 volts a.c. through a high resistance. A linearly varying negative sweep when applied as an input to this tube, produces a linearly increasing high voltage on the plate. These variations are made to appear across a condenser through a diode. The voltage across this condenser is the required G-M counter high voltage. It is necessary to connect a resistance across this condenser to let the charge leak away when the sweep flies back to the initial value.

Since the horizontal sweep on the scope should be in phase with the varying voltage across the G-M counter, it is necessary to feed the same negative sweep voltage, as applied to the high-voltage amplifier, to a power pentode, and the variations developed at the plate of this pentode are taken through a diode and applied to an X plate of the oscilloscope. The diodes in the above circuits act as buffers.

The linear negative sweep, required for the X sweep and the G-M counter (h.t.) supply, is obtained by charging a condenser to about 200 volts through a constant current device, such as a sharp cut-off pentode, and then discharging it through a thyratron. The required negative portion of this saw-tooth voltage taken through a diode supplies the necessary sweep voltage. The period of the sweep can be varied from 0.2 to 5 seconds.

The sharp positive pulses from the G-M counter due to a radioactive source are fed to a biased pentode and then passed on to a

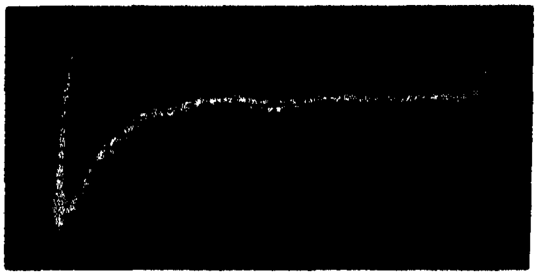

FIG. 2.

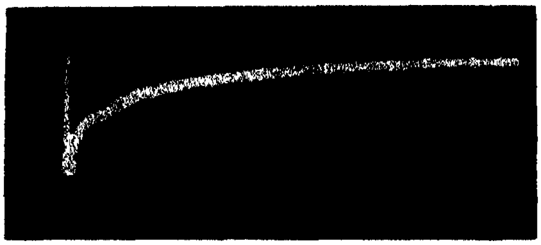

FIG. 3.

conducting pentode. The pulses from this pentode, broadened by a multivibrator circuit, charge a condenser through a diode. The voltage proportional to the counting rate built up across this condenser is used as the Y sweep. The integrating time of the circuit is 0.4 seconds.

Figures 2 and 3 are oscillograms of these curves. The name "PLATOSCOPE" has been suggested for the instrument and "PLATOGRAM" for the curves. These platograms are traced in a single sweep of five seconds.

Figure 2 is a platogram of a counter with a weak thorium source, the counting rate being 250 counts per second. The X sweep in this case varies from 900 to 1600 volts. The integrating time of the circuit being 0.4 seconds, the mean number of counts in this time interval is 100 and the expected fluctuation is of the order of 10 percent, in agreement with what is observed in Fig. 2. Figure 4 shows the plateau curve of the same counter but drawn from the readings taken in the usual way.

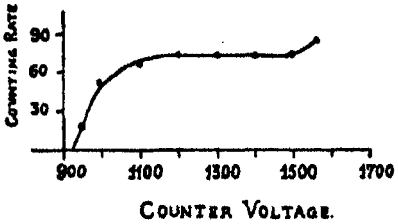

FIG. 4.

Figure 3 is the platogram of another counter taken with a radium source, the counting rate in this case being more than one thousand per second, and the X sweep varying from 900 to 1400 volts. This platogram taken with a strong source is smoother than the one in Fig. 2 taken with a weak source due to the relatively smaller statistical fluctuation.

A more detailed account of this instrument with circuit diagrams will be published elsewhere.

I wish to express my grateful thanks to Dr. Bhabha for his continued interest in this work. I would also like to express my thanks to Mr. K. B. McCabe who originally suggested this method and to Mr. A. B. Sahiar for helpful discussions throughout the work.

Empirical Balancing Procedure for FP-54*

F. C. ARMISTEAD
Massachusetts Institute of Technology, Cambridge, Massachusetts

June 16, 1949

THE FP-54 electrometer tube can be made both easy to balance and stable to operate, giving the high current amplification claimed by the manufacturer with no exceptional experimental difficulty. Stable operation is assured by the precautions prescribed in the G. E. descriptive sheets ETI-160.

The circuit, see Fig. 1, is essentially the Penick circuit,[1] which accomplishes automatic compensation for battery drift. The sensitivity with 10^{11} ohms on the grid was 1-cm deflection (at a meter) for 10^{-15} amp input. Characteristic curves such as that on the extreme right in Fig. 2 have the same wide maximum as Penick dealt with, and give the most stable operation. This procedure leads to the same balance on the characteristic curve as Penick's. The value of the procedure lies chiefly in the simplicity of the sequence of steps, such that it can be easily performed even by a person with no understanding of the circuit. Furthermore, whereas the Penick article dealt with the no longer available D-96475 tube, this procedure deals with an available tube. Stability with battery drift is excellent, being equally as good as that previously obtained by the author using the D-96475 and the Penick procedure.

Balancing Procedure: Provide leads convenient to the outside for testing as follows:

Points 1, 2, 3, 4, 5, 7, and 8, also the circuits at 1 and 3 should be easily opened for insertion of meter to measure i_{g1} and i_p.

Make all voltage measurements, E, with respect to point 4 using vacuum tube voltmeter.

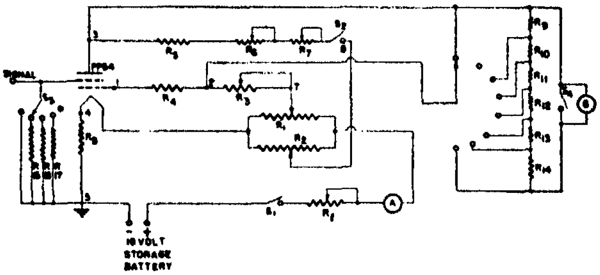

FIG. 1.

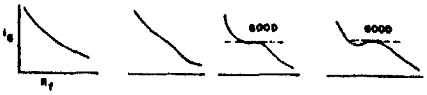

FIG. 2.

R_1: 200-ohm potentiometer; later replaced with fixed resistors.
R_2: 200-ohm potentiometer; later replaced with fixed resistors.
R_3: 10-K potentiometer; later replaced with fixed resistors.
R_4: 10 K.
R_5: 20 K.
R_6: 50-K potentiometer.
R_7: 1-K potentiometer.
R_8: 44.4 ohms.
R_f: 50 ohm potentiometer; later replaced with 6-ohm potentiometer and appropriate fixed resistor.
A: 0–100-ma meter.
S_1 and S_2: SPST toggle switches.
S_3: 8-position, shorting, selector switch, for shunt selection.
S_4: Key, normally closed.
S_5: n-position selector switch, for sensitivity selection. (Laboratory-made for high insulation).
G: Leeds and Northrup galvanometer, 2500f, 10^{-4} micro-amp./mm, C. D. R. X. 22 K.

Ayrton Shunt:
R_9: 250 ohms.
R_{10}: 1 K.
R_{11}: 2 K.
R_{12}: 4 K.
R_{13}: 10 K.
R_{14}: 20 K.

Sensitivity Selector:
R_{15}, R_{16}, R_{17}, etc.: 10^{11} ohms and less Victoreen Hi-Meg Resistors.

Start with galvanometer disconnected, also with R_1, R_2, R_3, and R_6 mid-range.

Always close S_1 before S_2, to avoid drift.

1. Ground FP-54 grid and turn Ayrton Shunt to open circuit position, i.e., the second position.
2. Adjust R_f until E_5 is -4.0 v.
3. Adjust R_1 until E_1 is 4.0 v (normally i_{g1} is 200 to 300 microamp.).
4. Adjust R_2 until E_2 is 6.0 v (normally i_p is 60 microamp.).
5. Successively re-perform steps 3 and 4 until both conditions are satisfied. R_3 and R_6 may be used in making final adjustment.
6. Measure E_2. If E_2-E_3 is greater than $\frac{1}{4}$ volt, reduce the filament current from the value set in step 2 so that E_5 is, say, -3.9 v, and repeat steps 3 through 6. If E_3-E_2 is greater than $\frac{1}{4}$ volt, increase filament current and repeat steps 3 through 6. When the difference is less than $\frac{1}{4}$ volt, proceed to step 7.
7. Connect a microammeter between points 2 and 3. Plot i_G microamperes *vs.* R_f settings, as filament current is varied both above and below the value chosen in step 2 or 6. A curve such as one of those in Fig. 2 should be obtained. To change curve shape to one on the right in this sequence, increase E_8 slightly, using slider on R_2; then bring E_2 and E_3 into equality again, using R_7; then re-perform step 7. Using R_6 move the whole curve vertically to make the flat portion correspond to zero microamperes.

Note: Record E_5, E_7, E_8, E_3, and E_1. These five numbers completely specify the curve which is observed. To re-establish a desired curve, set

E_5 by adjusting R_f,
E_7 by adjusting R_1,
E_8 by adjusting R_2,
E_3 by adjusting R_6,
and E_1 by adjusting R_3.

The last two will need to be successively re-performed until right.

When a good curve is obtained there is little advantage in seeking another one. Proceed immediately to step 11. However, if another curve is to be sought, in hope of a better, proceed to step 8.

8. Hold E_7 fixed and choose another value for E_8, using slider on R_2. Measure E_2 and E_3. Make them equal by adjusting R_6 alone, if possible, or start again at step 6, if not possible.
9. Same as step 7.
10. If still further balances are to be sought after exhausting the possibilities with fixed E_7 and various E_8's, it is better to start from the beginning again, but with R_3 and R_6 not at mid-range.
11. Re-set to those values of E_5, E_7, E_8, E_3, and E_1 which give the best curve for i_G *vs.* R_f. Make final adjustments as in step 7 except use galvanometer instead of microammeter, and adjust with R_f and R_7 only. Replace R_1, R_2, and R_3 with fixed resistors of the proper value, in order to keep the number of unsoldered connections in the circuit to a minimum. Also replace R_f with a 6-ohm potentiometer in series with a proper fixed resistor; this will facilitate later shifts in the filament current to follow any small drift of the balance point.

---

* This work was performed under Contract No. W-7405-eng-175 with the U. S. AEC in connection with the M. I. T. Metallurgical Project.

[1] D. B. Penick, Rev. Sci. Inst. 6, 115 (1935).

An Electrometer Amplifier

V. J. Caldecourt
The Dow Chemical Company, Midland, Michigan

June 30, 1949

THE advantages of the minature tube 12BE6 as an electrometer tube were pointed out by H. S. Anker.[1] Tubes of this type have a grid current of 10^{-13} to 10^{-14} amperes and a voltage gain between 200 and 300. They are compact and relatively non-microphonic.

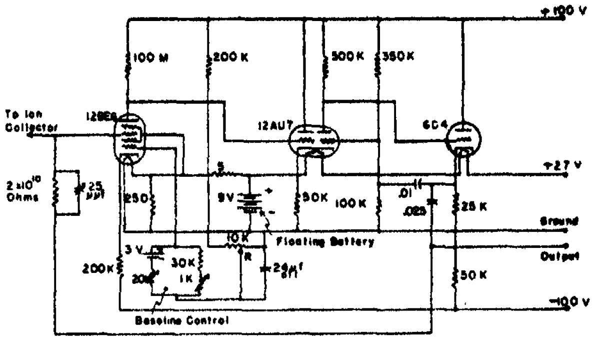

FIG. 1. Electrometer amplifier.

The grids 1, 2, and 4 in this pentagrid tube can be used to secure additional circuit stability over that inherent in the amplifier designed by H. S. Anker. The circuit shown in Fig. 1 has three features which improve circuit stability:

(1) The electron flow from the cathode of the 12BE6 tends to be maintained at a constant value because of degeneration in the large cathode resistor. The sensitivity of the circuit to filament current changes is reduced by a factor of seven without appreciable loss in amplifier gain.

(2) By proper choice of the setting of potentiometer R and then resetting the output to zero with the baseline control circuit a condition can be reached where the amplifier baseline is not affected by small changes in B supply voltage. This balance need not be made very accurately if a high stability power supply and a floating battery is used.

(3) A battery of dry cells (three Burgess 2F2H) is floated on the power supply to stabilize the filament temperature of the 12BE6 and to stabilize the potential of grids 2 and 4. The floating battery has been found worthwhile even when the regulated power supply prevents a 10 percent line voltage change from disturbing the amplifier baseline. Dry cells floated on a power supply provide high stability with little upkeep since the battery drain is nearly zero.

The d.c. amplifier in operation here shows a grid current of 10^{-13} amperes and a noise level of less than 0.1 mv as recorded by a Speedomax *A*. In obtaining a low noise level, care must be taken to avoid multiple grounds and low frequency vibration of the input grid lead. The power supply used is similar to the one described by H. S. Anker.[1] The gain of the d.c. amplifier without feedback is about 1000. A baseline drift of 1 to 2 mv per day is average. The unit is operated 24 hours per day and is used in conjunction with a mass spectrometer.

---

[1] H. S. Anker, "Stabilized d.c. amplifier with high sensitivity," Electronics (June, 1947), p. 138.

Improved Magnetic Focusing of Charged Particles

H. Hintenberger
Kaiser Wilhelm-Institut für Chemie, Tailfingen, Germany

July 18, 1949

IN this journal L. Kerwin[1] has recently published a theory of magnetic focusing of charged particles in which a formula for the shape of a uniform magnetic field is deduced[2] giving perfect focusing of an ion beam of wide divergence. Several special cases are discussed of second-order focusing in a uniform magnetic field whose edges are in the shape of straight lines or circles. About a year earlier nearly the same considerations were presented by the author in a letter to the Zeitschrift für Naturforschung.[3,4] To

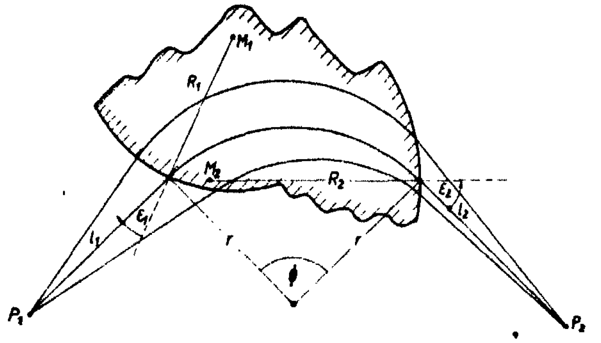

FIG. 1. General case of second-order focusing of an ion beam in a homogeneous magnetic field with curved field boundaries.

designers of second-order focusing instruments it should be of interest, that all cases of second-order focusing hitherto published,[1,2,3] are special cases of the following general second-order focusing condition:[4]

$$r\left\{\frac{\gamma_1}{R_1}+\frac{\gamma_2}{R_2}\right\}=c_1+c_2, \tag{1}$$

where the constants γ and c are given by

$$\gamma_{1,2}=\frac{1}{\cos^2\epsilon_{1,2}\left(\left[1+\left(\frac{r}{l_{1,2}}+tg\epsilon_{1,2}\right)^2\right]^3\right)^{\frac{1}{2}}}, \tag{1'}$$

$$c_{1,2}=\frac{r^2}{l_{1,2}^2}\cdot\frac{\left[\frac{r}{l_{1,2}}+3tg\epsilon_{1,2}\right]}{\left(\left[1+\left(\frac{r}{l_{1,2}}+tg\epsilon_{1,2}\right)^2\right]^3\right)^{\frac{1}{2}}}, \tag{1''}$$

and where $l_{1,2}$ and $\epsilon_{1,2}$ must fulfill the first-order focusing condition

$$r\sin\phi+l_1\frac{\cos(\phi-\epsilon_1)}{\cos\epsilon_1}+l_2\left[\frac{\cos(\phi-\epsilon_2)}{\cos\epsilon_2}-\frac{l_1}{r}\,\frac{\sin(\phi-\epsilon_1-\epsilon_2)}{\cos\epsilon_1\cos\epsilon_2}\right]=0, \tag{2}$$

first given by R. Herzog.[6]

For the notations used see Fig. 1. The radius of curvature of the piece boundary on the one side, for example, R_1 is then determined by (1). Especially, one boundary can be chosen as a straight line, *f.i.* $R_1=\infty$, then $r/R_2=(c_1+c_2/\gamma_2)$. If both boundaries are straight lines, second-order focusing can only be attained for certain values of l or ϵ which are given by $c_1+c_2=0$. A special solution of this equation is:

$$r/l_{1,2}=-3tg\epsilon_{1,2}. \tag{3}$$

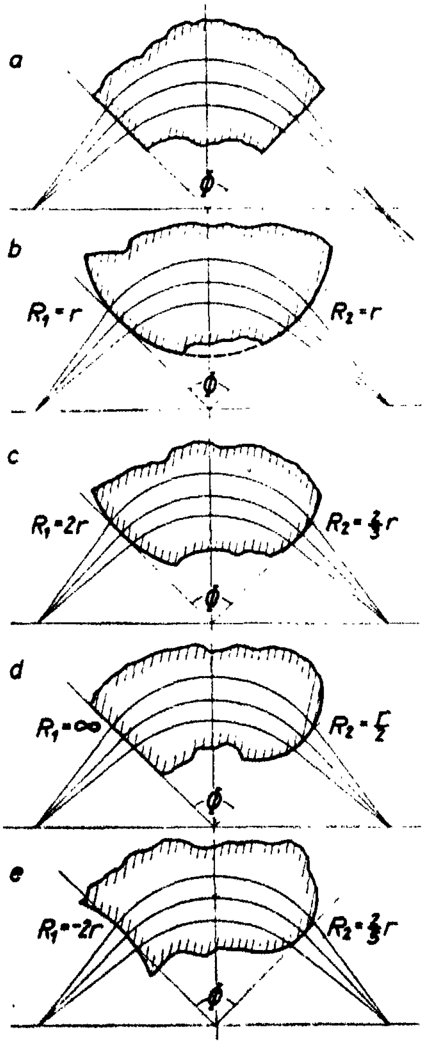

FIG. 2. Various possibilities of second-order focusing with $\Phi=90°$.

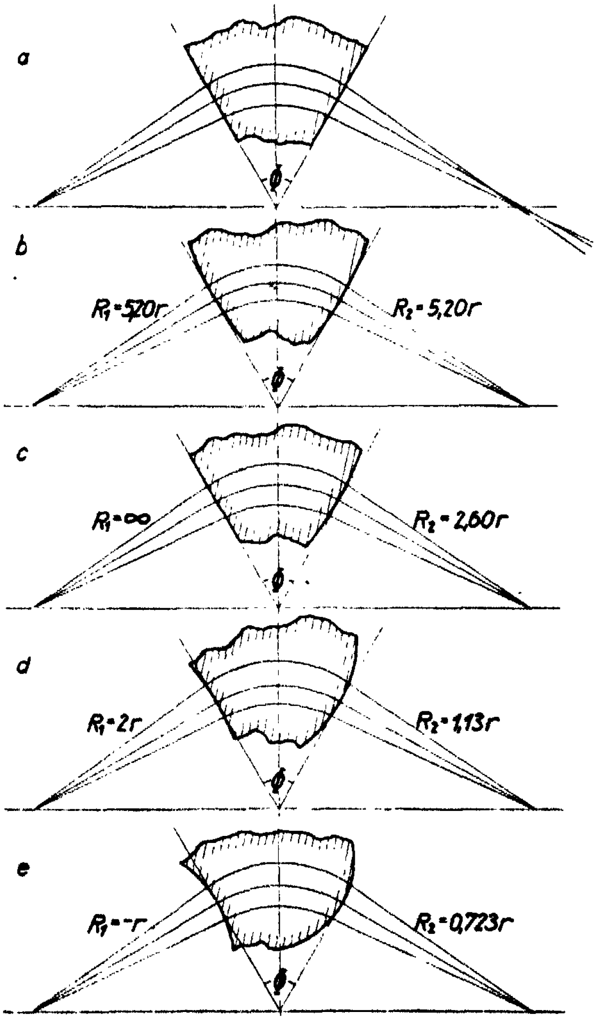

FIG. 3. Various possibilities of second-order focusing with $\Phi=60°$.

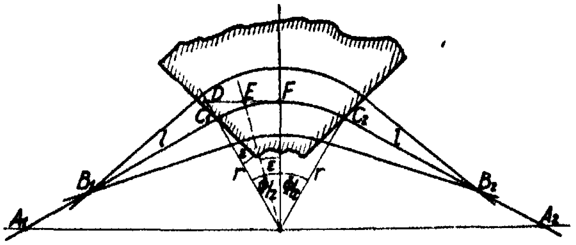

FIG. 4. Second-order focusing with straight lines as field boundaries.

In the symmetrical case ($l_1=l_2$, $\epsilon_1=\epsilon_2$, hence $\gamma_1=\gamma_2=\gamma$ and $c_1=c_2=c$) Eq. (1) becomes

$$r\left[\frac{1}{R_1}+\frac{1}{R_2}\right]=2\frac{c}{\gamma}=2\frac{r^2}{l^2}\left[(r/l)+3tg\epsilon\right]\cos^2\epsilon. \tag{4}$$

If moreover $\epsilon_1=\epsilon_2=0$ (entrance and exit of the beam normal to field boundaries) we can write the second-order focusing condition thus:

$$r\left[\frac{1}{R_1}+\frac{1}{R_2}\right]=2\frac{r^2}{l^2}=2tg^2\frac{\Phi}{2}. \tag{5}$$

In Figs. 2b–e and 3b–e several possibilities of second-order focusing are presented for $\Phi=90°$ and $\Phi=60°$ respectively and $\epsilon_1=\epsilon_2=0$. This may be compared with the first-order focusing shown in Figs. 2a and 3a.

In the symmetrical case with straight lines as field boundaries (inflection case $l_1=l_2$, $\epsilon_1=\epsilon_2\neq 0$, $1/R_1=1/R_2=0$, see Fig. 4) Eqs. (2) and (3) give the simple relations:

$$tg\epsilon=-\tfrac{1}{2}tg\frac{\Phi}{2},$$

$$\frac{l}{r}=-\tfrac{1}{3}\cot\epsilon=\tfrac{2}{3}\cot\frac{\Phi}{2}.$$

It is clear that second-order focusing may be applied advantageously in high intensity mass- and beta-spectroscopy.

A detailed report on the subject will be given in an article to be published in the *Zeitschrift für Naturforschung*.

[1] L. Kerwin, Rev. Sci. Inst. 20, 36 (1949).
[2] Smythe, Rumbaugh, and West, Phys. Rev. 45, 724 (1934).
[3] H. Hintenberger, Zeits. f. Naturforschg. 3a, 125 (1948).
[4] H. Hintenberger, Zeits. f. Naturforschg. 3a, 669 (1948).
[5] K. T. Bainbridge, Seventh Solvay Congress in Chemistry, September 1947.
[6] R. Herzog, Zeits. f. Physik 89, 786 (1934).

Mercury Vapor Trap to Protect Laboratory Workers

JAMES J. BROPHY
Physics Department, Illinois Institute of Technology, Chicago, Illinois

July 12, 1949

WHEN using glass vacuum systems, it frequently becomes necessary to repair punctures or cracks in the glass walls. If mercury is contained in the system, "blowing" the repaired point with a blow tube held in the mouth may become quite hazardous due to mercury vapor. Experience in this laboratory indicates that cool tubing between the joint under repair and the blow tube is not a safeguard against mercury vapor. Because of the frequency of such minor repairs and the hazards involved, it becomes imperative that some device be used to prevent mercury vapor from leaving the system and yet to allow the glass to be worked in the usual manner.

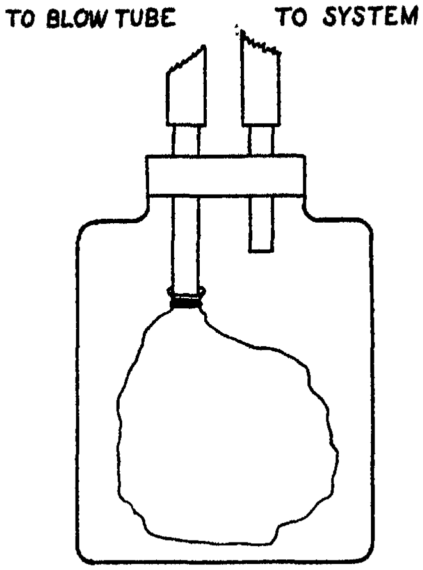

FIG. 1.

Allison[1] has described a satisfactory mouth-controlled valve for the use of compressed air to blow the glass, but it was felt that a less complicated device was needed. Traps containing water or oil proved ineffective. Finally, the device shown in the figure was devised and has been in use for some time.

A jar from vacuum-packed coffee was obtained and two pieces of copper tubing soft soldered to the metal cap. An ordinary toy rubber balloon is held to one of the tubes inside of the jar by a rubber band. Rubber tubing leads from the other end of the copper tube to the blowing mouthpiece, and from the other copper tube to the system. It can be seen that there is complete isolation of gas in the system from the atmosphere, yet the expansion of the balloon forces air into the system. The glass blower has the same control over the blowing as if the balloon were not present. It was found that a jar of the size described has sufficient capacity to allow working a system of average size.

This device has been in use for some time in this laboratory and has proven very effective in working mercury-filled systems. There is no maintenance other than the replacement of the balloon every few months to prevent its becoming contaminated.

[1] J. L. Allison, Rev. Sci. Inst., 12, 212 (1941).

Improved Multivibrator Quenching Circuit

C. V. ROBINSON
Biophysical Laboratory, Harvard Medical School, Boston, Massachusetts

July 15, 1949

THE multivibrator quenching circuit, though it is more complex than the Neher-Pickering or Neher-Harper circuits, has an important advantage in that it produces a quenching pulse whose size and duration are independent of the counter pulse. The multivibrator action of the original circuit by Getting[1] has been improved upon by Maier-Leibnitz,[2] but neither circuit has the advantage of permitting the counter cylinder to be grounded. One example in which this feature is necessary, is the use of metal-walled counters for biological experiments *in vivo*. The following circuit has good multivibrator action and permits the counter cylinder to be grounded.

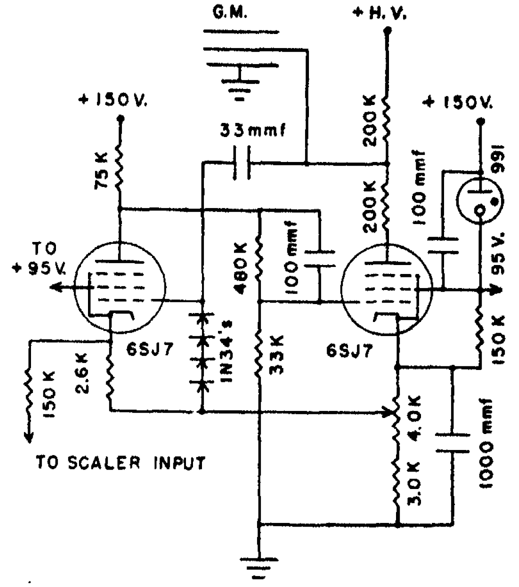

FIG. 1. Multivibrator quenching circuit.

The circuit is shown in Fig. 1. The right, or second, 6SJ7 in the figure is normally not conducting, and its plate supply is the positive operating voltage of the counter. The counter is connected into the plate resistor of this tube and coupled by a condenser to the grid of the first 6SJ7 which is normally conducting and has a 150 v plate supply. When a negative pulse appears on the counter wire, the multivibrator is triggered and the wire undergoes an approximately square negative quenching pulse (Fig. 2) which is one-half the pulse on the plate of the second 6SJ7. The voltage on the counter wire drops 240 volts initially, then rises to and remains at 170 volts below the operating voltage for the duration of the pulse and finally recovers in about 5 percent of this time. The recovery of the control grids to their steady bias values is considerably quicker than the recovery of the counter wire, so that the circuit is always ready for any pulse coming from the counter. The quick recovery of the circuit depends on the use of d.c. coupling from the first plate to the second grid and the use of crystal diodes for the first grid resistor (Fig. 1).

The duration of the quenching pulse is proportional to the capacitance of the condenser which couples the counter to the circuit. However the 5 percent recovery fraction is not affected by varying this capacitance. The potentiometer in the second cathode resistor varies the cut-off bias of the second tube, and hence the sensitivity of the circuit, without affecting the size or shape of the quenching pulse. Since the quenching pulse is likewise independent of operating voltage, the average plate current of the second 6SJ7 gives an accurate measure of the counting rate.

The circuit is sensitive to quite small pulses but will operate with a fair amount of capacitance across the input so that an input cable may be used. Some background may be caused by leakage pulses.

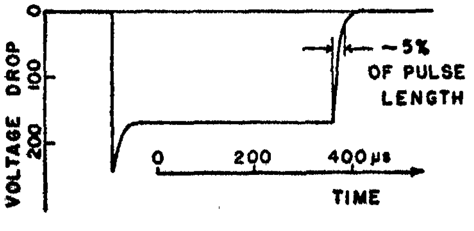

FIG. 2. Quenching pulse on the counter wire.

The voltages necessary to operate this circuit are supplied from outlets in most commercial scaling units. The proper value for the resistor which couples the circuit to the scaler depends on the sensitivity of the scaler to be used.

The author wishes to thank Mr. D. C. Caton for his friendly help and interest in working out this circuit. This work has been supported in part by the Atomic Energy Commission.

[1] I. A. Getting, Phys. Rev. 53, 103 (1938).
[2] H. Maier-Leibnitz, Rev. Sci. Inst. 19, 500 (1948).

Note on the Accuracy of the Buerger Precession Camera

HOWARD T. EVANS, JR.
Massachusetts Institute of Technology, Cambridge, Massachusetts

June 30, 1949

IN a recent communication[1] concerning the use of the Buerger precession camera in x-ray diffraction studies of single crystals, it was observed that in one test lattice measurements made with this instrument appeared to be accurate to within four parts in 10,000. Since there has been considerable interest in this point, it seemed worthwhile to survey the accuracy of the method to obtain a more reliable estimate than is afforded by this single observation. Several exposures were made of a quartz crystal (after Bradley and Jay),[2] using various x-ray wave-lengths and crystal-to-film settings (F). The results are summarized in Table I.

TABLE I.

Film	F, cm	Rad.	a_0, A	Error, p.p.t.	c_0, A	Error, p.p.t.
	Bradley & Jay		4.91278		5.40416	
1	6.00	Cu$K\alpha$	4.911	−0.37	5.406	0.37
2	5.50	Mo$K\alpha$			5.4077	0.65
		Mo$K\alpha_1$	4.9260	2.73		
		Mo$K\alpha_2$	4.9240	2.32		
		Mo$K\beta$	4.9260	2.73	5.4018	−0.44
3	6.00	Mo$K\alpha$			5.4102	1.11
		Mo$K\alpha_1$	4.9330	4.15		
		Mo$K\alpha_2$	4.9352	4.60		
		Mo$K\beta$	4.9266	2.81	5.4109	1.24
4	7.00	Mo$K\alpha$	4.9318	3.91	5.4134	1.70
		Mo$K\beta$	4.9312	3.79	5.4105	1.16

It is apparent that the original observation was optimistic, as was to be expected. The average error, uncorrected, is 2.50 parts per thousand, in agreement with the recent estimate of Barnes.[3] In some cases the error may be as high as 5 p.p.t.

Two factors probably account for most of the error: (1) error in F setting and (2) film shrinkage. The latter is probably responsible for the consistently high values shown. Evidently, in film No. 1, the two errors nearly cancel each other. It is suggested that in future models of this instrument the distance from film to crystal be fixed at 6.000 cm, so that the error due to this source may be eliminated.

The difference in average error in the a_0 and c_0 measurements is probably a result of crystal shape. The prismatic crystal is approximately 0.1×0.3 mm in size, and the resulting elongation of the x-ray spots would give rise to variations in error of judgment in setting a hairline in the two directions.

[1] Evans, Tilden, and Adams, "New techniques applied to the Buerger precession camera for x-ray diffraction studies," Rev. Sci. Inst. 20, 155–159 (1949).
[2] A. J. Bradley and A. H. Jay, Proc. Phys. Soc. 45, 507–522 (1933).
[3] W. H. Barnes, Am. Min. 34, 173–180 (1949).

Equipment for Measuring Light Scattering

M. Bier and F. F. Nord
Department of Organic Chemistry, Fordham University, New York, New York*

August 10, 1949

DURING our investigation by light scattering of aggregation phenomena in aqueous colloidal solution,[1] we have employed for two years a simple Tyndallometer in conjunction with a differential refractometer. The two instruments are similar to those described by P. P. Debye.[2] This description is presented because of the simplicity of construction and ease of use of our models, as well as because of the glass cells employed.

In the Tyndallometer presented in Fig. 1, the light from a mercury arc lamp (General Electric AH-4) is focused by a simple optical system on the center of the cell containing the solution to be examined. The optical system is conveniently placed in an optical tube, which contains light filters to isolate the desired band of the mercury arc spectrum (Wratten filters No. 2A and C5 for $\lambda = 4360$A. The tube can be equipped with a polarizer.

The housing of the cells containing the solutions is cylindrical, the cells containing the solution to be examined being centered by a system of semicircular double recesses. It is fitted with a double bottom for temperature regulation by water circulation. The heavy wall of the housing possesses radial apertures at angles of 45, 90, 135, and 180° to the incident beam of light. Into these circular apertures slides a short metal tube connected to the window of the search unit, which it supports. The search unit is part of an electronic photometer (Photovolt Corporation, New York, N. Y.: Model 512 with special multiplier search unit attachment), whose sensitivity is approximately 1×10^{-9} ft.-c. Thus, either the intensity of transmitted light or the scattering intensity at the three symmetrical angles can be measured. The window of the search unit is equipped with a photographic shutter and the above-mentioned short metal tube. This contains a reversed collimating system, consisting of a lens ($f = 5$ cm) and a screen with a central pin hole, placed in the focal plane of the lens. This system is necessary for accurate delimitation of the angle of scattering.

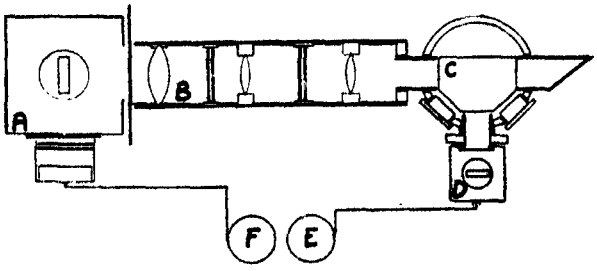

FIG. 1. Tyndallometer (top view): A = Light source; B = Optical system and light filters; C = Semioctagonal glass cell containing the solution; D = Search unit; E = Electronic photometer; F = Controlling photoelement.

The intensity of the primary beam of light is continually checked by a self-generating photoelement. The line voltage to the mercury arc lamp is regulated by a constant voltage transformer. The lamp housing is water cooled. A rotating plate with circular apertures of varying diameters is interposed between the light source and the optical tube. This offers a convenient way of regulating the intensity of the primary beam of light, thus extending the most useful range of the photometer.

For 90° scattering, rectangular cells are used. For angular measurements, semioctagonal cells have been introduced. To avoid reflection from the back wall of the cell, with consequent increase in measured dissymmetry of scattering, it has been found essential that this wall be either of black glass or provided with a dull black glass cement, fused on its outer surface.†

In the differential refractometer presented in Fig. 2, a mono-tic light beam is obtained by the use of a precision slit and a set of light filters identical with those used in the Tyndallometer. The beam is rendered as nearly parallel as possible, and, upon passage through the refractometer cell, is focused by a lens ($f = 65$ cm) on the cross hair of a microscope ocular. The ocular can be moved horizontally by a micrometer screw, measuring the displacement of the projection image of the slit with an accuracy of 2×10^{-4} cm. The whole optical system and the thermostated cell holder are conveniently placed in an optical tube.

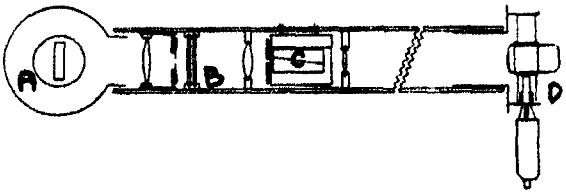

FIG. 2. Differential refractometer (top view): A = Light source; B = Optical system and light filters; C = Two-compartment cell for solvent and solution; D = Microscope ocular and micrometer.

The fused refractometer cell is rectangular, with optical glass windows and divided longitudinally by a thin glass wall, fused at an angle of about 77° to the front window. The cell is thus divided into two equal compartments, one containing the pure solvent and the other the solution. The beam of light, in passing through the cell, will be deflected proportionally to the difference of the refractive indices of the liquids in the two compartments. The sensitivity of the instrument is $\pm 2\times 10^{-6}\Delta\mu$. In calculating the index of refraction and calibrating the instrument, the deflection of the beam of light caused by the glass wall which divides the cell, must be taken into consideration. The original type of cell,[2] containing a hollow triangular prism, was found to give less reproducible results, due to the large difference in volume of the two compartments.

The calibration of both instruments must be carried out with samples of known turbidity, resp. index of refraction. Both instruments may be used in full light.

This work was carried out under the auspices of the Office of Naval Research. The instruments were built by W. H. Baker, Elmhurst, L. I., N. Y.

---

* Communication No. 184.

[1] M. Bier and F. F. Nord, Proc. Nat. Acad. Sci. 35, 17 (1949); Timasheff, Bier, and Nord, *ibid.* 35, 364 (1949).

[2] P. P. Debye, J. App. Phys. 17, 392 (1946).

† Such cells are manufactured by the Pyrocell Manufacturing Company, New York, N. Y.

Absorption Corrections in X-Ray Studies of Preferred Orientation

J. F. H. Custers
Diamond Research Laboratory, Johannesburg, South Africa

June 10, 1949

WITH reference to the paper by Smoluchowski and Turner,[1] I would like to draw attention to the fact that this problem was considered in some detail nearly a year ago. A paper embodying similar calculations appeared in Physica[2] as a supplement to "A New Method for the Determination of Preferred Orientations,"[3] where the treatment was somewhat fuller than in the paper by Smoluchowski and Turner. However, in general, their results confirm those obtained earlier, but the following points are worthy of mention.

In my paper not only the case of transmission (diffracted beams emerging at the back of the specimen, i.e., case of S. and T.) is considered, but formulas are also derived for the absorption factor for x-rays when these are reflected from the front of the flat specimen. Neglect of the absorption is not permissible in this latter case, as is evident both from the theoretical and experimental curves published by me.[3]

The formulas for $(E/E_0)_f$ and $(E/E_0)_b$, that is for the intensities of reflected and transmitted x-rays respectively were given by me in a somewhat complicated form. On substitution of

$$\sin\alpha_C = \cos\alpha_{ST} \quad \text{and} \quad \sin\varphi_C = -\cos\beta_{ST},$$

where the index ST refers to Smoluchowski and Turner, and the index C to Custers, it can easily be verified that the general formula for $(E/E_0)_b$ takes the form given by S. and T. (their formula 2).

If the formula for $(E/E_0)_f$ as given in my paper and which refers to reflected radiation, is transformed by making the abovementioned substitutions, it is found that the intensity of the reflected x-rays as a function of the angle of incidence α takes the form:

$$I = (A/A-\cos\alpha)e^{\mu t/A}\left[e^{-\mu t/A} - e^{-\mu t/\cos\alpha}\right].$$

The expressions for transmitted and reflected x-rays differ, therefore, only by the factor $\exp(\mu t/A)$.

In my article a formula is also given for the breadth of the Debye line as a function of the azimuth angle. This breadth turns out to be a sine-function.

---

[1] R. Smoluchowski and R. W. Turner, "Absorption corrections in x-ray studies of preferred orientation," Rev. Sci. Inst. 20, 173 (1949).

[2] J. F. H. Custers, "The intensity distribution along the Debye halo of a flat specimen in connection with a new method for the determination of preferred orientations," Physica 14, 461 (1948).

[3] J. F. H. Custers, Physica 14, 453 (1948).

New Instruments

W. A. Wildhack: Associate Editor
in Charge of this Section
National Bureau of Standards, Washington, D. C.

These descriptions are based on information supplied by the manufacturer and in some cases from independent sources. THE REVIEW *assumes no responsibility for their correctness.*

Ultrasonic Analyzer

A new panoramic system for ultrasonic spectrum analysis has been announced by Panoramic Radio Products, Inc. Called the Panoramic Ultrasonic Analyzer, Model SB-7, it reduces the analysis of ultrasonics to the simplest, fastest, and most direct procedures by enabling observation of the frequency and amplitude of one or many ultrasonic signals at one time.

Similar to other types of panoramic instruments, the SB-7 is an electronically tuned receiver in which the output is applied to a cathode-ray tube oscilloscope. Indications are obtainable for signals between 2 kc and 300 kc in the form of vertical deflections distributed across the cathode-ray tube screen, calibrated to provide direct readings of these values. The horizontal location of each deflection indicates the frequency of its corresponding signal.

The SB-7 has continuously variable resolution, enabling analysis of signals separated by as little as 500 c.p.s. Signal amplitude ratios as high as 300:1 are measurable, with full-scale deflections for input voltages between one millivolt and 50 volts. Scanning width is variable from zero to a 200-kc maximum.

Typical uses for the instrument include analysis of ultrasonic vibrations, monitoring telemetering subcarriers and communications carrier systems, evaluating harmonic and intermodulation distortion, measuring spectrum distribution of noise, checking transmission characteristics of lines and filters, Fourier analysis of complex ultrasonic wave forms and for countless other investigations where over-all observation of the ultrasonic spectrum is required.—PANORAMIC RADIO PRODUCTS, INC., *10 South Second Avenue, Mount Vernon, New York.*

Peak Voltage Rectifiers

Peak voltage rectifiers for use with Type 518 Electrostatic Voltmeters have been announced by the Rawson Electrical Instrument Company. Type 518P5 provides for measurement of voltages to five kilovolts, and Type 518P15, for voltages to 15 kilovolts.

With the combination of peak voltage rectifier and electrostatic voltmeter, the peak voltages of a wide variety of pulses, including microsecond pulses, can be measured. Radiofrequency high voltage measurements can be made; there is practically zero resistive current drain, and the input capacitances are approximately 5$\mu\mu$f for plus peaks and 18 $\mu\mu$f for minus peaks.

Suggested applications for peak meters are in induction heating units, television r-f power supplies, radio transmitters, testing transformers, and apparatus generating high voltages at low radio frequencies.—RAWSON ELECTRICAL INSTRUMENT COMPANY, INC., *Cambridge, Massachusetts.*

Binac

Binac, the world's second all-electronic brain, has been built to order by the Eckert-Mauchly Computer Corporation for Northrup Aviation, Inc. Designed especially for the solution of engineering problems, Binac is tiny in comparison with Eniac, its 30-ton parent which was built in 1946 for the U. S. Army. The computing unit of Binac is 5 ft high, 4 ft long, and 1 ft wide.

Binac operates in the binary system; it is required only to distinguish between zero and one. The computer converts automatically to binary numbers before beginning calculations and converts answers back to decimal form before printing them out on an electric typewriter. Actually, the computer receives and puts out figures in the octal system, from zero to seven, as this converts more easily to binary numbers than the decimal system does. Decimal numbers may be expressed using pairs of octal numbers.

The main reason for Binac's smaller size is the use of a mercury memory tube, which replaces 17,000 vacuum tubes and can store 15,000 binary digits. Electrical pulses representing numbers and instructions are sent through it at a rate of four million per second. They are held in the mercury column by being rerouted through it as many times as necessary.

Binac is expected to have great value in reducing preliminary design and test time on research and development projects. Calculations formerly impossible or impractical of solution can be completed rapidly, eliminating many costly and often destructive physical tests which were previously necessary.—ECKERT-MAUCHLY COMPUTER CORPORATION, *3747 Ridge Avenue, Philadelphia, Pennsylvania.*

Photo-Tube

The new, head-on, multiplier photo-tube 5819 is intended for use in scintillation counters for the detection and measurement of nuclear particle radiation and in other applications involving low level, large-area light sources. It has high sensitivity to blue-rich light and negligible sensitivity to infra-red radiation.

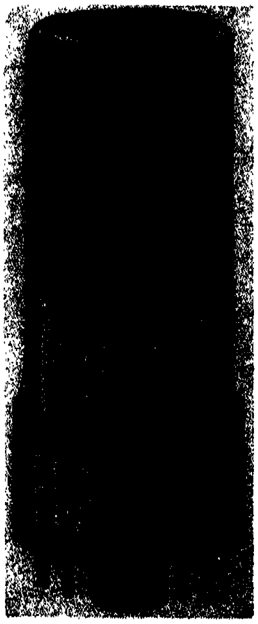

An outstanding feature of the 5819 is its semitransparent photocathode, which has a diameter of 1½ in. and an area of 1.8 square in. This relatively large cathode area permits very efficient collection of light from large-area light sources, such as are encountered in scintillation counters.

The spectral sensitivity characteristic of the 5819 peaks at about 4800A and cuts off at about 3100 and 6500A. It covers a region in which many organic and inorganic phosphors respond efficiently to radioactive emanations.

Utilizing ten electrostatically focused dynode stages, the 5819 operated at 90 volts per stage is capable of multiplying feeble currents produced at the cathode under weak illumination by an average value of 400,000 times.—TUBE DEPARTMENT, RADIO CORPORATION OF AMERICA, *Harrison, New Jersey.*

Aneroid Altitude Standard

In order to improve the procedure for calibrating and testing aircraft altimeters, Wallace & Tiernan Products, Inc., has developed a high precision aneroid indicator. The range is from minus 1000 ft to 30,000 ft altitude, with 10-ft graduations in the low altitude range. Although the instrument is compact, having a dial only 8½ in. in diameter, the scale is 45 in. long. Sensitivity and accuracy are respectively $\frac{1}{100}$ and $\frac{1}{10}$ of one percent, and the instrument is temperature-compensated. It is superior to a liquid column since it is portable, has a longer scale, has better readability, and eliminates hysteresis from the test procedure.—WALLACE & TIERNAN PRODUCTS, INC., *1 Main Street, Belleville 9, New Jersey.*

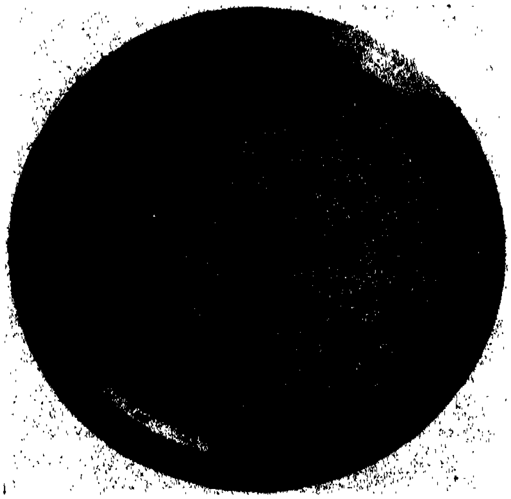

Dielectric Constant Meter

A new, compact dielectric constant meter for liquids, for demonstrating the principles related to this property, has just been announced by the Yellow Springs Instrument Company, Inc. It is the first low cost commercially available instrument of its kind and makes it possible, with one external probe, to measure the full range of dielectric constants from unity to 85. Basically the meter uses a calibrated condenser to measure changes in external capacitance (probe). A seven-position switch in the probe circuit introduces a predetermined

change in capacitance, the change being measured on the standard condenser as differences between readings. Readings of constants from one to 25 are accurate within one percent; the accuracy decreases to five percent at a constant of 80.

A pair of readings is made with the probe immersed in the liquid of unknown constant and a corresponding pair of readings is made with the probe in air. The difference in the readings taken in the liquid divided by the difference recorded in air is the dielectric constant for the liquid. Increments in external capacitance are read by tuning the circuit to resonance with the standard condenser, proper tuning being indicated by a sharp wink of the eye tube as oscillation begins.—Yellow Springs Instrument Company, Inc., *Yellow Springs, Ohio.*

Transmission Measuring Set

The Daven Company, manufacturers of precision electronic equipment, has introduced a moderately priced transmission measuring set Type 11A. Incorporating many of the features employed in many expensive models, this unit may be used to make all the precise measurements required by FCC.

Type 11A Transmission Measuring Set is a single meter instrument designed for specific use in checking frequency response, impedance matching characteristics, and gain and loss measurements, over a frequency range of 20 c.p.s. to 20,000 c.p.s. Measurements can be made to 111 db in steps of 0.1 db. Accuracy is ±1 percent.—The Daven Company, *191 Central Avenue, Newark 4, New Jersey.*

Spring-Coiling Machine

Carlson Spring Coiler No. 1 is a semi-automatic machine for winding both left-hand and right-hand compression, extension, and torsion springs. The machine is especially useful for coiling small quantities of springs and for making samples. The set-up time is only a few minutes, and springs may be wound from spring steel, music wire, stainless steel, phosphor bronze, or any other spring material.

The coiling machine will handle wire diameters up to 0.063 in. and will coil springs up to ¾ in. diameter; however, larger outside diameters are obtainable with special arbors. Springs up to 4 in. in over-all length and up to 25 coils can be produced; pitches are adjustable from zero up to a wide range. The end coils of compression springs are closed or squared automatically, and the springs are wound with a uniform pitch and to an exact length. Extended lengths for forming special ends or hooks can be made. The machine is hand-operated, but a motorized unit can be added if desired.

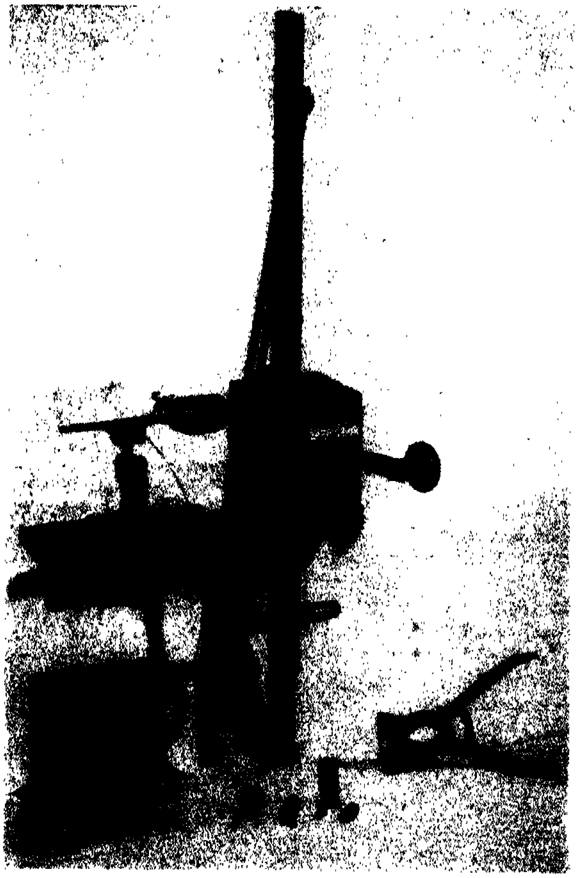

One turn of the handle produces three coils. Left-hand springs are made on the inner shaft, and right-hand springs are made on the outer shaft. The lower bar is adjustable horizontally to determine length. The long cam is adjustable at various angles to determine pitch. The short cam and distance from roller to long cam are adjustable to make any number of closed coils from one-half coil to three. The position and movement of the rack is adjustable to determine the number of coils. Arbors determine the spring diameters, and a friction-holding device on the tool post is adjustable to grip the wire. Complete instructions covering installation, operation, and set-up are supplied with each machine.—The Carlson Company, *277 Broadway, New York 7, New York.*

Resistohmeter

The Crown Industrial Products Company announces a new Electronic Resistohmeter. This unit is a Wheatstone bridge designed for measuring resistance and insulation resistance in both low and extremely high ranges.

The indicator used with the bridge is a 6E5 electron-ray tube. This tube, with an adjusting circuit and a balance switch, replaces the usual galvanometer. Sensitivity of the bridge does not suffer by the substitution, and the possibility of damage due to the large unbalance of the bridge when checking unknown resistance is eliminated.

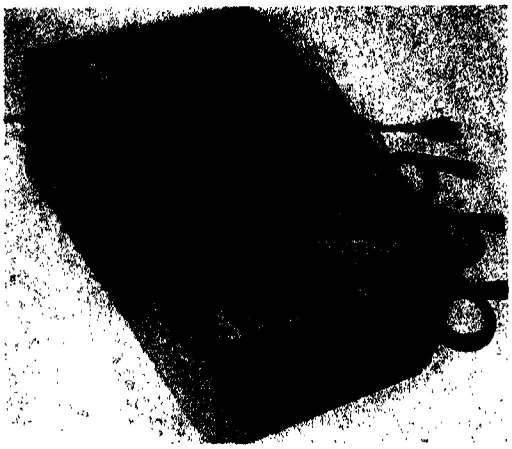

The Resistohmeter is guarded internally, so that leakage across the bridge components due to high humidity does not enter into or affect the operation of accuracy of the bridge. An external guard circuit guards specimens under test, so that leakage across paths other than the one under test is returned to a point in the bridge where it has no effect upon test measurement.

The Resistohmeter has a range from 1000 ohms to 100,000 megohms; d.c. test voltages used are 10, 100, and 500 volts. The unit operates on 115-volt, 60-cycle, a.c. current. Accuracy of operation of the unit is independent of power line voltage variations in both measurement of pure resistance and of leakage resistance of condensers.—Crown Industrial Products Company, *1315 West Sixty-Ninth Street, Chicago, Illinois.*

Gas Analysis

The Gow-Mac Instrument Company announces a new line of improved thermal conductivity units for low-cost gas analysis. Designated Type M by the manufacturer, these new units have the same precision of construction and close adherence to specifications as earlier products, but offer a far greater usefulness in gas analysis instrumentation as a result of greater bridge output and larger variety of available models.

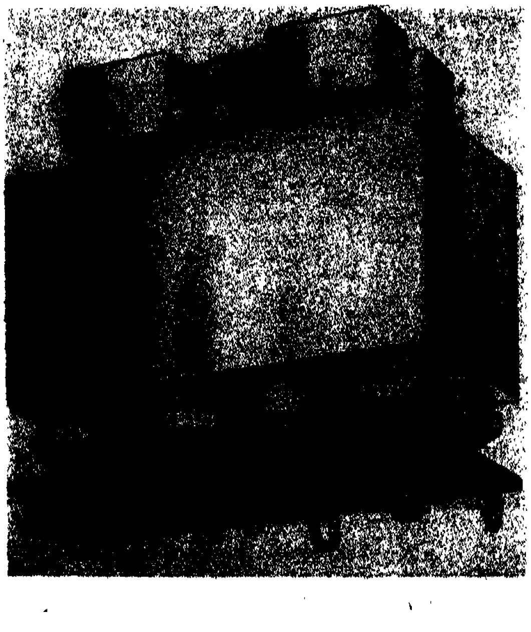

Type M cells offer a rugged, accurate, and extremely low-cost method of observing gases for purity or quantitative changes in gas mixtures under advanced, atmospheric, or partial pressures. Those concerned with special atmospheres, gas synthesis, inert gas distribution and generation, or the efficiency of furnaces and internal combustion engines, will find Gow-Mac Type M cells highly useful. In addition to industrial and research applications, the modest cost of Gow-Mac cells makes it possible for schools and colleges to include this equipment in their demonstration apparatus even where budgets are very conservative.

Type M/K is the most popular sensing element for continuous-service systems and gives a signal comparable to that originating with thermocouples. It can be incorporated into pyrometer circuits with only slight changes and recalibration. The bridge is monometallic and highly reliable. Housing is a handy sized steel cabinet, for bench or panel mounting.

Type M/K-SS has the same electrical and physical characteristics as Type M/K but is made of stainless steel for containing the more corrosive gases.

The model illustrated is the M/K-8, an eight-filament bridge with doubled output and highly satisfactory features for sensitive recording and control circuits. In gas-air tests, this unit has an output of 1.70 millivolts for one percent CO_2 in air and 11.8 millivolts for one percent H_2 in air.

The companion Model M/T-8 has an output of about five times that of the M/K-8. Both units are mounted in a steel cabinet 6 in.×6 in.×6 in. complete with gas-flow fittings and electrical terminal strips. Type M/T is a supersensitive four-spiral filament, selected by designers of portable and semiportable instruments because of the ease with which it can be used with many standard commercial galvanometers and standard power supplies.—Gow-Mac Instrument Company, *22 Lawrence Street, Newark 5, New Jersey.*

Wide-Band Amplifier

The -hp- 460A Wide-Band Amplifier is a new wide-band amplifier designed to make easier and faster a wide variety of measurements necessary in television, u.h.f., nuclear, oscilloscope, and general laboratory work.

This instrument offers true amplification without objectionable ringing or overshoot up to 200 mc. The pulse rise time is only 0.003 microsec., and a gain of 20 db is provided. As many as five instruments can be cascaded to provide additional gain.

The -hp- 460A is also designed for use with the -hp- 410A Vacuum Tube Voltmeter, and in this connection will increase voltmeter sensitivity 10 times at frequencies up to 200 mc. This makes possible fast, easy, mid-scale readings of voltages as low as 0.01 volt.

Since this instrument gives optimum performance through an impedance of 200 ohms, a 200-ohm coaxial system of connectors and cables is used with the -hp- 460A. Accessories include leads with fittings, panel jacks, plugs, and cables, adapters to connect the instrument into a standard 50-ohm Type N system, and a special adaptor for use with the -hp- 410A Vacuum Tube Voltmeter.—Hewlett-Packard Company, *395 Page Mill Road, Palo Alto, California.*

Radiation Counter

Model RC-1 Radiation Counter combines the functions of a scaling unit, a radiation survey meter, a count rate meter, and a contamination detector. The complete unit is extremely versatile. It measures only 12¼ in. by 9⅞ in. by 8¼ in. and weighs less than 24 lb.

Some of the features of the RC-1 are continuous 24 hr. per day stable operation without overheating; binary or decade scaler, choice of scaling values; self-contained high voltage supply from 500 to 1600 volts (higher voltage optional); resettable register mounted on panel; provision for elapsed and predetermined timers and preset count; count rate meter with ranges of 500. 5000, and 50,000 counts per min.; a special circuit keeping meter fluctuation minimum over the three ranges and permitting continuous variation of meter response.

Less space is required because of improved circuit design and choice of components. Provision is made for additional amplification, so that this unit may be used with proportional counters or with crystal scintillation counters.—Nucleonic Corporation of America, *499 Union Street, Brooklyn 31, New York.*

Wave Guide Test Equipment

Varian Associates have made available a microwave test set-up for operation at frequencies between 2600 mc and 3950 mc. Wave guide used is AN Type RG-48/U, 1½ in. by 3 in. by 0.080 in., with UG-53/U flanges.

Components of this test set-up are illustrated and are described, from left to right, in the following: (1) Coaxial cable to wave guide transition having voltage standing wave ratio less than 1.25 from 2700 mc to 3200 mc, and a connectorless coupling arranged to accommodate RG-5/U, RG-8/U, or RG-21/U flexible cable directly, utilizing the inner conductor as probe; (2) variable attenuator with range from 0.5 db to 10 db and power rating of 1 watt average, 1 kw peak; from 2600 mc to 3400 mc, the VSWR is less than 1.1; (3) standing-wave detector with precision-ground surfaces for continuing accuracy better than one percent; (4) termination which exhibits VSWR less than 1.05 from 2600 mc to 3400 mc, handles average power of 1 watt, peak of 1 kw.—Varian Associates, *93 Washington Street, San Carlos, California.*

Pyrometer Controller

The Loudon Electronic Controller is an entirely new instrument for medium and high temperature control applications. It is designed for use where precise control is needed or where vibration is severe, but the added cost of indicating or recording is not justified.

A thermocouple sensitive element is used. The measuring circuit is a null balance potentiometer with automatic cold junction compensation. Frequency of standardizing is greatly reduced by a new battery and circuit. Thirteen standard measuring ranges are available.

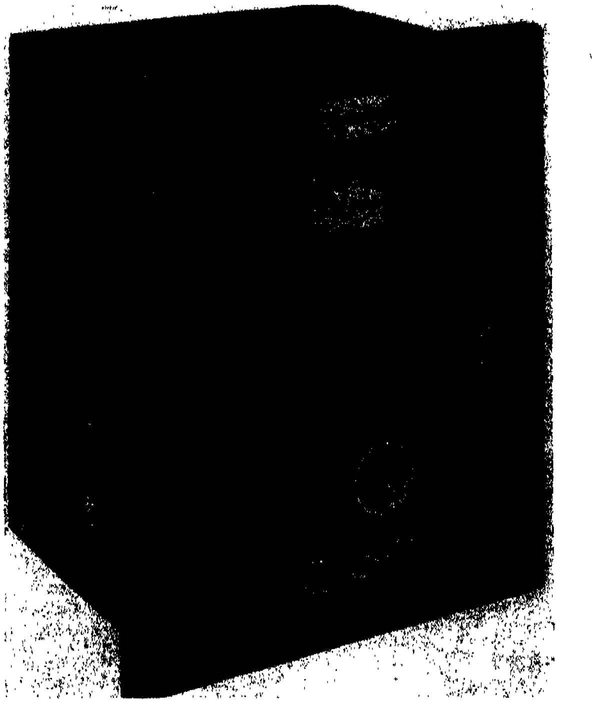

Unbalance voltages are converted to a.c. and amplified electronically. Control action is continuous and high speed. A two-position control relay is operated directly by the amplifier through a trigger circuit for high sensitivity. An antichatter circuit assures positive action. The relay contacts are suitable for operating valves, small heating elements, contactors, etc.

The entire unit is designed for industrial service under severe conditions of dust, fumes, and vibration. The case is compact and is designed for either wall or flush panel mounting.—Loudon Instruments, Inc., *5644 Lake Park Avenue, Chicago, Illinois.*

Torque Converter

The Zero-Max is a torque conversion structure for speed control variable from zero to maximum. Its operating principle involves the use of a crank motion on the input shaft creating linear motion which is absorbed on the output shaft by a series of one-way overriding clutches. A leverage mechanism is placed between the two shaft structures for varying the length of the stroke from zero to maximum, a continuous speed variation from zero to 4:1 ratio.

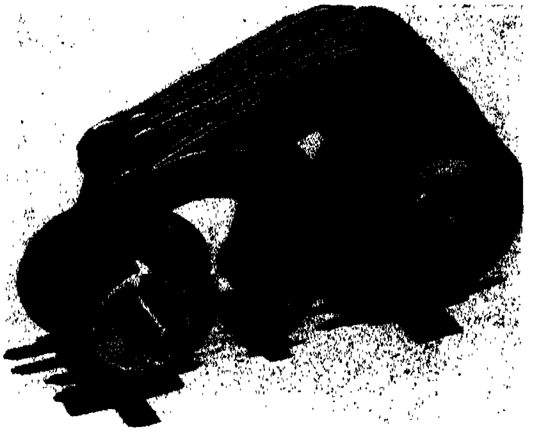

The principal advantages claimed for the Zero-Max are that it is compact, can be mounted in any position, provides level flow of power, has instant response to change of speed which can be made either while operating or stopped, excellent low speed as well as high speed performance, high starting torque, silent operation, and low cost.

The smallest unit which will handle loads up to 10 in. lb. output torque is now available. Its dimensions are 4 in.×2¾ in.×1½ in.—Revco Incorporated, *405 Thorpe Building, Minneapolis, Minnesota.*

Manufacturers' Literature

Instrument Notes—No. 9, May–June 1949, 4 pages, contains an article "Design parameters for linear accelerometers," including mathematical analysis.—Statham Laboratories, Inc., *9328 Santa Monica Boulevard, Beverly Hills, California.*

Tracerlog—No. 20, July 1949, 16-page publication features an article on Tracerlab beta-gaugés including topics on typical uses, radioactive source material, source rental and servicing, range and precision, speed of reaction, availability, calibration, and standardization.—Tracerlab, *55 Oliver Street, Boston 10, Massachusetts.*

Oscillographer—Vol. 11, No. 3, July–September 1949, features an article on the new DuMont Type 314-A Oscillograph-Record Camera. Also there is a description of Type 2542 Projection Lens and an article on a balanced-input adapter circuit.—Allen B. DuMont Laboratories, Inc., *1000 Main Avenue, Clifton, New Jersey.*

Experimenter—Vol. XXIV, No. 2, July 1949, 4 pages, features description of a new decade inductor, Type 1490, available in a range of one millihenry to 10 henries. Construction data, electrical characteristics, and safe operating limits are given.

Vol. XXIV, No. 3, August 1949, 4 pages, contains an article on measuring noise levels of f-m transmitters, and "the versatile voltage divider," Part III.—General Radio Company, *275 Massachusetts Avenue, Cambridge 39, Massachusetts.*

X-Ray Tube—A kit contains complete information and calculation charts for the new Amperex Rotating Anode X-Ray Tube "3000."—Amperex Electronic Corporation, *25 Washington Street, Brooklyn 1, New York.*

Radioactivity Instruments—New RCL Information Bulletin No. 8 includes description and illustrations of an extensive line of instruments for detection of radioactivity.—Radiation Counter Laboratories, Inc., *1844 West 21st Street, Chicago 8, Illinois.*

Photoelectric Cells—Bulletin PC-649, 4 pages, describes new line of selenium self-generating photoelectric cells. This bulletin contains diagrams, curves etc., describing the construction, performance characteristics, and applications of the photo-cells. A price list is also included.—International Rectifier Corporation, *6809 South Victoria Avenue, Los Angeles 43, California.*

Viscosimeter—Eight-page catalog describes the Brookfield Synchro-lectric Viscometer, acclaimed by users as offering the fastest and easiest method of measuring the viscosity or flow characteristics of materials—both in laboratories and at point of process.—Brookfield Engineering Laboratories, *Porter Street, Stoughton, Massachusetts.*

Pressure Gauge—Four-page, illustrated bulletin describes a compact gauge for measuring mechanical pressures or compressive loads. Full-scale readings of 100 lb. to 2500 lb. are available.—W. C. Dillon and Company, *5410 W. Harrison Street, Chicago 44, Illinois.*

Panel Instruments—Bulletin GEC-579 describes new line of 3½-in., long-scale panel instruments of internal-pivot-type construction. These instruments employ standard 3½-in. round and square cases, with 250 degree scale, 4.92 in. long, for good readability.—General Electric Company, *Schenectady 5, New York.*

Controllers—Thirty-two page bulletin, No. A120, illustrates and describes the company's new line of Series 500 air-operated controllers for automatically controlling temperature, pressure, flow, liquid level, humidity, and *p*H value. Complete data is given concerning on-off, proportional, reset, derivative and reset plus derivative models.—The Bristol Company, *Waterbury, Connecticut.*

Centrifuge—Form 25849L4 describes the new Spinco preparative centrifuge, having a top speed of 40,000 r.p.m. and equipped with vacuum chamber, vacuum pump, refrigeration unit, and related controls within a single enclosure.—Specialized Instruments Corporation, *612 O'Neill Avenue, Belmont, California.*

Volt-Ammeter—Catalog 109, 4 pages, describes the Amprobe pocket-sized, split-core voltammeter for measuring current without interrupting service. A pair of test leads is inserted in front-mounted pin-jacks for voltage measurements. Full scale current ranges of 6.5 amp. to 250 amp. are available. —Pyramid Instrument Company, *49 Howard Street, New York, New York.*

Resistors—Bulletin No. 4906, 4 pages, describes the 80X high voltage resistor. This resistor is rated at 4 watts, and is offered in values from 100 megohms to 100,000 megohms, established at 10,000 volts d.c. at 75°F and 50 percent relative humidity. Standard tolerance is plus or minus 10 percent.—S. S. White Industrial Division, *10 East 40th Street, New York 16, New York.*

Audio Sweep Generator—Bulletin 20A describes a new automatic audio sweep generator having a frequency of from 25 c.p.s. to 32,000 c.p.s. in one continuous range. The automatic sweep is adjustable from 500 cycles to 10,000 cycles, and sweep frequency is adjustable from 2 to 10 sweeps per second.—Clough Brengle Company, *6014 Broadway, Chicago 40, Illinois.*

Power Supply—Single catalog sheet describes Model 1210 Twin Power Supply, which has two regulated output voltages, each independently adjustable from 0 to 500 volts d.c. at

0–150 milliamp. Either positive or the common negative terminal may be grounded externally.—FURST ELECTRONICS, *12 South Jefferson Street, Chicago 6, Illinois.*

Relay—Four-page bulletin illustrates and describes type DO Amrecon power relay designed for exacting control requirements.—AMERICAN RELAY AND CONTROLS, INC., *4925 West Flournoy Street, Chicago 44, Illinois.*

New Materials

Forest K. Harris: Associate Editor
in Charge of this Section
National Bureau of Standards, Washington, D. C.

Scintillation Crystal

Clear crystals of cadmium tungstate, similar in physical and chemical properties to calcium tungstate, have recently been synthesized. Single crystals are grown in the form of slender, approximately square-section rods. The crystals are clear, pale yellow in color, having a density of 7.9 and a refractive index of 2.2–2.3. The emission spectrum has a peak just above 5000A, and the crystal is transparent to its own emission. Under γ-ray excitation this new tungstate possesses high phosphor efficiency throughout the temperature range 0–75°C. In addition, synthetic cadmium tungstate is a durable crystal of high physical and chemical stability, allowing its use in installations subject to the action of water or high humidity, solvents, or dilute acids. Because of its properties, it may be used as a phosphor in scintillation counters for the detection of high energy radiations such as x-rays, γ-rays and cathode particles. Unlike certain other phosphors it was found to have no appreciable long-time phosphorescence after exposure to massive dosages of radiation. Because of its very high refractive index, much of the generated light can be lost by total internal reflections. It is therefore necessary that the shape and mounting of this crystal with respect to the photomultiplier tube be designed to minimize these losses.

Linde synthetic cadmium tungstate is now available in research quantities, in ⅛-inch square-section rods, in lengths up to 2 inches. These rods can be readily fabricated into windows or mosaics for scintillation counters in the same manner as calcium tungstate. In special cases it may be possible to supply larger single pieces. Further information is available from the manufacturer.—THE LINDE AIR PRODUCTS COMPANY, NEW PRODUCTS DIVISION, UNIT OF UNION CARBIDE AND CARBON CORPORATION, *30 East 42 Street, New York 17, New York.*

Low Temperature Alloy Steel

Lebanon Grade 22 is an austenitic cast ferrous alloy containing 19.50 percent chromium and 9 percent nickel, among other alloying constituents. It has been used effectively in steel castings for pressure equipment in storing liquid oxygen. It is stated to show no structural changes down to −423°F, but an appreciable increase in hardness, proportional to the decrease in temperature, is shown. Ductility is lowered somewhat and the tensile strength is estimated to be approximately 200,000 p.s.i. at −423°F, with retention of adequate strength factors and resistance to embrittlement. The alloy is easily welded by gas or electric processes, without the need for subsequent heat treatment, since low temperatures do not seriously impair the as-welded impact resistance. This same alloy has also been successfully used in applications requiring heat-resistant characteristics at very high temperatures.—LEBANON STEEL FOUNDRY, *Lebanon, Pennsylvania.*

Mercury-Cleaning Process

The Bethelehem Mercury Oxifier is designed for the economical cleaning of metal-contaminated mercury. It consists essentially of a glass drum into which the mercury is poured, an agitator and motor, and a receptacle for the clean mercury. The cleaning process depends on the principle that base metal contaminations oxidize and precipitate from the mercury as metallic oxide powders. The agitator beats the mercury into a fine spray, providing maximum air contact with the mercury droplets. As the oxides form at the surface of the droplets, they are continually broken up into a dry, non-cohesive powder which can be readily separated from the mercury. After being agitated, the mercury is transferred to a receptacle where it is held for a sufficient time to allow the oxide particles to rise to the surface. After filtering, it is ready for use. Physical dusts, oils and greases are removed by the *Type F "gold-adhesion"* filter.

This cleaning process is stated to be so effective that the treated mercury is suitable for McLeod gauges, manometers, displacement devices and wherever high purity mercury is required. The apparatus handles up to 25 pounds at a time with a residual contamination of less than one part per million. Noble metals, such as gold, are not removed of course, but since gold is not detrimental to the value of mercury in physical apparatus there is no need for its removal except where absolute chemical purity is required. In this case a single distillation following the treatment is used in place of the usual triple distillation.—BETHLEHEM APPARATUS COMPANY, *Front and Depot Streets, Hellertown, Pennsylvania.*

High-Pressure Lubricant

Molykote-Type Z is a new and less expensive grade of molybdenum-compound lubricant peculiarly adapted to extreme bearing-pressure applications. It has exceptional chemical and thermal stability and its lubricating characteristics are not affected by temperatures up to 750°F, where its rate of oxidation assumes practical significance. (In the absence of air, experimental data indicate that lubricating and antiseizing properties are maintained at temperatures in excess of 750°F). Its affinity for metal surfaces combined with its film strength prevents galling and seizing at bearing pressures in excess of the yield strength of most metals. It may be applied dry in powder form or may be mixed with solvents, oils or greases. It is being used as a wear-in lubricant for dies, gears and machinery. It is stated to excel as a thread lubricant in connections subjected to sustained high temperatures, where it effectively prevents freezing of the threaded connection.

Molykote is a molybdenum-disulfide powder, whose tenacity and low coefficient of friction at high bearing pressures may be explained in part from its molecular structure. Each lamina is composed of a layer of molybdenum atoms with a layer of sulfur atoms on either side. One of these laminae adheres strongly to the metal surface because of the strong metal-to-sulfur bond. Other laminae slip easily because of the weakness of the sulfur-to-sulfur bond.

The manufacturer states that the following facts are shown by tests. (1) At contact pressures as high as 500,000 p.s.i. Molykote had the lowest coefficient of friction of more than twenty lubricants tested. (2) When applied to screw fasteners a predetermined tension was reached using one-half to one-third the torque required with conventional high pressure lubricants. Tightening took place with smoothly increasing torque, and the static and dynamic coefficients of friction differed less than seven percent. (3) When applied on surfaces to be press-fitted, the assembly force required was lower than with other high pressure lubricants. Assembly took place at a smoothly increasing load without the usual galling or seizing. In the absence of galling the distortion of press-fitted parts was greatly reduced. (4) Its use on conventional taper-collets increased gripping power by a factor as high as 5. (Lubricant was applied to threads, thrust washer and tapered surfaces, keeping the gripping surface free of lubricant.) (5) It is removed from surfaces only with difficulty. Even minute quantities adhering to the surface greatly improved the lubrication. Further particulars are given in the manufacturer's bulletin No. 52.—The Alpha Corporation, *Greenwich, Connecticut.*

Polystyrene Cement

Rez-N-Bond, previously used for cementing Lucite and other acrylic plastics, is now used for the permanent bonding of polystyrene. Setting time is a matter of seconds and finishing operations can be carried out within an hour. Joints are optically clear and the tensile strength of the bonded area is stated to be equal to that of the polystyrene material itself. This bonding agent is of the adhesive type and is non-flammable. Further information is available from the manufacturer.—Schwartz Chemical Company, *326 West 70 Street, New York 23, New York.*

Pre-Cementing Adhesive

H-511 Ubabond is a synthetic rubber cement which can be applied to surfaces that are to be joined together at a later time, even after shipment, without loss of adhesion efficiency. Upon application the adhesive dries to a non-tacky condition in fifteen to thirty minutes at room temperature. When the precemented surfaces are to be joined, reactivation is accomplished by infra-red, steam or dry heat, or by brushing or spraying solvent on the surfaces. The material is stated to provide a strong permanent bond and to be effective with a wide range of materials including fabrics, leather, glass, wood, paper, plastics, steel, galvanized iron, aluminum, and metal foils. Samples for testing may be obtained from the manufacturer.—Union Bay State Chemical Company, *50 Harvard Street, Cambridge, Massachusetts.*

Laboratory Products

Varno-Cement, softening at 80°C and melting at 100°C, may be used for leak-proof seals between glass and various types of tubing connections. It spreads rapidly and evenly when in a hot liquid state and sets at a moderate rate. It will adhere to carbon, porcelain, glass, metal, wood, plastics, cloth, transite, gypsum board, cork, and a variety of synthetic rubber materials. It has a low vapor pressure and can be used in vacuum work. It is easily stripped from a warmed surface, and can be recovered for reuse.

Varniton Stopcock Lubricant is made in 3 grades. *No. 1* is a general use lubricant suitable for precision analytical burettes. It is resistant to dilute acids and alkalis as well as many salt solutions. Its use is also suggested to eliminate the need for a glass rod in pouring from beakers—a thin film spread around the outside lip prevents the formation of drops. It is also an apparatus lubricant and rust-proofing compound and will successfully lubricate metal machine parts of apparatus submerged in constant-temperature baths or salt solutions.

No. 2 is a high melting lubricant for use where stopcocks must be operated near a combustion furnace. It is also used on stopcocks in lines carrying warm solutions.

No. 3 (*Organolube*) is useful for glass or metal stopcocks that are in contact with organic liquids. It is made of water-soluble materials that are generally non-reactive and insoluble in many classes of organic compounds. It is easily removed by washing with water.—The Varnitron Company, *416 North Varney Street, Burbank, California.*

Number-Coded Wire

Magic Wire has a code number printed in bright red along each inch of insulation. Compared with color-coded wire it is stated to have the following advantages: (1) The numerals do not wash or wear off, nor become discolored with age; and (2) there is no limit to the number of code numerals available. It is regularly available in No. 16 solid wire with plastic insulation and with code numbers from 1 to 35. Other sizes and types (with any code numbers) can be made up with cloth, rubber, or plastic insulation, in any gauge—solid or stranded.—Midwest Automatic Control Company, *510 Third Street, Des Moines 9, Iowa.*

THE
REVIEW OF SCIENTIFIC
INSTRUMENTS

VOLUME 20, NUMBER 11 *NOVEMBER, 1949*

A New Type of Diffusion Pump

E. L. HARRINGTON
University of Saskatchewan, Saskatoon, Saskatchewan, Canada

(Received March 1, 1948)

Certain features have been added to the standard diffusion pump which give to it certain definite advantages in both operation and control without introducing any new limitations.

THE two-stage mercury diffusion pump of the Kerth type has long been the most widely used one in laboratories generally. Indeed it meets quite satisfactorily the needs with respect to both speed and ability to work against appreciable fore-pressures. However, such pumps, and diffusion pumps in general, provide no seal between the high and the low vacuum sections; nor do they offer any indications as to the rate at which residual gases are being evacuated at any instant. Also, they are very dependent on the continuous action of the fore-pump.

The means by which the new type, herein described, overcomes these handicaps can be explained best through the aid of the diagram given in Fig. 1. Gas from the chamber to be evacuated, represented by *A*, passes in turn by the first-stage and the second-stage nozzles as in the standard pump, and is ejected into the water-cooled chamber, *B*. Here any mercury vapor is condensed far more completely than would be possible in the conventional outlet tube. From *B* the gases pass through cock *C* into the fore-pump. To this point the new pump is similar to, and functions like the standard pump, and retains all its virtues.

The new features are represented by *Y*, *K*, *P*, *S*, and *W*. After the fore-pump has reached and has operated for some time at its minimum attainable pressure, the cock, *K*, is closed. Thereafter the condensed mercury collects in the U-tube, *Y*, and soon effectively traps off the fore-pump. The outlet cock, *C*, is then closed and the fore-pump stopped. The auxiliary jet pump, *P*, thenceforth plays an important part by driving the traces of gases, collected by the first two stages, into the small bulb just below its nozzle. After *Y* is filled, mercury drops overflow into *P* and sweep out through *S*, in Sprengel pump fashion, any gases collected by *P*. The pump now operates as a three-stage vapor pump and Sprengel pump combination, having the speed of the former and the trapping action of the latter. The fore-pump will henceforth be required for only brief periods, if at all, whenever the mercury manometer indicates the collection of an appreciable quantity of gas. But the trap need not be opened. It is obvious that considerable pressure may develop beyond *Y* without affecting the action of the diffusion pump. *W* is an extension of the water jacket to make more certain the capture of backwardly diffusing mercury vapor. Experience has shown this added feature to be worth while even though it makes the construction a little more difficult. *G* contains a drying agent and is connected by a ground glass joint. *K* may be a simple cock as shown, lubricated with stopcock grease, though the author actually uses a mercury-sealed cock of the right-angle type, lubricated with only graphite, which may have some advantages.

Figure 2 is included to show how an already constructed pump of the ordinary type could be modified to include the new features. *G* is actually on a level with, but behind the manometer, not in the more elevated position shown in the diagram for the sake of clarity. The pumps shown in Figs. 1 and 2 are alike in principle. The one shown in Fig. 1 is neater and provides water cooling for both inlet and outlet tubes, but that shown in Fig. 2 is somewhat simpler to construct. In either type it is rather important that the nozzle of *P* be made rather small, a nozzle only 0.68 mm in diameter, has been found to be satisfactory. If too large, more vapor is driven through than can be condensed in the small bulb below. For the same reason the heater must not be run at too high a temperature. This would lead to a pressure sufficient to prevent the

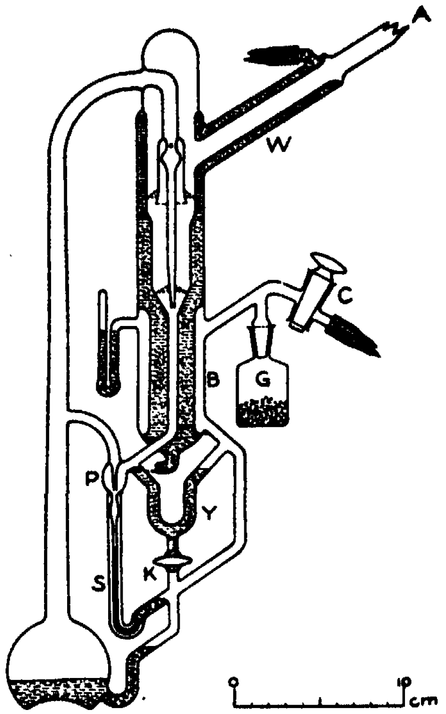

FIG. 1.

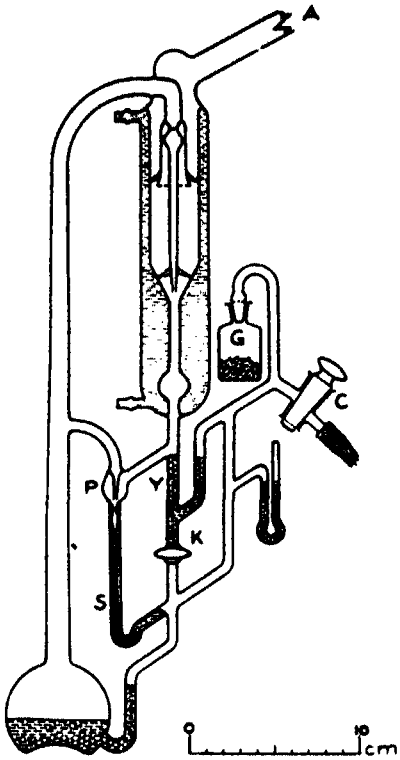

FIG. 2.

mercury drops from Y, needed to sweep out gases collected by P, from entering the latter. The capillary of S should have a diameter of between 2 and 3 mm. Other dimensions may be judged from the scales given, but are not critical.

Certain advantages of the new type of pump must be apparent. Through not having to operate the fore-pump continuously, wear, noise, and operating expense not only are reduced but the pump actually operates at a lower temperature than would be possible with a continuously operating pump. The traps provided by Y and by S prevent the return of captured gases to A, a very great advantage in case it becomes necessary or desirable to interrupt the operation of the diffusion pump, a step not possible with the conventional pump. In procedures requiring long periods the pumps may be stopped not only for noon periods or overnight, but for days or weeks, if desired, without losing all that has been accomplished. Gases or vapors once removed cannot get back and be readsorbed. When the trap first closes and the fore-pump is shut off, a Tesla coil will produce the same glow on either side of Y. Thereafter the pressure will increase beyond the trap while that in the tube leading to P falls progressively and eventually no discharge shows when the Tesla coil is applied. When this is the case, the first two stages are operating against a lower fore-pressure than the fore-pump alone could ever provide. Thus it is seen that the pumping action of P and of S are superimposed on the best the fore-pump can do. Also one is enabled from an observation of the spaces between mercury drops in S to judge directly, even only qualitatively, the degree of vacuum attained.

An X-Ray Camera for Obtaining Powder Pictures at High Pressures*

A. W. LAWSON AND N. A. RILEY**
Institute for the Study of Metals and Department of Geology, University of Chicago, Chicago, Illinois

(Received June 16, 1949)

Two methods are described of obtaining x-ray powder diffraction pictures of materials subjected to high hydrostatic pressures. Both techniques have been successfully employed to identify simple high pressure structures at pressures ranging up to 15,000 atmos. The essential feature common to both schemes is to encase the sample in a small beryllium bomb which serves to retain the pressure but permits the x-rays to be transmitted to the sample and diffracted to an external recording film. Sample data on cerium are given to illustrate the possibilities and limitations of this technique.

OUR knowledge of phase transformations at high pressures has been severely limited in the past by the lack of techniques for obtaining powder pictures of the various high pressure phases. This fact has been clearly demonstrated by Jacobs,[1] who has successfully obtained diffraction pictures up to 5000 atmos. in helium gas. His results revealed discrepancies with the volume changes associated with various transitions as previously determined by Bridgman. Later, Bridgman[2] redetermined some of the values in question and substantiated Jacobs' results. The superiority of the x-ray technique in studying transitions is obvious when one considers the detailed atomistic information obtainable directly only in this way. However, even when structures are too complicated to be readily unraveled from a powder picture, this technique has the advantage over straightforward dilatometry of permitting the investigator to establish, for instance, whether all of a phase has transformed. For this reason, it appeared worth while to design a method which would enable us to obtain diffraction pictures at the highest pressures possible. Such an apparatus, already successfully used,[3] is described below.

Jacobs' design was rejected as a starting point from the very first, because it appeared impractical to try to pack helium at pressures above those used by Jacobs. Furthermore, in Jacobs' apparatus the photographic film was exposed to the pressure—a delicate operation, since 24 hours were required to release the pressure without stripping the emulsion from the film.

As an alternative procedure, the possibility was explored of using a beryllium bomb and obtaining diffraction from samples with x-rays traversing the walls of the bomb. Two types of beryllium were examined: (a) fine grained, sintered beryllium and (b) large grained, cast beryllium. The scattering from the sintered material gave a much higher background than that from the large grained material and it was found impossible to obtain any results using sintered bombs. With the large grained material one is able to obtain many of the low angle intense transmission lines, but no high angle back-reflection lines may be discerned. This difference with grain size may account for the failure of Cohn[4] to obtain satisfactory diffraction pictures in an earlier attempt to utilize this technique. Examples of pictures obtained in this way are shown in Fig. 1. The well-defined rings in these pictures are diffraction lines obtained from highly divided cerium dispersed in Duco cement. The splotchy regions are individual Laue spots from the variously oriented grains in the beryllium. By comparing pictures taken through the beryllium, with and without a sample, one may easily eliminate the spurious beryllium spots and can, in general, identify at least five lines arising from the sample. In many cases, depending on the extinction coefficient of the sample for the particular wave-length used, more lines may be observed in the range of higher angles. With simple lattices even this limited information is usually enough, coupled with indirect information such as the density, to permit a structure determination.

Our preliminary experiments revealed that with cast beryllium several millimeters of beryllium in front of the specimen and at least a centimeter in back of the sample were tolerable. The grain size of the beryllium currently used in our laboratory is about 10 to 20 grains per cm^2.

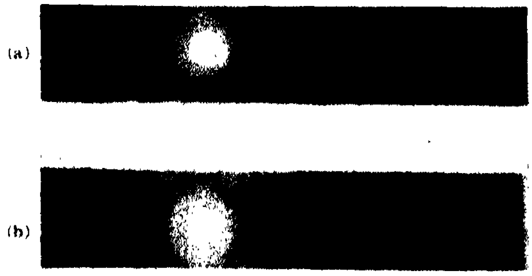

FIG. 1. Powder patterns of cerium taken with high pressure camera depicted in Fig. 4 and Fig. 5. (a) Face-centered Ce subjected to 10,000 atmos., (b) Face-centered Ce subjected to 15,000 atmos. Note the big change in volume, arising from the sudden collapse of the structure at about 12,500 atmos.

---

* This work was supported in part by the ONR under Contract ori-6-20-XX.

** Now with California Research Corporation, La Habra, California.

[1] R. B. Jacobs, Phys. Rev. 54, 325 (1938).

[2] P. W. Bridgman, Rev. Mod. Phys. 18, 1 (1946).

[3] A. W. Lawson and T. Y. Tang, Phys. Rev. 76, 301, 1949.

[4] W. Cohn, Proc. Am. Phys. Soc. 63 (June, 1922).

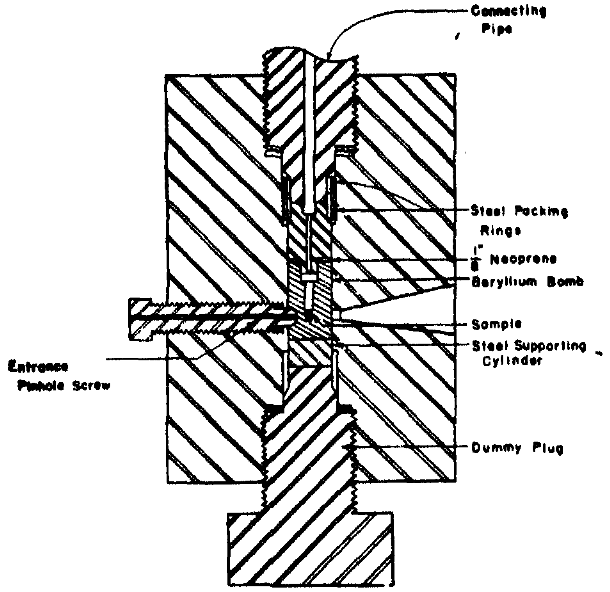

FIG. 2. Early model of high pressure camera illustrating packing of beryllium bomb in a larger steel container.

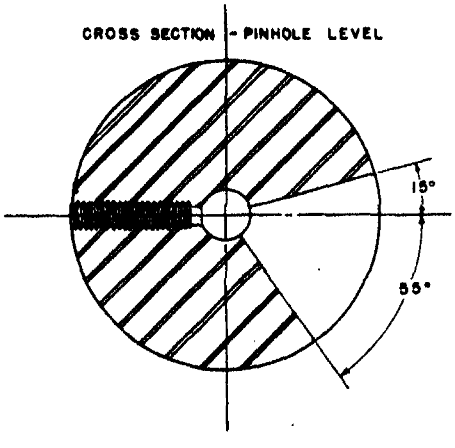

FIG. 3. Cross-sectional view of bomb shown in Fig. 2 (pinhole level).

Having ascertained the feasibility of using several millimeters of beryllium, we next tackled the mechanical design of the bomb. Two alternative techniques have been found satisfactory. The first technique consists in supporting the beryllium bomb externally with a heavy steel container and packing the bomb in such a way that hydrostatic pressure may be transmitted to the sample from a high pressure reservoir of the usual sort. The details of this packing are shown in Fig. 2 and Fig. 3. A "collar button" of hardened steel is inserted into the beryllium bomb near the top where the bore is widened to accommodate it. Between the collar and the beryllium bomb a rubber ring is inserted. The assembly is then screwed tightly down against a ledge in the reinforcing steel bomb by a plug under the beryllium bomb. This permits an initial compression of several hundred atmospheres to be applied to the rubber, thus packing the bomb assembly. This differential pressure appears to be sufficient in practice if SAE30 oil is used to apply the pressure. Although this oil is very viscous (if not frozen) at 10,000 atmos., the pressures should be very nearly hydrostatic within a few hours after the initial application of pressure owing to relaxation of the shearing stresses. In this way we have successfully maintained pressures up to 10,000 atmospheres for periods of many days. The reason for using this rather unconventional type of packing rather than the standard unsupported area type is to avoid the pinching off of the beryllium bomb, which has a rather low tensile strength compared to tool steel.

Using this assembly we have repeated Jacobs'[11] work on the transformation in AgI and completely substantiate his results within our error which is about 1 percent. The technique, however, has several disadvantages: firstly the thickness of the bomb requires rather long exposure times, and secondly, the difficulties encountered in properly aligning the x-ray beam with this cumbersome design are annoying and time-consuming. For these reasons it appeared desirable to sacrifice the principal advantage of this design, namely, the possibility of determining the pressure precisely, in the interests of simplicity and rapidity.

This decision led to the design of a very simple portable system, shown schematically in Fig. 4 and Fig. 5. In this design the beryllium bomb is completely unsupported and the thickness has been reduced by a

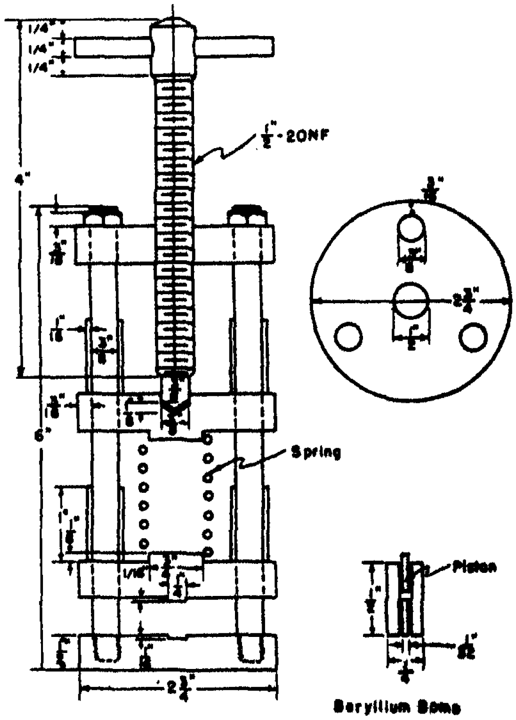

FIG. 4. Portable high pressure unit showing spring-loading device and miniature beryllium bomb. The bomb normally is seated below the cylindrical boss on the moving head driven by the spring.

TABLE I. Lattice spacings in face-centered cubic cerium* at 15,000 atmos.

hkl	$2r$	$2r-\delta$	d	a
111	2.02±0.03 cm	1.96 cm	2.75 ±0.05 cm	4.76±0.09 cm
200	2.30±0.01	2.24	2.42 ±0.01	4.84±0.02
220	3.23±0.01	3.17	1.71 ±0.005	4.84±0.02
311	3.78±0.02	3.72	1.46 ±0.01	4.85±0.03
420	5.14±0.02	5.08	1.077±0.003	4.82±0.02
		Average lattice constant a =		4.84±0.03

* These spacings were obtained using MoK_α radiation with a camera whose diameter equals 7.57 cm. *hkl* are the Miller indexes of the reflecting plane, r the radius of the diffraction ring, δ the correction (equal to 0.06 cm) for the thickness of the specimen as determined from similar patterns obtained at atmospheric pressure, d the calculated spacing, and a the calculated lattice constant.

factor of three. The outer diameter of the bomb, which is $\frac{1}{3}$ in. long, is only $\frac{1}{4}$ in. Unpacked pistons made of drill rod $\frac{1}{32}$ in. in diameter are pushed into the bomb by spring loading. The sample is mounted in Duco cement which transmits the hydrostatic pressure. The whole device weighs only a few pounds and may be mounted easily on any standard commercial x-ray unit. This device has been used for hundreds of hours above 15,000 atmos. without any failures owing to either leakage or fracture of the mechanical parts. The great advantage of this system is the fact that no expensive accessory equipment is necessary. The principal disadvantage is the uncertainty owing to friction in the pressure generated by the spring. Our normal procedure is to calculate the pressure in the bomb from the deflection of the spring, knowing the cross section of the piston and the Hooke's constant for the spring. In general, this procedure is not accurate to more than about 5 percent. This error may be reduced by a factor of two by plotting dead weight load *versus* piston displacement for increasing and decreasing load.

The camera is a semicylindrical film holder made light-tight by a filter for the particular wave-length employed in obtaining a picture. In general, we have found MoK_α radiation satisfactory. The exposure times, using 50 kv and 20 ma in a standard tube, then vary from one hour to about ten hours depending on the absorption of the sample for this radiation. The camera is mounted by means of clamps on the miniature press and is detachable to facilitate loading it with film.

Owing to the thickness of the sample ($\frac{1}{32}$ in.), an appreciable correction must be applied to the observed radii of the diffraction rings before calculating the lattice constant. A constant δ is subtracted from all the observed diameters $2r$, as illustrated in Table I. The constant δ may be determined in two different ways: firstly, it may be adjusted by trial and error until the lattice constant as computed from the Bragg relation is the same for all the observed rings, and secondly, it may be determined experimentally by comparing pictures taken through the beryllium bomb at atmospheric pressure with precision patterns obtained in the usual way. In our case, the agreement between the two values of δ so obtained is quite satisfactory.

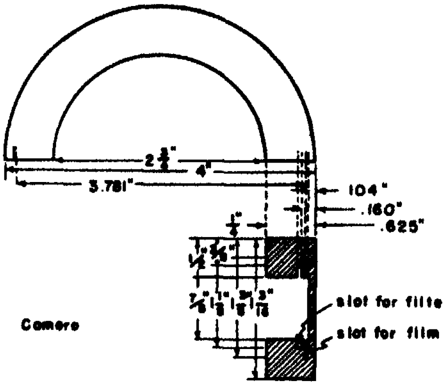

FIG. 5. The semicylindrical film holder which is mountable on the portable press shown in Fig. 4. The wide slot holds the film; the narrow slot holds a filter for the radiation employed and serves to make the film holder light-tight.

To date, three systems have been studied at high pressures, namely, AgI, Cd, and Ce. The structures of the high pressure modifications of Ce and AgI have been successfully resolved. In the case of Cd no transformation was discernible up to 10,000 atmos. However, the cadmium used by us was not particularly pure.

The authors would like to express their appreciation to their colleagues Dr. David Lazarus and Mr. Sumner Mayburg for assistance in a number of the tests.

THE REVIEW OF SCIENTIFIC INSTRUMENTS VOLUME 20, NUMBER 11 NOVEMBER, 1949

Fast Neutron Detector

W. G. MOULTON AND C. W. SHERWIN
Physics Department, University of Illinois, Urbana, Illinois

(Received June 27, 1949)

A simple fast neutron detector suitable for health physics applications has been constructed using two 931A photo-multiplier tubes in coincidence to reduce background. A "sandwich" made of Lucite and activated zinc sulfide is used to produce the scintillations. The efficiency of the instrument for fast neutrons from a Ra-Be source is 1.5 ± 50 percent$\times10^{-4}$. It detects a fast neutron flux of 20 neutrons/cm^2 sec. with a counting rate that is over ten times background.

RECENT appreciation of fast neutron hazards[1] makes a simple fast neutron detector desirable as a monitoring device. Photographic detection has been used, but has the disadvantage that the safe dosage may have been greatly exceeded before the film has been processed. A simple, reliable, and rugged instrument for counting fast neutrons has been constructed using 931A photo-multiplier tubes, which allows continuous checks to be made on the neutron flux.

Photo-multiplier tubes have been used for some time for the detection of alpha-, beta-, and gamma-radiation by placing a phosphorescent material in front of the window of a photo-multiplier tube.[2] Photo-multipliers can also be used to detect fast neutrons if a hydrogenous substance is placed in front of the phosphor so that the photo-multiplier will count scintillations produced by the recoil protons. However, the counter will have a low efficiency, resulting in a counting rate of the order of one count per hour for a fast neutron flux of one neutron/cm^2 sec. The pulses produced by this arrangement before amplification are quite high, above 0.3 volt for a good photo-multiplier operated at 1000 volts. However, there are also spurious large pulses. Even with a discrimination level set to pass only pulses above 0.3 volt produced by fairly energetic recoil protons, there are still enough large spurious pulses (never observed to be less than 50 counts/hr.) which cause a large background when weak neutron fluxes are being measured. Most of these spurious pulses come from the photo-multiplier tube, and not from the phosphor, since removal of the phosphor reduces their number only slightly.

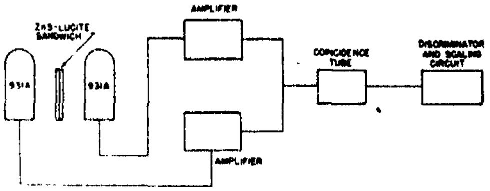

FIG. 1. Block diagram showing geometry and circuit components of the fast neutron detector.

Morton and Robinson have used two photo-multipliers in coincidence to reduce chance noise while counting particles.[3] The coincidence method was adopted here for detecting neutrons.

Figure 1 shows the geometry and circuit components used. The "sandwich" was prepared after the method of Sherr by spraying a small amount of shellac thinned with alcohol into the air and passing a sheet of Lucite $\frac{1}{16}$ in.$\times\frac{1}{2}$ in.$\times2$ in. through the vapor. A small amount of activated ZnS powder[4] was placed on the shellac film and the Lucite tapped until an even, transluscent layer was obtained. The Lucite was then passed through shellac vapor again, and another layer of Lucite of the same dimensions placed on top of the activated ZnS layer. The "sandwich" was then bound together at the edges. The photo-multipliers were placed as close together as possible with the "sandwich" between them.

Figure 2 shows the circuit used. The 931A photo-multipliers were selected to give approximately the same pulse heights. The inequality of pulse heights can be reduced by operating the photo-multipliers at different voltages. The circuit has a resolving time of the order of 50 microsec., and since there are a maximum of about six noise pulses per minute from one tube at the discriminator settings at which the circuit is used, the chance background rate is calculated to be one count in 280 hours. The actual background observed is approximately 1.5 counts/hr. The limiting factor in decreasing background probably is alpha-active contamination of the phosphor, since operating the counter 14 hours without the "sandwich" in place yielded no coincidence counts.

Figure 3 shows the response of the instrument. The fast neutron flux of 30 neutrons/cm^2 sec. was obtained from a calibrated 25-mg source of Ra and Be. The gamma-flux of 150 mr/hr. was obtained from a calibrated Ra source. It is noted that the effect of the

---

[1] The tolerable fast neutron dosage has been given as 200 fast neutrons/cm^2 sec. per eight-hour day. (T. C. Evans, Nucleonics, (March 1949), also Argonne National Laboratory Manual "Radiation hazard control," p. 3 (May 3, 1949)). However, an instrument should be capable of accurately measuring a flux of $\frac{1}{10}$ this value.

[2] R. Sherr, Rev. Sci. Inst. 18, 767 (1947); Marshal, Coltman, and Bennett, Rev. Sci. Inst. 19, 744 (1948).

[3] G. A. Morton and K. W. Robinson, Nucleonics (February 1949).

[4] The phosphor used was No. 33Z-20A obtained from the Radio Corporation of America, RCA Victor Division, Harrison, New Jersey.

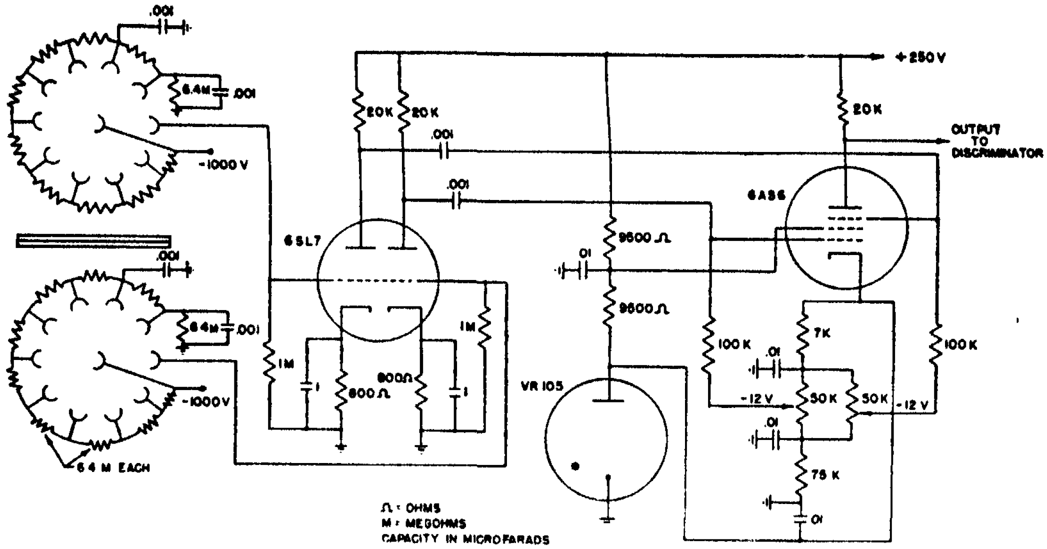

FIG. 2. Circuit diagram for the fast neutron detector. The pulses from the 931A's due to proton recoils are amplified by the 6SL7. The 6AS6 tube detects the coincidences.

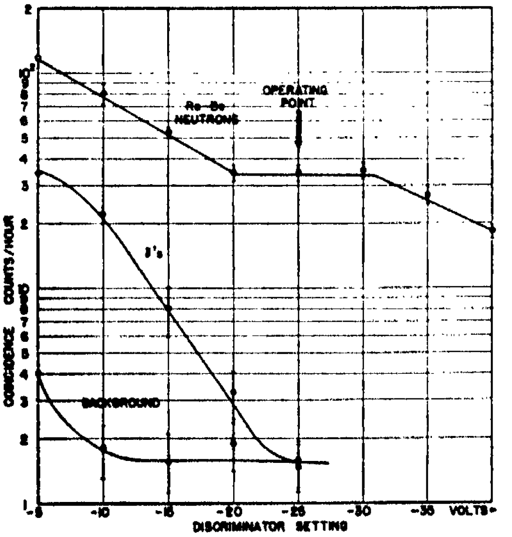

FIG. 3. Fast neutron sensitivity of the detector. The fast neutron flux is 30 neutrons/cm^2 sec., the gamma-flux 150 mr/hr.

gamma-radiation is almost completely removed by pulse height discrimination at the operating point. The discriminator circuit, not shown in Fig. 2, operates with the negative pulses coming from the plate of the 6AS6. The efficiency of the counter for fast neutrons at −25 volt discriminator bias is 1.5±50 percent $\times 10^{-4}$, since one observes a counting rate of 34 counts/hour with a neutron flux of 30 (neutrons/cm^2 sec.). The effective useful area of the sandwich was taken as 2 cm^2 in making the efficiency calculation.

The counter is constructed with all components, including the photo-multiplier tubes in a metal box for shielding. The output pulses can be fed into a circuit which will operate a mechanical counter. It is also possible to construct an alarm system which would be actuated when an eight-hour dose is exceeded. The efficiency might be greatly increased by using a large sandwich area and by using optical methods of focusing the scintillations on the photosensitive surfaces of the photo-multiplier.

THE REVIEW OF SCIENTIFIC INSTRUMENTS VOLUME 20, NUMBER 11 NOVEMBER, 1949

Instrumental Distortions in the Shapes of Continuous Beta-Spectra

GEORGE E. OWEN AND C. SHARP COOK
Department of Physics, Washington University, St. Louis, Missouri*

(Received August 1, 1949)

The positron spectrum of Cu^{61} and the negatron spectrum of P^{32} have been studied in a 5.7-cm radius of curvature magnetic spectrometer using a variety of vacuum chamber sizes and baffle designs. Conclusions are drawn from these data concerning the distortions in continuous beta-spectra caused by scattering from the finite geometry of the chamber.

I. INTRODUCTION

A NUMBER of possible sources of distortions in continuous beta-spectra have been indicated in a previous paper.[1]

The present experiments attempt to indicate those components of a beta-spectrometer which may or may not contribute distortions to such a spectrum.

When designing a chamber for beta-spectra investigations, one frequently must decide quite arbitrarily what type of chamber dimension and baffle arrangement will give the optimum spectrum. Since electrons are known to be easily scattered by exposed surfaces, the chamber design problem is then reduced to one in which the desired focusing is coupled with the minimum scattering of particles into the exit slit. Frequently the distance between the pole faces of the magnet is limited and the elimination of scattering is accomplished by one or more baffles introduced into the vacuum chamber.

The purpose of the present study is to investigate changes in the shape of a continuous spectrum as measured by a semicircular homogeneous field spectrometer when the number and positions of the baffles and the chamber size relative to the beam are varied. The beam is defined by apertures of the proper size cut in the baffles which are of the customary type extending completely across the chamber.

Studies of a somewhat similar nature have been made by Neary[2] using a number of diaphragms protruding from the chamber wall and a single defining slit.

II. EXPERIMENTAL DETAILS

The present investigation has been conducted using a uniform field semicircular magnetic spectrometer having a 5.7-cm radius of curvature. The instrument used in reference 1 has been rebuilt in order to allow sufficient flexibility for the current experiments. The distance between the pole faces has been increased and a vacuum tank open at the top (magnet has horizontal field) has been fitted between them. The lid of the vacuum tank is removable and carries the complete chamber geometry plus the flip coil, source air lock, counter, etc., The Lucite chamber geometry can be removed from the lid, thereby allowing complete flexibility in the choice of chambers. A cross section of the lid and chamber geometry is shown in Fig. 1, while Fig. 2 presents a photograph of the lid with Chamber #6 in place (the numbering of chambers will be explained later).

Five different chambers were constructed for the current experiments. These chambers differed in the distance between face plates. The term face plate is defined as the plate parallel to the pole face and secured to the baffles. Figure 3 shows a cross-sectional view of the baffles for each of five chambers used. The aperture in the baffles is identical in each chamber in order to allow a beam of constant dimensions to be used throughout the experiment.

Each chamber can be set up with five baffles at 30°, 60°, 90°, 120°, and 150° from the source. These baffles are denoted as 1, 2, 3, 4, and 5, respectively. All Lucite surfaces in the spectrometer chamber were coated with Aquadag and grounded in order to render them conducting and prevent charge from developing within the spectrometer.

The spectrometer in its present form using Chamber #6 with d/D (chamber height/beam height) $=5.9$ and, using Baffles 1, 3, and 5, was utilized in the recent investigations[3] of the radiations of I^{131}.

An end-window type G-M counter was used as indicated in Fig. 1. The filling mixture consisted of four cm argon and three cm ethylene. The window was a zapon window having a lower energy cut-off of approximately three kev.

The source holder consists of an aluminum ring held in position by two aluminum prongs as indicated in Fig. 1. The source is inserted into the spectrometer through the indicated vacuum gate. The vacuum techniques used throughout are of the types described by Kurie.[4]

Sources were mounted on zapon foils of approximately 0.03 mg/cm^2 thickness which in turn were mounted on the aluminum ring.

The solutions containing the radioactive material were deposited in a line on the zapon foils. Although by weight the average thickness was relatively small, in the initial experiments the deposit was not uniform. It was suggested[5] that small amounts of gelatin in the solution might reduce the mobility of the ions of the solid matter to such a point that a greater uniformity might be obtained. By adding gelatin to an amount which contributed approximately 0.01 mg/cm² to the source, sources of much greater uniformity were obtained.

---

* Assisted by the joint program of the ONR and the AEC.

[1] G. E. Owen and H. Primakoff, Phys. Rev. 74, 1406 (1948).

[2] G. J. Neary, Proc. Roy. Soc. A175, 71 (1940).

[3] Owen, Moe, and Cook, Phys. Rev. 74, 1879 (1948), Phys. Rev. 75, 1270 (1949).

[4] F. N. D. Kurie, Rev. Sci. Inst. 19, 485 (1948).

III. RESULTS

The types of study are the following:

A. the spectra of Cu^{61} as a function of the distance between face plates (three baffles),

B. the spectra of P^{32} as a function of the distance between face plates (three baffles),

C. the spectra of P^{32} as a function of the Z of the face plate and with the face plates adjacent to the beam (i.e., Chamber #1),

D. the spectra of P^{32} as a function of the number of baffles in a chamber of Type #2,

E. the spectra of P^{32} as a function of the type of a single baffle and of the face plate separation (single baffle).

A.

The initial studies of the effects of varying the ratio d/D within a spectrometer were made using the positron source Cu^{61}. Sources were prepared in the same manner as has been previously described.[6] All of the

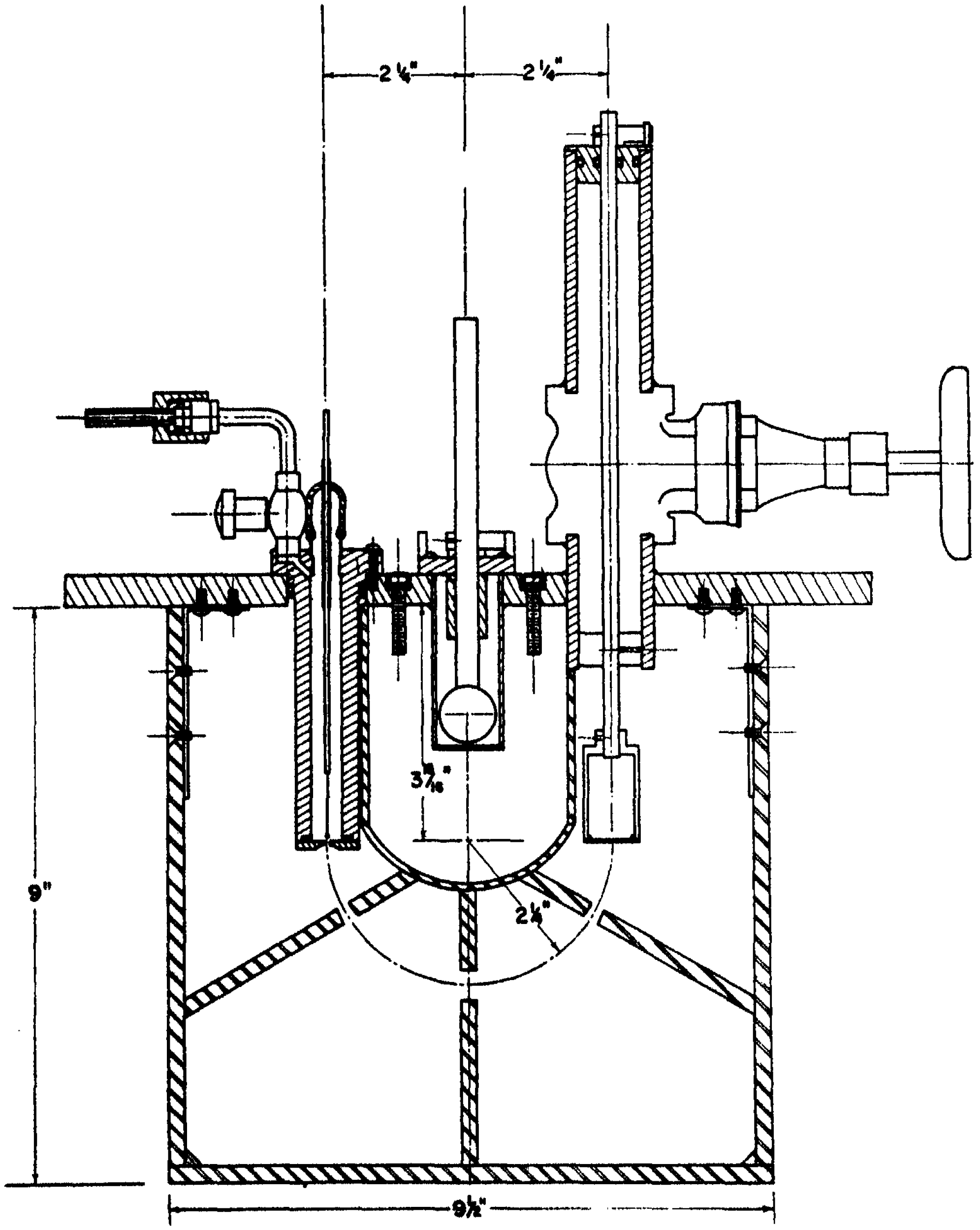

FIG. 1. Cross-sectional view of the vacuum chamber lid and the 180° beta-ray spectrometer chamber used in the current experiments. Chamber geometry is that used with three baffles in place. Source is inserted through vacuum gate at right of vacuum chamber lid. End-window G-M counter is at left. Flip coil for measuring magnetic field inserted into lead block in center.

---

[5] Professor A. Calandra, this department (private communication).

[6] C. S. Cook and L. M. Langer, Phys. Rev. 74, 227 (1948).

FIG. 2. Photograph of vacuum chamber lid and spectrometer chamber. Spectrometer Chamber #6 is in place. (For numbering of chambers see text.)

studies were performed using Baffles 1, 3, and 5. The similarity in the spectra as seen in Fig. 4 using various ratios d/D seems to indicate that the scattering of beta-particles from the face plates of a spectrometer chamber are essentially negligible.

The average source thicknesses in the case of Cu^{61} were in the range 0.02 to 0.06 mg/cm^2 as measured by weighing. However the sources did not deposit uniformly. This fact quite possibly accounts for the single spectrum from Chamber #3 which deviates at a higher energy than the others. A somewhat thicker source can account for this distortion.

Because of the relatively short half-life of Cu^{61} (3.33 hr.), it was necessary to prepare a new source for each run. In order to make certain that differences in source thickness did not affect the results, the same experiment was again performed using the negatron emitter P^{32}, which because of its longer half-life would allow the same source to be used throughout a set of runs.

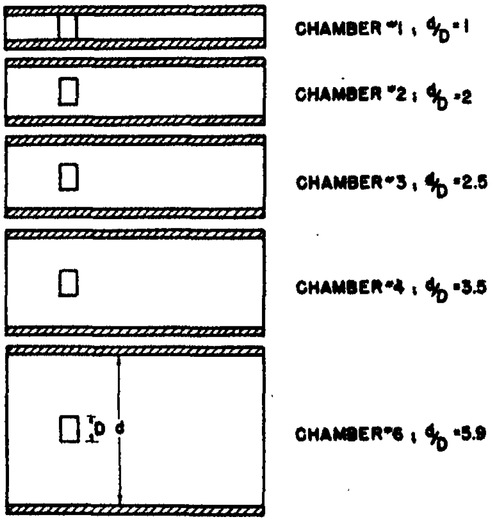

FIG. 3. Cross-sectional view of the baffles used in the various spectrometer chambers in the current experiments. Ratio of chamber height to beam height (d/D) and chamber number shown for each case.

B.

The result of the chamber height study using P^{32} is shown in Fig. 5. Again there is no marked difference between the largest chamber (#6) and smallest chamber (#1). There is however an almost negligible decrease of the deviation for the chambers whose $d/D>1$, which may or may not be real.

C.

This great similarity in the spectra led to a further study of face plate scattering. P^{32} was investigated in Chamber #1 ($d/D=1$) using face plates of different atomic number. Again Baffles 1, 3, and 5 were used. The results using face plates of Al, Cu, Sn, and Pb are shown in Fig. 6. There seems to be no marked difference in the spectra resulting from the four runs. This fact adds further confirmation to Parts A and B. If there is scattering from the face plates which can appear at the exit-slit, then a change in Z of the face plates should emphasize this effect.

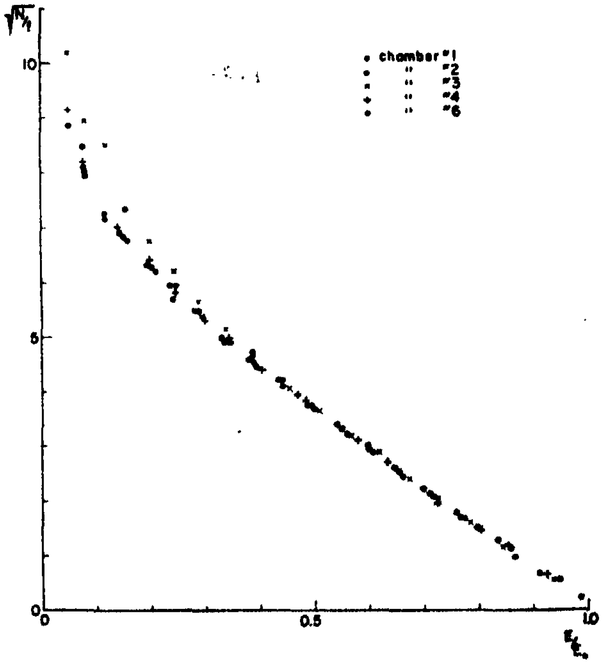

FIG. 4. Fermi-Kurie (FK) plots of Cu^{61} obtained using each of the Chambers #1, #2, #3, #4, and #6.

D.

The problem of minimizing scattering by a proper arrangement of baffles was investigated next. The re-

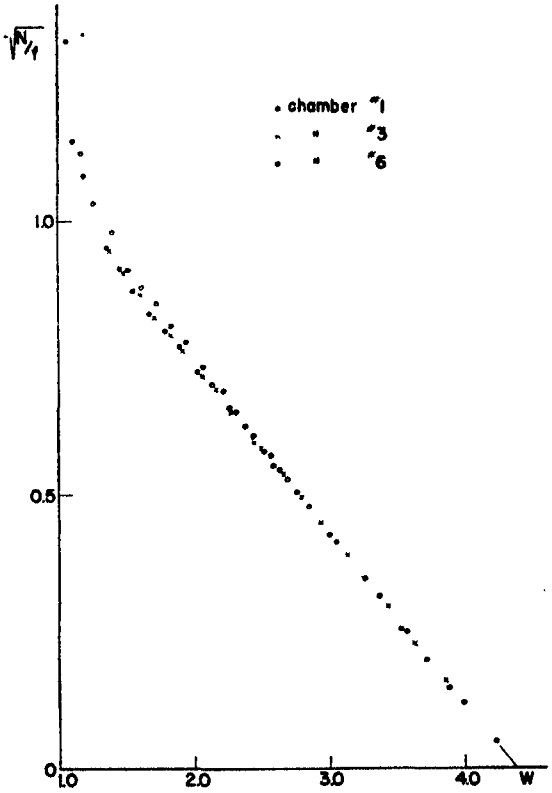

FIG. 5. FK plots of P^{32} using each of the Chambers #1, #3, and #6.

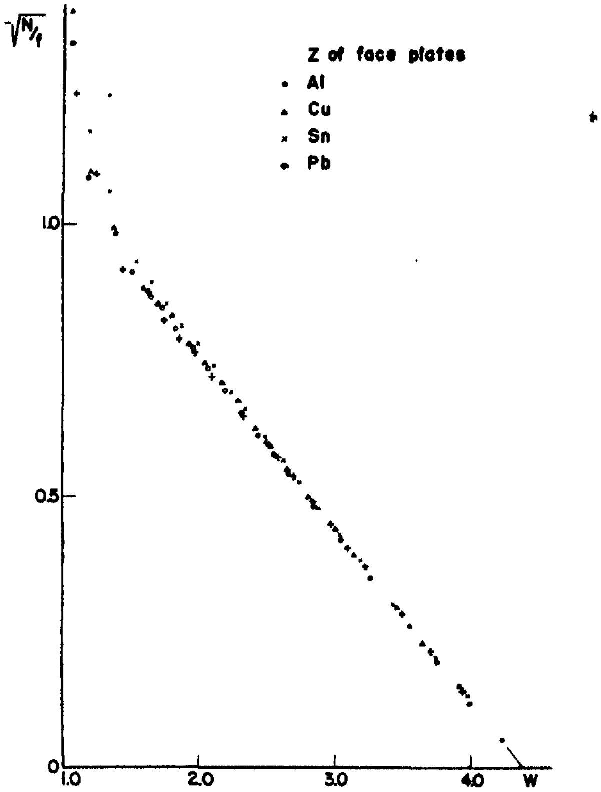

FIG. 6. FK plots of P^{32} using Chamber #1 and face plates of various atomic numbers as indicated.

sults are presented in Fig. 7. Five runs were made; a single baffle in the 30°, 90°, and 150° positions; three baffles at 30°, 90°, and 150°, and five baffles at 30°, 60°, 90°, 120°, and 150°.

The spectra fall into two distinct groups; all of the single baffle spectra lie in a group which is markedly above the group defined by the multiple baffle spectra.

Chamber #2 was used in these experiments because it has a d/D ratio which is close to that used in most spectrometers.

E.

It has been pointed out that baffle thicknesses and aperture design might have some effect upon the spectra; therefore, a series of studies were made on the single baffles. A single baffle in the #5 position at 150° was varied in thickness, and the aperture edge was varied from a bevel of 70° to the beam to an edge tangent to the beam. Figure 8 shows these results. The single baffle of $\frac{1}{4}$-in. Lucite having a 70° bevel; the single baffle of $\frac{1}{4}$-in. aluminum having an edge tangent to the beam; and the single baffle of $\frac{1}{8}$-in. lead having a tangent edge fall on the same curve which is markedly above that curve obtained using three baffles. It would appear therefore that the beveled edge and Lucite baffle do not account for the distortion.

Finally, a single Lucite baffle whose aperture edge is tangent to the beam was placed in Chamber #6 ($d/D=5.9$). In this instance the distortion was reduced roughly by a factor of two.

IV. DISCUSSION

A. Limitations of the Experiment

These experiments have been done using rather high energy spectra (P^{32} has a maximum beta-energy of 1.71 Mev, and Cu^{61} of 1.21 Mev).[7] It is quite possible that the effects of scattering would be more obvious with lower energy electrons.

Also any distortion in the beta-spectrum caused by the geometry is assumed to show over and above that caused by source thickness. In the case of the single baffle it can be seen that the differences are quite apparent. With regard to source thickness deviations the higher energy spectra are quite advantageous since possible deviations caused by source thickness occur over a small proportion of the spectrum.

Although no particular emphasis has been placed here on the shape of the spectrum, the sources were thin enough that the curves from the multiple baffle spectra agree quite well with curves taken from very thin sources.

B. Conclusions concerning Scattering

In the following discussion grazing angle scattering is defined as scattering in which either the angle of

---

[7] G. T. Seaborg and I. Perlman, Rev. Mod. Phys. **20**, 585 (1948).

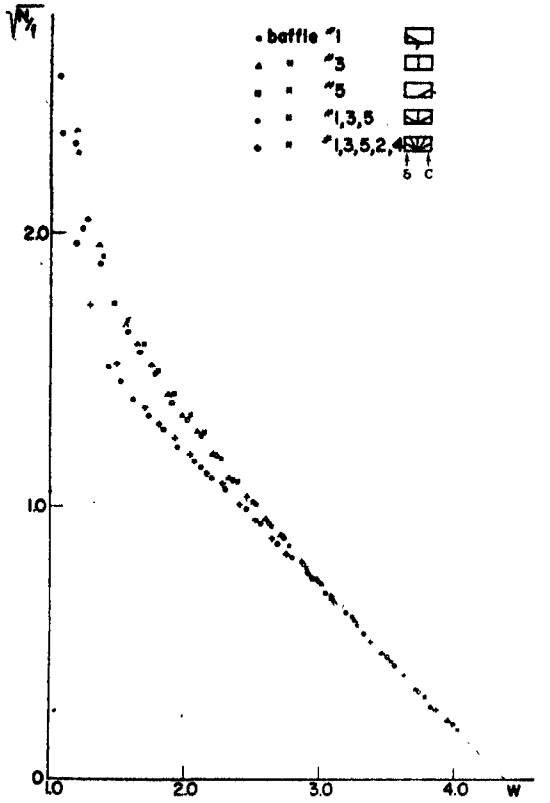

FIG. 7. FK plots of P^{32} using Chamber #2 and various Lucite baffle arrangements as indicated.

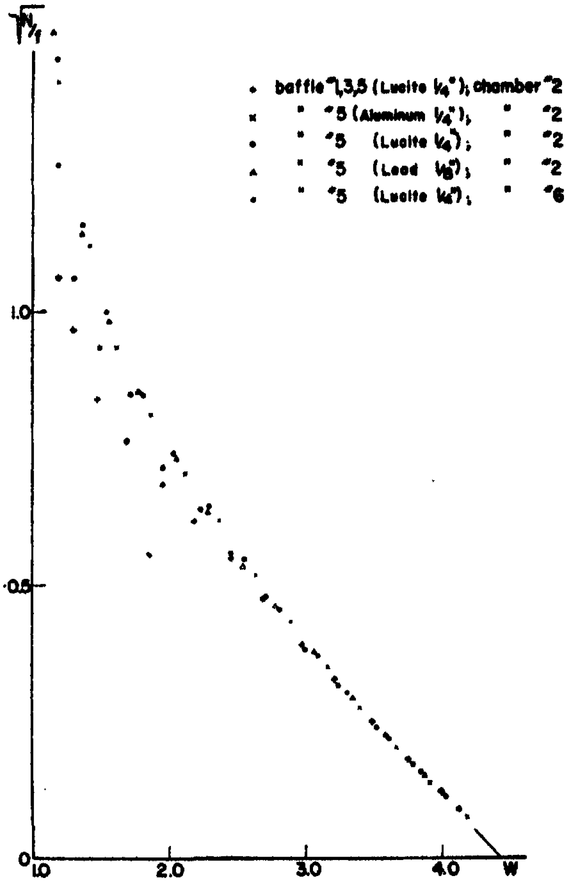

FIG. 8. FK plots of P^{32} using chambers and baffle arrangements indicated.

incidence or the angle of reflection or both are large. If grazing angle scattering is important, the experiments involving a variation of the *d/D* ratio should show large effects. Since there is no obvious change introduced in the spectrum by bringing the face plates down on the beam, it would seem that the grazing angle scattering is negligible. This conclusion is further supported by the ineffectiveness of a change of the atomic number of the face plate when that plate lies directly adjacent to the beam. However, the deviations introduced by the use of a single baffle indicate quite a large quantity of scattering of some type. Quite possibly this scattering is, as a result of the previous analysis, to a great extent large angle and multiple scattering.

In the experiments involving single baffles it was found that a single baffle in any one of three different positions gave identical results. A very rough qualitative description might be given as follows of the single baffle chamber. The single baffle chamber could be pictured as a cavity filled with an isotropic distribution of electrons, in which the number of particles within a given energy interval is a decreasing function of energy. With this picture the density of radiation would be a function of the volume and the wall area. Thus when the chamber height is increased the radiation density should decrease since the volume increases more rapidly than the exposed surfaces. This is borne out in Part E of the results wherein Chamber #6 is used instead of Chamber #2 thereby decreasing the distortion.

C. Conclusions on Spectrometer Design

From these studies it appears that once a beam of beta-particles has been sharply defined in a magnetic spectrometer by several baffles, the scattering of particles has been reduced to a minimum (in the region above 200 kev). The results also indicate that a single baffle does not sufficiently define this beam of electrons.

In the same energy region (>200 kev) it seems that once the beam is defined by several baffles the material of the spectrometer chamber contributes very little or no distortion to a spectrum.

The inability of grazing angle scattering to show any marked effects on the shape of the spectra seems to indicate that spectrometers of small chamber height can be utilized to a high degree of efficiency, provided a sufficient number of baffles are used.

We are greatful to Professor H. Primakoff for many helpful discussions and comments.

A Simplified Emission Regulator for Mass-Spectrometer Ion Sources*

E. B. Winn and Alfred O. Nier
Department of Physics, University of Minnesota, Minneapolis, Minnesota

(Received July 1, 1949)

A simplified electron emission regulator has been developed which operates by controlling the space current instead of the filament heater current. No vacuum tubes are used, but the performance is comparable with that of electronic regulators now in use.

A NEW type of electron emission regulator for mass-spectrometer ion sources has been developed which is considerably simpler and cheaper to construct than the electronic devices previously used.[1] Regulation is achieved by controlling the electric field at the filament by a control plate placed between the filament and the shield assembly, instead of by regulating the filament heater current. Electrically this is quite analogous to an ordinary triode vacuum tube operating with a positive grid. The voltage for the control plate is obtained by passing the emission current through a resistor and a 45-volt B battery connected in series, so that a change in emission causes a change in the control plate voltage which tends to oppose the emission change. This is illustrated schematically in Fig. 1, in which R_3 and R_4 are the control resistors and B_1 the biasing battery. The circuit adjusts itself so that the voltage between the filament and control plate is in the range 0 to 23 volts, depending upon the control resistance, for filament currents in the regulating range.

A diagram of the ion source components concerned in the circuit is given in Fig. 2. The control plate and filament cage are of Nichrome V, 0.015 in. thick. The control plate is mounted 1.0 mm from the shield on glass spacers, the mounting screws being insulated from the control plate by glass sleeves and additional spacers. The electrostatic shielding provided by the filament cage is necessary to eliminate the sensitivity of the emission current to the high fields existing between the source structure and the metal walls of the tube. The filament is of tungsten ribbon, 0.001 in.×0.030 in., stamped in the form of a hairpin and mounted so that the tip is approximately 0.5 mm from the plane of the control plate. This arrangement was found necessary to get an appreciable part of the total emission across to the trap. Since the potential of the control plate is above that of the filament, the uniform emission from a flat filament goes almost entirely to the control plate. The emission density from a hairpin-shaped filament is, however, considerably greater at the point than elsewhere, so that when the point is placed close to the hole in the control plate, a large fraction of the emission current will pass through, while still being subjected to the controlling field. With no magnetic field to collimate the electron beam, it was found that only about 2 percent of the total emission actually got across to the trap, about 80 percent going to the control plate and the remainder to the shield. For a source magnetic field of 250 gauss, the value used during most of the work, between 30 and 40 percent of the total emission was collected at the trap, most of the rest going to the control plate and serving only as the control current.

Since the total electron voltage comprises not only that applied between the control plate and shield but that between the filament and control plate as well, it should be borne in mind that a change in the emission will cause a change in the electron energy. During any one run the emission remains practically constant, of course, so that normally this factor need not be considered. For precise work, however, direct measurements of the voltage must be made to take into account changes in filament surface condition with changes in gas pressure and line voltage. The extent of these variations is discussed below.

With the range of control resistance indicated in the circuit diagram, 20,000 to 270,000 ohms, total emission

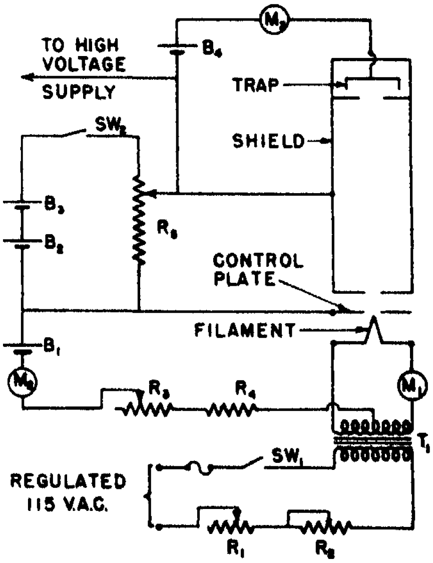

Fig. 1. Circuit diagram for space-charge regulator. R_1—150-ohm 50-watt rheostat; R_2—150-ohm 50-watt adjustable; R_3—250,000-ohm wire-wound potentiometer; R_4—20,000-ohm precision wire wound; R_5—50,000-ohm wire-wound potentiometer; B_1, B_2, B_3, B_4—45-volt B batteries; M_1—meter, 0–10 amp. a.c.; M_2—meter, 0–1.5 milliamp. d.c.; M_3—meter, 0–500 microamp. d.c.; T_1—filament transformer, secondary: 2.5 volts, 10 amp., 7500 r.m.s. volts insulation; SW_1—SPST toggle switch; SW_2—two position selector switch, 2500 volts insulation.

---

* Assisted by the Joint Program of the ONR and the AEC.

[1] Alfred O. Nier, Rev. Sci. Inst. 18, 398 (1947).

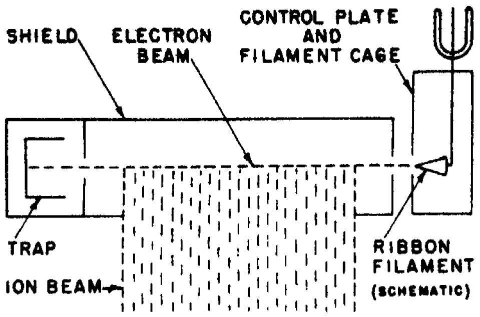

FIG. 2. Electron accelerating system for ion source equipped with space-charge control plate and filament cage. For complete diagram of a typical source see Fig. 2 of reference 1.

currents in the range 0.17 to 1.10 ma were obtained. The total emission was found to be practically independent of the accelerating voltage applied between the control plate and shield, a change in the latter from 0 to 90 volts, the maximum used, causing the emission to change by 0.2 percent.

The regulating range of the circuit, with the filament described above, begins at approximately 4.5 amp. filament current, and continues nearly flat up to about 6.0 amp., at which current the filament life is only a few hours. Because of the inherently low gain the characteristic is not perfectly flat, an emission change of the order of one percent resulting from a four percent change in filament current. This difficulty was eliminated by supplying the filament power through a Sola line regulating transformer. The resulting control was quite good, a five-volt line change at 115 volts resulting in a total emission change of 0.04 percent.

The effect on the regulation of using holes of different sizes in the control plate and shield was examined. Holes ranging from 0.5 mm to 2.0 mm in diameter were tried in the control plate, and, at the same time, the distance between the tip of the filament and the plane of the control plate was varied. It was found that the best control was achieved when the ratio of control plate hole diameter to control plate-filament spacing was approximately 2. The best ratio of trap current to total emission with this particular filament was given by a control plate hole diameter of 1.0 mm. The size of the hole in the shield had no effect on the regulation of the circuit. Shield hole diameters ranged from 0.34 to 2.0 mm, the former being chosen to determine whether this type of regulator would work satisfactorily with a gas-tight ion source. When the shield hole was equal to or larger than that in the control plate, its size had no discernible effect on the emission. However, when it was made smaller than the hole in the control plate, the trap current was restricted and the total emission current was affected somewhat by the electron voltage. For a control plate hole diameter of 1.0 mm and a shield hole diameter of 0.34 mm, a 90-volt change in the voltage applied between the control plate and shield caused a two percent change in the emission. At constant electron voltage, the regulation remained unimpaired.

The effect of a change in pressure in the ion source for a number of gases was investigated. Argon, helium, and nitrogen, which do not attack the hot filament, had no measurable effect on the emission in the pressure range 10^{-6} to 10^{-5} mm Hg. The presence of carbon dioxide exerted some influence on it, a tenfold change in pressure, from 10^{-6} to 10^{-5} mm Hg, causing the emission to fall by 0.5 percent. The effect of nearly pure oxygen was by far the worst, as one would expect, the same pressure change causing the total emission to drop about two percent. When the oxygen was pumped away, the emission did not recover immediately but required about three minutes to drift back to within 0.5 percent of its initial value.

The space-charge control regulator was compared with the electronic regulator already in use with this spectrometer, the control plate being attached to the shield for conventional operation of the source. Without the Sola transformer the effect of small line voltage changes was about the same for either circuit. The effect of gas pressure changes was somewhat more pronounced with the space-charge control regulator. A tenfold oxygen pressure change caused a 1.5 percent emission change with the electronic regulator, as compared with the two percent change found for the other. In spite of its lower gain, the space-charge control regulator is deemed acceptable as a substitute for the electronic regulator. In addition to its simplicity and ease of construction, all external circuit components being standard stock parts, it possesses the requisite stability for runs of long duration. During a three-hour test, using air at 2×10^{-6} mm Hg, the maximum emission current fluctuation was less than 0.5 percent. In another run in which carbon dioxide was introduced at a pressure of 7×10^{-6} mm Hg, the ion current showed the same degree of stability.

Although the batteries must be replaced occasionally, the elimination of an electronic power supply and the simplicity of the device are deemed adequate compensation for this slight inconvenience. An important feature resulting from the simplicity of the circuit is that the entire voltage drop to ground is across a simple filament transformer, which can be insulated for high voltage with no difficulty. One of the drawbacks of the older emission regulators is the fact that the unbalanced distributed capacity to ground in the several transformers introduces an a.c. ripple into the voltage applied to the ions. This effect, which usually is minimized by placing a suitable condenser between the shield and ground, is virtually non-existent in the present circuit.

THE REVIEW OF SCIENTIFIC INSTRUMENTS VOLUME 20, NUMBER 11 NOVEMBER, 1949

Electromechanical Lead Networks for A.C. Servo Mechanisms

DONALD MCDONALD
Aeronautical Research Center, University of Michigan, Ann Arbor, Michigan

(Received June 28, 1949)

The characteristics of conventional a.c. lead networks for a.c. servo mechanisms are compared to the characteristics of d.c. lead networks. Electromechanical lead networks for a.c. servo mechanisms having superior characteristics to those of the conventional a.c. lead networks are described and analyzed. A practical design for one of these electromechanical lead networks and its application to a servo system is shown.

ELECTRIC lead networks are used quite extensively to improve the response of servo mechanisms. The theoretical justification of the use of lead networks to improve the response of servo mechanisms and the general characteristics of basic lead networks has been considered thoroughly in several servo mechanisms texts.[1,2] In general, the notation used in this summary and in the following sections is that used in conventional servo mechanisms analysis. Such lead networks may operate on the error voltage, the input or output signal voltages separately, the feed-back voltage from an output tachometer, various internal loop voltages, and other signals. In many cases the input voltage to the lead network is a modulated, suppressed-carrier voltage, and it is necessary that the output voltage of the lead network also be a modulated, suppressed-carrier voltage of the same carrier frequency. Consequently, the basic d.c. lead network of Fig. 1, which is normally used where the output signal may be d.c. is not applicable by itself to these problems, and an a.c. lead network must be used.

The conventional a.c. lead networks do not operate on their input signals so effectively as does the network of Fig. 1 in a d.c. servo mechanism. Electromechanical a.c. lead networks as effective as the network of Fig. 1 can be designed and will be described following a brief summary of the characteristics of the convention a.c. lead networks.[3]

CONVENTIONAL A.C. LEAD NETWORKS

When the input and output voltages of a lead network must be modulated, suppressed-carrier voltages, two general types of a.c. lead networks are normally used. In the first type, the signal is demodulated, then the demodulated signal is passed through a d.c. lead network, like the one of Fig. 1, and lastly, the carrier is remodulated with the output voltage of the d.c. lead network. This type of a.c. lead network was probably the first to be used. The conventional tuned RLC and parallel-T networks are representative of the second type of a.c. lead network.[4] Regardless of the type of lead network, it may be stated that the essential characteristic of an a.c. lead network is that it produces a pronounced positive phase shift of the modulating envelope over specific portions of the modulating frequency band. As shown below, the two types of conventional a.c. lead networks do not meet these requirements so well as does the basic network of Fig. 1 when operating on a d.c. voltage.

The demodulator and modulator circuits of the first type of a.c. lead network produce noise. Filter circuits added to the demodulator and modulator tend to reduce the magnitude of this noise. Unfortunately the reduction in noise by this method is accompanied by a time delay or an effective negative phase shift of the modulating envelope. Such a negative phase shift may be partially compensated for by an increase in the attenuation of the d.c. lead network. This increase in the attenuation will result in an increase of the over-all noise-to-signal ratio. Hence, in the first type of a.c. lead network, an engineering compromise must be

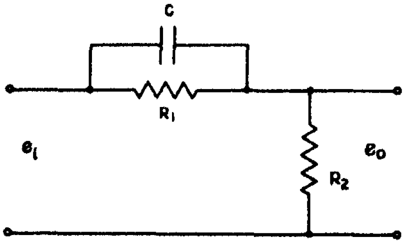

FIG. 1.

$r=\frac{R_1+R_2}{R_2}$

$T=R_1C$

$\phi=\angle\frac{e_0}{e_i}$

if

$$e_i=e\sin w_st \tag{1-1}$$

$$\frac{e_0}{e_i}=\frac{1}{r}\frac{1+jw_sT}{1+jw_s(T/r)}, \tag{1-2}$$

where maximum phase shift

$$\phi_{sm}=\sin^{-1}\left[\frac{r-1}{r+1}\right] \tag{1-3}$$

and occurs at

$$w_{sm}=\frac{(r)^{\frac{1}{2}}}{T} \tag{1-4}$$

$$\frac{e_0/e_i]_{w_s=\infty}}{e_0/e_i]_{w_s=0}}=r=\text{attenuation}. \tag{1-5}$$

---

[1] G. S. Brown and D. P. Campbell, "Principles of servomechanisms" (John Wiley and Sons, Inc., New York, 1948), p. 210.

[2] Albert C. Hall, "The analysis and synthesis of linear servomechanisms" (The Technology Press, Massachusetts Institute of Technology, Cambridge, 1943), p. 122.

[3] University of Michigan External Memorandum No. 25, "Improvements in the characteristics of a.c. lead networks for servomechanisms." This paper was also presented as a conference paper at the AIEE Mid-Winter Convention of 1949.

[4] Arthur H. Benner, "Phase lead for a.c. servomechanisms," J. App. Phys., 268–273 (1949).

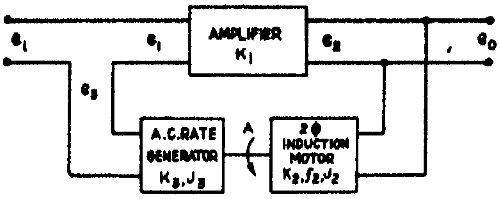
e_i
e_1
AMPLIFIER K_1
e_2
e_0
e_3
A.C.RATE GENERATOR K_3,J_3
A
2φ INDUCTION MOTOR K_2,f_2,J_2

FIG. 2.

$$e_0 = e_2 \tag{2-1}$$

$$e_1 = e_i - e_3, \quad e_1' = e_i' - e_3' \tag{2-2}$$

$$e_2 = K_1 e_1 \tag{2-3}$$

$$K_2 e_2' \cong [(J_2+J_3)p^2 + f_2 p]A, \quad \text{where } p = d/dt \tag{2-4}$$

$$e_3' = K_3 pA \tag{2-5}$$

$$J = J_2 + J_3, \quad f = f_2 \quad w_s \ll w_c \tag{2-6}$$

$$\frac{e_0'}{e_i'} \cong \frac{K_1 f}{f + K_1K_2K_3} \times \frac{1 + p(J/f)}{1 + p[J/(f + K_1K_2K_3)]} \tag{2-7}$$

(in general a primed variable denotes the envelope of the variable); let

$$\frac{f + K_1K_2K_3}{f} = r \quad T = J/f \tag{2-8}$$

$$\frac{e_0'}{e_i'} \cong \frac{K_1}{r} \frac{1 + pT}{1 + p(T/r)}, \tag{2-9}$$

if

$$e_i = e \sin w_s t \sin w_c t \tag{2-10}$$

$$\frac{e_0'}{e_i'} \cong \frac{K_1}{r} \frac{1 + jw_s T}{1 + jw_s (T/r)} \tag{2-11}$$

$$\phi_{sm} = \sin^{-1}\left[\frac{r-1}{r+1}\right] \tag{2-12}$$

$$w_{sm} = \frac{(r)^{\frac{1}{2}}}{T} \tag{2-13}$$

$$\frac{e_0'/e_i']_{w_s \to \infty}}{e_0'/e_i']_{w_s \to 0}} = r. \tag{2-14}$$

reached between (1) the amount of noise suppressed by filters in the demodulator and modulator and (2) the increase in noise-to-signal ratio resulting from the increase in attenuation required to offset the effect of the filters. These several factors cause this type of network to produce a smaller maximum positive phase shift than the d.c. lead network can produce by itself.

The a.c. lead networks of the second type are quite sensitive to changes in the carrier frequency which can reduce the effective lead developed by these networks and can, in some cases, produce lag instead of lead. This effect is more noticeable at 400 c.p.s. than at 60 c.p.s., because it is the absolute change in carrier frequency which affects the network, and, in general, 60 c.p.s. sources are, and can be, better frequency-regulated on an absolute basis than 400 c.p.s. sources. Also, the maximum value of the lead time constant T of the second type of a.c. lead network is limited, and this limits the minimum value of w_{sm}, the frequency at which the maximum positive phase shift of the modulating envelope occurs.[1,2] In some cases when the minimum value of w_{sm} is too large, it is possible to increase the phase shift at lower frequencies by increasing the attenuation. Unfortunately this increase in attenua-

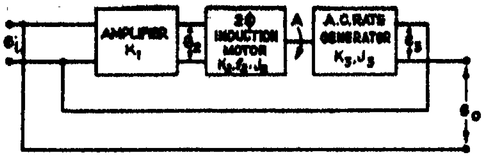
e_i
AMPLIFIER K_1
e_2
2φ INDUCTION MOTOR K_2,f_2,J_2
A
A.C.RATE GENERATOR K_3,J_3
e_3
e_0

FIG. 3.

$$e_2 = K_1 e_i \tag{3-1}$$

$$K_2 e_2' \cong [(J_2+J_3)p^2 + f_2 p]A, \quad \text{where } p = d/dt \tag{3-2}$$

$$e_3' = K_3 pA \tag{3-3}$$

$$e_0 = e_i - e_3, \quad e_0' = e_i' - e_3' \quad w_s \ll w_c, \tag{3-4}$$

$$J = J_2 + J_3, \quad f = f_2 \tag{3-5}$$

$$\frac{e_0'}{e_i'} \cong \frac{f - K_3K_2K_1}{f} \times \frac{1 + p[J/(f - K_1K_2K_3)]}{1 + p(J/f)} \tag{3-6}$$

(in general a primed variable denotes the envelope of the variable); let

$$\frac{f}{f - K_1K_2K_3} = r \quad T' = J/f \tag{3-7}$$

$$\frac{e_0'}{e_i'} \cong \frac{1}{r} \frac{1 + prT'}{1 + pT'} \tag{3-8}$$

or

$$\frac{e_0'}{e_i'} \cong \frac{1}{r} \frac{1 + jw_s rT'}{1 + jw_s T'} = \frac{1}{r} \frac{1 + jw_s T}{1 + jw_s (T/r)}, \tag{3-9}$$

where

$$rT' = T \tag{3-10}$$

$$\phi_{sm} = \sin^{-1}\left[\frac{r-1}{r+1}\right] \tag{3-11}$$

$$w_{sm} = \frac{(r)^{\frac{1}{2}}}{T}. \tag{3-12}$$

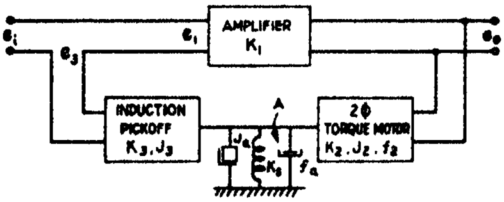

FIG. 4.

$$e_0 = K_1 e_1 \tag{4-1}$$

$$e_1 = e_i - e_3, \quad e_1' = e_i' - e_3' \tag{4-2}$$

$$e_3' = K_3 A \tag{4-3}$$

$$K_2 e_0' \cong [(J_2+J_3+J_a)p^2 + (f_2+f_a)p + K_s]A, \quad \text{where } p = d/dt, \tag{4-4}$$

$$J = J_2 + J_3 + J_a, \quad f = f_2 + f_a \tag{4-5}$$

$$\frac{e_0'}{e_i'} \cong K_1 \frac{Jp^2 + fp + K_s}{Jp^2 + fp + (K_s + K_1K_2K_3)} \quad w_s \ll w_c; \tag{4-6}$$

(in general a primed variable denotes the envelope of the variable); let

$$e_0 = e \sin w_s t \sin w_c t \tag{4-7}$$

$$w_n^2 = K_s/J \tag{4-8}$$

$$c = \frac{f}{2(K_s J)^{\frac{1}{2}}} \tag{4-9}$$

$$h^2 = \frac{K_s + K_1K_2K_3}{K_s} \tag{4-10}$$

$$u = \frac{w_s}{w_n} \tag{4-11}$$

then

$$\frac{e_0'}{e_i'} \cong \frac{K_1}{h^2} \frac{1 - u^2 + j2cu}{1 - (u/h)^2 + j2(c/h)(u/h)} = K_L G_L(ju). \tag{4-12}$$

tion may increase the noise-to-signal ratio of the lead network sufficiently to offset any improvement derived from an increase in positive phase shift at lower frequencies.

ELECTROMECHANICAL A.C. LEAD NETWORKS

By rearrangement of the elements of the lead network and by the choice of demodulators and modulators with excellent noise-to-signal ratios, it is possible to design an a.c. lead network which has performance comparable to the d.c. lead network in a d.c. servo mechanism. Such a lead network is shown in Fig. 2, and, because it contains electromechanical components, shall be referred to as an electromechanical lead network.[1] In the most general form, electromechanical lead networks are equally applicable for d.c. and a.c. operation, but in this article, only the a.c. form is discussed. (The network of Fig. 2 was described previously by the author in Electronics, November 1948. The meaning of the rearrangement of elements and the choice of the electromechanical components has been considered quite extensively in reference 3.)

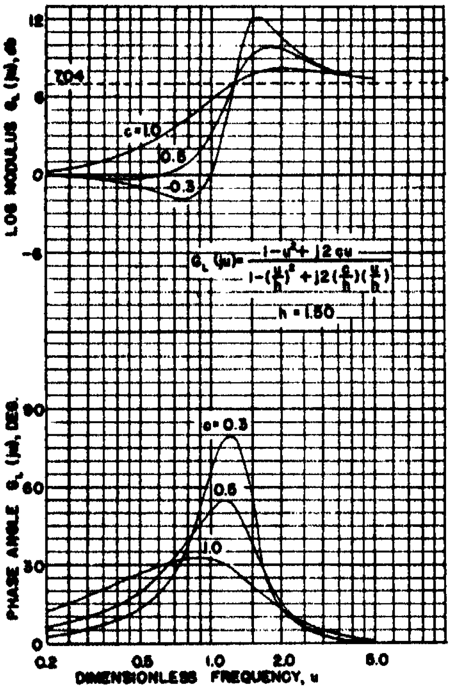

GRAPH 1.

In the system of Fig. 2 the motor functions as a demodulator, and the generator as a modulator. Both of these functions are approximate, with the limitations that w_s and the motor-generator speed be small compared to synchronous. The analytical expressions of (2–11), (2–12), and (2–13) of Fig. 2 show that the characteristics of this system are the same as for the conventional a.c. lead network.[2] By proper adjustment of K_1, K_2, and K_3, it is possible to establish any value of attenuation r, and the lead time constant T can be made as large as desired by the addition of inertia to the common motor-generator shaft. Unfortunately the minimum value of T is $(J_2+J_3)/f$, and this value may be too high for some servo applications.

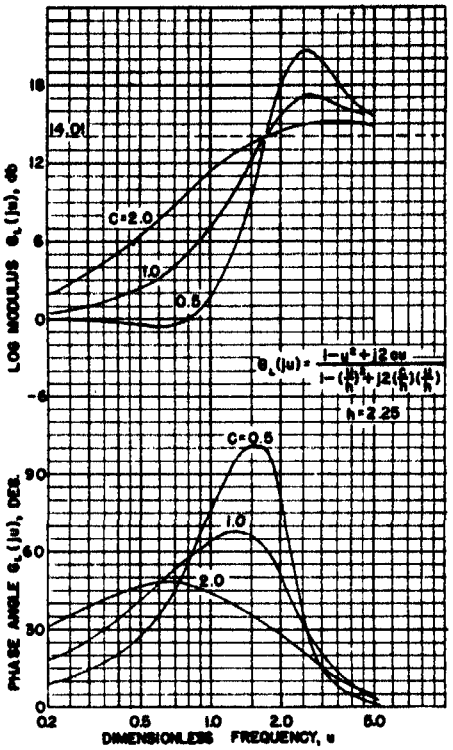

GRAPH 2.

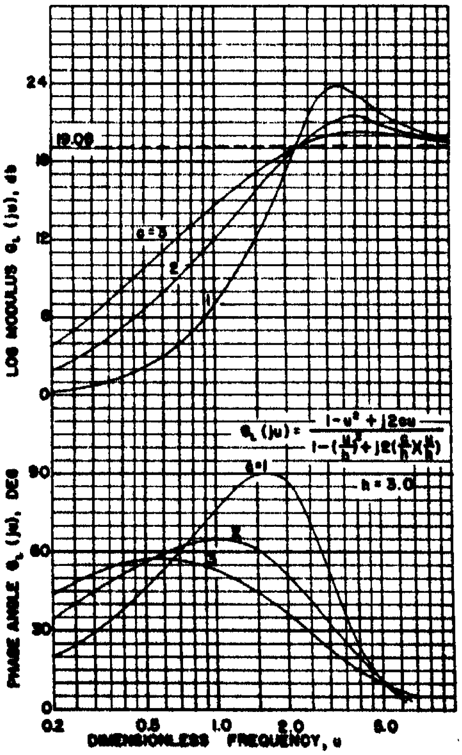

GRAPH 3.

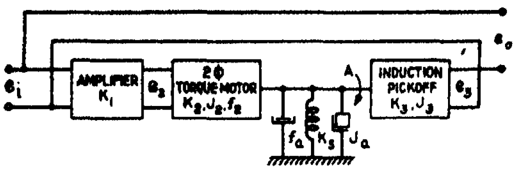

FIG. 5.

$$e_0 = e_i - e_3, \quad e_0' = e_i' - e_3' \tag{5-1}$$

$$e_3' = K_3 A \tag{5-2}$$

$$K_2 e_2' \cong [(J_2 + J_3 + J_a)p^2 + (f_2 + f_a)p + K_s]A, \quad \text{where } p = d/dt \tag{5-3}$$

$$e_2 = K_1 e_i \tag{5-4}$$

$$J = (J_2 + J_3 + J_a), \quad f = f_2 + f_a \tag{5-5}$$

$$\frac{e_0'}{e_i'} \cong \frac{Jp^2 + fp + (K_s - K_1K_2K_3)}{Jp^2 + fp + K_s} \quad w_s \ll w_c \tag{5-6}$$

(in general a primed variable denotes the envelope of the variable); let

$$e_0 = e \sin w_s t \sin w_c t \tag{5-7}$$

$$w_n^2 = K_s/J \tag{5-8}$$

$$c = \frac{f}{2(K_s J)^{\frac{1}{2}}} \tag{5-9}$$

$$q^2 = \frac{K_s}{K_s - K_1K_2K_3} \tag{5-10}$$

$$u = w_s/w_n \tag{5-11}$$

then

$$\frac{e_0'}{e_i'} \cong \frac{1}{q^2} \frac{1 - (qu)^2 + j2(qc)(qu)}{1 - u^2 + j2cu}. \tag{5-12}$$

The form of the electromechanical network of Fig. 2 will be referred to as a feed-back form because of the arrangement of the components in the circuit. Another arrangement of the components of Fig. 2 is shown in Fig. 3 and will be referred to as an electromechanical a.c. lead network of the parallel form. This parallel form of electromechanical network has characteristics similar to those of the feed-back form except that its lead time constant T is greater by a factor equal to the attenuation r. Consequently, in many cases the parallel form is not so useful as the feed-back form of electromechanical a.c. lead network. It is of interest to note that the amplifier K_1 can be omitted in the parallel form.

Figure 4 is a schematic of another electromechanical a.c. lead network. It is of the feed-back form but, as indicated by Eq. (4-12), does not have the phase and amplitude characteristics of the basic a.c. network. This network is a resonant lead controller.[2] Graphs 1, 2, and 3 show the phase and amplitude characteristics of this electromechanical system.

Figure 5 shows the parallel form counterpart of the electromechanical a.c. lead network of Fig. 4. Its characteristics are similar to those of the feed-back form.

Of the several types of electromechanical a.c. lead networks discussed, that of Fig. 4 appears to have the most desirable characteristics and also to be the simplest to manufacture. Figure 6 is a cut-away view of a pilot design of this electromechanical system. The main components of the system are (1) an induction torque motor, (2) a combination induction pickoff and electric spring, (3) an eddy-current damper, and (4) inertia weights. The induction torque motor and the combination induction pickoff and electric spring are made of simple, punched laminations and bobbin-wound coils and are called Microsyn elements.[3]

The induction torque motor is excited by a fixed a.c. reference voltage and by the signal voltage. It develops a torque proportional to the signal voltage which is virtually independent of the angular displacement of its rotor. The coils of the combination induction pickoff and electric spring are so arranged that there is a separate circuit for both the pickoff and electric spring. The pickoff circuit is excited with a.c. voltage and the circuit of the electric spring is excited with d.c. voltage. This combination then produces a signal voltage and a torque, both of which are proportional to the angular displacement of the rotor from neutral. By changing the d.c. excitation of the electric spring circuit, the torque gradient of the electric spring may be adjusted.

The eddy-current damper is made up of an aluminum damping disk and a multi-pole, Alnico permanent magnet with its poles parallel to the axis of rotation. This magnet is threaded axially into the housing; and therefore it is possible to adjust the spacing between the magnet and damping disk, thus changing the damping coefficient f.

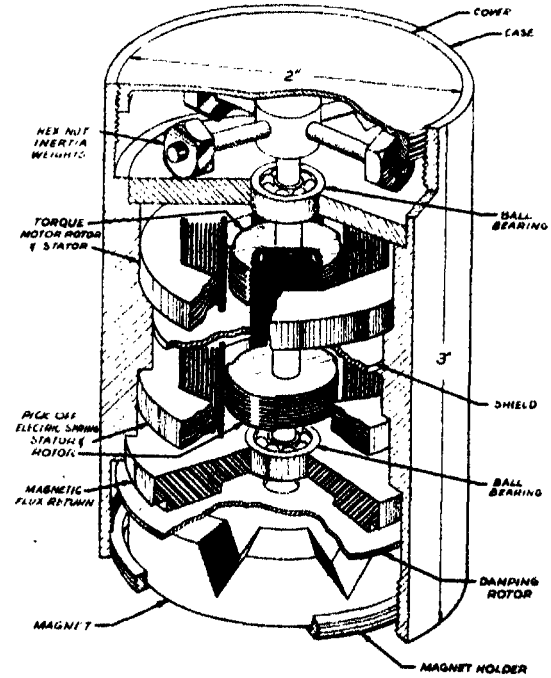

FIG. 6.

---

[3] The Microsyn elements were developed by the M. I. T. Instrumentation Laboratory and are more fully described in *Electronic Instruments* (McGraw-Hill Book Company, Inc., 1948), pp. 365–366. The combination of the induction pickoff and electric spring into one Microsyn element was developed by Mr. K. C. Mathews of the University of Michigan Aeronautical Research Center while he was a member of the Doelcam Corporation, Newton, Massachusetts.

FIG 7.

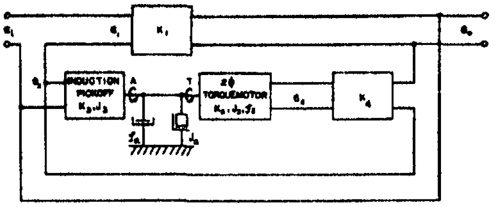

$$\frac{e_0'}{e_i'}\cong K_1\frac{Jp^2+fp+K_2K_3K_4}{Jp^2+fp+K_2K_3K_4(1+K_1)}. \tag{7-1}$$

Let

$$K_2K_3K_4=K_s. \tag{7-2}$$

Then

$$\frac{e_0'}{e_i'}\cong K_1\frac{Jp^2+fp+K_s}{Jp^2+fp+K_s(1+K_1)}. \tag{7-3}$$

The total moment of inertia of the system may be changed by adjusting the position of the inertia weights.

Thus as there are three continuously adjustable parameters—the spring constant, the damping, and the moment of inertia—it is possible to adjust the two variables w_n and c independently. The attenuation factor h^2 can also be adjusted independently by changing the pickoff sensitivity or the amplifier gain.

As planned, w_n and c are to be continuously adjustable from 1 c.p.s. to 6 c.p.s. and 0.5 to 1, respectively. Over these ranges of network parameters, the maximum power consumption of the torque motor should not exceed one-third of a watt.

If the electromechanical system of Fig. 6 is used in the circuit of Fig. 7, its natural frequency w_n can be increased and its design can be simplified. In Fig. 7 the spring K_s of Fig. 4 has been replaced by the amplifier K_4. It can be shown that if h^2 is set equal to $1+K_1$, Eq. (7-3) can be non-dimensionalized and will have the same form as Eq. (4-12) of Fig. 4. Hence the response of the circuit of Fig. 7 is the same as the response of the circuit of Fig. 4 and Eq. (4-12) and Graphs 1, 2, and 3 apply for both circuits.

FIG. 8.

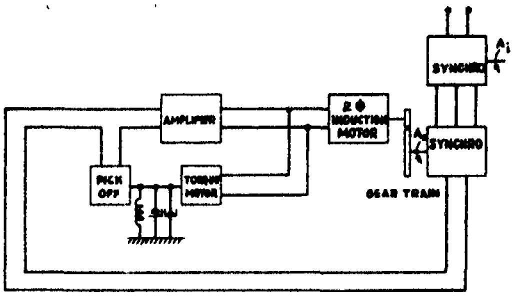

Changes in carrier frequency which will not prevent proper operation of any electromechanical components in the complete servo loop (such as motors and indicators) will not affect the operation of the electromechanical a.c. lead networks described. Graphs 1, 2, and 3 show that w_{sm} occurs near w_n, and, as noted above, w_n and hence w_{sm} may be adjusted to cover the region of frequencies required for almost every type of servo mechanism problem. Also the maximum value of phase shift ϕ_{sm} may be made larger for the network of Fig. 4 than for a single lead network having the same attenuation or noise-to-signal ratio.

An example of the application of the electromechanical lead network of Fig. 4 is shown in Fig. 8. Here a two-phase induction servo is being stabilized by the use of this electro mechanical a.c. lead network. As will be noted, the amplifier driving the servo motor is also used to drive the torque motor of the lead network. This is possible because of the very low power consumption of the torque motor.

In closing, if the feed-back paths of Figs. 2 and 4 are connected regeneratively, instead of degeneratively, and the parallel paths of Figs. 3 and 5 are connected so as to add, instead of subtract, these systems will become lag or integral networks instead of lead networks.

ACKNOWLEDGMENTS

I should like to thank Messrs. K. C. Mathews and P. E. Theobald of the University of Michigan Aeronautical Research Center for their assistance in the mechanical design of the system of Fig. 6.

THE REVIEW OF SCIENTIFIC INSTRUMENTS VOLUME 20, NUMBER 11 NOVEMBER, 1949

A High Power Attenuator for Microwaves

DANIEL ALPERT
Westinghouse Research Laboratories, East Pittsburgh, Pennsylvania

(Received July 1, 1949)

A high power variable attenuator has been developed for use in 10-cm wave guide transmission lines. The attenuating material is a liquid which serves also to transfer the absorbed energy. The attenuator can handle power levels up to 100 watts, has a power standing wave ratio less than 1.1 to 1, and an attenuation which is variable from 1.5 db to 40 db.

THIS paper describes a high power attenuator developed to vary the main power flow in a 10-cm wave guide. It was used in experiments on microwave breakdown potentials in gases, recently carried out at Westinghouse Research Laboratories. In these experiments it was necessary to vary the power level in a

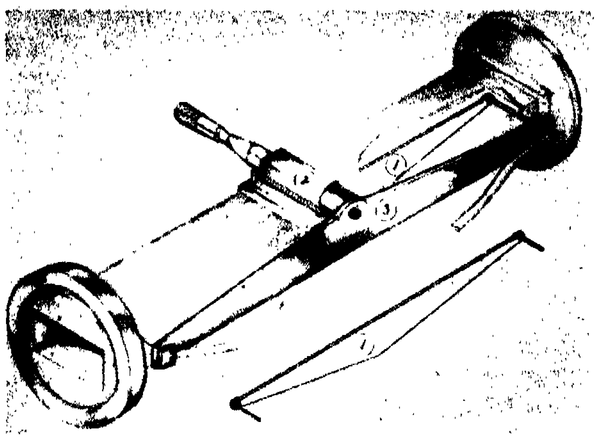

FIG. 1. High power liquid attenuator: 1. Lucite boat. 2. Spring-loaded drive mechanism. 3. Aluminum cross-bar supporting boat.

wave guide transmission line without introducing large reflections. During the war years a number of satisfactory low power variable attenuators were developed.[1] Such attenuators, however, cannot handle powers above about 1 watt, so that for higher power levels it has been customary to use power dividers which are highly reactive. The present attenuator, using a liquid both as the power absorbing material and as the means of heat transfer, can handle of the order of 100 watts of power with an attenuation variable from 1.5 to 40 db and a power standing wave ratio less than 1.1 to 1 at all settings.

The attenuator design is shown in Fig. 1. The liquid flows through a tapered plastic boat forming an attenuating sheet $\frac{1}{16}$ in. thick parallel to the small wave guide dimension. The length of the boat is 16¼ in. while the depth varies from ⅜ in. at the inlet to 1⅜ in. at the center. The losses in the Lucite container are negligible. Change in attenuation is accomplished by varying the distance between the attenuator boat and the wave guide side wall. The base inlet and outlet tubes which support the boat are clamped on the outside to a movable aluminum cross-bar. The drive mechanism consists of a cylindrical post sliding in a honed bearing and advanced by a spring-loaded micrometer head screw. Details of the construction and liquid seals are shown in Fig. 2.

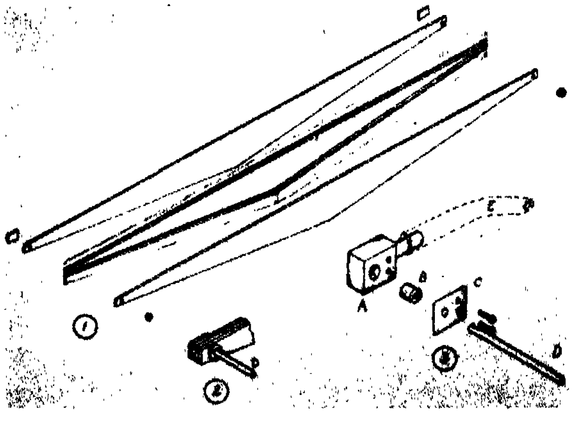

FIG. 2. Details of attenuator design: 1. Lucite parts: Spacer strips shown with wavy outlines cemented in place, then milled to correct outer shape. 2. Inlet construction. 3. Detail of inlet joint: A. Aluminum housing, B. Neoprene gasket, C. aluminum cover, D. brass tubing, E. rubber tubing to heat exchanger.

The choice of a cooling system for such an attenuator is a matter of taste. We used a closed system with an air cooled radiator and a small centrifugal pump. A flow rate of 5 to 10 cc per sec. is desirable as is a flow switch to turn off the incident power when the liquid is not circulating.

The liquid used in the attenuator is a mixture of ethylene glycol and water. Though any concentration ratio of these two liquids, including 100 percent water, will result in an excellent attenuator, we used a mixture of 60 percent to 70 percent of ethylene glycol in water. The choice was made empirically, based on the unusual attenuating properties of such mixtures as shown in Fig. 3: Varying concentrations of ethylene glycol in water were used to fill the plastic boat, and both the attenuation and standing wave ratio measured as a function of position. As is seen from the figure, the total attenuation passes through a maximum for a 70 percent–30 percent mixture, then falls considerably for

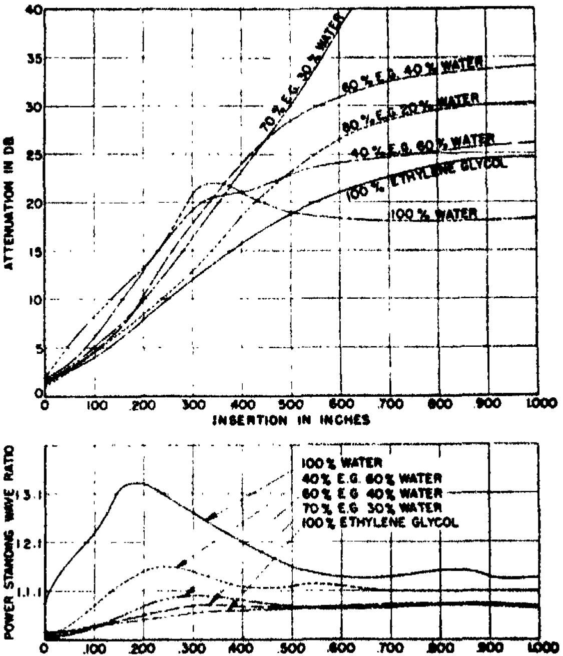

FIG. 3. Attenuation *vs.* insertion into wave guide for various liquid concentrations. The lower curve gives the power standing wave ratio as a function of position in the standard 10-cm *RG*$-48/U$ wave guide (outer dimensions 1.5×3 inches, wall thickness 0.080 in.).

---

[1] C. G. Montgomery, *Technique of Microwave Measurements* (McGraw-Hill Book Company, Inc., New York, 1947) pp. 720–803.

either undiluted ethylene glycol or plain water. Note that the total attenuation for the chosen concentration is almost twice that for water. The power standing wave ratio, shown in the same figure, is a maximum for pure water and drops to a minimum for ethylene glycol. For the 70 percent–30 percent mixture the maximum standing wave ratio is 1.07 to 1.

The curve for attenuation as a function of position cannot be considered an accurate calibration. The amount of attenuation varies considerably with liquid temperature; the direction of the shift as well as its magnitude depend on the attenuator position.

An interesting property of the liquids used is that the temperature variation of attenuation for water is generally in the opposite direction from that for ethylene glycol. Thus for a particular setting of the attenuator it is possible to choose a concentration of the two liquids which will reduce the temperature coefficient to a very small value. This would obviously be desirable for a high power fixed attenuator or buffer.

In the experiment for which the attenuator was developed, we used auxiliary methods for accurate power level measurement, and did not depend on an accurate calibration of the attenuator. In general, however, with the liquid reservoir maintained at room temperature the attenuator was very reliable and the readings were repetitive. For most measurements a flow rate of 6 cc per sec. was used. Thus for 40 watts input the average temperature rise in the attenuator itself was only 2°C. While 40 watts was our maximum available r-f power there is every indication that 100 watts could be readily handled. By increasing the rate of liquid flow or the size of the attenuator one could increase this power capacity considerably.

THE REVIEW OF SCIENTIFIC INSTRUMENTS VOLUME 20, NUMBER 11 NOVEMBER, 1949

A Flexible High Voltage Square Wave Generator*

LANGDON C. HEDRICK**
Mallinckrodt Chemical Laboratory, Harvard University, Cambridge, Massachusetts

(Received July 15, 1949)

Presented here is the design of a high voltage square wave generator suitable for modulating the absorption cell of a microwave spectrograph. Peak to peak voltages up to 1800 have been produced at 100 kc, feeding into an 800$\mu\mu$f capacitive load. The lower half of the cycle is kept automatically at ground potential and the adjustment of voltage from 0 to 1800 is controlled by a single variable.

THE instrument to be described was developed in response to a demand for a source of high voltage square wave modulation to be applied to a microwave absorption cell as described by Hughes and Wilson.[1]

Specifically, the instrument was required to supply a high (at least 1500V) amplitude square wave, automatically zero-based at all voltages, and amplitude-controlled with a single variable.

Modulation of the absorption cell reduces simply to charging and discharging a condenser at intervals appropriate to produce a square wave of voltage. Conventional amplifiers are unsuitable for the generation of the high voltages desired, and a switching technique similar to that employed in radar systems was devised.[2]

Inspection of Fig. 1 shows that alternately turning on T_1 and T_2 for short intervals will produce a square wave of voltage across the load condenser. Observe, however, that in charging the condenser, T_1 is acting essentially as a cathode follower while T_2 is simply a straight amplifier,[3] to use the term loosely. The result, with equal pulses on the switch tube grids, is an equi-

FIG. 1.

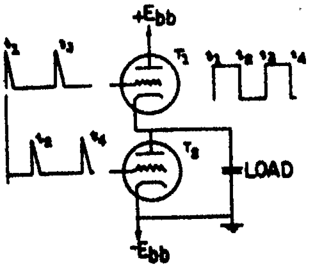

FIG. 2.

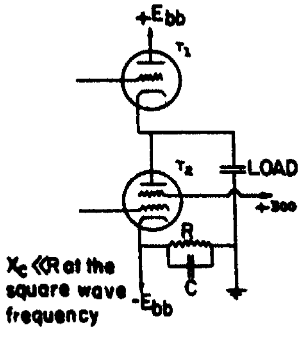

---

* The research reported in this document was made possible through support extended Harvard University by the Navy Department (ONR) under ONR Contract N5ori-76, Task Order V.

** Now with Baird Associates, Inc., Cambridge, Massachusetts.

[1] D. Hughes and E. B. Wilson, Phys. Rev. 71, 562 (1947).

[2] M.I.T. Radar School Staff, *Principles of Radar*, pp 6–38, 6–39.

[3] Considerations of input admittance of the switch tube grids govern. See F. E. Terman, *Radio Engineering* (McGraw-Hill Book Company, Inc., New York, 1947) pp. 309, 365.

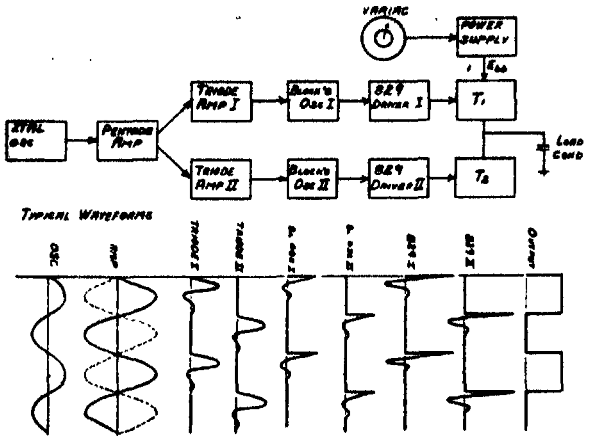

FIG. 3. Block diagram square wave generator.

librium with the bottom of the square wave well above the zero base. Using triode switch tubes, the limitations imposed by the requirements of automatic zero-basing and single dial control of amplitude eliminated, from a practical standpoint, the possibilities of (1) varying the amplitude and duration of the grid pulses so as to return the square wave to zero, or (2) floating the cathode of T_2 below ground sufficiently to produce the desired results.

Substitution of a tetrode for T_2 in Fig. 1 resulted in a significant improvement of the zero-seeking characteristic of the square wave. However, at low values of E_{bb}, the square wave base still drifted considerably above zero. This difficulty was eliminated by (1) tying the screen grid of T_2 to a fixed potential of 300 volts in order to sustain conduction by T_2 at low square wave amplitudes, and (2) reducing the drive to the grid of T_1 by reducing the screen potential on the driver tube for all values of E_{bb} less than 300 volts. Also, as E_{bb} was increased above 300 volts, a progressive drift of the square-wave base to a maximum of 20 volts was considered excessive. This drift resulted from the inability of T_2 to discharge the load condenser completely, regardless of the amplitude of the drive pulse. The use of a tetrode for T_2, however, makes it possible to develop sufficient automatic (negative) bias for the cathode of T_2 to give zero-basing within plus or minus 0.5 volts at all square wave voltages (see Fig. 2).

Figure 3 is a block diagram of the complete unit. Excepting the switch tube circuits, the design is conventional and none of the circuits is critical of adjustment. A crystal oscillator is used as the frequency-stabilizing element, followed by a pentode amplifier tuned to the crystal frequency. The push-pull triodes following the amplifier generate the out-of-phase pulses for synchronization of the blocking oscillators.[4] The precise triggering of the blocking oscillators, alternately every half-cycle, is essential to the stable timing of the rise and fall of the square wave, while the rapid response of the blocking oscillators to triggering is the key to obtaining sufficient drive for the switch tubes.

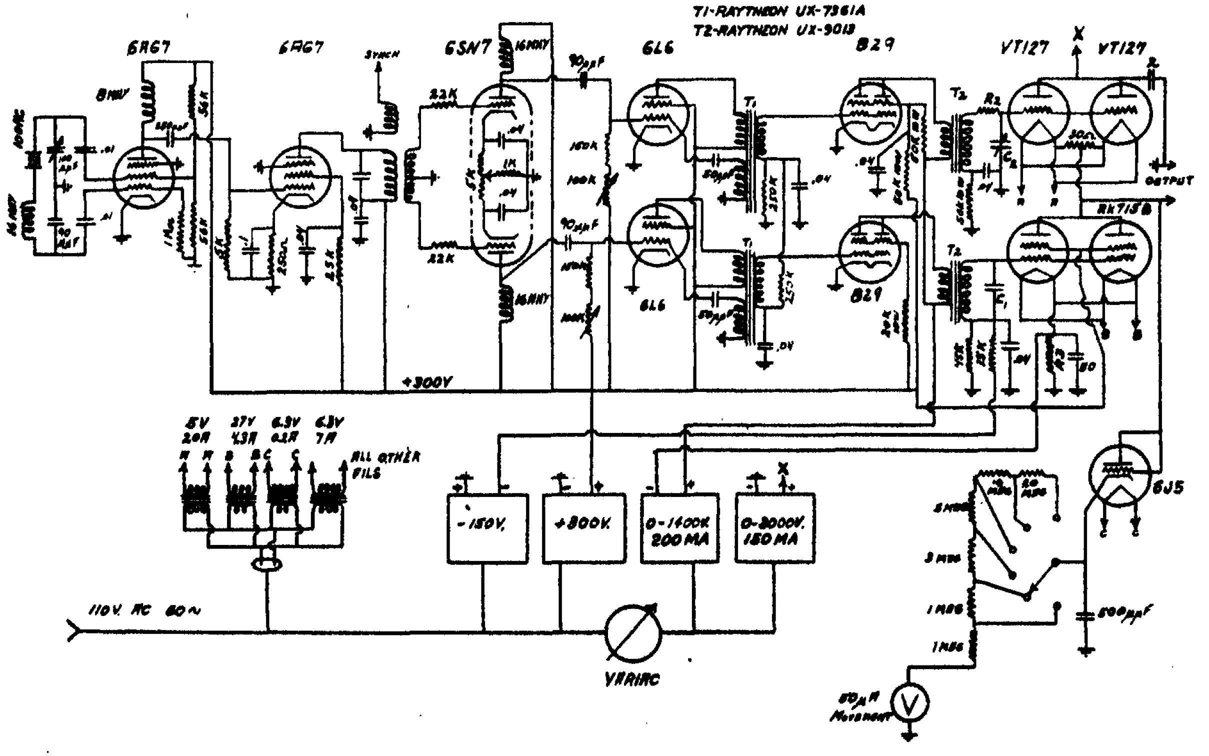

FIG. 4. Square wave generator. Condensers in μf unless otherwise noted; resistors in k = 1000 ohms; power supplies are conventional.

---

[4] H. J. Reich, *Theory and Application of Vacuum Tubes* (McGraw-Hill Book Company, Inc., New York, 1944), p. 395.

The sharp pulses out of the blocking oscillators are applied to the grids of the 829's (normally cut off). The sudden conduction of the 829's produces a very large voltage across the secondaries of the coupling transformers which triggers the switch tubes. E_{bb} is the variable which controls the amplitude of the square wave. The complete circuit diagram is shown in Fig. 4.

Design features which are important include a very low capacity (secondary winding to primary and ground) transformer for the filament of T_1, and critical adjustment for optimum wave shape of C_1, C_2 and R_2, in the switch tube grid circuits. The fixed and grid-leak components of the bias for T_1 must be adjusted to yield optimum wave shape at both high and near-zero values of square wave voltage, and R_3 must be adjusted for zero-basing.

The transformer driving the VT 127's is overloaded at high voltages. A conventional radar pulse transformer was stripped, rewound, (18 turns No. 14 wire on primary and 42 turns No. 20 wire on secondary) and was found to perform satisfactorily.

Results have justified the efforts in developing this instrument. R_2 and C_2 are adjusted, at maximum square wave voltage (1800 v), to limit the positive overshoot of the voltage rise to 20 volts and C_1 is adjusted to limit the negative overshoot of the voltage fall to 20 volts. With these damping conditions, the square wave rise and fall times are less than 0.2 microseconds at all square wave voltages while the time of the overshoots are less than 0.2 microseconds at maximum square wave voltage so that the top and bottom of the wave are essentially flat.

Currently in use is one unit as shown in Fig. 4, yielding 1800 volts of square wave across a Stark guide of 800 $\mu\mu$f capacity. Also, two smaller units produce 800 volts of square wave while meeting the original requirements. The smaller units use a single 811 in place of the parallel VT-127's, one RK-715B instead of two, and a single 1500 volt power supply for both the 829's and the switch tubes. Otherwise, circuits and construction are identical with the larger unit.

The upper frequency limit of the generators, consistent with good wave shape, appears to be in the region of 500 kc, while those in use and for which the values are specified operate at 100 kc. For frequencies below 100 kc, it is proposed to use a 100-kc crystal oscillator as the control element, dividing by blocking oscillators to twice the square wave frequency, and using an Eccles-Jordan[5] trigger circuit to obtain out-of-phase triggering of the blocking oscillators driving the 829's.[6]

---

[5] See reference 4, p. 353.

[6] In practice, type 3E29 tubes were used.

THE REVIEW OF SCIENTIFIC INSTRUMENTS VOLUME 20, NUMBER 11 NOVEMBER, 1949

Photo-Tube Input Impedance for a Voltage Stabilizer

E. N. Strait and W. W. Buechner
Laboratory for Nuclear Science and Engineering, Massachusetts Institute of Technology, Cambridge 39, Massachusetts

(Received August 1, 1949)

A circuit for stabilizing the voltage of an electrostatic generator is described. A photo-tube under constant illumination is used as an input impedance, eliminating the necessity for d.c. amplification of the error signal. This signal is impressed directly on the control grid of a 5693 pentode that is used to control corona-leakage current to the high voltage terminal of the generator. Convenience of operation and simplicity of construction are features of the circuit.

During the course of some recent efforts to improve the circuit used to stabilize the voltage of the open-air electrostatic accelerator at the M. I. T. High Voltage Laboratory, it occurred to the authors that a photo-tube under constant illumination might serve as an advantageous substitute for an input resistor in the first stage. Such a circuit has been constructed and has been in constant use for approximately three months. It has proved to be reliable and convenient in operation and is of very simple construction. Since the employment of a photo-tube in this fashion is not common, but nevertheless presents the possibility of numerous uses, it seems appropriate to give a brief description of its characteristics as applied to a voltage stabilizer.

Figure 1 is a schematic diagram of the circuit. The generator control features are similar to those described previously in the literature.[1] The positive-ion beam from the generator is deflected in the field of a large electromagnet and caused to pass between the jaws of a defining slit. Error signals set up by the beam current spilling onto the slit jaws are amplified and used to control a variable corona load facing the high voltage terminal of the generator. This control is accomplished by varying the potential of the control grid of a 5693 pentode, the plate of which is connected directly to a set of insulated corona needles facing the high voltage

---

[1] R. M. Ashby and A. O. Hanson, Rev. Sci. Inst. 13, 128 (1942); A. O. Hanson, Rev. Sci. Inst. 15, 57 (1944); McKibben, Frisch, and Hush, AEC Technical Information Division, Document MDDC 222 (1946).

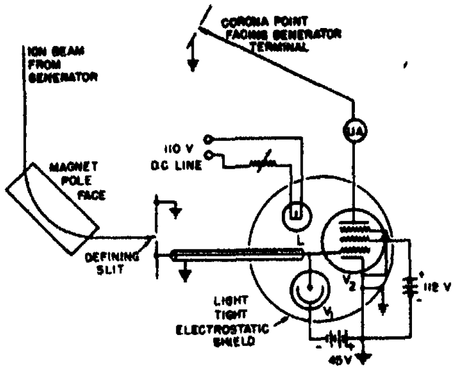

FIG. 1.

terminal. Each of these needles protrudes through a hole in a grounded shield. Placing a negative bias on the 5693 increases the impedance of the tube, thus causing the needle points connected to its plate to become more positive with respect to ground. This reduces the positive field in the neighborhood of the points; and, consequently, the corona current from the points is reduced. No additional high voltage power supply is required. The 5693 is similar in size and electrical ratings to the 6SJ7 but seems to be a more reliable tube for this rather strenuous service.

The novel feature of the circuit to be described here is the use of the photo-tube, which eliminates the necessity for a stage of d.c. amplification between the ion-beam slit jaws and the 5693 pentode. For simplicity of construction, only the signal from the lower jaw is used. Although this system is open to the objection that it may introduce voltage modulation with changes in ion-beam intensity, nevertheless, in practice this effect has been found to be negligible. The ion-beam intensity changes very little during continuous generator operation, and, with a sharply focused beam falling upon the defining slit, small changes in beam intensity result in only minute shifts in the median position of the beam. Large changes in beam intensity, as from one generator run to another, require adjustment of the circuit for optimum results, as will be described below; but similar adjustments, for example, in the magnitude of the input resistors, are also required in the case of a push-pull circuit employing signals from both jaws of the slit.

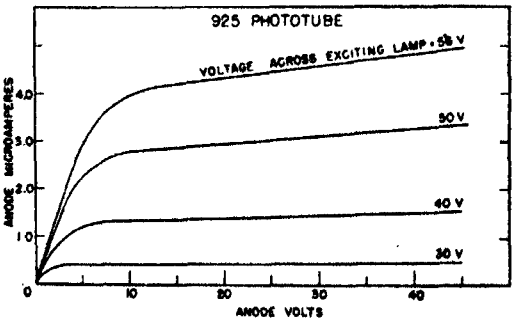

FIG. 2.

The advantages of the photo-tube impedance may be tabulated as follows:

(1). By operating the photo-tube in the region of cathode current saturation and with fixed illumination, the photo-tube may have a very high dynamic anode resistance. In the case of the 925 photo-tube, it may vary from 5×10^9 ohms at low levels of illumination to 4×10^7 ohms at moderate illumination. Figure 2 shows characteristic curves for a 925 tube in the region of interest to this discussion. This high resistance means that a change of a fraction of a microampere in the beam current falling on the lower slit jaw produces without further amplification a change of 10 volts or so in the potential of the control grid of the 5693. This is adequate to produce a change of 100 microamperes or more in plate current. The absence of an input stage of d.c. amplification eliminates the necessity of a separate power supply for this stage and simplifies the circuit construction.

(2). Despite high dynamic resistance, the photo-tube has only a moderate d.c. resistance, as shown by the slope of the chord drawn from the origin to the operating point (Fig. 2). Thus, the voltage drop across the tube is of the right magnitude to be readily bucked out by means of a 45-volt "B" battery. Since the current that the battery is required to carry is only the microampere or less in the ion beam spilling onto the lower slit jaw, the life of the battery is very close to its shelf life.

(3). Since the photo-tube normally operates in the region of fractions of a microampere up to a few microamperes, it is well suited to handling the currents encountered at the slit jaws. Furthermore, by changing the level of illumination, the photo-tube can be caused to give the same voltage drop when passing widely different currents. This adjustment can be made in a continuous fashion, in contrast to the usual situation with resistors in the range of 10^8 to 10^{10} ohms. In practice, this feature has been of great convenience, since it has reduced the operations needed to balance the circuit for various beam currents to one control, that of the current through the small lamp used to excite the photo-tube.

The circuit operates in the following manner. With the plate of the 5693 grounded, the spacing of the corona needles from the generator terminal is adjusted so that about 200 microamperes are drawn from the points. This current is not critical, but the needle spacing may need to be changed if the generator is to be operated at widely different voltages. With the plate ungrounded, the 5693 then controls the current from the needles. If the generator voltage tends to rise above its operating value, the ion beam is deflected less by the magnet; consequently, more current strikes the lower slit jaw. This causes the control grid of the 5693 to become less negative, and the tube therefore allows more current to pass from the needle points. This loads the generator and reduces the voltage. The most desirable operation is secured when, with about one-tenth of the total ion beam spilling on the lower slit jaw, the potential of the control grid of the 5693 is such as to allow about 100 microamperes to be drawn from the needle points. This may be accomplished for various ion-beam intensities by adjusting the illumination supplied by the 6-watt lamp, thus placing the operation on the appropriate branch of the photo-tube characteristic curves (Fig. 2). The 6-watt lamp is operated from a d.c. rather than an a.c. line to avoid a 120-cycle modulation of the photo-tube. Since this lamp never requires more than 30 milliamperes, it would be quite feasible to feed both the lamp and the 5693 screen grid from a common rectified power supply.

If the ion beam leaves the lower slit jaw altogether, the potential of the 5693 control grid becomes 45 volts negative to ground, which is more than enough to cut off the plate current. It is interesting to note that, although under these cut-off conditions the plate voltage on the 5693 may rise to about 5000 volts, which is far in excess of its maximum rating of 300 volts, the tube nevertheless performs very satisfactorily. Occasional sparking across the tube base occurs, but this is rare and does not interfere with the stabilizing action; and, since the current in the spark is limited to the 200 microamperes available from the corona points, the tube is not damaged. In any event, the plate-power dissipation is well within the 2.5-watt rating for this tube. A representative operation of the tube in this service is 100 microamperes at 2500 volts on the plate, or 0.25-watt dissipation.

The photo-tube, exciting lamp, and 5693 control tube are mounted inside a light-tight electrostatic shield as close to the defining slit as is convenient in order to minimize the input capacitance and thus keep the time constant low and also to protect against the pick-up of stray signals. The requirement for the light-tight feature is obvious.

This work has been supported by the Joint Program of the ONR and the AEC.

THE REVIEW OF SCIENTIFIC INSTRUMENTS VOLUME 20, NUMBER 11 NOVEMBER, 1949

An Absolute Noise Thermometer for High Temperatures and High Pressures

J. B. Garrison and A. W. Lawson
Institute for the Study of Metals, University of Chicago, Chicago, Illinois

(Received July 12, 1949)

A null device for determining the ratio of two absolute temperatures with an accuracy of 0.1 percent is described. This device balances the mean-square fluctuations in voltage across the terminals of two resistors arising from thermal agitation at the temperatures to be compared. The ratio of the resistances, when the noise voltages from the two resistors are equal, determines the ratio of their absolute temperatures. The limitation on the ultimate accuracy of the ratio of temperatures so determined is imposed by the relative value of the first and second moments of the voltage fluctuations observed, which in turn depends on the length of time utilized in averaging the fluctuations. With the apparatus described below, an observation time of two minutes is adequate to guarantee the accuracy claimed above for high temperatures, provided certain elementary precautions in constructing the noise thermometer are observed. Numerous tests have been conducted in the neighborhood of 1000°K which substantiate these claims. Extrapolation of the performance obtained at such temperatures indicates that material improvements in the accuracy of the absolute temperature scale above 2000°K may be obtained. The calibration of the thermometer is independent of the chemical composition and past physical history of the material from which it is constructed, in addition to being independent of the absolute pressure.

INTRODUCTION

SINCE the pioneer investigation of Schottky, Johnson, and Nyquist, our understanding of random noise in electrical circuits has been considerably enhanced. The urgency of a war, which required the ultimate in instrumentation, gave an added impetus to these studies with a concomitant realization of the maximum usable sensitivity in a wide variety of apparatus. Despite the enormous amount of labor expended on the reduction of noise, relatively few investigators have utilized this unavoidable background as a basis for measuring an observable quantity. Hull has determined a value for the charge of the electron by observing the fluctuations in plate current of a temperature-limited vacuum tube, attaining a precision of several percent and a surprising accuracy in view of our better understanding today. More recently, Dicke *et al.*[1] have used the microwave noise spectrum in studies of the temperature of interstellar space and the absorption of the atmosphere. This line of investigation is now being pursued in a number of different laboratories throughout the world. Cognizant of Dicke's investigations, Lawson and Long[2] published two discussions of the possibility of using thermal fluctuations in voltage across a resistor to measure very low temperatures. These discussions have been subjected to criticism by Gerjuoy and Forrester[3] and also by Brown and MacDonald.[4] Aside from specific warranted criticisms on matters not fundamental to the issue, these

---

[1] Dicke, Beringer, Kyhl, and Vane, Phys. Rev. **70**, 340 (1946).

[2] A. W. Lawson and E. A. Long, Phys. Rev. **70**, 220 (1946); Phys. Rev. **70**, 977 (1946).

[3] E. Gerjuoy and A. T. Forrester, Phys. Rev. **71**, 375 (1947).

[4] J. B. Brown and O. K. C. MacDonald, Phys. Rev. **70**, 976 (1946).

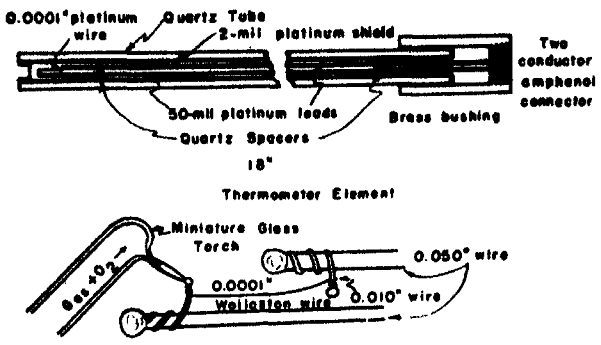

FIG. 1. Enlarged view of thermometer illustrating method of construction.

criticisms reduced in the main to a question of the practicability of determining temperature from noise measurements.* The device described below is an outgrowth of an attempt to ascertain the practicability of such measurements by a direct appeal to experiment. Although the original discussions of Lawson and Long pertained primarily to the determination of temperatures below 1°K, the device to be described appears to be even more useful and practical at very high temperatures where no satisfactory primary standards exist. This paper will deal principally with this phase of the problem where preliminary tests have been carried out at the present time.

To understand the operation of a noise thermometer, it is convenient to recall the Nyquist formula for the mean-square fluctuations in voltage arising from thermal agitation in a *passive* network, namely,

$$\overline{V^2}=4kRe(Z)T\Delta f. \tag{1}$$

In principle, if one knows Boltzmann's constant k, $Re(Z)$, the real part of the complex impedance of the network, and the magnitude of the mean-square fluctuations over a range of frequencies Δf, one has determined T, the absolute temperature of the resistor. Needless to say, such an approach is somewhat naive if a precision of 0.1 percent is desired, for in practice one must amplify the fluctuations and detect them. In this case even if one knows the characteristics of the amplifier and detector with a precision of 0.1 percent, one is still faced with the problem of their variations with time arising from changes in tube characteristics. If, however, one uses the same amplifier and detector to observe the noise generated by two independent circuits $Z_1(f)$ and $Z_2(f)$ which are different temperatures T_1 and T_2, and adjusts one of the impedances so that both circuits generate equal rectified noise voltages, then (assuming a noiseless amplifier).

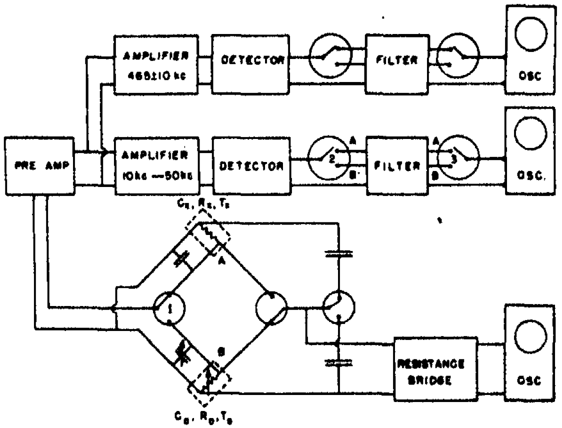

FIG. 2. Schematic circuit diagram of noise thermometer.

$$\frac{T_1}{T_2}=\frac{\int_0^\infty H(f)Re[Z_2(f)]df}{\int_0^\infty H(f)Re[Z_1(f)]df}. \tag{2}$$

If, furthermore, the $Re[Z]$ is independent of f wherever $H(f)$, a function determined by the characteristics of the amplifier and detector, is appreciable, then

$$\frac{T_1}{T_2}=\frac{Re[Z_2]}{Re[Z_1]} \tag{3}$$

and thus a comparison of the noise from two resistances may, in principle, provide the ratio of two absolute temperatures, i.e., an absolute temperature scale. In the device described below, the comparison of two noise voltages is made in such a way that Eq. (3) reduces simply to

$$T_1/T_2=R_2/R_1. \tag{4}$$

Actually, to insure that Eq. (4) is, in fact, valid to a sufficiently high degree of accuracy, it is necessary, for reasons discussed below, to adjust the corresponding input capacities C_1 and C_2 so that $R_1C_1=R_2C_2$.

In addition to the determination of the ratio of two absolute temperatures by the direct comparison of the noise from two independent resistors, one may also determine this ratio by another type of comparison, namely, by comparing the noise from R_1 and R_3 in parallel to the noise from R_3 alone. A balance can be achieved only when T_1 is greater than $2T_3$. In this case the balance condition is given by

$$T_1=[2+(R_3/R_1)]T_3 \quad T_3<T_1/2. \tag{5}$$

Because various types of errors enter in a different way into the two methods of comparison, these alternative balance schemes provide quasi-independent measures of the absolute temperatures of the hot resistance and consequently provide a stringent internal check on the accuracy of the instrument described below.

CRITERIA FOR ABSOLUTE THERMOMETRY

In order to insure an accuracy of 0.1 percent in noise thermometry the following criteria must be satisfied.

---

* In the meantime, Cook, Greenspan, and Wussler (Phys. Rev. 74, 1714 (1948)) have concluded that the use of thermal noise from quartz crystals to measure low temperatures is impractical.

A. Passivity of Thermometer

Element

The derivation of Nyquist's law is predicated on the assumption that the circuit is passive. This requires that no current be flowing through the resistor used as the thermometer element from an external power source and that, in addition, no spurious e.m.f. is generated in the element. This requirement is particularly important, even in metallic resistors, if thermionic emission is appreciable. For this reason one must avoid errors arising from the following sources:

1. *Thermoelectric effects.*—Junctions of dissimilar materials (even metals and insulators) should be avoided in the construction of the thermometer. In practice, any d.c. voltage at the terminals of the thermometer should be less than a few microvolts, a requirement not difficult to satisfy.

2. *Grid current.*—The need to amplify the fluctuations may give rise to two sources of error. Firstly, grid

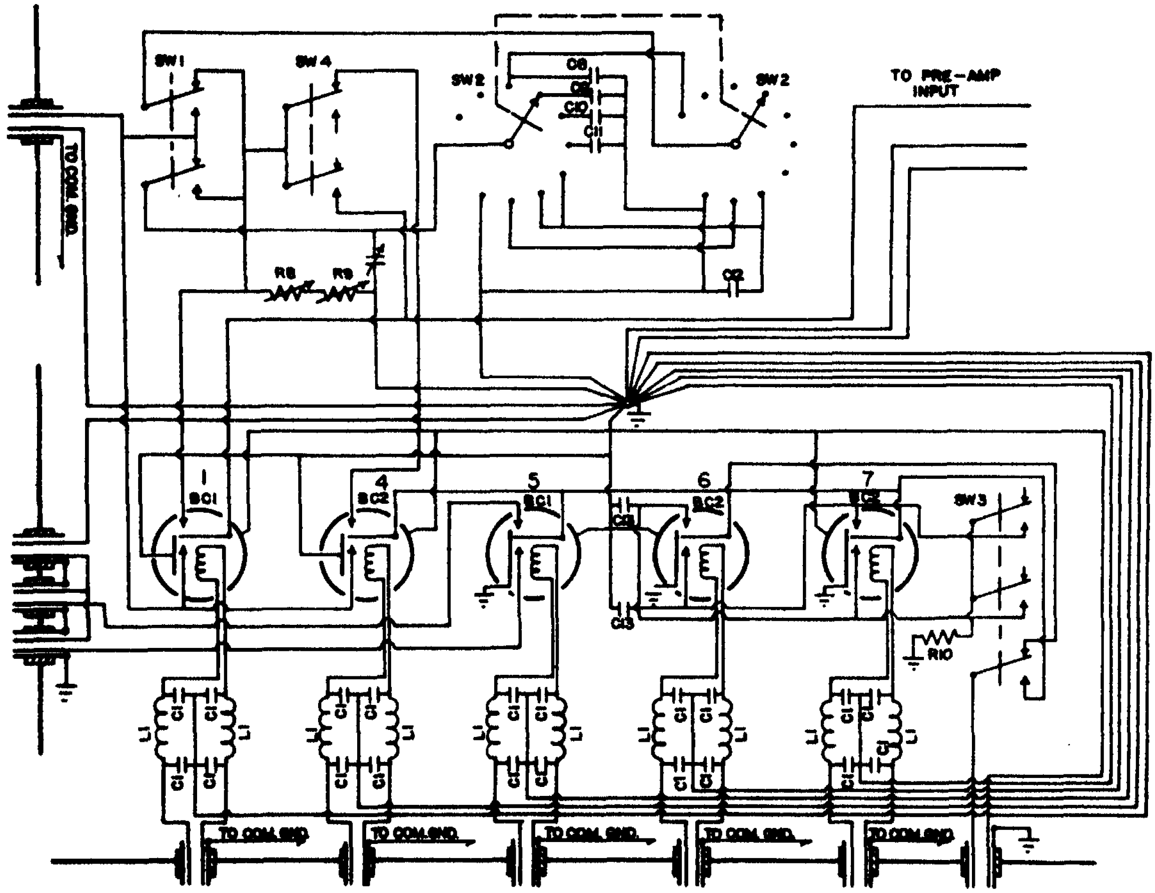

FIG. 3. Input switching circuit.

Parts list: (All resistances in ohms and capacities in microfarads)

*R*1	8*K*	*W. W.*	*C*1	0.1	400 v paper
*R*2	1.5*K*	½ *W*	*C*2	80	450 v elect.
*R*3	50*K*	*W. W.*	*C*3	40	450 v elect.
*R*4	100	½ *W*	*C*4	25	25 v elect.
*R*5	2.2*K*	½ *W*	*C*5	0.0008	
*R*6	500	1 *W*	*C*6	0.2	400 v paper
*R*7	25*K*	*W. W.*	*C*7	0.3	200 v paper
*R*8	10*K* Pot.	*W. W.*	*C*8	0.00002	
*R*9	100 Pot.	*W. W.*	*C*9	0.00004	
*R*10	500	½ *W*	*C*10	0.00006	
*R*81	30*K*	5 *W*	*C*11	0.000075	
			*C*12	0.0001	
*V*1	6*AU*6		*C*13	1	1000 v paper (Low leakage)
*V*2	6*J*6				
*V*3	6*AK*5		*L*1	2.5 mh	r-f choke
			*L*2	0.08 mh	r-f choke

SW 1	DPDT	Rotary, low capacity, isolantite
SW 2	DP 10 Pt.	Rotary, two gang
SW 3	3 PDT	Rotary, low capacity, isolantite
SW 4	DPDT	Rotary, low capacity, isolantite
BC 1	Brown converter	Standard
BC 2	Brown converter	Adjusted to open circuit during transit time

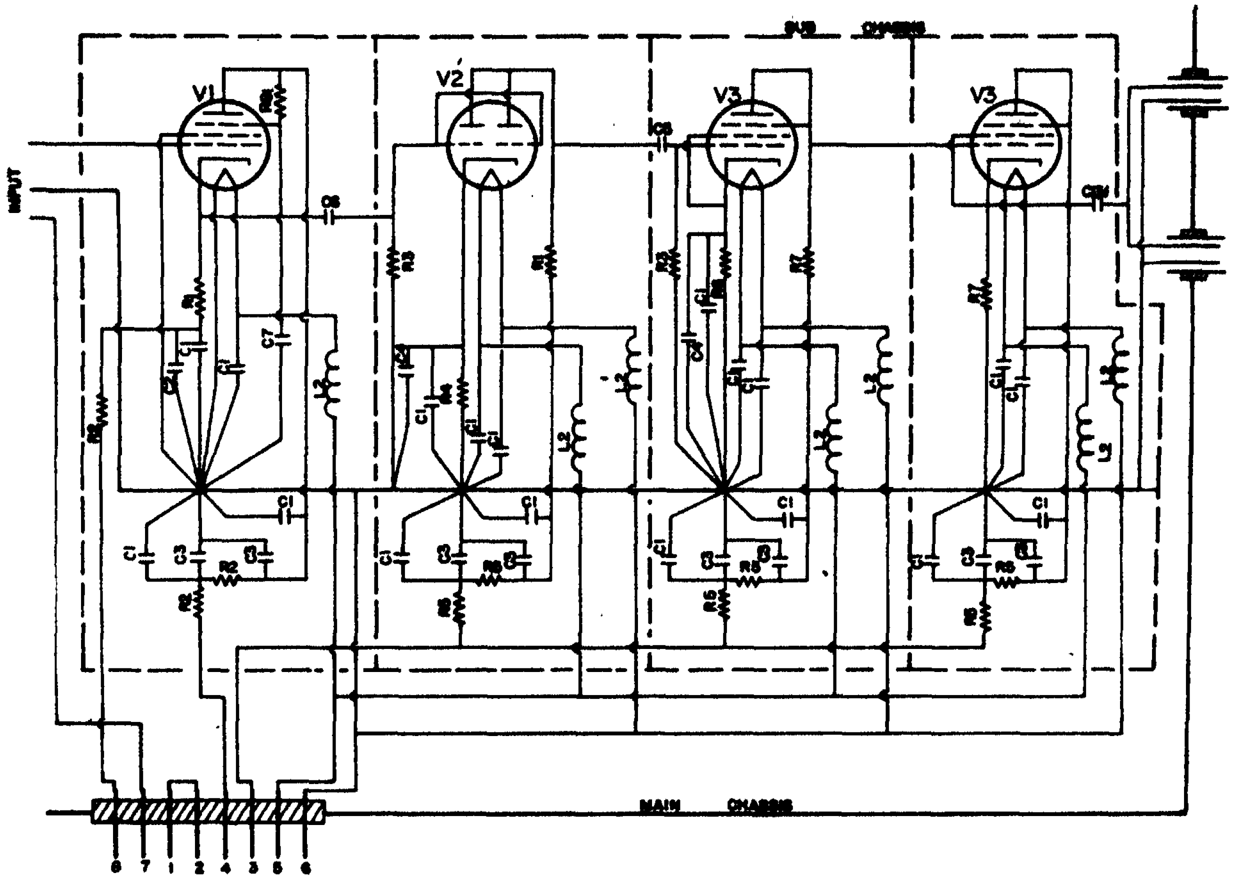

FIG. 4. Preamplifier (see Fig. 3 for parts list).

current fluctuations in the first amplifier tube may generate voltage fluctuations across the thermometer or the balance resistor. Since these two resistors must, in general, be unequal, a spurious unbalance signal will be generated. For the fractional error introduced (assuming wire wound resistors), one finds

$$\bar{V}_s^2/\bar{V}_T^2=(eIR/2kT), \tag{6}$$

where $\bar{V}_s^2$ is the shot noise generated in the resistor R by the grid current I, and $\bar{V}_T^2$ is the thermal noise generated at temperature T. For a resistor of 6000 ohms at room temperature, the error introduced is less than 0.03 percent provided the grid current is less than 10^{-9} amp.

However, the existence of grid current implies other sources of error at higher frequencies, since the dynamic grid resistance of an amplifier tube is, in general, smaller than the static grid resistance. The principal contribution to the dynamic grid conductance, other than the dielectric losses which can usually be made small, is the electronic loading of the grid owing to finite transit times. Thus, the grid resistance of a standard tube may be only 10^5 ohms at 3×10^7 cycles/sec. Accordingly, since the electronic loading varies as the square of the frequency, the grid resistance at 100 kc would be approximately 10^8 ohms. However, this resistance, which is in parallel with the thermometer element, has an effective noise temperature corresponding to two-thirds that of the cathode, so that the error from this source is the order of 0.02 percent, if the balance resistor is 10^4 ohms. This error is further reduced by the null method of making observations, by the use of miniature tubes, and by use of a cathode follower connection.

It is worthy of note that the considerations of this section limit the useful frequency spectrum of our thermometer to below 10^5 cycles/sec. and the magnitude of the hot resistor to a few thousand ohms, since in most tubes it is difficult to reduce the sum of the absolute magnitudes of the electron and positive ion grid currents below 10^{-9} amp.

3. Feedback.—The existence of feedback may contribute errors for two reasons. In general, it will make both the gain and the noise of the amplifier depend on the input impedance. (The noise of the amplifier, for this discussion, is defined as that noise observed when the input impedance is at 0°K.) It is, therefore, advisable to operate the first stage of amplification as a high gain cathode follower in order to minimize the feedback in the first tube. Under these conditions the principal source of feedback is the grid to cathode capacity in this stage, which, if smaller than a few $\mu\mu$f, meets the required conditions.

In view of the possibility of effecting a comparison of temperatures in two alternate ways (see above) in which the ratio of the impedance being compared is appreciably different, one is able to conduct an experimental test to ascertain that feedback is not a source of inaccuracy.

4. *Pick-up.*—A somewhat more troublesome source of error than feedback is pick-up. To avoid errors from the usual type of 60~ inductively coupled signals, the amplifier should be designed to pass only signals above about 10 kc. In addition, if high power induction furnaces in the vicinity are producing 60~ modulated high frequency signals, it is necessary to operate the thermometer in a shielded room, if the switch used to compare the two resistors is also to be operated at 60~. The most annoying limitation imposed by pick-up is the difficulty in using a temperature bath heated from an a.c. supply.

5. *Thermionic emission.*—At very high temperatures, where thermionic emission plays an important role, precautions must also be taken to prevent electrons emitted from a hot section of the element from condensing on a cooler section. In other words, the thermometer must be operated under "blackbody" conditions in order to avoid additional fluctuations being introduced by thermionic and photo-electrons.

For this reason it is desirable to surround the thermometer element as nearly as possible with a grounded shield constructed of similar material, which is at the same temperature as the bath.

B. Fluctuations in Noise

The accuracy attainable in noise measurements is fundamentally limited by statistics. If a white spectrum of noise is passed through a narrow band filter, the resulting noise may be roughly described as a sine wave of frequency equal to the center frequency of the filter, amplitude modulated by low frequency components whose maximum frequency is of the order of magnitude of one-half the pass band of the filter. Thus, if we average over a time long compared with Δf^{-1}, Rice has shown that

$$\bar{V}^2 - |\bar{V}|^2 = \bar{V}^2 (t\Delta f)^{-\frac{1}{2}}, \tag{7}$$

where t is the time of observation and Δf the band width of the filter. If, for instance, as in our case, $\Delta f = 4\times 10^4$ cycles/sec. and $t = 100$ sec., the resulting precision, which is given by $(t\Delta f)^{-\frac{1}{2}}$, will be of the order of 0.05 percent. This will also be the precision of the temperature measurement if the noise from the thermometer is large compared to the background noise in the amplifier. In principle, the precision may be increased indefinitely by increasing the time of observation. In general, however, a consideration of systematic

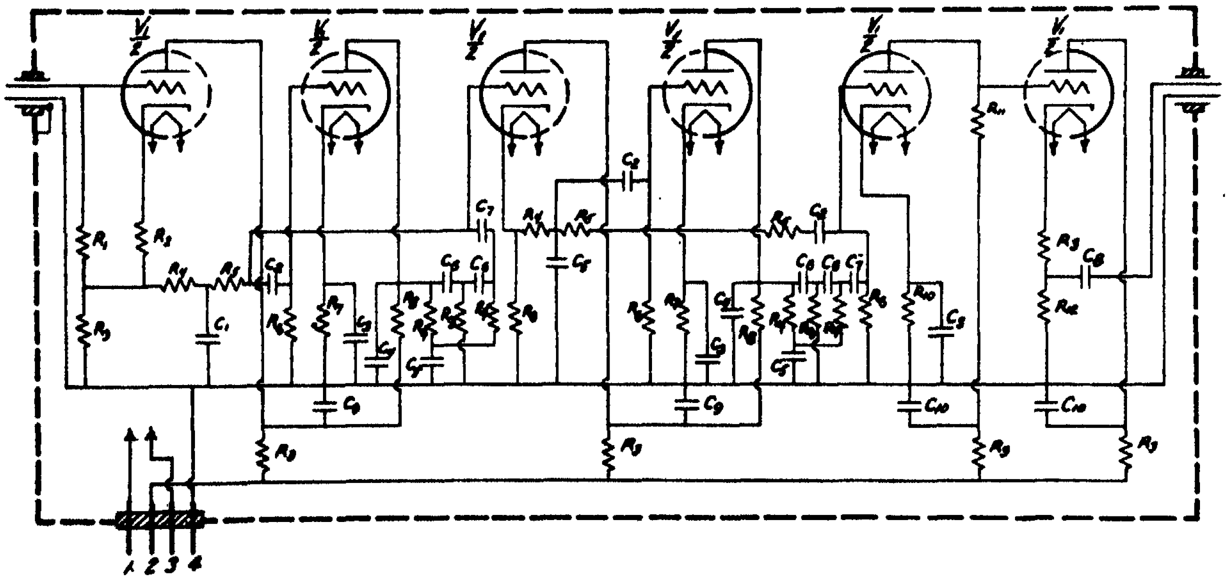

Fig. 5. 10–50-kc band pass filter.

Parts list: (All resistances in ohms and capacities in microfarads)

R1	50K	W. W.	C1	0.0003	
R2	500	½ W	C2	0.01	
R3	10K	1 W	C3	25	25 v elect.
R4	10K	½ W	C4	0.001	
R5	39K	½ W	C5	0.0002	
R6	470K	½ W	C6	0.0001	
R7	2.7K	1 W	C7	0.05	400 v paper
R8	90K	W. W.	C8	0.1	400 v paper
R9	5K	W. W.	C9	90	450 v elect.
R10	250	½ W	C10	40	450 v elect.
R11	25K	1 W			
R12	5K	1 W	V1	6SN7	

errors leads to the conclusion that such an increase in t is unwarranted in most cases.

C. Distributed Capacity in Input Circuit

In practice a certain amount of parallel distributed capacity is always associated with both the balance resistor and the thermometer element. Consequently, Eq. (4) yields the same result as Eq. (3) within 0.1 percent only if: (a) the time constants of the two impedances under comparison are nearly equal, i.e., $R_1C_1 = R_2C_2$, or (b) the high frequency cut-off ω_0 of the amplifier (assumed infinitely sharp) is sufficiently low so that $\tan^{-1}\omega_0RC=\omega_0RC$ within 0.1 percent. The latter requirement is equivalent to $\omega_0RC=0.055$. Thus, if the cut-off of the amplifier is 10^5 cycles/sec. and the input capacity is 25 $\mu\mu$f, the largest allowable balance resistor is only 3500 ohms. Thus, the latter requirement is very stringent on at least one of the design variables ω_0, R, and C. Accordingly, to achieve 0.1 percent accuracy in general, it is desirable to alleviate the restriction on the magnitude of the input capacities by satisfying condition (a) approximately. This may be accomplished in practice by adjusting a variable capacity in parallel with either the thermometer element or the comparison resistor until the noise in a narrow band at a high frequency is the same in the two

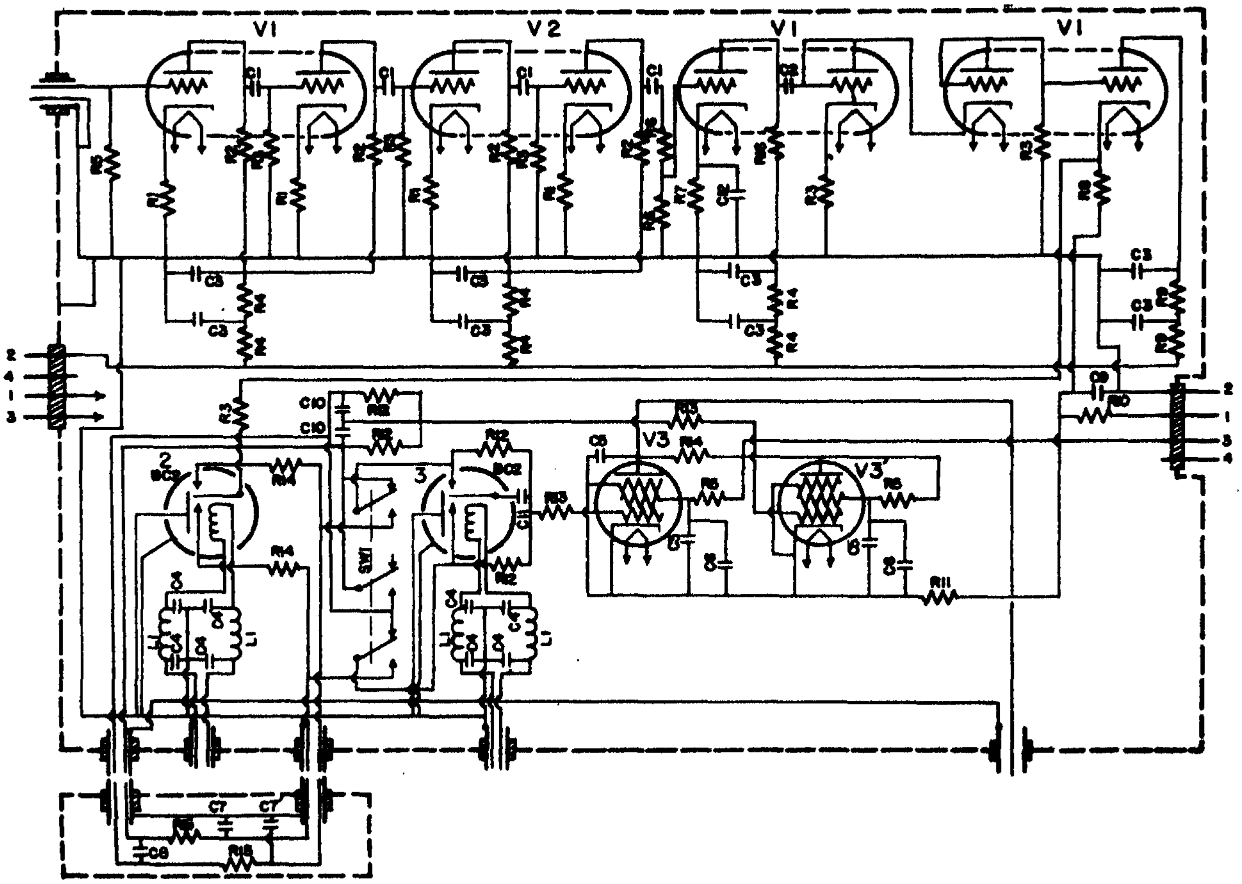

FIG. 6. Low frequency amplifier and balance detector.

Parts list: (All resistances in ohms and capacities in microfarads)

R1	500	1 W	C1	0.001	400 v
R2	22K	1 W	C2	0.0008	400 v
R3	47K	½ W	C3	40	450 v elect.
R4	2.2K	½ W	C4	0.1	
R5	50K	W. W.	C5	0.0001	400 v
R6	35K	½ W	C6	40	450 v elect.
R7	1.65K	½ W	C7	5	1000 v paper (low leakage)
R8	30K	5 W			
			C8	15	1000 v paper (low leakage)
R9	6.8K	1 W			
R10	1K	1 W	C9	40	450 v elect.
R11	13.5K	10 W	C10	0.005	400 v
R12	5M	½ W	C11	0.2	400 v
R13	100	½ W	C12	25	25 v elect.
R14	50	½ W			
R15	470K	½ W	V1	6SN7	
R16	25K	1 W	V2	6SL7	
			V3	6AC7	
L1	2.5 mh		r-f choke		
BC 2	Brown converter		Adjusted to open circuit during transit time		

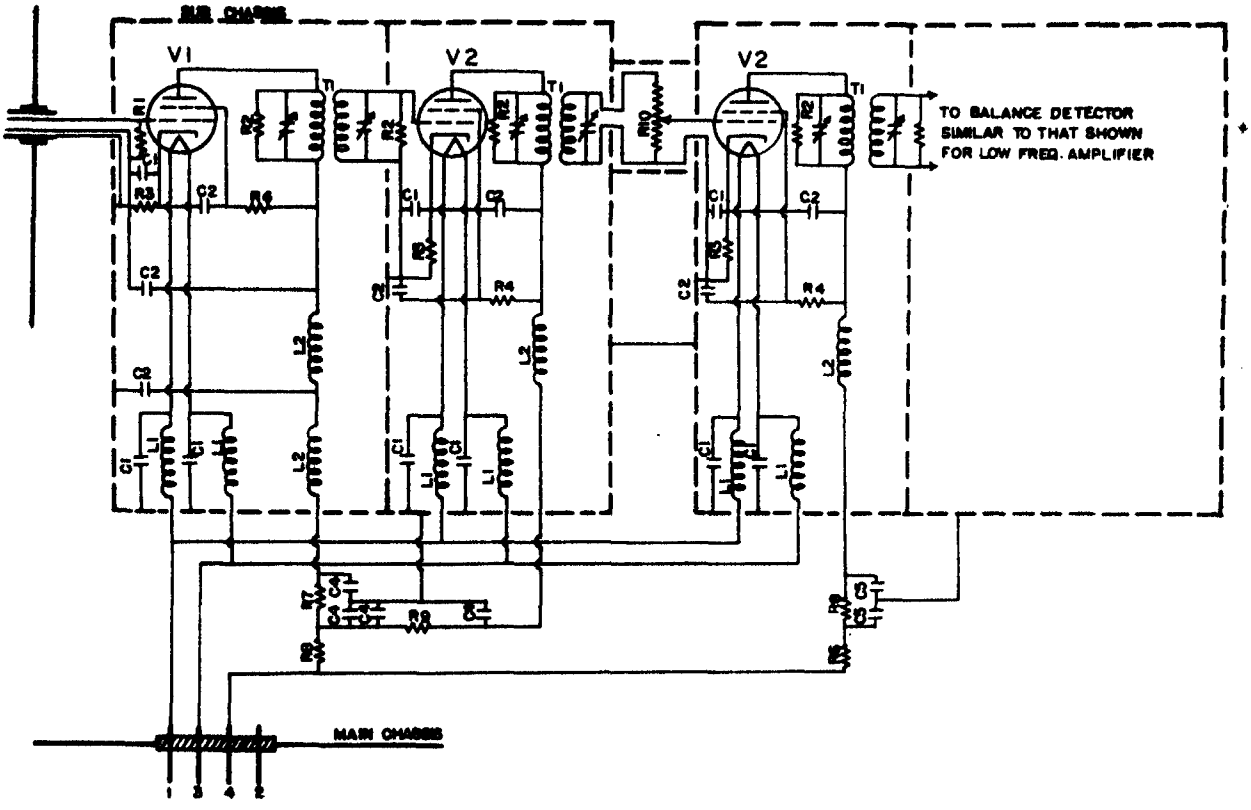
SUB CHASSIS
V1
V2
V2
T1
R1
R2
R3
R4
R7
R8
R10
C1
C2
C4
C5
L1
L2
TO BALANCE DETECTOR SIMILAR TO THAT SHOWN FOR LOW FREQ. AMPLIFIER
MAIN CHASSIS
1
3
4
2

FIG. 7. 465-kc amplifier and balance detector.

Parts list: (All resistances in ohms and capacities in microfarads)

$R1$	500K	½ W	$C1$	0.25	150 v paper
$R2$	47K	½ W	$C2$	0.2	400 v paper
$R3$	220	1 W	$C4$	20	450 v elect.
$R4$	25K	1 W	$C5$	40	450 v elect.
$R6$	2.7K	1 W			
$R7$	10K	1 W	$L1$	0.1 mh	r-f choke
$R8$	1.5K	5 W	$L2$	1 mh	r-f choke
$R10$	500K Pot.				
	$T1$	465 kc	I.F. transformer (interstage)		
	$V1$	6$AK5$			
	$V2$	6$AU6$			

input circuits, as observed by an auxiliary amplifier. In general, if such an adjustment is made with a precision of a few percent, the restrictions imposed on the magnitude of the input capacity by a sharp cut-off amplifier with a band width less than 10^5 cycles/sec. are not serious. If an accuracy of one percent is acceptable, the auxiliary adjustment of time constants is unnecessary.

D. Lead Corrections

Since the lead-in wires to the thermometer element are not at a uniform temperature in general, it is appropriate to inquire concerning the error so introduced. If we take the worst possible situation and assume that the leads are all at temperature T_2 when the thermometer is hot but that the resistance of the leads R_L is that which they have when at temperature T_1 of the thermometer R_1, then the error in T_1/T_2 is

$$\Delta\frac{T_1}{T_2}=\frac{R_L}{R_1}\left(\frac{T_2}{T_1}-1\right)\frac{T_1}{T_2}. \qquad (8)$$

Accordingly, the resistance of the leads should be less than 0.1 ohm.

E. High Frequency Resistance of Thermometer

The resistance of the thermometer element should be independent of frequency. For metallic resistances the primary variation of resistance with frequency arises from the skin effect. For this reason, the element should be made of sufficiently small wire to make this source of error negligible.

Furthermore, the wire should not be supported by ceramic materials such as Al_2O_3 which have a frequency dependent leakage at high temperatures.

F. Cross-Talk

In addition to errors arising from distributed capacity to ground across the input resistances, another source of error arises from distributed capacity in the switch used to effect the comparison of the two noise sources. Thus, because of finite values of the capacities in the switch the noise power observed in either position of the switch is not determined solely by the resistance to which the switch is connected but partially by noise coupled through the switch from the other resistor. To avoid this error, a large capacity may be switched synchronously across the circuit not being measured.

G. Non-Linearity in the Amplifier

If the two noise spectrums to be compared are identical, non-linearities in the amplifier giving rise to cross modulation are not a source of error. The two spectrums may be made identical by adjusting the time constants of the two input circuits to be the same in the manner described above.

THE THERMOMETER ELEMENT

The foregoing criteria dictate that the thermometer element have a resistance of no more than a few thousand ohms, a minimal parallel capacity, and leads whose resistance is less than a fraction of an ohm. Appreciable insulation leakage must occur only at places where the temperature is the same as that of the thermometer element and, furthermore, such conductance in parallel with the thermometer element must be the same at high frequencies as at low.

Such a thermometer is shown in Fig. 1. The thermometer element itself is made from 0.0001-in. platinum Wollaston wire, welded to heavy platinum leads 0.050 in. in diameter. To facilitate the welding, short sections of 0.010-in. platinum wire are wound around the heavy leads near their ends, as illustrated in Fig. 2. A small torch is used to melt a bead on the end of the heavy lead which fuses over the lighter wire, forming a good weld. A similar operation is performed on the light wire which has been wound with desilvered Wollaston wire.

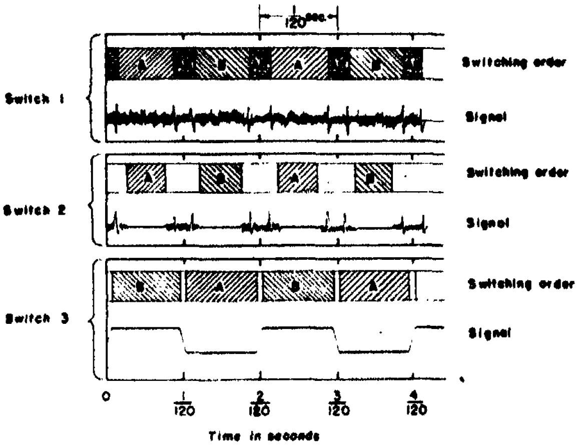

FIG. 8. Schematic diagram of switching order for converters # 1, 2, and 3.

The thermometer element is shielded completely by a 0.002-in. thick cylindrical platinum sheet supported by a quartz sheath. The leads are spaced from the platinum shield by short lengths of quartz tubing at the cold end, where leakage is negligible, and by a thin fused quartz disk near enough to the element so that its temperature is always the same as that of the element. To avoid electrical short circuits arising from sagging of the heavy leads at elevated temperatures, the thermometer is normally operated in a vertical position.

Because of the nature of its construction, this thermometer cannot be used above about 1400°C. It possesses the advantage of being operable in an air atmosphere, however, a factor which dictated this particular design. For operation at higher temperatures, a thermometer is now being constructed from tungsten. This thermometer is sufficiently rigid so that no insulating supports are required. However, it will of necessity be used only in furnaces with a neutral atmosphere.

THE BASIC CIRCUIT

The block diagram of Fig. 2 shows schematically the arrangement used to balance the noise voltages from two different resistors, and Figs. 3–7 show the circuits actually used. A Brown converter[**] is used to connect alternately each resistor to the input of an amplifier with a gain of the order of 10^6. When the noise level is of the order of several volts, it is rectified by a diode and the resulting direct current is used to charge a condenser with a time constant of the order of ten sec. Two such condensers are used, a Brown converter (#2) alternately charging one with the rectified noise output from resistance R_0 and then charging the other with the rectified noise output of R_x. If these condensers were isolated, one condenser would acquire an average voltage corresponding to the values R_0, T_0 while the other would acquire a different voltage in general characteristic of the values T_x, R_x. A third Brown converter (#3) is utilized to exhibit the difference between these average voltages on an oscillograph, and the null signal is obtained by adjusting the value of the variable resistor R_0.

As explained above, it is desirable to adjust $R_0C_0 = R_xC_x$. This adjustment is made by performing two independent noise balances in different frequency ranges. For this purpose, two separate channels are necessary as indicated in Fig. 2. One channel with a pass band from 10 kc to 50 kc is used to produce a noise balance which is almost independent of the input capacity. The other channel has a band width of approximately 20 kc centered at 465 kc and requires an adjustment of the variable condenser C_0 to achieve a rough balance. The final over-all balance of the system is then made by a second small adjustment of R_0.

During the instant when switching occurs, R_0 and R_x are in parallel and a spurious signal occurs. This spurious signal is eliminated by adjusting the second Brown converter feeding the filters so that it is open circuited during the switching period of the first Brown converter. The switching schedule and resultant signals are shown in Fig. 8. The principal limitation on the

---

[**] A Brown converter is a vibrating reed switch which operates synchronously from a 60~ a.c. power supply. It is made by Brown Instrument Company.

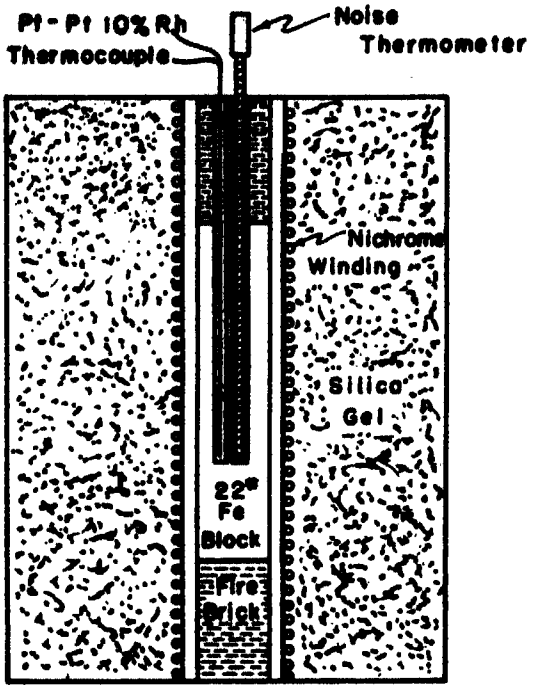

FIG. 9. Furnace for comparing calibrated thermocouple and noise thermometer.

use of such a mechanical switching device for the comparison of noise voltages is the variation of the contact potential in the switch. If the noise voltage is of the order of microvolts and must be detected with a precision of 0.1 percent, the variation in contact potential must be less than 10^{-9} volt. This criterion is satisfied by Brown converters at least for an appreciable fraction of their life which is said to be many years.

The switching cycle serves several essential functions in addition to affording a rapid mechanism for comparison of noise voltages from two different sources. Most important is the fact that it provides a scheme for subtracting out the additional noise generated continuously by the amplifier itself. If this were not the case, Eq. (2) etc., would not be applicable in such simple form. Secondly, the scheme eliminates the effects of all long term variations in gain in the amplifier and detector. Finally, it should be noted that this scheme makes the final balance essentially independent of variations of contact time in the converters.

The preamplifier (Fig. 4) consists of 4 stages, *RC* coupled. The first tube is a *6AU6* connected as a cathode follower for reasons mentioned above. This tube satisfies the requirements on grid current and in addition is neither particularly noisy itself nor subject to parasitic oscillation. The preamplifier is isolated in a separate well-shielded box and shock mounted in a large box which contains, in addition to the first five converters, the variable resistance R_0 and capacity C_0. Wire wound resistors are used exclusively. The output stage of the preamplifier is also a cathode follower to reduce interaction between the two channels which it drives.

Both amplifiers are of conventional design. All stages are operated from battery power, carefully filtered. The low frequency channel is limited in band width by two devices. The amplifier in this channel has a flat response (within three db) from about ten kc to 50 kc. The high frequency cut-off is sharply defined by two stages of the type of *RC* filtering described by Thiessen.[8] This filter cuts the response down 60 db at 100 kc. Frequencies below ten kc are considerably attenuated by choosing the interstage coupling condensers to be somewhat smaller than usual. This precaution avoids spurious errors from 60~ pick-up and extra noise arising from flicker effects in the tubes. The over-all design is such that the amplifier noise corresponds to Johnson noise from about a 1000-ohm resistor at 300°K in the grid circuit of the first stage of the preamplifier.

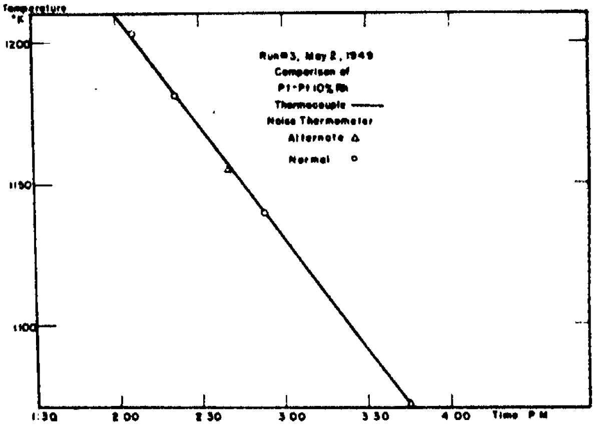

FIG. 10. Comparison between calibrated thermocouple and noise thermometer.

Detection of the noise is accomplished by the half-wave rectifier shown in Fig. 6. The output of the rectifier is fed to the filter-condensers through a cathode follower in order to avoid peak detection which would reduce the precision of the average. In principle, one can use the d.c. voltages on long time-constant filter-condensers directly to achieve a balance. However, if the filter-condensers tend to polarize, annoying time lags are introduced to the measuring technique. For this reason, the circuit of Fig. 6 is used to keep the polarization in the condensers negligible at all times. The two output condensers C_7 and C_7' have time constants of about ½ sec. so that there is little tendency for these to polarize. The long time constant for the filter is then derived by use of C_8 which takes the difference in voltage between C_7 and C_7' at all times and hence, in general, operates at a much lower voltage than either C_7 or C_7'. The tubes V_3 and V_3' are used to deliver this difference in voltage to an oscillograph and to cancel out the fluctuations on C_8 with respect to ground.

To evaluate the ratio of the temperatures of the resistors whose noise is under comparison, it is necessary to determine the ratio of their resistances. In

---

[8] G. J. Thiessen, J. Acous. Soc. Am. 16, 275 (1945).

TABLE I. Comparison of noise temperature and thermocouple temperature.

Temperature in °K observed by thermocouple	Temperature in °K observed by normal noise balance	Temperature in °K observed by alternative noise balance	Deviation in °K
1340	1342		+2
1299		1300	+1
1201	1203		+2
1181	1181		0
1156		1155	−1
1147	1147		0
1140	1139		−1
1079	1080		+1
1071		1071	0
991		995	+4
		Av. deviation	+0.8

order to simplify this measurement, the following circuit is used. Vibrator #4 shown in Fig. 3 switches between the two resistors 180° out of phase with vibrator #1, so that when one resistor is connected to the noise amplifier, the other is connected to the resistance bridge. The resistance being measured and the bridge form a potential divider which alternately provides charge for one of two condensers. When each of the two condensers are charged to the same potential the two resistors are in the same ratio as the two arms of the bridge. If one arm of the bridge is set at a value numerically equal to the temperature of the balance resistor R_0, the setting of the other arm at balance equals the unknown temperature, T. The balance of the bridge is easily detected by using another vibrator to compare the potentials of the two condensers. The bridge voltage is kept below 0.01 volt to avoid heating the sensitive Wollaston wire element appreciably.

HIGH TEMPERATURE TESTS ON THERMOMETER

To check the operation of the thermometer, comparisons were made with a Pt-Pt 10 percent Rh thermocouple calibrated at the melting points of NaCl and Au by Dr. Julian Goldsmith of the Department of Geology. The calibration was made by observing the melting point of a gold wire in a furnace whose temperature was controlled to within ±½°C. The thermocouple was then compared to the noise thermometer by placing them in juxtaposition in a 22-lb. iron block heated by a wire wound, well-insulated furnace, as shown schematically in Fig. 9. Owing to the lack of an adequate d.c. power supply, the block was initially heated to a high temperature using a.c. power. The power was then cut off, and measurements were made of the temperature of the block as it slowly cooled. The cooling rate varied from 2°C to 1°C per minute. The noise thermometer was approximately balanced and allowed to drift through a balance point. Interpolation in time was used to determine the thermocouple e.m.f. and the ratio of the hot resistance to the cold resistance at balance. This rather cumbersome technique was necessary to avoid pick-up from the power line.

The data thus obtained during a typical run are shown in Fig. 10. All the comparison points obtained in three runs on two successive days are shown in Table I.

It is apparent that the agreement between the two measurements is well within the experimental error and substantiates the accuracy claimed for noise thermometry. The authors believe that even better agreement would be obtained by making the comparison statically rather than dynamically.

TESTS AT HIGH PRESSURES

In order to confirm experimentally the theoretical prediction that noise thermometry should be independent of the ambient pressure, the temperature of a bomb in equilibrium with the room was measured with and without a pressure of 10,000 bars. The resistor inside the bomb was a 300-ohm coil of manganin wire of the type normally used as a pressure gauge. The pressure was transmitted to the coil by normal hexane and sufficient time was allowed for temperature equilibrium to be re-established before and after the application of pressure. No detectable change in the ratio of the high pressure resistor to the balance resistor was detected in this range of pressure.

SUMMARY

In conclusion, we would like to summarize the advantages of the noise thermometer described above.

(1) The accuracy and the precision of the thermometer is about 0.1 percent on an absolute scale above 100°K.

(2) The thermometer is independent of the material from which it is made or its previous thermal and mechanical treatment.

(3) The thermometer is independent of the absolute pressure.

The principal disadvantages of the thermometer are:

(1) The time required to obtain a precision of 0.1 percent.

(2) The difficulty in shielding the thermometer from extraneous pick-up.

(3) The limitations imposed on the input capacity, requiring the input stage to be reasonably close to the thermometer element.

While these disadvantages limit enormously the immediate use of the thermometer as a practical industrial tool, these limitations are considerably reduced if an accuracy of 1 percent is adequate.

Despite the disadvantages, noise thermometry appears capable of competing with any other laboratory absolute temperature scales at high temperatures and pressures. Its use to provide improved high temperature standards should be seriously considered by all those concerned with such problems.

ACKNOWLEDGMENTS

This work has been supported in part by the ONR under Contract No. N-6ori-20-XX with the University of Chicago. In addition, the authors desire to express their appreciation to Mr. Samuel Caldwell and Mr. David Zimmerman for assistance in construction of the circuits and to Mr. Frank Bruce, Mr. Karl Lindholm and Mr. Norman Nachtrieb for assistance in building the furnace, thermometer, and electrical shielding.

THE REVIEW OF SCIENTIFIC INSTRUMENTS VOLUME 20, NUMBER 11 NOVEMBER, 1949

An Apparatus for Measurement of Extremely High Internal Friction*

T'ING-SUI KÊ AND MARC ROSS
Institute for the Study of Metals, The University of Chicago, Chicago, Illinois

(Received June 27, 1949)

A simple torsion apparatus has been developed for measurement of extremely high internal friction by determining the angle by which strain lags behind the stress in forced cyclic vibration. The results of measurement were compared with torsion pendulum measurements using free decay method. The highest internal friction measured with this apparatus was 0.55. This apparatus can be used to measure internal friction at a constant given stress amplitude and at a constant frequency of vibration. The stress amplitude and frequency of vibration can easily be varied over a wide range. There is no theoretical limit to the lowest frequency of vibration that can be used with this apparatus. The feature that measurements can be made while the zero point is changing renders this apparatus very useful in the study of internal friction of freshly cold-worked metals.

INTRODUCTION

THE term internal friction means the capacity of a solid to dissipate its vibrational energy even though it is completely isolated from its surroundings. The conventional procedures of measuring internal friction at low stress level are (1) the free decay method, (2) the resonance method, and (3) the energy dissipation method. The correlation between these methods and their limitations has recently been discussed by Zener.[1]

In the past the magnitude of internal friction reported in the literature has been smaller than 0.1 when expressed by $1/\pi$ times the logarithmic decrement. In the measurement of internal friction of cold-worked aluminum under small stress, however, it has lately been found that the internal friction under appropriate conditions can be as high as 0.2.[2] Under these conditions the conventional methods of measurement mentioned above are no longer adequate either because the underlying concept is then ambiguous or because of the experimental difficulty of exciting the specimens to vibration.

If we consider that internal friction is a manifestation of strain lagging behind the applied stress, then the angle of phase lag α can be regarded as a measure of the internal friction. The internal friction can be conveniently reported as $\tan\alpha$. When the method of forced vibration is used, and the angle by which strain lags behind the stress directly measured, then the term internal friction is defined throughout the whole range from zero to infinity.

The purpose of this paper is to report a preliminary effort in developing an apparatus along this direction for measuring very high internal friction. The apparatus developed is to satisfy the following requirements: (1) measurements can be made at sufficiently low stress amplitude; (2) the frequency of the applied periodic stress can be varied through a wide range; (3) the apparatus is simple and easy to manipulate.

DESCRIPTION OF APPARATUS

A. "Strain Galvanometer" and "Stress Galvanometer"

The torsional method was chosen in the present development because it is much simpler experimentally than other methods when the strain to be measured or the stress applied is very small. The measurements of strain and of stress were made by two separate moving coil galvanometers.

In the strain or specimen galvanometer, the specimen, in wire form, constitutes the suspension of the galvanometer. Since experiments are conducted only at a low stress level, the current passing through the galvanometer coil is a measure of the shear stress acting on the wire specimen, the deflection of the galvanometer is a measure of the shear strain. The detailed description of such a galvanometer including the furnace surrounding the specimen has been previously given (Fig. 1).[3]

The current passing through the coil of this strain galvanometer was measured by another moving coil galvanometer with an 0.02-inch piano wire as its suspension. The internal friction of this suspension is very low and the phase lag in this "stress galvanometer" negligibly small. The deflection of this galvanometer is thus a measure of the applied shear stress.

The phase angle between stress and strain was measured by observing the deflections of the strain and the stress galvanometer on the same scale.

B. The Periodic Applied Stress

The driving potential was generated with a circular potentiometer linearly wound around its entire circumference with a constant potential maintained across opposite points C_1 and C_2 of the winding as shown in Fig. 2. The sliding contact P of the potentiometer was driven by a geared-down motor. The period used in

---

* This development has been supported in part by ONR (Contract No. N6ori-20-IV, NR 019 302).

[1] C. Zener, *Elasticity and Anelasticity of Metals* (University of Chicago Press, Chicago, 1948) pp. 60–63.

[2] T. S. Kê, "Internal friction of cold-worked metals at various temperatures," Comm. to J. of Metals, A.I.M.E.

[3] T. S. Kê, Phys. Rev. 71, 533 (1947).

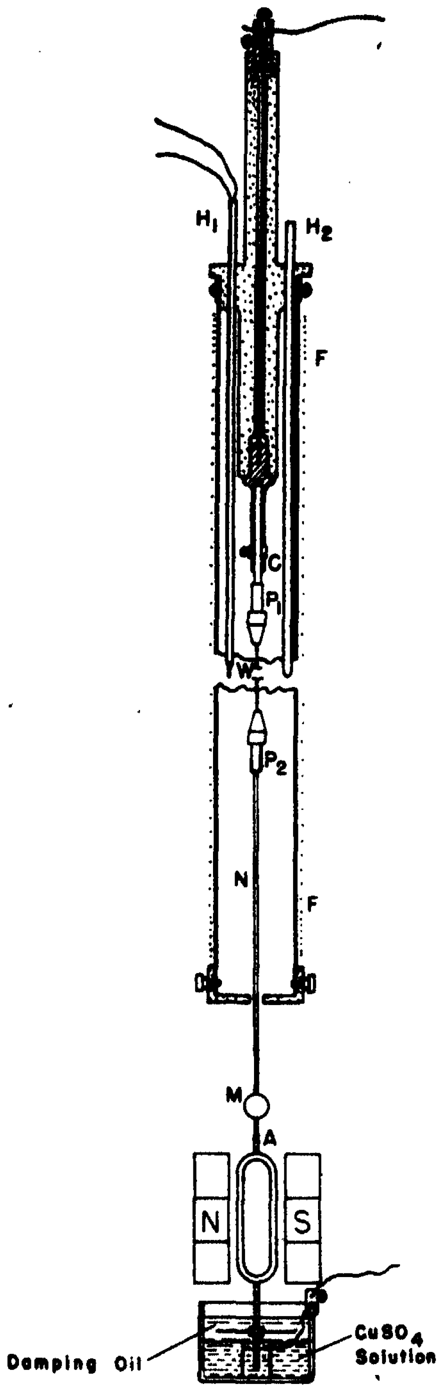

FIG. 1. The strain or specimen galvanometer (after Kê).

this experiment was 19.9 seconds. B_1 and B_1 are two identical storage batteries. Small variation in voltage was compensated by adjusting the variable resistances R_1 and R_2.

The wave form of the periodic voltage generated by this arrangement is shown in Fig. 3 as recorded by an Esterline-Angus graphic recording milliammeter. It is of saw-tooth form and each branch of the saw-tooth is linear.

C. Measurement of the Phase Lag

The saw-tooth periodic voltage described above was applied across the strain and stress galvanometers which are connected in parallel with each other. Since the inductance included in the circuit has negligibly small effect when the frequency of oscillation is so small, the currents passing through the moving coils of both galvanometers have the same phase and saw-toothed wave form. Accordingly the speed of the deflection of both galvanometers along the scale is essentially uniform.

There are several possible methods of determining the phase angle between the strain and the stress. The most direct method is to measure the time lag of the two deflections on the scale. With a period of vibration of twenty seconds, a time lag of one second would correspond to an internal friction of tan18°=0.325. Since it is difficult to measure time shorter than one second without using elaborate apparatus, the method of direct measurement of time lag is adequate only for very high internal friction or very long periods of vibration.

Another possible method is to measure the distance lag of the two deflections. The amplitude of vibration of the deflection on a scale three meters away from the galvanometers was 4 cm. For a wire specimen of 0.03 inch diameter and 1 foot length, this corresponds to a maximum shearing strain on the surface of the specimen of about 10^{-6}. In order to measure the distance lag with a reasonable accuracy, the minimum distance to be measured is 2 mm. A distance lag of 2 mm would correspond to an internal friction of tan4.5°=0.0787 which is still too high. The situation is even worse since the measurement of distance lag involves the difficult effort of observing the positions of two lines simultaneously when one of them is passing the zero mark of the scale.

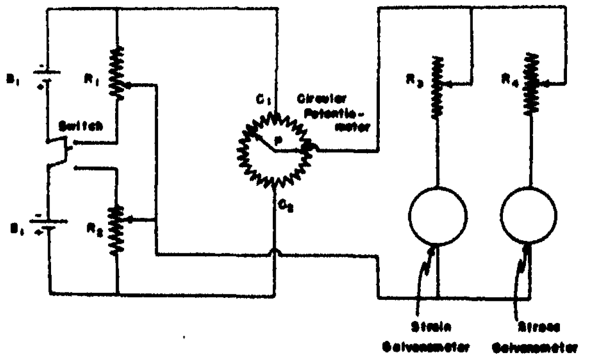

FIG. 2. The circular potentiometer for generating periodic applied stress.

In the method finally adopted, the line image (which is a bright line) representing strain was set vertical while that representing stress was set at 45° to the horizontal as shown in Fig. 4. A fiducial line was marked on the scale for occasional checks of the 45° line. The direction of motion of both the stress and strain lines is parallel to the horizontal scale. A small vertical scale was attached on the zero line of the horizontal scale. The speed of the stress line on the horizontal scale for a given stress amplitude (which can be varied by adjusting R_4 in Fig. 2) was previously determined when the stress line was set vertical. After the stress line was subsequently set at 45°, this measured speed is also the speed of the stress line along the vertical scale.

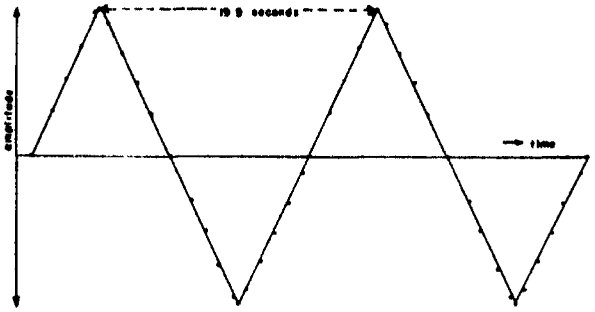

FIG. 3. The saw-tooth wave form of the periodic voltage generated by the circular potentiometer shown in Fig. 2.

Measurements were made with this arrangement as follows. With the periodic stress applied, the strain line was made to vibrate symmetrically about the zero line of the horizontal scale. This is accomplished by shifting the position of the horizontal scale. Readings are then made on the vertical scale of the position of the intersection of the stress and strain lines as it passes the zero line of the horizontal scale. One-half the difference between the readings for motion in one direction and motion in the opposite direction, is the mean distance between stress and strain deflections at the position of zero strain. With the known speed of the stress line on the scale, the time separation between the stress and strain lines is found, and thus the phase difference between stress and strain.

The position of the intersection of the stress and strain lines as it passes the zero line of the horizontal scale can be read with a fair degree of accuracy. With the optical system and the period of vibration used, the reading error causes an uncertainty in the value of internal friction of ±0.005 under good conditions.

COMPARISON WITH TORSION PENDULUM MEASUREMENTS

In order to test whether the internal friction measured by the phase difference method described above gives the true value, we can compare the results with those determined by a torsion pendulum by the free decay method. The latter method has been known to be very accurate for measuring internal friction having values lower than 0.1.

A. Internal Friction Peak Associated With Grain Boundary Relaxation in High Purity Aluminum

The internal friction of 99.991 percent aluminum measured with the phase difference method is shown in Fig. 5. The specimen was annealed at 450°C for two hours after it was cold-drawn to 95 percent reduction in area. The internal friction curve measured previously on an identical aluminum specimen with a torsion pendulum[3] is shown also in the figure for comparison. It is seen that the general shapes of the two curves are similar except that the curve determined by the phase difference method, which is at a lower frequency of vibration, was shifted to a lower temperature. From this relative shift of the internal friction maximum and the known ratio of the frequencies of vibration, the heat of activation associated with grain boundary relaxation in aluminum can be calculated according to the procedures previously outlined.[4] This gives a value of 37,000 calories per mole which is within 10 percent of the value previously determined.[3]

It is to be noticed that the higher temperature branch of the internal friction curve determined by the phase difference method has a higher value than the corresponding portion of the internal friction curve determined by a torsion pendulum. This appears to be caused by the amplitude effect since the aluminum specimen is very sensitive to stress amplitude at high temperatures. In torsion pendulum measurements, the stress amplitude was always reduced as we go to high temperatures so that the internal friction was always independent of stress amplitude. On the other hand, the stress amplitude used in the phase difference method was always kept at 4 cm as mentioned above. This stress amplitude is apparently large enough to cause amplitude effects at high temperatures.

B. Internal Friction Peak Associated With the Stress-Induced Interstitial Diffusion of Oxygen Atoms in Tantalum

The internal friction curve of a tantalum specimen containing oxygen was determined by the phase difference method and is shown in Fig. 6 with the previously reported curve by torsion pendulum.[5] It is seen that in this case the lower and higher temperature branches of the internal friction peak are quite symmetrical. This corroborates the statement made in the

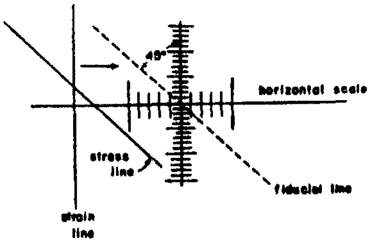

FIG. 4. Method for the measurement of the phase lag. The strain line image was set vertical while the stress line image was set at 45° to the horizontal scale. The direction of both line images is parallel to the horizontal scale during vibration.

---

[4] T. S. Kê, Phys. Rev. 72, 41 (1947).

[5] T. S. Kê, Phys. Rev. 74, 9 (1948).

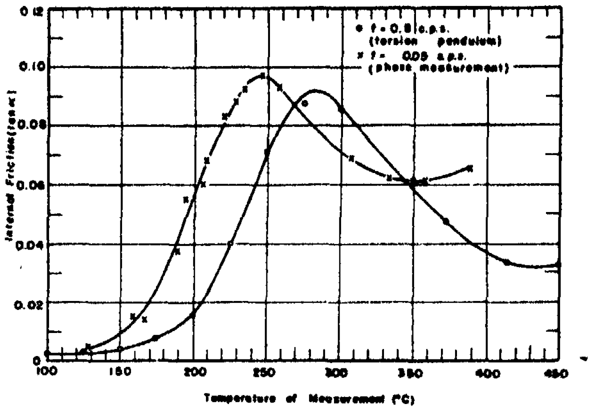

FIG. 5. Internal friction peak associated with grain boundary relaxation in high purity aluminum determined by phase lag measurement and by torsion pendulum measurement.

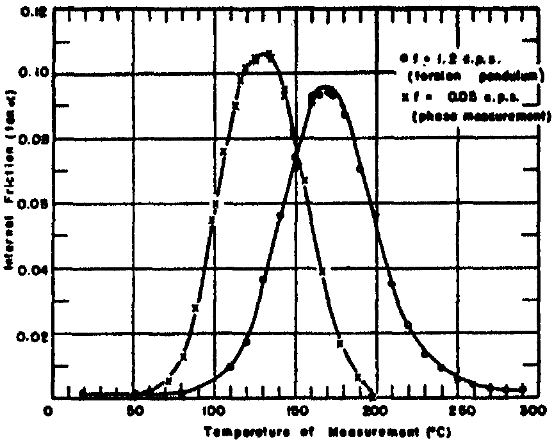

FIG. 6. Internal friction peak associated with the stress-induced interstitial diffusion of oxygen atoms in tantalum determined by phase lag measurement and by torsion pendulum measurement.

last section that the higher value of grain boundary internal friction observed for the high temperature branch was caused by amplitude effect. It is known that for the tantalum problem the amplitude effect is very small over a very large range of stress amplitude. The heat of activation determined from the relative shift of the two curves shown in Fig. 6 is 29,000 calories per mole. This is identical with the previously reported value.[5]

The reason that one curve has a higher peak than the other curve is because of the characteristic feature of this problem that the relaxation strength is larger at a lower temperature.[6]

SOME MEASUREMENTS OF EXTREMELY HIGH INTERNAL FRICTION

We have mentioned above that the internal friction of cold-worked, high purity aluminum under appropriate conditions can be as high as 0.2. In order to observe as high an internal friction as possible, a 99.991 percent aluminum specimen was heated fairly rapidly (the specimen temperature reached 250°C in about an hour) after it was subjected to cold-work of 95 percent reduction in area. The internal friction was measured while the temperature was going up. Figure 7 shows the value of internal friction at various annealing temperatures. It is seen that the highest internal friction observed is 0.55. Such a high value cannot be measured by other methods. The decrease of internal friction above 275°C indicates that the specimen has recrystallized at this temperature.

This example illustrates a great advantage of the method used in measuring the phase lag. While the cold-worked specimen is heating up, the specimen continues to recover from the twisting it was subjected during cold-drawing. This results in a constant shift of the zero point of the strain line. During the measurement, however, the horizontal scale can be shifted properly so that the strain line is always kept vibrating symmetrically about the zero line on the scale. Another way of correcting for the zero point shift is to take a series of consecutive readings and determining the mean value.

Figure 8 shows the decrease of internal friction of cold-worked 99.991 percent aluminum when annealed for various periods at 245°C. It is another illustration of the measurement of extremely high internal friction which cannot be done by other methods.

CONCLUDING REMARKS

We have described an apparatus for the measurement of extremely high internal friction. The highest internal friction measured with this apparatus was 0.55. This apparatus is simple and direct. It can be used to measure internal friction at a constant given stress amplitude and a constant frequency of vibration. The stress amplitude and frequency of vibration can easily be varied over a wide range. There is no theoretical limit to the lowest frequency of vibration that

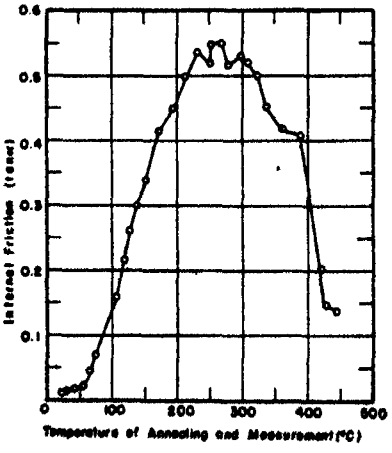

FIG. 7. Internal friction of cold-worked, high purity aluminum at various annealing temperatures.

---

[6] T. S. Kê, Phys. Rev. 74, 16 (1948).

can be used with this apparatus. The feature that the measurement can be made while the zero point is changing renders this apparatus very useful in the study of the internal friction of freshly cold-worked metals.

It is needless to say that the apparatus described is oversimplified. Many improvements to this apparatus suggest themselves. The optical method for reading phase difference can be refined by the use of photography, or more elaborately by the use of an oscilloscope or a recording oscillograph. This will extend the lower limit of internal friction that can be measured by this method. Another refinement is to use a sinusoidal applied stress. In using a saw-tooth wave form, an intrinsic error is involved when the phase difference is too large as the strain wave form may be, then, appreciably different from the stress wave form.

In conclusion, we are indebted to Dr. C. Zener and Dr. A. W. Lawson, both of this Institute for their interest in this development.

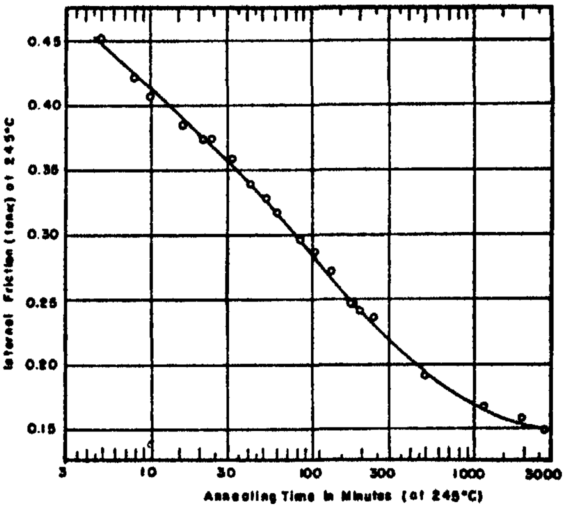

FIG. 8. Decrease of internal friction of cold-worked, high purity aluminum with annealing time at 245°C.

THE REVIEW OF SCIENTIFIC INSTRUMENTS VOLUME 20, NUMBER 11 NOVEMBER, 1949

A Device for the Measurement of Rotor Temperature in the Air-Driven Ultracentrifuge

PAUL GERARD ECKER,* JOSEF BLUM, AND C. W. HIATT**
Laboratories of the Rockefeller Institute for Medical Research, New York, New York

(Received July 12, 1949)

A device is described which permits the measurement of rotor temperature in the air-driven ultracentrifuge while the machine is in operation at speeds up to 60,000 r.p.m. A Thermistor situated inside the rotor changes its resistance as the temperature changes. Measurement of the Thermistor resistance by means of a Wheatstone bridge is accomplished with the use of needle contacts on the top of the turbine shaft and at the bottom of the rotor. Rotor temperature may be measured to within ±0.02°C and is believed to represent actual temperature of the rotating solution within 0.1°C.

AN important factor in determining the accuracy of sedimentation constants obtained in the ultracentrifuge is the precision with which the temperature of the solution is known. An error of 0.4°C, for example, in estimating the temperature of the solution may result in an error of one percent in the measured sedimentation constant. In sedimentation equilibrium experiments, which require continuous operation of the centrifuge for several days, unsuspected variations of temperature may constitute an even more significant source of error.

In an effort to improve the accuracy of the air-driven ultracentrifuge, the authors have constructed a device which permits the measurement of rotor temperature while the centrifuge is operating at speeds as high as 60,000 r.p.m. The determinations are made with an apparent precision of ±0.02°C and are believed to represent the actual temperature of the solution within ±0.1°C or less.

The apparatus employed is shown in schematic form in Fig. 1. A Western Electric Type V 578 Thermistor, *Th*, is used as the temperature-sensitive element of the circuit.[1] The Thermistor employed is a small bead of semiconducting material having a resistance of about 75,000 ohms at room temperature and a temperature coefficient of about −5000 ohm per degree. One of the platinum leads from the Thermistor is attached to the body of the rotor, the other is led through an insulating tube to the bottom contact *J2*, where the circuit is completed through a flexible needle guide tip as described below.

Thermistor resistance measurements are made with the Wheatstone bridge shown in the diagram. The bridge current is supplied by a 1.5-v air-cell, *B*, and is reduced to a value of five microamp. by the rheostat

---

* Present address: Peter Bent Brigham Hospital, Boston, Massachusetts.

** Merck Fellow in the Natural Sciences, 1948–50, under the National Research Council.

[1] The authors wish to express their appreciation of the assistance received from the Radio Division, Western Electric Company, New York, New York.

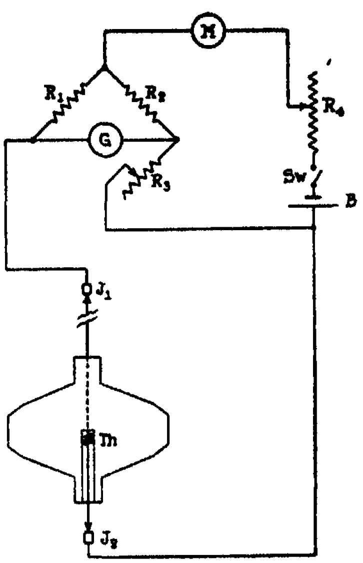

FIG. 1. Schematic diagram of the bridge circuit.

*R*1, *R*2—100,000-ohm wire wound precision resistors.
*R*3—Shallcross No. 827 resistance box, 0 to 1,111,000 ohms in 100-ohm steps.
*R*4—Wire wound rheostat, 200,000 ohms, with SPST switch (*Sw*) attached.
Th—Western Electric Type V 578 thermistor.
G—Leeds and Northrup mirror-type galvanometer.
M—Weston microammeter, 0 to 20 microamps..
B—1.5-v. Eveready air-cell, Type A-1300.
*J*1—Top contact (see Fig. 2).
*J*2—Bottom contact (see Figs. 3 and 4).

*R*4. When the bridge is in balance, the current passing through the Thermistor is only 2.5 microamp.

Electrical contact between the bridge and the turbine shaft is made at *J*1 through the needle contact shown in Fig. 2. A steel sewing needle, *G*, is mounted on the top end of the shaft by the brass cap, *H*, and rotates with the shaft. The tip of the needle presses against the concave bottom surface of an Oilite cylindrical brush, *F*, which is subjected to a downward pressure by the compression spring, *E*. The entire brush-mounting tube, *B*, may be adjusted in vertical position by sliding it up or down in the mounting frame, *C*, *D*. When placed so as to give proper pressure upon the needle tip, the tube is held by a set screw in the frame member, *C*. A hole in the brass cap, *A*, allows the introduction of small amounts of light oil occasionally to keep the Oilite brush lubricated. The arrangement shown affords a dependable, low resistance contact which functions satisfactorily at all speeds of shaft rotation, shows very slight evidence of wear, and imparts only a minimal friction drag upon the shaft.

From this contact the current passes down the turbine shaft and through the body of the rotor to one side of the Thermistor, as shown in *A*, Fig. 3. The Thermistor is mounted in a soft copper sleeve, *B*, which is affixed to the end of an insulating Bakelite rod, *C*. One lead wire from the Thermistor bead is crimped into a slot in the copper sleeve, which is pressed tightly against the material of the rotor. The lead wire from the other end of the Thermistor is pressed tightly into a slot on the end of the copper conducting rod, *D*, which is attached to the steel guide-tip assembly, *F*, *L*. The guide-tip assembly terminates in a steel needle tip,

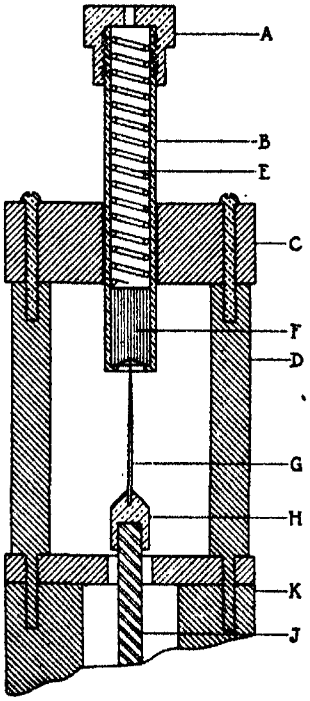

FIG. 2. The top contact.

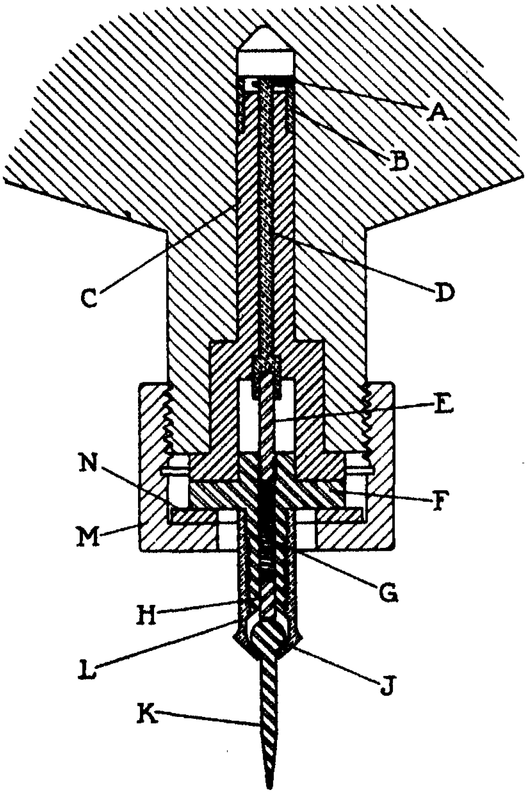

FIG. 3. The bottom contact and guide tip.

K, which is mounted in a ball joint, *J*. The compression spring, *G*, and plunger, *H*, maintain a constant pressure upon the spherical end of the needle and determine flexibility of the ball joint. The entire assembly is held firmly in place on the bottom of the rotor by the retaining cap, *M*, and fiber insulating washer, *N*.

When the rotor is lowered into operating position in the vacuum chamber, the guide-tip assembly descends into the bearing receptacle depicted in Fig. 4. The needle passes with ample clearance through the cap, *B*, and brass safety bearing, *C*, and rests upon the top, concave surface of the spring-loaded Oilite brush, *F*. The brush itself, along with its compression spring, *K*, is mounted in the floating bearing structure, *D*, *E*, which is free to move laterally to center itself beneath the descending needle. Electrical contact is made through the brush, *F*, and the current is conducted through the bearing mount to the brass washer, *G*, the binding post, *H*, and thence returns to the bridge circuit. The entire assembly is held in a Bakelite receptacle, *A*, which is mounted rigidly on the bottom plate of the vacuum chamber. The safety bearing, *C*, does not enter into the normal operation of the centrifuge, but is provided only to receive the weight of the rotor in the event of shaft breakage.

In addition to serving as an electrical contact, the needle functions as a guide tip to keep the rotor from precessing on its flexible shaft. By virtue of the ball-joint mounting, the needle is able to incline as required to keep its tip at all times on the center of rotation of the rotor. In so doing it acts in the same manner as the tool (called a "wiggler") used by machinists for precise centering operations. When the needle has sought and found the proper position for its tip upon the brush, it serves to guide the rotation of the rotor, there being sufficient rigidity at the ball joint to keep the rotor from precessing. Any slight change in the center of gravity of the rotor during rotation is rapidly accommodated by the needle, which merely inclines as required to bring its tip to the new center line of rotation. For optimal operation of the device it is necessary that the compression springs (*G*, Fig. 3, and *K*, Fig. 4) be properly matched in strength, and it is desirable that the freedom of motion at the ball joint be restricted to the minimum required (about two degrees of arc in the present case).

The Thermistor was calibrated by immersing the entire mounting assembly in an oil bath at accurately known temperatures between 0° and 30°C. The calibration curve obtained was reproducible within 0.02°C. No tendency for the resistance value to drift with time was observed. The current used in measurement has been limited to 2.5 microamp., this being the minimal value for adequate galvanometer response with the present equipment. Electrical heating under these conditions appears to be entirely negligible. Tests of the total contact resistance in the circuit showed that this quantity was ten ohms or less at all speeds of rotation up to 60,000 r.p.m., with no tendency to increase with moderate wear. The low value of the contact resistance allows it to be ignored in the measurement of Thermistor resistance, which is 75,000 ohms or greater.

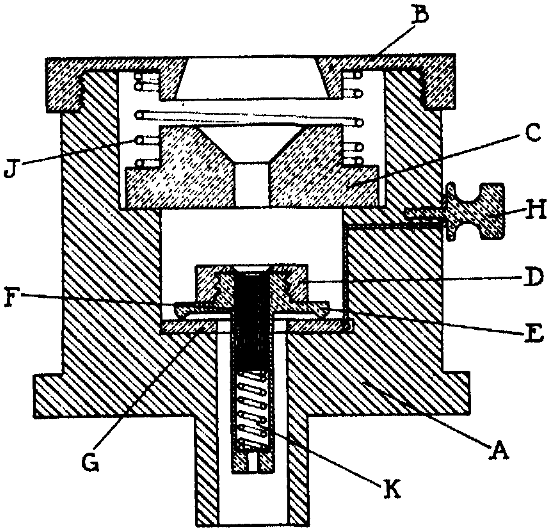

FIG. 4. The bottom bearing receptacle.

Resistance readings are taken continuously, or at arbitrary intervals during the operation of the centrifuge. When measured to the nearest 100 ohms, each resistance reading represents a temperature measurement which is reproducible within ±0.02°C. In conversion of resistance readings to temperature, which is done with reference to the calibration curve, the temperature values are rounded off to the nearest 0.1°C. After a more thorough investigation of the influence of gradients of temperature in the rotor, it may be possible to utilize the full precision of the apparatus and express temperature readings to the nearest 0.02°C. Efforts are being made at present to employ the Thermistor simultaneously as a thermoregulator to maintain the vacuum chamber and the rotor at a substantially constant temperature for sustained periods of operation.

THE REVIEW OF SCIENTIFIC INSTRUMENTS VOLUME 20, NUMBER 11 NOVEMBER, 1949

Application of the Electrical Analogy in Fluid Mechanics Research

PHILIP G. HUBBARD
Iowa Institute of Hydraulic Research, State University of Iowa, Iowa City, Iowa

(Received June 16, 1949)

The electrolytic bath and a modification thereof are presented as valuable tools in fundamental investigations of potential fluid flow. Principals and techniques are presented in full, together with some typical results which indicate the scope of the method and the accuracy obtainable. Particular emphasis is placed upon techniques which permit the high accuracy necessary in most studies.

INTRODUCTION

A TECHNIQUE is herein presented which permits determination of the dynamic characteristics of potential fluid motion around or between solid boundaries by measurements upon the electrical analog of the fluid system. The principles involved are, of course, not new. In the past, however, their practical application has been restricted to the determination of the flow pattern in two-dimensional systems and in a very limited number of three-dimensional systems for which the general velocity distribution is desired but highly accurate measurements are unnecessary. The present investigation was undertaken at the Iowa Institute of Hydraulic Research to determine the feasibility of the method for more accurate determinations of the pressure distribution along various three-dimensional boundary forms. The methods used to obtain the necessary precision are presented together with typical results from several specific problems.

THEORETICAL CONSIDERATIONS

Under certain conditions, the pattern of relative motion between a fluid and a boundary may be closely approximated through use of a function

$$\phi=\phi(x,y,z) \tag{1}$$

such that

$$\partial^2\phi/\partial x^2+\partial^2\phi/\partial y^2+\partial^2\phi/\partial z^2=0. \tag{2}$$

The function ϕ is commonly known as the velocity potential. Lines or surfaces of constant ϕ are everywhere normal to the velocity vector, and the gradient of ϕ in any direction is equal to the corresponding velocity component:

$$v_x=\partial\phi/\partial x;\quad v_y=\partial\phi/\partial y;\quad v_z=\partial\phi/\partial z. \tag{3}$$

Strictly speaking, the foregoing equations apply only to conditions of steady, irrotational flow, which are never wholly satisfied in actuality. However, when viscous effects are small in comparison with inertial effects, and when the flow pattern is determined solely by the boundary configuration, close agreement exists between the actual pattern and that indicated by the potential function for the corresponding boundary conditions. These conditions are satisfied especially well in zones where rapid acceleration of the fluid occurs, such as in well-faired conduit inlets and contractions and around the upstream face of streamlined bodies.

Since the velocity potential satisfies Laplace's equation [Eq. (2)], it also follows mathematical laws identical to those developed in theories of electricity, magnetism, and the conduction of heat. An examination of electric field theory reveals the following equations as the counterparts of those in hydrodynamics:

$$\partial^2 V/\partial x^2+\partial^2 V/\partial y^2+\partial^2 V/\partial z^2=0, \tag{4}$$

$$E_x=\partial V/\partial x;\quad E_y=\partial V/\partial y;\quad E_z=\partial V/\partial z. \tag{5}$$

E_x, E_y, and E_z (components of the vector representing the electric field strength) are obviously analogous to v_x, v_y, and v_z in Eq. (3), while V (the electric potential) is analogous to ϕ.

This similarity has long since suggested the possibility of examining the behavior of a fluid system by constructing its electrical analog and analyzing the performance of the latter with the aid of the more complete instrumentation available for electrical circuits.[1] For two-dimensional systems, various graphical and mathematical methods based on the potential theory have been used with worth while results, adequately fulfilling requirements for this type of study. For three-dimensional systems, however, graphical or mathematical solutions have been presented only for a very limited number of cases, and hence the electrical-analogy method is of greatest value in analyses of this type.

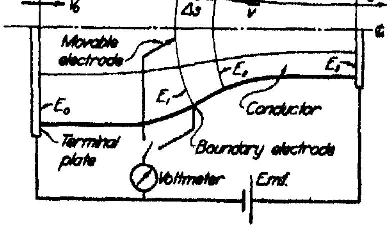

FIG. 1. Schematic representation of analogy between irrotational fluid flow and flow of an electrical current for a two-dimensional boundary contraction (see reference 2).

---

[1] E. F. Relf, "An electrical method for tracing lines in the two-dimensional motion of a perfect fluid," Phil. Mag. 48 (September, 1924).

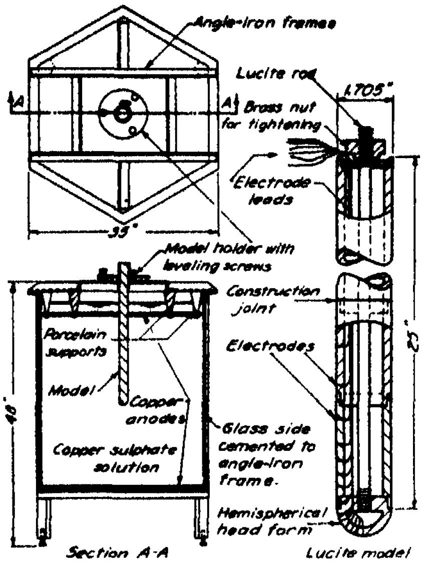

FIG. 2. Details of electrical-analogy tank and a typical model.

EXPERIMENTAL TECHNIQUE

The first step in constructing an electrical analog is to form a conductor or semiconductor (in this case an electrolytic solution) so that its boundary is geometrically similar to that of the flow system under consideration. The application of a voltage across this conductor, between zones representing the entrance and exit of the fluid in the system, then establishes within the conductor a potential pattern similar to that of its fluid prototype (see Fig. 1). A voltmeter or potentiometer circuit may thus be used to explore this potential pattern by means of electrodes in contact with the conductor. In most previous instances, the potential pattern throughout the electrolyte has been explored with the aid of a movable electrode which traces lines or surfaces of constant potential from which the approximate velocities are obtained.[2] Since, for the present study, conditions along the boundary only were desired and high accuracy was necessary, the movable probe was replaced by fixed electrodes flush with surface of the model. Their spacing could hence be measured with the requisite accuracy, usually with a machinist's precision surface gauge or by optical magnification and comparison with a standard scale.

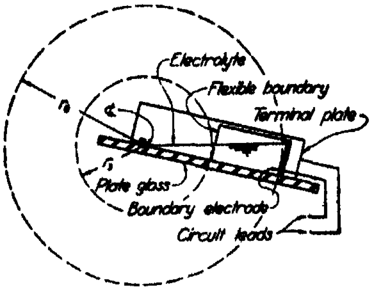

FIG. 3. Cross section of electrolytic bath simulating longitudinal segment of three-dimensional counterpart of Fig. 1.

Two construction techniques were adopted for the present studies, both using a 0.016-molar copper sulfate solution as the conductor. The first, for obtaining the flow pattern around bodies in otherwise parallel, uniform flow, consisted of a large tank filled with an electrolyte in which Luceti models of various bodies were immersed. An alternating voltage source was connected to the electrolyte by means of sheet-copper anodes, and the surface electrodes served for the determination of the potential distribution along the boundary. The major considerations in the design were (1) to make the model large enough so that small errors in construction would be relatively unimportant, and (2) to make the tank large enough so that the effect of the outer boundary would be negligible. Because of its non-conducting properties and transparency, plate glass was utilized for the sides of the tank. Although the cylindrical form is the most desirable from the standpoint of symmetry, a glass cylinder of the large dimensions desired could not be obtained readily, and a hexagonal prism was selected as the most practical substitute. A frame of angle iron was built, and the glass sides were cemented to the inside of the frame with aquarium cement. The lower anode rested on the bottom of the tank, and an angle iron frame supported the upper one just below the surface of the electrolyte (see Fig. 2). The Lucite models were introduced into the working section through a small hole in the center of the top anode, and the electrode leads were brought up through the hollow

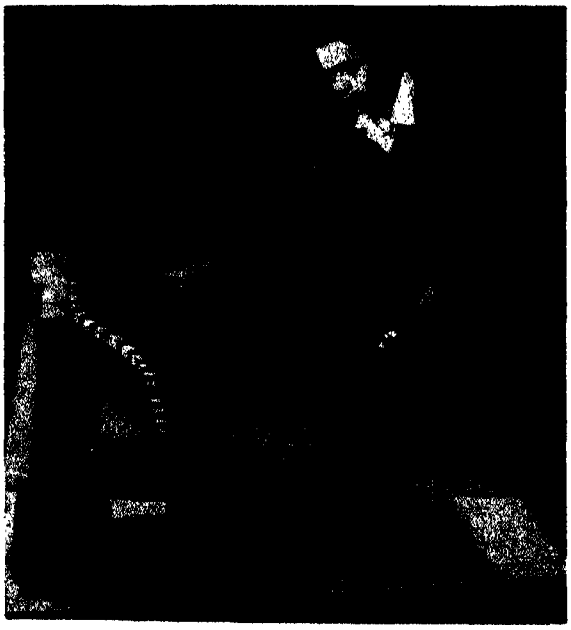

FIG. 4. Equipment used in electrical analysis of an axially symmetrical conduit transition.

---

[2] Cheers, Raymer, and Fowler, "Preliminary tests on electric potential flow apparatus," Aeronautical Research Council Tech. Report No. 2205 (1945).

interior of the model. The electrodes used were 0.012 inch in diameter, but even smaller ones are recommended to increase the relative accuracy.

The second construction technique was used to determine the boundary pressures for flow confined by various surfaces of revolution. In order to increase the accuracy of the measurements, models several times the size of the foregoing were necessary, but the construction of full models of the scale desired was quite impractical. For this reason only a small segment of the entire volume was used[2,3] since the flow pattern is identical for all longitudinal sections through the center line of an axially symmetrical body. A finite increment of the boundary surface of revolution, so narrow that in cross section its arc closely approximated a straight line, was represented by a strip of Pyralin, which could be bent longitudinally to any desired form. This strip, together with metal end plates, was assembled on an inclined pane of plate glass (see Fig. 3). When an electrolyte was poured into the space thus provided until the horizontal plane of the free surface intersected the plate glass at the predetermined axis of symmetry, the space it occupied was a representative segment of the entire volume. Hence, potentials obtained by means of electrodes along the Pyralin strip were essentially the same as would be obtained if the entire volume had been reproduced. The models were thus constructed without lathe work, and in such a way that the outline could be changed easily to any desired form (see Fig. 4).

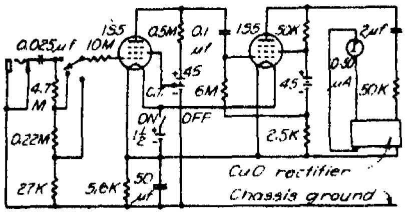

FIG. 5. Battery-operated millivoltmeter used as null detector.

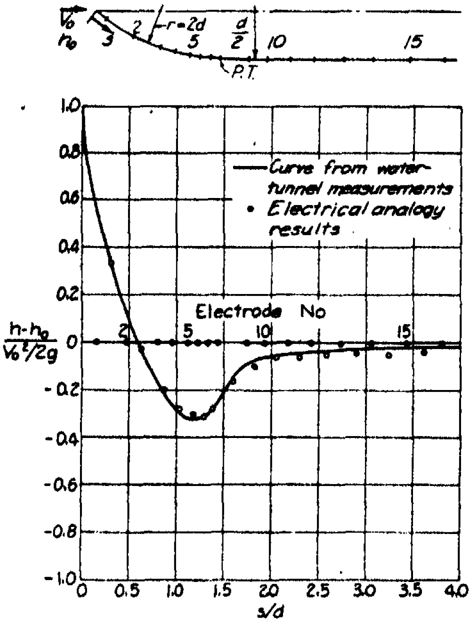

FIG. 6. Pressure distribution around a two-caliber ogival head form with cylindrical afterbody.

The segmental method of construction described in the preceding paragraph is not readily applicable to the study of bodies like those tested in the large tank, because the least accuracy would be obtained where the greatest accuracy is desired—i.e., the model would be located in the region where the electrolyte approaches zero depth and the measurements would be less reliable. The boundary would also necessarily be placed at a large distance from the model or bent to the form of a streamline.

In order to obtain consistent results with either construction technique, certain precautions must be observed in preparing and conducting the experiments. First, the electrolyte must be clean and homogeneous if the flow of current through it is to represent the flow of a non-viscous fluid. To insure this condition, the first solutions were made with distilled water, but later tests proved that tap water is satisfactory if it is first acidified with approximately 0.02 mole of sulfuric acid per liter, and then allowed to stand 24 hours before adding the copper sulfate. This eliminated most dissolved gases and converted the salts to compounds which did not precipitate or coat the electrodes and anodes. Copper was chosen as the anode material so that the electrochemical reaction would be reversible and the potential drop in the immediate vicinity of the anodes would be a minimum; both anodes and all electrodes were cleaned with dilute acid before each test. Polarization was avoided by using 60-cycle alternating current after tests showed that higher frequencies were unnecessary, and concentration gradients were eliminated by stirring the bath frequently. A filament transformer reduced the applied potential to six volts so that heating and the accompanying concentration gradients would be negligible.

Construction and measurement of the models is very important, of course, and careful consideration of the problem will be worth while. All boundary proportions, curves, and tolerances should be carefully controlled, but there is obviously no advantage in striving for a relative accuracy in the model which does not obtain in the prototype. The models must be thoroughly insulated and water-tight, because any leakage of the electrolyte will upset the readings. The spacing of the electrodes should be sufficiently close to measure the desired trends, the smallest spacing being necessary where rapid acceleration and high pressure gradients exist. The location of electrodes should be

---

[3] H. E. Babbitt and D. H. Caldwell, *The Free Surface Around, and Interference Between, Gravity Wells* (Engineering Experiment Station, Urbana, Illinois, January 7, 1948), Bulletin Series No. 374.

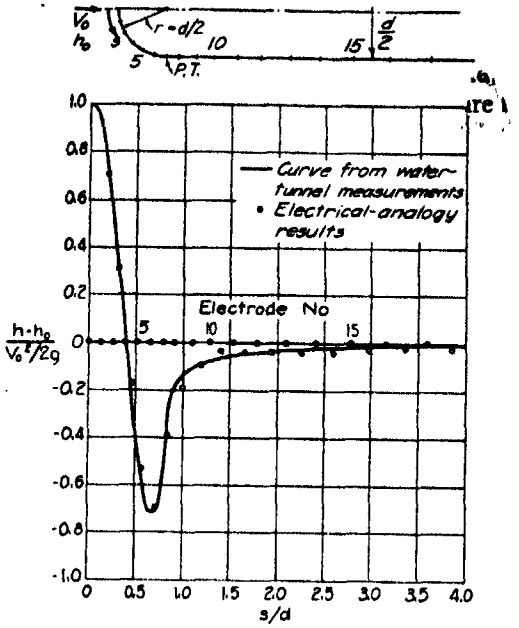

FIG. 7. Pressure distribution around a hemispherical head form with cylindrical afterbody.

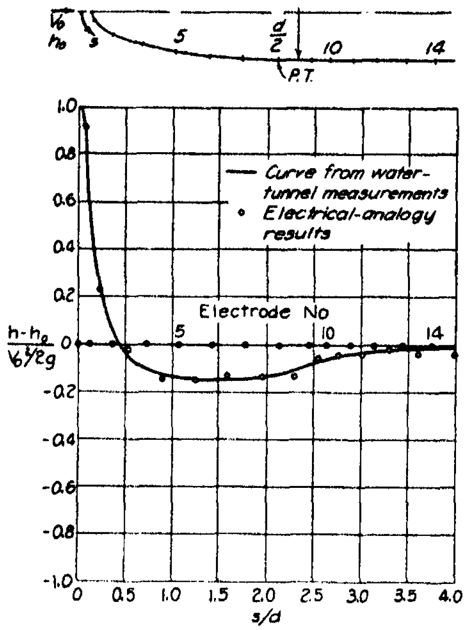

FIG. 8. Pressure distribution around a 4:1 ellipsoidal head form with cylindrical afterbody.

measured relative to a common point so that the errors compensate rather than accumulate as the differences are computed. Electrode diameters less than 2 percent of the minimum spacing are desirable to increase the accuracy in determining location, but this usually means using No. 30 wires or smaller. A special technique developed to place wires of this size in the boundary is as follows: A ⅛-inch Lucite rod is ground down on one side until its cross section is a semicircle, and a small groove is made down the center of the flat side. The wire is laid in the groove, and then a similarly formed rod is placed on top, clamped, and sealed with chloroform. The result is a ⅛-inch rod with the fine wire along its axis. Holes to admit the rod are then drilled in the model before the surface is finished, the rods are inserted and sealed with chloroform, and the surface is finished and polished. Heavier leads are finally soldered to the free end for connection to a selector switch.

The electrical measurements were made by means of a simple potentiometer circuit from which it was necessary to record only one quantity. A precision decade potentiometer was connected in parallel with the anodes, a high impedance millivoltmeter was inserted between the potentiometer tap and an electrode, and the potentiometer was adjusted until the voltage difference was a minimum. When necessary, a small capacitance was inserted across one arm of the potentiometer to compensate for the distributed capacity at the anodes and increase the sharpness of the null point. All electrode leads were connected to a rotary selector switch so that little time was lost in measuring their relative potentials. Although the potentiometer is actually a resistance-type device, the fact that the current through it is constant permits readings of fractional resistance to be interpreted directly as fractional potential with an accuracy of 0.01 percent of total potential.

The millivoltmeters used (see Fig. 5) were designed especially for this application, and were battery-operated to isolate them completely from all external influences. Miniature tubes and batteries were employed to keep size—and hence capacitance to ground—at a minimum, and wooden blocks further isolated the meter from its surroundings. The maximum sensitivity was sufficient to indicate reliably a potential difference of 3×10^{-4} volt, and less sensitive ranges for coarse adjustment were selected by a simple lever-type switch. A meter was selected as indicating element instead of the conventional earphones because of the low frequency used, the more complete isolation, and a general preference of the designer for visual indicators. Due to its very high input impedance, the meter drew negligible current from the electrodes even when the circuit was far from balance, and hence the potential field remained undistorted and gas did not accumulate on the electrodes.

To find the pressure distribution from the electrical measurements, only two quantities—the spacing Δs of the electrodes and the corresponding potential difference $\Delta\phi$—were needed, since

$$V=\Delta\phi/\Delta s, \tag{6}$$

and the change in piezometric head Δh is

$$\frac{\Delta h}{V_0^2/2g}=1-\left(\frac{V}{V_0}\right)^2\approx1-\left(\frac{\Delta\phi}{\Delta s}\right)^2\Big/\left(\frac{\Delta\phi}{\Delta s}\right)_0^2. \tag{7}$$

The quantity $(\Delta\phi/\Delta s)_0$ was evaluated from measurements between electrodes placed in a region of parallel

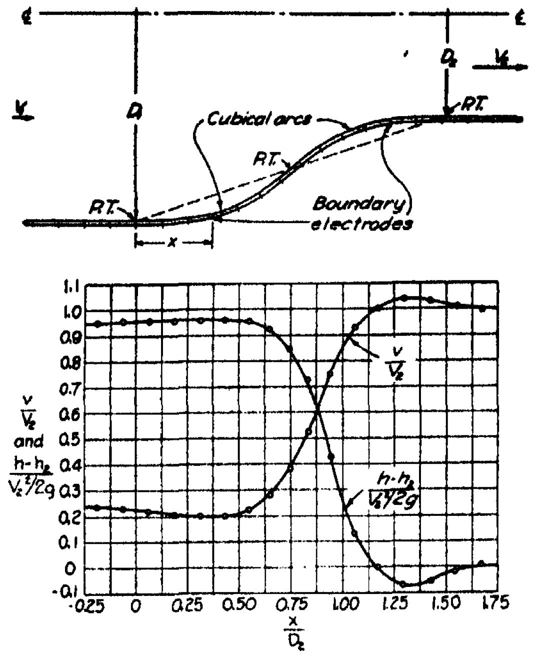

FIG. 9. Coordinate notation and typical results for cubical-arc contraction profile.

flow. Pressure-distribution curves were obtained by plotting the values from Eq. (7) midway between points corresponding to the electrode locations.

DISCUSSION OF RESULTS

The reliability of the immersion-tank measurements was determined by comparing the results for several different head forms with actual pressure distributions obtained in a water tunnel.[4] This comparison is shown in Figs. 6–8, and the agreement is certainly sufficient to justify use of the electrical-analogy results to predict actual performance for these bodies.

Two characteristics of the measurements should be noted: First, the points do not usually fall exactly on the water-tunnel curve, but alternate about it. This trend is undoubtedly due to very small errors in measuring the location of electrodes, and would be less for larger models; as already mentioned, such errors are self-compensating rather than cumulative. It should be noted that the electrodes used were much larger than those recommended in this paper, and their exact location was difficult to determine. The second characteristic is the failure to regain full static pressure along the cylindrical afterbody. This indicates that the reduction in cross-sectional area caused by introduction of the model was not negligible, though slightly less than one percent. For this reason, measurements between electrodes placed on a very slender rod inserted in place of the model were used for determining $(\Delta\phi/\Delta s)_0$. The over-all potential drop between the anodes was not sufficiently precise for this purpose because of capacity effects in the vicinity of each anode.

The reliability of the electrical measurements with the segmental method was checked in three different ways, and the errors were of the same order as those for the immersion-tank method. For example, the measured pressure gradient along a linear (i.e., conical) transition was compared with the theoretical curve; the maximum deviation was less than one percent, which is well within design limits for practical use.

Figure 9 shows the results of measurements on one of a series of nozzle models which were tested for design purposes.[5] The data obtained were adequate for determining optimum boundary shape to minimize the tendency toward cavitation. Similar tests have been performed on rounded reservoir inlets, with equivalent results. For all models, the location and magnitude of the maximum and minimum pressures were clearly shown.

Another highly useful application of the electrical analogy is to determine the form of the free surface in various flow systems where gravity plays a negligible role. The results of one such test are shown in Fig. 10, which indicates the form of the free surface and the velocity and pressure distributions in a liquid jet deflected by a normal boundary. The technique is simply to adjust the boundary curvature until the potential gradient is constant over its entire length, in accordance with the requirement that the pressure intensity must be zero (and the velocity hence constant) at all points on a free surface. The same procedure may be adapted to free-surface flow under gravitational influence through use of the Bernoulli relationship between velocity head and elevation along a surface of constant pressure.

CONCLUSIONS

The two methods described in this paper for applying the principles of the electrical analogy have proved

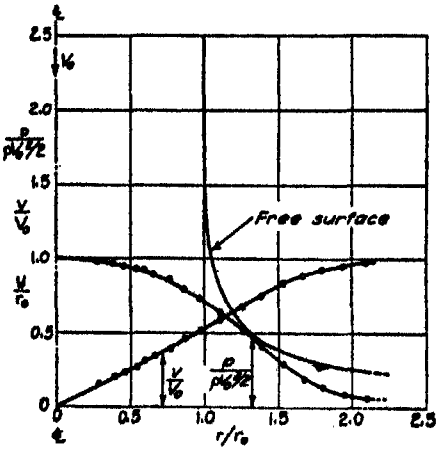

FIG. 10. Surface profile, velocity, and pressure distribution in a free jet striking a flat plate.

---

[4] H. Rouse and J. S. McNown, *Cavitation and Pressure Distribution—Head Forms at Zero Angle of Yaw* (University of Iowa Studies in Engineering, Iowa City, Iowa, 1948), Bulletin 32.

[5] H. Rouse and M. M. Hassan, "Cavitation-free inlets and contractions," Mech. Eng. (March, 1949).

satisfactory for determining velocity and pressure distributions in relative motion between fluids and boundaries under potential-flow conditions. Special attention should be directed to the following points to insure best results: (1) the electrolyte should be clean and homogeneous; (2) alternating current should be used to minimize polarization; (3) the electrochemical reaction between anodes and electrolyte should be reversible; (4) models should be sufficiently large to maintain a close relative tolerance in dimensions; (5) the finite distance to all boundaries must be considered, and their effects minimized by placing them as far as possible from critical zones; (6) electrode diameters should be very small relative to the spacing between electrodes to increase the over-all accuracy; (7) the potentiometer and null detector used must permit high accuracy in determining potential differences. With the requisite care in construction and technique of operation, results of any desired accuracy should be obtainable.

ACKNOWLEDGMENTS

The electrical-analogy tank and associated apparatus were originally designed at the Iowa Institute by Dr. S. W. Grinnell in 1945 and gradually improve during the subsequent four years of use. All measurements on the body forms were conducted by the writer, and initial evaluations of the results were made by Mr. E. Y. Hsu under the supervision of Dr. J. S. McNown. The curves for the nozzle form were taken from a University of Iowa Doctoral Dissertation by Mr. M. M. Hassan, and those for the free jet from a similar Master's Thesis by A. Leclerc, both of whom used techniques developed by the writer during the previous investigation. The method of simulating the entire flow passage by a small segment thereof was suggested by Dr. Hunter Rouse, under whose direction all portions of the research were performed. The project was supported by the Bureau of Ships and the ONR under Contracts NObs-24084, N7onr-495, and N8onr-500.

THE REVIEW OF SCIENTIFIC INSTRUMENTS VOLUME 20, NUMBER 11 NOVEMBER, 1949

The Shock Tube: A Facility for Investigations in Fluid Dynamics*

WALKER BLEAKNEY, D. K. WEIMER, AND C. H. FLETCHER
Palmer Physical Laboratory, Princeton University, Princeton, New Jersey

(Received June 20, 1949)

A qualitative description of the theory of the operation of a shock tube is given together with a discussion of its design. The construction of a particular tube 4 in.×18 in.×38 ft. is described as well as certain auxiliary equipment needed in its operation. The technique of operating the device and comparisons of its performance with expectations are discussed. This tube has been used to study certain properties of shock waves and to obtain a flow field of marked uniformity and freedom from turbulence. The Mach number of this flow may be adjusted at will from zero to the supersonic range without difficulty. An interferometer makes it possible to obtain an instantaneous picture of the density field so that the apparatus may be used as a very efficient transonic wind tunnel.

INTRODUCTION

THE propagation of sound, shock, and detonation waves in tubes has a long history beginning as far as we are aware with Davy in 1816. References to the early papers may be found in a paper by Dixon.[1] The elements of what we shall call "the shock tube" consist of a straight tube of arbitrary but uniform cross section separated into high and low pressure segments by a thin diaphragm. When the diaphragm is burst, disturbances are propagated in both directions, a rarefaction into the high pressure end and a compression rapidly becoming a shock in the low pressure end. Such an arrangement was used by Vieille[2] in 1899 to demonstrate the fact that shock waves are propagated with a speed greater than that of sound. More recent work includes that of Payman[3] and Payman and Shepperd.[4] During the war considerable work was done with shock tubes by a group at Princeton but reports were never given adequate publication.[5] This paper will be concerned with the operation of a shock tube and the description of a particular instrument. The quantitative relations involved will be given in the Appendix.

OPERATION

The behavior of the shock tube will first be described in a qualitative way. Let us suppose, for simplicity, that the gases in the low and high pressure sections are originally at the same temperature but different pres-

---

* This work received major financial support from the Navy Department through Contract N6ori—105 Task II.

[1] H. B. Dixon, Phil. Trans. A200, 315 (1903).

[2] P. Vieille, Comptes Rendus 129, 1228 (1899).

[3] W. Payman, Proc. Roy. Soc. A120, 90 (1928).

[4] W. Payman and W. C. F. Shepperd, Proc. Roy. Soc. A186, 293 (1946).

[5] An account of this work is to be found in reports to the Office of Scientific Research and Development; G. T. Reynolds, OSRD 1519 (1943), L. G. Smith, OSRD 6271 (1945), Fletcher, Read, Stoner, and Weimer, OSRD 6321 (1946).

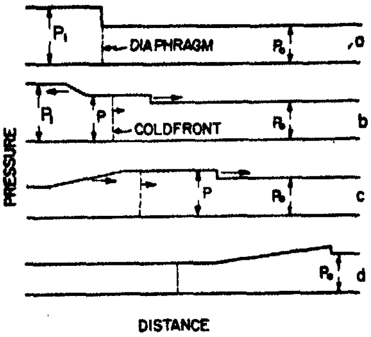

FIG. 1. Schematic diagram of the pressure distribution in the shock tube at different times. The drawings are not in scale. (a) Before the diaphragm breaks, (b) a short time after the diaphragm is burst, (c) after reflection of the rarefaction, (d) after the rarefaction has caught up with the shock.

sures. In practice this is usually the case. Suppose further that the diaphragm is suddenly eliminated. A compression immediately starts to propagate into the low end while a rarefaction goes the other way. The situation is sketched in a schematic way in Fig. 1. A boundary condition that must apply at the moving plane which separates the expanded from the compressed gas is that the velocity of the medium on either side of this plane must be the same. We may equate, therefore, the velocity acquired by an element of the fluid in front of the diaphragm passed over by the compression or shock wave to the velocity of an element of the fluid behind the diaphragm passed over by the rarefaction. Let the original pressures in the high and low ends be denoted by P_1 and P_0 and the ratio of the pressure in front of the shock to that just behind it be given by $P_0/P=\xi$. The quantity ξ is a convenient measure of the shock strength. Equating the velocities as indicated above yields a relation between ξ and P_0/P_1 (see Eq. (10) of the Appendix).

In the special case of air in both chambers originally at the same temperature and assuming the ratio of specific heats γ to be 7/5 and that the diaphragm disappears in an ideal manner, the result is

$$P_0/P_1=\xi[1-(1-\xi)/[\xi(7\xi+42)]^{\frac{1}{2}}]^7.$$

FIG. 2. A view of the shock tube from the high pressure end.

As will be seen presently the actual measured curve is of the same shape but differs quantitatively from this result by a few percent. The difference is attributed to the non-ideal way in which the diaphragm bursts. The ideal result therefore is a plane shock wave with a region of constant pressure behind it where the medium is in uniform motion and this region contains a plane marking the boundary between the two gases originally at different pressures in the two sections of the tube. This plane after the break represents a discontinuity in temperature and density but not in pressure. It will sometimes be referred to as the "cold front."

The rarefaction in the meantime is propagated in the other direction as indicated in Fig. 1. The leading edge of this wave is progressing into an undisturbed medium with the velocity of sound for that medium. The tail of the rarefaction or trailing edge is propagated, however, into a region at reduced temperature and moreover it is progressing against the stream velocity u acquired by the medium from the passage of the rarefaction. The velocity of the tail of the rarefaction with respect to the fixed tube is therefore c_2-u where c_2 is the local velocity of sound in the high pressure gas after expansion and u is the velocity of the fluid. The velocities of other phases of the rarefaction will fall between the two extremes. If the pressure fall is sufficiently great, the magnitude of u may exceed the local velocity of sound whereupon c_2-u becomes negative and the trailing edge actually moves forward with respect to the tube in the same direction as the shock is traveling.

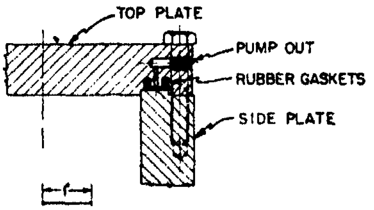

FIG. 3. Detail of the corner assembly of a typical section.

The disturbance which travels backward into the high pressure end will eventually reach the closed end of this section where it will be reflected as a rarefaction and will pursue the shock front down the tube. It will first overtake the temperature discontinuity between the two gases and eventually will overtake the shock itself if the tube is long enough. This is possible since the flow behind the normal shock is subsonic with respect to the shock itself. After the rarefaction overtakes the shock the pressure behind the front is no longer constant but falls off continuously and the strength of the shock dies off with time and distance.

When the shock front reaches the end of the low pressure section, another reflection takes place, a rarefaction if the end is open and a shock of more than twice the incident pressure jump if it is closed. In case the tube is of such dimensions that a region of constant pressure and uniform flow exists behind the incident shock then upon reflection at the closed end of the tube the reflected shock must progress upstream and its strength is such as to bring the flow to rest leaving a stagnant region of constant pressure behind it.

Very soon complications begin to arise from multiple reflections at the temperature discontinuity between the two gases and the two ends of the tube so that further prediction of the detailed behavior of the disturbances rapidly becomes more difficult. In designing a shock tube the lengths of the two sections must be chosen to give the desired durations of the flow before these complicating reflections arise.

As already mentioned, the conditions of the flow behind the incident shock but ahead of the cold front and the rarefaction wave should be very uniform in pressure, density, and velocity. As the shock strength parameter ξ goes from 1 to 0, the Mach number of this flow goes from 0 to a finite value which is supersonic with respect to coordinates fixed in the laboratory (see Appendix, Eq. (6)). For air and assuming the ratio of specific heats γ to be 7/5 this maximum Mach number is about 1.89. It will be noted that there is also a region of the same constant velocity behind the cold front. Since the temperature here is below that in front of this region, it follows that the Mach number must be greater. Investigation of the problem shows that there is no upper limit to the Mach number here as the pressure ratio P_1/P_0 is increased.

It will be noted that the strength of the shocks and the Mach numbers of the flow depend only on pressure ratios so that one may work over a large range by reducing the pressure in the low end as well as raising the pressure in the high end.

The foregoing qualitative discussion is predicated on the assumption that the diaphragm in the tube breaks in a highly idealized way. The quantitative relations and some comparisons with experiment will be given after the particular tube now in use has been described.

SHOCK TUBE CONSTRUCTION

In order to realize the properties in a shock tube discussed in the previous section it is necessary to maintain the correct ratio of the lengths of the two chambers and the cross section must be uniform throughout the length of the tube. Shock tubes have been made in our laboratory having circular, square, and rectangular cross sections, also some with one straight side and the remainder circular. In sizes they have ranged from 1 to 18 in. in the greatest transverse dimension and from 5 to 50 ft. in length. Some were crude and some were elaborate. The simplest one could be carried in the hand and inflated with a stirrup pump in the field for calibrating blast gauges. The most elaborate one so far constructed will be described below.

Experience has shown that the longer the tube the more nearly perfect is the shock front and the flow behind it. This is to be expected since the diaphragm

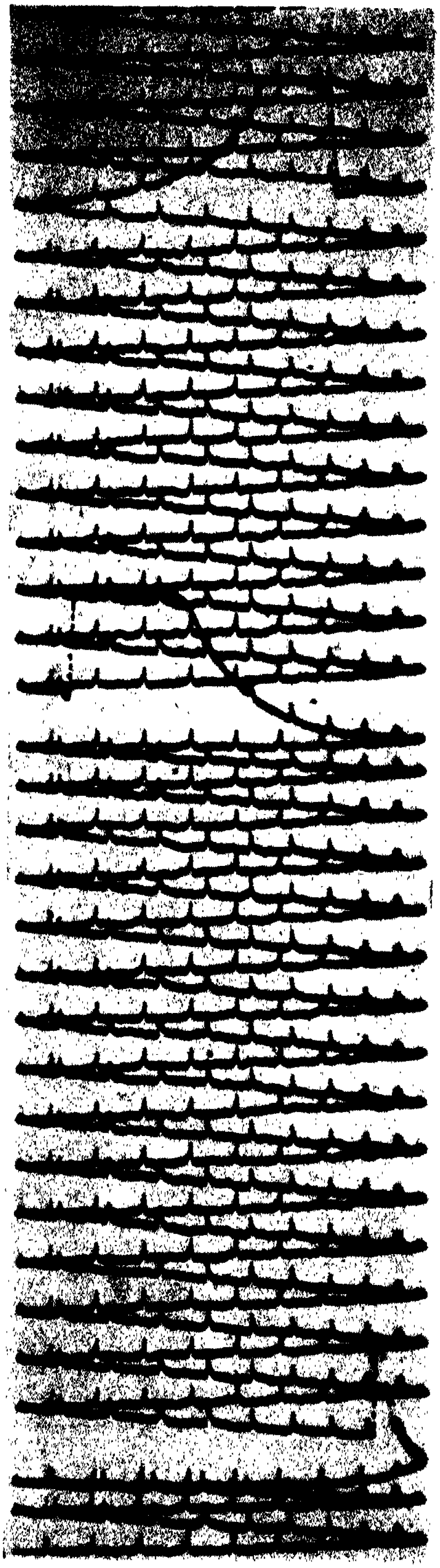

FIG. 4. A typical chronograph record showing in order from the top signals from the two light screens and the spark. For legibility in reproduction the first rise in each signal has been dotted on the print.

always breaks in a somewhat ragged fashion and a long expansion tube allows the irregularities to catch up and merge with the front. On the other hand if a given ratio is maintained between the lengths of the two chambers, this means that the high pressure section should be long also. A well-formed shock is found a few diameters from the diaphragm but in our work we have found it desirable to make our observations at a distance from the diaphragm of from 10 to 20 times the greatest dimension of the cross section.

In order to exploit the optical techniques it is desirable to have a channel with plane parallel sides in order to accommodate plane windows flush with the inside surface and in certain two-dimensional phenomena the height of the channel perpendicular to the direction of sight should be as large as conveniently attainable to delay interactions with the walls. The thickness along the light path must be sufficient to give measurable optical effects but not so thick that the light rays are deviated too far from their undisturbed paths within the tube. Certain other requirements must be considered such as the strength of materials and thickness of wall so that vibrations in the tube itself will not introduce undesirable effects.

All of these considerations were influential in the design of the present apparatus. Basically the tube is made up of seven 4-ft. rectangular sections, two 3-ft. sections, one 2-ft. section and two 1-ft. sections which may be bolted together to give a total length of 38 ft. The inside dimensions of all sections are 4 in.×17¾ in. An idea of the arrangement may be obtained by referring to the photograph in Fig. 2. In the foreground is the high pressure end, in this case 2 ft. long, the vacuum pump and gas handling manifold. The high pressure section may be rolled back and to one side giving full access to the remainder of the tube. The two chambers are faced with rubber where they join gripping the diaphragm between them. The two are held firmly together by a hydraulic clamping system operated by a hand pump.

FIG. 5. Shadow picture of a plane shock wave sweeping to the right over a horizontal plate.

The tube sections were fabricated from Dural plate 1⅛ in. thick. The inside surfaces were machined but not otherwise polished. The plates are bolted together with rubber gaskets in the seams to make a vacuum tight seal. Details of a corner are shown in Fig. 3 where it will be seen that the side plates are keyed into the top and bottom plates for added strength, and a double rubber seal is used. Provision is made for pumping out the space between these seals so that should a leak develop it can be quickly localized and the trouble corrected. Each side plate has a heavy cleat inset and bolted near each end. To join two sections, a flat rubber gasket is placed between them and longitudinal bolts through adjacent cleats draw the two sections together. Dowel pins insure proper alignment. The gasket is trimmed on the inside flush with the surface after the bolts have been drawn up tight.

Numerous ports 2 in. in diameter are distributed at points along the tube where various gauges and instruments may be mounted to investigate phenomena occurring within the tube. The test section, the last one on the low pressure end, is equipped with two observation windows 5 in. in diameter mounted in opposite walls flush with the inside surface. It is through these windows that all of the important optical studies are made. Two light screens are mounted to intercept the incident shock wave just before it enters the test section. Schematically they consist of miniature schlieren optical systems with light source, condensing lens, knife edge, and collimating lens on one side and field lens, knife edge, and photo-multiplier detector on the other side of the tube. The light passes through small windows in the 2-in. ports and traverses the tube in the form of a rectangular beam of parallel light about 5 mm wide and 20 mm high. When the knife edges are adjusted to cut off most of the light, the system is very sensitive and will detect the transit of a shock wave over the entire range of shock strengths from $\xi = 0.98$ to $\xi = 0.05$. The output signals have a sufficiently sharp rise to locate the shock in time to about 10^{-7} second. The two light screens are 16¾ in. (42.6 cm) apart and when the time interval between the two signals is measured, the velocity of the shock may be determined. From the velocity the shock strength ξ may be computed (see Eq. (4) in the Appendix).

There are many types of chronographs which could be used to measure the time interval. The one we use consists of a cathode-ray tube and drum camera combined with a sweep circuit which sweeps the beam back and forth at a frequency of 10 kilocycles with constant speed in both directions. Sharp "pips" are fed into the vertical amplifier at 5-microsecond intervals and the sweep is synchronized with the pips so that it begins and ends on a pip. The pip frequency is controlled by a quartz crystal oscillator in the usual fashion. The drum camera was improvised by attaching a strip of 35-mm film to the circumference of the sprocket only of the General Radio 651-AE camera. A contactor consisting of an insulated point near a flexible diaphragm is inserted in one of the ports prior to the light screens and on the passage of the shock front past this point the contactor closes a circuit which serves to turn on the spot on the CR tube which remains on for approximately one revolution of the film and hence prevents overlapping traces.

A typical velocity record is illustrated in Fig. 4. In addition to the two signals from the light screens which serve to determine the velocity of the shock a third signal is recorded at the time the spark is flashed to take a picture through the main observation windows thus fixing the time at which the observation was made. The velocity of the shock wave can be determined over a wide range with an accuracy of one part in 5000.

The windows in the test section are high quality optical flats with uniform optical thickness such as are required for interferometer applications. The windows are 5 in. in diameter, $\frac{3}{4}$ in. thick and mounted by means of Wood's metal seals to steel rings which in turn fit into the openings in the walls of the tube. The whole combination is flush with the inside surface and a rubber gasket on the outside seals the steel ring to the wall so that the system is vacuum tight. A similar pair of matched windows are mounted in a compensation chamber to equalize the optical paths in the interferometer. The whole test section, 3 ft. in length, has a quick-detachable connection with the remainder of the tube and may be rolled out on a carriage to facilitate adjustments on objects and models mounted in the observation region.

The interferometer needs little description since it is of the Mach-Zehnder type[6] and very similar to the one recently described by Winckler.[7] The two differ only in size, mechanical details in the mount, and methods of adjustment. The plates are 5 in. in diameter and inclined 45° to the optical axis. The instrument together with two optical benches supporting other components of the system used in the investigations rests on a steel table whose legs pass through holes in the floor to a concrete foundation independent of the laboratory building. The shock tube itself does not touch this table at any point so that mechanical vibrations in the tube do not disturb the optical system. The light source used in all the optical investigations is a spark having an effective duration of one microsecond or less. One of the signals used in the velocity measuring system also passes through an adjustable delay circuit and trips an auxiliary spark which serves to initiate the main discharge. The range of adjustment of the delay unit is from 0.2 to 2 milliseconds and the reproducibility is of the order of a few microseconds. Observations may be made by shadow, schlieren, or interferometry.[8]

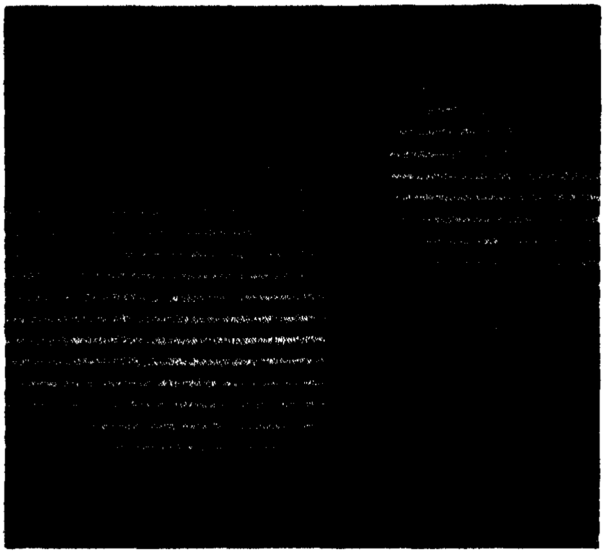

FIG. 6. Interferogram of the incident shock wave by the "offset" method and illustrating how the individual fringes may be traced through the shock.

A vacuum pump and gas handling manifold are provided so that different gases at any convenient pressure may be used in the system. For instance air and helium on the low and high pressure sides of the diaphragm respectively have been used to obtain a much stronger shock wave for the same initial pressures than one can obtain using air on both sides.

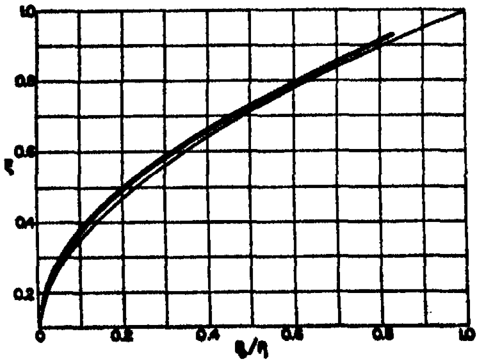

FIG. 7. Calibration curve for shock strength as a function of the starting pressure ratio.

PERFORMANCE

If the shock tube behaved in an ideal way the shock waves should be plane. A parallel shadow picture of an

---

[6] The optical flats for the interferometer and windows were prepared by Perkin-Elmer Corporation.

[7] J. Winckler, Rev. Sci. Inst. 19, 307 (1948).

[8] For a description of these techniques see, for example, Liepmann and Puckett, *Aerodynamics of a Compressible Fluid* (John Wiley and Sons, Inc., New York, 1947).

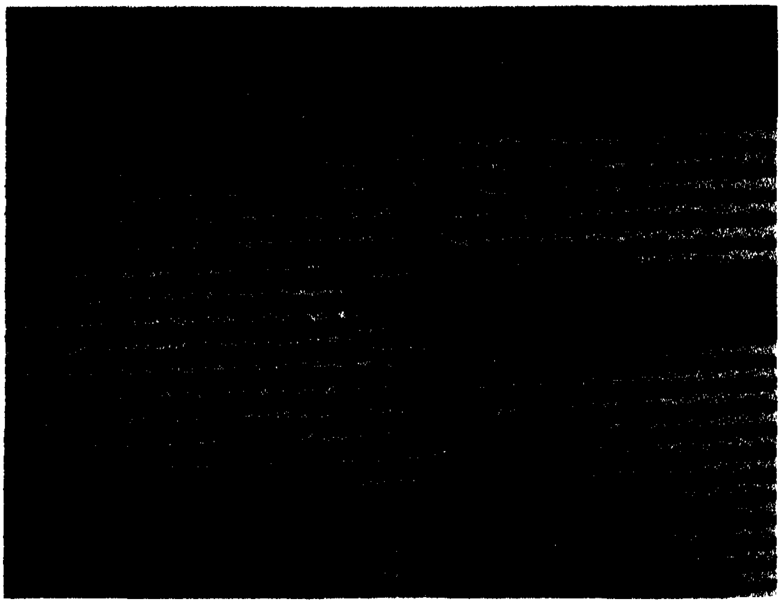

FIG. 8. Interferogram of an early phase of the flow over a wedge (10° half-angle). To the right of the shock $M=0$, and to the left, except near the tip of the wedge, $M=1$.

incident shock passing over a plane wall at grazing incidence is shown in Fig. 5. The ratio of the departure of this shock from a straight line to the length of the line is less than one part in *500*. It will also be noticed that the wall has no detectable effect on the shock where the two intersect.

It is clear that the strength of a shock $\xi=P_0/P$ can be determined both by its velocity and by the density ratio across the front. This density ratio is calculated from the fringe shift which occurs in the interferometer. The conventional method of identifying the fringes across the discontinuous shock front makes use of the white light fringes.[9] In dealing with two-dimensional configurations of density discontinuities we have found it more convenient to displace the light source so that the light is oblique to the shock by one or two degrees whereupon the fringes may be traced through the front as shown in Fig. 6. This method eliminates all the uncertainty concerning the exact location of the zero order of interference since this question is now irrelevant.

The idea of the offset light source has been carried one step further by installing two sparks, one centered on the optical axis of the system giving light in the interferometer parallel to the shocks and the other displaced as described above. The lens at the exit port of the interferometer forms separate images of the two sparks and a small mirror inserted here enables one to separate the two light beams so that two simultaneous pictures on two separate plates may be made. The one from the offset source is used to determine the strengths of the discontinuities and to identify the fringes on the other. Or by firing the sparks at different times the offset spark may be used to determine the strength of the incident shock and hence the Mach number of the flow while the second is available for analysis of phenomena occurring later in the flow.

The sensitivity of the interferometric method of measuring ξ depends on the difference of density on the two sides and hence on the absolute pressure and temperature at which the experiments are performed. The fringe shift approaches zero as $\xi\rightarrow 1$ and a constant value as $\xi\rightarrow 0$. We have found that a working range of pressures such that the fringe shifts lie in the range 0 to 20 is feasible and convenient and in the most favorable cases the shift can be measured to about 0.02 fringe. However, in using Eq. (13) to determine ξ for the incident shock, for example, other quantities enter including the wave-length, the width of the tube, the density of the undisturbed gas and the index of refraction.

From Eq. (14) of the Appendix we see that the computation of the shock strength ξ by the velocity method involves the velocity of sound c_0 in the undisturbed region. It would be advantageous to measure this quantity directly in the tube but so far we have used only air in the low pressure end and the c_0 was computed from the approximate relation

$$c_0/c_s=(T_0/T_s)^{\frac{1}{2}}(1+0.149P_w/P_a),$$

where c_s is the velocity of sound in dry air under standard conditions (331.6 m/sec.) and $T_s=273$°K, T_0 is the tube temperature and P_w and P_a are the partial pressures of water vapor and dry air in the low pressure section of the tube. The equation is valid only when $P_w \ll P_a$.

In comparing the two methods of measuring the shock strength ξ at which the tube is operated it is fair to say that each gives a nominal value which is accurate to 0.1 percent or better. However, since we have not bothered to determine the density and sound velocity of the undisturbed medium with high accuracy the absolute values of ξ as measured by the two methods differ by at most two percent in the range $(0.3<\xi<0.9)$.

---

[9] Ladenburg, Winckler, and Van Voorhis, Phys. Rev. 73, 1359 (1948).

The results of many velocity measurements on several tubes of different dimensions are shown in Fig. 7. The solid curve is obtained from Eq. (11) of the Appendix and the shaded band covers the region of experimental observations. The observed shock strength is always a little less (ξ a little more) than the simple idealized theory predicts. It should be noted also that ξ is not actually constant as the shock progresses down the tube.[10] In a tube 15 cm in diameter the velocity increased for several diameters beyond the diaphragm and thereafter decreased. At a distance of about 40 diameters the rate of loss in velocity with distance was less than 0.001 sec.^{-1}. These observations were made before the rarefaction reached the shock front.

For only moderate precision Fig. 7 may be taken as a calibration for any tube but if high precision is desired each tube should be calibrated individually or the shock strength should be measured in every experiment.

It has been found that successive "shots" in the tube taken with the same initial conditions reproduce one another to a surprising degree. The velocity of the incident shock can be reproduced to 0.1 percent which is about the accuracy of the measurement of the starting pressure P_1. Even little irregularities which appear if the point of observation is not far enough away from the diaphragm are often reproducible.

The flow behind the incident shock front as examined by all the standard optical methods appears to be very uniform with the exception, under some conditions of operation, of some very weak shocks which sometimes appear following the main shock. At first these were rather troublesome but doubling the length of the tube materially reduced the number and intensity of these subsidiary shocks. They are most evident in shadow pictures and represent the last traces of reflections from the walls which is the process by which the plane front is built up. A typical interferogram of a field of flow is shown in Fig. 8. Here air on the right is at rest while just to the left of the shock the flow is toward the right at about Mach number 1.0. A bow wave is just beginning to form ahead of the two-dimensional wedge. From the uniformity of the fringes on the left portion of the picture one can see that the flow is quite uniform. No detailed measurements have been made as yet so that limits on the degree of uniformity in the flow cannot be given.

The use of the tube as a transient wind tunnel[11] is well illustrated in Fig. 9 where the flow is supersonic at Mach number 1.4. This flow in air is in the region between the shock front which has already passed from view on the right and the cold front which has not yet reached the window. The tip of the wedge has been immersed in the flow for only about 100 microseconds and yet the flow appears to have reached a quasi-steady state. The boundary layer is clearly evident. The transition from the transient beginning of the flow to such a quasi-stationary state can be studied by taking pictures at intermediate times. It is worth noting that the Mach number of this flow can be determined independently from three different measurements; (1) the velocity of the incident shock wave, (2) the angle of

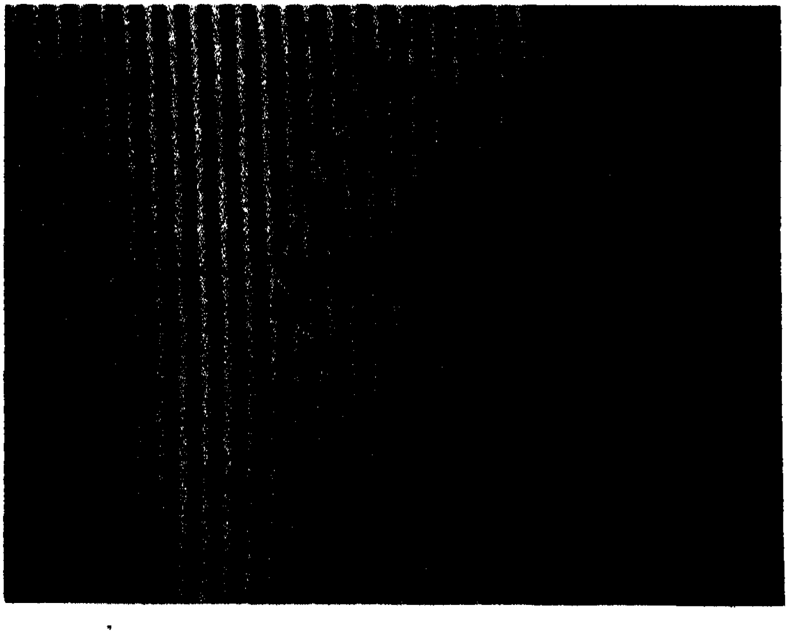

FIG. 9. Supersonic flow, $M=1.4$, over a wedge about 100 microseconds after the incident shock had passed the tip.

---

[10] R. J. Emrich and F. B. Harrison, Phys. Rev. 73, 1255(A) (1948).

[11] Another illustration of the supersonic flow in a shock tube may be found in the note by Mautz, Geiger, and Epstein, Phys. Rev. 74, 1872 (1948). The Mach number here is 2.5 and therefore must occur behind the cold front. This has been confirmed by private communication.

the attached bow wave, and (3) the fringe shift across the incident shock wave (by taking an earlier picture in which this shock front is visible). A detailed comparison of the bow wave method with the others has not yet been made but in the one case where we have data the agreement is satisfactory.

USES OF THE SHOCK TUBE

It will be readily apparent that the shock tube is a useful device for studying a great variety of problems in fluid dynamics. First may be mentioned the properties of shock waves themselves such as propagation, structure, interaction with other shock waves and with boundaries between different media or walls. In the field of chemical kinetics it lends itself to the investigation of problems of detonation and allied phenomena. The tube may be used as a wind tunnel with a Mach number variable over an enormous range, it being a particularly advantageous arrangement for the investigation of phenomena of a transient nature such as the growth of boundary layers and the approach of a flow toward a steady state. It is uniquely suited to the study of flows in the transonic region.

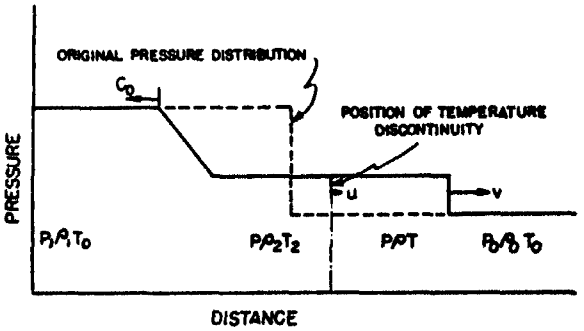

FIG. 10. Drawing to scale of the pressure configuration a short time after rupture of the diaphragm. $\xi=0.67$.

Among the more mechanical applications for which the tube has been used are the calibration of shock wave pressure gauges both of the kind that are immersed in the stream and those mounted flush with a wall, including mechanical and electrical types. Details of the mechanism of the deformation and bursting of diaphragms when struck by a shock wave have been elucidated with the help of this device. The damaging effects of blast waves on models and the diffraction of shock waves around obstacles may also be considered.

One can speculate on many other applications but those mentioned above have already been demonstrated by experiment.

The evolution of the shock tube technique at Princeton is the result of the contributions of a number of people working together on a project begun early in the war and supervised by one of us (WB). We particularly wish to acknowledge our indebtedness to the work of G. T. Reynolds, A. H. Taub, L. G. Smith, C. W. Lampson, J. C. Fletcher, W. T. Read, R. G. Stoner and R. J. Emrich.

APPENDIX. THEORETICAL RELATIONSHIPS

For convenience and completeness the quantitative or theoretical relations most useful in explaining the operation of the shock tube and in carrying out its design are summarized below. No attempt is made to give proofs since most of these may be found in standard texts on fluid dynamics. Although many of the elements of a theory of the shock tube have been worked out independently by several people we are indebted to A. H. Taub and his work with us in 1942 for the results given in this Appendix.[13]

Let us denote by $\rho'P'T'$ the density, pressure, and temperature on one side of any shock wave and let $\rho''P''T''$ denote the same quantities on the other side. Also let u', v' and u'', v'' be the components of the flow velocity perpendicular and parallel to the shock front on the two sides respectively. Considerations of the conservation of mass, momentum, and energy lead to the so-called Rankine-Hugoniot equations.[8]

$$\rho'(u'-V)=\rho''(u''-V)=m, \tag{1}$$

$$P'-P''=m(u'-u'') \quad v'=v'', \tag{2}$$

$$P'u'-P''u''=(m/2)(u'^2-u''^2)+m(E'-E''), \tag{3}$$

where V is the velocity of the shock wave, m is the rate at which matter passes through unit area of the shock front and E is the internal energy per unit mass. The direction of V is always into the region of lower pressure.

In the shock tube, of course, the medium ahead of the shock is at rest and its temperature and pressure are easily measured. The equation of state then fixes the density. The measurement of one other of the variables in Eqs. (1), (2), and (3) such as V completely determines all the others. In terms of the notation of Fig. 10 and assuming the equation of state to be that of a perfect gas

$$\begin{aligned}(V/c_0)^2&=[\gamma-1+(\gamma+1)/\xi]/2\gamma\\&=(1+6/\xi)/7 \quad \text{for} \quad \gamma=7/5,\end{aligned} \tag{4}$$

where $\xi=P_0/P$ and γ is the ratio of specific heats which for air may be taken as 7/5. The density ratio on the two sides of the shock is given by

$$\begin{aligned}\rho/\rho_0&=[\gamma+1+(\gamma-1)\xi]/[(\gamma+1)\xi+\gamma-1]\\&=(6+\xi)/(6\xi+1) \quad \text{for} \quad \gamma=7/5.\end{aligned} \tag{5}$$

The Mach number u/c of the flow behind the incident shock wave is given by

$$\begin{aligned}M^2=(u/c)^2&=2(1-\xi)^2/\gamma[(\gamma+1)\xi+\gamma-1]\\&=25(1-\xi)^2/7(6\xi+1) \quad \text{for} \quad \gamma=7/5.\end{aligned} \tag{6}$$

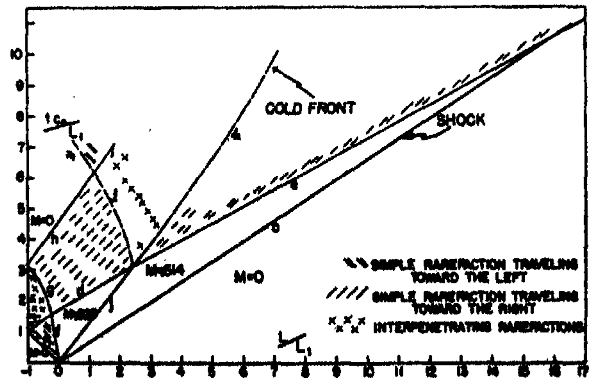

FIG. 11. Time-distance plot ($\xi=0.4$) of the various waves in the tube as computed from the theory. The conditions above the line *lm* involve both rarefactions and compressions.

---

[13] See also H. Schardin, Physik. Zeits. 33, 60 (1932).

For strong shocks ($\xi\rightarrow 0$) the Mach number approaches a limiting value of 1.89 for air assuming $\gamma=7/5$.

Again referring to Fig. 10 the velocity of the medium toward the right as a result of the rarefaction progressing toward the left (subscript 2) is given by

$$u/c_1=2[1-(P/P_1)^{(\gamma_1-1)/2\gamma_1}]/(\gamma_1-1), \tag{7}$$

where c_1 is the speed of sound in the undisturbed medium into which the rarefaction is going. c_1 is used in place of the c_0 used in the figure since the gases separated by the disphragm may have been different e.g., helium and air; this leads to the introduction of γ_1 for the gas originally at the higher pressure and γ for the other. If we let c_2 be the local velocity of sound after the rarefaction has passed, we may substitute c_2 for c_1 by the relation

$$c_1=c_2(P/P_1)^{-(\gamma_1-1)/2\gamma_1}, \tag{8}$$

and obtain the Mach number of the flow in this region

$$\begin{aligned} M_2=u/c_2&=2[(P_1/P)^{(\gamma_1-1)/2\gamma_1}-1]/(\gamma_1-1)\\ &=5[(P_1/P)^{1/7}-1] \quad \text{for} \quad \gamma_1=7/5. \end{aligned} \tag{9}$$

It will be noticed that as (P_1/P) increases without limit the Mach number does likewise to the approximation that γ remains constant.

Eliminating the velocity u in Eqs. (6) and (7) one obtains a relation between P_0/P_1 and ξ,

$$\begin{aligned} P_0/P_1=\xi[1-c_0(\gamma_1-1)(1-\xi)/c_1[2\gamma\xi\{\xi(\gamma-1)\\ +\gamma+1\}]^{\frac{1}{2}}]^{2\gamma_1/(\gamma_1-1)}. \end{aligned} \tag{10}$$

With air in both chambers at room temperature, $c_1=c_0$ and $\gamma_1=\gamma=7/5$, the equation reduces to,

$$P_0/P_1=\xi[1-(1-\xi)/[7\xi(\xi+6)]^{\frac{1}{2}}]^7. \tag{11}$$

From (10) or (11) the shock strength may be estimated from the starting pressures. A curve plotted from (11) is shown in Fig. 7.

If we let n be the fringe shift, measured in units of one fringe, caused by a change in density in the region of interest then

$$n=(Kl\rho_0/\lambda)(\rho/\rho_0-1), \tag{12}$$

where l is the width of the tube, ρ_0 the density in the undisturbed region, λ the wave-length and K the Gladstone-Dale constant. ($K\rho=\mu-1$, where μ is the index of refraction.) In terms of ξ,

$$\begin{aligned} n&=2(\mu_s-1)(l/\lambda)(\rho_0/\rho_s)(1-\xi)/[\gamma-1+(\gamma+1)\xi]\\ &=5(\mu_s-1)(l/\lambda)(\rho_0/\rho_s)(1-\xi)/(1+6\xi), \end{aligned} \tag{13}$$

where the subscript s refers to some standard condition.

A good way to picture the various effects which take place in the shock tube is to make a time-distance plot. This is done in Fig. 11 for a particular shock strength $\xi=0.4$ for air in both chambers of the tube. The abscissae are in terms of the ratio L/L_1 of the distance of the diaphragm from the point of observation to the length of the high pressure chamber while the ordinates are given by c_0t/L_1 also a pure number. The curves give the positions of various features as a function of time. It is assumed that the diaphragm breaks in an ideal manner and the computations are made using the relations given above together with the results in a paper by Taub.[13]

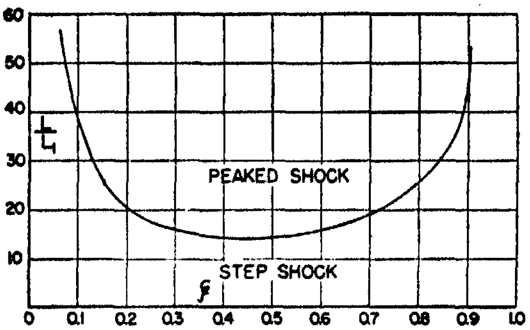

FIG. 12. Critical tube length for catch-up of the rarefaction.

The shock front (a) travels down the tube a long way with uniform speed. Behind it is a region of uniform flow of Mach number 0.614. The leading edge of the rarefaction (b) travels back to the closed end at uniform speed c_0, is reflected there and passes through the rarefaction along (c). It then proceeds at uniform speed (d) through the cold gas until it strikes the cold front where after some reflection it proceeds along (e) in the hot gas until it intersects the shock front. The trailing edge of the rarefaction follows in a similar way the path (f, g, h, i). For very strong shocks this edge starts forward instead of backward. The cold front moves forward at uniform speed along (j) leaving behind it a region of uniform flow of Mach number 0.825 until overtaken by the leading edge of the rarefaction after which it starts along a curved path (k). A reflection (l,m) occurs here. Since this is a somewhat idealized picture it is pointless to try to trace the events further. However, the chart is useful in predicting such things as the duration of the steady flow behind the shock front given by the vertical distance between (a) and (e) or behind the cold front given by the vertical distance between (j) and (d).

Similar plots may be made for other shock strengths and it will be found that the shape of the various curves varies considerably with this strength. For both weak and strong shocks the point at which the rarefaction catches the shock front occurs at larger values of L/L_1 than shown in Fig. 11. The way the catch-up point varies with shock strength is illustrated in Fig. 12 where the curve, for design purposes, has been estimated on a more conservative basis since the diaphragm does not break in the ideal way assumed in Fig. 11. Experimental results of Lampson[14] over a limited range of ξ agree with the curve of Fig. 12 within about five percent.

---

[13] A. H. Taub, Annal. Math. 47, 811 (1946).

[14] C. W. Lampson, OSRD Report 4754 (February, 1945).

THE REVIEW OF SCIENTIFIC INSTRUMENTS VOLUME 20, NUMBER 11 NOVEMBER, 1949

The Theoretical and Practical Sensitivity of the Pneumatic Infra-Red Detector*

MARCEL J. E. GOLAY
Signal Corps Engineering Laboratories, Fort Monmouth, New Jersey

(Received April 20, 1949)

Following an introductory sketch of the application of the pneumatic infra-red detector to spectrometry, the absolute sensitivity of a pneumatic detector is calculated for the case of an infinitely extended flat heat cell. The calculated r.m.s.e.n.i. is seen to be in good agreement with the experimental results.

INTRODUCTION

IN practical spectrometric applications the pneumatic infra-red detector[1] is utilized in an arrangement which embodies the so-called chopped beam method, and which presents the advantage of eliminating many sources of thermal drift. Figure 1 illustrates schematically this arrangement, as well as the essential elements of the detector. It will be observed that the chopping disk serves to interrupt not only the radiative beam from the infra-red source, but also the path between a photo-cell and its exciter. This serves to generate a synchronizing signal which controls the action of a flip-flop circuit, the two respective outputs of which are mixed on the grids of a double wave rectifier with the signal output and an inverted signal output. Thus, synchronous rectification (heterodyning down to d.c.) and linearity through zero are obtained, without the need of break-make contacts or other moving parts except the one chopping disk.

The d.c. output is fed to a commercial recorder, and it has been observed that when the optical line grid of the detector is shifted from the position of maximum sensitivity, at which the opaque portions of the line grid are imaged on the clear portions by the meniscus lens and the flexible mirror, to the position of zero sensitivity, at which the images of the opaque portions straddle the separations between the opaque and clear portions, the recorded noise decreases appreciably.

The circumstance just mentioned indicates that the thermal agitation of the flexible mirror, which, within the frequency band of observation, reflects the thermal agitation of the pneumatic cell, is directly observable and forms the essential component of the noise of the detector. Therefore, the attainable signal-to-noise ratio of a pneumatic detector designed for the frequency range utilized in the application mentioned above (10 c.p.s.) can be concluded from a study of the pneumatic circuit of the detector per se.

Incidentally, the displacement of the flexible mirror corresponding to the recorded noise is of the order of 10^{-10} in. This figure is obtained from an estimate of the amount of displacement of the flexible mirror within the band width of observation, and is considerably smaller than the total r.m.s. displacement of the flexible mirror representing the surface tension energy $\frac{1}{2}kT$ stored in it, on the average.

EQUIVALENT CIRCUIT OF A FLAT PNEUMATIC CELL

If it were possible to have a cell bounded by reflecting walls and an infra-red window made of perfect heat-insulating materials, and filled with a gas which is transparent to infra-red radiation, a radiation-absorbing membrane placed within this cavity would form the only means of heat interchange between the cell gas and other objects, in this case, the objects in the background viewed through the window. An optical system such as the one illustrated by Fig. 1 could then serve to obtain a measure of pressure changes of the gas due to known changes in the thermal background of the absorbing membrane, or due to the fluctuations of radiation interchange between the membrane and a background at constant temperature. Under these conditions it is expected that the signal-to-noise ratio of the detector would be limited essentially by the mean square radiation fluctuation $\langle \Delta J^2 \rangle_{\mathrm{Av}}$, between the absorbing membrane and its background, which is given by the classical formula:

$$\langle \Delta J^2 \rangle_{\mathrm{Av}} = 16kk_1T^5S\Delta f, \tag{1}$$

where k = Boltzmann constant, k_1 = Stephan-Boltzmann constant, T = absolute temperature of the background (and of the membrane and the cell gas), S = area of the membrane, and Δf = frequency band of observation.

Except for the small amount of additional noise introduced by the optical detecting system, the arrangement just postulated would form an ideal infra-red detector. For actual pneumatic detectors, the most important departure from an ideal detector is due to the circumstance that perfectly insulating walls are nonexistent. The heat conductivity as well as the specific heat of practical wall and window materials are both so much higher than those of any gas that it can be considered that the walls of the cell form a "thermal ground" in the equivalent thermal circuit. A relatively simple, yet rigorous theory of the effect of these thermal grounds on the absolute sensitivity of the pneumatic detector, i.e., its signal-to-noise ratio as a percentage of the signal-to-noise ratio of an ideal detector, can be derived for the case of a flat cell, the depth of which is negligibly small when compared to its other dimensions. A radiation-absorbing membrane is to be imagined in the median plane of this cell, at a distance x_0 from both top and bottom, and all field quantities such as temperature and gas density differentials can be expressed as functions of a single parameter x which represents the distance of the particular point considered to the median plane.

---

* The experimental phase of the work reported here was carried out at the Eppley Laboratory, Inc.

[1] Marcel J. E. Golay, Rev. Sci. Inst. 18, 347–362 (1947).

Figure 4 of reference 1 illustrates the equivalent circuit of a heat cell with lumped elements, in which a T transforming network has been inserted between the thermal and the pneumatic elements. By multiplication of, for instance, the thermal parameters, by proper coefficients, the transforming network can be dispensed with, and we obtain the simpler network illustrated by Fig. 5 of reference 1.

When account is taken of the distributed character of the various thermal and pneumatic elements, the more complicated network represented by Fig. 2 is obtained, underneath which the various symbols utilized are defined. The heat capacity at constant volume of the gas is continuously distributed along the temperature "divider" representing the heat conductivity of the gas. The difference between the heat capacities at constant pressure and at constant volume, which corresponds to the pneumatic work done (or received) by the gas, is represented by the multiplicity of condensers with a common terminal connected to the flexible mirror which forms the detecting element. For some purposes this detecting element will be imagined removed and replaced by an element 0 designed to measure the pneumatic impedance of the cavity.

The various elements of the equivalent circuit of Fig. 2 can be either thermal or pneumatic elements, depending upon whether the circuit is examined for its thermal or pneumatic properties. Both the thermal expression and the equivalent pneumatic expression have been given for each element, and these are connoted by the subscript th or pn appended to the brackets containing these various expressions. All these expressions refer to a cell having unit area, or to a cylindrical portion having unit cross section within an infinitely extended cell.

It will be recalled that R_r has the dimensions of a temperature differential over a heat flow differential (per unit area) *times the absolute temperature*, and that C has the dimensions of a heat capacity (per unit area) *divided by the absolute temperature*. This is for the purpose of maintaining the analogy between a thermal power (per unit area) $\Delta T^2/R_r$ and an electrical power V^2/R, or between a thermally stored available energy (per unit area) $\frac{1}{2}C\Delta T^2$ and an electrically stored energy $\frac{1}{2}CV^2$.

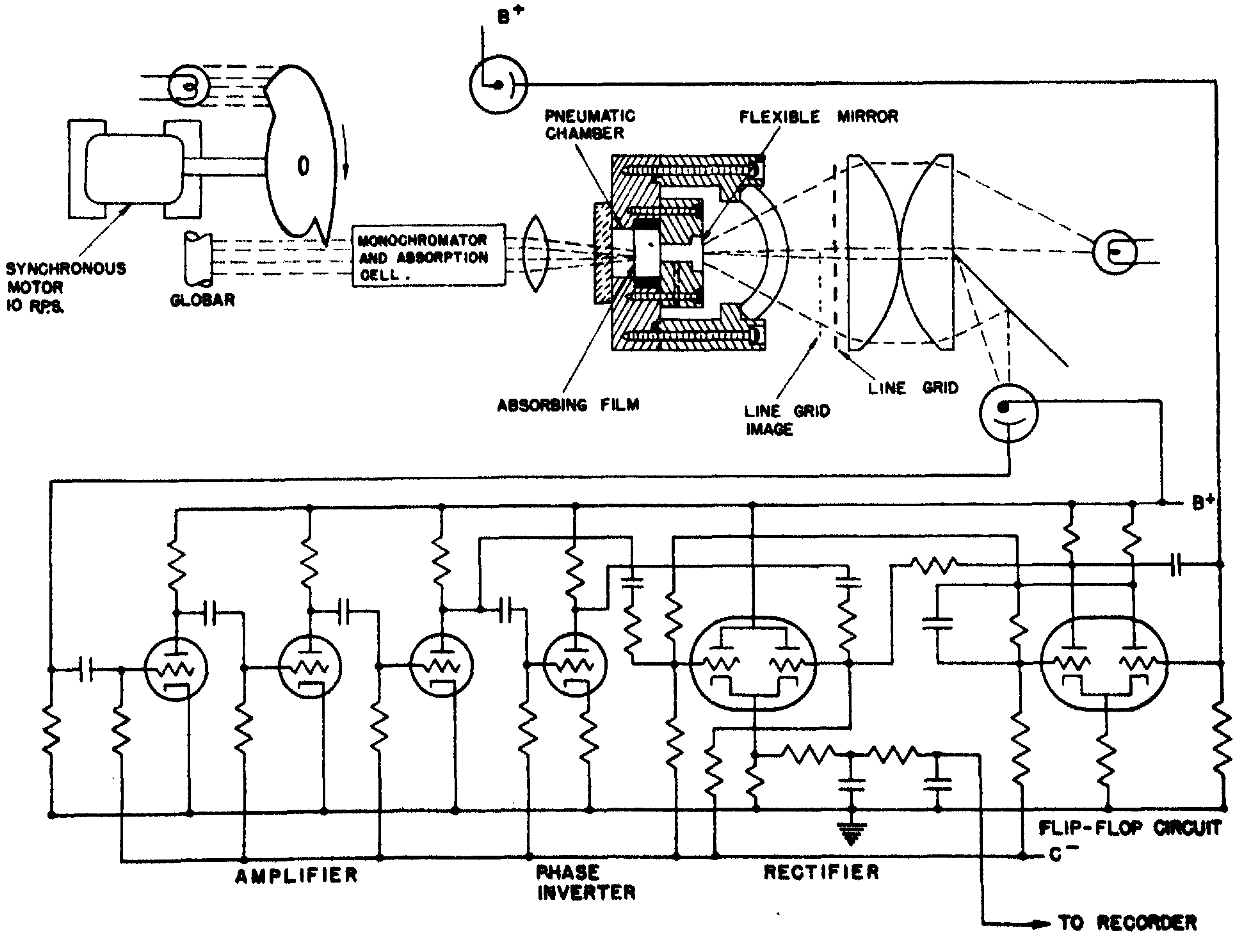

FIG. 1. Application of the pneumatic detector to I. R. spectrometry.

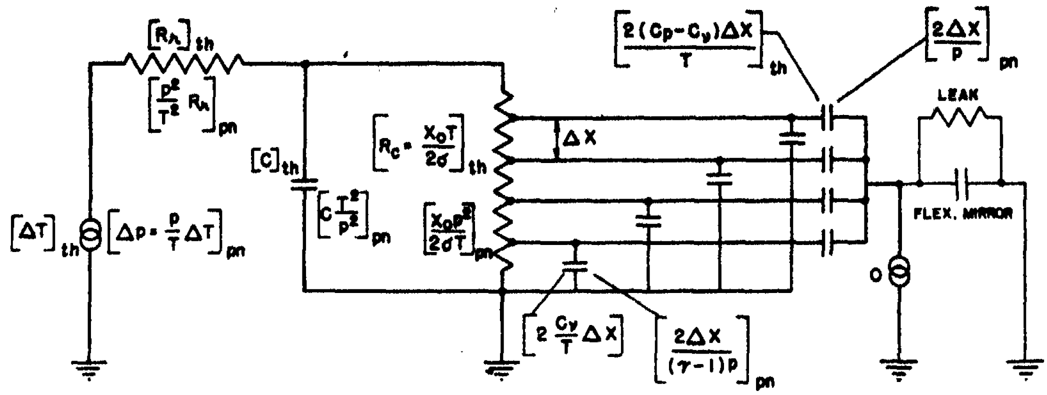

FIG. 2. Equivalent thermopneumatic circuit of a flat heat cell.

R_r—thermal radiation resistance between unit area of absorbing membrane and background, or heat resistance per unit area times absolute temperature (erg^{-1} cm^2 sec. T^2).

C—Thermal capacity per unit area of absorbing membrane, or heat capacity per unit area divided by absolute temperature (erg cm^{-2} T^{-2}).

c_p—Specific heat at constant pressure of unit volume of gas (erg cm^{-3} T^{-1}).

c_v—Specific heat at constant volume of unit volume of gas (erg cm^{-3} T^{-1}).

γ—Ratio of specific heats.

p—Gas pressure (erg cm^{-3}).

σ—Heat conductivity of gas (erg cm^{-1} sec.$^{-1}$ T^{-1}).

As an example of the qualitative use to which the circuit of Fig. 2 can be put, consider that the pneumatic impedance of the cell is measured by means of the device 0. At very low frequencies the impedance of the shunt resistance Rc will be negligibly small compared to the various capacities to ground $\Delta x/(\gamma-1)p$ and the capacity of the cell** will be $2x_0/p$, corresponding to isothermic compressions and expansions. Conversely, at very high frequencies the circuit to ground will be completed through the low impedance capacitive paths, and the capacity of the cell will be $2x_0/\gamma p$, corresponding to adiabatic compressions and expansions. Likewise, the effective thermal capacity of the gas elements distributed along Rc will be greater when 0 represents a straight shunt to ground, that is, when the cell is opened to the outside, than when 0 (and the flexible mirror), are disconnected, corresponding to a hermetically closed cell.

EFFICIENCY OF THE CELL

The thermal input to the cell is represented by the temperature differential ΔT in series with the radiative resistance R_r, and the available thermal power is given, in analogy to the electrical circuit, by the expression $\frac{1}{2}(\Delta T^2/R_r)$. The temperature differential ΔT will raise the pressure of the closed cell by an amount Δp_1. If the impedance of the cell, as measured by 0, is $R_{pn}+jX_{pn}$, the power derivable from the cell will be $\frac{1}{2}(\Delta p_1^2/R_{pn})$, since the imaginary lossless component of the impedance can be canceled by adding to the circuit another lossless element of opposite sign. The ratio of this last power to the former power will be the efficiency of the cell. As efficiency refers to energies while sensitivity refers to amplitude, the absolute sensitivity of the cell will be the square root of the efficiency.

It must be noted that considerations of thermal agitation need not be introduced in these calculations, for they are fully implied by the equivalent circuits. Thus, a temperature fluctuation, $\langle \Delta T^2\rangle_{Av}=4kTR_r\Delta f$ exists across any thermal resistance R_r; likewise, a pressure fluctuation $\langle \Delta p^2\rangle_{Av}=4kTR_{pn}\Delta f$ exists across any pneumatic resistance R_{pn}, and these expressions may be utilized to calculate the magnitude of the observable fluctuation. Conversely, the concepts of efficiency and absolute sensitivity are related to ratios of such fluctuations, and these ratios can be inferred directly from the circuit constants.

Since the amount of gas in the cell and, therefore, the value of the distributed capacity, are controllable, the values of these distributed capacities can be assumed to be so small as not to affect appreciably the time constant of the circuit which is then determined by R_r, R_c, and C.

The temperature differential ΔT_1 developed across R_c will therefore be equal to:

$$\Delta T_1=\frac{R_c}{R_r+R_c+jwR_rR_cC}\Delta T=\frac{1}{1+a+jb}, \tag{2}$$

where $a=R_r/R_c$ and $b=wR_rC$.

The pressure differential Δp_1 generated within the cell will be equal to the average temperature differential developed along R_c, $\frac{1}{2}\Delta T_1$, times p/T:

$$\Delta p_1=\frac{1}{2}\frac{1}{1+a+jb}\frac{\Delta Tp}{T}. \tag{3}$$

The determination of the cell impedance can be made by solving the differential equation relating the temperature distribution throughout the cell to the

---

** The expression "per unit area" is implied throughout.

flow of heat to or from the gas masses:

$$\sigma(d^2\Delta T/dx^2)=jw\Delta Q, \tag{4}$$

where ΔQ designates the quantity of heat delivered to a gas mass of unit volume.

The gas equation for a unit volume of gas undergoing small temperature and pressure fluctuations can be written:

$$(p+\Delta p)(1-\Delta\rho)=Ro(T+\Delta T), \tag{5}$$

where $\Delta\rho$ and Ro designate the fractional density change and the gas constant per unit volume, respectively.

The differential quantities involved in (5) are related by

$$\Delta p-p\Delta\rho=Ro\Delta T. \tag{6}$$

Furthermore, Ro and ΔQ satisfy the relations:

$$Ro=c_p-c_v \tag{7}$$

$$\Delta Q=c_v\Delta T-p\Delta\rho. \tag{8}$$

From (6)–(8) we obtain

$$\Delta Q=c_p\Delta T-\Delta p. \tag{9}$$

Substitution in (4) of this last expression for ΔQ yields

$$\sigma(d^2\Delta T/dx^2)=jwc_p\Delta T-jw\Delta p. \tag{10}$$

The general solution for ΔT:

$$\Delta T=A\sinh kx+B\cosh kx+(\Delta p/c_p) \tag{11}$$

where

$$k=(jwc_p/\sigma)^{\frac{1}{2}} \tag{12}$$

must satisfy the boundary conditions:

$$\Delta T=0 \quad \text{at} \quad x=x_0 \tag{13}$$

and

$$2\sigma(d\Delta T/dx)=\Delta T/Z \quad \text{at} \quad x=0, \tag{14}$$

where

$$1/Z=(T/R_r)+TjwC.$$

Solving for A and B we obtain

$$\Delta T=\frac{\Delta p}{c_p}\times\left[1-\frac{\sinh kx+\sinh k(x_0-x)+2k\sigma Z\cosh kx}{\sinh kx_0+2k\sigma Z\cosh kx_0}\right]. \tag{15}$$

Equations (5)–(7) and (15) give for $\Delta\rho$:

$$\Delta\rho=\frac{\Delta p}{p}-\frac{\Delta T}{T}=\frac{\Delta p}{\gamma p}\times\frac{\gamma-1}{\gamma}\frac{\Delta p}{p}\frac{\sinh kx+\sinh k(x_0-x)+2k\sigma Z\cosh kx}{k\sinh kx_0+2k^2\sigma Z\cosh kx_0}. \tag{16}$$

The volume of gas, Δv, introduced in the cavity as a result of the application of a pressure differential Δp, is given by the integral:

$$\Delta v=2\int_0^{+\infty}\Delta\rho dx=2x_0\frac{\Delta p}{\gamma p}+2\frac{\gamma-1}{\gamma}\frac{\Delta p}{p}\frac{2(\cosh kx_0-1)+2kZ\sinh kx_0}{k\sinh kx_0+2k^2\sigma Z\cosh kx_0}. \tag{17}$$

The capacitance of the cavity is equal to the ratio $\Delta v/\Delta p$ and is thus seen to consist of a fixed term $2x_0/\gamma p$ and of a variable and complex term. A plot of the real and imaginary components of this complex term can be found in Fig. 6 of reference 1.

The impedance $R_{pn}+jX_{pn}$ of the cavity is equal to the ratio:

$$R_{pn}+jX_{pn}=(\Delta p)/(jw\Delta v). \tag{18}$$

As we have seen above, the pressure of the gas can be made arbitrarily low, and the series development of $\sinh kx_0$ and $\cosh kx_0$ can be limited so as to introduce no terms containing powers of k higher than 4 in the numerator and in the denominator of the last fraction of (17). Carrying out these calculations yields for the second approximation of $R_{pn}+jX_{pn}$

$$\begin{aligned}R_{pn}+jX_{pn}&\cong\frac{p}{2jwx_0}+\frac{1}{24}p\left(1-\frac{1}{\gamma}\right)\frac{(c_pX_0/\sigma)+8c_pZ}{1+2(\sigma Z/x_0)}\\&\cong\frac{p}{2jwx_0}+\frac{p^2}{12T^2}\frac{R_c+4R_r+jwR_rR_cC}{1+(R_r/R_c)+jwR_rC}\\&\cong\frac{p}{2jwX_0}+\frac{p^2}{T^2}\frac{R_r}{12a}\frac{1+4a+jb}{1+a+jb}.\end{aligned} \tag{19}$$

When a thermal source causes a pressure differential Δp_1 within the closed cell, the available energy can be calculated as $\frac{1}{4}\Delta p_1^2/R_{pn}$. Recalling (3), the efficiency e of the cell can be calculated as:

$$e=\frac{\frac{1}{4}(\Delta T^2/R_2)}{\frac{1}{4}(\Delta p_1^2/R_{pn})}=\frac{3a}{(1+a)(1+4a)+b^2}. \tag{20}$$

Were the choice of a entirely at our disposal, this choice should be determined by the maximization of (20) which would give:

$$a=\tfrac{1}{2}(1+b^2)^{\frac{1}{2}}$$

and

$$e=3/[5+4(1+b^2)^{\frac{1}{2}}]. \tag{21}$$

DISCUSSION

The expression (21) given for e indicates that the efficiency of a flat pneumatic cell with walls forming a thermal ground can be as high as one-third, when b is negligibly small. This can be interpreted as meaning that the signal-to-noise ratio of a pneumatic infra-red detector embodying such a cell and having a perfectly absorbing central membrane has a ceiling equal to $1/\sqrt{3}=57$ percent of the signal-to-noise ratio of an ideal infra-red detector at room temperature.[***]

For spectrometric applications in which the chopped beam method is used, the parameter b is of the order of unity at 10 c.p.s., corresponding to a time constant, R_rC of the order of 0.02 sec. for the absorbing membrane in radiative equilibrium with its background. Thus an optimum value for a would be of the order of 0.7. Using one of the least conductive gases available, xenon, ($\sigma=0.000011$ cal. cm^{-1} sec.$^{-1}$ T^{-1}) this value of a would require a spacing of 0.09 in. between the radiation absorbing membrane and both walls of a flat cell.[****] As the thermal shunting effect of the side wall can be judged to become appreciable when the total depth of a round cell approaches its diameter, it can be expected that the ceiling of 57 percent of ultimate signal-to-noise ratio will be approached by cells which are 1 cm or more in diameter and which contain a black membrane.

Conversely, the expression for e is not critically dependent upon a for small departures from the optimum value. Round xenon-filled cells intended for spectrometric applications have been constructed, with a ¼-in. diameter and a 0.050-in. separation between the absorbing membrane and the infra-red window, the back portion of the cell being made hemispherical. Taking into account the thermal shunting effect of the walls, a value $a=2$ has been estimated for these cells, and taking $b=1$, the expression for e gives 6/28 or 0.46 for $(e)^{\frac{1}{2}}$.

It has been found experimentally that detectors with cells having the dimensions just indicated and a resistive radiation absorbing membrane have a r.m.s.e.n.i. of 5×10^{-11} watt, when utilized with the arrangement illustrated by Fig. 1. This r.m.s.e.n.i. was estimated from visual observation of the rectified output recorded by a Brown electronic recorder.

Estimating the value of Δf as 0.1 c.p.s. and the value of S as 7 mm^2 to allow for a narrow less sensitive portion near the edge of the cell, the value of $(\langle\Delta J^2\rangle_{Av})^{\frac{1}{2}}$ given by (1) is 5×10^{-12} watt. The order of magnitude difference between this and the observed value can be accounted for fairly well by the product of the following factors:

The theoretically expected fraction of ideal signal-to-noise ratio as determined above:	0.46
The estimated fraction of energy absorbed by a resistive sheet (theor. 68 percent when the back portion of the cell is perfectly reflecting):	0.65
The loss due to the use of the chopped beam method with utilization of the fundamental harmonic only (theor. $\sqrt{2}/\pi$):	0.45
The window reflection losses:	0.92
The product of all these factors is:	0.12

It may seem regrettable, at first glance, that the non-availability of gases having a lower heat conductivity than xenon does not permit the construction of efficient cells with a sensitive area having the shape and size of the image of the exit slit of a conventional infra-red monochromator. However, when the signal-to-noise ratio of the detector and the radiative output of the monochromator are at a premium, the multi-slit principle[2] can be used for the purpose of increasing the available infra-red radiative output of the monochromator without loss of resolving power, and the square or broadly rectangular bundle of radiation then obtained can fill fairly efficiently the sensitive area of a round cell.

[***] It will be recalled that the signal-to-noise ratio of an ideal detector at room temperature is limited by the radiation fluctuations *to* and *from* the detector, and that the elimination of the fluctuations of the *emitted* radiation of an ideal detector operating at absolute zero and viewing a thermal background at room temperature would increase its signal-to-noise ratio by the factor $\sqrt{2}$ over that of a room temperature device.

[****] It may be easily verified, and convenient to remember that the conductive heat interchange between two surfaces separated by a 0.03 in. thickness of xenon gas is equal to the radiative heat interchange between any black surface and its background. Hence, for $a=0.7$, the optimum half-thickness of a xenon-filled flat cell is calculated as 2(0.03/0.7) in.$\cong$0.09 in.

[2] Marcel J. E. Golay, J. Opt. Soc. Am. 39, 437 (1949).

THE REVIEW OF SCIENTIFIC INSTRUMENTS VOLUME 20, NUMBER 11 NOVEMBER, 1949

A Stark-Effect Microwave Spectrograph of High Sensitivity

K. B. McAfee, Jr., R. H. Hughes,* and E. Bright Wilson, Jr.**
Mallinckrodt Chemical Laboratory, Harvard University, Cambridge, Massachusetts

(Received June 2, 1949)

A microwave spectrograph is described in which the absorption of the gas being studied is modulated by the application of a periodic Stark-effect field so that the output of the crystal detector contains a radiofrequency component which can be amplified with a narrow-band amplifier. By using a very narrow bandwidth, achieved by employing phase-sensitive detection, high sensitivity is obtained. The klystron is swept mechanically over the frequency range. Details of the components are given.

INTRODUCTION

A NUMBER of investigators have described equipment for the study of the absorption spectra of gases in the centimeter wave-length region.[1] The earliest of these consisted of a klystron oscillator to supply the microwave energy, a wave guide section with mica windows (or a tuned cavity) to contain the gas, a crystal detector to rectify the ultra-high frequency radiation traversing the sample, and a low frequency or d.c. amplifier to amplify the rectified signal. The energy transmitted through the wave guide was measured as a function of frequency. Later most investigators have displayed the amplified voltage on the vertical plates of an oscilloscope while a saw-tooth voltage was used on the klystron reflector grid to sweep the tube over a narrow frequency range and was also used to sweep the oscilloscope spot horizontally. If a sufficiently strong and sharp absorption line of the gas occurs in the frequency region being covered, it will be seen as a pip on the oscilloscope trace. This arrangement has the advantage of simplicity, but it lacks the necessary sensitivity, unless additional refinements are introduced.

To provide greater sensitivity without losing in convenience, a system making use of the Stark effect to assist in the detection of weak absorptions has been described briefly.[2] It is the purpose of the present paper to describe in detail a more recent form of such a Stark effect spectrograph.

PRINCIPLE

The basic principle used is the modulation of the absorption of the gas at a low radiofrequency by the application of a square wave voltage to an electrode in the wave guide, thus creating a time-dependent, alternating Stark effect. This introduces a modulation of the microwave energy at a low radiofrequency in the vicinity of absorption lines. After rectification by a microwave crystal, the signal is amplified and detected by a narrow-band radio receiver or by a tuned radio frequency amplifier followed by a phase-sensitive detector, and applied to the vertical plates of an oscilloscope. The horizontal plates of the oscilloscope are swept by part of the saw-tooth voltage sweeping the reflector grid of the klystron. For the highest sensitivity a pen and ink recorder is used together with an amplifying and detecting system with a very narrow band width, the frequency being swept by a mechanical drive on the klystron. The spectrum observed is considerably more complicated than that given by the simpler spectrograph, but, on the other hand, correspondingly more information is displayed. Figure 1 gives the block diagram for the Stark-effect detection scheme.

CONSTRUCTION

In this section the construction of one spectrograph of the Stark-effect modulation type will be described in some detail. Alternate arrangements which have been found useful are given in the last section. The electronic apparatus generating the microwave energy is quite conventional. A QK33, *K*-band tube, operated by a TVN-8 power supply is used. A few percent change of

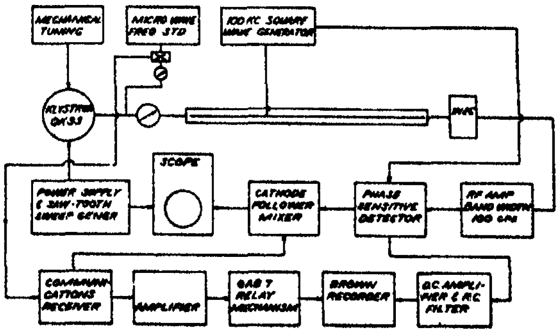

FIG. 1. Narrow band Stark effect spectrograph.

---

* Now at the Westinghouse Research Laboratory, East Pittsburgh, Pennsylvania.

** The research reported in this document was made possible through support extended Harvard University by the Navy Department (Office of Naval Research), under Office of Naval Research contract N5ori-76, T. O. V.

[1] B. Bleaney and R. P. Penrose, Proc. Roy. Soc. 189A, 358 (1947). R. Beringer, Phys. Rev. 70, 53 (1946). W. D. Hershberger, J. App. Phys. 17, 495 (1946). W. E. Good, Phys. Rev. 70, 213 (1946). C. H. Townes, Phys. Rev. 70, 665 (1946). W. Gordy and M. Kessler, Phys. Rev. 71, 640 (1947). Other types of spectrographs have been described by: G. E. Becker and S. H. Autler, Phys. Rev. 70, 300 (1946). Roberts, Beers, and Hill, Phys. Rev. 70, 112(A) (1946). C. K. Jen, Phys. Rev. 72, 986 (1947). W. Gordy and M. Kessler, Phys. Rev. 72, 644 (1947). R. J. Watts and D. Williams, Phys. Rev. 72, 1122 (1947). W. Gordy, Rev. Mod. Phys. 20, 668 (1948).

[2] R. H. Hughes and E. Bright Wilson, Jr., Phys. Rev. 71, 562 (1947). W. Low and C. H. Townes, Phys. Rev. 75, 529 (1949) briefly describe a recording Stark-effect spectrograph making use of phase-sensitive detection, mechanical sweeping and frequency markers.

frequency is accomplished by turning the tuning knob on the tube. By releasing the tuning set screw, a much larger range can be covered, usually from around 20,500 to 26,000 mc. Unfortunately, tubes are sometimes ruined on releasing this screw because of the development of internal short-circuits. A QK140 tube is used from 26,000 to 30,000 mc. Other tubes can be obtained to cover a wider frequency range. A saw-tooth voltage sweeps the tube over a mode which varies from around 5 to 50 mc in width.

Since components of the modulation frequency in the case of electronic sweeping are much too high to pass the narrowest filter, when it is used, tuning is accomplished by means of an electric motor connected mechanically to the ordinary tuning knob of the klystron. The arrangement consists of a 110 volt d.c. motor geared down 3600/1 driving the tuning shaft by means of a flexible coupling shaft. This allows sweeps as low as 0.1 mc/sec. to be employed. Brush contact noise will very likely produce interference unless precautions are taken to shield the receiver or to decrease the brush discharge. In addition, the klystron must be mechanically isolated from the driving motor.

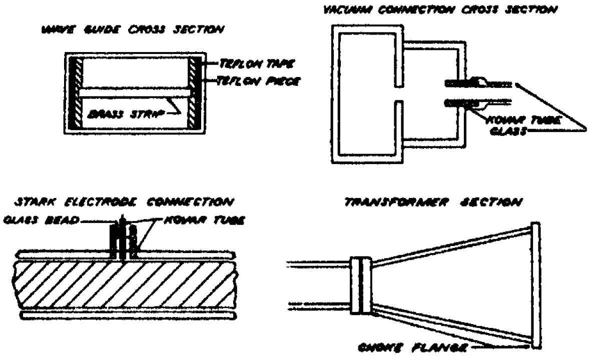

FIG. 2. Detail of wave guide cross section.

Absorption Cell

The absorption cell for the gas, which is the wave guide with the Stark electrode, consists of an X-band wave guide with outside dimensions $1\times\frac{1}{2}$ inches with an electrode installed in the center. See Fig. 2. The type of electrode which has been customarily used consists of a flat strip of brass parallel to the broad side of the wave guide, dividing the guide into two equal parts. The strip is a piece of flat soft brass 0.800 inches wide and 0.032 inches thick with a length almost that of the guide, which is 10 feet long. Pieces of Teflon, a plastic of low electrical loss and considerable chemical inertness, 0.394 inches by 0.0625 inches, 1 foot long, were provided with a groove 0.032 inches wide and 0.034 inches deep along the center of one face. The accuracy of the milling should be such that the central electrode is within 0.002 cm of the center of the wave guide. This groove was produced by completely enclosing the Teflon strip in a metal jig, the top of which has a slot through which the circular cutting tool may machine the groove. These pieces were placed along the narrow sides of the guide to hold the electrodes in place. In order to prevent arcing between the joints of these pieces, a continuous length of Teflon tape 0.394 inches wide and 0.020 inches thick was inserted between the pieces and the wall of the wave guide. As lengths of Teflon tape as long as the wave guide and 0.0625 inches thick are now available, a simpler construction could be employed by means of a single supporting Teflon strip. The electrical connection to the brass electrode was made by a wire soldered to its edge at one end and then passing through a small Kovar tube supported in a Kovar side tube by a glass bead. The details of this connection are shown in Fig. 2. A vacuum connection through a metal-to-glass Kovar seal was soldered to the broad side of the wave guide as shown in the figure. The opening through the guide was in the form of a slot 0.0625 inches by 3.75 inches. The ends of the cell were made gas tight with windows of mica sealed onto the flanges with a low-melting wax. Transformer sections as shown in Fig. 2 are needed in order to connect the X-guide to the normal K-band guide used for the rest of the microwave circuit. A K-band wave guide of the same general construction as that of the X-wave guide described above, has also been successfully used. The X-guide has the advantage of allowing lower pressures or higher powers to be used without encountering saturation effects, but has the disadvantage that a higher Stark voltage is necessary in order to secure the same potential gradient in the gas.

Detection System

After passage through the cell, the microwave energy is rectified by a 1N26 crystal using either a tuned or untuned crystal holder. The tuned one will increase the output over a small frequency range without retuning, but may decrease it for frequencies farther away. A microammeter is used to give a measure of the average current through the crystal and serves as a means of monitoring the power passing through the absorption wave guide. The signal strength depends roughly on the first power of this current. The microammeter is connected in series with a high impedance r.f. choke across the crystal output terminals. The crystal output is fed into a tuned 100,000 cycle amplifier[3] with a band width of about 100 cycles and a voltage gain of about a million. The 100 cycle band width prevents overloading the system with noise. The amplified signal is then rectified by a phase-sensitive detector locked to the 100 kc sine wave taken from the square-wave generator through the phase-adjusting circuit. A schematic diagram for the phase sensitive detector[4] is shown in Fig. 3. The time constant of the phase-sensitive detector is approximately 1 cycle per second. This output is recorded by a Brown Recording Potentiometer (Model No. 153x12v-x-9).

---

[3] Terman, *Radio Engineering* (McGraw-Hill Book Company, Inc., New York, 1947), p. 338 ff.

[4] Our circuit is a modification of M.I.T. Radiation Laboratory, Drawing No. B-14292-A, "Lock-in 30 cycle amplifier."

Although the pen and ink system with the narrow band width provides the highest sensitivity, it is more convenient when possible to operate at lower sensitivity with the 100 kc amplifier alone, without detection.

Square-Wave Generator

The interpretation of the spectra is much simpler when a square wave rather than when a sine wave is applied to the Stark electrode.[5] The square wave generator should be capable of providing a signal of appropriate frequency with a voltage adjustable from a few volts to about 1000 volts. Its power rating should be sufficient to permit it to feed the capacity of the wave guide which is of the order of 60 mmf per foot for the K-guide or 50 mmf per foot for the X-guide. The wave form should be of quite high quality if broadening of the lines is to be avoided. It is particularly convenient if this generator can be built so that it is automatically zero based; in other words, so that the voltage applied to the wave guide is zero for half the cycle and of high positive voltage for the other half. A complete unit was built starting with a hundred kc crystal oscillator, suitable amplifier, and switching stages to enable voltages up to 1500 to be applied to the guide. A detailed description of this square-wave generator is published separately.[6]

OPERATION

In order to make the adjustments for optimum power, a unidirectional coupler in the main line takes some energy which is rectified, amplified by a Ballantine meter used as an amplifier, and observed on the Y axis of an oscilloscope, the X axis being fed by the saw-tooth voltage. A variable attenuator should be inserted before the crystal to facilitate adjustment. The mode should be a half-circle without any sharp discontinuities except at the ends. As sufficient sensitivity for searching for lines and adjusting the equipment can sometimes be obtained by observing the amplitude of the envelope of the output of the 100 kc amplifier on the oscilloscope, not using the phase-sensitive detector and recorder, the operation of this part of the equipment is discussed first. The voltage on the reflector grid is varied until a mode is found and then a small adjustment is made so that the mode is symmetric about the center of the oscilloscope. Tuning of the plunger in the end of the

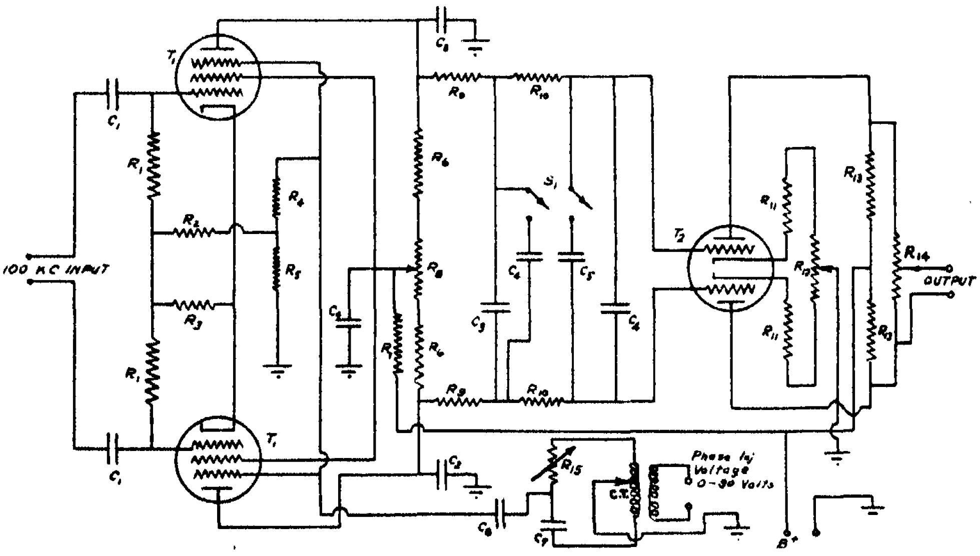

FIG. 3. Modified phase-sensitive detector.

C_1	0.0005 µf
C_2	1.0 µf
C_3	0.01 µf
C_4	0.1 µf
C_5	0.5 µf
C_6	0.0005 µf
C_7	0.00005 µf
T_1	5693 or 6SJ7
T_2	5692 or 6SN7

R_1	2 Meg Ω
R_2	1500 Ω
R_3	600 Ω
R_4	2 Meg Ω
R_5	10000 Ω
R_6	30000 Ω
R_7	20000 Ω
R_8	25000 Ω var.
R_9	0.5 Meg Ω
R_{10}	2 Meg Ω
R_{11}	4000 Ω
R_{12}	2000 Ω var. pot.
R_{13}	10000 Ω
R_{14}	50 Ω var. pot.
R_{15}	1 Meg Ω var. pot.

---

[5] The use of a square wave was suggested by Dr. Robert Karplus who designed and built the first generator used. B. P. Dailey Phys. Rev. 72, 84 (1947).

[6] L. C. Hedrick, Rev. Sci. Inst. 20, 781 (1949).

QK33 may increase the power output and also improve the mode shape. Sharp discontinuities in the mode give a signal which is displayed on the spectrum oscilloscope as a sharp pip. Although these signals can be seen not to be lines from their shape, they cause the scope trace to be very unstable and in many cases prevent observation of a true line. Discontinuities in the center of the mode are frequently caused by insufficient isolation of the tube from the Stark-effect guide. This is remedied by increasing the attenuation of the attenuator between the two. The discontinuities at the end of the mode are removed by decreasing the sweep voltage so that the complete mode is not quite covered.

When searching for weak lines for which the frequencies are not known, the order of the magnitude of the modulating square-wave voltage is important. A voltage should be chosen which will move the strongest Stark components about one line width. In general, a much higher voltage should be used if the substance shows a second-order Stark effect than if it shows a first-order Stark effect. Voltages from 1 to 10 volts are usually used with first-order effects whereas from 50 up to 1500 volts are used with second-order Stark effects.

The gas to be studied should be introduced into the cell at from 0.01–0.1 mm Hg pressure. If the pressure is too high, the line breadth will be so great that the available Stark effect voltage will be insufficient to separate the Stark components from the main line and the intensity will, therefore, be low. If the pressure is too low, saturation may occur, again reducing the intensity. Also, at low pressures the lines may be so narrow that frequency instability becomes a serious difficulty in connection with the pen recorder.

Difficulty may be experienced with the adsorption of the sample in the wave guide. If impure samples are used, the desired substance may be adsorbed to a large extent and the lines broadened by the impurity. The sample may have to be replaced often because of exchange of gas between the sample and the insulation.

When high sensitivity is required, for example to resolve a weak line viewed on the oscilloscope, the electronic sweeping is removed and the Brown recorder and phase-sensitive detector connected. Balancing controls then place the recording pen in the desired zero-signal position on the chart. Band width controls on the r.c. filter then select the desired band width while the speed of mechanical sweeping is adjusted so that the highest frequencies of modulation (depending upon anticipated line-widths) fall mainly within the pass band. Attenuation is carefully selected by adjusting the input to the Brown recorder since more gain can be employed with the recorder than with the oscillograph on account of the greatly inproved signal-to-noise ratio of the former system. If the purpose of high sensitivity is searching over a wide frequency range for weak absorptions, as much as 300 or more megacycles may be covered by first adjusting the power output over the range. When controls are set, operation is fully automatic, frequency pips being recorded every 2.5 megacycles. If ammonia has ever been present in the guide, it will probably be found that the lines previously concealed below the noise level will provide a very objectionable background on the chart. Considerably broadened, they may occupy a sizeable portion of the spectrum unless a method is found to reduce their intensity.

MEASUREMENT OF FREQUENCY

A K-band wave meter, either type TFK-6 or type TFK-2, can be inserted in the mode-monitoring side line, or in a separate one, for frequency measurements. If a tuned crystal holder is used, the plunger may be removed and a TFK-2 reflection-type wave meter connected to the end. The wave meter will then react giving a pip when the meter is in resonance. Two readings, one half-wave apart, are taken and by using the difference, the frequency is found in the calibration table. If the wave meter does not react strongly enough or if the pip is too broad, it may be desirable to use a transmission wave meter, TFK-6, before the crystal. Accurate frequency measurements may be made with the aid of a microwave frequency standard. Several of these have been described.[7] In our case a 5 megacycle crystal-controlled oscillator is employed as the basic standard, checked frequently against WWV. A chain of frequency multiplier units raises the frequency successively to 25, 125, and 675 megacycles, the last stage consisting of a pair of 2C40 tubes in push-pull. The 675 megacycles signal is carried by a cable to a crystal in a side branch where it is mixed with a portion of the main microwave signal. The beat frequency is amplified by a radio receiver (frequency range 1 to 42 mc) whose output is introduced into a cathode-follower mixer stage along with the output of the main signal amplifier so that sharp spikes are introduced onto the cathode-ray screen, superimposed on the spectral lines. Switches are arranged so that 5 and 25 megacycles can also be mixed on the crystal.

When the Brown recorder is to be used, frequency markers are placed on the side of the chart by means of a small d.c. relay to which a ball-point pen unit is attached. The relay is actuated by means of a plate circuit relay in the plate of a 6AB7 tube whose grid is controlled by the sharp frequency pips amplified by a Ballantine voltmeter. Thus a small ink mark appears upon the chart when the frequency difference of the klystron oscillator and a multiple of the frequency standard is equal to the receiver frequency setting. Another method which can be used is the actuation of the relay by means of a micro-switch controlled by the operator who views the frequency pips on the scope or listens to the output of the radio receiver.

---

[7] Strandberg, Kyhl, Wentink, and Hillger, Phys. Rev. 71, 326 (1947). W. E. Good and D. K. Coles, Phys. Rev. 71, 383 (1947). Robert Unterberger and W. V. Smith, Rev. Sci. Inst. 19, 580 (1948).

INTERPRETATION OF OSCILLOSCOPE PATTERN OR RECORDING TRACE

While it is experimentally simplest to use a sine-wave voltage on the Stark-effect electrode, the interpretation of the results is clearer and easier if a square-wave voltage is employed. Suppose the klystron to be swept over the small frequency range in the vicinity of an absorption line of the gas, and that a square wave voltage of say 100 kc is applied to the electrode in the wave guide in such a way that the voltage is zero for half of each cycle and has some positive value for the other half. During the zero-voltage half of the cycle the gas absorbs some of the microwave energy (usually less than 0.1 percent) at the frequency of the line. During the other half of the cycle, the absorption line is broadened, split, or displaced because of the Stark effect.[8] The absorption during the second-half of the cycle at the stated microwave frequency is, therefore, reduced. Consequently, a small fraction of the microwave energy at the original line frequency reaching the crystal detector is modulated at the frequency of the square wave. This modulated portion only is amplified and displayed on the oscilloscope screen or fed through the phase-sensitive detector and used as the input voltage to the recording potentiometer. Thus an absorption line on the oscilloscope or a similar displacement on the pen and ink recording is observed when the frequency of the klystron corresponds to the frequency of the absorption line.

On the other hand, when the microwave frequency coincides with that of the Stark components, modulation will correspondingly occur again, this time with opposite phase, i.e., the greatest absorption will occur when the Stark voltage is positive, none when the voltage is zero. Therefore, both unsplit lines and their displaced Stark components will be recorded. In the case of the oscilloscope pattern both the displaced and undisplaced lines will appear as similar pips while due to its ability to differentiate between the two phases, the phase-sensitive detector recording will show displaced and undisplaced components having opposite sense (see Fig. 4). As the 100 kc signal is proportional to the difference between the absorptions on the two halves of the modulation cycle, the intensities of both undisplaced lines and Stark components will be decreased, sometimes even to zero, when Stark components overlap the undisplaced line. Figure 4 shows the decrease in intensity due to the overlapping of Stark components and undisplaced line. It can be seen that as the Stark square-wave voltage is increased the Stark components spread out from the undisplaced line.

PERFORMANCE

The absolute sensitivity of the apparatus has been estimated by studying the various isotopic species of carbonyl sulphide. At room temperature a line due to $O^{18}C^{12}S^{34}$ has been found at 22,239.93 MC.* This should have a peak absorption coefficient of 4.5×10^{-9} cm^{-1}, based on the natural abundance of this isotope and the reported[9] peak absorption of $5.4\pm0.9\times10^{-5}$ cm^{-1} for the $J=1\rightarrow2$ transition of the principal isotopic species. Therefore, considering signal/noise ratios, it appears that this apparatus should be able to detect absorption coefficients as small as 2×10^{-9}. Without the phase sensitive detector and 1 cycle per second band width, lines can be detected with an absorption coefficient of approximately 10^{-8} per cm, using a band width of about 200 cycles.

The ultimate sensitivity of the spectrograph depends upon the frequency stability of the microwave frequency source, providing the balanced d.c. amplifier is sufficiently free from fluctuations in voltage output. Thus spurious frequency excursions of the microwave source when the source is mechanically tuned to the frequency of the absorbing line give rise to effects similar to ordinary noise in the very low frequency portion of the spectrum.

The sensitivity depends on the power transmitted through the absorption guide, the length of the absorption path, the frequency of the Stark modulation, the adjustment of the crystal and its inherent sensitivity, the band width of the amplifying system, and the noise level arising from the klystron, crystal, amplifier, and external sources. Increasing the power ultimately causes saturation in the gas. Lengthening the guide decreases the power reaching the crystal because of wall losses, etc. (Special designs of wave guide have been suggested which would permit quite long guides to be used and high power levels).[10] Increasing the frequency of modulation decreases the crystal noise (per unit band width) but ultimately causes broadening of the lines.[11] The question of the optimum values of the above vari-

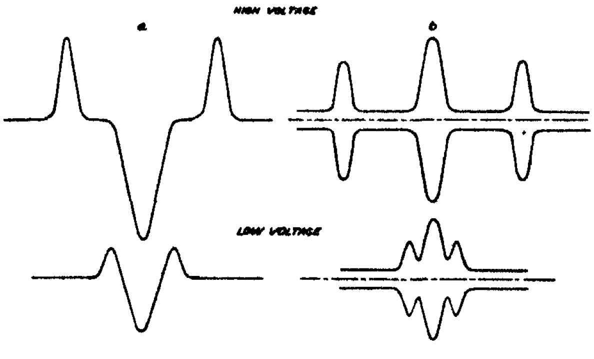

FIG. 4. (a) Recording trace of OCS transition $J-1$, $J-2$. Phase-sensitive detection separates Stark components (above axis) from undisplaced line (below axis). (b) Oscilloscope trace of same transition using T. R. F. receiver.

---

[8] Dakin, Good, and Coles, Phys. Rev. 70, 560 (1946).

* This absorption line has recently been reported by Bianco, Matlack, and Roberts, Phys. Rev. 76, 473 (1949) for enriched samples.

[9] Townes, Holden, and Merritt, Phys. Rev. 74, 1113 (1948).

[10] (a) W. D. Hershberger, J. App. Phys. 19, 411 (1948). (b) W. Gordy, Rev. Mod. Phys. 20, 668 (1948).

[11] (a) C. H. Townes and F. R. Merritt, Phys. Rev. 72, 1266 (1947). (b) R. Karplus, Phys. Rev. 73, 1027 (1948).

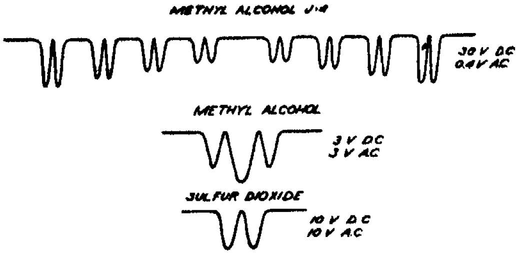

FIG. 5. Sine wave modulation.

ables and the ultimate possible sensitivity have been discussed by several authors.[10,12]

The line breadth and resolving power obtainable is limited by the gas pressure employed, the onset of saturation, the modulation frequency and ultimately by the Doppler effect.[10b] With X-guide and 100 kc modulation it has been possible to resolve lines 300 kc apart but doubtless better resolution can be obtained.

ALTERNATIVE ARRANGEMENTS

Besides the specific set-up described above, several spectrographs have been employed using certain modifications.

Use of Radio Receiver. The 100 kc amplifier can be replaced by a high quality communications receiver, such as a National HRO, Model 5TA1. Its crystal filter provides a narrow band width suitable for electronic sweeping and display of the output (taken from the second-detector of the receiver) on a cathode-ray oscilloscope. The receiver must have low noise characteristics.

Use of other Modulation Frequencies. The choice of 100 kc represents a compromise convenient for many purposes but use of frequencies as low as 6 kc and as high as 1 MC have been reported.[10,11a] The sensitivity increases with increased frequency but so does the minimum line breadth.

Use of Sine Wave Modulation. The Stark effect voltage used on the first spectrograph was a sine wave of from 50 to 100 kc. A 10 foot K-band wave guide has a capacity of around 600 mmf so that the guide has an impedance of around 2,000 ohms. By resonating the guide with a high Q coil, in parallel, the impedance to be driven by the sine wave generator is raised to around 200,000 ohms. It is much easier to apply a high voltage by sine wave than it is by square wave because the guide cannot be resonated when using square waves. The impedance for square waves is in the hundreds of ohms for the higher frequency components. Arrangements must be made to apply a d.c. voltage to the electrode also by means of an isolating resistor or choke.

The line shapes observed with sine-wave modulation are in general more complicated than those obtained with square-wave modulation. When high d.c. voltages, great enough to split a line into its components, and small a.c. voltages, just enough to move a component a fraction of its line width, are used, a pattern such as that in Fig. 5a is obtained.[13] Simple theory using a Taylor expansion shows that the first derivative of the line shape should appear for each component. Because the radio receiver is not phase sensitive, the double peaks are seen for each component. The linear Stark effect for this alcohol line gives rise to components which are equally spaced and symmetrically located about the line center frequency. At low a.c. and d.c. voltages, both small enough to deflect a first-order line a small fraction of its width, the second derivative of the line shape is seen as in Fig. 5b. The side lobes are inverted because the receiver is not phase sensitive. For lines with second-order Stark effect, the first derivative of the line shape is seen at low voltages as seen in Fig. 5c. When a.c. voltages large enough to move a component more than a line width are used, the spectrum observed from a single line with sine-wave modulation is very hard to interpret. As many as five or six separate pips have been obtained for the 3,3 transition in ammonia.

Wire Guide. This type of Stark effect guide has a simple wire down the center instead of the brass strip.[14] The model built by us contained a wire supported at both ends in a five foot guide. Some difficulty was experienced in keeping the wire from shorting on the sides of the guide. This type probably requires a square wave with one side at zero to give a good signal but no other modulation was tried. With ammonia and sulphur dioxide, the spectrum of a line consisted of a main line with a Stark effect line adjacent. The component line tapered out towards the high frequency range rather gradually, being several times as wide as the usual line so that it could not be confused with one. Because of the non-uniformity of the field, no components could be seen at large frequency differences from the undisturbed line as is possible with the strip guide. The picture was much simpler in this respect. It took two or three times as much voltage to get the same sensitivity in the wire guide as in the strip guide presumably because the non-uniform field has a low average value over the guide cross section. Because of the simplicity of the guide, the simplicity of the pattern, and the ease of evacuating it, a wire guide might be very useful for locating lines but not good for splitting lines into their components.

ACKNOWLEDGMENT

The experience of a number of investigators has been incorporated in the final apparatus described here. Mr. L. C. Hedrick designed and built the frequency standard, some of the power supplies, and the square wave generator. We should like to acknowledge particularly the assistance of Dr. B. P. Dailey, Mr. Robert Karplus, Mr. J. H. Goldstein, Mr. D. H. Baird, and Mr. A. A. Westenberg.

---

[12] C. H. Townes and S. Geschwind, J. App. Phys. **19**, 795 (1948).

[13] D. K. Coles, Phys. Rev. **74**, 1194 (1948).

[14] R. J. Watts and D. Williams, Phys. Rev. **72**, 980 (1947).

THE REVIEW OF SCIENTIFIC INSTRUMENTS VOLUME 20, NUMBER 11 NOVEMBER, 1949

Physical Instruments for the Biologist

Detlev W. Bronk
Associate Editor in Charge of this Section
Eldridge Reeves Johnson Foundation for Research in Medical Physics,
University of Pennsylvania, Philadelphia, Pennsylvania

A Double Pulse Constant Current Stimulator*

Robert L. Schoenfeld**

Department of Neurology, College of Physicians and Surgeons, Columbia University, New York
and
Electroencephalography Laboratories of the Neurological Institute of New York, New York

(Received May 14, 1949)

A double pulse stimulator for clinical use in testing refractory time periods of peripheral nerve and muscle is described. Two rectangular stimuli of variable width, time separation, and intensity are delivered from a high impedance source to the same pair of stimulating electrodes. Provision is made for initiating the horizontal sweep of a cathode-ray oscilloscope in synchrony with the stimuli. Action potentials produced may be picked up, suitably amplified and recorded on the vertical axis of the oscilloscope. The time interval between the stimuli at which the tissue is refractory may be observed as the distance between stimulus artefacts on the cathode-ray screen.

INTRODUCTION

In routine clinical testing of nerve and muscle, the response to a single stimulus—"twitch" or that to a maintained series of repetitive stimuli is used, the latter in order to produce a "tetanic" response which is similar to natural sustained movement. Following a single maximal stimulus a nerve or muscle is inexcitable for a measurable period of time, called the refractory period. This time is measured by subjecting nerve or muscle to two discrete stimuli, maximal or supramaximal and separated by a variable time interval.

The recovery of excitability may be measured by changes in magnitude of action potentials evoked by the stimuli. During the absolute refractory period, no action potential will be elicited by the second stimulus. As the time separation of the stimuli is increased, a second action potential will appear and increase in amplitude. These responses are amplified and recorded on the screen of a cathode-ray oscilloscope in synchrony with the stimuli so that the refractory properties of mammalian nerve and muscle may be tested (Fig. 1).

In order to provide for variable tissue impedances encountered with skin or needle electrodes, a constant current stimulator is required. The optimal stimulating wave form is a rectangular pulse of adjustable intensity and duration. The rectangular wave form facilitates comparison of test results in different clinical conditions. The intensity of the stimulus may be measured with a milliammeter at the longer pulse durations. The time interval between stimuli and their duration are determined with a timing oscillator used to calibrate the horizontal sweep of the oscilloscope.

THE STIMULATOR

The instrument, boxed in, is shown in the block diagram (Fig. 2). The horizontal sweep of the oscilloscope and the stimulator are triggered simultaneously by an external key. The keying voltage is differentiated to initiate the sweep and coupled directly through cathode followers to the delayer stages in both channels. The delayers provide a time delay between the start of the sweep and each of the stimuli. The output of the delayers, a step voltage similar to that produced by the key, is differentiated to trigger the pulse stages each of

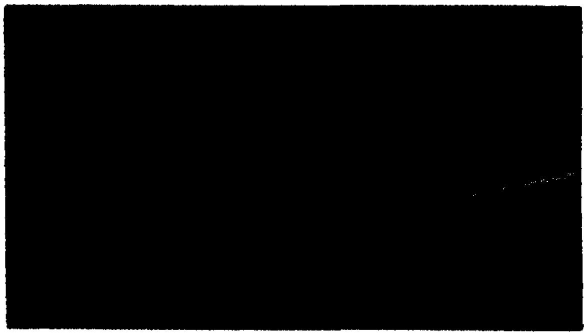

Fig. 1. Two successive muscle action potentials recorded from the frog's gastrocnemius, elicited in response to stimulation of the sciatic nerve. The stimulus artefacts precede each action potential. Time scale is approximately 40 milliseconds for full screen deflection. The refractory period for frog nerve is in the neighborhood of one millisecond.

---

* This paper is an abridgment of a thesis submitted in partial fulfillment of the requirements for the Degree of Master of Electrical Engineering at the Polytechnic Institute of Brooklyn, September 1948.

** The author wishes to express his appreciation to Dr. Paul F. A. Hoefer of the Neurological Institute for suggesting the problem and for elucidating the physiological applications.

which produces a rectangular pulse of adjustable duration. In the final stages, which act as high impedance sources, the pulses from each channel are mixed and coupled to the subject at the desired current intensity.

The key may be manual or a slow, free-running multivibrator giving a voltage excursion of from zero to +300 volts. The recording oscilloscope must have an externally driven single sweep. The delay time required, determined by the setting of the delayer (Fig. 3), is from 0–10 milliseconds to include normal as well as abnormal refractory time periods for mammalian nerves and muscles. The pulse duration, set in the pulse stages (Fig. 4), varies from 0.0001–3.0000 seconds with the longer pulses used for metering current intensity and for chronaxie determinations. The stimulating electrodes in the output of the final stages are maintained at ground potential between stimuli. Consequently, the two channels may be tied together and the stimuli applied successively through the same electrodes. The action potentials produced are suitably detected and recorded. The desired time relations may be determined from the separation of the stimulus artefacts on the cathode-ray screen.

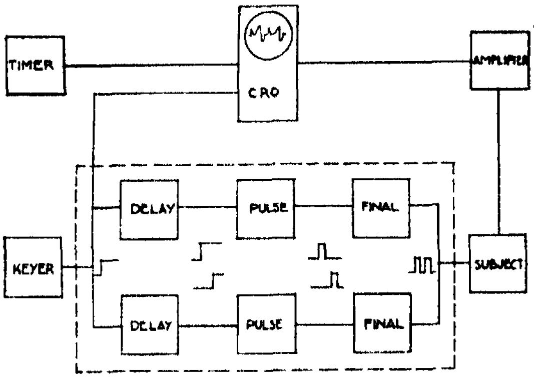

FIG. 2. Block diagram of stimulator and recording equipment.

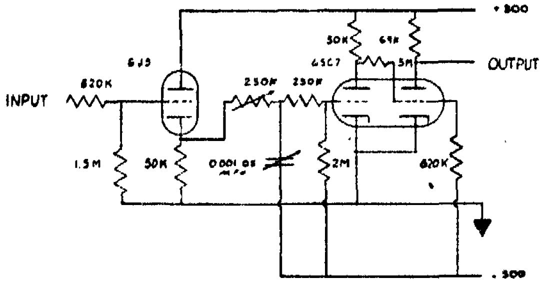

FIG. 3. Delay stage; tubes T_1, T_2, T_3 from left to right.

CIRCUIT DETAILS

In the delayer stage, modified from Toennies',[1] the two sections of the 6SC7 make up a bi-stable multivibrator (Fig. 3). Tube T_3 is saturated; tube T_2 is cut-off. The grid voltage of T_2 is maintained negative by the resistance divider in parallel with a condenser returned to −300. When the key is closed, the output voltage of the cathode follower rises to +200 volts. The grid voltage of T_2 begins to rise steeply as the condenser charges through the variable resistor. When T_2 conducts, its plate swings negative, driving the grid of tube T_3 rapidly below cut-off. Thus the keying voltage is reproduced at the plate of T_3 with a time delay determined by the setting of the variable resistance and capacity. When the key is released the tubes recycle to their original status, producing a negative swing at the plate of T_3, but this transition does not activate the following stages.

The pulse stages consist of two tubes arranged as a monostable multivibrator. Tube T_5 is conducting; tube T_4 is cut-off. The positive step from the delayer is differentiated providing a triggering voltage for the tubes to exchange limiting conditions. T_5 is cut-off until the condenser from the screen of T_4 to the grid of T_5 is charged. The grid resistor of T_4 is brought back to the common cathode facilitating a return to the initial stable state.

The use of a pentode for the normally quiescent tube enhances stability. The pulse width is adjusted by varying the coupling condenser and resistor in the grid of T_5. The output wave at the plate of T_5 is a positive pulse with good leading and trailing edges. The circuit is grounded at the plates and returned to the −300 supply for ease in coupling to the final stage.

The final stages, modified from Golseth's,[2] couple the stimuli to the subject and provide for control of stimulus strength (Fig. 5). Tube T_7 is a power pentode cathode follower designed to conduct heavily. Tube T_6 is cut off by the bias developed in the common cathode resistor as a result of the current through T_7. The signal from the pulse stage is directly coupled to the grid of T_6 causing this tube to conduct for the duration of the signal. A portion of the negative swing in screen voltage of this tube is directly coupled to the grid of T_7. Consequently, the current in T_7 decreases to the

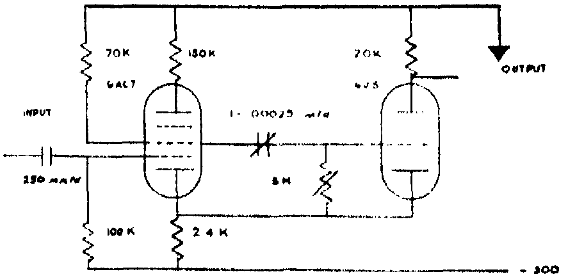

FIG. 4. Pulse stage; tubes T_4 and T_5 from left to right.

---

[1] J. F. Toennies (unpublished). Used in stimulators developed at the Rockefeller Institute of Medical Research in 1935.

[2] Mayfield, Oester, and Dillon, "Electrodiagnosis-examination of peripheral lesions by percutaneous stimulation of muscle," Percy Jones Hospital Center, Fort Custer, Michigan (1945).

extent that current flows in T_6. As a result, there is no net change in current and no degeneration in the common cathode resistor when the coupling between the screen of T_6 and the grid of T_7 is properly adjusted. The stimulating current intensity through the electrodes in series with the plate of T_6 is then determined by the input potentiometer setting which may be varied to give from 0–10 milliamperes in the output.

The plates of the final stages in both channels are joined since the output tubes are cut-off in the absence of a stimulus. The electrodes are thus initially at ground potential. The successive stimuli are independently formed in separate channels without intercoupling and pass through the same pair of electrodes with the desired time separation, pulse width, and current intensity.

PERFORMANCE

The output current remains constant for interelectrode impedances from 0–25 thousand ohms with a 20 percent decrease in intensity at 50 thousand ohms. The electrodes are fused with 1/25 ampere fuses to protect the subject in case of circuit failure. The maximum current carried by the fuses is safe for stimulation of peripheral nerve and muscle. A meter in series with the electrodes is used to measure the current intensity for the longer pulse durations.

Preliminary tests with the frog sciatic and gastrocnemius preparation as well as with normal human subjects have been made. The desired time relations may be determined by observation of the cathode-ray screen. A modified version of the output circuit, introducing degeneration, is advisable for the lower current intensities required for stimulation of exposed nerve and muscle tissue in physiological research.

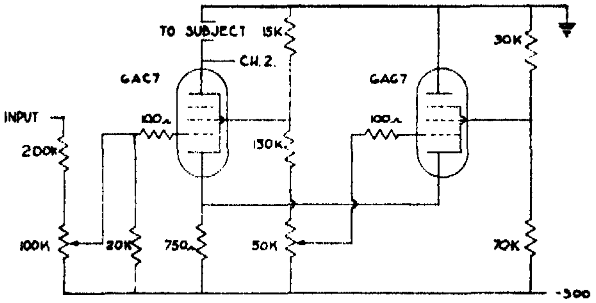

FIG. 5. Final stage; tubes T_6 and T_7 from left to right.

Laboratory and Shop Notes

An Iconoscope Electro-Optical Shutter for High Speed Photography

H. A. Prime and R. C. Turnock
Department of Electronics, University of Liverpool, England

June 16, 1949

ELECTRO-OPTICAL shutters of the Kerr Cell type have been used for many years in investigations of high speed optical phenomena. This type of shutter however suffers from a number of inherent disadvantages, due principally to the electrical and optical characteristics of the nitrobenzene which is used in the Kerr Cell.

In 1947, a proposal was put forward[1] for the application of the iconoscope type of television tube[2] as the control element of an electro-optical shutter. This technique depends on the storage characteristics of the mosaic. If a transient optical phenomenon is focused on the mosaic, the electron image formed on the mosaic may be stored with little distortion for several minutes before being "scanned off" by the electron beam of the iconoscope, and reproduced for examination on a separate display tube. During this storage period, the electron beam of the iconoscope is biased off. The reproduced image comprises the integrated effect of any variations in the phenomenon. However by suppressing storage, except for a short exposure period during the phenomenon, an image can be reproduced, representing changes occuring only within the exposure period.

The method of controlling the storage electronically is effected by suitably biasing the final anode of the iconoscope electron gun with respect to the mosaic potential. The operation of the iconoscope type of tube is based on "anode potential stabilisation" of the mosaic, so that the mean potential is the same as the potential of the final anode of the gun. If the final anode (normally at earth potential) is biased negative to the extent of 100–200 v, the emission of photo-electrons from the mosaic, when illuminated, can be largely suppressed, thus preventing image formation.

In order to permit storage and image formation during the exposure period, a positive-going pulse is superposed on the bias voltage. The amplitude of the pulse need only be sufficient to raise the final anode to earth potential again, although it has been established that the sensitivity of the system is greatly enhanced when the final anode is driven to 50–100 v positive with respect to earth. The duration of the pulse determines the exposure period. The image stored on the mosaic is subsequently reproduced on the display C.R.T. by scanning the mosaic raster once after the completion of the phenomenon. Finally, the display tube may be photographed and a permanent record obtained.

The technique has been investigated using an R.C.A. iconoscope tube Type 1846, and it has been established that in principle the operation of the system is as described above. Beside the usual distortions, common to iconoscope operation, there is a further cause for distortion in the present application, in that the mosaic does not assume a uniform potential distribution during the suppressed or "non-exposure" period. Thus, while the mosaic is illuminated, a redistribution of charge over the mosaic can occur. Since the emission of photo-electrons from the mosaic cannot be suppressed completely during the period that the collector anode is biased negative (an increase in the bias beyond −200 v does not appear to give improved suppression), a weak charge image is formed during the whole period of the phenomena. This spurious or "ghost" image can be investigated if the collector anode is not pulsed. The Kerr Cell shutter suffers from a similar defect, due to imperfect cut-off by the polarising elements.

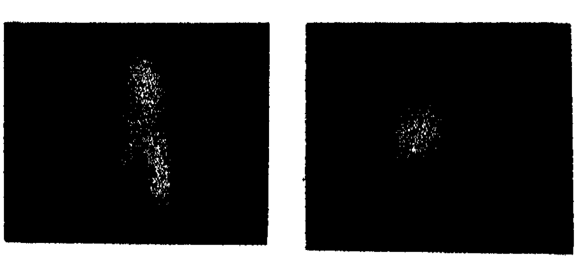

(a) (b)

FIG. 1. Records of sparks in air across a horizontal gap of 9-mm length. (a) Shutter open for duration of spark. (b) 2-μsec. exposure made 13 μsec. after initiation of spark.

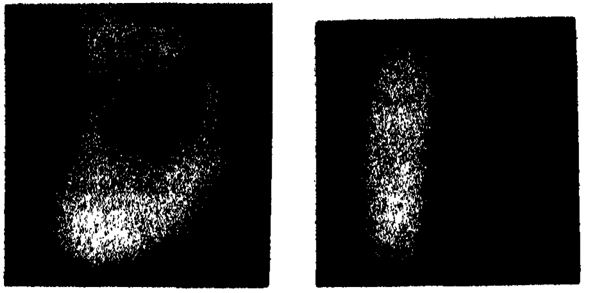

(a) (b)

FIG. 2. Records of neon lamp discharges. (a) Glow on "beehive" electrode. (b) Glow on "disk" electrode.

Experiments have also been carried out with the technique to record different types of phenomena.

Figure 1 illustrates the application of the technique to the high speed recording of discharge phenomena such as a spark. The source used was a 1000-amp. spark in air, of approximately 15 μsec. duration. The exposure time for Fig. 1(a) was the full duration of the spark so that the integrated effect is obtained. Figure 1(b) shows the result obtained when the exposure is reduced to approximately 2 μsec., and made 13 μsec. after the initiation. Figure 2 illustrates the application of the technique to the recording of recurrent phenomena, namely the recurrent discharges formed in a "beehive" type neon lamp, operated from the 50 c.p.s. mains. Exposures of 300-μsec. duration were made repetitively at the same phase in each cycle over a period of several seconds. The formation of the glow around either the "beehive," or the "disk" electrode, according to the particular half-cycle on which the exposure was made, is clearly shown.

A description of the technique will be published in greater detail in due course.

---

[1] R. F. Saxe and H. A. Prime, "The recording of optical transients," Proc. Inst. Elec. Eng. 96, Part II, 662 (August, 1949).

[2] J. D. McGee, *Electronics* (edited by B. Lovell) (Pilot Press, London, 1947).

Preparation of Samples of Active Metals

Donald F. Clifton
Institute for the Study of Metals, University of Chicago, Chicago, Illinois

August 22, 1949

THE problem of preparing oxide free specimens from metals that react with air at room temperature can frequently be solved by working under liquid nitrogen.

Filings for x-ray powder specimens sealed off in thin capillaries and briquetted specimens with a minimum of preferred orientation for use in an x-ray spectrometer are made under liquid nitrogen in a wide, fairly shallow container (crystallizing dish) in a shallow bath of nitrogen to prevent boiling so the filings can clump up for easier collecting. The larger container of liquid nitrogen need not be too well insulated as a fairly rapid evolution of gas helps to keep a dry atmosphere over the work dish and sweep away snow formed at the top of the container where the cold nitrogen comes in contact with the air. Working in a covered box with arm holes helps eliminate moisture.

The filings can be picked up from the liquid nitrogen in a thin glass capillary using a method of Dr. Edward Bicek. The capillary is held in a hole in a rubber disk in the end of a glass tube. The rubber is backed with a piece of filter paper, so the capillary will not be pulled through, and by a thick-walled glass capillary tube cemented in the glass tube. A glass wool plug in the upper end of the thin capillary keeps it free of filings so it can be sealed off. A rough vacuum readily pulls the filings up into the capillary. To seal in the specimen the capillary is lifted just above the liquid, the vacuum momentarily stopped so hot gas is not pulled over the filings, and the end sealed with a small flame. The upper end is sealed with the vacuum on.

Briquettes are made in a three-part die, a sleeve and two plungers. The sleeve, closed at the lower end with thin foil pierced with several small holes, is held about half-way in the nitrogen bath and the filings transferred to it with a medicine dropper. The upper plunger is then put in and the sleeve set down over the lower one, punching the foil in with it. This method keeps the filings under liquid nitrogen through all the steps, and prevents the filings being washed out of the die.

Soft metals can be extruded with a wire press under liquid nitrogen. Some others, too hard to extrude, can be drawn through wire dies under liquid nitrogen even when too soft to be drawn at room temperature.

A Glass Vacuum Valve

JOHN LAMBE
Airborne Instruments Company, Mineola, New York

August 19, 1949

IN constructing a high vacuum system that is to be frequently opened to the atmosphere and that employs an oil diffusion pump, it is highly desirable to insert a valve in the high vacuum line connecting the pump to the manifold. Such a valve will protect the hot oil from exposure to air at atmospheric pressure when the vacuum is broken. At the same time, it is important that the valve shall not seriously reduce the pumping speed of the system. To this end, metal gate valves with gaskets and packing of artificial rubber or other material are often used. Defects in the packing, either originally present or brought on by wear, sometimes cause leaks; the performance of the valve becomes erratic and troublesome.

To circumvent these difficulties and to avoid glass-to-metal joints at the valve connections, a completely sealed-in glass valve has been made. Because the only function of this valve is to protect the hot oil from the atmosphere when the vacuum chamber is opened, the ground-glass joint need not be a high vacuum seal. For use with octoil the valve is required to hold a vacuum of only about 100 microns against atmospheric pressure. Furthermore, the valve is operated only when the pressure on both sides is equal: it is closed before the vacuum manifold is opened to the atmosphere and opened when the manifold has been closed and roughed down by the forepump. (See Fig. 1.)

The valve consists of a ground-glass joint that can be opened and closed by a magnet. The valve was constructed in the following manner. A circular ground-glass butt joint was made; one section was sealed coaxially in the main exhaust line to an oil diffusion pump, while the other was capped and provided with a collar for coupling to a brass draw rod. A pocket with a side arm was provided in the main line just above the sealed-in section of the joint to accommodate the capped section when the valve is slid open. The capped section was placed inside the tubing, and the brass draw rod with its soft iron tip was connected to the collar through the side arm. The side arm was sealed off, and the valve was ready to install in the system. The side arm was made wide enough to allow for some lateral motion of the rod since a little twisting of the ground joint is necessary to pull it open with the magnet.

The valve was installed in a 2-inch main exhaust line. The valve constriction dimensions were 1 inch diameter and 1 inch length; the conductance of such a constriction is 35 liters per second. A gate valve having the full diameter of the line would require about 10 inches to be added to the line for connections; the conductance of such a section is 45 liters per second. The glass valve is therefore satisfactory from the point of view of maintaining pumping speed. In use it has proved to be reliable and easy to operate.

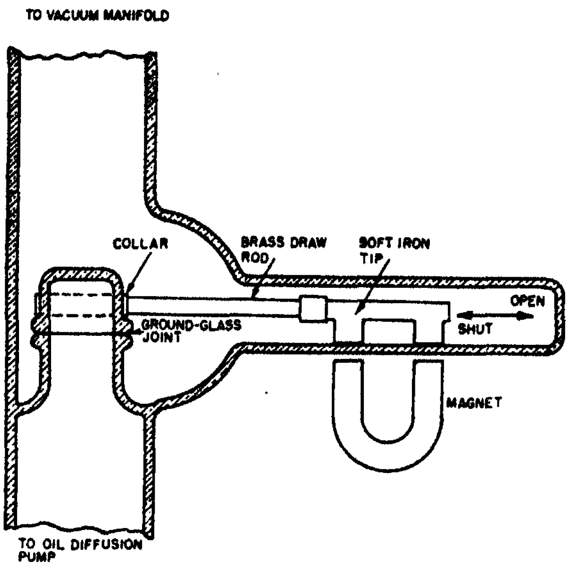

FIG. 1. Glass vacuum valve.

Straumanis' Method of Film-Shrinkage Correction Modified for Use without High Angle Lines

A. J. C. WILSON
*Philips Laboratories Inc., Irvington-on-Hudson, New York**

August 29, 1949

IN the normal Straumanis' method the film is arranged so that the x-ray beam enters through one punched hole and leaves through another diametrically opposite hole, the free ends of the film corresponding to a Bragg angle of approximately 45° (Fig. 1a). The position corresponding to 0° Bragg is obtained from the mean position of the low angle lines, and that corresponding to 90° from the mean position of the high angle lines. The Bragg angle of any reflection is then obtained by proportion, film shrinkage being automatically eliminated.[1]

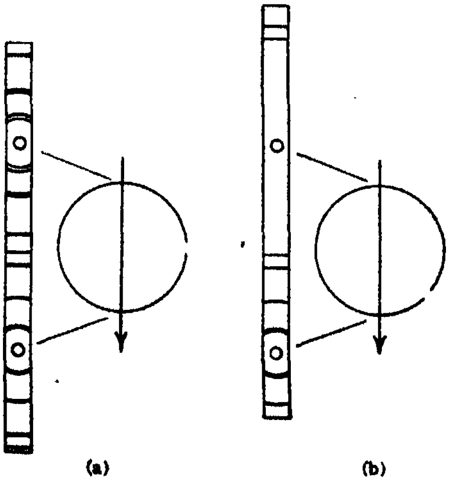

FIG. 1.

Many substances, however, have no high angle reflections, and the method fails because the position corresponding to 90° cannot be determined. This difficulty may be avoided by arranging that the free ends of the film lie in the low angle region, so that some of the low angle lines appear on each end of the film (Fig. 1b).

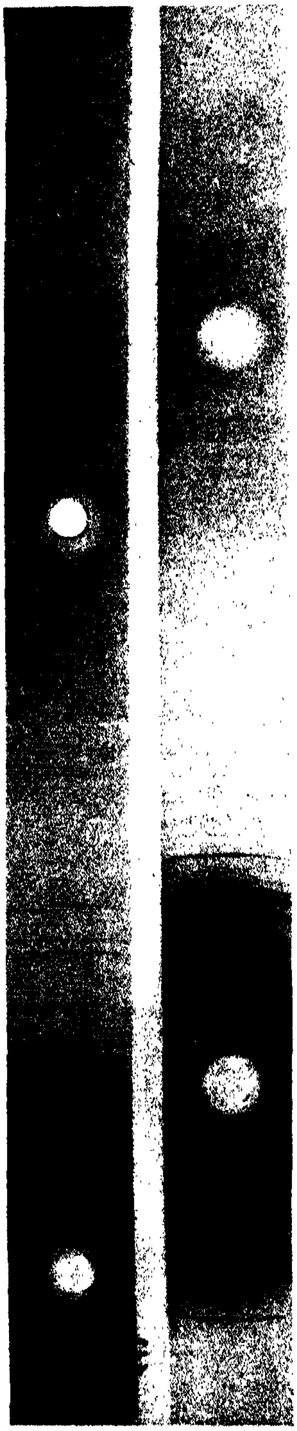

FIG. 2.

The position on the film corresponding to 90° can then be obtained from the mean position of certain of the low angle lines, while the position corresponding to 0° is obtained as before from the rest of the low angle lines. A suitable position for the free ends of the film is in the neighborhood of 20° Bragg.

A photograph of pentaerythritol taken with copper radiation and nickel filter is reproduced in Fig. 2, and it will be seen that there are easily measurable lines bracketing both holes in the film.

---

* On leave from University College, Cardiff, Wales.

[1] M. Straumanis and A. Ievins, *Die Prasisionsbestimmung von Gitterkonstanten Nach der Asymmetrischen Methode* (Virlag. Julius Springer, Berlin, 1940). (Now available through Edwards Bros., Ann Arbor, Michigan.)

A Helium Cryostat Temperature Control

I. Šimon*

*Research Laboratory of Electronics, Massachusetts Institute of Technology, Cambridge, Massachusetts***

September 8, 1949

DURING many experiments in low temperature physics it is desirable to maintain the temperature of the liquid-helium bath constant within narrow and adjustable limits. Several schemes have been used for this purpose. E. R. Andrew recently described[1] a servo mechanism which uses a motor-operated needle valve in the pumping line as a control device and a differential manometer with a photo-cell as an error voltage generator.

In the course of measuring the high frequency impedance of superconducting tin and mercury,[2] a simple device was found to be convenient for maintaining constant temperatures near the transition points. The method is suitable for keeping the vapor pressure in a liquid-helium cryostat at any desired value. The sensing device is again a differential manometer but an intermittent on-off system is used instead of a continuous-control servosystem. Satisfactory performance of such a system was made possible by the use of a rapidly operating control-valve in the pumping line. The response of this valve is practically instantaneous. There are oscillations of the pressure about a desired setting; these are due mainly to the time delay in the pressure equalization through the tubes which connect the cryostat with the pump and with the controlling differential manometer.

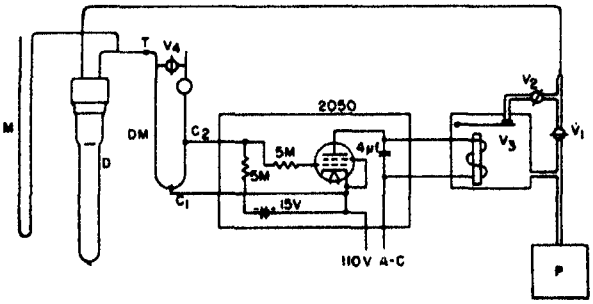

FIG. 1. Pressure control system for a liquid helium cryostat.

The complete set-up is shown schematically in Fig. 1. The Dewar vessel *D* containing the liquid helium is connected to the pump *P* via the coarse valve V_1, and the pressure of the vapor is read by means of a mercury manometer *M* and a differential oil-manometer (not shown in Fig. 1). As soon as the desired pressure is reached, the valve V_4 of the controlling differential manometer *DM* is closed, by-pass valve V_2 is opened and the main valve V_1 is closed. The pressure in the Dewar starts to increase and the rising column of mercury in the right-hand limb of *DM* reaches the contact C_2. The thyratron (type 2050) fires, the winding of the relay-valve V_3 is energized, and pumping is restored through the by-pass V_2, V_3. This process lasts as long as the contacts C_1, C_2 remain connected by the mercury column. By means of the needle valve V_2, the rate of pumping during the "on" period can be adjusted to minimize the amplitude of pressure oscillations.

The valve V_3 was made of a standard 10 M.A., 5000 ohm relay, by replacing the contacts by a nozzle ($\frac{1}{32}$ in. diam.) and a rubber-lined anvil. The relay was then sealed into a small can with an inlet tube.

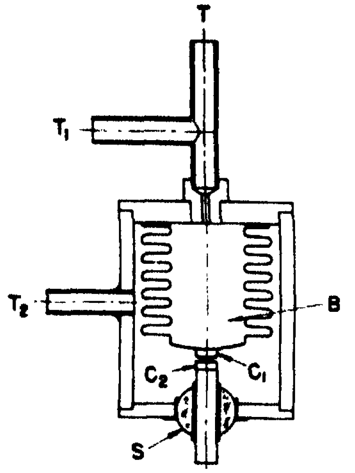

FIG. 2. Differential manometer with contacts for control of the grid voltage of a thyratron.

The mercury differential manometer was later replaced by a more convenient metallic manometer. As shown in the schematic drawing (Fig. 2), the bellows B is $1\frac{3}{4}$ in. o.d. with eight corrugations. Its deflection-*vs.*-pressure sensitivity is about 0.63 cm per 1-cm mercury pressure difference. Attached to it is a silver contact stud C_1 and the whole is enclosed in a vacuum-tight container with a kovar-to-glass-bushing S holding the fixed contact stud C_2. The tube T is the inlet for the pressure which is to be controlled; tubes T_1, T_2 are connected through a stopcock (V_4 in the Fig. 1). The width of the gap between the contacts C_1, C_2 is not critical, since the pressure adjusts itself to a value which keeps the contacts within a minimum operating distance.

With this equipment the pressure oscillations can be kept below 0.3-mm mercury by a proper adjustment of the valve V_3. The frequency of the oscillations is of the order of 1 c/sec. or more. The pressure can be set to any value between atmospheric pressure and about 2-cm mercury. The pressure oscillations of 0.3-mm mercury correspond to temperature variations of 0.00042°K at 3.9°K and to 0.0042°K at 2.0°K. The liquid helium bath and the immersed apparatus cannot, however, follow these rapid variations and remain at a constant mean temperature.

---

[*] Now with Arthur D. Little, Inc., Cambridge, Massachusetts.

[**] This work has been supported in part by the Signal Corps, the Air Materiel Command, and ONR.

[1] E. R. Andrew, J. Sci. Inst. 25, 416 (1948).

[2] I. Simon, Research Lab. of Electronics, M.I.T., Technical Report No. 126 (to be published).

A New Source of Radiation for Infra-Red Spectrometers

L. W. HERSCHER
The Dow Chemical Company, Midland, Michigan

August 29, 1949

THE purpose of this note is to describe a new source of radiation for infra-red spectrometers which has a number of advantages over the commonly used Globar.

The method of construction is indicated by the sketches Fig. 1 and Fig. 2. A length of porcelain rod is fitted with aluminum terminals. The middle portion of the rod is wound with 0.008-inch platinum wire at 25–50 turns per inch and the ends of the winding are fastened by 0–80 flat head screws tapped into the aluminum terminals. The rod is then covered with Sauereisen* cement No. 63 with a coating thick enough to cover the platinum wire. After coating, the source should be baked at 150°F for 24 hours before heating to operating temperature. Actual dimensions, of course, will depend on the particular spectrometer in which the source is to be used. The dimensions given in Fig. 2 are for a Baird Associates double-beam spectrometer.

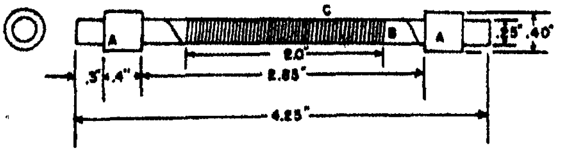

FIG. 1.

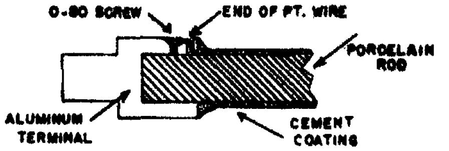

FIG. 2.

The new source maintains the desirable rugged and self-starting characteristics of Globars and in addition has the following advantages:

(1) Has lower emissivity in the 2–4μ region with equal emissivity throughout the remainder of the rock salt spectrum, therefore reducing short wave impurity in the long wave-length region.

(2) Does not change resistance with age.

(3) Has metal to metal contacts throughout the electrical circuit, therefore minimizing the possibility of variations in contact resistance.

(4) Very little ohmic heat is generated at the ends which permits cooler operation of the terminals and thus further reduces the possibility of contact failure.

(5) Has a positive temperature coefficient of resistivity so that power tends to be self-regulating with voltage fluctuations.

(6) By a choice of wire size and spacing the resistance can be controlled so that the source can be operated directly or in series with a ballast lamp at 115 volts; and since the resistance remains constant a variable voltage control is not necessary.

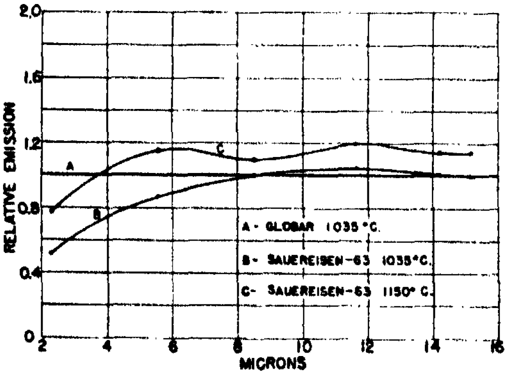

FIG. 3

Figure 3 shows some curves comparing the radiation of the new source at two different temperatures with a Globar at 1035°C. The temperatures were measured with an optical pyrometer. The curves indicate the cement coating has suppression of radiation in the short wave end of the spectrum with essentially equal emissivity elsewhere. As expected from observing these radiation characteristics, a given power input produces a higher equilibrium temperature for the cement coated source.

At present no tests have been made to determine the maximum temperature at which the new source will give satisfactory operation but at ordinary temperatures a long life is expected. The first one made has now been in operation for six months at about 1100°C in a Perkin-Elmer spectrometer and no measurable changes in its electrical or radiation characteristics have occurred.

---

[*] Sauereisen Cements Company, Pittsburgh, Pennsylvania.

A Statitron for a Small Nuclear Laboratory

D. R. Inglis,† R. W. Krone,‡ and S. S. Hanna
Department of Physics, The Johns Hopkins University, Baltimore, Maryland

August 8, 1949

THE statitron* here described was designed to fit the limits of both space and effort available in a small nuclear-physics laboratory. The techniques employed and the main features of design follow developments of more extensive programs elsewhere,[1,2] but a few new details have been incorporated.

The space available accommodates a tank 12 feet long and 6 feet in diameter, which rolls away temporarily in a horizontal direction into an adjacent hallway. No attempt was made to achieve the sort of compactness which characterizes some of the small vertical machines, the use of which usually requires the equivalent of two rooms one above the other. Textolite insulating supports are employed as in other horizontal statitrons which have followed the lead of Professor Herb in this respect. The single high potential electrode (dome) is supported from only one end in cantilever fashion, and the column of equipotential hoops is of uniform diameter throughout. This cylindrical array permits standardization of the hoops and leaves more room for work inside the tank than does a conical array. Because of the space limitation, it is found convenient for service and repair to use the manhole (Fig. 1) in the rear of the tank and avoid rolling the tank away except for major operations. There is room inside the tank to remove the dome with the tank in place. This arrangement has proved very satisfactory, for in over a year of operation it has not been found necessary to roll away the tank.

In order to provide some of the rigidity obtained by Herb with a conical tripod arrangement, a diagonal tension member, shown in Fig. 1, supports the dome assembly against gravity while three parallel compression members hold it rigid against rotation. These compression members also serve to support the steel hoops in the manner shown in Fig. 2. The upper horizontal rod (of ¾-in. aluminum stock) shown there provides two points of support by having its conical ends penetrate into ¼-in. holes in the hoop. A third support is supplied by the pin attached to the clamp of the lower horizontal rod. Assembly is facilitated by means of a simple spring extension built in a well in one end of the upper rod. Both horizontal rods serve also as shields to equalize the fields at the belts, the distance from belt to shield being half the distance between belts as is ideal for uniformly charged belts.

In addition to the usual accelerating tube, a similar evacuated tube which serves as a differential pumping tube is mounted in a symmetrical position, and the two tubes, connected by a rigid yoke at the high potential end, are supported and compressed by a second diagonal tension member (Fig. 1) pulling on the yoke midway between the two tubes and a little above their lower edges. This mounting is entirely independent of the cantilever support of the dome and hoop assembly, and the vacuum system is thus isolated from any vibration that might arise from the generator and belt pulley in the dome. Each tube consists of 27 porcelain sections, 9 in. o.d., 7 in. i.d., 2½ in. thick, making the insulating column about six feet long. These sections and the spun-steel re-entrant electrodes (Fig. 3) follow Herb's design with slight modifications.

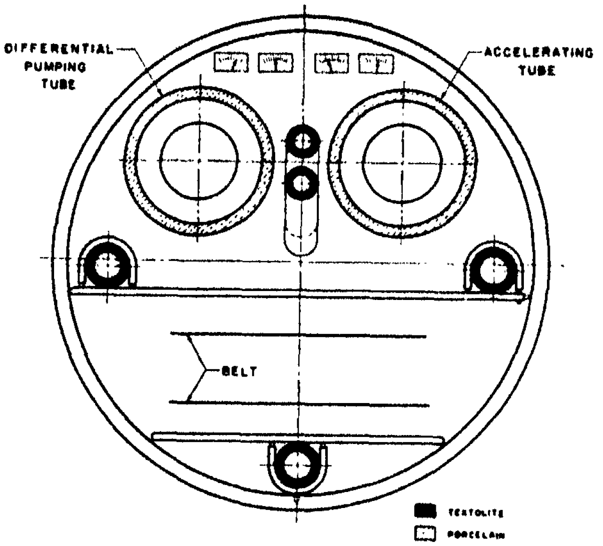

FIG. 2. Cross section of statitron.

The tubes were, however, assembled by the vinylseal baking technique approximately as developed by Trump. The use of vinylseal has caused some subsequent inconvenience as leaks were encountered, contrary to some experience elsewhere, but this may have been due to an inadequate equalization of oven temperature during the original baking procedure or to insufficiently flat ground surfaces at the joints. After the tubes were mounted horizontally, as described, in a manner perhaps dependent on the strength of the joints (though not so designed), tests revealed that the usual liquids used in leak hunting or repair seriously soften vinylseal. After helium leak detecting equipment had been put in operation the leaks were detected and most of them sealed by application of very small quantities of vinylseal without baking.

The ion source is of the Zinn type, and follows rather closely the design dimensions adopted by McKibbin in the "short tank" which was built at Madison at about the beginning of this decade. The only significant departure from his design is the mounting of the probe, which, as shown in Fig. 3, is held between internal Lavite insulators and is connected to the outside by a heavy copper rod capable of conducting away enough heat as well as providing an electrical connection. This alteration was made in an attempt to avoid some large ring seals in the vacuum housing, but turned out to be a dubious simplification. The filament and anode lead-throughs are sealed by means of a silicone (high temperature) rubber gasket squeezed between two Lavite insulators. The ion source is mounted on a differential pumping chamber (Fig. 3) from which a large pumping connection passes to a valve on the adjacent differential pumping tube. The pumping chamber is in turn attached to the first two porcelain sections of the accelerating tube, which contain a perforated focusing electrode. The low potential end of this electrode is constricted by a removable insert

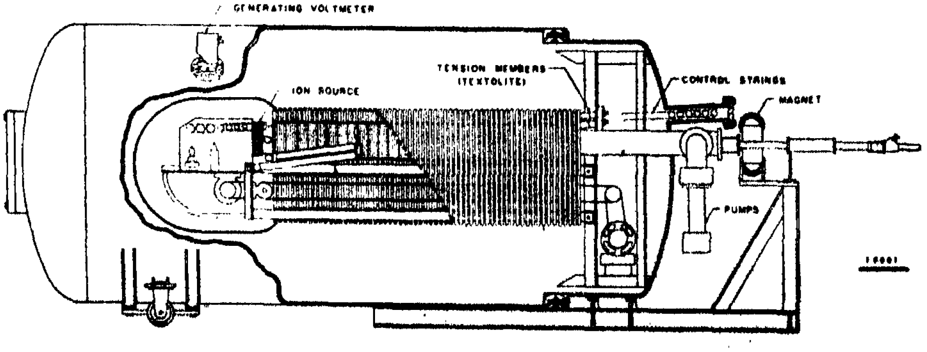

FIG. 1. Diagram of statitron.

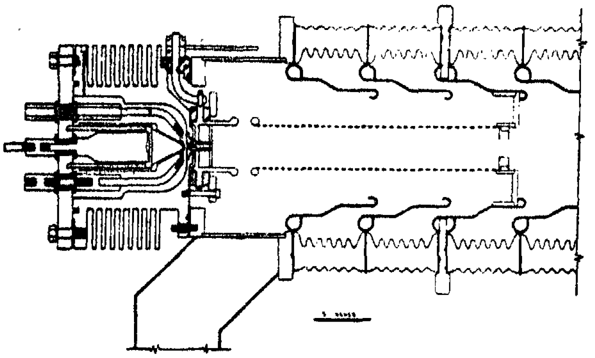

FIG. 3. Ion source, differential pumping chamber, and focusing assembly.

having an opening about ¾ in. in diameter, the pumping speed of which is presumably considerably less than that of the differential pumping tube. The complete focusing assembly is attached to a steel plate separating the first two porcelains from the rest of the column. In this case the seal is made with Neoprene gaskets to make possible alteration of the focusing arrangement without breaking vinylseal joints.

The geometrical arrangement of the control strings is considerably simplified over previous designs by providing a 6-in. pipe welded into the tank to hold the ground-potential pulleys, as shown in Fig. 1. This makes it possible to have simple straight-line coupling between pulleys on short shafts at both ends, in an entirely mechanical control system. Eight controls are provided: probe, paladium-leak, and filament variacs; focus and return-charging-current corona needles; arc switch, proton-deuteron shift, and nose spacing. The meters in the dome may be seen through a window beside the controls.

The position of the generating voltmeter of conventional design[3] is shown in Fig. 1, and in a symmetrical position on the opposite side of the tank is mounted an insulated set of corona needles protruding inside the tank wall for the purpose of electronic voltage control based on deflection of the beam by the magnet shown in Fig. 1. Charging current is supplied to the belt by means of a suitable high voltage transformer mounted inside the tank. A general view of the dome and hoop assembly is presented in Fig. 4.

This statitron replaces one[4] built in the same room around 1940 and partially dismantled during the war to make space for work for the Bureau of Ordnance. The reconstruction was started in 1946 with financial help from that source and completed in early 1948 with a grant from the University. It has been in use since then at voltages up to 1 mv, this limitation being set by the fact that the useful tank pressure was limited to about 50 lb., or half the rated pressure of the tank, by pressure-dependent leaks in the vacuum which until recently were pursued with insufficient zeal because of preponderant interest in research applications at the voltages easily attainable. Extensive construction was carried out in the Physics Shop by Messrs. Hill, Krause, Nemac, and Rogers. During the early part of the reconstruction, laboratory work was done by technician I. Brizendine, and in the final stages by technician Paul Milich. At various stages in the construction, valuable assistance was received from three graduate students, Messrs. I. Resnick, J. A. Neuendorffer, and C. M. Class.

FIG. 4. Statitron with pressure tank rolled away

[†] Now at Argonne National Laboratory, Chicago, Illinois.

[‡] Now at University of Kansas, Lawrence, Kansas.

[*] The name statitron is here applied to the instrument which is variously known also as a Van de Graaff "generator," electrostatic accelerator, or electrostatic "generator." In an informal poll among most of the users of these machines conducted some time ago by the editor of this Journal, the name statitron received majority but not unanimous approval.

[1] R. J. Van de Graaff, Phys. Rev. 38, 1919 (1931). Van de Graaff, Compton, and Van Atta, Phys. Rev. 43, 149 (1933). Van Atta, Northrup, Van Atta, and Van de Graaff, Phys. Rev. 49, 761 (1936). J. G. Trump and R. J. Van de Graaff, J. App. Phys. 8, 602 (1937). Trump, Merrill, and. Safford, Rev. Sci. Inst. 9, 398 (1938). J. G. Trump and R. J. Van de Graaff, Phys. Rev. 55, 1160 (1939).

[2] Herb, Parkinson, and Kerst, Rev. Sci. Inst. 6, 261 (1935), Phys. Rev. 51, 75 (1937). Parkinson, Herb, Bernet, and McKibben, Phys. Rev. 53, 642 (1938). Herb, Turner, Hudson, and Warren, Phys. Rev. 58, 580 (1940).

[3] Trump, Safford, and Van de Graaff, Rev. Sci. Inst. 11, 54 (1940).

[4] Jennings, Swartz, and Rossi, Rev. Sci. Inst. 15, 64 (1944). A charging belt and its pulleys from this statitron are in use in the present machine.

Pumping Speed of Diffusion Pumps below Limiting Pressure

CLIFFORD E. BERRY
Consolidated Engineering Corporation, Pasadena, California

August 1, 1949

IN a recent paper G. W. Sears[1] postulates that the true pumping speed of a diffusion pump should be a constant for all values of pressure below a critical value, and that the commonly used curves of pumping speed as a function of pressure are misleading at low pressures. According to Sears, the apparent pumping speed drops off at low pressures because the evolution of gas from the pump and the rest of the system eventually produces all of the measured pressure regardless of the amount of gas admitted to the system for measuring the pumping speed.

The fallacy in the present method of measuring pumping speed seems to lie in measuring the total system pressure rather than the partial pressure of the test gas itself. For a true pumping speed measurement, the test gas should be one which is not normally evolved from the system, and a mass spectrometer or the equivalent should be used to measure the partial pressure of the test gas.

Some data taken in this laboratory three years ago offer strong support of Sears' hypothesis. The experimental set-up is shown in Fig. 1. A VMF-20 air-cooled oil diffusion pump was used to evacuate a manifold, to which a small mass spectrometer tube was attached through a cold trap. The calculated pumping speed at the point of attachment was approximately 6 liters per second for air. The gas reached the mass spectrometer tube simply by diffusion. An ionization gauge was used to measure the total system pressure. Gas (helium) was admitted to the manifold through a molecular flow leak from a small sample volume *A*. In order to reduce the pressure in *A* and hence the helium introduction rate by reproducible fractions, an expansion chamber *B* was connected to *A* through a stopcock, and *B* was connected in turn to a mechanical pump through another stopcock. The leak rate and volume were so related that essentially no pressure reduction in *A*

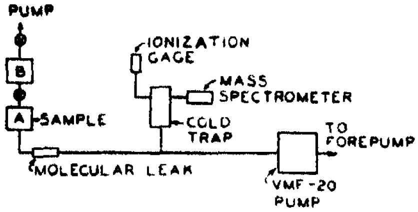

FIG. 1. Schematic diagram of system used for measuring pumping speed.

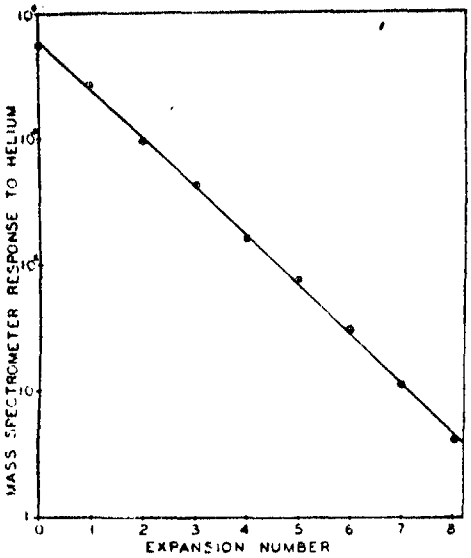

Fig. 2. Plot of mass 4 ion current in mass spectrometer vs. number of expansions of helium sample. Each expansion reduced the sample pressure by the same fractional amount.

took place because of leakage during the time required for the experiment.

The experiment was performed as follows: The system was pumped down until the residual or background pressure was 10^{-6} mm as indicated on the ionization gauge, which was calibrated for air. (Incidentally, this is the "blank-off" pressure given by the diffusion pump manufacturer's pumping speed curves.) Next, a sample of helium was introduced to *A* and the pressure adjusted to give a partial pressure of helium at the ionization gauge *of approximately* 2×10^{-5} *mm, using published calibration data* for the gauge. The reading of the mass 4 ion current produced by the mass spectrometer tube was noted. The sample in *A* was then back expanded *to B, which had been previously pumped out.* The helium ion current reading was again taken, with the mass spectrometer, and the process repeated until eight expansions had been made. The volume ratios were such that this process reduced the sample pressure by about 1000 times. Figure 2 shows the results, in which the log of the reading of the helium ion current is plotted against the number of expansions.

The curve shown is just what one would expect if the pumping speed of the pump for helium is a constant independent of pressure. The partial pressure of helium in the system is given by

$$P_{\mathrm{He}}=P_s\times\frac{S}{S_1}$$

where P_S is the pressure of helium in the sample volume, S is the speed of the leak, and S_1 is the speed of the pump. The linearity of the curve implies that S_1 is constant over a range of pressure from 2×10^{-5} mm down to 2×10^{-8} mm; the lowest pressure used. By comparison, the published speed curves for the pump used reveal that the speed begins to drop off below 8×10^{-6} mm, and is zero at 10^{-6} mm.

Further evidence is found in another test, in which a very small amount of helium is introduced through one leak and varying amounts of air through another. Varying the system pressure from 10^{-6} mm to 10^{-4} mm by varying the amount of air admitted produces no appreciable change in the reading of the helium current.

The clear inference from these data is that the blank-off pressure of diffusion pumps, as currently given, is not the pressure at which the pump stops operating, but the pressure at which gas is evolved from the system (including the pump itself) at such a rate as exactly to equal the inherent speed of the pump, and that the full-rated pumping speed, for gases not so evolved, may be retained at pressures several orders of magnitude lower than the rated "blank-off" pressure of the pump. This conclusion is of special importance in cases where the pumping speed for gases such as hydrogen and helium is of interest.

[1] G. W. Sears, Rev. Sci. Inst. 20, 458, 459 (1949).

Parallel Operation of Small Thyratrons

Paul G. Hansel
Servo Corporation of America, New Hyde Park, New York
September 22, 1949

SMALL thyratrons are often used in applications where the discharge current greatly exceeds the tube rating. Shortened tube life or erratic firing usually results from such overloaded operation.

Parallel operation of two thyratrons ordinarily fails to prevent overloading because of the tendency of one tube to fire first, thereby reducing the anode voltage on the second tube and preventing its firing.

Figure 1 illustrates a circuit which insures substantially simultaneous firing of parallel-operated thyratrons. In the case illustrated, a pair of 2D21 thyratrons in parallel were used to discharge a large condenser through the primary of a high voltage transformer to produce a high voltage trigger for a flashing light source.

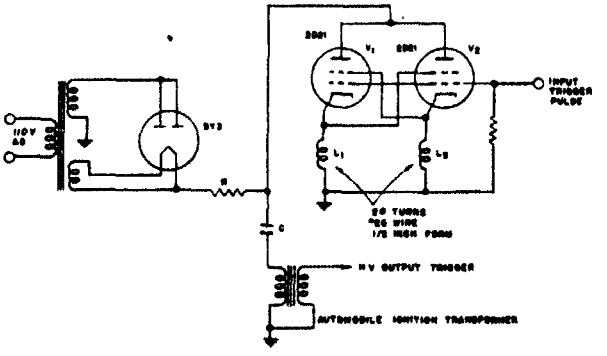

Fig. 1.

The two control grids are connected in parallel. A small inductance is inserted in each cathode and the shield grids are cross-connected to the cathodes as shown.

When the input trigger is applied to the control grids one tube, V_1 for example, may fire first. The surge of current through L_1 results in a positive pulse across L_1 which is applied to the shield grid of V_2, thereby causing V_2 to fire. The firing delay can be made very small by proper design of L_1 and L_2.

An Improved Embryological Micromanipulator

Howard H. Hillemann
Department of Zoology, Oregon State College, Corvallis, Oregon
July 12, 1949

THE improved version has a shorter stage from front to back (3½ in.) to provide more latitude in centering the object in the visual field. From side to side, the stage is somewhat longer (7 in.), for direct attachment of the vertical adjustment. Since the stage rests above the position of the original glass plate, it was necessary to attach 2 bars to the under surface for securing the instrument to the microscope. Depending upon which way the apparatus is oriented when slipped into the groove of the scope, it becomes either a right- or left-handed instrument.

The egg-holder attachment was modified in several ways. A knurled surface on the circumferential surface to provide friction for rotation with the finger tips was added. The three-coil pressure springs were enclosed in cylinders, each equipped with a knurled pressure adjustment knob. The egg-cup was made of a thicker metal (brass, $\frac{1}{16}$ in. thick) and in the form of a diamond-shaped parallelogram. The vertical adjustment knurl for the rotary stage was transferred to the right side along with all other adjustments.

The transverse bar of the horizontal adjustment (commercial mechanical stage) has two additions. One is an insulated electrode receptacle for transmission of current through the operating end of the instrument. There is also attached a secondary manipulator (from an obsolete foreign make of microscope) and is used for preliminary coarse adjustments. It can swing in an arc of 360° in the horizontal plane (horizontal lower bar) and 180° in a vertical plane (horizontal upper bar). In addition, the upper horizontal bar can swing through 360° and be made to slide in its sheath back and forth for a distance of about one inch.

The remaining details are much the same as those of the original instrument previously described.[1]

Figure 1 depicts the complete micromanipulator.

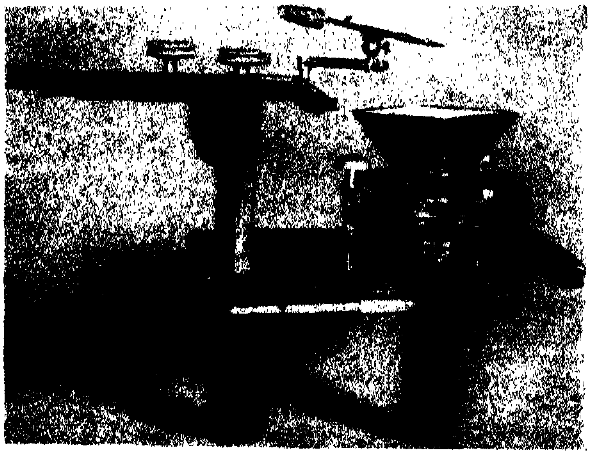

FIG. 1. Improved micromanipulator.

1. plain stage
2. vertical adjustment of manipulator
3. bar
4. rotary stage
5. pressure-spring cylinder
6. egg-cup
7. vertical adjustment of rotary stage
8. insulated electrode receptacle
9. secondary manipulator
10. lower horizontal bar
11. upper horizontal bar

The expense of manufacture came to about $135.00 exclusive of the price of a mechanical stage and two vertical racks and pinions, and was borne by a grant from General Research at Oregon State College. Mr. Charles J. Filz, mechanic in the department of Physics, is acknowledged for his skilled artisanship and for certain suggestions which improved the design.

[1] H. H. Hillemann, Anat. Rec. 84, 337 (1942).

Transient Response of High Voltage Resistance Dividers

HARRY J. WHITE
Research Corporation, 465 West Union Ave., Bound Brook, New Jersey

June 27, 1949

HIGH voltage resistance dividers as commonly used for d.c. or for low frequency a.c. measurements present no problems other than those of heat dissipation and mounting of the resistors. However, in the observation of transient or pulse voltages, considerable care in the design and arrangement of the divider is necessary in order to avoid serious distortion of the observed voltage waves. For the purposes of this paper, high voltage may be defined as 10 kv or higher, and it will also be assumed that a cathode-ray oscillograph is used as the observing means. The objects of the paper are to give theoretical and experimental data on the inherent distortion introduced by resistance dividers, and to provide design formulas and graphs for dividers to be used with transient voltages.

An ideal resistance divider would have neither capacitance nor inductance and would exactly reproduce the input voltage wave at its output terminals on a reduced scale determined by the divider ratio. Real dividers, on the other hand, have both capacitance and inductance associated with the resistance elements, and the capacitance in particular cannot be neglected when voltage waves having high rates of change are being studied. The inductance of modern surface-coated-type resistors is, however, very small and may be neglected for voltage dividers. Viewed from the energy standpoint, the stored energy of the electric field of the divider is important and can be the source of serious distortion, while the stored energy of the magnetic field is negligible.

Theoretical.—High voltage dividers are usually subject to electrostatic induction or pick-up effects from other high voltage apparatus in the immediate neighborhood, and it is therefore necessary to provide complete shielding of the resistance elements in order to avoid false indications. Perhaps the simplest and most satisfactory practical arrangement is to use cylindrical resistors with a coaxial cylindrical shield, as illustrated in Fig. 1. This has the advantages of providing complete shielding, good electrical clearances, avoidance of corona, and adequate cooling surface, and in addition is amenable to theoretical calculation.

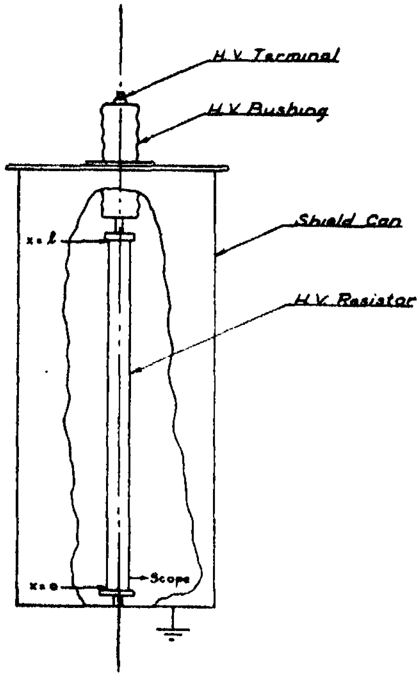

FIG. 1. Cylindrically shielded type H. V. resistance divider.

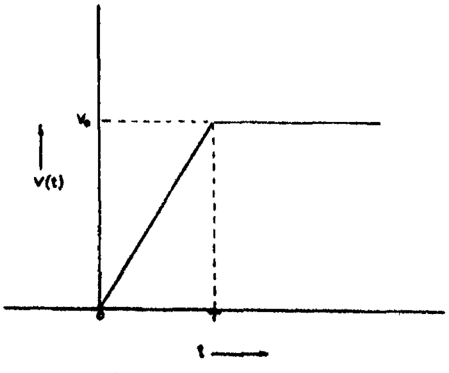

FIG. 2. Trapezoidal pulse.

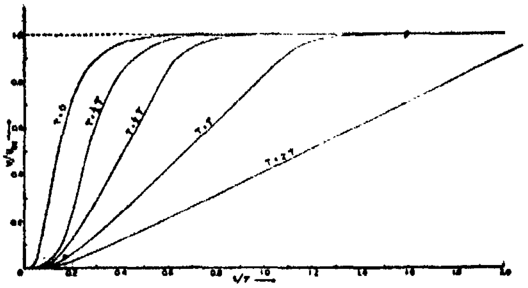

FIG. 3. High voltage resistance divider. Transient response curves for trapezoidal applied voltage; T = rise time of voltage; τ = RC = divider time constant; V_∞ = d.c. response voltage.

Many of the most useful transient voltage waves or pulses, such as those used in radar, can be characterized or simulated by the trapezoidal pulse shown in Fig. 2. Such a pulse rises at constant rate to its peak value V_0 in time T and is defined mathematically by Eq. (1)

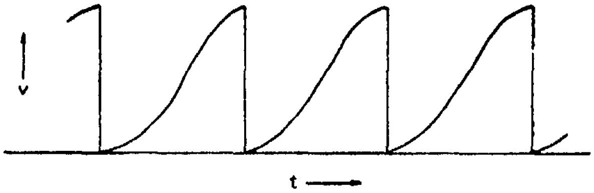

FIG. 4. Theoretical sine-wave charging voltage wave.

$$V(t)=\begin{cases}0 & \text{for } t<0\\ V_0(t/T) & \text{for } 0<t<T\\ V_0 & \text{for } t>T.\end{cases}\tag{1}$$

The response of the divider of Fig. 1 to this voltage pulse may be calculated by treating the divider as a transmission line having distributed resistance and capacitance, but negligible leakage and inductance. The capacity loading by the oscillograph may also be assumed negligible.

The partial differential equation and boundary conditions for the line are

$$\begin{aligned}&\partial V/\partial t=(1/rc)(\partial^2V/\partial x^2),\\ &V=0,\quad x=0,\\ &V=V_0(t/T),\quad x=l,\quad 0<t<T,\\ &V=V_0,\quad x=l,\quad t>T,\end{aligned}\tag{2}$$

where

$V=V(x,t)$, r = resistance per unit length, c = capacitance per unit length.

The solution is conveniently obtained by the Laplace transform method, with the steps briefly as indicated below. The Laplace transform of the applied voltage wave is

$$\bar{V}(\lambda)=(V_0/\lambda^2T)(1-\epsilon^{-\lambda T}),\tag{3}$$

while the transform $\bar{V}(x,\lambda)$ corresponding to (2) is

$$\bar{V}(x,\lambda)=\frac{V_0}{\lambda^2T}(1-\epsilon^{-\lambda T})\frac{\sinh x(rc\lambda)^{\frac{1}{2}}}{\sinh l(rc\lambda)^{\frac{1}{2}}}.\tag{4}$$

By the inversion theorem

$$V(x,t)=\frac{1}{2\pi i}\int_{\gamma-i\infty}^{\gamma+i\infty}\frac{V_0}{\lambda^2T}(1-\epsilon^{-\lambda T})\epsilon^{\lambda t}\cdot\frac{\sinh x(rc\lambda)^{\frac{1}{2}}}{\sinh l(rc\lambda)^{\frac{1}{2}}}d\lambda.\tag{5}$$

Integral (5) may be evaluated by contour integration and the calculus of residues and yields

$$V(x,t)=V_0\frac{\tau}{T}\left\{\frac{x}{l}\left[\frac{t}{\tau}-\frac{1}{6}\left(1-\frac{x^2}{l^2}\right)\right]+\frac{2}{\pi^3}\sum_{n=1}^{\infty}\frac{(-1)^{n+1}}{n^3}\exp[-n^2\pi^2(t/\tau)]\sin\frac{n\pi x}{l}\right\}\text{ for }0<t<T.\tag{6a}$$

$$V(x,t)=V_0\left\{\frac{x}{l}-\frac{2}{\pi^3}\cdot\frac{\tau}{T}\sum_{n=1}^{\infty}\frac{(-1)^{n+1}}{n^3}(\exp[n^2\pi^2(T/\tau)]-1)\times\exp[n^2\pi^2(t/\tau)]\sin\frac{n\pi x}{l}\right\}\text{ for }t>T,\tag{6b}$$

where $\tau=rcl^2$ = total resistance×total capacitance of divider = time constant of divider.

For observing high voltages, the divider ratio x/l will nearly always be 0.01 or less, so that $\sin(n\pi x/l)$ is closely approximated by $(n\pi x/l)$ if n is not too large. Using this approximation, (6a) and (6b) become

$$V(x,t)=V_0\cdot\frac{\tau}{T}\cdot\frac{x}{l}\left\{\frac{t}{\tau}-\frac{1}{6}+\frac{2}{\pi}\sum_{n=1}^{\infty}\frac{(-1)^{n+1}}{n^2}\exp[-n^2\pi^2(t/\tau)]\right\}\quad\text{for }0<t<T.\tag{7a}$$

$$V(x,t)=V_0\cdot\frac{x}{l}\left\{1-2\sum_{n=1}^{\infty}(-1)^{n+1}\times\frac{\exp[-n^2\pi^2(t-T/\tau)]-\exp[-n^2\pi^2(t/\tau)]}{n^2\pi^2(T/\tau)}\right\}\text{ for }t>T.\tag{7b}$$

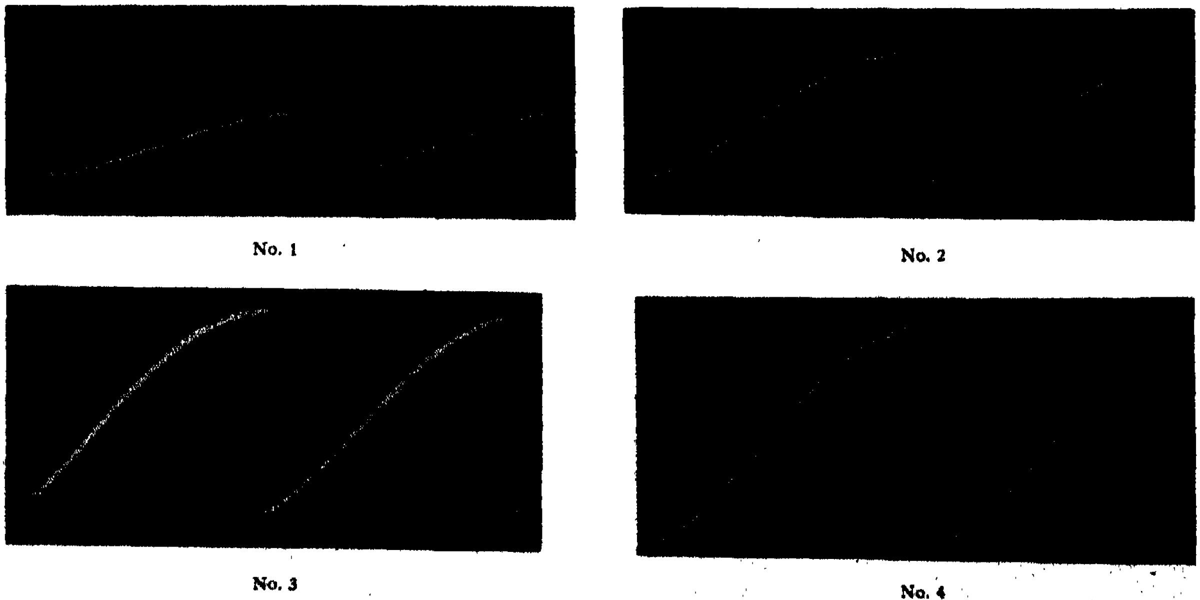

No. 1

No. 2

No. 3

No. 4

FIG. 5. Oscillograms showing charging voltage wave distortions for resistance dividers of Table I.

To obtain the response for a rectangular pulse (Heaviside unit function), let $T\rightarrow 0$ in (7b) and the limit is

$$V(x,t)=V_0\cdot\frac{x}{l}\left\{1-2\sum_{n=1}^{\infty}(-1)^{n+1}\exp[-n^2\pi^2(t/\tau)]\right\}. \quad (7c)$$

It may be noted that in these formulas $V_0\cdot x/l$ is the steady-state or d.c. response of the divider.

The response Eqs. (7) are plotted in Fig. 3 for a range of values of the parameter T/τ. Distortions of two types are introduced by the divider; namely, a change in the pulse shape, and a delay in reaching the final amplitude. For the case of a rectangular or step pulse ($T/\tau=0$), the time delay in reaching the peak amplitude amounts to about 0.65τ. As might be predicted, the distortions are less the slower the rate of rise of the voltage wave. These differences are clearly discernable in the response curves.

Experimental.—The validity and usefulness of the theoretical results have been checked for a typical application; namely, the observation of the pulse network charging voltage in a line-type radar modulator or pulse generator.[1] In this pulse generator circuit, an energy storage condenser is periodically charged from a d.c. power source through a charging inductance or choke, and periodically discharged into a load circuit by means of a pulse discharge switch, e.g., a hydrogen thyratron.

If the charging choke and pulse condenser are properly tuned to the pulse recurrence frequency, sine-wave charging is obtained as shown in Fig. 4. Such a charging wave is of great practical importance and is usually observed by means of a resistance divider and oscilloscope. In a typical radar case, the pulse condenser is discharged in about 1 μsec. and charged in about 1000 μsec. The discharge time is therefore exceedingly short, and the voltage wave across the pulse condenser approximates a step-voltage function in the neighborhood of the discharge point.

TABLE I. Resistance divider constants and time delays.

Resistance divider	a[a]	b	l	R[b]	C	τ[c]	Δt_1[d] Theor.	Δt_2[e] Exp.
No. 1	2 in.	16 in.	40 in.	60 meg.	27.2 $\mu\mu$f	1.63 milsec.	1.06 milsec.	0.80 milsec.
No. 2	2	16	20	30	13.6	0.41	0.27	0.26
No. 3	2	16	40	0.8	27.2	0.02	0.01	~0
No. 4	$\frac{1}{16}$	6	42	10	20	0.20	0.13	0.18

[a] a = H.V. resistor diam., b = shield can diam., l = shield can length.
[b] R = total divider resistance, C = total divider capacitance.
[c] τ = theoretical time constant of divider.
[d] Δt_1 = theoretical time delay of divider for step-voltage.
[e] Δt_2 = observed time delay of divider for step-voltage from Fig. 5.

An experimental line-type pulser was set up, using a 1 μsec. pulse-forming network and hydrogen thyratron pulse switch. Operation was at approximately 10 kv on the network and 250 p.p.s. recurrence rate. The charging voltage was observed with several resistance dividers having the theoretical time constants shown in Table I.

Oscillograms of the corresponding charging voltage waves are recorded in Fig. 5. The distortions are evident, especially in the cases of the longer time constant dividers. Table I summarizes the constants of the dividers together with the observed time delays in reaching minimum voltage after the pulse discharge as measured on the oscillograms. Agreement between the calculated and observed time delays are reasonably close, considering the theoretical and experimental approximations involved. These approximations could no doubt be reduced both in the theory and in the experimental test. But the value of the theory lies in establishing correct designs for H.V. resistance dividers rather than in predicting exact response functions, and in this sense a more exact and necessarily more involved theoretical treatment is not justified.

Conclusion.—Application of the curves of Fig. 3 will indicate the order of magnitude of the distortions to be expected with shielded H.V. resistance dividers for all cases where the applied voltage can be approximated by a step function or by a rising or falling trapezoidal wave. Resistance dividers must be used with care in observing transient or very high frequency voltages, but with proper design distortions generally can be kept to an acceptable minimum.

---

[1] Pulse Generators, M. I. T. Radiation Lab. Series, Vol. 5.

Voltage Stabilization for Electrostatic Generators Using an Electron Gun

S. J. Bame, Jr. and L. M. Baggett
The Rice Institute, Houston, Texas

July 18, 1949

An electron gun and auxiliary circuit for the control of a beam of positive ions accelerated by a Van de Graaff generator is described. A high degree of stabilization in energy is obtained with electron currents of from 10–20 microamperes sent back up the same vacuum tube which is used to accelerate the positive ions.

In the operation of a Van de Graaff high voltage generator, it is often desirable that some control mechanism be used to maintain the generator at a constant potential. A number of methods have been used.[1-3] The variable corona discharge method was the most satisfactory of these early systems, having a delay time of approximately 10^{-3} seconds. An improvement in the time constant can be made by sending an electron current up the accelerating tube to the high voltage electrode. The delay time for this method is of the order of 10^{-6} second. This principle has been made use of in a satisfactory system of stabilization.[4] This system, which we propose to modify, was composed of insulated jaws of a slit through which the beam from the analyzer passes. The potential of the jaws due to the beam of charged particles incident upon them controls a circuit (see Fig. 1) which in turn controls a source of electrons. The source sends current back up the accelerating tube to the high potential electrode. When the major part of the ion beam passes through the insulated slit, part of the current falls on each of the slit jaws. In equilibrium, when the potentials of the grids of the 6SJ7's are equal, the circuit sends an equilibrium value of electron current up the accelerating tube. This return current plus the losses due to insulation leakage and corona current must be balanced by the amount of current sprayed on

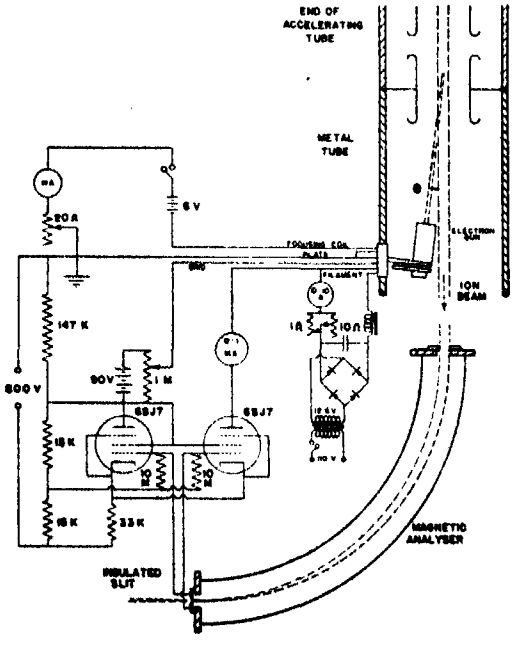

FIG. 1. Schematic diagram of the stabilization system. As installed in the Rice Institute Van de Graaff machine the angle θ, which the electron beam makes with the positive ion beam, is five degrees.

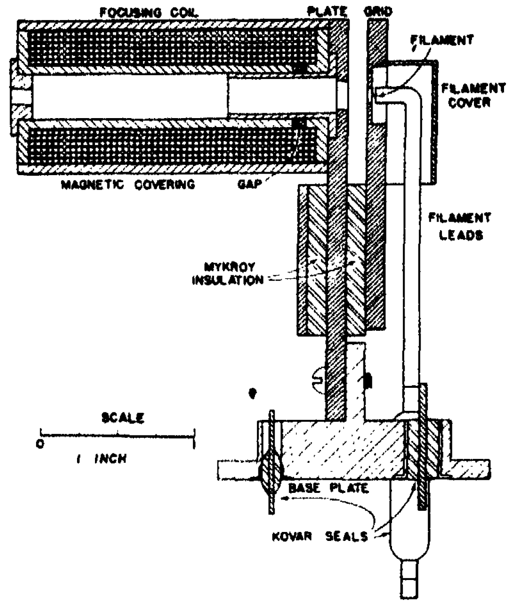

FIG. 2. Cross-sectional view of the electron gun.

the belt of the machine. If the energy of the beam deviates, resulting in a deflection of the positive ion beam on the slit jaws and a consequent change in the potential on the two grids of the 6SJ7's, both tubes operate to either increase or decrease the current sent up the tube, thus correcting the potential of the machine until the equilibrium value of the system is again reached.

The original electron source[4] was a triode adapted so that a divergent beam of electrons was directed up the accelerating tube. The diverging beam impinged upon the accelerating electrodes, resulting in electron multiplication. Since the multiplication depends on surface conditions of the metals and varies from time to time, it is not the most satisfactory method.

The object of the modification described in this paper was to improve the stabilization by replacing the triode with an electron gun of simple design which would send a well-defined beam of electrons back up the center of the accelerating tube, thus avoiding the electron multiplication effects.

The gun shown in Fig. 2 is of a simple single anode structure with a control grid and a magnetic focusing coil. All major elements of the gun are made of magnetic material in order to provide magnetic shielding for the filament and the electrostatic field between the grid and the anode. A tungsten filament is used to simplify the design of the gun and to avoid the possibility of poisoning the cathode.

Since helical filaments have a tendency to deform when heated, the filament used is a single straight piece of 10-mil wire 1 cm in length attached to the ends of heavy filament leads. Direct current was used for heating the filament in order to avoid an a.c. ripple in the beam current.

Ease in mounting new filaments and reproducing the characteristics of the gun results from constructing the grid, anode, and coil as a unit. The entire unit can be removed in order to replace an old filament. In order to insure that the new filament has the correct cathode to grid spacing of 0.05 cm, heavy, stationary filament leads are used; and filaments of the same geometry are attached in the same manner. This particular point is of importance, since a small deviation in filament to grid spacing can result in a large change in tube characteristics.

The gun is magnetically focused by a coil covered with monel metal. The fringing about the gap of non-magnetic material produces a small, localized focusing field of the proper shape for good focusing. One end of the coil winding is grounded and the other end is brought through the base plate by a Kovar seal.

The gun alone has the characteristics of a simple triode with an amplification factor of 25. By observing the beam on a zinc sulfide screen, it was found that a sharper focus was obtained as plate voltage was increased from 400 to 1600 volts. The focusing characteristics were reasonably good at 800 volts, giving a spot size of 5 mm at a distance of 18 inches.

In operation upon the Van de Graaff generator, the gun produced a high degree of stabilization. Without regulation the intensity of the heavy particle beam at the target varies over a wide range. With the stabilizer in operation the intensity is held constant to within 10 percent. The stabilization is a function of the electron beam current. Regulation is obtained with equilibrium electron beam currents of 5–20 microamperes. The regulation is satisfactory with an electron beam current of 5 microamperes but is somewhat steadier at 20.

A count of the x-rays in the control room of the high voltage laboratory showed that the x-ray intensity increased by a factor of 1.5 to 1.9 when electron beams of 20–25 microamperes of current were sent up the tube to the high potential electrode. This is not an excessive increase in the counting rate since it is only 10–20 times greater than the cosmic-ray background. This x-ray intensity could easily be reduced by substituting an Al or Be plate at the high potential end of the tube.

The authors wish to express their appreciation to Dr. T. W. Bonner for his advice and guidance. This work was assisted by the Joint Program of the ONR and the AEC.

---

[1] Parkinson, Herb, Bernet, and McKibben, Phys. Rev. 53, 642 (1938).
[2] A.O. Hanson, Rev. Sci. *Inst.* 15, 57 (1944).
[3] Fowler, Lauritsen, and Lauritsen, Rev. Sci. Inst. 18, 818 (1947).
[4] Bennett, Bonner, Mandeville, and Watt, Phys. Rev. 70, 882 (1946).

A Simple Automatic Water Distiller

NARCISO CORDERO AND IRINEO L. LAWAS
Laboratory of Biochemistry, College of Medicine, University of the Philippines, Manila, Philippines

September 8, 1949

THE distillation outfit here presented is a modification of the conventional glass distilling set which is available in practically all laboratories. By referring to the diagram, Fig. 1, the various parts may be appreciated.

The heating unit contains 50 ft. of nichrome wire (a) of gauge B & S 22, coiled to a spiral of about ⅛ in. diameter. The coil is laid horseshoe fashion at the bottom of a 1-liter Erlenmeyer flask of Pyrex glass, which serves as boiler. In this flask are also a feeder tube (b) and a glass siphon (c).

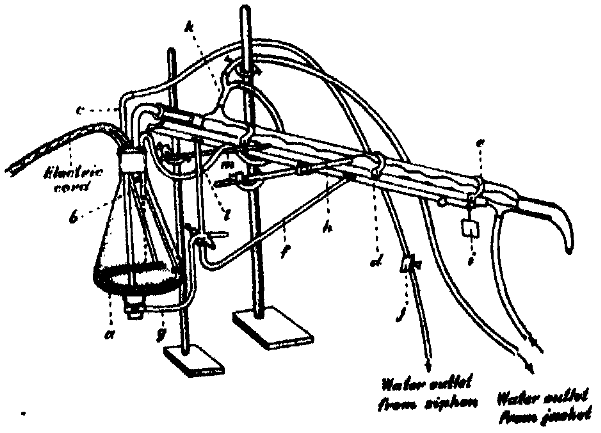

FIG. 1. Automatic water distiller.

(a) heating coil
(b) feeder tube
(c) siphon
(d) wooden strip mounting for condenser
(e) metal braces
(f) V-shaped metal rod
(g) bent clamp with cord
(h) metal rod serving as fulcrum
(i) counterpoise
(j) screw-clamp closing siphon outlet
(k) Y-tube from condenser jacket outlet
(l) rubber tubing of feeder tube
(m) metal rod serving as "rest"

The condenser is mounted by metal braces (e) on a grooved wooden strip (d) on the under surface of which are firmly attached:

1. A ½-in. metal rod (f) bent to a V, which, with the aid of cork at the tip of a clamp (g), supports the Erlenmeyer flask in position.
2. A ½-in. metal rod (h) passing at right angles to the condenser through 2 metal eyelets. Mounted on a sturdy iron stand, it is the sole support of the distiller assembly, and serves as fulcrum on which the whole outfit as a unit may swing see-saw fashion.
3. A 150-g weight (i) hangs from one of two hooks screwed 1 in. apart along the length at the distal end. It serves as counterpoise to obtain proper balance at the fulcrum during operation.

The feeder tube (b) receives water from the condenser jacket outflow through a y-tube (k) and a soft-walled rubber tubing (l) pressed between the under surface of the wooden strip (d) and another mounted metal rod (m) that serves as rest. When the flask is empty there should be no pressure exerted on the rubber tube, with a properly adjusted counterpoise, and fulcrum.

Operation. Starting with the boiler flask empty, the water supply is turned on. Part of the water from the condenser jacket enters the flask through the feeder tube (b). As the water in the flask rises high enough to submerge the heating coil and the binding posts, the wooden strip (d) tilts, compresses the rubber tubing (l), and decreases the water inflow into the flask. The siphon (c) is filled by suction from the flask and closed by screw clamp (j). The electric current is now turned on. As distillation proceeds the flask becomes lighter, pressure on (l) eases, and more water drops in, until the increasing weight of the flask slows the inflow again.

The automaticity is so effective that the inflow at the feeder tube maintains a nearly constant drip and the water level in the flask never changes more than 1 mm during distillation.

After several hours of operation the water in the boiler acquires a yellow color from concentrated soluble matter. Without stopping the electric current, the siphon is half-opened, and, as the hot water flows out, it is replenished by the feeder tube. The distillation slows down, but in 3 minutes the water in the boiler is clear again. The siphon is shut off, and in less than 1 minute the distillation goes on again full blast. Siphoning retards the accumulation of sediment. It is advisable to have an extra coil and Erlenmeyer flask always on hand for replacement during cleaning out, or in case of accidental failure of water supply.

The rate of distillation is about 2½ liters per hour. The distilled water has been tested and found to conform to the requirements for distilled water prescribed by the U.S.P.

The merits claimed for the set-up, in addition to its efficiency, are simplicity, and the ready availability of its component parts.

Measurement of Betatron Guiding Fields during Electron Ejection

E. C. Gregg, Jr.
Case Institute of Technology, Cleveland, Ohio

June 10, 1949

Due to the geometry and relatively unknown magnetic conditions, it has proved extremely difficult to calculate with any degree of accuracy the magnetic field strength as a function of radius and time in a betatron under typical orbit expansion or contraction conditions. Such factors are important not only when attempting to determine the optimum shape for conventional electron ejection but also for obtaining certain design parameters when considering beam removal and focusing.

A rather simple scheme for measurement of such fields is to use a small probe coil moveable along a radius and connected through an electronic integrating circuit to a cathode-ray oscilloscope operating with a linear sweep, as shown in Fig. 1.

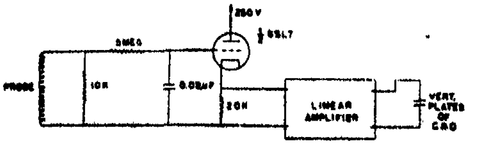

Fig. 1.

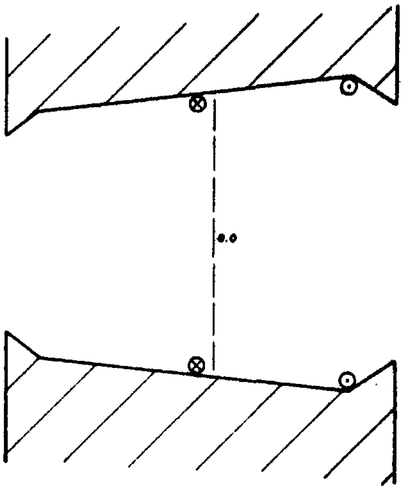

Fig. 2

The picture that is presented, of course, is the magnetic field as a function of time. If such patterns are measured (through photographs) for different positions of the probe, it is then possible to obtain H vs. r at any time t. If an expansion (or contraction) pulse is now added to the field by conventional betatron circuitry, this pulse will appear as a small but measurable pip on the pattern and will be the true field during the expansion pulse provided the integrator and oscilloscope are linear (both in amplitude and phase), over the required frequency band. Figure 2 shows the expansion coil arrangement relative to the pole faces and Fig. 3 log H vs. log r for the fields with and without expansion.

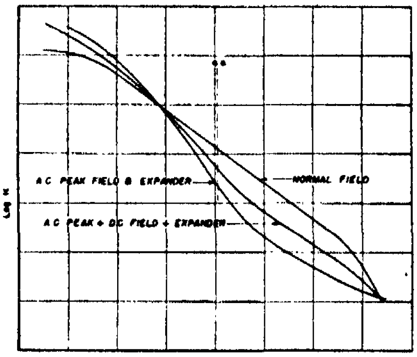

Fig. 3.

Measurements were made at the peak of the expansion pulse which was located in time at the peak of both the a.c. field (3200 oersteds) and the a.c.+d.c. field (5900 oersteds). Expansion currents were 640 amperes peak and 15μs half-width.

Delays in Rectangular Geiger Counters

G. E. Bradley and M. L. Wiedenbeck
Department of Physics, University of Michigan, Ann Arbor, Michigan

September 8, 1949

Recently Geiger counters of essentially rectangular geometry[1] have been used as high efficiency gamma-counters[2, 3] and in other applications in which their shapes are a convenience. When such counters are to be used for coincidence measurements, the delay in the initiation of the discharge will limit the resolving times which may be used.

We have measured the delays and efficiency of rectangular counters as a function of the position at which the ionizing particle passes through the counter. The counter which was used (Fig. 1) was 8 in.×4 in.×½ in. with a straight anode of 0.008-in. tungsten. The gas was a mixture of 9 cm argon and 1 cm ethyl alcohol.

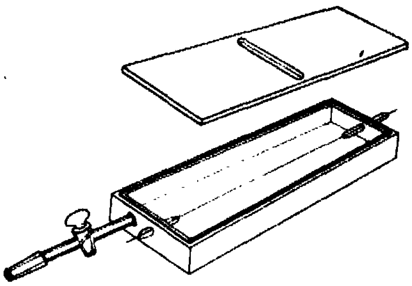

FIG. 1. Rectangular counter with inside dimensions 8×4×½ inches.

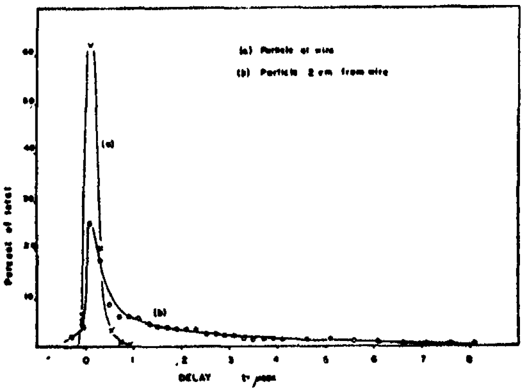

FIG. 2. Distribution of counts for various positions of the collimated beam of electrons.

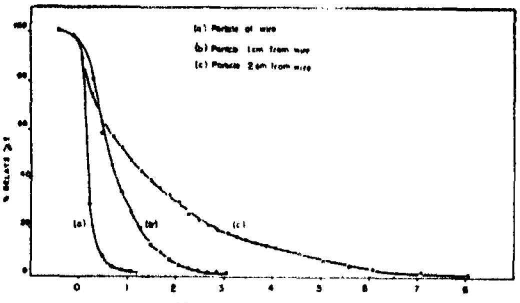

FIG. 3. Integral delay curves.

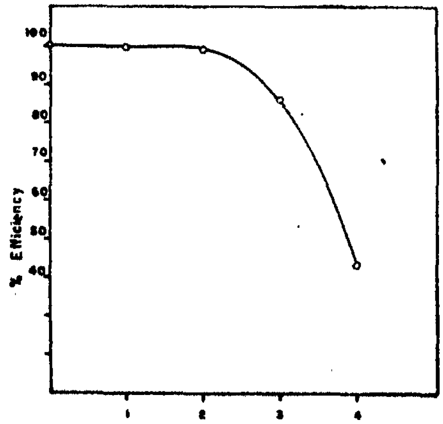

FIG. 4. Efficiency of the counter as a function of the position at which the electron passes through the counter.

A collimated beam of electrons was passed through a cylindrical Geiger tube near the anode and then through a mica window into the rectangular counter. The pulses from the cylindrical counter initiated the sweep of a synchroscope while the pulse from the rectangular counter produced a vertical deflection.

The delay curves are similar in shape to those obtained by Sherwin[4] for cylindrical counters. The peaks of these distribution curves fall at approximately 0.2 microsecond (Fig. 2). It should be noted that the position of the peak is essentially independent of the point at which the particle passes through the counter. A group of integral delay curves is shown in Fig. 3. The efficiency of the counter is plotted in Fig. 4 as a function of the distance from the wire at which the electron is sent through the counter. It is interesting to note that the efficiency is 100 percent for particles passing 2 centimeters from the wire although the delays at this position may be many microseconds.

---

[1] S. C. Curran and J. M. Reid, Rev. Sci. Inst. 19, 67 (1948).
[2] J. W. M. DuMond, Rev. Sci. Inst. 18, 626 (1947).
[3] J. R. Beyster and M. L. Wiedenbeck, Rev. Sci. Inst. 19, 819 (1948).
[4] C. W. Sherwin, Rev. Sci. Inst. 19, 111 (1948).

New Instruments

W. A. Wildhack: Associate Editor
in Charge of this Section
National Bureau of Standards, Washington, D. C.

These descriptions are based on information supplied by the manufacturer and in some cases from independent sources. THE REVIEW *assumes no responsibility for their correctness.*

Germanium Diodes Raytheon Types CK705, 706, 707, and 708 are new germanium diodes with excellent high frequency characteristics, and whose unusual features are small size (0.390 in. long and 0.160 in. diameter), distinctive marking using a color code, high ambient operating temperature rating of 100°C, and resistance to change in humid atmospheres. The higher temperature rating is obtained by using only glass and metal in the basic assembly, thus eliminating the necessity for a wax filler. In addition to total immersion, this design has withstood more than 72-hr. exposure to 95 percent humidity at temperatures from 25°C to 70°C.—RAYTHEON MANUFACTURING COMPANY, SPECIAL TUBE SECTION, *55 Chapel Street, Newton, 58, Massachusetts.*

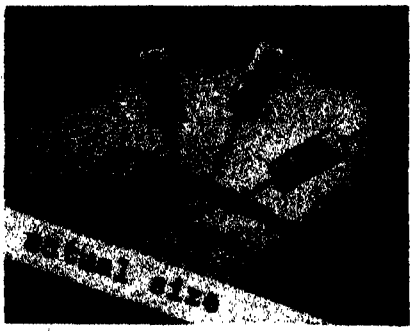

Secondary Frequency Standards Two new moderately priced secondary frequency standards, offering many of the advantages of expensive primary standards, are the -hp- 100C and 100D secondary frequency standards. They replace earlier -hp- models, and offer a number of important new advantages in addition to all the features of the old models 100A and 100B.

The new -hp- Model 100D offers rectangular wave output, timing pips at intervals of 100, 1000, and 10,000 microseconds, and an internal oscilloscope for convenient frequency comparison. This instrument may be conveniently standardized against Station WWV by using only a standard oscillator and a communications receiver. Thus the instrument provides most of the advantages of a primary standard at much less cost.

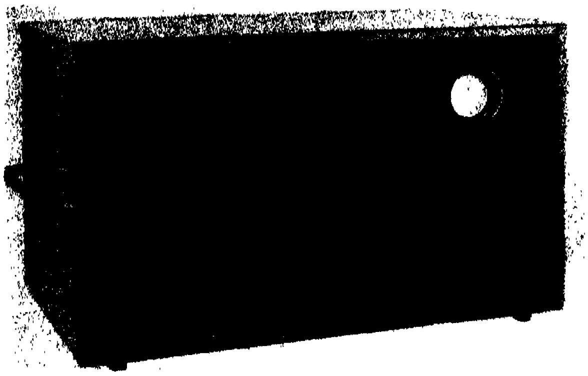

Both models employ crystal-controlled oscillator and divider circuits offering high stability and operational ease. Standard frequencies can be quickly selected on a front panel switch and may be employed simultaneously. Internal impedance has been held to around 200 ohms, so the standard frequencies can be delivered at some distance from the instrument. The output voltage is five volts, at all frequencies.

The -hp- 100D offers sine waves at five frequencies and rectangular waves at four frequencies. Accuracy is in the order of two parts in one million.

The 100C offers sine waves only, at four crystal-controlled frequencies. Accuracy is 0.001 percent.

Both instruments operate from a self-contained 115-volt regulated a.c. power supply.—HEWLETT-PACKARD COMPANY, *395 Page Mill Road, Palo Alto, California.*

High-Current Rectifiers

Dual selenium rectifier elements measuring 7¼ in.×12¾ in. have been developed by the International Rectifier Corporation. Each dual element consists of two of the company's largest size plates, 6¼ in.×7¼ in., strapped in parallel and rated in a three-phase bridge circuit at 34 amperes for continuous duty self-cooling, 85 amperes for continuous duty fan-cooling, and 340 amperes for highly intermittent duty. Dual elements are assembled in the company's three-phase bridge heavy duty 10 kw-rectifier, stack-rated at 1500 amperes.

Stacks are designed on the basis of 16 kw per cubic foot and are provided with an interlocked assembly to prevent lug misalignment and plate rotation. They are covered with a multiple-dipped black coating for improved heat radiation and protection against high humidity, excessive moisture, and other adverse atmospheric conditions. Operating efficiencies of 85 percent can be obtained, and when aluminum plates are used, the weight per dual element minus the hardware is nine ounces. Each 1500-ampere stack is 7¼ in. wide by 12 in. long by 14¾ in. high.

These dual rectifier assemblies are especially applicable for high current, intermittent duty, medium voltage applications (550 volts and below), and are being used to eliminate large storage battery banks with resultant elimination of maintenance costs and outage time.—INTERNATIONAL RECTIFIER CORPORATION, *6809 South Victoria Avenue, Los Angeles 43, California.*

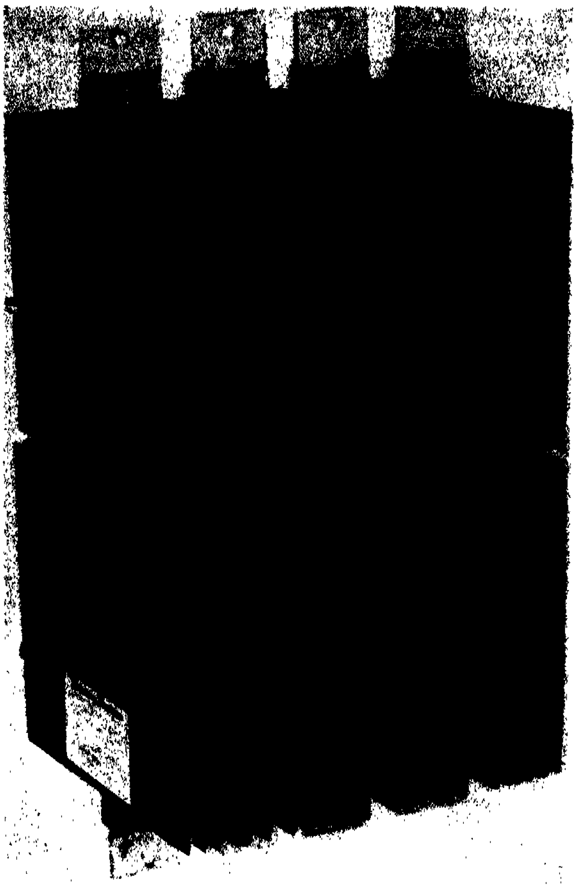

Spotwelder

Unimatic, a new automatic spotwelder, introduces a simplified "pushbutton spotwelding"; rheostats and other auxiliary adjustments have been eliminated. Designed primarily for use with light-weight stainless steels, the new Unimatic weld shows no evidence of burning, heat distortion, discoloration, or splattering.

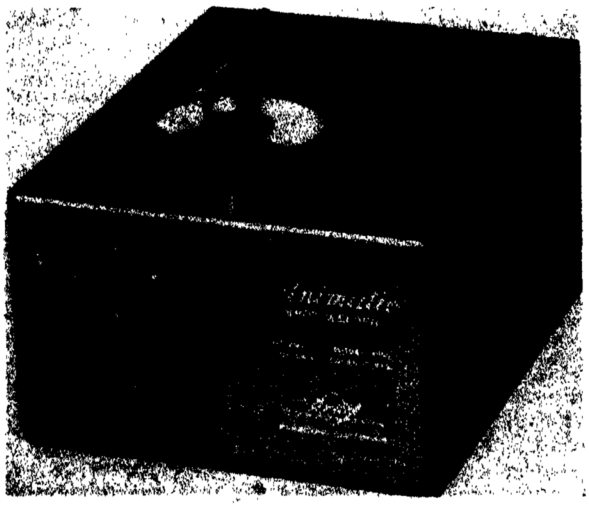

The "automatic" feature has been developed by incorporating in the welder a sensitive electronic circuit. When actuated by a touch of the welding button, the electronic brain instantly determines the amount of resistance heat required to homogeneously bond materials through a range of thicknesses. This automatic gauging and simultaneous welding eliminates guesswork on the part of the operator and results in burn-free welds of greater strength.

The Unimatic welder has been designed to meet the exacting requirements of the light-materials field. Uniform and dependable performance insures a strong, clean-finished weld.

The unit is sturdily built and compactly designed (9¾ in. long ×6¼ in. wide ×4½ in. in diameter), and operates on 110-120 volts a.c. 50–60 (cycle). Special models are available for other current supply.—UNITEK CORPORATION, *697 North Lake Avenue, Pasadena 6, California.*

Electron Microscope Accessories

Three new accessories permit specialized application of the electron microscope. They include a Type EMN-1 charge neutralizer, a Type EMX-1 focusing magnifier, and a self-bias gun kit.

The EMN-1 charge neutralizer is designed to neutralize charges produced on diffraction specimens by the primary electron beam of the microscope, which may cause distortion of the image. Essentially, the unit consists of a heated filament which sprays a low velocity stream of electrons into the diffraction specimen chamber. It is easy to install and operate, and is supplied complete with power supply which operates from a 115-volt, 50- or 60-cycle a.c. line, and draws approximately 60 watts.

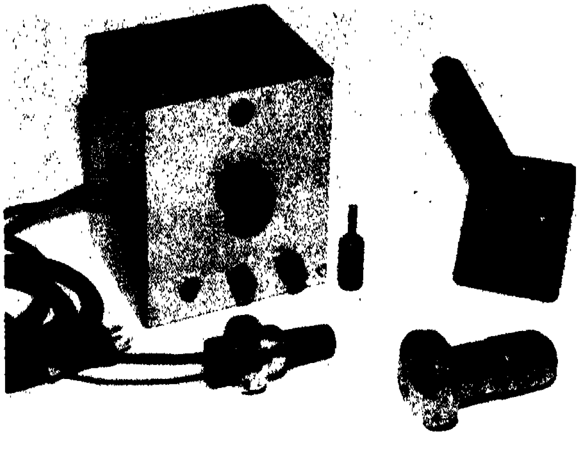

The Type EMX-1 focusing magnifier enables the microscope operator to focus upon a certain portion of the image field with greater precision. It permits direct viewing of the image at 150,000 magnifications, and greatly improves the quality of electron micrographs obtained. The attachment consists of a low power microscope mounted on a metal plate which may replace either of the viewing chamber side windows, a small prism coated on the upper face with fluorescent material, and a control handle to move the prism into and out of the electron beam path. The optical system consists of a 3.5-power objective lens and a 4-power eyepiece, providing a total magnification of 14 times. The attachment is 8 inches in over-all length and weighs 2¼ pounds.

Simplified alignment, greater stability, and improved over-all performance of the microscope are made possible by the self-bias gun kit, MI-12986. This attachment provides intense illumination with lower beam current. The intensity of the electron beam produced by the gun is controllable, making it possible to obtain maximum resolution in studies of a wide range of specimens.

The gun is useful when employing the diffraction adapter of the microscope to obtain diffraction patterns of specimens, since it supplies a high intensity, single-source electron beam that is most effective in this application. In conjunction with the focusing magnifier, the gun makes easy the detection of vibration, image drift, and magnetic field effects. The RCA self-bias gun is interchangeable with the zero-bias gun which is standard equipment for the Type EMU electron microscope.—SCIENTIFIC INSTRUMENT SECTION, RCA ENGINEERING PRODUCTS DEPARTMENT, *Camden, New Jersey.*

Direct Coupled Amplifier

The Type 112 direct coupled amplifier has a band width of d.c. to one megacycle when used at a maximum voltage gain of 5000. For voltage gain requirements of 166 and less, the band width extends to 2 megacycles. An output of approximately 150 volts (peak to peak) is available to a high impedance load such as CRT deflection plates. Continuously variable control of gain, 15 to 5000, is accomplished by the combination of a step and variable attenuator. Either single-ended or differential input may be employed.

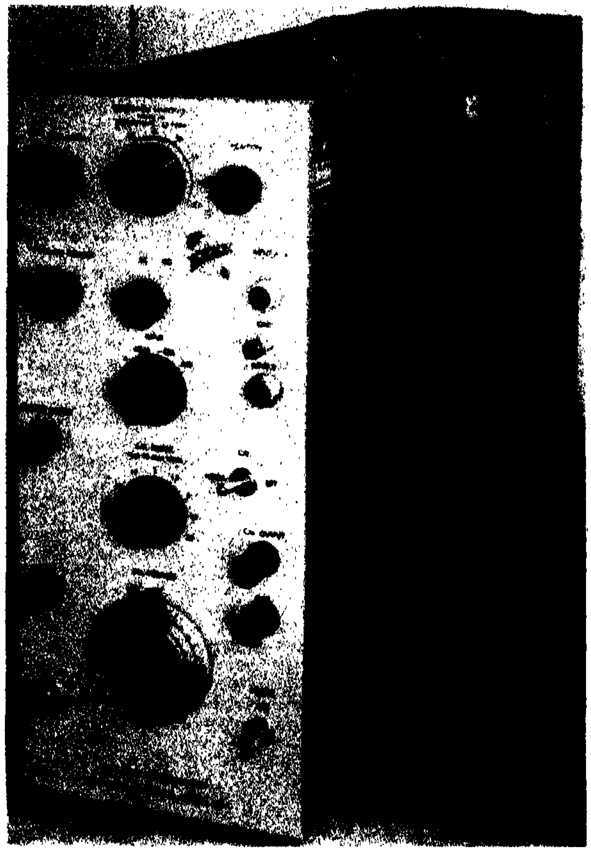

A one-kilocycle square wave calibrating voltage from 0 to 50 volts is available by a nine-position range switch in conjunction with a calibrated potentiometer providing an accuracy of plus or minus five percent, and the unit has unusually low drift characteristics.

This amplifier has been developed primarily as an accessory to the Tektronix Type 511-A, Type 511-AD, and Type 512 cathode-ray oscilloscopes. Its combination of high gain and wide band characteristics suggests other uses. Weight is approximately 30 pounds.—TEKTRONIX, INC., *712 S. E. Hawthorne Blvd., Portland 14, Oregon.*

Mica Window Counter

In the field of beta-ray counting, Radiation Counter Laboratories has produced a new RCL fusion seal mica window counter, the

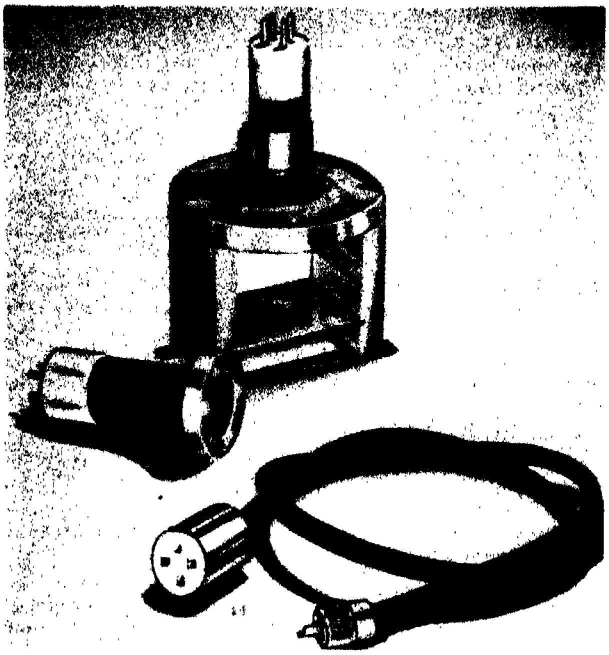

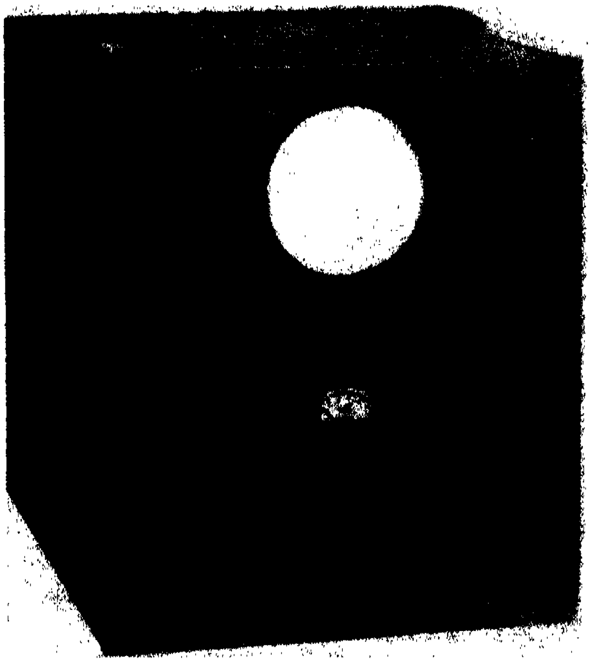

Mark 1, Model 3. In this counter the thin mica window is rigidly sealed by a direct mica to glass fusion—thus avoiding the leakage possibilities inherent in counters using cements, organic binders etc. A smooth, clear, lead borosilicate "seal bridge" is established, having a coefficient of expansion between that of lime glass and that of mica. A wide flange insures a large mica to glass area and the mica window is housed by metal fittings to provide against breakage.

The tube may be firmly supported on the standard RCL Lucite mount by a metal attachment which makes possible an accurate adjustment of the tube position. The convenient tube socket makes the tube adaptable to various commercially available shields.

The counters are available with mica window thicknesses of 3–4 mg/cm^2. For those experimenters using less energetic emitters such as C^{14} and S^{35}, mica window thicknesses of less than 2 mg/cm^2 are available.

Each counter tube is checked twice before it leaves the laboratory and complete threshold and plateau curves are provided with each unit tube. A shelf or storage life guarantee of six months accompanies the counter.—RADIATION COUNTER LABORATORIES, INC., *1844 West 21st Street, Chicago, 8, Illinois.*

Dual-Channel Oscilloscope

With the H-21 dual-channel oscilloscope it is possible to observe and analyze two independent and rapid phenomena occurring simultaneously. Such variables as speed and vibration, input and output signal of amplifiers, velocity and acceleration, or even a complete signal with an expanded portion of the signal can be compared.

The new H-21 contains two separate and complete electron guns in a single, five-inch flat face tube. Each channel has individual controls for intensity, focus, and X, Y, and Z axes. Vertical deflection sensitivity is less than 0.1 volt d.c./inch. Vertical amplifiers have conductive differential input in the 1X attenuator setting, allowing the use of push-pull preamplifiers for medical purposes. Vertical and horizontal amplifier outputs are interchangeable, thus allowing the connection of the more sensitive amplifier to the horizontal deflection plates for visual or photographic purposes. Triggering is in continuous sweeps of 2 c.p.s. to 50 kc; ½ second to 20 microseconds. Delay after triggering is less than one microsecond. Calibration voltage is continuous and indicated, 0 to 1 volt peak to peak, on a panel voltmeter. Range, up to 100 volts, is governed by the attenuator setting. Weighing only 65 pounds, and 14¼ in.×16¾ in.×21 in. in size, the H-21 should also prove valuable wherever weight and size are important factors. Designed for complete accessibility, every part can be brought into full view within 30 seconds.—ELECTRONIC TUBE CORPORATION, *1200 East Mermaid Lane, Chestnut Hill, Philadelphia 18, Pennsylvania.*

High-Speed Mechanical Sampler

A new high speed mechanical sampling device has sampling rates and performance far exceeding those of any known device of this type. Clean and reliable switching at sampling rates up to and exceeding 5000 cycles per minute is successfully achieved with good life. Sixty make-before-break contacts are sampled each cycle. Switches with 30 contacts are available with even higher sampling rates.

The switch is so designed that it may be driven by an external shaft thus permitting direct synchronization of electrical circuits with mechanical motion. The device may also be furnished in one unit with driving motor of any design or speed within the above

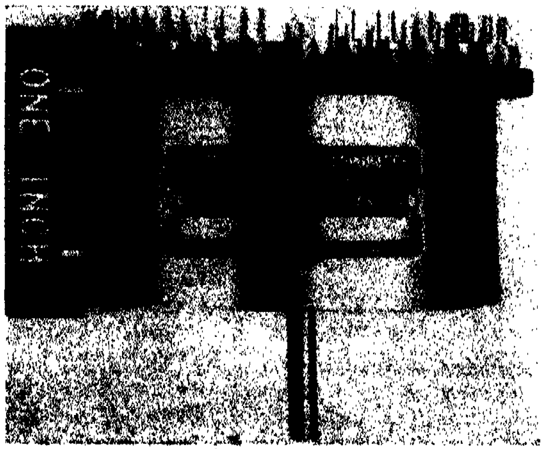

limits. Power drain is extremely low which renders it particularly attractive for many applications. The switch is completely encased as a protection against foreign material. It is operable at wide temperature ranges and under high forces of acceleration.—APPLIED SCIENCE CORPORATION OF PRINCETON, *P. O. Box No. 44, Princeton, New Jersey.*

Microscope

A new low-priced industrial microscope, Model 232, is available for general industrial and laboratory use. This instrument is a high quality, medium power microscope with built-in illumination and measuring scale (reticle), and high quality optics.

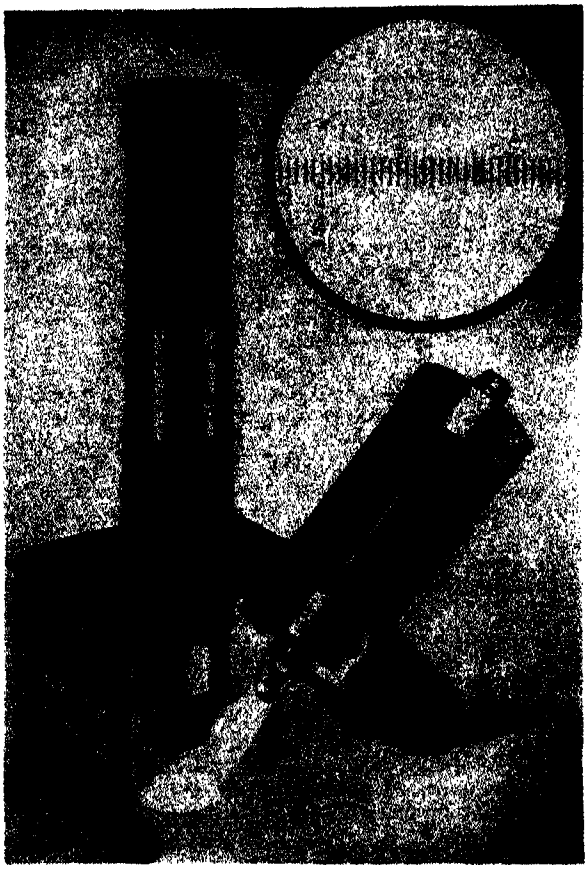

With a magnification of either 20× or 40×, this microscope has excellent resolving power and light efficiency.

For quantitive measurement and analysis of all types, a reticle has been incorporated for direct measurements with divisions of 0.004 in. and 0.002 in. for respective powers.

The eye point is more than one inch above the eyepiece. This enables the operator to work when wearing glasses, thus providing corrected vision for all examination. Focusing by means of the friction sliding tube is easy and positive.

Finish is in black Dulite, polished chrome, and deep maroon baked enamel. Ruggedly built, the instrument is light and portable with its own carrying case.—CLARKSTAN CORPORATION, *11927 West Pico Boulevard, Los Angeles 34, California.*

Manufacturers' Literature

Electronic Components—50-page Catalog No. 49 is a technical reference manual of tube sockets and shields, connectors, terminal strips, lugs, clips, brackets, and miscellaneous items.—CINCH MANUFACTURING CORPORATION, *Chicago 12, Illinois.*

Multipot—Technical data sheet on three series of small precision potentiometers, with power ratings of 1½ to 5 watts and linearities to within ±0.03 percent.—FORD ENGINEERING COMPANY, *Box 153, Los Angeles 41, California.*

Relays—Catalog D-20A describes and illustrates industrial and general-purpose relays and gives general information of the function of relays. Types of relays included are sensitive, midget metal base, heavy duty midget, midget magnetic, heavy duty power, thermal time delay, and motor-driven time delay relays.—WARD LEONARD ELECTRIC COMPANY, *31 South Street, Mount Vernon, New York.*

Spectrogram Comparator—Bulletin 168-49 describes and illustrates a comparator of the traveling microscope type intended for measuring spectrographic plates and similar records. The instrument reads to one micron over a range of 155 mm.—GAERTNER SCIENTIFIC CORPORATION, *1201 Wrightwood Avenue, Chicago 14, Illinois.*

Minature Standard Cell—Bulletin B-638-A. Design of cell radically departs from the classical-mechanical construction of the Weston standard cell, although retaining the original electrochemical design. Size is ⅞ in. square by 3½ in. high.—MUIRHEAD AND COMPANY, LTD., *Elmers End, Beckenham, Kent, England.*

Resistors and Sound Equipment—36-page Catalog No. 11-A illustrates and gives specifications on precision resistors, variable attenuators, and various items of electronic equipment including audio amplifiers and power supplies. Also included are mixer attenuation curves, mixer circuits pad formulas, and a voltage ratio table.—CINEMA ENGINEERING COMPANY, *1510 West Verdugo Avenue, Burbank, California.*

Mercury Switches—16-page Catalog No. 1343 describes a number of switches of two basic types, mercury-to-electrode and mercury-to-mercury. Their manufacture and testing is shown and typical applications are outlined.—MINNEAPOLIS-HONEYWELL REGULATOR COMPANY, BROWN INSTRUMENT DIVISION, *Wayne and Roberts Avenue, Philadelphia 44, Pennsylvania.*

Sheet Materials Testing—20-page Bulletin No. 1400 describes instruments and procedures for various methods of testing paper, paper-board, textiles, plastics, and other sheet materials.—W. AND L. E. GURLEY, *Troy, New York.*

Accelerometer—Single-sheet Bulletin No. 4.4 describes subminiature accelerometer Model F for detecting and measuring static or dynamic accelerations in applications requiring miniature components. It is ½ in. square by 2$\frac{7}{16}$ in. long, including terminals; weight, 23 g. Measures from ±4 g to ±25 g, depending upon the model.—STATHAM LABORATORIES, *9328 Santa Monica Boulevard, Beverly Hills, California.*

Optical Glass—24-page Catalog E-30 is the first optical glass catalog that Bausch & Lomb has issued since the start of World War II. It features the story of the manufacture of optical glass and lists technical specifications of available Bausch & Lomb glass.—BAUSCH & LOMB OPTICAL COMPANY, *Rochester 2, New York.*

Precisionomics—A new bi-monthly house journal contains items of interest to scientific and laboratory workers and to the general trade. Specialized fields, including petroleum, metallurgy, rubber, plastics, cement, soils and lime, plus laboratory utilities, will have articles of interest.—PRECISION SCIENTIFIC COMPANY, *3737 West Cortland Street, Chicago 37, Illinois.*

Colorimeter—Single-sheet Bulletin B-214 describes a new type of filter colorimeter differing from the ordinary precalibrated or visual colorimeter. Some of the features of the Coleman filter photoelectric colorimeter are a galvanometer scale panel calibrated in transmission and density, which is removable for insertion of other calibrated panels for a particular analysis; filters covering six uniform increments of spectral purity; selection of curvettes from 25 mm depth to capillary size; a photo-cell operating at extremely low sensitive levels, insuring better linearity, freedom from cell fatigue, and accompanying drift.—E. Machlett and Son, *220 East 23d Street, New York 10, New York.*

High Vacuum—Single-sheet describes and illustrates Type "R" 90° packless valve of the bellows type, compact but designed for minimum flow resistance in high vacuum service. Also on this sheet are described a packless throttle valve Type R62ST, couplings for glass-to-metal or metal-to-metal joints on vacuum systems, tubing for introducing a standard leak, a variable leak, and a sensitivity tester for leak detection.—Vacuum-Electronic Engineering Company, *316 37th Street, Brooklyn 32, New York.*

New Materials

Forest K. Harris: Associate Editor in Charge of this Section
National Bureau of Standards, Washington, D. C.

Hafnium

Hafnium (element 72) is very scarce in pure form but is usually present to some extent as an impurity in zirconium, from which it may be separated only with difficulty. There is no known chemical reaction which is possessed by one of these elements but not by the other, so that any method employed for their separation (crystallization, precipitation, distillation) is necessarily fractional in character. Hafnium is not easily obtained in the massive state by fusion because of its high melting point. The hot-wire technique may be used. Crude hafnium is heated in an atmosphere of iodine to obtain hafnium tetraiodide. The tetraiodide is vaporized at 600°C and, upon coming in contact with a tungsten filament at 1800–2000°C, deposits hafnium. In this way bright, ductile hafnium filaments 2–4 mm in diameter may be produced.

The important physical characteristics of hafnium are listed in Table I. Its properties are very similar to those of zirconium. It is a brilliant metal which is soft and pliable like copper. It can be cold-rolled, hammered, or drawn. It is gas sensitive, traces of oxygen or nitrogen ruining its malleability. There are no deoxidizers known for hafnium because it is so reactive itself. If a cold-worked piece of metal is annealed, the absorbed gases react to increase its electrical resistance and decrease its temperature coefficient of resistance.

Table I.

Melting point	*ca.* 2230°C
Specific gravity	12.1
Atomic volume	13.42A_3
Ionization potential	7.3 volts
Electrical resistance at 0°C	0.30×10^{4} ohm-cm
Temperature coefficient of resistance	0.44×10^{2}
Specific heat at 210°K	6.02 g cal./g atom
Atomic weight	178.6

Compared to most metals hafnium is relatively new, comparatively scarce (because of the difficulty in separating it from zirconium), and quite expensive. As a consequence its commercial possibilities are quite limited at present. Owing to its high melting point and electron emission it has been tested as a filament in lamps and vacuum tubes and as a cathode in x-ray tubes. Hafnium nitrate is added to tungsten oxide to the extent of 0.1–0.3 percent prior to the reduction of the oxide to tungsten. In this way grain growth is controlled with decreased tendency to offsetting. Special glasses have been prepared using hafnium. Patents have been issued for alloys prepared from hafnium with nickel, copper and silver; with manganese, chromium, iron, cobalt, nickel, and copper; and with 80 parts nickel, 20 parts chromium, and 0.5 parts hafnium in the production of electrical resistance heating elements.

The above material was abstracted from an article entitled "Hafnium" by D. R. Martin, in the current issue of *Foote-Prints* [21, No. 1 (1949)].—Foote Mineral Company, *18 West Chelten Avenue, Philadelphia 44, Pennsylvania.*

Laminated Metal

Inter-Weld is a process in which gold is permanently bonded to a non-ferrous metal base. Gold is welded to a barrier layer of pure nickel which is in turn silver-soldered to the base metal. The nickel barrier prevents the silver solder from bleeding through into the gold. Brass, nickel, monel, cupro-nickel, and beryllium-copper may be used as base metals. The entire assembly can be rolled to a thickness as small as six mils. Ratio of gold to over-all thickness can be as low as 1/600 with the gold measuring nine millionths of an inch. Strips four inches wide and in any length are available. The material is shipped in rolls interleaved with tissue or with the mirror finish protected by a strippable plastic coating that can be left in place for stamping and drawing operations.—American Silver Company, *36–09 Prince Street, Flushing, New York.*

Improved Carbide for Tools

Higher hardness, more wear resistance, greater cutting-edge strength and cratering resistance, and a more rapid dissipation of heat at the cutting edge are claimed for an improved *No. 905 Grade Carboloy* cemented carbide, used for light roughing cuts and finishing on non-ferrous metals and cast irons with hardness up to Brinell 550. The new material is stated to be fully as easy to braze and grind as was the old Grade 905, with increased service life and an improvement in holding size on long cuts and high production jobs. Performance tests have also shown that heat is carried away more rapidly from the cutting edge. Many sizes and types of standard tools and blanks in the new material are carried in stock.—Carboloy Company, Inc., *Detroit 32, Michigan.*

Metallurgical Products

Flawmaster is a thermoplastic compound which may be used to reclaim metal parts and castings with surface flaws, gas holes, faulty machine surfaces etc. It is applied manually, curing time being adjusted (between three minutes and 48 hours) by the addition of a polymerization agent. After curing it is machinable, chemically inert, and resistant to a wide range of temperatures (−75°F to 500°F). It is designed for the permanent stoppage of leaks in liquid and pressure-tight parts, and is applicable to both ferrous and non-ferrous metals.

Bonding Agent R-313 is designed for manually bonding dissimilar and similar materials such as glass, plastics, Neoprene, leather etc. to metals; and ferrous to non-ferrous metals. It is stated to meet high industrial requirements for pressure, chemical, and temperature resistance.

One advantage offered by both of these products is their simplicity of application, which is manual, no elaborate machinery being required. Descriptive literature may be obtained from the manufacturer.—Western Sealant, Inc., *9042 Culver Boulevard, Culver City, California.*

Rubber Seal

A change to a newly developed Neoprene for the rubber components of *Sealnut* (a combination mounting and sealing device for toggle switches and control shafts) provides greater flexibility at low temperatures and greater resistance to sunlight, weathering, and other aging factors. *Sealnut* is used extensively in equipment to prevent dirt, water, or gas from entering panels around switch and control shafts. A flexible elastic sleeve tightly grips the protruding shaft or toggle. An internal rubber ring seals the nut to the panel, yet permits metal-to-metal contact, insuring a solid mounting. It has been approved for various splash-proof and water-tight requirements and finds many indoor uses for protecting equipment in the presence of dusts or corrosive fumes. It can be readily substituted for standard mounting nuts now in service.—Radio Frequency Laboratories, Inc., *Boonton, New Jersey.*

Hydraulic Fluid

Lindol HF-X is a flame resistant hydraulic fluid with a tricresyl phosphate base. As it is not chlorinated it does not give off noxious fumes when exposed to high temperatures. Because of this feature, combined with its non-burning property, high lubricity, corrosion resistance, and low cost, it is expected to be widely incorporated in hydraulically operated installations. It is available in a wide range of viscosities and can be used in any system equipped for non-hazardous hydraulic fluid operation, or in any other system with but few changes. The manufacturer states that the initial cost of the material is lower than that of any comparable product and that lower maintenance costs offer added economies.—CELANESE CORPORATION OF AMERICA, *180 Madison Avenue, New York 16, New York.*

Paint Remover

A new paint remover has been developed which is believed applicable to high speed industrial processes. Aircraft camouflage enamels were so resistant to ordinary paint remover techniques that a special preparation was developed by the Air Force for this purpose. It was not, however, stable enough in storage to give satisfactory service. It is believed that revisions in the basic formula have met the storage problem, and that a specification now exists which is superior to special purpose proprietary items previously available. The material is applied by a spray method and is followed by a high pressure water wash.

This material is described in a report PB-97658, "Development and evaluation of paint remover," available from the Office of Technical Services at $1.75 per copy. (Checks or Money Orders should be made payable to the Treasurer of the United States.) The report also contains details of systematic tests made for the substitution of various components in the basic paint remover specification. As a result, a variety of satisfactory materials may be used.—OFFICE OF TECHNICAL SERVICES, *U. S. Department of Commerce, Washington 25, D. C.*

Cutting Oil Additive

501 Oilsaver is a product which, added in small concentration (1 in 400) to water, permits a 50 percent reduction in the water-soluble oil used, with no loss in coolant standards. This product also leaves an invisible protective film on surfaces it contacts with consequent rust protection of machines and machined parts. It is non-flammable, non-toxic, and does not have an unpleasant odor. It can be used in most water-soluble cutting oils and in a wide range of dilutions.

The manufacturer will supply a free test kit on request. It is suggested that the request be accompanied by a description of the machining operation, metal worked, cutting oil, and dilution formula.—THE BEACON RUST PROOFING MANUFACTURING COMPANY, *20 East 33 Street, New York 16, New York.*

Special Cooling Oil

Cyclotron Oil was developed especially for cooling the magnet coils of Carnegie Tech's synchro-cyclotron and was donated to the project by the Gulf Oil Corporation. It permits direct-contact cooling of the copper coils in channels as narrow as $\frac{1}{16}$ in. and therefore enables the coils to be more closely spaced than is possible in other designs, with a consequent reduction in magnet size. The oil is a good electrical insulator and has the unusual characteristic of resisting sludging and "breakdown" in contact with copper.—GULF OIL CORPORATION, *Pittsburgh, Pennsylvania.*

THE
REVIEW OF SCIENTIFIC
INSTRUMENTS

VOLUME 20, NUMBER 12 *DECEMBER, 1949*

Direct Calorimetry by Means of the Gradient Principle

T. H. BENZINGER AND C. KITZINGER
Naval Medical Research Institute, Bethesda, Maryland

(Received April 8, 1949)

A rapidly responding calorimeter for continuous recording of biological heat exchange has been described. The method is based on the enclosure of the subject in a shell completely lined with a uniform heat flow metering layer ("gradient layer") while ventilatory and respiratory heat losses are determined in heat exchange meters based on the same technic. The measurement comprises in one thermoelectric potential the sum of all components of heat loss (radiant, convective, conductive, and evaporative fractions). Partitioning measurements of respiratory and evaporative heat losses are readily obtained. Environmental conditions can be closely controlled, and widely varied.

The gradient calorimeter with its rapid response (time lag 42 seconds) is specifically designed for studies of reflex mechanisms involved in temperature control. It is, however, suggested that the characteristics described will, in general, encourage wider application of direct calorimetry in experimental and clinical studies.

I. BACKGROUND

IN the history of human calorimetry both indirect and direct methods have been shown to be of merit. Although direct calorimetry was first employed (A. Lavoisier, 1793), indirect chemical procedures introduced by Regnault and Reiset in 1849 attained wider use mainly because such measurements were less expensive and more convenient. New objectives required simultaneous application of both direct and indirect methods. Direct calorimetry was again resumed when Rubner compared heat loss and energy production from oxygen and food, in 1891. He formulated his results in the famous statement, that the law of conservation of energy is valid in the human body. Later on, direct calorimetry produced a wealth of knowledge in studies on nutrition (Graham-Lusk, Benedict, and others) and was finally extended to new fields, with the investigation of mechanisms involved in heat loss and the maintenance of internal body temperature. Dubois[1,2] and Hardy[3,4] achieved results of fundamental importance employing classical methods such as the Atwater-Rosa-Benedict and the Russell-Sage calorimeter.

The classical calorimeters, however, were difficult to operate. Many single readings had to be taken by several observers and many calculations and corrections were required after the experiment was completed. Long preparation was necessary before reliable measurements could be obtained, and the response of the calorimeter to changes in thermal output was extremely slow, requiring as much as an hour of full response time. Hence, for the clinical determination of energy exchange, direct methods have never competed successfully with indirect methods using gas analysis. If simpler methods for the thermal measurement of heat output could be developed, direct calorimetry would be the procedure of choice in many instances.

The recent trends in direct calorimeter design have been in the direction of automatic operation and a diminished inherent inertia in the instrument. The contributions made by Benedict,[5] Bothe,[6] Leschke,[7]

---

[1] E. F. DuBois, *Basal Metabolism in Health and Disease* (Lea and Febiger, Philadelphia, 1936), third edition.

[2] E. F. DuBois, *The Mechanism of Heat Loss and Temperature Regulation* (Lane Medical Lectures, Stanford University Press, Stanford University, California, 1937).

[3] J. D. Hardy and E. F. Dubois, "Regulation of heat loss from the human body," Proc. Nat. Acad. Sci. 23, 624 (1937).

[4] J. D. Hardy and G. F. Soderstrom, "Heat loss from the nude body and peripheral blood flow at temperatures of 22°C–35°C," J. Nutrition 16, 473 (1938).

[5] F. G. Benedict, "Zwei elektrisch kompensierte Emissionskalorimeter für kleine Tiere and Säuglinge, und für Erwachsene," Handbuch der biol. Arbeitsmethoden, Abt. IV, Teil 13, 689 (1934).

[6] W. Bothe and H. Wollschitt, "Neue Geräte für direkte und indirekte Kalorimetrie," Handbuch der biol. Arbeitsmethoden, Abt. IV, Teil 13, 943 (1937).

[7] E. Leschke, "Graphische Stoffwechselregistrierung," Handbuch der biol. Arbeitsmethoden, Abt. IV, Teil 10, Heft 5, 891 (1926).

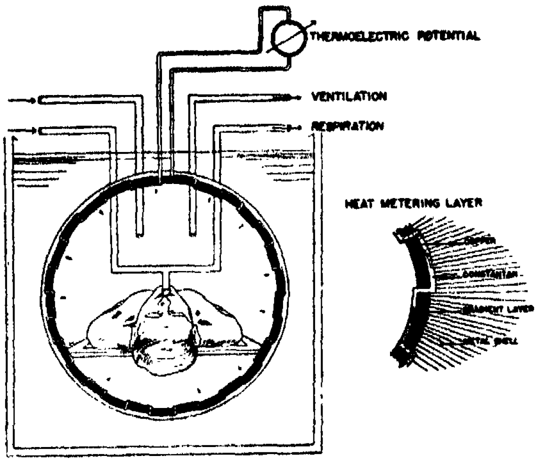

FIG. 1. Scheme of a gradient calorimeter.

Burton,[8] Burton and Bazett,[9] Barrows and Murlin,[10] Murlin and Burton,[11] Winslow, Herrington, and Gagge,[12,13] and Palmes and Park[14] are widely recognized and the description of their work needs no repetition.

Despite efforts to reduce the inertia in direct calorimetry, the response time has remained far slower than the rate of heat transfer from the subject to the measuring system, this latter rate being the limiting factor in the measurement of total heat output. Efforts to develop a human calorimeter with a shorter response time appear to be justified. Immediate changes of human heat loss must be expected when environmental conditions are suddenly altered. Changes of posture, effects of drugs, procedures used in physical therapy, and muscular exercise may result in rapid fluctuations of thermal output. Reflex responses to thermal stimuli, involved in the mechanisms of heat regulation and temperature control, might thus affect heat loss so rapidly that existing calorimeters could not adequately follow the course of physiological events. These objectives call for continuously recording procedures. However, direct immediate recording of the total heat exchange has not been achieved in the past. Certain components of the total have required separate measurement by various means, such as the determination of evaporative heat loss gravimetrically or by infra-red absorption of water vapor. Another example is the computation of radiant heat output as derived from average skin and wall temperatures. Such methods are cumbersome and liable to error. Therefore, it was made the object of the present study to develop an accurate and rapidly responding instrument for immediate, complete, and continuous recording of the human heat loss. Our method is based solely on the physical laws of heat transfer.

II. PRINCIPLES UNDERLYING THE OPERATION OF A HEAT-MEASURING SHELL WITH GRADIENT LAYER

When heat is transmitted across a layer of thermally conducting matter, a difference in temperature will be found to exist between the two surfaces of the layer. It follows from the definition of thermal conductivity, that

$$\vartheta_q = q \times D/\lambda,$$

where: ϑ_q = difference of layer surface temperatures (°C), q = heat flow (cal./sec.), D = thickness of layer (cm), λ = specific thermal conductivity of the layer material (cal./sec. cm °C). If D and λ are kept constant, the "gradient" ϑ_q can be used either for an instantaneous measurement or continuous recording of the heat flow, q. The gradient at any point of the layer may be measured by fixing one of a pair of electric thermometers on each side of the layer at that point. Such an arrangement may be called a "gradient layer."

The principle has formerly been used to determine local heat flows, or to establish thermal characteristics of materials (Nichols' heat flowmeter). It has also been used to determine local heat loss in humans (K. Büttner[15]).

Fewer attempts have been made to use the gradient principle in the measurement of total heat loss from biological or other sources of heat. J. D. Hardy and R. Day (1941)[16] have described an example of such an application to an infant calorimeter. This publication came to our attention after the war.

The Day-Hardy calorimeter consists of a copper shell built in the form of a box, inside of which 12 copper plates are mounted at a distance of 1 cm from the wall. The temperatures of these plates are measured against standard temperatures every 3 to 5 min., by means of one thermocouple for each plate, calculative comparison being made with the temperature of the surrounding air as measured with thermocouples above and underneath the copper shell at four different places. Under the conditions of their experiments, Day and Hardy found the average gradient of temperature over the two layers of air, including the intermediate copper shell, an appropriate measure of the heat output of calibrating units or of infants. Another instrument of this type was recently described in this journal by L. R. Prouty, M. J. Barret and J. D. Hardy.[16a]

---

[8] A. C. Burton, "The application of the theory of heat flow to the study of energy metabolism," J. Nutrition 7, 497 (1934).

[9] A. C. Burton, and H. C. Bazett, "Exchange of heat and vasomotor responses," Am. J. Physiol. 117, 36 (1936).

[10] W. M. Barrows, and W. R. Murlin, "A new automatic respiration calorimeter and a study of the influence of sugars on heat production in the rat," J. Nutrition 13, (Supp.), 17 (1937).

[11] J. R. Murlin and A. C. Burton, "Human calorimetry. I. Semi-automatic chambers," J. Nutrition 9, 233 (1935).

[12] Winslow, Herrington, and Gagge, "A new method of partitional calorimetry," Am. J. Physiol. 116, 641 (1936).

[13] Winslow, Herrington, and Gagge, "Physiological reactions of the human body to varying environmental temperatures," Am. J. Physiol. 120, 1 (1937).

[14] E. D. Palmes and C. R. Park, "A method of human calorimetry," Medical Dept., Field Res. Lab., Fort Knox, Kentucky, (April 1, 1947). Project No. 55, Report No. 3.

[15] K. Büttner, *Physikalische Bioklimatologie, Probleme und Methoden* (Akademische Verlagsgesellschaft M.B.H., Leipzig, Germany, 1938).

[16] J. D. Hardy and R. Day, "Respiratory metabolism in infancy and in childhood," Am. J. Dis. Child. 63, 1086 (1942).

[16a] Prouty, Barret, and Hardy, "Simple calorimeter for the simultaneous determination of heat loss and heat production in animals," Rev. Sci. Inst. 20, 357 (1949).

It was, however, the object of our work to measure continuously rates of heat loss from larger subjects which dissipate calories from different surface sites at different rates. Such a measurement requires further elaboration and attention to factors involved. The essential requirements for human calorimetry with gradient layers may be more adequately outlined by reference to Fig. 1.

The subject will be enclosed in a supporting metal shell, the inside of which is lined with a "gradient layer." The layer consists of a very thin sheet of material of determined thermal conductivity, λ, and thickness, D. Paired electric thermometers, in the form of copper-constantan thermocouples, are attached to the surfaces of the gradient material and will, at numerous points, measure the "gradient," which, under the conditions of biological heat exchange, will amount only to a few hundredths of a degree centigrade. The supporting metal shell, through its thermal capacity and conductivity, will prevent rapid changes of temperature at the outer (adjacent to the shell) surface of the layer. This outer layer temperature is the reference standard of the gradient measurement. Continued stability of the reference temperature, however, which simultaneously determines the thermal environment of the subject, will be attained by means of a temperature-controlled jacket (an open bath in the shown scheme).

The first requirement for quantitative calorimetry in such a heat measuring shell is *uniformity of response* of the gradient layer. Only if the subject is completely surrounded by a heat-sensitive layer of area n(cm^2) every square centimeter of which responds with the same potential, e(volts), to one unit of heat transfer (cal./sec./cm^2), will the total heat transfer q(cal./sec.) be represented by $e \times n$(volt) under every condition. In this case, the potential per calorie per second will be the same whether the shell be large or small, because the gradient will decrease proportionately as the thermosensitive area increases. Furthermore, the measured potential will be independent of the shape of the shell provided every unit of the surface yields the same potential, e volts, per calorie per second and square cm. Likewise, the response to heat loss in a calorimeter with a uniformly heat sensitive layer will be unchanged, regardless of the location of the subject within the calorimeter, the direction of flow of heat or its distribution as it is disseminated toward the heat-measuring wall. The response in electric potential of such an instrument for any given heat transfer, will be proportional to the number of measuring elements per unit area, not to their absolute count.

Gradient layers are sensitive to heat transfer in either direction. A *stable base* of the measurement (zero potential if there is no heat output) can be obtained only if the outside is maintained at a constant temperature, thus preventing sudden external heat changes from affecting the layer. Within reasonable limits the measurement will, however, not be affected by the absolute level of temperature at which the heat transfer takes place. Inherent compensation for different levels of temperature differentiates the gradient principle from other principles of human calorimetry.[a]

Stability of response is essential to a continuously recording method. Constancy of thermal conductivity, λ, and thickness, D, of the gradient layer are therefore required. It is undesirable to have within the gradient layer, air spaces of any magnitude allowing internal convection which may change the thermal conductivity, λ. The vertical distance, D, between the thermometers must be precisely set as it is small, for reasons to be mentioned below. Solid layer materials of sufficient rigidity are required. Penetration of water in the layer must be avoided.

Rapidity of response depends on the thickness and thermal diffusivity of the layer, as defined in Bothe's (1947)[17] theoretical treatise, by the equation:

$$T = 2D^2/\pi^2 a,$$

where: T = half-response time (sec.), D = thickness of the layer (cm), a = thermal diffusivity of the layer material (cm^2/sec.).

It is advisable to choose a material of quality and thickness such as to keep the rapidity of response parallel to the rapidity of physiological events or to the rate of heat transfer from the subject to the heat measuring layer. Since physiological changes of thermal output induced by reflex activities are presumably very fast, and radiant heat is transmitted from the skin to the wall at the velocity of light, the slowness of conductive, convective, and evaporative heat transfers will be the limiting factor. These transfers were found in a small calorimeter 8×8×16 in. to come to equilibrium within 30 to 120 sec. Such a response time in the gradient layer therefore seems to be sufficiently short for measurements in a full-scale human calorimeter where conductive and evaporative heat transfers will require even more time.

While the absolute level of temperature will not affect the measurement of thermal output, it will, however, greatly affect the *environment of the subject.*[b] Any source of heat that has an appreciable thermal capacity such as a human subject, will temporarily respond with an increased heat output to decreased environmental temperature, and vice versa. From this it follows that heat will be lost from or stored within the

---

[a] Rubner's air calorimeter, for example, needs a compensatory chamber which Bothe has improved by using two equivalent instruments, one of them for the subject, the other as a blank chamber.

[17] W. Bothe, Zur Planung des Schicht-Kalorimeters." AAF Aero Medical Center, Hq., 3rd Central Medical Establishment, Heidelberg, Germany (November 1946), Institute Report.

[b] We consider the inner surface of the layer as "environment" as there is no way to separate the subject from the air that surrounds him in a calorimeter. This air is subject to changes of temperature and moisture which will affect the physiological conditions. The radiant environment, however, is completely determined by the emissivity and temperature of the inner surface of the layer.

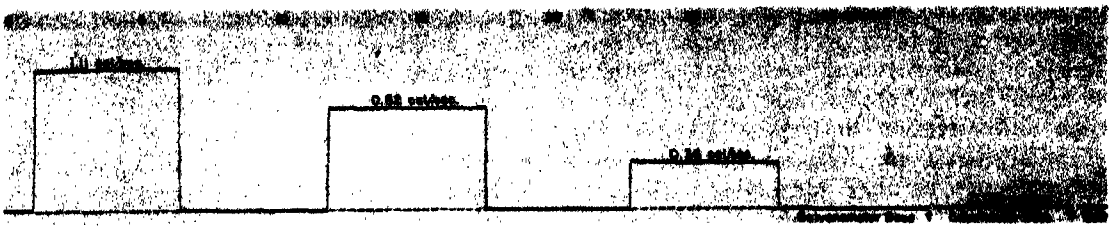

FIG. 2. Response of a heat metering shell to heat produced in a resistance coil. Voltages induced by various amounts of heat transfer recorded against time. Zero lines between the recordings have been obtained by switching the calorimeter out of the galvanometer circuit. In the right part of the record, zero response at zero heat output is indicated.

thermal capacity of the body, as the environment is cooled or warmed. These changes in heat output are of a physical nature and not manifestations of a physiological response. As gradient calorimeters are intended for investigation of rapid changes of heat output, they will necessitate more careful control of the thermal environment than has hitherto been required in calorimetry.

The temperature of the inner surface which faces the subject, will determine the thermal environment, whereas the thermal output of the subject will determine the gradient across the measuring layer. The outer surface of the layer can be maintained at a constant temperature by conventional means of temperature control. The inner surface temperature of the layer will deviate from this controlled temperature by the magnitude of the gradient. In order that the thermal environment be practically unaffected by the heat output, the gradient across the layer must be kept small. Only thin layers will fulfill this condition.

A high sensitivity (high voltage per calorie per second) could be obtained with gradient layers of poor thermal conductivity and considerable thickness, resulting in a substantial gradient and a correspondingly high thermoelectric potential. High gradients, however, are undesirable for the reasons mentioned above. It would therefore be preferable to employ more thermojunctions per unit area in order to obtain the desired sensitivity. By this means, a more uniform response is also achieved. With one copper constantan thermojunction per square inch, ten thousand thermojunctions can be installed in a human calorimeter seventy-five square feet in area. The heat output of a resting human would thus produce an electrical output of several millivolts from the layer, a potential adequate to operate, without preliminary amplification, commercially available recording potentiometers.

Plans to build a rapidly responding, continuously recording human calorimeter on the basis of these principles were started by one of us at Rechlin Aeromedical Laboratory in 1942. They were resumed by Benzinger, Bothe,[17] and Maier-Leibnitz at the AAF Aeromedical Center, Heidelberg, in 1945, and finally by the writers at the Naval Medical Research Institute, Bethesda, Maryland. The design for a human calorimeter including "plate meters" (Section VIII) was first outlined in a project proposal on June 21, 1947, for initiation of a project on "human calorimetry."

A human calorimeter of inner dimensions 32×32×84 in. is now under construction. The following description deals with a smaller calorimeter (8×8×16 in.) of similar design and construction, on which the experimental results reported here have been obtained.

The description of the small calorimeter consists of two separate parts: First, the design, construction, and testing of a heat-measuring shell will be described. Second, it will be shown how gradient measurement can be applied to the thermal exchange in ventilatory or respiratory circuits, so that direct recording of the total heat loss becomes possible.

III. CONSTRUCTION OF A HEAT MEASURING SHELL

A supporting shell of inner dimensions 8×8×16 in. was made of aluminum plates ¼ in. thick. One of the walls, 8 in. wide, 16 in. long, was removable, with a rubber gasket for sealing. The entire inner surface was enameled for electric insulation and then lined with a gradient layer as follows:

Strips of copper and constantan foil, 2/1000 in. thick, were interlaced through a layer of cellulose acetate sheet 30/1000 in. thick. Every square 2×2 in. was provided with one thermojunction. The foil elements were rectangular, 2 in. long, 1 in. wide, composed of two adjacent strips of metal, each of ½ in. width, copper and constantan, soldered together at one of their adjacent edges. These elements were placed on the plastic square with the soldered bonding in the middle. The elements were connected in series, with bridges at their corners, to form a continuous chain. The connecting bridges penetrate the plastic layer. All copper-constantan links of this thermopile (sequence in one direction of the electric circuit) were bonded to one side of the plastic layer, and all constantan-copper links to the other side of the plastic layer (schematic sketch in Fig. 1). Rubber cement was used to bond the foil and plastic surfaces. The total number of junctions was 160. The open surface of the layer was covered with enameled copper sheets, 5/1000 in. thick, and then coated with flat paint. The total internal resistance of the instrument amounted to 2.925Ω after the layers of the six walls had been connected in series. Two wires were brought out to connect the combined layers with the galvanometer or potentiometer used for testing.

IV. TESTS WITH A HEAT-MEASURING SHELL

For testing the characteristics of performance, the measuring shell was immersed in a water bath. Known sources of heat were established in the interior, and the potentials indicated at various rates of heat flow were either read from a precision null point potentiometer,[c] or recorded with a mirror galvanometer,[d] and photographic slit camera.

A. Constancy of Zero

Constancy of zero potential in the absence of heat output was tested by switching the heat measuring shell into and out of the circuit, while any existing potentials were recorded with the mirror galvanometer. Zero lines recorded when the heat measuring shell is in the circuit are designated in the figures as "calorimeter base," while the zero lines recorded when the heat measuring shell is out of the circuit, are designated as "galvanometer base."

Under the conditions of stable reference temperature, the "calorimeter base" was found to be stable and coincident with the galvanometer base (Fig. 2, right part). Such gradient measurements need no correction and lend themselves for immediate graphic recording of heat losses.

Rapid changes of temperature in the surrounding bath, however, would result in erroneous potentials as shown in Table I.

An error corresponding to one percent of a human metabolism at rest would be induced, if the bath temperature would increase or decrease at a rate of 3.6°C per hour. Such errors can be prevented by conventional means of temperature control.

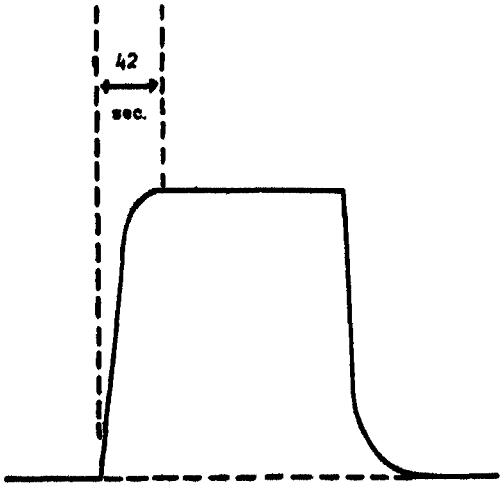

FIG. 3. Rapidity of response of heat metering shell to fast (radiant) heat transfer.

TABLE I.

Temperature increase of surrounding bath in °C/hr.	Response of calorimeter in cal./sec.	Response of calorimeter per 1°C/hr. in cal./sec.
0.00	0.00	—
9	0.74	0.82
12	1.00	0.83
24	1.93	0.81
39	3.11	0.81

B. Reproducibility of Response

Reproducibility of response was tested as shown in Fig. 2. A resistance coil[e] was suspended in the shell, and supplied with d.c. current. Current was read from a precision ammeter, and the rate of heat flow computed from current and resistance. (4.185 watts = 1 cal./sec.). In the majority of experiments the coil was covered with carbon paper to facilitate emission of low temperature radiation. Other arrangements for calibration will be described.

Figure 2 shows potentials indicated at various rates of constant heat flow, recorded over time with the mirror galvanometer. The shell responds to stable heat flows with stable potentials. With thermal outputs above 0.5 cal./sec., however, the transfer of heat from the coil to the measuring shell exhibits visible fluctuations as indicated in the recordings. This is a characteristic of thermal convection, which could not be observed in the absence of substantial air motion. The oscillations are indicative of variations in heat transfer, not in its measurement.

C. Linearity of Response

Linearity of response in potential to various rates of constant heat flow is demonstrated graphically in Fig. 10. The responses in potential were read from the null point potentiometer, and plotted against the caloric input into the calibration coil, computed from current and resistance. Rates of heat flow ranged from ¼ to 5 calories per second, in these tests. In a human calorimeter with a surface area 20 times larger than in the present calorimeter, these rates would correspond to ⅕ to 5 times the heat loss of a resting human.

D. Sensitivity

Once linearity of response is demonstrated, the "sensitivity" of a heat measuring shell can be expressed in volts per cal./sec. The sensitivity of our instrument is 135 microvolts per cal./sec. A human heat loss of 20 cal./sec. at rest would result in a potential of 2.7 millivolts when measured with a gradient layer of same construction characteristics in a full size calorimeter.

---

[c] Type K of Leeds and Northrup Company.

[d] Micro Moll, of Kipp and Zonen, Delft.

[e] The coil consisted of nickel alloy resistance ribbon, ¼ in. wide, 1Ω per foot. It was 10 in. long, 4 in. in diameter. The resistance was 29.0Ω. Four light adhesive cellulose tapes running lengthwise at the inner surface of the coil provided adequate strength, thus reducing its thermal capacity to a minimum.

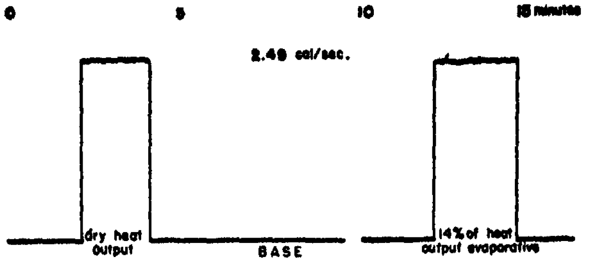

FIG. 4. Equal responses of a heat metering shell, to dry or wet heat transfers. *In the left part of the record, the calibrating heater* coil within the shell was partially covered with wet gauze. The gauze lost, as an average, 0.6 mg of water per second which required 0.348 cal./sec. or 14 percent of the total heat output of the coil. Such water was found condensed on the walls of the shell. The potential induced by such heat transfer is not visibly different from the potential induced by dry heat transfer of the same magnitude (right part of the record) after the wet gauze was removed.

E. Influence of the Gradient on the Radiant Environment of a Subject

It can be demonstrated by calculation rather than by testing, that the gradient produced in the layer will not induce an undesirable interdependence between the radiant temperature in the calorimeter and the heat loss of the subject. As the response of 80 active thermocouples was 135 microvolts to one calorie per second, each thermocouple yielded an average of 1.6 microvolts. The specific thermopotential between copper and constantan is approximately 40 microvolts per 1°C. The gradient across the layer at one calorie per second was therefore less than 0.05°C. The metabolic output of a human, when assumed to be 20 calories per second, would induce such a gradient in an 8-m^2 measuring shell of the same design and construction. Doubling of such heat loss would increase the radiant temperature of the environment by less than 0.05°C.

F. Rapidity of Response

Rapidity of response can be tested adequately only with radiant heat transfer to the meter. One rectangular side of the heat-measuring shell was removed. An electrically heated metal rod was placed above the open shell, at a distance of approximately 10 in. A shield was placed between the meter and the hot metal. When the shield was removed, heat was radiated to the layers. As shown in Fig. 3, the meter responded to the onset of radiation by full deflection within 42 sec. There is a slightly greater delay in response when exposure to radiant heat is interrupted.

G. Response to Evaporative Heat Transfer

The resistance coil used for calibration was dry in the tests described thus far. Biological subjects, however, lose a considerable fraction of their metabolic heat by vaporization of water. Therefore, another series of tests was run, with a source of heat involving evaporation: A light tray of insulated copper foil, 1/1000 in. thick, 3 in. wide, and 8 in. long, was placed at the bottom of the heating coil and covered with a 3×8-in. piece of cotton gauze. The gauze weighed about three grams and absorbed about three grams of water, when moderately wet. After each test, the average rate of evaporation could be determined from the weight loss of the tray and gauze and was expressed in terms of calories per second lost from the coil by evaporation. The loss was found to constitute 10 to 15 percent of the total when two calories per second were put into this calibrating instrument. Evaporative fractions as high as 30 percent were obtained when radiation and convection were suppressed. After the tests, the water was found as condensed moisture on the inner surfaces of the shell. Figure 4 shows that there was no appreciable difference in the records whether the heat was lost from the coil by radiation, conduction and convection alone, or whether as much as 15 percent of the total was transferred to the meter by evaporation and subsequent condensation of water.

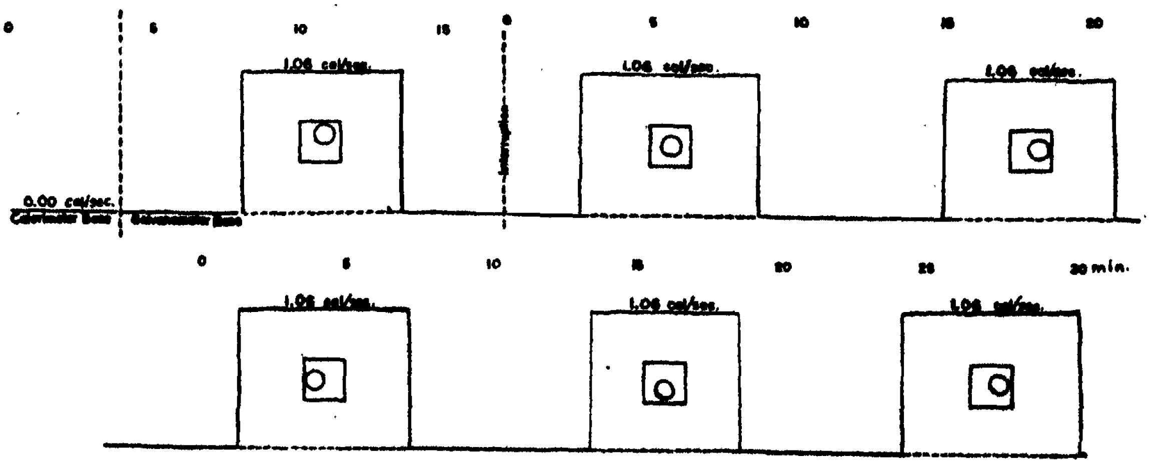

FIG. 5. Uniformity of response in a heat metering shell. The response of the shell to a given output of calories per second, as the location of the calibration resistance coil within the shell was changed. The various positions are indicated under each part of the record, by a scheme representing a cross section through the square shell and the cylindrical coil within it.

H. Uniformity of Response

Uniformity of response was tested in experiments with an equal known input of energy but with different location of the source of heat inside the meter. The calibration heater (resistance coil) could be moved without opening the shell. Suspended on light strings, the heater always dropped into the lowest possible position when the shell was turned at various angles. On the recordings (Fig. 5), five different positions (one twice) were tested and are schematically indicated on the corresponding parts of the record. Deviations, if any, amounted to less than ±1 percent of the indicated potential. Such uniformity of response allows the application of the gradient principle to heat exchange meters in which heat transfer is exponentially decreasing from a maximum at one end to almost zero at the other. Losses of calories from respiratory or ventilatory air can thus be recorded.

V. PRINCIPLES OF GRADIENT CALORIMETRY IN RESPIRATORY OR VENTILATORY AIR CIRCUITS

To function as a calorimeter for living subjects, a heat-measuring shell must permit exchange of respiratory gases. To prevent accumulation of moisture, a ventilatory air circuit must be established. Heat would be removed from, or conveyed into the calorimeter by these streams of air, unless such air would leave the calorimeter at the same temperature and humidity, which it had upon entering the calorimeter.

Actually, however, considerable amounts of heat will be transferred to the inspired air in the lungs. On the other hand, a substantial quantity of heat, reflected mainly by increased humidity, will be delivered into the ventilatory air, while it circulates through the calorimeter. Such heat must be removed, and measured, before it leaves the calorimetric system with the airflow.

Such measurement can be achieved if the heat is allowed to pass from the air into a cooling medium of constant temperature, which surrounds heat exchangers in both the incoming and outgoing air lines. While the heat passes through the walls of the heat exchangers, its rate of flow will be recorded by means of gradient layers.

Such an arrangement is shown in Fig. 6. The outlet exchanger, E_1, is lined with a gradient layer. The calories that have been delivered into the air while it circulated through the calorimeter (in the case of ventilatory air) or in the lungs of the subject (in the case of respiratory air) will pass through the layer into the cooling medium and thus be recorded. Such an exchange and measurement will take place regardless of whether the calories represented an augmented temperature or an increased humidity. The air temperature will be the same at point 2 of Fig. 6 where the air leaves the meter, and at point 1, Fig. 6, where the air enters the system. Also, the humidity of the air will be the same at points 1 and 2, provided the air at the inlet was moist and no cooler than the cooling medium.

The following requirements are essential: (1) exchange of heat in the connecting lines must be precluded. (2) The exchange of heat between the circulating air and the cooling medium must be practically complete. (3) The quantitative response of the gradient layers to heat flow must be linear, uniform, and equal in each part of the calorimeter.

Under these conditions, the potentials indicated can be made additive by serial wiring.

Recordings of the total heat exchange will then be obtained directly. Separate measurements can be made of respiratory heat losses, or heat removed by ventilation, which represents the evaporative fraction, under properly chosen conditions.

A more elaborate system of heat exchange meters designed to permit a wide flexibility of conditions with respect to temperature and humidity of respiratory or ventilatory air will be shown. First, however, construction and performance of heat exchange meters (plate meters) will be described.[f]

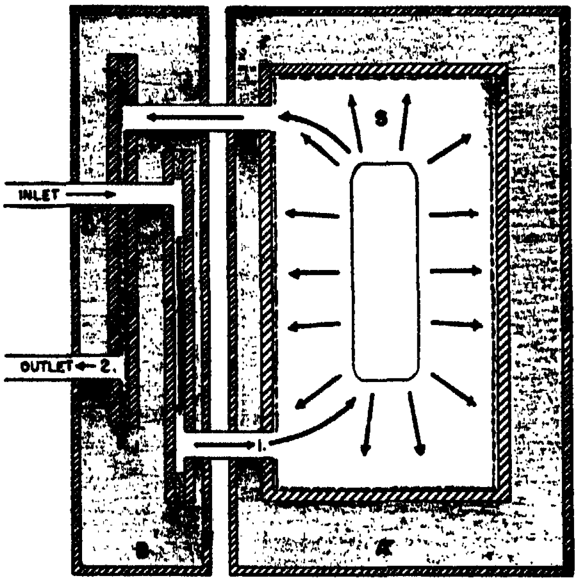

FIG. 6. Scheme of calorimeter with respiratory (or ventilatory) circuit. A heat metering air circuit through the heat measuring shell *S* is established by means of two heat exchangers, E_1 and E_2. The outlet exchanger E_1 allows the heat given off from the subject into the circulating air to pass into the water tank *B*. This heat is recorded by a heat metering layer at the walls of the exchanger E_1. The inlet exchanger E_2 only provides equality of temperatures in the circulating air at the points where it enters (1) and leaves (2) the metering system. Gradient layers are indicated by dotted lines.

---

[f] A correction is, however, required for seeming losses of calories induced by losses of matter.

Evaporated water leaves the body at lung or skin temperatures, but it leaves the measuring system at the temperature of the humidity setting plate meters. Calories liberated in this process are recorded, though they do not represent an actual heat loss. They need to be subtracted from the rates recorded. If the record shows a measured evaporative fraction of heat loss, H_m, the actual

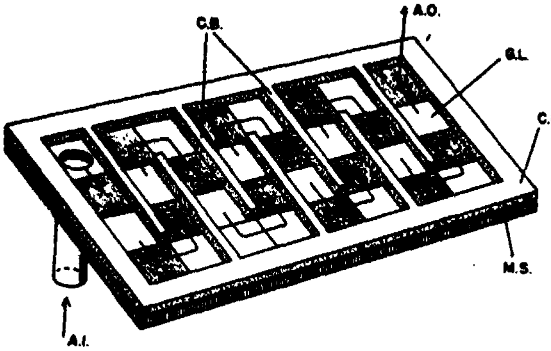

FIG. 7. Design of a "plate meter." Metering exchange of heat between circulating air and temperature-constant baths is achieved by close contact with gradient layers. The cork frame is to keep the layers at proper distance and to prevent heat transfer in side ways. The cover was removed. It carries the outlet and is also provided with a gradient layer. Arrows indicate direction of air flow.

A.I. = Air inlet.	C.F. = Cork frame.
A.O. = Air outlet.	G.L. = Gradient layer.
C.B. = Cork baffles.	M.S. = Metal shell.

VI. CONSTRUCTION OF A GRADIENT CALORIMETER WITH HEAT EXCHANGE METERS FOR CIRCULATING AIR

A. Plate Meter

An open plate meter is shown in Fig. 7. An aluminum plate, 10×18×¼ in., was enameled. A one-inch wide brim of the plate was lined with 30/1000-in. thick cellulose acetate sheet. A gradient layer, 16 in. wide, 8 in. long, was constructed on the open area within this plastic frame. Materials, methods, and dimensions were the same as applied in the construction of gradient layers for the heat-measuring shell. Instead of a continuous sheet, however, copper ribbons 5/1000×1⅞ in. were used for covering this gradient layer. The ribbons were placed parallel to the short side of the plate. An open space of ⅛ in. was left between adjacent ribbons to interrupt thermal conduction in the direction from the air inlet to the outlet. A round opening, 1 in. wide, was made as an air inlet in one corner of the plate and layer, and was provided with a short tubing, 1 in. in diameter, on the other side.

Upon the plastic frame, another 1-in. wide frame, consisting of ¼-in. thick cork plate, was mounted with rubber cement. Baffles of cork, ¼×¼ in. were then installed, as shown in Fig. 7.

Another aluminum plate, 10×18×¼ in. was similarly provided with a gradient layer, copper ribbons, air outlet, and plastic frame. The two plates, with their gradient layers facing each other and spaced by the cork frame and baffles, were bonded together and sealed around the edges by means of waterproof tape.

Between the in- and outlet, a narrow space thus remains which is subdivided, by the cork baffles, into a meandering flow passage for ventilatory or respiratory air. In such a "plate meter" no exchange of heat can occur except across the gradient layer. Thermal insulation of the connecting tubings was insured by inside lining made from balsa wood tubings of ¼-in. inner diameter.

B. The Calorimeter

Another plate meter with a mere mock-up of plastic and metal foil instead of the layer, was made for air inlet heat exchanger. The two plates and the heat-measuring shell were assembled, connected, and immersed as shown in Fig. 6. The gradient layers were wired as indicated in the diagram in Fig. 8. Potentials may be measured either separately or in serial wiring. If the potentials are recorded with the current sensitive mirror galvanometer, however, substitute resistors must be introduced for every layer that is switched off, in order to maintain the total resistance of the galvanometer circuit. With a supply of humid air at the inlet, slightly warmer than the bath surrounding the plates, this set-up is ready for testing.

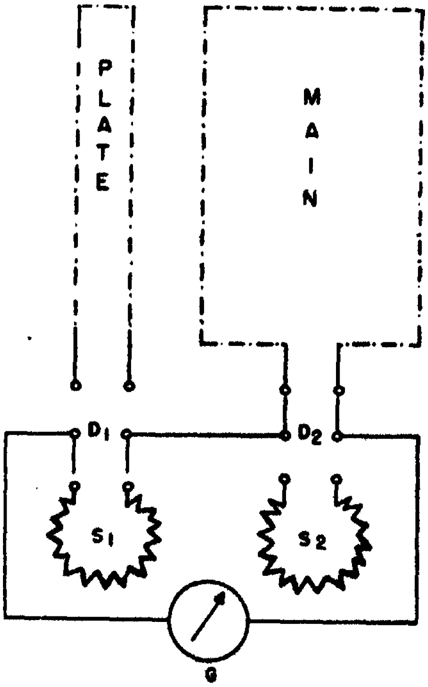

FIG. 8. Wiring diagram of calorimeter with ventilatory (or respiratory) circuit. *The heat meters of both main shell and plate* can be switched either separately or simultaneously into the galvanometer (*G*) circuit. *For recording of the potential in the* plate, a substitute resistor S_1 has to be introduced instead of the shell heat meter, and S_2 vice versa, in order to maintain the original internal resistances in the galvanometer circuit. Double throw double pole switches D_1 and D_2 serve this purpose.

---

evaporative fraction of heat loss, H_a, is:

$$H_a = H_m \frac{(578-\Delta t)}{578} \text{(cal./sec.)},$$

where Δt is the difference between the temperatures of the skin and the humidity setting plate, respectively.

Transportation of matter in the exchange of O_2 and CO_2 does not involve an appreciable exchange of heat.

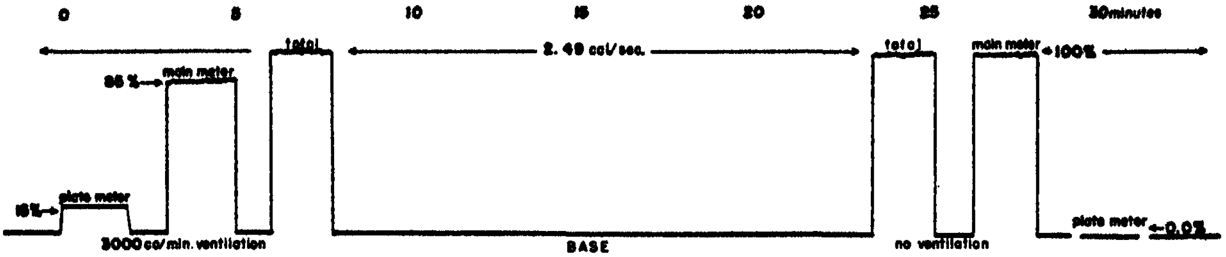

FIG. 9(a). Under the same, partially evaporative, heat output from the calibrating coil two records were taken for comparisons: One at no ventilation (right) and the other at 3000 cc/min. ventilation (left). In the experiment shown at left, 15 percent of the total heat loss was recorded in the respiratory circuit, and only 85 percent in the main shell. With no circulation (right) the total was recorded in the main shell, as the plate meter indicated zero.

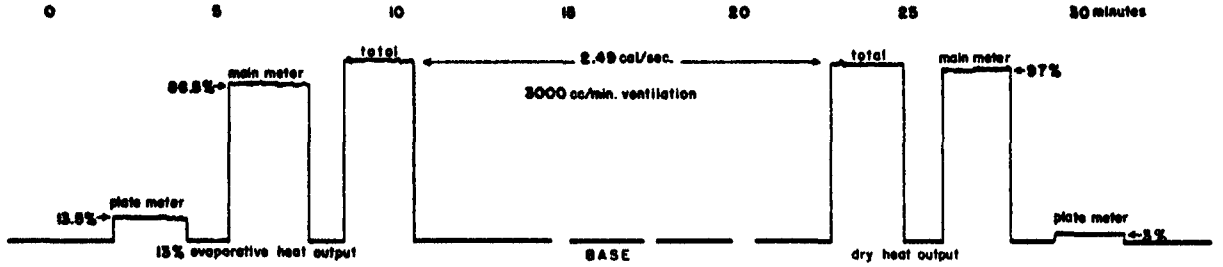

FIG. 9(b). Under a constant circulation of 3000 cc/min. partially evaporative heat output (left) was compared to dry heat output (right). Three percent only of the dry heat output was recorded in the plate, and 97 percent in the main shell, whereas 13.5 percent of the total passed to the plate, when the thermal output was partially evaporative.

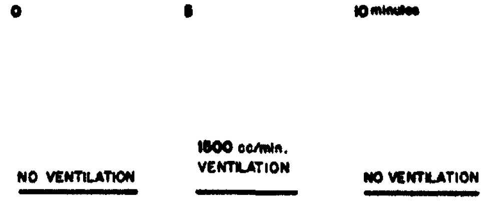

FIG. 9(c). The effect on the base of the calorimetric measurement of an air circulation which would correspond to 30 liters/minute of respiratory volume in a human calorimeter, with a 7°C difference in temperature between main shell and plates (essential for experiments at various temperatures of the inspiratory air).

VII. TESTING OF A CALORIMETER WITH A VENTILATORY (OR RESPIRATORY) AIR CIRCUIT

If the theoretical assumptions made on gradient calorimetry of circulating air are correct, and if the heat exchange meters are properly constructed, a gradient calorimeter with a ventilatory or respiratory circuit should respond to a certain rate of heat loss with the same potential whether or not circulation of air is present, whether the rate of circulation is high or low, and regardless of differences in distribution of heat between main shell and plate meter. This can be proven experimentally.

A. Tests with Presence or Absence of Air Circulation

In the first series of experiments an air circulation of 3000 cc/min. through the plate meter was established and later interrupted; the coil released a uniform and constant flow of calories during the entire period of experimentation. The responses of main and plate meters were made additive by serial wiring, and recorded as shown in Fig. 9(a), under the designation of "total." No difference could be seen between the totals, with and without air circulation. Separate recordings of potentials from main and plate meter, respectively, were taken in addition to ascertain the quantitative participation of the plate meter in the measurement of total heat loss.

The first part of the record shows that a substantial fraction of the total is transferred, with the circulating air, from the main shell into the plate meter under those conditions. In the second part of the record, taken while circulation was interrupted, the plate meter indicated no heat exchange and the total was reflected by the potential from the main measuring shell. The totals were the same in both cases.

B. Tests with Varied Distribution of Heat

In a different arrangement, the distribution of heat flow between the two parts of the calorimeter can be greatly modified without altering the rate of air circulation. Such tests were made for evidence of reproducible quantitative response under varied conditions. Even substantial circulation will not transfer a large fraction of heat from the main shell to the plate meter as long as the source of heat is dry. If however, the same constant source of heat suddenly begins to vaporize water, a large fraction of the total heat loss will appear in the plate meter and will be missing on the record of heat exchange obtained from the main measuring shell. This type of experiment is shown on the recording in

Fig. 9(b), in reversed sequence. Between the first (left) and the second (right) part of the test, a piece of wet gauze was removed from the interior of the calibration coil. The shift in distribution of heat flow among the parts of the calorimeter is demonstrated. As shown in the record, the totals are equal in both cases.

C. Tests with Various Kinds of Heat Transfer

In a third series of experiments, provisions were made to augment certain fractions of heat loss, at the cost of others: An evaporative fraction as high as 28 percent was obtained when the ventilatory air from the plate meter was drawn from the interior of the heating coil, which contained a piece of wet gauze, while the entire coil was wrapped in shining aluminum to suppress radiant and convective heat losses from the interior of the coil.

A maximum radiant fraction was expected from the blackened dry coil, with interrupted air circulation. The conductive fraction must be intensified when the dry coil is wrapped in bright aluminum. Under these conditions radiation is suppressed, evaporation excluded, and only thermal air motion induced. Finally, a high convective heat transfer was obtained by replacing the calibration coil with a 10-watt d.c. motor driving a fan, which caused a violent and turbulent convection in the calorimeter. In this instance, the energy was computed from the drop in voltage between the two poles of the running motor and from the current. The results of tests at various levels of energy input under these different conditions are plotted in graphic form as shown in Fig. 10.

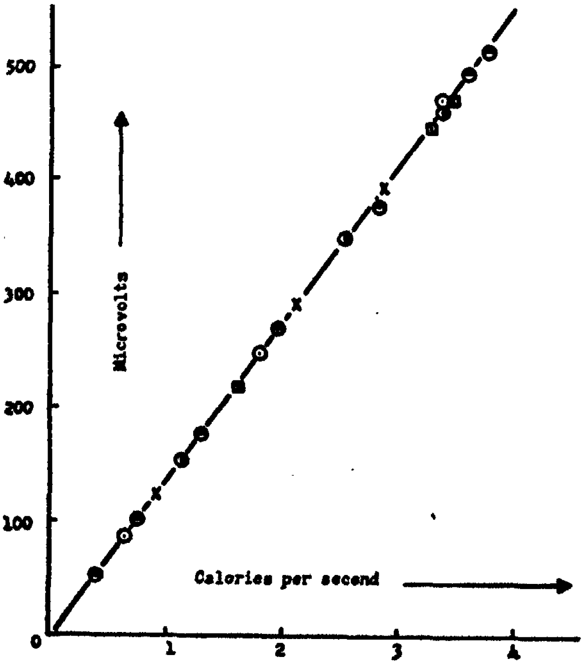

Fig. 10. Responses of gradient calorimeter in electric potential (microvolts) to transfer of heat (cal./sec.) lost in different ways. The following fractions were favored by different calibration sets;

◑ Radiant, measured in main shell.
● Radiant, 3.5 percent of total measured in plate meter.
× Conductive, measured in shell.
⊡ Convective, measured in shell.
⊙ Evaporative, 28 percent of total measured in plate meter.

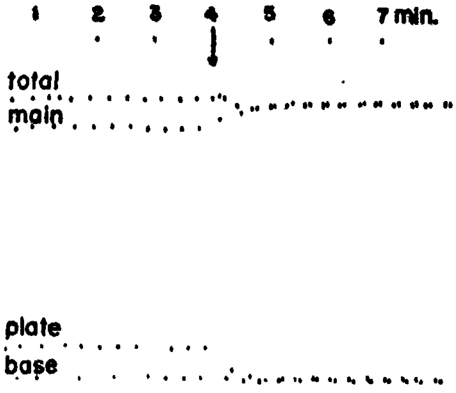

Fig. 11. Adjustment after a shift of heat transfer from the plate to main meter. The voltages of plate meter, main meter, and total were simultaneously recorded, as a circulation of 3 l/min. was interrupted (Arrow).

D. Constancy of Zero

The quantity of heat flow measured in a plate meter will be comparatively small. In such a system, however, the large thermosensitive area is liable to be affected by disturbing influences. It was, therefore, essential to test stability of base. Constancy of zero potential in the absence of thermal output is demonstrated in Fig. 9(c). Both plate meter and heat-measuring shell were connected in series and switched into and out of the galvanometer circuit, while air was circulating at the rate of 1500 cc/min. To make conditions of the test more severe, a difference of 7°C between the cooling media of plates, and main shell, was established. The circulating air, however, was protected in these tests from thermal exchange with the air in the heat-measuring shell, in a manner analogous to the necessary insulation of inspiratory and expiratory lines of the respiratory circuit. Without such insulation, the capacity of the large space of the heat-measuring shell to store moisture will induce slightly interfering gains and losses of heat from the circulating air. Therefore, humidity control will be essential once a ventilatory circuit is set up in addition.

E. Rapidity of Adjustment after Shifts of Heat Flow among Different Parts of the Calorimeter

The rapidity of response in potential to heat flow in a plate meter will not differ appreciably from that in the heat-measuring shell, since the construction of each is the same. Another question of rapidity, however, is involved in air circuit calorimetry. How rapidly will an adequate response be re-established after a sudden shift of heat flow from the main meter into the plate, as might occur following a change from dry heat loss to sweating? As shown in Fig. 11, the thermal exchange and its components were simultaneously recorded by periodic manual switching as a parallel to the mechanical performance of a multichannel-potentiometer. In the first period of the recording, there was a ventilation of three liters per minute, which would correspond to 60 liters per minute of human respiratory rate. Ten percent of the heat loss was recorded in the plate. At the arrow, the circulation was interrupted. The heat flow in the plate went down to zero within 45 sec. The main meter, after 2½ min., indicated the previous total. Meanwhile, there was only a slight transitory depression in the total as recorded by both meters in series. From this experiment it follows that neither changes in the rate of air flow nor shifts from dry to evaporative heat loss will disturb the quantitative measurement.

Experimental results with an instrument described in Sections III and VI have confirmed the theoretical outlines of gradient calorimetry given in Sections II and V. On the basis of these results a human gradient calorimeter was designed.

VIII. DESIGN OF A HUMAN GRADIENT CALORIMETER

The instrument shown schematically in Fig. 12 is designed for a wider flexibility of experimental conditions as compared to the simplified construction of Fig. 6. Ventilatory air of low relative humidity can be supplied at calorimeter temperature. Temperature or humidity of the inspiratory air can be independently varied. The system operates as follows:

In the ventilatory circuit, the incoming air must pass two heat exchangers (plate meters), one of which serves to establish a definite level of ventilatory humidity (cooling system *I*). The purpose of the other is to fix a certain ventilatory temperature (cooling system *II*) usually identical with the temperature of the main measuring shell. If cooling system *I* is kept at ice temperature, the ventilatory air will assume an absolute humidity of 4.58 mm Hg. During the passage through cooling system *II* the air will maintain its absolute humidity. The relative humidity, however, will decrease as the air will take up a substantial amount of heat from the tank. This negative exchange of heat will be recorded by a gradient layer in the plate exchanger. In the main meter, the ventilatory air will subsequently take up a part of the heat produced by the subject, some of it reflected by an increased temperature and some by an increased absolute humidity. The outgoing air will immediately re-enter cooling system *I* where the gradient layer will indicate a positive heat exchange. This heat exchange will include the amount of heat that has been acquired by the stream in cooling system *II*, as well as the amount that has been added by the subject in the main meter. If the heat meters in the incoming and outgoing exchangers are properly wired in series, the intake in *II* will be automatically subtracted from the output in *I* and the difference will represent the amount of heat given off by the subject into the ventilatory circuit. At the outlet in cooling system *I*, the ventilatory air will finally leave the calorimeter with the same temperature and humidity which it had when it entered between cooling systems *I* and *II*. It is, of course, necessary to prevent any exchange of heat along the lines that connect the various meters. These lines must be short and carefully insulated.

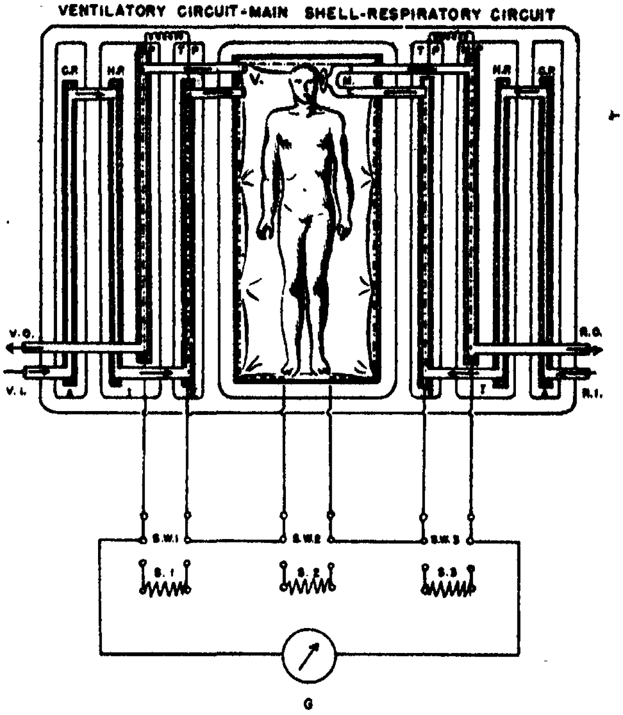

FIG. 12. Design of a human calorimeter.

CP —Compensatory plates.
G —Galvanometer.
HP—Humidity setting plates.
TP—Temperature setting plates with gradient layers.
MP—Metering plates for outgoing air.
M —Mouthpiece for respiration.
RI —Respiratory air inlet.
RO —Respiratory air outlet.

S_{1-3} —Substitute resistors.
Sw_{1-3}—Double pole double throw switches.
V —Ventilatory opening in main calorimeter.
VI —Ventilatory air inlet.
VO —Ventilatory air outlet.
I, *II*, *A* } Cooling systems.

There has been no indication in our tests so far that the exchange of heat in the plate meter will be incomplete to an extent which would cause measurable errors. If any such errors should be observed, they could be compensated, to a large degree, by preconditioning the ventilatory air in an accessory cooling system, *A*. The temperature in *A* would be adjusted to the temperature of the main measuring shell. If the condensation of water in the outlet exchanger in *I* should be deficient, a similar deficiency would occur in the inlet meter in cooling system *II* because the drop in temperature along the meter is approximately the same in both cases. The eventual escape of a small amount of heat would be balanced by the transfer of an equal amount of heat into the calorimeter.

The respiratory circuit is a mere duplication of the ventilatory one. Temperature of inspired air will be determined by the temperature in cooling system *II*. Humidity of inspired air may be varied from 100 percent to extremely low values by lowering the temperature in cooling system *I*. In Fig. 12 the cooling systems have been only schematically indicated. In actual construction it is advisable to incorporate them in the supporting shells of both main and plate meters. The cooling medium will circulate through wide shallow flow passages left between the two sheets of an aluminum double wall. Aluminum baffles arranged like cork baffles in plate meters will subdivide the space available into flow passages for the cooling liquid. Counterflow arrangements will provide uniformity of the reference temperature.

The wiring of the various meters is shown in Fig. 12. It is made to permit continuous, simultaneous recordings of the following components of heat flow:

(a) Respiratory heat exchange by individual recording of the respiratory plate meter.

(b) Evaporative heat loss from the skin under every condition that does not allow condensation of water within the main shell. Recording will take place in the combined ventilatory plate meters.[*]

(c) Total human heat loss, by serial wiring of the potentials of all meters.

This leaves only the radiant component of heat exchange, which is correctly included in the total, to be measured separately for complete partition. A method for continuous selective recording of radiant heat losses and average skin temperatures is under development.

It has been mentioned in the discussion of the principles that a man in a calorimeter of any dimension above body size cannot be isolated from the air that surrounds him. This air has a certain capacity for moisture and will thus cause a certain inertia in rate of heat transfer. Automatic humidity control, by means of commercially available instruments which would influence the ventilatory rate, is, therefore, considered in the plan. This was suggested by Dr. J. D. Hardy (in a personal communication). The exchange of oxygen and carbon dioxide will be continuously recorded together with the thermal exchanges. A way to obtain such recordings, is, for instance, the interferometric gas analysis (Bothe) with a recording system as described by the authors.[18] An additional method[19] makes it possible to record immediately the intake of oxygen and losses of carbon dioxide in liters per minute.

IX. DISCUSSION

It appears from the foregoing tests that gradient calorimetry will permit a sensitive and reliable determination of total heat loss from the human body. Direct calorimetry thus becomes comparatively simple. The many factors involved, such as radiation, conduction, convection, and evaporation from the skin, and respiratory losses of calories reflected either in temperature or humidity of expired air, have all been channeled into the determination of a single thermoelectric potential. Direct calorimetric measurements by this simple technic might well be applied not only to studies for which existing calorimeters have been used, but also to other studies for which the latter methods have been too cumbersome. This is not the place to enumerate such applications. In general there will be three categories:

(a) Direct and indirect calorimetry may be simultaneously applied when deviations from usual relationships between gaseous exchange and energy formation are expected.

(b) Direct calorimetry may be alternatively applied when indirect methods would be disturbed by alterations of respiratory control or experimental changes in respiratory gases (O_2, N_2, CO_2).

(c) The gradient measurement may replace determinations of metabolism from gaseous exchange because of its simplicity, once the instrument is set up.

Besides simplicity, the gradient calorimeter has the advantage of rapid response. Sudden and transitory alterations of heat loss may remain unnoticed in calorimeters of prolonged inertia. Since the response time of the gradient layer is less than one minute, this instrument can follow rapid changes in heat loss induced by thermal or other stimulation affecting the central and reflex mechanisms of human temperature control.

---

[*] This measurement comprises a small amount of convective heat transfer, which is in any case correctly included in the total. If the highest accuracy of partition is desired, this amount must be computed from the ventilatory rate, specific thermal capacity of air, and the difference between incoming and outgoing air temperatures in the ventilatory circuit.

[18] T. H. Benzinger and C. Kitzinger, "Photographic registration of interferometric gas analysis, AAF Aero Medical Center, Hq., 3rd Central Medical Establishment, Heidelberg, Germany (November 1946), Institute-Report.

[19] T. H. Benzinger, "Untersuchungen über die Atmung und den Gasstoffwechsel," Ergeb. d. Physiol. 41, 1 (1938).

THE REVIEW OF SCIENTIFIC INSTRUMENTS VOLUME 20, NUMBER 12 DECEMBER, 1949

Production and Measurement of Ultra-High Speed Impulses*,**

R. C. FLETCHER***
Laboratory for Insulation Research, Massachusetts Institute of Technology, Cambridge, Massachusetts

(Received August 1, 1949)

The capabilities and limitations of several impulse generators and voltage dividers, and a micro-oscillograph sweep circuit for dealing with kilovolt impulses in the millimicrosecond range, are described. The most successful combination produces and measures an impulse of a rise time equal to 4×10^{-10} sec.

INTRODUCTION

THE development of the micro-oscillograph[1] has made possible the production and measurement of impulses in the 20-kv range with rise times of the order of 4×10^{-10} sec. The techniques of working with such fast transients pose many new problems, for these transients may have frequency components over the range from 10 to 3000 mc/sec., requiring extremely broad-band ultra-high frequency circuits. The transients might justifiably be called ultra-high speed (u.h.s.) transients, and the corresponding circuits ultra-high speed (u.h.s.) circuits. This paper presents a description of the special u.h.s. circuitry investigated for the purpose of producing 20-kv u.h.s. impulses, and measuring them oscillographically.

I. TRANSMISSION LINE TECHNIQUES IN U.H.S. CIRCUITRY

As faster transients are employed, an increasing amount of difficulty is encountered with parasitic oscillations and other types of distortions due to lead inductance and stray capacity. This difficulty can be circumvented by distributing the inductance and capacity so that they act like a transmission line. The electrical length of such a line can be made longer than the signal being measured so that the resonant circuit of the parasitic elements is replaced by a pure resistance with a delay. Transmission line connections, therefore, have been used throughout the present investigation.

For the analysis of transmission lines in u.h.s. circuits it has been found convenient to use equivalent circuits to represent the interaction of the signals in the line with the circuit elements used as terminations. These equivalent circuits give the same answers as can be obtained with the more conventional reflection and transmission coefficients, but are much more adaptable to transient analysis, particularly if non-linear elements such as spark gaps are concerned. Figure 1 presents some basic equivalent circuits from which other combinations are easily derived. Additional equivalent circuits for special extended circuit elements will be described later.

II. GENERATION OF U.H.S. IMPULSES

Atmospheric Spark Gap

One of the most commonly used types of impulse generator is the atmospheric spark gap, which is generally believed capable of producing impulses with rise times of less than a millimicrosecond. This belief stems from the measurements of the formative time lags of the atmospheric spark, which have been reported to be as low as 1 mμsec. for high enough overvoltages (*ca.* 200 percent).[2] A first attempt in the present investigation was in this direction. The three-electrode trigger gap shown schematically in Fig. 2 was constructed. The left electrode is attached to a 52-ohm coaxial transmission line and is initially charged to a voltage V (of the order of 20 kv). The right-hand electrode was attached to another 52-ohm transmission line down which it is desired to produce the impulse. The center electrode is connected through a 10,000-ohm resistor to a trigger source. The left-hand (or long) gap is arranged so that its threshold is just a few per-

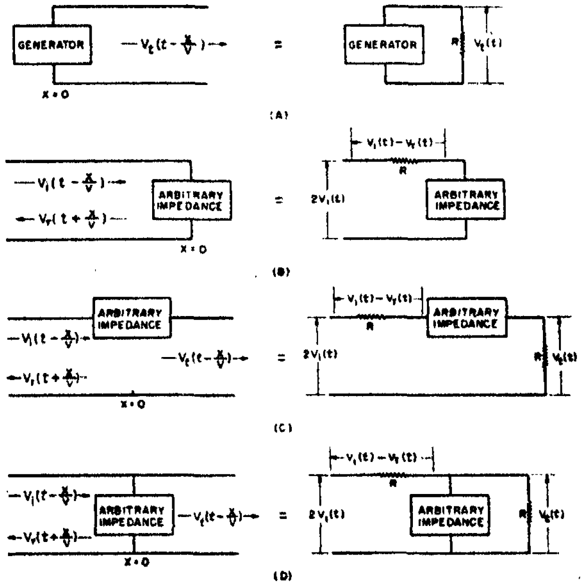

FIG. 1. Equivalent circuits for transmission line terminations (assumed to be located at $x=0$). R is the characteristic resistance of the line, and V_i, V_r, and V_t are the incident, reflected, and transmitted voltages, respectively, in the line.

---

* Sponsored by the ONR, the Army Signal Corps, and the Air Force under ONR Contract N5ori-07801.

** From a doctorate thesis in physics, Massachusetts Institute of Technology.

*** National Research Council Predoctoral Fellow.

[1] G. M. Lee, Proc. I.R.E. 34, 121W (1946).

[2] A summary of the measurements of the formative lag of the atmospheric spark is given by R. Strigel, *Elektrische Stossfestigkeit* (Verlag. Julius Springer, Berlin, 1939), p. 34.

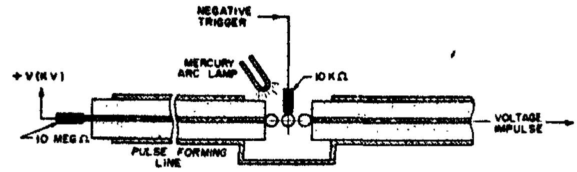

FIG. 2. Three-electrode trigger gap at atmospheric pressure.

cent above V, while the right-hand (or short) gap can be made much shorter, say one-fourth the length of the long gap. When a small trigger voltage of the opposite polarity to V is applied to the center gap, the long gap breaks down, charging the center gap up to the voltage V. The short gap thus finds itself with an overvoltage of approximately 400 percent, and should break down in less than 1 mμsec. Since no voltage appears on the transmission line to the right until the short gap breaks down, the breakdown of this gap should determine the shape of the impulse appearing on this transmission line.

When this trigger gap was built and tried, however, it was found incapable of generating impulses with shorter rise times than 20 mμsec. The rise time of the impulse was unaffected by the length of the short gap, nor was it affected by carefully arranging the gaps along the center conductor of a single coaxial transmission line to eliminate inductance of leads and capacity of electrodes to ground. It seemed to be a function of the long gap only. It was certain that the short gap was not firing first, because the trigger voltage was not capable of breaking down the short gap by itself (as could be tested by removing the voltage V and applying the trigger). The explanation of this rather unexpected result lies in the transient response of the long gap. Thus when the long gap breaks down first, it has to supply only enough current to cause a voltage drop V across the large resistance of the trigger generator, i.e., of the order of 2 amp. When the short gap breaks down, however, the current through both gaps must build up to cause the voltage drop V to appear across the characteristic resistance of the two transmission lines, i.e., 200 amp. Although the short gap might be capable of delivering this current very rapidly, the long gap takes a longer time. Thus, in spite of the fact that the short gap fires last, it is the building up of current from 2 to 200 amp. in the long gap which determines the shape of the impulse traveling down the right-hand transmission line.

Pulse Sharpener

In order to make use of the rapid firing of the short overvolted gap it is necessary to isolate it from the long gap. This can be accomplished by means of a transmission line between the two gaps which is sufficiently long to prevent reflections returning during the length of the impulse (Fig. 3). In practice it is necessary to use a three-electrode gap rather than the long gap alone in order to prevent loading the trigger generator with the low impedance of the transmission line. The operation proceeds as follows: The triggered gap, when fired, causes an impulse of rise time of the order of 20 mμsec. to travel toward the right on the center transmission line of Fig. 3. When this impulse arrives at the short gap, this gap has a large overvoltage on it and breaks down very rapidly after its normal lag time (consisting mostly of the time for an electron to arrive in the gap). If this time lag for firing of the short gap is longer than the rise time of the triggered gap, the impulse appearing on the right-hand transmission line will be determined by the breakdown characteristics of this short gap, causing a pulse-sharpening effect.

When this arrangement was tried for different lengths of the short gap, it was found that for gap-lengths short enough to produce impulses which rose in less than 1 mμsec., the lag time was shorter than the rise time of the trigger gap. This caused the top of the impulse to be rounded off to the slow rate of rise of the trigger gap. It is not known why this lag becomes so short for high overvoltages when there is no intentional source of electrons present (such as ultraviolet illumination). A clearing voltage of 200 volts between pulses seemed to have no effect on the time lag. To circumvent this difficulty the short gap was designed to hold higher pressures (up to 1500 p.s.i.) and to be adjustable down to 0.001-in. spacing. With these very short gaps under high pressure nitrogen it was found possible to have the gap long enough so that its time lag was long compared to the rise time of the trigger gap, and still short enough to produce an impulse which rose to 80 percent of full height in 0.3 mμsec.

In operation, this type of pulse-sharpening impulse generator has the disadvantage that the time lag for firing of the sharpening gap is statistical, with the finite probability of being shorter than the rise time of the trigger gap. This causes occasional impulses to have more rounded tops. In addition, the time lag seems to be affected by the previous discharge, if sufficient time is not allowed between pulses. A possible explanation of this effect might be the charging up of small insulating particles on the electrodes during the discharge which tend to emit electrons for long periods of time

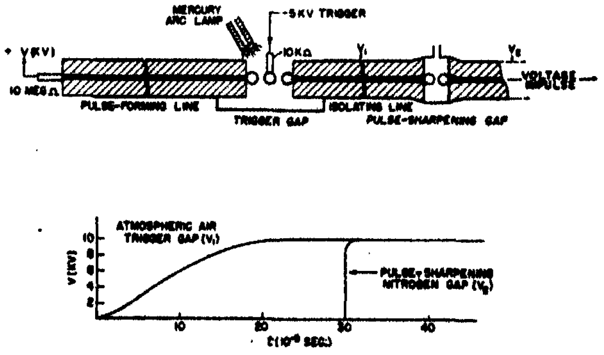

FIG. 3. Impulse generator using an isolated, overvolted spark gap for pulse sharpening.

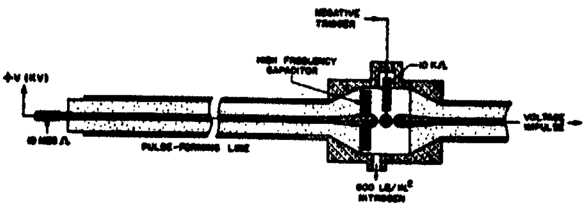

FIG. 4. Schematic drawing of high pressure trigger gap with capacitance sharpening.

after the discharge is over.[8] This time was found to be as long as 20 sec., making any set of measurements requiring many trials (such as the statistical distribution of time lags) very long and tedious.

High Pressure Trigger Gap

Observation of the operation of the high pressure-sharpening gap revealed that even for gaps which were only slightly overvolted fairly sharply rising impulses were produced. These impulses had the general characteristic of rising rapidly during the first part of the impulse and gradually slowing down as the voltage approached full height, causing the top part to be rounded. This observation suggested that a high pressure trigger gap would be successful in producing fast impulses if the top part could be sharpened.

It was thought that this sharpening could be accomplished with a high frequency capacitor as indicated schematically in Fig. 4. Thus this has the equivalent circuit shown in Fig. 5, where the resistors R represent the characteristic resistances of the transmission lines. If the trigger gap fired instantaneously, the voltage sent down the right-hand transmission line would be

$$\tfrac{1}{2}V[1+\exp(-2t/RC)],$$

producing a spike on the impulse which decays with a time constant of $RC/2$. If this time constant were made of the order of the rate of rise of the impulse from the trigger gap without the capacitor in place, one might expect that, with the condenser in place, an impulse would be obtained which had neither a spike nor a rounding-off.

The impulse generator shown in Fig. 6 was constructed following the above ideas. As one might expect, the sharpening condenser does not perfectly balance the rounding caused by the firing of the spark gap. The best compromise was an eight percent overshoot followed by a four percent undershoot. In addition, there were small (±4 percent) damped oscillations introduced by the condenser. The initial rise time was of the order of 0.4 mμsec. A photograph of a typical voltage pulse is presented in Section V, Fig. 19.****

FIG. 5. Equivalent circuit of trigger gap with capacitance sharpening. R is the characteristic resistance of the transmission line.

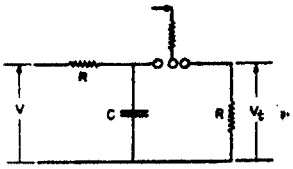

III. U.H.S. VOLTAGE DIVIDERS

In order to view these impulses (which were of the order of 20 kv) with the micro-oscillograph (which required about 200 volts for a reasonable deflection), a voltage divider is required. To accurately reproduce the rising characteristics of the previously described impulses as well as the flat part (which one might want to be as long as 100 mμsec.), we need a voltage divider with a uniform frequency response from 10 to over 3000 mc/sec. The construction of a suitable divider has proved even more difficult than the production of the impulses. The following is a description of some of the voltage dividers that have been tried, together with their limitations.

Capacity Divider

A capacity divider was constructed whose small capacitance (*ca.* 0.01 μμf) was a straight wire probe inserted into the transmission line down which the voltage impulse was sent, and whose large capacitance (*ca.* 1 μμf) consisted of the deflection plates of the micro-oscillograph together with the short coaxial lead to the deflection plates (Fig. 7). The deflection plates with their coaxial lead had a natural resonance of 3800 mc/sec. With the u.h.s. impulses described above, this resonance was excited to almost the full amplitude of the impulse voltage, making the observed voltage resemble a pulsed, undamped, microwave oscillation. Partial damping ($Q\simeq 3$) could be obtained with a graphite sleeve slipped over the center conductor of the coaxial lead. This resonance represents a fundamental limitation to this type of divider and could only be eliminated by redesigning the deflection chamber with the capacity divider built in. Therefore, this voltage divider is limited to viewing impulses with rise times greater than $10/\pi f_0=0.8$ mμsec. to keep the distortion less than ten percent.

Lumped Resistor Divider

A fairly good voltage divider can be constructed with small ($\tfrac{1}{4}W$) carbon resistors (e.g., Ohmite "Little

---

[8] L. Malter, Phys. Rev. **50**, 48 (1936).

**** For one planning to use this type of impulse generator, two characteristics are worth noting:

First, care must be taken to make the short gap short enough. A ratio of long-to-short gap of 5:1 at a pressure of 600 p.s.i. was found adequate. If this is not done, a spike will appear in front of the main impulse. This spike is probably due to the displacement current through the short gap when the long gap fires. By making the short gap short enough, it can be made to fire while the long gap is still in the process of breaking down. This causes the displacement current to add onto the breakdown current, producing a single impulse.

Second, the recovery time of the generator is very long. Normally the time of the recharging circuit had to be as long as 0.1 sec. to prevent multiple discharges, and under certain conditions even this time constant was insufficient to prevent them. For any application requiring a higher repetition rate than ten c.p.s. the recovery time of the generator would in some manner have to be decreased.

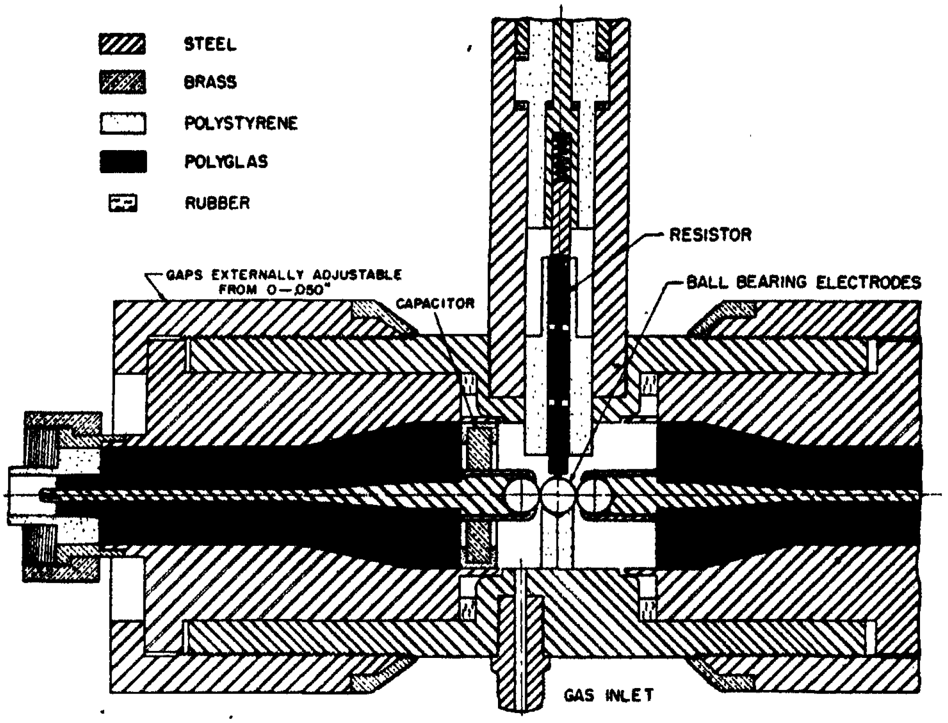

FIG. 6. High pressure nitrogen trigger gap with capacity sharpening (cross section).

Devil") arranged along the center of a coaxial line as indicated in Fig. 8. It was found necessary to have three resistors in series on the high voltage side to prevent voltage breakdown of the resistors at 20 kv. When this divider was tested with 10$k\Omega$ for the total resistance of the high voltage leg, it was found to produce a voltage pulse resembling that across a capacity being charged through a resistance with a time constant about 6 mμsec. This can be understood with the aid of steady-state transmission theory. Thus, if R_l is the large resistance of length l, R_s is the small resistance, R is the characteristic resistance of the line, and v is the normal propagation velocity, the dividing ratio as function of frequency ω is

$$\left\{\frac{1}{R_s}\left[\frac{R_l+j\omega(lR/v)}{j\omega(l/vR)}\right]^{\frac{1}{2}}\sinh\left[\left(R_l+j\omega\frac{lR}{v}\right)\left(j\omega\frac{l}{vR}\right)\right]^{\frac{1}{2}}+\cosh\left[\left(R_l+j\omega\frac{lR}{v}\right)\left(j\omega\frac{l}{vR}\right)\right]^{\frac{1}{2}}\right\}^{-1}.$$

For $\omega \ll (v/l)[(R/R_s)^{\frac{1}{2}}]$ and $R_l \gg R, R_s$, this expression reduces to

$$\{(R_l/R_s)(1+j\omega\tfrac{1}{6}(l/vR)R_l)\}^{-1}.$$

This is the frequency response of the equivalent circuit shown in Fig. 9, which has a time constant of $\frac{1}{6}(l/vR)R_l$. Since l/vR is the capacity of the large resistance to ground, this can be interpreted as the charging of the capacity of the middle of the large resistance by the front and back halves of the resistance. This equivalent circuit was checked experimentally by reducing both R_l and R_s by a factor of ten in order to reduce the time constant by a factor of ten and still keep the divider ratio. The shape of the observed impulse changed correspondingly. However, as this resistor is reduced, it has to dissipate more heat at the same voltage, causing the resistor to increase in temperature during the pulse. This increase in temperature caused a decrease in resistance and consequently an increase in the observed

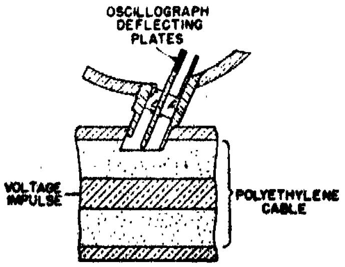

FIG. 7. Capacity divider consisting of transmission line probe and deflection plate leads.

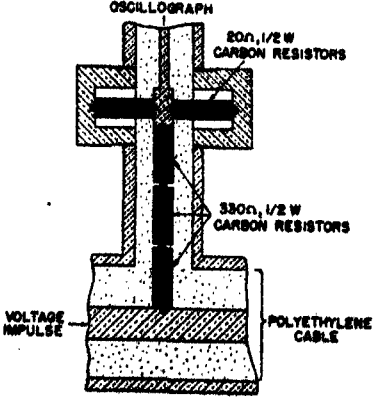

FIG. 8. Resistor divider using lumped carbon resistors.

voltage. For $R_l = 1000\ \Omega$ and $V_i = 10$ kv, this caused the voltage to rise ten percent in 10 mμsec., indicating that one would probably not want to use any smaller resistance. Therefore, for this particular kind of resistor and circuit arrangement, one is limited to viewing pulses of rise time greater than $10(lR_l/6vR) = 6$ mμsec. to keep the distortion less than ten percent.

Resistor-Cable Divider

Since transmission lines act like resistances for a time equal to twice their electrical length, these would appear ideal for a voltage divider. It is difficult, however, to design two transmission lines the ratio of characteristic impedances of which is the 100:1 required for the voltage divider (see, however, the following section), because the characteristic impedance changes so slowly with the geometric dimensions. For instance, for a coaxial line it changes as the logarithm of the ratio of the outer conductor diameter to the inner conductor diameter. An alternative possibility to using two transmission lines is to use one transmission line in combination with a lumped resistor. This would seem particularly useful if the transmission line could be used for the high voltage leg (which had previously limited the lumped resistor divider). This requires a ½-ohm lumped resistor of good characteristics as the low voltage leg. A thin, evaporated film of metal has been used successfully as a broad-band microwave attenuator.[4] This was successful because its thickness was smaller than the skin depth at the microwave frequencies, making the resistance independent of frequency. It was thought that this technique could be successfully applied to making the ½-ohm lumped resistor required here.

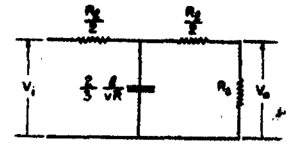

FIG. 9. Equivalent circuit for lumped resistor divider. R is the characteristic resistance of the line, l the length of the resistor R_l, and v the signal propagation velocity in the line.

The Microwave Research Institute, Polytechnic Institute of Brooklyn, kindly supplied us with two cylindrical ½-ohm resistors of size and material convenient for them to make (1 cm long, 1 cm diameter, of gold and platinum alloy). These were mounted in a coaxial line as shown in Fig. 10. The impulses observed with this arrangement had a sharp spike on the leading edge followed by a practically linear change in the voltage during the pulse, which was a decrease during the early part of the life of the resistor and an increase later in its life. In addition, the deflection did not correspond to the resistance measured initially with d.c., and had a tendency to change somewhat erratically from pulse to pulse, with a gradual decrease at first (down to a value corresponding to 0.2 ohm) and then an increase beyond the scale of the oscillograph (a resistance >3 ohm). This behavior was an indication that the resistors became overheated during the pulse. This overheating apparently caused the resistance to drop at first, presumably due to a rearrangement of the atoms. Later on, the resistance increased because the coating evaporated, as could be verified by observing that the transparency of the coating increased.

One might expect to minimize this heating effect by increasing the length and thickness of the resistive coating in order to increase the heat capacity. This can be done without changing the resistance value by keeping the ratio of length to thickness a constant. However, the following analysis of the initial spike will show that increasing the length increases the size of this spike.

The response of the circuit can be analyzed by steady-state transmission line theory. With the same nomenclature as before the transmission coefficient through the resistor is

$$T = \left\{ \cosh\left[\left(\frac{R_s}{R} + j\omega\frac{l}{v}\right)\left(j\omega\frac{l}{v}\right)\right]^{\frac{1}{2}} + \tfrac{1}{2}\left(\left[\frac{(R_s/R)+j\omega(l/v)}{j\omega(l/v)}\right]^{\frac{1}{2}} + \left[\frac{j\omega(l/v)}{(R_s/R)+j\omega(l/v)}\right]^{\frac{1}{2}}\right) \times \sinh\left[\left(\frac{R_s}{R} + j\omega\frac{l}{v}\right)\left(j\omega\frac{l}{v}\right)\right]^{\frac{1}{2}} \right\}^{-1}.$$

For $\omega \ll (R_s/R)(v/l)$ and $R_s \ll R$, this reduces to

$$T = \{1 + (R_s/2R) + j\omega(l/2v)\}^{-1}.$$

This is the response of the equivalent circuit shown in Fig. 11. Since lR/v is the inductance of the length of transmission line occupied by the resistor, it is seen that this inductance is the limiting circuit parameter. The equivalent circuit divides this inductance in two, and indicates that the observed voltage V_0 is the voltage across the resistance R_s and one-half the inductance lR/v. This was done on the assumption that half of the voltage drop due to the inductance is along the center conductor and half is along the outer conductor. With this and the previous assumptions the divider ratio as a function of frequency becomes $(R_s/R) \times [1 + j\omega(l/2v)(R/R_s)]$, with an inductive time constant of $(l/2v)(R/R_s)$. This inductance is thus the

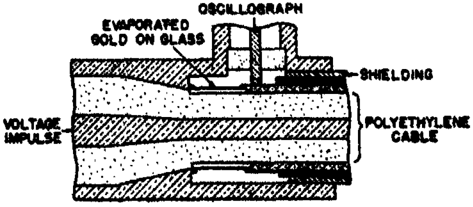

FIG. 10. Resistor divider using a transmission line with an evaporated metal resistor.

---

[4] Polytechnic Institute of Brooklyn, NDRC Div. 14, Reports 321 and 534 (1946).

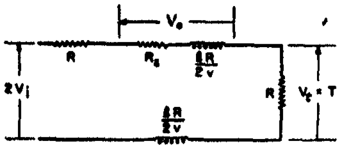

FIG. 11. Equivalent circuit for resistor cable divider. R is the characteristic resistance of the line, l the length of the resistor R_s, and v the propagation velocity in the line.

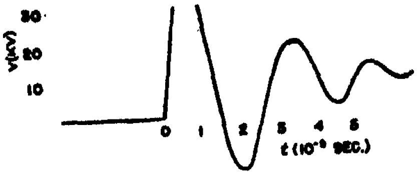

FIG. 13. Voltage impulse observed with inductive connection of Fig. 12.

source of the observed spike, and increasing the length of the resistance in order to decrease the heating effect would serve to increase the size of the inductance, and hence the size of the spike. This type of divider is therefore eminently unsatisfactory. Even if the resistive material were stable, a divider of these dimensions would be limited to rise times greater than $10(l/2v)(R/R_s) = 25$ mμsec. for less than ten percent distortion.

It is possible, however, that a semiconductor of shorter lengths (*ca.* 0.1 mm) and higher resistivity (*ca.* 0.1 ohm-cm) might be stable for these high currents and still accurately reproduce the u.h.s. transients. Initial investigations into this possibility were made with reduced TiO_2 ceramic resistors. A successful resistor could not be constructed, however, because of the mechanical difficulties of working with this brittle material of such small dimensions.

Transmission Line Divider

With the failure of lumped resistors as both the high and low voltage leg of a resistance divider, it would appear that lumped resistors would have to be abandoned if one expected to improve the response of the resistance divider. Transmission lines acting like ideal resistances for both legs offer a better possibility. The construction of two lines of a high enough ratio of characteristic resistances becomes simpler if one uses a high dielectric-constant material for the low impedance leg, because the characteristic resistance varies as $1/(\epsilon)^{\frac{1}{2}}$ and the electrical length as $(\epsilon)^{\frac{1}{2}}$. A suitable material is the TiO_2 ceramic, which has a dielectric constant of 85 (for a commercially available sample) independent of frequency up to at least 30,000 mc/sec. Although this material has the disadvantage of being hard and brittle, making it impossible to machine except with a grinding wheel, its high constant with uniform frequency response is not approached by any other known material.

In order to use this material in a voltage divider, the high voltage leg of which is a standard 50-ohm transmission line, it must be produced as a cylindrical tube the ratio of thickness to diameter of which is 0.0043, i.e., a thickness of 0.03 in. for a diameter of 0.7 in. (the diameter necessary for the TiO_2 to slip over the RG17/U cable used in these experiments). Initial efforts to produce a tube as thin as this by firing a thin wall on a ceramic Alundum tube failed because of the difficulty of having an electrode between the Alundum and the titanium dioxide. Thus, if this electrode (platinum to withstand the high firing temperature) is made too thin, the resistance of the electrode increases after the firing because of the loss of electrode material by diffusion. If the thickness is made too large, the TiO_2 does not bond to the Alundum so that it cracks upon cooling. No intermediate thickness which would eliminate both difficulties was found.

A second method to produce this thin-walled ceramic tubing is by extrusion. The American Lava Company managed to produce four tubes by this method whose average lengths were one foot and whose cross sections were less than 20 percent out-of-round. Silver electrodes were fired on the inside and the outside to form the coaxial transmission line.

The voltage shape observed with this type of divider was found extremely sensitive to the physical arrangements. Thus, a first attempt to connect the TiO_2 line through spring contacts is shown in Fig. 12. The voltage observed with this arrangement is shown in Fig. 13. The 500 mc/sec. oscillation is presumably due to a resonance between the inductance of the springs and the capacitance of the small section of line in front of the springs. A second (but less flexible) connection was achieved by pouring molten Woods metal into the gap between the outside of the TiO_2 and the circular brass connection (Fig. 14). (The gap is caused by the eccentricity of the TiO_2 tube.) The voltage is picked

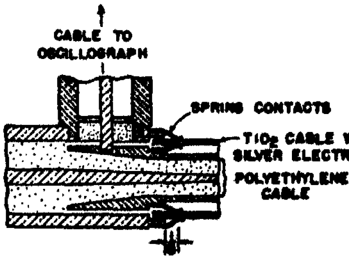

FIG. 12. Inductive connection to TiO_2 line in a transmission line divider.

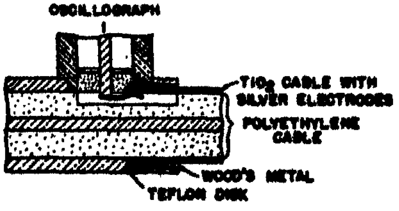

FIG. 14. Non-inductive connection to TiO_2 line in a transmission line divider with pick-up at the junction.

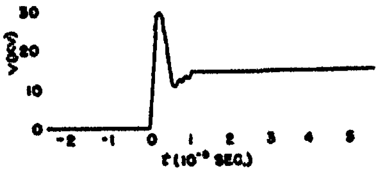

FIG. 15. Voltage impulse observed with non-inductive connection of Fig. 14.

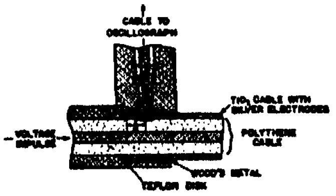

FIG. 16. Transmission line divider with pick-up one-fourth inch from junction.

off onto another transmission line through a spring contact to the inside electrode. The high currents of the voltage divider do not have to flow through this spring contact so that its inductance is not critical. The much improved voltage pulse is shown in Fig. 15. Even this impulse has a spike on it with an apparent inductive time constant of 0.3 mμsec.

It was believed that this remaining spike was due to the excitation of the higher modes of the coaxial lines by the transition from a low dielectric-constant material to a higher dielectric-constant material. This meant that steady-state transmission line theory would not predict the spike. In order to verify this belief, a short section of $\frac{1}{2}$-ohm coaxial line was built of the same dielectric material as the 50-ohm line. Although this was not suitable for general use as a divider because of its short electrical length (1 mμsec.), it was long enough to verify the non-existence of the spike, lending credence to the belief that the higher modes of the coax, which would only be excited by the high dielectric line, were the source of the spike.

This was at first thought to be a fundamental limitation of this type of voltage divider. However, further consideration indicated that the excitation of these higher modes might not materially affect the transmission of the TEM mode. Since these higher modes are exponentially damped as they travel away from the transition, at a large enough distance down the coaxial line it is possible to pick up the TEM mode without picking up the higher modes. The mode with the lowest attenuation constant in the TiO_2 line which would be excited by this transition is the TM_{01} mode with an attenuation constant of *ca.* π/b, where b is the thickness of the TiO_2. For the TiO_2 line used, this amounts to 36 db/cm. Thus one might expect, if the voltage were picked off a distance into the TiO_2 line of the order of 1 cm from the junction, that the distortion due to the excitation of these higher modes might be considerably less. It was found possible to construct such a pick-off by grinding a hole in the TiO_2 with carborundum embedded in a piece of brass tubing, and arranging the pick-off as shown in Fig. 16. This produced a pulse with no evidence of a spike on it (e.g., see Section V, Fig. 19).

Unfortunately, the rigorous solution of Maxwell's equations for these boundary conditions requires the solution of infinite determinants making it difficult to get enough information to indicate a figure of merit to compare with the other voltage dividers described. As judged from the reasonableness of the impulse which the divider reproduces when a parameter such as the sharpening condenser is varied, there would probably be less than ten percent distortion for impulses which were considerably shorter than the 0.4 mμsec. used here

FIG. 17. Schematic diagram of u.h.s. sweep circuit.

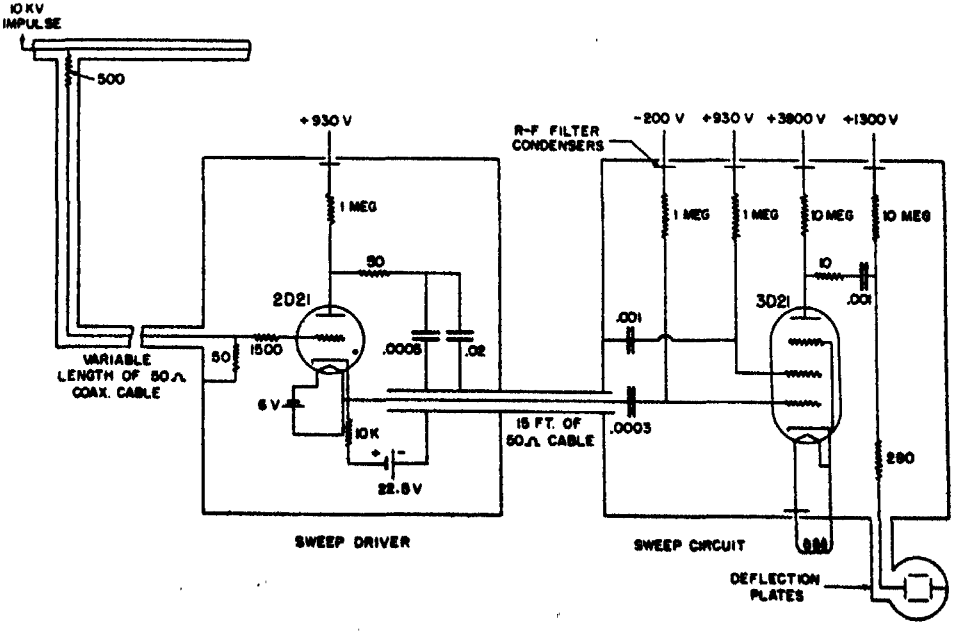

IV. U.H.S. SWEEP CIRCUITS

Generally speaking, it is not necessary to have a sweep speed any faster than to easily resolve the shortest time in which the transient changes appreciably. Thus, for viewing the previously described impulses, which had rise times of the order of 0.4 mμsec., a sweep speed with a full scale deflection in 10 mμsec. was entirely adequate to indicate the presence of spikes, oscillations etc. and to roughly determine the rise time. This sweep time is in a range which a vacuum tube can produce fairly well.

A more difficult problem than producing fast enough sweeps is to synchronize the sweep with the transient. Thus one of the first sweep circuits tried was a three-electrode trigger gap discharging a condenser through a resistor. This was capable of producing very fast sweep speeds, but even under illumination of a quartz mercury arc it could not be synchronized within 10 mμsec., so that many oscillograms were required before a single transient could be observed. A vacuum tube which is driven by the transient itself offers a chance for much more reproducible synchronization.

A schematic diagram of a successful sweep circuit is shown in Fig. 17. The sweep itself consists of a 3D21 pentode discharging the stray capacity attached to its plate. The pentode is driven by a 2D21 gas-filled thyratron, which drives the grid of the pentode positive enough to draw saturation current. The sweep speed is varied by changing the filament voltage of the 3D21. The sweep driver is necessary in order to isolate the sweep circuit from the impulse. This isolation is desirable to prevent the sweep speed changing with the shape and magnitude of the impulse and also to prevent the high frequencies contained in the impulse from feeding directly into the sweep circuit and exciting its parasitic resonances. Care had to be taken in the selection of a thyratron to make sure that its inherent time lag was not too long. Thus a 3C45 hydrogen thyratron (operating under the same conditions) was found to have a time lag of 130 mμsec. while the 2D21 has a lag of only 51 mμsec. Therefore, the 3C45 would require the impulse to be sent down 52 additional feet of polyethylene cable in order to get synchronization, greatly increasing the attenuation of the higher frequency components in the impulse. The whole circuit was completely shielded to prevent electrical pick-up from distorting the sweep. Synchronization was obtained by varying the length of cable leading to the sweep driver circuit.

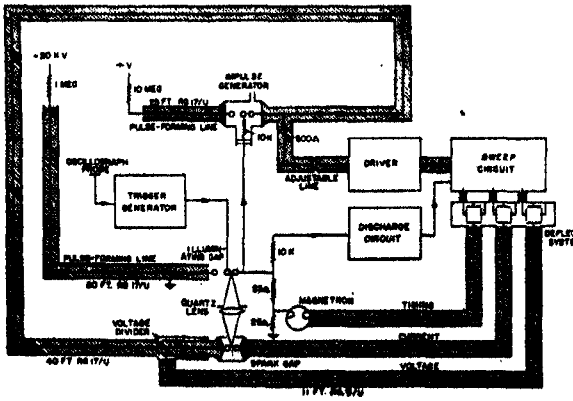

Fig. 18. Schematic circuit for testing impulse breakdown of air in the 10^{-9}-sec. region.

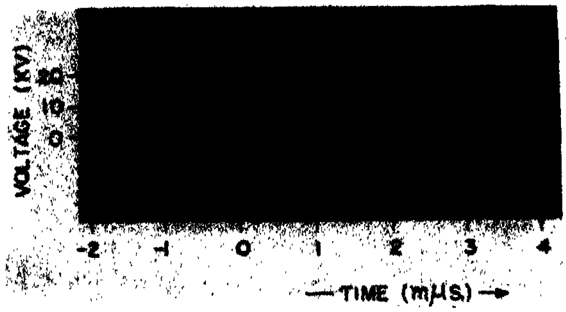

Fig. 19. Typical voltage oscillogram showing the arrival of voltage impulse at the left and breakdown of spark gap at the right. (The small oscillation in front of the impulse occurs because the voltage is viewed as the reflection from the spark gap superposed on the incident pulse; the oscillation is on the top of the incident pulse.)

This circuit provided sweep speeds with full scale deflection (1000 v) in times from 3 mμsec. up to 1000 mμsec., which were reproducibly synchronized with the high voltage impulse to within ±0.1 mμsec.

V. TYPICAL U.H.S. CIRCUIT

The use of the above u.h.s. circuit components can be illustrated with a circuit designed to test the impulse breakdown of an atmospheric spark gap (Fig. 18).

The process is started by turning on the beam of the microoscillograph for about one millisecond by means of a mechanical switch which dips quickly in and out of a pool of mercury. A probe is inserted into the beam path, so that when the beam is first turned on, a voltage is induced on the probe, which, when amplified, fires a thyratron ignition coil trigger generator. The output of the ignition coil triggers an illuminating gap which serves as ultraviolet illumination for the spark gap being tested. The illuminating gap simultaneously begins building up a photon intensity in the spark gap, sets off a magnetron timing wave, and triggers the u.h.s. impulse generator. When the impulse generator fires, a portion of the impulse is fed into the sweep driver while the main part proceeds down a 40-ft. transmission line (RG17/U) through the voltage divider to the spark gap. Current through the spark gap is observed by feeding the other side of the gap into the oscillograph through another transmission line. The cables from the voltage divider and the spark gap are so arranged that their signals arrive at the microoscillograph simultaneously. Synchronization of these with the sweep was obtained by varying the length of line to the sweep driver.

It was found that the plate of the sweep pentode began to recharge during the millisecond in which the oscillograph beam is turned on. To prevent this a hydrogen thyratron discharge circuit had to be built which turned off the power supply voltages leading to the sweep pentode after the sweep tube had been discharged. This discharge circuit was triggered from the illuminating gap.

In Fig. 19 there is reproduced a typical voltage oscillogram showing both the generated impulse and the breakdown of the spark gap.

ACKNOWLEDGMENT

The author is grateful to Professor A. von Hippel for making available to him the facilities of the Laboratory for Insulation Research and for his guidance and encouragement. He also wishes to acknowledge the constant cooperation and assistance of the members of the Laboratory.

THE REVIEW OF SCIENTIFIC INSTRUMENTS VOLUME 20, NUMBER 12 DECEMBER, 1949

Double Magnetic Lens Nuclear Spectrometer*

HAROLD M. AGNEW** AND HERBERT L. ANDERSON
Institute for Nuclear Studies, The University of Chicago, Chicago, Illinois

(Received July 4, 1949)

A large double magnetic lens spectrometer has been constructed for the study of gamma- and beta-ray spectra. The magnetic field is produced by two identical coaxial water-cooled coils, each 10.2 cm wide, 31.7 cm I.D., 73.7 cm O.D., and spaced 95.6 cm apart. The source is placed on the axis at the center of one coil and the detector is placed on the axis at the center of the other. The instrument is characterized by a large transmission with moderate resolution. Scattering is virtually absent because of the nature of the trajectories which are used, and because the large dimensions have made possible the removal of scattering material to a considerable distance from the source. The design has lent itself easily to the application of accelerating voltages at the detector admitting the detection of beta-rays down to 1 kilovolt. The maximum energy conveniently studied with the present arrangement is 2.8 Mev. Beryllium-coated Zapon films of thickness 0.01 mg/cm^2 have been used to mount sources. Charge does not accumulate on these sources. Observations with a Cs^{137} source 4 mm in diameter have shown a transmission of 1.4 percent with a resolution of 1 percent. The appearance of the internal conversion and Auger electron lines testifies to the absence of appreciable scattering.

INTRODUCTION

THE experimental study of beta- and gamma-ray spectra has, in many instances, been faulty because of scattering in the instrument and in the source. It seemed worth while to construct an instrument in which the scattering errors due to both causes could be reduced. In the double lens spectrometer described here, instrumental scattering has been markedly reduced by excluding scattering material over a fairly large region around the source, and by using a sufficiently complicated trajectory not easily followed by a series of chance scattering events. The spectrometer has a transmission which is large enough to allow the use of much thinner sources than is usually possible, thereby minimizing the effects of source scattering. The ratio, resolving power to transmission, in the present instrument, is more favorable than in most of the spectrometers which have been described thus far.

THEORY

The operation of the spectrometer is based on the behavior of a thin magnetic lens whose magnetic field has the form $H=H_0(1+z^2/a^2)^{-1}$ along its axis. This behavior has been studied rather completely by Glaser[1] who has shown that the paraxial ray equation has an explicit solution in this case. In our instrument, it was found that the electron trajectories could be predicted remarkably well using Glaser's results, even at a considerable distance from the axis. The design of the spectrometer was greatly simplified thereby.

The field produced by our coils as measured along their axis is shown in Fig. 1. A satisfactory fit of the formula

$$H=H_0(1+z^2/a^2)^{-1} \tag{1}$$

to these results was made with $a=19$ cm, and is shown in Fig. 2.

The radial distance r from the axis of particles with momentum p making not too large an angle with the axis is given by the usual paraxial ray equation,

$$d^2r/dz^2+(e^2/4p^2c^2)H^2r=0. \tag{2}$$

This is a form of the wave equation and for a field shape (1), the solution given by Glaser is

$$r=A(1+z^2/a^2)^{\frac{1}{2}}\sin\{(k^2+1)^{\frac{1}{2}}\arctan a/z+B\}, \tag{3}$$

where $k=eH_0a/2pc$. The constants of integration A

---

* This work was supported by a Joint Program of the ONR and the AEC.

** Now at Los Alamos Scientific Laboratory, Los Alamos, New Mexico.

[1] W. Glaser, Zeits. f. Physik 117, 285 (1941).

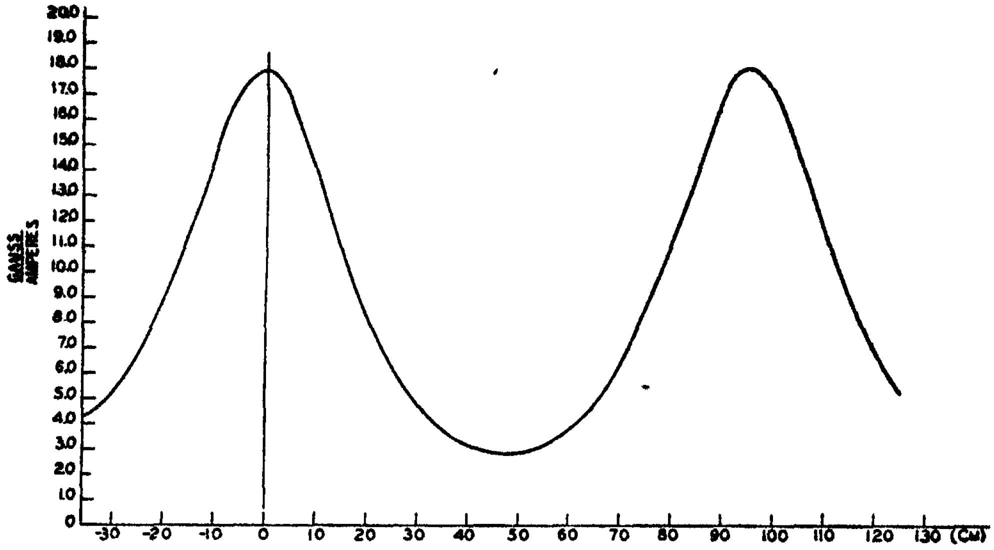

FIG. 1. The magnetic field as measured along the axis of the coils.

and B are determined by the boundary conditions which also determine the permissible values of the eigenvalue k.

In our arrangement, the source is placed at the center of one coil and the detector at the center of the other. If the coils were far enough apart, only those electrons from the source which are bent by the first coil so that they move parallel to the axis at large distances from the coil could be brought back to the axis at the detector by the second. The boundary condition imposed by this arrangement is that r remain finite for z very large. This requires that $B=0$. The eigenvalues of the momentum parameter are then determined by the condition that $r=0$ at $Z=0$, and are given by

$$k^2=4n^2-1; \quad n=1, 2, 3, \ldots. \tag{4}$$

The lowest value, $k^2=3$, establishes the value of the momentum which will be focused for a given value H_0. The values of k^2 obtained for $n=2, 3, \cdots$ correspond to lower values of momentum which will also be focused for the same H_0. These electrons cross the axis $n-1$ times before emerging from the field of the coil and must be eliminated by suitable baffles in order to make the instrument uniquely selective of a given value of momentum.

The value of the constant A is determined by the value of r at which the electrons move at large z and may be fixed by an annular baffle. It should be noticed that the value of A does not affect the value of momentum which is focused. Hence, a large aperture may be used without other impairment of the resolution than that which arises from the departure from the paraxial condition and the size of the source. The large intensity obtainable with this arrangement is due to this fact.

In our spectrometer, the coils are spaced 95.6 cm apart. The boundary condition $r=$finite at $z=\infty$ has to be replaced by $dr/dz=0$ at the mid-plane, $z=47.8$ cm. In this case, we have $k_1^2=3.24$ $(n=1)$, $k_2^2=18.27$ $(n=2)$, etc. To eliminate the second and higher harmonics, we made use of the fact that the orbit rotates with increasing z according to the relation,

$$\theta_2-\theta_1=\frac{k}{H_0a}\int_{z_1}^{z_2}Hdz. \tag{5}$$

Thus, the orbit $n=2$ rotates 2.37 times as much as that for $n=1$. We constructed a helical baffle placed in the center of the instrument which was designed to accept the orbit $n=1$, but not the $n=2$ or higher orbits. The use of a helical baffle in the center of the instrument frees the region around the source from scattering material.

There are also a series of eigenvalues which satisfy the condition $r=0$ at $z=47.8$, but these are eliminated by the presence of the solid core of the helical baffle.

The constant of the instrument was checked using the K conversion line of Ba^{137}(629 Kev). The annulus at the detector was fixed to accept electrons entering the detector (and leaving the source) at a mean angle of 29°. This line was detected at a current of 34.0 amperes corresponding to a value of $k^2=2.95$. This is somewhat smaller than the value calculated for paraxial trajectories because of the obliquity of the trajectory which was used. The calibration constant of the spectrometer in terms of the current I in amperes in the coils is given by the relation,

$$H\rho=100I \text{ gauss-cm}, \tag{6}$$

where $H\rho$ is the electron momentum in gauss-cm.

The trajectories in the spectrometer were checked by using the variable control shutter system and also by ray tracing near the detector using a series of annuli of varying diameter connected to a movable Geiger counter. Equation (3) with $k^2=2.95$ was found to give a quite accurate description of these observations.

ARRANGEMENT

The magnetic field is produced by two identical coaxial coils placed 95.6 cm apart. The coils have an inside diameter of 31.7 cm, and an outside diameter of 73.7 cm. Each coil consists of four pancakes connected in series. Each pancake is wound of 167 turns of 0.040-in.×1.0-in. copper strip. The pancakes are insulated from one another with 0.030-in. fabricated mica sheet, and the whole assembly is tightly clamped inside a Dural housing which has provision for water cooling. The cooling allows continuous operation at a current of 110 amperes, with a power dissipation of 10 kilowatts. At this current, the magnetic field at the center of each coil is 1980 gauss.

The coils are clamped to an iron shell, having a diameter of 73 cm with a wall thickness of ¼ in. This shell forms a part of the vacuum system, and also serves the useful purpose of shielding the spectrometer from the vertical component of the earth's field. The spectrometer is aligned in the direction of the horizontal component of the earth's field. The iron shell was carefully machined to be a true cylinder with uniform walls, and all other iron was kept remote from the coils. The cylindrical symmetry of the magnetic field was verified by observing with a fluorescent screen the low energy electrons produced with an electron gun. When these were emitted from a point on the mechanical axis of the instrument, they always remained symmetrically distributed about this axis, even at the lowest values of the magnetic field. The iron shell was found to perturb the axial magnetic field distribution in only a minor way. The proportionality of the field intensity to the current was found to be accurately maintained.

In all the work carried out with the instrument thus far, the source has been placed at the center of one coil and the detector at the center of the other. Other locations of the source and detector along the axis may be used to advantage. In particular, higher energies may be focused with improved dispersion, but with smaller transmission, if the distance between source and detector is increased.

The source is introduced into the spectrometer through a vacuum lock. The detector, usually a Geiger counter, is permanently placed at the other end of the instrument, and is filled *in situ*.

The aperture of the instrument may be controlled from the outside by means of two large adjustable iris diaphragms situated symmetrically between the coils at a separation of 39.1 cm. These are constructed of Dural after the fashion of those used in cameras. Each has 30 leaves of $\frac{1}{32}$-in. thickness, opens to a maximum diameter of 60 cm, and closes to a minimum diameter of 14.5 cm. The iris diaphragms are used in conjunction with fixed center disks having a diameter of 14.5 cm, thereby providing an annulus whose opening may be varied from zero to 22.7 cm.

The center of the instrument contains a helical baffle, the purpose of which is to eliminate second and higher order trajectories, and also to discriminate against either electrons or positrons, depending on the direction of the current in the coils. It is constructed on an aluminum-encased lead core 8 cm in diameter and 39 cm long. There are 9 aluminum fins bent to give an angle of rotation of 36½°. The loss in transmission due to these fins is about 5 percent.

The spectrometer is pumped at the source end. A Kinney VSD mechanical pump is used for rapid evacuation from atmospheric to a few microns pressure. Operating vacuum of 3×10^{-6} mm of Hg is maintained by means of a two-stage 4-in. oil diffusion pump backed by a small mechanical pump and using a liquid air trap. All vacuum joints are made with standard neoprene gaskets or "0"-rings. The "0"-rings were found to be particularly convenient and satisfactory. High vacuum is required to prevent the occurrence of high voltage discharges within the instrument.

The design of the spectrometer is shown in Fig. 3. Not shown are the aluminum castings in which the coils are mounted. These have bronze rollers which allow the movement of the coils over the top surface of a welded Dural table on which the whole is mounted. The easy assembly of the instrument is accomplished thereby.

CURRENT SOURCE

The current through the coils is supplied by means of two high-current ordinary portable welding generators and is electronically stabilized. The circuit of the regulator was developed here by Mr. Leonard Reiffel. A reference voltage and a voltage from an

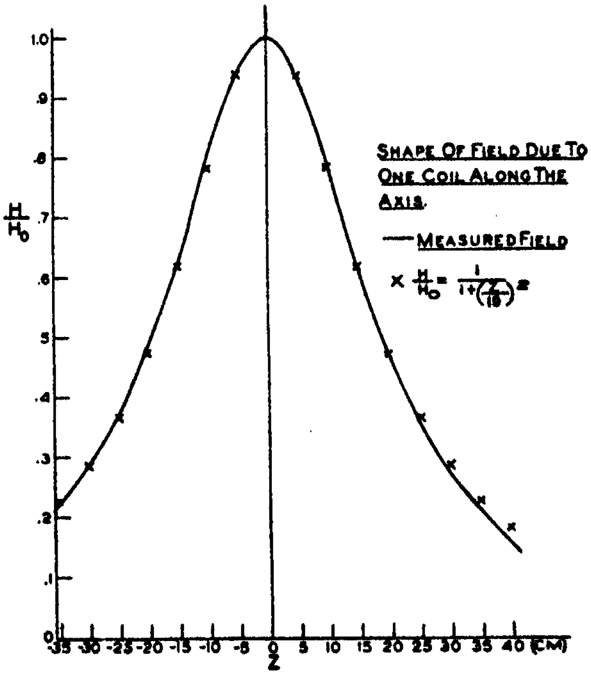

FIG. 2. A fit of the field measured along the axis of the coils to the expression $(1+(z/19)^2)^{-1}$.

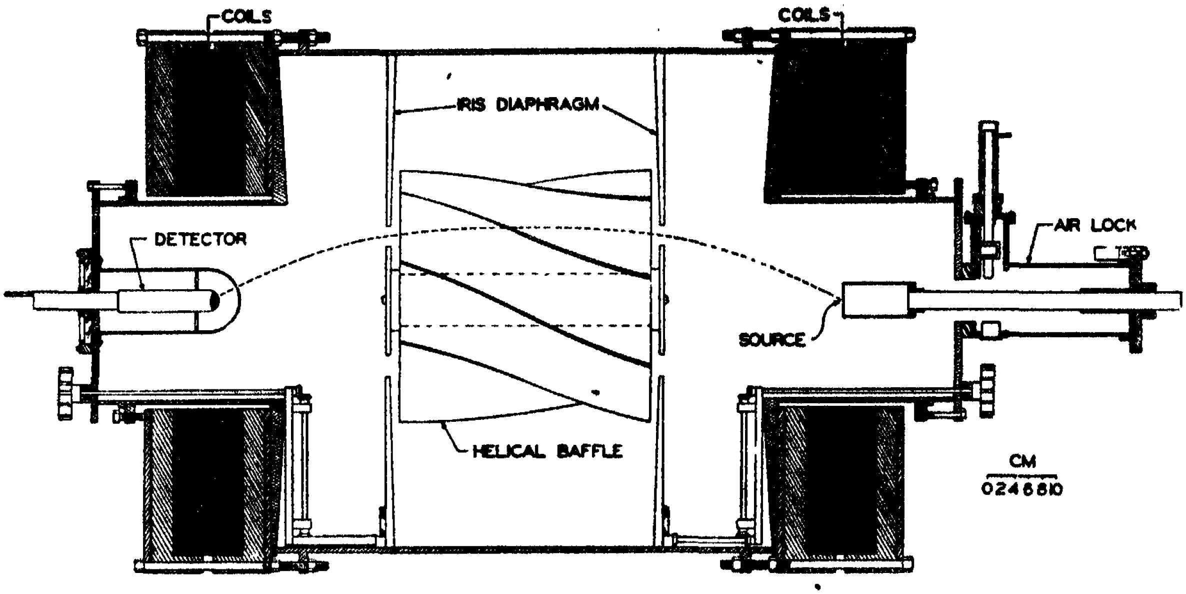

FIG. 3. Double magnetic lens spectrometer showing geometry used.

0.01-ohm Manganin resistance in series with the coil current are alternately fed into an a.c. amplifier by means of a Brown converter. The output of the amplifier is fed into a demodulator and the resulting d.c. voltage excites the field of an amplidyne, which in turn supplies the field of one of the welding generators. Using this system, the current can be held to within 0.05 percent for currents from 5 to 100 amperes. Storage batteries are employed for currents under 5 amperes.

DETECTOR

For the study of low energy beta-ray spectra, a special accelerating section has been constructed. From an analysis of the trajectories, it was found that within a small distance from the center of the coil, the trajectories are radial in a plane rotating with the electrons and have as their common center the center of the coil. Consequently, an accelerating section was constructed in which the field lines were radial. This was done by establishing a potential difference between concentric hemispheres; the counter, maintained at some voltage being the inner hemisphere, and a grounded shell with an annular slit, the outer. The end of the counter has No. 53 holes drilled radially in it between the angles of 20° and 40° such that it has a transmission of about 55 percent. A thin Nylon foil[2] is placed on top of this grid and then covered with an identical metal grid. At first it was thought that relatively thick foils could be used and enough accelerating voltage employed to compensate for their thickness. However, as was reported by Langer,[3] at high voltages spurious counts occurred which have no connection with the source. Plating the outer electrode with platinum and mirror-finishing had no effect on the value of the threshold at which these counts occurred. The spurious pulses could not be distinguished from the regular beta-ray pulses. As a compromise, a window approximately 9 kv thick was placed on the counter. With an accelerating voltage of 8 kv, one can measure down to 1 kv and can correct for window absorption quite accurately down to 10 kv. Figure 4 shows a typical result of the low end of a beta-spectrum with and without the accelerating voltage. This system has the advantage that the effect of the window can be measured and at the same time, the window is thick enough so that the counter can be used indefinitely and there is no necessity of changing counters and normalizing the data. Because of the thinness of the window, the counter is filled *in situ* to a total pressure of approximately 8 cm with a mixture of neon and amyl acetate. The counter is insulated from the rest of the machine by means of a polystyrene disk, through which the counter passes by means of an "0"-ring seal. The counter is connected to the glass filling system by means of Saran tubing and

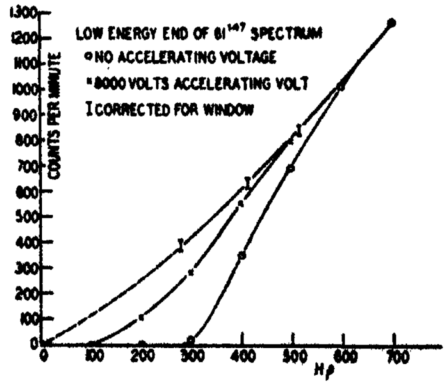

FIG. 4. Low energy end of β^- spectrum illustrating action of accelerator.

---

[2] Brown, Felber, Richards, and Saxon, Rev. Sci. Inst. 19, 818 (1948).

[3] L. Langer and C. S. Cook, Rev. Sci. Inst. 19, 257 (1948).

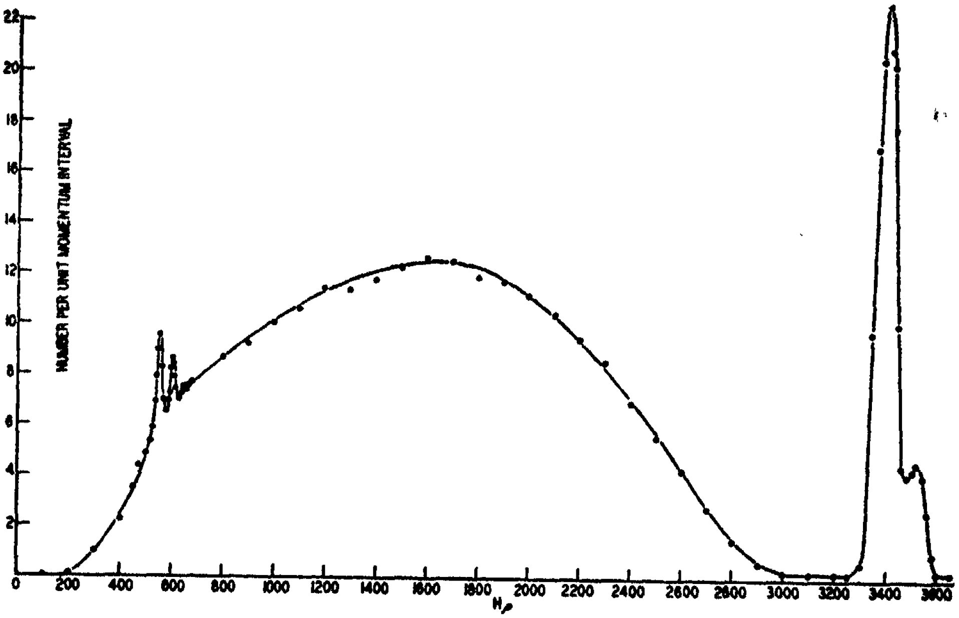

FIG. 5. Typical data showing β^- from Cs^{137} and Auger and internal conversion electrons from Ba^{137}.

standard flare fittings—providing insulation and flexibility.

SOURCES

Sources to be investigated in the instrument are usually mounted on thin Zapon[4] or LC600[5] films. At first, the foils were coated with a layer of Be by evaporation and then the source was placed on the side opposite to that having the Be. The resistance from the center of the foils on the side opposite to that on which the Be was evaporated to the foil edge was less than 800 megohms, and the resistance on the Be side was of the same order of magnitude. The Be seems to lodge inside the film. However, in some cases, when a source in a weak acid solution was applied to such a foil, the acid appeared to dissolve the Be just in the neighborhood of the source. Consequently, even though the source, which was approximately 4 mm in diameter, was surrounded by a conducting medium, it was found to charge up 2 to 3 kv. In these cases, the effect was overcome by preparing the sources on a plain film of Zapon or LC600 weighing about 0.01 mg/cm^2 and then, after the source was dry, covering it with a foil coated with Be. The covering foil with its Be weighed less than 0.01 mg/cm^2. The foils on which the sources are mounted are 2 in. in diameter and are mounted on a hard rubber stand consisting of a ring $\frac{1}{16}$ in.×$\frac{1}{16}$ in. supported by three $\frac{1}{16}$-in. square legs 4 in. long. Such a frame is made by milling the sides from a single piece of 2-in. diameter, $\frac{1}{16}$-in. wall hard rubber tubing. The hard rubber frame is made conducting by painting it with Aquadag. The sources are made to spread uniformly by first applying a very dilute drop of insulin over the desired area. Because of the large transmission of the instrument, it is possible to use sources weighing less than 0.05 mg/cm^2 for most substances.

The transmission and resolution of the instrument were checked using the internal conversion line of Ba^{137}. A thin source of Cs^{137} was measured in a known geometry. The absence of scattering was checked by verifying the $1/r^2$ law. Corrections were applied for window thickness and for the presence of the Ba^{137} gamma-ray. The number of electrons emitted from the source due to the conversion line of Ba^{137} was obtained from the fact that this line is 13 percent converted. Observation of the counting rate of the conversion electrons from this source in the spectrometer led to the result that the transmission of the instrument was 1.4 percent. The source used had a diameter of 4 mm and the half-width of the line at half-maximum was 1.1 percent. With a source one inch in diameter, the resolution was 9 percent obtained with a transmission of 11 percent. The latter measurement was made with a counter having a window the same size as the source and the baffles almost wide open. Figure 5 is a typical example of the type of data obtained using the accelerator section. This is a spectrum of Cs^{137}, and the resulting internal conversion lines of Ba^{137}. The appearance of Auger electrons from the Ba^{137} at the low end of the spectrum is particularly noteworthy and testifies to the small amount of scattering achieved in this instrument. Other spectra have been studied and will be reported in *The Physical Review*.

ACKNOWLEDGMENT

It is a pleasure to acknowledge the assistance of Mr. S. Hayashi during the initial construction of the instrument. We are grateful to Professor E. Fermi for his advice and continued interest in the work.

---

[4] John Backus, Phys. Rev. 68, 59 (1945).

[5] LC600 Synthetic Resin, Lithgow Corporation, Chicago, Illinois.

THE REVIEW OF SCIENTIFIC INSTRUMENTS VOLUME 20, NUMBER 12 DECEMBER, 1949

A Small Differential Analyzer with Ball Carriage Integrators and Selsyn Coupling

R. E. MEYEROTT AND G. BREIT
Yale University, New Haven, Connecticut*

(Received June 3, 1949)

A small scale differential analyzer is described which uses ball carriage integrators instead of the usual Kelvin disk integrators, and selsyn angle transmission instead of mechanical coupling of the rotating parts. The machine is inexpensive, easily constructed and is moderately accurate.

I. INTRODUCTION

THE practical value of a small scale differential analyzer was discovered by D. R. Hartree and A. Porter[1] when a model originally intended to be an aid in the design of a larger machine was assembled and tested. It worked so well that it was kept in operation. Since that time, several other model analyzers have been built following essentially the design of the earlier larger machines.[†, 2–4] The construction of all these small scale machines has been light and subject to vibration but worked well as long as no more than four or five integrators were coupled together. Their over-all accuracy has been stated to be around 2 percent.

The machine built in this laboratory differs from those previously built mainly in two ways: (a) the integrators are of the ball carriage type instead of the Kelvin disk type; (b) electrical transmission by means of selsyns replaces mechanical coupling of rotating

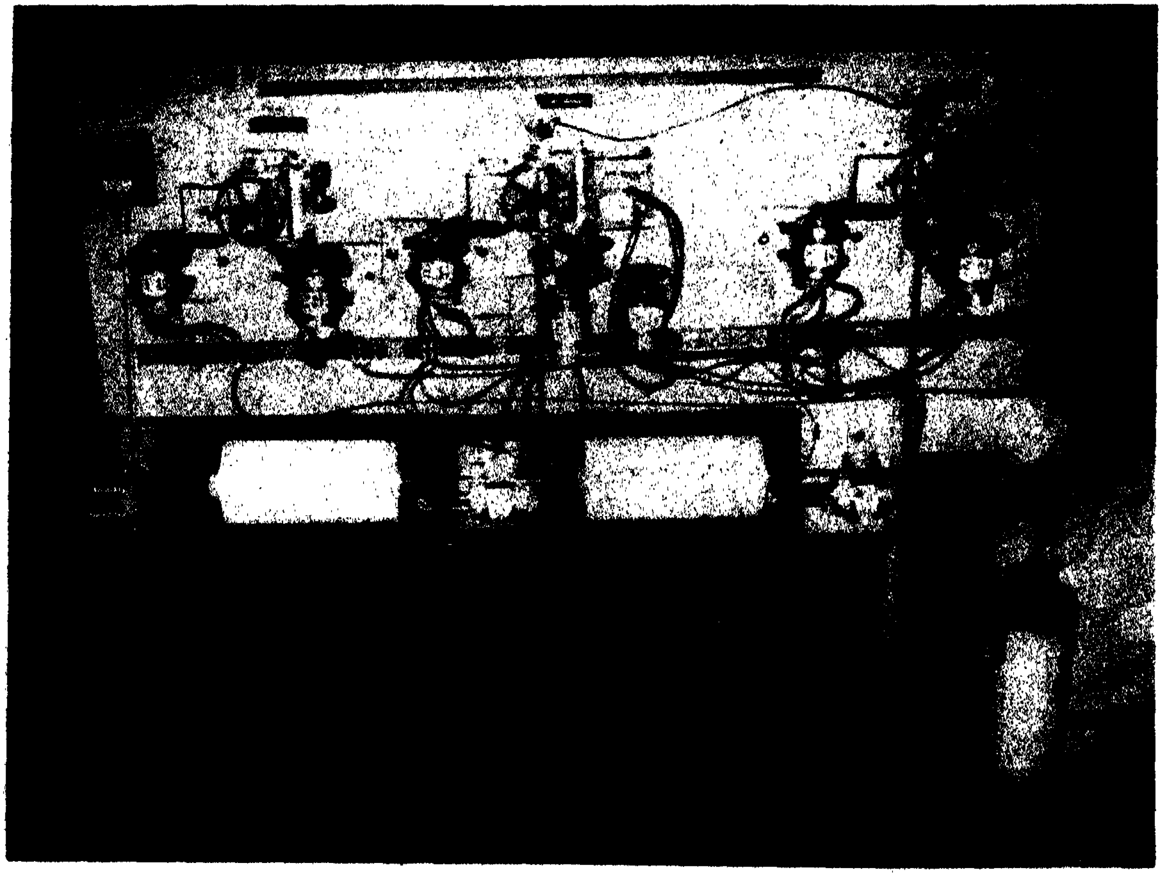

FIG. 1. Photograph of the differential analyzer. The independent variable shaft shown in Fig. 2 is below the table. The meter scale indicates relative dimensions.

---

* Assisted by Joint Program of the ONR and the AEC.

[1] D. R. Hartree and A. Porter, Mem. Proc. Man. Lit. Phil. Soc. 79, 5 (1935).

† For a more general discussion of differential analyzers see reference 4.

[2] Massey, Wylie, Buckingham, and Sullivan, Proc. Roy. Irish Acad. 45, 1 (1938).

[3] Lennard-Jones, Wilkes, and Bratt, Phil. Soc. Proc. 35, 485 (1939).

[4] V. Bush and S. H. Caldwell, J. Franklin Inst. 240, 255 (1945).

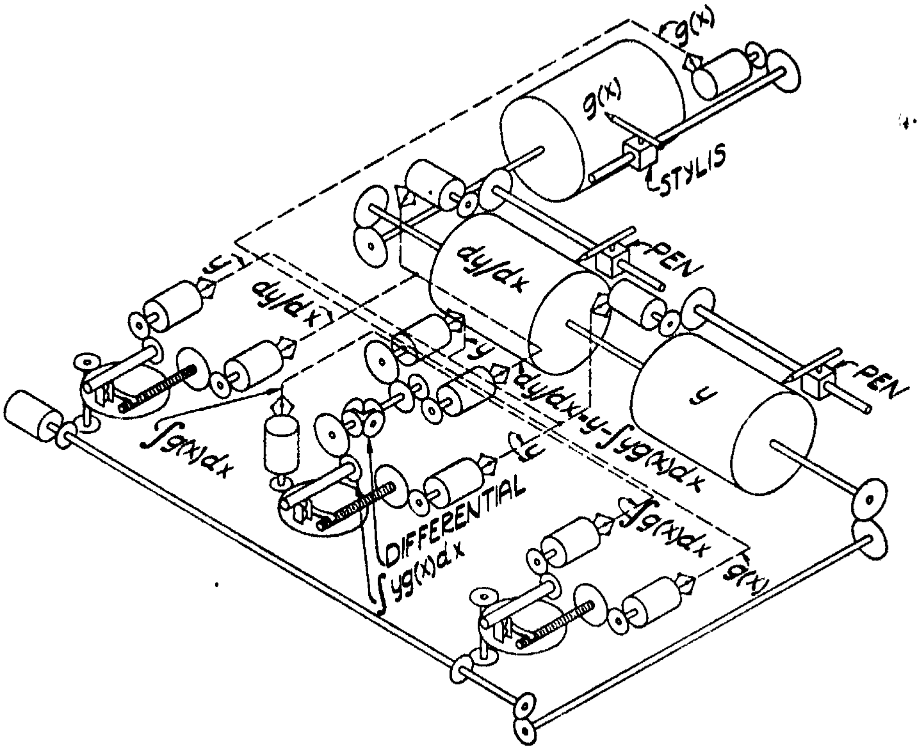

FIG. 2. Schematic diagram of the differential analyzer. The gear train used to position the ball carriage is here shown as a screw and a half-nut. Broken lines represent selsyn signal wires.

parts which is often accomplished by means of shafts. Advantages of the ball carriage type integrators are: (1) a good output torque which makes it possible to do without torque amplification, (2) a convenient way of adjusting the ratio of rotations of roller and disk; only the ball carriage has to be moved and the integrator table assembly remains fixed. Selsyn transmission has the following convenient features: (1) economy in precise shop work, (2) ease in changing connections between rotating parts. The latter feature is a time saver when the machine is being coupled for a new problem.

The main object of the present note is to call attention to the relative ease of construction of a differential analyzer of small or moderate accuracy which is being made possible by the availability of war surplus equipment in the form of ball carriage type mechanical integrators, servo mechanisms and other parts.

II. CONSTRUCTION

The machine contains three ball integrators, three function units and an adder unit. The term "function unit" is used here to denote a device capable of carrying an input function which can be coupled to other parts of the machine. It is also used to describe a device capable of recording an output function.

The function units were provided by a slight remodeling of two discarded kimographs and by the addition of a drum to a ruling engine. The adder unit is a differential geared to two selsyns. This unit is so arranged that when the adder is not used, one selsyn is disconnected and the differential then serves as an ordinary gear. This design feature makes it possible to permanently attach an adder to the output of an integrator and thus simplify the change-over for different equations.

A photograph and a plan of the machine are shown in Fig. 1 and Fig. 2 respectively. The connections are shown for the differential equation:

$$(d^2y/dx^2)-(dy/dx)+g(x)y=0.$$

Inspection of Fig. 2 shows that this equation requires the first integrator to drive the integrator table of the second. This means that sufficient torque must be available in the first integrator to drive the second integrator, five selsyns, and an adder unit. No slipping of parts was observed in ordinary operation. Inspection of Fig. 2 will show that the selsyns most likely to introduce errors are those which set the linear displacement of an integrator. Selsyns when used in the above manner, may introduce several degrees error. This effect has been eliminated by introducing an accurate gear reduction of 2500 to 1 between the selsyn and the integrator.

III. PERFORMANCE

The over-all backlash was tested by setting the machine to generate sine functions and noting the increase in amplitude per cycle. Sine functions were generated by making $g(x)=\text{constant}$ on the input function and disconnecting selsyn labeled y on the adder unit shown in Fig. 2. The increase in amplitude per cycle is about 0.2 percent which is only about 1/10 that reported for other small machines[3] and compares favorably with that of some more elaborate machines.[5] This error has been found to be due to the backlash of the integrator itself. To reduce this error it would be necessary to improve the integrator or else to provide a correction for backlash. No attempt was made to do either.

In order to investigate the performance when the input function was not constant it was found necessary to take considerable care in plotting the function $g(x)$. If this is done and $g(x)$ is large over most of the range of integration so that the first integrator is kept at a reasonably large displacement, the errors are about the same as those for sine functions. When no precautions are taken the error seldom exceeds 1 percent.

IV. CONCLUSIONS

The machine has proved satisfactory and convenient for the solution of problems with a nominal accuracy of one percent as described in the preceding section. Ball carriage type mechanical integrators do not require torque amplification when used with precautions described. Electric ("selsyn" or "synchro") angle transmission has proved reliable and convenient as a means of coupling functional units in the computing device.

ACKNOWLEDGMENTS

We wish to acknowledge the assistance of Mr. P. S. Jewett in making preliminary tests, of Mr. A. G. Petchar of the Sloane Physics Laboratory shop in the construction of the machine and of Mr. S. Geltman in performance tests. The Applied Physics Laboratory of The Johns Hopkins University has kindly supplied three mechanical integrators. Thanks are due also to Professors A. G. Conrad and J. L. Bower of the Electrical Engineering Department of Yale University for the loan of several selsyns, and to Dr. D. T. Sigley of the Applied Physics Laboratory for performance characteristics of mechanical integrators in similar computing devices.

---

[5] See for example H. P. Kuehni and H. A. Peterson, Elec. Eng. 63, 221 (1944).

THE REVIEW OF SCIENTIFIC INSTRUMENTS VOLUME 20, NUMBER 12 DECEMBER, 1949

A Slide Rule for Radiation Calculations

M. W. Makowski
Polish University College, London, England

(Received February 17, 1949)

A slide rule has been developed to facilitate rapid calculations based on the Planck radiation formula. Quantities such as the radiant flux density in a given wave-length region, the spectral radiant flux density at a given wave-length, or the corresponding quantities expressed in photon units, can be obtained readily for a black body over a range $\lambda T = 2\times 10^{2}$ to $\lambda T = 4\times 10^{4}$ micron degrees with an accuracy of about 1 percent. Simple extension rules can be used for larger values of λT.

I. INTRODUCTION

In the course of certain radiation calculations it was found that the available tables based on the Planck radiation formula were neither sufficiently comprehensive nor convenient for frequent reference. The need was felt for a device that would facilitate rapid calculations without involving too great a sacrifice in accuracy. Accordingly it was decided to develop a nomogram, based on the Wien displacement law, capable of giving rapidly approximate values for the radiation quantities most frequently encountered. Typical of such quantities is the radiation per unit area emitted by a black body at a given temperature in a given wave-length interval. The general features of the nomogram are shown in Figs. 1 and 2.

As the work proceeded the advantages of a slide rule arrangement became apparent, and it was decided to extend the computations already carried out with a view to the development of a radiation slide rule. This paper gives a description of the slide rule and the methods used in the associated calculations. The final form of the rule, the general arrangement of which can be seen in Fig. 3, includes the scales required for calculations involving spectral radiant flux density and radiant flux density, together with the corresponding quantities in photon units. The over-all dimensions are 19½ in.×3½ in. The stock carries the scales of maximum spectral radiant flux density, $H_\lambda$max.,[a] total radiant flux density, H, maximum spectral photon flux density, $Q_\lambda$max., total photon flux density, Q, temperature (centigrade and absolute), and wave-length. One side of the slide carries the scales required for calculations involving the first two of the above quantities, while the scales necessary for photon calculations are on the reverse of the slide. The back of the stock carries brief definitions and instructions, together with the scales relating wave-length, wave number, and electron volts.

---

[a] The symbols used throughout this paper have the usual significance. The subscripts λ, $\Delta\lambda$, ν, and $\Delta\nu$, refer to wave-length, wave-length interval, wave number, and wave number interval respectively. The symbol *cm* is used to denote unit of length referring to the surface of a black body. The values of the constants used follow Birge ($c_1 = 2\pi hc^2 = 3.7403\times 10^{-12}$ watt cm²; $c_1' = 2\pi c = 1.88355\times 10^{11}$ cm sec.$^{-1}$; $c_2 = hc/k = 1.43848$ cm deg. A).

II. THE PLANCK RADIATION FORMULA

If we consider unit area of a black body at temperature T and choose some wave-length λ, then the radiated energy for a wave-length interval 1 $\mathrm{cm}_{\Delta\lambda}$,[b] which we shall call the spectral radiant flux density, is given by the Planck radiation formula as

$$H_\lambda=\frac{c_1\lambda^{-5}}{e^{c_2/\lambda T}-1}\text{ watt } cm^{-2}\,\mathrm{cm}_{\Delta\lambda}^{-1}.$$

The corresponding expression for wave number interval $\Delta\nu=1\ \mathrm{cm}_{\Delta\nu}^{-1}$ is

$$H_\nu=\frac{c_1\nu^3}{e^{c_2\nu/T}-1}\text{ watt } cm^{-2}\,(\mathrm{cm}_{\Delta\nu}^{-1})^{-1}.$$

For a wave-length interval $d\lambda$ the energy radiated is $H_\lambda d\lambda$, and for a wave-length interval between λ_1 and $\lambda_2(\lambda_1<\lambda_2)$

$$H_{\lambda_1-\lambda_2}=\int_{\lambda_1}^{\lambda_2}H_\lambda d\lambda=\int_0^{\lambda_2}H_\lambda d\lambda-\int_0^{\lambda_1}H_\lambda d\lambda$$

$$=\int_{\lambda_1}^{\infty}H_\lambda d\lambda-\int_{\lambda_2}^{\infty}H_\lambda d\lambda\text{ watt } cm^{-2}.$$

For a given temperature T, the wave-length λ_m for which H_λ is a maximum, is obtained from $dH_\lambda/d\lambda=0$, which gives, of course, one case of Wien's displacement law,

$$\lambda_m=0.28972/T\ \mathrm{cm}_\lambda.$$

By substitution

$$H_\lambda\text{max.}=1.2875\times10^{-11}T^5\text{ watt } cm^{-2}\,\mathrm{cm}_{\Delta\lambda}^{-1}.$$

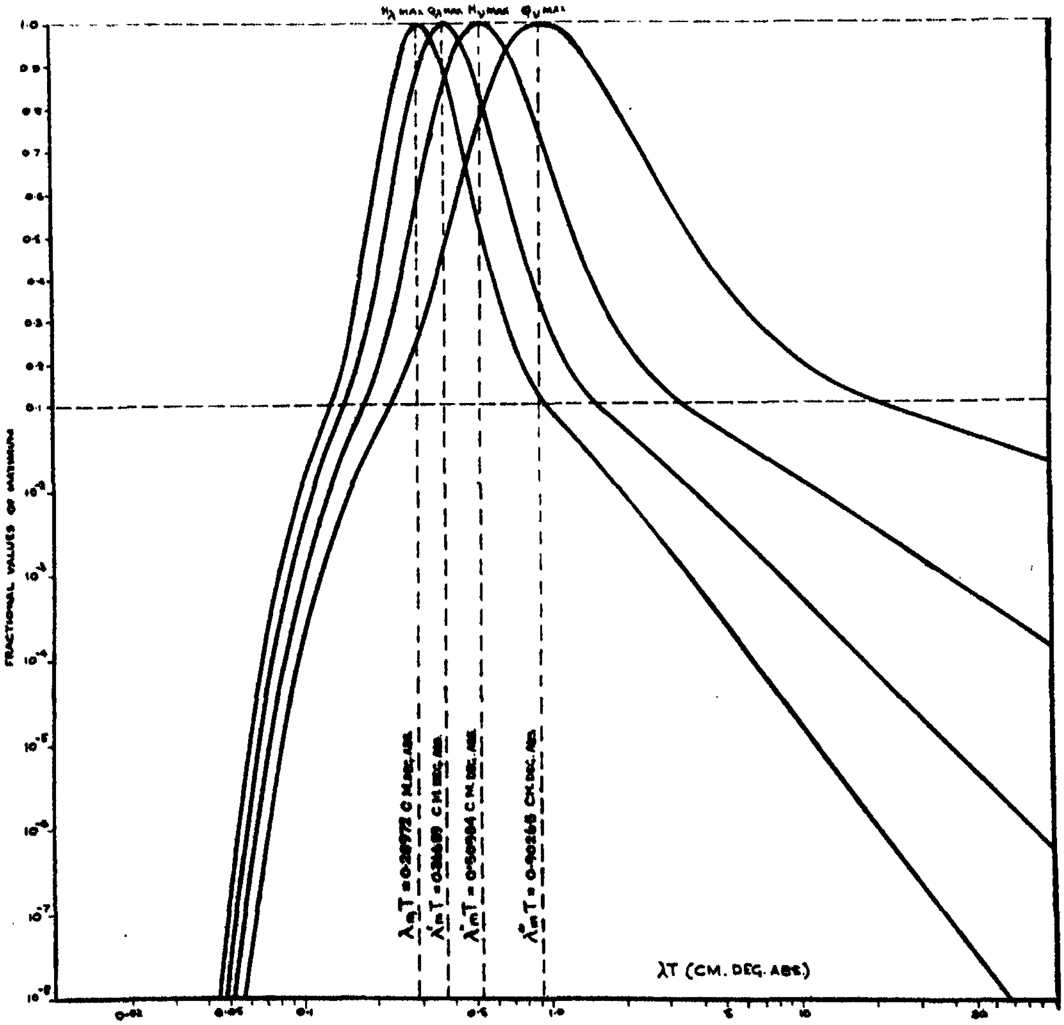

FIG. 1. Radiation nomogram—spectral curves.

---

[b] It is not possible to attach physical significance to the use of these wave-length and wave number intervals. The spectral quantities refer to a single point on a radiation curve and in all calculations involving a real wave-length interval, the centimeter interval disappears.

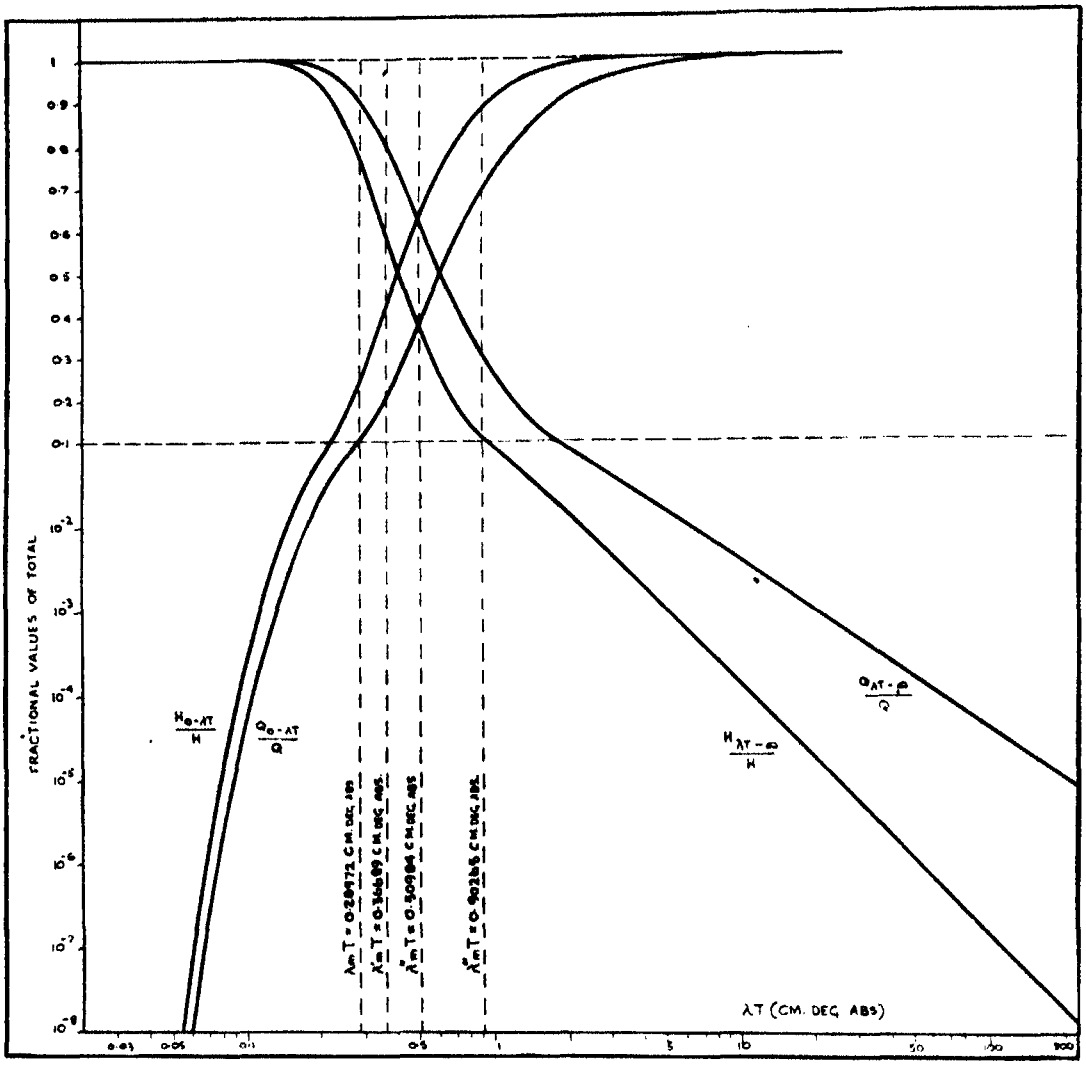

FIG. 2. Radiation nomogram—integration curves.

The total radiant flux density, H, is obtained by integrating H_λ over the wave-length range from zero to infinity, which process leads to the Stefan-Boltzmann law of radiation,

$$H = H_{0-\infty} = 5.67283 \times 10^{-12} T^4 = \sigma T^4 \text{ watt } cm^{-2}.$$

Since the energy associated with one photon is hc/λ, the corresponding formula for spectral photon flux density is

$$Q_\lambda = \frac{c_1'\lambda^{-4}}{e^{c_2/\lambda T}-1} \text{ photon sec.}^{-1}\ cm^{-2}\ \text{cm}_{\Delta\lambda}{}^{-1}.$$

The remaining formulas may be obtained in terms of photons:

$$Q_\nu = \frac{c_1'\nu^2}{e^{c_2\nu/T}-1} \text{ photon sec.}^{-1}\ cm^{-2}\ (\text{cm}_{\Delta\nu}{}^{-1})^{-1},$$

$$Q_{\lambda_1-\lambda_2} = \int_{\lambda_1}^{\lambda_2} Q_\lambda d\lambda = \int_0^{\lambda_2} Q_\lambda d\lambda - \int_0^{\lambda_1} Q_\lambda d\lambda$$

$$= \int_{\lambda_1}^{\infty} Q_\lambda d\lambda - \int_{\lambda_2}^{\infty} Q_\lambda d\lambda, \text{ photon sec.}^{-1}\ cm^{-2},$$

$$\lambda_m' = 0.366895/T \text{ cm}_\lambda,$$

$$Q_\lambda \text{ max.} = 2.1027 \times 10^{11} T^4 \text{ photon sec.}^{-1}\ cm^{-2}\ \text{cm}_{\Delta\lambda}{}^{-1},$$

$$Q = Q_{0-\infty} = 1.5213 \times 10^{11} T^3$$
$$= \sigma' T^3 \text{ photon sec.}^{-1}\ cm^{-2}.$$

If the radiating body obeys Lambert's law, quantities associated with the radiation in unit solid angle normal to the radiating surface may be obtained by dividing the above formulas by π. To avoid multiplicity of scales such quantities have not been included on the rule.

For shorter or longer wave-lengths the simple Wien or Rayleigh-Jeans formulas may be applied. These are approximations only, and it is necessary to have a method of determining the error introduced by their use. This error will, in general, be dependent on the range of λT involved, and a method of estimating it will be described later.

III. GENERAL METHOD AND TRANSFORMATIONS USED IN CALCULATIONS

Introducing the new variable $x=c_2/\lambda T$, and putting $X=(e^x-1)^{-1}$, the various formulas given in the preceding section may be written,

$$H_\lambda=c_1(T/c_2)^5x^5X, \tag{1}$$

$$H_\nu=c_1(T/c_2)^3x^3X=\lambda^2H_\lambda, \tag{2}$$

$$H_{\lambda_1-\lambda_2}=c_1\left(\frac{T}{c_2}\right)^4\int_{x_1}^{x_2}-x^3Xdx$$

$$=c_1\left(\frac{T}{c_2}\right)^4\left[\int_\infty^{x_2}-x^3Xdx-\int_\infty^{x_1}-x^3Xdx\right], \tag{3}$$

$$Q_\lambda=c_1'(T/c_2)^4x^4X, \tag{4}$$

$$Q_\nu=c_1'(T/c_2)^2x^2X=\lambda^2Q_\lambda, \tag{5}$$

$$Q_{\lambda_1-\lambda_2}=c_1'\left(\frac{T}{c_2}\right)^3\int_{x_1}^{x_2}-x^2Xdx$$

$$=c_1'\left(\frac{T}{c_2}\right)^3\left[\int_\infty^{x_2}-x^2Xdx-\int_\infty^{x_1}-x^2Xdx\right]. \tag{6}$$

On dividing each of the Eqs. (1)–(6) by T to the power appearing in the right-hand term, one obtains expressions of the form

$$BT^{-n}=f_1(c_1,c_2,c_1')f(x)$$

of which n takes the values 2, 3, 4, 5, and B is in order H_λ, H_ν, etc. f_1 is a function of the physical quantities only, and $f(x)$, treated as a function of the dimensionless variable x, is a purely mathematical expression which is specific for each quantity and independent of the chosen values of the physical constants.

From the general expression it can be seen that (a) Since each expression of the form BT^{-n} is dependent only on some function of $x=c_2/\lambda T$, it is possible to find for one particular value of BT^{-n} a set of pairs of λ and T such that $\lambda_1T_1=\lambda_2T_2=\lambda_3T_3=\cdots=\lambda_nT_n=c_2/x$. This is the general form of the Wien displacement law. If we take any maximum value of spectral quantity B_mT^{-n} we get $\lambda_mT=c_2/\beta=\text{const.}$, the form in which Wien's law is usually expressed. (b) In order to obtain the value of B for given values of λ and T, it is necessary to calculate $x=c_2/\lambda T$ and BT^{-n} from the product of $f_1(c_1,c_2,c_1')$ and $f(x)$ when finally $(BT^{-n})T^n=B$.

In the slide rule fractional values of the quantities are introduced. These are, for spectral quantities—the ratio of the given quantity to the corresponding maxi-

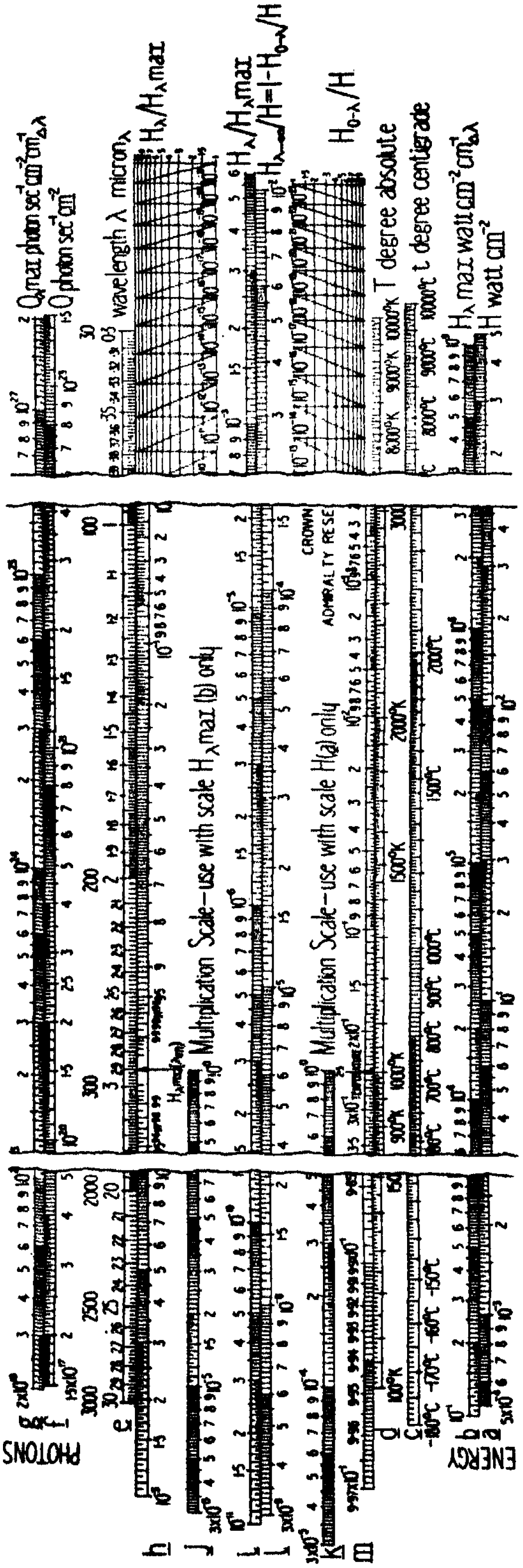
PHOTONS
ENERGY
3a
3b
3c
Q_λ max photon sec^{-1}cm^{-2}cm$_{\Delta\lambda}^{-1}$
Q photon sec^{-1}cm^{-2}
wavelength λ micron
H_λ/H_λmax
H_λ/H_λmax
$H_{\lambda-\infty}/H=1-H_{0-\lambda}/H$
$H_{0-\lambda}/H$
T degree absolute
t degree centigrade
H_λ max watt cm^{-2}cm$_{\Delta\lambda}^{-1}$
H watt cm^{-2}
Multiplication Scale—use with scale $H_\lambda$max (b) only
Multiplication Scale—use with scale H(a) only
CROWN
ADMIRALTY RESE
b
a
c
d
e
h
i
l
k
m

FIG. 3. Front of stock and energy side of slide. Only the ends and a central portion of the slide rule are shown. Scale *i* and *l* together with the corresponding longer wave-length figures on scale *e* are colored red.

TABLE I. Values associated with the maxima.

B	H_λ	Q_λ	H_ν	Q_ν
n	5	4	3	2
β	4.965114	3.920690	2.821439	1.593624
λ_m(symbol)	λ_m	λ_m'	λ_m''	λ_m'''
$\lambda_m T = c_2/\beta$ (cm deg. A)	0.28972	0.36689	0.50984	0.90265
Max. of $x^n/(e^x-1)$	$c_4 = 21.2013$	$c_4' = 4.77984$	$c_4'' = 1.42144$	$c_4''' = 0.64761$
Bmax.	$1.2875\times 10^{-11}T^5$	$2.1027\times 10^{11}T^4$	$1.7862\times 10^{-12}T^3$	$5.8950\times 10^{10}T^2$
Units of Bmax.	watt cm^{-2} $\text{cm}_{\Delta\lambda}^{-1}$	photon sec.$^{-1}$ cm^{-2} $\text{cm}_{\Delta\lambda}^{-1}$	watt cm^{-2} $(\text{cm}_{\Delta\nu}^{-1})^{-1}$	photon sec.$^{-1}$ cm^{-2} $(\text{cm}_{\Delta\nu}^{-1})^{-1}$

mum value, and for integration quantities—the ratio of the given quantity to the total value.

1. Spectral formulas

A general formula for H_λ, H_ν, Q_λ, and Q_ν may be written

$$B = f_1(c_1, c_2, c_1')T^n x^n/(e^x-1) \quad n = 2, 3, 4, 5.$$

The physical limits of x are zero and infinity; B is always positive and when x tends to either of these limits, B tends to zero. Hence there exists a value $x=\beta$ for which B is a maximum. This value is given by $dB/dx=0$ or

$$e^{-\beta}+\beta/n-1=0.$$

Knowing β we can find

$$\lambda_m T = c_2/\beta \tag{7}$$

where λ_m is the wave-length corresponding to the maximum value of B at temperature T; the maximum value of B

$$H_\lambda\text{max.} = (c_1/c_2^5)c_4T^5 \tag{8}$$

and

$$Q_\lambda\text{max.} = (c_1'/c_2^4)c_4'T^4, \tag{9}$$

where c_4, c_4', etc., represent the maximum values of $x^n/(e^x-1)$; the ratios

$$H_\lambda/H_\lambda\text{max.} = 1/c_4\cdot x^5/(e^x-1), \tag{10}$$

$$Q_\lambda/Q_\lambda\text{max.} = 1/c_4'\cdot x^4/(e^x-1), \tag{11}$$

$$H_\nu/H_\nu\text{max.} = 1/c_4''\cdot x^3/(e^x-1)$$

and

$$Q_\nu/Q_\nu\text{max.} = 1/c_4'''\cdot x^2/(e^x-1).$$

In the slide rule only the first two ratios are used since

$$H_\nu = (H_\lambda/H_\lambda\text{max.})\times H_\lambda\text{max.}\times\lambda^2,$$

and a similar expression holds for Q_ν. The graphs of the four fractions are given in Fig. 1 while the values associated with the maxima are listed in Table I.

2. Integration formulas

Formula (3) may be integrated by parts to give

$$H_{\lambda_1-\lambda_2} = \frac{c_1}{c_2^4}T^4\left|\sum_{n=1}^{\infty}\frac{1}{n^4}[(nx)^3+3(nx)^2+6nx+6]e^{-nx}\right|_{x_2}^{x_1}$$

from which we obtain

$$H_{0-\lambda} = \frac{c_1}{c_2^4}T^4\sum_{n=1}^{\infty}\frac{1}{n^4}[(nx)^3+3(nx)^2+6nx+6]e^{-nx},$$

$$H = H_{0-\infty} = (c_1/c_2^4)T^4\times 6\times(1^{-4}+2^{-4}+3^{-4}+\cdots),$$

and since

$$\sum_{r=1}^{\infty}r^{-4} = \pi^4/90$$

$$H = (c_1/c_2^4)T^4(\pi^4/15) = \sigma T^4$$
$$= 5.67283\times 10^{-12}T^4 \text{ watt } cm^{-2}. \tag{12}$$

The latter is the expression for the total power radiated per unit area of a black body at temperature T.

Further we have

$$\frac{H_{0-\lambda}}{H} = \frac{15}{\pi^4}\sum_{n=1}^{\infty}\frac{1}{n^4}[(nx)^3+3(nx)^2+6nx+6]e^{-nx}. \tag{13}$$

For larger values of λ, $H_{0-\lambda}\simeq H$, and in such cases it is better to use

$$H_{\lambda-\infty} = H - H_{0-\lambda} \quad\text{and}\quad H_{\lambda-\infty}/H = 1 - H_{0-\lambda}/H. \tag{13a}$$

Similarly in terms of photons

$$Q_{0-\lambda} = \frac{c_1'}{c_2^3}T^3\sum_{n=1}^{\infty}\frac{1}{n^3}[(nx)^2+2nx+2]e^{-nx},$$

$$Q = Q_{0-\infty} = \frac{c_1'}{c_2^3}T^3\times 2\times\frac{\pi^3}{25.79436\cdots}$$
$$= \sigma' T^3 = 1.5213\times 10^{11}T^3 \text{ photon sec.}^{-1}\ cm^{-2}, \tag{14}$$

$$\frac{Q_{0-\lambda}}{Q} = \frac{12.89718\cdots}{\pi^3}\sum_{n=1}^{\infty}\frac{1}{n^3}[(nx)^2+2nx+2]e^{-nx}, \tag{15}$$

and

$$Q_{0-\lambda}/Q = 1 - Q_{\lambda-\infty}/Q. \tag{15a}$$

The generalized curves for the four fractions over a range of λT are included in Fig. 2.

IV. THE SCALES OF THE SLIDE RULE

The general arrangement of the scales of the slide rule may be seen in Fig. 3. For convenience the scales are lettered from *a* to *s* and these letters will be used in referring to the various scales.

1. Stock

Taking as a basis the value of T, the equations listed below are obtained by taking logarithms of both sides of (7), (8), (12), (9), and (14):

$$\begin{gathered}\log\lambda_m=\log(c_2/\beta)-\log T,\\ \log H_\lambda\text{max.}=\log(c_1c_4/c_2^5)+5\log T,\\ \log H=\log\sigma+4\log T,\\ \log Q_\lambda\text{max.}=\log(c_1'c_4'/c_2^4)+4\log T,\\ \log Q=\log\sigma'+3\log T.\end{gathered}$$

If T is plotted as a logarithmic scale (d) with modulus m_T, the remaining scales are also logarithmic with moduli given by the second terms on the right-hand side of the equation:

$$\begin{gathered}m_\lambda=-m_T\ (\text{inverse scale } e),\\ m_{H_\lambda\text{max}}=\tfrac{1}{5}m_T\ (\text{scale } b),\quad m_H=\tfrac{1}{4}m_T\ (\text{scale } a),\\ m_{Q_\lambda\text{max}}=\tfrac{1}{4}m_T\ (\text{scale } g),\quad m_Q=\tfrac{1}{3}m_T\ (\text{scale } f).\end{gathered}$$

The constants in the various equations define the positions of the corresponding scales of the stock relative to the temperature scale. These constants are of two types, firstly those of purely mathematical conception and so invariant (e.g., β, c_4, c_4'), and secondly those derived from physical constants (c_1, c_2, c_1') which will depend on the values taken for c, h, and k. The latter define the relative positions of the scales on the stock, the former those on the slide. The values of the constants used have already been listed. The procedure necessary for the use of the slide rule with changed values of the constants will be given later.

Since in practical problems temperatures are usually expressed in degrees centigrade, the appropriate scale has been included (c). It has been assumed that 0°C = 273.18°K.

In the construction of the slide rule, a modulus for the temperature scale has been chosen $m_T=20$ cm, and about two decades taken covering directly the range 100°K to 10,000°K (−180°C to about 10,000°C). The same scale of wave-length is used to cover the two ranges, 0.3 to 30 microns (black figures) and 30 to 3000 microns (3 mm) (red figures).

All the scales on the stock, with the exception of scale e, are purely logarithmic, differing only by the moduli.

2. Slide

The slide is double-sided, one side (energy) for use in the $H_{\lambda_1-\lambda_2}$, H_λ, and H_ν calculations, the other (photon) for $Q_{\lambda_1-\lambda_2}$, Q_λ, and Q_ν. Since the two sides are similar, differing only quantitatively, only one will be discussed in detail.

As the slide scales are obtained from the fractions (13), (13a), (15), and (15a) in which the physical constants are eliminated, the scales themselves are independent of the values chosen for these constants. The scales are also independent of the stock except in so far as the moduli are determined by m_T. The two upper scales (h and i) are those of the fraction H_λ/H_λmax. for the two-wave-length ranges. For $x=\beta$, H_λ/H_λmax. = 1 and at this point lines marked "$H_\lambda$max." and "Temperature" have been added to the slide. If the slide is moved so that the latter line is opposite a given temperature, then the former line is opposite the corresponding value of λ_m on scale e. Scale h or i gives the values of H_λ/H_λmax. corresponding to any other value of λ. Three lines have been added to scale h giving also the wave-lengths corresponding to the maximum values of H_ν, Q_λ, and Q_ν.

If scale e is extended to longer wave-lengths by two decades, the corresponding values of scale h go down to 10^{-11}. The extended wave-length scale may be displaced to coincide with the original scale with values of λ 100 times larger, as given by the red figures. The appropriately displaced scale of H_λ/H_λmax., i, is also colored red. The fact that, in the direction of longer wave-lengths, scale i approximates to a logarithmic scale of modulus $\tfrac{1}{4}m_T=\tfrac{1}{4}m_\lambda$, permits the extension of the rule in this direction.

In the same way scale m (black) covers the fraction $H_{0-\lambda}/H$ (13) for the shorter wave-length range, and scale l (red) the fraction $H_{\lambda-\infty}/H$ (13a) for the longer range. Scale l approximates to a logarithmic scale of modulus $\tfrac{1}{3}m_T$.

On the photon side of the slide are the corresponding scales, n and o, of Q_λ/Q_λmax. (11) together with the scales, s and r, of $Q_{0-\lambda}/Q$ (15) and $Q_{\lambda-\infty}/Q$ (15a) respectively. Scales o and r approximate to logarithmic scales of moduli $\tfrac{1}{3}m_T$ and $\tfrac{1}{2}m_T$, respectively. The five lines mentioned above are, of course, repeated on the photon side of the slide.

In deriving the positions of the scale lines, involved fractions were calculated for round values of argument x, and then, with the aid of Interpolation Tables (HMSO, 1936), were inversely interpolated for round values of fractions using Bessel's interpolation formula including fourth and sometimes sixth differences. All calculations were made with two Brunsviga calculating machines by the method of balancing approximation.

For convenience in certain calculations, two logarithmic scales are included on each side of the slide, j and k on the energy side with moduli $\tfrac{1}{5}m_T$ and $\tfrac{1}{4}m_T$, and p and q on the photon side with moduli $\tfrac{1}{4}m_T$ and $\tfrac{1}{3}m_T$.

3. Back of stock

Scales relating wave-length, wave number, and electron volts are included on the back of the stock. For convenience in reading from these scales without

TABLE II. Accuracy of calculations using slide rule.

	Long wave-lengths	Vicinity of maximum spectral value	Shoft wave-lengths Values of fractions $\sim 10^{-3}$	10^{-4}–10^{-35}
H_λ/H_λmax.	1.5%	~0.5%	3.0%	5.0%
$H_{\lambda-\infty}/H$ or $H_{0-\lambda}/H$	1.25%	1.25%		
Q_λ/Q_λmax.	1.25%	~0.5%		
$Q_{\lambda-\infty}/Q$ or $Q_{0-\lambda}/Q$	1.0%	1.0%		

the use of the cursor, the wave number scale is given twice.

V. USE OF THE SLIDE RULE

In following the description of the use of the slide rule reference may be made to Fig. 3. The values given in brackets below refer to the actual settings of the scales in the figure. A straight edge should be used in place of a cursor.

(a) If the cursor line is set on a given value of temperature on scale *c* or *d* (say 727°C or 1000°K), then the following data may be read directly from the cursor line:

Scale *e*—wave-length λ_m (2.9 microns) corresponding to the maximum spectral radiant flux density, $H_\lambda$max.;
Scale *a*—total radiant flux density, H (5.7 watt cm^{-2});
Scale *b*—maximum spectral radiant flux density, $H_\lambda$max. (1.3×10^4 watt cm^{-2} $\mathrm{cm}_{\Delta\lambda}^{-1}$);
Scale *f*—total photon flux density, Q (1.52 photon $\mathrm{sec.}^{-1}$ cm^{-2});
Scale *g*—maximum spectral photon flux density, $Q_\lambda$max. (2.08×10^{20} photon $\mathrm{sec.}^{-1}$ cm^{-2} $\mathrm{cm}_{\Delta\lambda}^{-1}$).

(b) If the line marked "Temperature" is brought into coincidence with a given temperature (1000°K), and the cursor line placed against a given wave-length (say 1 micron or 100 microns), the values of the following fractions may be read directly from the cursor line:

For $\lambda=0.3-30$ microns:
Scale *h*—H_λ/H_λmax.(1.6×10^{-2}); Scale *m*—$H_{0-\lambda}/H$(3.3×10^{-4});
Scale *n*—Q_λ/Q_λmax.; Scale *s*—$Q_{0-\lambda}/Q$;
For $\lambda=30-3000$ microns:
Scale *i*—H_λ/H_λmax.(1.9×10^{-5}); Scale *l*—$H_{\lambda-\infty}/H$(1.45×10^{-4});
Scale *o*—Q_λ/Q_λmax.; Scale *r*—$Q_{\lambda-\infty}/Q$.

Further quantities may then be estimated using, if desired, the appropriate multiplication scales:

$$H_\lambda=(H_\lambda/H_\lambda\mathrm{max.})\times H_\lambda\mathrm{max.}(2.08\times10^{2}\ \mathrm{watt}\ cm^{-2}\ \mathrm{cm}_{\Delta\lambda}^{-1}),$$
$$H_\nu=(H_\lambda/H_\lambda\mathrm{max.})\times H_\lambda\mathrm{max.}\times\lambda_\mu^2\times10^{-8}(2.08\times10^{-6}\ \mathrm{watt}\ cm^{-2}\ (\mathrm{cm}_{\Delta\nu}^{-1})^{-1}),$$
$$H_{\lambda_1-\lambda_2}=[(H_{0-\lambda_1}/H)-(H_{0-\lambda_2}/H)]\times H=[(H_{\lambda_1-\infty}/H)-(H_{\lambda_2-\infty}/H)]\times H,$$
$$Q_\lambda=(Q_\lambda/Q_\lambda\mathrm{max.})\times Q_\lambda\mathrm{max.}$$
$$Q_\nu=(Q_\lambda/Q_\lambda\mathrm{max.})\times Q_\lambda\mathrm{max.}\times\lambda_\mu^2\times10^{-8},$$
$$Q_{\lambda_1-\lambda_2}=[(Q_{0-\lambda_1}/Q)-(Q_{0-\lambda_2}/Q)]\times Q=[(Q_{\lambda_1-\infty}/Q)-(Q_{\lambda_2-\infty}/Q)]\times Q.$$

In the formulas with square brackets only positive values of differences are taken. Both values of the fractions inside the bracket must be read from the same scale, or, if this is not possible since one wave-length is within the black range and the other within the red, then one of the fractions must be subtracted from unity.

The multiplication scales are so arranged that it is unnecessary to move the slide, when set at a given temperature, in order to carry out the operation of multiplication. Care must be taken, however, to use the correct multiplication scale for a given operation, as marked on the slide. When calculations of $H_{\lambda_1-\lambda_2}$ or $Q_{\lambda_1-\lambda_2}$ are being carried out for a narrow wave-length interval, the accuracy falls with decreasing interval, but may be increased by calculating the spectral values of H_λ, H_ν, Q_λ, or Q_ν for the middle point of the interval, and, assuming the spectral quantity to be constant over the interval, multiplying the quantity by the width of the interval.

VI. EXTENSION RULES AND CHANGE OF CONSTANTS

1. Temperature

The slide rule may be used for calculations involving temperatures outside the range 100°K to 10,000°K by a simple extension process. The temperature T is expressed in degrees absolute as $T_s=T\times10^n$, where n is a convenient integer such that T_s is within the compass of scale *d*. The corresponding wave-length $\lambda_s=\lambda\times10^{-n}$. By the processes already described, the values of the various quantities B_s are found for temperature T_s and wave-length λ_s, and the values appropriate to the original temperature obtained from the following formulas (the corresponding factors are given on the back of the rule):

$$H_\lambda=(H_\lambda)_s\times10^{-5n},\qquad Q_\lambda=(Q_\lambda)_s\times10^{-4n},$$
$$H_\nu=(H_\nu)_s\times10^{-3n},\qquad Q_\nu=(Q_\nu)_s\times10^{-2n},$$
$$H_{\lambda_1-\lambda_2}=(H_{\lambda_1-\lambda_2})_s\times10^{-4n},\qquad Q_{\lambda_1-\lambda_2}=(Q_{\lambda_1-\lambda_2})_s\times10^{-3n}.$$

A similar process may be applied to problems in which, although T is inside the normal range, the calculations move outside the limits of the slide.

2. Long wave-lengths

Since the red scales covering the longer wave-length range to 3000 microns (*i*, *l*, *o*, *r*) approximate to logarithmic, the slide rule may be extended to longer wave-lengths. The wave-length is replaced by a wave-length λ_s, such that $\lambda_s=\lambda\times10^{-n}$, where n is the smallest possible positive integer that will bring λ_s inside the normal red wave-length range of the rule. The corresponding quantities B_s may be calculated and transposed to the values for the original wave-length using the formulas given for the extension of the temperature scales.

3. Change of constants

From formulas (1) to (6) it can be seen that:

(a) the constant c_2 appears only in the ratio T/c_2, and
(b) the quantities related to energy and photons are proportional to c_1 and c_1', respectively.

Thus the use of the slide rule with different values of the physical constants is simple. If it is desired to introduce new values ${}_nc_1$, ${}_nc_2$, and ${}_nc_1'$, it is only necessary to make all calculations for a temperature T_n where $T_n = T\times c_2/{}_nc_2$ and multiply the values so obtained by the following factors:

$$\text{Energy} \quad {}_nc_1/c_1 = h'c'^2/hc^2$$
$$\text{Photons} \quad {}_nc_1'/c_1' = c'/c$$

where c' and h' are the new values of the constants.

VII. ACCURACY

The accuracy with which calculations can be made is limited by the accuracy with which the scales can be read. For any logarithmic scale the error is constant and approximately inversely proportional to the modulus of the scale. In the case of the scales of $H_\lambda$max.(b), H(a), $Q_\lambda$max.(g), and Q(f) (the scales with the smaller moduli) the error can be eliminated if desired by using the exact formulas given in Section II and included on the back of the rule:

$$H_\lambda\text{max.} = 1.2875\times 10^{-11}T^5, \quad H = 5.6728\times 10^{-12}T^4,$$
$$Q_\lambda\text{max.} = 2.1027\times 10^{11}T^4, \quad Q = 1.5213\times 10^{11}T^3.$$

The logarithmic scales limiting the accuracy of any calculations are those of temperature and wave-length. Both scales are of modulus 20 cm and the accuracy of reading is of the order of 0.25 percent. The other scales involved are those of the fractions (h, i, l, m, n, o, r, s) which are not logarithmic. In general, the relative accuracy will vary according to the region of the scale in use. However, for the longer wave-lengths (red scales) the errors are constant, the values being:

H_λ/H_λmax. (i)—about 1 percent
$H_{\lambda-\infty}/H$ and Q_λ/Q_λmax. (l and o)—about 0.75 percent
$Q_{\lambda-\infty}/Q$ (r)—about 0.5 percent

In the region of the respective maxima, the relative error for the fractions is reduced to a few tenths of one

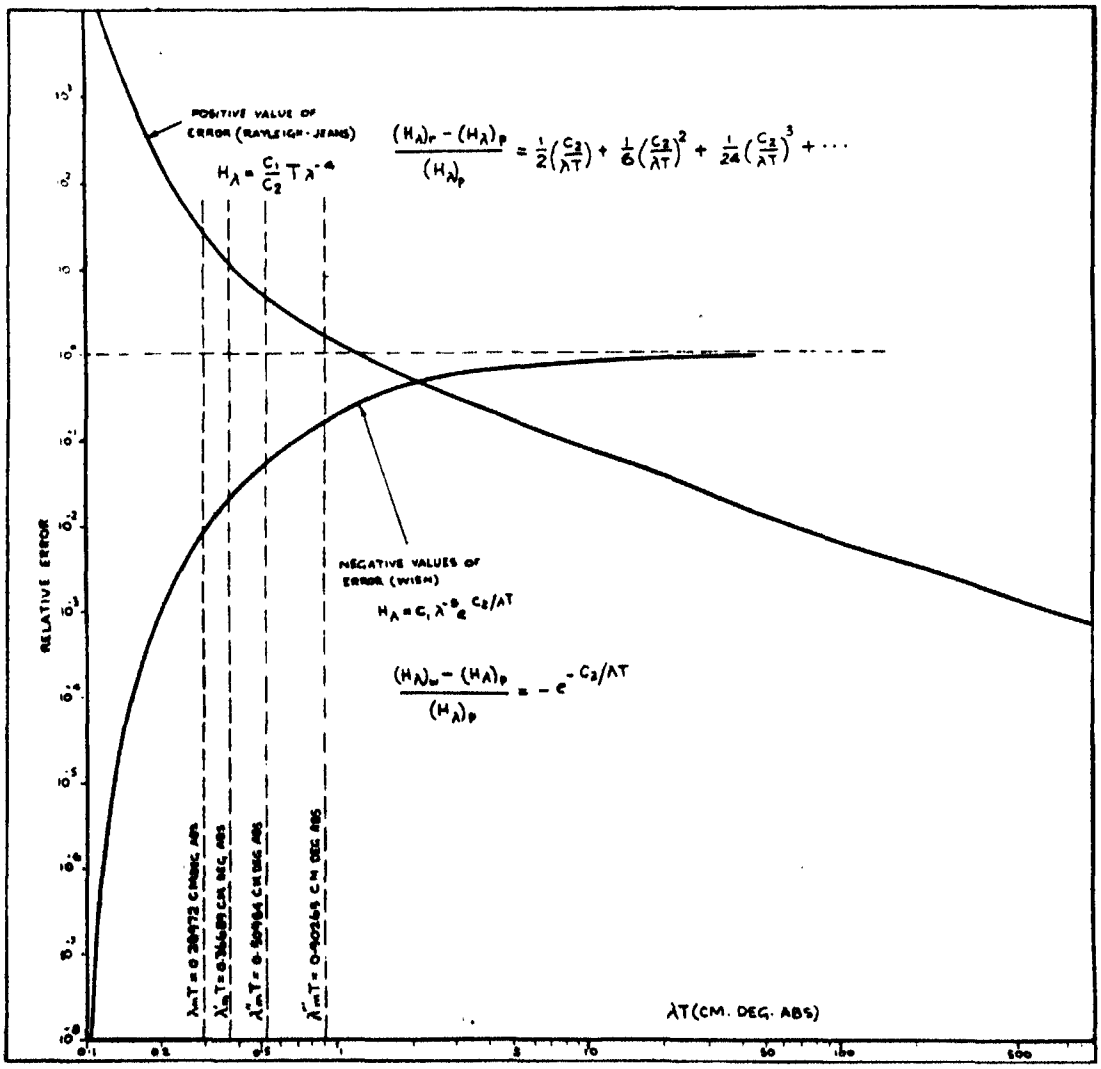

FIG. 4. Error introduced by application of Wien or Rayleigh-Jeans formulas.

percent, and increases from this value as shown in Table II, being approximately the same for all scales. The introduction of the diagonal scale présentation for the short wave-length ratio scales at one end of the slide prevents serious reduction of accuracy at the shortest wave-lengths.

In $H_{\lambda_1-\lambda_2}$ or $Q_{\lambda_1-\lambda_2}$ calculations the relative error is increased by taking differences, the error being greater for a narrow interval. For this reason it is better to assume a constant value of H_λ or Q_λ over the interval as described in Section V.

VIII. COMPARISON OF THE PLANCKIAN FORMULA WITH WIEN AND RAYLEIGH-JEANS FORMULAS

Both the Wien and Rayleigh-Jeans formulas may be treated as mathematical approximations of the exact Planck formula. The latter may be written in the form

$$(H_\lambda)_p T^{-5} = (c_1/c_2^5)x^5/(e^x-1).$$

It is possible to deduce either the Wien formula or the Rayleigh-Jeans formula and obtain the errors introduced by the use of these formulas in terms of x or T.

If $x \gg 1$ (λT very small) then e^x is sufficiently larger than unity for e^x-1 to be replaced by e^x, when

$$(H_\lambda)_w T^{-5} = (c_1/c_2^5)(x^5/e^x).$$

This is Wien's formula which is usually written in the form

$$(H_\lambda)_w = c_1\lambda^{-5}e^{-c_2/\lambda T}.$$

The error involved in using this approximation is

$$E_w = \frac{(H_\lambda)_w-(H_\lambda)_p}{(H_\lambda)_p} = \frac{x^5e^{-x}-x^5/(e^x-1)}{x^5/(e^x-1)}$$
$$= e^{-x}(e^x-1)-1 = e^{-x} = e^{-c_2/\lambda T}.$$

If, on the other hand, $x \ll 1$ (λT very large) then

$$e^x-1 = (1+x+\tfrac{1}{2}x^2+\cdots)-1 = x+\tfrac{1}{2}x^2+\cdots \simeq x$$

and

$$(H_\lambda)_r T^{-5} = (c_1/c_2^5)x^4.$$

This is, of course, the Rayleigh-Jeans formula and is usually written in the form

$$(H_\lambda)_r = (c_1/c_2)T\lambda^{-4}.$$

The relative error is

$$E_r = \frac{(H_\lambda)_r-(H_\lambda)_p}{(H_\lambda)_p} = \frac{x^4-x^5/(e^x-1)}{x^5/(e^x-1)} = \frac{e^x-1-x}{x}$$
$$= \frac{x}{2}+\frac{x^2}{6}+\cdots = \frac{1}{2}c_2/\lambda T+\frac{1}{6}(c_2/\lambda T)^2+\ldots$$

The corresponding formulas for H_ν, Q_λ, and Q_ν introduce similar errors as a function of x.

In the case of calculations involving $H_{\lambda_1-\lambda_2}$ or $Q_{\lambda_1-\lambda_2}$ estimation of the error is more complicated since the error is equivalent to some intermediate value of the error in the spectral quantity within the wave-length range involved. It can, however, be shown that the above formulas may be used to give the upper limit of the error if the largest value of λT (smallest value of x) in the interval is substituted in the expression for the error in the case of the Wien formula, or the smallest value of λT in the case of the Rayleigh-Jeans formula.

Figure 4 represents errors for both of the simplified formulas as a function of λT. The errors introduced by using either formula at given values of λ or λT can be estimated using this graph.

ACKNOWLEDGMENTS

The author wishes to acknowledge the valuable suggestions made in the course of many discussions by Dr. E. Lee, who initiated the work, Dr. A. Elliott, and Mr. T. H. Pratt, and is particularly grateful to Mr. L. A. J. Verra for assistance throughout the lengthy process of computing. In addition, the assistance of the Mathematics Division, N.P.L., in checking the calculations for the fractional scales was much appreciated.

Bibliography

(1) E. Q. Adams, J. Opt. Soc. Am. 37, 695 (1948).
(2) M. Bell, *Tables Numériques Universelles* (Dunod, Paris, 1947).
(3) F. Benford, J. Opt. Soc. Am. 9, 92 (1939).
(4) F. Benford, Gen. Elec. Rev. 46, 377, 433 (1943).
(5) R. T. Birge, Rev. Mod. Phys. 13, 233 (1941).
(6) H. G. W. Harding, Proc. Phys. Soc. 58, 1 (1946).
(7) *International Critical Tables* (McGraw-Hill Book Company, Inc., New York, 1929).
(8) E. Janke and F. Emde, *Funktionentafeln* (B. G. Teubner, Leipzig, 1933).
(9) P. Moon, *The Scientific Basis of Illuminating Engineering* (McGraw-Hill Book Company, Inc., New York, 1936).
(10) P. Moon, J. Math. Phys. 16, 133 (1937).
(11) P. Moon, J. App. Phys. 17, 506 (1946).
(12) P. Moon and D. E. Spencer, J. Math. Phys. 25, 111 (1946).
(13) P. Moon, J. Opt. Soc. Am. 38, 291 (1948).
(14) National Bureau of Standards, *Planck's Radiation Functions and Electronic Functions* (National Bureau of Standards, New York, 1941).
(15) F. K. Richtmyer and E. H. Kennard, *Introduction to Modern Physics* (McGraw-Hill Book Company, Inc., New York, 1942).
(16) *Smithsonian Physical Tables* (Smithsonian Institution, Washington, 1934).
(17) A. G. Worthing, J. Opt. Soc. Am. 9, 97 (1939).
(18) A. G. Worthing, J. Opt. Soc. Am. 9, 101 (1939).
(19) Zen'emon Miduno, Proc. Phys. Math. Soc. Japan, 20, 951 (1938) 3rd series.

THE REVIEW OF SCIENTIFIC INSTRUMENTS VOLUME 20, NUMBER 12 DECEMBER, 1949

Volumetric Respirometer for Aquatic Animals*

P. F. SCHOLANDER
Arctic Research Laboratory, Point Barrow, Alaska

(Received July 12, 1949)

The oxygen consumption of fish and other aquatic animals can be determined in the gas phase of a closed system provided the water is thoroughly equilibrated with the gas phase. The present respirometer employs a simpler and more efficient equilibration system than the earlier described model [Scholander, Haugaard, and Irving, Rev. Sci. Inst. 14, 48 (1943).] and permits a continuous recording of the oxygen consumption over a considerable range. The apparatus is well suited to be set up in banks and has been used extensively in temperature studies on arctic and tropical fishes and crustaceans.

PRINCIPLE

THE fish is kept in a respiration chamber where the air and the water are continually equilibrated by a turbine device. The gas volume is connected with a compensated manometer and a syringe with oxygen. The carbon dioxide is absorbed in the gas phase. As oxygen is used, new oxygen is introduced from the syringe so that the balance with the manometer is maintained. The oxygen consumed is read directly from the syringe.

APPARATUS

The apparatus consists of the following parts: respiration chamber; manometer block with oxygen syringe, taper plug, carbon dioxide absorption bucket, and compensating vessel; frame with equilibration turbine and drive; and water bath.

A glass jar furnished with a side arm serves as a respiration chamber. Valve grinding compound on copper tubing, mounted on a shaft and held in the drill press, was used to cut a one-inch hole in the side of a screw-cap jar. A short section of a one-inch screw-cap vial was cemented in the hole with de Kothinsky cement. An all-glass or plastic chamber would be preferable to the one described. The manometer is drilled out of a plastic $\frac{3}{8}$-in. block, with a No. 24 drill. The upper openings of the manometer bore are molded to fit the syringe tip and taper plug. This is accomplished by pushing a hot syringe tip or identical metal taper into the holes and removing it under the cold water faucet. A small plastic taper or rubber plug is made for one opening. Half-inch plastic buttons are cemented on to the bottom of the manometer block to hold the rubber stoppers for the respiration and compensating vessels. The bottom portion of a small vial serves as a bucket for the carbon dioxide absorbant. The bucket is suspended in a metal clip which hangs from a wire loop stuck into the bore of the manometer block. A cylindrical vial is used as a compensating vessel. The volume of this vial does not affect the accuracy, but increasing volume gives increasing sensitivity.

It is practical to mount several machines on the same angle brass frame having three wooden cross pieces (Fig. 1, B, C, D). The rubber stopper for the respiration chamber is screwed securely to B by means of long wood screws. A capillary glass tube passes through the stopper and through a large hole in B, and is supported by C. A stainless steel wire, to the end of which is attached a small plastic paddle, fits through the capillary. The paddle is separated from the stopper by a fiber washer (Fig. 2, B). A plastic cup is held over the paddle. This cup is made by pressing a piece of heated Plexiglass into a large hole with the bottom of a small jar. The hole may be drilled in a piece of wood. The edge of the cup is scalloped (Fig. 2) and holes are drilled through the center portion. The cup is held

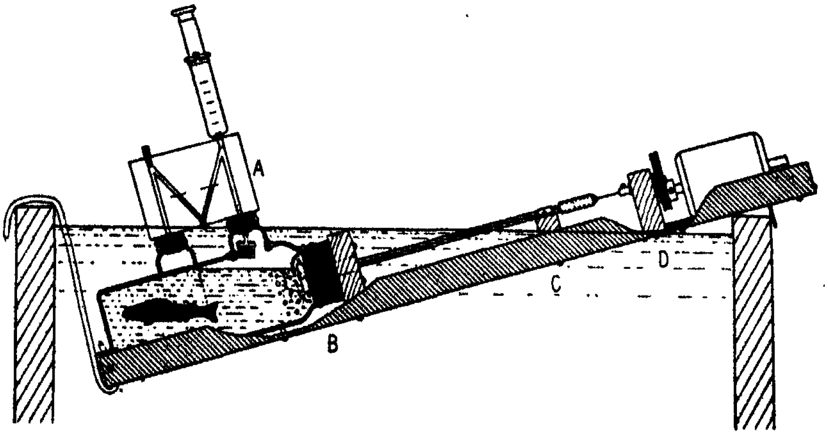

FIG. 1. Fish respirometer suspended in tank. A. Manometer block with compensating vessel, taper plug, oxygen syringe and absorption bucket. Manometer block is normally turned 90° to the chamber, not parallel as shown in the figure. B. Turbine bubbler. C. Support for capillary bearing with grease well. D. Pulley arrangement for driving several machines with one belt and one motor.

---

* Under contract with the ONR.

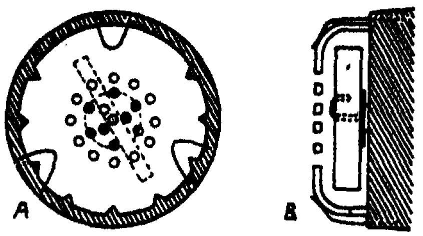

FIG. 2. A. Front view of turbine bubbler. B. Side view of turbine bubbler.

tightly against the rubber stopper by means of three stainless steel wire clips.

The upper end of the capillary is fitted with a piece of split Tygon tubing holding medium Nevastane grease (Keystone Company, Philadelphia). A small motor controlled by a rheostat drives the wire shaft either directly or through a belt and pulley arrangement (Fig. 1, D) if two or more machines are mounted on the same frame. We have been using banks of four machines.

When the paddle spins, water is sucked in through the center holes and is thrown out through the openings at the cup edge. If the water level is so adjusted that some of the holes are above water, the turbine will also draw in air. The degree of mixing and equilibration can be adjusted with the rheostat.

Any tank may be used as a water bath. Heavy wooden tanks are good insulators and maintain the temperature well. For accurate work the water bath should be regulated to within a few tenths of a degree.

REAGENTS

The manometer fluid consists of methyl orange-colored water with liquid potassium soap added until it runs easily in the manometer bore. We have been using Ascarite (A. H. Thomas, Philadelphia) for carbon dioxide absorption.

OPERATION

The respiration chamber is filled with aerated water of the proper temperature, the fish is put in, and the chamber is securely connected to the stopper. The frame is suspended in the water bath by a wire hook so that the side arm of the fish chamber protrudes out of the water. The turbine is started and the bubbling adjusted by adding or removing water with a syringe and by changing the tilt of the frame. The machine is left running open to the air until the temperature and gas tensions have equilibrated. This usually takes only a few minutes. The compensating vessel, containing a few drops of water, is attached to the manometer block, manometer fluid is filled to the mark, and the bucket, partially filled with Ascarite, is hung on the loop. The manometer block is then firmly connected with the respiration chamber. A slightly greased taper plug and a syringe filled with oxygen are placed in the proper manometer openings (see Fig. 1). The top of the syringe is sealed with a drop of glycerine and an arresting clip is put on.

At suitable intervals oxygen is delivered from the syringe to keep the manometer fluid at its mark. The amount of oxygen introduced into the respiration chamber equals the amount of oxygen consumed for that period, uncorrected for S.T.P. The S.T.P. factor applies only to the syringe. As the oxygen syringe is not protected by the water bath the smallest practical size syringe should be used and the determination should be run in a room of relatively constant temperature.

ACCURACY

The accuracy of the machine is determined by blank runs and by measuring the equilibration rates between the gas and the water. With 300 cc distilled and aerated water and 50 cc air, the system is stable to within plus or minus 0.01 cc per hour as read on a tuberculin syringe. Water badly contaminated with bacteria may give a positive blank. Runs made on the water after a fish has been in it for several hours sometimes give a positive blank, which is usually insignificant compared with the oxygen consumed by the fish.

The equilibration rate can be roughly estimated by

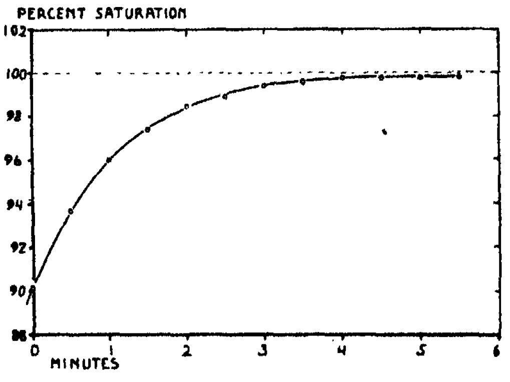

FIG. 3. Absorption rate of gasses into 90 percent saturated water running the bubbler at medium speed. The total amount of gasses re-absorbed agrees closely with the theoretical value.

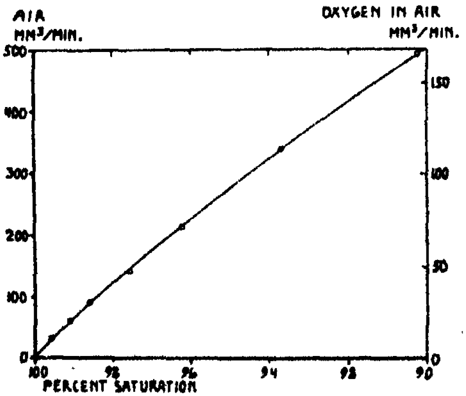

FIG. 4. Rate of oxygen absorption at various saturations estimated from the rate of air absorption.

determining the rate at which air is taken up by partially evacuated water. Two hundred and seventy cc water is equilibrated in the open machine. Water is boiled for ten minutes in a stoppered Erlenmeyer flask, the steam escaping through a hole in the stopper. While boiling, the water is drawn into a 50-cc syringe by means of a long needle inserted through the hole in the stopper. The initial gas bubble is expelled and the gas-free water cooled anaerobically in the syringe to the exact temperature of the water bath.

Thirty cc is added under the water in the fish machine with turbine off. The manometer is put on, a one-cc tuberculin syringe containing air is connected and the turbine is started. From Fig. 3 it will be seen that the amount of gas which was taken up by the water agrees closely with the air solubility for that temperature. In Fig. 4 the rate of air intake is plotted against the saturation. With 90 percent saturated water, the "air" was re-dissolved at the rate of 500 mm^3 per minute. Of this "air" approximately 34 percent would be oxygen and consequently, the rate of oxygen absorption into the same water was at least 34 percent of $500 = 170$ mm^3 per minute. This is more than sufficient for any fish or crustacean which can be put into 300 cc of water. At high temperatures foaming can be serious trouble, making the use of more water and a larger respiration chamber necessary. There does not seem to be any reason why the system cannot be adapted for continuous respiratory studies on very large forms.

THE REVIEW OF SCIENTIFIC INSTRUMENTS VOLUME 20, NUMBER 12 DECEMBER, 1949

Operation of the 184-In. Cyclotron

L. R. Henrich, D. C. Sewell, and J. Vale
Radiation Laboratory, University of California, Berkeley, California

(Received August 19, 1949)

The operation of the 184-in. synchro-cyclotron is reviewed in terms of the theory as developed by Bohm and Foldy. Certain relevant data on the properties of the magnet and rotating condenser are also presented.

1. INTRODUCTION

The general theory of the operation of a frequency modulated cyclotron—or synchro-cyclotron—has been discussed in earlier papers by Bohm and Foldy[1,2] among others. The purpose of the present paper is to present in more detail than previously reported[3] such operational data for the 184-in. Berkeley synchro-cyclotron as might be of interest. It is also intended to interpret the performance of the machine in terms of the theory. We mention first general characteristics of the machine and then investigate the operation when certain conditions are varied.

2. NORMAL ACCELERATION OF IONS

The final design of the 184-in. magnet determines such things as the energy of the ion as a function of the radius, r, while the design of the rotating condenser affects the mean rate of energy gain per turn. Since these and other related quantities will be needed in subsequent discussions of the performance of the machine, the expressions for these quantities are given below. The actual values for the machine are later tabulated (Table I) and graphed (Fig. 1a and 1b).

(a) $H(r)/H_c$—where $H(r)$ is the value of the magnetic field in the median plane and perpendicular to it as a function of the radius (r); and H_c is the value of the field at the center of the machine.

(b) $n(r) = -(r/H)(dH/dr)$, (1)

(c) $\beta^2(r) = [1+(M_0c^2/ZerH)^2]^{-1} = (v/c)^2$, (2)
where M_0 is the rest mass of the ion, c is the velocity of light, Ze is the charge on the ion, e is the unit electric charge, and v is the velocity of the ion.

(d) $E(r) = E_0/(1-\beta^2)^{\frac{1}{2}}$—the total energy of the ion, (3) including the rest energy (E_0).

(e) $\omega = ZeH/Mc$ where ω is the angular frequency (4) of rotation of the ion, and M the total mass of the ion.

(f) $K = 1+(n/1-n)(c^2/v^2)$: a necessary physical (5) quantity (see A-(16)),

$K = 1+hc^2/\omega^2$ an alternative expression of K (6) valid in a parabolic magnetic field (see B-(5)) where h expresses the rate of decrease of the magnetic field with radius, i.e.,

$$H = H_0(1-hr^2/2). \quad (7)$$

---

[1] D. Bohm and L. Foldy, "The theory of the synchrotron," Phys. Rev. 70, 249 (1946), herein after referred to as paper A. Equations and figures from this paper will be referred to as (A-(X) or A-Fig. (X)), respectively.

[2] D. Bohm and L. Foldy, "Theory of the synchro-cyclotron," Phys. Rev. 72, 649 (1947), referred to as paper B.

[3] Brobeck, Lawrence, MacKenzie, McMillan, Serber, Sewell, Simpson, and Thornton, Phys. Rev. 71, 449 (1947).

TABLE I. Data on 184-in. synchro-cyclotron. Deuteron energy, etc.

r (inches)	$H(r)/H_0$*	n	K	$1/\beta^2$	$E-E_0$ (Mev)	$\Omega\cdot 10^{-6}$/sec.	$-d\ln\omega_s/d\tau$	$\Delta E_s(100/C)$ kev	$V/\bar{V}$
0	1.0000	0.0000	6.37		0	11.465	1.43	3.7	0.955
5	0.9981	0.0026	3.83	1084.7	0.8	11.439	1.45	6.2	0.960
10	0.9957	0.0040	2.10	273.25	3.4	11.396	1.47	11.5	0.963
15	0.9937	0.0060	1.74	121.46	7.6	11.347	1.48	14.1	0.972
20	0.9913	0.0111	1.78	69.66	13.5	11.285	1.49	14.0	0.980
25	0.9883	0.014	1.66	45.21	21.0	11.206	1.49	15.2	0.990
30	0.9856	0.016	1.53	31.87	30.1	11.122	1.49	16.7	1.002
35	0.9829	0.020	1.49	23.79	41.1	11.027	1.46	17.0	1.014
40	0.9798	0.028	1.53	18.57	52.6	10.927	1.42	16.4	1.027
45	0.9763	0.031	1.48	14.98	65.9	10.813	1.38	16.7	1.043
50	0.9732	0.032	1.41	12.40	80.4	10.699	1.32	17.1	1.058
55	0.9698	0.040	1.44	10.50	96.2	10.576	1.25	16.2	1.070
60	0.9658	0.055	1.52	9.037	113.2	10.442	1.15	14.4	1.086
65	0.9614	0.055	1.46	7.912	131.0	10.319	1.07	14.2	1.097
70	0.9576	0.051	1.38	7.007	150.0	10.166	0.97	14.0	1.110
75	0.9540	0.057	1.38	6.272	170.0	10.028	0.87	12.9	1.122
76	0.9533	0.056	1.36	6.144	174.1	10.001	0.85	12.8	1.125
77	0.9526	0.057	1.36	6.013	178.5	9.972	0.83	12.5	1.128
78	0.9519	0.066	1.41	5.893	182.6	9.945	0.82	12.0	1.129
79	0.9510	0.081	1.51	5.779	186.8	9.915	0.80	11.0	1.130
80	0.9499	0.113	1.72	5.674	190.8	9.885	0.78	9.5	1.131
81	0.9482	0.176	2.19	5.575	194.7	9.848	0.76	7.3	1.135
82	0.9456	0.292	3.27	5.486	198.4	9.804	0.73	4.7	1.138
83	0.9413	0.424	5.00	5.423	201.1	9.747	0.70	—	1.140
84	0.9351	0.914	6.67	5.372	203.3	9.672	0.65	—	1.142
85	0.9219	1.080	—	5.393	202.4	9.540	0.64	—	1.145

* $H_0 = 15{,}000$ gauss (4-inch cones in center).

The above quantities depend on the shape of the magnetic field. In addition there are the quantities which depend on the physical characteristics of the rotating condenser that modulates the frequency of the dee voltage.[4] These may be expressed as a function of the phase τ of the rotating condenser, where we let $2\pi\tau$ represent the phase angle of the condenser and $\tau=0$ when the oscillation is at maximum frequency.

(g) $\omega_s(\tau)$ = the angular frequency of the oscillator. The subscript $_s$ denotes the angular frequency the ion must have if it is to be locked into the synchronous orbit at a fixed phase angle with no oscillations about this phase angle.

(h) $[V(\tau)]/\bar{V}$ = the ratio of the actual maximum dee voltage across the gap to the mean value during a modulation cycle.

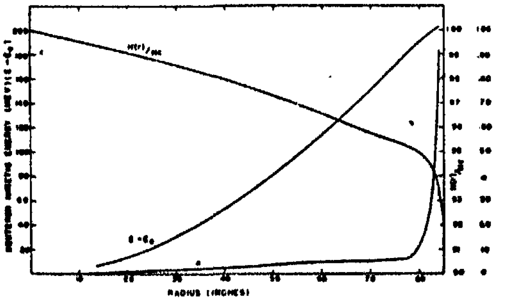

FIG. 1a. Deuteron energy, magnetic field and n as a function of the radius.

(i) $-(d\ln\omega_s)/d\tau$: a quantity used in computing mean energy gain per revolution.

The last three quantities have been expressed as a function of τ. However, the angular frequency of the ion is determined by the expression for ω given in (e) and depends on the magnetic field. For an ion to be in the synchronous orbit at any time its frequency must also be ω_s. This condition provides a unique correlation between the phase of the oscillator and the radius of an ion in the synchronous orbit. We accordingly denote the radius, energy, and angular frequency of such a synchronous particle by r_s, E_s, and ω_s. This correlation also permits us to express $V/\bar{V}$ and $-(d\ln\omega_s)/d\tau$ as a function of radius.

An ion will stay at the synchronous frequency only if it gains energy at the proper rate. This may be expressed using A-(15) by

$$\frac{dE}{dt}=-\frac{E_s}{K\omega_s}\frac{d\omega_s}{dt}=-\frac{CE_s}{K\omega_s}\frac{d\omega_s}{d\tau}, \tag{8}$$

where t is the time. To express the energy gain in terms of the rate of frequency modulation we have let $\tau=Ct$ where C is the number of frequency modulation cycles per second. Multiply (8) by the period of a revolution, $2\pi/\omega_s$, to get the energy gain per turn for the synchronous orbit, ΔE_s; so that

$$\Delta E_s/C=2\pi E_s/K\omega_s[-d\ln\omega_s/d\tau]. \tag{9}$$

The change in radius per turn will be given by A-(14),

$$\Delta r_s/C=[r_s/(1-n)\beta_s^2](\Delta E_s/CE_s). \tag{10}$$

---

[4] For the design of the frequency modulation equipment see F. H. Schmidt, Rev. Sci. Inst. 17, 301 (1946); MacKenzie, Schmidt, Woodyard, and Wouters, Rev. Sci. Inst. 20, 126 (1949).

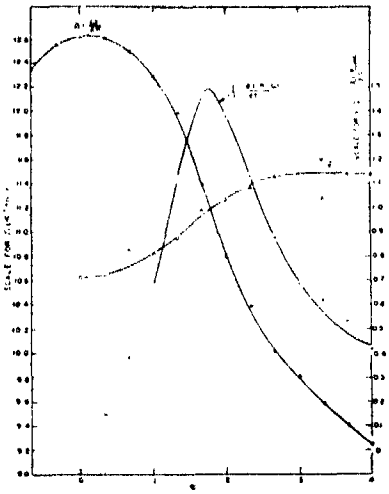

FIG. 1b. Variation of modulation frequency and applied voltage with time.

Now the phase angle, ϕ_s, for acceleration in the synchronous orbit is given by $eV\sin\phi_s=\Delta E_s$. Due to the change in ΔE_s and in V during the acceleration period the phase angle will change during the acceleration. The magnitude of the variation in $\sin\phi_s$ may be determined from the equation,

$$e\dot{V}\sin\phi_s=(\dot{V}/V)\Delta E_s. \tag{11}$$

3. OSCILLATIONS ABOUT THE SYNCHRONOUS ORBIT

The motion of a particle on the synchronous orbit is described by the expressions in the preceding section. Actually, few, if any, particles follow this orbit precisely. There are deviations from the orbit due to the fact that ions are not injected at the correct frequency corresponding to the central magnetic field, also due to the fact that ions are not injected at the synchronous phase angle, ϕ_s, but of necessity near a phase angle of 90° (see B-Appendix I). These causes will result in phase oscillations of the radius, energy and phase angle (see paper A).

The angular frequency of phase oscillation (A-(21)) is given approximately for small oscillations by

$$\omega_{ph}=(eVK\cos\phi_s/2\pi E_s)^{\frac{1}{2}}\omega_s. \tag{12}$$

The period of this oscillation will be

$$T_{ph}=2\pi/\omega_{ph}. \tag{13}$$

The amplitude of the energy oscillation will be (A-(19)),

$$\Delta E_{ph}=\pm(eVE_s/\pi K)^{\frac{1}{2}}[U(\phi_m)-U(\phi)]^{\frac{1}{2}}, \tag{14}$$

where

$$U(\phi)=-\cos\phi-\phi\sin\phi, \tag{15}$$

and ϕ_m is the maximum value of ϕ.

The amplitude of radial phase oscillation will be given using A-(14).

$$\Delta r_{ph}=\frac{r_s}{(1-n)\beta_s^2}\frac{\Delta E_{ph}}{E_s}. \tag{16}$$

There will also be additional radial oscillations—due, for example, to inhomogeneities in the magnetic field—which will be called "free radial oscillations". There will also be free vertical oscillations—i.e., oscillations perpendicular to the median plane of the magnet gap, denoted by a z coordinate—due originally to the ions starting their orbits at positions displaced from the median plane.

The general equations of motion of the ion may be obtained from the Hamiltonian

$$H=c\left\{M_0^2c^2+\left(p_r-\frac{e}{c}A_r\right)^2+\left(\frac{p_\theta}{r}-\frac{e}{c}A_\theta\right)^2+\left(p_z-\frac{e}{c}A_z\right)^2\right\}^{\frac{1}{2}}-e\Phi, \tag{16a}$$

where $\mathbf{A}=(A_r, A_\theta, A_z)$ is the vector potential in cylindrical coordinates and Φ is the accelerating potential, and $\mathbf{p}=(p_r, p_\theta, p_z)$ are the canonical momenta. The investigation of the free vertical and radial oscillations near any specified radius, r_0, may be carried out while neglecting the accelerating dee voltage. The mass may be taken as constant. The magnetic field may be taken as a function of r and z only, where z is the distance from the median plane. In this case it is possible to set $A_r=A_z=0$ and retain only $A_\theta=A(r, z)$. The equations of motion of the ion about a certain equilibrium orbit of radius, r_0, under these conditions can be written to the first approximation as

$$d^2(\Delta r)/dt^2=-(1-n)\omega_0^2\Delta r, \tag{17}$$

$$d^2z/dt^2=-n\omega_0^2z, \tag{18}$$

where $\Delta r=(r-r_0)$ is the deviation from the equilibrium orbit, ω_0 is the angular frequency in the equilibrium orbit and n is the value of n for the equilibrium orbit. The free radial oscillations will have the angular frequency $\omega_r=(1-n)^{\frac{1}{2}}\omega_0$ and the vertical oscillations will

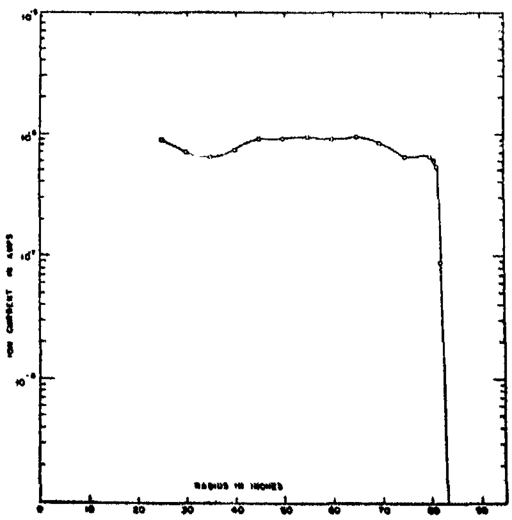

FIG. 2. Ion current as function of radius.

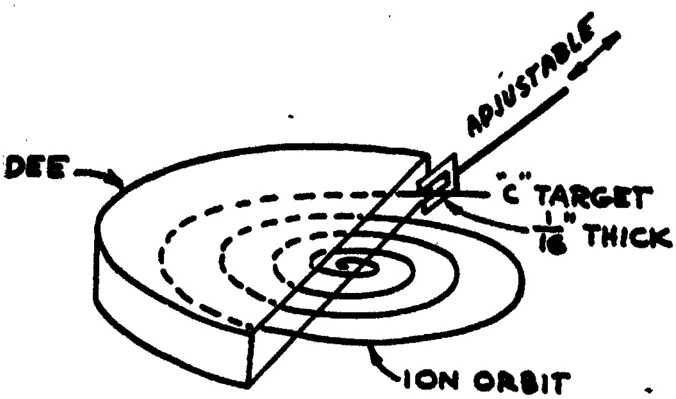

FIG. 3a. Diagram showing C shaped probe.

have the angular frequency $\omega_z = (n)^{\frac{1}{2}}\omega_0$. The vertical motion will be stable only for $n>0$ and the radial motion will be stable only for $n<1$. At $n=1$ there will be resonance between the periods of rotation and vertical oscillation, so in this region the vertical amplitude could build up due to resonance effects—in the same manner as the radial amplitudes could build up at $n=0$. Hence, for a stable orbit $0<n<1$. It follows that both ω_r and ω_z are smaller or slower than ω_0. Consequently, while the ion is performing one revolution, it will not complete a free radial or vertical oscillation. The result will be that the azimuthal position in the machine at which the ion has a maximum radial displacement will precess. The precessional period for radial oscillations will be

$$T_{pr} = 2\pi/\{\omega_0[1-(1-n)^{\frac{1}{2}}]\} \tag{18a}$$

and the precessional angular frequency will be

$$\omega_{pr} = \omega_0[1-(1-n)^{\frac{1}{2}}]. \tag{19}$$

The change in mean radius during a precessional period will be given by

$$\Delta r_{pr} = \{1/[1-(1-n)^{\frac{1}{2}}]\}[r_s/(1-n)\beta_s^2](\Delta E/E_s). \tag{19a}$$

4. OPERATION UNDER NORMAL CONDITIONS

Typical operating conditions (e.g., magnetic field, tank pressure, etc.) are given in Appendix I. Unless otherwise mentioned the discussion and data refer to operation with deuterons. The deuteron beam current received on an internal target as a function of the radius is plotted in Fig. 2. The minor variations in the ion current between 25 and 70 inches presumably are not significant and probably arise due to the method of reading the current. The factors that cause decrease of beam intensity (neglecting the effects at the maximum radius reached) are effective primarily at the small radii. These are (1) gas scattering which is unimportant at higher energies; (2) return of ions to center which takes place primarily during the first phase oscillation so that most of these ions never get beyond a radius of about 10 inches; (3) loss of beam because of the increase of the synchronous phase angle so that ions can no longer be retained in stable orbits (this occurs primarily before a radius of 20 inches is reached.); (4) loss of beam at small radii due to inadequate vertical focusing. Since the probe cannot go closer to the center than about 20 inches, the curve obtained (which starts at a radius of 25 inches) would not be expected to show any considerable change in beam intensity during acceleration.

5. LOSS OF BEAM AT LARGE RADIUS

Originally it was expected that the beam could be accelerated to the radius at which $n=1$, where the motion becomes radially unstable. Actually, however, most of the beam disappears at a radius of about 81.5 inches. Copper probes in the shape of a *C* (see Fig. 3a)—with the open end of the *C* toward the center of the tank—were placed in the path of the beam to find out what happened to the beam. Radioautographs were made of these probes (see Fig. 3b). They show that beam is received in the back part of the *C* at a radius of 75 inches. The radioautograph at the 82-inch radius shows most of the beam hitting on the top of the *C*. The lack of symmetry for top and bottom is probably due to not centering the probe in the surface of symmetry of the beam. This surface is determined as the surface about which the vertical oscillations of the ions take place. The loss of the beam could be considered as due to this surface being displaced. However, densitometer measurements of probe radioautographs at $r=75$ inches indicate that the surface of symmetry is displaced upwards only one-half inch while at $r=80\frac{1}{4}$, $81\frac{3}{4}$, and $82\frac{1}{4}$ inches this surface is very close to the median plane of the magnet gap. The radioautograph at 83 inches shows all of the beam hitting the top or bottom of the *C* probe before the 83-inch radius is reached and none hitting at 83 inches. It was also observed that there was a "hot" spot on the dee at about this radius where presumably the amplitude of vertical oscillations increases sufficiently to cause the ions to hit the dee. The hot spot was on the top of the dee due to the fact that the surface of symmetry is

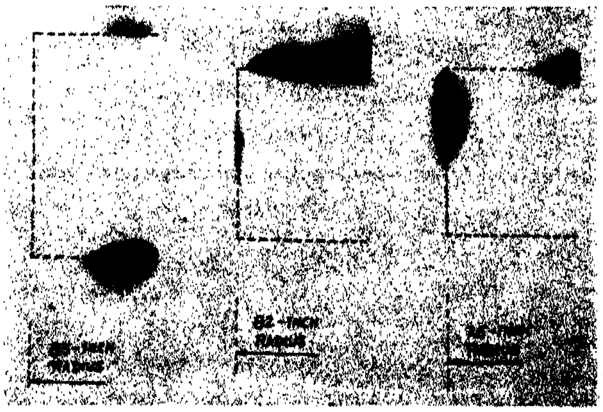

FIG. 3b. Radioautographs of beam taken with *C* shaped probe (taken at radii 75 inches, 82 inches, 83 inches).

about one-half inch above the median plane of the magnet gap while the dee is centered in the gap.

5a. Coupling at n = 0.2

It appears that the coupling between free radial and vertical oscillations at $n=0.2$ ($r=81.2$ inches) and the coupling between vertical oscillations and azimuthal inhomogeneities at $n=0.25$ ($r=81.7$ inches) is adequate to cause this loss of beam.

The amplitude, A_r, of the free radial oscillations is not known accurately but it is probably of the order on the average of one or two inches. The amplitude, A_z, of vertical oscillation is probably less than one inch. However, if all the energy of radial oscillation were fed into the vertical oscillation, the new amplitude of vertical oscillation, A_z', would be

$$A_z'=[A_z^2+(\omega_r/\omega_z)^2A_r^2]^{\frac{1}{2}}. \tag{20}$$

At $n=0.2$, $(\omega_r/\omega_z)=2$. Hence, if $A_r\geq 1$ inch and the energy in the radial oscillation were fed into the vertical oscillation, the amplitude A_z' would be at least 2 inches. Now the surface of symmetry at this radius is about one-half inch above the median plane of the magnet gap. The vertical clearance in the dee is 5 inches so that the distance from the surface of symmetry to the dee will be only 2 inches. Hence, all ions with $A_r>1$ inch would be intercepted by the dee if this process went on.

The extent to which this process goes on may be roughly calculated in two steps. We may first calculate the extent of coupling between the two modes of oscillation as follows. Let $r=r_0(1+\rho)$, $z=r_0\zeta$ and $\tau=\omega_0t$ where ω_0 is the angular frequency of rotation at the radius in question. (Note that τ as used in this section is not the same τ as used to denote period of frequency modulation.) Then the Hamiltonian, neglecting the accelerating voltage, may be written in the following form

$$H=\frac{M}{2}\left\{\frac{p^2}{M^2}+\frac{p_r^2}{M^2}+\frac{p_z^2}{M^2}+\omega_r^2r_0^2\rho^2+\omega_z^2r_0^2\zeta^2\right.$$
$$\left.-\alpha\omega_0^2r_0^2\rho\zeta^2+\cdots\right\}, \tag{21}$$

where p is the orbital angular momentum for the equilibrium orbit. The $\alpha=[(r^2/H)(\partial^2H/\partial r^2)]_{r_0}$ represents the coupling coefficient. Transforming to action and angle variables the Hamiltonian is averaged over the short term oscillations leaving only the long term oscillation due to the coupling term. It is found then that the duration of the coupling period, τ_J—i.e., the period of the long term oscillation in which period the amplitude of the z oscillation will change from its minimum value to a maximum value and back to its minimum value again—can be represented roughly by $\tau_J\simeq 2\pi(0.8r_0/-\alpha A_r)$. For $\alpha=-6.4$ and $A_r=1$ inch the coupling period is $\tau_J\simeq 2\pi\cdot 10$, i.e., the time it takes the ion to perform 10 revolutions, and during this coupling period at some time most of the energy of radial oscillation will be in the vertical oscillation. Hence, if the duration of the coupling is as large as τ_J, we can expect a considerable variation in the amplitude of A_z. Actually, when there is a considerable change in A_r, or A_z, this method of solution is not accurate. However, if the method indicates large changes, it is an indication of possible danger points.

Now actually as the ion increases its radius the value of n slowly increases. Whether much energy transfer takes place will depend on the length of time that the ion is close to resonance. An estimate of the effective period of resonance can be obtained as follows: let $n=n_0+\sigma\tau$ where n_0 is the value of n at the resonance. Then substitute this expression for n in the uncoupled Eqs. of motion, (17) and (18), and obtain the solutions for the uncoupled equation in ρ, ζ. Taking these as the solutions of the homogeneous equations we have to solve the non-homogeneous coupled equations

$$d^2\rho/dt^2=-(1-n)\rho+(\alpha/2)\zeta^2, \tag{22}$$

and

$$d^2\zeta/dt^2=-n\zeta+\alpha\rho\zeta. \tag{23}$$

The method of variation of parameters is used with the above approximate solutions. The variable coefficient in the solution then contains a term of large amplitude which is a Fresnel integral. The time taken to go from the minimum to the maximum value of this integral gives an approximation to the effective resonance period, τ_R—i.e., an approximation to the time during which the coupling may be considered effective as the particle passes through the resonance value $n=0.2$. It is found that

$$\tau_R=4[\pi n_0(1-n_0)^{\frac{1}{2}}/\sigma]^{\frac{1}{2}}. \tag{24}$$

Now

$$\begin{aligned}\sigma=dn/d\tau&=dn/dr\cdot dr/d\tau\\&=[(n+n^2-\alpha)/(1-n)\beta^2](\Delta E_s/2\pi E_s).\end{aligned} \tag{25}$$

The criterion may now be adopted that if $\tau_R>\tau_J$ most of the energy of radial oscillation will be transferred to vertical oscillation at least once as the ion goes through the resonance. Similarly, if a machine is being constructed and we wish to decide what physical condition must be met to have incomplete energy transfer for $n=0.2$, the condition would be approximately that $\tau_R<\tau_J$; i.e., we obtain the condition that

$$\frac{\alpha^2}{0.24-\alpha}<\frac{0.55r_0^2}{\beta^2A_r^2}\frac{\Delta E_s}{E_s}. \tag{26}$$

Calculation of τ_R for the 184-in. synchro-cyclotron with $E_s=2070$ Mev and $\Delta E_s=6$ kev gives $\tau_R=2\pi\cdot 100$, i.e., the passage through the resonance takes about 100 revolutions. Hence, we can expect almost complete energy transfer and so can expect that ions with amplitude of radial oscillation, A_r, greater than 1 inch will be lost near the $n=0.2$ radius due to striking the dee.

Now we have discussed above an experiment in which *C* shaped probes were used to detect the beam. In these experiments it was found that some of the beam struck the central part of the probe placed at a radius of 82 inches, but that none struck the central part of a probe placed at a radius of 83 inches. [In view of the data discussed in Section 15 as to the true center of rotation of the ions, we should probably correct these to 82.2 inches and 83.2 inches from the actual center of rotation of the ions.] Ions which strike in the central region of the probe may belong in one of two groups. If $A_r<1$ inch we may expect the ions to be accelerated past the radius at which $n=0.2$ without striking the dee. (The possible loss of these ions will be discussed below.) Ions with $A_r>1$ can be expected to get to a radial distance greater than where $n=0.2$ during part of their orbit, since the resonant coupling is effective where the average value of n during a revolution is 0.2. Calculation of the average value of n indicates that if $A_r>2\frac{1}{2}$ inches, the ion should get to a radius of 83 inches; if $A_r>5$ inches the ion should get to a radius of $83\frac{1}{2}$ inches. Hence, we may conclude that in the 184-in. cyclotron, ions with 1 inch$<A_r<5$ inches may indeed be lost by coupling near the radius where $n=0.2$ and not show up on the central part of a probe placed at a radius of $83\frac{1}{2}$ inches.

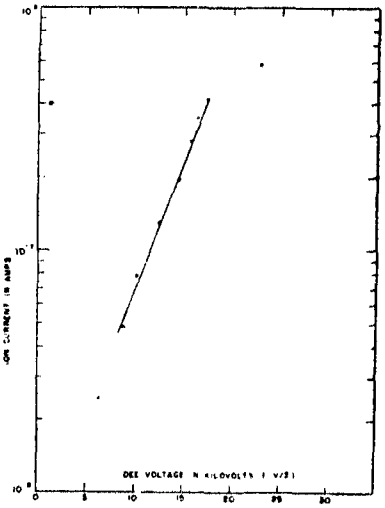

FIG. 4. Ion current as a function of the dee voltage.

It is possible by using (26) to determine a limit for α to insure that coupling be unimportant at $n=0.2$. For the 184-in. synchro-cyclotron letting $\Delta E=6$ kev and $A_r=1$ inch it is found that the coupling coefficient $(-\alpha)$ should be less than 0.14. Actually, it is about 6.4. Hence, if this is the reason for losing the beam at $n=0.2$, it would be rather difficult to correct the field in this case as this means determining $[-(1/H)(\partial^2H/\partial r^2)]_{r=r_0}$ so that it is less than 0.00002/in.^{2} which means very high accuracy in machine construction and field measurements. The physical process can be seen as follows. When $-\alpha$ is large, the strength of the vertical forces increases rapidly with radius since the field lines are more curved at the larger radii. Hence, when an ion is at large radii due to a radial oscillation, it will experience large vertical forces. At smaller radii the vertical forces will be weaker. With a suitable phase relation then it can be seen that the ion can have its vertical amplitude built up by the strong forces at large radii which are not counterbalanced by forces of similar strength at small radii.

In the case of the 37-in. synchro-cyclotron, with the same value of A_r and $\Delta E=5$ kev, at the radius where $n=0.2$, $(-\alpha)$ again should be less than 0.14. The actual value seems to be smaller than this. Radioautographs of *C* shaped probes show that the beam does not blow up in the 37-in. synchro-cyclotron at the radius where $n=0.2$ ($r_0=16$ inches) but that actually a considerable amount of the beam does reach the radius where $n=1$. The difference between the two machines may be due to the fact that the rate of decrease of the field is changing rapidly for the 184-in. synchro-cyclotron near this radius. This is not true in the case of the 37-in. synchro-cyclotron.

5b. Coupling at n = 0.25

The coupling here would be between the vertical oscillation and azimuthal inhomogeneities in the magnetic field, the ion performing two revolutions for each vertical oscillation. A term of the form $z\cos\theta$ would give coupling at $n=0.25$. It is possible to develop H_r, the radial component of **H**, in a series such that we can have

$$H_r=-(zH_z/r)n(1+h\cos\theta), \tag{27}$$

where h is a small quantity. We then must investigate the solution of

$$d^2z/dt^2=-(e/Mc)r\dot{\theta}H_r=-\omega_0^2n(1+h\cos\theta)z. \tag{28}$$

Letting $\omega_0dt=d\theta$, $\theta=2\phi$, $n=0.25$ the equation becomes

$$d^2z/d\phi^2+(1+h\cos2\phi)z=0, \tag{29}$$

which is a form of Hill's equation. An approximate solution can be obtained in the following form

$$z=\text{Const.}\exp[\pm(2/3)^{\frac{1}{2}}(h/2\pi)\theta]\cdot\Phi(\theta/2), \tag{30}$$

where $\Phi(\theta/2)$ is a periodic function. Hence z will change by a factor e when

$$\theta=2\pi[(3/2)^{\frac{1}{2}}(1/h)]. \tag{31}$$

Investigation of the available data on the field of the 184-in. magnet indicates that it is possible that such an inhomogeneity exists near $n=0.25$ with h of the order of 0.05. Hence, we may expect that in a period of 24 revolutions, ions could increase the amplitude of their vertical oscillation by a factor e.

The resonance time in this case is found to be

$$\tau_R=4(\pi n_0/\sigma)^{\frac{1}{2}}. \qquad (32)$$

Letting $\Delta E_s=5$ kev, $\alpha=-0.0015r^2$ it is found that $\tau_R=2\pi(104)$. Hence, the effective resonance time is sufficiently long to permit a considerable increase in the amplitude of vertical oscillation. Only particles with an initial $A_z\ll 1$ inch could be expected to get through this resonance in the 184-in. synchro-cyclotron. Hence, this coupling could be expected to account for the loss of practically all of the beam that might have gotten past the $n=0.2$ resonance.

There is insufficient data on the 37-in. magnet to investigate the effect of this coupling for that magnet. The effective resonance time, τ_R, is quite a bit shorter—only 27 revolutions. Radioautographs of a *C* shaped probe do indicate that there is some blowing up of the beam at $r=18$ inches near where $n=0.25$.

Investigation of the resonance at $n=0.1$ indicates that it is not dangerous. As we go to higher order resonances the coupling is probably much weaker so that the coupling period becomes longer. Hence, these resonances are probably unimportant.

5c. Coupling at n = 0.1

The coupling here would be between the vertical and radial oscillations with $\omega_r=3\omega_z$. Assuming a median plane of symmetry, the coupling term in the Hamiltonian (21) would be of the form $r_0^2\omega_0^2\mu_{2,6}\rho^2\zeta^6$, where $\mu_{2,6}\simeq(1/6.6!)[(r^7/H)(\partial^7H/\partial r^7)]_{r_0}=\alpha_7/6.6!$ Actually, $\mu_{2,6}$ will contain other terms but unless the lower derivatives are extremely large, this will be the important one to consider. We then find for the condition $\tau_R>\tau_J$ that we must have

$$6480(r_0^6/A_r^2A_z^4)>\alpha_7[2\beta^2(E_s/\Delta E_s)]^{\frac{1}{2}}.$$

Assuming $A_r=2$ inches, $A_z=1$ inch, $r_0=80$ inches, $\beta^{-2}=5.7$, $\Delta E_s=10$ kev, we find that the seventh derivative of (H/H_0) should be less than 0.1000/inch^7. Magnetic field measurements at each inch of radius might be used to estimate what the actual situation is by replacing derivatives by differences. However, the magnetic measurements are not good enough to give really significant values for the seventh difference. Even so, it appears that there is a large safety factor at this resonant frequency.

6. VARIATION OF ION CURRENT WITH VOLTAGE

The maximum obtainable ion current as a function of dee voltage is plotted in Fig. 4. All other conditions—such as condenser speed, etc.—were adjusted at each voltage to give the maximum current. The slope of the line between 9 and 17.5 kv indicates that the current varies as the third power of the voltage. As pointed out in the paper by Richardson *et al.*,[6] there are many factors that influence the variation of current with voltage, such as:

1. Source current. The ion current that can be pulled out of the source will depend on the accelerating dee voltage and might be expected to vary as $V^{\frac{3}{2}}$.
2. Loss of ions due to collision decreases with increasing ion energy. Hence, if the ion has a shorter path at low energies there will be less collision loss. With higher dee voltages the path length before a given energy is attained will be shorter.
3. The catching efficiency also varies with dee voltage. The Eq. B-(10) indicates for a fixed phase angle the efficiency will vary as $V^{\frac{1}{2}}$. Actually, the more detailed considerations of what ions are caught in phase stable orbits indicate that the ion current variation is even more sensitive to the voltage. This is related to the fact that with higher voltages the ions caught in phase stable orbits will reach larger radii in the first phase oscillation.

7. VARIATION OF ION CURRENT WITH CONDENSER SPEED

The ion current obtainable for fixed dee voltages but varying condenser speeds is plotted in Fig. 6. The figure is in terms of $I/I_{\max}$ *vs.* $C/C_{\max}$, where $I_{\max}$ is the maximum ion current for the given voltage and $C_{\max}$ is the condenser speed at which the beam disappears. This variation of *C* is equivalent to varying the synchronous phase angle.

The second paper by Bohm and Foldy gives a curve (B-Fig. 2) which represents the capture efficiency as a function of synchronous phase angle. However, this does not represent the above experimental data for the 184-in. synchro-cyclotron too well. This is primarily due to the fact that during a frequency modulation cycle of the 184-in. synchro-cyclotron the value of $\sin\phi_s$ varies by a considerable amount. The increase of ϕ_s from its value during the first phase oscillation to its value at the maximum (near $r=35$ inches) means that the range of ϕ_m, the maximum value of ϕ during the phase oscillation, in stable orbits will shrink. Hence, although the ϕ_m for a given ion may have been in a stable range during the first phase oscillation, it may be that at the maximum ϕ_s the ϕ_m is no longer stable. If we know the maximum value of ϕ_s during the f-m cycle, we can determine what range of ϕ_m will be stable at that ϕ_s. Since ϕ_m will not remain constant during the cycle it is necessary to be able to connect the value of ϕ_m at $r=35$ inches (ϕ_{mf}) with the value of ϕ_m in the first phase oscillation (ϕ_{ms}). (In the following the second subscript $_s$ denotes the value of the quantity at the start in the first phase oscillation and the subscript $_f$ the final value—or the value at $r=35$ inches.) An approximate relation between these two values of ϕ_m may be obtained as follows.

We know that during adiabatic changes the action integral as given in (A), $J=\oint I\dot{\phi}d\phi$ is invariant under such changes, where

$$I=E_s/\omega_s^2K \qquad (33)$$

and

$$\dot{\phi}^2=(eV\omega_s^2K/\pi E_0)[U(\phi_m)-U(\phi)],$$

or

$$\dot{\phi}^2=\dot{\phi}_0^2+(eV\omega_s^2K/\pi E_0)[\cos\phi+(\phi-\pi/2)\sin\phi_s]. \qquad (34)$$

---

[6] Richardson, Wright, Lofgren, and Peters, Phys. Rev. 73, 424 (1948).

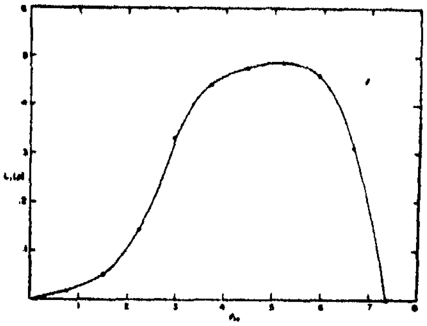

FIG. 5. Theoretical efficiency for constant dee voltage and varying condenser speed.

We shall assume that the change in ϕ on going from the first phase oscillation to the situation where $r=35$ inches is adiabatic. Now $\dot\phi$ varies between upper and lower limits and we assume that a crude approximation to the evaluation of J may be obtained by setting $\dot\phi=\dot\phi_m \sin\omega_{ph}t$ (see A-(22)). Then

$$J=I\dot\phi_m^2\oint \sin^2\omega_{ph}t dt=\pi(I\dot\phi_m^2/\omega_{ph}). \tag{35}$$

Hence, we assume for this approximation that $I\dot\phi_m^2/\omega_{ph}$ is constant in time. Now we are interested in the limiting $\dot\phi_m$ retained when $r=35$ inches. This will be for $\phi_m=\pi-\phi_s$. Hence

$$\dot\phi^2=(eV\omega_s^2K/\pi Mc^2)[\cos\phi+\cos\phi_s+(\phi+\phi_s-\pi)\sin\phi_s]. \tag{36}$$

Since $\dot\phi$ has its maximum value at $\phi=\phi_s$, we have

$$\dot\phi_{mf}^2=\left(2\frac{eV\omega_s^2K}{\pi Mc^2}[\cos\phi_s+(\phi_s-\pi/2)\sin\phi_s]\right)_f =\left(2\frac{eV\omega_s^2K}{\pi Mc^2}F_1(\pi/2,\phi_s)\right)_f, \tag{37}$$

where

$$F_1(\phi_0,\phi_s)=[\cos\phi_0+\cos\phi_s+(\phi_0+\phi_s-\pi)\sin\phi_s]. \tag{38}$$

The value of $\dot\phi^2$ at the start should be given by (B-(6))

$$\dot\phi^2=\dot\phi_0^2+\frac{eV\omega_s^2K}{\pi Mc^2}[\cos\phi-\cos\phi_0+(\phi-\phi_0)\sin\phi_s], \tag{39}$$

where ϕ_0 is the phase angle at the start of the acceleration and $\dot\phi_0$ is value of $\dot\phi$ at this angle. It is shown in B that the effective starting phase, ϕ, for all ions is $\pi/2$. Hence, setting $\phi=\phi_s$ to get $\dot\phi_{ms}$, we have

$$\dot\phi_{ms}^2=[\dot\phi_0^2+(eV\omega_s^2K/\pi Mc^2)F_1(\pi/2,\phi_s)]_s. \tag{40}$$

Using (35), (37), and (40) we then have

$$\dot\phi_{ms}^2=(\omega_{ph}/I)_s(I/\omega_{ph})_f\dot\phi_{mf}^2, \tag{41}$$

or

$$\dot\phi_{0s}^2=\left(\frac{\omega_{ph}}{I}\right)_s\left(\frac{I}{\omega_{ph}}\right)_f\left[\frac{2eV\omega_s^2K}{\pi Mc^2}F_1(\pi/2,\phi_s)\right]_f -\left[\frac{eV\omega_s^2K}{\pi Mc^2}F_1(\pi/2,\phi_s)\right]_s. \tag{42}$$

Substituting for I, ω_{ph} we get

$$\left(\frac{\pi Mc^2}{eV\omega_s^2K}\right)_s\dot\phi_{0s}^2=2\left[\frac{\cos\phi_{ss}\cdot V_fK_s\cdot E_{sf}^3\cdot\omega_{ss}^2}{\cos\phi_{sf}\cdot V_sK_f\cdot E_{ss}^3\cdot\omega_{sf}^2}\right]^{\frac{1}{2}} \times F_1(\pi/2,\phi_{sf})-F_1(\pi/2,\phi_{ss}). \tag{43}$$

This will give the limiting stable $\dot\phi_0$ which can start in the first phase oscillation and just be retained when $r=35$ inches. For small phase angles this may give a greater range of phase stability than is given by B-(8). Hence, the limiting $\dot\phi_0$ is determined by the smaller of the two quantities either B-(8) or (43) above, since the first one indicates ions that can be retained at small radii and the latter indicates those that can be retained at larger radii.

The calculation of $\dot\phi_{0s}^2$ depends on the value of certain quantities in the first phase oscillation. Now K varies considerably in the first few inches. A reasonable value to take seems to be that at the radius where $\dot\phi$ goes from positive values to negative values since only those where $\dot\phi$ becomes negative will be retained. We are interested in ions whose initial $\dot\phi_0$ is near the maximum positive value. A rough calculation indicates that for $\phi_{ss}<\pi/4$ a reasonable value of $r\simeq10$ inches. On this basis a capture efficiency curve $L_1(\rho)$ was computed and plotted against the maximum phase angle an ion might have in its orbit (see Fig. 5) where the relation

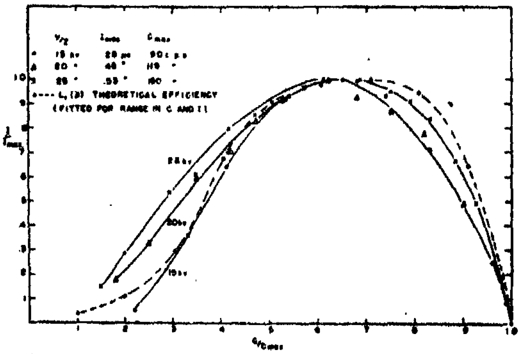

FIG. 6. Variation of ion current with condenser speed (or synchronous phase angle).

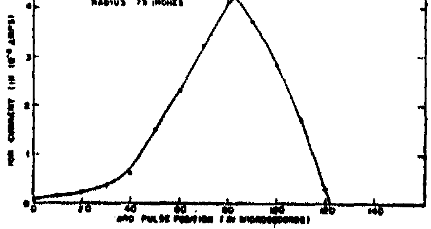

FIG. 7. Ion current received as a function of arc pulse position.

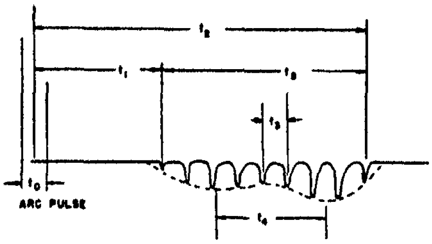

FIG. 8. Schematic drawing of oscilloscope pattern.

between the total range of ϕ_0 that may be captured into permanently stable orbits and $L_1(\rho)$ is given by

$$\Delta\omega_s=(\phi_0)_{\text{total}}=\left[\left(\frac{eV\omega_s^2K}{\pi Mc^2}\right)^{\frac{1}{2}}\right]_s 2L_1(\rho). \qquad (43a)$$

It will be noted that this capture efficiency drops to zero before $\sin\phi_{s,f}=1$. This is due to the fact that all ions captured start off with a certain minimum amount of phase oscillation—since they start at a phase $\phi_0=\pi/2$ which is different from $\phi_{s,i}$. As $\phi_{s,f}\rightarrow\pi/2$ the range of phase stability decreases rapidly toward zero. Hence, ions start with a ϕ_0 which may be stable when the ϕ_s for the ion is small at the start of the orbit—but then as ϕ_s increases as the radius increases, the ϕ falls outside of the range of stability. This capture curve is compared with experimental data in Fig. 6. The scales have been expanded so that the curves become zero at the same abscissa. There is good agreement in the general shape of the curves.

8. EFFICIENCY OR ACCEPTANCE TIME

An expression for the efficiency is given in B-(9). With the changes in notation introduced in this paper and using (37) the efficiency, ϵ, will be given now by

$$\epsilon=\frac{\Delta\omega_s}{(1/C)|d\omega_s/dt|}=\frac{1}{|d\ln\omega_s/d\tau|}\frac{\Delta\omega_s}{\omega_s}$$

$$=\left(\frac{eVK}{\pi Mc^2}\right)^{\frac{1}{2}}\cdot\frac{2L_1(\rho)}{|d\ln\omega_s/d\tau|}. \qquad (44)$$

The optimum value of $L_1(\rho)\simeq0.49$. At the start of acceleration $|d\ln\omega_s/d\tau|=1.47$ and $K\simeq2.10$, so that

$$\epsilon\simeq0.55[(eV/Mc^2)]^{\frac{1}{2}}. \qquad (45)$$

If $V=32$ kv, $\epsilon=0.0023$.

Some experimental data on the acceptance time is given in Fig. 7. This data was obtained by pulsing the arc for 2 μsec. and then measuring the ion current received on a probe at a radius of 75 in. The figure shows the ion current received when the arc was pulsed at different times in the frequency modulation cycle. A reasonable explanation of this curve would seem to be the following. Ions are created at the time the arc is pulsed. These ions can persist in the central region of the machine for a certain length of time, possibly undergoing radial phase oscillations. If, during this persistence time, the accelerating frequency comes into the range for acceleration into stable orbits, a certain fraction will be accelerated. If not, the ions are presumably lost to the top or bottom of the tank. Hence, the maximum length of arc pulse which can create ions that can be accelerated into stable orbits will be the sum of the persistence time plus the time that the frequency is in the range for acceleration into stable orbits. This latter time is what has been called the "acceptance" time in these papers. The data in Fig. 7 indicates a persistence time of about 60 μsec. (from $t=20$ μsec. to $t\simeq82$ μsec.) and an acceptance time of about 40 μsec. (from $t=82$ μsec. to $t=122$ μsec.). The observed "efficiency" will be the ratio of the "acceptance time" to the length of the cycle—so in this case where the cycle is 1/80 of a second, $\epsilon=(40\ \mu\text{sec.})/(1/80\ \text{sec.})=0.0032$ which is in reasonable agreement with the efficiency computed above. [The integrated current comes out to be 1.05 μa. This is also in fair agreement with the total current normally received.]

9. EFFICIENCY AS A FUNCTION OF RATE OF FREQUENCY MODULATION

The efficiency depends, as is indicated in (44), on the rate of frequency modulation during the first phase oscillation. It also depends on which ions caught in the first phase oscillation can be retained in stable orbits. The maximum frequency of the oscillator in the 184-in. synchro-cyclotron under normal operation is 12.61 megacycles (see Fig. 1). The frequency for catching deuterons is 11.47 megacycles for $H_c=15{,}000$ gauss. Hence, the frequency is changing fairly rapidly in the first phase oscillation. By making an appropriate adjustment it was possible to have the maxmum frequency in the f-m cycle only 11.63 mc so that the rate of frequency modulation was much slower during the first cycle. Hence, this factor would indicate a considerable increase in efficiency. The effect of this

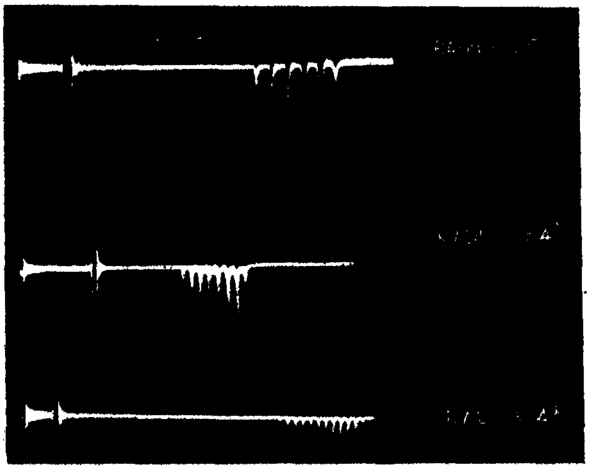

FIG. 9. Oscilloscope pictures. Radius 25 inches, 34 inches, 45 inches.

TABLE II. Oscilloscope pattern data (dee voltage≃19 kv).

Plate No.	Dee bias (kv)	Radius (inches)	Arc pulse duration (μsec.)	C sec.$^{-1}$	t_1 μsec.	t_2 μsec.	Time of flight μsec.	t_3 μsec.	No. of pips	t_5 μsec.	T_{pr} = precessional period μsec.	t_4 μsec.	T_{ph} phase period μsec.	$(\delta r)_{ph}$ inches
48		25 in.	5	92	156	192	158	36	4	12.0	12.9	—	41	3.9
51		34 in.	5	92	235	294	256	59	7	9.8	9.5	—	47	3.7
54		45 in.	5	92	450	535	473	85	12	7.7	6.1	45	47	2.8
83		25 in.	50	92	112	153	158	41	4	13.1	12.9	—	41	
80		34 in.	115	92	168	239	256	71	8	10.1	9.5	41	47	
88		45 in.	50	119	270	350	318	80	12	7.2	6.1	47	47	
70		34 in.	5	52	440	536	450	96	9	12.5	9.5			
73		34 in.	5	108	240	310	216	70	7	12.0	9.5			
76		34 in.	5	140	180	205	167	25	3	11.5	9.5			
64	0.5	34 in.	5	92	250	295	256	45	4	10.2	9.5			
66	2.0	34 in.	5	92	250	315	256	65	7	10.2	9.5			
68	4.5	34 in.	5	92	225	325	256	100	7	10.3	9.5			

change in $|d\ln\omega_s/d\tau|$ is to start ions off with a small phase angle, ϕ_s, and subsequently introduce a large change in it. But the function $L_1(\rho)$ will be small for very small values of $\rho(=\sin\phi)$. Thus the gain from other factors will be offset to some extent.

Data is not available to investigate thoroughly this effect. However, rough calculations indicate that the efficiency probably should be increased somewhat, say 20 percent in one of the cases investigated. The experimental data gave values of increase in efficiency ranging from 0 percent to 17 percent.

10. TANK PRESSURE

The 184-in. cyclotron dee will not hold voltage if the pressure in the tank is much above 2×10^{-5} mm Hg. On the other hand the normal operating tank pressures are in the neighborhood of 1×10^{-5} mm Hg. Hence, it has not been possible because of this limited range to obtain much satisfactory experimental data on the variation of ion current with tank pressure.

11. VERTICAL FOCUSING

Electrostatic focusing in cyclotrons has been considered by Rose[6] and Wilson.[7] It is due to the vertical components of the electric field near the dee gap. The formula derived by Rose is valid at larger radii, where the ion crosses the accelerating gap in a relatively short time. If the acceleration is averaged over one period of rotation, the mean acceleration is given by

$$\left\langle\frac{(d^2z)}{dt^2}\right\rangle_{Av}=-\frac{eV\omega^2z}{4\pi(E-E_0)}\cos\phi. \tag{46}$$

This expression breaks down for $E-E_0\simeq0$, i.e., at small radii, since here the ion spends most or all of its time in the accelerating region. For very small radii we can assume that the ion is in an electrostatic field uniform in the median plane. If there are two dees or a dee and a dummy dee so that the vertical component of the electrostatic field will be symmetrical about the center of the gap and zero at the center, an approximate formula for the electrostatic focusing in the central region is

$$\left\langle\frac{(d^2z)}{dt^2}\right\rangle_{Av}=-\frac{er^3z\cos\phi}{8M}\left[\frac{\partial^5V}{\partial z^2\partial x^3}\right]_{\rho=0,\,z=0}, \tag{47}$$

where x is measured in the median plane perpendicular to a center line between the dees. The derivative may be evaluated in two cases from the potential distribution given in Wilson's paper.

Now it has been pointed out before that the effective value of ϕ near the beginning of the orbit is $\phi_0\simeq90°$. Also, most of the ions that are caught have $\phi>0$ at the start. Hence, $\phi>\pi/2$ in the early part of the acceleration and we can expect a defocusing electrostatic force for most of the ions with which we are concerned.

A magnetic focusing force is the only force that can be used to counteract this defocusing force. The magnitude of the magnetic focusing force is given by (18). The value of n at the center is zero. Hence, to introduce magnetic focusing as rapidly as possible small cones of mild steel were put in the central part of the magnet on the pole faces. At first cones with base diameter 4 inches and 1¼ inches high were used, later cones with base diameter 6 inches were used.

With the cones in place the field is essentially constant to the 1-inch radius, then falls off about linearly

TABLE III. Maximum width for ions to hit on probe (all distances in inches).

		h_{max}				h_{max}		
r	Δr_{pr}*	A_r =1 in.	A_r =3 in.	A_r =5 in.	Δr_{pr}**	A_r =1 in.	A_r =3 in.	A_r =5 in.
20	1.56	—	0.10 in.	0.13 in.		—	—	—
40	0.33	0.06	0.12	0.16	1.1	—	0.23	0.30 in.
70	0.12	0.08	0.14	0.18	0.4	0.14	0.25	0.32
81	0.03	0.06	0.08	—	0.1	0.11	0.16	—

* Based on $\Delta E=eV\sin\phi_s$.
** Based on $\Delta E=40$ kev.

---

[6] M. E. Rose, Phys. Rev. 53, 392 (1937).
[7] R. R. Wilson, Phys. Rev. 53, 408 (1937).

with radius; however with the cones removed the field is constant to the 8-inch radius, then falls off linearly. With these cones removed, the ion current received on an internal target at the 80-inch radius is approximately 10 percent of the ion current obtainable with the cones in place. It, therefore, seems very desirable that such cones be used to produce vertical magnetic focusing at as small a radius as possible.

12. OSCILLOSCOPE DATA

It has been possible to examine the structure of the individual beam pulses that are received once each frequency modulation cycle, using a synchroscope and taking photographs of the oscilloscope pattern. Time markers were superposed on the beam pattern to permit determination of time intervals. A schematic picture is given in Fig. 8—with the notation which is to be used below. Typical photographs are given in Fig. 9. Data obtained from such photographs are given in Table II.

The ions as they are accelerated oscillate in various fashions about a synchronous orbit of steadily increasing radius. The time it takes for the ions to reach the probe radius is called the "time of flight". The time of flight to any specified radius can be computed by determining when the oscillator frequency corresponds to the natural frequency of rotation at the specified radius. This computed time in all cases lies within or close to the limits t_1, t_2. The cases where it lies outside the limits are understandable in terms of the arc being pulsed at a slightly too early time so that ions are not accelerated immediately but must stay for a short time in the central region of the machine before acceleration.

The actual motion of the ions which affect these oscilloscope patterns can be broken down into three components.

1. Expansion of the synchronous radius.
2. Phase oscillations about this radius.
3. Free radial oscillations about this radius.

The most noticeable thing about the pictures is the series of small pulses that occur every 7–13 microseconds, depending on the radius. The separation time, t_3, of these pulses agrees well with the precessional period, T_{pr} (Eq. (18a)). This precessional period will be apparent only for ions which have a free radial oscillation. The fact that the ions strike the probe in bunches—not continuously—indicates that the azimuthal angles at which the various ions have their maximum radial displacement are not distributed at random but are grouped together to a certain extent. Such a radial oscillation might be built up due to some sort of an azimuthal inhomogeneity at small radii where $n \simeq 0$, by the dee bias used, etc. If $n=0$, we can expect that the amplitude of such oscillations can be built up; for when $n=0$ displacements or forces acting at a certain azimuthal angle in the machine will be cumulative for successive revolutions; however, when $n>0$, the azimuthal angle of maximum displacement will precess around the machine so these successive displacements will come at different parts of the orbit and hence will not be cumulative. Some such condition appears to exist in this machine. The ions receive some radial displacement in a definite direction at the start of their acceleration so that the azimuthal angles of maximum displacement are pretty well bunched together in the early part of the acceleration. Calculation indicates that such a bunching could persist for several phase oscillations.

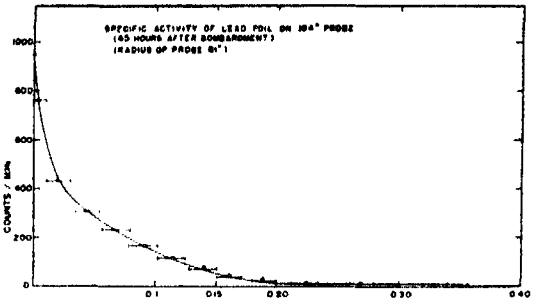

FIG. 10. Width of beam on probe.

If the envelope of the small peaks is drawn, two broad peaks may be seen on some photographs. The time separation of these peaks, t_4, agrees well with the period of phase oscillation, T_{ph} (see Eq. (13)). The fact that these are separated by the full period, T_{ph}, must mean that ions that strike the probe in the early group have an amplitude of free radial oscillation which is about as large as or larger than the amount that the radius increases in a period of phase oscillation.

It was also observed while making these oscilloscope pictures if the arc pulse was moved so that the arc was pulsed very late that these ions were received at the probe at a somewhat earlier time than the ions which start just before them. This effect probably is to be interpreted in the following manner. Ions that start late will have large phase oscillations. Hence, for most probe positions these late ions will be expected to strike the probe earlier than ions with smaller phase oscillations.

13. WIDTH OF BEAM ON PROBE

When the ions strike the probe, they will not be scraped off by the very edge of the probe, but will hit at various small distances in on the probe due to the combined effect of radial oscillation and precession. For radii where there are a large number of revolutions in a precessional period an approximate analytical formula can be obtained to give the maximum width, h, in on the probe at which ions will strike,

$$h_{\max}=A_r\{\sin f\theta_2\cdot\sin 2\pi f(1-f) + \cos f\theta_2[\cos 2\pi f(1-f)-1]\} \tag{48}$$

where A_r is the amplitude of free radial oscillation, $f=(1-n)^{\frac{1}{2}}$ and

$$\cos f\theta_2=1-\Delta r_{pr}/A_r. \tag{49}$$

A maximum value of Δr_{pr} may be obtained using (19a) and an energy gain per turn $\Delta E=eV$, the maximum possible increase in energy per turn. To get the distribution of the ions on the probe an energy gain per turn of $\Delta E=eV\sin\phi_s$ is more representative if the precessional period is a considerable fraction of the period of phase oscillation. (The relation (48) is valid only if $\Delta r_{pr}/A_r \ll 1$.) A first approximation to the solution of (48) indicates roughly the following dependence of $h_{\max}$ on n, A_r, and Δr_{pr}, as

$$h_{\max}\simeq\pi n(2A_r\Delta r_{pr})^{\frac{1}{2}}. \qquad (50)$$

Values of $h_{\max}$ based on this formula for $r=20$ inches, 40 inches and 70 inches and with both assumptions as to ΔE (with $V=40$ kv) are given in Table III. The value of $h_{\max}$ for $r=81$ inches was determined by a more detailed study of the orbits.

Various experiments have been performed to determine the distribution of the beam on the probe. In one experiment a lead probe was inserted into the beam at a radius of 81 inches. Thin slices also were taken off the leading edge of the probe and specific activity counts were made. The number of counts at various distances is shown in Fig. 10. The activity is almost all confined to $h<0.16$ inch—only about 5 percent of the measured activity shown on the curve having a greater h. The counts for $h>0.20$ inch can probably be attributed to ions which pass through the edge of the probe and then are scattered, or lose energy and precess with a large A_r.

14. AMPLITUDE OF FREE RADIAL AND VERTICAL OSCILLATION

A method of accurately determining the amplitudes of radial oscillation has not been found. There are various things which might give some indication of it. The radioautographs of the C shaped probes indicate an upper limit on it of maybe 5 inches. The oscilloscope data indicates that A_r may be of the order of 3 inches for a considerable fraction of the ions. The specific probe activity as a function of the distances from the leading edge seems to indicate somewhat the same thing. However, none of these data are very precise.

The amplitude of vertical oscillation is somewhat easier to observe by making an analysis of the distribution of activity on special probes, e.g., a grid of fine wires. Radioautographs of these wire probes indicate that the amplitude of vertical oscillation is of the order of three-quarters of an inch.

15. DISPLACEMENT OF THE CENTER OF ROTATION OF THE IONS FROM THE CENTER OF THE MAGNET

The position of the center of rotation was determined in two ways. The first method was based on magnetic field measurements. The vertical field strength was measured as a function of azimuthal angle for various radii. The field measurements could then be analyzed to give

$$H_z(r,\theta)=H_z(r)\left[1+\sum h_i(r)\cos(\theta+\delta_i)\right]. \qquad (51)$$

If we then let a be the displacement of the center of rotation, using only the first order harmonic, the value of a will be given by

$$a\simeq rh_1/n. \qquad (52)$$

The direction of displacement is indicated by δ_1 which is found to be about 105° away from the probe position. The magnitude of the displacement is about 0.6 inch at $r=10$ inches and increases to about 0.8 inch at $r=60$ inches. After 60 inches it increases somewhat due to the increase in $h_1(r)$. However, as soon as n starts to increase rapidly a drops and is about 0.2 inch from 81 to 82 inches.

This center was also determined by means of two extra non-current reading probes. The results of these measurements agree well with the results as calculated from the magnetic measurements.

If the energy of the ions is going to be determined from the radius of rotation, this effect should be taken into account.

ACKNOWLEDGMENTS

The authors wish to express their appreciation to Professor E. O. Lawrence for his encouragement of this work, to Professor Robert Serber for the many discussions and suggestions about this work, and to Mr. Robert Watt and the cyclotron operating crew for their assistance in collecting the experimental data.

APPENDIX I. TYPICAL OPERATING CONDITIONS

1. The magnetic field is 15,000 gauss at the center of the gap.
2. The dee voltage (average over the cycle) is 20 kv on the dee or a total maximum possible energy gain per turn of 40 kev.
3. A d.c. bias voltage of 1 kv negative with respect to ground is applied to the dee.
4. A dummy dee is used which is held at ground.
5. The r-f is modulated 100 times per second. This is accomplished by a variable capacitor which is rotated at 250 r.p.m. The capacitor has 24 teeth so that it then gives $250\cdot24/60=100$ cycles per second. The total frequency range is from 12.6 to 9.0 megacycles.
6. The pressure in the main vacuum tank and in the rotating capacitor tank is about 10^{-5} mm Hg.
7. The arc voltage of 150 volts is applied for 100 microseconds during each r-f modulation cycle. The arc current during this 100 μsec. pulse is about 20 amp.
8. The time average beam current is about 1 microampere.

THE REVIEW OF SCIENTIFIC INSTRUMENTS VOLUME 20, NUMBER 12 DECEMBER, 1949

A Fractional Microsecond X-Ray Pulse Generator for Studying High Explosive Phenomena

H. I. BREIDENBACH, JR.
Terminal Ballistic Laboratory, Aberdeen Proving Ground, Maryland

(Received July 12, 1949)

An x-ray pulse generator capable of producing short bursts of x-rays not greater than 3×10^{-7} seconds in duration has been constructed. These short bursts are obtained by supplying a negative 50 kv, 12.5 Joule trigger pulse to the cathode shield of a standard Westinghouse W.L. 389 flash x-ray tube. This pulse generates a pre-discharge plasma in the tube which blocks the main 100 kv, 290 Joule pulse until the cathode to anode gap impedance is lowered by ionization.

An arrangement is also described whereby 3 separate, successive radiographs of a single detonation may be taken at predetermined time intervals.

INTRODUCTION

THE value of short, intense pulses of x-rays for detonation studies has been generally accepted for the past eleven years. During that time several researchers have succeeded in reducing the pulse time duration from five microseconds to the present three-tenths microseconds.[1–7].

Each of these decreases in the pulse time duration greatly improved the definition of high speed objects as they appeared on radiographic plates until flash radiography advanced from the stage of an interesting but blurry curiosity to the well-defined, measurable recording technique of today.

The immunity of flash radiography to smoke and flame has made it peculiarly adaptable to studies of projectiles within and emerging from the tubes of weapons, shell fragmentation and armor penetration, high explosive detonation, explosion produced shock waves in metals and shape charge phenomena.[8] A few commercial applications such as investigations in the fields of fuel consumption in combustion engines, particle flow through tubes and studies of enclosed moving mechanical parts have been found, however, the major applications up to the present time have been military.

It is not surprising, therefore, to find that some of the latest advances in the field of flash radiography have been made in and for government research organizations. One of the most recent developments has been the discovery of a method for decreasing the x-ray pulse duration from a standard Westinghouse W.L.389 tube. This is accomplished with an unusual triggering arrangement.

THEORETICAL BASIS FOR CIRCUIT DESIGN

The design of the W.L.389 has been fully reported by Slack and Ehrke[4] but for the purpose of this discussion a sketch showing the electrode arrangement is shown in Fig. 1. The characteristics of this tube may be used to best advantage when it is connected into a circuit whose design is based upon the fundamentals of high vacuum spark phenomena as described by Drs. van de Graaff and Trump.[9]

They say in essence that when "an electron, starting from the cathode and accelerated by the voltage between the electrodes, impinges on the anode with the resultant possible emission of both a positive ion and photons, such positive ions and some photons return to the cathode and cause further electron emission. When the conditions are such that this interchange becomes cumulative, breakdown results."

It follows from the above statement, therefore, that if an abundant supply of electrons is introduced via the cathode shield into the tube before the main discharge occurs, these electrons will undergo the preliminary processes of the high vacuum breakdown until the ion-electron interchange becomes cumulative and the rapid deterioration of the over-all tube impedance induces the main discharge of the x-ray generating energy. It was decided to use condensers for storing the energy to be used in the trigger and main pulses, but the quantity of capacitor energy required by the WL389 for optimum performance was unknown. The magnitude of the required energy was partially governed by the 100-kv tube voltage, which tests had proven to be suitable for radiographing high explosive phenomena. Various combinations of condensers having different capacitance values were tried with the tube. These tests revealed that optimum performance was obtained by supplying a 12.5 Joule trigger and 290 Joule main discharge. The trigger was provided by a 0.01 microfarad 100-kv capacitor while the main discharge was stored in a 0.058 microfarad 100 kv series combination.

---

[1] K. H. Kingdon and H. E. Tanis, Jr., Phys. Rev. 53, 128 (1938).

[2] M. Steinbeck, Wissenschaftliche Veroffentlichen aus den Siemens Wirken 17, 263 (1938).

[3] W. J. Oosterkampf, Philips Tech. Rev., p. 22 (January 1940).

[4] C. M. Slack and L. F. Ehrke, J. App. Phys. 12, 165 (1940).

[5] V. A. Zuckerman, Comptes Rendus (U.S.S.R.), XL, No. 7, 267 (1943).

[6] H. Schardin and E. Schuman in several German reports. Office of Technical Intelligence Report 1622, 1627, 1628.

[7] J. C. Clark MDDC 768, Los Alamos Sci. Lab., New Mexico.

[8] J. C. Clark, "Flash radiography applied to ordnance problems," J. App. Phys. 20, 363 (1949).

[9] R. J. van de Graaff and J. G. Trump, J. App. Phys. 18, 327 (1947).

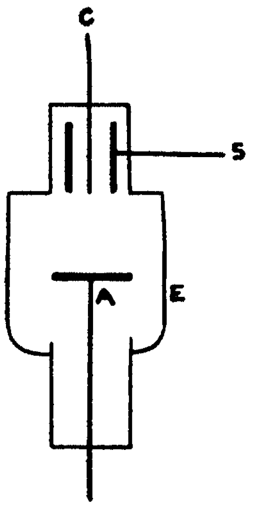

FIG. 1. Diagram of WL 389 tube showing arrangement of components.

Note: *C* to *S* gap 0.5 mm
C Cathode
S Cathode Shield
A Anode
E Pyrex

CIRCUIT DESIGN

A circuit has been constructed which fulfills the above requirements and consequently produces x-ray bursts of a few tenths of a microsecond in duration and of sufficient intensity to penetrate three-quarters of an inch of aluminum at 48 inches from the tube. Figure 2 shows the two main loops of the circuit. Figure 2a is the complete circuit including the triggering and the discharge loop while Fig. 2b shows the trigger loop alone. Looking first at Fig. 2a it can be seen that the two main storage condensers C_2 and C_4 are charged up to 100kv (±50kv) while at the same time the trigger condenser C_1 is charged to 100kv (±50kv). The power for the charge is obtained from a Westinghouse Style S.1.M. 982052 power-rectifier supply. Because of shunting resistor R_1, the cathode and cathode shield are equipotential during charging. The tube, therefore, remains inactive until this condition is changed by the generation of a high energy field in the gap.

The initial stages of the breakdown are started by impressing a 12.5 Joule, −50kv* pulse on the cathode shield of the tube. When it appears at the shield it creates a 105kv/cm field in the 0.5-mm cathode gap. At first a field emission spark occurs after which the high concentration of energy in the gap turns the spark into a high current arc. Samples of electrodes from used tubes show the fusing marks which were made at this stage of the discharge. This arc carries a copious supply of electrons which enter the cathode and tend to increase its temperature as well as its negative potential while at the same time it is decreasing the negative potential on the shield. This discharge generates a dense electron cloud or plasma in the vicinity of the cathode which temporarily blocks the main discharge until sufficient preliminary ionization has occurred. It is this electron cloud which is the key to high speed discharges in high vacuums. Its function is similar to that of a pump primer. It supplies the electrons which are consumed in generating photons and positive tungsten ions. These in turn pull secondary electrons from the heated cathode. The secondary electrons produce more photons and ions until the cumulative state is reached and the tube impedance rapidly approaches zero, causing the main discharge to ensue.

Let us return for a moment to view the source of the negative 50kv trigger pulse. Figure 2b shows the trigger generating loop alone. The d.p.d.t. switch is inserted merely to illustrate the operation of the triple sphere gap shown in Fig. 2a. The upward position of the switch places the +50kv charge on the trigger condenser C_1, while the downward position, which in reality occurs by sparking the gap with a 50 kv pulse transformer, throws the positively charged side of C_1 to ground. This results in a rush of electrons up from ground toward the positively charged side of C_1, and in flowing through it generates a negative −50kv drop across it. This is the initial negative pulse which appears at the cathode shield and triggers the tube.

The network composed of C_3, R_2 and L_1 is a low Q-resonant net which changes the resonant frequency of the trigger gap from 2 megacycles to 150 kilocycles. This net is necessary for preventing repeated triggering resulting from certain resonant characteristics in the trigger loop. The successive flashes which accompany repeated triggering cause undesirable repeated exposure of a single film. The function of the net is to shunt the gap with a low Q-resonant circuit having a long cyclical period, thereby delaying trigger repetition until the main discharge is completed. It was necessary to resort to this technique rather than the usual series resistive damping since any series resistance in the discharge loop would diminish the rise time and the energy of the trigger pulse.

Fractional microsecond discharges are not dependent upon preliminary ionization alone. A second factor is also important. This factor, the circuit impedance, is controlled by the internal characteristics of the circuit components, as well as the length of the discharge loop.

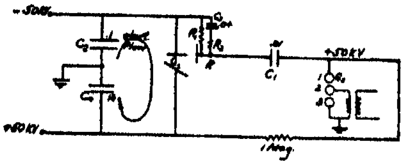

FIG. 2a.

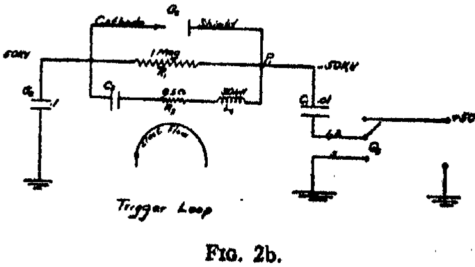

FIG. 2b.

---

* −50 kv with respect to the cathode, −100 kv with respect to the ground.

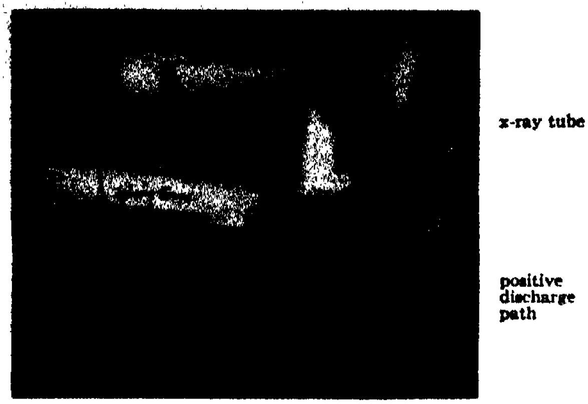

FIG. 3a. Tenth microsecond x-ray pulse generator, right side.

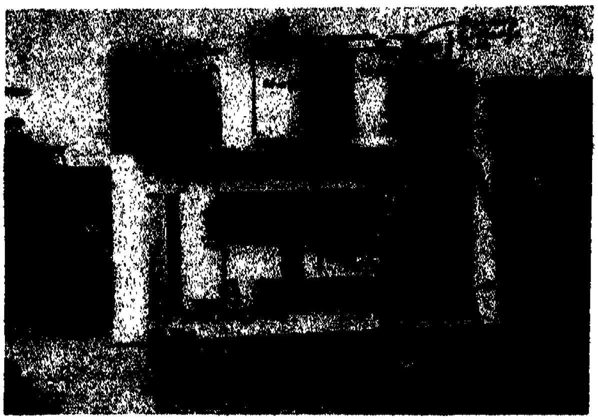

FIG. 3b. Tenth microsecond x-ray pulse generator, left side.

In our case we obtained storage condensers having the lowest internal inductance commercially available. These condensers were Solar type QPX tubulars having 0.3 microhenries. They were mounted as shown in Fig. 3 to give the shortest possible connections, which proved to be about 10 inches from the condensers to the extremities of the tube. This unit, embodying the circuit as described, is currently in use for making fractional microsecond detonation studies.

Figures 4, 5, and 6 show a series of three radiographs of a collapsing copper liner inside the cavity of a "shape charge." In these pictures, the charge was initiated from the left, causing the liners to collapse and form jets in a manner whose technical aspects are fully described in a recent paper by Drs. Birkhoff, MacDougall, Pugh, and Taylor.[10] Much interesting detail is visible in these pictures which has heretofore been obscured by blur.

FLASH TIME MEASUREMENTS

Two methods for measuring the effective duration of the x-ray bursts have been devised.[11] In one method an explosive stick having a known detonation velocity had a 0.002 inch thick by $\frac{1}{32}$ in. wide layer of lead foil cemented to its surface. The stick was detonated and radiographed before the detonation wave reached the end. This procedure yielded a picture of the lead foil being ejected at a measurable angle by the visible detonation front from the surface of the explosive. Figure 7a shows a $\frac{1}{2}$-in. diameter by 4-in. long cylinder of pentolite whose detonation velocity is 7.46 millimeters per microsecond. The detonation front marked by the dark vertical shadow in the stick is moving from left to right down the stick pealing off the lead foil. The sharpness of the angle made by the foil with the surface of the stick and the degree of blurring of the foil near the stick is an indication of the effective duration of the x-ray flash. In this case it appeared to be about 0.2 microseconds. Figure 7b is a radiograph of a similar explosive charge taken with a flash of about 1.5 microseconds duration. Much blurring is visible and the detonation front is completely obscured.

In the second method used, a photo-multiplier radiation detector[12] whose excitation was dependent upon the scintillations of a dyphenylacetylene crystal[13] was connected through a cathode follower to the vertical amplifier on a # 280 Dumont oscilloscope. The circuits used to synchronize the start of the high speed oscillographic time base with the flash of the x-ray tube are printed in a declassified AEC report[14] under the titles of "Neon tube trigger circuit" and "final photo-tube diagram." Our complete timing and synchronizing arrangement consisted of a photo-multiplier chassis similar to that reported by Fitz Hugh Marshall[12] except that a dyphenylacetylene crystal was substituted for his tungstate screen, a 10K anode resistor was substituted for his 1 meg. resistor in the 931A photo-multiplier in order to bring its resolution time constant down to 4×10^{-8} second, and a single cathode follower with high frequency response replaced his amplifier and cathode follower combination. Figure 8 shows the modified circuit, and Fig. 9 illustrates the arrangement of the components. The

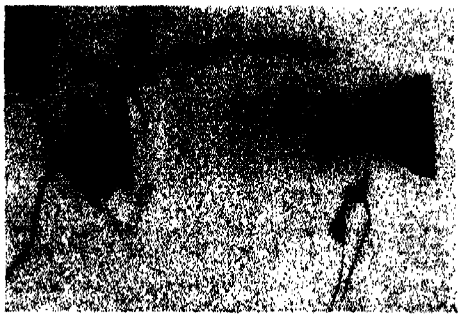

FIG. 4. 68 degree copper cone showing deformation 5 microseconds after detonation wave hit the vertex.

---

[10] Birkhoff, MacDougall, Pugh, and Taylor, J. App. Phys. 19, 563 (1948).

[11] See reference 8, p. 364.

[12] Marshall, Coltman, and Hunter, Rev. Sci. Inst. 18, 504 (1947).

[13] W. J. Koski, Johns Hopkins University, Baltimore, Maryland.

[14] Allen and Hudson, MDDC 447, Oak Ridge, Tennessee.

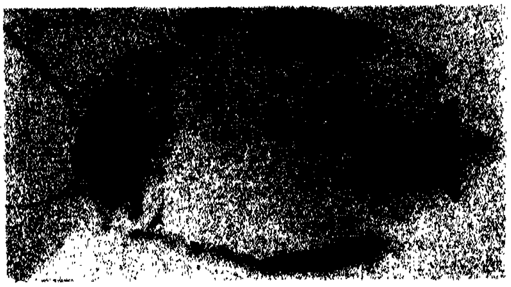

FIG. 5. 68 degree copper cone showing deformation 9.2 microseconds after detonation wave hit vertex.

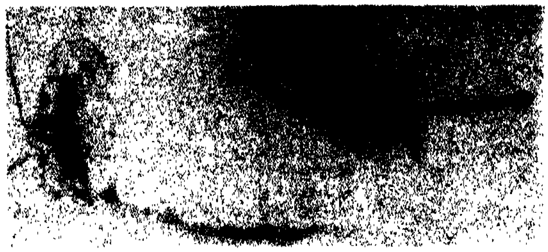

FIG. 6. 68 degree copper cone showing deformation 14.2 microseconds after detonation wave hit vertex. Collapse velocity in all three pictures approximately 1850 meters per second.

FIG. 7a. Pentolite cylinder showing sharp definition of foil strip and detonation wave. Taken with 10^{-7} second exposure.

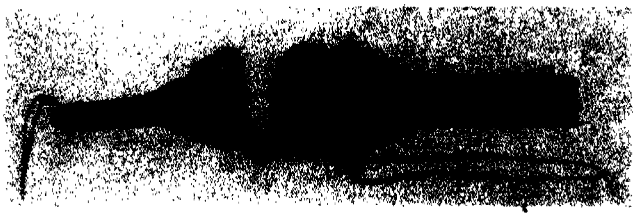

FIG. 7b. Pentolite stick showing blur and repeated exposure. Taken with 10^{-6} second oscillatory flash.

synchronizing and recording circuits were placed in a room apart from the x-ray equipment and all cables were double shielded coax with an outer sheathing of lead on those cables in the vicinity of the x-ray equipment. The photo multiplier and crystal were placed 41 inches from the x-ray tube and a 0.048 inch lead filter was placed between the crystal and the x-ray tube. The filter was necessary to prevent the high energy quanta in the burst from penetrating the crystal and hashing the photo-tube response. In addition to the filtering, it was also necessary to defocus the final dynode by means of the potentiometer shown in Fig. 8. Before these precautions were taken, the photo-multiplier noise was enhanced to such an extent as to obscure the signal produced by the main pulse. Figure 10 shows a picture of one of the many pulses recorded. The time markers are a 5 megacycle sine wave. The pulse rise time is about 0.05 μs, while the decay time is thought to be about 0.4 μs.**

Since the decay time of this crystal has not yet been ascertained, this cannot be considered a conclusive method of measuring the duration of the x-ray burst. It does, however, offer evidence as to the maximum possible time duration of the burst and a reliable means of recording its start.

THREE SUCCESSIVE RADIOGRAPHS

In the past, the inability to obtain more than a single radiograph of a single sample of high explosive was one of the greatest weaknesses of flash x-ray analysis. This shortcoming was a result of the inability to move or change the film quickly enough after each flash rather than to the difficulty of producing a series of flashes through a single tube.

The film and x-ray tubes and design of the blast chamber as shown in Fig. 11 permit the use of three

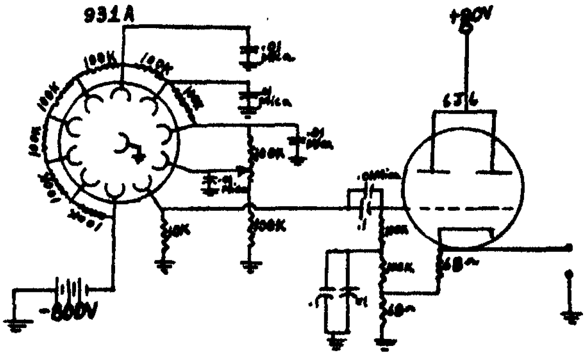

FIG. 8. Photo-multiplier and cathode follower circuit.

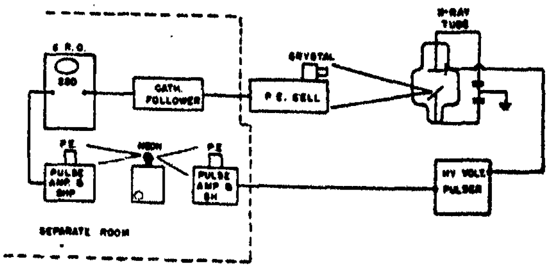

FIG. 9. Block diagram of pulse measuring equipment and x-ray pulse generator.

** Further work on the decay characteristics of this crystal is being undertaken, and it is hoped will be reported by Dr. Koski of Johns Hopkins University in the near future.

FIG. 10. Photo-multiplier pulse generated by x-ray flash on crystal detector. 5 megacycle time markers.

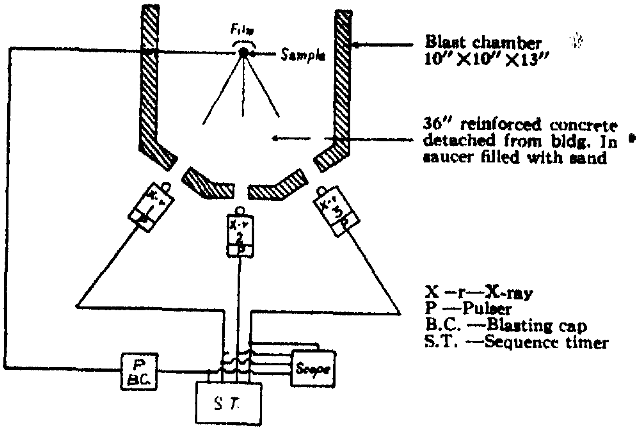
Film
Sample
Blast chamber 10"×10"×13"
36" reinforced concrete detached from bldg. In saucer filled with sand
X-r 1
X-r 2
X-r 3
X–r—X-ray
P—Pulser
B.C.—Blasting cap
S.T.—Sequence timer
P
B.C.
Scope
S.T.

FIG. 11. Blast chamber design and x-ray equipment arrangement as used for successive radiographs of high explosives.

separate films for three separate exposures of a single detonating charge. A lead diaphragm containing a 1.25 centimeter hole is placed between each x-ray tube and the port hole in the blast chamber wall. This allows a small cone of x-rays from each tube to pass into the blast chamber and expose only the film in its path. It is only necessary, therefore, to set a sequence timer at predetermined intervals, press the trigger button and start the four pulses which fire the high explosive charge and then trigger each one of the three x-ray units in their turn, thus obtaining three successive radiographs on separate films of the same sample at pre-set time intervals.

THE REVIEW OF SCIENTIFIC INSTRUMENTS VOLUME 20, NUMBER 12 DECEMBER, 1949

An Air Ionization Chamber for Soft X-Rays*

HERMAN E. SEEMANN
Kodak Research Laboratories, Rochester, New York

(Received July 15, 1949)

An ionization chamber is described which is nearly air-equivalent from 0.5 to 2.5A, "effective wave-length." It has been made adaptable for use with the electrometer and charging system of the Victoreen Minometer. Its sensitivity is of the order of 0.15 roentgen per scale division. Suggestions are made for possible improvements.

IN the course of an experimental study of the spectral sensitivity of x-ray films it became apparent that measurements of the intensity of the x-ray beam could not be made conveniently with commercially available instruments. At the longest wave-length used, 2.3A, the wall absorption of thimble chambers was too high. On the other hand, sensitive thin-walled chambers were so large as to present the geometrical problem of accurately measuring a beam, the cross section of which was small compared with the dimensions of the chamber, as well as the mechanical difficulty of properly placing such units near the x-ray source.

The schematic diagram of Fig. 1 will help to visualize the conditions to be satisfied. Filtered fluorescent x-rays were used to expose the film. Because of their low intensity, the fluorescent radiators had to be as close as practicable to the film and the radiating area had to be as large as possible. The result of efforts in these directions was that the center of the radiating area was about 6 cm from the film and, as viewed from the film location, appeared as a radiating circular disk about 2 cm in diameter. Thus, a quite divergent beam was incident on the film and allowance had to be made for this in the chamber design.

Since considerable work has been done on the design of both the standard air ionization chamber[1] and instruments intended for routine measurements in international roentgens, it seemed reasonable to proceed with the construction of a suitable chamber for this work. In order to meet the special requirements of our problem, compromises had to be made with well-established principles, but it was obvious that only by testing the finished instrument would it be known

---

* Communication No. 1270 from the Kodak Research Laboratories.

[1] L. S. Taylor and G. Singer, Bur. Stand. J. Research 5 (RP 211), 507 (1930). L. S. Taylor and C. F. Stoneburner, Bur. Stand. J. Research 9 (RP 505), 769 (1932).

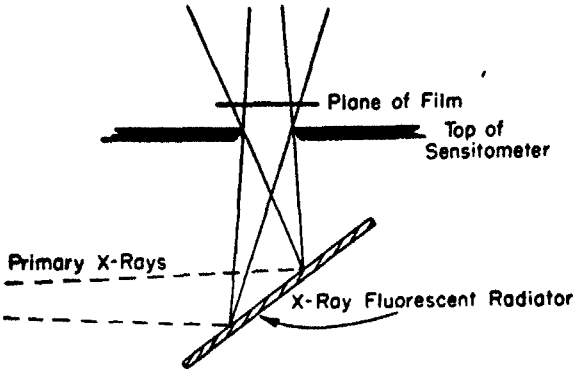

FIG. 1. Diagram showing conditions to be met by the ionization chamber described. The instrument was designed to measure divergent x-rays in the plane of the film.

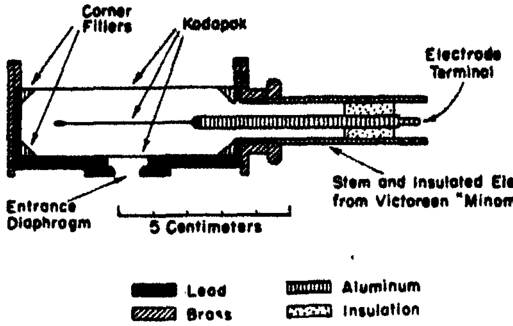

FIG. 2. The larger of the two ionization chambers, shown in section.

whether we had gone too far. In other words, it appeared likely that we could arrive more quickly at a satisfactory solution by constructing an instrument and testing it than by setting up the apparatus necessary to study the exact limitations of each principle involved in the design.

It was decided at the outset to try to adapt the ionization chamber for use with some commercially available electrometer and charging system. This part of the Victoreen Minometer[a] was chosen, since it is a simple and sufficiently accurate system. All that was necessary was to remove the insulated electrode and sleeve from the 0.01-roentgen chamber of a Minometer and build it as an integral part of the special chamber. Thus, the new chamber could be charged and its discharge read, using the Minometer in the way it is normally used with the chambers furnished by the manufacturer.

In the course of tests to determine the characteristics of this type of chamber, two chambers were built. The second and larger is shown in section in Fig. 2 and a photograph of it in the charging position in Fig. 3. The lead entrance diaphragm limits the x-ray beam to a diameter of 0.8 cm. The windows and electrode were made of Kodapak I,[b] 0.0022 cm thick, and were painted with India ink to render them conducting (see Notes on Construction). It will be noted that the metal ring of the electrode and the emergence window are both of large diameter to allow for the great divergence of the x-ray beam, as indicated in Fig. 1. Kodapak coated with India ink represents the culmination of tests to find a suitable conducting window material of approximate air-equivalence. One material which was tried out and may still have some applications in air ionization chambers is a fine silk netting, Silk Illusion No. 508, which was obtained from the David Dubin Company, New York. This material was sprayed with a suspension of Aquadag[c] in water after mounting. The water shrank the netting and, when dry, the netting was under sufficient tension to prevent sagging even under conditions of high humidity. Uncoated Silk Illusion No. 508 has a mass of 0.63×10^{-3} g/cm^2 (compared with 3.2×10^{-3} g/cm^2 for the uncoated Kodapak) and, since it consisted mostly of holes (!), it appeared to be a very desirable material from the standpoint of x-ray absorption and approximate air-equivalence. There were about six openings per centimeter. (Quimby[2] and her co-workers constructed a chamber using fine silk net impregnated with India ink.) Erratic readings were obtained when this netting was used and the evidence suggested that air currents prevented the collecting of ions at a constant rate, since no such trouble was experienced when both windows were closed with Kodapak.

Another serious difficulty arose from recording a very soft radiation emitted by the edge of the front entrance diaphragm which was, of course, almost completely transmitted by the netting. For experimental tests of this condition, an auxiliary limiting diaphragm was set up in front of the chamber and readings were taken at various separations and for 40- and 90-kvp x-rays emitted by a tungsten target tube.

Since the secondary radiation from the diaphragm was negligible at a large separation (inverse-square law), this procedure enabled us to distinguish between ionization originating in the air volume proper and that caused by the diaphragm. At 90 kv, the effect was much greater than at 40 kv and accounted for more than one-half the total radiation recorded by the instrument!

Tests at these two kilovoltages gave further support to the idea that emission from the edge of the lead diaphragm was responsible, since secondary effects increase rapidly with kilovoltage. One layer of Kodapak attached to the emergence side of the diaphragm reduced the effect to about six percent, but an additional layer made no further change. It seemed reasonable to conclude that the emission from the lead diaphragm consisted mostly of photo-electrons with probably a small amount of characteristic and scattered x-rays. Although the *total energy* of these photo-electrons must have been very small compared with the energy in the x-ray beam, they are so much more strongly absorbed in air that their ionizing effect was comparable to that of the entering x-rays.

---

[a] Made by the Victoreen Instrument Company, 5806 Hough Avenue, Cleveland, Ohio.

[b] Kodapak I is a wrapping material made by the Eastman Kodak Company. It consists of cellulose acetate and a plasticizer.

[c] A colloidal dispersion of graphite in water, made by Acheson Colloids Corporation, Port Huron, Michigan.

[2] Quimby, Lucas, Arneson, and MacComb, Radiology 23, 743 (1934). Improvements are indicated in a later paper, viz., E. H. Quimby and E. F. Focht, Am. J. Roentgenol. 50, 653 (1943).

The obvious way to get rid of effects from the limiting diaphragm is to mount it on the end of a tube extending a short distance in front of the chamber.[d] This arrangement could not be used for our experiments, however, because of the divergence of the x-ray beam, as shown in Fig. 1. For uses where the x-rays are more or less collimated, a projecting diaphragm should be attached and conducting silk netting might then be found satisfactory over the entrance to the chamber proper and on the electrode, but the large emergence window should be covered with Kodapak to stop air currents. If a chamber of this design were constructed for use with collimated x-rays, a projecting diaphragm and the use of netting should make its spectral response more nearly like that of the standard air chamber.

This chamber is much more sensitive to radiation coming from the rear than to that incident on the front, simply because the rear diaphragm is so much larger than the entrance diaphragm. Therefore, in actual use, precautions should be taken against *back-scattered* radiation, since its intensity will be exaggerated.

SATURATION

One of the first considerations in the design of an ionization chamber is to make sure that saturation conditions prevail for the ionized region and for the radiation intensities to be measured. Tests of the National Bureau of Standards chamber[1] indicate that a minimum field strength of about 60 v/cm is required. Tests of the electrometer of the Victoreen Minometer showed that, when fully charged, the potential difference was 153 v and when the fiber was at the end of the scale it was 112.5 v. The relation between scale readings and voltage was accurately linear. By using a very steady source of x-rays, it was then possible to test for saturation, since *scale readings (i.e., potential) should be directly proportional to the time of exposure.* Actually, the readings showed a slight falling off from strict proportionality, the difference being just detectable at the middle of the scale and increasing to five to seven percent at full scale. This was interpreted as indicating a lack of saturation. The smaller chamber (see Fig. 3) was the first one built, and the distance from electrode to windows was about 1.2 cm and the inside diameter of the case was 4.3 cm. Even with fillers in the corners, the apparent lack of saturation persisted and it was concluded that the "fringing" of the electric field between the electrode and the case might still be sufficient to give an intensity well below 60 v/cm in the ionized region, particularly near the discharge end of the scale.

This difficulty was the primary consideration leading to the construction of the larger chamber, the dimensions of which were made decidedly more favorable for saturation, but the lack of proportionality in the scale readings still persisted. Since the electrode-to-window spacing was now about 1 cm, the field strength would be 76 v/cm (ideally) at the discharge end of the scale or somewhat more than necessary for saturation. (Tests had shown that a full-scale reading on the *electrometer* was given by a potential of 76 v on the *ionization chamber*. The corresponding value for the small chamber was 67 v.) The lack of proportionality between scale readings and time of exposure seemed to be independent of the radiation quality, and this was surprising since there should be more ionization extending into the weaker parts of the field with hard radiations, because of the greater range of the photo-electrons. However, in view of the difficulty of detecting *changes in an error*, especially for an instrument with only ten scale divisions, some radiation quality effect may yet be found.

The normal procedure for use of the Victoreen Minometer consists in charging the chamber, indicated by the reading of "0" on the scale, then removing the chamber to expose it to x-rays, and finally reconnecting it to the electrometer and noting the scale reading. Thus, when the electrometer and the partially discharged ionization chamber are connected, they may be considered as two capacitances, C_e and C_i, at potentials, V_e and V_i, respectively, which share their charges, resulting in a final potential of V for the system. The

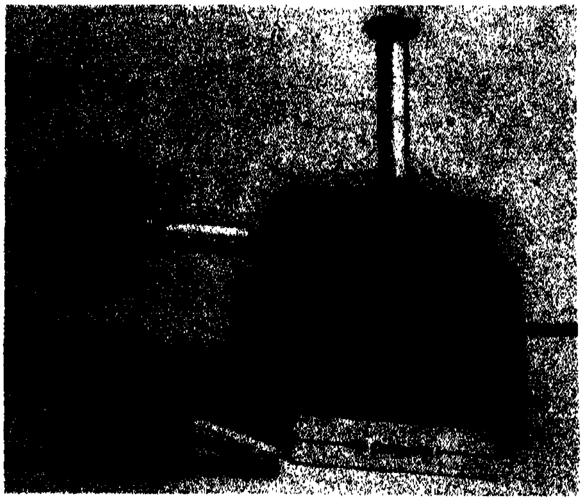

FIG. 3. Both ionization chambers, with the larger in the charging or reading position on the Minometer electrometer.

---

[d] This distance need not be great, since the mass of a square centimeter of the Kodapak was 3.2×10^{-3} g and thus was equivalent in electron absorption to the same mass per square centimeter of air. The corresponding distance through air is about 2.7 cm. The minimum distance between the diaphragm and the effective ionized volume in the National Bureau of Standards soft x-ray chamber is about 5 cm and thus utilizes air absorption and the inverse-square law to get rid of secondary radiations from the diaphragm.

charge, Q_x, lost from the chamber by x-ray ionization, is $C_i(V_e-V_i)$. The position of the electrometer fiber indicates a potential change, V_e-V, and, since this can be proved equal to $[C_i(V_e-V_i)]/[C_i+C_e]$, the readings are *proportional* to the charge lost by ionization. It is also true that $Q_x=(C_i+C_e)(V_e-V)$. Therefore, the instrument can be calibrated to read in roentgens. Since the principle of operation of the Minometer is on a sound basis, the need for a scale correction must arise from a lack of saturation.

CALIBRATION

Both the small and the large chambers were calibrated against the large standard chamber at the National Bureau of Standards. The standard chamber for low voltage x-rays was not available at the time so that a correction was applied to the readings of the large standard to allow for the air absorption between its diaphragm and its measured volume. The scale correction previously discussed was applied to readings of the Minometer and the calibration was expressed for a temperature of 22°C and a barometric pressure of 760 mm of mercury. Results are shown in Fig. 4. There may be some difference of opinion on the best unit for the abscissa scale. However, since continuous-spectrum x-rays were used and the filtration was increased with the kilovoltage, there is no truly adequate designation for the wave-length scale. In the lower kilovoltage range, no filter was used and the "effective wave-length" was taken to be 1.5 λ_0, since the wave-length of maximum energy, λ_m, is about 50 percent greater than the short wave-length limit, λ_0. The effective wave-lengths, λ_{eff}, for filtered rays were obtained from the slopes of their absorption curves in aluminum at the aluminum thicknesses used. Table I is a summary of the conditions used. The uniformity of response of both chambers is fairly satisfactory between 0.4 and 2.5A and they have quite similar characteristics. If this region were represented by a straight line parallel to the wave-length axis, no datum point would miss it by more than four percent. There is a slight loss in sensitivity in going toward longer wave-lengths, probably caused by the increasing absorption of the window and the electrode. The rapid increase in sensitivity at less than 0.5A may be caused by fluorescent and scattered x-rays from the edge of the lead diaphragm. (The K fluorescence of lead is excited at 87.6 kv and the point at $\lambda_{eff}=0.36$A was obtained with filtered 90-kv radiation.) Because of the increasing range of photo-electrons with decreasing wave-length, the walls of the chambers may be limiting the air ionization at the same time that lead fluorescence is increasing it, the latter perhaps becoming the greater factor.

Another factor, which we did not consider, is the possible influence of photo-electrons from the inside walls of the chamber. These would be excited by the x-rays scattered from the electrode and the air volume when the wave-length is short enough. The chamber might be used at shorter wave-lengths than originally intended if a cellulose layer or one of thin aluminum were used as a lining to absorb photo-electrons from the lead. Experiments reported by Hase and Küstner,[3] but not noted until this work was completed, show a considerable effect depending upon the wall material and suggest the possibility of compensating for the increase due to photoelectric ionization by a suitable restriction of the chamber volume. Certainly this idea has enough merit to justify further experimentation. The use of fairly homogeneous x-rays, such as the filtered K fluorescence of some of the elements, for calibrating experimental chambers would be of considerable advantage, since departures from air-equivalence would

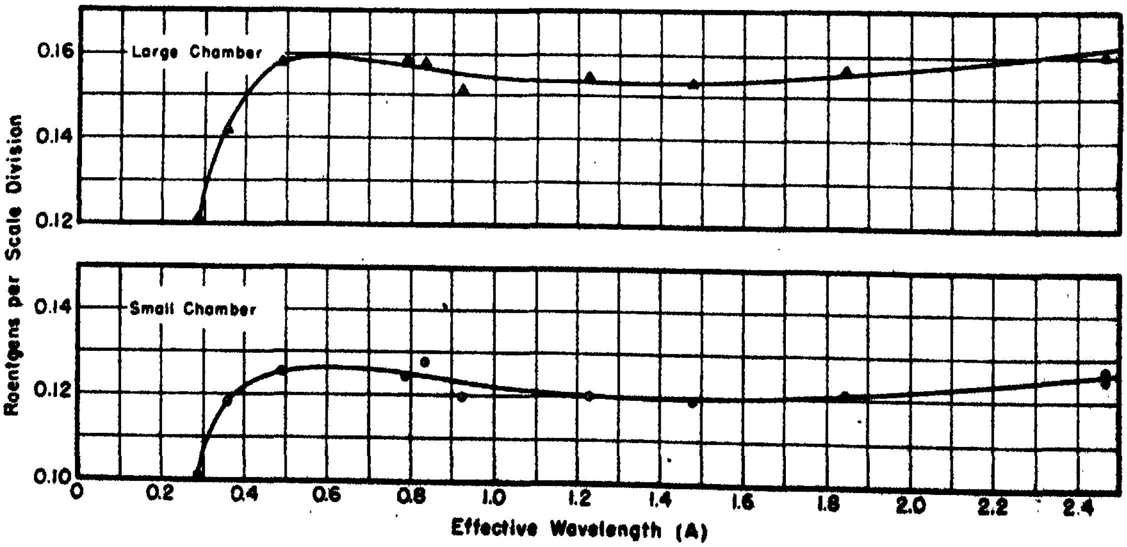

FIG. 4. Calibration curves for the ionization chambers. Full scale of the instrument is ten divisions.

---

[3] H. Hase and H. Küstner, Physik. Zeits. 39, 737 (1938).

be better "resolved" than with the filtered continuous spectrum and, therefore, indicate the cause more definitely. There are obvious difficulties, of course, but they might be overcome.

NOTES ON CONSTRUCTION

The Kodapak membranes were cemented to their metal supports with cellulose cement. Duco Household Cement or the cements used in the construction of model airplanes would probably serve just as well. A thin coating was first applied to the metal, which was then placed on a sheet of Kodapak lying on a flat metal surface. The sheet was held flat by weights but was under practically no tension.

Attempts to apply Aquadag or India ink by spraying were unsuccessful because the carbon tended to pile up in small "islands." The addition of wetting agents made little improvement. It was found that a coating of India ink which appeared to be continuous could be applied with a wad of cotton and was reasonably uniform. Dilution of the India ink with water in about 1:1 ratio was an aid in avoiding too thick a coating. Sufficient conductivity is obtained with very little carbon—a layer which obviously transmits some light is quite adequate.

Kodapak does not absorb much moisture but the coating of ink made it wrinkle. When dried, it was smooth and under appreciable tension. It remained flat during all but the most humid summer days, returning to flatness when the humidity dropped.

Since the use of fine netting, such as Silk Illusion No. 508, may be better in certain applications, some of its properties will be mentioned. It is very readily wetted by water and spraying with a water suspension of Aquadag was entirely successful. It expands when wet but shrinks to a good tension when dry. Spraying with an artist's air-brush is a convenient way to apply Aquadag but, because of the fineness of the netting fibers, estimation of the degree of coverage is difficult. If a sheet of white cardboard is placed behind the gauze during spraying, the rate of blackening will give some indication of the coating on the fibers. So little graphite is required for adequate conductivity that a good gray on the cardboard is sufficient.

It may be noted that a possible objection to the use of conducting netting is that it does not limit the electric field, as does a continuous conductor, but gives it a kind of tufted boundary. During discharge of the system, therefore, a small change takes place in the *effective* ionized volume because the boundary where *saturation* field strength exists moves. This effect might be negligible for the chambers described here and for fine netting, but could be large for the case of a relatively thin chamber, in which the netting forms a large proportion of the boundary of the ionized volume. A scale correction could be determined in the manner suggested for the saturation correction.

TABLE I.

Bureau of Standards conditions and results				"Wave-lengths"		
Kilo-volts*	Aluminum filter, centimeters	Roentgens per scale division, large chamber**	Roentgens per scale division, small chamber**	λ_0 angstroms	λ_m angstroms	λ_{eff} angstroms
7.5	0	0.1596	0.1242	1.65	2.47	
10.0	0	0.1565	0.1208	1.23	1.85	
12.5	0	0.1532	0.1188	0.99	1.48	
15.0	0	0.1545	0.1201	0.82	1.23	
20.0	0	0.1515	0.1196	0.62	0.92	
30.0	0.05	0.1574	0.1276	0.41		0.83
45.0	0.05	0.1584	0.1245	0.274		0.79
60.0	0.20	0.1580	0.1255	0.206		0.49
90.0	0.40	0.1419	0.1182	0.137		0.36
120.0	0.60	0.1209	0.1011	0.103		0.29

* Electrically filtered to give constant potential. Tungsten target tube with 1.5-mm beryllium window.

** The scale factor is believed to be in error by not more than ±2 percent.

The limiting diaphragm fits in guides and may be removed for insertion of other diaphragms (see Fig. 3). We have had no occasion to use more than one size.

The collector electrode consists of two thin metal rings with rounded edges, between which the Kodapak was cemented. A hole drilled in the ring permits it to be held by a small screw in a jaw filed into the end of the electrode stem. A locknut on the electrode stem is tightened so as to hold the electrode ring parallel to the chamber windows. This locknut is the knurled ring shown in Fig. 3.

The lead lining of the cylindrical part of the chamber is spot-soldered to the brass at a few points. The front lead plate rests against this lining and is held in place by three setscrews bearing against it through the brass wall. Similarly, the rear window frame of brass bears against the lead lining and is held by setscrews.

ACKNOWLEDGMENTS

It is a pleasure to acknowledge helpful suggestions made by J. A. Victoreen. Courtesies extended by L. S. Taylor and F. H. Day, at the National Bureau of Standards, are also greatly appreciated.

THE REVIEW OF SCIENTIFIC INSTRUMENTS VOLUME 20, NUMBER 12 DECEMBER, 1949

Instrument for Measurement of X-Ray Diffraction Patterns

JOHN A. BENNETT
National Bureau of Standards, Washington, D. C.

(Received July 13, 1949)

An instrument is described for measuring x-ray back reflection patterns for surface stress determinations. The chief feature of the apparatus is a curved slit in the optical system so that the beam of light which scans the diffraction ring is an arc having the same radius of curvature as the ring. This simple, inexpensive instrument has been found to be at least as precise as a microphotometer for these measurements and its use has resulted in a considerable saving of time. It is suggested that the instrument might appropriately be called a photomicrometer.

I. INTRODUCTION

In the determination of surface stress in metals by means of x-ray diffraction, the diffraction angle must be measured very accurately in order to achieve reasonable precision in the stress values. The technique used at the National Bureau of Standards for making these determinations was described in a previous publication.[1] Since the publication of this report, an instrument for measuring the diffraction patterns has been developed which has several advantages over the commercial microphotometer used previously.

The primary difficulty encountered in the x-ray measurement of stress or strain in metals is the lack of sensitivity. The diffraction angle is determined by measurement of two legs of a right triangle, R and S, where R is the radius of the diffraction ring on the film and S is the specimen-to-film distance. The lack of sensitivity is due to the small change in diameter of the diffraction ring (with change in stress) combined with the diffuseness of the ring itself. With a steel specimen, for example, the width of the ring (at a specimen-to-film distance of 60 mm) at half-maximum intensity is about 1 mm; a change in radius of 1 mm (even at the position of maximum sensitivity relative to the applied stress) represents a stress change of more than 60,000 psi. This condition is improved somewhat by making two patterns, one with the beam normal to the surface of the specimen and the other with the beam incident at 45°, but the need for accurate measurement of the ring radius is still apparent.

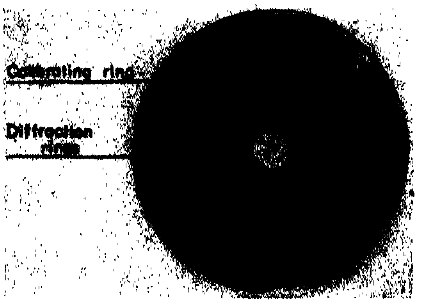

FIG. 1. Typical film used in surface stress determination. The calibrating ring is formed by exposure to the direct x-ray beam, the inside diameter being the shadow of a brass disk of known diameter.

Many investigators have measured the patterns visually, using a vernier film scale to obtain readings to 0.1 mm. In preliminary experiments with this method of measurement it was found that the readings could not be duplicated within 0.1 or 0.2 mm. For this reason, until recently, the measurements were made on a Knorr-Albers recording microphotometer. All of the data reported in reference 1 were obtained using this instrument, and it is doubtful that much more precise data could have been obtained from these patterns. However the use of this instrument had two disadvantages; the first was that the microphotometer, as its name indicates, scanned only a narrow sector of the ring. This scanning resulted in a jagged record on the chart, probably because of the graininess of the photographic emulsion. It is more difficult to determine the location of the maximum on such an irregular curve than it would be on a smooth curve. The second disadvantage in the use of the microphotometer was the time required to obtain measurements.

The instrument described in this paper was designed with a view to eliminating the above disadvantages without decreasing the accuracy obtained with the microphotometer. The method of making measurements of the diffraction angle (described more fully in reference 1) involves measuring the specimen-to-film distance, recording a calibrating ring of known inside diameter concentric with the diffraction ring (Fig. 1) and measuring the distance between the diffraction ring and the edge of the calibrating ring. It is this latter measurement which is made with the apparatus being described.

II. DESCRIPTION OF THE INSTRUMENT

A line sketch of the chief parts of the instrument is shown in Fig. 2. It consists essentially of a light source, slit, lens, film carrier, measuring and compensating photo-cells. The parts of the optical system are mounted in a standard 2-in.×2-in. slide projector in which the lens has been replaced by a 24-mm microscope objective. The slit is mounted in the slide carrier and the image of the slit is focused on the film with a reduction of five to one. This type of optical system has been used frequently in densitometers, for example, that described by Milligan.[2]

---

[1] J. A. Bennett and H. C. Vacher, "Calibration of the x-ray measurement of strain," J. Research Nat. Bur. of Stand. 40, 285 (1948).

In order to utilize all of the exposed portion of the diffraction ring in determining its dimensions, the scanning spot of light must have nearly the same radius of curvature as the ring. It is possible to satisfy this condition using only one slit because all of the patterns taken in the course of stress measurements on a particular specimen are exposed with nearly the same specimen-to-film distance, and the variation of ring diameter with stress is small. For the conditions of measurement, that is steel specimens, cobalt $K\alpha$-radiation, and film-to-specimen distance of 60 mm, the ring radius always approximates 20 mm. The curvature of the slit was chosen to give a reduced image on the film having a radius of 20 mm and an arc length of 15°. This length was chosen because in the technique used, readings were taken at 30° intervals around the ring and the amplitude of film oscillation was 7½°. Thus by scanning a 15° arc, all of the reflections have some effect on the result, but there is no overlapping between adjacent readings.

After passing through the film, the light is received on a barrier layer photo-cell. This cell is connected in the circuit shown in Fig. 3; the compensating cell receives its light directly from the bulb through a small hole in the top of the lamp housing. The amount of light reaching the compensating cell may be varied by rotating the adjusting screen (made from a piece of window screen of the sun-deflecting type) in front of the cell. All parts of the optical paths are covered with light shields to eliminate the effects of extraneous light.

The galvanometer has both a pointer and a light beam index, the latter having twelve times the sensitivity of the former. The galvanometer characteristics are as follows:

Coil resistance—1000 ohms;
Sensitivity—0.014 μa/mm;
Period—2.1 seconds;
External critical damping resistance—3200 ohms.

The resistance of 2000 ohms across the galvanometer gives a slightly over-damped condition which provides the most convenient operation.

The film carriage consists of the film holder described in reference 1 mounted on a cross slide moved by a rack and pinion. The knob shown at the left in Fig. 2 is used to traverse the film carriage, the movement of which is measured on a dial indicator calibrated in hundredths of a millimeter.

In order to determine the optimum width of slit for finding the location of maximum density of the diffraction ring, a series of slits was made up having different widths. It was found that a slit which gave an image on the film ½ mm wide resulted in the best combination of sensitivity and sharpness of the peak. Figure 4 shows the galvanometer deflections obtained as the K alpha-lines on a typical pattern were scanned with a slit of this width. It will be seen that the location of the maximum is quite sharp, and reproducibility of 0.01 to 0.02 mm is found experimentally.

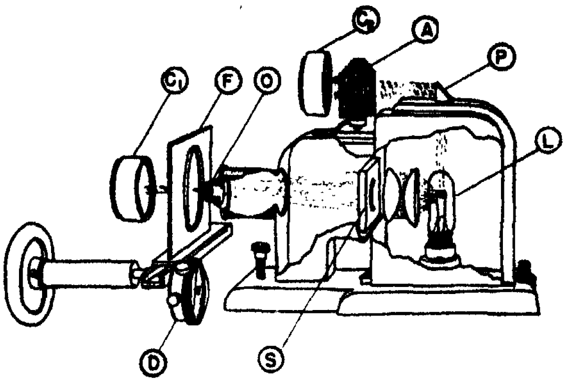

FIG. 2. Parts are identified on the sketch as follows: (L) light source, (S) slit, (O) 24-mm microscope objective, (F) film holder, (C₁) measuring photo-cell, (D) dial indicator, (P) prism, (A) adjusting screen, (C₂) compensating photo-cell.

As the radius of the calibrating ring is about 5 mm greater than that of the diffraction ring, the image of the slit does not fit the former. However, the density of the calibrating ring is nearly constant for several millimeters adjacent to its inner edge, so the edge is located as follows: The galvanometer reading is noted when the light beam is all on the calibrating ring and again when the beam is all inside the edge. The location of the edge is taken as the point where the galvanometer reading is midway between these two. The point located in this way is actually 0.01 mm outside the actual edge of the calibrating ring, but this difference is of no consequence as it is constant for all measurements.

III. RESULTS

In order to compare the precision of measurements made with this apparatus with the precision of those made previously with the microphotometer, the data from ten patterns, five of which had been measured with each instrument, were analyzed. The patterns were selected at random but all were obtained from two steel specimens which were identical as to composition and treatment. Measurements of the distance from the diffraction ring to the calibrating edge had been made at 30° intervals on each pattern, and the com-

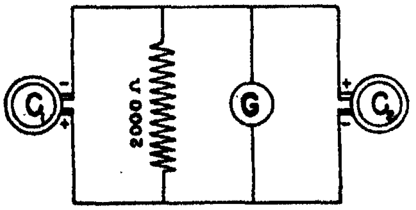

FIG. 3. Compensating type photo-cell circuit. C₁ is the measuring cell, C₂ the compensating cell.

---

[2] W. O. Milligan, "Recording photodensitometer for x-ray powder photographs," Rev. Sci. Inst. 4, 496 (1933).

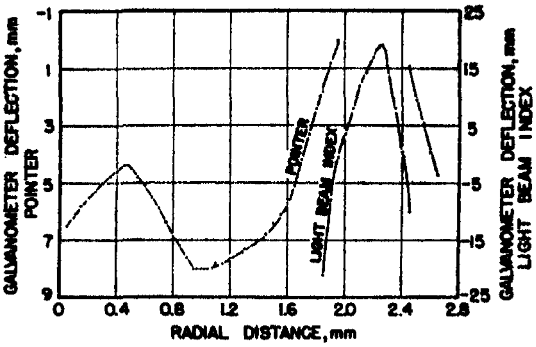

FIG. 4. Galvanometer deflections obtained as the CoKα-lines from a steel specimen were scaned.

parison was made using the standard deviation, σ,[3] for these twelve values. There was some overlapping of the values, but the average σ for the patterns measured with the microphotometer was 0.09 mm while that for the patterns measured with the new instrument was 0.07 mm. This is believed to be adequate evidence that the precision of the measurements with the new instrument is as good as that obtained with the microphotometer.

In order to determine whether or not there was a systematic difference between the measurements made by the two methods, three patterns were measured with both instruments. The data were analyzed by the methods described in reference 1 to obtain a single value from the twelve readings on each pattern. The differences between the values obtained from the microphotometer and the new apparatus were 0.06, 0.03, and 0 mm, respectively. These differences were not considered significant.

The time required to complete a set of observations with this apparatus is materially less than on the microphotometer, the saving being about 25 percent which represents 15 or 20 minutes per pattern. In addition, the apparatus is very simple so that virtually no time is required for maintenance.

Figure 5 shows typical results obtained with this apparatus in an investigation now underway at the National Bureau of Standards. A loading jig is arranged to apply a bending moment to a cylindrical steel specimen by means of a calibrated spring. The diffraction patterns were taken while the specimen was stressed and the tangent of the diffraction angle, θ, plotted against the bending moment. For comparison with data plotted in terms of stress, it may be noted that a maximum bending moment of 40 in./lb. corresponds to approximately 30,000 lb./in.^{2} stress in the surface of the specimen, and the total vertical height of the graph represents a change of ring radius of 0.84 mm at a specimen-to-film distance of 60 mm.

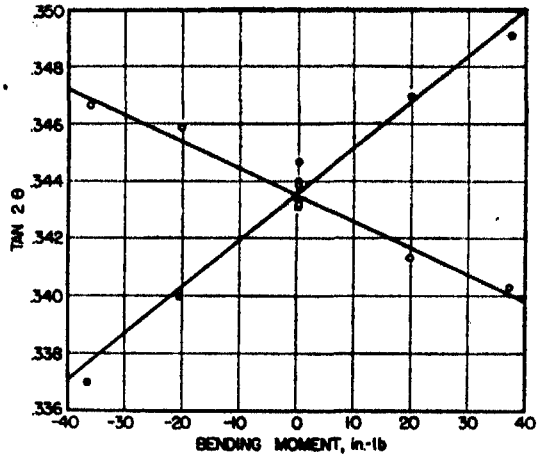

FIG. 5. Change in diffraction angle with the bending moment applied to a steel specimen.

IV. CONCLUSIONS

With the instrument described for measuring x-ray back reflection patterns it is possible to obtain at least as good precision as with a Knorr-Albers microphotometer. Furthermore the measurements can be made more rapidly. It appears to be the simplest and least expensive apparatus available for making these measurements with the necessary precision. The instrument might appropriately be called a photomicrometer.

While the instrument was designed primarily for stress determination work, it should also be useful for other laboratory measurements.

---

[3] *A. S. T. M. Manual on Presentation of Data* (American Society for Testing Materials, Philadelphia, 1947), p. 15.

THE REVIEW OF SCIENTIFIC INSTRUMENTS VOLUME 20, NUMBER 12 DECEMBER, 1949

Circuit for Rapid Determination of Resolving Power and Other Characteristics of Coincidence-Systems

H. DE WAARD
Natuurkundig Laboratorium der Rijks-Universiteit te Groningen, The Netherlands

(Received August 3, 1949)

A simple device is described in which pairs of pulses are produced that are moved continuously with respect to each other (wobbled) by an a.c. voltage that also sweeps an oscilloscope spot horizontally. The pulses are applied to both inputs of a coincidence system. Vertical deflection of the c.r. scope spot is caused by the output pulses of the system. Thus various characteristics can be made visible and the resolution can be read from the scope screen at a glance. With the instrument resolving powers from 3.10^{-6}–10^{-9} sec. approx. can be determined. The apparatus was calibrated by feeding the wobbling pulses into a radio receiver. The output of the receiver has a sharp minimum when the pulse distance (Δt) satisfies the condition $\Delta t=(1+2n)/2\nu$ where n is an integer, ν is the frequency to which the receiver is tuned.

INTRODUCTION

THE resolving power (τ) of a coincidence counting system is often derived from the number of chance coincidences recorded.[1,2] If there are two input terminals to which counters (1) and (2) are connected, counting an average of N_1, N_2 pulses per second, respectively, as a result of irradiation by photons or nucleons (while care is taken that no "coherent" particles or one single particle activate both counters), the average of the number of recorded "chance" coincidences per second is

$$N=2N_1N_2\tau. \tag{1}$$

From a value of τ determined by this formula a correction may be obtained for coincidence counts with different rates N_1 and N_2 and possibly with other counters by subtracting the number of chance coincidences. This method was probably applied for the first time by Dunworth.[3] As he remarked it can certainly be used when the apparatus is constructed in such a way that:

Within wide limits the resolving power (τ) is independent of

$$\begin{array}{l}(\alpha)\ N_1 \text{ and } N_2\\ (\beta)\ \text{form and size of the counter pulses.}\end{array} \tag{2}$$

Also for this reason in coincidence-counting systems size and form of the pulses are often standardized before they reach the coincidence mixing stage. This is accomplished for instance by the use of differentiating circuits[2] or triggered blocking oscillators.[1,4] Using these methods the pulse width may be made much smaller resulting in a better resolution. This can only be done when the resolving time is long compared with the fluctuation in the time-lag between passage of a particle through the counter and the resulting voltage pulse reaching a value sufficient to drive the coincidence system. Otherwise, real coincidences will also be lost.[3] This procedure is followed when gas-filled counters are used either in their Geiger or in their proportional regions and may also be used with crystal counters. Photo- or electron multipliers give very short pulses themselves. These counters may be connected directly to the coincidence mixing state.[5,6] Here the resolving time largely depends on the width of the pulses, and condition (2β) is not fulfilled. Nevertheless the relation (1) can be used to determine the average of τ and with it the chance coincidence rate in another experiment as long as condition (2α) is fulfilled and the *average* width of the counter pulses remains the same.

The greater the fraction of chance coincidences N of the total count, the more accurately τ must be determined to maintain the same accuracy in the number of real coincidences which is found by subtracting N. It is not always possible to keep N small compared with the number of real coincidences by improving the resolving power because the number of real concidences recorded also decreases when τ is made smaller than a certain value, especially with G-M counters (dependent on the construction of these).[2] So it may be necessary to evaluate τ with some degree of accuracy. Often the number of pulses per second a counter may give is

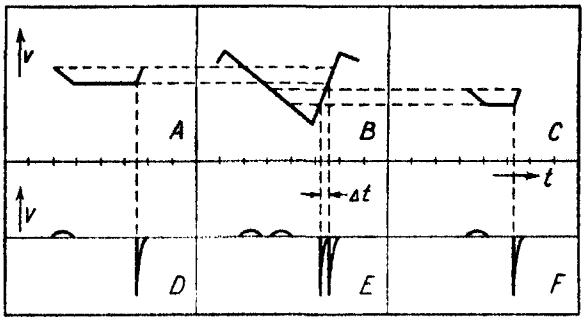

FIG. 1. Pulses (not to scale) at different points in the instrument. A. "Slice" cut out of sawtooth by V_2. B. Sawtooth produced by V_1. C. "Slice" cut out of sawtooth by V_3. D. Output at terminal A. E. Combined output at terminals A and B. F. Output at terminal B. (Fig. 2 shows meaning of letters.)

---

[1] H. L. Schultz and E. Pollard, Rev. Sci. Inst. 19, 617 (1948).
[2] H. Bradt and P. Scherrer, Helv. Phys. Acta 16, 251 (1943).
[3] J. V. Dunworth, Rev. Sci. Inst. 11, 167 (1940).
[4] H. L. Schultz and R. Beringer, Rev. Sci. Inst. 19, 424 (1948).
[5] Z. Bay and G. Papp, Rev. Sci. Inst. 19, 565 (1948).
[6] R. H. Dicke, Rev. Sci. Inst. 18, 907 (1947).

limited and then the determination of τ may require a considerable time. When, for instance, our system has $\tau=10^{-7}$ sec. and we wish to know τ within 10 percent while we must keep N_1 and $N_2<400$ sec.$^{-1}$, this means that the determination of τ takes about an hour. Thus it is impossible to see if by some instability of the circuit τ fluctuates in intervals of time shorter than an hour. Also it is difficult to make sure that τ is really independent of N_1 and N_2 because for lower counting rates the time required to evaluate τ gets even much longer. Yet another difficulty lies in the condition that one particle shall not activate both counters, necessitating a careful placing of counters and radioactive sources not always compatible with practical conditions. (When electron or photo-multipliers are used the rates N_1 and N_2 can be made much higher, so here the time required to evaluate the resolving power will be much shorter).

To avoid these difficulties sometimes a different method is used to determine τ. At a suitable spot in

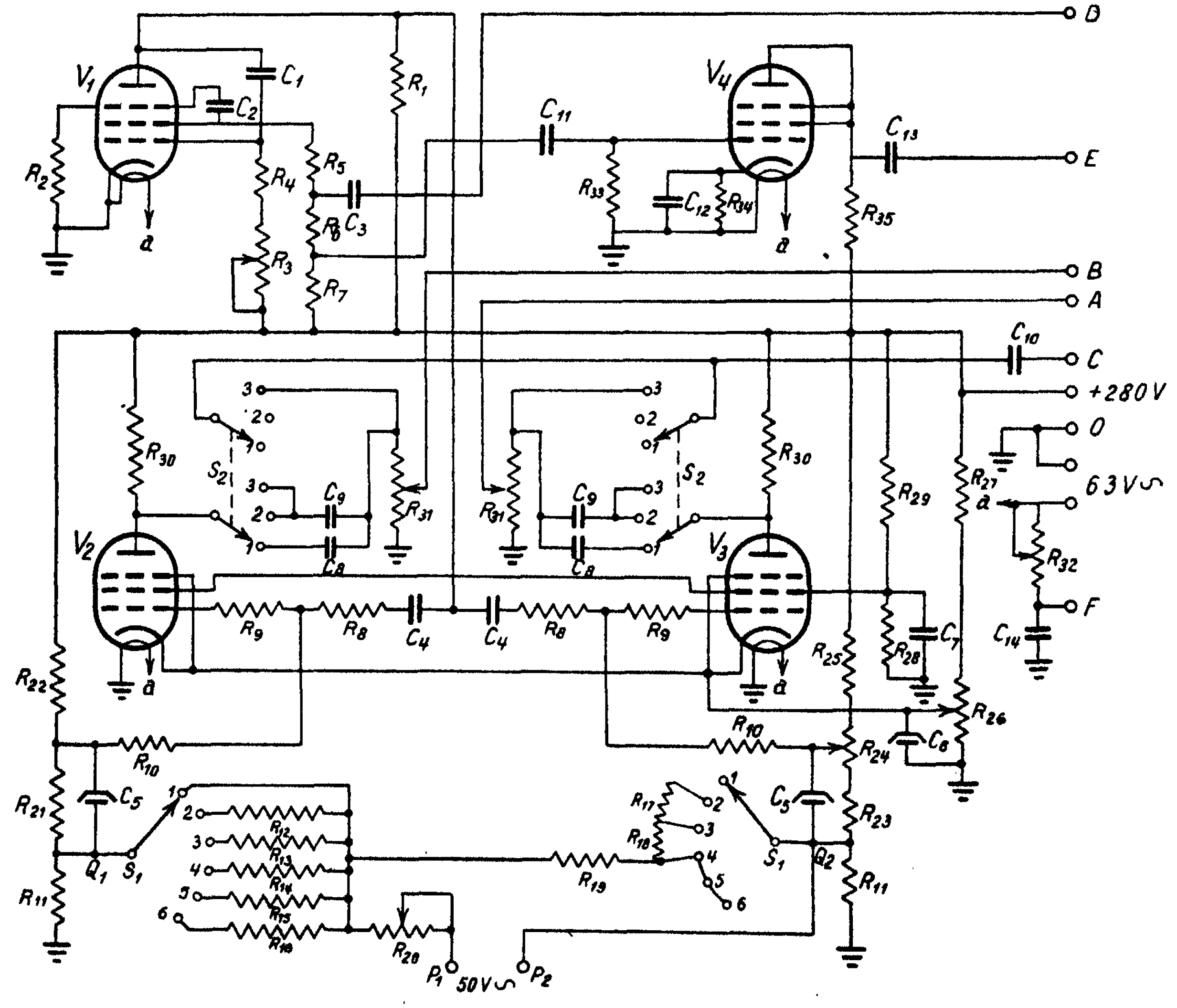

FIG. 2. Circuit of the resolving time indicator.

R_1—40K 2W
R_2—33K 1W
R_3—5m pot
R_4—0.5m ½W
R_5—20K 1W
R_6—2K ½W
R_7—0.2K ½W
R_8—5K ½W
R_9—100K ½W
R_{10}—22K ½W
R_{11}—1.05K 4W*
R_{12}—4.00K 2W*
R_{13}—18.0K 1W*
R_{14}—58.0K
R_{15}—198K
R_{16}—598K
R_{17}—0.80K*

R_{18}—0.20K*
R_{19}—2.02K*
R_{20}—0.6K pot*
R_{21}—10K ½W
R_{22}—75K 1W
R_{23}—5K ½W
R_{24}—10K pot (lin)
R_{25}—70K 1W
R_{26}—5K pot
R_{27}—27K 3W
R_{28}—22K 3W
R_{29}—3K 2W
R_{30}—10K 1W
R_{31}—5K pot (lin)
R_{32}—20K pot
R_{33}—0.2m ½W
R_{34}—0.1K ½W

R_{35}—10K 1W
C_1—500pf
C_2—200pf
C_3—0.01μf
C_4—0.5μf
C_5—12μf 50V (el)
C_6—50μf 50V (el)
C_7—1μf
C_8—150pf
C_9—25pf
C_{10}—200pf
C_{11}—0.01μf
C_{12}—12μf 10V.
C_{13}—0.01μf

* Low temperature coefficient.

3a

3b

FIG. 3. Form of maximum output pulses. A. S_2 (Fig. 2) in position 1. B. S_2 in position 2.

one of the channels, ahead of the coincidence mixer a line is inserted that delays the pulses. This line may be a length of cable[5] or an artificial delay line.[4] The same pulses are fed into both channels and the "length" of line that just makes the coincidences disappear is determined. This method also is rather complicated, especially when the system does not have a very high resolution. Then it is not practicable to use a cable because of the length required while an artificial line may cause a serious alteration of the pulse shape, making the calibration of this line dependent on the characteristics of the pulse amplifying and shaping circuits of the coincidence system.

In this article a simple device for direct determination of the resolving power of a system with two channels will be described that does not have the inconveniences of the methods just discussed. It also simplifies the testing and adjusting of coincidence systems. This apparatus can be used when the system fulfills conditions (2) and with the aid of it the validity of (2) can be checked. It enables one to see on a cathode-ray tube the behavior of the coincidence discriminator when pulses with varying time intervals are applied to the system. The resolving power can be read from the c.r. screen at any instant, e.g., when the coincidence rate is not high, even during a count.

PRINCIPLE OF THE INSTRUMENT

A sawtooth voltage (Fig. 1B) is fed into the grids of two pentodes. These have a grid space that is small in comparison with the sawtooth amplitude. So these tubes accept narrow "slices" of the sawtooth (Fig. 1A, 1C). RC-filters across the plate resistors of these tubes differentiate the plate voltage to sharp pulses produced during the flyback of the sawtooth voltage (Fig. 1D, 1F). (The pulses of opposite sign produced by the slow part of the sawtooth are small in comparison with these sharp pulses).

The grid bias of the two pentodes is varied continuously by an a.c. voltage applied to these grids in opposite phase. Thus the height of the sawtooth where the slices are cut, varies. This results in a varying distance between the pulses of Fig. 1D, 1F: a wobbling of the pulses relative to each other.

These pulses are applied to the two input terminals of the coincidence system to be examined. This apparatus only generates an output signal when the pulses are close enough to each other. This signal is fed to a vertical deflection plate of a c.r. oscilloscope. The horizontal plates of the scope accept an a.c. voltage in phase with the wobbling voltage. On the c.r. screen a number of pulses will appear extending to both sides of the picture as far as is dictated by the resolving power of the coincidence system and by the wobbling amplitude (Fig. 7, 8). Alternatively the output of the coincidence mixer can be connected to a vertical plate to show the variation of its output pulses as a function of input pulse distance (Fig. 9).

The time scale of the c.r. picture is determined by the wobbling amplitude and can be set at a number of values from about 3.10^{-6} to 10^{-9} sec.

Calibration of the time scale is obtained by feeding the pulses from both outputs of the instrument into the input of a radio receiver. When the pulse separation is half the inverse of the frequency to which this set is tuned its output will be a minimum.[6]

The pulses are wobbled while the receiver output is connected to a vertical deflection plate of the c.r. scope. A suitably phased a.c. voltage is applied to the horizontal deflection plates. A pulse pattern will appear which has minima when the pulse separation equals $1/2\nu$ (Fig. 4). ν is read from the receiver and because the time scale is linear its calibration is complete.

DESCRIPTION OF THE CIRCUIT

The Miller-dynatron or transitron circuit is used as a sawtooth generator (V_1 in Fig. 2). The flyback voltage-time curve obtained with this generator is exponential. It would be possible to make a sawtooth generator with linear flyback but this can only be done with a more complicated circuit. By choosing R_1, C_1, R_2, and C_2 the flyback time is adjusted to 8 μsec. approx. The sawtooth frequency can be varied from about 1.5 to 15 kc/s by varying R_3. This does not appreciably affect the flyback time. The sawtooth amplitude is about 60 volts.

The sawtooth voltage is applied to the grids of V_2 and V_3. R_8 serves to limit their grid current. The cathodes of these tubes are kept at a semi-fixed positive potential while the grid bias of V_3 may be varied by potentiometer R_{24}. This results in varying the difference in time (Δt) between the pulses appearing at the output terminals A and B. When both tubes have equal bias this difference is zero. If Δt is determined as a function of the setting of R_{24} the apparatus can be used in its simplest form: by feeding the pulses appearing at A

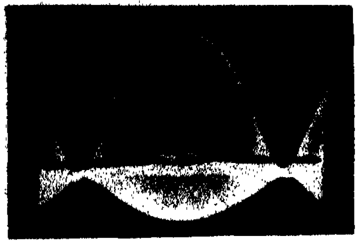

FIG. 4. Receiver tuned to 167 kc/*s*. Time scale not adjusted.

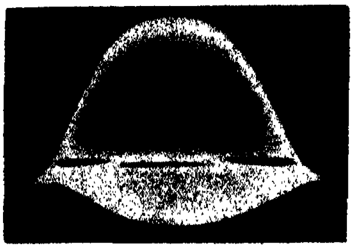

FIG. 5. Receiver tuned to 167 kc/*s*. Time scale adjusted to 3 μsec. (=pulse distance at the edges of the picture).

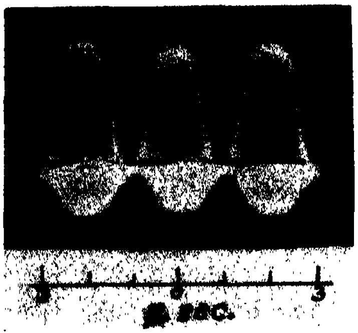

FIG. 6. Receiver tuned to 500 kc/*s*. Time scale =3 μsec.

FIGS. 4–6. Method of calibration. The photographs show the behavior of the output voltage of a radio receiver when pairs of pulses of varying separation from the resolving time indicator are applied to its antenna input. These pulses are wobbled by a 50 cycle a.c. voltage. Horizontal deflection is also caused by such a voltage.

and B to the coincidence system, connecting the output of this system to a c.r. oscilloscope and by then reading the position of R_{34} when pulses appear on the screen. The form of the pulses at A and B somewhat resembles that of a G-M counter pulse. Their width can be adjusted to two values (position 1 and 2 of S_2). Figure 3A shows the pulse form in position 1 of S_2 and Fig. 3B the form in position 2 of S_2. The amplitude of these (negative) pulses can be adjusted with R_{31}. Its maximum value is about 25 volts in position 1 and 8 volts in position 2 of S_2. By changing the amplitude and by switching S_2 the validity of condition 2β can be checked. Different shapes of the pulse can be obtained by putting parallel capacities across R_{30}, enabling a more severe test of condition 2β.

To obtain information about the behavior of the coincidence system more rapidly and also because the non-linear relationship between Δt and the setting of R (exponential flyback) would make calibration difficult, the pulse "wobbling" described above was introduced.

About 50 volts a.c., for instance taken from an extra winding of the power supply transformer, are applied to P_1 and P_2 (Fig. 2) causing a continuous variation of the bias of the grids of V_2 and V_3 in opposite phase. In this way the first order deviation from linearity of the flyback is eliminated from the v_w-Δt relation. (The bias difference between V_2 and V_3 is called v_w: the wobbling voltage). It should be noticed that the "effective" bias wobble (v_w) is about 0.3 of the a.c. voltage of Q_1 and Q_2 because of the shunting R_8C_4 combinations. Actually R_8 was inserted to enlarge the shunt impedance. The percentage deviation δ from linearity of the v_w-Δt relation can easily be evaluated. The maximum value of v_w will cause the largest δ. Now $v_{w\,\max}$ is ~ 20 volts. v_0 is the voltage across R_1 when the flyback cuts across the grid space of V_2 and V_3 (assuming $v_w=0$). Then with $v_0=180$ volts we have $v_{w\,\max}/v_0=\Delta t_{\max}/R_1C_1\sim 0.11$. Since first order deviation from linearity is eliminated by the balanced application of v_w we get $\delta_{\max}\sim 100/12(\Delta t_{\max}/R_1C_1)^2\sim 0.1$ percent. This is a smaller error than that inherent in the absolute calibration, as will be seen below.

The a.c. voltage that provides the horizontal oscilloscope sweep is derived from the 6.3-volt heater voltage. It is phased by the $R_{32}C_{14}$ combination and fed from terminal F into the sweep amplifier of the scope.

In order to get a better picture the cathode-ray beam is intensity-modulated by pulses from terminal E, connected to the c.r. tube control electrode, so that the picture is only made visible during the flyback of the sawtooth. These pulses are derived from those existing on the screen of the transitron tube V_1. A part of those negative pulses are applied to the grid of V_4, where their polarity is inverted.

CALIBRATION

To calibrate the instrument S_2 is switched to position 3 and terminal C is connected to a radio receiver. Thus the receiver accepts the combined pulses from V_2 and V_3 at its aerial input. R_1 is so adjusted that the sawtooth frequency is about 5 kc/*s*. As a receiver a Philips broadcast superheterodyne (type 695A) was used; any well calibrated commercial set with medium and long wave ranges and with an over-all band width of something like 12–18 kc/*s* will perform equally well. The output of the a.f. power amplifier of the set is connected to the vertical deflection amplifier of the oscilloscope. The horizontal deflection amplifier accepts an a.c. voltage from terminal E. S_1 is put in position 1 and the receiver is tuned to $\nu_1=167$ kc/*s*. When the horizontal sweep is properly phased by turning R_{32} the picture on the screen will be like Fig. 4. At the position of the minima Δt is now $1/2\nu_1=3$ μsec. Next R_{30} is adjusted so that the minima appear at the edges of the picture (Fig. 5). Thus the time scale, defined as Δt at

FIG. 7. Output of last stage (T_6) of system. Discriminator adjusted to give resolution $\tau = 0.012$ μsec.

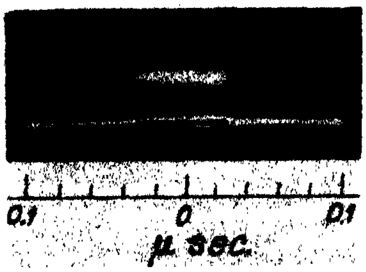

FIG. 8. Same as Fig. 7, but $\tau = 0.03$ μsec.

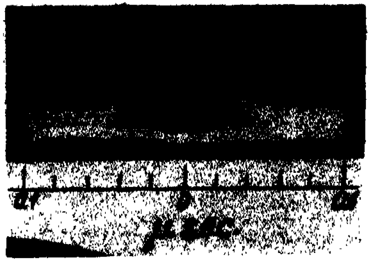

FIG. 9. Output of discrimination amplifier (T_5).

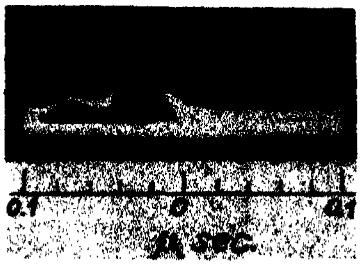

FIG. 10. Output of T_6 when coax cable. (590 cm) is in one channel of the system.

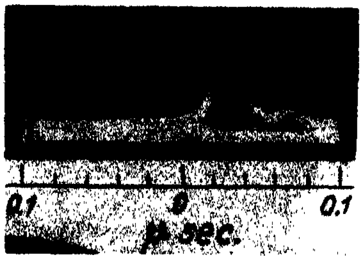

FIG. 11. Same as Fig. 10, but cable is in the other channel.

FIGS. 7–11. Photographs of c.r. scope screen of output under various circumstances at two different stages of a coincidence system, connected to the resolving time indicator.

the edges of the picture is fixed at 3 μsec. Now the wobbling voltage can be decreased in steps by switching S_1. The resistors R_{11}–R_{19} are selected so as to provide a voltage ratio: 1:0.3:0.1:0.03:0.01:0.003 at positions 1–6 of S_1, so the time scale ($\Delta t_{\max}$) is equal to 3, 1, 0.3, 0.1, 0.03, 0.01 μsec. at these positions respectively. It is not too difficult to choose R_{11}–R_{19} so that the deviation of any time scale does not exceed 2 percent. Thus we have a complete calibration. To obtain a higher accuracy or to check the v_w-ratio at different positions of S_1 the radio receiver can be tuned to $3\nu_1 = 500$ kc/s (position 2) or $10\nu_1 = 1666$ kc/s (position 3) and again a picture as shown in Fig. 5 must appear.

Also it is possible to utilize for calibration the minima of "higher order" in the receiver output, these will appear when $\Delta t = (1+2n)/2\nu_1$ ($n = 1, 2\cdots$). An example is given in Fig. 6 where S_1 is in position 1 and the receiver is tuned to $3\nu_1 = 500$ kc/s. This procedure can be followed when the receiver does not have a long wave range.

TESTING OF A COINCIDENCE SYSTEM

A coincidence system of medium resolution ($\tau = 10^{-7} - 10^{-8}$ sec.) has been tested with the instrument. This system has two channels, both containing a preamplifier (T_1, T_1') coupled to a special triggered multivibrator (T_2, T_2') that produces narrow pulses the width of which can be varied in steps. These are fed into the coincidence mixing stage (T_3, T_3') (a modified Rossi-stage). The output of this stage goes into a discriminator (T_4) followed by an amplifier (T_5). The output pulses of this amplifier trigger a multivibrator (T_6) when they are sufficiently large.

Terminals A and B (Fig. 2) of the resolving time indicator are connected to the inputs of T_1 and T_1' of the coincidence apparatus. Horizontal deflection on the oscilloscope is caused by the a.c. voltage from terminal F. Various signals are now applied to the vertical deflection plates of the scope (usually via the vertical deflection amplifier).

1. Output of T_6. Time scale = 0.1 μsec.; $\tau = 0.012$ μsec. (Fig. 7).
2. Output of T_6 but different discriminator (T_4) bias. Time scale = 0.1 μsec.; $\tau = 0.030$ μsec. (Fig. 8).
3. Output of T_5. Time scale = 0.1 μsec. (Fig. 9).
4. Output of T_6 when a length of coaxial cable (590 cm) has been inserted in one of the channels between T_2 and T_3. To the left of the peak a secondary peak is visible. This is caused by imperfect matching of the cable to the input and output impedances resulting in reflection at both cable terminals. Thus a second smaller pulse reaches the coincidence stage after traveling through the cable twice. In this way four more equidistant peaks of decreasing height have been observed. Time scale = 0.1 μsec. (Fig. 10).
5. Same as 4 but coax cable is in the other channel (Fig. 11). Figures 10 and 11 suggest another way of calibrating the resolving time indicator when a coincidence system with good resolution is at hand together with a length of coaxial line of which the propagation constant (f) is known. On the other hand we can conclude from Figs. 10 and 11 that $f = 0.60$ for the cable used there. The system was subjected to different pulse shapes and amplitudes and also the number of pulses per second was varied. This gave only a very slight change of the resolving time.

THE REVIEW OF SCIENTIFIC INSTRUMENTS VOLUME 20, NUMBER 12 DECEMBER, 1949

Design Curves for 180° Magnetic Spectrometers

GEORGE E. OWEN
Washington University, St. Louis, Missouri

(Received August 5, 1949)

The image shapes resulting from 180° focusing of charged particles in a homogeneous magnetic field have been computed. General curves are presented in terms of three variables for variable ρ-spectrometers (as in the case of photographic detection) and in terms of four variables for constant ρ-spectrometers (as in the case of detection with a fixed counter). The variables are source and exit-slit height, source width, angular selection, and exit-slit width.

The advantages of using sources and exit-slits with a large dimension parallel to the magnetic field (i.e., height) are noted.

I. INTRODUCTION

OF the many types of charged-particle spectrometers in use,[1] that which utilizes 180° focusing in a homogeneous magnetic field is perhaps the simplest and most widely used for various types of particle spectroscopy.

In preparation for work with this type of spectrometer, using electron sensitive plates as the detection apparatus, the problem of focusing has been reviewed in detail. Photographic line shapes have been computed as a function of the variable parameters involved, and, in addition, a general set of line shapes for constant radius spectrometers has been calculated. These curves have proven quite useful in this laboratory.

The theoretical aspects of this problem have been treated previously by several authors.[2] The problem as discussed here is set up in a manner similar to that of Lawson and Tyler.[2] However, in the following analysis, the distribution obtained for the particle-emitting source of infinitesimal width is analytic over the angular variation of particles coming from the source, and this results in a line shape which differs from that derived by Lawson and Tyler.

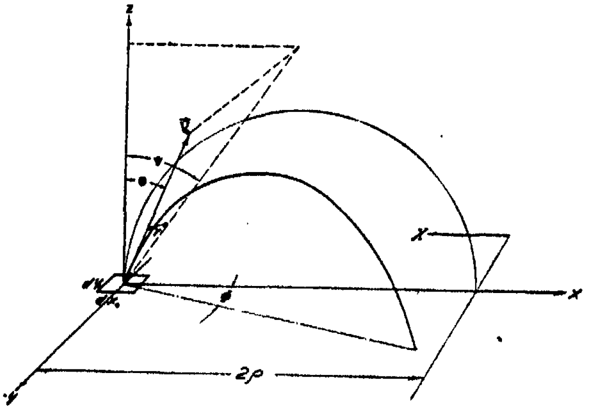

FIG. 1. The coordinate system used.

The photographic images[3a] are treated as functions of source and image height,[3b] width of source, and maximum angular selection about the normal to the source. The images for constant radius of curvature spectrometers are given in terms of these same parameters plus the width of the exit-slit. In all cases the linear dimensions are generalized by presenting them as a fraction of the radius of curvature.

II. THEORETICAL DEVELOPMENT

A. Equations of Motion

Since the equations of motion are derived in many books on electron optics, the procedure will merely be outlined here in order that the notation may be established.

Consider in Fig. 1 the case of the negatron with rest mass m_0 leaving the origin with a velocity $\mathbf{V}$, where[4]

$$\mathbf{V}=u_0\mathbf{i}+v_0\mathbf{j}+w_0\mathbf{k}, \tag{1}$$

and moving in an homogeneous magnetic field

$$\mathbf{B}=B_0\mathbf{j}. \tag{2}$$

The equation representing the motion of a negatively charged particle moving in a constant magnetic field is

$$\frac{d}{dt}\left\{\frac{m_0\mathbf{V}}{(1-V^2/C^2)^{\frac{1}{2}}}\right\}=-e(\mathbf{V}\times\mathbf{B}). \tag{3}$$

The solutions of Eq. (3) are of the form

$$[w_0-A^{-1}(x-x_0)]^2+[u_0+A^{-1}(z-z_0)]^2=w_0^2+u_0^2 \tag{4}$$

$$[y-y_0]=v_0t, \tag{5}$$

where

$$A=m_0(B_0e)^{-1}(1-V^2/C^2)^{-\frac{1}{2}}$$

and x_0, y_0, and z_0 = the initial displacement of the particle.

---

[1] K. Siegbahn and N. Svartholm, Arkiv. f. Mat. Astr. O. Fys. 33A, No. 21 (1946); L. M. Langer and C. S. Cook, Rev. Sci. Inst. 19, 257 (1948); Deutsch, Elliot, and Evans, Rev. Sci. Inst. 15, 178 (1944); Clifford W. Witcher, Phys. Rev. 60, 32 (1941); J. Backus, Phys. Rev. 68, 59 (1945).

[2] W. A. Wooster, Proc. Roy. Soc. (London) A114, 729 (1927); K. T. Li, Proc. Camb. Phil. Soc. 33, 164 (1937); J. L. Lawson and A. W. Tyler, Rev. Sci. Inst. 11, 6 (1940).

[3a] The term *photographic image* will be used to signify images formed in variable ρ-spectrometers in which photographic detection is most frequently used.

[3b] The term source height means the dimension parallel to the magnetic field (in the y direction, Fig. 1).

[4] **i**, **j**, and **k** are the conventional Cartesian base vectors.

To find the intersection of the orbit with the xy plane, we set $z=0$ and $z_0=0$ in (4), giving,

$$(x-x_0)_{z=0}=2Aw_0=2AV\cos\Theta.$$

To obtain the point of maximum displacement along the x axis, set $\Theta=0$

$$(x-x_0)_{\max}=2\rho=2AV.$$

This establishes the relation between the radius of curvature, ρ, and the momentum, p, and magnetic field, B_0,

$$p=B_0\rho/e. \tag{6}$$

The term t can now be eliminated from Eq. (5) by computing the time required for the particle to travel over the circular arc projected on the xz plane. The magnitude of the velocity along the arc is $(u_0{}^2+w_0{}^2)^{\frac{1}{2}}$. If the particle is emitted at the projected angle Ψ to the z axis, then the length of the projected orbit is $\rho(\pi-2\Psi)$. Equation (5) becomes

$$(y-y_0)_{z=0}=\frac{v_0\rho(\pi-2\Psi)}{(u_0{}^2+\omega_0{}^2)^{\frac{1}{2}}},$$

or, using the angle shown Fig. 1,

$$(y-y_0)_{z=0}=\rho(\pi-2\Psi)\sin\Psi\tan\Phi. \tag{7}$$

B. The Intensity Distribution from a Source of Infinitesimal Width

Consider the coordinate system given in Fig. 1. Let $n_v=$ the number of particles of velocity V leaving the source per unit solid angle per cm² per sec.

The total number leaving the source per sec. between x_0 and x_0+dx_0, y_0 and y_0+dy_0, Θ and $\Theta+d\Theta$, and Φ and $\Phi+d\Phi$ is,

$$dN=n_v\sin\Theta d\Theta d\Phi dx_0dy_0, \tag{8}$$

and the total number per sec. arriving at the image is,

$$N=\int_{-l_0/2}^{+l_0/2}\int_{-\Theta_0}^{+\Theta_0}\int_{-h/2}^{+h/2}\int_{-\Phi_0}^{+\Phi_0}n_v\sin\Theta dx_0d\Theta dy_0d\Phi, \tag{9}$$

where $h=$ the total height of the source (in the y direction), $l_0=$ the total width of the source (in the x direction), Θ_0 and Φ_0 are the limits on Θ and Φ imposed by the defining baffle.

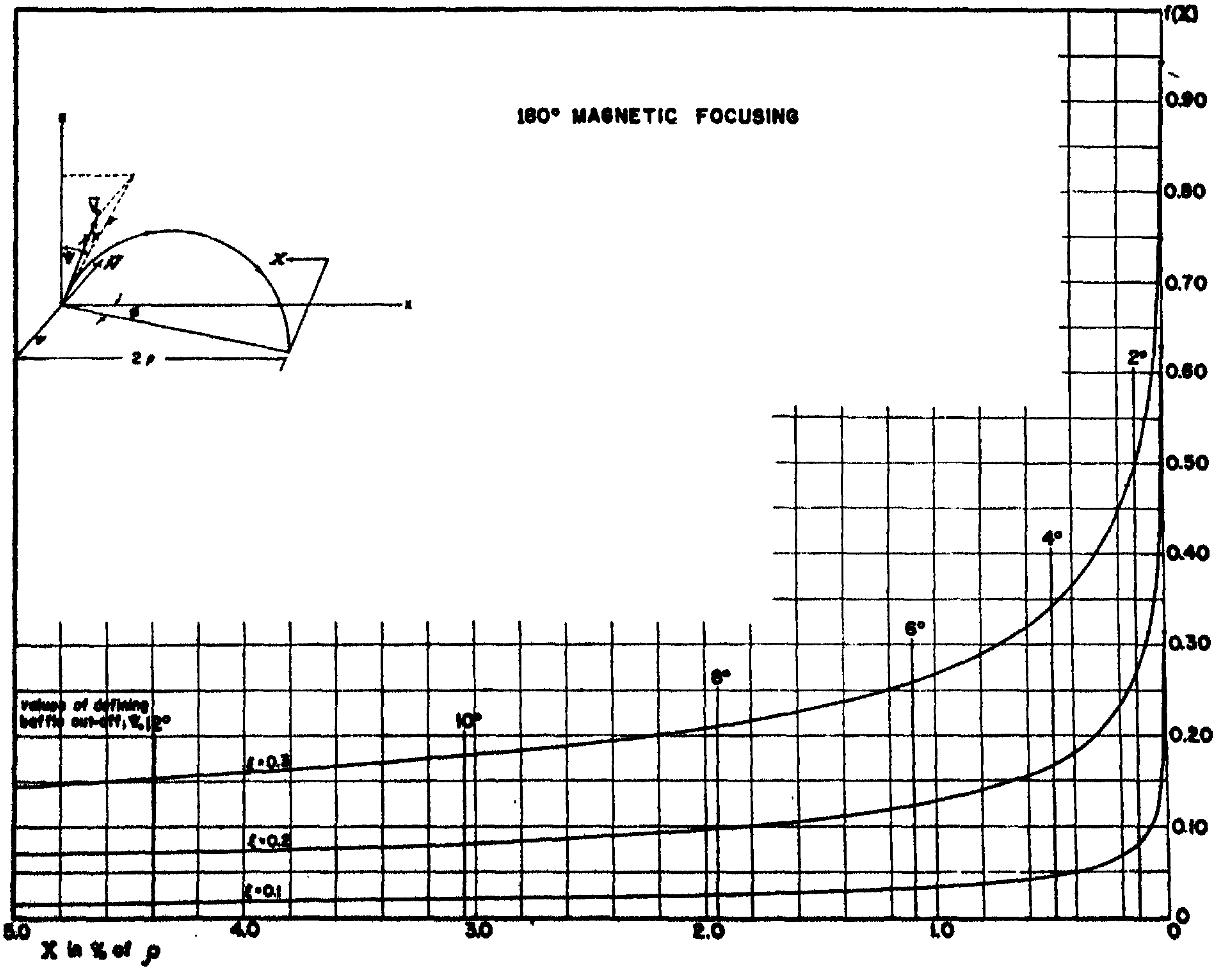

FIG. 2. The intensity distribution resulting from a source of infinitesimal width as a function of X.

From (7)

$$\Phi=\tan^{-1}\left\{\frac{y-y_0}{\rho(\pi-2\Psi)\sin\Psi}\right\} \tag{10}$$

and

$$d\Phi=d\left[\tan^{-1}\left\{\frac{y-y_0}{\rho(\pi-2\Psi)\sin\Psi}\right\}\right]. \tag{11}$$

Let

$$g(\Psi)=(\pi-2\Psi)\sin\Psi.$$

In the case discussed here, the source height is set equal to the image height. In general, however, these two dimensions may be handled in the same manner as shown below when they are not equal.

Expressing the limits of Φ in terms of Eq. (10), substituting Eq. (11) into Eq. (9), and integrating between

$$-\tan^{-1}\left(\frac{h/2+y_0}{\rho g(\Psi)}\right) \quad\text{and}\quad +\tan^{-1}\left(\frac{h/2-y_0}{\rho g(\Psi)}\right),$$

we now obtain (9) as

$$N=\int_{-l_0/2}^{+l_0/2}\int_{-\Theta_0}^{+\Theta_0}\int_{-h/2}^{+h/2} n_v\left[\tan^{-1}\left\{\frac{h/2-y_0}{\rho g(\Psi)}\right\} +\tan^{-1}\left\{\frac{h/2+y_0}{\rho g(\Psi)}\right\}\right]\sin\Theta dx_0 d\Theta dy_0. \tag{12}$$

Integrating Eq. (12) between the limits of the source height we obtain,

$$N=\int_{-l_0/2}^{+l_0/2}\int_{-\Theta_0}^{+\Theta_0} n_v\rho\left\{2\xi\tan^{-1}\left(\frac{\xi}{g(\Psi)}\right) -g(\Psi)\log\left[1+\left(\frac{\xi}{g(\Psi)}\right)^2\right]\right\}\sin\Theta d\Theta dx_0, \tag{13}$$

where

$$\xi=h/\rho.$$

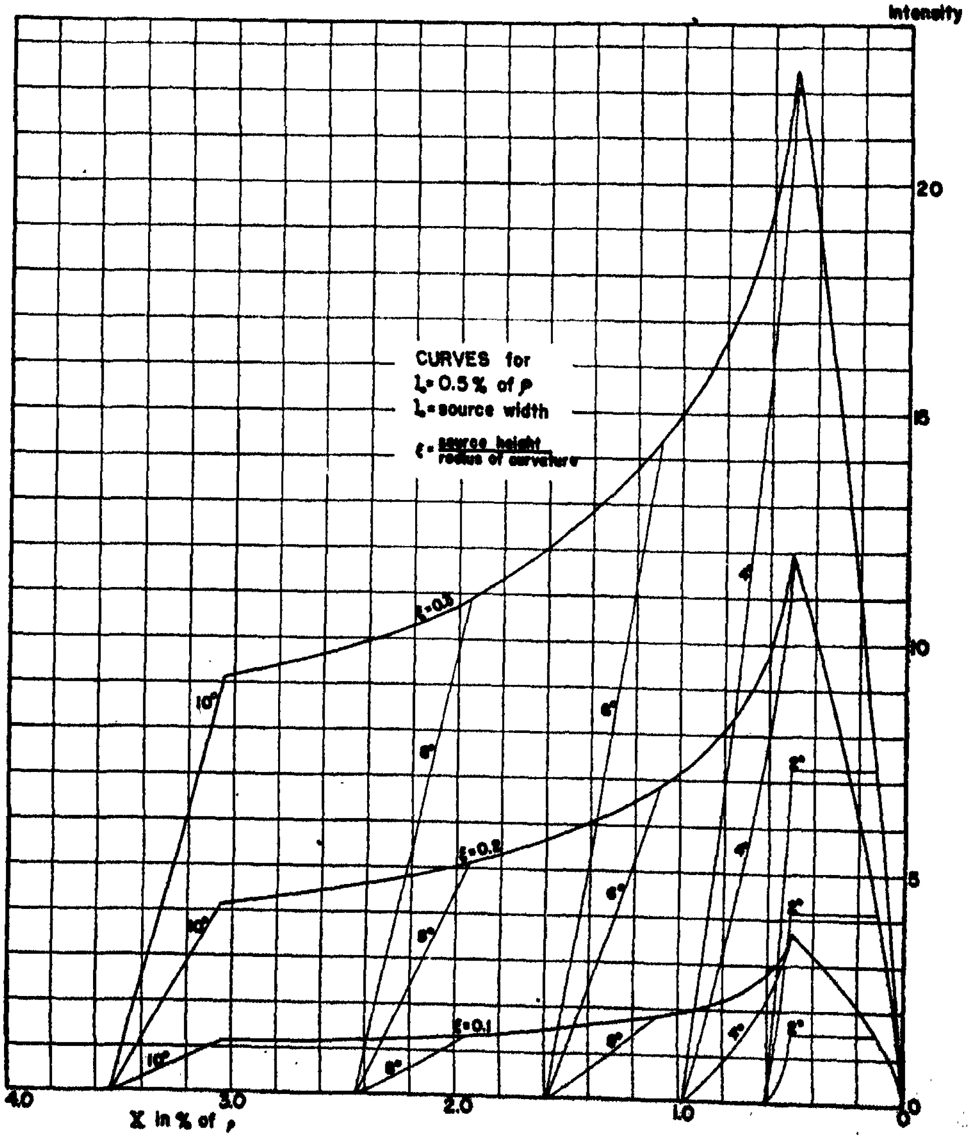

FIG. 3. Intensity distribution for a photographic image in the case where the source width is 0.5 percent of the radius of curvature.

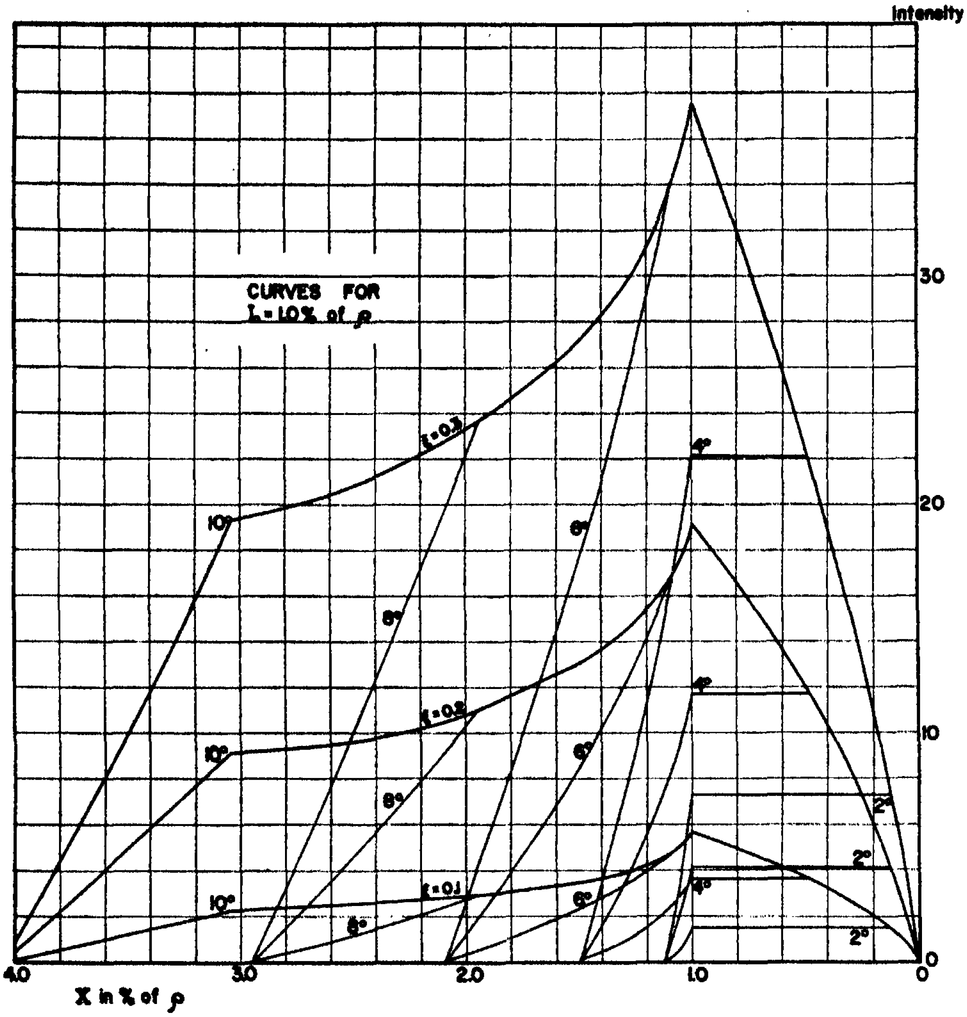

FIG. 4. Intensity distribution for a photographic image in the case where the source width is 1.0 percent of the radius of curvature.

When the source height is not equal to the image height, one obtains the same function as above with added terms in $\pm\Delta\xi$.

It should be noted at this point that Eq. (13) is analytic for all values of Θ, and Ψ. When $g(\Psi)\rightarrow 0$ the term, $\tan^{-1}(\xi/g(\Psi))$, approaches the limit $\pi/2$. It can be shown that

$$\lim_{g(\Psi)\rightarrow 0} g(\Psi)\log[1+(\xi/g(\Psi))^2]\rightarrow 0.$$

Since $\cos\Theta=\cos\gamma\cos\Psi$, and since $\gamma\leqslant\Phi$, where Φ is a small angle,

$$\sin\Theta d\Theta\cong\cos\gamma\sin\Psi d\Psi. \tag{14}$$

Insert Eq. (14) into Eq. (13). The factor $\cos\gamma$ can be taken outside the integral sign as an average value because it is approximately constant within the limits of integration.[5]

$$N\cong\langle\cos\gamma\rangle_{Av}\int_{-l_0/2}^{+l_0/2}\int_{-\Psi_0}^{+\Psi_0} n_v\left\{2\xi\tan^{-1}\left(\frac{\xi}{g(\Psi)}\right)\right.$$
$$\left.-g(\Psi)\log\left[1+\left(\frac{\xi}{g(\Psi)}\right)^2\right]\right\}\rho\sin\Psi dx_0 d\Psi. \tag{15}$$

Equation (15) can now be integrated between the limits, $-\Psi_0$ and $+\Psi_0$, set by the defining baffle. Since our interest lies in the photographic image, and since this image is distributed along the x axis in the negative direction from $x=2\rho$, let us define a new coordinate X, where

$$\mathrm{X}=2\rho(1-\cos\Psi) \tag{16}$$

$$d\mathrm{X}=2\rho\sin\Psi d\Psi. \tag{17}$$

Substitute from Eqs. (17) and (18) into Eq. (16) giving

$$N\cong\langle\cos\gamma\rangle_{Av}\int_{-l_0/2}^{+l_0/2}\int_{0}^{\mathrm{X}_0} n_v f(\mathrm{X})dx_0 d\mathrm{X}, \tag{18}$$

---

[5] $\langle\cos\gamma\rangle_{Av}$ is approximately one for all values of ξ used in spectrometers and does not become appreciably less than one until quite large angles are reached.

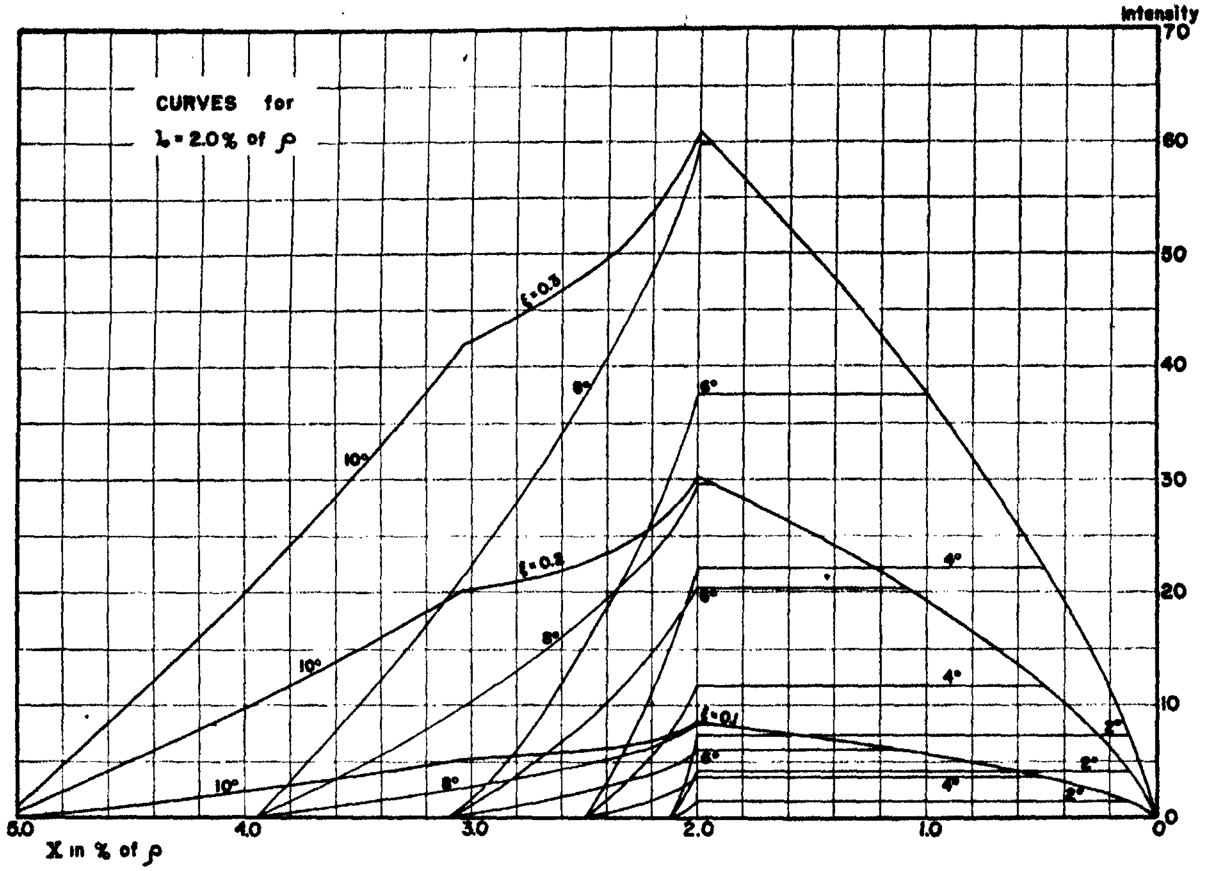

FIG. 5. Intensity distribution for a photographic image in the case where the source width is 2.0 percent of the radius of curvature.

where

$$f(X)=2\xi\tan^{-1}\left(\frac{\xi}{g_1(X)}\right)-g_1(X)\log\left[1+\left(\frac{\xi}{g_1(X)}\right)^2\right]. \quad (19)$$

For corresponding values of Ψ' and X',

$$g(\Psi')=g_1(X').$$

This relation allows one to compute $g_1(X)$ in terms of Ψ and obtain the corresponding value of X.

Setting $\langle\cos\gamma\rangle_{Av}=1$, it is seen that $f(X)$ in Eq. (18) is the distribution from a source of infinitesimal width dx_0. This distribution is shown in Fig. 2 for three values of ξ, i.e., for three different values of source height expressed as a fraction of the radius of curvature.

C. The Photographic Image Shape

The distribution from a source of finite width l_0 will be indicated as $F(X)$.

$F(X)=\sum$ of all the contributions from the infinitesimal widths dx_0 between the proper limits, or

$$F(X)=\int_{X_1}^{X_2} f(X')dX'. \quad (20)$$

Now define X_0[6] as $X_0=2\rho(1-\cos\Psi_0)$ where Ψ_0 is the maximum value of Ψ as determined by the defining baffles.

The three general cases are (1) $X_0<l_0$; (2) $X_0=l_0$; (3) $X_0>l_0$. Since the calculations of the images involved integrations of $f(X)$ within the proper limits, it was found convenient to integrate numerically the curves of Fig. 2. Let A_x be the area between $X=0$ and X; the method of calculation can then be indicated symbolically.

Case 1. $X_0<l_0$.
From $X=0$ to $X=X_0$
$F(X)=A_x$.
From $X=X_0$ to $X=l_0$
$F(X)=A_{x_0}$.
From $X=l_0$ to $X=l_0+X_0$
$F(X)=A_{x_0}-A_{x-l_0}$.

Therefore Case 1 provides the familiar flat-topped image indicating that Ψ_0 is small in relation to l_0.

Case 2. $X_0=l_0$.
From $X=0$ to $X=l_0$
$F(X)=A_x$.
From $X=l_0$ to $X=l_0+X_0$
$F(X)=A_{x_0}-A_{x-l_0}$.

---

[6] X_0 will be denoted as *image width*.

Curves of Case 2 give maximum intensity coupled with the optimum resolution.

Case 3. $X_0 > l_0$.
From $X=0$ to $X=l_0$
$F(X)=A_x$.
From $X=l_0$ to $X=X_0$
$F(X)=A_x - A_{x-l_0}$.
From $X=X_0$ to $X=X_0+l_0$
$F(X)=A_{x_0} - A_{x-l_0}$.

Case 3 gives a double-humped peak of poor resolution. In Figs. 3–6 the photographic image shapes are given in terms of three variable parameters. Each separate figure gives a set of images for a particular value of source width, l_0 (0.5 percent of ρ; 1.0 percent of ρ; 2.0 percent of ρ; and 4.0 percent of ρ, respectively). Also for each source width the images are shown as a function of three values of source and image height ($\xi=0.1$; $\xi=0.2$; and $\xi=0.3$) and as a function of five values of Ψ_0 (2°, 4°, 6°, 8°, and 10°).

Since resolution is computed on the basis of the total distance (2ρ) between source and image, and since the parameters are given in terms of percent of ρ; the widths of the images at one-half the intensity must be divided by two in order to provide the correct theoretical resolution. (This only applies to Figs. 3–6 for the photographic images.)

D. Image Shapes for Constant ρ-Spectrometers

In the case of constant ρ-spectrometers a fourth variable is added, that of exit-slit width L_0.

The diagrams are made up on the basis that 2ρ is the distance from the inner edge of the source to the inner edge of the exit slit. This specification allows the high energy terminus of the line to fall always at $X=0$. Other definitions of the limits of 2ρ may be made by an appropriate shift of the $X=0$ point.

In Figs. 7 and 8, the images for constant ρ-spectrometers were obtained by integrating the curves in Figs. 3–6. Because of marked similarities in shapes for differ-

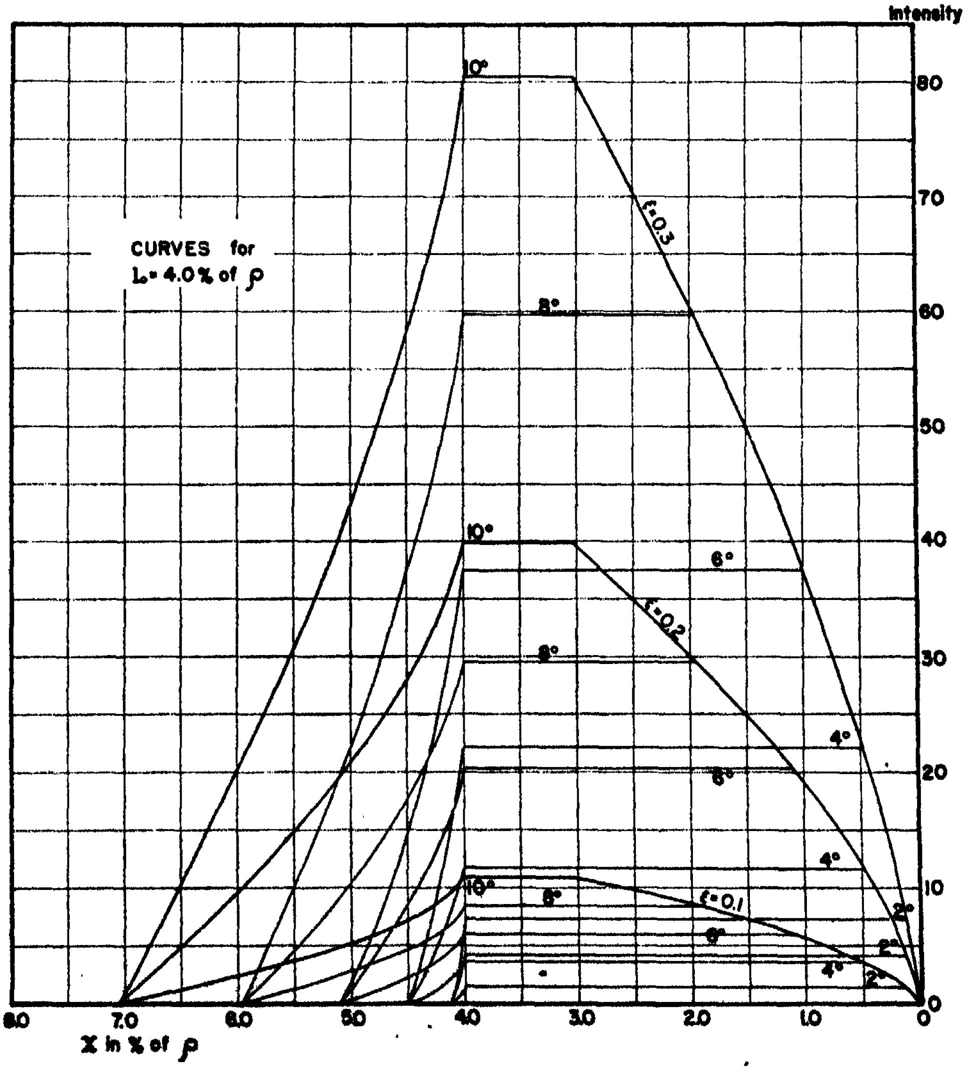

FIG. 6. Intensity distribution for a photographic image in the case where the source width is 4.0 percent of the radius of curvature.

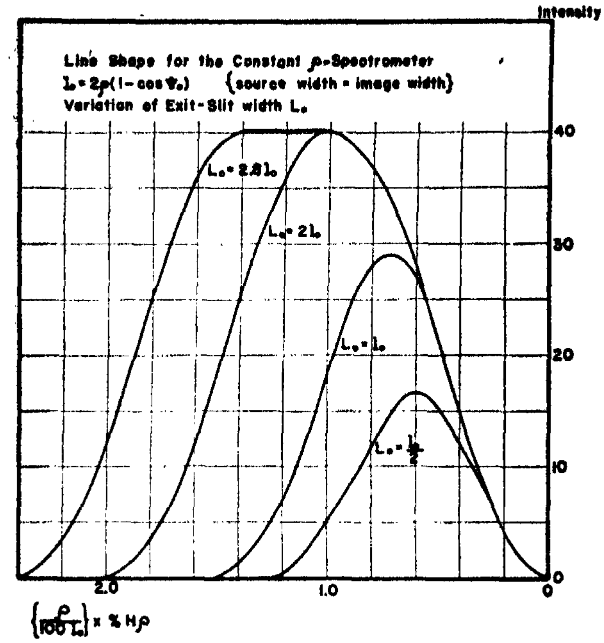

FIG. 7. Intensity distribution as a function of exit-slit width for a constant ρ-spectrometer in the case where the source width equals the image width. *Note.*—Multiply the abscissa by $100 l_0/\rho$ (using ρ and l_0 for a given spectrometer); the abscissa will then read in percent $H\rho$.

ent values of l_0 the results are given as functions of the ratio of source width to radius of curvature; thus, for specific cases these abscissas can easily be converted to percent $H\rho$ for any particular choice of ρ and l_0. The ordinates are given in units appropriate to a source width of 1.0 percent of radius of curvature, however, Fig. 9 provides the multiplication factor for conversion to cases where l_0 is different from 1.0 percent.

Figure 7 treats the effect of exit-slit width L_0 on the image in the special case where $l_0 = 2\rho(1-\cos\Psi_0)$ or $l_0 = X_0$ (Case 2).

Figure 8 indicates the effect of two variables, exit-slit width L_0 and Ψ_0. Ψ_0 is given in terms of Ψ_0' where Ψ_0' is that value of Ψ_0 such that $l_0 = 2\rho(1-\cos\Psi_0')$.[7] When l_0 and Ψ_0 are known the ratio of Ψ_0 to Ψ_0' is easily computed.

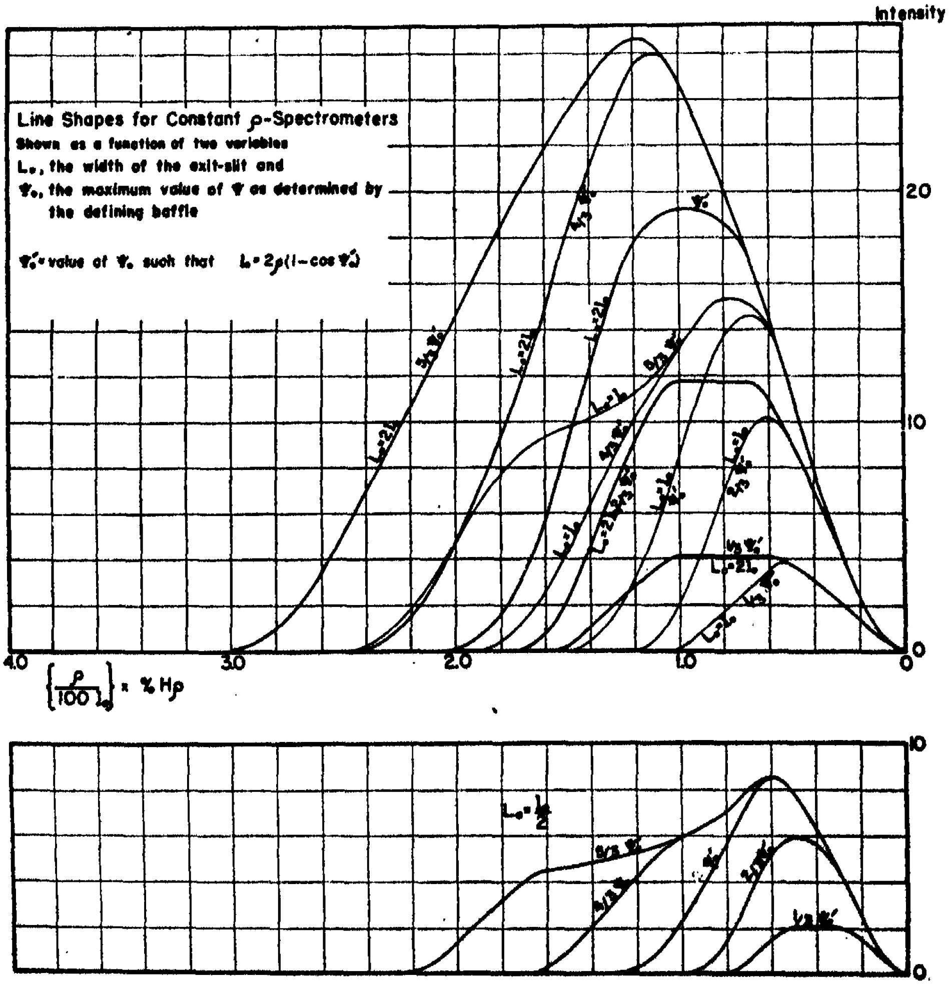

FIG. 8. Intensity distribution for a constant ρ-spectrometer as a function of l_0 and Ψ_0.

---

[7] Value of Ψ_0 when maximum intensity is coupled with optimum resolution. Ψ_0' fixes the ratio l_0/ρ.

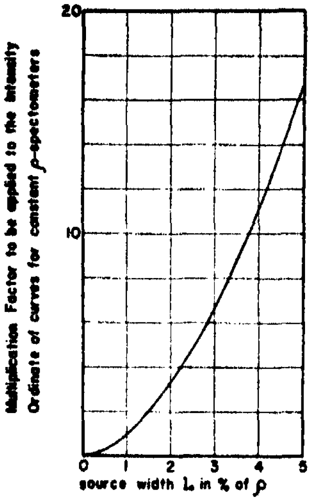

FIG. 9. Increase in intensity as a function of source width.

Figure 10 indicates the value of increased source and counter height. In Fig. 10 it is seen that the intensity increases very rapidly as ξ is increased, and that the resolution changes quite slowly.

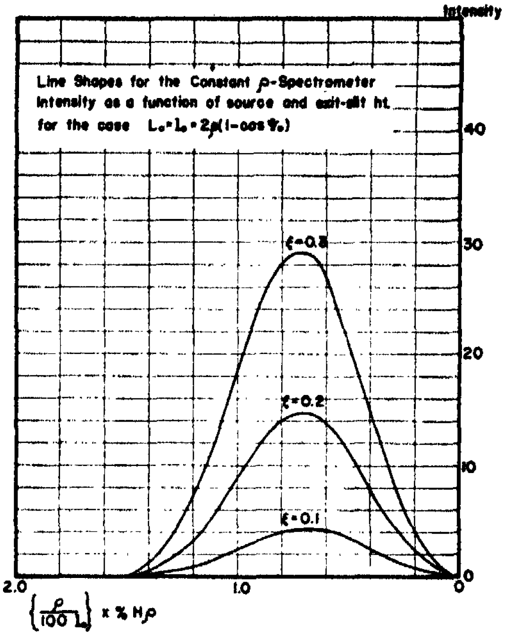

FIG. 10. Intensity distribution for a constant ρ-spectrometer as a function of the height of the source and exit-slit.

III. DISCUSSION

The use of a general set of curves of this type is convenient in both design and operation of spectrometers. In many cases ideal conditions cannot be realized in operation, and reference to a set of image curves can quickly tell one whether the sacrifice of resolution for intensity will actually result in an optimum operation of the instrument.

As an example, suppose that greater intensity is desired in a constant-radius spectrometer because of low specific activity of a beta-emitting source. This might be done by increasing the ratio of source width to exit-slit width from $l_0/L_0=0.5$ at $4/3\Psi_0'$ to $l_0/L_0=2.0$ at $\frac{3}{4}\Psi_0'$. Figures 8 and 9 show that this alteration triples the intensity at the expense of a loss of a factor of two in resolving power.

Another interesting result can be derived from Figs. 3–6 and 10. Intensity is seen to vary approximately as ξ^2, whereas resolving power is a slowly decreasing function of $\xi=h/\rho$. Thus the use of large heights for the source and the exit-slit is profitable in terms of a consequent gain in intensity.

It should be noted in conclusion that the theoretical shape of the monoenergetic line in the case of 180° focusing of beta-rays does not usually have the shape found experimentally. The theoretical line does not show the large low energy tail usually obtained in practice. This discrepancy can in large part be attributed to source thickness. Experimental indications of this have been observed in this laboratory.

A source of Th(B+C) was prepared by electrostatic deposition of thorium A on quarter-mil Al foil forming a very thin source. Another source of Th(B+C) was prepared from a solution providing a source of approximately 0.7 mg/cm^2. The F-line showed a marked symmetry about its point of maximum intensity and gave a resolution of 1.2 percent in the case of the source prepared by electrostatic deposition. In the case of the thicker source the F-line showed a marked low energy tail combined with a resolution of 2.5 percent.

I wish to thank Dr. F. B. Shull, Professor A. L. Hughes, and Dr. C. S. Cook for many helpful suggestions and comments.

This work was assisted by the Joint Program of the ONR and the AEC.

THE REVIEW OF SCIENTIFIC INSTRUMENTS VOLUME 20, NUMBER 12 DECEMBER, 1949

Apparatus for Isotope Separation by Thermal Diffusion

W. W. WATSON, L. ONSAGER, AND A. ZUCKER
Yale University, New Haven, Connecticut*

(Received August 10, 1949)

A compact, all-metal, multi-stage thermal diffusion apparatus for the separation of isotopes in quantity in non-corrosive gases at any pressure up to 175 lb/in.^{2} is described. For a particular gas the proper pressure may be well-enough calculated in advance as that giving maximum separation factor in the last column only. Operating with neon at 3 atmos. pressure, and using 12 meters of column consuming 4.9 kw for 260 hours, 7 liters of gas with a Ne^{22} content of 93.4 percent were produced.

IN an earlier note by one of us[1] brief mention was made of the operation of a six-column all-metal thermal diffusion apparatus, based on copper-clad G. E. Calrod heaters of ½-inch diameter and 200-cm effective heating length, for the enrichment of C^{13} in CH_4 gas at atmospheric pressure. Later, J. O. Buchanan coupled these same columns to a single 3-meter glass Clusius and Dickel hot-wire column to produce a considerable increase in the A^{36} content of a volume of argon gas.[2] We have recently rebuilt this equipment, noting and rectifying its deficiencies, and we have observed its performance under close to ideal conditions in the separation of the isotopes in a large batch of neon gas. Since very little information has appeared in the literature on the construction details and quantitative performance of producing thermal diffusion apparatus, a brief recital of our experience should be of some value. For a complete discussion of the theory of isotope separation by thermal diffusion the reader is referred to the review article by Jones and Furry.[3]

CONSTRUCTION FEATURES

The radius of the water-cooled copper pipe surrounding the Calrod heater in each column is such that the distance $2w$ between the hot and cold surface is for columns 1 and 2, 0.795 cm; for columns 3 and 4 it is 0.635 cm, and for columns 5 and 6 it is 0.476 cm. Fastened to the lower end of each cold pipe is a two-ply brass sylphon bellows to take up the differential expansion of the hot and cold surfaces. These bellows can hold a pressure of 175 lb/in.^{2}, and we solder them into place in the compressed state. Connection between the bellows and the lower end of the Calrod is made by means of two 2-inch lengths of thin-walled stainless-steel tubing, with one piece re-entrant inside the other, to minimize heat conduction. Similarly, at the top of each column 2½ inches of thin stainless steel connects the top of the cold wall to the Calrod at a point about ½ inch inside the insulating mica washer. All connections to the Calrod are of necessity silver-soldered. Figure 1 illustrates this end construction for each column.

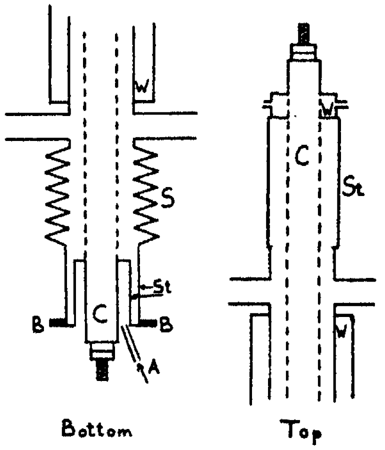

FIG. 1. End-construction of the columns. *S*—2-ply sylphon bellows, *St*—$\frac{1}{32}$ inch stainless steel, *C*—Calrod heater, *A*—cooling air, *B*—studs for counterweights, *W*—cooling water.

Also with the thought of minimizing heat losses, three thin stainless-steel centering fins, tapered nearly to a point at their outer ends, were soldered to each Calrod at 50-cm intervals along its length. The Calrods were then carefully straightened and the inner surfaces of the cold pipes were polished before assembly. That our precautions to lower heat losses could be improved upon are shown both by the power consumption when the columns are evacuated, as mentioned below, and by the fact that we found it necessary to add extra water cooling over the stainless-steel end plate connecting to the top of each column. Probably somewhat more than four inches of thin stainless-steel should be used between the hot and cold surfaces at each end of a column.

The columns are connected in series by means of ½-inch I.D. convective coupling pipes as shown schematically in Fig. 2. For compact arrangement the columns are mounted symmetrically around a center post, and the six hot convective couplers are wrapped there with a common heater. For the neon isotope separation, convective end volumes for the circulation of the proper amount of gas through the "light" and "heavy" ends of the apparatus are attached to the top of column 1 and to the bottom of column 6. The "light" end-volume consists of a square loop, six feet on a side, of 3-inch I.D. copper tubing coning down to one-inch diameter to join with the top of column 1. At the

---

* Assisted by the AEC.

[1] W. W. Watson, Science 93, 473 (1941).

[2] J. O. Buchanan, Phys. Rev. 75, 1332A (1949).

[3] R. C. Jones and W. H. Furry, Rev. Mod. Phys. 18, 151 (1946).

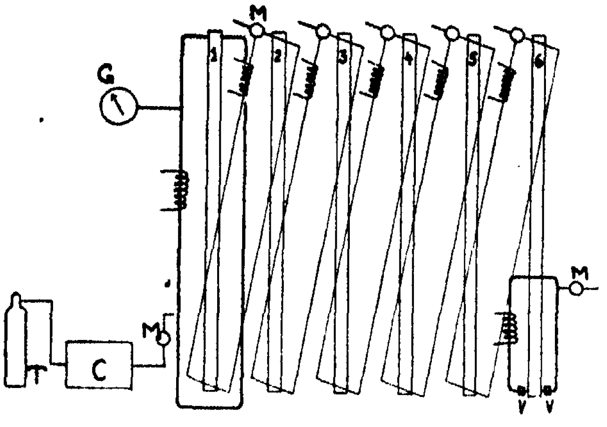

FIG. 2. Schematic diagram of thermal diffusion apparatus. C—compressor, M—McKay valves, V—sylphon bellows valves, G—pressure gauge, T—gas cyclinder.

"heavy" end is a shorter loop of 1½-inch copper tubing joined to the bottom of column 6 through sylphon valves by means of which the gas enriched in the heavy isotope may be isolated at the end of the operation. The size and appearance of the apparatus may be judged from Fig. 3.

All coupling pipes, end volumes and water pipes are joined with standard fittings, elbows and couplers and soft soldered. In a coupling pipe near the top of each of columns 2–6 and also at a convenient point in each end-volume McKay pressure valves are attached on T-joints for sampling, gas handling or evacuating. Whenever the Calrods are heated with the system evacuated we have found it necessary to hang a 20-lb. weight from studs soldered to the bottom of each sylphon bellows so that the unbalanced compressive force will not bend the Calrod.

Gas transfer between the commercial cylinders and the apparatus is effected with a small refrigerator compressor. These compressors are gas tight if they are in good condition with a new, well-worked-in universal sylphon shaft enclosure.

The Calrod heaters are powered by Δ connecting them in pairs across the 230-volt 3-phase a.c. circuit. Estimation of the temperature of any Calrod is best made by measurement of its extension with a cathetometer.

NEON ISOTOPE SEPARATION

Our objective was to produce 7 liters of neon gas with its Ne^{22} content at least 90 percent of the total. We arbitrarily decided to make the temperature difference between hot and cold walls 450°C. Therefore, in the notation of reference 3, $T_1=300°$, $T_2=750°$, $\bar{T}=525°$, $n=0.643$, $\nu=15$, $\eta=452.7$ micropoises at 525°K, $D=6.11\times 10^{-4}/\rho$, $\alpha=0.031$,[4] and, for columns 5 and 6, $2w=0.476$ cm, $B=5.484$ cm, $L=400$ cm. For the plane-wall approximation, we then computed with Eqs. (71) and (72) of reference 3, setting $K_c/K_d=2$ for maximum separation factor in columns 5 and 6, that the pressure should be about 3 atmos. This indicated that the "heavy" end-volume should have a capacity of about 2½ liters, and we decided to charge the apparatus with 150 liters (NTP) of neon in order to have a comfortable "factor of safety." Since the geometrical volume of the columns and coupling pipes is 8 liters, this dictated that the storage volume at the "light" end should have a capacity of about 30 liters.

Under these operating conditions our gauge pressure was 34 lb/in.², so that from the gas law $\rho=1.56\times 10^{-3}$ g/cm³ at 525°K. This makes $K_c^{(0)}/K_d^{(0)}=1.76$ for the last two columns, or close to the optimum value 2 for maximum factor. The transport $H^{(0)}$ is then 9.856×10^{-5} g/sec., $K_c^{(0)}=2.792\times 10^{-3}$ g.cm/sec. and $K_d^{(0)}=1.595\times 10^{-3}$ g.cm/sec. Corrections of these values for cylindricity by means of Eqs. (101)–(111) of reference 3 yield $H=1.1513\times 10^{-4}$ g/sec., $K_c=4.005\times 10^{-3}$ g.cm/sec. and $K_d=1.5681\times 10^{-3}$ g.cm/sec. Thus the K_c/K_d ratio is actually 2.5, a somewhat more efficient figure. Furthermore, experience indicates that a parasitic convection $K_p\cong 0.3K_c$ is unavoidable in cylindrical columns of this type. A parasitic convection current of this magnitude indicates azimuthal variations in temperature of 7° to 8° despite the good thermal conductivity of the copper sheath of the Calrod. Including this K_p, the total K is 6.775×10^{-3} g.cm/sec., $2A=0.017$, $2AL=6.8$ for columns 5 and 6 together, and hence they should have an equilibrium separation factor $q_e\cong 900$.

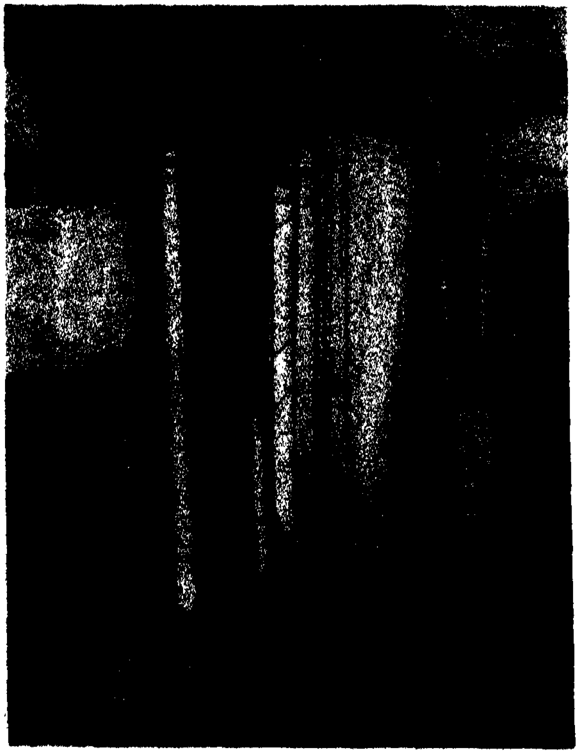

FIG. 3. General view of the assembled all-metal multi-stage thermal diffusion apparatus.

---

[4] L. Stier, Phys. Rev. 62, 548 (1942).

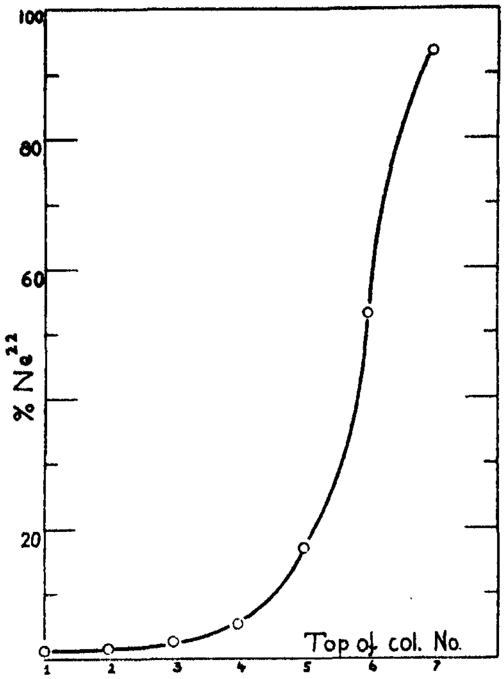

FIG. 4. Ne^{22} concentration at the top of each column after 262 hours of operation.

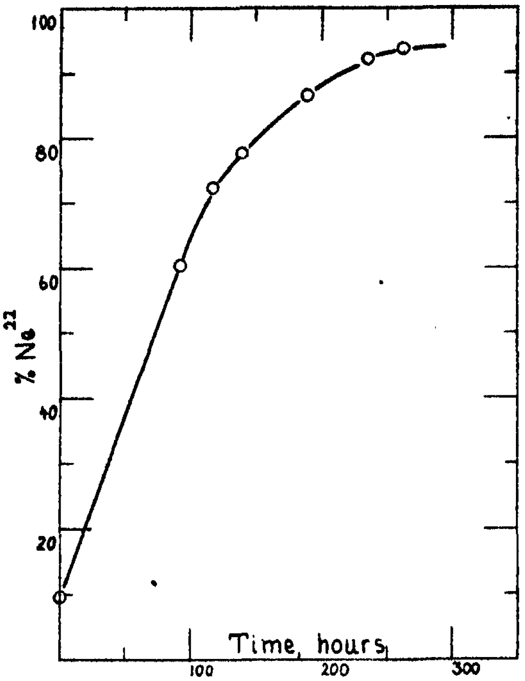

FIG. 5. Percentage abundance of Ne^{22} in the "heavy" end-volume as a function of time of operation.

One must be careful in setting the operating conditions in thermal diffusion apparatus such as this to avoid turbulence in the first columns. Since these columns have the largest value of $2w$, turbulence would occur first in them as the gas pressure is raised above a critical value characterized[5,6] by a Reynolds number R greater than about 25. For our neon gas pressure, $K_c/K_d = 12.3$ for columns 1 and 2, so that $R \cong 2(K_c/K_d)^{\frac{1}{2}} \cong 7$, or well below the value 10 recommended[7] as the maximum permissible value of R to guarantee the absence of turbulence. Since there is some evidence,[6,8] however, that the presence of a slight amount of turbulence does not decrease, and may even increase, the separation factor in Clusius and Dickel columns, it is possible that K_c/K_d ratios as high as 150 can be used. The effect of turbulence in thermal diffusion apparatus should be the subject of further investigation.

Figures 4 and 5 summarize the performance of the apparatus. Both curves indicate that when we isolated the end volume at the bottom of column 6 at 262 hours, this gas having then 93.4 percent neon 22, equilibrium had not yet been reached. For since columns 5 and 6 are identical, they should develop the same equilibrium separation factor (ratio of the isotope ratio at the two ends of the column). Figure 4 indicates that the over-all factor for these two columns at shut-down was about 70. One judges from the course of the curve in Fig. 5 that if the time of operation had been considerably lengthened, the neon 22 content might have risen to a maximum of 96 percent. The experimental q_e would then be in the range 100 to 200, but certainly not the expected 900. One can only conclude that parasitic convection currents were even larger than those suggested above. The loss of factor is probably accompanied by a gain in transport, however, thus increasing the yield of enriched product.

One would expect that at equilibrium, with the "heavy" end-volume containing mostly neon 22, the neon 21 isotope (0.27 percent abundant in the original gas) would be concentrated to the greatest extent at some intermediate point, say at the top of column 5. For the neon 21 should be set forward from the "light" end which contains mostly neon 20, and backward from the "heavy" end which is choked with the 22 isotope. Actually the samples taken at shut-down show that at the top of columns 3, 4, 5 and at the bottom of 6 the neon 21 content was 0.32 percent, 0.46 percent, 0.65 percent, and 0.62 percent respectively. Perhaps if these analyses were of equilibrium samples the expected greater neon 21 concentration at an intermediate point would be found.

With Eqs. (76), (99), and (411) of reference 3 we compute that the power consumption due to heat conduction through the neon gas in columns 3 or 4 should be 570 watts. Our actual power consumption in either of these columns was 770 watts. To maintain the ΔT of 450°C between surfaces when these columns were evacuated the power consumption was 225 watts per column. This last figure then includes all heat losses other than the heat conducted by the gas. The differ-

---

[5] L. Onsager and W. W. Watson, Phys. Rev. 56, 474 (1939).

[6] R. Simon, Phys. Rev. 69, 596 (1946).

[7] See reference 3, p. 173.

[8] A. Bramley and A. K. Brewer, Science 90, 165 (1939); J. Chem. Soc. 7, 972L (1939).

ence between these two experimental values agrees rather well with the calculated $Q=570$ watts.

It is to be concluded from these performance data that thermal diffusion apparatus constructed in this manner could produce quantities of well-separated isotopes for a number of the elements available in suitable gaseous compounds. The all-metal construction makes possible a choice in a wide range of pressures for most efficient operation. With continuous feed and bleed, separation and purification of certain commercial gaseous mixtures could undoubtedly be accomplished with properly designed thermal diffusion columns similar to these.

Most of the isotope analyses in this work were performed on our Thode-type[9] 60° mass spectrometer. We wish to thank Dr. H. D. Hoberman of the Department of Physiological Chemistry for making several mass spectrometer analyses supplementary to ours.

---

[9] Graham, Harkness, and Thode, J. Sci. Inst. 24, 119 (1947).

THE REVIEW OF SCIENTIFIC INSTRUMENTS VOLUME 20, NUMBER 12 DECEMBER, 1949

A Single Pulse Voltmeter

G. T. RADO, M. H. JOHNSON, AND M. MALOOF
Naval Research Laboratory, Washington, D. C.

(Received August 19, 1949)

The voltmeter described herein is capable of measuring the average amplitude of a *single* pulse with a random error of 0.2 percent of full-scale deflection. The instrument consists of a gated cathode follower bridge in conjunction with a ballistic indicator. In its present form the circuit responds to the average pulse amplitude over an arbitrarily selected interval of two milliseconds; thus, it measures the actual amplitude in the special case of a flat pulse of sufficient duration. The required input is 0.8 volt for full-scale deflection. The nonlinearity is less than 1 percent of any given deflection throughout the major part of the range of the instrument.

INTRODUCTION

IN the course of investigating the complex permeability of ferromagnetic metals at very high frequencies,[1] we encountered the problem of measuring the voltage amplitude of a *single* pulse to a relatively high degree of accuracy. Typical pulse voltmeters described in the literature[2] cannot be used for single pulses because they require a finite pulse repetition rate. Since the accuracy to be attained in our application makes it difficult to use a cathode-ray oscilloscope, we were obliged to develop a special instrument, called the "single pulse voltmeter" (SPVM), to fulfill our requirements. The applicability of this instrument is definitely limited with respect to admissible pulse shapes. Although the edges of a given pulse may be irregular, the top must be flat for a certain minimum time interval in the vicinity of the instant at which the amplitude is to be measured. If this condition is not fulfilled, the SPVM determines an average rather than the instantaneous pulse amplitude. However, the SPVM has a number of characteristic advantages that may be useful in applications related to ours. It is of interest, therefore, to describe the particular form of the circuit which is used in our experiments.

REQUIREMENTS

The SPVM was developed to fulfill the following requirements. It should be capable of measuring the amplitude of a positive *single pulse*, as well as the magnitude of a *d.c. voltage*, with an accuracy of about *one percent* without requiring calibration; if calibrated, the instrument should be accurate to one-half percent or better. The SPVM should make it possible, moreover, to determine the amplitude at an *arbitrary instant* within the duration of the single pulse, Δt_p. It is permissible, however, to require a certain finite "*viewing interval*," Δt_v, for "sampling" the amplitude in the vicinity of the instant in question. Since the SPVM is to be used primarily with pulses characterized by a flat top (and irregular edges), the resolution of the instrument does not need to be very sharp and values of $\Delta t_v (\Delta t_v \leq \Delta t_p)$ as large as two milliseconds are acceptable. The SPVM should require an input of less than 20 volts for full-scale deflection, and it should have an input impedance of at least 10^4 ohms. Finally, the instrument should not only respond to a single pulse but it should yield an accurate reading *without* requiring a repetition of the pulse.

METHOD

The ideal instrument for observing voltage pulses is undoubtedly the cathode-ray oscilloscope in conjunction with a video amplifier. Since the time dependence of the voltage may be examined in its entirety, the sampling process previously mentioned is clearly unnecessary. For precise measurements, however, this method is not generally satisfactory because there are several serious limitations on the accuracy attainable: (1) size of the screen, or rather, of the central portion of the screen, on the cathode-ray tubes ordinarily available; (2) thickness of the beam trace, particularly in the case of the long retentivity screens essential for the precise measurement of single pulses; (3) linearity of video amplifiers having a large voltage output. Although the accuracy of the oscilloscope method may be improved to some extent by photographing the beam trace,[3] the delay caused by developing and evaluating the film is an obvious disadvantage.

---

[1] For a complete description of the experimental method, as well as references to earlier communications, see M. H. Johnson and G. T. Rado, "Ferromagnetism at very high frequencies. II. Method of measurement and processes of magnetization," Phys. Rev. 75, 841–864 (1949).

[2] See, for example, Y. P. Yu, "An improved peak voltmeter for pulses," Rev. Sci. Inst. 19, 447–450 (1948); and R. Rudin, "A direct reading pulse length meter and shape analyzer," Rev. Sci. Inst. 20, 467–471 (1949).

The SPVM to be described here is based on a ballistic measurement of charge. In principle, the main circuit consists of a switch and a ballistic galvanometer in series with a fictitious generator. The latter represents the signal voltage to be measured and is assumed to have a finite internal resistance. The switch is normally open but an auxiliary circuit is arranged to close it for a single, arbitrarily selected time interval, Δt_v, whose magnitude is a *constant* of the SPVM. As a result, a current pulse of duration Δt_v passes through the galvanometer and causes it to deflect ballistically. If Δt_v is very small compared to the period of the galvanometer, the deflection is proportional to the total charge contained in the current pulse. Since Δt_v is constant, the deflection is proportional to the *average* current amplitude in the interval Δt_v and thus to the average amplitude of the signal voltage in this interval. In the special case of interest, however, the signal voltage pulse (whose duration is Δt_p) has a constant amplitude for an interval longer than Δt_v, so that the deflection of the galvanometer is now proportional to the *actual* signal amplitude. The SPVM may also be used to measure the magnitude of an ordinary d.c. voltage since this may be regarded as a special case characterized by an infinitely long Δt_p.

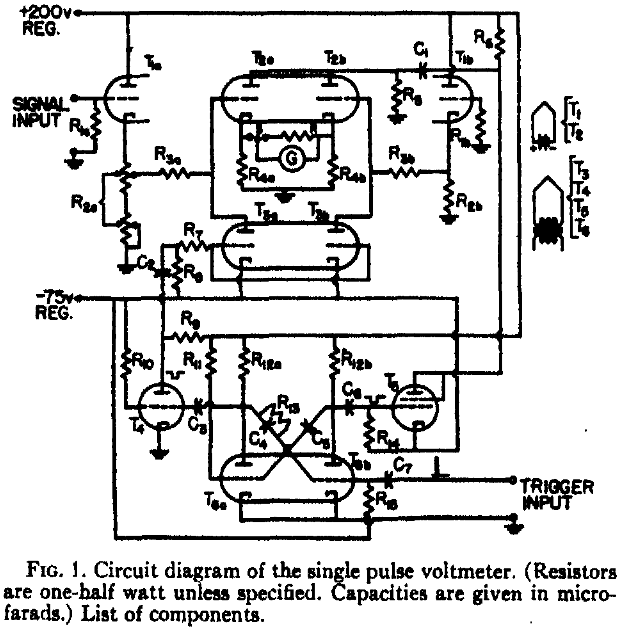

FIG. 1. Circuit diagram of the single pulse voltmeter. (Resistors are one-half watt unless specified. Capacities are given in microfarads.) List of components.

T_{3a}, T_{3b}—one-half 6SL7
T_5—6L6
All other tubes—one-half 6SN7
R—47K
R_{1a}, R_{1b}, R_{4a}, R_{4b}—22K
R_{2a}—1K and 5K potentiometers
R_{2b}—5.6K
R_{3a}, R_{3b}—220K
R_5, R_{10}, R_{11}—1 meg.
R_6—15K, 10 watt
R_7, R_{15}—100K
R_8—85K
R_9—100K, 1 watt
R_{12a}, R_{12b}—22K, 2 watts
R_{13}—150K
R_{14}—180K
C_1—1.0, 400 v, paper
C_2, C_3, C_6—0.05, 600 v, paper
C_4, C_7—0.0001, mica
C_5—0.004, mica
S—SPDT knife switch
G—ballistic galvanometer

Viewing interval: $\Delta t_v \approx 2$ milliseconds.
Galvanometer: Leeds & Northrup Company, Model 2285-D; sens. 3×10^{-10} coulomb/mm, CDRX 48K, period 32 sec., resist. 752 ohms.
Power supplies: +200 v electronically regulated; −75 v *VR*-regulated; filaments of T_1 and T_2: 6-v storage battery; filaments of T_3, T_4, T_5, T_6: 6-v transformer.

CIRCUIT

Figure 1 shows a schematic diagram of the SPVM circuit. The "switch" referred to in the previous section is seen to be replaced by two gated high vacuum triodes. These tubes are used as negative feed-back amplifiers of the cathode follower type in order that their performance be largely independent of voltage fluctuations and other instabilities. To obtain additional reliability, a bridge circuit is employed, and the ballistic galvanometer, *G*, is connected between the cathodes of two similar tubes, T_{2a} and T_{2b}. Normally these tubes are cut off but an auxiliary gating circuit makes them operative during an interval Δt_v. A voltage proportional to the signal is applied to the grid of one of these tubes T_{2a}, and the resulting unbalance of the bridge during Δt_v is measured as a ballistic deflection of the galvanometer. T_{2a} is isolated from the signal source by means of the cathode follower containing T_{1a}; a similar cathode follower (using T_{1b}) completes the symmetry of the arrangement. It may be noted that resistive coupling only is used in this part of the circuit in order to allow the measurement of d.c. voltages. The bridge is balanced by adjusting the potentiometer R_{2a} until the ballistic deflection in the absence of an input signal is zero.

The method of gating T_{2a} and T_{2b} is probably not conventional although it does involve some standard circuits. An external source supplies a trigger to the one-shot multivibrator, T_{6a} and T_{6b}, which generates a pair of single rectangular pulses, or "gates," of length Δt_v. The positive gate, taken from the plate of T_{6a}, is inverted in the stage containing T_4, and then used to drive T_{3a} and T_{3b} below cut-off. As a result, tubes T_{2a} and T_{2b} become conducting for the duration of Δt_v because their grid to cathode voltages are now above cut-off. In order to assure reproducible galvanometer deflections, these voltages should stay exceptionally constant; it is therefore important to note that their values during Δt_v are completely ***independent*** of the properties of the gating circuit. The negative gate, taken from the plate of T_{6b}, is inverted and amplified by T_5, and then applied to the plates of T_{2a} and T_{2b} during Δt_v. This process of pulsing the plate voltage on the cathode follower bridge may seem superfluous in view of the grid-gating described above. If the plate voltage is applied continuously, however, the zero reading of the galvanometer is found to drift due to leakage currents.

---

[3] Techniques for the periodic recording of single, fast traces on a cathode-ray tube are described by H. Goldstein and P. D. Bales, "High speed photography of the cathode-ray tube," Rev. Sci. Inst. 17, 89–96 (1946).

The filaments of tubes T_1 and T_2 are heated by a storage battery in order to improve the stability of the dynamic bridge balance (during Δt_v) and to avoid large discrepancies between the electrical and mechanical zero of the galvanometer. An electronic regulator is used to stabilize the +200-volt supply whereas a *VR* tube was found to be adequate for regulating the −75-volt supply. Most of the circuit components do not have critical values and are determined in a straightforward manner by tube ratings and the desired circuit characteristics. However, each of the resistances R_{4a} and R_{4b} should be approximately equal to one-half of the critical damping resistance of the galvanometer, and the constants of the multivibrator (particularly C_5, R_{11}, and R_{12b}) should be chosen to produce a Δt_v of the desired magnitude.

PERFORMANCE

Figure 2 shows a typical response curve of the SPVM taken with a d.c. input voltage obtained from a battery. It is seen that the required input is about 0.8 volt for full-scale deflection (≈ 50 cm), and that the non-linearity error computed from the data is less than one percent of any given deflection throughout the major part of the range of the instrument. At small deflections the errors are largely random errors (≤ 1 mm); at large deflections, on the other hand, the non-linearity of the bridge tubes becomes the limiting factor.

The accuracy of the SPVM may be improved by calibration and hence a reduction of the systematic errors due to non-linearity and the flat galvanometer scale. In this case the random error predominates; it is due to the limited precision with which the scale can be read because the stability of the bridge balance is better than one-half millimeter for periods up to about an hour. By using a calibrated SPVM and occasionally checking the bridge balance, it is possible to measure the ratio of two voltages with an accuracy of better that one-half percent over a range of about 6 db.

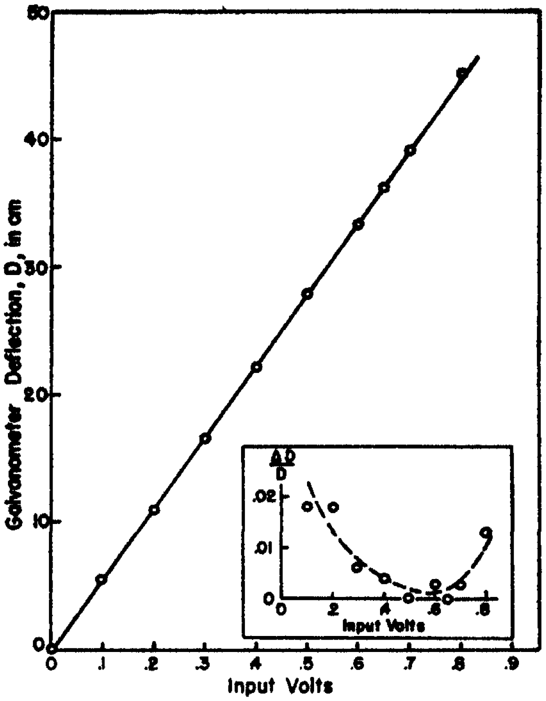

FIG. 2. Typical response curve of the single pulse voltmeter *without calibration*; the d.c. input voltage is obtained from a battery. Inset: the fractional error due to non-linearity, $\Delta D/D$, as computed from three sets of galvanometer deflections, D.

CONCLUSION

The SPVM described in this article represents the latest modification of an instrument which has been in use since September 1946. It fulfills all the requirements listed in a previous section and is best suited for the measurement of single pulses characterized by a flat top. The major disadvantages are the relatively slow operation necessitated by the ballistic indicator and the requirement of recalibration upon replacement of tubes T_1 or T_2. As implied previously, the SPVM may be used without modification for measuring the average amplitude or the total charge of a single pulse; it may also be used for measuring pulse length if the amplitude is constant. The resolution of the instrument may be improved by decreasing the time constant of the multivibrator and thus decreasing Δt_v.

THE REVIEW OF SCIENTIFIC INSTRUMENTS VOLUME 20, NUMBER 12 DECEMBER, 1949

Sliding Contacts to Transmit Small Signals

BILLY M. HORTON
Naval Research Laboratory, Washington, D. C.

(Received October 7, 1949)

Measurements have been made of root-mean-square noise voltage in the frequency range 0.5 to 200 c.p.s. generated by contacts sliding at low speeds using four arrangements of contacting bodies and various materials. Mercury with amalgamated probes gave the lowest noise levels. Some solid contacts operating with low friction on clean metal surfaces yielded values of generated noise below 1 microvolt at a sliding speed of 35 cm/sec. when two contacts were in parallel.

The noise increases with speed and varies with normal force. The r.m.s. generated noise voltage of a large number of independently mounted contacts in parallel is inversely proportional to the square root of the number of contacts.

IT is often necessary in experimental work to pass an electrical signal through a rotating joint. In the low frequency range this usually involves actual physical contact between the stationary and the rotating parts of the system; hence when rotation takes place some form of slippage must occur. Electrical impulses are usually generated by such sliding, and this electrical "noise" must be kept well below the level of the signal being passed.

Sliding contacts give rise to two main types of noise voltage. A contact which is carrying a sizeable current has variations in voltage corresponding to changes in its contact resistance. But even when practically no current is flowing through a sliding contact, electrical noise impulses still are generated by the sliding. Only this *generated* noise voltage is considered here. Its origin will not be discussed except to say that it is due partly to thermoelectric pulses from hot spots created by frictional heating and partly to effects of semi-conducting and insulating films. Its magnitude depends upon the materials used, the conditions of their surfaces, speed of sliding, normal force, and the number of contacts in parallel.

TABLE I. Generated noise voltage of brushes on solid rings (Two $\frac{1}{4}$-in.×$\frac{1}{4}$-in. brushes on each ring, sliding speed 35 cm/sec.).

Ring silver	Brush material	Generated noise microvolts	Normal force, g
Clean silver	G[a]	0.3	~50
	SG1	0.3	~50
	SG2	2.5	~50
Clean rhodium	G	0.8	30
	SG1	0.5	60
	RhG	0.4	50
Clean gold	G	0.6	40
Oxidized copper	G	11→1.0[b]	~50
Rhodium coated with silver sulfide	SG1	14	60
Electrographitic carbon	G	1.0→9[c]	900

[a] Symbols: G Natural graphite brush material, SG1 Silver-graphite, fine texture, low silver content, SG2 Silver-graphite, coarse texture, high silver content, and RhG Rhodium-graphite, 73 percent rhodium by weight.

[b] Generated noise voltage on oxidized copper was initially greater than value shown; it then decreased to approximately 1 microvolt after 100 rotations.

[c] Initial value of noise voltage was 1.0 microvolt; this increased to 9 microvolts as surface became glazed from sliding.

The generated noise voltage of a number of sliding contact arrangements has been measured. The conditions used in the work were chosen in order to find a suitable means for passing electroencephalograph signals out through the hub of a human centrifuge. In all of the tests two sliding contact arrangements were connected in series. The sliding speed used was 35 cm/sec. except where otherwise indicated.

In making the measurements the generated noise voltage was first amplified by a commercial electroencephalograph amplifier having a band pass of 0.5 to 200 c.p.s. The signal was then fed through a cathode-follower type amplifier into a thermo voltmeter having a time constant of 1.5 seconds for increasing and 3.0 seconds for decreasing deflection. The measuring apparatus had a noise voltage of 0.6 microvolt which was, in many cases, comparable in magnitude to the noise voltage generated by the contacts. It was necessary in these cases to make measurements of the noise voltage of the amplifying apparatus alone, in order that the average value of this noise could be eliminated from the measurements of the combined amplifier and contact noise.

The analysis and interpretation of the data was made according to the method which follows.

Let E_c = instantaneous voltage generated in the contacts, E_a = instantaneous noise voltage originating in the amplifying apparatus, and E_{a+c} = instantaneous total voltage of contacts and apparatus. We assume that E_a and E_c are independent, that E_a and E_c add linearly in the amplifier, and that the average value of each of them is zero (i.e., no d.c. component). Then it is easily shown that for a large number of observations

$$\langle E_c^2\rangle_{Av}=\langle E_{a+c}^2\rangle_{Av}-\langle E_a^2\rangle_{Av}. \tag{1}$$

Thus the expected value of $\langle E_c^2\rangle_{Av}$, which cannot be measured directly, can be determined from the measurable quantities $\langle E_{a+c}^2\rangle_{Av}$ and $\langle E_a^2\rangle_{Av}$.

An unbiased estimate of the variance σ_a^2 of $\langle E_a^2\rangle_{Av}$ is

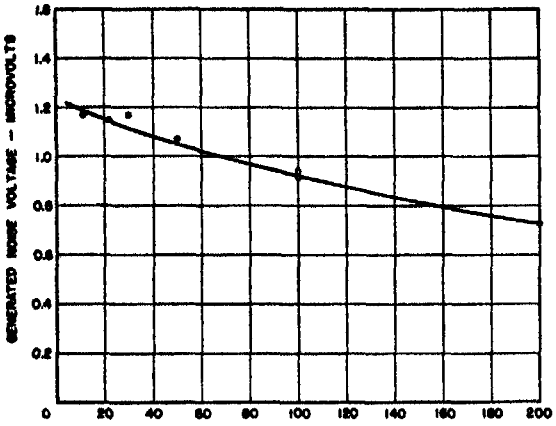

FIG. 1. Noise *vs.* normal force, ¼-in.×¼-in. rhodium-graphite brushes on rhodium-plated ring, speed 128 cm/sec.

given by

$$\sigma_a^2 = \frac{\sum_{i=1}^{n} \{E_a^2 - \langle E_a^2 \rangle_{\mathrm{Av}}\}^2}{n(n-1)}, \tag{2}$$

where n is the number of independent observations. A similar expression holds for the variance σ_{a+c}^2 of $\langle E_{a+c}^2 \rangle_{\mathrm{Av}}$. These variances can be used to obtain the variance σ_c^2 of $\langle E_c^2 \rangle_{\mathrm{Av}}$ according to the relation

$$\sigma_c^2 = \sigma_a^2 + \sigma_{a+c}^2, \tag{3}$$

which is valid for uncorrelated observations of E_a and E_{a+c}.

The usual procedure used for low noise contacts was to take, at 10-second intervals, 20 observations of E_a and then 20 observations of E_{a+c} until 100 readings of each had been obtained. These data were then used in expression (1) to determine $\langle E_c^2 \rangle_{\mathrm{Av}}$ and in expression (3) to determine σ_c^2.

It can be seen from expressions (1), (2) and (3) that it is possible for σ_c to be larger than $\langle E_c^2 \rangle_{\mathrm{Av}}$, and this was found to be the case with some of the materials used. For this reason the numerical values of generated voltage which are given correspond to the value $\{\langle E_c^2 \rangle_{\mathrm{Av}} + 2\sigma_c\}^{\frac{1}{2}}$ unless otherwise noted. This value is an upper fiducial limit on the noise voltage which is generated by the contacts. If it is assumed that the mean value $\langle E_c^2 \rangle_{\mathrm{Av}}$ follows a normal distribution, then the probability is approximately 0.98 that the actual r.m.s. values of generated noise voltage are less than the values given here.

The values of generated noise voltage obtained for solid brushes on metal and carbon rings are given in Table I. Clean metal surfaces used with brushes having satisfactory frictional properties can yield values of generated noise voltage below 1 microvolt under the conditions used. The coarse-textured silver-graphite SG2 had high friction when sliding on a clean silver surface and the generated noise of this combination was high. Several other metal-graphite brushes having 95 to 99 percent metal were tried, but these invariably had high friction, high wear, and high generated noise voltage. It may be seen from Table I that metal surfaces covered with corrosion films give much higher values of generated noise voltages than do clean surfaces. The electrographitic ring surface had a low value of noise immediately after sanding, but as rotation proceeded the surface became glazed and generated noise increased.

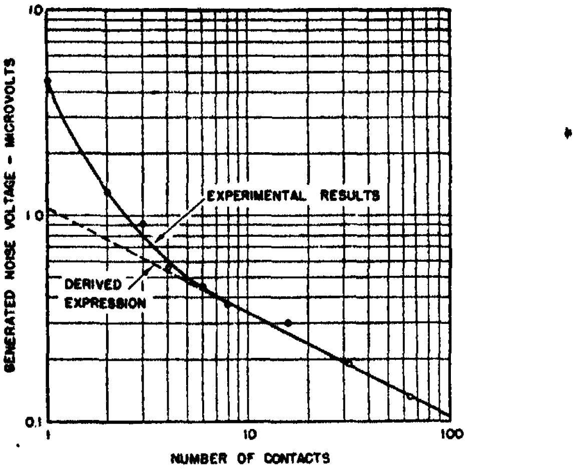

FIG. 2. Noise *vs.* number of contacts, natural graphite cubes between 45° beveled gold-plated rings, average weight of cubes 0.3 g.

Two types of liquid rings have been tried, one consisting of mercury and the other of sodium chloride solution. The liquid was poured into circular troughs which were then rotated, and contact to the rings was made by means of probes dipping into the liquid. Mercury rings with amalgamated copper probes gave values much below that of the measuring apparatus. From the dispersion in the experimental data the upper fiducial limit on the generated noise voltage can be set at 0.1 microvolt. Neither a scum of mercury sulfide nor a suspension of mercury sulfide in oil on the surface caused a measurable increase in noise when amalgamated copper probes were submerged in mercury. The sodium chloride solution with either gold or copper probes was found to generate voltages greater than 100 microvolts.

In order to minimize frictional heating, a "rolling-ball" apparatus was tried. This apparatus consisted of an inner ring, beveled on its outer edge at an angle of 45°, an outer ring similarly beveled on its inner edge, and balls which rolled in the V-groove between the rings. Two of these ball races were connected in series and up to 63 balls were placed in each groove. The whole apparatus was plated with gold to minimize the effect of corrosion films. Despite careful cleaning, this rolling-ball apparatus gave high values of generated noise and frequently developed an open circuit. With 63 balls in each of the grooves, the generated noise voltage was 1 microvolt.

All of the contact combinations were found to have a generated noise voltage which increased with speed. In the case of metal-graphite brushes on clean metal surfaces the generated noise voltage is very nearly proportional to speed in the range 35 to 130 cm/sec.

The normal force used to press the surfaces together also affects the amount of generated noise voltage, $\{\langle E_c^2\rangle_{Av}\}^{\frac{1}{2}}$. This relationship for rhodium-graphite brushes on a rhodium-plated ring is shown in Fig. 1. Not all materials, however, have a decreasing generated noise with increasing normal force. Natural graphite brushes on electrographitic rings, for example, showed an increase in noise with normal force up to the highest normal force used, 900 g.

When several contacts are operated in parallel, the generated noise voltage is less than that of a single contact. It can be shown that, for a large number of independently acting contacts, the r.m.s. generated noise voltage is inversely proportional to the square root of the number of contacts. In Fig. 2 values of $\{\langle E_c^2\rangle_{Av}\}^{\frac{1}{2}}$ are plotted against number of contacts. The gold-plated V-groove rings were used in these measurements, but in place of the rolling balls, $\frac{1}{4}$-in. cubes of natural graphite brush material were allowed to slide in the grooves. These cubes were able to act almost independently of each other since each was pulled down by its own weight, approximately 0.3 g.

In order to get an extremely large number of contacts coarse graphite flakes were poured into a deep circular trough and rings of gold-plated wire were submerged in the flakes. The generated noise of this combination is probably less than 0.12 microvolt, but the practical difficulty of sealing-in the mist of graphite flakes and the high resistance (6 to 8 ohms) compared with most of the other contact devices make this arrangement undesirable.

In conclusion, it can be stated that graphite or metal-graphite brushes operating with low friction on clean metal surfaces can yield very low values of generated noise voltage in the frequency range considered. High friction or corrosion films increase the generated noise. The noise increases with an increase in speed and can either increase or decrease with a larger normal force, depending upon the conditions in the rubbing surface. By operating a large number of contacts in parallel, a great reduction in generated noise voltage is possible. Mercury rings with amalgamated probes give lowest values of generated noise voltage.

THE REVIEW OF SCIENTIFIC INSTRUMENTS VOLUME 20, NUMBER 12 DECEMBER, 1949

The Gamma-Ray Counting Efficiency for a Lead-Cathode G-M Counter

E. T. JURNEY* AND FRED MAIENSCHEIN**
Indiana University, Bloomington, Indiana

(Received August 19, 1949)

The dependence of gamma-ray counting efficiency on energy has been determined in the range 0.17 Mev to 2.76 Mev for a G-M counter with a lead cathode. The efficiency for six energy values was found by coincidence measurements utilizing the disintegration of In^{111}, Au^{198}, Co^{60}, and Na^{24}. The result indicates a smooth increase in counting efficiency for increasing energy over the range of energies investigated.

THE application of coincidence counting techniques[1,2] to securing quantitative information about nuclear decay schemes demands a knowledge of the counting efficiency as a function of gamma-ray energy for the gamma-ray counters employed. Knowledge of this efficiency in fact enables one to test any particular proposed scheme by a simple determination of the ratio of the gamma-gamma-coincidence rate to the rate of counting gamma-rays in one of the two counters, although such a test is not always completely unambiguous.

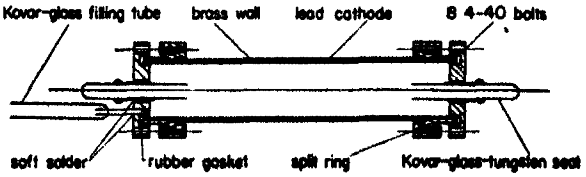

FIG. 1. Details of counter.

Norling[3] and Bradt, Gugelot, Huber, Medicus, Preiswerk, and Scherrer[4] have published gamma-ray counter efficiency curves for a number of different cathode materials. Such a curve for counters with lead cathodes has been obtained for use in conjunction with some coincidence experiments done in this laboratory, with results somewhat different from those of the published curves. Lead was chosen for the cathode material in order to get high counting efficiency, especially for gamma-rays having an energy of the order of a few hundred kilovolts.

---

* Now at Los Alamos Scientific Laboratory, Los Alamos, New Mexico.

** Now at NEPA Project, Oak Ridge, Tennessee.

[1] A. C. G. Mitchell, Rev. Mod. Phys. 20, 296 (1948).

[2] M. L. Wiedenbeck and K. Y. Chu, Phys. Rev. 72, 1164 (1947).

[3] F. Norling, Arkiv. f. Mat. Astr. o. Fys. 27A, No. 27 (1941).

[4] Bradt, Gugelot, Huber, Medicus, Preiswerk, and Scherrer, Helv. Phys. Acta 19, 77 (1946).

In the measurements to be described, the relative counter efficiency, i.e., that fraction counted of the total number of gamma-rays issuing from a source, was determined. We shall designate this relative efficiency by the symbol $\omega\epsilon$, which indicates that the quantity is the product of an absolute efficiency ϵ times a solid angle factor ω. This procedure obviates the necessity for determining the solid angle intercepted by the counter, but requires that the solid angle be kept constant for all the measurements.

The rate of counting beta-gamma- and gamma-gamma-coincidences arising from a particular radioactive disintegration depends directly on the counting efficiency for the gamma-rays which are emitted in the disintegrations. Thus, through the choice of simple, well-established decay schemes which involve gamma-rays with energies in the region of interest, one is able to deduce the counting efficiency for a wide range of energies.

I. DESCRIPTION OF THE COUNTERS

Figure 1 is a sketch of the counter details. The counter cathode is composed of a cylindrical brass jacket of 0.5-mm wall thickness inside of which is pressed a lead cylinder of the same wall thickness. It is likely that such a cathode might be more easily constructed by pouring the lead into a pre-tinned brass jacket and machining the surface to the proper thickness. The only surface treatment given the cathode was a cleaning with organic solvents and a rinsing with distilled water. The effective counting volume extends for 8.0 cm and is 2.2 cm in diameter. The counter anode is a 0.005-in. tungsten wire which is joined to short lengths of 0.020-in. tungsten wire at each end for sealing. The customary filling mixture of 1 cm Hg of ethyl alcohol vapor and 9 cm Hg of argon was employed. Each of the five counters which were constructed displayed good plateaus, but their background counting rates were somewhat higher than those of counters with more conventional cathode surfaces.

A. Cobalt 60

Cobalt 60 (5.3 yr.) decays by the emission of a single 300-Kev beta-ray group with the subsequent release in cascade of gamma-rays of 1.1 Mev and 1.3 Mev[5,6] energy from the resulting excited state of Ni^{60}. From such a cascaded pair of gamma-rays one expects the ratio of the gamma-gamma-coincidence counting rate to the rate of counting gamma-rays in one of the counters to be

$$\frac{N_{\gamma\gamma}}{N_\gamma}=\frac{2(\omega\epsilon_{1.1})(\omega\epsilon_{1.3})}{\omega\epsilon_{1.1}+\omega\epsilon_{1.3}}.$$

The energies are very nearly the same, however, and one is justified in considering this ratio to be the same as that given by two 1.2 Mev gamma-rays in cascade:

$$N_{\gamma\gamma}/N_\gamma=\omega\epsilon_{1.2}.$$

The experimentally determined value is $\omega\epsilon_{1.2}=(1.12\pm0.02)\times10^{-3}$.

B. Gold 198

It has been fairly well established[7] that the disintegration of Au^{198} is accomplished by the emission of a single beta-ray group which leads to an excited state of Hg^{198}, which in turn goes to the ground state through the release of a single 0.411-Mev[8] gamma-ray. The conversion coefficient α for this gamma-ray has been determined to be 0.025 by Peacock and Wilkinson.[9] For this simple mode of disintegration we expect the ratio of counting beta-gamma-coincidences to the rate of counting beta-rays to be

$$\frac{N_{\beta\gamma}}{N_\beta}\approx\frac{N_0(1-\alpha)F(0)\omega\epsilon_{.411}}{N_0F(0)(1+\alpha)}=0.95\omega\epsilon_{.411},$$

where $F(0)$ is the fraction counted of the electrons emitted by the source with no absorber before the beta-counter, and N_0 is the disintegration rate of the source.

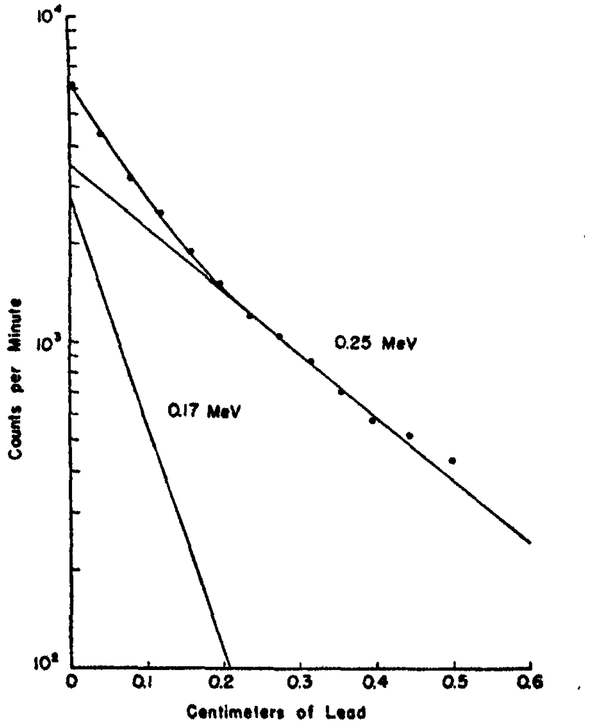

FIG. 2. Lead absorption curve for the gamma-rays from Cd^{111}.

---

[5] M. Deutsch and L. G. Elliott, Phys. Rev. 62, 558 (1942).

[6] Deutsch, Elliott, and Roberts, Phys. Rev. 68, 193 (1945).

[7] E. T. Jurney, Phys. Rev. 74, 1049 (1948).

[8] DuMond, Lind, and Watson, Phys. Rev. 72, 1271 (1947).

[9] C. L. Peacock and R. G. Wilkinson, Phys. Rev. 74, 1250 (1948).

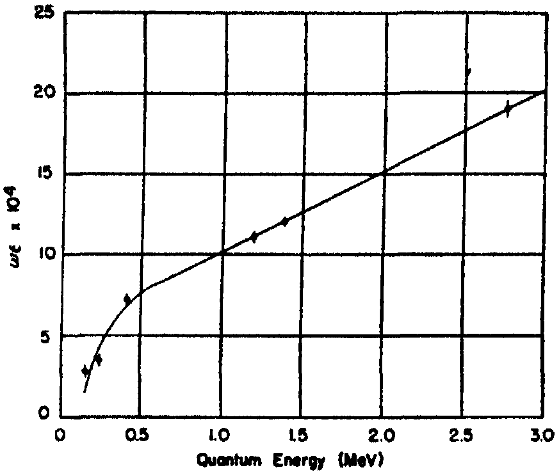

FIG. 3. Relative gamma-ray counting efficiency $\omega\epsilon$ as a function of energy.

One thus finds the relative efficiency for counting 0.411-Mev gamma-rays from a measurement of the beta-gamma coincidence rate. The quantity F cancels, furthermore, and the result is therefore independent of absorption or counting efficiency for the beta-rays.

In order to register beta-gamma-coincidences, one of the gamma-ray counters was replaced by an end-window type counter which had good transmission for the beta-rays. The resulting value for $\omega\epsilon_{.411}$ was $(0.736\pm0.01)\times10^{-3}$.

C. Indium 111

Indium 111 undergoes K-capture and the resulting Cd^{111} reaches the ground state by emitting in cascade gamma-rays of 0.17 Mev and 0.25-Mev[10] energy.

In this low energy region the dependence of relative efficiency on energy is likely to be critical, and one would like to be able to establish a point on the efficiency *vs.* energy curve for each of the gamma-rays. On the customary lead absorption curve the ratio of the counting rates for the two components at the initial part of the plot gives the efficiency for counting one of the gamma-rays relative to the efficiency for counting the other, if it is assumed that both gamma-rays are present in the same abundance. Actually, Boehm, Huber, Marmier, Preiswerk, and Steffen[11] report internal conversion coefficients of 0.09 for the 0.17-Mev gamma-ray and 0.042 for the 0.25-Mev gamma-ray. Figure 2 shows the lead absorption curve which was obtained; the ratio of the initial intensities is 1.30, and after correcting for internal conversion one finds that $\omega\epsilon_{.25}=1.23\omega\epsilon_{.17}$. The ratio of the rate of counting gamma-gamma-coincidences to the rate of counting gamma-rays in one of the counters is for this case:

$$\frac{N_{\gamma\gamma}}{N_\gamma}=\frac{2(\omega\epsilon_{.17})(\omega\epsilon_{.25})\times0.91\times0.958}{0.91\omega\epsilon_{.17}+0.958\omega\epsilon_{.25}}=1.15\omega\epsilon_{.17}.$$

The value of $N_{\gamma\gamma}/N_\gamma$ was found to be $(0.328\pm0.01)\times10^{-3}$; from it we obtain $\omega\epsilon_{.17}=(0.285\pm0.03)\times10^{-3}$ and $\omega\epsilon_{.25}=(0.350\pm0.03)\times10^{-3}$.

D. Sodium 24

Sodium 24 decays with the emission of a single beta-ray group of 1.39 Mev, and the resulting Mg^{24} nucleus emits two gamma-rays with 1.38 Mev and 2.76 Mev energy.[12] The expected gamma-gamma-coincidence ratio for the two gamma-rays is thus:

$$\frac{N_{\gamma\gamma}}{N_\gamma}=\frac{2(\omega\epsilon_{1.38})(\omega\epsilon_{2.76})}{\omega\epsilon_{1.38}+\omega\epsilon_{2.76}}.$$

The energy of the 1.38-Mev gamma-ray is near the 1.2-Mev value for which the efficiency was measured through the disintegration of the Co^{60}, and one expects the efficiency difference to be correspondingly small. Making use of the value of the efficiency at 1.2 Mev, as a first approximation, and the measured value of $N_{\gamma\gamma}/N_\gamma=(1.49\pm0.03)\times10^{-3}$, the efficiency for 2.76 Mev was determined as 2.23×10^{-3}. This value of the efficiency, together with the ones at 0.411 Mev and 1.2 Mev, determines a straight line. Therefore, the efficiency at 1.38 Mev can be more closely estimated and that at 2.76 Mev can be recalculated on the basis of the better approximation at 1.38 Mev. The efficiencies determined in this way are $\omega\epsilon_{1.38}=(1.22\pm0.02)\times10^{-3}$ and $\omega\epsilon_{2.76}=(1.91\pm0.05)\times10^{-3}$.

II. DISCUSSION

The complete curve of efficiency *vs.* energy is shown in Fig. 3. The shape of the upper portion of the curve (above 0.5 Mev) agrees quite well with that obtained by Bradt *et al.*[4] but there is marked disagreement in the low energy region. The Swiss group also made use of the disintegration of In^{111} in this region and found a sharp increase in efficiency for decreasing energy below about 0.5 Mev. This discrepancy in the results might be explained by the presence of a small amount of the positron-emitting activity of In^{109} in the source used by Bradt *et al.* for gamma-gamma-coincidences produced by annihilation radiation would occur at a rate which was greater by a factor of $1/\omega$ than the coincidences produced by two 0.51-Mev gamma-rays in cascade. The quantity $1/\omega$ amounts to about ten in the conventional coincidence counting geometry. This explanation is contradicted, however, by the fact that their lead absorption curve indicates a higher efficiency for counting the 0.175-Mev gamma-ray than it does for counting the 0.25 Mev one.

The authors are indebted to Professor A. C. G. Mitchell, who initially suggested the investigation and who gave valuable suggestions during the course of the work. This research was assisted by the joint program of the ONR and the AEC.

---

[10] J. M. Cork and J. L. Lawson, Phys. Rev. 56, 291 (1939).

[11] Boehm, Huber, Marmier, Preiswerk, and Steffen, Helv. Phys. Acta 22, 70 (1949).

[12] K. Siegbahn, Phys. Rev. 70, 127 (1946).

THE REVIEW OF SCIENTIFIC INSTRUMENTS VOLUME 20, NUMBER 12 DECEMBER, 1949

A Secondary-Emission Electron Multiplier Tube for the Detection of High Energy Particles*

ROBERT P. STONE
RCA Laboratories Division, Radio Corporation of America, Princeton, New Jersey

(Received September 2, 1949)

The requirements of high gain and low background current in an electron-multiplier tube for the direct detection of high energy particles are considered. The design and construction of an experimental electron-multiplier tube with a stable over-all gain of at least 10^8 and a background at room temperature corresponding to three or four electrons per minute released at the input is described. An 0.0008-inch thick nickel window is provided in the tube envelope to admit the high energy particles to the multiplier. The efficiency of this device is compared quantitatively with that of a Geiger tube as a detector of beta-particles. It is found that the over-all beta-particle counting efficiency of the tube is of the order of 1.3 percent, and that the efficiency of the oxidized silver magnesium target surface is 4.9 percent for a uranium source and 6.0 percent for a strontium source.

I. INTRODUCTION

THE main purpose of this investigation was to determine the feasibility of using a high gain secondary-emission electron-multiplier tube directly as a detector of high energy particles, particularly beta-particles, and to determine quantitatively the efficiency of its operation.

The use of electron multiplier tubes as detectors of high energy particles has been reported in the literature, but only in a rather qualitative form. Z. Bay[1, 2] has described briefly the use of the electron multiplier tube in counting photons and gamma-rays, and he has described in more detail[3] the application to alpha-, beta-, and x-rays. Bay reports[3] that he was able to count every alpha-particle and "perhaps" every beta-particle. The efficiency of counting gamma- and x-rays was about that obtainable with an ordinary Geiger-Müller counter.

J. S. Allen[4] has applied the electron multiplier to the mass spectrograph for counting of positive ions and electrons. He also reports[5] using a multiplier tube as an alpha-particle detector with near 100 percent efficiency. More recently, Allen has described[6] an electron-multiplier particle counter applied to an electron spectrometer and as an alpha-particle detector.

In an effort to minimize unwanted currents in their high voltage apparatus, Trump and van de Graaff[7] have made an experimental study of the secondary-emission ratio of several metals with primary electron velocities in the range of 30 to 340 kilovolts. Their data seem to indicate that the secondary-emission ratio is roughly inversely proportional to voltage in this region, being 0.12 for tungsten and 0.05 for aluminum at 300 kilovolts. The secondary-emission ratio is here defined as the ratio of the number of low velocity secondary electrons to the number of incident primary electrons.

From an extrapolation of Trump's data into the megavolt region it might be guessed that a secondary-emission beta-particle detector would have only a few percent efficiency, due to the small probability that an incident beta-particle would release a low velocity secondary electron. In a recent survey article on counting techniques Corson and Wilson[8] state: "With beta-particles the average number of secondaries per incident particle is small—. The result is a low counting efficiency for beta-particles, although quantitative data are not available." These quantitative data were sought in this investigation.

II. REQUIREMENTS OF THE MULTIPLIER TUBE

It is necessary for satisfactory detection of high energy particles that the electron-multiplier tube have sufficiently high gain and sufficiently low background noise that the incidence of a single electron at the input can be detected.

Assuming a secondary-emission ratio of greater than unity, the gain may be made as large as desired by using a sufficient number of stages. With a twelve-stage multiplier a stable gain of at least 10^8 was readily obtained.

The factor limiting the amount of gain which may be employed is the noise or "dark current" of the multiplier. Rajchman[9] has made a careful analysis of the sources of dark current in electrostatic electron multipliers. He lists the following as the main causes of dark current:

(1) ohmic leakage to the collector circuit,
(2) the effects of ionization of the residual gas,

---

[*] This report contains material presented as a thesis for the Doctor of Philosophy Degree in Electrical Engineering at Princeton University. The work was performed at RCA Laboratories in Princeton under the joint supervision of RCA and Princeton University.

[1] Z. Bay, Nature 141, 284 (1938).

[2] Z. Bay, Nature 141, 1011 (1938).

[3] Z. Bay, Rev. Sci. Inst. 12, 127 (1941).

[4] J. S. Allen, Phys. Rev. 55, 966 (1939).

[5] J. S. Allen, PB49548, U. S. AEC.

[6] J. S. Allen, Rev. Sci. Inst. 18, 739 (1947).

[7] J. G. Trump and R. J. van de Graaff, Phys. Rev. 75, 44 (1949).

[8] D. R. Corson and R. R. Wilson, Rev. Sci. Inst. 19, 207 (1948).

[9] J. A. Rajchman, Arc. des Sci. Phys. et Naturelles, 5e periode 20 (September–December, 1938).

(3) field emission from the conductors within the tube,
(4) thermionic emission of the electrodes.

The collector system must be appropriately designed, in both the internal tube structure and the external circuit, so as to minimize ohmic leakage. If present, this leakage may cause not only a varying d.c. component of the background current but also spurious pulses due to rapid fluctuations.

If there exists physically within the tube a direct path from output to input it may be possible to maintain a continuous current flow within the tube with no external excitation, due to ion feedback. The residual gas may be ionized by the electrons as they follow their normal paths through the multiplier. The positive ions so formed will tend to travel backwards in the multiplier structure from output toward input, releasing secondary electrons at the input if they strike the target surface. They thus constitute a positive feed-back link, which could be triggered by any residual electrons in the multiplier. Therefore, the tube design should be such as to best isolate the output from the input.

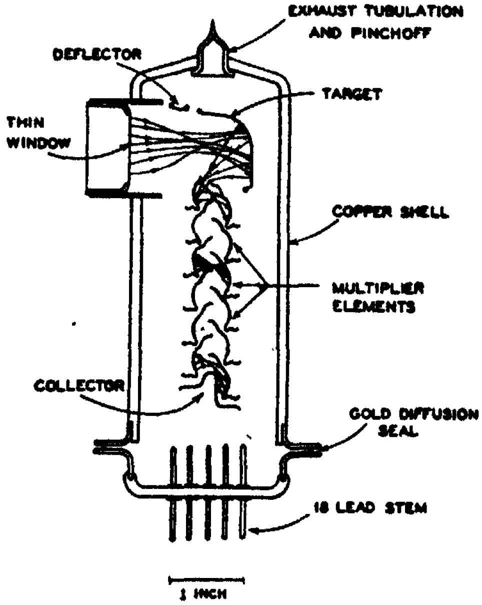

FIG. 1. Outline of tube structure and electron paths.

Field emission will occur at the surface of a conductor when the potential gradient is sufficiently large. It is thus necessary to physically design the multiplier structure to minimize the potential gradients, and to eliminate any sharp edges or projections from the parts at points of high gradient.

The foregoing causes of dark current may be reduced to a negligibly small value by exercising sufficient care in design and construction of the multiplier tube. The thermionic emission of the tube electrodes is, however, a fundamental limitation. This follows the standard Richardson equation for temperature-limited thermionic emission, with the temperature of the emitter being approximately room temperature. If the number of electrons released at room temperature is to be no greater than ten per minute, the work function of the emitting surface must be greater than 1.0 to 1.5 volts. For many of the commercially used secondary-emission surfaces the work function is considerably less than one volt. Thus the material for the secondary-emission surfaces must be selected with care.

If one must use a material of low work function for the secondary-emission elements, it is possible to reduce the thermionic emission by cooling of the multiplier structure. In a 931-A multiplier photo-tube, R. W. Engstrom[10] found that the room temperature thermionic emission from the first stage was of the order of 10^{-14} ampere. This is equivalent to about 10^6 electrons per minute. By cooling the tube to liquid air temperature the background count was reduced to about ten per minute.

While cooling of the multiplier tube may be practical in some cases, there may be experimental arrangements in which this would not be possible. Thus the use of a secondary-emitter material with a high work function is the more desirable solution to the problem.

III. DESIGN OF THE MULTIPLIER TUBE

Aside from the consideration of the general requirements of a high gain multiplier tube and the mechanical problems involved in its actual assembly, the main design problem is one of determining suitable electron optics. There are two general methods of accomplishing the proper focusing of electrons from stage to stage: by the use of either magnetic or electrostatic fields. In either case the electrons follow the paths indicated by simple ballistics.

In designing an electrostatic multiplier structure it is most useful, if not essential, to be able to predict the electrostatic field due to a given configuration of electrodes and the motion of an electron in this field. There are several quite useful experimental methods of determining electrostatic fields and electron trajectories. These are described in some detail by Zworykin and Rajchman[11] in their article on the development of the electrostatic electron multiplier.

The rubber model is a convenient experimental method which solves simultaneously the potential distribution and trajectory problems. Elevation on a suitably stretched rubber membrane corresponds to the potential field within the tube, and the trajectories of small balls are similar to the electron paths.

The rubber model technique was used in the development of the electrode structure for the multiplier tube used in these experiments. For the main multiplier chain it was decided to use a design known as the L16 element which had previously been developed by Rajchman for high gain, low dark current applications.

---

[10] R. W. Engstrom, J. Opt. Soc. Am. 37, 420 (1947).

[11] V. K. Zworykin and J. A. Rajchman, Proc. I.R.E. 27, 558 (1939).

In the design of the input system it is desired that a target as large as possible be exposed to the incident radiation, and that all secondary electrons originating at this target be focused into the multiplier chain. It is also necessary in the design of the input system to take into account the thin window in the vacuum envelope which admits the high energy particles into the multiplier. It is desired that any low velocity electrons which might be released at the inner surface of the thin window would also be directed into the multiplier chain. Thus each incident particle would have two opportunities to be detected, one by the release of secondary electrons as it passed through the window and another as it struck the target. The structure developed presents a useful target area of 0.8 square inch.

In the design of the collector electrode, it is desired to collect all the electrons from the last multiplier element, and not to disturb too badly the electron trajectories between the next-to-last and the last elements. Also, the collector should physically close the end of the multiplier chain, to minimize the possibility of ion feedback. Since the signal currents involved in this application are quite small it is not necessary to consider the effect of changing collector potential due to the ohmic drop caused by the signal current flowing in the load resistor. If this were not negligibly small, a much more complex collector system would be required to obtain a pentode characteristic.

The outline of the complete tube structure is shown in Fig. 1, together with the approximate electron paths. While the tube was designed for ready fabrication, it should be emphasized that it is entirely of an experimental nature and not available commercially.

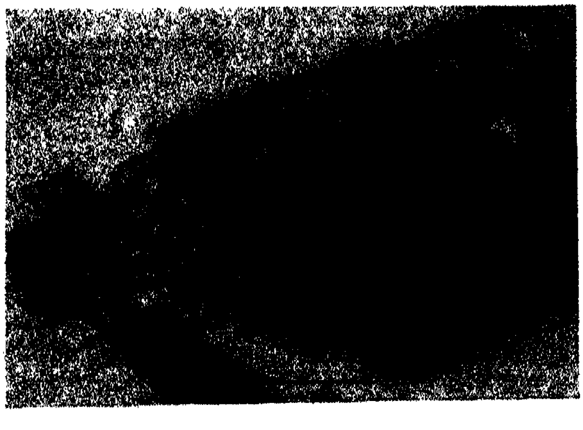

FIG. 2. Internal structure of multiplier tube.

IV. CONSTRUCTION OF THE MULTIPLIER TUBE

The details of the mechanical structure of the tube can also be seen in Fig. 1. A photograph of a sample internal structure is shown in Fig. 2. A photograph of a completed tube is shown in Fig. 3.

The multiplier electrodes are supported between ceramic rods, which extend through drilled holes in mica sheets on either side of the mount, so that the multiplier assembly is completely enclosed. The input system and collector electrode are supported by wires which also pass through the mica sheets. The entire assembly is supported from an 18-lead stem by the connecting leads. The width of the mica sheets and the length of the ceramic rods are so proportioned that the assembly will fit snugly inside the cylindrical envelope and thus be held together.

FIG. 3. Completed tube for beta-particle detection.

The target electrode and all the multiplier elements are made from 0.005-inch thick silver-magnesium sheet. Silver-magnesium was chosen for the secondary emission surfaces because of the stability of its secondary emission characteristics and because of the fact that it may readily be preprocessed (oxidized) before assembly. The preprocessed elements are relatively insensitive to exposure to dry air; in fact this type of element is quite useful in a demountable system. After the preprocessed elements are assembled, no additional activation is required. The tube is simply baked for degassing, and sealed off.

The remaining electrodes, namely the deflecting electrode in the input system and the collector are made of 0.005-inch thick cupro-nickel, a 70-30 copper-nickel alloy. The supporting wires for the input system and collecting electrode, as well as the connecting leads to the stem for all the electrodes, are made from nickel-chromium alloy wire (nichrome).

In the final tubes a copper envelope assembly was used. A copper shell was chosen because it would form a heavy, non-magnetic, light-tight shield. The side arm cylinder and cup were drawn from cupro-nickel sheet. The copper envelope assembly was made by silver soldering the various parts together in a hydrogen furnace. As a final stage in preparing the envelope, the cup containing the thin window is silver soldered into the arm of the envelope by RF heating in an atmosphere of hydrogen.

A gold diffusion seal was chosen for the final seal because it eliminates the possibility of contamination by sealing flames. This is thought to be a very necessary precaution in order to secure reproducible results with the secondary emission surfaces. Kovar was chosen as the base metal for the seal flanges because of the necessity of matching the thermal expansion of the adjacent glass section of the stem. It is possible to copper plate the Kovar and make the usual gold-to-copper diffusion seal to the copper plating.[13] In the final assembly of a tube, massive clamps are arranged to squeeze a ring of gold wire between the copper plated Kovar sections. The clamps contain a large copper section whose expansion on heating will increase the pressure on the gold ring. The actual diffusion of the gold into the copper is effected as the tube is baked out on the exhaust pumps.

A copper pinch-off tubulation was chosen to eliminate the possibility of contamination from gas released in the usual glass tip-off. In effecting the pinch-off, the copper tubulation is simply squeezed under great pressure until it is pinched in two. If the surfaces are clean, a vacuum tight seal invariably results.

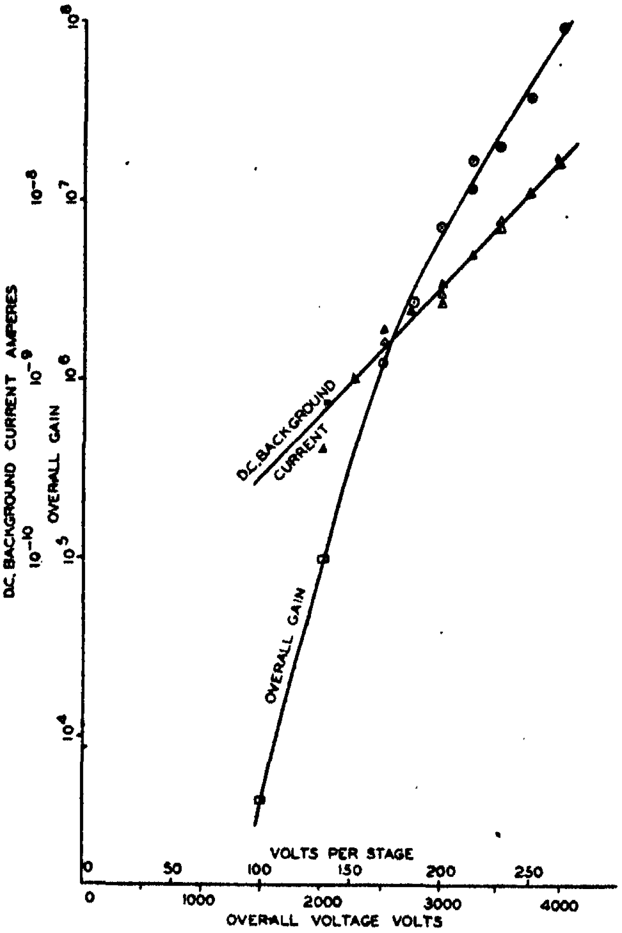

FIG. 4. Variation of over-all gain and d.c. background with voltage.

After the main features of the design had been worked out as outlined above, there still remained the problem of mounting a suitable thin window in the wall of the tube envelope for the admission of the beta-particles. The requirements on this window are twofold: that it be such that the high energy beta-particles may readily pass through it, and yet sufficiently strong mechanically to form part of the vacuum envelope of the tube.

The first requirement implies that the product of thickness times density be a minimum for the material used for the window. The second requirement implies that this thin foil be sufficiently strong mechanically to withstand evacuation, and rugged enough to form a reliable portion of the tube envelope. It is also necessary that the thin foil be capable of being suitably sealed to the envelope assembly, and moreover that it be capable of withstanding a bake of 450°C while evacuated.

For similar applications in Geiger tubes windows of thin mica or aluminum are used. They are usually clamped or waxed in place. Neither of these techniques would be satisfactory for the present tube. Grade A nickel was available in sheets 0.0008 inch thick. Disks of this material are readily silver soldered into the cupro-nickel cups in a hydrogen furnace. The windows so formed withstand evacuation and baking without oxidation and have shown no tendency to leak or rupture. The unsupported area of this window is $\frac{7}{8}$ inch in diameter.

Thus from the mechanical standpoint the nickel windows seem to be entirely satisfactory; they are quite easily fabricated and require no special techniques in handling. From the standpoint of transmission of beta-particles, the nickel should be slightly inferior to the aluminum. The thickness-density product for the 0.0008-inch thick nickel window is 0.0178 grams per square centimeter. This should just pass 130 kv beta-particles. This is a sufficiently low value for the tests contemplated. Therefore, because of their satisfactory mechanical properties the 0.0008-inch thick nickel windows were used on the tubes intended as beta-particle counters.

V. TESTS ON THE MULTIPLIER TUBES

The first two tubes constructed had substituted in place of the thin window a header containing leads which supported several small tungsten filaments just inside the envelope. By heating these filaments it was possible to introduce electrons into the structure as if they were originating at the back of the window. By this means it was possible to study the behavior of the multiplier and to measure its over-all gain. This is plotted in Fig. 4, together with the d.c. background current. This d.c. background was determined to be largely ohmic leakage to the collector system.

From the test data it was determined that the secondary emission ratio was quite constant from stage to stage in the multiplier. The variation with voltage of the secondary emission ratio of the oxidized silver magnesium surfaces is plotted in Fig. 5.

Having thus determined the d.c. characteristics of the multiplier, the possibility of detecting single electrons as its input was next investigated. The total charge deposited on the collector by a pulse originating as a single electron at the input will be the charge on the electron times the gain of the multiplier. The voltage pulse developed at the collector will be the quotient of this total charge divided by the capacity of the collector system. In order to avoid adding any cable capacity to the output capacity, a cathode follower stage was connected directly to the load resistor and all further observations made at the output of the cathode follower.

---

[13] Law, Whalley, and Stone, RCA Review 9, 643 (1948).

With the cathode follower in place the measured total output capacitance of the multiplier was $15.5 \cdot 10^{-12}$ farad. Thus with a multiplier gain of 10^7 a single electron should produce about a 0.1-volt pulse at the output. This could be readily observed with an ordinary laboratory oscilloscope containing an amplifier.

When the system was set up under these conditions and the filaments at the input heated slightly, a random "rain" of pulses of about the expected amplitude was observed on the oscilloscope. When the heating current was removed from the filaments it was found that there was still a scattering of pulses due to photoelectric emission caused by light entering the glass portions of the envelope. As these glass portions were progressively shielded the number of pulses decreased until with the structure in total darkness the background rate was 3 or 4 pulses per minute.

From the preceding tests it was concluded that the sensitivity of the multiplier was adequate to detect single electrons at its input, and that the number of background pulses was sufficiently low to permit room temperature operation.

In all, three tubes were assembled using the 0.0008-inch thick nickel window for the tests of efficiency of counting beta-particles.

The radioactive sources available were a small piece of uranium metal and a sample of strontium 90. Both of these are beta-emitters which are relatively free of other forms of radiation. The uranium source has a spectrum made up of several components with a maximum energy of 2.3 Mev. The spectrum of the strontium has a maximum at 0.3 Mev and a high energy cut-off of 2.4 Mev. The incident intensity of the sources was checked by observing the response of a thin mica window Geiger tube when given the same exposure as the window of the multiplier tube.

When the sources were placed before the window of the multiplier tubes pulses were observed at a rate considerably above the background pulse rate. These were analyzed with the aid of a pulse height discriminator and recorder. As the cut-off bias on the discriminator circuit was lowered, more and more pulses would have sufficient amplitude to be recorded within a given period of time. Thus a distribution curve of pulse height *versus* the number of pulses having this or greater height may be obtained.

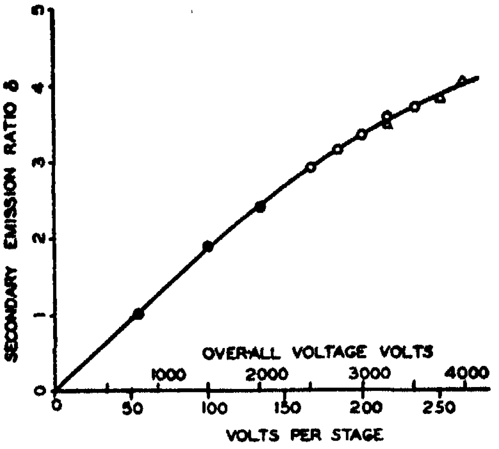

FIG. 5. Variation of secondary emission ratio with voltage.

The data were taken under two different conditions of test. The first was the normal connection in which low velocity electrons could be focused from both window and target. In the second the window was biased positive with respect to the target, so that no low velocity electrons would be focused from window to target. In this second condition the contribution from the target surface alone can be analyzed. Representative distribution curves are shown in Fig. 6.

From data of this sort the beta-counting efficiency may be readily determined. From the data one must assign some numerical value for the total number of counts observed for each curve. The number arbitrarily assigned to each curve is its intercept with the zero pulse height axis. This choice assumes that the observed distributions may be extrapolated to zero amplitude, and counts all pulses of greater than zero amplitude.

The over-all efficiency of the tube with the normal connection is defined as the ratio of the number of counts recorded by the multiplier tube to the number of beta-particles entering the window, the source being at a distance of 0.5 inch from the window. This over-all efficiency of the multiplier tube with the normal connection is:

Tube	Strontium source	Uranium source
No. 3	1.1 percent	1.6 percent
No. 5	1.1 percent	1.5 percent.

For the window-biased-off condition, the efficiency of the oxidized silver magnesium target surface is defined as the ratio of the number of counts observed with the multiplier to the number of beta-particles striking the active area of the target, the source being 0.5 inch in front of the window. This target efficiency is calculated to be:

Tube	Strontium source	Uranium source
No. 3	6.1 percent	4.7 percent
No. 5	5.9 percent	5.1 percent.

The target efficiency tabulated above is perhaps the more significant since it is a property of the target material itself, while the over-all efficiency is affected by scattering and solid angle dispersion between the window and target, and is thus a function of the particular geometry used.

The third thin window tube suffered a mechanical mishap during assembly and while its tests tended to confirm the results obtained with the other tubes they could not be placed on the same quantitative basis, and were thus omitted from the tabulation above.

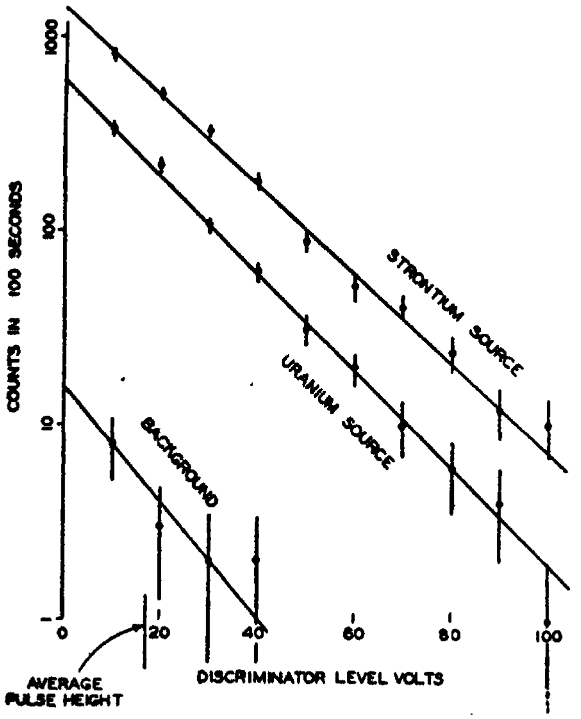

FIG. 6. Representative distribution curves for radioactive source.

The results with the various tubes are thus in good agreement, and moreover the secondary emission gain was quite uniform in all the tubes constructed.

VI. FURTHER TESTS AND CALCULATIONS

In all the pulse height distribution data at hand it appeared that the experimentally observed points could be reasonably well fitted by a straight line on the semilogarithmic plots presented. This would indicate an exponential pulse height distribution curve. This is not the form of distribution curve expected from an electron multiplier, which should show a leveling off at low pulse amplitudes.[18] Tests were then carried out to examine more carefully the shape of the observed distribution curves, and to determine why they were not of the expected shape.

First, the gain of the pulse amplifiers ahead of the pulse height discriminator was increased so that the fixed range of the discriminator was effectively shifted into the region of smaller pulse amplitude. The distribution curves obtained in this manner for the low amplitude pulses fitted smoothly onto the curves already presented, but instead of indicating any leveling off at low pulse amplitudes, showed that the observed curves actually rose a bit more steeply than an exponential at low pulse amplitudes.

Pulse height distribution measurements were then made on one of the early tubes with tungsten filaments at the head end, using the thermionic electrons as the input to the multiplier. It was then reasonably certain that the input thermionic electrons were striking only the target electrode, and that the observed output pulses were all originating at the target electrode. The pulse height distribution curve then showed the leveling off for low amplitude pulses, as would be expected for excitation confined to a single stage.

Tests were then made with essentially uniform excitation of all the stages of the multiplier. One of the early tubes had a glass section in its envelope. This was strongly illuminated, and the light was scattered throughout the interior of the tube by its bright internal parts. Pulse height distribution measurements were then made of the photoelectric pulses thus produced by the uniform excitation of all stages. The curve was the same shape as that for the radioactive samples for pulses of greater amplitude than the average pulse height. For decreasing pulse amplitudes, the curve rose rapidly as the contributions of successive stages of the multiplier became evident.

This is similar in form to the curves observed with radioactive excitation, although in this latter case the rise is not as steep as would be expected for uniform excitation of all stages. This suggests that in the radioactive case the main contribution is coming from the target (with the window-biased-off connection) but that there is some scattering of the primary particles to the following stages. That this scattering exists was verified by setting up the input system in air and measuring the intensity of scattered particles at the position of the multiplier stages by means of a Geiger tube. By this measurement it is estimated that 20 percent as many particles may strike the following stages of the multiplier as strike the target.

For the tubes under study it is difficult to arrive at a definite quantitative estimate of the detailed form of the target distribution curve from the observed window-biased-off curves. The factors involved are the proportion of the incident particles which strike the active region of each of the successive multiplier stages, and the efficiency of release of low velocity secondaries at each of these surfaces. However, the form of the observed distribution curves is now understandable. Because of this effect it is estimated that the true target efficiency may be as much as 20 percent below that indicated by the calculations based on the linear extrapolation. By the same reasoning the over-all efficiency of the multiplier may be as much as 10 percent higher than the value indicated by the linear extrapolation.

---

[18] G. A. Morton and J. A. Mitchell, RCA Review 9, 632 (1948).

From the foregoing analysis it seems reasonable to assume that the linear extrapolation to zero amplitude of the observed data for the window-biased-off condition will indicate approximately the total number of low energy electrons which come off the target surface. It should be possible to verify this number if the nature of the energy distribution of the radioactive source is known and if the variation of secondary emission ratio of the target with incident energy is known.

From data recently published by Meyerhof[14] the distribution of relative number of particles per increment of energy for the strontium source may be determined. The area under this curve is proportional to the total number of particles emitted from the source in a given time. Knowing the total number of counts observed with a Geiger tube, a scale of number of counts per unit increment of energy may be assigned. Thus, with this correlation, the number of incident particles per unit time at any given energy may be determined.

On a more detailed analysis of Trump's[7] data on the ratio of low energy secondary electrons to high energy primaries it was found that this secondary emission ratio appeared to be roughly inversely proportional to primary voltage in the high energy region. Also from Trump's data it was observed that a smooth curve was obtained on plotting the secondary emission ratio due to high energy primaries (at say 300 kv) against atomic number, the ratio increasing with increasing number. In this manner the secondary emission ratio at 300 kv was estimated to be 0.04 for magnesium and 0.09 for silver, and their variation with primary energy was assumed to be similar to that of the other materials measured by Trump.

Since these secondary emission ratios are less than unity, they may be interpreted as the probability that a primary particle will release a low energy secondary electron. Curves were thus deduced for the variation with energy of the number of primary particles, and of the variation with energy of the probability of releasing a secondary. If the product of number of primary particles times the probability of release of a secondary is summed point by point throughout the energy spectrum, the total number of counts expected per unit time would be determined.

By this method it was computed that, if the target were all silver, 1600 counts should be observed in the 100 second interval, when the multiplier tube was exposed to the strontium source in the window-biased-off condition. If the target were all magnesium about 750 counts would be expected under like conditions. The target is a mixture of silver and magnesium, and while the exact mechanism of release of secondary electrons is not known, it is at least certain that the primary particles must penetrate into the bulk of the material. Thus the observed number of counts, 1000, is between the computed extremes, and is thought to be a reasonable correlation. This indicates that the present determination of secondary emission ratio due to beta-particle excitation is in agreement with the data obtained by Trump on the secondary emission ratio with excitation by thermionic electrons accelerated by a van de Graaff generator.

VII. CONCLUSIONS

One of the initial objectives was the design and construction of an electron multiplier tube with sufficient over-all gain and sufficiently low background current so that single electrons released at its input might be detected. Having such a structure it was desired to mount a suitable thin window in its envelope to admit the beta-particles so that a sealed-off vacuum tube could be constructed. It may be said that all of these requirements were satisfactorily met by the tubes constructed.

Having this tool available, it was desired to determine quantitatively the efficiency of the electron multiplier in directly counting beta-particles. The results obtained from tests on three tubes with two different beta-particle sources are in good agreement. It is indicated that the over-all beta-particle counting efficiency of the electron multiplier tube is of the order of 1.3 percent. The efficiency of the oxidized silver magnesium target surface appears to be 6.0 percent for the strontium source and 4.9 percent for the uranium source. It is to be expected that the efficiency be higher for the strontium since it has stronger low energy components, and the secondary emission ratio is decreasing for increasing energy. The over-all efficiency is lower than the target efficiency because of solid angle dispersion and scattering within the tube between the window and the target. The target efficiency is a basic property of the material while the over-all efficiency is a characteristic of the particular tube structure employed.

This tube should be useful in applications where its low efficiency is not disadvantageous, such as high level monitoring. It should be particularly useful in monitoring high intensity radiation because it does not "block" at very high counting rates, but gives a steady output current whose magnitude is proportional to the intensity of radiation. This tube should also be useful where a very low background count is essential. In a demountable system, the multiplier structure could be inserted directly into the vacuum chamber without the intervening window and measurements made of all particles with energy of a few hundred volts or greater.

In conclusion, it is a pleasure to acknowledge the advice and helpful criticism from Professor C. H. Willis and the late Professor H. C. Rentschler of the Department of Electrical Engineering, Princeton University and from Drs. I. Wolff, E. G. Linder, and C. W. Mueller of the RCA Laboratories staff.

---

[14] W. E. Meyerhof, Phys. Rev. 74, 621 (1948).

THE REVIEW OF SCIENTIFIC INSTRUMENTS VOLUME 20, NUMBER 12 DECEMBER, 1949

A High Resolution Scale-of-Four

VAL FITCH
Pupin Physics Laboratories, Columbia University, New York, New York

(Received September 14, 1949)

A high resolution scale of four has been developed to be used in conjunction with the nuclear particle detection devices in applications where the counting rate is unusually high. Specifically, it is intended to precede the commercially available medium-resolution scaling circuits and so decrease the resolving time of the counting system. The circuit will function reliably on continuously recurring pulses separated by less than 0.1 μsec. It will resolve two pulses (occurring at a moderate repetition rate) which are spaced at 0.04 μsec. A five-volt input signal is sufficient to actuate the device.

INTRODUCTION

THE development of amplifiers of great band width and the use of inherently fast detection devices in the nuclear physics laboratory has emphasized the need for high resolution counting systems. In particular, counting equipment capable of resolving several events per microsecond is highly desirable in experiments performed with pulsed particle accelerators such as the Columbia synchrocyclotron. The present scale of four was devised to meet this requirement. Accepting signals from a pulse-height discriminator or "level-setter," the circuit, with its resolution time of less than 0.1 μsec., will normally provide sufficient "smoothing" of random pulse inputs[1] to drive the commercially available 5- to 10μsec. scaling units with a low counting loss. While designed primarily for use with nuclear particle detectors, the basic scale-of-two circuit is useful in other counting applications—e.g., counter chronographs, electronic computers, etc.

CIRCUIT CONSIDERATIONS

The scale of two in the present scaling circuit is a version of the familiar Eccles-Jordan trigger circuit. The selective diode switching, which Higinbotham found highly successful, is utilized.[2] To enhance the performance of the device at high frequencies, design considerations center around the basic ingredients of fast regeneration and appropriate "memory." The circuit must, on receipt of the initiating signal, pass quickly to the opposite stable condition and assume quiescence before the succeeding signal arrives. However, in any scaler there is one instant in the regenerative cycle when the circuit must be informed as to the direction the action should proceed. To enable the circuit to continue toward the opposite conducting position, some device is necessary to recall the previous situation and make conditions favorable for conduction starting in the proper tube. The minimum resolution obtainable depends to a high degree on the relative success of providing this memory. The memory must last sufficiently long after the triggering pulse to insure that the circuit passes to the opposite regime. In addition, it must be arranged that the circuit "forgets" the previous switching operation by the time the next triggering pulse arrives.

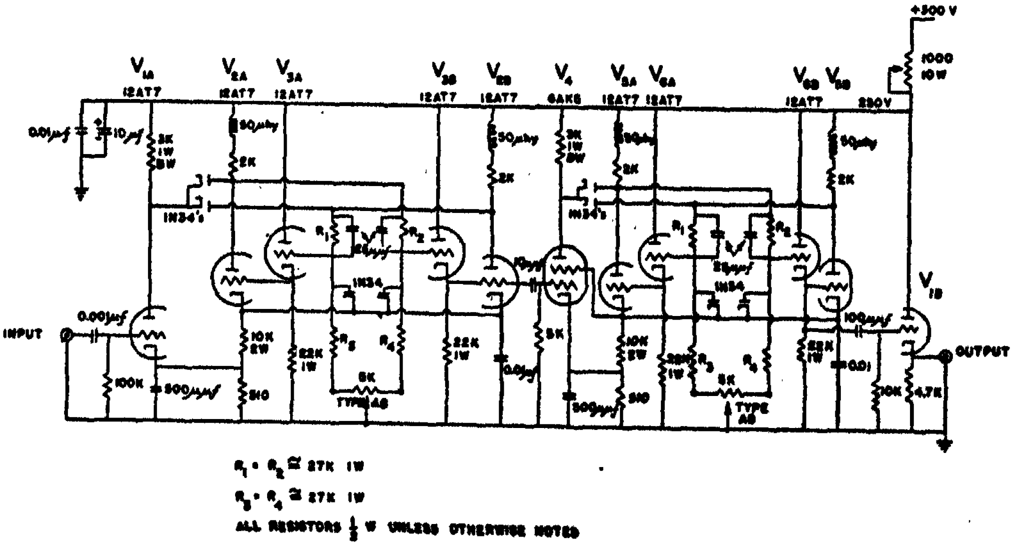

FIG. 1. Circuit diagram of scale of four.

---

[1] L. J. Rainwater and C. S. Wu, "Applications of probability theory to nuclear particle detection," Nucleonics 1, No. 10 (October 1947).

[2] Higinbotham, Gallagher, and Sands, "The model 200 pulse counter," Rev. Sci. Inst. 1, 706 (1947).

FIG. 2. Photograph showing layout and wiring on 7-in.×7-in. chassis.

In the original Higinbotham circuit, memory is achieved through the use of capacitors in parallel with the plate-to-grid cross-over resistors. Their capacitance is considerably higher (at least a factor of two) than is necessary for a frequency-independent compensation. The duration of the memory is determined by the grid-circuit *RC* time constant, and congruous with the comparatively slow action inherent in such a triode circuit the time constant is made fairly long.

In the present scaling circuit, a fast action is achieved by the standard wide-band techniques of using relatively low plate resistances (compensated) and high transconductance tubes. In the circuit diagram, Fig. 1, the switch tubes, V_{2A} and V_{2B}, and the cathode followers, V_{3A} and V_{3B}, comprise the first scale of two. The cathode followers employed in the plate-to-grid coupling network minimize the capacitive loading on the anodes of the switch tubes and hence speed the flip-over action. The crystal diodes in the grid circuits prevent overdriving the switch tubes and so limit their plate-voltage excursion.

Memory, however, is provided not only through capacitive but also through inductive effects. The capacitance in parallel with each cross-over resistor is comparatively low. To provide the additional memory necessary for reliable operation, the anode resistors are considerably overcompensated with 50-microhenry inductors.

The succeeding scale of two is identical with the first and is driven by the buffer tube V_4. The rectangular wave from the last scale of two is *RC*-differentiated with a 1-μsec. time constant and presented as the output through a cathode follower. The amplitude of the output pulse is approximately ten volts.

TESTING AND ADJUSTMENT

Fifteen scale-of-four units have been constructed and tested in this laboratory. They exhibit nearly identical characteristics, and the following remarks apply to their performance.

A measure of the reliability of any circuit is the allowable tolerance in components. The scale of four is found to operate despite a rather wide deviation from optimum values. Unfortunately, in a circuit of this general type, it is inevitable that *minimum* resolution is a function of the "balance" of the components. To facilitate compensation for unbalance in the fixed resistors, a linear potentiometer is provided as part of the cross-over network. A rough balance setting may be obtained with an ordinary high impedance voltmeter. The voltmeter is connected so as to measure the potential between ground and the cathode of the switch tubes; e.g., V_{2A} and V_{2B}. The circuit is then flipped from one stable regime to the other by momentarily touching to ground first one, then the other grid of the two cathode followers. The potentiometer is so adjusted that there is no change in the cathode voltage when the circuit switches to the opposite conducting position. Using the cathode of one of the cathode followers as a point of observation, the flip-over action may be verified with an additional voltmeter.

Response of the circuit to signal inputs may be checked with a sine wave or pulse generator and an oscilloscope. The amplitude of the sine wave should be at least five volts (r.m.s.) and the frequency higher than three megacycles. Pulse inputs may range from five to 20 volts with a duration less than 0.1 μsec. The first scale of two is checked with an oscilloscope by observing the plate signal of the buffer tube V_4; the second, by observing the output. Final setting of the balance potentiometer is effected by increasing the frequency until the scaling action falters (at 11 or 12 megacycles for the units tested) and then readjusting. When properly balanced, the circuit will respond to 13- or 14-megacycle signals. Tube replacement is found to have little effect on the resolution and does not necessitate readjustment.

Normal precautions should be taken in construction to minimize stray capacitance. The performance of the device is probably dependent on the arrangement of parts. Layout and wiring details of the units constructed in this laboratory are shown in Fig. 2. Five percent components should be employed throughout, and preliminary matching of the cross-over resistors (as noted in the circuit diagram) is suggested. The 50-μhenry inductors are *RF* chokes of the iron-core variety.

The scale of four requires an external power supply, preferably regulated, which can provide 60 ma at 300 volts.

ACKNOWLEDGMENTS

The author wishes to thank Dr. L. J. Rainwater for helpful discussion and Mr. S. Lipman for much laboratory assistance.

The work was performed under AEC government contract AT-30-1-Gen 72.

Erratum: A Wide Range Radiation Instrument

[Rev. Sci. Inst. 20, 711 (1949)]

Leonard Reiffel and Glenn Burgwald

On page 713 of this article under 2. of part V. Limitations the μr/hr. in the sentence "It was found that a 4°C change in temperature caused a shift of the order of 0.7 μr/hr." should be corrected to mr/hr.

THE REVIEW OF SCIENTIFIC INSTRUMENTS VOLUME 20, NUMBER 12 DECEMBER, 1949

A Sensitive Magnetometer for Very Small Areas

DARYL M. CHAPIN
Bell Telephone Laboratories, Inc., Murray Hill, New Jersey

(Received September 22, 1949)

A vibrating wire system for measuring weak magnetic fields is described for use in very small spaces. Quartz crystals are used for drivers to get sufficient velocity with very small displacements. To adjust the driving voltage to correspond exactly to the natural crystal frequency, the crystal is also used to regulate the oscillator.

EXPERIMENTAL work in the theory and in the practical application of magnetic phenomena frequently requires the measurement of a magnetic field at a point. With any actual measuring equipment, the size of the exploring coil or probe requires that the measurement be over an area—frequently a large area. This note reports the use of a quartz-driven loop probe, developed to reduce that area as far as possible and still to be sensitive enough to measure fields of one gauss or less. One of the tools developed measures in an area only 1 mm by about 0.15 mm and is sensitive to less than one gauss.

One such probe is a single loop of fine wire glued to a lightweight tube 1 mm in diameter and about $\frac{3}{4}$ in. long. The wire runs along one side, across the end, and back the other side. If this tube with its wire is constrained to move along its axis, the sides of the loop generate no voltage. The net voltage generated by this loop in a uniform field would be zero and hence its use is limited to such cases where the magnetic field is quite different at the two ends of the loop. In many such applications, the field at one end can be ignored and only that at the other end regarded as contributing to the generated voltage which will be proportional to the length of the end section, its velocity, and the field normal to the wire and motion.

FIG. 1. Bimorph crystal and probe.

For this probe, the mechanical driver is a bimorph crystal consisting of two quartz crystals joined together electrically reversed so that when one expands under the influence of an electric field the other contracts. A flexural motion of comparatively large motion and low frequency is produced. The supports for the crystal are placed at the nodes which by means of end-loading are made to appear at about seven-tenths of the distance from center to end. The center is the point of greatest motion. When a probe is mounted normal to the face at the center, it experiences pure translational motion along its axis as required. A picture of the bimorph crystal and its probe is shown in Fig. 1.

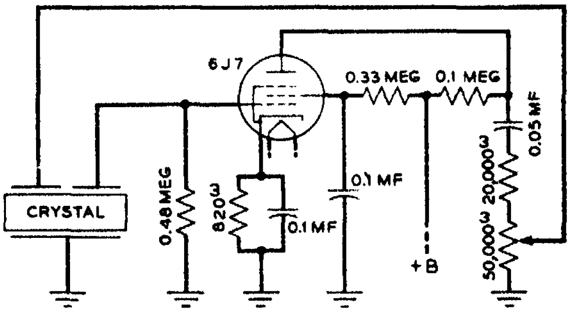

FIG. 2. Oscillator for bimorph crystal.

It is well known that a quartz crystal has a very high Q and its amplitude is very greatly affected by the driving frequency. It therefore appears that a reasonable way to control this frequency and keep it at the resonant frequency of the crystal is to control a vacuum tube oscillator by means of the crystal as shown in Fig. 2. The circuit reduces to a piezoelectric controlled oscillator with a probe mounted on the crystal. For maximum sensitivity, the amplitude of the oscillations should be increased to the maximum safe limit for the crystal.

The bimorph crystal used has a frequency of 872 cycles per second as loaded. Its calibrated sensitivity at the probe is 3.0×10^{-8} volt per gauss. Calling the sensi-

Fig. 3. A 49-kc crystal and probe.

tive length 1 mm, the maximum velocity is 42 cm per sec., the total travel is 0.154 mm, and the maximum acceleration is 235 g, where g is the acceleration of gravity. The noise level is the equivalent of 0.2 gauss.

With such a low voltage, it is necessary to minimize extraneous noise and pick-up. The electrostatic pick-up from the driving circuit is most easily decreased by grounding at the variable point of a 100-ohm potentiometer hung across the probe circuit. The impedance of the probe is less than one ohm, making it possible to use an input transformer of very high step-up ratio. The 52-db voltage gain obtained is enough to override the first tube noise so that sensitivity is limited by probe noises and not by tube noises. The rest of the measuring circuit needs no elaboration. The whole set was calibrated by observing the output voltage of the amplifier when the probe was in a known field.

A second type of probe uses the common longitudinal mode of a quartz crystal having a natural frequency of 49 kc. The crystal is shown in Fig. 3. At the fundamental frequency, a node appears at the center and antinodes at the ends. A loop of wire extending from the node up one side, across the end, and back on the other side to the node, differs in its motion from the probe described above in that only one end moves. Ideally, this unit measures absolute values of magnetic field at the antinode regardless of the field at the node and hence may be used to make measurements of a uniform field.

The oscillator circuit shown in Fig. 4 is of conventional form but shielding difficulties associated with the higher frequency resulted in a system a little less sensitive than for the bimorph crystal. Lead lengths had to be kept short with the crystal adjacent to the oscillator. A double metal shield around the oscillator decreased the unwanted pick-up. Another pick-up problem arises from the position of the loop. As shown in Fig. 3, only one-half of the loop is on the grounded face and the other half is on the ungrounded face. Hence there is considerable electrostatic pick-up which has to be balanced out. This might be avoided by laying the loop along the grounded face only.

The sensitivity of the 49-kc probe is 5.3×10^{-9} volt per gauss. The computed total motion is 0.5 micron. The maximum velocity is 7.6 cm per sec. and the maximum acceleration is 2380 g. The noise level is the equivalent of 4 gauss.

The structures illustrated were developed primarily for measuring fields close to flat surfaces such as magnetic recording tapes and their form is subject to modifications for other purposes.

Still smaller areas of measurement would appear possible by developing probes of finer wires or of thin conducting films a few atom diameters thick. The point is illustrated by the crystal of Fig. 3 where the probe wire is about 60 microns in diameter whereas the total travel is only about half a micron. After the probe dimension is sufficiently reduced, still higher frequency might be used to maintain sensitivity with smaller motion.

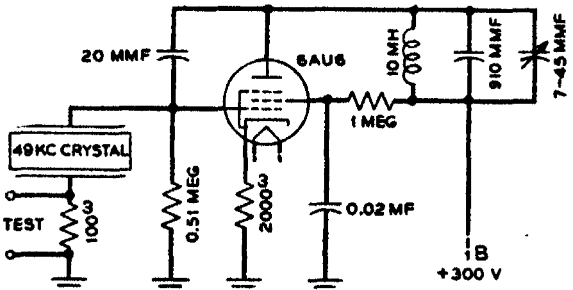

Fig. 4. Oscillator for 49-kc crystal.

As an indication of the possibilities, one interesting experiment may be cited. With the probe shown in Fig. 3, positive indications were obtained of the field that exists at the domain boundaries on the (10·1) surface of a demagnetized cobalt crystal. With the present crude probe, the observed field parallel to the surface and about 0.1 mm from it was 20 gauss.

THE REVIEW OF SCIENTIFIC INSTRUMENTS VOLUME 20, NUMBER 12 DECEMBER, 1949

Growing and Processing of Single Crystals of Magnetic Metals

J. G. Walker, H. J. Williams, and R. M. Bozorth
Bell Telephone Laboratories, Murray Hill, New Jersey

(Received September 22, 1949)

Single crystals of nickel, cobalt, and various alloys are grown by slow cooling of the melt. They are oriented by optical means and by x-rays, and ground to the desired shape using the technique described.

INTRODUCTION

IN the study of the ferromagnetic properties of single crystals a technique has been developed for growing rather large crystals and for cutting them in the desired form, properly oriented with respect to the crystal axes. The crystals prepared have been nickel, and the alloys of iron-nickel, copper-nickel, iron-silicon, iron-molybdenum, iron-aluminum and iron-cobalt-nickel, and cobalt in the hexagonal form. They have all been formed by cooling slowly from the melt, in much the way already described in a note by Cioffi and Boothby.[1] This article will describe the method in more detail, and then will explain the procedure that has been developed for cutting the crystal, determining its approximate orientation by reflection of light from etch pits and its accurate orientation by x-rays, grinding it to the desired shape, and etching it to remove deformed materials.

FURNACE

The furnace is intended only to melt and to cool slowly, and has no moving parts. It is cylindrical in form, mounted with its axis vertical, has a molybdenum heating element and operates with an atmosphere of pure dry hydrogen. Its construction is shown in Fig. 1. The casing is a 12-in. steel tube of ½-in. wall thickness, on the outside of which is brazed a thin steel jacket to form a water-cooling chamber of 1-in. thickness. The top and bottom are each held in place with 12 1-in. bolts and are sealed gas-tight with lead gaskets into which knife edges press. They are water-cooled, using several turns of copper tubing soldered in place. Near the upper end of the furnace, below the head, are a number of accurately bored and tapped holes. These provide means of mounting gas inlet valves, thermocouple leads, power leads and other necessary fittings, which are sealed with litharge and ⅛-in. lead gaskets.

The heating element is 0.070- to 0.100-in. molybdenum wire, wound with turns ⅜ in. apart on an alundum muffle (Norton RA-1139, 5-in. I.D., 5¾ in. O.D., 24 in. long). The total resistance of the winding is about 0.3 to 0.6 ohm when cold. Power leads are ¼-in. copper rods that pass through the furnace fittings inside of porcelain ferrules, made gas tight with porcelain cement. The inner ends of the copper leads are silver plated, and are connected to the furnace winding with ⅛-in. molybdenum rods.

Outside of the heating element is a 3-in. layer of 500 mesh acid-etched alundum, enclosed by a thin steel shell which permits easy removal of the inside of the furnace from its casing.

Through the center of the top is a steel fitting in which is cemented a Pyrex glass window 0.4 in. thick, for observing the melt. The temperature is checked with an optical pyrometer, calibrated to take account of the absorption of the glass. The window is protected from most of the direct radiation from the hot zone of the furnace, and the heat loss is reduced, by a metal baffle through which a hole is cut for observation.

The crucibles are of high purity alumina, usually Norton ATM-409 or RA-1139 alundum. They are placed in the heating zone so that the top is near the hottest part of the furnace. The difference in temperature between the top and bottom of a 5-in. crucible is about 40°C.

The material to be melted is obtained from various sources. Nickel of high purity, prepared by the carbonyl process, was obtained through the kindness of Mr. E. M. Wise of the International Nickel Company. Other materials were electrolytically purified cobalt, electrolytic iron, hydrogen reduced molybdenum and electrolytic cathode copper, kindly supplied by Mr. D. H. Wenny of the Bell Laboratories.

Temperatures up to 1550°C have been obtained with the use of a 220-volt 60-cycle supply, adjustable in steps of 2.2 volts. The power consumed is less than 11 kw.

ATMOSPHERE

Electrolytic hydrogen is purchased in tanks, and further purified by passing over pellets of palladinized alundum. These are contained in a 24-in. brass tube, 1 in. in diameter, which is soldered at each end to a ¼-in. copper tube lead and maintained at 75°C by a nichrome heating element enclosed with asbestos tape. The water vapor formed in the tube is removed in a drying tower of activated alumina also soldered at each end, and the hydrogen then goes through a diaphragm valve to its entrance near the top of the furnace. The exhaust gas leaves the furnace at the bottom. About 8 cubic feet per hour are normally used.

The dew point of the hydrogen is maintained at about −50°C or below. The entire system is checked for leaks with a pressure of 10 lb./in.^{2}

---

[1] P. P. Cioffi and O. L. Boothby, Phys. Rev. 55, 673 (1939).

A photograph of the furnace and associated apparatus is shown in Fig. 2.

MELTING AND COOLING

The crucible, of approximate diameter 1 inch and height 5 inches, is filled with the pure constituents or with a machined rod of alloy previously prepared. The air in the furnace is displaced with nitrogen and this in turn with hydrogen. The power is turned on and the voltage gradually increased to a point which is known to give the proper temperature for melting the charge. Melting occurs in about 5 hours. After the whole charge has been molten for about an hour the voltage is reduced about 1 percent every three hours until solidification is complete. This corresponds to about 5°C/hour and may take 10 to 20 hours. If the material is an alloy, it is homogenized by holding just below the melting point for 24 hours or more. The voltage is then reduced about 1 percent per hour to 1200°C, then more rapidly so that it cools to 50°C in about 20 hours. The furnace is then filled with nitrogen and opened to the air. The crucible is removed and carefully cracked from the ingot.

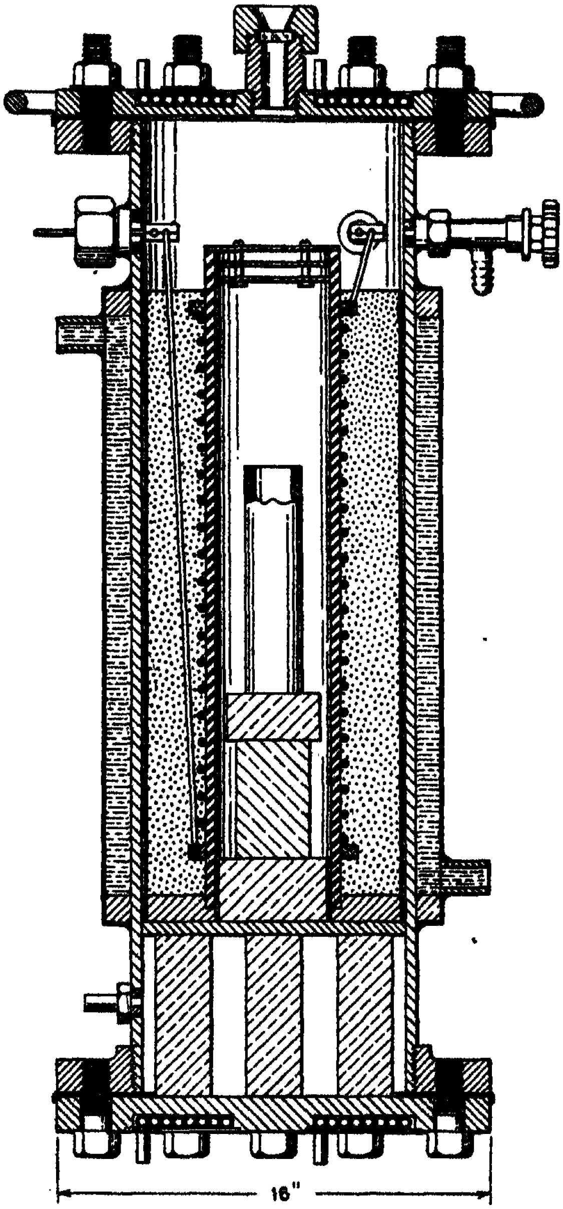

FIG. 1. Plan of molybdenum-wound furnace for growing crystals.

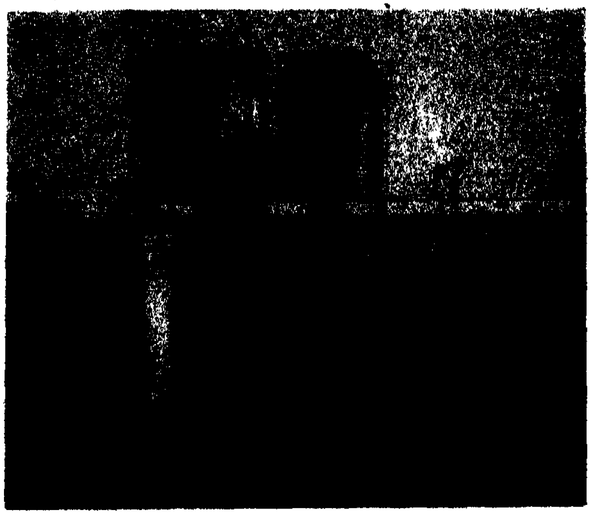

FIG. 2. Arrangement of furnace, power supply, and combustion and drying tubes for hydrogen.

ROUGH ORIENTATION

The ingot, weighing about 2 pounds, is sand blasted to remove the last bits of the crucible, and then etched in a suitable mixture of nitric and hydrochloric acids. An example of the result is shown in Fig. 3. A crystal is then selected and cut from the ingot with a jeweler's saw or with a wet cutting wheel of about $\frac{1}{16}$-in. thickness. Care must be taken to prevent straining of the crystal by excessive pressure or heat.

When etching shows that all but a single crystal has been cut away, the crystallographic axes are determined roughly from the reflections of light from the etch pits. In an otherwise dark room, light from a single source shines on the crystal over the observer's shoulder. By rotating the crystal an area of high reflectivity is located and a short piece of wire is fastened to this surface with modeling clay. When the surface is in the position of maximum reflection, the wire is placed so that it is directed about halfway between the light source and the observer's eye. The wire is then roughly normal to the etch plane. In the case of iron-silicon alloys there are 6 etch planes of the form [100]. In nickel there are 8 etch planes, [111], and these may be determined with an approximate error of 5° or more. A plane is then cut with the wet wheel approximately parallel to the desired plane and the surfaces are etched rather deeply (0.1 to 0.3 mm).

ACCURATE ORIENTATION

The surface so cut is mounted on a flat steel plate with sealing wax, applied after heating the parts in an oven at about 125°C. The steel plate has the form shown in Fig. 4 at (*a*), and can be screwed fast to the holder (*b*) in either of two positions at 90° to each other. The barrel-shaped holder is designed so that the crystal can be tipped by screwing the pin (*e*) or (*f*) and then locked into position by tightening the nut (*g*). It contains four V-grooves, (*c*) and (*d*), that permit its accurate location in a fixture connected to either an x-ray or a grinding machine. The holder is an adaptation of that used in the orientation of quartz and other crystals for piezoelectric use.

The next procedure is to orient the crystal surface with x-rays so that the required plane is accurately perpendicular to the axis of the holder, and then to transfer the holder to a surface grinder that will grind the surface accurately parallel to the plane. These two operations will now be described.

The x-ray spectrometer is shown in Fig. 5. The holder is mounted on one arm of the goniometer so that the crystal surface is on the axis, and the ionization chamber is set on another arm placed at the proper angle (2θ) calculated from Bragg's law. The holder is turned until maximum reflection is observed, and the scale is read. The crystal and holder are turned 180° about the holder axis and the operation repeated. The holder is then locked in the angular position halfway between the two scale readings, and the crystal turned in the holder, by the use of the screw (*e*) of Fig. 4, until the current through the ionization chamber is a maximum. The barrel is then turned 90° and again adjusted for maximum reading. The desired crystal plane is now perpendicular to the barrel axis.

The barrel is then removed from the spectrometer and mounted in a surface grinder as shown in Fig. 6, with the barrel axis carefully adjusted to be perpendicular to the travel of the cutting wheel. The crystal is ground in steps of 0.002 in. or less until a reasonably large surface is available. After etching, the x-ray spectrometer is used for a further checking. A surface can be cut accurately by this method in about a day's time after the ingot is taken from the crucible.

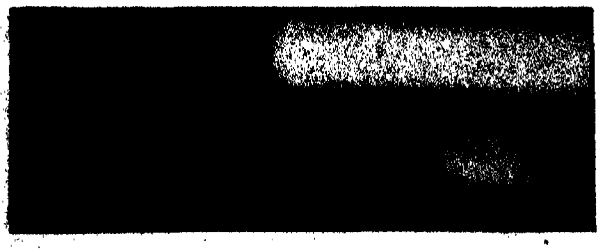

FIG. 3. Ingot showing several large crystals. Crucible is 5 in. long, and may be filled with alloy for melting (see portion of casting) or with unalloyed ingredients.

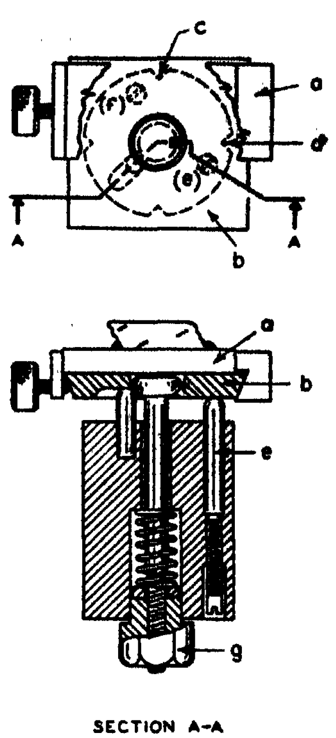

FIG. 4. Sketch of construction of barrel-shaped holder used in mounting and orienting crystal.

In order to determine the position of the crystallographic axes in the prepared surface, the crystal is unmounted and a back reflection Laue photograph is taken. Analysis of this gives the angle between an axis and some reference line on the crystal surface. The axis is then scribed on the crystal and it is mounted on a steel disk which has a square shank and threaded end. The shank is fitted into a square hole in a plate and screwed fast, and mounted on the surface grinder.

A new surface is then ground parallel to the crystallographic axis and perpendicular to the main surface. Using other positions of the square shank in the square hole, three more such surfaces can be ground. These can be checked with x-rays and corrected until the desired precision of cutting is attained. Accuracy can be as high as 5 min. or even higher if desired.

The method just described is the basis for cutting crystals of various forms. When a circular disk is wanted for measurement of magnetic torque,[2] the major surfaces are prepared as described. The crystal surface of required orientation is then fastened with wax to the end of a metal rod, with the surface aligned accurately perpendicular to the rod axis, and the rod held in a lathe. A ball bearing center is pressed against the crystal and the disk turned, taking very small cuts to avoid heating or straining the specimen.

More complicated shapes such as the "picture frame" previously described,[3] can be cut with care using a jeweler's saw and file.

---

[2] H. J. Williams and R. M. Bozorth, Phys. Rev. 55, 673 (1939).

[3] H. J. Williams, Phys. Rev. 52, 747 (1937).

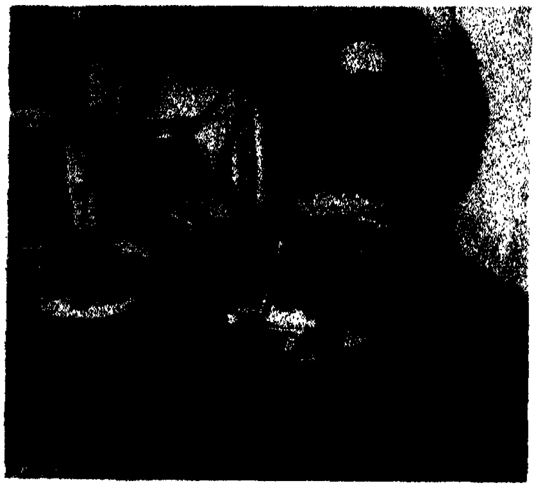

FIG. 5. Arrangement of barrel-holder and crystal in x-ray spectrometer.

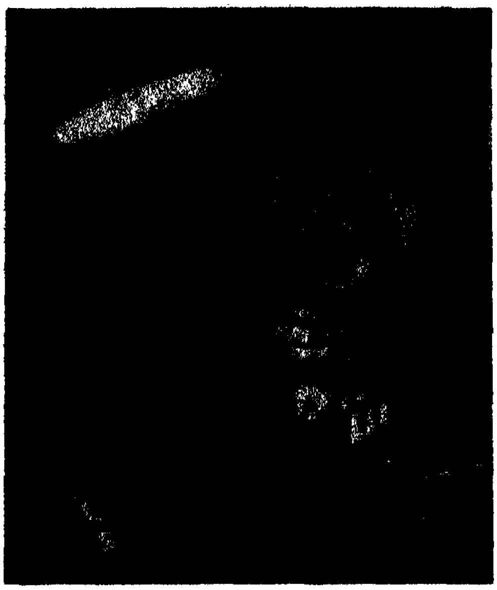

FIG. 6. Barrel-holder and crystal in position in surface grinder.

ETCHING AND POLISHING

For proper determination of crystal orientation by x-rays it is important that the surface be etched sufficiently deeply. An insufficient etch can always be detected by taking a back-reflection Laue photograph and noting the smeared appearance of the spots, or can be inferred from the lack of sharpness of the reflection on the spectrometer. When some work hardened material is present it may have an orientation appreciably different from that of the body of the crystal, consequently its complete removal is necessary. Worked material should also be removed before giving any heat treatment, to avoid recrystallization.

If repeated etching leaves an uneven surface the crystal may be hand lapped with 600 mesh abrasive cloth and re-etched. A particularly smooth surface can be maintained by electropolishing, using a bath of one part chromic trioxide, CrO_3, and 9 parts of 85 percent phosphoric acid, by weight. The specimen is used as the anode and two copper electrodes as cathodes and 18 volts applied. Usually one to five minutes operation, with the bath at about 80°C, is sufficient to remove strained material from surfaces that have had light mechanical polishing. Electropolishing is particularly important for the study of magnetic powder patterns.[4]

We are indebted to Mr. W. L. Bond for the opportunity to use the x-ray spectrometer and the barrel-shaped holder for orienting the crystals.

---

[4] Williams, Bozorth, and Shockley, Phys. Rev. **75**, 155, 178 (1949).

THE REVIEW OF SCIENTIFIC INSTRUMENTS VOLUME 20, NUMBER 12 DECEMBER, 1949

Physical Instruments for the Biologist

Detlev W. Bronk
Associate Editor in Charge of this Section
Eldridge Reeves Johnson Foundation for Research in Medical Physics,
University of Pennsylvania, Philadelphia, Pennsylvania

An Electromagnetic Blood Flow Meter

JOHN W. CLARK AND JAMES E. RANDALL
Research Division, Collins Radio Company, Cedar Rapids, Iowa

(Received July 18, 1949)

This report describes the design of an instrument for electrically measuring the rate of flow of blood passing through a glass cannula which has been inserted within a vessel of an anesthetized animal.

IT is frequently of interest in physiological research to study the variations of the blood flow rate as affected by drugs or by external stimuli such as heat. Accordingly, a reliable instrument which will indicate and record blood flow rate is of considerable utility to the physiologist. The instrument described below was developed for the use of the Department of Physiology at the State University of Iowa in connection with a study of the effects of diathermy upon blood flow and other physiological parameters. The results of this work will be published elsewhere.

A variety of instruments have been devised for the measurement of blood flow; the reader is referred to Potter[1] for a detailed study of this topic. Instruments which measure flow through a particular vessel (as opposed to perfusion systems, which measure the flow through an organ or a region of the body) may be classified into several types: drainage recorders, bubble flow meters, thermostrohmuhrs, rotameters, orifice flow meters,[2] and electromagnetic flow meters.

In the venous drainage recorder, one simply measures the quantity of blood drained from a vein in a measured time. This method obviously measures average flow only. The bubble flow meter introduces a long, coiled capillary in series with the vessel under study; a bubble of air is introduced and its motion timed with a stopwatch. This method is obviously not suitable for actuating a recorder. The thermostrohmuhr measures the temperature rise induced in the blood at a point downstream a short distance from a small heater. This method appears to be inherently inaccurate. The rotameter and the orifice flow meter are familiar devices for measuring flow of liquids; these, however, have a serious disadvantage as blood flow meters, in that both contain a constriction in the blood stream which tends to induce clotting with consequent errors in calibration.

The electromagnetic flow meter is free from most of the disadvantages of the instruments briefly described above. While this is not a new instrument, the writers feel that an account of a practical electromagnetic blood flow meter, together with the design problems and operating precautions associated with it, will be of interest. The electromagnetic flow meter was developed by Kolin[3–5] and used for blood flow studies in dogs by Kolin and Katz.[6] The principle of the instrument is illustrated in Fig. 1. The motion of the blood, which is a fairly good conductor, through the transverse magnetic field induces an e.m.f. which is proportional to its velocity. This small e.m.f. is amplified and actuates an indicating meter or a recorder. The linear velocity of the blood, multiplied by the cross-sectional area of the bore of the vessel, gives the volume rate of flow which is what one usually wants.

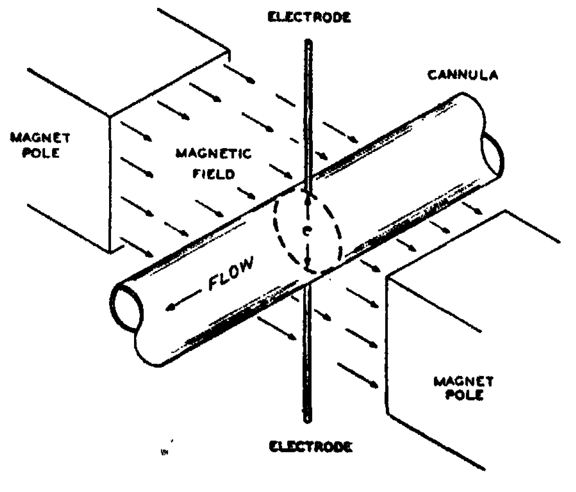

FIG. 1. Basic components of the flow meter.

---

[1] V. R. Potter, Editor-in-Chief, *Methods in Medical Research* (Year Book Publishers, Inc., Chicago, 1948), Vol. I, pp. 68–253.

[2] G. K. Moe, "A simple technique for continuous registration of blood flow," Science **109** (April 15, 1949).

[3] A. Kolin, "Electromagnetic flowmeter: principle of method and its application to blood flow measurements," Proc. Soc. Exper. Biol. and Med. 35, 53 (1936).

[4] A. Kolin, "An a.c. induction flowmeter for measurement of blood flow in intact blood vessels," Proc. Soc. Exper. Biol. and Med. 46, 233 (1941).

[5] A. Kolin, "Alternating field induction flow meter of high sensitivity," Rev. Sci. Inst. 16, 109 (1945).

[6] L. N. Katz and A. Kolin, "Flow of blood in carotid artery of dog under various circumstances as determined with electromagnetic flowmeter," Am. J. Physiol. 122, 788 (1938).

It is possible to place electrodes in contact with the exterior of the intact vessel; this method was used by Kolin[3,4,6] and also by Wetterer.[7] The technique of cannulating the blood vessel and inserting the flow meter is, however, simpler and is free from contact difficulties and errors due to changes in the lumen of the vessel with changes in the condition of the animal. The cannulation process is of course recommended only when it is permissible to inject anticoagulant drugs into the animal.

Because of the considerations outlined above, the cannula shown in Fig. 2 was designed. The platinum electrodes are sealed in the glass so as to contact the blood stream with a minimum of internal discontinuity. Indexing pins are provided to locate the cannula with respect to the electromagnet. Heparin is added intravenously to the animal's blood stream to inhibit clotting. The shape of the cannula was chosen to separate somewhat the magnet and the electrical circuit from the animal. This reduces grounding difficulties and also enables one to keep the contact area free of blood and other contaminants.

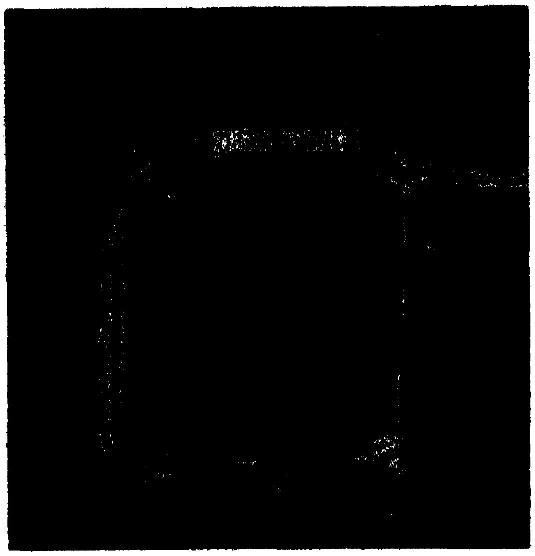

FIG. 2. The cannula with indexing pins.

The following brief outline of the theory of the instrument will aid in understanding its operation. Whenever there is relative motion between a conductor and magnetic lines of force, there is an induced e.m.f. proportional to the magnetic field, the length of the conductor and the relative velocity between the two:

$$e=-blv\cdot 10^{-8}, \tag{1}$$

where e is the induced e.m.f. in volts, b is the magnetic flux density in oersteds, l is the length of conductor in cm, and v its velocity with respect to the magnetic field in cm/sec.

In the electromagnetic flow meter the length l is represented by the diameter of the circle of the cross section of blood. This l will be determined by the internal bore of the vessel or cannula. If b is a fixed magnetic field as from a permanent magnet, then the induced e.m.f. is proportional to the linear velocity with which the blood flows through the vessel or cannula at the point of measurement. One is usually interested in the volume flow rate in cc per second rather than the linear flow rate in cm per second. These quantities are related as follows:

$$Q=v\cdot(\pi d^2/4), \tag{2}$$

where Q is the volume flow rate in cc per second, and d is the internal diameter of the tube.

Let $l=d$ in (1), and eliminate v between (1) and (2):

$$e=-b\cdot(4Q/\pi d)\cdot 10^{-8}. \tag{3}$$

We then see that for a given fixed magnetic field and a fixed rate of flow determined independently of physiological mechanisms it would be to our advantage, at least theoretically, to make the internal bore d as small as possible to produce a larger induced voltage.

When physiological considerations are made, we find that a small constriction will increase fluid friction at the site of the constriction, which results in an added "Peripheral Resistance" to the flow of blood. The rate of flow is thereby reduced;[8] or, in other words, we cannot assume a fixed rate of flow independent of constriction. It is thus necessary to have as little constriction as possible to insure the same conditions as though no instruments were present.

For the a.c. electromagnetic flow meter, the magnetic field varies approximately in accordance with the voltage applied to the electromagnet. This changing flux causes the voltage induced in the blood to alternate at the power supply frequency. Polarization at the electrodes is nullified and a stable a.c. amplifier may be used.[4,5]

However, with the use of an a.c. field a new complication arises. Auxiliary circuits must be added to bring the indicator to a zero reading when there is no flow. This occurs because the two probes with their leads form a single-turn transformer secondary. This difficulty may be analyzed as follows:

If the flux in Eq. (1) is varying sinusoidally, its instantaneous value may be represented by:

$$b=B\cos 2\pi ft. \tag{4}$$

in which B is the maximum flux density in gauss, and f is the frequency in c.p.s.

In order correctly to formulate the magnitude of the induced e.m.f. in this case, we must replace Eq. (1) by the more fundamental expression:

$$e=-10^{-8}(d\phi/dt), \tag{5}$$

---

[7] E. Wetterer, "New method of registering rate of blood circulation in unopened vessel," Zeits. f. Biol. 98, 26 (1937).

[8] R. E. Shipley and D. E. Gregg, "The effect of external constriction of a blood vessel on blood flow," Am. J. Physiol. 141, No. 2 (April, 1944).

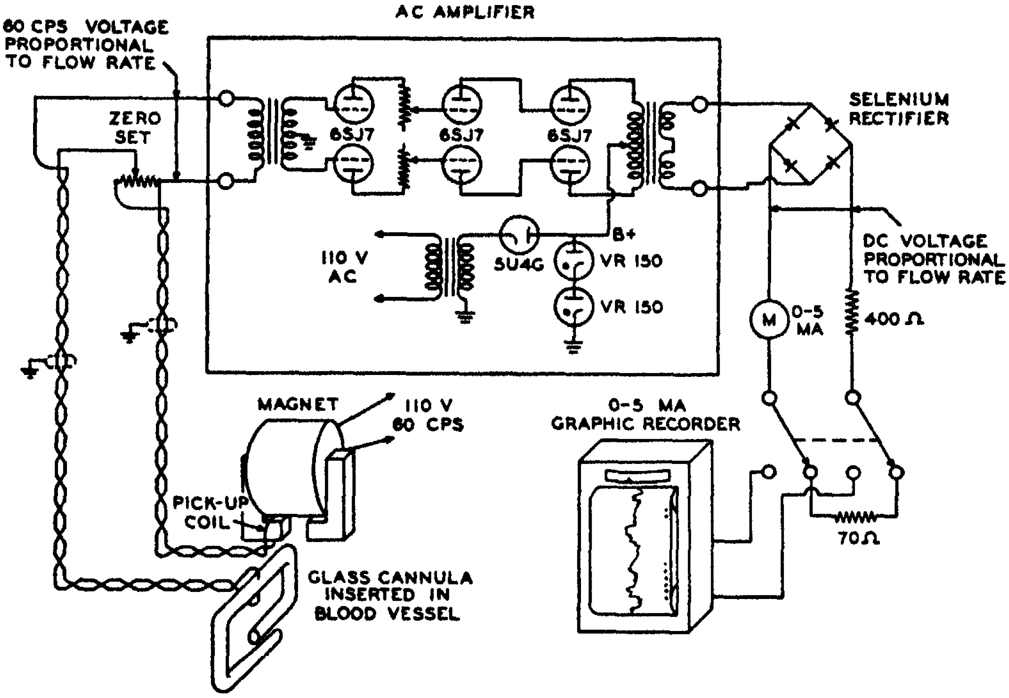

FIG. 3. Functional diagram of the blood flow meter circuits.

where ϕ is the total flux linked by the circuit formed by the leads to the cannula and the infinitesimal filament of blood which completes the circuit between the cannula electrodes. Since the blood stream is moving and the flux is changing:

$$-d\phi/dt=blv+A(db/dt). \qquad (6)$$

Here A is the effective area enclosed by the loop. Inserting (4) and (6) in (5) and, as before, eliminating v with the aid of (2), we get the following expression for the e.m.f. induced in an a.c. electromagnetic flow meter:

$$e=-4/\pi(QB/d)\cdot 10^{-8}\cos 2\pi ft-AB\sin 2\pi ft. \qquad (7)$$

This equation will be observed to have two terms, the first of which is similar to that encountered in the case of the steady magnetic field, while the second arises as a result of the time variation of the magnetic field in the a.c. case. The voltage expressed as the second term of Eq. (7) is that which arises by virtue of the electrodes and their associated leads acting as a one-turn transformer. This voltage has the unfortunate property of being independent of flow. Since it is of the same order of magnitude as the flow-induced voltage, it constitutes an undesirable zero-flow signal.

An obvious way to cancel out this undesired voltage is to place an auxiliary single-turn winding on the magnet. This winding is phased oppositely to the one formed by the cannula and its leads, and a potentiometer is used to reduce its magnitude to equality with that of the spurious voltages. This expedient would work perfectly were it not for non-linear phenomena in the transformer iron which give rise to harmonics in the generated voltage. The even harmonics do not cancel, so the only remedy is to limit the flux density to keep the harmonic content at a tolerable value. This, of course, is in conflict with one's wish to operate at high flux density to realize high sensitivity. A practical compromise must be arrived at between these two factors. For smaller flow rates and where the magnet must be small it may be necessary to accept the harmonic voltage and filter it out before the indicator amplifier.

For the developed instrument the magnet was made from stacked laminations of $\frac{1}{2}$-inch, 29-gauge L-4 special audio *A* iron. The coil was 1800 turns of No. 25 wire excited with 110 v a.c., 60 c.p.s. This gave a field of about 1000 oersteds across a $\frac{1}{2}$-inch cubed air gap between pole tips. Each cannula was provided with a mounting frame for uniform centering within the magnetic field.

Power from the a.c. line at 60 c.p.s. was used to excite the magnet coil because of its availability and because low loss magnet material is available for this frequency. This limits the frequency response of the

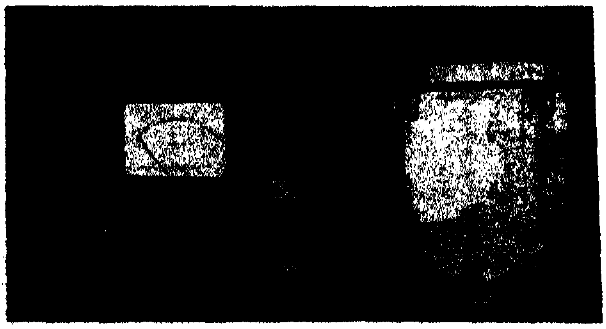

FIG. 4. The blood flow meter with its associated recorder.

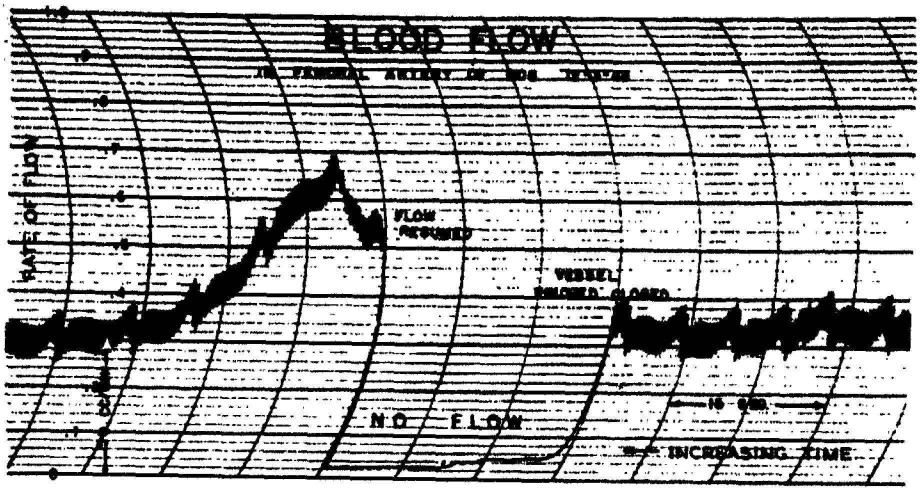

FIG. 5. A typical blood-flow record.

whole system to fluctuations less than 60 c.p.s. The frequency of pulsatile fluctuations appearing on the flow indicator is correct, but their amplitude is dampened by the recorder. Should a more faithful pulsatile picture be desired, it would be possible to increase the carrier frequency and also use an output recorder with the required higher response.

Figure 3 is a functional diagram of the blood flow meter. The a.c. amplifier is of conventional design, in this case for 60 c.p.s. use only. Since adequate plate supply filtering and low level shielding was used, no trouble was encountered by interaction of power supply ripple and signal. A gain control on the amplifier allowed for adjustment of the sensitivity. The output transformer was fed into a meter type selenium rectifier which gave best linearity in the operating range. This type of bridge rectifier will give an upward deflection regardless of the direction of blood flow. If the flow were of such a nature that its direction reversed completely, it would be possible to use a discriminator type detector which would give a reversed deflection for reversed flow.

Selection of an output recorder is determined by the over-all frequency response desired. For recording relatively slow fluctuations, an Esterline-Angus recording milliammeter was used. This is a highly damped instrument such that it probably is responsive to less than 5 cycles per second. The instrument with the best power sensitivity requires 5 milliamperes through an internal resistance of 70 ohms for fullscale deflection. Its chart can be driven at any convenient speed from ¾ in./hr. to 6 in./min., the choice depending upon the rapidity of change to be observed. Figure 4 is a photograph of the complete instrument with its associated recorder.

A large output meter is placed on the amplifier panel for viewing from a distance. Either of two ranges can be selected by a front panel switch. The chassis contains a meter and reference voltage for calibrating the amplifier. Energizing the magnet and the amplifier from a constant voltage transformer appeared to give adequate stability. Each cannula must be calibrated individually by running saline solution through the cannula, collecting it and dividing by the elapsed time to obtain flow rate. Two points, one of which may be the point obtained at zero flow, should be sufficient to establish calibration for the cannula. Calibration is independent of concentration of the solution provided that the amplifier input impedance is high enough and provided that salt or other contamination does not collect or crystallize on the electrodes. Salt solutions sometimes deposit crystals of the salt on rough edges with a slowly circulating system.

Figure 5 is presented as an example of the performance of this instrument. This is a typical chart record taken at 6 inches per minute, showing the blood flow in the femoral artery of a dog. Full scale deflection represents about 150 cc per minute. Several interesting phenomena may be observed on this record. The rapid fluctuations in blood flow caused by the heart beat are clearly seen. Superimposed upon these is a slower variation synchronous with the animal's breathing. Visceral pressure due to inhalation causes a momentary increase of flow. The instrument faithfully records the almost immediate cessation of flow when the artery is pinched off with a clamp, and the complex transient flow that occurs when flow is resumed. It takes almost 45 seconds for the arterial system to return to normal when flow is resumed.

ACKNOWLEDGMENTS

The writers wish to take this opportunity to acknowledge the contributions to this project of several of their co-workers. Mr. R. C. Kent (now on leave of absence from Collins Radio Company) was active in the early phases of this project, and contributed in particular to the problem of cannula design. The advice from the physiological standpoint of Prof. H. M. Hines and Mr. A. W. Richardson of the Department of Physiology of the State University of Iowa was invaluable. Finally, we would like to acknowledge the skill of Mr. H. Nunamaker, the glass blower at the Department of Chemistry of the State University of Iowa, who made the cannulas.

Laboratory and Shop Notes

An Electromagnetic Focusing Device for the Electron Microscope

HAROLD T. MERYMAN
Naval Medical Research Institute, Bethesda, Maryland

October 27, 1949

THE use of electromagnetic rather than electrostatic alternating fields in a beam deflection focusing device was first demonstrated by Ir. LePoole of Delft.[1] The Delft instrument has a very narrow neck between the condenser lens and the specimen chamber; the electromagnetic coils are placed around this neck outside the instrument. Bishop[2] has also described such an adaptation to the RCA instrument.

In adapting the electromagnetic system to the RCA e.m.u. electron microscope, it was decided at this laboratory, that the size of the specimen chamber and the nature of the metal casting made it both practical and advisable to place the coils inside the chamber in close proximity to the electron beam. The coils were wound without cores to eliminate the possibility of hysteresis and induced or residual magnetism. A description of such an adaptation to the RCA e.m.u. microscope follows:

A one and one-half inch O.D. brass tube (Fig. 1) is rigidly attached at its top by flanges to the screws which support the stage motion springs on the roof of the specimen chamber casting. The tube extends downward to within one-fourth inch of the stage and has a one-inch wide slot in front to permit the insertion of the specimen holder. Four pins are placed at 90° intervals around the outside of the tube one-quarter inch from the bottom, this arrangement reproduced three-fourths inch higher. On each side, around the upper and lower pairs of pins, are wound coils consisting of 400 turns each of 36-gauge Format Insulated Magnet Wire, care being exercised to avoid short circuits within the coils or to the brass tubes. With opposite polarity in top and bottom pairs, one side of each pair may be brought to a single terminal in a special bushing (Fig. 2) inserted between the casting and the vacuum manifold at the rear of the specimen chamber. To this terminal is brought one output lead from a 6-volt, 60-cycle, a.c. transformer which is in turn connected to the ground lead of the microscope chassis. The two remaining coil leads, top and bottom, are brought through separate terminals in the bushing to either side of a 40-ohm potentiometer through the rotor of which is fed the other lead of the 6-volt transformer. A double pole, double throw switch is used, one position energizes the primary of the transformer, the other position grounds the ungrounded side of the coils to prevent pick-up within the microscope column.

The positioning of the coils is not highly critical, balancing is achieved by adjustment of the potentiometer until there is no loss of illumination with the device energized. It is possible that square wave deflection may offer some advantages over sine wave at the expense of economy and simplicity.

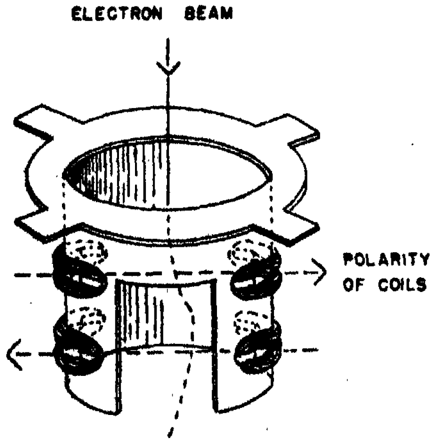

FIG. 1.

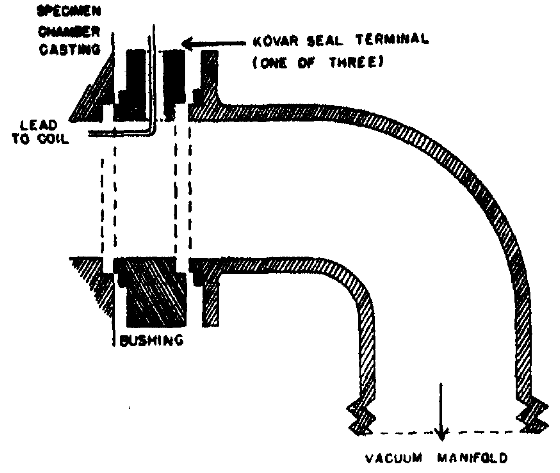

FIG. 2.

This device, by increasing the angular aperture of illumination, decreases the depth of field and increases the sensitivity of focusing. At an instrument magnification of 8000×, a departure from correct focus of one unit on the vernier adjustment results, with the focusing device energized, in a blurring over half a millimeter wide at any well-defined point. Accuracy in focusing is, however, closely dependent on alignment, particularly image rotation, which must be scrupulously centered.

Such increase in focusing sensitivity becomes particularly valuable at low intensities and in low contrast biological specimens. Although the use of this device does not obviate the need for through-focus studies where exceptional resolution is demanded, it does eliminate such precautions in routine work and places efficient operation and good quality results within the scope of the most inexperienced operator.

---

[1] Seen at the Institute for Electron Microscopy, Delft, Holland (April, 1949).

[2] F. W. Bishop, Rev. Sci. Inst. 20, 532 (1949).

Automatic Stabilization of the Overvoltage on a Geiger Counter

H. R. CRANE
Randall Laboratory of Physics, University of Michigan, Ann Arbor, Michigan

September 2, 1949

THE conventional Geiger counter circuit nearly always includes an electronic stabilizer which keeps the high voltage constant. However, this does not insure that the voltage will remain at the same value with respect to the plateau, because the latter may shift or change in length during an extended series of measurements. In many applications it is advantageous to eliminate the effect of drift in the characteristics of the counter tube by stabilizing the overvoltage rather than the absolute voltage. The purpose of this note is to describe a simple method by which this can be accomplished* and to suggest some specific applications.

As the voltage on a Geiger counter is increased from the lower to the upper limit of the plateau, the pulses can be seen to increase gradually in size. The pulse size is approximately proportional to the overvoltage, that is, to the excess of voltage over that corresponding to the lower limit of the plateau. Thus every time a count occurs, the size of the pulse gives information as to the value of the overvoltage. This fact is made use of in the circuit shown in Fig. 1, the high voltage being controlled automatically by the size of the pulse produced by the counter.

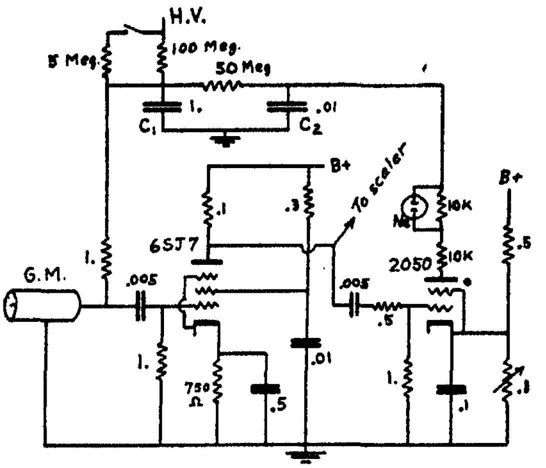

FIG. 1. All condenser and resistor values are in microfarads and megohms, respectively, except where otherwise specified. The circuit is designed for a B supply of 300 volts, and for a high voltage supply which gives up to about 400 volts in excess of the operating voltage of the counter tube.

The condensers C_1 and C_2 slowly charge from the high voltage supply. As the voltage on the counter tube rises above the threshold potential, the pulse height rises accordingly. The first pulse whose height exceeds a value determined by the bias on the thyratron, fires the thyratron, discharging C_2, which results in lowering the voltage on C_1 by about 10 volts. The thyratron will not fire again until after C_1 has recovered the 10 volts; the next pulse which comes along after that time will fire it. The circuit constants must be so chosen that the time required for C_1 to recover the 10 volts will be somewhat greater than the average time between counts, at the lowest counting rate to be expected. The component values given in Fig. 1 make the circuit suitable for use where the lowest counting rate to be expected is about 30 per minute. If the high voltage supplied to the circuit is 200 volts greater than the operating voltage of the counter tube, the thyratron will fire once every 5 seconds.

The "hunting" in the stabilizer appears as a saw-tooth oscillation of the high voltage, with a period of 5 seconds, and an amplitude of 10 volts. At high counting rates the upper and lower limits, which are 10 volts apart, are quite precisely defined. If the counting rate is reduced until it is not much greater than the hunting frequency, the voltage will make occasional excursions to values considerably above the upper limit just mentioned. If, in addition, the counter tube happens to be one whose plateau has considerable slope, an error in the number of counts will be introduced. There is, of course, nothing to prevent the voltage from making excursions clear to the region of continuous discharge, if the counting rate is low enough relative to the hunting frequency. A quantitative treatment of the hunting effects with proper regard for the shape of the plateau would be complicated. However, it may be remarked from the practical viewpoint that the difficulties just discussed can easily be avoided, since one is free to choose the hunting frequency sufficiently low to suit any application.

Some variations in the circuit may be mentioned: As a substitute for the thyratron a one shot multivibrator, a blocking oscillator, or a diode in a peak voltmeter circuit together with a triode regulator tube can be used. We chose the thyratron only because it seemed to be the simplest. The circuit is also adaptable to use with non-self-quenched counters. In that case the quench tube replaces the amplifier. If the quench circuit happens to be one which gives a negative signal, an inverter must be used between it and the thyratron.

The length of the warm-up period for the circuit presents a problem. Due to the small charging rate of C_1 the time required for it to rise from zero to the operating voltage when the power is first turned on is inconveniently long. Several easy solutions are possible. In the circuit shown a push button switch is provided, which increases the rate of charging by a factor 20. This is merely held down until the thyratron fires the first time, as indicated by flash of the neon bulb. Another solution is the use of the usual manual voltage control (unstabilized) at the start, with a switch to convert to the automatic control.

Several applications and advantages of the circuit are listed below:

1. Measurement of long duration, in which the characteristics of the counter are subject to drift due to changes in gas pressure, temperature, etc. The circuit will follow shifts of several hundred volts in the plateau.
2. Use of counters having narrow and sloping plateaus. Since the voltage is maintained at the same value with respect to the plateau, the counter efficiency remains essentially constant.
3. Coincidence and anticoincidence. Since the output pulse size is bracketed between close limits, the pulses from two or more such circuits can be combined directly to form coincidences without the use of auxiliary pulse shaping circuits to bring the pulses to uniform size.
4. Use with vibrator, multivibrator or radiofrequency high voltage supplies. Since the drain on the high voltage supply is of little importance, the circuit is well adapted to use with these types of high voltage supply.
5. Radiation monitors for safeguarding health, where it may be desirable to have the counter run for weeks or months without attention.
6. Measurements where attention is not possible, such as those in balloons or rockets.

The author is indebted to Mr. Earl McDaniel for assistance in developing the circuit described.

* Since writing this note it has come to my attention that a circuit which accomplishes the same result has been developed, independently, by the Radioactive Products Corporation of Detroit, Michigan.

Long-Lived Self-Quenching Counter Filling

LLOYD G. SHORE
Radiation Counter Laboratories, Inc., Chicago, Illinois
October 24, 1949

It has been found that counters filled with a suitably proportioned mixture of the four gases argon-xenon-oxygen-nitrogen are self-quenching when operated with the same counter circuits ordinarily used with conventional self-quenching counters (Fig. 1). Such counters may, furthermore, have long and flat plateaus and operate at reasonable voltages even up to near atmospheric filling pressures. Most important, these counters have shown no apparent deterioration in plateau characteristics after prolonged operation at rather high counting rates. Similarly, holding them at extreme overvoltages in "continuous" discharge for extended periods also has had no apparent adverse effect on subsequent performance.

Figure 2 indicates how the counter performance is affected by variations in the composition of the mixture. These data were taken with glass counters having 0.002-in. tungsten center wire, ¾-in. diameter silver cathode and 3-in. active length. The data given for "threshold" represent the triggering voltage for the scaling circuit at the usual 0.25 volt sensitivity. The data given for "approximate length of counting region" represent the approximate length in volts of that region above threshold wherein the counter was responsive to a radioactive (gamma) source and exhibited self-quenching behavior. This counting region does not represent, in every instance, a satisfactory counting plateau since in those cases where the filling parameters were far removed from optimum the oscilloscope pattern frequently showed erratic

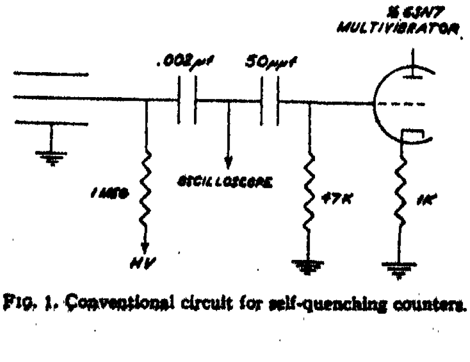

FIG. 1. Conventional circuit for self-quenching counters.

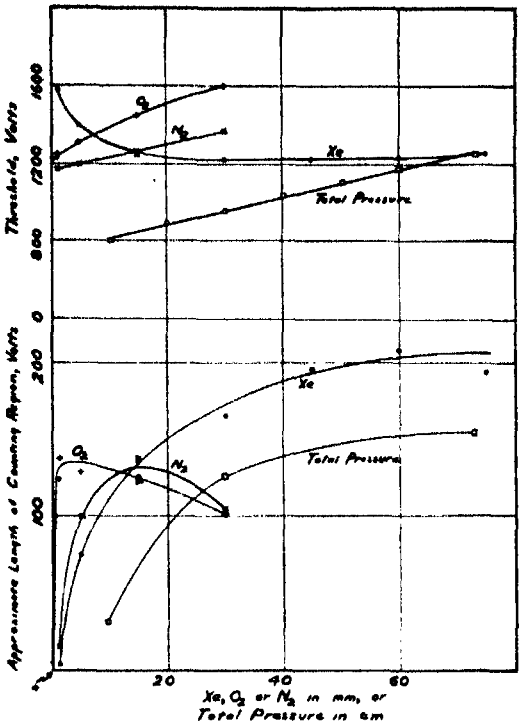

FIG. 2. Effect of mixture composition (for the particular case of 15 mm xenon, 1 mm oxygen, 15 mm nitrogen and argon the balance to 73 cm total pressure).

or multiple pulse formation. Nevertheless, in the many instances where the filling parameters were more or less optimum and particularly at the lower overvoltages, the observed pulses were discrete and even in size, reflecting proper self-quenching Geiger region performance. The curves show the effect of varying the partial pressure of a single component while keeping the remaining three components at the particular values of 15 mm xenon, 1 mm oxygen, 15 mm nitrogen and argon the balance to 73 cm total pressure. Similar trends are also obtained for other cases of workable mixture compositions. It is apparent that minimum values exist for each of the components below which most satisfactory performance is not achieved. The xenon, furthermore, exhibits a sharp threshold lowering effect until it is present in rather appreciable amounts.

Figure 3 shows the excellent plateau characteristics which may be obtained with a more or less optimum filling.

Although the exact self-quenching mechanism operating in the four-component mixture needs further consideration, the extended counting life and resistance to adverse overvoltage effects seem consistent with the relatively simple chemical nature of the filling. The life of the usual polyatomic quenched counters is known to be limited by decomposition and decomposition products of the polyatomic constituent and it has been the writer's experience that such counters are either rendered useless or show appreciable deterioration by 10^7 to 10^8 counts. In contrast, life testing of the new mixture has thus far shown no apparent deterioration at all after several weeks continuous operation at approximately 10^8 counts per day.

Promising applications for this long-lived counter filling appear to exist. It is felt that further studies on this and other noble-simple gas multicomponent mixtures would be desirable.

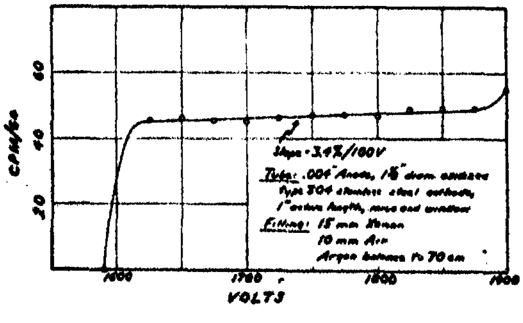

FIG. 3. Counter characteristic curve.

On the Vacuum Properties of Silastic*

G. D. ADAMS AND W. C. SHERWIN
Physics Department, University of Illinois, Urbana, Illinois
August 19, 1949

THE authors have independently investigated the vacuum properties of Dow-Corning Silastic rubber. Some attention was given to each of Silastic Nos. 122, 123, 125, 126, 150, and 160. The conclusion was reached that the material is not useful for vacuum below 10^{-5} mm Hg without very special precautions. It has a fairly high vapor pressure and the body is not completely impermeable.

I. In the course of developing vacuum seals for the 300-Mev betatron tube, it was hoped that some gasket material could be bonded to the porcelain section. This material should be workable into such condition as to permit a vacuum-tight joint and preferably should be relatively resistant to deterioration in the presence of ionization. To this end a series of experiments involving Silastic were conducted. In these the Silastic was bonded to the ends of porcelain sections and then faced to give a smooth Silastic-Silastic interface at the seal.

Silastic cured in our laboratory appears to have properties very similar to commercially cured sheet Silastic. More than twenty bonded seals were prepared and studied. Pumping a volume of about 3 liters through 1 meter of 2-in. glass tubing with a VMF-20 oil diffusion pump, almost every one of these seals allowed no better than 1 to 2×10^{-5} mm Hg to be reached. Heating while on the system liberated great quantities of gas but in the end did not help the vacuum materially. Testing for leaks with hydrogen indicated a transmission with a time delay of several minutes. This effect was not present in the absence of Silastic. Tests on the condition of the surfaces indicated the leakage was not entirely due to surface channels. This series used surfaces which were rough-cut, smooth-cut, dry, and coated with high vacuum grease. In another test, Silastic was directly bonded and cured between two porcelain sections. Vacuum tests on it gave substantially the same results as on seals containing an interface. We believe these experiments indicate diffusion through the body of the Silastic.

It was possible to use Silastic, either as cured by us or as commercial sheet, to obtain vacuum of the order of 10^{-6} mm Hg. This required compressing the Silastic to about one-half the original thickness, the sides not being constrained. It was noticed that the vacuum improves rapidly in the neighborhood of the critical compression. If the compression much exceeds the amount necessary to make a "tight" seal, it may rupture. Since several other tests also indicated that more compression would be required than that which we had available, this material was no longer considered.

II. Silastic is stable at moderately elevated temperatures at which ordinary rubber decomposes. This quality was desirable for gaskets in a metal vacuum system which could be outgassed by heating and also easily disassembled. The required ultimate pressure of the system was below 10^{-7} mm Hg. The experiments described in this section were performed to evaluate the material for this purpose.

A sample of Silastic was tested in a vacuum system whose ultimate pressure was 10^{-7} mm of Hg. With the Silastic inserted, the ultimate pressure was only 2×10^{-5} mm of Hg. When the Silastic was heated in the vacuum for 30 hours at 100°C, the ultimate pressure was reduced to 2×10^{-6} mm of Hg when hot, and

1×10^{-7} mm of Hg at room temperature. It thus appears that Silastic can be freed from the high vapor pressure fractions by vacuum heating.

A more serious problem with Silastic is its tendency to permit capillary-type leaks when used as an ordinary gasket. Gaskets were cut from sheets and compressed in smooth brass tongue-and groove-gasket assemblies. The system, with the gasket in place, was evacuated and heated to 100°C for 15 hours. All these gaskets contained leaks which required three to five minutes to show on a mass-spectrometer leak detector. This unusually long lag demonstrates the capillary nature of the leaks.

For further study, a seal made with two concentric gaskets was constructed. The air was pumped out and re-admitted to the space between the gaskets. In either case the pressure inside the vacuum system took several hours to reach a stable value. This slow approach to equilibrium suggests that some of the leaks are exceedingly fine capillaries, possibly indistinguishable from ordinary diffusion.

The total leak rate on a gasket two inches in diameter was measured and found to be 5 to 10 liters per second at 10^{-6} mm Hg.

It is seen that both authors have arrived at a similar conclusion: the material tested will not usually be applicable to vacuum below 10^{-6} mm Hg because of permeability.

* This work was supported by the Joint Program of ONR and AEC.

Formation of Insulating Layers by the Thermal Decomposition of Ethyl Silicate

Harold B. Law
RCA Laboratories, Princeton, New Jersey

August 22, 1949

IT has been found possible to produce highly insulating films on objects that are placed in a vacuum and heated to a high temperature in the presence of ethyl silicate vapor. Thermal decomposition of the vapor takes place at the high temperatures to produce silica and water.

The silica film builds up readily on hot objects and much more slowly on cold objects such as the walls of the vacuum chamber. The low temperature films are quite soft as they contain considerable water, but the hotter the object the less water will be included in the film.

The procedure that has been used is to place the object to be coated in a metal can and then arrange to heat the can by r-f in vacuum. A side tube containing liquid ethyl silicate is attached to the vacuum system with a stopcock or rubber hose and pinch clamp connection for the purpose of introducing ethyl silicate vapor. A fore pump vacuum is all that is required since the vapor pressure of ethyl silicate is 1.8 mm Hg at 20°C.[1] A trap has been used to freeze out excess vapor flowing through the system.

The rate of deposition of silica on hot surfaces depends very strongly on the temperature of the surface. To determine the rate, Ni strips were heated to various temperatures for a given time and the rate of deposition noted. Approximately 0.1 cc of liquid was vaporized into the system per minute during the tests. The curve obtained is given in Fig. 1.

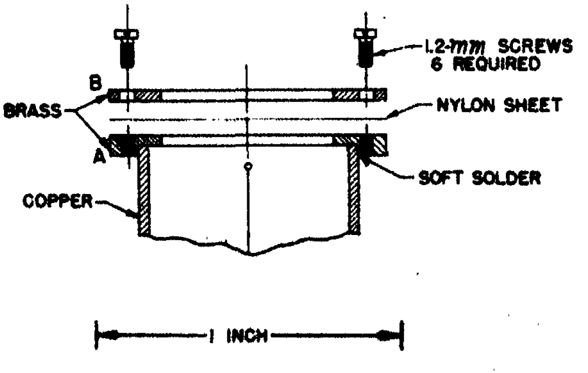

Fig. 1. Deposition of silica as a function of temperature.

While running the experiment on deposition rate, it was observed that the first four strips, or those processed below 870°C, had films that showed no visual structure of any kind, while all those from 900°C to 1100°C showed a milkiness that increased with the temperature of deposition. At the higher temperatures the surface contained a coating of very finely divided particles that could be brushed off. However, it was found later that if an object to be coated were heated below 850° until a perceptible layer of silica was deposited, the temperature could then be raised without the fine particle formation. Instead the films became translucent or opal in appearance when thick.

X-ray diffraction pictures show one broad line at 4.4A for both the high and low temperature deposition. Vitreous silica has a broad band at 4.33A.

A characteristic of the film is its tendency to shrink during formation. Since water is liberated when decomposition takes place, the shrinkage is probably associated with dehydration of the film that has been deposited.

Shrinkage of the film is well demonstrated by coating a fine mesh copper screen that has been mounted on a metal ring.[2] In order to keep the shrinkage of the coating from tearing the screen out of its mounting ring, it is necessary to drop the temperature of deposition shortly after the coating begins to form. Dropping the temperature tends to relieve the screen tension because the coated screen has an expansion coefficient characteristic of silica.

The excellent insulation provided by the coating makes it suitable for storage tubes that require insulating films for their operation.[3] It is also possible to make a fine mesh silica screen with tubular wires by first coating a fine metal screen with silica and then dissolving out the metal by prolonged exposure of the coated screen to acid.

---

[1] *Ethyl Silicate* (Carbide and Carbon Chemical Corporation of New York).

[2] H. B. Law, "A technique for the making and mounting of fine mesh screens," Rev. Sci. Inst. 19, 879–881 (1948).

[3] L. Pensak, "Conduction induced by electron bombardment in thin insulating films," Phys. Rev. 75, 472–8 (1949).

Vacuum Tight, Flexible Metal—Glass Seal

Kenneth M. Sancier
Chemistry Department, Johns Hopkins University, Baltimore 18, Maryland

October 10, 1949

A SLEEVE of Saran tubing can be used to form a vacuum tight, flexible seal between metal or glass tubing. The thermoplastic Saran tubing heated to the softening point is slipped over the hot metal or glass tubing; a snug fit is desirable. Further heating with finger pressure completes the bond between plastic and rigid tubing. If sufficient care is taken, an open flame can be used for the heating process; the hot gases above a flame are sufficient to soften the plastic. When metal tubing is part of the joint, thermal conduction can be utilized for the softening process. While the seal described above can easily be made satisfactory for vacuum of about 10^{-6} mm or better, any small leaks remaining may be sealed by painting the joint with Glyptal.

Such a seal was used where it was necessary to control the transfer of solutions of methanol and carbon tetrachloride from one part of a glass system to another, and where glass stopcocks lubricated with grease could not be tolerated. In this application a Hoke needle valve with copper tubing soldered to the inlet and outlet was sealed to the glass tubing using sleeves of Saran. In this way a flexible and completely vacuum tight assemble was constructed. Saran has the further advantage of absorbing less than 1 percent of carbon tetrachloride and 0.05 percent of methanol, by weight, thus no softening or swelling results from continued contact of such solutions with the seal.

A Procedure for the Solution of Certain Network Problems

John M. Kelso
Radio Propagation Laboratory, Pennsylvania State College, State College, Pennsylvania

September 29, 1949

THE following procedure was developed as a method for setting up network calculations to determine theoretically the distributed capacitance of coils. Actually the method is much more general than this, and is not restricted to electrical problems. However, it seems simpler to discuss it first in terms of the original problem, and then to make a few remarks concerning possible generalizations.

We wish to determine the capacitance existing between the ends of a coil of N turns, assuming that the capacitance between any pair of turns is known. This is equivalent to a set of points $1, 2, \cdots, N$, with the i-th and j-th points being connected by a capacitance C_{ij}. The equivalent circuit diagram becomes very complex for N greater than 5 or 6. Figure 1 shows the equivalent circuit for $N=5$, where we wish to know the total capacitance between the points 1 and 5.

In order to calculate the total capacitance of this network, the capacitances may be considered to be formed of parallel branches, each branch being made up of one or more capacitances in series. It is convenient to begin each parallel branch with the first conductor and end with the last. If this requirement is to be fulfilled, it frequently happens that some of the connections, say C_{ij}, must be used in more than one parallel branch. Suppose, for example, that C_{ij} is to be used Q times. The capacitance C_{ij} is replaced by Q capacitances, each of value C_{ij}/Q, in parallel. Then each time it is required to find a path from i to j, a different one of these Q capacitances is used.

The method given here for selecting a set of parallel paths is adapted to the use of unskilled computing help, since it does not require the use of a circuit diagram, and gives automatically the number of times that a particular capacitance has been used.

We denote the capacitance between two points by the number-pair corresponding to the subscripts used above. We may, then arrange these number pairs as the upper right, off-diagonal elements of an N by N square array. The principal diagonal is empty, and the lower left corner is filled by transposing the original elements across the principal diagonal. Such an array is shown in Fig. 2.

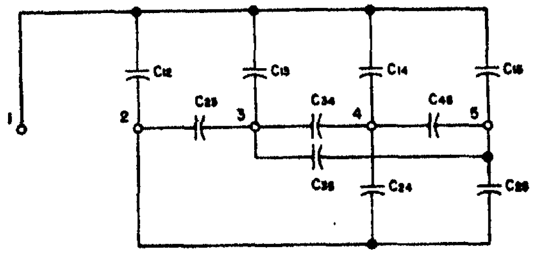

FIG. 1.

Using this array, suitable sets of paths can be obtained. The procedure to be followed in obtaining one such path is as follows:

(i) Choose as the first element, some element in the first row;
(ii) for the second element, choose any element in the *same column* as the first;
(iii) the third element lies in the *same row* as the second;
(iv) this alternation of rows and columns is continued until one of the elements chosen lies in the last row or column.

Each stopping point in such a path through the array forms one capacitance in a parallel branch. As each element in the upper half is used, it is checked off. Each time an element in the lower left portion is used, its transposed element in the upper right is checked. When all of the elements in the upper right have thus been checked, a complete set of paths has been obtained. The word "complete" is used in the sense that this set of paths is sufficient to calculate the total capacitance of the network, and it is not to be considered that the use of this word means that all possible paths have been found.

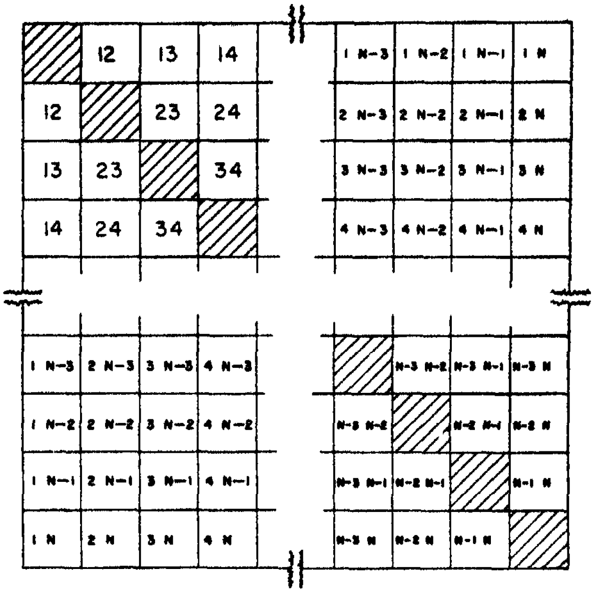

▨	12	13	14	1 N−3	1 N−2	1 N−1	1 N
12	▨	23	24	2 N−3	2 N−2	2 N−1	2 N
13	23	▨	34	3 N−3	3 N−2	3 N−1	3 N
14	24	34	▨	4 N−3	4 N−2	4 N−1	4 N
1 N−3	2 N−3	3 N−3	4 N−3	▨	N−3 N−2	N−3 N−1	N−3 N
1 N−2	2 N−2	3 N−2	4 N−2	N−3 N−2	▨	N−2 N−1	N−2 N
1 N−1	2 N−1	3 N−1	4 N−1	N−3 N−1	N−2 N−1	▨	N−1 N
1 N	2 N	3 N	4 N	N−3 N	N−2 N	N−1 N	▨

FIG. 2.

(A brief description of the above procedure may be given in terms of the game of chess: starting at a square on the first row, move to the last row or column by a series of "rook" moves, with row and column moves alternately.)

The elements of each single path are then added up in the appropriate manner as a series circuit, and finally the total group of paths is added as a parallel circuit.

As mentioned previously, the procedure discussed here is much more general than a method for calculating distributed capacitances. It is, in fact, really a method for selecting a set of parallel paths completely through a network. The set obtained is not unique, but is such that each element is used exactly once. If it is desired to sum the total effect of the paths, as in the capacitance problem, then the requirements on the quantity involved are that it can be added by first adding in series and then adding the parallel branches, and that a single element that must be used Q times may be considered to be formed of Q elements in parallel. The present method may be used for any quantity fulfilling these conditions.

It might also be noted that it is not necessary for all of the interconnections to exist. The lack of some particular connection would merely result in a gap in the array, which would not be serious as long as the circuit is such that a proper set of paths actually exists. In addition, some of the pairs of points may be connected by more than one element. In this case, the procedure would be the same as for the case where an element is to be used more than once. It is merely necessary to find several paths one of which includes each of these different elements.

We now give a proof, in words, of the principal assertions made above.

1. The upper right off-diagonal part of the square array contains all possible pairs ij for $i, j=1, 2, \cdots, N$, except $i=j$. Hence for each possible connection between the point i and the point j (i and j different) there is exactly one place in the upper right part of the array and a corresponding place in the lower left part. (As will be shown below, it is not necessary, however, that each element of the array be filled).

2. It is clear that making either a row or a column move entirely within one part of an array preserves one of the two subscripts. That is, we go from ij to ik, or from ij to kj. The effect of crossing the diagonal is not as evident.

The lower left part of the array is the lower left part of the transposed array of the original.[1] Thus, in the i-th column below the diagonal, we have the elements of the original i-th row; in the j-th row below the diagonal, we have the elements of the original j-th column. Further, in the upper right part of the array, the first subscript is always smaller than the second, since each row begins with the element $i(i+1)$. Because the order of subscripts has not been changed in writing the lower part of the array, it is always true that the second subscript is greater. Thus in crossing the diagonal, the following occurs:

(a) Going from the element ij in the j-th column above the diagonal, we may stop at any element jk in the same column below the diagonal. Since the second subscript is always greater, $k>j>i$.

(b) Going from the element pq in the q-th row below the diagonal we may stop at any element qr in the same row across the diagonal. Here also $r>q>p$.

So that we may say that all moves as described preserve one subscript. Moves across the diagonal invert the position of this subscript, and also insure that the altering subscript increases. This increase would be of interest if there is some type of problem where it is useful to move to progressively higher numbered elements of the circuit.

Consequently, a series of moves as described would give a sequence of subscripts, $1i-ij-jk-\cdots qN$. In the circuit this is equivalent to going from the point 1 to the point j; from the point i to the point j; $\cdots$; from the point q to the last point, N. If all of the possible connections of i to j exist, this is clearly one of several possible paths.

3. Let us consider what occurs if some of the connections are not made. We assume that an element may be used in more than one sequence of moves; hence, in order to be able to make a vertical move, it is only necessary that there be another element in the same column. But in the i-th column, the index i is one of the subscripts, while the other takes the values 1, 2, $\cdots$, N (excluding i). Thus, for a vertical move to be impossible in the i-th column, it would imply that the i-th element has only one connection to another element. Thus it would not be truly in the network we are considering, and can be neglected. (In the electrical case, a current would flow from the j-th element to the i-th, but there it would have no place to go.) Similar remarks apply to a horizontal move.

We have therefore shown that: (1) Each element in the circuit is represented in the array; (2) a sequence of moves as described gives a path through the circuit; and (3) it is always possible to make a proper move, unless some element which is included in the array is not truly in the circuit.

It might be noted that the transposed array need not be used if the circuit has sufficiently few gaps that special cases can be provided for by other means than the moves described. (The element 12 is always such a special case, as can be seen in Fig. 2.)

This work was done under the direction of Dr. A. H. Waynick, and was supported in part by Contract No. AF19(122)-44 with the U. S. Air Force, through sponsorship of the Geophysical Research Directorate, Air Materiel Command.

---

[1] A. A. Albert, *Introduction to Algebraic Theories* (University of Chicago Press, Chicago, 1942).

A Small Portable Reflectometer

William Liben* and Noel W. Scott
Engineer Research and Development Laboratories, The Engineer Center and Fort Belvoir, Fort Belvoir, Virginia

August 1, 1949

For measuring the reflectance of the 60-in. paraboloidal antiaircraft searchlight reflectors made at this laboratory, a small portable reflectometer has been used since 1942. The accuracy of the portable reflectometer for making measurements on the curved surfaces of 60-in. (25.5-in. focal length) and the 24-in. (10-in. focal length) paraboloids has been checked by cutting out and measuring the reflectances of small sections, both with it and with an absolute reflectometer. It gives consistent readings to at least one percent in reflectance, and has been used satisfactorily where it was inconvenient to use the absolute reflectometer.

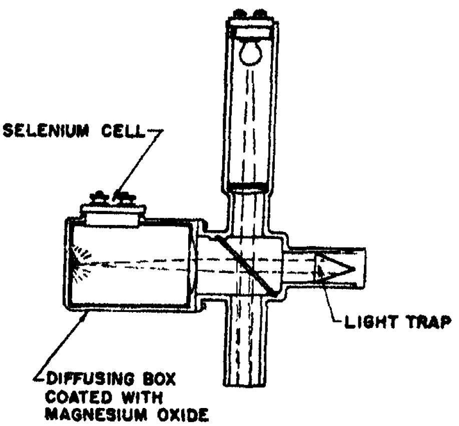

Fig. 1.

The instrument, shown in Fig. 1, projects a collimated beam of light from a light source through a semitransparent mirror to the reflecting surface, the reflected light being measured by a selenium-type photoelectric cell.

The light source, a 6- to 8-v lamp painted black except for a 3-mm diameter hole in the top, is operated from a 6.3-v filament transformer and a voltage regulator.

The current output of the selenium cell, which has a sensitive area of about 13 mm in diameter, is measured by a taut-suspension mirror "spotlight" galvanometer having a sensitivity of about 10^{-9} amp./mm. The sensitivity of the galvanometer, which has 100 scale divisions so that readings may be made directly in percentages, is controlled by a potentiometer between the cell and the meter.

Calibration is effected by using as standards two small, 2- by 2-in. mirrors of polished metal with differing reflectances. One of these, plated with rhodium, has a reflectance of from 70 to 75 percent, the other, plated with nickel, has a reflectance of from 60 to 65 percent. The reflectometer is calibrated by placing it upon one of the standards, and by adjusting the potentiometer across the galvanometer so that the scale reading equals the known reflectance of the standard. As a check it is then placed upon the second reflectance standard. This procedure both calibrates the reflectometer and checks it for proper operation. The presence of stray light may be detected by pointing the reflectometer into free space (zero reflectance).

---

* Now at Brookhaven National Laboratory, Upton, New York.

The Differential Pulse Transformer Bridge Circuit

John Alan Gledhill and Andrew Patterson, Jr.
Sterling Chemistry Laboratory, Yale University,
New Haven, Connecticut

June 10, 1949

In the course of devising a new method for the measurement of the Wien effect, we have evolved a bridge circuit suited for the study of the behavior of impedance elements when subjected to current or voltage pulses of widely varying amplitude and duration. The circuit, which resembles the differential transformer bridge mentioned by Hague,[1] is shown in Fig. 1. The use of pulsed instead of sine wave excitation permits a number of significant improvements in performance. The essential feature of the circuit is the differential pulse transformer, *Tr*. The identical twin primary windings are connected in opposition in series with the impedances Z_1 and Z_2. An oscilloscope is used to observe the voltage developed across winding 3. If Z_1 and Z_2 are equal pure resistances, for example, equal and opposite fluxes will be developed in the core when voltage is applied to the circuit and no voltage will be induced across winding 3. If Z_1 and Z_2 are unequal, the insertion or removal of the small resistances r_1 and r_2, as needed, or the varying of one of the impedances in terms of which the other is being measured will again result in no voltage being developed across winding 3. Thus, balance is indicated by a null in voltage from winding 3. The reversing switch, *Sw*, allows elimination of any small inequalities in the primary windings.

It may be shown mathematically that these same results will be obtained for any form of exciting voltage—sine wave, square pulse, or otherwise—so long as the transformer is suited to passing the band of frequencies involved. It may also be shown that the circuit is suited, under these circumstances, for use as an entirely general impedance bridge and that it may be balanced so long as any impedance Z_1 may be matched with a like impedance Z_2.

The sensitivity of the bridge is limited only by the input voltage applied and the gain available in the bridge amplifier, together with the transformer design requirements that the magnetizing inductance be as large and the coupling between the windings as close as possible. The close coupling has a further advantage in that the effect of differing earth admittances is minimized; unbalanced earth admittances will be reflected almost equally in both windings and thus cancel.

If square pulse excitation is applied, the ease of null detection (and hence of bridge balance) is greatly enhanced. First, both positive and negative pulse outputs may be obtained from winding 3 depending on the direction of the difference between Z_1 and Z_2; thus the direction in which one or the other must be altered to obtain balance is immediately indicated for any given bridge arrangement. With sine wave input this direction is not immediately apparent with ordinary oscilloscopic presentation. Second, *R*, *L*, or *C* components of an impedance affect the pulse shape differently. In the case of a parallel *R-L-C* combination, it may be shown that unbalanced *C* differentiates the pulse and produces humps at each end, oppositely directed; unbalanced *L* integrates the pulse and produces a slant on the top of the pulse; unbalanced *R* gives an output proportional to the unbalance and moves the pulse above or below the center line. In practise, it is not difficult to balance these three components separately, since the shape of the pulse observed indicates at once both the components out of balance and the direction of unbalance. This is in contrast to the case of a sine-wave excited bridge with either earphone or oscilloscope null detector. With the latter, an elliptical display may be employed to give separate indication of *R* and *C* components, for example, but in both the earphone or oscilloscope displays with sine wave input considerable time must be spent exploring for the direction of balance with reduced gain in the bridge amplifier; with pulse excitation the necessity of doing this is appreciably reduced.

The requirements outlined for suitable bridge transformers are not such as to require special transformer design. For pulses in the microsecond range, radar pulse transformers will often serve; in the millisecond pulse range, high quality audio transformers are well suited. In any case, two closely equal windings and a separate third winding are required and it must be established that the transformer has a frequency response adequate to pass the pulses to be used. We have used a bifilar wound magnetron input transformer (Western Electric D-163325, with one bifilar winding removed from the secondary) successfully. A much smaller microsecond-range transformer was made from a small 3-mil Hypersil core (Westinghouse No. 131 7996) with two windings each of No. 30 Formvar and one of 107 turns of No. 32 Formvar layer wound and distributed on both legs of the core.

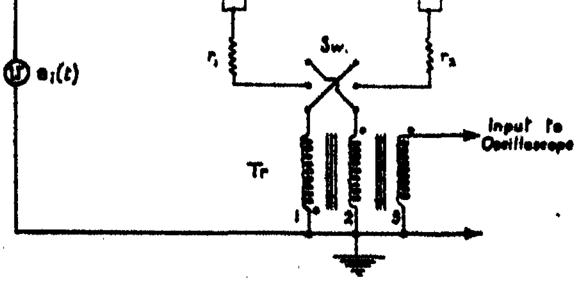

FIG. 1. Differential pulse transformer circuit.

To test the performance of the circuit, we have made impedance measurements with square pulse excitation at pulse lengths ranging from 1 to 1500 μsec. and voltages from 10 to 30,000 (for the shortest pulses) and have found it possible without difficulty to measure resistances, capacitances, and inductances as well as not too complicated series and parallel arrangements of these with accuracies comparable to those of the usual a.c. bridge methods. It has been found possible to employ the usual decade resistances and precision variable capacitors in making measurements on unknowns and still obtain accuracies in the range of 0.1 percent. If the residual inductances and capacities may be balanced out, this figure may be improved upon. Under special circumstances where very high voltages may be applied to the impedance elements, accuracies of 0.01 percent are readily achieved.

The following advantages of the circuit in application may be mentioned. By using short pulses at low repetition rates, down to one pulse only, heating of the measured elements is greatly reduced. This is particularly important in the investigation of elements with high temperature coefficients, of which the conductance of electrolytes is an example. The speed and ease with which balance may be reached is an important point in this same connection. If an appropriate pulse length is used, the method is capable of distinguishing parallel and series *R-C* circuits without requiring several measurements at different frequencies as is the case with the conventional sine-wave excited a.c. bridge. In cases where the field strength applied to the measured impedances must be accurately known or must be quite large, the facts that at balance the full pulse voltage is applied to the impedances and none across the transformer result in considerable economy in bridge excitation equipment and simplicity in field strength calculation. This result comes about because at balance the flux in the transformer is zero and accordingly no voltage exists across it. This is in contrast to the usual Wheatstone bridge circuit, where, in order to obtain maximum sensitivity, equal bridge arms are required, so that in such a case at most only half the input voltage may be applied to the measured elements.

[1] B. Hague, *Alternating Current Bridge Methods* (Pitman Publishing Corporation, London, 1938), fourth edition, pp. 421–422, and references cited there.

Preparation of Single Crystal Copper Ribbons from Single Crystal Copper Rods*

A. A. PETRAUSKAS, E. A. COOMBS, AND J. E. MACDONALD
Department of Physics, University of Notre Dame, Notre Dame, Indiana

August 9, 1949

IN connection with work on electronic emission from single crystal surfaces, a method was developed for processing single crystal ribbons of copper from single crystal rods. A rod having a known orientation of the crystallographic planes with respect to the axis of the rod was embedded in a block of brass. The rod was soldered in place for added mechanical support, and then the block was machined in the form of a strip approximately 0.04 inch thick. The block was mounted so that the surface which was cut exposed the desired crystallographic planes. The copper strip obtained in this manner was cemented on a steel block with Cenco Sealstick and the surfaces were ground parallel with a surface grinder. X-ray studies revealed that deformation of the single crystal strip extended to a depth of about 10 mil below the surface.

The deformed layer was oxidized and then the cupric and cuprous oxides were removed by the chemical process reported by Baker and Gibbs.[1] The strip of copper was oxidized for 10 minutes at 900°C and then transferred to another furnace at

500°C where it remained for one-half hour. It was found that the use of the second furnace at the intermediate temperature reduced the chipping off of the oxides when the strip was allowed to cool to room temperature.

Following the oxidation, the strip was placed in an alcoholic solution of HCl to which fresh stannous chloride has been added (40 cc of concentrated C.P. HCl to one liter of formula 12A denatured alcohol; 40 g C.P. fresh $SnCl_2 \cdot 2H_2O$). This solution dissolved both cupric and cuprous oxides. A non-polar medium of denatured alcohol was used since dilute aqueous solution of HCl attacks copper, and stannous chloride was added to reduce quickly the cupric ions to cuprous ions as the cupric ions attacked metallic copper.

An atmosphere of dry carbon dioxide above the alcohol solution prevented water vapor from dissolving in the alcohol. Vigorous agitation greatly speeded up the solution of oxides.

Approximately 10 mil of copper, 5 mil on each side, was removed in one oxidation procedure. This process was repeated until a smooth single crystal copper ribbon 5 inches long, 0.13 inch wide and about 0.003 inch thick was obtained.

This method of reducing the thickness of the strip was the most satisfactory one of the three methods attempted. Both straight chemical attack and electrolytic polishing pitted the copper producing minute holes which penetrated the ribbon.

---

* This work was sponsored by the Research Corporation.

[1] Irvin Baker and R. Stevens Gibbs, Ind. Eng. Chem., Anal. Ed. 18, 124–127 (1946).

Sensitivity of Schwarz-Hilger Thermopiles

E. SCHWARZ

Hilger and Watts, Ltd., London, England

January 3, 1949

IN his report on infra-red instrumentation and techniques, Williams[1] refers to the Schwarz thermopile made by Adam Hilger, Ltd., London, England, and he makes the ststement that although a sensitivity of 60 μv/μw is claimed by the makers, measurements made on two or three minimum area Schwarz thermopiles showed a sensitivity of only 8–12 μv/μw. No actual figures are given for the receiving area, the resistance of the couple, and the method of measurement. The sensitivity of 60 μv/μw is claimed for a vacuum thermocouple with an area of 2×0.2 mm and a resistance of 70–100 ohms, i.e., for 140–200 ohms for a compensated thermocouple of this type. All the measurements are made with a Hefner lamp as the light source at a distance of 50 cm from the receiver. The arrangement is similar to that described by Gerlach,[2] and a double-walled shutter is interposed to cut off the radiation. For vacuum thermopile No. F (1323301/49242), which contains two independent compensated elements with receivers of 2×0.2 mm behind a window of KBr, we found with the above method values of 72 μv/μw and a total resistance of 200 ohms for both elements. The same thermopile was tested by the N.P.L. which reports:

"The thermopile which bears the type and serial No. F (1323301/49242) is a vacuum thermopile with four receiving elements each approximately 2 mm by 0.2 mm. The elements are in line and lie parallel to the axis of the inner of two tubular envelopes. Radiation can reach the receiving elements through a longitudinal slot in the outer envelope and a potassium bromide window in the wall of the inner. Each of the outer receiving elements is electrically connected in series opposition with the adjacent inner element. The radiation is intended to be received on the inner element of the pair, the outer element providing compensation for temperature changes.

The sensitivity of each of the inner elements of the thermopile has been determined by comparison with Laboratory standards using as a source of radiation a blackened metal disk heated to a temperature of approximately 200°C. The thermopile was mounted vertically with the plane of the slot in the outer envelope perpendicular to the direction of the incident radiation. The compensating elements were shielded from direct radiation from the source by metal screens covering the upper and lower ends of the slot.

The source, which was about 4.0 cm in diameter, was situated about 50 cm from the thermopile and produced in the plane of the thermopile elements a uniform radiation intensity of approximately 0.5 mw/cm^2.

Under these conditions the sensitivities of the inner elements, expressed in terms of the open-circuit e.m.f. produced and the intensity of the radiation in the plane of the elements, were found to be: Sensitivity of upper element, 251 mv/w/cm^2; sensitivity of lower element, 251 mv/w/cm^2. The accuracy of the calibration is estimated to be ±1 percent.

These values were obtained after the thermopile vacuum had been improved by using the getter according to the instructions supplied with the thermopile."

As the area of the receiver is 4.10^{-3} cm^2 the sensitivity, expressed for a radiation of 1 μw falling on the receiver, is 62.8 μv/μw. These values are in fairly good agreement with the values measured with the Hefner lamp if one takes into account that the spectral distribution of the light sources is different.

The discrepancy between these values and the values reported by Williams may be due to the fact that the blackening of the receiver of the early types of thermopiles has not been adequate for the longer wave-length region.

---

[1] Van Zandt Williams, Rev. Sci. Inst. 19, 135 (1948).

[2] Gerlach, Physik. Zeits. 577 (1913).

A Technique for Cutting Metal Single Crystals

T. R. McGUIRE* AND ROBERT T. WEBBERT†

Sloane Physics Laboratory, Yale University,‡
New Haven, Connecticut

August 5, 1949

METALLIC single crystals grown by the Bridgman method are usually in the form of long cylinders. Ordinary methods for cutting pieces from such crystals are (1) to use a fine saw followed by an acid etch to remove the damaged and contaminated surface, or (2) to coat the crystal with paraffin which is then scribed along the line of the desired cut—the cutting process is then accomplished by etching with acid.

The first of these methods is rapid but involves the danger of severe damage to the crystal. Care must also be exercised to remove the last trace of ferromagnetic impurities left by the saw. The paraffin technique eliminates these objections, but, in

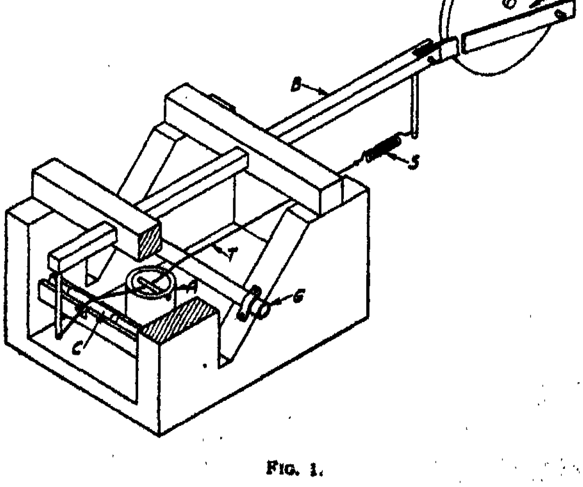

FIG. 1.

practice, cuts made by this method require many hours of almost constant attention and even then yield very poor looking results. Moreover, in many cases, the acid eats under the paraffin which then falls off because of the heat generated by the reaction.

Seeking to overcome these difficulties, a simple saw was built as shown in Fig. 1. The cutting action is due to acid carried by a Fiberglas[1] thread which passes through an acid bath, *A*, and over the crystal, *C*. The thread also passes over a glass rod, *G*, and is maintained under light tension by a small phosphor bronze spring, *S*. The bar, *B*, to which the thread is attached is constrained to move in slots, *L*, and is driven by an eccentric, *E*. The eccentric is rotated at about 8 r.p.m. by a geared electric motor.

The Fiberglas thread has high tensile strength, but sharp bends should be avoided, as the thread wears down quickly by abrasion. In the apparatus used by us, the thread must be replaced every 30 to 60 min. but no other attention is required.

The proper etch to use with each metal can be found by consulting *Metals Handbook*.[2] A few metals, such as aluminum, are cut very slowly as etching solutions containing hydrofluoric acid cannot, of course, be used in this device. About 5 hr. are required to eat through a 1-cm diameter tin crystal. The cut surface is square and somewhat roughened. With minor modifications, two or more cuts could easily be made simultaneously.

---

* Now at the Naval Ordnance Laboratory, White Oak, Silver Spring, Maryland.

† Now at the Naval Research Laboratory, Washington 20, D.C.

‡ Assisted by the ONR.

[1] This thread can be obtained from the Owens-Corning Fiberglas Corporation, Corning, New York.

[2] *Metals Handbook* (American Society for Metals, Cleveland, Ohio, 1949).

Pulse-Height Limiting Circuit for a Scintillation Detector

W. C. Elmore
Swarthmore College, Swarthmore, Pennsylvania

October 5, 1949

The modern scintillation detector of radiation consists of a phosphor used in conjunction with a photo-multiplier tube, such as the RCA 931-A, or the newer RCA 5819.* With such a detector the output voltage pulses have a considerable range in amplitude, and difficulty is often experienced in amplifying low level pulses, approaching in size the noise pulses from the photo-multiplier tube, without the amplifier being considerably overloaded, and therefore temporarily blocked by high level pulses. To meet this difficulty, one can design an amplifier of large dynamic range that is essentially overload-proof, no matter how great (within reason) the input signal. An alternative procedure is to limit the maximum pulse amplitude in the circuit between the photo-multiplier tube and the input stage of the amplifier (or preamplifier), thus permitting the use of a conventional pulse amplifier. Offhand one would surmise that existing non-linear circuit elements, such as the 1N34 crystal diode, do not have a sufficiently sharp bend in their voltage-current characteristic curve to make this method of limiting feasible at a level of perhaps 0.1 v. It is the purpose of this note to describe a simple circuit employing three crystal diodes that has proved to be very effective in limiting pulse amplitudes in the 0.1-v range. It is possible that the circuit may have other uses where a non-linear transfer characteristic is needed, having a sharp bend taking place in a few hundredths of a volt.

The basic limiting circuit is given in Fig. 1, where it is shown connected between a 931-A tube and a cathode-follower stage which serves as a preamplifier. With the supply voltage and resistance values given in the diagram, a steady current of about 0.1 ma flows at point *B* into the voltage-divider network consisting of the three diodes and the resistors R_1, R_2, and $R_3(R_1=R_2)$. Point *A* then has a potential with respect to ground of about 0.3 v positive, and diode D_3 is virtually non-conducting. If now a pulse of negative current is impressed on the network, as the result of a stream of electrons arriving at the anode of the photo-multiplier tube, point *A* drops in potential in proportion to this current until it reaches ground potential. Diode D_1 (and incidently D_2) is then cut off, and diode D_3 prevents point *A* from going negative to any great extent with a further increase of photo-multiplier current. Without D_3 the signal would not be limited, because of the finite, though high back resistance of D_1, and because of a possible capacitive feed-through of the signal.

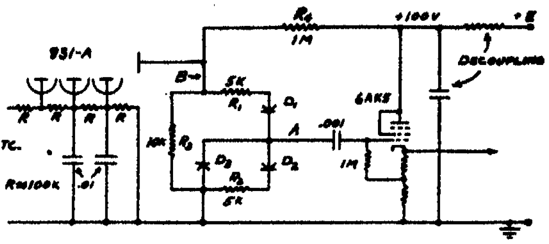

FIG. 1. Diagram of limiter circuit.

Static curves relating the potential V_A of point *A* to the net current I_B entering at point *B* are given in Fig. 2 for two values of the resistances $R_1=R_2$. These resistances are chosen equal to make the voltage-divider action of the circuit independent of voltage, except insofar as the diodes D_1 and D_2 differ in their characteristics. When $R_1(=R_2)$ has a low value, such as 1000 ohms, considerable curvature of the characteristic curve exists due to the increasing input resistance of the network as the input current is decreased. Part of the curvature may be due to dissimilarities in the diodes. The curvature is considerably reduced by increasing the series resistances to 5000 ohms, in fact, for the diodes used here, the curvature becomes almost negligible. The sharp bend in the curve occurs within 0.02 v.

The three diodes used for obtaining Fig. 2 were picked at random. The diode having the highest back resistance, as measured with an ordinary ohmmeter, was used for D_1, and the diode having the lowest forward resistance was used for D_3. Curves for other sets of diodes resemble the present curves, but differ in the degree of curvature and in the slope of the curve for negative currents.

The circuit values indicated in Fig. 1 have been chosen to give a speed of response that is suitable for use with an amplifier having a rise time of 1 or 0.2 μsec. Stray circuit capacitance should be kept at a minimum, particularly in the case of the lead from point *A* to the grid of the cathode follower. The magnitude of all the resistances in the limiter network can be reduced by as much as a

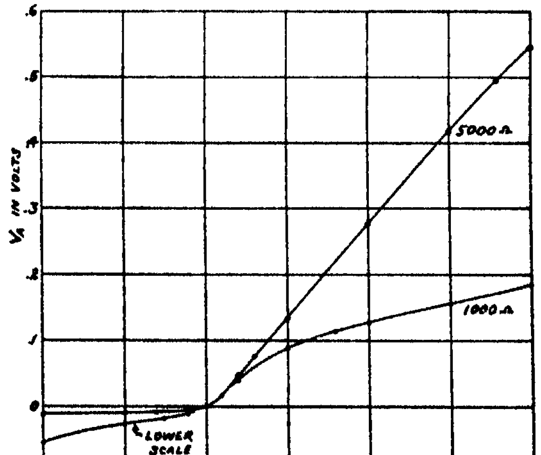

FIG. 2. Static curves showing the performance of the limiter circuit for two values of the resistances in series with the diodes D_1 and D_2.

factor of ten for greater speed, at the cost of decreasing the magnitude of the pulses.

The shape of the output pulses from the cathode follower depends on resistances and stray capacitances of the limiter circuit, provided the light flash from the phosphor is very short, as with anthracene and other organic phosphors. If the light decays with a time constant longer than about 0.1 μsec., as with the NaI(Tl) phosphor (which has a 0.25-μsec. decay constant) the trailing edge of the pulse then follows the decaying photo-multiplier current, provided limiting action is not taking place. Since pulse forming occurs at the input of the amplifier, the customary short time constant used for "clipping" pulses from an ionization chamber should not be used in the amplifier, otherwise "double differentiation" will result, with an attendant undershoot following each pulse.

The amplitude at which pulse-height limitation sets in can be controlled over a range of ten or more by varying the d.c. bias current through the network, i.e., by varying the resistance R_4 in Fig. 1. It is perhaps just as satisfactory to choose a suitable maximum amplitude, such as 0.2 v, and control the gain of the photo-multiplier tube by adjusting the high voltage supplied to the photo-multiplier bleeder resistors. The circuit described can be readily modified for use with a high voltage power supply having the positive side grounded. In this case the d.c. bias current for the crystal diodes can be obtained by connecting the resistor R_4 to the last dynode, instead of to the plate supply for the cathode follower.

The circuit described has been tested using a NaI(Tl) phosphor kindly supplied by Dr. R. Hofstadter. Pulses were examined with an oscilloscope having a fast triggered sweep and a delay line in the signal lead. It was found that the static curves of Fig. 2 adequately describe the limiting action of the circuit.

The author is indebted to the Research Corporation of New York for financial assistance.

---

* For a recent review of scintillation counters see J. W. Coltman, Proc. I. R. E. 37, 671–682 (1949).

A Portable Roentgenmeter for Field Use

C. C. Lauritsen
Kellogg Radiation Laboratory, California Institute of Technology, Pasadena, California

October 21, 1949

A PORTABLE roentgenmeter similar in size and shape to a fountain pen was first described at the December meeting of the Physical Society in 1932.[1] Such instruments are now in quite general use where personnel may be exposed to radiation hazards under normal working conditions and they have proved satisfactory for determining the integrated dose received during the day. The fact that batteries or some kind of charging device is required is usually not a disadvantage and may in fact be an advantage in routine operations where it is desired to keep a daily log for each worker.

However, in cases where extreme hazards may be encountered, particularly under field conditions, such accessories may not be available and would be inconvenient. For this reason we have developed an instrument which combines the usual elements with a frictional charging device. This instrument is shown schematically in Fig. 1 and the charging device and electroscope are shown in detail in the same figure.

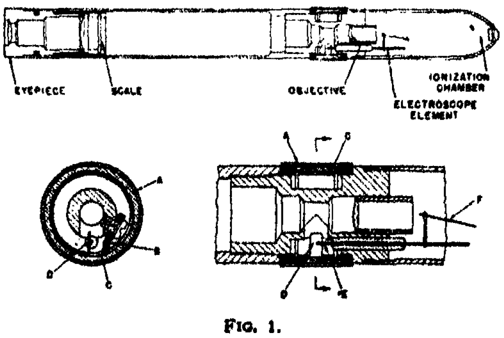

FIG. 1.

When the small sleeve, *A*, is rotated counterclockwise the friction pad, *B*, rubs against the inside of a polystyrene ring, *C*, and the collector spring, *D*, moves over to make contact with the electroscope support wire, *E*, thus charging the electroscope, *F*. A slight rotation in the opposite direction disconnects the collector spring from the electroscope and connects it to "ground." "0" ring seals effectively exclude moisture from the instrument.

As before, the instrument is so designed that full scale deflection represents one-tenth of a roentgen which was accepted as the maximum permissible daily dose. However, under conditions of extreme exposure one is not concerned with the permissible dose but with dangerous or even lethal doses and the electroscope must be observed and recharged at frequent intervals. For example, if the electroscope discharges in one minute a dangerous dose will be received in a few hours and a lethal dose in a few days. The possibility of recharging the instrument at will is a clear advantage in evaluating such hazards.

---

[1] C. C. Lauritsen, Phys. Rev. 43, 212 (1933).

Statistics of Counting Rate Meters

Ronald E. Burgess
Department of Scientific and Industrial Research, Radio Research Station, Ditton Parks, Slough, Bucks, England

October 10, 1949

THE indication of a counting rate meter exhibits statistical fluctuations due to the random arrival of the particles or events being counted. These fluctuations determine the standard deviation of a single reading and set a limit to the accuracy of the instrument. They may be reduced by the process of smoothing which can, for example, be effected by taking the mean of a number of uniformly spaced readings or by averaging the reading continuously over a length of time.

An analysis was given in 1936 in Sections 2–4 of the paper by Schiff and Evans[1] of the reduction of fluctuations by smoothing. Their results were in error due to an incorrect method of analysis and, since they are still accepted,[2] it seems desirable to give the correct expressions.

The general formula for the mean square fluctuation in the average of n values $(x_1, x_2 \cdots x_n)$ of a random variable is

$$\begin{aligned}\sigma_n{}^2 &= \left\langle\left[\frac{1}{n}\sum_{p=1}^{n}(x_p-\bar{x})\right]^2\right\rangle_{\mathrm{Av}}\\ &= \frac{1}{n^2}\left[\Sigma\langle(x_p-\bar{x})^2\rangle_{\mathrm{Av}}+2\mathop{\Sigma\Sigma}_{p\neq q}\langle(x_p-\bar{x})(x_q-\bar{x})\rangle_{\mathrm{Av}}\right]\\ &= \frac{1}{n^2}\left[n^2\sigma_1{}^2+2\sigma_1{}^2\sum_{m=1}^{n-1}(n-m)r_m\right],\end{aligned} \tag{1}$$

where σ_1 is the standard deviation of a single reading and r_m is the correlation coefficient between readings spaced $m(=p-q)$ apart.

If now the n readings are spaced at uniform intervals of time s, and since the correlation coefficient is determined, the exponential decay characteristic of the RC circuit

$$r_m = \exp(-ms/RC) = r_1{}^m, \tag{2}$$

where r_1 is the correlation coefficient $\exp(-S/RC)$ between adjacent readings.

The standard deviation of the average of the n readings is then given by

$$\frac{\sigma_n}{\sigma_1} = \frac{[n(1-r_1{}^2)-2r_1(1-r_1{}^n)]^{\frac{1}{2}}}{n(1-r_1)}. \tag{3}$$

This ratio lies between the value $1/n^{\frac{1}{2}}$ for zero correlation and unity for complete correlation as expected.

In the case of continuous observation over a time T, the summation in Eq. (1) is replaced by an integral and the variance of the average over T becomes

$$\sigma_T^2 = \frac{2\sigma_1^2}{T}\int_0^T (T-t)r(t)\cdot dt. \tag{4}$$

For the counting rate meter $r(t) = \exp(-t/RC)$ whence

$$\frac{\sigma_T}{\sigma_1} = \left\{\frac{2RC}{T}\left[1-\frac{RC}{T}+\frac{RC}{T}\exp\left(-\frac{T}{RC}\right)\right]\right\}^{\frac{1}{2}}. \tag{5}$$

---

[1] L. I. Schiff and R. D. Evans, Rev. Sci. Inst. 7, 456 (1936).
[2] Kip, Bosquet, Evans, and Tuttle, Rev. Sci. Inst. 17, 323 (1946).

Rapid Response Radiation Alarm*

R. L. Macklin and E. R. Rohrer
Carbide and Carbon Chemicals Corporation, K-25 Laboratories, Oak Ridge, Tennessee

August 29, 1949

CERTAIN alarm and safety control devices for radiation-producing equipment impose rather unusual requirements on the radiation-detecting instruments used to activate or trip them.

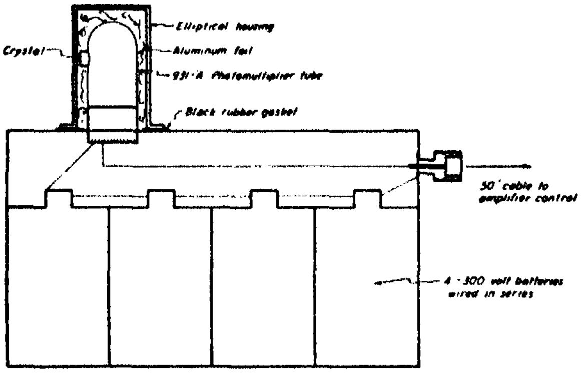
Elliptical housing
Crystal
Aluminum foil
931-A Photomultiplier tube
Black rubber gasket
50' cable to amplifier control
4 - 300 volt batteries wired in series

FIG. 1.

The instrument described here was designed to meet the following requirements.

(1) Activation of the alarm circuit within 0.5 sec. after the radiation intensity reaches a predetermined level.

(2) Assurance of operation even though much higher radiation levels were to be reached in as little as a few microseconds.

(3) Freedom from false alarms, i.e., reasonable ruggedness, stability and freedom from pick-up.

(4) Remote operation, if feasible.

The usual devices employed are ionization chambers, either argon-, freon-, or BF_3-filled. Pulse-operated devices are ruled out by the second requirement above as the amplifier tubes may become saturated or driven to cut-off, so that the rate meter circuit receives only a single pulse. Thus, a pulse-type circuit fails to trip if the radiation intensity rises high enough and fast enough.

The d.c. amplifiers used with ionization chambers have shown either a high pick-up sensitivity for switching transients or a slow response if transients were eliminated with a by-pass.

Design.—It appeared that a photo-multiplier tube might be satisfactory as a fast, transient insensitive, reasonably stable d.c. amplifier in this service. At current drains below 100 μa fatigue is not significant. At operating potentials above 120 v per stage, the over-all gain does not change rapidly and if desirable, special defocusing of an intermediate dynode may be used to give a nearly constant gain over a fairly wide range of voltages.

A single stage of d.c. amplification was used following the photo-multiplier to provide a signal of proper polarity to fire the thyratron and to reduce the effect of small changes in the thyratron-firing voltage. The signal fed to the grid of the thyratron was smoothed with the usual rate meter tank circuit employing a 0.05-sec. time constant. A crystal of anthracene is employed as the scintillator with an aluminum foil reflector as used by Bell.[1] A sketch of the photo-tube mounting and battery case is shown in Fig. 1. This is connected to the amplifier and relay by 50 ft. of microphone cable. The complete circuit with power supply and resetting device is shown in Fig. 2.

Performance.—Time of response tests have been made with a small (5 mg) radium gamma-ray source. This was held by an electromagnet against the pull of a long spring at a point considerably removed from the detector. Upon de-energizing the magnet, the source traveled rapidly to a position near the detector tube. The distance to the detector tube in this final position was such as to make the radiation intensity either 1½ or 3 times the tripping level. The intensity at the start of travel was about four percent of the tripping intensity. Timing contacts activated by the source started a clock which was stopped by the alarm circuit relay showing the time of response after the tripping level was reached.

For the standard 1½ times tripping level test, an average response time of 0.13±0.02 sec. was found. This compares with over 4 sec. for the ionization chamber circuits tested. At thrice tripping level, the response time was only 0.03 sec.

The tripping intensity used in these tests was 0.3 mr/sec. for exposures of a second or more. Using a 1P21 photo-multiplier tube and a 1-meg., 0.01-μf gridleak, the tripping intensity was 0.03 mr/sec. The lower thermal noise background with the 1P21 tube gave equal stability and freedom from false alarms. A further increase in sensitivity could no doubt have been achieved by applying a fixed bias to eliminate the average background signal and using an even larger input resistor for the 6SJ7.

The anthracene scintillator will also respond to fast neutrons, but the intensity required is rather beyond that available with

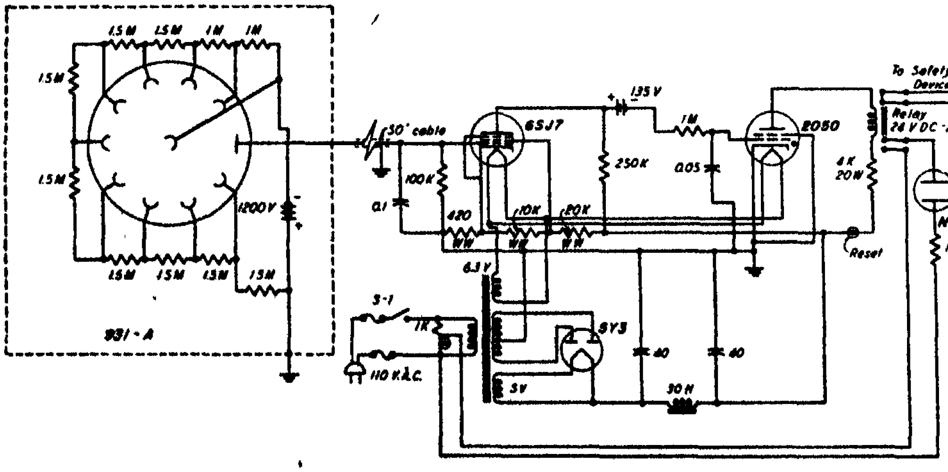

FIG. 2.

small gamma-ray free neutron sources. Thus, over-all operation checks are periodically made with a small gamma-ray source to ensure that the equipment is connected and functioning properly.

---

* This document is based on work performed for the AEC by Carbide and Carbon Chemicals Corporation, Oak Ridge, Tennessee.

[1] P. R. Bell, Phys. Rev. 73, 1405 (1948).

Note on Sealing Nylons Films to Geiger Counters*

ROBERT A. BECKER
Physics Research Laboratory, University of Illinois, Champaign, Illinois

August 22, 1949

IT was thought useful to report a very simple and certain method of attaching a thin Nylon sheet as the end window of a Geiger counter. As is evident from Fig. 1, the seal is of the compression type. The bonding material is ordinary rubber cement. (A commercial brand of the latter called "Neetstik" was employed.) The cement is diluted with several parts of benzene until it is sufficiently thin to be spread fairly uniformly with a small brush. The procedure is to apply two or three thin coats to the upper and lower surfaces, respectively, of the annular rings A and B in Fig. 1. To avoid later shrinkage, these are allowed to dry for about an hour. Following this, the Nylon sheet, cut oversize, is lightly laid on A, after which wrinkles are removed by pulling gently on the protruding edges. Finger pressure is then applied to the top surface of the Nylon to make it stick firmly to A. A heated piece of wire or other heated sharp instrument may be employed to clear the screw holes. This procedure, rather than punching with a cold instrument, avoids wrinkling the film. Ring B can then be attached in the obvious manner, with excess screw pressure being avoided. The purpose of the cement on B is to prevent cutting the Nylon by the ring. Surplus Nylon extending beyond the outer periphery of the rings can be melted off by means of the same heated wire.

The entire procedure, save for the initial drying of the cement, requires but a few moments, and is extraordinarily easy. No failures with this method have been experienced by the writer. A further advantage of the process is that the solvent will have evaporated from the adhesive before the sheet is applied, and thus does not weaken the edge of the window. With counters of the dimensions shown, and about 4 in. long protruding into an evacuated chamber, the writer has been able consistently to employ 6 cm pressure in the counter (1 cm alcohol and 5 cm argon) with $\frac{1}{2}$-mg/cm^2 Nylon windows. The counter plateaus are in excess of 200 v.

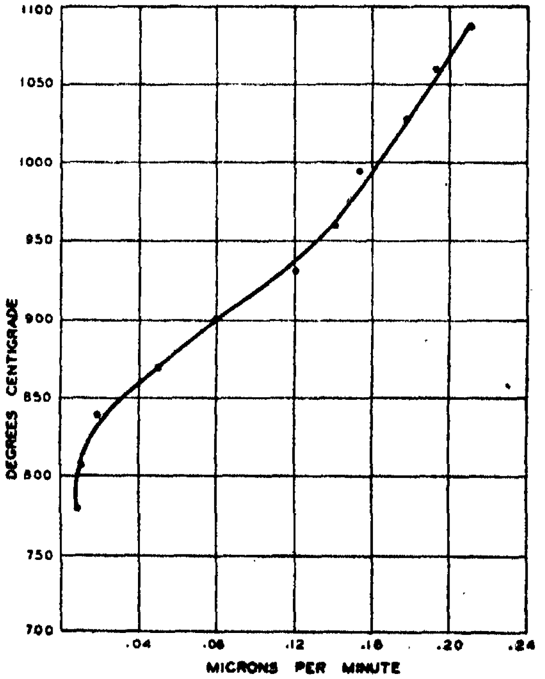

FIG. 1.

When employing Nylon window counters, it is necessary to take into account the diffusion of the counter gas through the Nylon. This effect for Nylon films has been described by others.[1] In the author's experiments this difficulty was reduced by keeping the counters open to a larger ballast volume and to a reservoir containing absolute alcohol maintained at melting ice temperature. The counter plateaus were checked from day to day.

The above bonding material has been employed also to attach zapon films to wire frames to be used as backing material for beta-spectrometer sources.

---

* This work was supported by the Joint Program of the ONR and AEC.

[1] J. A. Simpson, Jr., Rev. Sci. Inst. 19, 733 (1948). This author pointed out that water vapor may pass through the Nylon into the counter if the latter is immersed in a medium which bears water vapor.

Focusing in a Semicircular Magnetic Spectrometer

C. M. FOWLER, R. G. SHREFFLER, AND J. M. CORK
H. M. Randall Laboratory of Physics, University of Michigan, Ann Arbor, Michigan

August 19, 1949

THE line shape produced by a semicircular focusing spectrometer is currently of interest in the field of beta-spectroscopy. Although the boundary conditions imposed by a two-dimensional source and the defining slits have prohibited an exact solution of the three-dimensional problem, approximate solutions have been proposed by Wooster,[1] followed by Li[2] and by Tyler and Lawson.[3] A two-dimensional problem in which the particles are assumed to originate and remain in a plane perpendicular to the magnetic field, has been discussed in an approximate manner by Siegbahn.[4] The line shapes resulting from the two-dimensional treatment preserve the essential features predicted by the three-dimensional theories.

The purpose of this paper is to present an exact graphic treatment of the general two-dimensional problem. Using the technique discussed below, the line shape may be quickly determined for various arrangements of the sample and defining slits.

Figure 1 shows the circular trajectory of a particle projected at an angle θ from a point x, on the line source. The corresponding quantities ϕ and y define the trajectory at the image. Since mono-energetic particles are considered, the trajectory radii R, are the same for all particles. From Fig. 1,

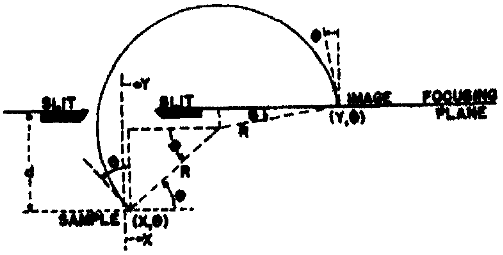

FIG. 1.

$$\theta = \sin^{-1}\left(\frac{d}{R} - \sin\phi\right) \tag{1a}$$

$$x = y - R\cos\phi - R\left(1 - \left(\frac{d}{R} - \sin\phi\right)^2\right)^{\frac{1}{2}}. \tag{1b}$$

The Jacobian of this transformation is

$$J\begin{pmatrix} x\theta \\ y\phi \end{pmatrix} = \frac{-\cos\phi}{\left(1 - \left(\frac{d}{R} - \sin\phi\right)^2\right)^{\frac{1}{2}}}. \tag{2}$$

Since the particles are assumed to be ejected isotropically from the source, the intensity I_0, of the particles per unit source length and

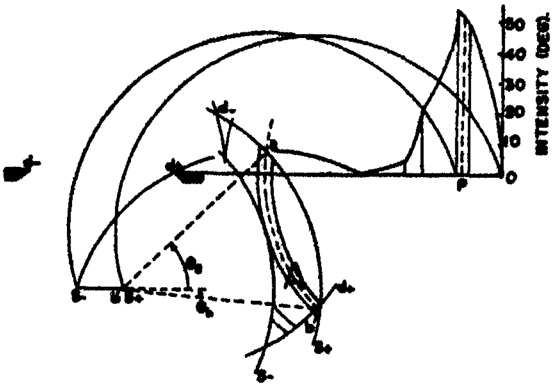

FIG. 2. Construction of two-dimensional line shape.

unit angle, is related to the corresponding intensity $I(y, \phi)$ at the image by the following equation:

$$I_0 dx d\theta = I_0 J\begin{pmatrix} x\theta \\ y\phi \end{pmatrix} dy d\phi = I(y, \phi) dy d\phi. \tag{3}$$

The line density $V(y)$, is obtained by substituting (2) into (3) and integrating over ϕ.

$$V(y) = I_0 \sin^{-1}\left(\frac{d}{R} - \sin\phi\right)_{\text{limits}} = I_0(\theta_a - \theta_b). \tag{4}$$

The determination of the θ limits of Eq. (4), and thus the construction of the line shape, is shown in Fig. 2. Here both sample

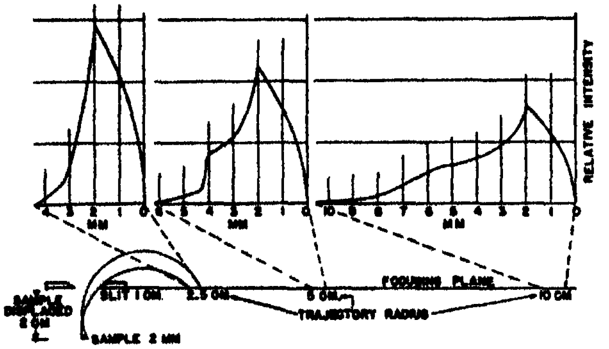

FIG. 3. Variation of line shape with focusing radius.

and slit widths have been exaggerated for clarity of construction. The intersections of the four circles, all with radius R, centered at $s+$, $s-$, $d+$, and $d-$ define an area A, which contains the centers of all the particle trajectory circles which can originate from the source and pass through the slits. To determine the intensity $V(y)$, at an arbitrary point P, of the image, a circle of radius R is constructed with P as center. The intersections, a and b, of this circle with the periphery of the area A, determine the limiting angles θ_a and θ_b. Since the point, a is an intersection with the $s+$ circle, θ_a is measured from the positive source limit, $s+$. On the other hand the positive slit, $d+$, determines θ_b, which is then measured from the intersection, b', of the source and a circle (radius R) with b as center. Other points of the image may be obtained in the same manner to complete the definition of the line shape.

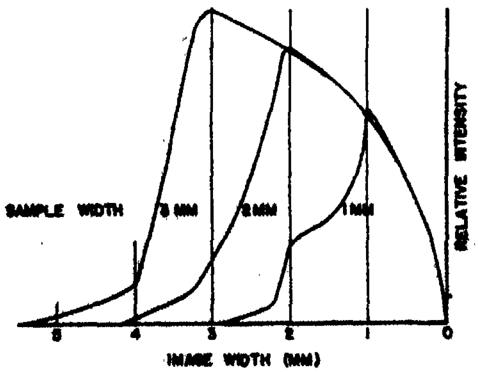

FIG. 4. Variation of line shape with source width. Trajectory radius 2.5 cm, sample displaced 2 cm, slit width 1 cm.

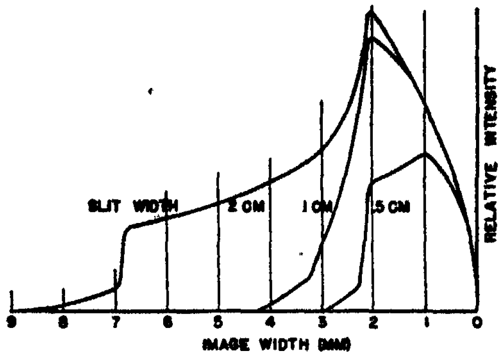

FIG. 5. Variation of line shape with slit width. Trajectory radius 2.5 cm, sample displaced 2 cm, sample width 2 mm.

In Fig. 2 the existence of five different topological zones forming the complete image presents no graphical difficulties. The number of zones depends upon the values of the various parameters: slit width, sample width, sample displacement, and trajectory radius. On the other hand the presence of a varying number of zones makes analytic expressions for the line shape awkward, although the functions are of a simple nature.

Figures 3-5 illustrate the effects of varying the parameters which determine the line shape. Figure 3 shows the typical line broadening and reduction of peak intensity with increasing trajectory radius. In Fig. 4 it can be seen that small increases in peak intensity, resulting from source widening, involve considerable loss in resolving power. Figure 5 stresses the importance of slit setting. As the slit width approaches the dimension of the sample, any appreciable increase in resolving power is gained only by a considerable loss in peak intensity.

In the conventional fixed radius spectrometer (Fig. 6) the sample and the focal line are colinear; i.e., in the above equations $d = 0$, and the Jacobian reduces to minus one. Since $\theta = -\phi$, Eq. (4) becomes: $V(y) \doteq I_0(\phi_b - \phi_a)$, where the points a and b determine ϕ_a and ϕ_b. The construction is simplified, since both angles are measured from P. By judicious choice of the spectrometer

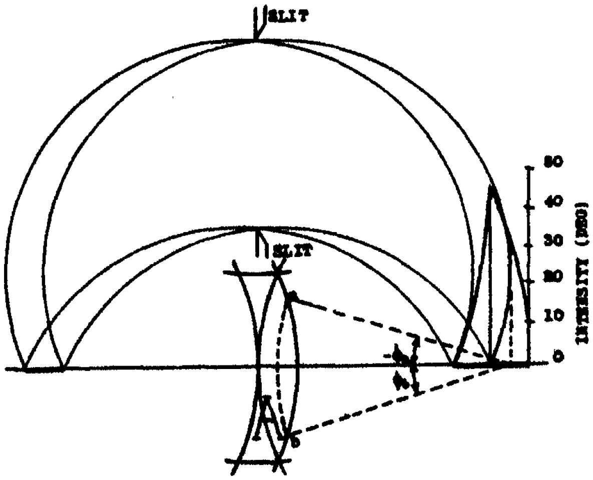

FIG. 6.

parameters, the line shape can be represented by only two zones (Fig. 6). For this special case, analytic expressions for the line shape may be advantageous.

This project was jointly supported by the AEC and the ONR.

---

[1] W. A. Wooster, Prog. Ray. Soc. A114, 729 (1927).
[2] K. T. Li, Proc. Camb. Phil. Soc. 33, 164 (1937).
[3] A. Tyler and J. Lawson, Thesis, Univ. of Michigan (1939).
[4] K. Siegbahn, Arkiv. f. Mat., Ostr., och Pysik, 30 (1944).

New Instruments

W. A. Wildhack: Associate Editor
in Charge of this Section
National Bureau of Standards, Washington, D. C.

These descriptions are based on information supplied by the manufacturer and in some cases from independent sources. THE REVIEW *assumes no responsibility for their correctness.*

Ultraviolet Microscope

Designed primarily for cancer research, an ultraviolet microscope for observing living, unstained body tissues is now in production.

The instrument's revolutionary objectives not only provide increased resolving power, but make it possible to photograph as well as view for the first time freshly prepared sections of live tissues and tissue cultures through three different ultraviolet wave-lengths. The photographs may also be projected or reproduced on color film through three visual color filters that provide densities, contrast and structural detail never before attained.

Developed during the past two years by Bausch & Lomb, and Polaroid Corporation, the microscope's objectives are of a reflecting type, and therefore, corrected chromatically throughout the entire ultraviolet and visible spectrum. Focusing can be done in visible light and photographs taken with other regions of the spectrum without disturbing the focal setting.

By using a band of wave-lengths, intensity of illumination in the image is high, allowing shorter photographic exposure than is required in a monochromatic objective system.

All of the elements, mirrors, and lenses have simple spherical surfaces, extremely precise, but relatively easy to produce by advanced grinding and polishing methods.

The microscope is particularly useful in the field of biochemistry for direct photographic recording of biological tissues, for microphotometric determination of biochemicals by photoelectric means, or for photo-densitometry.—BAUSCH & LOMB OPTICAL COMPANY, *635 St. Paul Street, Rochester 2, New York.*

Frequency Standard

A new frequency standard, employing a 100-kc crystal, has been announced by the Bliley Electric Company.

The equipment features a 24-hr. frequency stability of two parts in ten million, when subjected to line voltage fluctuation of as much as ten percent. Under adverse conditions of temperature humidity and semiportable operation, the instrument will maintain an accuracy of two parts in one million for a day period without resetting.

The frequency source employed is a Bliley GT cut quartz crystal unit temperature stabilized to within 0.1°C in a specially designed oven employing a mercury thermostat and external relay.

Long service life is assured by careful design and component selection. Long life tubes have been utilized in the crystal oscillator and automatic gain control circuits. Due to operation of the crystals at series resonance, and automatic gain control, the frequency is practically independent of line voltage and circuit component variations. Line voltage fluctuation of ±20 percent causes a frequency change of less than one part per million.

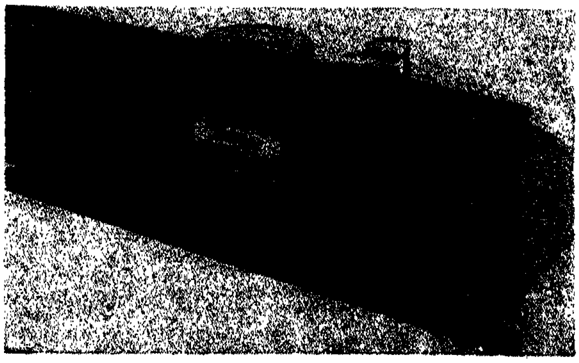

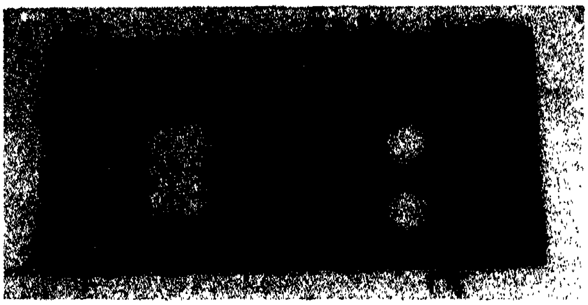

Terminals are provided for sine wave or harmonic output at both high impedance and low impedance. Power supply is self-contained and the equipment is designed for rack or cabinet mounting.

Universities, technical schools, military and commercial research laboratories, geophysical laboratories, and similar organizations will find the Bliley 100-kc frequency standard an indispensable instrument for frequency control and measurement. Inquiries are invited. Complete technical literature is available. —JOHN HARDER FENSTERMACHER, *Corry, Pennsylvania.*

Bridge and Amplifier

The BA-1 is a complete package of bridge elements, signal chopper, calibration system, amplifier, and power supply, designed for complete control of all SR-4 wire strain gauges and similar instrumentation.

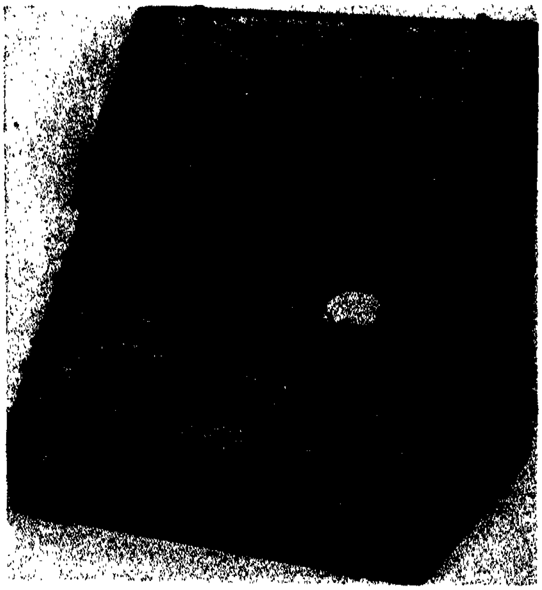

It drives any standard cathode-ray oscilloscope, and covers wide frequency range from static to high frequency. Calibrates at any time during test. High usable sensitivity and stability. Simple set-up and operation. Other resistive instrumentation in the form of displacement, load, pressure etc., pick-ups are handled effectively.

A unique feature of the BA-1 is the signal chopper which indicates the static unbalance of the bridge by intermittently shorting the bridge output. Static and very low frequency components of the signal are shown with the signal chopper on. High frequencies are observed with the chopper off. Chopper does not affect calibration.

Calibration is simple and fundamental by using the chopper to intermittently connect a calibration resistor across the active gauge. Built-in precision resistors cover the range of gauges and signal amplitudes normally used. Binding posts provide for an external calibration resistor. Calibration is checked readily at any time.

The amplifier faithfully reproduces the full range of frequencies likely to be encountered in practical engineering problems. Ample gain is provided to operate any standard cathode-ray oscilloscope at maximum usable sensitivity. Noise level is kept at a minimum by battery power, shock mounting, and selection of components.

Photographic records of transients, steady-state and static signals of short duration are easily made on a still camera. Dynamic signals of longer duration than the sweep period of the oscilloscope are recorded with a moving film camera.

Specifications.—Bridge input—50 to 2000 ohm resistive elements. Signal chopper frequency—100 c.p.s. Amplifier input—¼μf, 2 meg. Output—high impedance. Stages—3. Voltage gain—0, 10, 150, 3000. Frequency response—flat 5 to 20,000 c.p.s. Phase shift—negligible. Calibration—ten resistors, 10,000 to 10,000,000 ohms, one percent error. External resistor connection. Power supply—batteries, life 150 hr. Dimensions—12¼×9¾×7¾ in. Weight—22 lb. Price of the BA-1 is only $350.00 f.o.b. factory. ELLIS ASSOCIATES, *Box 77, Pelham 65, New York.*

Micro-Spectroscopy

A simple and convenient attachment for converting a standard infra-red spectrometer into a micro-spectrometer was described by Dr. E. R. Blout, associate director of research of Polaroid Corporation, at the annual meeting of the Optical Society of America.

With the device, scientists are able to make infra-red spectrographs or "fingerprints" of specimens only one-hundredth the weight of those required for analysis in standard instruments, particles so small that a single pound of material would be enough for 20 million samples. The attachment makes it possible to identify minute particles such as single hormone crystals and single fibers far too small to be examined with standard infra-red instruments. It is also expected to find use in the many situations in chemical and medical research in which only a few micrograms of material are available for study.

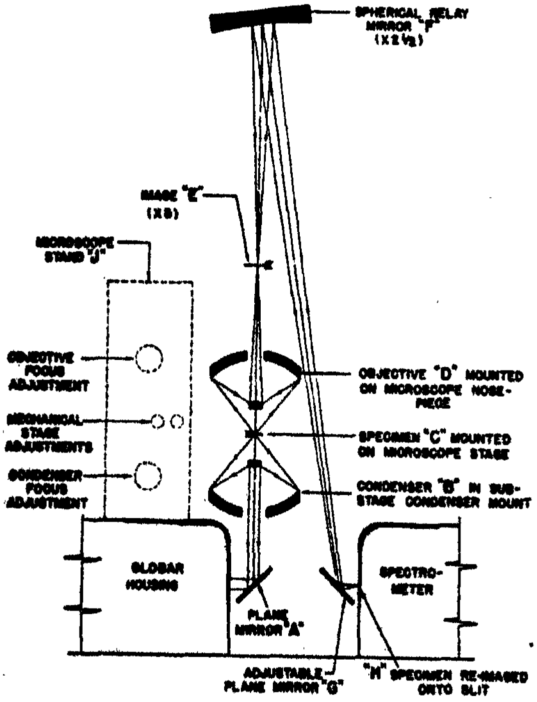
SPHERICAL RELAY MIRROR "F" (X2½)
IMAGE "E" (X8)
MICROSCOPE STAND "J"
OBJECTIVE FOCUS ADJUSTMENT
MECHANICAL STAGE ADJUSTMENTS
CONDENSER FOCUS ADJUSTMENT
OBJECTIVE "D" MOUNTED ON MICROSCOPE NOSE-PIECE
SPECIMEN "C" MOUNTED ON MICROSCOPE STAGE
CONDENSER "B" IN SUB-STAGE CONDENSER MOUNT
GLOBAR HOUSING
PLANE MIRROR "A"
SPECTRO-METER
ADJUSTABLE PLANE MIRROR "G"
"H" SPECIMEN RE-IMAGED ONTO SLIT

MICROSCOPE SPECTROMETER ASSEMBLY

The device was developed by Blout, G. R. Bird, and D. S. Grey of the Polaroid laboratories. They reported that the device is made possible by the use of reflective apochromatic microscope objectives designed by Grey. This lens focuses a magnified image of the object to be studied on the slit of a standard infra-red spectrometer. The complete attachment consists of the mirror-type lens together with auxiliary mirrors and a special stage for holding the specimens.

A somewhat similar technique was described earlier in the year by three British scientists (Barer, Cole, and Thompson). The British device made use of non-spherical mirrors in the microscope lens which were described as extremely difficult to manufacture. The new Grey-designed lens uses only sperical surfaces, relatively easy to produce by ordinary grinding and polishing methods. It is manufactured by Bausch & Lomb Optical Company in Rochester, New York.—POLAROID CORPORATION, *Cambridge 39, Massachusetts.*

Phase Monitor

The Clarke Model 109 high precision phase monitor for measuring phase relations at radiofrequencies has an absolute accuracy of ±1° and resolution and repeatability of ±0.1°. Phase is read directly from two dials calibrated in 0.1° increments. "Operator error" is eliminated since the answer obtained is not dependent upon the skill of the operator in making preliminary adjustments. The instrument continuously and automatically indicates the phase difference and requires no manipulation on the part of the operator. Provision is made to indicate antenna current in the various towers of a directional array, as well as to indicate the phase relations.

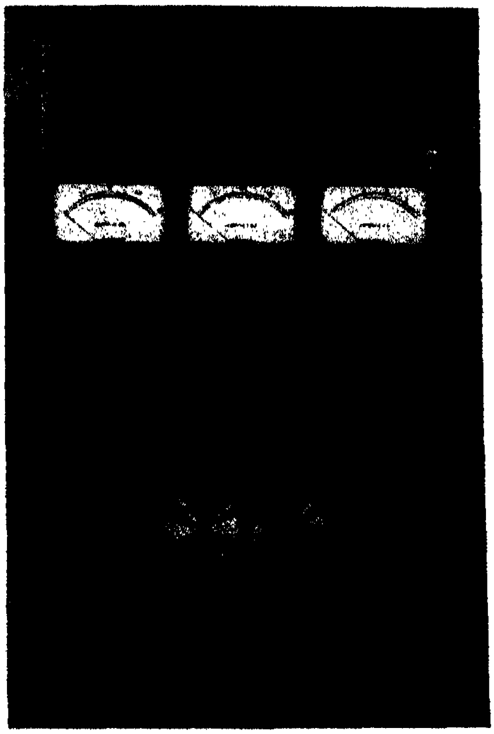

The Model 109 phase monitor requires 28 in. of panel space and is supplied with finishes to match those used by the various manufacturers of transmitting and associated equipment.—CLARKE INSTRUMENT CORPORATION, *910 King Street, Silver Spring, Maryland.*

Electronic Voltage Supply

A precision voltage regulator called the Electronic Standard Cell has been developed for instrumentation requiring accurate, highly stable d.c. voltage.

This electronic cell is available for any specified d.c. output voltage from 0 to 100 and for any load up to 30 ma. Output voltage is constant to better than 0.1 percent and with ripple less than 0.01 percent, throughout an input range of 75 to 135 volts a.c. at frequencies from 50 to 400 c.p.s.

Precise output voltages such as 0.10, 1.00, or 100.00 volts d.c., or the usual standard cell voltage of 1.018 can be supplied.

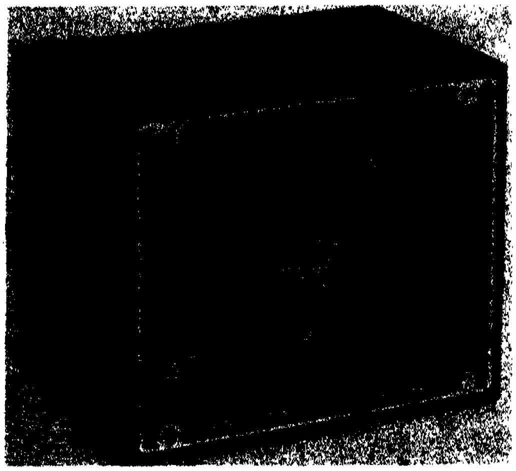

Simple electronic voltage regulators similar to the VR-150, VR-105, OA2, and OB2 are often used in electronic circuits, but in general are not accurate enough for reference voltages or instrumentation. However, by combining these regulators, that is, supply regulated voltage into a second regulator, the resulting voltage is extremely constant and independent of the supply voltage.

In the electronic standard cell, rectified voltage is initially filtered by an electrolytic capacitor and supplied to an OA2 regulator tube. The regulated output of this tube is then fed to an OB2 regulator. The output of this final regulator is extremely constant and is fed to the load through a variable dropping resistor to the binding posts. This dropping resistor allows any output to be obtained from 0 to 100 volts.

The electronic standard cell is designed for use with self-balancing potentiometers, recording oscillographs, resistance thermometers, wire strain gauges, position potentiometers, and many other industrial and laboratory instruments that require highly stable voltages for maximum dependability. It is well designed for use as an individual instrument and is sufficiently small and rugged to be used as a built-in component for larger instruments.—Hastings Instrument Company, Inc., *Hampton, Virginia.*

X—Y Recorder

A new Speedomax recorder now automatically plots the relationship between two variables, showing one as a function of the other. Tedious compilation and manual plotting by experienced personnel are eliminated. Instead, the variables to be plotted are converted d.c. signals, and connected to the instrument, one to the horizontal axis and the other to the vertical axis. The result is a permanent record, accurately plotting in minutes data that would require hours using the usual point by point method.

As compared to the usual recorder, which has only one measuring circuit and a constant speed non-reversing chart paper drive and which plots a variable as a function of time, this new recorder has two measuring circuits. Pen travel (*X* axis) is controlled by our well-known Speedomax G electronic circuit. A similar circuit controls the chart paper drive (*Y* axis) and makes it reversible. Thus, the new recorder makes it possible automatically to draw curves such as a hysteresis loop, temperature-*vs.*-temperature difference, stress-*vs.*-strain or other two variable curves.

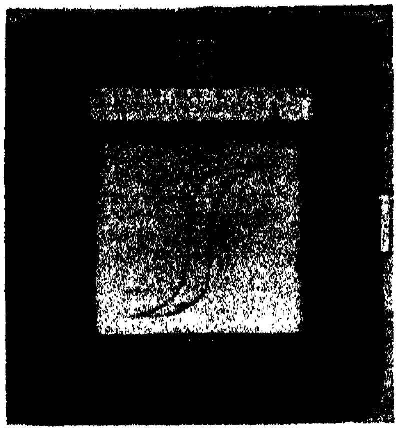

Response of the instrument is amply fast. The pen takes only 3 sec. for full scale travel of 9¾ in. Full chart travel is 10 in. and requires 4 sec. Standard minimum input voltage for full travel of the *X* coordinate is 2.5 mv, while the *Y* coordinate requires a minimum of 10 mv, for full travel.

For further information, write.—Leeds & Northrup Company, *4934 Stenton Avenue, Philadelphia 44, Pennsylvania.*

Wave Generator

A complex wave generator is now available, made by Alfred W. Barber Laboratories, under exclusive Patent License by Centre Research Laboratory. This device will generate any wave form which may be represented by a fundamental and second, third, fourth, and fifth harmonics in any percentage and any relative phase.

The frequency of the fundamental may be varied from 50 to 3000 cycles. The amplitude of any harmonic may be varied from zero to 100 percent of the fundamental. The phase of any harmonic may be varied through 360 degrees. The fundamental and all harmonics are derived from the same two beating oscillators so that no synchronizing problem exists. Phase shifting is done at a single frequency by means of simple, substantially linear phase shifting circuits. The output is one volt into 500 ohms at fundamental or any harmonic.

The complex wave generator is a new electronic generator with many important applications. It has proved itself in the rapid solution of many problems which hitherto were attacked in a very laborious manner. Its availability promises many interesting and useful applications in the future.—Alfred W. Barber Laboratories, *34-04 Francis Lewis Blvd., Flushing, New York.*

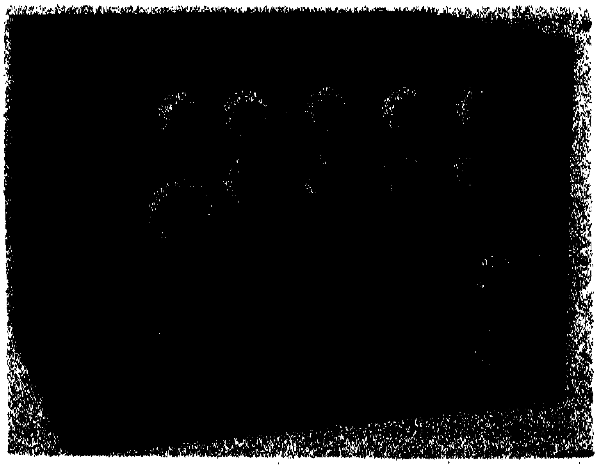

Platinum Resistance Thermometer

The platinum resistance thermometer units of conventional design are useful only to 500°C or thereabouts. At higher temperatures glass and mica become conductive and both materials lose their mechanical strength.

Platinum resistance thermometers are now manufactured which are entirely embedded in pure alumina and fired at a high temperature.

Alumina does not contaminate platinum as quartz does. It is still an excellent insulator at 1400°C. Its softening point is near 2000°C.

The units are 4 in. over-all length, 0.259 in. diameter, and provided with platinum lead stubs. Standard resistances are 25.5 and 60 ohms.

The units have no unsupported windings at any point. They are, therefore, very sturdy. In a conventional protection tube, they are expected to retain their accuracy for long periods.—PAUL G. WEILLER, *95 Broad Street, New York 4, New York.*

Manufacturers' Literature

Ultrasonic Reflectoscope—Bulletin 50-105 describes the Type UR reflectoscope, an ultrasonic instrument for instantaneously locating defects in metals and other materials by the application of a single "searching unit."—SPERRY PRODUCTS, INC., *Danbury, Connecticut.*

Current Data on High Vacuum Apparatus—Vol. 1, No. 2, 8 pages, contains a summary and 5-page article on "Production of low pressures" with graphical presentation of performance data on DPI pumps.—DISTILLATION PRODUCTS, INC., VACUUM EQUIPMENT DIVISION. *Rochester 13, New York.*

Announcer—No. 49 10 36, 16 pages, features an article on the brief history and modern trends in the analysis of gases. Included also are descriptions of three models of Burrell gas analyzers; the Speedigram, a new adaptation of a highly sensitive, accurate analytical balance; a microscope illuminator; and stainless steel automatic pipette washer.—BURRELL CORPORATION, *1942 Fifth Avenue, Pittsburgh 19, Pennsylvania.*

Optical Pyrometer (Potentiometer Type)—Catalog N-33D, illustrated, 16 pages, describes two special lens assemblies which are being increasingly used with the standard L & N optical pyrometer for measuring molten steel temperatures, or in the laboratory to make specialized temperature measurements.—LEEDS & NORTHRUP COMPANY, *4934 Stenton Avenue, Philadelphia 44, Pennsylvania.*

Combustibles Recorder—Bulletin 150-A, 16-page, illustrated, "Bailey combustibles recorder," features design improvements and new applications for this electronic equipment, which operates on the catalytic combustion principle and which provides either air or electrically-operated control of combustibles content. Typical applications to boiler furnaces, atmosphere producers, rotary kilns, industrial furnaces, and chemical processes are illustrated.—BAILEY METER COMPANY, *1050 Ivanhoe Road, Cleveland 10, Ohio.*

Tracerlog—October, 1949 issue features an article on the SU-5 beta-gamma-survey meter, a versatile new meter which is portable, battery-operated, and weatherproof, and which will serve the dual purpose of a radiation dosage rate meter and a monitoring instrument. A single sheet insert lists Tracerlab products and services etc.—TRACERLAB, *130 High Street, Boston 10, Massachusetts.*

Cenco News Chats—No. 65, 25 pages, presents an article on the organization of the National Science Teachers Association, a biographical sketch of Louis Agassiz, and descriptions of various items of laboratory equipment.—CENTRAL SCIENTIFIC COMPANY, *1700 Irving Park Road, Chicago 13, Illinois.*

Strain Gauges—New 12-page catalog describes Baldwin SR-4 bonded resistance wire strain gauges, illustrated by line drawings distinguishing 11 types of gauges and listing 102 standard gauges. The gauges are classified by types of wire and cementing materials to be used. A single table gives electrical resistances, gauge factors, dimensions, and prices.—THE BALDWIN LOCOMOTIVE WORKS, TESTING EQUIPMENT DEPARTMENT, *Philadelphia 42, Pennsylvania.*

Refractometer—News release on Precision-Dow Robomatic refractometer describes this instrument, which controls the flow of industrial process streams by refractive index instantaneously and continuously, and graphically records the results 24 hours a day.—PRECISION SCIENTIFIC COMPANY *3737 West Cortland Street, Chicago 47, Illinois.*

Radiation-Detection Densitometer—Bulletin No. 270 describes the Model 500-R Photovolt radiation-detection densitometer, a photoelectric instrument for the exact measurement of density of x-ray film employed in personnel monitoring for protection against radiation in nuclear, radioactive isotope, and x-ray work. Information on operation, applications, and price are included.—PHOTOVOLT CORPORATION, *95 Madison Avenue, New York 16, New York.*

Experimenter—September, 1949 issue features description of a new, general purpose, A-M, standard-signal generator, Type 1001-A, complete with photographs, sketches, and schematic diagrams and specifications. October, 1949 issue features a description of the Type 1701-AK Variac speed control, complete with photographs, curves, and schematic diagrams.—GENERAL RADIO COMPANY, *275 Massachusetts Avenue, Cambridge 39, Massachusetts.*

Automatic Circular Dividing Machine—Bulletin 182-49 describes and illustrates a fully automatic machine for production ruling of precision circular scales according to any standard pattern of lines having industrial or scientific application.—THE GAERTNER SCIENTIFIC CORPORATION, *1201 Wrightwood Avenue, Chicago 14, Illinois.*

Electro-Chemograph—Folder EM9-90(1), "An advanced electro-chemograph Type E," describes and illustrates an all a.c., or battery-operated, electro-chemograph, which includes, in one compact cabinet, a Speedomax Type G microampere recorder, a polarizer, and a power supply unit. Illustrations show the centralized control panel, typical recordings, and L & N dropping-mercury electrode assembly.—LEEDS & NORTHRUP COMPANY, *4908 Stenton Avenue, Philadelphia 44, Pennsylvania.*

Technique—Vol. 3, No. 4, Muirhead journal of instrument engineering, features articles on industrial instruments, improving the *pH* meter Type D-303, the rapid processing of photographic materials, and the miniature standard cell, Type D-550-A.—MUIRHEAD AND COMPANY, LIMITED, *Beckenham, Kent, England.*

High Vacuum Coaters—12-page booklet, "Vaporized metal-coatings by high vacuum," fully illustrated, describes DPI's entire line of vacuum chambers and vacuum coating equipment.—DISTILLATION PRODUCTS, INC., *755 Ridge Road West, Rochester 13, New York.*

New Materials

Forest K. Harris: Associate Editor
in Charge of this Section
National Bureau of Standards, Washington, D. C.

Ductile Cast Iron

The incorporation of a small amount of magnesium into cast iron produces a new graphite structure in the form of spheroids or compacted particles and eliminates a substantial amount of the flake graphite which weakens castings. The magnesium-treated cast iron combines the processing advantages of cast iron, such as fluidity, castability, and machinability, with many of the product advantages of steel—high tensile strength, elastic modulus, yield strength, toughness, and ductility. It behaves elastically like steel rather than cast iron under stress, with a modulus of about 25×10^6 p.s.i. This material is being produced by licensees under U.S. Patents No. 2,485,760 and No. 2,485,761.—INTERNATIONAL NICKEL COMPANY, *67 Wall Street, New York 5, New York.*

Magnet Materials

Alnico 5 DG (a modification of Alnico 5) has its crystal structure oriented in the direction of magnetization. It is stated to have the highest residual induction of any known permanent magnet material and permits the use of smaller magnets in applications.

Alnico 7 is designed for applications where a high demagnetization force is present, such as motors, generators, and variable gap devices. It has a higher coercive force than any other grade of Alnico.—GENERAL ELECTRIC COMPANY, *Schenectady, New York.*

Synthetic Wax

Ceramid, a synthetic wax now in commercial production, is an alkyl stearamide. It is hard, light yellow in color, and melts between 79.5 and 80.5°C. It is insoluble in water but more soluble in organic solvents than other commercial waxes, natural or synthetic. It is slower burning and higher melting than paraffin wax, and is compatible with asphalt, carnauba wax, cumarone resins, ethyl cellulose, microcrystalline wax, paraffin wax, and Acrawax C.

Its use is indicated in protective coatings and films deposited out of solution. It may be used as an antitack agent for resin organisols and as a mold lubricant for rubber and plastics. In most lacquers and enamels it dissolves clearly and serves as a gloss-reducing agent. It can be used for waterproofing textiles, paper, and leather, and may be blended with other waxes and hydrocarbons in polishes, insulating compounds etc. Samples and further data may be obtained from the manufacturer.—GLYCO PRODUCTS COMPANY, *26 Court Street, Brooklyn 2, New York.*

Insulating Film

Scotch-Weld No. 70 electrical insulating film is designed for use in coil construction. It is applied like tape and then heat-treated 1-2 hr. at 200-300°F, bonding itself into a unified layer of insulation. The cured film has high dielectric strength and is resistant to heat, moisture, oil, and most solvents. It is available in 60-yd. rolls, in widths up to 42 in., and in 2, 4, 6, and 8 mil thicknesses A manufacturer's bulleting is available on this product.—MINNESOTA MINING AND MANUFACTURING COMPANY, *900 Fauquier Avenue, St. Paul, Minnesota.*

Photographic Hypo

A new *acid fixer with hardener*, combining fixer and hardener in a single powder, is stated to have better keeping qualities and to be faster and easier to mix than the usual hypo, at no additional cost. It incorporates anhydrous sodium thiosulfate and is marketed in hermetically sealed cans. Being anhydrous, it does not cake or harden in storage during warm weather. Also it gives off heat during solution so that the hypo becomes slightly warmer instead of colder during the mixing.—ANSCO CORPORATION, *Binghamton, New York.*

Fireproofing Cement

A fireproofing cement for the protection of beams and other structural steel parts has been developed by the Eagle-Picher Company and rated by the Underwriters' Laboratories. The cement is produced as a powder which is mixed with water to form a stiff paste and then troweled onto a ribbed metal lath wrapped around the steelwork to be protected, without the use of forms. When applied in a layer 1¾ in. thick, it will afford fire protection for 3 hr., according to the manufacturer. It is much lighter than most other materials used for this type of fireproofing, and its cost is estimated to be one-fourth less than the methods commonly used. An added advantage is its ability to withstand spalling and crumbling. Its chief application is expected to be in chemical plants, refineries, and other industrial installations where exposed steelwork is part of the structure. A descriptive bulletin together with copies of the Underwriters' report are available from the manufacturer.—EAGLE-PICHER COMPANY, *Cincinnati 1, Ohio.*

Metal Cleaners

Surprep is designed for cleaning aluminum, steel, and zinc surfaces prior to organic finishing, It contains oil-displacing components that quickly dislodge oil, grease, and other organic material from metal surfaces. It also contains phosphating and other rust-removal chemicals that dissolve rust, oxide, and scale while the oil-removal agents are acting. It is applied by brushing or wiping, allowed to stand a few minutes and then wiped or rinsed off. The surface is given a light etch and a light phosphate film is deposited giving a good "tooth" for paint or organic finishes and resulting in greatly increased bond strength. No toxic vapors are evolved in use.

Zinc cleaner 20 is an anodic type of cleaner for preparing zinc-base die castings for electroplating. It does not contain silicates, surface-active materials, or other products which will react with zinc to form insoluble residues. It is a mild cleaner with very high detergent action.

Aluminum cleaner E is an etching type alkaline cleaner. It is used to produce a fine etched surface finish on aluminum as well as to prepare it for painting and electroplating.

Aluminum cleaner NE is a non-etching type of cleaner to degrease aluminum prior to organic finishing or electroplating. It does not react with highly polished aluminum.

Cleaner 100 is an alkaline, anodic electrocleaner for steel. It is designed for rapid cleaning action at low current densities, works well either anodically or cathodically, and can also be used effectively as a soak cleaner.

Brass cleaner is an alkali detergent for degreasing brass, copper, nickel-silver, lead, tin, and steel without attack. It can be used either as a soak or an electrolytic cleaner.

Manufacturer's literature is available on all of these products.—ENTHONE, INC., *442 Elm Street, New Haven, Connecticut.*

Glass for Lighting Fixtures

Foto-lite, designed for applications in louver lighting, is made from Corning's photo-sensitive glass. It is manufactured as a thin pane of transparent glass, in which white opalescent vanes in a symmetrical criss-cross pattern are incorporated throughout its depth by a photographic process. When used in a lighting fixture, this material allows direct light to pass through normal to the surface but blocks direct light at large angles to the normal. The translucence of the louvers, however, creates a diffusion of indirect light at side angles. Glare is eliminated as a result of the 45° light cut-off possessed by the material. The glass may be cut to size, fitting into almost any standard fixture calling for glass panels. Physically, the material is not affected by temperature changes and has no "sag" or cold flow. The louvers are a part of the glass and cannot lose their efficiency over an extended period. Also, they are not color-selective.—CORNING GLASS WORKS, *Corning, New York.*

Author Index to Volume 20

References with (L) are to Laboratory and Shop Notes

Adams, G. D. and C. W. Sherwin. On the vacuum properties of silastic—957(L)

Adams, Douglas P. and Howard T. Evans, Jr. Developments in the useful circular nomogram—150

—— (see Evans, Howard T., Jr.)—155

Agnew, Harold M. and Herbert L. Anderson. Double magnetic lens nuclear spectrometer—869

Allison, S. K., S. P. Frankel, T. A. Hall, J. H. Montague, A. H. Morrish, and S. D. Warshaw. Construction and calibration of a cylindrical electrostatic analyzer—735

Albert, Daniel. High power attenuator for microwaves—779

Amdur, I. and N. L. Brown. Effect of temperature on the steady-state sensitivity of vacuum radiation detectors—435

Anderson, Herbert L. (see Agnew, Harold M.)—869

Anderson, J. W. and R. Friedman. Accurate gas metering system for laminar flow studies—61

Andrews, Howard L. Book review—309

Angello, S. J. Book review—687

Anker, H. S. (see Sucher, I.)—321(L)

Armistead, F. C. Empirical balancing procedure for FP-54—747(L)

Arnold, James R. (see Robinson, Lawrence B.)—549

Bachman, C. H. New principle in controlled vacuum leaks—219(L)

—— Book review—453

Baggett, L. M. (see Bame, S. J., Jr.)—839(L)

Bailey, Carl, D. L. Drukey, and F. Oppenheimer. Magnetic ion source—189

Baker, Edward B. Variable temperature dielectric cell of wide frequency range for solids and liquids—716

Ballentine, Robert (see Bernstein, William—347

Bame, S. J., Jr. and L. M. Baggett. Voltage stabilization for electrostatic generators using an electron gun—839(L)

Bancroft, D. (see Elmore, W. C.)—136(L)

Barbour, Ian. Pantograph and tilting stage for use with nuclear plates—530(L)

Barrett, Martha J. (see Prouty, Lawrence R.)—357

Becker, Robert A. Note on sealing Nylon films to Geiger counters—966(L)

Benedikt, Elliot T. Errors in second-order measuring instruments—229

Benfield, A. E. Tachometer—663

Bennett, John A. Instrument for measurement of x-ray diffraction patterns—908

Benzinger, T. H. and C. Kitzinger. Direct calorimetry by means of the gradient principle—849

Bergmann, M. E. and I. Fankuchen. Modification of x-ray diffraction micro-camera to permit study of long spacings—696(L)

Bernstein, William and Robert Ballentine. Methane flow beta-proportional counter—347

Berry, Clifford E. Pumping speed of diffusion pumps below limiting pressure—835(L)

Bershader, Daniel. Interferometric study of supersonic channel flow—260

Bettis, E. S. and E. R. Mann. Servo employing the magnetic fluid clutch—97

Bier, M. and F. F. Nord. Equipment for measuring light scattering—752(L)

Bishop, Francis W. Device for producing an easily identified area on the electron microscope specimen screen—324(L)

—— Device to deposit automatically the proper thickness of metals used in shadow-casting in electron microscopy—527(L)

—— Technique for the production of silica-filmed electron microscope screens in quantity—529(L)

—— Magnetic beam-splitting focusing device for the electron microscope—532(L)

Blachman, Nelsen M. Counting volume of a cylindrical ionization chamber—477

—— **and Ernest D. Courant.** Dynamics of a synchrotron with straight sections—596

Bleakney, Walker, D. K. Weimer, and C. H. Fletcher. Shock tube: A facility for investigations in fluid dynamics—807

—— (see Mariner, Thomas)—297

Blizard, E. P. and S. DeBenedetti. Distant counting of scintillations—81(L)

Blum, Josef (see Ecker, Paul Gerard)—799

Bozorth, R. M. (see Walker, J. G.)—947

Brackmann, W. J. Book review—315

Bradley, G. E. and M. L. Wiedenbeck. Delays in rectangular Geiger counters—841(L)

Brainerd, J. G. Book review—312

Breidenbach, H. I., Jr. Fractional microsecond x-ray pulse generator for studying high explosive phenomena—899

Breit, G. (see Meyerott, R. E.)—874

Broersma, S. Inductance apparatus for diamagnetic measurements—660

Bronzo, J. A. and H. G. Cohen. Note on analog computer design—101

Brophy, James J. Mercury vapor trap to protect laboratory workers—750(L)

Brown, David R., William C. Galloway, Jack B. Robertson, and Gene A. Silvey. Self-contained recording pressure gauge—27

Brown, N. L. (see Amdur, I.)—435

Brown, Vinton A. and B. P. Ramsay. Maxwell bridge at low frequencies—236

Brubach, H. F. (see Specht, H.)—442

Buck, John B. Versatile microinjection and micropipetting syringe—676

Buechner, W. W. (see Strait, E. N.)—783

Burgess, Ronald E. Statistics of counting rate meters—964(L)

Burgwald, Glenn (see Reiffel, Leonard)—711, 944

Burkig, J. W., E. L. Hubbard, and K. R. MacKenzie. Pulsed oscillator for f-m cyclotron—135(L)

Calcote, Hartwell F. Ionization flame detectors—349

Caldecourt, V. J. Electrometer amplifier—748(L)

Cecconi, W. E. (see Coonrod, L. G.)—408

Chang, W. Y. and J. R. Winckler. Cloud-chamber equipment for study of infrequent cosmic-ray processes—276

Chapin, Daryl M. Sensitive magnetometer for very small areas—945

Chu, L. J. Book review—452

Clark, C. E. Statistical theory of the dead time losses of a counter—51

Clark, John W. and James E. Randall. Electromagnetic blood flow meter—951

Clifton, Donald F. Preparation of samples of active metals—830(L)

—— **and Cyril Stanley Smith.** Microsampling and microanalysis of metals—583

Cohen, H. G. (see Bronzo, J. A.)—101

Cole, Peter A. (see Wright, Barbara A.)—355

Cole, Robert H. and Paul M. Gross, Jr. Wide range capacitance-conductance bridge—252

Coltman, John W. (see McIntosh, Ralph O.)—135(L)

Colvin, Henry F., III. (see Goudy, Paul R.)—651
Cook, C. Sharp (see Owen, George E.)—768
Coomes, E. A. (see Petrauskas, A. A.)—961(L)
Coonrod, L. G., W. E. Cecconi, C. Gedraitis, K. R. Harper, and R. M. Lewis. Magnet coils—408
Cordero, Narcisco and Irineo L. Lawas. Simple automatic water distiller—840(L)
Cork, J. M. (see Fowler, C. M.)—966(L)
Courant, Ernest D. (see Blachman, Nelson M.)—596
Cowan, E. W. Large cloud chamber using rear illumination —492
Craig, R. S. (see Kerchen, Eugene E.)—524(L)
Craig, R. S. and W. E. Wallace. Vibration absorber for gas holders—369(L)
Cranberg, L. and J. Halpern. Calibration of photographic emulsions for low energy electrons—641
Crane, H. R. Automatic stabilization of the overvoltage on a Geiger counter—955(L)
Curtis, B. R., J. L. Fowler, and L. Rosen. Instrumentation for nuclear studies with externally focused deuteron beam from ten-mev cyclotron—388
Custers, J. F. H. Absorption corrections in x-ray studies of preferred orientation—752(L)

Darken, L. S. Modification of the Gouy modulator—323(L)
Daunt, J. G. and H. L. Johnston. Large helium liquefier —122
Davis, Leverett, Jr. Book review—691
Day, Allan R. Book review—310
DeBenedetti, S. (see Blizard, E. P.)—81(L)
deBretteville, A., Jr. (see Rosenblum, P.)—321(L)
de Waard, H. Circuit for rapid determination of resolving power and other characteristics of coincidence-systems—911
Dillon, J. H. (see Reichardt, C. H.)—509
Douglas, D. G. (see McPherson, A. I.)—457(L)
Drukey, D. L. (see Bailey, Carl)—189
Dubbert, Donald R. (see Schmitt, Otto H.)—170
DuMond, Jesse W. M. Conditions for optimum luminosity and energy resolution in an axial β-ray spectrometer with homogeneous magnetic field—160
—— Book review—308
—— Erratum: Conditions for optimum luminosity and energy resolution in an axial β-ray spectrometer with homogeneous magnetic field—616
Dunn, Harris W. (see Hagelston, Paul J.)—373(L)
Dushman, Saul. Use of characteristic curves for pump-speed *vs.* pressure—139(L)
—— Book review—690
Dyson, J. P. (see Graves, J. D.)—560

Ecker, Paul Gerard, Josef Blum, and C. W. Hiatt. Device for the measurement of rotor temperature in the air-driven ultracentrifuge—799
Edwards, James W., Rudolph Speiser, and Herrick L. Johnston. High temperature x-ray diffraction camera—343
Elmore, W. C. Pulse-height limiting circuit for a scintillation detector—963(L)
—— Book review—313
—— **and D. Bancroft.** Lock-in *RC* oscillator—136(L)
Evans, Howard T., Jr. Note on the accuracy of the Buerger precession camera—751(L)
——**, S. G. Tilden, and Douglas P. Adams.** New techniques applied to the Buerger precession camera for x-ray diffraction studies—155
—— (see Adams, Douglas P.)—150

Fankuchen, I. (see Bergmann, M. E.)—696(L)
—— (see Kaufman, H. S.)—733
Feld, Bernard T. Book review—689
Fitch, Val. High resolution scale of four—942
Fletcher, C. H. (see Bleakney, Walker)—807
Fletcher, R. C. Production and measurement of ultra-high speed impulses—861
Fowler, C. M., R. G. Shreffler, and J. M. Cork. Focusing in semicircular magnetic spectrometer—966(L)
Fowler, J. L. (see Curtis, B. R.)—388
Fowler, Richard C. Rapid infra-red gas analyzer—175
Fowler, William A. Book review—448
Frank, N. H. (see Twiss, R. Q.)—1
Frankel, S. P. (see Allison, S. K.)—735
Frémont, Claude. System for preparing semitransparent mirrors—620(L)
Friedman, R. (see Anderson, J. W.)—61
Fryburg, G. C. and J. H. Simons. Precision vacuum gauge —541

Gaerttner, E. R. and M. L. Yeater. An instrument for measuring curvature of cloud-chamber tracks—526(L)
—— **and M. L. Yeater.** Fast recycling cloud chamber and pulsed magnetic field equipment for use with pulsed accelerators—588
Galloway, William C. (see Brown, David R.)—27
Garrison, J. B. and A. W. Lawson. Absolute noise thermometer for high temperatures and high pressures—785
Gedraitis, C. (see Coonrod, L. G.)—408
Geoffrion, Claude. Optimum conditions for a 180° beta-ray spectrometer—638
—— (see Kerwin, Larkin)—381
Gillette, R. H. and M. H. Jellinek. Instrument for rapid determination of crystal orientation—480
Gilvarry, J. J. and D. F. Rutland. Operation of voltage-stabilizing elements with current-stabilized supplies—633
Gittings, H. T., Jr. Current integrator—325(L)
Glass, F. M. Methods for reducing insulator noise and leakage—239
Gledhill, J. A. and A. Patterson, Jr. Differential pulse transformer bridge circuit—960(L)
Golay, Marcel J. E. Theoretical and practical sensitivity of the pneumatic infra-red detector—816
Gold, Louis. Apparatus for the production of large metallic crystals by solidification at high temperatures—115
Goldblatt, M. (see Graves, E. R.)—579
Gosting, Louis J., Edwin M. Hanson, Gerson Kegeles, and Margaret S. Morris. Equipment and experimental methods for interference diffusion studies—209
Goudy, Paul R. and Henry F. Colvin III. Theoretical background of the multiple pressure tube anemometer—651
Graves, E. R., A. A. Rodrigues, M. Goldblatt, and D. I. Meyer. Preparation and use of tritium and deuterium targets—579
Graves, J. D. and J. P. Dyson. Scintillation counter for laboratory counting of alpha-particles—560
Greenblatt, M. H. Microwave secondary electron multiplier —646
Gregg, E. C., Jr. Measurement of betatron guiding fields during electron ejection—841(L)
Grill, E. J. and A. H. Weber. Simple punch for precision cutting of photographic film in a cylindrical x-ray diffraction camera—532(L)
Gross, Paul M., Jr. (see Cole, Robert H.)—252
Guimarães, Mario Alves and Palmyra Amazonas Sampaio. Circuit for the study of the operation of the Geiger-Müller counter—485
Gunn, Ross. Electronic apparatus for the determination of the physical properties of freely falling raindrops—291
—— Book review—688
Gutmann, F. and L. M. Simmons. Electrolytic thermistors —674

Haendler, Helmut M. (see Linnell, Robert H.)—364(L)

Hagelston, Paul J. and Harris W. Dunn. Method for preparing capillary tube samples for x-ray diffraction powder analysis—373(L)
Hall, T. A. (see Allison, S. K.)—735
Halpern, J. (see Cranberg, L.)—641
Halpern, W. (see Sommers, H. S., Jr.)—244
Hammer, F. Emmett and Frank E. Hoecker. New method of measuring the stopping power of several materials for alpha-particles—394
Hanna, G. C. (see Westcott, C. H.)—181
Hanna, S. S. (see Inglis, D. R.)—834(L)
Hansel, Paul G. Parallel operation of small thyratrons—836(L)
Hanson, Edwin M. (see Gosting, Louis J.)—209
Hanson, Marjorie (see Rothen, Alexandre)—66
Hardy, James D. (see Prouty, Lawrence R.)—357
—— (see Stoll, Alice M.)—678
Harper, K. R. (see Coonrod, L. G.)—408
Harrington, E. L. Use of gas traps in barometers, laboratory mercury lamps, etc.—368(L), 761
Harvalik, Zaboj V. (see Schwaneke, Alfred E.)—337
Hashimoto, K. (see Hayaski, C.)—524(L)
Havercroft, W. (seen Senftle, F. E.)—370(L)
Hayashi, C., K. Hashimoto, K. Kaneko, K. Okamoto, and R. Sagane. Several improvements on the "Philip's gauge"—524(L)
Hedrick, Langdon C. Flexible high voltage square wave generator—781
Henkel, R. L. and B. Petree. Stabilized high voltage power supply for electrostatic analyzer—729
Henrich, L. R., D. C. Sewell, and J. Vale. Operation of the 184-in. cyclotron—887
Hernandez, P. (see Senftle, F. E.)—370(L)
Herscher, L. W. Device for producing rate-proportional damping signal in servo systems—459(L)
—— New source of radiation for infra-red spectrometers—833(L)
Hiatt, C. W. (see Ecker, Paul Gerard)—799
Hickam, W. M. Design for a metal spectrometer tube—472
Hickman, J. W. and A. G. Kleinknecht. Sample scanning mechanism for x-ray diffraction—573
Higgs, Paul M. Recording mechanical pressure gauge of high range—23
Hillemann, Howard H. Improved embryological micromanipulator—836(L)
Hintenberger, H. Improved magnetic focusing of charged particles—748(L)
Hitchcock, Fred A. (see Hunter, Jack A.)—333
Hoadley, H. O. Multiple-reflection optical lever—30
—— (see Hammer, F. Emmett)—394
—— (see Kloepper, Robert M.)—17
Hoefer, Paul F. A. (see Markey, Charles)—612
Hoge, Harold J. Circuits for minimizing transient effects on energy measurements in calorimetry—59
Hopkins, N. J. Magnetic field strength meter using the proton magnetic moment—401
Horton, Billy M. Sliding contacts to transmit small signals—930
Hoyt, Rosalie C. Scintillation counter as a proportional device—178
Hubbard, E. L. (see Burkig, J. W.)—135(L)
Hubbard, Philip G. Application of the electrical analogy in fluid mechanics research—802
Hughes, R. H. (see McAfee, K. B., Jr.)—821
Hunter, Jack A., Ralph W. Stacy, and Fred A. Hitchcock. Mass spectrometer for continuous gas analysis—333
Huntoon, R. D. (see Thomas, H. A.)—516
Hurwitz, H., Jr. Electron trajectories in a gamma-ray spectrometer—318(L)
Hutchison, Clyde A., Jr. Book review—308
Iberall, Arthur S. Novel recording accelerometer—304
Inglis, D. R., R. W. Krone, and S. S. Hanna. Statitron for a small nuclear laboratory—834(L)
Irwin, John B. Book review—692

Jehn, Kenneth H. Wet bulb temperatures without a wick—668
Jellinek, M. H. Non-uniform shrinkage of x-ray films—368(L)
—— (see Gillette, R. H.)—480
Jennings, B. Large straight through vacuum valve for Van de Graaff generators—366(L)
Johnson, A. L. (see Shutt, R. P.)—398
Johnson, Carlton F. New vacuum gauge—364(L)
Johnson, Ellis A., Thomas Murphy, and P. F. Michelsen. New high sensitivity remanent magnetometer—429
Johnson, M. H. (see Rado, G. T.)—927
Johnston, H. L. (see Daunt, J. G.)—122
—— (see Edwards, James W.)—343
—— (see Ziegler, George W., Jr.)—367(L), 385
Jones, Sarah D. (see Lonberger, Rose E.)—454
Jurney, E. T. and F. Maienschein. Gamma-ray counting efficiency for a lead-cathode G-M counter—932

Kaneko, K. (see Hayashi, C.)—524(L)
Kaufman, H. S. and I. Fankuchen. Low temperature single crystal x-ray diffraction technique—733
Kê, T'ing-Sui and Marc Ross. Apparatus for measurements of extremely high internal friction—795
Kegeles, Gerson (see Gosting, Louis J.)—209
Kelso, John M. Procedure for the solution of certain network problems—959(L)
Kerwin, Larkin. Improved magnetic focusing of charged particles—36
—— **and Claude Geoffrion.** Further improvements in magnetic focusing—381
Ketchen, Eugene E., Forrest A. Trumbore, W. E. Wallace, and R. S. Craig. Dry box for handling alkali metals and other extremely hygroscopic materials—524(L)
Keuffel, J. Warren. Simplified chronotron-type timing circuit—197
—— Parallel-plate counters—202
Kirkpatrick, George P. Convenient method for checking the linearity of an electron multiplier circuit—81(L)
Kitzinger, C. (see Benzinger, T. H.)—849
Kleinknecht, A. G. (see Hickman, J. W.)—573
Kloepper, Robert M. and Frank E. Hoecker. Double-channel, direct reading, low frequency counting rate meter, and counting rate comparator—17
Knowles, Thomas (see Luckiesh, Matthew)—73
Koehler, James S. Book review—310
Kovásznay, Leslie G. High power short duration spark discharge—696(L)
Krone, R. W. (see Inglis, D. R.)—834(L)
Kuper, J. B. H. Book review—309

Lambe, John. Glass vacuum valve—831(L)
Lane, C. T. Kovar glass seals at liquid helium temperatures—140(L)
—— (see McGuire, T. R.)—489
Lander, J. J. High temperature x-ray diffraction techniques—82(L)
Langer, Lawrence M. Note on the preparation of beta-ray sources—216(L)
Larrabee, Martin G. Book review—454
Launer, Herbert F. Exposure meter for precision light dosage—103
Lauritsen, C. C. Portable roentgenmeter for field use—964(L)
Law, Harold B. Formation of insulating layers by the thermal decomposition of ethyl silicate—958(L)

Lawas, Irineo L. (see Cordero, Narcisco)—840(L)
Lawson, A. W. and N. A. Riley. X-ray camera for obtaining powder pictures at high pressures—763
—— (see Garrison, J. B.)—785
Lewis, Margaret N. Book review—313
Lewis, R. M. (see Coonrod, L. G.)—408
Liben, William and Noel W. Scott. Small portable reflectometer—960(L)
Liebson, Sidney H. Characteristics of halogen counters—483
Lind, David A. Design and performance of a multicellular Geiger counter for gamma-radiation—233
Linnell, Robert H. and Helmut M. Haendler. Simple electronic relay—364(L)
Lofgren, E. J., E. P. Ney, and F. Oppenheimer. Apparatus for cloud-chamber investigations with free balloons—48
Lonberger, Rose E. and Sarah D. Jones. Book review—454
Lorrain, Paul. On the design of a radiofrequency Cockroft-Walton accelerator—216(L)
Luckiesh, Matthew, A. H. Taylor, and Thomas Knowles. Sampling devices for determining the bacterial content of air—73

MacDonald, J. E. (see Petrauskas, A. A.)—961(L)
MacInnes, D. A. (see Ray, B. Roger)—52
Mackay, R. Stuart. Timer for short intervals—318(L)
MacKenzie, K. R., F. H. Schmidt, J. R. Woodyard, and L. F. Wouters. Design of the radiofrequency system for the 184-inch cyclotron—126
—— (see Burkig, J. W.)—135(L)
Macklin, R. L. and E. R. Rohrer. Rapid response radiation alarm—965(L)
MacRae, D. A. (see Minett, E. E.)—136(L)
Maienschein, F. (see Jurney, E. T.)—932
Makowski, M. W. Slide rule for radiation calculations—876
Maloof, M. (see Rado, G. T.)—927
Mann, E. R. (see Bettis, E. S.)—97
Mann, W. B. and G. B. Parkinson. Geiger-Mueller counting unit and external quenching equipment for the estimation of C^{14} in carbon dioxide—41
Mariner, Thomas and Walker Bleakney. Large mass spectrometer employing crossed electric and magnetic fields—297
Markey, Charles, Robert L. Schoenfeld, and Paul F. A. Hoefer. Frequency analyzer for bioelectric potentials in the sub-audio range—612
Marlow, Douglas and J. C. Pemberton. Automatic scanning and recording photometer for night sky studies—724
Marshall, F. R. (see Zarem, A. M.)—133
Martens, Frederick H. Differential counting with reversible decade counting circuits—424
Martinelli, Ernest A. (see Panofsky, Wolfgang, K. H.)—286
Matthews, F. W. and A. O. McIntosh. Apparatus for producing powder-like x-ray diffraction patterns from single crystals—365(L)
Mauer, Robert J. Book review—690
May, Joe Cyril. Book review—455
McAfee, K. B., Jr., R. H. Hughes, and E. Bright Wilson, Jr. Stark-effect microwave spectrograph of high sensitivity—821
McDonald, Donald. Electromechanical lead networks for a.c. servo mechanisms—775
McGuire, T. R. and C. T. Lane. Magnetic susceptibility balance for use at liquid helium temperatures—489
—— **and Robert T. Webber.** Technique for cutting metal single crystals—962(L)
McIntosh, A. O. (see Matthews, F. W.)—365(L)
McIntosh, Ralph O. and John W. Coltman. Toggle-operated valve—135(L)
McPherson, A. I. and D. G. Douglas. Measurement of the thickness of thin Nylon films—457(L)
Meryman, Harold T. Electromagnetic focusing device for the electron microscope—955(L)
Meyer, D. I. (see Graves, E. R.)—579
Meyerhof, W. E. Book review—451
Meyerott, R. E. and G. Breit. Small differential analyzer with ball carriage integrators and selsyn coupling—874
Michels, Walter C. and Esther D. Redding. Improved synchonous detector—566
Michelsen, P. F. (see Johnson, Ellis A.)—429
Minett, E. E., D. A. MacRae, and J. Townsend. Note on constant current regulators—136(L)
Monk, G. W. and G. K. Werner. Trochotron design principles—93
Montague, J. H. (see Allison, S. K.)—735
Moore, John W. (Simple stable d.c. amplifier for measurement of bioelectric potentials—698(L)
Morris, Margaret S. (see Gosting, Louis J.)—209
Morrish, A. H. (see Allison, S. K.)—735
Morrison, Adair and Fred Morton. Photomicrography of tracks in nuclear research emulsions—341
Morrison, P. Book review—693
Morton, Fred (see Morrison, Adair)—341
Moulton, W. G. and C. W. Sherwin. Fast neutron detector—766
Mouzon, J. C. Book review—687
Murdick, R. G. D.c. flat card resolver—137(L)
Murphy, George W. Use of anodized aluminum in the construction of calorimeter heaters—372(L)
Murphy, Thomas (see Johnson, Ellis A.)—429

Newell, Homer E., Jr. and Eleanor C. Pressly. Counting with Geiger counters—568
Ney, E. P. (see Lofgren, E. J.)—48
Nier, Alfred O. (see Winn, E. B.)—773
Nord, F. F. (see Bier, M.)—752(L)
Norton, Francis J. "Opener-upper" for gas samples—620(L)
Nuelle, R. E. (see Schulke, A. A.)—623(L)

Okamoto, K. (see Hayashi, C.)—524(L)
Olson, Harry F. Book review—314
Onsager, L. (see Watson, W. W.)—924
Oppenheimer, F. (see Bailey, Carl)—189
—— (see Lofgren, E. J.)—48
Owen, George E. Design curves for 180° magnetic spectrometers—916
—— **and C. Sharp Cook.** Instrumental distortions in the shapes of continuous beta-spectra—768

Panofsky, Wolfgang K. H. and Ernest A. Martinelli. Magnetic deflector for mesons produced in the 184-inch cyclotron—286
Pappenheimer, John R. Book review—450
Parkinson, G. B. (see Mann, W. B.)—41
Paterson, A. L. Book review—449
Patterson, A., Jr. (see Gledhill, J. A.)—960(L)
Pemberton, J. C. (see Marlow, Douglas)—724
Pepper, T. P. Octane vapor proportional counter—222(L)
Persico, E. Theory of the solenoid beta-ray spectrometer—191
Peterson, T. A., Jr. (see Rosenthal, L. A.)—426
Petree, B. (see Henkel, R. L.)—729
Petrauskas, A. A., E. A. Coomes, and J. E. MacDonald. Preparation of single-crystal copper ribbons from single-crystal copper rods—961(L)
Picard, Robert G., Perry C. Smith, and John H. Reisner. Operational features of a new electron diffraction unit—601
Pickering, W. H. Book review—451

Pollard, Ernest C. Book review—450

Powell, Wilson M. A 22-inch Wilson cloud chamber in a magnetic field of 21,700 gauss—403

Prescott, J. R. Use of multigrid tubes as electrometers—553

Pressly, Eleanor C. (see Newell, Homer E., Jr.)—568

Preuss, Luther E. Lead brick for shielding—534(L)

Prime, H. A. and R. C. Turnock. Iconoscope electro-optical shutter for high speed photography—830(L)

Prouty, Lawrence R., Martha J. Barrett, and James D. Hardy. Simple calorimeter for the simultaneous determination of heat loss and heat production in animals—357

Purcell, E. M. Book review—448

Quimby, S. L. Book review—689

Rado, G. T., M. H. Johnson, and M. Maloof. Single pulse voltmeter—927

Ramsay, B. P. (see Brown, Vinton A.)—236

Randall, James E. (see Clark, John W.)—951

Ray, B. Roger and D. A. MacInnes. Apparatus for determining the effect of centrifugal force on the potentials of galvanic cells—52

Redding, Esther D. (see Michels, Walter C.)—566

Reich, Herbert J. and Robert L. Ungvary. Transistor trigger circuit—586

Reichardt, C. H., H. Schaevitz, and J. H. Dillon. Stress-strain-time apparatus for fiber testing—509

Reiffel, Leonard. Thyratron square wave generator—218 (L)

—— Extended range d.c. bias control of thyratron plate current—699(L)

—— **and Glenn Burgwald.** Wide range radiation instrument —711; Erratum—944

Reisner, John H. (see Picard, Robert G.)—601

Retondo, Nadine (see Tobias, Julian M.)—519

Retzloff, Otto. Flexible vacuum seal—324(L)

Richards, J. (see Saxon, D.)—745(L)

Riley, N. A. (see Lawson, A. W.)—763

Robertson, Jack B. (see Brown, David R.)—27

Robinson, Charles F. Effect of space charge on the focusing properties of a 180° mass spectrometer—745(L)

Robinson, C. V. Improved multivibrator quenching circuit —750(L)

Robinson, J. Eugene (see Ter-Pogossian, Michel)—289

Robinson, Lawrence B. and James R. Arnold. Scintillation counter. I. Existence of plateaus—549

Rodrigues, A. A. (see Graves, E. R.)—579

Rohrer, E. R. (see Macklin, R. L.)—965(L)

Rosen, L. (see Curtis, B. R.)—388

Rosenblum, P. and A. deBretteville, Jr. Accurate, simple recording microphotometer—321(L)

Rosenthal, I. A. and T. A. Peterson, Jr. Measurement of the series-resonant resistance of a quartz crystal—426

Ross, Marc (see Kê, T'ing-Sui)—795

Rothen, Alexandre and Marjorie Hanson. Optical properties of surface films. II.—66

Rudin, Robert. Direct reading pulse length meter and shape analyzer—467

Rutland, D. F. (see Gilvarry, J. J.)—633

Sagane, R. (see Hayashi, C.)—524(L)

Sampaio, Palmyra Amazonas (see Guimarães, Mario Alves)—485

Sancier, Kenneth M. Vacuum tight, flexible metal—glass seal—958(L)

Sard, Arthur and R. D. Sard. Some statistical considerations on coincidence counting—526(L)

Saxon, D. and J. Richards. Vacuum lock for continuously evacuated systems—745(L)

Schaevitz, H. (see Reichardt, C. H.)—509

Schiff, L. I. Book review—687

Schmidt, F. H. (see MacKenzie, K. R.)—126

Schmitt, Otto H., and Donald R. Dubbert. Tissue stimulators utilizing radiofrequency coupling—170

Schoenfeld, Robert L. Double pulse constant current stimulator—827

—— (see Markey, Charles)—612

Scholander, P. F. Volumetric respirometer for aquatic animals—885

Schulke, A. A. and R. E. Nuelle. Note on removing the deuteron-induced color from quartz target plates—623(L)

Schwaneke, Alfred E. and Zaboj V. Harvalik. Microwave polarimeter—337

Schwarz, E. Sensitivity of Schwarz-Hilger thermopiles—962(L)

Scott, Noel W. (see Liben, William)—960(L)

Seaton, N. T. Precision automatic electrometer—500

Sears, G. W. Ultimate vacua of diffusion pumps—458(L)

Seemann, Herman E. Air ionization chamber for soft x-rays —903

Senftle, F. E., W. Havercroft, and P. Hernandez. Construction of beta-Geiger counters from prefabricated thin wall tubing—370(L)

Setlow, Richard B. High current ion source—558

Sewell, D. C. (see Henrich, L. R.)—887

Shenstone, A. G. Book review—315

Shepard, L. Rejuvenation of Geiger-Mueller tubes—217(L)

Sheppard, T. W. Book review—453

Sherwin, C. W. (see Adams, G. D.)—957(L)

—— (see Moulton, W. G.)—766

Shore, Lloyd G. Long-lived self-quenching counter filling—956(L)

Shreffler, R. G. (see Fowler, C. M.)—966(L)

Shutt, R. P., A. L. Johnson, and A. M. Thorndike. Cloud chamber of light weight for balloon flights—398

Silvey, Gene A. (see Brown, David R.)—27

Simmons, L. M. (see Gutmann, F.)—674

Šimon, I. Helium cryostat temperature control—832(L)

Simons, J. H. (see Fryburg, G. C.)—541

Simpson, O. C. and R. J. Thorn. New technique for the determination of heats of sublimation of slightly volatile substances—504

Slätis, Hilding. Experiments in the possibility of increasing the efficiency of gamma-counters—353

Smith, Cyril Stanley (see Clifton, Donald F.)—583

Smith, Perry C. (see Picard, Robert G.)—601

Smoluchowski, R. and R. W. Turner. Absorption corrections in x-ray studies of preferred orientation—173

Solomon, A. K. (see Steinberg, Daniel)—655

Sommers, H. S., Jr., P. R. Weiss, and W. Halpern. Conversion of a motor generator into a low noise power amplifier—244

Specht, H. and H. F. Brubach. Modified string flowmeter for measuring breath velocity—442

Speiser, Rudolph, George W. Zeigler, Jr., and Herrick L. Johnston. Regulation of temperature in the application of high frequency induction heating to thermodynamic measurements—385

—— (see Edwards, James W.)—343

—— (see Ziegler, George W., Jr.)—367(L)

Stacy, Ralph W. (see Hunter, Jack A.)—333

Stanton, John S. Method of assessing transient stresses in photoelastic substances—139(L)

Steinberg, Daniel and A. K. Solomon. Detection of Ca^{45}, I^{131}, P^{32}, and Zn^{65} by photographic film—655

Stoll, Alice M. and James D. Hardy. Direct experimental comparison of several surface temperature measuring devices—678

Stone, Robert P. Secondary-emission electron multiplier tube for the detection of high energy particles—935

Strait, E. N. and W. W. Buechner. Photo-tube input impedance for a voltage stabilizer—783

Sucher, I. and H. S. Anker. Vacuum-tube relay for thermostat control—321(L)

Suckling, E. E. Cardiotachometer based on the plethysmogram—518

Sultan, F. (see Yousef, Y. L.)—533(L)

Sulzer, Peter G. Wide-range saw-tooth generator—78

—— **and A. H. Waynick.** Improving the response characteristics of graphic recorders—320(L)

Taylor, A. H. (see Luckiesh, Matthew)—73

Taylor, Ralph C. and Carnot W. Ward. Lead-in seals for kinetic high vacuum systems using rubbers—457(L)

Teitel, Robert J. Design of equipment for thermal studies—575

Ter-Pogossian, Michel, J. Eugene Robinson, and J. Townsend. Pressure regulated thin window Geiger-Mueller counter—289

Thomas, C. D. Counter pulse shape—147

Thomas, H. A. and R. D. Huntoon. Amplitude bridge for detection of nuclear resonance—516

Thompson, A. Ralph. Book review—316

Thorn, R. J. (see Simpson, O. C.)—504

Thorndike, A. M. (see Shutt, R. P.)—398

Tilden, S. G. (see Evans, Howard T., Jr.)—155

Tint, H. Apparatus for electrode reversal in the Tiselius electrophoresis equipment—617

Tobias, Julian M. and Nadine Retondo. Syringe oxygen cathode for measurement of oxygen tension in solution and in respiratory gases—519

Townes, Chas. H. Book review—450

Townsend, J. (see Minett, E. E.)—136(L)

—— (see Ter-Pogossian, Michel)—289

Trott, W. J. Welder for attaching fine wires to massive metal bodies—624(L)

Trumbore, Forrest A. (see Ketchen, Eugene E.)—524(L)

Turner, R. W. (see Smoluchowski, R.)—173

Turnock, R. C. (see Prime, H. A.)—830(L)

Tweel, L. H. v. d. Vacuum-tube current integrator of improved design—323(L)

Twiss, R. Q. and N. H. Frank. Orbital stability in a proton synchrotron—1

Ufford, C. W. Book review—312

Ungvary, Robert L. (see Reich, Herbert J.)—586

Vale, J. (see Henrich, L. R.)—887

Valley, G. E. and J. A. Vitale. Counter controllable high pressure cloud chamber—411

van Heel, A. C. S. (see van Oort, W. P.)—319(L), 479

van Oort, W. P. and A. C. S. van Heel. New discharge tube for the hydrogen atom spectrum—319(L); Erratum—479

Vaze, G. H. Electronic instrument for rapidly tracing the plateaux of G-M counters—746(L)

Vitale, J. A. (see Valley, G. E.)—411

Vonnegut, Bernard. Capillary collector for measuring the deposition of water drops on a surface moving through clouds—110

Walker, J. G., R. M. Bozorth, and H. J. Williams. Growing and processing of single crystals of magnetic metals—947

Wallace, W. E. (see Craig, R. S.)—369(L)

—— (see Ketchen, Eugene E.)—524(L)

Ward, Carnot W. (see Taylor, Ralph C.)—457(L)

Warren, S. Reid, Jr. Book review—694

Warshaw, H. D. Rotor balancing with an electronic capacitor gauge—474

—— Measurement of the spin of a projectile in flight—507

Warshaw, S. D. Note on the preparation of uniform metallic foils—623(L)

—— (see Allison, S. K.)—735

Watkins, Dean A. Ten-channel electrostatic pulse analyzer—495

Watson, W. W., L. Onsager, and A. Zucker. Apparatus for isotope separation by thermal diffusion—924

Watts, R. J. Method of linearizing the voltage rise of a relaxation oscillator—81(L)

—— Method of asymmetrical pulse duration modulation—622(L)

—— Geiger tube quenching circuit for a negative high voltage supply—699(L)

Waynick, A. H. (see Sulzer, P. G.)—320(L)

Weber, A. H. (see Grill, E. J.)—532(L)

Webber, Robert T. (see McGuire, T. R.)—962(L)

Weimer, D. K. (see Bleakney, Walker)—807

Weiss, P. R. (see Sommers, H. S., Jr.)—244

Werner, G. K. (see Monk, G. W.)—93

Westcott, C. H. and G. C. Hanna. Pulse amplitude analyzer for nuclear research using pretreated pulses—181

White, Harry J. Transient response of high voltage resistance dividers—837(L)

Wiedenbeck, M. L. (see Bradley, G. E.)—841(L)

Wightman, A. S. Book review—692

Wilner, T. Cadmium trap for arresting mercury vapor—527(L)

Wilson, A. J. C. Straumanis' method of film-shrinkage correction modified for use without high angle lines—831(L)

Wilson, E. Bright, Jr. (see McAfee, K. B., Jr.)—821

Winckler, J. R. (see Chang, W. Y.)—276

Winn, E. B. and Alfred O. Nier. Simplified emission regulator for mass-spectrometer ion sources—773

Wollman, Seymour H. Absorption cell and loader for use in microanalysis by infra-red spectroscopy—220(L)

Woodyard, J. R. (see MacKenzie, K. R.)—126

Wouters, L. F. (see MacKenzie, K. R.)—126

Wright, Barbara A. and Peter A. Cole. Improved low angle x-ray diffraction camera—355

Wyman, Max. Book review—692

Yeater, M. L. (see Gaerttner, E. R.)—526(L)

—— (see Gaerttner, E. R.)—588

Yousef, Y. L. and F. Sultan. Vibration detection by a quartz oscillator—533(L)

Zarem, A. M. and F. R. Marshall. Method for measuring very high speed transient currents—133

Zerwekh, C. E., Jr. Percent transmission computer for infrared spectra—371(L)

Ziegler, George W., Jr., Rudolph Speiser, and Herrick L. Johnston. Cells drawn from tantalum, molybdenum, and platinum for high temperature research—367(L)

—— (see Speiser, Rudolph)—385

Zucker, A. (see Watson, W. W.)—924

Zworykin, V. K. Book review—311

Analytical Subject Index to Volume 20

References with (L) are to Laboratory and Shop Notes

Biophysical Instruments
  - Cardiotachometer based on the plethysmogram, E. E. Suckling—518
  - Direct experimental comparison of several surface temperature measuring devices, Alice M. Stoll and James D. Hardy—678
  - Double pulse constant current stimulator, Robert S. Schoenfeld—827
  - Electromagnetic blood flow meter, J. W. Clark and J. E. Randall—951
  - Equipment and experimental methods for interference diffusion studies, Louis J. Gosting, Edwin M. Hanson, Gerson Kegeles, and Margaret S. Morris—209
  - Frequency analyzer for bioelectric potentials in the subaudio range, Charles Markey, Robert L. Schoenfeld, and Paul F. A. Hoeffer—612
  - Improved embryological micromanipulator, Howard H. Hillemann—836(L)
  - Mass spectrometer for continuous gas analysis, Jack A. Hunter, Ralph W. Stacy, and Fred A. Hitchcock—333
  - Modified string flowmeter for measuring breath velocity, H. Specht and H. F. Brubach—442
  - Sampling devices for determining the bacterial content of air, Matthew Luckiesh, A. H. Taylor, and Thomas Knowles—73
  - Simple calorimeter for the simultaneous determination of heat loss and heat production in animals, Lawrence R. Prouty, Martha J. Barrett, and James D. Hardy—357
  - Simple stable d.c. amplifier for measurement of bioelectric potentials, John W. Moore—698(L)
  - Syringe oxygen cathode for measurement of oxygen tension in solution and in respiratory gases, Julian M. Tobias and Nadine Retondo—519
  - Tissue stimulators utilizing radiofrequency coupling, Otto H. Schmitt and Donald R. Dubbert—170
  - Volumetric respirometer for aquatic animals, P. F. Scholander—885

Bolometry
  - Effect of temperature on the steady-state sensitivity of vacuum radiation detectors, I. Amdur and N. L. Brown—435

Book Reviews
  - Anhorn, V. J. (see Barr, W. E.)—690
  - Arguimbau, Lawrence Baker, Vacuum-tube circuits—455
  - Arley, Niels, On the theory of stochastic processes and their application to the theory of cosmic radiation—691
  - Attwood, Stephen S., Electric and magnetic fields—694
  - Barr, W. E. and V. J. Anhorn, Scientific and industrial glass blowing and laboratory techniques—690
  - Beck, A. H. W., Velocity-modulated thermionic tubes—309
  - Boekelheide, V. (see Komarewsky, V. I., C. H. Riesz, W. A. Noyes, Jr., and S. Swann, Jr.)—310
  - Borden, Perry A. and Gustave M. Thynell, Principles and methods of telemetering—453
  - Brown, Gordon S. and Donald P. Campbell, Principles of servo mechanisms—315
  - Campbell, Donald P. (see Brown, Gordon S.)—315
  - Carlin, Benson, Ultrasonics—689
  - Chalmers, J. Alan, Atmospheric electricity—688
  - Chance, Britton, Frederick C. Williams, Vernon Hughes, Edward F. MacNichol, and David Syre, Wave forms—451
  - Dalton, Blanche H., Sources of engineering information—454
  - Dushman, Saul, Scientific foundations of vacuum technique—453
  - Griffith, Byron A. (see Synge, John L.)—691
  - Gurney, Ronald W., Introduction to statistical mechanics—687
  - Hamilton, Joseph G. (see Lawrence, John H.)—450
  - Harrison, Lord, and Loofbourow, Practical spectroscopy—315
  - Henisch, H. K., Metal rectifiers—687
  - Houston, William V., Principles of mathematical physics—312
  - Hughes, Vernon (see Chance, Britton, Frederick C. Williams, Edward F. MacNichol, and David Syre)—451
  - James, R. W., The optical principles of the diffraction of x-rays—449
  - Kamen, Martin D., Radioactive tracers in biology—309
  - Kirschbaum, Emil, Distillation and rectification—316
  - Komarewsky, V. I., C. H. Riesz, W. A. Noyes, Jr., V. Boekelheide, and S. Swann, Jr., Techniques of organic chemistry, Volume II—310
  - Kuiper, Gerard P., The atmospheres of the earth and planets—692
  - Lawrence, John H. and Joseph G. Hamilton, Recent advances in biological and medical physics—450
  - Livingston, Robert, Physico chemical experiments—308
  - London Institute of Physics, Measurement of stress and strain in solids—310
  - Loofbourow (see Harrison and Lord)—315
  - Lord (see Harrison and Loofbourow)—315
  - Mason, Warren P., Electromechanical transducers and wave filters—314
  - McLachlan, N. W., Modern operational calculus with applications in technical mathematics—692
  - MacNichol, Edward F. (see Chance, Britton, Frederick C. Williams, Vernon Hughes, and David Syre)—451
  - Newman, F. H. and V. H. L. Searle, The general properties of matter—308
  - Noyes, W. A., Jr. (see Komarewsky, V. I., C. H. Riesz, V. Boekelheide, and S. Swann, Jr.)—310
  - Pollard, E. C. and Julian M. Sturtevant, Microwaves and radar electronics—448
  - Potter, V. R., Methods in medical research, Volume I—454
  - Proprietors of instrument practice, The instrument manual—687
  - Ramberg, E. G. (see Zworykin, V. K.)—690
  - RCA Review, Radio at ultra high frequencies, Volume II—312
  - Rice, F. O. and Teller, E., Structure of matter—450
  - Riesz, C. H. (see Komarewsky, V. I., W. A. Noyes, Jr., V. Boekelheide, and S. Swann, Jr.)—310
  - Schiff, Leonard I., Quantum mechanics—693
  - Searle, V. H. L. (see Newman, F. H.)—308
  - Silver, Samuel, Microwave antenna theory and design—452
  - Smith, Arthur Whitmore, Electrical measurements in theory and application—313
  - Soller, Theodore, Merle A. Starr, and George E. Valley, Jr., Cathode-ray tube displays—311
  - Starr, Merle A. (see Soller, Theodore and George E. Valley, Jr.)—311
  - Sturtevant, Julian M. (see Pollard, E. C.)—448
  - Surugue, J., General techniques of the physics laboratory, Volume I—451
  - Sutton, George P., Rocket propulsion elements—448
  - Swann, S., Jr. (see Komarewsky, V. I., C. H. Riesz, W. A. Noyes, Jr., and V. Boekelheide)—310
  - Syre, David (see Chance, Britton, Frederick C. Williams, Vernon Hughes, and Edward F. MacNicol)—451

Book Reviews (continued)
- Synge, John L. and Byron A. Griffith, Principles of mechanics—691
- Taylor, Denis and C. H. Westcott, Principles of radar—450
- Teller, E. (see Rice, F. O.)—450
- Thynell, Gustave M. (see Borden, Perry A.)—453
- Valley, George E., Jr. (see Starr, Merle A. and Theodore Soller)—311
- Valley, George E., Jr. and Henry Wallman, Vacuum tube amplifiers—313
- Wallman, Henry (see Valley, George E., Jr.)—313
- Westcott, C. H. (see Taylor, Denis)—450
- Williams, Frederick C. (see Chance, Britton, Vernon Hughes, Edward F. MacNichol, and David Syre)—451
- Yagoda, Herman, Radioactive measurements with nuclear emulsions—689
- Zworykin, V. K. and E. G. Ramberg, Photoelectricity and its application—690

Bridge Circuits
- Amplitude bridge for detection of nuclear resonance, H. A. Thomas and R. D. Huntoon—516
- Differential pulse transformer bridge circuit, J. A. Gledhill and A. Patterson, Jr.—960(L)
- Maxwell bridge at low frequencies, Vinton A. Brown and B. P. Ramsay—236
- Wide range capacitance-conductance bridge, Robert H. Cole and Paul M. Gross, Jr.—252

Calorimetry
- Circuits for minimizing transient effects on energy measurement in calorimetry, Harold J. Hoge—59
- Direct calorimetry by means of the gradient principle, T. H. Benzinger and C. Kitzinger—849

Centrifuge
- Device for the measurement of rotor temperatures in the air-driven ultracentrifuge, P. G. Ecker, Josef Blum, and C. W. Hiatt—795

Cloud Chambers
- Apparatus for cloud-chamber investigations with free balloons, E. J. Lofgren, E. P. Ney, and F. Oppenheimer—48
- Cloud-chamber equipment for study of infrequent cosmic-ray processes, W. Y. Chang and J. R. Winckler—276
- Cloud chamber of light weight for balloon flights, R. P. Shutt, A. L. Johnson, and A. M. Thorndike—398
- Counter controllable high pressure cloud chamber, G. E. Valley and J. A. Vitale—411
- Fast recycling cloud chamber and pulsed magnetic field equipment for use with pulsed accelerators, E. R. Gaerttner and M. L. Yeater—588
- Instrument for measuring curvature of cloud-chamber tracks, E. R. Gaerttner and M. L. Yeater—526(L)
- Large cloud chamber using rear illumination, E. W. Cowan—492
- 22-inch Wilson cloud chamber in a magnetic field of 21,700 gauss, Wilson M. Powell—403

Computing Devices and Techniques
- Application of the electrical analogy in fluid mechanics research, Philip G. Hubbard—798
- Current integrator, H. T. Gittings, Jr.—325(L)
- D.c. flat card resolver, R. G. Murdick—137(L)
- Developments in the useful circular nomogram, Douglas P. Adams and Howard T. Evans, Jr.—150
- Errors in second-order measuring instruments, Elliot T. Benedikt—229
- Note on analog computer design, J. A. Bronzo and H. G. Cohen—101
- Percent transmission computer for infra-red spectra, C. E. Zerwekh, Jr.—371(L)
- Procedure for the solution of certain network problems, John M. Kelso—959(L)
- Slide rule for radiation calculations, M. W. Makowski—876
- Small differential analyzer with ball carriage integrators and selsyn coupling, R. E. Meyerott and G. Breit—874
- Some statistical considerations on coincidence counting, Arthur Sard and R. D. Sard—526(L)
- Statistical theory of the dead time losses of a counter, C. E. Clark—51
- Statistics of counting rate meters, Ronald E. Burgess—964(L)
- Vacuum-tube current integrator of improved design, L. H. v. d. Tweel—323(L)

Cosmic Rays
- Apparatus for cloud-chamber investigations with free balloons, E. J. Lofgren, E. P. Ney, and F. Oppenheimer—48
- Cloud-chamber equipment for study of infrequent cosmic-ray processes, W. Y. Chang and J. R. Winckler—276

Counters and Counter Circuits
- Automatic stabilization of the overvoltage on a Geiger counter, H. R. Crane—955(L)
- Characteristics of halogen counters, Sidney H. Liebson—483
- Circuit for rapid determination of resolving power and other characteristics, H. de Waard—911
- Circuit for the study of the operation of the Geiger-Müller counter, Mario Alves Guimarães and Palmyra Amazonas Sampaio—485
- Construction of beta-Geiger counters from prefabricated thin wall tubing, F. E. Senftle, W. Havercroft, and P Hernandez—370(L)
- Counter controllable high pressure cloud chamber, G. E Valley, and J. A. Vitale—411
- Counter pulse shape, C. D. Thomas—147
- Counting with Geiger counters, Homer E. Newell, Jr. and Eleanor C. Pressly—568
- Delays in rectangular Geiger counters, G. E. Bradley, and M. L. Wiedenbeck—841(L)
- Design and performance of a multicellular Geiger counter for gamma-radiation, David A. Lind—233
- Differential counting with reversible decase counting circuits, Frederick H. Martens—424
- Distant counting of scintillations, E. P. Blizard and S. DeBenedetti—81(L)
- Double-channel, direct reading, low frequency counting rate meter, and counting rate comparator, Robert M. Kloepper and Frank E. Hoecker—17
- Electronic instrument for rapidly tracing the plateaux of G-M counters, G. H. Vaze—746(L)
- Experiments in the possibility of increasing the efficiency of gamma-counters, Hilding Slätis—353
- Fast neutron detector, W. G. Moulton and C. W. Sherwin—766
- Gamma-ray counting efficiency for a lead-cathode G-M counter, E. T. Jurney and F. Maienschein—932
- Geiger-Mueller counting unit and external quenching equipment for the estimation of C^{14} in carbon dioxide, W. B. Mann and G. B. Parkinson—41
- Geiger tube quenching circuit for a negative high voltage supply, Richard John Watts—699(L)
- High resolution scale of four, Val Fitch—942
- Improved multivibrator quenching circuit, C. V. Robinson—750(L)
- Long-lived self-quenching counter filling, L. G. Shore—956(L)
- Measurement of the thickness of thin Nylon films, A. I. McPherson and D. G. Douglas—457(L)
- Methane flow beta-proportional counter, William Bernstein and Robert Ballentine—347

New method of measuring the stopping power of several materials for alpha-particles, F. Emmett Hammer and Frank E. Hoecker—394
Note on sealing Nylon film to Geiger counters, R. A. Becker—966(L)
Octane vapor proportional counter, T. P. Pepper—222(L)
Parallel-plate counter, J. Warren Keuffel—202
Pressure regulated thin window Geiger-Mueller counter, Michel Ter-Pogossian, J. Eugene Robinson, and J. Townsend—289
Pulse-height limiting circuit for a scintillation detector, W. C. Elmore—963(L)
Rejuvenation of Geiger-Mueller tubes, L. Shepard—217(L)
Scintillation counter as a proportional device, Rosalie C. Hoyt—178
Scintillation counter for laboratory counting of alpha-particles, J. D. Graves and J. P. Dyson—560
Statistical theory of the dead time losses of a counter, C. E. Clark—51
Statistics of counting rate meters, Ronald E. Burgess—964(L)

Dielectrics
Formation of insulating layers by the thermal decomposition of ethyl silicate, Harold B. Law—958(L)
Methods for reducing insulator noise and leakage, F. M. Glass—239
Variable temperature dielectric cell of wide frequency range for solids and liquids, Edward B. Baker—716

asticity
Apparatus for measurements of extremely high internal friction, T'ing-Sui Kê and Marc Ross—795
Stress-strain-time apparatus for fiber testing, C. H. Reichardt, H. Schaevitz, and J. H. Dillon—509
Vibration detection by a quartz oscillator, Y. L. Yousef and F. Sultan—533(L)
Electrical Machinery
Conversion of a motor generator into a low noise power amplifier, H. S. Sommers, Jr., P. R. Weiss, and W. Halpern—244
Modification of the Gouy modulator, L. S. Darken—323(L)
Electrical Measurements
Apparatus for determining the effect of centrifugal force on the potentials of galvanic cells, B. Roger Ray and D. A. MacInnes—52
Inductance apparatus for diamagnetic measurements, S. Broersma—660
Method for measuring very high speed transient currents, A. M. Zarem and F. R. Marshall—133
Sliding contacts to transmit small signals, Billy M. Horton—930
Variable temperature dielectric cell of wide frequency range for solids and liquids, Edward B. Baker—716
Wide range capacitance-conductance bridge, Robert H. Cole and Paul M. Gross, Jr.—252
Electrical Networks
Automatic stabilization of the overvoltage on a Geiger counter, H. R. Crane—955(L)
Circuits for minimizing transient effects on energy measurements in calorimetry, Harold J. Hoge—59
Electromechanical lead networks for a.c. servo mechanisms, Donald McDonald—775
Improved multivibrator quenching circuit, C. V. Robinson—750(L)
Improving the response characteristics of graphic recorders, P. G. Sulzer and A. H. Waynick—320(L)
Measurement of the series-resonant resistance of a quartz crystal, L. A. Rosenthal and T. A. Peterson, Jr.—426
Method of asymmetrical pulse duration modulation, Richard John Watts—622(L)
Method of linearizing the voltage rise of a relaxation oscillator, R. J. Watts—81(L)
Note on constant current regulators, E. E. Minett, D. A. MacRae, and J. Townsend—136(L)
Operation of voltage-stabilizing elements with current-stabilized supplies, J. J. Gilvarry and D. F. Rutland—633
Parallel operation of a small thyratron, Paul G. Hansel—836(L)
Photo-tube input impedance for a voltage stabilizer, E. N. Strait and W. W. Buechner—783
Pulse-height limiting circuit for a scintillation detector, W. C. Elmore—963(L)
Simple electronic relay, Robert H. Linnell and Helmut M. Haendler—364(L)
Transient response of high voltage resistance dividers, Harry J. White—837(L)
Transistor trigger circuit, Herbert J. Reich and Robert L. Ungvary—586
Electrometers and Electroscopes
Electrometer amplifiers, V. J. Caldecourt—748(L)
Methods for reducing insulator noise and leakage, F. M. Glass—239
Precision automatic electrometer, N. T. Seaton—500
Use of multigrid tubes as electrometers, J. R. Prescott—553
Electron Diffraction
Operational features of a new electron diffraction unit, Robert G. Picard, Perry C. Smith, and John H. Reisner—601
Electronic Instruments
Absolute noise thermometer for high temperatures and high pressures, J. B. Garrison and A. W. Lawson—785
Amplitude bridge for detection of nuclear resonance, H. A. Thomas and R. D. Huntoon—516
Circuit for rapid determination of resolving power and other characteristics of coincidence-systems, H. de Waard—911
Current integrator, H. T. Gittings, Jr.—325(L)
Differential counting with reversible decade counting circuits, Frederick H. Martens—424
Direct reading pulse length meter and shape analyzer, Robert Rudin—467
Double-channel, direct reading, low frequency counting rate meter, and counting rate comparator, Robert M. Kloepper and Frank E. Hoecker—17
Double pulse constant current stimulator, Robert L. Schoenfeld—827
Electromagnetic blood flow meter, J. W. Clark and J. E. Randall—951
Electrometer amplifier, V. J. Caldecourt—748
Electronic apparatus for the determination of the physical properties of freely falling rain drops, Ross Gunn—291
Electronic instrument for rapidly tracing the plateaux of G-M counters, G. H. Vaze—746
Exposure meter for precision light dosage, Herbert F. Launer—103
Flexible high voltage square wave generator, Langdon C. Hedrick—781
Geiger-Mueller counting unit and external quenching equipment for the estimation of C^{14} in carbon dioxide, W. B. Mann and G. B. Parkinson—41
A high resolution scale of four, Val Fitch—942
Improved synchronous detector, Walter C. Michels and Esther D. Redding—566
Lock-in *RC* oscillator, W. C. Elmore and D. Bancroft—136(L)
Magnetic field strength meter using the proton magnetic moment, N. J. Hopkins—401
Measurement of the spin of a projectile in flight, H. D. Warshaw—507

Electronic Instruments (continued)
- New vacuum gauge, Carlton F. Johnson—364(L)
- Precision automatic electrometer, N. T. Seaton—500
- Production and measurement of ultra-high speed impulses, R. C. Fletcher—861
- Pulse amplitude analyzer for nuclear research using pretreated pulses, C. H. Westcott and G. C. Hanna—181
- Rotor balancing with an electronic capacitor gauge, H. D. Warshaw—474
- Several improvements on the "Philip's gauge," C. Hayashi, K. Hashimoto, K. Kaneki, K. Okamoto, and R. Sagane—524(L)
- Simplified chronotron-type timing circuit, J. Warren Keuffel—197
- Simple stable d.c. amplifier for measurement of bioelectric potentials, John W. Moore—698(L)
- Simplified emission regulator for mass-spectrometer ion sources—E. B. Winn and A. O. Nier—773
- Single pulse voltmeter, G. T. Rado, M. H. Johnson, and M. Maloof—927
- Ten-channel electrostatic pulse analyzer, Dean A. Watkins—495
- Thyratron square wave generator, Leonard Reiffel—218(L)
- Timer for short intervals, R. Stuart Mackay—318(L)
- Tissue stimulators utilizing radiofrequency coupling, Otto H. Schmitt and Donald R. Dubbert—170
- Vacuum-tube current integrator of improved design, L. H. v. d. Tweel—323(L)
- Wide range radiation instrument, Leonard Reiffel and Glenn Burgwald—711; Erratum—944
- Wide-range saw-tooth generator, Peter G. Sulzer—78

Electron Microscope
- Device for producing an easily identified area on the electron microscope specimen screen, Francis W. Bishop—324(L)
- Device to deposit automatically the proper thickness of metals used in shadow-casting in electron microscopy, Francis W. Bishop—527(L)
- Magnetic beam-splitting focusing device for the electron microscope, Francis W. Bishop—532(L)

Electron and Ion Optics
- Conditions for optimum luminosity and energy resolution in the axial β-ray spectrometer with homogeneous magnetic field, Jesse W. M. DuMond—160
- Construction and calibration of a cylindrical electrostatic analyzer, S. K. Allison, S. P. Frankel, T. A. Hall, J. H. Montague, A. H. Morrish, and S. D. Warshaw—735
- Design curves for 180° magnetic spectrometers, George E. Owen—916
- Double magnetic lens nuclear spectrometer, Harold M. Agnew and Herbert L. Anderson—869
- Effect of space charge on the focusing properties of a 180° mass spectrometer, Charles F. Robinson—745(L)
- Electromagnetic focusing device for the electron microscope, H. T. Meryman—955(L)
- Electron trajectories in a gamma-ray spectrometer, H. Hurwitz, Jr.—318(L)
- Erratum: Conditions for optimum luminosity and energy resolution in an axial β-ray spectrometer with homogeneous magnetic field, Jesse W. M. DuMond—616
- Focusing in a semicircular magnetic spectrometer, C. M. Fowler, R. G. Shreffler, and J. M. Cork—966(L)
- Further improvements in magnetic focusing, L. Kerwin and Claude Geoffrion—381
- Improved magnetic focusing of charged particles, H. Hintenberger—748(L)
- Improved magnetic focusing of charged particles, Larkin Kerwin—36
- Instrumental distortions in the shapes of continuous beta-spectra, George E. Owen and C. Sharp Cook—768
- Large mass spectrometer employing crossed electric and magnetic fields, Thomas Mariner and Walker Bleakney—297
- Note on the preparation of beta-ray sources, Lawrence M. Langer—216(L)
- Optimum conditions for a 180° beta-ray spectrometer, Claude Geoffrion—638
- Theory of the solenoid beta-ray spectrometer, E. Persico—191
- Trochotron design principles, G. W. Monk and G. K. Werner—93

Electron Tubes
- Empirical balancing procedure for FP-54, F. C. Armistead—747(L)
- Extended range d.c. bias control of thyratron plate current, Leonard Reiffel—699(L)
- Parallel operation of a small thyratron, Paul G. Hansel—836(L)
- Photo-tube input impedance for a voltage stabilizer, E. N. Strait and W. W. Buechner—783

Fluid Dynamics
- Application of the electrical analogy in fluid mechanics research, Philip G. Hubbard—802
- Shock tube: A facility for investigations in fluid dynamics, Walker Bleakney, D. K. Weimer, and C. H. Fletcher—807

Gas Discharges
- Counter pulse shape, C. D. Thomas—147
- Erratum: A new discharge tube for the hydrogen atom spectrum, W. P. van Oort and A. C. S. van Heel—479
- Ionization flame detectors, Hartwell F. Calcote—349
- New discharge tube for the hydrogen atom spectrum, W. P. van Oort and A. C. S. van Heel—319(L)
- Parallel-plate counters, J. Warren Keuffel—202

Gas Handling and Measurement
- Accurate gas metering system for laminar flow studies, J. W. Andersen and R. Friedman—61
- Capillary collector for measuring the deposition of water drops on a surface moving through clouds, Bernard Vonnegut—110
- "Opener-upper" for gas samples, Francis J. Norton—620(L)
- Volumetric respirometer for aquatic animals, P. F. Scholander—885

High Voltage Techniques
- Flexible high voltage square wave generator, Langdon C. Hedrick—781
- Geiger tube quenching circuit for a negative high voltage supply, Richard John Watts—699(L)
- On the design of a radiofrequency Cockroft-Walton accelerator, Paul Lorrain—216(L)
- Stabilized high voltage power supply for electrostatic analyzer, R. L. Henkel and B. Petree—729
- Transient response of high voltage resistance dividers, Harry J. White—837(L)
- Voltage stabilization for electrostatic generators using an electron gun, S. J. Bame, Jr. and L. M. Baggett—839(L)

Illumination
- High power short duration spark discharge, Leslie S. G. Kovásznay—696(L)
- Large cloud chamber using rear illumination, E. W. Cowan—492

Infra-Red Technique
- Absorption cell and loader for use in microanalysis by infrared spectroscopy, Seymour H. Wollman—220(L)
- New source of radiation for infra-red spectrometers, L. W. Herscher—833(L)

- Percent transmission computer for infra-red spectra, C. E. Zerwekh, Jr.—371(L)
- Rapid infra-red gas analyzer, Richard C. Fowler—175
- Theoretical and practical sensitivity of the pneumatic infra-red detector, Marcel J. E. Golay—816

Interference and Interferometry

- Measurement of the thickness of thin Nylon films, A. I. McPherson and D. G. Douglas—457(L)

Ionization Chambers

- Air ionization chamber for soft x-rays, Herman E. Seeman—903
- Counting volume of a cylindrical ionization chamber, Nelson M. Blachman—477
- Methods for reducing insulator noise and leakage, F. M. Glass—239
- Portable roentgenmeter for field use, C. C. Lauritsen—964(L)

Ion Sources

- High current ion source, Richard B. Setlow—558
- Magnetic ion source, Carl Bailey, D. L. Drukey, and F. Oppenheimer—189

Isotope Separation

- Apparatus for isotope separation by thermal diffusion, W. W. Watson, L. Onsager, and A. Zucker—924

Laboratory Techniques

- Apparatus for the production of large metallic crystals by solidification at high temperatures, Louis Gold—115
- Cells drawn from tantalum, molybdenum, and platinum for high temperature research, George W. Ziegler, Jr., Rudolph Speiser, and H. L. Johnston—367(L)
- Construction of beta-Geiger counters from prefabricated thin wall tubing, F. E. Senftle, W. Havercroft, and P. Hernandez—370(L)
- Device for producing an easily identified area on the electron microscope specimen screen, Francis W. Bishop—324(L)
- Device to deposit automatically the proper thickness of metals used in shadow-casting in electron microscopy, Francis W. Bishop—527(L)
- Dry box for handling alkali metals and other extremely hygroscopic materials, Eugene E. Ketchen, Forrest A. Trumbore, W. E. Wallace, and R. S. Craig—524(L)
- Formation of insulating layers by the thermal decomposition of ethyl silicate, Harold B. Law—958(L)
- Glass vacuum valve, John Lambe—831(L)
- Growing and processing of single crystals of magnetic metals, J. G. Walker, R. M. Bozorth, and H. J. Williams—947
- Kovar glass seals at liquid helium temperatures, C. T. Lane—140(L)
- Lead-in seals for kinetic high vacuum systems using rubbers, Ralph C. Taylor and Carnot W. Ward—457(L)
- Mercury vapor trap to protect laboratory workers, James J. Brophy—750(L)
- Method for preparing capillary tube samples for x-ray diffraction powder analysis, Paul J. Hagelston and H. W. Dunn—373(L)
- Note on removing the deuteron-induced color from quartz target plates, A. A. Schulke and R. E. Nuelle—623(L)
- Note on sealing Nylon film to Geiger counters, R. A. Becker—966(L)
- Note on the preparation of uniform metallic foils, S. D. Warshaw—623(L)
- On the vacuum properties of silastic, G. D. Adams and W. C. Sherwin—957(L)
- "Opener-upper" for gas samples, Francis J. Norton—620(L)
- Preparation and use of tritium and deuterium targets, E. R. Graves, A. A. Rodrigues, M. Goldblatt, and D. I. Meyer—579
- Preparation of samples of active metals, Donald F. Clifton—830(L)
- Preparation of single crystal copper ribbons from single crystal copper rods, A. A. Petrauskas, E. A. Coomes, and J. E. MacDonald—961(L)
- Pressure regulated thin window Geiger-Mueller counter, Michel Ter-Pogossian, J. Eugene Robinson, and J. Townsend—289
- Simple automatic water distiller, Narcisco Cordero and Irneo L. Lawas—840(L)
- Simple punch for precision cutting of photographic film in a cylindrical x-ray diffraction camera, E. J. Grill and A. H. Weber—532(L)
- Sliding contacts to transmit small signals, Billy M. Horton—930
- System for preparing semitransparent mirrors, Claude Frémont—620(L)
- Technique for cutting metal single crystals, T. R. McGuire and R. T. Webber—962(L)
- Technique for the production of silica-filmed electron microscope screens in quantity, Francis W. Bishop—529(L)

Liquefaction of Gases

- Helium cryostat temperature control, I. Simon—832(L)
- Kovar glass seals at liquid helium temperatures, C. T. Lane—140(L)
- Large helium liquefier, J. G. Daunt and H. L. Johnston—122
- Magnetic susceptibility balance for use at liquid helium temperatures, T. R. McGuire and C. T. Lane—489
- Preparation of samples of active metals, Donald F. Clifton—830(L)
- Vibration absorber for gas holders, R. S. Craig and W. E. Wallace—369(L)

Magnetism

- Amplitude bridge for detection of nuclear resonance, H. A. Thomas and R. D. Huntoon—516
- Conditions for optimum luminosity and energy resolution in an axial β-ray spectrometer with homogeneous magnetic field, Jesse W. M. DuMond—160
- Design curves for 180° magnetic spectrometers, George E. Owen—916
- Double magnetic lens nuclear spectrometer, Harold M. Agnew and Herbert L. Anderson—869
- Electromagnetic focusing device for the electron microscope, H. T. Meryman—955(L)
- Erratum: Conditions for optimum luminosity and energy resolution in an axial β-ray spectrometer with homogeneous magnetic field, Jesse W. M. DuMond—616
- Fast recycling cloud chamber and pulse magnetic field equipment for use with pulsed accelerators, E. R. Gaerttner and M. L. Yeater—588
- Further improvements in magnetic focusing, Larkin Kerwin and Claude Geoffrion—381
- Growing and processing of single crystals of magnetic metals, J. G. Walker, R. M. Bozorth, and H. J. Williams—947
- Improved magnetic focusing of charged particles, H. Hintenberger—748(L)
- Improved magnetic focusing of charged particles, Larkin Kerwin—36
- Inductance apparatus for diamagnetic measurements, S. Broersma—660
- Magnet coils, L. G. Coonrod, W. E. Cecconi, C. Gedraitis, K. R. Harper, and R. M. Lewis—408
- Magnetic deflector for mesons produced in the 184-inch cyclotron, Wolfgang K. H. Panofsky and Ernest A. Martinelli—286
- Magnetic field strength meter using the proton magnetic moment, N. J. Hopkins—401

Magnetism (continued)
- Magnetic susceptibility balance for use at liquid helium temperatures, T. R. McGuire and C. T. Lane—489
- Measurement of betatron guiding fields during electron ejection, E. C. Gregg, Jr.—841(L)
- New high sensitivity remanent magnetometer, Ellis A. Johnson, Thomas Murphy, and P. F. Michelsen—429
- Optimum conditions for a 180° beta-ray spectrometer, Claude Geoffrion—638
- Sensitive magnetrometer for very small areas, Daryl M. Chapin—945
- Tachometer, A. E. Benfield—663
- Theory of the solenoid beta-ray spectrometer, E. Persico—191
- 22-inch Wilson cloud chamber in a magnetic field of 21,700 gauss, Wilson M. Powell—403

Mass Spectrograph and Mass Spectrometer
- Design for a metal mass spectrometer tube, W. M. Hickam—472
- Effect of space charge on the focusing properties of a 180° mass spectrometer, Charles F. Robinson—745(L)
- Large mass spectrometer employing crossed electric and magnetic fields, Thomas Mariner and Walker Bleakney—297
- Mass spectrometer for continuous gas analysis, Jack A. Hunter, Ralph W. Stacy, and Fred A. Hitchcock—333
- Simplified emission regulator for mass-spectrometer ion sources—E. B. Winn and A. O. Nier—773
- Trochotron design principles, G. W. Monk and G. K. Werner—93

Mechanics
- Apparatus for measurements of extremely high internal friction, T'ing-Sui Kê and Marc Ross—791
- Dynamics of a synchrotron with straight sections, Nelson M. Blachman and Ernest D. Courant—596
- Measurement of the spin of a projectile in flight, H. D. Warshaw—507
- Novel recording accelerometer, Arthur S. Iberall—304
- Rotor balancing with an electronic capacitor gauge, H. D. Warshaw—474
- Small differential analyzer with ball carriage integrators and selsyn coupling, R. E. Meyerott and G. Breit—874
- Stress-strain-time apparatus for fiber testing, C. H. Reichardt, H. Schaevitz, and J. H. Dillon—509
- Vibration absorber for gas holders, R. S. Craig and W. E. Wallace—369(L)

Meteorology and Meteorological Instruments
- Capillary collector for measuring the deposition of water drops on a surface moving through clouds, Bernard Vonnegut—110
- Electronic apparatus for the determination of the physical properties of freely falling raindrops, Ross Gunn—291
- Theoretical background of the multiple pressure tube anemometer, Paul R. Goudy and Henry F. Colvin, III—651

Micro Manipulation
- Improved embryological micromanipulator, Howard H. Hillemann—836(L)
- Microsampling and microanalysis of metals, Donald F. Clifton and Cyril Stanley Smith—583
- Versatile microinjection and micropipetting syringe, John B. Buck—676

Microwave Techniques
- High power attenuator for microwaves, Daniel Alpert—777
- Microwave polarimeter, Alfred E. Schwaneke and Zaboj V. Harvalik—337
- Microwave secondary electron multiplier, M. H. Greenblatt—646
- Stark-effect microwave spectrograph of high sensitivity, K. B. McAfee, Jr., R. H. Hughes, and E. Bright Wilson, Jr.—821

Monochromators
- Instrument for measuring curvature of cloud-chamber tracks, E. R. Gaerttner and M. L. Yeater—526(L)

Multiplier: Electron
- Automatic scanning and recording photometer for night sky studies, Douglas Marlow and J. C. Pemberton—724
- Convenient method for checking the linearity of an electron multiplier circuit, George P. Kirkpatrick—81(L)
- Fast neutron detector, W. G. Moulton and C. W. Sherwin—766
- Scintillation counter as a proportional device, Rosalie C. Hoyt—178
- Scintillation counter. I. The existence of plateaus, Lawrence B. Robinson and James R. Arnold—549
- Microwave secondary electron multiplier, M. H. Greenblatt—646
- Secondary-emission electron multiplier tube for the detection of high energy particles, Robert P. Stone—935

New Instruments
- Absolute pressure gauge—86
- Accelerometer—626
- Alpha-particle counter—375
- Aneroid altitude standard—754
- Atomic clock—141
- Automatic scaler—626
- Beta-gamma-scaler—88
- Beta-gauges—628
- Binac—753
- Bridge and amplifier—968
- Bridger—537
- Civilian walkie-talkies—143
- Coatingage—377
- Color computing device—326
- Continuous hydrogenation unit—85
- Counters—704
- Counter tube—629
- Deadtime and recovery of Geiger counters—627
- Dielectric constant meter—754
- Direct coupled amplifier—844
- Dual-channel oscilloscope—845
- Earth-shock acceleration detector—90
- Electronic microammeter—538
- Electronic motor control—462
- Electronic voltage supply—970
- Electron microscope accessories—844
- Electron multiplier photometer—377
- Fatigue tester—89
- Frequency standard—968
- Gamma-ray detection tube—628
- Gas analysis—756
- Geiger counter for prospecting—536
- Germanium diodes—842
- Graphic recorder—376
- Gyros—328
- Hand alpha-counter—225
- Hand torch—330
- High accuracy mercury manometer—89
- High current rectifiers—843
- High frequency voltmeter—626
- High speed mechanical sampler—845
- High stability carbon resistors—330
- Hivolt power supplies—327
- Hydrostatic impulse gauge—142
- Impedance bridge—704
- Induction tracer—630
- Infra-red analyzer—326
- Interpolator for UHF measurements—459
- Iron chamber—87
- Laboratory balance—330

Low frequency oscilloscope—625
Low range air cells—327
Magnetic flux meter—85
Magnetic test set—86
Mica window counter—844
Micromicroammeter—225
Microscope—846
Micro-spectroscopy—969
Microwave dielectrometer—224
Microwave power meter—377
Midget meter—87
Miniature adjustable-speed drive—463
Multichannel switch—327
Multirange kilovoltmeters—85
New alpha-particle counter—227
Noise generator—629
Nucleometer—374
Oscillator—702
Peak voltage rectifiers—753
Phase-contrast microscope—535
Phase meter—464
Phase meter and field strength meter—630
Phase monitor—969
Photo-tube—754
Piezoelectric gauges—90
Platinum resistance thermometer—971
Polinear recorder—702
Portable scaling-type radioactivity detector—536
Precision-regulated d.c. power supply—84
Precision Warburg apparatus—329
Preparative centrifuge—537
Projection oscilloscope—460
Proportional counter—705
Pulsed x-rays—86
Pyrometer controller—757
Radiation counter—757
Radiation meter—374
Radiation standards—225
Radioactivity demonstrator—142
Raychronometer—535
RCA electron diffraction unit—83
Recording system—461
Regulated power supply—83
Regulated power supply—538
Resistohmeter—755
R-f capacitance meter—227
R-f power supply—705
R-f Z-angle meter—88
Rouy photrometer—329
Secondary frequency standards—842
Selenium rectifiers—143
Sensitive integrator—464
Signal generator—461
Sky compass—460
Slotted line and standing wave indicator—144
Slotted line and video oscilloscope—461
Sound measurement—376
Speedigram—706
Spiral contractiometer—226
Spotwelder—843
Spring-coiling machine—755
"Super-Regulated" power supply—226
Tachometer—629
Temperature transmitter—627
Tensile tester—328
Thermoregulator—329
Toroidal coils—84
Torque converter—758
Transmission measuring set—755
Ultrasonic analyzer—753
Ultrasonic generator—375
Ultrasonic generator—703
Ultrasonic generators—141
Ultraviolet microscope—968
Vacuum pump—705
Vibration measurement equipment—143
Vibration measurements—462
Vibration meter—88
Viscosimeter—463
Wave generator—970
Wave-guide test equipment—757
Wave-guide windows—536
Wide-band amplifier—706
Wide-band amplifier—756
Wide-band chain amplifier—224
Wide-range power supply—375
X-Y recorder—970

New Materials
Asbestos tubing—709
Ashless filter material—710
Anti-fogging cleaning cloth—146
Bonding process—539
Carbide blanks—380
Carbide milling cutters—380
Carbide tubing—710
Castable refractory—92
Casting sealant—539
Cellulose ester thermoplastics—632
Cellulose gum—379
Centrifugal castings—380
Colloidal graphite—539
Conductive coatings—631
Copper-tungsten contacts—145
Core binder—539
Corrosion-resistant immersion heaters—632
Crystalline antibiotic—632
Cutting oil additive—848
Dry cell—332
Ductile cast iron—331, 972
Felt gaskets—466
Fire-retardant paint—332
Fireproofing cement—972
Flexible conduit—331
Flexible copper tubing—145
Gasket coating—540
Glass—379
Glass for lighting fixtures—972
Glass phenolic laminate—379
Glycol synthesis—632
Graded-glass seals—224
Graphite-filled Nylon—632
Hafnium—847
Heat exchange tubing—332
Heat resistant phenolic—540
Heat-resistant plastic tubing—146
Heat-resistant polystyrene—92
Hermetic seals—331
High pressure lubricant—759
High strength varnish—224
High temperature flexible tubing—332
High temperature plastic—540
Hydraulic fluid—848
Improved carbide for tools—847
Industrial preservative—465
Instrument-cleaning solutions—146
Insulating bushings—380
Insulating film—972
Laboratory products—760
Laboratory quartzware—540
Laminated metal—847

New Materials (continued)
- Lay-out plate—539
- Lens cleaner—92
- Lined steel pipe—632
- Low temperature alloy steel—759
- Magnet materials—972
- Mercury-cleaning process—759
- Metal cleaners—972
- Metal stripper—224
- Metallurgical products—847
- Neoprene floor mat—332
- New nickel alloys—466
- New resin—146
- Number-coded wire—760
- Nylon anode bags—466
- Paint remover—848
- Phosphor bronze wire—380
- Photographic hypo—972
- Plastic bell jar—379
- Plastic-coated steel tubing—710
- Plastic field lens—466
- Plastic for film or fabric—223
- Plastic pipe—92
- Polystyrene cement—760
- Pre-cementing adhesive—760
- Precision castings—710
- Protective coating for metals—466
- Protective coating for steel—709
- Relaxation machine—703
- Resistance alloy—710
- Rubber-insulated heating element—709
- Rubber seal—847
- Rust preventive wrapper—92
- Scintillation crystal—759
- Sealed terminal bushings—145
- Self-adhesive wire markers—146
- Silicone-coated carbon resistors—632
- Silicone Fiberglas sleeves—379
- Silicone rubber—223
- Small aluminum tubing—91
- Soldering and brazing—707
- Special cooling oil—848
- Stainless steel clad sheets—380
- Strapping tape—332
- Strippers for organic finishes—146
- Strong laminate—466
- Synthetic calcium tungstate crystals—145
- Synthetic wax—972
- Temperature indicators—332
- Thermosetting adhesive film—92
- Titanium—91
- Tungsten powder—380
- Ultra-fine abrasive powders—92
- Ultra-sensitive photographic emulsion—145
- Use for dri-film—540
- Wetting agent—146

Nomograms
- Developments in the useful circular nomogram, Douglas P. Adams and Howard T. Evans, Jr.—150

Non-Linear Elements
- Electrolytic thermistors, F. Gutmann and L. M. Simmons—674

Nuclear Machines
- *Betatrons*
  - Measurement of betatron guiding fields during electron ejection, E. C. Gregg, Jr.—841(L)
- *Cyclotrons and Synchrotrons*
  - Design of the radiofrequency system for the 184-inch cyclotron, K. R. MacKenzie, F. H. Schmidt, J. R. Woodyard, and L. F. Wouters—126
  - Dynamics of a synchrotron with straight sections, Nelson M. Blachman and Ernest D. Courant—596
  - Instrumentation for nuclear studies with externally focused deuteron beam from ten-Mev cyclotron, B. R. Curtis, J. L. Fowler, and L. Rosen—388
  - Magnetic deflector for mesons produced in the 184-inch cyclotron, Wolfgang K. H. Panofsky and Ernest A. Martinelli—286
  - Operation of the 184-inch cyclotron, L. R. Henrich, D. C. Sewell, and J. Vale—887
  - Orbital stability in a protron synchrotron, R. Q. Twiss and N. H. Frank—1
  - Pulsed oscillator for f-m cyclotron, J. W. Burkig, E. L. Hubbard, and K. R. MacKenzie—135(L)
- *Electrostatic Generators*
  - Large straight through vacuum valve for Van de Graaff generators, B. Jennings—366(L)
  - Stabilized high voltage power supply for electrostatic analyzer, R. L. Henkel and B. Petree—729
  - Statitron for a small nuclear laboratory, D. R. Inglis, R. W. Krone, and S. S. Hanna—834(L)
  - Voltage stabilization for electrostatic generators using an electron gun, S. J. Bame, Jr. and L. M. Baggett—839(L)
- *Linear Accelerators*
  - On the design of a radiofrequency Cockroft-Walton accelerator, Paul Lorrain—216(L)

Nuclear Technique
- Calibration of photographic emulsions for low energy electrons, L. Cranberg and J. Halpern—641
- Construction and calibration of a cylindrical electrostatic analyzer, S. K. Allison, S. P. Frankel, T. A. Hall, J. H. Montague, A. H. Morrish, and S. D. Warshaw—735
- Design and performance of a multicellular Geiger counter for gamma-radiation, David A. Lind—233
- Distant counting of scintillations, E. P. Blizard and S. DeBenedetti—81(L)
- Fast neutron detector, W. G. Moulton and C. W. Sherwin—766
- Instrumentation for nuclear studies with externally focused deuteron beam from ten-Mev cyclotron, B. R. Curtis, J. L. Fowler, and L. Rosen—388
- Lead brick for shielding, Luther E. Preuss—534(L)
- Magnetic deflector for mesons produced in the 184-inch cyclotron, Wolfgang K. H. Panofsky and Ernest A. Martinelli—286
- Note on removing the deuteron-induced color from quartz target plates, A. A. Schulke and R. E. Nuelle—623(L)
- Note on the preparation of beta-ray sources, Lawrence M. Langer—216(L)
- Pantograph and tilting stage for use with nuclear plates, Ian Barbour—530(L)
- Photomicrography of tracks in nuclear research emulsions, Adair Morrison and Fred Morton—341
- Portable roentgenmeter for field use, C. C. Lauritsen—964(L)
- Preparation and use of tritium and deuterium targets, E. R. Graves, A. A. Rodrigues, M. Goldblatt, and D. I. Meyer—579
- Pulsed amplitude analyzer for nuclear research using pretreated pulses, C. H. Westcott and G. C. Hanna—181
- Scintillation counter. I. The existence of plateaus, Lawrence B. Robinson and James R. Arnold—549
- Secondary-emission electron multiplier tube for the detection of high energy particles, Robert P. Stone—935

Optics, Geometrical
- Multiple-reflection optical lever, H. O. Hoadley—30
- Small portable reflectometer, W. Liben and N. W. Scott—960(L)

Optics, Physical
Apparatus for electrode reversal in the Tiselius electrophoresis equipment, H. Tint—617
Equipment and experimental methods for interference diffusion studies, Louis J. Gosting, Edwin M. Hanson, Gerson Kegeles, and Margaret S. Morris—209
Equipment for measuring light scattering, M. Bier and F. F. Nord—752(L)
Interferometric study of supersonic channel flow, Daniel Bershader—260
Optical properties of surface films, II., Alexandre Rothen and Marjorie Hanson—66

Oscilloscopes
Method for measuring very high speed transient current, A. M. Zarem and F. R. Marshall—133

Photoelasticity
Method of assessing transient stresses in photoelastic substances, John S. Stanton—139(L)

Photography
Calibration of photographic emulsions for low energy electrons, L. Cranberg and J. Halpern—641
Detection of Ca^{45}, I^{131}, P^{32}, and Zn^{65} by photographic film, Daniel Steinberg and A. K. Solomon—655
Iconoscope electro optical shutter for high speed photograph, H. A. Prime and R. C. Turnock—830(L)
Non-uniform shrinkage of x-ray films, M. H. Jellinek—368(L)
Pantograph and tilting stage for use with nuclear plates, Ian Barbour—530(L)
Photomicrography of tracks in nuclear research emulsions, Adair Morrison and Fred Morton—341

Photometry
Accurate, simple recording microphotometer, P. Rosenblum and A. DeBretteville, Jr.—321(L)
Automatic scanning and recording photometer for night sky studies, Douglas Marlow and J. C. Pemberton—724
Calibration of photographic emulsions for low energy electrons, L. Cranberg and J. Halpern—641
Exposure meter for precision light dosage, Herbert F. Launer—103

Piezoelectricity
Measurement of the series-resonant resistance of a quartz crystal, L. A. Rosenthal and T. A. Peterson, Jr.—426
Vibration detection by a quartz oscillator, Y. L. Yousef and F. Sultan—533(L)

Pressure Technique
Absolute noise thermometer for high temperatures and high pressures, J. B. Garrison and A. W. Lawson—781
Counter controllable high pressure cloud chamber, G. E. Valley and J. A. Vitale—411
Recording mechanical pressure gauge of high range, Paul M. Higgs—23
Self-contained recording pressure gauge, David R. Brown, William C. Galloway, Jack B. Robertson, and Gene A. Silvey—27
X-ray camera for obtaining powder pictures at high pressures—A. W. Lawson and N. A. Riley—763

Pyrometry
Ionization flame detectors, Hartwell F. Calcote—349

Radiation and Radiometry
Effect of temperature on the steady-state sensivity of vacuum radiation detectors, I. Amdur and N. L. Brown—435
Slide rule for radiation calculations, M. W. Makowski—876
Theoretical and practical sensitivity of the pneumatic infrared detector, Marcel J. E. Golay—816

Radioactive Techniques
Characteristics of halogen counters, Sidney H. Liebson—483
Counting with Geiger counters, Homer E. Newell, Jr. and Eleanor C. Pressly—568
Detection of Ca^{45}, I^{131}, P^{32}, and Zn^{65} by photographic film, Daniel Steinberg and A. K. Solomon—655
Gamma-ray counting efficiency for a lead cathode G-M counter, E. T. Jurney and F. Maienschein—932
Methane flow beta-proportional counter, William Bernstein and Robert Ballentine—347
New method of measuring the stopping power of several materials for alpha-particles, F. Emmett Hammer and Frank E. Hoecker—394
Rapid response radiation alarm, R. L. Macklin and E. R. Rohrer—965(L)
Some statistical considerations on coincidence counting, Arthur Sard and R. D. Sard—526(L)
Wide range radiation instrument, Leonard Reiffel and Glenn Burgwald—711; Erratum—944

Servo Mechanism
Conversion of a motor generator into a low noise power amplifier, H. S. Sommers, Jr., P. R. Weiss, and W. Halpern—244
Device for producing rate-proportional damping signal in servo systems, L. W. Herscher—459(L)
Electromechanical lead networks for a.c. servo mechanisms, Donald McDonald—775
Servo employing the magnetic fluid clutch, E. S. Bettis and E. R. Mann—97
Voltage stabilization for electrostatic generators using an electron gun, S. J. Bame, Jr. and L. M. Baggett—839(L)
Use of anodized aluminum in the construction of calorimeter heaters, George W. Murphy—372(L)
Vacuum lock for continuously evacuated systems, D. Saxon and J. Richards—745(L)
Welder for attaching fine wires to massive metal bodies, W. J. Trott—624(L)

Spectra and Excitation
New discharge tube for the hydrogen atom spectrum, W. P. van Oort and A. C. S. van Heel—319(L)
New source of radiation for infra-red spectrometers, L. W. Herscher—833(L)

Spectroscopy and Spectrometers
Absorption cell and loader for use in microanalysis by infra-red spectroscopy, Seymour H. Wollman—220(L)
Stark-effect microwave spectrograph of high sensitivity, K. B. McAfee, Jr., R. H. Hughes, and E. Bright Wilson, Jr.—821

Supersonics
Interferometric study of supersonic channel flow, Daniel Bershader—260

Surface Physics
Optical properties of surface films, II, Alexandre Rothen and Marjorie Hanson—66

Thermodynamics
New technique for the determination of heats of sublimation of slightly volatile substances, O. C. Simpson and R. J. Thorn—504
Regulation of temperature in the application of high frequency induction heating to thermodynamic measurements, Rudolph Speiser, George W. Ziegler, Jr., and Herrick L. Johnston—385
Theoretical and practical sensitivity of the pneumatic infrared detector, Marcel J. E. Golay—816

Thermoelectricity
Effect of temperature on the steady-state sensitivity of vacuum radiation detectors, I. Amdur and N. L. Brown—435

Thermometry and Temperature Control
Absolute noise thermometer for high temperatures and high pressures, J. B. Garrison and A. W. Lawson—785
Apparatus for the production of large metallic crystals by solidification at high temperatures, Louis Gold—115
Cells drawn from tantalum, molybdenum, and platinum for high temperature research, George W. Ziegler, Jr., Rudolph Speiser, and Herrick L. Johnston—367(L)
Design and equipment for thermal studies, Robert J. Teitle —575
Device for the measurement of rotor temperatures in the air-driven ultracentrifuge, P. G. Ecker, J. Blum, and C. W. Hiatt—799
Direct experimental comparison of several surface temperature measuring devices, Alice M. Stoll and James D. Hardy—678
Helium cryostat temperature control, I. Šimon—832(L)
High temperature x-ray diffraction camera, James W. Edwards, Rudolph Speiser, and Herrick L. Johnston —343
High temperature x-ray diffraction techniques, J. J. Lander —82(L)
Modification of the Gouy modulator, L. S. Darken—323(L)
Regulation of temperature in the application of high frequency induction heating to thermodynamic measurements, Rudolph Speiser, George W. Ziegler, Jr., and Herrick L. Johnston—385
Sensitivity of Schwarz-Hilger thermopiles, E. Schwarz —962(L)
Use of anodized aluminum in the construction of calorimeter heaters, George W. Murphy—372(L)
Vacuum-tube relay for thermostat control, I. Sucher and H. S. Anker—321(L)
Variable temperature dielectric cell of wide frequency range for solids and liquids, Edward B. Baker—716
Wet bulb temperatures without a wick, Kenneth H. Jehn —668

Time Measurement
Circuit for the study of the operation of the Geiger-Müller counter, Mario Alves Guimarães and Palmyra Amazonas Sampaio—485
Delays in rectangular Geiger counters, G. E. Bradley and M. L. Wiedenbeck—841(L)
Direct reading pulse length meter and shape analyzer, Robert Rudin—467
Fractional microsecond x-ray pulse generator for studying high explosive phenomena, H. I. Breidenbach, Jr.—899
Iconoscope electro-optical shutter for high speed photography, H. A. Prime and R. C. Turnock—830(L)
Production and measurement of ultra-high speed impulses, R. C. Fletcher—861
Simplified chronotron-type timing circuit, J. Warren Keuffel—197
Tachometer, A. E. Benfield—663
Timer for short intervals, R. Stuart Mackay—318(L)

Vacuum Technique
Cadmium trap for arresting mercury vapor, T. Wilmer—527(L)
Design of equipment for thermal studies, Robert J. Teitel —575
Flexible vacuum seal, Otto Retzloff—324(L)
Glass vacuum valve, John Lambe—831(L)
Large straight through vacuum valve for Van de Graaff generators, B. Jennings—366(L)
Lead-in seals for kinetic high vacuum systems using rubbers, Ralph C. Taylor and Carnot W. Ward—457(L)
Mercury vapor trap to protect laboratory workers, James J. Brophy—750(L)
New principle in controlled vacuum leaks, C. H. Bachman —219(L)
New type of diffusion pump, E. L. Harrington—761
New vacuum gauge, Carlton F. Johnson—364(L)
On the vacuum properties of silastic, G. D. Adams and W. C. Sherwin—957(L)
Precision vacuum gauge, G. C. Fryburg and J. H. Simons —541
Pumping speed of diffusion pumps below limiting pressure, Clifford E. Berry—835(L)
Several improvements on the "Philip's Gauge," C. Hayashi, K. Hashimoto, K. Kaneki, K. Okamoto, and R. Sagane —524(L)
Toggle-operated vacuum valve, Ralph O. McIntosh and John W. Coltman—135(L)
Ultimate vacua of diffusion pumps, G. W. Sears—458(L)
Use of characteristic curves for pump-speed *vs.* pressure, Saul Dushman—139(L)
Use of gas traps in barometers, laboratory mercury lamps, etc., E. L. Harrington—368(L)
Vacuum lock for continuously evacuated systems, D. Saxon and J. Richards—745(L)
Vacuum tight, flexible metal—glass seal, K. M. Sancier—958(L)

X-Ray Diffraction
Absorption corrections in x-ray studies of preferred orientation, J. F. H. Custers—752
Absorption corrections in x-ray studies of preferred orientation, R. Smoluchowski and R. W. Turner—173
Accurate, simple recording microphotometer, P. Rosenblum and A. DeBretteville, Jr.—321(L)
Apparatus for producing powder-like x-ray diffraction patterns from single crystals, F. W. Matthews and A. O. McIntosh—365(L)
High temperature x-ray diffraction camera, James W. Edwards, Rudolph Speiser, and Herrick L. Johnston—343
High temperature x-ray diffraction techniques, J. J. Lander—82(L)
Improved low angle x-ray diffraction camera, Barbara A. Wright and Peter A. Cole—355
Instrument for measurement of x-ray diffraction patterns, John A. Bennett—908
Instrument for rapid determination of crystal orientation, R. H. Gillette and M. H. Jellinek—480
Low temperature single crystal x-ray diffraction technique, H. S. Kaufman and I. Fankuchen—733
Method for preparing capillary tube samples for x-ray diffraction powder analysis, Paul L. Hagelston and Harris W. Dunn—373(L)
Modification of x-ray diffraction micro-camera to permit study of long spacings, M. E. Bergmann and I. Fankuchen—696(L)
New techniques applied to the Buerger precession camera for x-ray diffraction studies, Howard T. Evans, Jr., S. G. Tilden, and Douglas P. Adams—155
Non-uniform shrinkage of x-ray films, M. H. Jellinek—368(L)
Note on the accuracy of the Buerger precession camera, Howard T. Evans, Jr.—751
Sample scanning mechanism for x-ray diffraction, J. W. Hickman and A. G. Kleinknecht—573
Simple punch for precision cutting of photographic film in a cylindrical x-ray diffraction camera, E. J. Grill and A. H. Weber—532(L)
Straumanis' method of film-shrinkage correction modified for use without high angle lines, A. J. C. Wilson—831(L)
X-ray camera for obtaining powder pictures at high pressures, A. W. Lawson and N. A. Riley—763

X-Ray Equipment
Air ionization chamber for soft x-rays, Herman E. Seeman —903
Fractional microsecond x-ray pulse generator for studying high explosive phenomena, H. I. Breidenbach, Jr.—899

I.A.R.I. 75

INDIAN AGRICULTURAL RESEARCH
INSTITUTE LIBRARY, NEW DELHI.

Date of Issue	Date of Issue	Date of Issue
30·7·65		

GIPNLK—H-40 I.A.R.I.—29-4-55—15,000